

Yunmin Chen
Xiaowu Tang
Liangtong Zhan
Editors

Advances in Environmental Geotechnics

Proceedings of the International Symposium
on Geoenvironmental Engineering in
Hangzhou, China, September 8-10, 2009

 ZHEJIANG UNIVERSITY PRESS
浙江大学出版社

 Springer

**Yunmin Chen
Xiaowu Tang
Liangtong Zhan**

Advances in Environmental Geotechnics

**Proceedings of the International Symposium
on Geoenvironmental Engineering in
Hangzhou, China, September 8-10, 2009**

Yunmin Chen
Xiaowu Tang
Liangtong Zhan

Advances in Environmental Geotechnics

**Proceedings of the International Symposium
on Geoenvironmental Engineering in
Hangzhou, China, September 8-10, 2009**

With 1,091 figures

Editors

Prof. Yunmin Chen
Department of Civil Engineering
Zhejiang University
388 Yuhangtang Road, Hangzhou 310058
China
E-mail: chenyunmin@zju.edu.cn

Prof. Xiaowu Tang
Department of Civil Engineering
Zhejiang University
388 Yuhangtang Road, Hangzhou 310058
China
E-mail: tangxiaowu@zju.edu.cn

Prof. Liangtong Zhan
Department of Civil Engineering
Zhejiang University
388 Yuhangtang Road, Hangzhou 310058
China
E-mail: zhanlt@zju.edu.cn

ISBN 978-7-308-06597-9
Zhejiang University Press, Hangzhou

ISBN 978-3-642-04459-5 e-ISBN 978-3-642-04460-1
Springer Heidelberg Dordrecht London New York

Library of Congress Control Number: 2009934114

© Zhejiang University Press, Hangzhou and Springer-Verlag Berlin Heidelberg 2010

This work is subject to copyright. All rights are reserved, whether the whole or part of the material is concerned, specifically the rights of translation, reprinting, reuse of illustrations, recitation, broadcasting, reproduction on microfilm or in any other way, and storage in data banks. Duplication of this publication or parts thereof is permitted only under the provisions of the German Copyright Law of September 9, 1965, in its current version, and permission for use must always be obtained from Springer-Verlag. Violations are liable to prosecution under the German Copyright Law.

The use of general descriptive names, registered names, trademarks, etc. in this publication does not imply, even in the absence of a specific statement, that such names are exempt from the relevant protective laws and regulations and therefore free for general use.

Cover design: Frido Steinen-Broo, EStudio Calamar, Spain

Printed on acid-free paper

Springer is a part of Springer Science+Business Media (www.springer.com)

图书在版编目 (CIP) 数据

环境岩土工程新进展——国际环境岩土工程研讨会论文集：英文 / 陈云敏，唐晓武，詹良通主编. —杭州：浙江大学出版社，2009.9

书名原文：Advances in Environmental Geotechnics—Proceedings of the International Symposium on Geoenvironmental Engineering in Hangzhou, China, September 8-10, 2009
ISBN 978-7-308-06597-9

I. 环… II. ①陈…②唐…③詹… III. 环境工程：岩土工程—国际学术会议—文集—英文 IV. TU4-53 X5-53

中国版本图书馆 CIP 数据核字 (2009) 第 146026 号

Not for sale outside Mainland of China
此书仅限中国大陆地区销售

环境岩土工程新进展——国际环境岩土工程研讨会论文集
陈云敏 唐晓武 詹良通 主编

责任编辑 张 琛
封面设计 Frido Steinen-Broo
出版发行 浙江大学出版社
网址：<http://www.zjupress.com>
Springer-Verlag GmbH
网址：<http://www.springer.com>
排 版 杭州中大图文设计有限公司
印 刷 杭州富春印务有限公司
开 本 880mm×1230mm 1/16
印 张 60.25
字 数 3400 千
版 次 2009 年 9 月第 1 版 2009 年 9 月第 1 次印刷
书 号 ISBN 978-7-308-06597-9 (浙江大学出版社)
ISBN 978-3-642-04459-5 (Spring-Verlag GmbH)
定 价 320.00 元

版权所有 翻印必究 印装差错 负责调换
浙江大学出版社发行部邮购电话 (0571)88925591

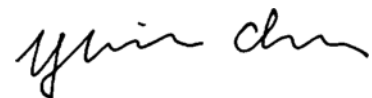
Preface

The International Symposium on Geoenvironmental Engineering (ISGE 2009) was held on September 8-10, 2009 in Hangzhou, China. ISGE 2009 was organized by MOE Key Laboratory of Soft Soils and Geoenvironmental Engineering, Zhejiang University, Chinese Institution of Soil Mechanics and Geotechnical Engineering (CISMGE), and Chinese Chapter of International Geosynthetics Society (CCIGS), under the auspices of ISSMGE TC5, sponsored by K. C. Wong Education Foundation, and National Natural Science Foundation of China, as well as Zhejiang University Zeng Guo-Xi Lecture Fund.

Issues associated with Environmental Geotechnics continue to be a major preoccupation for governments, public and private organizations and the general community worldwide. The Chinese Government has been putting great effort on environmental issues including sanitary disposal of solid waste, reuse of industrial wastes, remediation of contaminated land, prevention of groundwater contamination, environmental risk assessment, ecological techniques, etc. China also has much to share on the opportunities, challenges and responsibilities for environmental geotechnics with other countries, especially the developing countries.

Under the conference theme, “Reclamation of the Past and Toward a Sustainable Geoenvironment”, 168 abstracts in total were received and 125 papers in total were reviewed and accepted for publication in this proceeding. This proceeding encloses 2 Zeng Guo-Xi Lectures, 26 Invited Lectures and 97 papers. The topics covered include basic and advanced theories for modeling of geoenvironmental phenomena, testing and monitoring for geoenvironmental engineering, municipal solid wastes and landfill engineering, sludge and dredged soils, geotechnical reuse of industrial wastes, contaminated land and remediation technology, applications of geosynthetics in geoenvironmental engineering, geoenvironmental risk assessment, management and sustainability, ecological techniques and case histories. This proceedings include papers authored by core members of ISSMGE TC5 (International Society of Soil Mechanics and Geotechnical Engineering - Environmental Geotechnics) and geoenvironmental researchers from more than 23 countries and regions (i.e., Albania, Austria, Bengalese, Brazil, Canada, China, France, German, Hong Kong, India, Iran, Indonesia, Japan, Korea, Macau, Malaysia, Portugal, Russia, Taiwan, UK, USA, Uzbekistan, Vietnam).

It is our desire that the proceedings of International Symposium on Geoenvironmental Engineering (ISGE2009) provide an opportunity for the exchange of views among academic researchers, practical engineers and administration officers. “Advances in Environmental Geotechnics” presents the latest development in this interdisciplinary field.



Prof. Yunmin CHEN
Chairman, Organizing Committee of ISGE 2009

International Advisory Committee

Pedro Simão Sêco e Pinto (ISSMGE President)
William Van Impe (FedIGS President)
Fumio Tatsuoka (IGS President)
R N Taylor (Secretary General of ISSMGE)
Mario Manassero (Chairman of TC5)
Madhira Madhav (Vice President for Asia)
Zuyu Chen (President of CISMGE, China)
Chung-Tien Chin (President, Southeast Asian
Geotechnical Society)
Jiping Ru (NSFC, China)
Malek Bouazza (Australia)
Alain Holeyman (Belgium)
Peter Van Impe (Belgium)
Marcio Almeida (Brazil)
Luiz Guilherme Francisco Soares de Mello
(Brazil)
Maria Eugenia Gimenez Boscov (Brazil)
Delwyn G. Fredlund (Canada)
Kerry R. Rowe (Canada)
Zaiming Zhang (China)

Guangxin Li (China)
Xiurun Ge (China)
Chenggang Bao (China)
Jean-Pierre Gourc (France)
Richard Kastner (France)
Erwin Gartung (Germany)
Rolf Katzenbach (Germany)
Masashi Kamon (Japan)
Takeshi Katsumi (Japan)
Shigenori Hayashi (Japan)
Meindert Van (the Netherlands)
Farrokh Nadim (Norway)
Antonio Gens (Spain)
Richard Jardine (UK)
Stephan Jefferis (UK)
Hywel Thomas (UK)
Powrie William (UK)
Charles Shackelford (USA)
James K. Mitchell (USA)
Tuncer B. Edil (USA)

Technical Committee

Mike Sadler (Australia)
Xiang-Ling Li (Belgium)
Bruno Bussi ere (Canada)
Xiating Feng (China)
Chenggang Bao (China)
Yixin Dong (China)
Pinjing He (China)
Xianjin Kong (China)
Songyu Liu (China)
Hanlong Liu (China)
Maotian Luan (China)
Weimin Ye (China)
Liangtong Zhan (China)
Jianhong Zhang (China)
Jianmin Zhang (China)

Honglei Zhuo (China)
Wei Zhu (China)
John W. Cowland (Hong Kong, China)
Albert T. Yeung (Hong Kong, China)
Ming Hung Wong (Hong Kong, China)
Helmut Zanzinger (German)
Eun-Chul Shin (Korea)
Noriyuki Yasufuku (Japan)
Jinchun Chai (Japan)
Takeshi Katsumi (Japan)
M. Kitazume (Japan)
Dennes T. Bergado (Thailand)
Stephanie Glendinning (UK)
Susan E. Burns (USA)
Aigen Zhao (USA)

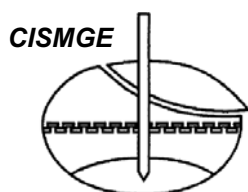
Organizing Committee

Yunmin Chen
Xiaowu Tang
Yanjun Du
Zhenshun Hong
Liming Hu
Minyun Hu
Han Ke
Lingwei Kong

Jianyong Shi
Shuilong Shen
Chao Xu
Liangtong Zhan
Mengxi Zhang
Zhenyin Zhang
Yuchao Li

Organized by

MOE Key Laboratory of Soft Soils and Geoenvironmental Engineering, Zhejiang University
Chinese Institution of Soil Mechanics and Geotechnical Engineering (CISMGE)
Chinese Chapter of International Geosynthetics Society (CCIGS)



Under the auspices of

ISSMGE TC5



Sponsored by

K. C. Wong Education Foundation
National Natural Science Foundation of China
Zhejiang University Zeng Guo-Xi Lecture Fund

王寬誠教育基金會
K. C. WONG EDUCATION FOUNDATION



Contents

The 2009 Zeng Guo-Xi Lecture

SYSTEMS ENGINEERING THE DESIGN AND OPERATION OF MUNICIPAL SOLID WASTE LANDFILLS TO MINIMIZE CONTAMINATION OF GROUNDWATER

C R. Kerry ROWE (3)

STATIC AND SEISMIC ANALYSIS OF SOLID WASTE LANDFILLS

Pedro Simão Sêco e PINTO (19)

Invited Lectures

MODELING APPLIED TO ENVIRONMENTAL GEOTECHNICS

Mario MANASSERO, Andrea DOMINIJANNI and Guido MUSSO (57)

MODELING DOMINANT TRANSPORT PROCESSES IN ONE-DIMENSIONAL CONTAMINANT TRANSPORT

E.C. Nirmala PETER, M. R. MADHAV, E. Saibaba REDDY and T. V. BHARAT (90)

THE VECTOR SUM METHOD: A NEW APPROACH TO CALCULATING THE SAFETY FACTOR OF STABILITY AGAINST SLIDING FOR SLOPE ENGINEERING AND DAM FOUNDATION PROBLEMS

Xiu-Run GE (99)

ACID MINE DRAINAGE FROM ABANDONED MINE SITES: PROBLEMATIC AND RECLAMATION APPROACHES

Bruno BUSSIÈRE (111)

EFFECT OF MgO ADDITIVE ON PREVENTING LEAKAGE OF Cr(VI) FROM A FLY ASH

Jin-Chun CHAI, Takanori HINO and Nobuyuki NISHINO (126)

ENVIRONMENTAL GEOTECHNICS RELATED TO LANDFILLS OF MUNICIPAL SOLID WASTES

Yun-Min CHEN and Tony L.T. ZHAN (132)

TDR MEASUREMENT SYSTEM AND THE APPLICATION OF TDR IN GEOENVIRONMENTAL ENGINEERING

Ren-Peng CHEN, Wei CHEN, Yun-Min CHEN (153)

THE STATUS OF ENGINEERING TECHNICAL STANDARDS OF WASTE SANITARY LANDFILL TREATMENT IN CHINA

Yi-Xin DONG (163)

CHALLENGES ASSOCIATED WITH THE DESIGN OF COVERS

Delwyn G. FREDLUND and J. STIANSON (168)

GEOTECHNICAL ASPECTS OF LANDFILL CLOSURE AND AFTERCARE

Erwin GARTUNG, Wolf-Ulrich HENKEN-MELLIES, Jürgen KANITZ and Hans-Günter RAMKE (188)

DEWATERING SLUDGE USING ELECTROKINETIC GEOSYNTHETICS

S. GLENDINNING, J. A. HALL, J. LAMONT-BLACK, C. J. F. P. JONES, D. T. HUNTLEY, C. WHITE and A. FOURIE (204)

FULL-SCALE PRACTICE OF ECOLOGICALLY BASED LANDFILL OF MUNICIPAL SOLID WASTE: TO ACCELERATE THE BIOLOGICAL CONVERSION INSIDE LANDFILL AND COVER LAYERS

Pin-Jing HE (217)

GASOLINE CONTAMINATED SITES: POLLUTANT TRANSPORT AND REMEDIATION

Li-Ming HU, Jay N. MEEGODA, Irene M. C. LO, Yan LIU, Sheng-Yan GAO and Zhao-Qun WU (221)

CONTAMINATED LAND AND ENVIRONMENTAL DAMAGE: AN ANALYSIS OF CURRENT REMEDIAL STRATEGIES AND FUTURE DEVELOPMENTS

Stephan A. JEFFERIS (236)

IN-SITU CONTAINMENT FOR WASTE LANDFILL AND CONTAMINATED SITES

Takeshi KATSUMI, Toru INUI and Masashi KAMON (248)

APPLICATION OF ELECTRICAL RESISTIVITY FOR CEMENT SOLIDIFIED/STABILIZED HEAVY METAL CONTAMINATED SOILS

Song-Yu LIU, Yan-Jun DU, Lei CHEN, Zhi-Bin LIU and Fei JIN (259)

RECENT RESEARCH ON THE HYDROGEOLOGICAL AND SETTLEMENT CHARACTERISTICS OF LANDFILLED MUNICIPAL SOLID WASTE

D. J. RICHARDS, W. POWRIE and R. P. BEAVEN (265)

GEOSYNTHETIC FUNDAMENTALS IN LANDFILL DESIGN

Gregory N. RICHARDSON and Aigen ZHAO (275)

APPLICATION OF SHEAR STRENGTH OF SOLID WASTE AND MULTILAYER LINER IN LANDFILLS

Jian-Yong SHI, Xue-De QIAN, Jun-Gao ZHU and Yu-Ping LI (286)

AN APPLICATION OF CENTRIFUGE MODEL IN ENVIRONMENTAL GEOTECHNICS ASSESSMENT OF SOFT GEOLOGICAL BARRIER SUBJECTED TO PILE CONSTRUCTIONS IN WASTE DISPOSAL SITE

Jiro TAKEMURA, Binod AMATYA and Osamu KUSAKABE (295)

REMOVAL OF HEAVY METAL FROM AQUEOUS SOLUTIONS USING CHINESE LOESS SOIL

Xiao-Wu TANG, Yan WANG and Zhen-Ze LI (314)

COUPLED THERMO-HYDRO-CHEMO-MECHANICAL MODELING FOR GEOENVIRONMENTAL PHENOMENA

Hywel R. THOMAS, Philip J. VARDON and Yu-Chao LI (320)

REMEDICATION TECHNOLOGIES FOR CONTAMINATED SITES

Albert T. YEUNG (328)

ADVANCES ON BUFFER/BACKFILL PROPERTIES OF HEAVILY COMPACTED GAOMIAOZI BENTONITE

Wei-Min YE, Qiong WANG, Yong-Gui CHEN and Bao CHEN (370)

A PRELIMINARY UNDERSTANDING ON PERFORMANCE OF BARRIERS FOR MSW LANDFILLS IN SOUTHERN CHINA

Tony L.T. ZHAN, Yun-Min CHEN and Xiao-Wu TANG (380)

ROLE OF SOIL WATER IN CEMENT-BASED TREATMENT OF DREDGED MATERIALS

Wei ZHU and C.F. CHIU (395)

Basic and Advanced Theories for Modeling of Geoenvironmental Phenomena

NUMERICAL SIMULATION OF ELECTRO-OSMOSIS IN SOFT CLAY

Liming HU, Wei-Ling WU and Zhao-Qun WU (407)

RESEARCH ON COEFFICIENT OF BRITTLE STRESS DROP OF BRITTLE-PLASTIC ROCKS AND ITS APPLICATION

Gui-Cai SHI, Xiu-Run GE and Yun-De LU (413)

DYNAMIC STABILITY ANALYSIS OF LANDFILL SLOPE IN DUSHANBE, TAJIKISTAN

Xue-Tao WANG, Tensay G. BERHE, Stephen WEBB and Wei WU (420)

HIGH-SPEED AND LONG RANGE FLOW ANALYSIS MODEL OF WASTE BODY AFTER SANITARY MSW LANDFILLS SLOPE UNSTABILITY

Zhan-Hong QIU, Yun-Min CHEN and Xiao-Gang WANG (426)

ONE-DIMENSIONAL CONSOLIDATION OF AQUITARD CONSIDERING NON-DARCY FLOW

Zhong-Yu LIU, Jin-Chao YUE and Li-Yun SUN (430)

SITE EFFECT ANALYSIS OF SHIRVAN GTL REFINERY, USING EQUIVALENT LINEAR SOIL BEHAVIOR (NE OF IRAN)

Ahmad ADIB, Naser EBADATI and Kobra HEYDARZADEH (435)

DATA DIVISION METHOD OF SAND LIQUEFACTION SAMPLES BASED ON SELF-ORGANIZING MAPS

Si-Si LIU and Ming-Hua ZHAO (443)

GOM-SVM PREDICTOR FOR LAND SUBSIDENCE AT FINISHED UNDERGROUND MINING

Zheng-Wen XIE and Xiao-Yu LIANG (449)

A FULLY COUPLED THERMO-HYDRO-MECHANICAL MODEL FOR METHANE HYDRATE RESERVOIR SIMULATIONS

Huo-Lang FANG (455)

NUMERICAL SIMULATION OF DYNAMIC RESPONSES IN TRANSVERSELY ISOTROPIC FLUID-SATURATED ELASTIC SEABED UNDER WAVE ACTIONS

Zhou-Yuan HENG, Wang-Yong HE, Sun ZHI and Chen-Ming WEI (462)

SOLUTIONS FOR A COMPLETELY SATURATED POROUS ELASTIC SOLID WITH IMPEDED BOUNDARIES

Ze-Hai CHENG, Jian-Zhong XIA, Yun-Min CHEN, Dao-Sheng LING and Bing ZHU (467)

THE THREE-DIMENSION SATURATED-UNSATURATED SEEPAGE ANALYSIS UNDER ATOMIZED RAIN OF HYDROPOWER PROJECT WITH HIGH SLOPE

Huan-Ling WANG and Wei-Ya XU (473)

STUDY ON UNLOADING ROCK MASS CONSTITUTIVE RELATIONSHIP

Jie LIU, Jian-Lin LI, Xiao-Hu WANG, Jian-Jun QU and Ting ZHU (480)

DESTRUCTURATION CONSTITUTIVE MODEL FOR SOFT CLAY

Xiao-Jun YU and Zhi-Hong QI (487)

IDENTIFICATION OF DAMPING RATIOS OF SOIL-STRUCTURE SYSTEM SUBJECTED TO AMBIENT EXCITATION

Zhi-Ying ZHANG, Qiang PAN, Chong-Du CHO and Zhan-Chao GAO (492)

Testing and Monitoring for Geoenvironmental Engineering

LABORATORY FLUME STUDIES ON CONSOLIDATION OF SOFT SILTY SEABED SOIL UNDER WAVE ACTIONS

Ying LIU, Hong-Jun LIU, Xiu-Hai WANG and Min-Sheng ZHANG (499)

CHARACTERISTICS OF SHEAR STRENGTH OF UNSATURATED WEAK EXPANSIVE SOIL

Wei-Min YE, Ya-Wei ZHANG, Bao CHEN and Shi-Fang ZHANG (505)

ON THE DETERMINATION OF THE SOIL-WATER CHARACTERISTIC CURVE USING THE PRESSURE PLATE EXTRATOR

Hui CHEN, Chang-Fu WEI, Rong-Tao YAN, Pan CHEN and Pan-Pan YI (511)

ZERO VALENT IRON TO REMOVE THE ARSENIC CONTAMINATION FROM NATURAL GROUNDWATER: BATCH AND COLUMN EXPERIMENT

M. A. ABEDIN, Takeshi KATSUMI, Toru INUI and Masashi KAMON (515)

SIMULATION TESTS OF BIODEGRADATION AND COMPRESSION OF MUNICIPAL SOLID WASTE

Jun-Long LIU, Han KE, Tony L.T. ZHAN and Yun-Min CHEN (521)

COMPATIBILITY OF TROPICAL SOIL AND BENTONITE MIXTURES SUBJECTED TO CHEMICAL SOLUTIONS

Thiago Luiz Coelho MORANDINI and Adilson do Lago LEITE (525)

DEVELOPMENT OF SEDIMENT MONITORING DURING HEAVY RAINFALLS

Chih-Ping LIN, Chih-Chung CHUNG, Yu-Chia CHANG and Tzong-Shen CHANG (531)

RESEARCH ON RELATIONS OF ENGINEERING INDEXES AND MICROSTRUCTURE FEATURE VALUES TO SATURATED SOFT SOIL

Yong XU, Ji-Chao ZHANG, Wu-Ping LI and He YI (537)

SHEAR STRENGTH BEHAVIOR OF BENTONITE MODIFIED BY TETRAMETHYLAMMONIUM CATIONS

Bate BATE and Susan E. BURNS (543)

MONITORING OF LANDFILL SETTLEMENT BY MEANS OF HORIZONTAL INCLINOMETERS

*Xiao-Bing XU, Hai-Yun WEI, Tony L. T. ZHAN, Yun-Min CHEN and Yao-Shang WANG (549)***Municipal Solid Wastes and Landfill Engineering**

EFFECT OF THICKNESS OF HYDRAULIC BARRIER ON THE INTEGRITY OF A COVER SYSTEM SUBJECTED TO DIFFERENTIAL SETTLEMENTS

Bhamidipati V. S. VISWANADHAM and Sathiyamoorthy RAJESH (555)

SEISMIC RESPONSE CHARACTERISTICS OF MUNICIPAL SOLID WASTE LANDFILLS

Xue-Jing DENG, Xian-Jing KONG and De-Gao ZOU (561)

STUDY ON SOIL PROPERTIES OF THE EARLY ECOLOGICAL RESTORATION FOR A CHEMICAL LANDFILL IN HUAINAN

Wen FAN, Jia-Ping YAN and Hui-Ping LIU (567)

GEOTECHNICAL SITE CHARACTERIZATION OF MUNICIPAL SOLID WASTE LANDFILL IN UZBEKISTAN

Kobiljon KHOLMATOV, Diana KHASHIMOVA, Wei WU and Marufdjan MUSAEV (571)

AMBIENT NOISE SITE INVESTIGATION OF A REPRESENTATIVE MSW LANDFILL IN BISHKEK, KYRGYZSTAN

Thiep DOANH, Xue-Tao WANG, Stephen WEBB and Wei WU (578)

ANALYSES ON APPLICABILITY OF ET COVERS IN HUMID AREAS

Wen-Jie ZHANG and Yun-Min CHEN (584)

IN-SITU TESTS AND SLOPE STABILITY ANALYSIS OF MUNICIPAL SOLID WASTE LANDFILL

Hsin-Yu SHAN and Tsuo-Hsien FAN (590)

EFFECT OF MUNICIPAL SOLID WASTE COMPOSITION ON PERMEABILITY

Harris RAMLI, Mastura AZMI, F. AHMAD and M. M. ALI (596)

STUDY ON THE DUNCAN-CHANG MODEL PARAMETERS OF STRESS COMPRESSION FOR MUNICIPAL SOLID WASTE

Zhen-Ying ZHANG, Chang-Fu WU and Yun-Min CHEN (602)

STUDY ON PARAMETER SENSITIVITY OF THE COMBINATION FAILURE OF LANDFILL WITH A DAM

Fan TU, Fang-Qiang CHANG, Zhao-Yun XIAO and Xiao-Jie WU (607)

MODEL TESTS ON DEFORMATION BEHAVIOR OF BENTONITE MIXED SOIL LAYER SUBJECTED TO A LOCAL SUBSIDENCE IN LANDFILL

Shigeyoshi IMAIZUMI, Yasuto SHINOZAKI, Kengo KUDO and Takuya YOSHINAO (615)

FACTORS AFFECTING SLOPE STABILITY OF LANDFILL COVERS

Manoj DATTA (620)

ONE-DIMENSIONAL SETTLING BEHAVIOR OF A GROUP OF SOIL MATERIALS IN STATIC WATER ASSUMING COASTAL LANDFILL

Shuichi NAGAOKA, Yuta NABESHIMA, Kenichi SATO, Shotaro YAMADA, Tomoaki HACHIMURA and Tetsuya MIYAHARA (625)

EXPERIMENTAL STUDY ON THE NONLINEAR CHANGE OF SATURATED HYDRAULIC CONDUCTIVITY OF WASTE SOIL

Ying ZHAO, Qiang XUE, Bing LIANG and Lei LIU (629)

LANDFILL GAS GENERATION AND TRANSPORT IN BIOREACTOR LANDFILL

Qi-Lin FENG, Lei LIU, Qiang XUE and Ying ZHAO (633)

DEVELOPMENT OF A COMPUTER SOFTWARE FOR PREDICTING LANDFILL SETTLEMENT AND ITS STORAGE CAPACITY

Yao-Shang WANG, Han KE, Tony L. T. ZHAN, Xue-Chen BIAN, Yun-Min CHEN and Zhe FU (637)

INFLUENCE OF RAINFALL PATTERN ON THE INFILTRATION INTO LANDFILL EARTHEN FINAL COVER

Guan-Wei JIA, Tony L.T. ZHAN, Yun-Min CHEN and D. G. FREDLUND (641)

MUNICIPAL SOLID WASTE MANAGEMENT AFTER WENCHUAN EARTHQUAKE

Hua TAO (646)

FIELD INVESTIGATION ON THE FEASIBILITY OF LEACHATE RECIRCULATION IN CHENGDU MSW LANDFILL, CHINA

Ji-Wu LAN, Tony Liang-Tong ZHAN, Yun-Min CHEN, Han KE, Zhao LIU and Guo-Qing LU (649)**Sludge and Dredging Soils**

REUSE OF POND SEDIMENT BY MIXING WITH STABILIZERS AND SHREDDED PAPER

Yasuyuki NABESHIMA and Seishi TOMOHISA (657)

LABORATORY STUDY ON ELECTROKINETIC DEWATERING OF SEWAGE SLUDGE

Yuan FENG, Tony L. T. ZHAN, Yun-Min CHEN and Quan-Fang ZHANG (662)

HYDRAULIC CONDUCTIVITY EVALUATION OF VERTICAL CUTOFF WALLS BEARING FILTER CAKE FROM SLUG TEST ANALYSIS

The-Bao NGUYEN, Chulho LEE, Yonghoon AHN and Hangseok CHOI (666)

FILTRATION PERFORMANCE OF TWO-LAYERED NONWOVEN GEOTEXTILES

Li-Fang LIU, Lian-Ying JI, Fa-Wen GUO, Qian-Li WANG and Xiao-Jie YANG (672)

REASONABLE CONSTRUCTION MANAGEMENT IN FILL LOADING WITH VACUUM CONSOLIDATION METHOD BASED ON FEM ANALYSES

Mohammad SHAHIDUZZAMAN, Yoshihiko TANABASHI, Hiroshi KAWABATA, Yujing JIANG and Satoshi SUGIMOTO (675)

FINITE ELEMENT NUMERICAL ANALYSIS TO INTERACTION OF BURIED SPIRAL STEEL PLASTIC COMPOSITE PIPE WITH SURROUNDING SOILS

Xiang-Yong ZENG, An-Fu DENG, Bing ZHENG and Xiao-Dong GUO (683)

EXPERIMENTAL STUDY ON ENGINEERING PROPERTIES OF A DREDGED SEDIMENT SOLIDIFIED BY COMMON CEMENTITIOUS MATERIALS

Ping CHEN and Bang-Min QIN (687)

IMPROVING SOFT GROUND AND SLUDGE BY OVER-PRESSURE VACUUM CONSOLIDATION SYSTEM

Ya-Wei JIN and Ben NIU (690)

CHANGING IN THE PHYSICAL PARAMETERS OF DUMPS OF THE COAL-MINING INDUSTRY OF KANSK-ACHINSK (SIBERIAN) COAL FIELD AND POSSIBILITY OF THEIR REMEDIATION

E.V. STANIS, E.N. OGORODNIKOVA and E.A. KARPUKHINA (694)

DYNAMIC REACTION ANALYSIS OF TAILING DAMS UNDER EARTHQUAKE

Bao-Lin XIONG, Xi-Liang WANG and Chun-Jiao LU (697)

Geotechnical Reuse of Industrial Wastes

USE OF RECYCLED COPPER SLAG IN CEMENT-TREATED SINGAPORE MARINE CLAY

S. H. CHEW and S. K. BHARATI (705)

EXPERIMENTAL STUDY ON THE ENGINEERING PROPERTIES OF TWO INCINERATION BOTTOM ASH OF MUNICIPAL SOLID WASTES

Jian-Ming ZHANG, Min-Yun HU and Si-Fa XU (711)

UTILIZATION OF COAL ASH AS RECYCLING MATERIAL OPTIONS IN VIEW POINT OF GEOENVIRONMENT

Ahmad RIFA'I, Noriyuki YASUFUKU, Kiyoshi OMINE and Kazuyoshi TSUJI (715)

STUDY ON THE ENGINEERING PROPERTY OF MIXED-SOIL FLY ASH

Ya-Sheng LUO, Jing LI and Andrew CHAN (721)

EXPERIMENTAL STUDY ON TREATMENT OF OVER-WETTED CLAYS USING CALCIUM CHLORIDE

Ying-Ying ZHANG, Yan-Jun DU, Song-Yu LIU and Fan ZHANG (728)

MECHANICAL AND CHEMICAL PROPERTIES OF ASH MOLTEN SLAG MIXED WITH BENTONITE

Fujio IGARI and Shigeyoshi IMAIZUMI (734)

AN APPLICABILITY OF DEHYDRATED CAKE PRODUCED FROM QUARRY TO IMPERMEABLE MATERIAL WITH HEAVY METAL ADSORPTION

Ryo SUETAKE, Kenichi SATO, Miyako TAKEDA and Morimoto TATSUO (740)

UNCONFINED COMPRESSIVE STRENGTH OF MIXTURE OF PHOSPHOGYPSUM-FLY ASH-LIME-CLAY

Zhi-Hong QI, Xue-Yuan XU, Mi-Lin ZHU and Yang HU (745)

ADSORPTION BEHAVIOR AND MECHANISM OF Cu(II) ON ACTIVATED FIRMIANA SIMPLEX LEAF

Qiang TANG, Xiao-Wu TANG, Man-Man HU, Yun-Min CHEN, Yan WANG and Nai-Yu KOU (749)

Contaminated Land and Remediation Technology

PURIFICATION OF Cr(VI)-CONTAMINATED SOIL BY FERMENTATION OF ORGANIC MATTER

Kiyoshi OMINE, Noriyuki YASUFUKU and Kazuya TAMURA (755)

AN OVERVIEW OF STABILIZATION/SOLIDIFICATION TECHNIQUE FOR HEAVY METALS CONTAMINATED SOILS

Yan-Jun DU, Song-Yu LIU, Zhi-Bin LIU, Lei CHEN, Fan ZHANG and Fei JIN (760)

CASE STUDY ON INFLUENCES OF OIL CONTAMINATION ON GEOTECHNICAL PROPERTIES OF COASTAL SEDIMENTS IN THE YELLOW RIVER DELTA

Yong-Gang JIA, Qiong WU, Xiang-Mei MENG, Xiu-Juan YANG, Zhong-Nian YANG and Geng-Cheng ZHANG (767)

BIOREMEDIATION OF WATER CONTAMINATED WITH BTEX, TPH AND TCE UNDER DIFFERENT

ENVIRONMENTAL CONDITIONS

C.K. LEI, J. H. LI, S.S. DONG and H. SHIM (772)

HYSTERETIC RETENTION OF Pb(II) IN KAOLIN COLUMN

Zhen-Ze LI, Yun-Min CHEN, Xiao-Wu TANG, Yan WANG and Qiang TANG (777)

EXPERIMENTAL STUDY ON THE MECHANISM OF ACTION OF IONIC SOIL STABILIZER ON RED CLAY OF WUHAN

Wei XIANG, De-Shan CUI and Fei AI (781)

EFFECTS OF SURFACE-ACTIVE AGENT ON MECHANICAL BEHAVIORS OF LOESS

Nai-Yu KOU, Xiao-Wu TANG, Quan-Fang ZHANG, Yun-Min CHEN and Qiang TANG (786)

EDTA-ENHANCED ELECTROKINETIC EXTRACTION OF CADMIUM FROM A NATURAL CLAY OF HIGH BUFFER CAPACITY

Ying-Ying GU, Albert T. YEUNG and Hong-Jiang LI (790)

Applications of Geosynthetics in Geoenvironmental Engineering

APPLICATIONS OF GEOGRID REINFORCED SOIL RETAINING WALL WITH WRAP-AROUND FACING IN RAILWAY

Guang-Qing YANG, Qiao-Yong ZHOU, Bao-Jian ZHANG and Jun-Xia DING (799)

TEST STUDY ON ENGINEERING PROPERTIES OF GABION STRUCTURES

Guo-Lin YANG, Xiang-Jing HUANG and Yu-Liang LIN (805)

PULLOUT TEST STUDY ON INTERFACE FRICTION CHARACTERISTICS OF REINFORCEMENTS WITH RED SANDSTONE AS FILLER

Yu-Liang LIN, Guo-Lin YANG, Yun LI and Xiang-Jing HUANG (812)

APPLICATION OF GEOMEMBRANE AS CARBON CAPTURE AT PALM OIL MILL

Andryan SUHENDRA and Amelia MAKMUR (817)

INTERFACE FRICTIONAL PROPERTY BETWEEN SAND AND GEOMEMBRANE

Jun-Li GAO, Meng-Xi ZHANG and Wen-Jie ZHANG (822)

COVERED ANAEROBIC LAGOONS WITH HDPE GEOMEMBRANE: EXPERIENCES IN DEVELOPING ASIAN COUNTRIES

Hoe-Boon NG, Chang-Wei QI and Xiao-Ming TAN (828)

LESSONS LEARNED FROM THE NUMERICAL MODELLING OF A RETAINING WALL WITH NON-UNIFORM REINFORCEMENTS

Xiang-Jing HUANG, Ze LIU and Vicari M (834)

EXPERIMENTAL STUDIES OF ARCHING EFFECT AND GEOSYNTHETIC DEFORMATION IN LOCAL SUBSIDENCE PROBLEM

Deng GAO, Bin ZHU, Yun-Min CHEN, Tony L. T. ZHAN and Xiang-Zhi WANG (840)

A LARGE-SCALE RAMP MODEL TEST ON COMPOSITE LINER SYSTEMS

Wei-An LIN, Tony L. T. ZHAN, Yun-Min CHEN and Sheng HE (846)

Geoenvironmental Risk Assessment, Management and Sustainability

URBAN NIGHT SOIL TRANSPORTATION AND TREATMENT IN CHINA

Ting LIU, Zhu-Lei CHEN and Lie YANG (853)

STUDY ON THE RELATIONSHIP BETWEEN LANDSLIDES, DEBRIS FLOWS AND THE MODERN

RIVER GEOLOGICAL PROCESSES

Ming-Xin ZHENG (859)

SEISMIC DAMAGE CHARACTERISTICS OF RURAL ADOBE-WOOD BUILDING IN GANSU PROVINCE INDUCED BY THE WENCHUAN GREAT EARTHQUAKE

Ai-Lan CHE, Zhi-Jian WU, Jun-Jie SUN and Jing-Hua QI (865)

EFFECTIVE FACTORS ON AMPLIFICATION IN CHABAHAR CITY, SOUTHEAST OF IRAN

Ahmad ADIB and Kobra HEYDARZADEH (872)

POST DISASTER INFORMATION MANAGEMENT: ISSUES RELATED TO MITIGATION ACTIVITIES IN IRAN

Ahmad ADIB and Vahid Hosseini JENAB (879)

ANALYSIS AND EVALUATION ON HYDROFRACTURE FAILURE IN AN ASPHALT CONCRETE CORE ROCK-FILL DAM: A MAOPINGXI DAM CASE

Xin-Hua Zhou and Xi-Bao RAO (883)

GEOENVIRONMENTAL RISK ASSESMENT IN ALBANIA

L. BOZO and G. J. IKONOMI (890)

STUDY ON DEBRIS FLOW HAZARD DISCRIMINANT ANALYSIS AND ZONING OF ONE DUMP

Shi-Guo SUN, Shao-Jie FENG, Ting-Ting JIANG, Hua XIAO and Sheng-Hua ZHANG (893)**Ecological Techniques and Case Histories**

SUSTAINABLE DESIGN BASED ON NEAR NATURE CONSTRUCTION METHOD—A CASE STUDY

Huat-Yoo CHUA, Hsiao-Chou CHAO and Chung-Tien CHIN (901)

ENGINEERING GEOLOGICAL PROPERTIES OF THE SATURATED CLAY FOUNDATION AT THE SOUTHERN EDGE OF MU US DESERT IN CHINA

Sheng-Rui SU and Fang-Qiang SUN (907)

GEOLOGY CONSIDERATION INFLUENTIAL IN URBAN DEVELOPMENT AND VULNERABILITY OF THE GORGAN REGION (NE IRAN)

Naser EBADATI, Ahmad ADIB and Reza MAGSOODLORAD (911)

PROTECTION TECHNOLOGY AND APPLICATIONS OF GABION

Guo-Lin YANG, Zhe-Zhe LIU, Gui-Lin XU and Xiang-Jing HUANG (915)

A PARAMETRIC STUDY ON EVALUATION OF STABILITY OF COLUMN TYPE DM IMPROVED GROUND

Masaki KITAZUME (920)

CASE STUDY ON GEOENVIRONMENTAL EFFECTS OF PRESS-IN PILES INSTALLATION

Jian-Xue SONG, Tong-He ZHOU and Yuan-Cheng GUO (926)

A CONSTRUCTION CASE OF RAMPS LOCATED ON THE EXPANSIVE SOIL FOR HIGHWAY INTERCHANGE

He-Ping YANG, Xiao NI and Jie XIAO (930)

ANALYSIS OF THE DEEP-SEATED CONCRETE SLAB FOR SETTLEMENT CONTROL AT BRIDGE APPROACH EMBANKMENT

Yun SUN, Yi-Qiang XIANG, Dong-Mei GUO and Ting-Ting ZHANG (935)

APPLICATION OF GEOCELL IN THE ECOLOGICAL PROTECTION OF ROCK SLOPE

Xin-Jun ZOU and Ming-Hua ZHAO (940)

The 2009 Zeng Guo-Xi Lecture

SYSTEMS ENGINEERING THE DESIGN AND OPERATION OF MUNICIPAL SOLID WASTE LANDFILLS TO MINIMIZE CONTAMINATION OF GROUNDWATER

R. Kerry ROWE¹

ABSTRACT: This paper discusses the need to adopt a systems engineering approach to the design and operation of municipal solid waste landfills. It discusses how the interaction between the different components affects the performance of the entire system and how, due to this interaction, the performance of the system as a whole is much greater than the individual contributions of each of the parts. Issues discussed in this context include: landfill covers and the role that they play, the effect of landfill operations such as the waste placement and leachate recirculation on liner temperature and leachate characteristics, leachate collection and the control of head on the liner, diffusion of contaminants through composite liners, the effect of geomembrane-clay liner interaction on leakage, the significance of wrinkles in a geomembrane, the effect of liner temperature on leakage, possible means of controlling liner temperature, geomembrane protection, the long-term performance of geomembranes and geosynthetic clay liners, and finally the contaminant transport implications of these issues. It is concluded that by taking a systems approach to design, construction and operations we can provide safer containment of waste and long-term environmental protection.

KEYWORDS: geosynthetics, landfills, leachate

INTRODUCTION

Despite reductions in waste generation, landfills will continue to be required for the safe disposal of municipal solid waste (MSW) for the foreseeable future. These landfills will generate both leachate and gas whose escape from the facility must be controlled to environmentally acceptable levels. The leachate is predominantly water but typically contains dissolved organic and inorganic chemicals and suspended solids (e.g. microbes, particulate matter etc.) whose escape from the landfill must be controlled to negligible levels. Landfill gas is predominantly comprised of methane and carbon dioxide which are of concern as greenhouse gases (especially methane) but it also contains trace amounts of volatile organic compounds. From an engineering perspective, the long-term performance of the modern MSW landfill will be governed by the performance of a system comprised of three primary subsystems: the barrier system below the waste, the landfill operations, and the landfill cover and gas collection system. To provide long-term environmental protection, this system must contain contaminants for what is called the contaminating lifespan of the landfill (i.e. the period of time during which the landfill will produce contaminants

at levels that could have unacceptable impacts if they were discharged into the surrounding environment). For large modern landfills this could be hundreds of years (Rowe et al. 2005).

The release of contaminants contained in landfill leachate can be reduced to environmentally acceptable levels with a suitable barrier system below the waste that includes a leachate collection system and a liner system. The leachate collection system minimizes the driving force for leachate escape (i.e. the leachate head acting on the underlying liner). The liner system provides resistance to the migration of contaminants both by the pressure driven movement of leachate containing contaminants (often referred to as leakage or advection) and the concentration driven movement of contaminants by a process of diffusion (those not familiar with the terminology and contaminant transport processes should refer to Rowe et al. 2004 for details). The leachate collection system typically involves a series of perforated pipes in a granular drainage layer together with a means of removing the leachate that is collected. The barrier system may involve a single liner or a double liner with a secondary leachate collection system (also called a leak detection system) between the two liners. In either case, the liner will typically be comprised of a

¹Vice Principal (Research), Queen's University and Professor of Geotechnical and Geoenvironmental Engineering, Geoenvironmental Centre at Queen's –RMC, Canada. Email: kerry@civil.queensu.ca

protection layer on top of a composite liner. The protection layer minimizes the damage from overlying coarse materials and the composite liner minimizes escape of contaminants. The composite liner involves a *geomembrane* (GM: 1.5-2 mm thick high-density polyethylene (HDPE) plastic sheet) overlying a *geosynthetic clay liner* (GCL: about 5-10 mm thick layer of low permeability clay, called bentonite, encased between two geotextiles) or a *compacted clay liner* (CCL: 600-1200 mm thick). In addition to controlling the escape of leachate and the contaminants in the leachate, the liner system also controls the escape of landfill gas to the subsurface.

The landfill cover and gas collection system will control both the ingress of moisture (which generates leachate) and egress of landfill gasses. In order to minimize the leakage of landfill gas to the atmosphere, the cover will include a liner system to provide resistance to gas escape and a gas collection system which reduces the driving force for gas escape by collecting the gas (thereby reducing gas pressures in the landfill). The liner system in the cover will often be similar to that in the bottom liner as described above. In addition to the liner and gas collection system, there may also be a moisture distribution system to provide moisture to the waste to encourage biodegradation and gas generation.

Landfill operations that can affect the performance of the entire system include: (a) the nature of waste that is accepted, (b) the sequence and location of waste placement, (c) operation and maintenance of the gas collection system, (d) the introduction of moisture or recirculation of leachate, (e) leachate-collection, (f) maintenances and cleaning of the leachate collection system, and (g) maintenance of the final cover.

This paper argues that in order to minimize the environmental impacts of this landfill, it is necessary to adopt a systems engineering approach to the design, construction and operation of the landfill. This will involve decomposing the entire system into subsystems as noted above. In turn, each subsystem is decomposed into simpler identifiable components, the performance of the individual components is examined, the interactions between different components of the system are assessed, and then the response of the entire system is assembled to quantify its overall engineering performance. It is essential that this evaluation consider how the interaction between different components affects the performance of the entire system and how, due to this interaction, the performance of the systems as a whole is much more than the individual contributions of each of the parts. In particular, it must be recognised that an action that may enhance the performance of one part of the system may have a negative effect on other parts of the system and the objective should be to ensure optimal performance of

the system as a whole as will be discussed in the following sections.

THE ROLE OF THE LANDFILL COVER

The generation gas and leachate is related to the movement of fluid through the waste. For example, the volume of leachate generated in a landfill is directly related to the movement of water through the cover. The leachate concentrations and the contaminating lifespan of a landfill are also related to the infiltration through the cover and this, in turn, may influence the performance of the underlying leachate collection system and bottom line (Rowe et al. 2004).

Before the relatively recent concerns about the effect of methane from MSW landfills on climate change, the primary consideration in cover design was the control of infiltration and hence leachate generation. Here there were two distinct philosophies and the cover would be designed to accommodate these philosophies.

One approach (e.g. MoE 1998) involves encouraging a modest amount of infiltration (0.15-0.2 m/a) through the landfill cover to encourage controlled biodegradation of the organic waste and flush out contaminants (e.g. chloride) that do not chemically stabilize with time. A simple soil cover that allows this level of infiltration is relatively cheap and, in an appropriately designed system, can reduce the contaminating lifespan of the landfill so that it is less than the service life of the barrier system. This provides good long-term environmental protection to the surface and groundwater. Experience indicates that landfills operated in this manner (e.g. the Keele Valley landfill in Toronto, Canada) generate a liner temperature in the 30-40 °C range (Rowe 2005, Rowe and Islam 2009). However, the downside to this approach is that a soil cover that permits the ingress of 0.15-0.2m of infiltration will not provide the same control on the egress of landfill gas as a low permeability cover.

The other approach is the dry tomb concept (e.g. US Subtitle D). This involved the desire for a very low permeability cover that would result in minimal leachate generation from infiltration though the cover (leachate would still be generated from the biodegradation of organic waste; e.g. see Fig. 1). This approach has the short-term operational advantage of reducing the amount of leachate that is generated (and the consequent cost of treating it) and minimizing the escape of landfill gas (provided there is a suitable gas collection system). This approach reduces the rate of gas generation by limiting availability of moisture needed to fuel the biodegradation processes, although, with time, enough moisture will accumulate in the waste to allow some biodegradation to occur (e.g. due to biodegradation of organic waste that

was moist when placed and by some leakage through the cover). Koerner and Koerner report a case with this type of cover where the temperature of the liner remained essentially constant at about 20°C for six years but then quickly increased to between 30-35°C. However, this approach has the unanticipated consequence that it substantially increases the contaminating lifespan of the landfill and the normal processes will commence as soon as the cover degrades. Thus, what appears to be good from the narrow perspective of minimizing leachate generation and treatment actually has negative environmental impacts when one examines it from a systems engineering perspective.

Landfill gas is comprised of methane and carbon dioxide in about equal proportions as well as small amounts of volatile organic compounds, nitrogen oxides, and carbon monoxide. For example, in the USA, landfills produce about 23 percent of the total anthropogenic methane emissions (USEPA 2008). As a result of concerns regarding the impacts of methane on climate change, there has been a concerted move to collect landfill gas and either flare (burn) the methane or use it for the generation of electricity. The latter has desirable environmental benefits. However, to effectively collect and use the landfill gas, there is a need for a suitable gas collection system to be installed below the liner in the landfill cover and one needs to ensure that there is sufficient moisture to provide economic quantities of gas. Thus, there is often a need to introduce moisture below a low permeability cover to accelerate biodegradation and consequent gas generation. If done, this has a beneficial effect in terms of making gas generation cost-effective. Within reason, more moisture results in more gas being generated and this has led to studies of the use of the landfill as an engineered bioreactor with a view to (a) maximizing gas generation, and (b) stabilizing the organic waste as quickly as possible. Thus, from this narrow perspective, the more moisture the better. From a slightly broader sub-system perspective there is a limit on what is a desirable moisture injection rate dictated by the need to avoid flooding the gas collection wells (which would then minimize gas production) and avoiding leachate seeps. However, to avoid unintended consequences such as shortening of the service life of both the leachate collection system and the underlying composite liner, a much broader systems engineering approach should be adopted in the design of bioreactors to ensure that the overall system performance, and hence environmental protection, is optimized even if it results in less than the preferred rates of gas generation. The interdependencies and potential implications of moisture addition on other aspects of the landfill system will be discussed in a following section.



Fig. 1 Leachate generated from biodegradation of organic waste at a landfill site located in a desert. Note black and brown leachate stain due the leachate leaking from the adjacent completed cell (upper left) into the operating cell (foreground)

LANDFILL OPERATIONS AND CONSEQUENT EFFECTS ON LEACHATE CHARACTERISTICS AND LINER TEMPERATURE

The manner and rate at which waste is placed can affect a number of aspects of the system performance. For example, with respect to providing the best performance of the GCL it is ideally hydrated (i.e. takes up moisture from the underling soil) when it has significant stress on it. This could be achieved by placing waste relatively quickly over a relative small part of the landfill. This also has the advantage of minimizing the size of the open operating area of the landfill at any time (thereby minimizing leachate generation). However there are a number of disadvantages from a broader systems perspective. For example, faster waste placement tends to result in the generation of higher liner temperatures (Collins 1993) which can substantially reduce the service life of the composite liner (Rowe 2005). Also, faster waste placement gives leachate with much higher levels of organic acids and inorganic contaminants such as calcium (Brune et al. 1991) which can rapidly clog the leachate collection systems (Rowe et al. 2004; Rowe 2009).

Armstrong and Rowe (1999) examined data relating to the effect of waste placement and total precipitation on the composition of the leachate produced at the Keele Valley landfill in Toronto, Canada. They observed that when fresh waste lifts are placed on older waste, the older waste acts as a bioreactor that "treats" the leachate generated by the newer waste. Thus, the beneficial effect of leachate percolation through older waste shown by

Ham & Bookter (1982) in a relatively small cell appears to be relevant to this large landfill site. These results suggest that planned waste placement and fluid addition (natural or irrigation) can play major roles in the treatment of leachate before removal from the landfill and hence reduction in clogging of the leachate collection system. However, to achieve this objective, one must have a much larger working area of the landfill with consequent increase in leachate generation.

The Solid Waste Association of North America has defined a bioreactor landfill as “a sanitary landfill operated for the purpose of transforming and stabilising the readily and moderately decomposable organic waste constituents within five to ten years following closure by purposeful control to enhance microbiological processes. The bioreactor landfill significantly increases the extent of waste decomposition, conversion rates and process effectiveness over what would otherwise occur within the landfill”. While there are undeniable benefits from this approach, as previously noted, Rowe et al. (2004) identified a number of concerns regarding this approach, as summarized below:

1. Limited effectiveness—The heterogeneity of waste may lead to significant variations in the moisture content throughout the waste body. The presence of preferential flow paths may lead to large portions of the waste mass not experiencing the beneficial effects of increased moisture content, and thus not degrading at an optimal rate. Furthermore, the current practice of disposing household waste in plastic bags limits the effectiveness of moisture addition (Jones-Lee and Lee 2000).
2. Inorganic contaminants—The operation of a landfill as a leachate recirculating bioreactor does not decrease the concentrations of many inorganic contaminants. Thus, although the organic loading may decrease, other pollutants may remain in the landfill at significant concentrations
3. Reduced service lives—The enhanced biological activity brought about by leachate recirculation may have an adverse effect on the service lives of engineered components of the lining system. Clogging of the leachate collection system may occur at greater rate with recirculation than for conventional operation. Additionally, the operation of a landfill as a bioreactor generally results in increased temperatures of 50°C -60°C (e.g. Koerner and Koerner 2006) which may reduce the service life of geomembrane liners (Rowe 2005; 2009).
4. Extended contaminant lifespan—The potential effects of inorganic contaminant loading noted in (2) above is compounded if the accelerated waste settlement achievable in landfills with leachate recirculation is used to increase landfill capacity and hence place more waste. Since leachate recirculation

is unlikely to have a significant effect on reducing many inorganic contaminants with the landfill, the placement of additional waste following settlement will serve to increase the total inorganic contaminant load and thus extend the contaminating lifespan of the landfill.

5. Optimal conditions—Recirculation of leachate is not, in and of itself, sufficient to achieve optimum conditions for bioreactor landfills (Phaneuf 2000).
6. Stability—Excess porewater pressures associated with leachate recirculation has led to instability in at least two cases. Additionally, increased densification and the placement of additional waste following settlement may lead to loading in excess of that for which lining systems and side slopes were designed if the landfill was not originally designed for recirculation.
7. Leachate seeps—Due to heterogeneity and anisotropy of waste, the addition of leachate during recirculation may give rise to leachate seeps created by lateral flow of leachate above relatively low permeability layers (e.g. intermediate cover soils).

Yuen et al. (1999) suggested that any consideration of operating a landfill as a bioreactor must be done in the context of an integrated waste management system and must consider the implications on all aspects of the system. The writer is in complete agreement of this statement.

The observed temperatures in different landfills reported in the literature range from 14°C to 87°C and at the liner from 7°C to 60°C (Rowe and Islam 2009). In all MSW landfill cases examined, peak temperatures in the range of 30°C -40°C were encountered at the top of the landfill liner with typical landfilling operations. Substantially higher peak liner temperatures (50°C - 60°C) were observed in the case where there had been moisture augmentation as noted above.

LEACHATE COLLECTION AND CONTROL OF HEAD ON THE LINER

The primary purpose of a leachate collection system (LCS) is to control the head acting on the underlying liner systems and, in so doing, minimize the driving force (head) that gives rise to leakage through the liner system. Failure of these systems can arise from clogging of the drainage layer and/or leachate collection pipes (due to a build-up of biofilm, inorganic precipitates such as CaCO₃, and small particulates such as silt and sand). Failure is said to occur when the hydraulic conductivity drops sufficiently that the LCS can no longer control the leachate head to the design value (even if considerable

leachate is still being collected). However, the same processes that can cause failure of these systems can also improve leachate quality by removing contaminants. The challenge is to design and operate these systems to take advantage of the microbial processes in treating leachate while avoiding an unacceptable build up of leachate head on the liner (i.e. failure). Thus, the LCS is a very important part of the overall landfill system. It is emphasised that both the design and the operations of the LCS are critical and at present there are many instances of both poor design and poor operations being implemented.

Rowe (2009) reviewed recent research and advances relating the design and long-term performance of LCS for modern MSW landfills. The key conclusions from that paper are reproduced below,

- If there is significant amount of organic waste, leachate with the potential to cause clogging of the leachate collection system can be generated even in arid climates.
- The leachate that is collected from modern landfills does not represent the leachate that enters the system. The biological processes that give rise to clogging of LCS also serve to reduce the concentration of both organic acids (COD, BOD) and inorganic contaminants that are susceptible to precipitation (e.g. calcium and some heavy metals). Thus, any predictions of the service life of LCS must be performed using estimates of the leachate characteristics of the leachate entering the LCS and should not be based on the characteristics of the effluent from existing LCS.
- Laboratory studies of clogging must use a leachate as representative as possible of that likely to be entering the system being examined. Generally this will not be the same as the leachate collected after it has passed through a modern LCS. The tests must also be run long enough to obtain realistic results; this likely means years, even for accelerated tests, except for tests on finer material (which clogs very quickly).
- A sand layer provides a good protection layer for the underlying liner and in so doing can perform a valuable function in this capacity. However, it should not be relied upon as a drainage layer for MSW leachate due its high potential for clogging. An optimal system is likely to involve a sand protection layer above the liner and a gravel leachate drainage layer above the sand.
- The coarser and more uniform the gravel, the longer will be its service life as a leachate drainage layer in a MSW landfill.
- Drainage layers are more prone to clog when kept saturated; thus it is recommended that leachate not be allowed to back-up in the leachate collection system since this (a) accelerates clogging of the LCS and (b) imposes a head on the liner that will increase leakage through any holes in the liner.
- The unsaturated gravel can perform a useful function in treating leachate (reducing the concentration of organic acids and calcium) before it reaches the saturated portion of the drainage layer. Other things being equal, the thicker the unsaturated portion of the drainage layer the greater the amount of leachate treatment and the longer the service life of the LCS.
- Clogging is related to the mass loading and is likely to be greatest near sumps and drainage pipes where the leachate flow is greatest. Clogging is also likely to be increased (other things being equal) when leachate is recirculated.
- When there is a continuous drainage layer, the placement of a suitable filter/separator layer between the waste and the underlying granular drainage layer will extend the service life of the LCS by (a) minimizing waste intrusion, (b) minimizing the migration of fines and other particulates into the drainage layer, and (c) providing some leachate treatment (reduction in organic acids and cations such as calcium) before it enters the drainage layer. In performing this role, the filter/separator layer will experience some clogging and a reduction of hydraulic conductivity (values of the order 6×10^{-8} m/s have been observed). However, one can design to deal with the level of perched leachate provided that there is a drainage layer below the filter and hence the head does not act on the liner and cannot escape to the environment.
- Considerable care is required in developing designs to replace gravel with tire shred. Gravel should be used in critical zones where there is a high mass loading (e.g. near leachate collection pipes or leachate sumps). Tire shreds could be used in less critical zones (e.g. side slopes) although, even then, an increased thickness of compressed tire shred will be needed to give a service life similar to that of a given thickness of gravel.
- Although there has been inadequate research regarding the effects of co-disposal of incinerator ash and MSW, the writer has been contacted in a number of cases by operators who are having problems with clogging of their LCS in situations where there has been co-disposal of incinerator ash (with high calcium, Ca^{2+}) and MSW (where the biodegradation of organic waste provides the CO_3^{2-}). More research is required on this topic; however, considerable caution should be exercised in the design of LCS for landfills where there will be co-disposal of incinerator ash and MSW.

DIFFUSION THROUGH COMPOSITE LINER SYSTEMS

Contaminant transport through a geosynthetic barrier system will involve (a) diffusive transport through the composite liner, and (b) advective transport (termed as leakage) through holes in the geomembrane. The latter transport mechanism is controlled by the clay component of the composite liner as discussed in the next section.

Geomembranes have been shown to be an excellent barrier to ionic contaminants (e.g. chloride, heavy metals etc.; Rowe et al. 2004). However, various researchers (most recently McWatters and Rowe 2007; 2009) have shown that volatile organic compounds (VOCs) could fairly readily diffuse, from both an aqueous and gaseous phase, through PVC, LLDPE and HDPE geomembranes. When these geomembranes are used in composite liners, the clay and attenuation layer provides the primary resistance to diffusive transport and contribute to a decrease the concentration of many organic contaminants due to biodegradation and sorption (Rowe et al. 2004).

An appropriate combination of geomembrane, clay liner and attenuation layer can provide sufficient resistance to diffusive contaminant transport for the various traditional contaminants found in leachate or landfill gas to control impact on an underlying aquifer to acceptable levels in a way that neither the geomembrane nor clay/attenuation layer could do alone.

Islam and Rowe (2009) examined the effect of ageing of HDPE geomembranes on their diffusion and sorption characteristics. They demonstrated that ageing of a HDPE geomembranes led to an increase in crystallinity, which actually had a beneficial effect with respect to diffusion, serving to reduce transport of VOCs through the geomembrane as it aged.

GEOMEMBRANE-CLAY LINER INTERACTION AND EFFECTS ON LEAKAGE

In the absence of holes in the geomembrane there would be no leakage (advection) of leachate or gas through a geomembrane liner (there would still be diffusion as discussed above). However it is not practical to construct a liner with no holes. Where there are holes and the geomembrane is in direct contact with the underlying clay liner, the leakage through the holes will be controlled by the clay liner and the transmissivity of the interface between the geomembrane and the clay liner. It can be shown (e.g. Rowe 2005) that the leakage through the composite liner will be substantially less than through either the geomembrane alone or the clay liner alone due to the composite action of the geomembrane and clay liner. Both theoretical

calculations and field monitoring demonstrate that the leakage through a geomembrane/GCL composite liner is one to two orders of magnitude lower than that of a geomembrane/CCL composite liner. This difference can be attributed to a combination of three things: (a) there is a lower probability of holes in the geomembrane due to underlying stones when underlain by a GCL than a CCL, (b) it is easier to get a relative smooth surface for the foundation layer below a GCL than for the surface of a compacted clay liner (which needs to be compacted 2-4% wet of standard Proctor optimum to achieve a suitable low hydraulic conductivity, Rowe et al. 2004), and, very importantly, (c) upon hydration, the bentonite in the GCL can close up small gaps between the GCL and geomembrane, giving much lower transmissivity of the interface between the geomembrane and GCL than can be achieved with a CCL. The latter two factors contribute to providing a much lower transmissivity for the geomembrane-GCL interface (θ) than for the geomembrane-CCL interface.

SIGNIFICANCE OF WRINKLES IN A GEOMEMBRANE

In the forgoing, it was emphasized that it was the composite action of the geomembrane and clay liner that resulted in low leakage through composite liner. However this is only true when the geomembrane and clay liner are in direct contact (Fig. 2). However, even if the geomembrane is placed with no wrinkles/waves as shown in Fig. 2, wrinkles usually develop due to thermal expansion of the geomembrane (Fig. 3) and if these wrinkles are present at the time the geomembrane is covered with the overlying ballast (e.g. granular drainage layer), it will provide local separation between the geomembranes and the clay liner since significant wrinkles (greater than about 3 cm high) present at the time they are covered generally do not disappear after the geomembrane is covered. Because wrinkles prevent intimate contact between the geomembrane and the underlying GCL or compacted clay liner, any leachate that enters through a hole in a wrinkle can freely move to any other point within the area of the wrinkle and the only hydraulic resistance is due to the clay liner. Thus, the combination of hydraulic conductivity and thickness (due to its effect on hydraulic gradient) of the clay liner becomes much more important where there are wrinkles than where there are no wrinkles. As a consequence, an increase in the hydraulic conductivity, k_s , of the clay liner due to clay-leachate interaction (see Rowe et al. 2004) will be much more significant where there are wrinkles than where the geomembrane and clay are in direct contact.

An equation to predict the leakage through a hole in a

wrinkle forming part of a interconnected wrinkle network of length L was published by Rowe (1998- Fig. 4). However until recently there was no data to assess the likely length of interconnected wrinkles.

To investigate the prevalence of wrinkles, a research study was conducted by the team at Queen's University to (a) quantify wrinkles over time at a specific field site and (b) at a numbers of other sites at the time of construction. Brachman et al. (2007) described the construction of the Queen's Experimental Liner Test Site (located at latitude $44^{\circ}34'14''N$, just north of Kingston, Canada) shown in Fig. 5. As far as we are aware, this is the only exposed and instrumented field geomembrane/GCL site in the world. New imaging techniques developed for wrinkle quantification (Take et al. 2007) have allowed the quantification of wrinkles at different sites by flying a blimp over the site and using high resolution, low altitude (30-70 m) aerial photography. Fig. 6 shows one such wrinkle network.

In addition to quantifying wrinkles on the base of landfills (Fig. 6), this technology also allows the examination of wrinkles on large slopes (Chappel et al. 2008). A paper that quantifies wrinkle properties and demonstrates the relationship between the percentage of a landfill that has significant wrinkles (ranging from a few % to almost 25%) and the time of day has just been submitted for publication. Another paper dealing with wrinkling at the Queen's Experimental Liner Test Site (Figs. 2, 3 and 5) is presently in preparation. When these papers are published designers will have a means of estimating the length of interconnected wrinkles. The findings are generally consistent with the length of wrinkles Rowe (2005) deduced would be necessary to explain the leakage through primary composite liners for landfills with double liner systems. Rowe (2010) will examine the question of leakage through composite liners with wrinkles in much greater detail than is possible here. While it is not essential to eliminate all wrinkles, the presence of wrinkles should be considered in calculating leakage through composite liners in the design. Construction procedures should be adopted to limit the length of interconnected wrinkles present at the time the geomembrane is covered.

IMPLICATIONS OF LINER TEMPERATURE ON CONTAMINANT TRANSPORT (LEAKAGE AND DIFFUSION)

As noted earlier, the temperature on a landfill liner varies with time and for a typical municipal solid wastelandfill the temperature may reach $30^{\circ}C$ - $40^{\circ}C$ and potentially up to about $60^{\circ}C$ for a landfill where there is significant moisture addition to accelerate biodegradation of organic waste. Rowe (2005) indicated that the service



Fig. 2 Geomembrane placed without any significant wrinkles at Queen's Experimental Liner Test Site, Godfrey Ontario. Geomembrane and clay are in direct contact. Note the almost imperceptible crease line (due to blown film process) in the middle of the photo. A similar crease line is shown later in the day (after thermal expansion of the geomembrane) in Fig. 3

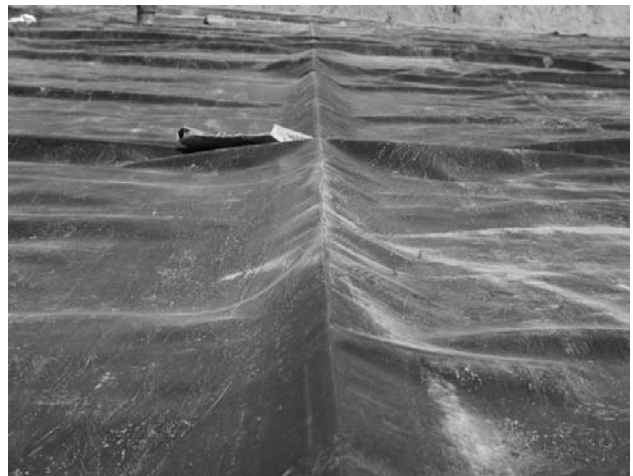


Fig. 3 Geomembrane was placed without any significant wrinkles at Queen's Experimental Liner Test Site. However if the geomembrane is exposed to solar radiation (before being covered) the increase in temperature and consequent thermal expansion lead to wrinkle formation. This photo shows the development of a wrinkle at a crease and subsidiary wrinkles. If there was a hole anywhere in this interconnected wrinkle network, leachate could readily move to any other point below the wrinkle network

life of a geomembrane liner used as part of a composite liner in these landfills will primarily depend on the liner temperature (as discussed in more detail in a later section). However, even before the geomembranes service

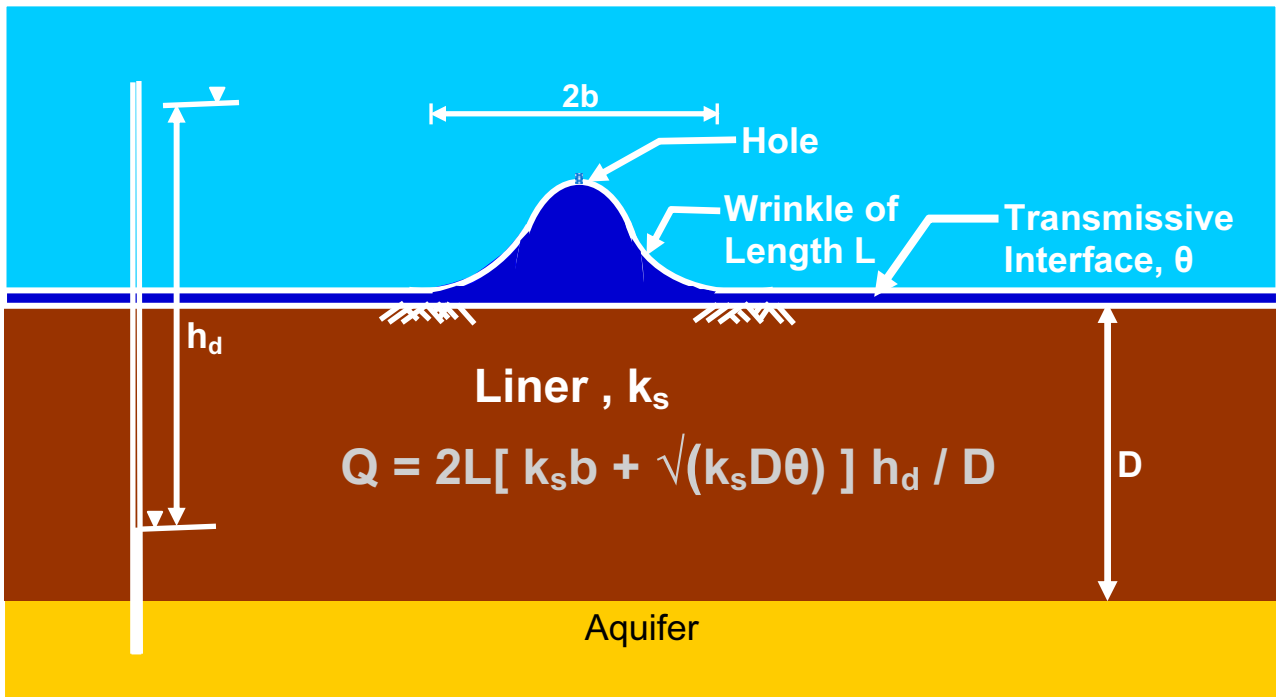


Fig. 4 Rowe (1998) Equation for calculating the leakage Q [m^3/s] from a hole in an interconnected wrinkle network of length L [m] and wrinkle width $2b$ [m], for a clay liner with hydraulic conductivity k_s [m/s], clay liner thickness D [m], geomembrane clay interface transmissivity θ [m^2/s], and head drop across the liner of h_d [m]. See Rowe et al. (2004) for more details

life is reached, temperature can affect both the hydraulic conductivity and diffusion coefficient of the geomembrane and clay liner (Collins, 1993; Rowe, 1998) and hence has the potential to affect the advective-diffusive transport through the liner system.

Contaminant transport analyses are typically performed using parameters obtained in the laboratory at laboratory temperatures (typically about 20°C). Prior to the recent work of Rowe and Arnepalli (2008b), no studies have been conducted to assess the potential effect of liner temperature on contaminant impact. Rowe and Arnepalli (2008b) performed a preliminary analyses of the potential implications of liner temperature for the case of a volatile organic contaminant (dichloromethane, DCM) found in landfill leachate (Rowe et al. 2004) through a composite liner comprised of a 1.5 mm thick HDPE geomembrane over a GCL resting on a 3.75 m thick attenuation layer which in turn is underlain by a 1 m thick aquifer. Most of the cases they considered were selected to correspond to conditions that might be expected in southern Ontario (Canada) where the ambient ground water temperature is about 10°C and the results suggested that, at least for these cases, the peak impact is very close to that predicted for the usual base case of 20°C . If confirmed for other contaminants, this is good news since it implies that the simple approach commonly used in Ontario for landfill design which neglects the influence temperature variation gives quite



Fig. 5 Queen's Experimental Liner Test Site (Brachman et al. 2007) during construction. Note the weather station and monitoring point in the upper centre of the photo. In this photo, the geomembrane has been placed over the GCL on the slopes and is presently being placed on the base. The GCL is not yet covered by geomembrane in the foreground

good results. However, Rowe and Arnepalli (2008b) cautioned that this conclusion should not be generalized until it has been confirmed for a wider range of cases. The one analysis run for a higher ambient groundwater temperature of 20°C gave a peak impact almost twice

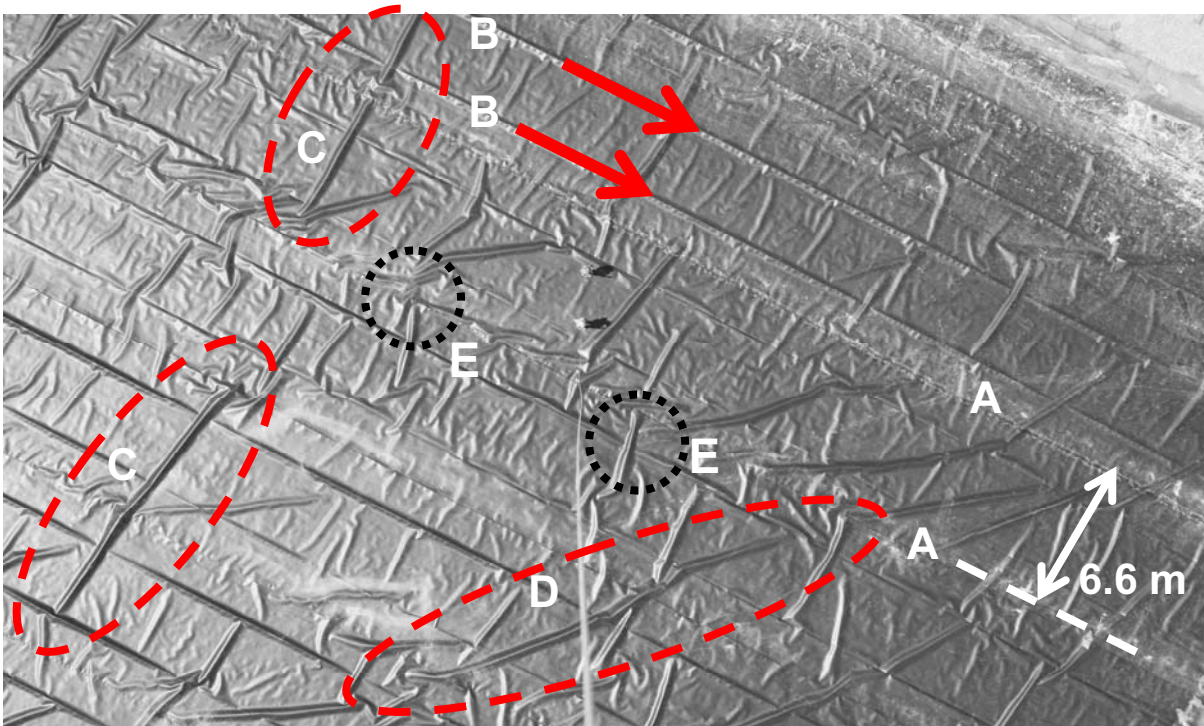


Fig. 6 Wrinkle network at a landfill site at latitude $43^{\circ}16' N$. Photo was taken at 1:20 pm on Aug 18 from a height of 65 m at an air temp $28^{\circ}C$. The width of a roll is shown for scale A-A. Note longitudinal wrinkle parallel to the geomembrane rolls at the creases (B) formed during manufacture as well as the wrinkle perpendicular to the roll direction (C) and at about 45° to the roll direction (D) and the interconnection between wrinkles (E) (Modified from Chappel et al. 2007)

that for the other time varying cases. Thus more investigation is needed to confirm how significant the average groundwater temperature may be with respect to contaminant impact.

POSSIBLE MEANS OF CONTROLLING LINER TEMPERATURE

In instances where it is considered necessary or desirable to operate the landfill in such a manner that it could, using a traditional design, raise the temperatures of the liner above $30^{\circ}C$ - $40^{\circ}C$, the system should be designed to ensure that the LCS and liner will still have an adequate service life to ensure environmental protection despite the elevated waste temperature. One approach to controlling liner temperature proposed by Rowe et al. (2007) involves application of heat exchanger technology. The system is comprised of a horizontal pipe array buried at the base of a landfill. Coolant circulated through the pipes absorbs the heat and reduces temperature in the landfill liner system. The hot coolant is pumped to facilities outside the landfill, where the excess heat is extracted, the coolant temperature is reduced, and the coolant is recirculated through the system.

The results of a preliminary numerical examination

of the feasibility of the proposed system for controlling liner temperature have been reported by Rowe et al. (2009a). They found that that introduction of cooling pipes can substantially reduce liner temperature. The influence of key design variables such as coolant flow rate and pipe spacing were examined. For the case studied, it was shown that the maximum liner temperature could be reduced by about $11^{\circ}C$. It also was found that the layout of cooling system may affect the temperature reduction. The study showed that a detailed examination of these design features is required and that full three-dimensional analyses are required since two-dimensional analyses overestimate liner temperature.

GEOMEMBRANE PROTECTION

The protection layer above a geomembrane serves two purposes: first to minimize the risk of damage to the geomembrane (e.g. holes) during construction, and second to minimize the strains and hence the risk for future holes forming due to environmental stress cracking. The first is well recognised but, except in Germany, the second is not so well recognised or accepted.

Gudina and Brachman (2006b) and Brachman and Gudina (2008b) examined the effect of different protection

layers in controlling the effect of physical stress on the strains developed in geomembranes. For the first time, this work showed that the presence of a wrinkle can increase the strains caused by gravel in the overlying drainage layer. This is important since current practice only considers a flat geomembrane (i.e. no wrinkles). The work of Brachman and Gudina (2008b) also provided the very first quantification of the strain in the geomembrane due to the indentation of the overlying gravel drainage layer through different protection layers under applied landfill stresses. Dickinson and Brachman (2006) looked at the effect different protection layers have upon the deformation of the GCL beneath the geomembrane. This work demonstrated that local thinning of a GCL occurs due to bentonite extrusion beneath gravel contacts and is exacerbated by the presence of a wrinkle.

The work of Gudina and Brachman (2006b) and Brachman and Gudina (2008a,b) clearly shows that geotextile protection layers that represent current North American practice are insufficient to limit the long-term tensile strains in the geomembrane. A study was conducted to examine why the geotextile cannot limit strain and they investigated alternatives to a thick sand layer (since in many applications this may be costly). This work (Dickinson and Brachman, 2008) demonstrates that slack in the geotextile stress-strain response prevents mobilization of force in conventional protection geotextiles until large deformations occur (i.e. it starts to work only after the strains in the geomembrane have increased beyond allowable limits). The work then went on to demonstrate that a 150 mm layer of either poor quality backfill (silty clay) or rubber tire shreds provide excellent protection to the geomembrane and GCL (i.e. inexpensive alternatives to potentially expensive sand have been found). The work also found that creating a composite protection layer with a thick nonwoven geotextile core between two layers of thin, but stiff geotextiles was able to reduce geomembrane strains to allowable levels at room temperature. However, the influence of time, temperature and chemicals on the composite protection layer still has to be assessed prior to use in a landfill.

Based on the work conducted to date, recommendations have been developed to minimize strains in geomembranes and deformations in GCLs. The research has demonstrated that a 150 mm-thick sand protection layer is sufficient to protect the geomembrane and GCL from 50 mm coarse gravel even when subjected to applied vertical pressures as large as 1,000 kPa (Gudina and Brachman 2006b; Brachman and Gudina 2008b; Dickinson and Brachman 2008).

LONG-TERM PERFORMANCE OF GEOMEMBRANE LINERS

The degradation of an HDPE GM liner is commonly

considered to have three stages (Hsuan and Koerner 1998). Stage I: Antioxidant depletion, Stage II: Induction time to the onset of polymer degradation, and Stage III: Polymer degradation involving the decrease in a GM property to an arbitrary level often taken to be 50% of the original value. These three stages will be referenced below.

Rowe et al. (2008a) examined the effect of MSW leachate composition on antioxidant depletion rates. It has been demonstrated that the key constituent of MSW leachate that accelerates antioxidant depletion is surfactant (e.g. soap). The volatile fatty acids and inorganic constituents which make up most of the chemical contamination in leachate had no significant effect (at the 95% confidence level) on the depletion of antioxidants.

Rowe et al. (2009b) examined the effect of geomembrane thickness on antioxidant depletion rates. This paper demonstrated that increasing the thickness of the geomembrane significantly increases the time for antioxidant depletion (other things being equal) but that the level of increase observed experimentally is less than might have been anticipated theoretically based on simple diffusion of antioxidants from the geomembrane. This discrepancy was attributed, in part, to the fact that even though the geomembranes were produced by the same manufacturer, they had different resins and antioxidant packages.

Rowe and Rimal (2008a) demonstrated that the rate of depletion of antioxidants is much slower in a full (simulated) landfill liner system (by about a factor of four) than in simple immersion tests that have previously been used to assess antioxidant depletion. Rowe and Rimal (2008b) showed that the choice of protection layer above the geomembrane significantly affected the rate of antioxidant depletion, with a 1.5 cm thick sand layer (or a GCL) decreasing antioxidant depletion compared to a conventional geotextile protection layer. Rimal and Rowe (2009) demonstrated that for the geomembrane they examined, which had hindered phenols and phosphites as the primary and secondary antioxidants, the depletion of antioxidants could be well modeled by diffusion theory. This theory, which gave good predictions of antioxidant depletion for a 1.5 cm sand protection layer, was used to demonstrate that increasing the sand protection layer to 30 cm would result in a decrease in the antioxidant depletion from the geomembrane and hence substantially increase the liner longevity (by about 100 years at 35°C).

The results obtained by Rowe and Rimal (2008a,b) were for composite liners under gravity stresses. Brachman et al. (2008) described the design of the geosynthetic landfill liner simulators (GLLSs) intended to physically examine the full liner system when subjected to field stresses. Rowe et al. (2009) demonstrated that the

antioxidant depletion was not significantly affected by the applied stresses and the rate of depletion in a composite liner was again about four times slower than in conventional immersion. Recent work (unpublished) experimentally confirmed the theoretical predictions of Rimal and Rowe (2009) that a thick (in this case 15 cm) sand protection layer would substantially reduce antioxidant depletion and extend geomembrane service life. Rowe and Rimal (2008a,b) examined one HDPE geomembrane while Rowe et al. (2009) examined another HDPE geomembrane to assess the importance of GM polymer and antioxidant package. These two studies provided considerable insight regarding the processes of antioxidant depletion in MSW liner systems for different geomembranes with different antioxidant packages. Many of these findings were summarized for the engineering community by Rowe (2009). Antioxidants are a critical component affecting the service life of HDPE geomembrane liners, and therefore these results both allow the best available predictions of the first stage (antioxidant depletion) of geomembrane service life and provide insight regarding design measures that will extend the service life of a given geomembrane.

Much less data is available for Stages II and III of geomembrane service life. Rowe et al. (2009c) have made the first estimates of Stages 2 and 3 of geomembrane degradation based on tests performed on geomembranes (previous estimates have been based on tests on plastic pipes). These estimates will be improved as more data becomes available.

The experimental data obtained above provided one aspect (the change in geomembrane properties with time at a given temperature) of the information needed to assess the service life of geomembranes. The other key factor is the change in the temperature of the liner in the field with time. Studies have been conducted to identify typical landfill liner time-temperature histories. Based on this, Rowe and Islam (2009) used the experimental results noted above to examine the effect of different landfill liner time-temperature histories on the likely service life of the geomembrane in a primary composite liner beneath the waste. Rowe and Hoor (2007) examined the effect of temperature on secondary geomembrane liners for different double liner configurations. Rowe and Hoor (2009) then extended this work and made predictions of the service life of the secondary geomembrane based on the temperature of the primary geomembrane. They demonstrated that for primary composite liners with only a GCL above the secondary leachate collection system, the temperature of the secondary geomembrane liner was only a few degrees below that of the primary liner geomembrane and hence would have a very similar service life unless (a) the secondary liner were thicker (e.g. include a foundation layer with the GCL), or (b) the secondary geomembrane was thicker (see effect of

thickness discussed above). It was recognised that the service life of the GM could be extended by reducing the liner temperature.

Rowe (2009) has provided a more extensive summary of the research noted above and reached the following conclusions regarding the long-term performance of HDPE geomembrane liners:

- The service life of one geomembrane will likely not be the same as that for another geomembrane under the same exposure conditions unless the geomembranes have both the same resin and antioxidant package. Since the antioxidant packages and resins used by geomembrane manufacturers change from time to time, the geomembrane service lives can be expected to change from manufacturer to manufacturer and even from time to time with the same manufacturer.
- The presence or absence of the volatile fatty acids and the typical primary inorganic constituent had negligible effect on the depletion of antioxidants for geomembranes immersed in synthetic MSW leachate. The constituent of leachate responsible for the significant difference in antioxidant depletion rate between geomembranes immersed in water and synthetic leachate was the surfactant (e.g. soap).
- Antioxidants were depleted at a faster rate in relatively acidic or basic immersion media (pH 4 and 10) than at typical MSW leachate (pH 6-8). This suggested that the service lives for geomembranes in contact MSW leachate may be different to that of geomembranes used for hazardous waste, where the pH can be high, or in heap leach pads where the pH can be very low.
- Other things being similar, a thicker geomembrane is likely to have a longer service life than a thinner geomembrane. Thus a thicker geomembrane may be appropriate when the 1.5mm geomembrane cannot provide adequate service life.
- Antioxidant depletion was about 2.2-4.8 times faster for a geomembrane immersed in leachate than for the same geomembrane in a simulated composite liner. Thus to obtain realistic estimate of geomembrane service life one needs to perform tests which simulate the expected conditions in a composite liner.
- Based on modelling of the diffusion of antioxidants, the antioxidant depletion time for a liner temperature of 35°C was predicted to be about 100 years (or more) longer for a 30cm sand protection layer than for the traditional case with just a geotextile protection layer or a thin (1.5 cm) sand protection layer.
- Tests conducted in new experimental apparatus that simulated the ageing of geomembranes under the combined effects of chemical exposure from

synthetic MSW leachate and an applied stress of 250 kPa at elevated temperatures, gave antioxidant depletion times about four times longer than for the same geomembrane immersed in leachate.

- For a geomembrane incubated at 85°C, there was an observed decrease in melt index with time attributed to the oxidative cross-linking even though the geomembrane was immersed in a highly reduced leachate. There was a corresponding decrease in stress crack resistance (SCR) and tensile properties at break. The SCR was more critical than tensile properties in terms of estimating the geomembrane service life (i.e. it gave shorter service lives). The service life at 85°C for the geomembrane was greatest immersed in air and least in leachate (8.75 years based on SCR and projected up to 17 years based on tensile break in air, 5.3-7.7 years in water, 3.4-5.6 years immersed in leachate).
- Based on the available data it was estimated that the service life of the geomembrane tested (immersed in leachate) is likely to exceed 700 years at 20°C, more than 150 years (and likely 225-375 years) at 35°C and more than 40 years (and likely 50-90 years) at 50°C. However, these are preliminary estimates and may change as more data becomes available over the next five years.
- Modelling of heat transfer from the primary to secondary geomembrane liner for different double liner systems, demonstrated that the steady state temperature profile was not very sensitive to thermal properties of liner materials but was highly dependant on the thickness of the soil component of the primary liner.
- For the geomembrane considered, the increase in the service life of the secondary geomembrane over that of an otherwise similar primary geomembrane liner was minimum of 40, 20 and 5 years at 30, 40 and 50°C respectively for an all-geosynthetic system and increased with increasing thickness of the primary liner to 120, 65 and 30 years at 30, 40 and 50°C respectively for a 1m thick primary liner.
- The service life of a geomembrane liner is extremely sensitive to the time-temperature history it experiences, with predicted service lives ranging between thousands of years and a few decades depending on this history. This range illustrates the important role that time-temperature history could play in terms of geomembrane service life and highlights the need for long-term monitoring of landfill liner temperature. It also demonstrated the significant potential effect of even a relatively short period of time at elevated temperatures above 50°C.

It can be inferred from the foregoing that the performance of the geomembrane is dependant on many other parts of the landfill system.

LONG-TERM PERFORMANCE OF GEOSYNTHETIC CLAY LINERS

The long-term performance of the GCL is predominantly governed by two considerations: (a) panel separation due to shrinkage of the GCL before the composite liner is covered with ballast (e.g. the granular drainage layer); and (b) clay-groundwater or clay-leachate interaction which can result in an increase in the hydraulic conductivity of the GCL.

The potential for GCL panel separation (Fig. 7) due to shrinkage of geosynthetic clay liners (GCLs) covered by a geomembrane and left exposed (i.e. with no overlying cover soil), first highlighted by Thiel and Richardson (2005), was emphasized by six reported cases where GCL panels, originally overlapped by 150 mm, had opened up leaving separations between GCL panels of between 200 and 1200 mm after periods of exposure of between 2 and 36 months (Koerner & Koerner 2005a, 2005b; Thiel et al. 2006). Laboratory studies (Thiel et al. 2006; Bostwick et al. 2007, 2008) have demonstrated that shrinkage of up to 23% could be induced in the laboratory by the application of cyclic wetting and drying. There is no documented evidence of loss of panel overlap for composite liners covered quickly and hence not subjected to wet/dry cycles. It is strongly recommended that composite liners involving GCLs be covered with the ballast layer as quickly as possible after placement.

The primary objective of the GCL in a composite liner system is to minimize leakage through holes in the geomembrane as discussed in an earlier section of this paper. This is largely achieved by limiting the lateral spreading of leachate once it gets through the hole in the geomembrane due to the low transmissivity of the interface between the geomembrane and GCL (Rowe 1998). It is well known (e.g. Petrov and Rowe 1997; Petrov et al. 1997; Ruhl and Daniel 1997; Rowe 1998) that interaction between the bentonite in a GCL and cations in a hydrating or permeating fluid can, in some cases, significantly increase the hydraulic conductivity of GCLs from the normal value with respect to water ($1 \times 10^{-11} \text{ m/s} < k < 5 \times 10^{-11} \text{ m/s}$) to values typically around $2 \times 10^{-10} \text{ m/s}$ but in extreme cases to as high as $3 \times 10^{-8} \text{ m/s}$. For a composite liner the hydraulic conductivity of the GCL is only really important in those zones where there is a significant head on the GCL (relative to the thickness of the GCL). Thus Rowe (1998) demonstrated that for a geomembrane in direct contact with a GCL, and provided that the transmissivity of the interface does not change significantly, a two order of magnitude increase in the hydraulic conductivity of the GCL only increased the leakage by a factor of about two. Therefore, even with significant chemical interaction between the GCL and leachate, the presence of the GCL can still substantially

decrease the leakage through holes in the geomembrane where there is direct contact between the GM and GCL. Thus the composite liner is still much better than a single geomembrane liner. As noted in a previous section, the change in hydraulic conductivity becomes much more significant where there are holes in wrinkles.



Fig. 7 Panel separation of a GCL in a composite liner in California (after Thiel and Richardson, 2005)

When dealing with GCLs resting on a less than ideal foundation (such as over a leak detection system or, to a lesser extent, gravel or coarse sand) there is the potential for internal erosion causing an increase in hydraulic conductivity as shown by Rowe and Orsini (2003) and also potentially causing clogging of the LDS (Giroud and Soderman 2000). This is a factor that should be considered where significant heads can develop over the primary GCL giving rise to high hydraulic gradients that could cause internal erosion. As long as the leachate collection system controls the leachate head to a low value (typically less than 0.3 m), this is unlikely to be a problem. However if the LCS fails or if its operation is discontinued, the build-up in leachate head could cause problems due to internal erosion. As indicated by Rowe and Orsini (2003), some GCLs are much more prone to this problem than others.

CONTAMINANT TRANSPORT IMPLICATIONS

Contaminant transport through landfill barrier systems is commonly modelled using the program POLLUTE (Rowe and Booker 1995; 1998; 2005). El-Zein and Rowe (2007; 2008a,b) described a new model developed for modelling 2D leakage through holes in the geomembrane and the effect of holes in wrinkles in the GM. They compared the predictions made with the new model with those obtained from conventional techniques using finite layer theory. They found that, in general, the

results from the conventional approach (e.g. using the program POLLUTE) were adequate for most engineering applications, but that the more sophisticated model may be required if the predictions from the conventional approach were close to regulatory limits (i.e. if the conventional predictions were within about 15%-20% of the regulatory limit then more accurate analysis would be required to provide a better prediction of potential impacts).

The various issues affecting the base barrier system discussed in this paper can generally be modeled using the program POLLUTE. For example, Rowe and Arnepalli (2008a) theoretically examined the effect of geomembrane ageing (using data obtained as indicated above) on diffusive transport and concluded that this factor could be ignored from a practical perspective. Rowe and Arnepalli (2008b) also theoretically examined the effect of landfill liner temperature on diffusive-advective transport of volatile organic compounds. They demonstrated that this could be an important consideration in landfill design, especially in climates where the groundwater temperature was of the order of 20°C. Currently, this aspect is neglected in design.

CONCLUSIONS

From an engineering perspective, the long-term performance of the modern MSW landfill will be governed by the performance of a system comprised of three primary subsystems: the barrier system below the waste, the landfill operations, and the landfill cover and gas collection system. This paper has argued that in order to minimize the environmental impacts of a landfill, it is necessary to adopt a systems engineering approach to the design, construction and operation of the landfill. This involves decomposing the entire system into subsystems as noted above. Each subsystem needs to be decomposed into simpler identifiable components, the performance of the individual components examined, the interactions between different components of the system assessed, and then the response of the entire system assembled to quantify its overall engineering performance. This evaluation must consider how the interaction between different components affects the performance of the entire system and how, due to this interaction, the performance of the system as a whole is better than the individual contributions of each of the parts. In particular, it was shown that an action that may enhance the performance of one part of the system may have negative effects on other parts of the system. The objective should be to ensure optimal performance of the entire system, not the components. This relates to both operations and the landfill design itself. For example, operational issues such as the waste placement sequence or recirculation of leachate can

impact on the service life of the underlying barrier system in either a positive or negative way depending on the details of how they are implemented. Also, the design of the leachate collection system and protection layer can have a significant effect on the leakage of contaminants through the underlying composite liner as well as on the service life of the composite liner. Furthermore, the time of placement of the protection and drainage layer over a composite liner (and the consequent wrinkles) can have a profound effect of leakage through the composite liner and factors such as interaction between a geosynthetic clay liner and the leachate will assume much greater significance if the geomembrane has significant interconnected wrinkles than if only a small proportion of the geomembrane is wrinkled due to the loss of composite liner action directly below wrinkles.

Considering all these issues, it is concluded that safe waste containment and long-term environmental protection can best be provided by taking a systems approach to the design, construction and operations of modern MSW landfills.

ACKNOWLEDGEMENTS

Funding for the research infrastructure used to obtain most of the results leading to the conclusions in this paper was provided by the Canada Foundation for Innovation and the Ontario Innovation Trust (OIT-MRI). Much of the research itself was funded by the Natural Sciences and Engineering Research Council of Canada. The research into the clogging of leachate collection systems was conducted in collaboration with Mr. M. Armstrong and Drs. I Fleming, A. Cooke, R. Cullimore, R. McIsaac and B. Rittmann. The investigation into the long-term performance of geosynthetic liner systems is being done in partnership with the Ontario Ministry of the Environment, Ontario Centres of Excellence, Terrafix Geosynthetics Inc., Solmax International Inc., AMEC Earth and Environmental, AECOM (Gartner Lee Ltd.), Golder Associates, CTT Group, Dr. Grace Hsuan from Drexel University, Drs. Richard Brachman, Andy Take, Greg Siemens, Mohammed Rayhani and Edwin Safari of the Geoengineering Centre at Queen's-RMC, Drs. N. Arnepalli, S. Dickinson, S. Gudina, Z. Islam, S. Rimal, H. Sangam formerly of the Geoengineering Centre at Queen's-RMC and present PhD students, F. Abdelaal, M. Chappel, A. Ewais, A. Hoor and R. McWatters. Many thanks to Ms. R. McWatters for carefully proof reading the paper.

REFERENCES

Armstrong MD & Rowe RK (1999). Effect of landfill

operations on the quality of municipal solid waste leachate, Proceedings of 7th International Landfill Symposium, S. Margherita di Pula, Cagliari, Sardinia, October, II: 81-88.

- Bostwick LE, Rowe RK, Take WA, Brachman RWI (2007). The effect of sample size on shrinkage of a non-scrim reinforced geosynthetic clay liner, 60th Canadian Geotechnical Conference, Ottawa, ON, 2123-2128.
- Bostwick LE, Rowe RK, Take WA, Brachman RWI (2008). Observations of the dimensional stability of four GCL products under combined thermal and moisture cycles, Geoamericas 2008, Cancun, Mexico: 435-443.
- Brachman RWI & Gudina S (2008a). Gravel contacts and geomembrane strains for a GM/CCL composite liner, Geotextiles and Geomembranes, 26 (6): 448-459.
- Brachman RWI & Gudina S (2008b). Geomembrane strains and wrinkle deformations in a GM/GCL composite liner, Geotextiles and Geomembranes, 26 (6): 488-497.
- Brachman RWI & Sabir A (2007). Preliminary assessment of the physical response of a double composite GM/CCL liner, 60th Canadian Geotechnical Conference, Ottawa, October: 2143-2148.
- Brachman RWI, Rowe RK, Take WA, Arnepalli N, Chappel MJ, Bostwick LE, Beddoe R (2007). Queen's composite geosynthetic liner experimental site, 60th Canadian Geotechnical Conference, Ottawa, October: 2135-2142.
- Brachman RWI, Rowe RK, Arnepalli DN, Dickinson S, Islam MZ, Sabir A (2008). Development of an apparatus to simulate the ageing of geomembranes under chemical exposure, elevated temperatures and applied stresses, Geoamericas 2008, Cancun, Mexico, March: 444-451.
- Brune M, Ramke HG, Collins H, Hanert HH (1991). Incrustation processes in drainage systems of sanitary landfills, Proceedings of the 3rd International Landfill Symposium, Sardinia: 999-1035.
- Chappel MJ, Take WA, Brachman RWI, Rowe RK (2008). A case study of wrinkles in a textured geomembrane on a slope, Geoamericas 2008, Cancun, Mexico, March: 452-458.
- Collins HJ (1993). Impact of the temperature inside the landfill on the behaviour of barrier systems. Proceedings of 4th International Landfill Symposium, Sardinia '93, 1: 417-432.
- Dickinson S & Brachman RWI (2006). Deformations of a geosynthetic clay liner beneath a geomembrane wrinkle and coarse gravel, Geotextiles and Geomembranes, 24(5): 285-298.
- Dickinson S & Brachman RWI (2008). Assessment of

- alternative protection layers for a geomembrane / geosynthetic clay liner (GM/GCL) composite liner, *Canadian Geotechnical Journal*, 45(11): 1594-1610.
- Dickinson S, Brachman RWI, Rowe RK (2009). Thickness and hydraulic performance of geosynthetic clay liners overlying a geonet, *ASCE Journal of Geotechnical and Geoenvironmental Engineering*, (Tentatively accepted)
- El-Zein A & Rowe RK (2007). Simultaneous leakage and diffusion of organic pollutants through damaged geomembranes, Tenth International Symposium on Numerical Methods in Geomechanics, NUMOG X, Rhodes, Greece, April 2007: 297-301.
- El-Zein A & Rowe RK (2008a). Parametric study of the effect on groundwater quality of leakage of benzene and toluene through composite liners, Euro-Geo 2008, Edinburgh, UK.
- El-Zein A & Rowe RK (2008b). Impact on groundwater of concurrent leakage and diffusion of DCM through geomembranes in landfill liners, *Geosynthetics International*, 15(1): 55-71.
- Giroud JP & Soderman KL (2000). Criterion for acceptable bentonite loss from a GCL incorporated into a liner system, *Geosynthetics International*, Special Issue on Liquid Collection Systems, 7(4-6): 529-581.
- Gudina S & Brachman RWI (2006a). Effect of boundary conditions on deflection of GM wrinkles in a GM/GCL composite liner, 8th International Geosynthetics Conference, Yokohama, Japan, September: 255-258.
- Gudina S & Brachman RWI (2006b). Physical response of geomembrane wrinkles overlying compacted clay, *Journal of Geotechnical and Geoenvironmental Engineering*, 132(10): 1346-1353.
- Ham RK & Bookter TJ (1982). Decomposition of solid waste in test lysimeters, *ASCE Journal of Environmental Engineering*, 108 (6).
- Hsuan YG & Koerner RM (1998). Antioxidant depletion lifetime in high density polyethylene geomembranes, *J. Geotech. Geoenv. Eng.*, 124(6): 532-541.
- Jones-Lee A & Lee GF (2000). Appropriate use of MSW leachate recycling in municipal solid waste landfilling, in *Proceedings Air and Waste Management Association 93rd National Annual Meeting*, CD-ROM paper 00-455, Pittsburgh, PA.
- Koerner GR & Koerner RM (2006). Long term temperature monitoring of geomembranes at dry and wet landfills, *Geotextiles and Geomembranes*, 24(1): 72-77.
- Koerner RM & Koerner GR (2005a). GRI White Paper #5 - In-Situ Separation of GCL Panels Beneath Exposed Geomembranes, *Geosynthetic Institute*, Folsom, PA, April 15, 2005, 21
- Koerner RM & Koerner GR (2005b). In-situ separation of GCL panels beneath exposed geomembranes, *GFR*, June-July 2005: 34-39.
- McWatters RS & Rowe RK (2007). Diffusive migration of volatile organic compounds through geomembranes, *Geosynthetics 2007, Proceedings Environmental Conference*, Washington: 106-120.
- McWatters RS & Rowe RK (2009). Transport of volatile organic compounds through PVC and LLDPE geomembranes from both aqueous and vapour phases, *Geosynthetics International*, (In press).
- Islam MZ & Rowe RK (2009). Permeation of BTEX through unaged and aged HDPE geomembranes, *ASCE Journal of Geotechnical and Geoenvironmental Engineering*, (In press).
- MoE (1998). Landfill standards: a guideline on the regulatory and approval requirements for the new or expanding landfill sites, Ontario Ministry of Environment, Ontario Regulation 232.98, Queen's Printer for Ontario, Toronto.
- Petrov RJ & Rowe RK (1997). Geosynthetic clay liner compatibility by hydraulic conductivity testing: Factors impacting performance, *Canadian Geotechnical Journal* 34(6): 863-885.
- Petrov RJ, Rowe RK, Quigley RM (1997). Selected factors influencing GCL hydraulic conductivity, *Journal of Geotechnical and Geoenvironmental Engineering ASCE*, 123(8): 683-695.
- Phaneuf RJ (2000). Bioreactor landfills – Regulatory issues, in *Proceedings 14th Geosynthetic Research Institute Conference*: 9-26.
- Rimal S & Rowe RK (2009). Diffusion modelling of OIT depletion from HDPE geomembrane in landfill applications, *Geosynthetics International*, (Accepted 24/3/09; in press).
- Rowe RK (1998). Geosynthetics and the minimization of contaminant migration through barrier systems beneath solid waste, Keynote Lecture, *Proceedings of the 6th International Conference on Geosynthetics*, Atlanta, March, 1: 27-103, Industrial Fabrics Association International, St. Paul, MN
- Rowe RK (2005). Long-Term Performance of Contaminant Barrier Systems, 45th Rankine Lecture, *Geotechnique*, 55 (9): 631-678.
- Rowe RK (2009). Long-term performance of leachate collections systems and geomembrane liners for MSW landfills, Keynote lecture, *GeoAfrica 2009*, Capetown, September 2009 (in press).
- Rowe RK (2010). A systems engineering approach to minimizing leachate leakage from landfills, Theme lecture at the 9th International Conference on Geosynthetics, Brazil.
- Rowe RK & Arneppalli D (2008a). Modelling the effects of aging of geomembranes on contaminant transport and the long-term performance of landfill composite liners, Theme lecture, 12th International Conference of International Association for Computer Methods

- and Advances in Geomechanics (IACMAG), Goa, India: 2334-2344.
- Rowe RK & Arnepalli D (2008b). The effects of landfill temperature on the contaminant transport through a composite liner, 12th International Conference of International Association for Computer Methods and Advances in Geomechanics (IACMAG), Goa, India: 2398-2404.
- Rowe RK & Booker JR (1995). A finite layer technique for modelling complex landfill history, *Can. Geotech. J.*, 32(4): 660-676.
- Rowe RK & Booker JR (1998). Modelling impacts due to multiple landfill cells and clogging of leachate collection systems, *Can. Geotech. J.*, 35(1): 1-14.
- Rowe RK & Booker JR (2005). POLLUTEv7 Pollutant migration through a nonhomogeneous soil, ©1983-2005, Distributed by GAEA Environmental Engineering, Ltd. 87 Garden Street, Whitby, Ontario, Canada L1N 9E7, Fax: 1-905-666-3744, e-mail: support@gaea.ca.
- Rowe RK & Hoor A (2007). Temperature of secondary liners in municipal solid waste landfills, *Geosynthetics 2007*, Washington, January: 132-146.
- Rowe RK & Hoor A (2009). Predicted temperatures and service lives of secondary geomembrane landfill liners”, *Geosynthetics International* (Accepted 6/12/08, in press).
- Rowe RK & Islam MZ (2009). Impact on landfill liner time-temperature history on the service life of HDPE geomembranes, *Waste Management*, (in press) doi:10.1016/j.wasman.2009.05.010.
- Rowe RK & Orsini C (2003). Effect of GCL and subgrade type on internal erosion in GCLs, *Geotextiles and Geomembrane*, 21(1): 1-24.
- Rowe RK & Rimal S (2008a). Depletion of antioxidant from HDPE geomembrane in a composite liner, *ASCE Journal of Geotechnical and Geoenvironmental Engineering* 134(1): 68-78.
- Rowe RK & Rimal S (2008b). Ageing of HDPE geomembrane in three composite liner configurations, *ASCE Journal of Geotechnical and Geoenvironmental Engineering* 134(7): 906-916.
- Rowe RK, Hoor A, Pollard A (2009a). Examination of a Method for Reducing the Temperature of MSW Landfill Liners, submitted for review.
- Rowe RK, Islam MZ, Hsuan YG (2008a). Leachate chemical composition effects on OIT depletion in an HDPE geomembranes, *Geosynthetics International*, 15(2): 136-157.
- Rowe RK, Islam MZ, Hsuan YG (2009b). Effect of thickness on the ageing of HDPE geomembranes, *ASCE Journal of Geotechnical and Geoenvironmental Engineering*, (In press)
- Rowe RK, Pollard A, Chong A, Chisholm E, Toda R, Tomson C (2007). Sustainable landfills—a technique for extracting heat to prolong service-life of geomembrane liners, 60th Canadian Geotechnical Conference, Ottawa, October: 1310-1315.
- Rowe RK, Rimal S, Sangam HP (2009c). Ageing of HDPE geomembrane exposed to air, water and leachate at different temperatures, *Geotextiles and Geomembranes*, 27(2): 131-151.
- Rowe RK, Quigley RM, Brachman RWI, Booker JR (2004). *Barrier Systems for Waste Disposal Facilities*, Taylor & Francis Books Ltd (E & FN Spon) London, 587.
- Ruhl JL & Daniel DE (1997). Geosynthetic clay liners permeated with chemical solutions and leachates, *Journal of Geotechnical and Geoenvironmental Engineering ASCE*, 123(4): 369-380.
- Take WA, Chappel MJ, Brachman RWI, Rowe RK (2007). Quantifying geomembrane wrinkles using aerial photography and digital image processing, *Geosynthetics International*, 14(4): 219-227.
- Thiel R & Richardson GN (2005). Concern for GCL Shrinkage when installed on slopes, *ASCE GeoFrontiers C Austin*, CD-ROM, Paper GRI-18, 7.
- Thiel R, Giroud JP, Erickson R, Criley K, Bryk J (2006). Laboratory measurements of GCL shrinkage under cyclic changes in temperature and hydration conditions, 8th International Conference on Geosynthetics, Yokohama, Japan (1): 21-44.
- USEPA (2008). *Inventory of U.S. Greenhouse Gas Emissions and Sinks: 1990-2006*. U.S. Environmental Protection Agency, Office of Atmospheric Programs, Washington, DC. USEPA #430-R-08-002.
- Yuen STS, Styles JR, Wang QJ, McMahon TA (1999). Findings from a full-scale bioreactor landfill study in Australia, in *Proceedings of 7th International Landfill Symposium*, Sardinia '99, Cagliari, Italy, 53 – 5 of French Assoc. for Computation. Grenoble.

STATIC AND SEISMIC ANALYSIS OF SOLID WASTE LANDFILLS

Pedro Simão Sêco e PINTO¹

ABSTRACT: The general characteristics of waste materials for static and seismic conditions are addressed. The static and dynamic response of barriers is presented. The performance of solid waste landfills during earthquakes is described. The analysis of solid waste landfills stability during earthquakes is presented. The advantages of quality assurance are pointed out. Instrumentation and monitoring to assess the safety control of waste landfills in order to detect any anomalies and to propose corrective actions is presented. The advantages of risk analysis to guide future investigations and to supplement conventional analyses in making decisions on waste landfills safety are discussed.

INTRODUCTION

The need of construction of high solid waste landfill in order to protect human health and the environment has created new engineering challenges.

In this framework the static and seismic behavior of solid waste landfills has deserved considerable attention.

The characterization of material properties for static and seismic design of solid waste landfills is a difficult task as due the heterogeneity of the material large samples are needed.

Also it is important to analyze the static and dynamic response of barriers.

The performance of solid waste landfills during earthquakes is described.

The analysis of solid waste landfills stability during earthquakes is presented.

The advantages of quality assurance are pointed out.

Instrumentation and monitoring to assess the safety control of waste landfills in order to detect any anomalies and to propose corrective actions is presented.

The advantages of risk analysis to guide future investigations and to supplement conventional analyses in making decisions on waste landfills safety are discussed.

GENERAL CHARACTERISTICS OF WASTE MATERIALS

The municipal solid wastes (MSW) are in general composed by a mixture of particules of different materials (i.e. plastic, wood, organics, etc.), and of different size. An industrial waste consists mainly of plaster.

Due to biodegradation and physic-chemical process the

mechanical properties of these waste materials are changing with time.

Different methods are used for the characterization of wastes, e.g. boring, test pits, SPT tests, CPT tests and sampling (De et al. 2004). It is important that these samples were representative of type and age of waste, placement techniques, acidic phase/stable methane phase (for municipal solid waste landfills).

A proposal for a geotechnical classification of different waste materials is given in Table 1.

Table 1 Geotechnical classification of waste materials according to GLR (1993)

Soil-like waste	Non Soil-like waste
Excavated soil	Municipal solid waste (MSW)
Industrial sludge	Bulky waste
Road construction debris	Green waste
Incineration residue & slag, ash, dust)	MSW-like industrial waste
Construction debris	Waste from construction sites
Sewage sludge	Solids Residues from mechanical-biological treated wastes

¹ Professor, National Laboratory of Civil Engineering(LNEC),University of Coimbra and University New of Lisbon, Portugal, President of the International Society for Soil Mechanics and Geotechnical Engineering. Email: pspinto@lnec.pt

The composition and characteristics of municipal solid wastes are also related with the status of the community and to cultural and dietary factor (Fig. 1). For instance the composition of MSW in USA integrates large proportions of paper, cardboard, plastic and textiles in comparison of South Africa that contains less paper and great proportion of organics waste (Blight, 2006).

SOLID WASTE CHARACTERIZATION

The shear strength properties of waste landfills are not easily determined since the physical composition of the mixture makes it unsuitable for the conventional laboratory strength testing. Testing equipment must withstand possible corrosive impacts, geometry of testing device must usually be 5 to 10 times larger than the maximum particle size of the tested waste material and in case of contaminated materials personnel protection must be guaranteed (Sêco e Pinto, 2008a). The size of testing equipment is too small relative to the normal size of the refuse. Also the shear parameters of municipal solid waste show a broad variety and a differentiation between fresh and old wastes.

To overcome this situation the waste properties are established based on the type of waste, the waste processing and the placement procedures.

Some properties are measured directly, such as dry density and water contents and other properties due the difficulties related with sampling are obtained from indirect methods combining with the existent knowledge of waste properties (Sêco e Pinto, 1997).

Total unit weights of the material are determined from in-place testing or laboratory compaction tests.

Kavazanjian (1995) has proposed an unit weight profile with depth (Fig. 2).

From literature survey the particle size distribution of municipal solid waste is shown in Fig. 3 (Jessberg, 1994).

Zekkos et al. (2006) using family curves developed on the basis of case weight versus depth curves the proposal of Fig. 4 after analysing several case histories.

From results of laboratory and field tests the shear parameters of municipal waste exhibits a diferentiation between fresh and old waste (Jessberg, 1996) (Fig. 5).

Also direct simple shear test laboratory tests on reconstituted large samples are used to determine large strain properties.

Machado et al. (2006a) based in triaxial tests conducted in MSW samples of 4 years old have obtained significant difference in the shear strength mobilization curves (Fig. 6).

Large scale shear tests were performed by Caicedo et al. (2002) in undisturbed samples of 0.9 m of diameter in Dona Juana Landfill located in city of Bogota. The tests were conducted in four stages. (i) a sample from the landfill was directly carved in place and the two pieces of

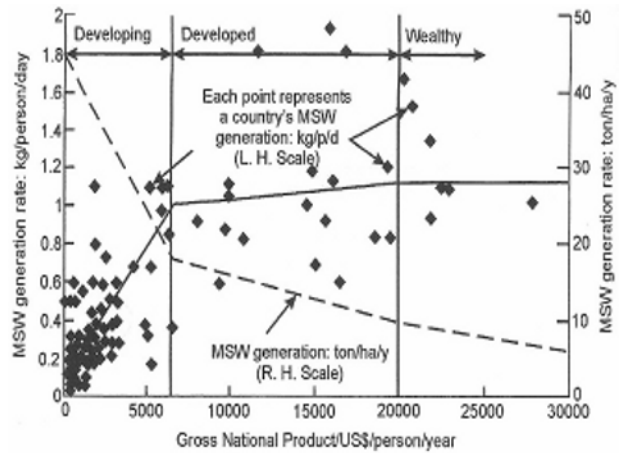


Fig. 1 Rate of generation of municipal solid wastes (after Medina, 1997 and Blight and Mbande, 1998)

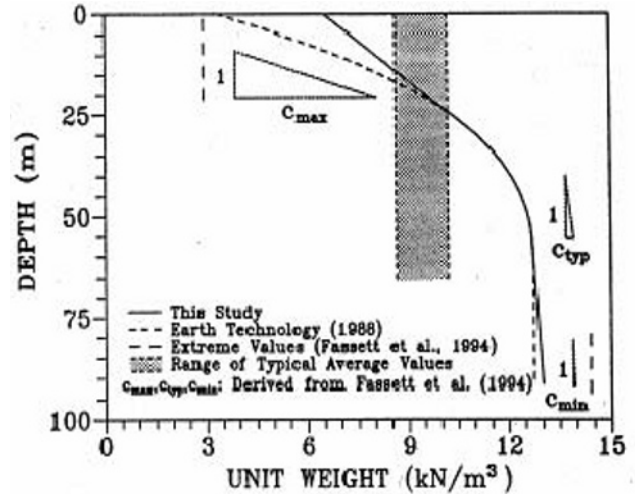


Fig. 2 Unit weight of MSW (after Kavazanjian, 1995)

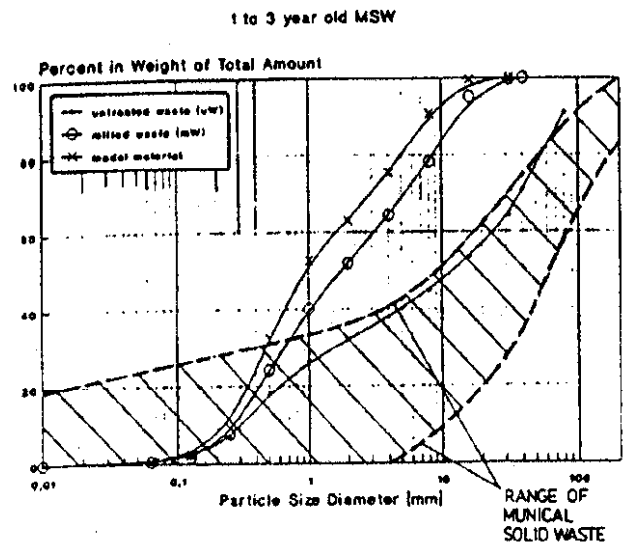


Fig. 3 Particle size distribution of waste for laboratory tests (after Jessberg, 1994)

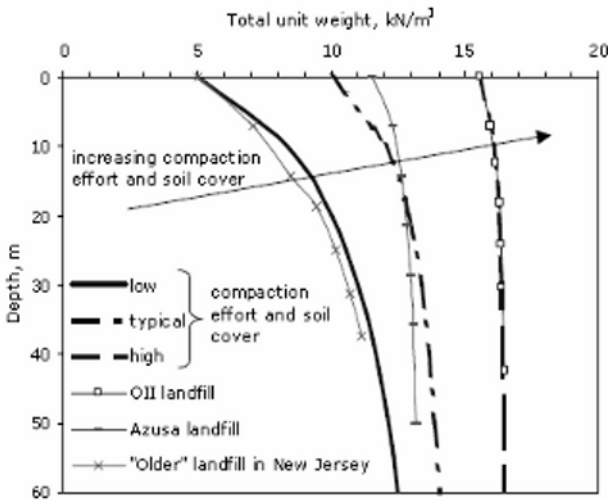


Fig. 4 Unit weight (after Zekkos et al. 2006)

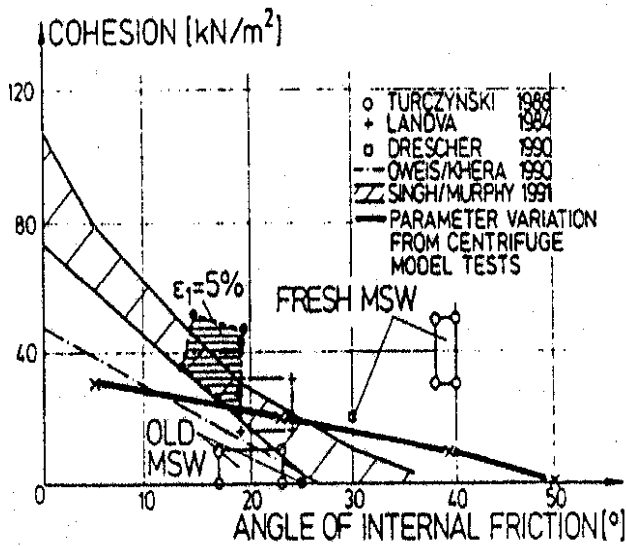


Fig. 5 Shear parameters of municipal solid waste (after Jessberg, 1996)

the shear box located around it, (ii) a loading frame is next set in place and instrumented. This frame permits the application of vertical and shear stresses, (iii) a normal stress is then applied and kept constant during of the test, (iv) the shear force is progressively applied increasing the load to the maximum stress, which is typically found for 60 mm of deformation.

The obtained results are shown in Figs. 7 and 8.

For the municipality solid waste landfills that are the most common, the stability analysis is affected by the uncertainties in the mechanical parameters, such as internal friction angle, cohesion and Young module, which are very difficult to determinate through laboratory or in situ tests.

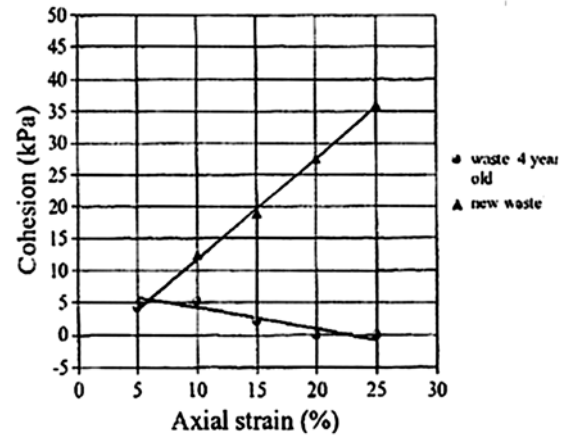
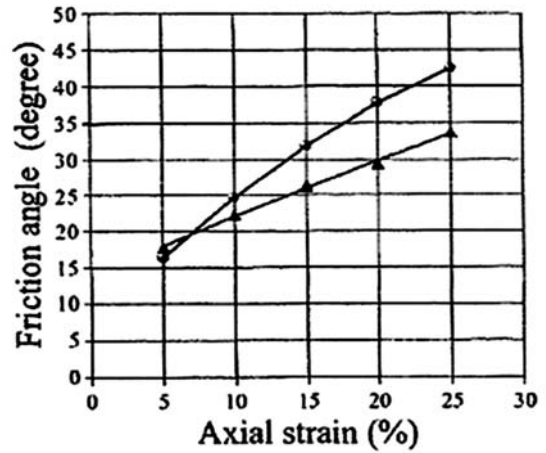


Fig. 6 MSW shear strength parameters mobilization as a function of axial strain (after Machado et al. 2006a)

A summary of the results obtained for the shear strength of MSW in Dona Juana landfill using different methodologies is presented in Fig. 9.

Numerous investigations of the waste behaviour have been conducted experimentally obtaining the following typical correlations reported in graphic form (Fig. 10).

Kavazanjian et al. (2001) compared bi-linear shear strength envelope with MSW shear strength envelope from back analysis of landfills and concluded in Fig. 11 that the former remain a lower bound effective stress envelope for MSW.

Bligh (2006) has illustrated in Fig. 12 the difficulties to measure the shear strength parameters of a MSW material due its heterogeneity and also high variable composition.

The mechanisms governing domestic waste settlement are complex. The term of consolidation suggested steps of MSW load-settlement curves, refers to settlement from the dewatering, shrinkage (decomposition of organic material) and compaction (overburden). This proposal is shown in Fig. 13 (Grisolia et al. 1992).

A composite rheological model and a computer program to calculate landfill settlements considering

primary and secondary mechanical compression from biodegradation of municipal solid waste were developed by Marques et al.(2002).

Machado et al. (2006b) have shown in Fig. 14 that are small changes in the initial young modulus and ultimate tensile stress in new samples, although samples 4 years old show a behaviour less plastic where the stress decrease after to reach the peak value.

Time effects on landfills behavior are the following (Mello and Boscov, 2002): (i) change in strength and compressibility behavior of MSW; (ii) clogging of drainage system; (iii) degradation of geo-membrane; (iv) change in water and gas pressure in the waste mass; (v) dissemination of pollutants.

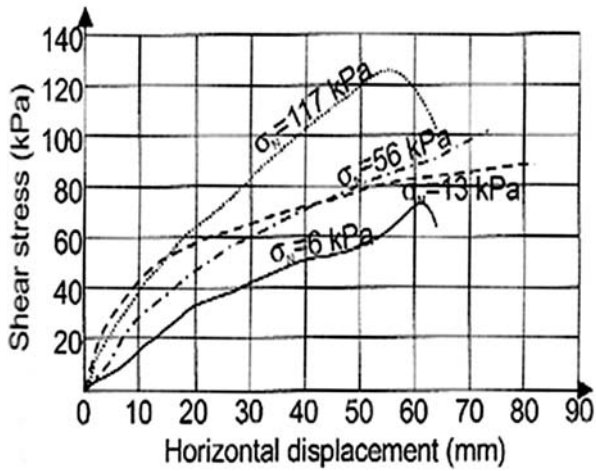


Fig. 7 Horizontal displacement versus shear strength for field direct shear tests in Dona Juana sanitary landfill (after Caicedo et al. 2002)

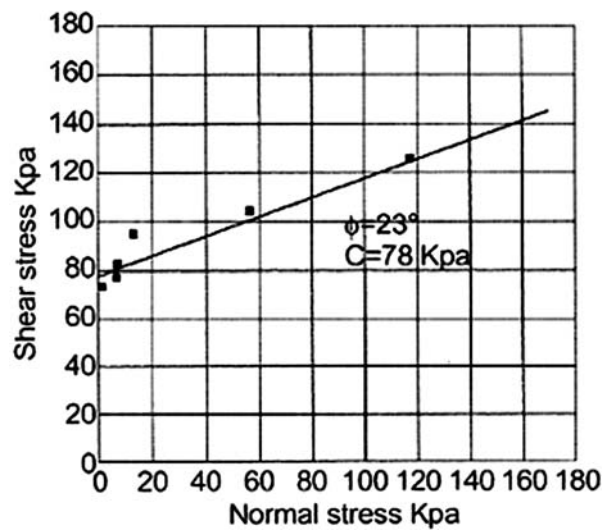


Fig. 8 Results of field direct shear tests in Dona Juana sanitary landfill (after Caicedo et al. 2002)

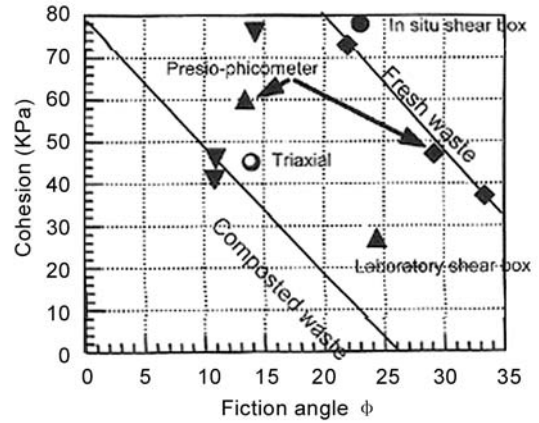


Fig. 9 Summary of shear strength results obtained for Dona Juana sanitary landfill (after Caicedo et al. 2002)

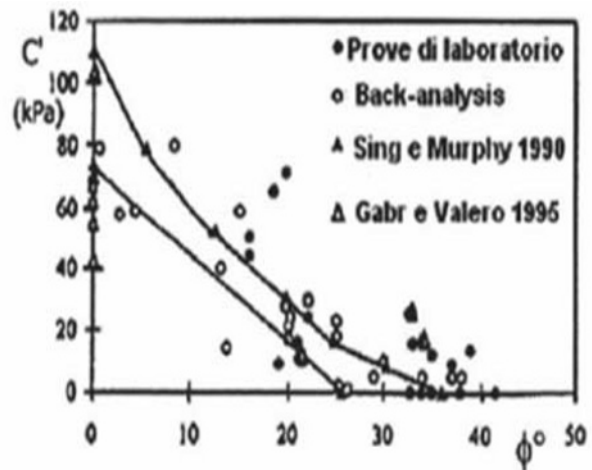
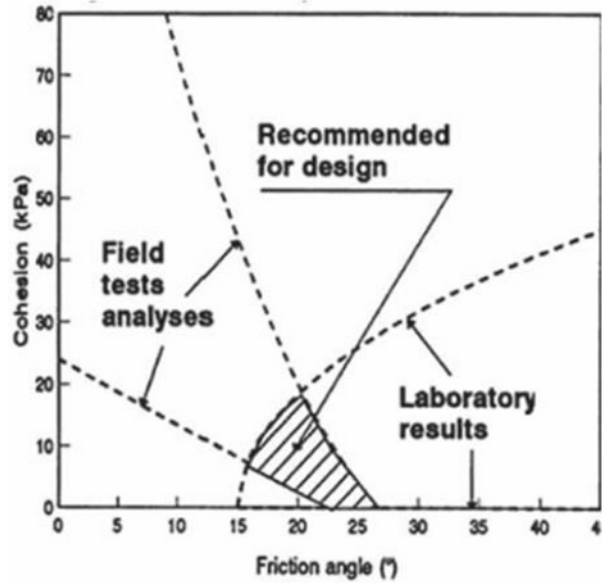


Fig. 10 Typical correlations for waste parameters

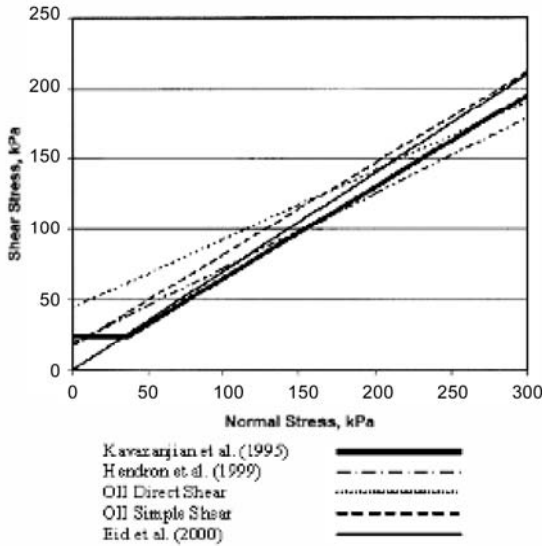


Fig. 11 MSW shear strength envelopes (after Kavazanjian et al. 2001)

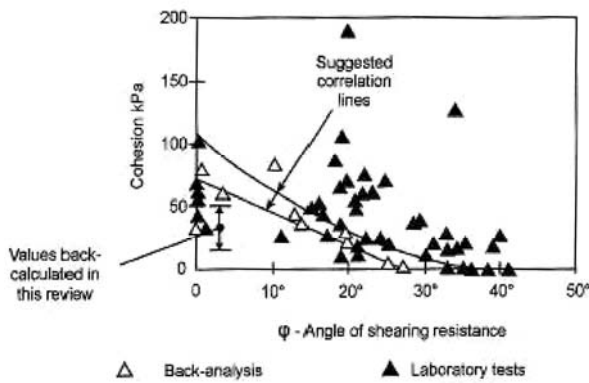


Fig. 12 Shear strength parameters for municipal waste (after Bligh, 2006)

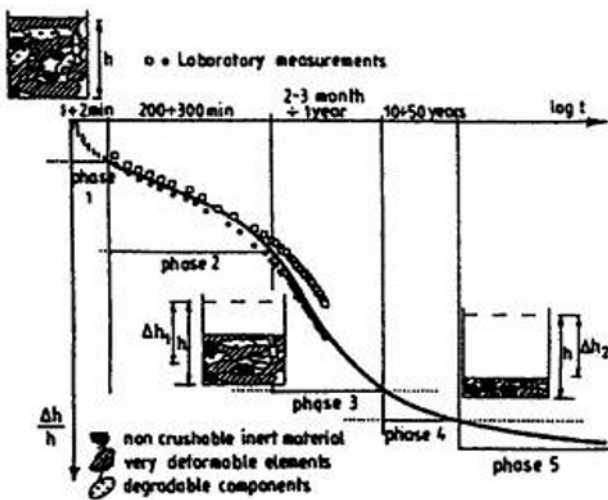


Fig. 13 General compression curve from MSW (after Grisolia et al. 1992)

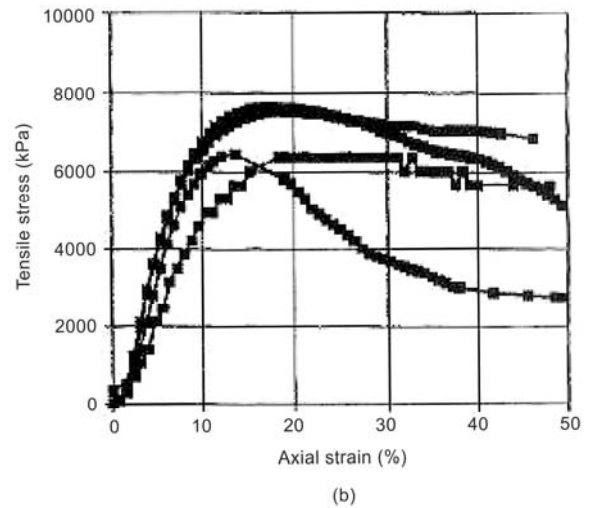
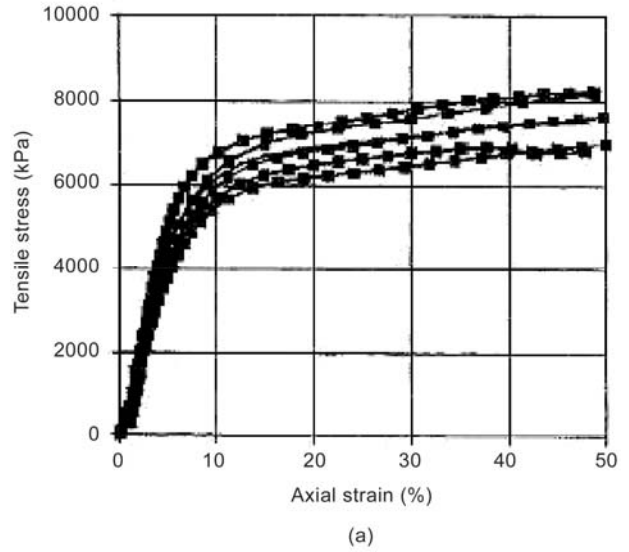


Fig. 14 Stress-strain curves obtained (a) new samples;(b) 4 years old samples (after Machado et al. 2006b)

Commoulos (2003) has shown based on observation that a landfill which is placed rapidly would yield higher settlements rates than a landfill with a longer construction period. In Fig. 15 is presented schematically that two waste columns A and B at the same landfill with different construction periods that the settlements rates of waste column A with the shorter construction period are higher than those of column B with the longer construction period.

Zekkos et al. (2007) have conducted stress-strain response tests of MSW materials under slow and rapid monotonic loading in large direct shear device (with 300 mm side and 180 mm height) and large triaxial shear device (with 300m diameter and 600-630mm height). The effect of composition, confining stress and loading rate were studied.

Variable strain rate direct shear and triaxial compression tests on waste materials of varying composition have shown that rate effects play an important role and dynamic shear strength of unsaturated MSW is about 20 % greater than the static shear strength.

Kavanjian (2008) has suggested based in data presented in Fig. 16 that, while predicting the total magnitude of post-closure settlement a priori may be problematic, long-term post-closure landfill settlement may be reasonably predicted, by monitoring post-closure settlement for a period on the order of 100 days and then extrapolating settlements on a log scale.

In situ determination of some MSW deformability parameters, such as shear and elasticity moduli and Poisson coefficient, is not yet a common practice. More frequent is the assessment of such parameters originated from back analysis. This can be understandable due to waste highly heterogeneous constituents and some site operational difficulties.

Bello et al. (2004) have developed a full displacement pressuremeter, specially designed for MSW landfill investigation. The system allows measurements of up to 100% radial deformation, which means approximately 5cm radial, possibly reaching the undisturbed waste matrix and allowing to incorporate the anisotropy effect.

The potentialities and limitations of SPT tests, CPTu tests and Plate load tests to characterize municipal solid waste landfills were discussed by Oliveira and Muriata (2004).

A wide range of reported Vs values for MSW compiled by Kavazanjian et al. (1996) is shown in Fig. 17.

Matasovic et al. (2004) have proposed the use of cone penetration test (CPT) to evaluate the undrained shear strength. For the determination of cone shear strength factor the authors have proposed the use of non intrusive SASW tests. A summary of the results of SASW profiles conducted in five waste landfills is presented in Fig. 18.

SASW is a particularly attractive method of investigation for landfill engineering where the nonintrusive nature of the methods eliminates many of the health and safety concerns typically associated with conventional borings for geoenvironmental investigations (Avsar et al. 2004).

The variation of shear modulus G and damping ratio λ with shear strain can be derived by laboratory tests (Sêco e Pinto, 1990).

For the variation of shear modulus and damping characteristics of waste materials, sandy silt material and silty material, with shear strain, the curves proposed by Singh and Murphy (1990) or by Vucetic and Dobry (1992) are presented in Fig. 19.

A very important aspect of linear elastic behavior by developing curves with much smaller reduction of shear modulus with strain is pointed by Singh (2002) in Fig. 20.

Singh (2002) suggested that the age and the state of decomposition of the refuse material be taken when selection a modulus reduction curve. Decomposed peat material may exhibit greater reduction in shear modulus with shear strain, however younger refuse material will

show very small reduction of shear modulus with shear strain.

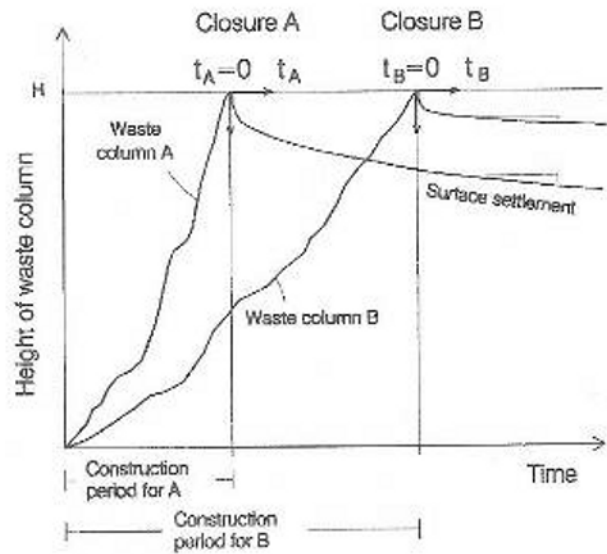


Fig. 15 Long-term settlements (after Commoulos, 2003)

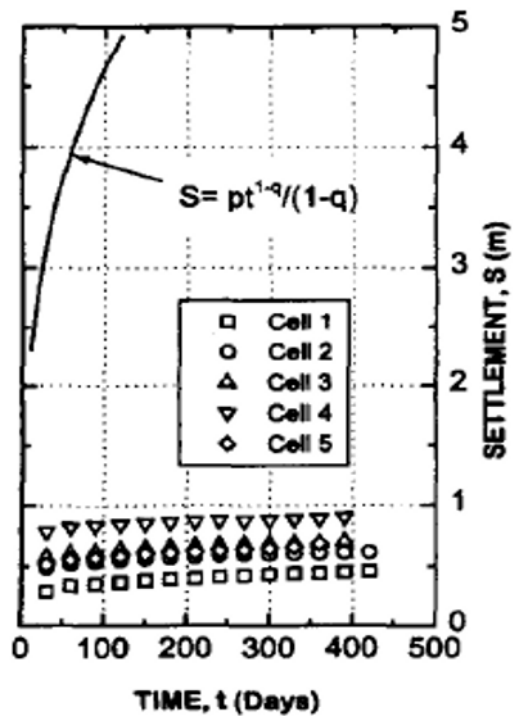


Fig. 16 Post-Closure Settlements (after Kavazanjian, 2008)

Towhata et al. (2004) have conducted cyclic triaxial tests. Figs. 21 and 22 show the variation of dynamic Young modulus and damping ratio with strain amplitude.

Back analysis of strong motion records captured at the base and crest of landfill provides the most reliable available information on modulus reduction and damping of MSW under seismic loading. Four different groups of reputable investigators came up with four

different sets of modulus reduction and damping curves, as shown in Fig. 23 (Kavazanjian, 2008).

The dynamic characteristics of municipal solid waste degradation in bioreactor landfills were analyzed by Hossain et al. (2007). The four different phases, namely anaerobic acidogenic phase, accelerated methanogenic phase and early and late decelerated methanogenic phases were investigated. The results of resonant column tests have shown that shear modulus and material damping curves versus shear strain are significantly affected by the degree of decomposition.

When solid waste landfills incorporate construction demolition debris the curves proposed for rockfill and gravel materials can be used.

DeJong et al. (2006) observed an increase in shear wave velocity from approximately 200 m/s to 540 m/s due to microbial treatment and pointed a similar shearing response to gypsum cemented soils under undrained conditions (Fig. 24).

The development of microbiological processes for improvement of the physical properties of soil is getting increase attention.

In Geomicrobiology the microorganisms play an important role in geological processes and the interactions between minerals.

Bioremediation has become an accepted remedy for soil and groundwater contaminated with hydrocarbons, especially with benzene, toluene, ethylbenzene, and xylene (BTEX). Natural attenuation relies upon native microorganisms to degrade and transform contaminants (Kavazanjian and Karatas, 2008).

Bench-scale experiments in progress at Arizona University are exploring the potential for microbially induced calcium carbonate precipitation through denitrification for improvement of engineering properties of granular soils (Karatas et al. 2008).

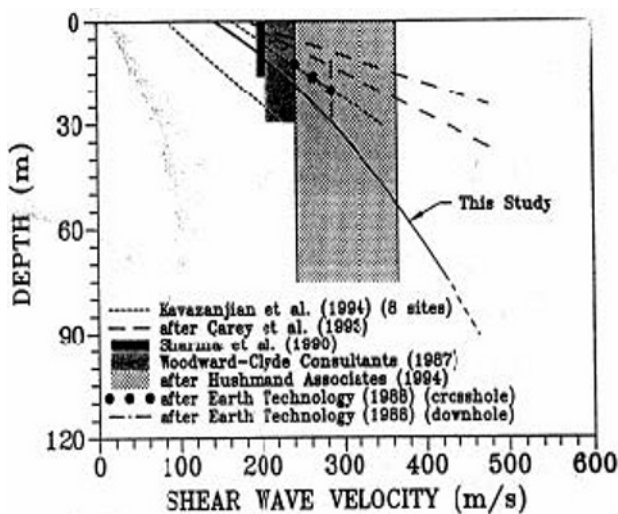


Fig. 17 Shear wave velocity of MSW (after Kavazanjian et al. 1996)

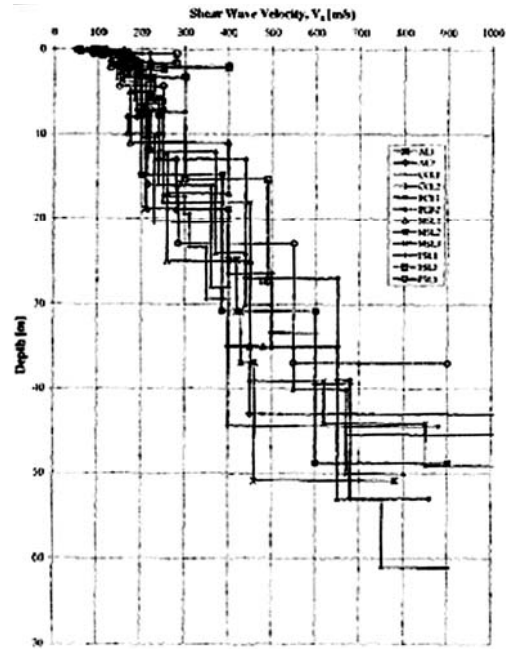


Fig. 18 SASW Database (after Matasovic et al. 2004)

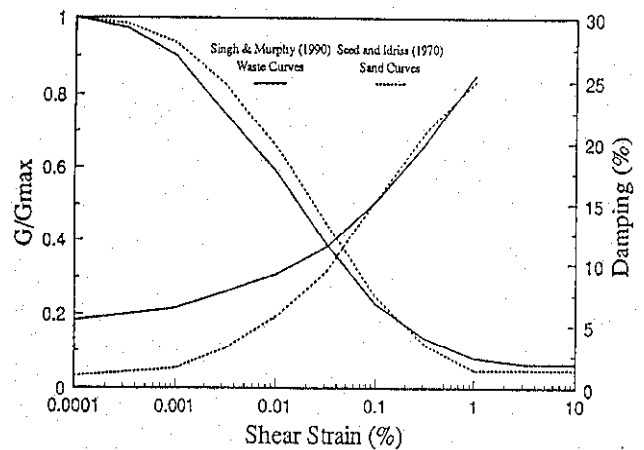


Fig. 19 Waste modulus degradation and damping curves used in study (after Singh and Murphy, 1990)

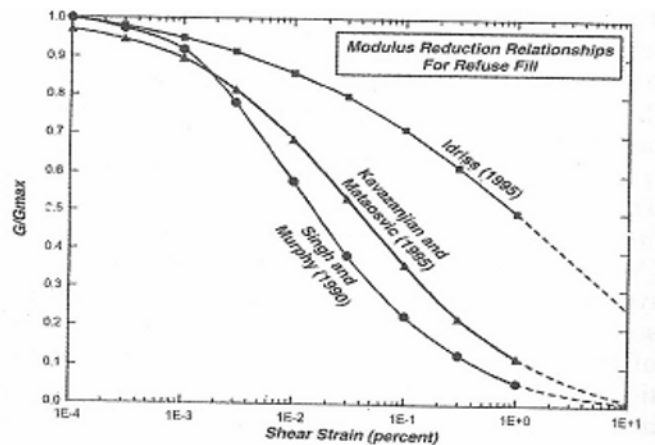


Fig. 20 Shear modulus reduction for refuse fill (after Singh, 2002)

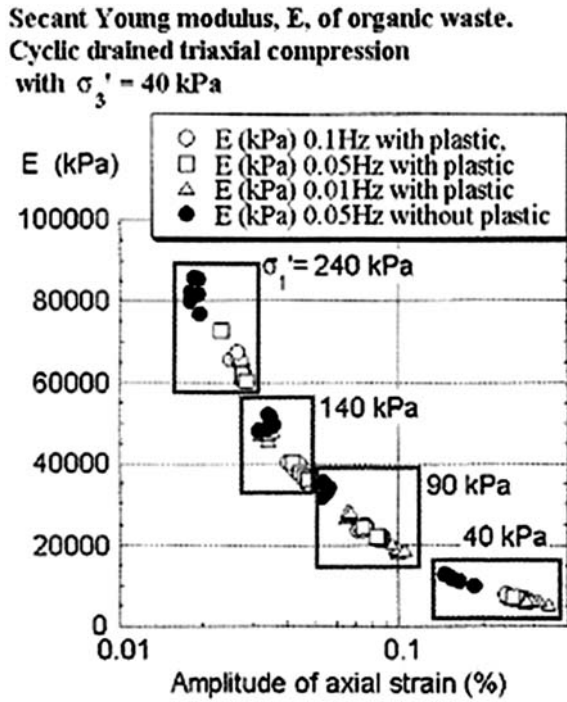


Fig. 21 Variation of dynamic Young modulus with strain amplitude (after Towhata et al. 2004)

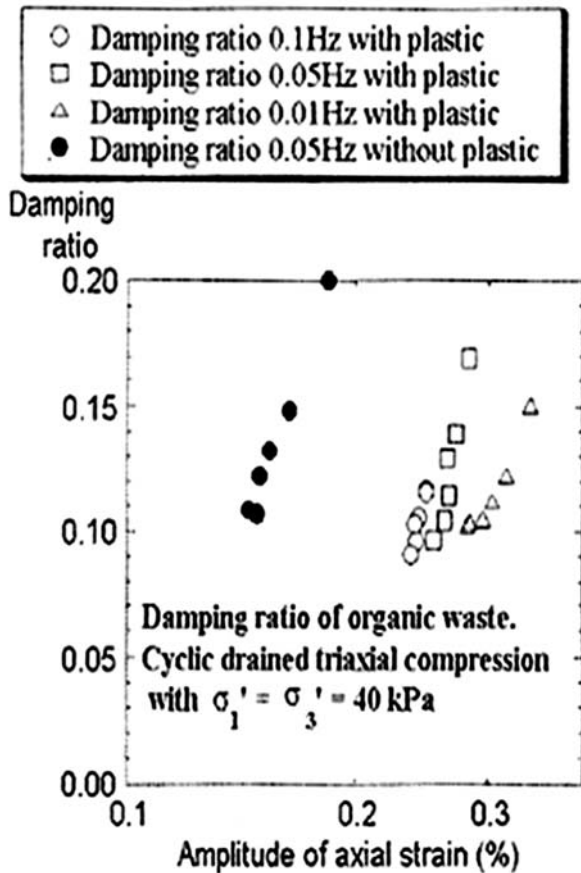


Fig. 22 Variation of damping ratio with strain amplitude (after Towhata et al. 2004)

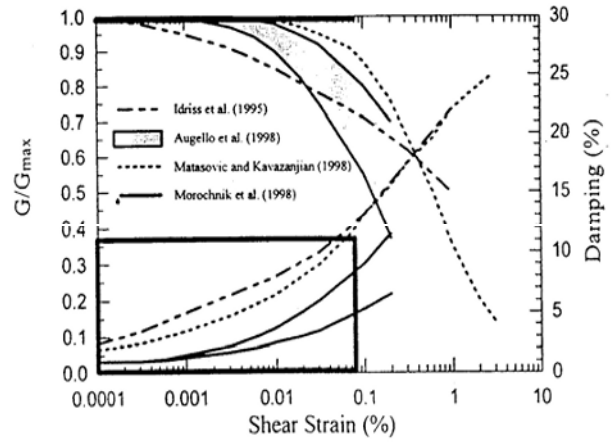


Fig. 23 Modulus and Damping ratio (after Kavazanjian, 2008)

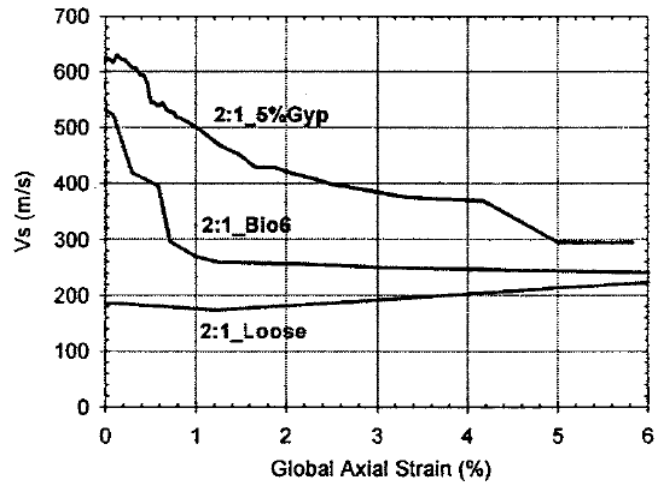


Fig. 24 Shear wave velocity measured during monotonic triaxial tests (after DeJong, 2006)

Until recently, the application of microbiological processes to improve the mechanical properties of soil for engineering purposes (e.g. increasing shear strength, decreasing compressibility, decreasing hydraulic conductivity) remained largely unexplored, in spite the potential benefits in geologic and anthropogenic processes. For example carbonate precipitation can result in cementation within soil increasing the shear strength and decreasing the hydraulic conductivity. The optimal microbial mineral precipitation mechanism should be calibrated taking into account the site characteristics.

Cabalar and Canakci (2005) based in a series of direct shear tests on sand mixed with different ratios of xanthan gum have shown an increase in average shear strength at failure from 30 kPa to 190 kPa when the xanthan gum content of the sample was increased from 1 percent to 5 percent.

Srivastava, RK et al. (2006) have explored the use of

GIS to identify the appropriate site locations through spatial analysis. The GIS database has integrated data acquisition (topographic maps, borehole data), scanning of maps, georeferencing and digitizing maps.

STATIC AND DYNAMIC RESPONSE OF BARRIERS

Introduction

The design of barriers of modern landfills should be based on the following main principles:

The mineral barrier is the basic component of traditional sealing systems referring in particular to the long-term performance. The requirements and characteristics of the mineral sealing layer in order of importance are: (1) low hydraulic conductivity (HC) at field scale, (2) long-term compatibility with the chemicals to be contained, (3) high sorption capacity, and (4) low diffusion coefficient.

Composite lining systems using geomembranes can give important advantages both in the short and long-term due to: (1) reduction of HC as a result of the attenuation of defects of both geomembrane and compacted clay (2) better biogas control; (3) minimization of desiccation problems; (4) enhancement of flow within the drainage layers toward the collection pipes (i.e. minimization of ponding leachate on the liner) and (5) the geomembrane on the top of the clay barrier delays contact between clay and leachate long enough for consolidation of the clay when the waste is landfilled, thus reducing compatibility problems. Construction procedures play a fundamental role in the final efficiency of the lining system in terms of field-scale HC.

Compacted Clay Liners

Compacted clay liners are clayey soils that have been remoulded and constructed to obtain a low hydraulic conductivity liner. Successful construction of a low hydraulic conductivity CCL using an adequate soil type and therefore design life of this system is highly dependent on: (a) water content control; (b) breakup of clods of soil and homogenization of non uniform soils; (c) lift thickness; and (d) method of compaction and equipment used. CCLs may experience an increase in hydraulic conductivity with time by several orders of magnitude if not adequately protected against desiccation cracking or frost damage. This is also a particular concern for CCL used as cover material in landfills.

Both desiccation cracking and frost damage protection are key to the design life of these barrier systems and can be mitigated through quality construction control and assurance.

Deformation of Compacted Soil Liner in a Geocentrifuge tests was analysed by Viswanadhan and Sergupta (2006). Fig. 25 shows that for SSL-3 shallow and wide cracks penetrating up to three fourth of the liner thickness, for SSL-4 wide and deep cracks penetrating up to full depth and in SSL-10 a number of small cracks were found to be distributed at the zone of maximum curvature.

The service life of a clay liner is the period of time during which the bulk hydraulic conductivity of the liner may be expected to fall within the design range. Provided the liner is properly designed and constructed and appropriate attention has been paid to clay-leachate compatibility (e.g. Rowe et al. 1995), it is expected that it will perform within the range of design hydraulic conductivity for thousands of years (MoE, 1998).

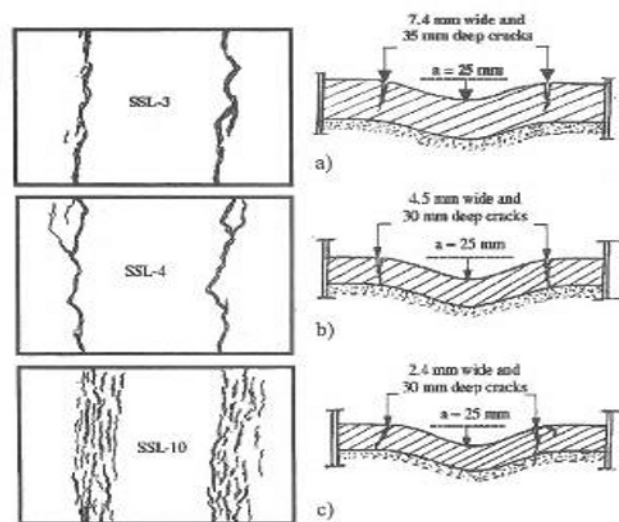


Fig. 25 Centrifuge results(after Viswanadhan and Sergupta, 2006)

Bentonite Enhanced Soils

Geosynthetic clay liners provide a convenient and potentially economical low permeability alternative to compacted clay liners both in covers and base liners in many situations. Due to the fact that it is a manufactured product, typically produced using either powdered or granular sodium bentonite, a high level of quality control can be achieved. The main advantages of GCLs are their limited thickness, improved resistance to differential settlement, ease of installation and low cost.

A database of 414 large-scale direct shear tests was assembled to evaluate variables governing geosynthetic clay liner (GCL) internal shear strength (Zornberg et al. 2004). Good repeatability of test results was obtained using same manufacturing lot GCL specimens, while comparatively high variability was obtained using different lot specimens.

Peak shear strength variability was found to increase linearly with normal stress, but to be insensitive to specimen conditioning procedures.

Geomembrane Liners

Geomembranes are planar, relatively impermeable polymeric sheets. Due to their low permeability, they make excellent liners for fluid retaining structures. There are many different types of geomembranes and the selection of a particular type depends upon the application in which it will be used.

The aging process of HDPE geomembranes can be envisioned as simultaneous combination of physical aging and chemical ageing. This includes chemical degradation, oxidative degradation, degradation by swelling, degradation by extraction, biological degradation and UV degradation. Oxidative degradation appears to be the most harmful to HDPE geomembranes, which are the most common geomembranes used in landfill liner applications due to their superior chemical resistance.

It was estimated that for the particular geomembrane examined, provided that the landfill is well maintained such that the liner (i.e. geomembrane) temperature is not higher than 15°C, the primary geomembrane would last at least 200 years whereas for the conditions where the temperature is at 33°C (an increase in temperature as a result of leachate mounding, discussed below), the service life is estimated to drop to about 70 years. It was also estimated that geomembranes used as secondary liners will last at least 400 years for a temperature range typical of groundwater, 7 to 10°C.

Concerns regarding the clogging of leachate collection systems have lead to the use of coarse drainage material in these systems. It is essential to ensure that the geomembrane is adequately protected against the potential detrimental effects of coarse gravel indenting the geomembrane, especially under the high overburden pressures in large landfills. The development of tensile strains within the geomembrane due to impingement of the coarse drainage material may have serious implications on the service life of the geomembrane and may impair its primary design function as a barrier to advective flow due to the development of holes.

Geomembrane liners are widely used in waste landfills mainly as base liner and cover liner to avoid water table and environmental contamination.

The results of centrifuge model tests provide useful information for the design of the spacing and placement of the reinforcement strips and the design and construction of actual prototype driving equipment (Zimmie, 2005).

polyurea is a material chemically similar to polyurethane can be separated in fluid form and then mixed during application to create a solid membrane. The material is applied using a spray technique or by pouring, depending on the desired thickness of the membrane. Curing time varies based the thickness of the membrane and on the temperature of the applied material, but the initial cure occurs relatively quickly and the final cure is several days (Burns and Parson, 2005).

Long term thermal regime of landfill liner systems using field temperature monitoring program and numerical analysis on heat transfer. Temperatures in liner system that contain geosynthetic clay liner (GCLs) were monitored prior and subsequent to waste placement. Temperatures in liners reached 30° C under 5-year old waste with an annual rate of temperature gradients decreased however, high variation in gradients remained subsequently to waste placement.

To analyse the long term sealing effect under field conditions test were conducted in lysimeter. The obtained results are summarized by Heerten (2006) in Fig. 26.

Yegian et al. (1995) by conducting shaking table tests have concluded that: (I) the geosynthetic interface reduces the level of the acceleration pulses of the ground motion; and (ii) the geosynthetic interface acts as base isolator absorbing the wave energy through interface slip.

Lee et al. (2007) have conducted large scale shaking table tests to understand the seismic behavior of geosynthetic reinforced slopes (GRS). In addition have performed numerical analyses using FLAC code. From the large scale shaking table tests the authors have concluded that GRS slopes with longer embedded length of reinforcement, smaller vertical reinforcement spacing and higher reinforcements stiffness exhibit better resistance to seismic loading (Figs. 27 and 28).

The estimated antioxidant depletion time for the HDPE geomembrane showing the critical importance of liner temperature and the nature of the chemical exposure proposed by Rowe (2006) is summarized in Table 2.

Table 2 Estimated antioxidant depletion time for the HDPE geomembrane (after Rowe, 2006)

Temperature	Air years	Water years	Leachate years	Simulated Liner
10	510	235	50	280
20	235	110	25	115
30	110	55	15	50
35	80	40	10	35
40	55	30	8	25
50	30	15	5	10
60	15	8	3	6

Landfill Drainage Layers

High transmissivity drainage layers may be used above liners to minimize the hydraulic head acting on the liner (and hence minimize flow through the liner). These drainage layers may be constructed from granular materials or geosynthetics or a combination of both. The maximum liquid thickness must be estimated for two reasons: (1) the liquid thickness is typically limited by regulations (e.g. the Resource Conservation and Recovery Act in the US requires a maximum liquid thickness of 0.3 m), and (2) good design requires that the liquid thickness be less than the thickness of the lateral drain (to avoid confined flow).

Special care is required to ensure adequate long-term drainage capacity. Geotextiles are often used as filters between the waste and the drainage layer—especially when either coarse drainage materials (e.g. gravel) or geonets are used to provide a drainage blanket. There has also been considerable debate regarding the use of carbonate drainage stone due to the potential for dissolution of the rock by leachate.

The clogging problem arises because municipal solid waste leachate contains nutrients that will encourage bacterial growth in geotextile filters, in granular drainage layers, around the perforations in the leachate collection pipes and within the pipes.

Details of experimental tests conducted in shaking table to analyse the behaviour of waste landfills with geotextile reinforcements is shown in Figs. 29 and 30.

Fig. 31 shows the schematic installation of sensor arrays in the cells.

Dynamic Geosynthetic Interface Behaviour

The key point of the geomembrane liners response to earthquake is the behaviour of geosynthetic interfaces. Slippage along interface could be possible; this may produce attenuation of earthquake induced acceleration to the cover liner but may cause some stability problems during and after earthquake loading.

To avoid this phenomenon it is necessary to control the interface strength, i. e. the limit value of the shear stress available along the interface in static and cyclic/dynamic condition, considering the different geosynthetic/geosynthetic and geosynthetic/soil combinations used in the field.

As far as the static interface strength analysis is concerned (Martin et al. 1984; Williams and Houlihan, 1986; Nigussey et al. 1989; Mitchell et al. 1990), it must be firstly emphasised that the friction angle between geosynthetic and soil is lower than the soil shearing resistance angle. Also the friction angle between geosynthetic and geosynthetic is lower than that between

geosynthetic and soil. Moreover, the residual interface strength is completely mobilised since a very low strain level. In any case, the static interface shear strength is influenced by different factors, such as the moisture, the geosynthetics disposition (in comparison with loading direction), the polishing grade in case of geomembrane use, the geosynthetic structure, the surface roughness, the soil nature (Jewell, 1990; Stark and Poeppel, 1992; O'Rourke et al. 1990).

The shear interface resistance of liner and cover systems landfills has deserved increasing attention.

The long term performance of geomembranes depends of their properties, tensile strains, exposure to chemicals in the leachate and temperature (Rowe, 2006). Chemical ageing of geomembranes has three distinct stages: (i) depletion time of antioxidants, (ii) induction time to the onset of polymer degradation; and (iii) degradation of the polymer to decrease some property to an arbitrary level (Hsuan and Koerner, 1998)

The dynamic properties of the geosynthetic liner can be replaced by the dynamic properties of the equivalent soil layer measured by shaking table tests.

Horizontal geosynthetic interfaces have a potential effect to modify the seismic response of overlying material.

Smooth HDPE geomembrane/geotextile liners reduce significantly the accelerations and shear stresses transmitted through the landfill profile, especially when the base acceleration exceeds 0.2g, as pointed by Yegian and Kadakal (1998). These effects should be taken into account to avoid unrealistic estimates of seismic acceleration, shear stresses and permanent deformations in a landfill.

From the comparison between the static and the cyclic/dynamic conditions it is possible to note considerable divergences in the interface shear strength, even if some factors, such as the moisture, have similar effects. Besides, for cyclic loads of small frequency, the shear strength is principally influenced by the number of cycles. For dynamic loads the difference in the shear strength from static to dynamic condition is due to the inertial and viscous effects linked to the load velocity and to its time variation (Carrubba and Massimino, 1998).

Particularly, to evaluate the frictional properties of the typical landfill interfaces, the most utilised device is the shaking table test (Hushmand and Martin, 1990; Yegian and Lahlaf, 1992; Strano, 2000). The normal stress on the considered interface is generated by means of a concrete block.

Until no block-table relative displacement occurs, the block moves in phase with the table. When the dynamic force reaches the interface limiting shear force, a relative displacement occurs. In this situation the block acceleration becomes lower than the table one and in the block acceleration/table acceleration curve it is possible

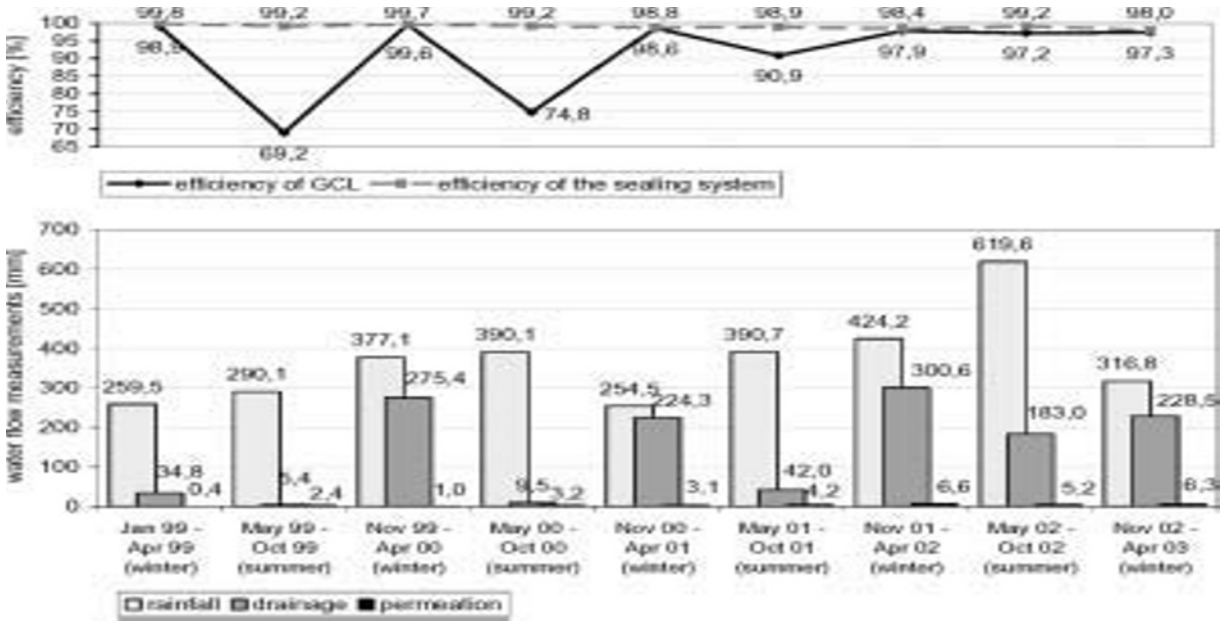


Fig. 26 The impact of summer and winter cycles on the sealing effect of single-layer standard Bentofix (after Heerten, 2006).

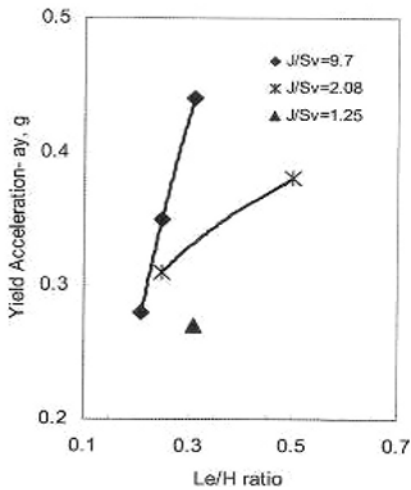


Fig. 27 Yield acceleration versus Le/H for modeled shaking tests (after Lee at al. 2007)

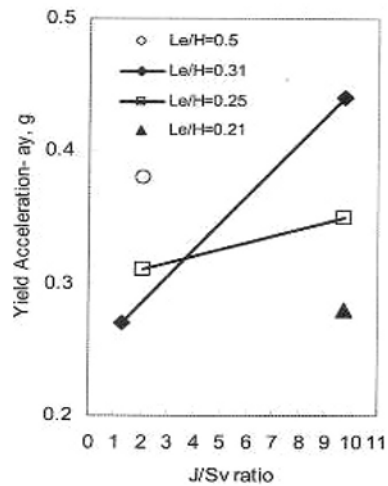


Fig. 28 Yield acceleration versus J/Sv value for modeled shaking tests (after Lee at al. 2007)

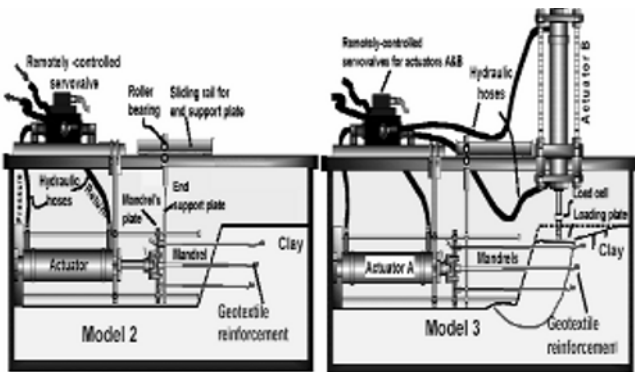


Fig. 29 Experimental equipment



Fig. 30 Details of the installation of the reinforcement

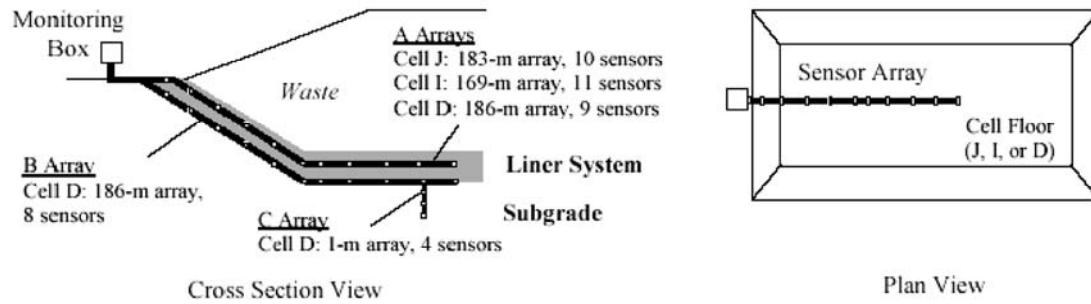


Fig. 31 Schematic Configuration of Sensor Arrays

to see a clear break. Considering the limit condition and assuming a Mohr-Coulomb failure criterion, it is possible to evaluate the friction angle ϕ_d , as:

$$\phi = \tan^{-1}(a / g) \quad (1)$$

being a_b the block acceleration and g the gravity acceleration.

Das and Shin (1999) carried out low frequency dynamic load test on a strip foundations resting on the geogrid reinforced saturated clay and concluded that the full geogrid reinforcement can reduce then permanent settlement of a foundation by about 20% to 30%.

Santhakumar et al. (2001) have conducted a series of dynamic plate loading tests and concluded that there is a considerable effect of the number of reinforcement layer, the size of the reinforcement, spacing of the reinforcement and frequency of loading on the dynamic bearing capacity of the subgrades. There is a substantial reduction in settlement of the reinforced subgrades as well due to inclusion of geogrid in the foundation soil.

As regards the other widely used cyclic/dynamic laboratory tests to check the geosynthetic/geosynthetic or geosynthetic/soil interfaces, it is important to mention the cyclic direct shear tests (Pasqualini et al. 1996; De 1996) and the shaking table tests on geotechnical centrifuge (Zimmie et al. 1994). The application of one test instead of another is mainly determined by the field use and the nature of the considered interface.

Table 3 reports the recommended tests to perform for eight typical geosynthetic/geosynthetic interfaces (De and Zimmie, 1998).

De and Zimmie (1998) suggest principally the use of cyclic direct shear device for seismic event problems, considering that for this event the first 5-30 cycles are the most important.

The shaking table tests on geotechnical centrifuge are very important to consider the same stress levels as prototypes. In landfill applications, for example, a bottom liner system may be subjected to normal stresses variable between 100 and 800 kPa, considering a waste height of 8-60 m respectively.

Table 4 shows the average values of the peak friction angle for different geosynthetics interface and different

tests in static and dynamic conditions

Analysing some typical geosynthetic/geosynthetic interfaces it is possible to point out the following observations (Carrubba and Massimino, 1998).

1) The initial values of friction angles in static and dynamic condition are very similar; even if due to the viscous nature of geosynthetics and the soil interface dynamic shear strength is influenced by the strain rate. This leads to lightly higher values of the friction angle in dynamic conditions than in static conditions.

2) For geotextile/smooth geomembrane inter-faces the peak dynamic friction angle decreases with the increase of the number of excitation cycles, especially for low values of the cycles number (Pasqualini et al. 1995; De and Zimmie, 1998). This reduction is very probably due to a polishing action. The polishing effect increases in moisture condition, common in landfill liners and covers because of the leachate or other fluid presence (Von Pein and Lewis, 1991). On the contrary, for smooth geomembrane/geonet interfaces and smooth geomembrane/smooth geomembrane interfaces it is possible to note a significant increase of the peak dynamic friction angle with cycle numbers. In the first case the increasing in peck dynamic friction can be due to a possible increased roughness of geomembrane caused by the geonet. In the second case the increasing in peck dynamic friction could be due to the occurrence of abrasion along the shaking direction (De and Zimmie, 1998). Finally, for the goetextile/geonet interfaces, the peak dynamic friction angle appears independent from the number of excitation cycles.

3) As far as the normal stress is concerned, its magnitude is not important for geotextile/smooth geomembrane and smooth geomembrane/smooth geomembrane; while it influences significantly the behaviour of smooth geomembrane/geonet and geotextile/geonet interfaces. In this last case, lower the normal stress higher the peak dynamic friction angle. The reason of the normal stress influence is until now completely understood; in some cases it could be related to the high deformability of no woven geotextile. The normal stress in relation to the material hardness can produce a penetration effect of one material to the other. This last phenomenon causes a

Table 3 Tests for estimating geosynthetic interface dynamic friction angles (after De and Zimmie,1998).

Interface description	Recommended testing procedures to estimate dynamic friction angle	
	Seismic excitation ⁽¹⁾	Machine foundation ⁽²⁾
Nonwoven geotextile over smooth geomembrane	ST or CDS consider reduction in ϕ	ST or CDS consider reduction in ϕ
Smooth geomembrane over geonet (oriented transversely)	CDS at proper σ	ST or CST at proper σ
Smooth geomembrane over geonet (oriented longitudinally)	CDS	ST or CST
Smooth geomembrane over geonet (oriented aligned)	CDS	ST or CDS
Nonwoven geotextile over geonet (oriented transversely)	CDS at proper σ and f	ST or CST at proper σ and f
Nonwoven geotextile over geonet (oriented longitudinally)	CDS at proper σ and f	ST or CST at proper σ and f
Nonwoven geotextile over geonet (oriented aligned)	CDS	ST or CDS
Smooth geomembrane over smooth geomembrane	CDS	ST/CST at proper f

Notes: ϕ = friction angle; σ = normal stress; f = frequency; ⁽¹⁾Seismic excitation = small number of cycles; ⁽²⁾Machine excitation = large number of cycles; CDS = cyclic direct shear for geosynthetics; ST = shaking table test; CST = centrifuge shaking table.

Table 4 Average peak friction angle of the interfaces (after De and Zimmie, 1998)

Interface Description	Static friction angle		Dynamic friction angle		
	Tilt table test	Direct shear tests	Direct shear tests	Shakingtable test	
				1g	10g to 40g
Nonwoven geotextile over smooth geomembraane	11.8°	12°	Decreases from 12.5° to 10.5°	12°	11°
Smooth geomembrane over geonet (transverse)	10.1°	11.3°	Increases from 11° to 18° (for low σ) or 14° (at high σ)	12°	7°
Smooth geomembrane over geonet(longitudinal)	9.8°	11.3°	Increases from 10° to 18° (for low σ) Or 16.5° (at high σ)	12°	11°
Smooth geomembrane over geonet (aligned)	8.1°	8.1°	Increases from 9° To 18° (for bot low and high σ)	---	---
Nonwoven geotextile over geonet (transverse)	24.5°	Ranges from 22° (at low σ) to 14.5° (at low σ)	Ranges from 24°(at low σ) to 17° at high σ)	24°	8°
Nonwoven geotextile over geonet (longitudinal)	13.9°	Ranges from 17° (at low σ) to 14° (at low σ)	15°	19°	11°
Nonwoven geotextile over geonet (aligned)	11.2°	10.5°	11° to 10°	---	---
Smooth geomembrane over smooth geomembrane	13.1°	8.8°	Increases from 10.3° to 19.5°	19°	13°

significantly non-linear behaviour of interfaces (Carrubba and Massimino, 1998).

4) For interfaces including geonet the mesh orientation can change greatly the results. Of course, the lower interface shear strength occurs when the strands are aligned in the same direction of the motion.

5) As in static conditions, the moisture has the effect to reduce the friction angle.

6) Interesting tests performed on HDPE geomembrane-nonwoven geotextile interface showed that the maximum slip displacement is higher than the permanent one.

Thus, for a safe design of landfill liners and leachate collection systems it is important to estimate not only the permanent slip displacement, as very frequently happens, but also the maximum dynamic displacement resulting from the displacement time history.

7) As far as the geosynthetic/soil interface behaviour is concerned, by shaking table test (Strano 2000), it is important to perform geotechnical test, to evaluate the angle of shearing resistance of the soil rather than the angle of friction. As well as dynamic soil properties, such soil relative density, shear modulus, damping ratio etc. (Cascone, 1995).

Lai et al. (1998) have performed cyclic shear tests on samples of a geomembrane supported geosynthetic clay liner. The dry material showed no degradation in shear strength during cyclic loading, on the other hand the hydrated material was found to reduce the shear strength by cyclic loading.

PERFORMANCE OF SOLID WASTE LANDFILLS DURING EARTHQUAKES

From the lessons learned from past earthquakes, such as Loma Prieta earthquake (Johnson et al. 1991; Buranek and Prasad, 1991; Sharma and Goyal, 1991) and Northridge earthquake (Matasovic and Kavazanjian, 1996; Stewart et al. 1994; and Augello, 1995) it is important to stress that modern solid waste landfills withstand the design earthquake without damages to human health and environment.

From well documented case histories the following failure mechanisms can be selected:

- Sliding or shear distortion of landfill or foundation or both;
- Landfill settlement;
- Transverse and longitudinal cracks of cover soils;
- Cracking of the landfill slopes;
- Damage to the gas system header pipes;
- Tears in the geomembrane liners;
- Disruption of the landfill by major fault movement in foundation;
- Differential tectonic ground movements;
- Cracks about the contact between refuse landfill and canyon;

- Liquefaction of landfill or foundation.

The damage modes listed are not necessarily independent of each other.

Experience has shown that well built waste landfills can withstand moderate shaking peak accelerations up to at least 0.2g with no harmful effects.

Nevertheless this scenario the integrity of solid waste landfills during strong earthquakes to achieve environmental and public health objectives deserves more consideration.

ANALYSIS OF SOLID WASTE LANDFILLS STABILITY DURING EARTHQUAKES

Introduction

The stability analysis of solid waste landfills will be introduced.

The behavior of solid waste landfills during the occurrence of earthquakes can be analyzed by experimental methods or mathematical methods.

Seismic design of solid waste landfills uses the same principles of seismic design of embankment dams (Sêco e Pinto, 1998a).

The capabilities and limitations of these methods are briefly summarized.

Experimental Methods

Experimental methods are used to test predictive theories and to verify mathematical models. The most popular techniques for solid waste landfills are shaking table and centrifuge models.

Shaking table tests, with the purpose of investigating the dynamic behaviour of reinforced structures with various boundary and surcharge condition, seismic input and reinforcement distribution were conducted by (Lo Grasso et al. 2006).

Centrifuge model tests have been carried out to understand the principle of waste-structure interaction and to investigate deformation induced stress redistributions within the waste body near a structure (Kockel et al. 1997).

Thusyanthan et al. (2004) from the results of centrifuge tests in municipal solid waste materials have concluded that the amplification of acceleration within the model waste depends mainly on the earthquake intensity.

Koseki et al. (2006) review recent physical model testing using shaking tables and summarizes lessons learned regarding seismic performance and potential failure mechanisms.

Mathematical Methods

The following dynamic analysis of embankment dams

are used (Sêco e Pinto et al. 1995):

- i) pseudo-static analyses;
- ii) simplified procedures to assess deformations;
- iii) dynamic analysis.

The slope stability of waste landfills is generally evaluated by limit equilibrium slope stability analyses.

For the pseudo-static analyses a seismic coefficient value equivalent to the peak ground acceleration divided by 1.5 can be considered (Sêco e Pinto et al. 1998a).

For solid waste landfills an acceptable seismic behaviour is anticipated if the calculated pseudo-static factor of safety ranges from 1.3 to 1.5.

Simplified procedures to assess landfills deformations were proposed by Newmark (1965), Sarma (1975) and Makdisi and Seed (1977) and have given reasonable answers in areas of low to medium seismicity.

Newmark's original sliding block model considering only the longitudinal component was extended to include the lateral and vertical components of earthquake motion by Elms (2000).

The use of dynamic pore pressure coefficients along with limit equilibrium and sliding block approaches for assessment of stability of earth structures during earthquakes was demonstrated by Sarma and Chowdhury (1996).

A new simplified semi-empirical predictive model for estimating seismic deviatoric-induced displacements based on the results of nonlinear fully coupled stick-slip sliding block analysis using a comprehensive database of hundreds of recorded ground motions was proposed by Bray (2007). The seismic displacements model are generally more consistent with documented cases of solid waste landfill performance.

A fully probabilistic assessment of sliding displacement incorporating the aleatory variability in the earthquake ground motion prediction was proposed by Rathje and Saygili (2008). The product of this analysis is a displacement hazard curve which provides the annual rate of exceedance for a range of displacement levels. The different deterministic and probabilistic methodologies to predict the sliding displacement of a slope are shown in Fig. 32.

Several finite element computer programs assuming an equivalent linear model in total stress have been developed for 1D (Schanabel et al. 1972; Idriss and Sun, 1992), 2D (Idriss et al. 1973; Lysmer et al. 1974) and pseudo 3D (Lysmer et al. 1975).

Since these models are essentially elastic the permanent deformations cannot be computed by this type of analysis and are estimated from static and seismic stresses with the aid of strain data from laboratory tests (cyclic triaxial tests or cyclic simple shear tests).

To overcome these limitations, nonlinear hysteretic models with pore water pressure generation and dissipation have been developed using incremental elastic or plasticity theory.

The incremental elastic models have assumed a nonlinear and hysteretic behavior for soil and the unloading-reloading has been modelled using the Masing criterion and incorporate the effect of both transient and residual pore-water pressures generated by seismic loading (Lee et al. 1978; Finn, 1987).

Sargent (1990) has introduced the concepts of verification and validation and the relations established between the three entities: the physical problem; the conceptual model; and the computer model and its numerical implementation are illustrated in Fig. 33.

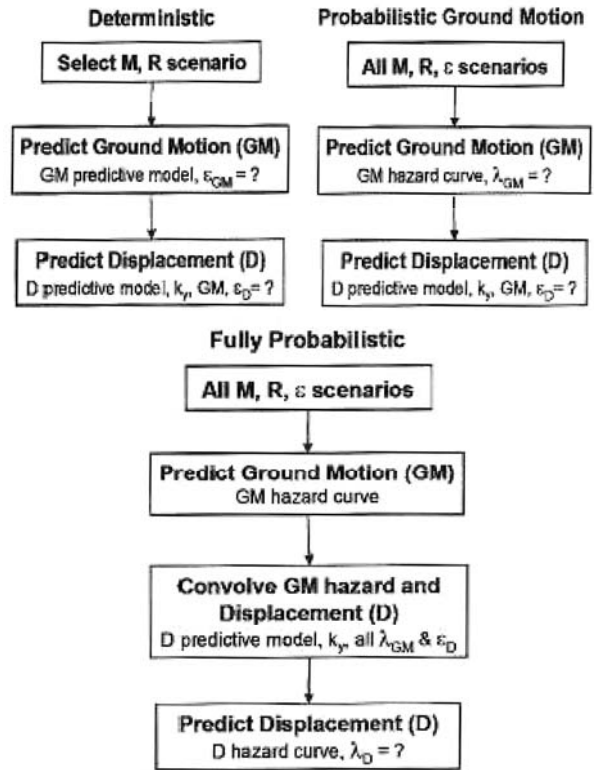


Fig. 32 Various methodologies for predicting sliding displacements (after Rathje and Saygili, 2008)

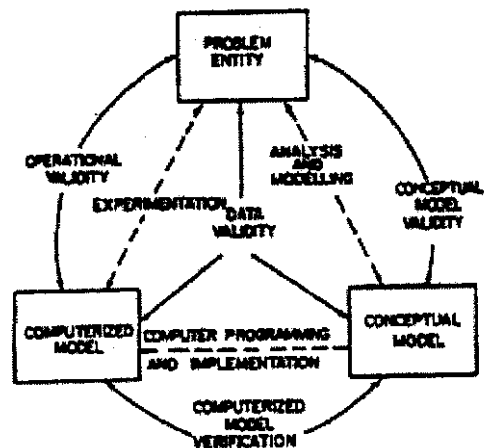


Fig. 33 Relations between physical problem, conceptual model and computer model (after Sargent, 1990)

Verification intends to ensure that the computer program is correct and its represents faithfully the conceptual model and validation applies essentially to the conceptual model, and its ability to reproduce satisfactorily the physical phenomena.

A slightly different terminology is adopted by ICOLD (1993) that considers that the numerical modelling process for dams should be checked in order to avoid unreliable results considering the following aspects:

- i) justification of the whole modelling method (the relevance to physical reality);
- ii) validation of the computer code;
- iii) quality assurance of the whole computation process.

A flowchart that integrates stability analysis of solid waste landfills, monitoring and safety analysis and lessons learnt from case histories proposed by Seco e Pinto and Maugeri (2005) is presented in Fig. 34.

Selection of Design Earthquakes

Introduction

The Code of Federal Regulations (United States, 1991) requires new municipal solid waste landfills to be designed either for a maximum horizontal acceleration taken from a published seismic map for a 10 percent probability of exceedance (90 percent probability of non exceedance) in a 250-year exposure period or on the basis of a site specific analysis. The related return period for the map-based acceleration is 2,375 years. The criterion of a site specific analysis is not specified in the regulation, but rather is left up to the individual states and may be probabilistic or deterministic. Because of the lower uncertainty, the return period for a site specific analysis may be less than 2,375 years.

The selection of seismic design parameters for municipal solid waste landfills, following the procedures used for dam projects, depends on the geologic and tectonic conditions at and in the vicinity of the site (Sêco e Pinto, 2007). Attenuation relations can be separated into 3 main tectonics classifications: (1) shallow crustal earthquakes in active tectonics regions, (2) regions subduction earthquakes, and (3) shallow crustal earthquakes in stable continental regions.

In terms of attenuation relations, the Idriss model (1995) and the Sadigh et al. model (1997) have only horizontal components, and Abrahamson and Silva (1997) relation has been used for vertical component. Overall, directivity has a significant effect on long-period ground motions for sites in the near-fault region.

EUROCODE n°8

The definition of the actions (with the exception of seismic actions) and their combinations is treated in

Eurocode 1 Action on Structures .

In general the national territories are divided by the National Authorities into seismic zones, depending on the local hazard.

In EC 8, in general, the hazard is described in terms of a single parameter, i.e. the value a_g of the effective peak ground acceleration in rock or firm soil called design ground acceleration (Fig. 35) expressed in terms of: a) the reference seismic action associated with a probability of exceeding (P_{NCR}) of 10 % in 50 years; or b) a reference return period (T_{NCR})= 475.

These recommended values may be changed by the National Annex of each country (e.g. in UBC (1997) the annual probability of exceedance is 2% in 50 years, or an annual probability of 1/2475).

where:

$S_e(T)$ elastic response spectrum,

T vibration period of a linear single-degree-of-freedom system,

α_g design ground acceleration,

T_B, T_C limits of the constant spectral acceleration branch

T_D value defining the beginning of the constant displacement response range of the spectrum,

S soil parameter with reference value 1.0 for subsoil class A,

η damping correction factor with reference value 1.0 for 5 % viscous damping.

The earthquake motion in EC 8 is represented by the elastic response spectrum defined by 3 components.

It is recommended the use of two types of spectra: type 1 if the earthquake has a surface wave magnitude M_s greater than 5.5 and type 2 in other cases.

The seismic motion may also be represented by ground acceleration time-histories and related quantities (velocity and displacement). Artificial accelerograms shall match the elastic response spectrum. The number of the accelerograms to be used shall give a stable statistical measure (mean and variance) and a minimum of 3 accelerograms should be used and also some others requirements. The seismic motion may also be represented by ground acceleration time-histories and related quantities (velocity and displacement). Artificial accelerograms shall match the elastic response spectrum. The number of the accelerograms to be used shall give a stable statistical measure (mean and variance) and a minimum of 3 accelerograms should be used and also some others requirements should be satisfied (Sêco e Pinto, 2009).

For the computation of permanent ground deformations the use of accelerograms recorded on soil sites in real earthquakes or simulated accelerograms is allowed provided that the samples used are adequately qualified with regard to the seismogenic features of the sources.

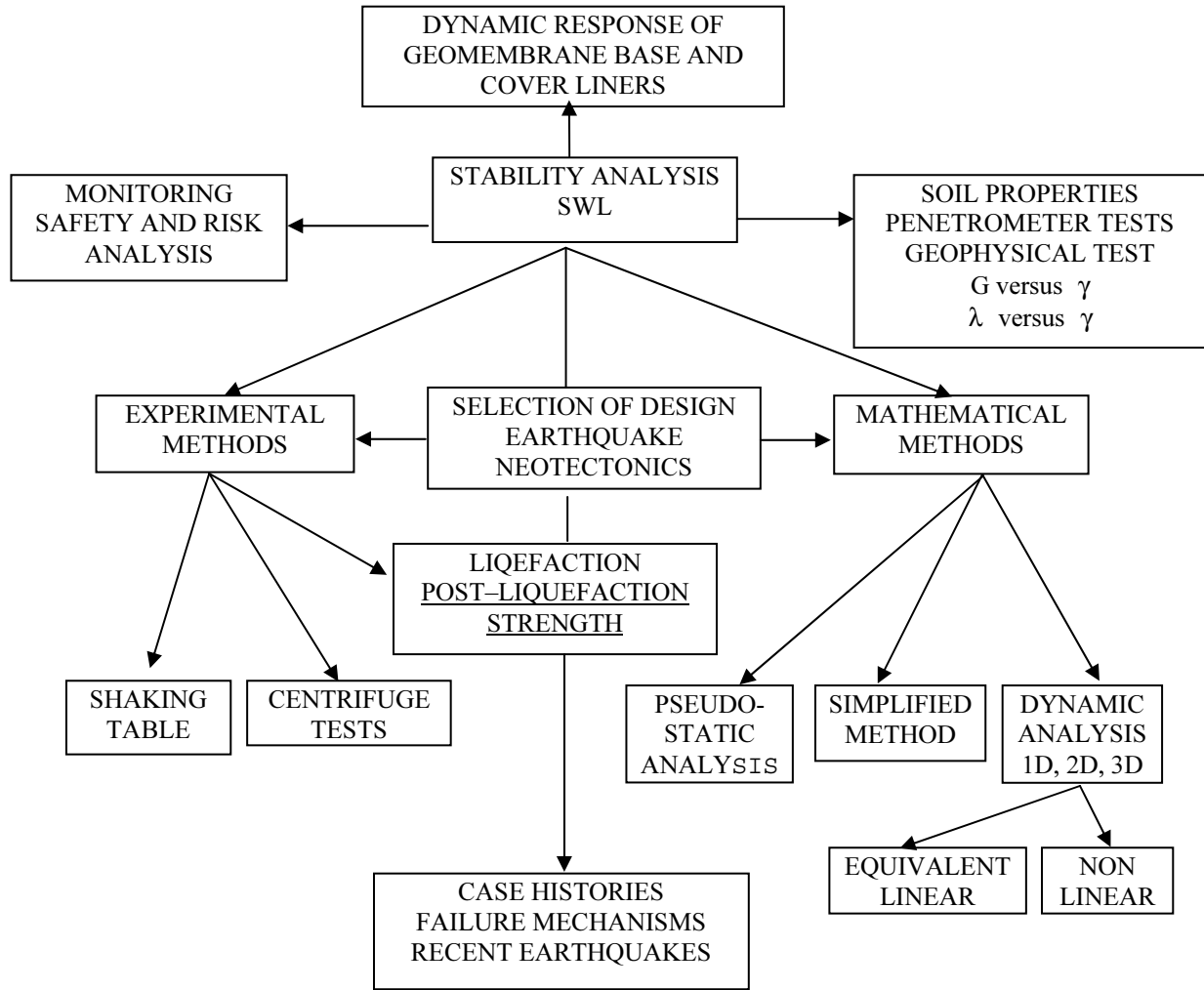


Fig. 34 Flowchart for solid waste landfills (after Seco e Pinto & Maugeri, 2005)

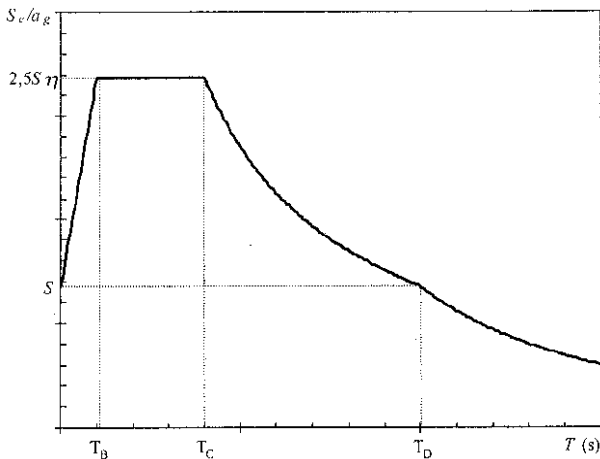


Fig. 35 Elastic response spectrum (after EC8)

For structures with special characteristics spatial models of the seismic action shall be used based on the principles of the elastic response spectra.

The selection of seismic design parameters for municipal solid waste landfill following the dam projects

depends on the geologic and tectonic conditions at and in the vicinity of the site.

The regional geologic study area should cover a 100 km radius around the site to include any major fault or specific attenuation laws.

The probabilistic approach quantifies numerically the contributions to seismic motion, at the landfill site, of all sources and magnitudes larger than 4 or 5 Richter scale and includes the maximum magnitude on each source.

The landfill should be designed for Operating Basis Earthquake (OBE) and Maximum Design Earthquake (MDE). Both depend on the level of seismic activity which is displayed at each fault or tectonic province.

For the OBE only minor damage is acceptable and is determined by using probabilistic procedures.

For the MDE only deterministic approach was used (ICOLD, 1983) but presently it is possible to use a deterministic and probabilistic approach. If the deterministic procedure is used, the return period of such an event is ignored, if the probabilistic approach is used a very long period is taken (ICOLD, 1989).

Neotectonics

Due to the fault tectonics and fracture mechanism, each earthquake possesses unique characteristics that are partly reflected in the obtained strong motion records and partly in the observed damage. Damage patterns and distribution in recent earthquakes have indicated that ground motion characteristics such as direction, pulse and duration could have significant influence and play important role in response of structures.

The tectonic conditions should include tectonic mechanisms, location and description of faults (normal, strike and reverse) and estimation of fault activity (average slip rate, slip per event, time interval between large earthquake, length, directivity effects, etc). These factors are important to assess the involved risk.

Determination of neotectonic activity implies first the qualitative geomorphologic analysis of air photos and topographic maps. The GPS system is another powerful means of monitoring the crustal mobility.

Cluff et al. (1982) have proposed the following classification for slip rates: extremely low to low for 0.001 mm/year to 0.01 mm/year, medium to high 0.1 mm/year to 1 mm/year and very high to extremely high 10 mm/year to 100 mm/year.

The current practice is the deterministic approach in which the seismic evaluation parameters were ascertained by identifying the critical active faults, which show evidence of movements in Quaternary time.

In general an active fault is a fault, reasonably identified and located, known to have produced historical fault movements or showing geologic evidence of Holocene (11 000 years) displacements and which, because of its present tectonic sitting, can undergo movements during the anticipated life of man-made structures.

The fault studies should considered various levels: (I) regional investigations should cover 150-200 km radius, in order to form a picture of the general tectonic setup; (ii) local investigations in 50 km radius; and (iii) faults intersecting the dam site with special significance for dam structure.

To assess if there is the potential for a significant amount of surface displacement beneath the structure several backhoe trenches are excavated with 3 to 4 meters deep and 30 to 50 meters long and should be inspected and log the exposures geologic features.

Recently a fault investigation method other than trenching has been developed, called the long Geo-slicer method in which long iron sheet piles with a flat U-shaped cross section are driven into an unconsolidated bed, iron plate shutters are inserted to face these iron sheet piles and the piles and shutters are pulled out to take undisturbed samples of strata of a certain width. This method is advantageous in regard to the ease of securing land for conducting investigations compared

with trenching and the ease of bringing the strata samples back to the laboratory for detailed observations (Tamura et al. 2000).

When active faults are covered with alluvium geophysical explorations such as seismic reflection method, sonic prospecting, electric prospecting, electromagnetic prospecting, gravity prospecting and radioactive prospecting can be used (Takahashi et al. 1997). Of these the seismic reflection method can locate faults if geological conditions are favourable, and confirm the accumulation of fault displacements based on the amount of displacements in strata that increases with strata age.

Together with the mentioned investigations of recent tectonic activity, historical and instrumental evidence complete the information body on the threat of fault breaks in the structure foundation.

For deterministic analyze median or 84th percentile ground motions are used for design ground motions for dams. The choice for median or 84th percentile is based on the slip rate of the fault and the downstream hazard and downstream hazard of the structure

The most dangerous manifestation concerning the landfill stability and integrity is the surface fault breaking, intersecting the landfill site.

To assess if there is the potential for a significant amount of surface displacement beneath the dam several backhoe trenches are excavated with 3 to 4 meters deep and 30 to 50 meters long and should be inspected and log the exposures geologic features.

For low slip rates (about 0.1mm/year or less) the medium ground motion is appropriate. For high slip rates (about 0.5 mm/year or greater) the 84th percentile ground motion is appropriate. Several scenarios are assumed and for near-source faults of the dam amplified motions resulting from source-rupture directivity effects should be included.

Site effects

The acceleration records registered during earthquakes contain significant information about source, path and site effects.

The geological differences, the variability of different soil and rock layers, the reflection and refraction of earthquake waves from the boundaries of these layers, the effect of earthquake waves passing through these layers, as well as the differences in the source mechanisms of each earthquake play an important related the comprehensive analysis of earthquake characteristics on the ground surface.

In Table 5 is presented the main factors that influence site effects

The influence of local conditions on site amplification proposed by Seed and Idriss (1982) is shown in Fig. 36. The initial response spectra proposed in the pre-standard

Table 5 Main factors that influence site-effects

Seismological	- Intensity and frequency characteristics of bedrocks seismic environment
	- Duration of bedrock motions
Geological	- Local geologic structure
	- Underlying rock type
	- Soil deposit thickness
	- Stratigraphical characteristics
	- Soil types in the stratigraphy
Geotechnical	- Elastic vibration characteristics of the soil deposit
	- Impedance contrast between the bedrock and overlying soil materials
	- Nonlinear behavior of soils in the stratigraphy, including fatigue-type effects by shaking duration
Geometrical	- Non horizontal soil-deposit layering
	- Topography of underlying bedrock
	- Basin configuration
	- Other inclusions that lead to two and three dimensional geometries

EC8 based in Seed and Idriss proposal was underestimating the design levels of soft soil sites in contradiction with the observations of the last recorded earthquakes.

Based on records of earthquakes Idriss (1990) has shown that peak accelerations on soft soils have been observed to be larger than on rock sites (Fig. 37). The high quality records from very recent earthquakes Northridge (1994), Hyogo-ken-Nambu (1995), Kocaeli (1999), Chi-Chi (1999) and Tottoriken (2000) have confirmed the Idriss (1990) proposal.

Based in strong motions records obtained during Hyogoken-Nambu earthquake in four vertical arrays sites and using and inverse analysis Kokusho and Matsumoto (1997) have plotted in Fig. 38 the maximum horizontal acceleration ratio against maximum base acceleration and proposed the regression equation:

$$\text{Accsurface}/\text{Accbase}=2.0 \exp(-1.7 \text{ Acc}/980) \quad (2)$$

This trend with a base in a Pleistocene soil is similar to the Idriss (1990) proposal where the base was in rock.

The downhole arrays are useful: (i) to understand the seismic ground response; and (ii) to calibrate our experimental and mathematical models.

The influence of directivity conditions is shown in Fig. 39.

In the last few years many studies have analyzed 2D site effects in the elastic range on ground motions (Aki 1993, Bard 1994), showing that differences relative to the 1D response due to the lateral propagation of surface waves and 2D resonance phenomena. Theoretical 3D elastic response studies indicate that differences relative to 2D are only quantitative.

It is well known that modern seismic codes (UBC 97, EC8) consider seismic site response as a 1D vertical wave propagation. Nevertheless, seismic response

coefficients and spectral shapes for different soil classes are used in order to quantify site effects. The site classification is based exclusively on the vertical soil profile.

In UBC 97 the uppermost soil layers are taken into account disregarding whether the total thickness of sediments is greater than 30m, and also their dynamic properties of the sediments and bedrock. The concept of the uppermost 30m Vs profile as a single parameter to evaluate the design response spectra for different shaking intensity levels (Borcherdt 1994). The main advantage is the simplicity and the unambiguous evaluation by conventional geotechnical surveys, but it is not accurate enough to estimate site effects.

Attenuation relations

Earthquakes are very complex and dangerous natural phenomena, which occurs primary in known seismic zones, although severe earthquakes have also occurred outside these zones in areas considered being geologically stable. As a result, regulatory agencies became more stringent in their requirements for demonstration of adequate seismic stability and design engineers responded by developing new and more convincing design approaches than had previously used. Thus the past years have seen a major change in interest and attitude towards this aspect of design (Sêco e Pinto, 2008b).

The lessons learned from recent earthquakes such as Mexico earthquake (1985), Armenia earthquake (1988), Loma Prieta earthquake (1989), Philippines earthquake (1990), Manjil earthquake (1990), Teleri-Limon earthquake (1991), Erzican earthquake (1992), Latur earthquake (1992), Northridge (1994), Kobe (1995), Marmara and Duzce earthquakes (1999), Athens earthquake (1999) and Chi-chi Taiwan, China earthquake

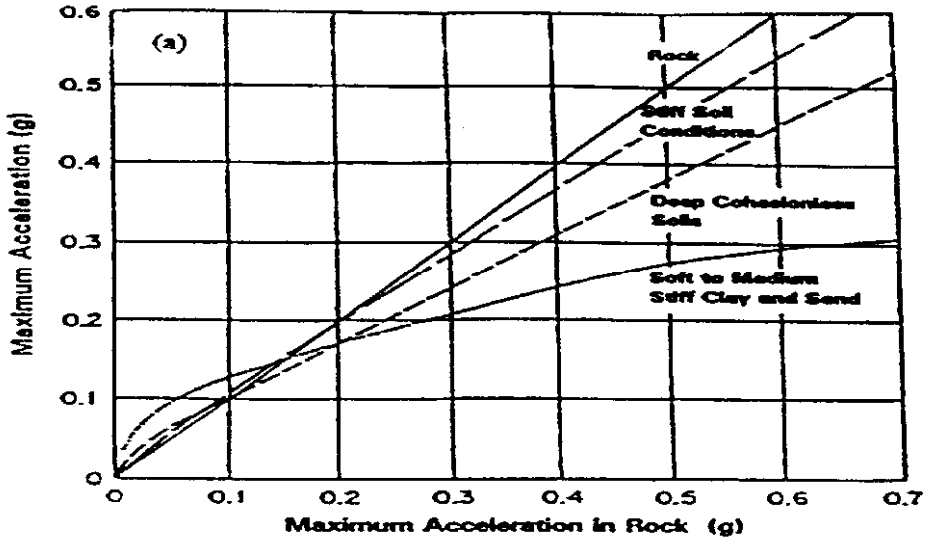


Fig. 36 Influence of local soil conditions on site response (after Seed and Idriss, 1982)

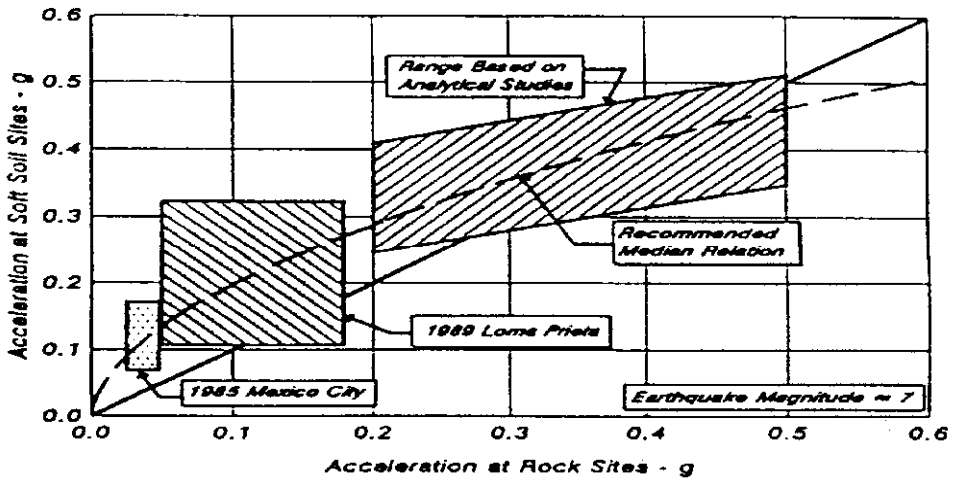


Fig. 37 Influence of local soil conditions on site response (after Idriss, 1990)

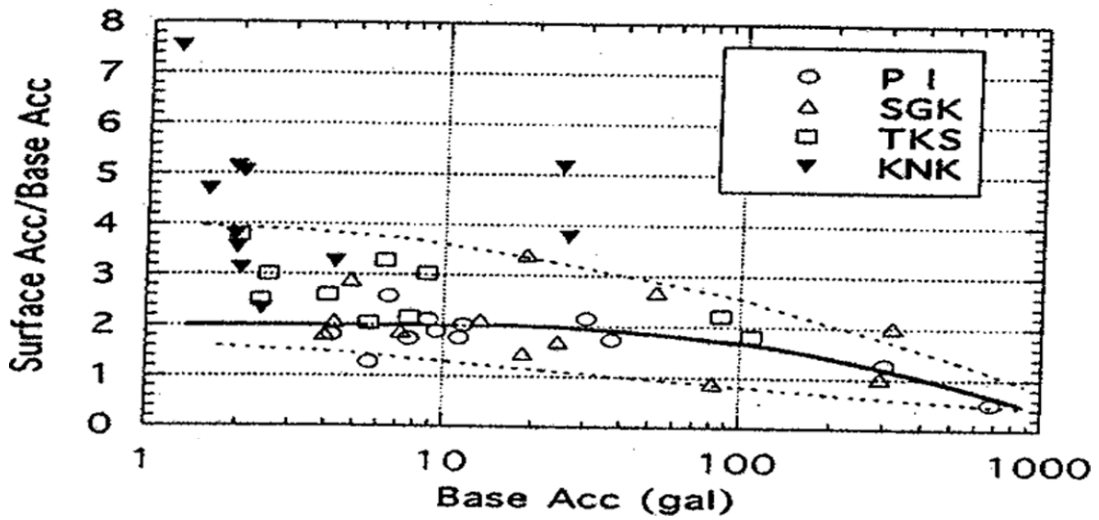


Fig. 38 Maximum horizontal acceleration ratio plotted against maximum base acceleration (after Kokusho and Matsumoto, 1997)

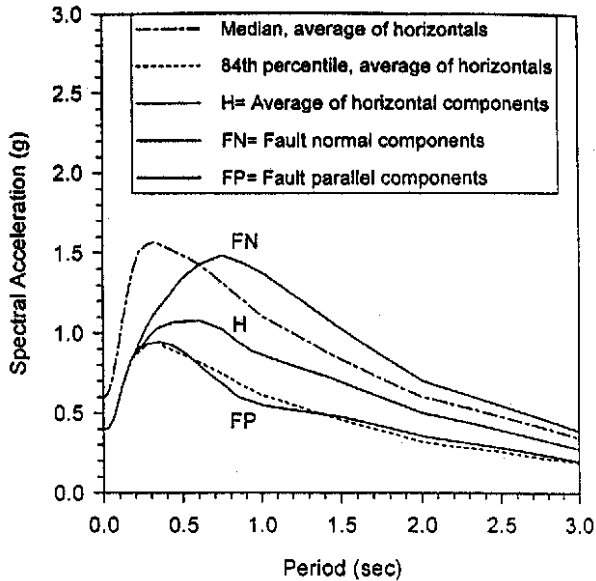


Fig. 39 Response spectra for forward directivity conditions for an $M=7$ earthquake at a distance of 5 km on soil (after Somerville, 1998)

(1999) have provided important observational data related with the seismic behavior of geotechnical structures.

Attenuation relations can be divided into 3 main tectonics classification: shallow crustal earthquakes in active tectonics regions, subduction earthquakes and shallow crustal earthquakes in stable continental regions.

The following attenuation relations were proposed:

Idriss model (1995) has only horizontal component and Sadigh et al. model (1997) and Abrahamson and Silva (1997) relation have been used for vertical component.

Somerville et al. (1997) has shown that directivity has a significant effect on long-period ground motions for sites in the near-fault region.

Earthquakes ground motions are affected by source mechanism, by path and by the local site conditions. The available procedures take these effects into account in varying degrees (Idriss, 1995).

Empirical analytical and fully empirical procedures have been developed to calculate these parameters.

These empirical analytical relationships were called attenuation relationships.

The attenuation relationships for estimating earthquake ground motions rely on recorded data and should incorporate ground motion parameters. The values of mean peak acceleration were presented by Trifunac and Brady (1975) and compared with recorded data in Fig. 40, has shown that the range of the recorded data is about a factor of 4 and the range of calculated mean values is closer to a factor of 10.

A comparison of eleven attenuation relationship and the peak horizontal acceleration of earthquake ground

motion recorded during the 1994 Northridge earthquake is shown in Fig. 41. The range of recorded data is still of 3 to 5 but the range of the calculated medium values has been reduced. This situation is due a significant increase in the data base.

The number of recording sites shown in Fig. 42 indicates that recordings are available from earthquakes with magnitudes from 4.6 to 7.4 and distances from 1 km to about 100 km, with a significant number of recording available at soil sites. It is important to mentioned that the data to be used in developing attenuation laws used only free field records.

The standard residuals are pointed in Fig. 43 as a function of earthquake magnitude and in Fig. 44 as a function of distances.

Seismic response analysis

During the past two decades landfill design and construction technology has advanced considerably in response to more stringent regulatory requirements and demands.

Because earthquakes could damage the waste containment system, with a consequent loss of sealing, one of the most important requirement of MSW landfills is that a landfill located in seismic impact zones be designed to resist earthquake hazards.

The seismic responses obtained by computer finite element 1D programs are considered reasonable (Bray et al. 1995; Mitchel and Mitchel, 2004).

These analyses are based on the solution of the equation of motion considering a homogenous and continuous soil deposit composed of horizontal soil layers and assuming a vertical propagation of shear waves. Since the slopes of landfills are usually flatter than slopes of earth dams, and landfill decks are larger than dam crests, two-dimensional response effects in landfills should be less significant than in earth dams. For the soil behaviour the equivalent linear method is used and the shear modulus and damping ratio are adjusted in each iteration until convergence has occurred.

Due to the uncertainties related to the material properties and the foundation geometry, the influence of the seismic action generally is evaluated via parametric and sensitivity studies.

The seismic response was also obtained by a computer finite element 1D program ESTOC developed in FORTRAN 77 (Vieira, 1995).

Input motions are incorporated by base horizontal and vertical acceleration power spectra. These can be obtained by direct records of seismic motions by response spectra or by trilogaritme diagram.

For the soil behaviour the equivalent linear methods is used and the shear modulus and damping ratio are adjusted in each iteration until convergence has occurred.

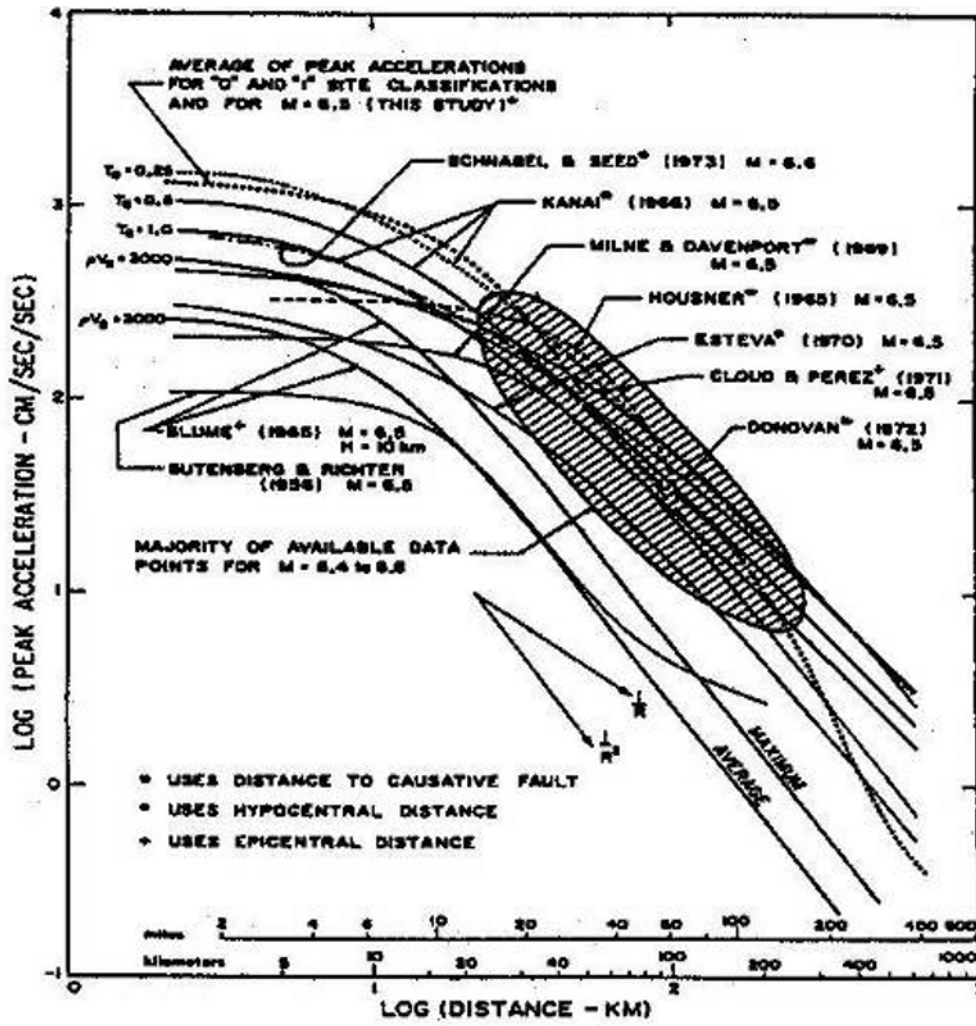


Fig. 40 Attenuation relationships (after Trifunac and Brady, 1975)

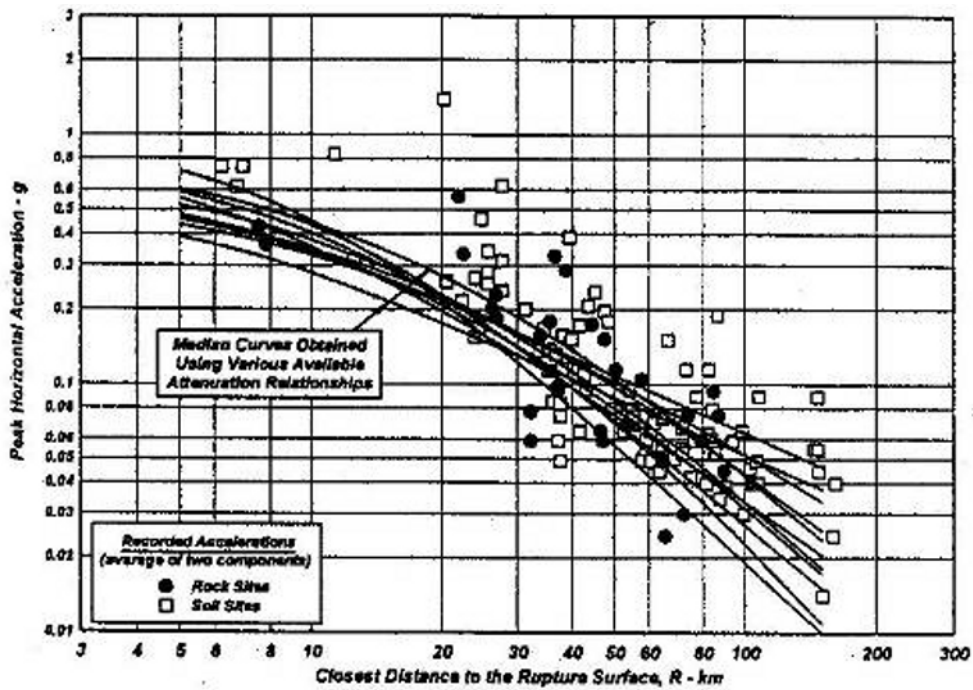


Fig. 41 Comparison of various attenuation relationships and motions recorded during Northridge earthquake

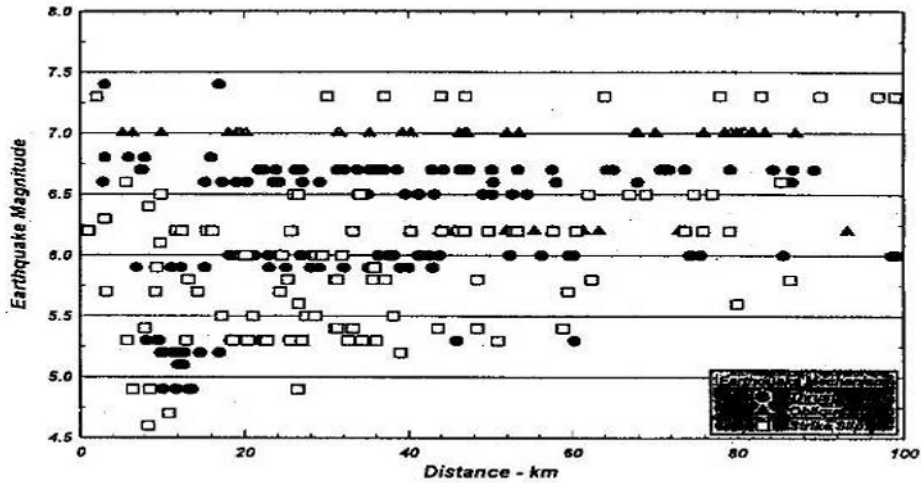


Fig. 42 Distribution of magnitude and distance of available peak acceleration data recorded in the free field at rock sites

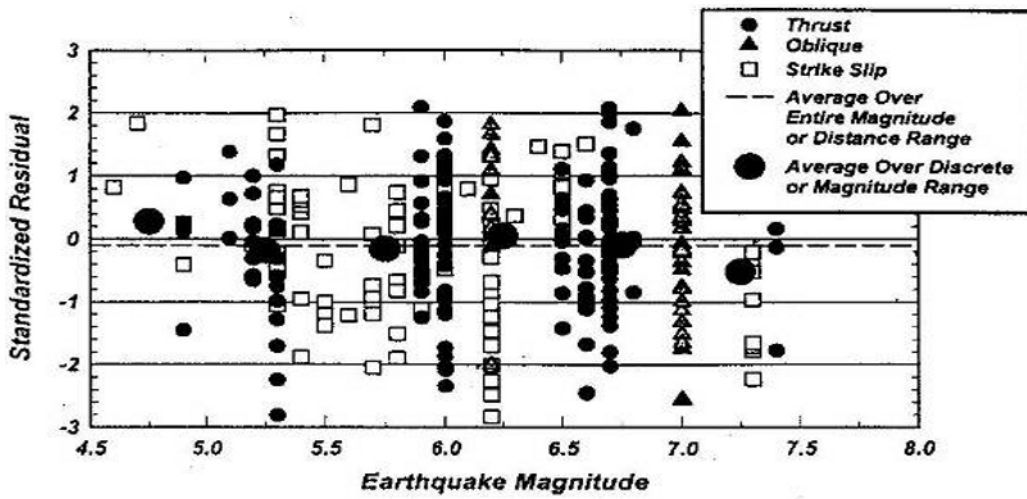


Fig. 43 Standard residuals calculated using the derived attenuation relationship for peak horizontal accelerations recorded at rock sites for magnitudes range 4.6 to 7.4

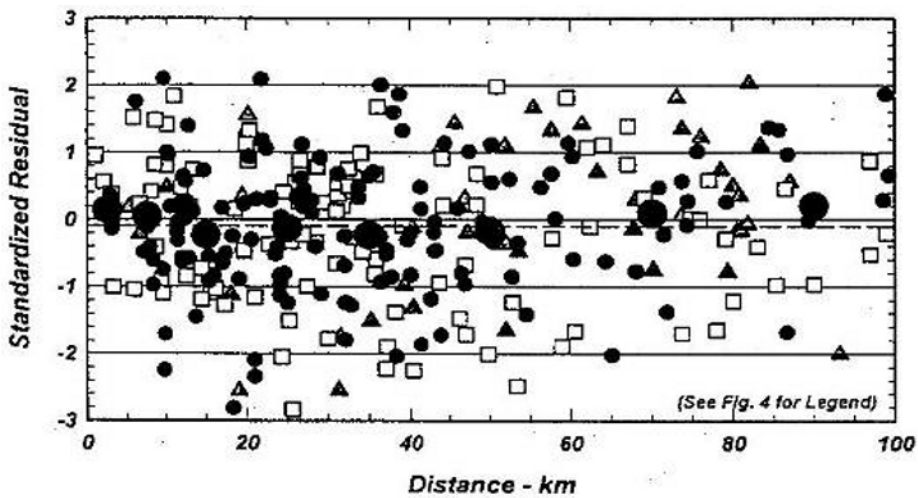


Fig. 44 Standard residuals calculated using the derived attenuation relationship for peak horizontal accelerations recorded at rock sites for distance range 2 to 100 km

The main profile for three foundation geometries (30 m, 40 m and 50 m depths), in order to check this influence, and for the seismic actions near and far source was analysed.

The shear stress distribution and the acceleration distribution for the solid waste at the Grandola solid waste landfill (SWL) for three foundation geometries are presented in Figs. 45 and 46 (Sêco e Pinto et al. 1999). The basic data for the Grandola SWL are reported by Sêco e Pinto et al. (1999).

Due to the geometry of the landfill (height and slopes), the effect of the HDPE geomembrane/geotextile liner was ignored; i.e. the dynamic properties of the geosynthetic liner was not replaced by the dynamic properties of the equivalent soil layer.

Table 6 summarizes for near source and far source the transference functions of acceleration (TFRA) between the bedrock and the ground level, the fundamental period of the layer (T_F), the maximum acceleration at the deck (MaxA), the acceleration at the bedrock (A) and the amplification ratio (AR).

Table 6 Summary of the seismic analyses results

	Near Source			Far Source		
	30	40	50	30	40	50
H(m)	30	40	50	30	40	50
TRFA	3.51	3.22	3.05	3.43	3.18	3.03
T_F (s)	0.35	0.43	0.51	0.35	0.43	0.51
MaxA	3.78	3.47	3.27	2.24	2.16	2.09
(m/s ²)						
A (m/s ²)	0.95	1.49	1.49	0.94	0.93	0.92
AR	2.54	2.33	2.19	2.38	2.32	2.27

A comparison the results of the analyses performed by SHAKE 91 and QUAD 4M codes Rathe and Bray (1999) have concluded that: (i) the maximum seismic loading for base sliding within a landfill can be estimated conservatively with 1D analysis; (ii) the 1D analysis underpredicts the surface maximum horizontal acceleration (MHA) along the slope of a landfill by 10% on average, and by as much as 40 %; (iii) at the crest, 1D analysis consistently under predicts the MHA by about 25%; (iv) along the deck, the analysis is only moderately unconservative and the effect of base rock topography is not captured with 1D analysis.

The analysis is carried out by using FLAC (Itasca, 2001), which is a two-dimensional explicit finite difference program for engineering mechanics computation. This program simulates the behaviour of structures built of soil, rock or other materials that may undergo non-recoverable deformation when their strength limits are reached. The dynamic option permits two-dimensional, plane strain, time domain dynamic analysis.

The program offers a wide range of capabilities to solve complex problems in engineering. FLAC dynamic

analysis considers time histories with the transient, irregular characteristics of design earthquake motions. This detailed ground response analysis will predict time histories of displacement and acceleration at various depths within a waste deposit. FLAC has been successfully used to analyse different types of dynamic problems (e.g. Bu, 2003).

It is important to stress that the dynamic characteristics of solid waste materials play an important role on the seismic response of landfill, and this area deserves more consideration (Sêco e Pinto et al. 1998a). It also is important to assess the dynamic shear strengths of liner materials due the effect of inertial forces in the refuse mass.

The influence of geometry and seismic input motion and material nonlinearity on the dynamic response of MSW landfills were investigated by Zania et al. (2007) by 2D finite element analyses (Fig. 47).

The authors have concluded that the circular slip surface (using the limit equilibrium method) leads in general to higher values of maximum horizontal equivalent acceleration compared to the base sliding case.

Liquefaction Assessment

The methods available for evaluating the cyclic liquefaction potential of landfills or foundation are based on laboratory tests and field tests.

In general the following laboratory tests are used: (i) cyclic triaxial test, (ii) cyclic simple shear tests, (iii) torsional cyclic shear tests. Due the difficulties in obtaining high quality undisturbed samples field test such as SPT tests, CPT tests, seismic cone, flat dilatometer and methods based on electrical properties of soil are used (Sêco e Pinto, 2003).

To estimate liquefaction resistance from shear wave velocity there are two procedures: (i) methods based on a combination in situ shear wave velocity measurements and laboratory tests on undisturbed tube and in situ freezing samples from Tokimatsu et al. (1991); (ii) methods based on in situ shear wave velocity measurement and a correlation between liquefaction resistance and shear wave velocity deduced from liquefaction degree in the field from Stokoe et al.(1999).

The assessment of liquefaction resistance from shear wave crosshole tomography was proposed by Furuta and Yamamoto (2000).

A new proposal presented by Cetin et al. (2001) is shown in Fig. 48 considered advanced in relation with the previous ones, as integrates: (i) data of recent earthquakes; (ii) corrections due the existence of fines; (iii) experience related a better interpretation of SPT test; (iv) local effects; (v) cases histories related more than 200 earthquakes; (v) Bayesian theory.

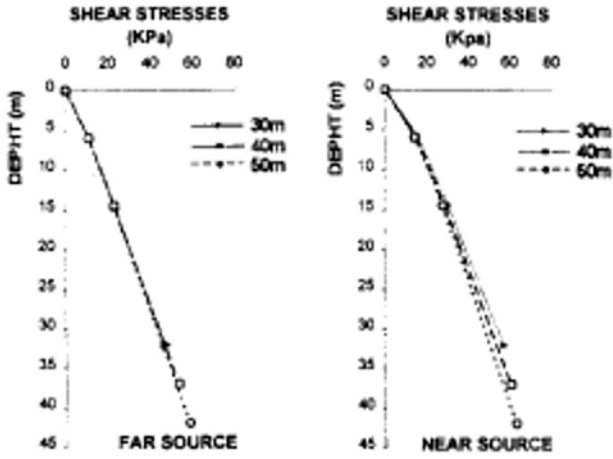


Fig. 45 Shear stresses distribution

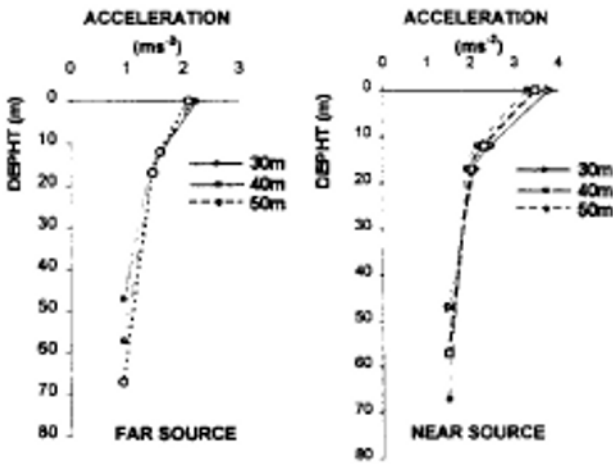


Fig. 46 Acceleration distribution

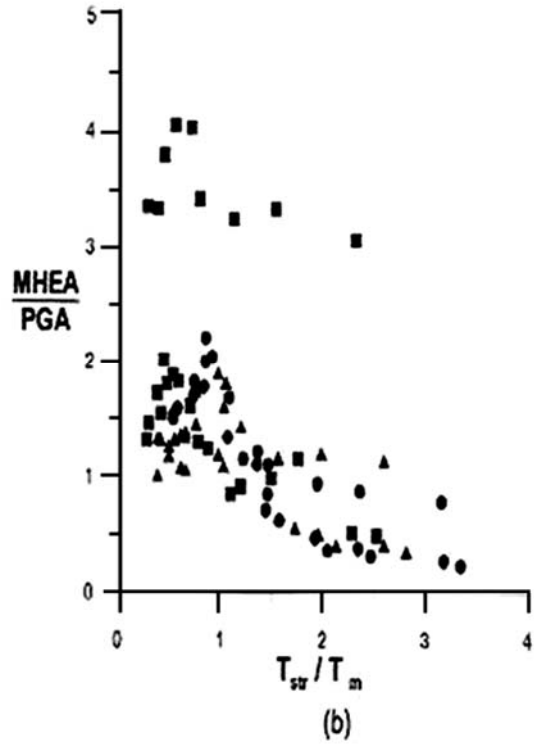
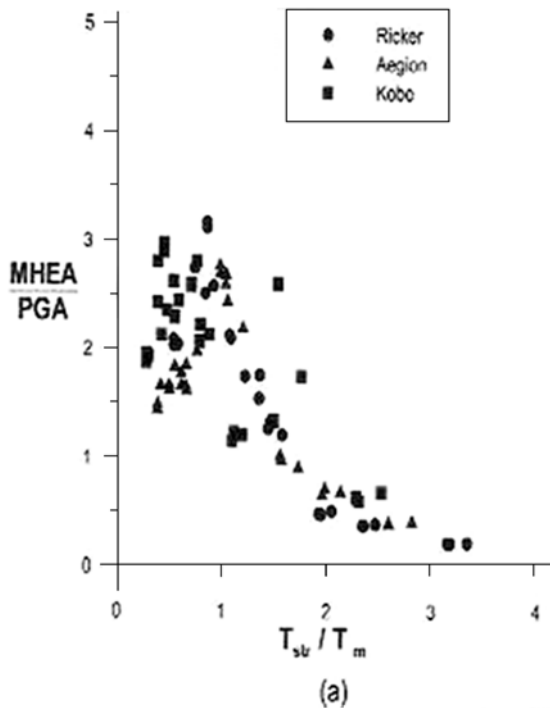


Fig. 47 Ratio of maximum horizontal acceleration (MHEA) to PGA is presented in variation to the ratio of the eigenperiod of the landfills to the mean period of the excitation for: a) circular slip surface and b) base sliding case (after Zania et al. 2007)

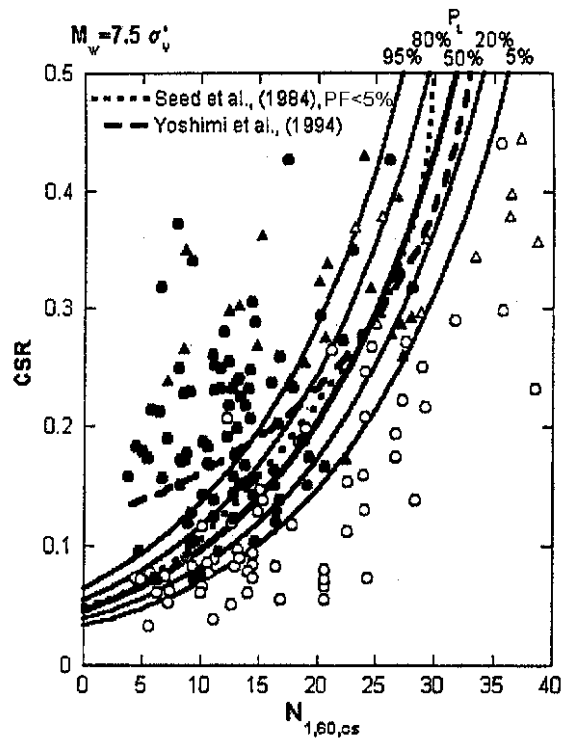


Fig. 48 Probabilistic approach for liquefaction analysis (after Cetin et al. 2001)

The post-liquefaction strength of loose silty sediments is commonly less than that of sands, but moderately dense silts at shallow depths are generally dilative, making them more resistant to ground deformation than cleaner sands (Sêco e Pinto et al. 1997; Youd and Gilstrap, 1999).

Two categories of remedial measures against liquefaction were proposed:

(i) Solutions aiming at withstanding liquefaction - Confinement wall: stiff walls anchored in a non liquefied layer (or a bedrock) to avoid lateral spreading in case of liquefaction; Soil reinforcement - transfer of loads to a non-liquefiable layer.

(ii) Solutions to avoid liquefaction: - Soil densification: compaction grouting to minimise the liquefaction potential; - Dewatering: to lower the water table in order to minimise the risk of liquefaction; - Drainage: to facilitate the dissipation of pore pressure; - Fine grouting: to increase the soil cohesion. Liquefaction resistance of silty sands during seismic liquefaction conditions for various silt contents and confining pressures was investigated by Amini and Qi (2000).

QUALITY ASSURANCE

The purpose of Quality Assurance (QA) and Quality Control are to ensure that the quality of the overall structure of a landfill or the implementation of a remediation project, and the individual components of these meet the required quality standards. QA and QC must relate to both the quality of the materials used and to the quality of the workmanship in accordance with the existing state of technology (Clark, 2005).

The following topics deserve attention:

Soil system (solid, liquid and gaseous phases);

- Groundwater system (perched water and aquifers);
- Surface water system (water courses, drainage, etc);
- Biological system (micro-organisms);
- Contamination (inorganic and organic);
- Other (land use, climate, temperature, regulatory controls, etc).

Quality control on site for geosynthetic placement should pay attention to the following main phases:

- proper storage on site;
- placement procedure;
- control after placement (inspection, possible repairs);
- placement of the upper layer.

To study the effects of compaction energy Fakher (2006) has conducted experiments using a compaction mold of 900mm of height and 550 mm of diameter with 5, 6 and 7 layers of waste. Each layer was impacted 56, 60 and 70 times. The obtained results are shown in Fig. 49.

Using a bulldozer for compaction the waste the number of passes versus density of wastes is shown in Fig. 50.

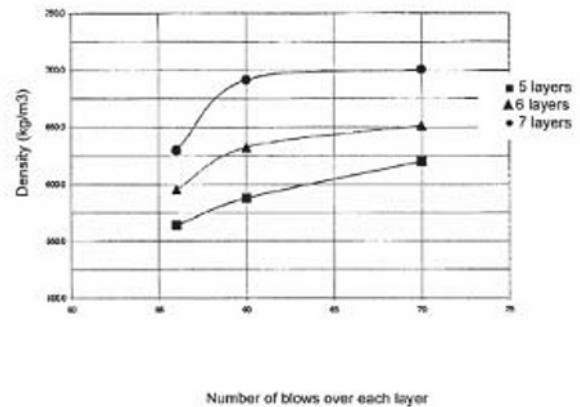


Fig. 49 Number of blows on each layer versus the density of compacted waste (after Fakher, 2006)

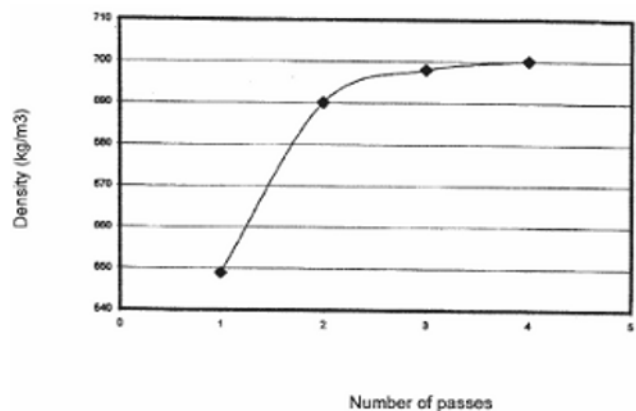


Fig. 50 Number of passages versus density of waste (after Fakher, 2006)

Santayana and Lopes (2003) appointed that for MSW landfills recent built in Portugal the CQA activity comprised: supervision of transport, marking, delivery and storage of the material; preliminary visual observations completed by tests to detect any defect that could endanger the performance of the geosynthetics; in situ verification of the seams quality, namely, as regards the high density polyethylene (HDPE) geomembranes, by assessing the non-destructive tests results performed by the installer (air pressure and vacuum tests), and by analysing the destructive tests results performed by the installer (peel and shear tests), complemented by the execution of the same tests by LNEC (in laboratory and in situ); examination of construction control documents (analysis of daily, weekly, final and acceptance reports produced during installation).

The quality of a compacted clay liner will depend on: (a) the characteristics of the clayey soil used; (b) the method of compaction and, in particular, the compaction water content; (c) the quality control during construction; and (d) the protection against desiccation after construction. Like most engineered liners, CCLs require protection from the elements (e.g. sun and frost) and

consideration must be given to the potential long term effects of differential settlements.

Rowe (2001) indicates that the construction of liner test pads prior to construction of the liner can ensure adequate construction practices without the risk of damage to the actual liner and enables the contractor to become acquainted with potential problems. They also provide a means of calibrating quality control and assurance procedures.

The fact that GCLs come in thin sheets that are seamed by overlapping does mean that considerable care is required during construction to avoid tearing the GCL sheets or opening the seams - especially when cover soil is being placed over the GCL.

The liner should be carefully installed in a manner that will avoid holes in the GCL. It is considered that GCLs have the capacity to effectively self-heal small holes but not large holes or tears. The potential for puncturing will depend on the robustness of the cover geotextile and/or other material.

Additional considerations include the need to place GCLs on a prepared foundation layer, and the stability of liner systems involving GCLs and other geosynthetics such as side slope stability and interface strengths between geosynthetics and/or soil surfaces. Additional concerns associated with the installation of GCLs are their shear strength unreinforced GCLs typically exhibit low internal shear strength upon hydration, making them unacceptable for use on steeper slopes; and the construction requirements associated with their use.

Kocevic et al. (2006) refer that the quality acceptance programme of GCLs of landfills located in the vicinity of Zagreb consists in analyzing the mineral composition (by X-ray powder diffraction), swell index, fluid loss and water absorption capacity.

INSTRUMENTATION AND MONITORING

Landfill behavior during construction and operation is monitored to check methods, results of analyses and model tests and to analyse it safety against deterioration of failure.

The detailed definition of the monitoring scheme cannot be made on the solid basis of the features of the solid waste embankment, because many external factors are to be taken into account when safety problems are considered.

The risk factors are classified in three classes, which are referred respectively to actions, to the structure or to values affected by hazards. The arithmetic average of all indices falling in a given class forms an overall risk factor for the class; in this way we define, respectively, an environmental factor E, a reliability factor F, a potential human/economic hazard factor R. Lastly a global risk index a_g , is developed by taking the

product of the three partially factors E, F, R.

A variety of non-intrusive monitoring methods are available. These include remote sensing such as aerial photography and satellite imagery as well as geophysical methods such as geomagnetics, electromagnetics, electrical resistivity, seismic, ground probing radar, induction and thermal.

From these it is possible to differentiate land use, vegetation, geology and hydrology, etc. Infra-red photography, for example, can be very effective in indicating where vegetation distress is occurring which may be caused by either gas migration or chemical contamination.

Non-intrusive methods are not generally sufficient on their own to characterise ground and groundwater conditions. However, the methods are generally less expensive than intrusive methods in relation to the areal extent of the information obtained and can be used as a reconnaissance tool to either plan future intrusive monitoring.

Grisola and Napoleoni (2006) based in the instrumentation of sanitary landfills have concluded that the evolution of the settlement over the time depends of the waste placing and the extraction of biogas.

Dellabianca et al.(2006) comparing the results of instrumentation and the values predicted by Plaxis using the model soft soil creep have obtained a reasonable agreement for the primary settlements.

Instruments should have the following characteristics: (i) sufficient accuracy; (ii) long-term reliability; (iii) low maintenance requirements; (iv) compatibility with construction techniques; (v) low cost; and (vi) simplicity.

- It is important to monitor the quality of groundwater flowing towards the landfill, namely colour, pH, turbidity, odour, dry mass, dissolved solids, electrical conductivity, biological oxygen demand (BOD), chemical oxygen demand (COD), ammonia, nitrogen, nitrite nitrogen, nitrate nitrogen, sulphides, chlorides, copper, lead, zinc, mercury, total hydrocarbons and total organic carbon (TOC). (Clark, 2005).

- Meteorological and hidric balance data are important to evaluate the leachate flux behavior in different periods of year. In general the leachate flux rate is obtained by the flux velocity measurement passing trough a specified section. Pore water pressures are measured by electric piezometers and hydraulic piezometers.

Municipal solid waste landfills superficial and depth settlements are measured by settlements plates and magnetic anchors. Inclinometers or slope indicators are routinely used for monitoring lateral deformations.

Thermopairs are used to monitor the degradation process evolution of solid waste landfills.

Referring to the shear resistance at the interface between compacted clay and smooth geomembrane, a constant trend of decrease in the shear strength with increasing temperature was observed, making this effect critical for stability of composite barriers (Benson et al. 2005).

To determine and evaluate geomembrane linear and surface deformation was studied, capping was attempted, and its applicability was confirmed. Brillouin Optical Time Domain Reflectometer (BOTDR) method capable of measuring distortions in meter increments using optic fiber sensors was used (Nakamura et al. 2006).

Optic fiber continuous distortion measurement technology, BOTDR, is a measurement method utilizing the principle that when light pulses through an optic fiber, the frequency of the Brillouin scattering light in the backscattered light returning to the incident side of the optic fiber, changes as shown in Fig. 51.

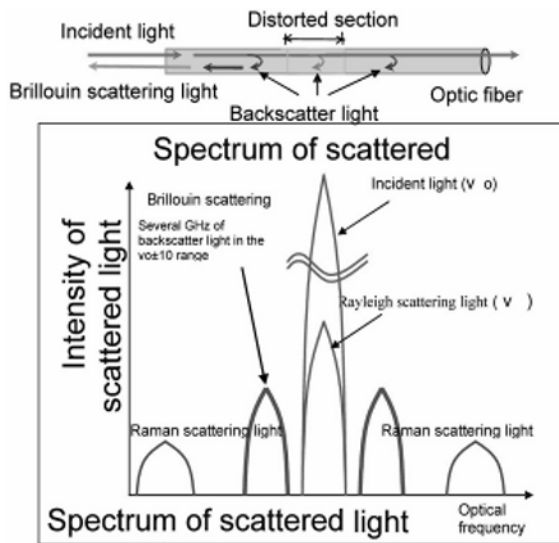


Fig. 51 Strain measurement principle of BOTDR (Nakamura et al. 2006)

Fig. 52 shows operations for installing sensor cable on the sheets.

Seismic downhole-array data provide an unique source of information on actual soil behavior over a wide range of loading conditions. Correlation and spectral analyses are performed to evaluate shear wave propagation characteristics, variation of shear wave velocity with depth, and site resonant frequencies and modal configurations (Elgamal et al. 1995).

In regard of seismic instrumentation of the response of the landfill to such seismic activity the type of instruments currently designated by accelerographs are strong - motion accelerographs, peak recording accelerographs and seismoscopes.

The seismic instrumentation and its maintenance, mandatory for dams, may be too expensive for landfills. However, the OII landfill has been instrumented with two accelerometers; one placed at the top of the landfill and another placed outside the landfill (Anderson et al. 1992).

In comparison with manual readings the automatic system allows a rapid data processing of results a great number of instruments. Once in operation an automatic

system allows a reduction of personal, both in the field and office. The automatic system and the central data processing allow a quicker updating of the information. An automatic system implies an increase of complexity, with the electronic equipment to be installed in unfavourable environment of temperature and humidity.

For data validation a preliminary check on the raw values (following the execution of function tests on measurement equipment) by comparing the actual values from the sensor readings with the established limits and data reduction (computation of engineering quantities) is performed.

For the interpretation of the measurements it is necessary to establish a procedure, a mathematic model that can be a statistical model a deterministic model or a hybrid model.

Safety control is the group of measures taken in order to have an up-to-date knowledge of the condition of the landfill and to detect in due time the occurrence of any anomalies to define actions to correct the situation or, at least, to avoid serious consequences.

The current trend is the development of systems to deal with automatic data acquisition, very flexible, that allows users to perform treatment of the information integrating tests and analysis, behavior models, visual inspections, documents data by any computer connect with Internet visualization



Fig. 52 Sheet installation condition

Application of expert system technology to safety control activities may contribute to improve its speed, provide higher levels of economy, robustness and efficiency.

Experience has shown that the rational and systematic control of dam safety should consist of several tasks (Sêco e Pinto, 1998):

- regular instrumentation measurements;
- data validation;
- data storage;
- visual inspections;

- safety evaluation;
- corrective actions.

RISK ANALYSIS

The first step is to consider what the risks could be. A list is give by Loxham, 2003):

- (i) Risk to Human Health either in the long or short term; (ii) Risk to Flora and Fauna including uptake in food chains; (iii) Risk to the Eco-system as a whole including diversity; (iv) Risk to the Asset Value of the Site even though realization is not necessarily planned; (v) Risk to the Use Value of the Site restricting its economic value; (vi) Risk of incurring Liabilities to others by cross boundary migration of site material; (vii) • Risk of Legislative non-compliance leading to fines or imprisonment; (viii) Risk to the Reputation of the owner or user of the site; (ix) Risk to groundwater; (x) Risk to surface water bodies; (xi) Risk of air pollution by vapors or dust.

Safety analysis for geotechnical structures, such as slopes, retaining walls, piles and shallow foundations implies the verification of limit states: ultimate limit states and serviceability limit states.

For dams also two levels of safety are considered, depending of whether they correspond to normal conditions for use of the structures(current scenario) or are associated with an exceptional occurrence (failure scenarios).From the above considerations it seems that for solid waste landfill a level of damage can be accepted provided there is no harmful discharge of contaminants to the environment.

The allowable value for the calculated permanent seismic displacement of geosynthetic liner systems is 150 to 300mm.

The upper value of 300 mm is appropriate for simplified analyses which use upper bound displacement curves for generic Newmark displacement charts, residual shear strength and/or simplified seismic analyses (Kavazanjian, 1998). The lower value 150 mm is more appropriate for more sophisticated analyses and formal Newmark displacement analyses.

For cover systems large displacements can be accepted taking into consideration that most cover failures can be detected and repaired at reasonable costs.

The allowable values of deformation of landfill systems, depends of several factors, namely of geosynthetic liner systems and gas recovery system.

Municipality waste landfills owners, regulatory authorities and consultants are interested in carrying out a risk analysis. Its purpose is to identify the main real risks associated with each type and height of landfill for all circumstances and can be conducted: (i) in extensive risk analysis of very large landfills, to substantiate

reliably the probabilities chosen in event trees; (ii) in simplified risk analysis of smaller landfills, to focus low-cost risk analysis on a few main risks; (iii) and in identifying possibilities for reducing these risks through low-cost structural or non-structural measures.

Although the annual failure probability of landfills is lower than 10^{-6} in most cases, it may be higher for landfills in seismic areas.

Risk management comprises the estimation of the level of risk and exercising adequate control measures to reduce the risk when the level is not tolerable (Caldeira et al. 2005). The essence of risk management and the role of quantitative risk assessment (QRA) within the context of risk management are shown in Fig. 53 (Ho et al. 2000).

There is a rich discussion related Failure Modes and Effect Analysis (FMEA), Failure Mode, Effects and Critically Analysis (FMECA), Event Tree Analysis (ETA), Fault Tree analysis (FTA) (ICOLD, 2005b).Structural Reliability Methods permit the calculation of failure probabilities of the mechanisms. Probabilities are calculated using the methods of the modern reliability theory such as Level III Monte Carlo, Bayesian theory, Level II advanced first order second moment calculations.

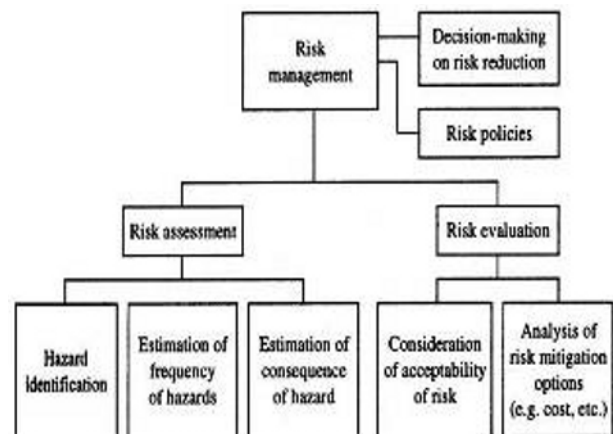


Fig. 53 Framework for risk management (after Ho et al. 2000)

Dam owners, regulatory authorities and consultants have been carrying out risk analyses for many years. Its purpose is to identify the main real risks associated with each type of structure and can be conducted: (i) in extensive risk analysis of structures, to substantiate reliably the probabilities chosen in fault trees using Monte Carlo simulation technique; (ii) in simplified risk analysis of smaller structures, to focus low-cost risk analysis on a few main risks; (iii) and in identifying possibilities for reducing these risks through low-cost structural or non-structural measures .It is important to stress that a higher factor of safety may not correspond to a lower probability of failure because it is important to take into account the

degree of uncertainty of the parameters.

Consideration of human behavior is essential when assessing the consequence of failures: well organized emergency planning and early warning systems could decrease the number of victims and so the study of human behavior plays an important role in assessment of risk analysis (Sêco e Pinto, 1991).

The results of a risk analysis can be used to guide future investigations and studies, and to supplement conventional analyses in making decisions on waste landfills safety improvements. With increasing confidence in the results of risk analyses, the level of risk could become the basis of safety decisions (Sêco e Pinto, 2002).

A probabilistic risk assessment addresses three fundamental questions (Salmon and Hartford, 1995): (I) what can go wrong? (ii) how likely is it?; (iii) what damage will it do?

FINAL REMARKS

In the precedent sections the characterization of solid waste landfills and lining systems during static and seismic conditions were presented. This information is very important to assist the design engineer in incorporating the adequate design measures to prevent deleterious effects of earthquake shaking.

All the essential steps of good analyses, whatever the type of material is involved shall be performed with a sufficient degree of accuracy that the overall results can be extremely useful in guiding the engineer in the final assessment of seismic stability. This final assessment is not made by numerical results but shall be made by experienced engineers who are familiar with the difficulties in defining the design earthquake and the material characteristics, who are familiar with the strengths and limitations of analytical procedures, and who have the necessary experience gained from studies of past performance.

To progress and to reach our goals we need leadership, development of news strategies, capacity and perseverance to fight against conservative practices, implementation of innovative solutions and courage to put in practice new policies.

If a man will begin with certainties, he shall end in doubts; but if he will be content to begin with doubts, he shall end in certainties.

(Francis Bacon - Advancement of Learning)

REFERENCES

ASCE: American Society of Civil Engineers
ICCHGE: International Conference on Case Histories in

- Geotechnical Engineering
ICOLD: International Conference on Large Dams or International Committee on Large Dams
ICRAGEESD: International Conference on Recent Advances in Geotechnical Earthquake Engineering and Soil Dynamics
ICSMFE: International Conference on Soil Mechanics and Foundation Engineering
JGED: Journal of the Geotechnical Engineering Division
JSMFD: Journal of the Soil Mechanics and Foundation Division
LNEC: Laboratório Nacional de Engenharia Civil
Abrahamson NA & Silva WJ (1997). Empirical response spectral attenuation relations for shallow crustal earthquakes. *Sei. Res. Lett.* 68(1): 94-127.
Aki K (1993). Local site effects on weak and strong ground motion. *Tectonophysics*, 218: 93-111.
Amini F & Qi GZ (2000). Liquefaction testing of stratified silty sands. *J.G.G.E.*, 126(3): 208-217.
Augello AJ, Bray JD, Seed RD, Matasovic N, Kavazanjian E, Jr, Solid waste landfill performance during the 1994 Northridge earthquake 1995. *Proc. 3rd ICRAGEESD*, St. Louis, 3: 1395-1401.
Avsar S, Bouazza A, Kavazanjian E (2004). Determination of optimum sampling locations in a solid waste landfill using PCSV Technique. *Proc. of In Situ Conference on Geotechnical and Geophysical Site Investigation*, 2: 1263-1266. Editors Viana de Fonseca and Mayne.
Bard PY (1994). Effects of surface geology on ground motion: recent results and remaining issues. *Proc. 10th European Conf. Earthq. Eng.*, Vienna, Austria, 1:305-323.
Bello LAL, Campos TMP, Júnior JT, Clarke BG (2004). Development of a full displacement pressurometer for municipal displacement solid waste site investigation in Brazil. *Proc. of In Situ Conference on Geotechnical and Geophysical Site Investigation*, 1: 657-663. Editors Viana de Fonseca and Mayne.
Benson CH, Bouazza A, Fratolocchi E, Manassero M (2005). Traditional and innovative barriers technologies. *Technical Committee Environmental Geotechnics Report*. CD-ROM.
Blight G (2006). A survey of lethal failures in municipal solid waste dumps and landfills. *Proc. 5th ICEG*, Cardiff, 1: 13- 37. Edited by H.R.Thomas .
Blight GE & Mbande C (1998). Waste management problems in developing countries in: *Solid Waste Management-Critical Issues for Developing Countries*. E. Thomas-Hope, Ed. Canoe Press, Kingston, Jamaica, 11-26.
Bray J (2007). Simplified seismic slope displacements procedures. *4th International Conference on Earthquake Geotechnical Engineering*, Thessaloniki. CD-ROM.
Bray JD, Augello AJ, Leonards GA, Repetto PC, Byrne RJ (1995). Seismic stability procedures for solid waste

- landfills. *JGE*, 121(2): 139-151.
- Bu S (2003). Local site effects on the seismic response of MSW landfills. *Proc. XII ECSMGE*, 1: 45-50.
- Buranek D & Prasad S (1991). Sanitary landfill performance during the Loma Prieta earthquake. *Proc. 2nd ICRAGEESD*, St. Louis, 2: 1655- 1660.
- Burns RL & Parson JJ (2005). Polyurea Repair of a MSW landfill Liner System, GRI-18. *Geosynthetics Research and Development in Progress. Geo Frontier, ASCE Conference*. Edited by E. Rathje.
- Cabalar AF & Canakci H (2005). Ground improvement by bacteria, *Proceedings of the Third Biot Conference on Poromechanics*, Norman, Oklahoma, Editors: Abousleiman, N. Cheng, A.H.-D, and Ulm, F.-J.
- Caicedo B, Yamin L Giraldo, Coronado O (2002). Geomechanical properties of municipal solid waste in Dona Juana sanitary landfill. *Proc. 4 ICEG*, 1: 177- 182.
- Caldeira L, Pimenta L, Silva Gomes A (2005). Framework of Risk Analysis and their Application to Embankment Dams (in Portuguese). *Seminar on Dams- Technology, Safety and Interaction with the Society*, Lisbon: 569- 585.
- Carrubba P & Massimino MR (1998). Dynamic geosynthetic interfaces behaviour. *Proc. XII Italian National Conference on Geosynthetic and Earth construction for Environmental protections*, In *Journal of Engineers and Architects*, 5(1-3): 33-36 (in Italian).
- Cascone E (1995). Shaking table test and modelling of retaining wall dynamic behaviour. Ph.D. Thesis, Faculty of Civil Engineering, University of Catania, Italy, (in Italian), p. 297.
- Cetin KO, e Seed RB, e Kiureghian (2001). Reliability based assessment of seismic soil liquefaction initiation, *XV ICSMGE TC4 Satellite Conference on Lessons Learned from Recent Strong Earthquakes*: 327-332. Edited by Atilla Ansal.
- Clark R (2005). Design basics and performance criteria chapter 1. *TC 5 Manual*, CD-ROM.
- Commoulos DG (2003). Long-term settlement behaviour of landfills. *Proc. of 13 European Conference of Soil Mechanics and Geotechnical Engineering*, 3: 137-142.
- Das BM & Shin EC (1999). Strip foundation on geogrid-reinforced clay: behaviour under cyclic loadings. *Geotextiles and Geomembranes*, 13: 657-667.
- De A (1996). Study of interfacial friction of landfill geosynthetics: static and dynamic. Ph.D. Thesis, Rensselaer, Polytechnic Institute, Troy, New York, USA:245.
- De A, Dunn RS, Matasovic N (2004). Site characterization, design and construction for closure of four hazardous waste landfills at a superficial site, *Fifth International Conference on Case Histories in Geotechnical Engineering*, New York, Edited by Shamsher Prakash, CD-ROM.
- Dellabianca SMA, Dellabianca LM, Muerieta PSN (2006). A field an numerical analysis on solid waste sanitary landfill settlement, *Proc. 5th ICEG*, Cardiff, 1: 423-429. Edited by H. R. Thomas.
- De A & Zimmie TF (1998). Estimation of dynamic interfacial properties of geosynthetics. *Geosynthetics International, Special Issue on Geosynthetic in Earthquake Engineering*, 5(1-2): 17-39.
- DeJong JT, Fritzges MB, Nusslein K (2006). Microbially Induced Cementation to Control Sand Response to Undrained Shear, *Journal of Geotechnical and Geoenvironmental Engineering*, ASCE, 132(11): 1381-1392.
- EC8 (Eurocode 8) (ENV 1998-5. 1994) Design provisions for earthquake resistance of structures-Part 5: Foundations, retaining structures and geotechnical aspects.
- Elgamal AW, Zeghal M, Parra E (1995). Identification and modelling of earthquake ground response. *First International Conference on Earthquake Geotechnical Engineering*, Japan.
- Elms D (2000). Refinements to the Newmark sliding block model. Paper No. 2132. *12th WCEE*, Auckland, New Zealand.
- Fahker A (2006). Experimental Study on the Compaction of Waste. *Proc. 5th ICEG*, Cardiff, 1: 445- 452. Edited by H.R.Thomas.
- Finn WDL (1987). *Finite Element Handbook—Chapter 3—Geomechanics*. McGraw-Hill Editors H. Hardestuncer.
- Furuta e Yamamoto (2000). Liquefaction assessment by shear wave crosshole tomography tests. Paper No. 831. *12th WCEE*, Auckland, New Zealand.
- GLR-Recommendations 1993 *Geotechnics of landfill. design and remedial works*, Technical Recommendations edited by the German Geotechnical Society for ISSMFE, Ernst & Sohn, Berlin.
- Grisolia M & Napoleoni Q (2006). Solid waste compressibility and settlements in sanitary landfills. *Proc. 5th ICEG*, Cardiff, 1: 461- 468. Edited by H.R.Thomas .
- Grisolia M , Napoleoni Q, Pagnoni A, Tancredi G (1992). Considerazioni sulla compressibilità del rifiuti solidi urbani. *Proc., 1st Italian-Brazilian Symposim on Sanitary and Environmental Engineering*, Rio de Janeiro.
- Hanson JL, Yesiller N, Swarbrick (2005). Thermal analysis of GCLs at a municipal solid waste landfills, *GSP 142. Waste Contaminant and Remediation*.*Geo Frontier, ASCE Conference*. Edited by E. Rathje.
- Heerten G (2006). Monitoring of Geosynthetics Long-Term behavior in landfill sealing system. *Proc. 5th ICEG*, Cardiff, 1: 525- 532. Edited by H.R.Thomas.
- Ho K, Leroi E, Roberbs B (2000). Quantitative Risk

- Assessment: Application, Myths and Future direction, GEO Eng, 2000, Melbourne: 269-312.
- Hossain MD, Haque MA, Qasim SR, Hoyos LL (2007). Dynamic characterization of municipal solid waste with degradation in bioreactor landfills. Proc. 4th ICEGE. Paper ID 1265.Thessaloniki.
- Hushmand B & Martin GR (1990). Final Report SBIR, Phase I study, Layered soil-synthetic linear base isolation system. Report submitted to the National Science Foundation Small Business Innovative Research Program, The Earth Technology Corporation, Long Beach, California, USA, p. 86.
- Hsuan YG & Koerner RM (1998). Antioxidant depletion lifetime in high density polyethylene geomembranes, ASCE, J.Geotech. Geoenv. Eng., 124(6): 532-541.
- ICOLD (1983). Seismicity and Dam Design. Bulletin (46).
- ICOLD (1989). Selection Seismic Parameters for Large Dams - Guidelines. Bulletin (72).
- ICOLD (2005). Risk Assessment in Dam Safety Management. Bulletin(130).
- Idriss IM (1990). Response of soft soil during soil earthquakes. Proc. H. Bolton Seed Memorial Symposium: 273-290.
- Idriss IM (1995). An overview of earthquake ground motions pertinent to seismic zonation. Proc. 5th Int. Conf. Seismic Zonation, Nice: 2111-2126.
- Jessberg HL (1994). Emerging problems and practices in environmental geotechnology. Proc. XIII ICSMFE, 1: 271-281.
- Jessberg HL (1996). TC5 activities - Technical Committee on Environmental Geotechnics, ISSMFE., Proc. 2nd. International Congress on Environmental Geotechnics, Osaka: 1-28.
- Jewell RA (1990). Strength and deformation in reinforced soil design, Proc. 4th Int. Conf. on Geotextiles. Geomembranes and Related Products, 3, The Hague, Netherlands, May 28 June 1.
- Johnson M, Lew M, Lundy J, Ray ME (1991). Investigation of sanitary slope performance during strong ground motion from the Loma Prieta Earthquake of October 17, 1989. Proc. 2nd ICORAGEESD, St.Louis, 2: 1701-1708.
- Karatas I, Kavazanjian E, Jr, Rittmann B (2008). Microbially induced precipitation of calcite using pseudomonas denitrificans. Proc. 1st International Conference on BioGeo Civil Engineering, Delft, The Netherlands.
- Kavazanjian E, Jr (1995). Evaluation of MSW properties for seismic analysis. Geoenvironmental Geotechnics: 1126-1141.Balkema, Rotterdam.
- Kavazanjian E, Jr (1998). Current issues in seismic design of geosynthetic cover systems. Proc. of the 6th Int. Conference on Geosynthetics, 1: 219-226.
- Kavazanjian E, Jr (2008). The indispensable role of Case Histories on landfill engineers SOAP 7, Proc. 6th International Conference in Case Histories in Geotechnical Engineering, Arlington.
- Kavazanjian E, Jr & Karatas I (2008). Microbiological improvement of the physical properties of soil, Proc. 6th International Conference on Case Histories in Geotechnical Engineering, Arlington, Paper N0.JKM 3.
- Kavazanjian E, Jr, Matasovic N, Stokoe K, Bray J (1996). In situ shear wave velocity of solid waste from surface wave measurements. Proc. of 2nd International Congress on Environmental Geotechnics, 1: 97- 102, Edited by Masashi Kamon.
- Kavazanjian E & Matasovic N (2001). Seismic design of mixed and hazardous waste landfills. Proc. 4th International Conference on Recent Advances in Geotechnical Earthquake Engineering and Soil Dynamics, SOAP 11, San Diego. Edited by Shamsher Prakash, CD-Rom.
- Kockel R, Konig D, Syllwasschy O (1997). Three basic topics mechanics on waste mechanics.Proc. 14th ICSMFE, 3: 1831- 1837.
- Kokusho Te & Matsumoto M (1997). Nonlinear site response during the Hyogoken-Nanbu earthquake recorded by vertical arrays in view of seismic zonation methodology. Proc of the Discussion Special Technical Session on Earthquake Geotechnical Engineering during 14th ICSMFE, Hamburg, Edited by Pedro S.Sêco e Pinto. Published by Balkema: 61-69. Kramer S. L. 1995. Geotechnical Earthquake Engineering. Prentice Hall.
- Koseki J, Bathurst RJ, Güler E, Kuwano J Maugeri M (2006). Seismic stability of reinforced walls. Proc. Geosynthetics Conference, Yokohama, 8 IGS Conference
- Kocevic ZB, Kovacic D, Matesic L, Velickovic B (2006). Quality acceptance testing of GCLs for landfill application. Proc. 5th ICEG, Cardiff, 1: 445-452. Edited by H.R.Thomas.
- Lee MK & e WLL Finn (1978). DESRA 2, dynamic effective stress response analysis of soil deposits with energy transmitting boundary including assessment of liquefaction potential. Soil Mechanics series n° 38. Department of Civil Engineering, University of British Columbia, Vancouver, Canada.
- Lee WF, Lin SS, Chen JW (2007). Seismic performance analysis of geosynthetic reinforced slopes. Proc. 4th ICEGE. Paper ID 1384.Thessaloniki.
- Lo Grasso AS, Maugeri M, Recalcati P (2006). Experimental seismic analysis of geosynthetic-reinforced soil structures with three-dimensional reinforcements by shaking table tests. Proc. of 8th International Geosynthetics Conference: 1489-1494.
- Loxham M (2003). Man made deposits – recent and ancient – risk analysis and environmental impact. Proc.XII ECSMGE: 125-130.
- Lysmer JT, Udaka CF Tsai, e HB Seed FLUSH 2 (1975).

- A computer program for approximate 3-D analysis of soil structure interaction problems. Report No. UCB/EERC 75-30. University of California, Berkeley, Machado SL, Carvalho MF, Nascimento JCF, Dourado KA (2006). Aging effect on MSW mechanical behaviour, Proc. 5th ICEGE, Cardiff 2: 1439-1446, Edited by H. R. Thomas.
- Machado SL, Carvalho MF, Nascimento JCF, Dourado KA, Rodrigues MB, Nascimento JCI (2006). Study of the MSW time differed compressibility in the Metropolitan Center Landfill, Proc. 5th ICEGE, Cardiff 2: 1447- 1454, Edited by H.R.Thomas.
- Makdisi FI & e HB Seed (1977). A simplified procedure for estimating earthquake induced deformations in dams and embankments. Report No. EERC 79-19. University of California, Berkeley.
- Marques aCM, Fliz GM, Vilar OM (2002). Landfill settlement calculations using a composite rheologic model, Proc. 4th ICEG, 1: 21- 26.
- Martin JP, Koerner RM, Whitty JE (1984). Experimental friction evaluation of slippage between geomembranes, geotextiles, and soils, Proc. Int. Conf. on Geomembranes, Denver, Colorado.
- Matasovic N & Kavazanjian E (1996). Dynamic properties of solid waste from field observations. Proc. of the First International Conference on Earthquake Geotechnical Engineering, 1: 549-554. Kenji Ishihara Editor.
- Matasovic N, De A, Dunn J, Kavazanjian E (2004). Slope stability at a hazardous waste site-Evaluation of the CPT cone factor N_k using dynamic property correlations. Proc. of the Third International Conference on Earthquake Geotechnical Engineering, 1: 478- 484. D. Doolin, A.Kammerer, T. Nogami, R. Seed and I. Towhata Editor.
- Medina M (1997). Informal recycling and collection of solid wastes in developing countries. Working paper 24. United Nations University 7 Institute of Advanced Studies, Tokyo, Japan.
- Mello LG & Boscov MEG (2002). Influence of time on design parameters of MSW, Proc. of 4th International Congress on environmental Geotechnics, Editors de Mello & Almeida, Rio de Janeiro: 913- 922.
- Mitchell JK & Mitchell R (2004). Environmental geotechnics. two Case Histories. SOAP 9. Prof. 5th International Conference on Case histories in Geotechnical Engineering, New York, SOAP 9. CD-ROM.
- Mitchell JK, Seed RB, Seed HB (1990). Kettleman hills waste landfill slope failure. I: liner-system properties, Journ. Of Geot. Eng., ASCE, 116(4).
- Mitchell, JK, Seed RB, Seed HB (1990). Kettleman Hills waste landfill slope failure I: Liner- System Properties. JGE 116(4): 647- 668.
- MoE (1998). Landfill standards: a guideline on the regulatory and approval requirements for the new or expanding landfilling sites. Ontario Ministry of the Environment May, Ontario Regulation 232/98. Queen's Printer for Ontario, Toronto.
- Nakamura J, Sakanishi M, Kitazawa, Kumagai K, Fujihashi K, Ogasawara TDM (2006). Deformation measurement technology of geomembrane at controlled landfills using optical fiber sensors. Proc. of 8th International Geosynthetics Conference: 203-206.
- Newmark NM (1965). Effects of earthquakes on dams and embankments. Geotechnique, 15(2): 139-160,
- Oliveira DAF e Murieta P (2004). Geotechnical site investigation of municipal solid waste landfills. Proc. of In Situ Conference on Geotechnical and Geophysical Site Investigation, 2: 1325-1330. Editors Viana de Fonseca and Mayne.
- O'Rourke TD, Druschel SJ, Netravali AN (1990). Journ. Of Geot. Eng., ASCE, 116(3): 451-469.
- Pasqualini E, Sani D, Roccato M (1995). Factors influencing geomembrane interface friction. Green '93, Sarsby, R.W., Editor Balkema, Proceedings of a conference held in Bolton, United Kingdom: 349-356.
- Pasqualini E, Stella M, Roccato (1996). Composite liners-improvements of the interface shear resistance. Proc. of 2nd International Congress on Environmental Geotechnics: Vol.1:591- 596. Edited by Masashi Kamon.
- Rathje EM & Bray JD (1999). Two dimensional seismic response of solid waste landfills. Proc. of 2nd International Conference on Earthquake Geotechnical Engineering Lisboa. 2: 655-660. Edited by Pedro S. Sêco e Pinto. Published by A. Balkema Rathje, E. and Saygili, G. 2008. Probabilistic seismic hazard analysis for the sliding displacement of slopes: scalar and vector approaches. Journal of Geotechnical and Geoenvironmental Engineering, June: 804-814.
- Rowe RK (2001). Liner Systems. Chapter 25 of Geotechnical and Geoenvironmental Engineering Handbook, Kluwer Academic Publishing, Norwell, U.S.A.: 739-788.
- Rowe RK, Armstrong MD, Cullimore DR (2000a). Mass loading and the Rowe, R.K. 2006. Some factors affecting geosynthetics used for geoenvironmental applications, Proc. 5th ICEG, Cardiff, 1: 41- 69. Edited by H.R.Thomas.
- Rowe RK, Quigley RM, Booker JR (1995). Clayey Barrier Systems for Waste Disposal Facilities. E & FN Spon (Chapman & Hall), London, p. 390.
- Sadigh K, Chang CY, Egan JA, Makdisi F, e RR Youngs (1997). Attenuation relationships for shallow crustal earthquakes based on California strong motion data. Seis. Res. Lett. 68(1): 180-189.
- Salmon GM & Hartford DND (1995). Risk analysis for dam safety. International Water Power & Dam Construction, March: 42-47.
- Santayana F Pardo & Lopes MG (2003). Geotechnical

- aspects and construction quality assurance plans for MSW landfills recently built in Portugal. Proc.XII ECSMGE: 199-204.
- Santhakumat AR, Verma AK, Rao AVSR (2001). Dynamic behavior of geogrid-reinforced soil. Proc. 4th International Conference on Recent Advances in Geotechnical Earthquake Engineering and Soil Dynamics, Paper 1.74, San Diego. Edited by Shamsheer Prakash, CD-ROM.
- Sargent RC (1990). Validation of mathematical models. Proc. Geoval-90, Conf. Stockholm Francisco Preprint.
- Sarma SH (1975). Seismic stability of earth dams and Embankments. *Geotechnique*, 25(4): 743-76.
- Sarma SH & Chowdhury R (1996). Simulation of pore pressure in earth structures during earthquakes. 11th WCEE, Acapulco, Mexico.
- Schnabel PB, Lysmer J, e Seed HB (1972). SHAKE A computer program for earthquake response analysis of horizontally layered sites. Report N UCB/EERC 72-12. University of California, Berkeley.
- Sêco e Pinto PS (1990). Dynamic characterization of soils. *Natural Hazards and Engineering Geology - Prevention and Control of Landslides and other Mass Movements*. European School of Climatology and Natural Hazard Course.
- Sêco e Pinto PS (1992). Dynamic analysis of embankment dams. *Soil Dynamics and Geotechnical Earthquake Engineering Seminar*. Edited by Sêco e Pinto. Balkema Publisher: 159-269.
- Sêco e Pinto PS (1997). Analysis of the behaviour of solid waste landfills (in Portuguese). Seminar on Geoenvironmental Aspects. of Industrial Solid Waste Landfills, Lisboa.
- Sêco e Pinto PS (1998). Instrumentation of embankment dams; Portuguese experience. Invited Lecture. International Conference on Dams and Reservoirs, Mexico: 117-132.
- Sêco e Pinto PS (2002). Some reflections about risk analysis of Geotechnical Structures. Proc. of 12th Danube- European Conference Geotechnical Engineering, Passau: 41-46.
- Sêco e Pinto P (2003). Seismic behaviour of geotechnical structures. Inaugural lecture, Proc. 13th Regional African Conference of Soil Mechanics and Geotechnical Engineering: 3-24. Marrakech, Edited by M. Sahli, L. Bahi & R. Khalid.
- Sêco e Pinto P (2007). Design of SWL and Lining Structures. Proc. of ISSMGE International Seminar, Beijing.
- Sêco e Pinto P (2008a). Seismic characterization of SWL and Lining Structures. Proc. of ISSMGE International Seminar, Accra.
- Sêco e Pinto P (2008b). Seismic behaviour of geotechnical structures. What lessons were learned? Proc. Indian Geotechnical Conference, 60 Anniversary, Bangalore.
- Sêco e Pinto PS (2009). Interaction between Eurocode 7 – Geotechnical Design and Eurocode 8 – Design for Earthquake Resistance of Foundations.
- Sêco e Pinto PS, Correia J, e Vieira A (1997). Evaluation of liquefaction potential of a site located in the South of Portugal. Proc of the Discussion Special Technical Session on Earthquake Geotechnical Engineering during 14th ICSMFE, Hamburg: 113-124. Edited by Pedro S.Sêco e Pinto. Published by Balkema.
- Sêco e Pinto PS, Lopes L Agostinho, Vieira A (1998). Seismic analysis of solid waste landfills. Proc. of 3rd. International Congress on Environmental Geotechnics, Lisboa. Edited by Pedro S. Sêco e Pinto. Published by A. Balkema.
- Sêco e Pinto PS & Maugeri M (2005). TC 5 Report. Osaka.
- Seed HBIM Idriss. (1982). Ground motions and soil liquefaction during earthquakes. Earthquake Engineering Research Institute, Oakland, California.
- Sharma HD & Goyal HK (1991). Performance of a hazardous waste and sanitary landfill subjected to Loma Prieta earthquake, Proc. 2nd ICORAGEESD, St. Louis, 2: 1717- 1725.
- Singh S (2002). Dynamic strength characteristics of municipal solid waste, Proc. of 4th International Congress on Environmental Geotechnics, Editors de Mello & Almeida, Rio de Janeiro: 157-161.
- Singh S & Murphy B (1990). Evaluation of the stability of solid waste landfill. *Geotechnics of waste landfills- Theory and practice*, ASTM STP 1070, Landva and G.D. Knowles, Eds: 259-284.
- Somerville (1998). Engineering art: earthquake ground motion. Proc. Geotechnical Earthquake Engineering in Soil Dynamics III. Edited by P Dakoulas, M Yegian , RD Holtz, Geotechnical Special Publication. No. 75, ASCE, 1: 1-38.
- Srivastava RK, Raddy M, Bala R, Tiwari MRP (2006). Landfill Site Selection Using GIS, Proc. 5th ICEG, Cardiff, 2: 1557- 1562. Edited by H. R. Thomas.
- Stokoe KHII, Darendeli MB, Andrus RD, Brown LT (1999). Dynamic soil properties: Laboratory, field and correlation studies. Theme Lecture. Proc. of 2nd International Conference on Earthquake Geotechnical Engineering, Lisboa. Edited by Pedro Sêco e Pinto. Published by A. Balkema, 3: 811-845.
- Stark TD & Poepfel AR (1992). Landfill linear interface strengths from torsional-ring-shear tests. *Journal. of Geot. Eng., ASCE*, 120(3).
- Stewart JP, Bray JD, Seed RB, Sita N (1994). Preliminary report on the principal geotechnical aspects of the January 17, 1994 Northridge Earthquake, Report No. UCB/EERC- 94/08, College of Engineering, University of California at Berkeley, Berkeley, California, p. 238.
- Strano A (2000). Soil-Geosynthetics interface shear

- strength evaluation by shaking table tests. Diploma Thesis, University of Catania, Italy (in Italian).
- Takahashi T, Mimoto K, Hayakawa T (1997). Present state of applications of geophysical methods to characterization of active faults. *Journal of Japan Society of Engineering Geology*, 38: 118-129.
- Tamura C, Kanyo S, Uesaka T, Nagayama I, e Y Wakizaka (2000). Survey and evaluation of active faults on dam construction in Japan. Paper No. 2493. 12th WCEE, Auckland, New Zealand.
- Thusyanthan NI Madabhushi & Singh S (2004). Modelling the seismic behaviour of municipal solid waste. *Proc. of the Third International Conference on Earthquake Geotechnical Engineering*, 1: 283-290. Doolin, A. Kammerer, T. Nogami, R. Seed and I. Towhata Editors.
- Towhata I, Kawano Y, Yonai Y, Koelsch F (2004). Laboratory tests on dynamic properties of municipal wastes. *Proc. of the Third International Conference on Earthquake Geotechnical Engineering*, 1: 688-693. Doolin, A. Kammerer, T. Nogami, R. Seed and I. Towhata Editors.
- Trifunac M & Brady G (1975). On the Correlation of Seismic Intensity Scales for the peaks of Recorded Strong Ground Motion. *Bulletin of the Seismological Society of America*, 65:139-162.
- UBC (Uniform Building Code) (1997). *International Conference of Building Officials*, Whittier, California, Vol. II.
- Vieira A (1995). Amplification of seismic movements for horizontal soil layers. Master thesis (in Portuguese). University New of Lisbon.
- Vilar OM & Carvalho MF (2002). Shear strength properties of municipal solid waste. *Proc. of 4th International Congress on Environmental Geotechnics*, Editors de Mello & Almeida, Rio de Janeiro: 59-64.
- Viswanadhan BVS & Sengupta SS (2006). Deformation of compacted soil liners in a geocentrifuge. *Proc. 5th ICEG, Cardiff*, 1: 809- 816. Edited by H. R. Thomas.
- Von Pein RT & Lewis SP (1991). Composite lining system design issues. *Geotextiles and Geomembranes*, 10(5-6): 125-131.
- Vucetic M Dobry R (1992). Effect of soil plasticity on cyclic response. *JGED, ASCE*, 117(GT1): 89-107
- Wijewickreme WKD & Vaid YP (1989). Geomembrane interface friction, *Canadian Geotechnical Journal*, 26.
- Williams ND & Houlihan M (1986). Evaluation of friction coefficients between geomembranes, geotextiles and related products, *Proc. 3rd Int. Conf. on Geotextiles*, Vienna, Austria.
- Yegian MK & Kadakai HV (1998). Seismic response of landfills with geosynthetic liners. *Proc. of the 6th Int. Conference on Geosynthetics*, 1: 227-230.
- Yegian MK & Lahlaf AM (1992). Dynamic interface shear strength properties of geomembranes and geotextiles. *Journal of Geotechnical Engineering, ASCE*, 118(5): 760-779.
- Yegian MK, Yee ZY, Harb JN (1995). Response of geosynthetics under earthquake excitations. *Proceedings of Geosynthetics '95*, 2: 677-689.
- Youd TL & Gilstrap SD (1999). Liquefaction and deformation of silty and fine-grained soils. *General Report. Proc. of 2nd International Conference on Earthquake Geotechnical Engineering, Lisboa*, 3: 1013-1020. Edited by Pedro Sêco e Pinto. Published by A. Balkema.
- Zania V, Tsompanakis Y, Psarrououlos P (2007). Slope stability of municipal solid waste landfills under seismic loading. *Proc. 4th ICEGE. Paper ID 1217.Thessaloniki*.
- Zekkos D, Bray JD, Athanasopoulos GA, Riemer MF, Kavazanjian E, Founta P, Grizi A (2007). Compositional and loading rate effects on the shear strength of municipal solid wastes. *Proc. 4th ICEGE. Paper ID 1525.Thessaloniki*.
- Zekkos D, Bray JD, Kavazanjian E, Matasovic N, Rathje E, Reiner M, Stoke KIII (2006). Unit weight of municipal solid waste. *ASCE Journal of Geotechnical and Geoenvironmental Engineering*, 132(40): 1250-1261.
- Zimmie TF (2005). Using geotechnical centrifuges for geosynthetic research and practice, GRI-18. *Geosynthetics Research and Development in Progress. Geo Frontier, ASCE Conference*. Edited by E. Rathje.
- Zimmie TF, De A, Mahumud MB (1994). Centrifuge modelling to study dynamic friction at geosynthetic interfaces. *Proc. of the Fifth Int. Conf. on Geotextiles, Geomembranes and Related Product, Singapore*: 1: 415-418.
- Zornberg JG, McCartney JS, Swan RH (2004). Internal Shear Strength of Geosynthetic Clay Liners. *Journal of Geotechnical and Geotechnical Engineering, ASCE*, 131.



Invited Lectures

MODELING APPLIED TO ENVIRONMENTAL GEOTECHNICS

Mario MANASSERO¹, Andrea DOMINIJANNI² and Guido MUSSO³

ABSTRACT: The paper deals with basic and advanced theories for modeling mechanical, hydraulic, chemical and electrical phenomena of growing practical interest involving mineral barriers, polluted subsoils and waste landfills. In particular, four related and very topical issues are focused on: (1) prediction of short and long term behavior of geosynthetic clay liners (GCLs) for pollutants control; (2) modeling of multiphase mass and energy flows for speeding up contaminant extraction by electrical potential and (3) high vacuum; and (4) assessment of mechanical behavior of lining systems on old landfill for allowing side and vertical extensions.

KEYWORDS: geosynthetic clay liner, contaminant vacuum extraction, cross-contamination, solid waste mechanical behavior

INTRODUCTION

Referring to the present state of the art, the theoretical modeling approaches applied to Environmental Geotechnics can be split in two main domains: flow-transport phenomena in porous media and mechanical behavior of particulate media. Only in few cases the two domains are fully coupled in order to set up more sophisticated models that theoretically should be able to result in a better representation of some actual problems.

Practical application aspects within the Environmental Geotechnics field require to model mass and energy flows in order to be able to cope with situations such as: 1) subsoil pollutant migration and control, 2) assessment of short and long term performances of mineral and polymeric barriers and 3) polluted sites contaminant treatment and extraction.

On the other hand, the theoretical prediction of particulate material mechanical behavior is often applied to Environmental Geotechnics problems involving: 1) waste landfill stability, management, extension and reclamation, 2) re-use of waste and by-products and 3) assessment of pollutant barriers performances subjected to large stress/strain variations.

Just a very basic treatment of the main general aspects related with mass and energy transport and mechanical behavior of porous and particulate media would require more than a textbook. Therefore, in the following, after a very short review of the basic

framework and equations concerning the two aforementioned main domains, a number of practical applications will be considered as illustrative examples including: (1) prediction of short and long term behavior of geosynthetic clay liners (GCLs) for pollutants control; (2) modeling of multiphase mass and energy flows for speeding up contaminant extraction by electrical currents and; (3) high vacuum; and (4) assessment of mechanical behavior of lining systems on old landfill for allowing side and vertical extensions

BASIC ASPECTS AND FUTURE DEVELOPMENTS OF THEORETICAL MODELING

In the following points the fundamental theories and related equations with reference to flow-transport phenomena and mechanical behavior of porous and particulate media are recalled.

Flow and Transport in Porous Media

The basic equations governing multiphase/multicomponent/ coupled mass and energy flows are today well known in their general form as synthesized below (Yong et al. 1992; Mitchell and Soga 2005).

Mass balance equations:

$$\frac{\partial(\theta^\alpha \rho_i^\alpha)}{\partial t} = -\nabla \cdot J_i^\alpha + \sum_{\beta} r_i^{\alpha \rightarrow \beta} \quad (1)$$

¹ Professor, Land, Environment and Geo-Engineering Department, Politecnico di Torino, Italy. Email: mario.manassero@polito.it

² Research Fellow, Environment and Geo-Engineering Department, Politecnico di Torino, Italy. Email: andrea.dominijanni@polito.it

³ Research Assistant, Structural and Geotechnical Engineering Department, Politecnico di Torino, Italy. mail:guido.musso@polito.it

where θ^α = volumetric fraction of the phase α ; ρ_i^α = density of the i -th component in the phase α ; $r_i^{\alpha \rightarrow \beta}$ = terms of partition and mass exchange from the phase α to the phase β for the i -th component.

Momentum balance equations:

$$\begin{aligned}
 J_i^\alpha &= \ell_{ii}^{\alpha\alpha} \nabla(-\mu_i^\alpha) + \ell_{ij}^{\alpha\alpha} \nabla(-\mu_j^\alpha) + \dots \\
 &\quad \dots + \ell_{ii}^{\alpha\beta} \nabla(-\mu_i^\beta) + \ell_{ij}^{\alpha\beta} \nabla(-\mu_j^\beta) + \dots \\
 J_j^\alpha &= \ell_{ji}^{\alpha\alpha} \nabla(-\mu_i^\alpha) + \ell_{jj}^{\alpha\alpha} \nabla(-\mu_j^\alpha) + \dots \\
 &\quad \dots + \ell_{ji}^{\alpha\beta} \nabla(-\mu_i^\beta) + \ell_{jj}^{\alpha\beta} \nabla(-\mu_j^\beta) + \dots \\
 &\dots \\
 J_i^\beta &= \ell_{ii}^{\beta\alpha} \nabla(-\mu_i^\alpha) + \ell_{ij}^{\beta\alpha} \nabla(-\mu_j^\alpha) + \dots \\
 &\quad \dots + \ell_{ii}^{\beta\beta} \nabla(-\mu_i^\beta) + \ell_{ij}^{\beta\beta} \nabla(-\mu_j^\beta) + \dots \\
 J_j^\beta &= \ell_{ji}^{\beta\alpha} \nabla(-\mu_i^\alpha) + \ell_{jj}^{\beta\alpha} \nabla(-\mu_j^\alpha) + \dots \\
 &\quad \dots + \ell_{ji}^{\beta\beta} \nabla(-\mu_i^\beta) + \ell_{jj}^{\beta\beta} \nabla(-\mu_j^\beta) + \dots \\
 &\dots
 \end{aligned} \tag{2}$$

where:

α, β = phases of the system; i, j = components distributed between the different phases; $\ell_{ij}^{\alpha\beta}$ = phenomenological coefficients of proportionality between the thermodynamic gradients and the associated fluxes; J_i^α = flux of the i -th component in the phase α ; $\nabla(-\mu_i^\alpha)$ = gradient of the generic thermodynamic potential that acts on the i -th component in the phase α (e.g. hydraulic, chemical, electric gradient).

The main assumptions adopted within the aforementioned equations are as follows:

- the system is governed by the linear irreversible thermodynamics principles;
- the state of the system is close to the equilibrium conditions;
- all the model phases (gas, liquid and solid) are continuous;
- fluid flows are slow and laminar.

In order to exploit the aforementioned equations for practical application it is necessary to evaluate the phenomenological coefficients of proportionality between the thermodynamic gradients and the associated fluxes. Today only the direct coefficient i.e. the main diagonal of the ℓ_{ij} matrix, representing hydraulic conductivity k , diffusion/dispersion coefficients D , electrical and thermal conductivity, can probably be considered reliable for consistent practical applications. Other parameters such as osmotic efficiency, electro-osmotic and thermal conductivity, in spite of their fundamental importance for assessing the pollutant

barrier performances and the electro-kinetic remediation efficiency are still unknown for most applications.

In Eqs. 2, the potential gradients are expressed by some among the unknowns of the model to be derived versus space and time (e.g. temperature, electric charge, component concentrations, phase density and pressure).

The interaction relationships ($r_i^{\alpha \rightarrow \beta}$) between the different components are taken into account by the summation terms of Eqs. 1. Using more or less sophisticated models, by these terms it is possible to express: chemical reactions among different components inside the same phase, degradation of the single component, source and sink contribution and/or phase changes and partitioning of the components among the different phases including volatilization, solution, sorption and the correspondent reverse reactions. These relationships, that link the different equations of the system, can be expressed at equilibrium, i.e. simulating instantaneous chemical reactions, or simulating non-equilibrium conditions versus time.

Beyond the aforementioned laws and relationships, in order to solve the multi phase and multi component coupled transport problem, further equations are necessary and they can be expressed through the state laws or constitutive equations of the single phases and the interaction relationships between phases.

Referring to the fluid phases, the state equations must relate pressure, temperature and volume while, for the solid phase, the theoretical modeling approach can be much more complex due to the existence of the stress-strain coupled tensors (instead of the pressure and volume simple scalars for fluids) and to the very sophisticated theoretical approach required in order to set up constitutive equations able to simulate, in a reliable way, the actual mechanical behavior of the particulate porous media.

For these reasons in most theoretical simulations of flow and transport within porous media the latter is considered rigid or as an alternative, simplified constitutive relationships are used (e.g. linear variation of volumetric strain versus effective isotropic stress).

As far as the interaction relationships between different phases are concerned, a distinction is to be made between fluid-fluid interactions, which can include both gas-liquid and aqueous-separate liquid (NAPL), and fluid-solid interactions.

In the first case, the pressure difference between fluids in contact, namely capillary pressure, can be expressed via the so-called retention or characteristic curves, i.e. as a function that relates the capillary pressure to the volumetric fraction of the fluids that occupy the porous medium (Bear, 1972; Charbeneau, 2000). The capillary pressure is in turn a function of the tension strength of the ideal membrane separating the two fluids, the different degree of affinity with the solid

phase (wetting potential) of the two fluids and of the pore size distribution of the porous medium (Bear, 1972). When the number of immiscible fluids is more than two the interaction problem becomes particularly complex and, in order to find a solution, it is necessary to refer to the scaling laws proposed by Leveret (1941) for three or more immiscible fluids with different wetting potential.

In the second case, the fundamental rules governing the interaction between the solid skeleton and the pore fluids in a particulate medium refer to the Terzaghi (1943) and Bishop (1954) basic and extended principle of the effective stress. The effective stress can be defined, in a first approximation, by the difference between the total applied normal stress and the pressure of the pore fluids. Similarly to the case of immiscible fluids interactions, also for solid-fluids interactions, it is then possible to relate, through appropriate constitutive equations, the effective stress variation to the volume fraction of the solid phase. Being the latter more currently expressed, within the geotechnical field, via the specific volume, the void index or the porosity.

Most of the parameters included in the aforementioned equations and relationships are not constant but are in turn a function of the problem unknowns (e.g. relative permeability versus fluid volumetric fraction, vapor tension versus capillary pressure, clay mineral fabric versus ion exchange phenomenon, osmotic efficiency of clayey materials versus ion concentration), leading, in the most general case, to a final highly non-linear very complex differential equations system to be solved. Another complicating factor to be mentioned is the non-uniqueness and irreversibility of some relationships describing the phase interaction (e.g. soil-water characteristic curves, precipitation and complexation chemical reactions)

In order to overcome the mathematical and numerical complexity and the difficulties in defining the input parameters, in most practical applications the aforementioned equations are simplified thanks to a series of further limiting assumptions:

- reduction of the number of phenomenological coefficients to the direct flow components only;
- reduction of the phase number and single phase mobility;
- reduction of component number of the single phase;
- reduction and simplification of chemical reactions and phase change involving the different component;
- linearization of functional relationships.

Some of the simplifications included in the list above have been exploited for implementing the models reported in the illustrative examples.

Mechanical Behavior of Particulate Media

Usually, when flow and transport phenomena must be simulated, the coupled constitutive equations describing the mechanical behavior of the solid particulate phase, namely the solid skeleton, can be partially simplified referring only to the volumetric strain variation due to mechanical stress changes and/or to thermo-chemical phenomena. Nevertheless, there are a lot of situations where the geotechnical problem to be faced requires the assessment of shear and tensional strains such as in the case municipal waste stability and settlement evaluation or in the case of possible cracks formation in a natural or artificial mineral barrier, for pollutant control, that in turn can produce a dramatic decrease of its efficiency with time.

In these cases the importance of the mechanical behavior of the waste or mineral materials could prevail on the other aspects and, in particular, on the flow and mass transport phenomena. Therefore, under these conditions most of the designer effort should be devoted to describe the mechanical behavior of the materials of interest not neglecting, if it is the case, the thermo-chemical stress that can play a significant role particularly in presence of fine grained materials (Hueckel, 1992a,b; Loret et al. 2002).

Just to show the complexity of the mechanical behavior of a particulate media, in the following a conceptual framework is proposed (Manassero and Shackelford, 1994). This framework allows the main aspects that influence the strength and deformability of any particulate material to be taken into account, even in the case of collapsible components and/or structured/cemented fabrics.

Most industrial and municipal solid wastes and by-products usually show stress-strain behavior of structured and lightly cemented particulate materials, as depicted in the qualitative model of Fig. 1. The main features of the proposed model are as follows:

- There are two basic boundary surfaces plotted in the $p - q$ and in the $p - \varepsilon_v$ planes (where p is the isotropic confinement stress, q is the deviatoric stress and ε_v is the volumetric strain). The first (1) surface describes the limit states of a particulate, frictional, non cemented, non structured (i.e. remoulded) material. This “frictional-dilatant state boundary surface” expands for increasing density values of the considered material (i.e. decreasing specific volume). The second surface (2) is a “structure surface” that describes the limit states when the particulate material is cemented or shows a structure that gives to the undisturbed material higher strength (at low confining stresses) than the remoulded material of the same density. This latter surface, as a first tentative

hypothesis, can be considered not to be significantly dependent on the material density.

- The p - ε_v plane is divided into four main zones by the projections of: (1) the well known critical state line and (2) the structure line that presents the intersection line between the structure surface and the friction-dilatant state boundary surface. The four main kinds of stress-strain behavior of the considered material can be obtained via the initial state parameters and, are therefore located inside one of the aforementioned zones acknowledged as brittle-softening zone (stress-paths A and E), brittle-hardening zone (stress-paths B and F), ductile-softening zone (stress-paths C and G) and ductile-hardening zones (stress-paths D and H).
- This proposed qualitative model can take into account the basic contributions (see the stress paths of Fig. 1) to the peak and residual strengths and the related stress-strain behavior of the considered material via: (1) the critical state surface for the pure friction contribution to the shear strength, (2) the frictional-dilatant state boundary surface for the locking (dilatancy) contribution and (3) the structure surface for the cementation and/or structure contribution.

The fundamental need of quantifying the stress-strain behavior of solid waste is outlined on the basis of the sketches of Fig. 1. This aspect is particularly important in the case of re-use of particulate by products involving diagenetic phenomena, in the case of cross contamination risk assessment when driven piles are foreseen to cross natural aquitards or aquicludes or in the case of vertical expansion of old landfill, where interactions between the old and new waste bodies and the related lining systems play a fundamental role in terms of safety and environmental impact.

Future Developments

As already mentioned, the complexity of a full and comprehensive coupling of the solid phase mechanical behavior of particulate media with the multiphase and multicomponent transport and interaction phenomena made practically impossible, at the moment, to set up a full purposes theoretical model. Some hydro-chemo-thermo-mechanical coupled model has been implemented by some author (Loret et al. 2002; Van Impe, 2002; Gens, 2007) within the general mixture theory, for colloid, micro and nano particle transport (Tiraferrri and Sethi, 2008) or for simulating the swelling and shrinking behavior of some clayey materials but always important simplifications or approximations have been adopted in order to solve the specific actual problem.

Given the aforementioned scenario it is almost obvious that the future research should continuing in the

direction of trying to couple in a more efficient and comprehensive manner the mechanical behavior with the energy and mass flow phenomena including the chemical, electric and thermal interactions. In doing this particular attention should be paid to improve the scale effects simulations (e.g. from the microscopic chemical compound interactions to the whole behavior of the lining system of a waste landfill) and to describe the discontinuity phenomena within the different systems that can occur during mass and energy flows, deformations of solid skeleton and phase transformations (Culligan, 2008). Some of the recent numerical modeling approaches based on the discrete element method (Itasca 2002; Itasca 2003; Camusso e Barla, 2009), instead of the continuous mechanics approach, seem to be rather promising referring in particular to the latter aspect.

GEOSYNTHETIC CLAY LINERS

Geosynthetic clay liners (GCLs) are factory manufactured liners that consist of a thin layer of bentonite (~5-10 mm thick) that is either sandwiched between two geotextiles or attached to a polymer membrane and held together by needle-punching, stitching or gluing with an adhesive. GCLs are increasingly used in covers and bottom liners for landfills because of their low hydraulic conductivity to water (i.e. k typically $\leq 3.0 \cdot 10^{-11}$ m/s). The main advantages of GCLs are the limited thickness, the material quality assurance, the ease of installation, the good compliance with differential settlements of underlying soil or waste and the low cost (Bouazza, 2002).

On the other hand, the limited thickness of this barrier can produce vulnerability to mechanical accidents, limited sorption capacity, and an increase of pollutant diffusive transport if an underlying attenuation mineral layer is not provided. Moreover, when exposed to water solutions containing high ion concentrations or di-valent cations, bentonite can undergo a significant increase of the hydraulic conductivity.

The evaluation of GCL performances as pollutant barriers needs an adequate theoretical approach for modeling the simultaneous migration of water and solutes through bentonite. Bentonite is a clay soil containing typically at least 70% of the three layered (2:1) clay mineral montmorillonite, which is characterized by a very high total specific surface (~760 m^2/g) and a negative electric charge. The ultra-fine pore size ($< 100 \text{ \AA}$) of this clay soil and the electric interaction between montmorillonite particles and ions in pore solution determine macroscopic phenomena that cannot be modeled on the basis of the advective-diffusive

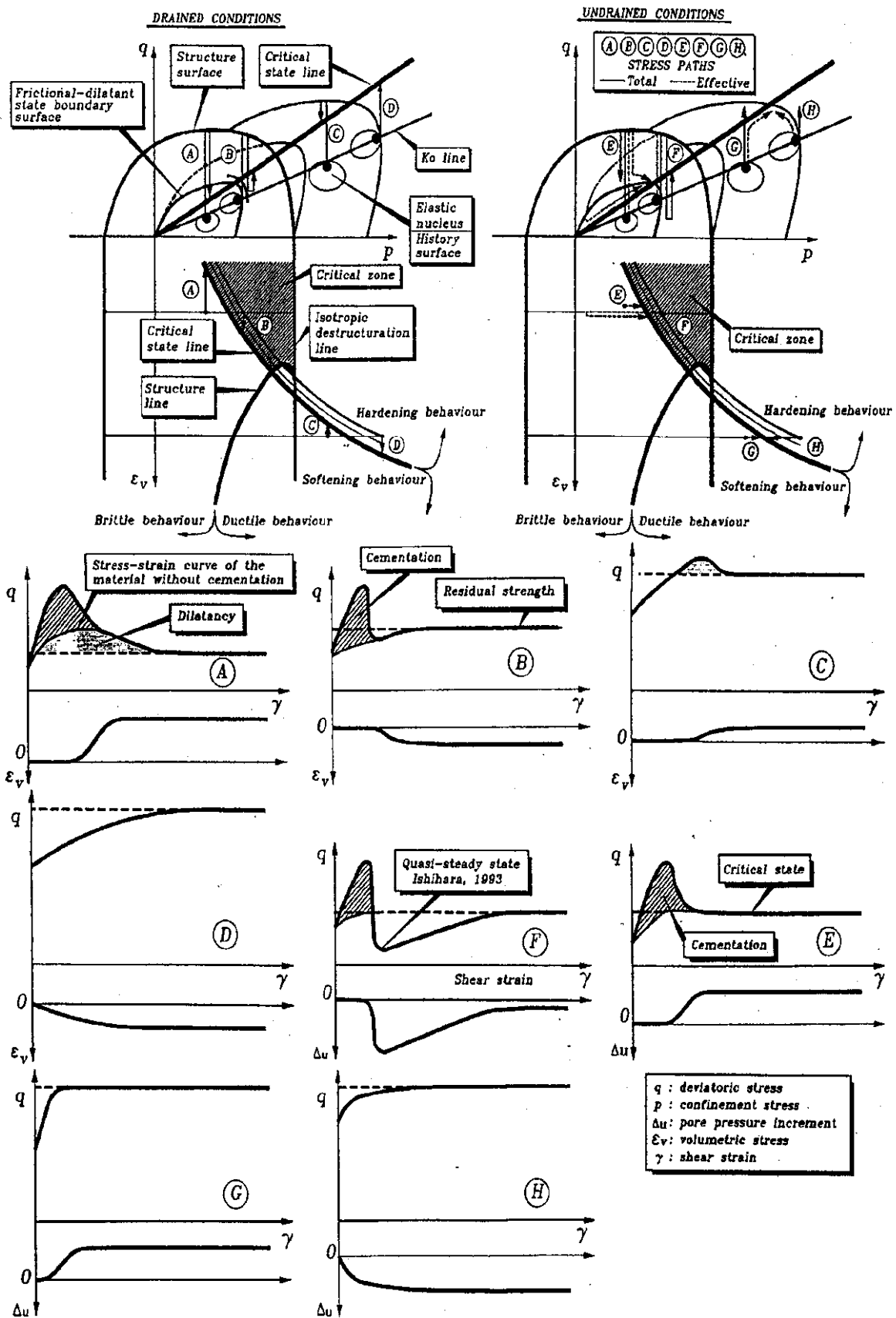
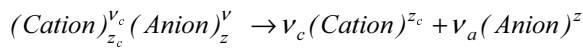


Fig. 1 Qualitative stress-strain relationships in pure shear of a particulate cemented (or structured) material (e.g. solid waste) in the framework of an elasto-plastic-work hardening model

transport theory, normally used to describe the movement of water and solutes through porous media. The more general coupled flux transport theory needs to be applied similarly to what is done for biological or reverse-osmosis membranes.

Before introducing the coupled flux transport theory, an analysis of equilibrium conditions is provided in order to separate partition effects, due to electric interactions between the ions in solutions and montmorillonite particles, from transport mechanisms, related to the motion of the different components of pore solution. Reference is made to the case of a pore solution containing a single salt, consisting of a cation (e.g. Na⁺ or Ca²⁺) and an anion (e.g. Cl⁻), assumed to be completely dissociated:



(v_c, z_c) and (v_a, z_a) are the stoichiometric coefficient and the electrochemical valence of the cation (index c) and the anion (index a), respectively (-).

The ionic concentrations, C_i , in the bulk solution are related to the salt concentration, C_s , as follows

$$C_i = v_i C_s, \quad (3)$$

Equilibrium Conditions and Partition Effect

If a porous medium is placed in contact with an external bulk solution, an equilibrium condition is reached after a sufficiently long time. When this condition is met and in the absence of partition mechanisms, the ion concentrations and the hydraulic pressure of the pore solution result to be equal to the ion concentrations and the hydraulic pressure of the external bulk solution. On the other hand, in the presence of partition mechanisms, this equality is not obtained and a discontinuity in ion concentrations and hydraulic pressure between the external bulk solution and the pore solution is observed.

In bentonite, the main partition mechanism is the electrostatic one. At the macroscopic scale, such effect can be accounted for by the Donnan's equations that define the equilibrium conditions between the pore solution of a charged porous medium and an external electrolyte solution. Donnan's equations establish the equality of the macroscopic electro-chemical potentials between the components of the pore solution and the components of the external bulk solution:

$$\bar{\mu}_w = \mu_w \quad (4a)$$

$$\bar{\mu}_i^{ec} = \mu_i^{ec} \quad i = a, c \quad (4b)$$

where $\bar{\mu}_w$ = chemical potential of water in the pore solution (N·m·mol⁻¹); μ_w = chemical potential of water in the external bulk solution (N·m·mol⁻¹); $\bar{\mu}_i^{ec}$ = electro-chemical potential of the i-th ion in the pore solution (N·m·mol⁻¹); μ_i^{ec} = electro-chemical potential of the i-th ion in the external bulk solution (N·m·mol⁻¹).

In order to find the relations between the pressure and the ion concentrations of the external bulk solution and the pore solution, the following definitions of the electro-chemical potentials, valid for dilute solutions, can be used (Katchalsky and Curran, 1965):

$$\mu = \mu + \frac{1}{C} (P - \Pi) \quad (5a)$$

$$\bar{\mu} = \bar{\mu} + \frac{1}{\bar{C}} (\bar{P} - \bar{\Pi})$$

$$\mu = \mu + RT \ln(C) + z F \Phi \quad (5b)$$

$$\bar{\mu} = \bar{\mu} + RT \ln(\bar{C}) + z F \bar{\Phi}$$

Where $\mu_b^0, \bar{\mu}_b^0$ (for b = w, a, c) = constants of integration in the external and the pore solution respectively (N·m·mol⁻¹); C_w, \bar{C}_w = water concentration in the external and the pore solution respectively; P, \bar{P} = fluid pressure in the external and the pore solution respectively (Pa); C_i, \bar{C}_i = ion concentration of the i-th ion in the external and the pore solution respectively (mol/m³); $\Phi, \bar{\Phi}$ = electric potential in the external and the pore solution respectively (V); $\Pi = RT \sum_{i=1}^{Nions} C_i$ = osmotic pressure in the external solution (Pa); $\bar{\Pi} = RT \sum_{i=1}^{Nions} \bar{C}_i$ = osmotic pressure in the pore solution (Pa); R = universal gas constant (8.314 J·mol⁻¹·K⁻¹); T = absolute temperature (K); F = Faraday's constant (96,485 C/mol).

Assuming that $\mu_b = \bar{\mu}_b$ (for b = w, a, c) and noting that the partition mechanism, based on the electrostatic interaction between the solid particles and the molecules in the pore solutions, acts only on the ion species and not on the electro-neutral water molecules, so that $C_w = \bar{C}_w$, Eqs. 5a, b can be expressed as follows:

$$\bar{P} - \bar{\Pi} = P - \Pi \quad (6)$$

$$\bar{C}_i = C_i \exp\left(-z_i \frac{F}{RT} \Psi\right) \quad (7)$$

where $\Psi = \bar{\Phi} - \Phi$ is the Donnan potential that represents the characteristic electric potential of the solid skeleton.

An ion partition coefficient, Γ_i (-), can be conveniently introduced as follows:

$$\Gamma = \frac{\bar{C}}{C} = \exp\left(-z \frac{F}{RT} \Psi\right) \quad (8)$$

In order to close the system, the equations that express the electro-neutrality condition within the external bulk solution, Eq. 9a, and within the pore solution, Eq. 9b, are used:

$$z_a C_a + z_c C_c = 0 \quad (9a)$$

$$z_a \bar{C}_a + z_c \bar{C}_c = \bar{C}_X \quad (9b)$$

where \bar{C}_X = concentration of the charge of solid particles within pore solution (mol/m^3), also called “fixed charge concentration”.

In the case of a solution containing a (1:1) electrolyte (e.g. NaCl or KCl), the ion partition coefficients result given by:

$$\Gamma = \Gamma^- - \frac{\xi}{2} + \sqrt{\left(\frac{\xi}{2}\right)^2 + 1} \quad (10)$$

where $\xi = \frac{\bar{C}_X}{C_s}$.

In Fig. 2, the cation partition coefficient, Γ_c , and the anion partition coefficient, Γ_a , are plotted as a function of the normalized salt concentration, $\chi = \xi^{-1} = C_s / \bar{C}_X$, for a solution containing a (1:1) electrolyte. Note that Γ_c is plotted on a logarithmic scale, while Γ_a is plotted on an arithmetic scale.

The coefficient $\Gamma_c \geq 1$ describes the accumulation of the cations within bentonite pores, whereas $0 \leq \Gamma_a \leq 1$ describes the exclusion of the anions. When $\Gamma_c = \Gamma_a = 1$, bentonite does not generate a partition of the ions and has not any selective capability; when $\Gamma_a = 0$ and $\Gamma_c \rightarrow \infty$ the membrane is “ideal” or “perfect”, being able to hinder completely the passage of the salt.

\bar{C}_X can be estimated on the basis of an idealised model for bentonite fabric. Bentonite can display a hierarchy of structures that are referred as lamellae at the finest level, tactoids or quasi-crystals or particles at the microscopic level, micro-aggregate or cluster at the mesoscopic level and macro-aggregates or peds on the macroscopic scale. A low hydraulic conductivity ($k < 10^{-9}$ m/s) is compatible only with the absence of micro and macro aggregates. If it is assumed that the tactoids are formed by packets of parallel lamellae (platelets) and the

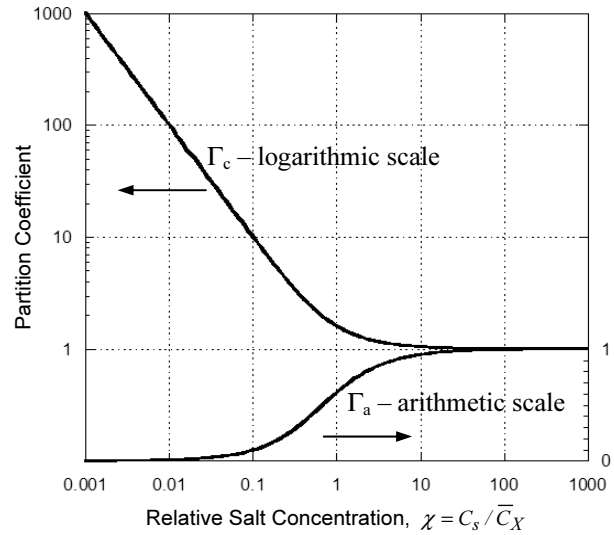


Fig. 2 Partition coefficients for a (1:1) electrolyte

only mobile fraction of pore solution is that located in the inter-tactoids pore space, while the pore solution within the tactoids is considered as part of the solid phase, than \bar{C}_X can be estimated as follows (Dominijanni and Manassero, 2008):

$$\bar{C}_X = \bar{C}_{X,0} \frac{1}{e'} = \frac{(1 - f_{Stern}) \sigma \rho_s S'}{F e'} \quad (11)$$

Where e' = void ratio referred to the void space between tactoids; $\bar{C}_{X,0}$ = concentration of the charge of solid particles evaluated at $e' = 1$ (mol/m^3); f_{Stern} = fraction of electric charge compensated by the cations specifically adsorbed in the Stern layer (-); σ = electric surface charge of lamellae (C/m^2), ρ_s = density of solid phase (g/m^3), S' = effective specific surface of tactoids (m^2/g).

The effective specific surface, S' , can be related to the total specific surface, S , (i.e. referred to the total surface of lamellae) through the average number of lamellae per tactoid, N_l , as follows:

$$S' = \frac{S}{N_l} \quad (12)$$

The void ratio, e' , referred to the inter-tactoids pore volume can be related to the total void ratio, e , and the number N_l of lamellae per tactoids as follows:

$$e' = e - b_l \rho_s \left(\frac{N-1}{N} \right) S \quad (13)$$

Where b_l = average half spacing between lamellae in tactoids as determined by X-ray measurements (4.5 \AA).

The inter-granular or effective stress, σ' , for bentonite can be expressed as follows (Dominijanni and Manassero, 2008a):

$$\sigma' = \sigma - \bar{P} = \sigma - P - \underbrace{(\bar{\Pi} - \Pi)}_{S_\pi} \quad (14)$$

Where S_π which is a function of the void ratio e' through Eq. 10, represents the swelling pressure.

In Fig. 3 theoretical values of swelling pressure are reported for $\bar{C}_X = 10^{-3}, 10^{-2}, 10^{-1}$ mol/L in the case of a solution containing a (1:1) electrolyte (e.g. NaCl).

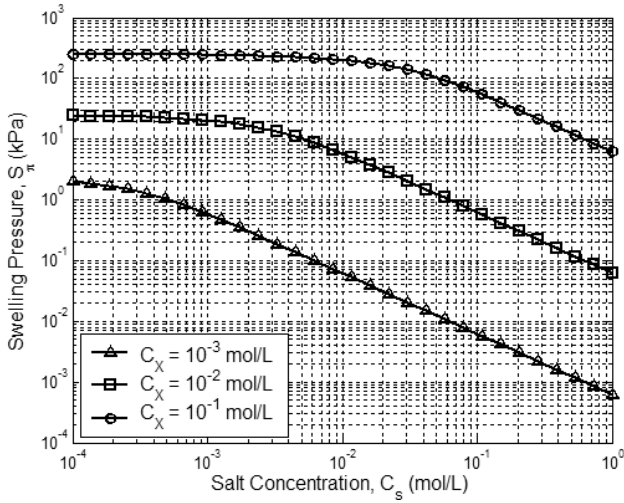


Fig. 3 Swelling pressure as a function of salt concentration and fixed charge concentration

When the salt concentration increases, the swelling pressure decrease up to negligible values. Higher values of swelling pressure are associated to higher values of \bar{C}_X .

At low salt concentrations, the swelling pressure tends to the theoretical maximum value, i.e. $S_\pi = RT\bar{C}_X$.

Under oedometric conditions, the void ratio e' can be related to the effective stresses as follows:

$$e' = e'_0 - a_v(\sigma' - \sigma'_0) \quad (15)$$

Where a_v = bentonite compressibility of intergranular contacts (Pa^{-1}); e'_0 = void ratio at a reference state (-); σ'_0 = effective stress at a reference state (Pa).

Using Eqs. 14 and 15 the void ratio results to be related, not only to the apparent effective stress $\sigma - P$, but also to the chemical composition of the pore solution through the swelling pressure S_π .

High salt concentration as well as substitution of di-valent for mono-valent cations determine a reduction of the swelling pressure and a consequent increase of the

effective stress. Such an increase of the effective stress produces a compression of bentonite, i.e. a reduction of the void ratio (this effect has been called “chemical consolidation” by Kaczmarek and Hueckel, 1998).

However local increase of effective stress at the microscopic scale can promote the aggregation of montmorillonite lamellae, causing the formation of thicker tactoids. The increase of the number of lamellae per tactoid determines a reduction of the effective specific surface, S' , and a possible increase of intergranular contact and, as a result, a decrease of the compressibility a_v . Such modifications of bentonite fabric result, at the macroscopic scale, in an enhance of mechanical characteristics, as rigidity and shear strength, and a worsening of barrier properties (i.e. an increase of hydraulic conductivity). This last effect is of particular concern for environmental applications and will be discussed deeper in the conclusions of this chapter.

Coupled Flux Transport Theory

The most general approach for modelling coupled fluxes is to invoke phenomenological equations by applying the formalism of the Thermodynamics of Irreversible Processes (Katchalsky and Curran, 1965; Yaroshchuk, 1995; Manassero and Dominijanni, 2003). The main advantage of this approach is to avoid any specification of physical properties of the membrane, maintaining the model as general as possible. Using such a formalism, Spiegler and Kedem (1966) derived the following equations for a semipermeable membrane permeated by a solution containing a single salt (e.g. NaCl or CaCl_2):

$$q = -P_{v\lambda} \left(\frac{dP}{dx} - \omega_\lambda \frac{d\Pi}{dx} \right) \quad (16)$$

$$J = (1 - \omega_\lambda)qC - P_\lambda \frac{dC}{dx} \quad (17)$$

Where q = volumetric solution flux ($\text{m}^3 \cdot \text{m}^{-2} \cdot \text{s}^{-1}$); J_s = salt flux ($\text{mol} \cdot \text{m}^{-2} \cdot \text{s}^{-1}$); $\Pi = (v_a + v_c)RT$; C_s = virtual osmotic pressure (N/m^2).

In Eqs. 15 and 16, there are three phenomenological coefficients: (1) $P_{v\lambda}$ is the specific hydraulic conductivity ($\text{m}^4 \cdot \text{s}^{-1} \cdot \text{N}^{-1}$), (2) ω_λ is the local chemico-osmotic efficiency coefficient (-), and (3) $P_{s\lambda}$ is the local salt permeability (m^2/s). The state variables are the virtual hydraulic pressure, P , and the virtual salt concentration, C_s , that represent the pressure and the salt concentration of a virtual external bulk solution that is assumed to be in thermodynamic equilibrium with the pore solution in correspondence to a given volume element of the porous medium. Virtual variables can be used to avoid the introduction of any physical assumption in the formulation

of flux equations. At the boundaries, the virtual solution coincides with the real bulk solution in contact with the porous medium. Therefore, the steady-state solutions of Eqs. 16 and 17 can be expressed using as boundary conditions the pressure and the salt concentration of the bulk solutions in contact with the membrane.

The phenomenological coefficients $P_{v\lambda}$, ω_λ and $P_{s\lambda}$ are unspecified functions of the salt concentration, C_s , and the hydraulic pressure, P (or the void ratio e).

The specific hydraulic conductivity can be expressed in terms of the more common local hydraulic conductivity, k_λ , as follows:

$$P_{v\lambda} = \frac{k_\lambda}{\gamma_w} \quad (18)$$

where γ_w is the water unit weight (N/m^3).

Based on this approach, all the phenomenological coefficients should be measured by suitable tests, without any assumption about their relation to physical properties of the membrane. However, the experimental determination of these parameters is particularly difficult due to their dependency on the salt concentration.

By linearizing the flux equations (Eqs. 16 and 17) an analytical solution at steady-state conditions can be obtained:

$$q = \frac{k}{\gamma_w} \left(\frac{\Delta P}{L} - \omega \frac{\Delta \Pi}{L} \right) \quad (19)$$

$$J = (1 - \omega)q \frac{C' \exp(P_\pi) - C''}{\exp(P_\pi) - 1} \quad (20)$$

where

$$P_\pi = \frac{(1 - \omega)qL}{P} \quad (21)$$

In Eqs. 19-21, the global coefficients k , ω , and P_s are average values of the local ones, or:

$$k = \frac{1}{L} \int k_\lambda \cdot dx \cong \frac{1}{\Delta C} \int k_\lambda \cdot dC \quad (22)$$

$$\omega = \frac{1}{L} \int \omega_\lambda \cdot dx \cong \frac{1}{\Delta C} \int \omega_\lambda \cdot dC \quad (23)$$

$$P = \frac{1}{L} \int P_\lambda \cdot dx \cong \frac{1}{\Delta C} \int P_\lambda \cdot dC \quad (24)$$

In order to obtain an understanding of the physical meaning of the phenomenological coefficients, although limiting the generality of the approach, Dominijanni and

Manassero (2005, 2007) and Dominijanni et al. (2006) proposed a model obtained by upscaling the modified Navier-Stokes equation and the Nernst-Planck equations and using the Donnan's equations to express the relations between real and virtual variables. The proposed model provides an interpretation of the experimental results of Malusis and Shackelford (2002a,b).

Based on the theoretical and experimental findings, the following observations were made.

First, the hydraulic conductivity, k , corresponding to relative low values of the salt concentration ($\leq 10^{-1}$ M), is dependent on the salt concentration due to the electroviscous effect and can be expressed as follows:

$$k = \frac{\tau}{3} \frac{e^3}{(1+e)} \frac{\gamma}{(\rho S')} \frac{1}{\mu (C', C'', \bar{C}_X)} \quad (25)$$

Where τ_m = matrix tortuosity factor (≤ 1) that takes into account the tortuous nature of the actual diffusive pathways through the porous medium due to the geometry of the interconnected pores; μ_e = electroviscous coefficient, which is related to the salt boundary concentrations C_s' , C_s'' and the fixed charge concentration \bar{C}_X .

However, the electro-viscous effect is not very significant for the range of parameters typical of GCLs, so that, at a first approximation, it can be neglected. Therefore, the electro-viscous coefficient can be considered almost equal to the viscous coefficient of water, μ_w , and, as a first approximation, it can be assumed $k_\lambda \cong k \cong cost$.

Second, the chemico-osmotic efficiency, ω , for a (1:1) electrolyte (e.g. Na Cl or KCl) can be expressed as follows:

$$\omega = 1 + \frac{\bar{C}}{2\Delta C} \left[Z_2 - Z_1 - (2t - 1) \cdot \ln \left(\frac{Z_2 + 2t - 1}{Z_1 + 2t - 1} \right) \right] \quad (26)$$

where

$$Z_1 = \sqrt{1 + (2C_s' / \bar{C}_X)^2}, \quad Z_2 = \sqrt{1 + (2C_s'' / \bar{C}_X)^2} \quad (27)$$

$$t_c = \frac{D_{0c}}{D_{0c} + D_{0a}} \quad (28)$$

In Eqs. 26-28, t_c is the cation transport number (-), D_{0c} is the cation free-solution diffusion coefficient (m^2/s), D_{0a} is the anion free-solution diffusion coefficient (m^2/s).

Third, the salt permeability can be expressed as follows:

$$P = (1 - \omega)nD^* \quad (29)$$

where D_s^* is the effective diffusion coefficient of the salt (m^2/s), given by:

$$D^* = \tau \frac{(\nu + \nu')D}{\nu D + \nu' D} \quad (30)$$

It can be observed that when $\bar{C} \rightarrow 0$, then $\omega \rightarrow 0$ and the flux equations 19 and 20 reduce to the expressions of the advective-diffusive transport theory.

Table 1 Bentonite selected physical and chemical properties for the GCL tested by Malusis and Shackelford (2002a,b)

Type	Bentomat®
Liquid Limit, LL (%)	478
Plasticity Index, PI (%)	439
Specific Gravity, G_s	2.43
Principal Minerals (%):	
montmorillonite	71
mixed-layer illite/smectite	7
quartz	15
other	7
Cation Exchange Capacity, CEC (meq/100g)	47.7

Table 2 GCL properties derived from the interpretation of Malusis and Shackelford (2002a,b) tests.

Hydraulic Conductivity, k (m/s)	$1.63 \cdot 10^{-11}$
Porosity, n (-)	0.79
Void Ratio, e (-)	3.76
Effective Diffusion Coefficient, D_s^* (m^2/s)	$2.7 \cdot 10^{-10}$
Thickness, L (m)	0.01
Fixed charge concentration, \bar{C}_X (mol/L)	0.0123

GCL Performances Based On Coupled Flux Transport Theory

From the interpretation of the experimental results obtained by Malusis and Shackelford (2002a,b) on a GCL, whose main characteristics are reported in Table 1, Dominijanni and Manassero (2005) derived the parameters reported in Table 2. These data represent a complete set of parameters obtained from an experimental investigation on a GCL. Unfortunately only a few of other data about GCLs are available from literature, so that it is not possible to generalise these results.

Using the steady-state fluxes given by Eqs. 19 and 20, the transport through a GCL can be evaluated taking into account the membrane behavior (i.e. partition and osmotic effects).

In Fig. 4 the steady-state mass flux, J_s , is plotted for a GCL with the properties in Table 2, with or without the membrane behavior. The flux through a GCL alone is compared with the flux through a compacted clay liner (CCL) 0.6 m thick and the flux through a composite barrier constituted by a GCL and a mineral attenuation layer (AL). AL can be a natural or manmade soil layer that can be characterized by a relatively high value of the hydraulic conductivity because its purpose is solely to reduce the concentration gradient by increasing the distance between the leachate pond and the bottom of the barrier. A scheme of the compared barriers is given in Fig. 4. The material properties for the CCL and the AL are reported in Table 3. At the bottom of the barrier, a perfectly flushing boundary condition has been assumed ($C_s''=0$). The choice of this boundary condition can be considered as a conservative approach because it maximizes the diffusive flux.

If the membrane behavior is not taken into account, the flux through the GCL is higher than through the CCL. If the membrane behavior is taken into account, the salt flux varies as a function of the leachate concentration ($C_s'=C_0$). The membrane behavior becomes more relevant and the salt flux is reduced with decreasing salt concentration.

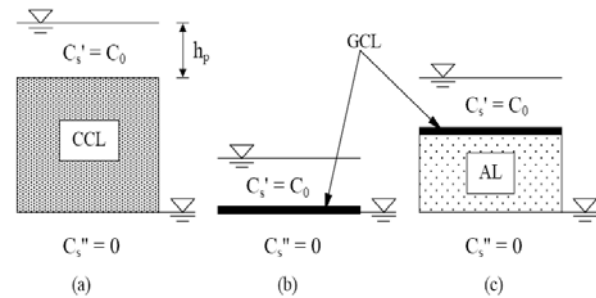


Fig. 4 Landfill barrier constituted by a: (a) compacted clay liner (CCL), (b) geosynthetic clay liner (GCL), (c) GCL and attenuation layer (AL)

Table 3 Properties of CCL and AL

	CCL	GCL	AL
Hydraulic Conductivity, k (m/s)	10^{-9}	10^{-11}	10^{-7}
Porosity, n (-)	0.4	0.7	0.3
Effective Diffusion Coefficient, D_s^* (m^2/s)	$6 \cdot 10^{-10}$	$2 \cdot 10^{-10}$	$9 \cdot 10^{-10}$
Thickness, L (m)	0.6	0.01	0.4

The salt flux through the GCL can be also lower than the flux through the CCL if the membrane behavior is accounted for.

The composite barrier (GCL+AL) has a salt flux lower than that of the CCL. If the membrane behavior is taken into account, the performance of the composite barrier is improved at low salt concentrations. The salt flux through a composite barrier may be obtained by imposing the conditions of equality of the volumetric and mass fluxes through all the layers of the barrier. The conditions of continuity of the fluxes allow the hydraulic pressures and salt concentrations to be evaluated at the boundaries between the layers. In the presence of membrane behavior, the solution of the flux continuity equations can be derived adopting an iterative procedure.

Membrane behavior can influence significantly the performance evaluation of a GCL with respect to a CCL. At low salt concentration ($< 10^{-1}$ M), the salt flux through a GCL is reduced because of (1) the presence of an osmotic volumetric flux of the solution directed from the bottom to the top of the liner, and (2) the ability of the solid particles to partially restrict the molecular diffusion of salt molecules through the bentonite pores. Therefore, an evaluation of GCL performance based on the advective-diffusive transport theory without membrane behavior can underestimate the ability of GCL to contain the contaminant.

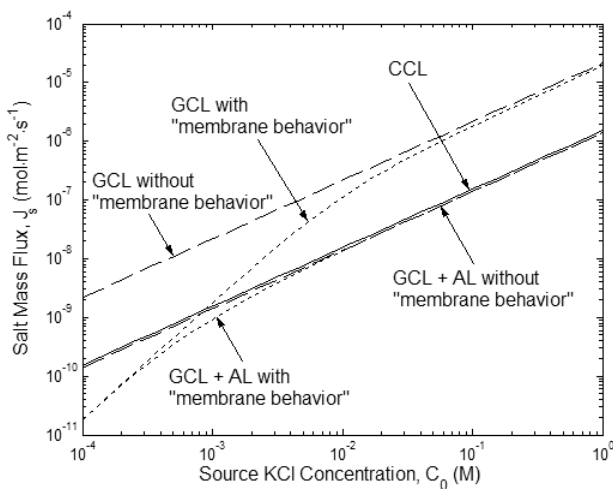


Fig. 5 Salt mass flux versus source KCL concentration for a CCL, a GCL and a GCL+AL

However, special attention must be paid to control the chemical composition of the leachate, because high salt concentrations or the presence of multivalent cations can produce fabric modifications that are not compatible with the assumption of constant hydraulic conductivity, k , and constant fixed charge concentration, \bar{C}_X .

Cation Exchange Effects

Clay used in GCLs is frequently sodium bentonite

(Na-bentonite), meaning that the dominant cation on the exchange complex of the montmorillonite particles is sodium (Na^+). Na-bentonite is generally preferred relative to calcium bentonite (Ca-bentonite) or magnesium bentonite (Mg-bentonite), because Na-bentonite is characterized by a higher swelling capacity and a lower hydraulic conductivity relative to either Ca-bentonite or Mg-bentonite. Presence of di-valent cations produces a reduction of swelling pressure, that, in turn, causes an increase of the effective or intergranular stress. At the microscopic scale, the increase of intergranular stress can not only determine the decrease of the void volume, but also promote the aggregation of montmorillonite lamellae and, consequently, the formation of thicker tactoids. Effects produced by substitution or exchange of di-valent cations (e.g. Ca^{2+}) for mono-valent cations (e.g. Na^+) on swelling pressure can be appreciated in Fig. 6 for a value of $\bar{C} = 10 \text{ mol/L}$.

Cation exchange is considered an issue of particular concern for GCLs used as hydraulic or contaminant barrier (Shackelford, 2007), due to the detrimental effect that can produce on containment properties of bentonite. In situ, cation exchange is mainly due to diffusion of calcium, commonly present in many natural soils, from adjacent layers to GCLs. The expected effects of exchange of calcium for sodium based on the proposed model can be summarized as follows:

- 1) reduction of swelling pressure and, consequently, increase of effective or intergranular stress; this effect tends to induce a compression of bentonite, i.e. a reduction of the void ratio (see Eq. 15);
- 2) increase of the number of lamellae per tactoids; this effect determines a reduction of the effective specific surface (see Eq. 12) and a possible decrease of intergranular compressibility (note that the increase of the rigidity of intergranular contacts tends to limit the void ratio reduction).
- 3) the reduction of effective specific surface implies a significant increase of the hydraulic conductivity (see Eq. 25) and a decrease of the electric charge of solid phase \bar{C}_{X0} (see Eq. 11).

The effect of an increase of the number of lamellae per tactoids, eventually induced by cation exchange, on the hydraulic conductivity of a bentonite characterized by a void ratio $e = 4$ ($n = 0.8$) can be appreciated in Fig. 7. The hydraulic conductivity results to be approximately proportional to the square value of N_l ; this means that when N_l changes from 1 to 100 a variation of almost 4 orders of magnitude can be expected for k . Larger increase of k should be attributed to the formation of micro and macro aggregates that needs a multi-porosity approach to be correctly modelled.

As a result, cation exchange effects can be modelled relating through empirical relations the effective specific surface S' and the electric charge of solid phase \bar{C}_{X0} to ion concentrations. Further research on this topic is necessary in order to evaluate suitable theoretical relations from the analysis of experimental data. However, it can be observed that two situations can be modelled adopting with different approaches:

- 1) bentonite with low void ratio, low ion concentrations, mono-valent cations prevailing on di-valent cations;
- 2) bentonite with high void ratio, high ion concentrations, di-valent cations prevailing on mono-valent cations;

Situation 1) need to be modelled with coupled flow theory. In the absence of significant change of chemical composition of pore solution, the effective specific surface S' and the electric charge of solid phase \bar{C}_{X0} can be assumed to be constant. This situation represents the condition of optimal operation for GCLs.

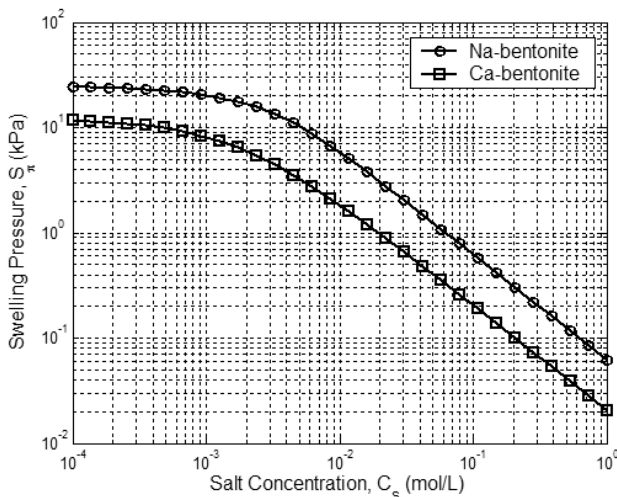


Fig. 6 Swelling pressure as a function of salt concentration for sodium and calcium bentonite ($\bar{C} = 10 \text{ mol/L}$)

Situation 2) is characterized by high hydraulic conductivity and low fixed charge concentration. Under these conditions osmotic phenomena are generally negligible, so that the advective-diffusive transport theory can be adopted to evaluate the movement of water and solutes through GCLs. This situation represents the condition of worst operation for GCLs.

As discussed previously, transition from situation 1) to situation 2) can be modelled by assuming a dependency of the effective specific surface S' and the electric charge of solid phase \bar{C}_0 on the ion concentrations. Unfortunately the determination of such dependency constitutes a formidable challenge. However,

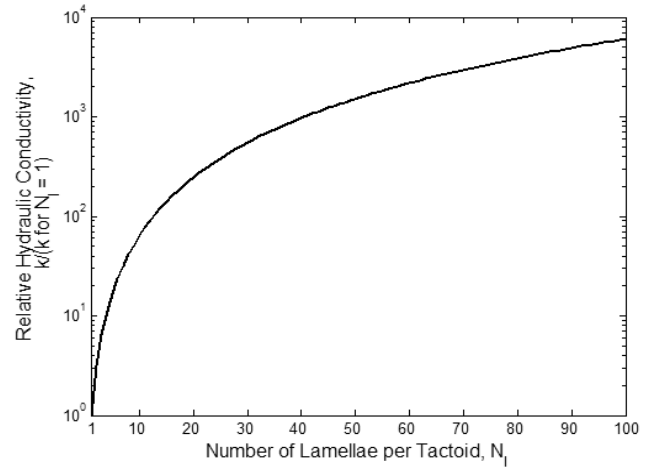


Fig. 7 Variation of hydraulic conductivity k as a function of the number of lamellae per tactoid ($e = 4, \rho_s = 2.41 \text{ g/cm}^3, S = 760 \text{ m}^2/\text{g}$)

modelling this transition situation has minor relevance from a practical point of view than modelling situation 1) and 2), which represent limit operative conditions for GCLs.

Conclusions

GCLs can represent a very attractive alternative to CCLs for cover and bottom liners of landfills. Use of GCLs should be evaluated critically taking into account the variability of bentonite properties under different boundary conditions (e.g. confining stress, leachate composition, calcium availability in confining layers). GCLs are found to perform excellently in situations characterized by low void ratio of bentonite, low ion concentrations, mono-valent cations prevailing on di-valent cations. Under such conditions the transport of water and solutes needs to be modelled by the coupled flow theory, instead of the more classic advective-diffusive transport theory, due to the relevance that the osmotic phenomena can have for the evaluation of GCL performances. However, due to the detrimental effects that can be produced by a modification of the boundary conditions in terms of both mechanical and chemical actions, GCLs should be always coupled with other barriers (e.g. geomembranes) or used in multiple barrier systems. On the other hand, it is very important to improve the chemo-mechanical coupling within the theoretical models in order to better simulate and predict the long term behavior of GCLs.

ELECTROKINETIC REMEDIATION

The low permeability of fine graded soils is a complicating feature for those remediation actions that

rely on the Darcian flow of the fluid phases, inasmuch even great pressure gradients cause very moderate seepage velocities and advective fluxes. In these geological conditions transport of contaminants shall be ensured by other driving processes and other techniques shall be used.

Electrokinetic remediation relies on the transport mechanisms that originate in the wet soil when imposing a low intensity DC electrical current. Couples of electrodes are placed in the soil mass, generating an electrical field that acts as a driving force to induce the movement of contaminants. The electrical field is effective in causing additional fluxes of the pore water (electroosmosis) and of the charged species in solution (electromigration), so that the technique has proved to be effective with respect to soils contaminated by heavy metals and polar contaminants. Since there is no competition between transport of the various species, the treatment is not selective and in principle can be used in sites contaminated with more than one contaminant. Contrarily to what occurs for electroosmotic consolidation, both electrodes allow drainage and a continuous flow of water is established in the treated soil mass.

Besides inducing the flow of water and charged species, the application of the electrical field promotes a number of complex phenomena of electro-chemical nature, such as electrolysis reactions at the electrodes, changes in pore water pH, adsorption and desorption processes, precipitation and dissolution. As a consequence of these processes, the mechanical properties of the treated soil mass can be modified permanently (e.g. Gray, 1970; Thomas and Lentz, 1990; Alshawabkeh et al., 2004).

In order to describe some peculiar aspects of the technique, first electroosmosis and electromigration will be introduced. Then, the main ingredients of the models available in the literature will be given.

Electroosmosis

Electroosmosis is assumed to arise as a consequence of the local electrical imbalance at the surface of the solid grains (see e.g. Sposito, 1984). Several theories have been proposed to model its occurrence at the pore scale (Schmidt, Helmutz – Smoluchowski). According to the Helmutz Smoluchowski theory, the velocity of water in a capillary tube under an electrical field is:

$$v_{eo} = \frac{\varepsilon \zeta}{\mu_w} \frac{\partial \phi}{\partial x} \quad (31)$$

where: ε is the dielectric constant of the water ($C \cdot V^{-1} \cdot m^{-1}$); ζ is the zeta potential of the solid – water interface (V),

or the electrical potential in the double layer at the point where the water starts to be free to move with respect to the solid phase; μ_w is the viscosity of water (Pa·s); ϕ is the imposed electrical potential (V).

In soils, the electroosmotic flow is conveniently written defining an electroosmotic conductivity K_{eo} :

$$q_{eo} = -K_{eo} \nabla \phi \quad (32)$$

The observed electroosmotic conductivity of most soils lays between $10^{-9} m^2 V^{-1} s^{-1}$ and $10^{-8} m^2 V^{-1} s^{-1}$, a quite narrow range with respect to the variations observed for the hydraulic conductivity. Electrical fields of about $100 V m^{-1}$ or less are therefore usually sufficient to mobilize water for remediation or consolidation purposes.

On basis of the Helmutz Smoluchowski theory, Mitchell and Soga (2005) express the electroosmotic conductivity as:

$$K_{eo} = -\frac{\varepsilon \zeta}{\mu_w} n \quad (m^2 V^{-1} s^{-1}) \quad (33)$$

n being porosity (-).

Expression (33) theoretically justifies the experimental observations suggesting that the electroosmotic conductivity does not depend on the size of the pores. Indeed, according to the Helmutz-Smoluchowski theory, the electroosmotic velocity along the radius of a capillary tube has a constant profile, except for a very thin area close to the tube's walls.

As the surface charge of clay minerals is normally negative, and so is ζ , electroosmosis in clays usually occurs from the anode (positive electrode) towards the cathode (negative electrode). Anyway, low pH conditions or other phenomena such as surface adsorption and complexation can invert the sign of the clay surface charge and of ζ . Lorenz (1969) found that in kaolinite ζ increased continuously with pH, being positive for pH values below 4 and negative at higher pH.

Electromigration and Electrical Conductivity

Electromigration indicates the mechanism by which charged species in solution are carried towards the electrode of opposite sign. In dilute solutions, the ionic mobility (velocity under a unit electrical field) can be expressed through the Nernst – Townsend – Einstein relation (Holmes, 1962):

$$u_k = \frac{z_k D_k F}{RT} \quad (34)$$

where u_k is the ionic mobility ($\text{m}\cdot\text{V}^{-1}\cdot\text{s}^{-1}$); z_k is the ionic valence, positive for cations and negative for anions (-); D_k is the diffusion coefficient ($\text{m}^2\cdot\text{s}^{-1}$); F is Faraday's constant (96,485 C/mol); R the universal gas constant ($8.314 \text{ J}\cdot\text{mol}^{-1}\cdot\text{K}^{-1}$) and T is the absolute temperature (K).

The effective ionic mobility in porous media u_k^* is usually obtained by substituting the diffusion coefficient D of the free electrolyte with the effective diffusion coefficient D^* , that takes into account the combined effect of porosity and tortuosity:

$$D_k^* = D_k n \tau \quad (35)$$

τ (-) being a tortuosity factor whose typical values are reported to range between 0.01 and 0.67 (Daniel and Shackelford, 1988; Shackelford and Daniel, 1991).

Since in electrolytes the electrical current is carried by the movement of ions, at low concentrations the electrical conductivity of an aqueous solution can be considered as a linear function of their mobility, molar concentration and ionic valence:

$$\chi_w = F \sum_{k=1}^n z_k u_k c_k \quad (36)$$

where χ_w (S m^{-1}) is the electrical conductivity of the water solution and c_k the molar concentration of the k^{th} species.

As for the electrical conductivity of soils, χ_s , existing models can be subdivided into 'non conductive particle' and 'conductive particle' models, the first group postulating that the electrical charge is transported only by the free pore water and the second group that the ions in the electrical double layer and the particles surface contribute as well (see e.g. Mitchell and Soga, 2005).

A "non conductive particle" expression of χ_s for a saturated soil is (Holmes, 1962):

$$\chi_s = F \sum_{k=1}^n z_k u_k^* c_k \quad (37)$$

Mualem and Friedman (1991) derived a theoretical function for the relative electrical conductivity, which is analogous to the ones existing for the relative permeability. Archie's law (Archie, 1942) is anyway often used:

$$\chi_s = \chi_w n^m S_r^p \quad (38)$$

where S_r is water saturation (-) and m and p are two empirical exponents that depend on the soil fabric.

Models for Electrokinetic Remediation

In principle, a complete model aimed at reproducing the effects of electrokinetic processes shall take into account the mass balances of the constituent phases (solid, water and air if in unsaturated conditions), the mass balance of the dissolved species and the electrical charge balance. Constitutive relations shall then be written for the solid skeleton, for the water retention properties (in unsaturated conditions), for the flow of water, air and chemical species in solution and for the electrical current.

Proper boundary conditions shall be imposed for the electrical current, for the pore fluid pressures, for the displacement field and for the transported species. As for the latter, the mass flux of the species is usually imposed (Neumann boundary conditions), in case also accounting for the effect of electrolytic reactions.

In order to reduce the number of unknowns, and of the equations to be solved, models initially focused only on the transport of the contaminant species of concern, assuming (i) constant electrical field, (ii) constant electroosmotic permeability, (iii) no reactions between species in water and (iv) linear adsorption isotherms. The following modified expression of the advection – dispersion – adsorption equation is then obtained in 1d conditions (Shapiro and Probstein, 1993):

$$n \frac{\partial c}{\partial t} = D^* \frac{\partial^2 c}{\partial x^2} - q_{eo} \frac{\partial c}{\partial x} - u_k \frac{\partial c}{\partial x} + \frac{\rho_b}{n} \frac{\partial F_a}{\partial t} \quad (39)$$

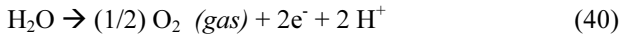
where F_a is the mass fraction of contaminant adsorbed on the solid fraction and ρ_b is the bulk density. Hamed et al. (1991) introduced an expression similar to (39) that did not account for adsorption; while Bruell et al. (1992), working with an uncharged specie, proposed an analogous expression without electromigration contribution.

The introduced assumptions have often been found to oversimplify the problem. A constant electrical field and a constant K_{eo} would induce a steady water flow, that under open drainages exclude mechanical strains. Therefore, assumptions (i) and (ii) exclude the possibility of simulating the mechanical effects of electrokinetic process. On their turn, assumptions (iii) and (iv) can have a deep effect on the simulation of the remediation process.

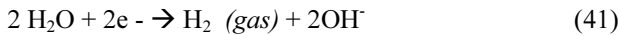
Many experimental evidences have showed temporal and spatial evolution of the electrical conductivity, mainly ascribed to chemical changes intervening in the pore fluid, and associated mechanical strains. The precipitation of hydroxides and salts formed by the contaminants (especially heavy metals) in proximity of

the cathode, severely limiting the success of remediation, has been detected as well.

Water splitting reactions occurring at the electrodes during the remediation process have been recognized to actively concur to the described electro-chemical changes. Such reactions, governed by Faraday's law, are an oxidation at the anode:



and a reduction at the cathode:



The oxidation reaction promotes the occurrence of an acid front migrating from the anode towards the cathode, while reduction induces a basic front that travels from the cathode towards the anode. A number of papers (see e.g. Acar and Alshawabkeh 1996, Kim et al. 2003; Al – Hadman and Reddy, 2008) showed the beneficial effect offered by the acidic front when remediating from cationic heavy metals. The acid front causes exchanges of protons with the heavy metal in the electrical double layer of the soil particles, so that the pollutant is desorbed from the soil surface and can be moved towards the cathode both by electroosmosis and electromigration.

In pure mineralogy soils such as those used in most laboratory studies (mainly kaolinite), a secondary effect of acidification is the relative increase of the electrical conductivity of the portion of sample on the anode side. Indeed, the ionic mobility of H^+ is about twice the one of the OH^- , and about one order of magnitude higher than the one of most ionic compounds. Moreover, high pH values in the cathode side favour precipitation of hydroxides and carbonates¹, removing ions from the pore solution and therefore locally decreasing the electrical conductivity. As a consequence, together with local porosity and permeability decrease due to pore clogging caused by precipitation, sharp electrical conductivity changes can arise. On their turn, these can locally induce negative pore pressures or consolidation (Esrig, 1968, Acar and Alshawabkeh, 1996, Eykholt, 1997), despite free drainage at the boundaries.

To take into account the effects of the evolving chemical conditions on the remediation process or on the mechanics of the soil, several models have been introduced (Corapcioglu, 1991; Alshawabkeh and Acar, 1996; Narasimhan and Sri Ranjan, 2000; Kim et al. 2003; Mascia et al.; 2007; Al Hadman and Reddy, 2008).

¹ A phenomenon that can affect the efficiency of remediation, and that is practically managed by controlling the pH of the catholyte through selective membranes that do not allow hydroxides to enter the soil or by introducing acid solutions at the catholyte.

Alshawabkeh and Acar (1996) extended the analysis to the mass balance equation of the soil mass and of H^+ and OH^- , so accounting both for pH changes and swelling or consolidation. A linear elastic behavior is assumed for the solid skeleton and the soil is assumed to be fully saturated.

The fluxes of water, electrical charge and of the k^{th} specie in solution are given by the equations:

$$q = -K_h \frac{\partial h}{\partial x} - K_{eo} \frac{\partial \phi}{\partial x} \quad (42 \text{ a})$$

$$i = -\chi_s \frac{\partial \phi}{\partial x} - F \sum_{k=1}^n z_k D_k^* \frac{\partial c_k}{\partial x} \quad (42 \text{ b})$$

$$j = -D \frac{\partial c}{\partial x} - c K \frac{\partial h}{\partial x} - c (u + K) \frac{\partial \phi}{\partial x} \quad (k = 1, 2, \dots, n) \quad (42 \text{ c})$$

where χ_s depends on the pore fluid chemistry as in (37) and n is the number of species in solution.

The first terms on the right hand side of the equations (42) are related to direct conduction phenomena (Darcy's law, Ohm's law and Fick's law), while the other terms represent coupled conduction phenomena (Yeung, 1990). It is of interest to notice that equation (42 c) differs from the usual advection – dispersion equation because of the contribution of the electrical field, that induces the transport of species both because of electromigration and of advective transport through electroosmosis. When the species is not charged the electromigrative term is dropped, since ionic mobility is equal to zero. Chemical osmosis and streaming potential (or an electrical field originated as a consequence of Darcian flow) are neglected.

The $n+2$ differential equations to be solved are the mass balance of the soil mixture, the conservation of the electrical charge, usually written neglecting the capacitance of the soil, and the mass balance of the dissolved species:

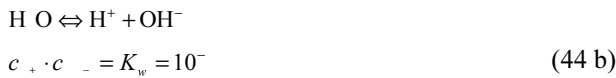
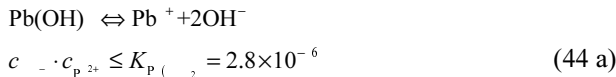
$$\frac{\partial \varepsilon_v}{\partial t} = m_v \gamma_w \frac{\partial h}{\partial t} = -\frac{\partial q}{\partial x} \quad (43 \text{ a})$$

$$\frac{\partial i}{\partial x} = 0 \quad (43 \text{ b})$$

$$\frac{\partial n c_k}{\partial t} = -\frac{\partial j_k}{\partial x} \pm n R_k \quad k=1, 2, \dots, n \quad (43 \text{ c})$$

where ε_v is the volumetric deformation (-), m_v is the volumetric compressibility of the soil (Pa^{-1}), γ_w is the unit weight of water (N m^{-3}), h is the hydraulic head (m). R_k is a generic production term due to (1) adsorption and desorption from the solid phase; (2) chemical reactions in the aqueous phase; (3) precipitation – dissolution phenomena.

Transported species can react one with the other, so models have to consider the related chemical equilibria. Saturation concentrations can indeed change drastically because of the pH variations. The concentration of the species is then further constrained by imposing the law of mass action for the reactions to which those could participate. Instant equilibrium is generally considered. As for lead, Alshwabkeh and Acar (1996) consider the precipitation of its hydroxide, so that the reactions and the mass action constants are:



Analogous expressions have been introduced by Kim et al. (2003) for Cadmium remediation in unenhanced and enhanced conditions. Here, enhancement consisted in manipulating the pH at the cathode reservoirs to values close to 5 for the entire duration of the treatment, to increase the solubility of Pb^{2+} and promote its desorption from the kaolinite particles.

To reduce the complexity of the problem, the number of modelled species can be lowered by neglecting the mass balance of those that do not take part to the reactions. Their concentration is then obtained by imposing the electroneutrality of the pore fluid (e.g. Alshwabkeh and Acar, 1996; Kim et al. 2003).

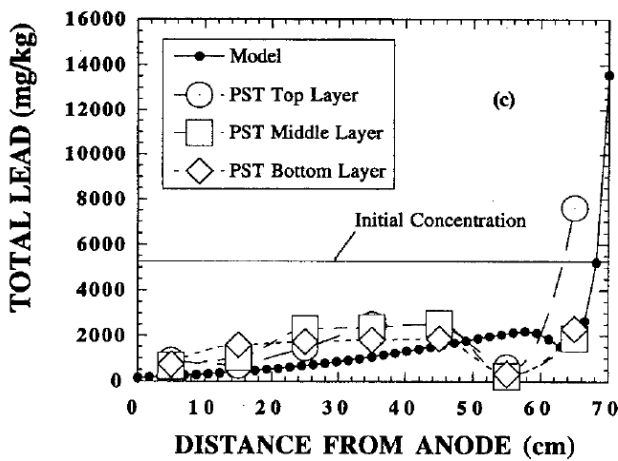


Fig. 8 Pb distribution in a Georgia kaolinite sample after 50 days of treatment (Alshwabkeh and Acar, 1996)

The system of equations (42 – 44), or analogous ones, have been shown mostly to satisfactorily reproduce a number of aspects such as the concentration of the contaminant (Fig. 8), the pH distribution (Fig. 9) and the electrical field (Fig. 10) in soils possessing a limited

buffering capacity.

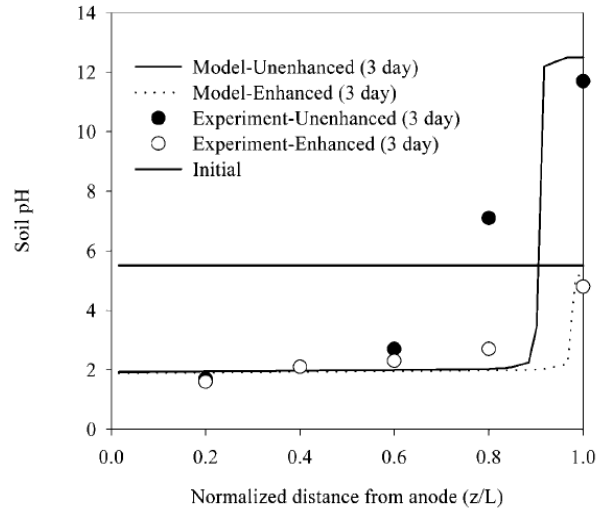


Fig. 9 pH distribution in un-enhanced and enhanced electrokinetic remediation of Cd contaminated kaolinite (Kim et al. 2003)

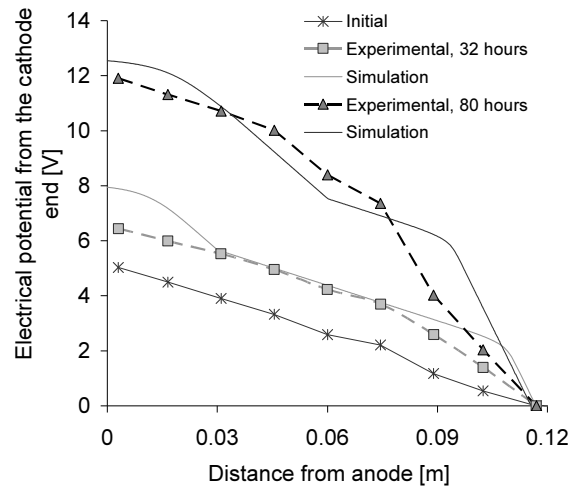


Fig. 10 Evolution of the electrical field within a Pisa Clay sample contaminated with Pb under constant electrical current conditions (Cattaneo et al. 2008)

Reactions terms

Several papers focused on the reaction term introduced in the mass balance equation of the chemical species. As stated previously the nR_k on the right hand side of equation (43 c) expresses rates of production due to different physico-chemical processes, such as: adsorption and desorption, reactions in the water phase and dissolution – precipitation reactions.

Experimental and theoretical studies showed that pH has an important impact on adsorption onto kaolinite particles. An increase of pH generally leads to higher adsorbed quantities of cationic metallic ions, as lead, cadmium or nickel, (Alshwabkeh and Acar, 1996; Kim

et al. 2003, Mascia et al. 2007). Conversely the adsorption of anionic species, such as those formed by chromium, has been found to decrease with pH (Reddy et al. 1997); and the same behavior has been noticed for some non ionic contaminants, such as 2, 6-dichlorophenol and 3-1, 1-dimethylurea (Diuron) (Polcaro et al. 2007).

The models proposed in the literature account for these effects both through linear adsorption isotherms adjusted in reason of the pH (Kim et al. 2003), or through more complex complexation models, that consider the effect of pH on the surface charge and the competition of sorption of the contaminant with other cations (Mascia et al. 2007).

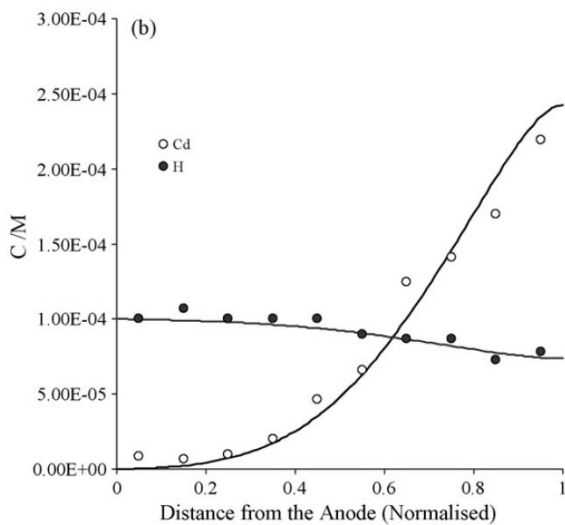


Fig. 11 Experimental (symbols) and model predicted (lines) concentrations of H^+ and Cd^{2+} in kaolinite after 340 h of electrokinetics. Electrical field $E = 1.5 \text{ V cm}^{-1}$ (Mascia et al. 2007)

In general, the penetration of the acid front has a beneficial effect on the removal of those metals whose adsorption is reduced at low pH. Desorption and transport of the contaminant can be more problematic if the soil possesses a certain buffering capacity that significantly hinders or retards the penetration of H^+ .

Yeung et al. (1997) compared the results of electrokinetic tests run on Georgia (pure) and Milwhite kaolinite (a commercial kaolinite with 4.3 % Fe_2O_3 and other impurities with an higher buffering capacity), where decontamination of the latter appeared to be feasible only if aided by the injection of EDTA. EDTA enhances the desorption and solubilisation of lead even at high pHs, making possible its removal in a less acid environment. In natural soils, carbonates are among the most important buffering agents, retarding the advancement of H^+ to a noticeable extent (Reddy et al. 1997).

On the other hand heavy metals precipitate as

carbonates in calcareous soils: Ottosen et al. (2001) noticed that in such conditions the dissolution of precipitates occurs at higher pH values, this enhancing the mobilization of contaminants. It is then not completely clear whether the presence of carbonates is detrimental for the electrokinetic remediation from cationic heavy metals or not; while in virtue of the imposed chemical equilibrium it favours the migration of anionic contaminants towards the anode (Reddy et al. 1997).

More in general, it seems that one of the main issues that complicates the modelling of electrokinetic remediation at the present extent is the fact that, in virtue of the pronounced pH and Eh gradients induced in the soil mass, complex equilibria can arise between the various dissolved substances and between those and the solid phase.

A more comprehensive approach has been proposed recently by Al – Hadman and Reddy (2008), by coupling a transport model (substantially eq. 42 c and 43 c, under a constant electrical field and null hydraulic field) with a geochemical model and library in charge of the reactive terms of eq. 43 c. Coupling is effectuated iteratively at each time step: the simulation of the fluxes is first implemented, then the geochemical model checks for the chemical equilibrium and imposes it locally. Finally the simulation proceeds to the following time step. Chemical processes considered are the electrostatic adsorption of charged ions on the soil (with consequent changes of the particles specific surface and ζ potential) and the equilibrium of the species formed by nickel, cadmium, chromium, potassium and chloride in a water environment, imposed through the law of mass action.

Non linearity of the water flow

The water flow during the electrokinetic remediation usually does not remain constant but, depending on a number of conditions, can decrease, stop or even invert direction

Constant hydraulic and electroosmotic conductivities in equation (43 a) can contribute to explain the decrease of the flow rate, if associated with a non homogeneous electrical field. In such conditions, to honour the mass balance of the soil, differential hydraulic pressures arise, contributing both to consolidation or swelling and to a net decrease of the water flow. Nevertheless, constant conductivities cannot explain the reversal of flow (cathode to anode), evidenced for instance by Eykholt and Daniel (1994) and by Garcia-Gutierrez et al. (2007). The dependency of K_{co} on pH has been imposed by Mascia et al. (2007) on experimental basis over a limited pH interval. Kim et al. (2003) relate ζ to the pH through an expression similar to the one provided by Lorenz (1969), and then K_{co} , to ζ as in eq. (33).

Besides pH changes, other mechanisms have been

demonstrated to affect the value of ζ in kaolin, such as the sorption of Co^{2+} , Cd^{2+} and Cu^{2+} (Hunter and James, 1992) or the sorption of Pb^{2+} (Stewart and West, 1996). In this perspective, the model proposed by Al-Hadman and Reddy (2008) sets a dependency of ζ on ionic strength, concentration of metal ions and pH (Fig. 12).

Although assuming a constant electrical field, and neglecting the contribution of Darcian flow, the predicted water flow compares reasonably well with the experimental data.

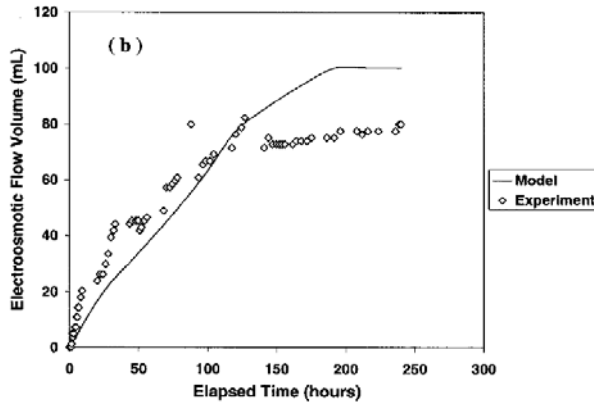


Fig. 12 Measured and predicted water flow in a kaolinite sample contaminated with Chromium, Nickel and Cadmium (Al – Hadman and Reddy, 2008)

Saturation / desaturation effects

Electrokinetic remediation could be effectuated in the vadose zone, and therefore on unsaturated soils. Nevertheless, little information on the influence of the saturation degree on the remediation process and on the transport parameters is available.

A few pilot tests have been performed in unsaturated soil layers to verify the optimum electro-chemical conditions for soil remediation (Mattson et al. 2002; Wiczorek et al. 2005, Chang et al. 2006). Mattson et al. (2002) suggested a model for electrokinetic ion transport through unsaturated sands, where a power law, calibrated on their experimental results, was assumed to describe the dependence of effective diffusion coefficient and effective ionic mobility on degree of saturation. As for the dependency of the electroosmotic conductivity on the saturation degree, to the writer's knowledge only the works by de Wet (1995) and by Gabrieli et al. (2008a) presented a few systematic laboratory data. Accordingly, it seems that the ratio $K_{\text{co}}(S_r) / K_{\text{co}}^{\text{sat}}$, where S_r is the water saturation and $K_{\text{co}}^{\text{sat}}$ is the electroosmotic permeability in saturated conditions, can be related to water saturation through a power law (Fig. 13).

For the natural illitic silt studied by Gabrieli et al. (2008), the effects of desaturation are stronger on the hydraulic conductivity than on the electroosmotic conductivity. On its turn, the electroosmotic conductivity is more affected

by saturation than the electrical conductivity.

The tests discussed by Gabrieli et al. (2008) have been simulated by Tamagnini et al. (2010). The model assumes constant electrical conductivity for the pore water. The electrical, water, air and electroosmotic conductivities in unsaturated conditions are described by power laws that depend on the saturation degree. Mass balance equations for the air, water and solid phases are introduced.

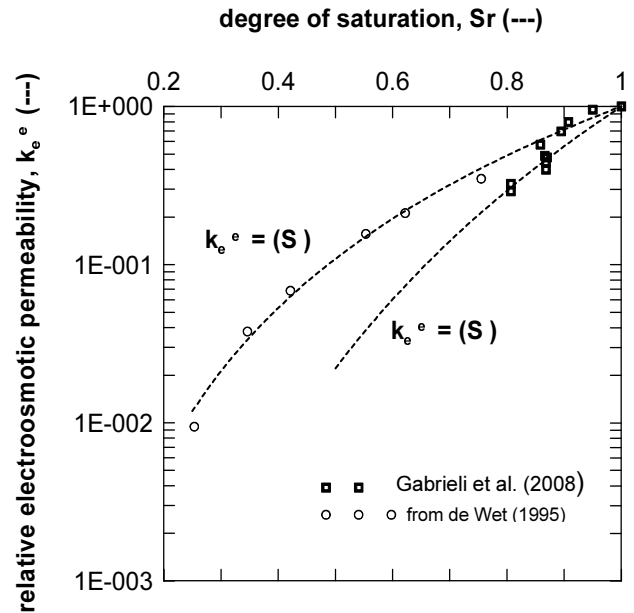


Fig. 13 Effects of the water saturation degree S_r on the electroosmotic permeability K_{co} of an illitic silt (modified from Gabrieli et al. 2008)

A desaturation front entering the sample is documented when the anode is in contact with the sample; as a consequence a non linear suction distribution arises within the samples, mostly significant for electroosmotic consolidation.

Desaturation can occur as well as a consequence of processes originating in the soil mass. Experimental findings showed this occurrence in natural illitic soils possessing a carbonate mass fraction ranging between 6 and 15 % (Chighini et al. 2002; Airolti et al. 2009). Indeed, the buffering action of carbonates derives from their dissolution reactions with H^+ . As a product of calcite dissolution, CO_2 is released in gaseous form (Appelo and Postma, 1993) locally desaturating the soil and sometimes leading to the generation of cracks. On its turn, desaturation is held responsible for an important local increase of the electrical field on the anode side, contrarily to what is found for most experimental tests on pure kaolinite (increase of the electrical field at the cathode side due to precipitation). A reasonable reproduction of these phenomena can be pursued by associating the transport model, including desaturation

effects, with a geochemical model that provides the equilibrium conditions of the carbonates in the soil (Airoldi et al. 2009). In this case, the geochemical model provides information on the CO_2 pressure due to calcite dissolution, information used to estimate the saturation degree on basis of the soil water retention curve. The electrical conductivity in unsaturated conditions, computed on basis of Eq. 38 where the calculated saturations have been introduced, appears reasonably capable of catching the experimental results (Fig. 14).

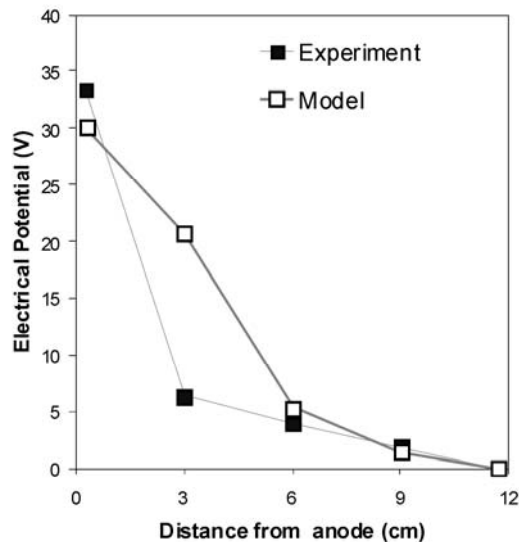


Fig. 14 Effects of desaturation induced by calcite dissolution on the electrical field in a natural kaolinite - illitic soil, after 2 weeks of treatment under an original homogeneous electrical field $E = 0.35 \text{ V cm}^{-1}$ (modified from Airoldi et al. 2009)

Conclusions

The electrokinetic technique appears as a viable tool for the remediation of contaminated clayey soils. Major induced phenomena, electroosmosis and electromigration, are effective in transporting both non ionic and ionic contaminants dissolved in the pore water.

Caution is anyway needed since electrokinetics significantly affects the original chemical equilibrium of the pore water. As for cationic contaminants, the technique is more effective in soils with a low buffer capacity, since water splitting at the anode provokes an acid front that migrating in the soil mass allows for desorption of cationic species. As for anionic contaminants, a higher soil buffering capacity appears more favourable, since the pollutant solubility is higher at higher pH.

In order to reproduce the mutating chemical equilibriums, it is not sufficient to model transport of the single contaminant object of remediation. Instead, it is required to compute jointly the transport of all the

species that could participate to significant reactions and of those that alter the adsorption and desorption processes (mainly H^+ and OH^-). Therefore, a proper modelling requires the knowledge of main chemical composition of the soil to be treated, and of the possible reactions of its elements with the contaminant of concern. As for the solid phase, critical components are carbonates and organic matter.

Transport parameters are affected as well by the evolving chemical environment. Although in some cases their evolution can be neglected when simulating only the flux of chemicals, their dishomogeneity has an impact on the mechanics of the treated soil, inducing swelling or consolidation. To this extent, further research is needed to clarify the geochemical - geomechanical interaction in a number of situations, such as for chemo-mechanical hardening, increase in strength due to precipitates and desaturation in carbonatic soils.

ENHANCED CONTAMINANT EXTRACTION BY HIGH VACUUM

The volatile organic compounds (VOCs) are a kind of contaminant that can be mainly found in the vadose zone under different phases i.e. as a separate liquid (NAPL), as a pore gas mixture component and adsorbed on the soil grain surface. Venting is one of the best available technologies that can be employed in order to remove the volatile or semi-volatile contaminants from the medium to high permeability subsoils. Basically, the technique consists of the pore air extraction by light vacuum applied to the head of a series of vertical wells. Sometimes, the extraction system can be enhanced by air injection wells located on an alternate pattern with respect to the one of the extraction wells.

High vacuum is applied in Multi-Phase Extraction (MPE) systems. This in-situ remediation technology is today rapidly emerging and allows a simultaneous extraction of vapour phase, dissolved phase and separate phase contaminants from vadose zone, capillary fringe, and saturated zone soils and groundwater. It is an advancement of soil vapor extraction (SVE) and is most commonly applied in moderate permeability soils.

Recently, a new contaminant extraction system (SGIBITI) has been proposed by Manassero (2003), Dominijanni et al. (2007). The system is fundamentally based on the well known technology of the vacuum consolidation that is currently used in the traditional geotechnical field for the improvement of the mechanical behavior of fine grained soft soils. It consists of a confinement of the polluted volume of soil by a capping geomembrane and side cut-off walls providing a series of injection and extraction wells for flushing fluids

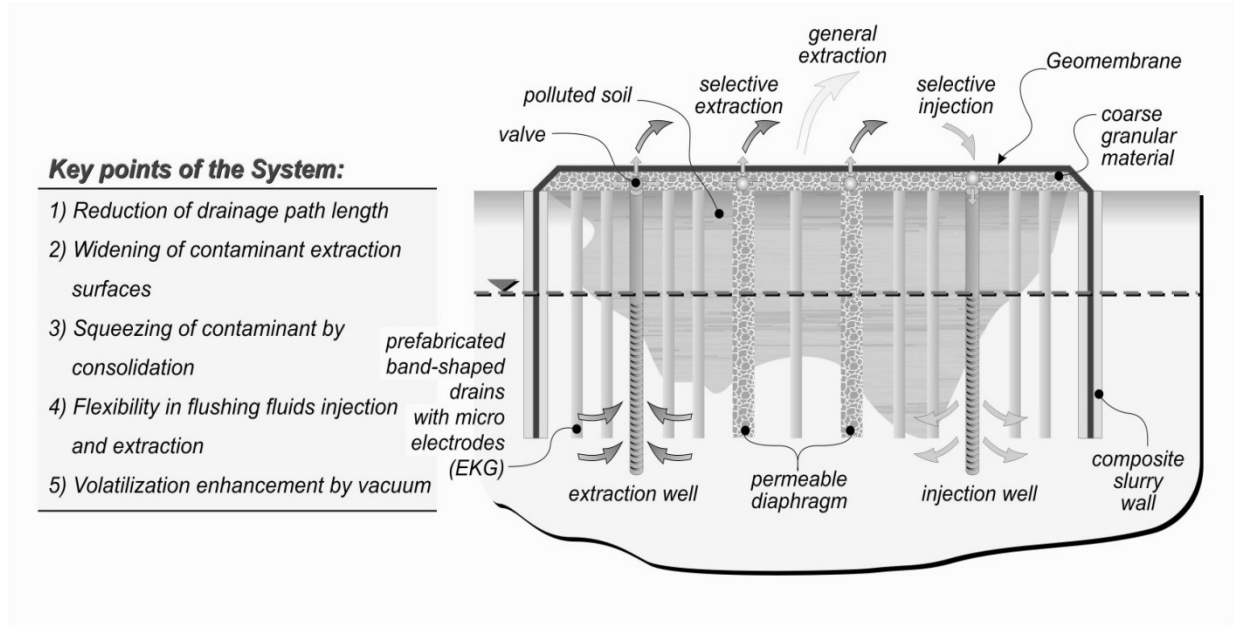


Fig. 15 High vacuum extraction system (SGIBITI)

(Fig. 15). The extraction of pollutant is enhanced by the high vacuum application that promotes the contaminant volatilisation and with the other components of the system is able 1) to reduce the drainage path length; 2) to widen the contaminant extraction surface including the ground surface; 3) to squeeze the contaminant from the pore fluids of fine grained soft soils; 4) to reverse the flushing fluid flow direction and 5) last but not list, to increase the contaminant concentration in the effluent gas phase.

Laboratory and field experimental programs are now in progress for the validation of the new proposed remediation technology. In the following, after an introductory illustration of the main aspects related to the theoretical modelling of the flow and transport phenomena related to this new technology, some recent laboratory test results are illustrated and preliminary discussed.

Theoretical Model for High Vacuum Extraction

In principle, the theoretical simulation of high vacuum induced fluid flows inside a sealed volume of soil and in presence of vertical wells and drainage layers for air injection and extraction, requires the use of a rather comprehensive model able to simulate multi-phase flows and multi-component transport.

Eqs. 1 and 2 can be used for these purposes adopting the explicit form reported here below for the different phase flows:

$$\frac{\partial[(1-n)\rho_s]}{\partial t} = -\nabla \cdot [(1-n)\rho_s v_s] \quad (45a)$$

$$\frac{\partial(nS_w\rho_w)}{\partial t} = -\nabla \cdot [nS_w\rho_w v_w] \quad (45b)$$

$$\frac{\partial(nS_a\rho_a)}{\partial t} = -\nabla \cdot [nS_a\rho_a v_a] \quad (45c)$$

$$\frac{\partial(nS_o\rho_o)}{\partial t} = -\nabla \cdot [nS_o\rho_o v_o] \quad (45d)$$

$$q_w = nS_w(v_w - v_s) = -\frac{K_w}{\mu_w} \nabla(P_w + \rho_w gz) \quad (46a)$$

$$q_a = nS_a(v_a - v_s) = -\frac{K_a}{\mu_a} \nabla(P_a + \rho_a gz) \quad (46b)$$

$$q_o = nS_o(v_o - v_s) = -\frac{K_o}{\mu_w} \nabla(P_o + \rho_o gz) \quad (46c)$$

where n is the soil porosity; ρ_i is the density of the i -th phase; S_i is the saturation degree, v_i is the effective velocity, q_i is the Darcy velocity, K_i the effective permeability, P_i is the pressure, μ_i is the dynamic viscosity of the i -th phase, g is the gravity acceleration and z is the vertical distance from the reference horizontal plane. The subscript s , w , a , and o define soil, water, air and oil (NAPL) respectively.

Form a practical point of view and looking at the specific soil type, it is usually possible to select what kind of phase flow will govern the contaminant extraction also in the case of a potentially complete multi-phase and multi-component flow scenario.

The high vacuum extraction system under consideration has been set up in order to speed up the extraction of residual volatile and semi-volatile contaminants (NAPL in particular) located inside a medium

to low permeability soils where also the water phase is at the residual content. Under these hypotheses, no-flow conditions occur for liquid phases (NAPL and water) and the contaminant extraction through the gas phase prevails by far on the liquid phase extraction. Therefore, the theoretical modelling can only consider the flow equation related to the gas phase.

For the sake of simplicity, in the following, the airflow is considered in steady state conditions, without source and sink contribution and, moreover air compressibility is neglected. The aforementioned assumptions lead to the following airflow equation:

$$\nabla \cdot q = \nabla \cdot \left[-\frac{K}{\mu} \nabla (P + \rho gz) \right] = 0 \quad (47)$$

The information required to handle the air phase in most models basically includes the air effective permeability that can be expressed by the following relation.

$$K_a = k_{ra} k_{int} \frac{\rho_r}{\mu_r} \quad (48)$$

where: k_{ra} is the air relative permeability; k_{int} is the intrinsic permeability of the porous medium; ρ_r is the density ratio between oil and water; μ_r is the relative viscosity between oil and water.

The relative permeability can be assessed by the relationships proposed by Manassero et al. (2005) on the basis of the Mualem model and the van Genuchten (1980) formulation for a two phases system:

$$k_{r,a} = \sqrt{1 - \frac{S_w + S_o - S_{w,r}}{1 - S_{w,r}}} \left[1 - \left(\frac{S_w + S_o - S_{w,r}}{1 - S_{w,r}} \right)^{1/m} \right]^{2m} \quad (49)$$

where: S_w is the saturation of water; $S_{w,r}$ is the residual saturation of water; S_o is the saturation of oil and m is the parameter of the van Genuchten original expression. Since, within the considered conditions water and oil are assumed in residual saturation conditions Eq. 49 can be simplified as reported below:

$$k_{r,a} = \sqrt{1 - \frac{S_{o,r}}{1 - S_{w,r}}} \left[1 - \left(\frac{S_{o,r}}{1 - S_{w,r}} \right)^{1/m} \right]^{2m} \quad (50)$$

where: $S_{o,r}$ is the residual saturation of oil.

Given the airflow scenario in partially saturated conditions, it is necessary to define the phase change relationships for the NAPL in order to assess its

extraction rate by the high vacuum system. Only the NAPL-gas phase change is taken into account within the considered model neglecting the NAPL-water and the NAPL-soil phase changes.

In the simplest case the component transport equations are usually set up using the partitioning coefficients among phases at equilibrium. This assumption can be considered reliable only for highly volatile compounds and at the very beginning of the extraction process with high saturation degree of the contaminant in the porous medium. On the other hand, in order to assess the advantages of the high vacuum extraction system in comparison with the more traditional soil venting techniques in enhancing residual contaminant extraction through the gas phase in medium permeability soil, it is mandatory to refer to non-equilibrium conditions for modeling the volatilization phenomena.

Referring to a first order phase transformation kinetics the mass transfer equation can be written as follows:

$$J = k_f (C_s - C_a) \quad (51)$$

being: J the contaminant mass flow among the different phases, k_f the phase transfer coefficient; C_a the contaminant concentration in the gas phase and C_s the contaminant concentration in the gas phase at equilibrium.

The phase transfer coefficient can be a function of: the gas flow velocity, the grain size distribution of the soil, the saturation degree of water, gas and NAPL itself and its expression can take the following form (van der Ham e Brouwers, 1998; Yoon et al. 2002):

$$K_{ao} = k_{ao}^i \left(\frac{S_o}{S_o^i} \right)^\beta \quad (52)$$

being: k_{ao}^i the initial value of the phase transfer coefficient, β an empirical parameter linked with the water saturation degree, S_o^i the NAPL initial saturation degree and S_o the NAPL saturation degree.

Given the aforementioned assumptions and simplifications, the governing transport equations for the gaseous contaminant component can be derived from the general ones (Eqs. 45 and 46) as follows:

$$\frac{\partial n S_a C_a}{\partial t} = -\nabla \cdot (-n S_a D_h \nabla C_a + q_a C_a) + K_{ao} (C_s - C_a) \quad (53)$$

$$\frac{\partial n \rho_o S_o}{\partial t} = -\nabla \cdot (q_o) + K_{ao} (C_a - C_s) \quad (54)$$

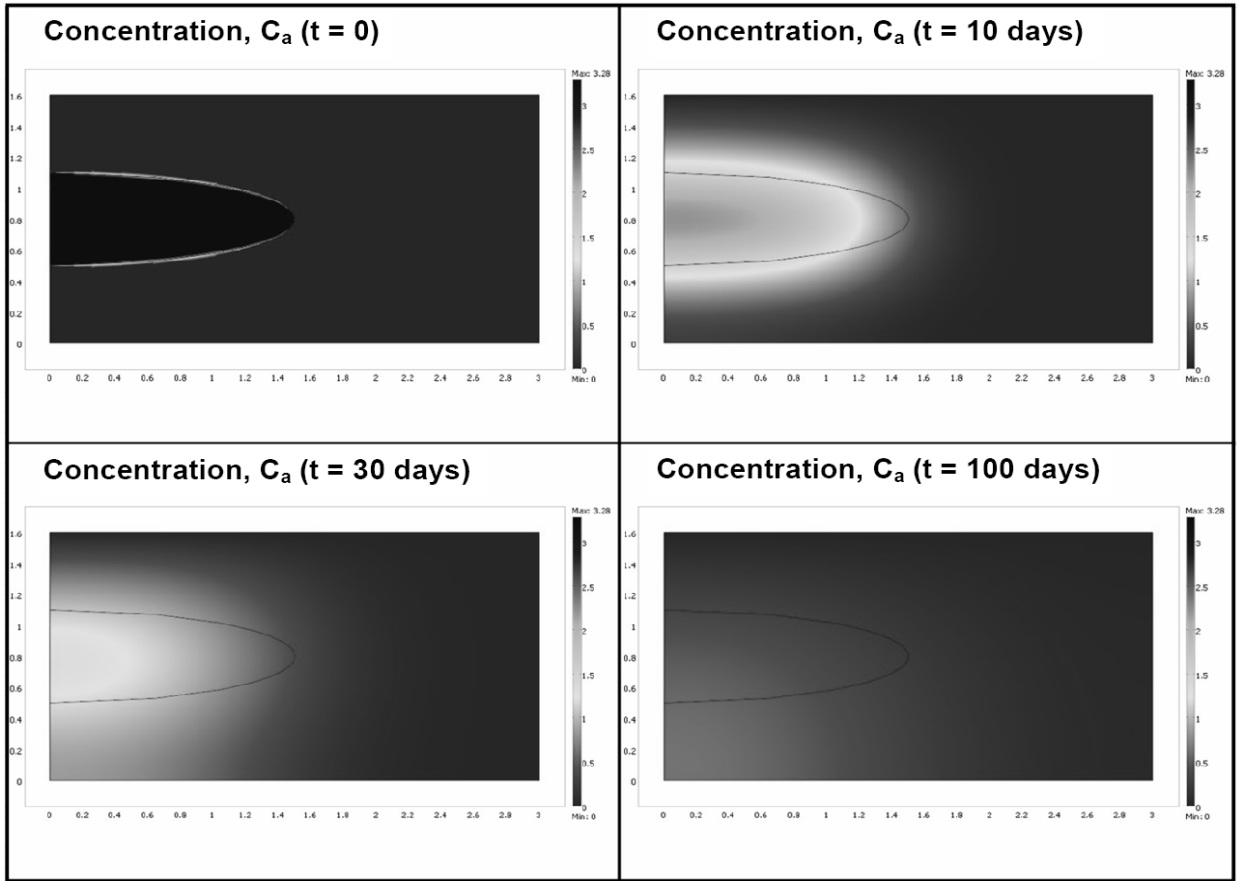


Fig. 16 Residual contaminant concentration at different times after venting extraction application ($\beta = 1$)

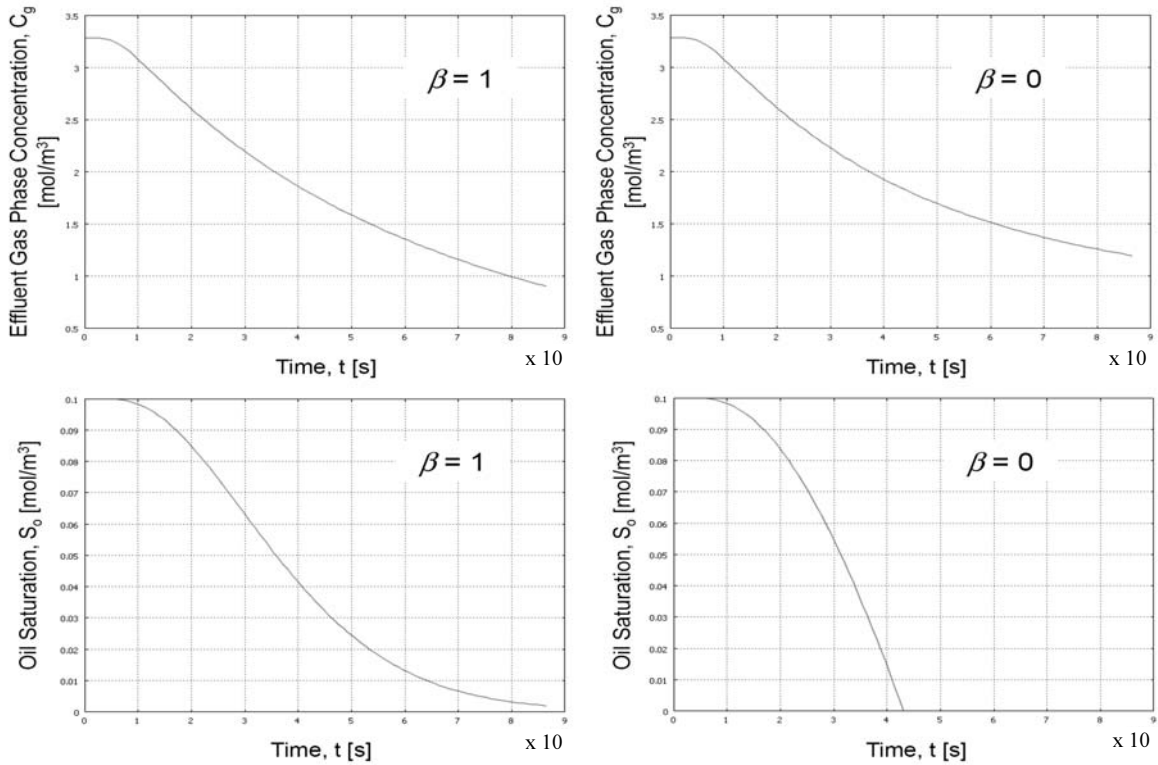


Fig. 17 The influence of the residual pore water content on the transfer coefficient and on venting extraction efficiency

being: ρ_o the contaminant density, S_a the air saturation degree and D_h the hydrodynamic dispersion coefficient.

By solving the differential equations system reported above, it is possible to evaluate the variation in time and space of the NAPL residual saturation in the soil pores and therefore the time necessary for the remediation and the related efficiency of this vacuum extraction technology.

An example of the solution of the NAPL extraction problem by volatilization with non linear variation of the transfer coefficient is shown in Figs. 16 and 17.

Observing the figures it is possible to appreciate the influence of the transfer coefficient variation through the exponent β that can take into account the amount of the current saturation degree of the different pore fluids (Harper et al. 1998; Yoon et al. 2002; Yoon et al. 2003)

Practical Advantages of The High Vacuum Application

In the most general case, the phase transfer mechanism from liquid to solid is also very sensitive to the absolute pressure of the pore gas phase and to the pressure difference from the gas and liquid phases (capillary pressure). Therefore, the NAPL-gas transfer coefficient is in turn a function of the absolute gas pressure through the equivalent diffusion coefficient from the kinetic theory of the perfect gas (Bird et al. 1960)

It is rather easy to realize the comparison between the liquid vaporization and extraction within a soil pore and the people living a train by an evacuation platform (see Fig. 18).

To reduce the gas absolute pressure is in principle equivalent to keep empty the train platform from standing blue people waiting for another train. In this way pink people can leave the train (phase transfer) in a very easy way and can evacuate the platform very quickly such as the pollutant can do leaving the pore space under high vacuum (i.e. low concentration of the other components of the pore gas mixture).

In order to prove and to quantify the aforementioned phenomena, a series of experimental investigations have been carried on small scale soil samples in the laboratory and some preliminary results are today available for the interpretation. All the laboratory tests have been carried out at the same gas mass flow.

Fig. 19 (Alferi 2009) shows a series of photos at different times from the beginning of the tests at different average vacuum pressures. It is possible to immediately observe that for a given time after the beginning of the test, the sample with the higher applied vacuum show a reduced residual NAPL (isooctane; vapor tension = 1.5 kPa at 20 °C) content.

Moreover, Fig. 20 also shows the time to the end of the treatment (i.e. in correspondence of the total

extraction of contaminant) versus the average vacuum pressure applied.

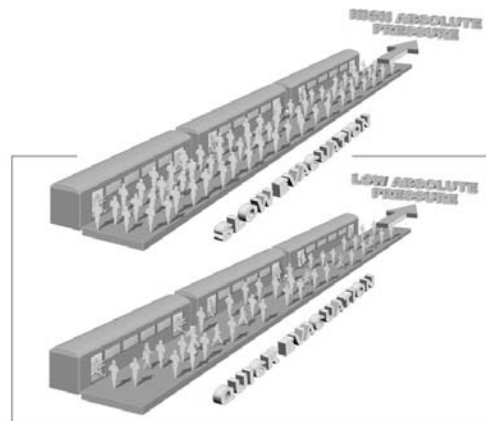


Fig. 18 Metaphoric exemplification of the phase change speed up by high vacuum application

It is possible to observe a reduction of more than 30% in extraction time from traditional low vacuum technologies (0.9 atm) to the high vacuum proposed system (0.1 atm), at a given mass gas flow rate.

A preliminary interpretation of laboratory test results has been carried out by Dominijanni et al. (2007) on the base of the differential Eqs. 53 and 54. The system is able to take in to account: advective and diffusive fluxes within the gaseous phase, NAPL non-equilibrium phase changes through the transfer coefficient $k_{g,o}$ and the progressive reduction of the surface contact gas-NAPL with NAPL saturation decrease with time.

Fig. 21 shows the interpretation of the experimental results of another series of laboratory tests carried out at different absolute gas pressures. It is possible to observe an important increase of the mass transfer coefficient also when the absolute pressure is reduced of just the 25-30%.

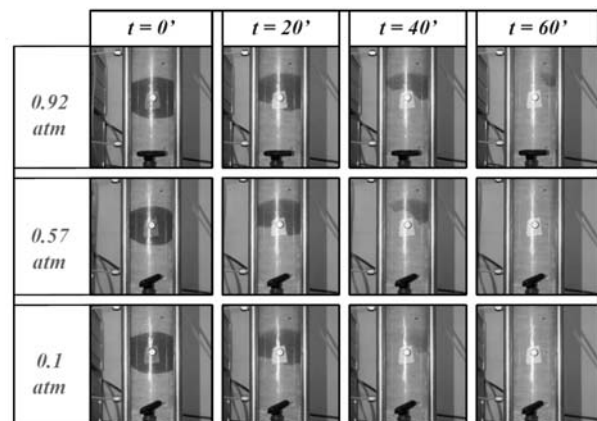


Fig. 19 Experimental contaminant extraction visualization at different times and absolute pressures

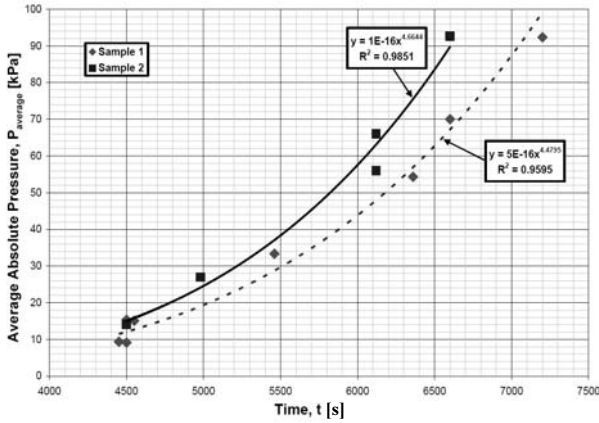


Fig. 20 Time for total contaminant extraction versus average absolute pressure

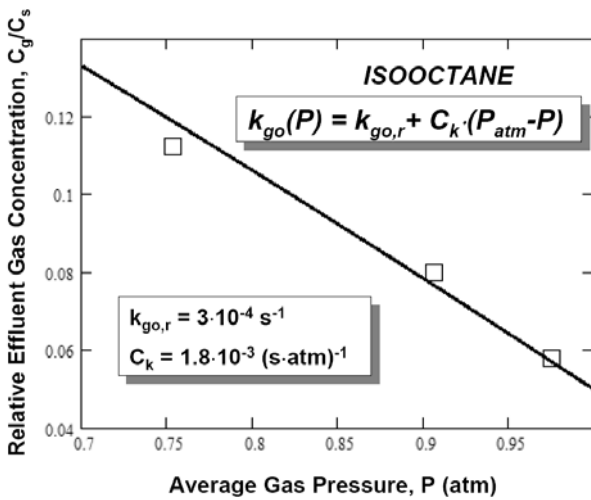


Fig. 21 Influence of the absolute pressure on transfer coefficient and on extraction system efficiency

Finally Fig. 22 shows a comparison between the traditional and SGIBITI systems when an important absolute pressure difference is imposed, without any limitation on the gas flow rate

It is possible to see that, thanks to the higher transfer coefficient, the asymptotic trend of contaminant extraction rate occurs at higher gas flow rate than in the case of traditional system i.e. it is possible to exploit by high vacuum application higher pressure gradient to further speed up the extraction rate beyond the improvement of volatilization efficiency.

In this example the decontamination time is around six times shorter by high vacuum application than with traditional venting systems.

Final Considerations

Future development, that are expected in order to improve the prediction capabilities of the theoretical models in the field of multi-phase multi-component

flows, concern the coupling processes both on the macro scale, in order to take into account the interaction between immiscible fluids under differential pressure gradients, and on the micro scale, in order to take into account the effect of osmotic and electrical potential on solute compound migration in fine grained soil.

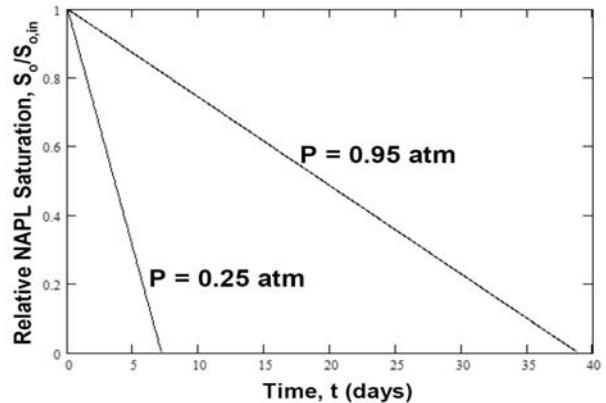
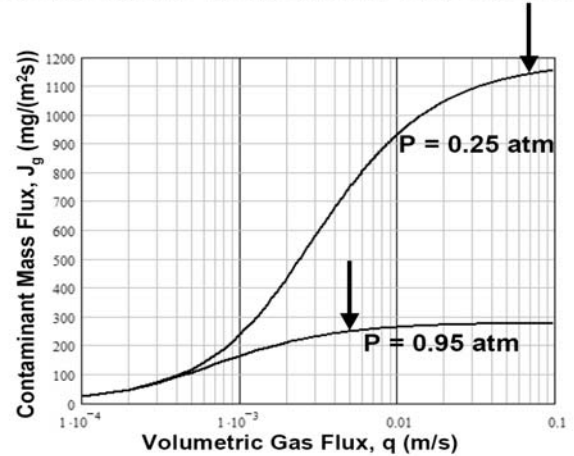
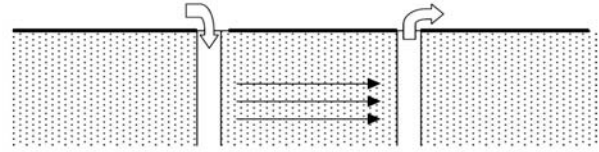


Fig. 22 Bulk effect of transfer coefficient increase on the efficiency of contaminant extraction system by venting

Also the coupled mechanical behavior can play a very important role specifically within fine-grained materials when high vacuum is applied. For instance, in some case tension cracks can occur promoting preferential flow paths that can lead in turn to a significant improvement of the advective extraction efficiency.

OLD LANDFILL EXPANSION IN THE VERTICAL DIRECTION

Old Landfill expansion in the vertical direction implies advantages in terms of (1) optimal use of landfill area, (2) high waste volume filled per unit area, (3) low

construction costs, (4) less public opposition, and (5) easier permitting (Qian et al. 2002). On the other hand, the safety and performances of a new landfill expansion mainly depend on the mechanical behavior of the old waste body. In fact, the additional waste fill from a vertical landfill expansion will cause settlement of the existing landfill and result in liner system and slope stability problems for both the existing and expanded landfills. A gas collection system in the existing landfill may also be of concern due to the large deformation of the solid waste surrounding the gas collection pipes. A liner and leachate collection system constructed on an existing landfill can experience large differential settlements. The long term performance of these systems should therefore be a major design consideration.

Example of a Performance Assessment on a New Lining System of a Piggy-back Landfill

A useful example of an appropriate assessments of stress-strain induced on a new lining system by the settlement of an old waste body is briefly described in the following (Golder Associate, 2006). The industrial waste landfill is located in southern Australia. The main vertical section and some details about the lining and capping system components of the new waste body are given in Fig. 23.

The first assessment was devoted to the study of the ability of the proposed reinforced spanning layer (consisting of a sandy gravel) to maintain structural integrity of the lining package over potential voids formed in the underlying old waste. A finite element model was developed to model the effect of any variations in the stiffness of the existing waste on the proposed liner system. Any variations of the stiffness of the existing waste would result in differential settlement near the liner. The input parameters, referring in particular to the mechanical behavior of the old waste, were estimated using the results of plate load tests, geophysical investigations and settlement monitoring systems during the former landfilling activity, which included a pre-load phase carried out just before the execution of the new lining system in order to speed up the old waste consolidation settlements.

The model predicts the behavior of the proposed reinforcement layers (geogrids) in the spanning layer below the liner. The purpose of the reinforcement layers is to distribute any differential settlement from the underlying waste over a larger area, and thereby reduce the strains on the liner system (Viswanadham and Jessberger, 2005). Two reinforcement layers were modelled and these represent the combined action of the two geogrids in the spanning layer and in the compacted clay, which in effect creates a soil beam.

The analysis shows that, according to the stiffness

used for the waste, if a large soft spot existed in the waste, the differential settlement around the soft spot would be around 300 mm over a period of 100 years, whereas the total settlement would be around 1m. The effect of the reinforcement layers in the spanning layer is to spread this differential settlement over approximately 10m (see Fig. 24).

According to the results of the analysis, the stresses in the geogrids increase over time, due to the creep deformation of the waste (see Fig. 25). The rate of the stress increase reduces with time and this rate is in line with the creep rate that decreases over time. The peak force after 100 years in the bottom geogrid and the GCL is 0.6 kN/m, which is less than 10% of the working strength of the adopted geogrid. Similarly, the peak force after 100 years in the upper geogrid (1.6 kN/m), is also less than 10% of the working strength of the adopted geogrid. The strength of the Geosynthetic Clay Liner (GCL) is not an issue, as the proposed GCL is a low stiffness GCL, and not a reinforcement unit. The loads are transferred to the geogrids.

The model also provides an indication of the strains that can be expected in the modelled materials (Fig. 26). The predicted horizontal strains that can be expected in the liner materials are less than 1%. These low strains are considered acceptable for the proposed liner components, with typical limits of 4% to 8% for materials such as High Density Polyethylene (HDPE) geomembrane, and higher strains for Linear Low Density Polyethylene (LLDPE) geomembrane and GCL's. The compacted and reinforced clay liner is also able to comply with this kind of elongation strain without approaching the threshold tensile strain value ($\epsilon=5\%$) which induces sudden and significant increases in the hydraulic conductivity in both reinforced and unreinforced clay barrier, as pointed out by Viswanadham and Jessberger (2005). According to these results, the proposed liner system can be considered sufficiently robust with significant additional capacity being available between the material performance of the proposed lining system, and the stresses and strains predicted in the rather conservative deformation model.

An additional Finite Difference Analysis (FDA) was carried out to simulate randomly located soft spots within the old waste underlying the new waste disposal (Fig. 27). The effect of a total loss of strength of the geogrid over an area, to assess the structural integrity of the base liner in this unlikely scenario, has also been modelled. In short, the results of the additional FDA analyses indicate the following:

- Removal of the geogrid, in order to model the effect of a total loss of strength of the geogrid (Fig. 28), causes only minor differences in the settlement results.
- Introduction of soft spots with 10% of the general modulus (Fig. 29) results in about a 30% increase in

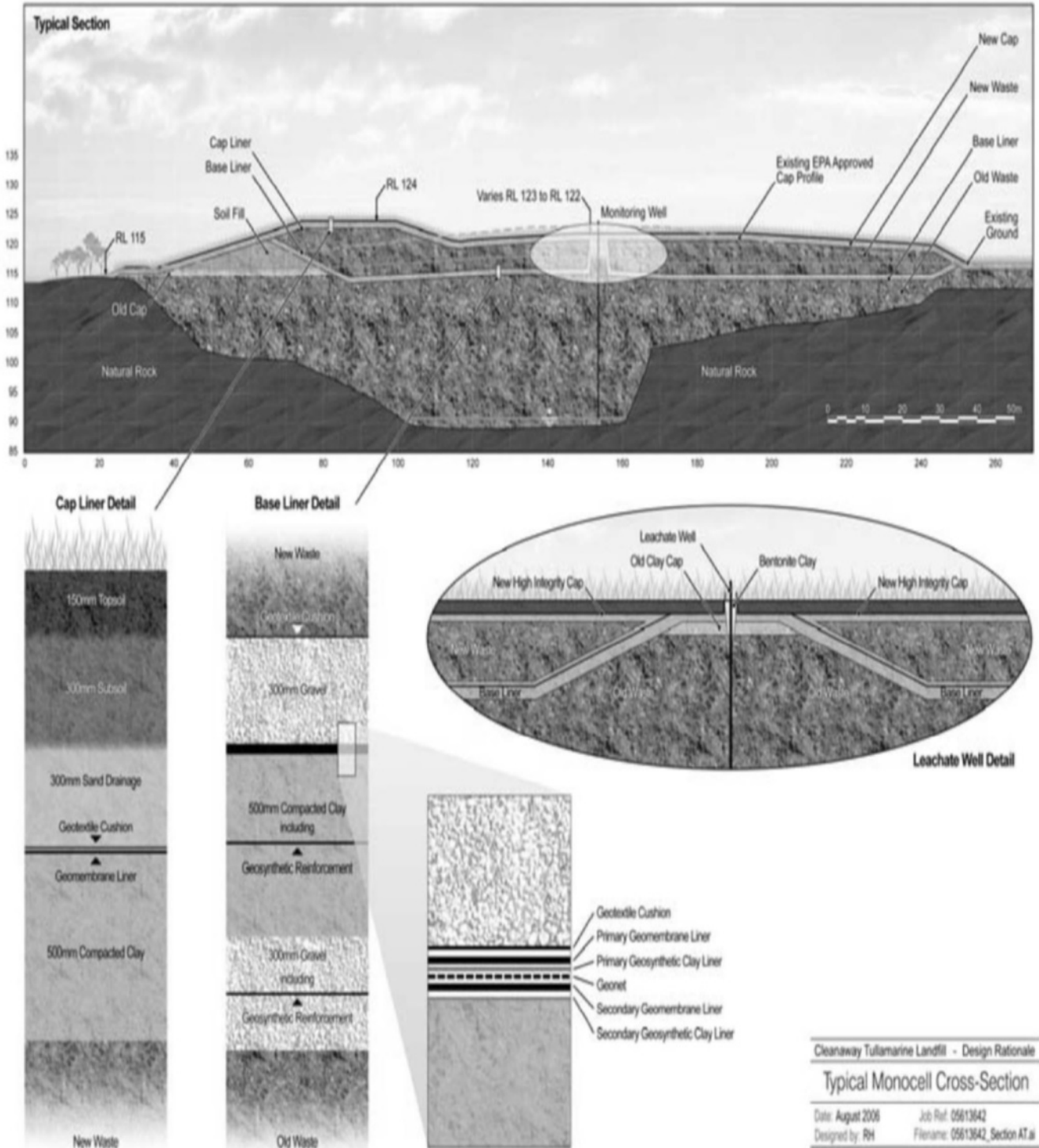


Fig. 23 Typical sections of the landfill

the maximum settlement. The increases in the axial loads and strains in the geosynthetic components of the liner system are generally less than 35%. The increase in the horizontal tensile strain in the clay liner is about 30%.

The material properties for the geogrids, the GCL and compacted clay were specified in the final design

documents according to the results of the modelling.

In conclusion, the previously illustrated example points out the importance of a complete and comprehensive knowledge of the mechanical behavior of waste. Unfortunately, most of the old landfill was filled without any kind of monitoring and/or measurement of the mechanical features of the stored wastes.

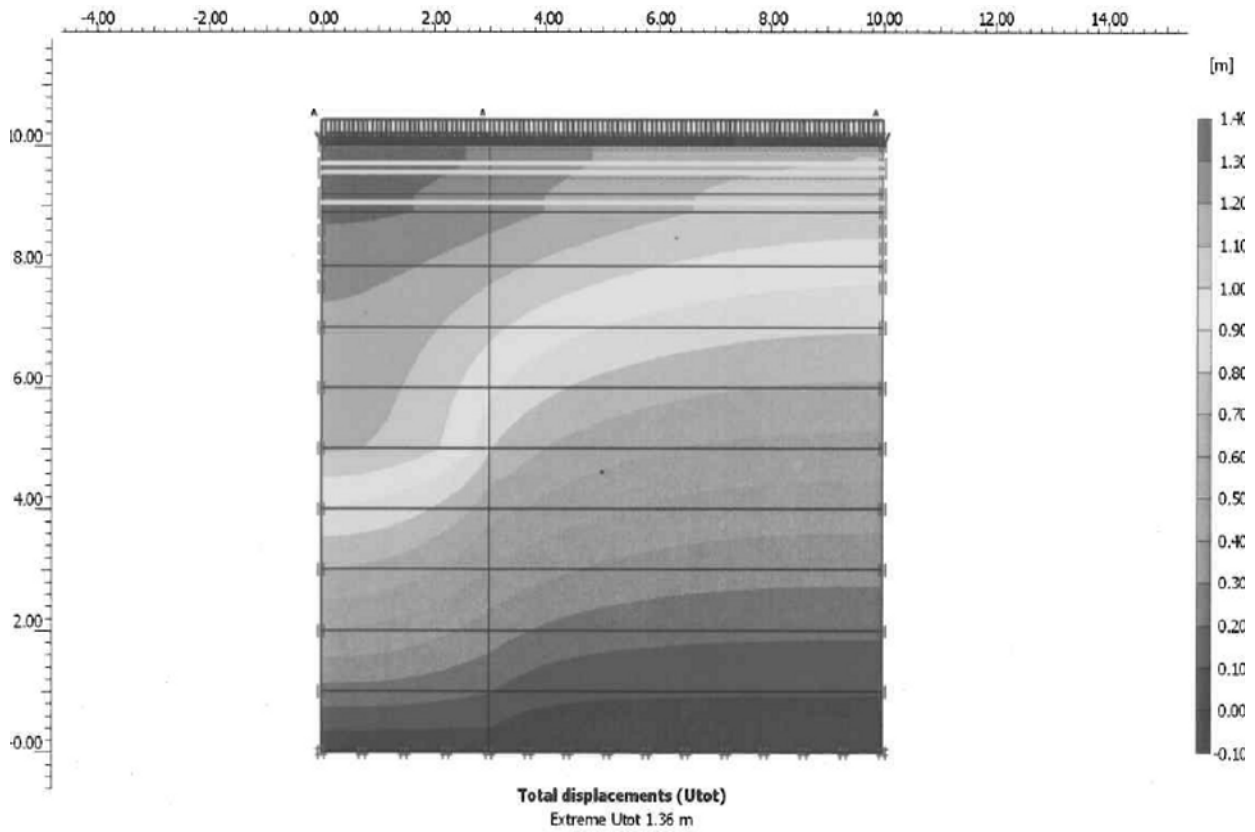


Fig. 24 Contour plot showing the waste settlements after 100 years

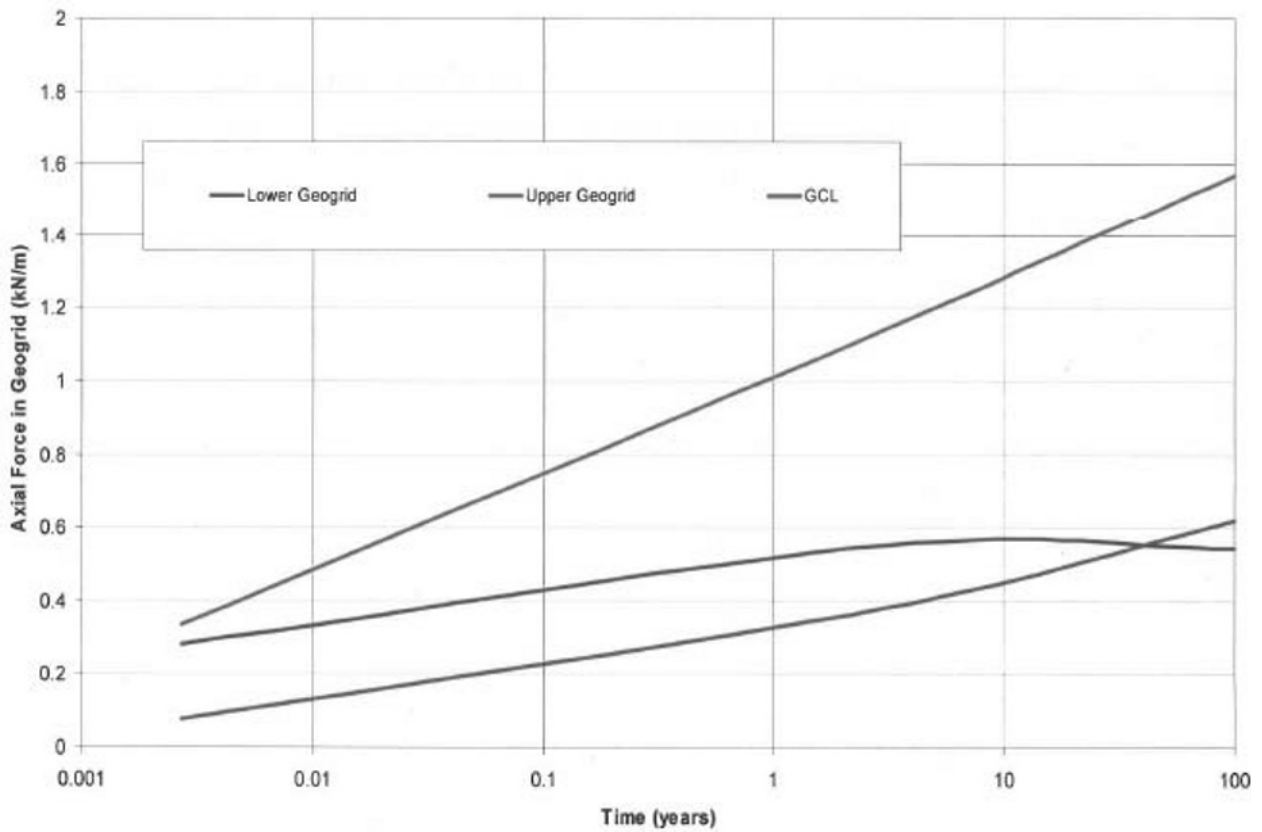


Fig. 25 Variation in the tension force in GCL and geogrids with time due to waste creep for a 5 m depth of “soft” waste

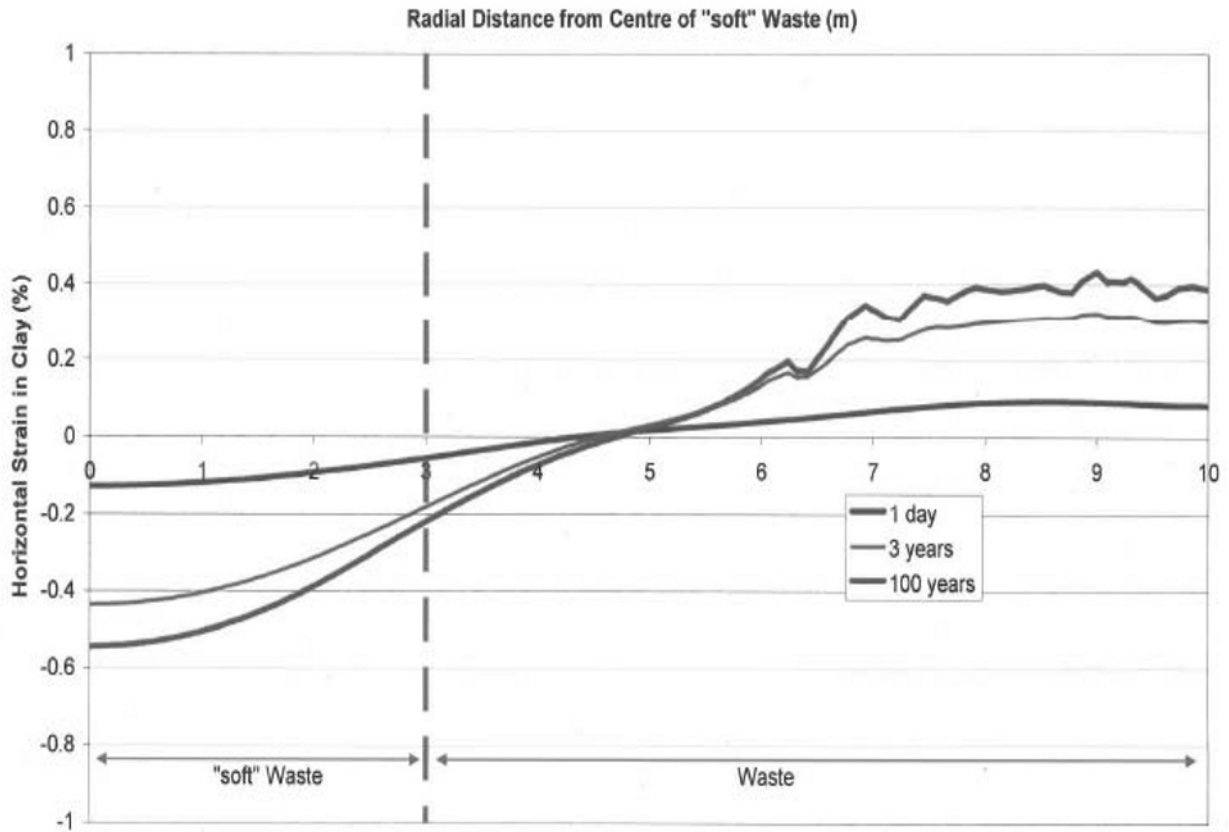


Fig. 26 Horizontal strain profiles in clay over time for a 5 m depth of “soft” waste

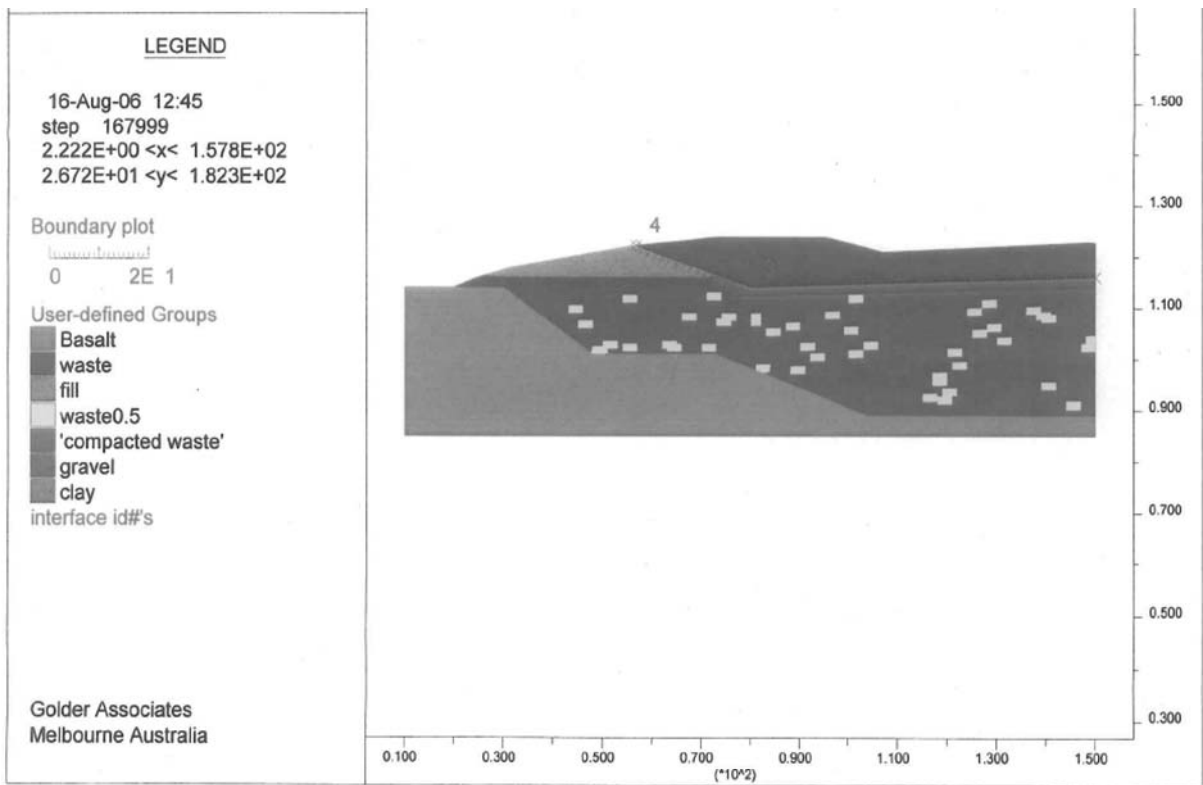


Fig. 27 FDA model with random soft spots

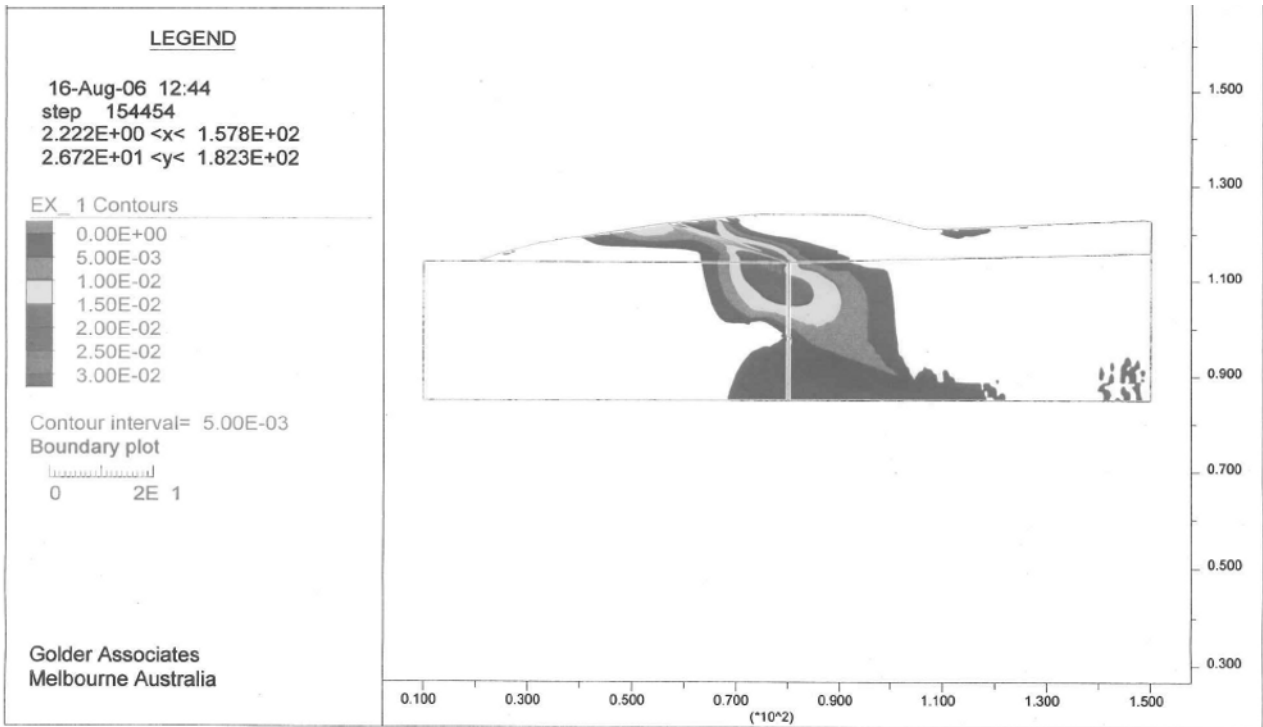


Fig. 28 Horizontal tensile strain contour without geogrid

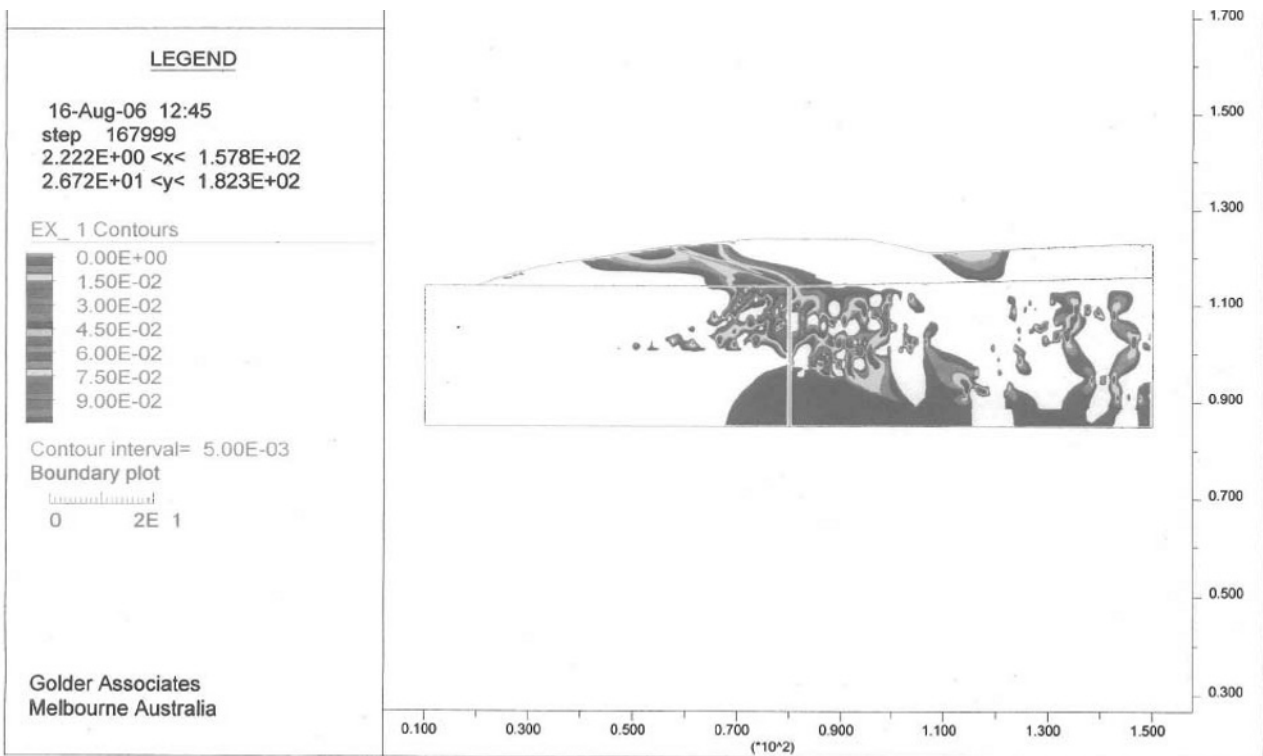


Fig. 29 Horizontal tensile strain contour with random soft spots

Therefore, in the case of need, the mechanical behavior of these rather peculiar materials should be investigated through in situ tests that at present are still in the initial setting phase and cannot be considered completely reliable, in particular, when used to predict

the full scale and long term behavior of different types of solid waste. For this reason any calculation model, even the most sophisticated, should be used with great care and the input parameters should cover the entire possible variation range in order to include the most adverse

possible conditions.

These variation ranges can be reduced in the near future, but only if monitoring of existing and new landfills becomes a normal procedure and if the field tests on these materials undergo significant improvements. In fact, even though significant progress has been made in the understanding of waste mechanics over the past 15 years, significant questions still remain unanswered concerning the appropriate parameters and the related variability of engineering interest, including shear strength and the compressibility of most municipal and industrial solid wastes (Kavanazjian, 2006). Furthermore, changes in waste streams due to recycling, waste reduction initiatives, and new products and processes, and changes in operational practices at landfills, including increased use of alternative daily covers, leachate re-injection, and the advent of bioreactor technology, suggest that the properties of our waste fills will continue to evolve in the foreseeable future. Thus field and laboratory investigations of the properties of solid waste will remain a very important part of landfill engineering and the improvement of their effectiveness and reliability at a large scale should be considered as one of the main challenges of Environmental Geotechnics for the future.

FINAL CONCLUSIONS

The importance of a reliable and consistent input parameters definition and scale effects are still outstanding in spite of the progress in modeling approaches. Therefore, experimental and theoretical research fields must advance together in order to allow any substantial progress within Environmental Geotechnics.

REFERENCES

- Acar YB & Alshawabkeh AN (1996). Electrokinetic remediation. I: pilot-scale tests with lead-spiked kaolinite. *J. Geotech. Engrg.*, 122 (3): 173-185.
- Airoidi F, Jommi C, Musso G, Paglino E (2009). Influence of calcite on the electrokinetic treatment of a natural clay. *J Appl. Electrochem.*
- Alferi M (2009). Report of Ph.D. research activity. (Thesis title: Multiphase pollutant extraction from subsoil by vacuum application). Politecnico di Torino.
- Al-Hamdan AZ & Reddy KR (2008). Electrokinetic remediation modeling incorporating geochemical effects, *J. Geotech. and Geoenv. Engrg.*, 134, (1): 91-105.
- Alshawabkeh AN & Acar YB (1996). Electrokinetic remediation II: Theoretical model. *J. Geotech. Engrg.* 122 (3): 186-196.
- Alshawabkeh AN, Sheahan TC, Wu X (2004) Coupling of electrochemical and mechanical processes in soils under DC fields. *Mechanics of Materials* 36: 453-465.
- Appelo CAJ & Postma D (1993). *Geochemistry, Groundwater and Pollution*. Balkema, Rotterdam.
- Archie GE (1942). The electrical resistivity log as an aid to determining some reservoir characteristics. *Trans. AIME*, 146: 54-63.
- Bear J (1972). *Dynamics of fluids in porous media*. Elsevier, New York.
- Bird RB, Stewart WE, Lightfoot EN (1960). *Notes on transport phenomena*. John Wiley & Sons, New York.
- Bishop AW (1954). The use of pore pressure coefficients in practice. *Geotechnique*, (4): 148-152.
- Bouazza A (2002). Geosynthetic clay liners. *Geotextiles and Geomembranes*, (20): 3-17.
- Bruell CJ, Sagall BA, Walsh MT (1992). Electroosmotic removal of gasoline hydrocarbon and TCE from clay. *J. Environ. Eng.*, 118 (1): 68-83.
- Camusso M & Barla M (2009). Micro parameters calibration for loose and cemented soil. *International Journal of Geomechanics*, (under publication).
- Cattaneo F, Jommi C, Musso G, Tamagnini C (2008). A model for electrokinetic transport in a contaminated clay. Presented at the 8th World Congress on Computational Mechanics – WCCM8 - Iacm Eccomas. Venezia, Italy, 30 June – 4 July 2008.
- Chang JH, Qiang Z, Huang CP (2006). Remediation and stimulation of selected chlorinated organic solvents in unsaturated soil by a specific enhanced electrokinetics. *Colloids and Surfaces A: Physicochem. Eng. Aspects.*, 287: 86-93.
- Charbeneau RJ (2000). *Groundwater hydraulics and pollutant transport*. Prentice-Hall, Upper Saddle River, New Jersey.
- Chighini S, Lancellotta R, Musso G (2002). Observations on the experimental behavior of Pisa clay during electroosmotic filtration tests. In: Vulliet L., Laloui L. and Schrefler B. A.(Editors), *Proc. of the International Workshop on Environmental Geomechanics*, EPFL-Press., Lausanne: 329-334.
- Corapcioglu MY (1991). Formulation of electroosmotic processes in soils. *Transp. Porous Media*, 6 (4): 435-444.
- Culligan PJ (2008). Understanding two-phase transport in porous media: what challenges still remain? *GeoCongress 2008. Characterization, monitoring, and modelling of geosystems*, Alshawabkeh A.N., Reddy K.R. and Khire M.V. (Eds.), GSP n.179, ASCE.
- Daniel DE & Shackelford CD (1988). Disposal barriers that release contaminants only by molecular diffusion. *Nucl. Chem. Waste Manag.*, 8: 299-305.
- De Wet M (1995). Electrokinetics, infiltration and unsaturated flow. In: Alonso E.E. and Delage P.

- (Editors), *Unsaturated Soils: Proceedings of the First International Conference on Unsaturated Soils*, A.A. Balkema, Rotterdam, (1): 361-366.
- Dominijanni A & Manassero M (2005). Modelling osmosis and solute transport through clay membrane barriers. *Waste Containment and Remediation* (ASCE Geotechnical Special Publication No. 47), Alshawabkeh, A., Benson, C.H., Culligan, P.J., Evans, J.C., Gross, B.A., Narejo, D., Reddy, K.R., Shackelford, C.D., Zornberg, J.G. (Eds), ASCE, Reston, VA, (CD-ROM).
- Dominijanni A & Manassero M (2008). Modelling the compressibility and the hydraulic conductivity of geosynthetic clay liners, *Proceedings of The First Pan American Geosynthetics Conference & Exhibition*, 2-5 March 2008, Cancun, Mexico, 59-68 (CD-ROM).
- Dominijanni A, Jones CJFP, Manassero M (2007). Sistemi di lavaggio/estrazione, in Manassero M. e Dominijanni A. (Eds.), *Atti delle Conferenze di Geotecnica di Torino, XXI Ciclo, Geosintetici e Ambiente*, Patron Editore, Bologna (CD-ROM).
- Dominijanni A, Manassero M, Vanni D (2006). Micro/macro modeling of electrolyte transport through semipermeable bentonite layers. *Proceedings of the 5th International Congress on Environmental Geotechnics*, Cardiff, Wales, UK, Thomas, H.R., Ed., Thomas Telford, London, Volume II: 1123-1130.
- Esrig MI (1968). Pore pressure, consolidation and electrokinetics. *Journal of the Soil Mechanics and Foundation Division*. (94): 899-921.
- Eykholt GR (1997). Development of pore pressures by nonuniform electroosmosis in clay. *J. of Hazard. Mater.* 55 (1-3): 171-186.
- Eykholt GR & Daniel DE (1994). Impact of system chemistry on electroosmosis in contaminated soils, *J. Geotech. Engrg.* 120 (5): 797-815.
- Gabrieli L, Jommi C, Musso G, Romero E (2008). Electrokinetic treatment of a natural silt in saturated and unsaturated conditions. *Geoproc 2008*.
- Garcia - Gutierrez MD, Gomez – Lahoz C, Rodriguez – Maroto JM, Vereda-Alonso C, Garcia-Herruzo F (2007). Electrokinetic remediation of a soil contaminated by the pyritic sludge spill of Aznacollar (SW, Spain). *Electrochimica Acta*, 52:3372-3379.
- Gens A (2007). Soil-environment interactions in geotechnical engineering: 47th Rankine Lecture. *Geotechnique* (in preparation).
- Golder Associates (2006). Report on Response to EPA Section 22(1) Notice to Supply Further Information Works Approval Application WA59144 Construction of New Lined Prescribed Waste Landfill Cells – Tullamarine Landfill, for Cleanaway Ltd Victoria, by Golder Associates Pty Ltd, Melbourne, Australia.
- Gray DH (1970). Electrochemical hardening of clay soils. *Geotechnique* 20 (1): 81-93.
- Hamed JT, Acar YB, Gale RJ (1991). Pb (II) removal from kaolinite using electrokinetics. *J. Geotech. Engrg.* 112: 241-271.
- Harper BM, Stiver WH, Zytner RG (1998). Influence of water content on SVE in a silt loam soil. *Journal of Environmental Engineering*, 124: 1047-1053.
- Holmes PJ (1962). *The Electrochemistry of Semiconductors*, Academic Press, London, U.K.
- Hueckel T (1992a). Water–mineral interaction in hygro-mechanics of clays exposed to environmental loads: a mixture approach. *Canadian Geotechnical Journal*, 29: 1071-1086.
- Hueckel T (1992b). On effective stress concepts and deformation in clays subjected to environmental loads. *Canadian Geotechnical Journal*, 29: 1120-1125.
- Hunter RJ & James M (1992) Charge reversal of kaolinite by hydrolysable metal ions: an electroacoustic study. *Clays and Clay Minerals*, 40 (6): 644-649.
- Itasca Consulting Group Inc (2002). PFC2D (Particle Flow Code in 2 Dimensions), Version 3.0. Minneapolis, ICG.
- Itasca Consulting Group Inc (2003). PFC3D (Particle Flow Code in 3 Dimensions), Version 3.0. Minneapolis, ICG.
- Kaczmarek M & Hueckel T (1998). Chemo-mechanical consolidation of clays: analytical solutions for a linearized one-dimensional problem. *Transport in Porous Media*, 32: 49-74.
- Katchalsky A & Curran PF (1965). *Nonequilibrium thermodynamics in biophysics*. Harvard University Press, Cambridge, MA.
- Kavazanjian E (2006). *Waste Mechanics: Recent Findings and Unanswered Questions*. Proceedings of Geo-Shanghai International conference hosted by Tongji University and the Shanghai Society of Civil Engineering, Shanghai, China: 82-103.
- Kim SO, Kim JJ, Yun ST, Kim KW (2003). Numerical and experimental studies on Cadmium (II) transport in kaolinite clay under electrical fields. *Water, Air, and Soil Pollut*, 150: 135-162.
- Leverett MC (1941). Capillary behavior in porous media. *Trans. AIME* 142, 341-358.
- Lorenz PB (1969). Surface conductance and electrokinetic properties of kaolinite beds. *Clays and Clays Minerals*, (17): 223-231
- Loret B, Hueckel T, Gajo A (2002). Chemo-mechanical coupling in saturated porous media: elastic–plastic behavior of homoionic expansive clays. *International Journal of Solids and Structures*, 39: 2773-2806.
- Malusis MA & Shackelford CD (2002a). Chemo-osmotic efficiency of a geosynthetic clay liner. *Journal of Geotechnical and Geoenvironmental Engineering*, 128(2): 97-106.
- Malusis MA & Shackelford CD (2002b). Coupling

- effects during steady-state solute diffusion through a semi-permeable clay membrane. *Environmental Science and Technology*, 36: 1312-1319.
- Manassero M (2003). Integrated systems for the remediation of polluted soils. Progetto di rilevante interesse nazionale (Project of relevant national interest). Ministero dell'Istruzione, dell'Università e della Ricerca.
- Manassero M & Dominijanni A (2003). Modelling the osmosis effect on solute migration through porous media. *Geotechnique*, 53(5): 481-492.
- Manassero M & Shackelford CD (1994). Classification of Industrial Wastes for Re-Use and Landfilling, I International Congress on Environmental Geotechnics, International Society of Soil Mechanics and Foundation Engineering Edmonton, Canada, Bi-Tech Publisher, Ltd, Vancouver, Canada.
- Manassero M, Musso G, Rabozzi C, Ribotta L (2005). Retention curves for a polluted soil. Proceedings of International Symposium, Advanced experimental unsaturated soil mechanics, 27-29 Giugno, Trento.
- Mascia M, Palmas S, Polcaro AM, Vacca A, Muntoni A (2007). Experimental study and mathematical model on remediation of Cd spiked kaolinite by electrokinetics. *Electrochimica Acta*, 52: 3360-3365.
- Mattson ED, Bowman RB, Lindgren ER (2002) Electrokinetic ion transport through unsaturated soils: 1. Theory, model development and testing. *Journal of Contaminant Hydrology* 54, (1-2): 99-120.
- Mitchell JK & Soga K (2005). Fundamentals of soil behavior. John Wiley and Sons, New York.
- Narasimhan B & Sri Ranjan R (2000). Electrokinetic barrier to prevent subsurface contaminant migration: theoretical model development and validation. *Journal of Contaminant Hydrology*, (42): 1-17.
- Ottosen LM, Hansen HK, Ribeiro AB, Villumsen A (2001). Removal of Cu, Pb and Zn in an applied electric field in calcareous and non-calcareous soils. *Journal of Hazardous Materials*, B85: 291-299.
- Polcaro AM, Vacca A, Mascia M, Palmas S (2007). Electrokinetic removal of 2,6-dichlorophenol and diuron from kaolinite and humic acid-clay system. *Journal of Hazardous Materials*, 148: 505-512.
- Quian X, Koerner, MR, Gray DH (2002). Geotechnical aspects of landfill design and construction, Prentice Hall, Upper Saddle River, New Jersey, USA.
- Reddy KR, Parupudi US, Devulapalli SN, Xu C (1997). Effects of soil composition on the removal of chromium by electrokinetics. *J. of Hazard. Mater.* 55 (1-3): 135-158.
- Shackelford CD (2007). Selected issues affecting the use and performance of GCLs in waste containment applications. In: Manassero, M., and Dominijanni, A., (Eds). *Geosynthetics and Environment*, Proceedings of the Geotechnical Engineering Conference of Torino (XXI Edition), Pàtron Editore, Bologna (CD version only).
- Shackelford CD & Daniel DE (1991). Diffusion in saturated soil: I. Background. *J. Geotech. Engrg.*, 117: 467-484.
- Shapiro AP & Probst RF (1993). Removal of contaminants from saturated clay by electroosmosis. *Environ. Sci. Technol.*, 27(2):283-291.
- Spiegler KS & Kedem O (1966). Thermodynamics of hyperfiltration (reverse osmosis): criteria for efficient membranes. *Desalination*, 1: 311-326.
- Sposito G (1984). *The surface chemistry of soils*, Oxford University Press, New York.
- Stewart DI & West LJ (1996). Discussion on the paper 'Impact of system chemistry on electroosmosis in contaminated soils' by Eykholt and Daniels. *J. Geotech. Engrg.* 122 (3): 250-251.
- Tamagnini C, Jommi C, Cattaneo F (2010). A model for coupled electro-hydro-mechanical processes in fine grained soils accounting for gas generation and transport. Accepted for publication in the *Anais da Academia Brasileira de Ciências*.
- Terzaghi K (1943). *Theoretical soil mechanics*, John Wiley and Sons, New York.
- Thomas TJ & Lentz RW (1990). Changes in Soil Plasticity and Swell Caused by Electro-Osmosis. In: K. B. Hoddinott and R. O. Lamb, Editors. *Physico-Chemical Aspects of Soil and Related Materials*, ASTM STP 1095, American Society for Testing and Materials: 108-117.
- Tiraferrri A & Sethi R (2008) Enhanced transport of zerovalent iron nanoparticles in saturated porous media by Guar Gum. *Journal Of Nanoparticle Research*, 324 (1-2): 71-79.
- Van der Ham AGJ & Brouwers HJH (1998). Modelling and experimental investigation of transient, nonequilibrium mass transfer during steam stripping of a nonaqueous phase liquid in unsaturated porous media. *Water Resources Research*, 34(1): 47-54.
- Van Genuchten MTh (1980). A closed form equation for predicting the hydraulic conductivity of unsaturated soil. *Soil Science Society of America Journal*, 44: 892-898.
- Van Impe PO (2002). Consolidation, contaminant transport and chemico-osmotic effects in liner materials. A theoretical and experimental study. PhD Thesis, Università Politecnica delle Marche, Ancona.
- Viswanadham BVS & Jessberger HL (2005). Centrifuge Modelling of Geosynthetic Reinforced Clay Liners of Landfill. *Journal of Geotechnical and Geoenvironmental Engineering*, 131(5):564-574.
- Wieczorek S, Weigand H, Schmid M, Marb C (2005). Electrokinetic remediation of an electroplating site: design and scale-up for an in-situ application in the unsaturated zone. *Engineering Geology*, 77 (3-4):

203-215.

- Yaroshchuk AE (1995). Osmosis and reverse osmosis in fine-charged diaphragms and membranes. *Advances in Colloid and Interface Science*, 60: 1-93.
- Yeung AT, Hsu C, Menon R (1997). Physicochemical soil – contaminant interactions during electrokinetic extraction. *J. of Hazard. Mater.*, 55 (1-3): 221-237.
- Yeung AT (1990). Coupled flow equations for water, electricity and ionic contaminants through clayey soils under hydraulic, electrical and chemical gradients. *Journal of Non Equilibrium Thermodynamics* 15 (3): 247-267.
- Yong RN, Mohamed AMO, Warkentin BP (1992). *Principles of contaminant transport in soils*. Elsevier, Amsterdam.
- Yoon H, Kim JH, Liljestrand HM, Khim J (2002). Effect of water content on transient nonequilibrium NAPL-gas mass transfer during soil vapor extraction. *Journal of Contaminant Hydrology*, 54: 1-18.
- Yoon H, Valocchi AJ, Werth CJ (2003). Modeling the influence of water content on soil vapor extraction. *Vadose Zone Journal*, 2: 368-381.

MODELING DOMINANT TRANSPORT PROCESSES IN ONE-DIMENSIONAL CONTAMINANT TRANSPORT

E.C. Nirmala PETER¹, M. R. MADHAV², E. Saibaba REDDY³ and T. V. BHARAT⁴

ABSTRACT: The present work investigates the impact of scale on dispersion coefficient for the transport of a non-reactive contaminant through a homogeneous medium. A scale-dependent dispersion coefficient which varies as a power law function of distance ($D_x = D_d + mx^n$, D_x – Dispersion coefficient, D_d – Diffusion coefficient, x – distance, and m and n are the multiplying and exponent factors which depend on the type of porous medium) was assumed. A numerical model with scale-dependent dispersion coefficient was developed and numerical experimentation carried out by varying the identified key parameters within the practical ranges. The effects of these parameters on the resulting break-through curves that describe the spread of the contaminant through the soil in one-dimensional flow and dispersion were studied. The key parameters, α_D , are the ratio of rate of diffusion per unit length of the porous medium to the measured seepage velocity ($\alpha_D = D_d/xV_x$), where V_x - measured seepage velocity) and parameter, β ($= mx^{(n-1)}/V_x$), dependent on the characteristics of the porous medium. Break-through curves indicate the dominant processes of transport such as diffusion, hydrodynamic dispersion and advection.

KEYWORDS: scale-dependency, dispersion coefficient, break-through curves, key parameters

INTRODUCTION

The classical Convection-Dispersion Equation (CDE) that assumes constant dispersion coefficient is generally used to describe contaminant transport through porous medium. Several field studies (Taylor and Howard, 1987, Domenico and Robbins, 1984, Toride et al. 1995) indicate scale-dependent dispersion, i.e., dispersion coefficient increases with distance 'x' from the source of pollution (Fig.1). Several solutions (Khan and Jury, 1990, Pachepsky et al. 2000, Pang and Hunt, 2001) have been developed incorporating the variation of dispersion coefficient with distance. Yates' (1990) analytical model was based on the assumption that dispersivity increases linearly with distance. Huang et al. (1995) developed a general solution with scale-dependent dispersion assuming that dispersivity, α , increases linearly with distance, beyond which an asymptotic value, α_L , is attained. Fractional Advection Dispersion Equation (FADE) developed by Zhou and Selim (2003) worked better than CDE to simulate scale effects. This paper presents a scale-dependent dispersion coefficient which

varies as a power law function of distance ($D_x = D_d + mx^n$, D_x – dispersion coefficient, D_d – diffusion coefficient, x – distance, and m and n are the multiplying and exponent factors which depend on the type of porous medium). A numerical model with scale-dependent dispersion coefficient was developed. Numerical

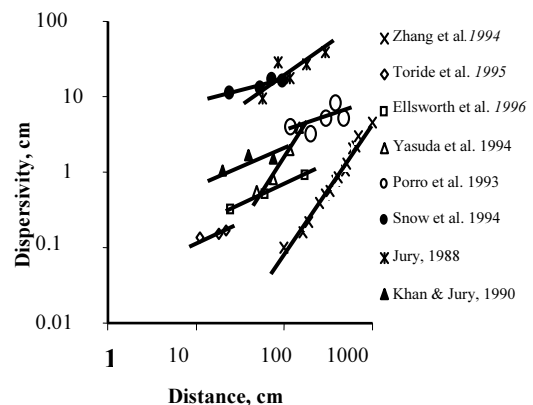


Fig. 1 Dependency of solute dispersivity on distance in soils

¹ Associated Professor, Department of Civil Engineering, Jawaharlal Nehru Technological University, Hyderabad, India. Email: ecnps@yahoo.co.uk

² Professor Emeritus, Department of Civil Engineering, Jawaharlal Nehru Technological University, Hyderabad, India. Email: madhavmr@gmail.com

³ Professor, Department of Civil Engineering, Jawaharlal Nehru Technological University, Hyderabad, India. Email: sbreddy@yahoo.com

⁴ Doctoral Student, Department of Civil Engineering, Indian Institute of Science, Bangalore, India. Email: tvbharat@gmail.com

experimentation of the model was carried out by varying the key parameters within the practical ranges. The study yielded a series of curves from which the dominant processes of contaminant transport can be identified.

PROBLEM DEFINITION AND MODEL

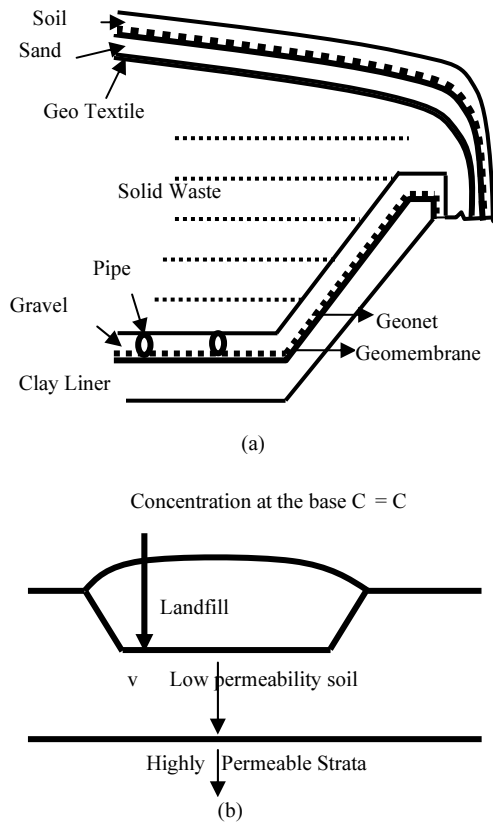


Fig. 2 (a) Schematic of landfill and (b) Problem description

Fig. 2(a) shows different components of the landfill. A simple schematic, Fig. 2 (b), shows a landfill resting on a low permeable soil layer of finite depth, overlying highly permeable strata. The concentration of the contaminant, C , at the base of the landfill is C_0 at any time greater than zero. The governing equation for one-dimensional convective-advective transport for non-reactive contaminant with scale-dependent dispersion coefficient is

$$D \frac{\partial C}{\partial x} - \left(\frac{\partial D}{\partial x} - V \right) \frac{\partial C}{\partial x} = \frac{\partial C}{\partial t} \tag{1}$$

where D_x is the dispersion coefficient, V_x - the measured seepage velocity, C - the concentration of the contaminant, t - time and x - the distance of travel of the contaminant. The dispersion coefficient, D_x is given by $D = \alpha v + D_d$ where α is the dispersivity, v - seepage velocity and D_d is the diffusion coefficient. Considering

a power law variation of dispersion coefficient, $D_x = D_d + mx^n$ the governing equation is

$$(D_d + mx^n) \frac{\partial^2 C}{\partial x^2} - (mnx^{n-1} - V_x) \frac{\partial C}{\partial x} = \frac{\partial C}{\partial t} \tag{2}$$

On normalizing Eq. 2 with $X = x/L$, $T = t/t_0$ and $t_0 = L/V_x$, and on substituting $D/LV = \alpha$ and $m.L^{-n}/V = \beta$, Eq. 2 transforms to

$$(\alpha_d + \beta X^n) \frac{\partial C}{\partial X} - (nX^{n-1} \beta - 1) \frac{\partial C}{\partial X} = \frac{\partial C}{\partial T} \tag{3}$$

Initial and boundary conditions are: $C(x, 0) = 0$ at $t = 0$; $C(0, t) = C_0$ for $t > 0$; $C(L_1, t) = C(L, t)$ for $L_1 > L$ where L is the total depth or thickness of the stratum.

FINITE DIFFERENCE METHOD OF SOLUTION

The total length of the column is divided into 'n' number of segments (Fig. 3). The governing equation in finite difference form transforms to

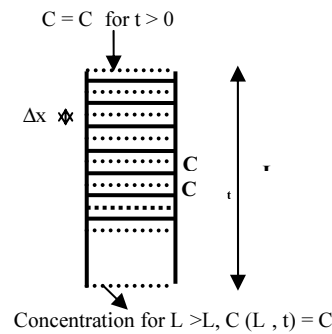


Fig. 3 Elements for finite difference analysis

$$(\alpha + \beta X^n) \left(\frac{C_+ - 2C + C_-}{(\Delta X)^2} \right) - (nX^{n-1} \beta - 1) \left(\frac{C_+ - C_-}{2\Delta X} \right) = \left(\frac{C_+ - C_-}{\Delta T} \right) \tag{4}$$

The above equation reduces to

$$C_{i+\Delta} = (\mu + \beta) C_{i-} + (1 - 2\mu) C_i + (\mu - \beta) C_{i+} \tag{5}$$

with $\mu = (\alpha_d + \beta X^n) \Delta T / (\Delta x)$ and $\beta = (nX^{n-1} \beta - 1) \Delta T / 2\Delta x$

CHECK FOR STABILITY AND CONVERGENCE

The input parameters (Table 1) resulted in the Break-Through curves (BTC) shown in Fig. 4 for $\alpha D = 1 \times 10^{-5}$,

Table 1 Input Parameters for Stability of the Model for Different Values of ΔX and ΔT

Input Parameters	1	2	3	4	5	6	7
α_D	1×10^{-5}	1×10^{-5}	1×10^{-5}	1×10^{-5}	1×10^{-5}	1×10^{-5}	1×10^{-5}
β	0.1	0.1	0.1	0.1	0.1	0.1	0.1
n	1.5	1.5	1.5	1.5	1.5	1.5	1.5
ΔX	0.02	0.02	0.02	0.02	0.02	0.01	0.01
ΔT	1×10^{-3}	1.5×10^{-3}	7.5×10^{-4}	9×10^{-4}	2×10^{-3}	4.5×10^{-4}	5×10^{-4}
μ_x	0.250	0.3750	0.18751	0.22502	0.5	0.45004	0.50005
β_x	-0.021	-0.0319	-0.01594	-0.01913	-0.0425	-0.01913	-0.02125
$\mu_x + \beta_x$	0.229	0.3432	0.17158	0.20589	0.458	0.43092	0.4788
$1 - 2\mu_x$	0.499	0.2499	0.624963	0.54995	-1×10^{-4}	0.09991	-1×10^{-4}
$\mu_x - \beta_x$	0.271	0.4069	0.20345	0.24414	0.543	0.46917	0.5213

$\beta = 0.1, n = 1.5, X = 0.02$, and ΔT equal to $1.5 \times 10^{-3}, 1 \times 10^{-3}, 9 \times 10^{-4}$ and 7.5×10^{-4} . The curves for all these values of ΔT converged to the same BTC. The values of $(\mu_x + \beta_x), (1 - 2\mu_x)$ and $(\mu_x - \beta_x)$ are positive for the above values of ΔT . Break-through curve couldn't be obtained for ΔT equal to 2×10^{-3} as $(1 - 2\mu_x)$ is negative even if the other two values are positive. The time step, $\Delta T \leq 1 \times 10^{-3}$ for $\Delta X = 0.02$ for convergence. The limiting value of ΔT varies with ΔX , e.g. for $\alpha_D = 1 \times 10^{-5}, \beta = 0.1, n = 1.5, \Delta X = 0.01, \Delta T$ was 5×10^{-4} .

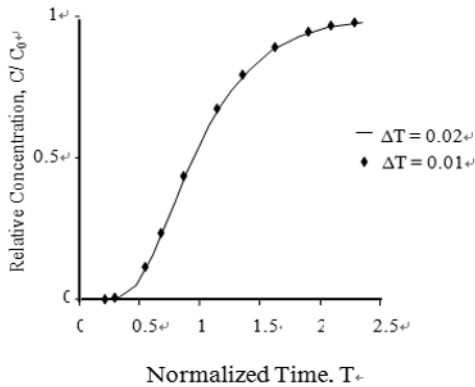


Fig. 4 Break-through curves for different values of ΔT

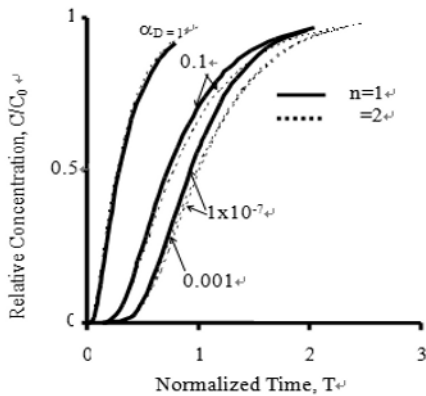


Fig. 5 Normalized time vs. relative concentration for $\beta = 0.1$

PARAMETRIC STUDY

The parameters α_D, n and β from Eq. (3) are identified as the key parameters that have the most influence on model calibration and predictions. The parameter $\alpha_D = D_d / LV_x$ for constant D_d , decreases with increases in the length /distance of travel (L) and/or with increase in the seepage velocity. In the present study three ranges of measured seepage velocities are $V_x > 10^{-3}$ cm/s, $10^{-3} > V_x > 10^{-6}$ cm/s and $V_x < 10^{-6}$ cm/s. Parameters n and $\beta = mL^{n-1} / V_x$ are dependent on the intrinsic properties of the porous medium and the length of travel of the contaminant. The effect of scale is more predominant on β and the impact is directly seen on the shape of the break-through curves.

The following values of D_d, L and V_x were assumed to obtain the maximum and minimum values of the parameters: 1. $D_d = 1.5 \times 10^{-6}$ cm²/s (Shackelford and Rowe, 1998); 2. L ranges from 1 cm to 200 cm; 3. The range seepage velocity, V_x , ranges between 1×10^{-2} and 1×10^{-9} cm/s. The minimum and maximum values of α_D considered are 1×10^{-7} and 1 respectively. The parametric study for the model was carried out considering a range of 'n' between 1 and 5, and β from 0.0001 to 1. The break-through curves are presented in Figs. 5 through 12.

EFFECT OF α_D, n AND β ON BREAK THROUGH CURVES

The effect of α_D on break-through curves was studied by varying parameter values from 1×10^{-7} to 1. Break-through curves with non-dimensional parameters of concentration (C/C_0) and normalized time ($T = t/t_0$ where t is any given time and t_0 is the time value corresponding to a relative concentration of 0.5) were drawn up to a relative concentration of 0.966. Fig. 5 shows the BTCs for different values of α_D , and for $\beta = 0.1$ and $n = 1, 2$. These curves indicate that the normalized time, T

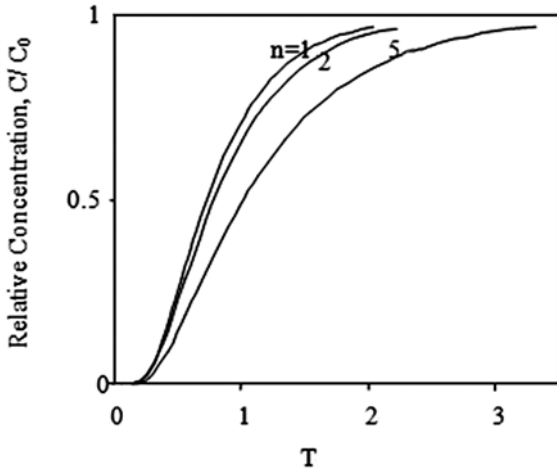


Fig. 6 Normalized time vs. relative concentration for $\alpha_D = 0.1$ and $\beta = 0.1$

required for a relative concentration, C/C_0 of 0.97, decreased with increase in the α_D value. The normalized time over which the relative concentration remains at zero increased with decrease in α_D value. The normalized time for obtaining a C/C_0 of 0.97, increases with increase in n value, for values of $\alpha_D < 1$, and for $\alpha_D = 1$, BTCs for $n = 1$ and 2 converged resulting in a single curve. Fig. 6 also illustrates the effect of n on break-through curves. If the rate of diffusion per unit length of the column is taken in to consideration, a seepage velocity of 1×10^{-6} cm/s or less yields a α_D value greater than or equal to 1. Therefore for soils with seepage velocity $\leq 1 \times 10^{-6}$ cm/s, the variation of the exponent 'n' on BTCs is ineffective (Fig. 7)

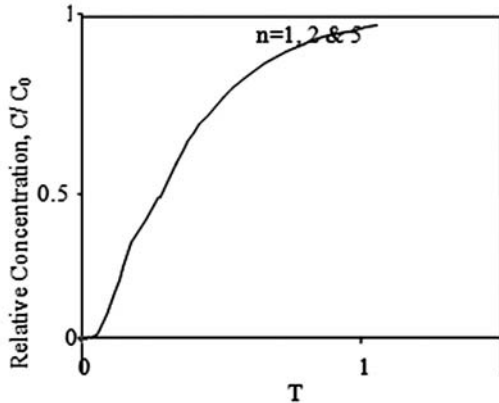


Fig. 7 Normalized time vs. relative Concentration for $\alpha_D = 1$ and $\beta = 0.1$

The normalized time with zero relative concentration also increases as β value decreases (Fig. 8). Especially for $\beta = 0.01$ and $\alpha_D \leq 0.001$, the relative concentration remains at zero almost up to a normalized time of 0.65 and then C/C_0 increases rapidly to a value of 0.96 at about a T value of 1.1. This may be due to the fact that the solute particles in soils may not follow Brownian motion but undergo Levy motion. Thus the Levy motion explains the stagnant zero relative concentration up to T

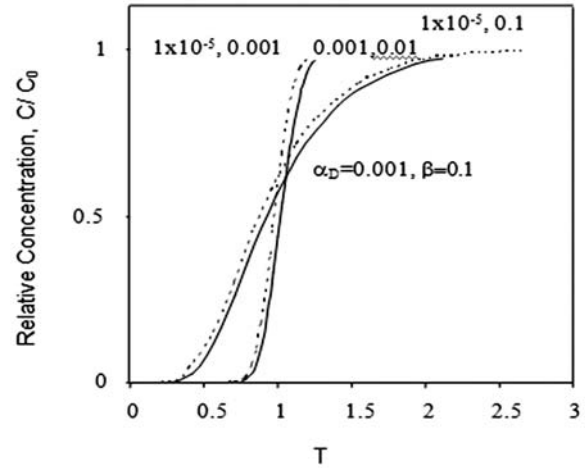


Fig. 8 Normalized time vs. relative concentration for $n = 1$

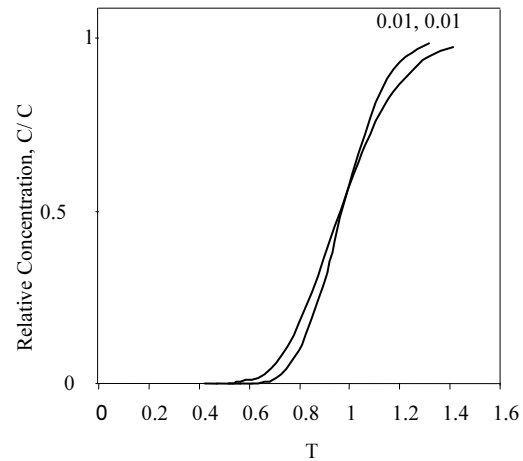


Fig. 9 Normalized time vs. relative concentration for $n = 1$

of 0.65, and the rapid increase in the relative concentration to reach a value of 0.96 at about a T value of 1.1. A α_D value of less than or equal to 0.001 can be obtained for measured seepage velocities greater than 1×10^{-2} cm/s. From Figs. 8 and 9 it is also observed that for the same values of α_D the shape of the curve changes resulting in increased normalized time values when β increases, and for a value of α_D greater than ten times the β value, the BTCs result in a single curve (Figs. 9 & 10). The ratio of α_D to β (D_d/mL^n) increases with decrease in the length of travel in a given porous medium. Therefore the effect β on BTC is more predominant for soils with larger lengths of travel resulting in ratios of α_D to β less than 10. Fig. 11 also illustrates the effect of β on the break-through curves.

DISCUSSION AND CONCLUSIONS

No break-through curve could be obtained for $\alpha_D \leq 0.001$ and $\beta \leq 0.001$ due to complete advective transport

process of the contaminant through the porous medium with seepage velocity greater than 1×10^{-2} cm/s. The BTCs for $\beta \leq 0.01$ and $\alpha_D \leq 0.001$ show Levy motion of the solute particles through the porous medium (Curves A, B and C Fig.12). Therefore the transport process may be advective-dispersive in nature with dispersion as the more dominant process than diffusion. Figs. 10 and 11 show that for $\alpha_D < 1$ and $\beta > 0.01$, $\alpha_D > 0.001$ and $\beta \leq 0.01$, elongated S – shaped curves are obtained for which the normalized time with zero relative concentration is greater than 0.1 but less than 0.5, with normalized time greater than 1.5 for a relative concentration of 0.96 (Curve D, Fig. 12). For $0.001 < \alpha_D < 1$, the measured seepage velocity is less than or equal to 1×10^{-2} , and more than or equal to 1×10^{-6} cm/s.

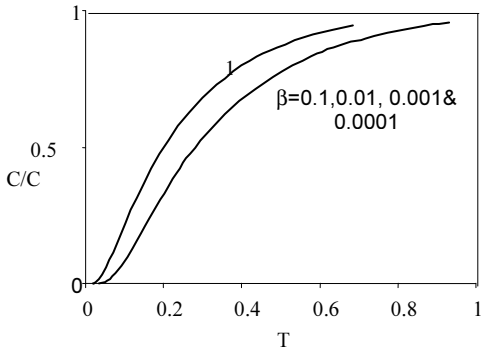


Fig. 10 Normalized time vs. relative concentration with $\alpha_D = 1$ and $n = 1.5$

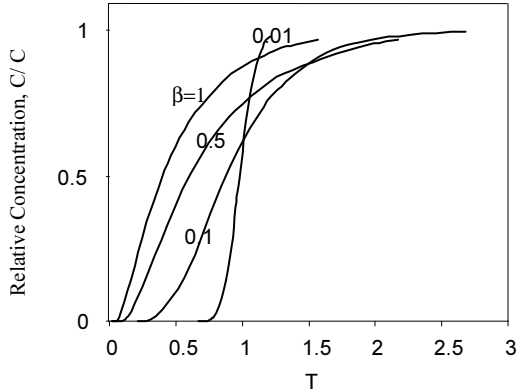


Fig. 11 Normalized time vs. relative concentration for $\alpha_D = 1 \times 10^{-5}$ and $n = 1$

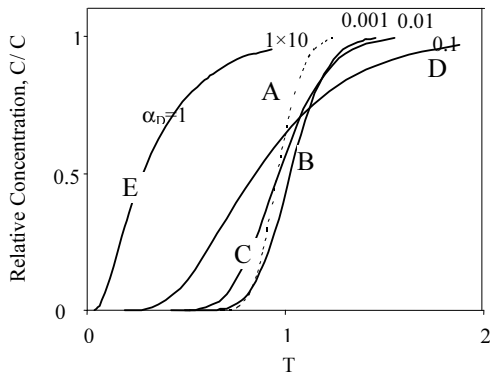


Fig. 12 Normalized time vs. relative concentration for $\beta = 0.01$ and $n = 1$

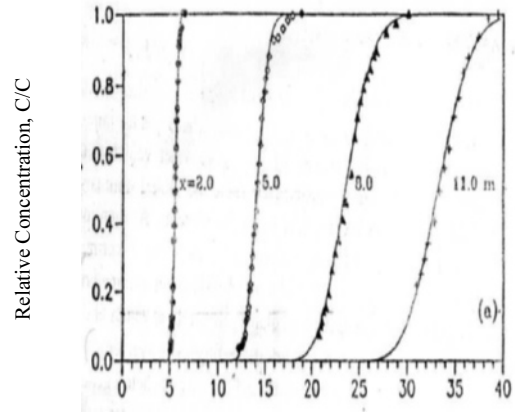


Fig. 13 Observed concentration distribution at several locations in homogeneous column (Huang et al. 1995)

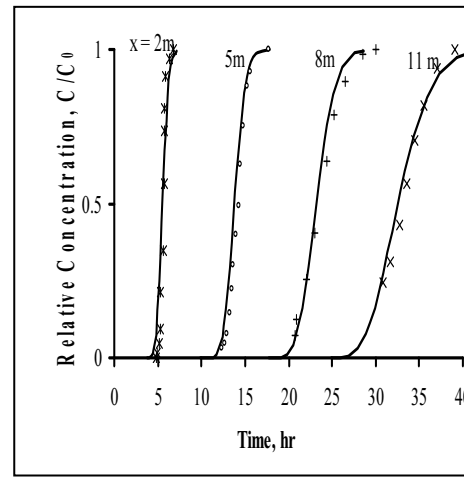


Fig. 14 Comparison of numerical solutions (using power law variation of dispersion coefficient with Length) with experimental data (Huang et al. 1995)

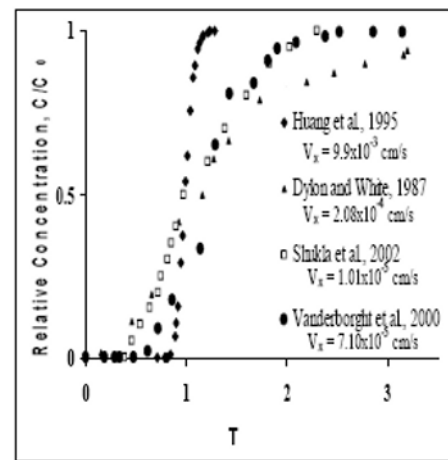


Fig. 15 Normalized Time vs. Relative Concentrations from Huang *et al.*, 1995, Dyson and White, 1987, Vanderborgh *et al.*, 2000 and Shukla *et al.*, 2002.

The curve indicates smooth movement of the contaminant through the porous medium. Therefore the probable transport processes may be dispersion-diffusion for soils with seepage velocity, $1 \times 10^{-2} \leq V_x \leq 1 \times 10^{-6}$ cm/s for long to short lengths of travel. Fig. 12 illustrates all the BTCs converging to a single curve for $\alpha_D \geq 1$ and $\beta < 1$. Similarly for $\alpha_D = 1$ and $\beta = 0.01$ also shows a BTC (Curve E, Fig. 12) with still less normalized time indicating that the probable process of transport may be purely diffusion for seepage velocity less than 1×10^{-6} cm/s, which agrees with Shackelford and Rowe (1998). Curves A, B, C, D and E show the transition of the transport processes from dominant advection-dispersion-through dispersion- diffusion to complete diffusion.

BTCs from laboratory tracer (NaCl) experiments conducted to investigate solute transport through 12.5 m long, horizontally placed homogeneous sand column are also in agreement with the curve A. The relative concentrations of the contaminant for various time periods at each of the locations (2 m, 5 m, 8 m and 11 m) were obtained to draw break-through curves as shown in Fig. 13 (Huang et al. 1995). Verification of the solution for power law variation of dispersion coefficient was carried out by developing break-through curves at different locations, i.e. at 2 m, 5 m, 8 m and 11 m, of the column. The model was calibrated (Fig. 14) to obtain solutions with values of 'm' equal to 5.01×10^{-6} , 2.9×10^{-6} , 2.15×10^{-6} and 2×10^{-6} , and an 'n' value of 1.5635 for 2 m, 5 m, 8 m, and 11 m lengths of the column respectively, which fitted well with the experimental data ($\alpha_D < 0.001$, $\beta < 0.01$ and $V_x < 1 \times 10^{-2}$). Fig. 15 shows the break-through curve obtained by Dyson and White, 1987 for a soil with a measured seepage velocity of 2.08×10^{-4} cm/s ($L = 16.4$ cm and $t_0 = 21.892$ h) for a near saturated structured clay soil in which steady state near saturated flow was created. This is similar to that of curve D of Fig. 12. Shukla et al. 2002 conducted tests on a short saturated soil column ($L = 10$ cm) of sandy loam using $MgCl_2$ solution. The break-through curve obtained was shown in Fig. 12. The break-through curve obtained by Vanderborght et al. 2000 for saturated loam soil column ($L = 95$ cm) from steady-state flow conditions with $CaCl_2$ as contaminant solution was also presented in Fig. 12. All these curves are in accordance with the observations presented above. Hence the dominant transport process can be easily identified from the shape of the break-through curve.

DIFFUSION STUDIES

The transient transport equation for diffusion of solute through a saturated porous medium is

$$nD \frac{\partial^2 c}{\partial x^2} = \alpha \frac{\partial c}{\partial t} \quad (6)$$

where α is a dimensionless parameter called the capacity factor which is porosity times the retardation factor. For a species with linear sorption behavior, α may be defined as

$$\alpha = n + \rho K \quad (7)$$

where ρ is the bulk density of solid; and K_d is the distribution coefficient. The initial and boundary conditions in the laboratory diffusion tests are: $c(x=0,0) = c$; $c(x,t=0) = 0$ and $c(x=L,t=0) = 0$.

INVERSE ANALYSIS

The estimation of mass transport parameters in geoenvironmental engineering is commonly performed using packages like Pollute. This "eye-fit" estimation is subjective and relies heavily on the insights of the modeler to evaluate the complex relationships between variations in model parameters and their effects on the model outputs. Consequently, this technique neither guarantees optimal parameters nor there exists a statistical framework for parametric uncertainty analysis. The classical techniques such as gradient-based search algorithms use the gradient information in the search space (parametric space) to converge to local optimum solutions. However, gradient-based optimizers can suffer from several important limitations. They are local rather than global by nature and so can be sensitive to the initial guess. Experimental or numerical noise can exacerbate this problem by introducing multiple local minima into the problem. Nevertheless nature inspired algorithms are gradient-free techniques which use heuristics to search for solutions.

An Optimization Approach

All the optimization techniques work based on minimizing or maximizing objective function which determines fitness or quality of the current solution. The objective function is formulated by solving the forward problem at a random location on the search space (i.e., a set of design parameters) and computing the error between the theoretical and the experimental ones.

Gradient based techniques

Gradient-based techniques are quick for analytically determined objective functions where the first and

second order derivatives can directly be transferred into a computer program. However, gradient-based optimizers can suffer from several important limitations. They are local rather than global by nature and so can be sensitive to the initial guess. Experimental or numerical noise can exacerbate this problem by introducing multiple local minima into the problem. In case of contaminant transport problems such as discussed in this work do not have explicit analytical solutions and since necessary gradients cannot be obtained analytically, gradients need to be computed numerically. The finite difference gradient calculations can be sensitive to the selected finite difference step size. Further, the use of design variables with different length scales or units can produce poorly scaled problems that converge slowly or not at all, necessitating design variable scaling to improve performance.

Nature-inspired Computation

Nature-inspired computation is the field of research that works with computational techniques inspired in part or fully by nature and natural systems. This makes use of nature as inspiration for the development of problem solving techniques. The main idea of this branch is to develop computational tools (algorithms) by taking inspiration from nature for the solution of complex problems. Simulated Annealing (SA), Genetic algorithms (GA) and Particle swarm optimization (PSO) are some of such nature-inspired algorithms used to find solution to an optimization problem in a given search space. To examine the performance of these algorithms a synthetic data is generated. The contaminant concentration data is obtained by solving the forward problem using the mass transport parameters $D=1.523 \times 10^{-6} \text{ cm}^2/\text{sec}$ and $\alpha = 34$. This data is used as an input for the nature-inspired algorithms to find the true design parameters which are assumed to estimate the contaminant concentration.

Simulated annealing (SA)

SA is a generic probabilistic and heuristic approach to solving global optimization problems. It uses a stochastic process based on probability, rather than a deterministic procedure, to seek the minima or maxima in the solution space. SA with threshold acceptance algorithm is applied to solve the chloroform diffusion data from the literature (Barone et al. 1992). Initial guess values are chosen at different locations on the search space similar to the gradient-based approaches and the above steps were followed. Simulated Annealing algorithm is implemented in Matlab 7.0 by integrating the forward model with simulated annealing and threshold acceptance call function. The SA algorithm needs an initial guess similar to gradient-based search

process and the process of searching is random. Thus, SA is run for five times independently for 200 iterations with different initial guess values. However, it is observed from the result that the algorithm fails to find exact global solution and only in few occasions the algorithm finds a good solution close to the global solution.

Genetic algorithms

Genetic algorithms (GA) are global optimization techniques that avoid many of the shortcomings exhibited by local search techniques on difficult search spaces. Genetic algorithms are heuristic global optimization methods that are based on the process of natural selection (Holland 1975; Mitchell, 1996). Starting from a randomly generated population of parameters, the optimizer seeks to produce improved parameters from one generation to the next. This is accomplished by using operators like selection, crossover and mutation. GA requires a genetic representation of the solution domain and a fitness function to evaluate the solution domain. The initial population is generated with 30 chromosomes covering the entire range of possible solutions (parametric space). In this work 0.95 crossover probability with two-point crossover and 0.03 mutation probability is used.

Particle swarm optimization (PSO)

PSO, similar to GA, is a class of derivative-free and population-based computational method. The foundation of PSO is based on the social behaviors of animals such as flocking of birds and fish schooling (Eberhart and Kennedy, 1995). The population size is set to 30 in both the algorithms. The maximum number of generations is set to 100 in each run. Acceleration coefficients of 0.5 each and constriction coefficient of 0.6 are used in the work. Recently a large number of theoretical studies have shown that particles get trapped into local optima when classical PSO algorithm (CPSO) is used (Bharat et al. 2008). To overcome the shortcomings of CPSO, a modified algorithm is used which introduces perturbation equation, for the global best particle found using standard PSO algorithm in each iteration. All the three, GA, CPSO and modified PSO are programmed in Fortran 90 on Alfa machine.

RESULTS AND DISCUSSION

The algorithms are tested on synthetically generated data with and without random noise. The performance of these algorithms on synthetic data for 10 independent runs with and without random noise is shown in Table 2. The results, shown in Table 2 for synthetically generated data, give best and worst values, success rate with tolerance.

When compared with SGA, the CPSO algorithm has better convergence rate and it converges to the exact global solution. However, the CPSO algorithm too suffers from immature convergence when the noise is introduced. When the perturbation is introduced for *gbest* particle PPSO algorithm, the particles escape from the local solutions and converge at global solution. It can be shown from Table 2 that in all the runs the algorithms converge to global solution which makes the success ratio 1. Finally, SGA, CPSO and PPSO algorithms are applied on Chloroform diffusion data to estimate the

transport parameters. All the three algorithms converge to the global solution. The theoretical profile representing the temporal variation of solute concentration in the source and collector reservoir obtained for the model parameters estimated by these methods are plotted against the Pollute based estimation from the literature (Barone et al. 1992) along with the experimental data is plotted in Fig. 16. This it shown from the results that modified PSO gives the reliable solution for inverse problem of parameter estimation in diffusion experiments.

Table 2 Performance of SGA, CPSO and PPSO algorithms on synthetic data

Algorithm	Data type	Tolerance	Success- rate	Best solution	Worst solution
SGA	Synthetic (without noise)	10%	0.60	1.4377E-05, 36.76 (rmse = 0.0038)	1.12E-05 42.84 (rmse = 0.01255)
	Synthetic (5% noise)	15%	0.30	1.33E-05, 37.2999 (rmse = 0.0145)	1.223E-06, 141.1999 (rmse = 0.0293)
CPSO	Synthetic (without noise)	10%	0.80	1.525E-05 34.0 (rmse = 0.0231)	1.2293E-05 42.8923 (rmse = 0.00891)
	Synthetic (5% noise)	15%	0.50	1.363E-05 37.39679 (rmse = 0.0143)	8.38E-06, 63.0482 (rmse = 0.01253)
mPSO	Synthetic (without noise)	10%	1.0	1.528E-05 34.0 (rmse = 1.28E-08)	1.526E-05 34.1036 (rmse = 1.38E-04)
	Synthetic (5% noise)	15%	1.0	1.4919E-05 34.0231 (rmse = 0.01366)	1.4918E-05 34.02304 (rmse = 0.01366)

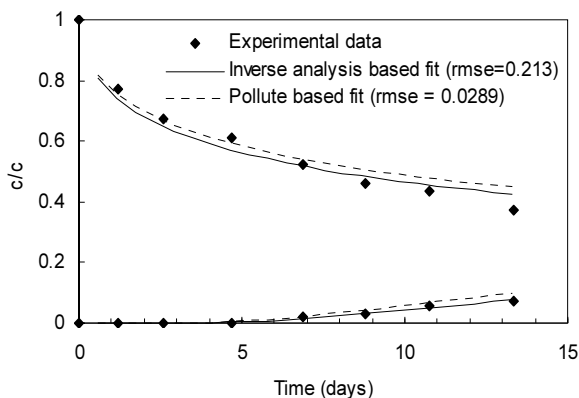


Fig. 16 Comparison between eye-fit calibration and the proposed solvers for chloroform diffusion data.

REFERENCES

Barone FS, Rowe RK, Quigley RMA. laboratory estimation of diffusion and adsorption coefficients

for several volatile organics in a natural clayey soil. *Journal of Contaminant Hydrology* 1992; 10: 225-250.

Bharat TV, Sivapullaiah PV, Allam MM, Accurate parameter estimation of contaminant transport inverse problem using particle swarm optimization, in: *Proceedings of IEEE Swarm Intelligence Symposium*, 1-7, 2008.

Domenico PA & Robbins GA (1984). A dispersion scale effect in model calibrations and field tracer experiments. *J. Hydrology*, 70:123-132.

Eberhart RC & Kennedy J (1995). A new optimizer using particle swarm theory, in: *Proceedings of the sixth International Symposium on Micro Machine and Human Science*, Nagoya, Japan, 1995: 39-43.

Holland JH (1975). *Adaptation in Natural and Artificial Systems*. University of Michigan Press: Ann Arbor, MI.

Huang K, Toride N, van Genuchten M, Th (1995). Experimental investigation of solute transport in large, homogeneous and heterogeneous, saturated

- soil columns. *Transport in Porous Media*. 18: 283-302.
- Khan AUH & Jury WA (1990). A laboratory study of the dispersion scale effect in column outflow experiments, *J. Contaminant Hydrology*, 5: 119-131.
- Mitchell M (1996). *An Introduction to Genetic Algorithms*, MIT Press.
- Pachepsky Y, David Benson, Walter Rawls (2000). Simulating scale-dependent solute transport in soils with the Fractional advective-dispersive equation. *Soil Sci. Soc. Am. J.*, 64: 1234-1243.
- Pang L & Hunt B (2001). Solutions and verification of a scale-dependent dispersion model. *Journal of Contaminant Hydrology*, 53(1-2): 21-39.
- Shukla MK, Kastanek FJ, Nielsen DR (2002). Inspectional analysis of convective-dispersion equation and application on measured break-through curves. *Soil Science Society of America Journal*, 66:1087-1094.
- Taylor SR & Howard KWF (1987). A field study of scale-dependent dispersion in a sandy aquifer. *Journal of Hydrology*, 90: 11-17.
- Toride N, Leij F, van Genuchten M, Th (1995). The CXTFIT code for estimating transport parameters from laboratory or field tracer experiments. Version 2, Research Report 137, US Salinity Lab., Riverside, CA.
- Yong RN & Warith MA (1989). Contaminant migration effect on dispersion coefficient. *ASTM, STP 1095*: 69-80.

THE VECTOR SUM METHOD: A NEW APPROACH TO CALCULATING THE SAFETY FACTOR OF STABILITY AGAINST SLIDING FOR SLOPE ENGINEERING AND DAM FOUNDATION PROBLEMS

Xiu-Run GE¹

ABSTRACT: A new approach, named the Vector Sum Method (VSM), is proposed in this paper, which can be used to study the safety factor of stability for slope and dam foundation problems. It is well known that the strength reduction method is generally applied in this field. Some disadvantages of slope and dam foundation stability analysis methods based on strength reduction principle are discussed. Several typical examinations calculated by the vector sum method are given. The comparison between results shows that the VSM is scientific and reasonable. For 2-D problems, it doesn't need trial calculations because the factor of safety can be represented as an explicit formula. The VSM can be applied easily for 3-D problems after the stress fields are acquired by finite element method or other methods. The VSM could be widely used in order to calculate the factor of safety against sliding for slope engineering and dam foundation problems in the future.

KEYWORDS: The vector sum method; Slope engineering; Dam foundation; The limit equilibrium method; The factor of safety of stability against sliding

INTRODUCTION

Since Limit Equilibrium Method (LEM) called classic Swedish method was put forward by Fellenius in 1927 (Fellenius 1939), the LEM has made great progress, after the development for more than 80a. Because Swedish slice method is based on the circle slip surface with free inter-slice forces, and Mohr-Coulomb's strength criterion is adopted. The safety factor can be easily represented as follows:

$$K = \frac{\sum (\sigma f + c) \Delta l}{\sum \tau \Delta l} \quad (1)$$

where, σ_i, τ_i are the average normal stress (assuming compressive stress is positive), shear stress on the slip surface of the i^{th} slice, respectively. Δl_i is the length of the slip surface of the i^{th} slice. f_i, c_i are the friction coefficient and the cohesive force of the i^{th} slice, respectively, and n is the slice number of the critical slip surface.

Eq.1 described as algebraic sum, is reasonable, for it satisfies the principle of moment balance. Eq.1 is also useful, even for the plane failure surface.

For a slope in engineering, the shape of the potential slip surface is not usually a circle, and it can be a curve or a piecewise line. The inter-slice forces of LEM cannot be ignored; different assumptions on the direction and the position of the inter-slice forces are made. Meanwhile, the loads applied on the slope are complicated, which include the groundwater, the earthquake, etc. All of these Factors promoted the development of the LEM. As is well known, the stress distribution of inter-slice forces and also on the potential sliding surface is a statically indeterminate problem and it can not be explicitly determined under no assumptions in general. The development of LEM for decades mainly focus on the division of slices, the magnitude, the direction and the position of force on the interface of slices, and the expression form of safety factor and so on. Many famous methods are formed under different assumptions, such as simplified Bishop method, Janbu method, Low-Karafiath method, Mongenstern-Price method, Spencer method and Sarma method.

The LEM has been extended from 2-D to 3-D recently in China, and has made great progress. Now the new no-slice LEM and strict 3-D LEM can be found (Zheng et al. 2007; Zheng 2007). With the popularization of FEM nowadays, the finite element analysis method based on the strength reduction

¹ Professor, Institute of Geotechnical Engineering, Shanghai Jiao Tong University, Shanghai 200030, P. R. China; Institute of Rock and Soil Mechanics, Chinese Academy of Sciences, Wuhan 430071, P. R. China. Email: gexiurun@whrsm.ac.cn

principle is also used in slope and dam stability analysis (Ducan 1996; Feng et al. 1990; Zheng et al. 2002; Zheng et al. 2005).

However, the safety factors analyses of stability against sliding of LEM and finite element method are commonly used, but are based on the strength reduction principle. The author has two basic viewpoints: one is that the rationality of the strength reduction principle seems to be doubtful. The other is that because force is a vector, the superposition principle of vectors should be hold in the solution of anti-sliding safety factor, the algebraic sum of force is hold only for some special cases. Based on the above viewpoints, the author and his colleagues have been seeking after a new calculation method for analysis of stability against sliding for more than twenty years which is called the Vector Sum Method (Ge 1987; Ge et al. 1995). Some developments on this method have been made recently (Liu 2007; Liu et al. 2007; Ge 2008).

DISCUSSION ON THE RATIONALITY OF THE SAFETY FACTOR OF STABILITY AGAINST SLIDING BASED ON STRENGTH REDUCTION METHOD

At present, the factor of safety against sliding for stability called FOS is widely used. Firstly a strength reduction value or strength reduction coefficient is assumed in this algorithm, then the shear strength of the potential slip surface (expressed by cohesion c and internal friction coefficient) is divided by F , and after a lot of trial calculations by adjusting the coefficient until the critical failure state on the slip surface is reached, the coefficient is adopted as the safety factor of the stability against sliding. According to the author's opinion, the rationality of this algorithm seems to be doubtful.

(1) c , $\tan\varphi$ divided by same F simultaneously is not very reasonable.

It is well known that, when the Mohr-Coulomb strength criterion is used, c and $\tan\varphi$ are two independent parameters of shear strength. These two parameters are different mechanical properties and play different roles in the Mohr-Coulomb strength criterion. Taking slope as an example, there are lots of different types of slope. The cohesive force c plays an important role to maintain the stability of slope, but in some other cases, internal friction angle φ but not the cohesive force c plays a key role. Meanings of the two parameters are different for different types of slopes.

(2) If c and $\tan\varphi$ are divided by different factors respectively, namely F_c and F_φ , it will be complicated and infinite combining solutions could be obtained.

(3) If only one parameter is unchanged in the analysis, only changing the other parameter, two answers will arise and they also cannot turn into the definition of the safety factor.

(4) When a potential sliding surface cuts many different materials with different properties, it is very unreasonable when all the strength parameters of different materials are still divided by the same coefficient F .

(5) If Mohr-Coulomb strength theory is adopted, the parameter φ can't be reduced freely. It has proved that when the strength parameters of material are reduced, the Poisson's ratio and the friction angle should maintain the following equation (Zheng et al. 2002):

$$\sin\phi \geq 1 - 2\mu \quad (2)$$

Then the reasonable results could be obtained. If the Poisson's ratio μ needs to be adjusted during the analysis, then the factor of safety will not be the definition by the original meaning. If μ is not adjusted, the result would be unreasonable.

(6) After strength reduction the mechanical state of slope is not in a real state but a virtual state. Frankly speaking, the factor of safety acquired from real state of stresses is much reasonable than from the virtual state.

(7) How to determine the field needed to be reduced when the finite element method is used? Because this strength reduction method often causes undesired plastic or damage zones in some regions, which will affect the overall state more or less, and effect on the factor of safety and its rationality.

(8) When the slope state is very close to its critical state in the reduction process, the finite element analysis will be very difficult to converge, then it is very natural to ask that whether the current state is in a critical state or not. On the other hand, this type of nonlinear calculation has a great relationship with selected constitutive model and the strength criteria etc. Different person adopt different constitutive relationship and strength criteria, which will have effect on the reliability and rationality of the factor of safety for stability against sliding with strength reduction method.

THE BASIC CONCEPT OF THE VECTOR SUM METHOD TO CALCULATE THE SAFETY FACTOR OF STABILITY AGAINST SLIDING FOR SLOPE AND DAM FOUNDATION PROBLEMS

(1) Force is a vector, here the sum doesn't mean algebraic sum but vector sum. The total sliding force vector is the vector sum of the sliding forces on the every section Δl_i of the potential slip curve. Similarly the total anti-sliding force vector is the vector sum of the

mobilized anti-sliding forces on the every section Δl_i of the potential slip curve.

(2) The two vectors must be projected to a certain direction when calculating the safety factor of stability against sliding.

(3) The projection direction should be reasonable and has a clear physical meaning.

(4) The total sliding force vector and the total anti-sliding force vector are in the same plane in 2-D state. It is reasonable that we take the potential sliding direction of the potential sliding body as the projection direction.

(5) For 3-D problems, taking the same principle as in 2-D problems, the total sliding force vector is the vector sum of the sliding forces on the every pieces ds_i of the potential slip surface. Similarly, the total anti-sliding force vector is the vector sum of the mobilized anti-sliding forces on the every pieces ds_i of the potential sliding surface. The total sliding force vector and the total anti-sliding force vector are projected to the potential sliding direction of the potential sliding body. The ratio of the projections is called the safety factor of stability against sliding by means of VSM, abbreviated as K .

CALCULATING THE SAFETY FACTOR AGAINST SLIDING FOR SLOPE AND DAM FOUNDATION PROBLEMS BY MEANS OF VSM IN 2-D CASES

(1) Some assumptions and principles in the Vector Sum Method

(a) For 2-D problems, the calculating region, the potential slip curve, and the sliding region are known. The search for critical slip surface is not included in this paper.

(b) Loads, boundary conditions of the slope or dam foundation, and the basic physical and mechanical parameters of rock and soil mass have been obtained through geological investigation and the field or lab testing. The current stress state in the slope or dam foundation has been acquired by finite element numerical method or other methods.

(c) The Mohr-Coulomb criterion is taken as the strength criterion of materials. When the current stress states are known, the anti-sliding shear stress on the slip curve can be represented as:

$$\tau_i = c + \sigma \tan \varphi \quad (3)$$

(d) The potential sliding direction of the potential sliding body can be considered as the projection direction. The angle between it and the x coordinate axis is θ , as is illustrated in Fig.1

(e) In plane problems, the definition of the factor of safety $k(\theta)$ by means of the VSM, is the ratio of the

projection of the total mobilized anti-sliding force vector and the total sliding force vector on the potential sliding direction:

$$K_{vs} = K(\theta) = \frac{\sum R(\theta)}{\sum T(\theta)} \quad (4)$$

where, $\sum R(\theta)$ represents the algebraic sum of projections of every anti-sliding force vector acting on the Δl_i ; $\sum T(\theta)$ represents the algebraic sum of projections on the potential sliding direction of every sliding force acting on the Δl_i .

(2) The expression of potential sliding direction for plane problems

As shown in Fig.1, for an arbitrary point on the slip curve under local coordinate system $o'x'y'$, the normal and shear stress are σ , τ respectively, and Δl_i is the length of section enclosed on the slip curve, The angle between x -axis(global coordinate system) and the tangent line at the point i on the slip surface is denoted as α .

The sign convention of stress is the same as in the rock and soil mechanics and for angle it is positive in anti-clockwise from the positive x -axis, and negative in clockwise. α is negative in Fig 1.

According to the Mohr-Coulomb criterion, the limited mobilized anti-sliding shear stress at the point i on the slip surface can be expressed as:

$$\tau_{fi} = c_i + \sigma_n \tan \varphi_i \quad (5)$$

The opposite direction of the vector of total anti-sliding forces will be taken as the direction of projection with the angle θ .

Therefore, the projection direction angle θ can be represented as:

$$\theta = \arctan \frac{\sum F_{yi}}{\sum F_{xi}} \quad (6)$$

where,

$$F_{xi} = \tau_{fi} \Delta l_i \cos \alpha_i \quad (7)$$

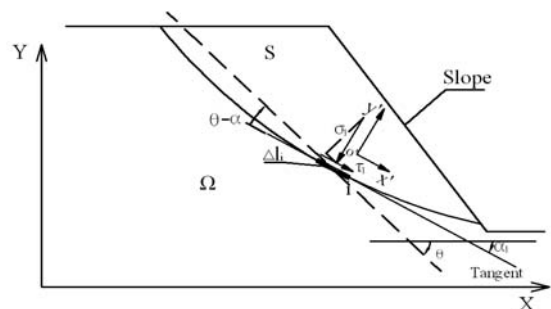


Fig. 1 The coordinate systems and the stresses state acting on the Δl_i

$$F_{yi} = \tau_{fi} \Delta l_i \sin \alpha_i \quad (8)$$

(3) The analytical expression for stability against sliding by the Vector Sum Method in plane problems

Fig.2 is a sketch for the solution of the safety factor by the Vector Sum Method. At any point i on the slip surface with cohesion c_i and internal frictional angle ϕ_i σ and τ are the normal stress and shear stress acting on the Δl_i of the potential slip curve, σ'_i and τ'_i are the normal stress and shear stress acting on the sliding mass by the bed rock. The relationships between them are:

$$\sigma = \sigma', \quad \tau = \tau' \quad (9)$$

The specific expression of Eq.4 is derived as following:

(a) The projection of $\tau_i \Delta l_i$ is:

$$T_\tau^i = \tau_i \Delta l_i \cos(\theta - \alpha_i) \quad (10)$$

The projection of $\sigma_i \Delta l_i$ is:

$$T_\sigma^i = \sigma_i \Delta l_i \sin(\theta - \alpha_i) \quad (11)$$

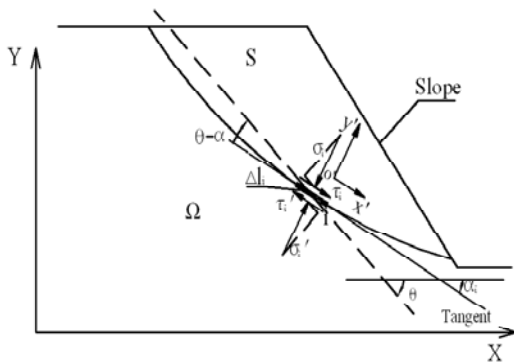


Fig. 2 Diagram of solving the safety factor of stability against sliding by vector sum method

Therefore,

$$\sum T(\theta) = \sum T_\sigma^i + \sum T_\tau^i \quad (12)$$

(b) The anti-sliding forces are mobilized by the cohesive forces, frictional forces of the rock and soil mass and the normal forces acting on the sliding mass by the bed rock. In the length Δl_i on the slip curve, the sum of the cohesive force and the frictional force are the shear strength of rock and soil mass, which is determined by the Mohr-Coulomb criterion:

$$\tau_{fi} = c_i + \sigma_i \tan \phi_i \quad (13)$$

The projection of $\tau \Delta l$ is:

$$R_\tau^i = \tau_{fi} \Delta l_i \cos(\theta - \alpha_i) \quad (14)$$

The projection of $\sigma' \Delta l$ ($= \sigma_i \Delta l_i$) is:

$$R_\sigma = \sigma \Delta l \sin(\theta - \alpha) \quad (15)$$

Therefore:

$$\sum R(\theta) = \sum R_\tau^i + \sum R_\sigma^i \quad (16)$$

(c) Substituting Eq.12 ~ Eq.16 into Eq.4, the safety factor of stability against sliding by the vector sum method can be represented as:

$$K = K(\theta) = \frac{\sum R(\theta)}{\sum T(\theta)} = \frac{\sum R_\tau + \sum R_\sigma}{\sum T_\tau + \sum T_\sigma} \quad (17)$$

where, K — the safety factor by the vector sum method.

Substitute the related Eqs. into Eq.17 and the expanded form is:

$$K_{vs} = \frac{\sum [(c + \sigma f) \cos(\theta - \alpha) + \sigma \sin(\theta - \alpha)] \Delta l}{\sum [\tau \cos(\theta - \alpha) + \sigma \sin(\theta - \alpha)] \Delta l} \quad (18)$$

If σ is tensile stress, the frictional force σf on the slip length Δl_i should be equal to zero.

THE SLOPE STANDARD EXAMINATIONS BY MEANS OF THE VECTOR SUM METHOD

The examples illustrated in Fig.3 and Fig.4 are EX1 (a) and EX1(c) from the standard examinations (1) of The Association for Computer Aided Design, Limited (ACADS) (Chen 2003).

Slope in EX1 (a) is a homogeneous, and its boundary conditions and field size are illustrated in Fig.3. EX1(c) is a non-homogeneous, and its dimension is the same with EX1 (a), However, the slope body is made up of 3 layers of soil shown in Fig. 4.

The search of the critical slip surface with the VSM is not discussed here. The critical slip surfaces in Fig.3 and Fig.4 searched (Chen 2003) with the STAB program are adopted as the potential failure surface here, and all layers of soil cut through by the surface are shown in EX1(c).

Based on the finite element method, the Vector Sum Method is applied for analysis of stability against sliding. The results from different methods are demonstrated in Table 1.

Through comparison of safety factors with different methods, the conclusions can be obtained. The safety factors with the VSM are in good agreement with the referee's answers with others. The relative errors of EX1 (a) and EX1 (c) between the results of the VSM and recommended method (Donald) are only 1.06%, 0.43%, respectively.

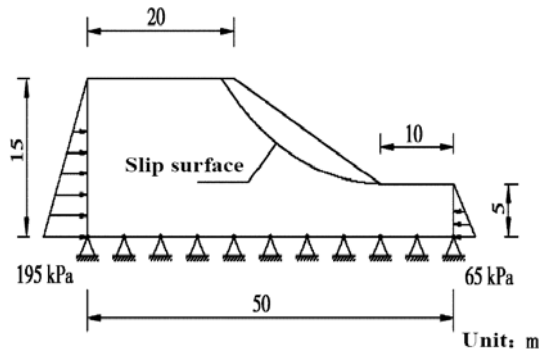


Fig. 3 Calculating model EX1(a) of ACADS

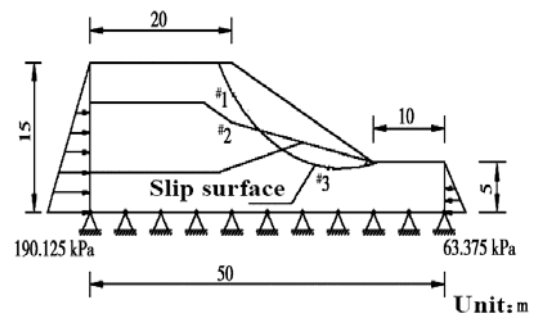


Fig. 4 Calculating model EX1(c) of ACADS

Table 1 Comparisons of safety factors for ACADS with different methods

Analysis method	Program	EX1(a)		EX1(c)	
		Safety factor	VSM / (θ) (°)	Safety factor	VSM / (θ) (°)
	Donald(recommendation)	1.000		1.390	
Referee's answer with LEM	SSA(Baker)	1.000		1.390	
	STAB(Chen)	0.991		1.385	
	GWEDGEM	1.000		1.390	
	EMU	1.000		1.390	
	Fredlund	0.990		1.406	
VSM	ANSYS (elastic stress)	1.011	-21.82	1.384	-21.51

SLOPE STABILITY ANALYSIS WITH THE VECTOR SUM METHOD FOR NON-CIRCULAR SLIP SURFACE IN PLANE PROBLEMS

(1) Computation Model

For further study on some characteristics of the Vector Sum analysis method, four kinds of slip surfaces are selected, and they are single straight-line, dual line, triple line and arbitrary curve. Material parameters, dimensions and boundary conditions of the four models are the same with EX1 (a) of ACADS standard test in previous part. The computation models are illustrated in Fig.5 (a) (b) (c) (d), and the slip surfaces of the specific shapes and locations are also indicated in these figures. Finite element method is still used in the vector sum analysis method.

(2) Comparison between the results obtained by VSM and other methods

The safety factors calculated by the vector sum method and the limit equilibrium methods are listed in Table 2, and they are very close to each other. The computation software used for limit equilibrium method is GEO-SLOPE Office 5. The M-P method means Morgenstern-Price method and L-K method means Low-Karafiath method.

DISCUSSION ON THE VECTOR SUM ANALYSIS METHOD

(1) The influence of element sizes on safety factor

Triple line slip surface are taken as an example, factors of safety, the mesh sizes and projection directions are shown in Table 3, from the table we can see that the element sizes made little influence on factor of safety. The K_{VS} slightly increases when the element size increases, and the relative difference is only 1.10%.

(2) The difference of K_{VS} between elastic stress state and elastic-plastic stress state with the vector sum analysis method.

In order to explore the influence of elastic stress state and elastic-plastic stress state on factor of safety, we calculate the safety factor under those two kinds of stress states respectively, as shown in Table 4. D-P strength criteria are taken and the inscribed and circumscribed circle of Mohr-Coulomb strength criterion is used here. Obviously the Mohr-Coulomb strength criterion lies between them.

It can be seen that the safety factor under the plastic stress state is slightly smaller than that under the elastic stress state. The difference of the safety factors between them is so small that it only has some differences in the second number after the decimal point.

In most cases, the elastic stress state and relative coarse mesh can meet the accuracy requirement of the safety factor calculation in the practical project.

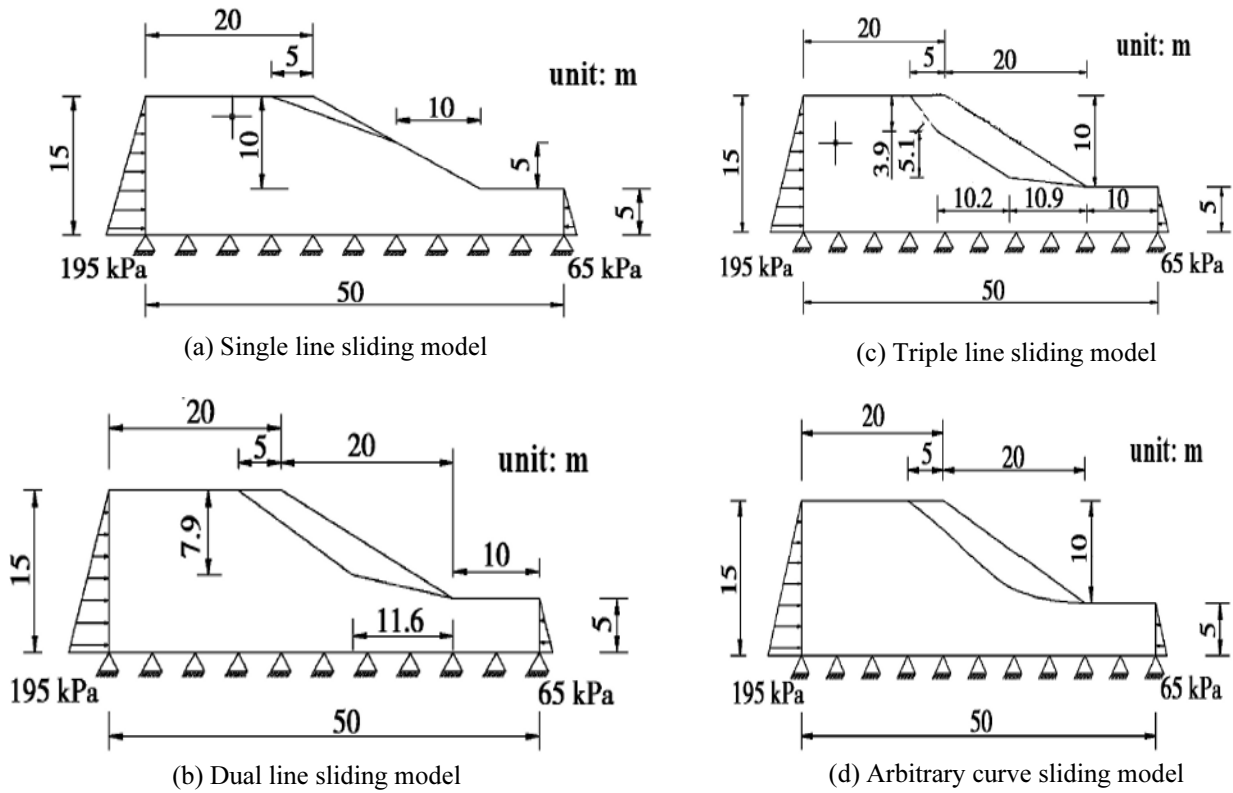


Fig. 5 Four kinds of non-circular slip surface

Table 2 Comparison between the safety factors obtained by the VSM and other methods according to different kinds of slip surfaces

sliding surface of computation model	safety factor with limit equilibrium method			Vector Sum method: finite element elasticity			
	M-P method	Bishop method	L-K method	Safety factor K_{VS}	Calculation direction $\theta /(^{\circ})$	Element number	node number
single straight-line	1.684	1.678	1.682	1.668	-18.43	4274	4447
dual line	1.071	1.139	1.076	1.091	-20.96	2195	2324
triple line	1.097	1.163	1.106	1.101	-20.00	2199	2328
Arbitrary curve	1.047	1.116	1.050	1.073	-20.45	2338	2467

Table 3 The influence of element sizes on the value of the safety factor with VSM

Element size/m	Element number	Safety factor K_{VS}	relative error /%	Calculation direction $\theta /(^{\circ})$	relative error /%
0.9	642	1.1116	1.10	-20.05	0.56
0.8	844	1.1086	0.83	-20.10	0.81
0.7	1107	1.1060	0.59	-20.04	0.51
0.6	1471	1.1033	0.35	-20.04	0.51
0.5	2085	1.1027	0.29	-19.98	0.21
0.4	3423	1.1011	0.15	-20.03	0.46
0.3	5902	1.1005	0.09	-20.03	0.46
0.2	13433	1.1012	0.15	-19.96	0.11
0.1	49986	1.0997	0.00	-19.938	0.00

Note: the relative error is based on the element size of 0.1 m

Table 4 Vector safety factors for the slip surfaces with different constitutive equations

calculation model	element number	node number	elasticity		Elasto-plastic (outer circle of D-P)		elasto-plastic (inner circle of D-P)	
			safety factor K_{VS}	calculation direction $\theta(^{\circ})$	safety factor K_{VS}	calculation direction $\theta(^{\circ})$	safety factor K_{VS}	calculation direction $\theta(^{\circ})$
Single line	4274	4447	1.668	-18.43	1.666	-18.43	1.665	-18.43
Double broken line	2195	2324	1.091	-20.96	1.086	-21.16	—	—
triple linear	2199	2328	1.101	-20.00	1.100	-20.33	—	—
Arbitrary curve	2338	2467	1.073	-20.45	1.067	-21.01	—	—

Note: — means no convergence

ANALYSIS OF STABILITY AGAINST SLIDING BY VECTOR SUM METHOD FOR 3-D PROBLEMS

(1) Preface

The stability analysis against sliding for 3-D problems is more complicated than that for 2-D problems. 3-D vector sum stability analysis method is based on the current stress state of slopes or dam foundations. Nowadays it is not difficult to acquire the stress state of 3-D object under various loads by numerical method. For this reason, the current trend to analyzing the stability against sliding should turn towards the more precise numerical method. The Vector Sum Method proposed in this paper is a new method in this field, which is based on that force is a vector, abandons the traditional concept of the strength reduction and uses 3-D finite element analysis or other numerical method as a tool.

(2) Definition of safety factor against sliding for 3-D vector sum method

The definition of safety factor of the VSM is: the ratio of the projection of total mobilized anti-sliding force vector and total sliding force vector on the potential sliding direction of the potential sliding mass. In this definition, total sliding force vector is a sum vector of normal forces and shear forces acting on the Δs_i of the potential slip surface. Similarly, total anti-sliding force vector is a sum vector of anti-sliding normal force and anti-sliding shear force acting on the Δs_i of the potential sliding surface by bed rock.

(3) Derivation of safety factor against sliding for 3-D problems with VSM

As shown in Fig. 6, σ_s , σ , σ_n are stress vector, shear stress and normal stress, respectively, which act on the slip surface at the point A. \hat{n} is the unit normal vector of tangent plane at the same point on the slip surface (positive pointing to outside of the sliding mass).

\hat{d} is the unit vector of the potential sliding direction. S is the slip surface. Then,

$$\sigma = \sigma \cdot \hat{n} \quad (19)$$

$$\sigma = (\sigma \cdot \hat{n}) \hat{n} \quad (20)$$

$$\sigma = \sigma - \sigma \quad (21)$$

Here, σ is the stress tensor at the point A on the potential slip surface.

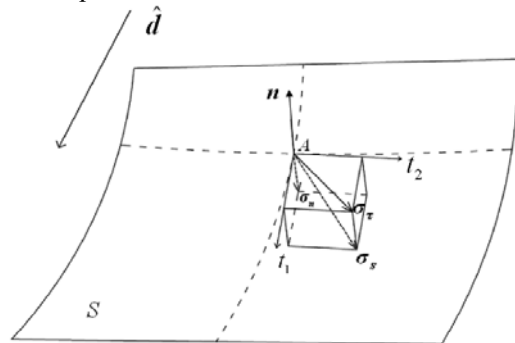


Fig. 6 The stress state at point A on potential slip surface

The normal stress acting on the sliding mass at the point A' can be expressed as:

$$\sigma' = -\sigma \quad (22)$$

To facilitate the derivation, the convention that the tensile stress is positive and the compressive stress is negative is adopted here. The safety factor of the vector sum method can be expressed:

$$K = \frac{R}{T} \quad (23)$$

where, R — the projection of total anti-sliding force on potential sliding direction \hat{d} ; T — the projection of total

sliding force on potential sliding direction \hat{d} . They can be expressed:

$$R = \int \sigma' \cdot (-\hat{d}) ds \quad (24)$$

$$T = \int (\sigma' \cdot \hat{d}) ds \quad (25)$$

In Eq. 24, limited anti-sliding stress vector σ' can be expressed:

$$\sigma' = \sigma' + \sigma' \quad (26)$$

If the Mohr-Coulomb criterion is accepted, the limited shear stress can be expressed:

$$\sigma'_\tau = (c - \sigma \operatorname{tg} \varphi) \hat{d} \quad (27)$$

where, \hat{d}_r — the unit direction of limited anti-sliding shear force of each section dS on the slip surface;

c — cohesive force;

φ — internal friction angle.

(4) Determination of unit direction \hat{d} of limited anti-sliding shear force

The direction \hat{d}_r is a unit direction, and is opposite to the projection direction of potential sliding direction on the tangent plane at the same point A on the slip surface.

(5) The basis for determination of direction \hat{d} .

The maximum and minimum principles proposed by Pan (Pan 1980) can be described as: (i) among all possible slip surfaces of a soil or rock structure, the real one renders the minimum resistance against the external load; (ii) the real internal force or stress distribution along the slip surface is the one that provides the maximum resistance against the external load. The principles were proved by Chen Zuyu [Chen 1998].

By now fixed slip surface has been discussed. According to the principles, for a certain slip surface, in order to render the maximum resistance against sliding, the direction \hat{d} of any point A should be taken as the opposite projected direction of the whole potential sliding direction on the tangent plane of the point A.

(6) Determination of whole potential sliding direction \hat{d}

There exists limited anti-sliding force at any point on the potential slip surface. According to the principle of friction, described as “the directions are always opposite to each other between the static friction force and relative sliding trend among two objects”, We define the opposite direction of the vector sum of all of limited anti-sliding forces on the slip surface as the potential sliding direction (Guo et al. 2009). And the whole potential sliding direction can be expressed as:

$$\hat{d} = \frac{-\int (c - \sigma \operatorname{tg}(\varphi)) \hat{d} ds}{\left\| \int (c - \sigma \operatorname{tg}(\varphi)) \hat{d} ds \right\|} \quad (28)$$

In this equation, the direction \hat{d}_r is determined by the potential sliding direction and the direction \hat{d} can be obtained by using the direction \hat{d} , so the implicit relationship between them can be set up. However, we can take the direction of integral of shear stress along the slip surface as the initial direction of potential sliding direction.

$$\hat{d} = \frac{\int \sigma_\tau ds}{\left\| \int \sigma_\tau ds \right\|} \quad (29)$$

where, \hat{d} — the initial direction of potential sliding direction.

Therefore, the next direction \hat{d}_i for each ds_i can be acquired by initial direction \hat{d} . Then, through Eq.28, the direction \hat{d}_1 can be obtained. It is a convergent sequence. The final direction of potential sliding direction can be obtained by above iteration when:

$$\left\| \hat{d}_{-1} - \hat{d} \right\| \leq \varepsilon \quad (30)$$

where, ε — convergence criteria for iteration, generally $1.0e-4$ can be used when Eq.(30) is satisfied, then $\hat{d} = \hat{d}_i$.

(7) Determination of safety factor of stability against sliding by the VSM for 3-D problems

Safety factor K of the Vector Sum Method for 3-D problems can be easily acquired by Eqs. 24 -27 and Eq. 23.

3-D EXAMPLES AND COMPARISON WITH RESULTS BY DIFFERENT METHODS

(1) To verify the rationality of the VSM for 3-D problems, three examples are used. Two of them are from the research of Zhang Xing (Zhang 1988), who proposed a 3-D ellipsoid example in 1988. Example 1 is a homogeneous slope, whose sliding surface is a part of simple ellipsoid surface; and in Example 2 the upper part of sliding surface is the same as example 1, but the bottom of the slip surface is cut by a weak intercalation. Model of the ellipsoid examples is shown in Fig.7. Many scholars have chosen these examples to test their procedures for 3-D problems. The last example is an asymmetric wedge slope stability problem in rock mechanics, which is used for many times as a verification when developing 3-D slope stability analysis programs.

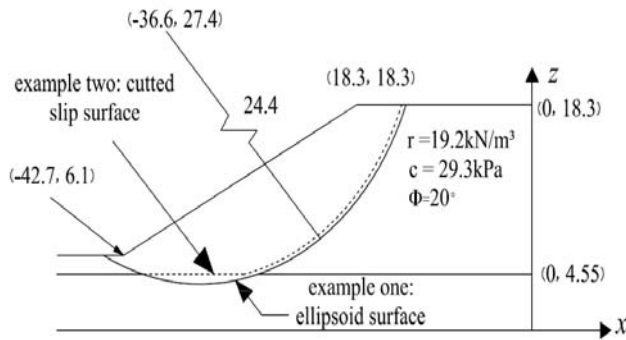


Fig. 7 Model of the ellipsoidal example (Zhang 1988)

(2) For example 1, gravity is the only load acting on the slope with two sides normally constrained and bottom fixed. the ideal elastic-plastic constitutive relationship of Mohr-Coulomb criteria and non-associated flow rule are adopted during computing the stress state by FEM. Meshes and the slip surface are shown in Fig. 8, and Fig. 9, respectively.

The safety factors of the VSM corresponding to different mesh densities of quadratic element in FEM are illustrated in Fig.10. Two different kinds of stress states (the elastic and elastic-plastic state) are also considered here.

The iterative process with the elastic stress state, which is given in Table 5, indicates that the convergence is very fast after the second iteration. In this example the 3-D element number of the slip surface is 7094. The safety factors by the limited equilibrium methods and the vector sum method are listed in Table 6.

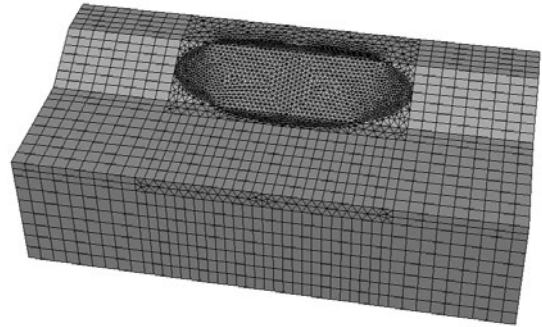


Fig. 8 Meshes of the ellipsoidal model in example 1



Fig. 9 Slip surface of ellipsoidal model

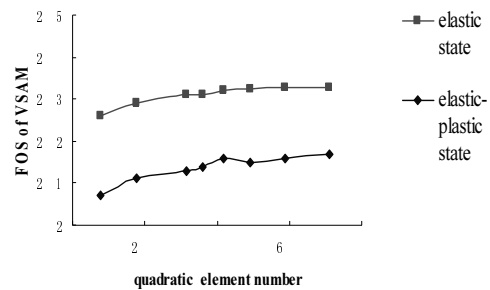


Fig. 10 The safety factors of the VSM with different numbers of quadratic element in example 1

Table 5 The iterative process of the VSM in example 1

iteration sequences	Safety factor k	$\ \hat{d}_- - \hat{d}\ $	Potential sliding direction \hat{d} (°)		
			α	β	γ
Initial value	2.302	—	-16.56	-89.99	-73.43
1	2.041	2.28e-3	-21.13	-89.99	-68.87
2	2.035	7.38e-5	-21.26	-89.98	-68.74
3	2.035	4.8e-5	-21.26	-89.98	-68.74

Note: α , β , γ are the angles between the axes of the global coordinate system x, y, z and the direction \hat{d} , respectively. “+” stands for the angles between the positive axis and the direction \hat{d} , “-” stands for the angles between the negative axis and the direction \hat{d} .

Table 6 Safety factors of different 3-D analysis methods in example 1

Zhang (1988)	Zheng (2007)	Chen (2001)	STAB-3D (Chen 2003)	Vector Sum Method
2.122	2.140	2.262	2.188	2.037

Table 7 Safety factors of different 3-D analysis methods in example 2

Zhang (1988)	Hunger (1989)	Lam & Fredlund (1993)	Huang & Tsai (2000)	STAB-3D (Chen 2003)	Upper bound (Chen, et al. 2001)	Zheng (2007)	Vector Sum Method
1.553	1.620	1.603	1.658	1.640	1.717	1.690~1.706	1.545 (Elasto-plastic state) 1.585(Elastic state)

The safety factor obtained under elastic stress state is about 2.04, which is slightly greater than that under the elastic-plastic stress state. Compared with other methods, the safety factors of the VSM are reasonable and acceptable in practice.

(3) Example 2

The ellipsoid is cut by a weak intercalation, and other conditions are the same as in Example 1 shown in Fig. 11.

The safety factors of the VSM corresponding to different numbers of linear element on the slip surface are illustrated in Fig. 12.

The safety factors of the VSM and other methods are listed in Table 7, which indicate that the safety factor is about 1.585 under the elastic stress state, and is about 1.545 under the elastic-plastic stress state. The results are consistent with the results from Zhang Xing.

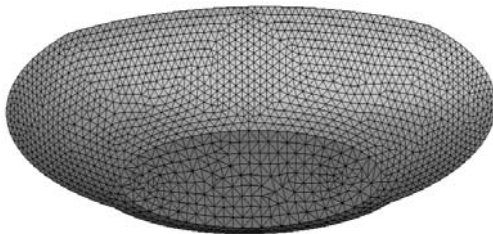


Fig. 11 The cut slip surface in example 2

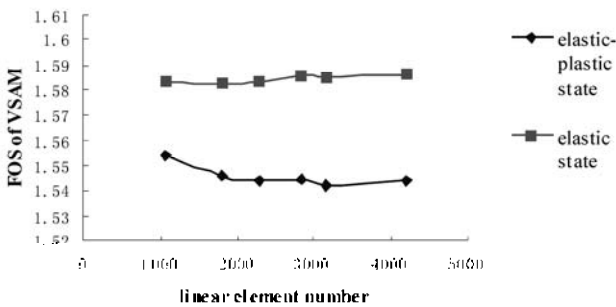


Fig. 12 The safety factors of the VSM with different numbers of linear element in example 2

(4) Example 3

Stability of the wedge-shaped body is a typical 3-D slope stability problem in rock mechanics. It is an asymmetric geometry of wedge in this example. There is analytical solution about simple wedge by Limit

Equilibrium Method, but it is based on the assumption that the direction of shear stress on the slip surface is parallel to the crest line of two structure faces shown in Fig.13. In this example, the same strength parameters are used in the left structure is the same as in the right structure plane. That is, $c = 0.05\text{Mpa}$, $\phi = 30^\circ$.

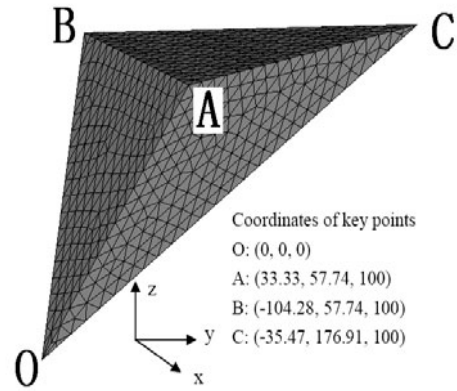


Fig. 13 Mesh of wedge

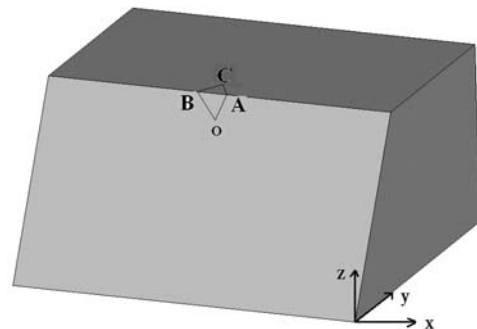


Fig. 14 Geometric shape of wedge

The mesh is shown in Fig.14. The scopes of calculating model in x-axis, y-axis, z-axis are $[-800,800]$, $[-400,1000]$ and $[-700,100]$, respectively. Deformation parameters of wedge and bedding rock are: $E = 8.0e10\text{ Pa}$ and $\nu = 0.3$, the density is 2600 Kg/m^3 . Boundary conditions: slope surface OAB and the top of wedge ABC are free and other sides is constrained in their normal direction. The safety factor of the wedge by the Vector Sum Method is 1.654, and the analytical

solution by limit equilibrium method is 1.64. It is consistent with each other very well.

Due to space limitation, applications of the VSM in practical engineering problems have not been included in this paper.

CONCLUSIONS

(1) The stability analysis problem of dam foundation and slope is a relatively old subject, but it is very important because of its close relationship with engineering construction. So, it is worth further studying and improving.

(2) Nowadays, it is still very popular that the safety factor of stability against sliding is acquired by the limit equilibrium method based on the strength reduction principle. With the increasing popularity of numerical analysis methods, it is not a problem to get the stress state of potential sliding mass on the slip surface. So, there are more and more examples computed by FEM with strength reduction method.

(3) There are many questions of safety factor defined by strength reduction method to need to be discussed. It should be noted that it uses a virtual state with reduced strength to evaluate the safety factor under current state, and its scientificness and rationality are worth discussing.

(4) Based on the basic characteristics of force vectors, current stress state and mechanical parameters of slope or dam foundation, the safety factor of the Vector sum method is defined as the ratio of the projection of total anti-sliding force vector and total sliding force vector on the potential sliding direction, which forms the basis of analysis of the Vector Sum Method for 2-D and 3-D problems.

(5) Some conclusions can be drawn from above examples:

① The consistency of safety factors gotten by Vector Sum Method and other methods shows that Vector Sum Analysis Method is reasonable and credible.

② Most of current technical instructions are based on limit equilibrium analysis method, they are also suitable to the Vector Sum Method.

(6) The advantages of the Vector Sum Method can be listed as follows:

① The definition of this new method is very clear in physics.

② The formula of the safety factor with this new method is explicit for plane problems. For 3-D problems the iteration converges very fast.

③ The Vector Sum Method can be applied together with the finite element method for 3-D problems. To plane problems, this new method can be used together with the finite element method, and also with the limit

equilibrium method. However, in the limit equilibrium method it needn't strength reduction method and iterations, but the force acting on the last slice need some special treatments.

④ The safety factor is not sensitive to the element size of FEM where the stress comes from.

⑤ There are very little difference between safety factors obtained under elastic state and elastic-plastic state.

⑥ The formula and the calculating process of this new method are very simple and clear in physics. It is easy to be programmed, and can be quickly mastered by the engineers and technical personnel and applied easily.

⑦ It is a fast and simple method when combined with FEM for 3-D problems. It has obvious advantages compared with other methods.

⑧ The Vector Sum Method is a new method in stability analysis against sliding of slope and dam foundation engineering, and this new method is worthy of further investigation, development and application.

ACKNOWLEDGEMENTS

I would like to express my gratitude to my students for their help, they are Dr. Li CG, Dr. GUO MW, Dr. Liu YZ and Dr. Hou M.X.

REFERENCES

- Chen ZY (2003). Earth slope stability analyses-theory, method and programs. China Water Power Press, Beijing, P. R. China (in Chinese).
- Chen ZY, Wang XG, Haberfield C, et al. (2001). A three-dimensional slope stability analysis method using the upper bound theorem Part I: theory and methods. *International Journal of Rock Mechanics & Mining Sciences*, 38(3): 369-378.
- Chen ZY (1998). On Pan's principles of soil and rock stability analysis. *Journal of Tsinghua University (Sci & Tech)*, 38 (1): 1-4 (in Chinese).
- Ducan J M (1996). State of the art: Limit equilibrium and finite-element analysis of slopes. *Journal of Geotechnical Engineering, ASCE*, 122(7):577-596.
- Feng DX, Wu JX, Ge XR (1990). Some Problems of Slope Stability Analysis. *Chinese Journal of Geotechnical Engineering*, 12(3): 1-9 (in Chinese).
- Fellenius W (1939). *Erdstatisch berechnungen*. Berlin.
- Ge XR (1987). The finite element analysis on rock mass and engineering with PC, In: *Proceedings of symposium on the 1st National Computational Mechanics on Rock and Soil*. Southwest Jiaotong University Press, Emei, P. R. China (in Chinese).
- Ge XR, Feng DX, Gu XR, et al. (1995). Stability and

- deformation analysis of complex rock foundations of several large dams and hydropower stations in China, In: Yoshinaka R, Kikuchi K eds. Rock Foundation: Proceedings of International Workshop on Rock Foundation[C]. Tokyo: AA BALKEMA, 1995: 243-248.
- Ge, XR (2008). Deformation control law of rock fatigue failure, real-time X-ray CT scan of geotechnical testing, and new method of stability analysis of slopes and dam foundations. Chinese Journal of Geotechnical Engineering 30(1): 1-20.
- Guo MW, Ge XR, Li CG, et al. (2009). Study on potential sliding direction in slope stability analysis based on vector sum method. Chinese Journal of Geotechnical Engineering, 31(4): 577-583 (in Chinese).
- Institute of Rock and Soil Mechanics, Chinese academy of sciences.(1981). Experimental study on rock slope stability analyses and calculation methods. Science Press, Beijing, P. R. China (in Chinese).
- Liu YZ (2007). Vector sum analysis method of slope and dam foundation stability against sliding. Ph.D. Thesis, Institute of Rock and Soil Mechanics, Chinese Academy of Sciences, P. R. China (in Chinese).
- Liu YZ, Ge XR, Li CG, et al. (2007). Stability analysis of slope and foundation based on vector method safety factor. Chinese Journal of Rock Mechanics and Engineering, 26(10): 2130-2140 (in Chinese).
- Pan JZ (1980). Stability analyses of structures and landslides. Water Resources and Hydropower Press, Beijing, P. R. China (in Chinese).
- Zhang X (1988). Three-dimensional stability analysis of concave slopes in plan view. Journal of Geotechnical Engineering, 114 (6): 658-671.
- Zheng H, Tham LG, Liu DF (2007). A slice-free method for stability analysis of slopes. Rock and Soil Mechanics, 28(7): 1285-1291 (in Chinese).
- Zheng H (2007). A rigorous three-dimensional limit equilibrium method. Chinese Journal of Rock Mechanics and Engineering, 26(8): 1529-1537 (in Chinese).
- Zheng H, Li CG, Lee CF, Ge XR (2002). Finite element method for solving the factor of safety. Chinese Journal of Geotechnical Engineering, 24(5): 626-628. (in Chinese).
- Zheng YR & Zhao SY (2005). Limit state finite element method for geotechnical engineering analysis and its applications. China Civil Engineering Journal. 38(1): 91-98,104 (in Chinese).

ACID MINE DRAINAGE FROM ABANDONED MINE SITES: PROBLEMATIC AND RECLAMATION APPROACHES

Bruno BUSSIÈRE¹

ABSTRACT: One of the most serious environmental issues related to the mining industry in Canada and elsewhere, is the pollution from abandoned mine waste disposal sites. The wastes containing sulphide minerals can oxidize and generate contaminants in the water drainage, a phenomenon called acid mine drainage (AMD). Different techniques are available to control the production of AMD. However, these techniques were mainly developed for the closure of operating sites, and are not as efficient for abandoned mine sites that were left exposed to natural conditions for years. The main differences between an operating and abandoned mine waste disposal site are the quality of the interstitial water, the presence of well implemented acidophilic bacteria, and the quality of the retaining infrastructures. To avoid contamination of surrounding ecosystems, it is necessary to take into consideration these particularities at the reclamation stage. The experience at the Lorraine mine site shows a slight improvement of the water quality in the waste disposal site 10 years after reclamation even if the oxygen barrier is working as expected. The addition of a passive treatment system to treat the contaminated pore water that will eventually flow out of the site is then a critical component of the reclamation at any abandoned AMD mine waste disposal site.

KEYWORDS: Acid Mine Drainage (AMD), AMD control methods, abandoned mine sites, passive treatment, case studies

INTRODUCTION

The mining industry is an important asset for the economy of many regions across Canada, particularly with respect to exports and employment, but also through numerous technological developments. Nevertheless, mining operations generate different types of wastes which are potentially environmentally harmful. Effective and efficient waste management programs are therefore required to ensure their long-term environmental stability.

Active mining operations must respect governmental environmental criteria and, by doing so, the production of contaminants in the environment is limited to a level considered acceptable by the overseeing governments. Nevertheless, some abandoned mine sites are not well controlled and have significant impacts on the environment. Two Canadian examples of sites affected by abandoned mine wastes are presented in Fig. 1a and b.

Before going any further, it is important to define what is an abandoned mine site. Several expressions (orphans, abandoned, retrocessed, inactive, closed, etc.) can be found in literature and currently there is no consensus on a unique definition. Identifying a clear definition is an important step since it will affect the

number of sites categorized as abandoned. In the following paper, a slightly modified version of the definition proposed by van Zyl et al. (2002) is used:

A mine site is considered abandoned if there are no solvable identifiable owners or operators for the facilities, or if the facilities have reverted to governmental ownership.

If we assume that having only one component of the mine is sufficient to categorize a site as an abandoned mine site (ex. a ramp, a shaft, an open cast, etc.), Canada has more than 10 000 abandoned sites (with more than 1,000 in the province of Quebec). In US, more than 550,000 sites are categorized as abandoned, while Sweden counts more than 1 000, 10,000 sites in Great-Britain and more than 5,500 in Japan (van Zyl et al. 2002).

It is well known that some components of the mine have a greater impact on the environment than others. Tailings impoundments and waste rock piles (called hereinafter mine waste disposal sites) are probably the most critical components; they can generate significant negative impacts on drainage water, on soils, and eventually on water drainage (e.g. Aguilar et al. 2004; Lee and Faure, 2007; Hakkou et al. 2008). To the knowledge of the author, no detailed and global statistics

¹ Professor, Department of Applied Sciences, University of Quebec in Abitibi-Témiscamingue (UQAT) Rouyn-Noranda, Québec, Canada. Email: Bruno.bussiere@uqat.ca

(or inventory) are available, at the planet scale, to quantify the volume and area of abandoned mine waste disposal sites.

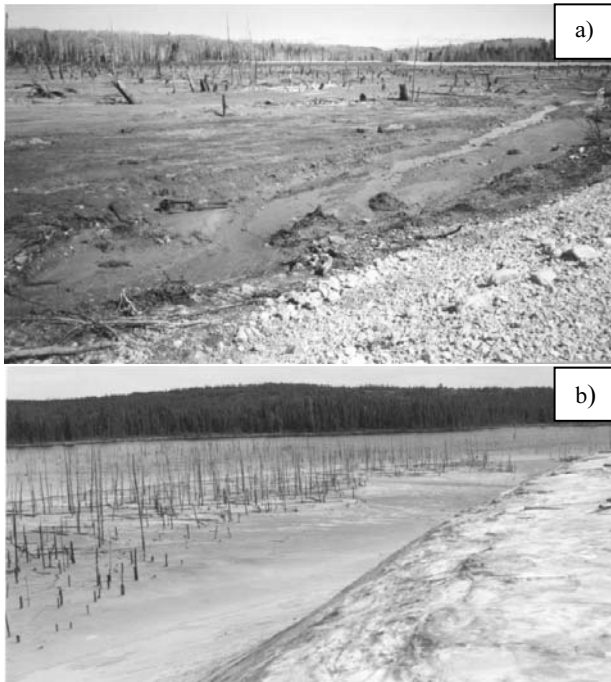


Fig. 1 Photographs showing environmental impacts from two Canadian abandoned mine sites a) Aldermac site, Rouyn-Noranda, Quebec, Canada, b) Manitou site, Val-d'Or, Quebec, Canada

To have a better idea of the challenge facing governments and the mining industry with abandoned mine waste disposal sites, some statistics of the province of Quebec, Canada are presented. In the province of Quebec, 50 abandoned mine waste disposal sites (having an area greater than 1 ha) are inventoried (see Fig. 2), which collectively cover an area of approximately 2 000 ha. Each site has a different level of impact on the environment. It is estimated that approximately 1 000 ha are covered by mine wastes that can generate contaminated drainage water. The estimated reclamation costs for these sites, using typical unit costs, are \$150 million (CDN). The picture depicted above for the province of Quebec is similar for the other Canadian hard rock mining provinces such as Ontario, British Columbia, and Manitoba.

These statistics show the importance of the problem. In the context of sustainable development, it is crucial for the mining industry to develop effective reclamation scenarios for existing and abandoned mine waste disposal sites, especially for those that generate acidic drainage (called acid mine drainage, AMD) in the environment. In the following, a description of the AMD problem will be given with some options available to rehabilitate waste disposal sites with AMD potential.

The main differences at the reclamation stage between abandoned and operating sites will be presented along with a case study of a rehabilitated abandoned acid generating mine waste disposal site. Finally, a short description of actions taken recently in Canada to reduce the environmental impacts of abandoned mine sites will be presented.

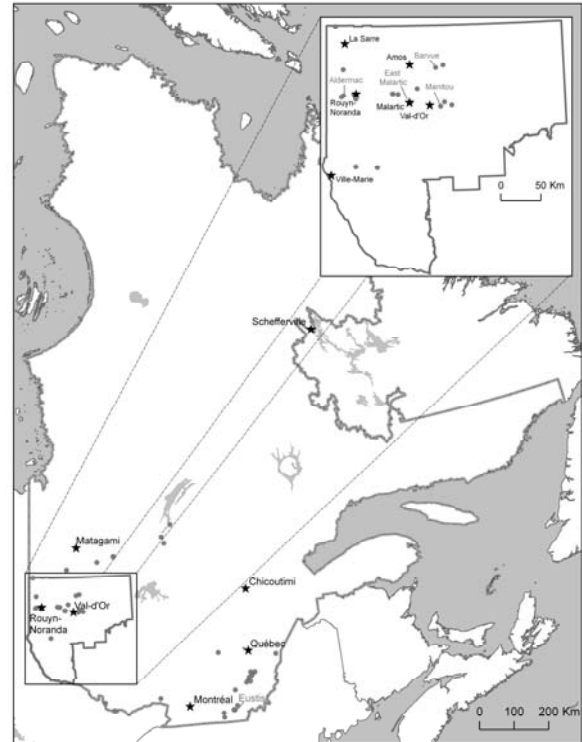
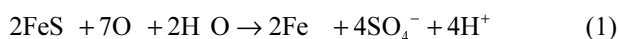


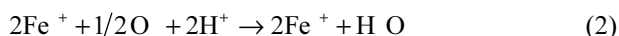
Fig. 2 Location of the abandoned mine waste disposal sites in the province of Quebec, with a close up on the Abitibi region (the main mining region of the province), that covers an area greater than 1 ha

AMD GENERATION

The AMD can be generated at or within a number of mine site components such as waste rock, tailings, open pit walls and underground workings (e.g. SRK, 1989; Morin and Hutt, 1997). The sulphide minerals such as pyrite and pyrrhotite oxidize in the presence of water and atmospheric oxygen producing AMD through a number of possible chemical and biochemical pathways. The oxidation of sulphide minerals (pyrite which is the more abundant sulphide mineral is taken here as reference) can be described by the following equations (e.g. Kleinmann et al. 1981; Ritcey, 1989; Blowes and Ptacek, 1994; Evangelou, 1995; Perkins et al. 1995; Morin and Hutt, 1997). The first step is the direct oxidation of pyrite (FeS_2) by oxygen which produces sulphates (SO_4^{2-}), ferrous iron (Fe^{2+}) and acidity (H^+):



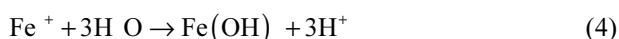
In the next step, the ferrous iron is further oxidized to ferric iron (Fe^{3+}).



Ferrous iron can also be oxidized to produce iron hydroxide (FeOOH) and acidity.



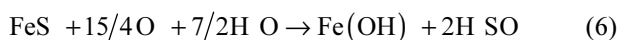
At a $\text{pH} > 4$, Fe^{3+} is precipitated out as ferric hydroxide ($\text{Fe}(\text{OH})_3$), which releases more acid in the environment.



At $\text{pH} < 4$, the ferric iron can remain soluble and can directly oxidize pyrite, liberating more acid into the surroundings.



The overall reaction for the complete oxidation of pyrite can be expressed as follows:



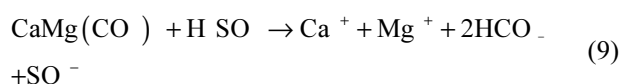
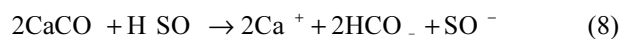
The oxidation of 1 mole of pyrite generates two moles of sulphuric acid. It is usually considered in the literature (e.g. Aubertin et al. 2002a) that direct oxidation by oxygen (Eq. 1) occurs at pH near neutrality ($5 < \text{pH} < 7$) while the indirect oxidation (Eq. 5) is predominant at lower pH values ($\text{pH} < 3$). The equations presented above are based on a stoichiometric equilibrium that does not take into account the kinetic of each reaction. The rate of oxidation is a function of additional factors (Morth and Smith, 1966 ; Lowson, 1982; Rogowski et Pionke, 1984 ; Nicholson et al. 1988 ; Frostad et al. 2000a,b ; Jerz and Rimstidt, 2004), including oxygen supply, temperature, pH, bacterial activity, mineral surface area, and crystallography.

It is usually considered that the rate of the reaction is controlled by Eq. 2. The reaction rate is slow at a low pH but increases rapidly as the pH drops due to the presence of bacteria. For example, *Acidithiobacillus ferrooxidans* bacteria have the capacity to catalyze the oxidation reaction of the ferrous iron into a ferric iron (Eq. 2); the rate of reaction can be increased by a factor up to 20 to 1,000 times (e.g. Berthelin, 1987). Some bacteria can also oxidize the sulfur produced during the sulphide oxidation:



The chemical quality of the drainage will also depend on the other minerals present in the mine waste. The acid can react by being neutralized by carbonates and (in a

lesser extent) silicate minerals, which are considered the main neutralizing minerals (e.g. Sverdrup, 1990; Kwong, 1993; Lawrence and Scheske, 1997). Eqs. 7 and 8 represent two possible reactions for the neutralization of sulphuric acid (at $\text{pH} > 6.3$) by calcite (CaCO_3) and dolomite ($\text{CaMg}(\text{CO}_3)_2$) respectively, which are two abundant carbonate minerals (Lapakko, 1994).



The equations show that two moles of calcite and 1 mole of dolomite are necessary to neutralize 1 mole of sulphuric acid. The capacity of the neutralizing mineral to limit the production of AMD is also dependent on different factors affecting the reactivity of the minerals (ex. temperature, pH, CO_2 pressure, mineral surface area and crystallography). The reactivity of carbonate minerals can be classified from the more reactive to the less: calcite > dolomite > Mg-ankerite > ankerite > siderite (Blowes et Ptacek, 1994). More details on the neutralization process in mine waste can be found in other publications (e.g. Sverdrup, 1990; Blowes and Ptacek, 1994; Lapakko, 1994; Sherlock et al. 1995; Aubertin et al. 2002a; Jambor et al. 2002; Bussière et al. 2005).

Finally, it is worth mentioning that other chemical reactions (other than oxidation and neutralization) can affect the rate at which AMD is generated. Precipitation of the secondary minerals can affect significantly the final water quality by reducing the concentration of certain elements at the effluent (elements are transferred from the liquid phase to the solid phase). For example, it is common to find secondary minerals that contain iron and sulfates in acid generating mine wastes (ex. goethite, jarosite, iron hydroxyde; references). Precipitation of secondary minerals can also affect the reactivity of sulphides and carbonates (references) by forming a coating on the particles. It is also documented that the accumulation of secondary minerals in tailings (called hard pan) can locally create a zone where the hydraulic conductivity is lower which can reduce oxygen migration and, consequently, the production of AMD (see Blowes et al. 1991; Aubertin et al. 2002a). The comprehension of all of these mechanisms relating to the secondary mineral formation is necessary when one wants to predict the evolution of AMD in a given mine site.

MAIN AMD CONTROL METHODS

When the neutralization potential of a given mine

waste is less than the acidification potential, AMD will occur and appropriate measures has to be taken at the mine waste storage site to mitigate it. Over the last few years, different techniques have been proposed to limit the environmental impacts of AMD. One approach is to control the production of AMD, from mine tailings or waste rocks, by eliminating one (or more) of the three main components of the oxidation reactions (see Eq. 1): oxygen, water and/or sulphide minerals.

Sulphide Extraction

The presence of sulphide minerals is essential to generate AMD. AMD can be controlled by extracting a sufficient portion of these minerals thus limiting the quantity of AMD generated in the environment. The necessary recovery of sulphide minerals will depend on the amount of neutralizing minerals. Different techniques such as flotation and gravimetric separation can be used to separate the sulphides from the tailings (e.g. McLaughlin and Stuparyk, 1994; Humber, 1995 ; Bussière et al. 1995, 1998). This control method is mainly applicable for operating sites but the recycling (sulphide extraction combined with metal recovery) of old abandoned mine wastes could also be an option in some particular cases. More information on sulphide extraction for environmental purposes can be found in Bussière et al. (1995, 1998), Benzaazoua et al. (1998, 2000), Benzaazoua and Kongolo (2003), Bois et al. (2005), and Mermillod-Blondin et al. (2005).

Oxygen Barriers

Oxygen is one of the key ingredients for the generation of AMD. Limiting oxygen availability for the reactive mine wastes is one of the most interesting approaches to control AMD, especially in humid climatic conditions (e.g. SRK 1989; MEND 2001). Different approaches can be used to create an oxygen barrier: placing a water cover or by elevating the water table, placing a cover with capillary barrier effects over the waste disposal site, or installing an oxygen consuming barrier (not discussed in this document).

Water cover and elevated water table technique

The water cover technique consists of completely covering the reactive mine wastes with water by submerging the mine waste in a lake or by building a dyke to hold both the mine waste and the water that submerges them. Because the oxygen diffusion coefficient is 10 000 times lower in water than in air, the flux of oxygen reaching the AMD mine wastes is usually sufficiently low and avoids AMD generation. However, a water cover is a complex, dynamic system subjected to

several factors such as tailings erosion and resuspension, oxygen migration, oxidation of sulphidic tailings by dissolved oxygen (DO), release of dissolved metals, water exchange with the surrounding environment, etc. Several studies on these aspects have been conducted to develop appropriate design tools for water covers (e.g. Adu-Wusu et al. 2001; Catalan and Yanful 2002; Yanful and Catalan 2002; Mian and Yanful 2004).

Water covers can raise serious stability concerns and can be difficult to maintain over the long term (Aubertin et al. 1997a). To reduce the geotechnical risks associated to a water cover, a new approach was proposed relatively recently for tailings: the Elevated Water Table (EWT) technique (MEND, 1996; Orava et al. 1997; Dagenais, 2005; Dagenais et al. 2006; Ouangrawa et al. 2006, 2009; Ouangrawa, 2007; Demers et al. 2008). The principle on which the EWT technique is based consists of maintaining a degree of saturation sufficiently high in the tailings above the water table in order to reduce the oxygen diffusion rate and prevent sulphide oxidation. A high degree of saturation is maintained by controlling seepage and capillary rise. Similar to water cover, the elevated water table technique is based on the fact that the effective diffusion coefficient of oxygen is very low in saturated (or nearly saturated) media (Mbonimpa et al. 2003, Aachib et al. 2004).

Cover with capillary barrier effects

Multi-layered covers with capillary barrier effects (CCBEs) use unsaturated soil properties to create the capillary barrier effects that maintain one of the layers at a high degree of saturation at all times. The high degree of saturation makes the moisture-retaining layer an efficient barrier against oxygen flow, by impeding gas advection and diffusion. By limiting oxygen flux, the cover limits AMD generation since oxygen is one of the constitutive elements of the sulphide mineral oxidation reactions.

The effectiveness of this type of cover is dependant upon a phenomenon called the capillary barrier effect. This effect is present when a fine grained material is placed over a coarser one. The two materials have different hydrogeological properties because of their different textures. In the initial desaturation stage, the fine grained material layer retains water more easily than the coarse layer because it has smaller interstitial pores. As the coarse material drains, the presence of gas in its pore space reduces the interconnectivity of the voids which reduces its hydraulic conductivity (k). This reduction of k in the coarse layer reduces the vertical water flow from the fine material and thus the latter layer can remain almost fully saturated at all times, creating the oxygen barrier. More details about capillary barrier effects and CCBE can be found in the literature (e.g. Nicholson et al. 1989; Akindunni et al. 1991; Aubertin et

al. 1995; Aachib 1997; Bussière 1999; Bussière et al. 2003).

Covers with capillary barrier effects usually contain three to five layers of different materials. Each layer has to play one (or more) specific role(s). Fig. 3 is a schematic illustration of a CCBE. The bottom layer is made of a fairly coarse material which functions as both a mechanical support and a capillary break. The fine grained material, utilized as the moisture retaining layer, is placed upon the first layer to create the capillary barrier effect. Another coarse material is placed upon the fine grained material layer to prevent water loss by evaporation and help lateral drainage. The other two layers (protection and surface layers) are protective layers against erosion and bio-intrusion for the CCBE; these are not discussed further in this paper.

Water Infiltration Barriers

As seen in Eq. 1, water is one of the essential components of AMD generation. Hence, one can control the production of acid by limiting water flow through the reactive mine wastes. To do so a water infiltration barrier must be built on top of the mine waste disposal area. To limit the influx of water, covers made of low hydraulic conductivity soils or synthetic materials (such as geomembranes or bentonite geocomposites) can be used. The configuration of these covers is similar to designs developed for the isolation of domestic and hazardous wastes (e.g. Oakley, 1987; Aubertin and Chapuis, 1991; Daniel and Koerner, 1993; Koerner, 1993, 1994; Aubertin et al. 1995; Rowe et al. 2004).

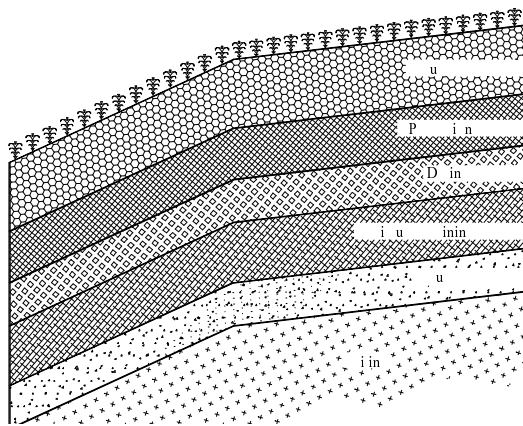


Fig. 3 Typical configuration of a CCBE used to limit the production of AMD (Aubertin et al. 1995)

Another option to limit water infiltration in arid and semi-arid conditions is the use of “Store-and-Release” SR covers (also bearing various other names such as “alternative”, “water balance”, or “evapotranspirative” covers). Such engineered systems are attracting considerable interest as they may represent an advantageous alternative to more traditional covers that

rely on materials having a low saturated hydraulic conductivity (e.g. Morris and Stormont 1997; Ward and Gee 1997; Dwyer 1998; Zhan et al. 2001; Scanlon et al. 2005).

A typical SDR cover includes a fine-grained soil layer placed on top of a coarser material. The capillary barrier effect at the interface between the fine and coarse materials allows the finer soil layer to store incoming water, which can later be released by evaporation. In sloping areas, a capillary barrier cover also acts as a lateral water diversion system. Additional layers can also be added to help the cover play its role(s) efficiently. Fig. 4 shows a typical water balance of a SDR cover. The objective of the cover is to have sufficient runoff, evapotranspiration, storage, and lateral percolation (in the case of inclined covers) to avoid water infiltration into the mine waste. The main advantages of a SR cover lie in its relative simplicity, long-term stability, and potentially lower construction costs compared to more traditional covers that rely on materials (natural soils and/or geosynthetics) with a low saturated hydraulic conductivity (e.g. Morris and Stormont 1997). More information on SR or SDR covers can be found in Williams et al. (2003), Benson et al. (2001), Fourrie and Moonsammy (2002); Bussière et al. (2007) and Aubertin et al. (2009).

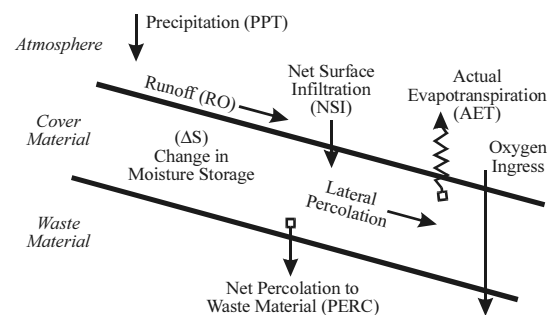


Fig. 4 Schematic representation of an SDR cover water budget (MEND 2001)

DIFFERENCES BETWEEN OPERATING AND ABANDONED MINE SITES

There are important differences between an operating mine and abandoned mine site (left exposed to natural conditions for years) and these differences influence the selection of the most appropriate reclamation scenario. These main differences are summarized in Table 1.

One of the main differences between abandoned and operating AMD mine waste disposal is the quality of the pore water. Sulphide oxidation in the mine wastes after the mine closure can significantly contaminate the pore water; typically, the pH of the water can be lower than 4, with high concentrations of sulphates and metals (in the order of thousands of ppm) such as iron, zinc, arsenic, etc. (see Aubertin et al. 2002a for examples). Moreover, a high concentration in iron can lead to indirect

oxidation of sulphide minerals (see for example Eq. 5) which would generate more acid even after the placement of an oxygen barrier. The addition of a neutralizing agent before the placement of the oxygen barrier could be a solution to reduce indirect oxidation (see Catalan et al. 2002). The objective is to precipitate iron ions and to reduce the concentration in ferric iron (Fe^{3+}) responsible of the indirect oxidation.

Table 1 Main differences between operating and abandoned AMD mine waste disposal sites (modified from Bussi re et al. 2005)

Characteristics	Operating sites	Abandoned sites
Pore water contamination	Low risk	High risk
Presence of AMD bacteria	Low activity	Highly active
Modern storage infrastructures	yes, in general	No, in most cases
Presence of water treatment system	yes	No

The main objective of AMD mine waste disposal sites is to limit the environmental impacts to an acceptable level. For abandoned mine sites, in addition to the future contamination, the reclamation must take care of the previous contamination. Hence, it is usually necessary to integrate into the reclamation scenario the treatment of the pore water that will flow out of the site. In the context of sustainable development, traditional chemical treatment of AMD is not considered a viable long term solution. The other option available is the use of passive treatment systems such as bioreactors with sulphate-reducing bacteria (e.g. Zaluski et al. 2003; Johnson and Hallberg, 2005; Neculita et al. 2007), wetlands (see Kalin, 1993 ; Gazea et al. 1996 ; Goulet and Pick, 2001), and oxic and anoxic limestone drains (e.g., Ziemkiewicz et al. 1997; Bernier et al. 2002; Cravotta, 2003). Because of metal concentrations and the volume of water that have to be treated during the wet season in humid climates, these approaches cannot usually reach (alone) the environmental regulation criteria for effluents coming from AMD abandoned mine waste disposal sites. However, these approaches could be an interesting option for sites where an oxygen or water infiltration barrier is placed as a primary AMD control method.

Other aspects also have to be taken into account for an effective abandoned AMD mine waste disposal site. Acidophilic bacteria are well implemented in mine wastes. As mentioned earlier, the presence of these bacteria can accelerate the production of AMD by a significant factor. Limiting their development can help to

reduce the environmental contamination, but cannot completely eliminate the problem (e.g. Kleinmann and Erickson, 1981; Watzlaf, 1986; Rastogi, 1996). The old infrastructures used to contain mine tailings are usually made of the tailings themselves and were built by experienced people that were taught empirically how to construct dykes, without necessarily taking into account state-of-the-art (at the time relatively poorly developed) geotechnical considerations. Moreover, hydraulic deposition produces a non-homogenous tailings mass, with unsaturated portions and low strength characteristics that induce difficulties with respect to final closure of the impoundment, especially when the tailings have the potential to generate AMD (Vick, 1990; Strachan, 2002; Aubertin et al. 2002b; Bussi re, 2007).

THE LORRAINE CASE STUDY

Different abandoned mine waste disposal sites were reclaimed worldwide in the last two decades or so. One of these sites (Lorraine site, Quebec, Canada) is described in more details. This case study allows for a better understanding of the technical challenges associated to the reclamation of an abandoned AMD tailings impoundment.

The Lorraine Mine Site

The Lorraine mine site, located in the T miscamingue region, Qu bec, Canada (see Fig. 5), was operated from 1964 to 1968. It generated approximately 600,000 tons of acid generating tailings disposed in a pond area covering approximately 15.5 hectares. The tailings thickness ranges from a few centimeters in the pond area up to 6 m (Aubertin, 1996). There was little mitigation work done at the end of the operation and the abandoned tailings were left exposed for 30 years. Chemical analysis of the seepage was characteristic of AMD with elevated concentrations of sulphates and metals, and by a pH ranging from 2.2 to 2.6.



Fig. 5 Lorraine mine site location



Fig. 6 Photographs of the site before and after reclamation work

Lorraine CCBE and Dolomitic Drains

The design of the CCBE was made using basic hydrogeotechnical properties of the soils located near the site and numerical modeling tools (see Nastev and Aubertin, 2000; Dagenais, 2005; Dagenais et al. 2005). The CCBE is composed of three layers: a base layer consisting of 30 cm of sand used as capillary break layer; a moisture-retaining layer made of silty material with a thickness of 50 cm that limits gas diffusion and water infiltration; and a 30 cm top layer consisting of sand and gravel to protect the silt layer from evaporation. Saturated hydraulic conductivity (k_{sat}) varies from 2×10^{-6} to 1×10^{-5} cm/s for the silt material and is about 7×10^{-3} cm/s for the sand. Suction tests done on the silt material gave an air entry value (ψ_a ; pressure at which a material starts to drain) ranging from 2.9 to 5 m of water for a void ratio between 0.85 and 0.62. The measured ψ_a for the sand is around 0.25 m of water. The contrast between the hydraulic properties makes possible the development of capillary barrier effects in the CCBE. More information on the construction, design and material properties can be found in Nastev and Aubertin (2000), Dagenais (2005), Dagenais et al. (2005), and Bussière et al. (2009).

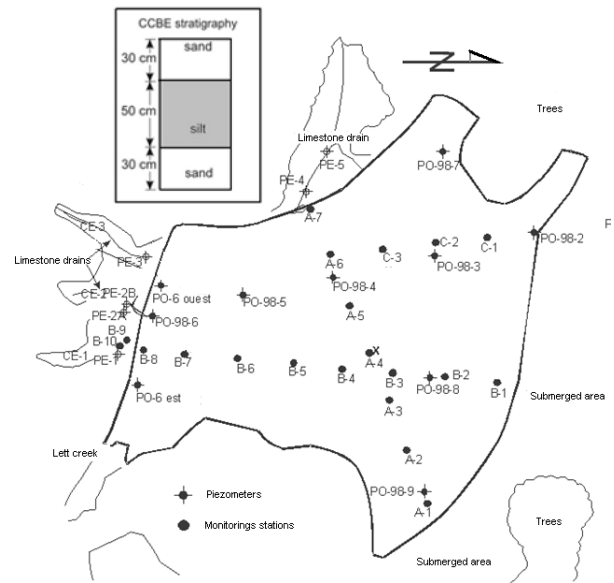


Fig. 7 Plan view after reclamation of the Lorraine Site showing the location of the instruments and the configuration of the CCBE

Even if the CCBE works as an oxygen barrier, the AMD presents in the pore water will have to be treated before discharging the water in the environment. At the Lorraine mine site, three dolomitic drains (Dol-1, 2, and 3) were built to treat the contaminated exfiltration from the south dykes. A fourth calcareous drain was installed near the west dykes but since the construction of the CCBE, the feed water draining to the drain was not contaminated by AMD, therefore this drain will not be discussed further.

The Lorraine dolomitic drains (see Fig. 7 for location) are trenches filled with coarse dolomitic stones (size of particles between 10 and 100 mm), with sides made of a silty material with a low saturated hydraulic conductivity (compared to the coarse dolomitic stones). The trench is isolated on top by a GCL liner. AMD flows by gravity into the drains that have a section of approximately 1.5 m^2 and a length of 65, 69, 55 m for Dol-1, 2, and 3 respectively. The hydraulic residence time was estimated using tracer tests at values between 700 and 2 000 minutes depending on the influx of water (the targeted value was 900 minutes). More information on the dolomitic drains can be found in Maqsood et al. (2007) and Bussière et al. (2009).

A monitoring strategy was developed to follow the performance of the CCBE and the dolomitic drains. TDR probes and Watermark sensors monitored volumetric water content and suction, respectively, in the different layers of the cover; the location of the 20 monitoring stations is presented in Fig. 7. Each station included four TDR probes (SoilMoisture) and four Watermark ceramic probes (Irrometer). A set of each was placed horizontally in both the sand layers and two sets were placed in the

silt layer of the CCBE. These instruments have been used previously by the authors to monitor the hydraulic behaviour of a CCBE during laboratory and test plot studies (Aubertin et al. 1995, 1997b, 1999; Bussière et al. 2003). The measurement of these characteristics gives insight into the hydrogeological behaviour of the CCBE and the development of capillary barrier effects. They also allow evaluation of the oxygen flux through the CCBE. Finally effluent flow and quality were also monitored. The frequency of the readings was similar for the CCBE and dolomitic drains monitoring: between 4 to 8 series of measurements per year. More information on the monitoring can be found in Dagenais et al. (2005) and Dagenais (2005).

Main Monitoring Results

To give a perspective on the performance of the CCBE to limit oxygen migrations, volumetric water content (θ) measurements from three representative monitoring stations (A3, A7 and B5) are presented with their corresponding oxygen flux calculated using the first Fick’s law. The water quality evolution will be presented using key physico-chemical parameters: pH, iron and nickel (the most problematic metals at the Lorraine mine site).

Volumetric water content and oxygen flux

Results presented in Fig. 8 show that the moisture-retaining layer usually had volumetric water content between 0.32 and 0.35, except for station A3 where values were usually between 0.35 and 0.4. Considering the porosity (n) of the layer estimated at 0.37 for stations A7 and B5, and at 0.4 for station A7, the degree of saturation ($S_r = \theta/n$) usually met the design criteria of 85%. It is also interesting to note in Fig. 7 that the bottom sand layers are desaturated at station B5 (θ usually between 0.10 and 0.20 for a porosity of 0.35), is closer to saturation at station A7 (θ usually between 0.15 and 0.25 for a porosity of 0.35) and is saturated at station A3 (θ values close to porosity at 0.35). This means that capillary barrier effects were present at station B5 and A7, and helped to maintain a high degree of saturation in the moisture-retaining layer while the phreatic surface at station A3 is close or in the CCBE.

The previous results showed that the CCBE hydrological behavior was working as planned and that the water retention layer maintained a high degree of saturation throughout the years of monitoring. To better assess the CCBE’s performance, the oxygen flux that was diffusing into the reactive tailings was calculated. Since the transient state is expected to be fairly short (approximately 10 days, e.g. Mbonimpa et al. 2003), Fick’s first law is used, for steady-state conditions, to

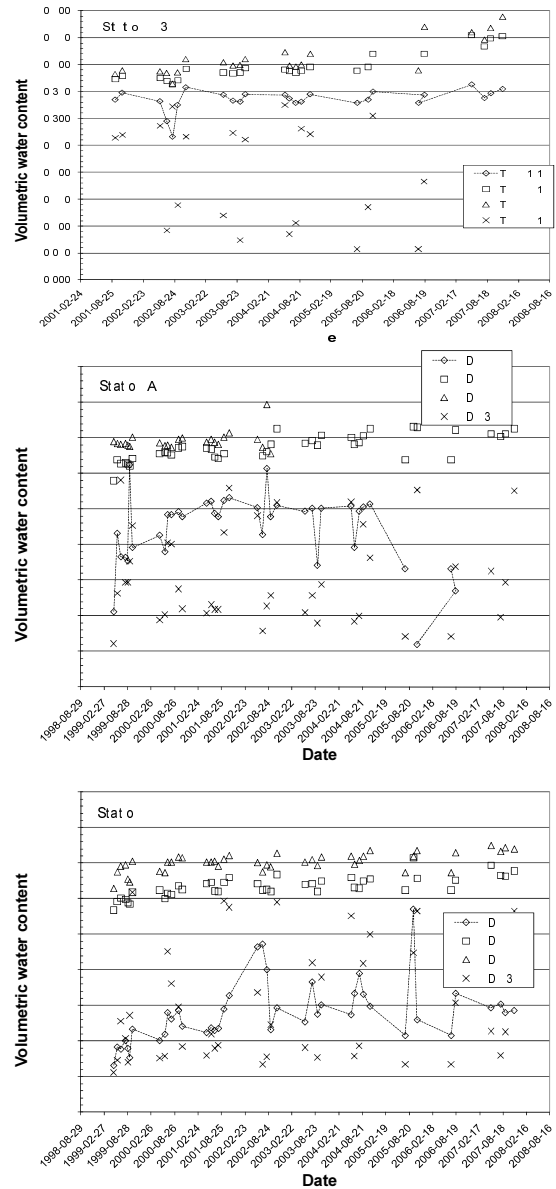


Fig. 8 Evolution of volumetric water content at monitoring stations A3, A7, and B5; TDR 1-1 is located in the bottom capillary break layer at 15 cm of the interface with the moisture-retaining layer, TDR 2-1 is located in the moisture retaining layer at 15 cm from the interface with the capillary break layer, TDR 2-2 is located in the moisture retaining layer at 15 cm from the interface with the top sand layer, and the TDR 3-1 is located in the top sand layer at 5 cm from the interface with the moisture-retaining layer (modified from Bussière et al. 2009).

calculate the oxygen flux to the tailings. The solution is expressed as:

$$F = D_e \frac{(C_0 - C_l)}{h} \tag{10}$$

where F is the gas flux, C_0 is 285 g/m³ (atmospheric oxygen concentration at the top of the cover), C_l is

0 g/m³ (oxygen consumed by sulfide tailings at the bottom of the cover), D_e is the effective diffusion coefficient and h is 0.5 m (silt layer thickness).

To estimate the parameter D_e in Eq. 10, the equation proposed by Aachib et al. (2002; 2004) was used:

$$D_e = \frac{1}{n^2} [D_a^0 \theta_a^{3.5} + HD_w^0 \theta^{3.5}] \quad (11)$$

where D_a^0 is the diffusion coefficient in air ($\approx 1.8 \times 10^{-5}$ m²/s) and D_w^0 is the diffusion coefficient in water ($\approx 2.5 \times 10^{-9}$ m²/s), n is the porosity, H is the Henry equilibrium constant (0.03 for oxygen at 20°C), θ_a represents the volumetric air content of the material and θ the volumetric water content of the material.

The estimated annual oxygen fluxes through the Lorraine CCBE (based on average annual volumetric water content in the moisture-retaining layer) are presented in Fig. 9. Results show that there is a transient period for the first two years after the CCBE construction. The higher oxygen flux for these first two years can be explained by a gradual saturation of the moisture-retaining layer. Since 2002, oxygen flux values were relatively stable at less than 5 g of O₂/m²/year for station A3, less than 12 g of O₂/m²/year for station A7 (except for 2006 where the flux was at 22 g of O₂/m²/year), and between 20 and 40 g of O₂/m²/year for station B5.

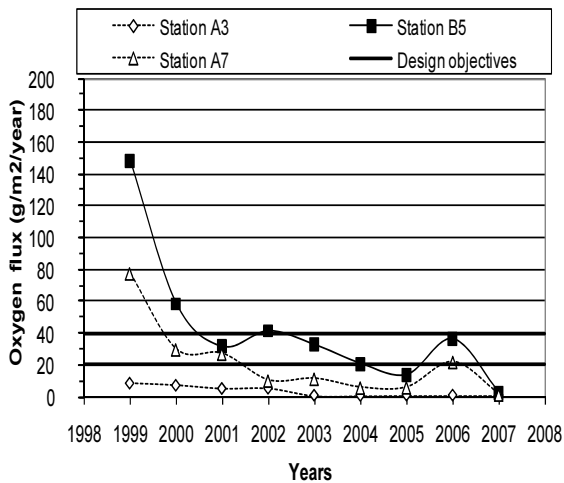


Fig. 9 Oxygen flux calculated using average values of volumetric water content in the moisture-retaining layer at monitoring stations A3, A7, and B5 (modified from Bussi re et al. 2009)

Considering the design objectives of having a flux between 20 and 40 g of O₂/m²/year (Nastev et Aubertin, 2000), the Lorraine CCBE is considered efficient to limit the diffusion of oxygen from the atmosphere to the reactive tailings.

Water quality

Improvement of the water quality at the effluent was also one of the objectives of the reclamation work at the Lorraine site. Fig. 10 presents the evolution of three critical parameters at the Lorraine site effluents: pH, iron and nickel. The influent pH (P0-6) slightly increased (typically from 3 to 4) between 1999 and 2007, even as the CCBE was working well as an oxygen barrier. The pH measurements at the effluent of the dolomitic drains were close to 6, 5.5 and 4.5 for Dol-1 Out, Dol-2 Out and Dol-3 Out respectively. One can also observe that the pH of Dol-3 Out had a decreasing tendency.

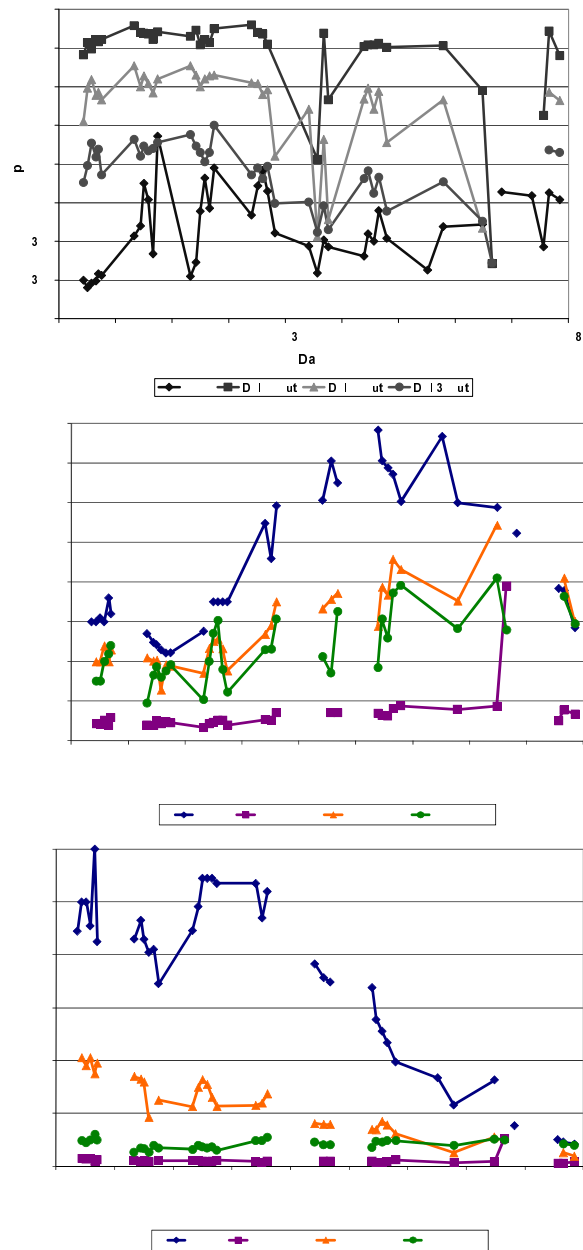


Fig. 10 Evolution of pH, nickel and iron at the effluent of the three dolomitic drains (identified as Dol-1 Out, Dol-2 Out, and Dol-3 Out) in the incoming water (P0-6) (modified from Potvin, 2009)

Iron concentrations at the influent (PO-6) went from 3,000 to 7,000 mg/L between 1999 and 2004. In 2000, a slight reduction to under 2,500 mg/L was observed. Between 2002 and 2006, iron concentrations increased to values close to 8,000 mg/L and decreased in the year following to a value of 3,500 mg/L in 2007. This increase between 2002 and 2006 is attributed to secondary mineral dissolution that could have remobilized the iron. Iron concentration at the effluent of Dol-1 is significantly reduced to values usually less than 1 000 mg/L. The capacity to reduce iron concentration is less for the other two drains.

Nickel concentrations in the influent and effluents of the drains showed a progressive reduction since the reclamation of the site. In the influent, nickel concentrations started at values between 8 and 11 mg/L during the period of 1999–2002 and reached values less than 1 mg/L the following year. At the effluent of Dol-1, nickel concentrations were usually less than 0.3 mg/L. Values at the exit of Dol-2 and 3 were slightly higher than in Dol-1 (between 0.5 and 1 mg/L in 2007).

The dolomitic drains allowed for improving the water quality at the final effluent, but have not been able to reach the environmental criteria of the provincial government. The drains have also different efficiencies (Dol-1>Dol-2>Dol-3) even if they were built using the same approach and the same materials. More work is presently underway to better understand the treatment mechanisms of the Lorraine dolomitic drains (Maqsoud et al. 2007; Potvin, 2009).

Lessons learned at the Lorraine mine site

The work at the Lorraine mine site allowed researchers to improve their knowledge on the reclamation of already oxidized abandoned acid generating mine waste disposal site. The main lessons learned were:

- The improvement of water quality at the effluent is not instantaneous even if an efficient oxygen barrier is placed on top of the acid generating materials. This is due to the contaminated pore water that has to flow out. In the case of the Lorraine site, a slight improvement was observed after 10 years.
- The placement of a water treatment system is essential if one wants to limit the contamination of the environment from the exfiltration of the site.
- At the Lorraine site, the dolomitic drains have improved the quality of the final effluent. However, the concentrations are still higher than the regulation criteria. Other techniques could be used in conjunction with the dolomitic drains (ex. passive bio-reactors using sulfate-reducing bacteria; see Neculita et al. 2007 for details) to improve further the quality of the exiting water.
- More information on indirect oxidation (by bacteria

and/or iron) and other geochemical reactions (ex. precipitation/dissolution of secondary minerals) below the cover would be useful to better assess the Lorraine CCBE performance.

In summary, the reclamation of the Lorraine site showed the numerous scientific challenges related to the reclamation of abandoned acid generating mine waste disposal areas.

GOVERNMENTAL ACTIONS TO REHABILITATE CANADIAN ABANDONED MINE SITES

Canada has made significant progress in the remediation of abandoned mine sites over the last 10 years. In the following, some of the recent initiatives are briefly described. The interested reader can consult the web site of the NAOMI (National Orphaned/Abandoned Mines Initiative) project for more information (<http://www.abandoned-mines.org/>).

In Ontario, the province created in 1999 a program to conduct reclamation work on Crown-held abandoned mine sites. The program will invest \$138 million (CDN) between 1999 and 2012. One of the prioritized sites is Kam Kotia located near the city of Timmins. The site (which contains three acid generating tailings impoundments) covers an area of approximately 500 ha. A five phase rehabilitation plan was proposed which integrated the construction of a chemical water treatment plant, relocation of tailings, the construction of engineered covers and the construction of a wetland. More information on Kam Kotia rehabilitation plan can be found in Hamblin and Kord (2003).

In Manitoba, the government has identified five high priority sites: Lynn Lake, Sherridon, Gods Lake, Snow Lake and Baker Patton. Environmental and risk assessments were completed in 2000 and at an additional 144 orphaned and abandoned sites (Tremblay and Hogan, 2009). 110 million dollars (CDN) has been committed to address the reclamation of Manitoban abandoned mines sites. More technical information on some of the abandoned mine sites of the province can be found in Moncur et al. (2005; Sheridan site) and Gunsigener et al. (2006a, b; Lynn Lake).

In British Columbia, the government has committed over \$190 million (CDN) for the management of the provinces contaminated sites and has spent \$35 million between 2002 and 2007; for the current year (2008-2009), the program has allocated \$27 million dollars

In Quebec, reclamation works are planned on different abandoned mine sites. The biggest site is Manitou, located near Val-d'Or. The 200 hectare acid generating mine waste disposal site will be rehabilitated using a non acid generating tailings coming from another mine (Goldex mine property of Agnico-Eagle). The non acid generating tailings (with a good neutralization

potential) will be used to cover the existing site and to create an oxygen barrier. Different cover scenarios are presently under investigation for the final reclamation. The overall costs related to the reclamation works at Manitou are estimated at \$40 to 50 million (CDN). Another acid generating site, Aldermac, will be rehabilitated in the next two years. The approximately 75 ha site is located near Rouyn-Noranda. The reclamation strategy selected at this site consists of isolating a portion of the site by a geomembrane and to use the elevated water table approach for the other portion. Other sites in the province of Quebec with different problematic occurrence have been rehabilitated in the last 15 years such as East Sullivan (Germain et al. 2003, 2004 ; Tassé and Germain, 2004), Lorraine (see the previous section), Canadian Malartic (Tassé et al. 1997), Candego (Aubertin et al. 2002a), Somex (Aubertin et al. 2002a), Wood Cadillac (Germain and Cyr, 2003 ; Tassé et al. 2003), Solbec-Cupra (Amyot et Vézina, 1997) and Poirier (Maurice, 2002).

LAST REMARKS

The present paper showed that the reclamation of abandoned mine sites is a significant challenge for most Canadian provinces and Territories. The challenge is technical, as shown in this paper, but also political since the sites are owned by the government and the decision to rehabilitate a given site must consider the availability of governmental financial resources. However, the last few years are encouraging since several millions of Canadian dollars have been engaged to reduce the pollution of the most problematic abandoned mine waste disposal areas.

The environmental problems related to abandoned mine sites are not restricted to Canada. Many other countries face similar problems and some of them have decided to tackle the problem. Some organizations have also started such as the Post-Mining Alliance. The Post-Mining Alliance is an independent not-for-profit organization with a mission to encourage and promote the regeneration of old mine sites for the sustainable benefit of the local community and the natural environment. More information can be found on their web site (<http://www.postmining.org/>).

ACKNOWLEDGEMENTS

My acknowledgments go to my collaborators at UQAT and the Ecole Polytechnique Montreal. I would like to thank Jill Baldwin and Isabelle Demers for helping improve the quality of the manuscript. Finally, I acknowledge the Natural Sciences and Engineering Research Council of Canada, the Canada Research

Chair program, and our various partners for their support.

REFERENCES

- Aachib M, Mbonimpa M, Aubertin M (2004). Measurement and prediction of the oxygen diffusion coefficient in unsaturated media, with applications to soil covers. *Water, Air and Soil Pollution*, 156:163-193.
- Aachib M, Aubertin M, Mbonimpa M (2002). Laboratory measurements and predictive equation for gaz diffusion coefficient of unsaturated soils. Proc. 55th Canadian Geotechnical Conference and 3rd joint IAH-CNC and CGS Groundwater Specialty Conferences, Niagara Falls, Ont., CD-Rom: 163-171.
- Aachib M (1997). Étude en laboratoire de la performance des barrières de recouvrement constituées de rejets miniers pour limiter le DMA. Ph.D. Thesis, Mineral Engineering Department, École Polytechnique de Montréal.
- Adu-Wusu C, Yanful EK, Mian MH (2001). Field evidence of resuspension in a mine tailings pond. *Canadian Geotechnical Journal*, 38: 796-808.
- Aguilar J, Dorronsoro C, Fernández E, Fernández J, García I, Martín F, Simón M (2004). Soil Pollution by a pyrite mine spill in Spain, evolution in time. *Environmental, Pollution*, 132: 395-401.
- Akindunni FF, Gillham RW, Nicholson RV (1991). Numerical simulations to investigate moisture-retention characteristics in the design of oxygen-limiting covers for reactive mine tailings. *Canadian Geotechnical Journal*, 28 :446-451.
- Amyot G & Vézina S (1997). Flooding as a reclamation solution to an acidic tailings pond – the Solbec case. Proc. of the 4th International Conference on Acid Rock Drainage, Vancouver, 2: 451-464.
- Aubertin M, Cifuentes E, Apithy S, Bussière B, Molson J, Chapuis RP (2009). Analyses of water diversion along inclined covers with capillary barrier effects. *Canadian Geotechnical Journal* (accepted and in print).
- Aubertin M, Bussière B, Bernier L (2002a). Environnement et gestion des résidus miniers. Presses Internationales de Polytechnique, Corporation de l'École Polytechnique de Montréal, Montréal.
- Aubertin M, Mbonimpa M, Jollette D, Bussière B, Chapuis RP, James M, Riffon O (2002b). Stabilité géotechnique des ouvrages de retenue pour les résidus miniers: problèmes persistants et méthodes de contrôle. Proc. of Défis & Perspectives: Symposium 2002 sur l'Environnement et les Mines, Rouyn-Noranda, on CD-ROM, paper s32a1019, p. 26, 526.
- Aubertin M, Bussière B, Joanes AM, Monzon M, Gagnon D, Barbera JM, Bédard C, Chapuis RP, Bernier L (1999). Projet sur les barrières sèches construites à partir de résidus miniers, Phase II:

- essais en place.” MEND Report 2.22.2c.
- Aubertin M, Dionne J, Marcoux L (1997a). Design guidelines and stability criteria of engineering works for water covers. Proc. of the 4th International Conference on Acid Rock Drainage, Vancouver, BC, 4: 1849-1866.
- Aubertin M, Bussière B, Barbera JM, Chapuis RP, Monzon M, Aachib M (1997b). Construction and instrumentation of in situ test plots to evaluate covers built with clean tailings. Proc. of the 4th International Conference on Acid Rock Drainage, Vancouver, BC, 2: 715-730.
- Aubertin M (1996). Recouvrement multicouche pour le parc à résidus du site minier Lorraine. Rapport soumis au MRNQ (SDM-R-96-23). p. 30.
- Aubertin M, Chapuis RP, Aachib M, Bussière B, Ricard J-F, Tremblay L (1995). Évaluation en laboratoire de barrières sèches construites à partir de résidus miniers. Rapport NEDEM/MEND Report 2.22.2a.
- Aubertin M & Chapuis RP (1991). Considération hydrogéotechniques pour l'entreposage des résidus miniers dans le nord-ouest du Québec. Proc. of the 1st International Conference on Acid Rock Drainage, Montréal, Québec, 3: 1-22.
- Benson CH, Abichou T, Albright WH, Gee GW, Roesler AC (2001). Field evaluation of alternative earthen final covers. *Int. J. Phytoremediation*, 3: 1-21.
- Benzaazoua M & Kongolo M (2003) Physico-chemical properties of tailing slurries during environmental desulphurization by froth flotation. *International Journal of Mineral Processing*, 69: 221-234.
- Benzaazoua M, Bussière B, Kongolo M, McLaughlin J, Marion P (2000). Environmental desulphurization of four Canadian mine tailings using froth flotation. *International Journal of Mineral Processing*, 6 : 57-74.
- Benzaazoua M, Bussière B, Lelièvre J (1998). Flottation non sélective des minéraux sulfurés appliquée dans la gestion environnementale des rejets miniers. Proc. of the 30th Canadian Mineral Processors Symposium, Ottawa: 682-695.
- Bernier LR, Aubertin M, Poirier C, Bussière B (2002). On the use of limestone drains in the passive treatment of acid mine drainage (AMD). Proc. of Défis & Perspectives: Symposium 2002 sur l'Environnement et les Mines, Rouyn-Noranda, on CD-ROM, paper s32 a1031, p.540.
- Berthelin J (1987). Des bactéries pour extraire des métaux. *La recherche*, 188 : 720-725.
- Blowes DW & Ptacek CJ (1994). Acid-neutralization mechanisms in inactive mine tailings. Short Course Handbook on Environmental Geochemistry of Sulfide Mine-Waste, Jambor, J.L., Blowes, D.W. (eds). Mineralogical Association of Canada. Special 22: 272-292.
- Blowes DW, Reardon EJ, Jambor JL, Cherry JA (1991). The formation and potential importance of cemented layers in inactive sulfide mine tailings. *Geochemica et Cosmochimica Acta*, 55: 965-978.
- Bois D, Poirier P, Benzaazoua M, Bussière B, Kongolo M (2005). A feasibility study on the use of desulphurized tailings to control acid drainage. *CIM Bulletin*, 98 : 78 (<http://www.cim.org>).
- Bussière B, Potvin R, Dagenais A-M, Aubertin M, Maqsoud A, Cyr J (2009). Restauration du site minier Lorraine, Latulipe, Québec: résultats de 10 ans de suivi. *Déchets, Sciences et Techniques*, 54: 49-64.
- Bussière B (2007). Colloquium 2004: Hydro-geotechnical properties of hard rock tailings from metal mines and emerging geo-environmental disposal approaches. *Canadian Geotechnical Journal*, 44: 1019-1052.
- Bussière B, Aubertin M, Zhan G (2007). Discussion: Design of inclined covers with capillary barrier effect, by S.-E. Parent and A. Cabral *Geotechnical and Geological Engineering*, 25:673-678.
- Bussière B, Aubertin M, Zagury GJ, Potvin R, Benzaazoua M (2005) Principaux défis et pistes de solution pour la restauration des sites miniers abandonnés générateurs de drainage minier acide. Proc. of the 2e Symposium sur l'Environnement et les Mines, organisé par l'ICM – Rouyn-Noranda, on CD-ROM, p. 29.
- Bussière B, Aubertin M, Chapuis RP (2003). The behaviour of inclined covers used as oxygen barriers. *Canadian Geotechnical Journal*, 40: 512-535.
- Bussière B (1999). Étude du comportement hydrique de couvertures avec effets de barrière capillaire inclinées à l'aide de modélisations physiques et numériques. Ph.D. Thesis, Mineral Engineering Department, École Polytechnique de Montréal.
- Bussière B, Benzaazoua M, Aubertin M, Lelièvre J, Bois D, Servant S (1998). Valorisation des résidus miniers : une approche intégrée – Phase II. Final report submitted to the Ministère des Ressources naturelles du Québec, p. 198.
- Bussière B, Lelièvre J, Ouellet J, Bois D (1995). Utilisation des résidus miniers désulfurés comme recouvrement pour prévenir le DMA: analyse technico-économique sur deux cas réels. Proceedings of Sudbury'95, Conference on Mining and the Environment, Ed. Hynes T.P. & Blanchette M.C., Sudbury, Ontario, 1: 59-68.
- Catalan LJJ & Yanful EK (2002). Sediment-trap measurements of suspended mine tailings in shallow water cover. *Journal of Environmental Engineering*, 128: 19-30.
- Catalan LJJ, Buset KC, Yin G (2002). Reactivity of oxidized sulfidic mine tailings during lime treatment. *Environmental Science & Technology*, 36: 2766-2771.

- Cravotta CA III (2003). Size and Performance of Anoxic Limestone Drains to Neutralize Acidic Mine Drainage. *Journal of Environmental Quality*, 32 : 1277-1289.
- Dagenais A-M, Aubertin M, Bussière B (2006). Parametric study on the water content profiles and oxidation rates in nearly saturated tailings above the water table. *Proceedings of the 7th International Conference on Acid Rock Drainage (ICARD)*, St. Louis, Missouri, R.I. Barnhisel (Ed.). The American Society of Mining and Reclamation, CD-ROM: 405-420.
- Dagenais AM (2005). Contrôle du drainage minier acide basé sur les effets de barrières capillaires. Ph.D. Thesis, Mineral Engineering Department, École Polytechnique de Montréal.
- Dagenais AM, Aubertin M, Bussière B, Cyr J (2005). Performance of the Lorraine mine site cover to limit oxygen migration. *SME Transaction*, 318: 190-200.
- Daniel DE & Koener RM (1993). *Cover Systems. Geotechnical Practice for Waste Disposal*, Chapman & Hall: 455-497.
- Demers I, Bussière B, Benzaazoua M, Mbonimpa M, Blier A (2008). Column test investigation on the performance of monolayer covers made of desulphurized tailings to prevent acid mine drainage. *Mineral Engineering*, 21: 317-329.
- Dwyer SF (1998). Alternative landfill covers pass the test. *Civil Engineering*, September 1998: 50-52.
- Evangelou VP (1995). *Pyrite Oxidation and Its Control*. CRC Press.
- Fourrie AB & Moonsammy M (2002). Store and release covers for landfills in semi-arid climates. *Unsaturated Soils*, Juca, de Campos & Marinho (eds), Swets & Zeitlinger, Lisse, 2: 823-826.
- Frostdad S, Klein B, Lawrence RW (2000a). Kinetic Testing 1. Effects of Protocol Variable on Rates of Weathering. *Proc. of the 5th International Conference on Acid Rock Drainage*, Denver, 1: 641-649.
- Frostdad S, Klein B, Lawrence RW (2000b). Kinetic Testing 2. Scaling Up Laboratory Data to Predict Field Rates of Weathering. *Proc. of the 5th International Conference on Acid Rock Drainage*, Denver, 1: 651-659.
- Gazea B, Adam K, Kontopoulos A (1996). A review of passive system for the treatment of acid mine drainage. *Mineral Engineering*, 9: 23-42.
- Germain D, Tassé N, Cyr J (2004). The East-Sullivan mine site : merging prevention and treatment of acid mine drainage. *Proc. of the 57th Canadian Geotechnical Conference and 5th joint CGS/IAH-CNC Conference*, Québec, Session 8D, CD-ROM.
- Germain D & Cyr J (2003). Evaluation of biofilter performance to remove dissolved arsenic : Wood Cadillac. *Proc. of Sudbury 2003, Mining and the Environment III, Session 1A Bacteria*, Paper on CD-ROM.
- Germain D, Tassé N, Cyr J (2003). Treatment of acid mine effluents using a wood-waste cover. *Proc. of Sudbury 2003, Mining and the Environment III, Session 3A Organic Amendments*, Paper on CD-ROM.
- Goulet RR & Pick FR (2001). Changes in dissolved and total Fe and Mn in a young constructed wetland: Implications for retention performance. *Ecological Engineering*, 17: 373-384.
- Gunsinger MR, Ptacek CJ, Blowes DW, Jambor JL, Moncur MC (2006a). Mechanisms controlling acid neutralization and metal mobility within a Ni-rich tailings impoundment. *Applied Geochemistry*, 21: 1301-1321.
- Gunsinger MR, Ptacek CJ, Blowes DW, Jambor JL (2006b). Evaluation of long-term sulfide oxidation processes within pyrrhotite rich tailings, Lynn Lake, Manitoba. *Journal of Contaminant Hydrology*, 83: 149-170.
- Hakkou R, Benzaazoua M, Bussière B (2008). Acid mine drainage at the abandoned Kettara mine (Morocco), 1: Environmental characterization. *Mine Water and the Environment*, 27: 149-159.
- Hamblin CD & Kord MG (2003). The rehabilitation of Ontario's Kam Kotia Mine: an abandoned acid generating tailings site. *Proc. of Sudbury 2003, Mining and the Environment III, Paper on CD-ROM*.
- Humber AJ (1995). Separation of sulphide minerals from mill tailings. *Proc. of Sudbury'95, Conference on Mining and the Environment*, Ed. Hynes T.P. & Blanchette M.C., Sudbury, Ontario, 1: 149-158.
- Jambor JL, Dutrizac JE, Groat LA, Raudsepp M (2002). Static tests of neutralization potentials of silicate and aluminosilicate minerals. *Environmental Geology*, 43:1-17.
- Jerz JK & Rimstidt JD (2004). Pyrite oxidation in moist air. *Geochimica et Cosmochimica Acta*, 68:701-714.
- Johnson DB & Hallberg KB (2005). Biogeochemistry of the compost bioreactor components of a composite acid mine drainage passive remediation system. *The Science of the Total Environment*, 338: 81-93.
- Kalin M (1993). *Treatment of Acidic Seepages Using Wetland Ecology and Microbiology: Overall Program Assessment*. Final Report, MEND project 3.11.1.
- Kleinmann RLP, Crerar DA, Pacellil RR (1981). Biogeochemistry of acid mine drainage and a method to control acid formation. *Mining Engineering*: 300-304.
- Kleinmann RLP & PM Erickson (1981). Field evaluation of a bactericidal treatment to control acid drainage. *Proceedings of the 1981 Symposium on Surface Mining Hydrology, Sedimentology and Reclamation*, D.H. Graves (ed.), Lexington, KY: 325-329.
- Koerner RM (1993). *Geomembrane liners. Geotechnical Practice for Waste Disposal*, Chapman & Hall: 164-186.

- Koerner RM (1994). *Designing with Geosynthetics*. 3rd edition, Prentice Hall, Englewood Cliffs, N.J.
- Kwong Y TJ (1993). Prediction and prevention of acid rock drainage from a geological and mineralogical perspective. (MEND Report 1.32.1 CANMET, Ottawa), p. 47.
- Lapakko KA (1994). Evaluation of neutralization potential determinations for metal mine waste and a proposed alternative. Proc. of the International Land Reclamation and Mine Drainage Conference and 3rd International Conference on the Abatement of Acidic Drainage, Pittsburgh, 1 : 129-137.
- Lawrence RW & Scheske M (1997). A method to calculate the neutralization potential of mining wastes. *Environmental Geology*, 32: 100-106.
- Lee G & Faure G (2007). Process controlling trace-metal transport in surface water contaminated by acid-mine drainage in the Ducktown mining district. *Water Air and Soil Pollution*, 186: 221-232.
- Lowson RT (1982) Aqueous oxidation of pyrite by molecular oxygen. *Chemical Reviews*, 5-82:461-497.
- Maqsoud A, Bussière B, Aubertin M, Potvin R, Cyr J (2007). Evaluation of the hydraulic residence time in the limestone drains of the Lorraine site, Latulippe, Québec. Proc. of the IV International Conference on Mining and the Environment, Sudbury, 1-11.
- Maurice R (2002). Restauration du site minier Poirier (Joutel) – expériences acquises et suivi des travaux. Proc. of Défis & Perspectives: Symposium 2002 sur l'Environnement et les Mines, Rouyn-Noranda, on CD-ROM, paper s32 a1021 p545.
- Mbonimpa M, Aubertin M, Aachib M, Bussière B (2003). Diffusion and consumption of oxygen in unsaturated cover materials. *Canadian Geotechnical Journal* 40: 916-932.
- McLaughlin J & Stuparyk R (1994). Evaluation of low sulphur rock tailings production at INCO's Clarabelle mill. Proc. of the Innovations in Mineral Processing Conference, Sudbury, 129-146.
- MEND (2001). Manual report 5.4.2, Volume 1: Summary, Volume 2: Sampling and Analysis, Volume 3: Prediction, Volume 4: Prevention and Control, Volume 5: Treatment, Volume 6: Monitoring. Canada Centre for Mineral and Energy Technology, Ottawa, Canada.
- MEND (1996). Review of use of an elevated water table as a method to control and reduce acidic drainage from tailings, Mine Environment Neutral Drainage Report 2.17.1. Canada Centre for Mineral and Energy Technology, Ottawa, Canada.
- Mermillod-Blondin R, Kongolo M, de Donato P, Benzaazoua M, Barrès O, Bussière B, Aubertin M (2005). Pyrite flotation with xanthate under alkaline conditions - application to environmental desulfurization. Proc. of the Centenary of Flotation Symposium, Brisbane, QLD.
- Mian MH & Yanful EK (2004). Analysis of wind-driven resuspension of metal mine sludge in a tailings pond. *Journal of Environmental Engineering and Science*, 3: 119-135.
- Moncur MC, Ptacek CJ, Blowes DW, Jambor JL (2005). Release, transport and attenuation of metals from an old tailings impoundment. *Applied Geochemistry*, 20: 539-659.
- Morin KA & Hutt NM (1997). *Environmental Geochemistry of Minesite Drainage. Practical Theory and Case Studies*. MDAG Publishing.
- Morris CE & Stormont JC (1997). Capillary barriers and Subtitle D covers: estimating equivalency. *Journal of Environmental Engineering*, 123: 3-10.
- Morth AH & Smith EE (1966). Kinetic of the sulphide-to-sulfate reaction. American Chemical Society, Division of Fuel Chemistry. Preprints. 10:83.
- Nastev M & Aubertin M (2000). Hydrogeological modelling for the reclamation work at the Lorraine mine site Québec. Proc. of the 1st Joint IAH-CNC-CGS Groundwater Specialty Conference, Montréal, Québec: 311-318.
- Neculita CM, Zagury GJ, Bussière B (2007). Passive treatment of acid mine drainage in bioreactors using sulfate-reducing bacteria: critical review and research needs. *Journal of Environmental Quality*, 36: 1-16.
- Nicholson RV, Gillham RW, Cherry JA, Reardon EJ (1989). Reduction of acid generation in mine tailings through the use of moisture-retaining cover layers as oxygen barriers. *Canadian Geotechnical Journal*, 26: 1-8.
- Nicholson RV, Gillham RW, Reardon EJ (1988). Pyrite oxidation in carbonate-buffered solution. *Geochimica Cosmochimica Acta*, 52:1077-1085.
- Oakley RE (1987). Design and performance of earth-lined containment systems. *Geotechnical Practice for Waste Disposal*, ASCE, 117-136.
- Orava DA, Tremblay GA, Tibble A, Nicholson R (1997). Prevention of acid rock drainage through the application of in-pit disposal and elevated water table concepts, Proc. of the 4th ICARD, Vancouver, Canada, 3: 973-983.
- Ouangrawa M, Molson J, Aubertin M, Bussière B, Zagury GJ (2009). Reactive transport modelling of mine tailings columns with capillarity-induced high water saturation for preventing sulphide oxidation. *Applied Geochemistry*, 24: 1312-1323.
- Ouangrawa M (2007). Étude expérimentale et analyse numérique des facteurs qui influencent le comportement hydro-géochimique des résidus miniers sulfureux partiellement saturés. Ph.D. Thesis, Department of Civil, Geological & Mining Engineering, École Polytechnique Montréal.
- Ouangrawa M, Molson J, Aubertin M, Zagury GJ, Bussière B (2006). The effect of water table elevation

- on acid mine drainage from reactive tailings: A laboratory and numerical modeling study. Proc. of the 7th International Conference on Acid Rock Drainage (ICARD), St. Louis, Missouri, R.I. Barnhisel (Ed.). The American Society of Mining and Reclamation, CD-ROM.
- Perkins EH, Nesbitt HW, Gunter WD, St-Arnaud LC, Mycroft JR (1995). Critical review of geochemical processes and geochemical models adaptable for prediction of acidic drainage from waste rock. Mine Environment Neutral Drainage (MEND) Report 1.42.1. Secretariat CANMET, Ottawa, Ont.
- Potvin R (2009) Évaluation à différentes échelles de la performance de systèmes de traitement passif pour des effluents contaminés par le drainage minier acide. PhD thesis, Université du Québec en Abitibi-Témiscamingue (to be published).
- Rastogi V (1996). Water quality and reclamation management in mining using bactericides. *Mining Engineering*, 48: 66-71.
- Rogowski AS & Pionke HB (1984). Hydrology and Water Quality on Strip-mined Lands. U.S. Environmental Protection Agency.
- Rowe RK, Quigley RM, Brachman RWI, Booker JR (2004). *Barrier Systems for Waste Disposal Facilities*, Taylor & Francis Books Ltd (E & FN Spon) London, p. 587.
- Ritcey GM (1989). *Tailings Management, Problems and Solutions in the Mining Industries*. Elsevier.
- Scanlon BR, Reedy RC, Keese KE, Dwyer SF (2005). Evaluation of evapotranspirative covers for waste containment in arid and semiarid regions in the Southwestern USA. *Vadose Zone Journal*, 4: 55-71.
- Sherlock EJ, Lawrence RW, Poulin R (1995). On the neutralization of acid rock drainage by carbonate and silicate minerals. *Environmental Geology*, 25: 43-54.
- SRK (Steffen, Robertson and Kirsten) (1989). *Draft Acid Rock Technical Guide*. BC AMD Task Force, Vol. 1.
- Strachan C (2002). Review of tailings dam incident data. *Mining Environmental Management, Tailings Management Guide*, January 2002: 7-9.
- Sverdrup HU (1990). *The Kinetics of Base Cation Release Due to Chemical Weathering*. Lund University Press.
- Tassé N & Germain D (2004). The East-Sullivan mine site : from abandonment to restoration. Proc. of the 57th Canadian Geotechnical Conference and 5th joint CGS/IAH-CNC Conference, Québec, Session 8D, CD-ROM.
- Tassé N, Isabel D, Fontaine R (2003). Wood Cadillac mine tailings: designing a biofilter for arsenic control. Proc. of Sudbury 2003, Mining and the Environment III, Session 1A Bacteria, Paper on CD-ROM.
- Tassé N, Germain D, Dufour C, Tremblay R (1997). Hard-pan formation in the Canadian Malartic mine tailings: Implication for the reclamation of the abandoned impoundment. Proc. of the 4th International Conference on Acid Rock Drainage, Vancouver. IV: 1797-1812.
- Tremblay GA & Hogan CM (2009). Approaches for the remediation of abandoned mines and NAOMI. *Déchets, Sciences et Techniques*, 54: 3-9.
- Van Zyl D, Sassoon M, Digby C, Fleury AM, Kyeyune S (2002). Mining for the future. Paper prepared for Mining, Minerals and Sustainable Development (MMSD), Appendix C: Abandoned Mines, p. 19.
- Vick SG (1990). *Planning, Design and Analysis of Tailings Dams*. BiTech Publishers Ltd. Vancouver, B.C.
- Ward AL & Gee GW (1997). Performance evaluation of a field-scale surface barrier. *Journal of Environmental Quality*, 26: 694-705.
- Watzlaf GR (1986). Control of acid drainage from mine wastes using bacterial inhibitors. Proc. of the 1986 National Meeting of the American Society for Surface Mining and Reclamation: 123-130.
- Williams DJ, Currey NA, Ritchie PJ (2003). Kidston waste rock dump design and "store and release" cover system seven years on. Proc. of 6th International Conference on Acid Rock Drainage, Cairns, Australia: 419-426.
- Yanful EK & Catalan LJJ (2002). Predicted and fieldmeasured resuspension of flooded mine tailings. *Journal of Environmental Engineering*, 128: 341-251.
- Zaluski MH, Trudnowski JM, Harrington-Baker MA, Bless DR (2003). Post-mortem findings on the performance of engineered SRB field-bioreactors for acid mine drainage control. Proc. of the 6th International Conference on Acid Rock Drainage, Cairns Australia: 845-853.
- Zhan G, Aubertin M, Mayer A, Burke K, McMullen J (2001). Capillary cover design for leach pad closure, *SME Transaction* 2001, 1: 104-110.
- Ziemkiewicz PF, Skousen J, Brant DL, Sterner PL, Lovett RJ (1997). Acid Mine Drainage Treatment with Armored Limestone in Open Limestone Channels. *Journal of Environmental Quality*, 26: 1017-1024.

EFFECT OF MgO ADDITIVE ON PREVENTING LEAKAGE OF Cr(VI) FROM A FLY ASH

Jin-Chun CHAI¹, Takanori HINO² and Nobuyuki NISHINO³

ABSTRACT: The effect of oxide magnesium (MgO) additive on preventing and/or reducing the leakage of Cr(VI) from a fly ash (coal ash) has been investigated by batch contact and column percolation tests. The test results indicate that MgO additive has an obvious effect of reducing Cr(VI) to Cr(III). For cases of adding 10 to 30% of Ariake clay into the fly ash, the test results indicate that Cr(III) was absorbed by the clay mineral. Comparing the results of the batch contact test and the column percolation test indicates that the column percolation test results in higher initial Cr(VI) concentration in the liquid phase. The main reason considered is that the column test had less water in contact with the ash at the early stage of the test. Also, the results of the column percolation test using the samples with different curing time indicate that with a cement additive, curing the sample can reduce Cr(VI) concentration, but with MgO additive, there is no obvious effect of curing the sample.

KEYWORDS: fly ash, hexagon chromium, magnesium additive, batch contact test, column percolation test

INTRODUCTION

From thermal power stations, large amount of fly ashes are generated every year, for example, in Japan, the amount was about 54 million Ton/year (RCUWGCM, 1999). How to treat and/or effectively use the fly ashes is an important environmental issue. One of the ways is to use them as construction material, such as for embankment construction. The fly ash can be used alone or mixed with waste clayey soils. However, fly ashes normally contain ions of heavy metals such as Cr(VI), Cd(II), Pb(II), etc, which may have a negative effect/impact to environment.

As for Cr(VI), the commonly used methods for preventing its leakage are: (1) stabilization/solidification, which uses cementation materials to bind the Cr(VI) within an insoluble matrix offering low leaking characteristics; (2) chemical process, which converts the toxic Cr(VI) to less environmentally hazardous forms, such as Cr(III). Cement is a widely used cementation material but it normally contains Cr(VI) and it is a strong alkaline material. Oxide magnesium (mainly MgO) can function as a cementation material and less alkaline than cement. Therefore, it can be expected to use MgO additive to prevent leakage of Cr(VI) from coal (fly) ashes.

In this paper, both batch contact and column percolation tests were conducted to investigate the effect of MgO additive on prevention the leaking of Cr(VI). For comparison, the tests of using cement as additive were also conducted.

LABORATORY TEST

Fly Ashes

The fly ashes tested have a brand name of Blair Athol (from Blair Athol coal, Australia). The chemical compositions of the ash are listed in Table 1. The chemical compositions were analyzed by fluorescent X-ray analysis method. The ignite loss was 2.31% and total Cr content was 3.2 mg/kg. The density of the fly ash particles was not tested for this batch, but the test result from a different batch (the same brand name) gives a value of 22.54 kN/m³ (Chai et al. 2009).

Ariake Clay

The Ariake clay used to mix with the fly ashes in this study was Ariake clay with a liquid limit (w_l) of 123.9% and plastic limit (w_p) of 56.2%. The dominant clay mineral in the Ariake clay is smectic one (Ohtsubo et al.

¹ Professor, Department of Civil Engineering, Saga University, Japan. Email: chai@cc.saga-u.ac.jp

² Associate Professor, Institute of Lowland Technology, Saga University, Japan. Email: hino@ilt.saga-u.ac.jp

³ Ube Material Industries Ltd., Japan. Email: nobuyuki.nishino@ube.materials.co.jp

Table 1 Chemical properties of the fly ash and the oxidized magnesium

Chemical component		SiO ₂	Al ₂ O ₃	Fe ₂ O ₃	TiO ₂	CaO	MgO	K ₂ O	Na ₂ O	P ₂ O ₃	SO ₄	H ₂ O
Content (%)	Fly ash	62.09	21.70	3.52	1.09	4.01	0.98	1.05	0.49	0.19	-	0.08
	Oxidized magnesium	0.18	0.06	0.10	-	0.55	82.6	-	-	-	4.06	1.29

1995). The pH value of the solution of the clay and distilled water with pH adjusted to about 6.0 and solid/liquid ratio of 1:10 was 7.4.

Additives

Two types of additives were used, namely oxidized magnesium (will be referred as MgO) and cement. MgO used was produced from sea water, and its chemical properties are listed in Table 1 also. The ignite loss is 11.16% and density is 6.86 kN/m³. All the data were provided by the manufacturer. The cement used was type B blast furnace cement (will be referred as the cement). The raw materials used to make it are blast furnace slag, clinker and gypsum.

Method for Batch Contact Test

The tests were conducted basically according to the regulation of the Public Notice No. 46, JEA (1991). The solid/liquid ratio adopted was 1:10. The liquid used was distilled water and the initial pH value was adjusted to about 6 by adding hydrochloric acid. The mixture was put into 1l glass bottles and mixed for 6 hours by rotating the bottles (upside down) with a speed of 30 rpm. Then the bottles were left for precipitation of solid particles for about 6 hours, and the liquid phase was further filtrated through a filter with an opening size of 0.45m. The concentration of Cr(VI) and total Cr, pH, and oxidation-reaction potential (ORP) of the liquid phase were measured.

Method for Column Percolation Test

The columns used have a diameter of 75 mm and height of 225 mm. The samples of the fly ash with or without additives for the column test were typically 20 mm thick. The samples were formed by compacting the material at near its optimum water content of about 30% (by A-method, JIS A 1210) (JSA, 1999) inside the column. The dry unit weight of the samples was about 11.4 kN/m³ (maximum dry unit weight of about 12.0 kN/m³). During the tests, the depth of distilled water on the top of the samples was kept as 150 mm and the

leakage was collected and the concentration of Cr(VI) and total Cr, pH and ORP were measured periodically.

For all samples, Cr(VI) and total Cr concentrations were measured by pack-text methods. To check the reliability of the pack-test results, about 20% of the samples, Cr(VI) concentration was measured by absorptiometric method using diphenyl carbazide (JIS K 0102 65.2) (JSA, 1998) and total Cr concentration by inductively coupled plasma-atomic emission spectrometry method (ICP-AES) (JIS K 0102 65.1.4) (JSA, 1998). It has been confirmed that the pack-tests gave acceptable results. pH was measured following the method specified by Japanese Geotechnical Society, JGS 0211-2000 (JGS, 2000). ORP was measured using Horiba pH/Cond meter D-54.

Cases Tested

The conditions for batch contact and column percolation tests are listed in Table 2.

Table 2 List of all tests conducted

Clay/fly ash ratio (C/F)	Batch contact test		Column test#	
	MgO (%)	Cement (%)	MgO (%)	Cement (%)
0:100	0, 5, 10	-	0, 5, 10	-
0:100	-	5, 10	-	5, 10
10:90	0, 1, 2, 3, 4, 5, 10	-	-	-
30:70	0, 5, 10	-	-	-

For each condition, 4 samples were prepared and tested at 4 different curing times, 0, 1, 2 and 3 weeks

RESULTS AND DISCUSSION

Batch Contact Test

To provide a reference for discussion, firstly, the batch contact tests using the cement and MgO as solid phase were conducted. For the cement, the equilibrium Cr(VI) concentration in the liquid phase was 0.5 mg/l and pH of 13.11. For MgO, there was no Cr(VI)

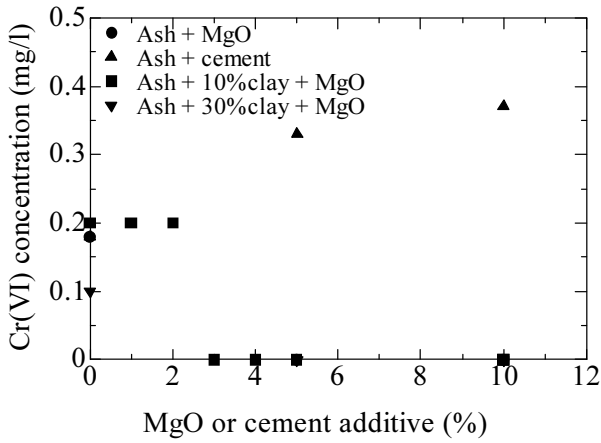


Fig. 1 Variation of Cr(VI) concentrations

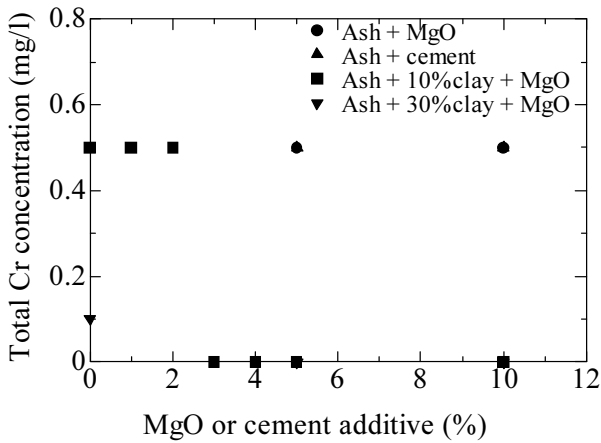


Fig. 2 Variation of total Cr concentration

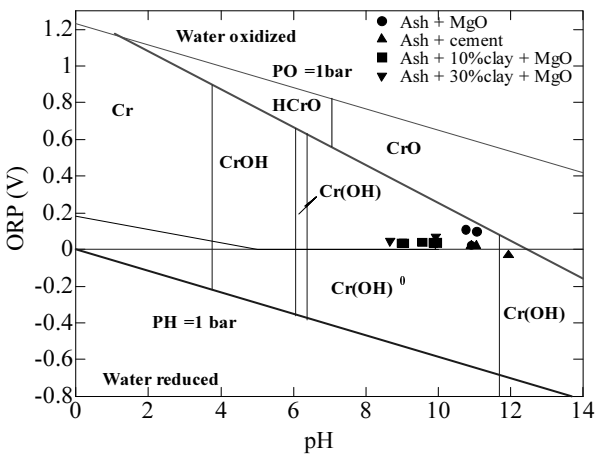


Fig. 3 pH-ORP diagram of Cr including the batch contact test results

detected (measuring low limit of 0.005 mg/l) and pH of the liquid phase was 10.24.

The equilibrium Cr(VI) concentrations are summarized in Fig. 1. For the fly ash alone case, the equilibrium Cr(VI) concentration was 0.18 mg/l. Then

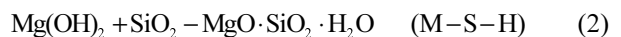
for the fly ash with additive cases, it can be seen that adding the cement increased Cr(VI) concentration because the cement used contains more Cr(VI) than the fly ash. Adding 5% and 10% MgO, there was no Cr(VI) detected. For the fly ash and the Ariake clay mixtures, in cases of no additive, adding 10% of the clay case almost resulted the same Cr(VI) concentration of without the clay case, and for adding 30% the clay case reduced Cr(VI) concentration to 0.1 mg/l. As expected that for the cases of adding 5% and 10% MgO into the fly ash and the clay mixtures, there were no Cr(VI) detected. To check the minimum amount of MgO additive to prevent the leakage of Cr(VI), the tests of adding 1%, 2%, 3% and 4% of MgO into the fly ash and 10% the clay mixture were also conducted. It is found that for the case investigated, 3% MgO additive is able to prevent the leakage of Cr(VI).

The results of total Cr concentrations are given in Fig. 2 and which can be used to explain the mechanism of the effect of MgO. First for all the cases of the fly ash with additives, the total Cr concentrations are almost the same and equals to about 0.5 mg/l. This clearly indicate that by adding MgO, Cr(VI) was reduced to Cr(III). However, for the fly ash and the clay mixtures, when the amount of MgO added is more than 3%, there was no Cr detected in the solution. It is considered that Cr(III) was adsorbed by the clay mineral.

The oxidation-reduction of Cr is influenced by the pH value as well as oxidation-reduction potential (ORP) of the solution. pH – ORP diagram for Cr (Pamer, 1994) is shown in Fig. 3 and the results of the batch contact test are included into the plot. It can be seen that for the fly ash and the clay mixture with MgO additive cases, the points are in the range of Cr(III). For the cases of the fly ash with the cement or MgO additives, the points are in Cr(III) side but near the Cr(VI) and Cr(III) boundary. From the figure, it can be seen that for the conditions tested, most possibly Cr(VI) was in a form of CrO_4^{2-} and it can be reduced to Cr(III) by the following reaction.



The possible reaction of MgO with the fly ash can be: when MgO meets water, it becomes $Mg(OH)_2$, and $Mg(OH)_2$ reacts with SiO_2 to form a substance of $MgO \cdot SiO_2 \cdot H_2O$ (M-S-H) and deposited.



Column Percolation Test

For easy to present the column percolation test results, a variable called the numbers of pore volume (NPV) is defined as follows:

$$NPV = \frac{V_L}{V_V}, \quad V_V = n \cdot V_T \quad (3)$$

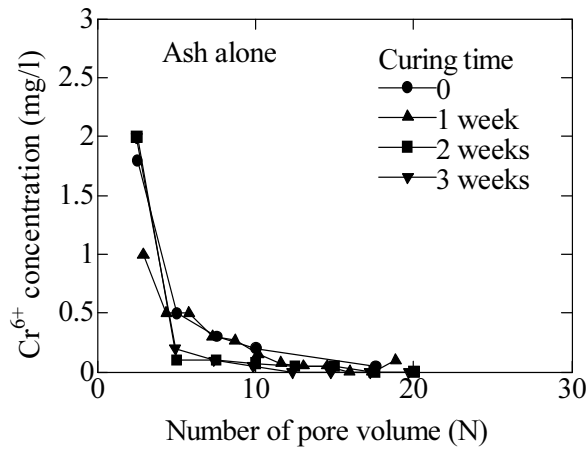


Fig. 4 Cr(VI) concentration variation (ash alone)

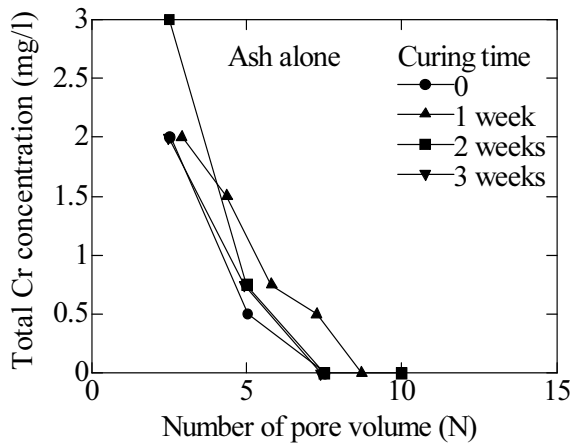


Fig. 5 Total Cr concentration variation (ash alone)

where V_L is the volume of the leakage collected, V_V is the volume of voids of a sample, V_T is the total volume of the sample (soil layer), and n is the porosity of the sample. The column tests were only conducted using the fly ash alone and with MgO or cement additives.

First as a reference, the variation of Cr(VI) and total Cr concentration with NPV of using the fly ash alone are given in Figs 4 and 5 respectively. From Fig. 4, it can be seen that Cr(VI) corresponding to NPV of about 2 is about 2 mg/l, which is much higher than the batch contact test results. For the samples tested, the ratio of the solid mass of the sample to 1 NPV of leakage by weight is approximately 1:0.5, which is much larger (less water) than the solid/liquid ratio of 1:10 adopted for the batch contact test, and it indicates that the amount of water in contact with the fly ash played an important role on Cr(VI) concentration (Chai et al. 2009). When NPV is larger than about 10, Cr(VI) concentration reduced below the environmental standard of (0.05 mg/l). This

result emphasizes that to investigate the possible environmental impact, it is important to select a test method which closely simulates the field condition. The total Cr concentration is higher than the corresponding

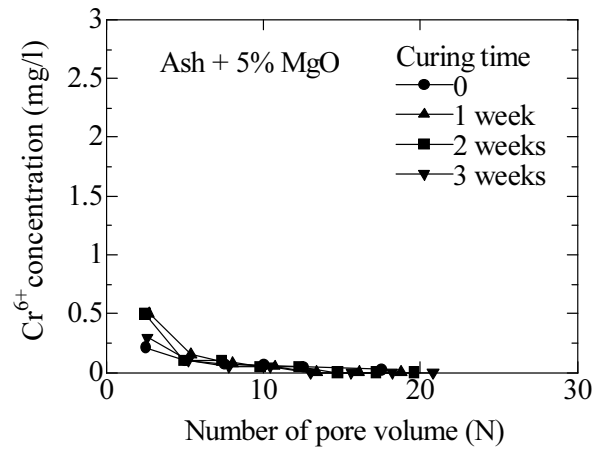


Fig. 6 Cr(VI) concentration variation (ash + 5% MgO)

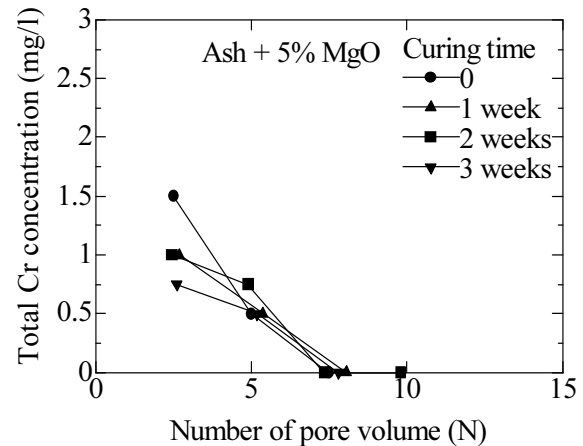


Fig. 7 Total Cr concentration variation (ash + 5% MgO)

Cr(VI) and reduced with the increase of NPV also. Another point is that the curing time had no obvious effect on both Cr(VI) and Cr concentrations.

The results of adding 5% MgO case are given in Figs. 6 and 7. Comparing with the results in Figs. 4 and 5 indicates that MgO additive reduced Cr(VI) concentration, but curing had no effect on reducing Cr(VI) concentration also. When NPV is larger than about 5, Cr(VI) concentration is less than the environmental standard. The total Cr concentration (Fig. 7) is little bit lower than that of without the additive case (Fig. 5), but the reduction is small. The results in Figs. 6 and 7 confirms the finding from the batch contact test with the fly ash (without the Ariake clay), that MgO reduced Cr(VI) to Cr(III). The results of adding 10% MgO is similar to that in Figs 6 and 7, but slightly lower Cr(VI) concentration.

For comparison, the Cr(VI) concentration of adding 5% the cement into the fly ash are depicted in Fig. 8. It

can be seen that without curing, adding 5% the cement had no effect on Cr(VI) concentration (comparing with the results in Fig. 4), but the curing time had an obvious

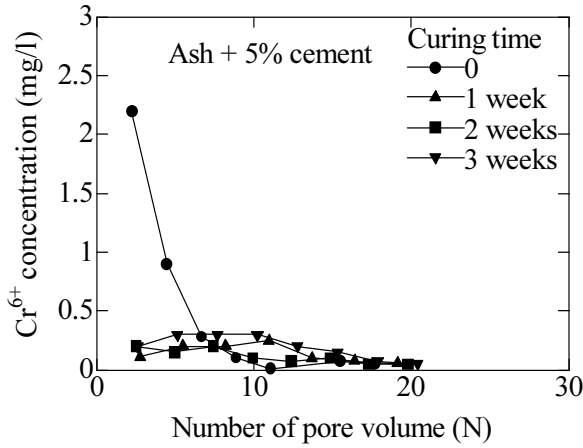


Fig. 8 Cr(VI) concentration variation (ash + 5% cement)

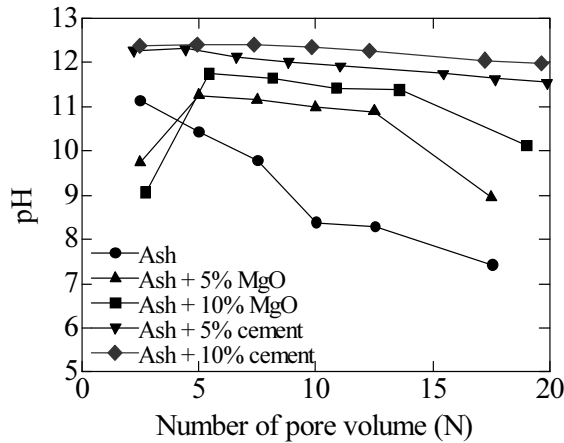


Fig. 9 Variation of pH value

effect on Cr(VI) concentration. However, in case of the total Cr concentration, the results of adding 5% the cement case is similar to that of the adding 5% MgO, and the curing time had no obvious effect. Although the exact mechanism is not clear, it seems that during curing period, the reaction between the fly ash and the cement reduced Cr(VI) to Cr(III).

The variations of pH value with NPV are compared in Fig. 9 for cases without curing time. It can be seen that comparing with the case of without additives, adding MgO initially reduced pH value about 2, and when NPV is larger than 5, reversely, pH value was increased and larger than that of without additive case. The results of adding MgO and with curing time cases show the same tendency. Although the exact mechanism is not clear, one of possible explanation is that when MgO reacted with water to form Mg(OH)₂ resulted in the increase of H⁺ in the solution, but during the subsequent

reaction of Mg(OH)₂ with SiO₂ to form M-S-H, there was certain decrease of H⁺ in the solution and the later reaction needs more time. However, during the whole process, pH values of adding MgO cases are lower than that of adding the cement case, and lower pH value favors the reduction of Cr(VI) to Cr(III).

CONCLUSIONS

The effect of oxide magnesium (MgO) additive on preventing and/or reducing the leakage of Cr(VI) from a fly ash (coal ash) has been investigated by batch contact and column percolation tests. Based on the test results, the following conclusions can be drawn.

(1) MgO additive has an obvious effect on preventing and/or reducing the leakage of Cr(VI) from the fly ash. By measuring the total Cr concentration, pH and oxidation reduction potential (ORP) of the equilibrium solution, the mechanism of reducing Cr(VI) concentration has been identified as reducing Cr(VI) to Cr(III). In cases of adding 10 to 30% of Ariake clay into the fly ash with MgO additive, both Cr(VI) and Cr(III) concentrations had been reduced, which implies that Cr(III) might be absorbed by the clay minerals.

(2) Comparing the results of the batch contact test and the column percolation test indicates that the column percolation test results in higher initial Cr(VI) concentration in the liquid phase because there was less water in contact with the ash at the early stage of the test. Therefore, to assess the possible environmental effect, a test method closely simulates the field condition is important.

(3) The results of the column percolation test using the samples with different curing time indicate that with a blast furnace cement additive, curing the sample can reduce the Cr(VI) concentration, but with MgO additive, there is no obvious effect of curing the sample.

REFERENCES

Chai JC, Onitsuka K, Hayashi S (2009). Cr(VI) concentration from batch contact/tank leaching and column percolation test using fly ash with additives. *Journal of Hazardous Materials*, 166: 67-73.

Japanese Geotechnical Society (JGS) (2000). Test Method for pH of Suspended Soils, JGS 0211-2000, Tokyo, Japan.

Japanese Standard Association (JSA) (1998). Testing Method for Industrial Waste Water, JIS K 0102 65.2 (Chromium), Tokyo, Japan.

Japanese Standard Association (JSA) (1999). Test method for soil compaction using a rammer, JIS A 1210, Tokyo, Japan.

- Japanese Environment Agency (JEA) (1991) Environment standards regarding to soil contamination. Public Notice No. 46 (in Japanese).
- Ohtsubo K, Egashira K, Kashima K (1995). Depositional and post-depositional geochemistry, and its correlation with the geotechnical properties of marine clays in Ariake Bay, Japan, *Geotechnique* 45 (3): 509-523.
- Palmer C & Puls R (1994). Natural attenuation of hexavalent chromium in ground water and soils. EPA/540/S-94/505, U.S. Environmental Protection Agency Ground Water Issue.
- RCUWGCM (1999). Activity report, Research Committee for Using Wastes as Geotechnical Construction Material (RCUWGCM), Japan (in Japanese).

ENVIRONMENTAL GEOTECHNICS RELATED TO LANDFILLS OF MUNICIPAL SOLID WASTES

Yun-Min CHEN¹ and Tony L.T. ZHAN²

ABSTRACT: Management of municipal solid waste (MSW) is one of the major environmental problems in China. Solid waste disposal in landfills remains the most economic form of disposal for most cases. In this paper, an attempt has been made to provide a review of four geotechnical issues associated with landfills of MSWs, including (1) water and leachate flow within landfills, (2) landfill gas generation, transport and control, (3) settlement of landfills and its impacts, and (4) stability of waste mass. The review is conducted primarily in the context of the waste composition characteristic and the current practice of landfills pertaining to China. The current status and major problems associated with the current landfill practice are identified and/or evaluated, and the areas required for future research and development are pointed out.

KEYWORDS: MSW, landfill, leachate, gas, settlement, stability

INTRODUCTION

With rapid industrialization and urbanization in the world, environmental issues have been a significant component of Geotechnical Engineering since about 1980. A new discipline called “Environmental Geotechnics” was born in an interdisciplinary context, and has become one of the most important subjects in the International Society on Soil Mechanics and Geotechnical Engineering (ISSMGE) as well as in all the regional Societies. In 1987, the Fifth Technical Committee (TC-5) was founded under ISSMGE. Following that, the International Congress on Environmental Geotechnics were organized almost as the same level of ICSMGE in Edmonton (1994), Osaka (1996), Lisbon (1998), Rio de Janeiro (2002) and Cardiff (2006). Although the scope of “Environmental Geotechnics” is becoming wider and wider, waste management remains as one of the most important and typical environmental issues in geotechnical engineering practice.

Management of municipal solid waste (MSW) is one of the major environmental problems in China. The total population is over 1.3 billion, occupying 22.3% of the global population. Most of the 661 cities daily generate thousands of tons of municipal solid wastes. Proper management of the huge amount of wastes becomes a critical and stringent environmental issue in most of the

Chinese cities. The lack of resources such as financing, suitable planning and civil infrastructures relative to the rapid increase of service demand has caused an adverse impact on the environment and human health.

Solid waste disposal in landfills remains the most economic form of disposal in the vast majority of cases. In Asia, depending on location, up to 90% of municipal solid wastes collected in cities and towns are currently disposed of in landfills. In most of the developed countries in Europe and America, the practice of MSW landfills has evolved from open dumping (~1970s) to controlled or sanitary landfill (~1990s), and to the modern bioreactor landfill. However, the standard of practice for MSW landfill disposal is still at a low-level. China has stipulated stringent regulations controlling adverse environmental impacts of MSW landfill disposal (i.e. controlled landfilling) since 1988. However, there is still a large gap between policy and implementation due to the lack of financing, research, pre-planning and suitable technology. Several lethal failures in MSW dumps and landfills happened (Chongqin in 1996). In addition, the impacts of landfill leachate and gas on the adjacent metropolitan environments, although being lack of data, are believed to be serious. Uncontrolled release of landfill gas (methane and carbon dioxide) from thousands of MSW dumps and landfills in China has become a non-negligible contributor to the global warming or the greenhouse effect (El-Fadel et al. 1997).

¹ Professor, MOE Key Laboratory of Soft Soils and Geoenvironmental Engineering, Zhejiang University, Hangzhou, China. Email: chenyunmin@zju.edu.cn

² Professor, MOE Key Laboratory of Soft Soils and Geoenvironmental Engineering, Zhejiang University, Hangzhou, China. Email: zhanlt@zju.edu.cn

In the present paper, an attempt has been made to provide a review of the environmental geotechnics associated with landfills of MSWs, including (1) water and leachate flow within landfills, (2) landfill gas generation, transport and control, (3) settlement of landfills and its impacts, and (4) stability of waste mass. The transport of leachate pollutant and landfill barriers will be discussed in another paper of this proceeding. The review is conducted primarily in the context of the characteristic of waste composition and the current practice of landfills pertaining to China. The current status and major potential problems associated with the landfill practice are identified and/or evaluated, and the points required for future research and development are proposed. The paper is concluded with a few constructive suggestions, which may be helpful to encourage the competent authorities/researchers/designers to work together further improvement of the present landfill technology.

WASTE COMPOSITION AND SOLID-LIQUID-GAS INTERACTIONS IN MSW LANDFILLS

Composition and Classification of Municipal Solid Wastes

Knowledge of waste composition of MSW is required to understand the performance of landfills. MSW typically consists of food and garden wastes, paper products, plastics, rubber, textiles, wood, ashes, and soils. These components exhibit a great variety in size, shape, degradability, compressibility and tensile strength. The proportion of these components, depending on living style and standard, will vary from one region to another. Even within a region, living standard changes, legislation, seasonal factors, pre-treatment and recycling activities may result in a changing waste stream over time. For example, a significant decrease in cinder content and an increase in the recyclable content and organic content happened to the Chinese MSW during the last decade (see Fig. 1). The significant change in cinder content was primarily the result of an increasing use of natural gas in kitchens.

Table 1 shows a comparison of waste composition among China, India, Korea, Singapore, UK and USA. The MSWs in China and India contain much more putrescible wastes (i.e. food and garden wastes, accounting for 40-50%) than the MSWs generated in UK, USA, Korea and Singapore. The content of mineral materials (cinder, dust, concrete etc.) in the Chinese countries is higher than those in UK and USA. These differences are likely attributable to the difference in the cooking styles between China and the other two continents as well as the difference in the living standard

among the countries. In addition, the recyclable content of MSWs in China is less than that in UK and USA, particularly with regard to paper waste. This is because there are many rag pickers in these two countries, who segregate and collect the recyclable materials (paper and plastics) at generation sources, collection points and disposal sites.

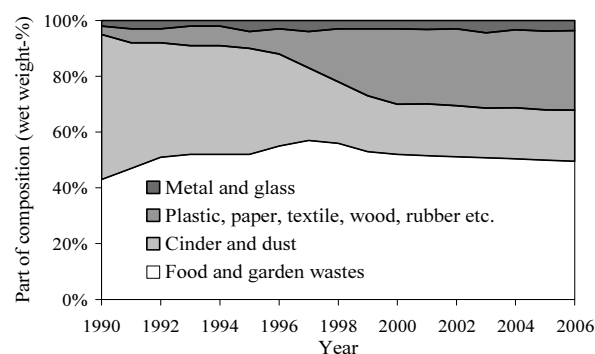


Fig. 1 Change in composition of MSW as generated in Suzhou, China over the last decade

Table 1 Comparison of Waste Composition Among China, India, Korea, UK and USA Generated in 2000

Country	Food, vegetable	Dust, cinder	Paper	Plastic, textile, wood, rubber	Metal, Glass	Others
China	43.6	23.1	6.7	16.7	3.4	6.5
India	41.8	40.3	5.7	8.2	4	0
Korea	24.6	NA	25.8	NA	13.5	NA
Singapore	23.5	17.1	21.6	11.1	24	2.7
UK	20	12	34	21	15	0
USA	15.3	10.9	29.8	29.4	12.7	1.9

Notes: China: data from Chinese Research Academy of Environmental Science (2003); India: data from Sharholly et al. (2007); Korea: data from Ministry of the Environment (2003); Singapore: data from Ministry of the Environment of Singapore (2000); UK: data from Watts et al., 2002; USA: data from US EPA (2005)

After being disposed in landfills, waste composition inevitably changes with time due to a biological degradation of the organics. The wastes embedded at different depths generally have experienced different degree of degradation, and hence pose different composition. Fig. 2 shows variations of MSW composition with fill age which was determined from the samples taken from the Suzhou landfill in China (Chen et al. 2009). It can be seen that the content of cinder and dust significantly increased with fill age. The other components (organics, plastics, paper, textiles, wood, glass, metal etc.) basically showed a decreasing trend with fill age. It should be pointed out that the change in the waste composition with fill age was partially attributed to the change in the original composition of MSW generated over the last decade (see Fig. 1).

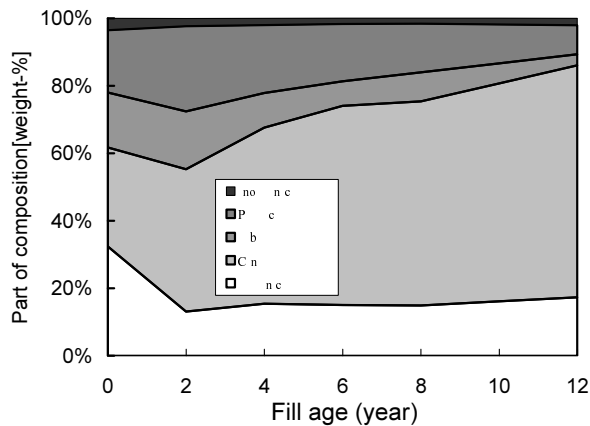


Fig. 2 Variations of MSW composition with fill ages of the samples (Chen et al., 2009)

The great variations in the composition of MSW inevitably produce a significant variety in waste engineering properties. This is the main reason why the experimental data of waste engineering properties (e.g. compressibility, shear strength and permeability) reported in the literatures vary widely. A better interpretation of published results requires an internationally agreed classification system (Dixon and Jones, 2005). Unfortunately, all the waste classification systems in common use were developed for the specific purposes such as assessment of calorific value and C/N ratio, rather than for geotechnical engineering purpose. It is inspiring that Dixon and Langer (2006) have recently developed a MSW classification system for the evaluation of mechanical properties. The classification system takes into account mechanical properties, size, shape and degradability potential of waste components. The classification system will be helpful to researchers involved in sharing and interpreting experimental data of waste mechanical properties. Further work is required to relate classification of waste components to mechanical behavior of waste mass.

Solid-Liquid-Gas Interactions in MSW Landfills

MSW landfill is a new form of infrastructure resulted from urbanization. Similar to other conventional earth structures such as dams, a landfill is concerned with three categories of traditional geotechnical problems, i.e. stability of waste mass, landfill settlement and water flow within landfill body. In addition to these, landfill is highly concerned with the prevention of landfill leachate and gas transporting into the adjacent environment. To prevent the environmental impacts, an engineered landfill differs from the conventional earth structures in that its design incorporates leachate and gas control systems such as covers, liners, drainage structures, gas

collection and leachate removal systems. The systems are composed of materials with markedly different properties and behavior. More importantly, the primary material building up a landfill (i.e. MSW) is much more complicated with respect to composition and properties than the mineral materials within the conventional earth structures. MSW consists of a wide variety of components from biodegradable organics to relatively inert materials as well as a significant portion of fibrous materials (e.g. plastics and fibers). The mechanical behavior of the fibrous materials is significantly different from that of particulate materials. Following waste placement, the landfill becomes a form of biochemical reactor in which the wastes together with moisture react to generate leachate, gases, heat and contaminants. These productions exert interactions with the parent wastes and other materials within the landfill such as drainage gravel, clay barrier and various kinds of geosynthetics. The solid-liquid-gas interactions result in changes in waste properties such as permeability, compressibility, decomposability and shear strength, and hence affect the transport of gas and leachate, settlement and slope stability of landfills (see Fig. 3). The solid-liquid-gas interactions also exert effects on the long-term performance of the landfill barrier system and the leachate drainage and collection system (Gartung et al. 1999; Rowe, 2005; Shackelford, 2006).

The solid-liquid-gas interactions in the MSW landfills are very complex, and an improved understanding on the interactions requires a methodology incorporating the multi phases and multi mechanisms in the landfills. For example, a hydro-bio-mechanical coupled model will help to obtain a better prediction of landfill settlement and stability. Several researchers on unsaturated soils and other similar porous media have successfully developed thermo-hydro-mechanical coupled models (Olivella et al. 1994; Thomas and He, 1995; Yang et al. 2000). In addition to that, the coupled model for MSW landfills should also account for the following features: (1) production of gas, leachate, heat and volume change as a result of decomposition of organics; (2) dependence of waste properties on fill age and strain level. Of course, the coupled model needs to be verified by physical model tests and full-scale field tests. A few researchers have started to make efforts along this direction (McDougall & Hay, 2005; Chen et al. 2006). The research work can be encouraged because it will improve our understanding on the multi-phase interactions in deformable and degradable porous medium. It will also promote the inter-discipline development among geotechnical engineering, environmental engineering and biological engineering.

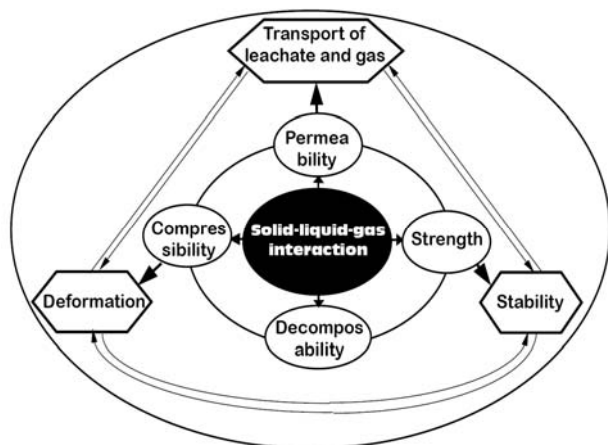


Fig. 3 Geoenvironmental aspects of solid-liquid-gas interactions in landfills of municipal solid wastes

WATER AND LEACHATE FLOW IN LANDFILLS

Thousands of open dumps or uncontrolled landfills in China are generally lack of effective facilities for water management and leachate control. The leachate mound within the landfills as well as leachate generation rate is quite high, particularly in humid regions (e.g. South-east China and Asia). The inappropriate management of water and leachate has resulted in several catastrophic failures of landfills, and caused a high level of environmental pollution risk around the landfills. The development of high leachate mound also has adverse effect on landfill gas control and recovery. Retro-fitted measures (e.g. retro-fitted leachate extraction wells) should be taken to lower down the high leachate level, and control leachate generation rate. For an engineered or controlled landfill, one important design criterion is that the leachate level within the landfill is kept below a specific elevation (e.g. a height of 30 cm as regulated by the EPA in USA). This is generally implemented by setting up a water management system (e.g. facilities for interception of rainwater and runoff) and a leachate control system (e.g. leachate drainage and collection system at the bottom or toe drains). In a modern bioreactor landfill, a leachate recirculation system is usually required to accelerate waste decomposition processes and enhance gas generation rate. Proper designs of all the above water/leachate management systems require an understanding on the water and leachate flow in the MSW landfills. Variables affecting water and leachate flow within a specific landfill include hydraulic properties of MSW (i.e. water retention capacity and hydraulic conductivity), local climate conditions, site hydrogeology, availability and effectiveness of water/leachate management systems and so on.

Water Retention Characteristic of MSW

The water retention characteristic of MSW is important in the prediction of leachate generation rate and leachate level in landfills. Only the water in excess of the field capacity of MSW will be released as leachate. The term “field capacity” is defined as the maximum moisture content that a porous medium can retain against gravity before it starts producing continuous downward flow. The field capacity of MSW is also an important indicator of the optimal water content for waste degradation in bioreactor landfill technology (Qian et al. 2002). However, it is surprising that so few detailed studies have been conducted on this aspect. This is probably a consequence of the heterogeneous nature of MSW, the difficulty of laboratory testing on MSW and the lack of standardization in reported experimental results (Zornberg et al. 1999).

Evaluation of the water retention capacity of MSW requires an understanding on the mechanisms of water retention within the waste mass. Zornberg et al. (1999) summarized three potential mechanisms of water retaining in the waste mass: (1) water within intra-particle voids (held by osmotic pressures); (2) water within inter-particle voids (held by capillary pressures); (3) water retained on low-permeability media (e.g. plastic bags and intermediate cover soils). The content of water retained by the first two mechanisms should be less than the field capacity of MSW. It is believed that the majority of intra-particle water is held in the organics. As the organics decomposes in landfills, this form of water will be released into the other two forms. This introduces an extra complexity to the water retention characteristic of MSW.

Water retention characteristic of MSW is highly dependent on several factors, including waste composition, waste placement method, degree of compaction, overburden pressure and degree of degradation. Fig. 4 shows a collection of water retention curves for the MSWs generated in different countries. As compared with the fine sand, the MSW materials pose a much higher volumetric water content at the full-saturation state as well as at the residual state. The high saturated water content is consistent with the macro-pore structure of the MSW. It is believed that the high residual water content is primarily attributed to the intra-particle water retained in the organic components of the MSWs. The Chinese MSW generated in 2000, having a higher organic content, poses a higher water retention capacity than that generated in 1992. The air entry values of all the MSWs are less than 1 kPa. A comparison of the water retention curves for the Korea MSW demonstrates that the desorption rate of the MSWs is highly dependent on the degree of compaction (DOC). It is generally

assumed that the field capacity is equivalent with the water content corresponding to a matric suction of 10 kPa. As shown in Fig. 4, the values of field capacity of Chinese MSWs range from 33% to 45%, being greater than the UK MSW. The volumetric field capacity reported in the other literatures covers a wide range from 20% to 55%. Zornberg et al. (1999) reported a bilinear decreasing trend of field capacity with the increasing burial depth of MSW in the Southern California landfill.

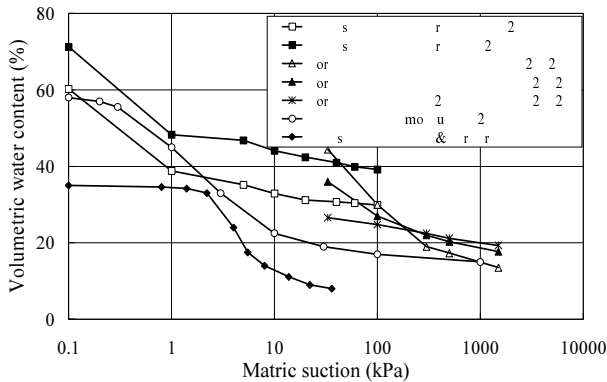


Fig. 4 Water retention curves for MSWs

Hydraulic Conductivity of MSW

The hydraulic conductivity of MSW is one of the key parameters in the design of a leachate control system and a leachate recirculation system particularly for bioreactor landfills. Variables affecting the hydraulic conductivity of MSW include waste composition, degree of compaction, waste structure orientation (e.g. anisotropy), degree of saturation etc. Numerous researchers have investigated this hydraulic property by performing large-diameter permeability tests in the laboratory or leachate pumping tests in the field (Landva and Clark, 1990; Oweis et al. 1990; Schroder et al. 1994; Rowe and Nadarajah, 1996; Powrie and Beaven, 1999; Jang et al. 2002; Chen et al. 2005). The values of hydraulic conductivity of MSWs reported in these literatures mostly fall into a range from 1.0×10^{-6} to 1.0×10^{-4} m/s, being in the same order as the fine sand and silty sand. Rowe and Nadarajah (1996) reported a trend of a decrease in hydraulic conductivity with the increasing burial depth of waste at the Fresh Kills landfill in New York. Powrie and Beaven (1999) used a large-diameter compression cell to investigate the relationship between hydraulic conductivity and overburden pressure for the UK MSW. The test results indicated that the hydraulic conductivity of the UK MSW could fall by over three orders of magnitude to $\sim 10^{-8}$ m/s due to the effect of compression alone when the burial depth of waste increased to a depth of 60 m. A similar laboratory investigation has been conducted on the Chinese MSW

by Chen et al. (2005), and the test results are shown in Fig. 5. The results show that the dependency of hydraulic conductivity on the overburden pressure is predominant at the pressures up to 300 kPa. The decrease of hydraulic conductivity at the high pressure range is relatively insignificant regardless of the further decrease in the void volume of waste. The decrease in hydraulic conductivity with the burial depth of MSW will exert an adverse effect on the performance of vertical leachate extraction wells when the drawdown in the wells is increased (Powrie and Beaven, 1999).

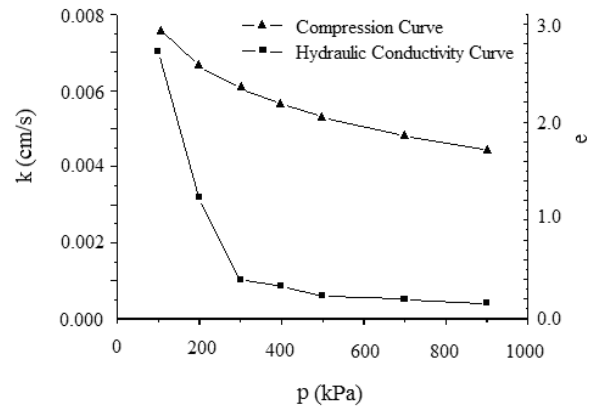


Fig. 5 Relationship of hydraulic conductivity (k) to Saturation density for the MSW generated in China

The hydraulic conductivity of MSW in a landfill is likely to be anisotropic. The anisotropic behavior may be related to the orientation of waste components in a two-dimensional shape (e.g. plastics, paper sheet). In addition, the vertical water permeability may be restricted by the presence of daily and intermediate covers that often contain some fine soils. The laboratory test results obtained by Landva et al. (1998) indicated that the vertical hydraulic conductivity of MSW could be less than the horizontal one by one order. The anisotropic behavior of hydraulic conductivity is likely to result in a perched leachate with a landfill. It is fortunate that the parametric study conducted by Rowe and Nadarajah (1996) showed that the vertical hydraulic conductivity did not play a significant effect on the performance of a vertical leachate extraction well as compared with the horizontal hydraulic conductivity.

Like most of porous media, the hydraulic conductivity of MSW will change with water content or degree of saturation. As experimental determination of unsaturated hydraulic conductivity is very difficult, even for conventional insert soils, little data is available for the MSW material. Probably one exception to this is Korfiatis et al (1984)'s laboratory study on water percolating through a column filled with unsaturated solid wastes. The experimental results, together with the numerical modeling, demonstrated that the change in hydraulic conductivity with water content was

insignificant once the water content of MSW exceeded the field capacity. Korfiatis et al. (1984) explained that the behavior was attributed to the large pore structure of MSW which inhibited a development of high suction heads. All the other researches on the unsaturated hydraulic conductivity of MSW were done in theoretical approaches (McCreanor, 1998; Jang et al. 2002; Kazimoglu et al. 2006; Zhang, 2007). The common principle of the theoretical approaches is to utilize the empirical pore-structure models developed by soil scientists (e.g. Van Genuchten-Mualem model) to predict the unsaturated hydraulic conductivity from the saturated conductivity and water retention curve. The numerical study conducted by Zhang (2007) suggested a power law function is of better representation for the unsaturated hydraulic conductivity of MSW. More experimental data are necessary for the validation of the theoretical approaches.

Another uncertainty in the hydraulic conductivity of MSW is its long-term behavior, which may be affected by the degradation process of MSW and the clogging of the pore spaces in MSW (including physical, chemical and microbiological clogging). As far as the authors are aware, no experimental data has been obtained on this aspect. This is an area of further research.

Water Balance in Landfills and Management of Water/Leachate

The information of leachate quantity and leachate level within a landfill is required to evaluate waste mass stability and environmental pollution risk, as well as to design a leachate control system. Both the quantity and level of leachate are directly related to a state of the dynamic water balance within a specific landfill. The main factors involved in the water balance system include climate conditions (i.e. precipitation, evaporation and evapotranspiration), hydraulic conditions of wastes (i.e. waste moisture content, field capacity and hydraulic conductivity), hydrogeological conditions of the surrounding environment and final cover conditions. The extent of influence from each of the factors is still dependent on landfill site topography (e.g. valley fill, plain ground fill), landfill operation stage (i.e. active stage and post-closure stage) and local climate condition (e.g. humid and arid climates). The water balance associated with the landfill sitting on a plain ground and its evaluation methods have been well documented (Schroeder et al. 1994; Qian et al. 2002). The water balance associated with the landfill locating in a valley is somewhat more complicated but being lack of detailed studies.

Fig. 6 shows a schematic diagram of water balance in a valley-fill landfill, which is the most common case in China. The input of water to the landfill includes

precipitation infiltration on the surface of the landfill, leachate generation caused by consolidation and degradation of waste, as well as surface and subsurface inflow from the surrounding environment. The output of water from the landfill mainly includes the actual evaporation from the surface of the landfill, and leachate discharge from any drains at the toe and bottom of the landfill. The level of leachate mound depends on a state of dynamic equilibrium between the water input and output. The influence from some of the major factors on leachate level and the corresponding control measures will be discussed in the following paragraphs.

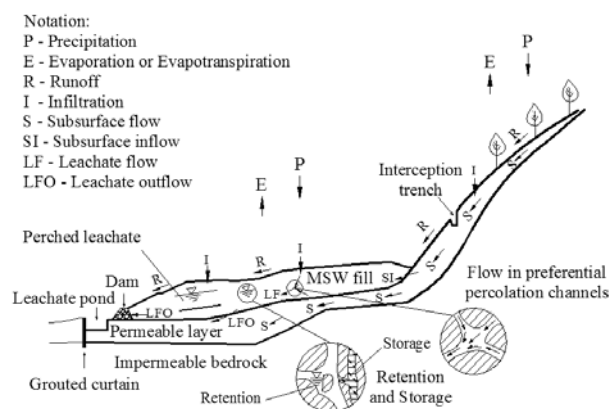


Fig. 6 A schematic diagram showing the water balance in a valley-fill landfill

(1) Precipitation infiltration on the surface of the landfill (i.e. notation of “I” in Fig. 6) generally represents the largest single contribution to the leachate quantity. As the MSW near the surface has a high value of water permeability (i.e. in the order of 10^{-4} m/s), it allows an easy entry of any forms of precipitation. Hence, the quantity of precipitation infiltration is highly dependent on the cover condition on the landfill surface. Many open dumps and uncontrolled landfills in the China are operated with the majority of area and time devoid of effective covers. In order to control the quantity and level of leachate, it is critical important to set up an effective cover system, including an intermediate cover on the active zone and a final cover on the zone to be closed. On this aspect, the experience in the developed countries, with respect to cover planning, design, construction and materials, will be beneficial to China (Qian et al. 2002; Gartung, 2006).

(2) The surface and subsurface inflow into a landfill from the surrounding environment (i.e. “R” and “SI”) can not be ignored when the precipitation catchment area upstream the landfill is relatively large. Precipitation falling on the upstream catchment area will either run off on the sloping surface or infiltrate into the subsoil. The inflow of surface runoff can be easily stopped by constructing an interception trench around the landfill. A

portion of the rainwater infiltrated into the subsoil will become a subsurface flow. The subsurface flow may exit at the downstream section and enter the landfill. It is usually difficult to intercept the subsurface flow. The amount of the subsurface flow depends upon factors such as the surface slope, the infiltrability of the shallow soil, and the vegetation condition at the upstream catchment area as well as the intensity and duration of rainfalls. The influence of the subsurface inflow on the leachate quantity should be assessed when making a decision on its control measures.

(3) The volume of leachate generation caused by consolidation and degradation of waste is primarily affected by waste compaction, waste moisture content, thickness of the waste and unit weight of the waste, as well as by landfill operation procedures such as waste compaction and fill speed. The MSWs in China generally have a high portion of putrescent food and garden wastes, and hence having a high water content. The leachate generation caused by consolidation and degradation of waste is one of the main sources of leachate, particularly in arid and semi-arid regions. This portion of leachate generation can be determined by conducting laboratory tests (Zornberg et al. 1999).

(4) The rate of leachate discharge from the toe and bottom of the landfill (i.e. "LFO") is one of the major factors controlling the leachate level within the landfill. Many open dumps and uncontrolled landfills in the China are generally devoid of a leachate drainage and collection system at the bottom. At some landfills, toe drains are installed at the retaining structure downstream the landfill. However, a clogging of the toe drains is generally observed after the landfills have been operated for several years. The lack of effective drainage facilities for leachate discharge will result in a continual accumulation of water input, and hence cause a high leachate mound within the landfill. Fig. 7 shows a distribution of leachate mound within the Suzhou landfill, which is plotted on the basis of field measurements of pore pressures and unsaturated-saturated seepage analyses (Zhan et al. 2008; Zhang, 2007). The maximum height of the leachate mound on the landfill bottom is 15 m. A high leachate level up to 15 m was also measured in the Kimpo landfill in Korea, in which a field monitoring program lasting three years was carried out (Jang and Kim, 2003). The field monitoring also indicated that the height of leachate level increased with an increase in fill height. To reduce the risk of landfill failure and environmental pollution, retro-fitted measures should be taken to lower the high leachate level within the landfill. This will be further discussed at the end of this section.

Apart from the above-discussed factors, the distribution of leachate mound as well as the leachate generation rate is also dependent on the storage capacity

of waste layers and the transient leachate percolation process through the waste body (see Fig. 6). Firstly, leachate can develop only after the increasing water content in the waste exceeds the field capacity. Secondly, because of the relatively large and heterogeneous pores of MSW, the leachate percolation through the waste is rarely a uniform wetting process, but exhibiting a preferential channeling flow (Korfiatis et al. 1984; McCreanor, 1998). Thirdly, the anisotropy and heterogeneity of hydraulic conductivity within the waste body usually result in a perched leachate mound on the low-permeability layers such as the intermediation cover layers (Lee et al. 1997; Jang, 2000; Jang et al. 2002). A significant perched leachate mound is also revealed by the field measurement of pore pressures in the Suzhou landfill in China (see Fig. 7). These behaviors bring an extra difficulty in developing a consistent model for simulating the leachate flow process within the landfill (Zhang, 2007). These behaviors should be taken into consideration when implementing the measures for controlling leachate level within the landfill.

Control of Leachate Head

For a new engineered landfill, a leachate drainage and collection system (LDCS) should be established to control the leachate head within the landfill. The LDCS at the bottom of a landfill generally consists of a coarse gravel drainage layer (≥ 30 cm), a network of leachate collection pipes, a filter layer (geotextile or mineral layer) and other accessories. The hydraulic conductivity of the drainage layer ($>10^{-3}$ m/s) and the diameter of the collection pipes must be large enough such that the maximum leachate head is smaller than the thickness of the drainage layer. The minimum gradients for the drainage layer and the collection pipes (longitudinal inclination $> 1\%$ and transverse inclination $> 3\%$) must be maintained even after the cease of settlement at the bottom of the landfill. Several researchers have developed analytic solutions for the estimation of maximum leachate head within the drainage layer (Qian et al. 2004; Ke and Chen, 2007). The solutions are able to assist in choosing the design parameters of the LDCS, including base grade, pipe gradient, horizontal drainage distance, hydraulic conductivity of drainage layer etc. At present, a great uncertainty associated with LDCS is that the LDCS may become ineffective in the long-term due to a clogging in the pore space (including physical, chemical and microbiological clogging). Several researchers have carried out field investigation, laboratory study and numerical modelling on the long-term performance of LDCS (Koerner and Koerner, 1995; Fleming et al. 1999; VanGulck, 2003; Rowe, 2005). The available laboratory and field evidence, combined with modeling, indicate that LDCSs in MSW landfills have

finite service life, which could range from less than a decade to more than a century depending on the design details, waste characteristics and mode of operation (Rowe, 2005). Rowe (2005) also provided several constructive suggestions for the extension of service life of LDCS. In Germany, a tunneling is constructed under the bottom of a landfill for the ease of cleaning leachate collect pipes (Gartung, 2006).

For an old landfill with a high leachate level, lowering of the leachate level is critical important for avoiding a landfill slide as well as reducing the environmental impact of leachate. In the developed countries, this is conventionally achieved by installing and pumping from vertical wells. Several researchers have carried out field and numerical studies on the efficiency of pumping leachate from vertical wells (Oweis et al. 1990; Rowe and Nadarajah, 1996; Jang, 2000; Al-Thani et al. 2004). Oweis et al. (1990) pointed out that leachate pumping may offer an attractive cost-effective alternative for leachate management in the uncontrolled landfills when compared to cutoff walls, toe drains, etc. On the basis of numerous assumptions, Rowe and Nadarajah (1996) developed an analytical solution for design engineers to estimating the well radius and spacing required to control the leachate mound to a specific level. The analytical solution can also be used aid the design engineers in assessing the viability of pumping wells as a leachate control measure. On the basis of field investigations and numerical modeling, Jang (2000) found that the low-permeability intermediate cover layer had an adverse effect on the efficiency of pumping. He suggested that a drainage path should be made through the intermediate cover soil before it is buried by another layer of waste. The numerical study conducted by Al-Thani et al. (2004) demonstrated that a seepage face would develop when the drawdown in the well is relatively large. The development of the seepage face together with the low hydraulic conductivity of the deep waste may result in a low yield from the pumping well. In addition, the long-term performance of the pumping wells may be affected by a gradual clogging of the filter pack and the waste around the well-bore. With a consideration of the uncertainty in the efficiency of the pumping method, Cox et al. (2007) investigated the

feasibility of using directional drilling to install horizontal wells for leachate control. The advantage of this method is that the horizontal wells are particularly effective in reducing leachate head near the bottom of the landfill, which is often the zone of most concern for regulatory and environmental purpose. The pilots and full scale field trials at Rainham, UK indicated the directionally horizontal wells could represent a viable, cost-effective alternative to conventional vertical wells.

GAS GENERATION, TRANSPORT AND CONTROL

The degradation of municipal solid wastes within a landfill can generate a great quantity of gas. The landfill gas consists predominantly (over 96%) of methane (CH_4) and carbon dioxide (CO_2), which are at more or less equal proportions. Both methane and carbon dioxide are greenhouse gases, and the greenhouse effect of methane is 21 times the effect from an equal amount of carbon dioxide. Methane is highly explosive in concentrations of 5 to 25 percent in air, and hence its migration to the surrounding areas may lead to fire and explosion hazards. In addition, the landfill gas has a significant value as an energy source (its heat value is about half that of natural gases). In order to control the air pollution and hazards from the landfill gases, the developed countries have issued policy and/or regulation to require a proper control of landfill gas as well as to encourage a recovery of energy from landfill gases. More and more attentions have recently been paid to the control and recovery of landfill gas in China. For example, the conversion of landfill gas into electrical energy has been implemented at several landfills in China under the financial support from the World Bank. The knowledge of gas generation and permeability is required for the design of landfill gas control and recovery systems.

Gas Generation Rate

The gas yield of MSW is defined as the total amount of gas produced by a unit weight of MSW over the landfill's gas generation time span. The gas yield is mainly a direct function of the total quantity of the waste

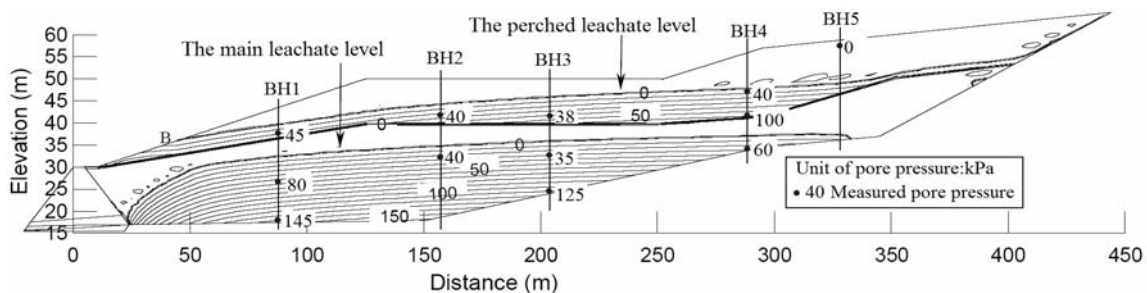


Fig. 7 Pore pressures measured in the field and distribution of leachate mound predicted by numerical simulation

available for decomposition (i.e. biodegradable wastes). Laboratory test results showed that the gas yield for the Chinese MSWs ranged from 300 to 400 L/kg (dry MSW), which is close to the gas yield of the American MSWs (He et al. 2007). The gas generation rate, however, is dependent not only on the waste composition characteristic but also on the environmental conditions such as moisture content, temperature, PH, the availability of nutrients and microbes within the landfill. In addition, the gas generation rate exhibits a highly time-dependent behavior, i.e. depending on the phases of waste degradation (i.e. aerobic phase, aerobic/acid generation phase, transition to anaerobic phase, anaerobic phase and transition to stabilization phase). Numerous theoretical and experimental studies have attempted to estimate or measure the gas yield as well as the gas generation rate. Comprehensive reviews of data from these studies have been presented in detail by several investigators (Barlaz et al. 1990; El-Fadal et al. 1997). However, because of the great spatial and temporal variations in waste composition and degradation conditions, how to properly describe the gas generation rate within a specific landfill is still a challenging and unsolved problem.

As discussed previously, the MSWs in China generally consist of much more putrescible food and garden wastes (40-50%) than the MSWs generated in UK and USA. The food and garden wastes are usually classified as the most easily biodegradable materials. The C/N ratio of the MSWs in China falls into the range from 20 to 30, which is believed as the optimal range for the anaerobic decomposition process. It is generally believed that the characteristic of waste composition generally lead to a relatively rapid decomposition process, hence a high rate of gas generation. Field evidence at most landfills in China indicates that the stabilization phase of gas generation generally starts half a year after placement of a waste layer, and 90% of gas yield occurs within the first two years after placement of the waste layer (He et al. 2007). This means that the stable gas generation period in the Chinese landfills is significantly earlier and shorter than that in the American landfills. This may facilitate the control and recovery of landfill gas.

A landfill typically takes many years to fill. This means, by the time when the landfill is closed, the wastes placed at different depths have already experienced different degree of degradation. In addition, the environmental conditions of degradation such as moisture content, temperature and oxygen concentration generally vary with the depth. Therefore, the waste layers at various depths have different values of gas generation rate. However, this characteristic is seldom taken into account in the published theoretical models for gas transport.

Gas Permeability of MSW

Landfill gas transport within a landfill occurs via two mechanisms, i.e. convection and diffusion. Convection is primarily induced by pressure gradients formed by gas generation in waste layers. Diffusion is the transport of substances induced by gas concentration gradients. It is generally accepted that gas diffusion within a landfill plays a relatively insignificant role in gas transport as compared with convection. This is true because the macro-porous MSWs at unsaturated conditions have much higher values of gas permeability than that of gas diffusion coefficient. Gas diffusion may become significant when the waste layer is saturated or nearly saturated with leachate. As the Reynolds number characterizing the flow of gases in landfills is typically smaller than 1, Darcy's law is assumed to be applicable in most of the theoretical models developed for the simulation of landfill gas transport (Arigala et al. 1995; Chen et al. 2003; Townsend et al. 2005).

The gas permeability of MSW is a key parameter in the design of a gas collection system as well as the design of an air ventilation system within a semi-aerobic landfill. However, much fewer experimental data for this parameter are available for the design as compared with those for the water permeability of MSWs. One exception to this is the laboratory study conducted by Kallel et al. (2004), in which the gas permeability and tortuosity for the processed MSWs and incinerator residue generated in Japan were investigated. The major findings from the laboratory study are as follows. The intrinsic gas permeability of the MSWs ranges from the order of 10^{-10} to 10^{-9} m², showing a trend of increase with the effective particle size (d_{10}). The relationship of gas permeability to the degree of saturation depends on the type of MSWs. For the coarse waste (i.e. shredded bulky MSW), the influence of the increasing water content on the gas permeability appears to be insignificant. However, for the incombustible waste, the gas permeability was observed to decrease with an increase in water content, particularly at the highly saturation state ($S_r \geq 0.85$). The tortuosity of the MSWs, ranging from 2 to 10, is clearly greater than that for a particulate material (e.g. sand). This is attributed to the presence of plastic films, paper and irregular shapes in the MSWs.

Recently, Wei et al. (2007) carried out a laboratory study on the gas permeability of the MSWs sampled from the Suzhou landfill in China. The influences of void ratio, degree of saturation and waste composition on gas permeability were investigated. The test results showed that the intrinsic gas permeability of the MSWs is in between 10^{-13} and 10^{-10} m². The influence of void ratio and degree of saturation is shown in Fig. 8 (where

θ_g is defined as the volume of gas-filled space per total volume of waste mass). A bilinear relationship is observed between gas permeability and volumetric gas content. At high values of degree of saturation (S_r), the decrease of gas permeability with a decrease in the volumetric gas content is much more significant than that at low values of S_r . It is found that the division point (i.e. $S_r=50\%$) is close to the degree of saturation corresponding to the field capacity of the MSW, which was measured in the laboratory. The influence of void ratio on the gas permeability is as much as 1-2 orders at the low range of S_r . The laboratory test results also show that the variation in waste composition with the burial depth does not imply so significant influence as void ratio and degree of saturation. This means the deep waste layer, generally having a lower void ratio and a higher degree of saturation, will pose a much lower value of gas permeability than the shallow waste layer. This is true because the deep waste layers in most of the landfills in China is saturated or nearly saturated by leachate. The experimental data indicate that, for the ease of gas collection, the water content of the waste within the landfills should be decreased to a value close to or below the field capacity. As discussed previously, this can be achieved by lowering the leachate level within the landfills.

Control of Landfill Gas

The control of landfill gas is generally implemented by a gas collection system combined with a cover system. The cover system is designed to prevent a free release of landfill gas as well as to maintain the environment suitable for the anaerobic gas production. The gas collection system generally consists of gas extraction well or extraction trench, network of gas collection pipes, condensate collection and pump station etc. The gas collection system is working in either passive way or active way (i.e. applying a vacuum pressure). Gas extraction well is the most important unit of a gas collection system. The major design parameters of gas extraction wells include well depth and diameter, well spacing and layout, and well working pressure. These parameters should be chosen such that the gas extraction wells will be capable of efficiently controlling gas pressures and extracting gas from all portions of the landfill. At present, no definite standards have been established for the design. EMCON (1998) had provided some recommendations on choosing well spacing based on engineering experience. The performance of gas extraction wells is also dependent upon gas permeability of wastes and performance of top cover. Scientific design of gas extraction wells requires more theoretical and experimental basis. Several researchers have developed analytical or numerical models for the

simulation of the landfill gas transport around gas extraction wells (Young, 1989; Arigala et al. 1995; Chen et al. 2003; Wei, 2007). The models were successfully used to predict the performance of gas extraction wells within a landfill, including the gas pressure distribution, the gas flow rate, etc. The influences of the above major parameters on the gas extraction performance have been studied by using the gas transport models. The major findings are summarized in the following paragraphs.

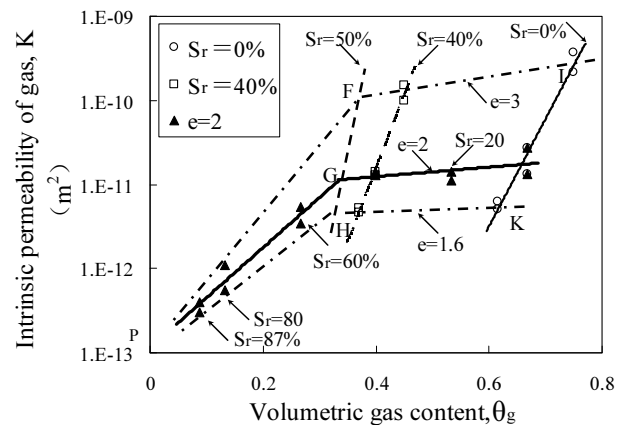


Fig. 8 Gas permeability for the MSW sampled from the Suzhou Landfill in China

Young (1989) suggests that the diameter of the gas extraction pipe is very important for increasing the gas extraction rate. The pipe diameter used in the current practice is generally greater than 180 mm, and the diameter of gas extraction wells is as large as 1 m. As the well diameter increases, the size of pump should be increased accordingly to maintain a fixed deficit pressure. In addition, covering landfills with relatively impermeable strata can enhance the efficiency of gas collection. Arigala et al. (1995) points out that the ratio of the total gas rate extracted from all the wells to the overall gas generation rate (κ) is an important parameter to optimize the number of wells and their spacing. Within a landfill with active gas extraction wells, an increase of κ tends to broaden the region of negative gauge pressures. A high value of κ (e.g. $\kappa \geq 1$) will result in a risk of drawing fresh air into the landfill, which increases the possibility of methane explosion and interferes with the anaerobic gas production processes. Decreasing the permeability of the cover layer or increasing its thickness tends to result in a higher gas pressure within the landfills when keeping the other parameters constant. The anisotropy in the gas permeability of wastes (i.e. horizontal versus vertical) exerts an influence on the flux through the landfill boundary (i.e. cover, bottom and lateral walls of landfill). Chen et al. (2003) found that under the passive venting condition the well's ability in capturing the landfill gas decays quickly with an increase in the distance from the

well. The simulation for the Fresh Kills landfill in USA indicates that the influence radius of the passive vent is generally less than 20 m. The parametric study also shows that the gas flow rate from the passive well is significantly affected by the well depth, the thickness and permeability of final cover.

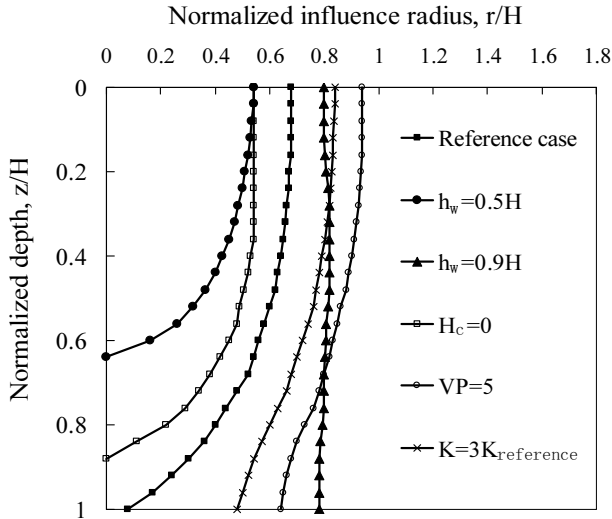


Fig. 9 Influence boundaries of the gas extraction well corresponding to different scenarios

Parameters for reference case:

Thickness of landfill (H); Length of well (h_w) = $0.7H$; Thickness of final cover (H_c) = $0.5m$; Gas permeability of final cover: $5.0 \times 10^{-14} m^2$; Vacuum pressure (VP) = $0kPa$; Gas permeability of waste: $K_h = 3.0 \times 10^{-12} m^2$; $K_v = 1.0 \times 10^{-12} m^2$; Gas generation rate (a) = $5.0 \times 10^{-17} kg/m^3 \cdot s$; Porosity of waste = 0.64 ; Temperature (T) = $40^\circ C$; Viscosity of gas mixture (μ) = $1.76 \times 10^{-5} kg/m \cdot s$; Gas density = $1.16 kg/m^3$

Recently, Wei (2007) carried out a more comprehensive parametric study on the performance of gas extraction wells within a landfill. In the study, the influences from all the above-mentioned major parameters are analyzed. The variations in gas permeability and gas generation rate with the burial depth of waste are also taken into account. Some representative results are shown in Fig. 9. The curves shown in this fig. represent different influence

boundaries of the gas extraction well corresponding to different cases. For each case, one variable is changed against the reference case. Here, it is assumed that the influence boundary can be defined as the locations where the pressure drawdown resulted from the gas extraction well is equal to 10% of the corresponding gas pressure for the scenario without a gas extraction well. Hence, the curves shown in Fig. 9 are actually the contour of pressure drawdown corresponding to a percentage of 10. As shown in Fig. 9, an increase in the well depth results in a significant enlargement of the influence zone, particularly in the vertical direction. Increasing the vacuum pressure in the active gas extraction well can also significantly enlarge the influence zone. An absence of landfill cover leads to a decrease in the influence zone. In addition, an increase in the gas permeability of waste tends to broaden the influence zone. On the basis of the parametric study, Wei (2007) recommended the depth of gas extraction wells should not be less than 70% of the thickness of landfill, and the spacing of wells can be adopted as 1.5-2.5 times the well depth. The study indicates that the values of well spacing recommended by EMCON (1998), ranging from 75 to 120 m, may be too large for the landfills with a thickness less than 30 m. The study also demonstrated that the existence of perched leachate or high leachate mound within a landfill would significantly interfere with the gas extraction. When this scenario occurs, a leachate pumping system should be installed in combination with the gas extraction wells.

SETTLEMENT OF MSW LANDFILL AND ITS IMPACT

MSW is a highly compressible and biodegradable material. The landfill settlement continues over an extended period of time, with a final settlement that can be as large as 30%-40% of the initial fill height. The settlement during the active life of a landfill will enlarge the storage capacity of the landfill, and affect the landfill operation and management. The post-closure settlement (particularly differential settlements) may cause damages

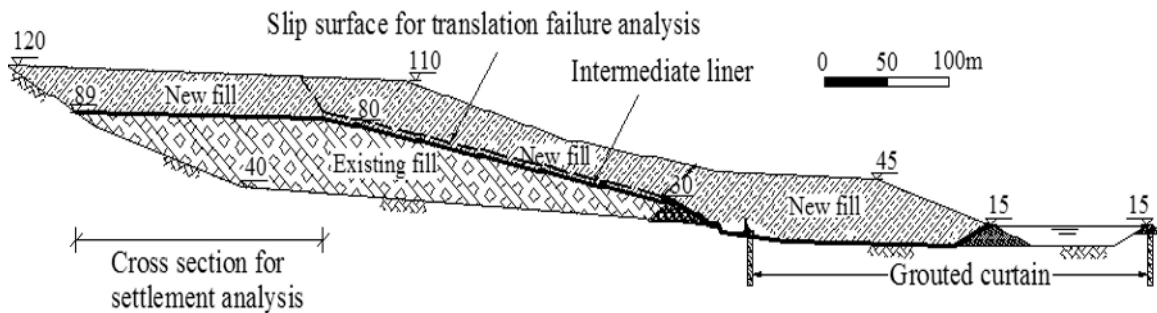


Fig. 10 A preliminary design of landfill expansion in Suzhou, China

(particularly differential settlements) may cause damages or malfunctions to the cover system and the gas collection system, and hinder post-closure reclamation of the landfill areas. The prediction of landfill settlement is required for assessing the above consequences and choosing proper remediation measures.

In addition, landfill expansion has now become a common practice at many landfills in China. To meet the new regulatory requirements, the expansion of an old uncontrolled landfill generally involves installation of an intermediate liner system in between the existing and expanded waste bodies (see Fig. 10). The serviceability of the intermediate liner system, being subjected to substantial differential settlements, is one of the critical issues associated with the landfill expansion. In addition, the differential settlements may alter the inclination of the leachate drainage layer, which is required for a gravity flow of leachate. The design of the intermediate liner system also requires the ability to predict settlement behavior of the existing landfill. Although the compressibility of municipal solid waste has been studied for several decades, the prediction of settlement at a specific landfill is still a challenging engineering problem due to the spatial and temporal variations of MSW materials.

Primary and Secondary Compression of MSW

It is generally accepted that there are three main mechanisms resulting in the compression of MSW, i.e. instantaneous compression and rapid consolidation in response to applied load, mechanical creep and compression due to waste decomposition. In the soil mechanics approach, the instantaneous compression and rapid consolidation is defined as primary compression, and the other two parts of time-dependent compression can be combined as secondary compression. For most cases, it is difficult to separate the compression due to mechanical creep from the compression due to waste decomposition.

The primary compression index (C_c) or the modified primary compression index (C_c') is commonly used to calculate the primary settlement of a landfill. The magnitude of C_c is primarily dependent on waste composition, degree of compaction and the stress level involved. As the waste composition varies from country to country, region to region and period to period, the values of C_c show a great variety in the literatures (Gabr and Valero, 1995; Wall and Zeiss, 1995; GeoSyntec, 1996; Landva et al. 2000). Even within a particular landfill with similar MSW input, the waste layers embedded at different depths generally have experienced different degree of degradation, and hence pose different composition. In addition, the void ratio of the waste layer generally shows a trend of decrease with the

increasing burial depth due to an increment of vertical effective stress. Hence, within a particular landfill, the value of C_c is highly dependent on the burial depth of the waste layer. However, the current engineering practice usually involves using a single value of C_c to describe the compressibility of all waste sub-layers. This practice may lead to inaccurate predictions of landfill settlement. A more rational approach is to measure material parameters for each of the sub-layers in the landfill, preferably taking undisturbed MSW samples from the landfill. A practice of this approach was conducted in the Suzhou landfill in China. The obtained experimental data are shown in Fig. 11. It is clear that the magnitude of C_c exhibits a trend of decrease with the burial depth. The deep waste layer, being composed of more cinder content and less compressible materials and being at a denser state, exhibits a lower compressibility than the shallow waste layer. The change in C_c is resulted from the variations in both waste composition and void ratio.

As indicated by field evidences and laboratory test results, the long-term compression due to waste decomposition is the major part of the secondary compression. Coduto and Huitric (1990) stated that the compression due to waste decomposition is probably 18%-24% of the waste thickness. Park and Lee (2002) stated that the decomposition-induced compression may continue for 10-20 years or more. The long-term compression of MSWs is mainly dependent upon the amount of biodegradable organic solids, initial void ratio as well as favorable decomposition conditions (e.g. leachate recirculation, PH buffer and microbial seed). Hence, the long-term settlement behavior is highly site-dependent. Since the late 1990s, there has been a strong thrust to upgrade the existing landfill technology from a storage/containment concept to an active bioreactor landfill. More attentions have been put on the long-term settlement behavior of bioreactor landfills. Settlement prediction techniques based on the modeling of the biodegradation process or the solid-liquid-gas interactions are under development and appear promising (e.g. McDougall and Pyrah 2001; White et al. 2004; Chen et al. 2006).

Prediction of landfill settlement requires a theoretical model that is capable of capturing both the primary and time-dependent compressions of wastes. Marques et al. (2003) developed a composite compressibility model, in which the time-dependent compressions due to waste decomposition and mechanical creep are considered separately. The model has five model parameters. However, the authors did not provide a clear presentation on how to determine the parameters. Recently, Chen et al. (2006) developed a practical model for the prediction of landfill settlement. In the proposed model, the time-dependent compressions due to waste decomposition and mechanical creep are combined together. The

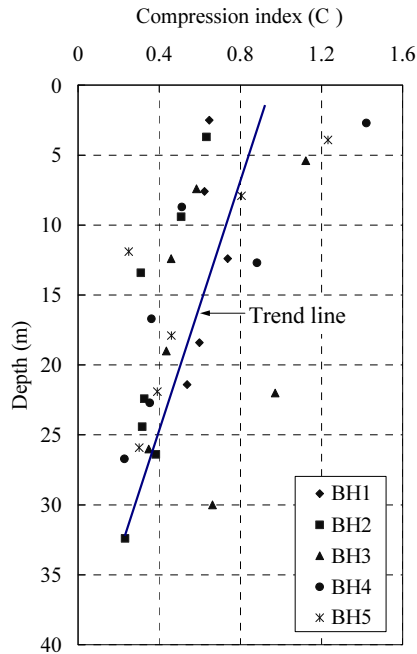


Fig. 11 Variation of compression index with depth measured from the samples taken from the Suzhou Landfill

expression of the model is

$$\varepsilon(\sigma, t) = \varepsilon(\sigma) + \varepsilon(\sigma) \left(1 - e^{-c(\sigma)t}\right) \quad (1)$$

where σ_i is the vertical stress of the waste layer at the time considered; t_j is time since placement of the waste layer in the landfill; $\varepsilon(\sigma_i, t_j)$ is the total strain corresponding to σ_i and t_j ; $\varepsilon_p(\sigma_i)$ is the primary strain of fresh waste resulting from the application of σ_i ; $\varepsilon_s(\sigma_i)$ is the ultimate secondary strain of the waste resulting from biological decomposition at a constant vertical stress of σ_i ; $c(\sigma_i)$ is a parameter representing rate of biological decomposition, which is dependent on the magnitude of σ_i .

There are three parameters to be determined in the model. Two of the parameters, i.e. $\varepsilon_p(\sigma_i)$ and $\varepsilon_s(\sigma_i)$, can be determined by conducting two one-dimensional mechanical compression tests (covering the maximum stress range involved) in the laboratory. One test is conducted on a fresh MSW sample, the other on a completely-decomposed MSW sample, which can be achieved by performing an accelerated decomposition test under a low stress level. $\varepsilon_p(\sigma_i)$ can be determined by the use of the primary compression curves obtained from the fresh waste. For a given stress (σ_i), $\varepsilon_s(\sigma_i)$ can be determined from the vertical distance in between the two compression curves obtained from the fresh and completely-decomposed MSW samples. The determination of $c(\sigma_i)$ requires field monitoring data representing the real rate of waste decomposition within a specific landfill (Chen et al. 2006).

Effect of Differential Settlement on Intermediate Liners and Mitigation Measures

As mentioned previously, vertical expansion of a landfill will cause a substantial settlement of the existing landfill (in particular differential settlement), which will inevitably affect the serviceability of the intermediate liner system in between the existing and expanded landfills. A safe design requires that the tensile strain level of the liner system resulted from the differential settlements is lower than the allowable tensile strains of the sealing materials in the liner system (e.g. compacted clay, geomembrane). The assessment of the potential tensile strain level requires not only a reliable settlement prediction but also an understanding the interactions between the intermediate liner and the underlying landfill. It is a very complex problem. At present, no solid methodology has been established for solving the problem. Qian et al. (2002) presented a simple equation for a rough estimation of the tensile strains of the liner subjected to differential settlements. The equation is based on the assumptions that the landfill has a negligible lateral movement and no any slippage occurs to the interface between the liner system and the underlying waste body.

Herein it is attempted to calculate the potential strains in the composite liner system induced by vertical settlements and lateral movements of the existing landfill by FLAC. The maximum and minimum MSW modulus for the component exponential model (Chen et al. 2009) was used for calculation. The composite liner system was modeled by beam elements without bending resistance. The main part of the Suzhou landfill is taken into consideration in the analysis. Fig. 12 shows the computed deformation of the existing landfill surface caused by the surcharge loading of the vertical expansion. It can be seen that the maximum lateral movement of the existing landfill is 2.44 m, which happens in the front slope, and the maximum settlement at the landfill surface is 4.55 m.

Fig. 13 shows the strain distributions of the intermediate liner system along the existing landfill surface. The maximum tensile strain ε in the liner is 2.06%, which appears near the anchor trench in the back slope of the existing landfill. It is interesting that compressive strains occur in the front slope of the existing landfill, which means that the liner system in these positions will be relaxed. The lateral movement of the existing landfill will have an apparent effect on the strain level and strain distribution of the liner at local positions. Further theoretical and experimental studies involved the time-dependent degradation of MSW are required for an improved understanding on this problem. Edelman et al. (1999) carried out a series of large-scale

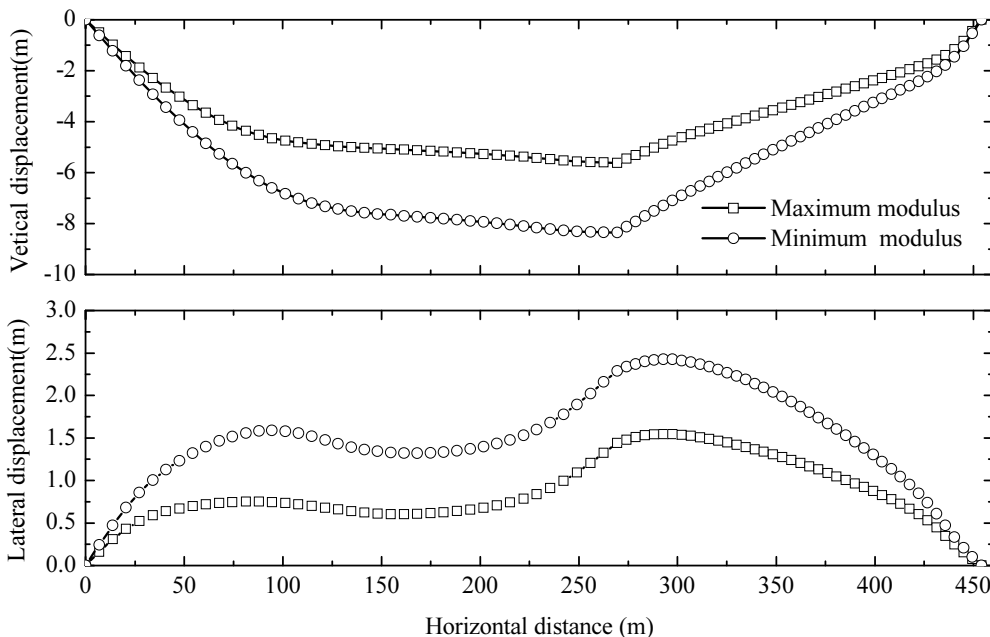


Fig. 12 Vertical and lateral deformation of the Suzhou landfill as a result surcharge loading of vertical expansion

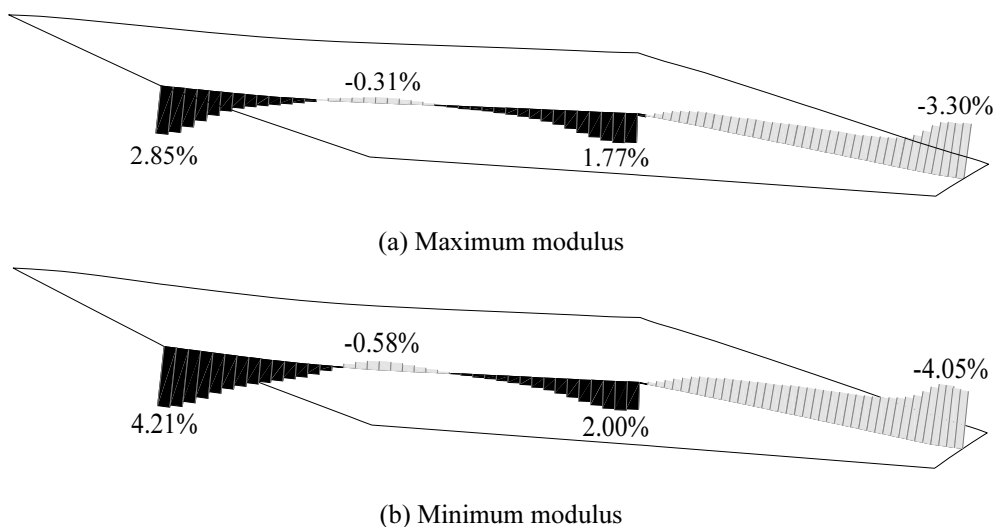


Fig. 13 Tensile strains of the intermediate liner system associated with the vertical expansion at the Suzhou landfill

model tests in attempt to define the ultimate state of horizontal and vertical compacted clay liners subjected to lateral movements or differential settlements. The test results in combination with field measurements provide a guideline for the overall design of the types of liners. The testing technique and equipment developed can be used to test other type of liners.

When the predicted tensile strain level of an intermediate liner system exceeds the allowable strain of the system, engineering measures should be taken to reduce the deformation of the liner system. At present, two measures are commonly used in engineering practice. One is to reinforce the liner system with a geogrid or high strength geo-textile, the other involves adjusting the thickness of the base backfill under the

liner system (i.e. increasing the backfill thickness at locations where settlement is anticipated to be greater). The design method for the geosynthetic reinforcement can be found in Qian et al. (2002). The key point of the latter measure is to obtain a reliable prediction of settlements of the old landfill. Both the above measures belong to a “passive” approach. An “active” approach, involving minimizing the settlements of the old landfill in advance, may be more attractive from economical view. Dynamic compaction technique has been employed in uncontrolled landfills to improve the waste density (Van impe and Bouazza, 1996; Mateos, 2006). As stated previously, high leachate level and pore pressures exist within most of the uncontrolled landfills in China. Lowering the high leachate level will cause a

significant settlement of the landfills as a result of an increment in the self-weight stress. Application of this measure before landfill expansion will be helpful to reduce the subsequent settlement caused by landfill expansion. A field testing program for this measure is carried out at the Suzhou landfill in China.

STABILITY OF MSW LANDFILLS

As mentioned previously, several lethal failures at the uncontrolled landfills took place in Asia during the last decade. The tragedies remind us that landfill stability is an issue that should not be overlooked. Blight (2006) conducted a survey on three lethal failures at the uncontrolled landfills in Asia. The survey suggests that the primary factor in all of the failures was lack of knowledge and technique regarding the effects of water and slope angle on the stability of waste mass. The secondary factor was the low strength of MSWs due to an absence of compaction or an abundance of plastic sheets. Koerner and Soong (2000) also pointed out that excessive moisture was invariably the triggering mechanism in all the landfill failures they had investigated. Hendon et al. (1999) reported a catastrophic landfill failure caused by leachate recirculation. At modern controlled landfills, composite liners, consisting of soil and geosynthetic materials, are widely used to prevent the contamination of the surrounding environment. The shear resistance at soil-geosynthetic and geosynthetic-geosynthetic interfaces is generally low, and the low interface strength has led to slippage and slope failure at many landfills (Koerner and Soong, 2000). For the landfills located in seismic impact zone, the effect of seismic forces on stability of landfills should be taken into account. The seismic forces usually produce relative movements within the waste, bottom liner system, cover system, foundations, and their interfaces, resulting in a loss or disruption of their functions (Anderson and Kavazanjian, 1995). This section tries to address the major factors influencing the static stability of landfills, including shear strength of MSW, leachate level and interface shear strength within a composite liner.

Shear Strength Characteristic of MSW

Information on the shear strength of the MSW is required for the assessment of slope stability since failures usually occur entirely or at least partially within the waste material. Numerous data on the shear strength of MSW have been obtained from both experimental measurements and back-analysis of field case histories over the last two decades (Landva and Clark, 1990; Jessberger, 1994; Gabr and Valero, 1995; GeoSyntec,

1996; Pelkey et al. 2001; Machado et al. 2002; Feng et al. 2005). However, the shear strength values reported in the literatures vary widely, with internal friction angle varying from 10° to 53° and cohesion varying from 0 to 67 kPa (Machado et al. 2002). The selection of appropriate shear strength parameters remains a challenging design issue for a site-specific landfill. Variability in the shear strength parameters is due to the variability of MSW compositions, the strain level at failure, the choice of representative samples and testing methods. The abundant fibrous materials in MSWs lead to a strain-hardening behavior upon shearing. Hence, the shear strength of MSWs is highly dependent on the strain level experienced by the waste mass. An additional factor affecting shear strength is the change in shear strength with the fill age of waste because of the biodegradation of the organic component (Dixon and Jones, 2005). As far as the authors are aware, little experimental data are available to evaluate the aging effect.

To facilitate the exchange and sharing of the published experimental data on shear strength of MSWs, an internationally agreed interpretation approach is required. Fig. 14 shows an effort along this direction. The experimental data selected from six of the literatures are plotted in terms of mobilized cohesion, c' , versus mobilized angle of internal friction, ϕ' . It should be noted that only data obtained from tests on relatively large-size specimens are presented in Fig. 13. The data sets from this study can be separated into two groups with one loci tending in a radial direction and the other tending in an annular direction. Each of the radial loci passes through data points corresponding to a same fill age (i.e. a synchronous locus). The synchronous loci sub-divide the rectangular coordinates into different zones corresponding to different ranges of fill age. The shear strength properties obtained from tests on the recent MSW are located in the left-upper zone with a high mobilized cohesion and a low mobilized angle of internal friction, and vice versa. Each of the annular loci passes through the data points corresponding to the same strain level (i.e. an iso-strain locus). The iso-strain loci sub-divide the rectangular coordinates into different zones corresponding to different levels of strain. As the strain level increases, both the mobilized cohesion and mobilized angle of internal friction increase, and hence the iso-strain loci expand outwards. The above chart consisting of synchronous and iso-strain loci can be used to interpret the experimental data from the six research papers. It is found that most of the data points fit reasonably to the above chart. The chart provides a useful reference for the interpretation of MSW shear strength data in the literature. Of course, more data and information are needed to improve the shear strength chart.

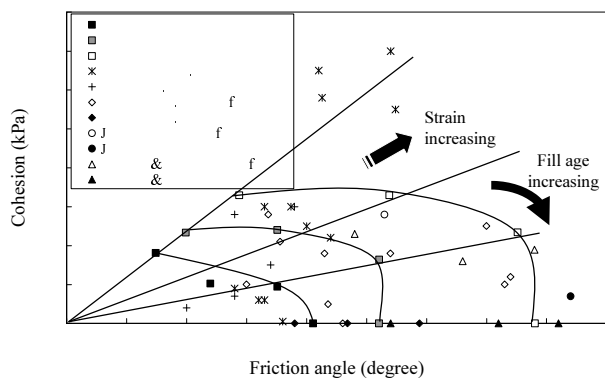


Fig. 14 Summary of shear strength parameters reported in six research literatures (Zhan et al. 2007)

Effect of Leachate Mound on Waste Mass Stability

As discussed previously, a high leachate level is present in most of uncontrolled landfills in the China. The influence of leachate level on the slope stability of the Suzhou landfill (before landfill expansion) was investigated by performing slope stability analyses by the use of the Bishop simplified method. The overall inclination at the sloping part of the landfill is 4H:1V (i.e. about 22°). The measurements of shear strength parameters at the two strain levels (10% and 20%) obtained by Zhan et al. (2007) were used for the analyses (refer to Fig. 14). Fig. 15 shows the change in F_s with the normalized height of leachate level (i.e. h/H), where H is the maximum thickness of the landfill. When the leachate level is located at the bottom of the landfill (i.e. totally unsaturated condition), the minimum F_s of the landfill is close to 3 (i.e. corresponding to the shear strength parameters at a strain level of 10%). An increase in the normalized height of the leachate level results in a significant decrease in the F_s . When the leachate level reaches the top surface of the landfill (i.e. totally saturated condition), the minimum F_s for the landfill is close to 1. The analysis results suggested that the leachate level in the landfill with a slope angle of 22° should be controlled at a height less than 70% of the landfill thickness if the F_s value is required to be greater than 1.4. The analyses also indicate that the use of shear strength parameters corresponding to a strain level of 20% seem to overestimate the factor of safety. On the basis of comparative analyses, Feng et al. (2005) suggested that a strain level of 10% is appropriate to define the shear strength parameters of MSWs for the evaluation of landfill stability. The analyses also indicate that the inclination of 4H:1V, as is the case for most of the landfills in China, is reasonable when the landfill is absence of an effective leachate control system. If the leachate level within a landfill can be controlled at a low

level (e.g. 30 cm in height), the landfill can be designed at a greater inclination. For example, some landfills in USA are designed at inclinations of 2H:1V~1.5H:1V. An increase in the inclination of a landfill will significantly enlarge its storage capacity.

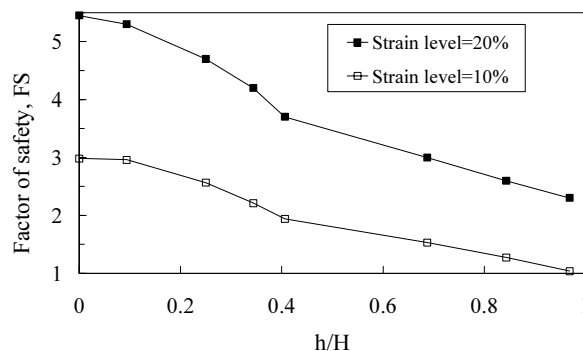


Fig. 15 Influence of leachate level on the slope stability of the Suzhou landfill

Slide of Waste Mass Along Weak Liners

For a controlled landfill lined with a composite liner system, landfill failure tends to be controlled by the weak shear strength at soil-geosynthetic and geosynthetic-geosynthetic interfaces. Fig. 16 shows a comparison of stress-deformation curves for different materials and interfaces, which are commonly found in landfills. The interfaces include textured geomembrane/ compacted clay (GM/CL), textured geomembrane/non-woven geotextile (GM-GT) and textured geomembrane/geosynthetic clay liner (GM/GCL). It can be seen that the MSW, exhibiting a strain-hardening behavior, poses higher ultimate shear strength than the compacted clay and the interfaces. The peak values of shear strength of the interfaces are close to that of the compacted clay. However, all the interfaces show a strain-softening, and hence have lower shear strength than the compacted clay when the shear displacement is large. A difference in the shear strength is also observed among different interfaces, particularly at a large shear displacement. The GM/GCL interface at a hydrated state has the lowest strength and exhibits a more significant strain-softening at a higher stress level. This is attributed to a bentonite extrusion from GCL to the interface. Fig. 17 shows the effect of bentonite extrusion on the changes in the shear strength envelopes of the GM/GCL interfaces (Chen et al. 2009). It can be seen that the values of interface friction angle at peak (ϕ_p) were 24.4° and 20.9° for the dry GM/GCL interfaces and the hydrated GM/GCL interfaces, respectively. The values of interface friction angle at large displacement (ϕ_{ld}) were 16.9° and 9.3° for the dry GM/GCL interfaces and the hydrated GM/GCL interfaces, respectively. A comparison of the two shear strength

envelopes corresponding to the large displacement conditions indicates that the bentonite extrusion at the large shear displacement caused a strength loss with a magnitude of 7.6° in terms of interface friction angle. The magnitude of strength loss is comparable to the combined effects of strain-softening, geotextile damage and geomembrane asperity removal on the post-peak strength reduction of the dry GM/GCL interfaces, which showed a magnitude of 7.5° in terms of interface friction angle. The influence of bentonite extrusion on the peak shear strength showed a magnitude of 3.5° in terms of interface friction angle. As compared with the peak strength envelope of the dry GM/GCL interfaces, the hydrated GM/GCL interfaces at the large shear displacement experienced a total strength loss with a magnitude of 15.1° in terms of interface friction angle. The shear strength parameters for some of the interfaces are shown in Table 2.

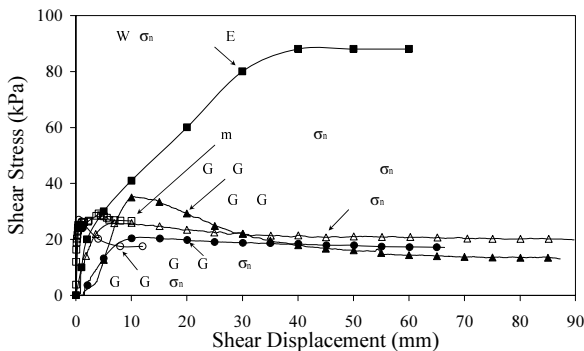


Fig. 16 Shear stress-displacement relationships for MSW, compacted clay and interfaces within composite liners

The shear strength parameters in Table 2 were used to evaluate the stability of the expanded waste body at the Suzhou landfill (see Fig. 10). For the purpose of comparison, a fixed slip surface mainly along the intermediate liner system was assumed for the translation failure analyses. The three-part wedge method proposed by Gao et al. (2007) was employed. The analysis results are also shown in Table 2. When the shear strength parameters at a large shear displacement are used, the factor of safety for the slippage against the hydrated GM/GCL interface is the lowest (i.e. $FS = 1.126$), followed by the GM/GT, the dry GM/GCL, and GM/CL in succession. It can be seen the factor of safety against the GM/GCL interface is significantly affected by both the hydration state of GCL and the shear displacement occurring to the interface. The analysis results indicate that the use of GM/GCL as a liner on the sloping ground should be very careful, particularly in a landfill absence of an effective water management system.

As the interfaces within a composite liner exhibit a strain-softening shear behavior, the failure mode of the

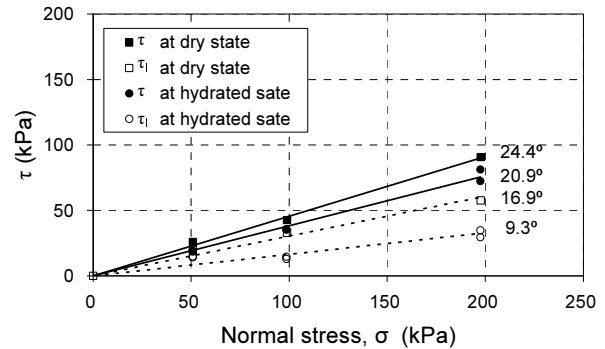


Fig. 17 Shear strength envelopes for the GCL/GM interfaces

lined landfill is usually in a progressive form (Filz et al. 2001). In addition, the differences in strength and stress-deformation behavior among MSWs, soil, geosynthetics and their interfaces tend to result in a strain incompatibility in between waste body and liner and/or within the composite liner (Mitchell et al. 1995; Jones and Dixon, 2005). The mechanical incompatibility as well as the progressive failure mode makes the failure mechanism of composite liners extremely complex, leading to much uncertainty in the choice of strength parameters for stability analyses. Although some efforts on this aspect have been made, the research work is far from complete.

SUMMARY

(1) As compared with the MSWs generated in Europe and USA, the MSWs generated in the China contain much more putrescent organic wastes (40%—50% on a wet weight basis), and are likely to have quite different behavior with respect to decomposition, gas generation, permeability, compressibility and shear strength.

(2) As a result of the biological decomposition process of the organic components, the hydraulic and mechanical properties of the MSWs tend to change with the age of fill. The aging effect should be taken into account when assessing the performance of MSW landfills.

(3) Water management and control of leachate level are a matter of the utmost concern with the current practice of MSW landfills in the China. High leachate level has caused several lethal landfill failures, and resulted in a high level of environmental pollution risk. Retro-fitted measures should be taken to lower down the high leachate level within the existing uncontrolled landfills.

(4) It is of great significance to control and recover landfill gas at thousands of open dumps and uncontrolled

Table 2 Factor of Safety for the Slide Along the Intermediate Liner at the Suzhou Landfill.

Interface	State	Shear strength parameters corresponding to large displacement		Factor of safety
		c (kPa)	ϕ (°)	
GM/GT	Dry	5	12.8	1.247
GM/CCL	Dry	11.4	23.6	2.141
GM/GCL	Dry	3.3	17.8	1.585
GM/GCL	Hydrated	0 (peak value)	20 (peak value)	1.724
		5	10	1.126

Note: GM: being textured with grains sprayed-on on both sides with a material identical to that of which the geomembrane is made (Textured, GSE Lining Technology, Inc., Houston, Tex.); GCL: having an intermediate layer of granular sodium bentonite with a mass per area of 4500 g/m², which held between a woven slit-film polypropylene geotextile (109 g/m²) and a nonwoven needle punched polypropylene geotextile (204 g/m²); GT: a polypropylene geotextile with a mass per area of 400 g/m²

landfills in Asia. The MSWs in the China generally exhibit a relatively concentrated gas generation behavior, which may facilitate the control and recovery of landfill gas. The interference of perched leachate or leachate mound with gas flow should be taken into account in the design of a gas extraction system.

(5) Expansion of the existing uncontrolled landfills usually involves the design an intermediate liner system in between the existing and expanded waste fills. There are two major technical difficulties associated with the design. One is the serviceability design of the intermediate liner system subjected to substantial differential settlement, the other is the stability design of the expanded landfill against the weak interfaces within the intermediate liner system.

ACKNOWLEDGEMENT

The authors would like to acknowledge financial support from research grants (50538080, 50425825 and 50878194) provided National Natural Science Foundation of China (NSFC), and the research funding from the Science and Technology Department of Zhejiang Province (2007C23038).

REFERENCES

- Al-Thani AA, Beaven RP, White JK (2004). Modelling flow to leachate wells in landfills. *Waste Management*, 24: 271-276.
- Anderson DG & Kavazanjian E, Jr (1995). Performance of landfills under seismic loading. 3rd Conf. on Recent Adv. in Geotech. Engrg. And Soil. Dyn, Univ. of Mo. At Rolla, St Louis, Mo. 3: 1557-1587.
- Arigala SG, Tsotsos TT, Webster IA, Yortsos YC, Kattapuram, JJ (1995). Gas generation, transport, and extraction in landfills. *J. Environ. Eng.*, 121(1):33-44.
- Barlaz MA, Ham RK, Schaefer DM (1990). Methane production from municipal refuse: a review of enhancement techniques and microbial dynamics, *CRC Critical Reviews in Environmental Control*, 19: 557-584.
- Blight G (2006). A survey of lethal failure in municipal solid waste dumps and landfills. *Proceedings of 5th International Congress on Environmental Geotechnics*, 1: 13-42.
- Chen Y, Chen K, Wu C (2003). Numerical simulation of gas flow around a passive vent in a sanitary landfill. *J. Hazard. Mater.*, 100: 39-52.
- Chen YM, Gao D, Zhu B (2009). Composite exponential stress-strain model of municipal solid waste and its application. *Chinese Journal of Geotechnical Engineering*, 2009(7).
- Chen YM, Ke H, Zhan LT (2005). Experimental Study on Engineering Properties of Municipal Solid Waste in China. *Proceeding of 2nd Germany conference on Geoenvironmental Engineering*: 116-127.
- Chen YM, Ling WA, Zhan LT (2009). Investigation of Mechanisms of Bentonite Extrusion from GCLs and Related Effects on the Shear Strength of GCL/GM Interfaces. Tentatively accepted by *Geotextiles and Geomembranes*.
- Chen YM, Xie Y, Zhan LT (2006). One-dimensional consolidation model for landfills considering solid-liquid-gas. *Chinese Journal of Geotechnical Engineering*, 28(2): 184-190 (in Chinese).
- Chen YM, Xie Y, Zhan LT (2006). One-dimensional consolidation model for landfills considering solid-liquid-gas interactions. *Chinese Journal of Geotechnical Engineering*, 28(2): 184-190 (in Chinese).

- Chen YM, Zhan Tony LT, Wei HY (2009). Mechanical compressibility of municipal solid wastes and its relationship to fill ages. *Waste Management*, 29(1): 86-95.
- Chinese Research Academy of Environmental Science (2003). Study on emission of greenhouse gases from municipal solid wastes in China. Chinese Research Academy of Environmental Science, Beijing, 2003.
- Cox SE, Beaven RP, Powrie W, Cole DJ (2007). Installation of Horizontal Wells in Landfilled Waste Using Directional Drilling. *Journal of Geotechnical and Geoenvironmental Engineering*, 132(7): 869-878.
- Dixon N & Jones DRV (2005). Engineering properties of municipal solid waste. *Geotextiles & Geomembranes*, 23(1): 205-233.
- Dixon N & Langer U (2006). Development of a MSW classification system for the evaluation of mechanical properties. *Waste Management*, 26: 220-232.
- Edelmann L, Hertweck M, Amannt P (1999). Mechanical behavior of landfill barrier systems. *Proceeding of Institution Civil Engineering Geotechnical Engineering*, 137: 215-244.
- Edincliler A, Benson CH, Edil TB (1996). Shear strength of municipal solid waste: Interim report-Year 1. *Envir. Geotechnics Res. Rep 96-2* Prepared for WMX Technologies, Inc. University of Wisconsin-Madison.
- El-Fadel M, Findikakis AN, Lechie JO (1997). Environmental impacts of solid waste landfilling. *Journal of Environmental Management*, 50: 1-25.
- Elzeftawy A & Cartwright K (1981). Evaluating the saturated and unsaturated hydraulic conductivity of soils, Permeability and Groundwater contaminant Transport, ASTM STP 746: 168-181.
- EMCON Associates (1998). Municipal solid waste landfill gas design plan review. Student Manual, APTI Workshop T018, First Edition, North Carolina State University, College of Engineering, Industrial Extension Service, Environmental Program, Raleigh, NC.
- Feng SJ, Chen YM, Zhan LT (2005). Study on shear strength parameters of municipal solid waste. *Journal of Zhejiang University (Engineering Science)*. 39(7): 987-991 (in Chinese).
- Filz GM, Esterhuizen JJB, Duncan JM (2001). Progressive failure of lined waste impoundments. *Journal of Geotechnical and Geoenvironmental Engineering*, 127(10): 841-848.
- Fleming IR, Rowe RK, Cullimore DR (1999). Field observations of clogging in a landfill leachate collection system. *Can. Geotech. J.*, 36(4): 685-707.
- Gabr MA & Valero SN (1995). Geotechnical properties of solid waste. *Geotechnical Testing Journal*, 18(2): 241-251.
- Gao D, Zhu B, Chen YM (2007). Three-part wedge method for translation failure analysis of landfills retained by a toe dam. *Chinese Journal of Rock Mechanics and Engineering*, 26(Supp.2): 1-8.
- Gartung E (2006). Landfill technology: German practice of geotechnical landfill design and construction. Compiled for Zhejiang University, 2006.
- GeoSyntec (1996). Static Deformation Analysis, Operating Industries, Inc. Landfill, Monterey Park, California. Report No. SWP-5, prepared by GeoSyntec Consultants on behalf of New Cure, Inc. for submission to the Environmental Protection Agency Region IX, San Francisco, California.
- He PJ, Qu X, Shao LM, Li GJ, Lee DJ (2007). Leachate pretreatment for enhancing organic matter conversion in landfill bioreactor. *Journal of Hazardous Materials*, 142: 288-296.
- Hendron DM, Fernandez G, Prommer PJ, Giroud JP, Orozco LF (1999). Investigation of the Cause of the 27 September 1997 Slope Failure at the Dona Juana Landfill. *Proceedings of the Seventh Waste Management and Landfill Symposium (Sardinia '99)*, Environmental and Sanitary Engineering Centre, Cagliari, Sardinia.
- Jang YS (2000). Analysis of flow behavior in a landfill with cover soil of low hydraulic conductivity. *Environmental Geology*, 31(3): 292-298.
- Jang YS & Kim YI (2003). Behavior of a municipal landfill from field measurement data during a waste-disposal period. *Environmental Geology*, 44:592-598.
- Jang YS, Kim YW, Lee SI (2002). Hydraulic properties and leachate level analysis of Kimpo metropolitan landfill, Korea. *Waste Management*, 22: 261-267.
- Jessberger HL (1994). Geotechnical aspects of landfill design and construction, Part 2: materials parameters and test methods. *Institution of Civil Engineers: Geotechnical Engineering Journal*, 107: 105-113.
- Jones DRV & Dixon N (2005). Landfill lining stability and integrity: the role of waste settlement. *Geotextiles & Geomembranes*, 23(1): 27-53.
- Kallel A, Tanaka N, Matsuto T (2004). Gas permeability and tortuosity for packed layers of processed municipal solid wastes and incinerator residue. *Waste Management & Research*, 22: 186-194.
- Kazimoglu YK, McDougall JR, Pyrah IC (2006). Unsaturated hydraulic conductivity of landfill waste. *Unsaturated Soils*, ASCE: 1525-1534.
- Ke H & Chen YM (2008). Estimation of Maximum Liquid Head over Multilayered Landfill Barriers *Journal of Environmental Engineering*, ASCE, 134(1):67-76.
- Koerner RM & Koerner GR (1995). Leachate clogging assessment of geotextile (and soil) landfill filters, Report CR-819371. Washington, DC US Environmental Protection Agency.

- Koerner RM & Soong TY (2000). Stability assessment of ten large landfill failures. Advances in transportation and geoenvironmental system using geosynthetics, Proceedings of sessions of Geodenvver 2000. ASCE Geotechnical Special Publication No. 103: 1-38.
- Korfiatis GP, Demetracopoulos AC, Boudodimos EL, Nawy EG (1984). Moisture transport in a solid waste column. *Journal of Environmental Engineering*, 110 (4): 789-796.
- Landva A & Clark JI (1990). Geotechnics of waste fills. *Geotechnics of Waste Fills—Theory and Practice*, ASTM STP 1070: 86-106.
- Landva AO, Pelkey SG, Valsangkar AJ (1998). Coefficient of permeability of municipal refuse. Proceedings of the 3rd International Congress on Environmental Geotechnics, Lisbon, 1: 63-72.
- Landva AO, Valsangkar AJ, Pelkey SG (2000). Lateral earth pressure at rest and compressibility of municipal solid waste. *Canadian Geotechnical Journal*, 37: 1157-1165.
- Lin WA, Zhan LT, Chen YM (2007). Shear strength of interfaces with composite liners. Proceedings of the 10th Chinese Conference on Soil Mechanics and Geotechnical Engineering (in Chinese).
- Ling HI, Pamuk A, Dechasakulson M, Mohri Y, Burke C (2001). Interactions between PVC geomembranes and compacted clays. *Journal of Geotechnical and Geoenvironmental Engineering*, 127(11): 950-954.
- Machado SL, Carvalho FM, Vilar OM (2002). Constitutive Model for Municipal Solid Waste. *Journal of Geotechnical and Geoenvironmental Engineering*, 128(11): 940-951.
- Marques ACM, Filz GM, Vilar OM (2003). Composite compressibility model for municipal solid waste. *Journal of Geotechnical and Geoenvironmental Engineering*, ASCE, 129(4): 372-378.
- Mateos T (2006). Dynamic compaction improvement in a MSW and in an inser waste landfills. Proceedings of 5th International Congress on Environmental Geotechnics, 1: 585-592.
- McCreanor & Philip T (1998). Leachate recirculation systems: mathematical modeling and validation, PhD dissertation, University of Central Florida, Orlando.
- McDougall JR & Hay J (2005). -Hydro- bio -mechanical modelling of landfilled waste: formulation and testing. Proc. Int'l. Workshop on Hydro-Physico-Mechanics of Landfills, University of Grenoble, March, 2005.
- Ministry of the Environment, Korea (2006). Generation of Wastes, http://eng.me.go.kr/docs/common/common_view.html?id=25&mcode=20&av_pg=2&classno=11.
- Ministry of the Environment, Singapore (2000). – Ministry of the Environmental: The Annual Report 2000, http://app.nea.gov.sg/cms/htdocs/category_sub.asp?cid=112.
- Mitchell JK, Bray JD, Mitchell RA (1995). Material interactions in solid waste landfills. *Geoenvironment 2000*, Geotechnical Special Publication No. 46, ASCE: 568-591.
- Olivella S, Carrera J, Gens A, Alonso EE (1994). Non-isothermal Multiphase Flow of Brine and Gas through Saline media. *Transport in Porous Media*, 15: 271-293.
- Oweis IS, Ellwood RB, Greene DS (1990). Hydraulic characteristics of municipal refuse. *Journal of Geotechnical Engineering*, 116(4): 536-53.
- Park HI & Lee SR (1997). Long-term settlement behavior of landfills with refuse decomposition. *Journal of Resource Management Technology*, 24(4): 159-165.
- Pelkey S, Valsangkar A, Landva A (2001). Shear Displacement Dependent Strength of Municipal Solid Waste and Its Major Constituent. *Geotechnical Testing Journal*, 24(4): 381-390.
- Powrie W & Beaven RP (1999). Hydraulic properties of household waste and implications for liquid flow in landfills. Proceedings of the Institution of Civil Engineers, *Geotechnical Engineering*, October 1999.
- Qian XD, Gray DH, Koerner RM (2004). Estimation of Maximum Liquid Head over Landfill Barriers. *Journal of Geotechnical and Geoenvironmental Engineering*, 130(5): 488-497.
- Rowe RK & Nadarajah P (1996). Estimating leachate drawdown due topumping wells in landfills. *Canadian Geotechnical Journal*, 33(1): 1-10.
- Schroeder PR, Dozier TS, Zappi PA, Aziz NM (1994). The Hydrologic Evaluation of Landfill Performance (HELP) Model: Engineering Documentation for Version 3. EPA/600/R- 94/168b, U.S. Environmental Protection Agency Office of Research and Development. Washington, DC, September.
- Sharholy M, Ahmad K, Mahmood G, Trivedi RC (2007). Municipal solid waste management in Indian cities – A review. *Waste Management*, 2007.
- Thomas HR & He Y (1995). Analysis of coupled heat, moisture and air transfer in a deformable unsaturated soil. *Geotechnique*, 45(4): 677-689.
- Townsend TG, Wise WR, Jain P (2005). One-Dimensional Gas Flow Model for Horizontal Gas Collection Systems at Municipal Solid Waste Landfills. *Journal of Environmental Engineering*, 131 (12): 1716-1723.
- United States Environmental Protection Agency (2005). Municipal Solid Waste in the United States: 2005 Facts and Fig.s (Full Report), <http://www.epa.gov/garbage/msw99.htm>.
- Van impe WF & Bouazza A (1996). Densification of domestic waste fills by dynamic compaction. *Canadian*

- Geotechnical Journal, 33: 879-887.
- VanGulck JF (2003). Biodegradation and clogging in gravel size material. Ph.D. thesis, Queen's University, Kingston, Ontario.
- Wall DK & Zeiss C (1995). Municipal landfill biodegradation and settlement. *Journal of Environmental Engineering*, 121(3): 14-224.
- Watts KS, Charles JA, Blaken NJR (2002). Settlement of landfills: measurements and their significance. *Waste 2002, Integrated Waste Management and Pollution Control: Research, Policy and Practice*: 673-682.
- Wei HY (2007). Study on gas flow in landfills of municipal solid wastes. Ph.D. dissertation, Zhejiang University, Hangzhou, 2007.
- Wei HY, Zhan LT, Chen YM (2007). Experimental study on gas permeability of municipal solid waste. *Chinese Journal of Rock Mechanics and Engineering*, 26(7): 1408-1415.
- White J, Robinson J, Ren QC (2004). Modeling the biochemical degradation of solid waste in landfills. *Waste Management*, 24: 227-240.
- Yang DQ & Shen ZJ (2000). Modeling of coupled flow of air, water, vapor and heat in unsaturated soils. *Chinese Journal of Geotechnical Engineering*, 22(3): 357-361 (in Chinese).
- Young A (1989). Mathematical modeling of landfill gas extraction. *J. Environ. Eng.*, 115(6): 1073-1087.
- Zhan LT, Chen YM, Ling WA (2007). Shear Strength Characterization of Municipal Solid Waste at the Suzhou Landfill, China. *Engineering Geology*, 97(2): 97-111.
- Zhan LT & Ng CWW (2006). Shear strength characteristics of an unsaturated expansive clay. *Canadian Geotechnical Journal*, 43(7): 751-763.
- Zhang WJ (2007). Study on water and leachate flow in landfills of municipal solid wastes. Ph.D. dissertation, Zhejiang University, Hangzhou, 2007.
- Zornberg JG, Jernigan BL, Sanglerat TR, Cooley BH (1999). Retention of free liquids in landfills undergoing vertical expansion. *Journal of Geotechnical and Geoenvironmental Engineering*, 125(7): 583-594.

TDR MEASUREMENT SYSTEM AND THE APPLICATION OF TDR IN GEOENVIRONMENTAL ENGINEERING

Ren-Peng CHEN¹, Wei CHEN², Yun-Min CHEN³

ABSTRACT: Time domain reflectometry (TDR) is a fast, accurate, and safe technology. The basic principle of time domain reflectometry (TDR) is the same as radar. The system sends an electromagnetic pulse along the waveguide and reflects on the mismatch impedance. Therefore, The position of mismatch impedance can be determined from the reflected signal which can be used to monitoring the underground water level. Commonly useful information from TDR signal includes the apparent dielectric constant and the electrical conductivity. The dielectric constant can be utilized to determine the water content of soils and the dry density. The electrical conductivity of pore fluid is a strong indicator of the ionic concentration of contamination in soils and has a strong relationship with the strength of soft soils treated by LKD or cement, therefore, the TDR method is widely used to control the effect of the treated soils and monitor the ionic contaminant.

KEYWORDS: Time domain reflectometry (TDR), dielectric constant, electrical conductivity

INTRODUCTION

As the development of the advance of project design and construction technology, it is important to monitoring the physical parameters of the soil in field. TDR (Time Domain Reflectometry) is a fast, accurate and safe technology filed technology. At the thirties of the last century, it was used to locate the position of the cable defect. Recently, people use it to measure the dielectric constant of the soil, water content and the monitoring of the landslides. On the basis of the study about the theory of TDR and the application in field, some researchers utilize the reflection signal of TDR to determine the water level.

TDR MEASUREMENT SYSTEM AND THE THEORY OF TRANSMISSION LINES

Time domain reflectometry (TDR) technology is a reliable, fast, and safe technology for measuring soil volumetric water content (Benson and Bosscher 1999; Noborio 2001). Fig.1 shows the main sections of TDR, including the step generator, data acquisition system, coaxial cable, and measurement probe. The step generator sends a step voltage to the coaxial cable, the input signal and the reflected signal are recorded by data acquisition system, and the apparent dielectric constant

and the DC electrical conductivity are estimated from the recorded signal.

The propagation of a TDR signal in the TDR system is described by transmission line theory. To account for the behavior of an unmatched system, the TDR system can be discretized as a lumped circuit consisting of uniform sections (Fig. 2). Each section accounts for the front panel, cable, probe head, and probe, respectively. Under the assumption of a transverse electromagnetic propagating wave mode, the general solution or transmission line equation in terms of voltage, V , and current, I , in complex phasor form is (Ramo et al. 1994).

$$V(z) = V^+ e^{-\gamma z} + V^- e^{\gamma z} \quad (1a)$$

$$I(z) = \frac{V^+}{Z} e^{-\gamma z} - \frac{V^-}{Z} e^{\gamma z} \quad (1b)$$

where z = position along the line; V^+ and V^- = two unknown voltage constants, which can be obtained using boundary conditions; γ = propagation constant, which is a complex quantity; and Z = characteristic impedance, depending only the geometry of the line and the material characteristics of the dielectrics between the two conductors. The variables of γ and Z can be expressed as:

¹ Professor, Department of Civil Engineering, Zhejiang University, China. Email: chenrp@zju.edu.cn

² MPhil. student, Department of Civil Engineering, Zhejiang University, China. Email: chenweizju@126.com

³ Professor, Department of Civil Engineering, Zhejiang University, China. Email: chenyunmin@zju.edu.cn

$$\gamma = \frac{j\omega}{c} \sqrt{K^*} \quad (2)$$

$$Z = \frac{Z}{\sqrt{K^*}} \quad (3)$$

In which $j = -1$; ω = angular frequency; K^* = relative dielectric permittivity (dielectric permittivity ϵ^* normalized by dielectric permittivity of free space ϵ [$\epsilon = 8.85418 \times 10^{-12}$ F/m]); c = velocity of light in vacuum ($c = 2.298 \times 10^8$ m/s); and Z = reference characteristic impedance, which is defined as the characteristic impedance of the transmission line insulated with air. The reference characteristic impedance can be calculated from the geometry of the line. For a coaxial transmission line, it can be derived as (Ramo et al. 1994)

$$Z = \frac{\ln(\frac{a}{b})}{2\pi} \sqrt{\frac{\mu}{\epsilon}} \quad (4)$$

where a is the out diameter of the inner conductor; b is the inner diameter of the outer conductor, ϵ (8.85418×10^{-12} F/m) is the vacuum dielectric permittivity, μ ($4\pi \times 10^{-7}$ H/m) is the vacuum magnetic permeability.

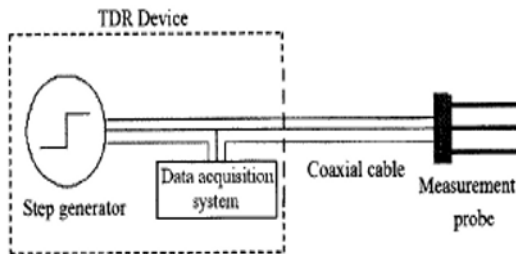


Fig. 1 Example of TDR system (adapted from Drnevich et al. 2001)

The propagation of a TDR signal in the TDR system is described by transmission line theory. To account for the behavior of an unmatched system, the TDR system can be discretized as a lumped circuit consisting of uniform sections. Lin (2003) introduced a procedure to use the transformed input impedance, the sampling voltage for TDR system, $V(0)$, can be expressed as

$$v(0) = \frac{Z(0)}{Z + Z(0)} V \quad (5)$$

Eqs. 2-5 are calculated in frequency domain. The process of calculation follows: first, take a Fourier

transformation of the source voltage, then change the time domain to frequency domain, obtain the frequency domain response by Eq. 5, then take an inverse Fourier transformation, change the frequency domain to time domain, finally, obtain the time domain response.

In addition, the phase velocity can be written as

$$v = \frac{c}{\sqrt{\epsilon_r}} \quad (6)$$

where c (2.298×10^8 m/s) is the speed of light and ϵ is the relative dielectric permittivity of the insulating material. Some electromagnetic wave is reflected and recorded by the TDR device if the impedance changes along the transmission line. If a transmission line with impedance Z is terminated by terminal impedance Z or connected to another section of transmission line with impedance Z , the reflected wave can be expressed as

$$V = \rho V \quad (7)$$

where V is the reflected wave, V is the incident wave, and ρ is the reflected coefficient. The reflection coefficient is related to the characteristic impedances as

$$\rho = \frac{Z - Z}{Z + Z} \quad (8)$$

If there is no impedance mismatch (i.e. $Z = Z$), $\rho = 0$ and no reflection adds to the step input; if $Z > Z$, $\rho > 0$, there is a positive reflection; if $Z < Z$, $\rho < 0$, there is a negative reflection. The position of the impedance mismatch measured from the source can be determined from the velocity of the wave propagation and returned time T as

$$x = v \cdot \frac{T}{2} \quad (9)$$

Then we can design different probes based on the position of the impedance mismatch, which is always the interface of different media.

MEASURING THE APPARENT DIELECTRIC CONSTANT

The relative dielectric permittivity is a frequency-dependent complex number, typically represented as

$$K(\omega) = K'(\omega) - jK''(\omega) \quad (10)$$

where the real part, K' , is a measure of the polarizability of the material; and the imaginary part, K'' , represents the energy absorption or dielectric loss. Several factors contribute to the energy loss, resulting from the fact that

constituent dipolar molecules require a finite time, or relaxation time, to adjust to the changing electromagnetic fields (Debye 1929). In addition to the dielectric loss of the material, the electromagnetic energy can also be dissipated by electrical conduction, which is sometimes referred to as Ohmic losses. This conduction can be in form of surface conduction via the electric charges on the surfaces of the solid and liquid phase ionic conduction via the dissolved electrolytes in water phase (Santamarina et al. 2001). The apparent dielectric constant K can be measured by these methods as follows:

The Method of Travel Time

The apparent dielectric constant K measured by TDR is based on travel time analysis, where the reflections are determined from an empirical tangent line or other constructions applied to the signal returning from the end of the probe. Von Hippel (1954) gives the relationship between dielectric constant and the apparent dielectric constant measured by TDR.

$$K(a) = \frac{K'(f)}{2} \left(1 + \sqrt{1 + \left(\frac{K''(f) + \frac{\sigma \cdot c}{\omega \epsilon}}{K'(f)} \right)^2} \right) \quad (11)$$

In which, K = the apparent dielectric constant; σ = DC electrical conductivity; and ω = angular frequency. The travel time can be calculated that the signal travels in two times of the probe length:

$$v = \frac{2L}{\Delta t} \quad (12)$$

Comparing Eqs. 6 and 12, the dielectric constant of the soil between the probes can be obtained:

$$K = \left(\frac{c \Delta t}{2L} \right) = \left(\frac{L}{L} \right) \quad (13)$$

In which, L = the length of the probe imbedded in the medium; L = the relative length. The unique unknown quantity Δt can be obtained by the travel time method.

Dielectric Constant From Surface Reflection

A model-based approach to determine dielectric constants from TDR measurement in highly conductive soils is presented. The approach utilizes information contained in the TDR signal from the reflection at the surface of the soil and employs the numerical model for the propagation of the TDR signals in a nonuniform line embedded in a dispersive material by Lin (2003). The

system parameters are first determined from a calibration process. After the system is calibrated, a two-parameter dielectric model is used to estimate the dielectric constants of soils by matching the predicted surface reflection versus the measured soil. This approach can potentially extend the application of TDR to the determination of water content and density in highly conductive soils such as chemically modified soils.

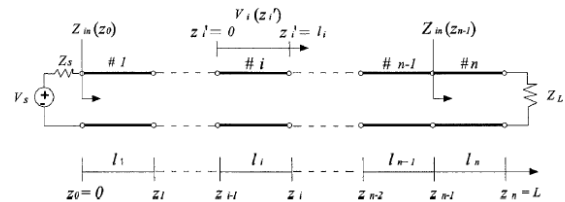


Fig. 2 Cascade of uniform sections used to represent a multisection transmission line

The matching process utilizes reflections from surface which are mostly influenced by highest frequency components (Heimovaara et al. 1994). The model used for inversion of the surface reflection is presented by Eq. 14.

$$K^*(\omega) = K - j \left(\frac{\sigma}{\omega \epsilon} \right) \quad (14)$$

where K^* - the dielectric constant in high frequencies; ω - highest frequencies in the surface reflections; K - surface reflection dielectric constant;

The advantage of using this approach is that it removes the influence of the DC electrical conductivity on K . Additional advantages of this model include its simplicity and the ability to be incorporated in inversion analysis to determine the most important information from the TDR signal, the real part of the dielectric permittivity at high frequencies.

Measure Ka by Surface Reflection Coefficient

The waveform frequency transmission model can consider the effect of dielectric relaxation and multiple reflections. The signal measured by TDR is signal in domain, so the signal must be transfer to frequency domain analysis from time domain analysis by Fourier transformation. Therefore, the whole process is so complicated to apply in the field. The method of surface reflection coefficient is a simply approach to analysis in time domain. It makes use of information contained in the reflection at the soil surface alone, without the need for the reflection at the end of the probe in travel time method.

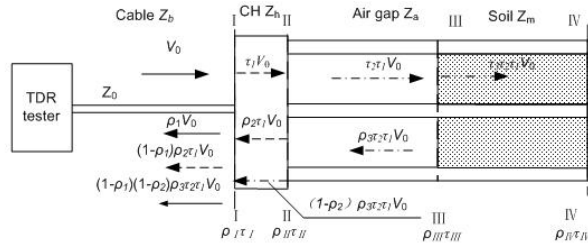


Fig. 3 Multiple reflections of step voltage in a TDR probe

The dominant mode of EM wave propagation in a coaxial cable is one-dimensional Transverse EM wave (TEM). The complex reflection coefficient, ρ_i , and transmission coefficient, τ_i , at the interface between section i and section $i+1$ is expressed as (Ramo et al. 1994):

$$\rho_i = \frac{Z_{c,i+1} - Z_{c,i}}{Z_{c,i+1} + Z_{c,i}} = \frac{\frac{Z_{p,i+1}}{\sqrt{K_{i+1}^*}} - \frac{Z_{p,i}}{\sqrt{K_i^*}}}{\frac{Z_{p,i+1}}{\sqrt{K_{i+1}^*}} + \frac{Z_{p,i}}{\sqrt{K_i^*}}} \quad (15)$$

$$\tau_i = 1 - \rho_i \quad (16)$$

where Z_c is characteristic impedance, depending only on the geometry of the transmission line and the material characteristics of the dielectrics between the two conductors; Z_p is reference characteristic impedance, which is defined as the characteristic impedance of the transmission line insulated with air. K^* is the relative dielectric permittivity of the insulating material in the cables or mold.

The amplitudes of transmission wave and reflection wave are calculated using the following equations:

$$V = \tau V \quad (17a)$$

$$V = \rho V \quad (17b)$$

where V and V are the amplitude of transmission wave and reflection wave at the impedance-mismatch interfaces, respectively.

For the standard probe specified by ASTM D6780, there are four impedance-mismatch interfaces: interface I-I (between the cable and the coaxial head), interface II-II (between the coaxial cable and the air gap), interface III-III (between the air gap and the soil), and interface IV-IV (probe end). If denoting the characteristic impedance of the cable, the coaxial head, the air gap, and the mold as Z , Z , Z , and Z , the reflection coefficients at the first three interfaces (ρ , ρ , and

ρ) and transmission coefficients at the first three interfaces (τ_I, τ_{II} , and τ_{III}) can be easily obtained.

The dielectric permittivity of soil can be expressed as:

$$K_{sc} = \left(\frac{Z}{Z}\right) \left(\frac{1-\rho}{1+\rho}\right) \quad (18)$$

where K_{asc} relative dielectric permittivity is calculated from the surface reflection coefficient ρ ; Z is the geometric impedance of the mold.

MEASURING THE ELECTRIC CONDUCTIVITY EC

Electrical conductivity is a measure of charge mobility in response to an electric field (Santamarina et al. 2001). Soils are generally regarded as a three-phased system (i.e. soil solids, water, and air). Therefore, many factors affect the bulk electrical conductivity of a soil, EC , including porosity, n , (or volumetric water content, θ), soil structure, composition of the pore fluid, surface conductance, and temperature (Friedman, 2005). The contribution of surface conduction of soil solids generally decreases as specific surface decreases. The surface conduction of sandy soils is small due to its relatively small specific surface. The air phase is also non-conducting (i.e. $EC = 0$). Therefore the pore fluid in the soil is the primary conducting phase for sandy soils. The volumetric water content, θ , and the electrical conductivity of pore fluid, EC , are the two dominant factors controlling bulk electrical conductivity, EC . By measuring the volumetric water content, θ , the electrical conductivity of the pore fluid, EC , can be estimated from the bulk electrical conductivity, EC . There are many models used to measure the electric conductivity of the soil, but most people measuring the electric conductivity of the soil for evaluating the porosity (n) or solution conductivity of water-saturated soils and rocks still use Archie's empirical law (Archie, 1942):

$$EC = n \cdot EC \quad (19)$$

where EC = the electric conductivity of the pore water, n = porosity.

Topp (1988) presented the Giese-Tiemann (G-T) method to determine the electric conductivity of the soil (EC):

$$EC = \left(\frac{K}{Z_u}\right) \left(\frac{1-\rho_\infty}{1+\rho_\infty}\right) \quad (20)$$

where K is the geometric constant of a probe (m^{-1}), Z_u the characteristic impedance of a cable (Ω), and ρ_∞ the reflection coefficient at a distant point from the first reflection on the waveform. It is defined as $\rho_\infty = (V_\infty - V) / V$, where V_∞ is the signal amplitude at the distant point (e.g. about 10 times larger than L) and V the signal amplitude from the TDR instrument. V and V_∞ can be determined conveniently from the waveform measured by TDR. We can determine the EC by TDR based on Eqs 18.

THE APPLICATION OF TDR

Measurement of water Content and Dry Density

Due to the large dielectric constant for water (around 81 at 20°C) in contrast to the relatively small dielectric constant for soil solids (around 3-5), it is possible to relate the apparent dielectric constant measured on a soil to its water content. Promotion of TDR technology for soil moisture monitoring is largely attributed to Topp et al. (1980), who established a relation between water content and soil apparent dielectric constant. The study by Siddiqui and Drnevich (1995) Siddiqui et al. (2000) utilized gravimetric water content along with soil dry densities as given in Eq. 21.

$$\sqrt{K} \frac{\rho}{\rho} = a + bw \quad (21)$$

where a and b are soil specific calibration constants; ρ is dry density of soil; ρ is density of water; and w is gravimetric water content.

Follows: to utilize the four rods probe to obtain the apparent dielectric constant of the soil in place K_a , field, excavate the soil from the location of the field test, compact the soil into the pre-weighed compaction mold, determine the mass of the soil-filled compaction mold, then calculate the wet density of the soil in mold and the dielectric constant of the soil in place. The water content of the mold can be determined as follows:

$$w = \frac{\sqrt{K} \frac{a\rho}{\rho} - \frac{a\rho}{\rho}}{b \frac{\rho}{\rho} - \sqrt{K}} \quad (22)$$

This method hypothesizes that the gravimetric water content of the soil in situ and in the mold are equal. The dry density of the soil in place can be calculated as follows:

$$\rho = \frac{\sqrt{K}}{\sqrt{K}} \frac{\rho}{1+w} \quad (23)$$

It is observed that we can obtain the apparent dielectric constant of the soil to calculate water content by travelling time method for different types of soils. However, in soils with electrical conductivities, the attenuation of the signal can eliminate the reflection from the end of the probe, which limits the application of travelling time method to these materials. Fortunately, the surface reflection method can be used in these materials.

Monitoring the Underground Water Level and the Electrical Conductivity

In this study, a TDR probe which can be used in high temperature and highly caustic environment was developed in attempt to simultaneously measure real-time leachate level and electrical conductivity of leachate. Fig. 3 shows the probe for measurement of leachate level. L_0 is the length between borehole surface and probe top, which can be read from the scale on the cable. d_k is the length of air section of the probe. ΔL is the length of leachate level change. As shown in Fig. 3, leachate level is $L=L_0+d_k$, in which d_k is a unknown parameter and can be determined by TDR waveform analysis.

When the probe is submerged in sample fluid, reflections mainly occur in two places due to impedance mismatch at cable-air interface and air-fluid interface. Although impedance mismatch also exists in the cable-probe connector filled with epoxy resin, the reflection here is not obvious for the epoxy resin part is really short. In this study, a particular calibration procedure is employed to eliminate this effect, and it is assumed that the characteristic impedance of epoxy resin section is the same as air section (Z for both). At the interface between cable and air section near probe top (Point A shown in Fig. 4), since Z (characteristic impedance of epoxy resin section or air section) $>$ Z (characteristic impedance of coaxial cable), positive reflection occur. At the interface between air and fluid (Point B shown in Fig. 4, 5), Z (characteristic impedance in test section) $>$ Z_g , negative reflection occur. Typical TDR waveform tested in water is shown in Fig. 5. As shown in Fig. 5, when leachate level changed, the air section length changes accordingly, represented as the time interval between point A and B in waveform. The connector between cable and probe, as represented by point A, do not move when water level changes. So the displacement of point B in TDR waveform (ΔT) represents the water level change (Δd_k).

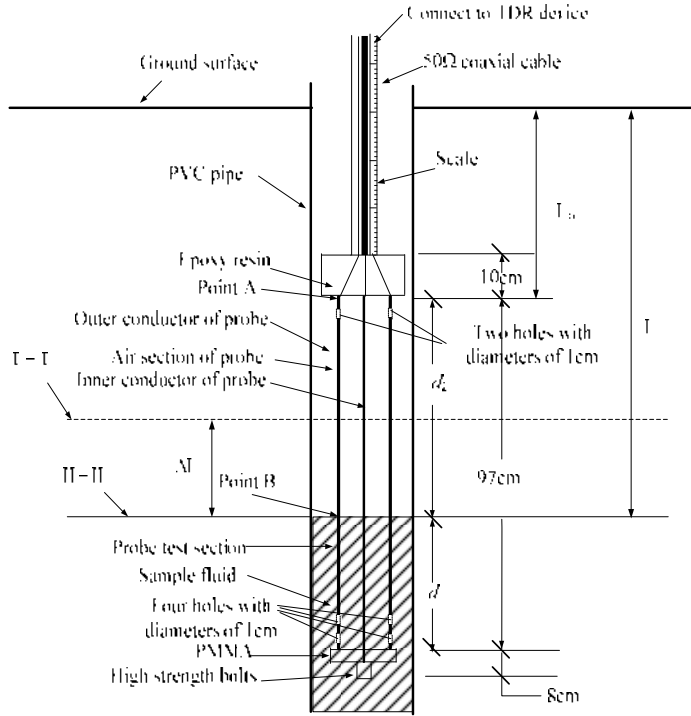


Fig. 4 Probe schematic diagram

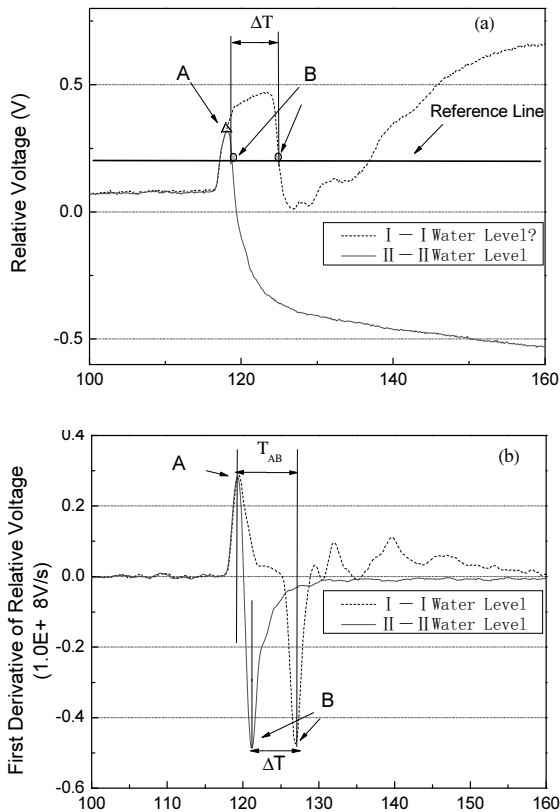


Fig. 5 Typical TDR waveform when air section in probe changed: (a) TDR waveform; (b) First derivative of TDR waveform

The methods to determine ΔT include reference line method and tangent line method, etc. (Svitzky et al. 1964; Timlin et al. 1996; Klemunes et al. 1997; Reece 1998). In reference line method, an appropriate line, called reference line, is selected to measure the time shift. The distance between intersections of the reference line and the TDR waveforms represents ΔT . Tangent line method, instead, tries to determine the accurate reflection point from the waveform.

A new method different from G-T method (Topp et al. 1988) is utilized to determine the electrical conductivity (EC). According to basic principles of electrical circuit, transmission line can be modeled as an equivalent lumped circuit. Especially at zero frequency, Heimovaara (1995) proposed a model for measuring EC. The EC of the sample can be derived as a function of the steady-state reflection coefficient ρ_∞ :

$$\sigma = M \frac{1}{d} \left(\frac{1 - \rho_\infty}{1 + \rho_\infty} \right) k(R, \rho_\infty) \quad (24)$$

where $M (= \epsilon cZ / R)$ is a probe constant; k is the correction factor for cable resistance, which is a function of ρ_∞ and R . Compared to traditional G-T method, the new method have considered transmission line loss and the effect from test section probe length. Since M and R can be determined by laboratory calibration

mentioned below, so that EC can be measured from steady-state reflection coefficient ρ_{∞} .

Monitoring the Landslides

A landslide is a major geohazard that often requires a monitoring system, in which the localized shear deformation is most important. Time domain reflectometry (TDR) has become an effective tool for detecting shear displacements and locating shear planes in rock (Dowding et al. 1988, 1989; Dowding and Huang 1994) and to some degree in soil slopes (Dowding and Pierce 1994; O'Connor et al. 1995; Dowding et al. 2001). An up-hole pulser launches a high-frequency electric pulse along a sensing coaxial cable grouted into the ground. Some portion of the electric pulse is reflected back to the TDR equipment as a result of the impedance (cable cross-sectional geometry) change due to the ground deformation. The time delay, amplitude, and shape of the reflected pulse provide a means to locate the deformation, determine the magnitude, and indicate the type of deformation. The relationship between shear displacement and intensity of reflection spike has been studied through calibration tests in an effort to quantify the shear displacement from the TDR measurement (Dowding, et al. 1988, 1989; Aimone-Martin et al. 1994). Fig. 6 illustrates a possible configuration of a TDR monitoring system for landslides.

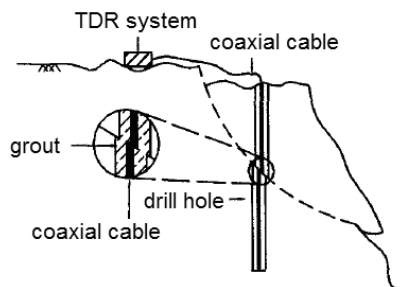


Fig. 6 The monitoring system of landslides

First, drill a hole at the location where the landslide will be measured, put the coaxial cable in the hole, then pour the grout into the hole in order to make sure that the deformation of the cable and the ground is equal. Second, through the laboratory calibration, the relationship between the TDR waveform and the effect of shear can be determined. Therefore, we can obtain the amplitude of the effect of shear and the locating the shear plane by the travel time method. Finally, the TDR system has a good prospect in monitoring the landslides in the place without anybody.

Control The Effect Of The Treated Soils

Soil stabilization and modification by addition of chemical admixtures are widely used to facilitate the construction and enhance the engineering properties of soil. Lime, lime kiln dust (LKD), and cement are being used for treating soft soils. Generally, the chemical changes in a system are associated with the simultaneous changes in its electrical properties. Boardman et al.(2001) suggested that the electrical conductivity of lime treated soil decreases with time and the measurement of electrical conductivity can be used as an effective quality control of lime stabilized subgrades. Yu and Drnevich (2004) showed that electrical conductivity measured by TDR was an accurate and effective indicator of the progress of hydration in the lime stabilized soils. Electrical conductivity measured by TDR was useful for quality assessment of LKD treated soils.

Electrical conductivity can be used to calculate the chemical soil dosage. Through the calibration experiment, we can get the relationship between the electrical conductivity and the chemical soil dosage. The experiment results demonstrated that the electrical conductivity can be fitted using hyperbolic equation perfectly.

$$EC = EC_1 - \frac{Bt}{A+t} \quad (25)$$

where EC_1 –the initial electrical conductivity (the electrical conductivity measured 5 minutes later after the compaction test); ECt –the electrical conductivity at t time, B and A –fitting constants. Transforming the Eq. 25, gives

$$\frac{EC_1 - EC}{EC_1} = \frac{B}{EC_1} \cdot \frac{t}{A+t} \quad (26)$$

Thus, Eq. 26 can be used to calculate the chemical soil dosage. When the chemical soil construction has been completely accomplished, testing the electrical conductivity of the soil at three different times, substituting it into Eq. 26, we can get the value of EC_1 , A and B . Therefore, the electrical conductivity increment can be determined at any time. In addition, we can use the calibration test results to confirm the chemical soil dosage.

The experiment results disclose that the electrical conductivity has a negative relationship with penetration resistance. Yu et. al. (2004) had discovered that two type of concrete have the same trend, the relationship between the unconfined compressive strength and the electrical

conductivity can be determined by the following equation.

$$f = \lambda \left[\frac{\pi}{2} - \tan^{-1}(\beta(EC - EC_1)) \right] P \quad (27)$$

where f is the unconfined compressive strength; λ is a empirical constant (zero dimension); β is a empirical constant (mS/m); EC - be obtained by calibration experiment (mS/m); P - atmospheric intensity of pressure ($P_a=0.098\text{MPa}$).

Doing a lot of experiments, we can fit every constant and get the relationship between EC_i and f . Therefore, we can use the electrical conductivity measured by TDR to obtain the penetration resistance by Eq. 27. Then, the strength of specimen can be determined.

Monitor the Ionic Contaminant

Determination of the ionic concentrations of soils in the field is important for the assessment of salinity (Rhoades, 1989), for the study of solute transport (Kachanoski et al. 1992; Ward et al. 1994; Vanclouster et al. 1995), and for the protection of groundwater resources influenced by land-applied chemicals (Franson, 1995). The electrical conductivity of the soil pore fluid, EC_w , has been found to be a reliable indicator of the total ionic concentration in soil pore fluids (with 1 dS/m being equivalent to approximately 10 meq/L (U.S. Salinity Laboratory Staff, 1954)). Variations in soil water ionic concentrations can therefore be measured by monitoring the electrical conductivity of the pore fluid. Unfortunately, the electrical conductivity of pore fluid is not easy to measure. As a result, the bulk electrical conductivity of the soil, EC , is frequently used to estimate the electrical conductivity of pore fluid by using a model to relate EC to EC_w .

The EC (EC, θ) method requires measuring the porosity together with the electrical conductivity of soil. Soil porosity is related to the specific gravity of soil grain and dry density:

$$n = 1 - \frac{\rho}{d \rho} \quad (28)$$

where ρ is the dry density of the soil; ρ is the density of water; and d is the specific gravity of soil grains.

The dry density in Eq. 28 can be determined using a new TDR method that measures both water content and dry density from a single measurement (Yu and Drnevich, 2004). Siddiqui and Drnevich (1995) and Siddiqui et al. (2000) developed the following relationship to relate TDR measured dielectric constant to the gravimetric water content along with soil dry densities:

$$\sqrt{K_a} \frac{\rho}{\rho} = a + bw \quad (29)$$

where a and b are the soil specific calibration constants; and w is gravimetric water content. The parameters, a and b , are obtained through laboratory calibration using a standard compaction tests [ASTM D698 (2000)]. Through use of commonly accepted values for K_a and extreme ranges of dry density, Drnevich et al. (2002) showed that a varies from 0.7~1.85, and b is approximately 9.

A similar relationship for the electrical conductivity of soil was proposed by Feng et al. (1999) and Lin (1999)

$$\sqrt{EC} \frac{\rho}{\rho} = c + dw \quad (30)$$

where: c and d are soil specific calibration constants. The parameters, c and d , can also be obtained from laboratory compaction tests, and are found to be dependent on the conductivity of the pore fluid. To avoid the effect of differences in the pore fluid between the laboratory sample and the field sample, Yu and Drnevich (2004) proposed a linear relationship between the apparent dielectric constant and soil electrical conductivity:

$$\sqrt{EC_b} = f + g\sqrt{K} \quad (31)$$

where f and g are soil specific calibration constants related to soil type, density, and pore fluid conductivity.

Combining Eqs. (29), (30) and (31), the soil dry density can be written:

$$\rho = \frac{(d - bg)\sqrt{K} - bf}{ad - cd} \quad (32)$$

Substituting Eq. 32 into Eq. 28, gives:

$$n = 1 - \frac{(d - bg)\sqrt{K} - bf}{(ad - cd)d} \quad (33)$$

Substituting the last part of Eq. 33 into Archie's law gives:

$$EC = \frac{EC}{\left(1 - \frac{(d - bg)\sqrt{K} - bf}{(ad - cd)d} \right)} \quad (34)$$

where: a , b , c , d , f , and g are the calibration constants obtained from laboratory compaction tests, d_s is the specific gravity of soil obtained from laboratory test, EC_b and K_a can be directly measured by TDR.

Eq. 35 indicates that the electrical conductivity of pore fluid can be estimated from a single TDR measurement (which gives K_a and EC_b), provided that the calibration constants are known. This set the basis for

using TDR to estimate the electrical conductivity of the pore fluid in saturated coarse grained soils

CONCLUSIONS

Time domain reflectometry has been gradually taken into account by the Academia and industry because of its convenience and accurate characteristic. With the invention of a variety of probes, the application of TDR test technology in the field has been greatly expanded. On base of the principle of TDR, we can use the reflected signal to determine the water level. Therefore, the water level and the electric conductivity of the water can be auto-monitored. TDR technology measures soil through measuring the dielectric constant and electrical conductivity of the soil and utilizing the calculating the dielectric constant modal to determine the water content and dry density of the soil. Since 1970s, TDR technology has been utilized in geotechnical engineering greatly. The most important application is monitoring the deformation of soils and rocks and the stability of the landslide. TDR has been paid attention to broadly because it's very convenient, safely, economic and digital. In addition, TDR measurement has been applied on soils treated by LKD. Through experiment the electrical characteristic of the treated soils and the rule of the strength increasing has been studied. Therefore, we can use the electrical conductivity measured by TDR to obtain the strength of the treated soils. The relationship between the electrical conductivity of the soil and the electrical conductivity of the pore water is the important base of the applying the electrical conductivity measurement to monitoring the ionic contaminant. Then, we can monitor the soil contaminant through the electrical conductivity of the pore water measured by TDR.

REFERENCES

- Archie GE (1942). The electrical resistivity log as an aid in determining some reservoir characteristics. *Trans. Sm. Inst. Min. Metall. Pet. Eng.* 146: 54-62.
- ASTM D698 (2000). Standard test method for laboratory compaction characteristics of soil using standard effort (12,400 ft-lbf/ft³ (600 kNm/m³)). *Annual book of ASTM standards*, 04: 08.
- Aimone-Martin CT, Oravec KI, Nytra TK (1994). TDR calibration for quantifying rock mass deformation at WIPP site, Carsbad, New Mexico. *Proc., Symp. on Time Domain Reflectometry in Environmental, Infrastructure, and Mining Applications*, U.S. Bureau of Mines, Special Publication SP 19-94: 507-517.
- Benson CH & Bosscher PJ (1999). Time domain reflectometry (TDR) in geotechnics: A review. *ASTM special technical publication*, 1350: 113-136.
- Boardman DI, Glendinning S, Rogers CDF, Holt CC (2001). In situ monitoring of lime-stabilized road subgrade, *Transportation Research Record*, No. 1757:3-13.
- Debye P (1929). *Polar molecules*, Chemical Catalog Company, New York.
- Dowding CH, Cole RG, Pierce CE (2001). Detection of shearing in soft soils with compliantly grouted TDR cable. *Proc., TDR 2001, Infrastructure Technology Institute*: 38-51.
- Dowding CH & Huang FC (1994). Early detection of rock movement with time domain reflectometry. *J. Geotech. Engrg.*, 120(8): 1413-1427.
- Dowding CH & Pierce CE (1994). Measurement of localized failure planes in soil with time domain reflectometry. *Proc., Symp. on Time Domain Reflectometry in Environmental, Infrastructure, and Mining Applications*, U.S. Bureau of Mines, Special Publication SP 19-94, NTIS PB95-105789: 569-578.
- Dowding CH, Su MB, O'Connor KM (1988). Principles of time domain reflectometry applied to measurement of rock mass deformation. *Int. J. Rock Mech. Min. Sci. Geomech. Abstr.*, 25: 287-297.
- Dowding CH, Su MB, O'Connor KM (1989). Measurement of rock mass deformation with grouted coaxial antenna cables." *Rock Mech. Rock Eng.*, 22: 1-23.
- Drnevich VP, Yu X, Lovell J (2002). A new method for water content and in situ density determination. *Proc., Great Lakes Geotechnical and Geoenvironmental Conference*, Toledo, Ohio.
- Feng W, Lin CP, Deschamps RJ, Drnevich VP (1999). Theoretical model of a multisection time domain reflectometry measurement system. *Water Resource Research*, 35(8): 2321-2331.
- Franson MA (1995). *Standard Methods for the Examination of Water and Wastewater*. 19th edition. American Public Health Association, Washington DC.
- Friedman SP (2005). Soil properties influencing apparent electrical conductivity: a review. *Computers and Electronics in Agriculture*, 46: 45-70.
- Heimovaara TJ, Bouten W, Verstraten JM (1994). Frequency domain analysis of time domain analysis of time domain reflectometry waveforms. II: A four-component complex dielectric mixing model for soils. *Water Resour. Res.*, 30(2): 189-199.
- Heimovaara TJ, Focke AG, Bouten W, Verstraten JM (1995). Assessing Temporal Variation in Soil Water Composition with Time Domain Reflectometry, *Soil Sci. Soc. Am. J.*, 59: 689-698.
- Kachanoski RG, Pringle E, Ward A (1992). Field measurement of solute travel times using time domain reflectometry. *Soil Science Society of America Journal*, 56: 47-52.

- Klemunes JA, Mathew WW, Lopez A (1997). Analysis of Methods Used in Time Domain Reflectometry Response, *Transportation Research Record*, 1548: 89-96.
- Lin CP (1999). Time domain reflectometry for soil properties. PhD thesis, School of Civil Engineering, Purdue University, West Lafayette, Ind.
- Lin CP (2003). Analysis of nonuniform and dispersive time domain reflectometry measurement systems with application to the dielectric spectroscopy of soils. *Water Resour. Res.*, 39(1), SBH61-SBH611.
- O'Connor KM (1991). Development of a system for highwall monitoring using time domain reflectometry. U.S. Bureau of Mines Summary Rep.
- Rhoades JD (1989). Intercepting, isolating and reusing drainage water for irrigation to conserve water and protect water quality. *Agricultural Water Management*, 16: 37-52.
- Ramo S, Whinnery JR, van Duzer T (1994). *Fields and waves in communication electronics*, 3rd Ed., Wiley, New York.
- Siddiqui SI & Drnevich VP (1995). A new method of measuring density and moisture content of soil using the technique of Time Domain Reflectometry. Rep. No.: FHWA/IN/JTRP-95/9, Joint Transportation Research Program, Indiana Department of Transportation-Purdue University.
- Siddiqui SI, Drnevich VP, Deschamps RJ (2000). Time domain reflectometry development for use in geotechnical engineering. *Geotech. Test. J.*, 23(1): 9-20.
- Santamarina JC, Klein KA, Fam MA (2001). *Soil and waves*, Wiley, New York.
- Svitzky A & Golay MJ, (1964), Smoothing and Differentiation of Data by Simplified Least Squares Procedures," *Analytical Chemistry*, 36(8): 1627-1639.
- Vanclouster M, Mallants D, Vanderborght J, Diels J, van Orshoven J, Feyen J (1995). Monitoring solute transport in a multi-layered sandy lysimeter using time domain reflectometry. *Soil Science Society of America Journal*, 59: 337-344.
- Von Hippel AR, ed (1954). *Dielectric materials and applications*, MIT Press, Cambridge, Mass.
- Timlin DJ & Pachepsky YA (1996). Comparison of Three Methods to Obtain the Apparent Dielectric Constant from Time Domain Reflectometry Wave Traces, *Soil Sci. Soc. Am. J.*, 60: 970-977.
- Topp GC, Davis JL, Annan AP (1980). Electromagnetic determination of soil water content: measurements in coaxial transmission lines. *Water Resour. Res.*, 6(3): 574-582.
- Topp GC, Zasovenko V, Zegelin SJ (1988). Determination of Electrical Conductivity using Time Domain Reflectometry: Soil and Water Experiments in Coaxial Lines," *Water Resources Research*, 24: 945-952.
- Ward AL, Kachanoski RG, Elrick DE (1994). Laboratory measurements of solute transport using time domain reflectometry. *Soil Science Society of America Journal*. 58: 1031-1039.
- Yu X & Drnevich VP (2004). Soil water content and dry density by time domain reflectometry. *Journal of Geotechnical and Geoenvironmental Engineering*. 130(9).
- Yu X & Drnevich VP (2004b). Time domain reflectometry for compaction control of stabilized soils, *Transportation Research Record*, No. 1868: 14-22.

THE STATUS OF ENGINEERING TECHNICAL STANDARDS OF WASTE SANITARY LANDFILL TREATMENT IN CHINA

Yi-Xin DONG¹

ABSTRACT: Chinese professional standards system of environmental sanitation was gradually formed in the late 1980s. The technical standard of waste sanitation landfill treatment is one of the earliest executive technical specifications. The basics of both landfill technology and standard formulation stem from sanitary landfill technical specification. During the development of the new standard, considerable attention is given to geotechnical engineering and landfill technology applied to landfill construction and development.

KEYWORDS: waste sanitary landfill, engineering technical standard, standard setting

INTRODUCTION

The technical standard of solid waste sanitary landfill treatment began in the middle period of 1980s in China. It developed in 1990s into a preliminary standard series applied to the guidance of construction of the domestic waste landfill site. In the late 1990s, the environmental sanitation professional standards system, which is technical standard system of waste sanitary landfill treatment, was formulated in the field of engineering construction. With the constant improvement and development of the system in an open state, it accomplished compilation and revision of the task by national annual plan. In the meantime, the system provided firm support to development and progress of waste landfill treatment engineering.

THE GENERAL SITUATION OF DOMESTIC SOLID WASTE SANITARY LANDFILL

According to statistics, there were 655 waste disposal cities in China at 2007. As far as the urban refuse treatment technology is concerned, Chinese cities have nearly 600 waste treatment facilities (66 incineration plants, 17 composting plants, and other facilities including sanitary landfills and simple landfills). Domestic waste disposal rate is 65%, and harmless treatment rate is about 35%. The main treatment is still landfill (Table 1, Fig.1).

Table 1 The number and the size of Chinese urban wastes treatment facilities (2001-2007)

Year	Harmless treatment plants (number)				Harmless treatment capacity (T / D)			
	Total	Sanitary landfill	Compost	Incineration	Total	Sanitary landfill	Compost	Incineration
2001	741	571	134	36	224736	192755	25461	6520
2002	651	528	78	45	215511	188542	16798	10171
2003	574	457	70	47	218603	187092	16511	15000
2004	559	444	61	54	238143	205889	15347	16907
2005	469	356	46	67	255862	211085	11767	33010
2006	413	324	20	69	256098	206626	9506	39966
2007	449	366	17	66	267751	215179	7890	44682

(① These data come from *The statistical yearbook of Chinese urban construction* during 2001-2007② Landfill facilities are only sanitary landfills)

¹ Senior engineer, Institute of standard rating, Ministry of housing and urban-rural construction, Beijing 100835, China. Email: dongyx@mail.cin.gov.cn

As small and simple landfills were closed in succession, the number of landfills in our country linearly decreased before 2006, but the total waste amount continued to rise. Moreover, average scale of landfill kept elevating, which was mainly concentrated in large cities.

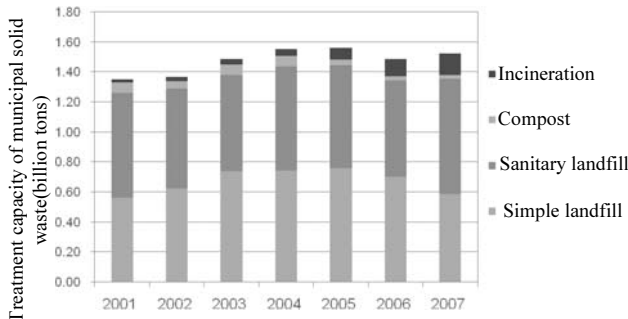


Fig. 1 The treatment capacity of Chinese municipal solid waste (2001-2007)

A number of sanitary landfills in small and medium-sized cities have been built since 2007. Meanwhile, waste landfill capacity in our country has been growing, but the size of landfill sites has a slight decrease in average (Fig.2). Normative sanitary landfills have been built in provinces and autonomous regions after the implementation of technical specifications. The distribution of sanitary landfills from 2001 to 2007 is shown in Fig. 3.

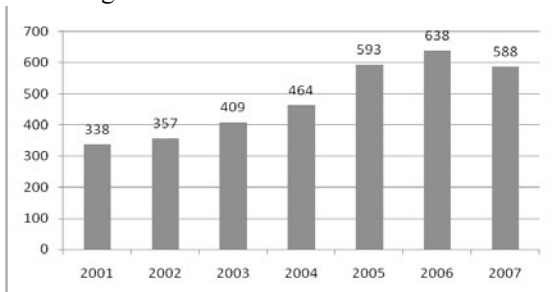


Fig. 2 The average treatment scale of Chinese solid waste sanitary landfill sites (2001-2007)

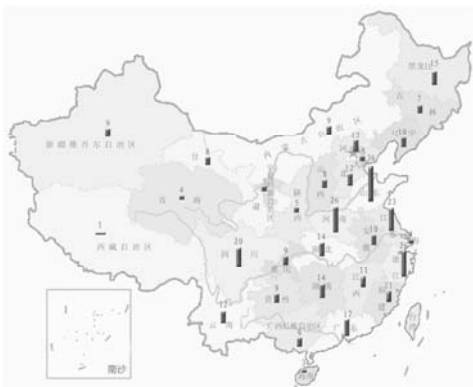


Fig. 3 The domestic distribution of the sanitary landfills in 2007

In general, the main trend of domestic waste sanitary landfill treatment has been formed, but the number of sanitary landfills, the scale and technological level still can not meet the requirements. There are still a large number of simple waste disposal sites, which is decentralized accumulation in the environment. There are still many technical problems in established landfill sites. Thus, in a long period, the construction of landfill is still very difficult. In order to guide the construction of new landfills and the closure or rebuild of simple waste landfills, the making of technical standard of landfill is facing new technical requirements.

TECHNICAL STANDARDS FOR CONSTRUCTION OF MUNICIPAL SOLID WASTE LANDFILLS IN CHINA

The technical standard of engineering construction is a very important basic work, which involves urban and rural planning, urban housing construction, transportation, water conservancy, electricity and other industries. For various types of work, regulations of investigation, planning, design, construction, installation, and inspection and operation maintenance are needed. The preparation of construction standards, in principle, is based on the standard system of construction projects. Nowadays, standard system of engineering construction published by China is “The People's Republic of China Engineering Construction Standard System (urban and rural planning, urban construction, housing construction part)”, which is an important part of the engineering construction standard system. It is consisted of comprehensive standards and three corresponding standards series. It's content with the national laws and regulations related to echoes (Fig.4).

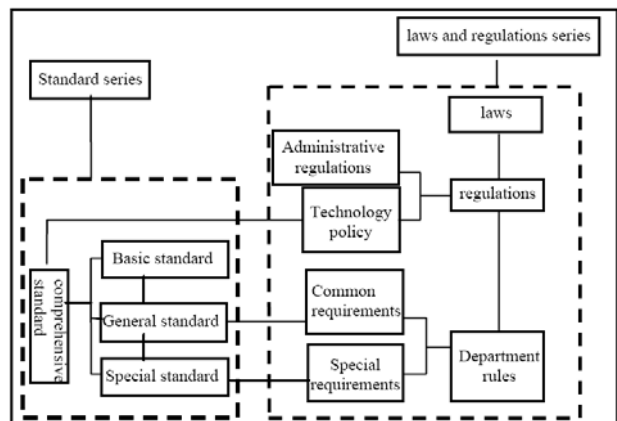


Fig. 4 The diagram of standard system in China

The comprehensive standards system involves necessary technology and management requirements of quality, safety, health, environmental protection and public

interest. It has a role of constraint and guidance towards professional standards at all levels.

The basic standard is widely used as the basis of other criteria in a certain professional scope, such as terminology, symbols, units of measurement, graphs, modules, basic classification, basic principles and so on. General standard refers to common standards of the standardization of a particular target. It can be used as the basis for the establishment of specific standards, such as general safety, general quality requirements of health and environmental protection, general design and construction requirements, general quality requirements, general design, construction requirements and test methods, as well as general management technology and so on.

Special standards refer to a specific standardization or supplementary and extended parts of general standards, which usually has small coverage, such as engineering investigation, planning, design, construction, installation, quality acceptance, and safety, environmental protection, requirements of a certain field and so on.

The technical standard of waste landfill is in the professional system of urban environmental landscape

sanitation. Fig.5 shows relation of city sanitation standards. Fig.6 shows the corresponding subsystem of the sanitation standards system. In the engineering construction standard system, city sanitation standards have been listed in(2)7,which are intricately linked with the history of urban sanitation industry and the city sanitation standard system established in the mid-eighties (Fig.2)

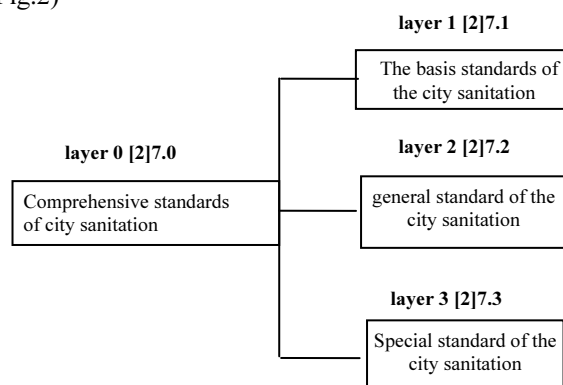


Fig. 5 The relation of city sanitation standards systems

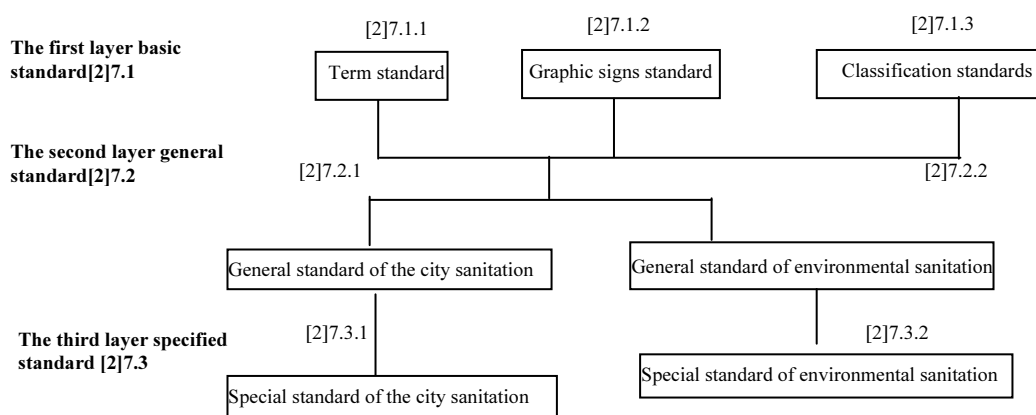


Fig. 6 Professional standard sub-system of the city sanitation

THE SCOPE OF APPLICATION FOR EXISTING SANITARY LANDFILL STANDARDS

In our solid waste sanitary landfill construction market, “Technical code for MSW sanitary landfill” is an important general specification. It was promulgated and implemented in 1988 by the ministry of construction. The relation of sanitary landfill standards and technology is mutual generation. So far, it has been revised four times. It is a general specification in sanitation standards systems. It is mainly applicable to newly building, rebuilding, and extension project of solid waste landfill. The technical contents of the standard contain whole process of landfill construction and various special technical requirements, and reflect

the standard and level of landfill construction, including site selection of landfill, foundation and anti-seepage facility of landfill, discharge and treatment of landfill leachate, emission and explosion-proof landfill gas, landfill cover, construction and acceptance of environmental protection and labor hygiene.

The special technical operations, such as the anti-seepage measure of landfill, treatment of landfill leachate, landfill gas power generation, landfill cover and so on, are also supported by the professional standards used to guide specific technical and operational implementation of landfill construction.

Following is a brief introduction of these special standards:

(1) Technical code for liner system of MSW landfill (CJJ113—2007)

Table 2 The professional standard system of landfill

[2]7.0 Comprehensive standards			
System code	The name of standard	Present standard	Remarks
[2]7.0.2	Technical code for municipal solid waste		Item at hand
[2]7.1 Basic standard			
System code	The name of standard	Present standard	Remarks
[2]7.1.1	Term standard		
[2]7.1.1.1	Standard for terminology of city appearance and environmental sanitation	CJJ65-2004	
[2]7.1.2	Graphic signs standard		
[2]7.1.2.1	Standards for figure symbols of environmental sanitation	CJJ/T125-2008	
[2]7.1.3	Classification standards		
[2]7.1.3.1	Classification and evaluation standard of MSW	CJJ/T102—2004	
[2]7.2 General standard			
System code	The name of standard	Present standard	Remarks
[2]7.2.2	The general standard of sanitation		
[2]7.2.2.7	Technical code for MSW sanitary landfill	CJJ17-2004	Revision in hand
[2]7.3 Special standards			
System code	The name of standard	Present standard	Remarks
[2]7.3.2	Special standard of environmental sanitation		
[2]7.3.2.12	Technical specification for operation and maintenance of municipal domestic refuse sanitary landfill	CJJ93-2003	Revision in hand
[2]7.3.2.13	Geotechnical engineering specification for MSW sanitary landfill		
[2]7.3.2.14	Technical specification for MSW sanitary landfill closure	CJJ112-2007	
[2]7.3.2.15	Technical specification of landfill liner leakage damage detection system		Item at hand
[2]7.3.2.16	Technical code for liner system of MSW landfill	CJJ113-2007	
[2]7.3.2.17	Leachate treatment project technical specification of MSW landfill		Item at hand
[2]7.3.2.18	Technical code for projects of landfill gas collection treatment and utilization	CJJ133	Item at hand
[2]7.3.2.19	The technical specification of operation and maintenance of landfill gas power plant		

(The numbers of standard system table denote standard system of engineering construction, professional number, layer number, classification number and standard serial number, respectively.)

It includes the design and material choice of landfill anti-seepage system, acceptance of construction techniques, and testing of anti-seepage system, etc.

(2) Technical code for projects of landfill gas collection treatment and utilization (CJJ133)

The specification includes collection and storage of biogas, gas power generation, gas generation technology,

environmental protection, and the design, construction and acceptance of gas power generation, etc.

(3) Technical specification for MSW sanitary landfill closure (CJJ112-2007)

The specification includes waste body shaping, discharge of landfill gas, cover, anti-seepage, surface water and sewage control, discharge and treatment of

landfill leachate, construction and management of landfill cover, environmental protection and labor sanitation, cover greening and land use.

Obviously, landfill construction is an integrated engineering technology. During the initial construction process, there are a number of imperfect technical requirements. The technical requirements always outgrow a standard with development of landfill technology. Meanwhile, matching special standards (mentioned earlier) are extremely favorable to landfill construction. In the past, the technical standards for landfill system were more concerned about environmental and health problems of landfills. Nowadays, geotechnical technology that goes with the general and special standards is imperative, which can consider the stability of landfill and pollution control.

The various environmental, geological and climate conditions of China caused different construction conditions of landfill sites, such as: leachate treatment of ultra-small size of the landfill, landfill site selection of alpine areas, the effect of groundwater to landfill for water network presented in plain areas, landfill construction of loess plateau region. The standard can consider characteristics of above region. There is an

urgent need to establish a landfill technical manual according to development of landfill technology and demand of landfill construction. It can guide landfill construction of various regions, and get accreditation in international standard.

From the opening of 2008, "Technical code for MSW sanitary landfill" will be revised again, and one of the new engineering standard of 2009 "Geotechnical engineering specification for MSW sanitary landfill" is under compilation, we look forward to accomplish as soon as possible. It will play an active role in furthering scientific, engineering and regulative developments of landfill in China.

REFERENCES

- The People's Republic of China Engineering Construction Standard System (urban and rural planning, urban construction, housing construction part), 2002. China building bookshop.
- The Statistical Yearbook of Chinese Urban Construction, 2001-2007.

CHALLENGES ASSOCIATED WITH THE DESIGN OF COVERS

Delwyn G. FREDLUND¹ and J. STIANSON²

ABSTRACT: The use of Cover Systems over top of mining wastes and industrial wastes has become a common solution for mitigating the release of contaminants into the environment. The design of single layer or multi layer cover systems appears to be quite straight forward from a conceptual standpoint. However, once the design procedure is embarked upon, it becomes clear that many assumptions are required as part of the design procedure. In addition, the numerical modelling procedure may prove to be a challenge because of the highly nonlinear nature of the partial differential equation that must be solved. The nonlinearity is generated because of the nonlinear permeability and water storage functions that are part of infiltration modelling. While the design of cover systems has proved to be challenging, there are also solutions that have been forthcoming. This paper attempts to describe the nature of the assumptions that need to be made as well as the solutions that have been developed for acceptable protocols for engineering design.

KEYWORDS: Cover design, Precipitation, Potential evaporation, Actual evaporation, Evapo-transpiration, Runoff, Unsaturated soil mechanics, Matric suction

INTRODUCTION

Cover systems have increasingly become a potential solution for many environmental concerns. Covers became a common solution around the 1980s, particularly for waste containment facilities and remediation of contaminated sites. Mining operations have two streams of waste material that need to be properly handled to mitigate damage to the environment. These two streams are waste rock and mine tailings. Cover systems provide a potential solution for both streams of waste materials.

The design of cover systems is easy to understand. However, there are issues and challenges associated with various aspects of design. There are issues related to the required input information and the solution of the moisture flow partial differential equation. There are also a large number of assumptions that need to be made at various stages of the design process. These assumptions can significantly influence the outcome of the cover design. The quantification of unsaturated soil properties for each material involved, (e.g. the permeability functions and the water storage functions), has proven to be a challenge for the geotechnical engineer (Fredlund, 2000; Fredlund, 2007).

Shackelford (2005) presented a summary of the primary current and future environmental issues associated with cover systems. The issues mentioned were: 1) long-term performance of waste containment

systems, 2) alternative barriers or covers (i.e. alternative to clay covers), and barrier materials, 3) innovative barriers (covers) and barrier materials, 4) forms of waste materials, 5) significance of biological waste processes, 6) the role of numerical modeling in cover design, and 7) professional identity. Of all these issues, it is *the role of numerical modeling as it relates to cover systems* that will be the primary focus of this paper.

The design of cover systems depends upon the ability to predict moisture fluxes in and out of the ground surface as well as through the unsaturated soils comprising the cover system. The analysis can be viewed as a “flux-driven” problem as opposed to a “head-driven” problem. Problems involving the predictions of hydraulic head are known to be easier to solve than problems involving the prediction of moisture fluxes. The boundary condition at ground surface needs to be described in terms of a moisture flux. The ground surface either has moisture coming down in the form of precipitation or going up in the form of evaporation and evapo-transpiration. The quantification of the moisture flux boundary conditions becomes almost as challenging as the solution of infiltration into the unsaturated soils.

The design of a cover system can be cast as a thin interface placed between the atmosphere and the underlying soil strata as shown in Fig. 1.

The climate imposed on top of the cover can vary widely from arid to humid conditions. It would not be expected that cover systems can function in a similar

¹ K.P. Chao Chair, Zhejiang University, Hangzhou, China. Email: unsaturatedsoil@yahoo.com

² Geotechnical Engineer, Golder Associates Ltd., Saskatoon, SK, Canada S7H 0T4

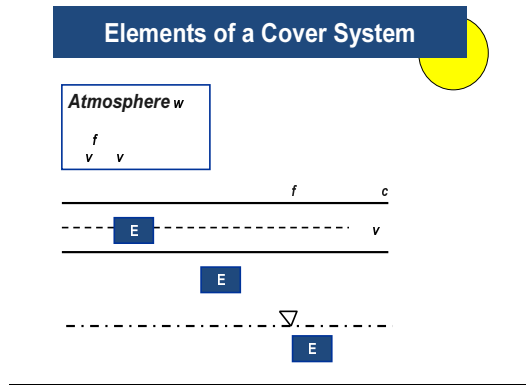


Fig. 1 Covers used as an interface between the material to be protected and the climatic environment

manner over a wide range of climatic conditions. Rather, it would be expected that covers could only perform satisfactorily under certain climatic conditions.

The purpose of the cover system can be viewed as functioning quite differently in differing situations. For example, the cover may operate as a “store and release” system in one case but it might be desirable to have it function as a saturation oxygen barrier in another situation. The location of the water table in the underlying materials will also have a strong influence on the functionality of the cover system. All elements of the cover system (i.e. atmosphere, cover and underlying soils), are highly variable and their material response behaviour can be viewed as being highly nonlinear, hysteretic and random (Fredlund, 2006). The challenges of solving such a problem are formidable but not impossible. At present, it is fair to say that it is difficult to give the same environmental problem to several geotechnical engineers and expect to get the same design solution for the cover system. It may also be difficult to get the same design solution for the cover system. It might also be difficult to get the same decision from two geotechnical engineers on whether a cover system will function satisfactorily in a particular environment.

CHALLENGES OF NUMERICAL MODELLING COVER SYSTEMS

Shackelford (2005) made several comments regarding the difficulties associated with the modeling of cover systems and these comments are worth repeating. He stated:

“The ability of models to accurately predict field performance of engineered systems has been and will continue to be an issue facing geotechnical engineers. This issue is particularly important when dealing with environmental problems because models are often used

as a tool to predict the future impacts and resulting risk from engineering activities.”

“The uncertainty in the accuracy of the model predictions can be considerable, particularly in cases where the time frame — design life is from hundreds to thousands of years.”

“There are accuracy problems associated with properties upon which the model is based as well as our knowledge concerning changes in the properties and processes with time.”

“The primary problem with numerical modeling is that the physical processes involved are governed by highly nonlinear unsaturated soil properties and the boundary conditions reflect natural randomness precipitation events as well as complex evaporative and evapo-transpiration phenomena.”

Numerical modelling associated with cover design appears to have presented more challenges than any other unsaturated soils application area. There appears to have been serious problems related to convergence when solving the partial differential equations and there are also questions related to the assumptions made at various stages of the analysis. The numerical modeling analysis is handled as a transient seepage analysis that may extend over a time period of several years (e.g. typically 10 years), using time steps in the order of a few minutes. The weather conditions can vary from being average conditions to extreme conditions and the soil properties can vary from being almost constant to being highly nonlinear. Needless to say, the numerical modeling challenges exceed those of other unsaturated soil mechanics problems.

CLIMATE CONTEXT FOR COVER SYSTEMS

The climatic context into which a cover system is placed should be understood before embarking on the numerical modeling aspects of cover design. “Store and Release” type covers are known to have the potential to function satisfactory in arid or semi-arid environments. However, there are situations where cover systems have been designed and used where the climate is not arid or semi-arid. The geotechnical engineer should have an appreciation of the significance of various climatic classifications.

Climatic classifications are based primarily upon a water balance calculation referenced to the ground surface. Calculations for climate classification provide the geotechnical engineer with information regarding the suitability of a particular type of cover system. The climatic classification provides information on whether a particular type of cover system has the potential to operate in a satisfactory manner. Once it has been decided that a particular cover system might function

satisfactorily, it is possible to proceed with a detailed cover design.

In geotechnical engineering, climate is usually determined using the Thornthwaite climate classification system (Thornthwaite, 1931, 1948). Thornthwaite published the first climate classification system in 1931. The classification system was revised in 1948 and it is the latter climate classification system that is generally used in geotechnical engineering. Climates are classified primarily based on temperature and precipitation. Temperature along with global setting (i.e. latitude) is used to estimate potential evapo-transpiration.

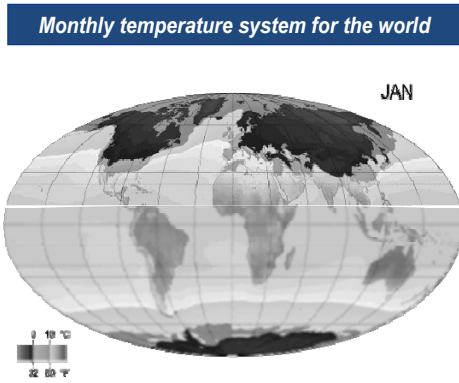


Fig. 2 Temperature is the primary factor controlling the evaporative flux from the earth's surface

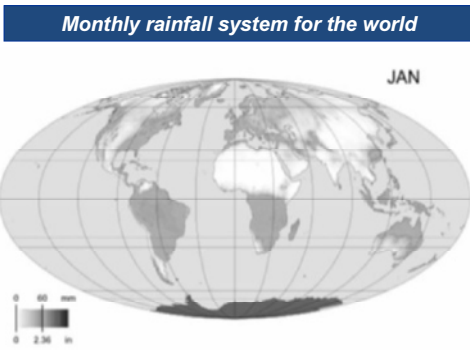


Fig. 3 Rainfall and snowfall are the contributors to precipitation falling the earth's surface

The Thornthwaite (1948) classification of climate was based on the calculation of a moisture index, I_m , that took into consideration total annual precipitation and annual potential evapo-transpiration. In 1948 it was assumed that the water surplus from one season might be carried forward to another season and therefore a weighting factor of 0.6 was applied to the water deficit calculation. However, in 1955, the 0.6 factor was omitted from the calculations of the moisture index which is now defined as follows.

$$I = 100(P / PE - 1) \quad (1)$$

where: I_m is the 1955 Thornthwaite moisture index, P is the total annual precipitation, and PE is the total annual potential evapo-transpiration calculated as the summation of the Thornthwaite (1948) monthly potential evaporations.

Thornthwaite (1948) incorporated the variables of length of daylight hours, mean monthly temperature, and an empirical constant, in the prediction of potential evaporation. The simplicity of the Thornthwaite equation has led to its usage for the classifications of global climate, as well as numerous other agricultural and engineering applications. The potential daily evaporation can be written using the Thornthwaite (1948) equation.

$$PE_d = 0.5333 \left(\frac{L}{12} \right) \left(\frac{N}{30} \right) \left(\frac{10T_a}{I} \right)^a \quad (2)$$

where: PE_d = potential evaporation in mm/day , L = length of daylight in hours, N = number of days in the month, T_a = mean monthly air temperature in $^{\circ}C$, I = sum for 12 months of the function $(T_d/5)^{1.514}$; (i.e. $\sum_{month=1}^{12} (T_d/5)^{1.514}$); Based on correlations to Pan Evaporation measurements, a = complex function of the variable I ; (i.e. $a = (6.75 \times 10^{-7}) I^3 - (7.71 \times 10^{-5}) I^2 + (1.79 \times 10^{-2}) I + 0.492$).

For a 30-day month and assuming that there are 12 hours of the day for evaporation, the potential evaporation equation can be written,

$$PE_m = 16.0 \left(\frac{10T_a}{I} \right)^a \quad (3)$$

where: PE_m = potential evaporation in $mm/month$. The potential monthly evapo-transpiration can be calculated for each of the 12 months and summed to give the total annual potential evapo-transpiration. For one year, the annual potential Thornthwaite evaporation can be written as follows:

$$PE = \sum_{i=1}^{12} PE_m \quad (4)$$

The total annual evapo-transpiration is used in conjunction with the total annual precipitation to classify the climate through use of Eq. (1). The climate classification criteria are shown in Table 1. The Thornthwaite classification is an empirical equation that was developed from limited climatic data collected in United States. However, it forms an adequate basis for establishing climatic types.

Table 1 Criteria for climate Classification¹

I_m (1955)	Category of Climate
> 100	Perhumid
20 to 100	Humid
0 to 20	Moist humid
-33 to 0	Dry subhumid
-67 to -33	Semi-arid
-100 to -67	Arid

¹ Moisture Index, I_m as defined in 1955.

It is important to establish the climatic type prior to embarking on a cover design because certain cover systems may be appropriate in one climatic setting but unsatisfactory in another setting. It is the ratio of the total annual precipitation, P , to the total annual evapo-transpiration, PE , which provides a guide to the suitability of a particular type of cover system.

BASIC FUNCTIONALITY OF A COVER SYSTEM

The first designed cover systems were predominantly made of compacted clays with an attempt to construct a relatively impervious cover over waste materials. However, the main problem that arose from the use of clay covers was the formation of cracks associated with drying and desiccation. Cracks made many of the clay covers quite permeable to the influx of water. As a result, a new generation of cover systems called “Alternative Covers” became more common. They were called “alternative Covers” because they were an alternative to clay covers. These cover systems were also referred to as “Store and Release” covers and ET (Evapo-transpirative) covers.

The engineering design of a “Store and Release” cover system involved the application of unsaturated soil mechanics principles (Fig. 4). The cover can change its degree of saturation with time and function in a manner that compensates for environmental fluctuations. Reductions in the degree of saturation reduce the hydraulic conductivity (or coefficient of permeability) of the cover system as long as the surface soil does not crack due to desiccation drying. The reduction in degree of saturation increases the storage capacity of the cover soil. The intent is for the cover to buffer the extreme climate forcing factors by storing water during wet periods and releasing it back to the atmosphere during dry periods.

Alternative covers can consist of a variety of soil types and often make use of sand and silt soils. The covers are designed on the basis of water storage and water release (i.e. a water balance design). There must be sufficient capability for the annual precipitation to be

removed from the cover on an annual basis. In other words, the cover must be in an area that tends towards being arid. However, an arid environment is not a sufficient criterion. The cover design must also take into consideration the distribution of precipitation throughout the year as well as the distribution of the thermal energy required to drive evapo-transpiration. Stated another way, the cover material must be able to provide sufficient water storage capacity and water release capacity to accommodate the climatic weather patterns that are likely to be imposed on the cover at any time of any year. It is necessary to test the functionality of the cover by subjecting the proposed design to several years of past climatic conditions. The cover may be subjected to 10 or more years of past climatic record data. The computer simulations may be reduced to time steps in the order of minutes and as a result the analysis becomes computationally intensive. There are also other factors that make the design analysis demanding and these will be later discussed. While the concept of “Storing” water and “Releasing water” throughout the year is simple, the analysis becomes dependent upon the assessment of many variables as well as several nonlinear unsaturated soil property functions.

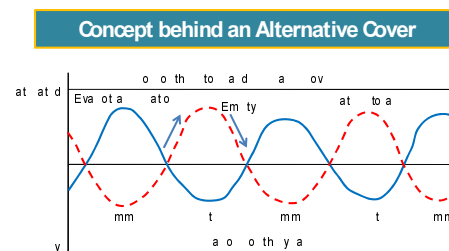


Fig. 4 Concept of “Store and Release” used in the design of Alternative Cover systems

Alternative covers can be classified into two main categories; namely, i.) MC or Monolithic covers, and ii.) CBC or Capillary Barrier Covers. Monolithic covers are also referred to as “Store and Release Covers”, “Soil-Plant Covers”, “ET or Evapo-transpirative Covers”, or “Phytocovers or Vegetated Covers”. Monolithic covers usually consist of a single, relatively thick layer of fine-textured soil with a relatively high water storage capacity. Alternative cover design requires there to be sufficient evaporative flux potential for the removal of water from the storage layer. Consequently, alternative covers require semi-arid or arid conditions to function as designed.

CBC or Capillary Barrier Covers usually take the form of two main layers. There will often be an additional organic layer placed over-top of the basic cover layers. The primary cover material usually consists of a fine-textured soil overlying a relatively coarse soil

layer. The fine layer is meant to store and release water from near the ground surface. The coarse layer is meant to function as a capillary break layer. These cover systems are meant to function under arid and semi-arid conditions. The criteria shown in Fig. 5 must be met in order for the CBC to function properly. The first design criterion states that the matric suction at the interface between the fine and coarse soil layers must always remain higher than the intersection of the permeability functions for the two materials. Failure to meet this criterion results in unwanted infiltration. The second design criterion states that the matric suction at the interface between the fine and coarse soil layers must be kept greater than the residual suction of the coarse layer. These two criteria are illustrated on the permeability functions shown for the fine and coarse soil layers (Fig. 5).

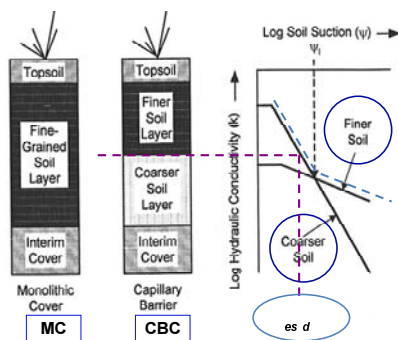


Fig. 5 Concept of a “Capillary Break” used in the design of Alternative Cover systems

Alternative covers have rapidly gained popularity because they have a lower susceptibility to cracking. The concept behind the design of alternative covers is simple and easy to grasp since the focus is on the storage of water rather than on the hydraulic conductivity of the materials involved. However, the design verification analysis is quite complex and involves a day by day numerical modelling simulation of typical climatic data. There are a wide range of possible soil cover materials that might possibly be used for soil layers. Once the alternative cover is constructed it usually has low post-closure maintenance requirements. There should; however, be post-closure studies to verify that the cover system is indeed functioning as it was designed to function. Post-closure verification of performance is an area where there does not appear to have been sufficient due diligence exercised.

Soil-water characteristic curves, SWCC, become the primary soils information required for alternative cover designs. There are two breaks on the SWCC that largely define the behaviour of the soils upon desaturation. These are the: i.) air entry value of the soil and ii.) residual suction of the soil. The SWCC for the soil defines the water storage capabilities of the cover system.

The infiltration and transmission ability of the cover system are largely dependent upon the permeability function for the soil (i.e. hydraulic conductivity versus soil suction). The permeability function for the cover material (and the underlying material), is also a function of the saturated hydraulic permeability and the SWCC of the soil.

The design of a cover system appears to be a relatively straight forward application of unsaturated soil mechanics principles. The inherent simplicity and straightforward concepts associated with the theory and design of cover systems can lead to unwarranted confidence in the design procedure. It is important to remember that the cover system has been put as an interceptor between the soil and the atmosphere. The cover systems are called upon to perform satisfactorily under an extremely wide range of diverse moisture and thermal flux boundary conditions.

Another class of cover systems are known as “innovative covers”. Innovative covers are classified mainly by their state of development. In other words, innovative covers are deemed to still be at a fundamental stage of research and development. Examples of innovative covers are: Clay Membrane Barriers, and Polymer-clay nanocomposites with superior mechanical, thermal and electrical properties. No further details are presented on innovative covers in this paper.

FRAMEWORK FOR COVER DESIGN AS A BOUNDARY VALUE PROBLEM

The design and performance of a cover system will be considered as a “boundary value problem”. There are many factors to balance in the design of a cover system. In this paper, the focus is on the complexity of the design and the detailed care that must be exercised when undertaking a cover system design.

The advent of the digital computer allowed the formulation of most geotechnical engineering problems as the solution of a partial differential equation where boundary conditions are specified. The information required for analyzing cover design is quite standard. It is necessary to know the ground surface geometry and have a fairly well-informed appreciation of the underlying stratigraphic sequence. It is necessary to be able to characterize the conditions at the designated boundaries of the problem. For unsaturated soils problems it is the characterization of the ground surface (net) moisture flux boundary condition that is of primary importance. The characterization of the (unsaturated) soil properties forms another important piece of input information. These are the primary factors that must be known in order to commence the design of a cover system. And it is in the context of a boundary value type

of analysis that a series of questions will be investigated. Attention will be paid to aspects associated with cover design and performance.

Geometry and Stratigraphy

Covers form the surface geometry of the problem to be analyzed. The stratigraphy associated with the pile has been built into the pile through the methods used to dispose of the waste materials. It is relatively easy to build a cover over tailings areas because they are generally relatively flat surfaces. Waste rock piles often have steep side slopes making it more difficult to construct and analyze a cover system on these surfaces. Both waste rock piles and tailings deposits are three-dimensional shaped structures (Fig. 6); however, design considerations are often limited to a one-dimensional analysis to simulate the relatively flat surface at the top of the pile. A two-dimensional analysis may sometimes be used for the simulation of the side-slope region.



Fig. 6 Illustration of varying evaporation conditions on the three-dimensional cover at Equity Silver (Weekes and Wilson, 2005)

The original one-dimensional modeling of a cover system was solved with the development of the SoilCover computer code (MEND, 1993) based on the Soil-Atmosphere formulation proposed by Wilson (1990). The first two-dimensional analysis of covers on a sloping surface to control oxygen fluxes was performed by Bussi re and Aubertien (2003). And more recently, a three-dimensional energy approach has been developed by Weeks and Wilson (2005). It might rightly be asked whether or not there is need for the sophistication of a three-dimensional analysis for cover designs. Recent studies by Weeks (2006) have shown that the computations of net evaporative flux from the soil surface can be significantly different depending upon the angle between the sun's rays and the orientation of the surface of the ground. Consequently, the performance of a soil cover can vary significantly from one part of the pile to another part.

In many cases, the geotechnical engineer needs to be aware that the ground surface is not level and that there is a potential for runoff and ‘‘ponding’’. The unevenness of the ground surface can result from differential settlement of the waste rock or the tailings with the result that the ground surface is highly susceptible to ‘‘ponding’’. In other words, the performance of the cover from one location to another can differ considerably from a simple one-dimensional characterization. There may not need to be much change in the orientation of the ground surface to bring about significant changes to the water balance over the surface of the pile.

Cover systems, particularly when viewed in a one-dimensional setting, have the appearance of being simple problems to numerically model. This is somewhat deceptive in that while the geometry is simple, the characterization of the soil properties is highly nonlinear and can lead to difficulties in obtaining convergence to a correct solution (Shackelford, 2005). It is important that checks be made on water balance calculations that are benchmarked against published known solutions (Gitirana, Jr., et al. 2005).

The Physics of Saturated-Unsaturated Water Flow for the REV

A Representative Elemental Volume called an REV must be selected within each of the continuum soil layers. It is necessary to first define the physics of saturated-unsaturated water flow through the REV while satisfying the conservation of mass requirement. The substitution of the constitutive behaviour for water flow and water storage, while satisfying conservation of mass, results in a partial differential equation, PDE, for saturated-unsaturated seepage through soil. The saturated-unsaturated water flow PDE is shown in Fig. 7 for the two-dimensional case.

The variable that must be determined from the PDE is the hydraulic head. In order to solve the PDE seepage equation it is necessary to have information on two soil properties; namely, the coefficient of permeability, k_w ,

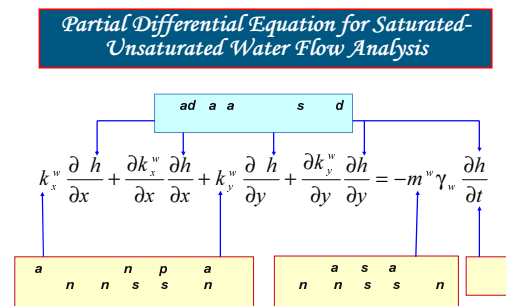


Fig. 7 The partial differential equation for saturated-unsaturated water flow for an REV (Fredlund and Rahardjo, 1993)

(or hydraulic conductivity) of the soil and the water storage, m_2^w , of the soil. Unfortunately, both of the soil properties are nonlinear functions of the matric suction of the soil (Fredlund et al. 1994; Fredlund et al. 1994).

The pore-water pressure term of matric suction constitutes one component of hydraulic head and as a result the PDE is nonlinear. The nonlinearity requires that the soil properties first be estimated while the hydraulic heads are computed. Then the soil properties must be adjusted to obtain more reasonable values and the hydraulic heads are once again computed. This process is repeated until the equation has converged. Convergence means that reasonably accurate soil properties were used when the hydraulic heads were computed. The iterative process may need to be repeated many times if the soil properties are highly nonlinear. It is also possible that the nonlinear PDE may not converge or even when the PDE has converged, the convergence may be to the wrong values of hydraulic head. Consequently, the solving of highly nonlinear PDEs has become an area of extensive research in mathematics and computing science.

The permeability and water storage functions are in reality more complex than what are shown in Fig. 8 since both functions exhibit hysteresis. In other words, there is one set of relationships that correspond to conditions when the soil is drying and another set of conditions that apply when the soil is wetting as shown in Fig. 9 (Phamet al. 2003). While hysteresis is known to exist in all soils, its effect is generally not taken into account in the design of cover systems. This is just one of many rather crude approximations that are made in the design of alternate covers. Generally it is the drying SWCC that is measured in the laboratory and this curve appears to be most commonly used in cover design analysis. In reality, the drying curve should be used when the soil is giving up water to the atmosphere and the wetting curve should be used when the soil is absorbing water. However, this does not appear to be the procedure normally used in cover design. It would also seem more reasonable to estimate a “mean” SWCC between the drying and wetting SWCC branches; however, this also does not seem to be usual engineering design practice.

The material(s) used for cover system may change considerably with time because of environmental influences. Cracking due to settlements and volume change is quite certain to occur. Furthermore, the growth of vegetation creates a network of root holes, fissures and cracks. Freezing and thawing cycles tend to produce a nugget-type structure particularly in fine-grained soils.

There may also be microbial contamination and other bio-intrusions that affect the soil structure. Changes in the soil structure tend to significantly change the soil-water characteristic curve for the materials involved.

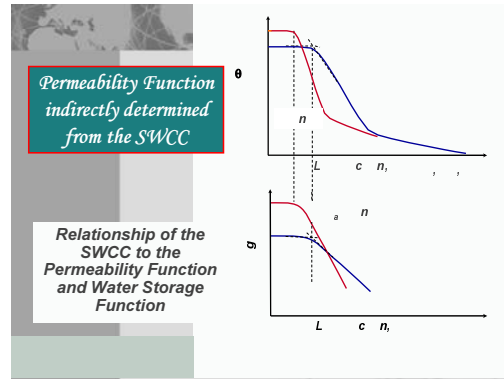


Fig. 8 Typical SWCCs and permeability functions for two soil types

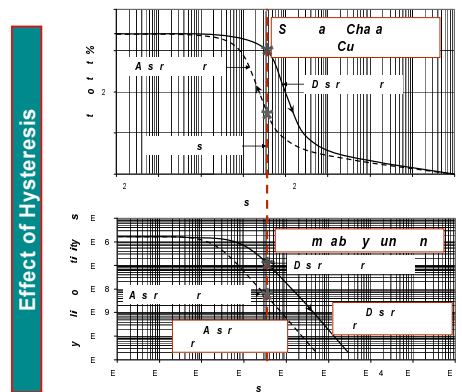


Fig. 9 Effect of hysteresis upon drying and wetting of a soil

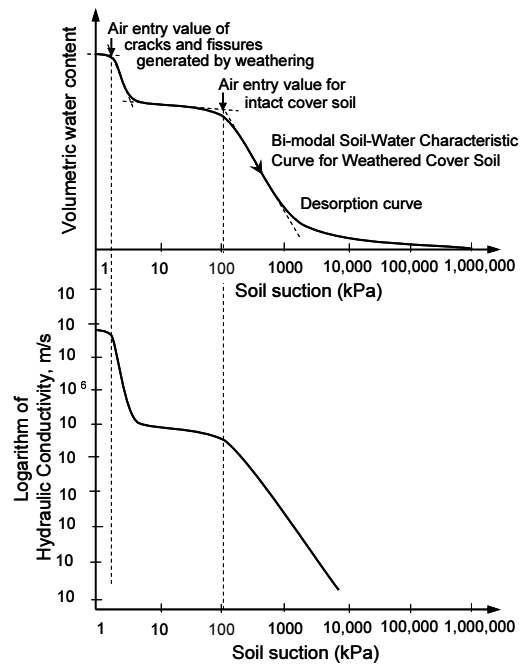


Fig. 10 Effect of cracking that may occur as a result of weathering of near-surface soils

Fig. 10 illustrates the type of changes that might occur in a typical SWCC that contains some clay content. It is possible that the SWCC will take on a bimodal character and that the saturated hydraulic conductivity may increase by several orders of magnitude. Consequently, numerical modeling simulations based on the properties of originally intact materials can be considerably different from the soils that develop near the ground surface with time.

Water Balance at Ground Surface

Analyses to compute net moisture flux conditions at the ground surface were not part of historical soil mechanics. The calculation of ground surface moisture flux based on climatic data is very much a part of unsaturated soil mechanics developments. It should be noted that the calculation of net moisture flux at the ground surface involves a number of assumptions and approximations. Some of the inherent difficulties are mentioned in the following sections. Other factors such as freezing and thawing are often not adequately taken into account.

The ground surface forms a flux boundary that interacts with the atmosphere. Water is either entering the ground surface boundary as a result of precipitation or it is leaving the ground surface through (actual) evaporation, AE , or evapo-transpiration, ET . Water may also be shed through runoff, R .

The components of moisture flux at the ground surface are illustrated in Fig. 11 and can be written in an equation as follows.

$$\text{Net Infiltration (I)} = \text{Precipitation (P)} - \text{Actual Evaporation (AE)} (\& \text{Evapo-transpiration (ET)}) - \text{Runoff (R)} \quad (5)$$

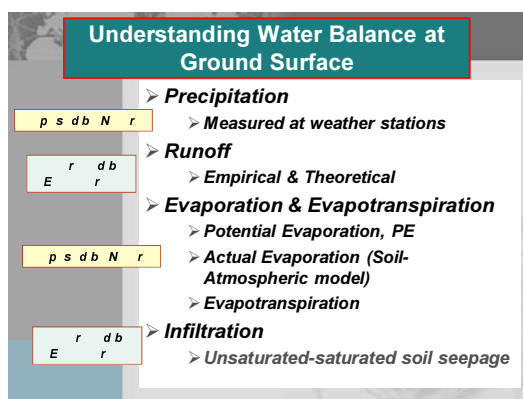


Fig. 11 Components of the moisture flux at the ground surface

In abbreviated form, the net infiltration at ground surface can be written,

$$I = P - AE - ET - R \quad (6)$$

The quantification of ground surface moisture flux conditions is a more recent analysis brought into soil mechanics. There has not been a long history of calculating ground surface moisture flux conditions because it is a complex problem and many assumptions must be made as part of the computational procedure. In particular, the calculations associated with determining actual evaporation, AE , are the most challenging. The elements of physics involved with the determination of potential evaporation should be fully understood prior to calculating actual evaporation. Potential evaporation occurs from the ground surface when there is an ample supply of water while actual evaporation can be thought of as evaporation from a ground surface where the soil is resisting evaporation (or holding back evaporation). Consequently, actual evaporation requires that the effect of soil suction be taken into account.

Each of the components of net infiltration must be assessed in order to determine the moisture entering at ground surface. Each of the components of net moisture flux will be discussed along with a brief description of the calculations and main assumptions required when performing the calculations. There are many factors that influence net infiltration at ground surface. The assessment of most variables is made using average soil conditions and average imposed moisture flux loads. The average and accumulated effects may not however, provide an accurate picture of long-term performance of the cover system. Extreme events or high intensity storms should probably be given more attention since extreme climatic conditions likely cause the most serious failures of cover systems.

Precipitation (rainfall and snowfall)

Precipitation can take the form of rainfall and snowfall. Its magnitude must be measured at or near the site under consideration. Temperature, relative humidity, wind speed and rainfall are usually the basic variables measured by an elementary weather station. The daily measurements of precipitation may have been measured over a period of many years. Each year of data should be considered as an independent record and used as such for analysis purposes. An accumulated annual precipitation record can be plotted for each year (Fig. 12). The accumulated annual precipitation can take one of several forms depending on the distribution of precipitation within the year as shown in Fig. 12.

Two differing scenarios are shown; namely, one where there is an even distribution of precipitation throughout the year and another where there are two distinct, short-lived monsoon seasons. Even though the total precipitation in a year might be the same for the two cases, the response of a cover system to each situation would be considerably different.

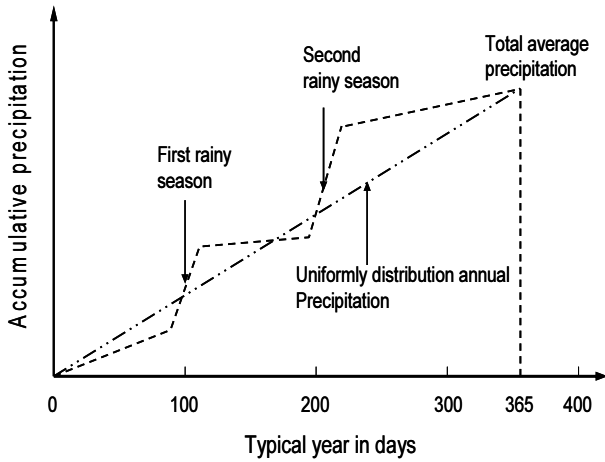


Fig. 12 Effect of a variation in precipitation distribution throughout the year

An unsaturated soil can only accept water at a particular rate and the rate is dependent mainly upon the present hydraulic conductivity and water storage capabilities. While it is possible for the soil to accept water at a rate in excess of the saturated hydraulic conductivity, it is quite likely that the intensity of rainfall during a storm can readily exceed the ability of the soil to accept water. Fig. 13 shows the intensity of rainfall versus time along with the capacity of the soil to accept water. When the intensity of precipitation exceeds the infiltration capacity the remainder of the moisture becomes runoff or “ponding” on the ground surface.

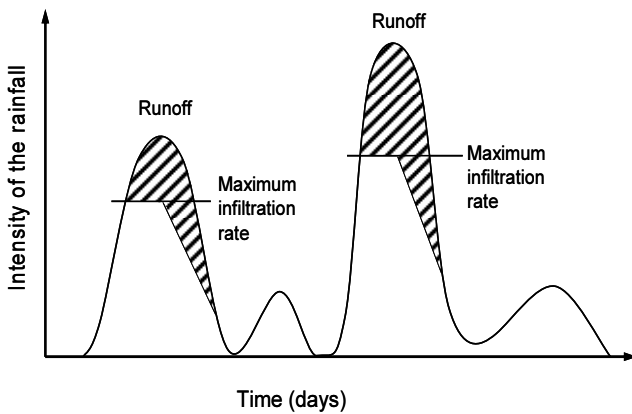


Fig. 13 Partitioning of rainfall based on the ability of the soil to accept water

The conventional collection of precipitation data does not allow for the character of a particular storm to be quantified. In other words, the rainfall for an entire day may be spread over most of one day with no consideration as to whether the storm was 10 minutes long or 10 hours long as shown in Fig. 14.

Generally the daily rainfall is spread out over most of

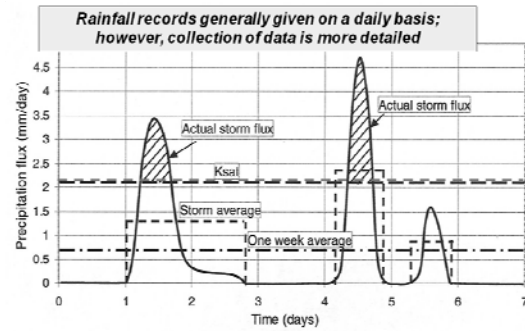


Fig. 14 Distribution of typical rainfall intensity diagrams

the day and as a result most of the precipitation will appear to infiltrate the soil. This is an inherent weakness in the conventional analysis of rainfall data that is collected and used in engineering design.

The primary driver for net ground surface moisture flux is precipitation and snowfall. This information is obtained from weather stations and Fig. 15 shows a typical plot of the daily rainfall records and the cumulative precipitation over the period of one year. There is a “resolution” problem associated with the collection of climatic data. Climate data typically includes daily data but a resolution of hours or even minutes should be known for a simulation that reflects reality. There are difficulties associated with designing a computer simulation that is capable of handling high intensity rainfall events in the context of a long-term simulation. For example, few software products permit mixing the resolution of input data (i.e. inputting hourly rainfall data but having a different time scale for other weather information). Convergence settings that provide reasonable accuracy for daily simulations might not provide reasonable accuracy for modeling to the fraction of a second.

While considerable attention has been given to the analysis of rainfall data, less attention has been directed towards the analysis of snowfall data. The analysis of snowfall data is unfortunately somewhat vague. An assumption must be made at the start of a spring infiltration season regarding how much snow exists (i.e. the volume of water to be distributed over each day of spring infiltration). A conservative assumption is to assume that all the snow that fell during the winter remains and contributes to the spring infiltration event. This type of assumption might prove to be overly conservative if actual snow depth measurements were available. The starting and ending time periods for the melting of the snow is also open to a somewhat arbitrary assumption on the part of the modeler.

Runoff

Runoff can be calculated as the water that cannot gain entrance into the soil when it falls to the ground.

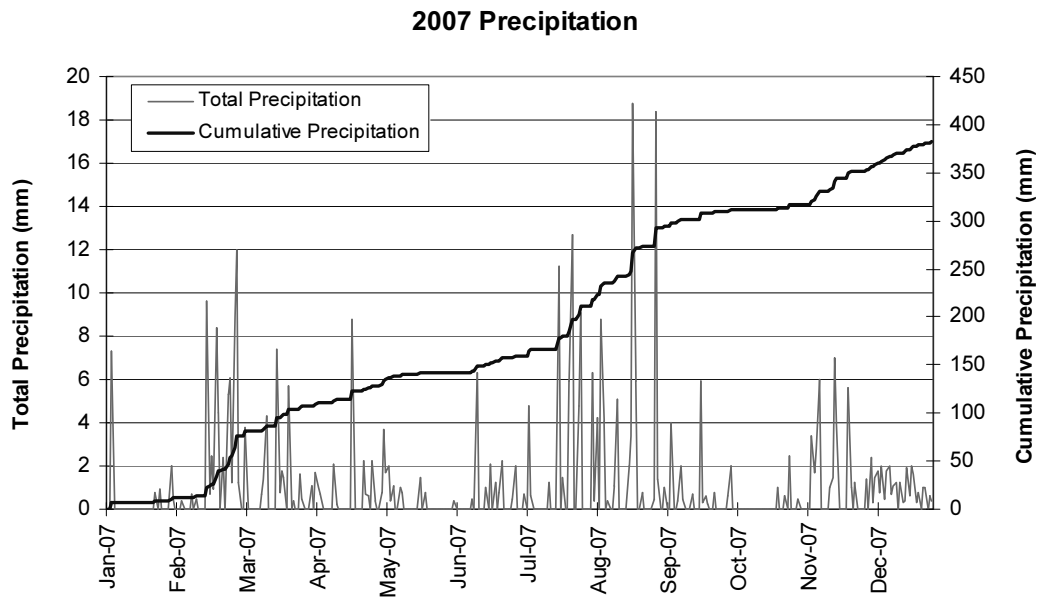


Fig. 15 Typical weather station record showing the daily precipitation and the cumulative rainfall at a particular site in Canada

The amount of moisture leaving the ground surface by actual evaporation is also taken into account. As well, the slope of the ground surface is taken into consideration when distributing the (vertical) rainfall onto a sloping surface. The water balance equation takes on the form shown below and its meaning is illustrated in Fig. 16.

$$NF = P \cos \alpha - AE - R \tag{7}$$

where: NF = the net moisture flux; P = precipitation; α = ground surface slope; AE = actual evaporation; R = runoff.

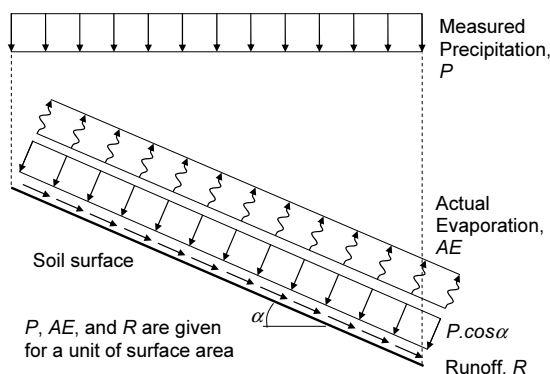


Fig. 16 Ground surface moisture flux associated with runoff

The term AE is a function of weather parameters and the soil suction at the soil-atmosphere boundary. Actual evaporation is discussed later and can be computed based

on potential evaporation and a limiting function (Wilson et al. 1997). Runoff must be computed in an interactive manner. If the soil surface being analysed has an efficient drainage system, any runoff water will be removed from the ground surface. In this case, the amount of net moisture flux, NF , should not produce pore-water pressures higher than zero at ground surface. The following set of equations can be used to represent runoff conditions (Gitirana Jr. et al. 2005):

$$NF = \begin{cases} P \cos \alpha - AE & \text{:if } P \cos \alpha - AE > 0 \text{ and } u_{ws} < 0 \\ EF(0 - u_{ws}) & \text{:if } P \cos \alpha - AE > 0 \text{ and } u_{ws} \geq 0 \\ P \cos \alpha - AE & \text{:if } P \cos \alpha - AE \leq 0 \end{cases}$$

where: u_{ws} = pore-water pressure at the surface; EF = a large number.

Runoff may take place when the value of $(P \cos \alpha - AE)$ is larger than the saturated hydraulic conductivity. The amount of runoff corresponds to the difference between the water available, $(P \cos \alpha - AE)$, and the amount of infiltration.

If the multiplier, EF , tends to infinity, the area flux boundary condition, $NF = EF(0 - u_{ws})$, becomes mathematically equivalent to a hydraulic head boundary condition the ground surface, $u_w = 0$. This approach is based on switching boundary conditions and can result in numerical oscillations due to an instantaneous change on the node value. This instantaneous change does not represent real-world conditions. Instantaneous changes in node values require mesh refinements that should theoretically be infinitesimal (Gitirana Jr., et al. 2005,

Nelson, 2005). Therefore, Eq. [6] appears to impose a more realistic condition.

The above-mentioned approach to the simulation of a rainfall event allows both the infiltration and the runoff components to be accurately simulated. Fig. 17 shows an accurate simulation of infiltration and runoff performed using SVFlux software (Fredlund, 1997) which utilizes the above-mentioned ground surface boundary condition (Gitirana Jr. et al. 2005).

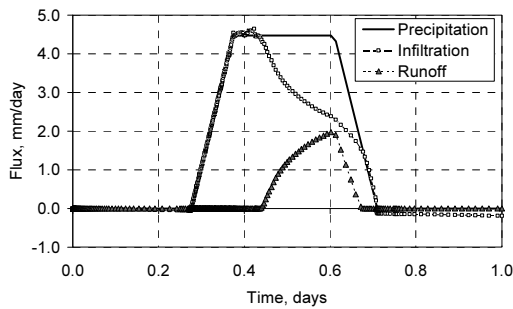


Fig. 17 Illustration of the ability to simulate infiltration and runoff conditions

There are also issues related to runoff when the soil is frozen or partially frozen. More research and guidance needs to be provided on handling climatic data during the winter and spring seasons.

Potential evaporative flux

The quantification of evaporation from the ground surface can be estimated using equations describing the physical processes involved. There have been numerous studies conducted since the 1920s that have attempted to predict the “potential evaporation” from the ground surface. It is; however, the “actual evaporation” and “evapo-transpiration” that are of primary interest in geotechnical and geo-environmental engineering. The physical laws affecting “potential evaporation” should be understood before calculating “actual evaporation”. Weather stations commonly record precipitation events, net radiation, temperature, wind velocity, relative humidity and possibly some other variables.

Potential evaporation is the amount of water removed by the atmosphere through evaporation if water is freely available at the ground surface. In general, about 80% of the energy required for evaporation comes from the sun (in the form of net radiation) while wind (in the form of a mixing term) and the vapor deficit of the air form a second important component contributing to evaporation. “Pan Evaporation” measurements (i.e. an open water surface) can be used to measure “potential evaporation”.

Researchers have attempted to develop empirical, mathematical equations that embrace the primary variables controlling the rate of evaporation from a free water surface (i.e. potential evaporation). Each proposed

“potential evaporation” equation uses specific weather-recorded data. The calculation of “potential evaporation” can be presented in units of *mm/day*; and the range of values is generally between zero and 10 *mm/day*. While the Thornthwaite (1948) equation is generally used to assess climatic conditions of aridity and humidity, it is the Penman (1948) equation that is generally used in geotechnical engineering for estimating *potential evaporation, PE*.

Penman (1948) incorporated a number of variables commonly collected at weather stations into the prediction of potential evaporation. The Penman equation combines a Dalton type formulation with the heat budget equation and as a result, the temperature at the evaporating surface is no longer required. Penman’s equation uses routine weather data as input (e.g. relative humidity, air temperature, wind speed, and net radiation).

$$PE = \frac{\Gamma Q_n + \eta E_a}{\Gamma + \eta} \quad (8)$$

where: *PE* = potential evaporation in *mm/day*, Γ = slope of saturation vapour pressure vs. temperature curve, $\text{kPa}/^\circ\text{C}$, Q_n = net radiation at the water (or saturated ground) surface, *mm/day*, η = psychrometric constant, $\text{kPa}/^\circ\text{C}$, $E_a = 2.625(1 + 0.146W_w)(u_{vo}^{air} - u_v^{air})$, *mm/day*, W_w = wind speed, *km/hr*, u_v^{air} = vapour pressure in the air above the water (or saturated ground) surface, *kPa*, u_{vo}^{air} = saturated vapour pressure at the mean air temperature, *kPa*,

The Penman equation shows that the vapour pressure gradient between the water surface and the air above the water becomes the primary driving mechanism for evaporation. There are two terms in the numerator of Eq. [8]. The first term involving *net radiation* characterizes the power of the sun to evaporate water. *Net radiation* quantifies the net effect of short and long wave radiation from the sun, surface reflectance (*albedo*) and surface temperature. The second term involves “*mixing*” of the air above the water or the drying power of the air.

The vapour pressure in the air above the water and the saturated vapour pressure at the water surface are the dominant variables driving evaporation. The saturated vapour pressure is a function of temperature while the actual vapour pressure in the air is related to the relative humidity. The two variables on the bottom of the Penman equation are also related to vapour pressure.

When solving the Penman (1948) equation it is not sufficient to use average daily values for variables such as temperature and relative humidity. Rather, it is necessary also know the minimum and maximum values for each day and then an assumption must be made regarding the variation of these variables throughout a 24 hour period. Fig. 18 shows the minimum, maximum and average air temperature readings at a particular site in

Canada for the year 2007. Fig. 19 shows the minimum, maximum and average relative humidity values for the same site in the year 2007. Minimum, maximum and average values are required for calculation purposes because of nonlinearity in evaporation behavior. Fig. 20 shows a typical annual plot of wind speed and Fig. 21 shows the net radiation for each day at the designated site. Net radiation values are not as commonly measured as other weather parameters and therefore, it is sometimes necessary to estimate net radiation values based on the latitude of the site under consideration. Figs. 18 to 21 show the information that is necessary for the

calculation of *Potential Evaporation, PE*, based on the Penman (1948) equation. Considerable information and computations are required even for the assessment of *potential evaporation*.

The *potential evaporation, PE*, calculation provides the engineer with an understanding of the evaporation that could occur from a water saturated surface. In the case of a soil cover system, the soil may be holding onto the water while the sun and wind are attempting to pull the water upward. The “struggle” between the climate and the soil gives rise to the *Actual Evaporation, AE*, from the ground surface.

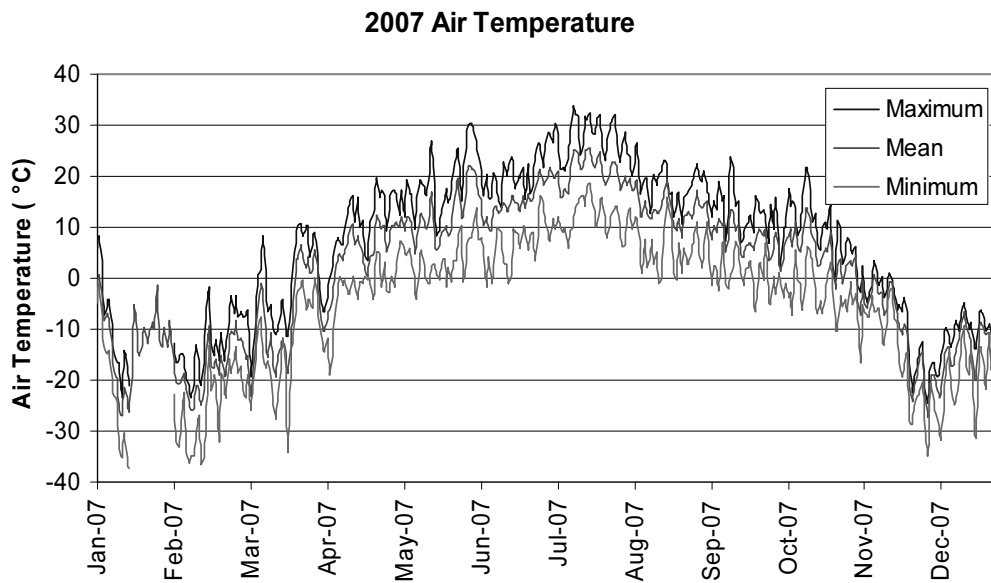


Fig. 18 Minimum, maximum and average air temperature readings for a particular site in the year 2007

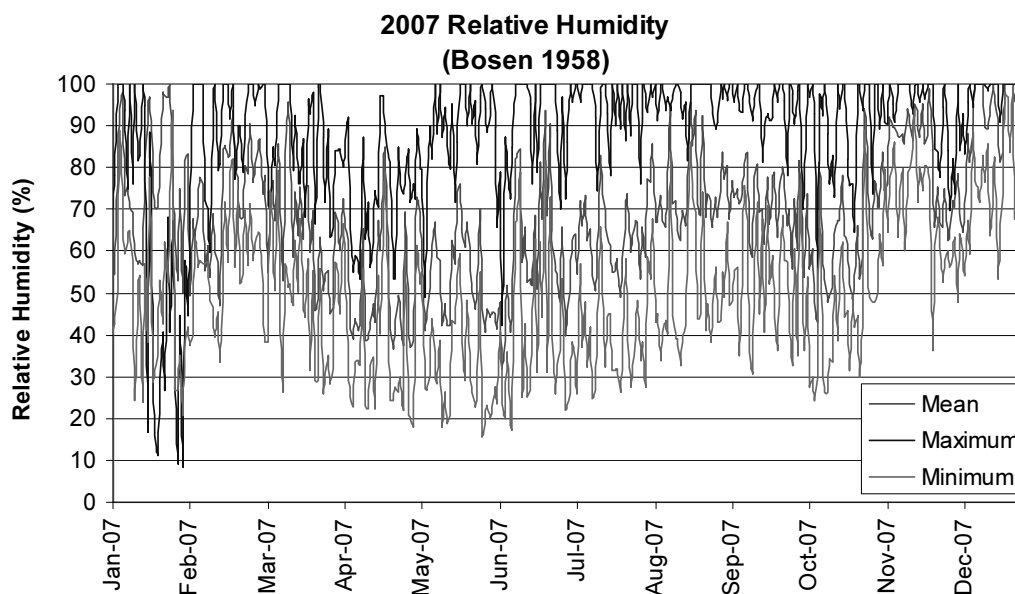


Fig. 19 Minimum, maximum and average relative humidity readings for a particular site in the year 2007

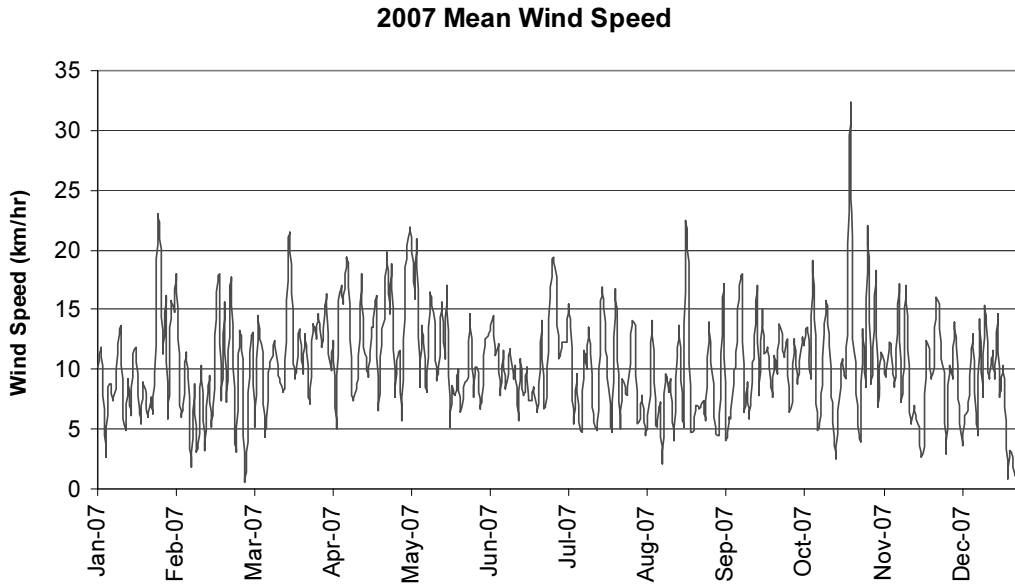


Fig. 20 Average wind speed readings for a particular site in the year 2007

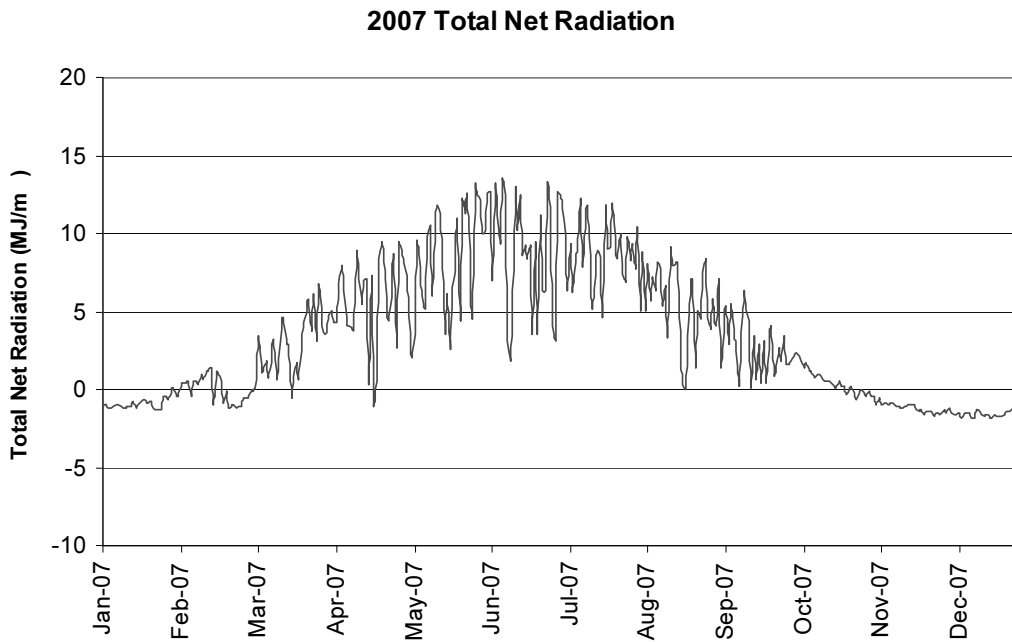


Fig. 21 Total net radiation readings for the same site in the year 2007

Actual evaporative flux

The *actual evaporation, AE*, from a soil surface might be considerable less than the *potential evaporation, PE*. The geotechnical engineer is more interested in calculating *actual evaporation, AE*, in order to compute the water-balances at the ground surface. Two equations are presented that can be used for calculating *actual evaporation, AE*, from a soil surface under varying soil suction conditions. Both equations are the outcome of research by Wilson (1990) who used evaporation from thin soil layers and sand column drying tests to verify the fundamental physical relationships used to extend the

Penman (1948) equation for the calculation of *actual evaporation, AE*.

Wilson’s (1990) first proposed equation takes the form of a modified Penman equation. The modification takes into consideration the reduced relative humidity (i.e. vapour pressure in the soil at ground surface), in the denominator of the Penman-Wilson equation (Wilson et al. 1994, 1997).

$$AE = \frac{\Gamma Q_n + \eta E_a}{\Gamma + \eta A} \tag{9}$$

where: AE = actual evaporation in mm/day , $A = u_{vo}^{soil}/u_v^{soil}$, $E_a = 0.35(1 + 0.15W_w)u_v^{air}(u_{vo}^{air}/u_v^{air} - u_{vo}^{air}/u_v^{soil})$, mm/day , u_v^{air} = water vapour pressure in the air above ground surface, mm Hg, u_{vo}^{air} = saturated vapour pressure at the mean air temperature, mm Hg, u_v^{soil} = vapour pressure in the soil at ground surface, mm Hg, u_{vo}^{soil} = saturated vapour pressure in the soil at ground surface, mm Hg, Γ = slope of saturation vapour pressure vs. temperature curve, mm Hg/ $^{\circ}C$, Q_n = net radiation at the water surface, mm/day , η = psychrometric constant, mm Hg/ $^{\circ}C$, W_w = wind speed, km/hr.

The relative humidity in the soil at ground surface, h_r is equal to u_v^{soil}/u_{vo}^{air} and the relative humidity of the air, h_{air} is equal to u_v^{air}/u_{vo}^{air} . The ratio of *actual evaporation* to *potential evaporation*, AE/PE , can be understood using the thermodynamic equilibrium relationship between relative humidity and negative pore-water pressure (or total suction) (Edlefsen and Anderson, 1943).

$$\frac{u_v^{soil}}{u_{vo}^{air}} = -\exp\left(\frac{u_w v_w \omega_v}{\rho_w g RT}\right) \quad (10)$$

where: hr = relative humidity in the unsaturated soil voids (i.e. vapour pressure in the soil divided by the saturation vapour pressure), u_{vo}^{air} = saturated air vapour pressure, kPa, u_v^{air} = vapour pressure in the soil at ground surface, kPa, u_w = pore-water pressure, kPa, ω_v = molecular weight of water, 0.018 kg/mol, v_w = specific volume of water, g = gravity acceleration, m/s, T = temperature, $^{\circ}K$

Eq. 9 can be re-arranged and used to compute the vapour pressure in the soil at ground surface.

$$u_v^{soil} = u_v^{air} e^{\left(\frac{u_w v_w \omega_v}{\rho_w g RT}\right)} \quad (11)$$

where: ψ = total suction (i.e. matric suction plus osmotic suction) or $(u_a - u_w) + \pi$ where u_a is the pore-air pressure and u_w is the pore-water pressure. If a reference temperature of $20^{\circ}C$ is selected the constants in the above equation give a value of 135,022. Therefore, the equation can be written as follows.

$$u_v^{soil} = u_v^{air} e^{\left(\frac{-\psi}{135022}\right)} \quad (12)$$

Another equation was proposed by Wilson et al. (1994, 1997) for calculating actual evaporation, AE . The equation takes the form of a “limiting function” between zero and potential evaporation depending on the vapor pressure in the soil at ground surface. The AE is scaled in accordance with Lord Kelvin’s equation. The “limiting function” equation is written as follows.

$$AE = PE \frac{u_v - u_v^{air}}{u_{vo} - u_v^{air}} \quad (13)$$

where: AE = actual evaporation in mm/day , PE = potential evaporation in mm/day , u_v = actual vapour pressure at the soil surface, u_{vo} = saturated vapour pressure at the soil surface temperature, u_v^{air} = vapour pressure in the air above the soil surface.

Assuming that the air, water and soil temperatures are approximately equal allows temperature to cancel and Eq. [13] to be written in terms of the relative vapour pressure (i.e. relative humidity) of the air above the evaporating soil and water surfaces and Lord Kelvin’s total potential equation.

$$AE = PE \frac{[-\exp\left(\frac{u_w v_w \omega_v}{\rho_w g RT}\right) - u_v^{air} / u_{vo}^{air}]}{[1 - u_v^{air} / u_{vo}^{air}]} \quad (14)$$

where: AE = actual evaporation in mm/day , PE = potential evaporation in mm/day , u_v^{air} / u_{vo}^{air} = relative vapour pressure (or relative humidity, h_{air}) of the air.

Soil suction at the ground surface is obtained by combining either Eq. 13 or 14 with the partial differential equation that models liquid and vapour flow in the soil. The combined solution is referred to as a “soil-atmospheric model”.

Wilson (1990) developed a Soil-Atmospheric model that combines heat and mass transport in the soil near to the ground surface and Lord Kelvin’s equation relating vapour pressure to total suction. The water flow partial differential equation (i.e. liquid and vapour flow) predicts the total soil suctions at the ground surface. The total suction predictions then make use of Lord Kelvin’s equation to yield the relative humidity (i.e. soil vapour pressure) at the ground surface. The vapour pressure in the soil provides an indication of the tenacity with which the soil is holding onto the water. Actual evaporation, AE , from the ground surface starts to be noticeably reduced from potential evaporation, PE when the soil suction in the soil at ground surface becomes greater than about 3000 kPa.

Wilson (1990) showed that it is the soil suction at the ground surface that primarily controls the actual rate of evaporation. Consequently, the soil type at ground surface is not a controlling factor when assessing the actual rate of evaporation as shown in Fig.22.

Evapo-transpiration flux

Plants can be viewed as small pumps that remove water more efficiently from the soil than can be done through evaporation from the soil surface (Tratch et al. 1995) (Fig. 23). Evapo-transpiration from plants can be

up to 10 times as high as actual evaporation. Therefore, it is important to take the ground surface vegetation into consideration. However, experientially the effect of vegetation has proven to be quite difficult. Evapo-transpiration is primarily a function of the root uptake zone and the leaf area index, LAI, of the plants. The growing season for the vegetation must be assumed and nutrients must be available in the soil to sustain plant growth. The long-term sustainability of plant growth has also proven to be a problem in some situations.

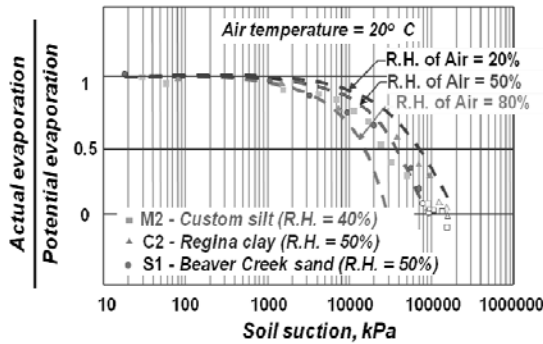


Fig. 22 Actual evaporation rate from sand, silt or clay soil surfaces as a function of the soil suction at ground surface

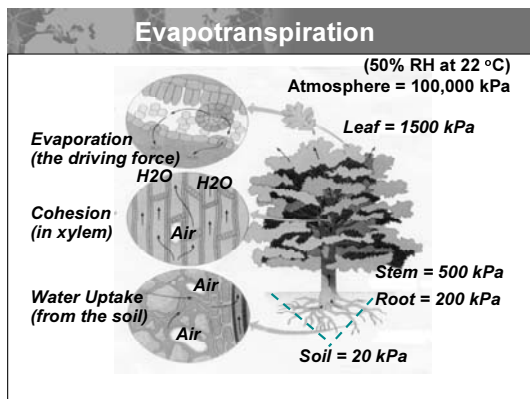


Fig. 23 Concepts associated with evapo-transpiration from vegetation

Numerical modelers are called upon to make numerous assumptions with regard to vegetation effects and these assumptions can have a significant affect on the outcome of the analysis. It is fair to say that more research is necessary with regard to the characterization of the effects of vegetation and how the results should be incorporated into a vegetation moisture flux model (Tratch et al. 1995).

Net moisture flux at ground surface

Each of the components that influence the net moisture flux at the ground surface has been described.

Once the information related to net moisture flux at the ground surface boundary is complete, then it is possible to proceed with the calculations of infiltration of water into the soil. However, it needs to be understood that the above-mentioned calculations for moisture flux are not independent of modeling soil infiltration. The actual evaporation, AE, is dependent upon knowing the total suction at ground surface. Actual evaporation is computed in the infiltration model and as a result there is a “coupling effect” between the infiltration model and the calculation of the moisture flux boundary conditions. Stated another way, the calculations combine the climatic ground surface moisture flux conditions with the solution of the nonlinear partial differential equation of unsaturated soil seepage. The combination of the unsaturated soil moisture flow and the climatic boundary conditions is called a “soil-atmospheric model”.

The soil-atmospheric model will need to be solved on an elapsed time scale that might be in the order of a few minutes. Each day is modelled and the time scale is continued for the entire year. However, one year may not be sufficient for design of the cover system. Rather, it may be necessary to perform these calculations for as much as 10 years or more. Needless to say, the design of the cover system is computationally demanding. As well, the high nonlinearity of the partial differential moisture flow equation makes convergence of the solution a challenge.

Fig. 24 shows the cumulative effects of precipitation, actual evaporation, and runoff for a portion of one year. The net effect is called “net infiltration” at the soil surface. Infiltration at the bottom of the cover system is generally referred to as “deep infiltration”. The magnitude of “deep infiltration” provides an indication of the amount of water that is likely to pass below the cover system into the underlying materials. There are many assumptions and calculations that have gone into the calculation of infiltration.

NUMERICAL MODELLING OF COVERS

There are several aspects of the cover design procedure that make the procedure an engineering challenge. The infiltration modelling involves the solution of a highly nonlinear partial differential equation that describes the seepage and water storage processes. The soil properties that produce nonlinearity in the PDEs are the permeability function and the water storage function. Both of these soil properties are related to the soil-water characteristic curve, SWCC.

If the SWCC has a relatively high air entry value and if the rate of desaturation of the soil is relatively slow, then there are usually few difficulties associated with convergence of the PDE. On the other hand, if the air

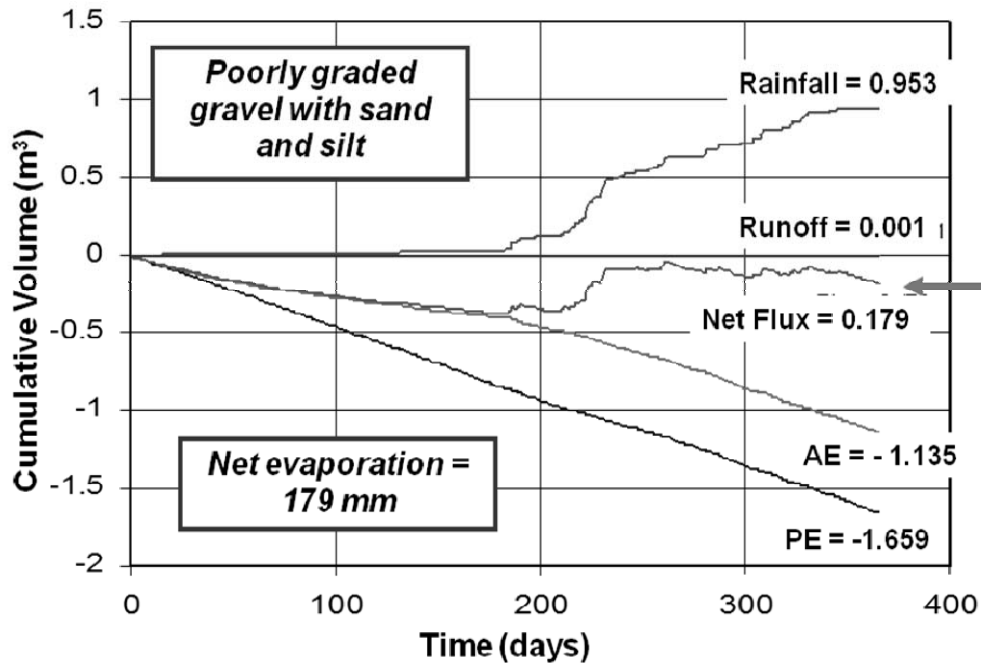


Fig. 24 Net infiltration computed after the ground surface moisture flux has been applied to the soil-atmospheric model

entry value is low (e.g. less than 10 kPa), or extremely low (e.g. less than 1.0 kPa), then convergence difficulties can be encountered with some software packages. The rate of desaturation also affects the nonlinearity of the PDE solution. If the rate of desaturation is steep, there can be considerable difficulties encountered in obtaining a converged solution.

There is also the possibility that the solution may have converged but the computer code has made compromising assumptions to assist in the convergence. It is possible that these assumptions will result in convergence to the wrong answer. However, there are special computational techniques that should be used when dealing with highly nonlinear PDEs. For transient type problems, it is possible to invoke convergence criteria that are related either to time steps or spatial distribution of computational nodes. It is relatively easy to make use of reduced time steps to encourage convergence; however, it is somewhat more difficult to reduce spatial changes as a solution moves towards convergence. The spatial changes technique is referred to as Adaptive Grid Refinement, AGR, and can be applied to the finite element numerical method.

Initial Conditions

The PDE being solved for unsaturated soils problems is nonlinear and consequently it is necessary to have a procedure to establish starting conditions. In other words, it is necessary to define the initial conditions for commencing the analysis.

One of the procedures that can be used to establish initial conditions is to create a situation that simulates average conditions over the past several years. In other words, an attempt is made to create a fictitious long-term steady state representation. There are several ways this can be accomplished. One procedure involves an averaging of all precipitation and weather conditions over a period of several years. For example, average conditions can be calculated over a 10-year period if weather records are available.

Fig. 25 shows the average precipitation conditions calculated from a 10-year record of weather conditions. The total precipitation for the year is also equal to the average precipitation over the 10-year period. The average conditions can be input into a preliminary infiltration model along with an arbitrary set of initial conditions (i.e. typically a hydrostatic suction profile). The calculations can be performed over a number of years until the suction profile at the end of back-to-back years is repetitive. It may take between two to four iterations for the suction profile to converge for simple cases and upwards of ten or more iterations for complex cases. It might even be necessary to “assist” convergence of the suction profile in cases where the response of the soil is slow. Convergence can be assisted by making favourable modifications to the suction profile between iterations. At this point, a “pseudo” steady state condition is established and the suction conditions with respect to depth can be used as the initial conditions for further modelling a series of actual weather conditions.

All Years: Daily Average

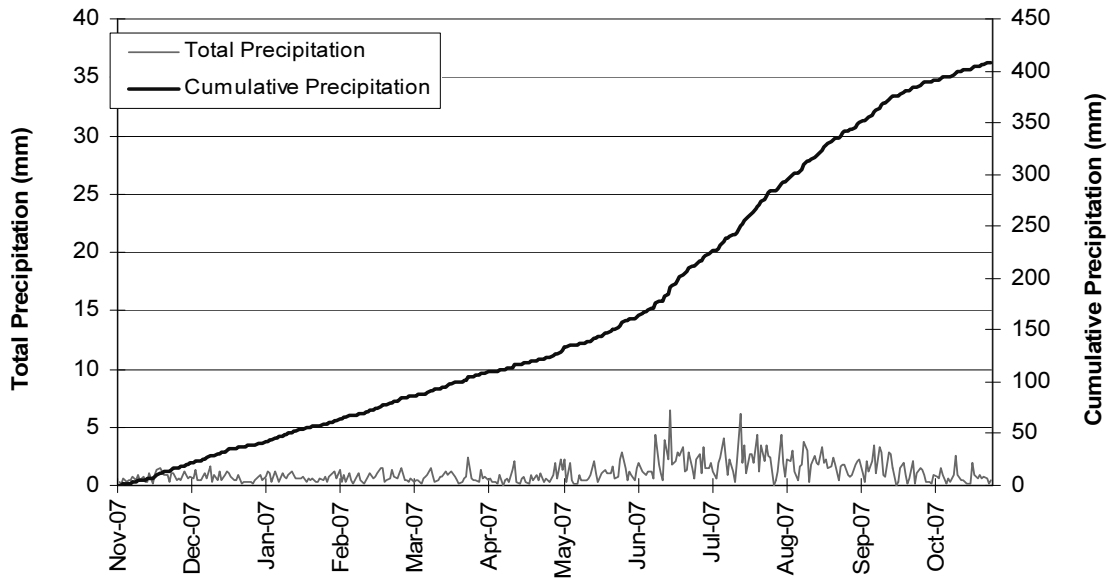


Fig. 25 Average daily precipitation over 10 years used to generate an initial steady state condition for the start of modelling

Convergence Difficulties

The convergence of the highly nonlinear partial differential moisture flow equation is the most pressing challenge facing soil cover modellers (Shackelford, 2007). However, significant advances have been made in resolving problems of non-convergence. There are two conditions that need to be satisfied in order to ensure that the correct modelling solution is attained. First, the solution of the PDE must converge for every time step of the lengthy design modelling period (e.g. 10 years). Secondly, the modeller needs assurance that the solution has converged to the correct solution. There are mathematical criteria that can be used to ensure that both of the mentioned criteria are met while solving the PDEs.

The most successful solutions to-date has involved the use of the Adaptive Grid Refinement, AGR, technique (Oden, 1989; Yeh, 2000). When using this technique, the finite element mesh is continually refined, as necessary, in order to meet the conditions that promote convergence to the correct solution. It is not possible for the geotechnical modeler to add the AGR feature to a particular software package. Therefore, it is important when modeling unsaturated soils problems that the modeler utilizes software packages that have AGR as a feature of the software. SoilVision Systems Ltd is an example of a software distributor that incorporates the AGR feature into all finite element modeling packages.

A simple finite difference formulation can be used to illustrate the adaptive time and space technique for solving nonlinear partial differential equations. Fig. 26

illustrates the finite difference solution of the one-dimensional consolidation equation. When solving the finite difference equation it is possible to define a variable called *Beta*, β . *Beta* is equal to the coefficient of consolidation times the time step, divided by the square of the spatial distance between nodes. In order for the finite difference solution to be correct, the β variable needs to be kept near to a value of 0.5. If β deviates too far from 0.5, errors can be incurred as described in Fig. 27.

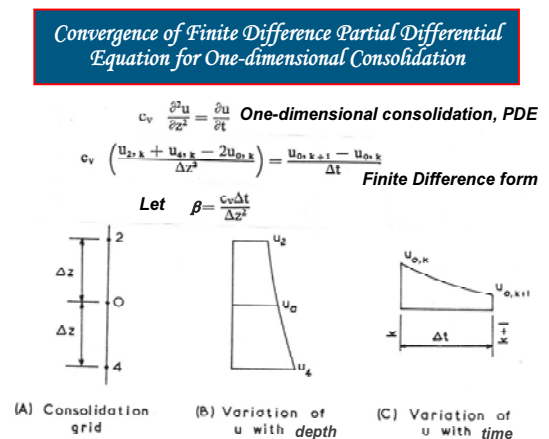


Fig. 26 Illustration of conditions necessary to ensure convergence in finite difference modelling

The coefficient of consolidation of a soil can change as the coefficient of permeability of the soil changes. Changes can be substantial and the variable can readily

go outside of acceptable limits and cause the solution to be in error. The problem should be solved by changing either the time interval or the spatial interval in order to bring the Beta variable into an acceptable range. It is easy to see how this can be accomplished when using a finite difference solution. When performing a finite element solution the spatial changes need to be accomplished by changing the size of the finite elements. This becomes a more challenging problem but the same basic technique has been incorporated into the solvers of all finite element solutions used by SoilVision Systems Ltd (SoilVision, 2005; PDE Solutions, 2005). Consequently, their solvers appear to meet the conditions necessary for convergence to the correct solution when solving highly nonlinear partial differential equations (e.g. SVFlux for moisture movement).

be in the order of 10 to 20 meters in length, of proper depth, and filled with appropriate material in order to yield accurate results (Benson et al. 2000).

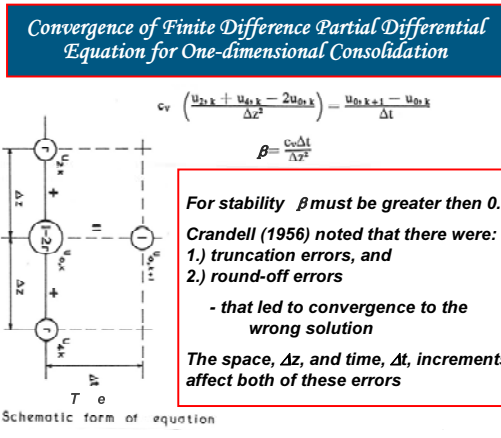


Fig. 27 Convergence can be controlled through use of adjustment of the time and space steps

VERIFICATION OF COVER DESIGNS

Field monitoring needs to be an essential part quality assurance, QA, for major cover systems. Measurements need to be taken to ensure that the cover system is performing as anticipated and as-designed. In fact, it is the field monitoring that has been performed on several cover systems that has given rise to the realization that closer attention may need to be given to various components of cover design.

A typical field monitoring system for a cover system would involve the installation of a: i.) lysimeter, ii.) weather station, iii.) soil suction measurements within the soil cover and iv.) water content measurements within the soil cover (Fig. 28). Equipment is available commercially for each of the mentioned measurements.

Design details for the lysimeter are extremely important in order that it will provide accurate measurements of infiltration. The lysimeter may need to

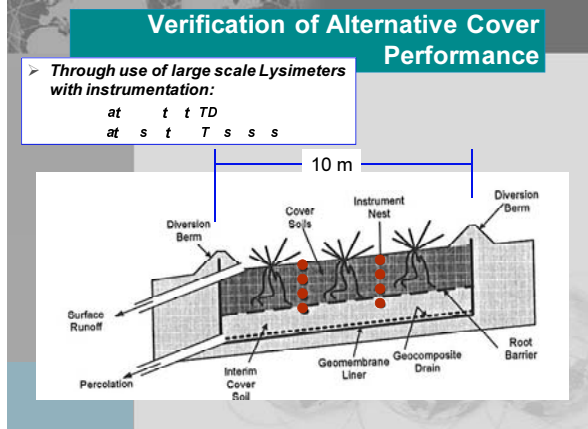


Fig. 28 Types of measurements required for verification monitoring of cover systems

Weather stations can be purchased for \$10,000 to \$15,000 and should be placed at the site of the cover system. While the cost of the weather station is modest, its maintenance and servicing may entail considerable expenditure. It must also be remembered that visual field inspections and reporting need to be an ongoing part the monitoring process.

UNIQUENESS OF COVER DESIGN PROCEDURES

There are many assumptions that need to be made as part of the design procedure for a cover system. The soil conditions can change with time due to the effects of weathering and freeze-thaw conditions with the result that the soil properties become far from the initially measured or assumed values. The changes can prove to differ by orders of magnitude from initial compacted or placement conditions. This does not make a realistic design impossible but simply shows that much greater care and detail must be given to the assessment of the unsaturated soil properties.

The climatic quantification that provides the final “net moisture flux” at ground surface has inherent many broad assumptions. The tendency to focus the analysis on average conditions may cause a deviation from the real performance of the cover system. In other words, maybe extreme weather conditions need to be more carefully evaluated during cover design. For example, extreme conditions where there is significant water runoff can result in serious erosion problems.

The effect of cracks forming in a clay rich soil can completely change the soil response to infiltration and exfiltration. Unsaturated soil properties are highly

nonlinear and may even change to be bilinear in character. These extreme conditions need to be given more attention and may even turn out to be a controlling factor once the clay content reaches a particular percentage.

LONG-TERM INTEGRITY

Long-term integrity of soil cover systems may increasingly become an activity within geotechnical and geo-environmental engineering. Soil cover designs have rapidly emerged and open-minded evaluation of their performance is essential for ensuring their long-term integrity and acceptability.

There appears to have been a strong dependence upon average or typical conditions for design purposes but the influence of extreme conditions needs to be given further consideration. This is true both for soil properties and weather conditions. Soils crack and their properties change on a logarithmic scale. Extreme weather conditions cause failures in cover systems. Simple models based on mean soil parameters and boundary conditions, might not be sufficiently conservative to ensure the long-term integrity of cover systems.

REFERENCES

- Benson CH (2002). Containment systems; lessons learned from North American failures. *Environmental Geotechnics* (4th ICEG), de Mello, L.G. and Almeida, M. (Eds), Swets & Zeitlinger, Lisse, The Netherlands, 2: 1095-1112.
- Bosen JF (1958). An approximation formula to compute relative humidity from dry bulb and dewpoint temperature. *Monthly Weather Review* 86:486.
- Bussiere B, Aubertin M, Chapuis RP (2003) The Behavior of Inclined Covers Used as Oxygen Barriers, *Canadian Geotechnical Journal*, 40: 512-535.
- Edlefsen NE & Anderson ABC (1943). *Thermodynamics of soil moisture*, Hilgardia, 15: 31-288.
- Fredlund DG (2007). Engineering design protocols for unsaturated soils. *Proceedings of the 3rd Asian Conference on Unsaturated Soils*, Editors: Zongze Yin, Junping Yuan, Abraham C.F. Chiu, Nanjing, P.R. China, Publisher: Science Press, 16 Donghuangchenggen North Street, 100717, China, April (21-23): 27-45, Beijing, China.
- Fredlund DG (2006). Unsaturated soil mechanics in engineering, *Journal of Geotechnical and Geoenvironmental Engineering*, ASCE, 132(3), March 1: 1-36.
- Fredlund DG (2000). The 1999 R.M. Hardy Lecture: The implementation of unsaturated soil mechanics into geotechnical engineering, R.M. Hardy Address. *Canadian Geotechnical Journal*, 37(5): 963-986.
- Fredlund DG & Rahardjo H (1993). *Soil Mechanics for Unsaturated Soils*, John Wiley & Sons, New York, N.Y.
- Fredlund DG & Xing A (1994). Equations for the soil-water characteristic curve. *Canadian Geotechnical Journal*, 31(3): 521-532.
- Fredlund DG, Xing A, Huang SY (1994). Predicting the permeability function for unsaturated soils using the soil-water characteristic curve. *Canadian Geotechnical Journal*, 31(4): 533-546.
- Gitirana G, Jr, Fredlund MD, Fredlund DG (2005). Infiltration-runoff Boundary Conditions in Seepage Analysis, *Proceedings of the 58th Canadian Geotechnical Conference, GeoSask2005*, Saskatoon, SK., Canada, Sept. 18-20, p. 8.
- PDE Solutions Inc (2005). *FlexPDE 5.0 - Reference Manual*. Antioch, CA, USA.
- SoilVision Systems Ltd (2005). *SVFlux User's and Theory Guide*. Version 5.55. Saskatoon, SK, Canada.
- Penman HL (1948). Natural evaporation from open water, bare soil and grass, *Proceedings of the Royal Society of London, Series A193*: 120-145.
- Pham HQ, Fredlund DG, Barbour SL (2003). A practical hysteresis model for the soil-water characteristic curve for soils with negligible volume change. *Technical Note, Geotechnique*, 53(2): 293-298.
- MEND (1993). *Soil Cover User's Manual*. University of Saskatchewan, Saskatoon, Canada.
- Nelson R (2004). Personal Communication. PDE Solutions Inc.
- Oden JT (1989). Progress in adaptive methods in computational fluid dynamics: 206-252. In J.E. Flaherty et al. (ed) *adaptive methods for partial differential equations*, Society for Industrial and Applied Mathematics, Philadelphia, PA.
- Sillers WS & Fredlund DG (2001). Statistical assessment of soil-water characteristic curve models for geotechnical engineering. *Canadian Geotechnical Journal*, 38(6): 1297-1313.
- Shackelford CD (2005). Environmental issues in geotechnical engineering, Keynote address, *Proceedings of the 16th International Conference on Soil Mechanics and Geotechnical Engineering*, Osaka, Japan, September 12 – 16, 1: 95-122.
- Thornthwaite CW (1931). Climates of North America according to a new classification, *Geographical Review*, 21: 633-655.
- Thornthwaite CW (1948). An approach toward a rational classification of climate, *Geographical Review*, 38: 55-94.
- Tratch DJ, Wilson GW, Fredlund DG (1995) The Prediction of Moisture Uptake in the Root Zone Due to Transpiration for Problems in Geotechnical Engineering, 48th Canadian Geotechnical Conference,

- Vancouver, B.C., September 25-27, 2: 771-780.
- Weeks B (2006). Prediction of Evaporation from Soil Slopes, PhD. Thesis, Department of Mining Engineering, University of British Columbia, Vancouver, Canada.
- Weeks B & Wilson GW (2005). Prediction of Evaporation from Soil Slopes. Canadian Geotechnical Journal. Accepted.
- Wilson GW (1990). Evaporation from Bare Soil Surfaces, PhD. Thesis, University of Saskatchewan, Saskatoon, Canada.
- Wilson GW, Fredlund DG, Barbour SL (1994). Coupled soil-atmosphere modelling for soil evaporation. Canadian Geotechnical Journal, 31(2): 151-161.
- Wilson GW, Fredlund DG, Barbour SL (1997). The effect of soil suction on evaporative fluxes from soil surface. Canadian Geotechnical Journal, 34(4): 145-155.
- Yeh G-T (2000). Computational subsurface hydrology: Reactions, transport, and fate. Kluwer Academic Publications, Boston, MA.

GEOTECHNICAL ASPECTS OF LANDFILL CLOSURE AND AFTERCARE

Erwin GARTUNG¹, Wolf-Ulrich HENKEN-MELLIES², Jürgen KANITZ³ and Hans-Günter RAMKE⁴

ABSTRACT: Municipal solid waste landfills are geotechnical structures. Essentially, they may be regarded as containments which serve the purpose of preventing harmful contaminants from migrating out of the waste pile towards the environment, menacing the bases of life in nature, surface water, ground water and the atmosphere. Inside the landfill municipal solid waste undergoes processes of bio-degradation associated with considerable volume changes and the generation of gas and leachate. During the phases of waste disposal, closure and aftercare the processes inside the waste fill, their effects on the components of the landfill structure, lining systems, drainage facilities and gas collectors, are monitored, and improvements or repair can be carried out conveniently, when necessary. However in the long-term, the landfill shall reach a stable condition, which requires no further observation, so aftercare can be rescinded. It may take long time to reach this desired final condition. Concepts for in-situ treatment of municipal waste during the closure- and aftercare phases may enhance bio-degradation by controlled gas extraction and leachate infiltration. For the time beyond the aftercare phase, the landfill has to be provided with a cover system, which functions adequately and reliably long-term under site-specific ambient conditions. When all pertaining specified technical criteria with respect to emissions, deformations and overall stability are met, the responsible competent authorities may establish that aftercare is complete, and the landfill can be released from aftercare.

KEYWORDS: landfill, closure, aftercare, surface cover, landfill gas, leachate, recultivation

INTRODUCTION

Municipal solid waste contains a large amount of degradable organic matter. Biological and chemical reactions start soon after deposition of the waste, altering the volume and the properties of the solid matter, generating landfill gas, odors and leachate. Municipal solid waste landfills are essentially bio-chemical reactors. The composition and the volume of solids, the shape and contours of the waste pile are changing with time according to differential degradation processes. Vertical and lateral movements take place inside the landfill. The distribution of moisture, water pressure and gas pressure vary with location and time. These physical parameters and their time dependent variations are of concern not only with respect to environmental issues but also with respect to the performance and structural integrity of the sealing systems, the leachate collection pipes and gas drains, as well as with respect to the stability of the entire waste pile.

In order to cope with the difficulties arising from the degradation of domestic waste in landfills, modern approaches of waste disposal request waste treatment before disposal of solids. Mechanical-biological waste

treatment methods and facilities, and waste incineration procedures and plants have been developed and are operating at large scale in many areas of the world. They facilitate waste management organizations to meet the standards of pertinent regulations, e.g. those of the European Landfill Directive (1999) which specify allowable contents of organics for solid waste. It may be expected that, in the future solid waste landfills will contain only small amounts of organics. Thus, most of afore mentioned problems associated with degradation of organics may be eliminated or at least eased to some degree in times to come.

However, in most European countries as well as in the rest of the world, untreated municipal waste is still being disposed of in landfills. And in countries like Germany where according to the "Ordinance on Environmentally Compatible Storage of Waste" (2001), since 2005 all waste material containing organics must be treated before disposal, many old municipal solid waste landfills do exist, where untreated domestic waste was deposited during the past 30 years. They have to be closed when the disposal phase ends, and they have to be provided with cover systems. Eventually, solid waste

¹ Senior Geotechnical Consultant, Altdorf, Germany. Email: e.gartung@t-online.de

² Senior Environmental Geologist, LGA Geotechnical Institute, Nuremberg, Germany, Wolf-Ulrich. Email: Henken-Mellies@lga.de

³ Chemical Engineer, CDM AG Bochum, Germany. Email:juergen.kanitz@cdm-ag.de

⁴ Professor, Hochschule Ostwestfalen-Lippe, University of Applied Sciences, Hoexter, Germany. Email: hg.ramke@gmx.de

landfills shall reach a stable state with respect to biochemical reactions, gas generation as well as hydraulic and mechanic properties, so they can be released from aftercare. Experience shows that, it may take very long time to reach this desired final condition.

After closure the performance of municipal solid waste landfills has to be monitored, gas drains and leachate collection systems have to be maintained. In order to minimize the time during which aftercare is required the degradation processes can be enhanced by technical means in the sense of in-situ treatment of the organic waste. Supervision, monitoring and controlling are mandatory until the recorded data justify release from aftercare, and a statement of no concern with respect to long-term environmental and structural safety can be issued by responsible experts, and subsequently decreed formally by the competent administration.

When a landfill is formally released from aftercare by decree of the competent supervising administration its legal status changes. The operator of the landfill is then dispensed from legal and financial responsibilities which were conferred upon him for the operational and the aftercare phases. The owner of the site - in many cases the public - takes over all responsibilities of the former waste disposal facility, without time limitation. According to German legislation, the landfill site is subject to the "Closed Substance Cycle and Waste Management Act" (Kreislauf- Wirtschafts- und Abfallgesetz) as long as it is in the operational and aftercare phases. After formal release from aftercare, the closed landfill is subjected to the jurisdiction of the "Federal Soil Protection Act" (Bundes- Bodenschutzgesetz). The legal implications connected with the release from aftercare demand very precise articulation of the technical requirements to be met. The technical specifications must be in agreement with both legal acts for rescinding aftercare of a closed landfill.

The "Technical Instructions on Waste from Human Settlements" promulgated in 1993 by Federal Law contain very little information on technical requirements for rescinding aftercare. The "Ordinance on Environmentally Compatible Storage of Waste from Human Settlements and on Biological Waste- Treatment Facilities" (2001), and particularly the "Ordinance on Landfills and Long-Term Storage Facilities" (2002), specify the objectives and contain detailed technical requirements for rescinding landfill aftercare.

The paper presented herewith, refers to the qualitative requirements of the existing Technical Instructions and Ordinances. However, at the present time, new comprehensive technical regulations for landfills are being prepared by pertinent experts for the German Federal Government. The basic philosophy of existing Ordinances will not be changed, but the new regulations will update the requirements, accounting for recent

technical developments, in particular with respect to long-term aspects of landfill cover systems.

LANDFILL CLOSURE AND AFTERCARE

In the lifetime of a municipal solid waste landfill four phases can be distinguished:

1. Construction and waste disposal phase
2. Closure phase
3. Aftercare phase
4. Final state when aftercare is complete

The first phase comprises construction and waste disposal activities. The bottom-liner is being constructed in one construction step or successively as waste is deposited and the waste pile is growing. At this state large surface areas of the waste fill are still unprotected, consequently due to ingress of rain water increasing quantities of leachate are generated, have to be collected and purified in treatment plants before they can be discharged into surface waters. The bio-degradation process begins. This is the most costly phase in the life of a landfill. It is also the most prosperous phase since payment for the delivery of waste provides the operator of the landfill facility with revenues to cover operational costs and to accumulate funds, needed as financial resources for expenses at later stages.

When the final design volume of waste has been placed, the disposal phase ends, and the phase of landfill closure commences. During this phase construction activities are carried out. Installation of gas wells and headers, maintenance of leachate collection facilities and placement of an efficient capping system aiming at a reduction of ingress of rain water and thus of the quantity of leachate are the main activities. The bio-degradation process continues. The construction work requests considerable funds. On the other hand there are very little - if any - revenues. To minimize overall cost, the operator of a landfill facility is interested in executing the landfill closure as soon and as quickly as possible to shorten the duration of the costly closure phase.

After landfill closure, the operational phase comprising disposal and closure phases ends, and the aftercare phase follows. Below the sealing cover biological degradation of organic waste material continues, landfill gas is generated, consolidation of the deposited waste induces flow of leachate by decreasing but still considerable quantity. Leachate has to be collected and treated before it can be discharged to surface waters in the nature. Gas has to be collected and conveyed to profitable use. The volume of solids is decreasing, thus the landfill structure is changing shape and material properties. These phenomena have to be monitored and to be controlled. Gas and leachate collection facilities have to be adapted accordingly

and must be maintained. The aftercare phase may last for a very long time depending on the size of the facility, the climatic conditions, the composition of the waste material, moisture content of waste and other factors. Revenues for sales of landfill gas used to generate energy may cover the expenses to some extent. Yet, the operator of the landfill is certainly interested in keeping the duration of the aftercare phase as short as possible, because as long as the landfill is not formally released from the aftercare phase it requires attention and supervision by the owner and by public authorities and it generates expenses continuously.

The duration of time during which a municipal solid waste landfill generates expenses for aftercare is often estimated at 30 years, equivalent to one generation in human life. An investigation into the state of degradation / mineralization of organics contained in old German landfills closed and provided with sealing covers in the seventies of the previous century revealed that, by no means have all waste piles achieved the desired stable, stationary conditions within 30 years (Stegmann et al. 2005). Even at relatively small landfills, the degree of degradation / mineralization of domestic waste obtained turned out to be not satisfactory. The investigations led to the conclusion that, in central European climate, efforts have to be made to enhance the degradation / mineralization process by controlled technical means in order to reduce the after-care period to an acceptable time (Henken-Mellies 2006).

At the end of the aftercare phase the condition of the deposited waste shall be such that, biological and chemical degradation processes and reactions have practically ceased and it can be assured that such processes will not be reactivated in the future under unfavorable conditions or unfavorable changes of the surrounding conditions. Any unavoidable long-term emissions from the landfill shall be very small to be tolerated, the public welfare shall not be impeded, and in particular ground water quality shall not be affected. Up to now, in Germany there is no municipal solid waste landfill for which the supervising authorities established that aftercare is complete. All closed German landfills are still in the aftercare phase.

CRITERIA FOR RELEASE FROM AFTERCARE

No more aftercare is required when the biological degradation processes of the organic waste material cease, the mineralization has reached an advanced level and emissions from the landfill do not impair public welfare. Furthermore, the deposited waste shall be in such a condition that, no substantial reactivation of biological processes shall occur in the future if environmental conditions undergo changes that may

favor biological reactions. The unavoidable long term emissions shall be small enough to be tolerable; in particular the ground water quality shall not be severely affected. This statement qualitatively highlights the goals to be reached.

Qualitative Criteria for Release from Aftercare

In more detail the following criteria have to be checked by the competent public authority (Ordinance on Landfills 2002):

1. Biological degradation processes, as well as other conversion reaction processes, have for the most part abated.
2. Gas formation has halted to the extent that no active degasification is required and harmful effects on the surrounding area as a result of gas migration may be excluded.
3. Subsidence has abated to such an extent that deformation-related damage to the surface sealing system can be excluded in future.
4. The surface seal and the recultivation layer are in a functional, stable condition which cannot be impaired by current and planned usage; measures must be taken to ensure that this is guaranteed even in the event of utilization changes.
5. Surface water is reliably discharged from the landfill.
6. Overall, the landfill is permanently stable.
7. The maintenance of structural and technical equipment is no longer required; dismantling has already been carried out, where applicable.
8. Where necessary, any leachate generated may be discharged in accordance with water legislation provisions.
9. The landfill does not incur any ground water pollution which should necessitate further monitoring or remediation measures.

If these qualitative criteria are applied too strictly, domestic waste landfills can never be released from aftercare, on the other hand if taken too easily, the environment may be exposed to unjustifiable effects, dangerous emissions and/or risks of structural instability of the waste pile, in the long-term.

Competent public authorities responsible for the environment as well as landfill operators need quantitative criteria. There has to be a basis for estimating the duration of time for the aftercare phase and the required funds. And there have to be quantitative criteria, trigger levels, for supervising agencies to justify the decision that aftercare can be rescinded. Quantitative criteria for rescinding aftercare of closed landfills are also needed with regard to probable legal disputes.

For general hydrologic situations in Germany trigger levels that can be monitored exist for many parameters

aiming at the protection of soil, ground water and surface water. However experience shows that, if these generally applicable values are employed to the situation of closed landfills strictly, and without any possibility for problem and site related deviations, rescinding aftercare of closed municipal landfills within acceptable time frames might probably be unlikely for most landfill sites. The question, how much emission from old landfills would be tolerable from the point of view of environment protection, initiated extensive research into environmental, hydrological, geotechnical and economic issues.

Guide Lines for Quantitative Criteria

As a result of these efforts, a first approach towards guide lines for quantitative criteria for rescinding aftercare of closed landfills was suggested by Stegmann et al. (2006). Based primarily on evaluations of recorded emission data from many old landfills, on scientific prognoses for the long-term performance of landfills and accounting for existing water protection regulations, Heyer et al. (2006) compiled limiting values for above criteria 1. 2. 3. 8. and 9. These values may be regarded as quantitative assessment criteria rather than as official trigger levels. They refer to actual emissions observed at the landfill site, to the emission potential of the waste fill which might be activated in the future, and to the anticipated efficiency of technical barriers. They take tolerable effects on the protected commodities—essentially soil, water and atmosphere—into account.

Quantitative aftercare criteria are specified for:

- Tolerable effects of contaminants from the waste fill onto ground water
- Tolerable effects of contaminants from the waste fill onto surface water
- Tolerable effects of landfill gas onto the atmosphere contributing to the green house effect
- Avoidance of immediate hazards at the landfill site and in its vicinity, e.g. explosions, health concerns etc.

Quantitative Criteria for Leachate Quality

Quantitative criteria for the emission of leachate from the landfill affecting ground water (items 8 and 9), regarding the source of emission (waste pile): Besides the concentration of contaminants, the mass flux as determined from concentration and quantity of leachate per hectare of waste deposit per year can be assumed.

Quantitative criterion for the limitation of effects onto water and ground water: Trigger levels of concentration of ground water are defined according to pertinent legislation.

For screening parameters, CSB, N_{total} , Cl and AOX the following scenarios with respect to leachate emission

are investigated:

- Direct discharge of leachate into surface waters
- Indirect discharge via sewage treatment
- Direct seepage into the ground

As an example the suggestions for acceptable residual emissions of the parameter CSB are explained as follows.

Direct discharge of leachate into surface waters:

According to pertinent regulations, the maximum permissible concentration is CSB 200 mg/l without limitation of mass flux, provided leachate collection and conduction facilities are maintained. It may take very long time to reach this value of permissible concentration although the emitted mass flux of contaminants may be small. For practicality in such cases, it is suggested to determine a permissible mass flux of contaminants particular to the site conditions in question, taking all important environmental issues into account. If the permissible mass flux of contaminants thus determined is not exceeded, it is justified to discharge the leachate into surface waters directly, even though afore mentioned limiting concentration of CSB may be exceeded.

Indirect discharge of leachate into surface waters via sewage treatment: According to pertinent regulations the limiting concentration is CSB 400 mg/l for discharge into sewage lines without mass flux limitation. However, complete release from aftercare would only be possible if the leachate collection and conduction facilities are maintained as requested by regulations. For practicality, it is suggested—as before in case of direct discharge—to specify a permissible mass flux of contaminants for the case in question, taking all relevant environmental issues into account. If the project specific permissible mass flux is not exceeded, then indirect discharge of leachate is acceptable, even though the limiting value of CSB concentration may be exceeded.

Direct seepage into the ground: Depending on local conditions at the site, permissible emissions from the waste fill can be specified in terms of mass flux in the order of 50 to 200 kg CSB / ha*a, for example. This is equivalent to 50 to 200 mg/l CSB concentration at a site where 100 mm/a natural ground water recharge is observed.

With respect to the effect onto the ground water the specified trigger level of concentration shall not be exceeded downstream of the landfill. It is defined by the permissible difference between upstream and downstream concentrations to be CSB = 11 mg/l. This criterion is derived from the permissible difference (downstream—upstream) for DOC of 4 mg/l and the relationship CSB: DOC of 2.75: 1 (according to pertinent German State Regulations NLO 2004).

The approach which combines limiting values of contaminant concentration and mass flux appears to lead to satisfactory solutions with respect to water protection and landfill aftercare aspects as well. The concentration

Table 1 Suggested quantitative aftercare release criteria with respect to leachate, ground water and direct discharge into surface waters

Parameter	Direct discharge into surface water		Indirect discharge via sewage line		Seepage towards groundwater	
	Concentration	Mass flux	Concentration	Mass flux	Difference of Concentration	Mass flux
	mg/l	kg/ha*a	mg/l	kg/ha*a	mg/l	kg/ha*a
CSB	200	50 – 200	400	50 – 200	12	50 – 200
N _{at}	70	25 – 100	> 70	25 – 100	NH 0.3 – 5	25 – 100
Cl	100	100 – 200	> 100	100 – 200	30	100 – 200
AOX	0.5	0.1 – 0.5	0.5	0.1 – 0.5	0.02	0.1 – 0.5

values were mainly taken from existing rather stringent regulations (e.g. AbwV 1996). Provided the anticipated long-term mass flux values are within the recommended order of magnitude, the supervising agency shall be free to permit higher concentrations near the source of emission. It is also justified to take natural attenuation into account when its effect is quantified by reliable prediction models. The goal shall be to keep long-term contamination of ground and surface water within acceptable limits.

Criteria for Landfill Gas

Uncontrolled emission of landfill gas must be strictly limited, because methane CH₄—the main component of landfill gas—contributes to the green house effect. So during the aftercare phase the landfill shall be operated and controlled in such a way that, the volume of gas migrating from the waste fill into the recultivation layer of the cover system shall be smaller than 0.5 l CH₄ / (m² *h) and the gas emission from the landfill surface into the atmosphere shall not exceed 25 ppm hydrocarbons, mainly methane. The fulfillment of these criteria has to be demonstrated for at least 10 years after landfill closure by monitoring in order to obtain the assessment for release from aftercare.

Criteria for Properties of the Deposited, Degraded Waste

Based on research into the elution behavior of municipal solid waste of different ages and different stages of decomposition (Kerndorff et al. 2006), trigger levels of certain parameters are recommended as presented in column 3 of Table 2. For comparison purposes Table 2 also lists values of permissible concentrations of the parameters for acceptance to deposition in solid waste landfills (allocation criteria)

according to pertinent German regulations in column 2 (Ordinance on Environmentally Compatible Storage of Waste, AbfAbIV, 2001).

The time required for degradation processes to reduce parameter values of column 2 to values of column 3 depends on the type of waste material and on the bio-reaction conditions, i. e. water content, temperature, rate of gas extraction, size of the landfill and others. Some of these conditional factors can be controlled and influenced in order to speed up the degradation process and achieve the permitted values for release from aftercare as soon as possible. According to the values listed on Table 2, dry landfills with mummified municipal waste cannot be released from aftercare because they inhibit a high potential for future biological degradation of organics which might be activated at a later time in central European climate.

Table 2 Quantitative criteria for solid waste with respect to release from aftercare

	1	2	3
Parameter		Acceptance criteria for waste disposal (AbfAbIV)	Target values for release from aftercare
Criteria of elution			
pH		5,5 – 13,0	6.0 – 9.0
el. Conductivity		≤ 50.000 µS/cm	≤ 2.500 µS/cm
TOC		≤ 250 mg/l	≤ 150 mg/l
Phenole		≤ 50 mg/l	≤ 0.5 mg/l
Arsenic		≤ 0.5 mg/l	≤ 0.1 mg/l
Lead (Pb)		≤ 1 mg/l	≤ 0.4 mg/l
Cadmium (Cd)		≤ 0.1 mg/l	≤ 0.05 mg/l
Chrome-VI (Cr)		≤ 0,1 mg/l	(≤ 0.1 mg/l)
Copper (Cu)		≤ 5 mg/l	≤ 1 mg/l
Nickel (Ni)		≤ 1 mg/l	≤ 0.2 mg/l
Mercury (Hg)		≤ 0.02 mg/l	≤ 0.005 mg/l
Zinc (Zn)		≤ 5 mg/l	≤ 2 mg/l
Fluoride (F)		≤ 25 mg/l	(≤ 25 mg/l)
Ammonium-Nitrogen		≤ 200 mg/l	≤ 50 mg/l
Cyanide, easily diluted		≤ 0.5 mg/l	≤ 0.1 mg/l
AOX		≤ 1.5 mg/l	≤ 0.5 mg/l
Ignition loss		-	-
TOC		-	-
Bio-degradability of dried residues of original material			
Determined as respiration activity (AT ₄)		≤ 5 mgO ₂ /gTS	≤ 2.5 mgO ₂ /gTS
Determined as gas generation rate in fermentation test (GB ₂₁)		≤ 20 l/kgTS	≤ 10 l/kgTS

Criteria for Settlement

In order to avoid damage to sealing layers of the cover system due to differential settlements, the final cover should be placed when 75% of the predicted total long-term settlement has occurred. For German domestic waste this may be the case about 8 to 16 years after landfill closure. The criterion for release from aftercare shall be that, 90% of the predicted total long-term settlements have occurred. This condition may be reached about 14 to 28 years after closure.

Technical Requirements for Release from Aftercare

For the assessment of release from aftercare the performance of the following technical items has to be checked and evaluated as being satisfactory:

- Ground- and hydrologic situation
- Sealing liner at the base
- Catchment, conduction and discharge of leachate
- Control of gas generation and minimized residual migration
- Cover system at the landfill surface and recultivation, vegetation
- Infrastructure, demolition of facilities no longer needed
- Geotechnical stability of the entire landfill and of its components.

The recommendations for quantitative criteria for release of domestic waste landfills from the aftercare phase compiled in this chapter are following lines of experience with long-term emissions from disposed waste, gained in Germany in practice and research (Heyer et al. 2006). They respect the concerns for protected commodities, soil, water, ground water and atmosphere. The recommendations try to find an acceptable compromise between “no emission” and “low emission” landfills in their final state, acceptable under environmental and under economic aspects, practicable and sufficiently clearly specified. This is a first attempt. It may need updating as new knowledge becomes available. These quantitative criteria are not directly applicable to landfills in other countries with different kinds of waste or in climatic zones other than central Europe.

CONCEPTS FOR THE AFTERCARE PHASE

Many landfills which were closed during the past two to three decades in Germany were provided with a sealing cover and with monitoring systems. The extraction of landfill gas was continued actively by application of low suction pressure as long as considerable amounts of gas could be recovered. Afterwards degasification occurred passively, small quantities of migrating gas were collected

in wells without the application of a vacuum and conducted to a flare. Leachate was collected and submitted to purification. Deformations of the landfill surface were monitored. Degradation of organics slowed down, but there were no indications that the biological processes inside the landfill would cease within a predictable period of time. In other words, if closed landfills are left by themselves with biological processes smoldering slowly on a very low level, the aftercare consisting mainly of monitoring and maintenance might continue forever. In order to reach a stable condition of the landfill within an acceptable time limit, concepts for systematic improvements of aftercare are necessary.

Sustainable minimization of long-term emissions is the major aim of domestic waste landfill aftercare. Suitable aftercare activities, summarized schematically on Table 3, deal with the installation and maintenance of a cover sealing system, with waste fill moisture content and leachate management, and last but not least, with degasification of the waste fill. Each one of these activities, discussed in more depth in following chapters, has an impact on the waste fill. In turn, the state and the properties of the waste, and especially their changes initiate feedback effects on cover system, on leachate generation and collection, and on gas generation - degasification. During the aftercare phase the landfill shall be controlled and managed in such a way that, afore mentioned criteria for release from aftercare into the final stable phase of no concern can be met within a reasonable time frame.

Table 3 Concept for landfill aftercare (in schematic chronological order from left to right).

- (a) main goal of the respective phase;
 (b) action concerning landfill gas;
 (c) action concerning leachate;
 (d) Action concerning landfill cover

Operational phase	Aftercare phase		Final phase
Waste disposal	Closure phase	Active aftercare	Transition phase of no concern
	Bio-reactor phase I	Bio-reactor phase II	Monitoring phase
(a)	Activation of anaerobic reactions	Activation of aerobic reactions	Monitoring
(b)	Optimized degasification deep gas wells	Aerobic reactions active degasification	Passive degasification
(c)	Leachate recirculation		
(d)	Temporary sealing cover		Permanent sealing cover

Bioreactor Phase I (Anaerobic)

Anaerobic degradation of organic waste material starts soon after waste deposition, provided the landfill contains enough moisture. During the closure phase and probably also during the early aftercare phase the municipal solid waste landfill shall be operated as a controlled anaerobic bio-reactor. Of course, landfills are no technical machines, so the biologic degradation processes can only be influenced to some extent. However, the following measures for enhancement of anaerobic reactions are usually quite successful:

- Increase of waste moisture content by leachate infiltration and/or by admission of some ingress of precipitation through a partly permeable temporary cover system
- Optimization of gas extraction by systematical degasification using gas wells with preferential filter zones at appropriate depth levels

The aim of controlling and technical management of the degradation processes of bio-reactor phase I, during the closure phase and partially during the aftercare phase is, to extract as much carbon in the form of landfill gas, Methane CH_4 and carbon dioxide CO_2 , from the waste fill as possible. In central European climate the bio-reactor phase I of municipal waste landfills of medium size may last for about 10 to 15 years.

Bioreactor Phase II (Aerobic)

When, in spite of active degasification, the decreasing generation of combustible landfill gas reaches very low levels with time, the process of organics degradation can efficiently be activated by air supply. The landfill is then operated in the aerobic bio-reactor phase II. Decisive for the efficiency of the extraction of carbon in the form of carbon dioxide CO_2 and the associated stabilization of the waste fill, is the total amount of gas flux. The greater the volume flux of gas, the more efficient is the stabilization of the landfill. In central European climate the bio-reactor phase II of municipal waste landfills of medium size may take about 5 to 10 years.

Final Monitoring Phase

When observations indicate the end of bio-reactor phase II, active degasification can be shut off. The operations are then changed to low level passive degasification. The final sealing cover is installed and the performance of the landfill is observed by a monitoring system for 10 years. When the recorded data prove that, stable conditions of the landfill have been achieved with respect to biological processes as well as to hydraulic and structural performance, the procurement of rescinding aftercare can begin. The competent supervising authority

will then examine whether all pertaining criteria mentioned in the previous chapter are met, and when all questions can be answered positively, the landfill may reach the desired final phase without need for further monitoring and with no concern for the environment.

The effects of activities listed on Table 3 are monitored continuously. By application of available computational prediction models in connection with the observational method, the processes occurring inside the waste fill and emissions of gas and leachate can be controlled in such a way that, targeted management of aftercare of closed municipal solid waste landfills becomes a reality.

LANDFILL GAS

Landfill gas is produced in domestic waste landfills due to biological degradation of organic waste. Anaerobic biological processes generate gaseous carbon compounds methane CH_4 and carbon-dioxide CO_2 . These gases contribute to the greenhouse effect and must be prevented from escaping into the atmosphere in an uncontrolled manner. At high concentrations landfill gas is toxic. A gas-mixture of methane and air with 4.4 to 16.5 % methane is explosive. It can menace human life, buildings or facilities in the vicinity of the landfill and must be avoided. Methane is combustible; it can be used for generation of electric energy. So there are several reasons for the need to collect landfill gas and to convey it to central treatment stations.

Landfill Gas Collection System

At well managed domestic waste landfills, gas collection facilities are installed a few months after the start of waste disposal. They are operated during the disposal phase, during the closure phase and during the aftercare phase of the landfill. Time dependent changes of physical, chemical and biological conditions inside the waste fill influence the biological processes and thus the generation of landfill gas during the different phases in the life of a landfill. These changes as well as the altering geometry of the landfill require adequate adaption of the gas collection facilities as time goes on.

Down to about 30 m below surface, landfill gas extraction facilities are operated at low vacuum of less than 3 kPa (30 mbar). Special care must be taken to avoid access of air from the atmosphere to the collectors in order to operate the system efficiently with respect to the volume of extracted gas, and to obtain landfill gas of good quality, which means gas with a methane content of 35 to 55 % and a calorific value of about 3.5 to 5.5 kWh/m³. An example of a gas collector head construction is shown on Fig. 1.

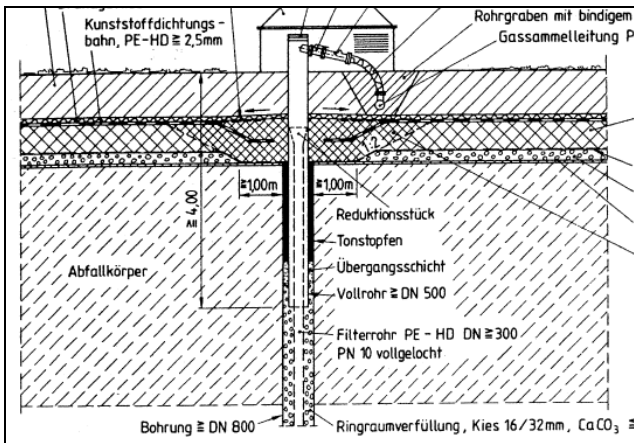


Fig. 1 Example of gas collector head

The installation of horizontal gas collectors, pervious blankets or trenches equipped with perforated pipes, are exceptional solutions nowadays. They were quite popular 20 years ago, but since these systems inhibit considerable technical disadvantages, they have been abandoned. More commonly, now gas wells, consisting of perforated plastic pipes of about 200 to 300 mm internal diameter, surrounded by coarse grained mineral filter material, are installed in vertical drilled shafts of 800 mm diameter. Their depth may reach 30 m, depending on the height of the waste fill. The upper section of the vertical gas collector, preferably down to at least 3 m, has to be sealed carefully to avoid ingress of air (Fig. 1). Similarly, the lower end of the vertical gas collector must keep a sufficient distance from the leachate collection drainage blanket at the bottom of the landfill. The distance should be greater than 10 % of the fill height or at least 2 m. Access of air to the gas collectors is indicated by the nitrogen N content of the landfill gas. Gas with high nitrogen content is called bad gas in landfill practice.

For landfills with heights in excess of about 30 m, two sets of vertical gas collectors are installed, one for the upper zone, which operates at a lower vacuum, and another one for the lower zone, which operates at a slightly higher vacuum. The vacuum applied to the deeper gas wells may be as high as 6 kPa (60 mbar). When the boundary between the upper and the lower gas drainage sections is properly sealed off, the two collectors extracting gas from different depths may be installed in the same drill hole.

For the design of gas collection facilities, often it is assumed that 1 Mg of domestic waste has the capacity to generate 150 to 200 m³ of landfill gas, and that the anticipated half life of the biological degradation process is 6 to 8 years. It is further assumed that about half the volume of the generated landfill gas can be collected. Accordingly, the members of the gas collection system are dimensioned for a rate of gas generation of 100 to

150 m³/h per gas well. At the beginning of operation, the gas production may meet these expectations. However, experience shows at many municipal waste landfills that, at depths below 10 m the apparent half life of the biological reactions may turn out to be 20 years or more, and the biodegradation process slows down considerably with time. Furthermore, at many old landfills it is observed that the quantity and the quality of the gas collected near the landfill surface down to 10 m is going down with time (Kanitz, 2007).

The observed decrease in the efficiency of gas collection with time cannot be attributed to consumption of organics and thus to lack of reactive organic carbon. It is rather due to unfavorable changes of the reaction conditions inside the landfill. Oxidative reactions of waste near the landfill surface may lead to a higher gas permeability in this zone and thereby facilitate ingress of air, which spoils the gas quality. The associated increasing nitrogen content may become as high as 20 %. It impedes the rate of anaerobic degradation of organics. If, at this stage in the life of the landfill, the landfill surface is sealed with an impervious cover and subsequently the water content of the waste fill decreases, anaerobic gas generation may slow down until it virtually ceases.

With respect to prevention of gas emissions into the atmosphere such a condition may appear desirable. However, the potential for future biodegradation with associated gas emissions as well as changes of the landfill volume and contours is kept at a very high level, because the amount of reactive organic carbon in the landfill remains very large. Decreasing gas production in spite of great quantities of degradable organics left inside the landfill is not a sustainably stable state. It does not justify release of the landfill from the aftercare phase.

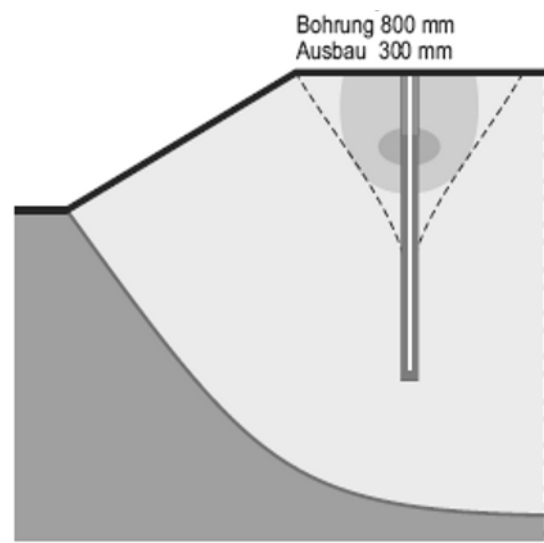


Fig. 2 Schematic section of degassed zone around a conventional gas collector during operational phase

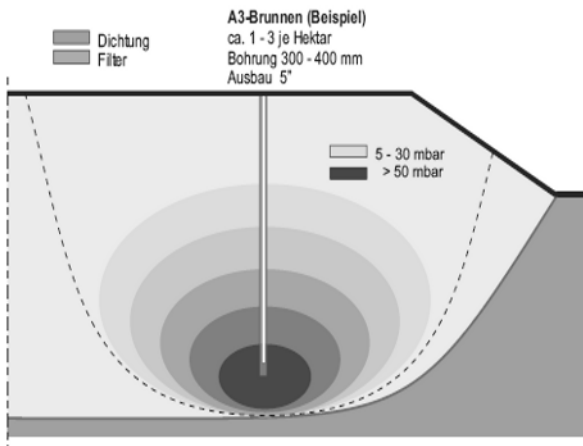


Fig. 3 Schematic section of degassed zone around a deep gas collector ("DEPO+"; patent of CDM-GmbH, Germany) during closure and aftercare phases

As schematically depicted on Fig. 2, the gas collection facilities being operated during the disposal phase affect a relatively narrow zone near the surface of the landfill in the vicinity of the vertical gas collector. The reach is unsatisfactory for longer-term degasification during the closure and aftercare phases. So at the beginning of the closure phase the existing gas collection facilities have to be amended in order to activate anaerobic degradation of organics at greater depth of the waste fill, and with greater reach.

Gas Collection System during Aftercare Phase

Fig. 3 schematically shows the objectives of activation of the anaerobic bio-reactions. The upper part of the gas collector pipe is inactivated to stop air intake. The gas collector extracts landfill gas from greater depth. A higher vacuum increases the reach of the gas collector. Anaerobic gas generation is activated and maintained at a high rate for a longer period of time. A considerable amount of organic waste material can be converted to gaseous carbon compounds, yielding combustible methane for electric energy generation.

The technical means needed for these objectives are gas collectors with packers which permit gas extraction from selected depth levels, equipment to generate and maintain vacuum pressures up to 8 kPa (80 mbar) and related appliances with adequate monitoring systems. The gas collection facilities must be operated by experienced engineers in the field who understand the processes well, and who are able to control and manage them successfully. Gas extraction facilities of this type require certain flexibility in design, construction and operation.

Fig. 4 shows a schematic section of a landfill with conventional gas collectors at the operative phase. The first step to improve the efficiency of gas extraction

often consists of installation of additional gas collectors as schematically shown on Fig. 5. The real improvement to be achieved in degassing the landfill during the closure and aftercare phases is sketched on Fig. 6; it indicates the results of deep collectors being operated at higher vacuum.

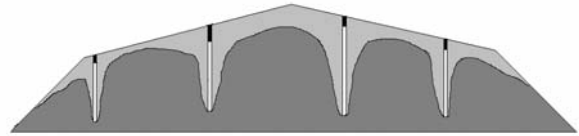


Fig. 4 Schematic section of a landfill with conventional gas collectors in the operative phase (vertical structures = gas collectors; light grey = part of landfill, which is degassed; dark grey = part of landfill, which is not reached by gas collection system)

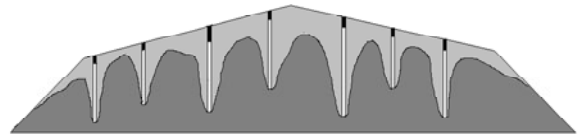


Fig. 5 Schematic section of a landfill with additional gas collectors in the operative phase



Fig. 6 Schematic section of a landfill with improved deep gas collectors at the end of the aftercare phase

Experience with improved gas extraction systems as described above has been very positive to date. With the concept of optimization of the degasification by deep gas wells, the perspectives to reduce the duration of the aftercare phase considerably are quite promising. At some old municipal waste landfills of smaller size, the gas collection facilities were used successfully for air supply to the organic waste, after the enhanced anaerobic degradation process had essentially reached its limits. Subsequent air circulation through the waste initiated aerobic reactions of the solid waste resulting essentially in the generation of carbon dioxide and in a sustainable stabilization and mineralization of the waste material. For smaller landfills the activation of aerobic reactions during the later part of the aftercare phase can be considered a very useful tool. Accordingly, it is recommended in Table 3. However, to date there is no experience yet with stimulation of aerobic reactions in very large landfills.

LEACHATE

During the closure and aftercare phases the main objectives of leachate management are:

- Minimization of leachate generation, in order to keep expenses for leachate treatment as low as possible, by placement of a cover seal and by surface water drainage
- Infiltration of leachate, to maintain an adequate moisture content inside the waste fill for efficient bio-degradation of organics and generation of landfill gas
- Prognosis of long-term leachate composition, aiming at fulfillment of the pertinent criteria for direct discharge into surface or ground water at the end of the aftercare phase

Experience at many German municipal solid waste landfills indicates that, after a few years of active anaerobic bio-degradation of organics, landfill gas generation is slowing down, particularly when the waste fill surface is covered with a seal and there is no supply of rain water to the waste fill. Since lack of moisture was identified as main reason for the decrease of biological activity, methods of supplying water were developed.

Leachate Reinfiltration Technology

The most economical method to improve the moisture content of covered waste fills consists of infiltrating leachate. 15 years ago, leachate infiltration was exercised for the first time at thoroughly monitored test fields. As an example of the studies, quantities of landfill gas harvested at test fields of equal size (2.400 m^2) with and without leachate infiltration are plotted on Fig. 7.

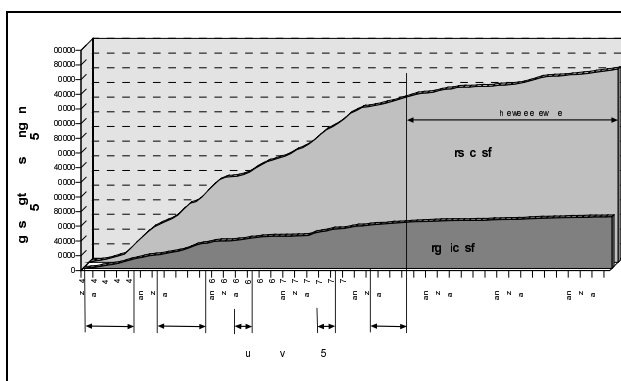


Fig. 7 Landfill gas quantities collected at test fields with (light grey) and without (dark grey) leachate infiltration (Bauer and Meisinger, 2006)

The upper curve of Fig. 7 shows the summation of landfill gas quantity collected in the test field with leachate infiltration. The lower curve applies to the test field without leachate infiltration (Bauer and Meisinger, 2006).

Very clearly, 6 months after the beginning of leachate infiltration, gas generation improved considerably.

The quality of the gas generated with leachate infiltration was very good with a methane content of 50 %. The properties and constituents of the leachate altered only slightly during the infiltration process. With increasing bio-activity the pH increased from 7.5 to 8.0. The electrical conductivity was slightly reduced. The high BSB_5 concentration of the leachate was reduced by percolation through the organic waste. The concentration of dissolved organic and inorganic constituents of the leachate did not show substantial changes during the infiltration test over several years. The content of heavy metal ions did not exceed the trigger values for direct discharge into surface or ground water.

Leachate infiltration technology as developed in test fields 15 years ago has become a routine at many German landfills, executed during closure and aftercare phases. As long as the landfill has not yet been provided with a final sealing cover, leachate infiltration can be carried out by means of horizontal fields or terraces filled with coarse grained mineral material as sketched schematically on Fig. 8. Below temporary covers infiltration trenches of the type shown on Fig. 9 may be used. When leachate infiltration is executed below existing final covers, perforated pipes penetrating the waste fill by 1 to 2 m are used for leachate infiltration.

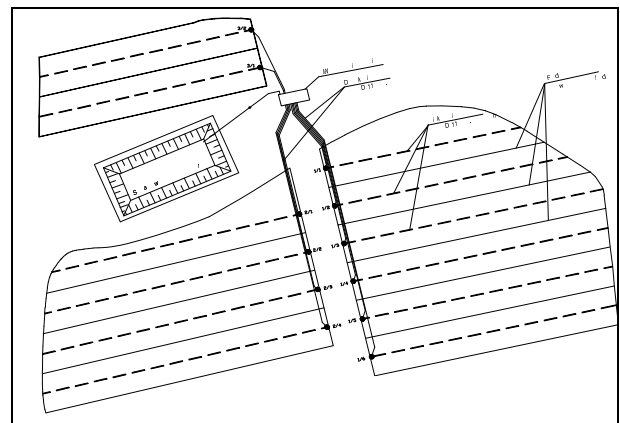


Fig. 8 Leachate infiltration field, landfill without cover, plan view (Bauer and Meisinger, 2006)

The infiltration pipes are supplied with leachate by gravity flow from intermediate storage tanks placed at the top of the landfill or from headers directly. The leachate is pumped up to the storage tank or header from the catchment pond at the toe of the landfill. The quantity of leachate to be infiltrated depends on many local parameters. It has to be determined by trial. In central European climate and for conventional domestic waste the order of magnitude of leachate quantity in liters l per day d to be designed for is 0.2 to 0.7 $\text{l}/(\text{d} \cdot \text{m}^3)$ per cubic meter m^3 of waste to be treated.

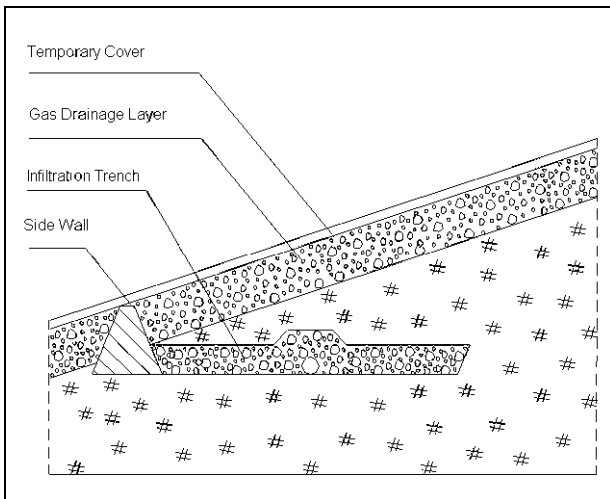


Fig. 9 Infiltration trench below temporary cover
(Bauer and Meisinger, 2006)

Individual control of each leachate supply valve equipped with an electric motor, control of electric pumps and control of all flows including generated landfill gas is usually carried out from the desk of the technical operator, where all measured data appear on the monitor. Evaluating the performance of the bio-reactor on the basis of measured and recorded data facilitates the operator to make his decisions concerning quantities of leachate as well as periods of infiltration and intervals. Generally, it is more effective to infiltrate smaller quantities many times than to infiltrate larger quantities fewer times. E.g. it is better to infiltrate 1 m³ of leachate 7 times per week, than 7 m³ of leachate once a week.

The methods of leachate infiltration and landfill gas extraction with adequate equipment and monitoring devices provide the operator with powerful tools to manage a domestic waste landfill as a controlled bio-reactor; directing the biological processes towards the goals of sustainable stabilization of the deposited organic waste, minimization of gas and leachate emissions and towards release from aftercare.

COVER SYSTEMS

After the disposal phase, landfills are closed and provided with a cover. During the closure phase and during the aftercare phase the cover shall prevent migration of dust, gas and odors from the waste fill into the atmosphere, and it shall prevent ingress of rain water into the waste fill in order to minimize the generation of leachate. Since, in domestic waste landfills biodegradation of organics causes changes in the volume of the deposited solid waste associated with differential settlements, the landfill cover undergoes substantial

strains. The deformations may impede the efficiency of the cover and even damage the sealing layer.

So, if very large deformations of the waste fill surface are anticipated, it may be advisable to install a temporary cover for the operational phase including the closure phase and to amend, or to replace it by a permanent cover at the time, the main deformations of the waste fill cease during the aftercare phase. During the closure and aftercare phases, the landfill surface is under continuous observation, and adaptations or repair work at the cover system can be carried out relatively easily, if necessary. However, in the final phase when the landfill shall be left by itself without concern for long-term safety, the cover system must be in a permanently stable and durably functioning state.

Based on the state of knowledge of the time, the German "Technical Instructions on Waste from Human Settlements" promulgated in 1993 by Federal Law, specified detailed requirements for landfill cover systems. According to these Technical Instructions, compacted clay liners were relied upon as the major sealing components of cover systems for long-term conditions. According to the regulations, the sealing elements in covers of hazardous waste landfills (class III), and of domestic waste landfill (class II), consist of a combination of a compacted clay liner and a geomembrane (Fig. 10). For inert waste landfills (class I), a compacted clay liner is considered sufficient. Technical requirements for cover systems and their components, compacted clay layers, geomembranes, coarse grained drainage layers and soil recultivation layers are specified in the Technical Instructions and subsequent Ordinances in detail.

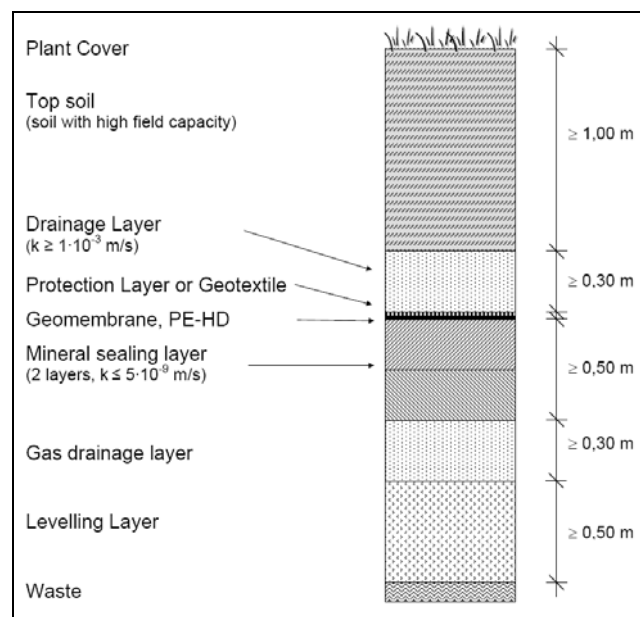


Fig. 10 Cover system for domestic waste landfills,
schematic

Experience with cover systems complying with all details of these regulations taught the lesson that, under conditions encountered in landfill covers, compacted clay liners are vulnerable to desiccation cracking. At several landfill sites and in special test fields it was observed that the sealing efficiency of the compacted clay liner decreased with time. Evidently, landfill cover systems which rely on the sealing function of compacted clay layers may not provide adequate safety long-term beyond the aftercare phase under all conditions which may occur in practice. So in Germany, it was necessary to amend the pertinent Technical Instructions in this regard.

The new "Ordinance on Landfills" (2009) contains only a general framework of technical instructions for landfill cover systems, without going into details. This enables specific solutions for each single case, gives back more responsibility to design engineers and the local authorities and is regarded more adequate than the past, tight regulations.

Research and Experience on Landfill Cover Systems

During the past two decades, extensive geotechnical research and development programs were carried out in Germany, aiming at a better understanding of the performance of various types of landfill cover systems under all anticipated boundary conditions. The objectives of the studies comprise the intention to provide a sound basis for technical recommendations for cover systems with appropriate long-term performance. In December 2006, researchers from geotechnical institutes, engineers from consulting firms and officers from competent governmental administrations gathered in a symposium at Hoexter University for Applied Sciences, under the auspice of the German Geotechnical Society, in order to sum up the results of research and development efforts achieved so far. The contributions to the symposium, discussions and conclusions drawn were compiled and edited by Ramke et al. (2007). Some of the key issues of the symposium will briefly be sketched, as far as they are referring to the topic of release of domestic waste landfills from aftercare.

Concept of Combined Cover Sealing System

In covers of domestic waste landfills the seal shall be composed of two components complementing each other with respect to redundancy. One of the two sealing components shall be a barrier that intercepts convective liquid flow and gas migration completely; this function is assigned to a geosynthetic barrier, commonly known as geomembrane. Asphalt liners may be used as alternative convection barriers instead of geomembranes provided the underlying layers meet the requirements for

placement and compaction of high quality asphalt.

The second sealing component shall be made of different material, commonly a mineral layer. Several alternatives are available for the mineral sealing layer; examples are given on Table 4. If the first component, the geomembrane, suffers from small damage, a hole or a tear, then – due to its very low hydraulic conductivity - the mineral seal prevents unacceptable amounts of flow of liquid from the drainage blanket of the cover system into the waste fill.

The mineral component shall have a longer service life than the geosynthetic barrier which supposedly may fail after – may be – several hundred years. After the service life of the geomembrane, the mineral liner has to act as the only reliable sealing layer of the landfill cover system. The mineral sealing component must not be as water tight as the geomembrane, but its permeability shall be so small that, for unlimited time after a conceivable failure of the geomembrane, the quantity of water that permeates into the waste fill is so small that it can be tolerated.

Table 4 Sealing components of cover systems for domestic waste landfills

1. Component: Convection barrier	2. Component: Mineral liner
Geosynthetic barrier (geomembrane) or Asphalt liner	a Compacted mixed in plant coarse grained mineral liners with sufficient amount of fines
	b Mineral sealing material with additives (polymers, water glass, other suitable chemicals)
	c Capillary barriers
	d Compacted clay liners
	e Geosynthetic clay liners (bentonite mats)

Mixed-Grained Mineral Liners

Compacted mixed in plant coarse grained mineral liners with a sufficient amount of fines can be composed in such a way that, the hydraulic conductivity is extremely low, shear strength (friction angle) is very high, there is practically no volume change with variations of water content, the liner does not experience fissuring due to desiccation, no impediments of the sealing function in the long-term are known. Well composed, placed and compacted coarse grained mineral liners request high quality workmanship in production. When properly executed they meet all technical requirements for permanent sealing function (Schick and Gartung, 2007).

Mineral Sealing Materials with Additives

If liners of mineral sealing material with additives (polymers, water glass or other suitable chemicals) consist mainly of a coarse grained soil skeleton with smaller amounts of fines in the coarse voids, they may have properties like under a., the afore mentioned compacted mixed in plant coarse grained mineral liners. If they consist mainly of clayey or silty soil, their properties may be essentially the same as those of compacted clay liners discussed below.

Capillary Barriers

Capillary barriers consist of two coarse grained soil layers of specified gradation curves. The relationship of size, shape and structure of the voids of the two soil layers, determining their capillarity, is crucial to the barrier function. It has to be determined by testing. The desired lateral conduction of water by capillary barriers is based on gravity flow. That is why the required minimum inclination of the landfill surface for capillary barriers is about 8°. Their barrier function is limited by the lateral flow capacity. It cannot be excluded that, due to precipitation of minerals from solution and/or migration of fines from overlying soil layers, and/or due to growth of microbes, the voids within the two coarse grained soil layers may change in size, structure and shape. If the relationship of the capillary characteristics of the voids of the two layers alters unfavorably with time, then the efficiency of a capillary barrier may be impeded in the long-term.

Compacted Clay Liners

Compacted clay liners are vulnerable to desiccation cracking. The geomembrane placed above the compacted clay layer may prevent the loss of moisture in the upwards direction - which is driven by capillary rise, convective transport of vapor and/or suction of plant roots. This protective function ends when the geomembrane loses its integrity (may be after several hundred years).

If there is a thermal gradient directed downwards due to lower temperatures inside the landfill than at the surface, a situation which may occur at a domestic waste landfill when all biological and chemical activities have ceased, then moisture movement is directed towards the waste fill, and the geomembrane has no effect in preventing the loss of moisture probably followed by formation of fissures. So it is very likely that the protective function of a geomembrane for the compacted clay liner will be lost in the long-term.

For the situation long time beyond the aftercare phase of domestic waste landfills, it has to be assumed that the compacted clay liner is the only sealing element

of the cover system. Hence, the boundary conditions for a compacted clay liner in a landfill cover system shall be such that, without accounting for the protective function of the geomembrane, long-term desiccation is avoided or at least minimized. In this sense, and for covers without geomembranes (landfill class I), the vulnerability of compacted clay liners in landfill cover systems to desiccation cracking can be reduced by the following measures (Witt, 2007):

- Use of soils of low or medium plasticity (clays of high plasticity are most sensitive)
- Placement and compaction at a water content below optimum Proctor water content
- Placement of a recultivation soil layer with high water storage capacity and great thickness
- Placement of a barrier against plant roots
- Placement of a sand layer of small thickness or of a suitable nonwoven geotextile immediately above the compacted clay layer in order to avoid direct capillary connection with the coarse grained drainage layer
- Use of sand or fine gravel for the drainage layer instead of coarse gravel or crushed stone

Geosynthetic Clay Liners

The sealing function of geosynthetic clay liners (bentonite mats) is based on the extremely low hydraulic conductivity of bentonite. Due to its high plasticity, hydrated bentonite is even more vulnerable to desiccation cracking than the clays of medium or low plasticity used for compacted clay liners, discussed above. So basically, geosynthetic clay liners pose the same problems as compacted clay liners. In addition, their hydraulic conductivity may be influenced by cation exchange, a chemical process that has to be expected to occur in nature when sodium-bentonite mats are used. The small layer thickness of geosynthetic clay liners of about 10 mm, in comparison with the thickness of compacted clay liners of 500 mm, further increases the probability of deficiencies in their sealing function in the long-term. In summary, it appears to be justified to assess only a limited sealing function to geosynthetic clay liners (bentonite mats) for the time beyond the service life of geomembranes.

The optional mineral sealing layers listed on Table 4 are characterized by differences in their long-term sealing performance. In principle, consisting of porous mineral materials, all of the seals are pervious; but there are differences in the parameters which determine the sealing function, that can be expressed as permittivity ($\psi = k/t$ hydraulic conductivity k divided by thickness of sealing layer t), quantity of seepage flow through the sealing layer per unit area and unit of time [$m^3/(m^2 \cdot m/s)$] for a certain head of water above the seal.

A comparison of the values of permittivity of different sealing materials may serve as one of the criteria for the design decision.

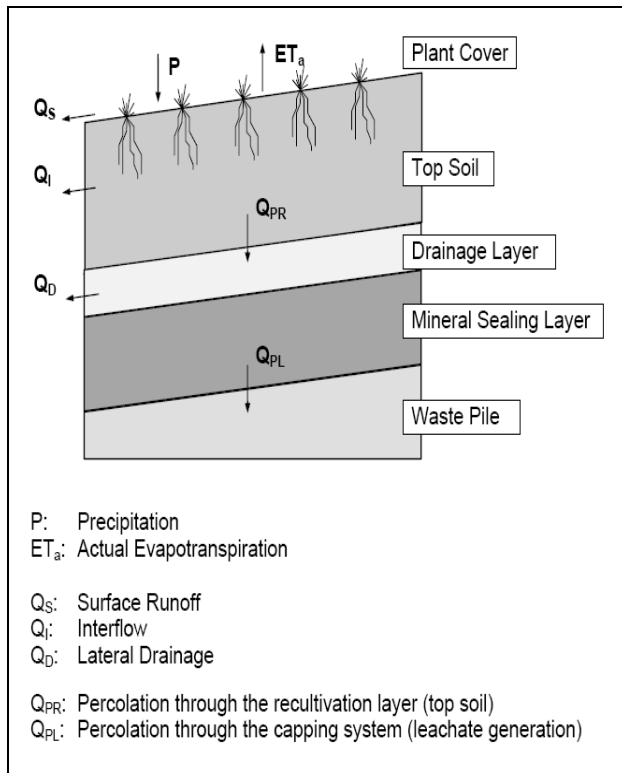


Fig. 11 Hydrologic concept of a landfill cover system, scheme

More elaborate bases for the design decision could be gained by site-specific predictions of the seepage quantity A_{sw} in millimeters per year for alternative cover systems to be compared (Fig. 11). Related to the annual precipitation N the external relative seepage rate $\epsilon_N = A_{sw} / N$ can be expressed; or, related to the seepage quantity A_{SR} that permeates through the recultivation layer, the internal relative seepage rate $\epsilon_{ASR} = A_{sw} / A_{SR}$ can be determined. The annual seepage quantity A_{sw} and the relative seepage rates ϵ_N or ϵ_{ASR} can be regarded as quantifications of the hydraulic efficiency of landfill cover systems. Their determination for short-term conditions with analytical and numerical modes poses no major problems (Ramke 2000). However, for long-term conditions the acquisition of reliable input values with respect to material parameters as well as to hydrological data is somewhat questionable. So, deterministic long-term forecasts of the performance of landfill cover systems seem to be doubtful. But parametric studies with analytical and numerical models can be very useful to support technical decisions, which otherwise would be based on records of past behavior and intuitive engineering judgment only.

Long-Term Aspects of Landfill Barrier Systems

Obviously, the assessment concerning the suitability of landfill cover systems under long-term aspects depends on site specific characteristics. These include the ground water regime at the site, the geological barrier, the bottom-liner system, the type of deposited waste and state of degradation of organics inside the waste fill, the type and state of the leachate collection system, the size of the waste disposal facility, local climatic conditions and others. The evaluation of the required long-term efficiency of the landfill cover system has to be elaborated specifically for each landfill site.

It would be inappropriate to standardize details of landfill covers by compulsory specifications in Ordinances promulgated by the government. Accordingly, the forthcoming German Landfill Ordinance will present a frame of principle requirements, rather than specifying technical details. The new regulations will permit a choice among cover systems, like those listed on Table 4, provided the suitability of the relevant components of the cover system can be demonstrated by adequate laboratory and/or field testing.

When the operator of a closed landfill applies for formal release from aftercare, the competent authorities have to examine whether the pertinent emission criteria are met; and they have to examine the cover system with respect to its actual state as well as to the expected long-term performance, along the lines sketched above. The assessment of sustainable functioning of the cover system is a prerequisite for rescinding from aftercare.

SUMMARY AND CONCLUSIONS

Municipal solid waste contains a great amount of organic matter which undergoes bio-degradation after disposal in a landfill. During biological degradation processes landfill gas is generated, the volume of solid waste is reduced and large differential deformations take place inside and at the surface of the waste fill. During the time when bio-reactions do occur, and further more, as long as the waste deposited in a landfill inhibits a considerable potential for bio-degradation which may be initiated at a later time by changes in moisture content or other ambient conditions, the landfill requires attention, monitoring of emissions, maintenance of systems for gas extraction and leachate collection and observation of deformations and slope stability of the waste fill. Eventually, each landfill shall reach a final, stable state in which bio-reactions have ceased and aftercare can be rescinded.

In order to minimize time and efforts for aftercare, according to modern landfill technology, municipal solid waste is treated by incineration or by mechanical-

biological methods, before it is disposed of in a landfill. So it may be expected that, landfills of the future which contain only very small amounts of degradable organics will cause less concern with respect to emissions and can be released from aftercare soon after closure. However, at the present time, many closed old municipal solid waste landfills in the aftercare phase do exist; and it is unforeseeable in most cases how long the aftercare phase will last, unless actions are taken to enhance the biological and mechanical stabilization of the waste fill.

In order to minimize the time required for aftercare, concepts for in-situ treatment of waste may be developed, enabling the operator to manage the landfill as a controlled bio-reactor. Optimization of landfill gas extraction and leachate infiltration are principle techniques applied for this purpose. In combination with adequate measurement systems, they facilitate controlled management of closed old domestic waste landfills, aiming at reaching a stable state which justifies release of the landfill from aftercare, as soon as possible. Monitoring of collected gas- and leachate quantities, and analyzing their compositions, together with deformation measurements at the landfill surface, provide a valuable data base for predictions of the anticipated performance of the waste fill and of future emissions. When these techniques are applied systematically and well understood, it is very likely that meaningful forecasts for the duration of the aftercare phase and plausible estimates for aftercare costs can be made.

Completion of the aftercare phase is a legal affair with consequences for the landfill operator and for the public. The competent authorities who are in charge of establishing the release of the landfill from aftercare by decree need technical criteria as a basis of their assessments. The criteria have to encompass aspects of emissions i.e. tolerable values of key parameters, requirements restricting long-term deformations, proof of structural stability of the waste fill, and requirements with respect to bottom liners and cover systems.

The long-term serviceability of bottom-liner systems for domestic waste landfills is considered established, when design, construction, quality control and monitoring data comply with detailed technical specifications of the pertinent regulations.

For cover systems the situation is more complicated. Landfill covers are exposed to site-specific ambient influences. Mineral components of cover systems experience repeated variations of their water content due to seasonal and daily weather cycles. Their sealing efficiency may be impeded in the long-run, especially when the seals consist of clayey soil layers which may be subject to cumulative desiccation damage. Since the lifetime of geosynthetic barriers (geomembranes) is considered limited, mineral sealing components of cover systems are of great importance with respect to the

evaluation of long-term safety. Different layer combinations and sealing materials are available for design and construction of cover systems. Their long-term, residual sealing efficiency differs; none of them is absolutely water tight. The question, how much ingress of water from precipitation can be tolerated without time limitation, cannot be answered solely on the basis of the observed performance of the cover. In order to assess adequate sealing performance to a landfill cover system, the long-term behavior of the landfill in question has to be regarded holistically. The ground water regime at the site, the geological barrier, the bottom-liner system, type and state of the waste fill, recorded emissions, and climatic conditions, all are interrelated and have to be examined. If the anticipated long-term seepage of water through the cover appears to be acceptable under all these aspects, the cover system is suitable for the case studied. Provided that all other pertinent criteria are met as well, the landfill in question may be released from aftercare.

REFERENCES

- AbwV (1996). Verordnung über Anforderungen an das Einleiten von Abwasser in Gewässer; AbwV—Abwasserverordnung, Anhang 51: Oberirdische Ablagerung von Abfällen.
- Closed Substance Cycle and Waste Management Act. German Federal Government (1994).
- European Landfill Directive (1999). The Council of the European Community.
- Federal Soil Protection Act. German Federal Government. (1998). (Bundes- Bodenschutzgesetz)
- NLÖ (2004). Abfallwirtschaftsfakten 9—Auslöseschwellen und Maßnahmenpläne nach § 9 DepV. Niedersächsisches Landesamt für Ökologie, Hildesheim, Oktober 2004.
- Ordinance on Environmentally Compatible Storage of Waste from Human Settlements and on Biological Waste-Treatment Facilities (2001) (Abfall-Ablagerungsverordnung AbfAbIV).
- Ordinance on Landfills and Long-Term Storage Facilities and Amending the Ordinance on Environmentally Compatible Storage of Waste from Human Settlements and on Biological Waste-Treatment Facilities (2002). (Deponieverordnung DepV 2002).
- Ordinance on Solid Waste Landfills (2009) (Deponieverordnung 2009).
- Technical Instructions on Waste from Human Settlements. German Federal Government (1993) (TA Siedlungsabfall).
- Bauer W & Meisinger S (2006). Erfahrungen aus dem Betrieb von Sickerwasser-Infiltrationsanlagen.
- Veröffentlichungen des LGA-Grundbauinstituts, Nürnberg, Heft 85: 193-208.

- Henken-Mellies U (2006). Strategien zur nachhaltigen Stilllegung und Nachsorge von Siedlungsabfalldeponien. Veröffentlichungen des LGA-Grundbauinstituts, Nürnberg, Heft 85: 175-192.
- Heyer KU, Hupe K, Stegmann R (2006). Kriterien für die Beendigung der Nachsorge—Resultate eines UFOPLAN-Vorhabens. Veröffentlichungen des LGA-Grundbauinstituts, Nürnberg, Heft 85: 233-247.
- Kanitz J (2007). Erhöhung der Deponiegasausbeute durch Optimierung der Gasbrunnen. Veröffentlichungen des LGA-Grundbauinstituts, Nürnberg, Heft 86: 235-251.
- Kerndorff H, Kühn S, Minden T, Orlikowski D, Struppe T (2006). Emissionsverhalten von Deponien und Identifikation von NA-Prozessen. Deponietechnik 2006, Hrsg.: Stegmann, Rettenberger, Bidlingmaier, Bilitewski, Fricke. Hamburger Berichte Band 29, Verlag Abfall aktuell, Hamburg 2006.
- Ramke H-G, Berger K, Stief K editors (2000). Wasserhaushalt der Oberflächenabdichtungssysteme von Deponien und Altlasten—Anwendung des HELP-Modells und Gestaltung der Rekultivierungsschicht. Fachtagung, Hamburg. Hamburger Bodenkundliche Arbeiten, Band 47—Institut für Bodenkunde, Universität Hamburg Ramke H-G, Witt KJ, Bräcker W, Tiedt M, Düllmann H, Melchior S (2007). Anforderungen an Oberflächen-abdichtungssysteme unterschiedlicher Deponieklassen—Ergebnisse des DGGT Status-Workshops 2006 in Hoexter. Veröffentlichungen des LGA-Grundbauinstituts, Nürnberg, Heft 86: 47-74.
- Schick P & Gartung E (2007). Gemischtkörnige Abdichtungsschichten in Oberflächenabdichtungssystemen. Anforderungen an Deponie-Oberflächenabdichtungssysteme, Hoexteraner Berichte zu angewandten Umweltwissenschaften, Heft 06. Herausgeber: Ramke H.-G. et al: 181-203.
- Stegmann R, Heyer KU, Hupe K, Willand A (2006). Deponienachsorge—Handlungsoptionen, Dauer, Kosten und quantitative Kriterien für die Entlassung aus der Nachsorge. Umweltforschungsplan des Bundesministeriums für Umwelt, Naturschutz und Reaktorsicherheit. Abfallwirtschaft, Förderkennzeichen (UFOPLAN) 204 34 327, im Auftrag des Umweltbundesamts.
- Witt KJ (2007). Tonmineralische Abdichtungselemente in Oberflächenabdichtungssystemen. Anforderungen an Deponie-Oberflächenabdichtungssysteme, Hoexteraner Berichte zu angewandten Umweltwissenschaften, Heft 06. Herausgeber: Ramke H.-G. et al: 165-180.

DEWATERING SLUDGE USING ELECTROKINETIC GEOSYNTHETICS

S. GLENDINNING¹, J. A. HALL², J. LAMONT-BLACK³, C. J. F. P. JONES⁴,
D. T. HUNTLEY⁵, C. WHITE⁶ and A. FOURIE⁷

ABSTRACT: Many industries create sludges as a waste product. Dewatering of these fine grained slurries is often problematic and the traditional outlets of lagoons or landfill may pose stability and environmental contamination issues. Sludges may be mineral based or organic based. Mineral based sludges created by mining processes are currently deposited into lagoons. These tailings are often very soft and poorly consolidated thus they may create an environmental hazard and even pose a severe safety threat, particularly in seismically active areas. The treatment and disposal of organic based sludges (sewage sludge) is one of the most problematical issues affecting waste water treatment in the developed world. The traditional outlets for sewage sludge are to spread it on agricultural land, or to form a cake for deposit to landfill or incineration. In order to create a sludge cake, water must be removed. Existing dewatering technology based on pressure can only remove a very limited amount of this water because of the way in which water is bound to the sludge particles or flocs. Sewage sludge lagoons, although smaller than tailings ponds still pose an environmental hazard or impede redevelopment.

Several researchers have shown that electrokinetic dewatering of sludge is more effective than conventional hydraulically driven methods. Electrokinetic dewatering involves the application of a D.C Voltage across the sludge, driving water under an electrical gradient from positive (anode) electrode to negative (cathode) electrode. However, there have been several reasons why this technique has not been adopted in practice, not least because the, normally metallic, anode rapidly dissolves due to the acidic environment created by the electrolysis of water.

This paper will describe experimentation using electrokinetic geosynthetics (EKG): polymer- based materials containing conducting elements. These have been used to minimise the problem of electrode corrosion and create a sludge treatment system that can produce dry solids contents in excess of 30%. It will suggest different options for the treatment of sludges both in situ in sludge lagoons and windrows, and ex situ as a treatment process using adapted filter press technology.

KEYWORDS: Sewage Sludge, Mine tailings, Dewatering, Electrokinetic Geosynthetics

INTRODUCTION

Electrokinetic geosynthetics (EKG) combine electrokinetics and geosynthetics providing a platform for dewatering technology which offers novel solutions to waste management challenges in many market sectors. These include treatment of high water content sludges, slurries, tailings, and dredgings, large volumes of which are produced by the construction, manufacturing, agricultural, mineral, water and sewage, and food processing industries. Many of these wastes are currently

deposited to land, either directly to landfill, into a lagoon, or by land spreading. Other wastes include liquids, currently requiring treatment before landfill. Such treatments, which include mixing with inert materials, thermal drying and chemical processing, are energy intensive and may involve a substantial increase in volume. In both cases, electrokinetic (EK) dewatering offers the potential for a major impact on the overall volumes of waste deposited to land. By separating solids from liquids, EK treatment can enhance resource recovery and re-use. For example: increasing solids content of

¹ School of Civil Engineering and Geosciences, Newcastle University, UK. NE1 7RU. Email: Stephanie.glendinning@newcastle.ac.uk

² School of Civil Engineering and Geosciences, Newcastle University, UK. NE1 7RU. Email: Jean.Hall@newcastle.ac.uk

³ Electrokinetic Ltd, Drummond Building, Newcastle University, Newcastle upon Tyne, UK. Email: john.lamont-black@electrokinetic.co.uk

⁴ Electrokinetic Ltd, Drummond Building, Newcastle University, Newcastle upon Tyne, UK. Email: colin.jones@electrokinetic.co.uk

⁵ Electrokinetic Ltd, Drummond Building, Newcastle University, Newcastle upon Tyne, UK. Email: david.huntley@electrokinetic.co.uk

⁶ Electrokinetic Ltd, Drummond Building, Newcastle University, Newcastle upon Tyne, UK. Email: chris.white@electrokinetic.co.uk

⁷ University of Western Australia, Australia. Email: fourie@civil.uwa.edu.au

sewage sludge permits its use as an autothermic fuel; dewatering of bentonite slurry reduces the need for chemical additives and enables its re-use; dewatering of dredgings permits reuse as a construction material. Additionally, EKG technology has the potential to enhance composting, thus improving the efficiency of an existing technology for reducing waste to landfill. Electrokinetics has also been additionally demonstrated to separate contaminants (both organic and inorganic) from fine-grained soils and thus can offer a technology for reducing the hazardous nature of contaminated soils.

This paper will explore the potential for EKG in the dewatering of organic and mineral sludges and demonstrate that this technology is feasible in many applications.

Mineral-Based Sludges

There are numerous industries that produce sludge-like wastes where the particulates are mineral based. Examples include potable water treatment sludge, producing a metalliferous rich sludge, tunneling applications, producing a mixture of bentonite, soil/rock and polymer additives and brewing, producing bentonite fines from the clarification process. However, by far the largest by volume worldwide is produced by the mining industry.

Metallurgical processing of diamond mine tailings, as an example, uses water as the processing and transport medium. The process results in two broad types of material, which are differentiated according to their dominant grain size: grits ($>75 \mu\text{m}$) and slimes ($<75 \mu\text{m}$). With the increasing importance of sustainable use of water in the mining industry, Welch, (2003), practices such as Paste and Thickened Tailings Disposal (P&TTD) are being adopted increasingly in the diamond mining sector Vietti, (2004). Dewatering prior to disposal offers a number of advantages including water recovery, reduction in size of the disposal facility or increased lifespan for a given facility, (Fourie, 2003; Welch, 2003). Whilst current P&TTD processes reduce disposal volumes and recover some water, the lack of a dewatering stage means that thickened tailings or pastes must be pumped in a liquid state to the disposal site using high pressure, high volume positive displacement pumps. It is apparent that the material has very low shear strength and high water content. However, the energy required to transport the tailings in this manner is very high as is the capital cost of the pumps required. Thus, a suitable dewatering technology, which could permit the transport of the tailings by conveyor in a drier, more solid state would reduce capital and operational costs and at the same time increase the quantity of water recovered, is highly desirable.

Organics-Based Sludges

A different range of industries produce sludges where the solid particulates are predominately organic in nature. These industries include the food industry, producing a range of sludges from vegetable washings to pulps and grains; paper manufacture, producing lignin pulp. However, the largest producer is the waste water industry where it is well understood that the dewatering of sewage sludge is one of the most challenging technical tasks. Current dewatering practice, based on mechanical pressure, is limited by the nature in which water is bound to the sludge flocs. Some of the dynamic in-process dewatering systems, such as the mechanical belt press, introduce an element of shearing of the flocs in process, increasing the dewatering effectiveness of the machine. However the process is still limited by the water trapped within a biological sludge cell. A dewatering system that could tackle bound water could enable more efficient disposal and re-use options in addition to volume reduction.

Electrokinetic techniques offer one potential cost-effective solution. The objective of the work described herein was to establish the susceptibility of a range of sludge materials to electrokinetic dewatering and to explore different means of application using electrokinetic geosynthetics (EKG).

Electrokinetic Phenomena

Electrokinetic phenomena have been studied extensively in the context of dewatering/consolidation of fine-grained (mineral-based) soils and are the result of the coupling between hydraulic and electrical potential gradients. These phenomena occur due to the presence of the diffuse double layer around the fine grained soil particles and involve the movement of electricity, charged particles and fluids (e.g. Yeung, & Mitchell (1993) and Mitchell (1993)). Of particular relevance is electroosmosis (E-O) where the applied electrical potential difference induces fluid flow in a charged particle matrix.

Typically electroosmotic dewatering of clay-rich materials is of the order of 1 to 4 orders of magnitude faster than hydraulic dewatering, with a typical value of electro-osmotic permeability (k_e) for a clay soil being $10^{-5} \text{ cm}^2/\text{Vs}$, as opposed to hydraulic permeability of $10^{-7} \text{ cm}^2/\text{s}$ to $10^{-9} \text{ cm}^2/\text{s}$ for silts and clays.

Like clay particles, organic-based sludge particles have a pH dependent surface charge, which is frequently negative. For this reason they too develop a diffuse 'double layer' of water surrounding the particles with the characteristic zeta potential at the boundary between the fixed and mobile portions of this layer. Because the flow of water induced by an electrical potential difference is not limited by pore size, electro-osmosis has the potential to remove interstitial water from sludge flocs,

thus greatly improving dewatering efficiency.

Indeed, Yaun & Weng (2002) noted a k_e value for sewage sludge of about 5 times that of many soils.

In order to determine whether or not any particular material is suitable for treatment using EK, the apparatus illustrated in Fig. 1 is used to determine coefficient of electroosmotic permeability, k_e .

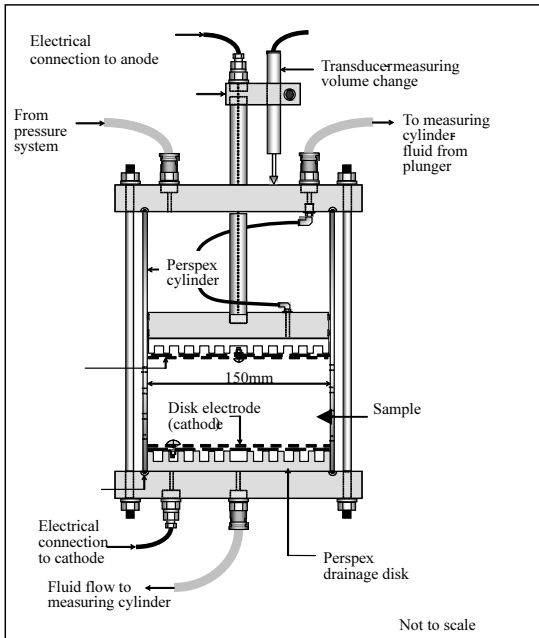


Fig. 1 Electrokinetic test set up

If the value of k_e is equal or greater than $1 \times 10^{-5} \text{ cm}^2/\text{Vs}$ then it is considered that the material has potential for treatment. The k_e for a range of mineral and organic materials is illustrated in Fig. 2.

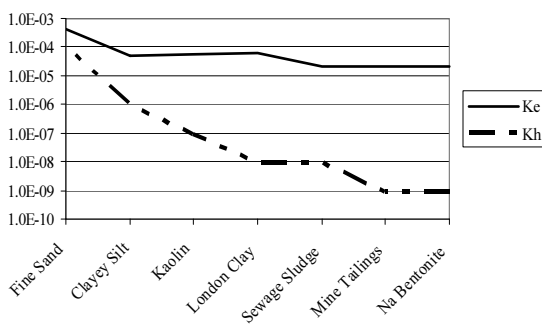


Fig. 2 k_e vs k_h for a range of materials

Electrokinetic Geosynthetics (EKG)

EKGs comprise conducting elements coated in a corrosion-resistant material, incorporated into a geosynthetic material. This patented design has overcome the problem of electrode corrosion. By encasing the metallic filaments in a relatively inert conductive material, electrode corrosion is effectively managed or eliminated.

By forming the electrode as a geosynthetic, EKG overcomes the problem of removing clean water by utilising the drainage and filtration functions of geosynthetics. Their ability to take on a wide variety of shapes and forms means that they can be manufactured to suit a range of different applications. A range of geosynthetic materials is illustrated in Fig. 3.

EKG can be applied in several ways:

- installed as vertical ‘wicks’ into sludge lagoons and used to draw water to the surface, removed by pumping, and discharged using form (3D materials in the form of d-g);
- formed as a fabric “bag” incorporating conducting elements as illustrated in (h)
- formed as the fabric in a belt or filter press to improve dewatering performance using form (i)
- installed as a combination of basal grid and fabric cover to increase dewatering rates in windrows (planar materials, a-c);

This paper will concentrate on the application using the illustrated planar forms and 3D drainage forms to treat both mineral-based and organic-based sludges and discuss more generally the application of other forms of EKG to date.

LAGOON APPLICATIONS

Tailings Lagoons

Extremely large volumes of mine waste are produced annually around the world. Recently Davies (2001) estimated that there are at least 3,500 active tailings storage facilities (TSF’s) worldwide and this likely to be an underestimate, due to lack of documentation. In some of these TSF’s, very wet tailings, with low solids content, have been deposited. Many years after placement, the water content remains relatively high, resulting in high risks of instability and extremely difficult rehabilitation. An example, from the Kimberley mine in SA is illustrated in Fig. 4.

In-situ dewatering of such problem material is highly desirable. Currently, the only available technology that can achieve this is the installation of prefabricated vertical drains. In order for these drains to work it is necessary to create a flow gradient in the tailings, which is usually achieved by the application of a surcharge load (e.g. by constructing a surcharge of imported fill). The drawbacks of this approach include the cost of importing and placing the fill, potential instability of the fill because of the low shear strength of the in-situ material and the fact that in some instances continuing and on-going deposition of tailings is required and this would not be possible if fill were imported and placed within the tailings impoundment.

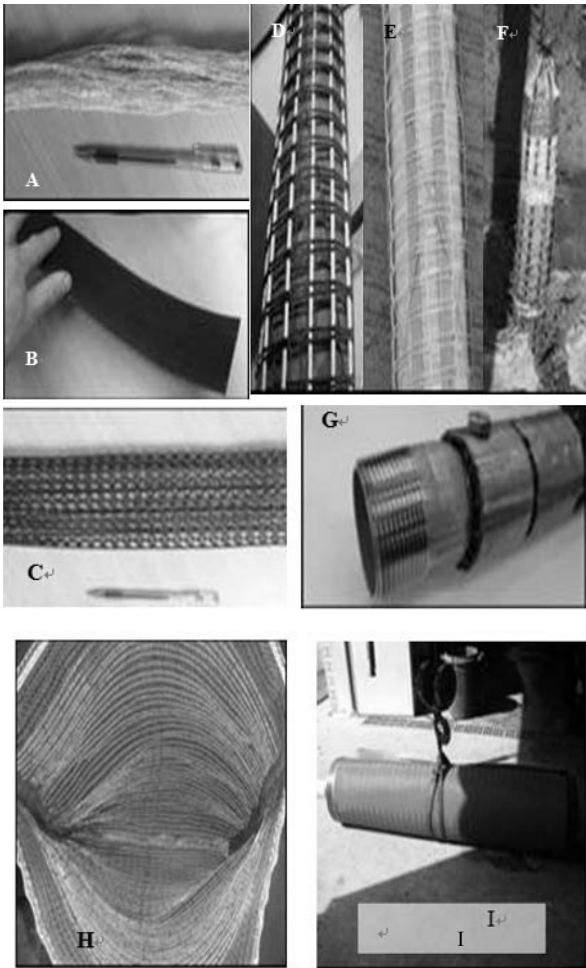


Fig. 3 EKG materials: - Planar materials (A-C), drainage materials (D-G), application materials (H-I)



Fig. 4 Tailings deposition at Kimberley mine, SA

Sewage Lagoons

Historically most water companies have disposed of large quantities of sludge in unengineered lagoons, constructed on sewage works sites, because this

represented the cheapest possible method for ‘dealing with’ this sludge. Until very recently in Europe it was in fact still legal to permanently deposit untreated sludge produced at a sewage works in a lagoon on that works, although it was not legal to do so with any imported sludge. Unfortunately these lagoons did not in fact deal with the sludge, they just postponed the time when it would have to be tackled properly. For some of these lagoons this time has now come, perhaps due to pollution of a watercourse or groundwater, or where the area of the lagoon represents the only possible space to expand the works, or in a few cases where there is development potential.

In both mineral and organic sludge lagoons, an EKG system has the potential to dewater in-situ either to facilitate removal of the sludge as a solid or to strengthen the sludge in-situ to free development potential; increase storage capacity and improve safety.

EKG Applications

Electroosmotic consolidation can be achieved by adapting prefabricated vertical drains (PVD) or wick drains to have an ‘active’ or electrokinetic component this creating an electrokinetic PVD or ePVD. e-PVDs utilise the higher flow rates that are achievable by E-O without the requirement for a surcharge load. The advantages of this approach are that it does not require the double-handling of large quantities of material demanded by the application of any load, and it is much faster. The speed advantage derives from the fact that electroosmotic permeability is higher than hydraulic permeability (for materials such as silts, clays and sludges), and that because no load is required, the full flow rate can be achieved immediately rather than needing to wait for gradual improvements in strength before additional load is applied as is the case with ‘staged loading’. A staged approach is normally required as soft, lagooned materials are too weak to support a significant load.

Laboratory testing

As previously discussed, initial laboratory trials are conducted to establish the k_c of a target material, to establish the suitability of a target material for EK treatment. Once established, further laboratory testing is undertaken in order to determine the suitability of the material for treatment using the chosen EKG application type. For lagoon applications this involves extended EK consolidation tests, either in the apparatus illustrated in Fig. 1 or in a small tank to determine whether EK treatment can effect volume reduction and strength increase in situ. The results of such consolidation trials on examples of both mineral-based and organic-based sludges will be described herein.

Mineral sludges

To evaluate the potential for electro-osmotic consolidation of mine tailings, an electro-osmotic testing cell similar to the device illustrated in Fig. 1 was used to establish the effect of voltage on consolidation. Tests were carried out on the materials detailed in Table 1.

Table 1 Properties of mine tailings tested

	Mineral sands	Kimberlite Slimes
Specific gravity	2.76	2.72
Liquid limit (%)	66	38
Plasticity index (%)	37	38
pH	8	8.5

Tests were run using a DC voltage of zero and 10V DC applied across the specimen height.

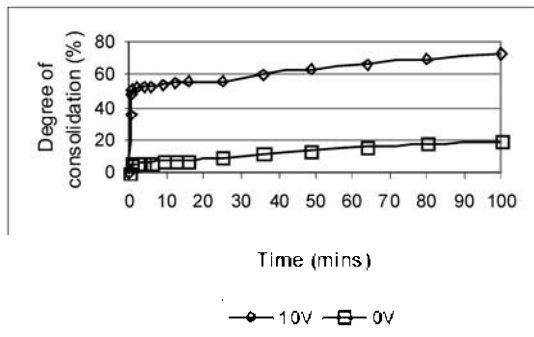


Fig. 5 Effect of electro-kinetic dewatering on rate of consolidation of mineral sands tailings

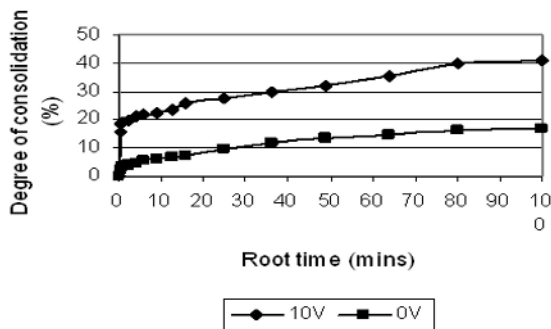


Fig. 6 Effect of electro-kinetic dewatering on rate of consolidation of kimberlite tailings

Results for the mineral sands tailings and the kimberlite tailings are shown in Figs. 5 and 6 respectively. Results are only shown for the first 100 minutes of the test as this clearly illustrates the benefit derived from the electro-dewatering. There is a very rapid initial effect, with up to 50% of the final consolidation occurring in less than 2 minutes for the mineral sand tailings and about 20% for the kimberlite tailings. The final amount of consolidation was relatively unaffected by the application of a voltage, but the rate of consolidation was significantly enhanced. A measure of

the efficiency of EK treatment is provided by the time taken to reach 90% of final consolidation. For the mineral sands and the kimberlite tailings, there was a reduction in time relative to conventional (i.e. unaided) consolidation of factors of 4.5 and 3.6 respectively.

Further EK consolidation tests were performed in two wooden tanks, 30cm x 20cm by 20cm deep, with the inside surfaces coated with an impermeable varnish. The tailings were mixed in a large paddle mixer for 15 minutes before being poured into the tanks. The electrodes, which were oriented vertically, were then inserted into the tailings. The 3D drainage electrodes used were similar to those illustrated in Fig. 3c with the exception that the EKG was wrapped in a non-woven heat-bonded geotextile when used as a cathode.

The electrodes were connected to a DC power source and the desired voltage of 5V set. Measurements were made throughout the tests of water collected (and withdrawn) from the cathode, the total mass of the tank (to determine total mass of moisture lost), evaporation from a control sample and current drawn. Within 15 minutes of switching on the power supply, water could be seen to be trickling slowly into the cathode void. Within a day, small eruptions (volcano-like) were evident in the vicinity of the anode and cracks began to appear in the surface of the tailings.

Figs. 7 and 8 show results for the mineral sands tailings. The results are presented in terms of total water lost, water decanted from the cathode and water lost to evaporation in Fig. 7. The sum of the two latter components is less than the total amount of water lost, with the remainder being water lost by electrolysis. The voltage gradient between the two nearest faces of the electrodes was 0.3 V/cm, which is significantly lower than most values reported in the literature. Even when the test was terminated after 7 days, the water content was still decreasing albeit at a slower rate than initially. It is quite clear that the electro-kinetic dewatering is having a very significant effect, with evaporation losses only accounting for about 32% of the total.

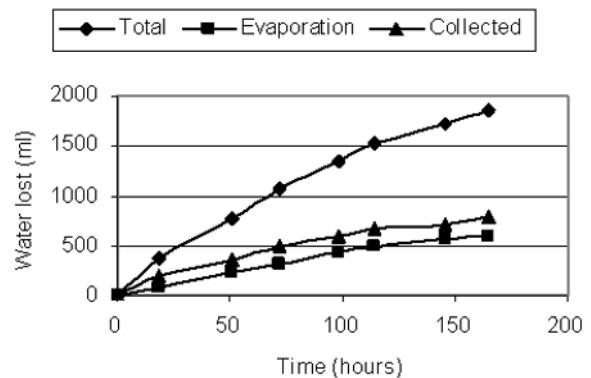


Fig. 7 Amount of water lost due to electro-kinetic dewatering and due to evaporation

The results are presented in terms of gravimetric water content in Fig. 8 and this again shows the very substantial benefit derived from the electro-kinetic dewatering. At a water content of over 140% (which is typical of the placement water content on the actual tailings facility), the tailings has an undrained shear strength significantly less than 1kPa, which presents particular stability concerns. Continuation of the test would soon bring about measurable undrained shear strengths in the tailings. It thus provides a relatively simple technique for dewatering tailings in-situ in order to achieve an improvement in undrained shear strength.

The power consumption during this test was 1.9kWh per dry tonne of tailings, which translates into a very low energy cost.

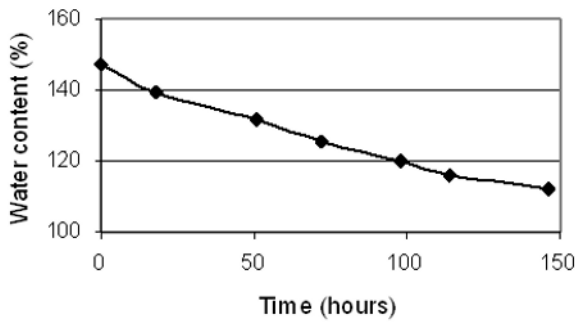


Fig. 8 Variation of water content with time for mineral sands tailings, laboratory tank test

Organic Sludge

Tests were again performed using the apparatus illustrated in Fig. 1 on two similar samples (A & B) of a cold digested thickened lagooned sewage sludge. This sludge had been resident in the lagoon for approximately 3 years. Tests were performed to determine the amount of volume reduction possible in 3 weeks of treatment. All tests were undertaken using an applied back pressure of 50kPa and an applied voltage gradient of 1V/cm, using parallel copper disc electrodes.

The sludge demonstrated a k_e value of 1.5×10^{-5} cm^2/Vs , which compares very favourably with the types of clay soils that are most amenable to this treatment. Results of the 21-day tests are summarised on Table 2, producing average solids contents of 27% (B) and 23% (A) and overall volume reduction of between 40% and 50%.

Table 2 Summary of long-term consolidation tests

	Test A	Test B
Initial moisture content	621 %	574 %
% dry solids	13.9% ds	14.8% ds
Test duration	21 days	21 days
Volume of extracted water	837 ml	1083 ml
% dry solids at cathode	31.8%	38.9 %
% dry solids at anode	64.5%	72.5%
Total volume reduction	-40%	-51.7%

Field Trials

Once laboratory trials have established the potential for treatment and the suitability of the chosen form of application, field trials are conducted to explore the mechanisms for up-scaling and to determine the operating parameters for full-scale treatment. Again, two different trials on both mineral and organic sludges will be described herein.

Mineral-based sludge lagoon

A 3m diameter container made from high density polyethylene (HDPE) was filled with mineral sands tailings similar to those described in section 2.1.1 directly from the thickener underflow. A view of the test tank is shown in Fig. 9.



Fig. 9 Large-scale test of in-situ consolidation of mineral sands tailings

The tailings was left to stand for three weeks, after which it was found to be at a water content of 158% and 750mm deep. This meant that the initial volume of material was 5.3m³. At the start of the field test, the undrained shear strength of the tailings was much less than 1kPa.

A single EKG cathode, wrapped in a non-woven, needle-punched geotextile was inserted by hand into the centre of the tank. Six anodes were inserted by hand in a hexagonal pattern around the cathode, at distances of 900mm from the cathode. All electrodes were connected to the power supply and the voltage increased to 30V over a ten-minute period, providing an initial voltage gradient of 0.33V/cm. The polarity was reversed whenever mine personnel visited the site, which was usually once a day, after the first week of more intensely monitoring. For operational reasons, the power supply was switched to a 12V rechargeable battery which meant that the voltage gradient for most of the test was reduced

to 0.11V/cm.

Water was regularly pumped out of the cathode using a small submersible pump. The volume, pH and conductivity of the water were measured regularly. Water that accumulated in the cathode overnight was only decanted the following morning. This sometimes resulted in water from the cathode discharging onto the tailings surface overnight, which could have decreased the effectiveness of this system because this free water was then able to flow into the cracks that formed around the electrodes. There were a few spells of light rain during the experiment and these are discussed later in the paper. Samples of the tailings were taken regularly for determination of water content.

The total volume of water lost over the 2 month test period is shown in Fig. 10.

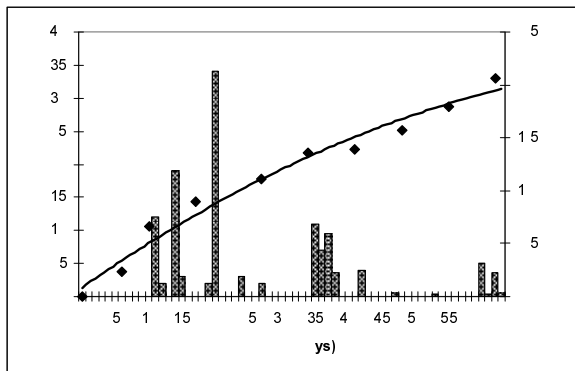


Fig. 10 Cumulative volume of water collected from the cathode

In excess of 2m³ of water was lost in total. A noticeable feature of the results in Fig. 10 is the gradual but consistent decline in the rate of water lost. This is due to the gradual decrease of the water content and thus water availability, plus the slight loss of contact between the upper part of the electrodes and the tailings over the period of the test. As can be seen from Fig. 10 there was a small effect of rainfall on the volume of water but this was not thought to be significant.

Equally, the effect of surface evaporation was not considered significant when compared to the effect of water removal by EK. At the end of the two-month period, the average water content of the tailings was 75%, varying from 54% near the top surface of the tailings (between cracks) to 92% at the bottom of the tank. The average value of 75% corresponds to an undrained shear strength of 18kPa, which is a very significant improvement over what was achieved merely by in-situ drying.

The voltage gradient used in the field test (0.11V/cm for most of the time) was about one-tenth of that used in the laboratory electroosmotic cell and about half that used in the laboratory tank test. It resulted in an energy consumption rate of 0.9kWh per dry tonne, compared

with rates of 1.9kWh and 30kWh per dry tonne for the tank test and the electroosmotic cell test respectively. Increasing the voltage gradient could have accelerated the rate of dewatering, but this would have been at the expense of decreased energy efficiency. The designer of an electroosmotic dewatering system thus has a great deal of flexibility in operational parameters that may be adjusted to suit a range of criteria, from maximising rate of dewatering to minimising energy consumption.

The total energy used during the two month test was approximately 2.5kWh. The initial dry density of the tailings at the start of the test was 510 kg/m³, so this translates into 0.9 kWh/dry tonne to dewater from a water content of 158% to 75%.

Full-scale trial using EKG to dewater sewage sludge in situ

The effectiveness of electrokinetic consolidation of lagooned sewage sludge cake by means of ePVDs was examined at pilot scale using two steel containers of 9.7m³ capacity with tailor-made butyl liners filled with approximately 8.5m³ of sludge. The sludge was in a liquid state with a low shear strength (unmeasurable using a hand vane, but estimated to be approximately 1kPa) and a solids content of only 10.6%. The skips were covered during the test to eliminate the potential for rainwater ingress. Two electrode arrays were evaluated:

- Rectangular array with Anode-Cathode spacing of 0.9m and Anode-Anode or Cathode-Cathode spacing of 0.4m – Skip A
- Hexagonal array with spacings of 0.7-0.9m (in practice an equilateral spacing would be chosen; here the hexagons were distorted to suit the containers) – Skip B.

The electrodes were composite EKG ePVDs (Fig. 3e and f), which comprised six different components including a central perforated drain, filter fabric, primary and secondary conducting elements, and integral and binding knitting yarns. The arrays were run at 30V, providing a voltage gradient in the order of 33V/m.

In all, 63 days of treatment, applying an intermittent voltage, resulted in a reduction in volume of 23% for skip A and 30% for skip B. It is considered that the potential for reduction however is much greater, as the method used to remove water from the cathodes was not particularly efficient and significant quantities of water collected at the surface of the sludge adjacent to the cathode from where it flowed back to the anode and effectively recirculated around the system. The effect of evaporation was considered to be negligible as the sludge had been taken from the near-surface a lagoon that had been open to the atmosphere, allowing all potential atmospheric drying to have taken place. Evaporation had been further reduced by the presence of the covers.

Shear strength was measured using a hand shear vane in a regular grid pattern across each skip. The average

shear strength for skip A was 7kPa and 16kPa for skip B. A before-and-after photograph of the Skip B is shown in Fig. 11. Again, it is felt that higher strengths can be achieved in the same time once the problem of water removal caused by the poor performance of the siphons is corrected.

Power consumption was calculated for the entire treatment period, from the readings made of current and voltage, with the lowest demand for power resulting from the electrode configuration in skip B averaging 128kWhr per cubic metre of wet sludge. Power consumption was expressed in this way as it was considered to be the most useful way of providing potential end-users with the likely cost of dewatering lagooned sewage sludge using this technique. However, it is felt to severely overestimate the amount of power required to treat this volume of soil if the overall treatment area is scaled up. These figures can be adjusted downwards by quantification of the following factors:

- Ineffective removal of water, which would lead to (i) reduced volume reduction and thus longer embedded lengths of electrodes and thus higher power demand and (ii) longer than necessary treatment duration thus higher overall power consumption over the duration of the trial.

- Addition of water during the filling of the skips. At 10.5% dry solids the sludge was wetter than the sludge in the lagoon and it is highly inefficient to use electroosmosis to remove water which could have been pumped clear of the surface of the lagoon at the beginning of the trial.

- Edge effects including (i) excessive current along the sludge/butyl liner contact (caused by water concentration due to ineffective water removal from some cathodes) and (ii) electrical field distortion meaning that the test arrays comprised a disproportionate number of electrodes that were at the edge of the overall array and thus part of 'partial cells'

An initial quantification of these factors has allowed an estimate of the 'true' power consumption for effective treatment:

- Grading the performance of siphons, and comparing this to the current drawn through the associated cathodes, showed that effective water removal from all cathodes would have the effect of reducing overall current for the array by approximately 33%;

- Removing the surface excess water could produce a saving of 42%–52%; and

- Accounting for edge effects (using an example of an array of 100 x 100 electrodes) would yield a saving of approximately 7%.

Compounding these factors yields an overall power saving of approximately 2/3. This means that the initial estimate of 128 kWhr/m³ to reach a volume reduction of 30% could be adjusted to 43kWhr/m³. This could be further refined as more effective water removal would

create a faster rate of volume reduction and thus shorten the overall treatment time. It is further noted that electroosmotic efficiency (volume of water moved per unit charge) varies according to voltage gradient such that a higher voltage gradient produces more rapid flow but is less efficient. The voltage gradient used in the trial was low relative to historically common values so there is scope to improve on the speed of treatment or to have a higher voltage over a larger electrode spacing to reduce the number of electrodes.

The laboratory testing has indicated that significant increases in shear strength and reductions in volume can be achieved by the application of E-O to lagooned sludges. The field trial has shown some improvement can be achieved by the application of E-O in situ using e-PVDs. However, some further development is required, particularly on the method of extracting the water from the cathodes before the full potential of E-O can be realised.

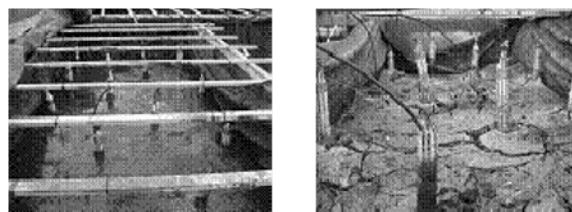


Fig. 11 Skip trial before and after treatment

BELT-PRESS APPLICATIONS

Many types of sludges are currently dewatered using mechanical means. Examples include both belt and filter presses. In the case of organic-based sewage sludge, it is firstly thickened using a polymer flocculant before being mechanically pressed. For reasons described earlier, the degree of dewatering achieved by these means is limited, at best achieving dry solids contents in the region of 15–20%. Therefore, the remit of the research in this market was to investigate the potential for applying electrokinetics to press technology to improve the dewatering of sewage sludge.

In the mineral sludges produced by the mining industries, the use of belt presses is far less prevalent. However, there exists a potential opening for a suitable dewatering technology and the aim of the research in this market was to investigate the potential for use of EK belt presses for use in the mining sector to aid water recover and reduce disposal volumes.

Laboratory Testing

The aim of the laboratory testing for this application was to establish whether the use of EK belts fabricated

from a combination of (belt) cloth and conducting elements could be used to effect EK dewatering, and to determine whether the relatively short duration of treatment (represented by the length of time that the sludge is resident in the belt press) is sufficient to produce EK dewatering. Additional objectives were to establish appropriate conducting element spacings and voltage gradients to apply.

Organic Sludges

Similar tests to those previously described were undertaken, using the apparatus illustrated in Fig. 1 with the exception of the form of the electrodes, the thickness of the sample and the duration of the test. Electrodes were cut from woven polyester material and electrified with carbon fibre strips at spacings of 5mm, 10mm, and 20mm. In this way these electrodes had very similar electrical and filtration properties to those that would be used in an operating press.

The sludge tested included the same ex-belt press humic sludge that was tested as part of the lagoon trial described earlier (15% dry solids) and ex-drum thickener activated sludge further dewatered by hand pressure (7.6% dry solids). The test set-up used two separate voltages of 15V and 30V applied to a 15mm thick sample with a back pressure of 70kPa for humic sludge and 25kPa for activated sludge. The tests lasted for 20 minutes. The higher pressure was used to simulate typical pressure exerted in a belt press and the 20-minute duration was considered to be approximately two to three times the typical residence time of sludge in a belt press.

The percentage dry solids achieved by treatment of the humic sludge after 20 minutes duration for the different electrode configurations and applied voltages is shown in Fig. 12.

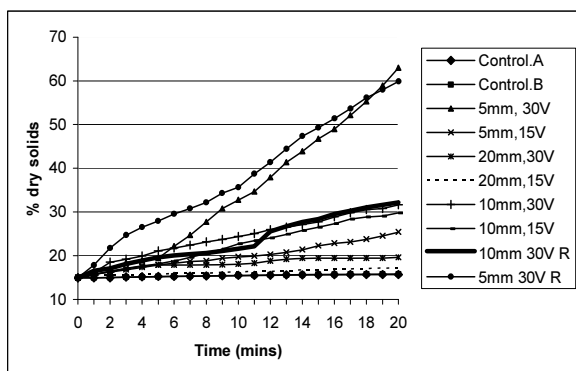


Fig. 12 Humic sludge: % dry solids from discharge. Test data followed by an "R" indicate a repeated test

This method calculates the dry solids in the material remaining in the cell from the volume of water collected. This calculation may underestimate % dry solids because

some water removed by electrolysis is not accounted for and may therefore be regarded as conservative. The most effective of the tests were repeated (denoted with an R) to ensure repeatability of the dry solids achieved. The results for similar tests on activated sludge are shown in Table 3.

Table 3 % dry solids after 20 minutes, activated sludge

	Electrode design and applied voltage			
	2.5mm 15V	5mm 30V	10mm 30V	Control
Discharge (ml)	63.00	126.00	93.00	0.00
Displacement (mm)	-0.07	-1.89	-1.32	0.00
% dry solids (discharge)	10.28	15.89	12.36	7.60

These results, although apparently less encouraging than those for the humic sludge were achieved using a back pressure of only 25kPa. This was necessary due to the very fluid consistency of the initial sludge material meaning that higher pressures forced the entire sample through the filter material. This low back pressure is of considerable significance here because it means that all the effective dewatering is attributable to E-O alone.

Mineral sludge

Standard filter belt material made from woven polyester was adapted to act as electrokinetic filter elements in a similar way to those formed for the sewage sludge except that the conducting elements were formed of single filament metallic elements. Kimberlite slimes were tested with properties illustrated in Table 4.

Table 4 Characteristics of thickened kimberlite slimes

Dry Solids Content (%)	Water Content* (%)	Bulk Density (Mg/m ³)	pH
57.2	74.8	1.581	9.53

* Water content defined in the geotechnical sense as (mass water/mass. solids) x 100

The slimes were placed in the electrokinetic cell between an anode and a cathode filter electrodes. The system was placed under a pressure of 70kPa and the resulting filtrate collected over a period of 35 minutes. The variables explored included:

- Sample thickness 10 mm, 20 mm, 35 mm and 50 mm
- Applied voltage 15 V and 30 V
- Spacing of conducting elements in the weave 7.5 mm, 10 mm, 15 mm and 20 mm.

Solids contents were calculated by subtracting the mass of collected filtrate from the original mass of sample

and the results were cross checked against changes in the volume of the sample, which were determined by use of an LVDT measurement of the cylinder piston displacement. An example of the solids content versus time for the 7.5 mm spacing filter electrodes at 15 and 30 V using 35 mm and 50 mm thick samples is shown in Fig. 13. The complete data set for the 15 V tests is shown in Fig. 14. A percentage dry solid content greater than 65% is required for transportation by conveyor belt (determined by further experimentation as the solids content above which liquefaction did not occur due to the vibration of the belt).

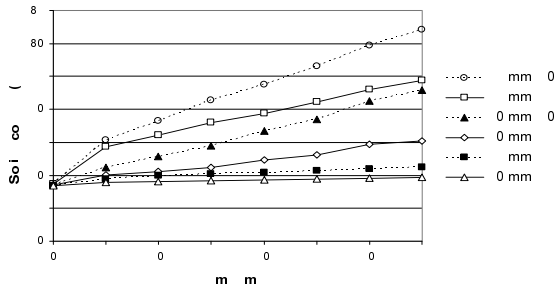


Fig. 13 Solids content versus time for 35 and 50 mm samples of kimberlite A slimes dewatered at 15 and 30 V using 7.5 mm filter electrode

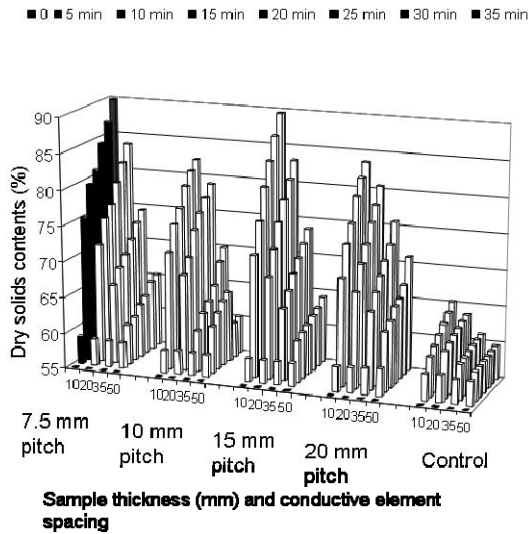


Fig. 14 Dewatering performance of kimberlite slimes from source A at 15 V using all the filter electrodes and control (0V) at 10 mm, 20 mm, 35 mm and 50 mm sample thicknesses

The data from the tests indicate that the dewatering performance was controlled by several factors including:

- Residence time
- Applied voltage
- Sample thickness.
- Design of filter electrodes

The data, as presented on Fig. 14 also indicate that for any given target solids content, the parameters can be

selected with a variety of different combinations to achieve the required end result. This flexibility means that there can be a balance struck between dewatering throughput, power consumption and cost of belts. Fig. 15 presents an example of such an analysis to identify an acceptable range of target solids contents for a working belt press equipped with belts having conductive elements at 7.5 mm spacing. This indicates that, based on these data, the optimum sample thickness for maximum throughput (derived from feed rate and belt speed) lies between 20 and 30 mm.

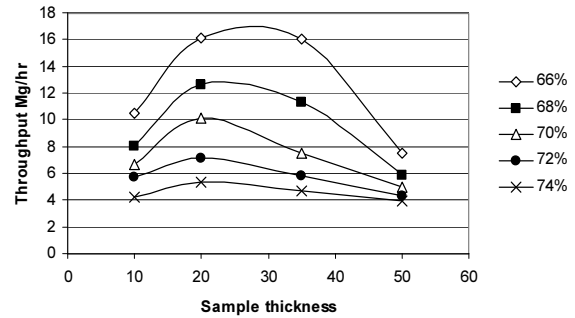


Fig. 15 Optimised throughputs to achieve different target solids contents using 7.5 mm pitch belts

Laboratory tests conducted were aimed at simulating the electrokinetic dewatering between a pair of woven electrokinetic geosynthetic (EKG) belts. A critical difference factor in the bench scale simulation is the absence of any shearing action, which is an important characteristic of a working belt filter press and which has been shown to increase dewatering performance over that indicated by static tests. Therefore it was critical to undertake field trials of belt-press applications in order to realise their full potential.

FIELD TRIALS

Organic–Sewage sludge trial UK

Full scale field trials have been conducted using a modified belt press fitted with EKG belts. The sludge tested was a mixture of Surplus Activated Sludge (SAS) and primary sludge. SAS is a biological waste by product from the waste water treatment industry and it is very difficult to dewater due to a very thick cell wall and thus it is common to blend with the more readily dewaterable primary sludges. The ratio of SAS to primary, although variable, is of the order of 40:60.

An unmodified standard belt press was producing 18 to 20% dry solids on this material. In order to achieve electrokinetic dewatering of the sludge, the only physical modifications made to the existing belt press were the replacement of the conventional belt with a new

conductive belt and the addition of voltage transfer equipment to apply voltage to the conductive belts (Fig. 16 and 17). Some further minor changes were made to the operation of the press, but these were limited to belt speed adjustment to obtain a satisfactory sludge residence time in the shear section. This necessitated a small adjustment in the sludge feed rate (~90% of the conventional mode flow) to the press to avoid flooding of the gravity drainage section.

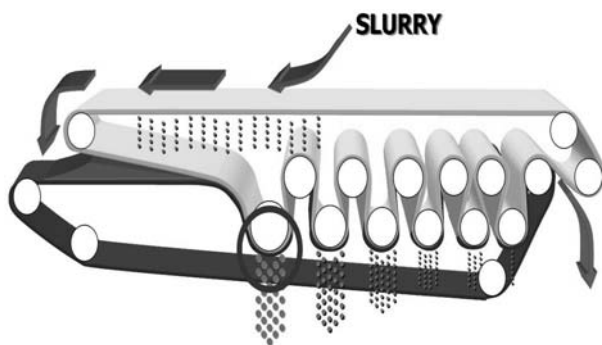


Fig. 16 Schematic of the Belt press system indicating the gravity feed section and subsequent rollers. Highlighted area close up is presented in Fig. 17

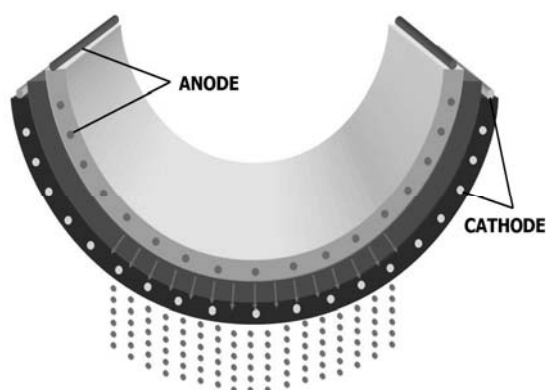


Fig. 17 Close up of sludge dewatering occurring in a belt press

Fig. 18 clearly demonstrates the increased cake dry solids that can be achieved by the combination of mechanical and electroosmotic dewatering. These results exceeded expectations based upon the laboratory results, and highlights the importance of the shear action within conventional dewatering. A cake dry solids of >30% was achieved with an applied voltage of 17V. This represents a significant improvement in cake dry solids over conventional dewatering. The increased cake dry solids obviously reduces the cake volumes for disposal and therefore transports and land disposal costs. Subsequent trials have produced results that concur with the original full scale results.

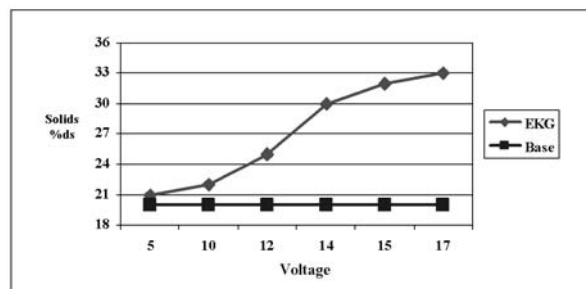


Fig. 18 Electrokinetic belt press dewatering performance

Electrokinetic sludge dewatering has a slightly higher energy requirement compared to a conventional belt press. At 14m³/h sludge feed rate, 2.5% DS feed sludge the power consumption yielded an additional electricity requirement of 19.5 kWh/day. However, the increase in electricity consumption is offset by the reduction in cake volume, cake transport costs and ultimate cake disposal costs. Overall there is a cost saving to water companies adopting this technology as presented in Table 5.

Table 5 Cost comparison between Belt Filter Press and EKG Dewatering

	BFP	EKG
Loading Kg dry solids/hr	540	540
Operating hours/year	8000	8000
Volume of cake m ³ /year	22,700	13,900
Disposal cost £/m ³	15	15
Total disposal cost £/year	340,500	208,500
Saving with EKG £/year		132,000

An additional benefit of raising the dry solids content of sludge above 33% – 35% is the possibility for sludge to become auto-thermic, which would mean significant savings on fuel oil for sludge incineration.

The performance of the full-scale trial was better than would have been predicted from the laboratory experiments. This is attributed to the additional effects of shearing and the thinner sample thickness in the field trial compared to the laboratory studies. Electrokinetic dewatering technology is well placed to compete with other methods of dewatering such as centrifuges, especially with the desire to reduce costs and energy consumption

Mineral–Diamond Mine Tailings SA

As a result of the positive results from the laboratory trials a series of full scale tests have been initiated in South Africa on diamond mine tailings. The dewatering trials were again based on a conventional belt filter press modified to permit the use of EKG belts, Figs. 16 and 17. The conductive belts were formed based on the dewatering performance of Kimberley slimes, as discussed in section 2.1.1.

Once the filter press had been delivered and commissioned at Kimberley (Fig. 19), paste from the bottom of the paste thickener was diverted to the press. The nature of the tailings was such that the material needed to be treated with flocculants; once a suitable flocculation dosage was found the trials started.

Fig. 20 shows the tailings on the top belt at the beginning of the cycle and Fig. 21 shows the dewatered tailings at the end of the cycle. The nature of the dewatered Kimberley tailings following belt press dewatering is shown in Fig. 22. The difference between the nature of the material in Fig. 20 and Fig. 22 is dramatic.

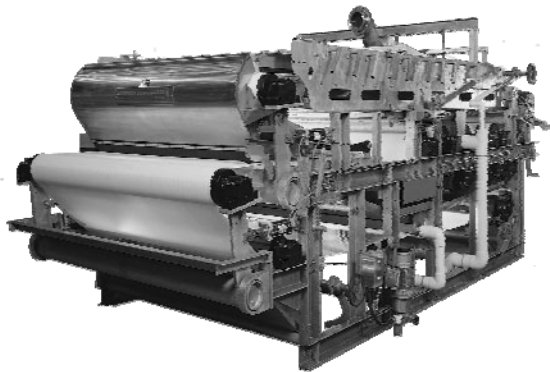


Fig. 19 Example of the form of belt press commissioned for the use of dewatering tailings



Fig. 20 Flocculated paste on top belt

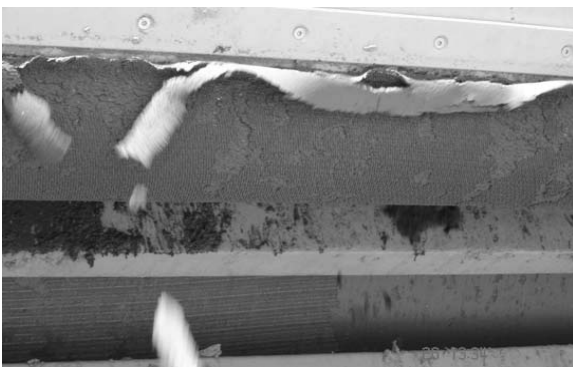


Fig. 21 Dewatered tailings at the distal end of the belt press



Fig. 22 Nature of the dewatered diamond mine tailings

The use of electrokinetic dewatering of kimberlite slimes has been shown to be possible and that the process can produce dewatered tailings suitable for transportation by conveyor. The process reduces the volume of the material needed to be deposited which has economic implications and also results in the recovery of water. The latter has major implications in some mining operations where the shortage of water is critical. The reduced volume permits more economic use of storage space and the lower water content of the deposited waste provides greater safety. Although the details of the cost savings are commercially sensitive at the moment, the anticipated cost of electrokinetic dewatering, to permit transportation by conveyor, is an order of magnitude less than the power costs involved in pumping slimes to the disposal site.

OTHER APPLICATIONS

Windrows

At present some humic sludge is treated by thickening, pressing (in a belt or filter press) and then drying in the open air in elongated stockpiles, or windrows. Wood waste is added in the proportion of approximately 30% – 40% by volume to improve the mechanical handling characteristics of the sludge. The mixing of wood waste has a cost implication for acquiring the material, mixing and handling of the bulk product, which increases markedly in volume on addition of the wood waste. Laboratory trials indicated that EK treatment had the potential to reduce the amount of wood-waste required for dewatering; a field trial established that EK had the ability to not only significantly improve drainage and volume reduction but also to improve microbial activity within the windrow, probably through electrolytical generation of oxygen. A field trial was conducted in order to assess the use of EKG in accelerating the conditioning process of the sludge. Fig. 23 shows the field trial windrow constructed on site. Part of the windrow was planted with grasses (RHS of picture) in order to assess and try to accelerate the potential phyto-conditioning process in the sludge. The remaining

half of the windrow was treated conventionally over an 8 week period.

Areas of increased drainage from the windrow can be seen on the concrete pad indicating that dewatering is taking place from the windrow and visual evidence of microbial activity was recorded. However the results from this field trial were inconclusive on the acceleration of the conditioning process. Further studies are planned before any wide-scale implementation can take place.



Fig. 23 Field trial windrow, sludge phyto-conditioning in the foreground, conventionally treated windrows in the far left.

EK Filter Bags

Many industries produce waste products from their processes as slurries (e.g. food industry and water treatment processes). Many of these slurries are heterogeneous in nature and particle size thus they pose dewatering challenges prior to disposal. Most of the established dewatering technologies require homogenous materials for application in the process; EK Filter bags offer another dimension to dewatering with a capability to treat heterogeneous materials. As with the belt press application, these filtration bags are an adaptation of an existing dewatering technology and laboratory testing bags are in the form of Fig. 3h. Large-scale laboratory trials on a metalliferous rich mineral water treatment sludge have indicated this technology has a potential application in batch dewatering. Furthermore, field trials are planned to demonstrate the flexibility of the system with a network of bags interconnected to expand the volume of slurry treated in each batch.

CONCLUSIONS

In this paper the application of electrokinetics to the dewatering of both mineral and organic sludge by means of electrically conductive geosynthetics (EKG) has been demonstrated through laboratory testing. Several different

methods of practical application have also been demonstrated through the successful execution of field trials. Although some applications are less well developed and proven, it is demonstrated that the role EKGs can have in enhancing the available technologies for the waste producing industries is significant and in many cases it has numerous benefits such as the ability to recover water during the process, power and cost savings on comparable dewatering technologies and a retrofitting capability.

ACKNOWLEDGEMENTS

The authors wish to thank De Beers and ACARP for the supply of mineral sludge samples and Severn Trent and Yorkshire Water for supply of organic sludge samples for testing. They also wish to thank Severn Trent Water for supporting the lagoon field trial, De Beers Consolidated Mines Pty and Ashbrook Simon Hartley for supporting the mine tailings field trial, Corpro Ltd, Engtex AB and GKD for development and supply of electrode materials, and WJ Groundwater Ltd for development of the water removal system. Further acknowledgement to the Technology Strategy Board for their ongoing funding of this research and development.

REFERENCES

- Davies MP (2001). Impounded mine tailings: what are the failures telling us?. CIM Distinguished Lecture 2000-2001. The Canadian Mining and Metallurgical Bulletin 94(1052): 53-59.
- Fourie AB (2003). In search of the Sustainable Tailings Dam: Do High-Density Thickened Tailings Provide the Solution, School of Civil Engineering and Environmental Engineering, University of Witwatersrand, South Africa.
- Mitchell JK. Fundamentals of Soil Behaviour, 2nd Edn., Pub. John Wiley & Sons Inc, New York, USA, 1993.
- Vietti A (2004). Know your chemistry—Suspension and Compaction behaviour of Paste. International Seminar on Paste and Thickened Tailings, Cape Town, South Africa.
- Welch D (2003). Advantages of Tailings Thickening and Paste Technology, Responding to Change—Issues and Trends in Tailings Management—Golder Associates Report: 5.
- Yaun C & Weng C. Sludge dewatering by electrokinetic technique: effect of processing time and potential gradient, Advances in Environmental research, 2002, www.elsevier.com/locate/aer, u.
- Yeung AT & Mitchell JK (1993). Coupled fluid, electrical and chemical flows in soil, Géotechnique, 43 (1): 121-134.

FULL-SCALE PRACTICE OF ECOLOGICALLY BASED LANDFILL OF MUNICIPAL SOLID WASTE: TO ACCELERATE THE BIOLOGICAL CONVERSION INSIDE LANDFILL AND COVER LAYERS

Pin-Jing HE¹

ABSTRACT: The application of bioreactor landfill with leachate recirculation was usually confronted with the problems of waste acidification and high ammonia content in leachate. A modified operation called “ecologically based landfill” was induced by recycling the pre-treated fresh leachate into landfill and sub-irrigating the stabilized leachate into the plant-soil system of cover layers. The former accelerated the methanization of biomass waste, whereas the latter converted the ammonia nitrogen into biomass nutrients. Secondary pollution from this system was expected to be minimized. The concept of ecologically based landfill was assessed and optimized in lab- and pilot-scale, and then validated in a full-scale landfill by 3 years of practice and monitor.

KEYWORDS: municipal solid waste, bioreactor landfill, ecologically based landfill, leachate recirculation, leachate irrigation

INTRODUCTION

The generation of municipal solid waste (MSW) in China in 2006 reached 407,000 t/d, among which food waste contributed to 60%~70%. Over 85% of these wastes were disposed in landfill. There was increasing interests in operating landfill as bioreactor with leachate recirculation to accelerate the decomposition of waste (Pohland and Al-Yousfi, 1994; Onay and Pohland, 1998; Reinhart et al. 2002). Nevertheless, successful cases were less reported than expected. Especially, when it faced to different wastes, the operation should be modified before transferred. A typical case was the landfill loaded with MSW rich in food / putrescible compositions in most of developing countries, such as China. After landfilled for 2 months, the weight of produced leachate can account for 1/3 landfilled wastes, and the COD concentration is more than 20–80 g/L (He et al. 2005). Our previous experiment had observed that an acidic environment (pH 4.8–5.4) was kept for more than one year when raw leachate from these landfills was directly recycled back (He et al. 2006a, 2007). As a result of acid tomb, the hydrolysis rate was low and the methanogenesis could not be started-up. It indicates that single operation like liquid recirculation might impose worse behavior. The kernel way of improvement is accelerating methanogenesis. Furthermore, ammonia could not be degraded under anaerobic environment, resulting in high ammonia concentration in the partially

stabilized leachate from bioreactor landfill with leachate recirculation – up to 3,000 mg/L.

In order to conquer the acid accumulation from direct liquid recirculation, it came to the concept of recycling leachate which has been removed of acids externally (i.e. ex-situ).

The partially stabilized leachate was biorefractory owing to great amounts of humic substance, ammonia and dissolved salt ions (He et al. 2006b; Lü et al. 2008). On the other hand, low water content and nutrient shortage in final cover soil were major limiting factors that restrict the vegetal restoration of landfill. Therefore, there came to the concept of irrigating biorefractory leachate onto vegetated covered soils, with expects that the leachate volume could be reduced by plant uptake and evapotranspiration, and that the leachate pollutants could be intercepted by soils and utilized by soil microorganisms or plants. However, the feasibility of leachate irrigation seriously depends on the leachate loading and the ecological effects of plant-soil ecosystem.

The combination of the above two concepts formed a modified operation called “ecologically based landfill”, with expect that the biological conversion both inside landfill and cover layers could be utilized and accelerated.

In this work, we experimentally investigated the optimal technologies for leachate pretreatment, so as to accelerate methanogenesis of landfill layers in initial

¹ Professor, Institute of Waste Treatment and Reclamation, State Key Laboratory of Pollution Control and Resource Reuse, College of Environmental Science and Engineering, Tongji University, China. Email: solidwaste@tongji.edu.cn

stages. Partially stabilized leachate was treated by plant-soil system, with aims, 1) to screen out suitable plants that can resist against leachate stress by lab-scale experiments, 2) to determine the capacity of hydraulic loading for irrigating leachate onto selected plants in lab-scale, and 3) to evaluate the long-term effect of leachate irrigation. A field strategy was then designed and validated by field practice and monitoring for more than 3 years.

LAB- AND PILOT-SCALE RESEARCH

Experimental Procedure

To assess the effect of leachate recirculation under different strategies, raw leachate was pretreated aerobically by sequential batch reactor (SBR, marked as A1), anaerobically by upflow filtration bioreactor (UFB, marked as AN1), or anaerobically by stabilized waste layers (AN2) or without pretreatment (FL). After pretreated respectively by these technologies, the effluent was recycled to landfill column, and tested for landfill performance. A column without leachate recirculation was established as contrast (marked as CR).

To experimentally determine the effects of landfill leachate irrigation on antioxidant system and physiological indexes related to stress, four grasses were selected, i.e. improved bermudagrass Dol sol (*Cynodon dactylon* cv. Dol sol), common hulled bermudagrass (*Cynodon dactyln* (L.) Pers), vetiver grass (*Vetiveria zizanioides* Nash) and bahia grass (*Paspalum notatum* Flugge). Four levels of leachate volume concentration were evaluated, i.e. 0, 15%, 35%, 70% and 100%. To determine the threshold of hydraulic loading for raw leachate irrigation on improved bermudagrass Dol sol (*Cynodon dactylon* cv. Dol sol), six levels of leachate hydraulic loading were set respectively at 2.77, 4.62, 6.46, 8.31, 10.15 and 12 mm/d.

Results and Discussion

Leachate recirculation in landfill layers

As shown in Fig.1, the COD concentration of CR maintained at 80 g/L for more than 50 weeks. Landfill columns with leachate pretreatment and recirculation had their highest COD of 60 g/L in 6th ~7th week. AN2 maintained this COD concentration until 20th week, while A1 and AN1's COD declined from 7th week on. The pH of CR was lower than 6 along the whole 50 weeks, while A1, AN1 and AN2 had their pH gradually climbed up to above 7.5 respectively from 10th, 17th and 26th week on. The generation of landfill gas (LFG) in CR stopped from 1st week on, while landfill columns with leachate pretreatment and recirculation could recover

their LFG generation respectively from 2nd, 13th and 16th week on. Furthermore, the LFG generation followed the descending sequence of AN2 > AN1 > A1. After 500 days of landfilling, the ratios of cellulose to lignin in the landfilled waste of CR, A1, AN1 and AN2 were about 1.69, 0.1, 0.23 and 0.39 respectively. Lower ratio of cellulose to lignin indicated that the landfilled waste was more stabilized in A1, AN1 and AN2.

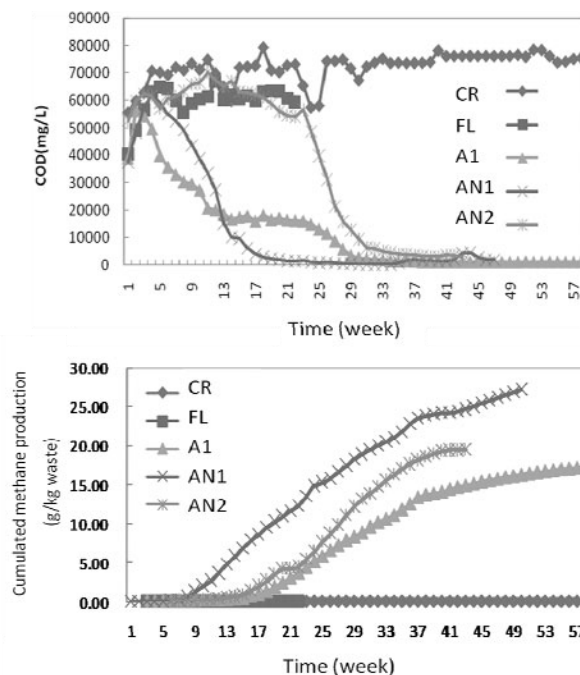


Fig. 1 Leachate COD and cumulated methane production under different strategies of leachate recirculation

In sum, external degradation of excessive volatile fatty acids (VFAs) in fresh leachate could facilitate the development of landfill layer environment favorable for methanogen. Therefore, under the scenario of landfilling waste rich in putrescibles, leachate pretreatment was required before leachate recirculation. Moreover, anaerobic pretreatment with UFB or stabilized waste could play a role of inoculation to landfill layers, stimulate the ecological shift of microorganisms, and have the benefit of biogas recovery, so that anaerobic pretreatment was more preferable than aerobic one. It was found that all biodegradable dissolved organic carbon (DOC) could be degraded in the form of LFG, COD in recycled leachate was less than 1500 mg l⁻¹, and the BOD₅/COD in recycled leachate was less than 0.1, after one year's operation with anaerobic pretreatment by stabilized waste.

Leachate treatment by plant-soil irrigation

All the grasses could survive with the irrigation loading of 12 mm/d for one growth season, except that bahia grass withered away at high volume concentration

of leachate. Most quantity of aboveground biomass was obtained when irrigated with 15% volume concentration. Once the concentration surpassed 15% and increased gradually, the vegetation biomass decreased, negatively related to volume concentration. The decreasing rate of biomass indicated that the resistant ability to leachate was: bermudagrass > vetiver grass > common bermudagrass > bahia grass. As shown in Fig.2, leachate of high volume concentration resulted in the imbalance between the production and consumption of activated oxygen, accelerated the process of lipid peroxidation and imposed on the grasses detrimentally. Leachate volume reduction of 61.3% – 91.2% and COD removal of 66.4% – 94.0% were obtained respectively by irrigating leachate into grass cover, while only 52.5% – 57.6% and 64.3% – 66.1% into bare cover (i.e. without vegetation). Under low volume concentration of leachate irrigation, the volume and COD reduction efficiency of bermudagrass were better than those of vetiver grass, while vetiver grass better than bermudagrass under high volume concentration of leachate irrigation. The high efficiency of leachate volume reduction and COD removal suggested that leachate treatment through irrigation on landfill vegetation was feasible. Besides, bermudagrass and vetiver grass were the plants suitable for vegetation.

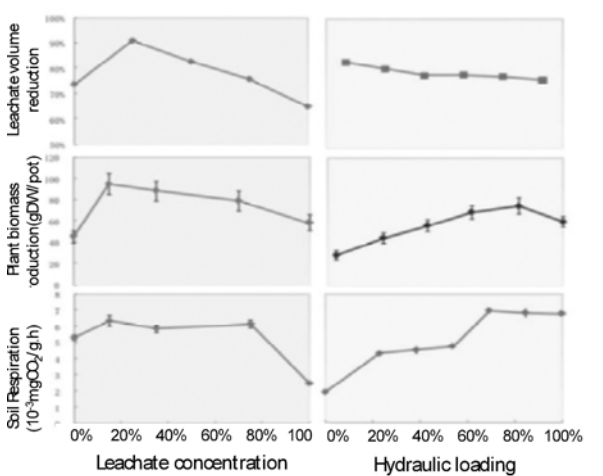


Fig. 2 Effects of the concentration and hydraulic loading of the irrigated leachate on plant and soil

Leachate irrigation led to high chlorophyll content, low proline content, as well as low MDA and H₂O₂ content of plant biomass. Soil enzyme activities, respirations, microbial biomass and ratio of biomass carbon to organic carbon (Cmic/Corg) were rather higher. Leachate irrigation with hydraulic loading of 6.46 – 10.15 mm/d led to declined proline, increased chlorophyll content, low POD activity and low content of MDA and H₂O₂. Soil bio-activity related parameters, such as soil enzyme activities, respirations, microbial biomass and

Cmic/Corg were all enhanced at 6.46 – 10.15 mm/d of hydraulic loading. However, when hydraulic loading increased to 12 mm/d or declined to 2.77 – 4.62 mm/d, the stress of irrigation on bermudagrass was aggravated, and soil bio-activity declined. The results revealed that leachate irrigation could alleviate the stress of environment on bermudagrass and improve the bio-activity of soil. The positive effect of leachate irrigation on the plant-soil system might be contributed to changes of soil water and physico-chemical property after leachate irrigated to the soil. It suggested that leachate irrigation could benefit plant-soil system, especially when controlled at suitable hydraulic loading (6.46 – 10.15 mm d⁻¹ in this work).

FULL-SCALE PRACTICE

Based on the lab-scale experiments, a field strategy was designed as presented in Fig. 3. First lift loaded with fresh waste was recycled with anaerobically pretreated leachate, so as to accelerate the methanogenesis and stabilization of landfilled waste. After operated for about half year when the landfilled waste approached partially stabilized, a second lift with fresh waste was established, and its leachate could be pretreated by the stabilized 1st lift, and then recycled back. Likewise, subsequent lifts could be set-up by utilizing precedent ones as external pretreatment units. Finally, the effluent from bioreactor landfill could be irrigated onto the final cover for ultimate disposal. By this procedure, a landfill could be ecologically self-sustained with pollutant accommodated in-situ.

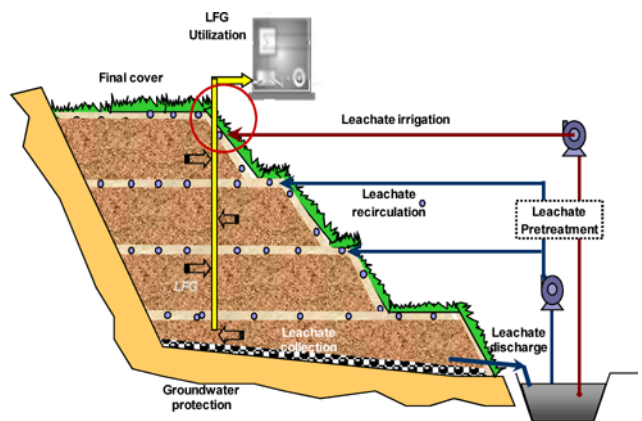


Fig. 3 Schematic diagram of field practice as ecologically based landfill

The above strategy was validated in field practice and monitored for more than 3 years. The field data confirmed that the COD of leachate declined and kept at 1060±240 mg l⁻¹ after operated for 17 months. From then

on, the BOD was kept at $120 \pm 50 \text{ mg l}^{-1}$, the BOD5/COD was about 0.11 ± 0.04 , the pH was 7.6 ± 0.3 , and the ammonia concentration was $1500 \pm 600 \text{ mg l}^{-1}$. The ratio of cellulose to lignin of landfilled waste kept declining, indicating the waste stabilization (Fig. 4). During field demonstration, $6 \sim 8 \text{ mm d}^{-1}$ of partially stabilized leachate was irrigated onto cover soils vegetated with common hulled bermudagrass (*Cynodon dactylo* (L.) Pers). Since the irrigation pipes were installed under 30 cm away from the surface, it was called as subsurface irrigation, so as to avoid aerosols from irrigated leachate. The reduction efficiency of leachate volume was highest around summer (from May to September), up to 54.7%~59.4% with the loading of 10 mm/d, followed by spring (March and April) and winter (January and February). The removal efficiency for leachate COD reached 96.5%. 91.3% of removed COD was contributed to soil interception. The organics of soil increased by 17.6%. The removal efficiency for leachate ammonia reached 97.1%. 19.9% of removed ammonia was transformed to nitrate, 15.6% was intercepted by soil. The ratio of ammonia volatilization was less than 2%. The nitrogen content of soil increased by 11.4%. The removal efficiency for leachate SS reached 95.3%.

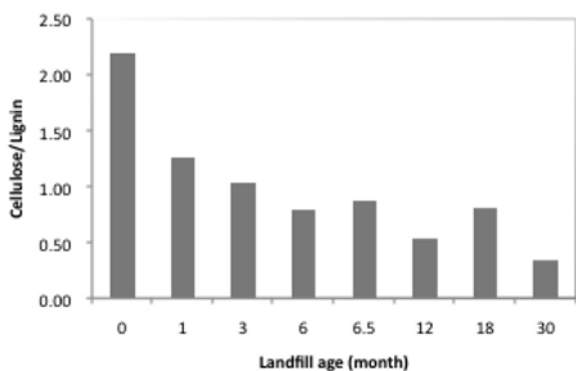


Fig. 4 Ratio of cellulose to lignin of landfilled waste

The field results implied that the strategy was effective for those landfills with more food waste. The strategy could also be applied in those old landfills or dumping sites that required restoration and recovery from methanogenesis. It also showed that it was feasible to irrigate the landfill final cover with partially stabilized leachate. By carefully selecting antioxidant plants and controlling proper leachate loading, landfill leachate

could meet the aims of leachate treatment and vegetation recovery simultaneously.

ACKNOWLEDGEMENTS

This work is partially supported by High-Tech Research and Development Program of China (2001AA644010, 2003AA644020, 2005AA644010-1); National Key Technology R&D Program (2006BAC06B05); National Natural Science Foundation of China (50538080, 50578115).

REFERENCE

- He PJ, Qu X, Shao LM, Li GJ, Lee DJ (2007). Leachate pretreatment for enhancing organic matter conversion in landfill bioreactor. *Journal of Hazardous Materials*, 142(1-2): 288-296.
- He PJ, Qu X, Shao LM, Lee DJ (2006a). Landfill leachate treatment in assisted landfill bioreactor. *Journal of Environmental Sciences-China*, 18(1):176-179.
- He PJ, Xue JF, Shao LM, Li GJ, Lee DJ (2006b). Dissolved organic matter (DOM) in recycled leachate of bioreactor landfill. *Water Research*, 40(7): 1465-1473.
- He PJ, Shao LM, Qu X, Li GJ, Lee DJ (2005). Effects of feed solutions on refuse hydrolysis and landfill leachate characteristics. *Chemosphere*, 59(6): 837-844.
- Lü F, Zhang H, Chang CH, Lee DJ, He PJ, Shao LM, Su A (2008). Dissolved organic matter and estrogenic potential of landfill leachate. *Chemosphere*, 72(9): 1381-1386.
- Onay TT & Pohland FG (1998). In-situ nitrogen management in controlled bioreactor landfill. *Water Research*, 32(5), 1383-1392.
- Pohland FG & Al-Yousfi B (1994). Design and operation of landfill for optimum stabilization and biogas production. *Water Science and Technology*, 30(12), 117-124.
- Reinhart DR, McCreanor PT, Townsend T (2002). The bioreactor landfill: its status and future. *Waste Management and Research*, 20(2): 172-186.

GASOLINE CONTAMINATED SITES: POLLUTANT TRANSPORT AND REMEDIATION

Li-Ming HU¹, Jay N. MEEGODA², Irene M. C. LO³, Yan LIU⁴, Sheng-Yan GAO⁵ and Zhao-Qun WU⁶

ABSTRACT: Gasoline type contaminants are a serious threat to soil and groundwater quality as well as health and welfare of general public. Most constituents of gasoline are volatile organic compounds. Soil vapor extraction and air sparging (SVE/AS) are the most efficient techniques to remediate soils and groundwater contaminated with volatile organic compounds. Hence in this state-of-the-art review paper the transport of gasoline-type contaminants in subsurface system and subsequent remediation process are introduced, discussed and summarized.

First the mechanism of contaminant transport in subsurface system is briefly introduced, and the mass transport equations, fluid flow equations, and the constitutive model of relative permeability - saturation - capillary pressure are discussed. Then the numerical method is introduced to simulate the process of multiphase flow and contaminate transport in porous media, and the tempo-spatial distribution of contaminants. Then the geotechnical centrifuge modeling, a convenient and efficient physical modeling technique is introduced.

Centrifuge model tests were conducted to study transport behavior of gasoline during contamination and remediation process, as well as air flow patterns during sparging process. The test results showed that gasoline infiltrated the vadose zone and moved downwards, forming a high concentration zone above the water table and then spreading out laterally. The water solubility and soil property influence gasoline transport behavior. The vapor pressure of contaminant seems to be an important factor affecting the efficiency of SVE. The zone of influence (ZOI) for air sparging is cone-shaped, and a stable ZOI can be maintained by the sparging pressure higher than a critical value. Based in the presentation it can be concluded that a combination of numerical simulation and centrifuge modeling can be used to understand the subsurface transport of LNAPLs and their remediation.

KEYWORDS: Subsurface contamination, remediation technology, centrifuge modeling, numerical simulation, soil vapor extraction, air sparging

INTRODUCTION

Gasoline type contaminants are posing serious threat to soil and groundwater quality as well as health and welfare of general public. Most constituents of gasoline are volatile organic compounds. Soil vapor extraction and air sparging (SVE/AS) are the most efficient techniques to remediate saturated soils and groundwater contaminated with volatile organic compounds. Hence in this state-of-the-art review paper the transport of gasoline-type contaminants in subsurface system and subsequent remediation process are introduced, discussed and summarized. Specifically this paper summarizes the research work on theoretical analysis, numerical modeling on contaminant transport behavior

and remediation and centrifugal modeling of the process to discuss the state-of-the-art.

STATE-OF-THE-ART OF NAPL TRANSPORT IN SUBSURFACE

NAPL Transport Behavior

Gasoline type contaminants are often regarded as LNAPLs (Light Non-Aqueous Phase Liquids). LNAPLs' transport in subsurface system is a complicated process (Philip et al. 1994, Reddi and Inyang 2001), as shown in Fig. 1. When LNAPLs are spilled they enter the unsaturated zone under gravity. Upon encountering a

¹ Associate Professor, Department of Hydraulic Engineering, State Key Laboratory of Hydro Science and Engineering, Tsinghua University, China. Email: gehu@tsinghua.edu.cn

² Professor, Department of Civil and Environmental Engineering, New Jersey Institute of Technology, Newark, NJ 07102, USA

³ Professor, Department of Civil Engineering, Hong Kong University of Science and Technology, HKSAR, China

⁴ MS student, State Key Laboratory of Hydro Science and Engineering, Tsinghua University, China

⁵ Research Assistant, Department of Civil and Environmental Eng., New Jersey Institute of Technology, Newark, NJ 07102, USA

⁶ Research Assistant, State Key Laboratory of Hydro Science and Engineering, Tsinghua University, China

capillary fringe, the LNAPL forms a pancake-like layer above the saturated zone. Groundwater flowing past the floating LNAPL dissolves soluble components, forming a dissolved plume down-gradient of the LNAPL zone.

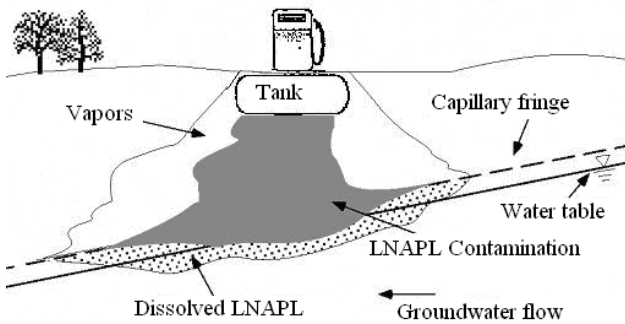


Fig. 1 LNAPLs release and Subsequent Migration

Multiphase Flow in Porous Media

Since free LNAPLs are independent liquid phase, the multiphase flow of air, water and LNAPL exists in subsurface system. Assuming that unsaturated flow of each phase follows Darcy’s law and Richards’ equation (Richards 1931), the velocity of each fluid phase can be written in terms of multiphase extension:

$$\mathbf{v} = -\frac{\mathbf{k}k_r}{\varepsilon S\mu} \cdot (\nabla P - \gamma \nabla z) \tag{1}$$

where \mathbf{v} is tensor of the mass average velocity, P is the fluid pressure, μ the dynamic viscosity of fluid phase, and γ the specific weight. The intrinsic permeability tensor \mathbf{k} is a function of medium fabric, and independent of fluid properties. k_r is the relative permeability, i.e. the ratio of the effective permeability of a fluid at a given saturation to the intrinsic permeability of the medium ($0 \leq k_r \leq 1$) which is a scaling factor.

The permeability of each fluid is one of the most important parameters that should be determined, which is related to fluid saturation and capillary pressure. The constitutive relationship between relative permeability, saturation and capillary pressure is the most important aspect governing the transport of LNAPLs in porous media.

Constitutive Relationship Between Relative Permeability—Saturation—Capillary Pressure

There exists substantial body of research describing the constitutive relationships of the three-phase flow in porous media. In water-LNAPL-air systems, it is often assumed that the fluid wettability governs the flow. Water is the most wetting phase, and it spreads as a film over the soil grains. LNAPLs have intermediate

wettability, and it spreads as a film over the water. Gas is the least wetting phase and it is surrounded by the total wetting phases, i.e. water and LNAPL. The three-phase k - S - P model can be idealized as two inter-related sub-models: saturation—capillary pressure, and relative permeability—saturation.

The S - P model describes the functional relationship between saturation and capillary pressure. Three-phase S - P model can be decomposed into two two-phase models. In water-LNAPL system, LNAPL is considered as a non-wetting phase, and in LNAPL-gas system, LNAPL is a wetting phase. Several S - P models were developed in past years in terms of unsaturated soil of water-air system (Brooks and Corey 1967, Stone 1973, Van Genuchten 1980, Fredlund, and Xing 1994), which are indicated by the soil-water characteristic curve. Moisture retention expressions in the unsaturated flow are extended to account for the presence of the LNAPL phase (Parker and Lenhard 1987, Lenhard and Parker 1988, Lenhard et al. 2004). By assuming that the pair capillary pressure in the three-fluid system is related to the interfacial tension and each fluid, the two phase S - P model can be extend to describe the three-phase system.

With respect to the LNAPL phase, since the trapping mechanisms are different for wetting and non-wetting phases, the magnitude of trapped LNAPL can be considered as a function of displacing phases. In water-LNAPL-air system, the residual saturation of LNAPL (S_{Nr}) can be defined as a linear function of water and gas saturations (Guarnaccia 1997):

$$S_{Nr} = S_w \left(\frac{S_{Nr}}{S_w + S_{Nr}} \right) + S_g \left(\frac{S_{Nr}}{S_g + S_{Nr}} \right) \tag{2}$$

where S_{Nr} indicates the LNAPL residual saturation as a non-wetting phase, and S_{Nwr} represents the LNAPL residual saturation as a wetting phase.

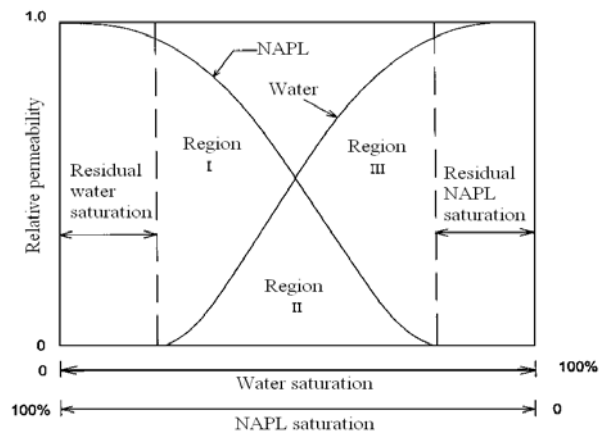


Fig. 2 Relative permeability of water and LNAPL as a function of saturation

The k - S model describes the functional relationship between relative permeability and saturation. Several k - S models were developed to describe the permeability for air-water-soil system of unsaturated soils (Gardner 1958, Kunze et al. 1968, Stone 1973, Mualem 1976, Fredlund 1994). Considering the two-phase system with water and LNAPL, the variation of the relative permeability with effective saturation should be that shown in Fig. 2. For the three-phase system, relative permeability of each fluid is usually presented in a ternary diagram, as show in Fig. 3 (Reddi and Inyang 2001).

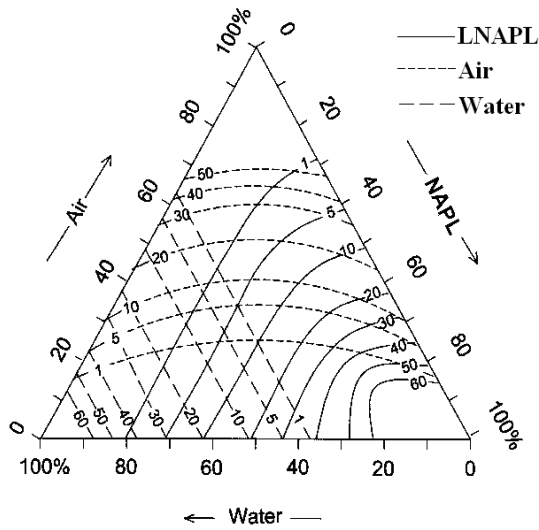


Fig. 3 Relative permeability for the three-phase flow in a ternary diagram

If we assume that the wetting and non-wetting phases become spatially segregated to the extent that their relative permeability functions become dependent only upon their respective saturations, the permeability for each fluid phase can be derived according to Van Genuchten S - P model (Van Genuchten 1980) and Mualem k - S model (Mualem 1976) as the following:

$$\begin{aligned}
 k_r(S_e) &= (S_e)^m \{1 - [1 - (S_e)^m]^2\} \\
 k_r(S_e) &= (S_e)^\psi \{1 - [1 - (S_e)^\psi]\} \\
 k_r(S_e, S_e) &= (S_e)^\zeta \{[1 - (1 - S_e)^\zeta] \\
 &\quad - [1 - (S_e)^\zeta]\}
 \end{aligned}
 \tag{3}$$

where m is the S - P model parameter for the water-air system, and ζ , ψ and ξ are fitting parameters. The subscript e indicates the effective saturation.

However, the functional relationships of the relative permeability (k_r) of fluids (air, NAPLs, and water), saturation (S), and pressure (P) are nonlinear and their direct experimental determination is very difficult. As

indicated above, the relative permeability of each fluid in three-fluid flow system is commonly derived from the two-fluid problem based on simplified assumptions, therefore it is needed to obtain physical modeling results to complement and verify the numerical simulation of the multiphase flow.

Mass Conservation in Subsurface System

The mass balance law for each fluid constituent can be expressed as the following equation (Hu 2007):

$$\frac{\partial(\varepsilon S \rho)}{\partial t} + \nabla \cdot (\varepsilon S \rho \mathbf{v}) = \rho Q
 \tag{4}$$

where ε is the porosity of the porous medium; S the fluid saturation; ρ is the fluid density, ρQ represents the point source or sink.

There are four different forms of LNAPL in subsurface system, free phase, LNAPL in gas phase due to volatilization, LNAPL in water phase due to dissolution, and LNAPL adsorbed in solid phase. There is mass transfer during the contamination and remediation process. The main processes of mass transfer pertinent to LNAPL are dissolution, volatilization and sorption.

The dissolved and volatized phases can transport together with the movement of pore-air and groundwater. The mass conservation for LNAPL can be expressed by the advection-dispersion equation,

$$\frac{\partial(\varepsilon SC)}{\partial t} = \nabla \cdot (\varepsilon S \mathbf{D} \nabla C) - \nabla \cdot (\mathbf{v} C) + \frac{\partial q}{\partial t}
 \tag{5}$$

where \mathbf{D} the second-order tensor of dispersion coefficient for LNAPL in the air or water phase; C is the LNAPL concentration.

Physical Modeling of LNAPL Transport

The soil column test is often used to simulation NAPL transport behavior (Pantazidou and Sitar 1993, Wu et al. 2002). However, it gives limited information due to its inability to represent the prototype stresses.

Geotechnical centrifuge modeling can be used to represent full-scale prototypes under normal field conditions and simulate the movement and remediation of contaminants. A $1/N$ scale model tested at N times centrifugal acceleration of the gravity experiences stress conditions identical to those in the prototype. Fluid flow occurs N^2 time faster in a centrifuge model. The use of a centrifuge can be a powerful physical modeling technique to study the long-term pollutant transport in soils (Culligan and Savvidou 1995).

One of the earliest uses of a centrifuge in geo-

environmental research was proposed by Arulanandan et al. (1988). They successfully modeled the pollutant transport process in saturated soils. Nimmo (1990) proved that unsaturated flow can be scaled in a centrifuge. Cooke and Mitchell (1991) verified that groundwater flow and moisture suction phenomena can be modeled by a centrifuge. Data obtained on the migration of a non-reactive contaminant have indicated that centrifuge modeling may provide a useful means to study contaminant transport in the unsaturated zone. Nakajima et al. (1998) found that mechanical dispersion can be modeled for low fluid velocity. Illangasekare et al. (1991) conducted model tests to investigate the 1-D movement of LNAPLs through unsaturated soils following a surface spill under a gravity of 20g. A reasonably sharp front was obtained between the advancing front and the displaced fluids. Mitchell and Stratton (1994) modeled an instantaneous 2000 L surface spill of light oil in dry medium sand and investigated the extent of the contamination. Hu et al. (2004) simulated soil venting extraction process for remediation of LNAPLs contaminated soils using centrifuge technique. These studies show that centrifuge modeling technique has the potential to study of the LNAPL transport in unsaturated soils.

Table 1 Scaling factors for pollutant transport problems

Parameter	Symbol	Dimension	Prototype	Model
Linear dimension	L	L	1	$1/N$
Volume	V	L^3	1	$1/N^3$
Mass	m	M	1	$1/N^3$
Density	ρ	ML^{-3}	1	1
Gravity	g	LT^{-2}	1	N
Pressure	P	MLT^{-2}	1	1
Surface tension		MLT^{-2}	1	1
Temperature	T	K	1	1
Flow velocity	v	LT^{-1}	1	N
Time	t	T	1	$1/N^2$
Viscosity	μ	$ML^{-1}T^{-1}$	1	1
Permeability	k	LT^{-1}	1	N
Intrinsic permeability	K	L^2	1	1
Concentration	C	ML^{-3}	1	1
Porosity	ϵ	1	1	1
Dispersion coefficient	D	L^2T^{-1}	1	1
Decay coefficient	κ	T^{-1}	1	1

The migration of LNAPLs in unsaturated soils is a complicated process. However, the centrifuge model is effective in simulating processes dominated by gravitation. The feasibility of using a centrifuge to model the transport of LNAPLs is yet to be validated. A good technique for checking scale effect is the "modeling of models" (Schofield 1980, Ko 1988). This technique is particularly useful when no prototype is available to

verify the model test results. With this technique, centrifuge models of different scales are tested at appropriate accelerations such that they can correspond to the same prototype. The models should predict the same behavior and thus provide a useful internal check on the modeling procedure. Some authors have reported similitude in centrifuge modeling tests of LNAPLs migration in unsaturated soils at relatively low gravitational levels. Chang et al. (1995) directly measured gasoline concentrations after a centrifuge test by collecting soil samples for gas chromatograph analysis. Gravelle et al. (1996) and Knight and Mitchell (1996) described the influence of two different constant rates of release on the penetration of the LNAPLs into an unsaturated granular medium. They modeled the release of 1000 L of silicon oil into unsaturated fine sand. A reproducible unsaturated moisture-suction profile was established and similar plumes at scale models of 15g and 30g were reported. Esposito et al. (1999) studied a 2-D spill of LNAPL from a transparent container that enabled direct visual observation of the oil infiltration. These tests took into account the influence of porosity on the migration of the LNAPL into the unsaturated sand and the spreading of the LNAPL at the saturated-unsaturated interface. The test results indicated good agreements of the unsaturated soil profile and the extent of contamination at both 20g and 30g. Culligan et al. (2002) reported the preferential flow of NAPLs in dry sands. Centrifuge modeling of NAPL transport behavior was reported by Kechavarzi (2000, 2002), Hu et al. (2002), Soga et al. (2003), Lo et al. (2003, 2004, 2005) by higher g-level tests, and the feasibility of the centrifuge modeling of LNAPL transport was verified by the modeling of models technique. Culligan and Soga (2006) gave the general introduction about the application of centrifuge modeling technique in NAPL transport problems.

STATE-OF-THE-ART IN RESEARCH OF IN SITU REMEDIATION TECHNOLOGY FOR VOCS

SVE/AS Remediation Technology

Soil/groundwater contamination is currently one of the major environmental problems in the world. Many remediation technologies have been developed to clean the contaminant in soils and groundwater. There are numerous cleanup technologies for gasoline-contaminated sites such as soil vapor extraction (SVE), air sparging, biosparging, landfarming, biopiles, bioventing, low-temperature thermal desorption, and natural attenuation (USEPA 1995). The SVE technology involves drawing or injecting air through the vadose soil region above the water table. It is an effective soil remediation method to

remove VOC mainly existing in LNAPLs. The remediation takes place by desorption and vaporization of VOCs in unsaturated soils and by carrying them in the gas-phase out of the contaminated soils. Air sparging is an *in-situ* soil/groundwater remediation technology, which involves the injection of air/gas under pressure into a well installed into the saturated zone. Air sparging technology extends the applicability of soil vapor extraction to saturated soils and groundwater through physical removal of volatilized groundwater contaminants and enhanced biodegradation in saturated and unsaturated zones. Air/oxygen injected below the water table volatilizes contaminants that are dissolved in groundwater, existing as a separate aqueous phase, and/or sorbed onto saturated soil particles. The volatilized contaminants migrate upward into the vadose zone, where they are removed, and generally using soil vapor extraction techniques. In addition to this air stripping process, air sparging also promotes biodegradation by increasing oxygen concentrations in the subsurface, stimulating aerobic biodegradation in the saturated and unsaturated zones. Air sparging systems must be designed with adequate air flow rates and pressures for the effective removal of contaminants from the site.

Theoretical Analysis for SVE/AS Remediation Technique

Air sparging is an emerging soil remediation method to decontaminate saturated granular soils and groundwater with volatile organic compounds (VOCs). The efficiency of in situ sparging system is controlled by the extent of contact between injected air and contaminated soil and pore fluid. Characterizing the mechanisms governing movement of air through saturated porous media is therefore critical to the design of an effective cleanup treatment (Kaleris and Croise 1999, Yang et al. 1999, El-Beshry et al. 2001).

A literature review of existing conceptual models, mathematical models of air sparging and microscopic research on porous medium was performed. It suggested that the air can not be simply treated as continuous phase flowing through the soil during air sparging. Investigation of the applicability of the capillary model shows that air bubbles flowing through the saturated soil during air sparging exhibit quite different characteristics from their motion in capillary tube. The factors accounting for this includes irregularities in channel geometry, non smooth surface of the interface between air and water film, and motion of fine particle during air sparging. Periodically constricted capillary tube or sinusoidally constricted capillary tube is recommended as prototype of pore-scale models for air sparging. The two phase flow theory was introduced to study the air

flow pattern and flow pattern transition during the air sparging. It was concluded that the flow pattern during air sparging is not only determined by the particle size, but also largely affected by the air injection pressure or air injection rate. The reported flow patterns of bubble flow and channel flow during air sparging are questionable. Bubble flow should be slug flow while the channel flow may be slug flow or churn flow. But further research is still needed to confirm this issue. The size and shape of the ZOI (zone of influence) can also be explained using microscopic perspective and network model is suggested for determining the size of ZOI. In a separate manuscript authors are presenting the basis for further microscopic research on air distribution, air saturation, flow patterns and air flow rate during the air sparging which are significant contributors to effective air sparging.

The determination of the size and shape of the ZOI is one of the critical steps in design of air sparging system (Reddy and Adams 2008). Reddy and Adams (2008) summarized the reported shapes and sizes of ZOI and categorized them into two types- parabolic shape (Adams 1999, Ji et al. 1993, McCray and Falta 1997) and conical shape (Lundegrad and Andersen 1996). As to the size of ZOI, the typical values of ZOI in 2-D experiments range from 15° for fine gravel ($D_{10}=2.5\text{mm}$) to 56° for well-graded sand ($D_{10}=0.2\text{mm}$) (Reddy and Adams 2008). Please note that our centrifugal test results confirm this conclusion. This is also conformed by the results reported in Nyer and Suthersan (1993), which is 15° for fine gravel and 60° for fine sand. The influence of heterogeneity on the ZOI has also been studied by many researchers (Reddy and Adams, 2001, Ji et al. 1993, and Lundegrad and Andersen (1996). Based on the research conducted by Reddy and Adams (2001), if the injected air entered the low-permeability strata from high permeability strata, the resulting zone of influence within the new strata resembled the zone of influence observed in a test using the particular soil in a homogeneous profile of the particular soil. But if the permeability ratio greater than 10:1 between adjoining soil strata, the migration of air will be prevented from moving into the lower-permeability media from the higher-permeability media.

Based on the experiments results mentioned above, it can be concluded that the size of ZOI is a function of size of soil and air injection pressure or air injection rate. With larger particle size of soil (e.g. gravels), the size of ZOI is smaller than that in the small particle size of soil (e.g. silty sand). Increase the air injection pressure, the size of ZOI will be enlarged. However, as to a certain particle size of soil, there is a limited size of ZOI independent on the air injection pressure.

To determine the ZOI by microscopic research, the network model which consists of pore bodies (nodes)

connected by a set of bonds (small tubes or throats) can be used. The simple network model consists of tubes with randomly chosen cross sectional areas connected to pores of fixed size and utilizes a two-dimensional diamond lattice structure with a unit length. Bubbles with initial velocity (the direction is determined by the orifice) migrate in the soil driven by buoyancy. The other external forces acting on a bubble rising in saturated porous medium includes drag force and clogging pressure at the throat, 'added mass' (Loubiere and Hebrard 2003, Wallis 1969). For low velocity of bubble, the drag force acting on a bubble rising in a porous medium can be expressed by the modified Ergun equation (Ergun 1952), in which the viscous energy losses are expressed by the Kozeny equation for laminar flow, proportional to the first power of the velocity. The clogging pressure is the pressure needed to move a bubble through a contraction of minimum diameter d , filled with a liquid of surface tension σ . The clogging pressure can be calculated at throat as shown in figure 4 based on Young-Laplace equation. The 'added mass' is accounted for the acceleration of bubbles relative to the surrounding fluid in the saturated soil.

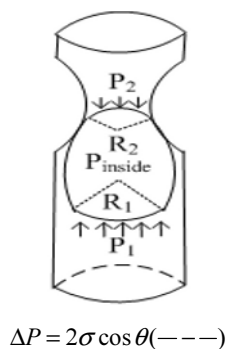


Fig. 4 Clogging pressure at throat in the soil

The ZOI can be determined by calculating the trajectory of a single bubble in the soil. At $t=0$, the bubble moves at the initial horizontal velocity (usually with horizontal direction). Later the horizontal air bubble flow rate decreases greatly due to drag force and resistant force at the throat while the vertical velocity of bubble increases by the driving force of buoyancy. The process continues until the horizontal velocity becomes close to zero. As a result, the trajectory of the bubble motion is like parabola. In the gravel or coarse sand, the driving force is greater than that in the fine sand, and then the direction of the bubble is changed fast. As a result, the ZOI in gravel or coarse sand is smaller compared with that in fine sand. It can be assumed that in extreme case the bubble is injected into tank full of water, then, the bubble moves almost vertically. As the injection rate is increased, the ZOI will be enlarged. However, when the initial injection rate is increased, the

drag force also increases correspondingly. As a result, the ZOI can not be enlarged infinitely. Based on physical equilibrium equation, there should be a limiting size for injection rate as shown in the experiment presented in Semer et al. (1998).

Physical Modeling For SVE/AS Remediation

The success of air sparging as a remedial technology for treatment of contaminated aquifers is well documented. However, there is no consensus, to date, on the mechanisms that control the flow of injected air through the saturated ground and the subsequent removal of contaminants. Therefore, it is difficult to develop design guide for site implementation. Currently, only qualitative results from laboratory experiments are available to predict the zone of influence of a sparging well.

Laboratory testing was conducted to investigate the efficiency of SVE and its influencing factors (Fischer et al. 1996, Widdowson et al. 1997, Harper et al. 1998, Reddy et al. 2000, Reddy and Adams 2000, Kirtland et al. 2001, Waduge et al. 2002, Yoon 2002, Adams and Reddy 2003). Hu et al. (2008) simulate the air flow in fine sands under different sparging pressure. However, the experiments were conducted under 1g and the in-situ stress condition could not be simulated.

In spite of the success of air sparging as a technique for the cleanup of contaminated soils, there is not, at present, a clear understanding of the manner in which the injected air pathways develop through saturated porous media. Design of air sparging facilities are based on results from pilot studies, and on generalized observations from a number of flow visualization studies currently available in the literature. Due to the empirical nature of these observations, they are not always transferable from one site to another.

NUMERICAL SIMULATION OF LNAPL TRANSPORT AND REMEDIATION

Numerical Simulation of LNAPL Transport Behavior

The software employing finite element method (FEM) was developed to simulate the transport and fate of LNAPLs in soils and groundwater during contamination and remediation (Pinder 1985). Hu et al. (2006) simulated the air-LNAPL-water multi-phase flow in subsurface system, and the transport behavior of LNAPL including its migration patterns, tempo-spatial distribution in soils and groundwater, and extent of contamination under different boundary conditions were investigated.

The calculation model used for LNAPL transport in subsurface system is shown in Fig. 5. Fine sand mass was used as an unsaturated zone, and the aquifer was

modeled as coarse sands. Their physical properties are listed in Table 2. Ethyl-benzene was adopted as LNAPL, and its physical properties are listed in Table 3.

Initially the soil was saturated by water. At the beginning of the numerical modeling, the soil was drained until reaching a stable moisture profile. Then, LNAPL was injected into the unsaturated soil mass, which then migrated into the unsaturated zone. The injection rate was $0.0375\text{cm}^3/\text{s}$, and the injection lasted for 3.9 months. The total injection of LNAPL was 0.38 m^3 . LNAPL continue to migrate in the subsurface system when the LNAPL supply stopped after LNAPL was depleted.

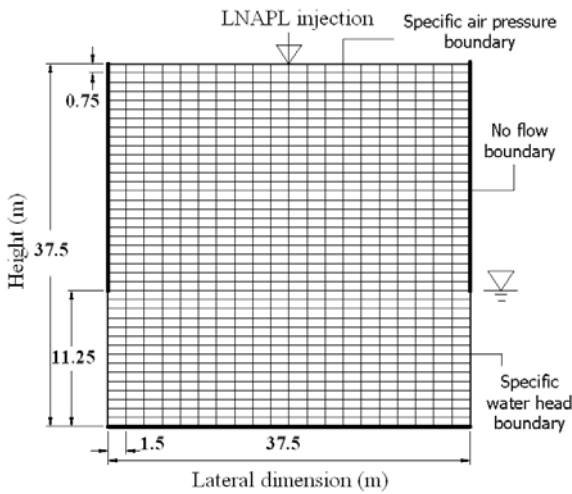


Fig. 5 Calculation model: LNAPL transport in subsurface system

Two types of boundary conditions were adopted: the groundwater table was stationary in one case, and groundwater flowing from right to left at the velocity of $2.0 \times 10^{-3}\text{ m/s}$ was the other.

Table 2 Physical properties of soil

Soil Type	Porosity	Dry density	Intrinsic permeability
Fine sand	0.42	$1.67\text{ (g/cm}^3\text{)}$	$1.46 \times 10^{-11}\text{ (m}^2\text{)}$

Table 3 Physical properties of air, LNAPL and water

Fluid phase	Density (g/cm^3)	Dynamic viscosity ($\text{Pa}\cdot\text{S}$)	Surface tension (g/cm)
Air	0.001196	0.0001785	/
LNAPL (Ethyl-benzene)	0.8670	0.0056	0.0449 (LNAPL-Water)
Water	1.0	0.01009	0.0742

Fig. 6 shows distribution of LNAPL after its migration in the subsurface system after 1, 2, 3 and 5 years. The groundwater was stationary, and the groundwater table was located on the top of aquifer. Fig. 7 shows the LNAPL distribution in groundwater at different times. Numerical results show that LNAPL moves downwards first and is retained to form a high concentration zone on top of the capillary fringe. The long-term migration behavior was also predicated using numerical modeling, demonstrating that LNAPL accumulates and spreads laterally along the capillary fringe.

Fig. 8 and Fig. 9 show the calculated results for spatial distribution of LNAPL after 1, 2, 3 and 5 years of migration in unsaturated soils and groundwater system. Groundwater flowed from right to left with a velocity of $2.0 \times 10^{-3}\text{ m/s}$.

It was shown that groundwater flow has little influence on transport behavior before LNAPL reaches groundwater table. However, after LNAPL reaches the groundwater table and starts migration into groundwater, the transport pattern in groundwater system is affected by groundwater flow, which also has impact on LNAPL distribution in unsaturated soils due to movement of the free phase with groundwater flow.

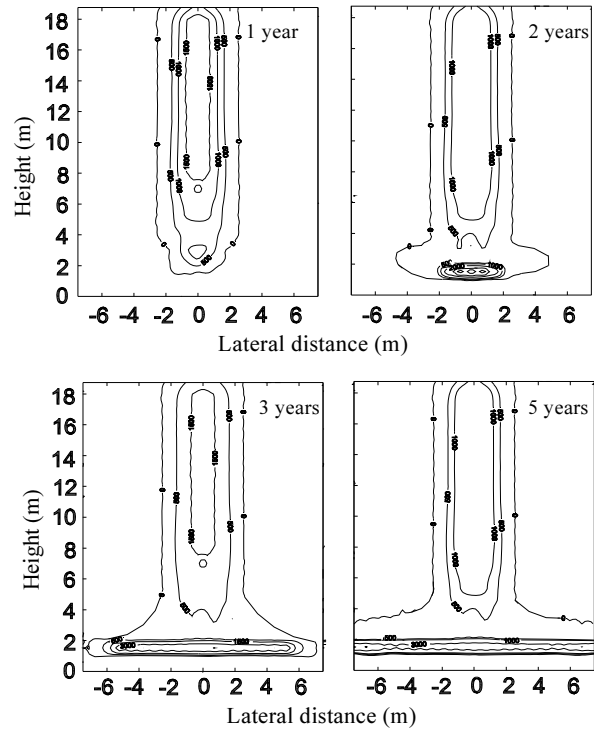


Fig. 6 Numerical results of tempo-spatial concentration of LNAPL in unsaturated soil (Unit: ppm)

Although numerical methods have many advantages in modeling long-term process and simulating various boundary/initial conditions, it requires verification using laboratory testing or field investigation. Conventional laboratory column tests, though relatively uncomplicated

to perform, are often found to be inadequate in simulating site conditions and the long-term transport of LNAPLs in the unsaturated zone and groundwater.

Therefore, centrifugal modeling is a powerful physical modeling technique for geo-environmental engineering problems such as transport and remediation of LNAPLs. The following section describes centrifugal tests which were performed to verify the results obtained from numerical simulation.

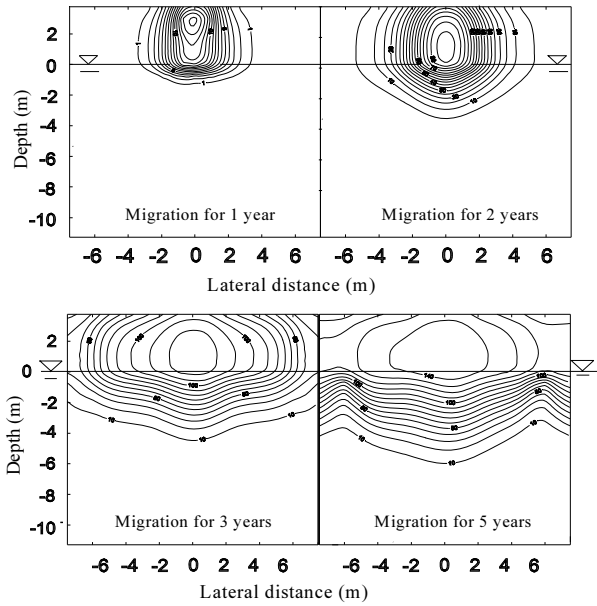


Fig. 7 Numerical results of tempo-spatial concentration of LNAPL in groundwater (Unit: ppm).

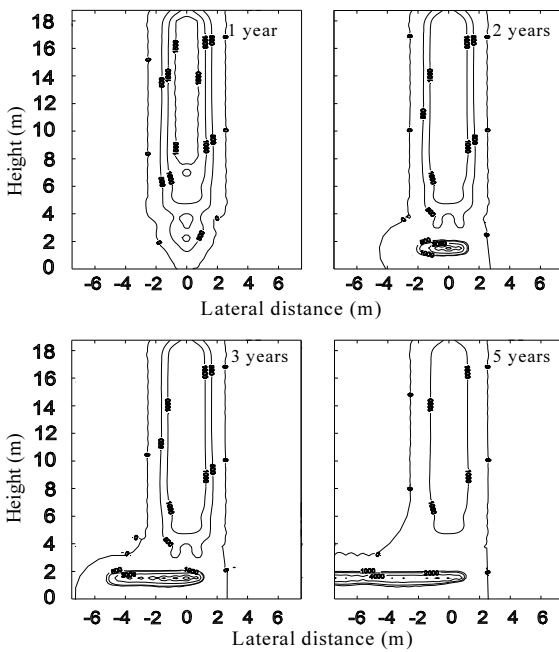


Fig. 8 Numerical results of tempo-spatial concentration of LNAPL in unsaturated soils (Groundwater flow) (Unit: ppm)

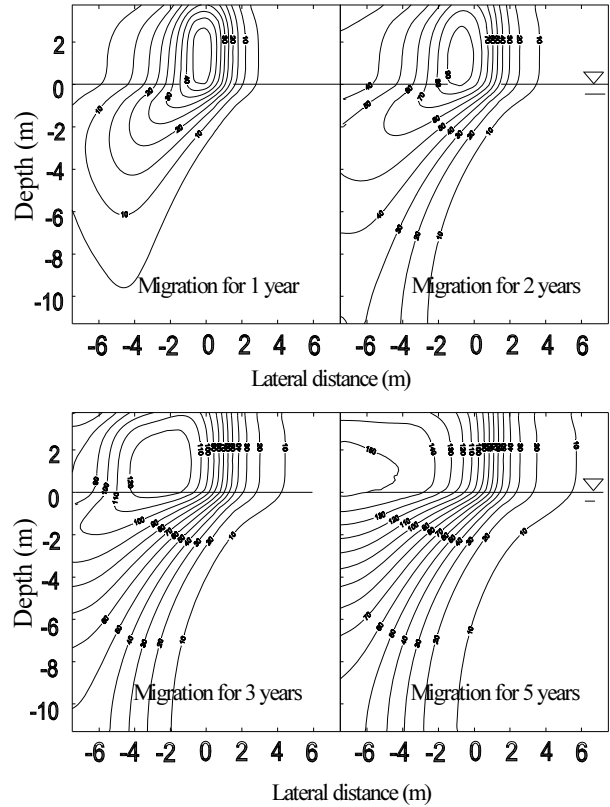


Fig. 9 Numerical results of tempo-spatial concentration of LNAPL in groundwater (Groundwater flow) (Unit: ppm)

CENTRIFUGE MODELING

Geotechnical centrifuges can be used to perform model tests that represent full-scale prototypes under field conditions. The use of a centrifuge can be a powerful physical modeling technique to study the long-term pollutant transport in soils.

Centrifugal Testing Procedure

The centrifugal tests were conducted to simulate LNAPL transport in unsaturated fine sands at a 75 g level in the Geotechnical Centrifuge Laboratory at Tsinghua University, which has an effective radius of 2m and payload of 50g-tons with a maximum acceleration of 250 g.

Ethyl-benzene was adopted as LNAPL in the centrifugal test. Fine sand (British Standard Fraction E), which was uniform quartz sands with a mean diameter D_{50} of 0.12 mm was used in preparation of the unsaturated soil samples to compare with numerical model results. The physical property of fine sand is listed in Table 2. Coarse sands with a mean diameter D_{50} of 0.40 mm were used as the aquifer material.

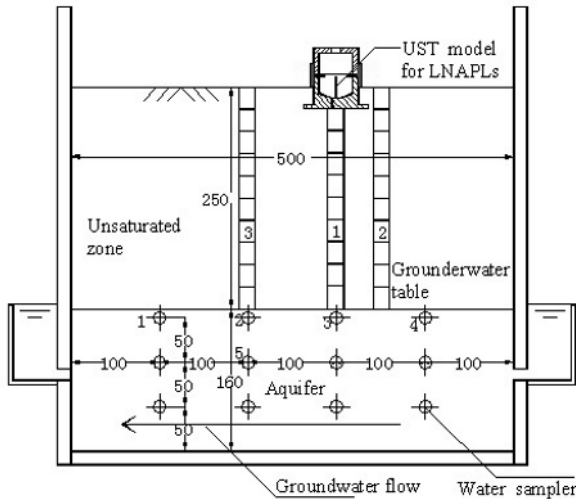


Fig. 10 Schematic of strongbox designed for centrifugal tests (Unit: mm)

The centrifugal tests were designed to match the numerical model as well as initial and boundary conditions, where a strongbox was used as shown in Fig. 10. The strongbox was made of steel with a 50 mm thick plexiglas front. The groundwater could be maintained stationary or flowing at the velocity of 2.0×10^{-3} m/s. A two-chamber container was designed to automatically release LNAPLs when the centrifuge acceleration reached the desired g level from an underground storage tank filled with LNAPLs (Hu et al. 2002). The groundwater sampling system with twelve syringes was installed in the strongbox, which could collect water samples during centrifuge flight by use of a driving piston connected with syringes.

The centrifuge test was conducted with several steps. Firstly, the prepared saturated soil model was mounted in the centrifuge for pre-consolidation for 23 minutes (equivalent prototype time of three months). Under the centrifuge acceleration, the soil sample was further compacted and homogenized until a stable moisture profile was formed in the unsaturated zone. After that, the centrifuge was stopped and a fixed volume of LNAPLs was injected into the upper chamber of the UST. Then, the centrifuge was spun again to release the LNAPLs and facilitate its transport into the unsaturated soil. After LNAPL migrated in soils for 0.25, 1, 2, 5 years (prototype time) individually, the centrifuge was stopped and soil samples were collected to determine contaminant concentrations using gas-chromatography.

In the centrifuge tests of the soil remediation, compressed air was injected into the soil mass for 15 minutes (equivalent prototype time of two months) and 30 minutes (equivalent prototype time of four months) after the 92-minutes (equivalent prototype time of one-year) LNAPLs migration, to extract the LNAPLs from the contaminated soil. The schematic design of

strongbox for SVE system is shown in Fig. 11. The mixture of BTEX was adopted as LNAPLs. The soil mass was then sampled and the contaminant distribution was analyzed.

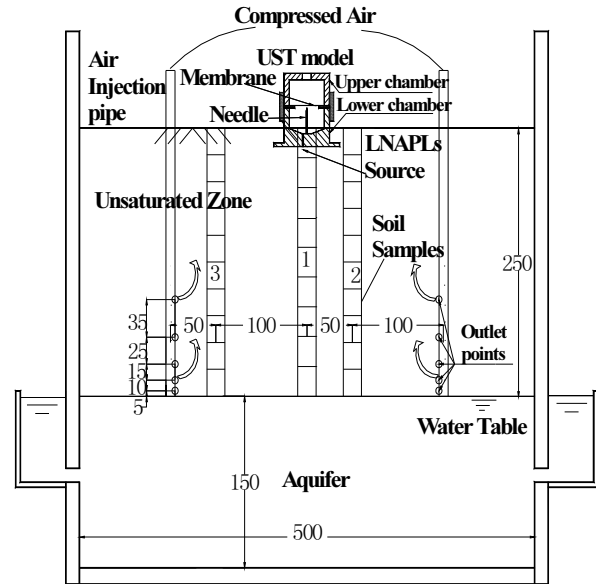


Fig. 11 Schematic Design of Strongbox (Unit: mm)

Centrifugal Test Results for Stationary Groundwater Table

The spatial distribution of LNAPLs after one year migration with stationary groundwater is shown in Fig. 12. The LNAPL concentration in water phase is shown in Fig. 13. LNAPLs moved downward and spread laterally 4m away from the leaking point. Majority of LNAPLs were retained in the capillary fringe and formed a high concentration zone on the top of the capillary fringe. Some dissolved LNAPL entered into the groundwater.

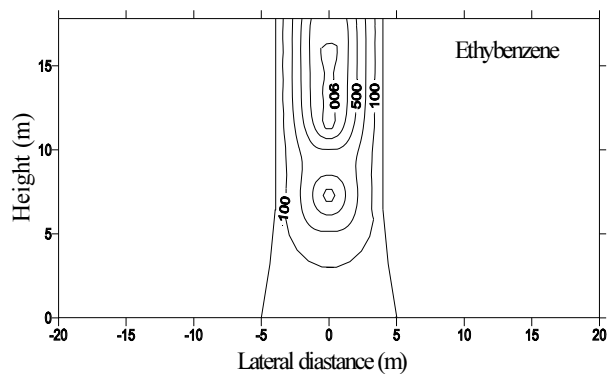


Fig. 12 Centrifugal test results: spatial distribution of LNAPL concentration in unsaturated soil after 1-year migration (Stationary groundwater table) (Unit: ppm)

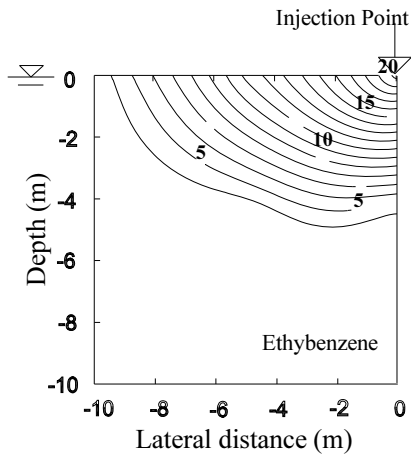


Fig. 13 Centrifugal test results: spatial distribution of LNAPL concentration in water phase after 1 year migration (Stationary groundwater table) (Unit: ppm)

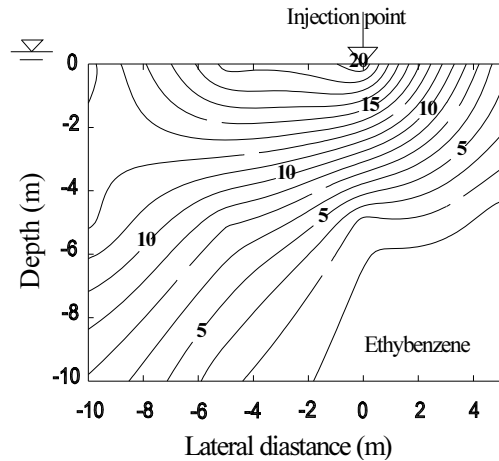


Fig. 15 Centrifugal test results: spatial distribution of LNAPL concentration in water phase after 1 year migration (Groundwater flow) (Unit: ppm)

Centrifugal Test Results for Flowing Groundwater

Fig. 14 and Fig. 15 show the spatial distribution of LNAPLs in the unsaturated zone and water phase after one year migration with groundwater flowing. Apparently, groundwater flow expedited the transport of LNAPL in subsurface system. Although the LNAPL spatial distribution in upper part of the unsaturated zone was little affected by the groundwater flow, the contamination pattern near the capillary fringe is quite different from that under the stationary groundwater condition. In groundwater system, the hydrodynamic dispersion due to water flow greatly accelerated migration of dissolved LNAPL, and the contaminated area is much larger. Similar findings were also obtained from the numerical model simulation.

It can be extrapolated from the above tests that LNAPLs will continue to move along the capillary fringe and more dissolved components will migrate into the groundwater.

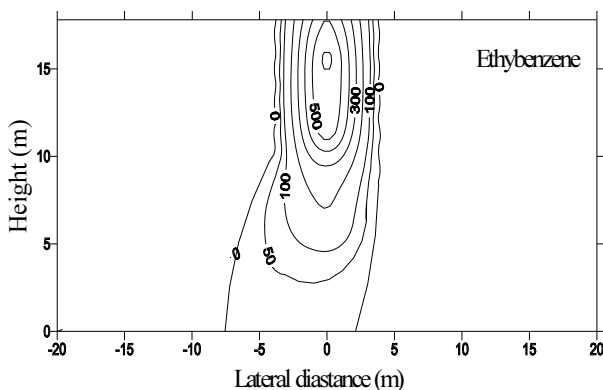


Fig. 14 Centrifugal test results: spatial distribution of LNAPL concentration in unsaturated soil after 1-year migration (Groundwater flow) (Unit: ppm)

The centrifugal modeling and numerical simulation produced similar transport behavior in subsurface system: LNAPL moved downwards, formed a high concentration zone on the top of the capillary fringe, and then spread laterally. The flow of groundwater accelerated the LNAPL migration, especially into groundwater. Because the volatilization of LNAPL is not adequately accounted in the numerical simulation, the extent of contamination in the unsaturated zone is much less than that obtained from centrifugal tests.

Centrifugal Test Results for SVE Process

During the first year of migration, as shown in Fig. 16, LNAPL concentrated along the vertical line of the leaking point and lateral spreading up to a radius of 4.0m around the line of the leaking point was detected.

For the SVE, the compressed air was injected into the soil mass, and air flow was intrigued from the injection pipe with higher pressure to the surface of the soil model where the air pressure is equal to the atmospheric pressure. The contaminants, specifically the BTEX from the contaminated soil were extracted from the air phase. The spatial distributions of the BTEX components before SVE and after SVE for 2 months and 4 months are presented in Fig. 17 and 18. It is quite clear that the high concentration zone moved upwards from 5 ~ 6 m above the water table before remediation to about 13 m above the water table after SVE remediation. This implies that most of contaminants moved upwards to the ground surface with the air flow in soil mass. The highest concentrations changed slightly, however the extent of contamination decreased significantly, and the severely contaminated soil mass near the water table was cleaned up by the SVE process.

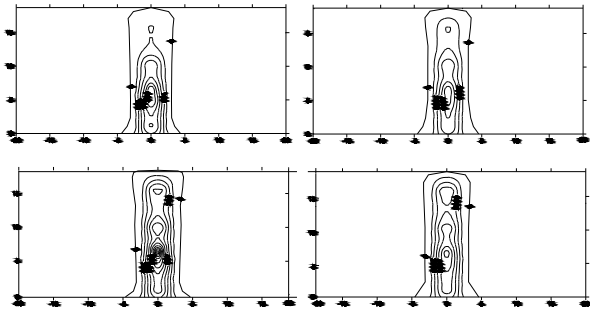


Fig. 16 BTEX Concentration after 1 Year Migration in Fine Sand (Concentration unit: ppm)

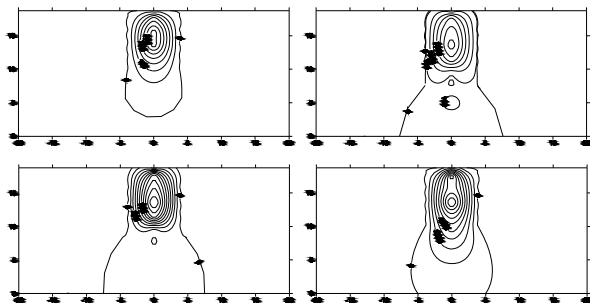


Fig.17 BTEX Concentration after SVE for 2 months (Concentration unit: ppm)

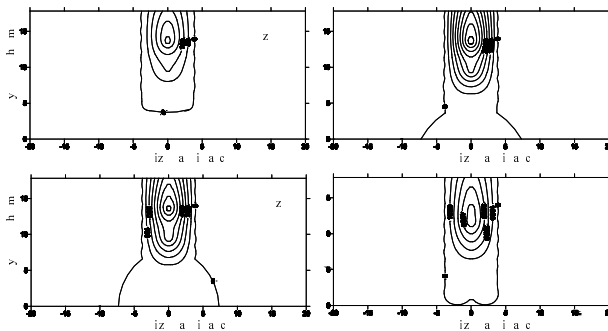


Fig. 18 BTEX Concentration after SVE for 4 months (Concentration unit: ppm)

The amount of BTEX retained in the soil mass was calculated to establish the loss of BTEX during the transport process and the effectiveness of SVE. Since the contaminant did not reach the boundary of the strongbox the pollutant transport in this centrifuge test was axisymmetric. Thus BTEX value can be calculated according to the concentration contours of the centrifuge test. The amount of BTEX can be estimated using the following equation:

$$\begin{aligned}
 M &= \int c(r, h) \cdot dm = \int c(r, h) \cdot \rho \cdot dv \\
 &= \int \int c(r, h) \cdot \rho \cdot 2\pi r \cdot dr \cdot dh
 \end{aligned}
 \tag{6}$$

where $c(r, h)$ is the contaminant concentration, which is a function of the radius r and the depth h of the plume; ρ_d is the dry density of the soil mass. The residual

amount of BTEX components in soil mass after SVE was roughly estimated in the same way for simplification of the calculation.

The residual amount of BTEX after SVE remediation for 2 and 4 months is also listed in Table 4. Approximately 47% of the BTEX mixture was removed from the contaminated site after 2 months of SVE. Only 13% of benzene was left in soil mass, while the residual percentages were 52%, 64%, and 58% for toluene, ethylbenzene, and o-xylene, respectively. This can be due to the fact that the vapor pressure of benzene is the highest among BTEX components, so benzene is much easier to be extracted into air phase. When SVE continued for 4 months, 68% of the total contaminant was removed. With additional clean air injected into the soil mass for flushing, more volatile organic contaminants can be removed. Moreover, the vapor pressure of contaminant components is found to play an important role on the effectiveness of SVE.

Table 4 Mass balance of BTEX in centrifuge tests

Contaminants	Migration for 1 year	SVE for 2 months	SVE for 4 months
Benzene	46%	13%	9%
Toluene	88%	53%	32%
Ethylbenzene	90%	64%	41%
O-xylene	100%	58%	36%
Total BTEX	88%	53%	32%

It appears that substantial amount of BTEX in soil phase and free phase were extracted into air phase and escaped from soil mass. These results apparently demonstrated that SVE is an effective soil remediation technology. However, the required air pressure, pipe spacing and location, and operation duration of the SVE technique to obtain the highest removal efficiency need further investigation.

Air Flow during AS Process

Based on the centrifuge tests employing glass beads as soil, the air sparging was simulated under a wide range of sparging pressures and centrifuge g levels. Four samples with different particle size distribution were prepared and tested under different g-levels of 15, 30, 40 and 50. The physical properties of glass beads used for centrifuge tests are shown in Table 5.

Table 5 Physical properties of glass beads used in tests

Sample No.	Particle Size (mm)	Dry density (g/cm ³)	Porosity (%)
1	0.8-1.0	1.617	35
2	1.5-2.0	1.684	33
3	4.0-5.0	1.676	33
4	0.8-5.0	1.953	22

The ZOI is cone-shaped for different samples under various g-levels. Fig. 19 shows the photos of stable ZOI in centrifuge tests at 15 g. It can be shown that for the uniform samples (Sample 1, 2, 3), the ZOI decrease with the increase of particle size.

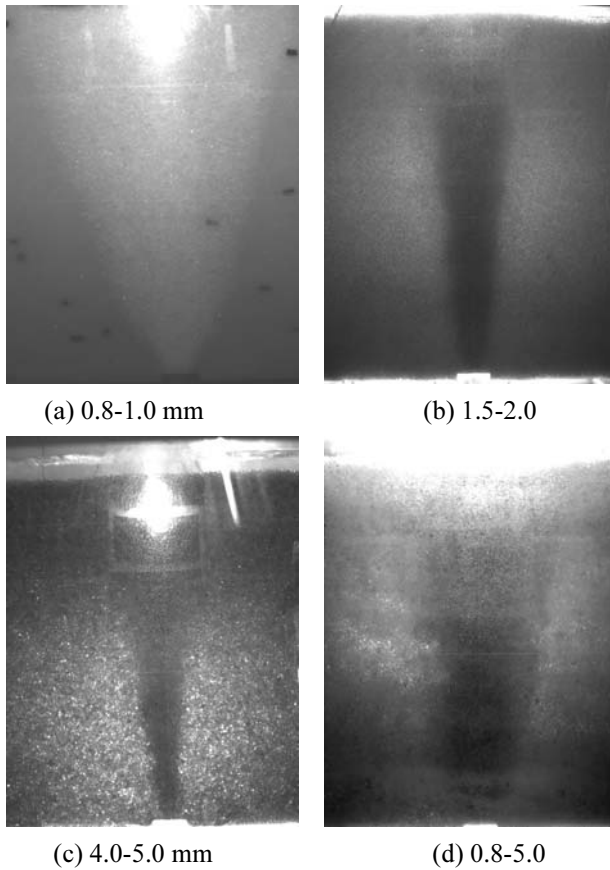


Fig. 19 Zone of influence in centrifuge tests at 15 g

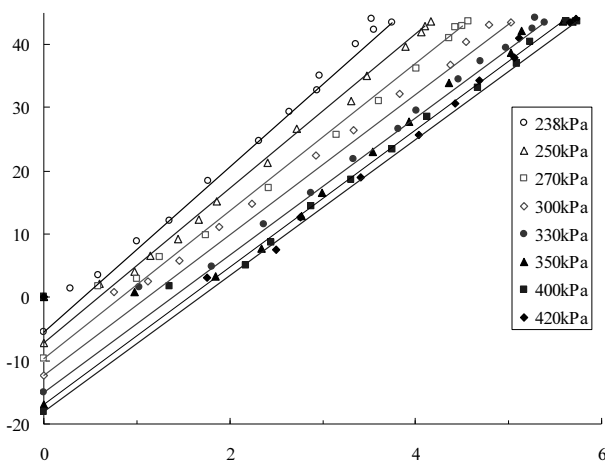


Fig. 20 Zone of influence for 1.5-2.0 mm sample under different air pressure in centrifuge tests at 50 g (Unit: cm)

Fig. 20 shows the boundary of ZOI under different air pressure for 1.5-2.0 mm sample under different air pressure in centrifuge tests at 50 g. The ZOI expanded with the increase of the inject air pressure at early stage.

While the sparging pressure is higher than the critical value, the ZOI decreased a little and then remained constant. The critical value of the air pressure is termed “critical sparging pressure”. Table 6 gives the value for critical sparging pressure for different samples at different g-level. It is show that the particle size has little influence on the critical sparging pressure. The g-level has substantial influence in critical sparging pressure, and the difference of critical sparging pressure and pore-water pressure increases with the increase of g-level.

Table 6 Critical sparging pressure from centrifuge tests

Sample No.	g level	Static water pressure (kPa) (1)	Critical AS pressure (kPa) (2)	(2)-(1) (kPa) (3)
1	15	64.8	100	35.2
	30	112.4	170	57.6
2	15	68.1	105.0	36.9
	30	134.2	180.0	45.8
	40	170.7	240.0	69.3
3	50	204.5	300.0	95.5
	15	72	110.0	38.0
	30	137.5	180.0	42.5
	40	178.3	230.0	51.7
4	50	211.6	290.0	78.4
	15	66.9	100.0	33.1
	30	129.8	180.0	50.2
	40	168.3	240.0	71.7
	50	203.3	300.0	96.7

Table 7 Virtual sparging point and cone angle from different tests

Sample No.	g-level	Virtual Sparging Point (cm)	Cone angel (°)
1	15	6.0	14.8
	30	5.4	7.4
2	15	27	5.7
	30	20	4.7
	40	23	4.4
3	50	18	5.3
	15	7.3	6.4
	30	6.2	6.8
	40	3.7	6.6
4	50	80	6.1
	15	24.6	9.9
	30	23.0	6.5
	40	25.0	6.5
	50	24.0	5.2

The stable ZOI can be described by use of the virtual sparging point and cone angle. Virtual sparging point means the intersection point of extension of ZOI boundary and axis of sparging well. The virtual sparging point and cone angle are shown in Table 7. The ZOI decreased with the increase of soil particle size and g level.

The above findings from centrifuge tests can provide useful references for design and application of air sparging for groundwater remediation.

CONCLUSIONS

Gasoline type contaminants are posing a serious threat to soil and groundwater quality as well as health and welfare of general public. Most constituents of the gasoline are volatile organic compounds. Soil vapor extraction and air sparging (SVE/AS) are most efficient techniques to remediate saturated soils and groundwater contaminated with volatile organic compounds. The state-of-the-art of transport behavior of gasoline-type contaminant in subsurface system and subsequent remediation are introduced, discussed and summarized in this paper.

The mechanism of contaminant transport in subsurface system is briefly introduced, and the mass transport equations, fluid flow equations, and the constitutive model of relative permeability - saturation - capillary pressure are discussed. Also, a theoretical analysis of bubble movement in soil and a methodology to compute the ZOI is presented.

The numerical simulation is a cost-effective method to investigate the complicated multi-physics issues. The numerical method was used to simulate the multiphase flow and contaminant transport in porous media, and the tempo-spatial distribution of contaminants was obtained.

Geotechnical centrifuge tests can reduce the sample dimensions and shorten the experimental duration. Also it is a convenient and efficient physical modeling technique. Centrifuge model tests were conducted to study transport behavior of gasoline during contamination and remediation process, as well as air flow patterns during sparging process.

The test results show that gasoline infiltrated the vadose zone and moved downwards, forming a high concentration zone above the water table and then spreading laterally. The water solubility and soil property influence gasoline transport behavior. The vapor pressure of contaminant seems to be an important factor affecting the efficiency of SVE. The zone of influence (ZOI) for air sparging was cone-shaped, and a stable ZOI can be maintained by the sparging pressure higher than a critical value. Hence a combination of numerical simulation and centrifuge modeling can be a useful means to study the subsurface transport of LNAPLs and their remediation.

ACKNOWLEDGEMENTS

The financial support from National Natural Science

Foundation of China (Project No. 50879038), Beijing Scientific Research Program (D07050601510000) and Program for New Century Excellent Talents in University (NCET-07-0480) from Chinese Ministry of Education are gratefully acknowledged.

REFERENCES

- Adams JA (1999). System effects on the remediation of contaminated saturated soils and groundwater using air sparging, University of Illinois at Chicago.
- Adams JA & Reddy KR (2003). Extent of Benzene Biodegradation in Saturated Soil Columns during Air Sparging. *Ground Water Monitoring and Remediation*, 23(3): 85-94.
- Arulanandan K, Thompson PY, Kutter BL, Meegoda NJ, Muraleetharan KK, Yogachandran C (1988). Centrifuge modeling of transport processes for pollutants in soils. *Journal of Geotechnical Engineering, ASCE*, 114(2): 185-205.
- Brooks RH & Corey AT (1967). Hydraulic properties of porous media. Colorado State University, Fort Collins, CO, *Hydrol. Pap.*, 3: 27-32.
- Chang IL & Ji Z (1995). Optimized analysis of gasoline (BTEX) in water and soil using GC/FID with purge and trap. Hewlett-Packard Company, Application note 228-324.
- Chang KG, Meegoda JN, Khera RP (1995). Centrifugal modeling of leaking underground storage tanks. *Transportation Research Record 1504, Pavement Design, Management and Performance; Soils, Geology and Foundations: 47-56.*
- Cooke B & Mitchell RJ (1991) Physical modeling of a dissolved contaminant in an unsaturated sand. *Canadian Geotechnical Journal*, 28: 829-833.
- Culligan PJ, Banno K, Barry DA, et al. (2002). Preferential flow of a nonaqueous phase liquid in dry sand. *Journal of Geotechnical and Geo-environmental Engineering, ASCE*, 128 (4): 327-337.
- Culligan P & Soga K (2006). Non-aqueous phase liquid behavior in the subsurface: transportation, source zone characterization and remediation In: *Physical Modelling in Geotechnics: the Sixth International Conference on Physical Modelling in Geotechnics - ICPMG'06* (ed. Ng, Zhang, and Wang), Hong Kong, China, 4-6 August 2006.
- Culligan-Hensley PJ & Savvidou C (1995). Environmental geotechnics and transport processes. In: *Geotechnical Centrifuge Technology* (ed. Taylor, R. N.), Blackie Academic & Professional, 196-263.
- El-Beshry MZ, Gierke JS, Bedient PB (2001). Practical modeling of SVE performance at a jet-fuel spill site. *J. Environ Eng., ASCE*, 127 (7): 630-638.
- Ergun S (1952). Fluid flow through packed columns,

- Chem. Eng. Prog., 48(2), 89-94.
- Espósito G, Allersma HGB, Selvadurai APS (1999). Centrifuge modeling of LNAPL transport in partially saturated sand. *Journal of Geotechnical and Geoenvironmental Engineering*, ASCE, 125(12): 1066-1071.
- Fischer U, Schulin R, Keller M, et al. (1996). Experimental and numerical investigation of soil vapor extraction. *Water Resour Res*, 32 (12): 3413-3427.
- Fredlund DG & Xing AQ (1994). Equations for soil-water characteristic curve. *Can. Geo. Journal*, 31(4): 521-532.
- Fredlund DG, Xing AQ, Huang SY (1994). Predicting the permeability function for unsaturated soils using the soil-water characteristic curve. *Can. Geo. J.*, 31: 533-546.
- Gardner WR (1958). Some steady-state solutions of the unsaturated moisture low equation with application to evaporation from a water table. *Soil Science*, 85: 228-232.
- Gravelle CF, Knight MA, Mitchell RJ (1996). Measurement of two-fluid saturations in a fine to medium sand. *Canadian Geotechnical Journal*, 33(6): 1014-1017.
- Guarnaccia J, Pinder G, Fishman M (1997). NAPL: Simulator Documentation, USEPA, EPA/600/R-97/102.
- Harper BM, Stiver WH, Zytner RG (1998). Influence of water content on SVE in a silt loam soil. *J. Environ Eng, ASCE*, 124 (11): 1047-1053.
- Hu L, Lo MC, Meegoda JN (2006). Numerical Analysis and Centrifuge Modeling on LNAPLs Transport in Subsurface System. *Progress in Natural Science*, 16(4): 416-424.
- Hu LM, Shu SZ, Lo IMC, et al. (2002). Centrifuge modeling of LNAPLs in porous media. In: *Inter. Conf. Physical Modeling in Geotechnics - ICPMG'02* (ed. Phillips, Guo and Popescu), Rotterdam: Balkema, 367-372.
- Hu LM & Liu Y (2008). Physical Modeling of Air-Sparging Technique for Groundwater Remediation. *Chinese Journal of Geotechnical Engineering*, 30(6): 835-839.
- Hu LM, Xing WW, Wu ZQ (2007). Numerical Modelling of NAPL Migration in Porous Media. *Rock and Soil Mechanics*, 28(5): 951-955.
- Illangasekare TH, Znidarcic M Al-Sheridda, Reible DD (1991). Multiphase flow in porous media. *Centrifuge 91*, Rotterdam: Balkema: 517-523.
- Ji W, Dahmani A, Ahlfeld D, Lin JD, Hill E (1993). Laboratory study of air sparging: air flow visualization, *Ground Water Monitoring Review*, Fall: 115-126.
- Kaleris V & Croise J (1999). Estimation of cleanup time in layered soils by vapor extraction. *Contam. Hydrol.*, 36 (1-2): 105-129.
- Kechavarzi C & Soga K (2002). Determination of water saturation using miniature resistivity probes during intermediate scale and centrifuge multiphase flow laboratory experiments. *Geotechnical Testing Journal*, 25(1): 95-103.
- Kechavarzi C, Soga K, Wiart P (2000). Multi-spectral image analysis method to determine dynamic fluid saturation distribution in to dimensional three-fluid phase flow laboratory experiments. *Journal of Contaminant Hydrology*, 46(3-4): 265-293.
- Kirtland BC, Aelion CM, Widdowson MA (2001). Long-term AS/SVE for petroleum removal in low-permeability Piedmont saprolite. *J. Environ Eng, ASCE*, 127 (2): 134-144.
- Knight MA, Mitchell RJ (1996). Modeling of Light non-aqueous phase liquid (LNAPL) releases into unsaturated sand. *Canadian Geotechnical Journal*, 33: 913-925.
- Kunze RJ, Uehara G, Graham K (1968). Factors important in the calculation of hydraulic conductivity. *Soil Science Society of America*, 32: 760-765.
- Lenhard RJ & Parker JC (1988). Experimental validation of the theory of extending two-phase saturation-pressure relations to three-fluid phase systems for monotonic drainage paths. *Water Resour. Res.*, 24(3): 373-380.
- Lenhard RJ, Oostrom M, Dane JH (2004). A constitutive model for air – NAPL – water flow in the vadose zone accounting for immobile, non-occluded (residual) NAPL in strongly water-wet porous media. *Journal of Contaminant Hydrology*, 71: 261-282.
- Lo IMC, Hu LM, Meegoda NJ (2004). Centrifuge modeling of LNAPL transport in unsaturated soils, *Journal of Geotechnical and Geoenvironmental Engineering*, ASCE, 130(5): 535-539.
- Lo IMC, Hu LM, Meegoda JN (2005). Feasibility study of using centrifuge for investigating LNAPL migration in unsaturated soils. *Soil & Sediment Contamination*, 14 (1): 85-103.
- Lo IMC & Hu LM (2004). Long-term Migration of LNAPL in Unsaturated Soils: Clayey Silt and Fine Sand. *Practice Periodical of Hazardous, Toxic and Radioactive Management*, ASCE, 8(4): 228-237.
- Loubiere K & G Hebrard (2003). Bubble formation from a flexible hole submerged in an inviscid liquid, *Chem. Eng. Sci.*, 58, 135-148, 2003.
- Lundgard PD & Andersen G (1996). Multiphase numerical simulation of air sparging performance, *Ground water*, 34(3), 451-460.
- McCray JE & Falta RW (1997). Numerical simulation of air sparging for remediation of NAPL contamination, *Ground Water*, 35(1): 99-100.
- Mitchell RJ (1998). The eleventh annual R. M. Hardy Keynote Address, (1997). *Centrifugation in geoenvironmental practice and education*. *Canadian Geotechnical Journal*, 35: 630-640.

- Mitchell RJ & Stratton BC (1994). LNAPL penetration into porous media. Centrifuge 94, Rotterdam: Balkema: 345-349.
- Mualem Y (1976). A new model for predicting the hydraulic conductivity of unsaturated porous media. *Water Resources Res.*, 12: 513-522.
- Nakajima H, Hirooka A, Takemura J, Marino MA (1998). Centrifuge modeling of one dimensional subsurface contamination. *Journal of the American Water Resources Association*, 34(6): 1415-1425.
- Nimmo JR (1990). Experimental testing of transient unsaturated flow theory at low water content in a centrifugal field. *Water Resources Research*, 26(9): 1951-1960.
- Nyer EK & Suthersan SS (1993). Air sparging: savior of ground water remediation or just blowing bubbles in the bathtub? *Ground Water Monitoring Review*, 13(4): 87-91.
- Pantazidou M & Sitar N (1993). Emplacement of Non-aqueous Liquids in the Vadoze Zone. *Water Resource Research*, 29(3): 705-722.
- Pantazidou M & Sitar N (1993). Emplacement of nonaqueous liquids in the vadose zone." *Water Resources Research*, 29: 705-722.
- Parker JC & Lenhard RJA model for hysteretic constitutive relations governing multiphase flow. *Water Resources Res.*, 1987, 23: 2187-2196.
- Philip BB, Hanadi SR, Charles JN (1994). Ground water contamination: transport and remediation. New Jersey: PTR Prentice Hall: 349-389.
- Pinder GF, and Abriola SC. (1986). On the simulation of non-aqueous phase organic compounds in the subsurface, *Water Resource Res.*, 22: 109-119.
- Reddi LN & Inyang HI (2001). *Geo-environmental Engineering: Principles and Applications*. Marcel Dekker, Inc.
- Reddy KR & Adams J (2008). Conceptual modeling of air sparging for groundwater remediation, Proceedings of the 9th international symposium on environmental geotechnology and global sustainable development, Hong Kong, China, June 2008.
- Reddy KR & Adams JA (2000). Effect of Groundwater Flow on Remediation of Dissolved-Phase VOC Contamination Using Air Sparging. *Journal of Hazardous Materials*, 72(2-3): 147-165.
- Reddy KR & Chinthamreddy S (2000). Comparison of Different Extractants for Removing Heavy Metals from Contaminated Clayey Soils. *Journal of Soil and Sediment Contamination*, 9(5): 449-462.
- Richards LA (1931). Capillary conduction of liquids through porous mediums. *Physics*, 1: 318-333.
- Semer R, Adams JA, Reddy KR (1998). An experimental investigation of air flow patterns in saturated soils during air sparging, *Geotechnical and Geological Engineering*, 16: 59-75.
- Soga K, Kawabata J, Kechavarzi C, et al. (2003). Centrifuge modeling of non-aqueous phase liquid movement and entrapment in unsaturated layered soils. *Journal of Geotechnical and Geo-environmental Engineering, ASCE*, 129(2): 173-182.
- Stone HL (1973). Estimation of three-phase relative permeability and residual oil data. *J. Canadian Pet. Tech.*, 12(4), 53-61.
- USEPA (1995). How to evaluate alternative cleanup technologies for underground storage tank sites: Chapter II Soil Vapor Extraction. EPA 510-95-007.
- Van Genuchten MT (1980). A closed-form equation for predicting the hydraulic conductivity of unsaturated soils. *Soil Sci. Soc. Amer. Journal.*, 44, 892-898.
- Waduge WAP, Soga K, Kawabata J (2002). Laboratory testing of air sparging/SVE system for remediation of NAPLs entrapped in heterogeneous soil. *Physical Modeling in Geotechnics - ICPMG'02*, Rotterdam: Balkema: 367-372.
- Wallis GB (1969). One-dimensional two-phase flow, pp. 219, McGraw-Hill, New York.
- Widdowson MA, Haney OR, Reeves HW, et al. (1997). Multilevel soil-vapor extraction test for heterogeneous soil. *J. Environ Eng, ASCE*, 123 (2): 160-168.
- Wu X, Tang J, Lu X (2002). Capillary-tube model and experiment of multiphase flow in capillary fringe, *Tsinghua Science and Technology*, 7(6): 584-590.
- Yang YJ, Gates TM, Edwards S (1999). SVE design: Mass transfer limitation due to molecular diffusion. *J. Environ Eng, ASCE*, 125 (9): 852-860.
- Yoon H, Kim JH, Liljestrand HM, Khim J (2002). Effect of water content on transient nonequilibrium NAPL-gas mass transfer during soil vapor extraction. *Journal of Contaminant Hydrology*, 54 (1-2): 1-18.

CONTAMINATED LAND AND ENVIRONMENTAL DAMAGE: AN ANALYSIS OF CURRENT REMEDIAL STRATEGIES AND FUTURE DEVELOPMENTS

Stephan A. JEFFERIS¹

ABSTRACT: Contaminated land management is now a mature discipline and geotechnical engineers are very familiar with desk studies and site investigation procedures. However, remedial practice varies very considerably with legal and financial instruments moving practice in many countries away from landfill. Sustainability also has become a topic for debate and the paper considers some aspects of sustainability as applied to contaminated land management. The paper then gives an overview the current status of the principal remedial technologies that are in use worldwide and seeks to identify the constraints both technical and regulatory that influence the selection of remedial actions. The avoidance of future contaminated land is obviously very important but has received rather little technical analysis. Future directions in environmental risk management are therefore considered and in particular questions such as: What will be the pollutants of the future? Should the geotechnical engineer be more involved in the design of industrial facilities to minimise risks of environmental pollution? How can the geotechnical engineer ensure that chemicals that are hazardous to the soil and groundwater environments are appropriately regulated and managed?

KEYWORDS: contaminated land, future contamination, sustainability, remediation.

INTRODUCTION

The management of contaminated land is now an established and mature discipline in many parts of the World. Furthermore, a substantial body of guidance literature is available and one of the purposes of this paper is to highlight some of the recent and important guidance. However, there are still evolving issues both in relation to historically contaminated land and the prevention of future contamination – a topic which tends to be more often addressed by way of regulation than pro-active thinking.

This paper will consider both historic and future contamination but before this it is appropriate briefly to consider what we mean by contamination. The author has considered this for many years and found that the ‘place’ in which some species is present is a key factor. Thus just as a weed may be defined as a plant in the wrong place so a chemical in soil may be in the wrong place and cause land contamination. However, the same chemical in an industrial process may be both useful and acceptable. Similarly grasses may be seen as weeds in a flower bed but useful when forming a lawn or as a cover layer for a mine waste pile. From consideration of place, the author has found that water can be a contaminant in deserts where its presence may lead to salts being drawn

up to the surface from deeper soils to the detriment of buildings and other construction. Similarly air can be a contaminant, for example, in unsaturated soils adjacent to tunnels where it may allow the oxidation of species such as pyrite with the production of acid and sulphate.

However, it does not follow that the prevention of future contaminated land is solely a matter of keeping chemicals in the right place. Experience has shown that escapes do occur and some chemical species are so persistent in the environment and/or can have such severe adverse effects that their introduction and/or use must be subject to strict regulation (see, for example, the European Union Registration, Evaluation, Authorisation and Restriction of Chemicals (REACH) regulations, Health and Safety Executive, 2009).

Of course contaminants need not be solely chemical and in the future, physical matter such as construction waste may become more significant as the desire to avoid disposal to landfill leads to the retention of more materials on redevelopment sites (crushed concrete etc.). Also it has long been recognised that energy in the form of heat/cold, light and noise can contaminate the environment. New technologies also may lead to new contamination. For example, although desirable from an energy efficiency perspective, there can be little doubt that ground sourced heat pumps will drive some new and

¹ Director, Environmental Geotechnics Ltd., UK. Email: egl@environmentalgeotechnics.com

unexpected contamination. Such risks may be described as countervailing risks as they run counter to the benefits of the technology. Geotechnical engineers must strive to identify and minimise countervailing risks resulting from new technologies that impact on the 'geo' environment.

We must be continually alert to new forms of contamination especially as land becomes more densely used and it is the author's opinion that geotechnical engineers should be prepared to be pro-active in preventing future pollution and not merely reactive to regulations developed by others. They should be prepared to involve themselves in the formulation of regulations which involve their areas of expertise – the 'geo' domain.

RISK ASSESSMENT AND REGULATION

The clean-up of an area of contaminated land may be required by local legislation/regulatory requirements or be a voluntary action by the owner or occupier of the land but whatever the drivers for the remediation it is likely to have to comply with some legislation. This legislation can vary significantly between countries (for UK legislation and regulations, see for example Sheppard et al. 2008) but however it is framed there is likely to be some consideration of the following:

- the source(s) and receptor(s) of the contamination;
- the actual and potential pathways between sources and receptors;
- that remedial targets should be determined by risk assessment and not because of the mere presence of potentially contaminating materials;
- the polluter pays principle.

Significant issues relating to these matters are considered below.

There can be little doubt that the source-pathway-receptor framework provides a valuable starting point for the analysis of environmental problems. However, its coupling with risk assessment merits some discussion. For example, typically in the context of contaminated land, risk is considered as:

$$\text{Risk} = \Sigma \text{Probability of occurrence} \times \text{Consequences}$$

The assessment must be carried out over each of the environmental media: air, water and land and consider the sub-compartments of these media such as human and ecological health, surface and groundwater as well as considering the generation of waste during remedial actions.

The aim of risk management is to reduce the overall risk to a level acceptable to society and thus by implication to ensure that no unacceptable risks occur in any sub-compartment. Acceptable risk is difficult to define in

regulations but in practice for human health only minimal risk is likely to be acceptable to lay society. For facilities perceived to present high risks such as nuclear installations, the risk may be required to be not only minimal but also to be as low as reasonably practicable (ALARP) – i.e. if it is practicable to reduce the risk then this should be done.

The definition of risk as the product of probability and consequence allows a distinction to be drawn between the procedures and regulations necessary for the management of contaminated land and facilities such as waste repositories. For municipal, industrial and nuclear waste repositories it is certain that the contents of the repository are sufficient to be source of harm if the containment fails (though the potential for contamination may reduce over time). Thus the consequences of an escape cannot be made minimal and protective measures must be focused on reduction of the probability of escape. Source removal is obviously not a practicable 'current' management option for repositories. Receptor management (prohibiting access to an area) may be desirable but difficult as it can be necessary to bind future generations beyond a time frame of about two generations (60 years) – longer than realistically can be achieved in most social/legal systems. Reduction of the probability of escape by pathway control thus becomes the only viable risk management procedure. Repository designs therefore tend to include multiple man-made barrier elements and where possible the repositories are/should be sited so as to take advantage of natural barriers such as clays and to avoid natural pathways such as aquifers.

For contaminated land, consequences may be reduced by source reduction or destruction and probabilities reduced by pathway management. Furthermore receptor control (reducing probability of exposure) may be achievable by permitting only certain types of development, for example, industrial use with hard cover and not housing. These trivial examples show that risk assessment, properly used, is not merely a numbers game but if logically applied, and this can be difficult, an important conceptual tool in the development of legislation and regulation.

As an aside we may also ask how often are contaminated land risk assessors properly trained in risk? Should all risk assessors be required to follow a course in accident investigation? This can bring a proper 'reality' to risk assessment and could radically extend the 'list' of risks that are generally considered in relation to contaminated land management.

A Riskier Society?

It is the author's view, that current risk assessment procedures allows us to take greater risks today than we

did yesterday. We have models for risk assessment which allow us better to understand source-pathway-receptor interactions. These models allow us to estimate the doses from sources and the responses of receptors (e.g. human health). We also have well developed groundwater models that allow detailed investigation of groundwater pathways and which are now perhaps more limited by available data than modelling capacity. Thus it can be argued that today risks are better quantifiable and that we can justify our actions when we ignore trivial risks. This is sometimes encapsulated in the phrase ‘risking it away’ but we must be cautious not to risk away significant issues and allow computer codes to overrule common sense. Furthermore computer codes may fail to consider the robustness of technologies, and the author is concerned that some technologies including containment and stabilisation in very challenging chemical systems and/or in very challenging environments rely on fragile and rather easily compromised concepts or components.

We also must allow that there are areas where despite our best modelling much uncertainty remains. Important problems include vapour exposure from volatile species in the ground and contaminant migration by/with dust. Ecological modelling was a source of substantial uncertainty but procedures are evolving (see for example Ashton et al. 2008).

Much remains to be done in the area of risk assessment both with regard to the assessment of the dose of contamination to the receptor and the response of receptor to the contamination – the harm or nuisance done. We also need more developed protocols for the assessment of the robustness of contaminated land management procedures.

STAKEHOLDER UNDERSTANDING

The requirement to reduce risk to a level acceptable to society requires that society must be able to understand the risk. For many situations, the test of acceptability is delegated, by legislation, to regulatory bodies. This is justified on the basis that lay understanding of technical issues can be limited and expert problems can properly be left to experts for answer. However, it should be remembered that environmental protection requires consideration of future outcomes where there cannot be certainty – an area where a narrowly focused expert may miss issues that concern the lay person who is in this case the key stakeholder. There is a risk that experts will focus on those areas where investigation and research can reduce uncertainty to low levels but ignore or be blind to areas of potentially high risk which are difficult to conceptualise or model.

THE POLLUTER PAYS PRINCIPLE

The polluter pays principle is a feature of many national and international regulatory frameworks. At first sight it seems an entirely appropriate starting point for regulation but there are some negative points that need to be considered. These include:

- Identifying the polluter and establishing liability may cause delay to investigative works and any necessary remediation;
- It can bring retrospective liability. Actions which were legal at the time they were carried out may become a source of future liability;
- How much of what we are doing today will be seen as having caused contamination by our children and grandchildren;
- The polluter if an individual may be dead or if a company may be a very different organisation with very different shareholders;
- Is it no more than retribution for the actions of our parents and grandparents?
- What remedy is appropriate for situations where clean-up is not possible (e.g. release of contaminants to the air)?

It follows that for historic contamination the polluter pays principle, if adopted, must be used with restrictions appropriate to the legal regime within which it is founded. However, if an individual or company knowingly causes pollution now or in the future then liability and the requirement for the polluter to remediate may seem to raise fewer issues but consider the following situation. A company knowingly releases a contaminant to a surface water drain. The release is entirely in compliance with a legal permit. Years later the contaminant is found to have polluted a water course. Should the company be held liable? Is this situation different to that relating to the liability for historic contamination under the polluter pays principle?

SUSTAINABILITY CONCEPTS

The World Commission on Environment and Development, 1987 (the Brundtland commission) statement on sustainability is perhaps the most often quoted statement on sustainability:

“Humanity has the ability to make development sustainable – to ensure that it meets the needs of the present without compromising the ability of future generations to meet their own needs”.

This is a statement which specifically considers humanity and intergenerational equity. Porritt (2005) finds that:

“... It’s the science of sustainability that provides the

rock-solid foundations upon which the structures of sustainable development are now being raised—still somewhat tentatively and haphazardly, it has to be said”.

He continues:

“For most businesses today, however, this remains far too unworldly: here, the language of the triple bottom line (economic, environmental and social bottom lines) still prevails, or 'stakeholder strategies', or corporate social responsibility, all jumbled together in a goulash of jargon and lofty aspiration that somehow still serves to keep physical reality at bay.”.

For Porritt sustainability is “best defined” as:

“as the capacity for continuance into the long-term future”.

For the engineer the potential conflict between Mr Porritt’s science of sustainability and the business triple bottom line approach must be recognised. There can be no doubt that it is essential to consider the sustainability of our actions but what does this mean on either basis? As we are currently able to practice it sustainability (or more strictly sustainable development) is a pathway to a sustainable future. The path that each of us must take will depend on our starting point.

Sustainability Assessment

As currently practiced a sustainability analysis can have similar steps to a life cycle assessment but will need to consider wider array of issues. The principal steps in an LCA (see British Standard BS EN ISO 14040: 1997 and also Jefferis, 2004) are:

- Goal and scope definition: defining the purpose and the boundaries of the analysis;
- Inventory analysis: Development of the process flow chart, selecting the indicators that are to be considered, collecting and processing the data;
- Interpreting the results: this may include development of weightings for the various indicators and some form of multi-criterion decision analysis.

Each of these steps can be a major operation. For example, Bardos et al. 2009 are amongst those who have identified very many potential indicators that might be used as part of a sustainability assessment. They found 2,421 individual indicators which they were able to categorise into 18 headline indicator categories but these categories were very broad and would have to be subdivided for application in contaminated land.

The multiplicity of indicators highlights another problem with sustainability assessment. Any workable procedure must be capable of readily displaying a multiplicity of indicators and their relative contribution to the overall assessment (see for example Bell and Morse, 2008).

Sustainability and Contaminated Land Management

For contaminated land remediation, to question sustainability at the level of individual clean-up procedures can fail to consider the fact that clean-up is seldom an aim in itself and is likely to be part of a larger scheme, the benefits/impacts of which may dwarf those of the clean-up stage. Furthermore, over the coming years, land contamination may prove to be a minor issue compared with the growing pressures on land from increasing urbanisation, from shortages of energy, food and water and the impacts of global warming. It also must be recognised that land will be subject to continuing cycles of development, redevelopment, abandonment etc. (see Fig. 1).

Furthermore, evolving land use may cause major changes in the pathways by which a source of contamination may reach a receptor and also introduce new receptors. Over what time-scale should sustainability be considered? A low cost, quick fix remediation in one generation may create greater problems for the next generation.

Another challenge is that currently there is no agreed assessment procedure for sustainability generally let alone for contaminated land. Indeed it is doubtful if there ever will be a single overarching procedure as value systems are continually changing and for example the social dimension properly requires consideration of ethics – an area constantly challenged by new developments. What is regarded as sustainable in one society or country at a particular stage of development may not be sustainable in another society/country at a different stage of development. It follows that we must seriously consider whether our present interpretation of sustainability will remain relevant to future generations. We have moved on from concepts separate regulatory bodies for individual environmental media: air, water and land. Today in many countries there is a more holistic approach of a single national body such as an environment agency with a remit to consider pollution of all environmental media—though noting that the creation of such agencies has been quite recent – only in 1996 in the UK. International bodies for seas etc. also exist but one wonders if they have sufficient powers. Will we move on yet again to national/international sustainability agencies?

It also must be asked is environmental protection always compatible with sustainability? What if the social benefits are great but there may be potential for short-term environmental harm? Consider for example a community where youth training centre is urgently required, a centre which will be operational for perhaps a decade but the only available site is potentially contaminated and very limited funds are available. Should these be deployed to build the centre or investigate the site,

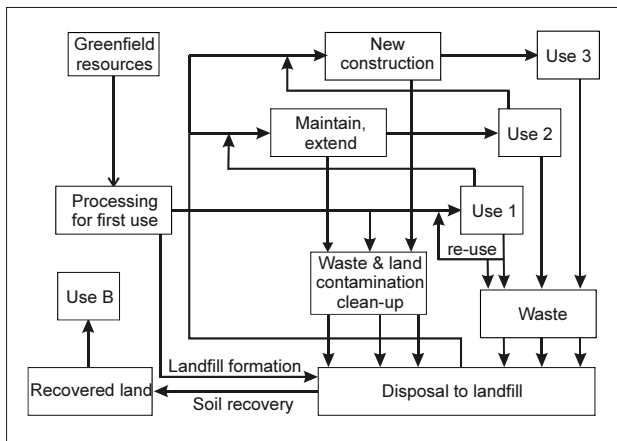


Fig. 1 Cycles of use of land from the original green field

there are insufficient funds to do both? Can urgent social needs outweigh possible environmental damage?

Some of the issues raised by sustainability are considered in more detail below. See also Azapagic, et al. 2004; Bartlett, H.V. and Guthrie, 2005; Jefferis, 2002a, 2004, 2008; Leiper, 2003 and Padiaditi et al. 2006.

MANAGEMENT OF CONTAMINATED LAND

The management of contaminated land may be divided into a number of phases of work

- Desk study;
- Intrusive site investigation;
- Remediation (if required);
- Verification of the remediation;
- Monitoring the performance of the remediation;
- Decommissioning and removal of remedial elements at the end of their required or functional lives. This may include the removal of permeable reactive barriers, in situ stabilised materials and barrier systems.

The first two phases of work, desk study and site investigation are well codified and one would not expect major issues to arise, though it must be allowed that the ready availability of desk study information varies greatly around the World. In some countries basic data such as historical map information is immediately available via the worldwide web (generally for a fee) whereas in other places data collection can be a complex and laborious task involving physical visits to data repositories.

There are also regular developments in site investigation enabling more information to be obtained in the field so that investigation strategies can be refined in real time. On-site and in-situ chemical analysis is available for a number of contaminating species and one can fully expect that within a few years in-situ toxicity testing will be a reality. Thus developments in desk study and site

investigation are flowing from advances in information technology and investigative technologies.

The remediation of contaminated land can raise issues beyond the simple question: will the procedure work? Issues may arise if remediation can cause harm to workers on the site and neighbours by exposure to contaminants uncovered by the works and dust from it. Furthermore it can cause nuisance (i.e. annoyance not amounting to actually harm) from dust, smells and noise and contribute large amounts of waste to landfill. It also can involve the movement of large volumes of soil and use significant amounts of energy with substantial exhaust emissions which in themselves may be an important source of secondary pollution.

There is also a continuing debate as to whether remediation should always remove the source of the contamination rather than merely protect receptors of the contaminant emissions by pathway control measures. If source removal is essential the problem still remains: what should be done with contaminants such as heavy metals that cannot be destroyed and asbestos for which there may be no economic procedure for its destruction.

There is also another key matter that must be addressed and that is the extent to which those currently involved in the management of historically contaminated land should involve themselves in the avoidance of future contaminated land. How should the experience developed in contaminated land management be deployed to prevent future contamination of land? Despite the array of guidance on the management of historically contaminated land, guidance is less widely available on the prevention of future contamination and in particular guidance addressed to people outside the "geo" domain.

Impact of Sustainability on Remediation

As discussed above, some geotechnical engineers and others involved in the management of contaminated land are questioning the sustainability of some remedial technologies. Problem holders (those who own or are responsible for contaminated land) may regard this questioning as little more than academic churning but there are some important underlying concerns which need to be addressed.

For example, the Brundtland commission statement on sustainability could be interpreted as requiring that contaminated sites should be cleaned up when they are identified and that no contaminated sites should be passed on to succeeding generations. This presents a number of problems:

- It implies a requirement for source removal within a generation;
- It denies the use of pathway control procedures unless the flux in the pathway is sufficient that clean-

up can be achieved within a generation or the source will decay within such a timescale;

- It thus denies the use of low intensity management procedures;
- It does not recognise the social and economic benefits that can be achieved from low intensity procedures;
- It does not recognise that source removal can be extremely disruptive and may even require the displacement of communities (consider the complex impacts on the communities at Love Canal in the USA (Mazur, 1998) and Lekkerkerk in Holland).

It follows that when setting goals (often necessarily short-term) for contaminated land remediation we should have regard to the long-term goals of sustainability. This will require not only appropriate use of appropriate remediation technologies but also prevention of future contaminated land and in particular it will require us to address the question: to what extent can we avoid future source creation. It is entirely reasonable to avoid dig and dump as a remedial technology of first choice for although it can provide certainty of remediation at the site of the original contamination it leaves a legacy to be managed. However, it is not reasonable to deny the potential of pathway control measures such as permeable reactive barriers on the basis that they are not sustainable as they are only control measures and may not destroy or render safe all contamination within a generation. Similarly when designing containment and in-situ stabilisation schemes we must accept that although they have a finite life they can bring current benefits. We live in a World of finite resources. Money spent on low risks denies money to higher risks and therefore makes the World less sustainable.

REMEDIAL TECHNOLOGIES

There is now a well developed armoury of remedial technologies available to the geotechnical/geoenvironmental engineer and for technical information the reader is referred to fuller texts such as the US Environmental Protection Agency remediation website, LaGrega et al. (2001) and Shackelford and Jefferis (2000). In addition to technical issues there are always regulatory issues and for a UK perspective on these see the UK Environment Agency Remediation Position statements (Peters, 2006).

However, it is appropriate also to consider current developments in the use remedial technologies. From a UK/European perspective, recent drivers for change have been:

- a) European Union legislative developments requiring treatment before landfill of all wastes including contaminated soil;
- b) Increasing tax on materials disposed to landfill;

- c) The focus of developers on certainty of clean-up and their preference for procedures with no on-going requirement for maintenance.

The legislative changes, (a) above, require that waste is pre-treated prior to landfill. Any potential treatment must fulfil all the following three criteria (but need only meet one of the four objectives of the third point):

- 1) It must be a physical/thermal/chemical or biological process including sorting.
- 2) It must change the characteristics of the waste.
- 3) It must do so in order to:
 - a) reduce its volume, or
 - b) reduce its hazardous nature, or
 - c) facilitate its handling, or
 - d) enhance its recovery.

Inert waste is exempted from the treatment requirement where treatment is not technically feasible. Where a waste to be landfilled is already the product of a waste treatment it is not necessary to further treat the residue prior to landfill. The key requirement is that the waste is subjected to a process that meets the three-point test (i.e. it changes its characteristics and some element of the waste is recovered).

The legislative changes have as intended reduced the opportunity for dig and dump as a remedial process. In the European Union dig, treat and dump is now mandated in place of dig and dump – though the treatment may be limited to segregation of clean and dirty soils with only the latter taken to landfill.

The increasing tax on materials disposed to landfill helps to make process based technologies which reduce the quantity of waste more viable as compared to landfill.

From a sustainability perspective, these are desirable changes landfilling waste merely transfers the contamination from one location to another and from one generation to another, though it must be allowed that within a landfill the waste will be in a designed containment environment and subject to stewardship – at least for the early part of its life as a source of contamination (note the difficulties of ensuring stewardship over multiple generations).

However, running counter to the legislative and financial drivers for landfill reduction is the developer's reasonable requirements for certainty and removal of long-term liability. In the UK, much contaminated land is redeveloped for housing and/or commercial or industrial use. The developer often sells the site and new facilities after development and does not want to retain any liability either for contamination left in the ground or the on-going operation and maintenance of process based technologies such as permeable reactive barriers as these will reduce the value and saleability of the development.

It follows that it always is important to consider commercial constraints as well as financial and technical issues when selecting remedial technologies. This means

that a site to be cleaned up for a commercial development use may use soil washing to recover clean material so that only contaminated residues are disposed. However, an identical site, in an identical setting which is to be cleaned up for public open space or non-commercial use may employ less intensive treatment such as receptor protection via a permeable reactive barrier or capping if groundwater contamination is not an issue.

Finally in relation to legislative developments it must be accepted that as more land is cleaned-up and legislation becomes more demanding, it becomes less tenable to seek to avoid contaminated land remediation on the basis that the site in question is within a wider area of contaminated land. The European Union Water Framework Directive (2000) sets obligations on member states in relation to achieving good ecological status for surface water bodies and good chemical status for groundwater. Good status is the focus of the directive and not just the reduction of risk to receptors/potential receptors of a particular land use or being no worse than the neighbours.

STATUS OF REMEDIAL TECHNOLOGIES

The following gives a brief overview of the current status of some remedial technologies in the UK.

Containment and Stabilisation

Containment by capping to prevent upward contaminant migration is widely used as is vegetative cover to prevent dust-blow for example from heavy metal contaminated sites.

Vertical slurry trench cut-off walls continue to be used but the level usage has declined significantly over the last two decade – possibly because of declining need rather than concerns about performance (indeed the author is not aware of any failure of a cut-off wall in service, as opposed to installation faults which do occasionally occur but can be largely eliminated by proper supervision during site works). A significant and continuing use for cut-off walls is landfill gas control. There is a UK National specification for slurry trench cut-off walls as barriers to pollution migration (Jefferis et al. 1999).

Soil stabilisation with cement and/or special admixtures has been widely researched and there is a substantial literature (see for example Bone et al. 2004). Despite the volume of research and associated publication, field take-up of the technology appears rather limited for contaminated land management though soil stabilisation with lime and/or cement or other binders is widely used for increasing the strength/ stiffness of soils for construction purposes (e.g. for road sub-bases). In these applications

considerable care is necessary with regard to sulphate induced heave which can be very large and which typically occurs on first wetting, for example, at the time of the first winter rains.

Stabilisation is also used to solidify and reduce leaching from the fine ash from waste incineration.

Bioremediation

Bioremediation continues to be widely used for the degradation of hydrocarbons. In the UK it is probably the most widely used process based technology (certainly by number of jobs undertaken if not by tonnes of soil treated).

Soil Washing

Soil washing, a separation technique based on particle size and/or density, is becoming more widely used as it allows material to be retained on site for re-use. It can be used for organic and inorganic contaminants though it may be more effective for the former. For commercial viability, the contaminated fraction must be no more than a modest fraction of the total material as it will require further treatment. It should be noted that soil washing is unlikely to achieve full removal of contaminants but it can allow regulatory limits to be achieved. High throughput processing plants are available.

Permeable Reactive Barriers (prbs)

The topic of permeable reactive barriers requires some discussion as it involves chemical reaction theory – an area of engineering which may not be familiar to all geotechnical engineers. A few key aspects of reaction engineering are considered below.

The simplest form of chemical reaction that may occur in a prb is:



That is there just a single reactant. For this reaction, assuming that the reaction is irreversible, the rate of change of mass of reactant, M_r can be written as:

$$\frac{dM_r}{dt} = -k_n M_r^n \quad (2)$$

Where n is the order of the reaction and k_n is the reaction rate constant. From Eq. 2 it can be seen that for all reaction orders other than zero (i.e. when $n > 0$) the rate of loss of reactant is a function of the current mass of reactant. The greater the current mass the greater the rate of reaction.

The degree of degradation achieved in a prb is a

function of the residence time t in the reactor, the reaction rate constant and the order of reaction. This is illustrated in Fig. 2 which shows the ratio of the effluent (treated) concentration to the influent (contaminated) concentration for a fixed input concentration to the reactor as a function of the reaction rate constant multiplied by the residence time in the reactor ($k_n t$). It can be seen that high values of ($k_n t$) are required to achieve significant reduction in concentration especially for high reaction orders ($n > 1$).

For a reactor of fixed bed volume, the residence time is inversely proportional to the flow rate. From Fig. 2 it can be readily deduced that the effluent to influent concentration ratio (an indicator of the degree of reaction) is very sensitive to the flow rate. It follows that when designing prb installations it is crucial to have an accurate assessment of the flow rate through the reactor. Unfortunately although we have groundwater models that can give very good information about groundwater levels, assessment of flow rates is much less reliable. This is because of the inherent uncertainty and heterogeneity of permeability in all but the most uniform soils. Because of the uncertainty in flow rate, prbs tend to be significantly over-designed. Field flow rates can prove to be markedly lower than worst case designed/modelled flow rates. Good data on flow rate can provide significant economies and indeed over-design as a result of poor flow data may be militating against the wider application of prbs.

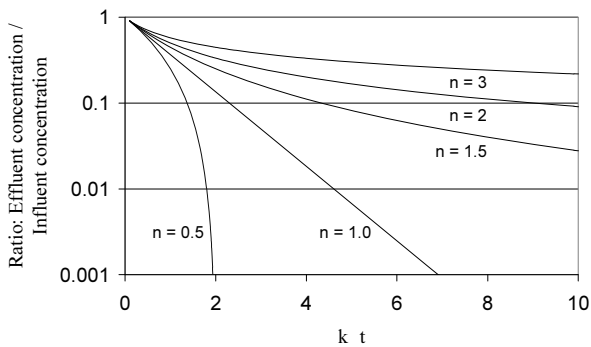


Fig. 2 Concentration reduction achieved in a reactor as a function of ($k_n t$)

It also should be noted that the reaction order has a major influence on the degree of reaction achieved. For low values of ($k_n t$) reactions may appear first order or pseudo first order. It is only at higher values that deviations become apparent. Furthermore many reactions have no simple order as they may involve multiple steps and/or pathways (as for example is the case for the reductive dechlorination of chlorinated solvents). It follows that when undertaking laboratory testing, tests must be continued until the required degree of reaction is achieved. One should never extrapolate from low values

of ($k_n t$) to estimate the degree of reaction at higher values of ($k_n t$). A fuller discussion of reactor kinetics is given in Levenspiel (1999). See also Jefferis (2002b).

In the UK, a variety of permeable reactive barriers (prbs) has been installed. Many of these have used the in-ground reaction vessel approach pioneered at Monkstown in Northern Ireland (Jefferis et al. 1997). Continuous wall systems where the reactive material is distributed along a length of permeable wall have found little application in the UK. Current designs tend to separate the reactor from the barrier wall (i.e. they adopt the reaction vessel concept but are neither funnel and gate designs nor continuous wall designs). The use of an in-ground reaction chamber allows better control of the reaction process, easier replacement of reactants and minimisation of short-circuiting of the flow through the reactor. Furthermore the separation of the reactor from the barrier wall can make construction markedly simpler as only a pipe has to pass through the wall and there is no need to seal the reactor to the wall (see Fig. 3). In this figure the collector may be a trench or pile bore filled with permeable materials such as sand or gravel. Its role is to collect the contaminated water from the source. The collector may be installed within the source zone as potentially this will lead to the greatest rate of source reduction and maximum utilisation of the reactor (see Eq. 2). However, excavation within the source zone may be undesirable because of the potential for harm to site workers, neighbours etc. The distributor returns the cleaned groundwater to the ground.

The flow through the reactor may be driven by the natural groundwater gradient or it may be pumped. Pumping allows the use of a by-pass to return the effluent to the contained zone if required during commissioning or if a malfunction of the reactor is detected.

It should be noted that in the reaction chamber configuration a prb becomes similar to a pump and treat operation except that (a) the flow may be the result of exploitation of a natural groundwater gradient rather than pumping, (b) the use of a cut-off wall prevents off-site migration rather than an hydraulic gradient achieved by pumping and (c) the cut-off wall, if fully enclosing the site, will reduce the volume of groundwater to be treated.

In the UK over the last few years the rate of prb installation appears to have declined. However, there has been considerable innovation and a number of low maintenance reaction chamber type prbs have been developed and deployed. Contaminants that are being treated include chlorinated solvents, gas works leachates and carbon disulphide. Media employed include iron metal, activated charcoal, slow release compounds and sand/gravel in aerobic or anaerobic reaction chambers. UK regulatory guidance on prbs is given in Carey et al. (2002).

VERIFICATION AND MONITORING

For all contaminated land management techniques both proven and innovative, it is important that the processes used on site are proven by verification during the works and if necessary by long term monitoring thereafter. The UK Environment Agency and Department of Environment, Food and Rural affairs document CLR11 defines verification as:

“The process of demonstrating that the risk has been reduced to meet remediation criteria and objectives based on a quantitative assessment of remediation performance”.

It is important that provision for verification and monitoring is built into the remedial designs. Otherwise they may be difficult and expensive to achieve. Guidance on verification is given in Bone (2007). For technologies which require the long term performance of a process such as a prb or barrier element such as a geomembrane it is important that the verification and monitoring programme considers the timescale over which the remediation is expected to endure.

The costs of long-term monitoring can be reduced if the monitoring system is designed and positioned so as to develop confidence in performance and permit long time intervals between monitoring rounds. Fig. 3 shows a conceptual diagram of a prb using a series of reaction chambers with a monitoring point installed between the second and third chambers (NB three chambers are shown for generality, more or less may be required). In this example it is assumed that the reaction chambers contain an absorbent material such as activated charcoal or other material which has a limited active life.

Samples for compliance testing will be taken at intervals at the point marked ‘X’. The role of the third chamber is to ensure that no contamination can reach the discharge point between sampling events at point X. The third chamber is specifically sized to allow sampling at long intervals, perhaps six monthly or longer. Without the third chamber there would be no quantitative basis on which to determine appropriate sampling intervals and the intervals would have to be based on the estimated lifetime of the media/ process in the first chamber. For a prb which does not use reaction chambers the same effect can be achieved by sampling within the prb rather than just at the prb effluent point. Without concepts such as the intermediate sampling point, for an innovative technologies very conservative (short) times between sampling events might be required by regulatory agencies. If sorbent materials are used in the reactors, a rather special problem can occur, the phenomenon of roll-up. This is a process whereby strongly sorbed (and therefore highly retarded species) desorb more weakly bound species which can be released as a spike at concentrations above the original

input concentration (this matter will be addressed in a later paper).

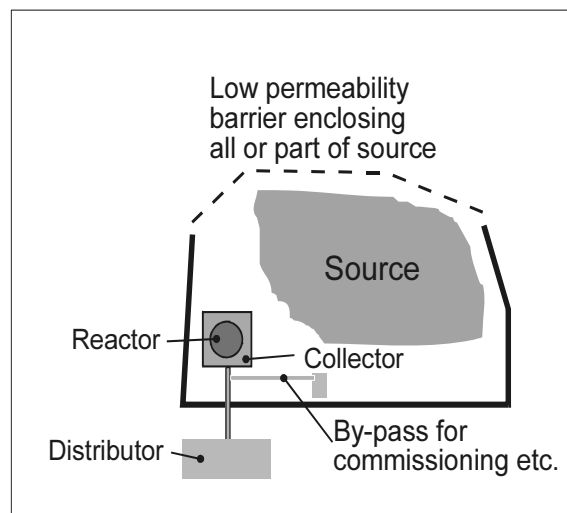


Fig. 3 Permeable reactive barrier using a reaction vessel separate from the barrier wall

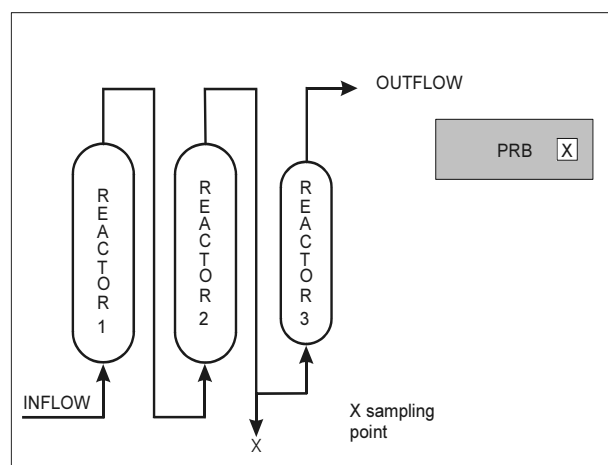


Fig. 4 Sampling location for a prb

INNOVATION IN CONTAMINATED LAND MANAGEMENT

Contaminated land investigation and management continues to be perceived, and indeed often is, an expensive process. Innovation therefore tends to be encouraged in terms of its potential for lower costs though certainty of performance is also important.

Site investigation and remediation costs can be significantly reduced by the timely availability of data. On site testing of soils can help to refine site investigations. It also gives real-time data for the classification of potentially contaminated material thereby ensuring that remedial measures are applied only where needed and where on-site clean-up technologies such as soil washing

or bioremediation are applied to confirm they are achieving the clean-up goals. If there are only a few contaminants known or expected to be present on a site then on-site testing techniques can be tailored to the expected contaminants. However, if such information is not available it may be preferable to use a general screening technique such as toxicity testing. The author has been involved with the development of a toxicity testing system based on bioluminescent bacteria. (see Weeks et al. 2004 and www.cysense.com).

Innovation in Remediation

Innovative processes continue to be developed and deployed. There have been applications of in situ heating to increase recovery of solvents, in situ chemical oxidation and much else besides. It is refreshing to see that clients continue to be willing to accept innovative technologies despite the fact that the construction industry is often regarded as very conservative.

PROBLEM SITES

There are a number of types of site which continue to be problematic as regards remediation. Examples include:

- Sites which are to be cleaned-up for use as public open space or other uses where there is little financial return – the costs may fall on the public purse and as public finance is finite this will deny other developments;
- Very large sites (mega sites) where the costs are so high as to be significant at a national expenditure level;
- Sites which are highly contaminated but too small to provide a financial return;
- Sites underlain by substantial depths of permeable soils and/or fractured/fissured rocks where there is no viable prb or containment procedure.

From the above it can be seen that groundwater management remains a problem for some sites but that otherwise the problems are mainly financial.

FUTURE CONTAMINATION

This may arise from current sources or from future operations. Current sources of contamination may cause future contaminated land if remedial measures fail and it is therefore necessary, when designing remedial measures which do not achieve full source destruction, to consider their durability and if possible the changes, both environmental and regulatory, that may occur during the design life of the remediation. This will be particularly important for permeable reactive barriers, passive barriers and stabilisation technologies.

In addition to failure of current remedial schemes other sources of future contaminated land/processes by which it may be created include:

- a) Existing pollution sources which are as yet undiscovered or unrecognised;
- b) Legislative changes which re-classify chemicals, exposure limits or remedial schemes;
- c) As a result of new knowledge about the behaviour of contaminative species becoming available;
- d) Release of chemicals or energy etc. in ignorance of their contaminative potential or as illegal acts;
- e) Major events such as landslides which allow contamination to escape from landfills etc.
- f) Change of environmental conditions, for example change of redox potential which may occur as a result of change changes in groundwater level. This may result in changes of speciation and thus changes in the solubility or phase of chemicals, for example sulphur species maybe reduced to the toxic and flammable gas hydrogen sulphide and carbonaceous material to the explosive and asphyxiating gas methane;
- g) Accidents including spills, fire and flood;

It is estimated that this year, 2009 the urban population of the World will for the first time exceed the rural population. Continuing urbanisation is likely to drive greater concerns regarding the environmental quality of soils and moves towards source removal rather than source management. There is also a significant risk that existing remedial schemes involving containment, stabilisation or pathway management will be revisited so that fuller use can be made of land. These are long-term changes and it is difficult for the geotechnical or the geoenvironmental engineer to make appropriate allowance for such developments and also those under (a) to (d) above. The engineer will be aware of the potential for impacts from (e) to (g) but may be unable to assess them as the 'source' zones may lie outside the areas to which he has access.

The risk from accidents may include fire and flood and these are becoming more significant as there is a tendency for manufacturing, storage and distribution facilities to become ever larger with single facilities serving a substantial fraction of a whole country or indeed several countries.

Fire provides an interesting example of a potentially developing role for the geotechnical engineer. When designing manufacturing or storage facilities the risk of fire is well recognised. However, it is perhaps less well recognised that a principal vector for the dispersal of contamination released in a fire will be the water used to fight the fire. This will mobilise soluble materials and also colloidal material and fine solid debris. This water may penetrate into the ground with the potential to contaminate the ground and the groundwater and/or run-

off via drains or other pathways to local receiving waters such as streams and rivers. The potential impact of fire fighting water can be greatly reduced if all the surfaces around the facility are designed to retain water and the buildings are set so as to be in a 'bowl' large enough to retain all the fire water (i.e. the buildings are set at a lower level than the surrounding area). In addition valves should be set in the surface water drains (drains for the removal of rainwater) to prevent the escape of fire water from the site. After a fire, the retained water can be tested and disposed of as appropriate to its level of contamination. This is a simple example of the more proactive role that the geotechnical engineer can take in relation to the reduction of the potential for future contaminated land.

CONCLUSIONS

Contaminated land management is now a mature discipline with several decades of practical experience and much published guidance indeed so much guidance that it is necessary in some countries to have guidance on the guidance.

Despite the array of guidance and the many developments in technology, there a number of problems remain. These include identifying the proper role of sustainability in contaminated land management. At present a sustainability assessment will be a rather costly exercise. When is it appropriate? How should sustainability be assessed? What are the key indicators to be employed? How do we ensure that engineers at all levels of a project from master planning to site supervision are empowered to minimise their environmental impact and improve project sustainability?

Some categories of sites, particularly the very small and the very large continue to cause problems but many of the problems relate to finance rather than technology and in particular the balancing of expenditure between contaminated land management, which for many is seen as a low risk problem against more 'deserving' expenditure such as community facilities, schools, hospitals etc. We live in a World of limited resources and money spent on low risks denies funds to higher risks.

It is the author's opinion that geotechnical engineers should be encouraged to pro-actively seek to minimise the risk of future contaminated land. For example by designing appropriate management schemes for fire water containment at industrial premises. They also should be prepared to use their accumulated experience of the behaviour of chemicals in the ground and groundwater environments to raise concerns about the widespread use or use without sufficient protection of chemicals which are manifestly dangerous to the environment.

Pollutants of the future may include:

- Any matter on energy in the wrong place in significant quantities (i.e. future concerns will not be limited to the present mainly chemical approach to contamination);
- Light, noise, and smells – at present these tend to be regarded as causing nuisance rather than actual harm. However, with increasing urbanisation and population densities sensitivities will increase;
- Poorly framed laws also may cause contamination by driving sections of industry or agriculture to take sub-optimal measures or loading parts of the environment beyond their carrying capacity.

It can be expected that there will be growing concern about effects without identifiable cause (e.g. childhood asthma) and causes without identifiable effects (e.g. overhead power lines).

REFERENCES

- Ashton D, Benstead R, Bradford P, Whitehouse P (2008). An ecological risk assessment framework for contaminants in soil. Environment Agency, UK.
- Azapagic A, Perdan S, Clift R (2004). Sustainable development in practice. Wiley.
- Bardos P, Lazar A, Willenbrock N (2009). A review of published sustainability indicator sets: How applicable are they to contaminated land remediation indicator-set development? ISBN 978-1-905046-18-8 Contaminated Land: Applications in Real Environments (CL:AIRE).
- Bartlett HV & Guthrie PM (2005). Guides to sustainable built environment development. Journal of Engineering Sustainability. Vol. 158, Issue ES4, Institution of Civil Engineers, London.
- Bell S & Morse S (2008). Sustainability indicators, measuring the immeasurable? Earthscan.
- Bone BD, Barnard LH, Hills CD (2004). Guidance on the use of Stabilisation/Solidification for the Treatment of Contaminated Soil. Science Report: SC980003/SR1, Environment Agency, UK.
- Bone BD (2007). Verification of remediation of land contamination. Science Report – NC/00/38/SR, in draft, UK Environment Agency.
- British Standards Institution (1997). BS EN ISO 14040:1997, Environmental management — Life cycle assessment – Principles and framework, BSI London.
- Carey MA, Fretwell BA, Mosley NG, Smith JWN (2002). Guidance on the Design, Construction, Operation and Monitoring of Permeable Reactive Barriers. National Groundwater & Contaminated Land Centre report NC/01/51, UK Environment Agency.
- EC Water Framework Directive (2000). 2000/60/EC,

- Official Journal L 327 , 22/12/2000 :1-73.
- Environment Agency and the Department for Environment, Food and Rural affairs (2004). Model procedures for the management of land contamination, Contaminated Land Report 11.UK.
- Health & Safety Executive (2009). REACH - Substances of Very High Concern, <http://www.hse.gov.uk/reach/svhc.pdf> - accessed June 2009.
- Jefferis SA, Norris GH, Thomas AO (1997). Contaminant barriers: from passive containment to reactive treatment zones. Fourteenth International Conference on Soil Mechanics and Geotechnical Engineering, Hamburg.
- Jefferis SA, Doe G, Tedd P (1999). UK National Specification for the construction of slurry trench cut-off walls as barriers to pollution migration. Institution of Civil Engineers, UK.
- Jefferis SA (2002a). Can we identify sustainable remediation techniques for contaminated land? Proc. 4th International Congress on Environmental Geotechnics, Rio de Janeiro, Brazil: 1039-1058.
- Jefferis SA (2002b). Engineering design of reactive treatment zones and potential monitoring problems. Advanced Ground water Remediation, Active and Passive Technologies. Simon, F.G., Meggyes, T., and McDonald, C. (Eds.). Thomas Telford Publishing, London, ISBN 0727731211: 75-86.
- Jefferis SA (2004). Geotechnology in harmony with the global environment: dream or deliverable? International Conference on Soil Mechanics and Geotechnical Engineering, Kyoto.
- Jefferis SA (2008). Moving Towards Sustainability in Geotechnical Engineering. Proc. GeoCongress 2008, Geotechnical special publication No.178. Reddy K.R., Khire M.V. and Alshawabkeh A.N. (Editors), American Society of Civil Engineers, New Orleans: 844-851.
- LaGrega M, Buckingham P, Evans J, Environmental Resources Management (2001). Hazardous Waste Management. McGraw Hill.
- Leiper Q, Fagan N, Engstrom S, Fenn G (2003). A strategy for sustainability. Engineering sustainability, Institution of Civil Engineers, London.
- Levenspiel O (1999). Chemical reaction engineering. 3rd ed, John Wiley and Sons.
- Mazur A (1998). A Hazardous Inquiry, The Rashomon Effect at Love Canal. Harvard University Press.
- Pediaditi K, Wehrmeyer W, Chenoweth J (2006). Sustainability evaluation for brownfield redevelopment. Proc. Institution of Civil Engineers Engineering Sustainability 159 March:3-10.
- Peters C (2006). Remediation position statements. Environment Agency, UK.
- Porritt J (2005). Capitalism as if the World matters. Earthscan.
- Shackelford C & Jefferis SA (2000). Geo environmental engineering for in situ remediation. Proc. GeoEng2000, Technomic Publishing Co., Inc:121-185.
- Sheppard C, Jefferis SA, Jacobs A (2008). Contaminated Land, Tolley's Environmental Law and Procedures Management, Lexis Nexis UK.
- US Environmental Protection Agency (USEPA) remediation website accessed June 2009:<http://www.clu-in.org/remediation/>.
- Weeks JM, Sorokin N, Johnson I, Whitehouse P, Ashton D, Spurgeon D, Hankard P, Svendsen C, Hart A (2004). Biological Test Methods for Assessing Contaminated Land, Science Group Report P5-069/TR1. UK Environment Agency.
- World Commission on Environment and Development. (1987). Our common future. Oxford University Press, UK.

IN-SITU CONTAINMENT FOR WASTE LANDFILL AND CONTAMINATED SITES

Takeshi KATSUMI¹, Toru INUI² and Masashi KAMON³

ABSTRACT: Management of waste landfill and contaminated sites has been a great concern in the discipline of geotechnical and geoenvironmental engineering. First, the current Japanese status of remediation of contaminated sites and waste containments are summarized in this paper, particularly focusing on the importance of development of in-situ remediation and containment technologies. Second, a construction technique for the vertical cut-off wall consisting of soil-bentonite mixture (SBM) which has been developed by the authors is presented. Third, environmental acceptability of pile installation through clay layer at closed landfill sites is discussed. The developed construction technique for SBM is implemented by employing the trench cutting and re-mixing deep wall method (TRD method) to achieve homogeneity of the wall. The trench cutting is first conducted supplying bentonite slurry to maintain the workability of the soil inside the trench, and then re-mixing with bentonite powder is conducted in the trench. In this paper, the construction method and the laboratory testing results on the hydraulic barrier performance of SBM focusing on its chemical compatibility is presented. Environmental acceptability of pile installation has been a concern when, in the redevelopment of closed waste landfills (e.g. the coastal landfill sites), steel pile foundation may be employed to obtain the bearing capacity of the facilities to be constructed. When piles are installed to reach the bearing layer beneath the clay layer, the leakage of leachate through the interface between the steel pile and the clay layer should be carefully considered to assure the barrier performance of clay layer, since the clay layer is intended to act as a barrier layer. This paper presents the research attempts to measure the interface transmissivity values between the steel and the clay, and confirms that the amount of leakage is negligible for the normally-consolidated state.

KEYWORDS: in-situ containment, bentonite, hydraulic conductivity, cut-off wall, pile foundation, clay liner

INTRODUCTION

Management of waste landfill and contaminated sites has been an important issue in the discipline of geotechnical and geoenvironmental engineering. Effective measures to promote the redevelopment of contaminated sites and waste landfill sites should be implemented.

Vertical cut-off walls are constructed at contaminated sites to contain the wastes and contaminants and prevent their transport in the aquifer. A hydraulic barrier material in the cut-off wall system needs to have a low hydraulic conductivity, and includes several types of materials such as geomembrane, steel (pipe) sheet pile, soil-cement, cement-bentonite, soil-bentonite, etc. Among them, soil-bentonite mixture (SBM) is one of the most widely used materials since it can provide low hydraulic conductivity values as well as sufficient deformability (e.g. Grube 1992). However, there are still several issues to be solved in order to promote the application of SBM, such as achieving the higher construction quality and

understanding the chemical compatibility.

Construction over the closed landfill sites has been a challenging issue. Particularly, whether the pile installation through the clay layer acting as a landfill bottom barrier is environmentally acceptable or not has been a great concern in the redevelopment of closed waste landfill sites in particular coastal landfill sites. The coastal landfill sites have been constructed in certain places around metropolitan areas in Japan, mainly because many coastal areas have thick clay layers with low hydraulic conductivity which can be used as landfill bottom barriers. After the completion of waste reclamation, these coastal landfill sites are expected to create new land space in urbanized areas where new space is difficult to find. In the redevelopment of such closed waste landfills, steel pile foundation may be employed to obtain the sufficient bearing capacity of the facilities to be constructed, because the waste layers are not suitable for bearing layer as well as the clay layers are usually too soft. When piles are installed to reach the bearing layer

¹ Professor, Graduate School of Global Environmental Studies, Kyoto University, Japan. Email: tkatsumi@mbox.kudpc.kyoto-u.ac.jp

² Assistant Professor, Graduate School of Global Environmental Studies, Kyoto University, Japan. Email: inui@mbox.kudpc.kyoto-u.ac.jp

³ President, Takamatsu National College of Technology, Kagawa, Japan; Professor Emeritus, Kyoto University, Japan

beneath the clay layer, the leakage of leachate through the interface between the steel pile and the clay layer should be carefully considered to assure the barrier performance of clay layer, since the clay layer is intended to act as a barrier layer.

First in this paper, the current Japanese status of remediation of contaminated sites and waste containments is reviewed. Second, a construction technique to install the SBM vertical cut-off wall which has been proposed by the authors (e.g. Kamon et al. 2006 and Katsumi et al. 2008b) is presented. The laboratory testing results on the hydraulic barrier performance of SBM focusing on its chemical compatibility is addressed. Third, environmental acceptability of pile installation through clay layer at closed landfill sites is discussed.

JAPANESE STATUS ON THE MANAGEMENT OF CONTAMINATED SITES

Several serious accidents and important events related to geoenvironmental engineering in Japan are listed in Table 1. The first case history of soil contamination discussed in Japan might be one occurred in a copper mining site in 1870s. However, many cases of soil and groundwater contaminations happened at the latter half of the 20th century, when rapid industrialization has been accomplished. In particular, groundwater contaminations with TCE (trichloroethylene) or PCE (tetra-chloroethylene) were detected at the various sites of several types of manufacturing facilities including chemistry, machinery, etc. in 1980s. In 1990s, soil and groundwater contaminations resulting from the improper barrier systems of waste landfills have been arisen at several sites. As a result, "Waste Management and Public Cleansing Law," which was originally established in 1970 to prescribe the framework for waste management, has been modified, and regulatory requirement for landfill bottom liners has been amended in 1998 as follows: The regulation permits that a natural clay > 5 m in thickness with hydraulic conductivity < 1×10^{-7} m/s could be utilized as a liner. Otherwise, it requires one of three following engineered liner systems: (1) two geomembranes (GMs) sandwiching a non-woven fabric or other cushion material, (2) a GM underlain by an asphalt-concrete layer > 5 cm in thickness with hydraulic conductivity < 1×10^{-9} m/s, or (3) a GM underlain by a clay liner > 50 cm in thickness and having hydraulic conductivity < 1×10^{-8} m/s.

Illegal dumping has also been becoming a serious environmental issue since 1990s. One of the serious case histories is that approximately 560,000 ton of wastes including toxic chemicals have been illegally dumped in Teshima Island in Setouchi Sea in the western part of Japan. At this illegal dumping site, the integrated measure

consisting of containment, excavation and removal, and vitrification treatment has been being conducted. There are several other illegal dumping sites which have caused

Table 1 Some important accidents and regulatory actions (in *Italic*) related to soil and groundwater contamination in Japan.

Year	Event
1877	<i>Soil contamination was first discussed in the National Congress.</i>
1955	Itai-itai disease (Cd)
1959	TCE production was increased.
1965	PCE production was increased. Cleaners' industry was increased.
1967	<i>Public Nuisance Countermeasures Basic Law (changed to Environmental Basic Law 1993)</i>
1970	<i>Law for Prevention of Soil Contamination in the Agriculture Sites</i>
1970	Soil contamination with Cr(VI) in Koto-ku, Tokyo
1980s	Soil contamination disclosure when national research institutes' movements.
1981	Groundwater contamination with TCE and PCE in Takatsuki-city (Osaka), Hino-city (Tokyo), etc.
1982	Groundwater contamination with TCE and PCE in Hachioji-city, Fuchu-city, Kumamoto, etc.
1983	<i>Groundwater investigation by the Environmental Agency</i>
1983	TCE contamination in Taishicho (Hyogo)
1986	<i>Guideline for Soil Contamination in Urban Area</i>
1991	<i>Environmental standards for soil were established for 10 chemicals. (Currently, 26 chemicals for urban area and 3 chemicals for agriculture site.)</i>
1992	<i>Guideline for Soil Contamination Measures for National Area.</i>
1999	<i>Environmental standards for groundwater were established.</i>
1999	<i>Guideline for Investigation and Remediation of Soil and Groundwater Contamination.</i>
1999	<i>Guidelines for DXNs. Law for DXNs.</i>
2000	Arbitration for the abandoned wastes site in Teshima island, Kagawa. (Illegal dumping started in 1978)
2001	Abandoned wastes in Aomori-Iwate area.
2002	<i>Soil Contamination Countermeasures Law (SCCL)</i>
2006	<i>"Guideline for the measure against petroleum contaminated soils – against oil smells and films" by Min. of Environment</i>

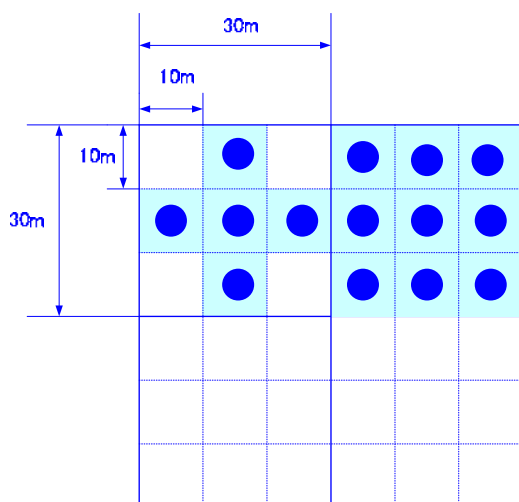


Fig. 1 Sampling point for site investigation of soil contamination according to Soil Contamination Countermeasures Law (SCCL)

serious environmental and social problems.

Construction works over old or closed landfill sites are of another great concern. These cases should be governed by 2 different governments. Waste management and environmental preservation are administrated by the Ministry of Environment, while construction works is administrated by the Ministry of Land, Infrastructure, and Transport. Recently, several regulatory guidelines and/or manuals have been issued cooperatively with two or more governmental bodies.

Environmental standards have been prescribed for soil and groundwater, as well as water and air. However, the environmental standards for soil and groundwater are rather new. Originally, the environmental standard for soil was prescribed only for the agricultural site in 1970. In 1991, the environmental standard for soil, which is no more limited to the agricultural site, has been prescribed. For this standard, leaching tests are conducted on 26 toxic chemicals (including heavy metals and volatile organic chemicals) for urban sites and 3 chemicals for agricultural sites (Cu, Cd, As).

Soil Contamination Countermeasures Law (SCCL), enacted in 2002, has brought various influences on the activities related to geo-environmental engineering. This law has been amended in 2009. Under this Law, two other criteria have been established in addition to the above-mentioned environmental standards; “composition value” and “leaching value (II).” Composition value, which is determined by the extraction using 1 N HCl, is used for the criterion against direct intake of soil. Leaching value (II) is for the criterion whether the contaminated soil can be measured by containment or immobilization.

SCCL requires the land owner to conduct the site investigation if the site of concern meets the designated

conditions; (1) land area is larger than 3000 m² and designated facilities were located and will be demolished due to the change of land use, or (2) there is some concerns of soil and/or groundwater contamination. The designated facilities are for example factories using toxic chemicals, and have been listed by the government. SCCL also presents the method how to conduct the site investigation; the investigation is conducted basically for 1 point per 100 m² (or 1 point per 900 m² if it can be proven from the records that there is low possibility for soil contamination) as shown in Fig. 1, and, if the soils do not satisfy the criteria, not only the top soil, but also soils at the depths of 1 m, 2 m, 3 m etc. should be tested. The reason why one unit has been decided 100 m² is from the previous statistics indicating that areas of the contaminated sites in Japan mostly exceed 100 m². Many researchers and practitioners have pointed out that this investigation method does not perfectly find the contamination, and also that there are some loopholes in the concept. Yet, this law has really been promoting the site investigation. Many land owners have been conducting site investigation voluntarily even if the site does not meet the designated conditions.

Table 2 Remediation measures applied to the contaminated soil and/or groundwater according to Soil Contamination Countermeasures Law

Measures		Numbers
Soil excavation & removal		296 (63.8%)
Bioremediation		18 (3.9%)
Chemical treatment		16 (3.4%)
In-situ remediation	Soil vapor extraction	20 (4.3%)
	Pump-and-treat	24 (5.2%)
	Soil washing	5 (1.1%)
	Other in-situ technology	3 (0.6%)
Immobilization and insoluble treatment		5 (1.1%)
In-situ Containment		14 (3.0%)
Pavements or embankments		34 (7.3%)
Others		29 (6.3%)

If the contamination exists, the land owner basically has a responsibility for measures. Since measures to prevent the human risks are required, not only contaminants removal including soil excavation/removal and contaminant removal but also containments, immobilization, or other technologies, can be applied. However, soil excavation and removal has been a most widely applied technology (more than 60%, as shown in Table 2), partly because of the preference of land owners and contractors. The amounts of excavated soils in Japan are estimated at 3,060,000 ton/year, and 73% of them are

used as a clay source in cement manufacturing. Other contaminated soils excavated are transported to landfill sites or soil treatment plants. Illegal dumping might exist. Considering such situations, in-situ technologies other than soil excavation and removal should be more widely applied. Thus, higher construction quality and performance are required for containment technologies including SBM discussed in this paper.

There are other emerging issues related to geo-environmental engineering listed below:

(1) To promote the resource recycling, utilizations of wastes, by-products, and soils generated through construction works have been promoted. Currently, 98-99% of waste cement concretes and asphalt concretes generated are utilized in construction works including earthen works. It is required to promote the further reuse of surplus soil; a large amount of the soil (195 million m³) was generated from construction sites, and 61 million m³ of it was reused at construction sites in 2005. Review on this issue is presented in Katsumi et al. (2008a).

(2) Natural contamination has been becoming of great concern. There are several excavation sites, in which the excavated soils are filled in the containment facility similar to waste landfills because these soils might naturally contain heavy metals such as As, Pb, etc. There have been discussions whether the current measures are reasonable or not. Protocol should therefore be established to evaluate the soils which have a possibility of natural contamination. Treatment and utilization methods should also be established (e.g. Dejima et al. 2008).

(3) Coastal landfill sites have been common in Japan, and are expected to create new land space. To build heavy facilities, pile foundations will sometimes be required to ensure the bearing capacity, and piles will reach the sandy layer below the clay layer, regarded as the barrier layer. Whether or not the installation of piles through the bottom clay barrier at coastal landfill sites would be environmentally acceptable has been a great concern, and has been discussed by many researchers. This issue is discussed in the latter chapter.

SBM (SOIL-BENTONITE MIXTURE) CUT-OFF WALL FOR IN-SITU CONTAINMENT

Construction Method

As discussed in the previous chapter, it is expected that containment technologies would be more widely applied. One of the great concerns on cut-off wall systems may include the quality assurance because they are constructed in-ground. Homogeneity is an important factor since the larger variability in the hydraulic conductivity

leads to the higher flux of contaminant out of the barrier system even though the average hydraulic conductivity values are equal (Britton and Filz 2007).

A new method for constructing the SBM vertical cut-off wall has been developed by employing the trench cutting and re-mixing deep wall (TRD) method, in order to achieve the high homogeneity of the in-ground wall (Kamon et al. 2006 and Katsumi et al. 2008b). Fig. 2 shows the construction sequence of the SBM vertical cut-off wall employing the TRD method. First, the trench cutting is conducted supplying bentonite slurry to maintain the workability of the soil inside the trench. Then, re-mixing with bentonite powder is conducted in the trench. The advantage of employing the TRD method is to construct the cut-off wall of high homogeneity even in the layered ground, since the cutter post which advances horizontally through the layers excavates, injects slurry or powder from its head, and mixes the soil, forming a continuous wall (e.g. Kamon et al. 1998).

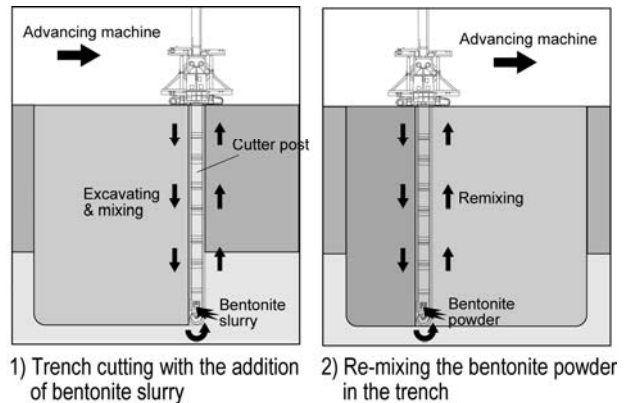


Fig. 2 Construction process of SBM vertical cut-off wall with TRD method

Chemical Compatibility of Bentonitic Barrier

It is well known that the hydraulic conductivity of bentonite-based material strongly depends on the chemical component of the permeants and/or the pore water (e.g. Shackelford et al. 2000, Katsumi et al. 2007) since the bentonite does not swell and/or the swelling is reversed in the presence of inorganic solutions or some organic liquids (Norrish and Quirk 1954). Particularly, inorganic solution containing polyvalent cations increased hydraulic conductivity with relatively lower concentration (~ 0.1 mol/L). This is because the existence of the polyvalent cations results in the development of thinner diffuse double layers and the less osmotic swelling. Fig. 3 illustrates the schematic drawings of the effects of valence of cations on osmotic swelling. Accordingly, the first wetting liquid dominantly affects the hydraulic performance of the clay barriers. When the SBM is employed as a barrier material, its chemical compatibility

should be assessed under the given conditions in the field. In the following sub-sections, the experimental results of hydraulic conductivity tests for the SBM specimens containing different concentrations of the divalent cation in the permeants as well as in the pore water are presented. Based on the test results, the effect of the divalent cation on the hydraulic conductivity of SBM was clarified.

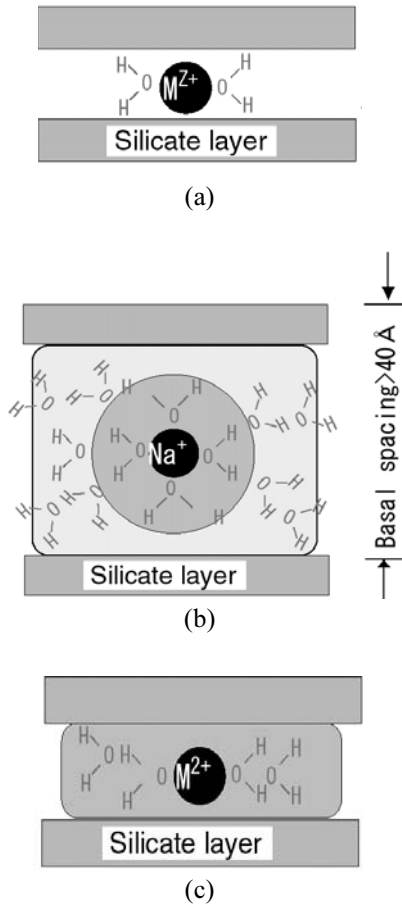


Fig. 3 Effects of valence of cations of osmotic swelling of smectite. (a) silicate layer, (b) osmotic swelling, and (c) restricted osmotic swelling due to the presence of divalent cations

Experimental Methods

Among three different soils used for the experimental study, experimental results on only one type of soil is presented in this paper. This soil is a mixture of volcanic cohesive soil and sandy gravel collected at a pilot scale test site (referred to composite soil in the following), presented in Kamon et al. (2006). The soil was sieved through a 4.75 mm-opening screen prior to the preparation of SBM specimen. The composite soil was prepared by mixing sandy gravel and volcanic cohesive soil at their natural water contents. The mixing ratio of 25:4 by dry weight (sandy gravel: volcanic cohesive soil)

was determined based on the thickness of each layer obtained from the boring log on the pilot test site. Ca^{2+} concentration in the pore water was adjusted to the target value by using the calcium chloride ($CaCl_2$) solution.

Simulating the process of the SBM cut-off wall construction by the TRD method, 10%-concentration hydrated bentonite slurry was blended with the soil first. The additive content of the bentonite slurry was determined based on the flowability of the soil-slurry mixture, approximately 150-mm flow value according to JIS R 5201. Once a mixture of suitable flowability was established, 50 to 150 kg/m^3 powder bentonite was then added and mixed using the soil mixer. The procedure for the preparation is summarized in Fig. 4.

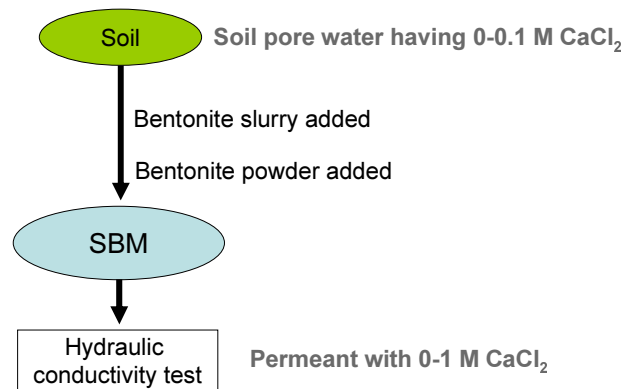


Fig. 4 Preparation of SBM specimen and hydraulic conductivity test

After consolidation at 30 kPa in the oedometer, SBM specimens having a 30 mm in height and 60 mm in diameter were subjected to the hydraulic conductivity tests. A flexible-wall permeameter with a fallen-head system according to ASTM D5084 was employed. A confining pressure of 30 kPa and a hydraulic gradient of approximately 30-40 were applied during the permeation. Permeation continued until the following requirements were confirmed: 1) the volume of the effluent and the influent were the same, 2) the change in hydraulic conductivity values with time was negligible, 3) pore volumes of flow were greater than 3, and 4) the electrical conductivity of the effluent was equal to that of the influent. Two test series are presented in this paper, namely P-series and N-series. P-series was designed to assess the chemical compatibility of SBM attacked by the solution containing $CaCl_2$. In this series, bentonite in SBM has been firstly wetted with pore water of original soil, and hydraulic conductivity tests were then conducted using $CaCl_2$ solutions as permeant. In the N-series, the expected detrimental effect of the $CaCl_2$ concentrations in original soil on the hydraulic conductivity was verified. In this case, swelling of the bentonite in SBM is impeded, due to the concentration of

inorganic chemicals in the soil and/or the groundwater at a contaminated site.

As the target level of hydraulic barrier performance, a laboratory hydraulic conductivity of 1×10^{-9} m/s might be one reference criteria based on the considerations of field performance required.

Effect of Inorganic Chemical

Fig. 5 illustrates the hydraulic conductivity values for the content of bentonite power (C_B) of 100 kg/m^3 , affected by the CaCl_2 concentration in permeant, c_p (Kamon et al. 2006). Hydraulic conductivity for $c_p = 0.1$ M is 3.5 times higher than that for distilled water. Another finding is that the difference in hydraulic conductivity is negligible for c_p higher than 0.1 M. For $c_p = 1.0$ M, hydraulic conductivity is slightly lower than those for $c_p = 0.1$ and 0.25 M probably due to the higher viscosity of the permeant. These observations confirm that hydraulic conductivity of SBM is not significantly increased even against the permeant containing the 1.0 M polyvalent cation if the bentonite in SBM is well hydrated with soil pore water. Prehydration of SBM with soil pore water will be very effective in obtaining the low hydraulic conductivity permeated with chemical solutions.

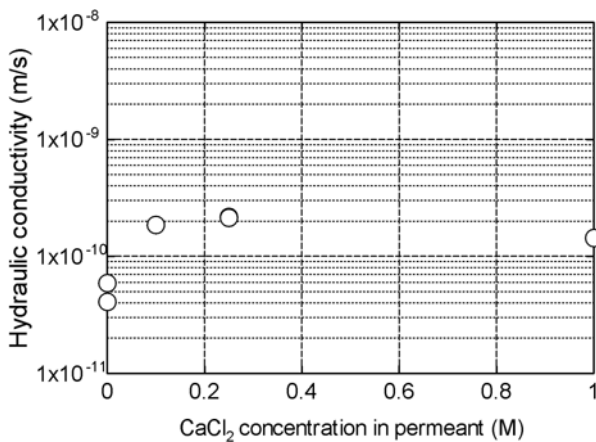


Fig. 5 Results of the hydraulic conductivity tests for $C_B = 100 \text{ kg/m}^3$ in P series: Effects of CaCl_2 concentration in permeant (Kamon et al. 2006)

The hydraulic conductivity values of SBM ($C_B = 100 \text{ kg/m}^3$) for different CaCl_2 concentrations in pore water of the original soil, $c_{c,sw}$ are shown in Fig. 6. The higher hydraulic conductivity values were obtained for the higher $c_{c,sw}$. Although the pore water containing calcium ions is diluted by the water fraction of the bentonite slurry, there was a significant increase in hydraulic conductivity. Hydraulic conductivity values were increased linearly for $c_{c,sw}$ lower than 0.05 M. However, for $c_{c,sw}$ higher than 0.05 M, they still increased but by

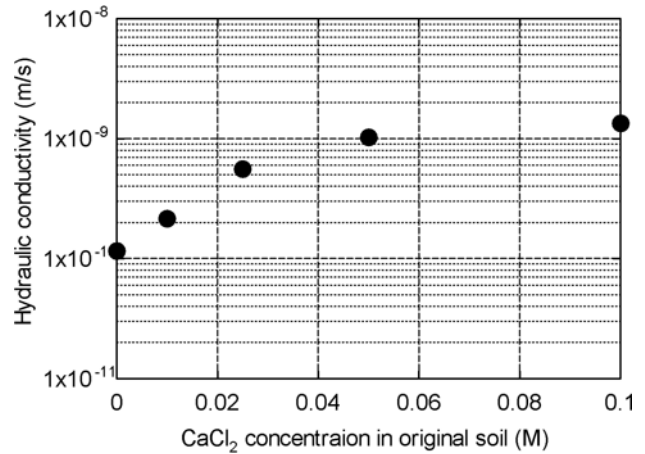


Fig. 6 Results of the hydraulic conductivity tests for $C_B = 100 \text{ kg/m}^3$ in N series: Effects of CaCl_2 concentration in original soil (Katsumi et al. 2008b)

the smaller rate. For 0.1 M, hydraulic conductivity reached higher than 1×10^{-9} m/s.

By comparing the effects of divalent cations on the hydraulic conductivity when they exist in permeant and in pore water of the original soil, it can be concluded that the cation in the pore water causes more significant increase in the hydraulic conductivity. The hydraulic conductivity for 0.1 M in permeant was 3.5 times as high as that for 0 M in permeant. In contrast, the increase in the CaCl_2 concentration in pore water from 0 to 0.1 M resulted in the increase in hydraulic conductivity by more than one order of magnitude. This difference indicates that the prehydration of bentonite is an important factor for the chemical compatibility of the SBM. Its effect is not minor even in the case that the divalent cation concentration in pore water is lower than 0.05 M as shown in Fig. 6. Thus, the concentration of the divalent cation and its variation in groundwater at the site of concern should be considered in evaluating the hydraulic barrier performance of SBM.

Effect of Bentonite Additive Content

The hydraulic conductivity values in N series for various C_B are shown in Fig. 7. Adding the larger content of bentonite was able to lower the hydraulic conductivity, even when the CaCl_2 concentrations in original soil were relatively high (0.05 or 0.1 M). Even for the highest CaCl_2 concentration of 0.1 M, hydraulic conductivity was lower than 1.0×10^{-9} m/s in case of $C_B = 150 \text{ kg/m}^3$. From these observations, when the SBM vertical cut-off wall is constructed at the contaminated site where the inorganic chemical concentration in soil/groundwater is high, its hydraulic barrier performance can be enhanced by adding the larger amount of bentonite. In the case that the SBM was prehydrated (CaCl_2 concentration in pore water = 0 M), hydraulic conductivity of lower 1.0×10^{-9}

m/s was achieved by adding 50 kg/m³ of powder bentonite for the composite soil used in this study.

Further investigations including design methods and the effects of soil types are discussed in Kamon et al. (2006) and Katsumi et al. (2008b, 2009).

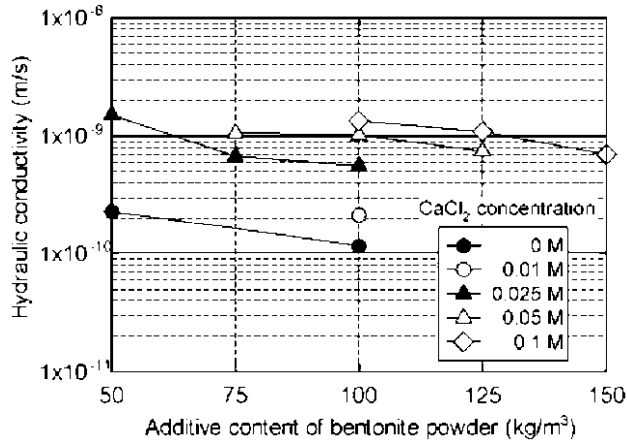


Fig. 7 Hydraulic conductivity vs. content of bentonite powder in N series (Katsumi et al. 2008b)

PILE INSTALLATION OVER CLOSED LANDFILL SITES

Possible Problems

Whether the pile installation through the clay layer acting as a landfill bottom barrier is environmentally acceptable or not has been a great concern in the redevelopment of closed waste landfill sites in particular coastal landfill sites, as previously mentioned (Fig. 8).

Before discussing the pile installation over closed landfill sited, pile foundations at soil reclamation sites are discussed. Reclamations have been conducted to develop new land space in metropolitan areas of Japan. Pile foundations have been applied in many cases to ensure the bearing capacity of the super-structures. These piles reach the sandy or gravel layer beneath the sea bed clay layer or reclaimed dredged clay layer. Fig. 9 shows the forces acting on the piles. When the consolidation is significant, negative skin friction occurs between the piles and the clay due to the settlement of these clay layers (Fig. 9 (b)). As a result, excessive axial compressive stress acts on piles due to the negative skin friction. The various field data at the reclamation sites have shown that a significant amount of axial compressive stress acted for the piles due to the negative skin friction (JSSMFE 1969, Saito et al. 1975, Miyazawa et al. 1981).

This axial compressive stress proves that clay and piles will strongly adhere to each other, if the clay is deformable enough. In addition, even if space was created between the clay and the piles, the space would

be difficult to maintain due to the lateral earth pressure and would close up as the consolidation proceeded and the clay deformed. Therefore, the amount of interface leakage will be expected negligible from the viewpoint of the barrier function of a clay layer with penetrating piles.

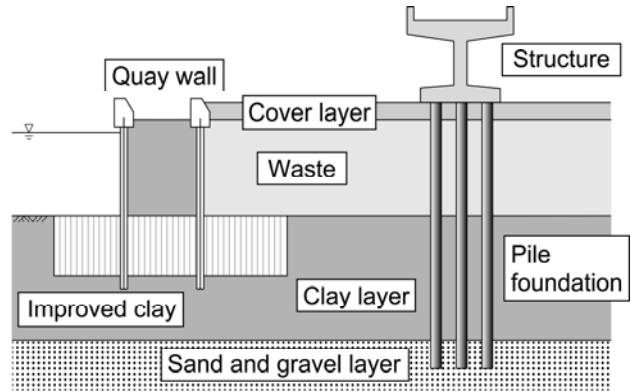


Fig. 8 Pile installation through the bottom clay layer at a coastal landfill site (Kamon et al. 2005)

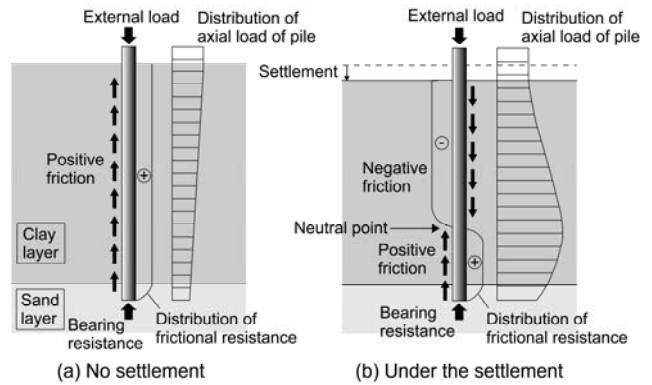


Fig. 9 Friction working at the interface between a pile and the clay (Kamon et al. 2005)

In the case of the installation of piles over coastal landfill sites, it is expected that friction between piles and surrounding clay will act similar to the reclaimed lands above mentioned. Several researchers including the authors have conducted the researches on this subject, and the findings from their researches may conclude that the pile installation does not significantly affect the barrier performance of bottom clay layer (e.g. Kamon et al. 2005, Boutwell et al. 2005, Amatya et al. 2006, Fuji et al. 2006, Manassero et al. 2007, Satyamurthy et al. 2008). In the following sub-sections, the experimental works to obtain the interface leakage are presented.

Modified Rigid-wall Permeameter

To measure the interface leakage between the clay and side wall which simulates the pile surface, modified

rigid-wall permeameter has been developed as shown in Fig. 10 by the authors (Katsumi et al. 2008c). This permeameter is able to measure the volume of water flow through the inner part of the clay specimen separately from the outer part in which the effect of the sidewall leakage may occur. This permeameter is also intended to evaluate the sidewall friction using the earth pressure gauges facilitated at the top and bottom caps.

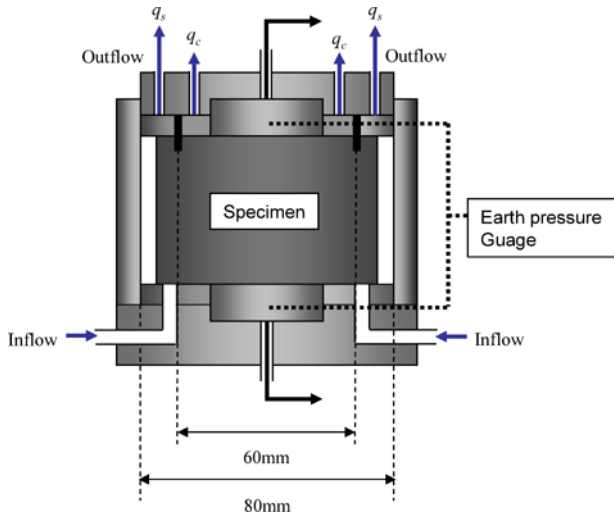


Fig. 10 “Modified” rigid-wall permeameter to measure the side-wall friction and interface transmissivity

To calculate the clay hydraulic conductivity, one-dimensional flow is assumed. It is also assumed that the cross-sectional area of the bullet (a) to induce the influent is virtually separated from inner and outer parts, and the ratio of cross-sectional areas of inner bullet (a_c) over outer bullet (a_s) is equal to the ratio of inner flow (q_c) over outer flow (q_s). Then, the clay hydraulic conductivity (k_c) and apparent hydraulic conductivity (k_s) including the interface leakage can be calculated using the following equation:

$$k = \frac{a \cdot L}{A \cdot (t_2 - t_1)} \ln \left(\frac{h_1}{h_2} \right) \quad (1a)$$

$$a = \frac{q_c}{q_c + q_s} a \quad (1b)$$

$$k = \frac{a \cdot L}{A \cdot (t_2 - t_1)} \ln \left(\frac{h_1}{h_2} \right) \quad (1c)$$

$$a_s = \frac{q_s}{q_c + q_s} a \quad (1d)$$

where L (m) is the length of the specimen, h_1 (m) and h_2 (m) are the water head in the bullet at time t_1 (s) and t_2

(s), and A_s (m^2) and A_c (m^2) are the cross-sectional areas of outer and inner parts in the permeameter.

Experimental Results and Discussions

Four different types of soils, namely Marine clay, Kaolinite, Fukakusa clay, and Mixed clay, were used. Clay specimens consolidated in an oedometer under a pre-consolidation pressure (p_{pre}) of 90 or 180 kPa were trimmed to be 2 mm smaller in diameter than the 80 mm interface transmissivity test cell (modified permeameter) to intentionally create a space between the clay and the sidewall. For all the cases, the consolidation pressures (p) during permeation were applied for 24 hours without applying a hydraulic gradient, and then a hydraulic gradient of about 30 was applied. Termination criteria of the permeation for each vertical pressure consist of equality of effluent against influent (0.75 to 1.25) and four stable values of hydraulic conductivity.

Examples of the experimental results are shown in Fig. 11. For the over-consolidation state of case-3, case-4, and case-5, since effluents were obtained only from the outer part, only k_s , which includes interface leakage, was plotted. (For case-5, intentional cylindrical water passway having 4 mm diameter was created.) For all the test cases, k_s was almost equal to k_c when p (x-axis) was equal to or larger than p_{pre} . Therefore, it was considered that intentional interface space was closed at the normally-consolidated state. The k_s values are always slightly larger than k_c . These slight differences between k_s and k_c are considered to be attributed to the interface leakage. For the case-5 in which intentional cylindrical water passway was created, the leakage was comparable to the one for other cases.

To evaluate the interface leakage, interface transmissivity, K_L (m^2/s), has been defined by Kamon et al. (2005) by the following equation:

$$Q = \left(\frac{\pi D}{4} k + \pi D \cdot K_L \right) \cdot i \quad (2)$$

where Q_{in} is influent volume (m^3/s), D is the diameter of the specimen (m), and i is the hydraulic gradient. Using Equation (2), the K_L values for Marine clay range from 1×10^{-13} to 1×10^{-12} m^2/s , while those for Kaolinite are higher ranging from 1×10^{-11} to 2×10^{-10} m^2/s both for the normally-consolidation state ($p > p_{pre}$).

The K_L values may vary with the soil type. Several factors, such as particle sizes, consistency, etc., have been evaluated in the relation to the K_L value, but the effects of these factors on the transmissivity was not clearly found. As plotted in Fig. 12, the K_L and the clay hydraulic conductivity of four different soils tested have a clear relationship. Note that only the data for the state

of normal consolidation are plotted in this Fig.. If the hydraulic conductivity of the clay is low, the interface transmissivity will be low.

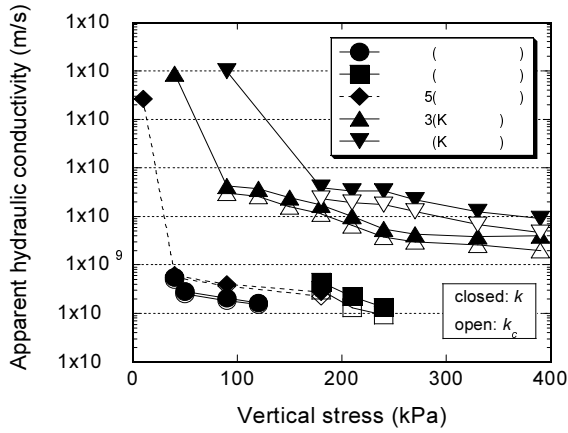


Fig. 11 Apparent hydraulic conductivity values measured using “modified” rigid-wall permeameters (90 kPa pre-consolidation pressure for case-1 and 3, and 180 kPa pre-consolidation pressure for case-2, 4, and 5)

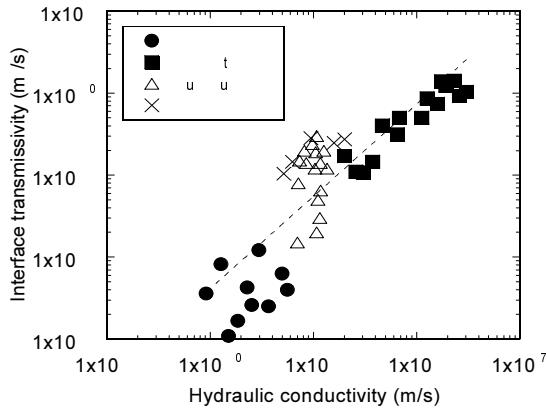


Fig. 12 Interface transmissivity versus hydraulic conductivity under the state of normal consolidation

Most countries including Japan have regulations of base liners with the thickness and hydraulic conductivity. Hydraulic conductivity lower than 1×10^{-7} m/s and thickness larger than 5 m are required for natural clay layer as a landfill bottom barrier in the Japanese regulation. Although interface transmissivity, K_L , can be used to evaluate the interface leakage, a direct comparison with the regulatory requirements is not possible because K_L has a different dimension (L^2/T) from the hydraulic conductivity (L/T). To evaluate the field performance and compare the regulations, two indices for the equivalent hydraulic conductivity, namely flow rate-equivalent hydraulic conductivity and velocity-equivalent hydraulic conductivity, have been proposed by Kamon et al. (2005). Since the velocity-equivalent hydraulic conductivity is still difficult to obtain from the current

experimental results, flow rate-equivalent hydraulic conductivity is discussed herein.

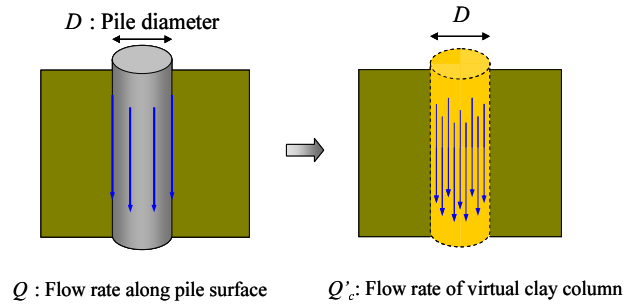


Fig. 13 Flow rates along the interface between the pile and the clay (left) and through the virtual clay column (right) for obtaining equivalent hydraulic conductivity, $k_{eq,f}$ (Kamon et al. 2005)

Flow rate-equivalent hydraulic conductivity is defined as the hydraulic conductivity of a virtual clay column which is assumed to have the same diameter as the pile and the same flow rate as the leakage flow rate from the interface between the clay and the pile as shown in Fig. 13. If the diameter of the pile is D_p (m), the flow rate along the pile surface, Q_L (m^3/s), can be calculated as:

$$Q = \pi D K i \tag{3a}$$

For the virtual clay column, flow rate, Q'_c (m^3/s), can be calculated as:

$$Q' = \frac{\pi D}{4} k i \tag{3b}$$

where $k_{eq,f}$ is the hydraulic conductivity of the virtual clay column (m/s). Since $Q_L = Q'_c$ is assumed, $k_{eq,f}$ is calculated by the following equation, and can be regarded as the flow-rate equivalent hydraulic conductivity.

$$k = \frac{4K}{D} \tag{3c}$$

Fig. 14 illustrates the relations of the $k_{eq,f}$ and K_L values when the pile diameter is 60, 70, or 100 cm. From the experiments conducted, the K_L value ranged from 1×10^{-13} to 1×10^{-10} m^2/s as shown in Fig. 12. Thus, the $k_{eq,f}$ value will range approximately from 1×10^{-12} to 1×10^{-9} m/s, which is significantly lower than the hydraulic conductivity of the regulatory requirements for bottom clay liners (1×10^{-7} m/s). Thus, it can be concluded that the installation of piles through the clay layer will have little adverse effect on the hydraulic barrier performance. Further discussions are made in Kamon et

al. (2005), Fuji et al. (2006), and Katsumi et al. (2008c).

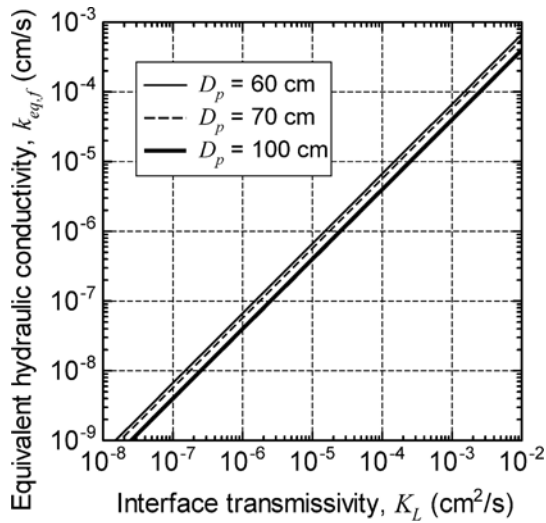


Fig. 14 Relations between interface transmissivity (K_L) and flow rate-equivalent hydraulic conductivity ($k_{eq,f}$) (Kamon et al. 2005)

CONCLUSIONS

This paper presents the review of current status of geoenvironmental engineering in Japan, installation methods of soil-bentonite mixture (SBM) and the results of hydraulic conductivity tests for the SBM focusing on its chemical compatibility, and environmental suitability of pile installation at closed landfill sites. The main conclusions can be summarized as follows:

Among several technological developments on the management of contaminated sites, there are still challenging subjects remained. Higher construction quality and performance are required for containment technologies including SBM.

A new technique for constructing the SBM vertical cut-off wall has been developed by employing the TRD (Trench cutting and re-mixing deep wall) method to attain the higher homogeneity of SBM. When no divalent cation exists in soil pore water, the hydraulic conductivity of the SBM permeated with 1.0 M CaCl_2 solution is only 3.5 times as high as that with the distilled water. Sufficient hydration of the bentonite will maintain the hydraulic barrier performance permeated with the water in which the divalent cations exist. Calcium ions in soil pore water have more significant effect on the hydraulic conductivity than those in permeant. However, hydraulic barrier performance can be enhanced by mixing the larger content of bentonite powder.

To discuss the environmental acceptability of pile installation at closed landfill sites, the modified rigid-

wall permeameter has been proposed to evaluate the interface leakage between clay and steel. Using the modified rigid-wall permeameter, the more accurate interface transmissivity was successfully obtained. For the normally-consolidation state ($p > p_{pre}$), the interface transmissivity values for Marine clay range from 1×10^{-13} to 1×10^{-12} m^2/s , while those for Kaolinite are higher ranging from 1×10^{-11} to 2×10^{-10} m^2/s . For the soils tested, the interface transmissivity values and the clay hydraulic conductivity have a clear relationship for the state of normal consolidation. Flow rate-equivalent hydraulic conductivity values range from 1×10^{-12} to 1×10^{-9} m/s for the tested soils for the state of normal consolidation. These values are sufficiently lower than the Japan regulatory values (1×10^{-7} m/s) for natural clay layer as a landfill bottom barrier. Thus, it may be concluded that the installation of piles through the clay layer will have little adverse effect on the hydraulic barrier performance.

ACKNOWLEDGEMENTS

Valuable support from Mr. S. Araki, Raito Kogyo Co., Ltd., is greatly acknowledged. The laboratory experiments were conducted with the cooperation of S. Hamada, Y. Ogawa, D. Matsushashi, A. Fuji, and A. Takai, former graduate students at Kyoto University.

REFERENCES

- Amatya BL, Takemura J, Khan MRA, Kusakabe O (2006). Centrifuge tests to evaluate effects of pile construction on post closure landfill sites with geological barrier, *5ICEG Environmental Geotechnics*, H.R. Thomas (ed.), Thomas Telford Publishing, London, UK: 353-360.
- Boutwell GP, McManis KL, Nataraj MS, Satyamurthy R (2005). Installation of driven piles in brownfields sites, 2005 PDCA Winter Roundtable.
- Britton JP & Filz GM (2007). High uniformity versus low hydraulic conductivity for vertical barriers in contaminant containment applications, *Geoenvironmental Engineering*, GSP No.163, S.E. Burns, P.J. Culligan, J.C. Evans, P.J. Fox, K.R. Reddy, N. Yesiller (eds.), ASCE: on CD.
- Dejima A, Inui T, Katsumi T, Kamon M (2008). Leaching characteristics of excavated soil containing arsenic by natural origin, *Geo-Environmental Engineering 2008 – Proceedings of the Eighth Japan-Korea-France Joint Seminar on Geoenvironmental Engineering*: 155-158.
- Fuji A, Katsumi T, Inui T, Kamon M (2006). Interface transmissivity between clay material and steel pile installed at coastal disposal site, *Geo-Environmental*

- Engineering 2006 - Proceedings of the Sixth Japan-Korea-France Joint Seminar on Geo-environmental Engineering: 23-27.
- Grube WE (1992). Slurry trench cut-off walls for environmental pollution control, *Slurry Walls: Design, Construction, and Quality Control*, ASTM STP 1129, D.B. Paul et al. eds., ASTM, Philadelphia: 69-77.
- JSSMFE (Japanese Society for Soil Mechanics and Foundation Engineering) (1969). Research on Negative Skin Friction of Piles (Committee Report) (in Japanese).
- Kamon M, Ohta H, Aoi M, Asada S (1998). Development of new river protection method by continuous inclined diaphragm wall, *Environmental Geotechnics*, P.S. Sêco e Pinto (ed.), Balkema, Rotterdam: 35-38.
- Kamon M, Katsumi T, Inui T, Hamada S (2005). Environmental acceptability of the installation of piles through the bottom clay barrier at coastal landfill sites, *Waste Containment and Remediation, Geotechnical Special Publication No.142*, A. Alshawabkeh, C.H. Benson, P.J. Culligan, J.C. Evans, B.A. Gross, D. Narejo, K.R. Reddy, C.D. Shackelford, and J.G. Zornberg (eds.), ASCE, (on CD).
- Kamon M, Katsumi T, Inui T, Ogawa Y, Araki S (2006). Hydraulic performance of soil-bentonite mixture barrier, *5ICEG Environmental Geotechnics*, H.R. Thomas (ed.), Thomas Telford Publishing, London: 733-740.
- Katsumi T, Ishimori H, Ogawa A, Yoshikawa K, Hanamoto K, Fukagawa R (2007). Hydraulic conductivity of nonprehydrated geosynthetic clay liners permeated with inorganic solutions and waste leachates, *Soils and Foundations*, 47(1): 79-96.
- Katsumi T, Inui T, Kamon M (2008a). Wastes and by-products used in geotechnical applications in Japan, *Geo-Environmental Engineering 2008 – Proceedings of the Eighth Japan-Korea-France Joint Seminar on Geoenvironmental Engineering*: 275-282.
- Katsumi T, Kamon M, Inui T, Araki S (2008b). Hydraulic barrier performance of SBM cut-off wall constructed by the trench cutting and re-mixing deep wall method, *GeoCongress 2008: Geotechnics of Waste Management and Remediation, Geotechnical Special Publication No.177*, M.V. Khire, A.N. Alshawabkeh, and K.R. Reddy (eds.), ASCE: 628-635.
- Katsumi T, Kamon M, Inui T (2008c). Environmental acceptability of pile installation at coastal landfill sites, *Proceedings of Second Japan-Korea Geotechnical Engineering Workshop—Geotechnics in Urban Areas*, Japanese Geotechnical Society & Korean Geotechnical Society: 151-156.
- Katsumi T, Inui T, Kamon M (2009). Effects of chemical exposure on the barrier performance of the soil-bentonite wall applied to in-situ containment, *Proceedings of 17th International Conference on Soil Mechanics and Foundation Engineering* (in press).
- Manassero M, Dominijanni A, Artico G, Biral L (2007). Field evaluation of the risk of cross contamination through a natural barrier due to foundation pile construction, *GEE07—Seventh Japanese-Korean-French Seminar on Geo-Environmental Engineering*: 311-318.
- Miyazawa K, Oishi S, Kubo S (1981). Long-term observation and experiment for negative friction at reclaimed land of Daikoku (Yokohama City Hall), *Tsuchi-to-Kiso, JSSMFE*, 29(4): 5-10 (in Japanese).
- Norrish K & Quirk J (1954). Crystalline swelling of montmorillonite, Use of electrolytes to control swelling, *Nature*, 173: 255-257.
- Saito T, Ishigami K, Kamei T, Fukuya T (1975). Vertical bearing capacity of steel piles installed in soft ground, *Tsuchi-to-Kiso, JSSMFE*, 23(7): 35-42 (in Japanese).
- Satyamurthy R, Nataraj MS, McManis KL, Boutwell GP (2008). Investigations of Pile Foundations in Brownfields, *Journal of Geotechnical and Geo-environmental Engineering, ASCE*, 134(10): 1469-1475.
- Shackelford CD, Benson CH, Katsumi T, Edil TB, Lin L (2000). Evaluating the hydraulic conductivity of GCLs permeated with non-standard liquids, *Geotextiles and Geomembranes*, 18(2-4): 133-161.

APPLICATION OF ELECTRICAL RESISTIVITY FOR CEMENT SOLIDIFIED/STABILIZED HEAVY METAL CONTAMINATED SOILS

Song-Yu LIU¹, Yan-Jun DU², Lei CHEN³, Zhi-Bin LIU⁴ and Fei JIN⁵

ABSTRACT: Electrical resistivity is a feature parameter of soils. It could be used to represent some fundamental geotechnical properties of soils. Based on the electrical resistivity study to cemented soil and contaminated soil, the electrical resistivity of cement solidified/stabilized contaminated soils was studied by laboratory test. Five types of artificial heavy metal contaminated soils (HMCS) were made up separately by mixing nitrate of Lead, Zinc, Cadmium, Nickel and Copper into the soils as the source of pollutant, and then treated by cement with different cement contents. Different concentration of heavy metal ions in HMCS was also considered during the test. Electrical resistivity of cement treated HMCS was measured at different curing time. The result shows that the electrical resistivity of cemented soils increases with the curing time and cement content no matter the soil is contaminated or not. The pollutant type and concentration are the main factors for electrical resistivity of contaminated soils no matter it has been treated by cement or not. More heavy metal ions in soil could lower the electrical resistivity of soil. Zinc contaminated soil and cement treated zinc contaminated soil have the highest electrical resistivity as comparing with other HMCS due to the high electrical conductivity of zinc ions. Unconfined compressive strength of cement treated Lead, Zinc, Cadmium, Nickel and Copper contaminated soils increased with the increase of their Electrical resistivity.

KEYWORDS: electrical resistivity, cemented soil, contaminated soil, unconfined compressive strength

INTRODUCTION

Electrical resistivity is a feature parameter of soils which very depends on soil microstructure properties, such as saturation degree, electrical conductivity of pore fluid, porosity, solid particle size and its distribution, ions concentration, and distribution in pore fluid of different soil layers etc. In recent years, the application of electrical resistivity in geotechnical engineering has been concerned by geotechnical researchers. It has been successfully used in ground survey and mapping by linking its value with the variety of stratum condition like the depth of aquifer or bedrock, salt or pollutant injection near the surface ground, underwater line, and thickness of the specific layers. Since the pollutant normally is electrolyte or organic such as heavy metal and hydro carbon oxide, electrical resistivity can easily distinguish the contaminated ground with those uncontaminated. The author's research group did some pilot work on using electrical resistivity to assess the property of specific soils and quality of deep mixing

piles (Liu, 2000, 2004, 2006, 2008; Yu, 2004; Gu, 2005; Han, 2006; Yu, 2007; Zha, 2007 etc.).

Solidification /Stabilization is a soil remediation technology using cement as an agent to mix with contaminated soils to lower the release tendency of pollutant in soils to the environment and strength its engineering property as a cement matrix. This paper discuss the electrical resistivity of cement Solidified/Stabilized heavy metal contaminated soils based on the prior study on the electrical resistivity of cemented soil and pollutant soil.

ELECTRICAL RESISTIVITY MEASUREMENT

Electrical resistivity of material defines as the value when current flow passes through a cube made up with this material with all sides 1m long. It is the reciprocal of electrical conductivity. The lower the electrical conductivity, the higher the electrical resistivity is. Soil is simply considered as a two phase material, solid framework and pore water. The electrical resistivity of

¹ Professor, Institute of Geotechnical Engineering, Southeast University, China. Email:liusy@seu.edu.cn

² Professor, Institute of Geotechnical Engineering, Southeast University, China. Email:duyanjun@seu.edu.cn

³ PhD student, Institute of Geotechnical Engineering, Southeast University, China. Email:clove.chenlei@gmail.com

⁴ PhD, Institute of Geotechnical Engineering, Southeast University, China. Email:seulzb@seu.edu.cn

⁵ MS Student, Institute of Geotechnical Engineering, Southeast University, China. Email:lhjinfei@163.com

soil is an integration of that of solid and liquid which simplified as a compound model of parallel connection and series connection. So the value of electrical resistivity is not only related to the characteristic of soil particles and pore water solution, the structure property and temperature can also impact on it. An electrical resistivity measuring box ESEU-1 working in an alternating current and two-phase electrodes condition was developed in the Institute of Geotechnical Engineering of Southeast University based on the double bridge principle (Liu, 2004). The electric frequency of the test apparatus was set as 50 Hz, which is consistent with that used in the daily life of China. The details of the test apparatus were discussed by Yu (2004).

ELECTRICAL RESISTIVITY OF CEMENTED SOILS

Lagoon clay with 60% water content from Yancheng City, Jiangsu Province was treated by 10%, 14% and 18% No.32.5 cement respectively with a designed water cement ratio of 0.5 in the laboratory. Table 1 is the fundamental property of soil. The 70.7mm*70.7mm*70.7mm cubic specimen were prepared and cured in a standard curing room with the temperature of 20 ± 3 °C and relative humidity of 100%. Unconfined compressive strength and electrical resistivity were tested at different curing time (Gu 2005).

Table 1 Fundamental property of soil from Yancheng City

Water content (%)	Organic content (%)	Density (g/cm ³)	Specific gravity
60	3.0	1.678	2.66
Void ratio	Liquid limit (%)	Plastic limit (%)	
1.681	66	31	

The result shows that the electrical resistivity of cemented soil increased with the increase of curing time and cement content (See Fig. 1).

Cement hydration reaction developed with the curing time and the degree of cement hydration mainly depends on the cement content. During this process, pore water in the soil was consumed, and the cementitious matrix bond with soil particles to form a more integrated solid, which resulted in a denser structure and more tortuous pore space. Since the electrical conductivity of pore fluid is much greater than that of soil grain particles, the electrical conductivity of pore fluid with good connectivity (e.g. larger pore size and less torturous path way) is better than those with poor connectivity. As a result, as compared with the untreated soil, the electrical resistivity of cemented treated soil was enlarged with the decreased water content and reduced connectivity.

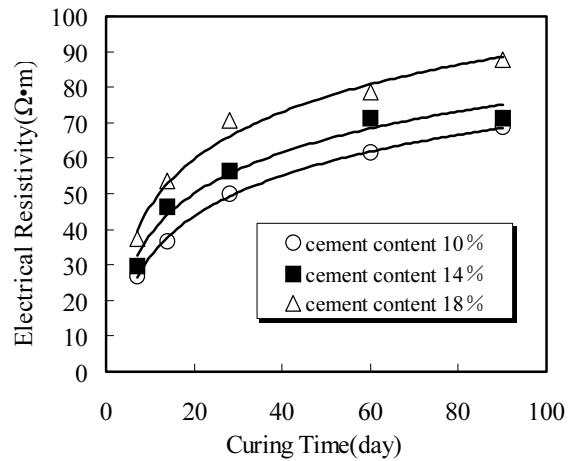


Fig. 1 The verity of electrical resistivity of cemented soil with curing time

Electrical resistivity of cemented soils has a linear relationship with unconfined compressive strength (see Fig. 2). It explains the workability of using electrical resistivity as a faster, easy, reliable and nondestructive tool to assess the quality of cement treated ground.

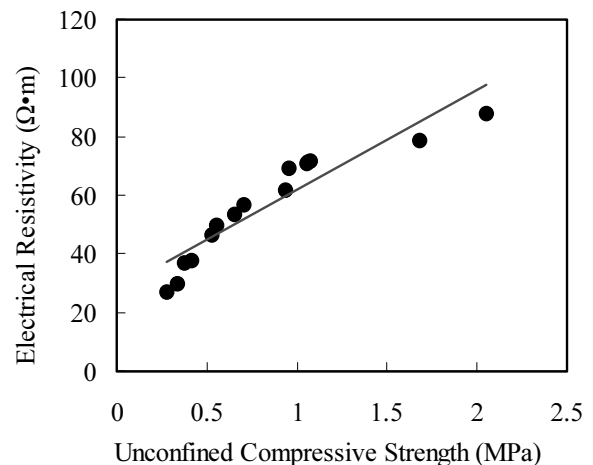


Fig. 2 The relationship of cemented soil between electrical resistivity and unconfined compressive strength

ELECTRICAL RESISTIVITY OF CONTAMINATED SOILS

Contaminated soils were prepared in the laboratory by mixing uncontaminated soils with heavy metal salt solutions. The soil was from Nanjing City, Jiangsu Province, and the fundamental property is shown in Table 2. Two types of typical heavy metal salts, zinc chloride (ZnCl₂) and nickel chloride (NiCl₂) were adopted as target contaminants with different contents (based on the weight of dry soil). Soils were oven-dried

and grounded to mix with heavy metal salt solution homogeneously, and then were allowed to dry in the oven again for 48 hours. After that, soils were crushed to powder. Designed amount pure water was added to the oven-dried soil powder. The soil was then compacted under the condition of its maximum dry density whereas water contents were controlled either greater or lower than the optimum water content. The thickness of each soil specimen was 20 mm while the diameter was 61.8 mm. Electrical resistivity of specimen was measured after that (Han, 2006).

Table 2 Fundamental property of soil from Nanjing City

Water content (%)	Specific Gravity	Liquid limit (%)	Plastic limit (%)	Clay content (%)
31.6	2.7	37	26.5	20.8

Figs. 3 and 4 show the variety of electrical resistivity of ZnCl₂ and NiCl₂ contaminated soils with different concentrations and water contents. No matter the pollutant is ZnCl₂ or NiCl₂, the electrical resistivity of soils decreased with the increase in concentration and water content. The change of electrical resistivity in the case of ZnCl₂ contaminated soil is much considerable than that in the case of NiCl₂ contaminated soil, especially when the contaminant concentration is in a small range. With the same concentration and water content, the electrical resistivity of ZnCl₂ contaminated soil is lower than that of NiCl₂ contaminated soil, especially when the water content is in a high value. That is mainly because the electrical conductivity of Ni²⁺ is poor than Zn²⁺.

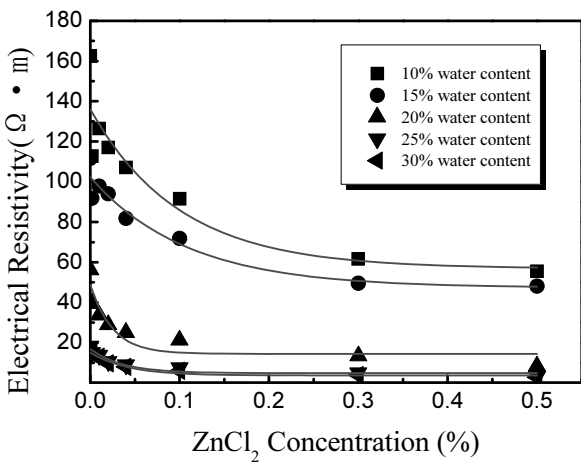


Fig. 3 The variety of electrical resistivity of Zn²⁺ contaminated soils with different ZnCl₂ concentration and water content

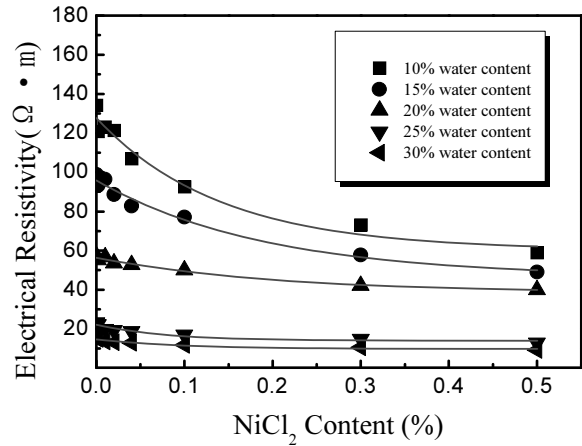


Fig. 4 The variety of electrical resistivity of Ni²⁺ contaminated soils with different NiCl₂ content and water content

Electrical resistivity of heavy metal contaminated soil decreased when comparing with uncontaminated soils due to the presence of active heavy metal ions. Since the electrical conductivity of pore fluid is a primary factor affecting the electrical resistivity of soils, the mobility of active heavy metal ions in the pore fluid would increase the soil electrical conductivity. As a result, the measured soil electrical resistivity decreased. It can be seen from Fig. 5 that the soil electrical resistivity of ZnCl₂ and NiCl₂ solution decreased with the increase of ZnCl₂ and NiCl₂ concentration. The electrical resistivity of NiCl₂ solution is higher than ZnCl₂ solution due to the less electrical conductivity of Ni²⁺ ion. The result presented in Fig. 5 can well explain why the values of measured electrical resistivity of ZnCl₂ and NiCl₂ contaminated soils are different although concentrations are the same.

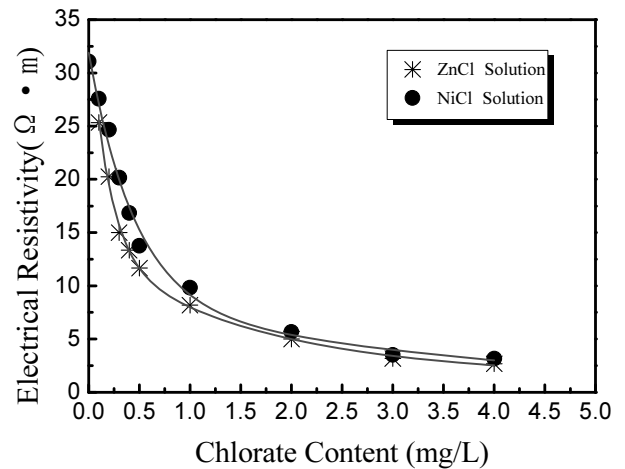


Fig. 5 The variety of electrical resistivity of chlorate solution with different concentration

ELECTRICAL RESISTIVITY OF CEMENT TREATED CONTAMINATED SOILS

The cemented contaminated soils were made up artificially in the laboratory by mixing cement, air-dried uncontaminated soils with heavy metal salt solution. The soil was a mixture of 15% pulverized kaolin and 85% commercial sand with particle size less than 1 mm. Five types of solutions, Lead nitrate (Pb(NO₃)₂), Zinc nitrate (Zn(NO₃)₂), Cadmium nitrate (Cd(NO₃)₂), Nickel nitrate (Ni(NO₃)₂) and Copper nitrate (Cu(NO₃)₂) were added to the predetermined amount of deionized water to form target contaminant solutions. Certain amount of solutions were added to cement, air dried kaolinite and sand admixtures until the water content reached the optimum water content of the kaolinite-sand admixture. Soils were then statically compacted under the condition of maximum dry density of the uncontaminated soil-sand admixture. Each soil specimen has the size of Φ5 cm* H10 cm. Unconfined compressive strength and electrical resistivity of these specimen were conducted at different curing time. Samples were prepared in triplicate denoted Mi-Cj, in which M is the type of heavy metal, C is the cement, i is the heavy metal content by the unit mg/kg, and j is the percentage of cement content.

Fig. 6 shows the relationship between electrical resistivity and unconfined compressive strength of cement treated lead contaminated soils with different lead content. Unconfined compressive strength, increased with the increase of electrical resistivity. Matrix with different Pb²⁺ concentration have nearly same increasing rate. For soil with very high Pb²⁺ content of 30,000mg/kg treated by 7.5% cement, the Pb²⁺ would seriously inhabit or retard the rate of cement hydration (Thomas, 1981), therefore, the soil matrix displayed very low electrical resistivity and poor strength properties.

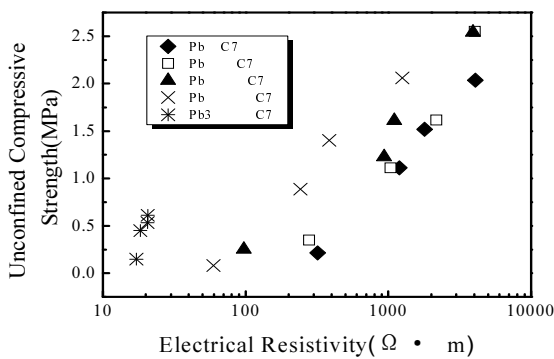


Fig. 6 The relationship between electrical resistivity and unconfined compressive strength with different Pb²⁺ content (1d, 7d, 14d, and 28 d curing time)

Fig. 7 shows the effect of the Pb²⁺ concentration on the value of electrical resistivity of cement treated lead contaminated soils and their variety with curing time. Similar with the case of untreated contaminated soils, the electrical resistivity of cemented contaminated soils decreased with the increase of lead concentration mainly due to the presence of greater amount of active heavy metal ions. The electrical resistivity increased with the curing time since cement hydration in soil had developed during the curing time.

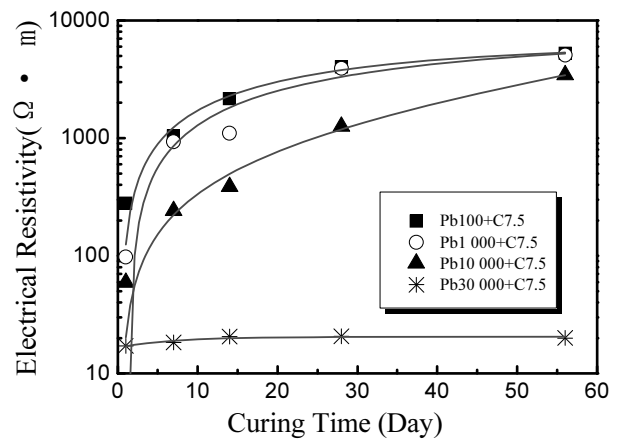


Fig. 7 The variety of electrical resistivity with different lead content and curing time (7.5% cement content)

Cement content is a primary factor for cement hydration as discussed above. Similar with cement treated uncontaminated soils, for cement treated Pb²⁺ contaminated soil, the electrical resistivity also increased with the increase of cement content (See Fig. 8).

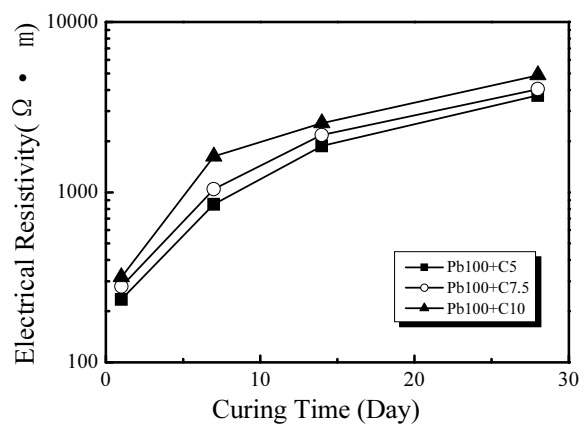
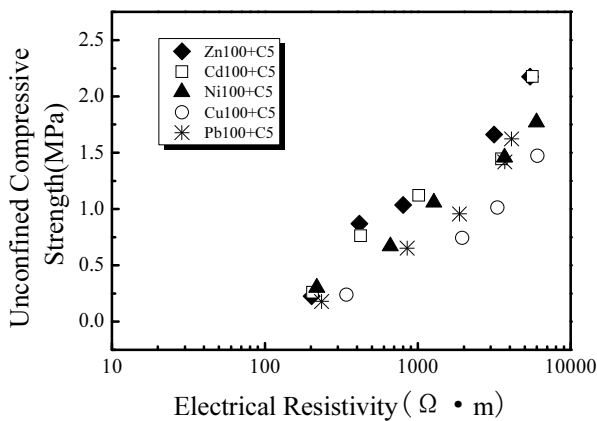


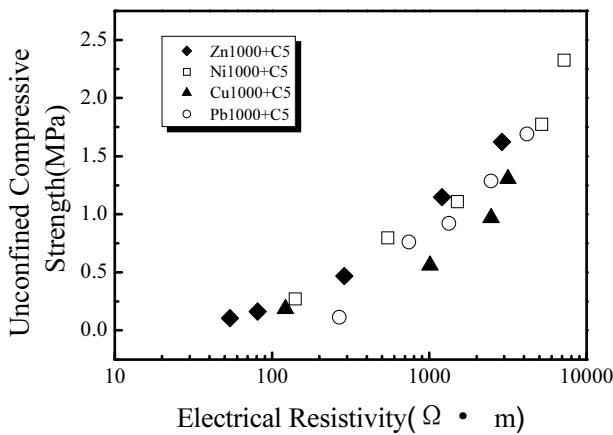
Fig. 8 The variety of electrical resistivity with different cement content (100mg/kg lead content)

Figs. 9a & 9b show the comparison of the electrical resistivity of cement treated soils contaminated by different types of heavy metals Zn²⁺, Cd²⁺, Ni²⁺, Cu²⁺

and Pb^{2+} , and their unconfined compressive strength. With the same pollutant concentration and cement content, 100mg/kg in Fig. 9a and 1,000 mg/kg in Fig. 9b, the unconfined compressive strength increased with the increase in electrical resistivity. Cement treated Cu^{2+} and Zn^{2+} contaminated soils have the highest and lowest electrical resistivity, respectively. This is because Cu^{2+} and Zn^{2+} have the lowest and highest metal activity among these metals. The electrical resistivity of cement treated contaminated soils with 100 mg/kg heavy metal pollutant concentration is higher than that with 10,000 mg/kg heavy metal pollutant. The aforementioned result is consistent with the case of cement treated Pb^{2+} contaminated soils.



(a) 100mg/L heavy metal pollutant



(b) 1 000mg/L heavy metal pollutant

Fig. 9 The relationship between electrical resistivity and unconfined compressive strength with different heavy metal pollutant (1 d, 7 d, 14 d, 28 d, and 56 d curing time)

CONCLUSIONS

(1) The electrical resistivity of cemented soils

increased with the increase of curing time and cement content because that cement hydration reaction changed the micro-structure of soils.

(2) The electrical resistivity of soils decreased with the increase of heavy metal pollutant concentration and water content. The electrical conductivity of pore fluid is the primary factor affecting the soil electrical resistivity. Zn^{2+} contaminated soil has lower electrical resistivity compared with Ni^{2+} contaminated soil due to that Zn^{2+} has higher electrical conductivity.

(3) Unconfined compressive strength of cement treated Pb^{2+} , Zn^{2+} , Cd^{2+} , Ni^{2+} and Cu^{2+} contaminated soils increased with the increase in electrical resistivity. Among these metals, cement treated Cu^{2+} and Zn^{2+} contaminated soils have the highest and lowest electrical resistivity respectively.

(4) Unconfined compressive strength of cement treated Pb^{2+} contaminated soils with different Pb^{2+} content has nearly same increasing rate with the increase of electrical resistivity. Electrical resistivity decreased with the increase of Pb^{2+} content, while increased with the curing time and cement content. For soil with very high Pb^{2+} content of 30 000mg/kg treated by 7.5% cement, Pb^{2+} would seriously retard the cement hydration. Therefore, the soil has very low electrical resistivity and poor strength.

ACKNOWLEDGEMENTS

The authors appreciate the support of the Specialized Research Fund for the Doctoral Program of Higher Education of China under Grant No. 20060286031, and National Natural Science Foundation of China under Grant No. 50878052 and No. 40802065.

REFERENCE

Gu MF (2005). Research on the cemented soil damage model base on the electrical resistance characteristics. Masters Degree Thesis, Southeast University, Nanjing, China.

Han LH (2006). Study on the application of electrical resistivity method in evaluation and reinforcement for contaminated soils. Ph.D. Thesis, Southeast University, Nanjing, China.

Liu SY & Yu XJ (2000). The electrical resistivity characteristic of the cemented soil. Proceedings of the 2nd International Symposium on Lowland Technology, Japan:185-190.

Liu SY & Yu XJ (2004). The circuit diagram of ESEU-1 soil electrical resistivity apparatus. China Patent: ZL03222401.X, 2004-6-30.

Liu SY, Han LH, Du YJ (2006). Experimental study on

- electrical resistivity of soil-cement. *Journal of Geotechnical Engineering*, 28(11):1921-1926.
- Liu SY, Du YJ, Han LH, Gu MF (2008). Experimental study on the electrical resistivity of soil-cement admixtures. *Environ Geol* 54:1227-1233.
- Thomas NL, Jameson DA, Double DD (1981). The effect of lead nitrate on the early hydration of Portland cement, *Cement Concrete Res.* 11(1):143-153.
- Yu M (2007). The application of electrical resistivity and CT method on cement-soil microstructure property. Masters Degree Thesis, Southeast University, Nanjing, China.
- Yu XJ (2004). On the theory and application of electrical resistivity method in geotechnical engineering. Ph.D. Thesis, Southeast University, Nanjing, China.
- Zha FS (2007). Electrical resistivity of structured unsaturated soils and its application. Ph.D. Thesis, Southeast University, Nanjing, China.

RECENT RESEARCH ON THE HYDROGEOLOGICAL AND SETTLEMENT CHARACTERISTICS OF LANDFILLED MUNICIPAL SOLID WASTE

D. J. RICHARDS¹, W. POWRIE¹ and R. P. BEAVEN¹

ABSTRACT: The paper starts with an overview of the changes in the philosophy of landfill design and waste composition that have taken place in the western world over the past 50 years. This provides a context for a summary of the natural processes within landfills that a modern landfill engineer must have knowledge of and take into account. The importance of fluid flow and waste settlement is highlighted; and some research that has led to an improved understanding of the factors governing these processes is described and discussed. Finally, the challenges associated with new waste types now being landfilled in the EU are considered.

KEYWORDS: landfill, hydraulic conductivity, settlement, biodegradation, creep

INTRODUCTION

Although now increasingly viewed as a last resort, landfill has been the primary means of municipal solid waste disposal in many countries for the past hundred years or more: archaeological evidence suggests that the practice dates back millennia. Over the past 50 years, changes in both the philosophy of landfill design and operation and the composition of municipal solid waste have led to the development of a more scientific approach, and the an improved understanding of the processes that take place within a landfill.

The paper starts with a brief description of the changes in the philosophy of landfill design and waste composition that have taken place in the western world over the past 50 years. This provides a context for a summary of the natural processes within landfills that a modern landfill engineer must have knowledge and take into account. The importance of fluid flow and waste settlement are highlighted; and some research that has led to an improved understanding of the factors governing these processes is described and discussed. Finally, the challenges associated with new waste types now being landfilled in the EU are considered.

LANDFILL PHILOSOPHY, PRACTICE AND PROCESSES

Although sanitary measures such as daily cover associated with landfills have been prescribed for some considerable time (since at least the 1920s in the UK),

landfills typically had little in the way of engineered controls (low permeability caps, liners or basal drainage systems) up until the 1960's or later. This was perhaps acceptable when much of the waste being disposed of into landfill was biologically inert: indeed, the use of such material to fill in unwanted holes in the ground (often left over from excavating clay for the manufacture of bricks, or sand and gravel for use in construction) might well appear to be sensible in resource efficiency terms. Prior to the introduction of the Clean Air Act in 1956 (HMSO, 1956), the general replacement of coal by gas as the main fuel for domestic heating and possibly a reduction in the average size of domestic gardens, the biodegradable proportion of municipal solid waste was a maximum of 30% with dust and cinders (ashes) making up over 50% (Watts & Charles, 1999). By the mid-1960's these proportions had been reversed, with the result that a significant component of the municipal solid waste being landfilled was not inert, but would gradually degrade over time, giving off gas and losing solid volume as it did so.

The realisation by the early 1960's that the passage of water through biodegradable or putrescible wastes would give rise to a potentially contaminating leachate led to landfills being located in areas where natural in-ground mechanisms would attenuate escaping leachate before it reached vulnerable ground or surface waters. By the late 1980's, increased regulatory controls on groundwater protection (e.g. the EU Groundwater Directive 80/68/EEC) together with a recognition of the need to control landfill gas (principally methane and carbon dioxide) following the destruction of a house by

¹ School of Civil Engineering and the Environment, University of Southampton, SO17 1BJ, UK. Email: djr@soton.ac.uk

an explosion of landfill gas at Loscoe in March 1986 (see e.g. Sarsby, 2000) had led to a philosophy of contaminant containment rather than any form of controlled release. The containment philosophy culminated in the concept of the dry tomb landfill, which aimed to isolate the waste from the environment by means of an impermeable liner and cap. The (hopefully) small amounts of leachate and gas generated are removed from the site by means of actively managed and pumped drainage and extraction systems.

The problem with the dry tomb approach is that it merely postpones the degradation of the waste, perhaps beyond the reliable life of the containment and gas/leachate management systems. When the waste does eventually degrade it will settle and the cap will subside and crack, allowing rainfall to infiltrate more rapidly. The resulting increase in the moisture content of the waste will lead to increased rates of waste degradation, leachate and gas generation and further settlement. Any landfill containing putrescible waste that has not fully degraded is likely to continue to generate potentially polluting leachate and greenhouse gases, possibly for hundreds of years before stable equilibrium conditions are achieved (Knox, 1990). Ongoing settlement of the waste is likely to result in a requirement for continued maintenance of any restorative cover, for both aesthetic and safety reasons.

It is now generally accepted that the only way in which landfilled wastes can be stabilised and their pollution potential removed within a reasonable timescale (i.e. years or a few decades, rather than hundreds of years) is by increasing the water content to enhance microbial degradation, and passing liquid through the waste to flush out recalcitrant (i.e. non-biodegradable) contaminants. Despite a possibly increased initial infrastructure cost, this has potential economic and environmental benefits in that the extraction and use of the degradation gas to generate electricity becomes more commercially viable; there is no long-term reliance on engineered containment and leachate/gas control measures; and the site should more rapidly reach a stable, non-polluting state in which the requirement for continued monitoring, maintenance and aftercare is reduced or eliminated. The last two of these are consistent with the requirements for a landfill to be viewed as sustainable, as enumerated by the Institute of Wastes Management (1998).

Reducing the polluting potential of wastes within a landfill by enhanced degradation and flushing requires a sound understanding of how liquid moves into and around the waste, and how the hydraulic conductivity of the waste is affected by waste processing, compression, degradation and gassing. Other aspects of landfill design and management, including the specification of final fill levels and the detail of the capping system, require

knowledge of the settlement characteristics of the landfill and the way that settlement will develop over time. The results of some recent research into development of long-term settlements over time and understanding fluid and flow within a landfill will now be presented and discussed.

SETTLEMENT

Fig. 1 shows data of settlement against $\log_{10}(\text{time})$ measured in three Consolidating Anaerobic Reactors (CARs) set up to investigate the linkages between waste degradation, gas generation and settlement. Full details of these experiments are given by Ivanova et al. (2008). CAR3 was a control reactor, in which biodegradation was successfully inhibited for the first 350 days or so of operation. This is evidenced by the gas generation curve shown in Fig. 2.

The slope of the initial graph of settlement against $\log_{10}(\text{time})$ for CAR3 can be used to determine the creep parameter C_c , where the creep strain ϵ_c , where

$$\epsilon_c = C_c \cdot \log \{t / t_0\} = \lambda_c \cdot \ln \{t / t_0\} \quad (1)$$

and $\lambda_c = C_c \div 2.303$. If it is assumed that creep effects are the same in CARs 1 and 2 as they are in CAR3, subtraction of the creep settlements from CARs 1 and 2 enables the biodegradation parameter C_b to be determined – assuming that degradation induced strains ϵ_b can be calculated using a relationship of the form:

$$\epsilon = C_b \cdot \log \{t / t_0\} = \lambda_b \cdot \ln \{t / t_0\} \quad (2)$$

where $\lambda_b = C_b \div 2.303$. This relationship is empirical, and is unsatisfactory in that it implies that degradation may continue indefinitely. In reality, degradation will stop when all of the putrescible material has gone.

The values of λ_c and λ_b determined from the CAR settlement data (Figs. 1 and 3) are compared with those given by Watts and Charles (1999) for recent domestic waste in Table 1. The range of the laboratory-measured degradation parameter λ_b (4.5 to 7%) is within that measured in the field (3 to 8%), but the relative importance of creep is much greater in the CAR experiments. This could be a result of the generally lower bulk densities. There is no obvious difference between the creep and degradation rates of the sample tested at 50 kPa (CAR2) and that tested at 150 kPa (CAR1).

HYDRAULIC CONDUCTIVITY

Tests in the Pitsea compression cell (Fig. 4; Beaven

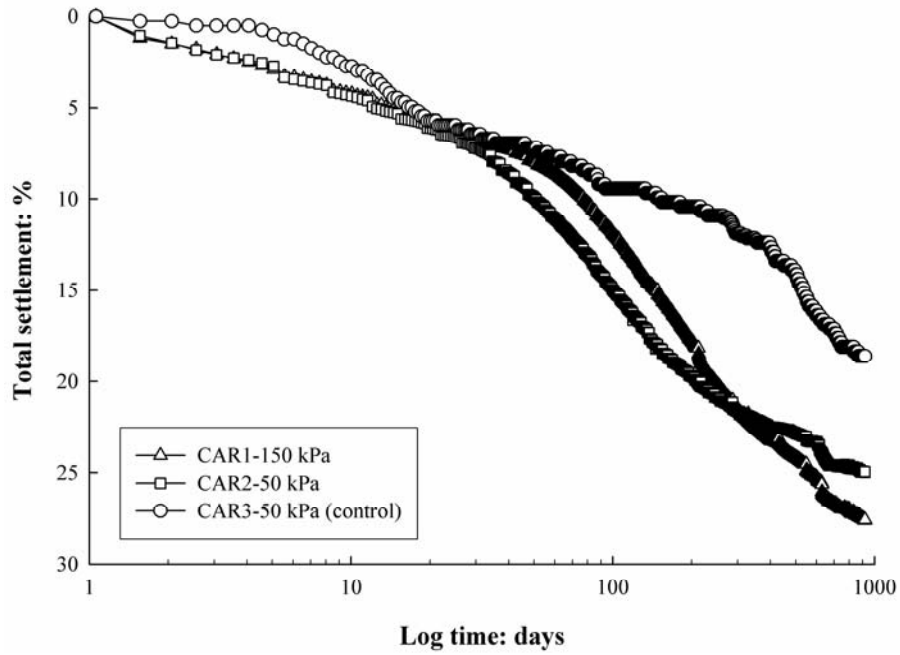


Fig. 1 Settlement against $\log_{10}(\text{time})$ observed in consolidating anaerobic reactor experiments (from Ivanova et al. 2008)

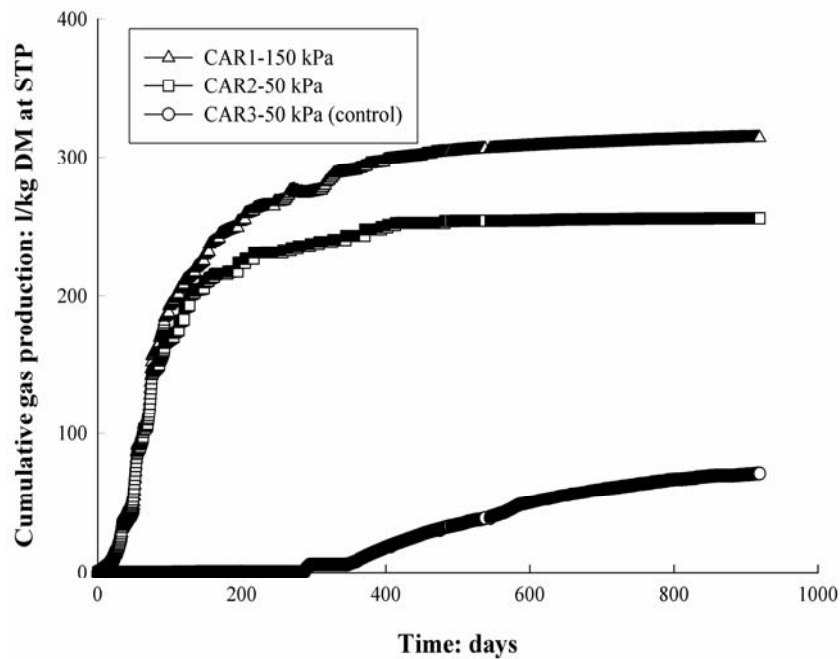


Fig. 2 Cumulative gas production against time observed in consolidating anaerobic reactor experiments (from Ivanova et al. 2008)

& Powrie, 1995; Powrie & Beaven, 1999) were carried out as part of a continuing programme of research into the compression and flow characteristics of wastes. The Pitsea cell is a purpose-built apparatus that accommodates a sample of waste 2 m in diameter and up to 2.5 m high – a size necessary to obtain representative results from samples of generally highly heterogeneous wastes. Overburden pressures are simulated by applying a vertical

stress via hydraulic rams acting on a platen on top of the waste. Typically, the applied stress is increased in five or six stages to a maximum of 600 kPa, representing landfill depths of up to 60 m. At the end of each compression stage, the bulk density, drainable porosity and saturated hydraulic conductivity of the waste are determined.

Detailed descriptions of the compression cell, including a correction to the applied stress to account for

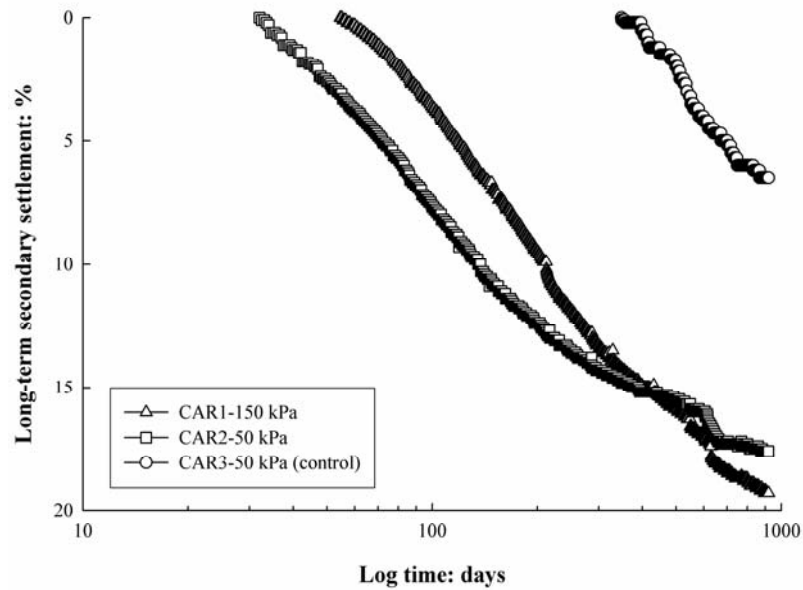


Fig. 3 Estimated degradation settlement against $\log_{10}(\text{time})$ (creep settlements removed) observed in consolidating anaerobic reactor experiments (from Ivanova et al. 2008)

Table 1 Measured degradation and creep parameters

Source of data	Bulk unit weight kN/m^3	Creep parameter λ_c , %	Degradation parameter λ_b , %	λ_b/λ_c
Brogborough (1, 2)	6	-	7.82	-
Calvert (1, 2)	8	0.868	7.82	9.0
Heathfield (1)	-	0.304	3.04	10.0
CAR1 (3)	5	1.80	7.00	3.9
CAR2 (3)	4	2.21	4.46	2.0
CAR3 (3)	4	2.18	5.43	2.5

(1) Watts and Charles, 1999; (2) Watts and Charles, 1990); (3) Ivanova et al. 2008

side friction, are given by Beaven & Powrie (1995), Powrie & Beaven (1999) and Beaven (2000). The general testing procedure may be summarized as follows. A waste sample is loaded into the cylinder, and its as-placed weight determined by means of the load cells on which the apparatus is mounted. The waste composition and as-placed water content are determined by sorting and oven drying sub-samples typically totalling ~2 tonnes. When compression in response to the application of a vertical stress has substantially ceased (i.e. compression is increasing at a rate of less than 1% of the sample thickness in 24 hours), the waste is saturated by allowing water to flow into the sample through the lower platen. After the refuse has been saturated it is allowed to drain under gravity to field capacity (defined as the water content of the waste in conditions of free downward gravity drainage), and the drainable porosity is calculated from the volume of leachate drained, per unit total volume. The bulk density can be calculated from the known mass and volume of the waste at any stage.



Fig. 4 Pitsea compression cell

The hydraulic conductivity of the refuse at each vertical load is measured in a constant head flow test. Water from the header tanks is allowed to flow upward through the refuse. The hydraulic gradient is determined by means of piezometers inserted through ports in the side of the column. Piezometers at the same horizon indicating the same hydraulic head confirm that flow is vertical and approximately uniform. The flow rate is measured using electromagnetic flowmeters, except at low flow rates when direct measurement of the (small) fall in water level in the header tanks with time has been found to be more reliable. The refuse is then drained, the applied stress increased and the cycle of operation and measurement repeated.

Tests were carried out on four different samples of domestic waste (DM3, PV1, DN1 and AG1) to investigate the effects of particle size reduction, degradation and compression on the bulk vertical hydraulic conductivity. DM3 was fresh, unprocessed waste; PV1 was fresh waste that had been pulverized and passed through a 150 mm screen and heavy fines (including some putrescibles) removed; DN1 was fresh waste that had been partly sorted and tumbled in a drum using the Dano system ; and AG1 which was a 25 year old partly degraded waste containing a mixture of soil, crude waste and pulverised waste that had been recovered from a depth of less than 5 metres from a landfill site. Further tests were carried out on sample DN1 to investigate the effects of partial saturation and gassing. Full characterization analyses are given by Powrie & Beaven (1999) for sample DM3, by Hudson et al. (2001) for waste DN1, and by Beaven (2000) for wastes PV1 and AG1.

Results

Raw data of hydraulic conductivity, drainable porosity and density at various vertical effective stresses are given for samples DM3, PV1 and AG1 by Beaven (2000), and for sample DN1 in high and low gas accumulation conditions and with high and low pore water pressures by Hudson et al. (2001). Fig. 5 shows the permeability in notionally saturated conditions for all four wastes plotted as functions of (a) vertical effective stress; (b) density and (c) porosity.

Fig. 6 shows the effect on hydraulic conductivity of gas accumulation in the Dano processed sample DN1, with the sample free to vent to atmosphere.

Analysis

1. There is a single correlation for all samples between vertical hydraulic conductivity and vertical effective stress in first loading. Differences in hydraulic conductivity resulting from particle size reduction and waste degradation are essentially second order, but

appear to become more significant at higher vertical effective stresses (with a spread of just over one order of magnitude in hydraulic conductivity at a vertical effective stress of 500 kPa).

2. There are individual correlations between vertical hydraulic conductivity and density for each waste type, with an essentially linear relationship between the logarithm of the vertical hydraulic conductivity and the dry density.

3. There is a single correlation between the vertical hydraulic conductivity and the drainable porosity of the waste. This is not surprising, as the drainable porosity represents a measure of the size and degree of connectivity of the voids, both of which will have a major influence on the bulk hydraulic conductivity. However, unlike the vertical effective stress, the drainable porosity is a difficult parameter to estimate a priori for design purposes, so the correlation between vertical hydraulic permeability and vertical effective stress is of more practical use.

4. Gas accumulation could reduce the hydraulic conductivity by between one and two orders of magnitude; at elevated pore water pressures, compression of the trapped gas will reduce its impact.

Powrie and Beaven (1999) point out that the expected variation in hydraulic conductivity with depth will have a profound impact on the pore pressure distribution in a landfill – even before such complicating factors as anisotropy and daily cover are considered. Even in simple downward flow to a pumped drainage blanket, pore pressures may well appear to be hydrostatic to a depth of 75% of the saturated waste thickness. This must be taken into account when measuring and interpreting leachate levels: for measurement purposes, piezometers with discrete, well defined response zones must be used in preference to fully-screened standpipes or observation wells, which will give a completely false picture.

LANDFILL: FUTURE CHALLENGES

Landfill has been the principal method of waste disposal throughout most of the developed world for the last 100 years or more. More than 80% of the UK's waste is currently disposed of to landfill. Recent and impending legislation and changes in resource management philosophy, in particular the EU Landfill Directive (European Council, 1999) are beginning to change this, but a major role for landfill in the disposal of residual (i.e. post treatment or energy recovery) wastes will remain. More importantly, the implementation of the EU Landfill Directive has had and will continue to have major implications for the nature of the waste that is disposed of to landfills throughout Europe, and hence for the way in which the receiving landfills should be managed.

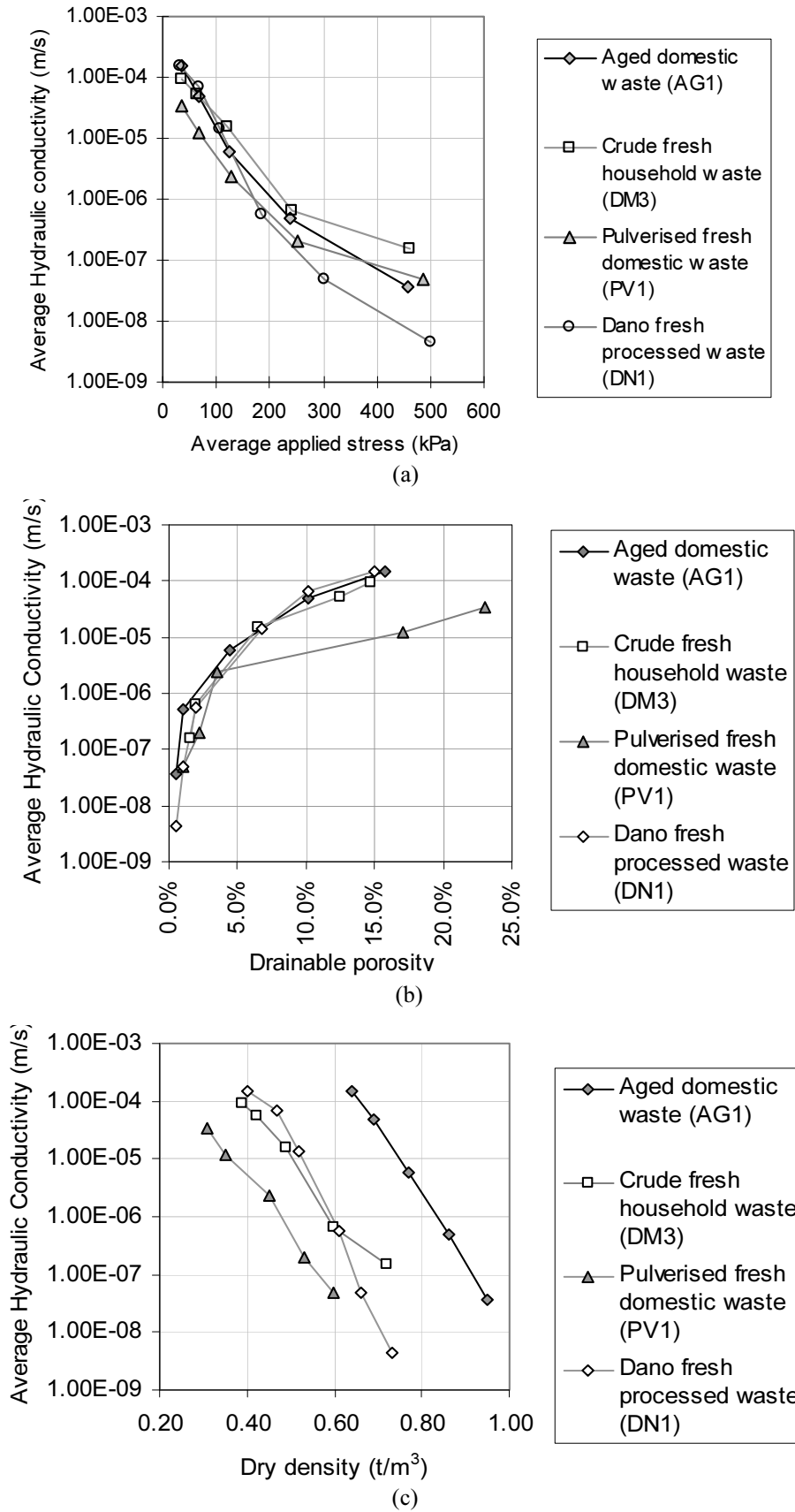


Fig. 5 Vertical hydraulic conductivity against (a) the logarithm of the vertical effective stress in first loading; (b) the drainable porosity; and (c) density, for wastes DM3, PV1, AG1 and DN1 (data from Beaven, 2000 and Hudson et al. 2001)

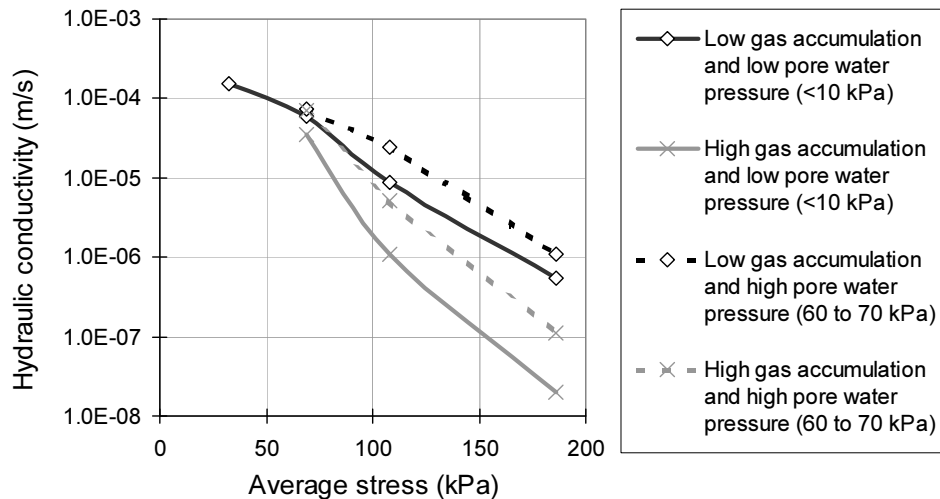


Fig. 6 Vertical hydraulic conductivity against vertical effective stress for sample DN1, showing the effect of gas accumulation (data from Hudson et al. 2001)

Perhaps the most immediate and obvious impact of the EU Landfill Directive will result from the required reduction in the amounts of biodegradable municipal waste (BMW) being disposed of to landfill to 75% of 1995 levels by 2006 (2010 in the UK), 50% by 2009 (UK 2013) and 35% by 2016 (UK 2020) and the requirement that landfilled wastes have been subjected to pre-treatment. The UK's waste strategy (DETR, 2000) sets targets for materials recovery from municipal solid waste (MSW) by recycling or composting of 25% by 2005, 30% by 2010 and 33% by 2015; with overall recovery rates (including energy) of 40%, 45% and 67% respectively.

Implementation of the EU Landfill Directive will require the large-scale treatment of MSW in some way to reduce the biological content. European experience suggests that treatment is likely to take one of two forms, either incineration or a treatment comprising of both mechanical and biological elements, together known generically as mechanical-biological treatment or MBT. The mechanical component of the treatment is likely to comprise sorting and removal of recyclables followed by particle size reduction of the remaining fraction by pulverizing or shredding. The biological component will probably be accelerated aerobic or anaerobic degradation. Processing will leave a residue which, though much less biodegradable than MSW, is not inert. German and Austrian experience with treated waste residues suggests that up to 20% of the original gas potential remains—up to 45 m³/Mg (Ziehmann & Meier, 1999; Stegmann & Heyer, 2001) compared with 200 to 250 m³/Mg for raw MSW (Leikam et al. 1999; von Felde & Doedens, 1999). In the UK, it is thought by some that there will be commercial or land improvement uses for treated waste residues. However in Germany, which has more experience and probably less biologically active residues,

they are deemed suitable only for disposal and 24%—40% by mass of the waste input is landfilled (Kühle-Weidemeier, 2004). Archer et al. (2005) confirm that the possibilities of markets for treated waste residues are limited, and a significant proportion is likely to be landfilled for the foreseeable future.

Waste residues treated to German standards have been well characterised in many respects, although the time required for full stabilisation and long-term settlement is unknown. However, Kühle-Weidemeier (2004b) and others suggest, counter-intuitively, that treated waste has a longer half-life in a landfill than raw MSW.

It has long been noted that shear tests on both fresh and aged MSW show little or no evidence of conventional geotechnical failure (i.e. continuing deformation at constant shear stress), even at shear strains of up to 50% (e.g. Jessberger et al. 1995 and Grisolia et al. 1995). In contrast, treated waste residues (e.g. Kühle-Weidemeier, 2003 and Scheelhaase et al. 2001) appear to reach conventional geotechnical failure. In addition to this apparent strain hardening, both aged and fresh MSW gain strength from fibre reinforcement effects (Kölsch, 1995), which are not present in treated waste residues. The way in which the strength of a treated waste will vary with the extent and nature of the treatment process is not well understood, but a significantly reduced capacity for strain hardening and minimal fibre reinforcement seem likely for any processed or treated MSW. Both of these will have a major impact on the stability of the waste body, in particular on the maximum slopes that can be achieved during waste placement. Unless the effects are understood and appropriate changes in working practice implemented, the consequences in terms of slope failure, and increased risk of environmental pollution could be severe.

Treated waste residues in the UK are likely to be of a lower standard (i.e. not as well sorted or processed, hence less homogeneous and with a wider range of particle shape and type) than in countries where waste pre-treatment processes are more advanced, such as Germany. They will therefore have rather different strength and settlement characteristics. Residues from wastes treated will continue to degrade, produce gas and settle over a long period of time (Raninger et al. 1999; von Felde & Doedens, 1999; Zichmann & Meier, 1999; Leikam et al. 1999); these problems will be worse with waste that has been treated to a lesser extent, as in the UK. Given that landfilling of treated wastes is likely to continue including deposition on top of existing landfills (Jones & Dixon, 2003), there is an urgent need to quantify and understand the bio-mechanical behaviour of waste residues resulting from a variety of standards of treatment, how this behaviour will evolve over time and the reasons for it.

Work at Southampton has recently begun to determine the degradation and settlement characteristics of a non-source segregated MSW. These wastes are subject to mechanical pre-treatment processes to remove inert materials and to reduce the particle size. They are then aerobically treated for up to 8 weeks within enclosed windrows undergoing regular turning of the waste pile in response to temperature and moisture measurements obtained from instrumentation probes embedded in the waste. A representative sub-sample of the biologically treated waste batch was placed, under a constant load, within a consolidating anaerobic reactor to replicate landfill conditions (Ivanova et al. 2003) (CAR2). A second sample was placed under identical conditions but with degradation inhibited through the addition of high acid concentrations within the leachate (CAR1). Initial results highlight the longer term degradability of these residual wastes in terms of settlement (Fig. 7) and the contribution of mechanical creep. The associated generation of landfill gas will be at rates that are not economically worthwhile to capture and may actually prove more problematic to long-term landfill management in terms of fugitive gas emissions. Therefore, although this waste treatment process may fulfil the letter of the Landfill Directive, the real benefits are less clear.

Other residual wastes likely to increase in volume but which will ultimately require disposal to landfill and may be problematic include incinerator ash and filter cake derived from emission control processes. These materials are likely to contain high concentrations of heavy metals and other contaminants that may become available through leaching processes due to conditions prevalent within landfills. Successive cycles of flushing have been shown to reduce the pollution potential of these materials. Hjelm and Hansen (2004) show that field data on the flushing of chloride from an incinerator

ash was in good agreement with models that predicted the reduction in chloride concentrations following a series of flushing cycles over the short term. What is less clear is the duration over which flushing must continue in order to achieve acceptable overall reductions in pollution potential, with model predictions ranging from 50—100 years (Fig. 8).

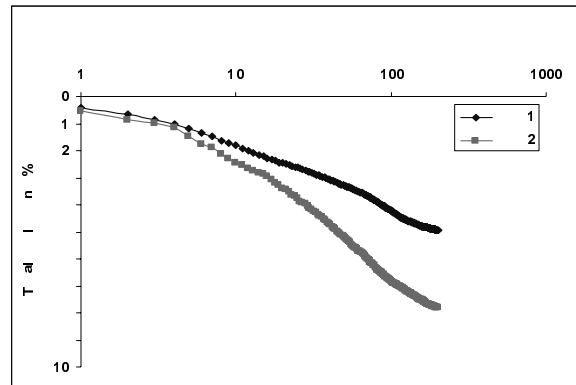


Fig. 7 (a) Settlement of MBT

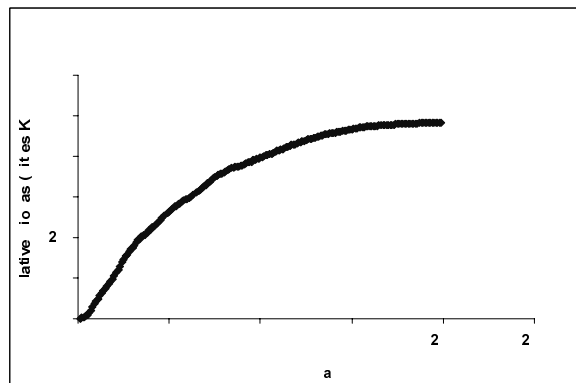


Fig. 7 (b) Gas generation of MBT (CH₄:62%; CO₂:38%)

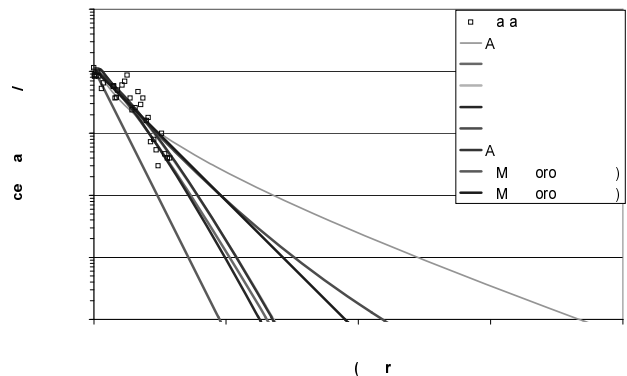


Fig. 8 Short term flushing field data and existing long-term model predictions (Hjelm and Hansen (2004))

CONCLUSIONS

The work presented in this paper has described some of the recent research activity and output of the University of Southampton Waste Management Research Group over the past six years. This work has been directed towards developing a fundamental understanding of the processes and conditions that control the behaviour of existing and old (post-closure) landfill and has provided simplified models that link the variability and anisotropy of waste hydraulic conductivity related to patterns of leachate head. It is evident that leachate level monitoring using fully screened observation wells will suggest a high hydrostatic pressure acting on the liner when in fact it is likely to be zero. For an active, gassing landfill, the hydraulic conductivity may be further reduced and considerable effort is currently being directed towards understanding and modelling the mechanism of gas generation and its effects on hydraulic conductivity. There is also a need to characterise more fully the structure of wastes and composition related to hydraulic conductivity.

The global drive towards alternative waste treatment processes and landfill diversion is likely to see an increase in post treatment residual wastes (incinerator ash and filter cakes) deposited to landfill. These wastes are likely to have increased pollution potential and require stabilisation, primarily by flushing. Reliable flushing models to predict late-time behaviour are required to predict stability. MBT residues will gas gently; at volumes and over periods that are likely to increase the difficulties of effective gas collection and management. It is clear that for sites receiving either type of residue, long term management will be required.

ACKNOWLEDGEMENTS

The University of Southampton Waste Management Research Group comprises many members past and present and has enjoyed considerable Research Council and industrial funding and support. The authors gratefully acknowledge the financial support provided by EPSRC and DEFRA and continued support from Veolia Environmental Services and W H White Plc. The authors gratefully acknowledge individuals from the wider WMRG who have contributed to this paper, in particular:

John Barker, Steve Cox, Andrew Hudson, Lucy Ivanova, Tristan Rees-White, Qingchao Ren, John Robinson, Asif Siddiqui, Dave Smallman, Anne Stringfellow, Jim White and Nick Woodman

REFERENCES

- Archer E, Baddeley A, Klein A, Schwager J, Whiting K (2005). *Mechanical-biological-treatment: a guide for decision makers processes, policies, markets*. Juniper Consultancy Services Ltd, Uley.
- Beaven RP (2000). *The hydrogeological and geotechnical properties of household waste in relation to sustainable landfilling*. PhD dissertation, University of London (Queen Mary and Westfield College).
- Powrie W & Beaven RP (1999). *Hydraulic properties of household waste and implications for landfills*. *Proceedings of the Institution of Civil Engineers (Geotechnical Engineering)* 137 (4): 235-247.
- Beaven RP & Powrie W (1995). *Determination of hydrogeological and geotechnical properties of refuse using a large compression cell*. *Proceedings of the 5th International Landfill Symposium, Sardinia 95* (eds T H Christensen, R Cossu and R Stegmann) II: 745-760. Cagliari: CISA Environmental Sanitary Engineering Centre.
- CIWM (1998). *Role and Operation of the Flushing Bioreactor*. Chartered Institute of Wastes Management, Business Services Ltd. Special report of the Sustainable Landfill Working Group.
- Clean Air Act (1956). HMSO, London.
- Coop MR & Atkinson JH (1993). *The mechanics of cemented carbonate sands*. *Géotechnique* 43(1): 53-67
- DETR (2000). *Waste strategy 2000 for England and Wales*. Department of the Environment, Transport and the Regions, London.
- Edil TB, Ranguette VJ, Wueller WW (1990). *Settlement of municipal refuse*. In *Geotechnics of waste fills—theory and practice*. ASTM STP 1070 (eds A Landva and G D Knowles). Philadelphia, USA: American Society for Testing and Materials.
- European Council Directive on the Landfill of Wastes 1999/31/EEC.
- von Felde D & Doedens H (1999). *Full scale results of landfilling mechanical biological pretreated MSW*. *Proceedings Sardinia 1999, Seventh International Waste Management and Landfill Symposium*. S. Margherita di Pula, Cagliari, Italy, 4-8 October 1999: 533-540.
- Grisolia M, Napoleoni Q, Tancredi G (1995). *The use of triaxial tests for the mechanical characterization of MSW*. *Proceedings Sardinia 1995*: 761-768.
- Hjelmar O & Hansen JB (2004). *Towards final storage quality in landfilling: an example*. *Proceedings of the Waste 2004 Conference*. 28-30 September, Stratford-upon-Avon, Warwickshire, UK.
- Hudson AP, White JK, Beaven RP, Powrie W (2004). *Modelling the compression behaviour of landfilled*

- domestic waste. *Waste Management* 24: 259-269.
- Hudson A, Beaven RP, Powrie W (2001). Interaction of water and gas in saturated household waste in a large scale compression cell. *Proc. Sardinia 2001, 8th International Landfill Symposium, Cagliari, Italy, III*: 585-593.
- Ivanova LK, Richards DJ, Smallman DJ (2003). An investigation into the factors affecting secondary settlement of wastes. *Proceedings Sardinia 2003*.
- Ivanova LK, Richards DJ, Smallman DJ (2008). The Long-Term Settlement of Landfill Waste. *Proc. Institution of Civil Engineers, Waste and Resource Management*, 161(3): 121-133.
- Jessberger HL, Syllwasschy O, Kockel R (1995). Investigation of waste body behaviour and waste-structure interaction. *Proceedings Sardinia 1995*: 731-743.
- Jones DRV & Dixon N (2003). Stability of Landfill Lining Systems – Report No. 1 Literature Review (P1-385/TR1). The Environment Agency, London.
- Kölsch F (1995). Material values for some mechanical properties of domestic waste. *Proceedings Sardinia 1995*: 711-729.
- Knox K (1990). The Relationship between leachate and gas. *Proceedings of International Conference Landfill Gas: Energy and Environment '90 held in Bournemouth ISBN 0-7058-1628-1 Session 8.1*: 367-386.
- Kühle-Weidemeier M (2003). Bedarf, konstruktionsgrundlagen und betrieb von deponien fuer mechanisch-biologisch behandelte siedlungsabfaelle. *Veroeffentlichungen des Institutes fuer Siedlungswasserwirtschaft und Abfalltechnik der Universitaet Hannover, Band 127. ISBN 3-921421-57-8*.
- Kühle-Weidemeier M (2004). Landfilling of mechanically-biologically pre-treated municipal solid waste. VIII. *International Symposium WASTE MANAGEMENT ZAGREB 2004. November 2004*.
- Kühle-Weidemeier M (2004b). Landfill properties of mechanically-biologically treated municipal solid waste. *Proc. Waste 2004 Conf.*: 601-614.
- Leikam K, Jahnke S, Raga R, Stegmann R (1999). Influence of water content and emplacement density on landfill emissions. *Proceedings Sardinia 1999*: 495-502.
- McDowell GR & Bolton MD (1998). On the micro-mechanics of crushable aggregates. *Géotechnique*, 48(5): 667-680.
- Mesri G, Febres-Cordero E, Shields DR, Castro A (1981). Stress-strain-time behaviour of clays. *Géotechnique* 31(4): 537-552.
- Mitchell JK (1993). *Fundamentals of soil behavior*, 2nd edition. New York: John Wiley & Sons.
- Powrie W (2004). *Soil mechanics: concepts and applications* (2nd edition). London & New York: Spon Press (Taylor & Francis).
- Powrie W & Beaven RP (1999). Hydraulic properties of household waste and implications for landfills. *Proceedings of the Institution of Civil Engineers (Geotechnical Engineering)* 137 (4): 235-247.
- Powrie W, Beaven RP, Harkness RM (1999). Applicability of soil mechanics principles to household wastes. *Proceedings of the 7th International Landfill Symposium, Sardinia 99* (eds T H Christensen, R Cossu and R Stegmann) III: 429-436. Cagliari: CISA Environmental Sanitary Engineering Centre.
- Raninger B, Pilz G, Gheser D (1999). Optimisation of mechanical-biological treatment of waste to achieve Austrian landfill requirements. *Proceedings Sardinia 1999*: 387-394.
- Sarsby RW (2000). *Environmental Geotechnics*. Thomas Telford Ltd, London, p. 594.
- Scheelhaase T, Bidlingmaier W, Klümper A, Maile A, Rechberger M (2001). Geotechnical behaviour of mechanically-biologically pretreated residual waste. *Proceedings Sardinia 2001*: 445-453.
- Soler ND, Maher A, Chae YS, Hamidi A (1995). A conceptual model for transient settlements in waste fills. *Unsaturated soils: Proceedings of the 1st International Conference, Paris, September 1995*, 1: 411-416. Rotterdam: A A Balkema.
- Stegmann R & Heyer KU (2001). Landfill concept for mechanically-biologically treated residual waste. *Proceedings Sardinia 2001*: 381-388.
- Watts KS & Charles JA (1990). Settlement of recently placed domestic refuse landfill. *Proceedings of the Institution of Civil Engineers* 88 (December): 971-993.
- Watts KS & Charles JA (1999). Settlement characteristics of landfill wastes. *Proceedings of the Institution of Civil Engineers (Geotechnical Engineering)* 137 (October), 225-233.
- Ziehmann G & Meier J (1999). Alternating aerobic/anaerobic treatment of MSW: large scaled experiments. *Proceedings Sardinia 1999*: 435-442.

GEOSYNTHETIC FUNDAMENTALS IN LANDFILL DESIGN

Gregory N. RICHARDSON¹ and Aigen ZHAO²

ABSTRACT: Contemporary design of lined landfills in the United States began in the early 1980's with Federal regulations focused on hazardous waste disposal. This regulatory framework was expanded to include municipal solid waste in the early 1990's. With nearly 30-years experience in the design of lined landfills, simple design practices have evolved to ensure the successful performance of lined landfills. Geosynthetic components play a critical role in the two main components of these landfills: (1) liners to limit the vertical migration of liquids, and (2) drainage field that collect the liquids and limit the potential for leaks to develop. Geomembrane liners provide a very stable barrier to the spread of liquids but must be built to very high standards, be protected from damage during construction and their service life, and come with the potential for stability problems generated by their slick surfaces. Geosynthetic drainage composites provide a means of draining the collected liquid from large areas of the liner surface. Properly designed, such geosynthetic drainage layers will add to the stability of the landfill by limiting hydrostatic forces due to the collected liquids. Past failures of lined landfills provide an effective means of demonstrating the inevitable consequences of not meeting fundamental design requirements for these components.

KEYWORDS: geosynthetics, landfill design, liners, drainage composites

INTRODUCTION

Over the past 25 years, design procedures for the liner and liquid collection systems have evolved with the development of both improved design methodology and geosynthetic components, and in response to observed failures in the field. A review of the more than 40 failure investigations performed by the authors indicates that failures can be minimized if design and construction fundamentals are observed. These fundamentals do not address the economics of the landfill or additional appurtenances that are also required. However, the fundamentals do protect the designer and owner from expensive failures.

Contemporary lined landfills rely on two key systems to control the migration of leachate draining from the waste: a low permeability liner system that limits the vertical and lateral movement of the leachate and a liquid collection/removal system (LCRS) to collect and remove the leachate that accumulates on the liner system. The design and construction considerations for these two systems are inherently very different and must be understood if landfill is to be a success.

An additional consideration not addressed in this paper is the need to operate the landfill in a manner consistent with its design. The operations manual

prepared by the designers must provide the owner with clear guidance on field operational practices that must be followed to ensure failure free operation. All contemporary landfills can be failed by field operations that are inconsistent with the design assumptions.

COMPOSITE LINER SYSTEM PERFORMANCE

Modern landfills rely on a composite liner system that depends on a synergistic relationship between the geomembrane liner (GM) and an underlying soil liner. A better understanding of the important design and construction considerations for these two components is obtained by examining the theoretical basis for estimating leakage through the composite liner. Empirical modeling and field observations (Giroud and Badu-Tweneboah 1992) have resulted in the "Giroud" equation for estimating leakage through a hole in the geomembrane portion of a composite liner. The empirical equation takes the form of:

good contact:

$$Q = 0.21h a k^{-4} \quad (1)$$

¹ Senior Consultant, Richardson Smith Gardner & Associates, USA. Email: greg@rsgengineers.com

² Vice-President Engineering, Tenax Corporation, USA. Email: azhao@tenax.com

for poor contact

$$Q = 1.15h a^1 k^4 \tag{2}$$

where “contact” refers to the contact between the soil liner and the geomembrane, e.g. no wrinkles in the liner and a properly smoothed clay surface contribute to a good contact, Q = rate of leakage through a defect (m^3/s); h = head of liquid on top of the geomembrane (m); t = thickness of the soil component of the composite liner (m);

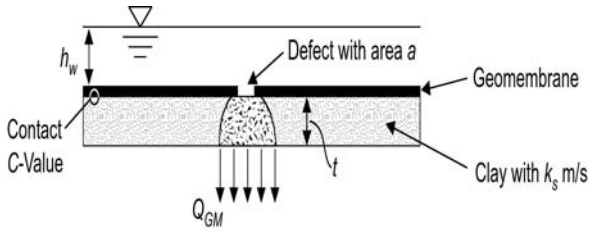


Fig. 1 Composite Liner Variables

a = area of defect in geomembrane (m^2); and k = hydraulic conductivity of the underlying clay liner (m/s). Eqs. 1 and 2 are incorporated into the latest versions of the HELP computer model (U.S. EPA 1994) used for predicting landfill leachate generation and leakage.

Leakage through a composite liner system increases with the following:

1. Increasing head, h , of leachate;
2. Decreasing soil liner thickness, t ;
3. Increasing soil liner permeability, k ;
4. Increasing area of defect in GM, a ; and
5. Decreasing lack of good contact between the two liner components.

Item 1 is the focus of the design of the LCRS system, Items 2 and 3 are typically specified by the regulatory agency, and Items 4 and 5 are minimized using a Construction Quality Assurance program (CQA). A discussion of CQA programs is beyond the scope of this paper but readers are directed to Koerner and Daniels (1993), and Daniels and Koerner (2007).

Eqs. 1 and 2 are generally not used in the actual design of a lined landfill but does provide a means of recognizing key factors that influence liner leakage. The limitations of Eq. 1 relate to the uncertainty as to the number of actual defects in the liner. With a comprehensive CQA program as outlined above, it is estimated that 1 to 3 $1cm^2$ defects remain per $4000 m^2$ area. This allows a rough estimate of potential leakage. Additionally, Eqs. 1 and 2 are frequently used to evaluate problems with excessive leakage in existing lined landfills. This means that Eqs. 1 and 2 should be considered an excellent forensic tool and not a design tool.

GEOMEMBRANE LINER DESIGN

While the hydraulic performance of the GM requires a field CQA program to minimize defects, the stability of the GM must be verified in the design. The typical GM is formed of a thermo-plastic that has a very low inherent interface shear strength, e.g. is very slick. Before the stability of the liner system can be calculated, the interface shear strength between each of the layers forming the liner and collection system must be evaluated.

Liner Interface Strength Testing

Within the United States, the interface shear strength is measured using the direct shear test (ASTM-D5321) on the interfaces of concern under project specific conditions. This test must be performed on each interface of the liner and LCRS system that will be placed beneath the waste. Typically, the controlling interface, i.e. having the lowest strength, is one of the two interfaces related to the geomembrane, i.e. GM to soil or GM to LCRS.

Fig. 2 show the results of a D5321 direct shear test to determine the interface shear strength between a textured GM and geosynthetic drainage composite, e.g. textured GM against a nonwoven geotextile. The test was performed

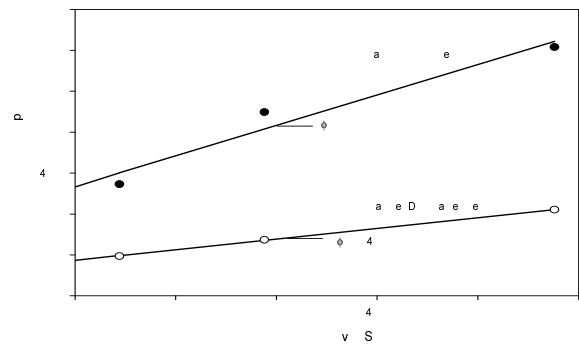


Fig. 2 ASTM D5321 Direct Shear Test Results
(1kPa = 20.5psf)

at three normal loads typical of what would be anticipated for a GM in a landfill final cover system. The maximum strength data represents the peak shear strength at displacements typically less than 12.5mm. The large displacement data reflects shear strengths that occur at displacements greater than 25mm. The large displacement strengths are typically lower due to abrasion damage to the texturing. The large displacement strengths are commonly used in seismic stability evaluations where the static factor of safety can drop below 1.0 during the event.

As shown on Fig. 2, the measured shear strength, τ , is typically represented by the Mohr-Coulomb equation

$$t = c + \sigma \tan \delta \tag{3}$$

where c is apparent adhesion, σ is the normal pressure on the interface, and δ is the interface friction angle. For liners placed on slopes, c should be a minimum of 2.5 kPa based on stability considerations during construction. The normal loads used in the ASTM D5321 direct shear test should be representative of the normal loads anticipated during the service life of the liner system.

Liner Stability Analysis

One of the greatest challenges facing the design engineer is to accurately estimate the density and shear strength of the waste and geometry of future waste placement. All of these parameters are beyond the direct control of the design engineer but must be conservatively estimated or failure can result.

Waste Properties

The density of waste can be estimated from historical data but can be impacted by local waste characteristics. Lacking local data on waste density, the authors recommend the use of densities presented on Table 1. Waste densities are obtained using annual surveys to establish waste volumes and truck scales to record the actual weight of waste received each year. The weight of waste must be increased to account for the daily cover soils applied to the waste to control vectors.

Table 1 Default Waste Total Unit Weights

Waste Type	Total Unit Weight, kN/m ³
Municipal Solid Waste	8-10
Construction/Demolition	6.5-9
Industrial	6-13
Coal/Fly Ash	9-12

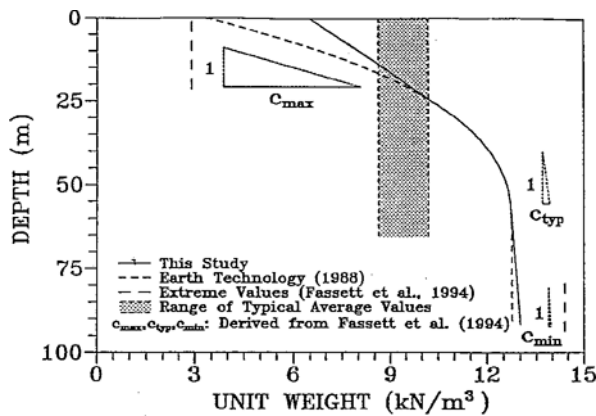


Fig. 3 Waste Unit Weight Increase with Depth

Note that waste densities generally increase with increasing normal loads so that the upper limits of density should be assumed for wastes having a height greater than approximately 45m. Fig. 3 shows this increase in density with depth for typical MSW (Kavazanjian, et.al, 1995).

Strength properties of common wastes are impossible to evaluate using typical geotechnical laboratory soil testing procedures due to the very large size gradation of the waste. What the design engineer must typically rely on is empirical strength values based on historic observation of both successful and failed waste placement conditions. Fig. 4 shows rotational stability failure of waste that allowed back calculation of the average shear strength of the waste at the time failure occurred. The nearly 30-m vertical faces of the waste require the waste to have an apparent cohesion even though the material is essentially



Fig. 4 Landfill Waste Stability Failure

non-plastic. For municipal solid waste, Fig. 5 shows a compilation of back-calculated shear strengths with a recommended design shear strength envelop for MSW (Kavazanjian, et al. 1995).

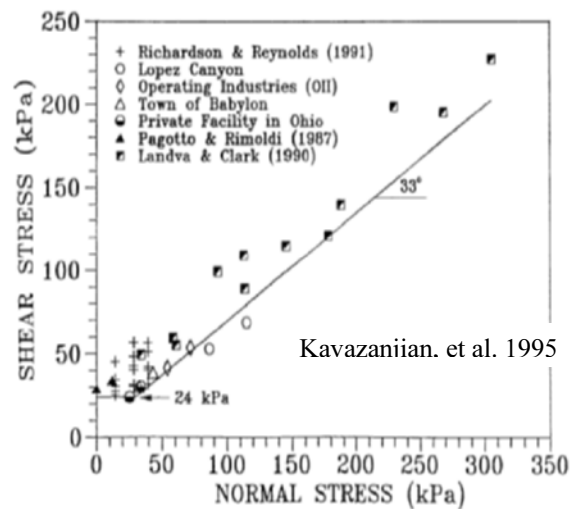


Fig. 5 Shear Strength of MSW Waste

Waste Geometry

The future geometry of the waste is beyond the direct control of the design engineer but can be influenced if the designer prepares an operational manual for the landfill that provides waste placement guidance to the operator. The design engineer must understand that all lined landfills can be failed from the improper placement of waste within the landfill. Thus, a properly prepared operations manual protects both the design engineer and the owner.

Correct placement of waste is typically controlled by specifying a maximum lift thickness and exterior slope for the lift. Stability can be improved if the operations manual requires full placement of each lift before subsequent lifts are begun. Additionally, the operations manual should provide the operator guidance on interim features that can influence localized stability such as

temporary roads for truck access during placement of each lift.

Numerical Analysis

Once the projected waste properties and geometry are defined, the stability analysis is performed using one of many slope stability programs commonly used by geotechnical engineers. The only real limitation on software selection is the need for the program to allow block type failures since the failure surface will follow much of the liner surface. Geotechnical programs that rely on circular failure surfaces cannot properly model the actual failure surface that will commonly along and rarely cross a portion of the liner surface. Fig. 6 shows the results of a typical waste stability evaluation. This evaluation was performed with the software program STABL.

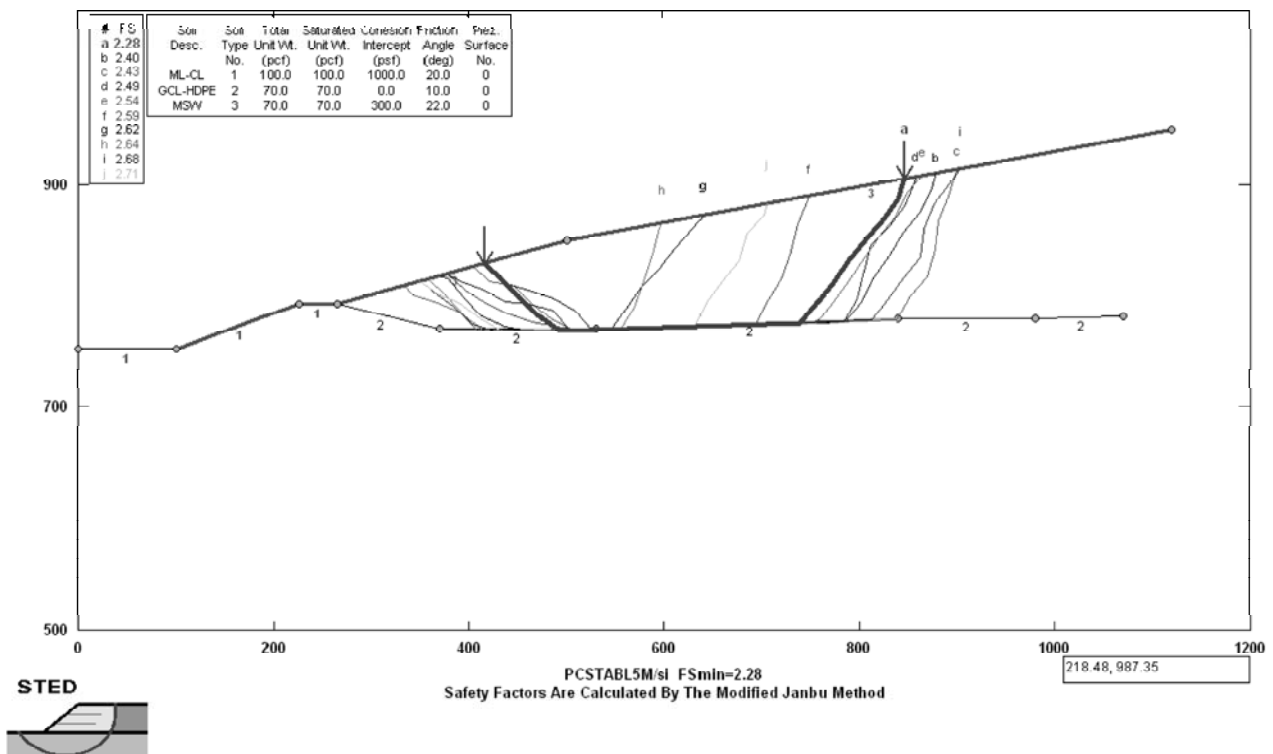


Fig. 6 Slope Stability Evaluation of Landfill

LEACHATE COLLECTION SYSTEM DESIGN

Recalling Eqs. 1 and 2, the impact of a defect in the liner system is minimized by maintaining a low head, h , of leachate acting on the liner system. In addition to minimizing leakage, the leachate head must be minimized to ensure stability of the waste. In the USA, the maximum head of leachate acting on a liner system is limited to 30-cm.

For the above reasons, the liners system must be

covered by a collector system that can withstand the normal loads generated by the weight of the waste and potential clogging due to both the suspended solids carried by the leachate and the biological clogging potential from the micro-organisms also carried by the leachate. The manner in which the landfill is operated will determine the potential for clogging of the leachate collection systems with landfills. Recirculation of leachate back into the waste has the greatest potential for clogging, thus demand an enhanced leachate collection system.

The LCS consists of two major systems: (1) an area collection system that covers the surface of the liner, and (2) a piping system that in turn drains the area collection system. The area collector is the primary mechanism for satisfying the regulatory limit on head acting on the liner while the piping system is responsible for draining the area system and directing the leachate to a sump for removal from the landfill.

Area Leachate Collection System

Area collection leachate collection systems were originally envisioned as sand layers placed immediately above the liner systems. In recent years, the sand layer is commonly replaced with a geocomposite drainage layer that consists of a geonet with a nonwoven geotextile bonded to one or both faces of the geonet. The variables in the analysis are shown on Fig. 7 below and include the impingement rate, q_h , at which leachate is draining from the waste, the liner slope β , and the slope base length L .

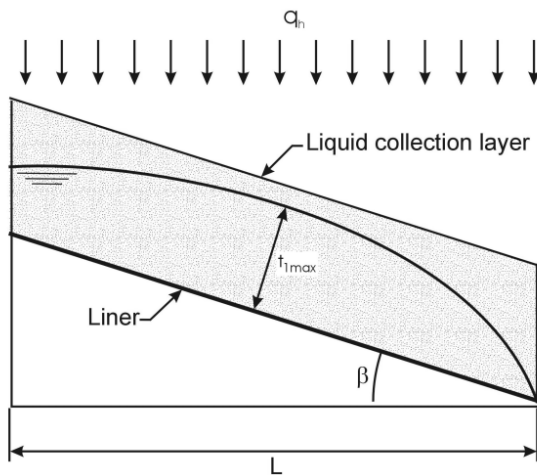


Fig. 7 Leachate Mounding Analysis

A simplified but accurate analysis for the maximum head in the above analysis was developed by Giroud et al. (1992) and is discussed in Giroud et al. (2000). The maximum head on the liner, termed t_{max} by Giroud, is given by the following equation:

$$t_{max} = j \frac{\sqrt{\tan^2 \beta + 4 q_h / k} - \tan \beta}{2 \cos \beta} L \tag{4}$$

where k is the permeability of the lateral drain. The j term is a numerical modifying factor whose value is always slightly less than 1 such that it can be neglected in the typical landfill analysis. Generally, the uncertainty regarding the impingement rate q_h does not justify the use of the j factor.

The total flow rate through the collector, Q , is equal

to $q_h L$ per unit width of the drainage layer. For lateral drains constructed using geocomposite drainage layers, Giroud (2000) has shown that Eq. (4) can be simplified due to the small flow thickness in drainage composites to the following:

$$t_x = \frac{q L}{k \sin \beta} \tag{5}$$

This greatly simplified equation is appropriate when the thickness of the geocomposite drainage layer is less than 20 mm over the range of slopes common to most landfills. This equation should not be used with thicker natural drainage layers. This allows the required transmissivity for a geocomposite drainage layer to be directly solved for as follows

$$\theta_u = \frac{q L}{\sin \beta} \tag{6}$$

Solutions based on Giroud’s numerical solution will be conservative and less than 5% in error. Again, the simplified solution in Eqs. 6 is applicable to geocomposite drainage systems only.

Published values of typical leachate generation values for non-arid regions show typical leachate generation rates of 11,000-20,000 liters/hector/day or a design rate of liquid supply of $1.3-2.3 \times 10^{-6}$ cm/sec during active placement of waste. This reduces to 2000-5600 liters/hector/day once a 30cm interim cover is placed, and 500-1500 liters/hector/day after placement of the final cover. The accuracy of these values was confirmed through discussions with solid waste regulators in the USA. Leachate generation rates will be dramatically impacted by the degree of leachate/storm water separation that is inherent in the facilities design and operational practices. The leachate generation rates referenced above reflect typical design and operational efforts. The 10^{-6} cm/sec design rate of liquid supply approximately represents the infiltration into a leachate collection system through a silty/clayey protective soil layer during initial waste placement. Facilities that employ supplemental 'rain sheets' may have less leachate, while those using porous operational covers will have significantly more. The design is obviously conservative for long-term flows if it is designed properly for the short-term operational flows.

Long-term performance

The long term performance of a lateral drain requires a larger allowed transmissivity, $\theta_{allowed}$, than that obtained from the design equations, $\theta_{req'd}$. This process was initially quantified by Koerner (1998) as follows:

$$FS_{dc} = \frac{\theta_{allowed}}{\theta_{req'd}} \tag{7}$$

where FS_{dc} is the overall safety factor for drainage, $\theta_{req'd}$ is the required transmissivity based on Eq. 6, and $\theta_{allowed}$ is the allowable transmissivity being determined under simulated condition for 100-hour duration using the following formula per GRI-GC8 standard (2001)

$$\theta = \theta_{allow} \frac{1}{RF_{CR} \times RF_{CC} \times RF_{BC}} \tag{8}$$

where θ_{allow} = allowable transmissivity, θ_{100} = laboratory measured transmissivity determined under simulated conditions for 100-hour duration, RF_{CR} = reduction factor for creep to account for long term behavior, RF_{CC} = reduction factor for chemical clogging, RF_{BC} = reduction factor for biological clogging.

The creep reduction factor RF_{CR} is based on 10,000 hour compressive creep data and calculated according to the following equation developed by Giroud et. al (2000) where:

$$RF_c = \left[\frac{(t_c / t_{virgin}) - (1 - n_{virgin})}{(t_c / t_{CR}) - (1 - n_{virgin})} \right]^3 = \left[\frac{t_c - \frac{\mu}{\rho}}{t_{CR} - \frac{\mu}{\rho}} \right] \tag{9}$$

t_{CO} = thickness after load application for 100hours, t_{virgin} = initial thickness, t_{CR} = thickness at the time period of interest (for instance, thickness at 50 year design life, extrapolated from the 10,000 creep curve), n_{virgin} = initial porosity, μ = mass per unit area of the considered geonet, ρ = density of the polymeric compound used to make the geonet

Range of clogging reduction factors is provided by GRI-GC8. Combining Eqs. 6, 7 and 8, a drainage safety factor, FS_{dc} , of the geocomposite drainage layer can then be calculated as follows:

$$FS = \theta \times \frac{1}{RF_{CR} \times RF_{CC} \times RF_{BC}} \times \frac{\sin \beta}{q_h \times L} \tag{10}$$

The selection of drainage FS-value is dependent upon the design life and criticality of the project, 2 – 3 is recommended by Giroud et al. (2000). The combination of drainage safety factor and reduction factors are sometimes called the Long-Term Services Factor.

Transmissivity testing

The in-plane flow capacity of a geocomposite is evaluated using a laboratory transmissivity test (ASTM D-4716). This test is performed using the transmissivity

box setup shown on Fig. 8. This apparatus allows a range of normal loads and boundary conditions, i.e. soil or geomembrane, to be applied to the face of the geocomposite. The head acting across the 300mm square sample can be varied to create a range of gradients that simulate field slope conditions. The flow gradient, i , is defined as the head divided by the flow length (300mm in the case of ASTM D4716).

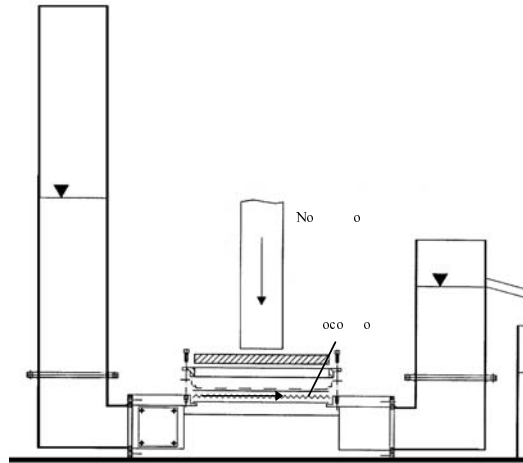


Fig. 8 ASTM D-4716 Transmissivity Test

Fig. 9 shows typical results from a laboratory transmissivity test. In general, transmissivity decreases with increasing normal loads and increases with decreasing flow gradients. Great care must be taken to properly specify the proper boundary conditions and load duration for this test. Boundary conditions on both the upper and lower faces of the drainage composite should reflect the actual material that will be encountered in the field. This allows a proper simulation of intrusion that may occur due to soft soils or large particles in the soils. The flow gradient used in the test must be equal to or larger than the actual anticipated flow gradient. The normal load should be allowed to seat for a time period of not less than 100 hours before performing the flow test. Additionally,

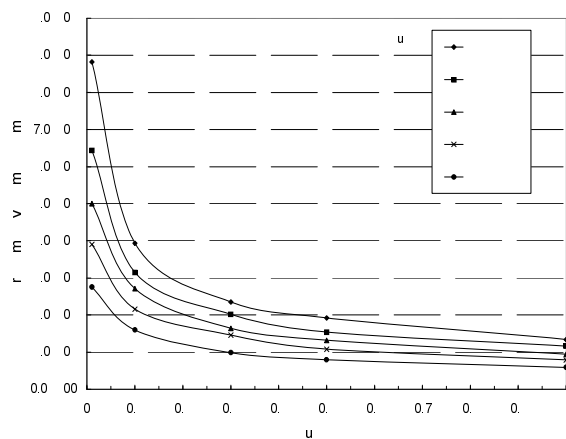


Fig. 9 Typical ASTM D-4716 Test Data

the manufacturer of the geocomposite drainage product should provide compressive creep test data indicating the performance of the specific product with a load duration of 10,000 hours. This effectively precludes the long-term collapse of the geonet core.

Pipe Collection System

While not a ‘geosynthetic’ system, the network of pipes that drain the area collectors have several unique design ‘geo’ considerations. Fig. 10 shows a typical collector pipe with an envelop of gravel placed around the pipe. This Fig. demonstrates two points should be understood by a designer: (1) the envelop of gravel not only filters leachate entering the pipe but significantly increases the normal load that the pipe can carry, and (2) no geotextile is ever placed between the waste and the drainage pipe. Typical leachate is rich in biological activity that can quickly clog a geotextile. Early work by Koerner et al. (1993) showed that biological growth due to the leachate quickly and dramatically reduced the permittivity of a geotextile. For this reason, a geotextile may be used beneath the pipe and stone to provide a cushion to protect the geomembrane but it is never used as a filter around the leachate collection pipes.

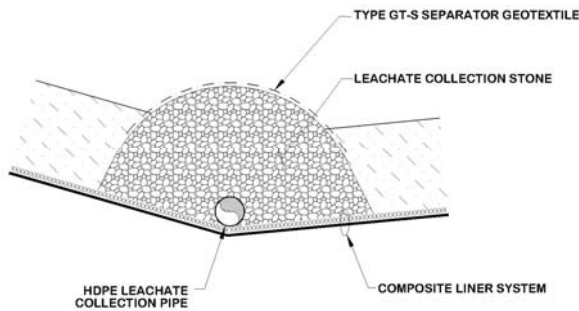


Fig. 10 Leachate Drainage Pipe Detail

FINAL COVER DESIGN

Since the 80’s, the convention in landfills in the USA is that a landfill cell that has a geomembrane liner must be closed with a final cover that also incorporates a geomembrane. The goal was to ensure that the final cover would allow less surface water infiltration than the anticipated leakage from the liner system. In recent years, this paradigm is changing and the control of gas emissions is now considered more important. This may result in fundamental changes in future designs of final cover systems.

Fig. 11 shows the two distinct designs that must be performed for a typical landfill: (1) a flat sloped top-

deck design with no slope stability concerns, and (2) the side slopes that may be as steep as 3 horizontal-to-1 vertical. The first general rule in final cover design is to prevent water falling on the top-deck from running onto the side slopes. This prevents excessive erosion on the slopes but requires the use of down pipes or swales to carry the water to the base of the landfill. The second general rule in final cover design is to avoid the use of compacted clay layers in the barrier design. Compacted clays will quickly desiccate in the final cover and provide no long term barrier to water or gas migration.

The cover design will usually consist of (1) a layer of soil compacted to provide structural support to the cover system, (2) a geocomposite gas venting layer (for MSW landfill), (3) a geomembrane to limit water and gas migration, (4) a drainage geocomposite drainage layer and (5) a vegetative soil layer to protect the geomembrane, limit erosion, and for esthetic reasons. The geomembrane component will require a rigorous CQA program as previously described for the geomembrane in a liner system.

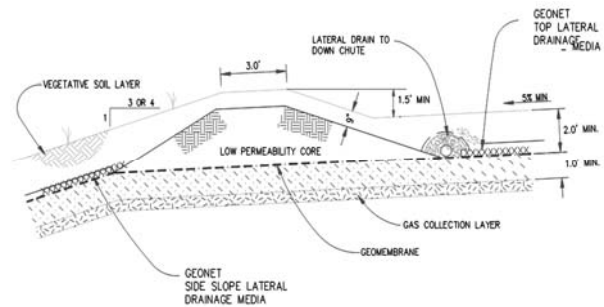


Fig. 11 Final Cover Systems

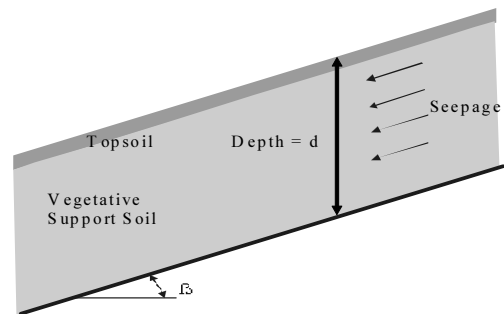


Fig. 12 Seepage Forces acting on Side Slopes

The design of side slopes presents the added complication of maintaining the slope stability of the veneer system on relatively steep slopes. Surface water percolating through the vegetative soil layer can produce seepage forces acting parallel to the slope if the soil layer saturates.

If the cover soil fully saturates and the drain layer is inadequate, the slope stability factor of safety is given as:

$$FS = \frac{\text{Resisting Forces}}{\text{Driving Forces}} = \frac{\gamma_b d \cos \beta \tan \delta}{\gamma_b d \sin \beta + \gamma_w d \sin \beta} \quad (11)$$

$$= \frac{\gamma_b \tan \delta}{\gamma_{sat} \tan \beta} \approx 0.5 \frac{\tan \delta}{\tan \beta}$$

where γ_{sat} is the saturated unit weight of the soil and γ_b is the buoyant unit weight of the soil, β is the slope angle, and δ is the interface friction angle.

When such seepage forces are eliminated by using high flow capacity geocomposite drainage layer, the slope safety factor, FS, becomes:

$$FS = \frac{\tan \beta}{\tan \delta} \quad (12)$$

Thus, the use of a geocomposite drainage layer doubles the sliding factor of safety under extreme surface water infiltration.

The geocomposite drainage layer must have sufficient transmissivity to carry the maximum anticipated percolation inflow and adequate interface friction with the adjacent geomembrane and vegetative soils. The design of the pore water pressure drain underlying a saturated cover soil layer was first presented by Thiel and Stewart at the Geosynthetics '93 conference in Vancouver, B.C. The rate of water infiltration into the geocomposite drain can be readily calculated under a unit gradient since the infiltration velocity is equal to the permeability of the vegetative layer. Typical permeability values for vegetative systems range from 1×10^{-3} to 1×10^{-5} cm/sec. Tighter soils do not allow root penetration and soils looser do not provide adequate water storage. The basic lateral drainage model developed by Thiel is shown on Fig. 13.

The quantity of water, Q_{in} , infiltrating into a unit width of drainage composite having a length L is given by

$$Q_n = k \times L \times 1 \quad (13)$$

The flow capacity of a drainage layer is solved for using Darcy's Law as follows:

$$Q_{out} = k_d \times i \times A = k_d \times i \times (t \times 1) = [k_d \times t] \times i = \theta \times i \quad (14)$$

where t is the thickness of the drainage layer, i is the flow gradient, and $[kt]$ is transmissivity. For slopes, the gradient i is equal to $\sin \beta$, where β is the slope angle. The transmissivity of a geocomposite drainage layer is obtained from laboratory testing as previously described. It is important that the transmissivity be obtained at

normal stress levels, boundary conditions, and gradients that reflect actual field conditions.

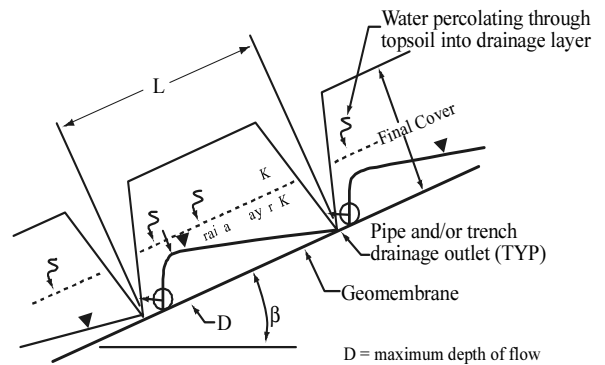


Fig. 13 Head Buildup in the Drainage Layer (Thiel and Stewart, 1993)

It is important to understand the impact of both L and D on the hydraulic factor of safety. Conveniently, the effective drainage length of the drain can be limited by draining it at each side slope swale commonly used to limit surface erosion. Such swales are commonly 30 to 50 m apart down the slope. The geocomposite drainage layer can be designed to drain into each swale as shown on Fig. 14.

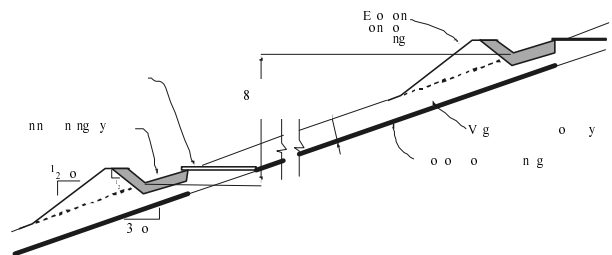


Fig. 14 Side Slope Swales and Geocomposite Drains

LESSONS LEARNED FROM FAILURES

Case A

This failure is particularly interesting in that it occurred on a relatively gentle slope. Fig. 14 demonstrates that cracks widening between sliding blocks. Fig. 15 shows that the vegetative supporting soil was washed to slope base. Initially this failure was thought to a surface erosion problem since the slope was minor. However no erosion ‘gullies’ running down the slope are visible and the vegetation on the cover is excellent. This led to suspect that something other than run off erosion was occurring.



Fig. 15 Cracks widening between sliding blocks

The details of the cover are as follows:

- slope angle = 8.5 degrees, slope length = 94 m
- cover profile: 15cm top soil, 45cm silty sands ($k=5 \times 10^{-4}$ cm/sec), single bonded geocomposite drainage net, and a smooth HDPE geomembrane.
- geocomposite transmissivity = 8×10^{-4} m²/sec



Fig. 16 Vegetative support soils washed to slope base

HELP analyses indicated that the topsoil and sand did not saturate and a peak flow into the geocomposite of 2.5 cm per day, $r = 2.9 \times 10^{-5}$ cm/sec. Thus the peak flow into the geocomposite was calculated $= 2.7 \times 10^{-5}$ m³/sec-m (2.9×10^{-7} m/sec * 94 m * 1). The drainage capacity of the geocomposite is calculated $= 1.2 \times 10^{-4}$ m³/sec-m (8×10^{-4} m³/sec-m * $\sin(8.5^\circ)$). This results in a predicted factor of safety of $1.2 \times 10^{-4} / 2.7 \times 10^{-5} = 4.5$. However, inspection of the failed cover clearly indicated that the cover had saturated. Thus the flow into the geocomposite should not have been calculated using HELP model and should have been calculated using the unit gradient design. This produces a peak inflow into the geocomposite of 4.7×10^{-4} m³/sec-m (5×10^{-6} m/sec * 94 m * 1) and an actual factor of safety of $1.2 \times 10^{-4} / 4.7 \times 10^{-4} = 0.26$! Clearly the drainage layer was under-designed and the final cover was subject to saturation. As a note, this cover was ‘repaired’ by removing all materials over the geomembrane and rebuilding with a larger capacity

geocomposite and perforated pipes that reduced the effective collection length of the geocomposite to approximately 30 m.



Fig. 17 Massive Soils Loss on Slopes

Case B

Massive sliding of cover soils occurred after a major storm dropped 120mm of rain on an East Coast municipal solid waste landfill cap construction project. The rainfall occurred within a span of 5 to 6 hours and damaged approximately 14 hectares of cover. Fig. 17 shows massive cover soil loss along the slope, and Fig. 18 demonstrates landfill gas pressure built-up under the geomembrane.

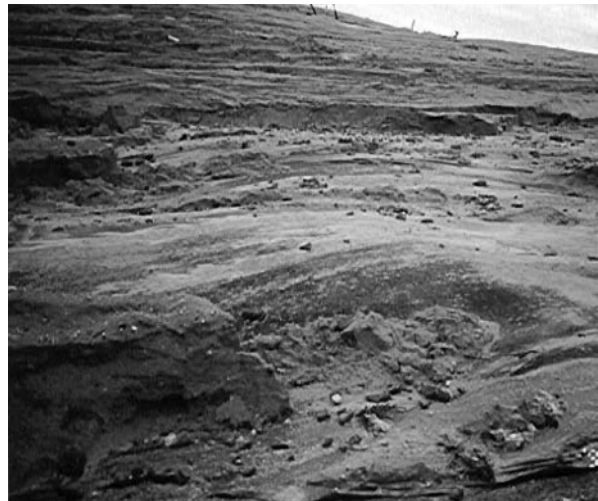


Fig. 18 LFG buildup under the geomembrane

Investigation showed that the failure likely resulted from one or more of the following mechanisms: (a) Inadequate transmissivity in the drainage layer, leading to excessive pore water pressures in the cover soil. Evaluation of the failure is based on the following field conditions that existed at the time of failure:

3:1 slope, $= 18.4^\circ$

Slope length = 122 m
 Cover soil permeability, $k=5 \times 10^{-3}$ cm/sec
 Saturated unit weight of soil $\gamma_{\text{sat}}=17.6$ kN/m³
 Transmissivity of the composite lateral drainage layer,
 $\theta=3.5 \times 10^{-4}$ m²/sec
 Geocomposite/texture geomembrane interface friction
 angle $\delta=22^\circ$

Field observations and laboratory testing indicated that the in-place soil was saturated. This soil was composed of fine sugar sand containing a high percentage of silt fines. The Unified Classification for this soil is SP-SM. The soil was to function as a vegetative support layer immediately above the final cover geomembrane and drainage geocomposite. The vegetative support layer was to be covered with 150 mm of topsoil supporting grass. Failure occurred before the topsoil layer and associated grass could be placed. Assuming saturation of the vegetative support sands, the factor of safety for the *drainage capacity*, FS_{dc} , of the geocomposite drainage layer can be calculated by the following equation:

$$FS = 3.5 \times 10^{-4} \times \frac{0.32}{5 \times 10^{-3} \times 122} = 0.018 \quad (15)$$

Clearly, with a safety factor of 0.018, the transmissivity of the geocomposite is inadequate. Using Eq. 11, site conditions at this project results in

$$FS = \frac{\gamma_b \tan \delta}{\gamma \tan \beta} = \frac{(17.6 - 9.8) \tan 22^\circ}{17.6 \tan 18.4^\circ} = 0.54 \quad (16)$$

Thus, the slope is unstable if the drainage capacity of the drainage net is exceeded. No existing geocomposite drains or geotextiles prove sufficient interface friction to enable a cover soil to remain in place for such a steep slope if the cover soil becomes saturated. However, when seepage forces are eliminated, the slope factor of safety of the cover soil per Eq. 12 was $= \tan \delta / \tan \beta$ or 1.21. Note that a minimum static sliding factor of safety of 1.5 is typically recommended. Thus, even the non-saturated condition was marginal at this site.

In addition to a lack of adequate transmissivity, there were problems of: (b) inadequate gas venting layer, causing LFG pressure buildup below the geomembrane; and, (c) highly erodible silty sands used in the vegetative support layer, causing soil mass loss, especially during storm events.

The failure of the cover soils highlighted significant design errors and construction sequence problems. Each of the mechanisms evaluated above are sufficient to have caused major damage to the partially constructed cover. With the exception of facilities in arid climates,

geocomposite lateral drainage systems must be designed assuming the overlying soils become saturated. Given the unusual weather trends that have dominated the past decade, long-term performance of these facilities must accommodate such weather extremes. The construction problems are related to construction in layers versus full sections. This construction practice leaves very large and highly erodible soil surfaces exposed for extended periods. Severe storms will cause major damage to construction when such practices are used. This is independent of the design adequacy of what is being constructed. Many contractors now limit the area of exposure allowed for erodible soil layers unless the contractor can demonstrate that excessive erosion will be mitigated. Incremental slope stability and soil loss evaluations will force this practice.

Based on the forensic analysis, revised analysis methods and repair techniques for this failure are proposed. These repair techniques include,

- Reduction of the effective slope length of the drainage layer
- Increase in transmissivity of the drainage layer.
- Decrease the erosion potential of the soils.
- Increase the capacity of the existing gas collection blanket.

SUMMARY

Geosynthetic components provide the only means for economically containing the waste byproducts of or cultures. Fortunately, these components are economical and made to very high standards. This paper has developed the simple but essential design considerations that must be evaluated for the successful development of a contemporary lined landfill.

REFERENCES

- ASTM (2002), D5321-02 Standard Test Method for Determining the Coefficient of Soil and Geosynthetic or Geosynthetic and Geosynthetic Friction by the Direct Shear Method, Annual Book of ASTM Standards, Vol 04.08.
- ASTM D4716 (2001). Test method for determining the (in-plane) flow rate per unit width and hydraulic transmissivity of a geosynthetic using a constant head.
- Carpenter JR (1986). STABL5/PCSTABL5 User Manual, Purdue University School of Engineering, Joint Highway Research Project JHRP-86/14, West Lafayette, IN 47907. Commercially available from Van Aller, Harald W., STEDwin (v. 2.80) Windows interface program, Queenstown, MD, Copyright 1999-2002.

- Daniels DE & Koerner RM (1993). Quality Assurance and Quality Control for Waste Containment Facilities, US-EPA, EPA/600/R-93/182.
- Daniels D & Koerner R (2007). Waste Containment Facilities: Guidance for Quality Assurance and Quality Control of Liner and Cover Systems, ISBN 13:978-0-7844-0859-9, ASCE Press.
- GRI-GC8 (2001). Standard guide for determination of the allowable flow rate of a drainage geocomposite. Geosynthetic Research Institute.
- Giroud JP & Badu-Tweneboah K (1992). Rate of Leakage through a Composite Liner due to Geomembrane Defects, Geotextiles and Geomembranes, Vol. 11.
- Giroud JP, Zornberg JG, Zhao A (2000). Hydraulic Design of Geosynthetic and Granular Liquid Collection Layers, Geosynthetic International, 7(4-75).
- Giroud JP, Zhao A, Richardson GN (2000). Effect of thickness reduction on geosynthetic hydraulic transmissivity, Geosynthetics International, Special Issue on Liquid Collection Systems, 7(4-6): 433-452.
- Koerner GR, Koerner RM, Martin JP (1993). Field Performance of Leachate Collection Systems and Design Implications, Proceedings of 31st Annual SWANA Conference, San Jose, Calif: 365-380.
- Koerner RM (1998). Designing with Geosynthetics , 4th Edition, Prentice Hall, New Jersey.
- Kavazanjian Edward, Matasivic Neven, Bonaparte Rudolph, Schmertman Gary (1995). Evaluation of MSW Properties for Seismic Analysis, GEOENVIRONMENT 2000, ASCE Specialty Conference, New Orleans, 24-26 February.
- Richardson GN & Zhao A (1998). Issues on Geosynthetic Drainage Systems in Landfills, Proc. of the 12th GRI Conf on Lessons Learned from Geosynthetics Case Histories, Philadelphia: 177-196.
- Thiel RS & Stewart MG (1993). Geosynthetic Landfill Cover Design Methodology and Construction Experience in the Pacific Northwest, Proceedings Geosynthetics'93, Vancouver, IFAI: 1131-1144.
- USEPA (1994). The Hydrologic Evaluation of Landfill Performance (HELP) Model, User's Guide and Engineering Documentation for Version 3, Office of Research and Development, United States Environmental Protection Agency, Report U.S. EPA/600/R-94/168b.

APPLICATION OF SHEAR STRENGTH OF SOLID WASTE AND MULTILAYER LINER IN LANDFILLS

Jian-Yong SHI¹, Xue-De QIAN², Jun-Gao ZHU³ and Yu-Ping LI⁴

ABSTRACT: The scope of this paper is to present the shear behaviors of municipal solid waste and interfaces of composite liner in landfills. The shear strength of solid waste was investigated by triaxial compression and direct shear tests. Triaxial tests are conducted using standard sand sample randomly reinforced by fabric to investigate the influence of fabric length, fabric content on their strength behavior. Test results showed that the sample strength increases with increasing of fabric length when the fabric length is smaller than a certain length threshold. Above this threshold, the fabric length has little effect on the sample strength. Similarly, the sample strength, especially the cohesion, increases dramatically with increasing of fabric content when the fabric content is below a content threshold. Above it, the fabric content has little influence on the strength. Comparison between the fabric length and content showed that the fabric content is more important, as satisfactory sample strength can be obtained even with a small fabric length when the fabric content is above a certain limit. All results of triaxial compression and direct shear tests show that the stress-strain or stress-displacement response for the solid waste has a steady hardening behavior without reaching peak stress condition due to the progressive contribution of the fibrous materials in the waste. It is suggested that the strength parameter of solid waste by triaxial compression test is obtained at the strain of 15%. The direct shear tests were performed to investigate the interface shear strengths for composite liners. The composite liner consists of nonwoven geotextile, HDPE geomembrane and compacted clay. The weaker interface in the composite liner can be transferred from the interface of geomembrane and nonwoven geotextile to the interface strength of geomembrane and saturated clay with increase of the normal pressure. Based on the test results, stability analysis for a failed landfill was conducted.

KEYWORDS: municipal solid waste, randomly reinforced sand, shear test, interface of composite liner, slope stability analysis

INTRODUCTION

Many landfill slope failures occurred in recent two decades, for example, Chongqing in China, Bandung in Indonesia, and other countries (Koerner & Soong, 2000). Similar to soils, cohesion and friction angle of solid waste are key parameters in landfill stability analysis. In landfill design, the laboratory and field tests, back-analysis from landfill failure case, and indirect in-situ tests are usually used to estimate the shear strength of solid waste (Singh & Murphy, 1990; Howland & Landva, 1992). Triaxial compression and shear box tests are convenient method used in laboratory to obtain the cohesion and friction angle of solid waste. Sometimes, unconfined compression and tensile tests are also used. Because of size limitation for apparatus, the

solid waste samples from samplers have to be reconstituted or totally disturbed (Zhang et al. 2000; Zhu et al. 2002). Based on research results, the strength behavior of solid waste is obviously different with soils. The testing results show that stress-strain relationship is hardening and not softening even for large strain (Zhang & Jie, 2006). Besides properties of solid waste, the landfill failure mode is another key factor for landfill stability analysis. The failure surface may be through subsoil base, waste mass or composite liner (Qian et al. 2002). It is necessary to investigate the interface shear strengths of composite liner. Shear box test is usually used to conduct this investigation (Xu et al. 2008; Shi et al. 2009). The shear strength of solid waste and interface shear strengths of composite liner are most important parameters for landfill stability analysis.

¹ Professor, Key Laboratory of MOE of Geomechanics and Dike Engineering, China. Email: soft-ground@hhu.edu.cn

² Professor, Key Laboratory of MOE of Geomechanics and Dike Engineering, China. Email: qianx@michigan.gov

³ Professor, Key Laboratory of MOE of Geomechanics and Dike Engineering, China. Email: zhujungao@hhu.edu.cn

⁴ Master student, Key Laboratory of MOE of Geomechanics and Dike Engineering, China. Email: g0801469@nus.edu.sg

SHEAR STRENGTH OF SOLID WASTE BY TRIAXIAL COMPRESSION AND SHEAR BOX TESTS

Triaxial Compression Tests for Artificial Waste

Based on statistical data from some landfills in China, the compositions of artificial solid waste used in research are shown in Table 1.

Table 1 Compositions of artificial solid waste

Content (%)	Food waste	Paper	Textiles	Plastics	Glass	Soil
	25.0	21.0	3.0	9.0	8.0	34.0

The samplers were prepared with diameter of 100 mm and height of 200 mm. The water content is 69%, dry density is 0.4 g/cm³. The C-D triaxial compression tests were performed under the cell pressures of 50 kPa, 100 kPa, and 200 kPa. The stress-strain relationship curves of triaxial compression tests are shown in Fig. 1

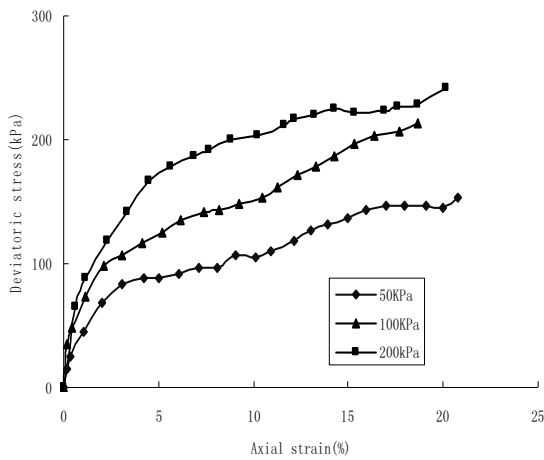


Fig. 1 Shear stress-strain curves of triaxial compression tests for artificial waste

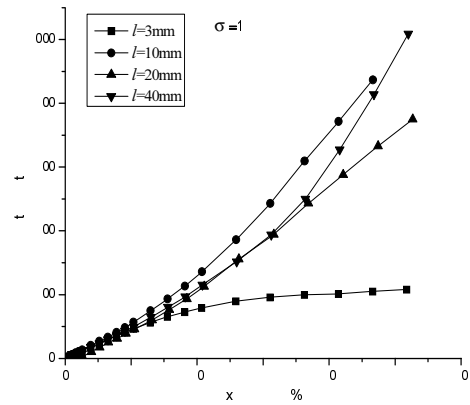
Triaxial Compression Tests for Standard Sand Mixed with Fibers

The samples are made by standard sand and fibers with same fiber weight content and dry density. The basic indexes of standard sand are listed in Table 2. The particle size distribution is shown in Table 3.

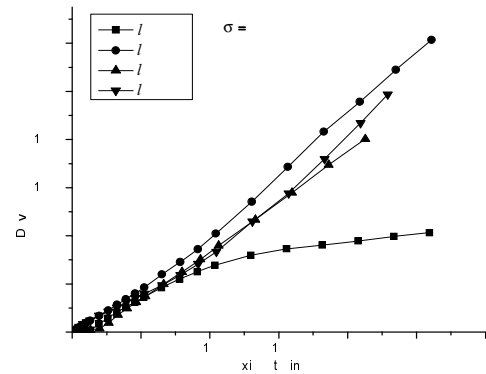
The void ratio, dry density, fabric content and fabric length are listed in Table 4. Tests are performed by conventional triaxial equipment and diameter and height of the samples is 39 mm and 80 mm, respectively.

Effect of fabric length on shear strength

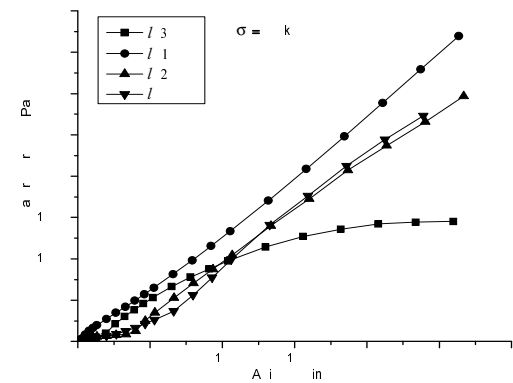
In order to investigate the effect of fabric length on shear strength of the solid waste, four groups of tests are conducted with different fabric length. Considering the limitation of conventional triaxial tests on the particle size of soil samples, the fabric length selected in the tests are chosen to be 3mm, 10mm, 20mm and 40mm. The stress-strain relationship curves for sample Nos. 3, 5, 6, 7, 10, 11, 12 and 13 are shown in Figs. 2 and 3.



(a) Results from CD triaxial test at $\sigma_3=100\text{kPa}$



(b) Results from CD triaxial test at $\sigma_3=200\text{kPa}$



(c) Results from CD triaxial test at $\sigma_3=400\text{kPa}$

Fig. 2 Results from CD triaxial test at 10% fabric content

Table 2 Basic indexes of standard sand

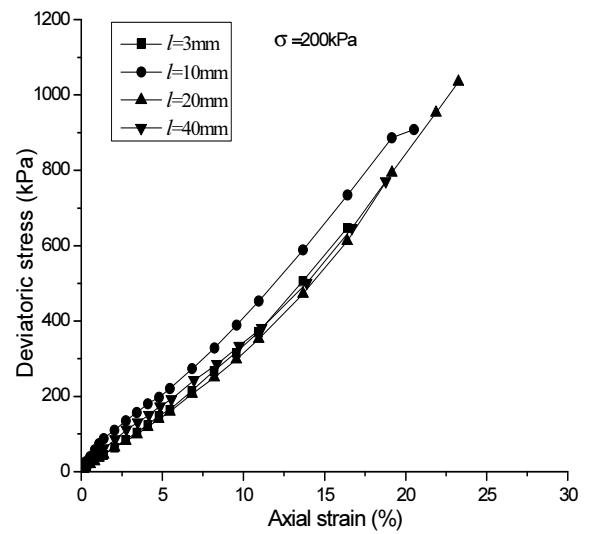
Max. dry density (g/cm ³)	Min. dry density (g/cm ³)	Specific gravity	Max. void ratio	Min. dry ratio	Dry density (g/cm ³)	Void ratio	Permeability (cm/s)
1.87	1.63	2.64	0.621	0.409	1.74	0.515	1.43 × 10 ⁻²

Table 3 Particle size distribution of standard sand

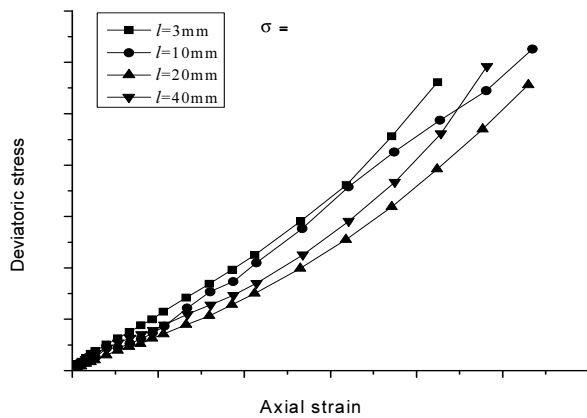
Diameter of particle (mm)	> 2	2-1	1-0.5	0.5-0.25	0.25-0.075	< 0.075
Content (%)	3.6	15.9	43.3	1.4	35.6	0.1

Table 4 Sample indexes of standard sand with fabric

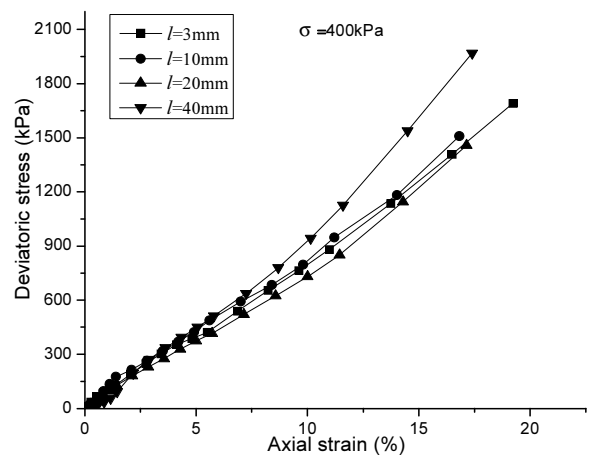
Sample	<i>e</i>	$\rho_{dm} / g / cm^3$	Content %	Length <i>l</i> /mm
1	0.601	1.65	0	-
2	0.510	1.75	0	-
3	0.601	1.16	10	3
4	0.510	1.23	10	3
5	0.601	1.16	10	10
6	0.601	1.16	10	20
7	0.601	1.16	10	40
8	0.601	0.89	20	10
9	0.601	0.89	20	20
10	0.601	0.72	30	3
11	0.601	0.72	30	10
12	0.601	0.72	30	20
13	0.601	0.72	30	40



(b) Results from CD triaxial test at $\sigma_3=200\text{kPa}$



(a) Results from CD triaxial test at $\sigma_3=100\text{kPa}$



(c) Results from CD triaxial test at $\sigma_3=400\text{kPa}$

Fig. 3 Results from CD triaxial test at 30% fabric content

It can be seen from Figs. 2 and 3 that, when the fabric content is 10%, the fabric length has an obvious effect on the strength behavior. Under the same confining pressure, the lowest strength is developed when the fabric length is 3mm compared to other fabric length values. Moreover, little difference is found on strength value when the fabric length ranges from 10mm to 30mm, which suggests that the fabric length has little effect on the strength of the reinforced soil when it is bigger than a certain threshold. This can be explained by the main function of the fabric which is to produce effective connections between soil particles. When the fabric is short, the connective effect becomes more and more evident as the fabric length increases. Thus, the soil strength, especially the cohesion is improved. And it increases with the increasing of fabric length. When one length threshold is reached, increased fabric length may have little impact on the strength as the connective effect between soil particles has been mobilized completely. When the fabric content is 30%, the fabric length has little influence on the strength behavior. Under the same cell pressure, little difference on the strength values is found for samples with different fabric length values. In general, when the fabric is short and with low content, the connective effect of soil particles cannot be developed significantly and some soil particles are still not connected. As the fabric content increases, soil particles which are not in the state of connection are connected effectively by short fabric. When a certain fabric content value is attained, the effective connection between the soil particles can be achieved with those short fabrics. Therefore, the influence of the fabric length becomes insignificant (in Fig. 3).

Table 5 Shear strength parameters of samples

Sam- ple	Content (%)	<i>l</i> (mm)	<i>c</i> (kPa)	$\varphi(^{\circ})$
3	10	3	24.26	36.27
5	10	10	142.91	37.12
6	10	20	115.54	36.75
7	10	40	112.53	37.33
10	30	3	2.66	36.48
11	30	10	22.01	35.38
12	30	20	13.65	35.6
13	30	40	10.00	36.80

Table 5, Figs. 4 and 5 show the variation of sample shear strength with different fabric length and content. It can be seen that with fabric length of 10mm, the cohesion

is six times as much as 3mm fabric length (142.91 kPa vs. 24.26 kPa). When the fabric length is 20mm and 40mm, the cohesion is 115.54 kPa and 112.53 kPa respectively, which are also much higher than the cohesion value with fabric length of 3mm. These results show that when a certain fabric length threshold is reached, shear strength of the reinforced sand will be kept in a constant level with little change. Also, the fabric length is shown to be of little impact on the sample friction angle

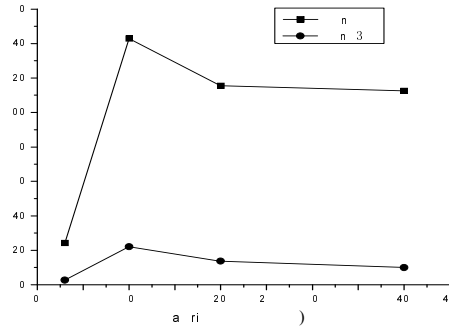


Fig. 4 Variation of cohesion with fabric length

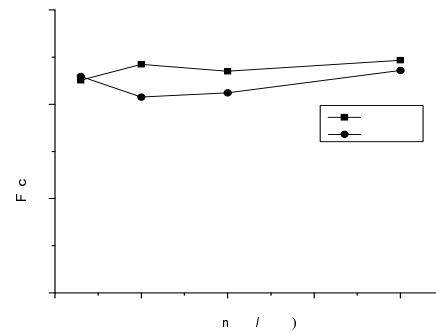


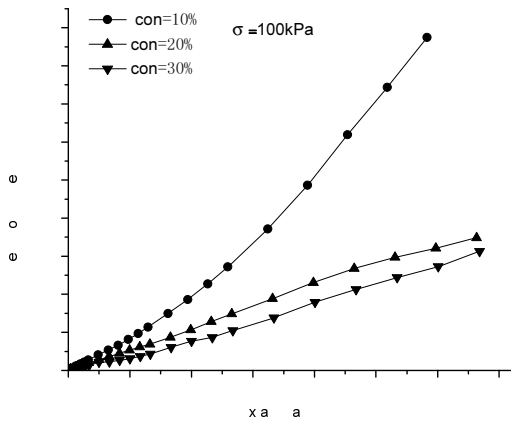
Fig. 5 Variation of friction angel with fabric length

Effect of fabric content on shear strength

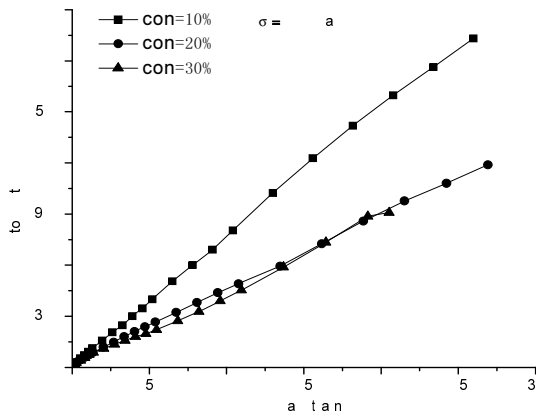
In order to investigate the effect of fabric content on shear strength of the solid waste, three groups of tests are conducted with different fabric content. The fabric contents used in this experimental program are chosen to be 10%, 20% and 30%. The stress-strain relationship curves for sample No.2, 3, 5, 6, 8 and 9 are shown in Figs. 6 to 7.

As shown in Fig. 6, the deviator stress increases continuously with the axial strain. With the same confining pressure, the strength of samples with 10% fabric content presents the rapidest increasing rate. The sample strength is shown to be decreased with increasing of the fabric content. When a certain fabric content threshold is reached, the fabric content may have little impact on the variation of shear strength. The same observations can be obtained from Fig. 7 for the fabric length of 20mm. It is also worthy to note that the deviator stress with fabric length of 20mm is larger than that of 10mm under the same

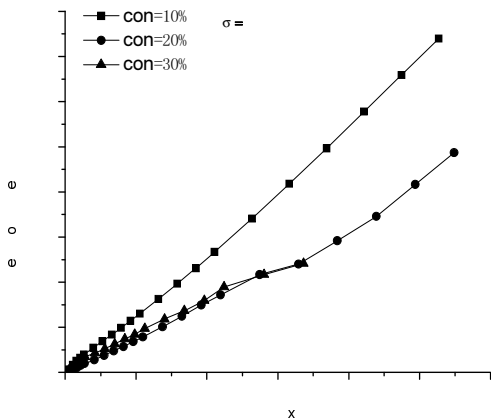
confining pressure. The shear strength parameters of the samples are presented in Table 6.



(a) Results from CD triaxial test at $\sigma_3=100\text{kPa}$

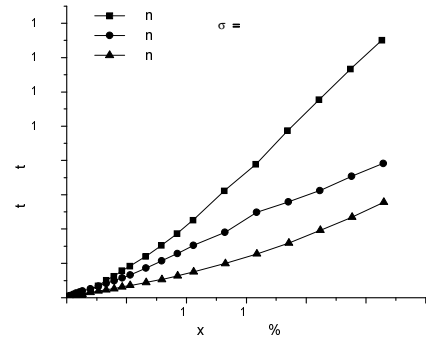


(b) Results from CD triaxial test at $\sigma_3=200\text{kPa}$

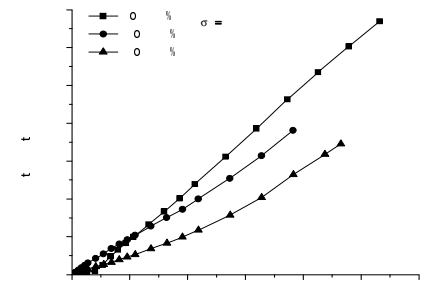


(c) Results from CD triaxial test at $\sigma_3=400\text{kPa}$

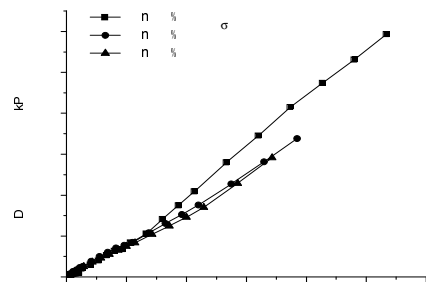
Fig. 6 CD test results at 10 mm fabric length



(a) Results from CD triaxial test at $\sigma_3=100\text{kPa}$



(b) Results from CD triaxial test at $\sigma_3=200\text{kPa}$



(c) Results from CD triaxial test at $\sigma_3=400\text{kPa}$

Fig. 7 CD test results at 20mm fabric length

Table 6 shows the variation of sample shear strength with different fabric content. It can be seen that the fabric can dramatically improve the soil cohesion, but has little impact on the friction angle (Figs. 8 and 9). Also, some reduction of the friction angle is observed with the increment of fabric content. At the beginning of the shearing process, the cohesion of soil particle is shown to be the main resistance, for clay the soil particle would experience the rearrangement from disorder to order; while the main behavior of sand is soil particle friction as it has no cohesive effect. However, the including of fabric into sand completely changes the mechanics, the reinforced sand gains cohesion for the connective effect of fabric, it is indicated that cohesive

property is observed in randomly reinforced sand. When the shear strain is large, friction is the main behavior between soil particles, for clay is interface friction as the soil particle has been rearranged along the shearing surface; for sand is friction between particles, while for the reinforced sand is the friction both between soil particles and fabric. After the increment of fabric content, the friction effect between soil particles and fabric will become the main behavior, which is lower than the friction between soil particles, consequently, the friction angle reduction is observed in the tests results.

Table 6 Shear strength parameters of samples

Sample	Length (mm)	Content (%)	<i>c</i> (kPa)	ϕ (°)
5	10	10	142.91	37.12
8	10	20	53.04	34.49
11	10	30	22.01	35.38
6	20	10	115.54	36.75
9	20	20	50.31	35.57
12	20	30	13.65	35.60

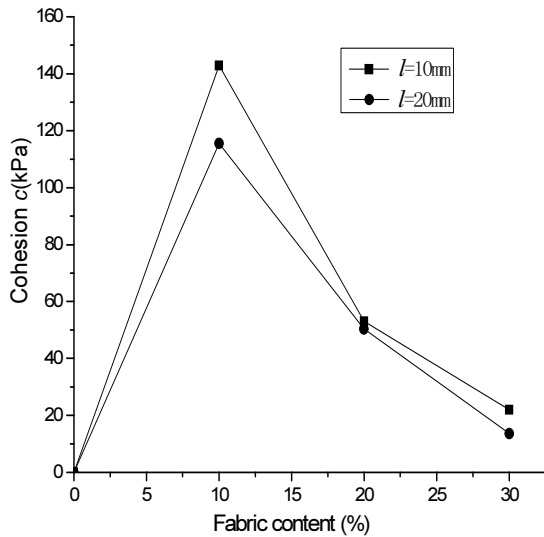


Fig. 8 Variation of cohesion with fabric content

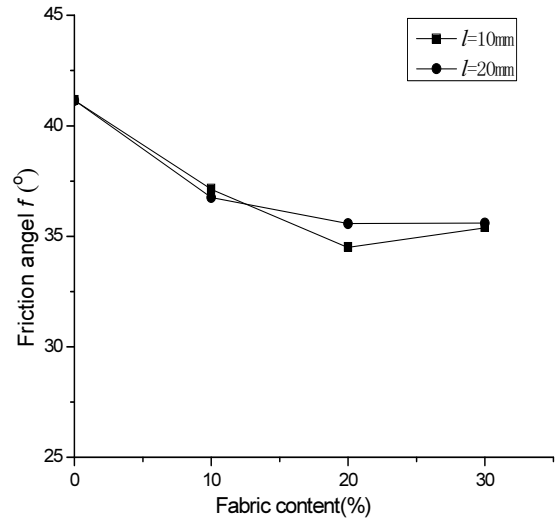


Fig. 9 Variation of friction angel with fabric content

It is analyzed that the fabric content plays a more important role than the fabric length, when a certain value of fabric content is reached, the reinforced effect can still be mobilized significantly even the fabric is not long enough. Essentially speaking, the main mechanics of fabric is to transfer the sand from cohesionless soil to cohesive soil.

From present data collected about solid waste composition, more than 40% of solid waste is organic ingredient and its length is usually more than 10mm, the results of this experimental program are basically consistent with the values obtained from the tests (Qian & Guo, 1998).

Triaxial Compression Tests for Remolded Waste Samples from Landfill

The waste samples taken from the field were dried. The waste compositions of the samples are listed in Table 7.

The samples from landfill were air-dried and remolded. The testing samples were compacted in 5 layers. The diameter and height of the samples are 100 mm and 200 mm, respectively. Their dry density is 0.84 g/cm³. Before test, the samples were saturated by vacuum for 1 hour. The stress-strain curves of triaxial compression test are shown in Fig. 10.

Table 7 Compositions of waste samples from field

Content (%)	Ash, soil	Wood	Plastic	Textile	Glass	Ceramics	Rubber
	57.8	15.3	12.5	4.7	4.3	2.7	2.7

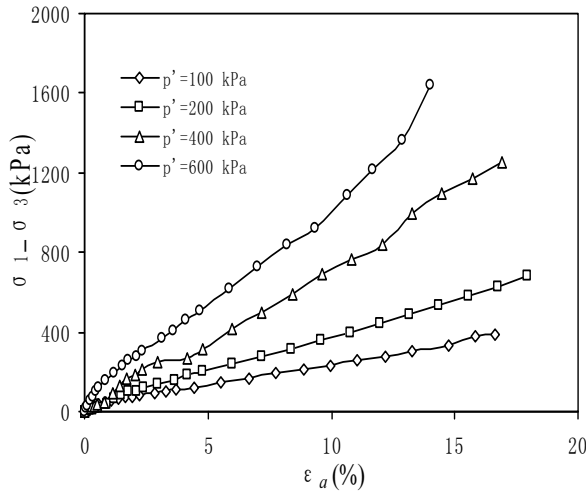


Fig. 10 Shear stress-strain curves of triaxial compression test for remolded waste samples

Direct Shear Tests for Remolded Waste Samples from Landfill

The samples taken from the landfill were air-dried and remolded. The testing samples were compacted in 3 layers. Their dry density is 0.84 g/cm³. The diameter and height of the samples are 61.8mm and 20 mm, respectively. The stress-strain curves of direct shear box tests are shown in Fig. 11.

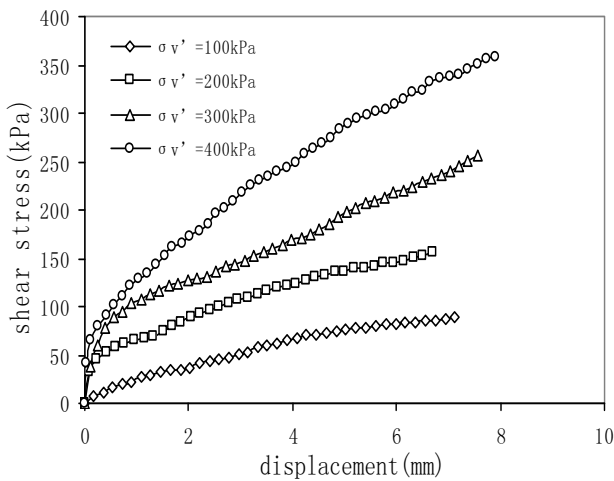


Fig. 11 Shear stress-displacement curves of direct shear tests for remolded waste samples

The stress-strain response in Figs. 1-10 and stress-displacement response in Fig. 11 exhibit a steady hardening behavior without reaching peak stress condition, even for the strain greater than 15% in triaxial compression test and the displacement greater than 4 mm in direct shear test. The similar results have been also reported by other researchers (Zhang et al. 2000; Zhang & Jie, 2006). This steady hardening behavior for the solid waste samples is

attributed to the progressive contribution of the fibrous materials in the shear resistance of the solid waste. Because the shear strength of the solid waste increases with increase of shear strain or shear displacement without reaching peak shear stress and post-peak reduction condition, selection a reasonable strain or displacement to determine the allowable shear strength of waste is very important in the landfill stability analysis. Considering the impact on other structures, such as liner system, leachate and gas pipes in landfills due to waste deformation, using the shear strength corresponding to the strain of 15% as the strength parameter in the stability analysis is acceptable based on current and previous researches (Zhu et al. 2002). This strength criterion for solid waste is also the same as the strength criterion for soil.

INTERFACE SHEAR STRENGTH OF COMPOSITE LINER BY DIRECT SHEAR BOX TEST

The apparatus used to investigate the interface behavior of geosynthetic materials in landfill composite liners is shown in Fig. 12. The size of the geosynthetic material sample is 150 mm × 250 mm. The vertical pressures applied in the tests were 100 kPa, 200 kPa, 350kPa, and 500kPa, respectively. The shearing rate was kept in 0.005 mm/sec until large displacement is reached. The curves of shear stress versus displacement and interface strengths were obtained.

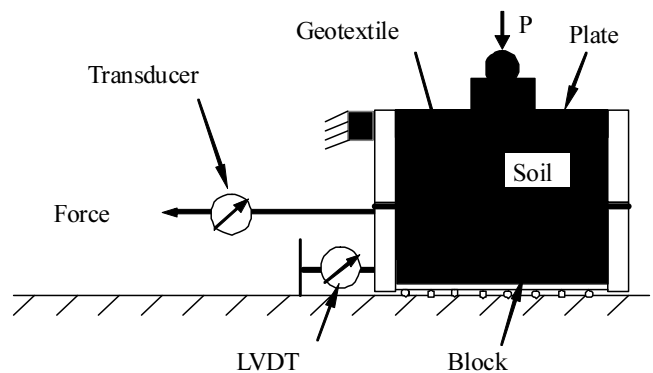


Fig. 12 Schematic diagram of direct shear apparatus

The curves of stress versus displacement of the interface of HDPE geomembrane and saturated clay under different normal pressures are shown in Fig. 13. The strength envelop of the interface of geomembrane and saturated clay is presented in Fig.15. It can be seen in Fig. 15 that the cohesion is $c = 62.42$ kPa and the frictional angle is $\phi = 11.6^\circ$.

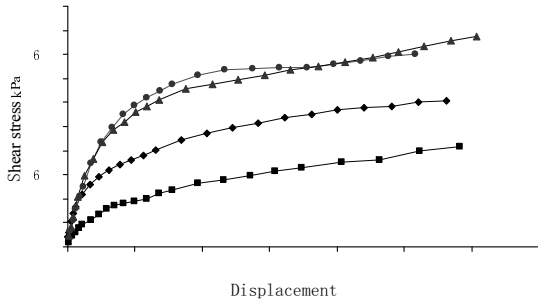


Fig. 13 Curves of shear stress versus displacement of interface of geomembrane and saturated clay

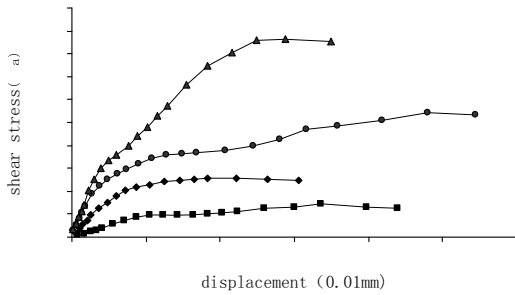


Fig. 14 Curves of shear stress versus displacement of interface of geomembrane and nonwoven geotextile

The curves of stress versus displacement of interface of geomembrane and nonwoven geotextile under different normal pressures are shown in Fig. 14. The strength envelop of interface of geomembrane and nonwoven geotextile is also presented in Fig.15. Fig. 15 shows that the cohesion is $c = 0$ kPa and the frictional angle is $\varphi = 27.8^\circ$

The comparison of strength envelopes between the interface of geomembrane and saturated clay and the interface of geomembrane and nonwoven geotextile is shown in Fig. 15. It can be seen in Fig. 15 that the interface strength of geomembrane and saturated clay under low normal pressure is higher than the interface of geomembrane and nonwoven geotextile. However, under high normal pressure, the interface strength of geomembrane and nonwoven geotextile becomes to be higher than the interface strength of geomembrane and saturated clay. The crossing point of these two curves is at the pressure of 185 kPa. Generally, there is at least a layer of nonwoven geotextile placed over and/or beneath geomembrane in a composite liner. This interface may become a weaker interface in the composite liner when the normal pressure is lower than 185 kPa, especially in the new waste filling portion. The weaker interface may be transferred to the interface of geomembrane and saturated clay when a certain fill height is reached.

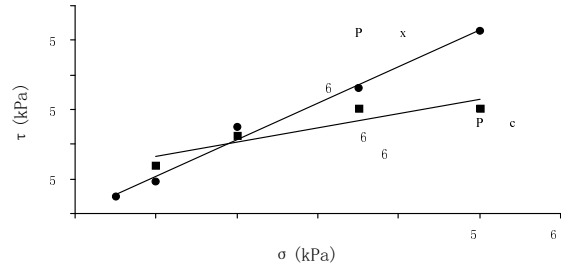


Fig. 15 Comparison of strength envelopes between two different geosynthetic interfaces

LANDFILL STABILITY ANALYSES

Some phenomena showed a municipal solid waste landfill located in southern China is in critical condition with a very low factor of safety. Based on the field investigation, there is no any soft or weak soil layer beneath the landfill. The shear strengths of the solid waste and liner interfaces were also investigated by using triaxial compression and shear box tests, respectively. The potential failure face passes through both the waste mass and the interface of the composite liner by simple calculation method. A two-wedge method developed by Qian et al. (2004) was used to conduct slope stability analysis for this landfill. The waste mass was divided into the active wedge and passive wedge. The limited equilibrium method is used to stability analysis for two wedges. The equilibrium equations of active and passive wedges were calculated. The factor of safety can be obtained. The strength parameters of the solid waste are determined from Fig. 10 and the strength parameters of the interfaces in the composite liner are from Fig. 15. The normal forces acting on the interfaces between two blocks are shown in Fig. 16. The calculated factor of safety for this slope is 1.07. This slope is in limited state.

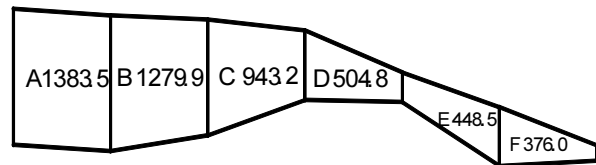


Fig. 16 Normal forces acting on the interfaces between two blocks

To prevent sliding failure for this slope, the surcharge at toe of slope was applied. A soil surcharge berm with height of 5 m and top width of 3 m was constructed. After completion of construction, the factor of safety was increased to 1.36.

CONCLUSIONS

(1) When the fabric is short, the strength is shown to be increased significantly with the increment of fabric length; while when a certain fabric length threshold is reached, little effect on the strength can be observed. Also the fabric length is shown to be of little impact on the strength when the fabric content is in high percent;

(2) When the fabric content is low, obvious increment on strength is observed with the fabric content increases, especially for the increment of cohesion. When a certain value of fabric content is reached, the increment of fabric content may have little effect on strength, and higher percent of fabric may lead to lower strength. It is also found that fabric content is more crucial than fabric length, when some value of fabric content is reached, the reinforced effect can still be mobilized significantly even the fabric is not long enough;

(3) There are different strength behaviors between soil and municipal solid waste. Both stress-strain response and stress-displacement response for solid waste exhibit a steady hardening behavior without reaching peak stress condition, even for the strain greater than 15% in triaxial compression test and the displacement greater than 4 mm in direct shear test. It is suggested that the strength parameter of solid waste by triaxial compression test is obtained at the strain of 15%. The strength criteria of solid waste are same as that of soil.

(4) The strength envelopes of the interfaces of the composite liner show that the weaker interface in the composite liner may be transferred from one to another under different normal pressures. The test results showed that the weaker interface in the composite liner is transferred from the interface of geomembrane and nonwoven geotextile to the interface of geomembrane and saturated clay with increase of the normal pressure.

(5) The potential failure face for a municipal solid waste may pass through waste mass and the interfaces of the liner. Thus, both shear strength of the solid waste and interface shear strengths of the composite liner are key parameters for landfill stability analysis. Selecting suitable apparatus to investigate these parameters are also important.

ACKNOWLEDGEMENTS

This research is financially supported by NSFC (No. 50879022) and NSF-JS(No. 20082890).

REFERENCES

- Howland JD & Landva AO (1992). Stability Analysis of a Municipal Solid Waste Landfill. Proceedings of ASCE Specialty Conference on Stability and Performance of Slope and Embankments-II. Berkeley CA, June 28-July 1: 1216-1231.
- Koerner RM & Soong TY (2000). Stability Assessment of Ten Large Landfill Failures. Advances in Transportation and Geoenvironmental Systems Using Geosynthetics, Proc. of Sessions of GeoDenver 2000. ASCE Geotechnical Special Publication. 103:1-38.
- Qian X, Koerner RM, Gray D H (2002). Geotechnical Aspects of Landfill Design and Construction. Prentice Hall, Upper Saddle River, New Jersey, U.S.A.
- Qian X & Koerner RM (2004). Effect of Apparent Cohesion on Translational Failure Analyses of Landfills. Journal of Geotechnical and Geoenvironmental Engineering, ASCE. 130(1): 71-80.
- Shi J, Qian X, Zhu Y (2009). Shear Behavior of Composite Liner of Landfills by Simple Shear Test. Accepted for publication by Rock and Soil Mechanics (in Chinese).
- Singh S & Murphy B (1990). Evaluation of the Stability of Sanitary landfills. Geotechnics of Waste Fills-Theory and Practice. ASTM STP 1070, Arvid Land, G. David Knowles, Eds. Philadelphia: 240-258.
- Xu C, Liao X, Ye G, Li Z (2008). Research on Interface Frictional Characteristics of Geosynthetics by Laboratory Tests. Rock and Soil Mechanics, 29(5): 1285-1289 (in Chinese).
- Zhang B & Jie Y (2006). Strength and Deformation Characteristics of Municipal Solid Wastes. Engineering Mechanics, 23(II): 14-22 (in Chinese).
- Zhang Z, Wu S, Chen Y (2000). Experimental Research on the Parameter of Life Rubbish in City. Chinese Journal of Geotechnical Engineering, 22(1): 35-39 (in Chinese).
- Zhu J, Shi J, Yan Y (2002). Tests of Strength Properties of Solid Waste in Landfills. Proceedings of 1st Chinese Symposium on Geoenvironment and Geosynthetics, Hangzhou, Bao C & Chen Y, (eds.): 192-196 (in Chinese).

AN APPLICATION OF CENTRIFUGE MODEL IN ENVIRONMENTAL GEOTECHNICS ASSESSMENT OF SOFT GEOLOGICAL BARRIER SUBJECTED TO PILE CONSTRUCTIONS IN WASTE DISPOSAL SITE

Jiro TAKEMURA¹, Binod AMATYA² and Osamu KUSAKABE³

ABSTRACT: In this paper, performance of natural clay barrier subjected to massive pile constructions is investigated using laboratory scale models on a geotechnical centrifuge. Model grounds comprising either thick barrier of soft clay or stiff clay were made and pile construction, pile lateral loading were simulated both in 1-G and High-G environments besides conducting advective-diffusive transport modeling for very long prototype design period in the centrifuge. Two types of pile namely open end and closed end steel piles were used as model piles. Deformation of the ground due to pile deflection under lateral loading and its impact on leakage, and the change in resistivity of ground in the vicinity of pile due to contaminant movement were monitored. Assessments of flow and transport around piling area and pile free area were done on completion of the centrifuge test by thorough model excavation, sampling and chemical analysis. Test results reveal that soft ground is secure from its deterioration irrespective of the types of pile and their stiffness but stiff ground is susceptible to some amount of deterioration. However the degree of damage can be reduced by using open end piles for stiff ground provided that the piles are installed under appropriate surcharge pressure. So the stiffness of the ground and its thickness are very important parameters to be considered for the safety against possible environmental deterioration due to the mentioned activities.

KEYWORDS: natural clay barrier, waste disposal landfill, piling, contaminant transport, centrifuge

INTRODUCTION

Proper solid waste disposal for sustainable environment is a greater concern these days. Many design standards for waste disposal structure can be found around the world as per the local needs. Some standards and specifications allow using natural geological barrier in landfill design for protection of subsurface environments, e.g. French regulatory (Manassero et al. 1997), Japanese regulatory (Kamon, 2001). Relatively thick marine clay deposits, which are normally found in the seabed of coastal areas in Japan, are used as a liner of offshore landfills for municipal and industrial waste in Tokyo and Osaka (Aburatani et al. 1996; Shimizu, 1996).

In the context, an issue has been now how to effectively use these reclaimed offshore land in the post closure landfill stage. The port of Tokyo is planning to develop urban infrastructures like network of highway through these areas. The major concern is that the new development in such waste prone zone could be environmentally critical and may pose long term negative impact. In order to construct seaside roads through such a reclaimed land covered with waste, huge pile foundation structures are

unavoidable due to very low bearing capacity of the (waste and subsurface) ground. The concern raised by such massive pilings is the disturbances to the natural clay barrier underneath the landfill. As the piling structures need complete penetration through the natural clay barrier and resting over sand or gravel bearing stratum, such penetration could deteriorate the barrier providing an access for contaminant leakage and may trigger ground water pollution ultimately. A conceptual diagram for the case is shown in Fig.1.

To investigate the problem, knowledge of contaminant transport in porous media is essential besides pure geotechnical background. Contaminant transport mechanism in porous media is well established now (e.g. Bear & Verruigit, 1987; Freeze and Cherry, 1979). The flow in porous media is very slow for a typical ground comprised of clay and the pollutant migration phenomena is diffusion dominant (Shakelford, 1989). Thus modeling contaminant leakage in the mentioned type of ground is very time consuming. As such modeling in real field condition or full scale modeling is practically not possible as the flow and transport process will be continued for decades.

¹ Associate Professor, Dept. of Civil & Environmental Engrg, Tokyo Institute of Technology, Japan. Email: jtakemur@cv.titech.ac.jp

² Post Doctoral Fellow, Schofield Centre, University of Cambridge, UK. Email: bla23@cam.ac.uk

³ Professor, Dept. of Civil & Environmental Engrg, Tokyo Institute of Technology, Japan. Email: kusakabe@cv.titech.ac.jp

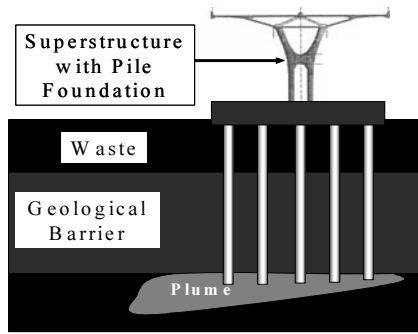


Fig. 1 Conceptual diagram of pile construction and its possible impact

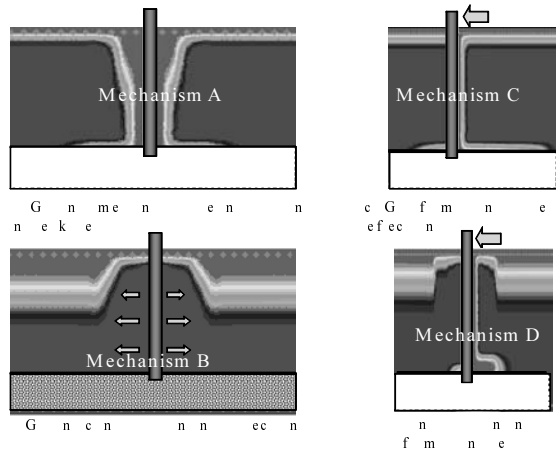


Fig. 2 Some of the possible hypothetical mechanisms of leakage through piles

In the glimpses of such reality, an option could be physical modeling approaches. It is now a well established fact that centrifuge modeling could properly simulate diffusion dominant advection-dispersion phenomena. A fundamental concept and similitude of centrifuge model, including the flow and transport modeling can be found in many literatures (e.g. Arulanandan et al. 1988; Gariner et al. 2007; Hensley and Schofield, 1991).

In geotechnical engineering, an issue of soil pile interaction is not a new topic. However the issue could be reviving as such interaction phenomena could be associated to the deterioration of barrier quality provided to landfills. There could be expected several scenarios about the effects of piles on the barrier quality and possible mechanisms of leakage of pollutants as shown in Fig. 2. A lot of centrifuge research conducted for soil pile interaction behavior under lateral loading can be found (e.g. Hamilton et al. 1991; Terashi et al. 1989; Craig, 1985). As a centrifuge model can generate prototype stress condition in the model ground, prototype soil-pile interaction behavior and its ultimate impact or change in the ground condition can be modeled properly. In order to investigate the possible

leakage along the pile surface, Kamon et al. (2005) measured interface transmissivity between clay and the side wall of oedometer mold. Although these laboratory tests can provide variable information about the effects of soil stiffness and overburden stress on the transmissivity, it cannot simulate the deformation of clay adjacent to the pile by piling process and the deflection of pile caused by environmental loads, such as earthquake loading. Numerical modeling of such problem is also cumbersome as induced critical failure mechanisms of leakage are unknown and governing parameters are uncertain.

Thus the main objective of this research is to investigate and assess the damages caused by piling structures in the barrier system of landfill using centrifuge model tests. Model grounds comprising either thick barrier of soft normally consolidated clay or stiff clay with overconsolidation ratio (OCR) of 2 to 5 were made and pile construction, pile lateral loading were simulated besides conducting advective-diffusive transport modeling for very long prototype design period. Two types of pile namely open end and closed end steel piles were used as model piles. Deformation of the ground due to pile deflection under lateral loading and its impact on leakage, and resistivity change in a pile vicinity ground due to contaminant movement were monitored by using a strain-gauged pile and a resistivity pile respectively. Assessment of flow and transport around piling area and pile free area was done after the centrifuge test by thorough model excavation, sampling and chemical analysis.

PHYSICAL MODELING OF CONTAMINANT TRANSPORT

Principles of Contaminant Transport in Clay

Contaminant transport in porous media is classically described by a form of partial differential equation referred to as the advection-dispersion equation (Bear & Verruijt, 1987; Freeze and Cherry, 1979; Ogata, 1970). For one dimensional flow in a homogenous, isotropic media, the mentioned equation becomes as:

$$R_d \frac{\partial C}{\partial t} = D_{hl} \frac{\partial^2 C}{\partial x^2} - V_{int} \frac{\partial C}{\partial x} \tag{1}$$

where C is the concentration of solute in fluid phase, t and x are time and direction of transport, and, D_{hl} is the coefficient of hydrodynamic dispersion in the longitudinal direction. Average interstitial flow velocity (V_{int}) is defined as $V_{int} = V/n$ (V : Darcy's flow velocity, n : porosity) for fully saturated condition. R_d is retardation factor given by the following equation:

$$R_d = 1 + \frac{\rho_d K_d}{n} \quad (2)$$

where ρ_d is dry density of soil, K_d is linear distribution coefficient.

$$K_d = \frac{dC_s}{dC} \quad (3)$$

where dC_s is change in sorbed concentration, dC is change in the dissolved concentration. The model ground in the study was made by kaolin clay of low specific surface, which is very low reactive. Contaminant source used in the model was sodium chloride which is also non reactive chemical. So chloride sorbed in the clay mineral surface was insignificant and didn't form any insoluble precipitates. Under these conditions;

$$R_d = 1 \quad (4)$$

As the porous media used in the model is pure clay (kaolin) with very low hydraulic conductivity, the Peclet number (P_L) (Eq.5) in the model becomes very small (less than one under high centrifugal acceleration with hydraulic gradient one which is the possible highest hydraulic gradient in the field).

$$P_L = \frac{d_{50} \cdot V_{int}}{D_m} \quad (5)$$

d_{50} is the mean particle size, D_m is the coefficient of molecular diffusion. In such a condition, the dispersion of solute in the model clay can be regarded as the molecular diffusion (Perkins and Johnson et al. 1963, Bear and Verruijt, 1987; Hensley and Randolph, 1994). Thus,

$$D_{ht} \approx D_m \quad (6)$$

Beside P_L , there is another definition of Peclet number denoted by P_e

$$P_e = \frac{L \cdot V_{int}}{D_m} \quad (7)$$

where L is distance from the boundary to reference point or flow path length.

So the partial differential equation (Eq.1) can be modified into following form:

$$\frac{\partial C}{\partial t} = D_m \frac{\partial^2 C}{\partial x^2} - V_{int} \frac{\partial C}{\partial x} \quad (8)$$

Non reactive soil of homogenous character and non-reactive contaminant which are used in the model test may not be analogous to the field condition. But the behavior of normally consolidated clay which could be normally found in the offshore site can be modeled in the laboratory condition using remolded clay. Non reactive clay and conservative contaminant are chosen simply to observe the most critical condition which could prevail in the site. This is also very critical to simplify the phenomena and achieve the contaminant movement to reasonable depth for studying the various effects in relatively short time.

Principle of Centrifuge Modeling and Scaling Law

The mechanical behavior of a prototype soil mass under the earth's gravity '1-G' can be replicated in a small-scale model of $1/N$ experiencing a centrifugal acceleration of ' NG '. If the product of the depth and acceleration is the same in the model and the corresponding prototype, the stress distribution throughout the model will be identical with that throughout the prototype. In such condition, the local seepage velocity at any point within a centrifuge model is N times that experiences at a similar point in a prototype giving a scale factor of $1:N$, i.e.

$$V_m = N \cdot V_p \quad (9)$$

If the flow paths along which pore fluid travels have a scale factor for length of $1:N$, the time for seepage flow is then:

$$t_m = \frac{1}{N^2} t_p \quad (10)$$

This means that the advection in a centrifuge model will occur at N^2 times the rate of the equivalent migration in the prototype and that the level of contamination in both model and prototype will be identical. This scaling factor is also required for the dispersion process. Several researches show that such scaling laws for contaminant migration are valid provided tests are done at low Peclet number (P_e) (e.g. Arulanandan et al. 1988). Therefore, centrifuge model tests can offer means of carrying out small-scale accelerated physical modeling of contaminant migration in clay at stress levels similar to those experienced by the prototype. One of the advantages in the centrifuge model is that porosity variation can be modeled in the ground similar to the prototype during test and this feature is an

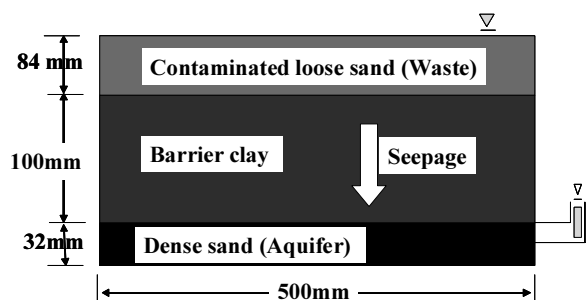


Fig. 3 Model ground with three basic layers

Table 1 Properties of kaolin clay

Specific Gravity (G_s)	2.61
Liquid Limit (W_L)	77.5%
Plastic Limit (W_P)	30.3%
Plasticity Index (I_P)	47.2
Compression Index (C_c)	0.65
Swelling Index (C_s)	0.10
Void ratio at 10 kPa effective pressure	2.23
Permeability at void ratio 1.6	1.6×10^{-9} m/sec
CEC (meq/100g)	1 ~ 15

Table 2 Chemistry of pore fluid in pure kaolin clay model ground

Test	Moisture Content %	pH	EC mS/cm	TDS ppm	Na ppm (meq/100g)	Ca ppm (meq/100g)	K ppm (meq/100g)	Mg ppm (meq/100g)	Cl ppm (meq/100g)	SO ppm (meq/100g)
CM-3	71.6	3.96a	1.294	647	150 (0.47)	39 (0.14)	3 (<0.01)	3 (0.02)	19 (0.04)	455 (0.67)
CM-4	58	4.44b	1.473	670	222 (0.56)	100 (0.29)	5 (<0.01)	0	30 (0.05)	646 (0.78)

Note: CM-2 pore fluid properties were expected to be similar with CM-3 as all test conditions were similar.

a: pH of 4.5 times diluted solution

b: pH of 27 times diluted solution

important issue while working with normally consolidated clay ground.

Among the various advantage of the centrifuge modeling, accelerating the contaminant movement through the media is the major advantage for this study. In this test series, centrifuge model was designed for 100G centrifugal field, under which 1 hour centrifuge model operation time could simulate the phenomena for 1.14 years of prototype time.

CENTRIFUGE MODEL TEST PROGRAM

A series of model tests were conducted in geotechnical laboratory of Tokyo Institute of Technology using Mark III centrifuge. Specifications and details of the Mark III centrifuge are given by Takemura et al. (1999). Test series namely CM-1, CM-2, CM-3 and CM-4 are presented in this paper. Each model test had 10 to 11 piles. Steel piles of 10 mm diameter (D) and 0.5mm thickness with smooth surface (normal stainless steel surface without any further polishing) were used. As tests were programmed for 100-G, such dimension simulates 1m diameter pile. As the pile construction in such waste prone zone is dubious, it is preferred to make as low disturbance to the natural barrier as possible. In such intension, open end piles (hollow tubular pipe) with smooth surface and with 81% opening area were used primarily. However, to see the extent of ground disturbance, closed end piles with cone tip at the base were also used.

Table 3 Physical properties of silica sand

Specific Gravity (G)	2.56
D (mm)	0.235
D (mm)	0.174
Coefficient of Uniformity (C_u)	1.46
Coefficient of Curvature (C_c)	0.99
Max. Void Ratio (e_{max})	1.13
Min. Void Ratio (e_{min})	0.67

The general test procedures involved preparation of model ground with desire strength, OCR and effective stress profile in the barrier ground followed by series of pile constructions and full phase advection-diffusion transport. The following sections describe the modeling approaches, test layouts, model preparation, model pile construction, pile loading, soil sampling and chemical analysis.

Modeling Approaches

Modeling approaches were developed to investigate governing factors influencing the contaminant leakage around the vicinity of piles and trace resulting leakage due to pile construction and also due to its life time serviceability. Different ground conditions: Normally consolidated ground (NC ground) (Soft clay deposit) and Over-consolidated ground (OC ground) (Stiff clay deposit) which are quite common features of clayey ground, were modeled to have an insight in the role of a ground (barrier) in the leakage mechanism. Similarly two types of steel pile: Closed end (CE) pile and Open end (OE) pile were considered to have an insight in the

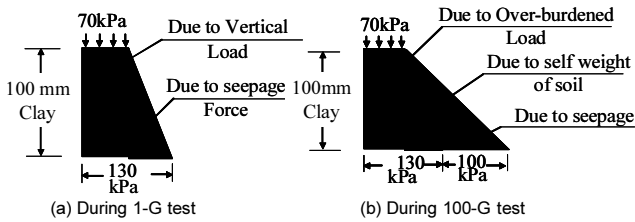


Fig. 4 Effective stress profile for soft geological barrier modeling

role of piles in the leakage mechanism in such grounds. For OE piles, steel tube with external diameter of 10mm and internal diameter of 9mm was used. Similarly for CE pile, 10mm diameter steel tube with cone tip was used. They are considered as partial displacement pile and displacement pile respectively.

Model Ground Description

A three layered model ground was prepared; a dense sandy layer at base (as aquifer) with dry density of 15.0 kN/m^3 , soft/stiff thick clay layer at mid (as natural clay barrier) and loose sandy layer at top (as waste layer) with dry density of about 13.7 kN/m^3 . The dimensional details of the model are shown in Fig.3. All the tests were carried out in a strong box which has inside dimension of 150 mm width, 500 mm length and 350 mm depth. Model barrier was constructed using kaolin clay. The general properties of the kaolin clay are shown in Table 1 and the chemical properties of pore fluid in pure kaolin clay, which was prepared by mixing kaolin powder with de-ionized water, are shown in Table 2. Such clay has low ion exchange capacity and is less reactive in nature. Thus selecting such clay, the complication due to sorption of ground can be reduced. A dense porous ground underneath the clay layer was modeled using uniformly graded silica sand (grade VI). The physical properties of the silica sand are given in Table 3. The silica sand was also used for loose sandy ground over the clay layer as waste deposits. This layer was provided to simulate overburden weight due to waste deposits on the barrier ground and was inundated with synthetic solution made of red ink and NaCl mixture (Model Contaminant Solution). A mixture of pilot red ink (INK-350-R) about 15 times diluted with pure water and NaCl (approximately 0.05 mol/lit) was used for the synthetic solution. The purpose of red ink solution was to trace the flow path and visualize the leakage plume if any in the smeared zone around piles or any other induced leakage due to soil-pile interaction phenomenon. NaCl could act as a nonreactive tracer as both Cl^- and Na^+ are nonreactive ion with very low sorption capacity. Combination of such tracers and the ground could much simplify the flow and transport mechanism in the ground.

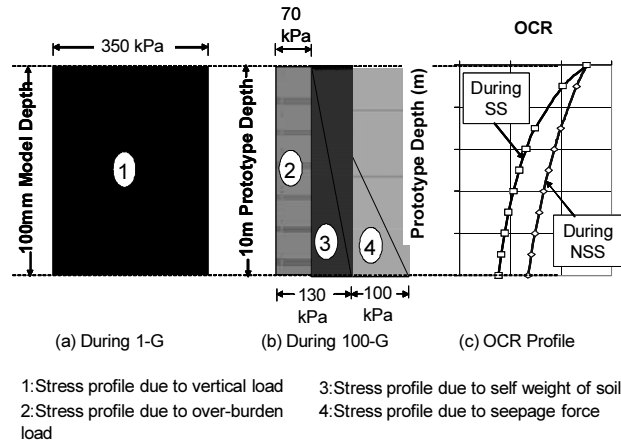


Fig. 5 Stress and OCR profile for stiff geological barrier modeling

For a soft natural clay barrier (NC ground) model, effective stress profiles were developed in the ground during tests as shown in Figs. 4. Vertical stress of 70 kPa was generated by a bellofram cylinder in the laboratory floor (1-G) and by over burden load (top sand layer) in 100-G acceleration. The varying stress profile was generated by seepage force in 1-G and by self weight and seepage force in 100-G. A porosity variation or strength variation from the top to bottom is an important feature of soft ground and such feature can be easily modeled in centrifuge. As the stress developed in the ground in 1-G was always less than or equal to the stress developed in 100-G, the ground remained as NC soft ground. The details regarding model ground preparation for soft geological barrier, instrumentation technique in the model ground can be found in Amatya et al. (2006) and Amatya (2006).

For developing a stiff clay type natural clay barrier (OC ground), the kaolin clay was consolidated by the consolidation pressure of 350kPa in 1-G. During 100-G centrifugal consolidation, the stress profile generated was about the same as that of NC case (Fig.4). The imposed load was quite high during 1-G stage than that of the 100-G stage. This difference of loading generated OC ground. The stress and OCR profile for these different stages are shown in Figs. 5. Once such barrier ground of expected strength, OCR and thickness was prepared, it was covered up by a loose sandy layer by slumping sand and then the model solution was supplied from the bottom of the top sand.

Model Implementations and Test Setup

(1) Test setup

Basic features of model instrumentation are shown in Fig. 6. Basically, instrumentations were done to monitor pore pressure, settlement, resistivity and temperature variations in the ground which were measured by pore

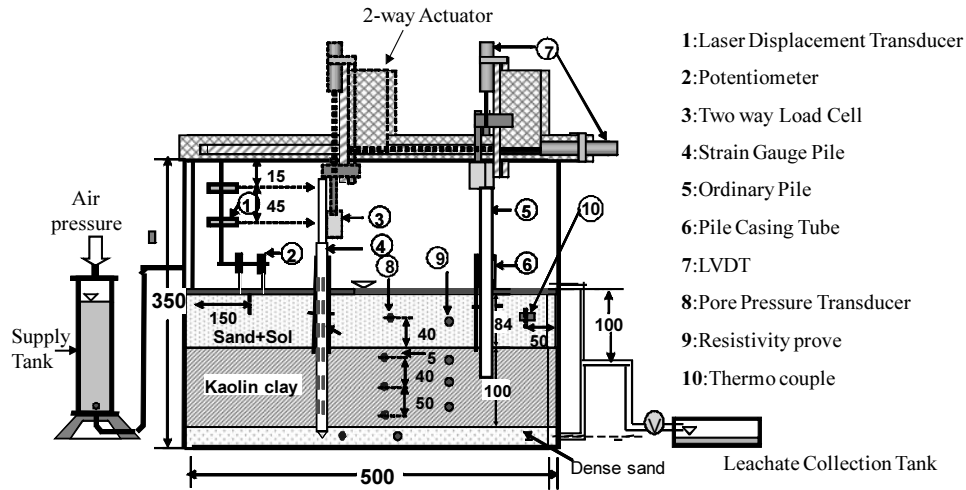


Fig. 6 Test setup and instrumentations

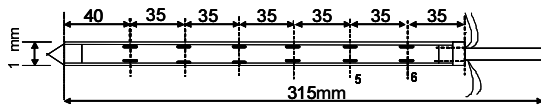


Fig. 7 (a) Model strain gauge (SG) pile

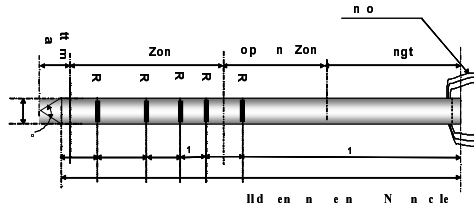


Fig. 7 (b) Model resistivity pile

pressure transducer, potentiometer, resistivity prove and thermo-couple respectively. In addition to them, two-way actuator was equipped with two potentiometers (LVDTs) to locate the positioning of actuator in vertical and horizontal direction. Two-way load cell was also attached with the actuator to measure horizontal and vertical loads applied to the model piles. Besides there were two Laser Displacement Transducers installed on a stand to detect and measure the movement or rotation of a strain gauged pile.

(2) Strain Gauged Pile

A model pile instrumented with strain gauges at the internal surface of the pile along its length was used in the tests. It is a closed end pile with 10 mm external diameter with six strain gauge pairs at spacing of 35mm as shown in Fig. 7(a). Two strain gauges are affixed to each level (one for bending in tension and the other for bending in compression) and are connected as a fully active bridge circuit for measuring bending strain. Before use in tests, the pile was loaded as a cantilever beam to calibrate gauges in bending strain. Calibration was also done for known induced strain.

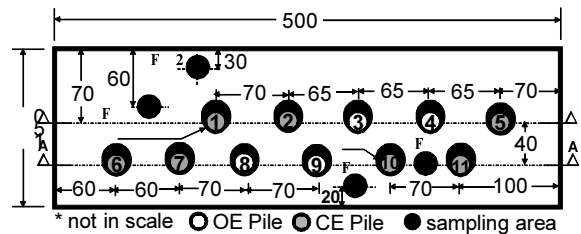


Fig. 8 Pile configuration in the model ground (CM-3)

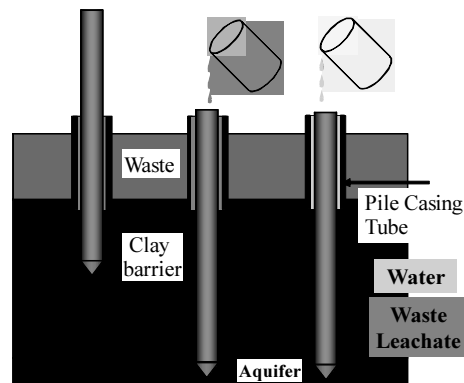


Fig. 9 Various field conditions during pile installation

(3) Resistivity Model Pile

A Resistivity model pile made of Acrylic plastic with 10 mm diameter and 5 resistivity sensors (2-pole type) shown in Fig. 7(b) was made. A 2-pole type sensor was chosen specifically due to restriction of external diameter of pile to 10 mm. These sensors were powered by AC current. An AC/DC converter with amplifier was used to measure outputs in term of potential difference to obtain the resistivity of the surrounding ground at various sensor depths. Difficulties related with measuring electrical resistivity of ground are that it is influenced by many factors like mineralogical constituents, microstructure, fabric and external parameters like quality and amount of pore fluid, packing density, temperature etc. (Kate, 1995;

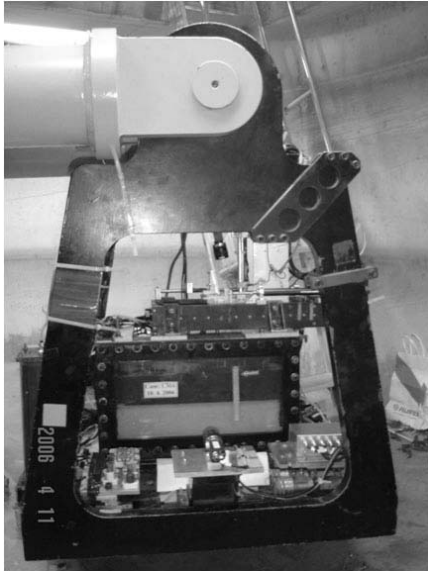


Fig. 10 Complete model ground and accessories mounted on centrifuge platform

Fukue et al. 2001). Despite these many influencing factors, such sensor could still be a useful device under control environment where only a few influencing parameters will vary. This means that contaminated front/plume can be detected by comparing the measured resistivity and the resistivity of uncontaminated soil with similar physical properties.

Model Pile Installation

Pile installation process was categorized into two parts; one as 1-G pile installation and the other as High-G pile installation. Pile installation was done basically in a configuration as shown in Fig. 8. As shown in Fig. 6, the pile driving areas were separated from surrounding loose contaminated sandy area (waste) by casing tubes (inner diameter 10.5mm and length 120mm) while preparing the top layer in the model. This casing tube also served as a guide for keeping piles upright while driving. Before pile driving, the sand layer was fully inundated with the model synthetic solution. The solution was initially supplied through a perforated plastic tube placed at the bottom part of the layer. As mean particle size of silica sand used in the layer was large enough, high degree of saturation of the layer was obtained within a few minutes. All the casing tubes were filled with the solution to consider possible leachate stagnation in the pile driving area before pile installation. But to confirm the effect of possible scenarios in the field, various conditions were modeled in CM-1 as shown in Fig. 9.

In the later stage during centrifugation, the solution was simply supplied over the layer. Piles were driven by a two-way actuator as shown in Fig. 6 through continuous pushing technique till it reached the bottom

sand layer. The amount of forced applied during pile driving can be determined from the load cell attached to the actuator. As 2-way actuator can move in a line with a limited length, the piles in the row A-A (Fig. 8) were driven in 1-G and the piles in the other row B-B were driven in-flight (High-G). In the test CM-3 and CM-4, a pile (P-1) in the row B-B was strain gauged (SG) pile and the SG pile was installed in 1-G due to the difficulty in driving it with chords in High-G. The piles driven in unit gravity are designated as 1-G pile and driven in high gravity are designated as High-G pile. Some of these piles were closed end (CE) pile and some of the others were open end (OE) piles. The 1-G piles were driven once the three layered model ground was basically ready. Driving pile in 1-G can't stimulate the field condition stress history in the model ground and an overburden load induced by the top sand layer was also very small in magnitude whereas driving piles in high gravity (like 100-G) could induce expected prototype stress condition in the ground and also around the pile vicinity. To drive the pile in high gravity, the model was first mounted in the centrifuge platform as shown in Fig. 10 and centrifuged for certain hours in order to allow the model ground to settle under self weight consolidation process or reconsolidated the swelled ground. The degree of ground consolidation can be ascertained instantaneously in-flight from the ground surface settlement data as well as the response of pore water pressure transducers installed at various depths in the barrier ground. Once an adequate degree of ground reconsolidation occurred (for example more than 90% of primary consolidation), the pile driving process was initiated in High-G. Both 1-G and High-G piles were driven in the ground without inducing seepage flow in the model.

Lateral Loading of Model Pile

Pile lateral loading is an important part of this research as it is suspicious that such loading could deteriorate further the barrier, by disturbing the ground around and also creating a gap between pile and surrounding clay, which might promote an easy access of leachate down to the aquifer through the barrier. As the centrifuge can simulate prototype effective stress condition, lateral loading behavior of piles in the ground can be well simulated. This is one of the major advantages of centrifuge in this research. However, due to some limitation of the accessories, lateral loadings were performed in two categories; one in 1-G and the other in High-G. As actuator can only move in the alignment B-B (Fig. 8), the piles in the alignment A-A were loaded in 1-G. In both 1-G and High-G cases, once all piles of relevant gravity were driven vertically, the lateral loading was conducted for each pile separately. All piles (except strain gauged pile) were loaded laterally

Table 4 Conditions of model pile

CM-1					
Pile No.	Pile Type	Gavity level	Deflection of pile head		Remark
			R → L % of Dia.	L → R % of Dia.	
P-1	OE	1-G	0	0	
P-2	OE	1-G	0	>250*	
P-3	OE	High-G(30G)	0	0	
P-4	OE	High-G(30G)	0	0	
P-5	OE	1-G	0	>100*	
P-6	OE	1-G	0	0	
P-7	OE	1-G	0	0	
P-8	OE	1-G	0	0	
P-9	OE	1-G	0	0	
P-10	OE	1-G	0	0	

R→L: right to left, L→ left to right
 *sand intrusion occurred due to large deflection in 1-G

CM-2					
Pile No.	Pile Type	Gavity level	Deflection of pile head		Remark
			R → L % of Dia.	L → R % of Dia.	
P-1	OE	1-G	0	0	
P-2	OE	High-G(50G)	25	27	
P-3	OE	High-G(50G)	23	18	
P-4	OE	High-G(50G)	23	16	
P-5	OE	High-G(50G)	0	0	
P-6	-	-	-	-	
P-7	OE	1-G	42	20	
P-8	OE	1-G	13	14	
P-9	OE	1-G	7	13	
P-10	OE	1-G	4	4	
P-11	OE	1-G	0	0	

CM-3					
Pile No.	Pile Type	Gavity level	Deflection of pile head		Remark
			R → L % of Dia.	L → R % of Dia.	
P-1	CE	High-G(100G)*	200	0	SG Pile
P-2	CE	High-G(100G)	50	0	
P-3	OE	High-G(100G)	80	0	
P-4	OE	High-G(100G)	48	0	
P-5	CE	High-G(100G)	0	0	
P-6	CE	1G	60	0	
P-7	CE	1-G	36	0	
P-8	OE	1-G	64	0	
P-9	OE	1-G	0	0	
P-10	CE	1-G	0	0	R-Pile
P-11	CE	1-G	0	0	

*pile installed in 1-G and laterally loaded in High-G

CM-4					
Pile No.	Pile Type	Gavity level	Deflection of pile head		Remark
			R → L % of Dia.	L → R % of Dia.	
P-1	CE	High-G(100G)*	50	0	SG Pile
P-2	OE	High-G(100G)	81	0	
P-3	OE	High-G(100G)	64	59	
P-4	OE	High-G(100G)	0	0	
P-5	CE	High-G(100G)**	0	0	
P-6	CE	1-G***	71	78	
P-7	OE	1-G	76	95	
P-8	OE	1-G	43	96	
P-9	OE	1-G	0	0	
P-10	CE	1-G	0	0	R-Pile
P-11	CE	1-G	0	0	

*pile installed in 1-G and laterally loaded in High-G
 **partial sand intrusion occurred accidentally during pile driving
 ***significant sand intrusion occurred accidentally during pile driving

at the pile head by the two-way load cell (L.C.) attached to the two-way actuator as shown in Fig. 6. Horizontal displacement were applied at constant displacement rate of 0.21mm/sec both in 1-G and High-G until certain expected range of pile head displacement was achieved. In CM-2 and CM-4, two-way lateral loadings (loading back and forth) and in CM-1 and CM-3, one-way lateral loading (single push) were performed for a short duration.

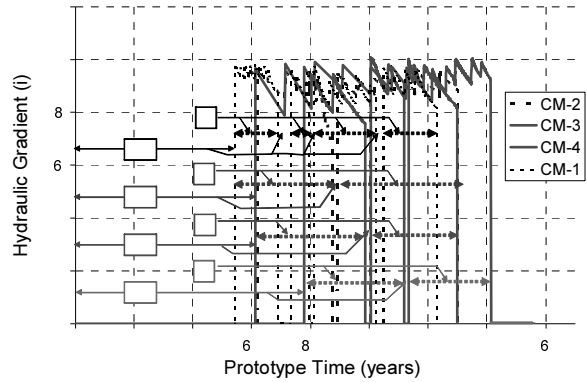


Fig. 11 Hydraulic gradient variation

The amount of lateral loads applied and horizontal displacements at the pile head were measured by L.C. and the potentiometer attached to the actuator respectively. Special measures were taken to laterally load a SG model pile. This pile was laterally loaded in High-G (100-G) at the extended pile head (extended portion) as shown in Fig. 6. From the strain gauges of the pile, bending strain data along the pile length can be obtained and the deflection profile can be generated using integration technique graphically or analytically. The SG pile (P-1) in test CM-3 and CM-4 was designated as High-G pile as it was laterally loaded under the elevated centrifugal field in-flight condition though the vertical installation was performed under 1-G condition. In the model, instrumentations were also included for measuring SG pile head rotation using two laser displacement transducers (LDT) at different elevations. The casing tube was not drawn out during pile lateral loading. It was still in the place. This is also an expected scenario in real construction site. Thus, there might have significant effect on the pile lateral resistance by the tube. However, load-displacement behavior of pile is not a main concern in this research; rather lateral pile deflection behavior is a major concern to predict ground deformation and such prediction can be done once strain profile along the pile length is available. The pile conditions of all tests are summarized in Table 4.

Modeling Advective-Diffusive Transport

Diffusion dominated transport was maintained during pile driving and lateral loading process. During such processes, no seepage flow in the model was allowed. Actually a couple of hours (sometimes even 2 to 4 days) was consumed to set the model in the centrifuge platform with complete accessories and events including driving piles in 1-G, allowing some time for centrifugal consolidation and driving pile in High-G. Such complete no seepage flow stage from the instant of supplying model contaminant to the top sand layer to the instant of inducing seepage flow is considered as No Seepage Stage (NSS). After all pile installation and required

lateral loading, seepage flow was induced in the model by about a unit hydraulic gradient. Such stage from the instant of activating seepage flow in the model to the instant of stopping it is considered as Seepage Stage (SS). The total SS stage was maintained at least for 53 hrs model time which will be about 60yrs prototype time. During such stages, hydraulic gradient and settlement of the ground were fully monitored. The NSS also come out during a short stop of centrifuge between seepage stages for filling the solution to the supply tank. Fig. 11 shows the variation of hydraulic gradient in the entire process of diffusion and advection with the prototype time. Some amount of hydraulic gradient fluctuation during test was inevitable due to continuous draw down and frequent supply of model solution at the top layer.

Soil Sampling and Chemical Analysis

On completion of a desired SS duration, the centrifuge was stopped. The model container was removed from the centrifuge platform. Soil samples were collected at different locations as shown in Fig. 8 using thin wall sampling tube of 27 mm diameter. Samplings were done at pile driven area (PDA) and some other free area designated as pile free areas (PFA) at various depths. Collected soil samples are chopped down in number of layers and separated into two parts, one for chemical analysis and the other for moisture content determination. About 50 gm of pure water was mixed with the collected soil sample for the chemical analysis and agitated thoroughly using a magnetic stirrer. Once thorough mixing was achieved, soil and liquid parts were separated by using a table centrifuge. The collected liquid was sent for chemical analysis. The concentration of anion, such Cl^- and SO_4^{2-} and cation, such as Na^+ , were measured using Ion Chromatography machines. From the concentrations of the diluted liquid and void ratio estimated from the measured moisture contents, the concentrations of tracer chemicals in pore water were calculated. pH, total dissolved solid (TDS) and electric conductivity of the diluted pore water were also measured by a water proof mater (HI 98130: Hanna Instruments). Details of the chemical analysis including the sample processing are given by Amatya (2009).

RESULTS AND DISCUSSIONS

In the following discussions, the test results are given in prototype scales.

Strength and Settlement History of the Barrier Ground

The main characteristics of the four model tests are summarized in Table 5. Fig. 12 shows the void ratios at

Table 5 Main characteristics of models

Model	Type of Barrier	Types of pile used	Lateral pile loading
CM-1	Soft/ NC	OE	1-way loading
CM-2	Soft/ NC	OE	2-way loading
CM-3	Soft/ NC	OE & CE	1-way loading
CM-4	Stiff/ OC	OE & CE	1-way or 2-way loading

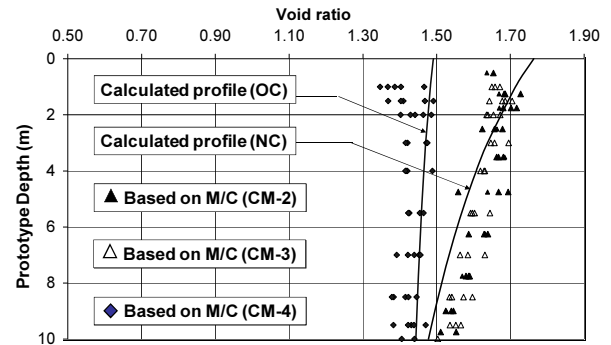


Fig. 12 Calculated and observed void ratio profile at PFA in the barrier ground

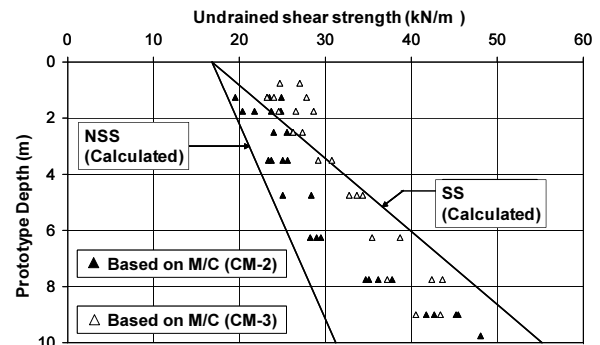


Fig. 13(a) Strength profile of the soft barrier ground (CM-2 & CM-3)

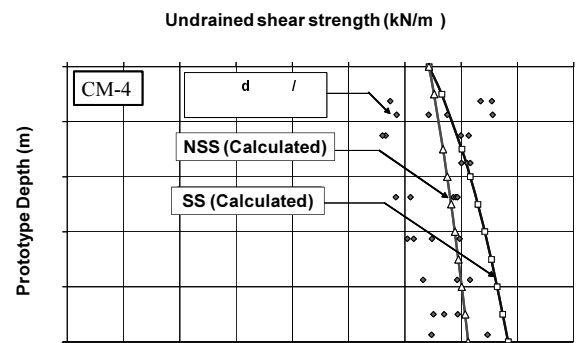


Fig. 13(b) Strength profile of the stiff barrier ground (CM-4)

pile free area (PFA) obtained from the moisture contents measured after the tests for the soft barrier ground (the models CM-2 & 3) and stiff barrier ground (the model CM-4). The depth variation of void ratio calculated from the stress histories are also depicted in the figure. Strength profiles estimated from the equivalent consolidation pressure, which is derived from the void ratio (Fig. 12), are shown in Figs. 13 for the soft and stiff

grounds together with the calculated ones from the stress history for the two stages NSS and SS. The undrained shear strength for the soft barrier are obtained by strength increasing ratio, $(c_u/\sigma'_v)_{NC}$ of K_0 normally consolidated kaolin clay for NC ground, which is 0.24. For the stiff ground (the model CM-4), the expected undrained shear strength (c_u) is derived according to the following expression by Wroth (1984):

$$\frac{c_u}{\sigma'_v} = \left[\frac{c_u}{\sigma'_v} \right]_{NC} OCR^m \tag{11}$$

where, $m=0.83$ for the model clay.

From Fig.12 and Fig.13(a), it can be confirmed that the centrifuge generated a barrier ground having the strength gradually increasing and the porosity decreasing with depth. This is an important property of a soft ground and also one of the important features that the centrifuge model can generate. In case of the stiff barrier ground, it had almost uniform porosity and strength throughout the depth (Fig. 12 and Fig. 13(b)).

Consolidation settlement observed at the ground surface during the whole test duration for the models CM-3 and CM-4 are shown in Fig.14 and Fig.15 respectively. Each figure has two sets of settlement data designated as PM-1 and PM-2 and both of them were nearly of same location. These two figures show that settlement of the stiff ground model was very low and smaller than that of the soft model ground during test duration. In the soft model ground, significant settlement (almost half or more than half of the total settlement) occurred after in-flight pile driving and lateral loading, whereas in stiff model ground, very small amount of ground settlement occurred after the pile loading activities. The compression of clay due to consolidation possibly has an effect on gradual sealing of gaps/deformation which could have occurred during pile deflection.

Pile Responses in Vertical and Lateral Loadings

(1) Pile installation

Fig. 16 shows typical responses of closed end (CE) and open end (OE) piles on their penetration into the OC ground in 1-G. Sudden increase of pile driving load upon an arrival of pile to the bottom dense sand layer could be observed very clearly for both types of piles. Such changes occurred earlier for the CE piles than the OE piles, which indicated the difference in the deformed area by pile installation between displacement piles and partial displacement piles. Due to intrusion of sand happened very accidentally during the pile driving, one CE pile responded differently particularly at the upper part of penetration. Due to such intrusion, the pile driving

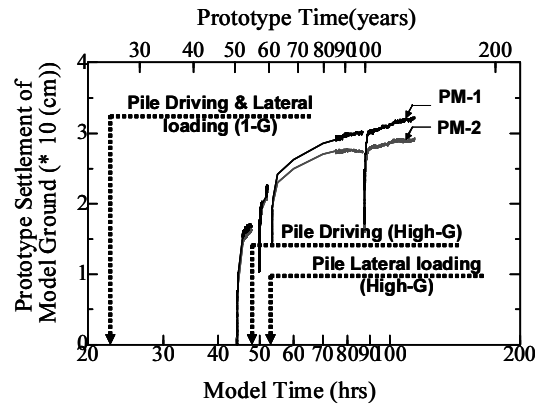


Fig. 14 Settlements of the soft barrier ground (CM-3)

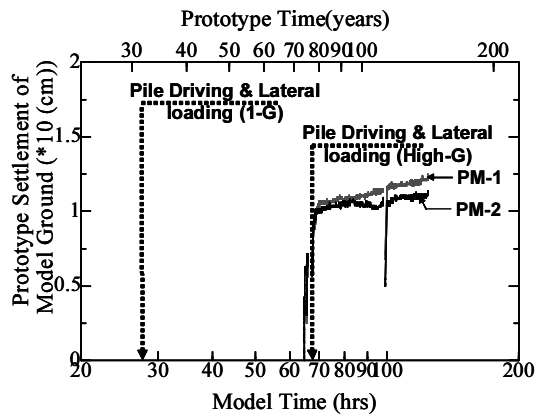


Fig. 15 Settlements of the stiff barrier ground (CM-4)

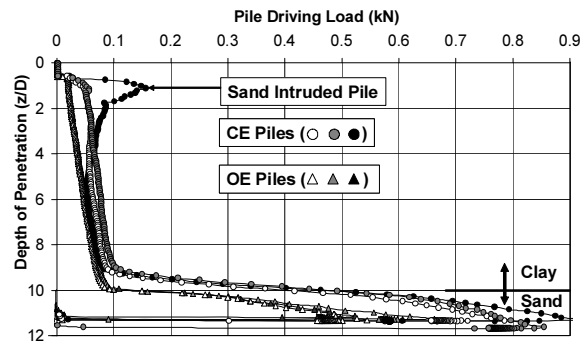


Fig. 16 Pile driving load versus depth of penetration in 1-G (CM-4)

load increased significantly and such effect existed at least for upper 3m prototype depth.

(2) Lateral loading

Pile responses on lateral loading for the piles driven in 1-G and High-G for various tests are shown in Figs.17 to Figs.19. The amount of pile head displacements for various piles in these tests are shown in Table 4. In the model CM-2, lateral displacements were applied to the pile head alternately with the displacement by up to 42% of pile diameter in 1-G loading cases and up to 27% pile diameter in High-G loading cases. The load displacement responses for the various piles seemed reasonably linear

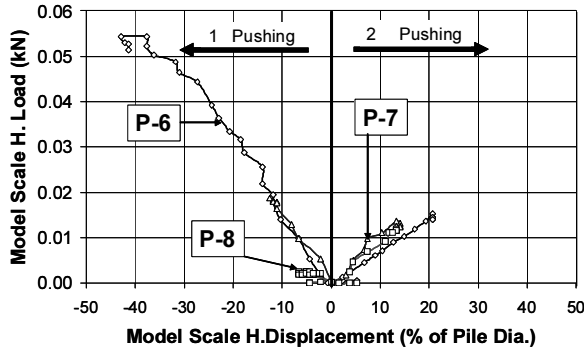


Fig. 17(a) Load versus displacement at loading point under 1-G (CM-2)

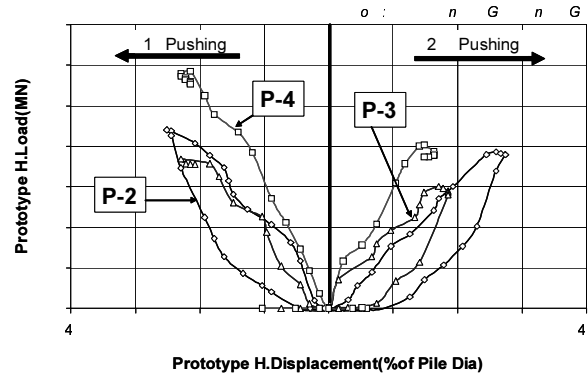


Fig. 17(b) Load versus displacement at loading point under High-G (CM-2)

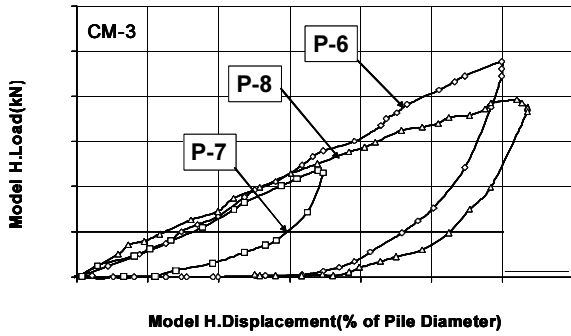


Fig. 18(a) Load versus displacement at loading point under 1-G (CM-3)

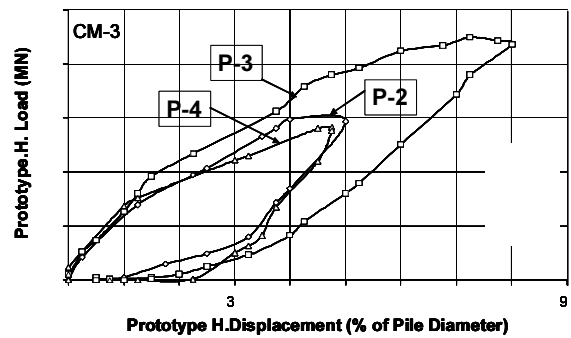


Fig. 18(b) Load versus displacement at loading point under High-G (CM-3)

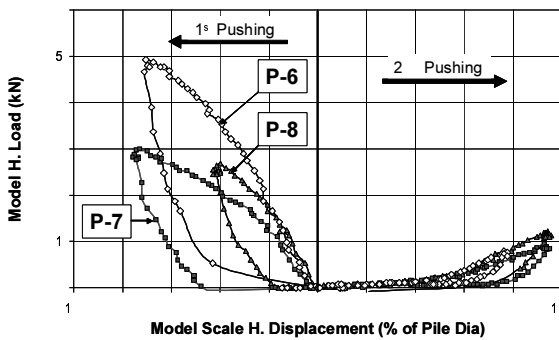


Fig. 19(a) Load versus displacement at loading point under 1-G (CM-4)

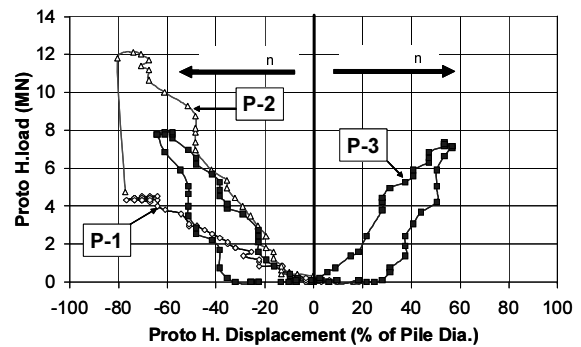


Fig. 19(b) Load versus displacement at loading point under High-G (CM-4)

till the maximum loading imposed. However, the responses of unloading stage were strongly nonlinear. Thus the behavior was obviously not elastic even for the linear behavior in the loading stage. Although the piles in the model CM-3 were loaded and unloaded only rightward, a similar trend in the load-displacement curves to that of the model CM-2 was also observed in 1-G lateral loading cases (Fig. 18(a)). In these cases, the lateral loading was applied up to about 60% of pile diameter.

Nonlinear load-displacement behavior was observed in the loading stage for High-G piles in the model CM-3. Hysteresis loops in the loading and unloading processes show that the residual pile head displacements were larger for 1-G piles than High-G piles, implying that larger plastic deformation took place in the former than

the latter. In the High-G lateral loading cases of the model CM-3, the pile head displacement was applied up to 80% as shown in Fig. 18(b), except of pile P-1 which was accidentally displaced by 200% of the pile diameter due to some problem in two-way load cell. Such a big horizontal displacement on the pile could have perhaps yielded the damage in the barrier and caused a leakage.

In the case of stiff ground model (CM-4) in which some piles were laterally loaded alternately, a unique behavior of load displacement behavior was observed for the 1-G loading case (Fig. 19(a)). Lateral resistance of the pile dramatically decreased in the second loading to the opposite direction of the first one. In the second loading, the lateral load increased very little up to the displacement of 50% of pile diameter and then the load

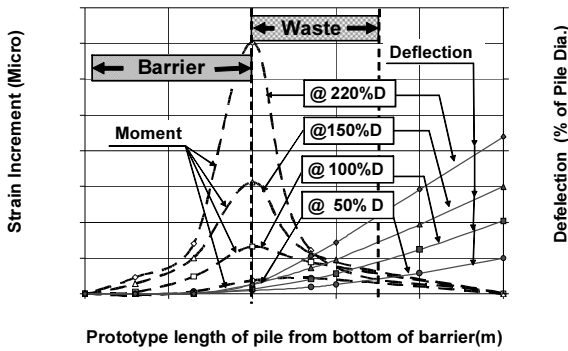


Fig. 20 Strain and deflection profile for SG pile at various amount of lateral deflection (CM-3)

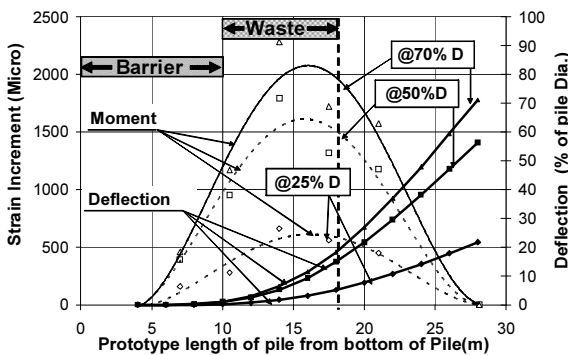


Fig. 21 Strain and deflection profile for SG pile at various amount of lateral deflection (CM-4)

increment rate showed some increase. This dramatic decrease of the resistance could be explained by significant softening or gap formation at the right side of pile when it was loaded from right to left in the first loading (Matlock, 1970). This could also happen in the left side in the second loading. Such deterioration of clay could make a significant impact on the ability of barrier to protect leakage. The larger resistance of pile P-6 than the other piles (P-7 and P-8) could be attributed to the sand intrusion in the barrier ground during the vertical pile driving process, which happened accidentally as mentioned before. On the other hand, the lateral resistances in the first and second loadings were more or less similar for the case of High-G loading as the clay was subjected to an adequate overburden stress on the surface. Because of some problem in the actuator due to mentioned reasons, the piles P-1 and P-2 were loaded only in one direction. In this model, pile heads were displaced up to 95% pile diameter in 1-G and up to 80% in High-G respectively.

In these tests, the pile lateral resistances recorded during the lateral loading were not much different even though the undrained shear strength of the stiff clay layer of model CM-4 was much larger than that of the soft clay models (CM-2 and CM-3). It implies that the top sand layer significantly contributed in the lateral resistance. Many researchers mentioned that in most cases, the properties of the soil between the ground surface and a

depth of 6 to 10 diameters will govern the behavior of a pile subjected to lateral loading (e.g. Fleming et al. 1998; Reese and Van Impe, 2001). As the layer was prepared just by slumping sand without much care, it is expected that such process may have contributed in some discrepancy of the resistance value at different locations as well as in different tests. However, the lateral loading intensity is not main concern in this research. Rather imposed deflection of pile should be emphasized as such deflection could generate gap or deterioration in the barrier. In order to counter such top layer resistance problem and impose some deformation at the barrier, relatively large amount of deflection at the pile head was imposed which could be seen in Table 4.

In order to assess the deformation occurred at the barrier ground throughout the depth while a pile was deflected by the load at its head, the deflection profile for the SG pile was estimated from the bending strain data at various stages of loadings. Strain increment at each SG level and deflection profiles generated based on such data are shown in Fig. 20 and Fig. 21 for the pile P-1 of the models CM-3 and CM-4 respectively. In both cases, though significant displacement was imposed at the pile head, 200% and 70% pile diameter respectively, the pile seemed to be displaced at the barrier surface (waste-barrier interface) by only about 13% of pile diameter for CM-3 and by only about 1% of pile diameter for CM-4. Although the deflections of at the interface were relatively small compared to those imposed at the pile head, these deflections at the head and interface were much more than those expected in the actual sites. For example, according to the foundation design of the Design Specification of Highway Bridges (JRA, 2002), the allowable deflection of pile head is only 1%.

Contaminant Migration and Leakage Assessment at Pile Free Area

Chloride (Cl⁻) concentrations of pore water measured by Ion Chromatography are plotted against the depth in Fig. 22 as the concentration depth profile (CDP). In the figure CDP predicted by using numerical code (GMS, 2000) is also shown. The concentration at the top of barrier is about 2,100mg/lit, which is higher than the Cl⁻ concentration of about 1,800mg/lit for the model contaminant solution (0.05mol NaCl solution with the red ink). Similarly higher concentration was obtained from the water in the top sand, which is the most probably caused by the evaporation of the solution in the top sand layer during centrifugation with the rotational speed of 210 rounds per minutes. Gradual change of the output from the resistivity probe embedded in the top sand clearly indicates the continuous rise in concentration during the in-flight time (Fig.23). This rise from C_{0i}=1800mg/lit to C_{0e}=2,100mg/lit, was considered in the numerical analysis

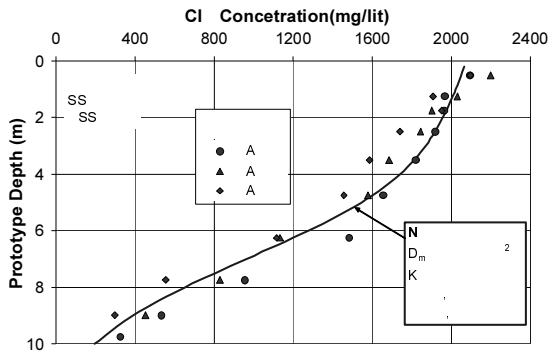


Fig. 22 Cl⁻ concentration depth profile measured at pile free area in centrifuge model and predicted by numerical (CM-2)

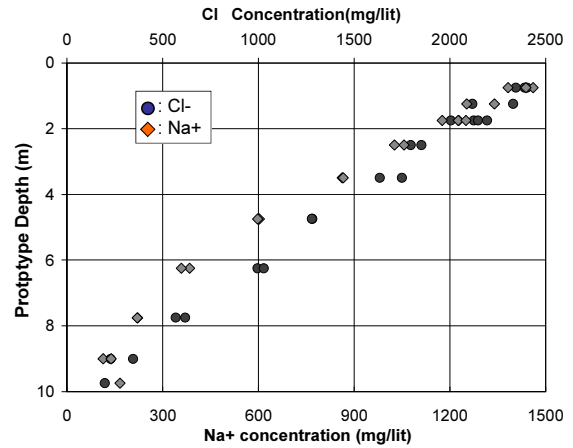


Fig. 25 Cl⁻ and Na⁺ concentration depth profiles measured at pile free area in centrifuge model (CM-2)

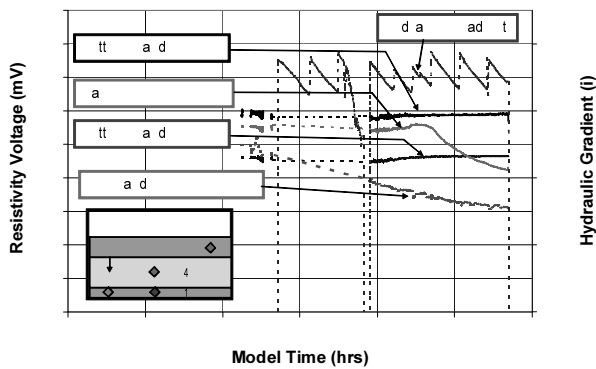


Fig. 23 Responses of resistivity probes in the model ground (CM-2)

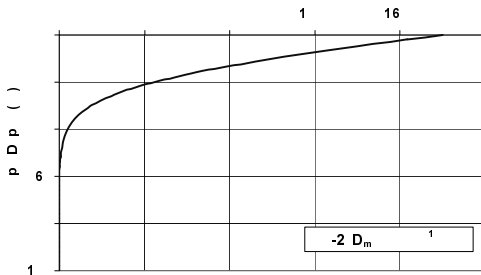


Fig. 24 Cl⁻ concentration due to diffusion in NSS stage estimated by POLLUTE (CM-2)

as a boundary condition. Furthermore, the CDP by the diffusion during non seepage time (NSS) was also estimated using POLLUTE (Rowe and Booker, 1991) as shown in Fig. 24 and used as the initial condition in the numerical analysis. Molecular diffusion coefficient used in the simulation, $D_m=7.5 \times 10^{-10} \text{ m}^2/\text{s}$ was estimated by back calculation and hydraulic conductivity, $K=1.7 \times 10^{-10} \text{ m/s}$, was estimated from the results of falling head permeability tests using oedometer samples. The numerical prediction agrees well with the observation, supporting the assumed D_m value. These Cl⁻ CDPs indicate that performance of the barrier ground was very

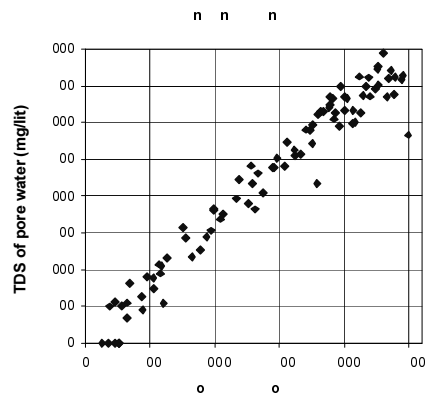
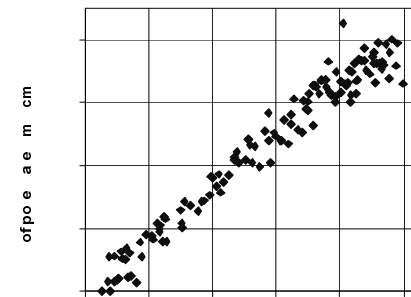


Fig. 26 Comparisons of Cl⁻ concentration with electric conductivity (EC) and total dissolved solid (TDS) of pore water (CM-3)

good and only 10% of the top concentration had reached the bottom part for 60 years time of diffusion and 60years time of advection and diffusion. The downward advective flow with unit hydraulic gradient modeled in this study is considered a quite conservative for the aquitard underlain by the confined aquifer in a seabed.

For the model CM-3, sodium (Na⁺) concentrations were also measured at PFA. The CDP of Na⁺ is compared with that of Cl⁻ in Fig. 25. Although the shape of the profile are similar for the two ions, the advancement of Cl⁻ was a little faster than that of Na⁺, suggesting some sorption occurred for the sodium. The relatively higher

value of Na^+ concentration at the bottom most layer was due to the inherent Na^+ not due to advective –diffusive flow (see Table 2).

In Fig. 26, electric conductivity (EC) and total dissolved solid (TDS) of pore water are compared with the Cl^- concentrations of the same samples. Although there were some scatterings especially for those with high values at the upper layer of the barrier, both ED and TDS had a linear relation with Cl^- concentration, implying that the variation of concentration with depth could be estimated using these quantities measured by a simple method, like the water proof meter used in this study.

Contaminant Migration and Leakage Assessment Due to Pile Driving

(1) Visual inspection

The contaminant migration and leakage assessment were done at first by visual inspection of the red color in the model ground during model excavation after the test. Typical photos of the cross section of the clay taken during such inspection are shown in Fig. 27 and Fig. 28. No extended red color seepage was observed along the pile length in the barrier zone in all model tests (with some exceptions). The color tracer transport in the barrier seemed to be basically consistent irrespective of the pile free area or the area subjected to pile driving with different pile types and loading categories. In the model CM-4 (Fig. 28), one pile (P-6 (1st pile from left)) showed extraordinary leakage behavior but it was mainly due to a massive sand intrusion during pile driving process happened accidentally as discussed before.

(2) Effect of Pile Installation Process

To discuss the effect of pile installation process, especially for the condition in the casing tube, various conditions were modeled in the model CM-1 as shown in Fig. 9. Though in the real field condition, no waste leachate is kept inside the casing tube during pile driving process, some possibilities were modeled by filling casing tubes with contaminant or water before or after pile driving. Above mentioned cases were done to make sure the effect under different possibilities and trace the critical one if any. The chloride CDPs at PDA with the different condition are compared together with those at PFA in Fig.29. Although the results in the figure only limited for 1-G driven OE piles, the chloride CDPs with the different conditions were almost the same as those at PFA even for the piles driven in 1-G. The effect of gravitational field in pile installation for soft clay has been found very little. From these facts it can be said that no contaminant will be carried down by the pile even if the piling will be done in the leachate filled area. The adherence between clay and pile surface is adequate to protect the side wall seepage along the pile if the pile is installed statically keeping in the upright position as done in the test.

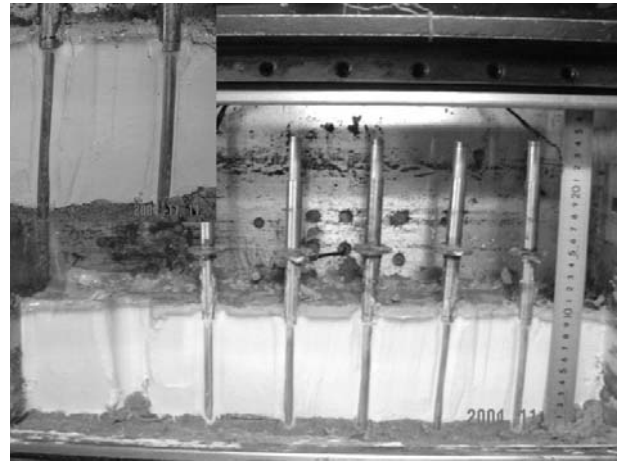


Fig. 27 Typical model X-section (B-B (CM-3))



Fig. 28 Typical model X-section (A-A (CM-4))

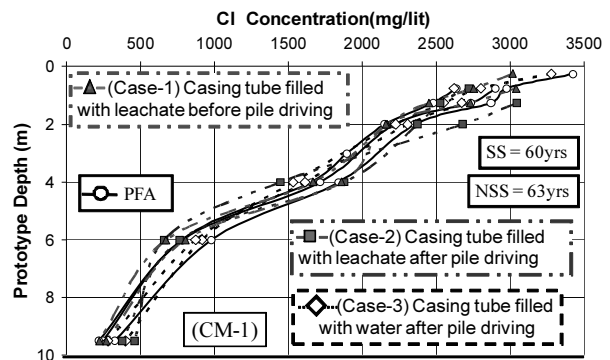


Fig. 29 Comparison of various field conditions (CM-1)

(3) Effects Of Pile Type And Lateral Loadings In Soft Barrier Ground

Figs. 30 shows the Cl^- CDP for various categories (1-G, High-G, normal piles without lateral loading and laterally loaded piles) of OE pile measured in the model CM-2. The results showed that Cl^- concentrations at PDA was either similar to those of PFA or slightly lower. In general, no any piles showed significantly more Cl^- concentration than PFAs. This finding reveals that there

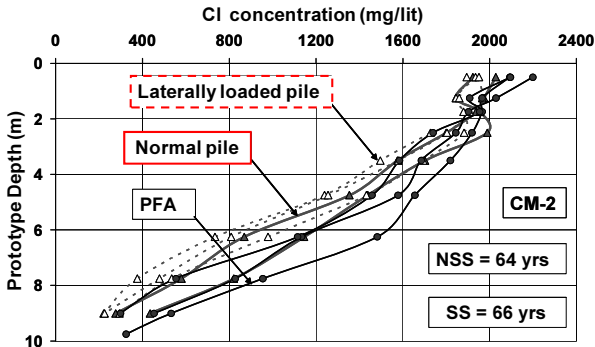


Fig. 30(a) Cl concentration depth profile for 1-G, OE piles with PFA in soft ground (CM-2)

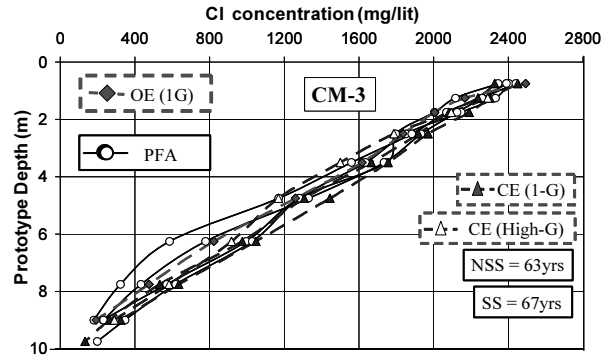


Fig. 31(a) Cl concentration depth profile for OE and CE piles with PFA in soft ground (CM-3)

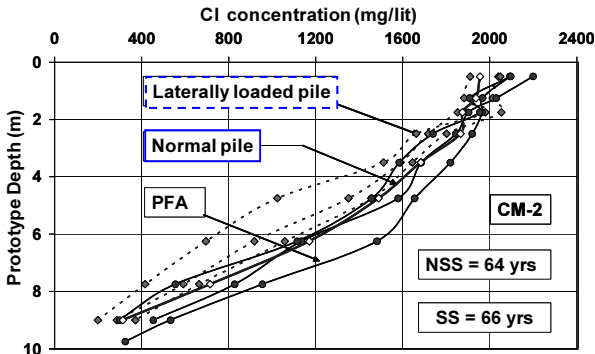


Fig. 30(b) Cl concentration depth profile for High-G, OE piles with PFA in soft ground (CM-2)

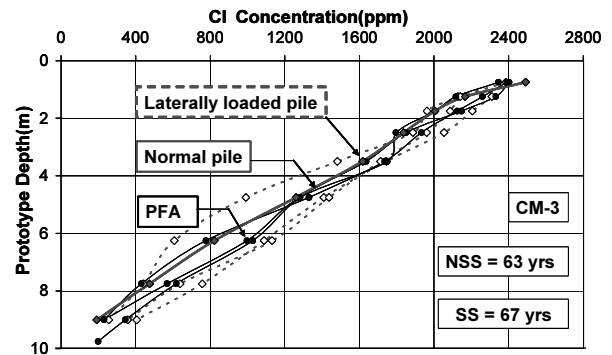


Fig. 31(b) Cl concentration depth profile for OE piles with PFA in soft ground (CM-3)

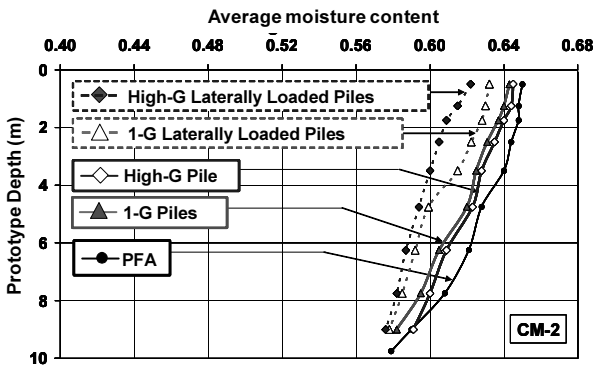


Fig. 32 Average moisture content profiles in soft ground (CM-2)

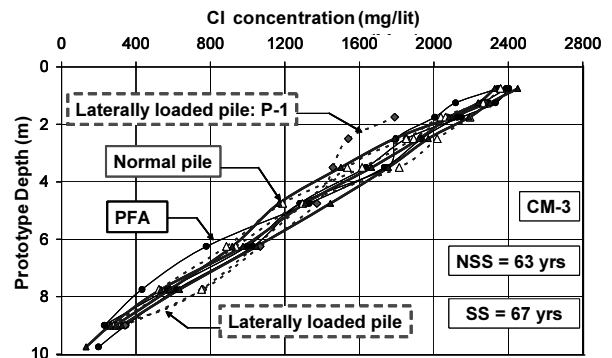


Fig. 31(c) Cl concentration depth profile for CE piles with PFA in soft ground (CM-3)

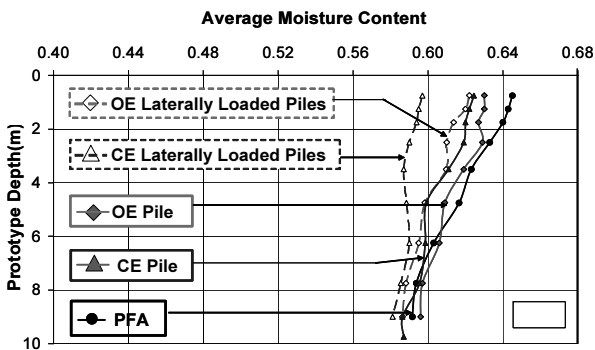


Fig. 33 Average moisture content profiles in soft ground (CM-3)

was no extra flow or leakage due to pile driving or due to some amount of pile deflection in a soft ground. A similar result was observed in the model CM-3 also. The result of CM-3 is shown in Figs. 31. The 1-G lateral loading was expected to create significant gap/deformation or failure zone as stiffness of pile would be very high compared to that of the ground and the overburden load would be also significantly low. However no adverse effect was found for both in 1-G and High-G for up to given lateral displacement (Table 4) and both the tests showed no any such gap formation or any leakage penetrating down to the bottom aquifer. The massive

lateral displacement up to 200% of pile diameter at pile head level applied to the pile (P-1) in the model CM-3 created displacement of pile by up to about 13% of pile diameter at the waste barrier interface. However such significant displacement didn't create any significant leakage or flow. This could be assured from Fig. 31(c). It must be because of the soft ground easy to deform as well as monolithic movement of pile and surrounding ground due to good adherence between them. It should be noted here that the settlement of the soft ground was considerably high too. The pile used in the experiment has prototype stiffness (EI) of 3376 MN.m². So, relative stiffness of pile to that of soil was relatively high from practical aspect. From above discussion, it could be confirmed that, the results could be extended to stiffer piles as well, provided that pile lateral displacements at the waste-barrier interface are limited to certain range for example up to 10% of pile diameter.

As void ratio or porosity is one of the governing factors influencing flow and transport, its evaluation was done at various locations and depth by determining moisture content. Figures 32 and 33 show the average moisture content profiles for PDAs under various categories of pile loading and PFA for the models CM-2 and CM-3 respectively. Pile driving definitely caused some radial consolidation in the ground. The degree of radial consolidation was higher for CE piles (displacement piles) than OE piles (partial displacement piles). The m/c of surrounding ground was found further decreased with lateral loading. However these effects due to such changes could not be seen in the CDP shown in Figs.30 and 31. The net porosity change in the vicinity ground of PDAs was so small that probably it did not create any major significant differences in the flow and transport in these zones. Besides, the sampling area was large enough that the possible delicate change in the ground in the pile periphery was overlooked. However, from the above results and discussion, it could be concluded that for the soft barrier ground, there was rather less flow around the piling area and has not created negative effects by ground smearing or ground displacement by the pile deflection. It may be worth to note that the adopted sampling technique at various locations already generated around 150 samples each for moisture content and chemical analysis in each test. So despite a desire to refine the sample collection at very delicate area, it became simply unrealistic to follow because of physical nature, abundant samples, risk of deterioration of model ground due to dehydration itself unless sampled quickly and need of an adequate soil amount for m/c and chemical analysis.

(4) Effects of stiffness of the barrier and sand intrusions

Figs. 34 show the results of Cl⁻ CDPs for the stiff barrier ground (model CM-4). Figs. 34 (a) and (b) show the comparative results of Cl⁻ CDPs at PFAs and PDAs

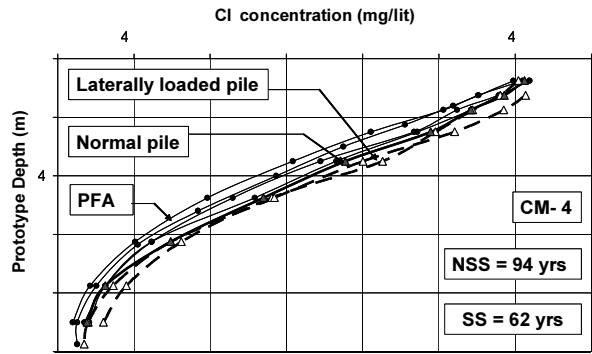


Fig. 34(a) Comparison of Cl⁻ concentration depth profile for 1-G, OE piles with PFA in stiff ground (CM-4)

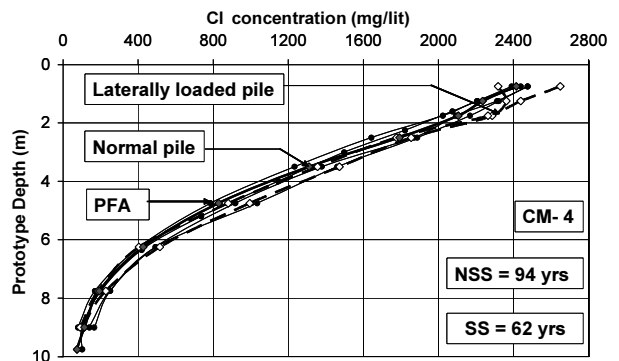


Fig. 34(b) Comparison of Cl⁻ concentration depth profile for High-G, OE piles with PFA in stiff ground (CM-4)

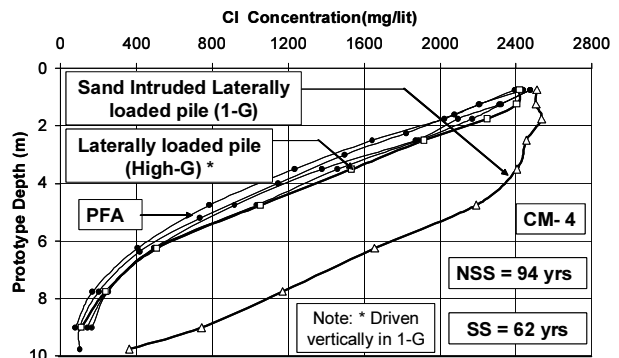


Fig. 34(c) Comparison of Cl⁻ concentration depth profile for laterally loaded CE piles with PFA in stiff ground (CM-4)

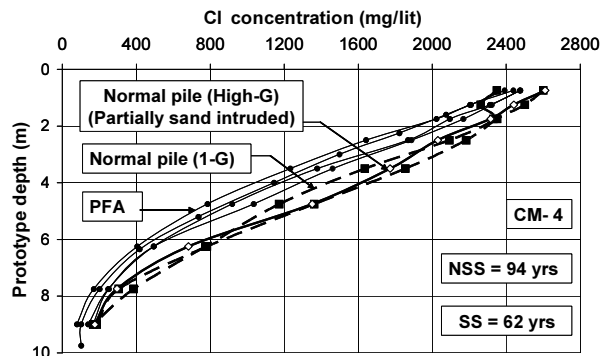


Fig. 34(d) Comparison of Cl⁻ profile for CE piles (without lateral loading) with PFA in stiff ground (CM-4)

for 1-G OE piles and High-G OE piles respectively. The piles driven in 1-G seemed created a very thin smear zone causing CI CDP for such piles slightly more than PFA (Fig. 34(a)). Such effect was not seen in High-G pile (Fig. 34(b)). This difference reveals that driving the OE piles in such ground in real field scale condition is acceptable. The difference was most possibly because of unrealistically very stiff ground (very high OCR) in 1-G. Driving pile in 1-G condition creates very high OCR in the ground as the ground could not generate the prototype inherent stress condition. Such a condition no longer remains effective in High-G pile driving or field scale pile driving. Also, there was an appreciable deterioration of the barrier strength/quality upon two-way loading done in 1-G as shown in Fig. 19(a). Such effects could not be diminished by the following reconsolidation in the centrifuge as discussed in Fig.15. It may be worth to remind here that for the soft NC clay model, such difference between 1-G and High-G pile was not observed.

Figs. 34(c) and (d) show the comparative result of CI CDPs at PFAs and PDAs with the CE pile. The similar trend of gravity (scale) effect as in the OE cases could be observed. In these cases, however, a negative effect is more noticeable (Fig.34(d)). The CI CDP result for the pile (P-1) of known deflection profile (Fig. 21) is shown in Fig. 34(c) with a designation of “Laterally loaded pile (High-G)”. The pile didn’t show significant negative effect despite significant pile head displacement due to lateral loading. This was possibly happened due to relatively small amount of ground displacement at waste-barrier interface which was only about 1% of pile diameter.

A major ground disturbance and massive deterioration of the barrier quality was found for Sand Intruded Laterally loaded pile (Fig. 34(c)). Such deterioration could also be seen in Fig. 28. The red color plume penetrated more than half of the barrier thickness in the pile surrounding. Thus the prevention of possible intrusion of permeable material (e.g. waste, sand) during pile driving is very important and an adequate thickness of barrier ground should be considered in order to prevent such intrusion during pile construction.

Fig. 35 shows moisture content results for all categories of piles in the model CM-4. The results were quite consistent with the previous model tests showing ground densification as per the pile types (Figs.32 &33). The densification of the ground by CE pile driving should have slowed down the pollution movement around the pile vicinity to some extent. However, to the contrary, slightly more contaminant migration was observed throughout the depth for the CE piles than the OE piles particularly for the 1-G driven piles. This indicates that there may be a formation of thin micro-cracks or a smeared zone or a gap between pile and

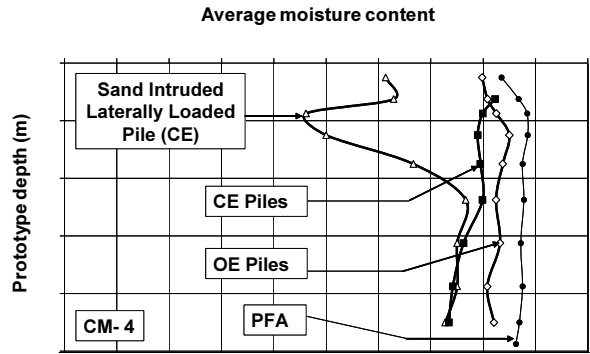


Fig. 35 Average moisture content profiles (CM-4)

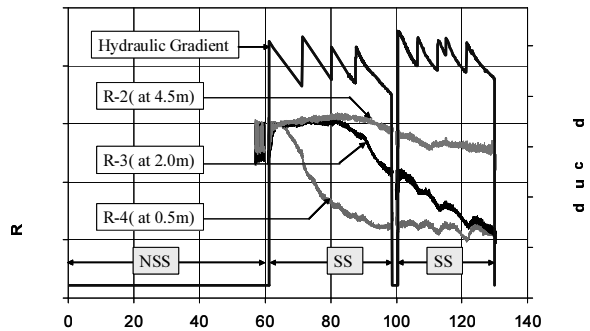


Fig. 36 Response of resistivity pile sensors (R) (CM-3)

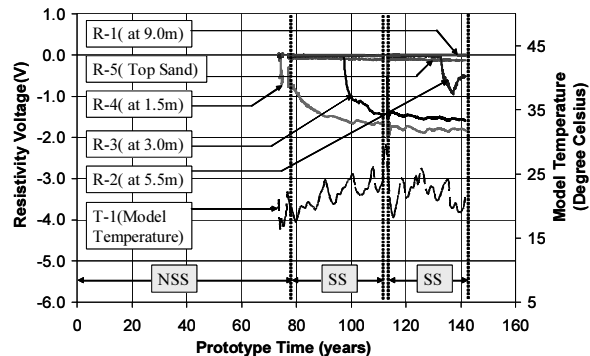


Fig. 37 Response of resistivity pile sensors (R) (CM-4)

adjacent surrounding clay accelerating the leakage rate. The ground was no softer enough to maintain the adherence between pile and clay or to mold itself to seal the gap formed during the various soil pile interactions. Also the ground settlement in the following reconsolidation in the centrifuge was significantly low in this case. However, such deterioration was most possibly happened due to 1-G pile driving/lateral loading. In 1-G condition, as the inherent stress condition in the prototype ground cannot be generated, OCR of the ground becomes very high and stiffness ratio of pile and soil also becomes very high. Thus, most possibly such deterioration or problem will not happen in the field scale work.

Contaminant Migration and Leakage Assessment by Resistivity of the Ground

Fig. 36 show the contaminant plume movement around PDA on a real time basis in term of resistivity voltage for soft ground (model CM-3) with the variation of hydraulic gradient during the test with stages NSS and SS. The results correspond to a CE 1-G pile without lateral loading. The corresponding depths of the sensors are also shown in the figure. The resistivity voltage-time curves at various depths show that the resistivity of surrounding ground was changing very gradually. This indicates that there was no gap in the pile soil interface or smearing zone otherwise the curve could have shown abrupt break through due to quick arrival of contaminant front. Thus ground disturbance by pile construction in soft NC clay and life time serviceability of pile on such ground have no adverse effects. This result is quite consistent with the previous results.

Fig. 37 shows the result of the resistivity measurement along the pile in the model CM-4. The sensors of the pile responded a bit differently for the stiff ground. A sudden jump in the resistivity curve for depth 1.5m, 3.0m and 5.5 m were found. This indicates that there must have been either micro level gap or thin smearing zone around pile allowing advective flow to reach the influence zone of sensor quickly. The temperature variation in the model is presented in the figure. Some small fluctuations in the resistivity response were consistent with those of model temperature fluctuations. However the resistivity voltage change in the ground can give an idea of pollution movement and thus the leakage in spite of many influencing parameters on the output, like temperature, density of ground etc. In Fig. 37, the sensor 'R-1' (at 9.0m) showed the almost constant resistivity voltage throughout the test. This indicates that in spite of some deterioration of the barrier at upper parts, the leakage did not reach bottom parts or it was still negligible as confirmed in Figs.34. The chemical tests of the discharged seepage solution stored in leachate collection tank (Fig. 6) also confirmed the same result. Thus the thick clay barrier seems to be strong enough to prevent any pollution in the local hydrogeology (aquifer).

CONCLUSIONS

Successful centrifuge modeling techniques for pile construction in geological barrier coupled with flow and transport modeling were developed. A soft ground having strength gradually increasing with depth and a stiff ground having uniform strength throughout the depth were successfully made in centrifuge models to simulate different types of thick natural clay barrier. The deteriorations of barrier ground due to the pile construction as well as due to

pile deflection upon lateral loading were investigated. The following conclusions are drawn in this study:

- (1) Visual observation by the red color tracer gave a very quick and an approximate idea that pile construction in soft/stiff geological barrier is basically safe enough and doesn't cause subsurface ground water pollution.
- (2) Soil investigation and chemical analysis of pore water reveal that for soft barrier grounds, there is no extra flow or leakage due to pile driving or some amount of pile deflection. Driving pile in 1-G or High-G using open end pile or closed end pile doesn't make significant difference on ability of such barrier ground in preventing the contaminant leakage. Thus it can be inferred that soft ground is strong enough to prevent its deterioration irrespective of the types of pile or their stiffness. This finding may also suggest that for the soft ground, a similar model test could be done in simple laboratory floor as a relatively conservative way.
- (3) In the case of stiff barrier ground, for both closed end and open end piles driven in 1-G showed a slight deterioration of the barrier ground, which is probably attributed to thin a smear zone or micro cracks. Such deterioration was not seen in the piles driven in High-G. This difference reveals that driving piles under the stress conditions equivalent to a real field scale is acceptable even for the stiff ground tested in this study. Some amount of pile deflection was also found very minor effects on the barrier quality.
- (4) A major ground disturbance and massive deterioration of the barrier quality was found while intrusion of high permeable materials occurred during pile driving. Thus protection of pile driving area from waste layer, drainage layer or cover materials is very essential. Adequate thickness of barrier ground should be considered in order to minimize the effect of such intrusion during pile construction.

RECOMMENDATIONS

Concentration depth profiles of the chemicals analyzed in the models, such as Cl^- , varied from each other as each test was unique in itself. Furthermore the input concentration at the leachate source also varied from test to test. Some degree of gradual evaporation loss of the solution during centrifugation was observed, causing gradual increase of the concentration at the top boundary of the barrier, which was not noticed in the beginning. There were also inevitable errors in the chemical analyses. Therefore, cross correlation between the data measured from various methods (chemical analyses, proves) for various samples as much as possible are essential to have a confidence in data reliability. Mass balance calculation about the retained chemical in the model is also very useful to check the reliability of the measured data.

REFERENCES

- Aburatani S, Hayashi Y, Nishikawa T (1996). Offshore waste disposal by Osaka Bay Phoenix Project, Proc. of 2nd Int. Congress on Environmental Geotechnics, Osaka, Kamon (eds.) 1: 623-628.
- Amatya BL(2006). Performance of Geological Barrier with Piles in Post Closure Landfill, PhD thesis, Tokyo Institute of Technology.
- Amatya BL, Khan MRA, Takemura J, Kusakabe O (2006). Centrifuge model test of groundwater pollution due to construction of pile foundations in waste disposal site, International Journal of Offshore and Polar Engineering 16(1): 65-72.
- Arulanandan K, Thompson PY, Kutter BL, Meegoda NJ, Muraleertharan KK, Yogachandran C (1988). Centrifuge modelling of transport processes for pollutants in soils, J. Geotech. Engng Am. Soc. Civ. Engrs 114(2):185-205.
- Bear J & Verrujit A (1987). Modelling ground water flow and pollution, Dordrecht, Holland: D.Reidel.
- Craig WH (1985). Modelling pile installation in centrifuge experiments, 12th ISSMFE 2: 1101-1104.
- Fleming WGK, Weltman AJ, Randolph MF, Elson WK (1998). Piling Engineering, Surry University Press, Glasgow and London.
- Freeze R Allen & John A Cherry (1979). Groundwater, Eaglewood Cliffs, NJ: Prentice Hall.
- Fukue M, Minato T, Matsumoto M, Horibe H, Taya N (2001). Use of a resistivity cone for detecting contaminated soil layers, Engineering Geology 60: 361-369.
- Garnier J, Gaudin C, Springman SM, Cullican PJ, Goddings D, Konig D, Kutter B, Phillips R, Randolph MF, Thorel L (2007). Catalogue of scaling laws and similitude questions in geotechnical centrifuge modeling, IJPMG 7(3): 1-23.
- GMS 3.1 (Ground Water Modeling System) (2000). Tutorial manual, the Environmental Modeling Research Laboratory of Brigham Young University.
- Hamilton JM, Dunnavant TW, Murff JD, Phillips R (1991). Centrifuge study of laterally loaded behavior in clay, Centrifuge 91, Ko (ed.), 285-292.
- Hensely PJ & Randolph MF (1994). Modeling contaminant dispersion in saturated sand. Proc. 13th ICSMFE, New Delhi: 1557-1560.
- Hensely PJ & Schofield AN (1991). Accelerated physical modelling of hazardous-waste transport, Geotechnique 41(3): 447-465.
- Japan High Association (2002). Foundation Design, the Design Specification of Highway Bridge.
- Kamon M (2001). Environmental issues of geotechnical engineering, Proceedings of the fifteenth international conference on soil mechanics and geotechnical engineering, Istanbul 4: 2629-2674.
- Kaomon M, Katsumi T, Inui T, Hamada S (2005). Environmental acceptability of the installation of piles through the bottom clay barrier at coastal landfill sites, Waste Containment and Remediation, Geotechnical Special Publication, No. 142, ASCE, CD-ROM.
- Kate JM (1995). Consolidation and electrical resistivity behavior of clays, Compression and Consolidation of Clayey soils, Hiroshima, Yoshikuni & Kusakabe (eds.): 87-92.
- Manassero M, Van Impe WF, Bouazza A (1997). Waste disposal and containment, Proc. of 2nd Int. Congress on Environmental Geotechnics, Osaka, Kamon (eds.) 3: 1425-1474.
- Matlock H (1970). Correlations for the design of laterally loaded piles in soft clay, Proc. 2nd Offshore Technology Conference. Paper OTC1204.
- Ogata A (1970). Theory of dispersion in a granular medium, U.S. Geological Survey Professional Paper, p. 411.
- Perkins TK & Johnson OC (1963). A review of diffusion and dispersion in porous media. Society of Petroleum Engineers Journal 3: 70-84.
- Reese LC & Van Impe WF (2001). Single Piles and Pile Groups under Lateral Loading. A.A. Balkema/ Rotterdam/Brookfield.
- Rowe RK & Booker JR (1991). Pollution migration through a liner underlain by fractured soil. Journal of Geotechnical Engineering, ASCE 118(7): 1031-1046.
- Shackelford CD (1989). Diffusion of Contaminant through waste containment barriers, Transportation Research Record 1219: 169-182.
- Shimizu K (1996). Geotechnics of waste landfill, Proc. of 2nd Int. Congress on Environmental Geotechnics, Osaka, Kamon (eds.) 3: 1475-1491.
- Takemura J, Kondoh M, Esaki T, Kouda M, Kusakabe O (1999). Centrifuge model tests on double propped wall excavation in soft clay, Soils and Foundation, 39(3) 75-87.
- Terashi M, Kitazume M, Kawabata K (1989). Centrifuge modelling of a laterally loaded pile, 12th ICSMFE 2: 991-994.
- Wroth CP (1984). The interpretation of in situ soil tests. 24th Rankine Lecture, Geotechnique 34(4): 449-489.

REMOVAL OF HEAVY METAL FROM AQUEOUS SOLUTIONS USING CHINESE LOESS SOIL

Xiao-Wu TANG¹, Yan WANG² and Zhen-Ze LI³

ABSTRACT: Loess soil, a relatively abundant and inexpensive material in China, is being investigated as an adsorbent to remove heavy metals from aqueous solutions. Pb(II), Cu(II) and Zn(II) can be removed very efficiently with loess soil, and the adsorption capacity of loess soil towards those three heavy metal ions follows the order: Pb(II) (270.3 mg g⁻¹) > Zn(II) (215.9 mg g⁻¹) > Cu(II) (108.9 mg g⁻¹). Factors relevant to adsorption process such as reaction time, pH and loess dosage were discussed in this paper. The clay minerals and organic matter were found to play important roles in adsorption process and the adsorption mechanism included ion exchange, surface complex and surface precipitation.

KEYWORDS: loess soil, heavy metal, adsorption, removal, kinetics, isotherm

INTRODUCTION

Nowadays, environmental pollution has aroused considerable attention throughout the world. Heavy metal contamination is one of the most hazardous contamination types and has been causing worldwide concern. Heavy metal ions can be released into environment by means of various industrial processes such as mining, metallurgical engineering, battery manufacturing, nuclear power operations, chemical manufacturing, etc. The heavy metal ions are stable and persistent in the environment since they cannot be degraded and destroyed. These metal ions can be harmful to many living lives and organisms once spread through food chain.

Conventional methods for removing metal ions include membrane filtration, adsorption, oxidation /reduction, ion exchange, precipitation, reverse osmosis, electro dialysis, etc. However, few of them were put into practice due to high cost, low efficiency, sensitive operating conditions and production of secondary sludge (Ahluwalia 2005). In recent years, a lot of researchers have focused their interest on all kinds of adsorbents because of the low cost and high efficiency of adsorption method. Loess soil is one of the promising materials for removing heavy metal ions among the numerous adsorbents.

CHARACTERISTICS OF LOESS SOIL

Loess is a widely distributed soil over the world (Xie 2001, Smalley et al. 2005). Chinese Quaternary loess

covers approximately 640,000 square kilometers stretching from the Northwest to the Northeast in China. Loess soil samples in our study were taken from the suburban area of Xi'an, China, which belong to typical Quaternary Loess deposited in Chinese Loess Plateau (Liu 1985).

Table 1 shows the grain size distribution and basic parameters of loess soil. Silt particle, 65.4%, has the largest percentage. The loess also has minor organic matter (5.5 mg g⁻¹) and a low cation exchange capacity (8.6 meq/100g). As shown in Table 2, the major constituents of tested samples are silicon dioxide (63.68 %), aluminum oxide (12.77 %) and calcium oxide (9.56 %).

It was observed from the scanning electronic microscope (SEM) (Fig. 1) that the surface of the particle was coarse with ample pits and protuberance. The abundant angular and broken particles in loess suggest the involvement of rich crystalline defects in sand grains (Smalley et al. 2005). Accordingly, these crystalline defects may provide plenty of active adsorption sites for heavy metals. Fig. 2 shows the transmission electron microscope (TEM) image of loess soil particles. The diameters of most particles were observed to be less than 0.3 μm. These particles can be specified as clay colloids and probably contribute to the large specific surface area of loess soil (24.1 m² g⁻¹), which may have close relation with the high adsorption capacity of loess soil. The surface of loess soil was not slippy or regular but uneven with hollows and bulges according to the morphology of soil particles.

In general, loess soil is easily available, cost effective,

¹ Prof., MOE Key Laboratory of Soft Soils and Geoenvironmental Eng., Zhejiang University, China. Email: tangxiaowu@zju.edu.cn

² Ph.D. student, ditto. Email: wy027@zju.edu.cn

³ Ph.D., Research Associate, Faculty of Engineering, Utsunomiya University, Japan. Email: lazyhero@live.cn

and has good physical and chemical properties. There is chance for loess soil to be developed as a promising adsorbent in developing countries. Our work group has done a series of researches to study the adsorption capacity of loess soil towards heavy metal ions. In this paper, removal of heavy metals (i.e. Pb(II), Cu(II) and

Zn(II)) using loess soil from China was summarized in order to find the mechanism of adsorption of heavy metals by loess soil. In view of the high adsorption capacity of loess soil towards heavy metals, loess soil could be a potential liner material for contaminant barrier system.

Table 1 Grain size distribution and basic characteristics of loess soil

Sand % 0.25-0.05mm	Silt % 0.05-0.005mm	Clay % <0.005mm	Organic (mg g ⁻¹)	CEC (meq/100g)	Specific surface area (m ² g ⁻¹)	Natural pH
13.2	65.4	20.5	5.5	8.6	24.1	8.2

Table 2 Chemical constituents of loess soil (after Tang et al. 2008a)

Constituent	SiO ₂	TiO ₂	Al ₂ O ₃	Fe ₂ O ₃	FeO	MnO	MgO	CaO	Na ₂ O	K ₂ O
Weight by Percentage	63.68	0.78	12.77	2.74	0.89	0.09	3.14	9.56	2.35	3.01

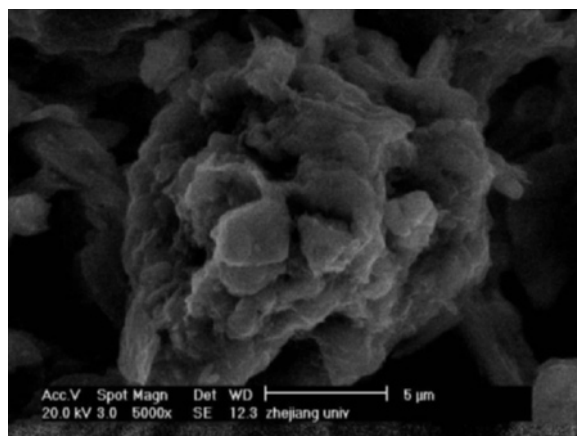


Fig. 1 SEM photo of loess soil (after Tang et al. 2008a)

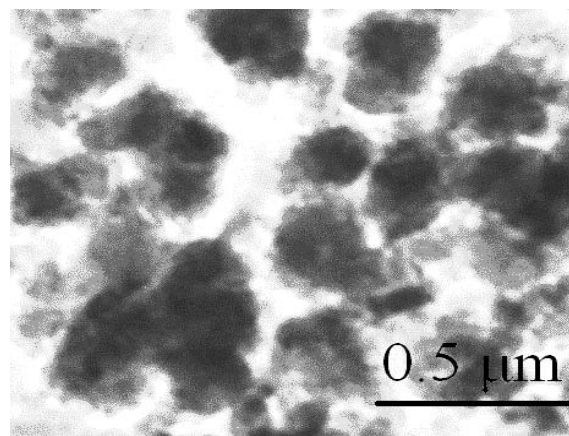


Fig. 2 TEM photo of dispersible loess particles in water (after Tang et al. 2008b)

ADSORPTION KINETICS

In the industrial usage of adsorbents, the time dependence of adsorption on solid surfaces is named as adsorption kinetics. Predicting the rate at which adsorption takes place for a given system is probably the most important factor in adsorption system design. Three kinetic models (i.e. pseudo-first order kinetics, pseudo-second order kinetics and intraparticle diffusion model) were used to describe the adsorption process.

The pseudo-first order kinetic equation is given by (Do 1998):

$$q_t = q_e(1 - e^{-k_1 t}) \quad (1)$$

The above equation can be linearized as

$$\log(q - q_e) = \log q_e - \frac{k_1}{2.303} t \quad (2)$$

where q_e and q_t are the amount of solute adsorbed on per unit adsorbent at the equilibrium and elapsed time, t respectively (mg g⁻¹) and k_1 is the pseudo-first order rate constant for the adsorption process (min⁻¹).

The pseudo-second order kinetic equation is written as (Do 1998):

$$\frac{t}{q} = \frac{1}{k_2 q_e^2} + \frac{1}{q_e} t \quad (3)$$

where k_2 is the pseudo-second order rate constant (g mg⁻¹ min⁻¹).

The equation for the intraparticle diffusion model is (Ho and McKay 1998):

$$q = k_{in} t^{1/2} + C \quad (4)$$

where k_{int} is the relevant rate constant ($\text{mg g}^{-1} \text{min}^{-1/2}$) and C is the intercept.

The test results of Zn(II), Cu(II) and Pb(II) adsorption on loess soil in separate Zn-loess, Cu-loess and Pb-loess system showed that the pseudo-second order kinetics model was the most appropriate model to interpret the adsorption process due to the highest correlation efficient of all (Tang et al. 2008ab, Li et al. 2009). When the initial concentration of Zn(II) was 50, 100, 200 mg L^{-1} , the pseudo-second order rate k_2 was 9.1×10^{-4} , 5.1×10^{-4} and $1.5 \times 10^{-4} \text{ g mg}^{-1} \text{min}^{-1}$ respectively (Tang et al. 2008b), indicating that the pseudo-second order rate decreased with increasing the concentration of heavy metal ions. Through experiments of Cu(II) adsorption on loess soil, k_2 increased from 3.66×10^{-3} to $19.98 \times 10^{-3} \text{ g mg}^{-1} \text{min}^{-1}$ as the solution pH increased from 3.0 to 7.0 (Tang et al. 2008a), indicating that higher pH benefited adsorption process. The adsorption kinetics of Pb(II) by loess soil at different temperature was studied. The pseudo-second order rate increased from 0.000261 to 0.01712 $\text{g mg}^{-1} \text{min}^{-1}$ with increasing the temperature from 10 to 55 °C (Li et al. 2009), suggesting that higher temperature was conducive to the rapid adsorption process.

In a word, adsorption of heavy metal ions can be conducted under the condition of smaller solute concentration, higher pH and higher temperature.

ADSORPTION ISOTHERMS

Three general isothermal adsorption models including the Langmuir, Freundlich, and Dubinin-Radushkevich (D-R) models were used to evaluate the test data and to interpret the possible adsorption mechanism.

The Langmuir isotherm model assumes that homogeneous monolayer surface adsorption occurs and can be written as (Do 1998)

$$\frac{C}{q} = \frac{1}{bQ} + \frac{C}{Q} \quad (5)$$

where q_e is the mass ratio of the adsorbed solute on the adsorbent (mg g^{-1}), C_e the equilibrium solute concentration (mg L^{-1}), Q the maximum adsorption capacity of the adsorbent (mg g^{-1}), and b the Langmuir constant (L mg^{-1}).

The Freundlich isotherm model assumes a heterogeneous and patch-wise surface that is independent from one another. The equation can be written as (Do 1998)

$$q = K C^n \quad (6)$$

where K_F is the Freundlich constant (mg g^{-1}) indicating the adsorption capacity and strength of the adsorptive

bond and n is the heterogeneity factor.

The D-R (Dubinin-Radushkevich) isotherm model assumes a uniform pore-filling adsorption and can predict the free adsorption energy change. The D-R model can be written as (Do 1998)

$$\ln q = \ln q_m - k\varepsilon^2 \quad (7)$$

where q_m is the maximum adsorption capacity (mol g^{-1}), k a model constant related to the free adsorption energy and the Polanyi potential, which is written as

$$\varepsilon = RT \ln \left(1 + \frac{1}{C} \right) \quad (8)$$

where the unit of C_e should be translated into mol L^{-1} . The mean free energy of adsorption E is

$$E = -\frac{1}{\sqrt{2k}} \quad (9)$$

The adsorption is basically ascribed to surface adsorption by means of ion exchange when $|E|$ is between 8.0 and 16.0 kJ mol^{-1} , while, the mechanism is physical adsorption for $|E|$ ranging from 1.0 to 8.0 kJ mol^{-1} .

Fig. 3 shows the adsorption isotherm of Zn(II), Cu(II) and Pb(II) on loess soil. Following the definition of Gilles and Smith (1974), all the three isothermal can be designated as type "H", suggesting that loess soil has a high affinity for these heavy metals. Table 3 shows the predicted parameters calculated by isothermal models. The simulated results by Langmuir, Freundlich, and D-R models showed that Langmuir model was the best model to analyze the adsorption behavior of Zn(II), Cu(II) and Pb(II) (Tang et al. 2008ab, Li et al. 2009). The Langmuir monolayer adsorption capacity of Zn(II), Cu(II) and Pb(II) on loess soil was 215.9, 108.9 and 270.3 mg g^{-1} respectively. Loess soil showed an excellent adsorption capacity with very large adsorption amounts. It is apparent that the adsorption capacity of loess soil towards those three heavy metal ions follows the order: Pb(II) > Zn(II) > Cu(II).

EFFECT OF LOESS DOSAGE

Fig. 4 shows Zn(II), Cu(II) and Pb(II) adsorption capacity at different loess dosage. As can be seen in Fig. 4, the adsorption density, the amount adsorbed per unit mass (q_e), presents a decreasing trend with increasing loess dosage.

It can be readily understood that when the loess amount is small, the metal ions can easily arrive at the adsorption sites, and accordingly, the loess has high adsorption capacity. As the loess dosage is increased, it

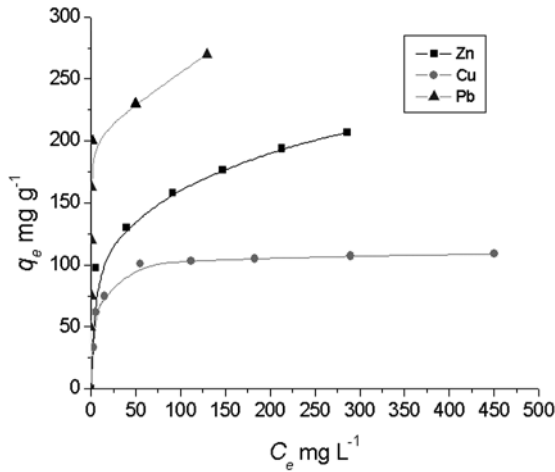


Fig. 3 Adsorption isotherm of heavy metal on loess soil

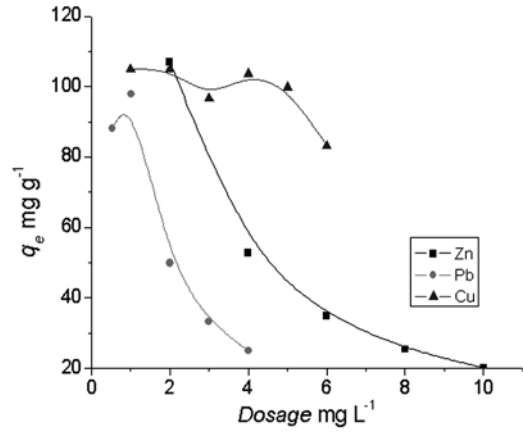


Fig. 4 Effect of loess soil dosage on heavy metal adsorption capacity

Table 3 Predicted isothermal constants by Langmuir, Fredunlich and D-R isotherm models

Heavy metal	Langmuir			Freundlich			D-R			
	Q mg g ⁻¹	b L mg ⁻¹	R^2	K_F mg g ⁻¹	n	R^2	q_m mol g ⁻¹	k mol ² kJ ⁻²	E kJ mol ⁻¹	R^2
Pb	270.3	0.51	0.99	123.93	6.1	0.74	0.0027	0.002	-16.67	0.7
Zn	215.9	0.04	0.995	65.39	5	0.99	0.0054	0.003	-12.91	0.999
Cu	108.9	0.18	0.976	45.67	6.4	0.834	0.0027	0.006	-8.70	0.855

is hard to approach the adsorption sites for heavy metal ions due to overcrowding of loess particles (Bhattacharyya and Sen Gupta 2008). In addition, high adsorbent dosage can form particle aggregation, which will lead to a decrease in the total surface area and an increase in diffusional path length (Shukla et al. 2002). Therefore, the heavy metal adsorption amount per unit mass decreases with increasing the loess dosage. It is apparent that the adsorption efficiency increases along with increasing the loess dosage (Fig. 5) because of the increase of available adsorption sites. When the loess dosage reaches certain value, the heavy metals can be nearly completely removed from aqueous solutions.

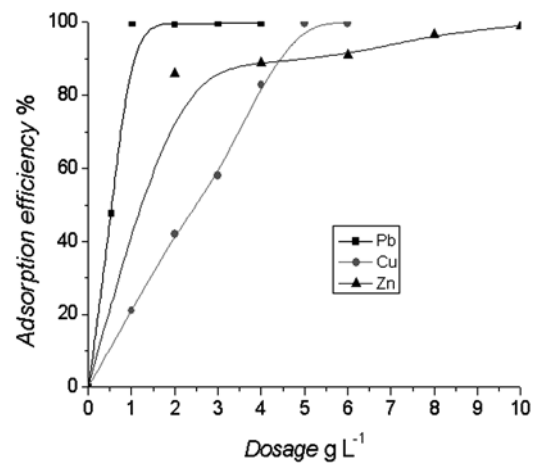


Fig. 5 Effect of loess soil dosage on heavy metal adsorption efficiency

EFFECT OF PH

Fig. 6 shows the effect of pH on heavy metal removal efficiency. In general, the removal efficiency of Zn(II), Cu(II) and Pb(II) increased with increasing the initial pH of the aqueous solution till the heavy metals were nearly completely removed. The removal efficiency of Zn(II) increased from 91.2 to 99.8 when the pH increased from 1.0 to 5.0. The Zn(II) removal efficiency shows a linear form increase and loess soil has a high affinity for Zn(II) at very low pH. The removal efficiency of Cu(II) was

5% at pH=2.1, and then there was a sharp increase in removal efficiency from 5% to 97% with increasing the pH from 2.7 to 4.4. The removal efficiency of Cu(II) could reach 99.1% at pH=6.3. Similar with removal of Cu(II), at low pH, around 1.5, small amount of Pb(II) was removed, with a removal efficiency 8.6%. The removal efficiency of Pb(II) increased rather quickly, removing 99.4% of Pb(II) at pH=3.2. Adsorption of

Cu(II) and Pb(II) with increasing pH can be divided into three stages: i) At very low pH, a small amount of heavy metals was removed; ii) At a certain pH range, the adsorption of heavy metals was a rather rapid process and the removal efficiency increased quite a lot; iii) Heavy metals were removed nearly completely, and the removal efficiency basically remained constant with increasing the pH value of the solution continuously.

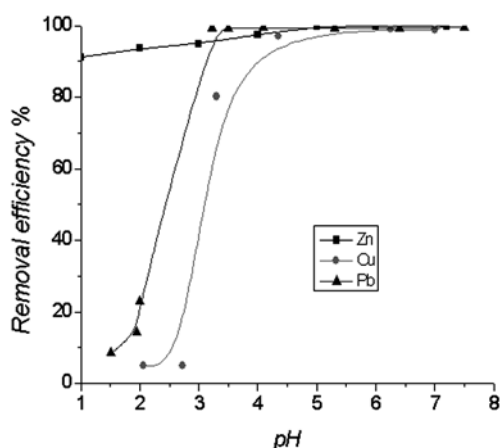


Fig. 6 Effect of pH on heavy metal removal efficiency

DISCUSSION ABOUT THE MECHANISM INVOLVED

Heavy metal adsorption by loess is a rather complex process affected by several factors. In order to better understand the adsorption behavior of heavy metals on loess soil surface, the mechanism of heavy metals on loess was studied (Tang et al. 2009ab, Li et al. 2009). Fig. 7 shows the XRD spectra of loess and heavy metal loaded loess. The main minerals in loess soil were determined to be quartz, calcite, albite, goethite and kaolinite on the basis of the band intensity. After loaded with heavy metals such as Pb(II), Cu(II) and Zn(II), the pattern of XRD had some changes as can be seen in Fig. 7.

Under proper conditions, the calcite in loess could react with heavy metals to form surface precipitation on loess soil surface. After loaded with Pb(II), the bands relevant to calcite disappeared and the strong bands relevant to cerussite (PbCO_3) was observed, which could be explained by



Similar carbonate also was found in other heavy metal loaded loess soil, which demonstrated that calcite in loess soil can help heavy metals to form surface precipitation on loess soil surface.

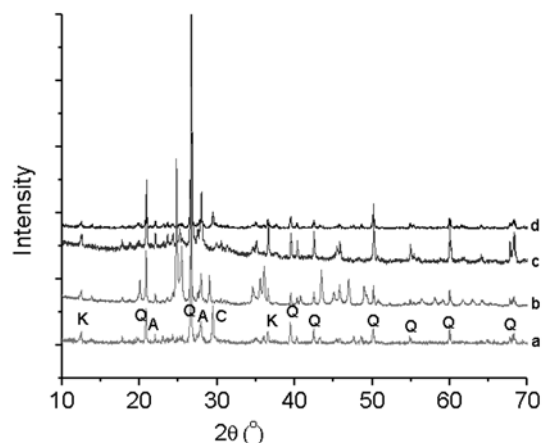
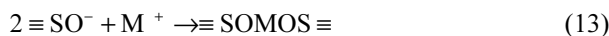


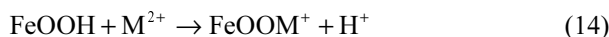
Fig. 7 XRD spectra of loess and heavy metal loaded loess (a: loess, b: Pb(II) loaded loess, c: Cu(II) loaded loess, d: Zn(II) loaded loess; A: Albite, C: Calcite, G: Goethite, K: Kaolinite, Q: Quartz)

Heavy metals could be adsorbed on clay minerals by penetrating into clay layers in the form of ion exchange with originally contained K^+ ions or through electrostatic force with permanent negative sorption sites, which can be expressed as



where S denotes mineral constituents and M denotes Pb, Cu and Zn.

The patterns related to quartz changed when loess soils were loaded heavy metals, indicating that quartz has played an important role in the adsorption process. Goethite was also a very important component in loess contributing to remove heavy metals from aqueous solutions and many researchers have studied the adsorption behavior of goethite towards heavy metals (Ostergren et al. 2000, Trivedi and Axe 2001, Mustafa et al. 2004). The reaction between heavy metals and goethite can be written as



In addition, there was a little organic matter in loess soil, and the carboxyl group has been confirmed to contribute the adsorption of heavy metals (Tang et al. 2008ab, Li et al. 2009). The carboxyl group can complex with heavy metals in the following form:



CONCLUSIONS

Loess soil has proven to be a promising material for removal of heavy metals from aqueous solutions. Not only is loess soil abundant, but also it is really an

efficient and economic adsorbent that is effective to many heavy metals such as Pb(II), Cu(II) and Zn(II). Loess soil could be developed as a potential liner material for contaminant barrier system.

(1) Adsorption process of Pb(II), Cu(II) and Zn(II) on loess soil can be best interpreted with the pseudo-second order kinetic model and the Langmuir isothermal model.

(2) Loess soil has high affinities for heavy metals and the adsorption capacity of loess soil towards heavy metal ions follows the order: Pb(II) (270.3 mg g^{-1}) > Zn(II) (215.9 mg g^{-1}) > Cu(II) (108.9 mg g^{-1}).

(3) pH and loess soil dosage both have great influence on the removal of heavy metals from aqueous solutions.

(4) Clay minerals and organic matter in loess soil contribute a lot to the heavy metal adsorption process, and the main adsorption mechanisms include ion exchange, surface complex and surface precipitation.

ACKNOWLEDGEMENTS

The authors would like to express their sincere gratitude to the Key Project of National Science Foundation of China (NSFC) (grant 50538080) for their financial support of this study.

REFERENCES

- Ahluwalia SS & Goyal D (2005). Removal of heavy metals from waste tea leaves from aqueous solution. *Eng. Life Sci.* 5: 158-162.
- Bhattacharyya KG & Sen Gupta S (2008). Kaolinite and montmorillonite as adsorbents for Fe(III), Co(II) and Ni(II) in aqueous medium. *Appl. Clay Sci.* 41: 1-9.
- Do DD (1998). *Adsorption Analysis: Equilibrium and Kinetics*, Imperial College Press, London.
- Ho YS & McKay GA (1998). A comparison of chemisorption kinetic models applied to pollutant removal on various sorbents, *Trans. Inst. Chem. Eng. B* 76: 332-340.
- Li ZZ, Tang XW, Chen YM, Wang Y (2009). Sorption behavior and mechanism of Pb(II) on Chinese loess. *J. Environ. Eng.-ASCE.* 135: 58-67.
- Liu DS (1985). *Loess and Environment*. Science Press: Beijing.
- Mustafa G, Singh B, Kookana RS (2004). Cadmium adsorption and desorption behaviour on goethite at low equilibrium concentrations: effects of pH and index cations, *Chemosphere* 57: 1325-1333.
- Ostergren JD, Trainor TP, Bargar JR, Brown GE, Parks GA (2000). Inorganic ligand effects on Pb(II) sorption to goethite (α -FeOOH): I. Carbonate. *J. Colloid Interface Sci.* 225: 466-482.
- Shukla A, Zhang YH, Dubey P, Margrave JL, Shukla SS (2002). The role of sawdust in the removal of unwanted materials from water. *J. Hazard. Mater.* B95: 137-152.
- Smalley IJ, Kumar R, O'Hara Dhand K, Jefferson IF, Evans RD (2005). The formation of silt material for terrestrial sediments: Particularly loess and dust. *Sedimentary Geol.* 5, 179(3-4): 321-328.
- Tang XW, Li ZZ, Chen YM, Wang Y (2008a). Removal of Cu(II) from aqueous solution by adsorption on Chinese Quaternary loess: Kinetics and equilibrium studies. *J. Environ. Sci. Heal. A* 43: 779-791.
- Tang XW, Li ZZ, Chen YM (2008b). Behaviour and mechanism of Zn(II) adsorption on Chinese loess at dilute slurry concentrations. *J. Chem. Technol. Biotechnol.* 83: 673-682.
- Trivedi P & Axe L (2001). An analysis of zinc sorption to amorphous versus crystalline iron oxides using XAS. *J. Colloid Interface Sci.* 244: 230-238.
- Xie DY (2001). Exploration of some new tendencies in research of loess soil mechanics. *Chinese J. Geotechnical Eng.* 23(1): 3-13.

COUPLED THERMO-HYDRO-CHEMO-MECHANICAL MODELING FOR GEOENVIRONMENTAL PHENOMENA

Hywel R. THOMAS¹, Philip J. VARDON² and Yu-Chao LI³

ABSTRACT: Coupled thermo-hydro-chemo-mechanical (THCM) behavior of soils is important in a number of geoenvironmental engineering applications including nuclear waste disposal, landfill engineering, freeze-thaw cycles and fate and contaminant transport. As part of ongoing research and development in this field a number of key developments have been undertaken at the Geoenvironmental Research Centre (GRC), Cardiff, UK, with particular focus on the numerical simulation of these phenomena. This paper outlines some of these developments set within the context of the numerical finite-element model developed at the GRC – COMPASS, and discusses the theoretical and numerical implementation and comparison of numerical simulations with experimental data. In particular the development of the effects of temperatures elevated above 100°C on gas pressure and water phase change and consequently the moisture movement; frozen ground behavior with particular reference to seasonal freeze-thaw cycles with frost heave and ice segregation possibly leading to solifluction; reactive thermo-hydro-chemical-mechanical models including geochemical behavior with focus on the osmotic potential; and High Performance Computing (HPC) have been included.

KEYWORDS: THM modeling, temperature effects, frozen soil, chemistry, HPC, numerical modeling

INTRODUCTION

In a number of engineering applications coupled thermo-hydro-chemo-mechanical behavior is of interest. These include: i) the performance assessment of High-Level nuclear Waste (HLW) repositories, ii) leachate and clay barrier modeling in landfill engineering, iii) high and low temperature regions, especially where seasonal variations encounter water phase change, and iv) the fate and contaminant transport through saturated and unsaturated regions of the ground. A large volume of work exists on a wide variety of aspects included within this topic (e.g. Thomas, 2006). It is furthermore possible to link sophisticated mechanistic models of the performance of soils to design criteria or risk based models assessing system performance in terms of risk and/or human health. The reliability of such model linkages is dependent upon the mechanistic model capturing complex phenomena with the soils.

This paper outlines recent research undertaken in this field in the Geoenvironmental Research Centre (GRC) at Cardiff University, building upon a large volume of work (e.g. Thomas and He, 1994; Thomas et al. 2003; Cleall et al. 2006a, b; Thomas et al. 2009a, b, c; and Thomas and Rees, 2009) of which many of the numerical

aspects are included within the bespoke transient finite-element code COMPASS (COde for Modelling PARTially Saturated Soils).

A brief treatment of the theoretical and numerical aspects of the computational code COMPASS is followed the recent developments. These entail the freeze-thaw behavior of soils including the development of ice lenses and summer heave phenomena; the high temperature behavior of soils in particular the development of gas pressures due to elevated temperatures directly and moisture phase change; an investigation into the vapor migration behavior; the development of the chemical model to include the osmotic potential; and the development of a high-performance computer algorithm developed for hybrid distributed-memory machines made up of discrete shared-memory nodes.

THEORETICAL AND NUMERICAL MODEL

The governing equations for COMPASS are formulated from the primary variables, pore-water pressure, u_l , temperature, T , pore-air pressure, u_a , displacement, \mathbf{u} , and chemical component concentration, c_d^i , to describe the thermo-hydro-chemical-mechanical behavior. In

¹ Professor, Geoenvironmental Research Centre, Cardiff University, UK. Email: ThomasHR@Cardiff.ac.uk

² Research Fellow, Geoenvironmental Research Centre, Cardiff University, UK. Email: VardonPJ@Cardiff.ac.uk

³ Research Associate, Geoenvironmental Research Centre, Cardiff University, UK. Email: LiY24@Cardiff.ac.uk

general terms the flow variables are formed into governing equations by consideration of the conservation of mass/energy and the mechanical formulation is formed by consideration of stress equilibrium, with more details of the THM model found in Thomas and He (1994). Chemical behavior considers advection, diffusion and dispersion and in addition geochemical reactions including sorption, ion exchange and precipitation/dissolution via a geochemical model, MINTEQA2, with the detailed formulation of the model found in Cleall et al. (2007).

Numerically, a Galerkin weighted residual finite-element scheme is used to discretise the equations spatially and an Eulerian finite-difference scheme is used for temporal discretisation. The governing equations after spatial discretisation is expressed in matrix form as:

$$\mathbf{A}\phi + \mathbf{B}\frac{\partial\phi}{\partial t} + \mathbf{C} = \{0\} \quad (1)$$

where \mathbf{A} is the matrix of flux coefficients, \mathbf{B} is the matrix of storage coefficients, \mathbf{C} is the vector of gravitational coefficients and ϕ is the vector of primary variables.

After temporal discretisation the system can be expressed concisely as:

$$[a]\phi^{n+1} = [b] \quad (2)$$

where $[a]$ and $[b]$ are the system matrices and ϕ^{n+1} is the vector of primary variables for the new time.

A number of direct and iterative solution schemes have been implemented including the LU, Cholesky, Frontal, PCG, CGS and BiCG, with a number of different preconditioners for the iterative solvers (Owen, 2000).

FREEZE/THAW BEHAVIOR

In cold localities the upper region of soil can be subject to freeze-thaw cycles in response to seasonal variations. Frost heave and ice segregation often occur as the ground freezes which cause potential engineering problems including pavement cracking, foundation damage and pipeline fracture. Moreover, periglacial solifluction may occur on slopes during the thaw phase of the freeze-thaw cycle (e.g. Harris, 1996).

The THM model is developed so that phase change, moisture movement due to cryogenic suction and the development of ice lenses are included. Full details can be found in Thomas et al. (2009b).

It is well established that when freezing the spatial thermal gradient causes pore-water movement in the direction of the lower temperature under uniform pressure

fields (e.g. Hoekstra, 1966; Mageau and Morgenstern, 1980). This thermally induced driving force can be thermodynamically determined using the Clapeyron equation (Henry, 2000). Therefore, assuming that the pore-water velocity can be split into two components based upon the driving force, the pore-water velocity can be written as:

$$\mathbf{v} = \mathbf{v}_i + \mathbf{v}_T = \mathbf{v} - \frac{k}{\gamma} \frac{\rho L}{T} \nabla T \quad (3)$$

where \mathbf{v}_i represents the pore-water velocity; \mathbf{v}_T is the velocity induced by liquid gradient using a Darcian formulation; \mathbf{v}_T^i represents pore water velocity induced by temperature gradient for freezing soils; k_i is the hydraulic conductivity which is assumed to be a function of the temperature; γ_i is the unit weight of water; ρ_i is the density of pore water; T and T_0 are the temperature and the freezing point of pore water respectively; and L is the latent heat of fusion.

Maintaining energy conservation in the heat formulation requires the inclusion of the latent heat of fusion. Therefore the heat content of the soil can be expressed as:

$$\Phi = H_c (T - T_r) - LnS \rho \quad (4)$$

where H_c is the volumetric heat capacity of the soil; T_r is the reference temperature; n is the porosity; S_i refers to the degree of moisture respect to ice and ρ_i is the density of pore ice.

To initiate the creation of a new ice lens a stress criterion is adopted (e.g. Gilpin, 1980; Nixon, 1991). For a one-dimensional case these approaches consider that the soil skeleton separates and an ice lens forms when the pore-water pressure exceeds the sum of the overburden stress, p_{ob} , and the separation strength of the freezing soil, p_{sep} , i.e. the vertical effective stress, σ' , is less than $-p_{sep}$ (minus sign signifying tension):

$$\sigma' \leq -p_{sep} \quad (5)$$

Typically, p_{sep} is in the range of 20 ~ 150 kPa (Nixon, 1991). This approach could be developed into a more general approach by the approach proposed by Konrad and Duquenois (1993).

Two seasonal scenarios are considered: soils which overlie a permafrost, and soils which do not. Soils overlying a permafrost freeze are subject to bi-directional freezing and a hydraulically closed system, whereas soils not overlying a permafrost subject to one-sided freezing with pore-water availability governing ice lens formation. The predicted ice-lens formation and

heave are illustrated in Fig. 1 for a column of soil initially 100mm tall with a 20% initial water content, under a range of stress and strength conditions. The grey portion of the Fig. represent the soil and the white the ice lenses.

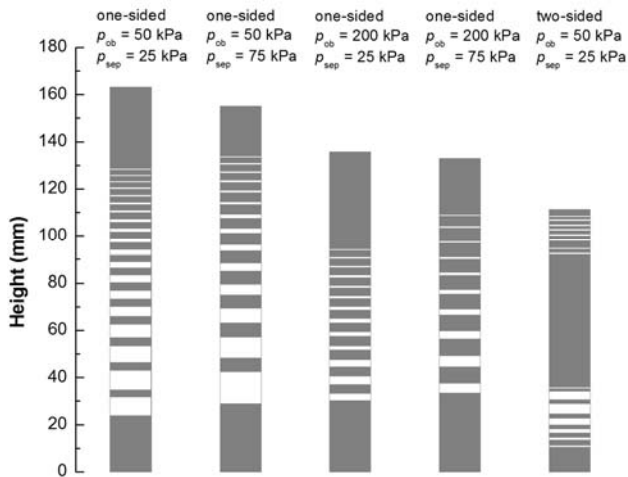


Fig. 1 Predicted ice lens distributions for typical freezing condition (ice lens region – white)

The numerical results for one-sided freezing are consistent with experimental results observed in step-freezing tests (Konrad, 1994). In two-sided freezing a single frozen fringe is found in the lower region initially, due to the permafrost, with pore-water moving vertically down due to the thermal gradient. Rainfall is simulated on the top surface of the column with the water drawn towards the frozen fringe, causing thicker ice lenses and consistent with the observed summer heave behavior (Mackay, 1983). When the top surface then freezes a second frozen fringe at the top of the column occurs with the frozen fringes both moving towards each other until they meet. Thin ice lenses are observed in the upper region and consolidation due to pore-water pressure loss are found in the central region of the column. The results of a typical analysis for two-sided freezing are shown in Fig. 2 where by seasonal variation is simulated over 3 days. In the summer period there is only a single frozen fringe near the base of the sample with the pore-water being drawn towards this frozen region causing ice lenses and summer heave. When the surface of the soil column freezes the lower frozen front move upwards due to a flux of thermal energy leaving the sample and a new frozen front is created in the upper region moving quickly downwards. These frozen fronts then meet and the whole column is then below 0°C. The proposed model has been also employed to simulate two small-scale laboratory freezing and thawing tests performed in a centrifuge and shown to be able to represent the development of both the thermal field and ice segregation observed in the physical models; further details of these

tests and simulations are available in (Thomas et al. 2009b).

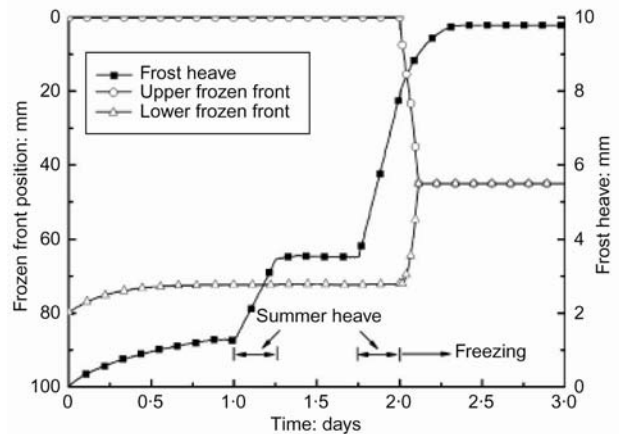


Fig. 2 Frozen front position and the frost heave for the two-sided freezing example

HIGH TEMPERATURE BEHAVIOR

In the context of nuclear waste disposal the behavior of a porous media in temperatures over 100°C may be important. The thermal output of deposition-holes within a repository interact with each other forming a three-dimensional thermal field (e.g. Cleall et al. 2006a). The spacing is then governed by the maximum allowable temperature which is at present set at 100°C for performance assessment, with some allowance for unknowns (e.g. Werme, 1998). However, this limit is adopted due to a lack of rigorous scientific understanding of the processes occurring above this limit. Significant cost savings in the construction of HLW repositories could be made should this performance assessment limit be relaxed. In addition, regardless of the spacing design anisotropic hydration and clay desiccation may cause temperatures to rise locally to over 100°C at the canister/buffer interface.

Importantly, at higher temperatures the gas pressures can become large due to pore-water phase change and change in gas pressure due to temperature. Significant moisture movement may then occur as the vapor content of the pore-gas increases due to temperature driven phase change.

The approach to this problem is that the governing equations are formed in terms of phase conservation as opposed to mass conservation and the sink/source terms between phases evaluated to ensure that mass conservation is also satisfied.

The conservation of pore-gas phase, following the approach of Luikov (1966), may be written as:

$$\frac{\partial}{\partial t}[\rho_g \theta_g] + \frac{\partial}{\partial t}[\rho_{da} H \theta_l] = -\nabla \cdot \mathbf{J}_g + S \quad (6)$$

where t is time, ρ_g is the density of the gas, θ_g is the volumetric gas content, ρ_{da} is the density of the dry air, H is Henry's constant, \mathbf{J}_g is the pore-gas flux and S is a sink/source term.

The pore-gas flux can be expressed following the approach proposed by Thomas and Sansom (1995) as:

$$\mathbf{J}_g = -\nabla \cdot [\rho_g \mathbf{v}_g] - H \nabla \cdot [\rho_{da} \mathbf{v}_l] \quad (7)$$

where \mathbf{v}_g is the gas velocity, which is determined following Darcy's Law as shown by Geraminegad and Saxena (1986) as:

$$\mathbf{v}_g = -\frac{k_{int} K_{rg}}{\mu_g} \left[\frac{P_g}{T} \nabla T + \nabla P_g \right] \quad (8)$$

The sink/source term S from Eq. 6 is included following the approach of Luikov (1966) where S is considered to be equal to the time derivative of the volumetric vapour content which in turn is equal to the diffusive flux of vapour. Based on the Philip and de Vries theory (Philip and de Vries, 1957), the flux can therefore be expressed as:

$$S = -\rho_g \nabla \cdot \left[D_{atms} \tau_v \theta_g \nabla \left(\frac{\rho_v}{\rho_g} \right) \right] \quad (9)$$

This theory has been validated against experimental work carried out by Commissariat à l'énergie atomique (CEA), France on a highly compacted bentonite column (Gatabin and Billaud, 2005) with experimental and numerical results for the region of the soil column closest to the heater shown in Fig. 3. More details can be found in (Thomas et al. 2009c).

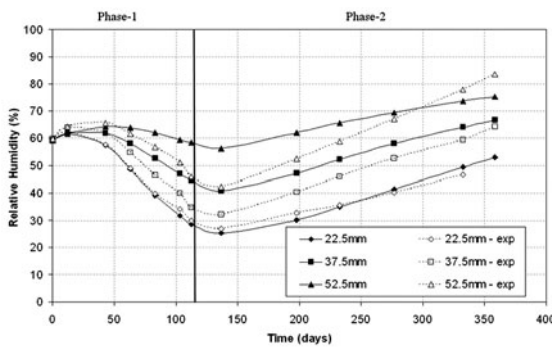


Fig. 3 Relative humidity evolution at 22.5, 37.5 and 52.5mm from heater

VAPOR MIGRATION

Vapor migration through soils is an important thermo-hydraulic coupling and critical to understanding the thermo-hydraulic behavior of the majority of geoenvironmental engineering problems when temperature gradients are apparent. In a number of these problems highly-compacted clays, with a low hydraulic conductivity, are used for barrier purposes.

Traditional rules of vapor flow such as the Philip and de Vries (1957) approach were based upon vapor flow through sand and often over-predict the simulation of vapor flow through the highly-compacted clay. This over-prediction is often compensated for by the inclusion of coefficients (e.g. Olivella and Gens, 2000).

A series of experiments were designed to investigate this phenomenon for both Kaolin and MX-80 bentonite under isothermal and thermo-hydraulic conditions. Full details of the experimental work and numerical simulation can be found in Singh (2007). A key experimental premise was that the liquid flow of pore-water would include advective flow of chloride ions whereas vapor flow would not allow this movement. Therefore, by measurement of water content and chloride ion concentration both the liquid and vapor flows could be identified.

The original Philip and de Vries (1957) theory of diffusive vapor movement can be written as:

$$\mathbf{v} = -D \nabla T - D \nabla \theta \quad (10)$$

where \mathbf{v} is the velocity of vapour, T is the temperature, θ_l is the volumetric liquid water content and D_{TV} and D_{MV} are the thermal and isothermal vapour diffusivities respectively. The diffusivities can be written consistent with the Philip and de Vries theory but including two factors, η_1 and η_2 , to allow for the incorporation of experimental evidence. These then become:

$$D = \eta_1 \frac{D_v}{\rho} f \frac{(\nabla T)}{(\nabla T)} \left(h \frac{d\rho}{dT} \right) \quad (11)$$

and

$$D_v = \eta_2 \frac{D_v \tau \theta}{\rho} \left(\rho \frac{dh}{d\theta} \right) \quad (12)$$

where D_{atms} is the molecular diffusivity of vapour through air, v_v is a mass flow factor, τ , is the tortuosity factor, ρ_l is the density of water, $(\nabla T)_d/(\nabla T)$ is the microscopic pore temperature gradient factor, h is the relative humidity and ρ_o is the saturated vapour density. The thermal and isothermal diffusivities revert to the

original Philip and de Vries theory if η_1 and η_2 are unity.

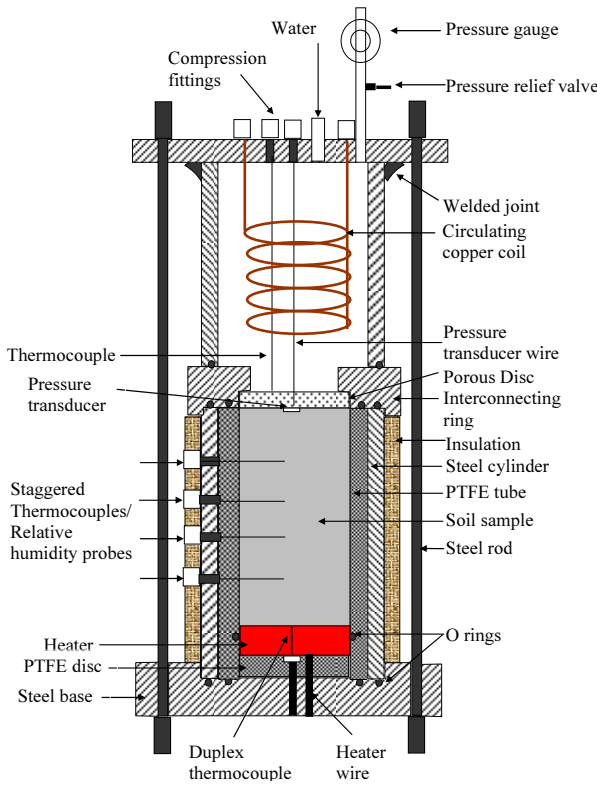


Fig. 4 Schematic diagram of the thermo-hydraulic cell

Experimental results undertaken at the GRC by Singh (2007) involved the design and use of a new thermo-hydraulic cell which can be seen in Fig. 4. Of note is the low corrosion grade 316L stainless steel, fluoroelastomer O-rings installed at the interfaces to provide a good seal designed to withstand temperatures up to 200°C and have a good chemical resistance. A polytetrafluoroethylene (PTFE) tube was used within the cell to reduce heat loss. PTFE has a low thermal conductivity, low coefficient of friction, good compressive strength and high chemical resistance. Temperature control at the top of the cell was achieved by the circulation of water at a fixed temperature and in addition pressurized water of up to 0.6MPa could be added at the top of the sample. At the base of the cell temperature control is provided by an electric heater. A number of relative humidity and thermocouple instruments are provided throughout the soil sample.

A large number of experiments were undertaken and a number of key aspects could be identified. The ion accumulation towards the hot end of the samples was found and the circulation of moisture via vapor and liquid flow could be isolated. It is indicated that appropriate values for inclusion into the Philip and de Vries vapor law for Kaolin were $\eta_1=0.22$ and $\eta_2=1.00$ and $\eta_1=0.17$ and $\eta_2=0.60$ for MX-80 bentonite.

CHEMICAL BEHAVIOR

The chemical and geochemical behavior of an unsaturated soil is complex and this section represents the most recent developments of ongoing work to capture a number of these phenomena. A number of both chemical and geochemical phenomena are already included into the COMPASS model including multi-component chemical transport based upon advection, dispersion and reaction. The geochemical reactive aspects of the formulation are incorporated via the use of an established speciation model and calculated at the end of the coupled transport-mechanical model (Cleall et al. 2007).

The soil suction comprises a number of potentials, namely the matric potential, the osmotic potential, the electric potential and the gravitational potential. For most situations the electric potential has been found to be negligible and within most literature and for most soils, the osmotic potential is also neglected, leaving the total potential to be made up of matric (capillary) potential and gravitational potential.

In the particular case of active compacted clay soils such as bentonites, used heavily as buffer material in HLW repositories, the osmotic potential may represent a large aspect of the total suction. A number of chemicals are subject to dissolution/precipitation and ion-exchange dependent upon the water content, ingress of water into the micro-pores, which governs the swelling behavior, and the chemical concentration gradients that exist.

Incorporating the osmotic potential, the Darcian velocities of the liquid and vapor movement become:

$$\mathbf{v}_l = -k_l \left[\frac{\nabla u_l}{\gamma_l} + \nabla z + \sum_{i=1}^{nc} \frac{-1000RT\gamma_i\omega_o}{\rho_l g} \nabla c_d^i \right] + \frac{-1000R\omega_o}{\rho_l g} \sum_{i=1}^{nc} \gamma_i c_d^i \nabla T \quad (13)$$

and

$$\mathbf{v}_v = -\frac{D_{atms} v_v \tau_v \theta_a}{\rho_l} \nabla \cdot \left[\rho_0 h_o \left(\frac{\partial h_m}{\partial s} \nabla s + \frac{\partial h_m}{\partial T} \nabla T \right) + \rho_0 h_m \sum_{i=1}^{nc} \frac{\partial h_o}{\partial c_d^i} \nabla c_d^i + \rho_0 h_m \frac{\partial h_o}{\partial T} \nabla T + h_m h_o \frac{\partial \rho_0}{\partial T} \nabla T \right] \quad (14)$$

where k_l is the unsaturated hydraulic conductivity, γ_l is the unit weight of liquid, z is the elevation, ω_o is the osmotic efficiency, γ_i is the activity coefficient of the i^{th}

chemical component, ρ_l is the density of liquid moisture, g is the gravitational constant, R is the gas constant, T is the temperature, c_d^i is the dissolved concentration of the i^{th} chemical component, nc is the number of chemical components, ρ_o is the density of saturated water vapour, h_m is the relative humidity due to matric potential and h_o is the relative humidity due to osmotic potential.

HIGH PERFORMANCE COMPUTING

Incorporating the higher order coupling behavior and the simulation of realistic field-scale domains with realistic timescales yields computational expensive simulations. In particular, the three-dimensional simulation of a fractured rock mass of a full scale HLW repository yields simulations with approximately 1,000,000 finite elements, with 6 degrees-of-freedom at each nodal location, for a Thermo-Hydro-Mechanical simulation and many more degrees-of-freedom with the inclusion of chemical behavior. High-Performance Computing (HPC) is one method to reduce the computational time by increasing the amount of computation undertaken at any one time.

A number of computational techniques exist and in this work parallel computation has been used designed to be undertaken on a purpose built HPC machine with, in particular, a high-performance interconnect designed to allow fast communication between processors. Most HPC machines can be generally fitted into either shared-memory or distributed memory. Share-memory machines have a number of processing-cores with access to a single memory resource whereas in distributed-memory machines each processor has its own dedicated memory. A number of key differences in terms of computational algorithms are apparent. Shared-memory machines do not require communication between processing cores, although due to memory bus saturation the number of processors available is generally limited. In distributed-memory machines communication is required where a processor requires information that has been calculated by another processor which requires careful management. It must also be noted that computational technology changes quickly and that various architecture components progress at different rates and change the dynamic of a computer system. This means that previous HPC algorithms that gave good speed-up performance may then not work well on modern computational facilities (Vardon et al. 2008).

In recent times a hybrid architecture has become common with shared-memory ‘nodes’ of up to 8 processing cores formed into a distributed-machine architecture made up of any number of these nodes. A parallel algorithm for COMPASS has been developed to take advantage of this architecture. Details of this approach

can be found in Vardon et al. (2009).

A hybrid parallel modeling approach is used with a multi-threaded model on the shared-memory nodes and message passing across multiple nodes. The multi-threaded approach is used for all parallelizable calculations and the message-passing approach is used only when parallelizable calculations are large enough so that calculation time is much greater than the communication of the result.

Within the COMPASS code, the matrix-build section, where the sparse non-symmetric system matrices i.e. [a] and [b] from Eq. 2 are calculated, is inherently parallelizable and the computation to communication ratio is high. In this section both multi-threaded and message-passing are used. In the solver section, where Φ^{n+1} from Eq. 2 is evaluated by use of an iterative Krylov sub-space solver (Barrett et al. 1995), many results are required throughout each iteration of the solver, of which it is likely to be many within each solution.

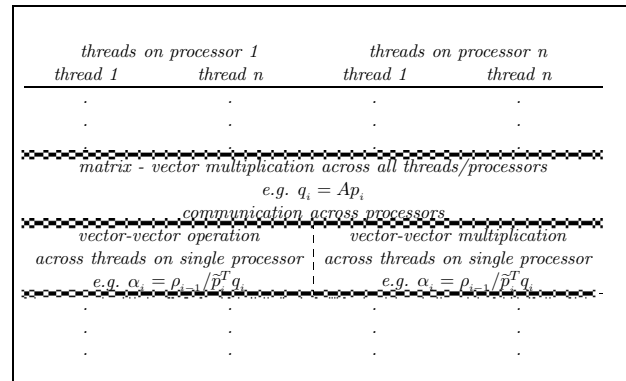


Fig. 5 Schematic of the multi-level parallelism used in the Krylov subspace solver. A is a matrix, q and p are vectors and α and ρ are scalars

In general the calculations that occur within Krylov sub-space solvers can be characterized in two ways, i) a vector-vector operation, or equivalent where the number of scalar values in a vector undertake a mathematical operation; ii) a matrix-vector operation. Option (ii) then has the size of the vector times more individual operations. In most cases the resultant is a vector taking the same time to communicate. The matrix-vector multiplications are then calculated across all possible processing cores with the vector-vector operations calculated only using the multi-threaded model on shared-memory nodes. This is schematically seen in Fig. 5.

This approach has been implemented and tested across a number of machines with some results found in Vardon et al. (2009). A sample of the results for a 350,000 finite-element analysis undertaken on Merlin, a HPC machine situated at Cardiff University, is shown in Fig. 6. Merlin is formed from 2048 Intel Xeon (Hapertown/

Seaburg) processing cores, using quad-core technology with eight processing cores per node. The interconnect is an InfiniBand Connect-X with 20Gbps bandwidth.

The results show that using 16 processing cores a speed-up of over 5 times is found. This enables analyses to be undertaken that otherwise would take significant periods of time.

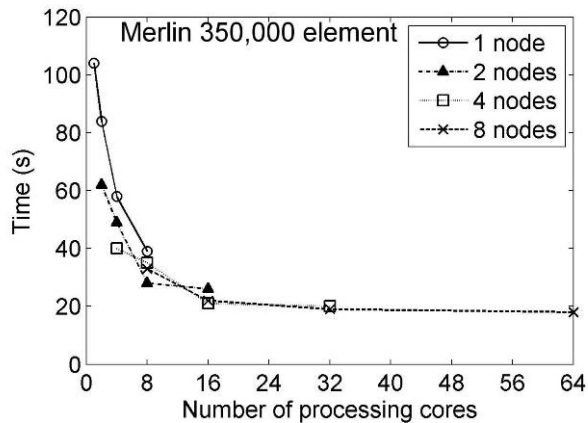


Fig. 6 Wall-time of the Krylov sub-space for a 350,000 finite-element simulation on the Merlin HPC machine

CONCLUSIONS

The work presented in this paper represents an overview of the developments into the understanding of coupled thermo-hydro-chemo-mechanical behavior of soils undertaken at the Geoenvironmental Research Centre at Cardiff University. Extreme temperature behavior such as freezing and thawing of the ground and the impact of temperatures over 100°C are investigated and incorporated into the numerical model COMPASS. The vapor flow in compacted clays is investigated experimentally and the impact of these results included within the numerical model. The osmotic potential is included within the chemical behavior of the model, with the effects on the moisture velocities noted. Finally a high-performance computing algorithm to enable analyses to be undertaken in reduced time is presented.

ACKNOWLEDGEMENTS

The work that has been carried out in the paper has been partly supported by the European Commission under the sixth EURATOM Framework Programme for nuclear research and training activities (2002-2006) within the THERESA project, under contract FP6-036458 and the UK Engineering and Physical Sciences Research Council (EPSRC) through grant number GR/T22964. The use of High-Performance Computing facilities is gratefully acknowledged both at the

Advanced Research Computing @ Cardiff (ARCCA) at Cardiff University and the High Performance Computing Collaboratory (HPC²) at Mississippi State University.

REFERENCES

- Barrett R, Berry M, Chan T, Demmel T, Donato J, Dongraa L, Eijkhout V, Pozo R, Romine C, Van der Vorst H (1995). *Templates, for the solution of linear systems: building blocks for iterative methods*. John Wiley & Sons, New York.
- Cleall PJ, Melhuish TA, Thomas HR (2006a). Modelling the three-dimensional behaviour of a prototype nuclear waste repository. *Engineering Geology*, 85(2): 212-220.
- Cleall PJ, Seetharam SC, Thomas HR (2007). Inclusion of some aspects of chemical behaviour of unsaturated soil in thermo/hydro/chemical/ mechanical models. I: Model development, *ASCE Journal of Engineering Mechanics*, 133(3): 338-347.
- Cleall PJ, Thomas HR, Melhuish TA, Owen DH (2006b). Use of parallel computing and visualisation techniques in the simulation of large scale geoenvironmental engineering problems. *Future Generation Computer Systems*, 22: 460-467.
- Gatabin C & Billaud P (2005). Bentonite THM mock up experiments, sensors data report, CEA, Technical report NT DPC/SCCME 05-300A.
- Geraminegad M & Saxena S (1986). *Finite elements in plasticity: Theory and practice*. Pineridge Press Ltd., Swansea.
- Gilpin RR (1980). A model for the prediction of ice lensing and frost heave in soils. *Water Resources Research*, 16: 918-930.
- Harris C (1996). Physical modelling of periglacial solifluction: Review and future strategy. *Permafrost and Periglacial Processes*, 7: 349-360.
- Hoekstra P (1966). Moisture movement in soils under temperature gradients with the cold-side temperature below freezing. *Water Resources Research*, 2: 241-250.
- Konrad JM (1994). 16th Canadian Geotechnical Colloquium —Frost heave in soils—Concepts and engineering. *Canadian Geotechnical Journal*, 31: 223-245.
- Konrad JM & Duquenois C (1993). A model for water transport and ice lensing in freezing soils. *Water Resources Research*, 29: 3109-3124.
- Luikov AV (1966). *Heat and mass transfer in capillary—porous bodies*. Oxford: 233-303.
- Mageau DW & Morgenstern, NR (1980). Observations on moisture migration in frozen soils. *Canadian Geotechnical Journal*, 17: 54-60.
- Nixon JFD (1991). Discrete ice lens theory for frost heave in soils. *Canadian Geotechnical Journal*, 28: 843-859.

- Olivella S & Gens A (2000). Vapour transport in low permeability unsaturated soils with capillary effects. *Transport in Porous Media*, 40: 219-241.
- Owen DH (2000). Preconditioned parallel iterative solution methods for coupled finite element analyses, PhD Thesis, University of Wales, Cardiff.
- Philip JR & de Vries DA (1957). Moisture movements in porous materials under temperature gradients. *Transactions, American Geophysical Union*, 38(2): 222-232.
- Singh RM (2007). An experimental and numerical investigation of heat and mass movement in unsaturated clays. Ph.D. thesis, Cardiff School of Engineering, Cardiff University, UK.
- Thomas HR ed (2006). 5th ICEG Environmental geotechnics. Opportunities, challenges and responsibilities for environmental geotechnics. Thomas Telford.
- Thomas HR, Cleall PJ, Chandler N, Dixon D, Mitchell HP (2003). Water infiltration into a large scale in-situ experiment in an underground research laboratory—physical measurements and numerical simulation. *Géotechnique*, 53(2): 207-224.
- Thomas HR, Cleall PJ, Dixon D, Mitchell HP (2009a). The Coupled Thermal-Hydraulic-Mechanical Behaviour of a Large Scale In-Situ Heating Experiment. *Géotechnique*, 59(4): 401–413.
- Thomas HR, Cleall PJ, Li Y, Harris C, Kern-Luetschg M (2009b). Modelling of cryogenic processes in permafrost and seasonally frozen soils, *Géotechnique* 59(3): 173-184.
- Thomas HR & He Y (1994). A coupled heat-moisture transfer theory for deformable unsaturated soil and its algorithmic implementation. *International Journal for Numerical Methods in Engineering*, 40: 3421-3441.
- Thomas HR & Rees SW (2009) Measured and simulated heat transfer to foundation soils. *Géotechnique* 59(4): 365-375.
- Thomas HR & Sansom MR (1995). Fully Coupled Analysis of Heat, Moisture and Air Transfer in Unsaturated Soil. ASCE, *Journal of Engineering Mechanics*, 121(3): 392-405.
- Thomas HR, Siddiqua S, Seetharam SC (2009c). Inclusion of higher temperature effects in a soil behaviour model, *Géotechnique* 59(3): 279-282.
- Vardon PJ, Cleall PJ, Thomas HR, Philp R (2008). “Three-dimensional field-scale coupled thermo-hydro-mechanical modeling” In Proceedings of the 12th International Conference of the International Association for Computer Methods and Advances in Geomechanics, Goa: 2419-2425.
- Vardon PJ, Banicescu I, Cleall PJ, Thomas HR, Philp RN (2009). Coupled thermo-hydro-mechanical modelling: A new parallel approach, In the proceedings of the PDSEC-09 workshop of the IEEE IPDPS 2009 conference, Rome.
- Werme L (1998). Design premises for canister for spent nuclear fuel. Technical Report TR-98-08, SKB.

REMEDICATION TECHNOLOGIES FOR CONTAMINATED SITES

Albert T. YEUNG¹

ABSTRACT: Contaminated sites can pose a significant risk to public health and the environment. Many different *in-situ* or *ex-situ* remediation technologies have been developed throughout the years to mitigate the risk imposed by soil contamination. These technologies may be contaminant and site specific. Remediation can be achieved by contaminated soil removal, contaminant removal, containment, stabilization/solidification, transformation, or different combinations of these mechanisms. It may also be necessary to apply these technologies in combination to achieve remediation goals, in particular, for cases of contamination by multiple contaminants. Some of the remediation technologies currently available are presented in this invited lecture, in particular, the theory, state of development, applicability, limitations, remediation efficiency, cost effectiveness, and potential side effects of the remediation technologies are presented. Details of performance monitoring are described, criteria on selection of the appropriate remediation technology are given, and remediation cost estimate procedure is outlined. As innovative remediation technologies are being developed continually to satisfy various needs, the technologies presented in this invited lecture are by no means exhaustive. Nonetheless, a comprehensive list of references is given for readers interested in particular technologies to conduct their further exploration.

KEYWORDS: contaminated sites, remediation technologies, performance monitoring, selection of remediation technologies, remediation cost estimate

INTRODUCTION

Contaminated sites are always a public concern for its potential damage to living organisms including human beings, the ecology, the environment, and even property value. If the contamination problem is not adequately identified, recognized, delineated, studied, and practically resolved, it can pose a considerable risk to public health and the environment. It may also adversely affect current or proposed land uses and development of the site. Therefore, it should be carefully considered in the subdivision, development, and redevelopment of land; any change in land use, such as from commercial to residential, or from one form of commercial to another, e.g. from service station to office; where additions and alterations may be proposed to the existing landscape and/or infrastructures; and the transactions of land and properties.

Remediation of soil contamination can be achieved by: (1) *in-situ* removal of contaminants from the contaminated site for further off-site treatment of the contaminants removed; (2) *ex-situ* removal of contaminants from the contaminated soil after the soil has been excavated from the contaminated site; (3) *in-*

situ containment of the contaminants with the toxicity of the contaminants remains unchanged but the contaminants are isolated from human contacts for a predetermined period of time; (4) excavation of the contaminated soil and transport it to an engineered containment system for long-term isolation; (5) *in-situ* transformation of the contaminants so that the mobility and/or the toxicity of the contaminants are significantly reduced so as to reduce the risk of soil contamination to public health and the environment; and (6) any contaminations of these remediation mechanisms. All these mechanisms have their advantages and limitations. Moreover, they are contaminant specific and heavily dependent on the subsurface environmental conditions of the site. Therefore, it is very important to recognize that there is not a single technology or a single combination of technologies that would be applicable to all contaminants under all subsurface environmental conditions.

An attempt is made in this invited paper to give an overview of some of the remediation technologies, in particular, the theory, state of development, applicability, limitations, remediation efficiency, cost effectiveness, and potential side effects of these technologies. Details of performance monitoring of remediation progress are

¹ Associate Professor, Department of Civil Engineering, The University of Hong Kong, Pokfulam Road, Hong Kong Special Administrative Region, China. Email: yeungat@hku.hk

described, criteria on selection of the appropriate remediation technology are given, and remediation cost estimate procedure is outlined. As innovative remediation technologies are being developed continuously, the technologies presented in this invited paper are by no means exhaustive. Nonetheless, a comprehensive list of references is given for readers interested in particular technologies to conduct their further exploration.

References are listed under either the "General" sub-section or sub-sections specific to the respective section or sub-section headings. Moreover, many handbooks, special publications, and textbooks covering a great variety of remediation technologies such as Freeze and Cherry (1979), U.S. EPA (1985), LaGrega et al. (1994), National Research Council (1994), Wilson and Clarke (1994), Evans (1997), Otten et al. (1997), Suthersan (1997), Sellers (1999), Reddi and Inyang (2000), Hyman and Dupont (2001), Rowe (2001), Stegmann et al. (2001), Yong (2001), Lehr et al. (2002), Boulding and Ginn (2004), Nathanail and Bardos (2004), Sharma and Reddy (2004), Hudson (2006), Domínguez (2008), Dubois (2008), Khire et al. (2008), Nemerow et al. (2009), etc. are included in the sub-section "General" in the references to provide a wealth of information for researchers and practitioners interested in the subject.

SUBSURFACE CONTAMINATION

Contaminants can exist in different chemical states and different forms in the subsurface. The physical and chemical interactions of contaminants with the existing soil dictate the fate of contaminants in the subsurface. The environmental conditions of the soil depend on the hydrogeology of the contaminated site. The problem is further complicated by the large number of possible geochemical and biogeochemical reactions and the fact that the outcome of these reactions is heavily dependent on the existing environmental conditions, such as pH, Eh (redox potential), salinity, mineralogy of soil solid particles, temperature, pressure, etc. Moreover, these soil-contaminant interactions are dynamic, reversible, and inter-dependent. Nonetheless, these geochemical processes largely determine the feasibility of remediation technologies required if cleanup of the site becomes necessary. Therefore, a thorough understanding of the soil-contaminant interactions under different environmental conditions is essential. Discussion of the mechanisms and modeling of these soil-contaminant interactions are beyond the scope of this paper, interested readers should refer to the references in environmental chemistry such as Sawyer and McCarty (1978), Devlin et al. (1990), Sequeira (1994), Rajeshwar and Ibanez (1997), Evangelou (1998), Sparks (2003), and Manahan (2005); in aquatic chemistry such as Snoeyink and Jenkins

(1980), Stumm and Morgan (1996), and Benjamin (2002); in soil chemistry such as Cresser et al. (1993), McBride (1994), Sposito (1994, 2004, 2008), Bohn et al. (2001), Essington (2004), Selim and Kingery (2003), and Kirk (2004); in hydrogeology such as Freeze and Cherry (1979), Domenico and Schwartz (1990), Palmer (1996), and Fetter (1999), and in geochemical and biogeochemical reaction modeling such as Krešić (2007), and Bethke (2008), as listed at the end of this paper.

REMEDIATION TECHNOLOGIES

Different *in-situ* and *ex-situ* remediation technologies are detailed in this section, in particular, the theory, state of development, applicability, limitations, remediation efficiency, cost effectiveness, and potential side effects of the remediation technologies are presented. However, readers should note that the boundaries among different remediation technologies sometimes can be very vague due to considerable overlapping of different technologies. Therefore, the categorizing of remediation technologies may be subjective and/or unconsciously arbitrary.

Excavation and Off-site Disposal

Excavation followed by off-site disposal, often known as dig and haul, is a well proven and readily implementable remediation technology. It is applicable to practically all contaminants. Contaminated soil is physically excavated and transported to permitted off-site treatment and disposal facilities. Pretreatment of the contaminated soil excavated may sometimes be required to satisfy the ultimate land disposal requirements (Lehr et al. 2002). Prior to 1984, excavation and off-site disposal was the most common method for remediating hazardous waste sites in the U.S. Nonetheless, excavation of contaminated soil is the first step of all *ex-situ* remediation technologies. However, the technology can be expensive when costs of transportation, and off-site treatment and/or disposal are included.

It should be noted that there are hazards implicitly associated with the handling of contaminated soil. The soil may be contaminated with explosive, flammable, or combustible materials, e.g. carbon disulfide, hydrogen sulfide, methane, tetraethyl lead, etc., any sparks generated during excavation may ignite these materials to cause a fire or explosion. Excavation workers may be exposed to volatile organic compounds (VOCs), semi-volatile organic compounds (SVOCs), and particulates contaminated with semi-volatile organics, and/or inorganic contaminants. Hazards of inhaling contaminated airborne dusts are particularly evident during warm and dry periods. Workers may also be exposed to the risk of dermal contact with waste materials when handling such

materials. Workers may inadvertently ingest contaminants or waste materials that collect on their hands and clothing in the form of dust during excavation, as dust ingestion may occur when workers take water and/or meal breaks, or after they have left the contaminated site if established hygiene procedures, e.g. washing hands, are not strictly followed. Microorganisms in contaminated soil may pose biological hazards at sites containing medical wastes or sewage sludge. Workers may be exposed to inhalation, ingestion and/or dermal contact with pathogens such as *Coccidioides sp.*, *Histoplasma sp.*, *Mycobacterium sp.*, etc.

Other factors that may limit the applicability and effectiveness of the technology include: (1) generation of fugitive emissions may be a problem during excavation and transportation; (2) remediation cost is heavily dependent on the distance between the contaminated site and the nearest disposal/treatment facility with the required permit(s), therefore, the logistics of excavation and transportation of contaminated soil is extremely important in the economic consideration of the technology (Sellers 1999); (3) depth and composition of the materials requiring excavation must be considered, the remediation technology is typically restricted to shallow soils less than approximately 3 m below ground surface, as backhoes can generally excavate to a maximum depth of approximately 6 m and soil excavation at greater depth requires larger and more powerful earth moving equipment; excavation in the vicinity of infrastructures may require the installation of temporary lateral support systems for safety reasons, which increase the cost and duration of the remediation project substantially; (4) transportation of the contaminated soil through populated areas may affect community acceptability; (5) disposal options for certain waste, such as mixed waste, radioactive or transuranic waste, may be very limited; (6) contaminants can potentially migrate from disposal/treatment facilities through different pathways, such as effluent discharge to surface water, rainfall surface runoff, leaching into groundwater, volatilization to the atmosphere, and dike uptake; and (7) disposal/treatment facilities without proper design and maintenance can develop odor, mosquito, and insect problems.

In-situ Natural Attenuation

In-situ Natural attenuation is a component of all remedial solutions to subsurface contamination. It refers to the natural physical, chemical, and biological processes that reduce the concentration of contaminants in the subsurface (Sellers 1999). Examples are advection, dispersion, and dilution of contaminants by infiltration; transfer of contaminants in groundwater to the air in soil pores by volatilization; bioremediation of organic

contaminants; or reduction of contaminant mobility by sorption onto soil particle surfaces (Wiedemeier et al. 1999).

In-situ natural attenuation can be an appropriate remediation technology when the contaminants degrade or disperse readily and do not pose a significant risk to public health and/or the environment while they attenuate, in particular when the contamination source has been removed or contained. It is generally not an appropriate technology when (1) the site contains a significant amount of non-aqueous phase liquids (NAPLs); (2) concentrations of contaminants are so high that they pose an unacceptable risk to public health and/or an ecosystem, or become toxic to microorganisms; and (3) the rate of attenuation is unacceptably slow.

In-situ natural attenuation has several advantages and disadvantages in comparison to other remediation technologies (Boettcher and Nyer 2001). The advantages include: (1) less remediation waste products are generated, therefore the possibility of cross-media transfer of contaminants and human exposure is considerably less than that of most typical *ex-situ* technologies; (2) less intrusion and few surface operational facilities are required; (3) can be applied to all or part of a site depending on site conditions and remediation goals; (4) can be used in conjunction with, or as a follow up to other remediation technologies; and (5) the overall remediation costs are lower than those of active remediation. However, the potential disadvantages include: (1) remediation time may be longer than that required by a more active remedial solution; (2) characterization may be more complex and costly; (3) degradation of parent compounds may generate more toxic degradation products; (4) long-term performance monitoring is often required; (5) institutional controls may be required for risk management; (6) contaminant migration and/or cross-media transfer may occur if the hydrology and geochemistry of the site change over time; and (7) there may be a negative public perception of the technology, and public outreach and education may be required before the technology can be accepted by stakeholders.

Dispersion, sorption, and volatilization are important processes of *in-situ* natural attenuation. However, biodegradation is very likely to be the most effective process in most cases (Park et al. 2007; Jordan et al. 2008). An aquifer is a complex ecosystem that contains a variety of microorganisms competing for food and striving to reproduce. Variables of the system include: temperature, contaminant distribution, pH, soil type, nutrient levels, hydraulic conductivity, geochemistry, and availability of electron acceptors. These variables affect the occurrence and rate of contaminant biodegradation. Details of bioremediation and biodegradation are given in a later sub-section.

In-situ natural attenuation can be enhanced by the

introduction of selected chemicals into the subsurface to stimulate or enhance one or more of the natural attenuation mechanisms, in particular biodegradation. These processes will be discussed in detail in the subsections on soil flushing and reactive zone remediation (Yong and Mulligan 2004).

In-situ Containment Systems

Remediation or cleanup of many contaminated sites may be technically impossible, financially unviable, cost-ineffective, impossible to complete within a given time frame, and/or unnecessary when the risk posed to public health and the environment is acceptably low. As a result, attention has been given to the control of subsurface contamination so as to isolate the public from these toxic chemicals. Containment of the subsurface contamination zone using physical barriers may thus be a viable option. Moreover, a contained contamination zone can be used as an *in-situ* reactor for trials of new *in-situ* remediation technologies without exposing the public to unnecessary risk associated with unbounded treatment zones.

As shown in Fig. 1, *in-situ* containment systems are composed of: (1) vertical containment barriers of various types (walls); (2) natural or artificially engineered and emplaced bottom containment barriers (floors); and (3) surface containment barriers (caps or covers) (Mitchell and Rumer 1997).

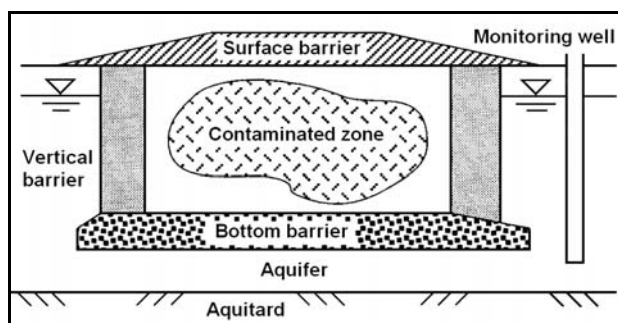


Fig. 1 Components of an *in-situ* containment system (after Rumer and Ryan 1995)

The functions of walls and floors are to prevent the waste and contaminated groundwater or leachate within the contaminated zone from coming into contact with the and clean groundwater in the surrounding. The functions of caps or covers are to prevent uncontrolled escape of leachate and gases from the contaminated zone; to prevent infiltration of precipitation and runoff into the contaminated zone; to separate the materials in the contaminated zone from humans, animals, and plants; and to serve as the foundation for different types of development and land use atop the contaminated zone.

These containment system components must be compatible to the contaminated materials to be contained,

ground deformations, and the effects of cycles of wetting and drying and of freezing and thawing. Design and construction of these containment system components require: (1) definition of objectives; (2) assessment of the existing and future site conditions expected; (3) evaluation of the options; (4) selection of the systems; (5) design of the systems; (6) supervision of construction; (7) post-construction performance monitoring; and (8) cost estimate.

The steps taken in the analysis and design of an *in-situ* containment system to ensure the system will serve the intended functions should include: (1) establishment of the geometry of the containment system; (2) evaluation of the potential movement of adjacent ground; (3) selection of construction materials for the different components of the wall, floor and cap; (4) evaluation of the suitability of potential construction methods; (5) design of joints; (6) cost estimate; (7) development of construction program; and (8) consideration of QA/QC requirements (Mitchell and Rumer 1997). Details of the different components of the containment system are discussed as follows.

Vertical containment barriers

Vertical containment barriers are typically constructed as cutoff walls of hydraulic conductivity of 1×10^{-9} m/s or less. When the hydraulic conductivity of the barrier wall is very low or when the hydraulic gradient across the wall is very small, significant contaminant transport by advection is practically prevented. However, it should be noted that migration of dissolved contaminants through the vertical containment barriers can still occur in the absence of advection as shown in Fig. 2.

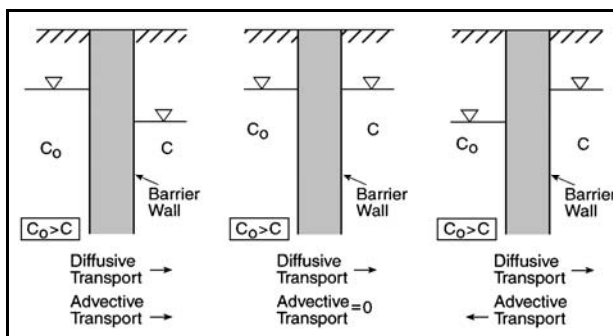


Fig. 2 Advective and diffusive contaminant transport across a vertical containment barrier (after Rumer and Ryan 1995)

When the contaminant concentration in the contaminated zone C_0 is higher than that outside the containment system C as shown in Fig. 2, molecular diffusion through the pores induced by the concentration gradient may result in significant migration of low molecular weight solutes across soil-bentonite barriers (Mott and Weber 1991; Shackelford and Daniel 1991a,b;

Shackelford and Redmond 1995). Therefore, sorbents may have to be added to the barrier to reduce the effective diffusivity of the contaminant in the barrier so as to retard diffusive contaminant transport and to extend the effective design life of a vertical containment barrier.

Soil- and cement-based vertical containment barriers include soil-bentonite slurry trench cutoff walls; cement-bentonite slurry trench cutoff walls; plastic concrete cutoff walls; cutoff walls backfilled with mixtures of cement, bentonite, fly ash, ground granulated blast furnace slag, and/or natural clay; cutoff walls constructed by deep soil mixing; and cutoff walls constructed by different grouting techniques. Geomembranes can also be installed as vertical containment barriers. Details of the construction materials and procedures of these vertical containment barriers are given by Ryan (1987), Cavalli (1992), Davidson et al. (1992), Grube (1992), Evans (1993, 1995), Filz and Mitchell (1995), Koerner and Guglielmetti (1995), Rumer and Ryan (1995), Mitchell and Rumer (1997), and Woodcock and Miller (1997).

The selection of the type and materials of vertical containment barriers depends on many factors including: (1) depth and length of vertical containment barriers required; (2) specified maximum allowable hydraulic conductivity; (3) type and extent of contamination; (4) soil types; (5) conditions of bottom containment barriers; (6) depth to groundwater table; (7) local availability of construction materials and equipment; (8) prior local experience; (9) local weather conditions; (10) construction schedule; (11) response of local residents; and (12) costs.

The structural or hydraulic performance of vertical barrier systems can be evaluated by proper quality control and testing specimens excavated from within the barrier constructed (Tamaro and Poletto 1992). However, less is known about the integrity of vertical barrier systems constructed for environmental remediation purposes. Construction QA/QC, box-outs, pumping tests, injection tests, geophysical evaluation, and post-construction sampling and testing are used for monitoring and performance evaluation.

Bottom containment barriers

The bottom containment barriers (floors) underneath a contaminated zone to minimize downward migration of leachate into the environment may be indigenous, i.e. a naturally occurring low hydraulic conductivity geologic formation. The barriers can also be artificially engineered and emplaced, i.e. constructed using admixtures and/or specially engineered construction techniques. They are usually the most uncertain components of an *in-situ* containment system in terms of their effectiveness as perimeter seal.

The use of native soil and rock strata as the bottom containment barriers depends heavily on the reliable

determination of their compositional and physical properties, and the anticipated stability of these properties after prolonged exposure to the contaminants (Boutwell and Hueckel 1995). If the naturally occurring low hydraulic conductivity geologic formation is not a practical solution, it is not always easy to construct the bottom containment barriers below the contaminated zone without disturbing it. However, it can be accomplished by many proven construction techniques such as permeation grouting, non-directional jet grouting to form overlapping cylinders as shown in Fig. 3, directional jet grouting to form slanted panels as shown in Fig. 4, directional drilling and scarifying as shown in Fig. 5, hydrofracturing and grouting, micro-tunneling techniques, etc. (Peterson et al. 1995). Less proven techniques include ground freezing to control groundwater flow (Powers 2007), and the installation of electrokinetic barriers to contaminant transport across compacted clay liners (Mitchell and Yeung 1991).

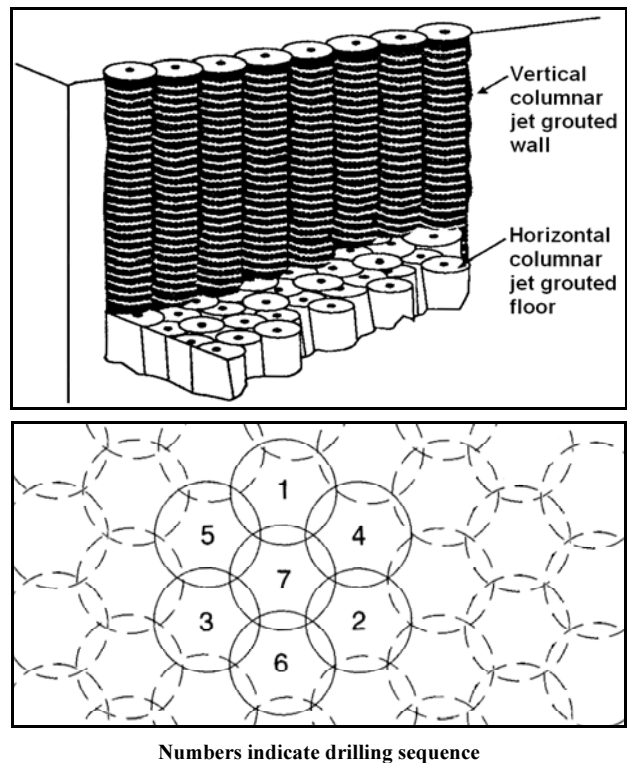


Fig. 3 Barrier floor formed by overlapping grout columns

The concept of constructing low hydraulic conductivity bottom containment barriers below a contaminated zone is comparatively new relative to the construction of vertical containment barriers. Whatever quality control and assurance procedures and techniques are employed to evaluate the quality of the constructed barriers, detection of any defects in the constructed barriers, provisions for capture and recovery of any leachate leakage through the barriers, and possibility of repairing the leaky barriers, if necessary, are issues that need to be

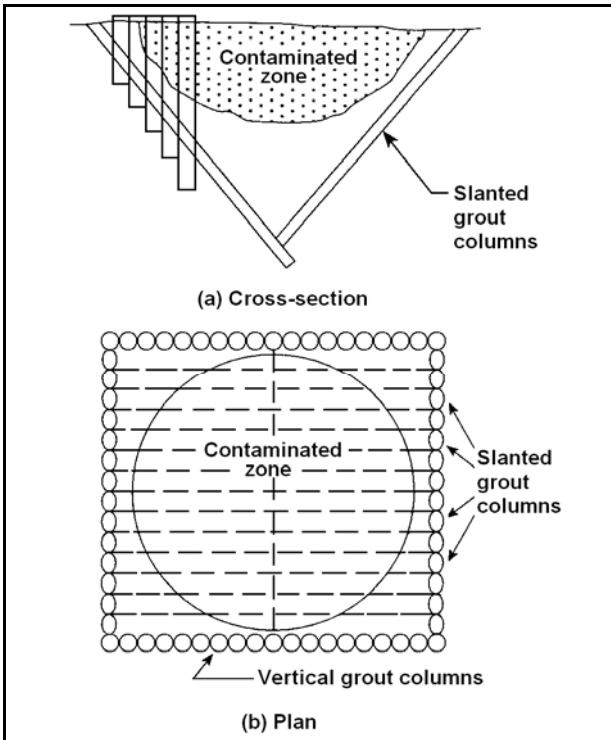


Fig. 4 Barrier floor formed by slanted grout columns

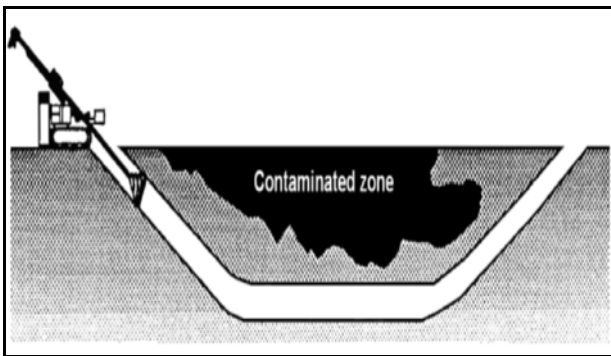


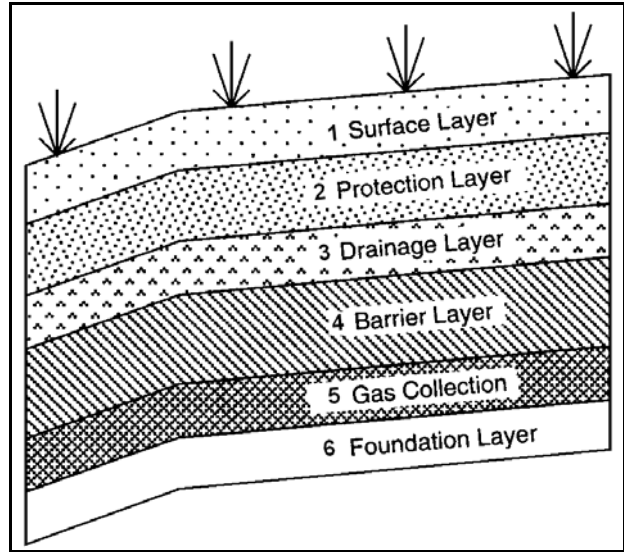
Fig. 5 Barrier floor constructed by directional drilling and scarifying technique

addressed. In fact, specific future studies have been recommended for the continued advancement of bottom containment barrier technologies by Rumer and Ryan (1995).

Surface containment barriers

The surface barriers (cap) of a containment system may contain six basic components. The functions and typical construction materials of these components are depicted in Fig. 6. Depending on the characteristics of the contaminants contained in the system, materials available to construct the cap, and site conditions, not all the components shown in Fig. 6 may be required for all sites. In fact, caps must be tailored to the specific requirements of each particular remediation project. In fact, these components are practically identical to those used in landfill covers with very similar design considerations (Crawford and Smith 1985; Bonaparte

1990; Boschuk 1991; Sharma and Lewis 1994; Daniel and Koerner 1995; Koerner and Daniel 1997; McBean et al. 1995; Qian et al. 2002; Hollingsworth 2004).



Layer no.	Primary functions	Typical materials
1	Separate underlying layer from ground surface; resist erosion; reduce temperature and moisture extremes in underlying layers	Topsoil; geosynthetic erosion control mat; cobbles; paving material
2	Store infiltration water before removal; separate waste from humans, animals, and vegetation; protect underlying layers from wetting and drying, and freezing and thawing	Soil; recycled or reused waste material; cobbles
3	Reduce water head on barrier layer; reduce uplift water pressure on overlying layers; reduce period overlying layers are saturated after rain	Sand or gravel; geonet or geocomposite
4	Impede water percolation through cap; restrict outward movement of gases from waste	Compacted clay; geomembrane; geosynthetic clay liner; waste material; asphalt
5	Collect and remove gases	Sand or gravel; soil; geonet or geotextile; recycled or reused waste material
6	Foundation for the cap, especially during construction	Sand or gravel; soil; recycled or reused waste

Fig. 6 Components of final cap (after Rumer and Ryan 1995; Mitchell and Rumer 1997)

The factors affecting the performance of the surface barriers include: (1) types of layers included; (2) materials and thicknesses of individual layers; (3) annual precipitation;

(4) surface slope angle of the cap; (5) compressibility of the contained waste; (6) time-dependent deformation of the contained waste; (7) gas generation of the contained waste; and (8) presence of burrowing animals. The design of surface containment barriers thus should consider: (1) design life of the cap; (2) expected routine and major maintenance of the cap; (3) nature of the contained waste; (4) site conditions; (5) materials available; (6) temperature extremes, including possibility of freeze-thaw conditions; (7) precipitation extremes that: (a) affect the design slope angle of the cap surface to promote runoff and control drainage of surface water; and (b) may lead to cyclic wetting and drying that can cause shrinkage cracks in some soils; (8) penetration of plant roots, burrowing animals, worms, and insects into the soil; (9) inadvertent human excavations into the cap; (10) subsidence of the waste, leading to change in drainage contours and formation of cracks in some soils; (11) down-slope slippage or creep, resulting in landslides or cracking; (12) vehicular movements on the cap that can damage the cap; (13) deformation caused by earthquakes; and (14) wind or water erosion of materials. Detailed design considerations and possible alternative configurations for each layer are given in Rumer and Ryan (1995).

It should be noted that cap failures are not uncommon and most have occurred during or shortly after construction. Primary causes of failures are: excessive erosion; buildup of excessive pore water pressure in the cap layers; lack of a drainage layer; a drainage layer of insufficient flow capacity; and/or incorrect estimation of the shear resistance between the cap layers (Boschuk 1991). Although most failures did not cause rupture of the barriers, the repair was quite costly.

Stabilization and Solidification

Stabilization is the process by which reagents are mixed with the contaminated soil or sludge to minimize the mobility of the contaminants and/or to reduce the toxicity of the waste (Conner 1990). Solidification is the process by which sufficient quantities of solidifying reagents are added to solidify the waste material. The stabilization/solidification process thus refers to either chemically binding or physically trapping the contaminants in soils (Anderson 1994). Stabilization/solidification is used in remediation projects to: (1) improve the handling and physical characteristics of wastes; (2) minimize the rate of contaminant migration into the environment; and (3) reduce the toxicity of certain contaminants. Stabilization/solidification is a more permanent remedial solution than *in-situ* containment. It is sometimes referred to as immobilization, fixation, or encapsulation.

The technology may require the contaminated soil or sludge be dewatered or large-size particles or debris be removed or crushed, as there are always operational limits on the maximum size of particles that can be handled by the equipment used to mix contaminated soil with reagents. Contaminated soil or sludge may be treated *in-situ*, in containers, or in a mobile processing unit. For sites requiring relatively deep *in-situ* stabilization/solidification or more thorough mixing, modified augers with mixing blades as shown in Fig. 7 can be employed.

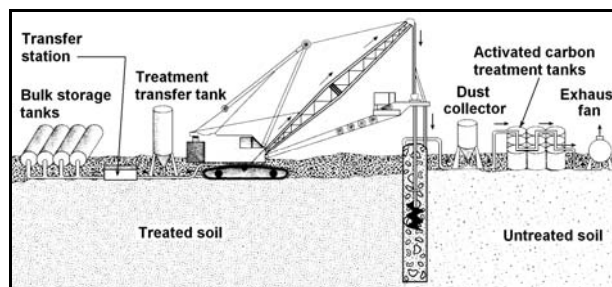


Fig. 7 Schematic of an *in-situ* mixing process with modified augers (after LaGrega et al. 1994)

The advantages of the technology include: (1) low cost; (2) applicable to a wide range of contaminants; (3) applicable to different soil types; (4) uses readily available equipment; (5) simple operation; and (6) higher throughput rates than many other remediation technologies. However, the disadvantages of the technology also include: (1) contaminants are not destroyed or removed; (2) the volume of treated soil may be increased significantly by the addition of reagents; (3) emissions of VOCs and particulates may occur during the mixing process, rendering the requirement of extensive emission control; (4) delivery of reagents to the subsurface and achieving uniform mixing *in-situ* may be difficult; (5) *in-situ* solidification may limit future uses of the site; and (6) long-term efficiency of the process may be uncertain, in particular when the subsurface environmental conditions change over time.

Reagents used in stabilization/solidification of waste can be broadly categorized into two types: (1) binder; and (2) sorbent. Binder is a reagent that increases the strength of the product, and sorbent is a reagent that primarily retains contaminants in the stabilized matrix. There is an extensive range of binders and sorbents commercially available, including several proprietary reagents. Some of the non-proprietary reagents include cement (Paria and Yuet 2006); pozzolans such as fly ash (Dermatas and Meng 2003), pumice, ground blast furnace slag, and cement kiln dust; lime; soluble silicates; organically modified clays; modified lime; thermosetting organic polymers; thermoplastic materials; etc. Moreover, the waste may also be pretreated by chemical additives to reduce the solubility of

contaminants prior to solidification. For example, Cr^{6+} may be pretreated with ferrous sulfate to reduce the chromium to the less soluble and less toxic Cr^{3+} . Arsenic can be immobilized by oxidizing As^{3+} to the less toxic and less mobile As^{4+} , and then treated with ferrous sulfate to form the insoluble FeAsO_4 . Lead can be pretreated and immobilized by trisodium phosphate Na_3PO_4 to become lead phosphate $\text{Pb}_3(\text{PO}_4)_2$ (U.S. EPA 1985).

The stabilization/solidification technology employs one or more of these mechanisms: (1) macroencapsulation; (2) microencapsulation; (3) absorption; (4) adsorption; (5) precipitation; and (6) detoxification. Detailed description of these mechanisms is given by LaGrega et al. (1994). However, the stabilization/solidification process is heavily dependent on the type of reagent used.

Cement-based stabilization/solidification is a process that mixes contaminated soil with type I or II Portland cement followed by addition of water, if necessary, for hydration (Paria and Yuet 2006). The hydration of cement forms a crystalline structure consisting of calcium aluminosilicate. The contaminants are bound into the cement matrix and undergo physicochemical changes that reduce their mobility. As a result of the high pH environment generated by cement, the metals are retained within the hardened structure in the form of insoluble hydroxide or carbonate salts. Moreover, acidic waste can be neutralized. The process is applicable to metals, PCBs, oils, and other organic compounds (Sharma and Reddy 2004). Extensive dewatering of wet sludges and waste is typically unnecessary as water is required for cement hydration. The disadvantage is the sensitivity of cement to the presence of certain contaminants that may retard or prohibit hydration and the resulting setting and hardening of the material.

Pozzolanic or silicate-based processes involve siliceous and aluminosilicate materials that are not cementitious by themselves. However, they form cementitious substances when react with lime or cement and water. However, pozzolanic reactions are generally slower than cement reactions. The primary immobilization mechanism is the physical entrapment of contaminants in the pozzolan matrix. The treated soil can vary from soft fine-grained material to a hard cohesive material similar to concrete in appearance. The process is applicable to metals, waste acids, and creosotes. Unburned carbon in fly ash may sorb organics from the waste. As a result, a pozzolan such as fly ash may have beneficial effects in the stabilization of both organic and inorganic wastes (Sharma and Reddy 2004).

Organic polymerization stabilization/solidification relies on polymer formation to immobilize the contaminants in soil. The process is applicable primarily to special wastes such as radionuclides, but it is also applicable to

metal and organic contaminants.

Thermoplastic stabilization/solidification is a microencapsulation process by which the contaminants do not react with the encapsulating material chemically, but is covered with a relatively impermeable layer. For example, the contaminants can be bound into a stabilized/solidified mass by a thermoplastic material such as asphalt (bitumen) or polyethylene. The process is applicable to metals, organics, and radionuclides.

A variety of tests is being used to evaluate the long-term stability of the stabilized/solidified waste. The primary objective of the stabilization/solidification technology is to reduce the rate of contaminant migration into the environment. However, contaminants in the treated waste can migrate into the environment as leachate when precipitation infiltrates the treated waste. The fluid to which the contaminants are leached is called the leachant. After the leachant has become contaminated, it becomes leachate. The overall ability of a treated waste to leach contaminants is denoted as leachability. Available tests used to gauge the leachability of the treated material include: (1) paint filter test; (2) liquids release test; (3) extraction procedure toxicity characteristics (EPTox); (4) toxicity characteristic leaching procedure (TCLP); (5) modified uniform leach procedure; (6) maximum possible concentration test; (7) equilibrium leach test; (8) dynamic leach test; (9) sequential leach test; and (10) multiple extraction procedure. Details of these leaching test methods are discussed by LaGrega et al. (1994). It should be noted that the test method affects the leachability of the specimen determined experimentally, in particular, test variables that affect the contaminant concentrations in the leachate include: (1) leachant-to-waste ratio; (2) surface area of the waste; (3) type of leachant; (4) pH of the leachant; (5) contact time; (6) extent of agitation; (7) number of replacements of fresh leachant; (8) extraction vessel; and (9) temperature. The impact of these test variables should be self-evident. It should also be noted that the selection of the type of chemical analysis and the analytical procedures for the leachate is not a trivial exercise.

Additional physical and engineering property tests are required to evaluate the physical integrity and engineering properties, such as strength, compressibility, and hydraulic conductivity, of the treated material. These tests include: (1) moisture content; (2) bulk and dry unit weight; (3) specific gravity of the solid component; (4) particle size distribution; (5) laboratory cone index; (6) pocket penetrometer; (7) microstructural examination; (8) supernatant formation during curing and rate of setting; (9) unconfined compressive strength; (10) consolidation characteristics; (11) hydraulic conductivity; (12) wet/dry durability; and (13) freeze/thaw durability. Details of these tests are discussed by LaGrega et al. (1994) and appropriate testing standards.

Pump-and-Treat

Pump-and-treat remediation is to extract groundwater from contaminated site and process it through a water treatment system. The pump-and-treat technology relies on the advection of water through the contaminated zone, transfer of contaminants to the water, and extraction of the water from the subsurface for further treatment (Mackay and Cherry 1989; Cohen et al. 1997; Nyer 2001). A typical pump-and-treat system for the remediation of a leaky underground storage tank is depicted in Fig. 8.

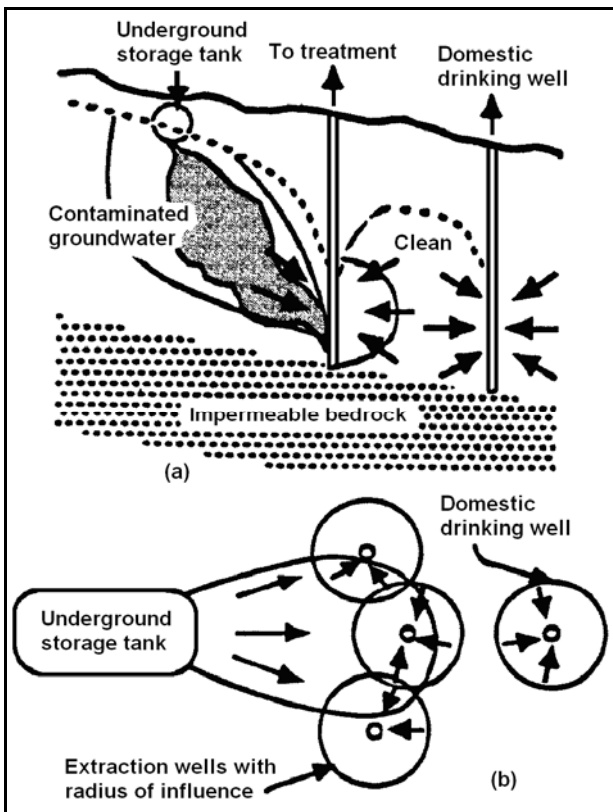


Fig. 8 Pump-and-treat system for the remediation of a leaky underground storage tank: (a) cross-section; (b) plan

A groundwater pumping system combined with a treatment system, i.e. a pump-and-treat system, is often designed for a specific groundwater contamination problem. The hydrology of the site, the source of contamination, and the characteristics of contaminants must be understood before an efficient and cost-effective pump-and-treat program can be implemented (Chang et al. 2007; Endres et al. 2007; Guo et al. 2007; Bau and Mayer 2008). The system requires the removal of many pore volumes of groundwater for a long period to meet the mandated allowable contaminant levels in the subsurface (Rowe 2001). As a result, a pump-and-treat cleanup is a relatively slow and expensive process. It usually lasts at least five to ten years, but can last for decades. The time it takes depends on: (1) the type and

amount of harmful contaminants in the subsurface; (2) the size and depth of the contaminated aquifer; and (3) the geological conditions of the contaminated site. Cleaning up contaminated water in the subsurface is often very difficult and sometimes not possible. Pump-and-treat is thus the best remediation technology available for such cases. Pump-and-treat can also be used to help keep contaminated groundwater from spreading into nearby drinking water wells while other kinds of cleanup actions are being taken (Bau and Mayer 2007). The U.S. EPA has been using pump-and-treat at over 500 superfund sites.

The contaminant source must first be removed to make the pump-and-treat technology effective. For example, leaking oil drums or tanks must be removed and the contaminated soil in the vicinity must be cleaned up.

An extraction system usually consisting of one or more wells equipped with pumps is built to extract contaminated groundwater from the subsurface. The pumps draw the contaminated groundwater into the wells and up to the ground surface where the water goes into a holding tank and then to a treatment system for treatment. Treatment technologies for the contaminated groundwater extracted can be grouped into three broad categories: physical, chemical, and biological. Physical treatment methods include adsorption, density separation, filtration, reverse osmosis, air and stream stripping, and incineration. Chemical treatment methods include precipitation, oxidation-reduction, ion exchange, and neutralization. Biological treatment methods include activated sludge, aerated surface impoundments, anaerobic digestion, trickling filters, and rotating biological discs. Details of these treatment methods are given by Boulding and Ginn (2004). The treated water can then be returned to the subsurface, a public sewer, or a pond.

When a significant amount of free product of a LNAPL exists in an aquifer, the system must be designed to maximize the recovery of the free product (Rivett et al. 2006). Caution must be exercised during the recovery of light non-aqueous phase liquid (LNAPL) when an extraction well is used to control the local hydraulic gradient so as to collect the free product in the cone of depression. If the pumping rate is excessive and the cone of depression becomes too deep, residual LNAPL globules can be trapped below the groundwater table due to capillary forces exerted on LNAPL globules by the aquifer material. The LNAPL globules constitute a persistent source of contamination to groundwater after completion of contaminant removal from the aquifer.

The most difficult aspect of pump-and-treat remediation is to achieve efficient extraction of contaminants that are strongly sorbed on the aquifer matrix (Ishimori et al. 2006; Saez and Harmon 2006; Parker et al. 2008).

Soil Flushing

Soil flushing is an *in-situ* remediation technology that uses an aqueous solution to purge or leach contaminants from the soil into the solution. The flushing solution can be plain water or a carefully designed solution, such as a surfactant or cosolvent, that optimizes desorption of contaminants from soil particle surfaces and solubilization of contaminants in the flushing solution (Martel et al. 2000).

A schematic of soil flushing is presented in Fig. 9. The flushing solution is pumped into the aquifer via injection wells. The solution then flows down-gradient through the contaminated zone where it desorbs contaminants from soil particle surfaces, solubilizes them in the solution, and flushes them towards the extraction wells where the solution is extracted. The contaminated solution is treated using typical wastewater treatment methods and then recycled by pumping it into the injection wells again. The technology can also be applied to treat soil in the vadose zone as shown in Fig. 10. The flushing solution is sprayed on the ground surface, which then infiltrates through the contaminated zone by gravitational force to the groundwater. The leachate is finally removed by the groundwater extraction well.

In-situ soil flushing can be applied to many types of organic and inorganic contaminants. The hydraulic conductivity of the contaminated zone is a dominant controlling factor on the applicability of the technology. Regions of hydraulic conductivity higher than 1×10^{-5} m/s are considered optimal, and regions of hydraulic conductivity lower than 1×10^{-7} m/s are poor candidates for soil flushing (Roote 1997). Soils with carbon contents less than 1% by weight are good candidates while soils with carbon contents higher than 10% by

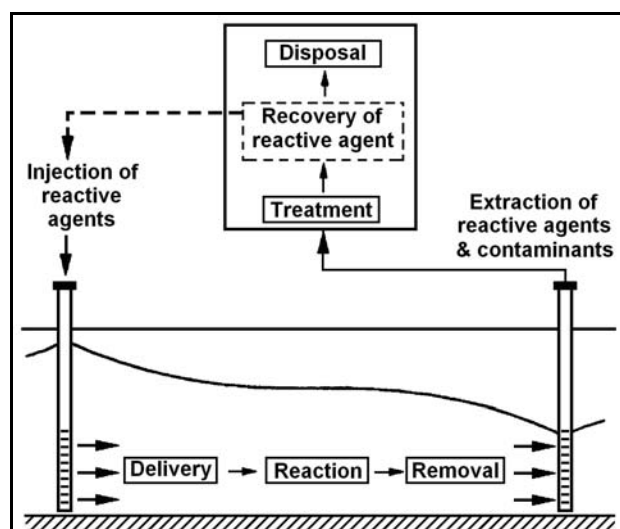


Fig. 9 Schematic of soil flushing (after Sharma and Reddy 2004)

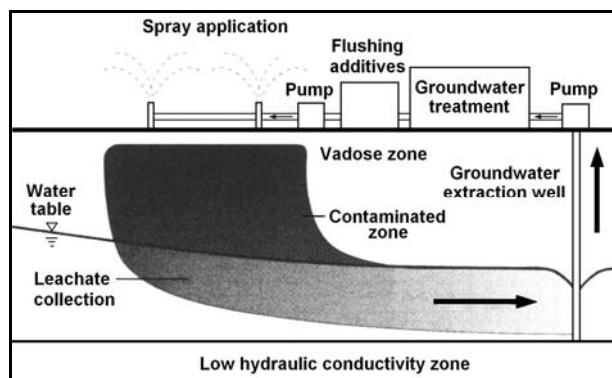


Fig. 10 Schematic of soil flushing in vadose zone (after Sharma and Reddy 2004)

weight are generally difficult. Other variables affecting application of the technology include: (1) depth of the contaminated zone; (2) concentration and volume of contamination; (3) distribution coefficients of contaminants between soil particle surfaces and flushing solutions; (4) presence of geologic heterogeneities in the soil horizon; (5) interactions of flushing solutions with contaminated soil; (6) suitability of contaminated site for installation of wells for delivery and recovery of flushing solutions; and (7) design factors such as sizing the delivery and recovery systems to ensure complete recovery of the elutriate. Flushing of NAPLs may be difficult due to: (1) low water solubilities of NAPLs; (2) high interfacial tension between NAPLs and soil particles; and (3) relatively low hydraulic conductivities of NAPLs because of their relatively high viscosity (Boulding and Ginn 2004).

The advantages of the technology include: (1) it is an *in-situ* technology, therefore it causes less exposure of the cleanup personnel and the environment to contaminants; (2) it is a relatively simple and economical operation to implement; (3) it is applicable for a wide variety of contaminants, both organic and inorganic (Francis et al. 1999; Lee et al. 2004); (4) it is applicable for both saturated and unsaturated zone; and (5) it may be used with many other remediation technologies. However, it may have these disadvantages: (1) it may be a slow process when geologic heterogeneities or free products are located within the soil horizon; (2) solubilized contaminants may be transported beyond the influence zone of the extraction well, and unintentional and uncontrolled spreading of contaminants may occur; (3) remediation times may be long; and (4) when the contaminated zone is deep, flushing solution is expensive, and/or remediation time is long, the process may be costly.

The technology can be enhanced using different flushing solutions (Anderson 1993; Mann 1995; Roy et al. 1995; McCray and Brusseau 1998). Moreover, the technology can be modified by using other innovative remediation technologies simultaneously. For example,

soil fracturing may be used in fine-grained soils to increase interactions among flushing solution, soil, and contaminant (Alfaro and Wong 2001). *In-situ* steam injection can stimulate volatilization and solubilization of sorbed contaminants in the subsurface (National Research Council 1994).

Reactive Zone Remediation

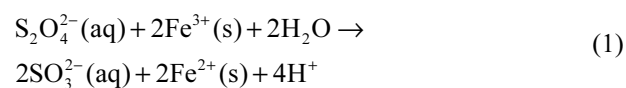
The soil flushing technology can be modified to create *in-situ* reactive zones. The technology focuses on manipulating the *in-situ* chemistry and microbiology by injecting selected reagents into the subsurface to accelerate natural attenuation of the contaminant. *In-situ* chemical oxidation/reduction reactions can then be stimulated to detoxify the contaminated zone. *In-situ* reactive zone are applicable for a wide range of contaminants, and they have been applied or are being evaluated on heavy metals such as chromium, zinc, mercury, copper, arsenic, lead, and cadmium; chlorinated aliphatic hydrocarbons (CAHs) such as trichloroethene, tetrachloroethene, 1,1,1-trichloroethane, carbon tetrachloride, and daughter products of these compounds; pentachlorophenol; and halogenated organic pesticides such as 1,2-dichloropropane, and 1,2-dibromo-3-chloropropane (Lenzo 2001).

Reactive zones used to remediate subsurface contamination can be created by two different methods: (1) by injecting chemical reagents that impact the redox conditions or react with the contaminant in the subsurface; or (2) by injecting electron acceptors and electron donors to enhance microbial growth in the subsurface under aerobic or anaerobic conditions. Depending on the nature of the contamination and the existing subsurface environmental conditions, reactive zones can be oxidizing or reducing.

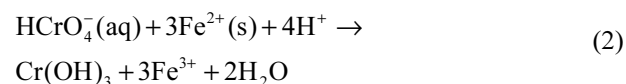
Oxidizing reactive zones are artificially enhanced subsurface treatment zones where the environment is maintained as strongly oxidizing, i.e. the redox potential is maintained well above 0.0 mV and dissolved oxygen is above 2.0 mg/l (Seol et al. 2003). The environment is created by injecting air or oxygen, or chemical oxidants, such as hydrogen peroxide H_2O_2 (Bower et al. 2000; Beltrán 2003; Vitolins et al. 2003; Siegrist et al. 2008), potassium permanganate $KMnO_4$ or sodium permanganate $NaMnO_4$, ozone, chlorine, or oxygen releasing compounds, into the subsurface (Fischer et al. 2001). Contaminants are chemically or microbially oxidized. For example, hydrogen peroxide H_2O_2 can be injected with ferrous sulfate to produce hydroxyl radicals to oxidize chlorinated organic compounds into carbon dioxide, water, and chloride ions (Huang and Weber 2005). Potassium permanganate $KMnO_4$ or sodium permanganate $NaMnO_4$, possibly in combination with H_2O_2 , may be used to remediate VOCs, SVOCs, and

polychlorinated biphenyls (PCBs) (Greenberg et al. 2000; Mott-Smith et al. 2000; MacKinnon and Thomson 2002; Ferguson et al. 2004; Li and Schwartz 2005; Crimi and Taylor 2007; Ferrarese et al. 2008; Thomson et al. 2008; Crimi et al. 2009). These oxidants have an additional benefit of enhancing a down-gradient naturally aerobic environment to promote bacterial growth so as to accelerate biological oxidation of readily biodegradable compounds such as petroleum hydrocarbons, benzene, toluene, ethylbenzene, xylene (BTEX), and vinyl chloride. However, it should be noted that some geological materials, e.g. pyrite, may release a large amount of iron and acid when exposed to oxidants. These potential negative impacts must be considered before the application of oxidizing reactive zones.

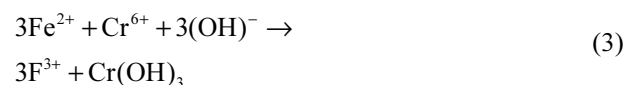
Reducing reactive zones are artificially enhanced subsurface treatment zones where the environment is maintained as strongly reducing, i.e. the redox potential is maintained well below 0.0 mV and dissolved oxygen is above 1.0 mg/l. Cr^{6+} may be reduced to Cr^{3+} using reducing agents such as Fe^{2+} , Fe^0 , calcium polysulfide, or sodium dithionite (Fruchter 2000). Dithionite is a sulfur-containing oxyanion that breaks down rapidly in aqueous solution to form two sulfoxyl radicals. These radicals react rapidly to reduce naturally occurring ferric iron to ferrous iron,



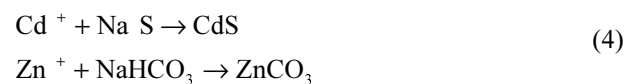
Aqueous chromate reacts with Fe^{2+} and precipitates as a solid hydroxide $Cr(OH)_3$ as depicted in Eq. (2),



Similarly, hexavalent chromium can also be reduced by ferrous sulfate at neutral pH (Walker and Pucik-Ericksen 2000; Khan and Puts 2003)



Moreover, cadmium can be precipitated using sodium sulfide and zinc can be precipitated using sodium bicarbonate as depicted in Eq. (4) (Suthersan 1997),



In-situ immobilization or fixation can thus be achieved by injection of reagents that transform metal or radionuclide contaminants into an immobile form, such as precipitate (Khan and Puts 2003).

Aerobic or anaerobic conditions can be enhanced and engineered by a manipulation of the natural environment to create a microbial reactive zone to achieve the

remediation goals using *in-situ* bioremediation and biodegradation of organic contaminants, in particular petroleum hydrocarbons and halogenated aliphatic hydrocarbons. Details of bioremediation and biodegradation are given in a later sub-section.

Design considerations for a reactive zone include: (1) hydrogeology of the contaminated site; (2) groundwater chemistry of the contaminated site; (3) microbiological conditions of the contaminated site; (4) reactive zone layout; (5) baseline definition; (6) regulatory issues; (7) reagents to be used; (8) well design such as type, number, depth, screen zone(s), and layout; (9) reagent feed such as feed rate, solution strength, and frequency of injection; and (10) performance monitoring program.

Soil Washing and Solvent Extraction

Soil washing is an *ex-situ* technology that uses aqueous solutions to separate organic, inorganic, and radioactive contaminants from excavated soil (Anderson 1993; Deshpande et al. 1999; Torres et al. 2005; Kuhlman and Greenfield 2006). It can be used as a pretreatment process to reduce the volume of feedstock for other remediation technologies. The process includes excavation of the contaminated soil, mechanical screening to remove various oversize materials, separation processes to generate coarse- and fine-grained fractions of the contaminated soil, treatment of the individual fractions, i.e. soil washing, and management of the residuals generated. The extracting fluid requires further treatment afterwards to remove and destroy the contaminants. The process also reduces the volume of contaminated soil by washing out fine-grained soil particles where contaminants are sorbed onto and disposed them of as sludge. The technology has been applied successfully to remediate soils contaminated by petroleum hydrocarbons, polycyclic aromatic hydrocarbons (PAHs), polychlorinated biphenyls (PCBs), pentachlorophenol, pesticides, heavy metals, creosotes, and radioactive wastes (Sellers 1999).

Advantages of the technology include: (1) the technology significantly reduces the volume of contaminated soil as the contaminants are concentrated in a relatively small portion of material, typically 10%; (2) the technology employs a closed system, permitting full control of the environmental conditions, such as pH and temperature, under which the contaminated soil is treated; (3) clean soil after treatment can be backfilled at the same site; (4) potential to remove both organic and inorganic contaminants; and (5) high throughput rate. However, disadvantages of the technology include: (1) ineffective for soils containing 30%–50% of silt, clay, or organic matter as contaminants tend to sorb onto these materials; (2) relatively expensive as a result of the additional costs associated with treating wastewater and

air emissions; (3) washing fluid may be difficult to formulate for complex mixed waste; (4) small volumes of residual contaminated sludge and wastewater require further treatment or disposal; (5) soil excavation and handling may expose the public and/or cleanup personnel to contaminants; (6) a large space is required to accommodate the soil washing system, system throughput rate, and site logistics.

Solvent extraction technology is similar to soil washing but uses organic solvents to dissolve contaminants and remove them from excavated soil (Anderson 1995; Mulligan et al. 2001; Silva et al. 2005; Kakitani et al. 2006, 2007; Murena and Gioia 2009). The technology is based on chemical equilibrium separation techniques being utilized in many industries. It effects the preferential separation of one or more constituents from one phase into a second phase. Typical solvents include liquefied gases, such as propane or butane, and triethylamine. Several additional concerns must be addressed when using a solvent extraction system: (1) solvents must be handled with extreme care as they may be inflammable and of extreme pH; (2) solvent loss during treatment affects emissions to the environment and remediation cost; and (3) amount of residual solvent remains in the treated soil may be of concern due to residual toxicity (Sellers 1999).

Permeable Reactive Barriers

As shown in Fig. 11, a permeable reactive barrier (PRB) is an engineered barrier of reactive treatment material placed across the flow path of a contaminant plume in aquifer that removes or degrades contaminants in the groundwater flowing through it (Vidic and Pohland 2000; Palmer 2001). It relies on the natural hydraulic gradient to move groundwater through the barrier. Therefore, there is no continuous input of energy and manpower into the remediation process and there is no mechanical breakdown, thus minimizing long-term operation and maintenance costs of remediation projects. Moreover, technical and regulatory issues relating to the discharge of treated groundwater are avoided or minimized. However, the applicability and effectiveness of the PRB may be limited by: (1) lengthy treatment time relative to other active remediation technologies; (2) potential for losing reactivity of the reactive treatment material, requiring replacement of the material; (3) potential for decrease in hydraulic conductivity of the reactive treatment material due to biological clogging and/or chemical precipitation; (4) potential of plume bypassing the PRB as a result of seasonal fluctuations in the flow regime; (5) currently limited to shallow depths; and (6) longevity of PRB performance is uncertain (Sharma and Reddy 2004; Henderson and Demond 2007).

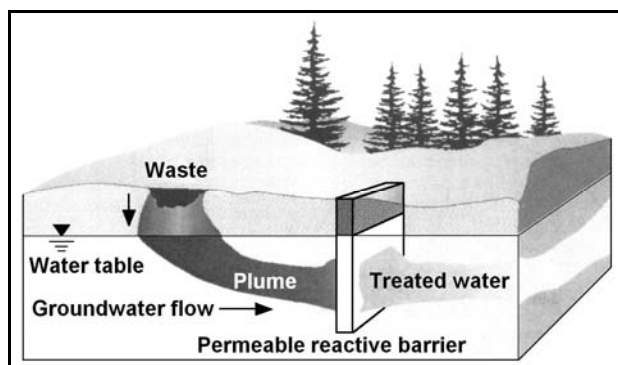


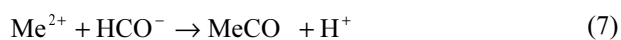
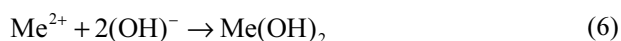
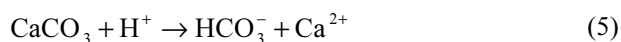
Fig. 11 Schematic of permeable reactive barrier (after Tratnyek et al. 2003)

A PRB can be installed as a continuous reactive barrier or as a funnel-and-gate system. A continuous reactive barrier consists of a permeable reactive cell containing the reactive treatment material. A funnel-and-gate system has an impermeable section, i.e. the funnel, that directs the captured groundwater towards the permeable reactive cell, i.e. the gate. The methods to emplace PRBs include: (1) conventional excavation; (2) trenching machines; (3) tremie tube/mandrel; (4) deep soil mixing; (5) high-pressure jetting; and (6) vertical fracturing and reactant sand fracturing (U.S. EPA 1999).

Permeable reactive barriers use many different treatment mechanisms to remediate contaminants in the groundwater, including: (1) transformation by abiotic and biotic processes; (2) physical removal; (3) pH or Eh modification; (4) metal precipitation; and (5) sorption or ion exchange. These mechanisms are discussed as follows.

Transformation by abiotic and biotic processes

Crushed limestone has been used in PRBs since 1970s to remediate acid mine drainage and metal-contaminated groundwater (Cravotta and Watzlaf 2002; Waite et al. 2002; Jones et al. 2002). Dissolution of calcite CaCO_3 , the principal component of limestone, can neutralize acidity, and increase pH, concentrations of alkalinity ($\text{CO}_3^{2-} + \text{HCO}_3^- + \text{OH}^-$), and calcium (Ca^{2+}) concentration in the mine water as described by Eq. (5). Metal contaminants can precipitate as hydroxides or carbonates as described by Eqs. (6) or (7), respectively if the pH of the environment is sufficiently high.



where Me = metal.

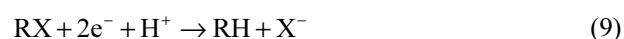
The use of zero-valent iron to dehalogenate chlorinated aliphatic organic compounds in groundwater was pioneered by the University of Waterloo in 1992

(Gillham 2008). The degradation process is an abiotic process and the mechanism is attributed to the direct electron transfer on the iron surface. Therefore, the reaction rates are proportional to the surface area of the iron. Zero-valent iron produces a low oxidation potential in groundwater, resulting in precipitation of low-solubility minerals that remove some redox-reactive contaminants such as uranium, chromium, and nitrate.

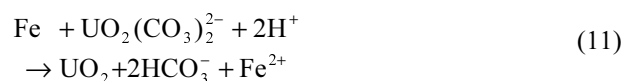
Corroding zero-valent iron Fe^0 provides electrons by (Matheson et al. 2002; Tratnyek et al. 2003)



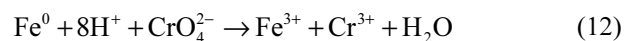
which can reduce halogenated or nitroaromatic compounds as described by Eq. (9) or metals/inorganic species as described by Eq. (10)



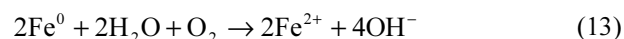
For example, uranium may precipitate as uraninite UO_2 or less crystalline precursor (Morrison et al. 2002)



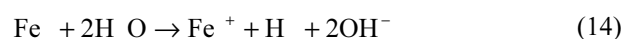
and Cr^{6+} can be reduced to Cr^{3+} , and Cr^{3+} forms sparingly soluble hydroxide minerals containing a solid solution of Cr^{3+} and Fe^{3+} ,



Water can compete for the electrons produced in the corrosion process. In aerobic aqueous systems, Fe^0 reacts with water according to



Under anaerobic conditions, Fe^0 reacts with water according to



Both of these reactions decrease the redox potential and increase the solution pH within the PRB.

The main criteria for proper functioning of aerobic biological PRBs to treat organic contaminants are availability of surface area and oxygen in the PRB, as bacteria need the surface area to attach and interact with the contaminants in the plume. Oxygen can be supplied in different ways. For example, an air sparging curtain can be installed in the PRB to supply oxygen to enhance degradation of aerobically biodegradable compounds such as BETX (Kao et al. 2001a,b, 2003; Kalinovich et al. 2008). Solid phase oxygen release compounds (ORC) can also be installed in PRBs to enhance degradation of contaminants (Hicks 1999). Biotic reduction of inorganic contaminants in PRBs has to be supported by supplying electron donor and nutrient materials for microbial

growth. Leaf mulch, sawdust, wheat straw, and alfalfa hay have been used as electron donors, and municipal waste or compost has been used as nutrient sources. Dissolved sulfate is an electron acceptor. Oxidation of organic material by sulfate, consumption of acidity, and the coupling to metal reduction are given by (Christensen et al. 1996)



where CH_2O = solid organic. The reducing environment generated in the PRB results in the precipitation of metals and other redox-reactive inorganic contaminants. PRBs that employ biotic reduction have successfully remediated metal, sulfate, nitrate, and acid contamination (Morrison et al. 2002). However, it should be noted that groundwater temperature affects the population of microorganisms and the rate of sulfate reduction significantly.

Physical removal

The PRB can be a series of air sparging points injecting air into a plume of volatile organics to remove the contaminants vertically for release them into the atmosphere or for capture by a soil vapor extraction system. The hydraulic conductivity of the subsurface is increased to make air sparging applicable.

A pilot-scale evaluation of the application was performed at the East Garrington gas plant in Alberta, Canada. The target contaminants were BTEX, and air sparging was the preferred remediation technology. However, the contaminants were situated in a low hydraulic conductivity glacial till at shallow depth. Two 44-m long trenches were dug and backfilled with pea gravel to overcome the geological limitation. Air sparging was then performed within these trenches and the results were good (U.S. EPA 1999).

pH or Eh modification

Modification of the pH in the contaminant plume is primarily used to precipitate dissolved metals in a plume. A PRB was installed at the Tonolli Superfund Site in Pennsylvania, U.S.A. to remove lead, cadmium, arsenic, zinc, and copper by conveying the groundwater through a limestone bed (U.S. EPA 1999).

The technique is often used in the first barrier of a multiple barrier system to generate the necessary environment for the reactions in the subsequent barriers. An example of the application is to adjust the pH to within a range in a pre-barrier so that bacteria may grow or bacterial reaction can occur in the biological reaction barrier.

Modification of the Eh of a system involves the exchange of electrons between chemical species that

affects a change in the valence state of the participating species. The redox reactions must occur readily under the natural temperature and other environmental conditions of the PRB. Blowes and Ptacek (1992) successfully used fine-grained zero-valent iron to generate a highly reducing environment to change the state of dissolved hexavalent chromium to the less soluble trivalent chromium and the metal was then precipitated as chromium hydroxide.

Metal precipitation

Precipitation of metals can be accomplished by altering the pH or Eh conditions, or by addition of chemicals to a PRB. Limestone is the most common chemical used in PRBs to treat acid mine drainage. Hydroapatite was used in a PRB as a source of phosphate to precipitate lead (Schwartz and Xu 1992). Apatite, zero-valent iron, and amorphous ferric oxide have also been used in a PRB to promote chemical precipitation and to accumulate uranium at Fry Canyon, Utah, U.S.A. (U.S. EPA 1999; Naftz et al. 2002). After one year of operation, all three were able to remove uranium. Zero-valent iron has demonstrated the highest removal efficiency of 99% and the other two treatment materials of approximately 90%. Sulfide can be used to precipitate metals, as metal sulfides are generally less soluble than metal hydroxides. When calcium or iron sulfide is used in the construction of PRBs, metals that have lower solubility as sulfides, such as silver, mercury, etc., would take the sulfide from the calcium or iron and precipitate. The calcium and iron would be released to the groundwater.

The key to the design for precipitation of metals in PRBs is to have the necessary chemical in solid form so that it can be used in the construction of PRBs. Moreover, the chemical must be able to interact effectively with the dissolved metal in the contaminant plume.

Sorption or ion exchange

Sorption is a process by which a chemical in the dissolved phase is sorbed onto solid particles. Most sorption reactions are reversible, pH-dependent, chemical specific, sorbent specific, concentration-dependent, and occur at relatively rapid rates. Surface complexation models are often used to describe the reaction chemistry of various sorption processes (McBride 1994; Sposito 2004, 2008; Bethke 2008). Common sorbents include activated carbon, amorphous ferric oxyhydroxide, zeolites, and ion exchange resins. Most metal contaminants dissolved in groundwater are in the divalent or trivalent state and thus are amenable to ion exchange.

Activated carbon has been widely used to remove organics from groundwater. Its large internal surface area sorbs organics by surface tension. A PRB was installed at

the Marzone Superfund site in Georgia, U.S.A. using 815 kg of activated carbon to remediate groundwater contaminated with pesticides including benzene hexachloride (BHC), β -BHC, dichlorodiphenyldichloroethane (DDD), dichlorodiphenyltrichloroethane (DDT), lindane, and methyl parathion. The contaminant concentrations in the treated groundwater are below detection levels (U.S. EPA 1999). However, it should be noted that the sorption process is reversible. Therefore, the used activated carbon must be removed from the subsurface and managed properly after it has been consumed or the plume is remediated. Otherwise, the sorbed organics can be released to the clean groundwater afterwards. The activated carbon in a PRB thus has to be retrievable. Moreover, the presence of other dissolved ions may compete with organics for sorption sites within activated carbon, reducing the sorption efficiency of activated carbon for organics. Bacterial growth can also foul activated carbon, reducing its effectiveness to remove organics.

Amorphous ferric oxyhydroxide has a high affinity for uranium and metal contaminants. However, the affinity is dependent on the concentrations of carbonate and hydrogen ions in the solution (Hsi and Langmuir 1985; Waite et al. 1994). The predominant uranium removal mechanism in the Oak Ridge and Durango projects may be sorption onto ferric oxides and oxyhydroxides that form from oxidation of zero-valent iron (Matheson et al. 2002).

Zeolites are hydrated alumino-silicates with a large internal surface area and high sorption capacity. They have been used in PRBs to treat inorganic contaminants by sorption and cation exchange, i.e. a contaminant molecule replaces another molecule at the zeolite particle surface. A pilot-scale demonstration project using a surfactant-modified zeolite was performed by the Large Experimental Aquifer Program near Portland, Oregon, U.S.A. The project was designed to demonstrate the technical feasibility of the technology to remediate hexavalent chromium, and the results indicate the PRB functioned as designed with retardation factors on chromium transport in the order of 50 (U.S. EPA 1999).

As in the case of activated carbon, sorption is a physical process and thus reversible. Therefore, the consumed material must be removed from the PRB and managed properly. Moreover, naturally occurring constituents such as dissolved iron and bacterial growth can foul the ion exchange material, thus reducing its sorption efficiency. It should also be noted that ion exchange treatment can be expensive.

Bioremediation and Biodegradation

The most important principle of bioremediation is the use of microorganisms (mainly bacteria) to decompose

hazardous contaminants, transform them to less harmful forms, and/or immobilize them under suitable environmental conditions (Anderson 1995; Hinchee et al. 1995a,b; Head et al. 2003). As bioremediation takes advantage of natural processes, it is thus a very safe technology. The microorganisms existing in soil pose no threat to human at the site or in the community. No dangerous chemicals are used in the process. The nutrients used to make microorganisms grow are fertilizers commonly used on lawns and gardens. When the environmental conditions are favorable, contaminated soil and/or groundwater are remediated *in-situ*. Therefore, cleanup workers do not need to make direct contact with the contaminated soil and/or groundwater. Moreover, there are practically no harmful byproducts generated by the cleanup process. The process does not need to mobilize as much equipment or labor as most remediation technologies. As a result, the operating cost is relatively low. Bioremediation has been used successfully to cleanup many contaminated sites and is being used at 50 Superfund sites across the U.S.

Although microorganisms live virtually everywhere, their ability to decompose man-made contaminants in the subsurface depends on three factors: (1) types of microorganisms; (2) types of contaminants; and (3) geological and chemical conditions at the contaminated site (Banwart et al. 2007).

Bioremediation is currently used commercially to cleanup mostly hydrocarbons found in gasoline. However, microorganisms have the capacity to biodegrade almost all organic contaminants and many inorganic contaminants (National Research Council 1993). When microorganisms have access to a variety of chemicals to help them generate energy and nutrients to build more cells, they can do their work to "bioremediate" harmful contaminants. Organic contaminants serve microorganisms in two ways as shown in Fig. 12: (1) they are a source of carbon for the building of new cells; and (2) they provide electrons for microorganisms to obtain energy, as microorganisms gain energy by catalyzing energy-producing chemical reactions that involve breaking chemical bonds and transferring electrons away from contaminants.

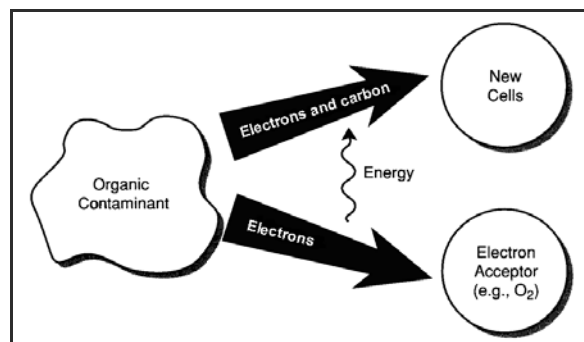
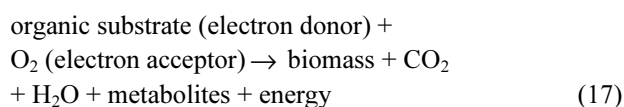
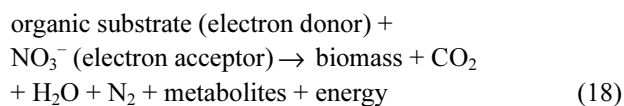


Fig. 12 How organic contaminants serve microorganisms (after National Research Council 1993)

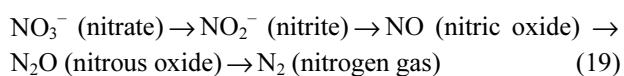
Under normal environmental conditions, many microorganisms use molecular oxygen O_2 as the electron acceptor, and the process of decomposing organic contaminants using O_2 is called *aerobic respiration*. Microorganisms use O_2 to oxidize part of the carbon in contaminants to carbon dioxide CO_2 to generate energy, and the remaining carbon to produce new cell mass. In the process, O_2 is reduced to water H_2O . Therefore, the byproducts of aerobic respiration are carbon dioxide, water, and an increased population of microorganisms. The biochemical reaction is depicted by



In reduced or low molecular oxygen environments, facultative anaerobes can use *facultative respiration* to shift their metabolic pathways and use nitrate NO_3^- as the terminal electron acceptor. The process is called denitrification and is generally depicted by



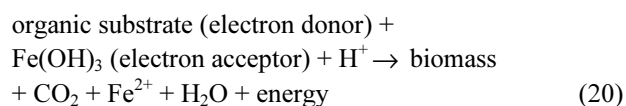
The reduction of NO_3^- to nitrogen gas N_2 is completed through a series of electron transport reactions as follows:



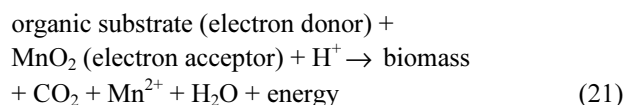
Most denitrifiers are existing in soil and heterotrophic. A large number of species can reduce nitrate to nitrite in the absence of oxygen, with a smaller number of species can complete the reaction by reducing nitrous oxide to nitrogen gas.

Many classes of microorganisms can survive in the absence of molecular oxygen, using a process called *anaerobic respiration*, where metals such as Fe^{3+} and manganese Mn^{4+} , sulfate SO_4^{2-} , or even CO_2 can be used in lieu of oxygen to accept electrons from contaminants being degraded (Leahy et al. 1997; Hicks 1999). The anaerobic microorganisms that are important to environmental remediation include iron and manganese reducing bacteria, and sulfanogenic and methanogenic bacteria. Anaerobic growth is less efficient than aerobic growth. However, these bacteria complete important geochemical reactions including bacterial corrosion, sulfur cycling, organic decomposition, and methane production. In addition to new cell mass, the byproducts of anaerobic respiration depend on the electron acceptor, and may include reduced forms of metals, carbon dioxide CO_2 , hydrogen sulfide H_2S , and methane CH_4 . The simplified biochemical reactions performed by these classes of microorganisms are depicted as follows:

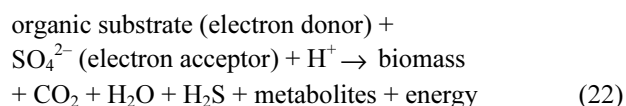
Iron reduction:



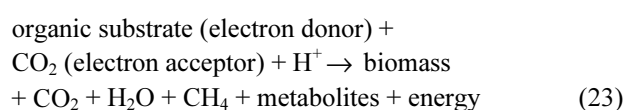
Manganese reduction:



Sulfanogenesis:



Methanogenesis:



Fermentation is a metabolism that can play an important role in oxygen-free environments, where organic contaminants serve as both electron donor and electron acceptor. Through a series of internal electron transfers catalyzed by microorganisms, organic contaminants are converted to innocuous fermentation products, such as acetate, propionate, ethanol, hydrogen, and carbon dioxide. These products can be biodegraded by other species of bacteria to carbon dioxide, methane, and water ultimately. In some cases, microorganisms can transform contaminants with little or no benefit to the cell by the process of *cometabolism* (Aulenta et al. 2006). For example, when microorganisms oxidize methane, toluene, and phenol, they produce certain enzymes that decompose chlorinated solvents even though the solvents itself cannot support microbial growth. Methane, toluene, and phenol are the primary substrates as they are the microorganisms' primary food sources, while the chlorinated solvents are the secondary substrates. Microorganisms can detoxify halogenated organics contaminants by the process of *reductive dehalogenation*. Microorganisms catalyze a reaction that replaces a halogen atom on the contaminant molecule by a hydrogen atom, and thus adds two electrons to the contaminant molecule to reduce it. A substance other than the halogenated contaminant, such as hydrogen and low molecular weight organic compounds including lactate, acetate, methanol, or glucose, must exist to serve as the electron donor. In most cases, the reductive dehalogenation process cannot generate energy but is an incidental reaction that may benefit the cell by eliminating a toxic material.

Regardless of the metabolism mechanism that microorganisms use to decompose contaminants, the elemental cellular components of microorganisms are relatively constant as tabulated in Table 1. If any of these or other elements essential to cell building is in short

supply relatively to the carbon content provided by organic contaminants, microbial growth may be limited and rate of bioremediation may be retarded. Therefore, a bioremediation system must be properly designed to supply appropriate concentrations of these nutrients if the natural habitat does not supply them adequately.

Table 1 Molecular composition of a bacterial cell

Element	Dry mass by proportion (%)
Carbon	50
Oxygen	20
Nitrogen	14
Hydrogen	8
Phosphorus	3
Sulfur	1
Potassium	1
Sodium	1
Calcium	0.5
Magnesium	0.5
Chlorine	0.5
Iron	0.2
Others	0.3

When the natural environmental conditions at the contaminated site can adequately provide all the essential materials, *intrinsic bioremediation* can occur *in-situ* without human participation. However, *in-situ engineered bioremediation* may be required to supply microorganism-stimulating materials and to optimize the environmental conditions so as to accelerate the desired biodegradation reactions (Toffoletti et al. 2005; Rodzewich et al. 2006; Rojas-Avelizapa et al. 2007).

The favorable environmental conditions do not always exist and cannot be developed in the subsurface, for example, the site temperature is too cold or the soil is too dense. At these sites, the contaminated soil has to be dug up for cleanup above ground where heaters and soil mixing can help improve environmental conditions (Turrell et al. 1998; Al-Daher et al. 1998, 2001; Perfurmo et al. 2006, 2007). The proper nutrients and oxygen can be added by stirring the mixture or by forced air circulation. However, some microorganisms work better under anaerobic conditions. Mixing soil can sometimes cause harmful contaminants to evaporate before the microorganisms can decompose them. Under these circumstances, the contaminated soil has to be mixed inside a special tank or building where evaporating contaminants can be collected and treated, so as to prevent them from polluting the air.

Existing microorganisms can detoxify many contaminants. However, some compounds, such as petroleum hydrocarbons, alcohols, ketones, and esters, are more easily biodegraded than others (Balba et al. 1996, 1998). Technologies to stimulate the growth of microorganisms to degrade a wide range of other

contaminants, such as PAHs, ethers, halogenated compounds, PCBs, and nitroaromatics, are emerging (McQueen et al. 1999; Atagana et al. 2003; Makkar and Rockne 2003). Reactions and products of biodegradation of these compounds are given by Alexander (1999). Microorganisms cannot destroy metals, but they can change their reactivity and mobility. Schemes using microorganisms to mobilize metals from one location and scavenge them from another location have been applied to remediate sites contaminated by mining activities (Abdelouas et al. 2000; Evans and Trute 2006; Diels and Lookman 2007; Groudev et al. 2008).

Microorganisms can also demobilize contaminants by three basic ways: (1) Microbial biomass can sorb hydrophobic organic molecules. Sufficient biomass grown in the path of contaminant migration may stop or slow contaminant transport in the form of a biocurtain. (2) Microorganisms can produce reduced or oxidized species that cause metals to precipitate. Examples are oxidation of Fe^{2+} to Fe^{3+} , which precipitates as ferric hydroxide $\text{Fe}(\text{OH})_3$; reduction of SO_4^{2-} to sulfide S^{2-} , which precipitates with Fe^{2+} as pyrite FeS , or with mercury Hg^{2+} as mercuric sulfide HgS ; reduction of hexavalent chromium Cr^{6+} to trivalent chromium Cr^{3+} , which can precipitate as chromium oxides, sulfides, or phosphates; or reduction of soluble uranium to insoluble U^{4+} , which precipitates as uraninite UO_2 . (3) Microorganisms can biodegrade organic compounds that bind with metals to keep the metals solubilized. Unbound metals often precipitate and become immobilized.

Phytoremediation

Phytoremediation is the removal, stabilization, and degradation of organic and inorganic contaminants in soils by green plants as shown in Fig. 13 (Carman and Crossman 2001; Suresh and Ravishankar 2004; Kvesitadze et al. 2006). Water and nutrients are taken up by plants, and carbon dioxide, oxygen, water, and photosynthates are released to the environment. Utilizing plants to control

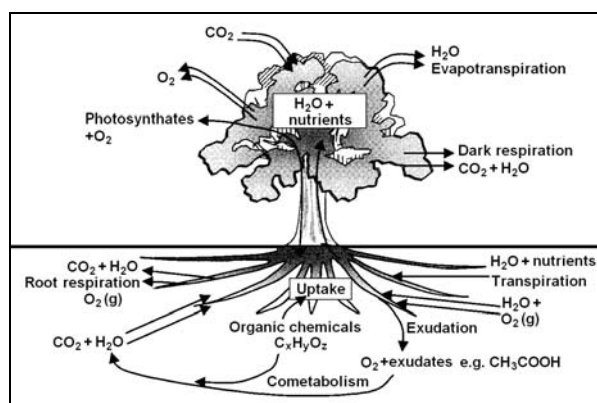


Fig. 13 Concept of phytoremediation (after Carman and Crossman 2001)

soil and water degradation has a long history. Many early agriculturalists developed plant-based systems to minimize soil erosion, restore disturbed environments, and cleanse water.

The U.S. EPA (U.S. EPA 1998) has defined six mechanisms of phytoremediation. Three of these mechanisms are applicable to the remediation of organic contaminants: (1) phytodegradation; (2) rhizodegradation; and (3) phytovolatilization. The other three are applicable to inorganic contaminants: (4) phytoextraction; (5) rhizofiltration; and (6) phytostabilization.

Phytodegradation, also known as phytotransformation, is the breakdown of contaminants taken up by plants through metabolic processes within the plant, or the breakdown of contaminants external to the plant through the effect of constituents, such as exudates and enzymes, produced by the plants. Organic contaminant molecules are degraded into simpler molecules and incorporated into plant tissues by various biochemical reactions caused by enzymes within the plant.

Rhizodegradation, also known as enhanced rhizosphere biodegradation, phytostimulation, or planted-assisted bioremediation/degradation, is the breakdown of contaminants in the soil through microbial activities enhanced by the rhizosphere, i.e. the root zone. It is much slower than phytodegradation. Microorganisms can breakdown organic contaminants such as fuels or solvents into harmless products by biodegradation. Exudates released by plant roots provide nutrients for microorganisms to enhance their activities. Biodegradation is also aided by plants through loosening the soil and transporting water to the root zones.

Phytovolatilization is the uptake and transpiration of contaminants by plants, with release of the contaminants or modified forms of the contaminants to the atmosphere. It occurs as plants take up water and organic contaminants to the leaves and evaporate, or volatilize, them into the atmosphere.

Phytoextraction, also known as phytoaccumulation, is the uptake and translocation of metal contaminants in the soil by plant roots into the above ground portions of the plants. Certain plants, called hyper-accumulators, absorb unusually large amounts of metals (Padmavathamma and Li 2007). After these plants have grown for some time, they are harvested and then either incinerated or composted to recycle the metals. If plants are incinerated, the residual ash must be disposed of in a hazardous waste landfill, but the volume of ash will be less than 10% of the original volume of the contaminated soil. Metals such as nickel, zinc, and copper are the best candidates for removal by phytoextraction as it has been shown that they are preferred by a majority of the approximately 400 known hyper-accumulators.

Rhizofiltration is the adsorption or precipitation onto plant root surfaces, or absorption into the roots of

contaminants that are in the soil solution in the root zone. It is similar to phytoextraction, but the plants are used primarily to remediate contaminated groundwater rather than soil. The plants to be used are raised in greenhouses with their roots in water. Once a large root system has been developed, contaminated water is used to substitute their water source so as to acclimate the plants. The plants are then transplanted in the contaminated zone where the roots take up the contaminated water. As the roots become saturated with contaminants, they are harvested. For example, sunflowers were used successfully to remove radioactive contaminants from pond water in a test at Chernobyl, Ukraine.

Phytostabilization is the use of certain plant species to immobilize contaminants in the soil and groundwater through absorption and accumulation by roots, adsorption onto root surfaces, or precipitation within the rhizosphere. The process reduces the mobility of contaminants to minimize contaminant migration to the groundwater or air, so as to reduce bioavailability for their entry into the food chain. The technique can be used to re-establish a vegetative cover at sites where natural vegetation is lacking due to high metals concentrations in surface soils or physical disturbances to surficial materials. Metal-tolerant species can be used to restore vegetation to the sites, thereby decreasing the potential migration of contaminants through wind erosion and transport of exposed surface soils, and leaching of contaminants to groundwater.

The processes occurring within the rhizosphere are integral to phytoremediation. Contaminants in contact with plant roots in the root zone must permeate the root membranes by the process of rhizofiltration before they can be absorbed by plants. Uptake of contaminants by plant roots is a direct function of contaminant concentrations in the soil solution and usually involves chemical partitioning on root surfaces followed by transport across the cortex to the plants' vascular systems. The contaminant may be bound or metabolized at any point during transport.

The technology is effective for the remediation of soils contaminated with moderately hydrophobic organic contaminants such as BTEX, chlorinated solvents, and nitro-toluene ammunition wastes with $1.0 \leq \log K_{ow} \leq 3.5$ (Carman and Crossman 2001; Susarla et al. 2002; Gao et al. 2007). The octanol-water partition coefficient K_{ow} of an organic compound is the concentration of the organic compound dissolved into octanol divided by the concentration dissolved into water when the organic compound is shaken with a mixture of n-octanol and water. Generally, constituents with $\log K_{ow} < 0.5$ are too water soluble to be taken up into roots, and constituents with $\log K_{ow} > 3$ are bound too tightly to soil particles or roots to be taken up into plants. Examples of organic compounds with $\log K_{ow} < 0.5$ include methyl tertiary

butyl ether (MTBE) and 1,4-dioxane, and constituents with $\log K_{ow} > 3$ include most PAHs. Organic contaminants taken up by plants can be degraded by phytodegradation, accumulated in the plant tissue by phytoaccumulation, or transpired through the leaves by phytovolatilization (Schnoor et al. 1995; Shirdam et al. 2008). Phytodegradation of organic contaminants continues in root zones through the process of rhizodegradation (Sharma and Reddy 2004). The fate of organic contaminants can generally be predicted using the octanol-water partition coefficient K_{ow} of the particular constituent using Briggs' Law as tabulated in Table 2.

Table 2 Fate of organics predicted by Briggs Law

Log K_{ow}	Mechanisms
< 1.0	Possible uptake & transformation
1.0 - 3.5	Uptake, transformation, volatilization
> 3.5	Rhizosphere bioremediation or phytostabilization

The technology is also effective for the remediation of soils contaminated with excess nutrients such as nitrate, ammonium, or phosphate; and heavy metals (Lin et al. 2000, 2008; Barbaferi 2001; Asada et al. 2006; Claus et al. 2007; King et al. 2008; Mendez and Maier 2008; Tiwari et al. 2008). Inorganic contaminants can be incorporated in plant tissues through the process of phytoaccumulation (Padmavathamma and Li 2007). The tendency of plants to uptake, immobilize, or exclude metals is highly contaminant- and soil-specific. Soil factors that influence the tendencies include: (1) soil pH - increases in soil pH generally reduce solubility of metals and uptake by plants; (2) cation exchange capacity (CEC) - increases in CEC of soil reduces plant uptake; (3) organic matter - inorganic forms of metals are generally taken up more readily by plants than organic forms; and (4) natural and synthetic complexing agents - the presence of complexing agents such as ethylenediaminetetraacetic acid (EDTA) and diethylenetriaminepentaacetic acid (DPTA) generally increases the solubility of metals, making them more available to roots and more likely to be taken up by and accumulated in plants (Meers et al. 2005).

Metals can also be bound to soil within the rhizosphere, or to the root tissue itself. Exudates released in the rhizosphere can increase the soil oxygen content and the soil pH up to 1.5 pH units, change the redox conditions of the soil, promote oxidation of metal contaminants, and reduce mobility and bioavailability of metals.

Phytoremediation technologies offer these advantages: (1) it is an *in-situ* technology; (2) it is relatively inexpensive as it uses plants; and (3) it is a safe and passive technology driven by solar energy, and eye-pleasing, hence it is more likely to be accepted by

the public (Wolfe and Bjornstad 2002). However, they have these disadvantages: (1) relatively shallow cleaning depths, less than 1 m for grasses, less than 3 m for shrubs, and less than 6 m for deep-rooting trees; (2) the process is slow and it requires three to five growing seasons to achieve remediation goals; (3) knowledge to optimize phytoremediation technologies is still experimental; (4) the technology is site specific and the choice of plants is critical, and the cleanup strategy requires detailed site characterization to maximize plant growth and contaminant uptake; (5) potential contamination of the food chain; and (6) the technology may relocate contaminants from the subsurface to the plant, creating residual waste to be disposed of.

Although many mechanisms of phytoremediation are not fully understood, there are many reported applications of phytoremediation in China, Portugal, Russia, India, New Zealand, and Australia (Willey 2007).

Air Sparging / Soil Vapor Extraction

Air sparging is an *in-situ* process where air is bubbled through contaminated soil via air injection wells (sparge points) to create a subsurface air stripping system to remove volatile contaminants through volatilization as shown in Fig. 14 (Marley et al. 1992; Anderson 1994; Parsons et al. 1997; Smith 1998; Bass et al. 2000). In a typical field setup, compressed air is delivered to an array of air injection wells through a manifold system to inject the air into the subsurface below the known lowest point of the contaminated zone. The injected air rises toward the ground surface through the contaminated zone due to buoyancy, and the contaminants are partitioned into the vapor phase. The contaminant-laden air eventually reaches the unsaturated vadose zone where the contaminated air is collected by a soil vapor extraction system for further treatment above ground (Bass et al. 2000).

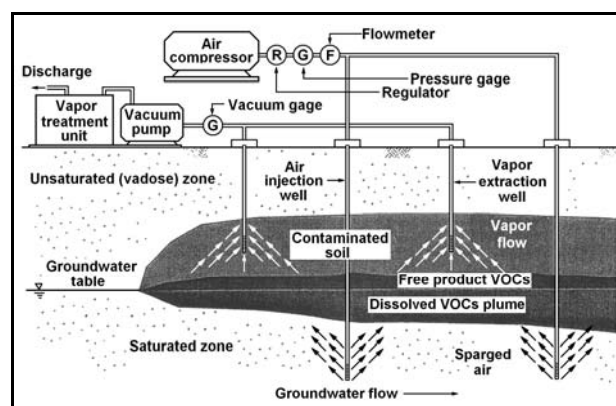


Fig. 14 Schematic of *in-situ* air sparging/soil vapor extraction system (modified from Reddy and Adams 2002)

Soil vapor extraction by itself is a technology for removal of VOCs and SVOCs from unsaturated soils or the vadose zone. A vacuum is applied to the contaminated soil through vapor extraction wells to generate a negative pressure gradient in the subsurface that drives the vapor to move towards the wells by advection (Hsu and Yeung 1996; Braida and Ong 2000; Zhao and Zytner 2004). The contaminant-laden vapors extracted from the wells are then treated above ground using standard air treatment techniques such as carbon filters or combustion.

Different processes including volatilization, diffusion, advection, and desorption occur during soil vapor extraction. Volatilization of contaminants occurs as the contaminated air in soil pores is removed. When the concentration of the volatile organic compound in the pore air is decreased, the shift in chemical equilibrium drives the dissolved and free-phase contaminants to partition from the saturated zone into the unsaturated vadose zone for removal by the soil vapor extraction system.

Advantages of the air sparging technology include: (1) ability to remove VOCs and SVOCs from groundwater including less volatile and sorbed contaminants that are not amenable to soil vapor extraction alone; (2) enhancement of biodegradation by injection of oxygen; (3) enhancement of co-metabolism of chlorinated organics when methane is added to the groundwater; and (4) most effective for relatively permeable and homogeneous sites. Limitations of the technology include: (1) very limited effectiveness in fine-grained and low hydraulic conductivity soils; (2) site geology and depth to contaminants must be known; (3) potential for uncontrolled flow of dangerous vapors through the saturated zone; (4) potential for free product migration from groundwater mounding; and (5) may be ineffective if air flow does not reach the contaminated zone due to soil heterogeneities.

Advantages of the soil vapor extraction technology include: (1) equipment is readily available and easy to install; (2) minimum disturbance to the site; (3) short treatment duration ranging from six months to two years under optimal conditions; (4) economical relative to other remediation technologies; (5) effective for treating both dissolved and free-phase (free-product) contaminants; and (6) very easy to couple with other remediation technologies. However, disadvantages of the technology include: (1) contaminant removal is very rapid at the beginning, and then lingering contaminants are found to exist for a prolonged period of time; (2) it is ineffective in low hydraulic conductivity soils, stratified soils, and high-humic-content soils; (3) air emission treatment systems and permits are often required; and (4) it is applicable to unsaturated soils only.

The soil vapor extraction process can be enhanced by

the use of hot air injection (Kaslucky and Udell 2005), electric heating, or pneumatic fracturing of soil (Frank and Barkley 1995; Schulenberg and Reeves 2002), etc. (Liang and Lee 2008) to increase the mobility of volatile organics and improve the efficiency of the soil vapor extraction process.

Electrochemical Remediation

Contaminants in fine-grained soils cannot be efficiently or effectively removed by the pump-and-treat or soil flushing technology because of the low hydraulic conductivity and large specific area of the soil. Too low a hydraulic gradient applied to fine-grained soils will take too long to complete the cleanup process, as the rate of permeation of flushing fluid through the soil is too low. Too high an applied hydraulic gradient may induce hydraulic fractures in the soil. These fractures may provide paths for contaminants to spread randomly in the subsurface and aggravate the situation. In hydraulically heterogeneous fine-grained soils, the flushing fluid permeates contaminated soils preferentially through paths of the least hydraulic resistance, rendering zones of low hydraulic conductivity practically untreated during the flushing process. The large specific area of fine-grained soil further complicates the situation by providing numerous active reaction sites for soil-contaminant interactions such as surface complexation and sorption/desorption of contaminants. Electro-chemical remediation may be a viable remediation solution under these given complex site conditions (Sah and Lin 2000; Kim et al. 2005; Yeung 2006).

The electrochemical remediation processes rely heavily on the electrokinetic phenomena in fine-grained soils, which stem from the molecular structure of clay. The surfaces of clay particles are normally negatively charged because of isomorphous substitutions and the presence of broken bonds (Mitchell 1993; Yeung 1994). Adsorbed cations are held tightly to clay particle surfaces by strong electrostatic forces to maintain electrical neutrality. Surplus cations and their associated anions exist as salt precipitates. When clay particles are in contact with water, the salt precipitates go into solution. As the adsorbed cations generate a much higher concentration near clay particle surfaces, they are driven by a concentration gradient to diffuse away from clay particle surfaces to homogenize the ion concentration in the pore fluid. The escaping tendency is counteracted by the electrical attraction of the negatively charged clay particle surfaces. A diffuse double layer is thus formed. Governing equations describing the behavior of the diffuse double layer are given by Hunter (1981), Sposito (1984), Yeung (1992, 1994), and Mitchell (1993).

The diffuse double layer provides a mobile layer of cations in the vicinity of the soil particle surface.

However, the electrokinetic behavior and thickness of the layer depends heavily on the chemistry of pore fluid (Hunter 1981; Sposito 1984; Yeung 1992; Mitchell 1993). If the interconnecting soil pores are idealized as a bundle of capillaries, the wall surface of the capillary is negatively charged and the mobile cations form a concentric shell in close proximity of the wall surface within the capillary. The behavior of the shell depends on the electrokinetic properties of clay particle surfaces, chemistry of the pore fluid, and their interactions. Several electrokinetic phenomena thus arise in clay when there are couplings between hydraulic and electrical driving forces and flows. The electrokinetic phenomena of direct relevance to electrochemical remediation are electroosmosis, electromigration or ionic migration, and electrophoresis, in which the liquid, dissolved phase, and solid phase moves relative to each other under the influence of an externally applied direct-current (dc) electrical field.

Electroosmosis is the advective movement of the pore fluid from the anode (positive electrode) towards the cathode when a dc electric field is imposed on a wet clay. Electromigration or ionic migration is the advective movement of the charge-carrying dissolved phase relative to that of the liquid phase under the influence of an imposed dc electric field. Anionic species (negatively charged ion) moves towards the anode (positive electrode) and cationic species (positively charged ion) towards the cathode (negative electrode). Electrophoresis is the advective transport of charged particles, colloids, or bacteria in suspension under the influence of an imposed dc electric field. Details and milestone developments of these electrokinetic phenomena are given in Yeung (1994).

Electrochemical remediation technologies of contaminated soils may include electrochemical mobilization of contaminants, electrokinetic extraction of contaminants from fine-grained soils, electrochemical injection of decontamination agents, electrochemical transformation of contaminants in soils and their various combinations and modifications. All these remediation technologies involve basically the application of a direct-current (dc) electric field across the soil and utilization of the resulting electrokinetic flow processes, geochemical processes, and electrochemical reactions to remediate the contaminated soils. These electrokinetic flow processes, geochemical processes, and electrochemical reactions include flow of electric current through the soil; electroosmotic migration of pore fluid; electromigration of ions, charged particles, colloids and bacteria; electrolysis of pore water in soil at the electrodes and subsequent migration of hydrogen and hydroxide ions into the soil, resulting in a spatial and temporal change of soil pH; gas generation at electrodes; development of non-uniform electric field; occurrence of reverse

electroosmotic flow; changes in electrokinetic properties of soil; hydrolysis; phase change of contaminants; soil-contaminant interactions such as sorption and desorption of contaminants onto and from soil particle surfaces; formation of complexes of contaminants; precipitation of contaminants etc., and interactions of these processes (Yeung 2009). The migration of pore fluid, ions, charged particles, colloids, and bacteria can be utilized to remove contaminants from polluted soil and/or to inject enhancement agents, nutrients, etc. to facilitate various remediation processes. The geochemical processes can be used to provide the necessary environmental conditions to control the direction of electroosmotic flow and to solubilize contaminants in the soil, so as to enhance the efficiency of the electrochemical remediation processes.

Electrokinetic extraction is an emerging technology developed to remove inorganic and organic contaminants from fine-grained soils as an electrical gradient is a much more effective force in driving fluid flow through fine-grained soils (Iyer 2001; Lageman et al. 2005). It involves the application of a dc electric field through electrodes embedded in the subsurface across the contaminated soil. The contaminant is removed by the combination of (1) electroosmotic advection of the pore fluid flushing the contaminants; (2) electromigration or ionic migration of contaminants that carry charges; and (3) electrophoresis of charged particles and colloids that are binding contaminants on their surfaces as shown in Fig. 15. Moreover, these chemical transport mechanisms can be utilized to inject cleansing fluid, enhancement agents such as complexing agents and surfactants, nutrients, and/or bacteria to improve the effectiveness and efficiency of the process (Yeung et al. 1996; Acar et al. 1997; Budhu et al. 1997; DeFlaun and Condee 1997; Thevanayagam and Rishindran 1998; Rabbi et al. 2000; Lee and Lee 2001; Reddy et al. 2003a,b; Saichek and Reddy 2005a,b; Yeung and Hsu 2005; Maturi and Reddy 2008; Kim et al. 2008; Murillo-Rivera et al. 2009).

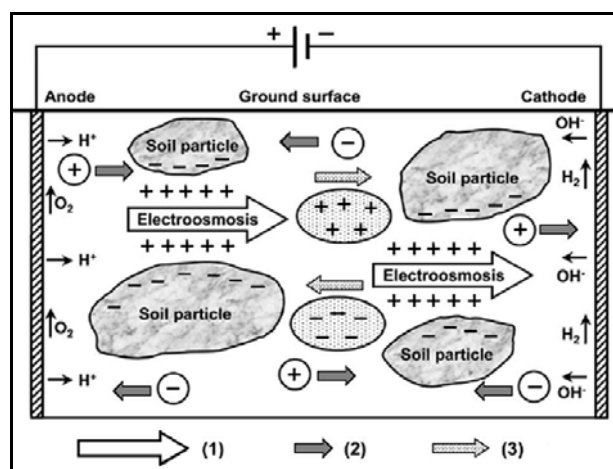


Fig. 15 Concept of electrokinetic extraction of contaminants from soil

Extractability of contaminants from soil primarily depends on the mobility of contaminants within the soil matrix, which is a function of the chemical state of the contaminants, surface characteristics of soil particles, chemistry of pore fluid, and their interactions. In addition to electroosmotic advection, electrokinetic extraction also makes use of the transport mechanisms of advective electromigration and electrophoresis. Therefore, the contaminants must exist as a mobile phase within the soil matrix, such as a dissolved phase in the pore fluid, a colloidal phase suspended in the pore fluid, and/or a mobile immiscible liquid phase co-existing with the pore fluid in soil pores. It is difficult to remove contaminants from a soil that exist as a separate solid phase such as precipitates in soil pores, or as a sorbed phase on soil particle surfaces. Therefore, electrochemical reactions associated with electrokinetic extraction that would affect the mobility of contaminants are of paramount importance on the extractability of contaminants. Factors affecting contaminant extractability by electrokinetics includes: (1) soil type; (2) contaminants type and concentrations; (3) soil pH; (4) acid/base buffer capacity of soil; (5) zeta potential of soil; (6) electroosmotic flow direction; (7) sorption/ desorption characteristics of soil particle surfaces; (8) operating parameters; and (9) enhancement techniques. Detailed discussion of these factors is given in Yeung (2006).

The pertinent geochemical processes affecting the electrochemical remediation processes include: (1) generation of pH gradient; (2) change of zeta potential of soil particle surfaces; (3) change of direction of electroosmotic flow; (4) sorption and desorption of contaminants onto/ from soil particle surfaces; (5) buffer capacity of soil; (6) complexation; (7) oxidation-reduction (redox) reactions; and (8) interactions of these processes. These processes are discussed in detail in Yeung (2009).

Electrokinetic extraction is an emerging remediation technology applicable to fine-grained soils of low hydraulic conductivity and large specific area. As with many other remediation technologies, electrokinetic extraction has its own drawbacks including: (1) migration of contaminants is not highly selective; (2) acidification of soils to promote mobility of contaminants may not be technically feasible and/or environmentally acceptable; (3) the technology is not very cost-effective when the target contaminant concentration is low and the background non-target ion concentration is high; among many others. Successful application of the technology primarily depends on mobility of the contaminant in the soil matrix. However, the efficiency and effectiveness of electrokinetic extraction can be improved by combining the technique with other remediation technologies such as the Fenton treatment process, Lasagna process, biodegradation, phytoremediation process, etc. Some of these techniques are discussed as follows.

Ek-Fenton process

The Fenton reaction involves two steps: (1) decomposition of H_2O_2 catalyzed by Fe^{2+} or other transition elements to generate hydroxide radicals; and (2) oxidation of organic pollutants by hydroxide radicals. Yang and Long (1999), and Yang and Liu (2001) studied the feasibility of coupling electrokinetic extraction with a Fenton-like treatment process using a permeable reactive wall of scrap iron powder to remove and oxidize organic contaminants experimentally. Their bench-scale laboratory experimental results indicate that it is feasible to combine electrokinetic extraction and the Fenton-like process to treat TCE and phenols in soils. The overall contaminant remediation efficiency is contributed by two mechanisms: (1) organic contaminant destruction by the Fenton-like process; and (2) contaminant removal by electrokinetic extraction.

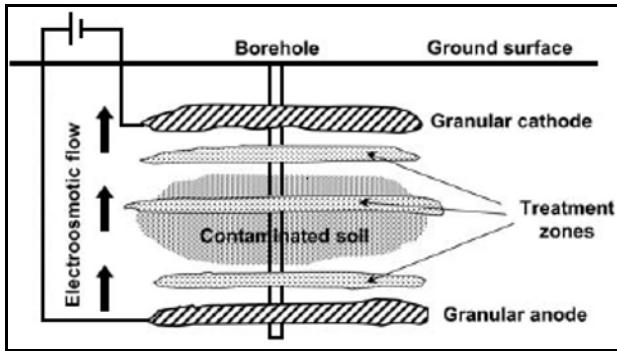
Lasagna process

The Lasagna process is an Integrated *In situ* Remediation technique (Ho et al. 1995, 1999a,b). Electrokinetics is coupled with sorption/degradation of contaminants in treatment zones that are installed directly in contaminated soils. A dc electric field is applied to mobilize the contaminants in contaminated soils to the treatment zones where the contaminants are removed by sorption, immobilization, or degradation as shown in Fig. 16. The technique is called Lasagna because of the layered appearance of electrodes and treatment zones. Conceptually, it can treat organic and inorganic contaminants as well as mixed wastes. Electrodes and treatment zones can be of any orientation depending upon the emplacement technology used and the site-contaminant characteristics as shown in Fig. 16.

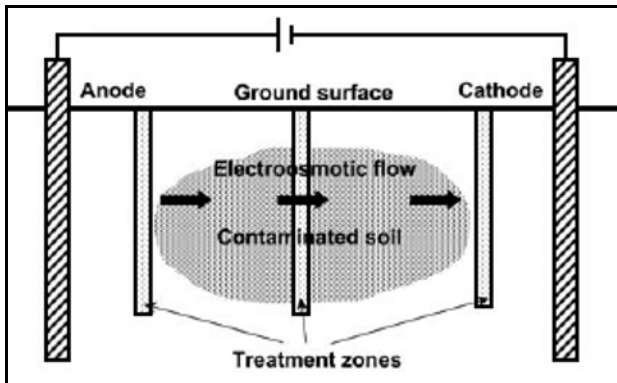
Generation of in-situ reactive iron-rich barriers

Faulkner et al. (2005) have successfully generated subsurface barriers of continuous iron-rich precipitates *in-situ* by electrokinetics in their laboratory-scale experiments. Continuous vertical and horizontal iron-rich bands up to 2 cm thick have been generated by applying an electrical voltage of less than 5 V over a period of 300-500 hours, with an electrode separation of between 15 and 30 cm. The iron-rich barrier is composed of amorphous iron, goethite, lepidocrocite, maghemite, and native iron. The thickness of the iron-rich band increases with an increase in the applied voltage. The barrier is generated using sacrificial iron electrodes installed on either side of a soil/sediment mass as shown in Fig. 17. The applied dc electric field dissolves the sacrificial anode and injects the iron ions into the system, and re-precipitation of the iron ions in an alkaline environment forms the barrier. The iron-rich band so produced is of hydraulic conductivity of 1×10^{-9} m/s or

less and unconfined compressive strength of 10.8 N/mm². The barrier may function as an impervious barrier to contaminant transport or a reactive barrier to degrade contaminants. By monitoring the dc electric current intensity passing through the barrier, the integrity of the iron-rich band may be assessed. Moreover, the barrier may 'self-heal' by continuing application of a dc electric current.



(a) Horizontal configuration



(b) Vertical configuration

Fig. 16 Principle of Lasagna Process (after Ho et al. 1995)

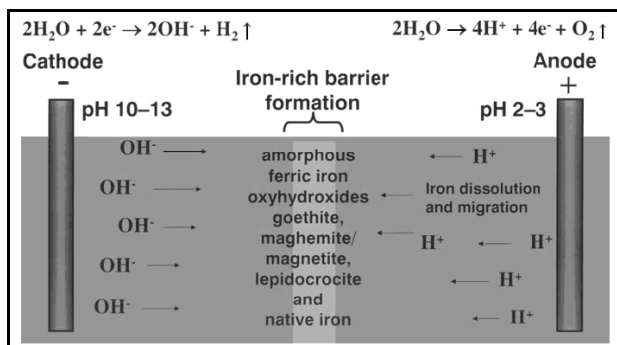


Fig. 17 Principle of iron-rich barrier generation by electrokinetics (after Faulkner et al. 2005)

Bioelectrokinetic remediation

The feasibility of injecting benzoic acid to enhance the biodegradation of TCE by electroosmosis for neutral benzoic acid and electromigration for benzoate anion was explored by Rabbi et al. (2000). Their experimental

results demonstrate the feasibility in principle for using electrokinetic injection to engineer the degradation of recalcitrant hydrocarbons, or other difficult to degrade contaminants. A similar study on phenol was conducted by Luo et al. (2006).

Bioremediation is a process for remediation of metal-contaminated soil. Indigenous sulfur-oxidizing bacteria convert reduced sulfur compounds to sulfuric acid which acidifies the contaminated soil and mobilize the metal ions. Experimental results on remediation of copper-contaminated soil by Maini et al. (2000) indicate that the effectiveness of electrokinetic extraction was enhanced by pre-acidification of the contaminated soil by sulfur-oxidizing bacteria. The electrokinetic treatment also appeared to stimulate the activity of sulfur-oxidizing bacteria by the removal of inhibitory ions and other positive effects of the electric current upon soil microbial activities. The synergistic methodology appears to be promising for a range of contaminated sites including former gasworks and wastes from mining.

Ek-Phytoremediation process

The use of a combination of electrokinetic remediation and phytoremediation to decontaminate soils contaminated by copper, cadmium, and arsenic was investigated by O'Connor et al. (2003) in laboratory-scale reactors. Their results indicate that a dc electric field can migrate metallic contaminants from the anode towards the cathode, accompanied by significant changes in soil pH. Moreover, perennial ryegrass could be grown in the treated soils to take up a proportion of the mobilized metals into its shoot system.

Other possible uses of electrokinetics in environmental management include (Yeung 2008): (1) concentration, dewatering and consolidation of wastewater sludge, slimes, coal washeries, mine tailings, or dredging (Vijh 1995; Barton et al. 1999; Buckland et al. 2000; Yuan and Weng 2002); (2) injection of grout to control groundwater flow; (3) injection of cleaning agents into contaminated soils (Acar et al. 1997; Jiradecha et al. 2006); (4) injection of vital nutrients to stimulate the growth of microorganisms for biodegradation of specific contaminants (Kim and Han 2003; Chen et al. 2006); (5) electrokinetic barriers to contaminant transport through compacted clay landfill liners of slurry encapsulation walls (Mitchell and Yeung 1991; Yeung 1993; Faulkner et al. 2005); (6) electrokinetic extraction of contaminants from polluted soil (Chang et al. 2006; Alshwabkeh et al. 1999; Yeung 2006); (7) modification of flow pattern of groundwater, and manipulation of the movement and size of contaminant plumes; (8) enhancement of flow through permeable reactive contaminant barriers (Ho et al. 1995, 1999a,b); (9) real-time and reliable detection and delineation of subsurface contamination (Campanella 2008); (10) rapid and reliable in-situ determination of

hydraulic conductivity of compacted clay landfill liners; (11) *in-situ* generation of reactants for cleanup, electrolytic decomposition and/or solidification of contaminants; and (12) retrofitting of leaking in-service geomembrane liner (Darilek et al. 1996; Yeung et al. 1997a,b).

Thermal Treatment

Thermal treatment technologies are destruction and removal types of heat treatment of contaminated soil including thermal desorption, vitrification, thermal destruction, and incineration (Anderson 1993, 1994; Lee et al. 2008).

Thermal desorption is a technology that heats contaminated soil or sludge *in-situ* or *ex-situ* to volatilize contaminants and remove them from the soil. Volatile and semi-volatile organics are removed from contaminated soil in thermal desorbers at 100 to 300°C for low-temperature thermal desorption, or at 300 to 550°C for high-temperature thermal desorption (Soesilo and Wilson 1997). The vapors are collected and treated in a gas treatment system. The gas treatment units can be condensers or carbon adsorption units that trap organic compounds for subsequent treatment or disposal. The units can also be afterburners or catalytic oxidizers that completely destroy the organic contaminants. The basic components of a thermal desorption system include: (1) pretreatment and feed; (2) thermal processor and discharge; and (3) air emissions control. Critical factors controlling the performance of the technology are: (1) soil type and moisture content; and (2) temperature, residence time, mixing, and the sweep gas flow rate in the thermal processor (Sellers 1999). The technology is effective in the remediation of soils contaminated with oil refining wastes, coal tar wastes, wood-treating wastes, creosotes, hydrocarbons, chlorinated solvents, fuels, PCBs, mixed wastes, synthetic rubber processing waste, pesticides, and paint wastes (Sharma and Reddy 2004).

Vitrification is a thermal stabilization/solidification process that does not require the addition of reagents. It can be performed *in-situ* or *ex-situ*. The process involves melting and fusion of materials at temperatures normally in excess of 1200°C followed by rapid cooling to glass-like materials. During the process, non-volatile metals are immobilized within the glass; volatile metals, such as lead, cadmium, and zinc, volatilize, and they must be captured in the off-gas treatment system; and organic compounds pyrolyze or combust. The process requires an extraordinary amount of energy of 800 to 1,000 kWh per ton of soil treated *in-situ* (Sellers 1999). As a result, it is only used to treat relatively small quantities of wastes that are difficult to treat by other remediation technologies. It can be used to treat radioactive wastes, metal sludges, asbestos-containing waste, or soil or ash contaminated with metals. Although soil or waste

containing organic contaminants can be treated by the process, vitrification technologies are usually directed towards inorganic contaminants. Although the gas structure is generally a relatively strong and durable material resistant to leaching, proper disposal of the vitrified slag is required. It should be noted that vitrification is a complex process and requires a high degree of specialized skill and training.

Thermal destruction is *ex-situ* processes that thermally destroy organic contaminants by oxidation, pyrolysis, hydrogenation, and reduction (Renoldi et al. 2003).

Catalytic oxidation has been used for emission control of organic compounds from industrial sources and/or remediation of contaminated sites for a long time. However, oxidation catalysts have been poisoned by halogens, certain metals, particulates, phosphorus, and sulfur compounds in the past, thus limiting their applications to non-halogenated contaminated air streams. Recently, new catalysts have been developed to overcome these obstacles and to achieve high destruction efficiencies.

Catalytic oxidation units for the destruction of halogenated compounds typically consist of: (1) a gas or electric preheater to raise the air-stream temperature to the catalyst temperature of < 450°C; (2) a catalytic reaction; (3) a shell and tube heat exchanger to recover approximately 50% of the heat in the reactor exit gas; and (4) a scrubber to remove halogens and hydrogen halides from oxidation products before their release to the atmosphere, as shown in Fig. 18. In an air sparging/soil vapor extraction operation, the contaminated vapors are extracted from wells through a manifold and pumped to the catalytic oxidation unit. In a groundwater remediation operation, the contaminants are air stripped from the groundwater and the contaminated vapors are directed to the catalytic oxidation unit.

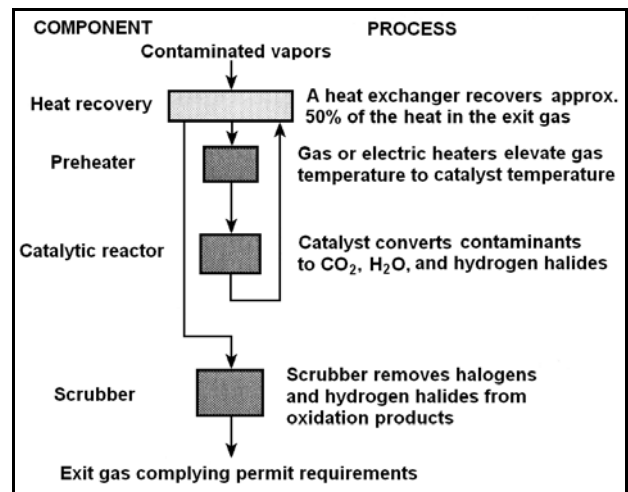


Fig. 18 Catalytic oxidation unit flow chart (after Anderson 1994)

Catalytic oxidation is cost competitive with other processes as the fuel costs are lower. However, a potential disadvantage of the technology is that the catalyst may be deactivated or poisoned by various volatile chemicals. Nonetheless, it is anticipated that development of new catalysts will expand the range of halogenated organic compounds that can be effectively treated by catalytic oxidation.

Pyrolysis is an *ex-situ* chemical decomposition process by which the wastes are heated in the absence of oxygen as shown in Fig. 19. As it is impossible to achieve a completely oxygen-free environment in practice, nominal oxidation occurs. Pyrolysis involves a two-step process to remediate contaminated soil in a chamber at temperatures 400 to 1200°C: (1) wastes are heated to separate the volatile components from the non-volatile char and ash; and (2) the volatile components are burnt to assure incineration of all the hazardous components.

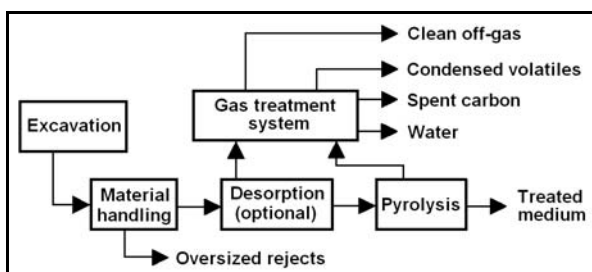


Fig. 19 Schematic of pyrolysis (after Soesilo and Wilson 1997)

Incineration is intended to permanently destroy organic contaminants. It is a complex system of interacting pieces of equipment, representing an integrated system of components for waste preparation, feeding, combustion, and emissions control as shown in Fig. 20. The most important component of the system is the combustion chamber, or the incinerator. There are four major types of incinerator: (1) rotary kiln; (2) fluidized bed; (3) liquid injection, and (4) infrared. Details of these four types of incinerators are given by Soesilo and Wilson (1997).

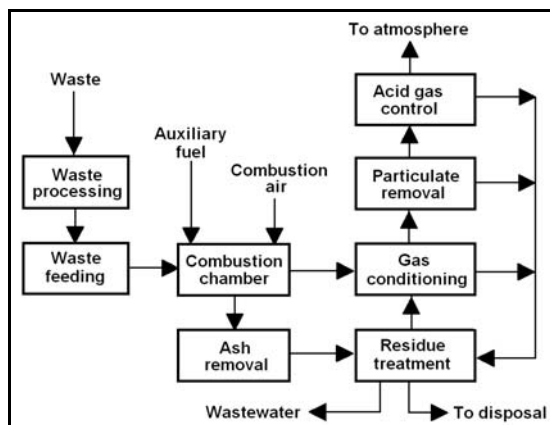


Fig. 20 Incineration system concept flow diagram (after Soesilo and Wilson 1997)

Other Remediation Technologies

Many innovative remediation technologies at different stages of development are emerging and not covered in this invited paper. These technologies include: (1) supercritical extraction of contaminants from soils (Jayaweera 2003); Nagpal and Guigard 2005; Anitescu and Tavlarides 2006; Rivas et al. 2009; Sunarso and Ismadji 2009); (2) *in-situ* injection of nanoscale zero-valent iron particles into dense non-aqueous phase liquid (DNAPL) source of groundwater contamination (Chang et al. 2007; Kovalick 2008); (3) emulsion pertraction process (Bringas et al. 2006; Alguacil et al. 2008); (4) UV photodegradation/photolysis (Annapragada et al. 1997; Pichat 2003; Wen et al. 2009); (5) membrane-assisted processes; (6) non-thermal plasma discharge; (7) sediments remediation phase transition extraction (Ludmer et al. 2009); (8) microwave induced oxidation (Guo et al. 2009); (9) pneumatic fracturing to enhance bioremediation of VOCs (Venkatraman et al. 1998; Christiansen et al. 2008); (10) deep well stripping (Otten et al. 1997); (11) sonochemical degradation of contaminants (Destailats et al. 2003); (12) the electron beam process for radiolytic degradation of contaminants (Mincher and Cooper 2004); (13) microwave-induced plasma (Dawson et al. 2009); (14) CO₂ sequestration in deep sedimentary formations (Benson and Cole 2008).; among many others. Interested readers are referred to the cited literature.

PERFORMANCE MONITORING

Performance monitoring is used to ensure that the behavior of the contaminant plume does not deteriorate over time and/or the remedial action is progressing as intended. It collects a subset of parameters used in the site characterization monitoring focusing on the most significant parameters of the site as a function time during the remediation process. Performance monitoring wells should be located up-gradient from, within, transverse to, and just down-gradient from the contaminated zone. Specimens collected from these wells are used to verify that the concentrations of individual chemicals or parameters of concern, contaminated zone boundaries, and overall progress towards remediation goals are acceptable over time and space (Wiedemeier et al. 2006).

The minimum goals of performance monitoring of remediation processes are to: (1) demonstrate that remediation is occurring as expected; (2) detect changes in subsurface environmental conditions that may reduce or enhance the efficiency of the remediation technology; (3) verify that the contamination situation is not deteriorating; (4) verify that there has been no

unacceptable impact to down-gradient receptors; (5) detect any new releases of contaminants to the environment that may pose an unacceptable risk to public health and/or the environment or impact the effectiveness of the remediation technology; (6) demonstrate the efficacy of institutional controls already in place to protect the public health and the environment; and (7) verify progress towards achievement of remediation objectives. In addition to meeting these goals, a site-specific contingency plan must be prepared in case the remediation technology fails to perform as anticipated.

On completion of the remediation process, a verification sampling and analysis program is typically implemented to confirm that cleanup goals have been met. The verification data are compared with the final remediation goals using statistical methods. Additional remediation may be necessary if the remediation goals are not met (ASCE 1999).

Detailed planning and implementation of performance monitoring programs are beyond the scope of this paper. Interested readers are referred to the literature. Detailed description of environmental monitoring programs is given by ASCE (1999), and Wiedemeier et al. (2006). Detailed monitoring system design to obtain groundwater and soil parameters are given by Gavaskar et al. (2000), Nielsen and Nielsen (2006), Sara (2006), and Sevee (2006). Different monitoring techniques are given by Askari et al. (1996), Roh et al. (2000), McNab and Ruiz (2001), McAndrews et al. (2003), Bromage et al. (2007), Sacile (2007), Rivett and Thornton (2008), Wilson et al. (2008), McCobb et al. (2009), among many others. Special precautions required for environmental drilling are described by Ruda and Farrar (2006), and groundwater sample analyses are detailed by Vitale and Braids (2006).

SELECTION OF REMEDIATION TECHNOLOGIES

A contaminated site is an unusable resource. However, the site can be restored for productive use with adequate site remediation planning and proper executive of remediation technologies. Therefore, upon identification of a contaminated site, these planning questions should be posed to address the remediation aspects of the site: (1) Under which law or statute should the remediation be conducted? (2) What is the extent of contamination and what is the likelihood that the contaminants will migrate? (3) If remediation is necessary, what level of cleanup is required to restore the site to be a *clean* site? (4) What remediation technologies are available and which options are the preferred technologies for the site?

The applicability and effectiveness of a remediation technology to treat a particular site depends on four

major factors: (1) the local factor: the acceptability of the technology to local community; (2) the regulatory factor: the statutes and regulations applicable to the operation of the technology, for example, laws that regulate discharges to surface waters and emissions to the atmosphere, as discharges and/or emissions may be necessary for the operation of the technology; (3) the technology factor: the technical, cost, and performance characteristics of the technology; and (4) the site factor: the hydrogeology of the contaminated site; and the structure, particle size distribution, organic content, pH, and moisture content of the soil at the site.

Evaluation of remediation technologies may be in three phases: (1) general response actions; (2) assembly of technologies as alternatives; and (3) screening of alternatives (ASCE 1999). A general response action is defined as one approach to remediation of contaminants in one medium. It can be active remediation or institutional actions. Remediation alternatives to be assessed are scenarios for the total remedial action. Each may include several individual remedial actions for different parts of the contaminated site and different media. Each alternative scenario may include several general response actions and many remediation technologies.

If a technology is considered to be applicable for the contaminated site, the implementation feasibility at the particular site can be evaluated by analyzing whether the technology can achieve: (1) overall protection of public health and the environment; (2) compliance with applicable or relevant and appropriate requirements; (3) long-term effectiveness and permanence; (4) reduction of toxicity, mobility, and volume of contaminants; (5) short-term effectiveness; (6) no insurmountable implementation barriers; (7) relatively cost-effective; (8) compliance with legal requirements; and (9) community acceptance.

A screening matrix using 13 factors was developed to evaluate qualitatively the performance of different remediation technologies by the U.S. Environmental Protection Agency (U.S. EPA 1993). Eight of these 13 factors involve a comparative rating: better, average, or worse. The eight comparative rating factors are: (1) overall cost including the design, construction, and operation and maintenance costs of the main processes of the technology; (2) commercial availability; (3) minimum contaminant concentration achievable by the technology; (4) time to complete remediation of a "standard" site of 18,200 tons for soil or 3,785,000 liters for groundwater using the technology; (5) degree of system reliability and maintainability when using the technology; (6) level of awareness of the remediation consulting community regarding the availability of the technology; (7) degree of regulatory and permitting availability of the technology; and (8) level of community acceptability to

the technology. The remaining five factors demonstrate performance-related questions. The five technology performance factors are: (1) Is the technology capital intensive or operation and maintenance intensive? (2) Is the technology typically part of a treatment train? (3) What is the physical form of the residuals generated when the technology is applied? Is it solid, liquid, or vapor? (4) What parameter of the contaminated media is the technology primarily designed to address? (5) What is the long-term effectiveness of the technology? Does the use of the technology maintain the protection of public health and the environment over time after the remediation objectives have been met? The matrix provides a screening of prospective technologies in a rapid way (Soesilo and Wilson 1997).

Detailed procedure for remediation design is beyond the scope of this paper. Interested readers may refer to Soesilo and Wilson (1997), and ASCE (1999).

COST ESTIMATE

A cost estimate for a remediation project can be developed through seven basic steps: (1) develop the project description; (2) classify project sites; (3) identify the remediation technologies and treatment trains to be used; (4) estimate the quantity of work and direct cost of each technology; (5) estimate sampling and analysis and professional labor costs required to support the project; (6) identify miscellaneous direct costs required to complete the project; and (7) estimate indirect costs, general conditions, overhead, and profit (Rast and Rast 2003). However, it should be noted that there are many ways to develop cost estimates and the exact steps to be performed vary from project to project, depending on the nature of the project, reporting requirements, and the personal preference of the estimator. Small adjustments to these steps may be necessary to meet specific needs of individual projects.

SUMMARY

Many available remediation technologies are reviewed in this invited paper, in particular, the theory, state of development, applicability, limitations, remediation efficiency, cost effectiveness, and potential side effects of the remediation technologies are presented. Details of performance monitoring are described, criteria on selection of the appropriate remediation technology are given, and remediation cost estimate procedure is outlined. As innovative remediation technologies are being developed continually to satisfy various needs, the technologies presented in this invited

lecture are by no means exhaustive. Moreover, there are so many remediation technologies, combinations of remediation technologies, and their variations to suit particular site conditions, it is practically impossible to give a thorough overview of all the remediation technologies for contaminated sites in a single paper. In fact, many of the remediation technologies reviewed in this paper can be elaborated in detail as the thesis of a single paper by itself. Nonetheless, an overview of many existing remediation technologies is given. Readers interested in particular technologies are referred to the references so that they can conduct further exploration.

ACKNOWLEDGEMENTS

It is a formidable task to give an overview of so many proven and emerging remediation technologies in a single paper. The author is humbled by the wealth of information available in the literature. It is impossible to mention, or even to be conscious of all the people whose work, talk, and publications have affected one's thinking or implanted ideas which have later flourished. Therefore, the author would thank all the researchers and practitioners working diligently on different aspects of different remediation technologies, who have contributed selflessly to the literature for the advancement of these technologies to better the quality of our environment. Moreover, the author would thank the Organizing Committee of the International Symposium on Geoenvironmental Engineering (ISEG 2009) for their trust and confidence bestowed on the author for inviting him to prepare the manuscript for the Symposium.

REFERENCES

General

- Benjamin MM (2002). *Water chemistry*. McGraw-Hill, Boston, MA, U.S.A.
- Bethke CM (2008). *Geochemical and biogeochemical reaction modeling*, 2nd edition. Cambridge University Press, Cambridge, U.K.
- Bohn HL, McNeal BL, O'Connor GA (2001). *Soil chemistry*, 3rd edition. John Wiley & Sons, New York, NY, U.S.A.
- Boulding JR & Ginn JS (2004). *Practical handbook of soil, vadose zone, and ground-water contamination: Assessment, prevention, and remediation*, 2nd edition, Lewis Publishers, Boca Raton, FL, U.S.A.
- Cresser MS, Killham K, Edwards T (1993). *Soil chemistry and its applications*. Cambridge University Press, Cambridge, U.K.
- Deviny JS, Everett LG, Lu JCS, Stollar RL (1990).

- Subsurface migration of hazardous wastes. Van Nostrand Reinhold, New York, NY, U.S.A.
- Domínguez JB (2008). Editor. Soil contamination research trends. Nova Science Publishers, New York, NY, U.S.A.
- Dubois AN (2008). Editor. Soil contamination: New research. Nova Science Publishers, New York, NY, U.S.A.
- Domenico PA & Schwartz FW (1990). Physical and chemical hydrogeology. John Wiley & Sons, New York, NY, U.S.A.
- Essington ME (2004). Soil and water chemistry: An integrative approach. CRC Press, Boca Raton, FL, U.S.A.
- Evangelou VP (1998). Environmental soil and water chemistry: Principles and applications. John Wiley & Sons, New York, NY, U.S.A.
- Evans JC (1997). Editor. In situ remediation of the geoenvironment. Geotechnical Special Publication No. 71, ASCE, Reston, VA, U.S.A.
- Fetter CW (1999). Contaminant hydrogeology, 2nd edition. Prentice Hall, Upper Saddle River, NJ, U.S.A.
- Freeze RA & Cherry JA (1979). Groundwater. Prentice-Hall, Englewood Cliffs, NJ, U.S.A.
- Hudson RC (2006). Editor. Hazardous materials in the soil and atmosphere: Treatment, removal, and analysis. Nova Science Publishers, New York, NY, U.S.A.
- Hyman M & Dupont RR (2001). Groundwater and soil remediation: Process design and cost estimating of proven technologies. ASCE Press, Reston, VA, U.S.A.
- Khire MV, Alshawabkeh AN, Reddy KR (2008). Editors. Geotechnics of waste management and remediation. Geotechnical Special Publication No. 177, ASCE, Reston, VA, U.S.A.
- Kirk GJD (2004). The biogeochemistry of submerged soils. Wiley, Hoboken, NJ, U.S.A.
- Krešić N (2007). Hydrogeology and groundwater modeling, 2nd edition. CRC Press, Boca Raton, FL, U.S.A.
- LaGrega ND, Buckingham PL, Evans JC (1994). Hazardous waste management. McGraw-Hill, New York, NY, U.S.A.
- Lehr JH, Hyman M, SeEVERS WJ, Gass T (2002). Handbook of complex environmental remediation problems. McGraw-Hill, New York, NY, U.S.A.
- Manahan SE (2005). Environmental chemistry. CRC Press, Boca Raton, FL, U.S.A.
- McBride MB (1994). Environmental chemistry of soils. Oxford University Press, New York, NY, U.S.A.
- Nathanail CP & Bardos RP (2004). Reclamation of contaminated land. John Wiley & Sons, Chichester, U.K.
- National Research Council (1994). Alternatives for ground water cleanup. National Academy Press, Washington, D.C., U.S.A.
- Nemerow NL, Agardy FJ, Salvato JA (2009). Editors. Environmental engineering: Water, wastewater, soil, and groundwater treatment and remediation, 6th edition. Wiley, Hoboken, NJ, U.S.A.
- Otten A, Alphenaar A, Pijls C, Spuij F, de Wit H (1997). In situ soil remediation. Kluwer Academic Publishers, Dordrecht, the Netherlands.
- Palmer CM (1996). Principles of contaminant hydrogeology, 2nd edition. CRC Lewis Publishers, Boca Raton, FL, U.S.A.
- Rajeshwar K & Ibanez J (1997). Environmental electrochemistry: Fundamentals and applications in pollution abatement. Academic Press, San Diego, CA, U.S.A.
- Reddi LN & Inyang HI (2000). Geoenvironmental engineering: Principles and applications. Marcel Dekker, New York, NY, U.S.A.
- Rowe RK (2001). Editor. Geotechnical and geoenvironmental engineering handbook. Kluwer Academic, Boston, MA, U.S.A.
- Sawyer CN & McCarty PL (1978). Chemistry for environmental engineering, 3rd edition. McGraw-Hill, New York, NY, U.S.A.
- Selim HM & Kingery WL (2003). Editors. Geochemical and hydrological reactivity of heavy metals in soils. Lewis Publishers, Boca Raton, FL, U.S.A.
- Sellers K (1999). Fundamentals of hazardous waste site remediation. Lewis Publishers, Boca Raton, FL, U.S.A.
- Sequeira CAC (1994). Editor. Environmental oriented electrochemistry. Elsevier, Amsterdam, the Netherlands.
- Sharma HD & Reddy KR (2004). Geoenvironmental Engineering. John Wiley & Sons, Hoboken, NJ, U.S.A.
- Snoeyink VL & Jenkins D (1980). Water chemistry. John Wiley & Sons, New York, NY, U.S.A.
- Soesilo JA & Wilson SR (1997). Site remediation planning and management. Lewis Publishers, Boca Raton, FL, U.S.A.
- Sparks DL (2003). Environmental soil chemistry, 2nd edition. Academic Press, San Diego, CA, U.S.A.
- Sposito G (1994). Chemical equilibria and kinetics in soils. Oxford University Press, New York, NY, U.S.A.
- Sposito G (2004). The surface chemistry of natural particles. Oxford University Press, New York, NY, U.S.A.
- Sposito G (2008). The chemistry of soils, 2nd edition. Oxford University Press, New York, NY, U.S.A.
- Stegmann R, Brunner G, Calmano W, Matz G (2001). Editors. Treatment of contaminated soil - Fundamentals, analysis, applications. Springer, Berlin, Germany.

- Stumm W & Morgan JJ (1996). *Aquatic chemistry: Chemical equilibria and rates in natural waters*, 3rd edition. John Wiley & Sons, New York, NY, U.S.A.
- Suthersan SS (1997). *Remediation engineering design concepts*. CRC Press, Boca Raton, FL, U.S.A.
- U.S. EPA (1985). *Handbook—Remedial action at waste disposal sites (revised)*. Report No. EPA/625/6-85/006, Office of Emergency and Remedial Response, U.S. EPA, Washington, D.C., U.S.A.
- Wilson DJ & Clarke AN (1994). Editors. *Hazardous waste site soil remediation: Theory and application of innovative technologies*. Marcel Dekker, New York, NY, U.S.A.
- Yong RN (2001). *Geoenvironmental engineering: Contaminated soils, pollutant fate, and mitigation*. CRC Press, Boca Raton, FL, U.S.A.
- In-situ Natural Attenuation**
- Boettcher G & Nyer EK (2001). *In situ bioremediation. In situ treatment technology*, 2nd edition. CRC Press, Boca Raton, Florida, U.S.A.: 259-326.
- Jordan F, Waugh WJ, Glenn EP, Sam L, Thompson T, Thompson TL (2008). Natural bioremediation of a nitrate-contaminated soil-and-aquifer system in a desert environment. *Journal of Arid Environments*, 72(5): 748-763.
- Park DK, Ko NY, Lee KK (2007). Optimal groundwater remediation design considering effects of natural attenuation processes: pumping strategy with enhanced-natural-attenuation. *Geosciences Journal*, 11(4): 377-385.
- Wiedemeier TH, Rifai HS, Newell CJ, Wilson JT (1999). Natural attenuation of fuels and chlorinated solvents in the subsurface. John Wiley & Sons, New York, NY, U.S.A.
- Yong RN & Mulligan CN (2004). Natural attenuation of contaminants in soil. Lewis Publishers, Boca Raton, FL, U.S.A.
- In-situ Containment Systems**
- Bonaparte R (1990). Editor. *Waste containment system: Construction, regulation, and performance*. Geotechnical Special Publication No. 26, ASCE, New York, NY, U.S.A.
- Boschuk J, Jr (1991). Landfill covers: An engineering perspective. *Geotechnical Fabrics Report*, 9(4):23-34.
- Boutwell GP & Hueckel T (1995). Floors and bottom barriers: Indigenous. Assessment of barrier containment technologies—A comprehensive treatment for environmental remediation applications. Proc., International Containment Technology Workshop, Baltimore, Maryland, U.S.A., Rumer R.R. and Mitchell J.K., (eds.): 141-184.
- Cavalli NJ (1992). Composite barrier slurry wall. Slurry walls: Design, construction, and quality control. Paul D.B., Davidson R.R. and Cavalli N.J. (eds.) ASTM STP 1129, ASTM, Philadelphia, Pennsylvania, U.S.A.: 78-85.
- Crawford JF & Smith PG (1985). *Landfill Technology*. Butterworths, London, U.K.
- Daniel DE & Koerner RM (1995). Waste containment facilities: Guidance for construction, quality assurance and quality control of liner and cover systems. ASCE Press, New York, NY, U.S.A.
- Davidson RR, Denise G, Findlay B, Robertson RB (1992). Design and construction of a plastic concrete cutoff wall for the Island Copper Mine. Slurry walls: Design, construction, and quality control. Paul D.B., Davidson R.R. and Cavalli N.J. (eds.) ASTM STP 1129, ASTM, Philadelphia, PA, U.S.A.: 271-288.
- Evans J (1993). Vertical cutoff walls. *Geotechnical practice for waste disposal*. Daniel D.E. (eds.) Chapman & Hall, London, U.K.: 430-454.
- Evans JC (1995). Soil- and cement-based vertical barriers with focus on materials. Assessment of barrier containment technologies—A comprehensive treatment for environmental remediation applications. Proc., International Containment Technology Workshop, Baltimore, MD, U.S.A., Rumer R.R. and Mitchell J.K. (eds.): 5-43.
- Filz G & Mitchell JK (1995). Design, construction, and performance of soil- and cement-based vertical barriers. Assessment of barrier containment technologies – A comprehensive treatment for environmental remediation applications. Proc., International Containment Technology Workshop, Baltimore, MD, U.S.A., Rumer R.R. and Mitchell J.K. (eds.): 45-75.
- Grube WE, Jr (1992). Slurry trench cut-off walls for environmental pollution control. Slurry walls: Design, construction, and quality control. Paul D.B., Davidson R.R. and Cavalli N.J. (eds.) ASTM STP 1129, ASTM, Philadelphia, PA, U.S.A.: 69-77.
- Hollingsworth S (2004). Cover systems for land regeneration: Thickness of cover systems for contaminated land. BREbookshop, Garston, U.K.
- Koerner RM & Daniel DE (1997). Final covers for solid waste landfills and abandoned dumps. ASCE Press, New York, NY, U.S.A.
- Koerner RM & Guglielmetti JL (1995). Vertical barriers: Geomembranes. Assessment of barrier containment technologies—A comprehensive treatment for environmental remediation applications. Proc., International Containment Technology Workshop, Baltimore, MD, U.S.A., Rumer R.R. and Mitchell J.K. (eds.): 95-118.
- McBean EA, Rovers FA, Farquhar GJ (1995). *Solid waste landfill engineering and design*. Prentice Hall PTR, Englewood Cliffs, NJ U.S.A.

- Mitchell JK & Rumer RR (1997). Waste containment barriers: Evaluation of the technology. In situ remediation of the geoenvironment. Evans, J.C., Editor, Geotechnical Special Publication No. 71, ASCE, Reston, VA, U.S.A.: 1-25.
- Mitchell JK & Yeung AT (1991). Electro-kinetic flow barriers in compacted clay. Geotechnical Engineering 1990. Transportation Research Record 1288, Transportation Research Board, National Research Council, Washington, D.C., U.S.A.: 1-9.
- Mott HV & Weber WJ, Jr (1991). Factors influencing organic contaminant diffusivities in soil-bentonite cutoff barriers. Environmental Science & Technology, 25(10): 1708-1715.
- Peterson ME & Landis RC (1995). Artificially emplaced floors and bottom barriers. Assessment of barrier containment technologies—A comprehensive treatment for environmental remediation applications. Proc., International Containment Technology Workshop, Baltimore, MD, U.S.A., Rumer R.R. and Mitchell J.K. (eds.): 185-208.
- Powers JP (2007). Construction dewatering and groundwater control: New methods and applications. John Wiley & Sons, Hoboken, NJ, U.S.A.
- Qian X, Koerner RM, Gray DH (2002). Geotechnical aspects of landfill design and construction. Prentice Hall, Upper Saddle River, NJ, U.S.A.
- Ryan C (1987). Vertical barriers in soil for pollution containment. Geotechnical practice for waste disposal '87. Woods R.D., Editor, Geotechnical Special Publication No. 13, ASCE, New York, NY, U.S.A.: 182-204.
- Rumer RR & Ryan ME (1995). Editors. Barrier containment technologies for environmental remediation applications. John Wiley & Sons, New York, NY, U.S.A.
- Shackelford CD & Daniel DE (1991a). Diffusion in saturated soil. I: Background. Journal of Geotechnical Engineering, ASCE, 117(3):467-484.
- Shackelford CD & Daniel DE (1991b). Diffusion in saturated soil. II: Results for compacted clay. Journal of Geotechnical Engineering, ASCE, 117(3):485-506.
- Shackelford CD & Redmond PL (1995). Solute breakthrough curves for processed kaolin at low-flow rates. Journal of Geotechnical Engineering, ASCE, 121(1):17-32.
- Sharma HD & Lewis SP (1994). Waste containment systems, waste stabilization, and landfills: Design and evaluation. John Wiley & Sons, New York, NY, U.S.A.
- Tamaro GJ & Poletto RJ (1992). Slurry walls - Construction quality control. Slurry walls: Design, construction, and quality control. Paul D.B., Davidson R.R. and Cavalli N.J., Editors. ASTM STP 1129, ASTM, Philadelphia, PA, U.S.A.: 26-41.
- Woodcock JC & Miller KR (1997). Slurry wall construction in deep mined area. In situ remediation of the geoenvironment. Evans, J.C., Editor, Geotechnical Special Publication No. 71, ASCE, Reston, VA, U.S.A.: 197-211.

Stabilization and Solidification

- Anderson WC (1994). Editor. Innovative site remediation technology. Vol. 4—Stabilization/solidification. American Academy of Environmental Engineers, Annapolis, MD, U.S.A.
- Conner JR (1990). Chemical fixation and solidification of hazardous wastes. Van Nostrand Reinhold, New York, NY, U.S.A.
- Dermatas D & Meng XG (2003). Utilization of fly ash for stabilization/solidification of heavy metal contaminated soils. Engineering Geology, 70(3-4):377-394.
- Paria S & Yuet PK (2006). Solidification-stabilization of organic and inorganic contaminants using Portland cement: A literature review. Environmental Reviews, 14(4):217-255.

Pump-and-Treat

- Bau DA & Mayer AS (2007). Data-worth analysis for multiobjective optimal design of pump-and-treat remediation systems. Advances in Water Resources, 30(8):1815-1830.
- Bau DA & Mayer AS (2008). Optimal design of pump-and-treat systems under uncertain hydraulic conductivity and plume distribution. Journal of Contaminant Hydrology, 100(1-2):30-46.
- Chang LC, Chu HJ, Hsiao CT (2007). Optimal planning of a dynamic pump-treat-inject groundwater remediation system. Journal of Hydrology, 342(3-4):295-304.
- Cohen RM, Mercer JW, Greenwald RM, Beljin MS (1997). Design guidelines for conventional pump-and-treat systems. Report No. EPA/540/S-97/504, Office of Solid Waste and Emergency Response, U.S. EPA, Washington, D.C., U.S.A.
- Endres KL, Mayer A, Hand DW (2007). Equilibrium versus nonequilibrium treatment modeling in the optimal design of pump-and-treat groundwater remediation systems. Journal of Environmental Engineering, ASCE, 133(8):809-818.
- Guo X, Zhang CM, Borthwick JC (2007). Successive equimarginal approach for optimal design of a pump and treat. Water Resources Research, 43(8):Article Number W08416.
- Ishimori H, Katsumi T, Yoshikawa M, Fukagawa R (2006). Performance evaluations of pump-and-treat system using advection-dispersion analysis: Effects of clay layer on remediation duration. Soils and

Foundations, 46(1):45-59.

Mackay DM & Cherry JA (1989). Groundwater contamination: Pump-and-treat remediation. *Environmental Science & Technology*, 23(6):630-636.

Nyer EK (2001). Limitations of pump and treat remediation methods. In situ treatment technology, 2nd edition. CRC Press, Boca Raton, FL, U.S.A., 1-39.

Parker BL, Chapman SW, Guilbeault MA (2008). Plume persistence caused by back diffusion from thin clay layers in a sand aquifer following TCE source-zone hydraulic isolation. *Journal of Contaminant Hydrology*, 102(1-2):86-104.

Rivett MO, Chapman SW, Allen-King RM, Feenstra S, Cherry JA (2006). Pump-and-treat remediation of chlorinated solvent contamination at a controlled field-experiment site. *Environmental Science & Technology*, 40(21):6770-6781.

Saez JA & Harmon TC (2006). Two-stage aquifer pumping subject to slow desorption and persistent sources. *Ground Water*, 44(2):244-255.

Soil Flushing

Anderson WC (1993). Editor. Innovative site remediation technology. Vol. 3 – Soil washing/soil flushing. American Academy of Environmental Engineers, Annapolis, MD, U.S.A.

Francis CW, Timpson ME, Wilson JH (1999). Bench- and pilot-scale studies relating to the removal of uranium from uranium-contaminated soils using carbonate and citrate lixivants. *Journal of Hazardous Materials*, 66(1-2):67-87.

Lee SW, Kim JY, Lee JU, Ko I, Kim KW (2004). Removal of arsenic in tailings by soil flushing and the remediation process monitoring. *Environmental Geochemistry and Health*, 26(4):403-409.

Mann MA (1995). Soil washing and soil flushing. American Academy of Environmental Engineers, Annapolis, MD, U.S.A.

Martel R, Gélinas PJ, Lefebvre R, Hébert A, Foy S, Saumure L, Roy A, Roy N (2000). Laboratory and field soil washing experiments with surfactant solutions: NAPL recovery mechanisms. *Emerging technologies in hazardous waste management 8*. Tedder D.W. and Pohland F.G. (eds.) Kluwer Academic/Plenum Publishers, New York, NY, U.S.A., 55-67.

McCray JE & Brusseau ML (1998). Cyclodextrin-enhanced in situ flushing of multiple-component immiscible organic liquid contamination at the field scale: Mass removal effectiveness. *Environmental Science & Technology*, 32(9):1285-1293.

Roote DS (1997). Technology overview report: In-situ flushing. *Groundwater Remediation Technologies*

Analysis Center, Pittsburgh, PA, U.S.A.

Roy D, Kommalapati RR, Valsaraj KT, Constant WD (1995). Soil flushing of residual transmission fluid - Application of colloidal gas aphron suspensions and conventional surfactant solutions. *Water Research*, 29(2):589-595.

Reactive Zone Remediation

Anderson WC (1994). Editor. Innovative site remediation technology. Vol. 2 – Chemical treatment. American Academy of Environmental Engineers, Annapolis, MD, U.S.A.

Beltrán FJ (2003). Ozone-UV radiation-hydrogen peroxide oxidation technologies. *Chemical degradation methods for wastes and pollutants*. Tarr M.A. (ed.) Marcel Dekker, New York, NY, U.S.A., 1-75.

Bower KC, Durik S, Miller CM (2000). Development of an enhanced ozone-hydrogen peroxide advanced oxidation process. *Emerging technologies in hazardous waste management 8*. Tedder D.W. and Pohland F.G., Editors, Kluwer Academic/Plenum Publishers, New York, NY, U.S.A., 167-176.

Crimi ML & Taylor J (2007). Experimental evaluation of catalyzed hydrogen peroxide and sodium persulfate for destruction of BTEX contaminants. *Soil & Sediment Contamination*, 16(1):29-45.

Crimi M, Quickel M, Ko S (2009). Enhanced permanganate in situ chemical oxidation through MnO₂ particle stabilization: Evaluation in 1-D transport systems. *Journal of Contaminant Hydrology*, 105(1-2):69-79.

Ferguson SH, Woinarski AZ, Snape I, Morris CE, Revill AT (2004). A field trial of in situ chemical oxidation to remediate long-term diesel contaminated Antarctic soil. *Cold Regions Science and Technology*, 40(1-2):47-60.

Ferrarese E, Andreottola G, Oprea IA (2008). Remediation of PAH-contaminated sediments by chemical oxidation. *Journal of Hazardous Materials*, 152(1): 128-139.

Fischer NM, Reed T, Camrud D, Madsen C (2001). BTEX/TVPH remediation using an oxygen release compound. In situ aeration and aerobic remediation. Leeson A., Johnson P.C., Hincee R.E., Semprini L. and Magar V.S. (eds.) *Bioremediation Series*, Battelle Press, Columbus, OH, U.S.A., 6(10):15-22.

Fruchter J (2000). In situ redox manipulation for treatment of chromate and trichloroethylene in ground. *Proceedings of the Abiotic In Situ Technologies for Groundwater Remediation Conference*, Dallas, Report No. EPA/625/R-99/012, Office of Research and development, U.S. EPA, Cincinnati, OH, U.S.A., 96-97.

Greenberg RS, Thomas A, Kakarla PKC, Watts RJ

- (2000). In situ Fenton-like oxidation of volatile organics: Laboratory, pilot and full-scale demonstrations. *Emerging technologies in hazardous waste management* 8. Tedder D.W. and Pohland F.G. (eds.) Kluwer Academic/Plenum Publishers, New York, NY, U.S.A., 153-165.
- Huang Q & Weber WJ, Jr (2005). Peroxidase-catalyzed oxidative coupling of phenols in the presence of geosorbents. *Subsurface contamination remediation: Accomplishments of the Environmental Management Science Program*. Berkey E. and Zachry T. (eds.) American Chemical Society, Washington, D.C. U.S.A., 64-81.
- Khan FA & Puts RW (2003). In situ abiotic detoxification and immobilization of hexavalent chromium. *Ground Water Monitoring & Remediation*, 23(1):77-84.
- Lenzo F (2001). Reactive zone remediation. In situ treatment technology, 2nd edition. CRC Press, Boca Raton, FL, U.S.A., 327-389.
- Li XD & Schwartz FW (2005). Using phosphate to control the Mn oxide precipitation during in situ chemical oxidation of chlorinated ethylenes by permanganate. *Subsurface contamination remediation: Accomplishments of the Environmental Management Science Program*. Berkey E. and Zachry T. (eds.) American Chemical Society, Washington, D.C. U.S.A., 82-95.
- MacKinnon LK & Thomson NR (2002). Laboratory-scale in situ chemical oxidation of a perchloroethylene pool using permanganate. *Journal of Contaminant Hydrology*, 56(1-2):49-74.
- Mott-Smith E, Leonard WC, Lewis R, Clayton WS, Ramirez J, Brown R (2000). In situ oxidation of DNAPL using permanganate: IDC Cape Canaveral demonstration. *Chemical oxidation and reactive barriers - remediation of chlorinated and recalcitrant compounds*. Wickramanayake G.B., Gavaskar A.R. and Chen A.S.C., Editors. Battelle Press, Columbus, OH, U.S.A., 125-134.
- Siegrist RL, Crimi ML, Munakata-Marr J, Illangasekare T, Dugan P, Heiderscheidt J, Petri B, Sahl J (2008). Chemical oxidation for clean up of contaminated ground water. *Methods and techniques for cleaning-up contaminated site*. Annable M.D., Teodorescu M., Hlavinek P. and Diels L. (eds.) Springer, Dordrecht, the Netherlands, 45-58.
- Seol Y, Zhang H, Schwartz FW (2003). A review of in situ chemical oxidation and heterogeneity. *Environmental & Engineering Geoscience*, 9(1):37-49.
- Thomson NR, Fraser MJ, Lamarche C, Barker JF, Forsey SP (2008). Rebound of a coal tar creosote plume following partial source zone treatment with permanganate. *Journal of Contaminant Hydrology*, 102(1-2):154-171.
- Vitolins AR, Nelson BR, Underhill SA, Thomas LMH (2003). Fenton's reagent-based in situ chemical oxidation treatment of saturated and unsaturated soils at a historic railroad site. *Soil & Sediment Contamination*, 12(1):139-150.
- Walker WJ & Pucik-Ericksen LE (2000). In situ reduction of hexavalent chromium in groundwater and surface soil using acidified ferrous sulfate. *Proceedings of the Abiotic In Situ Technologies for Groundwater Remediation Conference*, Dallas, Report No. EPA/625/R-99/012, Office of Research and development, U.S. EPA, Cincinnati, OH, U.S.A., 99-100.

Soil Washing and Solvent Extraction

- Alfaro MC & Wong RCK (2001). Laboratory studies on fracturing of low-permeability soils. *Canadian Geotechnical Journal*, 38(2):303-315.
- Anderson WC (1993). Editor. *Innovative site remediation technology*. Vol. 3—Soil washing/soil flushing. American Academy of Environmental Engineers, Annapolis, MD, U.S.A.
- Anderson WC (1995). Editor. *Innovative site remediation technology*. Vol. 5—Solvent/chemical extraction. American Academy of Environmental Engineers, Annapolis, MD, U.S.A.
- Choy CC, Korfiatis GP, Meng X (2006). Removal of depleted uranium from contaminated soils. *Journal of Hazardous Materials*, 136(1):53-60.
- Deshpande S, Shiao BJ, Wade D, Sabatini DA, Harwell JH (1999). Surfactant selection for enhancing ex situ soil washing. *Water Research*, 33(2):351-360.
- Kakitani T, Hata T, Kajimoto T, Imamura Y (2006). A novel extractant for removal of hazardous metals from preservative-treated wood waste. *Journal of Environmental Quality*, 35(3):912-917.
- Kakitani T, Hata T, Katsumata N, Kajimoto T, Koyanaka H, Imamura Y (2007). Chelating extraction for removal of chromium, copper, and arsenic from treated wood with bioxalate. *Environmental Engineering Science*, 24(8): 1026-1037.
- Kuhlman MI & Greenfield TM (2006). Simplified soil washing processes for a variety of soils. *Journal of Hazardous Materials*, 66(1-2):31-45.
- Mulligan CN, Yong RN, Gibbs BF (2001). Surfactant-enhanced remediation of contaminated soil: A review. *Engineering Geology*, 60(1-4):371-380.
- Murena F & Gioia F (2009). Solvent extraction of chlorinated compounds from soils and hydrodechlorination of the extract phase. *Journal of Hazardous Materials*, 162(2-3):661-667.
- Silva A, Delerue-Matos C, Fiuza A (2005). Use of solvent extraction to remediate soils contaminated with hydrocarbons. *Journal of Hazardous Materials*, 124(1-3):224-229.

- Torres LG, Aguirre AL, Verdejo A, Iturbe R (2005). Enhanced soil-washing treatment for soils which are highly contaminated with crude oil. *Ecosystems and sustainable development V. Tiezzi E., Brebbia C.A., Jorgensen S.E. and Gomar D.A. (eds.) WIT Press, Southampton, U.K., 541-550.*
- Permeable Reactive Barriers
- Blowes DW & Ptacek CJ (1992). Geochemical remediation of groundwater by permeable reactive walls: Removal of chromate by reaction with iron-bearing solids. *Proc., Subsurface Restoration Conference, Dallas, TX, U.S.A.*
- Christensen B, Laake M, Lien T (1996). Treatment of acid mine water by sulfate-reducing bacteria; results from a bench scale experiment. *Water Research, 30(7):1617-1624.*
- Cravotta CA, III, & Watzlaf GR (2002). Design and performance of limestone drains to increase pH and remove metals from acidic mine drainage. *Handbook of groundwater remediation using permeable reactive barriers. Naftz, D.L., Morrison S.J., Fuller C.C. and Davis J.A. (eds.) Academic Press, Amsterdam, the Netherlands, 19-66.*
- Gillham RW (2008). Development of the granular iron permeable reactive barrier technology (good science or good fortune). *Environmental Geotechnology and Global Sustainable Development 2008. Yeung A.T. and Lo I.M.C. (eds.) Advanced Technovation Limited, Hong Kong, China, 5-15.*
- Henderson AD & Demond AH (2007). Long-term performance of zero-valent iron permeable reactive barriers: A critical review. *Environmental Engineering Science, 24(4):401-423.*
- Hicks P (1999). The use of oxygen release compound (ORC[®]) for enhanced bioremediation. *Proc., the 1998 National Conference on Environmental Remediation Science and Technology, Greensboro, NC, U.S.A., 63-79.*
- Hsi CD & Langmuir D (1985). Adsorption of uranyl onto ferric oxyhydroxides: Application of the surface complexation site-binding model. *Geochimica et Cosmochimica Acta, 49(9):1931-1941.*
- Jones WE, Denham ME, Phifer MA, Sappington FC, Washburn FA (2002). Permeable reactive barrier/geosiphon treatment for metals-contaminated groundwater. *Handbook of groundwater remediation using permeable reactive barriers. Naftz, D.L., Morrison S.J., Fuller C.C. and Davis J.A. (eds.) Academic Press, Amsterdam, the Netherlands, 105-132.*
- Kalinovich I, Rutter A, Poland JS, Cairns G, Rowe RK (2008). Remediation of PCB contaminated soils in the Canadian Arctic: Excavation and surface PRB technology. *Science of the Total Environment, 407(1):53-66.*
- Kao CM, Chen SC, Liu JK (2001a). Development of a biobarrier for the remediation of PCE-contaminated aquifer. *Chemosphere, 43(8):1071-1078.*
- Kao CM, Chen SC, Su MC (2001b). Laboratory column studies for evaluating a barrier system for providing oxygen and substrate for TCE biodegradation. *Chemosphere, 44(5):925-934.*
- Kao CM, Chen SC, Wang JY, Chen YL, Lee SZ (2003). Remediation of PCE-contaminated aquifer by an in situ two-layer biobarrier: laboratory batch and column studies. *Water Research, 37(1):27-38.*
- Matheson LJ, Goldberg WC, Bostick WD, Harris L (2002). Analysis of uranium-contaminated zero valent iron media sampled from permeable reactive barriers installed at U.S. Department of Energy sites in Oak Ridge, Tennessee, and Durango, Colorado. *Handbook of groundwater remediation using permeable reactive barriers. Naftz, D.L., Morrison S.J., Fuller C.C. and Davis J.A. (eds.) Academic Press, Amsterdam, the Netherlands, 343-367.*
- Morrison SJ, Naftz DL, Davis JA, Fuller CC (2002). Introduction to groundwater remediation of metals, radionuclides, and nutrients with permeable reactive barriers. *Handbook of groundwater remediation using permeable reactive barriers. Naftz, D.L., Morrison S.J., Fuller C.C. and Davis J.A. (eds.) Academic Press, Amsterdam, the Netherlands, 1-15.*
- Naftz DL, Fuller CC, Davis JA, Morrison ST, Felcorn EM, Rowland RC, Freethey GW, Wilkowske C, Piana M (2002). Field demonstration of three permeable reactive barriers to control uranium contamination in groundwater, Fry Canyon, Utah. *Handbook of groundwater remediation using permeable reactive barriers. Naftz, D.L., Morrison S.J., Fuller C.C. and Davis J.A. (eds.) Academic Press, Amsterdam, the Netherlands, 402-434.*
- Palmer PL (2001). Permeable treatment barriers. *In situ treatment technology, 2nd edition, Lewis Publishers, Boca Raton, FL, U.S.A., 459-482.*
- Schwartz FW & Xu Y (1992). Modeling the behavior of a reactive barrier system for lead. *Modern Trends in Hydrogeology, Proc., 1992 Conference of the Canadian National Chapter, International Association of Hydrogeologists, Hamilton, Ontario, Canada.*
- Tratnyek PG, Scherer MM, Johnson TL, Matheson LJ (2003). Permeable reactive barriers of iron and other zero-valent metals. *Chemical degradation methods for wastes and pollutants: Environmental and industrial applications. Tarr M.A. (ed.) Marcel Dekker, New York, NY, U.S.A., 371-421.*
- U.S. EPA (1999). Field applications of in situ remediation technologies: Permeable reactive barriers. Report No. EPA 542-R-99-002, Technology Innovation Office,

- U.S. EPA, Washington, D.C., U.S.A.
- Vidic RD & Pohland FG (2000). In situ groundwater remediation using treatment walls. *Emerging technologies in hazardous waste management* 8. Tedder D.W. and Pohland F.G. (eds.) Kluwer Academic/Plenum Publishers, New York, NY, U.S.A., 119-139.
- Waite TD, Davis JA, Payne TE, Waychunas GA, Xu N (1994). Uranium(VI) adsorption to ferrihydrite: Application of a surface complexation model. *Geochimica et Cosmochimica Acta*, 58(24):5465-5478.
- Waite TD, Desmier R, Melville M, Macdonald B (2002). Preliminary investigation into the suitability of permeable reactive barriers for the treatment of acid sulfate soils discharge. *Handbook of groundwater remediation using permeable reactive barriers*. Naftz, D.L., Morrison S.J., Fuller C.C. and Davis J.A. (eds.) Academic Press, Amsterdam, the Netherlands, 67-104.
- ### Bioremediation and Biodegradation
- Abdelouas A, Lutze W, Gong W, Nuttall EH, Strietelmeier BA, Travis BJ (2000). Biological reduction of uranium in groundwater and subsurface soil. *Science of the Total Environment*, 250(1):21-35.
- Al-Daher R, Al-Awadhi N, El-Nawawy A (1998). Bioremediation of damaged desert environment using the windrow soil pile system in Kuwait. *Environment International*, 24(1-2):175-180.
- Al-Daher R, Al-Awadhi N, Yateem A, Balba MT, El-Nawawy A (2001). Compost soil piles for treatment of oil-contaminated soil. *Soil & Sediment Contamination*, 10(2):197-209.
- Alexander M (1999). *Biodegradation and bioremediation*, 2nd edition. Academic Press, San Diego, CA, U.S.A.
- Anderson WC (1995). Editor. *Innovative site remediation technology*. Vol. 1—Bioremediation. American Academy of Environmental Engineers, Annapolis, MD, U.S.A.
- Atagana HI, Haynes RJ, Wallis FM (2003). Optimization of soil physical and chemical conditions for the bioremediation of creosote-contaminated soil. *Biodegradation*, 14(4):297-307.
- Aulenta F, Majone M, Tandoi V (2006). Enhanced anaerobic bioremediation of chlorinated solvents: environmental factors influencing microbial activity and their relevance under field conditions. *Journal of Chemical Technology and Biotechnology*, 81(9):1463-1474.
- Balba MT, Al-Awadhi N, Al-Daher R (1998). Bioremediation of oil-contaminated soil: microbiological methods for feasibility assessment and field evaluation. *Journal of Microbiological Methods*, 32(2):155-164.
- Balba MT, Al-Awadhi N, Al-Daher R, Chino H, Tsuji H (1996). Remediation and rehabilitation of oil-lake beds in Kuwait. 1. Bioremediation of oil-contaminated soil. Restoration and rehabilitation of the desert environment. Al-Awadhi N., Balba M.T. and Kamizawa C. (eds.) Elsevier Science, Amsterdam, the Netherlands, 21-40.
- Banwart SA, Thomson S, Rees H, Lerner D, Wilson R, Romero-Gonzalez M (2007). In situ bioremediation by natural attenuation: from lab to field scale. *Water dynamics*. AIP Conference Proceedings, 898:207-210.
- Carnegie D & Ramsay JA (2009). Anaerobic ethylene glycol degradation by microorganisms in poplar and willow rhizospheres. *Biodegradation*, 20(4):551-558.
- Diels L & Lookman R (2007). Microbial systems for in-situ soil and groundwater remediation. *Advanced science and technology for biological decontamination of sites affected by chemical and radiological nuclear agents*. NATO Science Series IV Earth and Environmental Sciences, 75:61-77.
- Evans PJ & Trute MM (2006). In situ bioremediation of nitrate and perchlorate in vadose zone soil for groundwater protection using gaseous electron donor injection technology. *Water Environment Research*, 78(13):2436-2446.
- Gallagher JR & Sorensen JA (2001). Biological treatment of amine wastes from the gas industry. *Ex situ biological treatment technologies*. Magar V.S., VonFahnestock F.M. and Leeson A. (eds.) Bioremediation Series, Battelle Press, Columbus, OH, U.S.A., 6(6):141-148.
- Groudev S, Spasova I, Nicolova M, Georgiev P (2008). Bioremediation in situ of polluted soil in a uranium deposit. *Methods and techniques for cleaning-up contaminated site*. Annable M.D., Teodorescu M., Hlavinek P. and Diels L. (eds.) Springer, Dordrecht, the Netherlands, 25-34.
- Gunderson CA, Kostuk JM, Gibbs MH, Napolitano GE, Wicker LF, Richmond JE, Stewart AJ (1997). Multispecies toxicity assessment of compost produced in bioremediation of an explosives-contaminated sediment. *Environmental Toxicology and Chemistry*, 16(12):2529-2537.
- Hartley W, Uffindell L, Plumb A, Rawlinson HA, Putwain P, Dickinson NM (2008). Assessing biological indicators for remediated anthropogenic urban soils. *Science of the Total Environment*, 405(1-3):358-369.
- Head IM, Singleton I. and Milner M.G. (2003). *Bioremediation: A critical review*. Horizon Scientific Press, Wymondham, U.K.
- Hicks P (1999). The use of oxygen release compound (ORC[®]) for enhanced bioremediation. *Proc., the 1998 National Conference on Environmental Remediation*

- Science and Technology, Greensboro, NC, U.S.A., 63-79.
- Hinchee RE, Leeson A, Semprini L (1995a). Editors. Bioremediation of chlorinated solvent. Battelle Press, Columbus, OH, U.S.A.
- Hinchee RE, Means JL, Burris DR (1995b). Editors. Bioremediation of inorganics. Battelle Press, Columbus, OH, U.S.A.
- Leahy MC, Nelson CH, Fiorentine AM, Schmitz RJ (1997). Ozonation as a polish technology for in situ bioremediation. Proc., 4th International In Situ and On-Site Bioremediation Symposium, New Orleans, LA, U.S.A., 479-483.
- Livingston RJ & Islam MR (1999). Laboratory modeling, field study, and numerical simulation of bioremediation of petroleum contaminants. *Energy Sources*, 21(1-2):113-129.
- Lynch JM & Moffat AJ (2005). Bioremediation—Prospects for the future application of innovative applied biological research. *Annals of Applied Biology*, 146(2):217-221.
- McQueen D, Joshi CJ, Thongkheung A, Jordan TL (1999). Isolation and growth of glycol degrading bacteria. Proc., the 1998 National Conference on Environmental Remediation Science and Technology, Greensboro, NC, U.S.A., 131-140.
- National Research Council (1993). *In situ bioremediation: When does it work?* National Academy Press, Washington, D.C., U.S.A.
- Makkar RS & Rockne KJ (2003). Comparison of synthetic surfactants and biosurfactants in enhancing biodegradation of polycyclic aromatic hydrocarbons. *Environmental Toxicology and Chemistry*, 22(10):2280-2292.
- Perfurmo A, Banat IM, Marchant R (2006). The use of thermophilic bacteria in accelerated hydrocarbon bioremediation. *Environmental problems in coastal regions VI: Including oil spill studies*. Brebbia C.A. (ed.) WIT Press, Southampton, U.K., 67-77.
- Perfumo A, Banat IM, Marchant R, Vezzulli L (2007). Thermally enhanced approaches for bioremediation of hydrocarbon-contaminated soils. *Chemosphere*, 66(1):179-184.
- Pinelli D, Nocentini M, Fava F (1999). In situ bioremediation of a soil contaminated by mineral oil: A case study. Proc., 5th International In Situ and On-Site Bioremediation Symposium, San Diego, CA, U.S.A., 313-318.
- Rayner JL, Snape I, Walworth JL, Harvey PM, Ferguson SH (2007). Petroleum-hydrocarbon contamination and remediation by microbioventing at sub-Antarctic Macquarie Island. *Cold Regions Science and Technology*, 48(2):139-153.
- Rodzewich C, Belanger C, Moreau N, Pouliot M, Fellows N (2006). Treatment of PCP-contaminated soil using an engineered ex situ biopile process on a former wood treatment superfund site. *Contaminated soils, sediments and water volume 10: successes and challenges*. Calabrese E.J., Kostecki P.T. and Dragun J. (eds.) Contaminated Soils Series, Springer, New York, NY, U.S.A., 327-338.
- Rojas-Avelizapa NG, Roldan-Carrillo T, Zegarra-Martinez H, Munoz-Colunga AM, Fernandez-Linares LC (2007). A field trial for an ex-situ bioremediation of a drilling mud-polluted site. *Chemosphere*, 66(9):1595-1600.
- Srinivasan U & Glaser JA (1999). The validity of ergosterol-based fungal biomass estimate in bioremediation. Proc., 5th International In Situ and On-Site Bioremediation Symposium, San Diego, CA, U.S.A., 103-109.
- Suko T, Fujikawa T, Miyazaki T (2006). Transport phenomena of volatile solute in soil during bioventing technology. *Contaminated sediments: Evaluation and remediation techniques*. Fukue M., Kita K., Ohtsubo M. and Chaney R., Editors. ASTM STP 1482, ASTM, West Conshohocken, PA, U.S.A., 374-379.
- Thomas AO and Lester JN (1993). The microbial remediation of former gasworks sites—A review. *Environmental Technology*, 14(1):1-24.
- Toffoletto L, Deschenes L, Samson R (2005). LCA of ex-situ bioremediation of diesel-contaminated soil. *International Journal of Life Cycle Assessment*, 10(6):406-416.
- Tsai TT, Kao CM, Yeh TY, Liang SH, Chien HY (2009). Application of surfactant enhanced permanganate oxidation and biodegradation of trichloroethylene in groundwater. *Journal of Hazardous Materials*, 161(1):111-119.
- Turrell J, Clark L, Berbenni P, Nobili F (1998). Remediation of groundwater and aquifer material at the Rho Oil Refinery, with particular reference to the use of ex situ bioremediation. Proc., 6th International FZK/TNO Conference on Contaminated Soil, Edinburgh, Scotland, U.K., 1185-1186.
- Weesner B, Acree S, McAlary T, Salvo JJ (1998). Design and operation of a horizontal well, in situ bioremediation system. Proc., 1st International Conference on Remediation of Chlorinated and Recalcitrant Compounds, Vol 6.—Designing and Applying Treatment Technologies, Monterey, CA, U.S.A., 9-14.

Phytoremediation

- Asada M, Parkpian P, Horiuchi S (2006). Remediation technology for boron and fluoride contaminated sediments using green plants. *Contaminated sediments: Evaluation and remediation techniques*.

- Fukue M., Kita K., Ohtsubo M. and Chaney R. (eds.) ASTM STP 1482, ASTM, West Conshohocken, PA, U.S.A., 304-310.
- Barbafieri M (2001). Heavy metal chemical species in soil in relation to plant uptake for phytoremediation strategies. Water-rock interaction, Vols. 1 and 2. Cidu R. (ed.) A.A. Balkema, Leiden, the Netherlands, 1039-1042.
- Carman EP & Crossman TL (2001). Phytoremediation. In situ treatment technology, 2nd edition. CRC Press, Boca Raton, FL, U.S.A., 391-435.
- Claus D, Dietze H, Gerth A, Grosser W, Hebner A (2007). Application of agronomic practice improves phytoextraction on a multipolluted site. *Journal of Environmental Engineering and Landscape Management*, 15(4):208-212.
- Gao YZ, Ling WT, Zhu LZ, Zhao BW, Zheng QS (2007). Surfactant-enhanced phytoremediation of soils contaminated with hydrophobic organic contaminants: Potential and assessment. *Pedosphere*, 17(4):409-418.
- King DJ, Doronila AI, Feenstra C, Baker AJM, Woodrow IE (2008). Phytostabilisation of arsenical gold mine tailings using four Eucalyptus species: Growth, arsenic uptake and availability after five years. *Science of the Total Environment*, 406(1-2):35-42.
- Kvesitadze G, Khatisachvili G, Sadunishvili T, Ramsden JJ (2006). Biochemical mechanisms of detoxification in higher plants: Basis of phytoremediation. Springer, Berlin, Germany.
- Lin Q, Shen KL, Zhao HM, Li WH (2008). Growth response of *Zea mays* L. in pyrene-copper co-contaminated soil and the fate of pollutants. *Journal of Hazardous Materials*, 150(3):515-521.
- Lin ZQ, Schemenauer RS, Cervinka V, Zayed A, Lee A, Terry N (2000). Selenium volatilization from a soil-plant system for the remediation of contaminated water and soil in the San Joaquin Valley. *Journal of Environmental Quality*, 29(4):1048-1056.
- Meers E, Ruttens A, Hopgood MJ, Samson D, Tack FMG (2005). Comparison of EDTA and EDDS as potential soil amendments for enhanced phytoextraction of heavy metals. *Chemosphere*, 58(8):1011-1022.
- Mendez MO & Maier RM (2008). Phytostabilization of mine tailings in arid and semiarid environments - An emerging remediation technology. *Environmental Health Perspectives*, 116(3):278-283.
- Padmavathiamma PK & Li LY (2007). Phytoremediation technology: Hyper-accumulation metals in plants. *Water Air and Soil Pollution*, 184(1-4):105-126.
- Schnoor JL, Licht LA, McCutcheon SC, Wolfe NL, Carreira LH (1995). Phytoremediation of organic and nutrient contaminants. *Environmental Science & Technology*, 29(7):A318-A323.
- Shirdam R, Zand AD, Bidhendi GN, Mehrdadi N (2008). Phytoremediation of hydrocarbon-contaminated soils with emphasis on the effect of petroleum hydrocarbons on the growth of plant species. *Phytoremediation*, 89(1):21-29.
- Suresh B & Ravishankar GA (2004). Phytoremediation - A novel and promising approach for environmental clean-up. *Critical Reviews in Biotechnology*, 24(2-3):97-124.
- Susarla S, Medina VF, McCutcheon SC (2002). Phytoremediation: An ecological solution to organic chemical contamination. *Ecological Engineering*, 18(5):647-658.
- Tiwari KK, Dwivedi S, Mishra S, Srivastava S, Tripathi RD, Singh NK, Chakraborty S (2008). Phytoremediation efficiency of *Portulaca tuberosa* rox and *Portulaca oleracea* L. naturally growing in an industrial effluent irrigated area in Vadodra, Gujrat, India. *Environmental Monitoring and Assessment*, 147(1-3):15-22.
- U.S. EPA (1998). A citizen's guide to phytoremediation. EPA 542-F-98-011, Office of Solid Waste and Emergency Response, U.S. EPA, Washington, D.C., U.S.A.
- Willey N (2007). Editor. *Phytoremediation: Methods and reviews*. Humana Press, Totowa, NJ, U.S.A.
- Wolfe AK & Bjornstad DJ (2002). Why would anyone object? An exploration of social aspects of phytoremediation acceptability. *Critical Reviews in Plant Sciences*, 21(5): 429-438.

Air Sparging / Soil Vapor Extraction

- Anderson WC (1994). Editor. *Innovative site remediation technology*. Vol. 8—Vacuum vapor extraction. American Academy of Environmental Engineers, Annapolis, MD, U.S.A.
- Bass DH, Hastings NA, Brown RA (2000). Performance of air sparging systems: a review of case studies. *Journal of Hazardous Materials*, 72(2-3):101-119.
- Braida W & Ong SK (2000). Modeling of air sparging of VOC-contaminated soil columns. *Journal of Contaminant Hydrology*, 41(3-4):385-402.
- Frank U & Barkley N (1995). Remediation of low permeability subsurface formations by fracturing enhancement of soil vapor extraction. *Journal of Hazardous Materials*, 40(2):191-201.
- Hsu HT & Yeung AT (1996). Development of a mathematical model for design of multiple-well soil vapor extraction systems. *Environmental toxicology and risk assessment: biomarkers and risk assessment—Fifth volume*. Bengtson D.A. and Henshel D.S. (eds.) ASTM STP 1306, ASTM, PA, PA, U.S.A., 441-455.
- Kaslusky SF & Udell KS (2005). Co-injection of air and steam for the prevention of the downward migration of DNAPLs during steam enhanced extraction: An

- experimental evaluation of optimum injection ratio predictions. *Journal of Contaminant Hydrology*, 77(4):325-347.
- Liang CJ & Lee IL (2008). In situ iron activated persulfate oxidative fluid sparging treatment of TCE contamination—A proof of concept study. *Journal of Contaminant Hydrology*, 100(3-4):91-100.
- Marley MC, Hazebrouck DJ, Walsh MT (1992). The application of insitu air sparging as an innovative soils and ground-water remediation technology. *Ground Water Monitoring and Remediation*, 12(2):137-145.
- Parsons EG, Barclay C, Thirumirathi D (1997). In situ air induction as an innovative technology for bioremediation in the capillary zone. Proc., 4th International In Situ and On-Site Bioremediation Symposium, New Orleans, LA, U.S.A., 277-282.
- Reddy KR & Adams JA (2002). Cleanup of chemical spills using air sparging. *The handbook of hazardous materials spills technology*. M. Fingas (ed.) McGraw-Hill, New York, NY, U.S.A., Chapter 14.
- Schulenberg JW & Reeves HW (2002). Axi-symmetric simulation of soil vapor extraction influenced by soil fracturing. *Journal of Contaminant Hydrology*, 57(3-4):189-222.
- Smith W (1998). Use of AS/SVE to remediate chlorinated solvents. Proc., 1st International Conference on Remediation of Chlorinated and Recalcitrant Compounds, Vol. 1—Risk, Resource, and Regulatory Issues, Monterey, CA, U.S.A., 187-192.
- Zhao L & Zytner RG (2004). The application of FEMLAB in modeling soil vapor extraction. Proc., World Engineers' Convention 2004: Vol. D Environment Protection and Disaster Mitigation, Shanghai, China, 115-119.
- ### Electrochemical Remediation
- Acar YB, Rabbi MF, Ozsu EE (1997). Electrokinetic injection of ammonium and sulfate ions into sand and kaolinite beds. *Journal of Geotechnical and Geoenvironmental Engineering*, ASCE, 123(3):239-249.
- Alshwabkeh AN, Yeung AT, Bricka MR (1999). Practical aspects of in-situ electrokinetic extraction. *Journal of Environmental Engineering*, ASCE, 125(1): 27-35.
- Barton WA, Miller SA, Veal CJ (1999). The electrode-watering of sewage sludges. *Drying Technology*, 17(3):497-522.
- Bonilla A, Cuesta P, Zubiaga R, de Baranda MS, Iglesias J (1999). In situ contaminated soil remediation and contaminated soil containment using electrokinetic techniques. Proc., Global Symposium on Recycling, Waste Treatment and Clean Technology, San Sebastian, Spain, 2571-2581.
- Buckland DG, Shang JQ, Mohamedelhasan E (2000). Electrokinetic sedimentation of contaminated Welland River sediment. *Canadian Geotechnical Journal*, 37(4):735-747.
- Budhu M, Rutherford M, Sills G, Rasmussen W (1997). Transport of nitrates through clay using electrokinetics. *Journal of Environmental Engineering*, ASCE, 123(12):1251-1253.
- Campanella RG (2008). Geo-environmental site characterization. The 3rd James K. Mitchell Lecture, Geotechnical and geophysical site characterization. Proc., 3rd International Conference on Site Characterization, Taipei, China 3-15.
- Chang JH, Qiang ZM, Huang CP (2006). Remediation and stimulation of selected chlorinated organic solvents in unsaturated soil by a specific enhanced electrokinetics. *Colloids and Surfaces A—Physicochemical and Engineering Aspects*, 287(1-3):86-93.
- Chen XJ, Shen ZM, Lei YM, Zheng SS, Ju BX, Wang WH (2006). Effects of electrokinetics on bioavailability of soil nutrients. *Soil Science*, 171(8):638-647.
- Darilek GT, Corapcioglu MY, Yeung AT (1996). Sealing leaks in geomembrane liners using electrophoresis. *Journal of Environmental Engineering*, ASCE, 122(6):540-544.
- DeFlaun MF & Condee CW (1997). Electrokinetic transport of bacteria. *Journal of Hazardous Materials*, 55(1-3):263-277.
- Faulkner DWS, Hopkinson L, Cundy AB (2005). Electrokinetic generation of reactive iron-rich barriers in wet sediments: Implications for contaminated land management. *Mineralogical Magazine*, 69(5): 749-757.
- Ho SV, Athmer C, Sheridan PW, Hughes BM, Orth R, McKenzie D, Brodsky PH, Shapiro A, Thornton R, Salvo J, Schultz D, Landis R, Griffith R, Shoemaker S (1999a). The lasagna technology for in situ soil remediation. 1. Small field test. *Environmental Science & Technology*, 33(7):1086-1091.
- Ho SV, Athmer C, Sheridan PW, Hughes BM, Orth R, McKenzie D, Brodsky PH, Shapiro AM, Sivavec TM, Salvo J, Schultz D, Landis R, Griffith R, Shoemaker S (1999b). The lasagna technology for in situ soil remediation. 2. Large field test. *Environmental Science & Technology*, 33(7):1092-1099.
- Ho SV, Sheridan PW, Athmer CJ, Heitkamp MA, Brackin JM, Weber D, Brodsky PH (1995). Integrated in situ soil remediation technology: The Lasagna process. *Environmental Science & Technology*, 29(10): 2528-2534.
- Hunter RJ (1981). *Zeta potential in colloid science: Principles and applications*. Academic Press, London, U.K.

- Iyer R (2001). Electrokinetic remediation. *Particulate Science and Technology*, 19(3):219-228.
- Jiradecha C, Urgan-Demirtas M, Pagilla K. (2006). Enhanced electrokinetic dissolution of naphthalene and 2,4-DNT from contaminated soils. *Journal of Hazardous Materials*, 136(1):61-67.
- Kim GN, Jung YH, Lee JJ, Moon JK, Jung CH (2008). Development of electrokinetic-flushing technology for the remediation of contaminated soil around nuclear facilities. *Journal of Industrial and Engineering Chemistry*, 14(6):732-738.
- Kim SO, Kim WS, Kim KW (2005). Evaluation of electrokinetic remediation of arsenic-contaminated soils. *Environmental Geochemistry and Health*, 27(5-6): 443-453.
- Kim SS & Han SJ (2003). Application of an enhanced electrokinetic ion injection system to bioremediation. *Water, Air, & Soil Pollution*, 146(1-4):365-377.
- Lageman R, Clarke RL, Pool W (2005). Electro-reclamation, a versatile soil remediation solution. *Engineering Geology*, 77(3-4):191-201.
- Lee HS & Lee K (2001). Bioremediation of diesel-contaminated soil by bacterial cells transported by electrokinetics. *Journal of Microbiology and Biotechnology*, 11(6): 1038-1045.
- Luo QS, Wang H, Zhang XH, Fan XY, Qian Y (2006). In situ bioelectrokinetic remediation of phenol-contaminated soil by use of an electrode matrix and a rotational operation mode. *Chemosphere*, 64(3): 415-422.
- Maini G, Sharman AK, Sunderland G, Knowles CJ, Jackman S (2000). An integrated method incorporating sulfur-oxidising bacteria and electrokinetics to enhance removal of copper from contaminated soil. *Environmental Science & Technology*, 34(6):1081-1087.
- Maturi K & Reddy KR (2008). Cosolvent-enhanced desorption and transport of heavy metals and organic contaminants in soils during electrokinetic remediation. *Water Air and Soil Pollution*, 189(1-4):199-211.
- Mitchell JK & Yeung AT (1991). Electro-kinetic flow barriers in compacted clay. *Geotechnical Engineering 1990. Transportation Research Record 1288*, Transportation Research Board, National Research Council, Washington, D.C., U.S.A., 1-9.
- Mitchell JK (1993). *Fundamentals of soil behavior*, 2nd Edition. John Wiley & Sons, New York, NY, U.S.A.
- Murillo-Rivera B, Labastida I, Barrón J, Oropeza-Guzman MT, González I, Teutli-Leon MMM (2009). Influence of anolyte and catholyte composition on TPHs removal from low permeability soil by electrokinetic reclamation. *Electrochimica Acta*, 54(7): 2119-2124.
- O'Connor CS, Lepp NW, Edwards R, Sunderland G (2003). The combined use of electrokinetic remediation and phytoremediation to decontaminate metal polluted soils: A laboratory-scale feasibility study. *Environmental Monitoring and Assessment*, 84(1-2): 141-158.
- Rabbi MF, Clark B, Gale RJ, Ozsu-Acar E, Pardue J, Jackson A (2000). In situ TCE bioremediation study using electrokinetic cometabolite injection. *Waste Management*, 20(4):279-286.
- Reddy KR, Chaparro C, Saichek RE (2003a). Iodide-enhanced electrokinetic remediation of mercury-contaminated soils. *Journal of Environmental Engineering, ASCE* 129(12):1137-1148.
- Reddy KR, Chinthamreddy S, Saichek RE, Cutright TJ (2003b). Nutrient amendment for the bioremediation of a chromium-contaminated soil by electrokinetics. *Energy Sources*, 25(9):931-943.
- Sah JG & Lin LY (2000). Electrokinetic study on copper contaminated soils. *Journal of Environmental Science and Health Part A—Toxic/Hazardous Substances & Environmental Engineering*, 35(7):1117-1139.
- Saichek RE & Reddy KR (2005a). Electrokinetically enhanced remediation of hydrophobic organic compounds in soils: A review. *Critical Reviews in Environmental Science and Technology*, 35(2):115-192.
- Saichek RE & Reddy KR (2005b). Surfactant-enhanced electrokinetic remediation of polycyclic aromatic hydrocarbons in heterogeneous subsurface environments. *Journal of Environmental Engineering and Science*, 4(5):327-339.
- Thevanayagam S & Rishindran T (1998). Injection of nutrients and TEAs in clayey soils using electrokinetics. *Journal of Geotechnical Engineering, ASCE*, 124(4): 330-338.
- Vijh AK (1995). Electrochemical aspects of electroosmotic dewatering of clay suspensions. *Drying Technology*, 13(1&2):215-224.
- Yang GCC & Liu CY (2001). Remediation of TCE contaminated soils by in situ EK-Fenton process. *Journal of Hazardous Materials*, 85(3):317-331.
- Yang GCC & Long Y-W (1999). Removal and degradation of phenol in a saturated flow by in-situ electrokinetic remediation and Fenton-like process. *Journal of Hazardous Materials*, 69(3):259-271.
- Yeung AT (1992). Diffuse double layer equations in SI units. *Journal of Geotechnical Engineering, ASCE*, 118(12):2000-2005.
- Yeung AT (1993). Electro-kinetic barrier to contaminant transport. *Proc., International Conference on Environmental Management: Geo-water & Engineering Aspects*, Wollongong, Australia, 239-244.
- Yeung AT (1994). Electrokinetic flow processes in porous media and their applications. *Advances in porous media*. Corapcioglu M.Y. (ed.) Elsevier, Amsterdam, the Netherlands, 2, 309-395.

- Yeung AT (2006) Contaminant extractability by electrokinetics. *Environmental Engineering Science*, 23(1): 202-224.
- Yeung AT (2008). *Electrokinetics for soil remediation. Environmental Geotechnology and Global Sustainable Development 2008*. Yeung A.T. and Lo I.M.C., Editors. Advanced Technovation Limited, Hong Kong, China, 16-25.
- Yeung AT (2009). Geochemical processes affecting electrochemical remediation. *Electrochemical remediation technologies for polluted soils, sediments and groundwater*. Reddy K.R. and Cameselle C. (eds.) John Wiley & Sons, New York, NY, U.S.A., in press.
- Yeung AT, Chung M, Corapcioglu MY, Stallard WM (1997b). Impoundment liner repair by electrophoresis of clay. *Journal of Environmental Engineering, ASCE*, 123(10):993-1001.
- Yeung AT, Darilek GT, Corapcioglu MY (1997a). Electrophoresis: Innovative technique to repair leaking impoundments. In *situ remediation of the geoenvironment. Geotechnical Special Publication No. 71*, ASCE, Reston, VA, U.S.A., 560-573.
- Yeung AT & Hsu C (2005). Electrokinetic remediation of cadmium-contaminated clay. *Journal of Environmental Engineering, ASCE*, 131(2), 298-304.
- Yeung AT, Hsu C, Menon RM (1996). EDTA-enhanced electrokinetic extraction of lead. *Journal of Geotechnical Engineering, ASCE*, 122(8):666-673.
- Yuan C & Weng CH (2002). Sludge dewatering by electrokinetic technique: Effect of processing time and potential gradient. *Advances in Environmental Research*, 7(3):727-732.

Thermal Treatment

- Anderson WC (1993). Editor. *Innovative site remediation technology. Vol. 6—Thermal desorption*. American Academy of Environmental Engineers, Annapolis, MD, U.S.A.
- Anderson WC (1994). Editor. *Innovative site remediation technology. Vol. 7—Thermal destruction*. American Academy of Environmental Engineers, Annapolis, MD, U.S.A.
- Lee WJ, Shih SI, Chang CY, Lai YC, Wang LC, Chang-Chien GP (2008). Thermal treatment of polychlorinated dibenzo-p-dioxins and dibenzofurans from contaminated soils. *Journal of Hazardous Materials*, 160(1):220-227.
- Renoldi F, Lietti L, Saponaro S, Bonomo L, Forzatti P (2003). Thermal desorption of a PAH-contaminated soil: a case study. *Ecosystems and sustainable development IV, Vols. 1 & 2*. Tiezzi E., Brebbia C.A. and Uso J.L. (eds.) WIT Press, Southampton, U.K, 1123-1132.

Other Remediation Technologies

- Alguacil FJ, Alonso M, Lopez F, Lopez-Delgado A (2008). Uphill permeation of Cr(VI) using Hostarex A327 as ionophore by membrane-solvent extraction processing. *Chemosphere*, 72(4):684-689.
- Anitescu G & Tavlirides LL (2006). Supercritical extraction of contaminants from soils and sediments. *Journal of Supercritical Fluids*, 38(2):167-180.
- Annapragada R., Leet R., Changrani R. and Raupp G.B. (1997). Vacuum photocatalytic oxidation of trichloroethylene. *Environmental Science & Technology*, 31(7):1898-1901.
- Benson SM & Cole DR (2008). CO₂ sequestration in deep sedimentary formations. *Elements*, 4(5):325-331.
- Bringas E, San Roman MF, Ortiz I (2006). Separation and recovery of anionic pollutants by the emulsion pertraction technology. *Remediation of polluted groundwaters with Cr(VI)*. *Industrial & Engineering Chemistry Research*, 45(12):4295-4303.
- Chang MC, Shu HY, Hsieh WP, Wang MC (2007). Remediation of soil contaminated with pyrene using ground nanoscale zero-valent iron. *Journal of the Air & Waste Management Association*, 57(2):221-227.
- Christiansen CM, Riis C, Christensen SB, Broholm MM, Christensen AG, Klint KES, Wood JSA, Bauer-Gottwein P, Bjerg PL (2008). Characterization and quantification of pneumatic fracturing effects at a clay till site. *Environmental Science & Technology*, 42(2): 570-576.
- Destailhats H, Hoffmann MR, Wallace HC (2003). Sonochemical degradation of pollutants. *Chemical degradation methods for wastes and pollutants*. Tarr M.A. (ed.) Marcel Dekker, New York, NY, U.S.A., 121-163.
- Dawson EA, Parkes GMB, Bond G, Mao R (2009). A system to investigate the remediation of organic vapors using microwave-induced plasma with fluidized carbon granules. *Review of Scientific Instruments*, 80(3), Article Number: 034102.
- Fatemi F, Liu L, Mahabadi OK, Satish M (2008). Investigating the effect of implementing heating rods within a ZVI-PRB to enhance performance, improve design and reduce costs. *Water Air and Soil Pollution*, 190(1-4):231-243.
- Gong ZQ, Alef K, Wilke BM, Li PJ (2007). Activated carbon adsorption of PAHs from vegetable oil used in soil remediation. *Journal of Hazardous Materials*, 143(1-2):372-378.
- Guo W, Gao D, Wang X (2009). A study of kinetic modeling of the degradation of acid orange 7 by microwave induced oxidation process. *Environmental Engineering Science*, 26(2):327-332.
- Jayaweera I (2003). Supercritical water oxidation

- technology. Chemical degradation methods for wastes and pollutants. Tarr M.A. (ed.) Marcel Dekker, New York, NY, U.S.A., 121-163.
- Kovalick WW, Jr (2008). Review of characterization and remediation of technologies for NAPL's in groundwater. Methods and techniques for cleaning-up contaminated site. Annable M.D., Teodorescu M., Hlavinek P. and Diels L. (eds.) Springer, Dordrecht, the Netherlands, 165-175.
- Ludmer Z, Golan T, Ermolenko E, Brauner N, Ullmann A (2009). Simultaneous removal of heavy metals and organic pollutants from contaminated sediments and sludges by a novel technology, sediments remediation phase transition extraction. *Environmental Engineering Science*, 26(2):419-430.
- Mincher BJ & Cooper WJ (2003). The electron beam process for the radiolytic degradation of pollutants. Chemical degradation methods for wastes and pollutants. Tarr M.A. (ed.) Marcel Dekker, New York, NY, U.S.A., 305-341.
- Moreno E, Reza J, Trejo A (2007). Extraction of polycyclic aromatic hydrocarbons from soil using water under subcritical conditions. *Polycyclic Aromatic Compounds*, 27(4): 239-260.
- Nagpal V & Guigard SE (2005). Remediation of flare pit soils using supercritical fluid extraction. *Journal of Environmental Engineering and Science*, 4(5):307-318.
- Pichat P (2003). Photocatalytic degradation of pollutants in water and air: Basic concepts and applications. Chemical degradation methods for wastes and pollutants. Tarr M.A. (ed.) Marcel Dekker, New York, NY, U.S.A., 77-119.
- Rivas J, Gimeno O, Mantell C, Portela JR, de la Ossa EJM, de la Calle RG (2009). Supercritical CO₂ extraction of PAHs on spiked soil Co-solvent effect and solvent regeneration by ozonization. *Journal of Hazardous Materials*, 162(2-3):777-784.
- Sunarso J & Ismadji S (2009). Decontamination of hazardous substances from solid matrices and liquids using supercritical fluids extraction: A review. *Journal of Hazardous Materials*, 161(1):1-20.
- Venkatraman SN, Schuring JR, Boland TM, Bossert ID, Kosson DS (1998). Application of pneumatic fracturing to enhance in situ bioremediation. *Journal Of Soil Contamination*, 7(2):143-162.
- Wen H, Bergendahl JA, Thompson RW (2009). Removal of estrone from water by adsorption on zeolites with regeneration by direct UV photolysis. *Environmental Engineering Science*, 26(2):319-326.
- Reports on Engineering Practice No. 99, ASCE, Reston, VA, U.S.A.
- Askari MDF, Maskarinec MP, Smith SM, Beam PM and Travis CC (1996). Effectiveness of purge and trap for measurement of volatile organic compounds in aged soils. *Analytical Chemistry*, 68(19):3431-3433.
- Bromage ES, Vadas GG, Harvey E, Unger MA, Kaattari SL (2007). Validation of an antibody-based biosensor for rapid quantification of 2,4,6-trinitrotoluene (TNT) contamination in ground water and river water. *Environmental Science & Technology*, 41(20):7067-7072.
- Gavaskar A, Rosansky S, Naber S, Gupta N, Sass B, Sminchak J, DeVane MP, Holdsworth T (2000). DNAPL delineation with soil and groundwater sampling. Treating dense nonaqueous-phase liquids (DNAPLs) - remediation of chlorinated and recalcitrant compounds. Wickramanayake G.B., Gavaskar A.R. and Gupta N. (eds.) Battelle Press, Columbus, OH, U.S.A., 49-58.
- McAndrews B, Heinze K, DiGuseppi W (2003). Defining TCE plume source areas using the Membrane Interface Probe (MIP). *Soil & Sediment Contamination*, 12(6):799-813.
- McNab WW & Ruiz R (2001). In situ measurement of electroosmotic fluxes and conductivity using single wellbore tracer tests. *Ground Water Monitoring and Remediation*, 21(4):133-139.
- McCobb TD, LeBlanc DR, Massey AJ (2009). Monitoring the removal of phosphate from ground water discharging through a pond-bottom permeable reactive barrier. *Ground Water Monitoring and Remediation*, 29(2):43-55.
- Nielsen DM & Nielsen GL (2006). Ground-water sampling. Practical handbook of environmental site characterization and ground-water monitoring, 2nd edition, Nielsen D.M. (ed.) Taylor & Francis, Boca Raton, FL, U.S.A., 959-1112.
- Rivett MO & Thornton SF (2008). Monitored natural attenuation of organic contaminants in groundwater: principles and application. *Proceedings of the Institution of Civil Engineers—Water Management*, 161(6):381-392.
- Roh Y, Lee SR, Choi SK, Elless MP, Lee SY (2000). Physicochemical and mineralogical characterization of uranium-contaminated soils. *Soil & Sediment Contamination*, 9(5): 463-486.
- Ruda T & Farrar J (2006). Environmental drilling for soil sampling, rock coring, borehole logging, and monitoring well installation. Practical handbook of environmental site characterization and ground-water monitoring, 2nd edition, Nielsen D.M. (ed.) Taylor & Francis, Boca Raton, FL, U.S.A., 297-344.
- Sacile R (2007). Remote real-time monitoring and control of contamination in underground storage tank

Performance Monitoring

ASCE (1999). Environmental site characterization and remediation design guidance. ASCE Manuals and

- systems of petrol products. *Journal of Cleaner Production*, 15(13-14): 1295-1301.
- Sara MN (2006). Ground-water monitoring system design. *Practical handbook of environmental site characterization and ground-water monitoring*, 2nd edition, Nielsen D.M. (ed.) Taylor & Francis, Boca Raton, FL, U.S.A., 517-572.
- Sevee J (2006). Methods and procedures for defining aquifer parameters. *Practical handbook of environmental site characterization and ground-water monitoring*, 2nd edition, Nielsen D.M. (ed.) Taylor & Francis, Boca Raton, FL, U.S.A., 913-958.
- Vitale RJ & Braids OC (2006). Ground-water sample analysis. *Practical handbook of environmental site characterization and ground-water monitoring*, 2nd edition, Nielsen D.M. (ed.) Taylor & Francis, Boca Raton, FL, U.S.A., 1113-1134.
- Wiedemeier TH, Barden MJ, Haas PE, Dickson WZ (2006). Designing monitoring programs to effectively evaluate the performance of natural attenuation. *Practical handbook of environmental site characterization and ground-water monitoring*, 2nd edition, Nielsen D.M. (ed.) Taylor & Francis, Boca Raton, FL, U.S.A., 573-637.
- Wilson RD, Yip WC, Naas CN (2008). Assessing performance of a permeable biobarrier. *Proceedings of the Institution of Civil Engineers—Water Management*, 161(6):375-379.
- Zolla V, Freyria FS, Sethi R, Di Molfetta A (2009). Hydrogeochemical and biological processes affecting the long-term performance of an iron-based permeable reactive barrier. *Journal of Environmental Quality*, 38(3):897-908.
- Selection of Remediation Technologies**
- ASCE (1999). *Environmental site characterization and remediation design guidance*. ASCE Manuals and Reports on Engineering Practice No. 99, ASCE, Reston, VA, U.S.A.
- Bage GF, Samson R, Sinclair-Desgagne B (2004). A proactive approach can make site remediation less expensive. *Environmental Management*, 34(4):449-460.
- Efroymsen RA, Peerson MJ, Giffen NR, Ryon MG, Smith JG, Hargrove WW, Roy WK, Welsh CJ, Druckenbrod DL, Quarles HD (2008). Investigating habitat value to inform contaminant remediation options: Case study. *Journal of Environmental Management*, 88(4):1452-1470.
- Efroymsen RA, Peterson MJ, Welsh CJ, Druckenbrod DL, Ryon MG, Smith JG, Hargrove WW, Giffen NR, Roy WK, Quarles HD (2008). Investigating habitat value to inform contaminant remediation options: Approach. *Journal of Environmental Management*, 88(4):1436-1451.
- Faw RE & Shultis JK (1993). *Radiological assessment: Sources and exposures*. PTR Prentice-Hall, Englewood Cliffs, NJ, U.S.A.
- Greenberg R & Cervino D (2002). Fixed price cleanups as useful tools to eliminate risks in brownfields redevelopment. *Brownfield sites: Assessment, rehabilitation and development*. Brebbia C.A., Almorza D. and Klapperich H. (eds.) WIT Press, Southampton, U.K., 307-314.
- Hightower M, Armstrong J, Beam P, Ingle D, Steimle R, Trizinsky M (1998). Cooperative approach in implementing innovative technologies at the Pinellas STAR Center. *Proc., 1st International Conference on Remediation of Chlorinated and Recalcitrant Compounds*, Vol. 1—Risk, Resource, and Regulatory Issues, Monterey, CA, U.S.A., 229-233.
- Klaffke D (2006). Recent approaches for urban groundwater pollution prevention and remediation - Analysis and recommendations. *Urban groundwater management and sustainability*. NATO Science Series IV Earth and Environmental Sciences, 74:357-373.
- Knowlton RG, Peterson DM, Zhang HB (2003). The use of decision support systems to address spatial variability, uncertainty, and risk. *Spatial methods for solution of environmental and hydrologic problems—science, policy, and standardization*. Singhroy V., Hansen D.T., Pierce R.R. and Johnson A.I. (eds.) ASTM STP 1420, West Conshohocken, PA U.S.A., 109-121.
- Ko NY & Lee KK (2008). Reliability and remediation cost of optimal remediation design considering uncertainty in aquifer parameters. *Journal of Water Resources Planning and Management*, ASCE, 134(5):413-421.
- Liu L, Hao RX, Cheng SY, Guo HC (2004). An integrated feasibility study on designing remediation systems for petroleum-contaminated sites. *Water Air and Soil Pollution*, 156(1-4):83-95.
- Peralta RC, Kalwij IM, Wu SJ (2008). Practical remedial design optimization for large complex plumes. *Journal of Water Resources Planning and Management*, ASCE, 134(5):422-431.
- Porter A, Sadek A, Hayden N (2006). Fuzzy geographic information systems for phytoremediation plant selection. *Journal of Environmental Engineering*, ASCE, 132(1):120-128.
- Qin XS, Huang GH, Chakma A (2007). A stepwise-inference-based optimization system for supporting remediation of petroleum-contaminated sites. *Water Air and Soil Pollution*, 185(1-4):349-368.
- U.S. EPA (1993). *Remediation technologies screening matrix and reference guide*. U.S. EPA, Washington, D.C., U.S.A.

Yoon H, Werth CJ, Barkan CPL, Schaeffer DJ, Anand P (2009). An environmental screening model to assess the consequences to soil and groundwater from railroad-tank-car spills of light non-aqueous phase liquids. *Journal of Hazardous Materials*, 165(1-3):332-344.

Cost Estimate

Rast RR & Rast JC (2003). *Environmental remediation estimating methods*, 2nd edition. Construction Publishers & Consultants, Kingston, MA U.S.A.

ADVANCES ON BUFFER/BACKFILL PROPERTIES OF HEAVILY COMPACTED GAOMIAOZI BENTONITE

Wei-Min YE^{1,2}, Qiong WANG¹, Yong-Gui CHEN^{1,2} and Bao CHEN^{1,2}

ABSTRACT: Compacted bentonite is considered as buffer/ backfill materials for geological disposal of high-level radioactive wastes in many countries. Through a national screening and comparison, GMZ bentonite is selected as the first choice of Chinese buffer materials for high-level radioactive waste repository. Many studies were conducted on GMZ bentonite, however, its still in the primary stage compared with other candidate bentonites. In order to better orientate the future research work, the progress on researches of GMZ bentonite was summarized, which consist of studies on mineralogy and chemical composition, mechanical properties, hydraulic behavior, swelling behavior, thermal conductivity, microstructure and volume change behavior. Based on analysis of the current studies, the key issues to be explored in the future were also proposed, that is the influence of temperature on behavior of the GMZ bentonite; the migration law of nuclide in compacted bentonite and sealing properties of GMZ bentonite based materials under coupled T-H-M-C conditions..

KEYWORDS: GMZ bentonite, mechanical properties, hydraulic properties, thermal conductivity, microstructure characteristic, volume change behavior

INTRODUCTION

Important attention has been devoted over recent years to safety dispose of high level radioactive waste (HLW) (Wu 2005). Deep geological disposal is considered worldwide as the most safely and feasible method (Pusch 1979; Shen 2001b). This disposal concept is based on a multi-barrier system, which comprises the natural geological barriers and the engineering barriers.

Engineering barriers represents the man-made engineering materials placed with in a repository, which aims to seals the possible escape path for the radionuclide to the environment. As the final barriers in the repository, buffer/backfill materials are expected to have the following properties: very low permeability, high exchange capacity, sufficient mechanical resistance, high thermal conductivity, moderate swelling potential, low shrinkage in response to the drying, suitable swelling pressure, et al. Due to its favorable properties, the bentonite is considered as the buffer/backfill material in HLW depository in many countries.

In the real repository, the buffer/backfill material will undergo complex and coupled thermo-hydro-chemo-mechanical processes. As a result, the characteristics of buffer/backfill material in the field are quite different from that in general conditions. Thus, the study about

these is essential to safely dispose the high-level radioactive wastes (Wang 2006).

Presently, lots of studies have performed all over the world on other candidate bentonites, including MX80 (America), FoCa (France), S-2 (Spain) and Kunigel VI (Japan) et al. useful experimental and theoretic experience for the further study are obtained. The techniques generally used include lab tests, physical models, and field tests and so on. However, under T-H-M-C conditions, the influence of chemistry on sealing behavior of bentonite is extremely complex, and related studies were still in the primary stage; so most studies of coupled T-H-M-C effects are conducted by numerical simulating methods (Liu 2008).

China is among the latecomers to the study on buffer/backfill materials, but some progresses have been made. Gaomiaozi (GMZ) bentonite has been selected as the first choice as buffer/backfill materials for Chinese high-level radioactive waste repository, after a nationwide screening. Also, many contributions have been made to the study of mineralogy and chemical composition, mechanical property, hydraulic behavior, swelling behavior, thermal conductivity, microstructure, and volume change behavior about GMZ bentonite. Based on a comprehensive review on the results have been achieved about the studies of GMZ bentonite, all the

¹ Key Laboratory of Geotechnical Engineering, Tongji University, Shanghai 200092, China

² United Research Center for Urban Environment and Sustainable Development, the Ministry of Education, China, Shanghai 200092, China. Email: ye_tju@tongji.edu.cn

achievements have been summarized, and the key issues to be explored in the future are also proposed here.

BASIC PROPERTIES OF GMZ BENTONITE

Mineralogy and Chemical Composition

The quantitative minerals composition of GMZ01 (Na-bentonite) analyzed by X-ray diffraction is summarized in Table 1. It appears that the proportion of montmorillonite is dominant in GMZ01 bentonite, with a high smectite content of 75.4% (Liu 2001). The bulk chemical component of GMZ01 bentonite was analyzed by X-ray fluorescence spectrometry: Al₂O₃ 14.20%, SiO₂ 67.43%, P₂O₅ 0.02%, CaO 1.13%, K₂O 0.73%, TiO₂ 0.12%, FeO 0.29%, TF₂O₃ 2.40%, MgO 0.10%, Na₂O 1.75%, MnO 0.02%. Besides that, GMZ bentonite also contains some lanthanon, like La, Ce, Nd (light rare earth elements) and Y (heavy rare earth elements) (Wen 2005a).

Table 1 Mineral composition of GMZ01

Mineral	% (in mass)
Quartz	11.7%
Cristobalite	7.3%
Feldspar	4.3%
Calcite	0.5%
Kaolinite	0.8%
Montmorillonite	75.4%

Basic Physico- Chemical Properties

As buffer/backfill materials, engineering properties of bentonite are mainly influenced by its physico-chemical properties, especially the CEC (cation exchange capacity) and exchanged cation species, which directly affect the adsorption capacity of nuclide (Liu Yue-miao 2001). Table 2 shows the basic physico-chemical properties of GMZ01. The dominant cation is sodium (37.52 mmol/100g). The high CEC (77.06 mmol/100g) and the large specific surface (570 m²/g) are in good agreement with a big plastic index (Ip = 275).

MECHANICAL PROPERTIES

Compaction Characteristics

For the construction of engineering barrier in HLW repository, pure bentonite or sand-bentonite mixtures have to be densely compacted to a form of brick or pellet. Quality of bentonite bricks compacted directly influence

Table 2 Basic properties of GMZ01

Sample	GMZ bentonite	Sodium
Particle density G _s (Mg/m ³)	2.66	
Liquid limit w _L (%)	313	
Plastic limit w _P (%)	38	
Plastic index I _p	275	
Specific surface S (m ² /g)	570	
Cation exchange capacity (meq./g)	77.06	
Exchange capacity of K ⁺ (meq./g)	0.55	
Exchange capacity of Na ⁺ (meq./g)	37.52	
Exchange capacity of Ca ²⁺ (meq./g)	23.18	
Exchange capacity of Mg ²⁺ (meq./g)	10.17	
Alkali Index	1.14	

the function of engineering barriers, so study on the compaction characteristic of bentonite is of great engineering importance.

Generally, the uniaxial static compaction method is employed for producing of the bentonite block. Results show that under the same compaction pressure, the higher the water content, the higher the dry density. However, when the water content increases to higher than a certain value, some like the optimum water content to the dynamic compaction, the dry density turns to decrease with the increase of water content (Guo 2004).

GMZ01 bentonite with 15% water content is more easily to be compacted to a high density block than that of below 10% or above 20% (Liu 2007b).

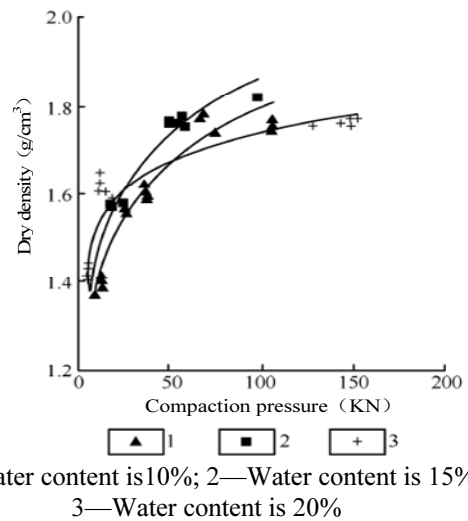


Fig.1 Relationship between dry density and compaction pressure (Liu 2007b)

Compressive Strength

At room temperature, the unconfined compressive strength and the elastic modulus of GMZ Na-bentonite both increase with its dry density. Unconfined strength for GMZ01 reaches maximum at its optimum water content (close to $\omega=13\%$) (Wen 2005b, Liu 2007b) (Figs. 2 & 3).

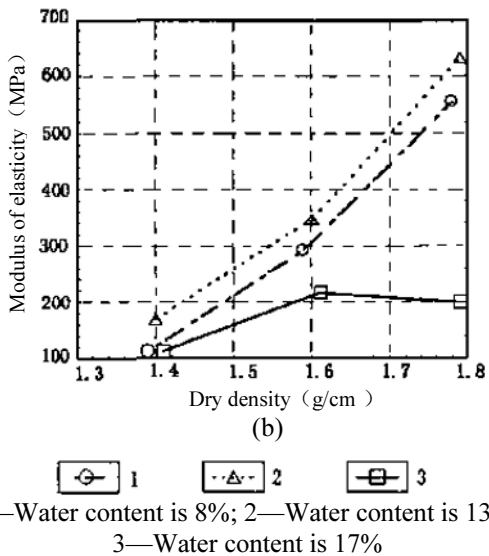
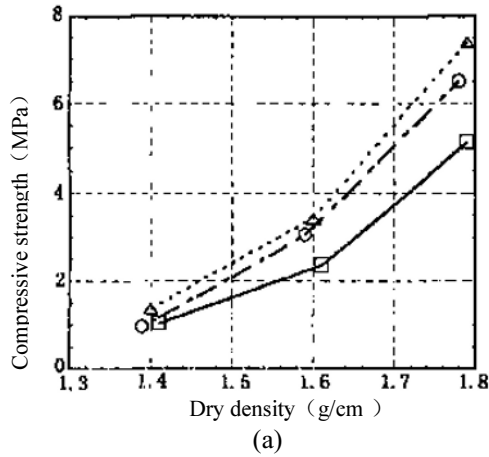


Fig. 2 Compressive strength, Modulus of elasticity vs. dry density (Wen 2005b)

Swelling Properties

During the formation process of artificial barrier, buffer/backfill materials must have the ability to swell by water intake, in order to fill in the voids between bentonite bricks and bricks, bricks and canister, and bricks and host rock. However, during the operation of repository, excessive swelling pressure developed as bentonite's wetting should be avoided, which might cause damage to the repository. So, the swelling behavior is a key property of buffer/backfill materials.

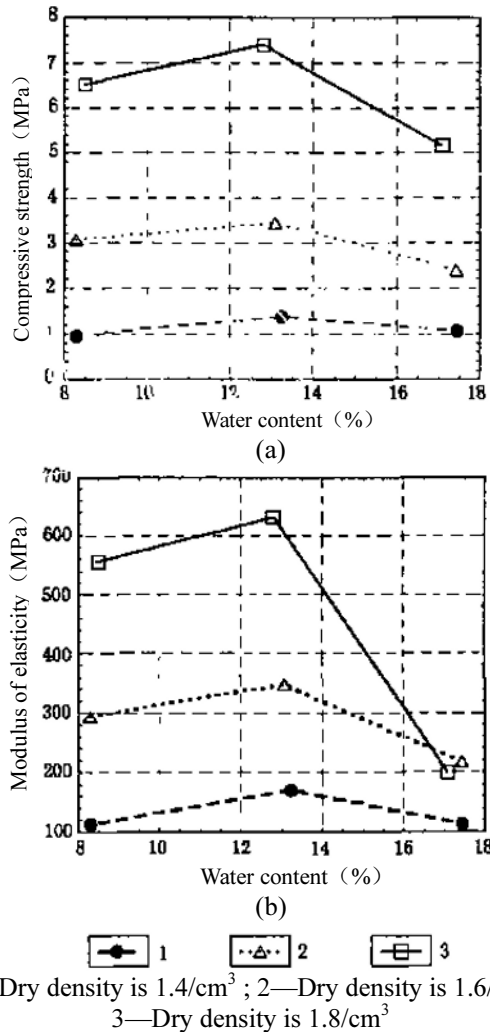


Fig. 3 Compressive strength, Modulus of elasticity vs. water content (Wen 2005b)

It's widely accepted that the swelling pressure of compacted bentonite is influenced by its mineralogy composition, structure, and initial dry density et al. Results indicate that influencing factors on the swelling pressure of bentonite can be classified into internal ones including specific surface area, cation exchange capacity, property of pore water (ion type and concentration) et al. and external ones such as dry density, water content and compaction method et al. (Ye 2007). The maximum swelling pressure increases with increase of montmorillonite content and initial dry density (Komine, & Ogata 1999; Wang 2000; Agus 2005), but the maximum swelling pressure and expansion ratio are almost independent of the initial water content (Wang 2000; Liu 2002).

The curves of swelling pressure vs. time for compacted GMZ bentonite clearly develop in step-phase (Fig. 4). For the specimen with same moisture content, the higher the initial dry density, the faster the swelling velocity; and the more obvious the step-phase character of the swelling pressure curve develops. Specimen with

density of 1.75 g/cm³ shows the maximum swelling velocity and swelling pressure.

The swelling pressure changes with time nonlinearly, but there is a linear relationship between time/swelling-pressure and time. There is an exponential relationship between swelling pressure and dry density for GMZ01. (Ye 2007).

$$P = 0.0194 \exp(7.4197 \rho) \quad (1)$$

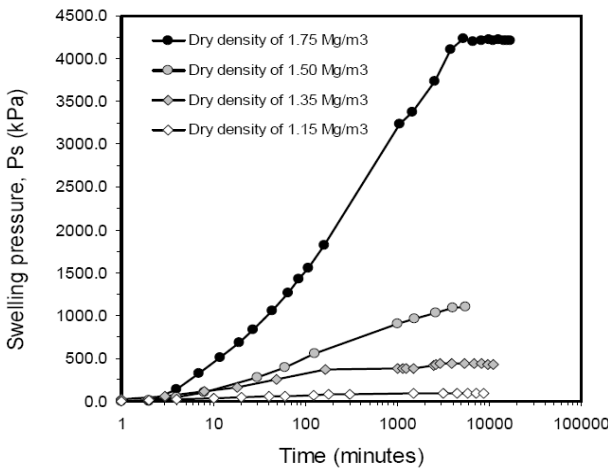


Fig. 4 Curves of swelling pressure vs. time (Ye 2007)

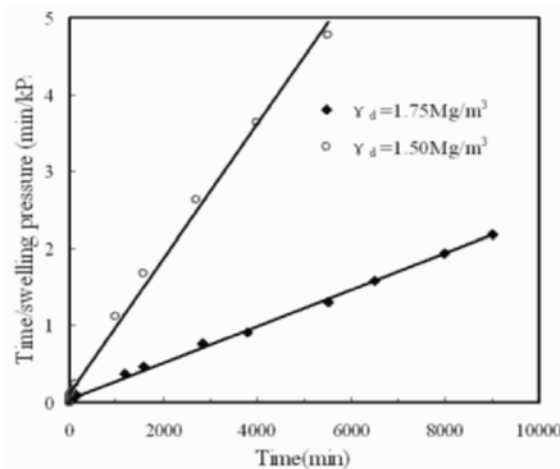


Fig. 5 Relationships between Time/Swelling-Pressure and Time (Ye 2007)

HYDRAULIC BEHAVIORS

Compacted bentonite must have low hydraulic conductivity in order to prevent groundwater from flowing into the repository. It is recommended by IAEA that the hydraulic conductivity of buffer/backfill materials must be less than 10⁻¹³ m/s. Results indicate that, during the construction and operation process, water content of compacted bentonite keeps changing, at the same time, the hydraulic conductivity of bentonite

varies with water content. So, lots of experimental studies have been conducted to investigate the hydraulic conductivity of densely compacted bentonite with different water content.

Saturated Hydraulic Properties

It is reported that, the hydraulic conductivity of densely compacted bentonite or sand-bentonite mixtures is significantly influenced by its dry density and compaction water content. When bentonite is compacted on the dry side (2%—4%) of optimum water content, the hydraulic conductivity reaches minimum (Huang 1992; Goran 2002; Met 2005). While, compacted slightly on the wet side, due to aggregation of the clay matrix forms lots of larger pores, results in higher hydraulic conductivity (Komine 2004).

Saturated hydraulic conductivity of GMZ01 bentonite shows in Table 3. The hydraulic conductivity of GMZ01 significantly decreases with increase of dry density, while increases as the increase of temperature (Wen 2006).

Unsaturated Hydraulic Properties

Table 3 Saturated hydraulic conductivity of GMZ bentonite (Wen 2006)

Dry density (g/cm ³)	Temperature (°C)	Hydraulicity(m/s)
1.4	25	1.12×10 ⁻¹²
	60	1.87×10 ⁻¹²
	90	2.91×10 ⁻¹²
1.6	25	1.94×10 ⁻¹³
	60	3.61×10 ⁻¹³
	90	5.75×10 ⁻¹³
1.8	25	9.99×10 ⁻¹⁴
	60	1.99×10 ⁻¹³
	90	3.00×10 ⁻¹³

In fact, during the construction and operation process, buffer/backfill materials in the repository experiences drying and wetting cycles (Alonso 2005). Accordingly, the buffer/backfill materials undergoes a limitative amplitude of expansion and shrinkage cycles coupling with micro-structural changes, due to the extremely large stiffness of the host formation (granite for instance). It is obvious that in repository, the cyclic expansion and shrinkage process and its influencing mechanism on the unsaturated hydraulic properties of bentonite are very complex. Therefore, it is necessary to investigate the unsaturated hydraulic behavior and its coupling microstructure changes of bentonite under confined and unconfined conditions, based on a clear understanding of its soil-water characteristics.

Soil-water characteristic

Water retention curve (WRC) for a soil is defined as the relationship between suction (ψ) and water content [gravimetric water content (ω), or volumetric water content (θ)] or degree of saturation. Substantively, WRC stands for the water retention (i.e. water storage) capacity of unsaturated soil in the form of water content and suction. That is to say, WRC is a basic constitutive relation for explaining the engineering characteristics of unsaturated soil, it works as a bridge for organically integration of theory, test and prediction methods for study on unsaturated soils (Lee 1998).

There are many methods for obtaining water retention curves of unsaturated soils, among them vapor phase technique and osmotic technique are mostly used for unsaturated bentonites. Shen et al. (1998, 2001a) determined the soil water characteristic curve of compacted bentonite by using the method of saturated saline solution, results show that the corresponding water content to certain suction is not influenced by initial dry density and initial water content, but determined by micro-pores in bentonite. They also noted that the salt solution method can be used for measuring high suction.

The water retention curves of GMZ01 bentonite under confined and unconfined conditions and room temperature was measured using the vapor phase technique and osmotic technique by Chen et al. (2006, Fig. 6). Fig. 6 shows that for high suctions ($s > 4$ MPa) the two curves are almost the same, while for lower suctions ($s < 4$ MPa) difference between different confining conditions becomes more significant as the suction increases: under unconfined conditions, the water content increase quickly with increasing in suction; when suction is 0.01MPa, the water content (164%) is much higher than that of in confined condition (26%).

The temperature effects on soil water characteristic of GMZ01 bentonite was reported by Wan et al. (2009). Results indicate that under both confined and unconfined conditions, for a constant suction, the water retention capacity of GMZ01 bentonite decrease as temperature increases, and the influence of temperature become more obvious with the decrease of suction.

For high suctions, no obvious difference was observed between the two water retention curves at the same temperature; however, for low suctions, the water retention capacity of confined sample is significantly lower than that of unconfined sample (Fig.7a). The hysteretic behavior of compacted bentonite decreases with the increase of temperature. For suction higher than 4MPa, the hysteretic behavior of GMZ bentonite became more obvious with decrease of suction.

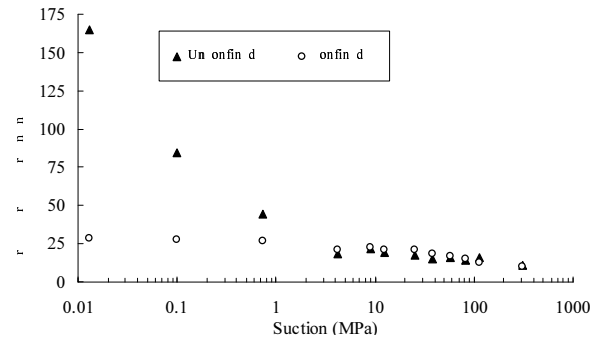
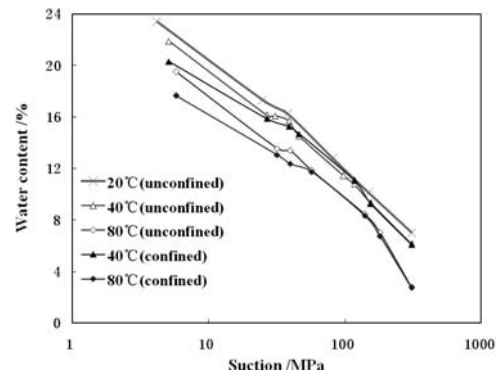
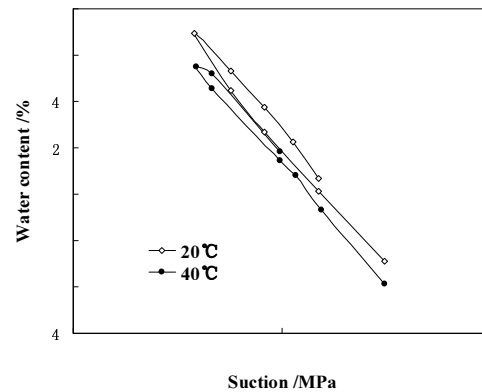


Fig. 6 WRC of GMZ bentonite (1.70g/cm³)(Chen 2006)



(a) Wetting curves



(b) Hysteretic characteristic curves

Fig. 7 Comparison of the WRC in unconfined/confined wetting paths at different temperature (Wan 2009)

Unsaturated hydraulic properties under confined condition

The hydraulic conductivity of GMZ01 bentonite with dry density of 1.70g/cm³ under confined conditions was determined by transient profile method (Ye et al. 2009a). The variation of hydraulic conductivity with suction is presented in Fig. 8. It shows that the unsaturated hydraulic conductivity of GMZ01 bentonite is between 1.13×10^{-13} m/s and 8.41×10^{-15} m/s, and it does not evaluate linearly with soil suction. When the suction decreases from the initial value of about 80 MPa, the hydraulic conductivity of GMZ01 bentonite firstly decreases ($68 \text{ MPa} \leq s \leq 80 \text{ MPa}$) then turns to increase with the decrease of suction ($0 \leq s < 70 \text{ MPa}$).

Unsaturated hydraulic properties under unconfined condition

Niu (2008) investigated the unsaturated hydraulic conductivity of GMZ01 bentonite with dry density of 1.70g/cm^3 under unconfined conditions (Fig. 9). Results show that under unconfined conditions, the unsaturated hydraulic conductivity of GMZ01 bentonite is stabilized between $1.0 \times 10^{-14}\text{m/s}$ and $1.0 \times 10^{-13}\text{m/s}$, except some fluctuation at the initial stage of the test.

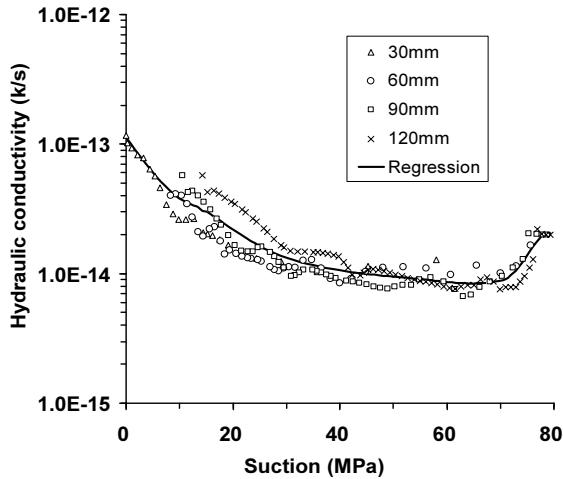


Fig. 8 Variation of hydraulic conductivity of GMZ bentonite with suction under confined conditions (Ye 2009a)

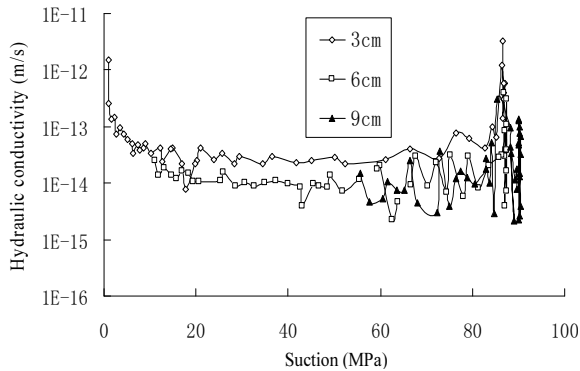


Fig. 9 Unsaturated hydraulic conductivity of GMZ01 bentonite evaluates with suction under unconfined conditions (Niu 2008)

Figs. 8 and 9 suggest that for certain suction, the unsaturated hydraulic conductivity under unconfined condition is higher than that of under confined condition. The difference in values of hydraulic conductivity could be explained by the possible difference in microstructure that caused by hydration under different conditions.

THERMAL CONDUCTIVITY

Thermal conductivity of buffer / backfill materials is a key index for the design of high-level radioactive waste (HLW) repository (JNC, 2000). It directly determines the dissipation of decay heat released by high-level radioactivity waste in repository.

Liu et al. (2007a) found that the thermal conductivity of GMZ01 increases significantly with the increase of dry density. And for low dry density, water content slightly influence the thermal conductivity. While with the increase of dry density, the influence of water content on the thermal conductivity will gradually increase (Fig. 10).

When the saturation is more than 20%, a linear relationship between the thermal conductivity of compacted GMZ01 bentonite and saturation was observed (Fig. 11).

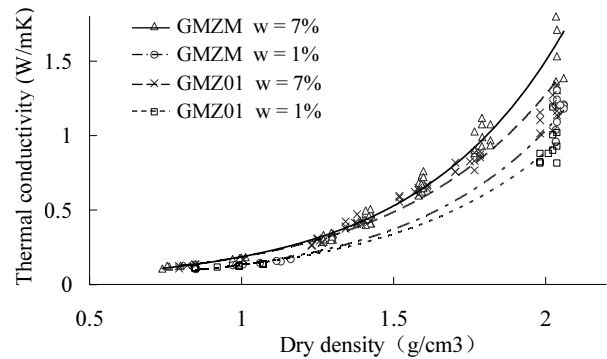


Fig. 10 Thermal conductivity vs. dry density (Liu 2007a)

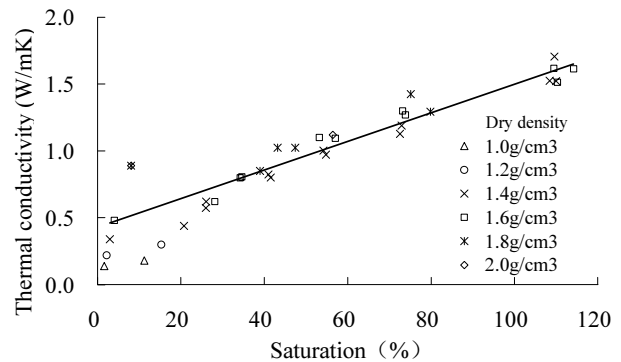


Fig. 11 Thermal conductivity vs. saturation (Liu 2007a)

It is reported that the presence of quartz sand obviously improves the thermal conductivity of pure bentonite (Moss 1983; Ould-Lahoucine 2002; Liu 2003). Ye (2009) found that for same dry density, the thermal conductivity of sand-bentonite mixture (GMZM) increases with the increase of sand ratio; and for different dry density, the higher the dry density, the more obvious the effect of sand ratio (Fig. 12). The thermal conductivity increases with increasing of sand ratio in the case that the water content is higher than 0%.

However, for specimen with water content of 0%, the thermal conductivity increased with sand ratio until 30% and decreased thereafter. This result agrees with the conclusion of other researchers.

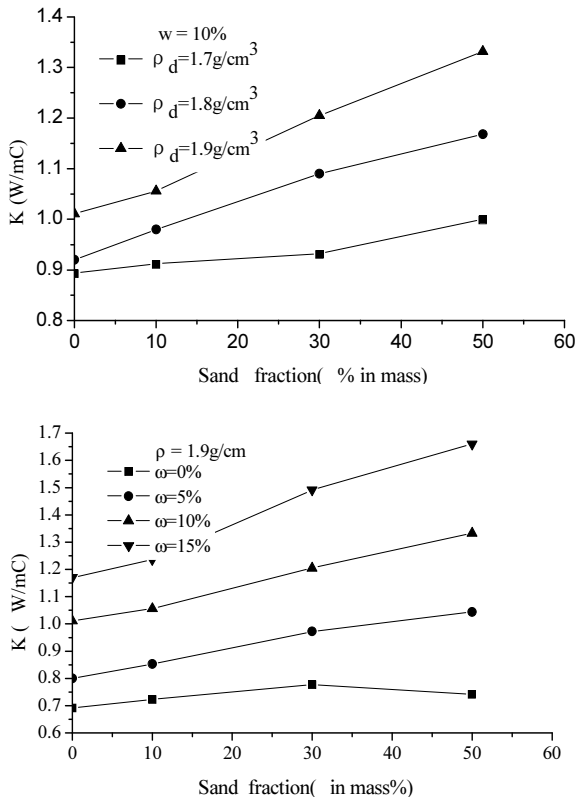


Fig. 12 Thermal conductivity versus mass fraction of sand

MICROSTRUCTURE CHARACTERISTIC

Properties of soils depend on its structure, i.e. soil fabric and arrangements of soil particles. For unsaturated soils, the arrangement of particles influences the suction distribution. The micro-structure of bentonite determines its thermal, hydraulic and mechanical properties, so the study of microstructure and its varying properties are of great importance for bentonite. Nowadays, several techniques could be used for investigation of the microstructure of soil, among which Environmental Scanning Electron Microscope (ESEM) can be used for qualitative analyzing the microstructure; whereas Mercury Intrusion Test (MIP) technique could be employed for determination of Pore Size Distribution (PSD) curve of soils (Yu 2006).

Microstructure of GMZ01 Bentonite under Unconfined Conditions

Fig.13 presents the cumulated PSD data of four unconfined GMZ01 bentonite specimen hydrated at

different suction. The low cumulative intruded pore volume for 309MPa indicates that compacted bentonite was relatively denser under high suction. This is consistent with the observation made by ESEM (Fig.14): no intra-aggregate pore was observed under high suction. However, the cumulative intruded pores increase rapidly with decrease of suction; this indicates that both the total pore volume and diameter of pores increase rapidly as suction decreases.

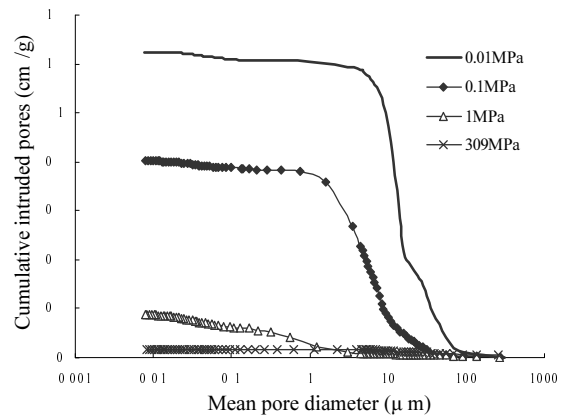


Fig. 13 Pore-size distribution of confined compacted Gaomiaozi bentonite (Ye 2009b)

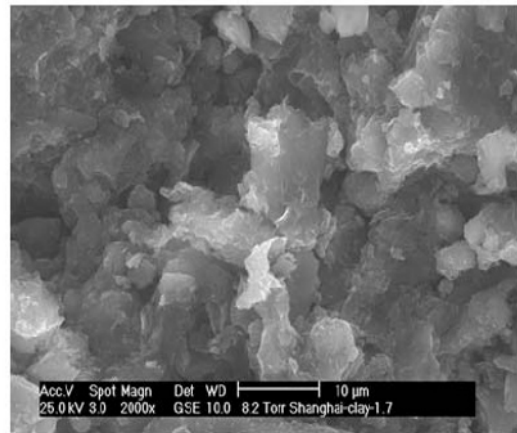


Fig. 14 ESEM photos of GMZ bentonite under Suction of 309MPa (Ye 2009b)

Fig. 15 shows the pore-size distribution (PSD) data of the three specimens under unconfined condition. It is shown that the PSD curve for the specimen under suction of 1MPa is unimodal, and radii of pores varies from 0.1 to 3micrometers; as suction decreases to 0.1MPa, the PSD curve is bimodal and radii of pores varies in the range of 0.5—5micrometers and 5—90micrometers; when suction decreases to 0.01MPa, the PSD curve presents trimodal characteristic, and radii of pores ranges from 0.5—6micrometers, 6—15micrometers and 30—120micrometers, respectively. This indicates that under unconfined conditions, the volumetric strain of GMZ01 bentonite caused by hydration mainly due to

swelling of macro-pores in the soil. EMES photo (Fig.16) also indicates that macro-pores in the bentonite increased evidently.

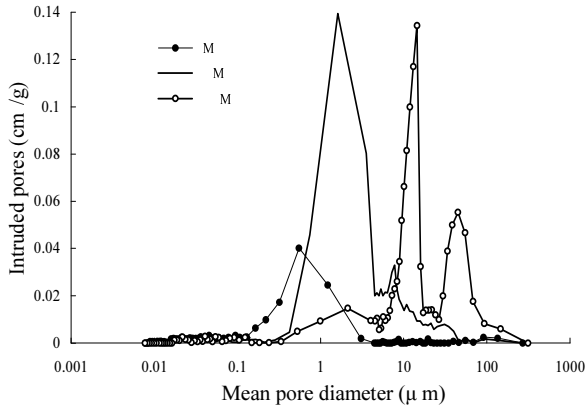


Fig. 15 Pore-size distribution of unconfined compacted Gaomiaozi bentonite (Ye 2009b)

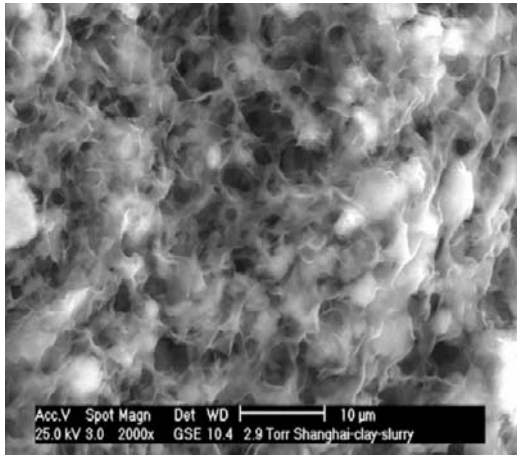


Fig. 16 ESEM photos of GMZ bentonite under Suction of 0.01MPa (Ye 2009b)

Microstructure of GMZ01 Bentonite under Confined Conditions

The micro-structure of GMZ01 bentonite under confined conditions is completely different from that of unconfined conditions. Under confined conditions, the PSD curves of the specimen hydrated at suction of 1.0MPa and 0.1MPa, are bimodal distributed at radii of pores range 0.3—4μm and 80—340μm (Fig. 16 & Fig. 17). With decrease of suction, the bentonite swells, while the total volume of inter-aggregate pores were reduced and amount of inter-aggregate pores were increased. That means radii of pores in compacted GMZ01 bentonite become uniformly with decreasing of suction. The ESEM photo also shows that the overall structure of the soil is homogeneous with no clear big inter-aggregates pores (Fig. 18).

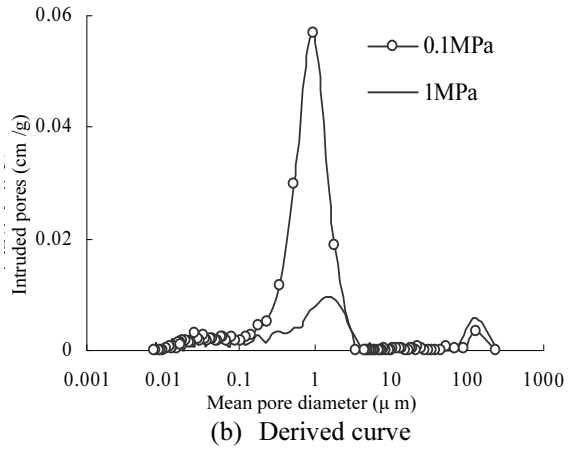
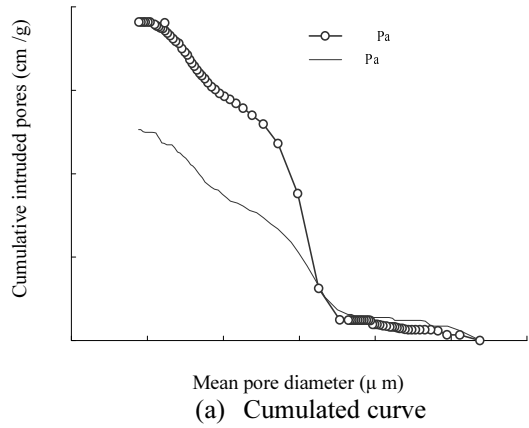


Fig. 17 Pore-size distribution of Compacted GMZ01 bentonite under confined conditions

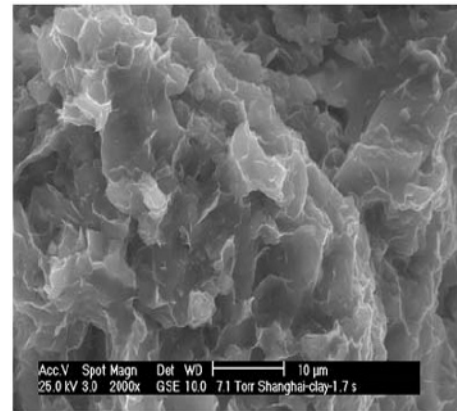


Fig. 18 ESEM photos of GMZ bentonite under Suction of 0.1MPa (Ye 2009b)

VOLUME CHANGE BEHAVIOR

As buffer/backfill materials, bentonites may experience cyclic drying and wetting paths caused by coupled T-H-M effects. While bentonite swells with water intake and shrinks with water loss, so drying and wetting cycles will result in the swelling and shrinkage deformations of

bentonite.

As high plastic clay, the swelling of compacted bentonite is mainly caused by the absorbing of water into the interlayers of montmorillonite inducing the matric suction decreases and repulsive force (i.e. osmotic pressure) increase. So, the volume change of bentonite under unconfined conditions can be computed using diffuse double layer (DDL) theory. For GMZ01 bentonite with dry density of 1.70g/cm^3 , the void ratio after swelling could be estimated using the following equation (Yu 2006):

$$e = 10^{[1.5-0.2a \cosh(2.02p+1)]} \quad (2)$$

Where, e is void ratio; p repulsive force of double layer (suction) ; $a \cosh$ is inverse hyperbolic cosine function.

For the higher suction range, the attractive forces between particles are greater than that of the repulsive forces, so the attractive forces (Van der Waals forces) play a dominant role; however, attractive forces were ignored in the DDL theory. Therefore, the DDL theory is not suitable for samples in higher suction. In the former studies, this theory was only applied in the suction range less than 1MPa (Schanz 2005).

The calculated and experimental data of volume change of GMZ01 bentonite under unconfined conditions were shown in Fig.19 (Yu 2006). The theoretical curve shows a good agreement with the experimental results, but, the discrepancy increases with the decreasing of suction.

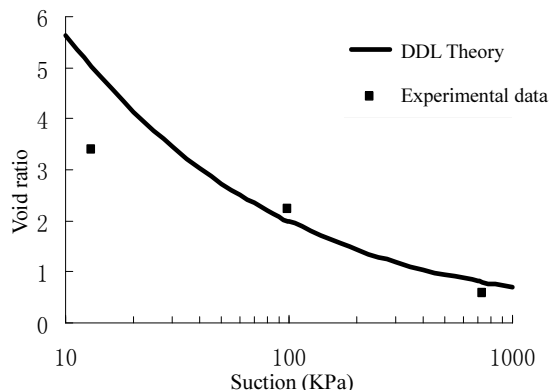


Fig. 19 Relationship between void ratio and suction of GMZ bentonite under unconfined conditions (Yu 2006)

CONCLUSIONS

The deep geological disposal based on multi-barrier system is considered as the most safety and effective way for disposal of high level radioactive wastes (HLW). The bentonite was selected as buffer/backfill materials due to its excellent properties. Significant work has been performed over the world on many candidate bentonite.

At present, many works consist of studies on mineralogy and chemical composition, mechanical properties, hydraulic behavior, swelling behavior, thermal conductivity, microstructure and volume change behavior were performed on GMZ bentonite, which is selected as the first choice of Chinese buffer materials for high-level radioactive waste repository.

However, compared to other bentonites in the world, the study on GMZ bentonite used as buffer/backfill materials is still in the primary stage. Problems related to the influence of temperature on behavior of the GMZ bentonite; the migration law of nuclide in compacted bentonite and sealing properties of GMZ bentonite based materials under coupled T-H-M-C conditions et al. should be key issues to be explored in the future.

ACKNOWLEDGEMENTS

The authors are grateful to the National Natural Science Foundation of China for the financial supports (No. 40772180, No. 40572161, No.40728003), Project from State Administration of Science and Technology for National Defense ([2007]831), and Shanghai Leading Academic Discipline Project (B308).

REFERENCES

- Alonso EE & Romero E (2005). Expansive Bentonite-Sand Mixtures in Cyclic Controlled-Suction Drying and Wetting, *Engineering Geology*, 81: 213-226.
- Agus SS (2005). An Experimental Study on Hydro-Mechanical Characteristics of Compacted Bentonite-Sand Mixtures, *Bauhaus-University Weimar*.
- Barbour L (1998). The Soil Water Characteristic Curve: a Historic Perspective. *Nineteenth Canadian Geotechnical Colloquium*.
- Chen B, Qian LX, Ye WM, Cui YJ, Wang J (2006). Soil-Water Characteristic Curves of Gaomiaozi Bentonite, *Chinese Journal of Rock Mechanics and Engineering*, 21(7):1054-1058.
- Goran S et al. (2002). Determination of Hydraulic Conductivity of Sand-Bentonite Mixtures for Engineering Purposes, *Geological and Geological Engineering*, 20:65-80.
- Guo MF (2004). *Compaction Properties of Sand-Bentonite Mixtures*, Taiwan, China (in Chinese).
- Haug MD & Wong LC (1992). Impact of Molding Water Content on the Hydraulic Conductivity of Compacted Sand-Bentonite Liner Material. *Canadian Geotechnical Journal*, 29,253-262.
- Komine H & Ogata N (1999). Experimental Study on Swelling Characteristics of Sand-Bentonite Mixture for Nuclear Waste Disposal. *Soils and Foundations*

- 39 (2), 83-90.
- Komine H (2004). Simplified Evaluation on Hydraulic Conductivities of Sand-Bentonite Mixture Backfill, *Applied Clay Science*, 26:13-19.
- Liu YM & Chen ZR (2001). Bentonite from Gaomiaozi, Inner Mongolia as an Ideal Buffer/ Backfilling Material in Handling Highly Radioactive Wastes—a Feasibility Study, *Acta Mineralogica Sinica*, 21(3): 541-543 (in Chinese).
- Liu QS & Wang ZJ (2002). Influence Factors of Sand-Bentonite Mixtures on the Swelling Pressure, *Chinese Journal of Rock Mechanics and Engineering*, 21(7):1054-1058 (in Chinese).
- Liu JZ (2003). Thermal Conductivity of Granite Gravel-Bentonite Mixture, Taiwan, China (in Chinese).
- Liu YM & Cai MF (2006). On the Thermal Conductivity of GMZ Bentonite, The Second Rock and Engineering Conference, China:742-746 (in Chinese).
- Liu YM & Cai MF Wang J(2007a). Thermal Conductivity of Buffer Material for High-Level Waste Disposal, *Chinese Journal of Rock Mechanics and Engineering*, 26(S1):3891-3896 (in Chinese).
- Liu YM & Cai MF (2007b). Compressibility of Buffer Material for HLW Disposal in China, *Uranium Geology*, 23(2):91-95 (in Chinese).
- Liu DY(2008). Numerical Analysis of the Coupled Thermo-Hydro Effects on Buffer/Backfill Materials under Unsaturated Conditions, Taiwan, China (in Chinese).
- Moss M (1983). Thermal Conductivity of Bentonite/Quartz High Level Waste Package Backfill, *Scientific Basis for Nuclear Waste Management 6*, Materials Research Society, 719.
- Met,A et al. (2005). Environmental Geological and Geotechnical Investigations Related to the Potential Use of Ankara Clay as a Compacted Landfill Liner Material, *Environmental Geology*, 47:225-236.
- Niu WJ (2008) The Unsaturated Permeability Test of Highly Compacted Bentonite under Free Swelling Condition, Tongji university, Shanghai (in Chinese).
- Ould-Lahoucine C, Sakashita H, Kumada T (2002). Measurement of Thermal Conductivity of Buffer Materials and Evaluation of Existing Correlations Predicting it, *Nuclear Engineering and Design*:1-11.
- Pusch R (1979). Highly Compacted Sodium Bentonite for Isolating Rock-Deposited Radioactive Waste Products, *Nuclear Technology*, 45:153-157.
- Scientific Basis for Nuclear Waste Management XVIII (Part 1).(1994). Materials Research Society Symposium Proceedings.
- Shen ZY & Li GD (1998). Determination of SWCC of Compacted Bentonite, *Geotechnical Investigation and Surveying* (4):331-334 (in Chinese).
- Shen ZY, Chen JR, Ma BH (2001a). Determination of SWCC of Unsaturated Bentonite using Salt Solution Method, *Hydrogeology and Engineering Geology*, (4): 6-8 (in Chinese).
- Shen ZY (2001b). Research Progress of Geological Disposal of High-Level Wastes. *Chinese Geology* 28(12): 19-21 (in Chinese).
- Wang ZJ & Liu QS (2000). Experimental Study of Swelling Characteristics of Compacted Sand-Bentonite Mixture, *Rock and Soil Mechanics*, 21(4):331-334 (in Chinese).
- Wu BL (2005). Compaction Properties of Sand-Bentonite Mixture for High-Level Waste Disposal. Taiwan, China (in Chinese).
- Wen ZJ (2005a). Selection and Basic Properties of China's Buffer Materials for High Level Radioactive Waste Repository, *Acta Petrologica et Mineralogica*, 24(6):584-588 (in Chinese).
- Wen ZJ & Shen DJ (2005b). Preliminary study on static mechanical property of GMZ Na-bentonite, *World Nuclear Geoscience*, (22):211-214 (in Chinese).
- Wen ZJ (2006) Physical Property of China's Buffer Material for High-Level Radioactive Waste Repositories, *Chinese Journal of Rock Mechanics and Engineering*, 25(4):794-800.
- Wang J & Chen WM (2006). Geological Disposal of High-Level Radioactive Waste and its Key Scientific Issues, *Chinese Journal of Rock Mechanics and Engineering*, 25(4):801-812.
- Ye WM, Huang Y, Cui YJ, Tang YQ, Delage P (2005). Micro-structural Changing Characteristics of Densely Compacted Bentonite with Suction under Unconfined Hydrating Conditions, *Chinese Journal of Rock Mechanics and Engineering*, 24(24):4570-4575 (in Chinese).
- Yu C (2006). Volume Change Behavior and its Micro-Structural Mechanical Of Unsaturated GMZ Bentonite, Tongji University (in Chinese).
- Ye WM & Schsnz T (2007). Characteristics of Swelling Pressure of Densely Compacted Gaomiaozi Bentonite GMZ01, *Chinese Journal of Rock Mechanics and Engineering*, 26(2): 3861-3865 (in Chinese).
- Ye WM & Qian LX (2009a). Laboratory Test on Unsaturated Hydraulic Conductivity of Densely Compacted Gaomiaozi Bentonite under Confined Conditions, *Chinese Journal of Geotechnical Engineering*, 31(1):105-108 (in Chinese).
- Ye WM, Qian LX, Chen B, Yu C (2009b) Characteristics of Microstructure of Densely Compacted Gaomiaozi Bentonite, *Journal of Tongji University (Natural Science)*, 37(1):31-35 (in Chinese).

A PRELIMINARY UNDERSTANDING ON PERFORMANCE OF BARRIERS FOR MSW LANDFILLS IN SOUTHERN CHINA

Tony L.T. Zhan¹, Yun-Min Chen² and Xiao-Wu Tang³

ABSTRACT: A barrier system, consisting of bottom barrier, lateral barrier and top cover, is the most important component of a controlled MSW landfill. Numerous research efforts have been put to study the performance of the basal liners for MSW landfills. However, relatively few studies were carried out on the resistance of basal liners to a high leachate mound, which is commonly present at landfills in Southern China. In addition, the investigation on the performance of vertical barriers is relatively scarce. This paper tried to present some preliminary understanding on the performance of landfill barriers in the south of China. The paper firstly presents a field investigation on the transport of leachate pollutant at the Suzhou MSW landfills with vertical barrier installed. Then, the performance of four regulatory liner systems subjected to a high leachate mound will be discussed, and some implications on the barrier design are given. The paper also includes a review on the recent advances on alternative earthen covers for MSW landfills.

INTRODUCTION

A barrier system, consisting of bottom barrier, lateral barrier and top cover, is the most important component of a controlled MSW landfill. The bottom and lateral barriers are intended to control leachate transport into the surrounding soils and groundwater. The top cover is meant to control precipitation infiltration into landfills as well as to prevent free release of landfill gas into atmosphere. It is relatively easy to repair any failures or malfunctions in the top cover because it is accessible. However, a failure of bottom and lateral barriers will result in serious environmental impacts and substantial clean-up and repair costs. Two types of barriers, i.e. basal liners and vertical barriers, are commonly used in MSW landfills. The applicability of them at a specific landfill is primarily dependent on the local geological and hydro-geological conditions, the availability of materials and techniques. Most countries in the world have issued stringent regulations or guidelines on the design and construction of the barriers. Numerous research efforts and investigation have been carried out on the performance of the basal liners for MSW landfills (Giroud and Bonaparte, 1989; Foose et al. 2002; Rowe, 2005; Rowe, 2006; Shackelford, 2005). However, relatively few studies were carried out on the resistance of basal liners to a high leachate mound, which is

commonly present at landfills in Southern China. In addition, the investigation on the performance of vertical barriers is relatively scarce (Karmon et al. 2006). This paper tried to present some preliminary understanding on the performance of landfill barriers in the south of China. The paper firstly presents a field investigation on the transport of leachate pollutant at the Suzhou MSW landfills with vertical barrier used. Then, the resistance of four commonly-used liner systems to a high leachate mound will be discussed, and some implications on the barrier design are given. The paper also includes a review on the recent advances on alternative earthen covers for MSW landfills.

MECHANISM OF LEACHATE TRANSPORT THROUGH LANDFILL BARRIERS AND CRITICAL DESIGN POINTS

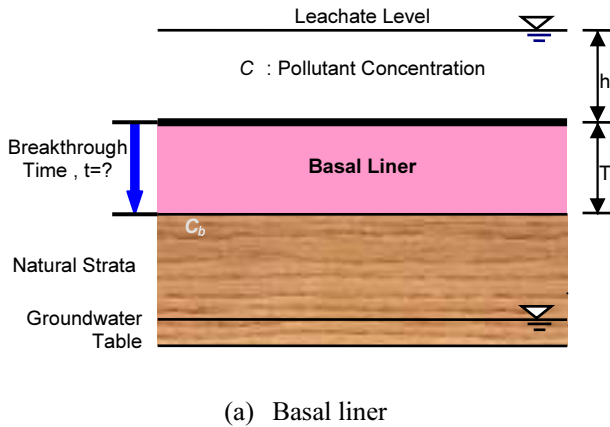
Leachate is a liquid that has seeped through a MSW landfill and has accumulated bacteria and other possibly harmful dissolved or suspended materials. The leachate composition of MSW landfills, controlled by the anaerobic microbial degradation of organic substances, is very complex. The contaminants in the leachate included organic contaminants such as COD, BOD, VOCs, dioxin, and inorganic contaminants such as heavy metal

¹ Professor, MOE Key Laboratory of Soft Soils and Geoenvironmental Engineering, Zhejiang University, Hangzhou, 310058, China. Email: zhanlt@zju.edu.cn

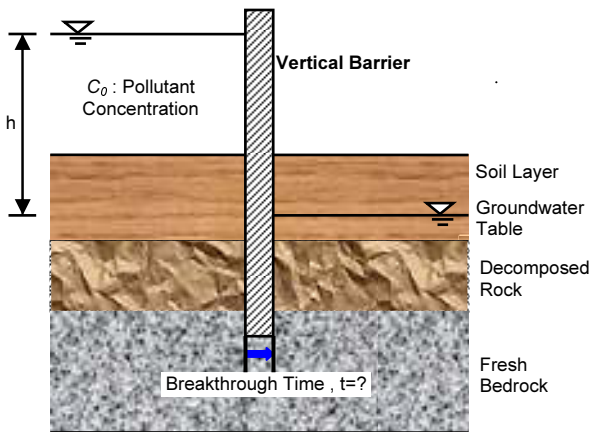
² Professor, MOE Key Laboratory of Soft Soils and Geoenvironmental Engineering, Zhejiang University, Hangzhou, 310058, China. Email: chenyunmin@zju.edu.cn

³ Professor, MOE Key Laboratory of Soft Soils and Geoenvironmental Engineering, Zhejiang University, Hangzhou, 310058, China. Email: tangxiaowu@zju.edu.cn

(Cd, Pb, Hg etc.). The concentration of most of these contaminants is related to the phases of the degradation process and changes with time accordingly.



(a) Basal liner



(b) Vertical barrier

Fig. 1 Conceptual models for leachate transport through landfill barriers

Fig. 1 shows a conceptual model for the transport of contaminants in the leachate through a landfill barrier. The transport process depends on the hydraulic head of leachate (*h*), the concentration of contaminants in the leachate (*C*₀), the thickness (*T*) and performance of the barrier, and the bottom/downstream boundary condition. The time (*t*) required for the contaminants to breakthrough the barrier is a key design parameter. For the time being, debate still exists on the design criterion of the breakthrough time. It is generally accepted that a barrier should be designed such that the concentrations of both inorganic and organic contaminants in a receptor aquifer beneath/downstream the barrier are compliant with the minimum regulatory requirements during the full lives of the involved contaminants. The full live of contaminants within a MSW landfill depends on the total operation period (e.g. 15~30 years), the post-closure

period with further management of leachate (e.g. 30 years required by the EPA in USA) and the fate of inorganic and organic contaminants. From the above point of view, the breakthrough time of the MSW landfill barrier should be designed to be no less than 50 years.

The transport process of contaminants through mineral barriers (e.g. natural stratum, compacted clay liner, concrete diaphragm wall etc.) involves three kinds of mechanisms, i.e. advection, diffusion and adsorption. The advection mainly depends on the leachate head and the hydraulic conductivity of the mineral barriers. Diffusion represents a combination of molecule diffusion and mechanical dispersion. The adsorption represents the retarding effect of the mineral barrier with respect to a specific pollutant. The one-dimensional transport process of a reactive contaminant is usually described by the following simplified equation:

$$n \frac{\partial c}{\partial t} = nD \frac{\partial^2 c}{\partial z^2} - \rho K \frac{\partial c}{\partial t} + S^+ \quad (1)$$

where, *c* is the concentration at depth *z* and time *t*, *n* is the effective porosity, *D_e* is the effective diffusion coefficient, *ρ_d* is the dry density, *K_d* is the partitioning coefficient, and *S⁺* is the reaction item representing biodegradation of organic contaminants, precipitation and chemical reactions that may mobilize a contaminant and others.

The first requirement for the design of a landfill barrier is to minimize the advection flow of leachate (i.e. leakage). As a result, diffusion essentially dominates the transport process through the barrier for most cases. However, it should be noted that the advection flow may become comparative to diffusion or even dominant for the cases: 1) a build-up of high leachate head above the barrier due to ineffective management of water, gradual clogging of leachate drainage system or a failure/termination of leachate collection; 2) the hydraulic conductivity of the mineral barrier exceeds the design value (e.g. 1×10⁻⁹ m/s) as a result of poor construction quality or a decay in the barrier material with time.

The above discussions indicate that the design of a barrier should not be isolated from the design of a leachate head control system. The characteristic and performance of one of them have an impact on that of the other. In addition, it is needed to take into account the potential decay in the barrier materials (e.g. geomembranes, GCL, compacted clays etc.). This is because the barrier materials are keeping on experiencing an interaction with the complex leachate, and suffering from a multi-field geoenvironment (high pressure, high temperature, high concentration etc.).

Another critical design point is that the performance-based design of landfill barriers should be based not only on leakage rate but also contaminant transport (Rowe, 1998; Foose et al. 2002). The performance of the MSW landfill barriers should usually be assessed on the basis of the mass flux of VOCs, which are generally toxic at lower concentration than many inorganic contaminants (Edil, 2003). For a detailed design, the self-biodegradation characteristic of VOCs can be taken into account (Rowe and Brachman, 2004).

The design of MSW landfill barriers in each country should be strictly complied with the relevant regulation or guideline issued by the country. When the standard forms of barriers are not applicable for a specific landfill site, it is generally required for the designer to demonstrate the “equivalence” of alternative barrier designs. In other words, the performance of the alternative barrier should be at least equivalent to the regulatory prescribed barrier. Several researchers have offered good demonstrations on how to perform assessment of equivalence and what factors influencing the assessment of equivalence (Katsumi et al. 2001; Foose et al. 2002; Rowe and Brachman, 2004).

The design of a barrier should be site-dependence, i.e. being based on the local geological and hydro-geological conditions, the availability of materials, construction technique and equipments, the local quality assurance/control systems. For example, in a region where the construction quality of CCL is not guaranteed, the GM/GCL/AL composite liner is more applicable than the GM/CCL.

VERTICAL BARRIERS FOR MSW LANDFILLS

When a landfill site has a continuous and sufficiently thick stratum with low permeability, the use of vertical barrier is usually more cost-effective than the use of basal liners. Vertical barriers were commonly used for the first-generation controlled landfills in China. Most of the landfills are located in a valley or canyon. The low permeability bedrock generally forms a shape of “dustpan” with an opening downstream the landfills. Vertical barriers, extending to the underlying fresh bedrock, are constructed at the downstream opening. The vertical barrier and the bedrock are expected to constitute a closed barrier system against the leachate in the landfills.

The forms of vertical barriers include concrete diaphragm wall, composite diaphragm wall, steel sheet pile wall and grout curtain. For example, low permeability soil-bentonite or cement-bentonite slurry walls are widely used as vertical barriers in both UK and USA (Grube, 1992; Evans, 1994; Karmon et al. 2006). Inazumi et al. (2006) presented a new type of H-jointed

steel pipe sheet pile wall with H-H joints. Fig. 2 shows one typical structure of vertical barriers used at the valley landfills in China. The vertical barriers are made up of two sections, i.e. a concrete diaphragm wall embedded in the upper soil layers and a grout curtain developed in the cracked bed-rock.

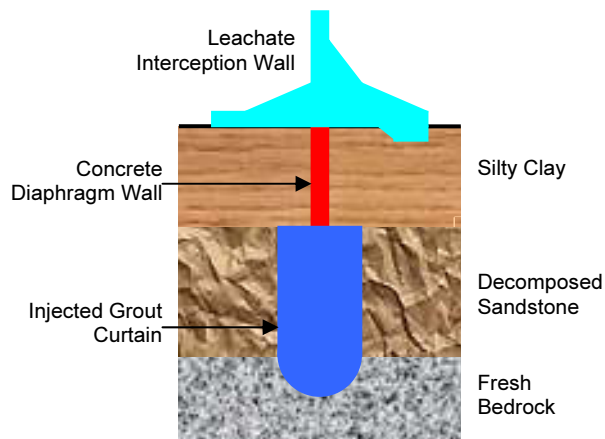


Fig. 2 Typical structure of vertical barriers used at the valley landfills in China

Vertical barriers are also often used as a remediation measure for the uncontrolled MSW landfills and other contaminated sites. This measure shows its advantages for the case that it is technically or economically difficult to clean up the contaminants in soil and/or groundwater. Vertical barriers are commonly used in other engineering fields such as hydro-power engineering and underground engineering, and hence the technique is readily available even in the developing countries. However, it is surprising to find out that the published research work on vertical barriers is much less than that on various liners for landfills. The relevant regulation or guideline is not available in most countries. At present, engineers are still lack of a scientific methodology and special testing techniques for the performance evaluation of vertical barriers. Recently, there is a trend of increase in the relevant research work such as Evans and Opdyke (2006), Fratolocchi et al. (2006), Karmon et al. (2006). A preliminary investigation on the performance of the vertical barrier at the Suzhou landfill will be presented in the following section.

INVESTIGATION OF LEACHATE TRANSPORT AT THE SUZHOU LANDFILL

Site Description and Hydro-Geological Conditions

The Suzhou landfill is located about 13 km southeast of Suzhou City in China. The layout of the landfill is shown in Fig. 3. The landfill was put into operation in

July, 1993. At the time of the field investigation (April, 2006), the landfill has received 4.6 million m³ municipal solid wastes from the Suzhou city. Fig. 4 shows the main cross-section of the landfill at the time of field investigation. The landfill consists of a number of filled platforms that are set back at an embankment slope of 4H/1V. A rockfill dam retains the lowest platform. As shown in Fig. 4, neither sealing liners nor leachate drainage and collection systems were constructed at the base of the landfill. A vertical barrier was installed under the interception wall of the leachate pond to limit downstream movement of leachate. The vertical barrier consisted of a concrete diaphragm wall and an injected grout curtain (see Fig. 2). The vertical barrier was designed and constructed to obtain a hydraulic conductivity lower than 1.0×10^{-6} cm/s. The vertical barrier was made to extend to the underlying fresh rock. The natural soil strata below the landfill bottom was comprise of a layer of alluvial-colluvium deposit, highly-decomposed sandstone along with slightly-decomposed and fresh sandstone. The alluvial-colluvium deposit was composed of gravelly silty clay with a thickness ranging from 5 to 27 m. The water permeability for the silty clay ranged from 1×10^{-6} cm/s to 5×10^{-6} cm/s. Joints were well developed in the highly-decomposed sandstone, resulting in a high hydraulic conductivity. However, the fresh rock at the bottom had a high integrity and a water permeability less than 1×10^{-9} m/s. The vertical barrier and the fresh rock were expected to constitute a closed barrier system against the leachate in the landfill.

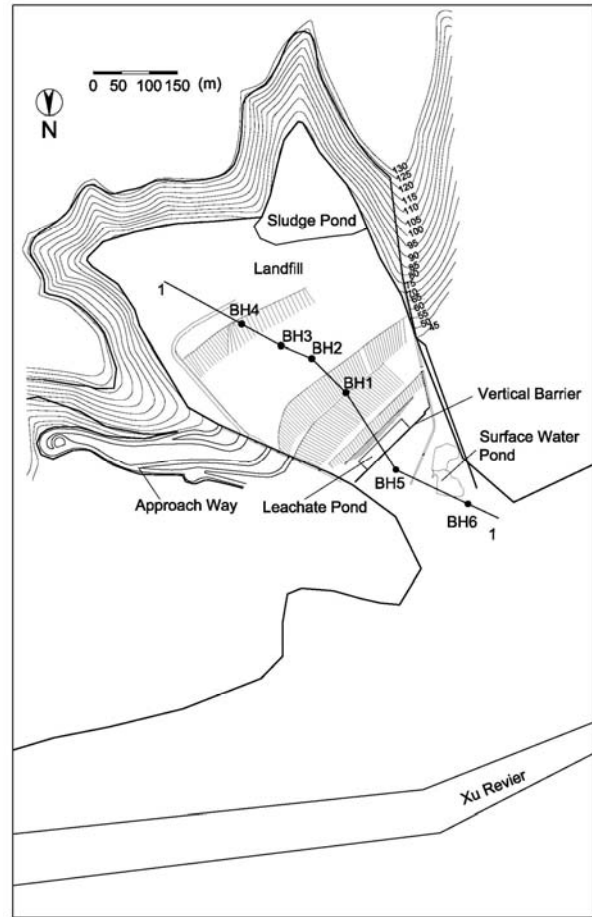


Fig. 3 Layout of the Suzhou landfill and locations of boreholes

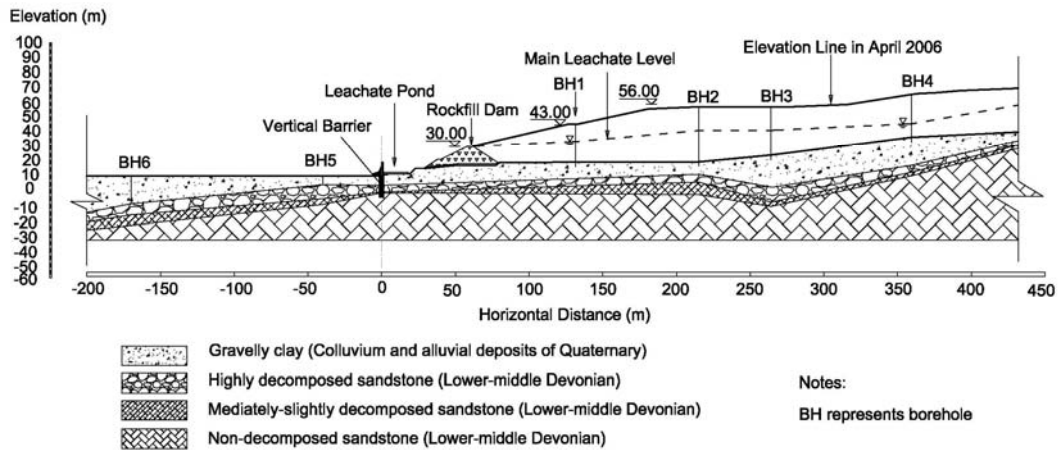


Fig. 4 Cross section of the landfills and natural strata beneath the landfill bottom (adapted from Zhan et al. 2008)

The height of leachate mound within the landfill has an important influence on the transport of leachate pollutant. The field investigation also included measurements of hydraulic pressures at different depths into the landfills. Pore pressure transducers were installed in the four boreholes (i.e. BH1 to BH4). In each borehole, there were three transducers located at different depths (e.g. 8 m, 17 m and 25 m). After instrumentation, all the boreholes

were backfilled so as to recover the original hydro-geological conditions. Sealing clay was used as backfill materials for the sections corresponding to the intermediate and top soil covers. It was expected that the two transducers separated by the sealing clay could register the leachate heads within different hydrological regimes. The “steady-state” pore pressures recorded by the transducers are shown in Fig. 5, together with the perched and

main phreatic lines deduced from the measurements. It can be seen that the transducers installed near the bottom of the landfill registered high hydraulic pressures (145, 125 and 60 kPa in boreholes BH1, BH3 and BH4 respectively). It indicated that the height of leachate mound on the base of the landfill was up to 14.5 m, which is substantially greater than the allowable leachate head regulated by the developed countries (i.e. 30 cm). The variation of pore pressure with the depth revealed a perched leachate

mound (up to 8 m high) on the intermediate soil cover. The development of high leachate mound at the landfill was attributed to the following reasons: 1) no leachate drainage and collection layer installed at the base; 2) the toe drains at the rockfill dam was seriously clogged shortly after landfill operation (less than 5 years); 3) ineffective management of income water during landfill operation. More details about the hydro-geological conditions of the landfill can be found in Zhan et al. (2008).

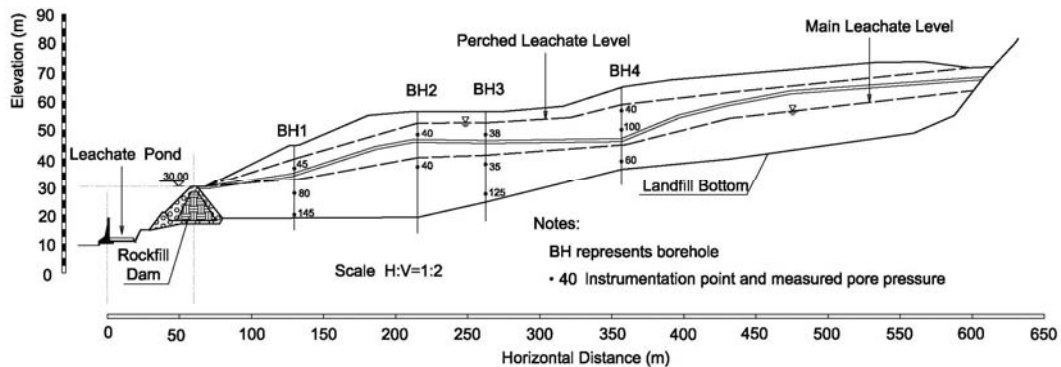


Fig. 5 The measured pore pressures and the deduced leachate levels within the Suzhou landfill

Soil Sampling and Laboratory Analyses

A field and laboratory program was carried out to investigate the transport of leachate pollutant through the natural soil layer at the base of the landfill. The field investigation consisted of borehole investigation (six boreholes: BH1 to BH6) and soil sampling. Four of the boreholes (BH1 to BH4) on the upstream of the vertical barrier were drilled down to the bottom of the landfill, and then entered the underlying silty clay layer to the depths of 3.9, 1.9, 1.95, and 10.35 m, respectively (Fig. 4). The other two boreholes at the downstream (i.e. BH5 and BH6) were drilled to depths of 6 and 20 m, respectively. The drilling was performed without the introduction of drilling mud and liquids. A system of steel casings was installed in each bore-hole to avoid the contamination of the soil samples by the leachate in the boreholes. Continuous sampling was carried out within the silty clay layer in the four boreholes (BH1 to BH4). Fig. 6 shows a picture of the first soil sample taken in BH1. Soil sampling in boreholes BH5 and BH6 were executed at a spacing of 2 m. It is believed that the soil samples taken from BH5 and BH6 were free from leachate contamination, at least for the deep soil layer.

All soil samples recovered from the boreholes were taken to the laboratory for the determination of soil composition, soil properties and soil contamination. The measured soil composition and properties for the silty clay is shown in Table 1. X-ray diffraction analysis of

the soil samples identified quartz as the primary mineral constituent with lesser proportions of albite, clinocllore and muscovite. The cation exchange capacity (CEC) was 9.1 meq/100 g. The pH value, as determined from the diluted soil sample with a soil-water ratio of 1:5, indicated that the silty clay was slightly acidic. Atterberg limit tests indicated that the silty clay had a liquid limit of 35.2% and a plastic limit of 20.8%. The in situ moisture content of the soils was determined to be an average value of 25%. The hydraulic conductivity of the silty clay, as measured using flexible wall hydraulic conductivity tests, was about 1.0×10^{-6} cm/s.



Fig. 6 Picture showing the first soil sample taken at the base of the landfill and in BH1

Table 1 Mineralogical and chemical data for the silty clay

Parameter	Mean
Property	
Porosity	0.41
Liquid limit (%)	35.2
Plastic limit (%)	20.8
Moisture content (%)	25
Wet unit weight (kN/m ³)	19.8
Hydraulic conductivity (cm/s)	1.1×10 ⁻⁶
pH (soil-water ratio: 1:5 w/v)	6.0
Mineralogy (<74 μm)	
Quartz	59.6%
Albite	15.3%
Clinochlore	5.7%
Muscovite	19.4%
Cation exchange capacity	9.1 meq/100 g

Table 2 Physicochemical characteristics of leachate from the Suzhou landfill

Parameter	Mean	Parameter	Mean
Cl ⁻ (mg/L)	3638	Cd (mg/L)	0.004
SO ₄ ²⁻ (mg/L)	15	Zn (mg/L)	0.03
K ⁺ (mg/L)	1666	Hg (mg/L)	<0.001
Na ⁺ (mg/L)	2080	COD (mg/L)	20 400
Cu (mg/L)	0.16	BOD (mg/L)	8800
Pb (mg/L)	0.08	pH	8.0
Cr (mg/L)	0.29		

Chemical analyses were carried out to determine contaminants in the silty clay layer, including chloride (Cl⁻), COD, copper (Cu), lead (Pb) and chromium (Cr). Chloride (Cl⁻) was chosen to represent the inorganic contaminants in the leachate for the reason that it is not easily adsorbed by soil, difficult to decompose, and easy to measure (Kjeldsen, 1986; Chen and Wang, 1997). The chemical oxygen demand (COD) represented the organic matter of the contaminants from the leachate. In addition, three common heavy metals, namely, copper, lead and chromium represented the heavy metals in the leachate. The total contents of Cu, Pb and Cr in the soil samples were determined following the methods described by NSPRC (1997a; 1997b). The water-extractable content of COD was determined following the methods recommended by NSPRC (1997c). The water-extractable content of Cl⁻ was measured by an ion chromatograph. The solute for testing COD and Cl⁻ was prepared by diluting 100 g air-dried soil sample with 1 L de-ionized water. Leachate samples were also collected from the leachate pond and taken to the laboratory for chemical analysis. The leachate quality as determined is shown in Table 2. It can be seen that the COD value of the

leachate was as high as 20000 mg/L. The leachate also contained a high concentration of chloride (i.e. 3638 mg/L). The values of concentration of Cu, Pb and Cr in the leachate are relatively higher than the other heavy metals.

Preliminary Results

Figs. 7 and 8 shows the distribution of chloride ion (Cl⁻) and COD along the depth measured from soil samples of the six boreholes, respectively. It can be seen that both the content of Cl⁻ and COD at the base of the landfill (i.e. from BH1 to BH4) are significantly greater than those downstream the vertical barrier (i.e. from BH5 and BH6), particularly for the first 2m soil layer. The data of BH6 can be regarded as the background value of the silty clay layer since the borehole is 180 m away from the vertical barrier. The Cl⁻ content measured from the soil samples upstream the barrier ranged from 300 to 6000 mg/kg, and showed a decreasing trend with depth in most of the boreholes. The Cl⁻ content measured from BH1 was kept to be greater than 500 mg/kg even at the depth of 9 m under the landfill bottom. The Cl⁻ content downstream the vertical barrier was less than 100 mg/kg. It seems that the Cl⁻ content at the downstream showed a decreasing trend with the distance from the vertical barrier.

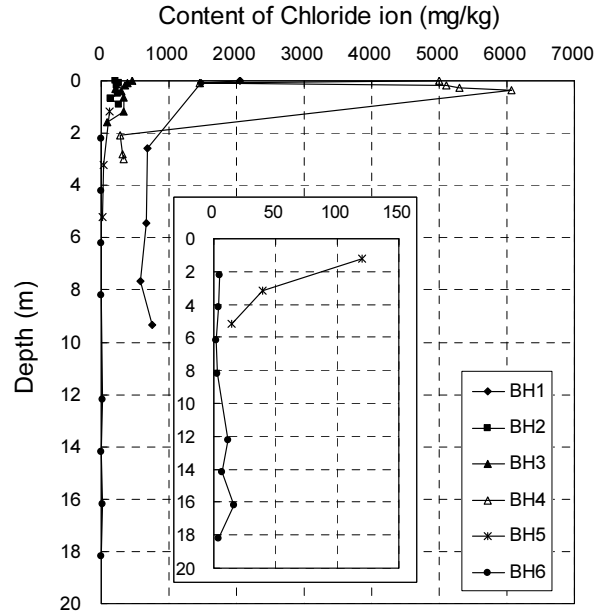


Fig. 7 Variations of Cl⁻ with depth at the six boreholes (BH1-BH4, BH5-BH6)

The COD content measured from the first 0.1 m soil layer adjacent to the landfill bottom ranged from 750 to 3700 mg/kg. The COD content measured from BH1 showed a decreasing trend until the depth increased to 5 m. The COD content measured at the downstream ranged

from 150 to 500 mg/kg. The interpretation of the above data implied that, after 13 years of landfill operation, the chloride ion (Cl^-) in the leachate had migrated to a depth greater than 9 m, and the COD reaching a depth of 5 m. The deep migration of chloride ion (Cl^-) may be attributed to the high leachate mound (>10 m) present on the base of the landfill. In addition, chloride is a non-reactive solute, and its migration is faster than organic contaminants and heavy metals. The less migration depth of COD is likely related to its slower migration speed and its greater adsorption capacity by the silty clay. More data are required for further verification of the transport distance.

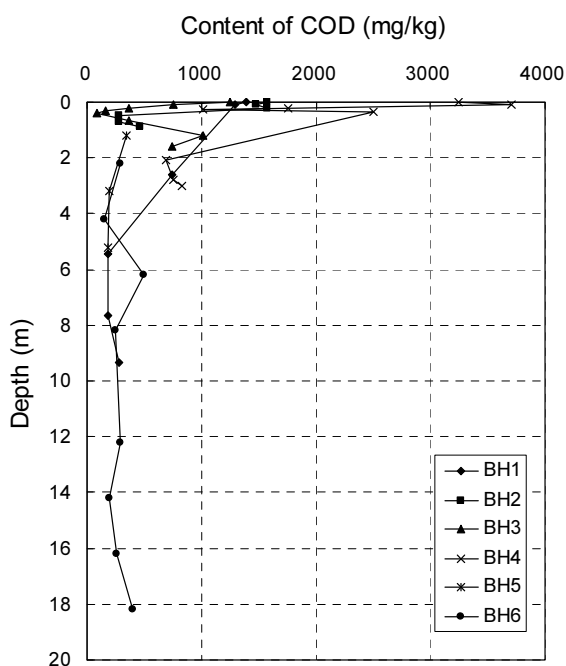


Fig. 8 Variations of COD value with depth at the six boreholes (BH1-BH4, BH5-BH6)

Table 3 shows variations in the total content of three heavy metals (lead, copper, and chromium) with depth (0 to 3 m), which were obtained from the six boreholes (i.e. BH1 to BH6). As before, the data of BH6 can be regarded as the background value the site. The total contents of the three heavy metals followed the order: $\text{Cr} > \text{Pb} > \text{Cu}$. For each of the heavy metals, the total content at the base of the landfill was generally greater than the corresponding background value, especially for the shallow depth. The discrepancy against the background value for lead and chromium seemed to be greater than that of copper. Table 3 also shows the allowable values of heavy metal content for the Chinese and European standards (NSPRC, 1995; Marzougui and Mammou, 2006). It can be seen that the total contents of chromium and copper did not exceed the allowable values regulated in the Chinese standards, even at the shallow depth. The content of lead exceeded the first-level allowable value of NSPRC (1995) only at the

shallow depth. The total contents for all the three heavy metals were less than the upper bound values regulated by the European standard.

Table 3 Total content of Pb, Cu and Cr measured from the soil samples taken from the Suzhou landfill

	Depth (m)	Cu (mg/kg)	Pb (mg/kg)	Cr (mg/kg)
BH1	0—0.2	27.2	27.5	67.8
	0.2—0.4	19.4	39.8	76.3
	2.0—2.2	28.6	26.1	64.7
BH2	0—0.2	20.8	23.0	60.5
	0.45—0.65	13.9	58.9	52.6
	1.7—1.9	17.0	19.9	48.8
BH3	0—0.2	25.3	37.4	54.0
	0.5—0.7	21.1	35.8	41.7
BH4	0.9—1.1	22.6	26.4	46.6
	0—0.2	20.1	33.6	66.3
BH5	2.6—2.8	20.1	35.2	72.6
	0—0.2	29.1	39.0	69.4
BH6	1.0—1.2	30.5	18.4	41.2
	0	27.6	35.0	62.5
A	2	20.4	28.0	67.2
		35	35	90
B		30—60	50—100	50—100

Notes: A: Chinese soil quality standard (first-level values); B: European soil quality standard

It is acknowledged that the data were not enough to make a conclusion on the performance of the vertical barrier. Because of the uncertainty in the performance of the vertical barrier, a composite liner system is used in the vertical expansion projects of this landfill, which is under construction. Apart from the composite liner system to be installed at the bottom of the expanded waste body, another vertical barrier is built downstream to cut off the potential leakage and diffusion of leachate through the original cut-off wall. The new vertical barrier was designed to be a cement-bentonite slurry wall.

BASAL LINERS FOR MSW LANDFILLS AND ITS PERFORMANCE UNDER A HIGH LEACHATE MOUND

Types of Basal Liners

Various types of basal liners have been proposed, regulated and utilized at modern landfills. The types include single geomembrance liner, single clay liner (natural or compacted), composite liner and double liners. Among them, double liners, consisting of two single or composite liners, are generally used at hazardous waste landfills with a high level of contamination risk.

Composite liners are currently the most commonly used type of liners at MSW landfills in most countries. The currently-used composite liners generally consist of either a geomembrane (GM) and compacted clay (CCL, at least 60 cm) or a geomembrane and geosynthetic clay liner (GCL). The regulations or guidelines in almost all the countries require a geomembrane as a component of composite liners, but the requirement on the thickness and hydraulic conductivity of CCL exhibits a variety in various countries (Karmon, 2001). Some countries require an additional attenuation layer underlying a composite liner. Fig. 9 shows the forms of liners regulated by the respective EPAs in China, Germany and USA. As GCLs possess many advantageous properties such as low hydraulic conductivity, easy installation, limited thickness, relatively low cost and so on, the products have been extensively used in the GM/GCL composite liners at the MSW landfills in China. “Technical code for municipal solid waste sanitary landfill (CJJ17-2004)” in China states that GCLs are allowed to be used to replace the clay liner beneath the geomembrane liner at a particular scenario. The designer is usually required to demonstrate that the replacement complies with the “equivalence” rule and will not cause slope stability problem along the basal liners.

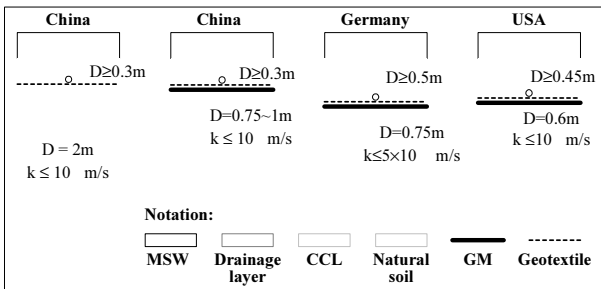
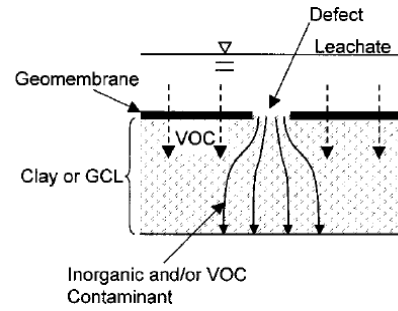


Fig. 9 Regulatory prescribed liners in China, Germany and USA

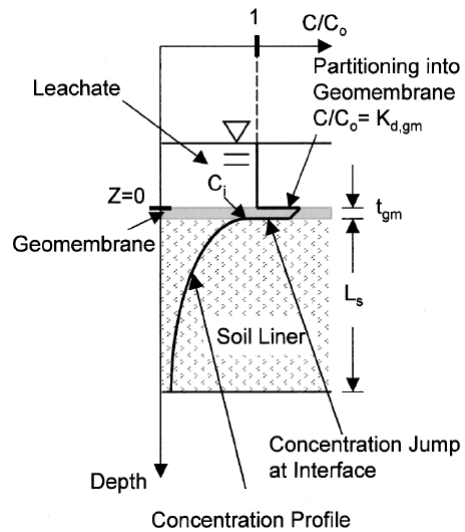
Mechanism of Leachate Transport through Composite Liners

When a composite liner with a geosynthetic barrier (e.g. GM and GCL) is considered, the transport mechanism of contaminants depends on the type of contaminants (i.e. organic and inorganic). There are two pathways for contaminant transport through composite liners (see Fig. 10): (a) advection and diffusion of inorganic and organic contaminants through defects in the geomembrane (GM) and subsequently the CCL or GCL, and (b) diffusion of organic contaminants through the intact geomembrane and subsequently through the CCL or GCL (Foose et al. 2002). The most significant pathway for inorganic contaminants is through defects in the geomembrane (holes, defective seams, etc.). In contrast to inorganic contaminants, organic contaminants

can diffuse through intact geomembrane at appreciable rates.



(a) Advection and diffusion



(b) Diffusion of organic contaminants

Fig. 10 Pathways for contaminant transport through composite liners (Foose et al. 2001)

Composite liners for MSW landfills are generally designed to be very effective at controlling advection flow such that diffusion essentially dominates the transport process for most cases. It should be noted that the advection flow through composite liners may become comparative to diffusion or even dominant for the cases: (a) the leachate head on the liners exceeds 10 m; and (b) the defect Peclet number in geomembranes (indicating the number of defects per hectare of area) exceeds 0.6 (Foose et al. 2002). As discussed previously, the leachate head greater than 10 m does exist in the landfills in southern China. In addition, the construction quality of composite liners in the developing countries is still at a relatively low standard. It is quite likely that the number of defects in the installed geomembranes is greater than the above boundary value, and that the hydraulic conductivity of the compacted clay liner is greater than the regulatory value. As far as the authors are aware, the performance of composite liners under the above scenarios is not enough studied and understood. Almost

all the published research studies on the performance of composite liners are based on the assumptions that diffusion essentially dominates the transport process. One exception to this may be Rowe and Brachman's study (2004), in which the leachate head at the base of the modeled landfill is assumed to build up to 6 m and 12 m at the times of 30 years and 50 after landfill closure.

A Review on Performance of Composite Liners for MSW Landfills

Extensive research work has been carried out to investigate the performance of various composite liners, especially for the cases of diffusion-dominated transport process (Foose et al. 2002; Rowe, 2005; Rowe, 2006; Shackelford, 2005). This section is intended to make a review on the major findings:

(1) Both field monitoring data and theoretical calculations have demonstrated that composite liners are substantially better than single liners in terms of controlling leakage (i.e. advection flow) from landfills, and that although there will typically be some leakage, the measured leakage rates through composite liners are very small (Rowe, 2005). This is because contaminant transport through the geomembrane is firstly limited to leakage through small defects in the GM, and the underlying CCL or GCL further reduces the leakage through the defects in the GM.

(2) The quantity of advection flow (often referred to as leakage) through defects in geomembranes is strongly influenced by the nature of the contact between the geomembrane and the underlying CCL or GCL. Gaps along this interface may arise from wrinkles in geomembranes and uneven surface of the underlying CCL or GCL. The gaps result in a significant increase in the transmissivity of the interface. Field evidence shows that the leakage rate through GM/CCL is 1-2 orders of magnitude greater than that through GM/GCL (Bonaparte et al. 2002; Rowe et al. 2004). This is because the interface contact of GM/CCL is usually worse than that of GM/GCL, and hence the interface transmissivity for a GM/CCL is much greater than that for a GM/GCL.

(3) Geomembrane is an excellent diffusive barrier to water and inorganic solute such as heavy metals, but is not a good diffusion barrier for volatile organic compounds (VOCs) such as toluene and dichloromethane. This is consistent with the field evidence that a wide variety of VOCs in various concentrations were detected in 91 leachate collection lysimeters installed beneath the liners of the landfills in Wisconsin, USA, and that the concentration of dichloromethane collected beneath the GM/CCL composite liners do not tend to be any lower than those collected beneath the single CCL (Shackelford, 2005). The service life of geomembrane depends on the

exposure conditions including temperature and contact solutes. On the basis of laboratory tests, the service life of HDPE geomembrane is estimated to be 120 years if the temperature at the base of a landfill is 20°C, and 70 years if the temperature is 33°C (Sangam and Rowe, 2002).

(4) As the thickness of GCL (i.e. 6-7 mm) is much less than that of CCL (at least 60 cm) stipulated by the regulations in various countries, the attenuation function of the conventional GCL is much less than that of the regulated CCL. When the transport of VOCs (which is dominated by diffusion) is considered, the mass flux through the GM/GCL composite liner can be two or three orders greater than that through the GM/CCL liner with a thickness of CCL greater than 62 cm (Foose et al. 2002). An attenuation layer (AL) is required under the GM/GCL composite liner to act as a partial diffusion barrier as well as to provide a greater opportunity for a self-biodegradation of VOCs. Theoretical calculations demonstrated that the GM/GCL/AL liner can provide the same or even greater environmental protection as compared with the GM/CCL/AL liner provided that the total thickness of the two kinds of liners is made the same (Rowe and Brachman, 2004).

(5) The performance of GCL as a barrier is affected by many factors, including the method of manufacture, the effect of freeze-thaw cycles, the susceptibility to desiccation and shrinkage, the potential for internal erosion of GCL, the clay-leachate interactions, and so on (Rowe, 2006). Many of the influences can be mitigated by choosing appropriate GCL products and adopting appropriate design and construction methods. The long-term hydraulic conductivity of GCL can be significantly affected by the clay-leachate interaction, in particular cation exchange (Shackelford, 2005). The magnitude of the influence depends on the type and concentration of solutes and the duration of the interaction. The laboratory test results obtained by Lee (2004) show that the ultimate hydraulic conductivity of GCL increases by 1-2 order of magnitude when the GCL was permeated with calcium chloride (CaCl₂, concentration up to 100 mM). However, the time require to reach the ultimate state (i.e. reaching chemical equilibrium) may be very long in the field conditions with a controlled leachate head (Lee and Shackelford, 2005).

(6) The performance of CCL as a barrier is also affected by many factors, including the available fine-grained materials, the influence of clods and gravel content, the quality of construction, the effect of freeze-thaw cycles, the susceptibility to desiccation and shrinkage, the clay-leachate interactions, and so on (Qian et al. 2002; Rowe, 2006). It is generally more difficult to control the quality of CCL than that of GCL, particularly in the developing countries being absence of construction equipments and quality assurance/control systems. The long-term per-

formance of CCL was investigated by Gartung et al. (1999). The authors recovered many undisturbed clay samples from the single CCL liner (60 cm in thickness) under a MSW landfill in Bavaria of Germany that had been operated for 12 years. The hydraulic and mechanical properties of the clay samples were measured, and the biological, chemical and mineralogical studies were also carried out. It was found that the density of the compacted clay had increased with time, and the hydraulic conductivity had decreased by two orders of magnitude from the originally-controlled value of 1.0×10^{-7} m/s. No desiccation was observed in the CCL even though a high temperature up to 53°C was measured at the base of the landfill. Careful chemical analyses did not indicate any trace of contaminants within the CCL. There was a considerable population of aerobic and anaerobic microbes within the CCL, and a membrane of bio-slime covering the surface of the CCL. The observed excellent performance of the CCL appears to be the result of a combined effect from the good quality of CCL, the low leachate head (a few millimeters) at the site and the positive microbiological influences.

Preliminary Study on Performance of Basal Liners Subjected to a High Leachate Head

As discussed previously, field evidences at the landfills in humid regions of southern China indicated that the leachate mound on the landfill bottom was likely to build up to a high level shortly after landfill operation (< 5 years). The performance of basal liners for this case is not enough studied and understood. The geoenvironmental research group in Zhejiang University performed an analytical study on the performance of basal liners subjected to a high leachate mound (Xie, 2008; Chen and Xie, 2009). The analytical study involves four kinds of contaminants (i.e. lead, chromium, dichloromethane and benzene) and four types of regulatory prescribed basal liners (i.e. 2 m CCL, GM+75 cm CCL, GM+GCL, and

GM+75cm AL). The conceptual model use for the analytical study is shown in Fig. 1(a). The study considered a semi-infinite bottom boundary condition, representing a deep groundwater table. The advection flux (leakage) of the contaminants through defects in geomembrane of composite liners was calculated by using the analytical solution provided by Rowe (1998). The mass flux of inorganic and organic contaminants through mineral or composite liners was calculated by using the analytical solution obtained by Xie (2008).

The analysis results for two kinds of contaminants (i.e. lead and dichloromethane (DCM)), representing inorganic and organic contaminants respectively, were chosen to present in this paper. The concentration of lead on the base liners (C_0) was assumed to keep as 12.3mg/L, and its allowable concentration level beneath the liners (C_b) is 0.01mg/L ($C_b/C_0=0.0008$). The concentration of DCM on the base liners (C_0) was assumed to a constant of 4.15 mg/L, and its allowable concentration level beneath the liners (C_b) is 0.005mg/L ($C_b/C_0=0.0012$). Herein, it is assumed that the number of defects for the GM is 20 holes/ha, and the area of each defects is 1 cm². Table 4 shows a list of material and chemical parameters relevant to the transport of the two contaminants through the four liner materials. More detailed information can be found in Xie (2008).

Parts of results from the analytical study are presented in the following sections. Table 5 shows a comparison of the calculated leakage rate through the four types of basal liners (i.e. 2 m CCL, GM+75 cm CCL, GM+GCL, and GM+75cm AL). For each of the composite liners with GM, the calculated leakage rate increases proportionally with an increase in the leachate head (h). When the leachate head (h) increases from 0.3 m to 10 m, the leakage rate increases by 24-31 times. For the 2m CCL, although the influence of leachate head on leakage rate is not so significant, the leakage rate through it is significantly greater than that through each of the of the GM+GCL is the best, followed by the GM+75 cm

Table 4 Material and chemical parameters for the considered contaminants and the liner materials (Rowe and Brachman, 2004)

Parameters		GM	CCL	GCL	AL
Thickness (m)		0.0015	1.0	0.007	0.75
Porosity		--	0.32	0.86	0.40
Hydraulic conductivity (m/s)		--	1.0×10^{-9}	5.0×10^{-11}	1.0×10^{-7}
Dry density (g/cm ³)		--	1.79	0.79	1.62
Diffusion coefficient (m ² /s)	Pb	6.0×10^{-15}	4.0×10^{-10}	5.9×10^{-10}	8.9×10^{-10}
	DCM	5.0×10^{-13}	8.0×10^{-10}	3.3×10^{-10}	8.9×10^{-10}
Sorption coefficient K_d (ml/g)	Pb	--	1.37	1.0	0
	DCM	--	1.5	0	0.28
Partitioning coefficient S (-)	DCM	5.0	--	--	--

Table 5 Calculated leakage rate through four types of basal liners subjected to different leachate heads

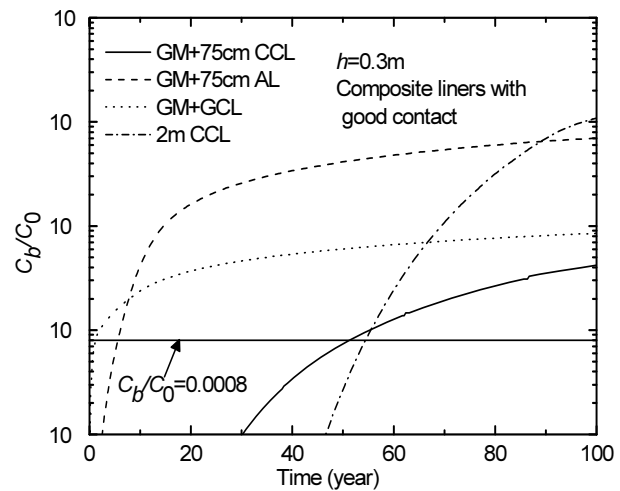
Type of liner	θ (m ² /s)	Leakage rate (m/year)			
		$h=0.3$ m	$h=1.0$ m	$h=3.0$ m	$h=10.0$ m
GM+75 cm CCL	1.6×10^{-8}	3.8×10^{-4}	1.2×10^{-3}	3.2×10^{-3}	0.01
GM+75 cm AL	1.6×10^{-8}	6.5×10^{-4}	1.9×10^{-3}	5.0×10^{-3}	0.0158
GM+ GCL	6.0×10^{-12}	3.5×10^{-7}	1.1×10^{-6}	3.4×10^{-6}	1.1×10^{-5}
2m CCL	---	0.036	0.047	0.079	0.189

Note: the values of θ listed indicate a good contact in between the GM and the underlying layer

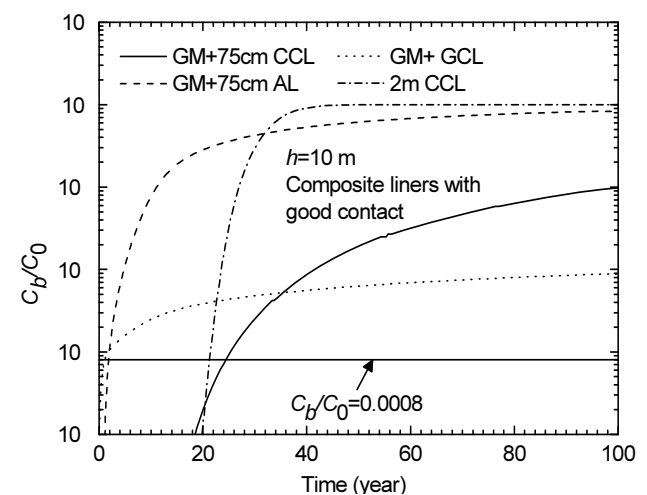
CCL or AL, and the worst for the 2m CCL. This is consistent with the previous understanding that the GM in conjunction with either the CCL or GCL is very effective in controlling leakage, especially when the GM are short of defects and in good contact with the underlying layer (Rowe, 2005). The analysis results also indicate that the control of leachate head is effective in controlling leakage through composite liners.

Fig. 11 (a) and (b) show the calculated concentration of lead released at the bottom of the four basal liners subjected to leachate head of 30 cm and 10 m, respectively. It can be seen that the rise in the leachate head exerts a significant influence on the performance of the basal liners. Herein defines the time required for the released contaminant reaching the allowable concentration level ($C_b/C_0=0.0008$) as a breakthrough time (t). As the leachate head increases from 0.3 m to 10 m, the breakthrough times for the liners decrease to 1/3-1/2 of the reference durations, with the exception of the GM+GCL. With respect to the breakthrough time for lead, the performance of the GM+GCL is the worst, followed by the GM+75 cm AL, and the best for the GM+75 cm CCL and the 2 m CCL. The influence of leachate head on the long-term concentration is also significant. As the leachate head increases from 0.3 m to 10 m, the concentration released at the time of 100 years for the liners increases by more than one order, with the exception of the GM+GCL.

Fig. 12 (a) and (b) show the calculated concentration of DCM released at the bottom of the four basal liners subjected to leachate head of 30 cm and 10 m, respectively. It can be seen that the rise in the leachate head exerts a significant influence on the performance of the 2 m CCL. As the leachate head increases from 0.3 m to 10 m, the breakthrough time for the 2 m CCL decreases to 1/2 of the reference duration, and the concentration released at the time of 100 years increases by nearly one order. However, it is unexpected that the influence of leachate head on the composite liners with GM is not so significant. With respect to the breakthrough time for DCM, the order in the performance of the four liners is: 2 m CCL > GM+75 cm CCL > GM+75 cm AL > GM+GCL.



(a) $h = 30$ cm



(b) $h = 10$ m

Fig. 11 Calculated concentration of Pb released at the bottom of the four basal liners: (a) $h = 30$ cm; (b) $h = 10$ m (Assumption: the number of defects in geomembrane is 20 per ha and the area of each defects is 1 cm²)

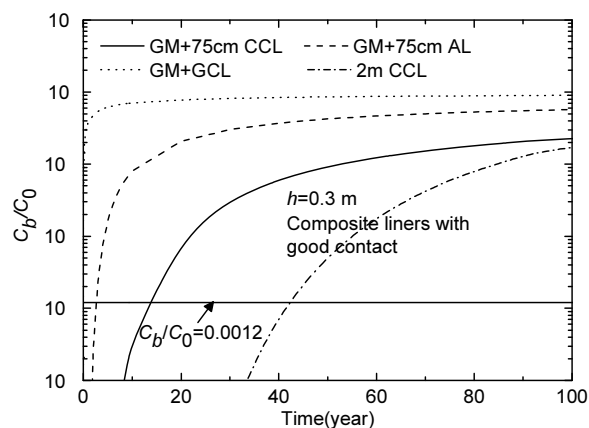
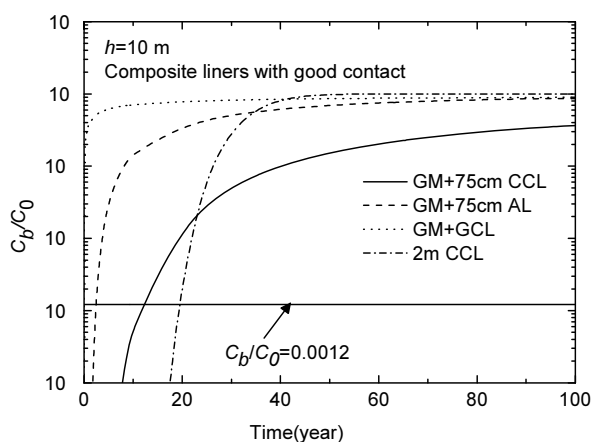
(a) $h = 30 \text{ cm}$ (b) $h = 10 \text{ m}$

Fig. 12 Calculated concentration of DCM released at the bottom of the four basal liners: (a) $h = 30 \text{ cm}$; (b) $h = 10 \text{ m}$ (Assumption: the number of defects in geomembrane is 20 per ha and the area of each defects is 1 cm^2)

The analysis results above demonstrated that the rise of leachate head will result a proportional increase in the leakage rate and a significant decrease in the breakthrough time. Under a high leachate mound (e.g. 10 m), the overall performance of the GM+75 cm CCL is the best among the four regulatory liners considered, but its service life may still be not long enough to meet the serviceability requirement of MSW landfills (at least 50 years). Therefore, the control of leachate head at a low level will be very important to make the service life of the basal liners meet the serviceability requirement. For the landfills in which the leachate head is not guaranteed to be controlled at a low level, it may be required to use an enhanced form of liners with respect to the current regulatory prescribed ones. The GM/GCL/CCL or GM/GCL/AL could be an alternative option. The analytical study reported by Rowe and Brachman (2004) indicates that GM+0.6m CCL+3.15m AL and GM+GCL+3.743m

AL are able to control the released concentration of contaminants below the allowable level throughout the time frame of the landfill modeled (200 years). In Rowe and Brachman's study (2004), it is assumed that the leachate head is built up to 6 m and 12 m at the times of 30 years and 50 after landfill closure. As discussed before, field evidences in southern China indicated that the leachate head at the base of the landfills started to build up shortly after landfill operation. Further study is required on this aspect.

ALTERNATIVE EARTHEN FINAL COVERS

When a landfill or part of it reaches the elevation as design, a final cover is installed to limit precipitation infiltration as well as to prevent free release of landfill gas into atmosphere. The function of the final cover is an important factor controlling leachate production rate and leachate mound within the landfill. Compacted clay covers or composite covers are commonly used in the current engineering practice. Field observations show that compacted clay covers, being susceptible to climate changes, do not function as well as expected due to desiccation and cracking. Composite covers, consisting of soils and geosynthetics such as geomembrane, geocomposite and geotextile, are relatively high in costs. In addition, the long-term performance of composite covers, which are exposed to complex climate changes, is not sufficiently understood. Because of these reasons, alternative earthen covers have gained interest recently (Shackelford, 2005). Alternative earthen covers (AEC) comprise entirely of soils and are designed on the basis of water balance principles. Shackelford (2005) has summarized the advantages of AECs: (a) AECs are typically less susceptible to desiccation and cracking since they can be constructed using relatively non-plastic soils; (b) AECs are relatively simple to construct since the focus of design is to achieve a high water storage capacity rather than to use heavy compaction to obtain a low hydraulic conductivity; (c) AECs are more economical since they can be built using a wide range of soil types, usually with the local vicinity of the site; and (d) AECs require relatively low post-closure maintenance.

The basic concept for AECs is to provide a water storage capacity within the cover that is greater than that needed to store water at any time of the year so that the amount of water percolating into wastes is minimized. At present, there are two most common types of AECs, i.e. monolithic covers and capillary barrier covers (see Fig. 13). Monolithic covers or MCs (also called store-and-release covers, soil-plant covers, evapotranspirative covers, or phytocovers) consist of a relatively thick, single layer of a fine-grained soil with a relatively high water storage capacity. The infiltrated water during a rain

period is stored in the MCs, which will subsequently be released by evaporation or evapotranspiration during a dry period. A capillary barrier cover (CBC) is a two-layered system consisting of a relatively fine-grained soil overlying a relatively coarse-grained soil. The barrier effect is caused by the contrast in the unsaturated hydraulic conductivity between the fine-grained and coarse-grained soil layers. Capillary barrier is effective as long as the matric suction at the interface is higher than the suction corresponding to the intersection of the hydraulic conductivity versus suction curves for the two soils. It is generally believed that this condition could be maintained only in arid and semi-arid climates. Recently, Rahardjo et al. (2007) carried out laboratory and numerical study on the applicability of the CBC in humid regions. The preliminary results show that the condition for capillary barrier can be achieved under a relatively humid climate by providing good lateral drainage within the overlying fine-grained soil layer.

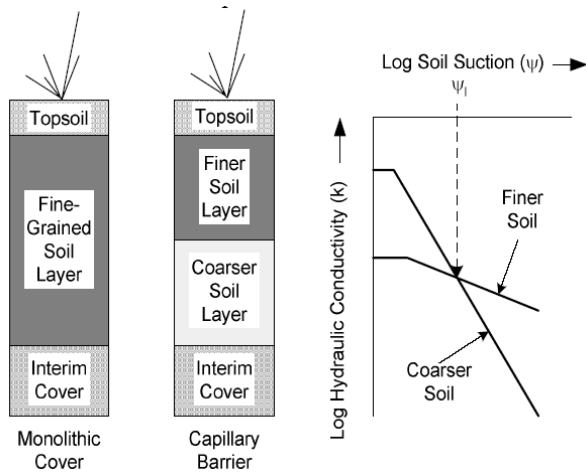


Fig. 13 Typical cross sections of the two main types of alternative earthen final covers (Shackelford, 2005)

The performance of the alternative earthen covers was investigated in USA through the Alternative Cover Assessment Program (Albright et al. 2004). The program consists of the monitoring of relatively large (10×20 m), fully instrumented drainage lysimeters with cross-sections representing conventional and alternative covers constructed at 11 field sites with various climate conditions (i.e. arid, semiarid, sub-humid and humid). The field monitoring results for semiarid and sub-humid climate conditions indicate that the AECs have performed extremely well in terms of limiting percolation, with very low percolation rates (<1.5 mm/yr) measured. The field observation also shows that the vegetation on the AECs plays an important role in the storage-and-release process. As the climate conditions show spatial and temporal variations in different countries and regions, further work is require to confirm the observed performance. In addition to field work, numerical modeling is usually

used as a good tool to predict the future performance of AECs subjected to a variety of climate conditions as well as the global climate change being taken place. It should be noted that the physical processes involved in the AECs are governed by highly nonlinear unsaturated soil properties and the boundary conditions reflect natural randomness precipitation events as well as complex evaporative and evapo-transpiration phenomena (Shackelford, 2005). A sophisticated numerical modeling software is required to predict the complex soil-atmosphere interaction and the transient flow process, and the predictions should be verified by comparison with field data.

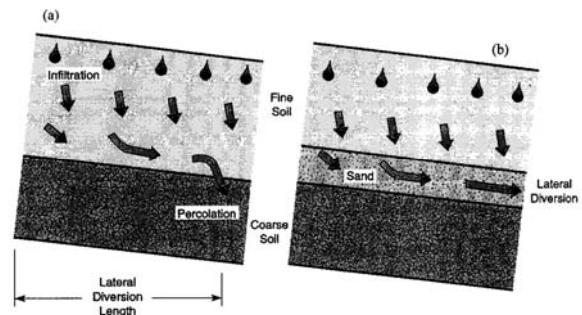


Fig. 14 An improved form of capillary barrier cover with lateral diversion (Stormont Morris, 1997)

It is generally believed that the alternative earthen final covers are effective only in arid and semi-arid climates. The field investigation reported by Albright et al. 2004 indicates that the earthen covers performed well under sub-humid climate condition. The laboratory and numerical study reported by Rahardjo et al. (2007) showed that an improved capillary barrier cover may be effective under a relatively humid climate. The proposed improvement is to provide good lateral drainage within the overlying fine-grained soil layer. Stormont and Morris (1997) reported an improved form of capillary barrier cover by inclusion of a sand layer (called unsaturated drainage layer) within the overlying fine soil layer (see Fig. 14). Stormont and Morris (1997) demonstrated that the sand layers are effective in providing a lateral diversion of infiltrating water and preventing a water breakthrough the underlying coarse layer. Further study is required for the performance of the improved capillary barrier cover, including the lateral diversion capacity of the unsaturated drainage layer, the short-term responses to critical meteorologic condition and the long-term response to climate changes (including seasonal and global ones).

SUMMARY

(1) Field evidences at the landfills in humid regions of southern China indicated that the leachate mound on the landfill bottom was likely to build up to a high level

shortly after landfill operation (< 5 years). The high leachate head would result in a high level of environmental pollution risk at the landfills. Water management and control of leachate level are a matter of the utmost concern with the current practice of MSW landfills in southern China.

(2) Vertical barrier is likely to be the most economic form of barriers for MSW landfills sitting on a good-quality bottom geological barrier. Several types of vertical barriers, including concrete diaphragm wall, composite diaphragm wall, steel sheet pile wall and grouted curtain, have been utilized in MSW landfills. Further research work is required in the performance assessment for the vertical cutoff walls, particularly in the long-term performance.

(3) The analytical study in this paper demonstrated that the rise of leachate head on the basal liners will result in a proportional increase in the leakage rate and a significant decrease in the breakthrough time. Under a high leachate mound (e.g. 10 m), the overall performance of the GM+75 cm CCL is the best among the four regulatory prescribed liners, but its service life may still be not long enough to meet the serviceability requirement of MSW landfills (at least 50 years). The control of leachate head at a low level will be very important to make the service life of the basal liners meet the serviceability requirement. For the landfills in which the leachate head is not guaranteed to be controlled at a low level, it may be required to use an enhanced form of liners (e.g. GM/GCL/CCL or GM/GCL/AL). Further study is required on this aspect.

(4) Two types of alternative earthen final covers, i.e. monolithic cover and capillary barrier cover, have been used in the current practice of landfills. The alternative covers have many advantages with respect to performance, economy and workability. The feasibility in the use of an improved capillary barrier cover in humid regions should be further investigated.

ACKNOWLEDGEMENTS

The authors would like to acknowledge financial support from research grants (50538080 and 50878194) provided National Natural Science Foundation of China (NSFC), the financial support from the National Key Technology R&D Program funded by the Ministry of Science and Technology of China (2006BAJ06B02), and the research funding from the Science and Technology Department of Zhejiang Province (2007C23038).

REFERENCES

Albright WH, Benson CH, Gee GW, Roesler AC,

- Abichou T, Apinmantragoon P, Lyles BF, Rock SA (2004). Field water balance of landfill covers. *Journal of Environmental Quality*, 33(6): 2317-2332.
- Bonaparte R, Daniel D, Koerner RM (2002). Assessment and recommendations for improving the performance of waste containment systems, EPA Report CR-821448-01-0. Washington, DC: US Environmental Protection Agency.
- Chen YM & Xie HJ (2009). A study on contaminant transport in soils and the performance of barrier systems. *Proceedings of International Workshop on Environmental Geotechnics*, Wuhan, 2009.
- Chen PH & Wang CY (1997). Investigation into municipal waste leachate in the unsaturated zone of the red soil. *Environment International*, 23(2):237-245.
- Edil TB (2003). A review of aqueous-phase VOC transport in modern landfill liners, *Waste Management*, 23: 561-571.
- El-Fadel M, Findikakis AN, Lechie JO (1997). Environmental impacts of solid waste landfilling. *Journal of Environmental Management*, 50: 1-25.
- Evans JC (1994). Hydraulic conductivity of vertical cut-off walls. *Hydraulic Conductivity and Waste Contaminant Transport in Soils*. ASTM STP 1142: 79-94.
- Evans JC & Opdyke SM (2006). Strength, permeability and compatibility of slag-cement-bentonite slurry wall mixtures for constructing vertical barriers. *Proceedings of 5th International Congress on Environmental Geotechnics*, 1: 118-125.
- Foose GJ, Benson CH, Edil TB (2002). Comparison of solute transport in three composite liners. *Journal of Geotechnical and Geoenvironmental Engineering*, 128(5): 391-403.
- Fratolocchi E, Pasqualini E, Balboni P (2006). Performance of a cement-bentonite cut-off wall in an acidic sulphate environment. *Proceedings of 5th International Congress on Environmental Geotechnics*, 1: 133-139.
- Gartung E, Mullner B, Defregger F (1999). Performance of compacted clay liners at the base of municipal landfills: The Bavarian experience. *Proceedings Sardinia '99, 7th International Waste Management and Landfill Symposium*, 3: 31-38.
- Giroud JP & Bonaparte R (1989). Leakage through liners constructed with geomembranes. Part II: Composite liners. *Geotextiles and Geomembranes*, 8(2): 71-111.
- Grube WE (1992). Slurry trench cut-off walls for environmental pollution control, *Slurry Wall: Design, Construction, and Quality Control*, ASTM STP 1129: 69-77.
- Inazumi S, Kimura M, Nishiyama Y, Yamamura K, Tamura H, Kamon M (2006). New type of hydraulic cutoff walls in coastal landfill sites from H-jointed steel pipe sheet piles with H-H joints. *Proceedings of 5th International Congress on Environmental Geotechnics*,

- 1: 725-732.
- Karmon M (2001). Environmental issues in geotechnical engineering. Proceeding of the 15th conference on soil mechanics and geotechnical engineering, 1: 2629-2674.
- Karmon M, Katsumi T, Inui T, Ogawa Y, Araki S (2006). Hydraulic performance of soil-bentonite mixture barrier. Proceedings of 5th International Congress on Environmental Geotechnics, 1: 733-740.
- Katsumi T, Benson CH, Foose GJ, Karmon M (2001). Performance-based design of landfill liners. *Engineering Geology*, 60: 139-148.
- Kjeldsen P (1986). Attenuation of Landfill Leachate in Soil and Aquifer Material. PhD Thesis, Technical University of Denmark.
- Lee JM (2004). Long-Term Hydraulic Performance of Geosynthetic Clay Liners Subjected to Inorganic Salt Solutions. PhD dissertation, Colorado State University, Fort Collins, Colorado, USA.
- Lee JM & Shackelford CD (2005). Impact of bentonite quality on hydraulic conductivity of geosynthetic clay liners. *Journal of Geotechnical and Geoenvironmental Engineering*, 131(1): 64-77.
- Marzougui A & Mammou AB (2006). Impact of the dumping site on the environment: Case of the Henchir EI Yahoudia Site, Tunis, Tunisia. *Comptes Rendus Geosciences*, 338(16):1176-1183.
- NSPRC (National specifications of the People's Republic of China), 1997a. Soil Quality—Determination of Copper, Zinc—Flame Atomic Absorption Spectrophotometry. GB/T 17138-1997 (in Chinese).
- NSPRC (National Specifications of the People's Republic of China), 1997b. Soil Quality—Determination of Lead, Cadmium—Graphite Furnace Atomic Absorption Spectro-photometry. GB/T 17141-1997 (in Chinese).
- NSPRC (National Specifications of the People's Republic of China), 1997c. Test Method Specification for Leaching Toxicity of Solid Wastes — Horizontal Vibration Extrac-tion Procedure. GB 5086.2-1997 (in Chinese).
- NSPRC (National Specifications of the People's Republic of China), 1995. Environmental Quality Specifications for Soils. GB 15618-1995 (in Chinese).
- Qian XD, Koerner RM, Gray DH (2002). Geotechnical aspects of landfill design and construction. Prentice-Hall, Inc, New Jersey, 2002.
- Rahardjo H, Krisdani H, Leong EC (2007). Application of Unsaturated Soil Mechanics in Capillary Barrier System. Proceeding of the 3rd Asian Conference on Unsaturated Soils. Nanjing, 2007: 127-137.
- Rowe RK. Geosynthetics and the minimization of contaminant migration through barrier systems beneath solid waste. In: Proceedings of the Sixth International Conference on Geosynthetics, Atlanta: Industrial Fabrics Association International, 1998: 27-102.
- Rowe RK (1998). Geosynthetics and the minimization of contaminant migration through barrier systems beneath solid waste. Proceedings of the 6th International Conference on Geosynthetics, March, Atlanta, GA: 27-102.
- Rowe RK (2005). Long-term performance of contaminant barrier systems. *Geotechnique*, 55(9): 631-678.
- Rowe RK (2006). Some factors affecting geosynthetics used for geoenvironmental application. Proceedings of 5th International Congress on Environmental Geotechnics, 1: 43-69.
- Rowe RK & Brachman RWI (2004). Assessment of equivalence of composite liners. *Geosynthetics International*, 11(4): 273-286.
- Rowe RK, Quigley RM, Brachman RWI, Booker JR (2004). *Barrier Systems for Waste Disposal Facilities*, E & FN Spon, London, 2004, p. 579.
- Sangam HP & Rowe RK (2002). Effects of exposure conditions on the depletion of antioxidants from high-density polyethylene (HDPE) geomembranes. *Canadian Geotechnical Journal*, 39(6): 1221-1230.
- Shackelford CD (2005). Environmental issues in geotechnical engineering. Proceeding of the 16th conference on soil mechanics and geotechnical engineering, 1: 95-122.
- Stormont JC & Morris CE (1997). Unsaturated drainage layers for diversion of infiltrating water. *Journal of Irrigation and drainage engineering*, ASCE, 123(5): 364-366.
- Xie HJ (2008). A study on contaminant transport in layered media and the performance of landfill liner systems. PhD thesis, Zhejiang University, Hangzhou.
- Zhan Tony LT, Chen YM, Ling WA (2008). Shear strength characterization of municipal solid waste at the Suzhou landfill, China. *Engineering Geology*, 97(2): 97-111.

ROLE OF SOIL WATER IN CEMENT-BASED TREATMENT OF DREDGED MATERIALS

Wei ZHU¹ and C.F. CHIU²

ABSTRACT: Cement-based solidification/stabilization is one of the popular technologies to remediate dredged materials (DM). This paper presents a laboratory study which investigates the relationship between the development of hydrates within the cement-treated soil matrix and its mechanical properties. The effects of cement content, curing period, clay content and humic acid content on the soil water composition and mechanical behavior of the cement-treated DM are evaluated. A soil water transfer model is proposed for the cement-based treatment from which two new water content parameters: change in hydration water content (Δm_{hw}) and change in bound water content (Δm_{bw}) are identified. Δm_{hw} and Δm_{bw} can be related to the amount of resultant hydrates and the development of the amorphous hydrates in the cement-treated soil matrix, respectively. It is found that Δm_{hw} and Δm_{bw} may be used to correlate some mechanical properties (such as unconfined compressive strength, yield stress and effective cohesion) of the cement-treated DM.

KEYWORDS: dredged materials, cementation, bound water, hydration water

INTRODUCTION

The demand for the dredging operations in China has increased tremendously in recent years, for instance the volume of dredged materials (DM) involved in the ocean disposal follows an increasing trend in the last decade and the annual volume reached around 200 million m³ in 2007 (Fig. 1). Besides ocean disposal, land disposal is another option, in particular for disposing the DM from the inland lakes and rivers. However, many land disposal sites are reaching their capacity and there is a shortage of land for constructing new disposal facilities due to recent economic development in China. Thus, utilization of the DM for beneficial use is one of the options under consideration to reduce the need for new disposal facilities.

Cement-based solidification/stabilization is one of the popular technologies for the treatment of DM and hazardous materials (Connor 1990). Cement is used as a binding agent and mixed with the soft or hazardous material to produce a mechanically stable soil matrix that exhibits higher strength and stiffness, and can also encapsulate possible contaminants (Mitchell 1981, Meegoda et al. 2000). Different approaches have been adopted to interpret the mechanical behavior of cement-

treated soils. Parameters like cement content and water-cement ratio are widely used to evaluate the strength of the cement-treated soils (Tatsuoka et al. 1997, Tremblay et al. 2001, Chew et al. 2004, Lee et al. 2005, Horpibulsuk et al. 2005). On the other hand, the microstructural studies of cement-treated clays have revealed that the hydrates produced from the cement hydration and pozzolanic reactions contribute to the modification of their mechanical properties (Connor 1990, Dermatas et al. 2003a & 2003b, Chew et al. 2004). Recent findings (Zhu et al. 2007a, 2007b & 2009, Chiu et al. 2009) have shown that the resultant hydrates formed in the cement-treated soils may be correlated to their soil water composition. Hence, it is important to understand the role of soil water in controlling the performance of the cement-based treatment of DM.

This paper summarizes the findings of three series of laboratory tests, from which the key factors that influence the cement-based treatment of DM are studied. The soil water composition and mechanical behavior of the cement-treated DM are evaluated. A soil water transfer model is proposed for the cement-based treatment. Two new water content parameters derived from the proposed model are used to correlate some mechanical properties of the cement-treated DM.

¹ Professor, College of Environmental Science and Engineering, Hohai University, China. Email: weizhu@hhu.edu.cn

² Associate Professor, Key Laboratory of Ministry of Education for Geomechanics and Embankment Engineering, Hohai University, China, Email: acfchiu@yahoo.com.cn

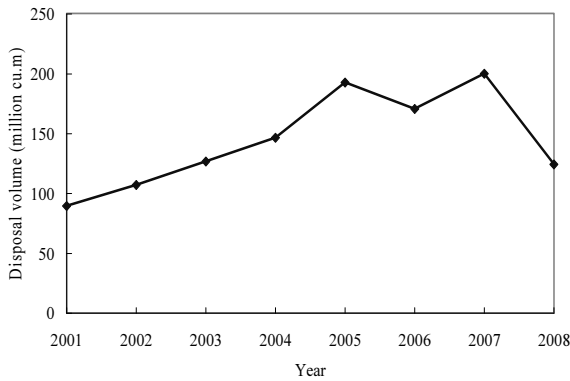


Fig. 1 Ocean disposal of DM in China (SOA 2008)

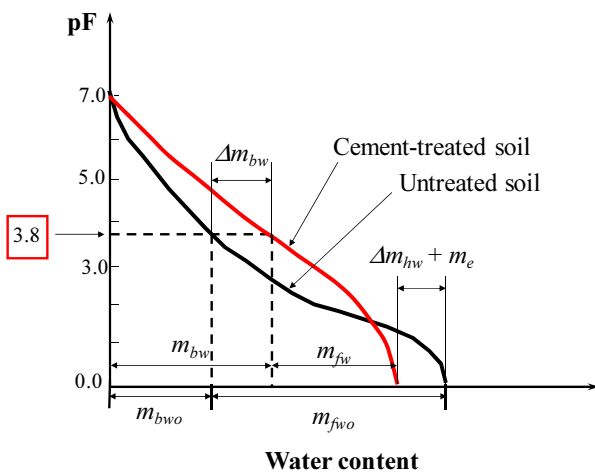


Fig. 2 Water retention curves for untreated and cement-treated soil

Table 1 Basic physical properties of tested soils

Physical index	L	M	R	S
Liquid limit (%)	75	73	62	72
Plastic index	47	41	27	40
Clay content (%)	20	32	30	89
Initial water content (%)	108	93	95	96
Organic content (%)	0.45	0.31	0.32	-

SOIL WATER TRANSFER IN CEMENT-BASED TREATMENT

Based on the energy state of the water molecules in the soil matrix, soil water can be classified into: (1) hydration water; (2) bound water; and (3) free water (Mitchell, 1992). Hydration water (HW) is chemically bonded to the soil minerals. Bound water (BW) is physically attracted to the vicinity of soil particles by adhesive forces. Free water (FW) is the loosely held water mainly controlled by surface tensional forces and gravity. In conventional soil mechanics, the pore water (PW) in the soil matrix is comprised of BW and FW.

Fig. 2 shows the water retention curves of an untreated soil and the corresponding cement-treated soil. The soil water transfer process during the cement hydration and pozzolanic reactions can be illustrated by the differences between the two water retention curves. The initial masses of FW and BW per unit volume of the untreated soil are represented by m_{fw0} and m_{bwo} , respectively. After cement hydration and pozzolanic reactions, the masses of FW and BW per unit volume of the cement-treated soil are represented by m_{fw} and m_{bw} , respectively. Thus, the change in the mass of BW per unit volume of the cement-treated soil (Δm_{bw}) is evaluated as follows:

$$\Delta m_{bw} = m_{bw} - m_{bwo} \quad (1)$$

The cement hydration reactions consume part of the PW which becomes the HW bounded into the newly formed hydrates. In addition, some water evaporates by the heat of hydration. As a result, the loss of PW can be evaluated by the following equation:

$$\Delta m_{hw} + m_e = (m_{fw0} + m_{bwo}) - (m_{fw} + m_{bw}) \quad (2)$$

where Δm_{hw} and m_e are the change in the mass of HW and the mass of water loss in evaporation per unit volume of the cement-treated soil, respectively. Δm_{hw} is the amount of HW bounded in the hydrates during the cement hydration which may reflect the amount of the hydration products found in the cement-treated soil. In addition, part of the FW is transferred to BW because more water is attracted around the surfaces of the newly formed amorphous calcium silicate hydrates (CSH) and calcium aluminate (CAH). Thus, Δm_{bw} may reflect the extent of the hydrates (products from cement hydration and pozzolanic reactions) developed within the cement-treated soil matrix.

LABORATORY STUDIES

Tested Soils

The tested soils used in the study were taken from four different locations in China: (i) a lake sediment L; (ii) a marine sediment M; (iii) a river sediment R; and (iv) a soft clay S. Detailed description and classification of the soils are given by Zhu et al. (2007a & 2007b). The basic physical properties of the soils are summarized in Table 1. According to the Unified Soil Classification System (USCS), L, M and S are classified as clay of high plasticity (CH) and R is classified as silt of high plasticity (MH). The predominant clay minerals found in the soils are kaolinite, illite and montmorillonite.

Specimens Preparation

Type I Ordinary Portland cement (OPC) was used as the cementing binder. The initial water content of the soil slurry was maintained around 93% – 116%. The cement-treated samples were formed by mixing the soil slurry with dry OPC powder to achieve cement contents (a_c) ranging from 38 kg/m³ to 700 kg/m³, which correspond to 5% to 91% of the dry weight of soil. The mixing was carried out as fast as possible inside a domestic mixer to avoid hardening of the cement-soil mixture. After mixing thoroughly, the mixture was placed into stainless steel molds 39 mm in diameter and 80 mm in height. The mixing and placing was completed at room temperature and took approximately 20 minutes. The specimens were wrapped by plastic sheet and put inside an environmental chamber for curing where the ambient temperature and relative humidity were maintained at 20±2°C and higher than 90%, respectively.

Testing Program and Procedures

Three series of the laboratory tests were conducted. The first series was conducted on soils L, M and R. The second series was conducted on the artificial materials made by adding different proportions of clay (S) into a silty soil such that the clay content of the samples varies from 15% to 89%. The third series was conducted on the soil L mixed with different proportions of humic acid. The testing conditions of the three series of tests are summarized in Table 2. After curing the specimens to the target period, unconfined compression tests and consolidated undrained tests were performed; and PW and BW contents of the specimens were determined.

The PW content (sum of m_{fw} and m_{bw}) was determined by oven drying the soil specimen to 105°C for at least 24 hours. Lebedev (1936) suggested that a soil potential of 3.8 pF can be used to distinguish between BW and FW. pF is defined as $-\log(h)$ where h is the water head expressed in cm. m_{bw} was determined by the centrifuge method (Gardner, 1937). The pF of soil water under centrifugal force is evaluated by the following equation:

$$pF = 2 \log(n) + \log(r_1 - r_2) + \log\left(\frac{r_1 + r_2}{2}\right) - 4.95 \quad (3)$$

where r_1 is the radial distance to the free water surface (cm), r_2 is the radial distance to the midpoint of the soil specimen (cm) and n is the angular velocity (rpm). Eq. 3 shows that pF is a function of the angular velocity. A compact centrifuge (Hitachi CR21) with an operable radius of 98 mm was used in the study. The diameter and height of the specimen holder is 50 mm and 51 mm, respectively. The trial run showed that a duration of 180 minutes is sufficient for the specimen to attain equilibrium

condition under the centrifugal acceleration. All tests were conducted at a controlled temperature of 20°C. The specimens in the centrifuge were subjected to angular velocities of 6,000 and 9,000 rpm, which correspond to 3.5 pF and 4 pF, respectively. BW content at 3.8 pF was determined by linear interpolation.

The unconfined compression test was conducted at a deformation rate 1.18 mm per minute. During each test, the specimen was covered by a rubber membrane to minimize water loss due to evaporation. The test was terminated when the peak strength was attained or 5% axial strain was reached for specimens exhibiting contractive behavior. The triaxial specimen was 39 mm in diameter and 80 mm in height. Drainage was allowed at the top platen and the excess pore water pressure was measured at the bottom of the specimen. Before installation in the triaxial cell, the specimen was initially saturated inside a vacuum chamber filled with de-aired water for at least 24 hours. After installation in the triaxial cell, the pore pressure coefficient B was measured. If the B value was smaller than 0.97, a back pressure would be used to saturate the specimen inside the triaxial cell. Isotropic compression test was carried out using incremental loading. Each loading stage was terminated after confirming the completion of consolidation by using the root time method. Thereafter undrained shear test was conducted at an axial compression rate of 0.05% per minute.

SOIL WATER COMPOSITION FOR CEMENT-TREATED DM

Fig. 3 shows the variation of soil water composition with a_c for the cement-treated samples of L after 7 and 28 days of curing. The PW content (sum of m_{fw} and m_{bw}) decreases linearly with a_c . The reduction of PW content is assumed to transfer partly into HW during cement hydration (Δm_{hw}) and partly loss in evaporation (m_e). The average value of m_e was around 13 kg/m³ for a_c ranging from 38 to 700 kg/m³ based on a control experiment. Δm_{hw} is evaluated from Eq. 2 and the following linear relationship between Δm_{hw} and a_c is emerged:

$$\Delta m_{hw} = k_1 \times a_c \quad (4)$$

Table 2 Testing conditions

Series	I	II	III
Soils	L, M, R	S	L
Cement content (kg/m ³)	50-700	38-114	100-200
Curing days	7-90	1-28	3-28
Clay content (%)	18-29	15-89	20
Humic acid content (%)	-	-	0.4-7.6

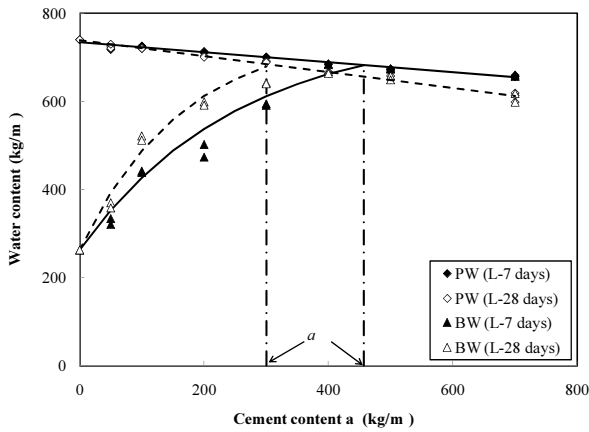


Fig. 3 Effect of cement content on soil water composition for cement-treated samples of L

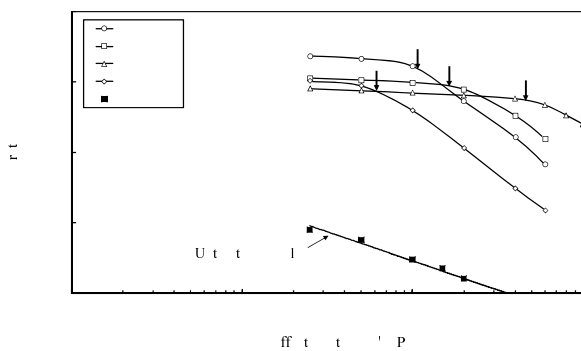


Fig. 4 Isotropic compression lines of cement-treated samples of L

Table 3 Parameters for soil water transfer model

DM	L		M		R	
Curing days	7	28	7	28	7	28
k (-)	0.10	0.16	0.12	0.16	0.13	0.21
k (m/kg)	0.004	0.006	0.006	0.009	0.006	0.008
a (kg/m)	457	300	376	259	304	218

k_1 increases from 0.1 to 0.16 as the curing period increases from 7 days to 28 days. It seems that k_1 may be used to estimate the extent of hydration reactions. Based on the chemical analysis of cement hydration, the water consumption is approximately about 0.2 to 0.25 of a_c (Lea 1970). Thus it is postulated that the hydration reactions may be far from completed after 28 days of curing. Fig. 3 also shows that m_{bw} increases nonlinearly with a_c , which indicates the increasing extent of the amorphous CSH and CAH developed within the cement-treated soil matrix. Δm_{bw} is evaluated from Eq. 1 and the following nonlinear relationship between Δm_{bw} and a_c is emerged:

$$\Delta m_{bw} = k_3 \cdot (1 - e^{-k \cdot a}) \text{ for } a_c \leq a_{co} \quad (5)$$

where a_{co} is a threshold cement content beyond which FW is eliminated, k_2 is a parameter that governs the rate of increment in BW and k_3 is a fictional value of Δm_{bw} at $a_c > a_{co}$ which is taken as 500 kg/m^3 in this study. k_2 increases from $0.004 \text{ m}^3/\text{kg}$ to $0.006 \text{ m}^3/\text{kg}$ as the curing period increases from 7 days to 28 days. Correspondingly, a_{co} reduces from 457 kg/m^3 to 300 kg/m^3 . Based on Eqs. 4 and 5, a soil water transfer model is proposed for the evaluation of the transfer of HW and BW during the cement-based treatment of DM. Four parameters (k_1 , k_2 , k_3 and a_{co}) are required in the model where k_1 governs the rate of increment in HW, k_2 governs the rate of increment in BW, k_3 is a fictional value of Δm_{bw} at $a_c > a_{co}$ which is assumed as 500 kg/m^3 in this study and a_{co} is a threshold cement content beyond which PW exists only as BW. Table 3 summarizes the values of k_1 , k_2 and a_{co} for the three DM used in this study. It is evident that k_1 and k_2 increase with the curing period, but a_{co} decreases with increasing curing period. Thus, the two new water content parameters (Δm_{hw} and Δm_{bw}) are functions of cement content and curing period.

KEY FACTORS FOR CEMENT-BASED TREATMENT ON DM

Cement Content and Curing Period

Fig. 4 shows the isotropic compression test results of cement-treated samples of L as void ratio (e) plotted against mean effective stress (p'). The isotropic compression line of untreated samples of L is also shown in the figure for comparison. The symbol L-100-07 in the figure represents samples of L treated with a a_c of 100 kg/m^3 and cured for 7 days. It is seen from the figure that the compression lines of the cement-treated samples lie above that of the untreated samples, i.e. the void ratio of the cement-treated soil is higher than that of the untreated soil for a given stress level. The arrows in the figure indicate the yield stresses (p'_y) determined by Butterfield's method (1979). It appears that the yield stress increases with increasing cement content and curing period. Similar to natural clay, the observed high yield stresses of the cement-treated DM are evidences of structure resulted from cement hydration and pozzolanic reactions.

Previous studies (Horpibulsuk et al. 2005; Kasama et al. 2006) have shown that the yield stress is also influenced by the initial water content. Horpibulsuk et al. (2005) have postulated to use the soil water/cement ratio to combine the effects of cement content and water content on the strength development of cement-treated soft clay. Fig. 5 shows the relationship between p'_y and soil water/cement ratio for cement-treated soils cured for

28 days. The test results of this study (L, M and R) are in consistent with those of Ariake clay (Horpibulsuk et al. 2005, Kasama et al. 2006) and Hudson river DM (Dermatas et al. 2003b). It is evident that the yield stress decreases with increasing soil water/cement ratio for a given soil. The figure also shows the yield stresses measured from three specimens curved for 7 days. It is apparent that the yield stress increases with curing period for a given soil water/cement ratio. It seems that no single equation can be used to best fit the test data of all five DM or soft soil, i.e. the extent of enhancement in mechanical behavior is different for different soil types. Previous studies (Chew et al. 2004, Zhu et al. 2007a) have shown that the extent of hydrates developed in the cement-treated soil is significantly affected by the clay minerals and amount of clay content found in the soft soils. Thus, the discrepancy between the test data of different soils may be attributed to the different extent of hydrates formed and eventually affecting their mechanical properties. The effect of clay content on the strength of cement-treated soils will be discussed in the next section.

Figs. 6 and 7 show the effects of cement content and curing period on the peak strength envelope of the cement-treated samples of L, respectively. The failure line of the untreated samples of L is also shown in the figures for comparison. It is evident that a linear failure envelope can be used to represent the peak shear strength of each test series for the range of confining pressure considered in the study. The values of the angle of internal friction (ϕ') for the cement-treated samples are in general slightly greater than that of the untreated samples, except for the one cured for 90 days. However, the effect of cement content and curing period on the effective cohesion (c') is more apparent; c' increases substantially with increasing cement content and curing day.

Fig. 8 shows the relationship between c' and percentage of cement (by weight) for cement-treated soils cured for 28 days. The test results of the study (L, M and R) are in good agreement with those of four other DM or soft soils reported in the literature, i.e. c' increases nonlinearly with increasing cement content for a given soil. The figure also shows c' measured from some specimens curved for 7 days. It is apparent that c' also increases with curing period for a given percentage of cement (by weight). It seems that no single equation can be used to best fit the test data for all seven DM or soft soils. The amount of clay content and plasticity are different for all seven soils presented in Fig. 8 (Chiu et al. 2009). Hence, it is anticipated that the scatter of data may be caused by the different extent of hydrates formed and developed in soils with different clay content and clay minerals; and eventually affecting their shear strength properties.

Fig. 9 shows the relationship between unconfined compressive strength (q_u) and a_c for the cement-treated samples of L after 7 and 28 days of curing. A minimum cement content (a_{cm}) is required for an apparent strength improvement. The values of a_{cm} range from 30 to 70 kg/m^3 for the three DM (L, M and R) used in the study. When a_c is between a_{cm} and 300 kg/m^3 , q_u increases linearly with a_c . Beyond 300 kg/m^3 , q_u increases nonlinearly with a_c . In addition, q_u increases with the curing time for a given a_c .

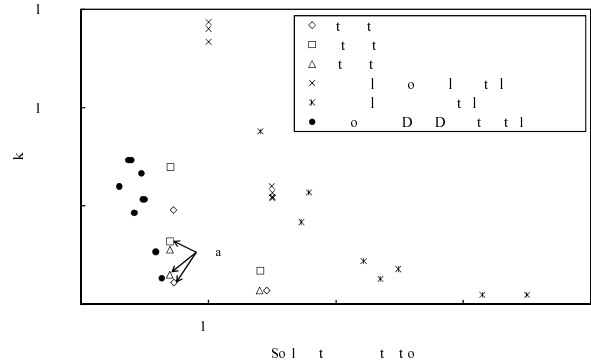


Fig. 5 Relationship between yield stress and soil-water/cement ratio for cement-treated soils cured for 28 days

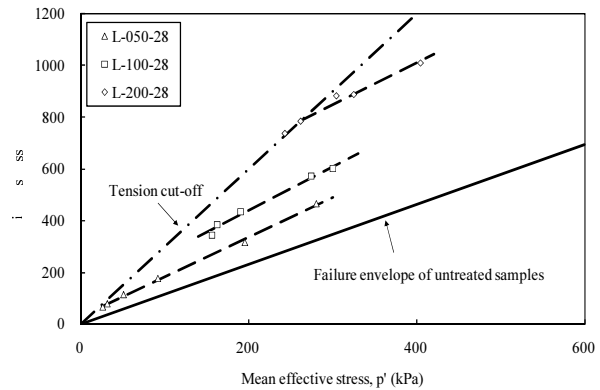


Fig. 6 Effect of cement content on peak strength envelope of cement-treated samples of L

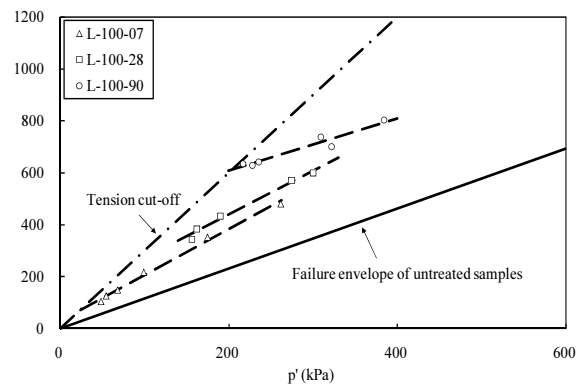


Fig. 7 Effect of curing period on peak strength envelope of cement-treated samples of L

Clay Content

The effect of clay content on the strength of cement-treated soils was studied by conducting unconfined compression tests on the artificial materials made by adding different proportions of clay (S) into a silty soil (series II in Table 2). The clay content of the samples varies from 15% to 89%. Fig. 10 shows the effect of clay content on q_u for the cement-treated samples cured for 7 days. There is an optimum clay content (CC_{opt}) at which a peak value of q_u is observed for a given cement content. CC_{opt} is 36, 47 and 51% for cement content of 57, 76 and 114 kg/m^3 , respectively. Similar to the discussion of the test results presented in Figs. 5 and 8, the difference in q_u may be attributed to the different extent of hydrates formed and eventually affecting the strength of the cement-treated soil. Fig. 11 shows the relationships between the change in BW (Δm_{bw}) and clay content for the cement-treated samples curved for 7 days. A trend similar to that shown in Fig. 10 is observed. There is also an CC_{opt} at which a peak value of Δm_{bw} is observed. For a given cement content, both Δm_{bw} and q_u reach their peak values at a similar value of CC_{opt} . As Δm_{bw} reflect the extent of the hydrates (products from hydration and pozzolanic reactions) developed in the cement-treated soil, it may be an appropriate parameter to quantify the effect of hydrates on the strength of the cemented soils. The proposed correlations will be discussed in the next section.

Humic Acid Content

Humic acid is one of the major components found in the organic matter in DM. The effect of humic acid content on the strength of cement-treated soils was studied by conducting unconfined compression tests on the soil L mixed with different proportions of humic acid (series III in Table 2). The humic acid content of the samples varies from 0.4% to 7.6%. Fig. 12 shows the effect of humic acid content on q_u for the cement-treated samples curved for 7 days. It is evident that q_u decreases with increasing humic acid content. In addition, there is a threshold humic acid content (HA_{th}), beyond which q_u reduces to a relative low and steady value. Such low strength can be attributed to a negligible formation and development of hydrates in the cement-treated soil. For specimens cured at 7 days, HA_{th} are 3.6 and 5.8% for a_c of 100 and 200 kg/m^3 , respectively, thus HA_{th} increases with a_c . As expected, a higher amount of humic acid is required to retard the formation of hydrates at a higher cement content. Past studies ((Kamon et al. 1989, Tremblay et al. 2002, Dermatas et al. 2003a) have shown that humic acid may hinder the cement-based treatment process by retarding the hydration reaction through reducing the pH of the pore solution. The cement

hydration normally takes place under a high alkalinity environment. If the pH is too low, fewer hydrates will be formed. In addition, humic acid may react with the hydrated lime (calcium hydroxide) produced by the cement hydration to form insoluble reaction products. As a result only part of the calcium ions is available for the subsequent pozzolanic reactions and the amount of pozzolanic products will also be reduced. Hence, the understanding of the formation and development of the resultant hydrates in the cement-treated soil may be useful in interpreting the effect of humic acid. Fig. 13 shows the effect of humic acid content on Δm_{bw} for the cement-treated samples curved for 7 days. It is apparent that similar trend is observed as compared with that shown in Fig. 12. Both q_u and Δm_{bw} increase with a_c for a given humic acid content. Besides, both parameters decrease with increasing humic acid content for a given a_c , and reach a steady value around a similar threshold humic acid content (HA_{th}).

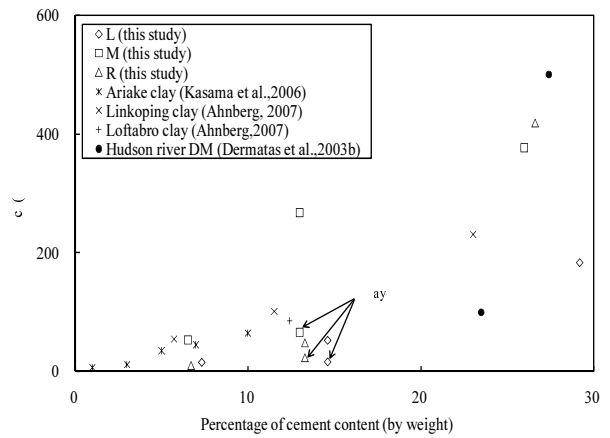


Fig. 8 Relationship between effective cohesion and percentage of cement (by weight) for cement-treated soils curved for 28 days

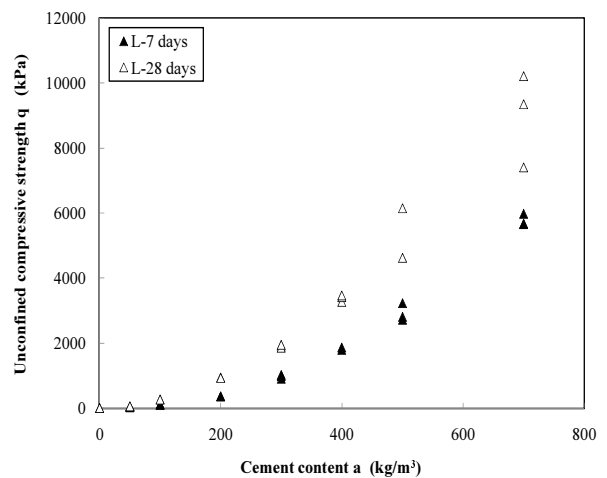


Fig. 9 Effect of cement content on unconfined compressive strength of cement-treated samples of L

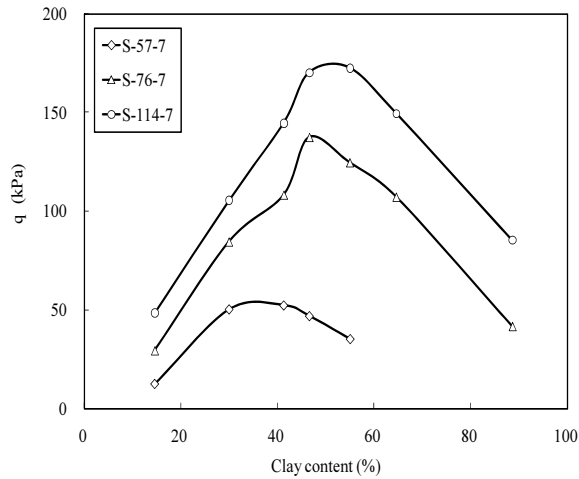


Fig. 10 Effect of clay content on unconfined compressive strength of cement-treated samples of S

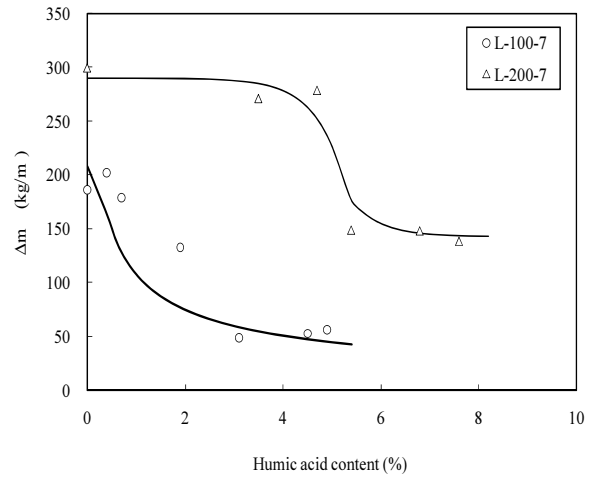


Fig. 13 Effect of humic acid content on change in BW content (Δm_{bw}) of cement-treated samples of L

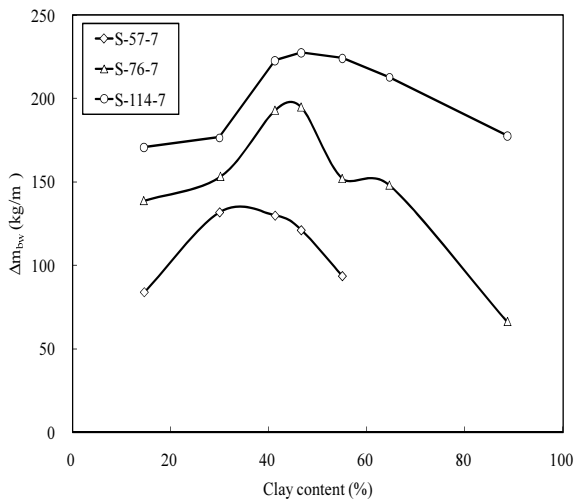


Fig. 11 Effect of clay content on change in BW content (Δm_{bw}) of cement-treated samples of S

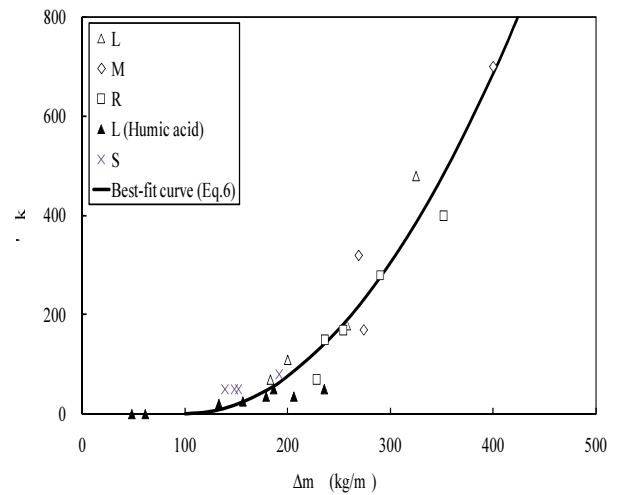


Fig. 14 Relationship between yield stress and change in BW content for cement-treated DM

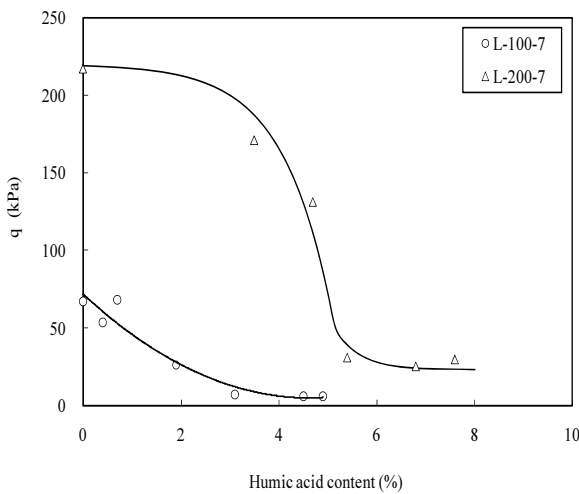


Fig. 12 Effect of humic acid content on unconfined compressive strength of cement-treated samples of L

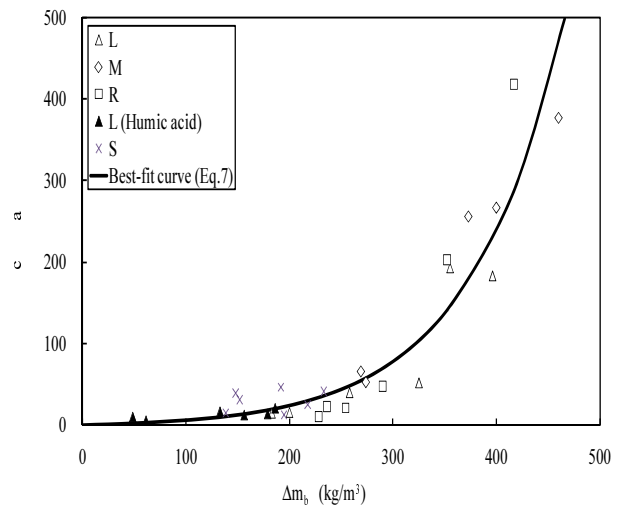


Fig. 15 Relationship between effective cohesion and change in BW content for cement-treated DM

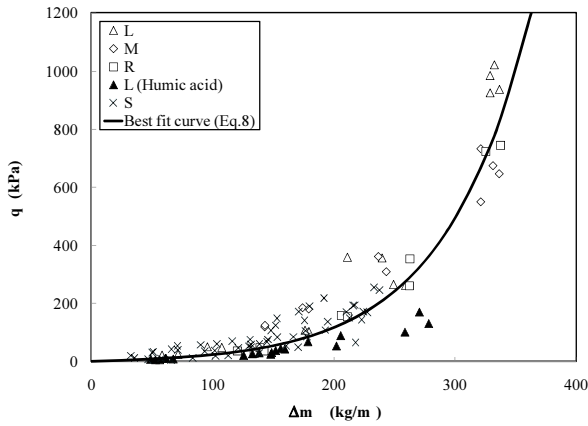


Fig. 16 Relationship between unconfined compressive strength and change in BW content for cement-treated DM

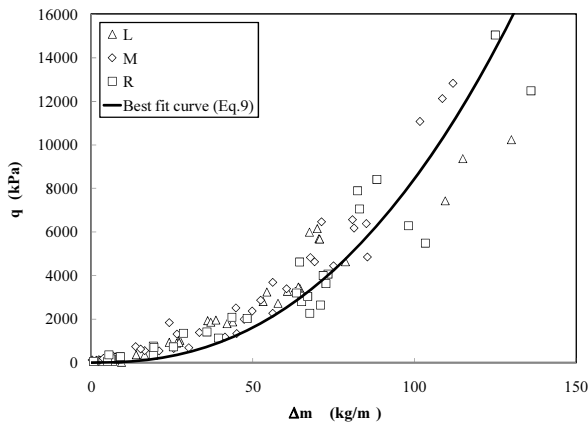


Fig. 17 Relationship between unconfined compressive strength and change in HW content for cement-treated DM

CORRELATIONS BETWEEN MECHANICAL PROPERTIES AND WATER CONTENT PARAMETERS

It has been shown in the previous section both the mechanical properties and soil water composition of the cement-treated soil can be related qualitatively to the extent of the resultant hydrates developed in the cement-treated soil matrix. For instance, key factors like cement content, curing period, clay content and humic acid content influence both the mechanical properties (yield stress, effective cohesion and unconfined compressive strength) and the soil water composition (Δm_{hw} and Δm_{bw}) in a similar manner. Thus, it is suggested that Δm_{hw} or Δm_{bw} may be used to correlate some mechanical properties of the cement-treated DM. Eq. 5 is valid only if a_c is smaller than a threshold cement content (a_{co}). Further the value of Δm_{hw} is much smaller than that of Δm_{bw} , for example, Δm_{hw} and Δm_{bw} are in the orders of

10 kg/m³ and 100 kg/m³, respectively, for a_c of 100 kg/m³ and a curing period of 7 days. Hence, the measurement errors of Δm_{hw} are much more significant for a_c smaller than 100 kg/m³. It is suggested that Δm_{bw} can be used to correlate the yield stress (p'_y), effective cohesion (c') and unconfined compressive strength (q_u) of the cement-treated DM at $a_c \leq 200$ kg/m³.

Figs. 14, 15 and 16 show the relationships between p'_y and Δm_{bw} , c' and Δm_{bw} , q_u and Δm_{bw} , respectively. The figures show that Δm_{bw} increases nonlinearly with p'_y , c' and q_u , in other words, these mechanical parameters are proportional to the extent of hydrates developed in the cement-treated soil matrix. The following empirical expressions can be used to best-fit the test data shown in the figures:

$$p'_y = 4 \cdot 10^{-6} \cdot \Delta m_{bw}^{3.18} \tag{6}$$

$$c' = 3 \cdot (e^{0.011 \cdot \Delta m} - 1) \tag{7}$$

$$q_u = 7.5 \cdot (e^{0.014 \cdot \Delta m} - 1) \tag{8}$$

For $a_c > a_{co}$, Δm_{hw} is a better option than Δm_{bw} because Δm_{bw} reduces with increasing a_c (see Fig. 3). Fig. 17 shows the relationship between q_u and Δm_{hw} for a_c ranging from 50 to 700 kg/m³. The following empirical expression is used to best-fit the test data:

$$q_u = 0.14 \cdot \Delta m_{hw}^{2.39} \tag{9}$$

Despite the scatter of data, it seems that unique correlations can be obtained between Δm_{bw} and some mechanical parameters (p'_y , c' and q_u) for $a_c < a_{co}$ for four different natural DM and artificial materials which exhibit different basic physical properties, like clay content and humic acid content. For $a_c > a_{co}$, an unique relationship is also emerged between Δm_{hw} and q_u .

ENGINEERING APPLICATIONS

Eqs. 6-9 clearly demonstrate the potential use of a single water content parameter (Δm_{hw} or Δm_{bw}) in evaluating the mechanical properties of cement-treated DM, such as yield stress, effective cohesion and unconfined compressive strength, from which the performance of the cement-based solidification/stabilization can be assessed. Either Δm_{hw} or Δm_{bw} can combine the effects of cement content and curing time as it is empirically related to the extent of hydrates developed during the cement hydration and pozzolanic reactions, which is the fundamental cause for the physical modification of the cement-treated DM. Besides, it seems that unique relationships (Eqs. 5-8) may be obtained from soils with different clay content and

humic acid content.

One of the potential applications of the proposed empirical correlations is the assessment of the field performance of cement-based solidification/stabilization treatment. In the conventional design approach, the field properties can be obtained by multiplying a modification factor to the laboratory properties because of heterogeneous nature of DM, non-uniform mixing of cement and different curing conditions in the field (Tang et al. 2001). The proposed parameters has the following advantages: (i) it is easily determined by commercially available compact centrifuge; (ii) it can be related to several mechanical parameters like yield stress, effective cohesion and unconfined compressive strength; (iii) no modification factor is required because it is empirically correlated to the extent of hydrates formed in the cement-treated DM.

CONCLUSIONS

Three series of laboratory tests were conducted to study the effects of cement content, curing period, clay content and humic acid content on the soil water composition and mechanical behavior of four cement-treated dredged and artificial materials. It is found that the aforementioned factors influence both the mechanical properties (like yield stress, effective cohesion and unconfined compressive strength) and the soil water composition of the cement-treated soils in a similar manner. The enhancement of the mechanical properties of the cement-treated soils is related to the extent of hydrates developed in the soil matrix from the cement hydration and pozzolanic reactions, which also alter their soil water composition by changing the content of hydration water (HW) and bound water (BW). A soil water transfer model is proposed for the cement-based treatment from which two new water content parameters: change in HW content (Δm_{hw}) and change in BW content (Δm_{bw}) are identified. It is found that both Δm_{hw} and Δm_{bw} can be correlated to the mechanical properties (such as unconfined compressive strength, yield stress and effective cohesion) of the cement-treated soils in a coherent manner.

ACKNOWLEDGEMENT

This study is sponsored by the Ministry of Water Resources of China through Grant No.200701045.

REFERENCES

Ahnberg H (2007). On yield stresses and the influence of

- curing stresses on stress paths and strength measured in triaxial testing of stabilized soils. *Canadian Geotechnical Journal* 44(1):54-66.
- Butterfield R (1979). A natural compression law for soils. *Géotechnique* 29(4):469-480.
- Chiu CF, Zhu W, Zhang CL (2009). Yielding and shear behaviour of cement-treated dredged materials. *Engineering Geology* 103(1-2):1-12.
- Chew SH, Kamruzzaman AHM, Lee FH (2004). Physicochemical and engineering behavior of cement-treated clays. *J. Geotech. Geoenviron. Engrg. ASCE*. 130(7):696-706.
- Connor JR (1990). *Chemical fixation and solidification of hazardous wastes*. Van Nostrand Reinhold, New York.
- Dermatas D, Dadachov M, Mirabito M, Meng X (2003a). Strength development of solidified/ stabilized organic waste and optimum treatment design. *Journal of the Air and Waste Management Association* 53(11):1363-1372.
- Dermatas D, Dutko P, Balorda-Barone J, Moon DH (2003b). Evaluation of engineering properties of cement treated Hudson River dredged sediments for reuse as fill materials. *Journal of Marine Environmental Engineering* 7(2):101-123.
- Gardner RA (1937). The method of measuring the capillary tension of soil moisture over a wide moisture range. *Soil Science* 43:277-283.
- Horpibulsuk S, Miura N, Nagaraj TS (2005). Clay-water/cement ratio identity for cement admixed soft clays. *J. Geotech. Geoenviron. Engrg. ASCE*. 131(2):187-192.
- Kamon M, Tomoshisa S, Sawa K (1989). On the stabilization of hedoro by using cement group hardening materials. *Journal of the Society of Materials Science Japan* 38(432):1092-1097 (In Japanese).
- Kasama K, Zen K, Iwataki K (2006). Undrained shear strength of cement-treated soils. *Soils and Foundations* 46(2):221-232.
- Lea FM (1970). *The chemistry of cement and concrete*. 3rd Ed., Edward Arnold Ltd., London.
- Lebedev AF (1936). *Soil and Groundwaters*. The Academy of Sciences of the USSR (In Russian).
- Lee FH, Lee Y, Chew SH, Yong KY (2005). Strength and modulus of marine clay-cement mixes. *J. Geotech. Geoenviron. Engrg. ASCE*. 131(2):178-186.
- Meegoda JN, Partymiller K, Richards MK, Kamolpomwijit W, Librizzi W, Tate T, Noval BA, Mueller RT, Santora S (2000). Re-mediation of chromium contaminated soils—a pilot scale investigation. *ASCE practice periodical of hazardous, Toxic Radioactive Waste Manage* 4(1):7-15.
- Mitchell JK (1981). Soil improvement state of the art report. *Proc. 10th International Conference on Soil*

- Mechanics and Foundation Engineering, Stockholm, 4:509-565.
- Mitchell JK (1992). Fundamentals of soil behavior, 2nd Ed., John Wiley & Sons, New York.
- State Oceanic Administration P.R. China (2008). China Marine Environmental Quality Report 2008. State Oceanic Administration People's Republic of China, Beijing (In Chinese).
- Tang YX, Miyazaki Y, Tsuchida T (2001). Practices of reused dredgings by cement treatment. *Soils and Foundations* 41(5):129-143.
- Tatsuoka F, Uchida K, Imai K, Ouchi T, Kohata Y (1997). Properties of cement treated soil in Trans-Tokyo Bay Highway project. *Ground Improvement* 1(1):37-57.
- Tremblay H, Duchesne J, Locat J, Leroueil S (2002). Influence of the nature of organic compounds on fine soil stabilization with cement. *Canadian Geotechnical Journal* 39:535-546.
- Tremblay H, Leroueil S, Locat J (2001). Mechanical improvement and vertical yield stress prediction of clayey soils from eastern Canada treated with lime or cement. *Canadian Geotechnical Journal* 38:567-579
- Zhu W, Chiu CF, Zhang CL, Feng ZC (2007a). Soil-water transfer mechanism for cemented clay. Proc. 13th Asian Regional Conference on Soil Mechanics and Geotechnical Engineering, Kolkata, India 1:765-768.
- Zhu W, Zhang CL, Chiu ACF (2007b). Soil-water transfer mechanism for solidified dredged materials. *J. Geotech. Geoenviron. Engrg. ASCE*. 133(5): 588-598.
- Zhu W, Chiu CF, Zhang CL, Zeng KL (2009). Effect of humic acid on the behavior of solidified dredged material. *Canadian Geotechnical Journal* 46(8) in press.



**Basic and Advanced Theories for Modeling
of Geoenvironmental Phenomena**

NUMERICAL SIMULATION OF ELECTRO-OSMOSIS IN SOFT CLAY

Liming HU¹, Wei-Ling WU² and Zhao-Qun WU³

ABSTRACT: Electro-osmosis consolidation seems to be a potential technique for improvement of soft clay. The traditional electro-osmosis theory cannot provide satisfied solution since the hypothesis of constant parameters of mechanical and electrical properties of soils. In this paper, FEM software is developed to couple the Laplace's equation for electrical field with Biot's consolidation equation, and the displacement of soil mass and pore-water pressure can be obtained during electro-osmosis process. The non-linear variety of hydraulic permeability of soil mass during consolidation is incorporated in the control equations. The boundary conditions for electrical field, seepage flow and displacement can be adequately simulated. The calculation results agree well with the monitoring data from analytical model. The software can predict the displacement behavior of soil mass and provide useful data for system design of electro-osmosis treatment.

KEYWORDS: electro-osmosis, consolidation, pore-water pressure, FEM, Biot's theory

INTRODUCTION

Electro-osmosis consolidation provides a potentially attractive soil improvement technique, which involves the application of a direct current (DC) potential across electrodes embedded in the soil and cause the flow of pore water from the anode toward the cathode.

Following the pioneering work of Casagrande on the beneficial effects of electrical treatment on the shear strength and stability of fine-grained soils, the electro-osmotic consolidation technique has been used in various geotechnical engineering applications, including stabilization of slopes, excavations, and embankments, controlling groundwater flow, increasing pile capacity and the strength of clays, and dewatering tailings and sludge (Casagrande 1948, Perry 1963, Bjeruum et al. 1967, Fetzer 1967, Davis and Poulos 1980, Casagrande 1983, Eggstad and Foyne 1983, Lo et al. 1991, Shang and Dunlap 1998, Bergado et al. 2000, Weiss et al. 2005, Fourie et al. 2007, Glendinning et al. 2008). Meanwhile, numerous laboratory studies have been published (Bernatzik 1948, Wang 1953, Esrig and Gemeinhardt 1967, Banerjee et al. 1984, Feldkamp and Belhomme 1990, Lo and Ho 1991, Laursen 1997, Nettleton et al. 1998, Chen and Murdonch 1999, Micic et al. 2001, Lefebvre and Burnotte 2002, Mohamedelhassan and Shang 2002, Hong and Hu 2007, Glendinning et al. 2005, Zhuang and Wang 2007, Jones et al. 2008).

Ersig (1968) proposed analytical solutions to calculate the excess pore water pressure in a one dimensional uniform electric field. The control equation is similar to Terzaghi's consolidation theory since the electrical field intensity is constant. Wan and Mitchell (1976) derived analytical solutions to calculate the excess pore water pressure for the electro-osmotic treatment in a uniform electric field with a surcharge pressure. Shang (1998) developed an analytical solution for the electro-osmotic consolidation process in a uniform electric field in anisotropic soil with a surcharge pressure.

However, the analytical solutions for a one-dimensional uniform electric field may not be applicable for most applications in the vicinity of electrodes. Lewis and Humpheson (1973) established the governing equations of electric current and electro-osmotic flow in soil mass based on the conservation law of water mass and electric charge, and formulated a finite element model to analyze the electro-osmotic flow in two-dimensional electric fields. Su and Wang (2003) established analytical solutions of ultimate excess pore-water pressure in a hypothetical two-dimensional electric field for different boundary conditions based on governing equations used by Lewis and Humpheson (1973).

Previous studies assumed that the soil electrical and mechanical properties remain constant during electro-osmotic consolidation process. However, the soil electrical conductivity in the vicinity of electrodes decreases

¹ Associate Professor, Department of Hydraulic Engineering, State Key Laboratory of HydroScience and Engineering, Tsinghua University, China. Email: gehu@tsinghua.edu.cn

² MS Student, ditto

³ Research Assistant, ditto.

significantly and rapidly during the electro-osmotic treatment, which results in significant voltage drop in the vicinity of soil-electrode interface (Bjerrum et al. 1967; Wade 1976; Lo et al. 1991). Rittirong and Shang(2008) proposed a 2D finite difference model to analyze the electro-osmotic consolidation considering voltage drop in the vicinity of the soil-electrode interface and change of soil compressibility. The permeability of the soil varies according to water content change and consolidation of soil mass. Effects of the change in the soil conductivity and permeability during electro-osmotic consolidation have not been studied systematically in the literature. Furthermore, the deformation of soil mass has not been coupled in the governing equations for the electro-osmosis process. Therefore, the subsurface settlement can not be obtained directly during numerical simulation.

The purpose of this study is to develop a numerical model to analyze the electro-osmotic consolidation process of soil mass subjected to various electric fields. Effects of the electrode dimensions and change of soil conductivity are incorporated in the analysis of distribution electric field intensity. The permeability change of soil during consolidation is considered to simulate the groundwater flow. Most important of all, the soil deformation is coupled in analyzing the electro-osmosis process, which gives the direct solution of ground surface settlement. Since the electro-osmosis generates a non-uniform pore water pressure and deformation in soil, a time-dependent finite element model is developed to simulate the mechanical and hydraulic behavior of soft soil under electro-osmosis treatment.

GOVERNING EQUATIONS FOR ELECTRO-OSMOSIS CONSOLIDATION

Consolidation of Soil

For the saturated soil, Biot's theory is used to describe the consolidation behavior of soil based on the Terzaghi's theory for the effective stress,

$$-\nabla^2 \mathbf{u} - \frac{\lambda + G}{G} \nabla(\nabla \cdot \mathbf{u}) + \frac{1}{G} \nabla(H - z) = 0 \quad (1)$$

in which, \mathbf{u} is the displacement vector of soil mass, λ and G is the elastic constants for soil skeleton, $H-z$ is hydraulic head of pore water pressure, among which H is total head, and z is position head.

Hydraulic Flow

Hydraulic flow is intrigued by the energy differential, and the flow of fluid through a porous media is given by Darcy's law,

$$v = -k i = -k \frac{\partial H}{\partial x} \quad (2)$$

in which k_h is hydraulic permeability, H is the total hydraulic head equal to the sum of the position and pressure heads, and v_h is velocity of pore water flow.

The equation can be extended to describe three dimensional problems.

$$\bar{v} = -k \nabla H \quad (3)$$

Electro-osmosis Flow

Casagrande (1948) showed that flow through porous media induce by a voltage gradient had the same form as Darcy's law, i.e.

$$v = -k_e i = -k_e \frac{\partial V}{\partial x}, \text{ or } \bar{v} = -k_e \nabla V \quad (4)$$

in which V is the electric potential, and k_e is the electro-osmosis conductivity.

Coupling of Electrical Field and Seepage Field

It has been shown both theoretically and experimentally that electro-kinetic and hydrodynamic flows may be superimposed, giving the combined fluid flow equation.

$$\bar{v} = \bar{v}_h + \bar{v}_e = -k \nabla H - k_e \nabla V \quad (5)$$

Applying the law of conservation of mass and using the continuity equation, the following equation can be derived for the saturated soil,

$$\frac{\partial q}{\partial t} = \text{div}(\bar{v}) = -\frac{\partial \varepsilon}{\partial t} \quad (6)$$

in which ε is the volume strain of soil mass.

Combining Eqs. 5 and 6, we can obtain the mass conservation equation of water flow during electro-osmosis,

$$\nabla \cdot (k \nabla H + k_e \nabla V) = \frac{\partial \varepsilon_v}{\partial t} = \frac{\partial}{\partial t} (\nabla \cdot \mathbf{u}) \quad (7)$$

According to the law of conservation of charge the governing equation for the electric field can be represented by the following equation,

$$\sigma_e \nabla V = C_p \frac{\partial V}{\partial t} \quad (8)$$

in which σ_e is the electric conductivity and C_p is the capacitance per unit volume.

Governing Equations for Electro-osmosis Process

Based on the above analysis, the governing equations for electro-osmosis process can be expressed as follows:

$$\begin{aligned}
-\nabla \mathbf{u} - \frac{\lambda + G}{G} \nabla(\nabla \mathbf{u}) + \frac{1}{G} \nabla(H - z) &= 0 \\
\nabla \cdot (k \nabla H + k \nabla V) &= \frac{\partial}{\partial t} (\nabla \mathbf{u}) \\
\sigma \nabla V &= C \frac{\partial V}{\partial t}
\end{aligned} \tag{9}$$

The basic variants for the coupled equation are displacement, total hydraulic head, and electrical potential.

Moreover, the mechanical, hydraulic and electrical parameters for soil can be expressed as the function of the physical properties of soil.

DEVELOPMENT OF NUMERICAL MODELING

Based on the above theory, a numerical model is developed to simulate the electro-osmosis consolidation process for soft clay. The spatial discretization is based on finite element method, and the time discretization uses the finite differential method. The basic variables for this software are displacement of soil mass, hydraulic head and voltage potential. Superior to the previous research on numerical simulation for electro-osmosis, the developed software can directly obtain the displacement of soil, i.e. the ground settlement.

Boundary Conditions

There are two types of boundary conditions for displacement, seepage and electrical fields respectively.

Dirichlet conditions specify values or function for the basic variants at boundary, which is,

$$\begin{aligned}
u &= \hat{u} \\
v &= \hat{v} \\
w &= \hat{w} \\
H &= \hat{H} \\
V &= \hat{V}
\end{aligned} \tag{10}$$

where u^s , v^s and w^s is the three components of displacement vector \mathbf{u} .

Neumann conditions give the constraint force and flux conditions at boundary, which is,

$$\begin{aligned}
l\sigma + m\tau + n\tau &= \bar{F} \\
l\tau + m\sigma + n\tau &= \bar{F} \\
l\tau + m\tau + n\sigma &= \bar{F} \\
lv + mv + nv &= v \\
lj + mj + nj &= j
\end{aligned} \tag{11}$$

where j is the electric current density, and (l, m, n) is the normal vector at boundary.

Initial Conditions

To get an exclusive solution initial values of the basic variants should be provide, usually expressed as follows:

$$\begin{aligned}
\mathbf{u}(\mathbf{x}, 0) &= 0 \\
H(\mathbf{x}, 0) &= H \\
V(\mathbf{x}, 0) &= V(\mathbf{x})
\end{aligned} \tag{12}$$

RESULTS OF NUMERICAL SIMULATION

1D Consolidation Result and Comparison to Esrig's Theory

Esrig (1968) proposed a 1-D theory that consolidation due to electro-osmosis induced water flow is governed by a diffusion equation,

$$\frac{\partial u}{\partial x} + \frac{k}{k} \cdot \gamma \cdot \frac{\partial V}{\partial x} = \frac{1}{C} \cdot \frac{\partial u}{\partial t} \tag{13}$$

in which u is excess pore water pressure. According to the hypothesis of constant electrical field intensity, the second item of left side is equal to 0, so the equation is in the same form as Terzaghi's consolidation equation. The analytical solution for the Esrig's theory was presented by Mitchell and Soga(2003).

The comparison of calculation result and analytical solution is illustrated in Fig. 1 and Fig. 2, in which the hydraulic conductivity is assumed to constant. The calculation result shows good agreement with the analytical solution.

Furthermore, the developed software can simulated the effect of variant soil parameters during electro-osmosis process. The values for k_h , σ_c and k_e always change due to the change of void ratio e of soil mass, which has a significant effect on electro-osmosis process. In Fig. 1 the dotted line shows the nonlinear change of excess pore water pressure along x-axis when time factor $T_{V=\infty}$, in which the linear relationship between k_h and $e^3/(1+e)$ is incorporated into calculation. Electro-osmotic flow stops at this time, and water flow velocity, i.e. \vec{v} , is zero. Thus Eq. 5 is presented as,

$$\frac{\partial u}{\partial x} = -\frac{k}{k} \gamma \frac{\partial V}{\partial x} \tag{14}$$

According to the above equation, the excess pore pressure at equilibrium ($T_{V=\infty}$) at any location is given by,

$$u = -\frac{k}{k} \gamma V + k \gamma \int V \frac{\partial}{\partial x} \left(\frac{1}{k} \right) dx \tag{15}$$

The second item on the right side of the above equation results in the nonlinear change of u at $T_V = \infty$. Series of ' $k_h \propto e^3/(1+e)$ ' in Fig. 2 shows delayed consolidation progress due to the decreasing hydraulic conductivity during electro-osmosis process, compared with the result of constant k_h . T_V is calculated using the initial value of k_h .

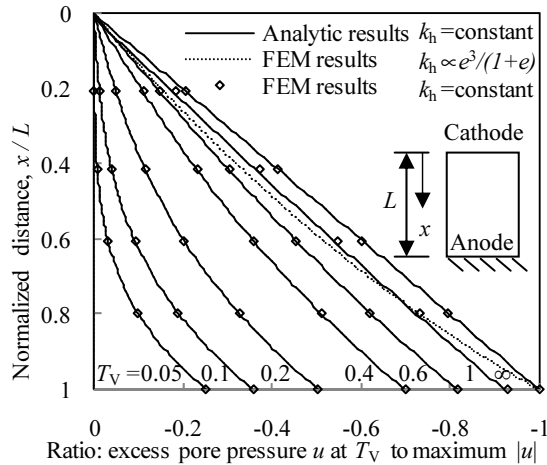


Fig. 1 Dimensionless excess pore water pressure as a function of dimensionless time and distance for 1-D consolidation by electro-osmosis

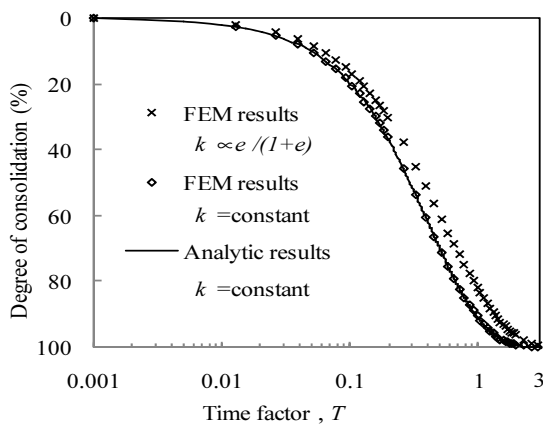


Fig. 2 Average degree of consolidation versus dimensionless time for 1-D consolidation by electro-osmosis

FEM Results for 2D Electro-Osmosis Consolidation

Fig. 3 gives a 2D calculation model for electro-osmosis treatment of soft soil. The left and right boundaries are placed by electrodes, and cathode is open for free water drainage. The soil surface is free drained and can be surcharged by load. The parameters for soil are listed in Table 1. Three cases are simulated by the developed FEM software:

Case (a): with uniform surcharge of 1×10^5 N/m on top, no electric field;

Case (b): with electric field, no surcharge;

Case (c): combined surcharge of 1×10^5 N/m on top with electric field.

Table 1 Input parameters used in the 2D electro-osmosis consolidation model

Parameter	Value
Unit weight of water, γ_w (N/m ³)	9810
Poisson ratio, ν	0.3
Drained elastic modulus, E (Pa)	2×10^{-6}
Capacitance per unit volume of soil, C_p (Farad/m ³)	0
Hydraulic conductivity, k_h (m/s)	3×10^{-9}
Electro-osmotic permeability, k_e (m ² /s/V)	8×10^{-9}
Electric conductivity, σ_e (S/m)	0.15

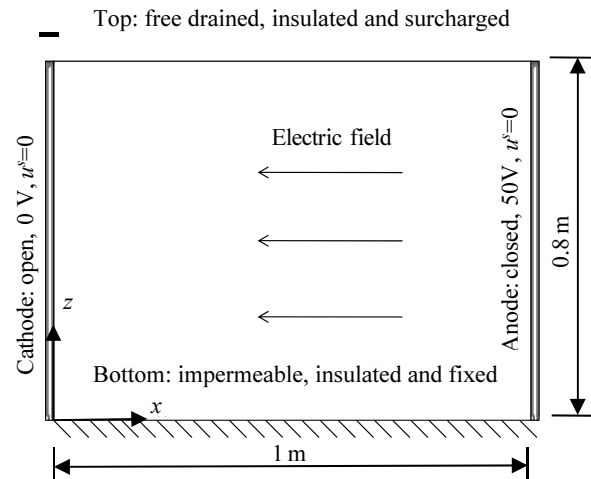


Fig. 3 Schematic of the 2D electro-osmotic consolidation problem

Excess Pore Water Pressure Distribution at Equilibrium

Case (a) is the consolidation process described by Biot's theory. When consolidation process reaches an equilibrium, the excess pore pressure induced by surcharge drops to zero all over the studied field in Fig.3. No particular figures of pore pressure distribution are presented for this case.

The contour of normalized excess pore water pressure at equilibrium for case (b) is illustrated in Fig. 4. Case (b) and (c) have the same draining boundaries but different initial values for excess pore pressure. As we know, final steady solution to a time dependent system, will not be influenced by initial conditions, therefore case (c) has the same excess pore pressure distribution as case (b).

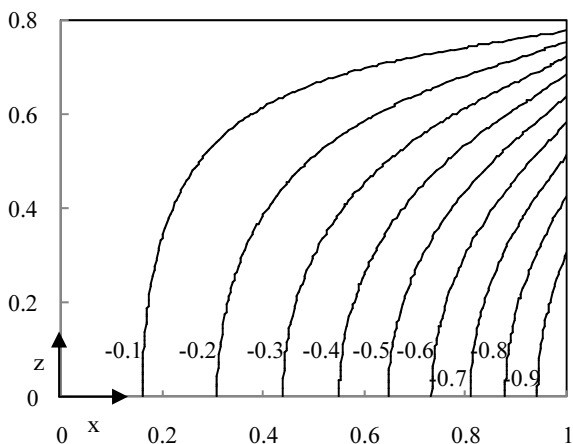


Fig. 4 Contour of normalized excess pore water pressure at equilibrium for case (b)

Settlement Distribution during Electro-Osmosis

To investigate settlement during electro-osmosis progress, the normalized settlement distribution of soil surface at different times is shown in Fig. 5. At the location $x=1$ which the anode is placed, the normalized settlement is nearly the same for case (a) and (b), which means these two cases have the same consolidation rate at anode point on the surface. The consolidation rate is mainly related to hydraulic conductivity but not the electric-osmotic permeability.

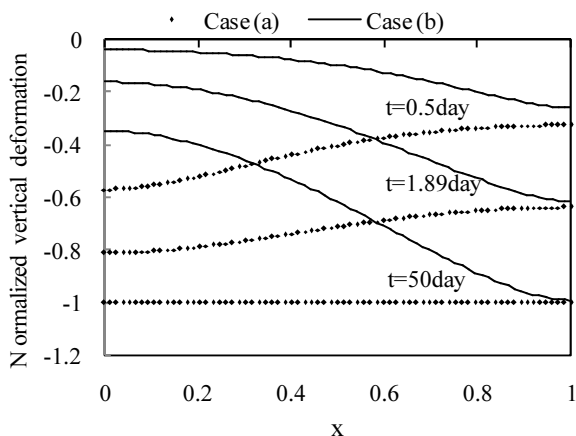


Fig. 5 Normalized settlement distribution on soil surface at different times

Fig. 6 gives the settlement distribution of case (c) and the combination of cases (a) and (b). It can be shown that the result for case (c) is equal to the direct summation of case (a) and (b). As mentioned before, soil deformation is governed by the stress equilibrium equation, where excess pore pressure plays an important role. According to Eq. 7, the excess pore pressure and electrical voltage together contribute to the change of volumetric strain of soil skeleton. Due to dissipation of positive excess pore pressure due to surcharge or the

accumulation of the negative excess pore pressure due to electro-osmosis, vertical deformation, i.e. surface settlement is induced.

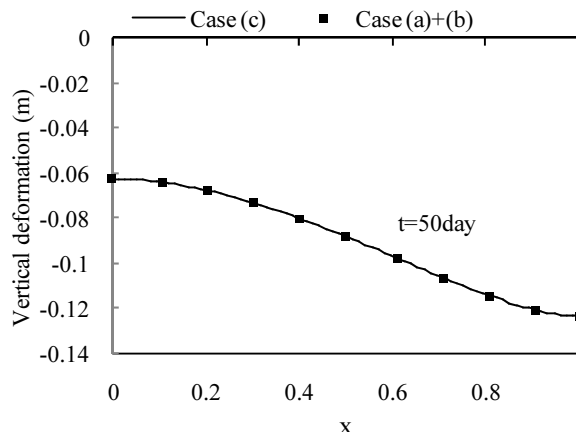


Fig. 6 Settlement distribution on soil surface at equilibrium

CONCLUSION

A numerical model was developed to analyze electro-osmotic consolidation of soft soil using finite element method. The model is used to predict the ground settlement and groundwater movement during electro-osmotic treatment.

Settlement can be obtained directly by the developed software, which shows great advantage in coupling soil deformation with seepage field and electric field.

The accuracy of the numerical model is verified by comparison to the theoretical solution and enhanced by incorporating effects of hydraulic conductivity change of soil mass during treatment.

Coupling effects of soil deformation, groundwater flow and electric field are further investigated to enrich the research on electro-osmosis consolidation, which is beyond the scope of this paper.

ACKNOWLEDGEMENTS

The financial support from Key Scientific Project (Project No. 109006) and Program for New Century Excellent Talents in University (NCET-07-0480) from Chinese Ministry of Education are gratefully acknowledged.

REFERENCES

Banerjee S & Vitayasupakorn V (1984). Appraisal of electro-osmotic oedometer tests. *Journal of Geotechnical Engineering*, 110(8): 1007-1023.
 Bergado DT, Balasubramaniam AS, Patrawaran MAB, et al. (2000). *Electro-osmotic Consolidation of Soft*

- Bangkok Clay with Prefabricated Vertical Drains. *Ground Improvement Journal*, (4): 153-163.
- Bernatzik W (1948). Contribution to the problem of seepage pressure in electro-osmosis, *Proceedings of the 2nd International Conference on Soil Mechanics and Foundation Engineering*, 7: 65-66.
- Casagrande L (1983). Stabilization of soils by means of electroosmotic state-of-art. *Journal of Boston Society of Civil Engineering, ASCE*, 69(3): 255-302.
- Casagrande L (1948). Electroosmosis in soils. *Geotechnique*, 1: 159-177.
- Chen JL & Murdonch L (1999). Effects of electro-osmosis on natural soil: field test. *Journal of Geotechnical and Geo-environmental Engineering*, 125(12): 1090-1098.
- Davis EH & Poulos HG (1980). The relief of negative skin friction on piles by electro-osmosis. *Proceedings of the 3rd Australian and New Zealand Conference on Geomechanics*, 1: 71-77.
- Eggestad A & Foyn T (1983). Electro-osmosis improvement of a soft sensitive clay. *Proceedings of the 3rd European Conference on Soil Mechanics and Foundation Engineering*: 597-603.
- Esrig MI & Gemeinhardt JP (1967). Electrokinetic stabilization of an illitic Clay. *Journal of the Soil Mechanics and Foundations Division, ASCE*, 93 SM3(5): 109-128.
- Feldkamp JR & Belhomme GM (1990). Large-Strain Electrokinetic Consolidation - Theory and Experiment in One Dimension. *Geotechnique*, 40(4): 557-568.
- Fetzer CA (1967). Electroosmotic stabilization of west branch dam. *Journal of the Soil Mechanics and Foundations Division, ASCE*, 93 SM4 (7): 85-106.
- Fourie AB, Johns DG, Jones CJFP (2007). Dewatering of mine tailings using electrokinetic geosynthetics. *Canadian Geotechnical Journal*, 44(2): 160-171.
- Glendinning S, Jones CJFP, Pugh RC (2005). Reinforced soil using cohesive fill and electrokinetic geosynthetics. *International Journal of Geomechanics, ASCE*, 5(2): 138-146.
- Glendinning S, Lamont-Black J, Jones CJFP, Hall J (2008). Treatment of lagooned sewage sludge in situ using electrokinetic geosynthetics. *Geosynthetics International*, 15(3): 192-204.
- Hong HQ & Hu LM (2007). Experimental study of electro-osmosis by reversing polarity in kaolin clay. *The 1st Sri Lankan Geotechnical Society International Conference on Soil and Rock Engineering, Colombo*.
- Jones CJFP, et al. (2008). Recent research and applications in the use of electro-kinetic geosynthetics. Keynote paper, the 4th European Geosynthetics Conference, Edinburgh, UK.
- Laursen S (1997). Laboratory investigation of electro-osmosis in bentonites and natural clays. *Canadian Geotechnical Journal*, 34(5): 664-671.
- Lefebvre G & Burnotte F (2002). Improvement of electro-osmotic consolidation of soft clays by minimizing power loss at electrodes. *Canadian Geotechnical Journal*, 39(2): 399-408.
- Lo KY, Ho KS, Incullet II (1991). Field Test of Electro-Osmosis Strengthening of Soft Sensitive Clay. *Canadian Geotechnical Journal*, 28(1): 74-83.
- Lo KY & Ho KS (1991). Electroosmotic strength of soft sensitive clays. *Canadian Geotechnical Journal*, 28(1): 62-73.
- Micic S, Shang JQ, Lo KY, et al. (2001). Electro-kinetic strengthening of a marine sediment using intermittent current. *Canadian Geotechnical Journal*, 38(22): 287-302.
- Mitchell JK & Soga K (2003). *Fundamentals of soil behavior*. The 3rd Edition, John Wiley & Sons, Inc, USA.
- Mohamedelhassan E & Shang JQ (2002). Vacuum and surcharge combined one-dimensional consolidation of clay soils. *Canadian Geotechnical Journal*, 39(5): 1126-1138.
- Nettleton IM, Jones CJFP, Clark EBG, et al. (1998). *Electrokinetic geosynthetics and their applications*. The Sixth International Conference on Geosynthetics, USA.
- Perry W. Electro-osmosis dewaterers foundation excavation *Construction Methods and Equipment*, 1963, 45(9): 116-119.
- Rittirong A & Shang JQ (2008). Numerical analysis for electro-osmosis consolidation in two-dimensional electric field. *Proceedings of 18th International Offshore and Polar Engineering Conference, Vancouver, Canada*: 566-572.
- Shang JQ & Dunlap WA (1998). Pullout resistance of high voltage strengthen ground anchors. *Journal of Geotechnical and Geoenvironmental Engineering, ASCE*, 124(9): 840-845.
- Weiss CA, Malone PG, Hock VF, et al. (2005). Use of small-scale electro-osmotic systems in controlling groundwater movement around structures. *Environmental & Engineering Geoscience*, 11(1): 53-60.
- Zhuang YF & Wang Z (2007). Interface electric resistance of electro-osmotic consolidation, *Journal of Geotechnical and Geoenvironmental Engineering, ASCE*. 133(12): 1617-1621.

RESEARCH ON COEFFICIENT OF BRITTLE STRESS DROP OF BRITTLE-PLASTIC ROCKS AND ITS APPLICATION

Gui-Cai SHI¹, Xiu-Run GE² and Yun-De LU³

ABSTRACT: The complete stress-strain curve of rock could be divided into pre-failure and post-failure regions according to the peak stress. The post-failure mechanical characteristics of rock are corresponding to many rock engineering, such as underground excavation, pillar, rock burst and so on. Therefore, the research on the post-failure characteristics of rock is of important significance both in theory and in practice. In general, the post-failure region of rock shows instability in the mechanical response, which is difficult to be described by the strength softening model, and should be described by the elastic-brittle-plastic model. Keeping the strain rate of axial as a constant, a series of triaxial conventional compress failure tests about marble of Ya'an, red sandstone of Guixi and granite of Dawu were performed by RMT-150B rock mechanics test system, and the complete stress-strain curves of rock specimens under different confining stresses were obtained. Utilizing the stress-strain curves, the relation function between brittle stress drop and confining stress of marble was obtained. Based on this, elastic-plastic constitutive model, ideal elastic-brittle-plastic constitutive model and non-ideal elastic-brittle-plastic constitutive model are employed to analyze the deformation and plastic zone of the rock mass surrounding the underground workshops of some hydroelectric power station after the completion of excavation. Therefore, the beneficial reference was provided when applied elastic-brittle-plastic model to numerical analysis about brittle-plastic rock medium and its structures as well.

KEYWORDS: elastic-brittle-plastic constitutive, post-failure, coefficient of brittle stress drop, numerical calculation

INTRODUCTION

The complete stress-strain curve of rock could be divided into pre-failure and post-failure regions according to the peak stress. The post-failure mechanical characteristics of rock are corresponding to a good many rock engineering, such as underground excavation, pillar, rock burst and so on. Therefore, the research on the post-failure characteristics of rock is of important significance both in theory and in practice.

Via yielding and hardening phases, after its peak strength, tension reinforcement will necking-down, also called deformation localization or deformation gradient effect. The failure of rock is different from metal, and its deformation of softening phase after peak strength is because of the expanding and communicating of cracks. But we still can apply the conception of deformation localization or deformation gradient in the research of its characteristic of softening phase. Till now, some efforts are achieved, but disputing exists as well (Pan 2002, Wang & Pan 2003), so that their application in complex geotechnical engineering need more impenetrate works.

In general, the post-failure region of rock shows instability in the mechanical response, which is difficult to be described by the strength softening model, and should be described by the brittle-plastic model. As is now well known, the basic feature of brittle-plastic material is the abrupt, uncontrollable brittle stress drop in its stress-strain curve. Generalized to complex stress condition is, as soon as the stress loading to the peak strength from the initial elastic state, it will drop to residual strength abruptly and rapidly.

How to describe rock's stress drop after failure in numerical simulation reasonably becomes very important. To some brittle rocks, make a study of a reasonable method to describe the stress drop of rock after failure is more practicable than to describe strain softening (Zheng 1997).

In order to slide over the uncertainty of stress drop mode, some scholars insist on dealing brittle failure with continuous strain softening model (Yin 1987), what disobey the deformation characteristic of brittle rocks obviously. Brittle-plastic material's stress drop from peak stress surface to residual stress surface is not a continuous process, but an abrupt and uncontrollable

¹ Ph.D, Department of Civil Engineering, Shanghai Jiaotong University, China. School of Civil Engineering and Architecture, Changzhou Institute of Technology, China. Email:shigc@sjtu.edu.cn

² Professor, Department of Civil Engineering, Shanghai Jiaotong University, China. Email:xiurunge@public.wh.hb.cn

³ Mr., Department of Civil Engineering, Shanghai Jiaotong University, China. Email:luyd@sjtu.edu.cn

process, and the peak strength is beyond retrieve as well. All those characteristics cannot be described by continuous strain softening model. What's more, even though deal it with continuous strain softening model, the historical softening model cannot be adopt. Some scholars, such as Pietruszczak (1981), Prevost (1984), and so on, have proved from theory and computation: when the soften rate of material is relatively great, it will bring on more than one solutions of plasticity problem. Zheng (1997) proved that when the soften rate of material is relatively great, the classic constitute integrate will can't carry out. Fortunately, brittle material still obey Il'yushin postulate, and based on plastic potential theory, the method to describe stress drop history is bring out (Liu 1989).

NUMERICAL COMPUTATION MODEL OF BRITTLE-PLASTIC ROCKS

Main characteristics of brittle-plastic rocks' complete curves are (Ren 1999): (1) curves can be linearized before peak strength; (2) yield region is very stricture; (3) stress abruptly drop to residual strength after peak; (4) residual phase is stable.

In order to come at some proper function expression, following obviously fundamental assumptions given: (1) under a certain stress state, the curve is unique, without regard to rate of loading and creep; (2) curve is continuous, and curvilinear function is monotone; (3) material will not occur any potential harden after residual strength.

Three assumptions mentioned above is truthfulness. Aplling those three assumptions, make peak strength region quickness, linearized elastic region and stress drop region, ignore the minor gradient of stress drop and residual stress decline, the complete stress-strain curve can be predigested as three phases: linear elasticity-brittle stress drop -ideal plasticity, and two yield strength: peak strength and residual strengthen, what is named as brittle-plastic constitutive model. In practice, almost all brittle materials' stress drop is not absolutely vertical. So vertical stress drop can be called ideal brittle-plastic model, and gradient of stress drop considered can be called Non-ideal brittle-plastic model, see Fig. 1.

DEFINE THE METHOD OF STRESS DROP BY PLASTIC POTENTIAL THEORY

Ge (1997) applied plastic potential theory in defining the method of stress drop of non-ideal brittle-plastic model.

If $F(\sigma)=0$ is peak strength function and $f(\sigma)=0$ is residual strength function. When stress loads from an

initial elastic state to a certain point of peak strength surface, marked as *A*, if meets the conditions of loading, stress will abruptly drops to a certain point of residual strength surface, marked as *B*. Fig. 2 described the typical stress drop forms in two-dimension Mohr stress space. *B*₁ corresponds to center invariant assumption, *B*₂ corresponds to shortest path assumption, and *B*₃ corresponds to principal stress invariant assumption. Obviously, different method of stress drop will comes out different results, and adopt center invariant assumption sees to be a more general method.

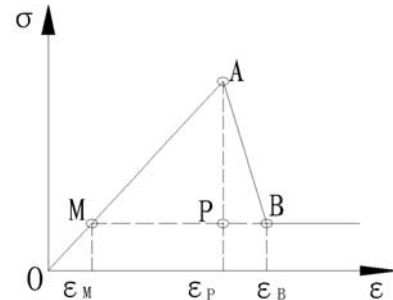


Fig. 1 Non-ideal brittle-plastic model

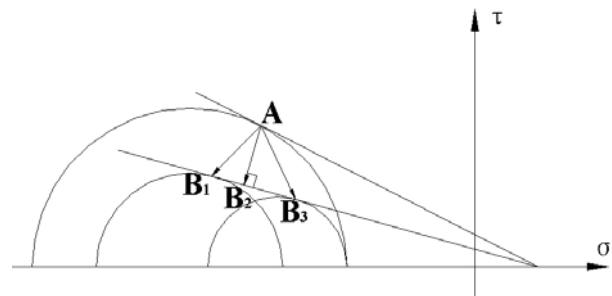


Fig. 2 Three typical mode of stress drop

Because of its brittleness, rock's yield surface has a discrete change in stress space, which will bring a plastic strain increment. Meanwhile, brittle materials still obey Il'yushin postulate, so plastic strain increment during stress drop meet plastic potential theory, i.e.

$$\Delta \epsilon = \Delta \lambda \frac{\partial F}{\partial \sigma} \quad (1)$$

where $\Delta \lambda$ is plastic multiplier, under the condition of small strain, during any increment of stress, the changes of strain are assumed to be divisible into elastic and plastic components, so that

$$\Delta \epsilon = \Delta \epsilon + \Delta \epsilon \quad (2)$$

When stress drop brings to a nonzero complete strain increment, i.e.

$$\Delta \epsilon \neq 0 \quad (3)$$

then we can assume that

$$\Delta\varepsilon + \Delta\varepsilon = \Delta\varepsilon = -R\Delta\varepsilon \quad (4)$$

where R is an undetermined non-negative parameter termed the coefficient of brittle stress drop, which needs to be determined by specific rocks' uniaxial or triaxial compression tests.

Fig. 3 is a typical complete curve of brittle rocks got by uniaxial compression tests. Combined with Fig. 3, we can determine the coefficient of brittle stress drop R by some characteristic parameters.

$$R = \frac{b}{a} \quad (5)$$

where

$$b = \varepsilon_B - \varepsilon_P, a = \varepsilon_P - \varepsilon_M$$

According to ideal brittle-plastic model, then $b=0$.

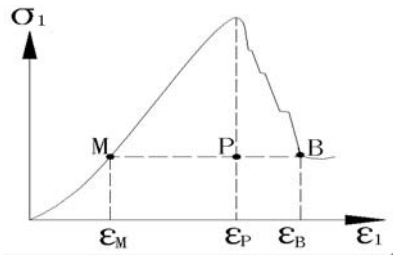


Fig. 3 Typical complete curve of brittle rocks

On the other hand, the brittleness of rock is relative, so the coefficient of brittle stress drop is relative also. During triaxial compression test, with the increasing of confining pressure, the brittleness of rock change to ductility, so the coefficient of brittle stress drop should be a function of confining pressure, so that

$$R = f(\sigma_c) = \frac{\varepsilon(\sigma_c) - \varepsilon(\sigma_r)}{\varepsilon(\sigma_c) - \frac{\sigma_r(\sigma_c)}{E(\sigma_c)}} \quad (6)$$

where $\sigma_c = (\sigma_2 + \sigma_3)/2$, and during conventional triaxial test $\sigma_c = \sigma_2 = \sigma_3$.

Then on use of Eq. 4,

$$\Delta\varepsilon = -\theta\Delta\varepsilon \quad (7)$$

where

$$\theta = 1/(1+R) \quad (8)$$

For ideal brittle-plastic model, it is a particular case that $\theta=1$.

The relationship between stress and strain is given by the standard linear elastic expression

$$\Delta\sigma = D_k \Delta\varepsilon_{k1} \quad (9)$$

Then we can get the stress increment of stress drop easily,

$$\Delta\sigma = \sigma - \sigma = -\theta\Delta\lambda\tau \quad (10a)$$

namely

$$\sigma = \sigma - \theta\Delta\lambda\tau \quad (10b)$$

where

$$\tau = D_{k1} \left. \frac{\partial F}{\partial \sigma_k} \right| \quad (11)$$

and $\Delta\lambda$ determined by following Eq.

$$f(\sigma^B) = f(\sigma - \theta\Delta\lambda\tau) = 0 \quad (12)$$

The different of ideal and non-ideal brittle-plastic model is the very non-zero coefficient of brittle stress drop. In order to get the coefficient of brittle stress drop based on the complete stress-strain curves, triaxial compression test research on different brittle rocks carried on.

EXPERIMENTAL SYSTEM AND SPECIMEN

Experimental System

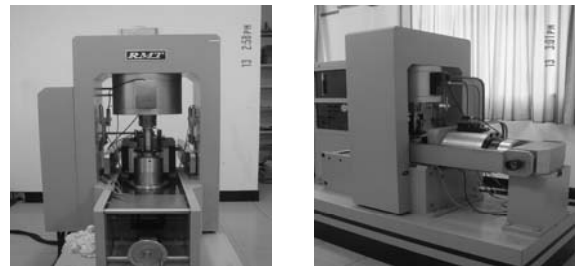


Fig. 4 Outlooks of RMT-150B rock mechanics test system

Keeping the strain rate of axial as a constant, the tests accomplished on RMT-150B rock mechanics test system equipment by laboratory of rock and soil mechanics of Shanghai Jiaotong University. This system's full name is Microcomputer Servo-Control Rock Mechanics Multifunction Testing System. RMT is the shortened

form of “Rock Mechanics Testing System”, and its max axial loading is 1,000 kN, max level is 500 kN. It is improved on RMT-64, whose behavior was introduced by Ge (1994).

Specimen

Red sandstone quarried from Guixi, Jiangxi Province, China, marble quarried from Ya’an, Sichuan Province, China, and granite quarried from Dawu, Hubei Province, China.

Cylindrical specimens used in tests commonly prepared by close drilling and coring. Diameters are 50 mm, heights are 100 mm, and surface evenness beyond ± 0.02 mm. In order to avoid the different stress history and stress state of rock specimens, because of their different collection depth, we applied the method of trepan in getting a set of rock specimens from one rock mass. What’s more, we do our best to avoid the effect of external disturbance during the process of sampling and transportation. Therefore, a set of rock specimens belongs to the same rock layer, and the mechanics characteristics of them are rather identical.

OUTCOMES OF TEST

Principle of Data Processing

In order to embody the anisotropy of rock specimens, we apply regression analysis in each rock specimen’s test data, and each uniaxial compression test is dealt with a particular case of triaxial compression test, that’s to say confining pressure is zero.

Combined Fig. 3 with Eq. 6, when applying experiment in determining the coefficient of brittle stress drop, the strains ϵ_M , ϵ_P and ϵ_B of character point M, P and B are required. ϵ_P and ϵ_B can be gained directly, and ϵ_M equals to the elastic strain calculated by residual strength, so that

$$\epsilon = \sigma_r / E \tag{13}$$

That is to say, nothing remained but to determined σ_r , E , ϵ_P and ϵ_B , the coefficient of brittle stress drop can be determined accurately.

Coefficient of Stress Drop Tests of Marble

Confining pressure of triaxial compression test change from 0 to 30 MPa, Fig. 5 shows the typical complete curves of conventional triaxial compress tests of marble (Shi 2006).

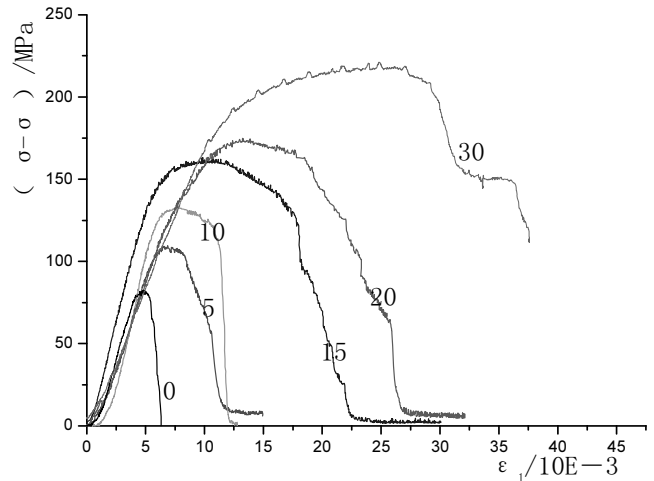


Fig. 5 Complete curves of conventional triaxial compress tests of marble

Table 1 shows the characteristics parameters of typical complete curves of marble.

Based on the characteristics parameters of above 13 marble specimens under different confining pressures, applying regression analysis, the coefficient of brittle stress drop under conventional triaxial compress is found to be

$$R(\sigma) = \frac{-59\sigma + 6133\sigma + 17621}{154\sigma + 1233\sigma + 45556} \tag{14}$$

Table 1 Characteristic parameters of complete curves of marble.

Test Number	σ_p MPa	ϵ_p 10^{-3}	σ_r MPa	ϵ_B 10^{-3}	E GPa	σ_3 MPa
m-1-1	85.95	4.125	1.804	6.696	20.84	0
m-1-2	92.51	3.965	0.129	6.630	23.33	0
m-1-3	91.22	4.193	0.259	6.620	21.76	0
m-11-1	82.29	4.774	0.129	6.312	17.24	0
m-11-2	81.06	4.372	0.773	6.173	18.54	0
m-b-6	109.50	8.094	8.438	11.664	14.15	5
m-b-8	109.63	6.856	13.785	12.347	16.72	5
m-b-7	134.45	7.590	17.130	12.028	19.03	10
m-b-5	132.03	8.623	17.003	12.003	16.47	10
m-2-3	163.80	10.726	23.281	22.379	16.67	15
m-10-1	193.69	15.202	29.704	29.393	14.06	20
m-10-2	176.93	13.364	29.278	27.161	14.74	20
m-9-1	221.38	25.715	58.077	38.700	9.78	30

Coefficient of Stress Drop Tests of Red Sandstone

Confining pressure of triaxial compression test change from 0 to 40 MPa, Fig. 6 shows the typical complete

curves of conventional triaxial compress tests of red sandstone.

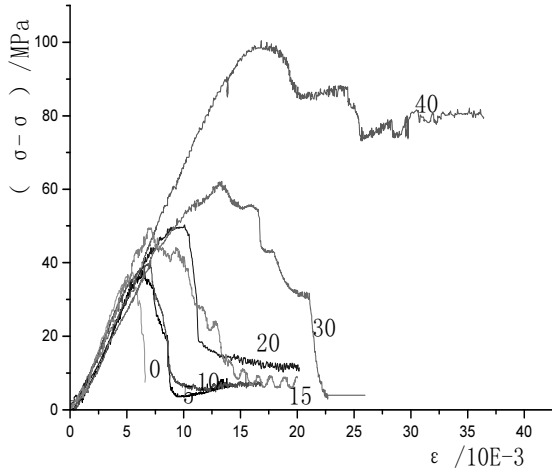


Fig. 6 Complete curves of conventional triaxial compress tests of red sandstone

Table 2 Characteristic parameters of complete curves of red sandstone.

Test Number	σ_p MPa	ϵ_p 10^{-3}	σ_r MPa	ϵ_B 10^{-3}	E GPa	σ_3 MPa
r-s-1-1	37.43	5.309	1.655	7.305	7.05	0
r-s-1-2	38.82	6.149	4.399	7.317	6.31	0
r-s-1-3	37.78	5.415	1.294	6.602	6.98	0
r-s-12-1	42.38	5.049	3.829	6.688	8.39	0
r-s-12-2	44.00	4.778	4.846	5.923	9.21	0
r-s-b-1	39.47	4.464	6.876	5.941	8.84	0
r-s-b-2	37.69	4.607	4.966	7.222	8.18	0
r-s-b-3	37.82	6.344	8.947	9.275	6.75	5
r-s-b-7	39.85	6.112	8.692	9.363	7.34	5
r-s-b-10	35.78	5.975	13.692	10.088	7.66	10
r-s-b-9	37.43	6.632	13.183	9.803	7.15	10
r-s-c-13	38.58	8.304	16.494	10.605	5.85	10
r-s-10-2	39.71	6.850	16.838	9.896	7.26	10
r-s-c-21	49.53	7.119	27.096	14.225	9.06	15
r-s-9-1	51.86	10.07	38.990	11.286	7.14	20
r-s-9-2	50.98	10.60	30.998	17.329	6.69	20
r-s-c-2	62.13	13.36	72.781	17.991	6.90	30
r-s-c-6	100.3	18.82	114.74	27.503	7.46	40

Table 2 shows the characteristics parameters of typical complete curves of red sandstone.

Based on the characteristics parameters of above 18 red sandstone specimens under different confining pressures, applying regression analysis, the coefficient of brittle stress drop under conventional triaxial compress is found to be

$$R(\sigma) = \frac{\sigma - 1722\sigma - 16925}{22\sigma - 545\sigma - 45987} \quad (15)$$

Coefficient of Stress Drop Tests of Granite

Fig. 7 shows the typical complete curves of conventional uniaxial compress tests of granite.

Table 3 shows the characteristics parameters of typical complete curves of granite.

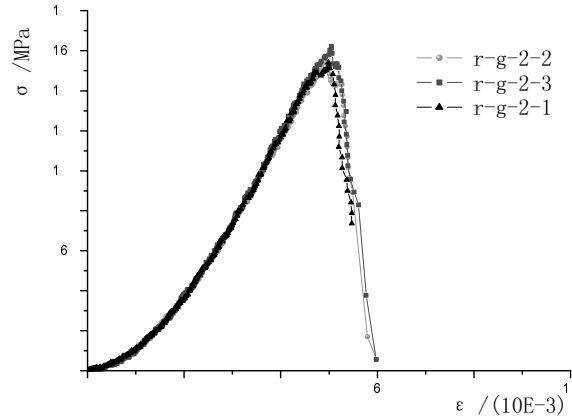


Fig. 7 Complete curves of uniaxial compress tests of granite

Table 3 Characteristic parameters of complete curves of granite.

Test Number	σ_p MPa	ϵ_p 10^{-3}	σ_r MPa	ϵ_B 10^{-3}	E GPa	R
r-g-2-1	154.15	4.985	5.391	5.950	30.92	0.201
r-g-2-2	154.36	4.935	5.693	5.982	31.28	0.220
r-g-2-3	162.00	5.046	5.586	5.977	32.10	0.191
r-g-1-1	143.11	4.413	8.403	5.849	32.43	0.346
r-g-1-2	137.20	5.624	8.728	7.358	24.40	0.329

Learn from Figs. 5-7, with the increasing of confining pressure, the brittleness of rock change to ductility, the peak strength point rearwards shift gradually, and the yield phase before failure becomes distinct gradually. That's to say, there will bring to distinct plastic strain, and brittle stress drop will not take place, so that brittle-elastic-plastic model shown as Fig. 1 will be out of time, and should be replaced by bilinear elastic-linear softening-residual plastic model (Four-line calculation model) shown as Fig. 8 (Lu 2004). The gradient of brittle rock after failure is far grater than mid-lower strength rock, and the whole deformation is far smaller, thus shows grate brittleness. However, the post failure region is still controllable, and can get its post failure curve. If the strengthen of the rock is stronger, its brittleness is more obviously.

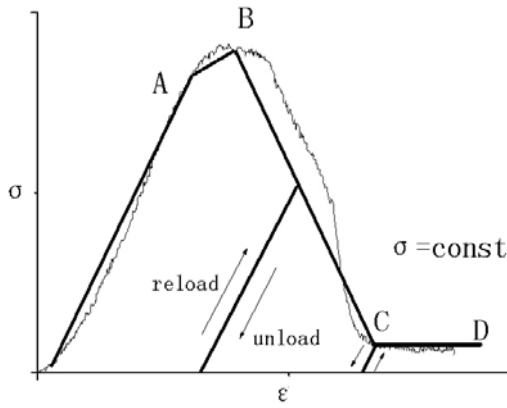


Fig. 8 Four-line calculation model

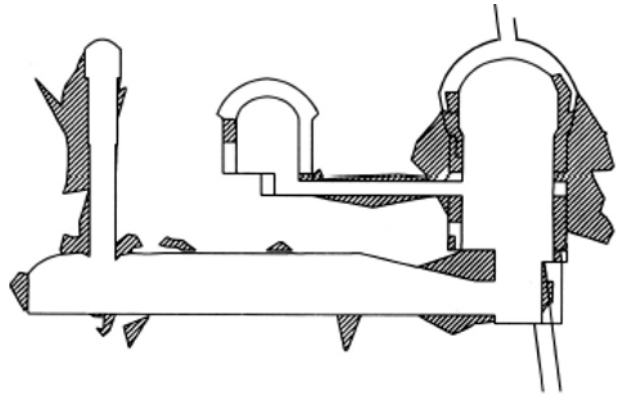


Fig. 11 Plastic zone under non-ideal elastic-brittle-plastic model

CALCULATION APPLICATION

Based on above theories and tests, elastic-plastic constitutive model, ideal elastic-brittle-plastic constitutive model and non-ideal elastic-brittle-plastic constitutive model are employed to analyze the deformation and plastic zone of the rock mass surrounding the underground workshops of some hydroelectric power station after the completion of excavation. Its 3D finite element mesh of underground caverns is shown below. The material parameters of the underground caverns adopt Eq. 14.

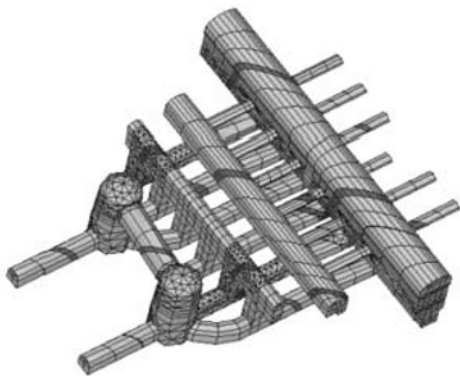


Fig. 9 3D finite element mesh of underground caverns

Plastic zones of the rock mass under different calculation constitutive models are shown as Figs. 10-12.

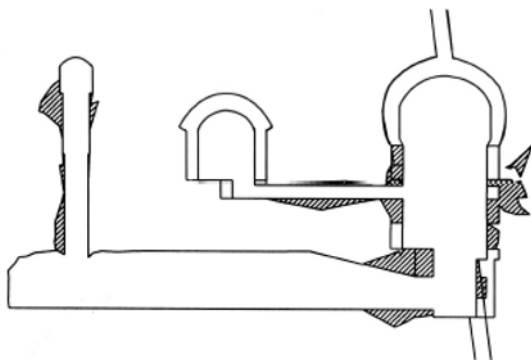


Fig. 10 Plastic zone under elastic-plastic model

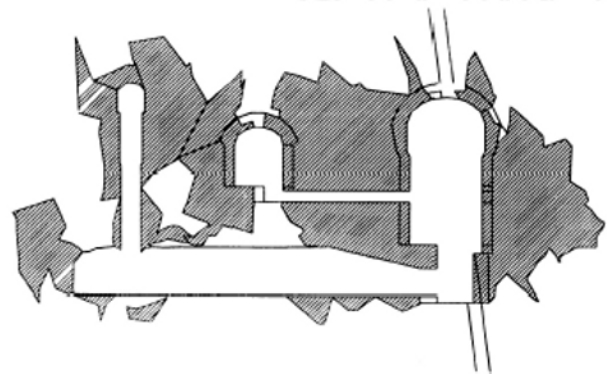


Fig. 12 Plastic zone under ideal elastic-brittle-plastic model

CONCLUSIONS

1. Based on the uniaxial compression test and conventional triaxial compression test, the relation function between coefficient of brittle stress drop and confining stress of marble of Ya'an, red sandstone of Guixi and granite of Dawu were obtained, and the beneficial reference was provided when applying brittle-elastic-plastic model in numerical analysis about brittle rocks and theirs structures as well.

2. The brittle stress drop is conditional happen. The coefficient of brittle stress drop is a function of confining pressure, and it will increase gradually with confining pressure.

3. With the increasing of confining pressure, the brittleness of rock changes to ductility. If the confining pressure is low, applying brittle-elastic-plastic model shown as Fig. 1 in numerical analysis is reasonable, and it is seems to be one of the few choices. However, if the confining pressure is high, brittle stress drop will not happen, and the model should be replaced by bilinear elastic-linear softening-residual plastic model shown as Fig. 8.

4. The gradient of brittle rock after failure is far grater than mid-lower strength rock, and the whole

deformation is far smaller, thus shows grate brittleness. However, the post failure region is still controllable, and can get its post failure curve. If the strengthen of the rock is stronger, its brittleness is more obviously.

REFERENCE

- Ge XR & Zhou BH (1994). New advance in indoor experimental equipment in rock mechanics-experimental system of RMT-64. *Rock and Soil Mechanics* 15(1): 50-56.
- Ge XR (1997). Post failure behaviour and a brittle-plastic model of brittle rock. *Computer Methods and Advances in Geomechanics*. Rotterdam: Balkema, 151-160.
- Liu WZ (1989). Limit load computation of brittle-plastic structure and its application to engineering. Beijing: Tsinghua University.
- Lu YD, Ge XR, Jiang Y (2004). Study on conventional triaxial compression test of complete process for marble and its constitutive equation. *Chinese Journal of Rock Mechanics and Engineering* 23(15): 2489-2493.
- Pan Y & Shen JH (2003). Discussion on 'Size effect analysis on strain softening of quasi-brittle materials considering strain gradient effect. *Chinese Journal of Rock Mechanics and Engineering* 22(12): 2104-2107.
- Pan YS & Wei JM (2002). Experimental and theoretical study on size effect on strain softening of rock materials. *Chinese Journal of Rock Mechanics and Engineering* 21(2): 215-218.
- Pietruszczak ST & Mroz Z (1981). Finite element analysis of strain softening materials. *International Journal of Numerical Methods In Engineering* 10: 327-334.
- Prevost JH & Hughes TJ (1984). Finite element solution of elasto-plastic boundary value problems. *Journal of Applied Mechanics* 48: 69-74.
- Ren F & Shen Q (1999). Elastic-brittle-plastic Theory and Numerical Simulation of Excavation for Permanent Lock of TGP. *Journal of Yangtze River Scientific Research Institute* 16(4): 6-14.
- Shi GC & Ge XR & Lu YD (2006). Experimental study on coefficients of brittle stress drop of marble principle for rock mass with brittle-plasticity and its applications. *Chinese Journal of Rock Mechanics and Engineering* 25(8): 1625-1631.
- Wang XB, Pan YS, Yang XB (2003). Size effect analysis on strain softening of quasi-brittle materials considering strain gradient effect. *Chinese Journal of Rock Mechanics and Engineering* 22(2): 188-191.
- Yin YQ (1987). Introduction to Nonlinear Finite Element Method for Solid Mechanic. Beijing: Peking University Press, Tsinghua University Press.
- Zheng H, Ge XR, Lee CF (1997). Analysis principle for rock mass with brittle-plasticity and its applications. *Chinese Journal of Rock Mechanics and Engineering* 16(1): 8-21.

DYNAMIC STABILITY ANALYSIS OF LANDFILL SLOPE IN DUSHANBE, TAJIKISTAN

Xue-Tao WANG¹, Tensay G. BERHE², Stephen WEBB³ and Wei WU⁴

ABSTRACT: The dynamic analysis of the landfill slope was carried out on a typical landfill in Tajikistan. The site investigation consists of sampling from boreholes, geotechnical laboratory tests and geophysical tests in field. Based on the results of the site investigation, dynamic analysis of the selected landfill in Tajikistan was carried out with the finite-difference programme FLAC3D and GEOSLOPE. Features, advantages and disadvantages of these programmes are discussed and the results of the response analysis of the selected landfill, subjected to an earthquake with a peak ground acceleration of 0.5g, are presented in this paper. The results of the analysis showed that the slope instabilities will occur approximately after 12 seconds of shaking.

KEYWORDS: Stability analysis, landfill, dynamic analysis, strong ground motion

INTRODUCTION

Municipal solid waste landfills subjected to strong ground motions may cause severe environmental damages or possess various risks, such as groundwater and soil contamination, threat of human lives or damage to operational facilities. The present paper reports the results of a stability analysis of a Municipal Solid Waste (MSW) landfill slope in Tajikistan with the consideration of strong ground motion. Tajikistan is one of the seismically active regions in Central Asia.

The cooperative project NISMIST (Management of environmental risks associated with landfills in seismically active regions in the New Independent States of Central Asia) within the 6th Framework Program of the European Commission, was launched in 2005. One of the objectives of this project is the analysis of the dynamic behaviours of municipal solid waste landfills in the seismically active regions of the New Independent States (NIS) of Central Asia.

Tajikistan is bordered on the south by Afghanistan, on the east by China and on the west and north by Uzbekistan and Kyrgyzstan. Dushanbe, the capital of Tajikistan is located on a southern slope of Hissar Mountains in a picturesque fertile valley at an elevation of 750-840 meters above mean sea level. The project area is located 12 km south-east in the outskirts of Dushanbe city. There are two landfills in the study area,

one is relatively new and the second one is old landfill.

New Landfill

The new landfill (currently operating) is located in a natural depression at the head of a small valley surrounded by terraced and partially tilled grassland. The immediate subsoil is loess of varying thickness (40-100m). There is no barrier between the waste and the subsurface. The waste is typically unsorted household refuse, construction debris and metal wastes. Organic waste content appears to be relatively low. The main problems identified during the preliminary site investigation are: groundwater contamination, slope failure of landfill, gas and heat production, waste toxicity and air pollution. Steep landfill slopes could collapse under large earthquakes.

Old Landfill

The old landfill site is located at about 8.5 km east of Dushanbe city on right bank of the Shuraksaïy river. It is about 2 km to the east from the new landfill site located on the left bank of the Shuraksaïy river. The landfill area extends approximately 700 m in the north-south direction and 230 m in the east-west direction and occupies a contiguous area of about 16 ha of agricultural land. The landfill was closed in 1979 and had an estimated volume of about 1 million m³ of municipal solid waste (MSW)

¹ MSc., Institute of Geotechnical Engineering, Universität für Bodenkultur Wien, Austria. Email: xuetao.wang@boku.ac.at

² MSc., Institute of Geotechnical Engineering, Universität für Bodenkultur Wien, Austria. Email: gebremehinberhe.tensay@boku.ac.at

³ Dr., Institute of Geotechnical Engineering, Universität für Bodenkultur Wien, Austria. Email: stephen.webb@boku.ac.at

⁴ Professor, Institute of Geotechnical Engineering, Universität für Bodenkultur Wien, Austria. Email: wei.wu@boku.ac.at

deposited.

After preliminary site investigation, the identified problems in the old (closed and covered) landfill site are: risk of collapse of the side slopes of the landfill facing the river during flooding and / or major earthquake, flow of leachate (chemicals) directly into the river or into the ground water, emissions of toxic gases and odours and heat production.

In the present stability analysis calculations, taking seismic event as a triggering potential, the scenario of the landfill and surrounding hills under severe seismic event are analysed using finite-difference program FLAC3D and QUAKE/W.

SITE INVESTIGATION

The site investigation consists of sampling from boreholes, geotechnical laboratory tests and geophysical tests in field. Two boreholes were drilled to a depth of 18m. Both disturbed and undisturbed soil samples were taken to the laboratory and various soil properties were determined. Shear tests and triaxial consolidation tests were also conducted. The basic soil parameters at the landfill site are presented in Table 1.

Geologically, the area is combined from alluvial deposit of quaternary loam of loess with a thickness of

Table 1 Basic soil parameters of Dushanbe landfill site

Soil parameters	Units	Mean values
Unit weight	[kN/m ³]	17.5-21.0
Saturated unit weight.	[kN/m ³]	19.0-21.0
Porosity (n)	-	0.351-0.455
Moisture content (w)	%	13.9 - 28.9
Liquid limit	%	25.4 – 31.4
Plastic limit	%	19.7 – 23.3
Natural compressibility	-	0.08-0.13
Compressibility at saturated condition	-	0.15-0.92
Shear strength	[MPa]	3.1-35.6
Friction angle (ϕ)	[°]	23.3-24.2
Cohesion (c)	[KPa]	10 - 17

more than 30 m. However on the Shuraksaiy side, new deposits combined with loams and transported clays are observed. As per hydro-geological investigation, groundwater is not observed up to the drilling depth of 18.0 m. The ground water level in the area is possibly more than 80 m below the surface. It seems that the

ground water will not have any influence on the stability of the landfill slope.

In addition to the boreholes, the geophysical investigation of the land fill site is also carried out using the ambient noise technique. The geophysical site investigation was conducted by T. Doanh (ENTPE) with the help of local scientists, Mr. Hamza, Dr. Farrukh and Dr. Ischuk (CHI). Using ambient noise technique the landfill site was investigated for different material characteristics. The whole waste body including underlying natural loess was investigated. This investigation was aimed at evaluating some dynamic characteristics of waste and loess deposits, mainly for the determination of fundamental resonance frequency and seismic amplification.

Two all-in-one state of the art digital seismic noise measurement systems from Micromed, Tromino were used in this geophysical site investigation. To facilitate the ambient noise measurements, the old landfill site is artificially separated into two elongated zones along the broken water pipe in the middle of the landfill. Primarily, we performed 36 tests along 4 measurement lines inside the landfill area and 3 short measurement lines on natural loess outside the landfill area. The coordinates of all measurement points are obtained with the integrated GPS of the Tromino devices. The distance between measurements points along four lines is approximately 50 m. With the ambient noise technique, some dynamic characteristics like the resonance frequency f_0 , the seismic amplification $A_{H/V}(f_0)$ and also the shear wave velocity V_s profiles can be obtained.

The V_s profiles at a site are usually obtained through conventional and expensive geophysical methods, i.e. seismic refraction technique. These profiles have an important role in controlling the site response during earthquakes. Ambient noise measurements combined with inverse analysis technique offers an alternative and economical way to determine the V_s profiles. It is successfully used in the case of sedimentary deposits. The V_s profiles of landfill sites can be estimated with the same method.

The global interpretation of the landfill is presented in Fig. 1. The horizontal axis is not to scale to emphasize the details of the subsoil. The compacted final loess top cover is indicated with dark green colour. This shallow soil layer has a higher velocity than the main waste body due to presumably from compaction effort. The actual ambient noise measurements can detect this velocity inversion with the reversal of the UD component in the power spectral diagrams.

The ambient noise technique can resolve the multiple strata problem with relatively low contrasts between two adjacent layers as in the case of waste deposits on loess. The main dynamic characteristics of the old Dushanbe

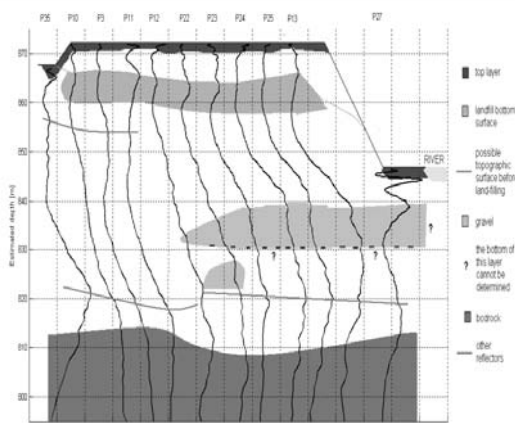


Fig. 1 Global profile of Dushanbe old landfill

landfill using noise ambient technique are summarized in Table 2. The shear wave velocity V_s of the loess substratum is of about 650 m/s. A resonance frequency of about 1.5 Hz was identified on intact loess, along a secondary road outside the old landfill site, and 4.0 Hz inside Dushanbe city.

Table 2 Ambient noise site investigation results of Dushanbe old landfill

Material	Waste	Loess
f_0 [Hz]	1.2 - 2.2	1.4 - 1.6
$A_{H/V}(f_0)$	2.0 - 5.5	4.0 - 5.0
Frequency range [Hz]	1.0 - 2.7	1.0 - 2.5
V_s [m/s]	240	320 - 350

DYNAMIC ANALYSIS USING NUMERICAL MODELING

The dynamic analysis of landfills can be performed using different numerical methods. Here the analysis is performed using the FLAC 3D and QUAKE/W software.

FLAC3D (Fast Lagrangian Analysis of Continua in three dimension) is a three-dimensional explicit finite-difference program for engineering mechanics computation designed by Itasca Consulting Group, Inc. FLAC3D extends the analysis into three dimensions, simulating the behaviour of three-dimensional structures built of soil, rock or other materials that undergo plastic flow when their yield limits are reached. Materials are represented by polyhedral elements within a three-dimensional grid that is adjusted by the user to fit the shape of the object to be modelled. Each element behaves according to a prescribed linear or nonlinear stress-strain law in response to applied forces or boundary restraints.

QUAKE/W is the part of the software GeoStudio. GeoStudio applications can be used to model almost any geotechnical problem, including: slope stability problems involving earth and rock slopes, embankments with anchors, soil nails and geo-synthetics; seepage affected by infiltration, drains, and injection wells; earthquake-induced deformation and pore-water pressure generation etc. QUAKE/W is a geotechnical finite element software product for the analysis of earth structures subjected to earthquake shaking and other sudden impact loading. The numerical modelling for the dynamic analysis calculation is based on a 2-D finite element scheme.

FLAC 3D Modelling

There are twelve built-in material models in FLAC3D. Each model is developed to represent a specific type of constitutive behaviour commonly associated with geologic materials. FLAC3D is used here to estimate the response of these existing landfill subjected to an earthquake with a peak ground acceleration (PGA) value of 0.5g. The evaluation of the results should help to get an insight on the possible effects of the seismic loading on the slopes of the landfills and whether remediation measures are necessary. An additional analysis is also conducted to evaluate the possible behaviour of buried gas collection pipes under the existing stress and deflection conditions. The selected slope is located beside a river, which could cause intrusion of refuse material in case of a landfill slope failure. The basic characteristics of waste, loam and alluvial material of the Dushanbe landfill used in FLAC3D analysis are presented in the Table 3.

Table 3 Characteristics of different material at Dushanbe landfill

Parameters	Waste	Loam	Alluvium
E [MPa]	8.5	20	80
Poisson ratio, ν	0.3	0.25	0.2
Density, ρ [kg/m ³]	750	1900	2100
Cohesion, c [kPa]	10	14	0
Friction angle, ϕ [°]	23	20	35
Dilation angle ψ [°]	0	0	0

For the purpose of the static analysis of these models, the boundary conditions are assumed to be rigid and they are represented by fixed boundaries. The model for the Dushanbe landfill consists of three layer block, namely alluvium, loam and waste material. The slope at the river is assumed to have an angle of inclination of 30 degrees to the vertical and is founded on the loam layer with a maximum thickness of 15 m which is itself underlain by 20 m thick layer of alluvial material. The origin of the

coordinate system is located at the bottom of the alluvium.

The resulted displacements in x and z directions are shown in Figs. 2 and 3. The calculations stopped after 14 seconds of the total 16 seconds because of the unacceptable mesh distortion. A maximum displacement of 8m is occurred in x-direction at the middle of the slope of the loam. This large displacement in x-direction is due to plastic flow of the slope material. For this reason, the slope is considered to be unstable in the case of earthquake of an equivalent magnitude greater than 0.5g. The maximum vertical settlement of 2.8 m occurred at the top of the landfill and at the bottom of the loam slope facing the river.

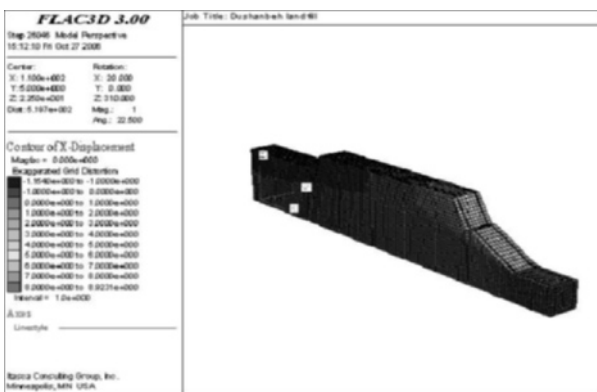


Fig. 2 Displacements of Dushanbeh landfill in z-direction (towards river)

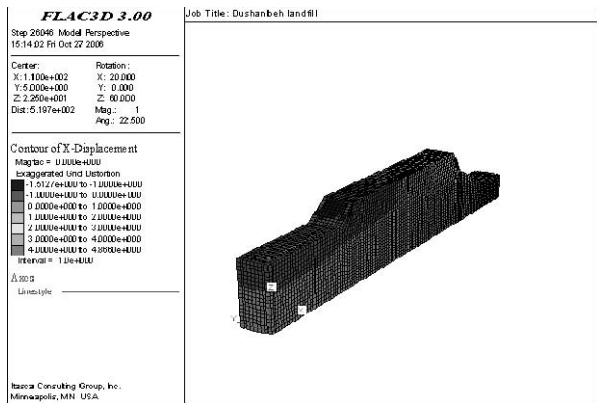


Fig. 3 Displacements of Dushanbeh landfill in x-direction (towards road)

In order to detect the amplification and attenuation states in the numerical model, the x-acceleration response of the refuse and the soil material was analysed using monitoring locations at the top and the bottom of each material. From the analysis, it can be concluded that the soil deposit as well as the waste are seemed to amplify the ground motions. The results of the simulation by the numerical modelling show that the modelling by FLAC3D can be utilised to understand the

effects of earthquake loading on landfills, physical damage to landfill and its acceleration response. This numerical modelling of landfills can capture the realistic damage that occurs in a landfill under earthquake loading.

During the shaking, there is considerable plastic flow in the landfill material, which results in irrecoverable displacements. This can be visualized using the comprehensive view of the final displacement field as contours superimposed on the landfill surface which shows the x-displacements at the different places of the landfill.

From the test results, the maximum accelerations experienced by the model waste and loess subjected to the model earthquake were used to understand the amplification or attenuation characteristics of landfill and loess. The comparison between the acceleration amplitude for the top and the bottom of the waste material and the top of the loess material with the base acceleration of the model indicates that the waste material as well as the loess material attenuates the input motion.

QUAKE/W Modelling

Basically there are four boundary conditions supported by the QUAKE/W software. Among these the Nodal displacement boundary conditions are relevant for the present analysis. These nodal displacement boundary conditions are meant as a frame of reference during the analysis of the problem. Usually the displacements at the node of interest are set to be zero. In this problem the horizontal motion are allowed at the nodes but restrained in the vertical direction.

While using the QUAKE/W, one is able to calculate:

- the motion and inertial forces that occur during the shaking,
- the generation of excess pore water pressures,
- the potential reduction of the soil shear strength,
- the effect on stability created by the inertial forces, excess pore-water pressures and possible shear strength losses, and
- the redistribution of excess pore-water pressures and possible strain softening of the soil after the shaking has stopped.

In addition, QUAKE/W can couple the dynamic formulation to structural element model and hence permit soil-structure interaction.

The earthquake intensity used for both analyses is taken from earthquake records of Uzbekistan which has a total length of 16 seconds and a peak ground acceleration of 6 m/s² or 0.6g which corresponds quite well with the intensity of 0.5g suggested by local seismologists. This digital record was scaled to the required peak value. The time-history of the earthquake

was then applied to the bottom of each model.

Usually earthquake records have some drift in the data. This does not have a great effect on the dynamic response, but it sometimes leads to unrealistic picture of the displacement computed from double integration of the acceleration record. Therefore the raw data require some modifications. The raw data can be modified by removing the minor vibrations at the ends. A base line correction is applied here so that the positive and negative area under the curve is the same. Fig. 4 shows the finite element mesh together with the boundary conditions. That is the problem is fixed at the bottom in both directions. The same material properties are used in the analysis as in case of FLAC3D analysis.

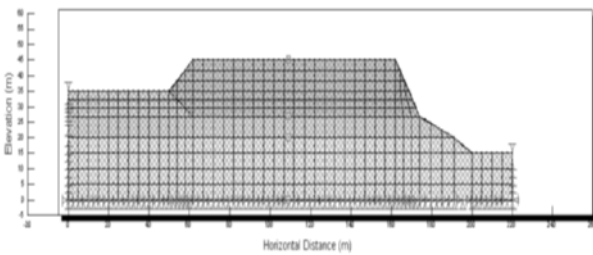


Fig. 4 The finite element mesh with boundary conditions of the Dushanbe landfill

Before the analysis, four history nodes for slope are identified. The locations of these history nodes are at the interface of two soil layers and at the bottom most level of the slope. The soil shear stiffness G and the Poisson's ratio are assumed to be constant for each soil layer for both slopes.

Fig. 5 shows the distorted model of the Dushanbe landfill. The maximum displacement (in the x-direction) of 20 cm occurred at the bottom of the slope of the landfill (Fig. 5). A maximum settlement (displacement in z-direction) of 1.5 cm occurred at the middle of the slope.

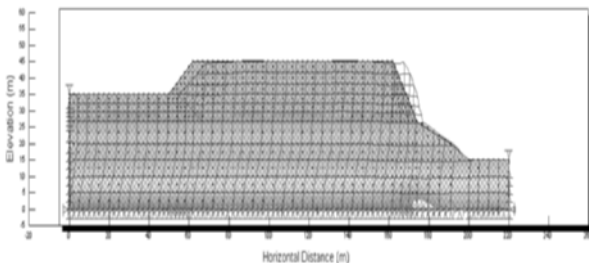


Fig. 5 The distorted model of the Dushanbe landfill

Figs. 6–8 show the acceleration histories of loam, alluvial and waste deposits respectively. From the acceleration time histories diagrams, it can be concluded that the loess material attenuates the input motions whereas the waste seems to amplify it.

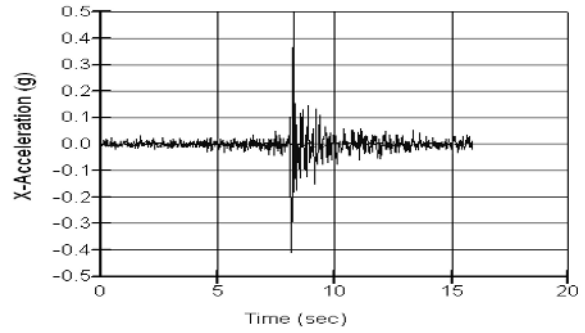


Fig. 6 Acceleration histories at the top (red line) and at the bottom (blue line) of the loam deposit

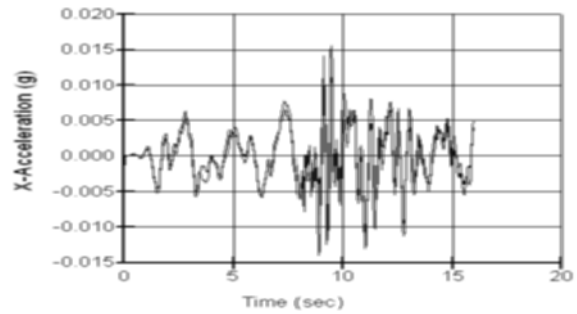


Fig. 7 Acceleration histories at the top (red line) and at the bottom (blue line) of the alluvial deposit

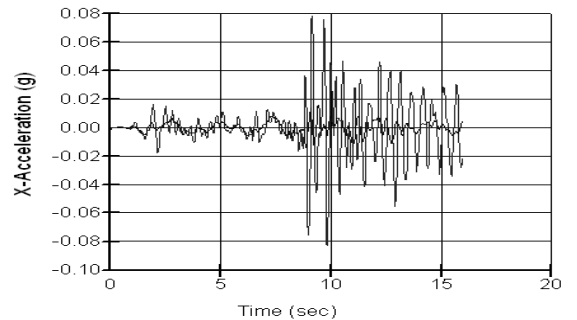


Fig. 8 Acceleration histories at the top (red line) and at the bottom (blue line) of the waste deposits

CONCLUSIONS

The results of dynamic analysis using QUAKE/W and FLAC3D are quite similar except the displacement magnitudes, which show significant variations. This may be attributed by the fact that there is a difference in the basic numerical method used by each of these two software applications and material modeling. QUAKE/W uses the finite element and FLAC3D uses finite difference schemes where the latter is still advanced in tracking all possible state of the soil medium. QUAKE/W uses equivalent linear material behaviour whereas FLAC3D handles the problem using the non-linear material behaviour. The slight differences in the other results could be as a result of the 2D and 3D analysis. Therefore,

the values of the displacements obtained from FLAC3D analysis are considered to be more realistic. The basic findings from the numerical analysis of Dushanbe landfill are:

- There is considerable plastic flow of the landfill material in the results of FLAC3D analysis.
- The results showed that the input acceleration is significantly attenuated by the soil layer immediate to the input level and the attenuated response is amplified by the waste material.
- Both analyses showed instability starting from 12 seconds of the input motion.

ACKNOWLEDGEMENTS

The NISMIST project (Contract 516732) is funded by the EU Sixth Framework Programme within the International Cooperation (INCO) especially for Russia and New Independent States (Call identifier FP6-2003-INCO-Russia + NIS-1).

REFERENCES

Abrahamson NA & Silva WJ (1996). Empirical Ground Motion Models, Report prepared for Brookhaven

- National Laboratory, New York, USA, p.144.
- Anderson DG & Kavazanjian E, Jr (1995). Performance of Landfills Under Seismic Loading, Proceedings of the Third International Conference on Recent Advances in Geotechnical Earthquake Engineering and Soil Dynamics, University of Missouri-Rolla, Vol. 3, St. Louis, Missouri, USA, pp. 277-306.
- Bray JD, Rathje EM, Augello AJ, Merry SM (1998). Simplified Seismic Design Procedure for Geosynthetic-Lined, Solid-Waste Landfills, Geosynthetics International, 5(1-2): 203-235.
- Kavazanjian E, Jr & Matasovic N (1995). Seismic analysis of solid waste landfills, Proceedings, Geoenvironment 2000, ASCE specialty conference, New Orleans, Louisiana.
- Makdisi FI & Seed HB (1978). Simplified Procedure for Estimating Dam and Embankment Earthquake-Induced Deformation, Journal of the Geotechnical Engineering Division, 104(GT7): 849-867.
- Thusyanthan NI, Madabhushi SPG, Singh S, Haigh S, Brennan A (2004). Seismic behaviour of Municipal Solid Waste (MSW) landfills, 13th World Conference on Earthquake Engineering Vancouver, B.C., Canada, August 1-6, Paper No. 2702.

HIGH-SPEED AND LONG RANGE FLOW ANALYSIS MODEL OF WASTE BODY AFTER SANITARY MSW LANDFILLS SLOPE UNSTABILITY

Zhan-Hong QIU¹, Yun-Min CHEN² and Xiao-Gang WANG³

ABSTRACT: If the leachate level is excessively high within sanitary MSW Landfills, it's failure shows high-speed and long range flow with liquid phase (leachate) carrying about solid phase(waste body) after landfills slope unstability, which likes mud-rock flow. Based on structure two-phase flow theory, and taking consider of the initial conditions, the boundary conditions and the storage condition of waste body flow, the mathematical model of waste mass's flow has been established. The discretization model can be established by finite calculus of differences. The high-speed and long range flow of waste mass after landfills slope unstability with high leachate level can be simulated by this model, and the flow distance and the area affected by failed waste mass can be predicted based on simulated results.

KEYWORDS: sanitary MSW Landfill, high leachate level, high-speed and long range flow

INTRODUCTION

Sanitary MSW landfills usually were built in the village, which catchment area usually is very large. Surface runoff and subsurface runoff will form in catchment area when there is rainfall, and which will run into landfill sitting at low side. At the present time, there are not valid separating rain water and sewage systems in the working face of almost all sanitary MSW landfills in our country. So, huge amounts of rainwater will infiltrate into waste body when there is heavy rain in landfill site [shown as Fig.1].

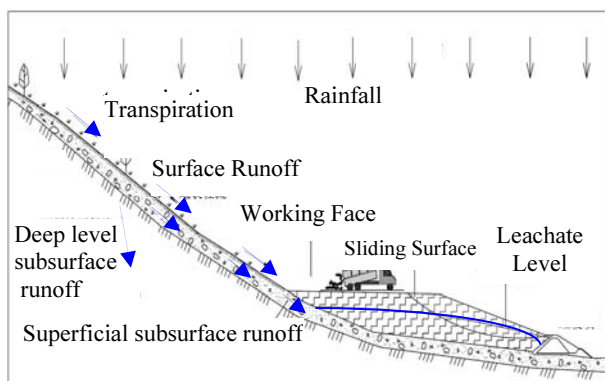


Fig.1 the Hydrologic Cycle Model of Sanitary MSW Landfill

At the present time, there are not valid collection and drainage system of leachate in almost all sanitary MSW Landfills in our country, even though advanced large-scale landfills such as Tianziling landfill in Hangzhou city. So, under the rainfall infiltration for many years, the leachate level is very high in sanitary landfill. For example, the leachate level is about 50 meters in Tianziling landfill in Hangzhou city (Zhejiang Province Engineering Investigation Institute, 2002). The probability of slope unstability is very great in sanitary MSW landfills with the high leachate level. The reason of slope unstability of ten landfills all over the world were analyzed by Koerner and Soong (Koerner & Soong, 2000), analysis results show that the main inducement of seven failed landfill is that the leachate level is excessively high.

If the leachate level is excessively high within sanitary MSW landfills, because bulk density of waste mass is less than that of general soil far and away, it's failure form is not same as that of general soil slop, but shows as high-speed and long range flow with liquid phase (leachate) carrying about solid phase (waste body) after landfills slope unstability, which likes mud-rock flow. For example, the Dona Juana landfill in Colombia, because the leachate level is excessive high which is caused by leachate recirculation, 1.8 million tons of solid wastes flow 1-1/2 km into a river at low side of landfill within a very short time. The elevation of this river is

¹ Associate Professor, Architectural and Civil Engineering College, Taizhou University, China. Email: qiuzhanhong@tzc.edu.cn

² Professor, MOE Key Laboratory of Soft Soils and Geoenvironmental Engineering, Zhejiang University, China. Email: chenyunmin@zju.edu.cn

³ Professor, Architectural and Civil Engineering College, Taizhou University, China. Email: wangxg824@tzc.edu.cn

about 200 m below the base elevation of the landfill. The flow slide intersected and filled the river (David M. Hendron, P.E., 2006) [shown as Fig.2].

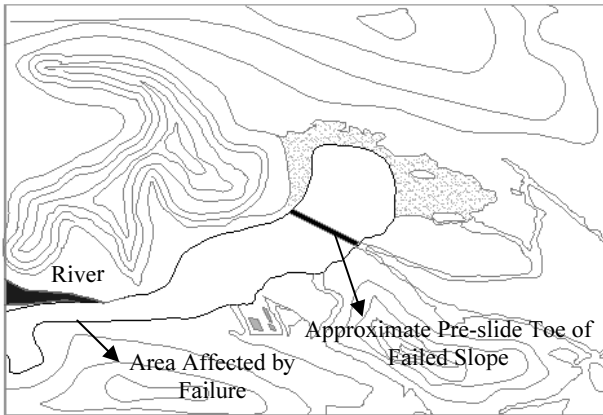


Fig.2 High-speed and long range flow of waste body in Dona Juana Landfill

At the present time, waste body was supposed to be rigidity in the most papers focused on slope stability analysis of landfills, and limiting equilibrium method was been adopted in these papers, e.g. (Qian 1997; Wang et al. 2004; Chen. et al 2000; Chen et al. 2008; Zhan et al. 2008). And the analyses of these papers all focused on the stability safety factor of waste landfill slope, the shear strength characterization of waste mass, and unstability condition of MSW landfill slope so on, these are very seldom papers studying the high-speed and long range flow of waste body after landfill slope unstability.

The leachate is complicated and high concentration organic waste water, which consists of ammonia nitrogen, volatile phenol, mercury, lead, chromium and other potentially hazardous substances. Once the landfill fail under the high leachate level, the failed waste body will flow in a very long range with carrying about much leachate, and the poisonous and harmful substance in these leachate will pollute our environments which we live by all means. So, it is very important to analyze the high-speed and long range flow of waste body and predict the area affected by failed waste mass after landfill slope unstability with the high leachate level.

FUNDAMENTAL EQUATION OF MOTION

At the present time, there are a large numbers of papers on studying numerical simulation of mud-rock flow motion, e.g. (WANG Guang-qian et al. 1998), (O'brien, J. S. et al. 1993), (HU Jian et al. 2006), (Ni Jinren et al. 1998). But the paper on high-speed and long range flow study of waste body in MSW landfill is very seldom. Because the high-speed and long range flow of waste body is almost same as that of mud-rock flow, the

analysis methods of mud-rock flow motion can be used to analyze the high-speed and long range flow motion of waste body. Based on the theory of solid-liquid two phase flow (WANG Guang-qian et al. 1998), the fundamental equation of high-speed and long range flow of waste body can be established, which can be expressed as the following equation.

$$\frac{\partial h}{\partial t} + \frac{\partial(hU)}{\partial x} + \frac{\partial(hV)}{\partial y} = 0 \quad (1)$$

$$\begin{aligned} \frac{\partial U}{\partial t} + U \frac{\partial U}{\partial x} + V \frac{\partial U}{\partial y} \\ = -g \frac{\partial h}{\partial x} - g(S_x + S_y) + \frac{\mu}{\rho} \left(\frac{\partial^2 U}{\partial x^2} + \frac{\partial^2 U}{\partial y^2} \right) \end{aligned} \quad (2)$$

$$\begin{aligned} \frac{\partial V}{\partial t} + U \frac{\partial V}{\partial x} + V \frac{\partial V}{\partial y} \\ = -g \frac{\partial h}{\partial y} - g(S_x + S_y) + \frac{\mu}{\rho} \left(\frac{\partial^2 V}{\partial x^2} + \frac{\partial^2 V}{\partial y^2} \right) \end{aligned} \quad (3)$$

In which, h is the depth of waste mass flow, U and V are the average vertical flow velocity in x and y direction respectively, S_x and S_y are the elevation gradient of runway surface of waste body flow in x and y direction respectively, S_x and S_y are the friction gradient of runway surface of waste body flow in x and y direction respectively, μ is the synthesized viscosity coefficient of waste body flow, ρ is the average vertical density of waste body flow.

S_x and S_y can be expressed by the following equation.

$$S_x = -\frac{\partial z}{\partial x}, \quad S_y = -\frac{\partial z}{\partial y} \quad (4)$$

In which, z is the elevation of runway surface of waste body flow.

Because these are one or more phenomenon in sanitary MSW landfills in our country, such as leachate collection and drainage system is fail to work, these is no valid separating rain water and sewage systems, the permeability coefficient of the level drainage liner is very small in vertical direction, and the ditch holding up rainwater is fail to work so on, the leachate level is usually very high in sanitary MSW landfills in our country. At the same time, the contents of organic and fiber are usually very great in waste body. So, the high-speed and long range flow of waste body shows very obvious viscosity.

In the exiting papers, the best friction resistance model to simulate viscosity flow of waste body is O'Brien model (O'brien, et al. 1993), which can take

consider of the effect of yield stress, viscosity stress, disperse stress and turbulent flow. It can be expressed as the following equation.

$$S = \frac{\tau_B}{\gamma h} Sgn(u) + \frac{2\mu_B u}{\gamma h^2} + \frac{k u \sqrt{u^2 + v^2}}{gh} \quad (5)$$

$$S = \frac{\tau_B}{\gamma h} Sgn(v) + \frac{2\mu_B v}{\gamma h^2} + \frac{k v \sqrt{u^2 + v^2}}{gh}$$

In which, S and S are the friction gradient of runway surface of waste body flow in x and y direction respectively, τ is Bingham stress, γ is the bulk density of liquid phase, μ is viscosity coefficient of waste body flow, $Sgn(\cdot)$ is the symbol function, k is the friction coefficient of waste mass flow.

THE DEFINITE CONDITION

Eq. 1 is nonlinear hyperbolic type partial differential equation, and it is very difficult to solve by analysis method. At the present time, it is usually solved by finite calculus of differences. The definite condition includes the initial condition, the boundary condition and the storage condition of waste body flow (Hu et al. 2006).

The Initial Condition

The initial value of both flow velocity and depth of flow are zero in whole calculation zone of waste body flow.

The Boundary Condition

The boundary conditions include the bottom boundary condition, the entrance boundary condition and the free boundary condition.

Bottom boundary condition

On the bottom boundary, the motion of waste body flow has no reflection to happen, so the normal velocity of flow is zero, and the tangential velocity of that is the one half of original velocity due to the loss of kinetic energy.

Entrance boundary condition

The values of flow velocity and depth of flow are fixed at the entrance boundary of waste body flow. These values can be defined by the amount of sliding waste body, during time of waste body flow and energy conservation law.

Free boundary condition

Free boundary condition of waste body flow can be defined by freezing method. The fundamental idea of

freezing method is defining boundary based on the deepness of waste body flow. The whole calculation zone is divided dry zone, wet zone and shallow water zone based on the deepness of waste body flow. The nodes of dry zone are not calculated, the nodes of wet zone are calculated by different scheme, and the nodes of shallow water zone are not calculated directly, but are modified based on the value change of the nodes of wet zone around.

The Storage Condition of Waste Body Flow

According to the existing documents at present, we take consider of the most simple storage condition of waste body flow, which is that the velocity of waste body flow is 0.0001m/s.

CONCLUSIONS

The high-speed and long range flow of waste mass is a very complex motion after landfills slope instability, and which will pollute our environments which we live by all means. So, it is very important to analyze the high-speed and long range flow of waste body and predict the area affected by failed waste mass after landfill slope instability with the high leachate level.

(1) If the leachate level is excessively high within sanitary MSW Landfills, it's failure form is not same as that of general soil slop, but shows as high-speed and long range flow with liquid phase (leachate) carrying about solid phase (waste body), which likes mud-rock flow.

(2) Because the high-speed and long range flow of waste body is almost same as that of mud-rock flow, the analysis methods of mud-rock flow motion can be used to analyze the high-speed and long range flow motion of waste body.

(3) Based on the theory of solid-liquid two phase flow, the fundamental equation of high-speed and long range flow of MSW was established. This two-dimension model can be solved by using finite calculus of differences.

(4) Based on contents of waste mass in landfill, the solid-liquid two-phase characteristic parameters of waste body flow must be studied in the future, which including Bingham stress τ , bulk density γ of liquid phase, viscosity coefficient μ of waste body flow, friction coefficient k .

ACKNOWLEDGEMENTS

This Project was supported by the Natural Science

Foundation of Zhejiang Province, China (Grant No. Y108792).

REFERENCES

- Zhejiang Province Engineering Investigation Institute (2002). Engineering hydro geological survey report of second landfill in Hangzhou city[R].
- Koerner RM & Soong TY (2000). Stability Assessment of Ten Large Landfill Failures, Advances in Transportation and Geoenvironmental systems Using Geosynthetics, Proceedings of sessions of Geo Denver, ASCE Geotechnical Special Publication No.103:1-38.
- David MH (2006). Large Landslide Risks in Solid Waste Facilities... Geotechnical Fundamentals Count. *Geo-Strata*: 28-30.
- Qian XD (1997). Stability Analysis of Cover Soil over Geosynthetic Layered Slope with Seepage Force. Michigan Department of Environmental Quality, Waste Management Division, Lansing, MI.
- Wang XQ, Zou WL, Zhu RG (2004). Stability analysis of cover soil slope on waste landfill under seepage with limit equilibrium method. *Chinese Journal of Rock Mechanics and Engineering*. 23(11): 1939-1943.
- Chen YM, Wang LZ, HU YY (2000). Stability analysis of a solid waste landfill slope. *China civil engineering journal*, 33(3):204-212.
- Chen YM, Gao D, Zhu B, Chen RP (2008). Stability and permanent displacements analysis of waste landfills along the underlying liner surface during Earthquake. *Science in China E*, Vol. 38 (1): 79-94.
- Zhan Tony LT, Chen YM, Ling WA (2008). Shear strength characterization of municipal solid waste at the Suzhou landfill, China. *Engineering Geology* 97: 97-111.
- Wang GQ, Shao SD, Fei XJ (1998). Simulation of debris flow: I-Model. *Journal of Sediment Research*, (3): 7-13.
- O'Brien JS, Julien PY, Fullerton WT (1993). Two-dimensional water flood and mudflow simulation. *Journal of Hydraulic Engineering*, 119(2): 244-261.
- Hu J, Kuang SF, Xu YN (2006). 2-D numerical simulation of viscous debris flow. *Journal of Sediment Research*, (6): 60-64.
- Ni JR & Wang GQ (1998). Conceptual Two-phase Flow Model of Debris Flow (I). *Acta Geographica Sinica*, (1):66-85.

ONE-DIMENSIONAL CONSOLIDATION OF AQUITARD CONSIDERING NON-DARCY FLOW

Zhong-Yu LIU¹, Jin-Chao YUE² and Li-Yun SUN³

ABSTRACT: There sometimes exists the notable difference between the solution of one-dimension consolidation of aquitard based on Terzaghi's theory and the field settlement observations, which can be in a certain extent ascribed to that the flow of pore water in the aquitard may not obey Darcy's law. In order to improve the precision of consolidation computation, the non-Darcy flow equation described by the power function for the lower velocity of flow and the linear function for the higher velocity of flow is introduced to modify Terzaghi's one-dimensional consolidation equation, and the presented equation is generalized to take account of the consolidation case due to the falling of the water head in the confined aquifer. The numerical analysis is performed by using the finite volume method. The effects of the parameters of non-Darcy flow on the consolidation process are investigated. The numerical results indicate that the non-Darcy flow delays the dissipation of pore water pressure in the aquitard; thereby the consolidation time of aquitard is longer than that of the solution based on Terzaghi's theory.

KEYWORDS: aquitard, consolidation, non-Darcy flow, finite volume method, pore water pressure

INTRODUCTION

It's a global problem that the exploitation of the groundwater will bring on the compression of the water-bearing stratum and thereby does on the land subsidence, which has been paid more and more attention by the environmental engineers and protectionists. Since the field settlement observations illustrate that the proportion of the compression deformation of aquitard to the land subsidence in some regions is greater than 50% (Zhang 2002), the precision of prediction on the latter is dependent on the accuracy of prediction on the former to a great extent, and even only the former is taken into account for the preliminary estimate of the latter in some regions (Roland et al. 1987). Therefore, the consolidation computation of aquitard is worthy of our research in depth, and is usually carried out based on Terzaghi's one-dimensional consolidation theory at present. However, there sometimes exists the notable difference between the solution of one-dimension consolidation of aquitard based on Terzaghi's theory and the field settlement observations, which can be in a certain extent ascribed to the assumption of Terzaghi's theory that the flow of pore water in the porous media follows Darcy's law. In fact, the non-Darcy flows occur in a lot of saturated clay layers, and there exists the visible difference among their mathematical expressions

for the non-Darcy flow based on their different experimental results (Deng 2007; Hansbo 1997; Qi 2007; Wang 2003; et al.), of which the applicability of Hanbo's formula as Eq. 1 is regarded as the most comprehensive

$$\left. \begin{aligned} q &= ci^m, & (i \leq i_1) \\ q &= K(i - i_0), & (i > i_1) \end{aligned} \right\} \quad (1)$$

where q is the velocity of flow; i is the hydraulic gradient; i_1 is the threshold hydraulic gradient for the linear flow; c and K are the permeability coefficients for the lower velocity of flow described by the power function and for the higher velocity of flow described by the linear function respectively; i_0 is the computed threshold hydraulic gradient for linear flow; m is the parameter described by experiment. And the relationships among these parameters are

$$i_0 = i_1 \frac{m-1}{m}, \quad c = \frac{K}{mi_1^{m-1}} \quad (2)$$

If $m = 1$, then $i_0 = 0$, $c = K$, and Eq. 1 reduces to Darcy law. If the power function for the lower velocity of flow or the linear function for the higher velocity of flow is left out of account respectively, then Eq. 1 reduces to the expression introduced by Liu et al. (2006, 2007) and Liu and Yang (2006) or by Xie et al. (2007).

¹ Professor, School of Civil Engineering, Zhengzhou University, China. Email: zhyliu@zzu.edu.cn

² Professor, School of Water conservancy and Environment Engineering, Zhengzhou University, China. Email: yuejc@zzu.edu.cn

³ Ph.D Student, ditto. Email: liyunjia@zzu.edu.cn

Therefore, it is improper that Darcy law is adopted to describe the flow during the consolidation of these saturated clay layers. Thus, in order to make the influence of non-Darcy characteristic of flow in the process of consolidation clear, Liu et al. (2006, 2007) and Liu and Yang (2006) modified Terzaghi's one-dimensional consolidation theory by introducing the flow equation only considering the threshold hydraulic gradient i_1 , i.e. taking no account of the power function for the lower velocity of flow in Eq. 1, and the influence of i_1 on the consolidation of saturated clay layer was investigated. Xie et al. (2007) introduced Eq. 1 describing the flow to deduce the new consolidation equation, but the linear function for the higher velocity of flow in Eq. 1 was taken no account of when they solved their equation.

In this paper, in order to improve the precision of consolidation computation of aquitard due to the falling of water head in the artesian aquifer under the aquitard, the non-Darcy flow described by Eq. 1 is incorporated in the Terzaghi's one-dimensional consolidation equation. Then the influences of the parameters of non-Darcy flow on the consolidation of aquitard are investigated by introducing the finite volume method to solve the presented equation.

GOVERNING EQUATION

The problem studied herein deals with one-dimensional consolidation of an aquitard composed of clayey soil, on which top and bottom there exist aquifers composed of sand. Fig. 1 is the schematic diagram, where H is a half of thickness of the aquitard; h is the initial confined head of water in the bottom confined aquifer on the condition of the hydraulic balance. Now let its confined head fall suddenly Δh , and then the compression deformation of the aquitard will emerge because the pore water pressure in the aquitard diminishes.

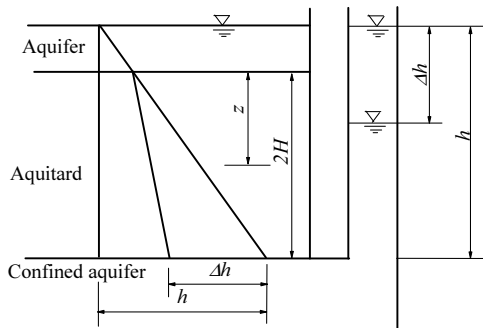


Fig. 1 Sketch map of soil layer structure and boundary condition

The main assumptions are made as follows:

1. Solid particles and water phase are incompressible,

the soil is homogeneous and fully saturated, and the consolidation of aquitard under the initial condition has ended.

2. The flow in the aquitard is governed by the non-Darcy flow described by Eq. 1, and takes place only in a one-dimensional vertical direction.

3. These parameters m , i_1 and K of non-Darcy flow in Eq. 1 and the coefficient of compressibility a are constants.

In this way, the governing equations for one-dimensional consolidation of aquitard can be written as

$$\frac{C_v}{\gamma_w^{M-1} i_1^{M-1}} \left(\frac{\partial u}{\partial z} \right)^{M-1} \frac{\partial^2 u}{\partial z^2} = \frac{\partial u}{\partial t} \tag{3}$$

where $u(z, t)$ is the excess pore water pressure; z is the depth; t is the time; γ_w is the unit weight of water; C_v is the coefficient of consolidation of soil, and $C_v = K(1+e)/(a\gamma_w)$; e is the void ratio of soil; $M = m$ if $i \leq i_1$ and $M = 1$ if $i > i_1$. It is evident that Eq. 3 reduces Terzaghi's one-dimensional consolidation equation if $m = 1$.

The initial condition is

$$u(z,0) = \Delta h \gamma_w z / (2H), \quad 0 \leq z \leq 2H \tag{4}$$

The boundary conditions are

$$u(0,t) = 0, \quad u(2H,t) = 0, \quad t > 0 \tag{5}$$

For the convenience of the following research, the dimensionless parameters are introduced as follows

$$U = \frac{u}{\Delta h \gamma_w}, \quad Z = \frac{z}{H}, \quad T = \frac{C_v t}{H^2}, \quad I = \frac{iH}{\Delta h}, \quad I_1 = \frac{i_1 H}{\Delta h} \tag{6}$$

Whereupon Eqs. 3-5 can be rewritten as

$$\frac{1}{I_1^{M-1}} \left(\frac{\partial U}{\partial Z} \right)^{M-1} \frac{\partial^2 U}{\partial Z^2} = \frac{\partial U}{\partial T} \tag{7}$$

$$U(Z,0) = Z/2, \quad 0 \leq Z \leq 2 \tag{8}$$

$$U(0,T) = 0, \quad u(2,T) = 0, \quad T > 0 \tag{9}$$

where $M = m$ if $I \leq I_1$ and $M = 1$ if $I > I_1$.

DERIVATION OF NUMERICAL SOLUTIONS

Since it is difficult to obtain the analytical solutions of the aforementioned differential equation because of its nonlinearity, the finite volume method is introduced to obtain its numerical solutions.

Discretization of Equation

Divide the aquitard into N cells from the top down by

the proportional spacing ΔZ , and fix up a node at the midpoint of every cell. At the same time, let the time step equal to ΔT . Then the integral calculation for Eq. 7 is done in the j th cell during the k th time interval (from the time T_k to the time T_{k+1})

$$\int_T^{T+1} \int_{\Delta Z} \frac{1}{I_1^{M-1}} \left(\frac{\partial U}{\partial Z} \right)^{M-1} \frac{\partial^2 U}{\partial Z^2} dZ dT = \int_T^{T+1} \int_{\Delta Z} \frac{\partial U}{\partial T} dZ dT \quad (10)$$

Eq. 10 can be rewritten as

$$\int_{T_k}^{T_{k+1}} \left(\frac{1}{MI_1^{M-1}} \left(\frac{\partial U}{\partial Z} \right)^M \Big|_X - \frac{1}{MI_1^{M-1}} \left(\frac{\partial U}{\partial Z} \right)^M \Big|_S \right) dT = \int_{\Delta Z} \left[\int_T^{T+1} \frac{\partial U}{\partial T} dT \right] dZ \quad (11)$$

where the subscripts X and S denote the bottom and top boundaries respectively.

Let the backward difference substitute for the partial derivative of U with respect to T on the right of Eq. 11, and the central difference do for the partial derivative of U with respect to Z on the left of Eq. 11. Thus

$$\frac{1}{MI_1^{M-1}} \left[\left(\frac{U_{j+1,k+1} - U_{j,k+1}}{\Delta Z} \right)^M - \left(\frac{U_{j,k+1} - U_{j-1,k+1}}{\Delta Z} \right)^M \right] \Delta T = (U_{j,k+1} - U_{j,k}) \Delta Z \quad (12)$$

That is

$$U_{j,k+1} = U_{j,k} + \alpha \left[(U_{j+1,k+1} - U_{j,k+1})^M - (U_{j,k+1} - U_{j-1,k+1})^M \right] \quad (13)$$

where $\alpha = \frac{1}{MI_1^{M-1}} \frac{\Delta T}{\Delta Z^{M+1}}$.

Disposal of Initial and Boundary Conditions

The initial conditions described by Eq. 8 can be expressed as

$$U_{j,0} = 2j / N \quad (14)$$

In view of the boundary condition described by Eq. 9, the gradient of the pore water pressure on the top boundary of the first cell can approximate to

$$\frac{\partial U}{\partial Z} \Big|_S = \frac{U_{1,k+1}}{\Delta Z / 2} \quad (15)$$

Then Eq. 11 for the first cell can be rewritten as

$$U_{1,k+1} = U_{1,k} + \alpha \left[(U_{2,k+1} - U_{1,k+1})^M - 2^M U_{1,k+1}^M \right] \quad (16)$$

In a similar way, Eq. 11 for the bottommost cell can be rewritten as

$$U_{N+} = U_{N-} + \alpha \left[2 U_{N+} - (U_{N+} - U_{N-+}) \right] \quad (17)$$

ANALYSIS

The system of equation composed of Eqs. 13, 16 and 17 is solved by the iterative method on account of its nonlinearity when $m > 1$, and let $N = 100$ and $\Delta T = 10^{-6}$ in the following analysis.

Influence Of Non-Darcy Flow Properties On The Dissipation of Excess Pore Water Pressure

First, the influence of m on the dissipation of excess pore water pressure is investigated. The curves of the dimensionless excess pore water pressure U versus the dimensionless depth Z at the dimensionless times $T = 0.05$ and 1.00 for the cases that $m = 1.5, 2.0$ and 3.0 respectively while $I_1 = 1.0$ are figured in Fig. 2, in which the corresponding curve based on Terzaghi's theory is also done by the solid line to contrast with each other. It is evident that the value of U based on the non-Darcy flow is greater than that based on the Darcy flow with $m > 1.0$, and furthermore the greater the value of m , the greater the difference of excess pore water pressure between based on the Darcy and non-Darcy flows. Therefore, the dissipation rate of excess pore water pressure based on the non-Darcy flow is slower than that based on the Darcy flow. Moreover, the almost correspondence of the upper and lower segments of the curves for $T = 0.05$ in Fig. 2 indicates that the value of m has a little influence on the dissipation rate of excess pore water pressure in the zones near the drainage surfaces at the early stage of consolidation.

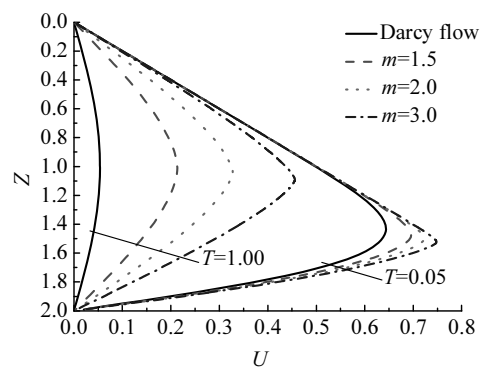


Fig. 2 Influence of m on dissipation of pore water pressure ($I_1=1.0$)

In order to investigate the influence of I_1 on the dissipation of excess pore water pressure, the curves of the dimensionless excess pore water pressure U versus the dimensionless depth Z at the dimensionless times $T = 0.05$ and 1.00 for the cases that $I_1 = 0.5, 1.0$ and 5.0 respectively while $m = 2.0$ are figured in Fig. 3. It is evident that the influence of I_1 on the dissipation of excess pore water pressure is similar to that of m , that is,

the value of U based on the non-Darcy flow is also greater than that based on the Darcy flow with $I_1 > 0.0$, and furthermore the greater the value of I_1 , the greater the difference of excess pore water pressure between based on the Darcy and non-Darcy flows.

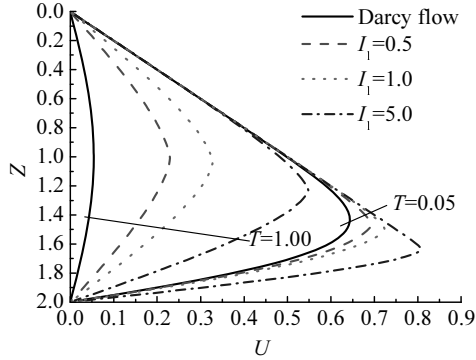


Fig. 3 Influence of I_1 on dissipation of pore water pressure ($m=2.0$)

Influence Of Non-Darcy Flow Properties On The Degree of Consolidation

Since the degree of consolidation based on the effective stress is the same as that based on the deformation considering the assumption that the coefficient of compressibility a are constants, the degree of consolidation U_t in the following analysis is based on the former, that is

$$U_t = \frac{\int_0^H \sigma' dz}{\gamma_w \Delta h H} = 1 - \int_0^H U(Z, T) dZ \tag{18}$$

The curves of the degree of consolidation U_t versus the dimensionless time T for the cases that $m = 1.5, 2.0$ and 3.0 respectively while $I_1 = 1.0$ or the cases that $I_1 = 0.5, 1.0$ and 5.0 respectively while $m = 2.0$ are figured in Fig. 4 or 5 respectively. These Figures show that the rate of consolidation will slow down if the flow in the aquitard obeys the non-Darcy law compared with Darcy law, and the difference will increase with the increasing of m and I_1 , that is, the time corresponding to a given degree of consolidation U_t will be delayed. For example, corresponding to $U_t = 70\%$, the dimensionless time $T = 0.403$ if the flow of the pore water obeys Darcy law, but $T = 0.830, 1.562$ and 7.686 respectively if $m = 2.0$ and $I_1 = 0.5, 1.0$ and 5.0 respectively. Therefore, according to the definition of I_1 described by Eq. 6, it can be obtained that the thicker the aquitard or the less the confined head fall Δh , the less the rate of consolidation of the aquitard, that is, the greater the deviation from the calculated value based on the Terzaghi's one-dimensional consolidation theory. Thus, the parameter I_1 composed of the threshold hydraulic gradient i_1 , the half thickness of aquitard H

and the confined head fall Δh is also important to characterize the consolidation of aquitard besides the coefficient of consolidation C_v .

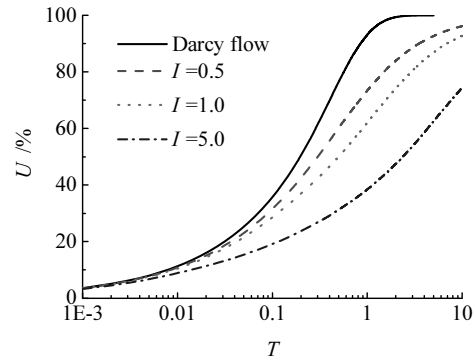


Fig. 4 Influence of m on the degree of consolidation ($I_1=1.0$)

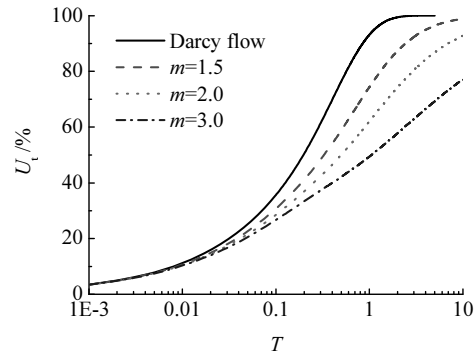


Fig. 5 Influence of I_1 on the degree of consolidation ($m=2.0$)

CONCLUSIONS

By substituting the non-Darcy flow equation described by the power function for the lower velocity of flow and the linear function for the higher velocity of flow for Darcy law, Terzaghi's one-dimensional consolidation equation is modified and generalized to take account of the consolidation case due to the falling of the water head in the confined aquifer, and the finite volume method is introduced to solve the presented equation. Based on this study, the following conclusions can be drawn:

- (1) The non-Darcy flow delays the dissipation of pore water pressure in the aquitard, thereby the rate of consolidation is less than that of the solution based on Terzaghi's theory.
- (2) The rate of the dissipation of pore water pressure and the rate of consolidation of the aquitard will decrease with the increasing of m or I_1 . Therefore, the parameter I_1 is important to characterize the consolidation of aquitard besides the coefficient of consolidation C_v .

ACKNOWLEDGEMENTS

This research was partly supported by the Science Program of Henan Expressway Development Co. Ltd. (Grant No. 2007GF009).

REFERENCES

- Deng YE, Xie HP, Huang RQ, et al. (2007). Law of nonlinear flow in saturated clays and radial consolidation. *Applied Mathematics and Mechanics (English Edition)*, 28(11): 1427-1436.
- Hansbo S (1997). Aspects of vitical drain design: Darcian or non-Darcian flow. *Geotechnique*, 47(5): 983-992.
- Liu ZY & Yang RG (2006). One-dimensional consolidation of double-layered ground considering the intial hydraulic gradient. *Journal of Hefei University of Technology (Natural Science)*, 29(5): 568-572 (in Chinese).
- Liu ZY, Zhang TH, Ma CW (2007). Effect of initial hydraulic gradient on one-dimensional consolidation of saturated clays. *Rock and Soil Mechanics*, 29(3): 467-470 (in Chinese).
- Liu ZY, Liu ZG, Ma CW (2006). One-dimensional consolidation of saturated clays considering intial hydraulic gradient. *Journal of Zhengzhou University (Engineering Science)*, 27(3): 21-24 (in Chinese).
- Qi T, Xie KH, Hu AF, et al. (2007). Laboratorial study on non-Darcy seepage in Xiaoshan clay. *Journal of Zhejiang University (Engineering Science)*, 41(6): 1023-1028 (in Chinese).
- Roland WL & Bornard AS (1987). *The finite element method in the deformation and consolidation of porous media*. New York: John Wiley & Sons, 1987: 100-115.
- Wang XY & Liu CL (2003). New Understanding of the Regularity of Water Seepage in Cohesive Soil. *ACTA Geoscientia Sinica*, 24(1): 91-95 (in Chinese).
- Xie HL, Wu Q, Zhao ZM, et al. (2007). Consolidation computation of aquitard considering non-Darcy flow. *Rock and Soil Mechanics*, 28(5): 1061-1065 (in Chinese).
- Zhang Y (2002). One-dimensional general model of land subsidence and its solution. *Journal of Engineering Geology*, 10(4): 434-437 (in Chinese).

SITE EFFECT ANALYSIS OF SHIRVAN GTL REFINERY, USING EQUIVALENT LINEAR SOIL BEHAVIOR (NE OF IRAN)

Ahmad ADIB¹, Naser EBADATI² and Kobra HEYDARZADEH³

ABSTRACT: Site effect is one of the important factors which should be evaluated before constructing any important structure. Gas refinery is a sensitive structure that is should be studied seismicity and effect of soil characteristics on earthquake hazard increasing or decreasing in study region. In this study, site effects of the gas refinery site in Shirvan, NE of Iran, studied and evaluated by numerical method and soil equivalent linear behavior using EERA program. To obtain soil characteristics, 4 borholes excavated and soil mechanics tests done on the samples of these boreholes. Generally, ground type of the region in shallow depth is gravel (G) and in deep is clay (CL). S-wave velocity obtained by downhole test. By regarding to these primary information, ground surface response resulted in all boreholes and the results show by isoacceleration, isoamplification, isofrequency and isoperiod maps. Maximum acceleration in the ground surface, is 0.422 g in recurrent period 475y. Mean amplification factor in the region is 2.3. The region is amplified in mean frequency range 12-14 Hz, and period range 0.070-0.085 (s). Then, the result differentiated according to Iranian Code of Practice for Seismic Resistant Design of Buildings, Standard No. 2800. Finally, the results compared by ground type obtained according Standard 2800. By comparing, it is observed that surface acceleration, amplification factor, and amplification frequency and period are compatible with ground type of all sites according Standard 2800. Acceleration response and amplification spectra are compatible in all sites. Regarding to compatible results and ground characteristics in all boreholes and by regarding to the restricted study region then one can suppose the region is uniform with small variations.

KEY WORDS: Shirvan-, Site effect-, GTL refinery-, Amplification factor

INTRODUCTION

The study site (site of Shirvan GTL refinery) is located at 8 km of western Shirvan, at geographic coordinate 57°49' to 57°51' eastern longitude and 37°24' to 37°25' northern latitude. Fig. 1 shows its geography location and geology map. This refinery, is geologically located on alluvium and Pleistocen deposits. Around the refinery, 3 formations outcropped, Limston of Tirgan formation (ktr), Alluvium Traces (Qt1) and Alluvium deposits of Low and agricultural ground (Qt2) (Jafarian, 2005). A large part of the site is located on Qt1 and its geotechnic properties are affected by this deposit.

Geotechnic and sedimentary properties of the alluvium deposits in the site, imply that they are member of river and fan deposits. To study soil geotechnic properties, 4 boreholes drilled whose properties are shown in Table 1.

Borehole A, drilled at south eastern part of the site. It has silty gravel to depth 1m, with low fine percent. With

increasing fine percent from depth 1 to 4 m, increases plasticity and moisture (GC). There is silty and clayey sand from depth 4 to 8 m (Adib et al. 2008).

Borehole B, drilled at south western of the site up to 10 m depth that has gravely sand to 2m with clay and fine percent lower than 15%. From 2 to 4m, fine percent and plasticity increased (ML, CL). From depth 5 m, drilling stopped because of existence of very competent ground and coarse block of rock (GM) (Adib et al. 2008).

Borehole C, drilled in north of the site with depth 9 m. It has clayey gravel to depth 1 m, and to depth 3 m includes clay and silt with low plasticity. From 3-6m, gravel with silt and low fine percent is found (Adib et al. 2008).

Borehole D, drilled in center of the site and with 20 m depth that to depth 2 m has silt and clay with low plasticity, and to depth 9 m, gravel with clay or silt. From 9—19 m, gravely clay (CL) is found (Adib et al. 2008).

¹ Islamic Azad University, South Tehran Branch, Iran. Email: dr_a_adib@yahoo.co.uk

² Islamic Azad University, Islamshar Branch, Iran. Email: drebadati@yahoo.com

³ Zaminkav Research Group, Iran. Email: k.heydarzadeh@yahoo.com

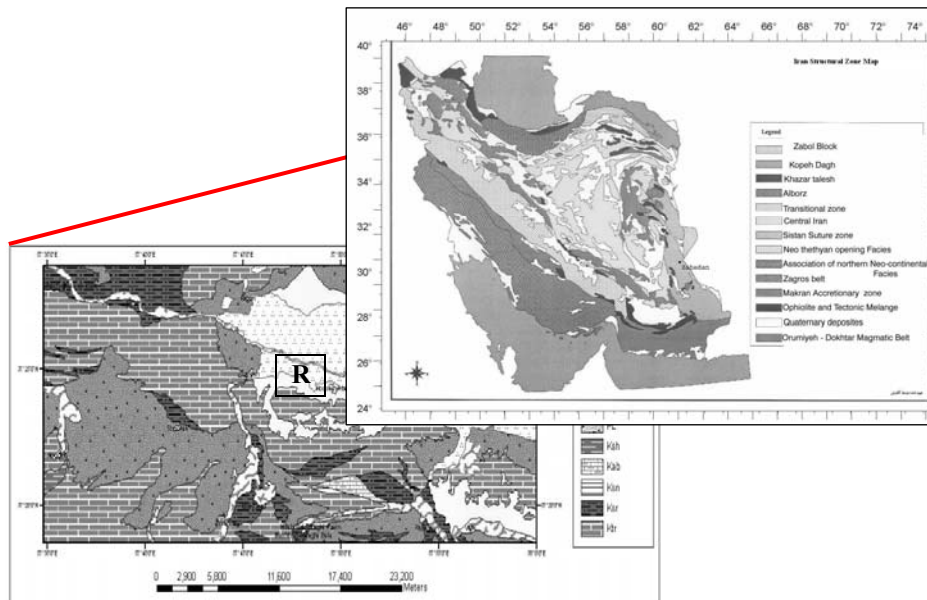
Table 1 Boreholes coordinates of the study site

Boreholes name	X(E)	Y(N)	Depth (m)
A	570155	4140378	11
B	569190	4140223	10
C	569555	4140902	9
D	569857	4140418	20

About seismicity of the region, we can say that in this region, many historical and instrumental earthquakes happened. Most important earthquake reported in Garmkhan at 1996 with magnitude 6.1 and intensity VIII (MMI) (Ambraseys & Melville, 1982). We used accelerogram of this earthquake in Bojnoord station for ground response analysis. Values of horizontal and vertical components of ground motion acceleration obtained 0.35 (g) and 0.15 (g), respectively. According these values, the site locates in the region of high

earthquake risk (Adib et al.2008).This value is used for site effect analysis as arrival acceleration on seismic bedrock of the site.

In seismic geotechnic, evaluation of wave propagation in the earth and its variation from seismic bedrock to ground surface will analyze. Seismic wave properties such as amplitude and frequency change when it propagates from bedrock to ground surface. Soft sedimentary deposits, amplify special frequency of the ground motion and hereby, they increase destructive effects and damages of earthquakes (Ishibashi, 1992 & Vucetic et al. 1991). The amplification evaluated by ground response analysis which is representative of soft deposit behavior into bedrock motion. Response of sedimentary deposits depends on frequency of bedrock motion and geometry of soil layers above bedrock. In case of soil amplifying, the accelerations will be more destructive when frequencies of the seismic wave are similar to amplification frequency of sites (Kramer, 1996).

**Fig. 1** Geology map and site location of the Shirvan GTL Refinery(R)

STUDY METHOD

Different techniques have developed as one, two or three dimensional methods. One dimensional method used when soil layering is relatively horizontal and soil response resulted due to SH wave and its vertical propagation. For one dimensional ground response analysis, is used one of the three methods, linear, equivalent linear (local nonlinearity) and nonlinear analysis.

In linear method, a defined time history of bedrock is shown at Fourier domain using fast Fourier transformation (FFT). Every expression in Fourier series of bedrock, multiply at transfer function to make ground

surface motion. Ground surface motion analyze in time domain using inverse fast Fourier transfer motion. In equivalent linear method, nonlinearity properties of shear and damping modulus applied to define soil equivalent linearity using iterative calculation to find shear and damping values compatible with effective strain in any layers. In this method, first a defined motion series consider in Fourier domain, then transfer function obtain for different layers using existing properties of soil profile. Transfer functions define variation of amplification factor with frequency in a soil profile. In third step, to find amplification spectrum transferred to a special layer of soil, Fourier spectrum multiply at transfer function of soil profile. In forth step, acceleration time

history for that layer, obtain by inverse fast Fourier transformation. Shear stress and strain of the layer obtain in fifth step using maximum acceleration resulted from acceleration time history, and the layer properties. In six step, new shear modulus and damping obtain by damping ratio and decreasing curves of shear modulus resemble with effective strain of strain time history. With these new properties of the soil, new transfer functions obtain and processing iterate to find difference between new and old properties in a defined range (Kramer, 1996).

Ground motion analysis in the GTL refinery of Shirvan site is down using geotechnic information and velocity profile of soil in the boreholes, existing accelerogram in frequency domin and use of FFT and FFF-inverse algorithm. Passing information from time to frequency domain obtained by doing as following:

- Studying scientific history about the object;
- Drilling borehole and gathering information;
- Analyze and drawing soil response in Fourier domain and drawing relevant curves.

DISCUSSION

To analyze soil behavior, definition of all layers of the soil profile and properties of primary motion operated to the profile, is necessary. Most important parameters of the soil profile to approximate soil behavior in dynamic state are thickness, natural density, maximum shear modulus, ground gravity acceleration in the location of boreholes and soil type (Seed et al. 1986). Seismic characteristic and shear wave velocity of the site determined by downhole test. Based on downhole test and data of borehole D which is in center of the site, depth of seismic bedrock (velocity 750 m/s) obtained 42 m.

According to the Study shear wave velocity at

different depth, it is found that velocity increases from east to west.

1. Physic and dynamic properties

Geotechnic and dynamic properties of the soil have main role to define site effect. These properties determined in 4 boreholes, A to D shown in tables 2to5.

2. Site effect

Dynamic properties of the soil in the region calculated using shear wave velocity and with association of standard shear modulus and damping curves. Data analyzed using modeling program of one dimensional ground response, and maximum acceleration, ground response spectrum and period of soil profile obtained as outputs [5]. The values apply to define potential regions of amplification and variation of spectral acceleration with different frequency and period for soil profile. To study site effect on diffusive waves of earthquake and approximate linear one dimensional of soil nonlinearity in frequency domain, first geotechnic properties of the soil and shear wave velocity obtained in selected profiles by applying earthquake acceleration in selected recurrent period and applying it to the soil column, then dynamic behavior of the soil obtained in one dimension (depth) and by equivalent – linear method. Accelerogram of ground motion on bedrock of Deyhook station in 1979 Tabas earthquake (because of high acceleration) and accelerogram of Garmkhan earthquake in Bojnoord station (L and T components), because of nearity to the site, is used to response analysis. Ground response spectrum at ground surface, amplification frequency of seismic wave amplitude, amplification factor and acceleration values with depth are the results of analysis. Analysis of soil dynamic behavior in the location of the boreholes presented in continue. The results in every of the boreholes are shown in following tables and figures:

Table 2 Geophysic and Dynamic properties of borehole A

Layer No.	Thickness (m)	Soil type	Shear Modulus	Damping Ratio	V_s (m/s)	Total density (KN/m ³)
1	2	G	Gravel (Seed et al.)	Gravel (Seed et al.)	159.7	19
2	4	G	Gravel (Seed et al.)	Gravel (Seed et al.)	362.6	18.70
3	5	SM	Sand (Seed & Idriss) Upper Bound	Sand (Seed & Idriss) Upper Bound	472.5	20
4	3	CL	Clay, (Sun, et al.) PI=10-20	Clay, (Sun et al.) Average	521.8	17
5	3	G	Gravel (Seed et al.)	Gravel (Seed et al.)	544.7	18.50
6	3	CL	Clay, (Sun,et al.) PI=10-20	Clay, (Sun et al.) Average	564.7	18
7	8	CL	Clay, (Sun,et al.) PI=10-20	Clay, (Sun et al.) Average	576.2	18
8	6	CL	Clay, (Sun,et al.) PI=10-20	Clay, (Sun et al.) Average	675.4	18
9	Bedrock	----	-----	-----	700	19

Table 3 Geophysical and Dynamic properties of borehole B

Layer No.	Thickness (m)	Soil type	Shear Modulus	Damping Ratio	V_s (m/s)	Total density (KN/m ³)
1	3	G	Gravel (Seed et al.)	Gravel (Seed et al.)	242.5	19.70
2	3	G	Gravel (Seed et al.)	Gravel (Seed et al.)	406.2	17.30
3	4	G	Gravel (Seed et al.)	Gravel (Seed et al.)	500.6	17.30
4	4	CL	Clay, (Sun, et al.) PI=10-20	Clay, (Sun et al.) Average	551.2	17
5	3	G	Gravel (Seed et al.)	Gravel (Seed et al.)	579.2	18.50
6	3	CL	Clay, (Sun, et al.) PI=10-20	Clay, (Sun et al.) Average	599.2	18
7	5	CL	Clay, (Sun, et al.) PI=10-20	Clay, (Sun et al.) Average	634.7	18
8	5	CL	Clay, (Sun, et al.) PI=10-20	Clay, (Sun et al.) Average	679.5	18
9	Bedrock	----	-----	-----	700	18

Table 4 Geophysical and Dynamic properties of borehole C

Layer No.	Thickness (m)	Soil type	Shear Modulus	Damping Ratio	V_s (m/s)	Total density (KN/m ³)
1	2	G	Gravel (Seed et al.)	Gravel (Seed et al.)	205.5	18.50
2	4	G	Gravel (Seed et al.)	Gravel (Seed et al.)	387.2	17.50
3	4	G	Gravel (Seed et al.)	Gravel (Seed et al.)	496.7	20
4	4	CL	Clay, (Sun, et al.) PI=10-20	Clay, (Sun et al.) Average	547.3	17
5	3	G	Gravel (Seed et al.)	Gravel (Seed et al.)	575.3	18.5
6	3	CL	Clay, (Sun, et al.) PI=10-20	Clay, (Sun et al.) Average	595.3	18
7	5	CL	Clay, (Sun, et al.) PI=10-20	Clay, (Sun et al.) Average	630.8	18
8	5	CL	Clay, (Sun, et al.) PI=10-20	Clay, (Sun et al.) Average	675.6	18
9	Bedrock	----	-----	-----	700	18

Table 5 Geophysical and Dynamic properties of borehole D

Layer No.	Thickness (m)	Soil type	Shear Modulus	Damping Ratio	V_s (m/s)	Total density (KN/m ³)
1	3	CL	Clay, (Sun, et al.) PI=10-20	Clay, (Sun et al.) Average	187	16.5
2	4.5	G	Gravel (Seed et al.)	Gravel (Seed et al.)	360.3	18.7
3	3	G	Gravel (Seed et al.)	Gravel (Seed et al.)	446.2	22
4	3	CL	Clay, (Sun, et al.) PI=10-20	Clay, (Sun et al.) Average	481	17
5	3	G	Gravel (Seed et al.)	Gravel (Seed et al.)	507.1	18.5
6	2.5	CL	Clay, (Sun, et al.) PI=10-20	Clay, (Sun et al.) Average	526.8	18
7	8	CL	Clay, (Sun, et al.) PI=10-20	Clay, (Sun et al.) Average	573.9	18
8	10	CL	Clay, (Sun, et al.) PI=10-20	Clay, (Sun et al.) Average	652.4	18
9	Bedrock	----	-----	-----	700	18

Table 6 Mean results of ground response analysis in borehole A

mean surface acceleration	mean amplification factor	mean ampli frequency	mean ampli period
0.36g	2.85	11.8	0.085

Table 7 Mean results of ground response analysis in borehole B

mean surface acceleration	mean amplification factor	mean ampli frequency	mean ampli period
0.36g	1.86	12.5	0.080

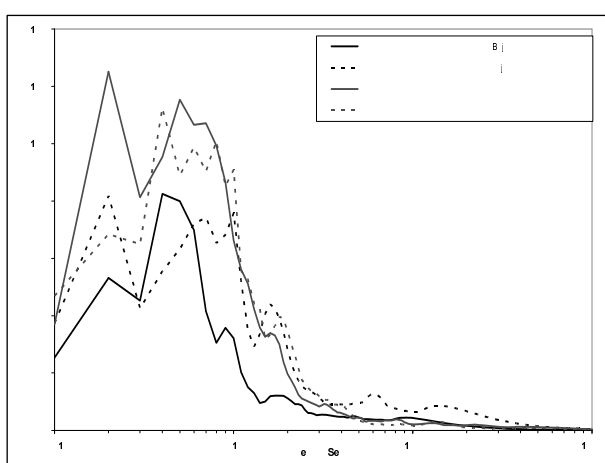


Fig. 2 Response spectra resulted by operating 2 accelerograms, Bojnoord and Deyhook (L,T component in borehole A)

According to Fig. 2, main peak obtained by operating L component of Bojnoord and T component of Deyhook accelerograms at period 0.04 s and by operating two other components at period 0.02 s.

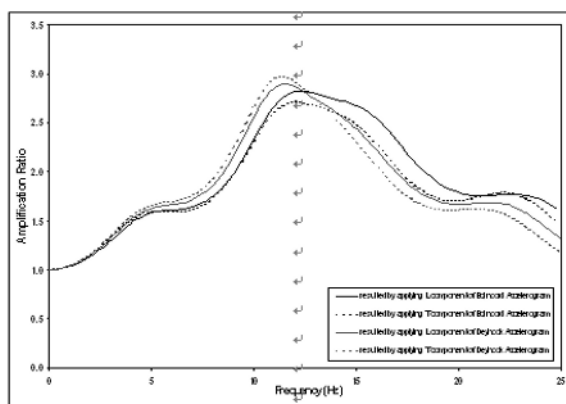


Fig. 3 Amplification spectra resulted by operating 2 accelerograms, Bojnoord & Deyhook (L,T component) in borehole A

Table 8 Mean results of ground response analysis in borehole C

mean surface acceleration	mean amplification factor	mean ampli frequency	mean ampli period
0.42g	2.16	14.6	0.069

Table 9 Mean results of ground response analysis in borehole D

mean surface acceleration	mean amplification factor	mean ampli frequency	mean ampli period
0.38g	2.35	12.2	0.083

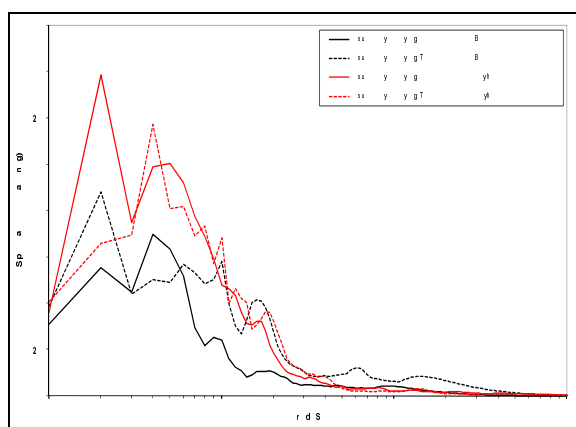


Fig. 4 Response spectra resulted by operating 2 accelerograms, Bojnoord and Deyhook (L,T component) in borehole B

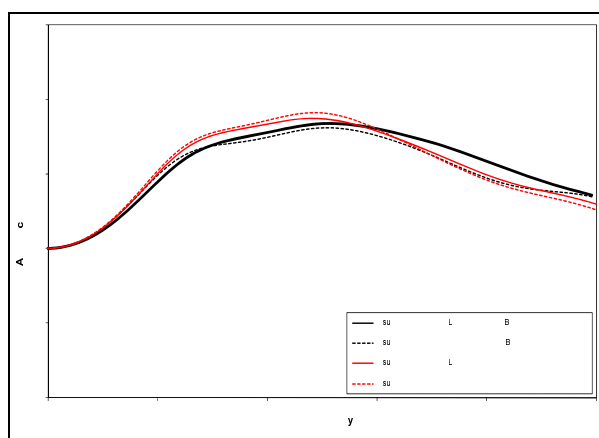


Fig. 5 Amplification spectra resulted by operating 2 accelerograms, Bojnoord and Deyhook (L,T component) in borehole B

Acceleration values obtained by operating Deyhook accelerogram, are generally, more than Bojnoord. Of course, results of operating Bojnoord accelerogram are more reliable because it is nearer to the site.

Amplification spectra has a clear peak in frequency about 12 Hz

According to resulted response spectra for borehole B, it is found that main peak obtained by operating L and T component of Bojnoord and Deyhook accelerogram, respectively, are at period 0.04 s, and in two other components are at period 0.02 s. Its amplification spectra show a peak at frequency about 12 Hz.

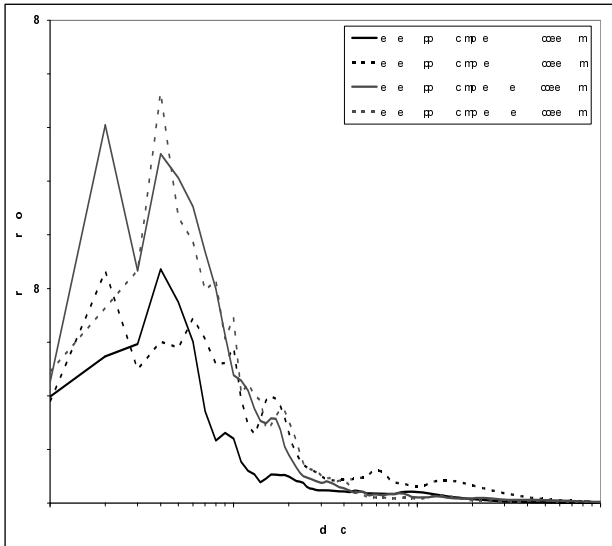


Fig. 6 Response spectra resulted by operating 2 accelerograms, Bojnoord and Deyhook (L,T component) in borehole C

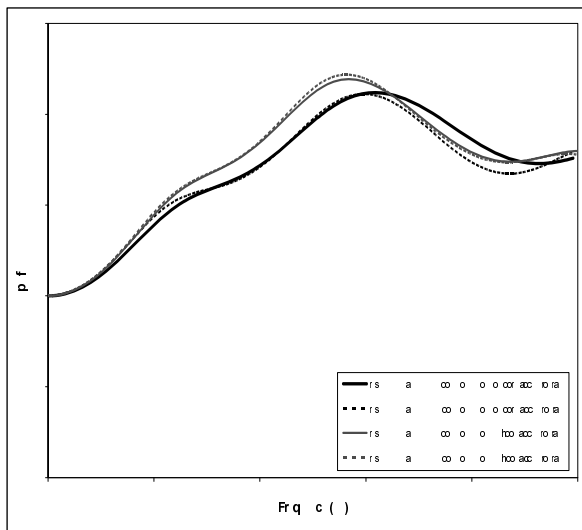


Fig. 7 Amplification spectra resulted by operating 2 accelerograms, Bojnoord and Deyhook (L,T component) in borehole C

Main peak of acceleration response spectra resulted by operating T and L components of Bojnoord, is at period 0.02 s and at two other components is at period 0.04 s. Its amplification spectra has a main peak at frequency about 15 Hz.

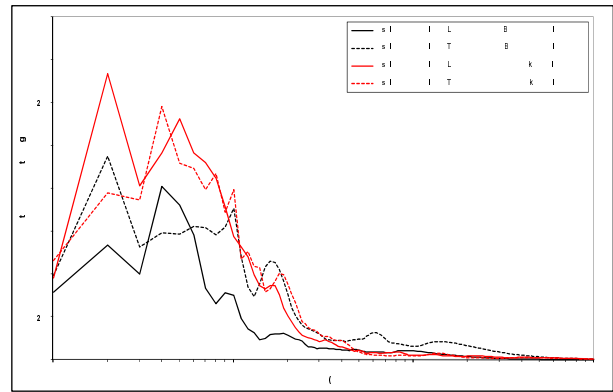


Fig. 8 Response spectra resulted by operating 2 accelerograms, Bojnoord and Deyhook (L,T component) in borehole D

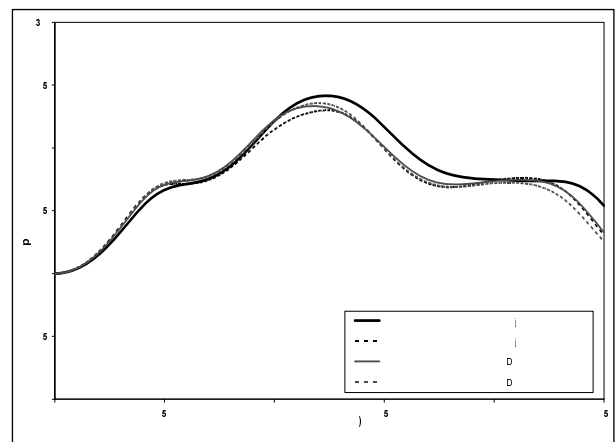


Fig. 9 Amplification spectra resulted by operating 2 accelerograms, Bojnoord and Deyhook (L,T component) in borehole D

According to Fig. 6, response acceleration spectra obtained by operating L component of Bojnoord accelerogram is similar to resulted spectra of T component of Deyhook accelerogram, with lower acceleration values. Also response spectra obtained by operating L component Deyhook accelerogram, is similar to them, but in this one, first peak is the main peak. Amplification spectra resulted by operating both accelerograms have a clear peak at mean frequency 12.2 Hz. Mean amplification factor is 2.35.

RESULTS

Based on the results of site effect, isoacceleration, isoamplification, isofrequency and isoperiod maps of the site by applying Bojnoord accelerogram are presented. According to the maps, generally ground surface acceleration is lower at the east. Maximum acceleration, resulted from applying L component, is at north and resulted

from applying T component is at center of the site. Difference between acceleration values, is very small. Amplification factor increases from the west to the east. Minimum frequency is observed at the east and the south of the site. Generally, frequency increases from east and south to north, and period increases from north to south and east (Figs. 10—13).

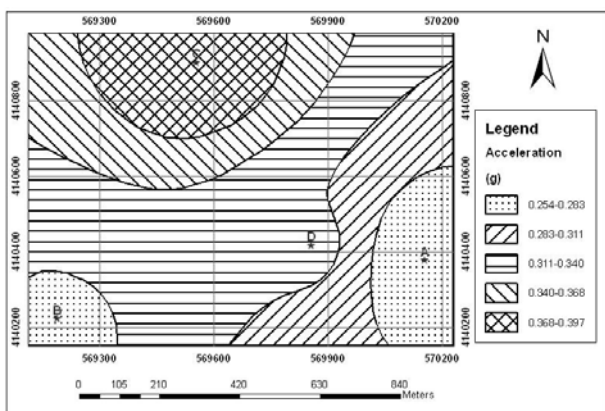


Fig. 10 Isoacceleration map of the site ground surface resulted by applying L component of Bojnoord accelerogram

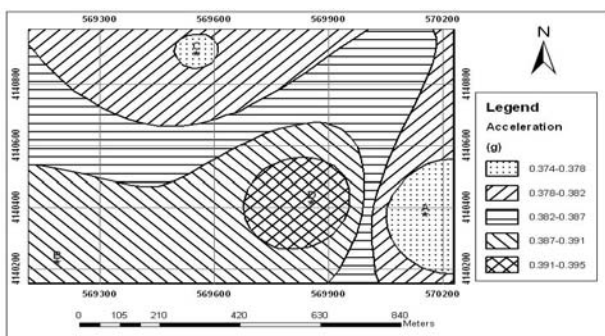


Fig. 11 Isoacceleration map of the site ground surface resulted by applying T component of Bojnoord accelerogram

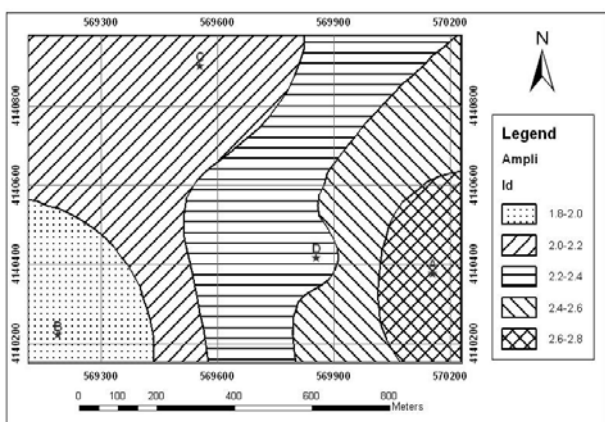


Fig. 12 Isoamplification map of the site ground surface resulted by applying L component of Bojnoord accelerogram

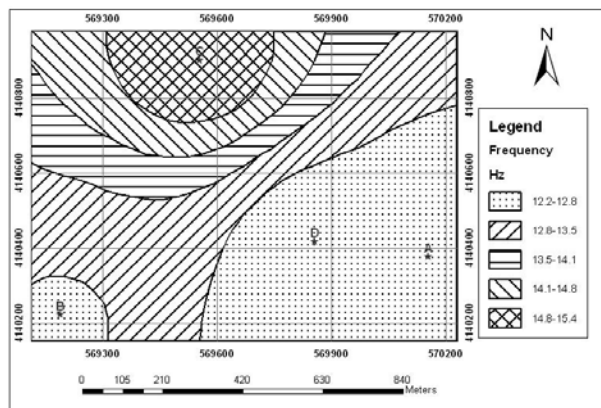


Fig. 13 Isofrequency map of the site ground surface resulted by applying L component of Bojnoord accelerogram

CONCLUSIONS

The ground of the site classified (Table 11) based on Iranian Code of Practice for Seismic Resistant Design of Buildings, standard 2800 (Table 10). Mean results in all boreholes compare with their ground type based on standard 2800 and presented in Table 12. According to

Table 10 Ground classification of Iran standard 2800 (Iran Building and Housing Research Center, 2005)

Ground type	Deposits description	V_s^{30} (m/s)
I	a) Igneous rocks (with fine and coarse texture), hard and very competent sedimentary rocks and massive metamorphism rocks and Conglomerate beds.	More than 750
	b) hard soil (dense Gravel and Sand, very hard Clay) with thickness less than 30 m.	$750 > V_s \geq 375$
II	a) loose igneous rocks (such as Tuff), loose sedimentary rocks, foliated metamorphism rocks and generally all rocks that are loosened under weathering and foliation (declare and destroy) situation.	$750 > V_s \geq 375$
	b) hard soils (dense Gravel, Sand, very hard Clay) with thickness more than 30 m.	$750 > V_s \geq 375$
III	a) weathered rocks	$375 > V_s \geq 175$
	b) moderate dense soils, Gravel and Sand with intergranular connection and moderate dense Clay.	$375 > V_s \geq 175$
IV	a) soft deposits with high moisture because of high elevation of ground water surface.	
	b) any soil profile including minimum 6 m Clay with plastic index more than 20% and moisture more than 40%.	Less than 175

Table 11 Ground type of the site based on Iran Standard 2800

Class	Thickness(M)	Vs30 _(m/s)	Y	X	ID
Ib	34	462.75	4140378	570155	A
Ib	30	496.47	4140223	569190	B
Ib	30	491.75	4140902	569555	C
Ib	36	423.03	4140418	569857	D

Table 12 Comparing mean results in boreholes with their ground type gained by Iran standard 2800

borehole	Ground surface acceleration (g)	Amplification factor	Amplification frequency	Amplification period	Ground type (Standard 2800)
A	0.367	2.85	11.8	0.085	Ib
B	0.366	1.86	12.5	0.080	Ib
C	0.429	2.16	14.6	0.069	Ib
D	0.389	2.35	12.2	0.083	Ib

the mean results, the results of all boreholes are very similar, that is because of similarity of their properties.

Acceleration values in boreholes are very similar and are accommodated with their ground type, except borehole C (B (Ib) < A (Ib) < D (Ib)). Borehole A and then D have maximum amplification, that they have ground type Ib. Maximum frequency is in borehole C (Ib) and minimum value is in borehole A (Ib). Amplification frequency and period values are reliable according to the ground type of standard 2800.

REFERENCES

- Adib A, et al. (2008). Shirvan seismic zonation report, Zaminkav research Group, reports of seismic geotechnic microzonation of Shirvan.
- Ambraseys NN & Melville CP (1982). A History of Persian Earthquakes, Cambridge Univ. Press, New York.
- Iran Building and Housing Research Center (2005). Iranian Code of Practice for Seismic Resistant Design of Buildings, standard 2800, 3rd Ed, BHHRC, Tehran.
- Ishibashi I (1992). Discussion to Effect of soil plasticity on cyclic response, by M. Vucetic and R. Dobry, Journal of Geotechnical Engineering, 118(5): 830-832.
- Ishibashi I & Zhang X (1993). Unified dynamic shear moduli and damping ratios of sand and clay, Soils and Foundations, 33(1): 182-191.
- Jafarian MB(2005) Geology map of Shivan, sheet 1:100000, Geological Survey of Iran.
- Kramer SL (1996). Geotechnical Earthquake Engineering, Prentice Hall, Upper Saddle River, New Jersey, 653.
- Seed HB, Wong RT, Idriss IM, Tokimatsu K (1986). Moduli and damping factors for dynamic analyses of cohesionless soils, Journal of Geotechnical Engineering, ASCE, 112(11): 1016-1032.
- Vucetic M & Dobry R (1991). Effect of soil plasticity on cyclic response, Journal of Geotechnical Engineering, ASCE, 117(1): 89-107.

DATA DIVISION METHOD OF SAND LIQUEFACTION SAMPLES BASED ON SELF-ORGANIZING MAPS

Si-Si LIU¹ and Ming-Hua ZHAO²

ABSTRACT: To some extent, artificial neural networks (ANNs) had been successfully applied to the classification of sand liquefaction. In majority of which, data division was carried out on an arbitrary basis. However, the way on how data were divided may have a significant effect on model performance. In this paper, data division and its impact on ANN model were investigated through evaluating the possibility of sand liquefaction on condition of shallow foundations. And a new data division method was investigated: data division using self-organizing maps (SOMs). Results indicated that a statistical property of data in training, testing, and validation sets needs to be taken into account for ensuring optimal model performance. Obviously, the SOM clustering method was suitable for data division.

KEYWORDS: sand liquefaction; seismic settlement evaluation; neural network; self-organizing map; back propagation

INTRODUCTION

Seismic settlement of foundation soil was one of the main causes of foundation failure that had done great harm to building structures. Three reasons may cause foundation failures: (1) settlement caused by nonsaturated sandy soil seismic desiccation (2) seismic settlement of saturated sand liquefaction, (3) soft soil plastic deformation. To building construction, if there exists no earthslide dangers caused by sites lateral spreading, main seismic damages caused by sand liquefaction were excessive settlement of buildings. Therefore, as predicting on static settlement values, predictions of sand liquefaction settlement values on different conditions were important evidences for finding anti-seismic measures.

Neural networks (NNs) (Zurada 1992; Fausett 1994) was a kind of artificial intelligence that named by its network structures were similar with human brain's. The NNs was learning from samples, then mapping relationships between inputting data and outputting data could be found. Similarity between neural networks and traditional statistical model lied in that model parameters were adjusted to such a state that output error minimizations between measuring data and network data could be obtained. Different from traditional model, the NNs contained a large number of parameters, therefore over-fitting could be generated especially when learning data had noises. Cross validation method (Stone 1974) was usually used to avoid over-fitting in the NNs, in which data were divided into 3 subsets: training subset, testing subset, and validating subset. Training subset was

used to adjust connecting right value. Testing subset was applied to test networks prosperities in different stages and stop networks learning when error increased. Validating subset was taken to evaluate model prosperities when training finished. Cross validation method was usually considered to be the most effective method in avoiding network's over-fitting (Smith 1993).

As an effective predicting method, the NNs had been successfully used in geotechnical engineering, for which had capabilities of nonlinear mapping between inputting and outputting. When the NNs were used in engineering prediction, data based on random selection were divided into training subset, testing subset, and validating subset. However, recent researches showed that data division method had great effect on network calculating results (Tokar and Johnson 1999). Generally believed that properties of the NNs were the most reliable method when only samples had extrapolating calculation extreme values were used (Minns and Hall 1996; Tokar and Johnson 1999). Therefore, training, testing and validating subsets should have similar statistical properties in order to obtain better network properties (Masters 1993).

This paper discussed clustering analysis of sand liquefaction sample by self-organizing neural network, including three parts:

1. Introduced clustering analysis methods of learning sample based on SOM network
2. Discussed statistical properties contained in clustering results
3. Compared network calculating results by using random data division with the above results

¹ Research Student (Ph.D), College of Civil Engineering, Hunan University, Changsha, 410082, China. Email: liusi1949@sina.com

² Professor, College of Civil Engineering, Hunan University, Changsha, 410082, China. Email: mhzhaohd@21cn.com

SELF-ORGANIZING MAP

The self-organizing map (SOM) algorithm by Kohonen was a method for creating a topologically correct nonlinear projection of a high dimensional data set onto a prototype grid of lower dimensionality. The SOM was typically used to discover groups of similar patterns by transforming a large amount of data into a simple visual presentation.

Competitive Process

Let m denote the dimension of input data. Let an input vector selected at random from the input space be denoted by

$$X = [x_1, x_2, \dots, x_m] \tag{1}$$

Each of the SOM nodes was associated with a m -dimensional weight vector W which defined the neuron as a point in the input space R^m .

$$W_j = [w_{j1}, w_{j2}, \dots, w_{jm}]^T, \quad j = 1, 2, \dots, l \tag{2}$$

where l was the number of neurons in the network.

In this study, given an assumption that the same threshold value was applied to all the neurons, the threshold was the negative of bias. Furthermore, through finding the neuron with the largest inner product $W_j^T X$ to determined the location where the topological neighborhood of excited neurons was to be centered.

In mathematical sense, the maximal inner product $W_j^T X$ was equivalent to the minimal Euclidian distance between vector X and W_j . The best matching unit $i(x)$ was

$$i(x) = \arg \min_j \|x - w_j\|, \quad j = 1, 2, \dots, l \tag{3}$$

Cooperative Process

Let $h_{j,i}$ denote the topological neighborhood centered on winning neuron i , let $d_{i,j}$ denote the lateral distance between winning neuron i and excited neuron j . Then gave an assumption that the topological neighborhood $h_{j,i}$ was a unimodal function of the lateral distance $d_{i,j}$, such that it satisfied 3 distinct requirements:

- (1) $h_{j,i}$ = maximum, when $d_{i,j} = 0$;
- (2) $h_{j,i}$ monotone decreased, when absolute value of $d_{i,j}$ increased.
- (3) $h_{j,i} = 0$, when $d_{i,j} \rightarrow \infty$.

Using Gaussian function to satisfying these requirements mentioned above:

$$h_{j,i} = \exp\left(-\frac{d_{i,j}^2}{2\sigma^2}\right) \tag{4}$$

where σ was the width of $h_{j,i}$ which decrease with time

goes. Using an exponential function to describe this decay process:

$$\sigma(n) = \sigma_0 \exp\left(-\frac{n}{\tau_1}\right), \quad n = 1, 2, \dots, \tag{5}$$

where σ_0 was the initial value of σ , τ_1 was the time constant. Then the Eq. (4) became

$$h_{j,i}(n) = \exp\left(-\frac{d_{i,j}^2}{2\sigma(n)^2}\right), \quad n = 1, 2, \dots, \tag{6}$$

Adaptive Process

In Kohonen model, weight vector of neuron i in network could be expressed as follows:

$$\Delta w_j = \eta y_i x_j - g(y_j) w_j \tag{7}$$

where η was learning-rate parameter of the algorithm; $g(y_j)$ was the positive scalar function of response y_j ; w_j is the weight vector of neuron j .

$g(y_j)$ was set to be a linear function in order to simplified calculation, as shown by

$$g(y) = \eta y \tag{8}$$

$$\text{Let } y_i = h_{j,i} \tag{9}$$

Using Eqs. 7&8 in Eq.9, obtain

$$\Delta w_j = \eta h_{j,i} (x_j - w_j) \tag{10}$$

So, the updated weight vector $w_j(n+1)$ at time $n+1$ was defined by:

$$w_j(n+1) = w_j(n) + \eta(n) h_{j,i}(n) (x_j - w_j(n)) \tag{11}$$

To obtain a better network performance, learning-rate parameter function $\eta(n)$ could be set as time varying formal. The same as $h_{j,i}$, beginning with initial value η_0 , and then, $\eta(n)$ decreased gradually with increasing time n . So, $\eta(n)$ was set as a exponential function, as shown by

$$\eta(n) = \eta_0 \exp\left(-\frac{n}{\tau_2}\right), \quad n = 1, 2, \dots, \tag{12}$$

where τ_2 was another time constant of the SOM algorithm.

DATA COLLECTION AND NORMALIZATION

Data in this paper sourced from 61 groups of various building foundation seismic settlement examples, collected by Chen Guoxing (2008). And these seismic settlement data come from Niigata earthquake in Japan, Haicheng earthquake and Tangshan earthquake in China.

Details of the range of values for these records were summarized in Table 1. These data would also be used in training and testing the BP network. Because the output neuron of BP network was the ratio of earthquake-induced settlement to liquefaction soil depth, the data for using in cluster analysis by SOM network included earthquake intensity for describing earthquake ground

motion characteristics, average pressure of foundation base, foundation type, ratio of liquefaction soil depth to width of foundation, ratio between length and height of building for describing building characteristics, relative density of sand, non-liquefaction soil thickness covered above and underground water level for describing ground characteristics.

Table 1 Data Ranges Used for Developing Artificial Neural Network Models

Model variables	Mean	Standard deviation	Minimum	Maximum
Earthquake intensity, I	7.951	0.717	7	10
Foundation type, T	1.967	0.793	1	4
Ratio between length and height of building, L/H	2.843	1.162	0.7	6.8
Average pressure of foundation base, p (kPa)	79.944	26.844	18	160
Ratio of liquefaction soil depth to width of foundation, B_D	1.103	0.492	0.14	2.75
Relative density of sand, D_r	0.530	0.063	0.36	0.65
Non-liquefaction soil thickness covered above, D_n (m)	7.752	2.455	1.6	14
Underground water level, d_w (m)	1.707	0.861	0.4	4.1
Ratio of earthquake-induced settlement to liquefaction soil depth, s/D_1	0.069	0.042	0	0.239

Data Normalization

To improve training, preprocessing of the data to values between 0-1 was carried out before presenting the patterns to the SOM network. The following normalization procedure (Masters 1993) was used.

For a variable with maximum and minimum values of V_{max} and V_{min} respectively, each value, V , was scaled to its normalized value, A , using

$$A = (V - V_{min}) / (V_{max} - V_{min}) \quad (13)$$

CLUSTERING ANALYSIS OF SEISMIC SETTLEMENT LIQUEFACTION SAMPLE BY SOM

SOM network equipments in NeuroShell 2 (Ward Systems Group 1993-1998) were used to analyze Sand liquefaction Sample. According to Forte and Pages (1995, 1997), SOM neural network would converge to a unique state on condition of one-dimensional grid that ensured

determinism and repeatability of clustering analysis results. 61 groups of pile sample were classified as 4 types to ensure enough samples in each cluster, so there were also 4 output neurons. Learning ratio function was set to be $\eta_0=0.1$, then decreases gradually. To guarantee better statistical precision, $\eta(n)$ must be a minor value but more than 0.01 to escape metastable state. SOM network was converged after 3000 iteration.

8 input modules were included in the SOM network, and they were earthquake intensity, foundation type, ratio between length and height of building, average pressure of foundation base, ratio of liquefaction soil depth to width of foundation, relative density of sand, non-liquefaction soil thickness covered above, underground water level. As far as foundation sample to be measured, ratio of earthquake-induced settlement to liquefaction soil depth was unknown. Therefore, it was not included in input modules in clustering analysis. Results of clustering analysis on seismic settlement liquefaction sample by SOM were listed in Table 2.

Table 2 Input and Output Statistics Obtained Using Self-Organized Map

Model variables and data sets	Statistical parameters				
	Mean	Standard deviation	Minimum	Maximum	Range
Earthquake intensity, I					
Training set	8.111	0.716	7	10	3
Testing set	7.750	0.750	7	9	2
Validation set	7.250	0.775	7	8	1
Foundation type, T					
Training set	2.000	0.856	1	4	3
Testing set	1.875	0.875	1	4	3
Validation set	1.875	0.875	1	3	2
Ratio between length and height of building, L/H					
Training set	2.927	1.039	1.1	5.8	4.7
Testing set	3.213	1.588	0.9	5.2	4.3
Validation set	2.800	0.950	1.0	5.3	4.3
Average pressure of foundation base, p (kPa)					
Training set	80.69 3	20.663	30.0	160	130.0
Testing set	73.73 8	18.828	31.2	150	118.8
Validation set	81.93 8	19.797	34.2	155	120.8
Ratio of liquefaction soil depth to width of foundation, B_D					
Training set	1.099	0.562	0.27	2.75	2.48
Testing set	0.771	0.541	0.25	2.55	2.30
Validation set	0.898	0.521	0.24	2.35	2.11
Relative density of sand, D_r					
Training set	0.526	0.064	0.36	0.65	0.29
Testing set	0.554	0.060	0.46	0.65	0.19
Validation set	0.524	0.055	0.45	0.60	0.15
Non-liquefaction soil thickness covered above, D_n (m)					
Training set	7.811	2.506	2.6	14.0	11.4
Testing set	8.350	2.600	2.5	12.0	9.5
Validation set	8.125	2.619	2.8	13.4	10.6
Underground water level, d_w (m)					
Training set	1.644	1.215	0.4	4.1	3.7
Testing set	1.625	1.250	0.5	4.0	3.5
Validation set	1.638	1.172	0.4	3.8	3.4

NEURAL NETWORK PREDICTION ON SEISMIC SETTLEMENT LIQUEFACTION

In order to validate that better predicting properties could be obtained by using SOM network in data division, back propagation (BP) network was applied twice in calculating seismic settlement samples in this paper. In addition, these two BP models had the same initial settings. The input data to the BP network consisted of 8 impact factors. It required an input layer of 8 neurons. For the problem described herein, a single hidden layer consisting of 12 neurons had been adopted.

The output information was only ratio of earthquake-induced settlement to liquefaction soil depth, so the out layer consisting of 1 neuron was required. And initial weight was 0.3, and learning ratio was 0.1.

Firstly, training data, testing data and validating data were selected by random sample selection method, and according calculating results of validating data were recognized as BP1. Secondly, SOM network clustering method was applied in data division, and according calculating results of BP networks were recognized as BP2. At last, calculating results from BP1 and BP2 validating data were compared and listed in Fig.1.

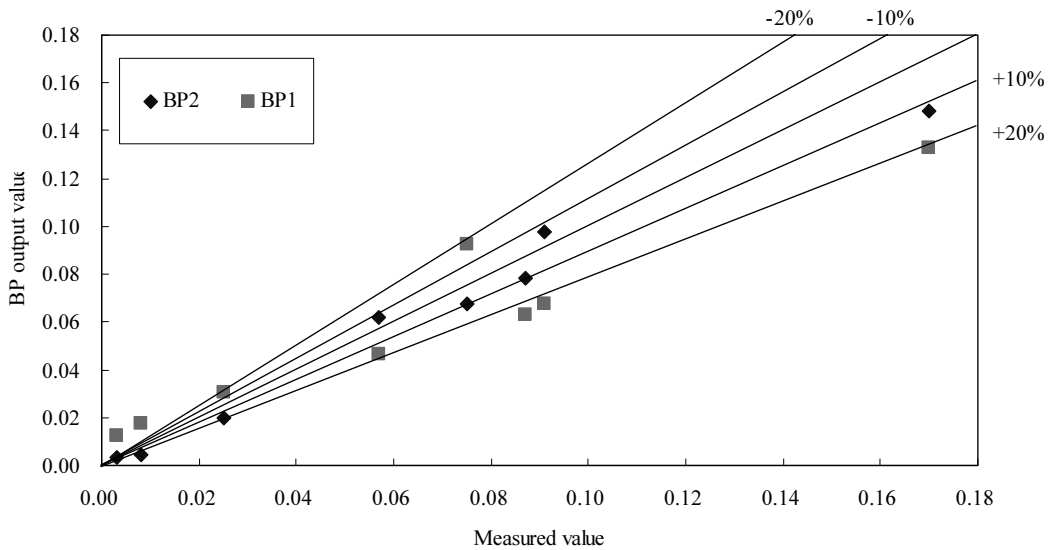


Fig. 1 Comparison of computed (BP2&BP1) and measured value

The BP network output and the measured value were compared in Fig.1. Correlation coefficients of the network were listed in Table 3. It suggested that most of the predicted values were lying within $\pm 20\%$ error from the line of perfect agreement with BP1, and most of the predicted values were lying within $\pm 10\%$ error from the line of perfect agreement with BP2.

Table 3 Correlation coefficients of BP1 and BP2

Performance measures	BP1	BP2
Correlation coefficient r	0.8771	0.9473

CONCLUSIONS

Data division by SOM networks was discussed in this paper, and its calculating results were also compared with that of traditional random selection method. When data were divided into training, testing and validating subsets, each one's statistical properties had great effect on calculating results. Training, testing and validating

subsets would represent similar statistical properties when one-dimensional SOM network was used in sample clustering analysis, and better network results could be obtained by using learning subset having similar statistical properties. As one of seismic settlement prediction methods, method used in this paper could deduce comparatively accurate predicting results and provide related auxiliary in formations for engineering practice.

REFERENCES

Kohonen T (2001). Self-organizing Maps, Springer-Verlag, Berlin.
 Goser K (1997). Self-organizing map for intelligent process control, in Proceedings of WSOM'97, Workshop on Self-Organizing Maps, Espoo, Finland, June 4-6, Helsinki University of Technology, Neural Networks Research Centre, Espoo, Finland: 75-79.
 Cigizoglu HK (2005). Application of generalized regression neural networks to intermittent flow forecasting and estimation. J. Hydrol. Eng., 10(4):

- 336-341.
- Kurup PU & Griffin EP (2006). Prediction of soil composition from cpt data using general regression neural network. *J. Comput. Civ. Eng.*, 20(4): 281-289.
- Lok TMH & Che WF (2004). Axial capacity prediction for driven piles using ann: Model comparison. *Geotrans 2004, Geotechnical Engineering for Transportation Projects (GSP No. 126)*, M. K. Yegian and E. Kavazanjian, eds.
- Middendrop P (2004) Thirty years of experience with the wave equation solution based on the method of characteristics. *7th Int. Conf. on the Application of Stress Wave Theory to Piles*.
- Pal M & Goel A (2006). Prediction of the end depth ratio and discharge in semicircular and circular shaped channels using support vector machines. *Flow Meas. Instrum.*, 17(1): 50-57.
- Pal M (2006). Support vector machines-based modeling of seismic liquefaction potential. *Int. J. Numer. Analyt. Meth. Geotech.*, 30(10): 983-996.
- Feng ZL, Sun HT, Wang SJ (1999). Prediction of vertical ultimate bearing capacity of single pile by using artificial neural networks. *Journal of Tongji University*. 27(4): 397-401.
- Ahmad I & Akhtar NK (2006). Kinematic seismic response of piles-importance and modeling. *GeoCongress 2006, Geotechnical Engineering in the information Technology Age*.
- Che WF (2003). Axial bearing capacity prediction of driven piles using artificial neural network. M.S. Thesis, FST, University of Macau.
- Chen GX & Li FM (2008). Seismic settlement estimation of sand liquefaction based on RBF neural network model. *Journal of Natural Disasters*. 17(1): 180-185.

GOM-SVM PREDICTOR FOR LAND SUBSIDENCE AT FINISHED UNDERGROUND MINING

Zheng-Wen XIE^{1, 2} and Xiao-Yu LIANG³

ABSTRACT: Underground mining is one of the causes of land subsidence. The process of the land subsidence caused by underground mining is complicated and systematicness. Accurate prediction the land subsidence has important practical or immediate significance to avoid the harm of land subsidence. Grey system theory was applied extensively and had gained a series of achievements in land subsidence prediction, but our preliminary study showed that the general GM(1,1) model was inadequate to handle prediction as its only adapt to the data with exponential law. The advantages and disadvantages of general GM (1, 1) model and support vector machine (SVM) are analyzed respectively. A new land subsidence forecasting model based on GOM (1, 1) and SVM model was put forward. The new model develops the advantages of accumulation generation in the grey forecasting method, weakens the effect of stochastic disturbing factors in original sequence, strengthens the regularity of data, and avoids the theoretical defects existing in the grey forecasting model. The advantage of support vector machine which can fit nonlinearity time series data efficiently was also used. The example shows that the prediction accuracy has been improved quite a lot in comparison with general grey model.

KEY WORDS: land subsidence, underground mining, GOM (1, 1), SVM, prediction

INTRODUCTION

Land subsidence is an environmental geology phenomenon that the land surface elevation falls down due to ground compression. It is a slow movement and it may break the pipelines and subsidize and/or tilt the buildings in the affected area. The causes of land subsidence include natural factors and human activities. The natural factors are the collapsing of the loess, the drainage consolidation of the organic soils, the development of mining activities, compression of the sediments, and so on. The human activities consist of the underground construction and the withdrawal of liquid and/or solid from the underground. Prediction of the land subsidence is very important for our environment. Many researchers developed the land subsidence prediction methods, 'Regression Analysis' (Moghaddas, 2008), 'FEM' (Suzuki, 1994), 'Grey Theory' (Nichol, 1998; Xie, 2005), 'Neural Network' (Kim, 2008; Kerh, Hu, 2003), etc. Grey theory is one of the most widely used methods. Grey theory, developed originally by Deng, is a truly multidisciplinary and generic theory that deals with systems that are characterized by poor information and/or for which information is lacking. The fields

covered by grey theory include systems analysis, data processing, modeling, prediction, decision making and control. Grey forecasting models have been extensively used in many applications, and it was improved by many researchers (Dong, 2008; Zhang, 2002).

The advantages and disadvantages of grey forecasting methods (Guo, 2001; Zhou, 2002) and support vector machine(SVM)(Xie,2007)were analyzed respectively, an new land subsidence forecasting model GOM-SVM predictor which combined with grey theory and support vector machine technology was put forward in the purpose of improve the prediction accuracy.

GREY PREDICTION MODEL

Deng proposed Grey theory to deal with indeterminate and incomplete systems (Deng, 1982) Unlike conventional stochastic forecasting theory, Grey theory simply needs few sample data inputs to construct a Grey model. Since the poor regularity for the tested land subsidence data, the *AGO* technique in Grey forecasting is suitable to reduce the randomization of the raw data efficiently. Generally, the procedure for *GM* (1, 1) forecasting is

¹ Lecturer, Safety and Environment Institute, China Jiliang University, China. Email: xiezhengwen@cjlu.edu.cn

² Ph.D Student, School of Resources and Safety Engineering, Central South University, China.

³ Lecturer, Safety and Environment Institute, China Jiliang University, China.

explained as follows:

Denote the original data sequence by

$$x = \{x(1), x(2), \dots, x(n)\} \tag{1}$$

where n is the number of data observed.

The AGO formation of $x^{(0)}$ is defined as:

$$X = \{X(1), X(2), \dots, X(n)\} \tag{2}$$

where $X(1) = x(1)$,

$$\text{and } X(k) = \sum_{i=1}^k X(i), k=1, 2, 3, \dots, n \tag{3}$$

The GM(1, 1) model can be constructed by establishing a first order differential equation for $X(k)$ as:

$$dX(k)/dk + aX(k) = b \tag{4}$$

Therefore, the solution of Equation (4) can be obtained by using the least square method. That is,

$$\hat{X}(k) = \left[X(1) - \frac{b}{a} \right] e^{-ak} + \frac{b}{a} \tag{5}$$

$$\text{where } [a \ b] = (B \ B)^{-1} X \tag{6}$$

And

$$B = \begin{bmatrix} -Z(2) & 1 \\ -Z(3) & 1 \\ \dots & \dots \\ -Z(n) & 1 \end{bmatrix} \tag{7}$$

where

$$Z(k) = \alpha X(k) + [1 - \alpha] X(k-1) \tag{8}$$

$$X_n = [x(2), x(3), \dots, x(n)] \tag{9}$$

We obtained $\hat{x}^{(1)}$ from Equation (5). Let $\hat{x}^{(0)}$ be the fitted and predicted series,

$$\hat{x} = (x(1), x(2), \dots, x(n), \dots) \tag{10}$$

where $\hat{x}(1) = x(1)$

$$\hat{X}(k) = (1 - e^{-ak}) \left[X(1) - \frac{b}{a} \right] e^{-ak} + \frac{b}{a} \tag{11}$$

where $\hat{x}(1), \hat{x}(2), \dots, \hat{x}(n)$ are called the GM(1, 1) fitted sequence, while $\hat{x}(n+1), \hat{x}(n+2), \dots$ are called the GM(1, 1) forecast values.

Support Vector Machines

The SVM proposed by Vapnik. The time-series

problems can be brought down to support vector regression (SVR) problems. Suppose that we are given a set of observation data (samples) $(X, y), (X_2, y_2), (X_k, y_k), X \in R, y \in R$. For the regression problem based on the SVM, our goal is to find a linear function $f(X) = w \cdot X + b$ that has at most ϵ deviations from the actually obtained targets y for all the training data, and is also as flat as possible.

We describe the linear function f , in the form

$$f(X) = w \cdot X + b \tag{12}$$

One way to ensure this is to minimize the squared Euclidean norm, i.e. $\|w\|^2$. Formally we can write this problem as a convex optimization problem by requiring:

$$\begin{aligned} &\text{minimize } \frac{1}{2} \|w\|^2 \\ &\text{subject to } \begin{cases} y - w \cdot X - b \leq \epsilon \\ w \cdot X + b - y \leq \epsilon \end{cases} \quad i=1, 2, \dots, n \end{aligned} \tag{13}$$

According to statistics learning theory, we want to obtain the optimal generalization. Allowing for some errors, we can introduce the slack variables $\xi \geq 0$ and $\xi^* \geq 0$. Hence we arrive at the following:

$$\begin{aligned} &\text{minimize } \frac{1}{2} \|w\|^2 + C \sum_{i=1}^k (\xi + \xi^*) \\ &\text{subject to } \begin{cases} y - w \cdot X - b \leq \epsilon + \xi \\ w \cdot X + b - y \leq \epsilon + \xi^* \end{cases} \quad i=1, 2, \dots, n \end{aligned} \tag{14}$$

The constant $C > 0$ determines the tradeoff between the flatness off and the amount up to which deviations big r than e is tolerated. Using the optimal method, we can obtain the dual optimization problem, maximize

$$\begin{aligned} W(\alpha, \alpha^*) = &-\frac{1}{2} \sum_{i=1}^k (\alpha - \alpha^*)(\alpha - \alpha^*)(X, X) \\ &+ \sum_{i=1}^k y(\alpha - \alpha^*) - \epsilon \sum_{i=1}^k (\alpha + \alpha^*) \end{aligned} \tag{15}$$

$$\text{subject to } \begin{cases} \sum_{i=1}^k (\alpha - \alpha^*) = 0 \\ 0 \leq \alpha, \alpha^* \leq C, i=1, 2, \dots, n \end{cases} \tag{16}$$

Solving the above optimal problems, we can obtain the regression function of the SVM.

$$f(X) = \sum_{i=1}^k (X \cdot X_i) + b \tag{17}$$

Based on the Karush–Kuhn–Tucker (KKT) conditions for quadratic programming, only a small number of

coefficients $(\alpha - \alpha^*)$ will be assumed to have nonzero values, and their data points could be referred to as support vectors (Pijush S, 2008).

We can solve the nonlinear problems by mapping the data into a high feature dimension space. In high feature dimension space, the inner product can be replaced by the kernel function, i.e. $K(X, X') = \phi(X)\phi(X')$, we do not need to know the specific formulation of the nonlinear mapping ϕ . So Eqs. (14)– (16) can be changed into the following formulation:

$$\text{Maximize } W(\alpha, \alpha^*) = -\frac{1}{2} \sum_{i=1}^n (\alpha - \alpha^*)(\alpha - \alpha^*)K(X_i, X_i) + \sum_{i=1}^n y_i(\alpha - \alpha^*) - \varepsilon \sum_{i=1}^n (\alpha + \alpha^*) \tag{18}$$

$$\text{subject to } \begin{cases} \sum_{i=1}^n (\alpha - \alpha^*) = 0 \\ 0 \leq \alpha, \alpha^* \leq C, i = 1, 2, \dots, n \end{cases} \tag{19}$$

$$f(X) = \sum_{i=1}^n (\alpha - \alpha^*)K(X, X_i) + b \tag{20}$$

The following is three general kernel functions:

(1) Polynomial kernel

$$K(X, Y) = ((X \cdot Y) + 1)^d, d = 1, 2, \dots, n \tag{21}$$

(2) Radial kernel

$$K(X, Y) = \exp\left\{-\frac{|X - Y|^2}{\sigma^2}\right\} \tag{22}$$

(3) Sigmoid kernel

$$K(X, Y) = \tanh(\phi(X \cdot Y) + \theta) \tag{23}$$

We can solve the quadratic optimal problem of Eqs.(15), (16), (18), and (19) by a variety of methods, including the interior point algorithm, the sequential minimal optimization, and decompression algorithms, etc.

GOM-SVM Model for Fire Prediction

Combined grey theory prediction method with support vector machine is a new prediction method. First use the opposite direction accumulated generating operation (OD-AGO) technique to identify the systematic regularity of the original time series data. Using the opposite direction accumulated generating operation technique efficiently reduces noise in the discrete time series data by converting ambiguous original time-series data to a monotonically increased series. Then the advantage of support vector machine which can fit no linearity time series data efficiently is use to establish prediction model.

Finally the Inverse opposite direction accumulated generating operation (OD-I-AGO) technique is used to get the prediction results. The arithmetic design as follow:

Step 1. Denote the original data sequence by

$$x = \{x(1), x(2), \dots, x(n)\} \tag{24}$$

where n is the number of data observed.

Step 2. The λ ($0 < \lambda < 1$) exponent formation of x is defined as:

$$x' = \{(x(1))^\lambda, (x(2))^\lambda, \dots, (x(n))^\lambda\} \\ (x(i))^\lambda > 0, i = 1, 2, \dots, n \tag{25}$$

Step 3. The opposite direction AGO formation of x' is defined as:

$$x = \{x(1), x(2), \dots, x(n)\} \tag{26}$$

$$\text{while } x(k) = \sum_{i=1}^k x(i), k = 1, 2, \dots, n$$

Step 4. Choose $K(X, X')$

Step 5. Solve optimize result (15), (16), use support vector machine, and find the support vector $X, i = 1, 2, \dots, N$;

Step 6. Construct function

$$f(X) = \sum (\bar{\alpha}^* - \bar{\alpha})K(X, X_i) + \bar{b}; \tag{27}$$

Step 7. Calculate the OD-AGO time series data X prediction result \hat{X} ;

Step 8. Inverse opposite direction (OD-I-AGO) \hat{X}^1 , get the prediction model of the original time series data;

$$\hat{X}(k+1) = \hat{X}(k+1) - \hat{X}(k), \\ k = n+1, n+2, \dots \tag{28}$$

Step 9. The $1/\lambda$ ($0 < \lambda < 1$) exponent formation of $\hat{X}(k+1)$

Step 10. Check precision of the model.

$$MAPE = \frac{1}{n} \sum_{t=1}^n \left| \frac{y_t - \hat{y}_t}{y_t} \right| \tag{29}$$

Step 11. Turn to Step 1.

Land Subsidence Prediction

In order to show the precision of the GOM-SVM predictor, an actual example of HUNAN province is used to testify it (Xie, 2007), land subsidence date used as table 1.

The procedure for the GOM-SVM model was showed in Fig. 1

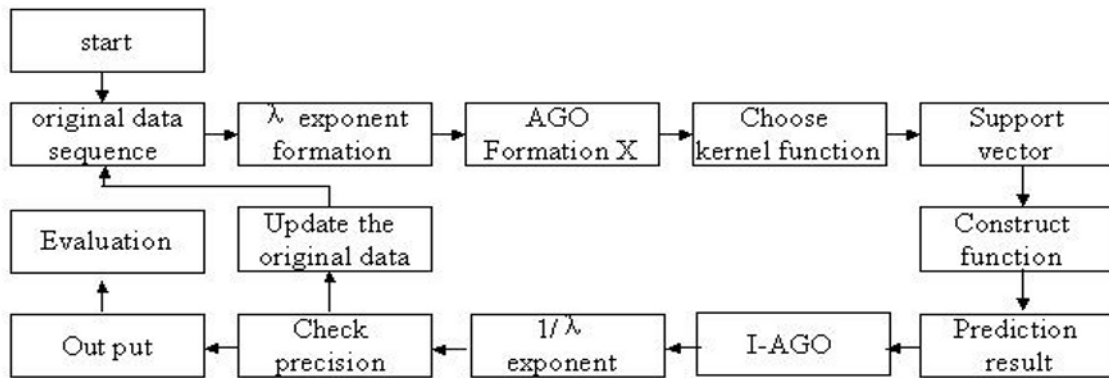


Fig. 1 Procedure for GOM-SVM model

Table 1 Land subsidence observation data

Time/d	Observation place 1				Observation place 2			
	Tested Land subsidence/mm	Time/d	Tested Land subsidence/mm	Time/d	Tested Land subsidence/mm	Time/d	Tested Land subsidence/mm	
0	630	1020	867	0	604	927	949	
51	645	1199	880	57	657	1176	963	
243	682	1387	884	191	720	1408	986	
437	816	1581	891	373	830	1784	985	
624	857	1779	893	602	870	1971	987	
831	868	1960	896	740	896	2011	990	

Choose the data of the observation place 1 between 0-1199 days and observation place 2 between 0-1176 days, the traditional GM (1, 1) model and GOM-SVM

model are put forward and the fitting results of the land subsidence are showed in Table 2, Figs. 2 and 3.

Table 2 Comparison of different fitting results with different model

time /d	Tested Land subsidence /mm	Observation place 1				Time /d	Tested Land subsidence /mm	Observation place 2			
		General Grey predictor		GOM-SVM predictor				General Grey predictor		GOM-SVM predictor	
		fitting results /mm	Relative Deviation /%	fitting results /mm	Relative Deviation /%			fitting results /mm	Relative deviation /%	fitting results /mm	Relative deviation /%
0	630	630.0	0.0	645	2.38	0	604	604.0	0.0	615.1	1.84
51	645	725.9	11.1	652	0.03	57	657	750.2	14.2	646.9	1.54
243	682	746.6	8.7	709.6	2.31	191	720	776.1	7.8	730.1	1.40
437	816	767.9	6.3	801.9	0.50	373	830	803.1	3.2	813.3	2.01
624	857	789.8	8.5	871.2	0.83	602	870	830.8	4.5	868.8	0.14
831	868	812.3	6.9	872.9	0.11	740	896	859.5	4.1	904.7	0.97
1020	867	835.5	3.8	868.9	0.80	927	949	889.3	6.3	936.5	1.32
1199	880	859.3	2.4	877.7	0.78	1176	963	920.0	4.5	960	0.31

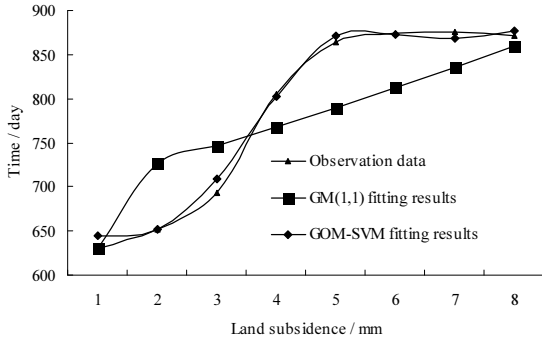


Fig. 2 Fitting results with different model (place 1)

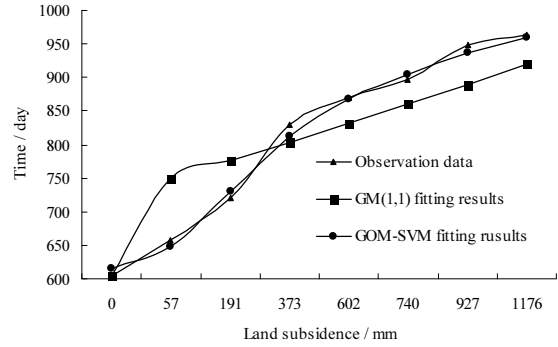


Fig. 3 Fitting results with different model (place 2)

From the Figs. 2 and 3 we can see that the new predictor GOM-SVM model have better fitting results than traditional GM (1, 1) predictor. And calculate the relative deviation of two predictor, we can found that the traditional GM (1, 1) predictor had bad fitting results, as it max relative deviation was 11.1% and 14.2% in place 1 and 2, fitting results turn to be invalidation. The

GOM-SVM predictor’s max relative deviation was 2.38% and 2.01% in place 1 and 2, it can use for land subsidence prediction.

In virtue of the high fitting precision of the GOM-SVM predictor so we choose it predict the land subsidence between 1387—1960 days in place 1 and 1408-2011days in place 2, results showed in Table 3.

Table 3 Land subsidence prediction and detection

Observation place 1				Observation place 2			
time/d	Tested Land subsidence/mm	Predicting results/mm	Relative deviation/%	time/d	Tested Land subsidence/mm	Predicting results/mm	Relative deviation/%
1387	884	887.2	0.36	1408	986	977	0.91
1581	891	892.4	0.16	1784	985	982	0.30
1779	893	893.8	0.09	1971	987	989	0.20
1960	896	894.2	0.20	2011	990	994	0.40

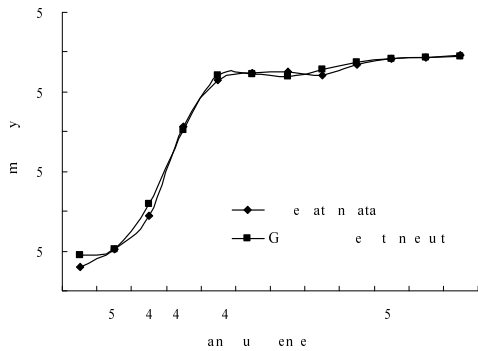


Fig. 4 Prediction results with different model (place 1)

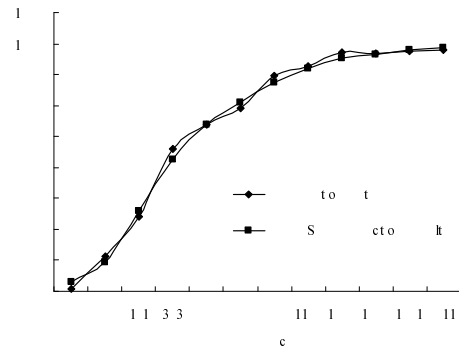


Fig. 5 Prediction results with different model (place 2)

From the Table 3, Figs. 4 and 5 we can see that the new predictor GOM-SVM model have better prediction results, the max relative deviation was only 0.91%, it’s proved to be fit for land subsidence prediction.

The actual example is showed that the improved Grey model can improve the defect.

CONCLUSIONS

The general GM (1, 1) prediction with all given data for forecasting the land subsidence proved that is far away from practical, do not reflect the system’s change.

This paper develops a GOM-SVM model to predict the land subsidence, and it can provide promising prediction results. The new model develops the advantages of accumulation generation in the grey forecasting method, weakens the effect of stochastic disturbing factors in original sequence, strengthens the regularity of data, and compared with the conventional SVM model; it can improve the convergence speed greatly. The example of Hunan province in China showed that the prediction

accuracy has been improved quite a lot in comparison with general grey model.

REFERENCES

- Moghaddas SN, Gh T, Tavakoli M (2008). The use of neural network to predict the behavior of small plastic pipes embedded in reinforced sand and surface settlement under repeated load, *Engineering Applications of Artificial Intelligence*, 6(21): 883-894.
- Suzuki M & Ishii K (1994). Parameter identification and probabilistic prediction of settlement of embankment, *Structural Safety*, 14(1): 47-59.
- Douglas N & Ian WF (1998). Settlement over peat on the A5 at Pant Dedwydd near Cerrigydrudion, North Wales, *Engineering Geology*, 50(3):299-307
- Kim YS & Kim BT (2008). Prediction of relative crest settlement of concrete-faced rockfill dams analyzed using an artificial neural network model, *Computers and Geotechnics*, 35(3): 313-322.
- Xie ZW, Hu HH, Hu YF (2005). Application of improved Grey prediction model for settlement prediction of roadbed. *rock and mechanics*, 26(S2): 227-230.
- Kerh T, Hu YG, Wu CH (2003). Estimation of consolidation settlement caused by groundwater drawdown using artificial neural networks, *Advances in Engineering Software*, 34(9): 559-568.
- Dong YF, Li YM, Lai M, Xiao MK (2008). nonlinear structural response prediction based on support vector machines. *Journal of Sound and Vibration*, 311(3): 886-897.
- Zhang DH, Jiang SF, Shi KQ (2002). Theoretical defect of grey prediction formula and its improvement. *Systems engineering theory and practice*, 8: 140-142.
- Guo HM & Ma PX (2001). Deformation of composite Htpimf. *Geotechnical Investigation and Surveying*, 1: 14-16.
- Zhou QN & Wang X (2002). The use of the gray theory in the prediction of land subsidence. *Soil Eng. and Foundation*, 16(4): 31-33.
- Deng JL (1982). *Grey system fundamental method*. Huazhong University of Science and Technology Wuhan, China.
- Xie ZW & Hu HH(2007). Improved Grey Prediction Model for Land Subsidence at Finished Underground Mining. *Proceedings of ICMHPC 2007*, Shandong: Shandong University of Science and Technology, 1000-1005.
- Pijush S (2008). Support vector machine applied to settlement of shallow foundations on cohesionless soils, *Computers and Geotechnics*, 35(3): 419-427.

A FULLY COUPLED THERMO-HYDRO-MECHANICAL MODEL FOR METHANE HYDRATE RESERVOIR SIMULATIONS

Huo-Lang FANG¹

ABSTRACT: A fully coupled thermo-hydro-mechanical model is proposed to simulate the complex performances of methane hydrate reservoirs during gas production. The model is based on the fully coupled theories of multiphase fluid flow, heat transfer and deformation in methane hydrate media. With this model, a robust numerical simulator is developed by use of the Galerkin finite element method and the hybrid Eulerian-Lagrangian approach. The simulator can consider the phase change due to hydrate dissociation, the flow of pore water and gas, the heat transfer due to convection and conduction, and the geomechanical phenomena of reservoirs such as compaction, subsidence, casing damage and wellbore stability, etc. Numerical analyses of a methane hydrate reservoir by a depressurizing well are performed by using this simulator. Results reveal some thermal and mechanical characteristics of reservoirs and also indicate the capability of the simulator in designing gas production schemes.

KEYWORDS: methane hydrate, reservoir, gas production, numerical simulation

INTRODUCTION

Methane hydrates are ice-like compounds in which methane molecules are lodged within the lattices of ice crystals under high pressure and low temperature. They mainly exist beneath the permafrost of arctic regions and below the seabed offshore. The amount of methane gas in hydrates is estimated to be much greater than all worldwide conventional gas resources. Recent discoveries of large accumulations around the world, such as the Mallik in Canada, the Nankai Trough in Japan, the North Slope of Alaska in USA and the Messoayakha gas field in Russia, have confirmed that methane hydrates may be a potential energy resource in the future.

Apart from the great energy potential of methane hydrate, there are some serious safety and environmental problems. The pre-historic landslides of some marine hydrate deposits in the world show the possibility of seafloor landslides affecting facilities and there exist the inherent challenges in drilling and producing the hydrate resource. In addition, there is a problem that disruption of hydrate deposits could release methane, a powerful greenhouse gas into the atmosphere. In order to develop methane production from hydrate under these severe environmental conditions, it is necessary to investigate in detail the physical, chemical, thermal and mechanical properties of hydrate bearing sediments and predict precisely thermo-hydro-mechanical behavior and gas production. Recently, some numerical simulators such as

the MH21-HYDRES, STOMP-HYD, CMG- STARS and TOUGH+HYDRATE (Masuda et al. 2003, Wilder et al. 2008) have been developed to evaluate gas production from hydrate. These simulators consider mainly both fluid flow and heat transfer while the solid phase is assumed to be immobile. Kimoto et al. (2007) proposed a chemo-thermo-mechanical finite element model to investigate the geomechanical effects of hydrate dissociation without considering the effect of convection in the energy conservation equation. Ng et al. (2008) developed a geomechanical model in FLAC2D code to study the wellbore stability during gas production. More recently, Rutqvist and Moridis (2008) proposed a numerical method by coupling the simulator TOUGH+HYDRATE with the geomechanical code FLAC3D and investigated the coupled thermal, hydraulic and geomechanical behaviors of hydrate deposits.

In this paper, a fully coupled thermo-hydro-mechanical model is presented to predict the complex behaviors of methane hydrate reservoirs during gas production. The model is based on the fully coupled theories of multiphase fluid flow, heat transfer and deformation in methane hydrate media. With this model, a robust numerical simulator is developed by use of the Galerkin finite element method and the hybrid Eulerian-Lagrangian approach. The simulator can consider the phase change due to hydrate dissociation, the flow of pore water and gas, the heat transfer due to convection and conduction, and the geomechanical phenomena of

¹ Fellow, Department of Civil Engineering, Zhejiang University, Hangzhou 310058, P.R. China. Email:fanghl5991@live.jp

reservoirs such as compaction, subsidence, casing damage and wellbore stability, etc. As an example, numerical analyses of a methane hydrate reservoir by a depressurizing well are carried out by use of this simulator. The distributions of pressure, temperature, and deformation in the reservoir, as well as the gas production and stress in casing are evaluated.

MODEL FORMULATION

The fully coupled thermo-hydro-mechanical model for methane hydrate simulation is derived based on the mass, energy, and momentum conservation principles in porous media, which account for the effects of multiphase flow and heat transfer, and their interaction with geomechanics. The main characteristics of the model are as follows: (1) hydrate is assumed to be an immobile substance which can make phase change from solid to fluid, (2) the flow of water and gas is governed by the two-phase mass conservation equation in which the transport is governed by Darcy's law, and the relation of relative permeability and capillary pressure is governed by the effective saturation, (3) the heat transfer is governed by the energy conservation equation including conduction and convection, and (4) the interaction between the mechanical behavior of a deforming solid matrix and fluid dynamics is governed by the equilibrium equation based on the Biot's two-phase mixture theory.

Governing Equations

Considering the effect of deformation in the solid skeleton, the water mass conservation equation is given by

$$\frac{\partial(\rho_w n S_w)}{\partial t} + \nabla \cdot (\mathbf{k} k_{rw} \rho_w / \mu_w (-\nabla p_w + \rho_w \mathbf{g})) + \rho_w n S_w \partial \varepsilon_v / \partial t = q_w \quad (1)$$

where ρ_w , S_w , k_{rw} , μ_w , p_w and q_w are the density, saturation, relative permeability, dynamic viscosity, pressure and source term for water phase, respectively, n is the porosity, ε_v is the volumetric skeleton strain, \mathbf{k} is the intrinsic hydraulic permeability tensor, \mathbf{g} is a vector for the acceleration resulting from gravity, and t is time. ρ_w and μ_w depend on pressure and temperature.

Similarly, the gas mass conservation equation is given by

$$\frac{\partial(\rho_g n S_g)}{\partial t} + \nabla \cdot (\mathbf{k} k_{rg} \rho_g / \mu_g (-\nabla p_g + \rho_g \mathbf{g})) + \rho_g n S_g \partial \varepsilon_v / \partial t = q_g \quad (2)$$

where ρ_g , S_g , k_{rg} , μ_g , p_g and q_g are the density, saturation, relative permeability, dynamic viscosity, pressure and source term for gas phase, respectively. ρ_g and μ_g depend on pressure and temperature. The supporting equation

for water and gas saturations is given by $S_w + S_g = 1$.

The hydrate mass conservation equation is given by

$$\frac{\partial(\rho_h n_0 S_h)}{\partial t} = q_h \quad (3)$$

where ρ_h , S_h and q_h are the density, saturation and source term due to hydrate dissociation for hydrate phase, respectively, and n_0 is the initial porosity.

Considering all contributions to the heat storage and flux over all phases, the energy conservation equation is given by

$$\frac{\partial(h_c(T - T_0))}{\partial t} + \nabla \cdot ((\rho_w c_w \mathbf{v}_w + \rho_g c_g \mathbf{v}_g)(T - T_0) - \lambda \nabla T) = q_T \quad (4)$$

where c_w and c_g are specific heat capacities for water and gas, respectively, \mathbf{v}_w and \mathbf{v}_g are velocities for water and gas, respectively, T is the reservoir temperature, T_0 is the reference temperature, h_c is the effective specific heat define as

$$h_c = (1 - n - n S) \rho_s c_s + n S \rho_w c_w + n S \rho_g c_g + n S \rho_h c_h \quad (5)$$

in which c_s and c_h are specific heat capacities for solid skeleton and hydrate, respectively, q_T is the heat source term, λ is the effective thermal conductivity tensor, which is written in an linear combination of the thermal conductivities for different components of the system as

$$\lambda = (1 - n - n_0 S_h) \lambda_s + n S_w \lambda_w + n S_g \lambda_g + n_0 S_h \lambda_h \quad (6)$$

in which λ_s , λ_w , λ_g and λ_h are the conductivities for solid skeleton, water, gas and hydrate, respectively.

Neglecting the inertial effects over all phases, the momentum conservation equation reduces to the static stress equilibrium as

$$\nabla \cdot (\boldsymbol{\sigma}' - \alpha p \mathbf{m}) - \rho \mathbf{g} = \mathbf{0} \quad (7)$$

where $\boldsymbol{\sigma}'$ is the effective stress tensor, p is the averaged pore pressure defined as $p = S_w p_w + S_g p_g$, α is the Biot's coefficient, \mathbf{m} is an identity vector, and ρ is the average density of the mixture defined as

$$\rho = (1 - n - n_0 S_h) \rho_s + n S_w \rho_w + n S_g \rho_g + n_0 S_h \rho_h \quad (8)$$

The relation between effective stress and strain can be given by

$$d\boldsymbol{\sigma}' = \mathbf{D}(d\boldsymbol{\varepsilon} - d\boldsymbol{\varepsilon}_p - d\boldsymbol{\varepsilon}_T) \quad (9)$$

$$d\boldsymbol{\varepsilon}_p = -dp / (3K_s) \mathbf{m} \quad (10)$$

$$d\boldsymbol{\varepsilon}_T = \beta_s / 3dT \mathbf{m} \quad (11)$$

where D is the tangent stiffness matrix, $\boldsymbol{\varepsilon}$ is the total skeletal strain vector, $\boldsymbol{\varepsilon}_p$ is the strain caused from compression of grains by internal pore pressure, $\boldsymbol{\varepsilon}_T$ is the thermal strain due to temperature changes, K_s and β_s are bulk modulus and thermal expansion coefficient for solid skeleton, respectively.

Capillary Pressure and Permeability

The capillary pressure and relative permeability are considered with the following van Genuchte model (van Genuchte 1980):

$$p_c = (S_e^{-1/m} - 1)^{(1-m)} / a \quad (12)$$

$$k_{rw} = S_e^{1/2} \left(1 - (1 - S_e^{1/m})^m \right)^2 \quad (13)$$

$$k_{rg} = (1 - S_e)^{1/3} (1 - S_e^{1/m})^{2m} \quad (14)$$

where p_c is the capillary pressure defined as $p_c = p_g - p_w$, a and m are material parameters, and S_e is the effective saturation defined as

$$S_e = (S_w - S_{wr}) / (1 - S_{gr} - S_{wr}) \quad (15)$$

where S_{wr} and S_{gr} are residual saturations of water and gas, respectively.

Change in the intrinsic permeability due to changes of hydrate saturation and porosity is accounted by the following equation:

$$k = k_0 (1 - S_h)^N \left((n - n_c) / (n_0 - n_c) \right)^N \quad (16)$$

where k is the intrinsic permeability, k_0 is the intrinsic permeability without hydrate, N and N_n are permeability reduction indexes depending on pore structure, temperature and hydrate saturation, and n_c is the reference porosity.

Kinetics of Hydrate Dissociation

The dissociation kinetics of hydrate is modeled with the following Kim-Bishoni equation (Kim et al. 1987):

$$dn_g/dt = k_d \exp(-\Delta E / (RT)) A_d n_0 S_h (f_e - f_g) \quad (17)$$

where dn_g/dt is the molar gas generation rate, k_d is the intrinsic hydration reaction constant, ΔE is the hydration activation energy, R is the universal gas constant, A_d is the specific surface area of hydrate particles, f_e and f_g are

values of gas fugacity at V-H-Lw equilibrium and for the pressure at temperature T , respectively. The fugacity is calculated by the Peng-Robison equation of state (Peng and Robison 1976). The V-H-Lw equilibrium pressure is evaluated by use of the method proposed by Sloan (1998).

The source terms for different phases due to hydrate dissociation can be given by

$$q_g = M_g dn_g / dt \quad (18)$$

$$q_w = M_w N_h q_g / M_g \quad (19)$$

$$q_h = -(M_g + M_w N_h) q_g / M_g \quad (20)$$

$$q_T = -\Delta H_d q_g / M_g \quad (21)$$

where M_g , M_w and M_h are molecular masses for gas, water and hydrate, respectively, N_h is the hydrate number, and ΔH_d is the heat of hydrate dissociation.

SPATIAL AND TEMPORAL DISCRETIZATIONS

Usually, the mass conservation equations of water and gas, and the momentum conservation equation of solid skeleton can be numerically solved by using the standard Galerkin method. But, the energy conservation equation is difficult to solve for higher Peclet number when using the standard Galerkin method. Numerical instability or strong oscillation occurs in the region of higher pressure gradient. In order to overcome this problem, the hybrid Eulerian-Lagrangian approach proposed by Yeh et al. (1992) for the energy conservation equation is used. With the standard Galerkin method and hybrid Eulerian-Lagrangian approach, the following coupled nonlinear equation can be discretized spatially as

$$\mathbf{C}\dot{\mathbf{X}} + \mathbf{K}\mathbf{X} = \mathbf{F} \quad (22)$$

where \mathbf{C} and \mathbf{K} are the corresponding matrices of governing equations, \mathbf{X} is the primary variable vector defined as displacement, water pressure, gas pressure and temperature, and \mathbf{F} is the prescribed load vector resulted from the nodal force and source or sink.

To discretize the governing equation temporally, the time differential is replaced by a finite difference formulation, resulting in the following equation:

$$\left(\mathbf{C}^{(i)} + \Delta t \boldsymbol{\theta} \mathbf{K}^{(i)} \right) \Delta \mathbf{X} = \Delta t \mathbf{C}^{(i-1)} \mathbf{X}^{(i-1)} + \Delta t \left((1 - \boldsymbol{\theta}) \mathbf{F}^{(i)} + \boldsymbol{\theta} \mathbf{F}^{(i+1)} \right) \quad (23)$$

where $\boldsymbol{\theta}$ is an integration factor which defines the required time interval, and Δ means the increment. Since

the equation is highly nonlinear, the solution is obtained by using iterative procedures such as the Picard method or the Newton-Raphson method.

EXAMPLE OF SIMULATION

The simulator described above is used to investigate the performances of methane hydrate reservoirs during depressurization. An idealized cylindrical volumetric methane hydrate reservoir with 10 m thick stratified sediments of the alternating sand with hydrate and clay without hydrate layers is considered as shown in Fig. 1. The upper layer from the sea bottom to the surface of the hydrate layer is 200 m thick, and the lower layer extends to a great depth. The upper and lower layers are clay deposits without hydrate. The water depth at the sea bottom is 620 m. The reservoir has a single well with casing and cement at the center and is modeled by a two-dimensional radial model. The finite element model for simulation is 30 m in thickness and 100 m in radius, where the thickness of each layer is same. The schematic of casing and cement is shown in Fig. 1. In general, shear force along the interface between cement and sediment or between casing and cement may cause relative displacement. Because shear strength between cement and casing is much higher than that between cement and sediment, slippage is assumed to occur only along the interface between cement and sediment where interface element is used.

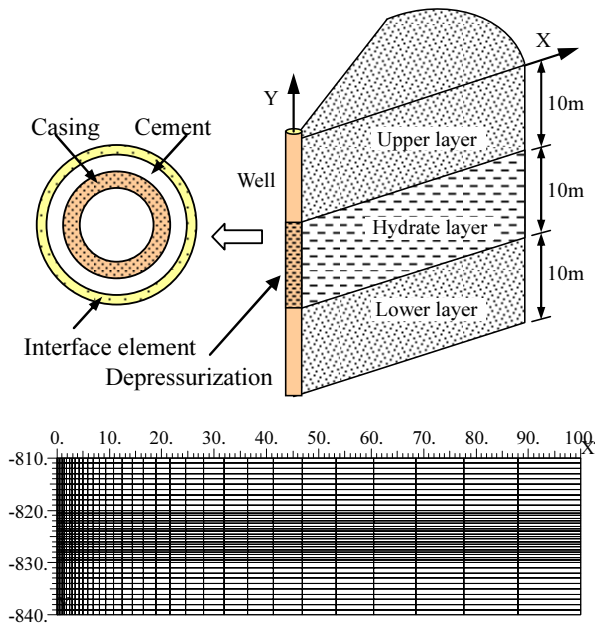


Fig. 1 A two-dimensional radial model

The initial reservoir pressure is given in accordance with the hydrostatic pressure and the initial reservoir temperature is assumed to be 282.15 K. The external, top

and bottom boundaries of the model are constant in pressure and temperature. The depressurization of 7 MPa is given along the inner boundary of the hydrate layer. The external boundary is constrained to move only vertically and the bottom of the model is constrained to allow lateral motion only. The top boundary is free in deformation.

The main material properties are listed in Table 1. The Young's modulus E of deposits is determined based on the triaxial compression tests of natural hydrate sediments obtained from the Nankai Trough site (Masui et al. 2005, 2008) and the Poisson's ratio ν is assumed. The friction angles of the interface between cement and sediment are assumed to be 5°, 10°, 15° and 20°, respectively, to investigate its effect on casing stress.

Table 1 Main material parameters

Parameter	Value
Sand deposits	$E=1238S_h+212$ MPa, $\nu=0.30$
Clay deposits	$E=80$ MPa, $\nu=0.35$
Casing	$E=2.1 \times 10^5$ MPa, $\nu=0.30$
Cement	$E=8.3 \times 10^3$ MPa, $\nu=0.25$
Initial porosity	0.4
Initial hydrate saturation	0.4
Sand permeability, mD	100.0
Clay permeability, mD	1.0
van Genuchte model	$\alpha=5.81 \times 10^{-4}$ 1/Pa, $m=0.81$
Permeability reduction	$N=5, N_n=0$
Interface strength	$c=0, \varphi=5^\circ, 10^\circ, 15^\circ, 20^\circ$
Residual saturation	$S_{wr}=0.1, S_{gr}=0.1$
Density, g/cm ³	$\rho_s=2.650, \rho_h=0.913$
Specific heat, J/(kg.K)	$c_w=4190, c_g=2100$ $c_s=800, c_h=2010$
Thermal conductivity, J/(m.s.K)	$\lambda_w=0.59, \lambda_g=0.03$ $\lambda_s=2.09, \lambda_h=0.45$

Fig. 2 shows the time evolution of cumulative gas production by using depressurization method. The cumulative gas during 500 days is equal to about 120,000 m³ under the standard condition. The figure also indicates that the magnitude of the strength between cement and sediment does not significantly change the cumulative gas production.

Fig. 3 illustrates the subsidence along the surface of the hydrate layer after 500 days of depressurization. The maximum subsidence occurs near the wellbore and its value is equal to about 20 cm. The change of the friction angle between cement and sediment does not affect the subsidence substantially.

Fig. 4 shows the shear stress distribution along the centerline of the hydrate layer after 500 days of depressurization. Shear stress near the wellbore is proportional to the friction angle between cement and sediment.

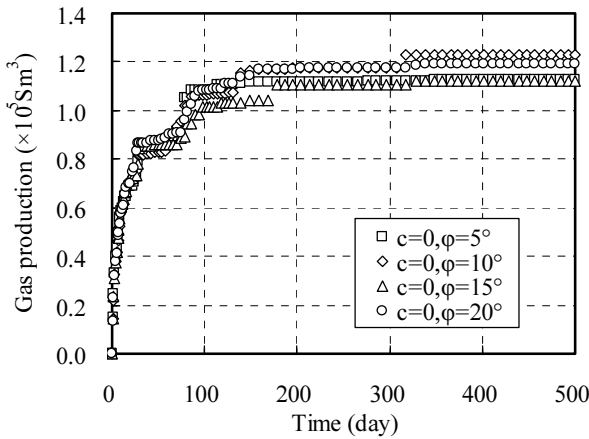


Fig. 2 Gas production by depressurization method

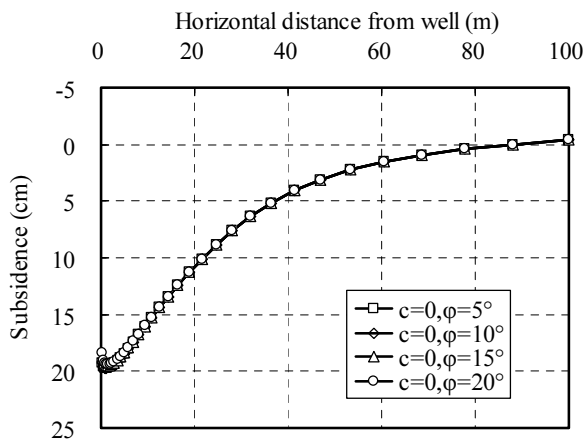


Fig. 3 Subsidence distribution along the surface of the hydrate layer after 500 days of depressurization

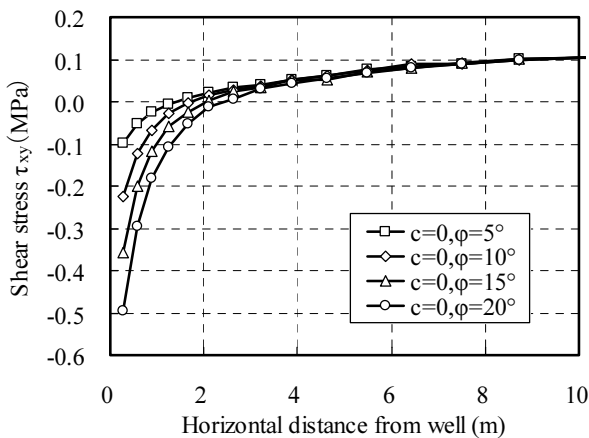


Fig. 4 Shear stress distribution along the centerline of the hydrate layer after 500 days of depressurization

Fig. 5 displays the axial stress distributions of casing in depth for different friction angles between cement and sediment after 500 days of depressurization. As can be seen, high compressive stress may be induced within the

depressurization interval due to large vertical strain associated with reservoir compaction, which then may exceed the compressive strength of the casing material. The figure also indicates that relative slippage tends to decouple the sediment with cement and reduce the load shifting from the sediments to the casing during depressurization. Therefore, frictional slippage will greatly reduce axial casing stress and then the occurrence of slippage can significantly enhance the safety of casing.

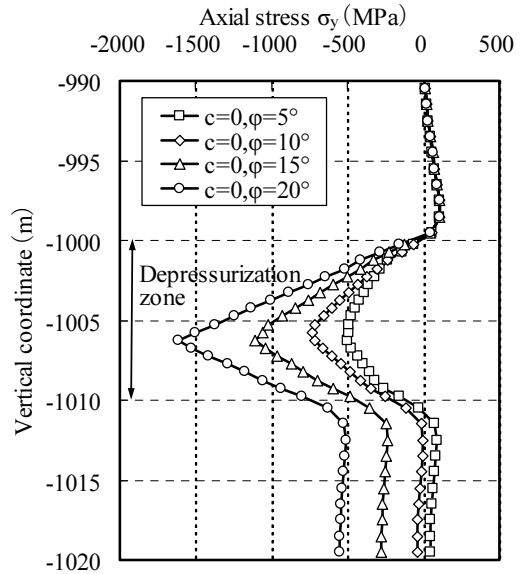


Fig. 5 Axial stress distribution of casing in depth after 500 days of depressurization

Fig. 6 shows some reservoir performances after 500 days of depressurization. The spatial distribution of water pressure is shown in Fig. 6(a). Near the wellbore in the hydrate layer, pressure drops sharply to well pressure. Moreover, although the pressure declines peripherally in the hydrate layer, a large pressure drop is also found in the upper and lower layers. This indicates that a depressurization of the hydrate layer can be recharged not only by the peripheral water influx from the hydrate layer but also by the influx from adjacent upper and lower non-hydrate layers.

Fig. 6(b) illustrates the spatial distribution of hydrate saturation. As can be seen, more hydrates are dissociated at the center of the hydrate layer than other regions. The maximum distance from well to dissociation front is equal to about 8 m.

Fig. 6(c) shows the spatial distribution of temperature. The hydrate dissociation leads to cooling of the hydrate layer near the well owing to the strongly endothermic nature of the hydrate reaction.

Figs. 6(d) and 6(e) illustrate the distribution of horizontal and vertical displacements, respectively. As can be seen, the maximum horizontal and vertical displacements

occur on the surface of the model. Moreover, vertical sediment displacement is greater than horizontal sediment displacement.

Fig. 6(f) displays the porosity distribution. The porosity at the region of dissociation changes from 0.4 to 0.36 due to the compaction of the reservoir induced by a reduction in pressure and hydrate dissociation.

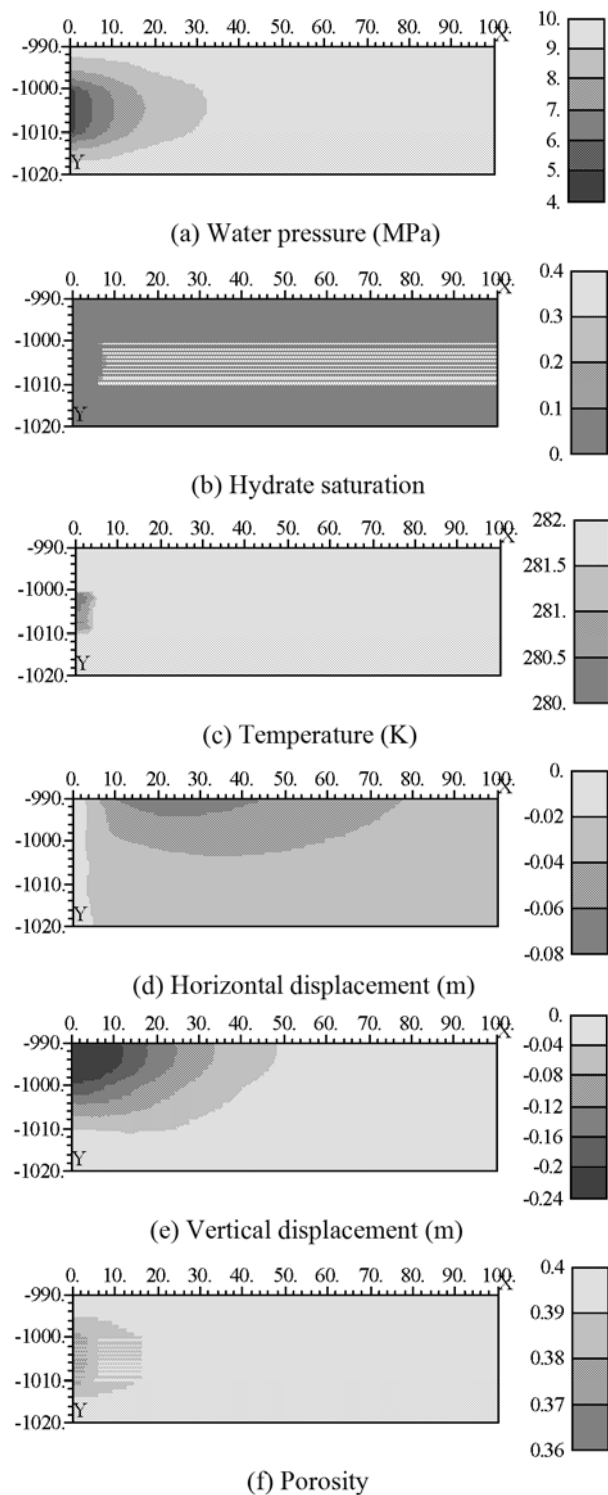


Fig. 6 Reservoir performances after 500 days of depressurization

CONCLUSIONS

In this study, the interacting phenomena of two-phase flow, heat transfer and geomechanical behavior for methane hydrate reservoirs during depressurization was investigated by using the proposed fully coupled thermo-hydro-mechanical model. Based on the results of this study, the following conclusions can be summarized.

(1) The fully coupled thermo-hydro-mechanical model can simulate the phase change due to hydrate dissociation, the flow of pore water and gas, the heat transfer due to convection and conduction, and the geomechanical phenomena of reservoirs.

(2) A robust numerical simulator was developed by use of the Galerkin finite element method and the hybrid Eulerian-Lagrangian approach. With this simulator, the accurate solution can still be obtained even very large time-step and coarse global mesh are used.

(3) Gas extraction from methane hydrate reservoirs may result in severe sediment compaction during gas production by use of the depressurization method.

(4) High compressive stress in casing may occur as a result of relatively rapid compaction in reservoirs. Frictional slippage between sediment and cement tends to reduce the axial compressive stress in casing and enhance casing safety significantly.

(5) The simulator can predict the complex behaviors of methane hydrate reservoirs including wellbore and casing stability during gas production and then can be used for designing production strategies for optimized production.

REFERENCES

- Kim HC, Bishnoi PR, Hedemann RA, Rizvi SSH (1987). Kinetics of methane hydrate decomposition. *Chemical Engineering Science*, 42(7): 1644-1653.
- Kimoto S, Oka F, Fushita T, Fujiwaki M (2007). Chemo-thermo-mechanically coupled numerical simulation of the subsurface ground deformations due to methane hydrate dissociation. *Computers and Geotechnics* 34: 216-228.
- Masuda Y, Kurihara M, Ohuchi H, Sato T (2003). A field-scale simulation study on gas productivity of formations containing gas. *Proc. of the 4th Inter. Conf. On Gas Hydrates, Yokohama, Japan.*
- Masui A, Haneda H, Ogata Y, Aoki K (2005). The effects of saturation degree of methane hydrate on the shear strength of synthetic methane hydrate sediments. *Proc. of the 5th Inter. Conf. On Gas Hydrates, Trondheim, Norway.*
- Masui A, Miyazaki K, Haneda H, Ogata Y, Aoki K (2008). Mechanical characteristics of natural and artificial gas hydrate bearing sediments. *Proc. of the*

- 6th Inter. Conf. On Gas Hydrates, Vancouver, British Columbia, Canada.
- Ng MYA, Klar A, Soga K (2008). Coupled soil deformation-flow-thermal analysis of methane production in layered methane hydrate soils. OTC 19364, Offshore Technology Conference, Houston, Texas, U.S.A.
- Peng DY & Robison DB (1976). Two and three phase equilibrium calculations for systems containing water. *Can. J. Chem. Eng.*, 54: 594-599.
- Rutqvist J, Moridis GJ, Grover T, Collett T (2008). Geomechanical response of known permafrost hydrate deposits to depressurization-induced production. Proc. of the 6th Inter. Conf. On Gas Hydrates, Vancouver, British Columbia, Canada.
- Sloan, ED (1998). Clathrate hydrates of natural gases. Second ed. Marcel Dekker Inc., New York.
- van Genuchten MT (1980). A closed-form equation for predicting the hydraulic conductivity of unsaturated soils. *Soil Sci. Soc. Am. J.*, 44: 892-898.
- Wilder JW, Moridis GJ, Wilson SJ, Kurihara M, White MD, Masuda Y, Anderson BJ, Collett TS, Hunter RB, Narita H, Pooladi-Darvish M, Rose K, Boswell R (2008). An international effort to compare gas hydrate reservoir simulation. Proc. of the 6th Inter. Conf. On Gas Hydrates, Vancouver, British Columbia, Canada.
- Yeh GT, Chang JR, Short TE (1992). An exact peak capturing and oscillation-free scheme to solve advection-dispersion transport equation. *Water Resource Research*, 28: 2937-2951.

NUMERICAL SIMULATION OF DYNAMIC RESPONSES IN TRANSVERSELY ISOTROPIC FLUID-SATURATED ELASTIC SEABED UNDER WAVE ACTIONS

Zhou-Yuan HENG¹, Wang-Yong HE², Sun ZHI³ and Chen-Ming WEI⁴

ABSTRACT: The seabed is assumed to be transversely isotropic fluid-saturated elastic porous medium. Based on the anisotropy theory and Biot dynamic consolidation equations, this paper has established a 3D-dynamic seabed model in $u-w-p$ form and defined anisotropic indicators ξ_α, ξ_β, m for the first time. The governing equations are solved by the Wilson- θ finite element program of DSFEM, and the numerical model is verified by test results. The computation results indicate that the amplitude of the pore water pressure decays more quickly with higher wave heights, shorter wave periods, or in shallower water depths.

KEYWORDS: transversely isotropic, seabed, wave action, dynamic equation, finite element, pore water pressure

INTRODUCTION

The natural seabed is composed of complex three-phase medium of soil, fluid and gas. When fluid fills with all pores of soil, it is called the fluid saturated porous medium. Under normal circumstances, natural seabed is made up of different geological layers formed during deposition process with the preferential orientation of soil particle and its fabric units. The deformation modulus, Poisson's ratio and the shear modulus of the seabed medium are different between the horizontal and vertical directions of soil layers. The performance of soil's stress-strain relation is mostly anisotropic. Therefore, treating the natural seabed as a transversely isotropic medium is more realistic in many cases.

Biot (1962) set up the anisotropy dynamic equations of porous medium, assuming that the solid skeleton of the saturated porous medium is in the performance of being statistically transversely isotropic. Some scholars have researched on the issue by using numerical solutions, such as Laplace domain boundary element, and analytical solutions of Fourier transform. However, those studies only focus on land-based foundation. Few studies have been made on the anisotropic seabed under wave actions. Recently, scholars began to study the anisotropy permeability of seabed (Lin 1997, Zheng 2006).

In this paper, the seabed is assumed to be transversely isotropic saturated porous medium, and based on the anisotropy theory and Biot consolidation equations (Biot

1962), with the analysis of dynamic responses of the transversely isotropic fluid-saturated elastic seabed under wave actions, the program of dynamic finite element method is explored and the numerical model is verified by test results.

CONSTITUTIVE THEORY

Constitutive Relation

The stress-strain relation of any point in the anisotropic elastic medium can be expressed as:

$$\{\sigma\}=[C]\{\varepsilon\} \quad (1)$$

where $\{\sigma\}$ and $\{\varepsilon\}$ are the stress and the strain matrixes, respectively; $[C]$ is the stiffness matrix with 36 flexibility parameters.

But a transversely isotropic stress-strain relation may be derived from Eq.1 with only 6 elastic parameters in the stiffness matrix $[C]$ as follows:

$$c_{11}=\lambda m(1-m\mu_2^2), c_{12}=\lambda m(\mu_1+m\mu_2^2) \quad (2a)$$

$$c_{13}=\lambda m\mu_2(1+\mu_1), c_{33}=\lambda(1-\mu_1^2) \quad (2b)$$

$$c_{44}=G_2, c_{55}=E_1/(1+\mu_1) \quad (2c)$$

where E_1 , μ_1 are the horizontal elastic modulus and Poisson's ratio of transversely isotropic plane,

¹ Ph.D. Student, School of Civil and Architecture Engineering, Central South University, Changsha, China. Email:381766254@qq.com

² Professor, School of Civil and Architecture Engineering, Central South University, Changsha, China.

³ Postgraduate, School of Water Conservancy, Changsha University of Science and Technology, Changsha, China.

⁴ Postgraduate, School of Water Conservancy, Changsha University of Science and Technology, Changsha, China.

respectively; E_2, u_2, G_2 are the elastic modulus, Poisson's ratio and the shear modulus in the vertical plane, respectively, and

$$m = E_1/E_2 \tag{3}$$

$$\lambda = E_2/(1 + \mu_1)(1 - \mu - 2m\mu_2^2) \tag{4}$$

Stress-Displacement Relation

Geometric equations of transversely isotropic elastic medium are expressed the same as the isotropic ones. The stress-displacement equations are as follows:

$$\begin{cases} \sigma_x = c_{11} \frac{\partial u}{\partial x} + c_{12} \frac{\partial v}{\partial y} + c_{13} \frac{\partial w}{\partial z}, \tau_{xy} = c \left(\frac{\partial v}{\partial z} + \frac{\partial w}{\partial y} \right) \\ \sigma_y = c_{12} \frac{\partial u}{\partial x} + c_{11} \frac{\partial v}{\partial y} + c_{13} \frac{\partial w}{\partial z}, \tau_{yx} = c \left(\frac{\partial w}{\partial x} + \frac{\partial u}{\partial z} \right) \\ \sigma_z = c_{13} \frac{\partial u}{\partial x} + c_{13} \frac{\partial v}{\partial y} + c_{33} \frac{\partial w}{\partial z}, \tau_{xz} = c_{66} \left(\frac{\partial u}{\partial y} + \frac{\partial v}{\partial x} \right) \end{cases} \tag{5}$$

SEABED DYNAMIC EQUATION

Consolidation Equation

The assumptions of the transversely isotropic saturated soil body are basically the same as the Biot's: 1) Soil skeleton is an ideal medium of elastic body and is compressible; 2) The incompressible pore fluid and flow in soil follow the generalized Darcy's flow law; 3) Soil pores are connected with each other; 4) The impacts of some factors such as temperature, etc. are neglected; 5) Saturated soils are of statistical transversely isotropic properties.

Based on the above assumptions and the principle of effective stress, by employing Biot dynamic consolidation equations, the transversely isotropic elastic saturated seabed dynamic equations can be finally set in $u-w-p$ form as follows:

$$\begin{aligned} & \left[c_{11} \left(\frac{\partial^2}{\partial r^2} + \frac{1}{r} \frac{\partial}{\partial r} \right) + \frac{1}{2} (c_{11} - c_{12}) \frac{1}{r^2} \frac{\partial^2}{\partial \theta^2} + c_{44} \frac{\partial^2}{\partial z^2} \right] u + [(c_{11} - c_{12}) \frac{1}{r} \times \\ & \frac{\partial^2}{\partial r \partial \theta} - (c_{11} + c_{66}) \frac{1}{r^2} \frac{\partial}{\partial \theta}] u_\theta + (c_{13} + c_{44}) \frac{\partial^2 u_z}{\partial r \partial z} - \frac{\partial p}{\partial r} = \rho \frac{\partial^2 u_r}{\partial t^2} + \rho_w \frac{\partial^2 w_r}{\partial t^2} \end{aligned} \tag{6a}$$

$$\begin{aligned} & \left[(c_{11} - c_{66}) \frac{1}{r} \frac{\partial}{\partial r \partial \theta} + (c_{11} + c_{66}) \frac{1}{r} \frac{\partial}{\partial \theta} \right] u + \left[\frac{1}{2} (c_{11} - c_{12}) \left(\frac{\partial}{\partial r} + \frac{1}{r} \frac{\partial}{\partial r} - \frac{1}{r} \right) \right. \\ & \left. + c_{11} \frac{1}{r} \frac{\partial}{\partial \theta} + c \frac{\partial}{\partial z} \right] u_\theta + (c_{13} + c_{44}) \frac{1}{r} \frac{\partial u}{\partial \theta z} - \frac{1}{r} \frac{\partial p}{\partial \theta} = \rho \frac{\partial u_\theta}{\partial t} + \rho \frac{\partial w_\theta}{\partial t} \end{aligned} \tag{6b}$$

$$\begin{aligned} & (c + c_{44}) \left(\frac{\partial}{\partial r \partial z} + \frac{1}{r} \frac{\partial}{\partial z} \right) u_r + (c + c_{44}) \frac{1}{r} \frac{\partial u_\theta}{\partial z} + \left[c_{44} \left(\frac{\partial}{\partial r} + \frac{1}{r} \frac{\partial}{\partial r} + \frac{1}{r} \frac{\partial}{\partial \theta} \right) \right. \\ & \left. + c \frac{\partial}{\partial z} \right] u - \frac{\partial p}{\partial z} = \rho \frac{\partial u}{\partial t} + \rho \frac{\partial w}{\partial t} \end{aligned} \tag{6c}$$

where u_i ($i=r, \theta, z$) is the soil skeleton displacement; w_i ($i=r, \theta, z$) is the fluid displacement relative to solid skeleton ; ρ_s, ρ_w, ρ are the soil particle's density, the fluid's density and the total density of saturated soil, respectively; their relation are as follows:

$$\rho = (1-n) \rho_s + n \rho_w \tag{7}$$

where n is the porosity; p is the pore water pressure.

Pore Flow Equation

The fluid balance equation can be obtained as follows by putting geometric equations, the stress Eq. 5 and fluid flow equation together:

$$\begin{cases} \rho \frac{\partial u}{\partial t} + \frac{\rho}{n} \frac{\partial w}{\partial t} + \frac{\eta}{k} \frac{\partial w}{\partial t} + \frac{\partial p}{\partial r} = 0 \\ \rho \frac{\partial u_\theta}{\partial t} + \frac{\rho}{n} \frac{\partial w_\theta}{\partial t} + \frac{\eta}{k} \frac{\partial w_\theta}{\partial t} + \frac{1}{r} \frac{\partial p}{\partial \theta} = 0 \\ \rho \frac{\partial u}{\partial t} + \frac{\rho}{n} \frac{\partial w}{\partial t} + \frac{\eta}{k} \frac{\partial w}{\partial t} + \frac{\partial p}{\partial z} = 0 \end{cases} \tag{8}$$

where k_{dr}, k_{dz} are the permeability in transversely isotropic plane and its vertical plane, respectively; η is the dynamic viscosity of pore fluid.

The continuity equation of soil pore flow is as follows:

$$k_x \frac{\partial^2 p}{\partial x^2} + k_y \frac{\partial^2 p}{\partial y^2} + k_z \frac{\partial^2 p}{\partial z^2} - \gamma_w n \beta \frac{\partial p}{\partial t} = \gamma_w \frac{\partial}{\partial t} (\epsilon_{vx} + \epsilon_{vy} + \epsilon_{vz}) \tag{9}$$

where k_x, k_y, k_z are the permeability in x, y or z ,respectively; n is the porosity; β is the compressibility of pore fluid.

When the seabed is taken to be transversely isotropic, there are that $k_x = k_y = k_{dr}, k_z = k_{dz}$.

Simultaneous Equation

Combing Eq. 6, Eq. 8 and Eq. 9, we get the simultaneous three-dimensional dynamic equation group in $u-w-p$ form for the first time, which can be applied to the transversely isotropic fluid-saturated elastic seabed under wave actions. In accordance with the specific conditions of wave actions and boundary, by using this group of the dynamic equation model, the corresponding solution of soil skeleton displacement u_i , the fluid displacement relative to soil skeleton w_i and pore water pressure p can be obtained theoretically. Then, from the stress-displacement Eq. 5, the effective stress of natural

seabed could be calculated.

For two-dimensional problems, all variables (only when $i=y$, θ) are zero. If $E_1=E_2$, $\mu_1=\mu_2$, k and G are same in all directions, the model will degrade to be the dynamic equations of isotropic seabed.

In many cases, analytical methods and numerical methods are jointly utilized to obtain a better solution.

NUMERICAL ANALYSIS METHOD

Overall Equation

The overall matrix equation of the balance and the continuity matrix equation in computational domain is deduced as follows:

$$\begin{bmatrix} \bar{K} & K' \\ K & \tilde{K} \end{bmatrix} \begin{Bmatrix} \delta \\ \beta \end{Bmatrix} + \begin{bmatrix} M & 0 \\ 0 & 0 \end{bmatrix} \begin{Bmatrix} \ddot{\delta} \\ \ddot{\beta} \end{Bmatrix} + \begin{bmatrix} C & 0 \\ 0 & 0 \end{bmatrix} \begin{Bmatrix} \dot{\delta} \\ \dot{\beta} \end{Bmatrix} = \begin{Bmatrix} R \\ S \end{Bmatrix} \quad (10)$$

where, $\{R\}$ is the matrix of node loads; $[\bar{K}]$, $[K']$, $[M]$, and $[C]$ are the superposition matrixes of the unit matrixes of $[\bar{K}]^e$, $[K']^e$, $[M]^e$, $[C]^e$; $\{\delta\}$ are the displacement vector of various points; $\{\beta\}$ is the pore water pressure vector.

The stiffness matrix consists of three parts, but the values are greatly different. The magnitude of E is about 10^7 , the permeability k is below 10^{-4} , γ_w is about 10^4 , the time step Δt is below 1.0, all in terms of N, m, s for the basic units of force, length and time. Therefore, the ratio of the values of the elements of $[\tilde{K}]$ and $[\bar{K}]$ reaches around 10^{14} , the value of $[K']$ is between $[\bar{K}]$ and $[\tilde{K}]$. This paper adopts the adjusting coefficient by both sides of Eq.7 multiplied 10^n , where n takes the half magnitude of the ratio of elements of $[\bar{K}]$ and $[\tilde{K}]$.

Numerical Method

For the dynamic finite element problem, there are many solutions, and the integration method does not need to transform the motion equation. And not only can it be used to solve linear problems, but also could be effectively applied to the nonlinear one at every moment directly. According to the different formats in time domain, the integration method can be divided into two methods of the explicit and the implicit. Wilson- θ method is an unconditionally stable implicit method and the time step can be selected at random, but too large time step will lead to errors increasing gradually. The solving time cycle will be longer as more precise solution required. Therefore, a reasonable selection of the time step is very important. With the above analysis, combining the characteristics of the load on seabed by wave actions and boundary conditions, this paper adopted the Wilson- θ method and developed a dynamic

finite element program of DSFEM.

EXAMPLE AND ANALYSIS

For numerical computation, we assume the dynamic permeability $k_{dr}=k_{dz}=k=0.11 \times 10^{-3} \text{ m} \cdot \text{s}^{-1}$, porosity $n=0.30$.

Then transversely isotropic non-dimensional elastic parameters are introduced as follows:

$$\zeta_1 = C_{33}/C_{44} \quad (11a)$$

$$\zeta_2 = C_{11}/C_{44} \quad (11b)$$

$$\zeta_3 = C_{13}/C_{44} + 1 \quad (11c)$$

and defined anisotropic indicators are as follows:

$$\zeta_\alpha = C_{11}/C_{33} = \zeta_2/\zeta_1 \quad (12a)$$

$$\zeta_\beta = (C_{33} - C_{13} - C_{44})/C_{44} = \zeta_1 - \zeta_3 \quad (12b)$$

When m, λ, μ_1, μ_2 are 1.67, 1.26×10^7 , 0.35, 0.25, respectively; we have $c_{11}=1.88 \times 10^7$, $c_{13}=0.71 \times 10^7$, $c_{33}=1.11 \times 10^7$, $c_{11}=G_2=0.36 \times 10^7$; $\zeta_1=3.05$, $\zeta_2=5.22$, $\zeta_3=2.97$; $\zeta_\alpha=1.71$; $\zeta_\beta=0.11$.

The numerical simulation results and analysis are as follows by putting above all in DSFEM.

Model Verification

As Figs. 1 and 2 show, the pore water pressure values between the numerical results and the test results (ZHOU 2005) meet well within 5.0%. The analysis point is shown in Fig. 3.

In Fig. 1, the linear wave height H is 14cm, wave period T is 1.4s, the water depth h is 50cm. In Fig. 2, the conoidal wave H is 12cm, T is 2.0s, h is 30cm.

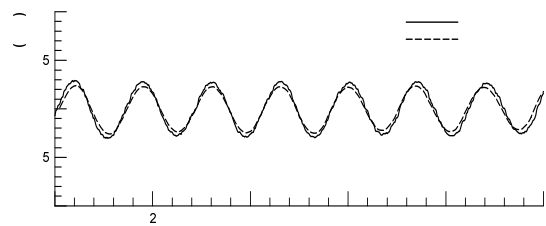


Fig. 1 Comparison of pore water pressures in seabed under linear wave actions

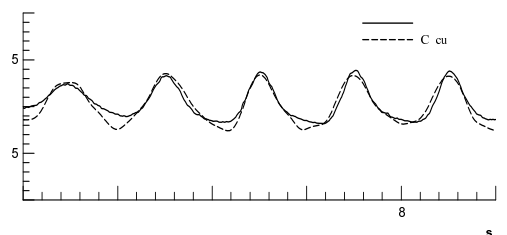


Fig. 2 Comparison of pore water pressures in seabed under conoidal wave actions

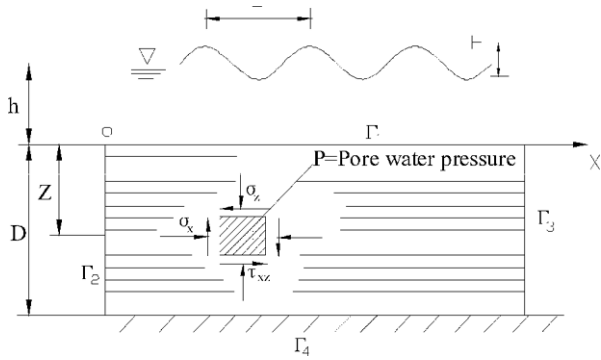


Fig. 3 Transversely isotropic seabed model

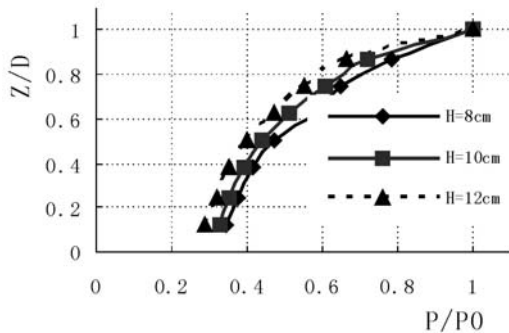


Fig. 4 The seabed pore water pressure responses with different wave heights

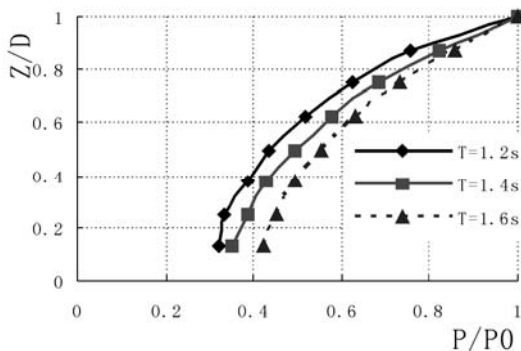


Fig. 5 The seabed pore water pressure responses with different wave periods

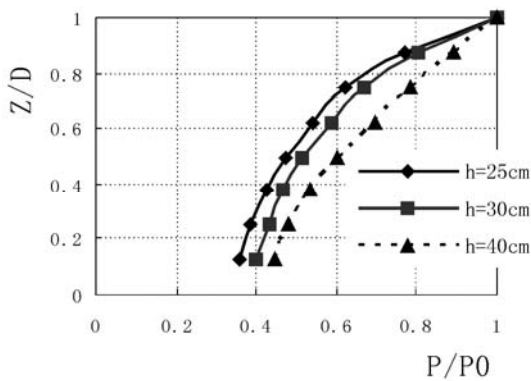


Fig. 6 The seabed pore water pressure responses in different water depths

Numerical Result

Under linear wave actions, the numerical results of pore water pressures are given, where in Fig. 4, h is 40cm, T is 1.2s; in Fig. 5, h is 50cm, H is 14cm; in Fig. 6, H is 12cm, T is 1.4s. The solution is as follows:

(1) From Fig. 4, the pore water pressures with different values of H but the same h and T are obtained; the pressures caused by high-height wave decay more rapidly than that by low-height one.

(2) Fig. 5 shows the pore water pressures with different values of T ; the pressures caused by short-period wave decay more rapidly than that by long-period one; in addition, because wave pressure on seabed surface is larger under long-period wave actions than under short ones, the absolute value of pore water pressure is larger under long-period wave actions than under short ones.

(3) Fig. 6 shows the pore water pressures with different values of h ; the pressures in shallow water decay more rapidly than that in deep one.

(4) From the definition of the anisotropic indicators, it shows that when $m=\zeta_\alpha=\zeta_\beta=1$, the seabed is isotropic medium; when $m=1.67$, $\zeta_\alpha=1.71$, $\zeta_\beta=0.11$, as these examples used, the seabed is transversely isotropic; the values of the indicators reflect the anisotropy degree. When $k_{dr}=k_{dz}=k_{d\theta}$, it means that the penetration anisotropy of seabed is not taken into consideration.

CONCLUSIONS

(1) This paper has discussed the anisotropy concept, from the inherent anisotropy of seabed soil, analyzed and gave the transversely isotropic constitutive relations and dynamic controlling equations, furthermore, defined the anisotropic indicators ζ_α , ζ_β , m , to reflect the degree of anisotropy intuitively.

(2) Based on Biot dynamic consolidation equations, for the first time, a 3-Dimensional model of transversely isotropic fluid-saturated elastic seabed is established in $u-w-p$ form. This paper has probed the realization of the Wilson- θ method and has developed the finite element program, which can be used in the computation and analysis of the dynamic responses of the seabed under wave actions.

(3) The test results have verified the numerical model. The computation results show that: the amplitude of the pore water pressure decays more quickly with higher wave heights, shorter periods, or in shallower water depths.

REFERENCES

Biot MA (1956). The theory of propagation of elastic wave in fluid saturated porous solid. J Acoust Soc

- Am, 28(2):168-191.
- Biot MA (1962). General theory of acoustic propagation in porous dissipative media. *J Acoust Soc Am*, 34(9):1254-1264.
- Biot MA (1962). Mechanics of deformation and acoustic propagation in porous media. *J Appl Phys*, 33(4): 1482-1498.
- Lin YS & Jeng DS (1997). The effect of variable permeability on the wave-induced seabed response. *Ocean Engineering*, 24(7): 623-643.
- Zhang JF, Zhang QH, Qin CR (2006). Numerical simulation of wave-induced response of inhomogeneous and anisotropic seabed. *Journal of Tianjin University*. 39(2): 159-164.
- Lekhnitskii SG (1963). *Theory of elasticity of an anisotropic elastic body*. Holden-Day Inc. San Francisco.
- Zhou YH (2005). The numerical simulation of pore water pressure responses in elastic seabed under wave actions. *Journal of Waterway and Harbor*. 2(6): 623-643.
- Jeng DS & Seymour BR (1997). Response in seabed of finite depth with variable permeability. *Journal of Geotechnical and Geoenvironment Engineering*, 123(10): 902-911.
- Philip LF (1999). Numerical modeling of wave interaction with porous structures. *Journal of water port coastal, and ocean engineering*. December: 216-222.

SOLUTIONS FOR A COMPLETELY SATURATED POROUS ELASTIC SOLID WITH IMPEDED BOUNDARIES

Ze-Hai CHENG¹, Jian-Zhong XIA², Yun-Min CHEN³, Dao-Sheng LING⁴ and Bing ZHU⁵

ABSTRACT: Axisymmetric solutions, which are applied in the consolidation calculations of a semi-infinite clay stratum with impeded boundaries, are derived. Laplace and Hankel integral transforms are utilized with respect to time and radial coordinates, respectively in the analysis. The derivation of fundamental solutions considered two boundary-value problems involving unit point loading and ring loading in the vertical direction. The solutions are extended to circular distributed normal load. The computation of settlements, shearing stress and excess pore pressure in the consolidating layer subject to circular distributed loading are presented.

KEYWORDS: consolidation, integral transform, impeded boundaries

INTRODUCTION

Biot's consolidation theory was proposed from continuous medium fundamental equations (Biot 1941). The theory taking into account the coupling between the solid strains and pore pressure dissipation is called "coupled consolidation theory". The solution of the governing equations of a porous solid is more complicated than those involving ideal elastic solids. A solution for plane and axially symmetric problems in terms of two displacement functions was presented (McNamee et al. 1960). The general solution for displacement functions is obtained through the application of Laplace and Fourier integral transforms for plane problems and Laplace and Hankel integral transforms for axisymmetric problems. The analysis was extended to consolidation of a finite clay layer on a smooth impervious base (Gibson et al. 1970). Axisymmetric fundamental solutions for completely saturated porous elastic solid were presented (Puswewala et al. 1988). Gu and Jin (1992) analyzed the consolidation problems for an axisymmetric vertical loaded multi-layer base. A method through expanding the field of solution was adopted to obtain an analytical solution for finite layer (Huang et al. 1996). The state vector solution of the axisymmetric Biot's consolidation problems for multilayered poroelastic media was derived by the use of the Laplace-Hankel integral transform and the Cayley-Hamilton theorem (Wang et al. 2001). A

radial point interpolation method (meshless method) to solve Biot's consolidation problem was adopted (Wang et al. 2002). Particular internal formulations for two- and three-dimensional soil consolidation (poroelasticity) analysis was presented (Park et al. 2002). Cavalcanti and Telles (2003) solved Biot's plane strain consolidation equations for poro-elastic saturated media by application of BEM.

All the above investigations assumed that the surface of the consolidating layer is fully permeable or impermeable, but that the surface might be affected by geotechnical engineering impediments such as a sand cushion used in preloading, the soil layer within the pile length in settlement calculation of substratum below piles or a replacement layer of embankment impeding permeation of the consolidating layer. The impeding layer has enough stiffness in the vertical direction and its deformation can be ignored. The impeding layer can be simplified as an impeded boundary of the sub-consolidating layer. Xie et al. (1996, 1999) studied one-dimensional consolidation of layered soils with impeded boundaries. However results for two-dimensional problem with impeded boundaries have not been reported.

This paper deals with the derivation of axisymmetric fundamental solutions that are applied in the consolidation calculations of a semi-infinite clay stratum with impeded boundaries. The derivation of fundamental solutions considers two boundary-value problems involving unit

¹ Associate Prof., School of Civil Engineering and Architecture, Zhejiang University of Science and Technology, China. Email: chengzh2008@163.com

² Prof., School of Civil Engineering and Architecture, Zhejiang University of Science and Technology, China

³ Prof., Department of Civil Engineering, Zhejiang University, China

⁴ Prof., Department of Civil Engineering, Zhejiang University, China

⁵ Associate Prof., Department of Civil Engineering, Zhejiang University, China

point loading and ring loading in the vertical direction. The solutions are extended to circular loading and other distributed loading. The calculation and analysis of settlements, shearing stress and excess pore pressure in the consolidating layer subject to circular loading are presented.

GOVERNING EQUATIONS AND GENERAL SOLUTION

Following Biot (1941), the displacement equations for axisymmetric deformations of a completely saturated isotropic and homogeneous poroelastic solid in a cylindrical coordinate system are expressed in the following:

$$(\nabla^2 - \frac{1}{r^2})u_r + (2\eta - 1)\frac{\partial \varepsilon}{\partial r} + \frac{1}{G}\frac{\partial p_f}{\partial r} = 0 \tag{1}$$

$$\nabla^2 u_r + (2\eta - 1)\frac{\partial \varepsilon}{\partial z} + \frac{1}{G}\frac{\partial p_f}{\partial z} = 0 \tag{2}$$

$$c\nabla^2 \varepsilon = \frac{\partial \varepsilon}{\partial t} \tag{3}$$

where $\nabla^2 = \frac{\partial^2}{\partial r^2} + \frac{1}{r}\frac{\partial}{\partial r} + \frac{\partial^2}{\partial z^2}$, $\varepsilon = \frac{1}{r}[\frac{\partial}{\partial r}(ru_r) + r\frac{\partial u_z}{\partial z}]$, $\eta = (1 - \nu)/(1 - 2\nu)$, $c = 2G\eta k$

In the above equations, $u_r(r, z, t)$ and $u_z(r, z, t)$ denote displacements in r and z directions, respectively; $p_f(r, z, t)$ is the excess pore pressure; G and ν denote shear modulus and Poisson’s ratio of the bulk material; k is the coefficient of permeability of the medium; ε is the dilatation of the bulk material.

The stress-strain relations are expressed as

$$\frac{\sigma_{rr}}{2G} = \varepsilon_{rr} + (\eta - 1)\varepsilon + \frac{p_f}{2G} \tag{4}$$

$$\frac{\sigma_{\theta\theta}}{2G} = \varepsilon_{\theta\theta} + (\eta - 1)\varepsilon + \frac{p_f}{2G} \tag{5}$$

$$\frac{\sigma_{zz}}{2G} = \varepsilon_{zz} + (\eta - 1)\varepsilon + \frac{p_f}{2G} \tag{6}$$

$$\frac{\sigma_{zr}}{2G} = \varepsilon_{zr} \tag{7}$$

where $\sigma_{rr}(r, z, t)$, $\sigma_{\theta\theta}(r, z, t)$, $\sigma_{zz}(r, z, t)$ and $\sigma_{zr}(r, z, t)$ are non-zero stress components of the bulk material; $\varepsilon_{rr}(r, z, t)$, $\varepsilon_{\theta\theta}(r, z, t)$, $\varepsilon_{zz}(r, z, t)$ and $\varepsilon_{zr}(r, z, t)$ are bulk strain components.

Following McNamee and Gibson (1960), displacements $u_r(r, z, t)$ and $u_z(r, z, t)$ and pore pressure $p_f(r, z, t)$ are expressed in terms of two functions ϕ and ψ in the following form:

$$u_r = -\frac{\partial \psi}{\partial r} + z\frac{\partial \phi}{\partial r} \tag{8}$$

$$u_z = -\frac{\partial \psi}{\partial r} + z\frac{\partial \phi}{\partial r} - \phi \tag{9}$$

$$p_f = -2G(\frac{\partial \phi}{\partial z} - \eta\nabla^2 \psi) \tag{10}$$

It is convenient to non-dimensionalize all quantities with respect to length and time by selecting a certain length “ R ” as unity, and “ R^2/c ” as a unit of time, respectively. The substitution of Eqs. (8)~(10) in Eqs. (1)~(3) yield the following governing equations for functions ϕ and ψ :

$$\nabla^4 \psi = \nabla^2 \frac{\partial \psi}{\partial t} \tag{11}$$

$$\nabla^2 \phi = 0 \tag{12}$$

Laplace and Hankel transforms of Eqs. 11 and 12 result in the following two ordinary differential equations. Define ϕ_{hl} and ψ_{hl} as zero-order Hankel transform and Laplace transform of functions ϕ and ψ , respectively.

$$(\frac{\partial^2}{\partial z^2} - \zeta^2 - p)(\frac{\partial^2}{\partial z^2} - \zeta^2)\phi_{hl} = 0 \tag{13}$$

$$(\frac{\partial^2}{\partial z^2} - \zeta^2)\psi_{hl} = 0 \tag{14}$$

where p is Laplace transform parameter; ζ is Hankel transform parameter; $\gamma = \sqrt{\zeta^2 + p}$.

Solutions of the above two equations are

$$\psi_{hl} = A(\zeta, p)e^{-z\zeta} + B(\zeta, p)e^{-z\gamma} + C(\zeta, p)e^{z\zeta} + D(\zeta, p)e^{z\gamma} \quad (15)$$

$$\phi_{hl} = E(\zeta)e^{-z\zeta} + F(\zeta)e^{z\zeta} \quad (16)$$

where $\gamma = \sqrt{\zeta^2 + p}$

Based on Eqs. 4~16, general solutions for displacements, excess pore pressure and stresses for axisymmetric deformations of a completely saturated porous elastic solid can be written as follows:

$$\bar{u} = \int_0^\infty \zeta J(r\zeta) [\zeta A e^{-\zeta} + \gamma B e^{-\gamma} - \zeta C e^\zeta - \gamma D e^\gamma - (z\zeta + 1)E e^{-\zeta} + (z\zeta - 1)F e^\zeta] d\zeta \quad (17)$$

$$\bar{u} = \int_0^\infty \zeta J_1(r\zeta) (A e^{-\zeta} + B e^{-\gamma} + C e^\zeta + D e^\gamma - z E e^{-\zeta} - z F e^\zeta) d\zeta \quad (18)$$

$$\bar{p} = 2G \int_0^\infty \zeta J(r\zeta) (\eta p B e^{-\gamma} + \eta p D e^\gamma + \zeta E e^{-\zeta} - \zeta F e^\zeta) d\zeta \quad (19)$$

$$\bar{\sigma} = 2G \int_0^\infty \zeta J(r\zeta) [-\zeta A e^{-\zeta} - \zeta B e^{-\gamma} - \zeta C e^\zeta - \zeta D e^\gamma + (z\zeta + 1)E e^{-\zeta} + (z\zeta - 1)F e^\zeta] d\zeta \quad (20)$$

$$\bar{\sigma} = 2G \int_0^\infty \zeta J_1(r\zeta) (-\zeta A e^{-\zeta} - \gamma B e^{-\gamma} + \zeta C e^\gamma + \gamma D e^\gamma + z\zeta E e^{-\zeta} - z\zeta F e^\zeta) d\zeta \quad (21)$$

where the superposed bar denotes the Laplace transform of the relevant quantity.

Combining the above general solutions with different boundary conditions, fundamental solutions can be obtained.

FUNDAMENTAL SOLUTIONS FOR POINT LOADING

In Fig.1, a vertical point load P_0 is applied over the surface of the semi-infinite consolidating layer. H

denotes the thickness of the impeding layer; k_1 is the coefficient of permeability of the impeding layer; k_2 is the coefficient of permeability of the consolidating layer. It is assumed that the impeding layer has enough vertical stiffness and permeation only takes place vertically in the impeding layer not considering shearing stress over the plane ($z=0$). Following Terzaghi one dimensional consolidation theory, the boundary conditions for the surface of the consolidating layer are derived in the following forms.

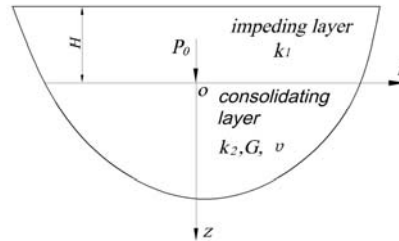


Fig. 1 Semi-infinite stratum subject to a point loading

$$k_2 \frac{\partial p_f}{\partial z} = k_1 \frac{p_f}{H} \quad (22)$$

$$\sigma_{rz} = 0 \quad (23)$$

$$\sigma_{zz} = p_0 \delta(r) / (2\pi r) \quad (24)$$

By using Laplace transform and the zero order Hankel transform, the boundary conditions are as follows:

$$k_2 \frac{\partial \bar{p}_f}{\partial z} = k_1 \frac{\bar{p}_f}{H} \quad (25)$$

$$\bar{\sigma}_{rz} = 0 \quad (26)$$

$$\bar{\sigma}_{zz} = p_0 / (2\pi p) \quad (27)$$

Base on Eqs. 17 ~27, the fundamental solutions in the Laplace domain can be obtained in the following form.

1) Displacement in the radial direction:

$$\bar{u} = -\frac{P_0}{4Gp\pi} \int_0^\infty (e^{-r+\zeta}) \zeta (e^\zeta \zeta (k_1 + Hk \zeta) + e^\gamma (k_1 (-\gamma + pz\eta) + Hk \gamma (-\zeta + pz\eta))) J_1(r\zeta) / (k_1 (-\gamma\zeta + \zeta + p\eta) + Hk (-\gamma\zeta + \zeta^3 + p\eta)) d\zeta \quad (28)$$

2) Displacement in the vertical direction:

$$\bar{u} = -\frac{P}{4Gp\pi} \int_0^\infty (e^{-\gamma+\zeta} (e^\zeta \gamma \zeta (k + Hk \zeta) + e^\gamma (k (-\gamma \zeta + p\eta + pz\zeta\eta) + Hk \gamma (-\zeta + p\eta + pz\zeta\eta))) J(r\zeta)) / (k (-\gamma \zeta + \zeta + p\eta) + Hk (-\gamma \zeta + \zeta + p\eta)) d\zeta \quad (29)$$

3) Vertical total compressive stress:

$$\bar{\sigma} = -\frac{P}{2p\pi} \int_0^\infty (e^{-\gamma+\zeta} \zeta (e^\zeta \gamma \zeta (k + Hk \zeta) + e^\gamma (k (-\gamma \zeta + p\eta + pz\zeta\eta) + Hk \gamma (-\zeta + p\eta + pz\zeta\eta))) J(r\zeta)) / (k (-\gamma \zeta + \zeta + p\eta) + Hk (-\gamma \zeta + \zeta + p\eta)) d\zeta \quad (30)$$

4) Shearing stress:

$$\bar{\sigma}_r = -\frac{P_0}{2p\pi} \int_0^\infty (e^{-\gamma+\zeta} \zeta (e^\zeta \gamma (k + Hk \zeta) + e^\gamma (k (-\gamma + pz\eta) + Hk \gamma (-\zeta + pz\eta))) J(r\zeta)) / (k (-\gamma \zeta + \zeta + p\eta) + Hk (-\gamma \zeta + \zeta + p\eta)) d\zeta \quad (31)$$

5) Excess pore-water pressure:

$$\bar{p}_f = \frac{p \eta}{2\pi} \int_0^\infty (e^{-\gamma+\zeta} \zeta (-e^\gamma (k + Hk \gamma) + e^\zeta (k + Hk \zeta)) J(r\zeta)) / (k (\gamma \zeta - \zeta - p\eta) + Hk (\gamma \zeta - \zeta - p\eta)) d\zeta \quad (32)$$

SOLUTIONS FOR CIRCULAR RING LOADING

The vertical ring loading, whose intensity is equal to the Heaviside unit step function $H(t)$ per unit arc length applied along a circular ring of radius R on a horizontal plane at $z=0$, is shown in Fig. 2. Application of Laplace transform and Hankel transform yields the following boundary conditions over the plane ($z=0$):

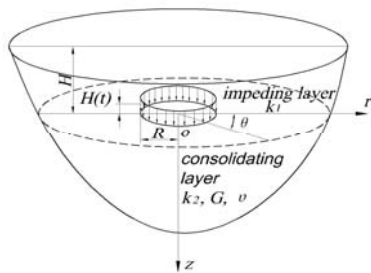


Fig. 2 Semi-infinite stratum subject to axisymmetric ring loading

$$k_2 \frac{\partial \bar{p}_f}{\partial z} = k_1 \frac{\bar{p}_f}{H} \quad (33)$$

$$\bar{\sigma}_{rz} = 0 \quad (34)$$

$$\bar{\sigma}_{zz} = RJ_1(R\zeta) \quad (35)$$

By replacing $P_0 / 2\pi$ in the fundamental solution for point load with $RJ_0(R\zeta)$, the fundamental solution for ring loading can be obtained.

SOLUTIONS FOR CIRCULAR LOADING

The vertical circular loading configuration, whose intensity is equal to q applied over a circular area of radius “ R ” at $z=0$, is shown in Fig. 3. Use of Laplace transforms and Hankel transforms yields the following boundary conditions over the plane ($z=0$):

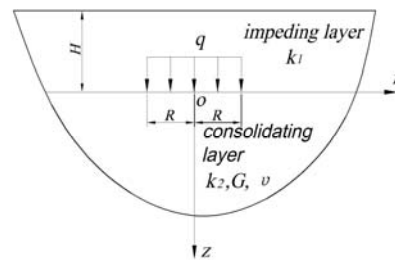


Fig. 3 Semi-infinite stratum subject to axisymmetric circular loading

$$k_2 \frac{\partial \bar{p}_f}{\partial z} = k_1 \frac{\bar{p}_f}{H} \quad (36)$$

$$\bar{\sigma}_{rz} = 0 \quad (37)$$

$$\bar{\sigma}_{zz} = qRJ_1(R\zeta)/(p\zeta) \quad (38)$$

By replacing $P_0 / 2\pi$ in the fundamental solution for point loading with $qRJ_1(R\zeta)/\zeta$, the fundamental solution for ring loading can be obtained.

NUMERICAL COMPUTATION AND ANALYSIS

All the above solutions should be evaluated numerically. In the numerical quadrature scheme, all infinite integrals

with respect to the Hankel transform parameter ζ are evaluated by using the Simpson rule and time domain solutions are computed using the approximate Laplace inverse formula suggested by Shapery (1962)

Vertical unit circular loads acting over a unit circle at $z=0$ for a semi-infinite stratum are considered. Solutions were used in the numerical study, where $k_1/k_2=1$, $R=1$, $h=1$, $q=1$, $v=0$, H from 0 to 5. The consolidation degree, excess pore pressure and shearing stress were analyzed. Non-dimensionalized time T is used to denote the time of solution, where $T=ct/R^2$.

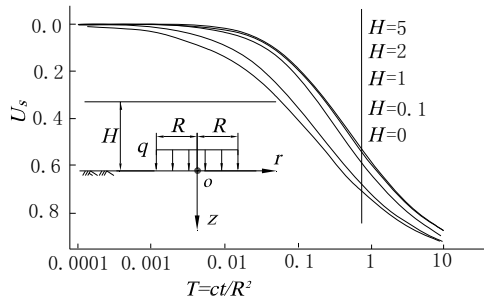


Fig. 4 Effect of the impeding layer on consolidation

It is apparent that the impeding layer has an obvious influence on the consolidating layer (in Fig. 4). The impeding layer impedes the permeating process of the consolidating layer. The thicker the impeding layer is, the longer the permeating line and the lower the consolidation process develops. When the impeding layer thickness is zero, the boundary then become fully permeable.

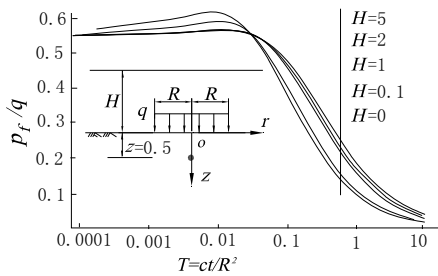


Fig. 5 Effect of the impeding layer on excess pore pressure

The change of excess pore pressure at $z=0.5$ under the center of the loaded area is shown in the Fig.5. The results have been plotted in the form of curves of p_f/q against $T=ct/R^2$. The Mandel-Cryer effect is obvious. The peak value appears when T is 0.01~0.1. But the peak value time become late when H from 0 to 5. The Mandel-Cryer effect is weakened while the thicker of the impeding layer increases.

The change with time of shearing stress at the place which of $z/R=0.5$ and $r/R=1$ is shown in the Fig.6. The

results have been plotted in the form of curves of σ_{rz}/q against $T=ct/R^2$. It can be seen that the shearing stress decreases during the consolidation. The peak value appears when T is about 0.1. The change of the shearing stress become smaller while the thickness increases in the semi-infinite stratum. The distribution of the shearing stress at the level of $z=0.5$ is shown in Fig.7. The shearing stress reaches the maximum when $r/R=1$.

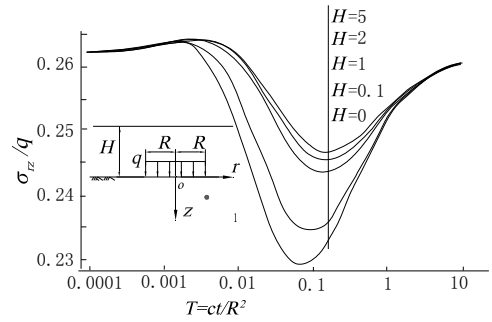


Fig. 6 Effect of the impeding layer on shearing stress

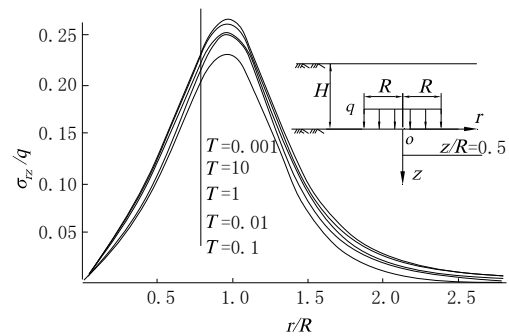


Fig. 7 Shearing stress distribution at $z=0.5$ with different time

CONCLUSIONS AND DISCUSSION

Explicit solutions for Laplace transforms of displacements, tractions and pore pressure were derived for a semi-infinite stratum with impeding boundaries and subjected to axisymmetric point loads and ring loads, respectively. The Laplace and Hankel transforms utilized in this paper are powerful. The solutions can be extended to deal with circular distributed and other distributed normal loadings. The result is convergent.

As a result of the calculation and analysis, it is apparent that the thickness of the impeding layer has an important influence on settlement, pore pressure and shearing stress of the consolidating layer. The thicker the impeding layer is, the weaker the Mandel-Cryer effect. The impeding layer delays the settlement progress of the consolidating layer. The shearing stress reaches biggest at the edge of the loading area.

REFERENCES

- Biot MA (1941). General theory of three-dimensional consolidation. *J. Appl. Phys.* 12: 155-164.
- McNamee J & Gibson RE (1960). Plane strain and axially symmetric problems of the Consolidation of a Semi-infinity Clay Stratum. *Q. J. Mech. and Appl. Math.*, 8(2): 210-227.
- Gibson RE, Schiffman RL, Pu SL (1970). Plane strain and axially symmetric consolidation of a clay layer on a smooth impermeable Base. *Q. J. Mech. Appl. Math.*, 13 (4): 505-519.
- Puswewala UGA & Rajapakse RKN (1988). Axisymmetric fundamental solutions for a completely saturated porous elastic solid. *Int. J. Engng. Sci.*, 26(5): 419-436.
- Gu YZ & Jin B (1992). Biot consolidation analytical solutions for multi-layer base subject to axisymmetric loading. *J. Geotechnical Engineering*, 20: 17-21.
- Huang CZ & Xiao Y (1996). Analytical solutions for two dimensional consolidation problems. *J. Geotechnical Engineering*, 18: 47-54.
- Wang JG & Fang SS (2001). The state vector solution of axisymmetric Biot's consolidation problems for multilayered poroelastic media. *Mechanics Research Communications*, 28: 671-677.
- Wang JG, Liu GR, Lin P (2002). Numerical analysis of Biot's consolidation process by radial point interpolation method. *International Journal of Solids and Structures*, 39: 1557-1573.
- Park KH & Banerjee PK (2002). Two-and three-dimensional soil consolidation by BEM via particular integral. *Comput. Methods Appl. Mech. Engrg.*, 191: 3233-3255.
- Cavalcanti MC & Telles JCF (2003). Biot's consolidation theory—application of BEM with time independent fundamental solutions for poro-elastic saturated media. *Engineering Analysis with Boundary Elements*, 27: 145-157
- Xie KH (1996). One dimensional consolidation analysis of layered soils with impeding boundaries. *J. Zhejiang University (Chinese)*. 30: 567-575.
- Xie KH, Xie XY, Gao X (1999). Theory of one-dimensional consolidation of two-layered soil with partially drained boundaries. *Computers and Geotechnics*, 24: 265-278.
- McNamee J & Gibson RE (1960). Displacement function and linear transforms applied to diffusion through porous elastic media. *Q. J. Mech. Appl. Math.*, 13: 89-111.
- Schapery RA (1962). Approximate methods of transform inversion for viscoelastic stress analysis. *Proc. 4th U.S. Nat. Cong. on Appl. Mech.* 1075.

THE THREE-DIMENSION SATURATED-UNSATURATED SEEPAGE ANALYSIS UNDER ATOMIZED RAIN OF HYDROPOWER PROJECT WITH HIGH SLOPE

Huan-Ling WANG¹ and Wei-Ya XU²

ABSTRACT: Based on the background of Goupitan Hydropower Project high slope to research saturated-unsaturated seepage problems under atomized rain. Firstly, influence factor of flood discharge atomization is analyzed, the rainfall intensity and distribution of flood discharge atomization is researched by fuzzy mathematics, using the measured data, and a membership function of flood discharge atomization is built on the basis of statistical analysis and expertise, and then forecast the rainfall intensity and range by the fuzzy comprehensive judge. Secondly, According to the control equation of saturated-unsaturated state, the integral saturated-unsaturated unsteady seepage control equation is constituted on the connection of saturation degree. The FEM computation format of mathematic model is deduced by Galerkin weighing margin method, the compute iterate mode of nonlinear FEM is developed, and the three dimensional FEM program of computing saturated-unsaturated unsteady seepage under ground seepage condition by FORTRAN language, the solving technical methods and convergence speed are improved. At last, based on the slope geological characteristics, the slope geological model and calculation model are building, the saturated-unsaturated seepage field under ground seepage condition for the high rocky slope is simulated, and the result could provide important scientific references for seepage control measures and safety estimate in Hydropower Project.

KEYWORDS: flood discharge atomized rain, saturated-unsaturated seepage, high rocky slope, Goupitan hydroelectric station

INTRODUCTION

In the 21st century, the applied research to resource development is still one of the main tasks of fractured rock seepage mechanics. Scholars of different countries to study the conception model and the characteristics of fractured rock mass saturated unsaturated seepage, For example, Flint et al. (1993)、Pruess et al. (1999) carried out a detailed study on the possible conceptual model of non-saturated fractured rock mass seepage at U.S. underground nuclear waste storage of to Yucca Mountain area; Dragila and Wheatcraft (2001) researched the non-saturated flow characteristics of fractured rock mass; Tokunaga and Wan (1997) researched the fluid speed under non-saturation through the laboratory test. In addition, the seepage research of oil and gas has developed rapidly with the rise of the oil industry, the problem of low permeability, thermal exploitation of heavy oil and other issues made more complex task to study seepage. All of these applied research to promote the saturated and unsaturated seepage of fractured rock mass development. At present, along with the development of hydropower resources, the center of the world high

dam construction quickly shifts to China. Since the construction of Ertan Hydropower Station, china has been successively designing and constructing a large number of high and ultra-high dams. The heights of these dams are close to 300m or even more than 300m, such as the Xiao wan Hydropower Station (height is 292.0m), Xiluodu Hydropower Station (height is 278.0m), Jinping Hydropower Station (height is 305.0m), Goupitan Hydropower Station (height is 232.5m) et al. The flood discharge and energy dissipation of these high dam always get the characteristics of “high-head, the large flux, steep slopes, narrow valleys”. The largest single-wide flux of flood discharge exceeded 200m³/s with a single-wide energy dissipation power over 300 MW/m. In a word, to analysis the flood dissipation problem is very important to these projects; the atomized rain phenomenon is inevitable within the vicinity of hydropower project when the high dam flood discharge (Liu et al. 2001; Su et al. 2002).

Generally speaking, the higher the water head, the greater the flux, the greater the rainfall intensity, the greater the flood discharge atomization (Sun, S.K et al. 2003; Zhang, H et al. 2003). Flood discharge atomized

¹ Lecturers, Key Laboratory of Coastal Disaster and Defence, Ministry of Education, Hohai University, China. Email: whl_hm@163.com

² Professor, Institute of Geotechnical Engineering, Hohai University, China. Email:weiyaxu@hhu.edu.cn

rain infiltrate through rocky slope back to the water table is a saturated and unsaturated seepage process. Natural rainfall is different from the flood discharge atomized rain in that the intensity of flood discharge atomized rain is much greater than the natural rainfall. Rainfall intensity is not the same at the infiltration border when atomized rain infiltrates (Wang 2006). The differences in external condition make the study of rock mass saturated-unsaturated seepage under seepage a quite particular problem. Atomized rain cause slope rock saturated-unsaturated seepage is a common phenomenon of hydropower projects. As to the seepage control measures and the slope stability analysis, the study of slope rock saturated-unsaturated seepage under atomized rain has a very significant practical meaning.

The largest flood discharge capacity of Goupitan Hydropower Project is 29100 m³/s and the flood discharge power of the dam is 42200MW, which is to the forefront of arch dams in the world. The atomized phenomenon could be very serious during flood discharge, and to analysis the slope saturated-unsaturated seepage is very important both to the slope stability analysis and the engineering measures.

GEOLOGICAL MODEL AND CALCULATION MODEL CONSTRUCTION OF DOWNSTREAM SLOPE

Goupitan hydropower station is the largest water resource conservancy of Wujiang River. The dam is located in the middle of the Wujiang River, Yuqing Xian in Guizhou Province. The drainage area the project controlled is 43250km² which is 49.2% of the entire valley. The total capacity is 6.451 billion m³, and the dam's design height is 230.5m. The power Station capacity is 3000 MW and the design capacity annual is billion KW/h (Changjiang Water Resources Committee 2001).

The valley shape of Goupitan is a symmetrical V shaped canyon. According to the slope type, the lithology and structure, the karsts development features, the unloading features and the influence extent of flood discharge, the natural slope is divided into five zone shown in Fig. 1, in the picture, I, II, III zone is flood discharge atomized region, IV, V zone are not affected by the flood discharge atomized rain.

based on the analysis of the right bank slope rock group, rock mass structure and the rock mass development environment, the calculation model is established, which is shown in Fig. 2. The interlayer in the bedrock is simulated by 1m entities element, the drainage hole of 2m entities element simulation. The model generated a total of 29,594 elements, 25,409

nodes. The elemental scales range between 1-10m and the largest is about 20m.

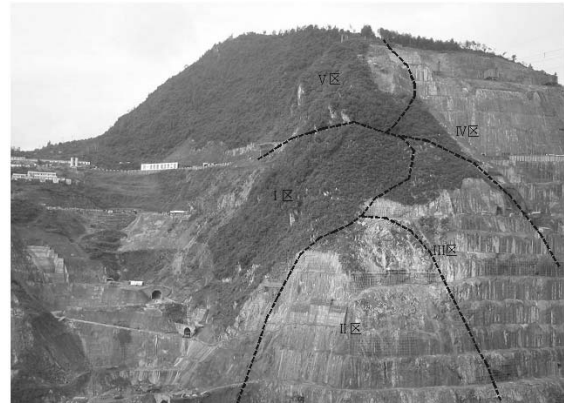


Fig. 1 Engineering geological general picture of downriver slope at Goupitan hydraulic station

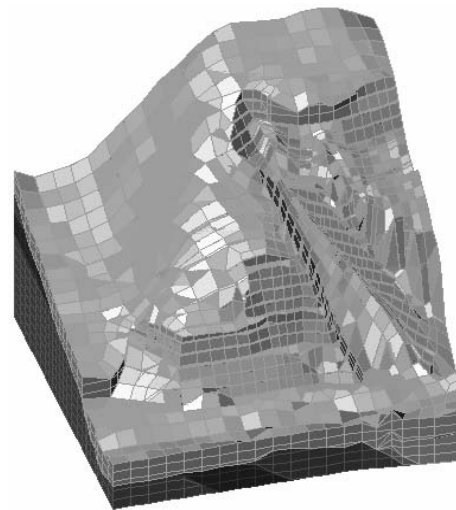


Fig. 2 Model network of right slope

FLOOD DISCHARGE ATOMIZATION INTENSITY AND DISTRIBUTION SCOPE FORECAST

Flood discharge atomization is a very complex physical process and has many impact factors. At present, the theoretical analysis methods used to study it is confronted with certain difficulties. Besides, physical modeling method is not mature. This paper is based on the methods of literature (Wang 2006) proposed flood discharge atomization problem, the fuzzy math theory is introduced, then forecast the rainfall intensity and range by the fuzzy comprehensive judge (the max degree of membership rule).

Slope Atomized Rainfall Fuzzy Comprehensive Evaluation Model

The rainfall intensity of flood discharge atomized

region of any point could be expressed as:

$$S=f(Q, H, h, a, b, c, x, y, z) \tag{1}$$

where, Q is flood discharge capacity, H is water level difference between upstream and downstream; h is elevation difference of the end of outshoot to downstream surface; a is terrain conditions influencing factors; b is flow exports boundary conditions and water tongue movement factors; c is influencing factors of weather conditions; x, y, z are space coordinates of be studied points, where x is along the water tongue flow direction, z is along the vertical direction.

It is not considered Parameters a, b, c impact for Goupitan dam flood discharge atomization, at the same time, the non-dimensional coordinates is considered. Set up $\beta=h/H, \lambda=x/H, \mu=y/H, \gamma=z/H$. Therefore, the formula (1) is simplified:

$$S=f(Q, H, \beta, \lambda, \mu, \gamma) \tag{2}$$

In these conditions, the factors set of atomized rainfall intensity and distribution is $(Q, H, \beta, \lambda, \mu, \gamma)$. Because of the weight distribution difficulty, it uses two judge methods: firstly, a comprehensive judge of the characteristics rainfall intensity order in flood discharge atomization, and its impact factor set is $\{Q, H, \beta\}$; Secondly, evaluating the distribution of rainfall intensity, and its impact factor set is $\{\lambda, \mu, \gamma\}$. The weight is obtained by fuzzy equation on basis of the prototype data and membership function established (Song, et al. 2003).

Rainfall intensity order $S_0=f(Q, H, \beta)$ judgment

The impact factors of rainfall intensity, Q, H, β is divided into 7 grade to judge, each distribution is get primarily on the basis of expert-level experience and the same projects analogy, the specific distribution shown in Table 1. The membership function of Rain-order shown in Table 2. According to the membership function in Table 2, the single factor evaluation matrix of experts, the comprehensive evaluation set of the first-class judge is obtained by A and synthesis computing. Finally, the max S evaluation result is made by the max degree of membership rule.

Table 1 Classification of S_0, Q, H, β

classification	1	2	3	4	5	6	7
S_0 /mm/h	1000	850	750	650	500	350	200
Q /m ³ /s	18000	16000	13000	10000	6000	2000	500
H /m	260	220	190	150	110	70	30
β	0.6	0.55	0.5	0.4	0.3	0.2	0.1

Where, Q_i is classification index of Q, H_i is classification index of H, β_i is classification index of β .

Table 2 Classification of S_0, Q, H, β

factors	weight \tilde{A}	Membership function
Q /m ³ /s	0.35	$\mu(Q)=exp((-2.8e-7)(Q-Q_i)^2)$ ($i=1,2,\dots,7$)
H /m	0.35	$\mu(H)=exp((-3.7e-4)(H-H_i)^2)$ ($i=1,2,\dots,7$)
β	0.3	$\mu(\beta)=exp(-50(\beta-\beta_i)^2)$ ($i=1,2,\dots,7$)

Comprehensive evaluation of atomization distribution scope

At $\{Q, H, \beta\}$ conditions, the grade of S_0 atomization characteristics rain intensity has drawn in the first-class judgment. Rainfall in space would show certainly distribution in the atomized rain-affected regions. Factor sets of rainfall intensity distribution could be expressed as $S=f\{\lambda, \mu, \gamma\}$. The judging steps of S have the same evaluation process of characteristics rainfall intensity order. The impact factor of the classification and membership function are shown in Tables 3 and 4.

Table 3 Classification of S, λ, μ, γ

classification	S /mm/h	λ	μ	γ
1	$S \geq S_0$	0.5	0.3	0.1
2	$S_0 > S \geq 1/2S_0$	0.7	0.5	0.15
3	$1/2S_0 > S \geq 1/10S_0$	1.0	0.75	0.25
4	$1/10S_0 > S \geq 1/50S_0$	1.5	1.05	0.35
5	$1/50S_0 > S \geq 1/100S_0$	2.2	1.4	0.5
6	$1/100S_0 > S \geq 1/500S_0$	3.2	1.85	0.7
7	$1/500S_0 > S$	4.5	2.35	1.0

Table 4 Distribution of membership function and weight of λ, μ, γ

factors	weight \tilde{A}	Membership function
λ	0.32	$\mu(\lambda)=exp((-4.5(\lambda-\lambda_i)^2)$ ($i=1,2,\dots,7$)
μ	0.35	$\mu(\mu)=exp(-7.0(\mu-\mu_i)^2)$ ($i=1,2,\dots,7$)
γ	0.33	$\mu(\gamma)=exp(-50(\gamma-\gamma_i)^2)$ ($i=1,2,\dots,7$)

Where, λ_i is classification index of λ, μ_i is classification index of μ, γ_i is classification index of γ .

Fuzzy Comprehensive Evaluation of Slope Atomized Rainfall.

A certain point of slope is used to the forecast point. The corresponding hydraulic conditions and boundary conditions are shown in Table 5.

Table 5 Hydraulic condition and boundary condition of a slope certain point

factors	Q/m ³ /s	H/m	β	λ	μ	γ
Measure point	10230	151.73	0.466	1.4	4.84	0.5

According to the table above that lists the hydraulic conditions {Q, H, β} and boundary conditions {λ, μ, γ} of slope of a certain point, the atomized rainfall is comprehensively evaluated based on the aforementioned two judges.

S₀ and its impact factor classification shown in Table 1, according to the membership function in Table 2, then the single factor evaluation matrix and comprehensive evaluation set B could be got.

$$\tilde{R} = \begin{bmatrix} 4.56E-08 & 8.94E-05 & 1.17E-01 & 9.85E-01 & 6.67E-03 & 5.80E-09 & 3.07E-12 \\ 1.31E-02 & 1.78E-01 & 5.82E-01 & 9.99E-01 & 5.25E-01 & 8.45E-02 & 4.16E-03 \\ 4.07E-01 & 7.03E-01 & 9.44E-01 & 8.04E-01 & 2.52E-01 & 2.91E-02 & 1.23E-03 \end{bmatrix}$$

$$B = A \circ \tilde{R} = \begin{pmatrix} 5.91E-02 & 1.27E-01 & 2.46E-01 & 4.37E-01 \\ 1.22E-01 & 8.40E-03 \end{pmatrix}$$

According to the max membership rule, the characteristics rainfall intensity is the fourth grade, that is, S₀=650mm/h.

Rainfall intensity distribution and its impact factors classification criteria are shown in Table 3. Membership function of single factor evaluation matrix \tilde{R} is obtained from Table 4.

Comprehensive evaluation set S is:

$$B = A \circ \tilde{R} = \begin{pmatrix} 8.33E-03 & 3.52E-02 & 1.67E-01 & 4.05E-01 \\ 3.41E-01 & 4.37E-02 & 0.00E+00 \end{pmatrix}$$

The distribution of characteristics rainfall intensity is the fourth grade in Table 1 by the max membership rule, that is, distribution ranges from 65mm/h to 13mm/h. Therefore, a forecast of the rainfall intensity distribution of flood discharge atomized areas ranges form 65mm/ to 13mm/h. The rain intensity of concentrated strong rainfall areas is 650 mm/h.

According to the above study on the atomized rainfall intensity, its distribution, and together with the classification of flood discharge atomization, the slope rain intensity distribution of these three atomization areas are as follows: the rain intensity of zone I is

13mm/h, which is in the downstream of cross-cutting steep slopes 615-645m elevation; the rain intensity of II zone is 65mm/h, which is in the north of I zone and 555m elevation of the ridge below; the rain intensity of III zone is 650mm/h, which is in the west zone II and 610m elevation of the slope below; The other two zones IV and V would be little effected on flood discharge atomization.

ANALYSIS OF SLOPE SATURATED-UNSATURATED SEEPAGE

Seepage Mathematical Model

The rock flow was also considered to comply with the law of Darcy in the process of unsaturated seepage (Gray et al. 1991a; Prues et al. 1999; Zhang et al. 2004).The whole equation of saturation and unsaturated seepage is (Mao 1999):

$$\frac{\partial}{\partial x} \left(k_j k_r(\theta) \frac{\partial h}{\partial x_j} + k_3 k_r(\theta) \right) = \left(C + \frac{\theta}{n} S \right) \frac{\partial h}{\partial t} \quad (3)$$

where, k^s is the hydraulic conductivity coefficient tensor for the saturation; k_{i3} is the hydraulic conductivity coefficient value with only number 3 coordinate axis in saturated hydraulic conductivity coefficient tensor; k_r is the relative permeability rate, which is the ratio of unsaturated hydraulic conductivity coefficient with the same kind of media of saturation hydraulic conductivity coefficient, $k_r = 1$ in saturation areas, $0 < k_r < 1$ in the unsaturated areas; n is the porosity; θ is the water content; C is specific water capacity, in the positive-pressure area $C = 0$; S_s is units storage; h_p is the pressure head; n is the porosity; t is the time.

The application of Galerkin finite element method to solve the above equation and deducing the domination equation is:

$$[D]\{h\} + [S]\left\{\frac{\partial h}{\partial t}\right\} = F \quad (4)$$

where, $[D]$ is the overall permeability matrix; $\{hp\}$ is the head column vector of unknown head node; $[S]$ is the capacity matrix; $\{\partial h / \partial t\}$ is the differential coefficient of node head to time; $[F]$ is the known constants, which is obtained by the known head node;

According to the FEM format and the time difference format and the boundary conditions, the three dimensional FEM program of computing saturated and unsaturated unsteady seepage under ground seepage condition by FORTRAN language is developed.

Boundary Conditions and Hydraulic Parameters

Initial volume water content or the initial suction of rock mass media is also need when unsaturated seepage calculation, as well as unsaturated hydraulic parameters $h\sim\theta$ and $kr\sim\theta$ relations curve (Panda, et al. 1999a; Panda, et al. 1999b). Initial volume water content is from tests, but $h\sim\theta$ and $kr\sim\theta$ curve could not reached by test and commonly used experience formula fitting. In this paper, introduce the formula of Van Genuchten model, the Van Genuchten model parameters is fitted by the least square in accordance with the corresponding materials analogy, and then the obtained fitting parameters would be as material information of medium to include the data document. The specific water capacity of procedures calculation is gained using linear interpolation method by $h\sim\theta$ and $kr\sim\theta$ curve. The weathered rock, because of its weathered serious and more basically tend to homogeneous, it would be as homogeneous material and to establish a hydraulic coefficient, its saturated hydraulic conductivity could be established by water pressure test method, that is, $\omega = 1L/min \cdot m \cdot m$. Unsaturated hydraulic parameters in weathering zone would be confirmed to refer the Three Gorges unsaturated hydraulic parameters of whole weathering zone (Zhang, et al. 2001).

The known head boundary: slope external water head boundary is normal water level 630.0m; the slope internal water head is 430.0m which is water level of rivers.

Analysis of Computer Result

The seepage fields of different duration under atomized rainfall, the seepage field decline condition after rainfall stopped in four days, as well as the seepage field where the slope was protected (spray the surface slope in the 10cm thick concrete.) were simulated. Cut two sections from the three-dimensional model to analyze, one is for the horizontal flow section1; the other is for vertical flow section2, which is shown in Fig. 3-6.

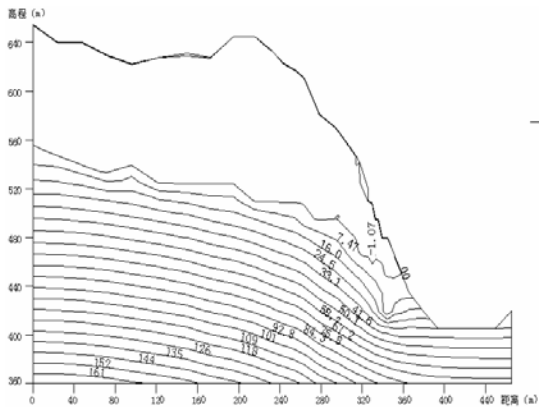


Fig. 3 Pressure contours of section 2 in flood discharge 1 hour

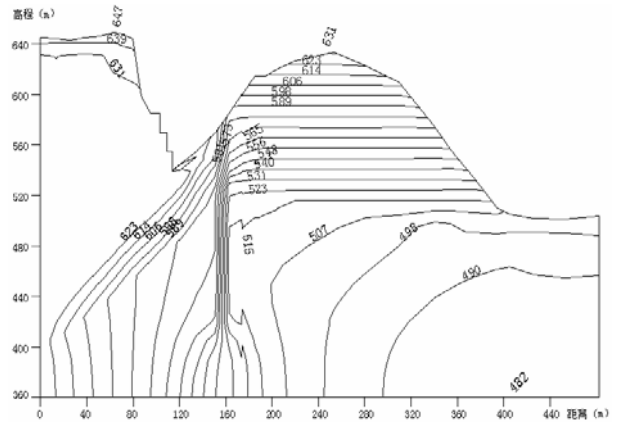


Fig. 4 Water head contours of section1 in flood discharge 1 hour

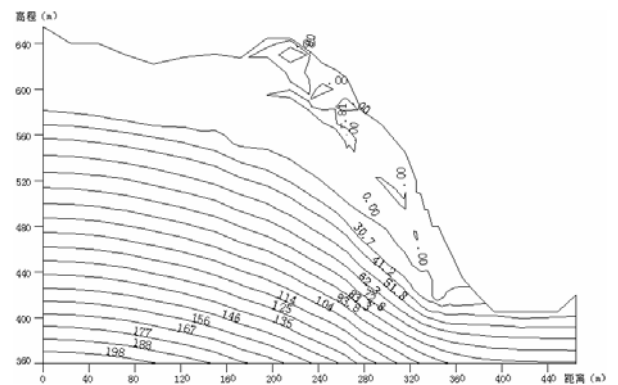


Fig. 5 Pressure contours of section2 in pro-rainfall 48 hour and flood discharge 24 hour

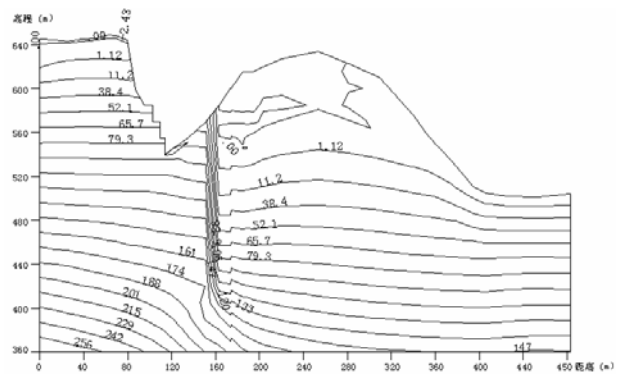


Fig. 6 Pressure contours of section1 in pro-rainfall 48 hour and flood discharge 24 hour

The results of these analyses are: 1) With the atomized rain continued, the slope surface water infiltration peak has been decreasing and the ground water level rising; Transient saturated zone of slope surface is gradually from local small regional into a large with the atomization continued to rain, and the transient saturated zone is in the slope surface, its maximum depth from the ground close to 30~40m; 2) Transient saturated zone caused by atomized rain infiltration is mainly in the shallow slope, so the stability of slope shallow is negative, especially in

the atomized area and the gentle slope site; 3) Drainage holes of slope saturated zone really played a focus on drainage and reduce the role of head, the impermeable curtain make the hydraulic gradient saltate, the infiltration surface greatly reduced, and its reducing rate is about 30~55m. The setups of impermeable curtain near the drainage holes could reduce the infiltration ratio-drop, which is very favorable to prevent the permeability failure of drainage holes. 4) If it has early rainfall, the water content has been increased in the slope at this time, the groundwater level has increased to a certain extent, then if it has flood discharge again, the ground water level of the slope rise faster, and the slope surface would be form a large transient saturated zone. Therefore, this condition has relatively large impact on slope stability; 5) The slope in the atomized zone were applied to protection measure, which could reduce the rate of groundwater level increase and is conducive to the slope anti-seepage. However, because the slope was protected by concrete, concentrated atomized rain make the slope surface water would not be discharged promptly and infiltration, so a large transient saturated zone were formed and these transient saturated zone is not conducive to stability. Therefore, the protect measures to slope is propitious to anti-seepage but make against drainage, and should increase the drainage measures of slope.

CONCLUSIONS

Rocky slope saturated-unsaturated seepage problem under flood discharge atomization is a major scientific issue in the construction of almost every high dam Project. For it is directly related to the layout of hydropower seepage control measures and slope safety and stability, the study on rocky slope saturated-unsaturated seepage problems under atomized rain is very important and of practical significance. Presently many theoretical problems need to be solved on the saturated-unsaturated seepage of rock, for example, the unsaturated hydraulic parameters problem, the mathematical modeling of rock seepage problem, and the numerical program problem, et al. In this research, fuzzy math is used to comprehensively forecast the atomized rain intensity and its distribution, which provided external convenience for the slope seepage calculation. The mathematical model of saturated-unsaturated seepage is built by equivalent continuous medium model, and then a corresponding numerical procedure is programmed and also the procedure for calculation make certain optimize; Applying the established geological model and seepage program, the saturated-unsaturated seepage to atomized slope of Goupitan hydropower project had been calculated the result could provide important scientific

references for seepage control measures and safety estimate in Hydropower Project.

ACKNOWLEDGEMENTS

The financial support provided by the Natural Science Foundation of Hohai University (Nos. 2008429411) and National Natural Science Foundation of China (Nos.50128908) for this work is gratefully acknowledged.

REFERENCES

- Pruess K, Faybishenko B, Bodvarsson GS (1999). Alternative concepts and approaches for modeling flow and transport in thick unsaturated zones of fractured rocks *Journal of Contaminant Hydrology* 38: 281-322.
- Flint LE, Flint AL, Hevesi JA (1993). Shallow infiltration processes in arid watersheds at Yucca Mountain, Nevada. In: Fifth International High Level Radioactive Waste Management Conference, Las Vegas, Nev., MA Proceedings. La Grange Park, III: American Nuclear Society: 2315-2322.
- Dragila MI & Wheatcraft SW (2001). Free-surface films: CGER, Conceptual Models of Flow and Transport in the Fractured Vadose Zone. Washington, D.C.: National Academy Press 217-242.
- Tokunaga TK & Wan J (1997). Water film flow along fracture surfaces of porous rock. *Water Resources Research* 33(6): 1287-1295.
- Liu SH & Liang ZC (2001). Prediction and prevention of atomized flow in hydroelectric engineering. *Engineering Journal of Wuhan University*, 34(3):1-5 (in Chinese).
- Su JM & Li HR (2002). The effects of atomization by flood discharge on downstream slope of Ertan hydroelectric station. *Hydrogeology and Engineering Geology* (2):22-25.
- Sun SK & Liu ZP (2003). Longitudinal range of atomized flow forming by discharge of spillways and outlet works in hydropower stations. *Shuili Xuebao*. (12): 53-59 (in Chinese).
- Zhang H, Lian JJ, Wang SD (2003). Numerical calculation of over flow atomization for Wantang Hydropower Station. *Shuili Xuebao* (4): 8-15(in Chinese).
- Wang HL (2006). Stability study on saturated—unsaturated fracture rock slope under atomized rain of high dam. Ph.D. Thesis, Hohai university. Nanjing, China.
- Changjiang Water Resources Committee (2001). Wujiang Goupitan Hydropower Station feasibility study report for the third fascicule-engineering geology. Ministry

- of water resources Changjiang Water Resources Committee.
- Song HC, Xu WY, Shao JF, Xu RC (2002). Stability analysis of unsaturated soil slope under atomized rain. *Journal of Hohai University* 30(6): 16-21(in Chinese).
- Gray WG & Hassanizadeh SM (1991a). Paradoxes and realities in unsaturated flow theory. *Water Resources Research*. 27(8): 1847-1854.
- Pruess K (1999). A mechanistic model for water seepage through thick unsaturated zones in fractured rocks of low matrix permeability. *Water Resources Research* 34(4): 1039-1051.
- Zhang YT (2004). The theory and application of rock hydraulics. *Chinese rock mechanics and engineering century achievements*. Hohai university press: 278-303 (in Chinese).
- Mao CX, Duan XB, Li ZY (1999). Numerical computation in seepage flow and programs application. Hohai university press (in Chinese).
- Panda BB & Kulailake PHSW (1999a). Influence of discontinuity geometry parameters and transmissivity on hydraulic behavior of discontinuous rock. *J. of Engrg. Mech.*, 125 (1): 41-50.
- Panda BB & Kulailake PHSW (1999b). Relations between fracture tensor parameters and permeability tensor parameters for discontinuous rock. *J. of Engrg. Mech.*, 125(1): 51-59.
- Zhang JF, Xu CM, Wang MX (2001). Seepage parameters of the completely weathered granite at the Three Gorges dam site. *Journal of Rock Mechanics and Engineering* 20(5): 705-709 (in Chinese).

STUDY ON UNLOADING ROCK MASS CONSTITUTIVE RELATIONSHIP

Jie LIU¹, Jian-Lin LI², Xiao-Hu WANG³, Jian-Jun QU⁴ and Ting ZHU⁵

ABSTRACT: The model experiment is applied to the geology material models, plaster cast models and sand syrup models. With analysis and fitting of the results got from model experiments, an initiatory increment constitutive relationship of jointed unloading rock masses is put forward. Fully considering the deficiency of the constitutive relationship, a new one is established with change on parameter choosing and physical meaning. Afterwards the constitutive relationship is put into ADINA, and an analysis is made for the high slope model of Geheyan hydropower station. By comparing the calculation results with those which were got by loading method, the rationality of the constitutive relationship is proved.

KEYWORDS: model experiments, constitutive relationship, jointed unloading rock masses

FOREWORD

With the unloading theories at the present time, for the single direction unloading experiments, theories on the unloading magnitude subsection decay process that modulus and poisson's ratio resulted from the main unloading direction have been put forward. And many satisfied experimental results have been obtained (Ha et al. 1998).

But this subsection unloading method also has some deficiencies. They are dealing with the continuous process into section, regarding the modulus and poisson's ratio of stress phases as constants, providing the instant parameters being difficult. It is mainly for the single direction unloading (Jian-lin LI 1999), and it takes the weather the single direction stress decreases or not as the unloading judgments criterion. Therefore, the stress fluctuation of rock mass in the practical engineering is spatial and poly directional. It also includes vulnerable area of joint plane. The subsection unloading is hard to meet the requirement. Then it need to study the correlation between spatial loading variation and the characteristics of rock mass (geometry characteristic and mechanical characteristic). It sets up three dimensional unloading constitutive relationships by providing the instant parameters to rock mass. It also gives the corresponding unloading judgments and still homogenizes rock mass on each block area as the isotropic material.

EXPERIMENTAL MODEL

The cube sample 250mm×250mm×250mm blocks are employed in the experiment. It simulates four in-situ rock mass sizes: 0.75m×0.75m×0.75m, 2.25m×2.25m×2.25m, 6.75m×6.75m×6.75m and 20.25m×20.25m×20.25m. The geometrical similarity scale CL is 3、9、27 and 81 (Jian-lin LI 2003) separately. The experiment is mainly for the main structure plane rock masses which have one group, two groups and three groups of joint planes. To simplify the model, the end region bonding is used in the combination of different groups of joint plane (Fig. 2b).

Geometrical Parameters of Experimental Model

One group of joint plane (Fig. 1a):

- ① NWW (angle 8°) A1 group space 2 meters.
- ② NEE (angle 38°) A2 group space 1 meter.
- ③ EW (angle 21°) A3 group space 2 meters

Two groups of joint plane (Fig. 1b):

- ① NEE+NWW B1 group.
- ② NEE+EW B2 group.
- ③ NWW+EW B3 group

The joint planes above are shown in the Fig.1.

Three groups of joint plane (Fig. 1c)

- ① NEE+NWW+EW C₁ group

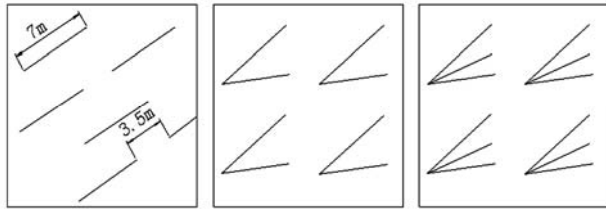
¹ Associate Professor. College of Civil & Hydropower Engineering, Three Gorges University, China. Email: liujiea@126.com

² Professor, Key Laboratory of Geological Hazards on Three Gorges Reservoir Area, Ministry of Education, Three Gorges University, China. Email: ljl@ctgu.edu.cn

³ Assistant engineer, Hubei Qingjiang Hydropower Development Co., Ltd., China. Email: wxh15714@126.com

⁴ Graduate student, Three Gorges University, China. Email: qujianjun493@163.com

⁵ Graduate student, ditto. Email: titi0915@yahoo.com.cn



a. One group of joint plane b. Two groups of joint plane
c. Three groups of joint plane

Fig. 1 The conventional diagram of joint planes

Parameters of Experimental Material

Three kinds of molding material are used (Jian-lin LI 2003) in the experiment. They are geomechanics molding material, sand pulp molding material and plaster molding material. The plaster molding material is mainly used to simulate one group of joint plane. The geomechanics molding material is mainly used to simulate two and three groups of joint plane. And the sand pulp molding material can simulate the three groups of joint plane at the same time. The mixture ratio and mechanical parameters of geomechanics molding material is shown in the Table 1.

Table 1 The mixture ratio of sand pulp molding material and its mechanical parameters

mixture ratio					Bulk density	Compressive	Modulus
barite powder	iron powder	gypsum	water	admixture	/kN·m ³	strength /MPa	/GPa
2.39	2.39	0.48	1	/	28.9	5.5	1.2

Table 2 The correlated data of NWW direction structure

points	1	2	3	4	5	6	7	8	9	10	11
E_t (Gpa)	25.904	25.116	18.234	15.255	12.884	9.978	7.409	5.203	4.659	4.553	3.947
J_2 (MPa) ²	6.363	2.216	0.473	0.485	0.996	1.481	2.078	2.772	3.461	4.107	4.961
T(MPa)	6.751	4.925	3.546	2.625	1.846	1.371	0.968	0.615	0.308	0.049	-0.259
P(MPa)	7.638	5.813	4.433	3.512	2.734	2.258	1.855	1.503	1.195	0.936	0.628
d	2.000	2.000	2.000	2.000	2.000	2.000	2.000	2.000	2.000	2.000	2.000
θ	-0.637	-0.321	0.322	0.409	0.179	0.323	0.423	0.497	0.548	0.583	0.617
E_t / E_0	1.000	0.970	0.704	0.589	0.497	0.385	0.286	0.201	0.180	0.176	0.152

Table 3 The statistical table of displacement differences between the scheme II and the scheme III

Category	100 platform	128 platform	150 platform	165 platform	180 platform	206 highway
Axial line section of 4# diversion tunnel						
Displacement of Vertical river direction	0.58	0.81	0.57	0.42	0.46	0.29
Displacement of along river direction	-1.7	-1.0	-0.2	-0.9	-1.15	0.8
Displacement of plumb direction	3.6	6.3	4.4	4.88	4.55	4.2
Axial line section of 3# diversion tunnel						
Displacement of Vertical river direction	0.81	0.52	0.56	0.50	0.46	0.72
Displacement of along river direction	-1.5	-1.7	-1.3	-1.3	-1.5	-0.4
Displacement of plumb direction	3.2	6.7	5.1	4.8	4.9	4.5

THE FITTING AND IMPROVEMENT OF CONSTITUTIVE RELATIONSHIP

According to the original statistic data, it selects the

tangent modulus E_t to be the main limiting quantity of unloading displacement of rock mass. It acquires the relation conventional diagram between the tangent modulus E_t and the others' variables. And it also ascertains the increase and decrease relationship of variables approximately. Then it uses the MATLAB to write the program. The

experimental data with multiple regression analysis(Wei-Song XIE 2003) will be analyzed according to the least cube method. With deleting the redundant parameters, it ascertains each parameter and the experiential constitutive. The following analyses are all based on the isotropic homogeneity of rock mass.

Experimental Data

The experiment makes three directional loading & unloading of each sample. The stress and strain of each direction in several periods are memorized. Then the tangent modulus is calculated, three-dimensional principal stress, triaxial strain, three-dimensional principal stress invariants, three-dimensional deviatoric stress invariants and Lode's parameters of each block; the positive stress and shear stress, attenuation ratio of tangent modulus of each structure plane are also calculated. Some correlated calculating quantities of sand pulp component which includes one group of structure plane are shown in the Table 2.

Fitting Constitutive Relationships

(1).The formula used in the unloading process:

$$\frac{20 - \sin(\theta)}{2 + \sqrt{J} / 2R} \times \frac{e^{\times}}{4\pi - d^{-} \arctan(T/P)} \times \frac{5c \cos \varphi + 4R \sin \varphi}{(\pi - \sin \varphi)(2R + c)} - \frac{2c \cos \varphi + 1.5R \sin \varphi}{(\pi - \sin \varphi)(2R + c)} = \frac{E}{E} \tag{1}$$

(2).The condition of entering the unloading process:

- ① There are structure planes in the divided block.
- ② There are no states such as pull damage, press damage, tensile-shear damage and compress-shear damage in the divided block. If there are these situations, the elastic modulus to be zero will be chosen.
- ③ $T > \frac{R}{2}$, T_{max} are the historical maximum positive stresses.
- ④ When the variable T decreases and if it satisfies the four conditions, it will enter the unloading process.

Condition of Dapping the Unloading Process

When the variable T augments, it will dap the unloading process. After dapping the unloading process, the false deteriorated E_t of tangent modulus used in the loading calculation (the tangent strength of rock mass during the unloading process) should use the E_t which is dapping the unloading process.

Deficiency and Improvement of Model

The status in application of constitutive relation above is in the reference (Jie LIU et al. 2005). During the calculating analytical process, it have been found that there are some deficiencies as follows.

(1). The attenuation coefficient of tangent modulus E_t doesn't always change in the interval. $[0,1]$. When the attenuation coefficient E_t / E_0 is less than zero, it indicates that the tangent modulus E_t is negative. And when the attenuation coefficient E_t / E_0 is more than one, it indicates that tangent modulus E_t is more than the original modulus. The above two situations don't agree with the practical engineering.

(2). It have been found that some parameters such as Lode's parameters and the attenuation coefficient E_t / E_0 are not definite during the further experimental analysis. It needs a further parameter sensibility analysis.

(3). It doesn't compound the there failure modes well. The fitting formula which is improved should meet the following conditions:

ws. If $T \geq (c + P \tan(\varphi))$, the rock mass occurs shearing damage. If $P \geq Rc$, the rock mass occurs compressive damage. If $P \leq Rt$, the rock mass occurs tensile damage. Therefore, the fitting formula should satisfy $T < (c + P \tan(\varphi))$ and $P < Rc, P > Rt$. And the relative variables combination will be used in the following fitting formula.

(4). When the attenuation coefficient E_t / E_0 is less than zero, it will have a situation that the stiffness matrix is negative. Moreover, the numerical amplitude of fluctuation of multi-parameter is too high. It will easily result in the calculating divergent phenomena.

Improved Constitutive Relationship

Some improvements have been made as follows based on the deficiencies of constitutive relationship above.

Parametric Affection Analysis

According to the experimental data, some parameters have been deleted basing on the sensibility analysis. The final chosen parameters and the relation points of E_t and their fitting chart are as follows.

It can be seen from the Fig.2 that the positive stress on the structure plane affects the variation of deformation modulus E_t directly. The deformation modulus E_t reduces with the positive stress decreasing on the structure plane. This indicates that the positive increases on the structure plane. It results in expansion of crack.

And the cross correlation attenuate that occurs on the Structure plane in both sides of crack. And then it results in the shear resistant and deformation resistant abilities

of rock mass decrease. Therefore, according to the concentration region of points in the Fig. 2, it can be fitted to the model: $E_t=6.975+2.363P$ by Straight-line. And its maximum relative error is 17% with the mean square deviation 8.39. From the linear fitting results it is known that the positive stress on the structure plane and deformation modulus of rock mass are linear relations basically.

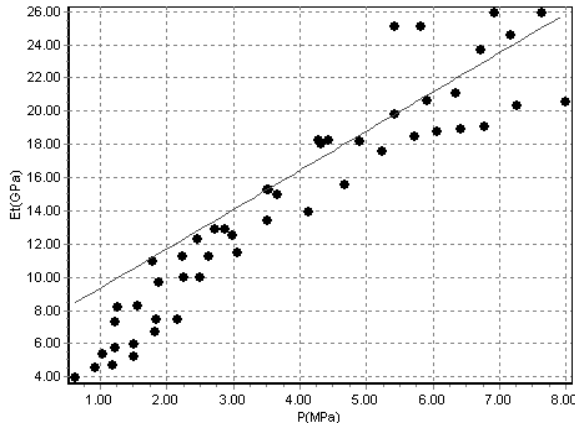


Fig. 2 P and E_t points

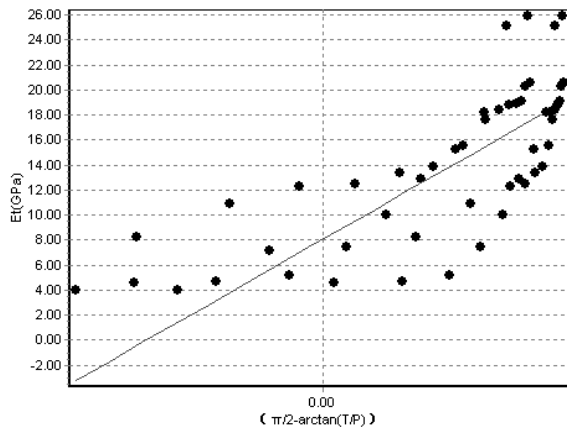


Fig. 3 $(\pi/2-\arctan(T/P))$ and E_t points

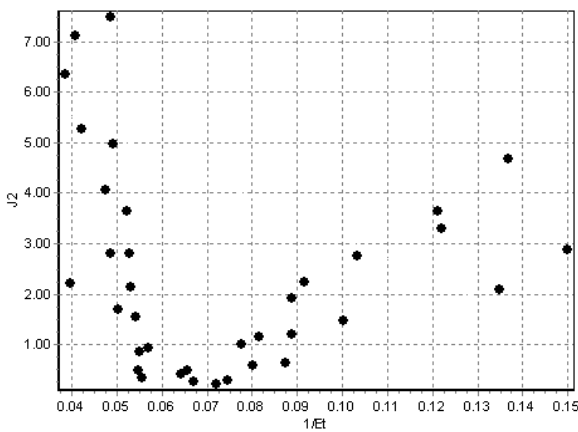


Fig. 4 Chart of J_2 and $1/E_t$ points

The $(\pi/2-\arctan(T/P))$ indicates the angle between the resultant force on the structure plane and the tangential direction of the structure plane. From the Fig. 3, it is known that the positive stress on the structure plane affects the variation of deformation modulus E_t directly. The deformation modulus E_t decreases resulted from the positive stress on the structure plane reduces. The explanation in physics is: under the resultant force in variable condition, if $(\pi/2-\arctan(T/P))$ is smaller, the tangential component on the structure plane is bigger. The shear slide trend on the structure plane increases resulted from it. But the normal component on the structure plane decreases at the same time. It results in contact alteration on the structure plane. The result getting from them is the deformation modulus of rock mass decreasing. Then according to the concentration region of points, it can be fitted to the model: $E_t=8.058+15.16(\pi/2-\arctan(T/P))$ by straight-line. As its maximum relative error is 22%, its mean square deviation is 18.70. It is only a little bigger than the square deviation 15.34 which is fitted by quadratic fitting. In order to simplify the final fitting formula, it is known that the variable $(\pi/2-\arctan(T/P))$ and the deformation modulus of rock mass are basically linear relations.

J_2 is the second invariant of stress deviator tensor. According to the concentration region of points, it can be fitted to the model: $J_2=972.43(1/E_t)^2+(-212.253)(1/E_t)+12.320$ by quadratic curve. And its maximum relative error is 15%, with the mean square deviation 24.20. From the fitting results, it is known that the positive stress on the structure plane and the deformation modulus of rock mass are non-linear relations of quadratic curve basically. Then based on this, the constitutive relationship below is in the first power formula of deformation modulus. And the denominator will be displaced by $J_2^{1/2}$.

Analysis under the Destroyed Condition of Rock Mass

Considering the three kinds of failure modes of rock mass at the same time, when the $T \cong (c+P\tan(\varphi))$, shear damage of the rock mass will occur. When the $P \cong Rc$, compression damage of the rock mass will occur. And when the $P \cong Rt$, tensile damage of the rock mass will occur. Therefore, the fitting formula should satisfy the $T < (c+P\tan(\varphi))$ and $P < Rc, P > Rt$. The relative variables combination will be displaced into the fitting formula as follow.

Fitting Constitutive Relation Ships

Based on the data and analysis above, according to adopting cut-ami-try method and inserting variables combination of different modes, the following formula finally can be acquired.

$$E = E \times \frac{(c + P \tan \phi) [\frac{\pi}{2} - \arctan(T / P)]}{(T + c + P \tan \phi) (\frac{\pi}{2} + \frac{\sqrt{J}}{2R_c})} \times \frac{P + R}{R_c} \tag{2}$$

Inserting the formula

$$E_t = d\sigma / d\varepsilon \tag{3}$$

The constitutive of unloading augmentation can be acquired.

$$d\sigma / d\varepsilon = E \times \frac{(c + \tan \phi) [\frac{\pi}{2} - \arctan(T / P)]}{(T + c + \tan \phi) (\frac{\pi}{2} + \frac{\sqrt{J}}{2R})} \times \frac{P + R}{R} \tag{4}$$

APPLICATION EXAMPLE

Computational Scheme

This constitutive relationship was inserted into the finite element analytical program ADINA into. The three-dimensional model analysis of high slope for the Geheyan power station on Qingjiang River is shown in the Fig. 5 and Fig. 6. And we do some finite element analysis based on it.

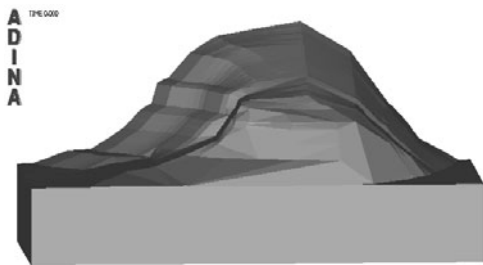


Fig. 5 The view along the river of 3D calculating model

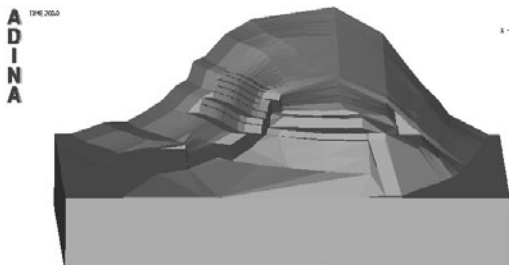


Fig. 6 The view along the river after excavation of 3D calculating model

We consider several computational schemes below during the analysis.

Scheme I: The finite element analysis is under the original stress state.

Scheme II: The finite element analysis is under the excavation state without considering the fracture damage.

Scheme III: The finite element analysis is with considering the fracture damage state.

We mainly list some calculating achievements of scheme II and scheme III.

Comparing the results of scheme II with the results of scheme III, we subtract the calculating displacement results of scheme II based on the calculating displacement results of scheme III. And the final results are shown in the Table 3.

CALCULATING ANALYSIS

It takes the displaced position after stress subsidence of the original state as zero point. It is different from the situation that the rock mass of common slope after excavation deforms to the hollow plane side (it is inclined to the downstream direction). The slope of the water transmission tunnel exit deforms to the upstream side. These calculating results accord with the monitoring data of several monitoring points on the exit slope. The monitoring data shows that the top of downstream slope after excavation has abnormal displacement inclined to the upstream. It takes the point PL32019 on the top of slope for example in the Fig.7. The negative value of displacement indicates that it is inclined to the upstream. And the positive value of displacement indicates that it is inclined to the downstream.

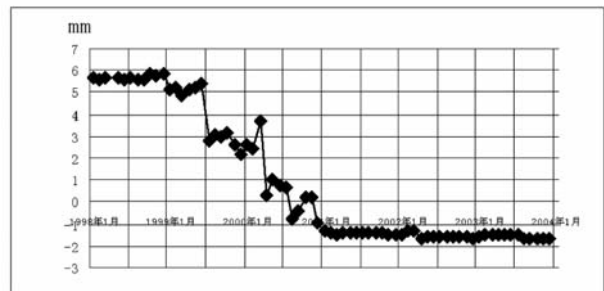


Fig. 7 The deformation conditional curve along the river of PL32019 point

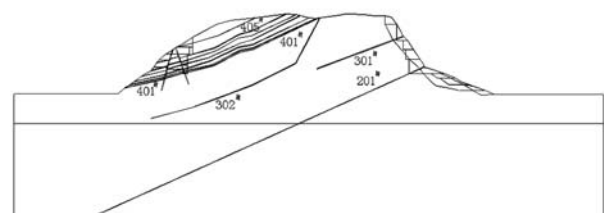


Fig. 8 The conventional diagram of main structure plane about the high slope of Geheyan power station

This phenomenon is mainly decided by the geological structure of slope (shown in the Fig. 8). That is to say, the bottom of 201 interbed is the weak shale. And the elastic modulus is less than 0.35 GPa. The region between the top of 201 interbed and 301 interbed is the heavy layer or thin-layer argillaceous limestone with fine particle oolitic limestone. Its elastic modulus is close to 5 GPa. The region between 301 interbed and the regolith on the top of slope is thin-layer argillaceous limestone with fine particle oolitic limestone. And its elastic modulus is close to 12 GPa. It comes into being hardened rock mass gradually from up e to down, because of the 201 interbed and the 301 interbed are both the countertendency bedded planes. This situation results in that the deformation of the higher slice hardened rock mass inclined to the hollow plane(the downstream direction) is less than the deformation inclined to the upstream resulted from lower slice hardened rock mass rebounded. This deformation is a component of the deformation resulted from lower slice hardened rock mass rebounded. Under the same excavated unloading magnitude, if the elastic modulus is smaller, the rebounded magnitude is bigger. On the other hand, the rearward shift of slope will cause the rearward shift of gravity center. It manifests that the weak shale on the bottom of 201 interbed will be crowded out. It accelerates the deformation inclined to the upstream of top calcareous rock resulted from the weak shale. The action of the two aspects causes the deformation on the top of slope expanding to the upstream side.

The unloading leads to the rock mass quality near the excavation plane deterioration and the deformation parameter decreases. The decrease mainly indicates that the elastic modulus reduces and the poisson ratio increases. For the vertical excavation plane on the top of slope, the decrease of deformation parameter will accelerate the displacement inclined to the downstream. For the rock mass on the bottom of interbed, especially for the weak shale on the bottom of the 201 interbed, the unloading will lead to the slippage, developing and even expansion(in the tensile stress region) of its internal crack. And it characterizes expansion phenomenon macroscopically. This expansion accelerates the rock mass on the top of interbed inclined to the upstream. Then it increases the displacement inclined to the upstream of the rock mass on the top of the slope. According to the calculating results, the action effect of the latter is more than the action effect of the former. The maximum displacement inclined to the upstream under the unloading state is still on the top of slope. But it is bigger by 2.97 cm than the excavation state is.

Considering the state after unloading, it indicates the diminution of vertical stress after the excavation causes the crack expansion paralleled with the ground. Then it occurs the expansion bulging phenomenon of rock mass.

Without considering fracture damage, that is to say, without considering attenuation of rock mass mechanical parameter, the rebound of rock mass only includes elastic rebound, and it doesn't include fracture damage expansion.

Considering the unloading state, it causes the rock mass quality near the excavation plane deterioration. And the deformation parameter decreases. The decrease mainly indicates that the elastic modulus reduces and the poisson's ratio increases. For the vertical excavation plane on the top of slope, the decrease of deformation parameter will accelerate the displacement inclined to the downstream. For the rock mass at the bottom of interbed, especially for the weak shale at the bottom of the 201 interbed, the fracture damage of rock mass will result in the slippage, developing and even expansion(in the tensile stress region) of its internal crack. And it characterizes expansion phenomenon macroscopically. This expansion accelerates the rock mass on the top of interbed inclined to the upstream. Then it increases the displacement inclined to the upstream of the rock mass on the top of the slope. According to the calculating results, the action effect of the latter is more than the action effect of the former. The maximum displacement inclined to the upstream under the fracture damage state is still on the top of slope. But it is bigger by 1.7 cm than the excavation state.

Considering the elastic modulus decrease resulted from unloading, it improves the stress concentration phenomenon. The tensile stress of rock mass decreases from 1.3 MPa to less than 0.54 MPa. For the rock mass with minimal tensile strength, when the tensile stress is more than the tensile strength, it may result in the fracture damage of rock mass. With the stress redistribution resulted from the fracture damage, it will decrease the tensile stress in this region.

CONCLUSIONS

(1) The improved jointed unloading rock mass constitutive is based on parameter sensibility analysis. the positive stress P on the structure plane, the angle $(\pi/2 - \arctan(T/P))$ between resultant force on the structure plane and tangential direction of structure plane are defined and also the influence of the second invariants of stress to the attenuation coefficient E/E_0 about a point of the rock mass.

(2) The improved jointed unloading rock mass constitutive satisfies the three kinds of single stress distributions of rock mass damages well. They are shearing damage, compression damage and tensile damage.

(3) The improved jointed unloading rock mass

constitutive keeps the attenuation coefficient E/E in the region $[0,1]$ well. It conforms with the practical engineering. It also makes the stiffness matrix be non-negative. Then it enhances the astringency of calculation.

(4) According to the three dimensional model analysis, the fact that the deformation on the top of downstream slope about the Geheyan power station is different from the common slopes which is putting forward. And the main factors are analyzed.

ACKNOWLEDGMENTS

The research has been supported in part by National Natural Science Foundation of P.R. China (No. 90610029), The Higher School Imbursing Project of Three Gorges University of P.R. China (No. 00956).

REFERENCES

- Ha QL, Li JL, Zhang YX (1998). The Non-linear Rock Mass Mechanics of Jointed Unloading Rock Mass. China Architecture Industry Publishing Company: 100-102.
- Li JL (1999). Unloading Rock Mass Mechanics Theory and Application, China Architecture Publishing Company: 156-158.
- Li JL (2003). Unloading Rock Mass Mechanics. Beijing, China Water Resources and Hydropower Engineering Publishing Company: 50-51.
- Xie WS (2000). Numerical Analysis. Tianjing University Publishing Company: 92-94.
- Liu J, Li JL, Huang YS (2005). Study on Unloading Rock Mass Constitutive. Earth and Environment, 3:112-116.

DESTRUCTURATION CONSTITUTIVE MODEL FOR SOFT CLAY

Xiao-Jun YU¹ and Zhi-Hong QI²

ABSTRACT: Considering the test results, a developed destructuration, is presented, and results from undrained triaxial shear tests show that the model can well describe the stress-strain characteristics. In this model, the stress-induced anisotropy of soft soil is taken into account. Meanwhile, electrical resistivity method, which is convenient, continual, economical and practicable, is taken to define and measure the destructuration variable. In addition, the destructuration evolvement law employed is established by the test results. The model has advantages comparing with the traditional models.

KEYWORDS: soft clay, destructuration variable, anisotropy, constitutive model, electrical resistivity anomalies

INTRODUCTION

Natural clays have their structure which must be spoiled during the deformation process. In previous studies, constitutive models often neglected the soil structure affection, and accordingly model calculated results deviated from engineering practice.

Recently, there are two kinds of macro-constitutive models considering soil structure, the one is solid mechanical method, and another is damage mechanical method. The familiar destructuration models are Gens & Nova (1993) model, Rouainia & Wood (2000) model, Cudny (2003) model, and S-CLAY1S model (Karstunen et al. 2005). In defining and determining the quantitative structure parameters of destructuration constitutive models, some of the conventional soil testing methods have lacked appropriate equipment to probe into soil samples, and some are very difficult to operate while the others are too costly.

Electrical resistivity of the soil can be considered as a proxy for the spatial and temporal variability of some physical properties such as structure, water content, or fluid composition. Because the electrical resistivity method has some remarkable superiority such as rapid, economy, convenient, continuous, practicable and nondestructive, consequently, recently, some experts applied for the electric resistivity method in studying quantification structure and its variability. For example, Tabbagh et al. (2000) applied for the electrical resistivity method to describe the horizontal and vertical variability of soil structure and properties at the scale of interest. Jackson (2000) identified electrical resistivity anomalies in a roadside embankment following the repeated

measurement of resistivity over 18 months. Samouelian et al. (2003) monitored artificial cracks as they deepened and observed an increasing apparent electrical resistivity anomaly over time.

These achievements indicate that soil electrical resistivity parameters can reveal the variability of soil structure and properties, and has the preferable foundation to define and determine the quantitative structure parameters.

In existing destructuration constitutive models, the destructuration evolvement functions either have too many hypothesize or are very complicated in calculation. In addition, anisotropy of soft soil is often neglected in the traditional constitutive models, and accordingly model calculation results were far away from engineering practice.

In this paper, electrical resistivity anomaly is firstly taken to define and measure the destructuration variable, and destructuration evolvement law employed is established by the test results. Additionally, Stress-induced anisotropy of soft clay is considered in establishing the destructuration constitutive model. Drained triaxial shear tests show that the proposed model can reflect the deformation of soft clays and is satisfactory in its application.

TEST RESEARCH

Test Scheme

Undisturbed soil used for the tests is Lianyungang marine clay. The index properties for the soil are

¹ Associate Professor, Key Laboratory of Ministry of Education for Geomechanics and Embankment Engineering, Hohai University; Yancheng Institute of Technology, Civil Engineering, China, Email: flyingfish7101@126.com

² Engineer, College of Architectural & Civil Engineering, Jinling Institute of Technology, China, Email: qzh@jlit.edu.cn

summarized in Table 1.

For establishing the destructuration evolution function, the triaxial drained shear test with the simultaneous electrical resistivity test is used.

Table 1 Index properties of the soft soil

ω / %	ρ	G_s	e	ω_L /%	ω_p /%	C /kPa	Φ ($^\circ$)
65.4	1.68	2.64	1.68	65.2	29	2.0	13.4

Test Results and Discussion

Definition and measurement of destructuration variable

The proposed definition for the destructuration variable is

$$\omega = \frac{\Delta\rho_{t0} - \Delta\rho_t}{\Delta\rho_{t0} - \Delta\rho_{ta}} \tag{1}$$

Parameters $\Delta\rho_{t0}$ 、 $\Delta\rho$ and $\Delta\rho_{ta}$ are respectively electrical resistivity anomalies of undisturbed samples and disturbed samples and remolded soil samples,

$$\Delta\rho = \frac{\rho - \rho}{\rho} \tag{2}$$

Parameters ρ_{t0} 、 ρ_t are respectively average electrical resistivity of undisturbed samples and disturbed samples, and

$$\rho = \frac{\rho_v + 2\rho_H}{3} \tag{3}$$

Parameters ρ 、 ρ_H are respectively vertical and horizontal electrical resistivity of samples.

Destructuration evolution function for the stress-strain relationship

Results from triaxial drained shear tests on the soft soil show that there is a good relationship between plastic volumetric strain and destructuration variable gotten from electric resistivity anomalies. Fig.1 illustrates that parameter ω will increase with the development of the plastic volumetric strain of the soils.

Considering the results from triaxial drained shear tests and electric resistivity tests, the destructuration evolution function has the following form,

$$\ln(1 - \omega) = -(a\varepsilon^2 + b\varepsilon) \tag{4}$$

Parameter ω is destructuration variable; ε_v^p is plastic volumetric strain; parameters a, b are soil parameters obtained by tests.

Eq. 4 shows that ω is zero when ε_v^p is zero, and it

will develop and trend to 1 with the increase of the plastic volumetric strain, as shown in Fig. 1.

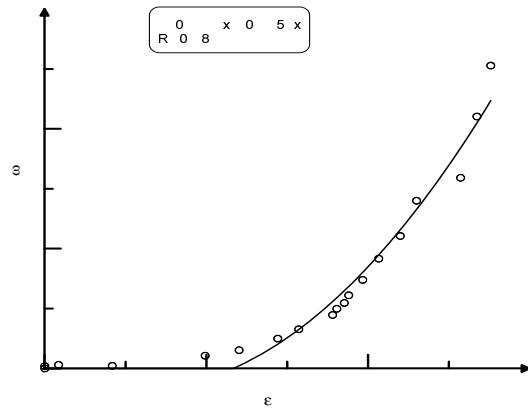


Fig. 1 The relation between ω and ε_v^p

CONSTITUTIVE MODEL

The Yield Surface

Considering the stress path tests' results and S-CLAY1S model (Karstunen, 2005), the yield surface of natural soft clay can be given as Fig. 2. Assume that the hardening variable α in the model keeps its original value α all the time.

In the simplified stress space of the triaxial test, the yield surface expression is given by

$$p' = p' + \frac{(q - \alpha p')}{M - \alpha} \frac{1}{P'} \tag{5}$$

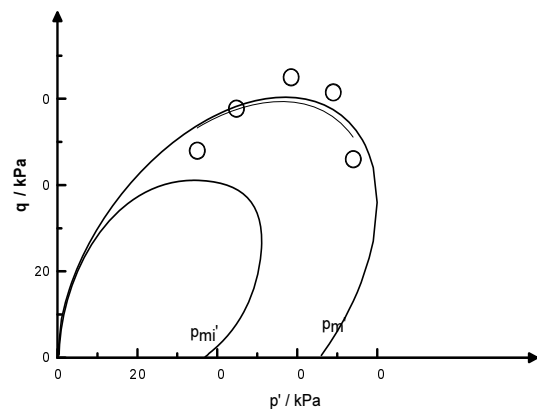


Fig. 2 The yield surface

The Relationship Between ω and p'_{mi} / p'_m

The notional intrinsic yield surface for the remolded soil is assumed to be of the same shape and orientation as the yield surface of natural soil, but size is smaller, as shown in Fig. 2. The size of the yield surface for the remolded soil is specified by a parameter p and this is

related to the size of the yield surface for the natural soil.

The results of the tests show that the yield stress ratio p' / p_m' relates well to the destructuration variable ω and the relationship is given as Fig. 3 and Eq. 6 (Yu 2009). The expression of ω is shown as Eq. 1

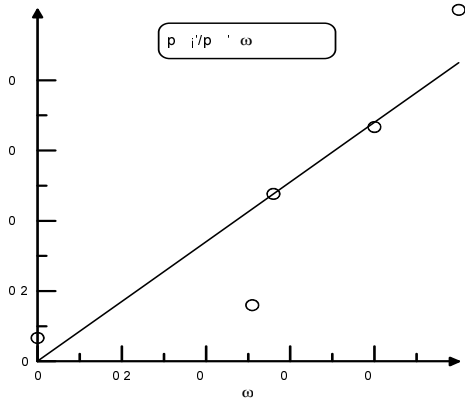


Fig. 3 The relation of ω and p'_{mi}/p'_m

$$p'_{mi} / p'_m = \omega \tag{6}$$

Destructuration Evolvement Function

Destructuration evolvement function, describing the gradual damage process of soil structure with the development of plastic strain, is shown in Eq. 4.

Hardening Law

Volumetric hardening law is the same equation as of the Modified Cam Clay model, and the change in size of the intrinsic yield surface relates well to the plastic volumetric strain increment:

$$dp'_{mi} = \frac{vp'_{mi}d\varepsilon_v^p}{\lambda - k} \tag{7}$$

Stress-strain Relationship

Combining Eq. 6 and Eq. 7, following expression is obtained:

$$d\varepsilon = \frac{(\lambda - k)dp'_m}{vp'_m} + \frac{(\lambda - k)(d\omega)}{v\omega} = d\varepsilon^I + d\varepsilon^{II} \tag{8}$$

The increment of plastic volumetric strain can therefore be considered as consisting of two components. The one is related to the increase of size for the yield surface, and another is the additional plastic volumetric strain occurring because of destructuration. The increment of plastic volumetric strain is expressed as:

$$d\varepsilon = \frac{(\lambda - k)dp}{vp} \tag{9}$$

$$d\varepsilon = \frac{(\lambda - k)(d\omega)}{v\omega} \tag{10}$$

Transforming Eq. 5, and combining Eq. 9, we can get:

$$d\varepsilon = \frac{\lambda - \kappa}{v} \left[\frac{(M - \alpha) - (\eta - \alpha) \frac{dp'}{p'}}{(M - \alpha) + (\eta - \alpha) \frac{p'}{p'}} + \frac{2(\eta - \alpha)}{(M - \alpha) + (\eta - \alpha) \frac{p'}{p'}} \frac{dq}{p'} \right] \tag{11}$$

Substituting Eq. 4 into Eq. 10, it can be written as:

$$d\varepsilon_v^{p(II)} = \frac{\lambda - \kappa e^{-(ae^2 + b\varepsilon)}}{v} \frac{(2a\varepsilon_v^p + b)d\varepsilon_v^p}{1 - e^{-(ae^2 + b\varepsilon)}} \tag{12}$$

$$v = 1 + e \tag{13}$$

$$e = e^{-(\lambda - \kappa) \ln p' - \kappa \ln p'} \tag{14}$$

where λ is compression index, κ is swelling index, e_0 is the original void ratio.

The elastic increment of volumetric strain is

$$d\varepsilon = \frac{1}{K} dp' \tag{15}$$

Parameter K is tangent volumetric modules of the soil in the elastic state.

Eq. 11 and Eq. 12 are substituted into Eq. 8; the incremental form of stress-plastic volumetric strain relationship is given by

$$d\varepsilon = \frac{\lambda - \kappa}{v} \left[\frac{(M - \alpha) - (\eta - \alpha) \frac{dp'}{p'}}{(M - \alpha) + (\eta - \alpha) \frac{p'}{p'}} + \frac{2(\eta - \alpha)}{(M - \alpha) + (\eta - \alpha) \frac{p'}{p'}} \frac{dq}{p'} + \frac{e^{-\varepsilon^2 + \varepsilon} (2a\varepsilon + b)d\varepsilon}{1 - e^{-\varepsilon^2 + \varepsilon}} \right] \tag{16}$$

$$d\varepsilon = d\varepsilon + d\varepsilon^p \tag{17}$$

Eq. 15 and Eq. 16 are substituted into Eq. 17, the incremental form of the stress- strain relationship is obtained.

The Determination of Model Parameters

The proposed model involves eight parameters, as shown in Table 2.

Table 2 Parameters of model

elastic	plastic	destructuration
e_0, K	$\lambda, \kappa, M, \alpha_0$	a, b

Elastic deformation parameter of soil

Parameter K is the tangent volumetric modulus, and it can be gotten from the tangent inclination of the original elastic part of curve, which is volumetric strain-stress curve.

Plastic deformation parameter of soil

Parameters M , λ , κ are basic parameters of the Modified Cam-Clay model. Considering the stress path test results and referring to achievements of Nakano (2005), the following equation can be gotten,

$$\alpha_0 = \eta_0 = \frac{3(1-k_0)}{1+2k_0} \tag{18}$$

Parameter η_0 is original stress ratio.

Destruction parameter of soil

An optimum procedure is needed in determining parameter b and a .

With the optimized value of b and a , triaxial test can be simulated.

MODEL VALIDATION

To investigate the performance of the proposed model, the triaxial drained shear test on the soft soil from Lianyungang was carried out. The model parameters are shown in Table 3.

Table 3 Model parameters of Lianyungang soft clay

e_0	K (kPa)	λ	κ	M	α_0	a	b
1.681	522	0.439	0.032	0.77	0.45	12.71	29.57

The parameters are substituted into the partial differential equations Eq. (15) and Eq. (16). In the model of triaxial drained tests, $\eta = q / p' = 3$ so the increment formulation of elastic volumetric strain and plastic volumetric strain can be respectively written as,

$$d\varepsilon = \frac{dp'}{K} = \frac{dp'}{522} = 0.0019dp' \tag{19}$$

Eq. 19 and Eq. 20 are substituted into Eq. 17; the stress-strain increment formulation can be gotten.

$$d\varepsilon = \frac{0.407}{(1.511 - 0.439 \ln p')} \left[\frac{e^{-\varepsilon^2} \cdot \varepsilon (25.42\varepsilon - 29.57)d\varepsilon}{1 - e^{-\varepsilon^2} \cdot \varepsilon} + 1.333 \frac{dp'}{p'} \right] \tag{20}$$

The partial differential equation is integrated, and the original condition is considered, so the model expression of stress-volumetric strain can be obtained.

The validation result of model indicates that the experimental data can be well predicted by the proposed model, as shown in Fig. 4.

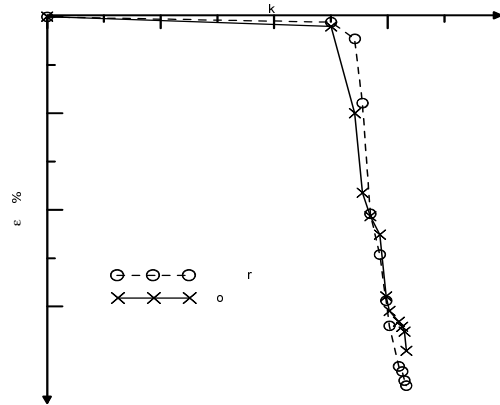


Fig. 4 Validation of model

CONCLUSIONS

- (1) A destructuration constitutive model for soft clay, considering stress-induced anisotropy, is established.
- (2) The electric resistivity anomaly is introduced to define and measure the destructuration variable, and it helps to overcome the disadvantages of traditional measurements.
- (3) Destructuration evolution law employed is established by the test results, and it helps to improve the applicability and rationality of the model.
- (4) Tests show that the proposed model can reflect the deformation of soft clays.
- (5) The uncertainty of the proposed model is mainly from model imperfect and test imprecision.

ACKNOWLEDGMENTS

This work was supported by Jiangsu Province Science Technology Council (BK2007070).

REFERENCES

Cudny M (2003). Simple multi-laminate model for soft soils incorporating structural anisotropy and destructuration. In P.A. Vermeer, H. F. Schweiger, M. Karstunen & M. Cudny, Proc. Int. Workshop on Geotechnics of Soft Soils: Theory and Practice, Noordwijkerhout. VGE.
 Gens A & Nova R (1993). Conceptual bases for a

- constitutive model for bonded soils and weak rocks. In A. Anagnostopoulos, F. Schlosser, N. Kalteziotis & R. Frank, Proc. Int. Symp. On Geomechanical Engineering of Hard Soils and Soft Rocks, Athens: 485-494. A. A. Balkema.
- Jackson PD, Northmore KJ, Meldrum PI, Gunn DA, Hallam JR, Wambura J, Wangusi B, Ogutu G (2002). Noninvasive moisture monitoring within an earth embankment – a precursor to failure. *NDT&E Int.* 35, 107-115.
- Karstunen M, Krenn, Wheeler SJ, Koskinen M, Zentar R (2005). Effect of anisotropy and destructuration on the behavior of Murro test embankment, *International Journal of Geomechanics, ASCE*, 5(2):87-97.
- Nakano M, Nakai K, Noda T (2005). Simulation of shear and one-dimensional compression behavior of naturally deposited clays by super and sub loading the yield surface Cam-clay model. *Soils and Foundations*. 45(1):141-151.
- Rouainia M & Muir Wood D (2000). A kinematic hardening constitutive model for natural clays with loss of structure, *Que.* 50(2):153-164.
- Samouelian A, Cousin I, Richard G, Tabbagh A, Bruand A (2003). Electrical resistivity imaging for detecting soil cracking at the cent metric scale, *Soil SCI. Soc. J. Am.* 67: 1319-1326.
- Tabbagh A, Dabas M, Hessen A, Panissod C (2000). Soil resistivity: a noninvasive tool to map soil structure horizonation , *Geoderma* 97: 393-404.
- Yu XJ & Shi JY (2009). Research on the disturbed state concept for the soft clay roadbed. *GeoHunan International Conference 2009*.

IDENTIFICATION OF DAMPING RATIOS OF SOIL-STRUCTURE SYSTEM SUBJECTED TO AMBIENT EXCITATION

Zhi-Ying ZHANG¹, Qiang PAN², Chong-Du CHO³ and Zhan-Chao GAO⁴

ABSTRACT: Accurate evaluation of damping ratios of a system is a prerequisite for seismic design involving soil-structure interaction (SSI) effects. The investigations on determining the damping ratios of soil-structure systems, however, lack robustness due to the complexity of such systems. This study proposes a combined approach to obtain accurate damping ratios of SSI systems. Peak-picking (PP) method is employed to extract natural frequencies of the SSI system and damping ratios are derived using the stochastic subspace method. The advantages of the proposed approach are discussed with detailed description of the principle, experiments, and formula. In effort to demonstrate the feasibility and validity of the proposed technique, a practical example is presented. The results indicate the proposed method can effectively identify the damping ratios of soil-structure system subjected to ambient excitation. It is directly useful in damping ratios identification of an SSI system.

KEYWORDS: damping ratio, soil-structure interaction system, ambient excitation, modal parameter identification

INTRODUCTION

Damping level of a system is essential to its dynamic response analysis. In civil engineering, damping ratio is commonly employed in characterizing the damping level of structure and is of great importance in seismic design (Kareem and Gurley 1996). But in conventional building seismic designs, the influence of the soil-foundation under the structures is neglected and the damping ratio adopted in current design is also based on rigid soil-foundation. But, an in-situ civil structure is always working with soil-structure interaction (SSI) effect. Therefore the interaction effect should be accounted in the dynamic analysis and thus the seismic designs will be more practical. It is difficult to perform dynamic analysis with sufficient accuracy for SSI systems because of its complex mechanism and the lack of experimental studies for dynamic properties of in-situ SSI systems. Based on the energy dissipation mechanism, the composition of the damping in SSI system could be classified into three types: material damping, motion coordination damping and radiation damping. The damping is so complex that it's very difficult to be separated. To develop the building seismic design involving SSI effect, it's a prerequisite for achieving the equivalent damping ratios of SSI system by in-situ experiments.

As to assess damping ratio of a system, conventional tests require both known input and output signals of the system and then get the damping ratio through some identification methods. But in practice, it is not easy to apply artificial excitation to an actual SSI system, and there always exists non-controlled and unknown external excitations such as passing vehicles, winds and so on. Hence there is a growing interest in present work to use ambient excitation technique (Siringoringo and Fujino 2008; Ren and Zong 2004) which requires no input excitation and measures only the output to predict the dynamic behavior of system. However, the response is significantly influenced by noise when the input employs ambient excitation, it seems difficult to assess damping ratio accurately. So far, many identification methods have been proposed and developed, but most of them cannot achieve success in identifying accurate damping ratios of SSI systems under ambient excitation. The peak-picking (PP) method (Bishop and Fladwell 1963) is one of the most widely used ambient modal analysis method known as a reliable extraction of natural frequencies. But its utilization is still limited due to its inaccurate estimation on damping ratios (Abdel-Ghaffar and Housner 1978).

The stochastic subspace identification algorithm (Overschee and Moor 1991; Peeters and Roeck 1999)

¹ Professor, Human Settlements and Civil Engineering College, Xi'an Jiaotong University, China. Email: zhangzhy@mail.xjtu.edu.cn

² State Key Laboratory for Disaster Reduction in Civil Engineering, Tongji University, Shanghai 200092, China

³ Department of Mechanical Engineering, Inha University, Incheon 402751, Korea

⁴ Human Settlements and Civil Engineering College, Xi'an Jiaotong University, China

shares the advantages of both ARMAV and ARV models (Peeters and Roeck 1999; Reynders and Roeck 2008). But in this algorithm, the illusive modes, which should be distinguished and removed from the identification results, are observed among real modes. Stochastic subspace algorithm had been applied to civil structures for model identification (Peeters and Roeck 2000; Yu and Ren 2005) based on empirical mode decomposition of the structure subjected to ambient excitation.

Although some site SSI system, or the full-scale damping ratios have been measured (mainly in the small amplitude region) and discussed in Japan (Satake et al. 2003), it is insufficient to serve other territory and they did not show the identification method of damping ratio for SSI system. It is expected, through the existed model identification algorithms, to select and develop a new identification method which could apply to SSI systems for the system damping ratio identification more successfully. After comparison of different identification methods, this work presents a combined identification method to get a relatively accurate damping ratio for SSI system under ambient excitation. The paper briefly reviews theoretical formulation. In the end, damping ratios of a 9 stories frame-shear wall structure with SSI effect are obtained on the basis of the proposed method in order to illuminate the practical application procedures and the applicability. The method might serve as a means to perform a preliminary assessment of the damping ratios of 82 in-situ buildings located in Xi'an, China, which will be discussed in authors' another paper.

DAMPING RATIO IDENTIFICATION METHODOLOGY

Here introduces the basic methodology which helps understanding how the two identification methods are combined and applied to the extraction of the damping ratios of SSI system.

The PP method is rather simple and widely used to determine the eigenmodes of a structure based on output-only measurements. In this method, the eigenfrequencies are simply observed by the peaks of the spectra. It is proved that this method is of certain precision in identifying eigenfrequencies but lacks of accurate on estimating damping ratios. The stochastic subspace algorithm is another one which is working on output-only and regarded as a more advanced identification method. But it's extremely difficult to distinguish and eliminate the illusive modes. Though the two independent numerical techniques are not latest, it is verified that if the two methods are combined as a new one, the complementary technique will be applied with increasing the accuracy and reliability to achieve the damping ratios of SSI system.

IDENTIFICATION OF NATURAL FREQUENCIES

The Discrete Fourier Transform (DFT) is fundamental to signal processing and also a key step for identification of modal parameters in the PP method. The finite Fourier transform with the signal length T can be written as

$$X_T(\omega) = \int_0^T x_T(t) e^{-j\omega t} dt \quad (1)$$

Considering the sampling of finite signal $x_T(t)$ with sampling interval of $\Delta t = T/N$, which satisfies the sampling theorem, the finite sequence of discrete Fourier transform can be expressed as

$$\tilde{X}_T(n) = \sum_{k=0}^{N-1} \tilde{x}_T(k) e^{-j \frac{2\pi n}{N} k} \Delta t = \Delta t \sum_{k=0}^{N-1} \tilde{x}_T(k) e^{-j \frac{2\pi n k}{N}} \quad (2)$$

where N is sampling number and ω is frequency resolution.

There always exists signal leakage and occurring errors in Fourier transform. The leakage rate is direct related to the two side-lobes of the frequency spectrum of the window functions. It can be approximated to the real frequency spectrum if the height of the side-lobes tends to be zero and leads to the energy focusing on the main lobe. To minimize the energy leakage, we used Hanning window function in the discrete signal processing of present PP method.

In order to avoid the occurrence of illusive modes caused by the mixing between high and low frequency signals, signal filtering is required by anti-mix filter during the sampling, as well as the selection of sampling frequency based on Shannon sampling theorem. Besides the efforts to decrease the influence of high frequency signals during sampling, as mentioned above, the test results are usually disturbed by noise. The reduction of noise contamination can also be implemented through averaging technique during signal processing. In the test here, considering the random noise, the linear average technology for spectrum is adopted. In the average process, each signal with given length in time domain is calculated by Fast Fourier Transform (FFT), and then the frequency spectrum of each point is linearly averaged with equal weight. The increase of average times may be accompanied with the decrease of relative standard deviation. The natural frequencies are then simply obtained by peak picking on the curve of average spectrum.

IDENTIFICATION OF DAMPING RATIOS

Unlike the frequency domain identification method, the stochastic subspace identification method doesn't require transferring the measured time history responses

into frequency domain, which avoids the truncation error caused by FFT so that relatively high accuracy damping ratio assessment will be achieved, compared to the frequency domain method.

The response signals under ambient excitation will be influenced inevitably by the noise and will not be smooth enough to identify the damping parameters. In order to reduce the effect of noise disturbance, 5 points cubic smoothing function method is used in present work. It is an effective way to eliminate high-frequency random noise and improve signal-to-noise ratio. Based on least square method and polynomial approximation, the functions are given by

$$\begin{aligned}
 y_1 &= 1/70[69x_1 + 4(x_2 + x_4) - 6x_3 - x_5] \\
 y_2 &= 1/35[2(x_1 + x_5) + 27x_2 + 12x_3 - 8x_4] \\
 &\vdots \\
 y_i &= 1/35[-3(x_{i-2} + x_{i+2}) + 12(x_{i-1} + x_{i+1}) + 17x_i] \quad (3) \\
 &\vdots \\
 y_{m-1} &= 1/35[2(x_{m-4} + x_m) - 8x_{m-3} + 12x_{m-2} + 27x_{m-1}] \\
 y_m &= 1/70[-x_{m-4} + 4(x_{m-3} + x_{m-1}) - 6x_{m-2} + 69x_m]
 \end{aligned}$$

where $i = 3, 4, \dots, m - 2$, y_i is the smoothing value with respect to x_i .

The discrete-time stochastic state-space model under ambient excitation can be described as follows

$$\begin{cases} x_{k+1} = Ax_k + w_k \\ y_k = Cx_k + v_k \end{cases} \quad (4)$$

The natural frequencies and the damping ratios can be extracted from the state equations if the state transition matrix A is derived. Hankel matrix is constructed based on the test response data and the row vector space is split into past and future blocks.

$$H = \frac{1}{\sqrt{j}} \begin{bmatrix} y_0 & y_1 & \dots & y_{j-1} \\ y_1 & y_2 & \dots & y_j \\ \vdots & \vdots & \ddots & \vdots \\ y_{i-1} & y_i & \dots & y_{i+j-2} \\ y_i & y_{i+1} & \dots & y_{i+j-1} \\ y_{i+1} & y_{i+2} & \dots & y_{i+j} \\ \vdots & \vdots & \ddots & \vdots \\ y_{2i-1} & y_{2i} & \dots & y_{2i+j-2} \end{bmatrix} = \begin{bmatrix} Y_{past} \\ Y_{future} \end{bmatrix} \quad (5)$$

Consider the QR-decomposition of Hankel matrix

$$\begin{bmatrix} Y_{past} \\ Y_{future} \end{bmatrix} = \begin{bmatrix} R_{11} & 0 \\ R_{21} & R_{22} \end{bmatrix} \begin{bmatrix} Q_1^T \\ Q_2^T \end{bmatrix} \quad (6)$$

Then the orthogonal projection of the row vector space is obtained

$$O_i = Y_{future}/Y_{past} = Y_{future}Y_{past}^T(Y_{past}Y_{past}^T)^{\dagger}Y_{past} = R_{21}Q_1^T \quad (7)$$

Introducing singular value decomposition (SVD) into the projection matrix, we derived

$$W_1O_iW_2 = USV^T = (U_1 \ U_2) \begin{pmatrix} S_1 & 0 \\ 0 & 0 \end{pmatrix} \begin{pmatrix} V_1^T \\ V_2^T \end{pmatrix} = U_1S_1V_1^T \quad (8)$$

The subspace system identification theory indicates

$$O_i = \begin{bmatrix} C \\ CA \\ \vdots \\ CA^{i-1} \end{bmatrix} [\hat{x}_i \ \hat{x}_{i+1} \ \dots \ \hat{x}_{i+j-1}] = \Gamma_i \hat{X}_i \quad (9)$$

where $\Gamma_i = U_1S_1^{1/2}$, $\hat{X}_i = \Gamma_i^{\dagger}O_i$. Similarly, we have

$$O_{i-1} = Y_{future}^-/Y_{past}^+ \Rightarrow O_{i-1} = \Gamma_{i-1}\hat{X}_{i+1}, \hat{X}_{i+1} = \Gamma_{i-1}^{\dagger}O_{i-1} \quad (10)$$

O Deriving from least square method, the matrix

$$\begin{pmatrix} A \\ C \end{pmatrix} = \begin{pmatrix} \hat{X}_{j+1} \\ H_{i/j} \end{pmatrix} \hat{X}_i^{\dagger} \quad (11)$$

Separating eigenvalues of the system matrix A ,

$$A = \Psi \Lambda \Psi^{-1} \quad (12)$$

where Ψ is eigenvector matrix and Λ is a diagonal matrix representing the eigenvalues of the discrete time system. The eigenfrequencies ω_i and damping ratios ξ_i are found from

$$\mu_i = e^{\lambda_i \Delta t}; \lambda_i, \lambda_i^* = -\xi_i \omega_i \pm j \sqrt{1 - \xi_i^2} \omega_i \quad (13)$$

where Δt is the sampling time.

APPLICATION

As practical application procedure of the basic methodology, an illustrative example is given in this section. It is a 9-story shear-wall structure with type II soil-foundation in Xi'an.

Natural frequencies and damping ratio are calculated by PP method, the first frequency is 1.80Hz, but the accuracy of extracted damping ratio is not satisfying.

After removing the higher frequencies, the frequency response signals in time domain are utilized to identify the damping ratios of SSI system via stochastic subspace method. Then the modal parameters are derived by varying the orders of the modes and row numbers of the

Hankel matrix. The corresponding results, including extracted natural frequencies and damping ratios, are shown in Tables 1 and 2.

The results obtained from stochastic subspace method usually involve illusive modes which can be observed by the irregular data in Tables 1 and 2. Since the natural frequency of the frame-shear wall structure has been determined by PP method as 1.80 Hz, the data which are

closed to this value (adopted as 1.78-1.83 Hz) in Table 1 is recognized as the results extracted from real modes. Consequently, the modal damping ratios corresponding to these frequencies in Table 2 are addressed as the correct results. Taking advantage of equal average algorithm, the damping ratio of the frame-shear wall SSI system is determined as $\xi = 2.64$, which is in good agreement with previous experimental results.

Table 1 Frequencies derived from stochastic subspace method

Natural frequencies											
2.691	0.000	0.968	0.000	3.640	0.000	1.408	0.000		0.000		0.000
2.432	6.827	2.307	6.734	2.156	6.042	1.985	6.221		3.540	3.004	4.072
2.165	6.647	2.346	6.669	3.041	6.902	1.980	6.248	2.282	6.560	3.280	6.885
	4.929	1.931	4.670		4.571	3.040	6.836	1.836	4.344	1.787	4.139
1.548	3.887		4.556	1.148	3.745	1.733	4.111	1.773	4.128	1.786	4.125
1.817	4.079	1.803	4.166	1.640	4.060	1.791	4.122	1.790	4.132	1.805	4.118
1.789	4.192	1.783	4.318	1.795	4.109	1.787	4.113	1.795	4.119	1.795	4.118
1.781	4.163	1.793	4.166	1.799	4.117	1.798	4.103	1.794	4.122	1.795	4.123
1.790	4.167	1.786	4.144	1.794	4.105	1.793	4.125	1.793	4.122	1.793	3.353
1.792	4.158	1.787	4.125	1.792	4.123	1.794	3.489	1.793	2.587	1.793	4.122
1.792	4.158	1.785	3.916	1.784	2.169	1.796	2.607	1.795	3.631	1.793	3.149
1.792	4.159	1.786	4.121	1.791	3.351	1.792	3.280	1.793	3.072	1.792	3.083
1.790	4.160	1.788	3.905	1.791	3.238	1.785		1.794	3.120	1.676	1.792
1.787	4.159	1.788	4.167	1.791	3.163	1.786	2.072	1.793	3.129	1.792	3.205
1.787	4.161	1.785	4.134	1.789	3.332	1.789	3.225	1.792	3.126	1.791	3.017

Table 2 Damping ratios derived from stochastic subspace method

Damping ratios											
23.924	0.000	65.590	0.000	8.002	0.000	41.072	0.000	14.386	0.000	14.386	0.000
27.207	3.298	6.570	3.031	14.282	4.317	8.603	2.208	31.423	27.833	6.196	13.215
13.007	3.281	7.566	4.523	7.878	1.637	8.552	1.987	26.666	45.486	12.325	2.857
33.869	18.435	18.447	20.235	13.243	8.009	7.139	1.543	6.418	2.545	3.964	1.243
6.295	-8.617	10.743	3.411	5.862	13.867	1.562	1.397	3.628	0.992	3.434	1.513
3.590	0.655	3.398	4.592	8.154	7.071	2.097	1.483	3.802	0.815	3.275	0.478
3.503	-0.546	1.821	3.169	2.598	0.879	2.873	0.648	3.162	0.453	2.432	0.132
2.243	-0.323	2.903	0.223	2.669	0.485	3.087	-0.243	2.805	0.237	2.690	0.278
2.318	0.081	2.757	0.469	2.247	0.697	2.634	0.249	2.680	0.227	2.642	71.893
2.442	0.199	2.662	-0.089	2.515	0.217	2.732	-9.429	2.777	44.080	2.648	0.266
2.420	0.195	2.668	36.229	2.394	83.782	1.470	8.333	2.726	21.930	2.653	-1.413
2.411	0.164	2.688	0.048	2.207	-3.029	2.696	-46.22	2.674	6.578	2.637	-1.454
2.398	0.122	2.350	-4.979	2.313	1.498	2.143	-94.46	2.677	3.546	76.996	2.650
2.390	0.040	2.462	-1.265	2.205	8.960	2.258	-90.40	2.690	2.539	2.664	1.711
2.340	0.058	2.476	-0.419	2.215	11.097	2.224	14.741	2.753	2.240	2.699	36.713

CONCLUSIONS

Accurate evaluation of damping ratios of soil-structure system is a prerequisite for seismic design of structures involving SSI effect. So far, most parameter identification methods cannot be independently used.

Hence a new approach to identify the damping ratios of SSI system subjected to ambient excitation is proposed to seek a potential solution. The new approach relies on PP method to identify natural frequencies and extracts damping ratios from stochastic subspace method. This approach may greatly increases accuracy of identified damping ratios of the SSI system.

The tests on a 9 stories frame-shear wall structure considering SSI effect is presented to demonstrate the feasibility and validity of the proposed approach. The response signals are firstly anti-mix filtered to remove high frequencies, and then de-noised through 5 points cubic smoothing method. Resulting from PP method, all test points have closed natural frequencies of 1.80 Hz. And modal damping ratio of 2.64 is derived from stochastic subspace method, in which the illusive modes are removed based on outcome of PP method.

The proposed approach is expected to be beneficial to identify the damping ratios of SSI system subjected to ambient excitation, therefore provides a potential solution for seismic structure design.

ACKNOWLEDGEMENTS

This work was supported by State Key Laboratory for Disaster Reduction of China and Inha University of Korea. The authors would like to thank Xi'an Jiaotong University for providing the experimental apparatus.

REFERENCES

- Kareem A & Gurley K (1996). Damping in structures: Its evaluation and treatment of uncertainty. *Journal of Wind Engineering and Industrial Aerodynamics* 59 :131-157.
- Siringoringo DM & Fujino Y (2008). System identification of suspension bridge from ambient vibration response. *Engineering Structures*.30(2) : 462-477.
- Ren WX & Zong ZH (2004). Output-only modal parameter identification of civil engineering structures. *Structural Engineering and Mechanics*.17: 429-444.
- Bischoff P & Fladwell G (1963). An investigation into the theory of resonance testing. *Philosophical Transactions of the Royal Society of London* 255 (1055) : 241-280.
- Abdel-Ghaffar AM & Housner GW (1978). Ambient vibration tests of suspension bridge. *Journal of the Engineering Mechanics Division ASCE*, 104(5): 983-999.
- Overschee PV & Moor BD (1991). Subspace Algorithms for the Stochastic Identification problem. *Proceedings of the 30th IEEE Conference on Decision and Control*, Brighton: 1321-1326.
- Peeters B & de Roeck G (1999). Reference-based stochastic subspace identification for output-only modal analysis. *Mechanical Systems And Signal Processing*. 13: 855-878.
- Peeters B & Roeck GD (1999). Reference-based stochastic subspace identification for output- only modal analysis. *Mechanical Systems and Signal Processing*, 13 (11): 855-878.
- Reynders E & Roeck GD (2008). Reference-based combined deterministic–stochastic subspace identification for experimental and operational modal analysis. *Mechanical Systems and Signal Processing*. 22 (4): 617-637.
- Peeters B & Roeck GD (2000). Reference based stochastic subspace identification in civil engineering. *Inverse Problems in Engineering*. 8: 47-74.
- Yu DJ & Ren WX (2005). EMD-based stochastic subspace identification of structures from operational vibration measurement. *Engineering Structures* 27:1741-1751.
- Satake N, Suda K, Arakawa T, Sasaki A, Tamura Y (2003). Damping evaluation using full-scale data of buildings in Japan. *Journal of Structural Engineering, ASCE*. 129: 470-477.



**Testing and Monitoring for
Geoenvironmental Engineering**

LABORATORY FLUME STUDIES ON CONSOLIDATION OF SOFT SILTY SEABED SOIL UNDER WAVE ACTIONS

Ying LIU¹, Hong-Jun LIU², Xiu-Hai WANG³ and Min-Sheng ZHANG⁴

ABSTRACT: In this paper, tests on silty soil obtained from the Yellow River Delta under waves were conducted in a wave flume (size: $15(L) \times 1.0(H) \times 0.5(W)$, unit: m) to investigate characteristics of its consolidation behaviors. In addition, soil penetration strength was measured with a mini-penetrometer, and variations of pore water pressure were analyzed to study the mechanisms. Results indicated that the sliding interface between the oscillatory layer and the underlying layer would move downwards under another round of wave actions after a period of time's consolidation under self-weight in static water, while the magnitude of the oscillation would be much smaller than that of the last time. Analytical results of pore water pressure variations clearly illustrated that the liquefaction tended to be initiated in the surface layer and spreading fast into lower layers. The penetration strength data revealed that there was a layer of extremely high strength in the sliding zone, which might be the embryo of the hard crust in the tidal flat of the Yellow River Estuary. All in all, the strength of such silt soil increased unequally along the depth continuously under wave loadings, and the consolidation speed was much higher than that in the static water.

KEYWORDS: consolidation, soft silty seabed soil, sliding interface, pore water pressure, penetration strength

INTRODUCTION

Water waves, propagating over the sea floor from deep seas to coastal zones and interacting continuously with the seabed, give rise to a wide variety of phenomena in the marine environment. Many of these phenomena are very complex and the associated physical mechanisms are far from being understood, and the consolidation of seabed soil is one of them.

Soil consolidation is often caused by external loadings. The consolidation theory was originally developed by Terzaghi (1924) for the one dimensional case. Biot (1941) later extended his theory to two- and three-dimensional cases in saturated soil. From then on, formulations based on Biot's theory assuming linear responses for both elastic solid skeleton and compressible fluid were respectively developed (e.g. Yamamoto et al. 1978, Madsen 1978). They subsequently verified in several experimental studies with different sandy soils (Yamamoto et al. 1978, Tzang 1992). These linear formulations particularly gave light in fundamental behaviors of seabed soil under wave loadings. However, works on the non-linear responses such as silty soil have been relatively insufficient in both experimental studies and theoretical studies.

The Yellow River is famous throughout the world for

its high sediment carrying capacity as well as its high frequency of changing channels. And the modern Yellow River Delta began to develop since 1855 when the river migrated to flow to Bohai Sea (Li 1993). The rapid deposition together with the complicated hydrodynamic conditions firstly formed a layer of relatively homogeneous deposits above the older ones, which are mainly composed of silty soil (Li 1998). The responses of silty seabed (including tidal flat) to wave loadings in Yellow River Delta had been studied for years (Chen et al. 2006, Zhang et al. 2007). In spite of those beneficial progress, more details should be noted, especially the consolidation process, which is almost impossible to be detected in situ, and flume experiment is a better method to get continuous data under controlled wave loadings.

In this paper, the whole process of the consolidation about soft silty seabed soil under wave loading was investigated in the laboratory flume experiments, and the variations of soil strength and pore water pressure were analyzed to study the mechanism of the process.

LABORATORY FLUME TESTS

Fig.1 shows the present configuration of the experimental wave flume ($15(L) \times 1.0(h) \times 0.5(w)$, unit: m).

¹ Ms, College of Environmental Science and Engineering, Ocean University of China, China. Email: jimijijiao@yahoo.com.cn

² Professor, College of Environmental Science and Engineering, Ocean University of China, China. Email: hongjun@ouc.edu.cn

³ Engineer, College of Environmental Science and Engineering, Ocean University of China, China. Email: showseas@ouc.edu.cn

⁴ Engineer, College of Environmental Science and Engineering, Ocean University of China, China. Email: minshengzhang@ouc.edu.cn

It is equipped with a piston-type wave generator on one end and a dissipating gravel beach on the other end.

The soil trench is under the middle part of the regular wave segment. Only half part of the soil trench was used to save labor. The water level was set at 0.45 m. After

being calibrated with static water, four pore water pressure transducers were deployed every 10 cm below the soil surface. Pore water pressure signals were acquired by the data acquisition software DASyLab. And the coordinate system defined in this paper is also displayed in Fig. 1.

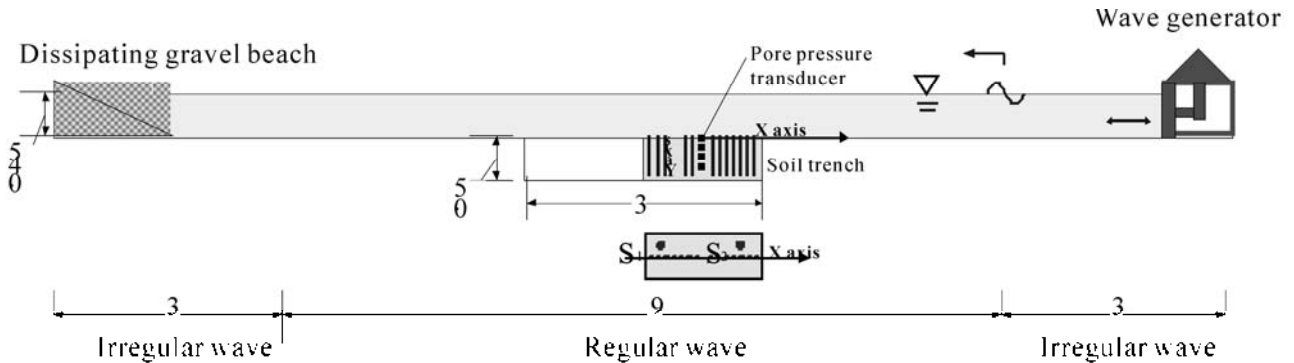


Fig.1 Experimental flume setups (unit: m)

Table 1 Grain size composition of the soils (%)

Name	Grain size (mm)		
	>0.075	0.005~0.075	<0.005
Silty soil	19.3	75.1	5.6

The soil was first blended with water in a tank and then displaced to the soil trench. As shown in table 1, the clay content (P_c) of prepared soil was 5.6%. The moisture content was 33 %, density $\rho=1.85 \text{ g/cm}^3$, specific gravity $\rho_s=2.71$, porosity $n=0.49$, degree of saturation $S_{at}=94\%$. After being left undisturbed for 1 day, the flume was then subsequently filled with water until reaching the designated depth of 45 cm. This flume experiment was conducted in three parallel tests, among which one had some erroneous measurements due to malfunction of the pore pressure transducers while the other two were good in consistency. For each test, information on voltage and period of harmonic signals were first transmitted from a control unit to wave maker to generate monochromatic waves in the flume for about 120 min. Before and after the wave actions, the mini-penetration test was implemented at two fixed sites (S_1, S_2) to investigate the variations of seabed soil's strength. Next the seabed was left consolidated in static water for about 22 hr before waves were generated again for 120 min. This work was repeated five times in all, and the phenomena were observed during the wave actions. At last, the mini-penetration test was implemented on the whole traverse section plane of the soil seabed. The detailed information of the mini-penetration test sites is also displayed in Fig.1. Wave conditions were constant in the whole test, wave height $H=14.8 \text{ cm}$, wave length $L=180.0 \text{ cm}$, wave period $T=1.13 \text{ s}$. Considering the positions of buried transducers and sites for mini-penetration test, the influences of the flume ledge were neglected in this paper.

RESULTS OF THE FLUME TESTS

Formation and Evolution of Sliding Interface

Waves will induce cyclic stresses within the seabed soils which may cause a progressive buildup of pore water pressure (Seed 1978). When the pore water pressure accumulates to a stage where it becomes equal to the vertical effective stress, the liquefaction happens. In the tests, the surface layer of soils became fluidize as soon as waves arrived there, and this zone of liquefaction would expand with the wave actions. Because of the dissipation of wave energy and the increasing degree of the consolidation of seabed soil in the profile, this expanding course would stop at a certain depth after about an hour of wave actions. This liquefied layer, surging with waves and leading to a visible interface from the underlying seabed soil, is defined as oscillatory layer in this paper. The visible interface is defined as sliding interface, while the underlying layer is called steady layer. Fig. 2 is the photo of the soil trench sustaining wave loading at the fourth day, and the shapes and locations of sliding interface in the last three days were traced out on the front glass, while the whole evolution of the sliding interface is given in the accessorial schematic. The sliding interface would move deeper when subjected to waves again after almost a day of consolidation, but the amplitude was smaller than last time. As illustrated in Fig. 2, water layer became turbid as soon as waves arrive the soils, and a layer mainly constituted by clay particles ($P_c>60\%$) was formed at the surface of the seabed when the waves had subsided. It must be admitted that there was a loss of clay particles in the soil seabed.

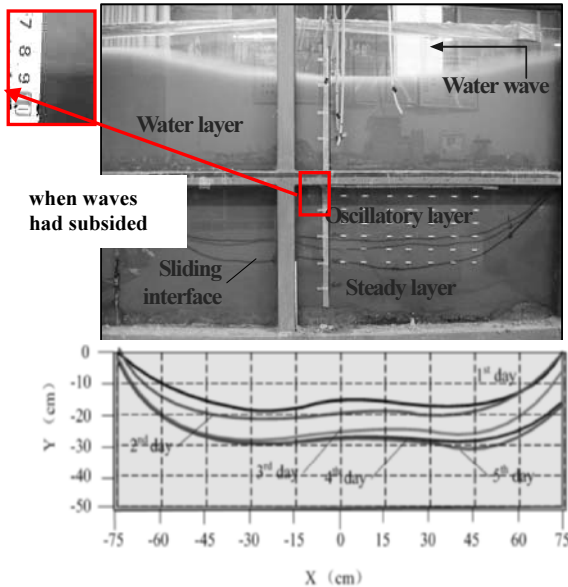


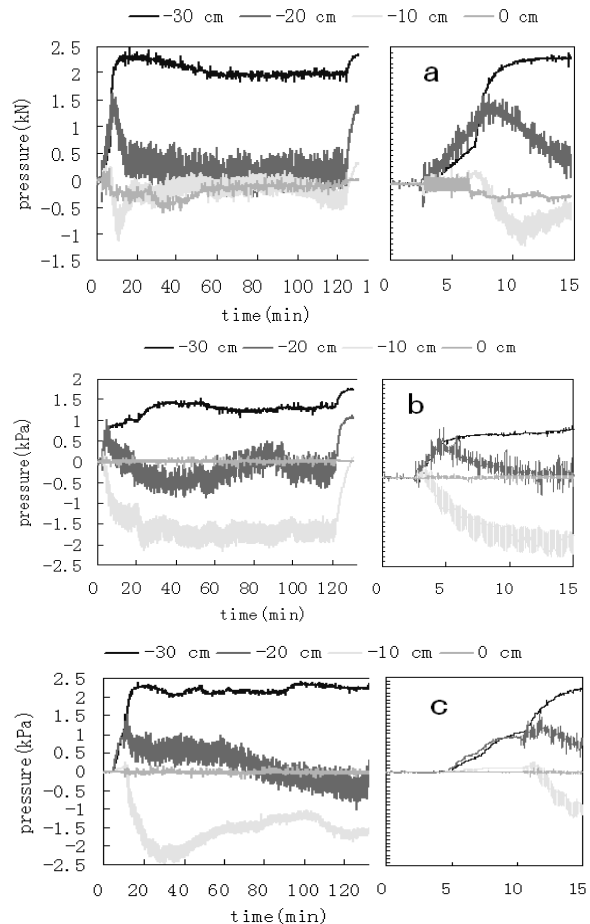
Fig. 2 Photo of the soil trench sustaining waves at the fourth day and evolution sketch of sliding interface

The wave vibration would drive the soil particles to a position with lowest potential energy (Wang 2002). After the wave actions, the particles were rearranged more densely, and this might prompt people to speculate that the whole seabed tended to be more stable and would result in the upward-going of the sliding interface. Otherwise, from the perspective of energy conservation, the energy of waves dissipated by the surging of the oscillatory layer. After the consolidation for nearly one day's time, soil particles arranged much tighter. When the waves of same energy were re-exerted on the seabed, the amplitude of the oscillatory became smaller, and this would undoubtedly involve more soil to the surging process. On the other hand, the loss of clay particles in the seabed soil led to the reduction of internal cohesive force between particles, so the dynamic shear strength was weakened and the soil particles slipped more easily (LI et al. 2005). The above speculation is a good explanation to the phenomena of the down-going of the sliding interface. In addition, the subsiding of the seabed soils caused from consolidation and erosion of the surface layer helped to this down-going.

Pore Water Responses

The pore water pressure transducers buried at different depths of the seabed ($d=0$ cm, -10 cm, -20 cm, -30 cm) kept a good record of the temporal variations of pore water pressure in the whole experiment. The measured pore water pressure data was seen to have consisted of two temporal components, i.e., the excess and the oscillating. It is clearly seen from (a)~(e) in Fig. 3, there was a initial stage (for $t_{in}<t<t_{ma}$; t_{in} : occurrence time of initiation of pore water pressure amplification; t_{ma} :

occurrence time of the maximum excess pore water pressure ΔP) of tempestuous varieties in both amplitude and excess as soon as the waves were employed. After this stage, two typical pore water pressure responses from different depths were displayed. Pore water pressure data from depth of -30 cm showed a stage (for $t_{ma}<t<t_{fi}$; t_{fi} : finish time of the wave loadings) of steady excess after reaching the maximum value. Data from -10 cm and -20 cm showed a decreasing stage (for $t_{ma}<t<t_{st}$; t_{st} : occurrence time of the steady excess pore water pressure) before the steady stage(for $t_{st}<t<t_{fi}$). The sharp decline of excess pore water pressures suggested a possible collapsing process in soil structures. The causes are not fully understood, and Tzang (2006) has also found a momentary period of depressions of excess pore water pressure at the initial stage. He thought this was due to overshooting the stress limit by pore water pressure's dynamic oscillations or due to upward pressure gradients during phase of wave trough. But his deduction can't explain the consecutive negative excess pore water pressure at $d = -10$ cm (even in the steady stage) sufficiently. Considering the continuous erosion of seabed surface by waves, 10 cm could stand for the pore water responses of surface layer. The continuous dislocations between soil particles might induce a vacuum, which resulted in a continuous negative excess pore water pressure. Furthermore, there was a stage of sharp increase in the excess at



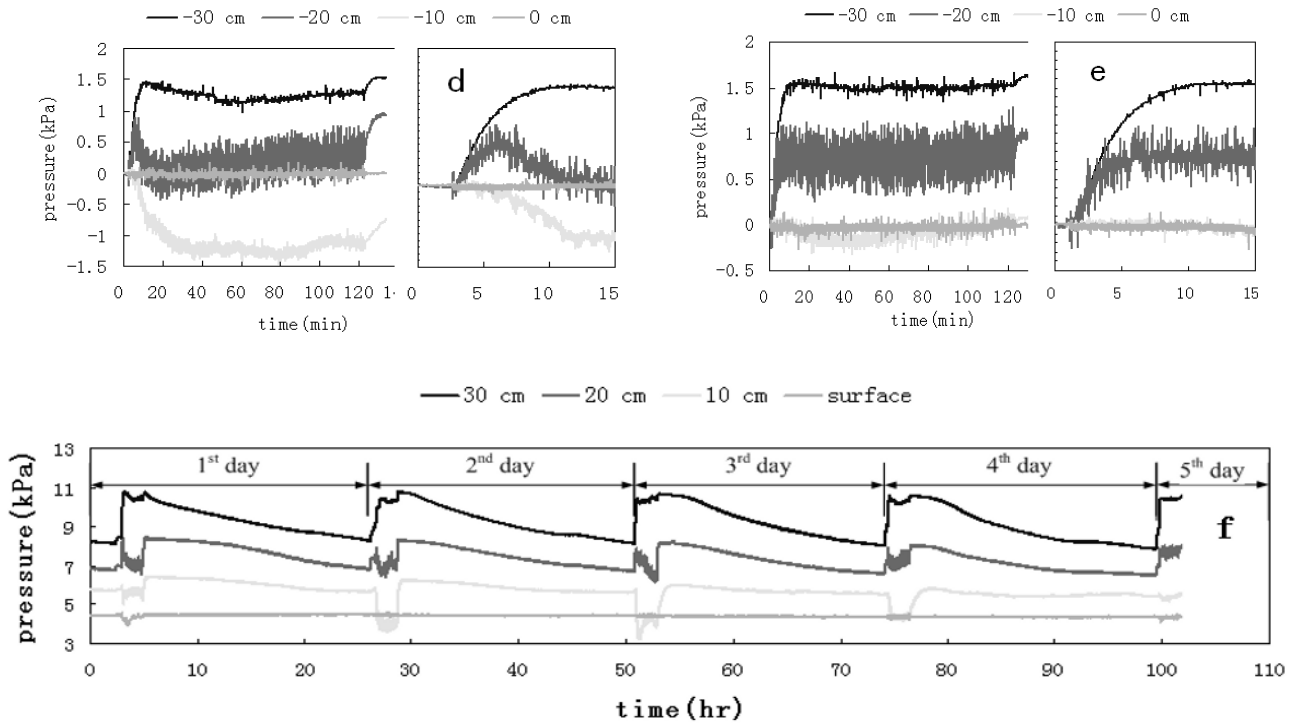


Fig. 3 Temporal variations of wave-induced pore water pressure responses in soft silty seabed of (a) 1st day, (b) 2nd day, (c) 3rd day, (d) 4th day, (e) 5th day, (f) whole consolidation without deduction of the static water pressure.

the end of the wave actions in (a), (b) and (d), and it's an obvious evidence of the compact deposit of the soil particles when waves subsided.

To further investigate the pore water responses, the influence of the erosion should not be ignored. According to (e) in Fig. 3, the 0 accumulation of excess pore water pressure of the 10 cm proved the erosion had at least reached there. The whole consolidation of the five days are shown in (f). The dissipation in excess pore water pressure began when the waves stopped, and the dissipating speed gradually slowed down.

The concept of liquefaction ratio N was employed. N is the specific value between excess pore water pressure ΔP and theoretical static stress P_s . P_s at a given depth d can simply be expressed as (Tzang 2007)

$$P = (1-n)(\rho - \rho')gd \quad (1)$$

Some important times and ΔP with liquefaction ratio N are summarized in Table 2.

The results illustrated that the excess pore water pressures were initiated almost simultaneously across the whole depth and then attained to increasing maximum values with depth in a short period. For example, in third day, $t_{in} = -10$ cm, -20 cm, -30 cm are 275 s, 282 s, 288 s; $t_{ma} = 10$ cm, 20 cm, 30 cm are 769 s, 806 s and 1185 s. The occurrence time of both the initiation and maximum of pore water pressure could be seen to slightly lead at shallower depths to downwards. This suggested that the fluidized responses occurred from surface to deeper layers.

Table 2 Key times, ΔP and N of the seabed soil at different depths in five day when sustaining wave actions

day		0 cm	-10 cm	-20 cm	-30 cm
1	$t_{in}(s)$	170	179	180	185
	$t_{sr}(s)$	213	374	487	828
	$\Delta P(kPa)$	0.21	0.27	1.41	2.29
	N	*	0.25	0.69	0.72
2	$t_{in}(s)$	*	151	161	165
	$t_{sr}(s)$	*	193	292	2045
	$\Delta P(kPa)$	*	0.07	0.68	1.41
	N	*	0.08	0.36	0.47
3	$t_{in}(s)$	*	275	282	288
	$t_{sr}(s)$	*	769	806	1185
	$\Delta P(kPa)$	*	0.16	1.19	2.30
	N	*	0.21	0.70	0.81
4	$t_{in}(s)$	*	166	165	174
	$t_{sr}(s)$	*	280	357	691
	$\Delta P(kPa)$	*	0.02	0.67	1.45
	N	*	*	0.44	0.54
5	$t_{in}(s)$	*	*	80	100
	$t_{sr}(s)$	*	*	369	894
	$\Delta P(kPa)$	*	*	0.81	1.53
	N	*	*	0.60	0.61

“ * ” stand for data being not available

The maximum excess pore water pressure ΔP and liquefaction ratio N showed similar increasing trends with depth in five days' wave loadings. Contrary to Tzang's experiment (the deeper layer is much more stable under wave loading), this indicated a bigger potential of liquefaction in deeper layers. The causes for this difference may be the less consolidation seabed soils and bigger wave energy in this paper's experiment.

In the five days' period, the liquefaction ratios N at -30 cm depth are 0.76, 0.47, 0.81, 0.54 and 0.61. This fluctuate was a idiographic phenomena in soft silty seabed, which suggested that the liquefaction and condensation were carried on alternately because of the erosion of seabed's surface when subjected to waves.

Variations of Soil Strength

The penetration strength of the seabed soil at S_1 and S_2 was measured with a mini-penetrometer everyday as soon as waves had subsided, and strength data was recorded every 2.5 cm in depth. It is shown in Fig. 4 that the penetration strength of the soil increased greatly with the wave loadings implemented times. All of the curves have a similar trend of firstly increase and secondly decrease. Additionally, the depth (D_m) of the maximum value (N_m) of the soil penetration strength varied in different days. For example, the maximum value N_m in the third day, fourth day and fifth day are about 27 kN, 55 kN, 70 kN, and the corresponding depth D_m are about -25 cm, -29 cm, -38 cm. This down-going trend of the maximum value N_m has a good coincidence with the development of the sliding interface, while D_m of each day has some spatial consistency with the location of the sliding interface. The results illustrated that the zone of the sliding interface had high strength. On the other hand, the initial curve in Fig.4 stands for the initial strength values of seabed soils after one day's consolidation by self-weight, and they had a slight increase compared with the 0 penetration strength when the mixed soils was displaced to the soil trench. Nevertheless, as mentioned above, after five days' wave loadings, the maximum value had increased to 70 kN. This indicated a great consolidation speed of soil when sustained wave loading.

After one day's consolidation of seabed soil since waves subsided, the penetration strength of soil was measured in the profile every 10 cm. The distribution of the soil penetration strength is displayed in Fig. 5.

Fig. 5 demonstrated again that there was a hard-layer in the zone where the sliding interface had passed. The existence of the hard-layer was also found in Foda's flume experiment (1994). Besides, Lin Mian (2001) found that the displacement of soil skeletal frame was 0 at some depth in the silt through theoretic calculation, and that is to say, a relatively hard layer was formed there under wave actions. Even with these findings, the

causes regarding the hard-layer are still not clear. But the relations between sliding interface and hard-layer give us some clues to put the axe in the helve.

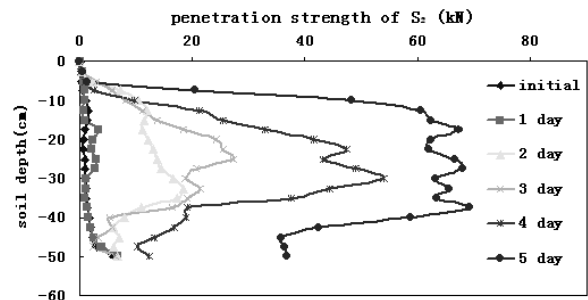


Fig. 4 Variations of penetration strength of seabed soil for five days

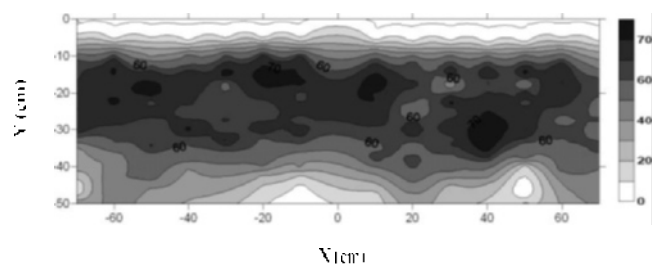


Fig. 5 Isograms of penetration strength of seabed soil (kN)

When the seabed is subjected to wave actions, the sliding interface between oscillatory layer and steady layer inevitably became the main channel of seepage flow, while soil particles will be dislocated from their initial position and re-arranged under the joint action of seepage flow and shear stress induced by waves. In this procedure, soil particles find the steadiest place to settle down and lead to the optimized arrangement of soil particles in this zone. At the same time, better drainage conditions here accelerate the consolidation of the soil at this part. With the down-going of the sliding interface, the hard-layer has formed.

DISCUSSION AND CONCLUSIONS

When the liquefaction happened in silty soil, the structure of the soil skeleton would be destroyed, and the soil lost its strength to behave as fluid and surge with the waves. The surface layer sustained stronger wave loadings, and the negative excess pore water pressure in it indicated that the continuous dislocations between soil particles might induce a vacuum.

In the five-day's period, the settlement of seabed soil induced by consolidation and erosion of the surface layer led to an increase of wave energy exerted on deeper layer. Additionally, the consolidation in static water

between two wave actions caused soil particles to arrange more densely. Their joint results were the down-going trend of sliding interface and the fluctuation of the deeper layer's liquefaction ratio N . The zone where sliding interface had passed would form a layer with extremely high strength, and it was called hard layer in this paper. Overall, the strength of such silt soil increases unequally along the depth continuously under wave loading, and the consolidation speed is much quicker than in the static water.

In-situ investigation data show that the hard crust is ubiquitous in the tidal flat of Yellow River Estuary. Soil particles in this hard crust arrange relatively densely and the hard crust usually has high strength. The underlying layer is a soft soil layer with high clay content, high moisture content, high porosity and low strength. Considering these same features between hard crust at the Yellow River Estuary and hard layer in the flume tests, it can be pointed out that the hard layer is the embryo of the hard crust of Yellow River Estuary. So results in the flume test may be used to explain the formation and characteristics of the hard crust. According to the similarity theory in model test, the responses of seabed with 5 m thickness to waves of $H=1.48$ m, $L=18$ m, $T=3.57$ s can be inferred. After a period (about 3.16 hr) of wave actions, a sliding interface will be formed at some depth (about 2 m to 3 m) in the seabed, and the zone around this sliding interface usually has relatively high strength (named hard crust) when waves have subsided. While subjected to even the same waves again, a new sliding interface will develop in a deeper depth, so the upper layer may move along this new sliding interface. As a result, the old hard crust will deviate from the original location. The mobility of the hard crust is a perplexity to the coastal engineer, and results in this paper's research could give some clues to understand the process and then to solve this problem.

Flume experiment is a good method to study the evolution process of the seabed under controlled conditions. However, it has to be mentioned that only the consolidation process of homogeneous soft silty soil under monochromatic wave is considered in this paper. However, for engineering practice, the situation is very complex, so more research for different wave conditions and inhomogeneous seabed soil is still in great need.

ACKNOWLEDGEMENTS

Financial support from Natural Science Foundation of Shandong Province (Con. No.Y2007E07) is gratefully acknowledged.

REFERENCES

- Terzaghi KD (1924). Theorie der hydrodynamischen Spannungsercheinungen und ihr erdbautechnisches anwendungsgebiet. In: Proceedings, first international congress of applied mechanics, Delft, Netherlands, 1: 288-294.
- Biot AM (1941). General theory of three-dimensional consolidation. *J Appl Phys.*, 12(2): 155-64.
- Yamamoto T, Koning HL, Sellmeijer H, Van Hijum E (1978). On the response of a poro-elastic bed to water waves. *Journal of Fluid Mechanics* 87: 193-206.
- Madsen OS (1978). Wave-induced pore pressures and effective stresses in a porous bed. *Geotechnique*. 28 (4): 377-393.
- Tzang SY (1992). Water wave-induced soil fluidization in a cohesionless fine-grained seabed. Ph.D. University of California, U. S. A.
- Li GX & Xue CT(1993). Sediment thickness, sedimentation rate and slit body shape of the Yellow River Subaqueous Delta Lobe. *Marine Geology & Quaternary Geology*. 13(4): 35-44.
- Li GX, Wei HL, Han YS, Chen YJ (1998). Sedimentation in the Yellow River delta, part I: flow and suspended sediment structure in the upper distributary and the estuary. *Marine Geology*. 149: 93-111.
- Seed HB & Rahman MS (1978). Wave-induced pore pressure in relation to ocean floor stability of cohesionless soils. *Marine Geotechnology* 3(2):123-150.
- Chen YY, Liu HJ, Jia YG, Cong YP (2007). Qualitative study on mechanism of liquefaction and seepage of seabed structure silty soil under cyclic loads. *Rock and Soil Mechanics* 28(8): 1631-1635.
- Zhang JM, Shan HX, Jia YG, Liu HJ, et al.(2007). An experimental study of nonuniform consolidation of rapid sediment seabed soils at Yellow River mouth subjected to wave and tide wave loading. *Rock and Soil Mechanics*, 28(7): 1369-1380.
- Tang SY & Ou SH (2006). Laboratory flume studies on monochromatic wave-fine sandy bed interactions Part 1. Soil fluidization. *Coastal Engineering* 53: 965-982.
- Lin M (2001). Analysis of Silt Soil Prosperities by Water Waves. *Science of China(E)*. 31(1): 86-96.
- Foda MA (1994). Resonant fluidization of silty soil by water waves. *J G R*. 99(10): 20264~20475
- Wang CJ (2002). *River Dynamics*, Beijing: China Communications Press.12, 5-8.
- Li LY, Cui J, Jing LP, Du XL (2005). Study on liquefaction of saturated silty soil under cyclic loading. *Rock and Soil Mechanics*, 26(10): 1663-1666.

CHARACTERISTICS OF SHEAR STRENGTH OF UNSATURATED WEAK EXPANSIVE SOIL

Wei-Min YE¹, Ya-Wei ZHANG², Bao CHEN³ and Shi-Fang ZHANG⁴

ABSTRACT: The strength properties of unsaturated soil are far more complicated than those of saturated soil. As a kind of typical and widely spread unsaturated soil, expansive clay shows a very close relationship between its shear strength and water content, for its high content of hydrophile, such as montmorillonite, illite and etc. The shear strength of soil is of much significance in the design of foundation and slope in expansive soil area. The determination of shear strength for expansive soil is always an important issue in this aspect. Based on the investigation of expansive clay in a slope along Han-Shi highway, Hubei Province, some unsaturated shear tests with suction control have been conducted, and then, unsaturated mechanical parameters have been obtained using double-variables strength theory, and characteristics of the unsaturated shear strength of the specimen have been explored. Results indicate that slight shear dilatation appeared during the unsaturated shearing course and its value decreases with the increase of confining pressure and suction. For lower suction, the cohesion of the tested soil specimen linearly increases with suction increases. The shear coefficient ϕ^b for testing specimen is 10.7°.

KEYWORDS: unsaturated soil, weak expansive soil, shear strength, shear test

INTRODUCTION

The Mohr-Coulomb strength theory can be used for the accurately determination of shear strength for saturated soils, which has been proved by experiments and engineering practices. But the strength properties for unsaturated soils are far more complicated. This may be because that the surface tension of the water-air interface in unsaturated soil causes different pressures in water and air, and mostly the pore water pressure is a negative value. So, the effective stress for unsaturated soil is no longer equal to the pressure between grains, because pore air pressure and negative pore water pressure appear simultaneously (Ye et al. 2006). Therefore, many formulas for description of saturated soil cannot be simply extended to unsaturated soil.

Expansive soil is a kind of typical unsaturated soil which distributes widely in many arid and semiarid areas in the world, such as Australia, Canada, China, India, Israel, South Africa, the United States and so on. The shear strength of expansive soil is highly related to its high content of hydrophilic clay minerals which include montmorillonite and illite. Therefore, from different aspects, a lot of experimental studies and theoretical

explorations have been carried out on shear strength of expansive soil. Melinda F et al. have investigated the strength and deformation characteristics of a residual soil of the Bukit Timah Granitic Formation with infiltration, which leads to slope failure. At the beginning of the infiltration process, the soil deformation is small but matric suction decreases rapidly. When failure approaches, soil deformation increases sharply (Melinda et al. 2004). Using conventional saturated shearing technique, YANG et al. (2005) tested some saturated compacted specimens of Ningming expansive soil after experiencing drying-wetting circles. After comparing the test results obtained to some other similar shearing tests, they explored the influence of dry-wet circling effects on expansive soil strength. Based analysis of the shear test results of an expansive soil, Kong and Tan (2000) established a relationship between the shear strength parameters and initial water content of an unsaturated compacted expansive soil. Zhan et al. (2006) carried out a lot of experimental and theoretical explorations to the shear strength of expansive soil by performing suction-controlled direct shear tests on both natural and compacted specimens. And based on the direct shear test results of several groups of Nanning expansive soil specimen

¹ Professor, Key Laboratory of Geotechnical and Underground Engineering of Ministry of Education, Tongji University, China.
Email: ye_tju@tongji.edu.cn

² Ph.D Student, ditto. Email: zhyaowei2006@163.com

³ Vice-Professor, ditto. Email: chenbao@tongji.edu.cn

⁴ Master Student, ditto. Email: zhangshifang512@163.com

using improved direct shear apparatus, Xiao et al. (2007) analyzed the influences of vertical load, water content and dry density on the ultimate shear stress and residual shear stress of the test soil.

Based on a comprehensive review of information related to shear strength of unsaturated expansive soil, suction-controlled shear tests on unsaturated soil specimen obtained from side slope along the Han-Shi Expressway in Hubei province have been done and test results have been analyzed using double-variable theory. Based on these, some unsaturated shear strength parameters are obtained and the shear strength characteristics of tested unsaturated weak expansive soil have been analyzed.

SHEAR STRENGTH THEORY FOR UNSATURATED SOIL

Based on Terzaghi's principle of effective stress for saturated soils, Bishop proposed one of the well-known shear strength equation for unsaturated soils (Bishop 1959).

$$\tau = c' + [(\sigma - u_a) + \chi(u_a - u_w)] \tan \phi' \quad (1)$$

where c' = effective cohesion; u_a = pore air pressure; u_w = pore water pressure; $u_a - u_w$ = matric suction; ϕ' = effective friction angle; parameter χ depends on the degree of saturation, χ equals zero corresponding to perfectly dry conditions and χ equals unity corresponding to saturated conditions. When χ equals unity Eq. (1) reduces to Terzaghi's classic effective stress equation for describing the behavior of saturated soil ($\sigma' = (\sigma - u)$).

As the parameter χ in Bishop's formula is difficult to be measured and influenced by lots of factors, also the determination of suction ($u_a - u_w$) is not so easy, Croney and Coleman, Aitchison and Jennings latterly proposed respective formulas of effective stress which are some similar to Bishop's formula (Barbour 1998).

After that, Huat et al. (2005), Vilar (2006) and Fredlund et al. (1996) etc, made their contributions to the study on the shear strength of unsaturated soil from different aspects, such as improvements on testing apparatus and theoretical models, as well as shear strength prediction using SWCC and so on.

At the same time, a large amount of researches have been done on stress variable and shear strength theory for unsaturated soils in China. Chen et al. (1994) derived effective stress formula for anisotropic porous media, based on discussions of the effective stress variable of unsaturated soil, and determined the effective stress parameters by tri-axial tests. Miao et al. (2001) explored the relationship between shear strength and water content (or matric suction) of unsaturated soil based on

the investigation of components of matric suction. Chen et al. (2004) developed a set of direct shear apparatus for unsaturated soil and studied the relationship between strength, deformation and water content of loess with this apparatus. Based on a self developed fractal model, Xu (2004) easily estimated the unsaturated shear strength using surface fractal dimension and air-entry value. At the same time, Miao et al. (2007), Sheng et al. (2006), Luan et al. (2006), and Lu et al. (2006), also made a lot of experimental and theoretical explorations to the shear strength theory for unsaturated soils and the tri-axial strength of unsaturated expansive soil. Ye et al. (2006) investigated the unsaturated shear strength of Shanghai soft clay through unsaturated tri-axial tests. Results show that, in lower suction, the tri-axial strength for unsaturated Shanghai soft clay is linear to suction, which certifies the applicability of double-variable strength theory to unsaturated soft soil. The tri-axial shear coefficient ϕ^b of Shanghai soft clay (layer ④) is 10.6° .

But until recently, the double-variables shear strength formula, proposed by Fredlund et al. (1978) for unsaturated soils, has been considered as comparatively more mature in theory and popular in applications.

$$\tau = c' + (\sigma - u) \tan \phi' + (u_a - u_w) \tan \phi^b \quad (2)$$

where c' = effective cohesion; ϕ' = effective angle of internal friction related to net normal stress variable ($\sigma - u_a$), ϕ^b = effective angle of internal friction related to shear strength depending on matric suction ($u_a - u_w$). Based on typical values of ϕ^b for various soils, Fredlund (1997) found that the value of ϕ^b is often less than or equal to the value of internal friction angle ϕ' . While Gan (1988) proved that when suction is lower than a certain value, such as the air-entry value, $\phi^b = \phi'$. And when matric suction exceeds a certain value, ϕ^b is non-linear and decreased with the increase of suction. That is to say, for most soils, ϕ^b is a non-linear variable.

SHEAR TESTS FOR UNSATURATED SOIL

Soil Specimen

The tested soil was obtained from a side slope along Han-shi highway at Laohekou, Hubei Province, with a depth of 1-1.5m. According to the geological investigation report of this project, the soil features are alluvial and diluvial cohesive soil of quaternary pleistocene, dark-yellow, rigid-plastic, containing a little Fe, Mn oxide tuberculosis and a little incanus kaolin bands. It has low natural water content and relatively high allowable bearing capacity.

According to results of X ray diffraction and infra-

red spectrum analysis, the specimen mainly composed of quartz, illite, and also some albite, montmorillonite, potash feldspar and kaolinite, etc.

Table 1 Chemical components of tested specimen

Component	%
SiO ₂	67.4
Al ₂ O ₃	16.4
Fe ₂ O ₃	5.75
K ₂ O	2.38
Na ₂ O	0.93
MgO	1.30
TiO ₂	0.84
CaO	0.93
MnO	0.06
Cl	0.07
BaO	0.07
NiO	0.04
ZrO ₂	0.03
Cr ₂ O ₃	0.04

Some physical properties of the test soil are shown in Table 2. According to “the Chinese State Standards for ‘the Construction Techniques in Expansive Area’ (GBJ112-87)”, tested soil belongs to weak expansive soil.

The process of specimen preparation was strictly controlled according to the Standard for Soil Test Method (GB/T 50123-1999). The dimensions of the specimen were 61.8 mm in diameter and 20mm in thickness.

Testing Apparatus

The 4FDJ-20 direct shear test equipment for unsaturated soil, which was developed by CHEN et al. (2004), was employed here. Setup of the direct shear apparatus is shown in Fig.1. It mainly includes a bench, an air chamber, a shear box, vertical loading system, drainage system and measuring system, etc. Vertical load is applied through a lever loading system.

Compared to conventional shear test equipments for saturated soil, this apparatus has an additional set of

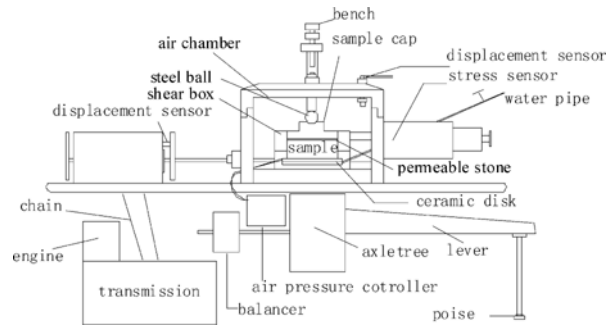


Fig. 1 Sketch of the direct shear apparatus for unsaturated soil (Chen 2004)

sealed container, air pressure control system and exhausts device drive by water. At the same time, axis parallel translation technique was used for suction control in soil specimen. More specialties of this device can be found from literature (Chen 2004).

Testing Procedure

Soil-water characteristic curve (SWCC) for the test soil is given in Fig. 2. Fig. 2 shows that, for the desorption curve of the test specimen, the boundary effect zone and the transition zone are clear, whereas the residual zone is unobvious. The air entry value of the test soil is about 120~200kPa. Therefore, for the unsaturated direct shear test, the selected controlling suction is 120kPa, 300kPa and 400kPa. Simultaneously, the selected confining pressures in this test are 100kPa, 200kPa and 300kPa (Table 2).

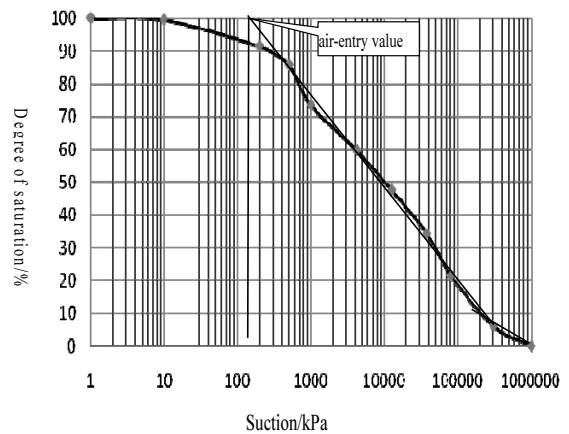


Fig. 2 SWCC of test soil

Table 2 Some basic physical properties of test soil

Liquid limit/%	Plastic limit/%	Natural water content/%	Montmorillonite mass fraction/%	Illite mass fraction /%	Free swelling ratio/%	Specific gravity/(g cm ⁻³)
42.08	23.68	20.64	5	22	58	2.71

Table 3 Parameters for unsaturated shear test

Specimen	Confining pressure /kPa	Suction/kPa
A	100	120
B	200	300
C	200	400
D	300	400

This test is a consolidation drained direct shear test with suction control, and the test was carried out in the following steps: ceramic disk saturation, suction control consolidation and suction control shearing. The whole procedure was seriously controlled according to requirements of the Standard for Soil Test Method (GB/T 50123-1999).

- a. Ceramic disk saturation.
- b. Soil consolidation

Soil specimen was consolidated with suction and confining pressure control until the consolidation deformation reaches stable. According to requirements of the Standard for Soil Test Method (GB/T 50123-1999), consolidation course can be stopped when the deformation rate reaches 0.005mm/h.

- c. Unsaturated shearing

Based on the same standard mentioned above, after consolidation, the specimen is sheared with suction and confining pressure control. The shearing velocity is designated at 0.00192mm/min. When the shear stress peak appeared and the shear displacement reached 4mm stopped the shearing course. If there wasn't shear stress peak, the shearing course should be continued to the shear displacement reached 6mm.

RESULTS AND DISCUSSIONS

Shear Dilatations

Relationship between vertical displacement and shear displacement is given in Fig. 3. It shows that there are slight differential shear dilatations during the shear course for all the soil samples, and the shear dilatation value decreases with the increase of confining pressure and matric suction.

Relationship between Shear Displacement and Shear Stress

Curves in Fig. 4 describe the relationship between shear displacement and shear stress under different combination of confining pressure and suction. According to the Standard for Soil Test Method (GB/T 50123-1999), the failure shear stress and the shear stress at shear displacement 4mm when failure not happened were recorded as the shear strength. So, the shear stress of the

soil 4 specimen tested are 127kPa, 200kPa, 218kPa and 256kPa respectively.

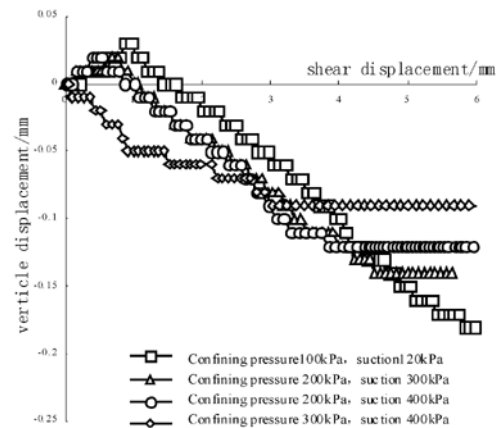


Fig. 3 Relationship between vertical displacement and shear displacement

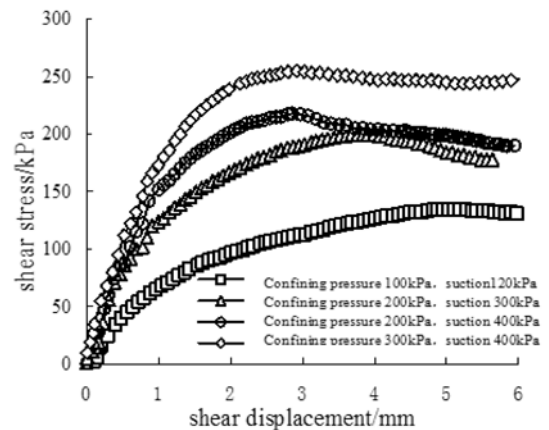


Fig. 4 Relationship between shear stress and shear displacement

Fig. 4 also shows that the shear strength of unsaturated soil increases with suction increases for constant confined stress, and increases with confined stress increases under the same suction. It clearly shows that the failure shear stress increases with the increase of shear stress and vertical stress.

Shear Strength of Unsaturated Soil

Based on the test results and the double-variables shear strength theory for unsaturated soil, the Mohr-Coulomb's failure envelope for the test soil can be drawn in Fig. 5. It shows that in low suction scope, the cohesion of the soil sample increases with suction linearly, and the effective angle of internal friction related to matric suction is a constant. Therefore, the double-variable theory is suitable for the evaluation of the unsaturated weak expansive clay tested in this paper. Some unsaturated

mechanical parameters for the test soil are, $\phi^b = 10.7^\circ$, $c' = 66.5 \text{ kPa}$, $\phi' = 20.81^\circ$.

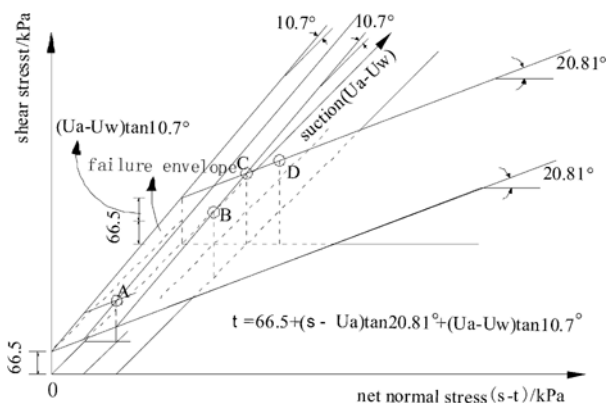


Fig. 5 Mohr-Coulomb's failure envelope for tested soil

CONCLUSIONS

1) Slight shear dilatation occurred during the unsaturated shear test with confining pressure and suction control, and the shear dilatation value decreases with the increase of confining pressure and suction.

2) Under constant confined stress, the unsaturated shear strength of test soil increases with suction increases. While under the same suction, the unsaturated shear strength of test soil increases with confining pressure increases.

3) For low suction, the cohesion of the tested soil specimen linearly increases with suction increases. The double-variable theory is suitable for the evaluation of the unsaturated weak expansive clay tested in this paper. Some unsaturated mechanical parameters for the test soil are, $\phi^b = 10.7^\circ$, $c' = 66.5 \text{ kPa}$, $\phi' = 20.81^\circ$.

ACKNOWLEDGEMENTS

The study was supported by the National Basic Research Program (2006CB403200) and Shanghai Leading Academic Discipline Project (B308).

REFERENCES

Barbour SL(1998). Nineteenth Canadian Geotechnical Colloquium: The soil-water characteristic curve: a historical perspective [C]// Canadian Geotechnical Journal, 35 (5): 873-894.
Bishop AW (1959). The principle of effective stress. Lecture delivered in Oslo, Norway, in 1955, published in *Tecknish Ukeblad*. 106 (39): 859-863.

Chen ZH, Wang YS, Xie DY (1994). Effective stress in unsaturated soil. *Chinese Journal of Geotechnical Engineering*, 16(3): 62-69 (in Chinese).
Chen ZH (2004). Development & application of consolidation apparatus and direct shear apparatus for unsaturated soils. *Chinese Journal of Geotechnical Engineering*, 26(2): 161-166 (in Chinese).
Deng G & Shen ZJ (2006). Numerical simulation of crack formation process in clays during drying and wetting. *Geomechanics and Geoengineering*, 1(1): 27-41.
Fredlund DG, Morgenstem NR, Widger RA (1978). The Shear Strength of Unsaturated Soils. *Canadian Geotechnical Journal*, 15(3): 313-321.
Fredlund DG, Xing A, Fredlund MD, Barbour SL (1996). The relationship of the unsaturated soil shear strength to the soil-water characteristic curve. *Canadian Geotechnical Journal*, 33(3): 440-448.
Fredlund DG & Rahardjo H (1997). *Soil Mechanics for Unsaturated Soil*. Beijing: China Architecture and Building Press.
Gan KM, Fredlund DG, Rahardjo H (1988). Determination of the shear strength parameters of an unsaturated soil using the direct shear test. *Canadian Geotechnical Journal*, 25(3): 500-510.
Huat BBK, Ali FH, Hashim S (2005). Modified Shear Box Test Apparatus for Measuring Shear Strength of Unsaturated Residual Soil. *American Journal of Applied Sciences*, 2(9): 1283-1289.
Kong LW & Tan LR (2000). Study on shear strength and swelling-shrinkage characteristic of compacted expansive soil. *Proceedings of the Asian Conference on Unsaturated Soils*, Singapore, 515-519.
Lu ZH, Chen ZH, Fang XW, Guo JF, Zhou HQ (2006). Structural damage model of unsaturated expansive soil and its application in multi-field couple analysis on expansive soil slope. *Applied Mathematics and Mechanics (English Edition)*, 27(7): 891-900.
Luan MT, Li SQ, Yang Q (2006). Matric suction, tension suction and their equivalent in four-grain packed unsaturated soils with isolated pore water. *Proceedings of the Fourth International Conference on Unsaturated Soils*, 2162-2173.
Melinda F, Rahardjo H, Han KK, Leong EC (2004). Shear strength of compacted soil under infiltration condition. *Journal of Geotechnical and Geoenvironmental Engineering*. 130(8): 807-817.
Miao LC, Sandra LH, Ying C, Yuan JP (2007). Relationship between soil structure and mechanical behavior for an expansive unsaturated clay. *Canadian Geotechnical Journal*, 44(2): 126-137.
Miao TD, Mu QS, Liu ZY, Ma CW (2001). Effective stress and shear strength of unsaturated soil with low water content. *Chinese Journal of Geotechnical Engineering*, 23(4): 393-396 (in Chinese).

- Vilar OM (2006). A simplified procedure to estimate the shear strength envelope of unsaturated soils. *Canadian Geotechnical Journal*, 43(10):1088–1095.
- Xiao HB, Zhang CS, He J, Fan ZH (2007). Expansive soil-structure interaction and its sensitive analysis. *Journal of Central South University of Technology*. 14(3): 425-430.
- Xu YF (2004). Fractal approach to unsaturated shear strength. *Journal of Geotechnical and Geoenvironmental Engineering*. 130(3): 264–273.
- Yang HP & Xiao D (2005). The influence of alternate dry-wet effect on the strength characteristic of expansive soils. *Journal of Changsha University of Science and Technology (Natural Science)*. 2(2): 1-5 (in Chinese).
- Ye WM, Chen B, Bian ZX, Zhu HH, Bai Y (2006). Tri-axial shear strength of Shanghai unsaturated soft clay. *Chinese Journal of Geotechnical Engineering*. (3): 317-321 (in Chinese).
- Zhan TLT & Ng CWW (2006). Shear strength characteristics of an unsaturated expansive clay. *Canadian Geotechnical Journal*, 43(7): 751–763.

ON THE DETERMINATION OF THE SOIL-WATER CHARACTERISTIC CURVE USING THE PRESSURE PLATE EXTRATOR

Hui CHEN¹, Chang-Fu WEI², Rong-Tao YAN³, Pan CHEN⁴ and Pan-Pan YI⁵

ABSTRACT: The pressure plate extractor is commonly used to measure the soil water characteristic curve (SWCC). In the measurement, two methods are adopted to determine the soil water content, through weighing the soil sample and the outflow, respectively. With the first method, part of soil mass may lose during the operation, while with the second method air bubbles may accumulate under the ceramic plate, inducing the air-water interfacial effect. All these factors may result in error in the measurement. To resolve these issues, a modified method for weighing the outflow is introduced. By comparing the data obtained with these three methods, it is found that the method of weighing soil is suited for the case when matric suction is large or testing time is long, whereas the method of weighing outflow is suitable only when matric suction is small and testing time is short. It is also found that the proposed adjusted method of weighing outflow can be effectively used to determine the soil water characteristics for all soils.

KEYWORDS: the pressure plate extractor, the soil water characteristic curve, the method of weighing soil, the method of weighing outflow, the adjusted method of weighing outflow

INTRODUCTION

The water content in the unsaturated soil is a function of matric suction. This constitutive relationship is commonly referred to as the soil-water retention curve in soil sciences, and well known as the soil-water characteristic curve (SWCC) in geotechnical engineering. Using the SWCC, we can compute or determine the hydraulic conductivity function (Van Genuchten 1980; Mualem 1976; Brooks and Corey 1964; Burdine 1953), the volumetric variation of the soil (Wang 2007), the shear strength in the unsaturated soil (Fredlund et al. 1995; Vanapalli et al. 1996; Babu et al. 2005; Huang and Wu 2007), and the attribution of the water content in subsurface (Fredlund and Rahardjo 1997; Jing 2004; Wang 2008). Apparently, this relationship plays an important role in the research and engineering practice related to unsaturated soils.

Numerous laboratory apparatus have been developed to measure the SWCC independently. These instruments include the pressure plate extractor (Sun et al. 2006), the tempe cell and the constant flow laboratory system (Lu et al. 2006) which concurrently measure the SWCC and

the hydraulic conductivity function. Among these instruments, the pressure plate extractor is the most common apparatus due to its high efficiency, convenience for operation, cost effectiveness, and so forth. Usually, two methods are adopted in using the pressure plate extractor, namely, including the method of weighing soil (WSM), which measures the water content by weighing the soil sample when equilibrium is reached, and the method of weighing outflow (WOM), which measures the water content by weighing the outflow from the soil sample after equilibrium is attained. In the measurement, however, there are some factors that can adversely influence testing results. For example, with the WSM, part of soil mass may lose, and in using the WOM, the outflow could be overestimated because air bubbles accumulate under the ceramic plate due to the diffusion of dissolved air at a high pressure or for a long period of time. All these factors may result in error.

In this paper, we address how to accurately determine the water content of unsaturated soils by using a pressure plate extractor. To this end, an adjusted method of weighing outflow (WOAM) is introduced to minimize the error in measuring the water content of a soil sample.

¹ Ph.D Student, State Key Laboratory of Geomechanics and Geotechnical Engineering, Institute of Rock and Soil Mechanics, Chinese Academy of Sciences, China. Email:chenhuifang3589@163.com

² Professor, ditto. Email: cfwei@whrsm.ac.cn

³ Ph.D Student, ditto. Email: yrt301@163.com

⁴ Ph.D Student, ditto. Email:chenpan0203@163.com

⁵ Ph.D Student, ditto. Email:ppan2003 @163.com

MATERIALS AND METHODS

Two different types of soils were used in the experiment, whose properties were given in Table 1.

Table 1 Physical properties of soils used in the testing

Soil type	Particle size distribution %			Dry density g/cm ³
	Sand	Silt	Clay	
silty sand	63.5	36.5	0	1.55
clayey silt	13.8	75.2	11	1.54

Each soil was air dried, sieved through a 0.002m screen and packed to predetermined dry bulk densities in 0.0618m-inner diameter and 0.02m-high cutting rings. To make sure that all the soil samples have the same structure for all tests, we adopted a unique compaction procedure, in which predetermined sample mass was pressed into the 0.0618m-inner diameter and 0.02m-high cutting ring. After a soil sample was compacted, it was then saturated by using the vacuum saturation method. Then the sample was weighed to determine the initial amount of water. The sample was assembled on the saturated ceramic disk in the pressure plate extractor. All experiments were conducted at room temperature 20°C. During the test, the air pressure was increased when outflow is less than a level of 0.05 gram per hour. After each test, the soils were removed from the cell and weighed, oven dried at 105°C for 24 hours, and weighed again to determine the water content.

Because the WSM and the WOM are very well recognized, only the WOAM is introduced hereinafter. The testing principle of the WOAM is similar to that of the WOM. Namely, they both measure the soil water content by weighing the outflow mass. In the WOAM, however, two saturated ceramic disks with the same properties were assembled in the pressure plate extractor, one of the disks were used to host the soil sample, while the other used for the calibration purpose. In the experiment, we first record the initial readings of balances connecting with the two saturated ceramic disks, respectively; the air pressure is then elevated, and when equilibrium is attained, the readings of balances connecting with the two saturated ceramic disks are recorded. Based on these measurements, we can compute the saturation of the sample according to these readings of balances. With the WOAM, those issues occurring in the WOM, such as air-bubble accumulation, existence of the air-water interface and evaporation of outflow, can be avoided.

RESULT AND DISCUSSION

Figs. 1-2 illustrate the SWCCs for the silty sand and the clayey silt, respectively, determined by using the

three methods. It can be seen that the difference between the saturations obtained by the WOM and the WOAM increases gradually with the increase in the matric suction, and the saturation by the WOM can become negative for the clayey silt (see Fig. 2). Clearly, use of the WOM may induce error in determining the SWCC, and the error stems from the air-bubble accumulation and the formation of the air-water interface within the ceramic disk. From Fig. 2, it can also be seen that the difference between the saturation obtained by the WSM and the WOAM is small for the clayey silt. In addition, it is evident that, at the same matric suction, the saturation of the WOAM is generally larger than that of the WSM and the WOM.

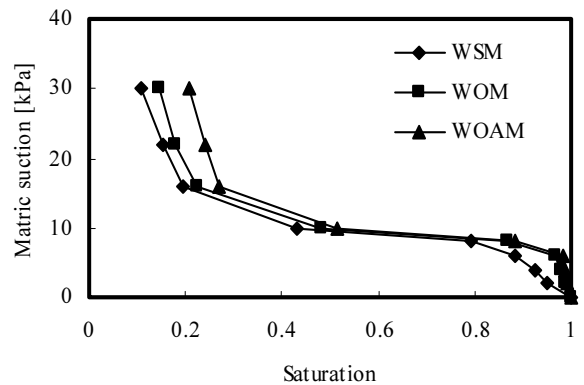


Fig. 1 Soil-water characteristic curves of silty sand

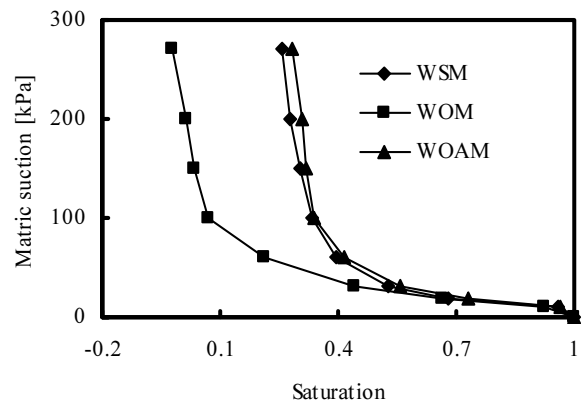


Fig. 2 Soil-water characteristic curves of clayed silt

To explore the reasons for these discrepancies, we refer to the formulations used to calculate the saturation. In the WSM, the saturation is obtained by

$$S_i = 1 - \frac{m_i - m_1}{nV} \quad (1)$$

where S_i is the saturation of the sample corresponding to the i th matric suction p , n is the porosity, V is the total volume of the sample, m_i and m_1 are the sum of

the mass of the cutting ring and the soil when the matric suction is zero and p , respectively. After the equilibrium is attained, the sum of the mass of the cutting ring and the soil is measured. In weighing the soil sample, part of soil mass may inevitably lose. As a result, the measured value of m_1 is less than the actual value. According to Eq. 1, it can be concluded that the measured value of saturation is less than the actual value of saturation.

In the WOM, the relationship between the saturation and the outflow is given by

$$S_2 = 1 - \frac{m_2 - m_0}{nV} \tag{2}$$

where S is the saturation of the sample at the matric suction p , m_0 and m_2 are the balance readings when the matric suction are zero and p , respectively. Because air bubbles accumulate under the ceramic plate due to the diffusion of dissolved air at a high pressure or a long period of testing time and the existence of the air-water interface, the measured value of m_2 is larger than the actual value. According to Eq. 2, it can be seen that the measured value of saturation is less than the actual value of saturation.

In the WOAM, the relationship between the saturation and the outflow is given by

$$S_3 = 1 - \frac{(m_3 - m_0) - (m_1 - m_{10})}{nV} \tag{3}$$

where S_3 is the saturation corresponding to p , m_0 and m_3 are the readings of balances connecting to the saturated ceramic disk without the sample when the matric suction are zero and p , respectively. m_1 and m_{10} are the readings of balances connecting to the ceramic disk on which the saturated soil was assembled when the matric suction are zero and p , respectively.

It is worthy to note that, the WOAM inherits the advantage of the WOM, i.e., avoiding repeatedly weighing soil, and discards disadvantages of the WOM, such as air-bubbles accumulation, formation of air-water interface and evaporation of outflow. Hence, the WOAM yields the best results.

Table 2 summarizes the mass losses of the soil samples before and after testing for the three methods, and Table 3 compares the computed and measured values of the water content after testing. From Table 2, one can see that with the WSM, the loss of the soil mass in silty sand is more than that in clayey silt. The reason for this is that the silty sand contains no clay content (see Table 1) so that the soil particle is prone to lose. From

Table 3, it can be seen that the difference between the measured value and the computed value of the water content for silty sand is more than that for clayey silt, since the loss of soil mass has been considered as part of the outflow from the soil sample. Hence, the WSM is suitable for clayey soils or for the cases that matric suction is large or the testing time is long.

With the WOM, the loss of soil mass is small for both silty sand and clayey silt, and the computed value of the water content can even be negative for clayey silt. Hence, the WOM may induce error in determining the SWCC. The error arises because air bubbles accumulate under the ceramic plate due to the diffusion of dissolved air at a high pressure or a long period. Hence, the WOM is only suitable for the case when the matric suction is small and testing time is short.

With the WOAM, the loss of soil mass is small and the computed value of the water content after testing is close to the actual value for both silty sand and clayey silt. The reason for this is that the WOAM inherits the advantage of the WOM, i.e., avoiding repeatedly

Table 2 The sample masses before and after testing for the three methods

Soil type	Method	The sample mass (g)	
		Before testing	After testing
silty sand	WSM	93.05	90.37
	WOM	92.98	92.14
	WOAM	92.98	92.14
clayey silt	WSM	92.54	91.70
	WOM	92.58	92.10
	WOAM	92.58	92.10

Table 3 Comparison of the water masses after testing

Soil type	Methods	The water mass after testing (g)	
		Computed value	Measured value
silty sand	WSM	2.57	5.49
	WOM	3.81	6.12
	WOAM	5.46	6.12
clayey silt	WSM	6.70	7.50
	WOM	-0.53	7.04
	WOAM	7.38	7.04

weighing soil, and discards disadvantages of the WOM, such as air-bubbles accumulation, formation of air-water interface and evaporation of outflow. As a consequence, the WOAM yields the best results.

CONCLUSIONS

The pressure plate extractor is commonly used to measure the soil water characteristic curve. Two methods are usually adopted by using the pressure plate extractor, including the method of weighing soil and the method of weighing outflow. This paper discusses the issues related to the use of these two methods. In using the method of weighing soil, part of soil particle may be lost so that the measured value of saturation is less than the actual value, and in using the method of weighing outflow, the measured value of saturation is less than the actual value because air bubbles accumulate under the ceramic plate by diffusion of dissolved air at a high pressure or a long period. In order to resolve these issues, an adjusted method of weighing outflow is adopted. It inherits the advantage of the WOM, i.e., avoiding repeatedly weighing soil, and discards disadvantages of the WOM, such as air-bubbles accumulation, formation of air-water interface and evaporation of outflow. As a consequence, the WOAM yields the best results.

By comparing the data obtained with the three methods, it is found that the WSM is suitable for clayey soils or for the cases when matric suction is large or testing time is long, whereas that the WOM is only suitable for the cases when matric suction is small and testing time is short. It is also found that the adjusted method of weighing outflow is applicable to determine the SWCC for all soils.

ACKNOWLEDGEMENTS

The research were supported by Natural Science Foundation of China (Contract #10872211).

REFERENCES

- Van Genuchten MT (1980). A closed-form equation for predicting the hydraulic conductivity of unsaturated soils. *Soil Sci. Soc. Am. J.*, 44: 892-898.
- Mualem Y (1976). A new model for predicting the hydraulic conductivity of unsaturated porous media. *Water Resour. Res.* 12(3): 513-522.
- Brooks RH & Corey AT (1964). Hydraulic properties of porous media. Hydraulic Paper no.3, Civil Engineering Dep., Colorado State Univ., Fort Collins, Colo. flow. J. Irrig.
- Burdine NT (1953). Relative permeability calculations from pore-size distribution data. *Petr. Trans., Am. Inst. Mining Metall. Eng.* 198: 71-77.
- Wang DL, Luan MT and Yang Q (2007). Experimental study on volume change of unsaturated soils and its application to estimation of subsidence. *Journal of Disaster Prevention and Mitigation Engineering.* 27(3): 307-311.
- Fredlund DG, Xing A, Fredlund MD, Barbour SL (1995). The relationship of the unsaturated soil shear strength function to the soil water characteristic curve. *Canadian Geotechnical Journal.* 32: 440-448.
- Vanapalli SK, Fredlund DG and Pufahi DE (1996). The relationship between the soil-water characteristic curve and the unsaturated shear strength of a compacted glacial till. *Geotechnical Testing Journal,* 19(3): 259-268.
- Babu GLS, Rao RS and Peter J (2005). Evaluation of shear strength functions based on soil water characteristic curves. *Journal of Testing and Evaluation.* 33(6): 461-465.
- Huang RQ & Wu LZ (2007). Study on the shear strength of unsaturated expansive soils. *Journal of Chengdu University of Technology (Science & Technology Edition),* 34(3): 221-224.
- Fredlund DG & Rahardjo H (1997). *Soil mechanics for unsaturated soils.* Wiley-interscience.
- Jing HJ (2004). Study on water infiltration pattern into loess subgrade. *Journal of Highway and Transportation Research and Development.* 21(4): 40-42.
- Wang TH (2008). Moisture migration in unsaturated loess subgrade. *Chinese Journal of Geotechnical Engineering.* 30(1): 41-45.
- Sun SG, Chen ZH, Zhu YQ, Liu YH, Wang L (2006). Coordinated ceramic plate extractors and some problems of SWCC test. *Journal of Logistical Engineering University,* 4: 1-5.
- Lu N, Wayllance A, Carrera L, Likos WJ (2006). Constant flow for concurrently measuring soil water characteristic curve and hydraulic conductivity function. *Geotechnical Testing Journal,* 29(3): 230-241.

ZERO VALENT IRON TO REMOVE THE ARSENIC CONTAMINATION FROM NATURAL GROUNDWATER: BATCH AND COLUMN EXPERIMENT

M. A. ABEDIN¹, Takeshi KATSUMI², Toru INUI³ and Masashi KAMON⁴

ABSTRACT: Groundwater with high levels of arsenic has received much attention in some Asian countries due to its massive environmental alarm. Groundwater flowing throughout As-rich geologic stratum may become contaminated with high concentrations of toxic As, which can make its way into private and public water supply wells. So it is urgently needed to overcome the silent arsenic disaster to feed arsenic free drinking water to the people. Presently, zero valent iron (ZVI) is to be studied as an effective tool for cleanup of groundwater containing heavy metals. Thus, it has special attention due to its high adsorption capacity and strong affinity to remove arsenic from contaminated groundwater. This paper highlights the burgeoning use of zero valent iron for mitigation of arsenic from groundwater. A series of both batch and column experiments were conducted to evaluate arsenic removal capacity by ZVI with the effect of pH, Eh and Dissolved Oxygen (DO) content. The results showed that more than 99% arsenic was removed in both batch and column experiment. In column experiment, efficient removal of arsenic was observed concentrations below the limit of 10 µg /L (WHO's Standard) in the treated waters. Arsenic removal capacity of zero valent iron was determined to be 2.5 mg As/g ZVI.

KEYWORDS: Arsenic, zero valent iron, groundwater

INTRODUCTION

The natural contamination of groundwater by arsenic is thought to be highly valuable passing with time. Arsenic contamination in groundwater, in fact, has become a global issue of public health as it has been encountered in many countries and regions of the world under varying conditions (Bhattacharya et al. 2002, Smedley and Kinniburgh 2002). Since the first detection of As contamination in Bangladesh in 1993, various studies have provided information regarding origin, distribution and factors controlling the presence of As in groundwater (Bhattacharya et al. 2006).

At the end of the 20th century, the arsenic contamination in groundwater in Bangladesh has been documented as a serious environmental health disaster with severe socioeconomic consequences; a great challenge for the Government of Bangladesh is to provide safe drinking water for the urban and rural population. Studies have also been undertaken cost-effective, sustainable and environment friendly approaches to mitigate the As problem in Bangladesh (Jakariya et al. 2007, von Bromssen et al. 2007). However, there is no

single solution to the problem and mitigation strategies would differ from the area to area based on the local geology and culture. In the considering remediation approaches, new concerns such as possible change of arsenic concentrations with time, and transfer of As from the water plants through irrigation, need to be addressed.

Recently, the versatility of ZVI material has been demonstrated for the potential use in environmental engineering. Due to the small particle size, large surface area and high in-situ reactivity, these materials have great potential in a wide array of environmental applications such as soil, waste water and groundwater remediation. In addition due to small size and high adsorption capacity, ZVI can be effectively used in groundwater treatment. To the best of our knowledge, however, the application of ZVI to the removal of arsenic from natural contaminated groundwater in developing countries such as Bangladesh, India, Nepal has not been well documented. Arsenic contamination in these countries has recently been detected not only in drinking water but also in agricultural products such as rice (Meharg and Rahman 2003). However, information about systematic

¹ Doctoral Student, Graduate School of Global Environmental Studies, Kyoto University, Japan. Email: masumagriculture@yahoo.com

² Professor, Graduate School of Global Environmental Studies, Kyoto University, Japan. Email: tkatsumi@mbx.kudpc.kyoto-u.ac.jp

³ Assistant Professor, Graduate School of Global Environmental Studies, Kyoto University, Japan. Email: inui@geotech.mbox.media.kyoto-u.ac.jp

⁴ President, Takamatsu National College of Technology, Japan, Email: koucho@takamatsu-nct.ac.jp

redox potential, suitable pH values and clear knowledge about use of most efficient and cost effective types and amount of zero valent iron is unknown.

The aim of this study is to investigate the application of zero valent iron for the remediation of arsenic from naturally contaminated groundwater with reference to pH, Eh and DO content and to determine the rate and extent of As adsorption by ZVI. Finally find out the use of most efficient and cost effective types and amount of zero valent.

MATERIALS AND EXPERIMENTS

The chemicals used in this study were analytical grade and all the stock solutions were prepared with deionized water (DI). The arsenic stock solution was prepared by $\text{Na}_2\text{HAs}_4 \cdot 7\text{H}_2\text{O}$ in DI water. Three zero valent iron materials viz. KB-90, TK-H and K-100T were obtained from JFE Steel Corporation, Japan. The characteristics of zero valent iron from JFE Steel Corporation are shown in Table 1. Toyoura sand, with particle density of 2.55 g/cm^3 , compacted state void ratio of about 0.87, and saturated density of 2.01 g/cm^3 was used in column experiment. The grain size distribution of Toyoura sand is shown in Fig. 1

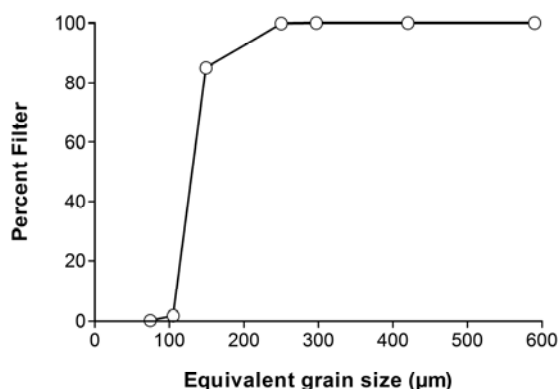


Fig. 1 Grain size distribution of Toyoura sand

Batch Experiment

The batch experiments utilized ZVI and were conducted on 500 mL conical flasks. In all cases, 500 ml of arsenic contaminated water was loaded with different levels of iron. Then the conical flask containing different levels of arsenic contaminated water and different levels of iron were placed on an orbital shaker at room temperature (24°C) for different time periods. In case I, 1 mg/L arsenic contaminated water was mixed with 1.0 g/L of three types of above mentioned ZVI without any adjustment of pH. The sampling periods were 1, 5, 10 and 24 hrs later. In case II, 1 mg/L arsenic contaminated water was mixed with 1.0 g/L iron (KB-90). In this experiment, control, pH 5.0 and pH 7.0 were adjusted using 0.1 M NaOH and HCl. The sampling periods were 1, 2, 3, 4, 5, 10, 15 and 24 hrs later. In case III and IV, 0.2 mg/L arsenic contaminated water was loaded with 1.0 and 2.0 g/L iron (KB-90) respectively with three levels of pH viz. control, 5.0 and 7.0. The sampling periods were similar to case II.

Column Experiment

Column experiments were conducted using acrylic columns packed with zero valent iron. The test columns were 5 cm inner diameter by 30 cm length with side sampling port. The column contained inlet, outlet and three side sampling ports at 8.0, 16.0 and 24 cm from the influent end (Fig. 2). The side sampling port is extended upto 4.5 cm in the end of the column and must be porous of the extended area. The inner diameter of the side sampling port is 1.0 cm. Two column filtration tests with different contents of iron and sand were conducted in this study. Column A was filled with 550 g of 50% ZVI (KB-90) and 410 g of 50% sand (Toyouura) mixture, while column B consisted of 75/25 (v/v) ZVI and sand mixture. A well-homogenized ZVI and sand mixture funneled into the column in five increments to ensure that column A and column B were packed homogeneously. The initial concentration of artificial arsenic spiked water

Table 1 The characteristics of zero valent iron

Types of ZVI	Chemical composition %		Particle size distribution %							
	Metal Fe	Total Carbon	> 250 μm	>180 μm	>150 μm	>106 μm	>75 μm	>63 μm	>45 μm	<45 μm
KB-90	93.5	0.482	0	0.2	0.9	25.5	32.9	8.6	13.9	18.0
TK-H	98.1		0	16.0	40.1	23.2	7.3	1.3	2.5	9.6
K-100T	94.8		0	0	2.7	36.3	20.9	6.7	10.9	22.5

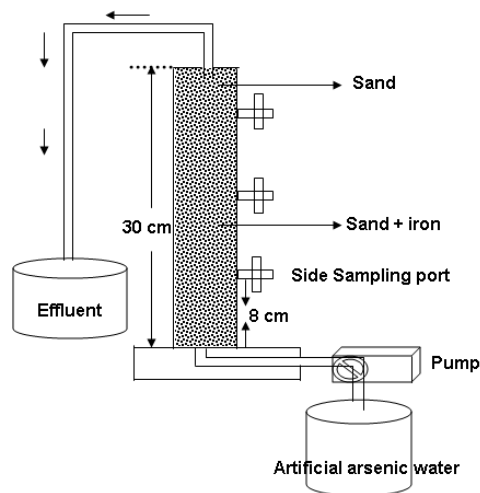


Fig. 2 Set up for column experiment

was 200 $\mu\text{g/L}$ and passed through both columns upward direction at a 30 mL/hr flow rate using peristaltic pump.

Arsenic Adsorption Capacity

Arsenic adsorption capacity was also evaluated for KB-90 zero valent iron. Duplicate samples of 1.0 g KB-90 ZVI were mixed in 500 mL conical flask for 12 hours at initial arsenic concentration 1, 5, 10, 15, 20, 25, 30 and 40 mg/L in a shaker at 100 rpm and allowed to settle. After 12 hours, 3, 5 and 7 days settlement, 20 mL of the suspension was collected with the help of syringe sampler and then filtered through syringe filter with 0.20 μm pore size before As determination.

Measurements and Chemical Analysis

The pH, Eh and DO content were measured immediately after collection of samples by combined pH and Eh meter and DO meter respectively. The pH meter was calibrated with three buffers (pH 4.0, 7.0 and 10) daily. Then the suspension was filtered through syringe filter with 0.20 μm pore size. Arsenic concentrations were measured by Graphite furnace atomic absorption spectrophotometer and Hydride generation atomic absorption spectrophotometer.

RESULTS AND DISCUSSION

Batch Studies

The performance of three different types of ZVI is shown in Fig. 3. Arsenic removal on a mass basis followed the order, KB-90 > K-100T > Tk-H when the initial As concentration was 1.0 mg/L. Among the three ZVI types, KB-90 shows best performance to remove arsenic from the water source.

The removal of arsenic by ZVI was largely affected by contact time, types of zero valent iron and lesser degree of amount of iron. In all the ZVI system, arsenic concentration decreased exponentially with time. From Fig. 4, it is revealed that after 15 hrs elapsed time 99% of arsenic is removed, where the initial arsenic concentration was 0.2 mg/L and ZVI 2 g/L and in the same time 97.5% of arsenic is removed using 1.0 g/L zero valent iron. After 10-hour elapsed time the result meets the Bangladesh drinking water standards (0.05 mg/L) using 1.0 g/L ZVI where WHO (0.01 mg/L) as well as Bangladesh Standards meets using 2.0 g/L ZVI.

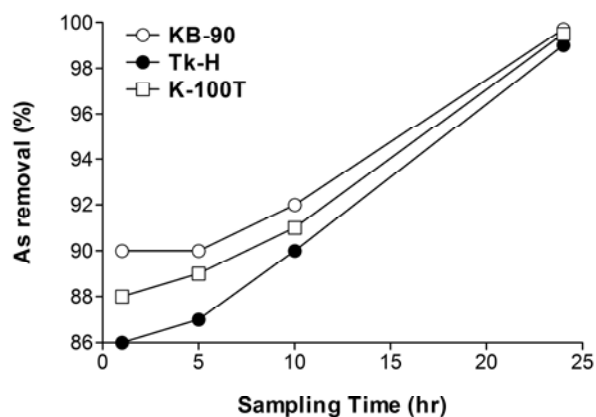


Fig. 3 Arsenic removal by ZVI (As conc. 1.0 mg/L and ZVI 1.0 g/L)

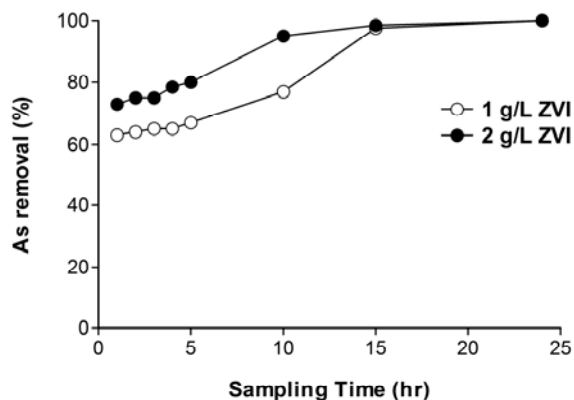


Fig. 4 Arsenic removal by ZVI (As conc. 0.2 mg/L, without pH adjustment and ZVI type KB-90)

The pH dependence of arsenic removal is due to differences in arsenic adsorption in terms of ionization of both adsorbates and adsorbents (Su and Puls 2001a). The effect of pH on arsenic removal from arsenic contaminated water using zero valent iron is illustrated in Figs. 5 and 6. The removal of arsenic occurred prominently at pH 7 than other two cases. More than 99% of the arsenic was removed after 15 hours of reaction at pH 7. Similar, results have been reported from other investigators; Biterna et al. (2007) reported over 99% of As(V) was removed in 6 hrs when initial pH was controlled at 7.2

and nearly 90% at pH 4.2 and Bang et al. (2005) found 99.8% removal of arsenate under oxic conditions at pH 6.0 after 9 hrs of reactions and Sun et al. (2006) observed over 95% removal at pH 8.28. The pH 7.0 also showed the best performance when initial arsenic concentration was 1.0 mg/L.

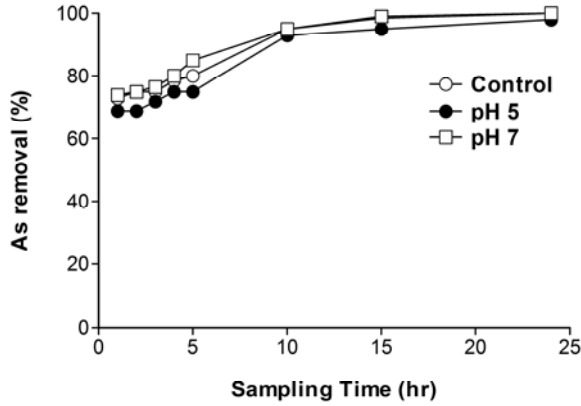


Fig. 5 Arsenic removal by ZVI (As 0.2 mg/L & ZVI (KB-90) 2.0 g/L)

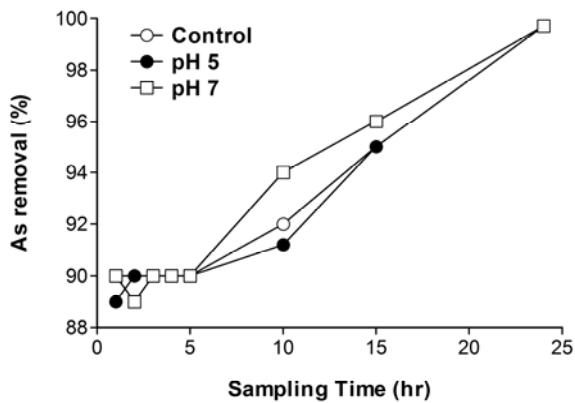


Fig. 6 Arsenic removal by ZVI (As 1.0 mg/L & ZVI (KB-90) 1.0 g/L)

The effect of Redox reactions (Eh) and DO content on the removal of arsenic was evaluated by comparing the experimental results obtained under a series of batch tests (Figs.7 and 8). The result showed that the redox potential (Eh) in the KB-90 ZVI system decreased with time from positive values of 284 to 76 mV and DO content varies between 5.19 and 2.96 mg/L. Redox reaction (Eh) is directly related to the pH of the solution and important in controlling As concentrations by their effects on As speciation and reduction of metal oxides which adsorb or precipitate arsenic. High DO content will increase the rate of iron oxidation and subsequently improve the removal of arsenic by zero valent iron.

Column Experiments

Column experiments were conducted continuously for 175 days to investigate the removal of arsenic by ZVI

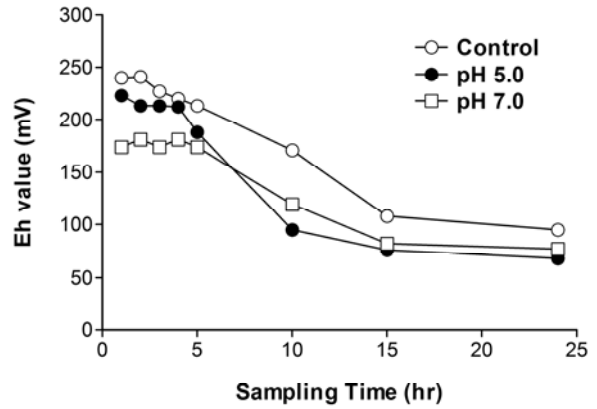


Fig. 7 Eh variation with time (As 0.2 mg/L & ZVI (KB-90) 2.0 g/L)

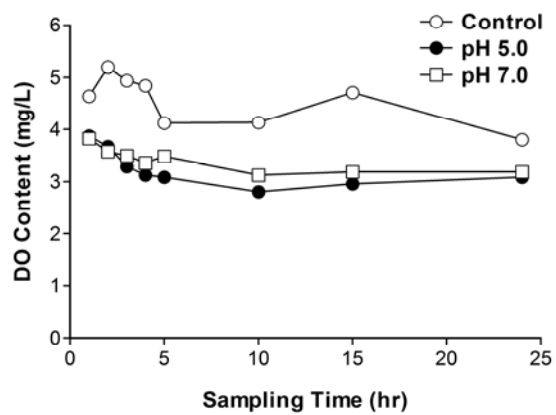


Fig. 8 DO variation with time (As 0.2mg/L & ZVI (KB-90) 2.0 g/L)

materials. As expected, total As concentrations in different positions of the up flow mode column followed an order; column influent > bottom port effluent > middle port effluent > top port effluent > Column effluent (Figs.9 and 10). ZVI efficiently eliminated arsenic from water. The arsenic concentration remained below 2 µg/L during the first 30 days after elapsed time

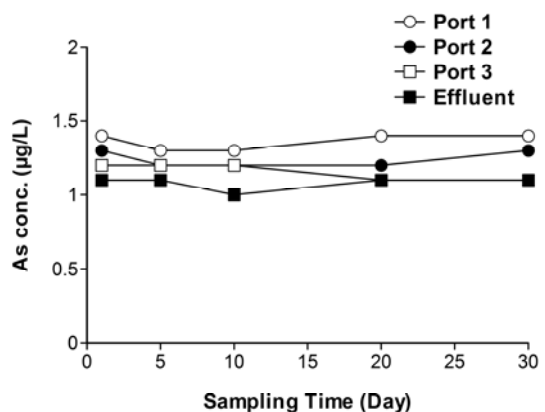


Fig. 9 Arsenic removal by zero valent iron (As conc. 200 µg/L and 50% sand and 50% KB-90 ZVI)

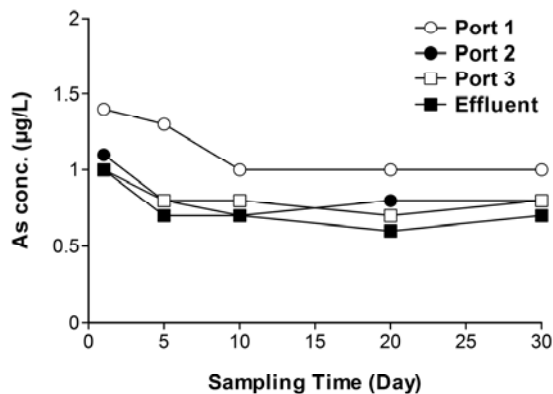


Fig. 10 Arsenic removal by zero valent iron (As conc. 200 µg/L and 75 % sand and 250% KB-90 ZVI)

and the arsenic concentrations in drinking water standard of WHO and Bangladesh were not exceeded. Seven hundred twenty milliliter water was treated on daily basis. Till now 75% sand + 25% ZVI exhibited better removal efficiency than 50% sand +50% ZVI.

Treated water by ZVI showed higher pH than that of influent water. The increase of pH values has been attributed to water decomposition by ZVI and adsorption reaction of arsenic which release OH⁻ groups from the absorbents as a result of ligand exchange. The pH of influent and effluent waters is shown in Fig. 11. The Eh values in effluent water showed a decreased trend with time up to -131 (Fig. 12). The similar observations for pH and Eh have been reported by other investigators (Su and Puls 2001a, b).

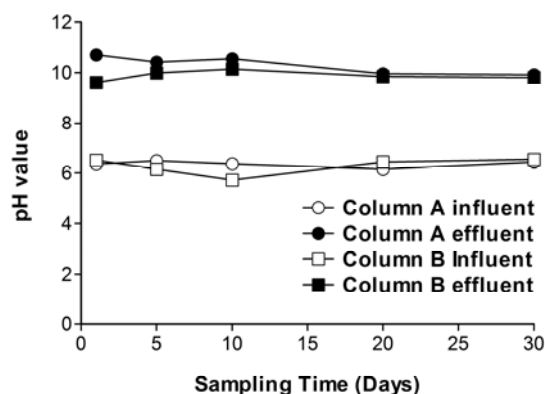


Fig. 11 pH variation with time

Arsenic Adsorption Capacity

An attempt was also made to determine the highest capacity of ZVI to adsorb As from contaminated water through batch experiment. This experiment helped to estimate each gram of ZVI can adsorb how much amount of arsenic. This implies that the arsenic adsorption capacity should be a better design parameter

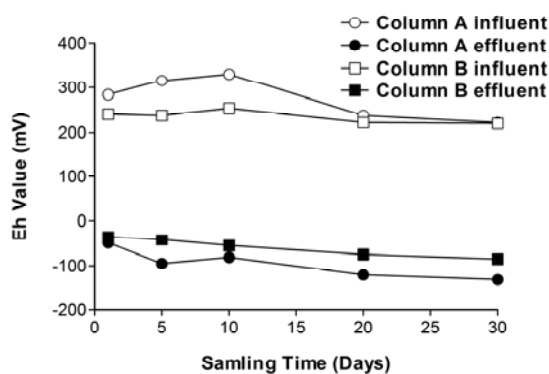


Fig. 12 Eh variation with time

for the estimation of the amount of ZVI required for field application of filtration system. Furthermore, compared with other similar studies, this study showed a comparatively high As removal capacity.

Time dependence As adsorption reaction with ZVI was analyzed by reacting 1.0 g ZVI with varying levels of As concentrations. It is clear from Fig.13, the As adsorption by zero valent iron increases with As concentration in solution upto a certain limit and then decreased. The total As adsorption by 1 gram ZVI reaches peak with 2.5 mg As when settled for 12 hours. Moreover, 3, 5 and 7 days settlement shows an excellent variation with 12 hrs settlement which supports the coprecipitation of As with iron (Table 2 showed the similar results from other researchers). Therefore, the total As removed from the solution through adsorption and coprecipitation was increased to 4.33 mg/g (Fig.13) which is almost double of adsorption. It can be concluded that the As removal capacity (through adsorption and co precipitation) of ZVI is 4.33 mg/g.

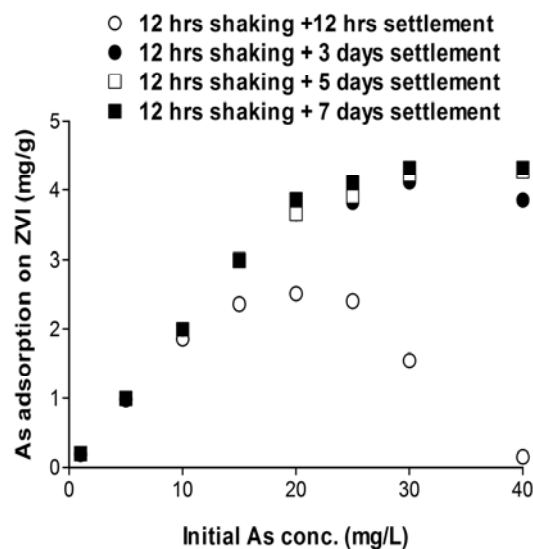


Fig. 13 Arsenic adsorption capacity (ZVI (KB-90) 1.0 g/ 200 mL)

Table 2 Arsenic removal capacities by ZVI as determined in Batch and Column studies

Iron material	Removal capacity (mg/g)	Reactors	References
Peerless	1.77	Batch	Su and Puls (2001)
Peerless	0.73	Batch	Su and Puls (2001)
Peerless	7.5	Column	Lien and Wilkin (2005)
Nanoscale iron	3.5	Batch	Kanel et al. (2005)

Source: Su (2006)

CONCLUSIONS

Arsenic free water supply is the most crucial goal of As mitigation Program. The hydrological situation of Bangladesh and other arsenic affected countries, aquifer lithologies and water chemistry vary from region to region as well as season to season. Particularly, water chemistry is important in developing As removal technologies because performance of a number of As removal technologies depends on water quality, specially pH and redox potential.

This study confirms that zero valent iron is effective to remove arsenic from contaminated groundwater or water resources. Among the ZVI materials, KB-90 showed the best performance. Around neutral pH is the optimal condition of the effluent water to treat arsenic contamination. Efficient removal of arsenic ($< 10 \mu\text{g/L}$ in the treated waters) by employing ZVI was observed.

A filtration system ex-situ water treatment plant or filter using zero valent iron and sand mixture can be used to remove arsenic from contaminated water at a short contact time in presence of dissolved oxygen and in a near neutral pH range.

REFERENCES

- Bang S, Kortiaty GP, Meng X (2005). Removal of arsenic from water by zero valent iron. *Journal of Hazardous Materials*. 121: 61-67.
- Bhattacharya P, Frisbie SH, Smith E, Naidu R, Jacks G, Sarkar B (2002). Arsenic in the environment: A global perspective. *Handbook of Heavy Metals in the Environment*. B. Sakrar (Ed.), Marcell Dekker Inc., New York: 145-215.
- Bhattacharya P, Ahmed KM, Hasan MA, Broms S, Fogelstrom J, Jacks G, Sracek O, von Bromssen M, Routh J (2006). Mobility of arsenic in groundwater in a part of Brahmanbaria district, NE Bangladesh. *Managing Arsenic in the Environment: From Soil to Human Health*. R. Naidu, E. Smith, G. Owens, P. Bhattacharya and P. Nadebaum (Eds.) CSIRO Publishing, Melbourne, Australia: 95-115.
- Biterna M, Arditoglou A, Tsikouras D (2007). Arsenate removal by zero valent iron. Batch and column tests. *Journal of Hazardous Materials* 149(3): 548-552.
- Jakariya M, von Bromssen M, Jacks G, Chowdhury AMR, Ahmed KM, Bhattacharya P (2007). Searching for suitable arsenic mitigation strategy in Bangladesh: experience from two Upazilas. *International Journal of Environmental Pollution* 31 (3-4): 415-430.
- Meharg AA & Rahman MM (2003). Arsenic contamination of Bangladesh paddy field soils: implications for rice contribution to arsenic consumption. *Environmental Science and Technology* 37: 229-234.
- Smedley PL & Kinniburgh DG (2002). A review of source, behavior and distribution of arsenic in natural waters. *Applied Geochemistry* 17(5): 517-568.
- Su C (2006). Utilization of zero valent iron for arsenic removal from groundwater and wastewater. Chapter 9. *Zero Valent Iron Reactive Materials for Hazardous Waste and Inorganics Removal*. I.M.C. Lo., R.Y. Surampalli and K.C.K. Lai (eds.) American Society of Civil Engineers.
- Su C & Puls RW (2001a). Arsenate and arsenite removal by zero valent iron: kinetics redox transportation and implications for insitu groundwater remediation. *Environmental Science and Technology* 35:1487-1492.
- Su C & Puls RW (2001b). Arsenate and arsenite removal by zerovalent iron: effects of phosphate, silicate, carbonate, borate, sulfate, chromate, molybdate, and nitrate, relative to chloride. *Environmental Science and Technology* 35: 4562-4568.
- Sun L, Wang H, Zhang R, Sui J, Xu G (2006). Treatment of groundwater polluted by arsenic compounds by zero valent iron. *Journal of Hazardous Materials* 129: 297-303.
- von Bromssen M, Jakariya M, Bhattacharya P, Ahmed KM, Hasan MA, Sracek O, Jonsson L, Lundell L, Jacks G (2007). Targeting low arsenic aquifers in groundwater of Matlab Upazila, Southeastern Bangladesh. *Science and the Total Environment* 379: 121-132.

SIMULATION TESTS OF BIODEGRADATION AND COMPRESSION OF MUNICIPAL SOLID WASTE

Jun-Long LIU¹, Han KE², Tony L.T. ZHAN³ and Yun-Min CHEN⁴

ABSTRACT: In this paper, biodegradation-compression tests were carried out to investigate the dependence of long-term settlement behavior of municipal solid waste (MSW) on stress level. Three biodegradation-compression test apparatuses were purposely developed. The apparatuses were equipped with units for vertical loading, leachate recirculating, gas collecting, and temperature controlling. Fresh MSW samples were compacted the prescribed density in the test apparatus, and then subjected to three different stress levels (100,200 and 400 kPa). Biodegradation processes of the MSW samples were simulated at the controlled temperature (41 °C) and under a leachate recirculation condition. The compression and gas production of the samples were recorded. The experimental results indicated that the secondary compressibility parameters of the MSW are dependent on the vertical stress level. It seems that the gas production rate of the MSW is independent of the stress level.

KEYWORDS: municipal solid waste, landfill, compression, settlement, leachate

INTRODUCTION

Estimation of settlement for municipal solid waste (MSW) landfills is critical to the successful site operation and the future development as well as to the maintenance of the sites (Park et al. 2007). Bioreactor landfills with leachate recirculating are expected to become more widely adopted in the future (Hossain et al. 2003). A considerable amount of settlement occurs due to the decomposition of municipal solid waste in landfills over a period of years (Park et al. 2002). Therefore, it is of special importance to estimate the settlement of MSW landfills accurately as well as to explore the effects of MSW decomposition on long-term landfills settlement.

The heterogeneous nature of MSW particles, coupled with biodegradation of organic solids, make the estimation of settlement of MSW landfills extremely difficult. Much progress has been made in the prediction of MSW landfills settlement, and numerous settlement estimation methods have been proposed in the literature (Edil et al. 1990; Marques et al. 2003; Park et al. 2007; Sharma et al. 2007). Most settlement models cited in the literatures can be classified into four broad categories: soil-mechanics based models, rheological models, empirical models, and biodegradation-induced settlement models (El-Fadel and Khoury 2000). Brief discussions of three

of the more significant methods are presented below.

Sowers (1973) used the following equations that similar to those used for primary and secondary consolidation of soils to estimate settlement of a landfill.

$$\Delta H = \Delta H_1 + \Delta H_2 \quad (1)$$

$$\Delta H_2 = H C_c' \log \frac{p_0 + \Delta p}{p_0} \quad (2)$$

$$\Delta H_2 = H_1 C_{\alpha}' \log \frac{t_2}{t_1} \quad (3)$$

where, ΔH =total settlement; ΔH_1 =primary settlement; ΔH_2 =secondary or long-term settlement; H = initial thickness of waste; H_1 =thickness of waste at the beginning of the secondary settlement; $C_c' = C_c / (1 + e_0)$, where C_c =modified compression index and e_0 =void ratio; C_{α}' =modified secondary compression index; p_0 =initial stress; Δp =stress increment; t_1 =starting time for secondary compression; and t_2 =ending time for secondary compression.

Edil et al. (1990) applied Gibson and Lo's model to estimating the long-term settlement of MSW landfills.

¹ Master Student, MOE Key Laboratory of Soft Soils and Geoenvironmental Engineering, Zhejiang University, China

² Associate Professor, MOE Key Laboratory of Soft Soils and Geoenvironmental Engineering, Zhejiang University, China
Email :boske@126.com

³ Professor, MOE Key Laboratory of Soft Soils and Geoenvironmental Engineering, Zhejiang University, China

⁴ Professor, MOE Key Laboratory of Soft Soils and Geoenvironmental Engineering, Zhejiang University, China

The following expression is used to predict total settlement.

$$\varepsilon(t) = \Delta\sigma(a + b\{1 - \exp[-(\lambda/b)t]\}) \quad (4)$$

where, $\varepsilon(t)$ =total strain; $\Delta\sigma$ =compression stress; a =primary compression parameter; b = secondary compression parameter; λ/b =rate of secondary compression; t =time since load application; $\Delta\sigma a$ =initial amount of compression; and $\Delta\sigma b$ =long-term secondary compression.

Edil et al. (1990) proposed the power creep model, uses the following equation to estimate settlement of a landfill.

$$S(t) = H \cdot \varepsilon(t) = H \cdot \Delta\sigma \cdot m \cdot (t/t) \quad (5)$$

where, m =reference compressibility; n =coefficient of compression; t =reference time; t =time since load application; and $\Delta\sigma$ =loading pressure.

In comparison of settlement models cited above and other settlement predicting approaches, the influence of stress on long-term settlement of MSW landfills has not been identified. Creep power and rheological models assumed that the long-term settlement is proportional to stress, while Sowers (1973) models, Bjarngard (1990) model, and some other models assumed that long-term settlement has no relationship with stress level.

The objective of this study was to investigate changes in settlement and biodegradation of MSW subjected to different vertical stress levels. Three biodegradation-compression test apparatus for MSW were specially developed. Artificial waste samples were filled in the test apparatus and allowed to degrade to different conditions for compressibility testing, which can simulate the biodegradation and settlement processes of a bioreactor landfill.

TEST APPARATUS

There has been no standard experimental apparatus and methods for the compression of MSW. In a conventional sanitary landfill, refuse biodegradation proceeds at suboptimal rates for decades or even centuries. To accomplish the tests, Efforts need to be made to accelerate the decomposition rate of the fresh refuse. Leachate recirculating, neutralizing, 41 °C temperature controlling, and the addition of an inoculum of anaerobically digested sewage sludge would accelerate the biodegradation rate of MSW (Barlaz, et al. 1987).

A biodegradation-compression test apparatus for MSW were specially developed by Xie et al. (2005), which was equipped with units for vertical loading, leachate recirculating, gas collecting, and temperature

controlling. The apparatus had been modified and upgraded, and three test apparatus were specially developed to perform three compression tests. One of the test apparatus is indicated in Fig.1, and brief introductions of the test apparatus are also presented below.

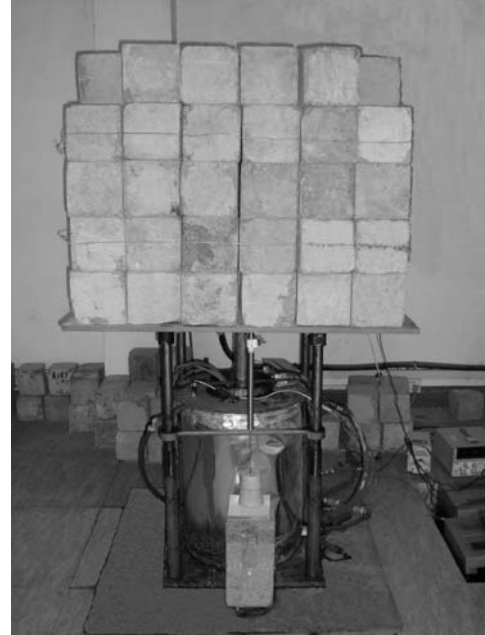


Fig. 1 Test apparatus

A temperature control system was designed for this experiment. The temperature of the samples was controlled by water placed around the cells, and the samples were incubated in the sample cells maintained at 40-41 °C to produce optimal waste biodegradation conditions. The leachate with the addition of an inoculum of anaerobically digested sewage sludge was recycled everyday to accelerate biodegradation rate of the refuse samples. A seal system is also designed to keep the samples in appropriate decomposition conditions. Gas was collected in Tedlar gas sampling bags and the volume was measured by pumping into a calibrated carboy using water displacement. The component of biogas can be measured through Thermoquest Trace 2000 GC/MS. The LVDT (linear variable differential transformer) and dial indicator were both used to measure the settlement of waste samples.

EXPERIMENTAL METHODS

Experimental Design

According to other compression tests of MSW cited in the literatures, the range of loading pressures is predominantly from 50kPa to 1000kPa. Vertical stresses of 100kPa, 200kPa, 400kPa were applied to 1#, 2#, and 3# samples, respectively. To accelerate the decomposition

rate of the refuse samples, 41 °C temperature controlling, leachate recirculating, neutralizing, and the addition of an inoculum of anaerobically digested sewage sludge were used in the test.

Experimental Materials

The refuse samples adopted in the tests were artificial samples that had been prepared in the environmental laboratory, and the composition of the solid waste samples was referred to statistics bureau of Hangzhou, 2000. All the components of waste samples were shredded to keep the grain size diameter of all particles less than 30 mm. The specific gravity of waste particles was 2.04, which was measured by a siphonic tube. The void ratio was 4.96, and the moisture content was about 61.4%. Physical characteristics of MSW adopted in the tests are shown in Table.1.

Table 1 Physical characteristics of MSW samples

Moisture content (%)	Wet density (g/cm^{-3})	Dry density (g/cm^{-3})	Specific gravity	Initial void ratio(e)
61.4	0.88	0.34	2.04	4.96

Test Procedures

The temperature controlling system, loading system, seal system, and leachate recirculating system of the three test apparatus had been well examined before the tests were conducted. Artificial waste samples with the same physical characteristics were than filled in the three test cells respectively. The waste samples were preloaded to obtain a prescribed density. Vertical pressures of about 100kPa, 200kPa, 400kPa were applied to the samples, respectively, and vertical settlement was measured consecutively. The leachate generated was collected in the leachate collector. Leachate with the addition of an inoculum of anaerobically digested sewage sludge was recirculated a week after the tests were conducted. Gases generated from biodegradation of waste samples were collected in Tedlar gas sampling bags.

RESULTS AND DISCUSSIONS

In this paper some preliminary results of laboratory tests are presented. The settlement-time curves of the tests were shown in Fig. 2. 100kPa, 200kPa, 400kPa in the figure representative of 1#, 2#, 3# MSW samples that suffered different vertical stresses. Vertical stress levels have considerable effects on primary settlement, and increasing vertical stress level can raise the capacity of a

landfill. The strain-time curves of the three samples were approximately parallel to each other, and the sample subjected to a lower vertical stress has a relative greater slope. In the early stage of compression, settlement is dominated by mechanical interactions such as reorientation and delayed compression of the waste. The strain-time curves of the three samples were relatively flat. However, in the last stage of compression, the settlement rate becomes large because of the effects of decomposition. Good agreement is shown between test results and other research cited in the literatures. The practice of using a single compressibility value when performing a settlement analysis may lead to inaccurate predictions (Chen 2009).

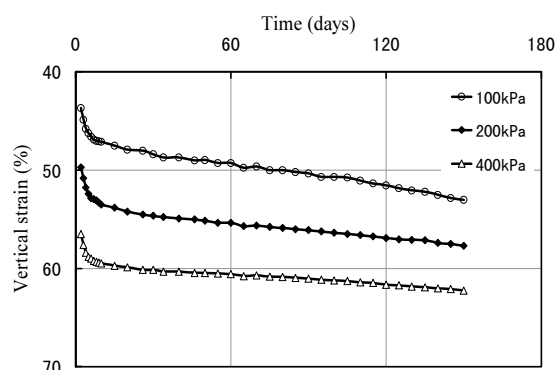


Fig. 2 The variation of settlement with time

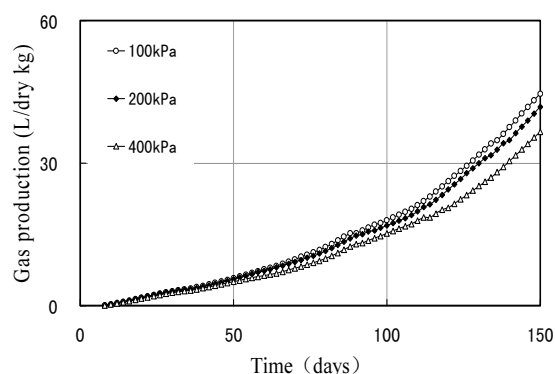


Fig. 3 Cumulative biogas production of the samples

Biogas production is characteristic of municipal solid waste landfills (Manna et al. 1999). Gases generated from the biodegradation of MSW samples were collected after leachate recirculating was performed. The cumulative biogas production of the three samples was indicated in Fig. 3. Gas production of MSW samples in the tests was almost independent with vertical stresses, and the sample subjected to a lower vertical stress generated more biogas to a slight degree. In the early stage of the tests, the gas production rates of three samples were relatively slow. However, in the last stage of compression, biogas production rate of the three samples subjected to different vertical stresses increased instantaneous as biodegradation rates of refuse were accelerated.

SUMMARY AND CONCLUSIONS

Three test apparatus equipped with units for vertical loading, leachate recirculating, gas collecting, and temperature controlling were specially developed to conduct the compression tests. The tests can simulate settlement and biodegradation processes of bioreactor MSW landfills.

Vertical stress levels have significant effects on settlement of a landfill. Primary settlement varied directly as stress level, and the secondary (or long-term) settlement decreased as vertical stress level increased. As a result, the total settlement difference showed a decreasing trend with increasing loading pressures.

In the early stage of long-term compression, settlement is dominated by mechanical interactions such as reorientation and delayed compression of the waste, and the strain-time curves of the three samples were relatively flat. However, in the last stage of compression, the settlement rate becomes large because of the effects of decomposition.

There is no significant relationship between vertical stress level and the biogas production of MSW landfills. Total biogas production of the three MSW samples was approximately the same. With respect to the early stage of long-term compression, biogas production rate of the three samples subjected to different vertical stress levels increased instantaneously as biodegradation rates of refuse were accelerated in the last stage of long-term compression.

ACKNOWLEDGEMENTS

This work were supported by the funding from National Natural Science Foundation (research grant: 50538080; 50508039), and financial support from Bureau of Science and Technology of Suzhou (research grant: SS0733).

REFERENCES

Barlaz MA, Milke MW, Ham RK (1987). Gas production

- parameters in sanitary landfill simulators. *J. Waste Management & Research*. 5 (1): 27-39.
- Edil TB, Ranguette VJ, Wuellner WW (1990). Settlement of municipal refuse: Geotechnics of waste fills—Theory and practice. ASTM Spec. Tech. Publ. 225-239.
- EI-Fadel M & Khoury R (2000). Modeling settlement in MSW landfills: A critical review. *J. Critical Reviews in Environmental Science and Technology*. 30(3): 327-361.
- Hari D Sharma & Anirban De (2007). Municipal Solid Waste Landfill Settlement: Postclosure Perspectives. *Journal of Geotechnical and Geoenvironmental Engineering*. 133(6): 619-629.
- Hossain MS, Gabr MA, Barlaz MA (2003). Relationship of Compressibility Parameters to Municipal Solid Waste Decomposition. *Journal of Geotechnical and Geoenvironmental Engineering*. 129 (12): 1151-1158.
- Park HI & Lee SR (2002). Long-term settlement behavior of MSW landfills with various fill ages. *J. Waste Management and Research*. 20(3): 259-268.
- Park HI, Park B, Lee SR, Hwang DJ (2007). Parameter evaluation and performance comparison of MSW settlement prediction models in various landfill types. *Journal of Environmental Engineering*. 133(1): 64-72.
- Manna L, Zannetti MC, Genon G (1999). Modeling biogas production at landfill site. *J. Resources Conservation and Recycling*. 26: 1-14.
- Marques ACM, Filz GM, Vilar OM (2003). Composite compressibility model for municipal solid waste. *Journal of Geotechnical and Geoenvironmental Engineering*. 129(4): 373-379.
- Sowers GF (1973). Settlement of waste disposal fills[C]. Proceedings of the 8th International Conference on Soil Mechanics and Foundation Engineering, Moscow: 207-210.
- Xie Y, Chen YM, Tang XW, Ke H, Zhan LT (2005). Development and application of biodegradation compression test apparatus for municipal solid waste. *Chinese Journal of Geotechnical Engineering*. 27(5):571-576 (in Chinese).
- Chen YM, Zhan LT, Wei HY and Ke H (2009). J. Aging and compressibility of municipal solid wastes. *Waste Management*. 29(1): 86-95.

COMPATIBILITY OF TROPICAL SOIL AND BENTONITE MIXTURES SUBJECTED TO CHEMICAL SOLUTIONS

Thiago Luiz Coelho MORANDINI¹ and Adilson do Lago LEITE²

ABSTRACT: Tropical soils cover vast regions of the globe and have great potential to be use as compacted clay liner in waste disposal facilities. When required, bentonite clay can be added to these soils so as to improve their hydraulic properties and contaminant retention capacity. One of the important issues to be addressed when evaluating bentonite as additive material is the compatibility of the mixture when exposed to waste liquids, once the liner properties can be affected after waste disposition. This paper focus on the compatibility of mixtures of a tropical soil sample plus bentonite exposed to different chemicals solutions. This parameter is evaluated through modified Atterberg limits determination. The proportions used to compose the mixtures were 3, 6, 9 and 12% (dry weight basis). The chemical solutions applied were sodium hydroxide (pH11), nitric acid (pH3) and sodium chloride (5 g/L). The results indicate a small decrease in the plasticity of the mixtures when exposed to acidic and alkaline solutions, while greater variations were observed when the mixtures were exposed to the salty solution. The incompatibility index (IC_p) shows that the addition of bentonite did not exert so much influence on the compatibility of the samples, especially at high proportions and for salty solutions.

KEYWORDS: tropical soils, bentonite clay, chemicals solutions, plastic index, compatibility

INTRODUCTION

Tropical lateritic soils cover vast regions in the globe and are characterized by low activity, high content of quartz, iron and aluminum oxides/hydroxides and kaolinite as the dominant clay mineral. When compacted, they usually present relatively high dry unit weights and low hydraulic conductivities. Therefore, they have great potential to be use as liner in waste disposal facilities, such as sanitary/industrial landfills and waste ponds (Anderson and Hee, 1995).

On the other hand, compacted clay liner (CCL) composed of tropical soils sometimes may not attend required design properties, particularly hydraulic conductivity and contaminant retention capacity. In this way, bentonite seems to be a good additive material to improve the properties of lateritic soils, because of its intense swelling and cation exchange capacity (CEC) (Anderson and Hee, 1995; Osinubi and Nwaiwu, 2002).

As pointed out by Madsen & Mitchell (1989), Acar and Olivieri (1989) And Schackelford (1994), besides the mechanical and the contaminant transport requirements, other important issue that must be addressed for choosing suitable CCL materials is the clay/waste interaction, which is called liner compatibility. A good compatibility

means that no significant changes will take place when the liner material is exposed to waste solutions (organic or inorganic).

This paper evaluates the compatibility of admixtures of a tropical soil sample and bentonite through modified Atterberg limits determination. The proportions used in the laboratory tests were 3, 6, 9 and 12% (dry weight basis). The waste liquids were typified by different chemical solutions, such as HNO₃ (pH 3), NaOH (pH 11) and NaCl (5 g/L).

SOILS CHARACTERISTICS

The sodium bentonite sample used in the tests (Brasgel) is commercially available in Brazil. It was chosen from four different samples by means of CEC tests. The chosen sample was that of higher CEC.

The lateritic soil (SN sample) was collected from a road slope, in the vicinities of Mariana, southeastern Brazil. In place, the weathering profile was composed mainly by a typical dark red oxisoil. In the laboratory it was submitted to ordinary disturbed sample preparation, according to the Brazilian standard ABNT-NBR6457 (1986), which consisted of air drying at room temperature,

¹ Doctoral student, Núcleo de Geotecnia, Universidade Federal de Ouro Preto, Brazil. e-mail: thiagomorandini@yahoo.com.br

² Doctor, Universidade Federal de Ouro Preto, Brazil. e-mail: alleite@em.ufop.br

sieving, homogenization and reduction.

The admixtures were prepared according to the following proportions (dry weight basis): 3, 6, 9 and 12%, receiving the convenient denominations of SN3, SN6, SN9 and SN12. These proportions were based on

the studies by Anderson and Hee (1995), Shackelford and Jefferis (2000), Farnezi (2005) And Batista (2006). The bentonite sample received the denomination of BK. Some geotechnical and physicochemical properties of the samples are presented in Table 1, including the references

Table 1 Sample properties

PROPERTY	SN	SN03	SN06	SN09	SN12	BK
Bentonite (%)	0	3	6	9	12	100
¹ Grain-size analysis						
Clay (%)	42	42	42	42	42	91
Silt (%)	6	3	6	6	6	9
Fine Sand (%)	6	13	10	8	10	0
Médium Sand (%)	36	30	32	32	32	0
Coarse Sand (%)	8	10	8	10	8	0
Gravel (%)	2	2	2	2	2	0
^{2,3} Atterberg Limits						
Liquid Limit LL (%)	51,9	77,7	96,6	117,0	156,0	682,5
Plastic Limit PL (%)	29,6	27,6	28,7	26,8	27,8	90,6
Plasticity Index PI (%)	22,3	50,1	67,9	90,2	128,2	591,9
Activity (Skempton, 1952)	0,53	1,19	1,62	2,15	3,05	6,50
⁴ Specific Gavity						
Gs(g/cm ³)	2,84	2,828	2,817	2,803	2,791	2,452
⁵ Physicochemical						
Cation Exchange Capacity CEC (meq/100g)	6,9	13,5	18,6	25,3	36,0	99,4
Specific Surface SS (m ² /g)	53,8	105,3	145,6	197,3	281,3	775,9

¹ ABNT (1984) NBR 7181; ² ABNT (1984) NBR 6459; ³ ABNT (1984) NBR 7180; ⁴ ABNT (1984) NBR 6508; ⁵ Pejon (1992)

used for the tests.

Table 1 shows that the clay content of the mixtures was not affected by the addition of bentonite, as expected. On the other hand, the Atterberg limits, the activity and the CEC/SS experimented a great increase, as expected. According to the classification of Skempton, the SN and SN3 samples are considered, respectively, inactive and normal clays, while samples SN6, SN9, SN12 and BK are active clays.

Fig. 1 depicts the increase of both the liquid limit and plasticity index with the addition of bentonite. It can be

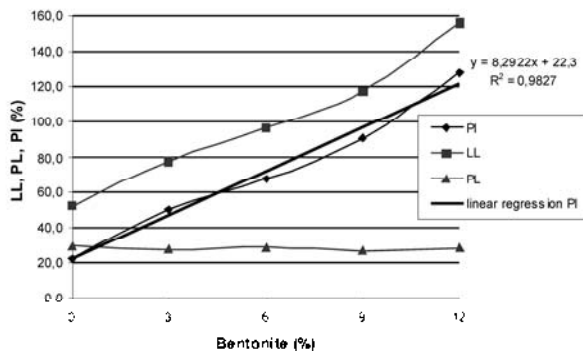


Fig.1 Atterberg limits variation of the SN sample and mixtures with bentonite addition

seen also that the plastic limit practically was not affected by the addition of bentonite. A quasi-linear trend was observed for the plastic index with the addition of bentonite, as demonstrated by the high determination coefficient of the linear regression in Fig. 1 ($R^2 = 0,963$).

Fig. 2 shows the variation of CEC and SS of the SN sample with the addition of bentonite. As can be noted, the increase of these parameters is linear from 0 to 12% of bentonite, and above this the rate of increase is greater.

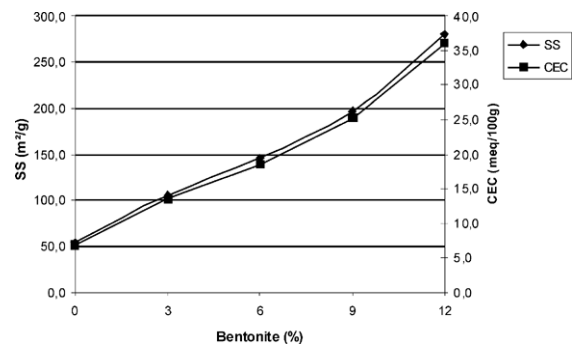


Fig. 2 Variation of SS and CEC of the SN sample and mixtures with bentonite addition

COMPATIBILITY TESTS: METHODS

The compatibility of the samples was evaluated through modified Atterberg limits. These tests are intended to determine these limits with different fluids other than water, and then compare the results with the ordinary Atterberg limits determined with water. The methods used are the same routinely adopted in any geotechnical laboratory, which are mentioned in the precedent item. Of course, careful handling was needed due to the dangerous that chemical solutions represent.

The studied solutions were nitric acid - HNO_3 (pH = 3), sodium hydroxide - NaOH (pH = 11) and sodium chloride (5 g/L). It is recognized that actual waste liquids are complex and may not be completely represented by these solutions. However, they were meant to typify some of the most aggressive conditions to which a liner is exposed to in waste disposal facilities. ACAR and Olivieri (1989), Farnezi (2005) And Farnezi and Leite (2007) reported the same approach to evaluate the compatibility of soils to different chemicals.

The Plastic Incompatibility Index (IC_p), proposed by Farnezi and Leite (2007), was estimated according to equation 1. It demonstrates how plasticity of soils change when they are exposed to fluids in comparison to water. Greater values of IC_p indicate greater variations in the plasticity, which means more incompatibility.

$$IC_p (\%) = \frac{PI_w - PI_f}{PI_w} \times 100 \quad (1)$$

where PI_w means the plasticity index with water and PI_f the plasticity index with the analyzed fluid.

COMPATIBILITY TESTS: RESULTS

Table 2 depicts the compatibility tests results for all the studied samples, including the calculated IC_p values. It is worth to note the higher IC_p values for NaCl compared to the other chemicals. This fact was not observed in the work of Farnezi and Leite (2007), but they studied different soils samples.

Figs. 3, 4 and 5 shows respectively the variation of LL , PL and PI with the increasing proportions of bentonite.

Some observations can be extracted from Fig. 3: 1) as expected, LL increased with the addition of bentonite; 2) the rate of increase is greater for water in comparison to the other fluids, especially for higher bentonite contents and 3) the liquid limit decreased for all the fluids in comparison to water.

Fig. 4 shows that there was no expressive change in the PL for all the fluids and bentonite proportions used. In this way, the PI curves (Fig. 5) are very similar to the LL curves and the same observations made in the precedent paragraph can be stated for them.

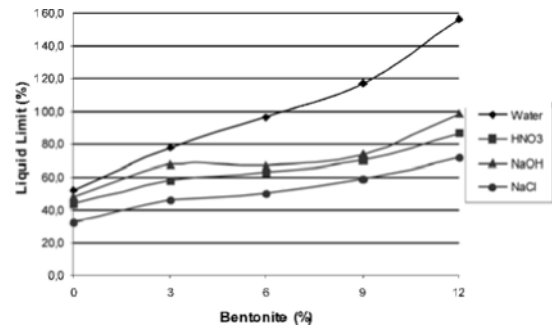


Fig. 3 Variation of the liquid limit (LL) of the SN sample and its mixtures with bentonite

Table 2 Results of the compatibility tests

Fluid	LL (%)	PL (%)	PI (%)	ICp (%)
SN Sample				
Water	51,9	29,6	22,3	0,0
HNO ₃	43,7	25,9	17,8	20,1
NaOH	47,6	27,7	19,9	10,6
NaCl	32,2	22,3	9,9	55,5
SN03 Sample				
Water	77,7	27,6	50,1	0,0
HNO ₃	58,3	27,8	30,5	39,1
NaOH	67,3	28,3	39,0	22,2
NaCl	45,6	23,7	21,9	56,3
SN09 Sample				
Water	117,0	26,8	90,2	0,0
HNO ₃	70,5	31,2	39,3	56,4
NaOH	73,3	30,4	42,9	52,4
NaCl	58,4	23,7	34,7	61,5
SN06 Sample				
Water	96,6	28,7	67,9	0,0
HNO ₃	62,7	28,8	33,9	50,1
NaOH	67,1	30,1	37,0	45,5
NaCl	49,7	22,4	27,3	59,8
SN12 Sample				
Water	156,0	27,8	128,2	0,0
HNO ₃	86,4	35,2	51,2	60,1
NaOH	98,6	37,7	60,9	52,5
NaCl	71,3	24,1	47,2	63,2
BK Sample				
Water	682,5	90,6	591,9	0,0
HNO ₃	495,2	140,5	354,7	40,1
NaOH	470,6	83,0	387,6	34,5
NaCl	310,9	82,8	228,1	61,5

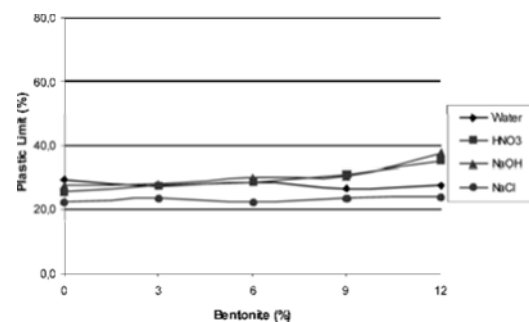


Fig. 4 Variation of the plastic limit (PL) of the SN sample and its mixture with bentonite

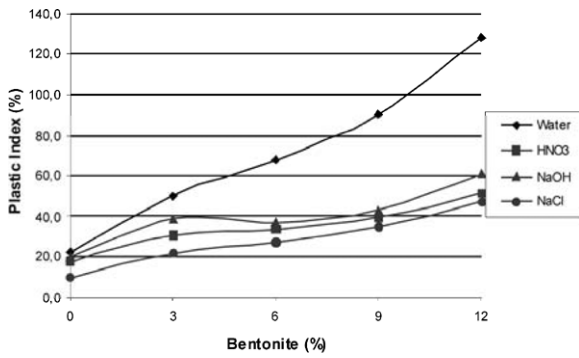


Fig. 5 Variation of the plastic index (*PI*) of the SN sample with bentonite percentage

Figs. 6 and 7 show bar diagrams with the results for BK and SN samples, respectively. The BK (bentonite) sample diagram (Fig. 6) clearly demonstrates the decrease in the plasticity with the application of fluids other than water. On the other hand, for the natural soil (SN) sample an expressive change in the plasticity was only observed for the NaCl solution.

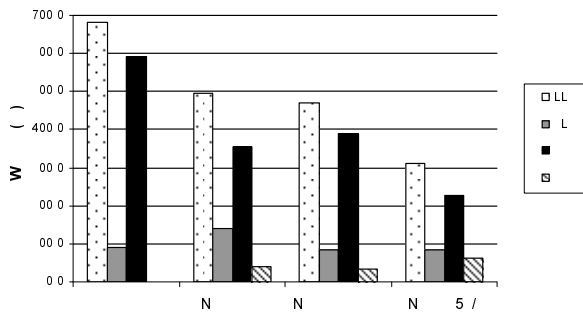


Fig. 6 Bar diagrams for Atterberg Limits and *IC_p* values: BK sample

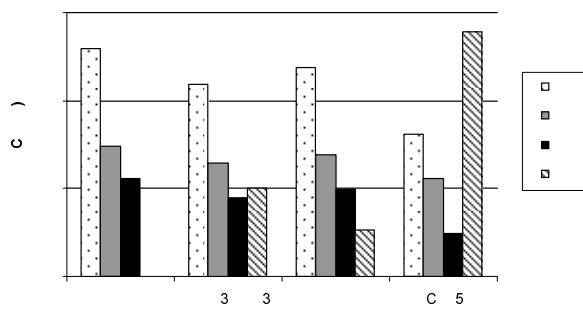


Fig. 7 Bar diagrams for Atterberg Limits and *IC_p* values: SN sample

Fig. 8 depicts bar diagrams for the mixtures samples. The same trend can be observed for all the studied samples in terms of *LL*, *PI* and *IC_p* variation in comparison with water: 1st NaCl; 2nd HNO₃; 3rd NaOH.

Fig. 9 shows the *IC_p* variation with the addition of bentonite for all the samples and chemical solutions.

Despite the lack of data between 12% and 100% of bentonite, it is clear that the *IC_p* reaches its maximum around 12%, then it follows a decreasing trend until 100%. The decreasing rate is even accentuated for the HNO₃ and NaOH solutions. Farnezi and Leite (2007) reported a general trend of increasing the compatibility (reducing the incompatibility) of a lateritic soil when the proportion of bentonite was 6% or more.

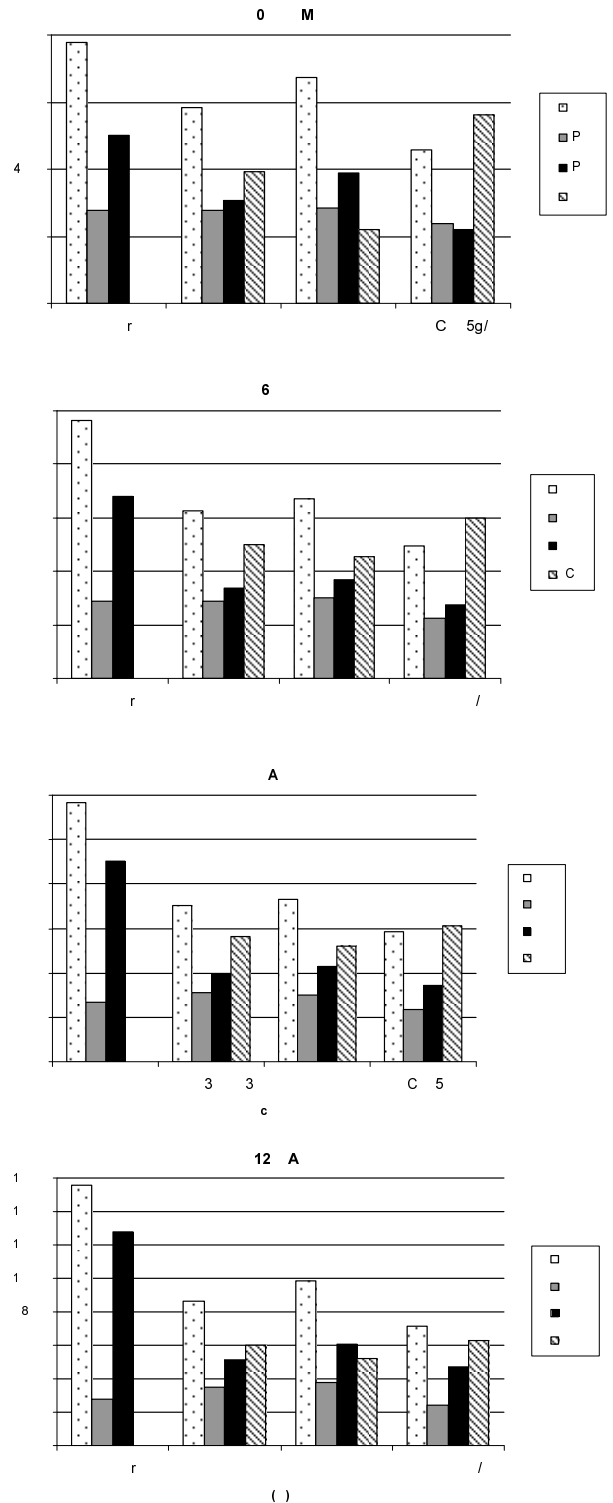


Fig. 8 Bar diagrams for Atterberg Limits and *IC_p* values: (a) SN03 sample; (b) SN06; (c) SN09 and (d) SN12

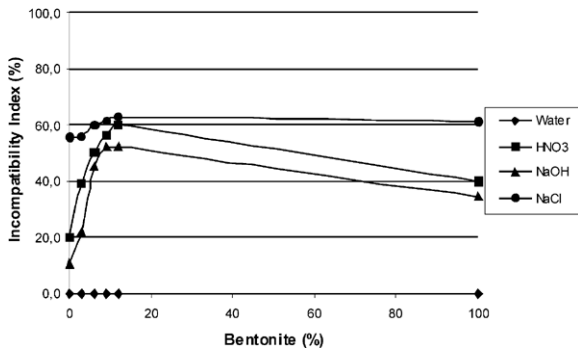


Fig. 9 IC_p variation with the percentage of bentonite

The IC_p variation was not so expressive when NaCl was the fluid used in the test. It means the bentonite addition does not exert so much influence on the plasticity of the samples with all the studied fluids.

CONCLUSIONS

The following is a list of some important conclusions of this study:

- 1) For all the fluids, including water, the liquid limit experimented greater variations than the plastic limit, which remained practically constant over the increasing rate of bentonite;
- 2) The exposition to the fluids other than water has decreased the plasticity of the samples, leading to positive IC_p values;
- 3) The IC_p values clearly indicates that the NaCl solution has more effect over all the studied soil samples than the other solutions. It is well known the effect of salty solutions on the electric double layer of clay minerals (LAMBE, 1958) and that must be the case. Considering the high content of salts of leachates from sanitary landfills, caution should be exercised when evaluating long term quality of liner materials;
- 4) In spite of the high IC_p values for NaCl, the addition of bentonite did not bring significant changes on that for any of the studied samples.

The results presented in this paper do not indicate the end of this research. So future issues to be addressed are:

- Compatibility should be evaluated through different laboratory testing, including hydraulic conductivity, consolidation and shear strength;
- Different chemical solutions, including actual leachate, should be applied in these tests;
- Liner exhumation is suggested to verify the long term quality of CCL composed of tropical soils, including lateritic and non-lateritic.

ACKNOWLEDGEMENTS

The authors would like to thank the Coordenação de Aperfeiçoamento de Pessoal de Nível Superior (CAPES), which provided a grant to the first author. Special thanks is given to Bentonit União Nordeste S/A, represented by Pedro Paulo Furtado Gouveia, who gently donated the bentonite samples used in this research.

REFERENCES

- ABNT NBR 6508 (1984). Grãos de solos que passam na peneira 4,8 mm—Determinação da massa específica. São Paulo, SP.
- ABNT NBR 6459 (1984). Solo - Determinação do limite de liquidez. São Paulo, SP.
- ABNT NBR 7181(1984). Solo - Análise Granulométrica. São Paulo, SP.
- ABNT NBR 7180(1984). Solo – Determinação do limite de plasticidade. São Paulo, SP.
- ABNT NBR 6457(1986). Amostras de solo – preparação para ensaios de compactação e ensaios de caracterização. Rio de Janeiro.
- Acar YB & Olivieri I (1989). Pore fluid effects on the fabric and hydraulic conductivity of laboratory-compacted clay. Transportation Research Record, v. 1219: 144-159.
- Anderson SA & Hee BH (1995). Hydraulic conductivity of compacted lateritic soil with bentonite admixture. Environmental & Engineering Geoscience, 1(3): 299-312.
- Batista P (2006). Avaliação geotécnica de misturas de um solo laterítico com cimento e bentonita para uso em cortinas verticais. Dissertação de Mestrado. Universidade Federal de Ouro Preto. Ouro Preto.
- Farnezi MK (2005). Alternativa de melhoramento técnico de solos tropicais para uso em sistemas basais de selagem, através da aplicação de bentonita. Dissertação de Mestrado. Universidade Federal de Ouro Preto. Ouro Preto.
- Farnezi MK & Leite AL (2007). Lateritic soil and bentonite mixtures assessment for liner usage purpose. Soils and Rocks. 30(2): 102-112.
- Lambe TW (1958). The structure of compacted clay. Journal of the Soil Mechanics and Foundations Division SM2, n. 1654: 1-34.
- Madsen, FT & Mitchell JK (1989). Chemical effects on clay fabric and hydraulic conductivity. The Landfil. Ed. Berlin / Heidelberg. 20: 201-251.
- Osinubi KJ & Nwaiwu CMO (2002). Compacted lateritic soils as hydraulic barriers in waste containment systems. In: INTERNATIONAL CONGRESS ON ENVIRONMENTAL GEOTECHNICS, 4TH, Rio de Janeiro, Balkema, Rotterdam: 225-230.

Pejon OJ (1992). Mapeamento geotécnico da Folha Piracicaba -SP (escala 1:100.000): Estudo de aspectos metodológicos, de caracterização e de apresentação dos atributos. Tese de Doutorado -Escola de Engenharia de São Carlos - Universidade de São Paulo.

Shackelford CD (1994). Waste-soil interactions that alter

hydraulic conductivity. Hydraulic Conductivity and Waste Contaminant Transport in Soil, ASTM STP 1142, p. 111-166. Philadelphia.

Shackelford CD & Jefferis SA (2000). Geoenvironmental engineering for in situ remediation. GEOENG. Melbourne, Australia, Preprint.

DEVELOPMENT OF SEDIMENT MONITORING DURING HEAVY RAINFALLS

Chih-Ping LIN¹, Chih-Chung CHUNG², Yu-Chia CHANG³ and Tzong-Shen CHANG⁴

ABSTRACT: Due to geological weathering and climate change, soil erosion in watershed is becoming a serious problem in Taiwan. Sediments affect water quality during heavy rainfalls and their deposition reduces reservoir capacity. Monitoring of sediment movement is crucial to estimate sediment yield and analyze watershed dynamics related to slope stability. It also plays an important role in reservoir management during heavy rainfalls. While suspended-sediment concentration (SSC) can be observed by manual sampling and lab testing, it is difficult to predict the right sampling timing and mobilize field crew during storms. Currently, there are no effective measuring techniques for automatic SSC measurement, particularly in fluvial environment. Existing methods provide an accuracy much influenced by particle sizes of suspended sediments, function only in a limited range of measurement and are not cost effective for field maintenance and wide spatial coverage. This paper introduces an innovative method based on time domain reflectometry (TDR) that may lead to an effective solution for monitoring of sediment movement. TDR is a monitoring technique based on transmission lines, in which a time domain reflectometer transmits an EM wave and receives a reflected EM wave, and wherein various TDR sensing waveguides can be designed to monitor different physical quantities, such as soil moisture content (based on dielectric permittivity), electrical conductivity, water level, and displacement. A TDR SSC probe is designed and a new travel time analysis method with temperature correction procedure is proposed for accurate determination of SSC. Unlike optical and acoustic method, TDR measurement is shown to be insensitive to sediment particle size. Other advantages of the TDR method include low-cost transducers, durability, and multiplexing capability. Results of laboratory evaluation and field monitoring are introduced.

KEYWORDS: Time Domain Reflectometry, Suspended Sediment Concentration

INTRODUCTION

Soil erosion in watershed is becoming a serious problem in Taiwan because of the geological weathering and dramatically climate changing. Monitoring of sediment movement is crucial to estimate sediment yield. It also plays an important role in land or reservoir management during heavy rainfalls. Therefore, accurate suspended sediment concentration (SSC) monitoring, especially for high SSC condition in a runoff event, is essential when studying catchment hydrology and land management. The SSC can be determined by directly taking samples for direct measurements or by using automated measuring techniques, such as optical and acoustic methods (Wren et al. 2002). However, the optical and acoustic methods are easily affected by particle sizes of suspended sediment or limited to a narrow measurement range (Sutherland et al. 2000; Thorne and Hanes 2002). Moreover, the sophisticated instruments used in the automated methods

are easily damaged during heavy runoffs by the speedy flows and the rocks and debris entrained. Still further, the instruments are often too expensive to be deployed with wide spatial coverage.

Time domain reflectometry (TDR) is a measurement technique based on transmission line theory. A time domain reflectometer transmits an electromagnetic (EM) wave into a transmission line connected to a sensing waveguide and receives a reflected EM wave, which responds to the physical parameter to be monitored. It is widely applied in soil water content measurement (Topp et al. 1980), which is related to SSC measurement in principle. Unlike other techniques having a transducer with a built-in electronic sensor, TDR sensing waveguides are simple and durable mechanical device without any electronic components. When connected to a TDR pulser above water for measurement, the submerged TDR sensing waveguide is rugged and can be economically replaced when damaged. Multiple TDR sensing waveguides

¹ Professor, Department of Civil Engineering, National Chiao Tung University, Taiwan, China. Email: cplin@mail.nctu.edu.tw

² Postdoctor, Natural Hazard Mitigation Research Center, National Chiao Tung University, Taiwan, China. Email: ccchung.cv91g@nctu.edu.tw

³ M.S., Department of Civil Engineering, National Chiao Tung University, Taiwan, China. Email: kidobear@gmail.com

⁴ Ph.D. Student, Department of Civil Engineering, National Chiao Tung University, Taiwan, China. Email: markchang.cv89g@nctu.edu.tw

can be connected to a TDR data acquisition system through a multiplexer and automated, hence increasing the system functions and spatial coverage.

This paper introduces the methodology of TDR approach for SSC measurement, and investigation of influence factors and performance in laboratory experiments and field tests.

THEORETICAL BACKGROUND

Principle of TDR

A TDR measurement setup is composed of a TDR device and a transmission line system. A TDR device generally consists of a pulse generator, an oscilloscope, a sampler, and the transmission line system which consists of a leading coaxial cable and a measurement waveguide (or probe) as Fig. 1 shows. The pulse generator sends an electromagnetic (EM) pulse along a transmission line and the sampler is used to record returning reflections from the measurement probe due to impedance mismatches. TDR has been used since 1930s for cable fault locating. Over the last 20 years, TDR has become a valuable tool for measuring dielectric properties of soil and other materials.

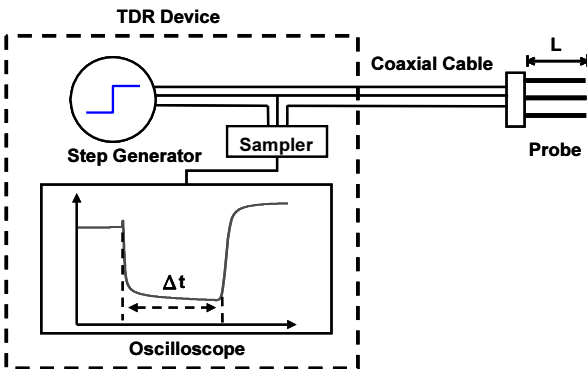


Fig. 1 Time Domain Reflectometry (TDR) measurement setup

Topp et al. (1980) showed that the apparent propagation velocity V_a of an EM wave in a transmission line is related to the apparent dielectric constant ϵ_a . Furthermore, the apparent propagation velocity V_a of the EM wave traveling through the probe can be obtained by determining the time difference between two reflections due to impedance mismatches of the probe. So the apparent dielectric constant ϵ_a proposed by Topp et al. (1980) can be formulated as

$$\epsilon = \left(\frac{c}{V}\right)^2 = \left(\frac{c\Delta t}{2L}\right)^2 \tag{1}$$

where c is light velocity at free space (2.998×10^8 m/s), time difference Δt is between the arrivals of the two reflections as the round-trip length of the probe L as shown in Fig. 2.

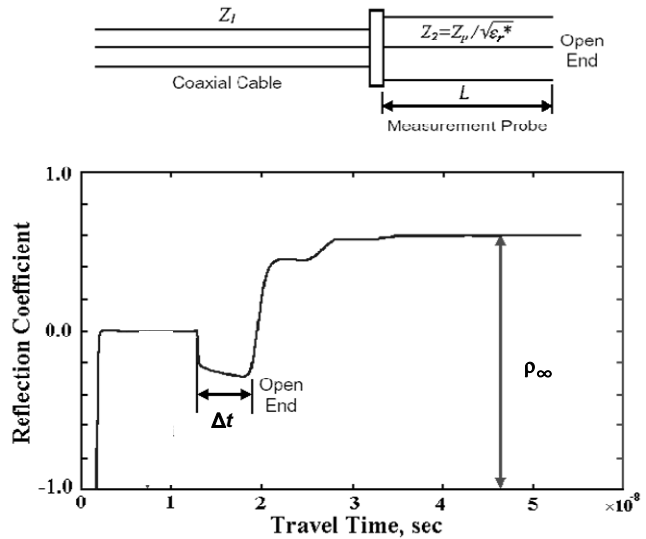


Fig. 2 Typical TDR waveform

Dielectric Mixing Model

The apparent dielectric constant of soil solid ϵ_s varies from 3 to 5 typically, depending on its composition, while the apparent dielectric constant of water ϵ_w is about 80, depending on temperature (Pepin et al. 1995). The bulk dielectric permittivity of water with suspended sediments may be expressed as a function of SSC by the volumetric mixing model as: (Dobson et al. 1985)

$$\sqrt{\epsilon} = (1-SS)\sqrt{\epsilon} + SS\sqrt{\epsilon_{ss}} \tag{2}$$

where ϵ is bulk apparent dielectric constant of the water with suspended sediments; SS is the volumetric percentage of suspended sediment, which ranges from zero to 1, and ϵ_{ss} is the apparent dielectric constant of the sediment.

The SS can be transferred into the unit of ppm (or milligram per liter), which is commonly used in hydrology as

$$ppm(mgl^{-1}) = \frac{SS \cdot G}{1 - SS} 10 \tag{3}$$

where G s is the specific gravity of suspended sediment.

TDR Travel Time Analysis

To precisely determine the apparent dielectric constant ϵ_a as listed in Eq. (1), Heimovaara (1993) proposed a calibration method for obtaining the travel time between some apparently defined start time and the

actual probe head start time (t_0 , as defined in Fig. 3) and probe length L . as the calibration method utilizes experiments on materials of known dielectric constant (typically air and water) and the following relation

$$\Delta\tau = t + \Delta t = t + \frac{2L}{c}\sqrt{\epsilon} \quad (4)$$

where $\Delta\tau$ is the measured travel time including t_0 from time mark to the end of probe head and the round-trip travel time Δt of probe section. The probe constants including travel time t_0 and probe length L can be solved with air and water measurements once the $\Delta\tau_{\text{air}}$ of air and $\Delta\tau_{\text{w}}$ of water are obtained. The travel time is conventionally determined by the tangent line method in soil water content measurement. Chung and Lin (2009) shows that the derivative method is more clearly defined for automation and works well in non-dispersive media, which is supposed to be the case in sediment suspensions. Both methods are illustrated in Fig. 3 and will be evaluated for their performance in SSC measurements.

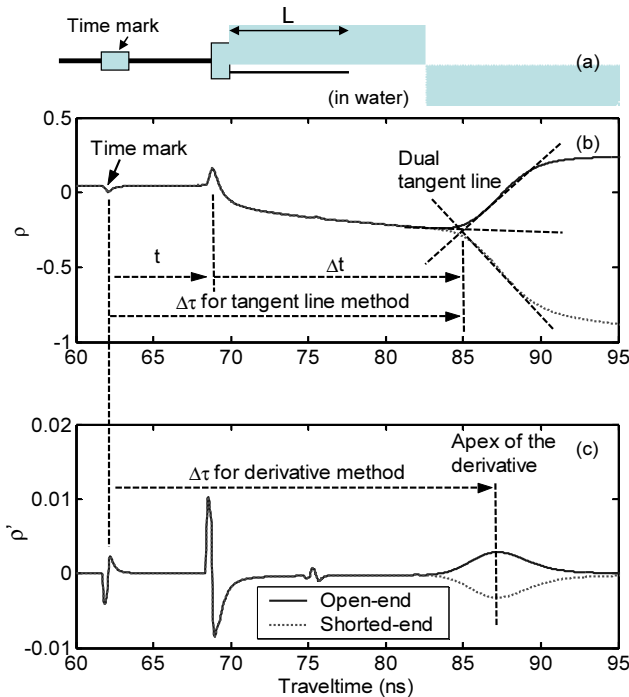


Fig. 3 The schema of TDR probe in water (a) and corresponding waveform (b) and the derivative (c). The definition of travel time parameters are also shown in (b) for the dual tangent line method and (c) for the derivative method

MATERIAL AND METHODS

TDR Probe Design for SSC Measurement

SSC measurements require accuracy much greater than water content measurements. Different probe design

and data reduction methodology may be needed. Six TDR probe designs for SSC measurement are shown in Fig.4, and these probes are further tested for determining the optimal type for TDR SSC measurements.

The selection of the trial probes in Fig.4 include difference in probe configuration (balanced vs. unbalanced), boundary condition (open-end vs. shorted-end), and probe length. U-shape probe are also evaluated to reduce the probe size while maintaining the desired sensing length.

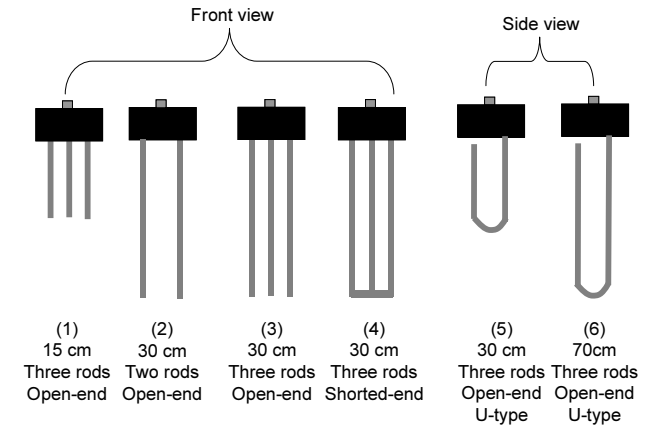


Fig. 4 Six types of the TDR probe for SSC measurement

TDR SSC Calibration, Temperature Correction, and Measurements

Since the apparent dielectric constant of water is temperature dependent, a temperature correction method for TDR SSC measurements is proposed in this study. Based on the TDR travel time analysis as mentioned in the previous section, the TDR travel time in water containing suspended sediment at certain temperature can be rewritten based on Eqs. (2) and (4) as:

$$\Delta\tau(T) = t + \Delta t = t + \left(\frac{2L}{c}\right) \left[\sqrt{\epsilon_w(T)}(1-SS) + \sqrt{\epsilon_w(T)}(SS) \right] \quad (5a)$$

$$\epsilon_w(T) = 78.54 \cdot \left(\begin{array}{c} 1 - 4.58 \cdot 10^{-7} (T - 25) \\ + 1.19 \cdot 10^{-5} (T - 25) \\ - 2.8 \cdot 10^{-9} (T - 25) \end{array} \right) \quad (5b)$$

in which the TDR travel time $\Delta\tau$ (measured in T Celsius degree) is composed of travel time between the electrical marker and start point of sensing waveguide t_0 and the actual travel time Δt in the probe section. The Eq. (5b) shows how the apparent dielectric constant of water ϵ_w depends on temperature T (Pepin et al. 1995).

Therefore, a temperature correction method for TDR SSC measurements has the following steps:

- A. Calibrate the system parameters L and t_0 by

measuring TDR travel times along the TDR sensing waveguide in air and in water and the water temperature.

- B. Calibrate the dielectric permittivity of suspended sediment ϵ_{ss} in Eq.(6) with known concentrations.
- C. Based on steps A and B, the volumetric percentage of suspended sediment can be determined by the equation:

$$SS_s = \frac{(\Delta\tau(T) - t) - \frac{2L}{c} \sqrt{\epsilon(T)}}{\frac{2L}{c} (\sqrt{\epsilon_{ss}} - \sqrt{\epsilon(T)})} \quad (6)$$

The resolution of SSC measurement is determined by the resolution of travel time analysis and probe length, as can be inferred from Eq. (6).

Influence Factors and Performance Evaluation

To evaluate the performance of TDR SSC measurements, various influence factors, such as water salinity, soil type, and particle size, are systematically examined. A Campbell Scientific TDR100 device with SDM50 multiplexer were used as a typical TDR measurement system, and several trial TDR probes as shown in Fig. 4 are connected via 25m CommScope QR320 cable to the SDM50 multiplexer. In addition, the sampling interval dt of each probe is chosen for the greatest resolution possible.

Both the dual tangent line method and the derivative method are used to obtain the end reflection point, as shown in Fig. 3, Furthermore, numerical interpolation is used to achieve time resolution to about half the sampling interval dt of the TDR sampler.

Effect of water salinity is examined for all probes. Probes were immersed into water (SSC = 0) with various electrical conductivity (EC or σ) from 5 ~ 600 $\mu\text{S cm}^{-1}$. Eq. (5) is used to check the variation due to EC effect, then a probe with lowest error and least affected by EC is selected for further evaluations.

Shihmen clay ($G_s = 2.73$) and ChiChi silt ($G_s = 2.71$), and one man-made silica silt ($G_s = 2.67$) grinded from glass materials were selected for tests. The particle size of Shihmen clay is the finest. The mean particle size of ChiChi silt and silica silt are most identical, except that the ChiChi silt is composed of some sand and clay size particles. Calibration tests for the travel time – SSC rating curve are conducted on sediment suspensions with various SSC from 0 ~ 150,000 ppm.

RESULTS AND DISCUSSIONS

Effect of Water Salinity

In measurements of water with different salinity, the

range of variation in the TDR travel time is transferred to variation of SSC (by assuming $G_s = 2.75$ and $\epsilon_{ss} = 4$). TDR travel times with different water salinity are corrected to the 25 Celsius degree. The measured travel time and corresponding SSC of the 70 cm open probe using the derivative method is shown in Fig. 5 for example. Fig. 5a shows the mean value and error bar of travel time $\Delta\tau$. Using the case of 5 $\mu\text{S cm}^{-1}$ as the reference, Fig. 5b transforms the differences in travel time into relative errors in sediment concentration. The mean error is less than 2100 ppm (about 0.7 theoretical resolution).

The resolution and variation range due to water salinity are shown in Table 1. For all probes, the derivative method of travel time analysis performs significantly better than the dual tangent method. The three-rod probe performs much better than the two-rod probe, suggesting the importance of balanced configuration of the probe. The shorted-end probe does not show improvement over open-end probe, and the U-shape dose not affect the measurement performance.

For the same or similar resolution, accuracy seem to increase with measuring probe length, waveform examination reveals that the reflections from electrical marker or mismatch in the probe head may interfere with the end reflection in short probes. Therefore, a pure and clear end reflection is important and should be ensured by placing the electrical marker at an appropriate location relative to the probe length and minimizing the reflection in the probe head. Among all the probes, the 70 cm U-shape probe with the derivative method of travel time analysis is least affected by water salinity, This probe will be used for further evaluations.

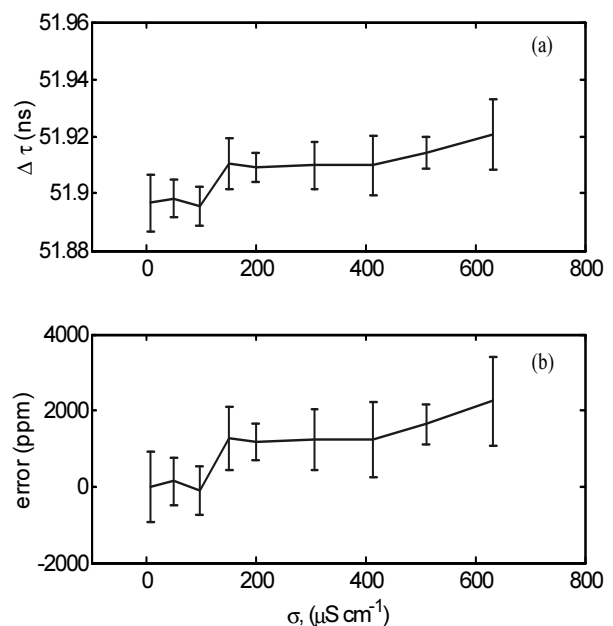


Fig. 5 The salinity effect for (a) travel time $\Delta\tau$ and (b) estimated error of the 70cm open probe using the derivative method

Table 1 Comparisons of derivation range due to salinity effect for each probe types

Deviation Range (ppm)	Probe type	15 cm	30 cm	30 cm	30 cm	30 cm	70 cm
		Three rods Open-end	Two rods Open-end	Three rods Open-end	Three rods Open-end U-type	Three rods Shorted-end	Three rods Open-end U-type
Resolution		7000	3200	3200	3200	3200	2500
Dual tangent line (deviation range / resolution)		29,700 (4.2)	27,000 (8.4)	12,000 (3.8)	22,000 (6.9)	11,000 (3.4)	7000 (2.8)
Derivative (deviation range / resolution)		14,700 (2.1)	16,800 (5.3)	5200 (1.6)	4600 (1.4)	7300 (2.3)	2100 (0.84)

Travel Time - SSC Rating Curve

Based on the optimal probe design in last section, travel time – SSC rating curve of Shihmen clay was first established with the 70 cm probe. TDR waveforms are recorded with various SSC from 0 to 150 000 ppm in water with two different EC ($\sigma = 200$, and $400 \mu\text{S cm}^{-1}$), and the ravel times were determined by the derivative method.

The temperature corrected travel time $\Delta\tau$ (corrected to $T = 25$ in Celsius degree) are shown in Fig. 6. The apparent dielectric constant of the sediment estimated by regression has similar value for the two cases of different water salinity ($\epsilon_{ss} = 8.47$ for $\sigma = 200 \mu\text{S cm}^{-1}$, and $\epsilon_{ss} = 7.53$ for $\sigma = 400 \mu\text{S cm}^{-1}$). The difference in the resulting slopes of the rating curves is less than 3 percent, showing that water salinity has a insignificant effect on SSC measurements.

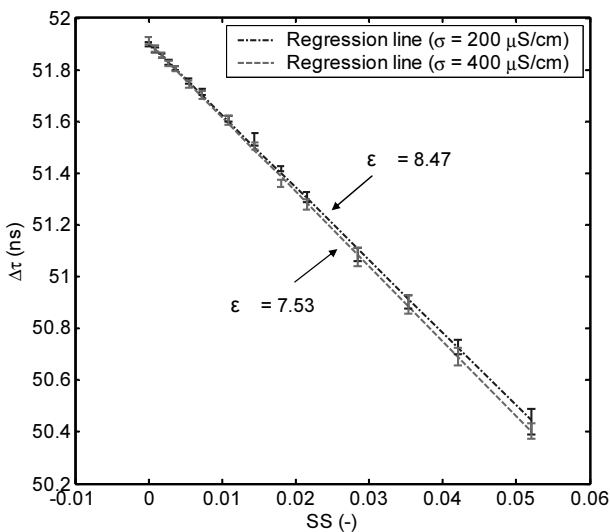


Fig. 6 Rating curve of travel time $\Delta\tau$ and Shihmen clay volumetric content SS. Error bars represent experimental data with 2 standard deviation

Effect of Soil Type and Particle Size

The travel time – SSC rating curves for the silica silt

and ChiChi silt were then established. Due to limited amount of samples, the highest SSC for ChiChi silt was only 0.02 (50,000 ppm).

Fig. 7 shows the travel time – SSC rating curves for the three types of sediments (water with $\text{EC} = 400 \mu\text{S cm}^{-1}$), and Fig. 8 shows mean errors estimated from the difference between measured data and the regression lines of three different types of measured samples. The rating curve of ChiChi silt almost overlaps with that of Shihmen clay, showing no signs of particle size effect.

However, the calibrated ϵ_{ss} of silica silt is 3.61, significantly different for that of ChiChi silt and Shihmen clay, resulting in about 14 % difference in the slop of the travel time – SSC rating curve. This difference may be attributed to different mineralogy of the silica from natural soils. It is believed that the bulk dielectric permittivity of the natural sediments does not vary significantly with time. Hence, it can be calibrated with a few actual SSC measurements. Comparing with particle size dependency in acoustic and optical methods, this sediment (mineralogy) dependency is not significant.

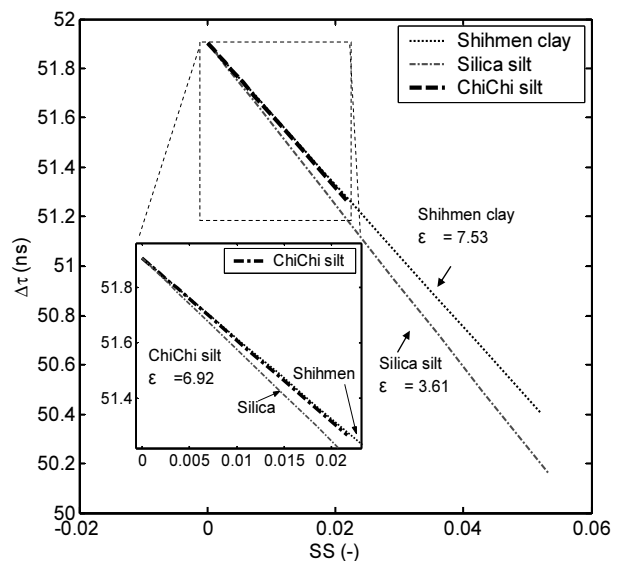


Fig. 7 Rating curve of travel time $\Delta\tau$ with Shihmen clay, silica silt and ChiChi silt

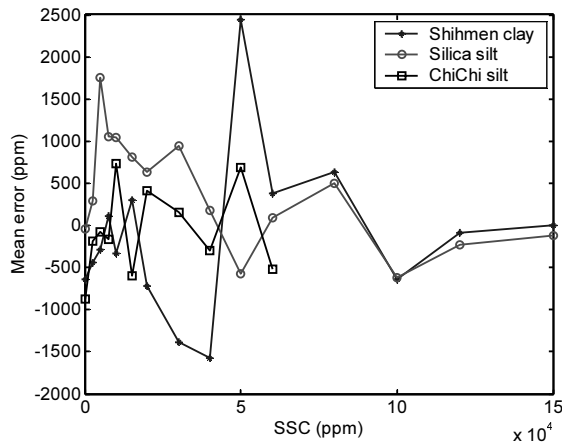


Fig. 8 The measurement error from rating curve of travel time Δt with Shihmen clay, silica silt and ChiChi silt

PILOT TEST IN-SITU

An extensive SSC monitoring program which mobilize manual samplings during the typhoon event was established at the inflow and outflow locations of Shihmen reservoir in northern Taiwan. An automatic monitoring station using TDR sensing technology developed in this study was established in one outlet.

This program started in summer, 2008, and SSC hydrographs were obtained for four typhoon events, including Kalmaegi, Fung-Wong, Sinlaku, and Jangmi.

Of the four typhoons recorded, Fung Wong has the lowest inflow and SSC in the outlet. To show the performance of TDR SSC measurements, the results of Fung Wong typhoon is shown in Fig. 9. The hydrograph of TDR SSC generally agree well with that of manual sampling (bottle sampling of surface water). The difference is about ± 2000 ppm, which is consistent with what was observed in the laboratory.

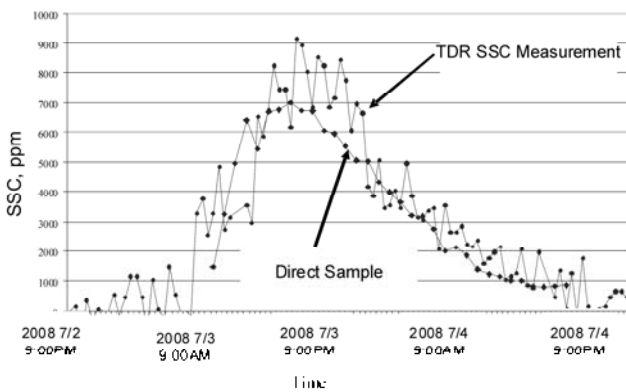


Fig. 9 SSC hydrographs of Shihman outlet during Fung Wong typhoon, 2008

CONCLUSIONS

Time Domain Reflectometry (TDR) is a measurement technique based on transmission line with several advantages, such as durability, low cost transducers, and multiplexing, an innovative TDR SSC measurement method is developed in this study. The sensitivity and resolution of the TDR method were theoretically derived based on dielectric mixing model, and their influencing factors including probe length, material properties, and temperature were identified. The calibration method and temperature compensation method were developed accordingly.

These developments improve the TDR SSC accuracy drastically and the measurement is insensitive to electrical conductivity and particle size. Compared with traditional SSC method, the measurement range of the TDR method is theoretically unlimited, and the TDR probe is simply a waveguide which can be easily made to fit different environments. Both laboratory and field testing suggest its feasibility and great potential.

REFERENCES

- Dobson MC, Ulaby FT, Hallikainen MT, L-Rayes MA (1985). Microwave dielectric behavior of wet soil - part II: dielectric mixing models. *IEEE Trans. Geoscience and Remote sensing*, GE-23: 35-46.
- Heimovaara TJ (1993). Design of triple-wire time domain reflectometry probes in practice and theory. *Soil Sci. Soc. Am. J.* 57: 1410-1417.
- Chung CC & Lin CP (2009). Apparent dielectric constant and effective frequency of TDR measurements: influencing factors and comparison. *Vadose Zone Journal*, 8 (In press).
- Pepin S, Livingston NJ, Hook WR (1995). Temperature-dependent measurement errors in time domain reflectometry determinations of soil water. *Soil Sci. Soc. Am. J.* 59: 38-43.
- Sutherland TF, Lane PM, Amos CL, Downing J (2000). The calibration of optical backscatter sensors for suspended sediment of varying darkness levels. *Marine Geology*, 162: 587-597.
- Topp GC, Davis JL, Annan AP (1980). Electromagnetic determination of soil water content and electrical conductivity measurement using time domain reflectometry. *Water Resou. Res.* 16: 574-582.
- Thorne PD & Hanes DM (2002). A review of acoustic measurements of small-scale sediment processes. *Continental Shelf Research*. 22: 1-30.
- Wren DG, Barkdoll BD, Kuhnle RA, Derrow RW (2000). Field techniques for suspended-sediment measurement. *J. Hydr. Engrg., ASCE*. 126: 97-104.

RESEARCH ON RELATIONS OF ENGINEERING INDEXES AND MICROSTRUCTURE FEATURE VALUES TO SATURATED SOFT SOIL

Yong XU¹, Ji-Chao ZHANG², Wu-Ping LI³ and He YI⁴

ABSTRACT: The microstructure feature values included fractal dimension of grains, fractal dimension of holes, porosity, total area of poles, number of holes, average circle of holes, average area of holes, complicated degree of holes, and average diameter of holes. A new technology comprised of the liquid nitrogen refrigeration sample-made technique (LNRSM), the scan electronic microscope technique (SEM), and the image processing, analysis, computer vision technique (IPACV) introduced in geotechnical engineering research. Using this technology, the microstructure feature values extracted from 46 groups samples. Meanwhile, the engineering indexes which included compression coefficient, compression module, cohesion and internal friction angle have also withdrawn based on traditional experiment method. The research results between microstructure feature values and engineering indexes discovered there are some relations which proved effective to explain engineering properties of saturated soft soil with microstructure feature values.

KEYWORDS: saturation soft soil, micro-structure, quantitative analysis, LNRSM, SEM, IPACV, fractal geometry

INTRODUCTION

Current civil engineering researches commonly reveal that soil engineering properties not only rest on their microstructure, but also depend on their micromechanics (Shen 1996). To build up calculate models in linear analysis methods, the complex soil structures were commonly simple treated as continuous media before. With these suppose, developing of current soil mechanics meet many troubles for lacking of the description to the evolutes laws of soil structure and the structure characteristics to the soil microstructure (Henkel 1959; Liu et al. 2002).

Restricted by traditional soil sample-made techniques, meanwhile, research on microstructure characteristics which were still not consider the soil micro composition have done at perturbation soil, not saturated soil, sandy soil, or loess. As a result, lower accuracy which sometimes may be up to decuple times is certain in use of the theories and in engineering practices.

Thanks to advances in technologies of LNRSM, SEM, IPACV and fractal geometry theory in 1990's, researches on microstructure feature values of saturated soft soil have access to quantitative analysis (Shen 1996). Some quantitative and quality relations between major microstructure feature values and the macroscopic engineering property feature values of Guangdong scientific

center saturated soft soil have discussed based on the new experimental technology (Xu 2006).

EXTRACT PROCEDURE OF MICROSTRUCTURE FEATURE VALUES TO SATURATED SOFT SOIL

Sampling in Place

To avoid big perturbation of the samples in saturated soft soil, the stainless steel drill machine whose diameter is 107mm and whose wall is thinner has adopted in sampling procedure of Guangdong science center. There are two kinds of comparison samples took from 13 holes, one kind is for the normal soil test, and the other is for the microstructure analysis. The sampling depths are from 2.2m to 2.5m, from 4.2m to 4.5m, from 6.2m to 6.5m, from 8.2m to 8.5m, and from 10.2 to 10.5m.

LNRSM in Lab

When the right dry method for the hydrated saturated soft soil would not get (Chai 2005; Xu 2006), the bulge or constringency will unavoidable, which would cause many tiny cracks and ruin the samples microstructure. During the samples refrigeration procedure, LNRSM is the best way to keep the natural microstructure of

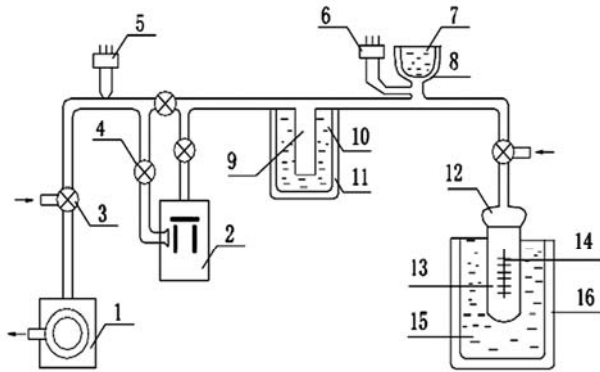
¹ Instructor, School of Civil Engineering, Guangzhou University, China. Email:xyjerry1975@126.com

² Professor, School of Civil Engineering, Guangzhou University, China. Email:zhangjichao1956@126.com

³ Professor, School of Civil Engineering, Guangzhou University, China. Email:wupingli@126.com

⁴ Professor, Guangdong scientific center, China, Email:yihegdsc@163.com

saturated soft soil. With this technology, 46 groups saturated soft soil samples which size were $2\text{mm} \times 4\text{mm} \times 10\text{mm}$ have made. (Chen et al. 2000; Chai et al. 2005; Zhang 2005; Xu 2006). The theory chart of LNRSM shows in Fig. 1.



- 1: MECHANICAL PUMP
- 2: DIFFUSION (VACUUM) PUMP
- 3: ADMISSION VALVE
- 4: VALVE
- 5: THERMOCOUPLE WELL
- 6: IONIZATION GAUGE
- 7: LIQUID NITROGEN
- 8: COLD TRAP
- 9: PIPE COLD TRAP
- 10: LIQUID NITROGEN
- 11: DEWAR'S BOTTLE
- 12: GROUND CONNECTION
- 13: SAMPLE ROOM
- 14: SAMPLE HOLDER
- 15: LIQUID NITROGEN
- 16: DEWAR'S BOTTLE

Fig. 1 LNRSM construction

SEM Analysis

Treated by LNRSM, each sample broke into two parts by hand along the cross-section and kept in natural state. Keeping natural cross-section upward, all samples stamped firmly on sheets copper with electric gum, and then they numbered. When the electron beam bombards the untreated sample surface, the dust which would pollute microscope lens would arise from the samples surface. Meanwhile, the electrical discharge which would strongly influence the watching and imaging quality in the electron microscope room will also appear, so the samples surface must treated. Before put into the electron microscope room, gold powder must spray on the samples in vacuum evaporation spraying gilt machine. The spray layers' thickness was between 20nm and 30nm which proved to be the best to watch and

image when samples were in the high vacuum circumstance. (Chen et al. 2000; Jiang et al. 2001).

After spraying gold powder treatment, all samples put into the electron microscope room of the NS-3500 scan electron microscope made by Hitachi Company of Japan to watch and take photographs at all selected natural broken cross-section. Typical microstructures found out at higher multiple times at first, and 96 photographs that half were 3000 times and the others were 300 times have took at last.

Extraction of Saturated Soft Soil Microstructure Feature Values

IPACV, which include noise removal, histogram equalization and histogram regularization, etc., has used to pretreat the photographs that took in the scan electron microscope room to achieve saturated soft soil microstructure feature values.

Microstructure fractal geometry values usually express with Hausdorff dimension. Provided E is the assembly of points, and $I_1, I_2, I_3, \dots, I_n, I_{n+1}, \dots$, are open zone that assemble into E , a is a real number which is no less than zero, δ is the maximum zone length, $H_\delta^a(E)$ is the outside measure degree of E , then:

$$H_\delta^a(E) = \inf \left\{ \sum_{i=1}^{\infty} |I_i|^a : \bigcup_{i=1}^{\infty} I_i \in E, |I_i| \leq \delta \right\} \quad (1)$$

If exist D , when $0 < a < D_H$, $H_\delta^a(E) \rightarrow \infty$, when $D < a < \infty$, $H_\delta^a(E) \rightarrow 0$, then D will be the Hausdorff dimension of E (Xie 1996; Zhang et al. 2005; Kennech 2000; Xu 2006).

With similar measure ε , if a picture divided into $N(\varepsilon)$ respective comparability parts which are also similar with the whole picture, then its fractal dimension value can calculate as Eq.2.

$$D = -\lim_{\varepsilon \rightarrow 0} \frac{\ln N(\varepsilon)}{\ln \varepsilon} \quad (2)$$

According to the Eq.2, the calculation method of saturated soft soil microstructure fractal dimension geometry feature values lists in Table 1 (Xu 2006).

After pretreating the microstructure photographs which based on porosity, the microstructure photographs were breaking up, sieving and tag with the calculation method given in Table 1, and the fractal geometry values show in Table 2.

According to composite of soil, other microstructure feature values also extracted by breaking up, sieving and tagging samples microstructure photographs. Typical microstructure feature values and their matching engineering indexes list in Table 2.

Table 1 Microstructure fractal calculation method

Fractal geometry value	ε /nm	$N(\varepsilon)$
Grain fractal dimension (D_d)	Picture divide grid length	The whole grid number with grain according to ε
Hole fractal (D_d)		The whole grid number with hole according to ε

Table 2 Microstructure feature values and engineering indexes of typical saturated soft soil samples

Sample number	1	2	3	5	6	7	...	45	46
Grain fractal D_{pd}	1.734	1.737	1.721	1.720	1.785	1.826	...	1.757	1.774
Hole fractal dimension D	1.768	1.783	1.782	1.850	1.754	1.897	...	1.782	1.826
Number of holes n	419545	419510	419550	419507	419841	419543	...	419533	419568
Average area of holes \bar{A} (μm)	0.03005	0.03021	0.03001	0.03023	0.02988	0.03004	...	0.03009	0.02999
Average diameter of holes Φ (μm)	0.19561	0.19610	0.19546	0.19618	0.19504	0.19556	...	0.19573	0.19540
Average circle of holes (μm)	0.5174	0.5187	0.5170	0.5189	0.5159	0.5173	...	0.5177	0.5169
Complicated degree of holes D	2.60282	2.60198	2.60308	2.60183	2.60378	2.60290	...	2.60262	2.60318
Porosity n	0.502	0.576	0.562	0.610	0.492	0.572	...	0.510	0.600
Compression coefficient α_s (MPa^{-1})	0.581	1.867	0.898	1.377	0.704	1.571	...	0.898	1.632
Compression module E (MPa)	3.46	1.26	2.54	1.86	2.80	1.49	...	2.27	1.53
Cohesion c (kPa)	5.7	5.7	2.8	15.1	25.7	7.3	...	6.6	3.8
Internal friction angle φ ($^\circ$)	8.6	4.3	2.2	8.2	3.5	3.2	...	6.4	4.3

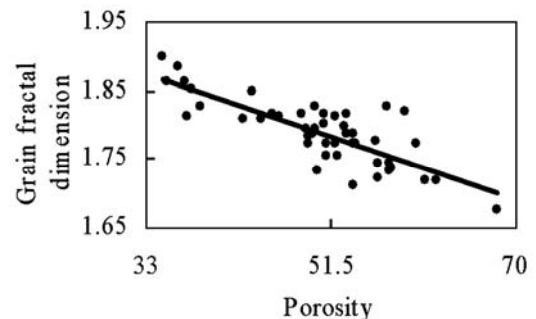
RELATIONS BETWEEN GRAIN FRACTAL DIMENSION AND POROSITY

The scattered data diagram of all samples between grain fractal and porosity gives in Fig. 2. The most commonly conclusion from Fig. 2 can classify as follows:

1) Grain fractal values arrange from 1.65 to 1.90, and the average value is about 1.7901.

2) There is an obvious linear relation between grain fractal dimension and porosity in saturated soft soil. When $R^2 = 0.6463$, provide n is the porosity, it is possible to express the results as Eq.3.

$$D = 2.0388 - 0.0049n \quad (3)$$

**Fig. 2** Relations between grain fractal dimension and porosity

In which D_d is the grain fractal dimension, n is the porosity, and R is the correlation coefficient.

3) Grain fractal dimension can explain the compactness of saturated soft soil in microstructure. The larger the grain fractal dimension value is, the denser the soil is. In another word, the porosity becomes smaller, and the grain fractal dimension gets bigger, which means the grain distribution appear more complicated.

RELATIONS BETWEEN HOLE FRACTAL DIMENSION AND POROSITY

The scattered data diagram of all samples between hole fractal dimension and porosity gives in Fig. 3. The most commonly conclusion from Fig. 3 classify as follows:

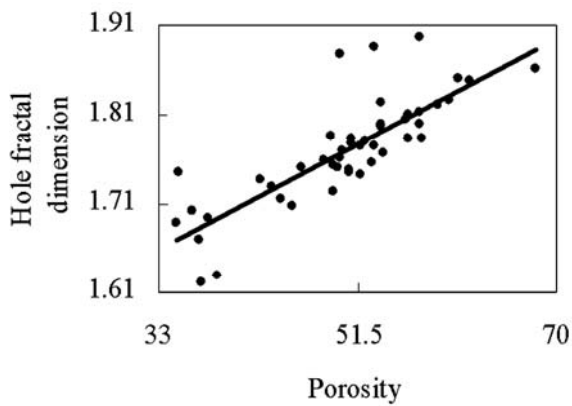


Fig. 3 Relations between hole fractal dimension and porosity

1) Hole fractal dimension values arrange from 1.61 to 1.91, and the average value is about 1.7696.

2) There is an obvious linear relation between hole fractal dimension and porosity. When $R^2 = 0.6581$, it is possible to express the results as Eq.4.

$$D = 1.449 + 0.064n \tag{4}$$

In which D is the hole fractal dimension, n is the porosity, and R is the correlation coefficient.

3) With the decrease of porosity, hole fractal dimension values are also drop. So hole fractal dimension values present the compactness of saturated soft soil too. In a word, the denser the soil is, the smaller the hole fractal dimension value is.

RELATIONS BETWEEN COMPRESSION COEFFICIENT AND MICROSTRUCTURE FEATURE VALUES

Compression coefficient is one of the important indexes which sign the compressibility of soil. When significance level is 0.05, it is possible to express the

results for the microstructure feature values and compression coefficient as Eq.5 by adopting multivariable gradually linearization go back analysis method.

$$\alpha_{-2} = 703.481 + 4.573n - 0.017n_h \tag{5}$$

In which α_{-2} is the compression coefficient, n is the porosity, and n_h is the number of holes.

It is obvious from Eq.5 the compression coefficient of saturated soft soil is a linear function of the soil porosity and the number of holes, so the microstructure characteristics can use to explain the engineering compressible property.

RELATIONS BETWEEN COMPRESSION MODULE AND MICROSTRUCTURE FEATURE VALUES

The scattered data diagram of all samples between compression module and porosity gives in Fig.4.

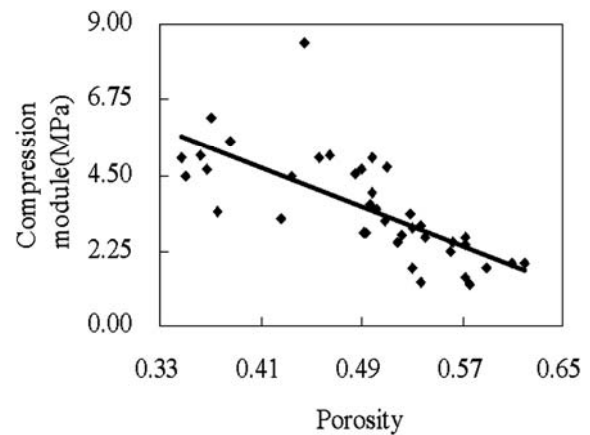


Fig. 4 Relations between compression module and porosity

When the significance level is 0.05, it is possible to express the results for the microstructure feature values and compression module as Eq.6 using multivariable gradually linearization go back analysis method.

$$E_{-2} = -14.068n + 10.439 \tag{6}$$

In which E_{-2} is the compression module, n is the porosity.

Fig.4 and Eq.6 provides a clear sign of the relative severity of all microstructure feature values. There is an obvious linear role between compression module and porosity.

RELATIONS BETWEEN COHESION AND MICROSTRUCTURE FEATURE VALUES

When the significance level is 0.05, it is possible to

express the results for the microstructure feature values and cohesion as Eq.7 by adopting multivariable gradually linearization go back analysis method.

$$c = -21731.05 - 38.029n + 0.0519n \quad (7)$$

In which c is the cohesion, n is the porosity and n_n is the number of holes.

Eq.7 provides a clear sign of the relative severity of all microstructure feature values. Only the number of holes and porosity have obvious linear relations with cohesion, while the linear influence of others microstructure feature values were unobvious. There is intersectional influence in these 9 microstructure feature values, and the subordinate feature values can gradually pick out and then got rid of by gradually linearization go back analysis.

RELATIONS BETWEEN INTERNAL FRICTION ANGLE AND MICROSTRUCTURE FEATURE VALUES

When the significance level is 0.05, it is possible to express the results for the microstructure feature values and internal friction angle as Eq.8. using multivariable gradually linearization go back analysis method,

$$\varphi = 2672.8D - 6951.4 \quad (8)$$

In which φ is the internal friction angle, and D_c is the complicated degree of holes.

As seen from the Eq.8, the complicated degree of holes is the major feature which influenced the internal friction angle. The scattered data diagram of all samples between internal friction angle and complicated degree of holes gives in Fig. 5.

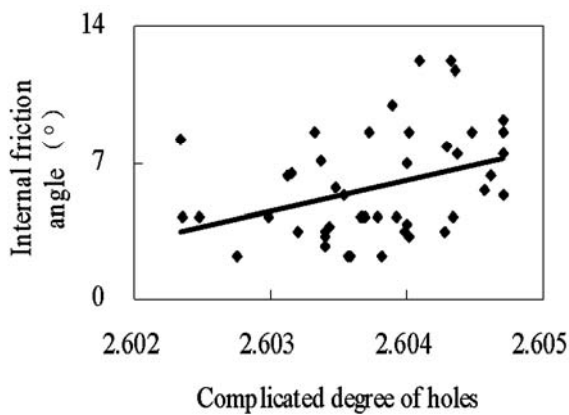


Fig. 5 Relations between internal friction angle and complicated degree of holes

Fig. 5 provides an obvious linear role between internal friction angle and complicated degree of holes.

While the linear influence of others microstructure feature values were relatively unobvious. There was a positive relativity between complicated degree of holes and internal friction angle, with the decrease of internal friction angle of soil, the complicated degree of holes drop. In another word, when the complicated degree of holes increases in some action, the shearing strength of saturated soft soil would also strengthen.

CONCLUSION

With LNRSM, SEM and IPACV, the microstructure feature values and engineering indexes of 46 groups saturated soft soil samples of Guangdong scientific center have been analysis, and some conclusions come into being as follows:

- 1) In statistics meaning the saturated soft soil microstructure fractal dimension feature values have the self-similar character. In geometry the saturated soft soil microstructure have obvious fractal dimension geometry characteristics. So it possible to pick up microstructure photographs quantitative with fractal dimensions geometry method.
- 2) Different microstructure feature values have different influence on the engineering property indexes of saturated soft soil. Grain fractal dimension is the linear function of porosity Hole fractal dimension is the linear function of porosity. Compression module is the linear function of porosity. Internal friction angle is the linear function of complicated degree of holes. Compression coefficient is the linear function of porosity and number of holes. Cohesion is the linear function of porosity and number of holes.
- 3) To bridge between microstructure feature values and engineering indexes of saturated soft soil, compound use of some techniques such as LNRSM, SEM, and IPACV might be an effective way to develop the microstructure mechanics.

REFERENCES

Chai SX, Han WF, Wang P, Wei HZ (2005). Experiment on artificially-prepared clay samples by freeze-drying for SEM. *Coal Geology & Exploration*. 33(2):46-48.

Chen JO, Ye B, Guo SJ, Li ZM (2000). Quantitative analysis on SEM image of soft ground microstructure in Zhu Jiang delta. *Journal of Chinese Electron Microscopy Society*. 20(1):72-75.

Henkel GJ (1959). The relations between the strength, pore-water pressure, and volume change characteristics of saturated clays. *Geotechnique*. 9(3).

Hu RL, Wang SJ, Li XQ, Guan GL (1999). A growing point of engineering geology in 21st century soil

- micromechanics. *Hydrogeology and Engineering Geology*. 1999(4):5-8.
- Jiang XQ, Wang SY, Mo HH (2001). Test for microstructure of Soft Soil, *Geotechnical Investigation and Surveying*. 2001 (4):5-8.
- Kenneth J Falconer (2000). *Fractal Geometry - Mathematical Foundations and Applications*. Shenyang: North-eastern University Press, China.
- Li XQ, Hu RL, Zhang L (2000). The variation of microstructure during soft soil solidification. *Earth Science Frontiers*, 7(1):147-152.
- Liu HS & Xu XZ (2002). 283 questions in ground and foundation engineering. Beijing: China Planning Press, China.
- Milan Sonka, Vaclav Hlavac, Roger Boyle (2003). *Image Processing, Analysis, and Machine Vision*. Beijing: Post and telecom press, China.
- Shen ZJ (1996). Mathematics model of soil structure—soil mechanic core problems in 21st century. *Chinese Journal of Geotechnical Engineering*, 18(1):95-97.
- Xie HP (1996). *Introduction to Fractals in Rock Mechanics*. Beijing: Science Press, China.
- Xu Y (2006). *Research and Application on Dynamic Consolidation Pretreatment Technique of Saturated Soft Soil*. MA.D. Guangzhou Univ. Guangzhou, China.
- Zhang JC, Xu Y, Li WP, Zhu LH, Yi H, Wang LF (2005). Quantitative Analysis on Saturation Soft Soil Microstructure for Guangdong Scientific Center, *Building Science*, China, 21(3):34-38.

SHEAR STRENGTH BEHAVIOR OF BENTONITE MODIFIED BY TETRAMETHYLAMMONIUM CATIONS

Bate BATE¹ and Susan E. BURNS²

ABSTRACT: Over the past decades, bentonite exchanged with quaternary ammonium cations to form organobentonite has gained increasing attention. Due to its high sorption capacity for organic contaminants and low friction angles, organobentonite has many applications, including in the areas of contaminant site remediation, landfill clay liners, and as a pipe jacking lubricant and drilling mud. Although many properties of organobentonites have been studied in detail, such as sorption capacity, swelling, and hydraulic conductivity, little data are available on the strength of this engineered clay. This study presents the results of the shear strength behavior of tetramethylammonium cations exchanged bentonite (TMA-bentonite) as a function of organic loading. TMA-bentonites had higher shear strength and higher hydraulic conductivity than the unmodified bentonites. The initial shear modulus increased with the amount of TMA loaded on the bentonite surfaces, i.e. as the organic loading was increased. The tested samples were normally to lightly overconsolidated, but always exhibited peak behavior and positive pore pressures in the stress strain curve. This study sets the stage for further investigation of more complicated organic cations, such as tetramethylammonium (TEA) and hexadecyltrimethylammonium (HDTMA).

KEYWORDS: bentonite, hydraulic conductivity, organobentonite, organoclay shear strength, tetramethylammonium

INTRODUCTION

Over the past decades, bentonite exchanged with quaternary ammonium cations to form organobentonite has gained increasing attention. Organobentonites, or organoclays, demonstrate high sorptive capacity and have been proposed as sorptive amendments in contaminant remediation applications. Additionally, the interfacial friction of an organoclay can be engineered, making it an attractive lubricant material in applications like pipe jacking.

Numerous studies on the sorptive capacity of organoclays for organic and inorganic contaminants have been performed, and in general, organoclays are highly sorptive for organic contaminants (Bartelt-Hunt et al. 2003, Burns et al. 2006). For organoclays with long alkyl chains such as hexadecyltrimethylammonium (HDTMA), the sorption is due to partition between the aqueous solution and the organic medium created by the alkyl chains (Smith et al. 1990). For HDTMA organoclays, as the organic carbon content was increased the sorption increased, indicating the presence of a partitioning mechanism. In contrast, shorter alkyl chains or cations

with benzyl functional groups in their structures acted as a surface sorption medium (Burns et al. 2006), where the organic contaminants were held at specific sites on the clay surface. An increase in organic carbon content led to the decrease in surface area, which in turn decreased the sorptive capacity of the clay (Burns et al. 2006).

Lorenzetti et al. (2005) reported hydraulic conductivity tests on GCLs amended with two different types of organobentonites: BTEA-bentonite and HDTMA-bentonite. It was found that the addition of both types of organobentonites led to increased hydraulic conductivity. As the quantity of organobentonite amendment was increased from 10% to 90%, increases of three orders of magnitude in hydraulic conductivity were obtained. The increased hydraulic conductivity was due to the fact that the organobentonites were hydrophobic and did not swell as much as untreated bentonites in the presence of water. Less swelling led to larger voids available for hydraulic flow, which increased the hydraulic conductivity compared to unmodified bentonite. However, when the permeant was changed to an organic contaminant, the hydraulic conductivity would be expected to remain

¹ Graduate Research Assistant, School of Civil and Environmental Engineering, Georgia Institute of Technology, USA. Email: bate@gatech.edu

² Associate Professor, School of Civil and Environmental Engineering, Georgia Institute of Technology, USA. Email: susan.burns@ce.gatech.edu

relatively unchanged due to the hydrophobic interaction between the contaminant and the organic phase in the clay. BTEA-bentonite resulted in a significant improvement in benzene transport when compared to the conventional GCLs based on one-dimensional solute transport simulation (Burns et al. 2006). Although the hydraulic conductivity of the BTEA-bentonite modified GCLs was larger than that of the conventional bentonite, the increase in sorptive capacity resulted in considerable retardation of solute transport through the GCL, without a significant increase in the mass of benzene transported through the GCL. In contrast, modifying the GCLs with HDTMA-bentonite did not improve solute transport. Although the sorptive capacity of HDTMA-bentonite was larger than that of conventional bentonite, the increase in hydraulic conductivity in the HDTMA-amended GCLs resulted in a steady-state benzene flux that was an order of magnitude larger than that for the conventional GCL (Lorenzetti et al. 2005).

Although many properties of organobentonites have been studied, such as sorption capacity, swelling, and hydraulic conductivity, little data were available for the strength of organoclays. Burns et al. (2006) carried out direct shear tests on HDTMA-bentonite and BTEA-bentonite where surface coverage of the organic cation varied from 50% cation exchange capacity (CEC) exchanged to 100% CEC exchanged. The measured direct shear peak friction angle was lower as the surface coverage of HDTMA was increased, as would be expected for a shift from solid/amorphous behavior to amorphous/liquid behavior as the monolayer coverage was increased (Burns 2006). However, BTEA clay showing an increase in strength as the total organic carbon content was increased. The mechanisms behind the increase in friction, or chemical adhesion, in BTEA were not clear; however, it was hypothesized that the degree of disorder in the packing of the benzene ring, in addition to a component of chemical adhesion, was responsible for the increase in measured strength for the BTEA clays. Surfactant packing density was critical in the frictional behavior of the organoclays; surfactant monolayers can exhibit three different phase states as a function of packing density: solid-like, amorphous, and liquid (Yoshizawa et al. 1993). At low surface coverages of HDTMA, the monolayer acts characteristically like a solid; however, as surface coverage is increased, the surfactant packing density increases, resulting in a monolayer that behaves more like a liquid (Yoshizawa et al. 1993).

This study presents the results of the shear strength behavior of tetramethylammonium cation-exchanged bentonite (TMA-bentonite). Consolidated undrained triaxial shear tests at effective confining pressures of 50, 100, and 200 kPa were performed. Organic loadings of 30%, 60%, and 100% of CEC of bentonite were selected

to create different packing density on the clay surface.

MATERIALS

Wyoming bentonite (CG-50, CETCO), composed primarily of sodium montmorillonite, was the base clay for the study and was used as received. The natural-organic carbon content of the material was 0.2% (Huffman Laboratories, Inc., Golden, CO), and its cation exchange capacity (CEC) was 69.1 meq/100g (Hazen Research Inc., Golden, CO). Tetramethylammonium (TMA) chloride ($(\text{CH}_3)_4\text{NCl}$), a type of quaternary ammonium cation, was chosen for study. TMA chloride and sodium chloride (NaCl) were obtained from Fisher Scientific, and were used as received. The water used in all experimentation was deionized (Barnstead E-pure).

EXPERIMENTAL METHOD

The TMA bentonite used in this study was synthesized in the laboratory by exposing the particle surfaces of the bentonite to an aqueous solution containing the TMA cation at 30%, 60%, and 100% of the cation exchange capacity of the clay. The organic compound was dissolved in 40 liters of deionized water, and 2 kg of the clay were added to the aqueous solution. The resulting suspension was mechanically stirred for 1 hour and allowed to stand for a minimum of 24 hours to allow settlement. The supernatant was then siphoned off, and the deposits were rinsed with deionized water to remove any salts or loosely bound cations, until the conductivity of the supernatant was below 600 $\mu\text{S}/\text{cm}$. Mineralogical impurities were separated by gravity settling.

Then the slurry was poured, slowly to prevent entrapped air bubbles, into a stainless steel slurry consolidometer. The consolidometer was 10.2 cm (4 inch) in diameter and 45.7 cm (18 inch) in height. Axial load was placed on the slurry in increments of 3.5, 7, 14, 28, 56, and 100 kPa, until consolidation was achieved at each load step. The stress was applied to the slurry using pneumatic loading (Karol Warner, Inc). Once the ultimate preloading stress was achieved, the slurry was unloaded by the same increments in the reverse order. The duration of each load step was typically 1 day; however, at maximum load, the duration was increased depending on the rate of settlement. Filter paper (P5 Grade, Fisher Scientific) and a nonwoven geotextile were placed on top and bottom of the samples to facilitate drainage. To ensure the sample was saturated and to maintain the ionic strength within the sample throughout the compression, the top of the consolidometer was filled with 0.001M NaCl, and the bottom was connected to a 0.001M NaCl tank. After

consolidation was completed, the samples were extruded from the consolidation tube, and the compressed samples were then split into 3 pieces for strength testing. Samples were trimmed with a soil lathe and wire saw into 3.6 cm (1.4 inch) diameter and 7.6 cm (3 inch) height samples. The final water contents of the consolidated samples ranged from 164% to 257%.

Consolidated undrained (CUIC) triaxial shear tests were performed using Geotac load trac systems (Geotac, Texas, USA). All shear tests were strain rate controlled tests and were performed in accordance with ASTM D4767-04. According to the consolidation results, a strain-rate of 0.5% /hr was selected. Samples were reconsolidated to effective confining pressures of 50, 100, or 200 kPa, with a backpressure of 140 kPa during shear. All samples were sheared with a minimum B-value of 0.95. Standard corrections (surface area change, membrane stiffness, and friction between loading rod and bushing) were performed in calculating the stresses from the measurements. The corrected heights and diameters of the samples were used in the shearing test calculation by assuming right cylindrical deformation.

For samples consolidated to 100 kPa, hydraulic conductivity was tested according to ASTM D5084-03 before undrained shearing. The inflow and outflow fluids used in sample compression and shear tests were 0.001M NaCl solution in order to maintain a background ionic strength for the clay surface and the bulk solution. To prevent corrosion within the panel controls, the salt solution was isolated from the de-aired (Nold deaerator) water by two P620000 bladder accumulators (Trautwein Soil Testing Equipment, Houston, Texas, USA).

RESULTS AND DISCUSSIONS

Specimens of the TMA-bentonite resulted in organoclay samples with either 30, 60, or 100% of its inorganic cations exchanged with the TMA organic cation. Theoretical and measured total organic carbon contents were within predicted ranges (data not shown).

As shown in Table 1, the water contents for all three TMA-bentonites decreased after extrusion from the slurry consolidometer and reconsolidation and shear in the triaxial cell. For all soils, during reconsolidation to the effective confining pressure of 50 or 100 kPa, or primary consolidation to 200 kPa, there was a decrease in sample volume. The loss of volume indicates either that there was significant swell and water sorption as the sample was extruded (not observed), or that the actual stress transferred in the consolidometer was lower than anticipated.

Table 1 Water Content of Organobentonites Before and After Isotropic Consolidation

Soil	After Slurry Consolidation*	After Triaxial Shear		
		50kPa	100kPa	200kPa
	w/c (%)	w/c (%)	w/c (%)	w/c (%)
30TMA	164	144	121	105
60TMA	257	190	166	125
100TMA	184	172	152	126

* (Nominal 100 kPa)

General Features of TMA-Modified Organobentonites

The results from the CUIC shear strength tests are shown in Figs. 1-3. The results are presented in terms of four variables: (1) Effective mean normal stress $p' = (\sigma_1' + 2\sigma_3')/3$, (2) deviatoric stress $q = (\sigma_1' - \sigma_3')$, (3) axial strain, and (4) pore water pressure. The shear behavior of the organic modified clays demonstrated several notable trends: all clays tested demonstrated peak shear strength, even though the samples were normally consolidated and demonstrated positive pore water pressure throughout the duration of shearing. Although the tests were performed to a strain of approximately 25%, many of the tested samples did not completely achieve critical state condition, which is reflected in the shear stress parameters (Table 2). The predominant mode of failure in the testing program was shear banding, with displacement along the failure surface. Also notable was the presence of an intercept in the p' - q diagrams. In all cases, the p' - q diagram had an intercept on the y-axis, indicating either: critical state was not achieved at 20-25% strain, or bonding between the organic molecules recovered during prolonged shear.

Table 2 Summary of Shear Strength Behavior

	30TMA	60TMA	100TMA
	Peak (Critical)	Peak (Critical)	Peak (Critical)
M	1.26 (1.06)	1.63 (1.44)	1.80 (1.16)
ϕ (deg)	31.3 (26.9)	40.0 (35.6)	43.9 (29.2)
y-int (kPa)	21.8 (26.9)	22.0 (20.2)	18.6 (34.3)
r^2	0.9992 (0.9997)	0.9992 (0.9998)	1.0000 (0.9640)

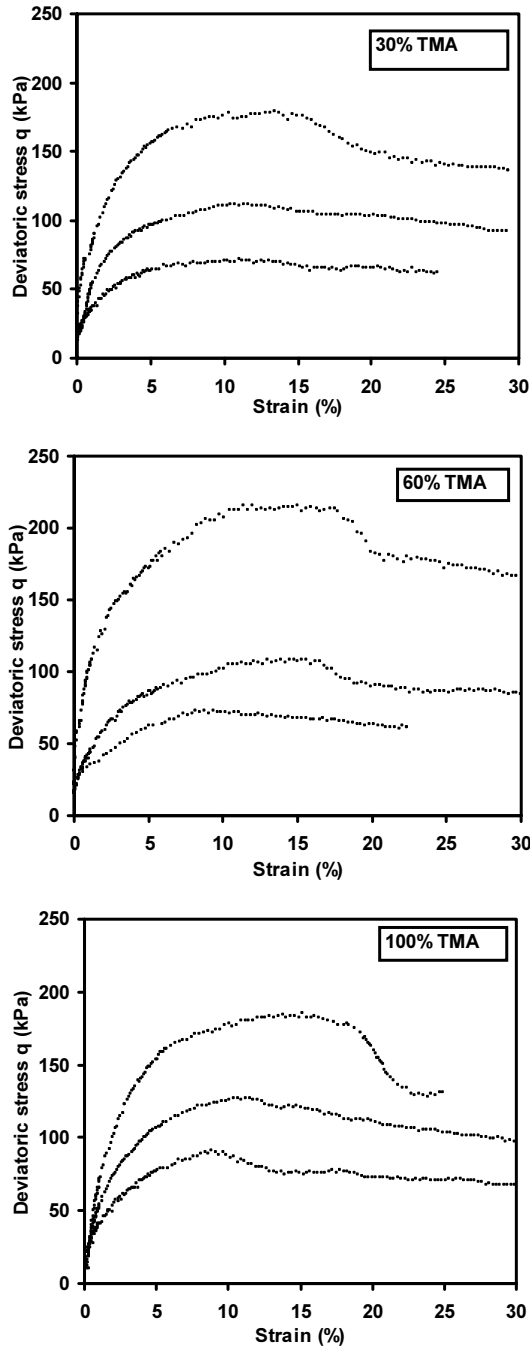


Fig. 1 Shear strength behavior of TMA-bentonite: (a) 30% CEC exchanged; (b) 60% CEC exchanged; (c) 100% CEC exchanged.

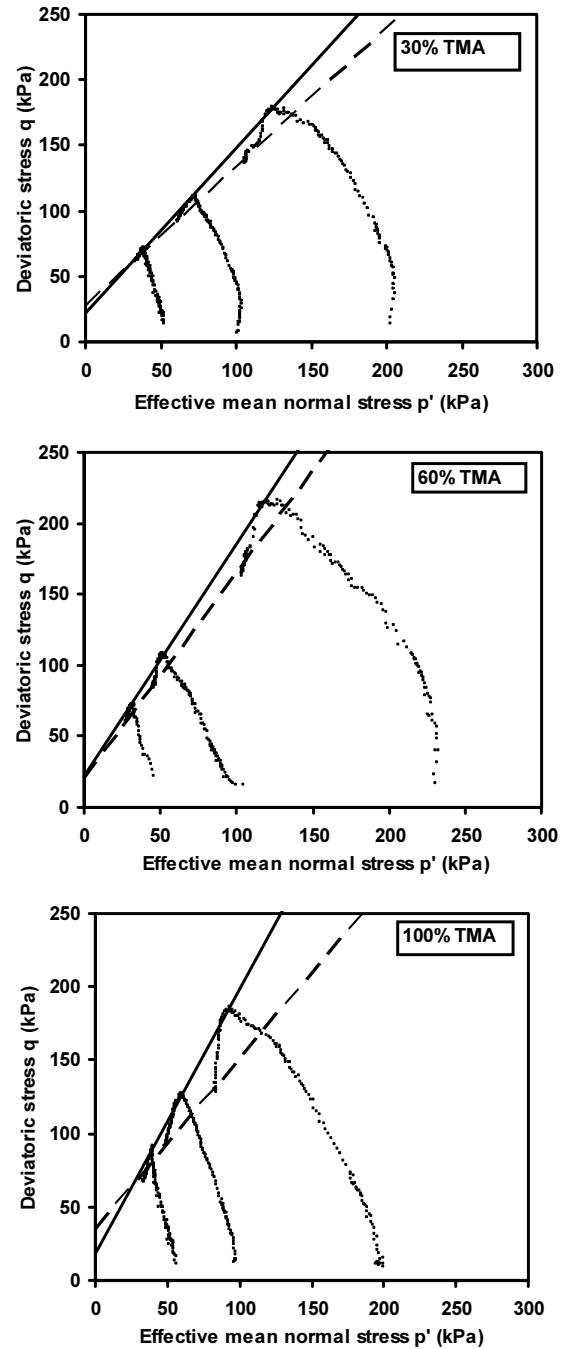


Fig. 2 p' - q diagrams for TMA-bentonite: (a) 30% CEC exchanged; (b) 60% CEC exchanged; (c) 100% CEC exchanged.

Effects of Organic Cation Loading

The effect of increasing organic content was observed in the increase of the measured peak friction angle. As the total organic carbon content increased, the effective peak friction angle increased the effective peak friction angle increased from 31.3° at 30% CEC to 43.9° at 100% CEC (Table 2), which represents a substantial increase in interfacial friction due to the presence of the TMA cations on the clay surface. The results are

reasonably consistent with the results of direct shear tests by Soule and Burns (2001), which measured a direct shear friction angle of 34° for 85% CEC TMA-exchanged bentonite.

Mesri and Olsen (1970) reported that the angles of internal friction of calcium and sodium montmorillonite at low stress levels were 15° and 4° , respectively. In this study, the increase in shear strength for the organoclay is due in part to the decrease in water content at given effective confining pressure (Table 1). The addition of

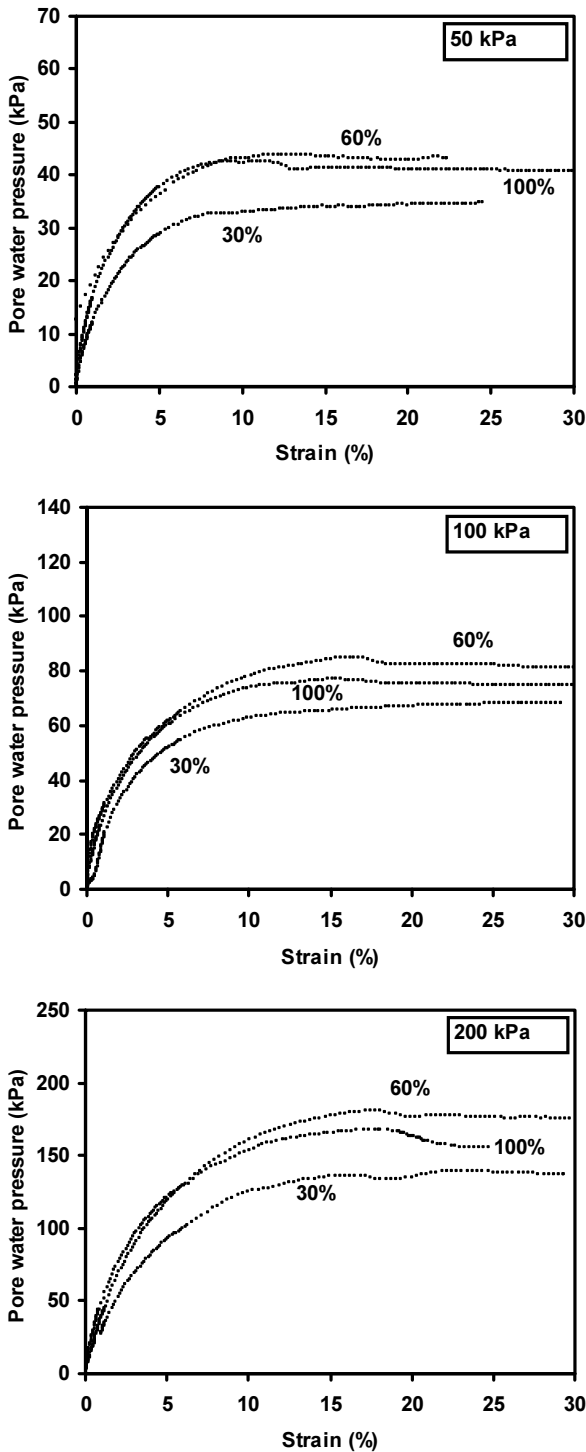


Fig. 3 Pore pressure measured during triaxial shear: a) confining stress = 50 kPa; b) confining stress = 100 kPa; and c) confining stress = 200 kPa

the organic phase creates a hydrophobic surface which repels water and acts to increase the density of the clay, which in turn leads to the observed increase in strength. In the context of electrical double layer theory, the adsorbed TMA cations bond more strongly to the bentonite surface than inorganic cations (e.g. Na^+ , Ca^{2+}), reducing the electrical repulsive forces between bentonite particles.

Hydraulic Conductivity

The hydraulic conductivities of TMA-bentonite were measured under 100 kPa effective confining pressure at organic loading of 30%, 60%, and 100% of CEC (Fig. 4). As was anticipated, the hydraulic conductivity increased as the organic loading was increased. This trend is attributable to the fact that the organobentonites were hydrophobic and did not exhibit the same swelling characteristics as untreated bentonites in the presence of water (Lorenzetti et al. 2005). At the microscopic level, the electrical repulsive forces between TMA-bentonite particles are lower than those between pure bentonite particles, and the attractive forces are higher due to increased hydrophobic interaction between the organic cations attached to the particle surfaces. As a result, at a given effective confining stress, TMA-bentonite particles tend to form larger aggregates than pure bentonite particles, leaving larger pore voids, which in turn increase the hydraulic conductivity.

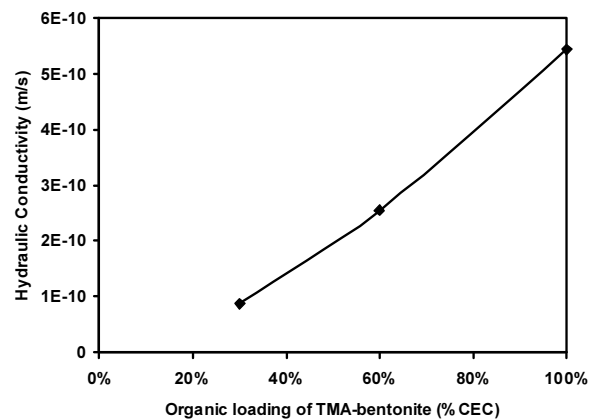


Fig. 4 Hydraulic conductivity of TMA-bentonite as a function of organic loading

SUMMARY

This study investigated the stress-strain behavior of TMA exchanged bentonite at 30%, 60%, and 100% of the clay's CEC using consolidated undrained triaxial tests. It was found that: (1) TMA-bentonites demonstrated higher shear strength and higher hydraulic conductivity than the unmodified bentonites; (2) As the organic loading was increased, the peak effective stress friction angle increased and the initial shear modulus also increased; and (3) The normally to lightly-overconsolidated modified organoclays demonstrated peak behavior in the stress-strain curves, coupled with positive pore water pressures throughout the duration of shearing.

This study sets the stage for further investigation of

more complicated organic cation structure, such as tetraethylammonium (TEA) cations and hexdecyltrimethylammonium (HDTMA) cations.

REFERENCES

- American Society for Testing and Materials (2003). D5084 - Standard Test Methods for Measurement of Hydraulic Conductivity of Saturated Porous Materials Using a Flexible Wall Permeameter.
- American Society for Testing and Materials (2004). D4767 - Standard Test Method for Consolidated Undrained Triaxial Compression Test for Cohesive Soils.
- Bartelt-Hunt SL, Burns SE, Smith JA (2003). Nonionic organic solute sorption onto two organobentonites as a function of organic-carbon content. *Journal of Colloid and Interface Science* 266: 251-258.
- Burns SE, Bartelt-Hunt SL, Smith JA, Redding AZ (2006). Coupled mechanical and chemical behavior of bentonite engineered with a controlled organic phase. *Journal of Geotechnical and Geoenvironmental Engineering* 132(11).
- Lorenzetti RJ, Bartelt-Hunt, SL, Burns SE, Smith JA (2005). Hydraulic conductivities and effective diffusion coefficients of geosynthetic clay liners with organobentonite amendments. *Geotextiles and Geomembranes* 23: 385-400.
- Smith JA, Jaffe PR, Chiou CT (1990). Effect of ten quaternary ammonium cations on tetrachloromethane sorption to clay from water. *Environmental Science and Technology*, 24(8): 1167-1172.
- Soule NM & Burns SE (2001). Effects of organic cation structure on behavior of organobentonites. *Journal of Geotechnical and Geoenvironmental Engineering*, 127(4):363-370.
- Mesri G & Olson RE (1970). Shear strength of montmorillonite. *Geotechnique*, London, 20(3):261-270.
- Yoshizawa H, Chen YL, Israelachvili J (1993). Fundamental mechanisms of interfacial friction. 1. Relation between adhesion and friction. *Journal of Physics and Chemistry*, 97:4128-4140.

MONITORING OF LANDFILL SETTLEMENT BY MEANS OF HORIZONTAL INCLINOMETERS

Xiao-Bing XU¹, Hai-Yun WEI², Tony L. T. ZHAN³, Yun-Min CHEN⁴ and Yao-Shang WANG⁵

ABSTRACT: Waste settlement will affect the liner system and ultimate usage of the municipal solid waste landfill significantly. Settlement at different depths of a landfill cell in Shanghai Laogang Landfill, China, is monitored by means of horizontal inclinometers. The settlement profiles at different elevation of the landfill were obtained to investigate the settlement behavior of the Chinese MSW landfill. The monitoring results for the bottom horizontal inclinometer showed that the settlement monitoring method used in the landfill cell has a good accuracy. Large secondary settlement is found for the top horizontal inclinometer near the surface of the landfill cell.

KEYWORDS: settlement, MSW, landfill, horizontal inclinometer

INTRODUCTION

Settlement measurements derived from the survey of surface benchmarks is related to secondary compression after landfill closure, and it can be difficult to interpret these measurements since secondary settlement of lower waste layers had started long time before (Oliver and Gourc 2008). As considerable amount of settlement occurs during the filling and construction stages, the accurate prediction of primary and secondary settlement of layers at different depths (with different age) during filling process would allow estimation of air space, planning of construction sequence, design of both intermediate and final covers as well as planning for expansions (Hunte et al. 2007). A program to monitor waste settlement was conducted at a field-scale landfill cell in Shanghai Laogang Landfill since September 2006. The objective of the program is to collect quantitative data on settlements at different depths of the landfill cell during filling and after closure, and to calibrate a model for predicting future settlement and the remaining air space of the landfill. Settlement data have been collected through six horizontal inclinometers installed at different depths. About two years' monitoring of the bottom and top horizontal inclinometers are reported in this paper.

SITE DESCRIPTION AND MONITORING PROGRAM

As shown in Fig. 1, the pilot project covers an area of

200 m×125 m. The whole landfill cell is divided into two areas by an embankment. In the western area (1#), two cross-sections which are 30 m apart from each other are selected to install horizontal inclinometers for settlement monitoring.

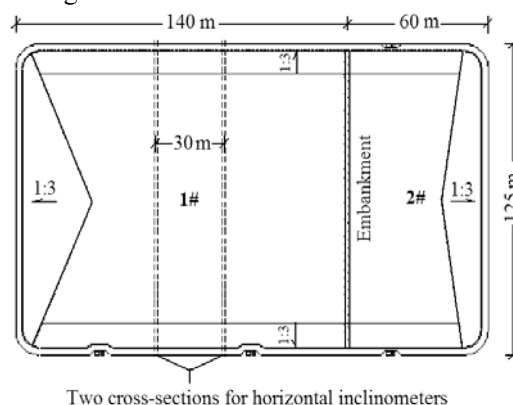


Fig. 1 Plan view of landfill cell

As shown in Fig. 2, a maximum thickness of about 8m wastes are deposited in the landfill cell. The cell accepted about 100,000 tones of municipal solid waste from Shanghai. A 1.5 mm thick HDPE geomembrane and a 500 mm gravel drainage layer are constructed at the bottom of the landfill cell. The waste is divided into three layers by two 300 mm thick intermediate soil covers and finally covered with a 650 mm thick clay liner.

Working principle of the horizontal inclinometer is shown in Fig. 3. A flexible HDPE pipe which has a 63 mm

¹ Ph.D Student, MOE Key Laboratory of Soft Soils and Geoenvironmental Engineering, Zhejiang University, 310027, China

² Engineer, Zhejiang Institute of Hydraulics and Estuary, 310020, China; Formerly Ph.D. Student of Zhejiang University, 310027, China.

³ Professor, MOE Key Laboratory of Soft Soils and Geoenvironmental Engineering, Zhejiang University, 310027, China. Email: zhanlt@zju.edu.cn

⁴ Professor, MOE Key Laboratory of Soft Soils and Geoenvironmental Engineering, Zhejiang University, 310027, China

⁵ Master Student, MOE Key Laboratory of Soft Soils and Geoenvironmental Engineering, Zhejiang University, 310027, China

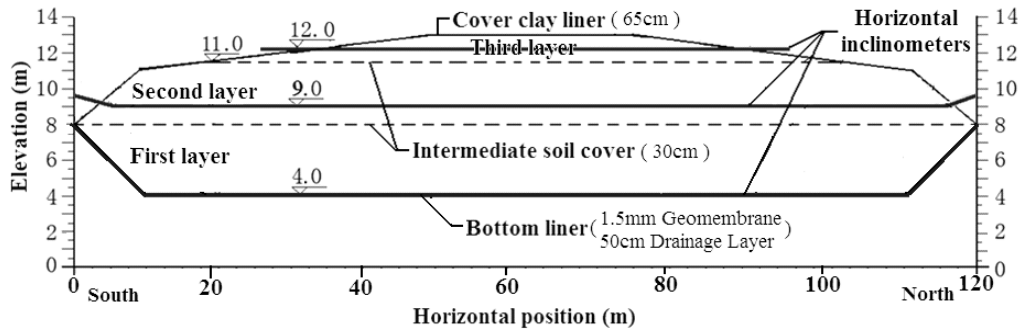


Fig. 2 Section view of landfill cell

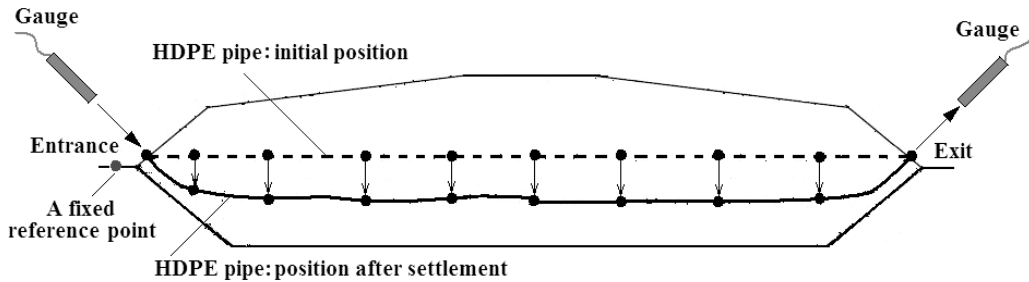


Fig. 3 Working principle of the horizontal inclinometer

outside diameter and 53 mm inside diameter is buried in a trench in the wastes, with two exits on the landfill sides. A measuring probe with a water pressure gauge is sent into the HDPE pipe through a pre-installed string in that pipe. Original data monitored from the horizontal inclinometer is a water pressure head recorded by the probe. The water pressure head represents the difference in elevation between the position of the measuring probe and a fixed reference point outside the pipe. When the measuring probe is sent to the prescribed point of the HDPE pipe, the difference in elevation between the measuring point and the fixed reference point is registered, and the waste settlement indicated by the position of the HDPE pipe at any time is possible to be obtained. The accuracy of the water pressure head gauge used is ± 7 mm.

The first two horizontal inclinometers are installed at the bottom of the first waste layer in the two cross-sections. The second two in the second waste layer are about 1 m above the first intermediate soil cover. The last two in the third waste layer are just beneath the cover clay liner. Composition of the municipal solid waste from Shanghai is shown in Table 1. Table 2 shows the timeline of the landfill cell construction and filling processes.

Table 1 Composition of municipal solid waste from Shanghai (Sun et al. 2008)

Waste composition	Organic	Plastics, textile, wood	Glass, metal	Others
Content (Wet weight %)	65	30	2.5	2.5

Table 2 Timeline of landfill cell construction and filling

Date	Waste thickness above the bottom (m)	Description
2006.9.1	0	Bottom liner, horizontal inclinometer
2007.1.8	3	Intermediate soil layer
2007.2.7	5	Horizontal inclinometer
2007.2.16	6	Intermediate soil layer
2007.3.1	8	Clay liner cover (closure)
2007.4.5	8	Horizontal inclinometer

MONITORING RESULT AND DISCUSSION

The horizontal inclinometer beneath the first waste layer was installed on Sep 1st 2006, and its first monitoring was made on Nov 7th 2006. The settlement during the filling of the first 1m thick wastes between Sep 1st 2006 and Nov 7th 2006 was not recorded. About 7m thick wastes were deposited after Nov 7th 2006, and the landfill cell was closed on March 1st 2007. Latest monitoring was made on Nov 22nd 2008.

The first monitoring results on Nov 7th 2006 (Fig. 4(a)) show us the profile of the bottom HDPE pipe which is consistent with the actual bottom contour of the landfill cell. At the horizontal position from 0 m to 20 m and that from 110 m to 120 m, there are two significant inclines as constructed. The slope of the bottom from 20 m to 110 m is about 2.2%. It also indicates that the settlement monitoring method through the horizontal inclinometer has a good accuracy of ± 1 cm.

As shown in Fig. 4(b), about two years' monitoring from Nov 7th 2006 to Nov 22nd 2008 shows an average value of 5.9 cm settlement for the bottom horizontal inclinometer, and the maximum settlement is about 29.1 cm. As there is relatively loose soil layers (0~50 cm thick) under the bottom horizontal inclinometer, the settlement consist of both compression of soil layers and consolidation of the ground under the landfill cell.

The top horizontal inclinometer is just beneath the

cover clay liner. As the first monitoring was made after landfill closure, settlement monitored is secondary compression due to creep and biodegradation. Evolution of the top horizontal inclinometer at the horizontal positions from 30 m to 90 m is shown in Fig. 5(a) and Fig. 5(b). The maximum settlement on Nov 22nd 2008 from April 5th 2007 occurs in the middle of the landfill cell which is about 185.9 cm.

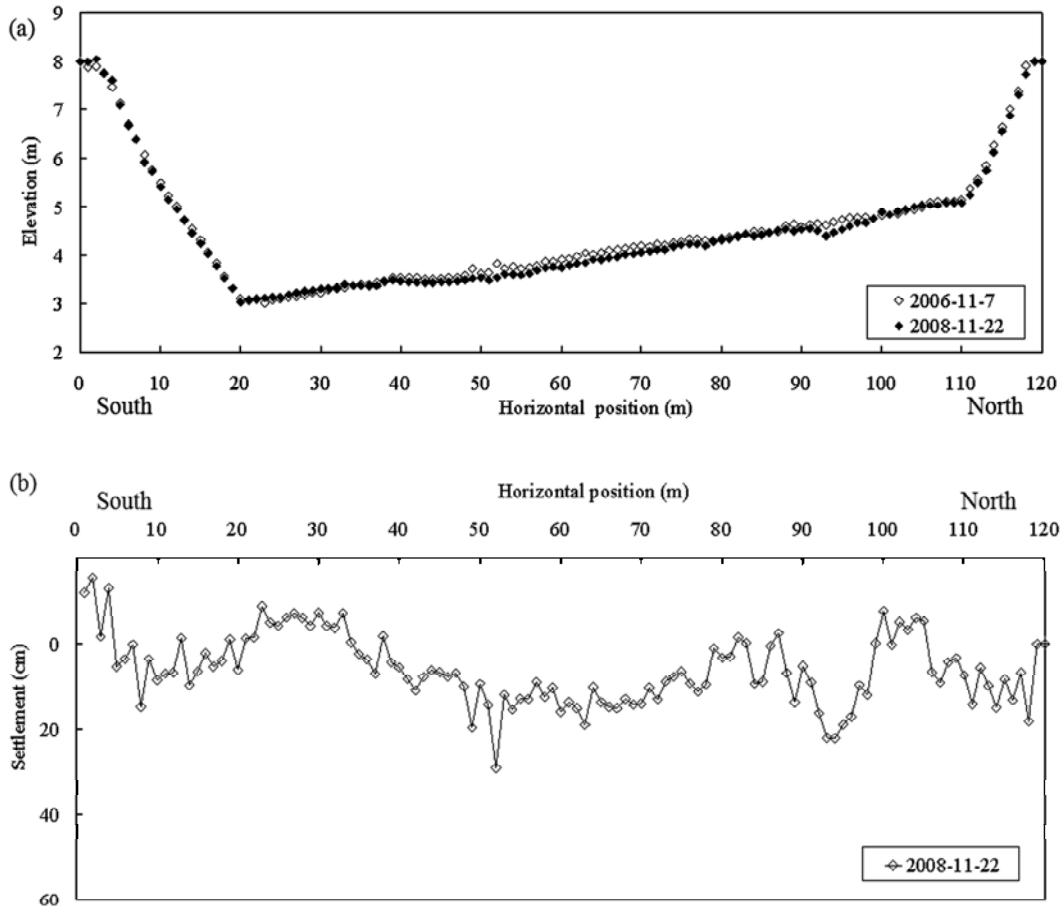
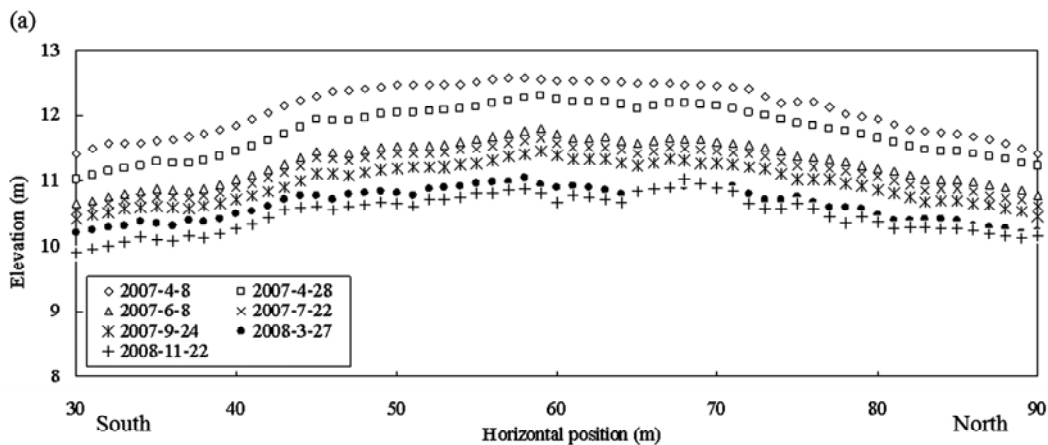


Fig. 4 Evolution of bottom horizontal inclinometer at the eastern cross-section



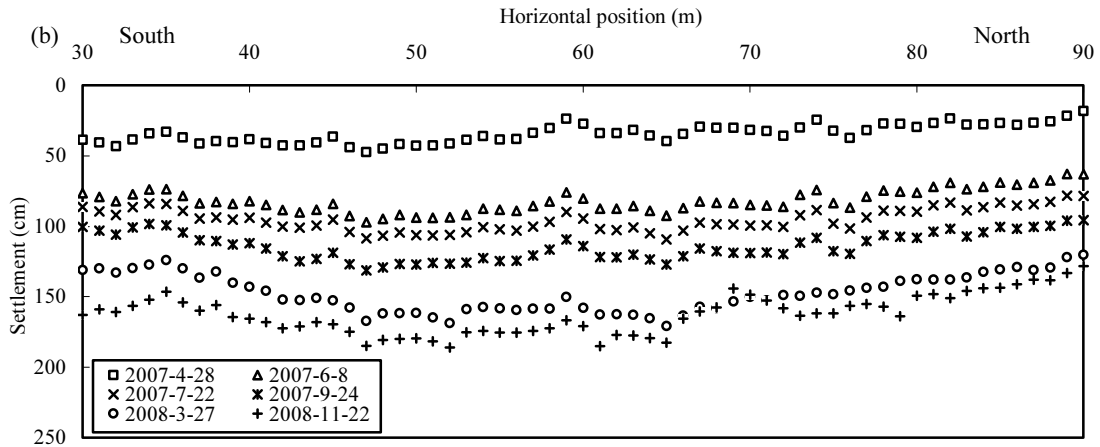


Fig. 5 Evolution of the top horizontal inclinometer at the eastern cross-section

As shown in Fig. 6, the average settlement within a period of about 594 days (from April 5th 2007 to Nov 22nd 2008) is about 162.4cm which is 20.3% of the finished level (i.e. about 8m thick wastes beneath the top inclinometer). Further monitoring of settlement in the landfill cell and the analysis associated with the calibration of a settlement model is in progress.

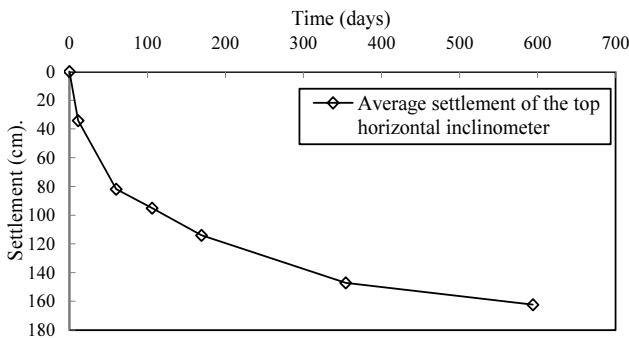


Fig. 6 Average settlement of the top horizontal inclinometer at horizontal positions from 30 m to 90 m at the eastern cross-section

CONCLUSION

Monitoring results of the bottom horizontal inclinometer indicates that the settlement monitoring method has a good accuracy of ± 1 cm. About two years' monitoring from Nov 7th 2006 to Nov 22nd 2008 shows that an average value of 5.9cm settlement occurred for the bottom horizontal inclinometer. This settlement consists of both the compression of relatively loose soil

layers under the bottom horizontal inclinometer and consolidation of the ground under the landfill cell. Within a period of about 594 days after the first monitoring on April 5th 2007, the average secondary settlement monitored near the surface of the landfill cell is large which is about 144cm, and it is 20.3% of the finished level (i.e. about 8m thick wastes beneath the top inclinometer).

ACKNOWLEDGEMENTS

This work were supported by the key fund of the National Natural Science Foundation (research grant: 50538080), the National High Technology Research and Development Program of China (2003AA644020) and financial support from Bureau of Science and Technology of Suzhou (research grant: SS0733)

REFERENCES

Hunte C, Hettiaratchi P, Meegoda JN, Hettiarachchi CH (2007). Settlement of bioreactor landfills during filling operation. *New Peaks in Geotechnics*. Geo-Denver.

Oliver F & Gourc JP (2008). Geomechanical monitoring of sanitary landfill sites: control of settlement and associated parameters. 1st Middle European Conference on Landfill Technology. Budapest. Hungarian Academy of Sciences.

Sun XJ, Xu DM, Li X, Li B (2008). Analysis of composition and caloric value of municipal solid waste in Shanghai. *Journal of Tongji University (Natural Science)*. 36(3): 356-360 (in Chinese).



**Municipal Solid Wastes and
Landfill Engineering**

EFFECT OF THICKNESS OF HYDRAULIC BARRIER ON THE INTEGRITY OF A COVER SYSTEM SUBJECTED TO DIFFERENTIAL SETTLEMENTS

Bhamidipati V. S. VISWANADHAM¹ and Sathiyamoorthy RAJESH²

ABSTRACT: The objective of this paper is to study the performance of a compacted soil barrier of the cover system of municipal solid waste landfills. The risk of initiation and propagation of cracks of the soil barrier subjected to differential settlements due to underlying waste particularly was examined. Centrifuge tests were performed on model soil barrier subjected to continuous differential settlement at 40 gravities. The model soil barrier material has been selected in such a way that it envelopes the material characteristics of the soil barriers available in various parts of the world. Model soil barriers were moist-compacted towards the wet side of its optimum moisture content. The thickness of soil barrier varied is 0.6, 0.8 and 1.2 m. With the help of extensive instrumentation and the digital image analysis, the deformation profile, strain distribution and the water breakthrough of the soil barrier were analyzed throughout the deformation process to assess their performance. Soil barrier of 0.6 m thick registered a catastrophic nature of water breakthrough when the distortion level approaches 0.075 whereas 1.2 m thick soil barrier had a progressive failure once the distortion level approach 0.112 and 0.8 m thick soil barrier tends to fail when distortion level approach 0.093. All the three model soil barriers were observed to lose their integrity when subjected to maximum level distortion of 0.125.

KEYWORDS: cover systems, landfills, cracking, centrifuge models, model tests

INTRODUCTION

An impervious barrier formed with clay-rich soil is being used widely in cover systems to contain municipal and hazardous wastes safely. The barrier layer is intended to control infiltration into the waste and hence leachate from the waste to the ground water. Clay-rich soils can be considered as an effective and economical barrier material provided it has a coefficient of permeability of 1×10^{-9} m/s or less. However, soil barrier is susceptible to cracking due to moisture fluctuations (desiccation cracks) and differential settlements (mainly due to readjustments and decomposition of the contained wastes). Excessive differential settlements lead to cracking of clay barrier and impair the main function of a soil barrier. Sowers (1972) estimated that waste settles 10%–30% of its original height under its own weight within one to two years of its burial. Jessberger (1994) reported that settlement can be as much as 40%–50% of original height of a landfill. In Bioreactor landfills due to non-uniformity of recirculation of leachate by horizontal and vertical trenches, the occurrence of the differential settlements is quite natural and more pronounced. The problem due to differential settlements is more pronounced in case of a cover system than the bottom

lining system because the former is subjected to low overburden pressure as well as settlement due to readjustments and ongoing bio-degradation of the wastes that lies underneath. Hence, the present study is to focuses to investigate the effect of artificially induced differential settlements on the integrity and deformation behavior of soil barriers of varying thickness in a large beam centrifuge available at Indian Institute of Technology Bombay (IIT Bombay), India.

Application of centrifuge modeling technique to the present study is relevant because the loss of integrity of soil barrier is highly influenced by the presence of prototype stress conditions. Centrifuge scaling factors relevant to modeling of soil barriers and errors due to high acceleration field have been described elsewhere extensively by Viswanadham and Mahesh (2002). The centrifuge tests reported here were performed at an acceleration field of 40 g. The 4.5 m radius large beam centrifuge at IIT Bombay is being used for studying number of problems of importance in geotechnical and geo-environmental engineering. The centrifuge capacity is 250 g-ton with a maximum payload of 2.5 t at 100 g and at the higher acceleration of 200 g the allowable payload is 0.625 t (Chandrasekaran 2001).

¹ Professor, Department of Civil Engineering, Indian Institute of Technology Bombay, Powai, India. Email: viswam@civil.iitb.ac.in

² Research Scholar, ditto. Email: rajesh.s@iitb.ac.in

EXPERIMENTAL TEST SETUP

In the present study, model soil barrier material was chosen such a way that it represents the properties of CCL material used in construction of lining systems for landfills (Benson et al. 1999). A mixture of commercially available kaolin clay and locally available poorly graded sand in proportion of 80:20 (by dry weight) was used to serve as a model soil barrier material. The properties of the material are in the same range as those of CCL material characteristics used in actual practice in many landfills in USA. The model soil barrier was found to have a liquid limit of 38%, plasticity index of 16%, maximum dry unit weight and OMC with standard Proctor compaction energies are 15.9 kN/m^3 and 22%.

Thickness of the soil barrier used for containing municipal solid waste ranges from 0.6 to 1.2m. As per EPA (1989), for the semi-arid region, the minimum thickness recommended for an impervious layer of a cover system is 0.6m. Hence, in the present study, thickness of impervious layer is selected as 0.6, 0.8 and 1.2m respectively. In majority of the landfill sites, thickness of the cover soil placed above the soil barrier in the cover system ranges from 1m to 1.5 m thick. This cover soil can induce an overburden pressure of 25 kN/m^2 . Four centrifuge tests at 40 g have been conducted to study the influence of thickness of the soil barrier on the deformation behavior of soil barrier when it is subjected to differential settlements. Parametric study involving two cases are discussed in the present study. *Case 1*, one centrifuge test was carried out to study the cracking pattern of 1.2 m thick soil barrier having water as an overburden (12.5 kN/m^2). In the *case 2*, three centrifuge tests were carried by varying thickness of soil barrier such as 0.6, 0.8 and 1.2m along with constant overburden pressure equal to 25 kN/m^2 obtained by placing a saturated sand layer and standing water above soil barrier. The maximum central settlement of 1m is induced at a settlement rate of 0.85 mm/min (in model dimensions). The performance of 0.6 m and 1.2 m thick soil barrier has been reported in detail by Viswanadham and Rajesh (2009). In the present study, centrifuge test results corresponding to 0.8 m thick barrier has been addressed and its performance is compared with 0.6 m and 1.2 m thick clay barrier.

Test Procedure

Fig. 1 shows a cross-section of the test set-up used in the present study. Hydraulic trap-door system was custom designed to induce differential settlements to the model soil barrier in enhanced gravity. The model was prepared at normal gravity with the cylinder at its full stroke. Desired settlement rate was achieved by withdrawing the air pressure in the tank in steps and allowed the oil to

flow out of the cylinder through a needle flow control valve. On an average, a settlement rate of 0.85 mm/min (in model dimensions) was achieved for all the tests and non-uniform settlements were induced continuously. A miniature potentiometer (P3) was attached to the trap-door plate to monitor the movement of the trap-door plate, which would provide the central settlement values starting from zero to a maximum of 25 mm in model dimensions during the centrifuge test.

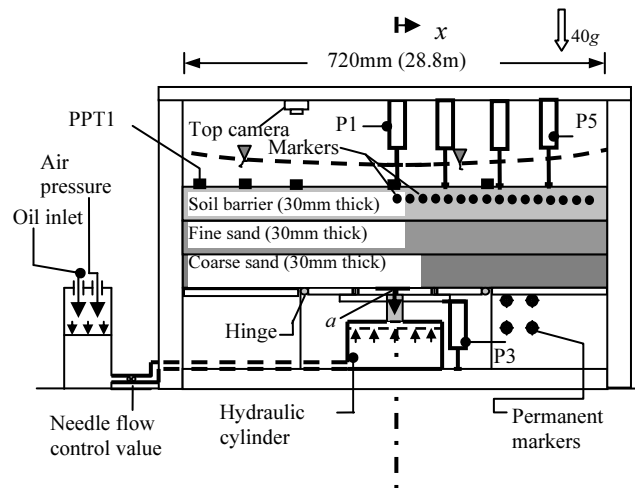


Fig. 1 Cross-section view of model test package

Model Preparation

The model preparation involves placement of a thick non-woven geotextile layer cut into three pieces along the length of the container. A 30 mm thick saturated coarse sand layer followed by 30 mm thick saturated fine sand layer was placed at a relative density of 55%. These layers were introduced to eliminate any stress concentration, which may arise due to abrupt discontinuity at hinge locations and are referred herein as sacrificial layers. The kaolin-sand mixture was moist-compacted with OMC+5% and corresponding dry unit weight (14.2 kN/m^3).

Four numbers of potentiometers were used in all models placed on the right half cross section of the barrier at every 100 mm interval starting from the center line of the barrier (starting from P1, as shown in Fig. 1). Discrete markers were prepared using transparency strips and are placed 5mm below the top surface of the barrier to provide some confinement effect to the markers such that displacement of markers are purely due to the material behavior of the soil barrier. Two Charge Coupled Device (CCD) video cameras, one on the front side of the model and the other on the top over the model surface were installed to monitor the performance of the soil barrier during the centrifuge test. At various stages of central settlements, photographs were taken through an image acquiring software and were later used for

image analysis to compute deformation profiles and strain distribution along the top fiber of the soil barrier.

ANALYSIS AND INTERPRETATION

The information recorded from the potentiometers, throughout the centrifuge testing was used to monitor the movement of the hydraulic trap-door assembly and the deformation profile of the top surface of the soil barrier. The settlement values obtained from the potentiometers was plotted with respect to time (see Fig. 2) to know the relative movement of the soil barrier. From this figure, it can be observed that the settlements measured from the potentiometer P3 (placed at the trap-door plate) and P1 (placed at the centre of the clay barrier) are almost identical, which implies the trap-door system works very efficiently, devoid of any stress concentration. It can also be observed that constant settlement rate of 0.85mm/min has been achieved. Moreover, when the centrifuge was stopped, the settlement values were observed to be constant.

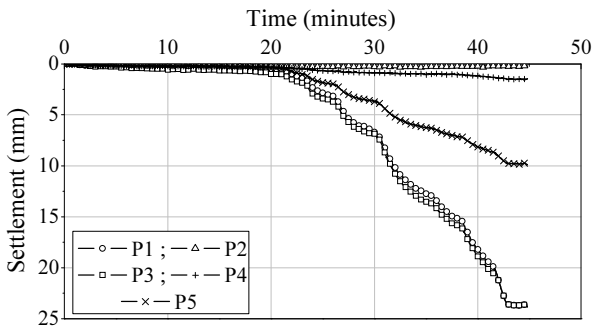


Fig. 2 Variation of measured settlement with time [Case1]

Deformation Profile and Strain Variation

Strain distribution along the clay barrier surface was analyzed optically by measuring the integral displacement of the discrete markers embedded in the soil (Fig. 1). The images were captured with the help of an image capturing software during centrifuge tests. Pictures captured at various settlement stages were digitized by using a module map edit of GRAM++ package (GRAM++ 2004). Position of permanent markers relative to each other was pre-measured and was used to scale and control the images captured. In the next step, tracking the location and analyzing the displacement of markers at each settlement stage was carried-out. The measured co-ordinates of a row of markers fixed in the soil in all settlement stages are approximated with an exponential equation of the normal distribution to get the deformation at various stages, curvature and strain computations along the longitudinal axis of the soil

barrier. Fig. 3 shows the deformation profile of the soil barrier under various stages of central settlement for the model case1. Even though only one half of the soil barrier was analyzed, for the sake of visibility, full section is plotted by considering it as symmetry.

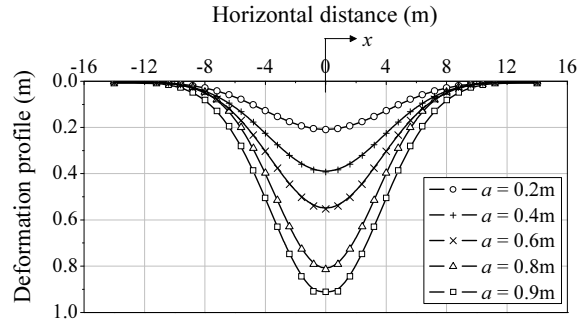


Fig. 3 Variation of measured deformation profile with horizontal distance [Case1]

When the horizontal distance from centre of the soil barrier x is zero, the value of settlement is defined as a central settlement a (Figs. 1 and 3). Distortion level is the ratio of central settlement a at ant particular stage of centrifuge testing to the horizontal distance (l).

The computation of the strain along the top fibre of the soil barrier can be arrived using combined bending and elongation method (Lee and Shen 1969, Scherbeck and Jessberger 1993). Let $w(x)$ be the function of deformation profile of the deformed soil barrier, where $w(x)$ gives the settlement of the deformed barrier at any horizontal distance x . Consider an element of length dx in the original un-deformed state of the barrier. Let the element is subjected to a differential settlement of du in the vertical direction. Then increase in length due to the settlement difference can be written as:

$$\delta x = \sqrt{dx^2 + ((du / dx)dx)^2} - dx \tag{1}$$

Elongation strain: The elongation strain in the deformed soil barrier is due to change in length and it can be computed from $\delta x/dx$. By simplifying the equation (1), the elongation strain or the strain due to change in length ϵ_l can be computed as follows:

$$\epsilon = \sqrt{1 + [w'(x)]^2} - 1 \tag{2}$$

Fig. 4 shows the variation of elongation strain for the case1 type clay barrier.

Curvature strain: Curvature strain or bending strain ϵ_c along the top surface of the barrier can be written as (based on theory of pure bending):

$$\epsilon = R_{of} \kappa(x) d \tag{3}$$

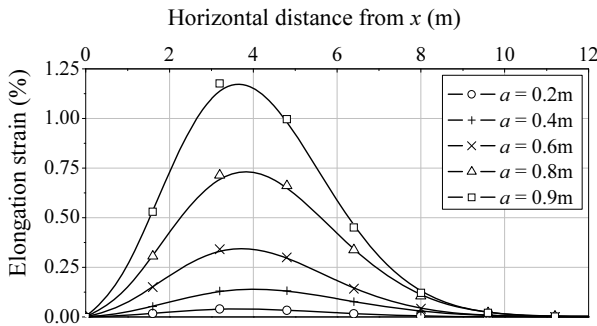


Fig. 4 Variation of elongation strain with horizontal distance [Case I]

where, d = thickness of soil barrier, $\kappa(x)$ = Curvature at any horizontal distance X . It can be obtained by differentiating the settlement contour function $w(x)$ twice:

$$\kappa(x) = \left(\frac{w''(x)}{(1 + w'(x))^2} \right) \tag{4}$$

R_{of} = Neutral axis factor (assumed as 0.67)

Fig. 5 shows the variation of curvature strain for the case I type soil barrier.

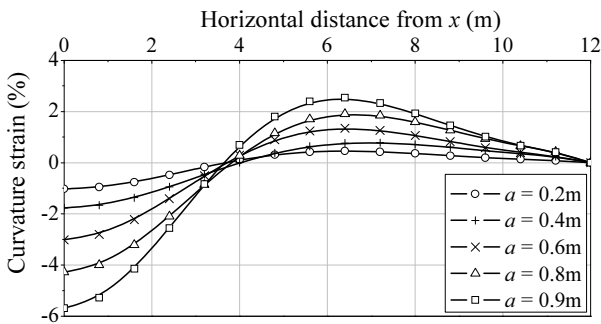


Fig. 5 Variation of curvature strain with horizontal distance [Case I]

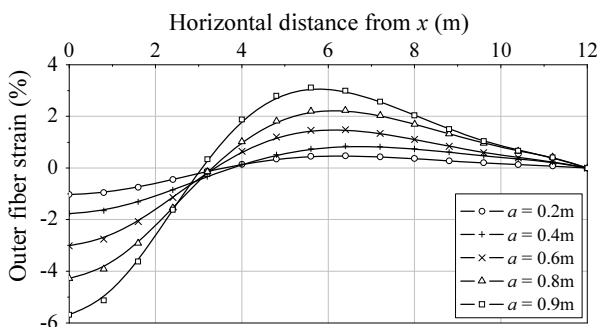


Fig. 6 Variation of outer fibre strain with horizontal distance [Case I]

Outer fibre strain: Outer fibre strain along the top surface of the barrier ϵ_{of} is the algebraic summation of elongation strain and curvature strain. It is given by:

$$\epsilon_{of} = \epsilon_l \pm \epsilon_c \tag{5}$$

Fig. 6 shows the variation of outer fiber strain for the case I type soil barrier. It can be observed that as the central settlement increases the strain levels also increases and the maximum strain were observed to be occurred near the location of hinges.

Computation of Water Breakthrough

In 1.2 m thick soil barrier (Case I), overburden pressure of 12.5 kN/m² was generated by placing the 30mm height of water above clay barrier. The thickness of the clay barrier for Case 2a, 2b, 2c is 1.2, 0.8 and 0.6 m respectively. In all these three tests, overburden pressure corresponding to 25 kN/m² was created by 27 mm thick layer of fine sand and 10 mm free standing water above this sand layer. The severity of the water breakthrough can be quantified using infiltration rate which is directly observed by the reduction in the height of the water column at the various stages of differential settlement. The change in height of the water level can be determined using the change in water pressure measured using PPTs (PPT 1 to 5), installed at the top surface of the clay barrier placed at mid-width of the container (Fig. 1). Fig. 7 shows the variation of water pressure along the length of the barrier for the case I type soil barrier. It can be observed that at various stages of central settlement, water level takes the curvilinear shape mainly because the model is subjected to radial acceleration field.

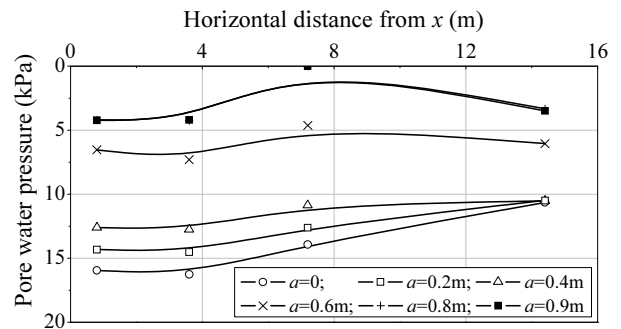


Fig. 7 Variation of water pressure along horizontal distance [Case I]

Moreover, it can also be observed that as the central settlement increases, accumulation / ponding of water take place on the central portion of the soil barrier. When the central settlement is between 0.4 m to 0.6 m, it can be noticed from Fig. 7 that the reduction in the water pressure, (i.e. height of water) has taken place mainly due the infiltration of water through the development of cracks in the clay barrier.

INFLUENCE OF THICKNESS OF SOIL BARRIER

When the central settlement is plotted against maximum curvature $\kappa(x)$ (i.e. near the hinge locations, as shown in Fig. 1), as shown in Fig. 8, distinct linear variation was obtained. It can be noticed that for the same distortion level, thin barrier experiences higher curvature (i.e. minimum radius) when compared to a thick soil barrier. Moreover, it can also be noticed that as the thickness of the soil barrier increases, the maximum curvature also increases.

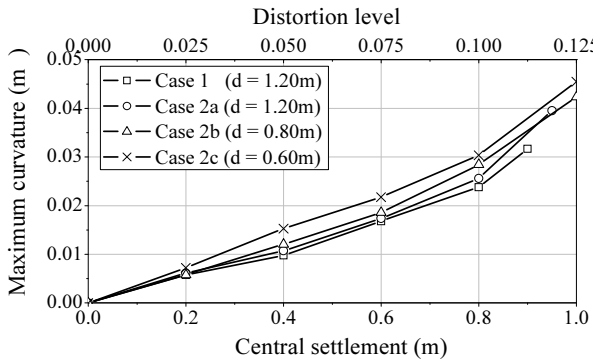


Fig. 8 Variation of maximum curvature with distortion level and central settlement

Fig. 9 shows the variation of maximum outer fiber strain for all four soil barriers tested corresponding to a central settlement and distortion level *a/l*. As the thickness of the soil barrier and the central settlement increases, the strain values also increases significantly. It can be observed that thin soil barrier tends to experience lower strain values when compared to thick barriers.

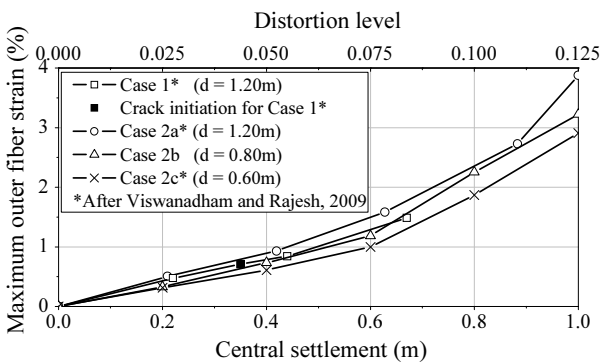


Fig. 9 Variation of maximum outer fiber strain with distortion level and central settlement

From the water pressure measurements, as shown in Fig. 7, the prototype height of water present above soil barrier can be determined at various settlement stages. The model height of the water column can be determined by dividing the prototype height with the scale factor (i.e. $h_p/h_m=N=40$ in the present case). Before the commencement

of inducing movement to trap-door plate, initial height of the water present at various locations was determined. The corrections in the initial model height of water have to be done such that computed value from PPT is same as initial height of the water level. Infiltration Rate (IR) of the soil barrier can be computed using the expression of falling head permeability test. The area of the stand pipe is considered same as the area of the soil sample because the water can infiltrate all along the surface of the soil barrier, Length of the sample is taken as thickness of the soil barrier. Since the reduction in the height of the water column is coupled with the ponding of the water because of the depression above the clay barrier (due to continuous differential settlement), the term infiltration rate is used instead of coefficient of permeability. In this centrifuge testing, the infiltration rate of the soil barrier model dimension is N times that of the prototype as per the governing scaling law (Schofield, 1980).

The prototype infiltration rates at various distortion levels have been plotted for various models as shown in Fig. 10. It can be observed that there exists a gentle variation in IR up to a certain distortion level followed by a steep variation. Steep variation of IR indicates water breakthrough of the soil barrier. Since the water sealing in the form of thick bentonite paste was applied on the sides of the container, infiltration of the water may only be possible either due to pore spaces present in the soil barrier or due to the crack formation.

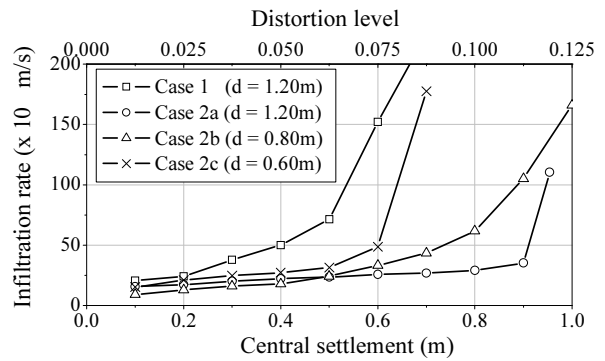


Fig. 10 Variation of maximum curvature with distortion level and central settlement

From the post-test examination of deformed soil barrier for all the model tests, it was confirmed that side leakage was prevented by water sealing arrangement. When the strain level due to deformation exceeds the permissible limit of the soil barrier, hydraulic barrier has a tendency to crack. Water infiltration may not be occurring immediately at the time of crack initiation; however, it can happen when the cracks extend to sufficient depth and width.

As can be noted from Fig. 10, up to a central settlement equal to 0.55m, variation of IR is less and

beyond this, a sharp decrease in IR is registered for *case 1* soil barrier (barrier of 1.2 m thick & water as an overburden). Identical observation was registered for *case 2c*, (barrier of 0.6 m thick and overburden pressure of 25 kN/m²). For this case, sharp decrease in IR was recorded immediately after inducing central settlement of 0.6m. Slight delay in water breakthrough can be observed for model *case 2c*, may be due to the presence of confining stresses developed by the overburden pressure. In the *case 2b* (barrier of 0.8 m thick & overburden pressure of 25 kN/m²) decrease in IR was recorded immediately after inducing central settlement of 0.75 m. However, for model *case 2a* (clay barrier of 1.2 m thick & overburden pressure of 25 kN/m²), water breakthrough was seen at the settlement of 0.9 m. However, formation of crack would have got initiated well prior to this settlement ratio. Confining stresses resulting due to the presence of overburden would have suppressed the tendency of widening of crack. In view of this, severity of water breakthrough is observed to be progressive in nature. From Fig. 10, it can be justified that crack depth and width at settlement ratio of 0.5 is sufficient for the thin model clay barrier to lose its integrity.

CONCLUSIONS

The performance of a soil barrier as an effective hydraulic barrier and the information about the status of soil barrier was monitored throughout the deformation process. The application of centrifuge modelling technique in combination with digital image analysis to study the deformation behavior of clay based engineered barriers subjected to differential settlements has been demonstrated. Based on the analysis and interpretation of centrifuge test results, the following conclusions are drawn:

All the four model soil barriers tend to lose their integrity once the outer fiber strain due to differential settlements exceeds the ultimate strain of a clay barrier material. Higher the thickness, higher is the resistance to deformation. It can also be observed that maximum strain for all the settlement stages occur about 5.5 m to 6.5 m from the centre of the clay barrier, which is the zone of a maximum curvature. Moreover, as the thickness of the clay barrier increases, the strain values are also increased significantly for the corresponding settlement ratio. It can be observed that thin clay barrier tends to experience lower strain values when compared to thick barriers. Soil barrier of 0.6 m thick registered a catastrophic nature of water breakthrough when the distortion level approaches 0.075 whereas 1.2 m thick

soil barrier had a progressive failure once the distortion approach 0.112 and 0.8 m thick soil barrier tends to fail when distortion level approach 0.093. All the four model soil barriers were observed to lose their integrity when subjected to maximum distortion level of 0.125 and hence suitable strengthening measures need to be considered for clay barrier based cover systems subjected to differential settlements.

REFERENCES

- Benson CH, Daniel DE, Boutwell GP (1999). Field performance of compacted clay liners. *Journal of Geotechnical and Geoenvironmental Engineering*, ASCE. 125 (5): 390-403.
- Chandrasekaran VS (2001). Numerical and centrifuge modelling in soil structure interaction. *Indian Geotechnical Journal* 31(1): 30-59.
- EPA (1989). EPA technical guidance document: Final covers on hazardous waste landfills and surface impoundments, EPA/530- SW-89-047. U.S. Environmental Protection Agency, Washington, D.C.
- GRAM++ (2004). Technical document, CSRE, Indian Institute of Technology Bombay <http://www.csre.iitb.ac.in/gram++/>.
- Jessberger HL (1994). *Geotechnical Aspects of Landfill Design and Construction*. Part 1, Part 2 and Part 3. Proceedings of the Institution of Civil Engineers-Geotechnical Engineering. 107: 99-122.
- Lee KL & Shen CK (1969). Horizontal movements related to subsidence. *Journal of Soil Mechanics and Foundation division*, ASCE. 94 (6): 139-166.
- Scherbeck R & Jessberger HL (1993). Assessment of deformed mineral sealing layers. In: Sarsby, R.W. (Ed.), *Waste Disposal by Landfill*. Proceedings, Green'93, Geotechnics of Related to the Environment, Bopltan, U.K. A. A. Balkema, Rotterdam: 477-486.
- Schofield AN (1980). Cambridge geotechnical centrifuge operations. *Geotechnique*. 30 (3): 227-268.
- Sowers GF (1972). Settlement of waste disposal fills. *Proc., 8th Int. Conf. On Soil Mechanics and Foundation Engineering*, Moscow: 207-210.
- Viswanadham BVS & Mahesh KV (2002). Modeling deformation of clay liners in a small centrifuge. *Canadian Geotechnical Journal*. 39 (6): 1406-1418.
- Viswanadham BVS & Rajesh S (2009). Centrifuge model test on clay based engineered barriers subjected to differential settlement. *Applied Clay Science*. 42 (3-4): 460-472.

SEISMIC RESPONSE CHARACTERISTICS OF MUNICIPAL SOLID WASTE LANDFILLS

Xue-Jing DENG¹, Xian-Jing KONG² and De-Gao ZOU³

ABSTRACT: As a new type of geo-engineering, municipal waste landfills had a number of characteristics, such as low density, high compressibility of MSW and existence of liner system, which distinguished them from natural slopes and other types of artificial dams. In order to investigate the seismic response characteristics of landfills, 8 physical model experiments of landfills were conducted on shaking table, and nonlinear numerical simulation for the test were performed subsequently. The experimental results and numerical calculation could verify and supplement one another, and also indicated that experiencing excessive relative displacement between the specific interfaces within base and cover liners was primary failure patterns of landfill under earthquake. However, waste itself collapse was seldom a concern problem. There were obvious two parts of wedges named “active wedge” and “passive wedge”, while landfill cover slop sliding. Further results could also be got: (1) the landfill height, density of MSW and spectral characteristics of input motions were the primary factors that effected acceleration response at the top of landfill. (2) Significant acceleration attenuation of a motion could occur when earthquake wave transferred through landfill base liner containing HDPE geo-membrane. Furthermore, larger acceleration was the input motion, more obvious was the attenuation. (3) The inclination angle of landfill cover had significant effects on the critical sliding of cover liner. However, the friction coefficient of the HDPE interface within the bottom liner system was the primary factor effecting the critical sliding acceleration of bottom liner system with relatively small base slope angle.

KEYWORDS: municipal waste landfills, shaking table test, seismic response, numerical simulation

INTRODUCTION

Along with attention to sustainable development of urban, more and more municipal solid waste landfill were built in the world over the past few decades. As a new type of geotechnical engineering, it had already become the most important means of municipal solid waste disposal. Although, landfills might not seriously danger people's lives and property like other buildings in earthquake, a strong earthquake might destroy the internal structure of the landfill. Then, landfill lost its normal anti-seepage function, or even led to landslides. In addition, these damages caused by earthquake usually could not be repaired.

Concerns about the seismic performance of landfills had motivated a number of recent studies on seismic response characteristics of landfill. Because of a few landfill damage cases in earthquake, conducting shaking table test and performing numerical simulation of landfill were the most common research methods. The previous studies of landfill shaking table test mainly aimed at the

simulation of a simple composite slop or Newmark sliding system, in order to investigate the dynamic properties of interface included in these system.

Yang et al. (2002) conducted a series of shaking table tests on the composite slop containing geomembrane. They investigated the effects of the slop angle, predominant period and peak acceleration of input motion etc. on the shear strength parameters between interfaces within the slop. Chen & Gao (2008) presented a three-part wedge limit equilibrium method for translational failure analyses of landfills retained by a toe dam. 1-D equivalent linear dynamic response analysis and NewMark method were combined to evaluate the earthquake induced permanent displacement in base liner interface. Kramer and Matthew (1997) and Wartman (2005) investigated the seismic stability of soil slopes and the accuracy of the Newmark procedure calculating permanent displacement.

A series of shaking table tests on eight large scale landfill models were conducted in this paper and nonlinear numerical simulation of these tests were performed subsequently, in order to investigate the seismic response

¹ Lecturer, Department of Engineering Mechanics; China University of Petroleum; China. dengxuejing@gmail.com

² Professor, School of Civil and Hydraulic Engineering, Dalian University of Technology, China. Kongxj@dlut.edu.cn

³ Associate professor, School of Civil and Hydraulic Engineering, Dalian University of Technology, China. Zoudg@dlut.edu.cn

characteristics of landfills.

BRIEF INTRODUCTION OF SHAKING TABLE TEST

Landfills had a number of characteristics that distinguished them from natural slopes and other types of constructed soil slopes and dams. The most significant were the relatively low density of material placed within them and the existence of liner systems including low shearing resistance interface, which introduced planes of weakness into a landfill slope. Taking into account these engineering characteristics of landfills, eight large-scale landfill physical models were designed for shaking table test. The model geometry and materials were determined according to the method of traditional earth dam test.

The “garbage” of the models was replaced by a mixture of coarse fly ash, bentonite and fine sawdust. The contents of each components and water content of the mixture were carefully adjusted, so that the mixture’s density was in the reasonable range of the real garbage soil. Then the mixture was tested by the direct shear apparatus to study its shear strength envelope. As a result, two kinds of mixture with different density of 5.5kN/m³ and 7.5kN/m³, whose shear strength envelope were similar to the real refuse, were selected for the shaking table test. Model base and cover were all composed of silty sand. The landfill models were constructed and tested in rigid box containers with dimension of 4.0 m×1.0 m×1.4 m that were bolted to the shaking table. Fig. 1 illustrated eight profiles of landfill model used in shaking table test by changing the slope angle of cover (β) and base (θ), and by selecting a mixture with different densities. The geometry and material parameters of the landfill models were summarized in Table 1.

A non-woven polypropylene fabric (PPF) and a low-density polyethylene (LDPE) geomembrane were selected as the interface materials. The PP fabric was black, rough and with the thickness of 0.1mm, and its two sides had a “fuzzy” appearance with short loose protruding fiber, the geomembrane was a smooth, white, 0.2mm thick material. The two surfaces of the geomembrane had identical textures. The static friction angle of the mixture-geomembrane interface and the dense sand PP fabric were measured using the direct shear apparatus. The more details of the models design, input earthquake and displacement measurement strategy had been expressed in published literature (Kong and Deng 2008).

According to the typical landfill configuration, eight physical models were designed, and the following conclusions were drawn from shaking table test: (1) Experiencing excessive relative displacement within the

specific interfaces of landfill liner and cover systems was the primary observed failure patterns induced by earthquake, however, waste itself collapse was seldom a concern problem. (2) When other parameters were fixed, seismically induced permanent displacement of landfill liner were shown to be approximately proportional to the amplitude of input motion. (3) Significant acceleration attenuation of motion took place when earthquake wave transferred through landfill base liner including LDPE geomembrane. Moreover, larger was the peak acceleration of input motion, more obvious was the attenuation.

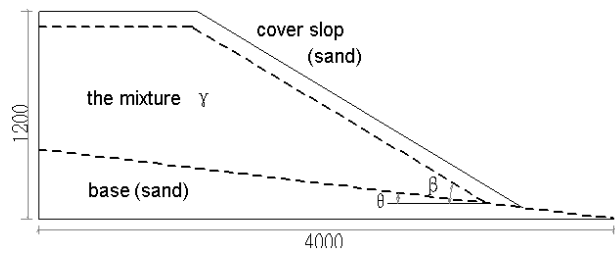


Fig. 1 Profile of the Landfill model for shake table test unit: mm

Table 1 geometry and material parameters of the models

name	$\gamma/\text{kN/m}^3$	$\theta/^\circ$	$\beta/^\circ$	Input motion	geomembrane
ZG21	5.5	11	27	sinusoidal	LDPE
ZC21	5.5	11	27	sinusoidal	PPF
ZC11	5.5	6	27	sinusoidal	PPF
ZC12	5.5	6	34	sinusoidal	PPF
ZC120	7.5	6	34	sinusoidal	PPF
KG21	5.5	11	27	Kobe	LDPE
TG21	5.5	11	27	Tangshan	LDPE
TG11	5.5	6	27	Tangshan	LDPE

NON-LINEAR NUMERICAL SIMULATION OF SHAKING TABLE TESTS

Shaking table test needed a lot of money and time, therefore, only a few well designed and representative models could be tested on shaking table. Non-linear numerical simulation played an irreplaceable role in further research. The following research was to perform non-linear seismic response analyses on the 8 models, in order to study how the factors, including wastes properties, landfill heights, input motion and site conditions etc., to influence the seismic response of landfills, and be prepared to validate the proposed stability evaluation method.

Configuration of Landfill Models

2D configurations of landfill models used in this study were shown in Fig. 2, which Geometric dimensions were consistent with the test models. Configurations 1 and 2, with the same cover slop angle of 27° and different base slop angle, were named model *a* and *b* respectively. Model *c* illustrated by configuration 3 had the same base slop as model *b*, but more steep cover slop than model *b*.

Considering that the silt sand which composed the model base and cover had not plastic deformation in shaking table test, these two parts of models were supposed as elastic materials. However, there was apparent plastic deformation in the “garbage” while inputting strong earthquake (e.g. MHA = 0.4g), so it was reasonable that the mixture were simulated by using a Mohr-Coulomb elastic-plastic constitutive model.

In numerical calculation, contact elements were adopted to represent the effects of geomembrane between sand and “garbage”. All parameters of the material used in calculation were selected according to the test results.

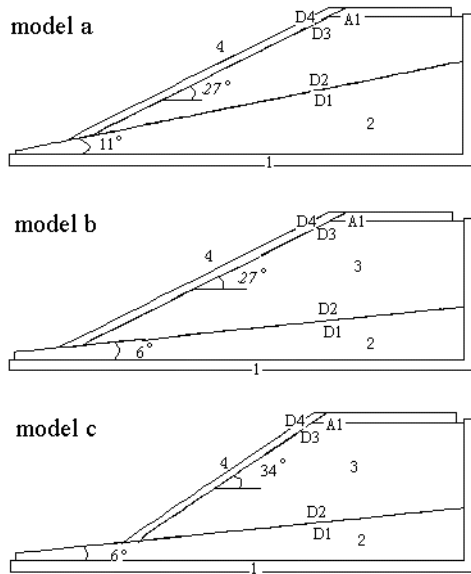


Fig. 2 Landfill configurations used in nonlinear numerical analysis

Two kinds of input motions were used in the numerical simulation. The sinusoidal input motions with frequencies 10Hz could cause landfill model instability easily in shaking table test. In numerical simulation, more sinusoidal input motions with frequencies 5/10/15/20/25/30/35/40Hz were selected to excite the models *a*, *b* and *c*. The sinusoidal motion linearly ramped up for 1.5 seconds followed by full amplitude motion for 6 seconds and 1.5 seconds of ramping down.

According to the integral relationship of acceleration and displacement, maximum horizontal displacement of the shaking table (MHD) could be expressed as:

$$MHD = \frac{MHA}{2\pi f} \tag{1}$$

where *f* was the sinusoidal motion frequency, *MHA* was the maximum horizontal acceleration; *MHD* was the maximum horizontal displacement of the shaking table. Noted that, according to the formula (i), while fixing the peak acceleration, as the frequency of a sinusoidal motion was different, there was difference of 1/*f*² times between the maximum horizontal displacements of the motion inputting to shaking table.

In order to make the calculation results comparable to the shaking table model test, two recorded earthquake motions selected to numerically calculate were identical to the input motions used in the model test, which were named Kobe and Tangshan motion. Fig. 3 and Fig. 4 shown FFT amplitude of the two earthquake motions.

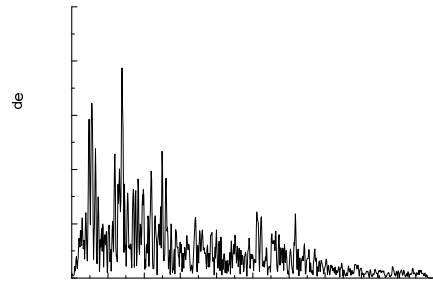


Fig. 3 FFT of Kobe motion recorded on shake table

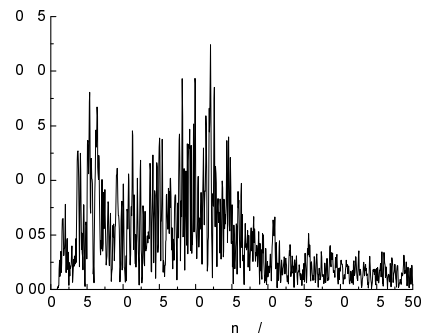


Fig. 4 FFT of Tangshan motion recorded on shake table

SEISMIC RESPONSE CHARACTERISTICS OF MUNICIPAL WASTE LANDFILLS

The dynamic acceleration response at top of landfill model and the permanent displacement between interface within models would be illustrated below, in order to investigate the effects of the following factors, such as landfill height, spectral characteristics of input

motions, the base and cover slop of landfill model and, the density of the “garbage” on the acceleration at top of landfill and the permanent displacement of the interface in landfill.

Acceleration Response of Landfill Model

The natural frequencies of landfill significantly depended on the density of MSW and the height of landfill. Then, both of the two factors were generally considered as the main factors affecting landfill acceleration response. Moreover, such an influence would be different while inputting motions with the different main frequency.

Fig.5 and Fig.6 respectively showed the maximum acceleration response at top of model *a* and model *b* with the shaking table inputting the different frequencies sinusoidal motion. The values at solid marker points, representing the maximum acceleration response at top of models while inputting 10 Hz sinusoidal motion, were found near to the corresponding results from numerical calculation.

In addition, Fig. 5 also indicated that the models amplified the base motion at 10 Hz and 20Hz significantly, perhaps as a result of resonance of the triangular-shaped “garbage” on the inclined base composed of the compacted soil and covered by stiff sand.

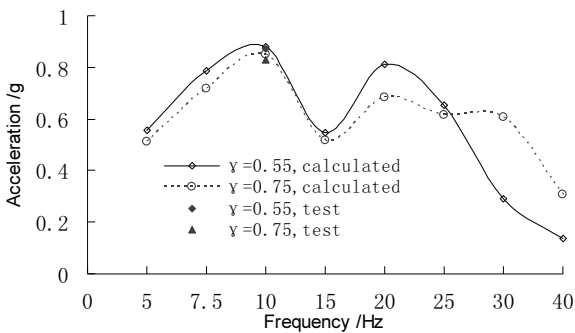


Fig. 5 The maximum acceleration response at top of model *a* from different MSW density under sinusoidal motions with different frequencies

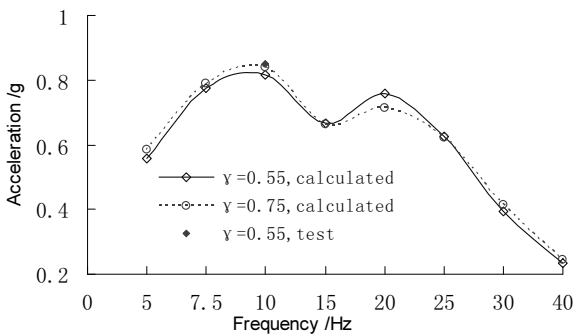


Fig. 6 The maximum acceleration response at top of model *b* from different MSW density under sinusoidal motions with different frequencies

Fig. 7 shown a smoothed FFT graph of the acceleration at top of model *a* and *b* during the Kobe and Tangshan motions with the same peak acceleration of input motions. The maximum response acceleration at top of model *b* while shaking by Tangshan motion was higher than by Kobe motion. This result indicated that the spectral characteristics of input motions impacted the dynamic response of landfills significantly. In addition, with similar to the results shown in Fig. 6, it was found that there were two main frequencies at which the base motion could be amplified by models.

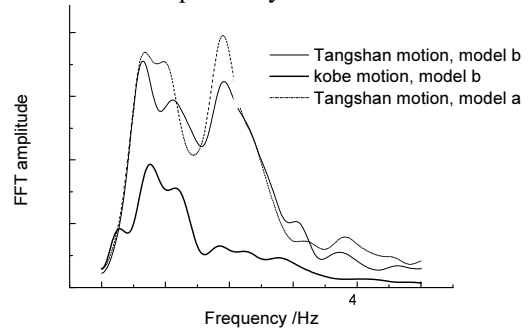


Fig. 7 Comparison of top acceleration response of model *b* from different MSW density under Tangshan and Kobe motions

Permanent Displacement of Base Liner and Cover

Fig. 8 and Fig. 9 given the permanent horizontal displacement results of base liner and cover, which respectively recorded by D2 to D1 and D4 to D3 marked in Fig. 2. For comparison, corresponding displacement amplitude of shaking table, calculated from formula (i), were given by those points closest to the horizontal axis. It seemed that the permanent displacement of landfill base liner and cover were proportional to the displacement amplitude of shaking table, while fixing the acceleration amplitude of sinusoidal motion. In other words, larger the displacement amplitude of input motions was, the greater the permanent displacement could occur between in the base and cover interfaces. This was a very interesting conclusion.

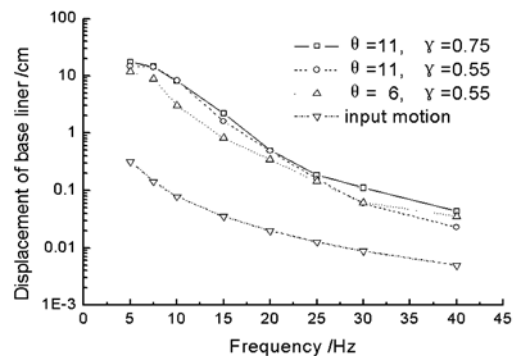


Fig. 8 Base liner permanent displacement of landfill model from different MSW density, different cover and liner slop under sinusoidal motions with different frequencies

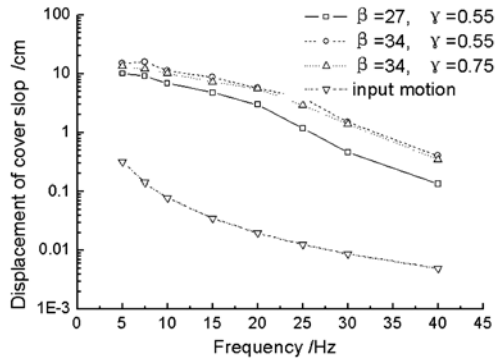


Fig. 9 Cover slop permanent displacement of landfill model from different MSW density, different cover and liner slop under sinusoidal motions with different frequencies

Figs. 10-15 shown displacement time histories for D1-D4 points, which Located on both sides of interface illustrated by Fig. 2. Actually, the relative sliding of D2 to D1 and D4 to D3 could represent the permanent displacement of landfill0 base liner and cover slop.

The maximum horizontal permanent displacement of base liner (D2 to D1) and cover slop (D4 to D3) of model *a* after inputting Tangshan motion were 3.69 cm and 3.14 cm respectively, according to Fig.10. For comparison, the maximum horizontal permanent displacement for base liner (D2 to D1) and cover slop (D4 to D3) of model *a* after inputting Kobe motion are 5.43 cm and 2.73 cm respectively, according to Fig. 11. MSW density was 550 kg/m³.

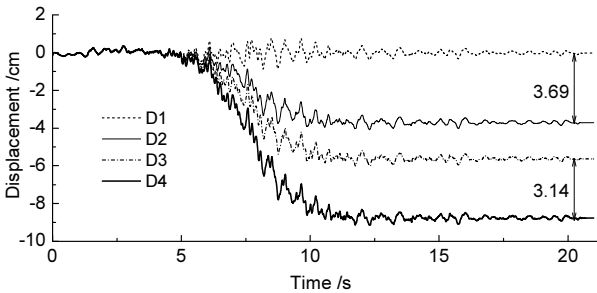


Fig. 10 Horizontal displacement time history for D1-D4 of model *a* with input Tangshan (a). MSW density was 550 kg/m³

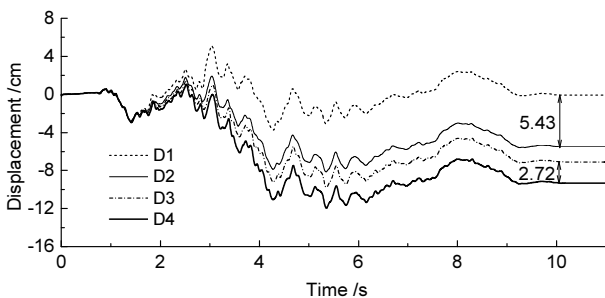


Fig. 11 Horizontal displacement time history for D1-D4 of model *a* with input Kobe motion. MSW density was 550 kg/m³

Although, the acceleration response with inputting Tangshan motion for point A1 at top of model *a* was significantly larger than inputting Kobe motion with the same peak acceleration, the permanent displacements of landfill cover slop induced by the two motions were comparable with each other. Meanwhile, the permanent displacement for landfill liner of model *a* caused by Kobe motion were found significantly larger than by Tangshan motion. Thus, Considering predominant period of Tangshan motion was shorter than Kobe motion (Figs. 3 and 4), we might get a conclusion that long period motion tended to make larger permanent displacement in landfill base liner, however, the peak acceleration of ground motion could affect the permanent displacement in landfill cover slop significantly.

Calculated displacement time histories for D1-D4 of model *b* by Tangshan motion were shown in Fig. 12, while the density of “garbage” was 5.5kN/m³. The permanent displacements of landfill base liner and cover were 1.83 cm and 2.54 cm respectively. The corresponding results were shown in Fig. 13, while the “garbage” density was increased to 7.5kN/m³. It could be found that the permanent displacement of landfill base liner and cover were decreased to 1.47 cm and 1.58 cm respectively.

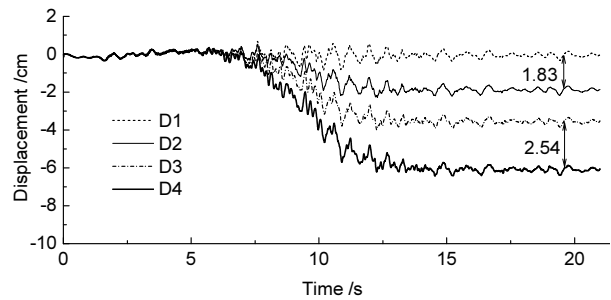


Fig. 12 Horizontal displacement time history for D1-D4 of model *b* with input Tangshan motion. MSW density was 550 kg/m³

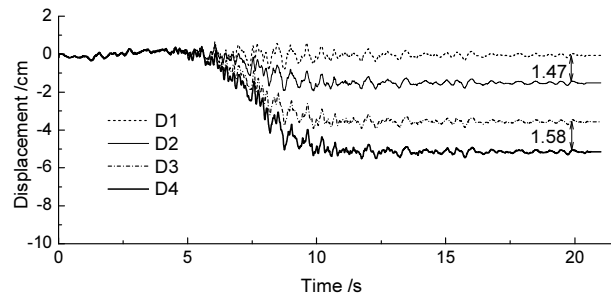


Fig. 13 Horizontal displacement time history for D1-D4 of model *b* with input Tangshan motion. MSW density was 750 kg/m³(*b*)

Fig. 14 indicated that the Kobe motion with 0.86 g peak acceleration produced much larger displacement (5.97 cm) than by Tangshan motion (1.83 cm, Fig. 12). Therefore, the same conclusion as Fig. 8 was provided. The displacement time histories of model *c* were shown in Fig. 15, in contrast to Fig. 12, the cover slop angle played a main role to effect the cover's sliding.

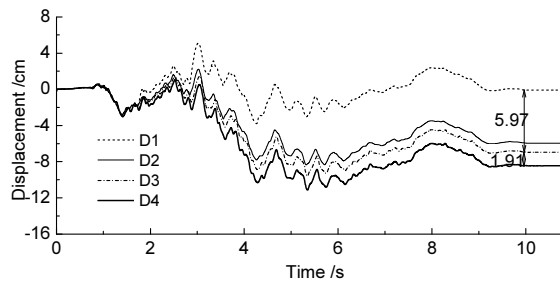


Fig. 14 Horizontal displacement time history for D1-D4 of model *b* with input Kobe motion (*a*). MSW density was 550 kg/m^3

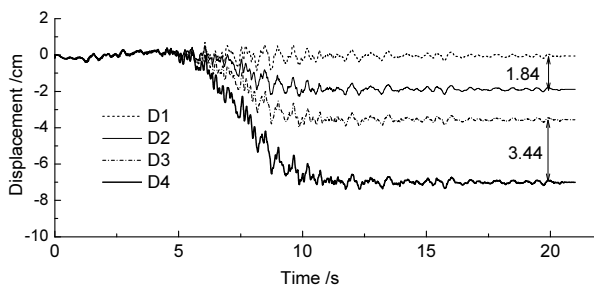


Fig. 15 Horizontal displacement time history for D1-D4 of model *c* with input Tangshan motion (*b*). MSW density is 550 kg/m^3

CONCLUSIONS

As a supplement verification of the physical model test, and also in order to investigate the seismic response characteristics of landfills, nonlinear numerical simulation of the landfill models used in shaking table test was performed. The following conclusions could be drawn. The landfill height, density of MSW and spectral characteristics of input motions were the primary factors that affected acceleration response at the top of landfill. Significant acceleration attenuation of a motion could occur when earthquake wave transferring through landfill base liner containing HDPE geomembrane. Furthermore, larger acceleration was the input motion, more obvious

was the attenuation. The inclination angle of landfill cover had significant effects on the critical sliding of cover liner. However, the friction coefficient of the HDPE interface within the bottom liner system was the primary factor which could affect the critical sliding acceleration of bottom liner system with relatively small base slope angle mostly. The permanent displacement of landfill base liner and cover slop were proportional to the displacement amplitude of input motions with same acceleration amplitude. In other words, the large displacement amplitude of input motion tended to cause the large the permanent displacement in liners of landfill.

ACKNOWLEDGEMENTS

Financial support was provided by National Science Foundation (No. 50538080). This support has been gratefully acknowledged.

REFERENCES

- Jiang BY (2002). Studies on soil slop containing geomenbrane. Dalian University of Technology.
- Chen YM, Gao D, Zhu B, Chen RP (2008). Analysis of stability and permanent displacement of landfill base liner. Science in China, 38(1): 79-94.
- Augello AJ (1997). Seismic response of solid-waste landfills. Berkeley: University of California.
- Kramer SL & Smith MW (1997). Modified Newmark Model for Seismic Slope Displacements of Compliant Slopes, Journal of Geotechnical Engineering, 123(7): 635-644.
- Wartman J, Raymond B Seed M, Bray JD (2005). Shaking Table Modeling of Seismically Induced Deformations in Slopes. Journal of geotechnical and geoenvironmental engineering ASCE 2005, 131(3): 610-622.
- Deng XJ (2007). Shaking Table Test on Seismically Induced Deformation Mechanism and Seismic Stability Evaluation of Municipal Waste Landfills. Dalian, Dalian Uuniversity of Technology.
- Kong XJ & Deng XJ (2008). Shaking Table Test on Seismically Induced Deformation Mechanism of Municipal Waste Landfills, China Civil Engineering Journal, 41(5): 64-71.
- Hoe IL (2001). Recent applications of sliding block theory to geotechnical design. Soil Dynamics and Earthquake Engineering, 21: 189-197.

STUDY ON SOIL PROPERTIES OF THE EARLY ECOLOGICAL RESTORATION FOR A CHEMICAL LANDFILL IN HUAINAN

Wen FAN¹, Jia-Ping YAN and Hui-Ping LIU

ABSTRACT: The soil properties after ecological restoration for 16 months for a chemical landfill in Huainan should be monitored for the purpose of making sure the early restoration work was going on in an effective way. On the basis of field investigation, the related parameters of soil properties were evaluated by various techniques, including AAS (Atomic Absorption Spectroscopy), pH analyzer and soil organic matter analysis. The results showed that the physical nature of soil had got certain improvement. The pH value had remarkably decreased from 10.3~10.6 to 7.76~8.28 by pH analyzer and the soil contained highly organic matter and nitrogen, but lack of phosphorus and potassium. The effects of heavy metals such as Cu, Cd, Pb, Zn were also discussed in detail on the basis of ecological risk assessment. The concentration of heavy metals were higher than the background value in different extent, and it was calculated that there are approximately 61.5% of this area in slight ecological risk grade and only Cd was in slight ecological hazard.

KEYWORDS: ecological restoration, soil organic matters, heavy metals, ecological risk

INTRODUCTION

Huainan, as one of coal resource-rich cities in China, so many years mining has not only provided necessary energy security for China's economic development, also brought mine collapse, soil erosion and other environmental issues, which damaged the local ecosystem seriously. Therefore abandoned mining areas in Huainan should be restored imperatively. The chemical landfill in this paper is just one of the most serious pollution sites in a restoring area. In order to make sure the restoration work goes in an effective way in future, the paper, at the base of monitoring results, has analyzed the soil fertility and done ecological risk assessment for heavy metals, at the same time given some suggestions for latter restoration work.

MATERIALS AND METHODS

The Generality of the Study Region

The area of this chemical landfill is 2.039 hm², and its waste resource comes from construction waste and chemical castoff. This area, with not film topography, density vegetation, is a natural oxygen bar, showing

beautiful ecologic landscape. There is a Mestasequoia forest on the north and a Ligustrum nursery on the west. The pre-processing of this landfill is: first, to cover the surface with 30~40 cm soil; then add impermeable layer in 20~30 cm; at last, cover soil about 30 cm. Meanwhile, construct a leachate treatment system. The field investigation showed that this area had a large number of shrubs and herbaceous plants in good growing tendency, such as honeysuckle, Melia azedarach, holly, ligustrum, Broussonetia papyrifera, Robinia Pseudoacacia, Photinia, Pittosporum, Ailanthus altissima, axillaris and so on, the vegetation coverage had reached more than 95% .

Samples Collection

Soil is heterogeneous in horizon and vertical, so in order to make samples representative, taking full account of heap, slope, as well as peripheral influences, we set up 6 sampling lines and collect 13 samples for testing in all. The sampling depth is 0~30 cm. Observe the color, structure, humidity, roots and so on. Each site collect the soil about 1 kg. After natural drying for half a month, sieve the soil samples in size of 2 mm and 0.25 mm respectively for testing the chemical properties. Different size use in different indexes.

¹ Master student, School of Earth Science and the Environment, Anhui University of Science and Technology, China. Email: ffww1234@126.com

² Professor, School of Earth Science and the Environment, Anhui University of Science and Technology, China. Email: jpyan@aust.edu.cn

³ Master student, School of Earth Science and the Environment, Anhui University of Science and Technology, China. Email:lhpla2003@yahoo.com.cn

Monitoring Methods

The items include pH, total nitrogen(TN), total phosphorus(TP), total potassium (TK), organic matter(OM) and heavy metals of Cu,Cd, Pb, Zn and so on. 2.5:1

Potential of water extraction for pH; Semi-micro Kjeldahlfor TN; Anti-mono-molybdenum colorimetry for TP; flame atomic absorption spectrophotometry for TK and heavy metals; potassium dichromate oxidation titration for OM. Each item for one sample should be tested twice. Monitoring results are shown in Table 1 and Table 2.

Table 1 Physical and chemical properties of the soil

Sample No.	Depth (cm)	pH	OM (g/kg)	TN (%)	TP (%)	TK (%)
I -1	0~30	7.79	14.3	0.147	0.0063	0.0599
II -1	0~30	7.87	13.62	0.133	0.007	0.0594
III-1	0~30	8.04	15.66	0.133	0.0065	0.0582
III-2	0~20	8.26	16.34	0.105	0.0056	0.0525
III-3	0~20	7.85	15.66	0.147	0.0061	0.0541
IV-1	0~30	8.12	14.98	0.175	0.0057	0.0573
IV-2	0~30	8.19	14.3	0.147	0.0063	0.0588
IV-3	0~20	8.02	17.03	0.147	0.0052	0.0555
IV-4	0~20	7.98	15.66	0.119	0.0053	0.0549
V -1	0~30	8.16	21.11	0.189	0.0065	0.0574
V -2	0~20	8.28	16.34	0.091	0.0058	0.054
VI-1	0~30	7.89	11.58	0.105	0.0073	0.0596
VI-2	0~20	7.76	12.94	0.119	0.0035	0.0549

Table 2 Concentration of heavy metals

Sample No.	Cu (mg/kg)	Cd (mg/kg)	Pb (mg/kg)	Zn (mg/kg)
I -1	58.33	0.34	39.94	91.51
II -1	48.64	0.24	35.63	82.69
III-1	50.14	0.43	35.96	80.67
III-2	39.6	0.39	35.38	63.1
III-3	43.14	0.36	36.29	74.05
IV-1	44	0.26	35.93	81.75
IV-2	51.96	0.22	36.54	81.01
IV-3	46.38	0.21	35.16	75.6
IV-4	45.63	0.33	36.22	78.7
V -1	61.22	0.27	40.76	88.48
V -2	46.66	0.19	39.88	71.54
VI-1	49.62	0.25	45.52	94.52
VI-2	45.81	0.31	40.61	70.14
Background value	22	0.19	24.8	76.8

RESULTS AND DISCUSSION

Physical and Chemical Properties of the Soil

pH value

The pH value in this area ranged from 7.79~8.28, compared with the past 10.3~10.6 has a great decrease

from strong alkaline to alkaline, that may be for the ion interaction in soil-vegetation system and the flush and infiltration of rainwater, which can reduce the content of soluble hydroxide compounds. Under the condition of alkaline, there is no serious damage to the soil structure, meanwhile, from the field investigation the good growth of vegetation has shown that the existing vegetation has a very good mechanism patience on the soil with high pH value.

Soil Nutrient Reserves

Soil nutrient reserves mainly means the content of organic matter, total nitrogen, total phosphorus and total potassium, which is an important factor reflecting the level of soil fertility. We can know the results from Table 1, the content of OM is 15.35 g/kg, TN is 1.35 g/kg, total phosphorus is 0.059 g/kg and total potassium is 0.566 g/kg. Compared with the average content of OM(14 g/kg)

and TN(0.86 g/kg) of soil in Anhui province(Xi et al. 1998), this chemical landfill is rich in C and N. But the contents of TP and TK are much lower than normal content in China. According the classification of soil fertility in China in Table 3, results show that the content of C and N can meet the need for plants growth basically, at the same time soil of this chemical landfill has a certain keeping fertility and buffering.

Table 3 Classification of soil fertility in China

Grade	OM (%)	TN (%)	P ₂ O ₅ (%)	K ₂ O (%)
lower	<0.7	<0.06	<0.04	<0.1
low	0.7-1.1	0.06-0.09	0.04-0.07	0.1-0.2
middling	1.1-1.5	0.09-0.13	0.07-0.10	0.2-0.4
high	1.5-2.2	0.13-0.20	0.10-0.25	0.4-0.5
higher	>2.2	>0.20	>0.25	>0.5

Evaluation for soil heavy metals Contamination

Evaluation of ecological risk for heavy metals

The ecological analysis and evaluation on water sediment has a more widely application than evaluation of soil heavy metals contamination (Wu et al. 2003). In this paper, the method of potential ecological risk index is used to evaluate the potential ecological risk of heavy metals. The formula of calculation is:

$$RI = \sum_{i=1} E_r = \sum_{i=1} T_r P \quad P_i = \frac{C_d^i}{C_r^i} \quad (1)$$

P_i is the single factor contaminated index; C is the

measured value; C_r^i is the background value; T_r^i is the coefficient, which can reflect the heavy metal's toxicity and the biological sensitivity on its pollution; E_r^i is one heavy metal's potential ecological risk coefficient of number i ; RI is the ecological risk index for whole area(Yang et al. 2006).

According some relevant literatures and the characteristics of heavy metals pollution in reclamation, kinds of toxic coefficients are set up in Table 4 (Liu et al. 1999).

There is a classification in Table 5 (Li et al. 2006) , which is Ecological risk index and its classification

Table 4 Index of ecological hazard for different heavy meta

Element	Cu	Cd	Pb	Zn	Cr	Hg
Toxicity coefficients	5	20	5	1	2	28

Table 5 Ecological risk index and its classification

E_r^i	RI	Ecological risk	Risk grade
<=40	<=50	slighter	A
40-80	50-120	slight	B
80-160	120-240	middling	C
160-320	240-480	serious	D
>320	>480	more serious	E

Analysis and Discussion of Evaluation Results

From above table, there is only 15.4% Cd in slight ecological hazard grade, others in slighter. All of the area there are 61.5% in slight ecologic risk grade. Some research have indicated that organic matter's early

application can accelerate the adsorption and fixation of Cd in soil and reduce the absorption of plants .But with the passage of time, this effect will go opposite because of the organic acid, produced form organic matter's mineralization and decomposition, which can accelerate the solubility of Cd. However, in high pH value this

effect doesn't work remarkably. The result is that the complexes of humic acid and metals have a more stability in high pH value, then metal ions' release be prevented. Thus, despite Cd is much higher than the

background value, there is no influence on plants growth. However, because of its potential ecological hazard, specific measures should be taken in latter restoration.

Table 6 Result of ecological risk for heavy metals

Samples No.	Ecological hazard coefficient E_r^i				RI	Risk grade
	Cu	Cd	Pb	Zn		
I -1	13.26	35.8	8.05	1.19	58.3	B
II -1	11.05	25.26	7.18	1.08	44.57	A
III-1	11.39	45.26	7.25	1.05	64.95	B
III-2	9	41.05	7.13	0.82	58	B
III-3	9.8	37.89	7.32	0.96	55.97	B
IV-1	10	27.37	7.24	1.06	45.67	A
IV-2	11.81	23.16	7.37	1.05	43.39	A
IV-3	10.54	22.11	7.09	0.98	40.72	B
IV-4	10.37	34.74	7.3	1.02	53.43	B
V -1	13.91	28.42	8.22	1.15	51.7	B
V -2	10.6	20	8.04	0.93	39.57	A
VI-1	11.28	26.32	9.18	1.23	48.01	A
VI-2	10.41	32.63	8.19	0.91	52.14	B

CONCLUSIONS

(1) pH value in this chemical landfill soil have a remarkably reduce, so there will be more kinds of plants to survival; There is rich of organic matter and nitrogen, but lack of phosphorus and potassium.

(2) The Concentrations of heavy metal are higher than the background value in different degree. Only Cd is in slight ecological hazard. All of the area there are 61.5% in slight ecologic risk grade.

Basically, the soil nutrient is able to maintain normal plant growth, as well as the heavy metal pollution is not so serious that having toxic effect on plant growth. It means the ecological rehabilitation in this area is feasible, and the existing plants growth situation indicates that the early ecological rehabilitation has gained some effects.

Suggestion for the latter ecological rehabilitation: monitor the precipitation regularly, oil fertility, species diversity and the development condition in this area. Improve the condition of soil phosphorus and potassium deficiency through the imposition of fertilizers, strictly control the discharge of pollutants to prevent the concentration of heavy metal growing, at the same time,

should reinforce the artificial trim and strengthen safeguards and prevent to herd and cut.

REFERENCES

- Xi CP (1998). Soil of China. Agricultural Press of China.
- Wu XM, Li LQ, Pan GX (2003). Soil Pollution of Cu, Zn, Pb and Cd in Different City Zones of Nanjing. Chinese Journal of Environmental Science. 24(3): 105-111.
- Yang XH, Hu ZQ, Zhang XL (2006). Risk Assessment of Reclaimed Land Filled with Fly Ash and Stabilization Remediation Technology. Science & Technology. 24(3):33-34.
- Liu WX, Luan ZK, Tang HX (1999). Environmental Assessment on Heavy Metal Pollution in the Sediments of Le An River with Potential Ecological RiskIndex. ACTA ECOLOGICA SINICA. 19(2): 207-208.
- Li ZB, Luo YM, Song J, et al. (2006). Ecological Risk Assessment of Heavy Metal Polluted Soil: A Case Study. Soils. 38(5):566-567.

GEOTECHNICAL SITE CHARACTERIZATION OF MUNICIPAL SOLID WASTE LANDFILL IN UZBEKISTAN

Kobiljon KHOLMATOV¹, Diana KHASHIMOVA², Wei WU³ and Marufdjan MUSAEV⁴

ABSTRACT: In geotechnical engineering the techniques of site investigation for soils are well established and little is known for the characterisation of municipal solid waste landfills. This paper presents the findings of geotechnical investigations for characterization of landfills situated in vicinity of large cities of seismically active regions of Central Asia. The site investigations using boreholes and geotechnical laboratory tests have been conducted on the landfill site Ahangaranskaya situated at Tashkent Region, Uzbekistan.

KEYWORDS: landfill, loess, borehole, geotechnical lab tests

INTRODUCTION

In geotechnical engineering the techniques of site investigation for soils are well established and little is known for the characterisation of municipal solid waste landfills. The most landfills were put into operation in quarries and depressions without any site investigation or technical documents, the waste depth and ground conditions beneath the waste are not known.

This paper presents the findings of geotechnical investigations for characterization of landfills situated in vicinity of large cities of seismically active regions of Central Asia. The site investigations using geotechnical techniques have been performed on the landfill site Ahangaranskaya situated at Tashkent Region, Uzbekistan, at latitude 41°05'50.9" N and longitude 69°28'54.0" E about 32 km south-west from the limits of Tashkent city. Tashkent city is the capital of the Republic of Uzbekistan, the most cosmopolitan Central Asian city, has a population over 2.4 million citizens and spreads over 326 km². Tashkent city is the largest waste producer, and landfill Ahangaranskaya is the best equipped MSW landfill in Central Asia. Nowadays landfill Ahangaranskaya is a main MSW landfill of Tashkent city, it equipped with modern equipment, including waste trucks, compactors and excavators. Landfill operation is well organised including waste registration, emplacement records and the adequate control of the landfill territory.

Ahangaranskaya landfill was put into operation in 1967 with projected capacity of about 7.5 million m³. It

was founded on an existing excavated pit and further developed to a final trapezoidal embankment of waste deposits above the ground. Nowadays it is topped with a final protective cover of approx. 50 cm thick of compacted loess taken from inside the landfill area. The landfill area occupies a contiguous area of about 59 ha of land. It is separated inside by four loading concreted platforms into four zones bounded by linear asphalt access road. Annually landfill accepts 733 000 tons of waste. The nearest Urta-Saray settlement is located about 6 km north-west of the landfill.

GEOMORPHOLOGY AND DRAINAGE SYSTEM

The investigated area is situated on the plain at the left bank of the river Chirchik. The topography is represented by alluvial-proluvial plains. They are mainly characterised by complanate relief with many weakly expressed slopes in Golodnaya Steppe. On watersheds the relief of these plains is slightly-hilly, and in band of foothills is aslope- corrugated, which is divided by wide fluvial valleys and shallow lateral arid dales. There are ravines in some sites of plain as well as canals, drainages and collectors within the irrigated tracts of lands. Altitudes range between 230-650 m.

The landfill area is located on slightly hilly territory of foothill plain characterised by ravine beam system. Altitudes range between 456 - 482 m. There is no hydrographic net inside of landfill area.

¹ Research Associate, Hamburg University of Technology, Germany. Email: k.kholmatov@tuhh.de

² Research Associate, Hamburg University of Technology, Germany. Email: khashimova@tuhh.de

³ Professor, Universität für Bodenkultur Wien, Austria. Email: wei.wu@boku.ac.at

⁴ Professor, Tashkent State Technical University, Uzbekistan. Email: promecologiya@mail.ru

METEOROLOGICAL CONDITIONS

Climatic conditions of Tashkent Region are characterized by its geological location, is far from sea basins and close to sandy deserts. It results in high dryness of air, especially in summer time. High position of sun characterized by relatively low geographic latitude results in high air temperature, which in July month 42°C-44°C in shadow. Also in some periods of winter time the temperature riches up minus 22°C. This abrupt amplitude of annual temperature ranges together with the abrupt variation of daily temperature and dryness of air allows characterizing the climate of Tashkent Region as abrupt continental.

Average monthly temperature of the air ranges from -7.2°C (January) to +42.8°C (July). The hottest season is a period from May to September. The coldest period is observed from November to February. Duration of frost-free period in average is 224 days. Average duration of daylight hours are 12 hours 12 minutes.

The relative annually air humidity is 58%. The absolute air humidity ranges in the following limits: maximal absolute air humidity ranges from 12.8 to 13.4% (observed in June-August), minimal absolute air humidity is 4.3%-7.0% (observed November - March).

Atmospheric precipitations during the year are irregular, and their highest amounts take place in winter and spring time. In summer time the precipitations are insignificant and almost not existing. Blanket of snow lies 38 days annually in average. Average height of snow blanket is 16 cm, and sometimes up to 23.2 cm. Maximal depth of soil freezing is 0.66 cm.

On the territory of Tashkent Region the winds of north and north-west direction predominate. The highest average wind velocity is in north-west direction (2 m/sec). The strong winds having velocity more than 15 m/sec are observed in July.

REGIONAL GEOLOGY

The geological structure consists of two geological-structural floors: lower Paleozoic and upper Meso-Cenozoic. Lower structural floor in central part is in depth 3000 m. Upper structural floor consists of Meso-Cenozoic stratum. Main constructional environment is Neogene and quaternary stratums with thickness up to 1800 m.

Deposits of molasses formation of Neogene are widely spread almost all over the surface under the quaternary deposits, and represented by continental, mainly red, marly and aleuritic clays, aleurolites (siltstones) and marls.

Geological-genetic complex of upper-Quaternary

alluvial-proluvial stratum is composed by complanate, essentially by Golodnaya Steppe plain situated on the right bank of river Sirdarya—the third terrace of rivers Chirchik and Ahangaran. This stratum represented by loess, gravels, loams, and clay sands.

Geological-genetic complex of undifferentiated quaternary proluvial stratum is on south of Golodnaya Steppe within Lomakinskiy plateau. This complex is represented by homogeneous sediments of macroporous straw-colored (pale-yellow) loess stratum (consisting of pulverescent tenacious clay sands and loams) with high slump characteristics. The thickness of this complex ranges between 4-5 m to 60-80 m.

Geological-genetic complex of undifferentiated quaternary alluvial stratum in upper part of cross-section is represented by group of loess, and in bottom part by conglomerate of peddle stone. The thickness of loess blanket of Golodnaya Steppe terraces is 20-40 m, and Sirdarya terraces is 2.7 m. The total thickness of peddle stones in valley of river Ahangaran is up to 150 m.

Geological-genetic complex of undifferentiated quaternary deluvial-proluvial loess stratum is represented by upper part of terrace. The thickness is 10-25 m. This complex lies on conglomerate and pebble stone.

Geological-genetic complex of anthropogenic stratum has been formed as a result of constructional and human activity. This complex consists of various types of fill-up soils.

COVER SEQUENCES AND SOILS

The local geology of Tashkent is dominated by massive coarse soil (sand and gravel) and loess deposits and can be divided into two parts. The eastern third of Tashkent is underlain by QIII-IV, a sequence of Late Quaternary sand and gravel along the main valley of the Chirchik River. The coarse soil formations have a thickness of about 500 to 600 m. Towards West the coarse soils gradually change into older loess sediments ranging from 30 to 40 m thick of QII age (Middle Pleistocene). The loess blankets the rolling topography in the west of Tashkent with its broad hills and valleys. The Quaternary sediments are separated from underlying folded Neogene and Paleogene clays by an angular unconformity.

SITE SPECIFIC UNDERGROUND CONDITIONS

The underground at the landfill site Ahangaranskaya is represented by three quaternary strata. The first stratum is the upper Quaternary sediment of Golodnaya Steppe complex QIII (gl) and consists of loam and loamy sand with gravel bands down to 10-15 m. This layer is followed by the middle Quaternary sediment of Tashkent

complex with two sections: the top section QII (ts2) and the bottom section QII (ts1). These two sections consist of loess loams with gravel bands of 60-70 m total thickness. The third layer is under Quaternary sediment of Soh complex QI (sh1) and consists of proluvial and dealluvial stony loam, pebble stone with sandy-argillaceous filler, conglomerates on argillaceous cement with marl with of 150-200 m.

The Quaternary sediments are followed by the upper Pliocene sediment of Neogene consisting of compact plastered light-brown aleurolite (siltstone), marl, argillaceous sandstone.

HYDROGEOLOGY

The area of investigations, according to hydrogeological zoning, completely enters in Tashkent artesian pool and it is located on border mountain and platform areas. The mountain part of the area combined by Paleozoic sediments, enters in Chatkal-Kurama group of pools waters. The flat area covered with a powerful cover of Meso-Cenozoic rocks is a part of Tashkent artesian pool.

In the following sections the spatial distribution as well as the lithological and hydrochemical properties of the water bearing horizons within the investigation area are described in stratigraphic sequence.

Recent (QIII+IV) Alluvial Sediments

It is advanced in valleys of the rivers of Chirchik, Akhangaran and Dalverzin steppes. Water horizon in the top part of a valley of Chirchik river from Gazalkent city up to Chirchik city is supervised by floodplain area I and II terraces that frequently on width makes 1-2 km. In the middle part from Chirchik city up to Yangiyul city also covers and the area of III up-floodplain terraces. Due to expansion of a valley its width increases up to 6-20 km. In the bottom part of the valley from Yangiyul city up to Syr-Darya river the water horizon is traced not only in limits actually valley of Chirchik river but also due to development of alluvial sediments in limits of Chirchik-Keles watershed in upper Pliocene, bottom and middle Pleistocene borrows a part of the area of a watershed.

In the top part of a valley are pebbles with boulders with sand-gravel filler of modern age. Sometimes they are spread with conglomerates and gravels of QIV. The thickness of water horizon is up to 20 m. In middle part of valley modern pebbles with boulders with sand-gravel filler with boulders with sand-gravel and sandy filler with layers of conglomerates of QIV age. Total thickness of horizon is 50-80 m. In bottom part of valley water bearing are pebbles with sandy filler of modern sedimentation and pebbles with boulders with sandy-gravel fillers of upper Quaternary age. The total thickness of horizon is

90-100 m. Filtration properties (permeability) of water bearing sediments are fluctuate in wide range (diapason).

Modern pebbles with boulders with sand-gravel filler in the top and middle part of a valley have factor of a filtration (permeability) of 100-150 m/day and 150-200 m/day respectively. Less permeable QIV alluvial pebbles with layers of conglomerates (permeability <25 m/day) and pebbles with boulders with sand-gravel and sandy filler with layers of conglomerates (permeability 25-50 m/day) which are covered by very friable pebbles with thickness 5-10 m having permeability more than 250 m/day.

In the bottom part of valley the pebbles with sandy thin and fine-grained filler characterized by permeability 10-21 m/day and 35-160 m/day respectively. The main source of feed of groundwater horizon is surface infiltration irrigation waters from the irrigated lands and linear infiltration irrigation waters from irrigated lands, and linear is from an irrigating network, and less is underground inflow from the side of large lateral rivers especially on Ahangaran branches of the valley of Ahangaran river. The insignificant role is played by atmospheric precipitation. During passage of flood a underground waters are filled in a narrow strip from a channel of the river.

The expenditure of groundwater occurs by drainage network of Syr-Darya river, channel of Chirchik river, regional drain, operation by water-fences, and in the summer period by transpiration and evaporation.

The general direction of groundwater flow is from North-East to South-West aside of Syr-Darya river. The angle of their mirrors ranges from 0.004 in the top part of a valley up to 0.001 in bottom part.

Groundwater is fresh, their mineralization basically up to 0.5 g/liter and total hardness up to 7.0 mg-equal/liter. In the bottom part of a valley, and also in a narrow strip lengthways left part of valleys from Gazalkent city up to mouth Bashliksay, mineralization of groundwater is from 0.5 up to 1.0 g/l at the total hardness 7-10 mg-equal/liter. Directly along foothills of the left coast of Chirchik river there are groundwaters with the solid residue (dry particles) 1.0-1.5 g/l with the total hardness more than 10 mg-equal/liter.

In valley of Ahangaran river, the water bearing horizon is in limits of floodplain, I and II up floodplain terraces. Down from Turk village transversal dimensions (size) of water bearing horizon ranges from 0.5 up to 1.0 km. This width is up to outfall of Karabau and Gushsay, below which till Karahtay village water bearing horizon if gradually increasing till 3-4 km, and below Sartamgalin near the Kerauchi village where valley of Ahangaran river is dividing to Ahangaran and Gedjigen branches rich 10 km. The thickness of water bearing horizon is also increase in the same direction. In the area around Angren city is 10-15 m, from Angren city up to

Sartamgalin is 15-20 m, and increases up to 25-30 m in the area of valley dividing. Actually in Ahangaran branch of valley the thickness of horizon is from 10-15 up to 25-40 m, and in Gedjigen is 50-70 m.

The water bearing strata composing water horizon are represented by one, two and sometimes three layers with various permeability (filtration properties). It pebbles with boulders with sand-gravel very friable filler of modern age (permeability 100-200 and more m/day), pebbles with sand-gravel a filler with dense packing pebbles (permeability 40-50 m/day), pebbles with a sandy and sandy filler of the bottom part QIV age (permeability 10 m/day). In area of a Tujabuguz water reservoir alluvial pebbles modern age have conductivity of 280 m/day, permeability up to 150 m/day. In Dalverzin steppe described the horizon of groundwater lithologically is consist of gravel- pebble strata and overlapping them loams and sandy loams frequently with the significant content of gravel and pebble. It is advanced in limits of I-III up-floodplain terraces of Syr-Darya river. The thickness reaches 100 m.

Strata consist of high level of water. Specific debits of wells range from 13.98 up to 24.08 liter/sec. In southern and south-west part, closer to Syr-Darya river, specific debits is decreased up to 2.3-7.15 liter/sec. Permeability from 22.5 up to 54.8 m/day.

Mineralization of groundwater from 1.0 up to 3.0 g/l, total hardness from 13.5 up to 35.0 mg-equal./l. Reduction of mineralization and total hardness, according to the data of previous investigations, is marked with depth. So, on the depth 30-40 m solid residue (dry particles) is 1.24-1.45 g/l, total hardness is 14.0-15.4 mg-equal./l, and on the depth below than 60-70 m mineralization is 0.54-0.73 g/l at total hardness 7.0-8.6 mg-equal./l.

Recent Alluvial-Proluvial (Fluvial) Sediments

It spread on valleys of large channels and aryks (irrigation ditches) Karakamish, Burata, Salar, Bozsu, Karakulkuduk, Djun, as well as on the valleys of large left tributaries of rivers Chirchik-Aksakatasay, Uyzuruksay, Karamanassay. On Kokaral loessial massif it is in limits of talus train Ummati, Sardobsay, narrow 0.1-1.5 km valleys of Kuruksay and Chaulisay.

Water bearing stratums in valleys of channels and aryks is represented mostly by loess-like loams with inclusions of gravel, sand, rare - gravel with sand-loam filler, in valley of Keles river loess-like loams and gravel with sand-loam filler. The thickness of water bearing horizon from 1.5-5.0 to 16.5-19.5 m. Ground waters are on the depth from 0.1-1.0 to 5.0-15.0 m.

Upper Quaternary Alluvial-Proluvial (Fluvial) Sediments

It spread on right- and left-bank valley of Chirchik

river, left-bank valley of Ahangaran river to south-west from Pskent loessial massif, and also on right and left board of Ahangaran river valley, in valleys of Belyautsay and Bamkis Middle Quaternary (QIII) alluvial sediments ay.

Middle Quaternary (QIII) Alluvial-Proluvial (Fluvial) Sediments

Developed in plain zone of Chirchik-Keles watershed, within the limits of foothill Karzhantau plain of southern slope Karzhantau mountain system, on left-blank of valley Chirchik river between Parkentsay river and Ahangaran river, on Pskent, Kokaral loess massifs, in Dalvarzin steppe. The section of water bearing sediments is represented by two types: crushed rock and gravel with loamy and sand-loamy filler and loess-type loams without underlying layer of friable clastic stratum. In the first type section the thickness of water bearing sediments tangs from 3-19 to 22-28 m and rarely reaches 37-45 m. Depth of opening of water bearing sediments under the cover of loess-type loams from 8-20 to 40-60 m, and rarely up to 80 m. In second type of section the thickness of water bearing loams varies in limits from 2 up to up to 60-80 m.

In Ahangaran valley to Pskent loessial massif water bearing horizon lies mainly on aleuolite (siltstone) clays, rarely - conglomerates of upper Pliocene, especially in Ahangaran branch of valley on loams and pebbles of lower Quaternary age. Water bearing sediments represented by pebbles with sand-loam, sand-gravel filler among which traced interlayers and lenses of loams with thickness from 5-7 to 13-20 m. The thickness of water bearing horizon ranges from 40 to 60-85 m.

TECTONICS AND SEISMICITY

Tashkent is located in the seismically most active region in Central Asia. Since 1868 there are about 27 earthquakes with magnitude greater than the magnitude of 4.5 (Erdik 2005). The seismicity is dictated by the two major thrust zones, the Tian Shan and Pamir. These two thrust zones slip in response to the stress release resulting from the collision of India with Asia. Tashkent, the most cosmopolitan city of all Central Asia, has a population over 2.4 million and spreads over 326 km². It is built on massive loess deposits and it was devastated in the last historical 1966 earthquake (7.5 on the Richter scale), leading to a nearly complete reconstruction of the city. This earthquake was well documented and circulated in the international scientific community.

Several earlier earthquakes in the 20th century also significantly damaged the city. The probability of the next earthquake with the magnitude $M = 6.1$ for the next 20 years is very high for Tashkent city (Nurtaev 2004). It

is well-known that the intersection of several active faults in the Tashkent region is just located in the north-east vicinity of the city. To estimate the seismic hazard at the regional level, the Peak Ground Acceleration (PGA) maps of the whole East Asia with 10 % of probability of exceed in 50 years return period was produced within the Global Seismic Hazard Assessment Program (GSHAP), with the participation of local scientists. A large PGA value of about 4.8 m/s² was found for Tashkent region.

GEOTECHNICAL SITE INVESTIGATIONS

The following types of field and laboratory investigations were carried out:

- Drilling of boreholes d=250 mm with loess sampling;
- Sampling of loess borehole undisturbed samples;
- Installation of observation wells for ground water monitoring;
- Design and installation of safety constructions;
- Construction of landfill plan and landfill cross-section;
- Geotechnical lab tests;
- Statistical treatment of the laboratory test results;

Table 1 Lithological units, observations during drilling

Nr	Lithologic description of soils	Borehole 1, depth in m	Borehole 2, depth in m
1	Soil-vegetative layer	0.0 – 0.3	0.0 – 0.3
2	Loess-type loams, brown, moistened, with inclusion of calcareous concretions	0.3 – 13.0	0.3 – 30.0
3	Grass with loamy filling	13.0 – 13.3	30.0 – 30.5
-	Groundwater level	7.4	24.68
-	Total depth	13.3	30.5

For determining the physical-mechanical properties of loess-type soils the boreholes d=250 mm have been drilled by boring machine PBU (ПБУ) and sampling of loess borehole undisturbed samples with interval 1.0 m have been done by soil-sampler GOU-2 (ГОУ-2). Table 1 shows lithological units observed during drilling.

Further boreholes were completed as observation wells by drilling with boring machine URB-2A2 (УРБ-2А2) with a rolling cutter bit d=246 mm.

Laboratory testing of loess borehole undisturbed

samples has been conducted according to Interstate Standards nrs. 30416-96 (general requirements), 25100-95 (classification), 12248-96 (soil strength), and 12248-78 (shear strength). Strength properties were determined by means of slow (sluggish) shear with previous compression (precompression) and water saturation at loadings $P = 0.1, 0.2$ and 0.3 MPa.

Slump properties and deformation behaviour of loamy soils were determined on compression tests by the two-curve method. Compression tests were conducted at final loading 0.3 MPa. Pre-consolidation pressures of soils were determined according to Braja (2005). Compression index (coefficient) of soils was determined according to lab test results for the void ratio and pressure by using procedure described by Braja (2005). Statistical treatment of the laboratory test results were conducted according to Interstate Standard nr. 20522-96.

RESULTS

Ahangaranskaya landfill area is located in a submontane zone characterized by ravine relief on a slightly hilly territory in the Golodnaya / Hungry Steppe, and altitudes range from 456 m to 482 m. In respect of lithology the investigated area consists of loams, covered by soil-vegetable layer with thickness 0.3 m. Cavities of relief are filled with municipal solid wastes from Tashkent City.

During the site investigations the groundwater level has been reached in depth 7.40-24.68 m (December 2006) below the ground surface (altitudes 448.8 - 457.7 m). According to long-term observations of Tashkent Region the groundwater reaches the maximal level in October-December and minimal level in April-May months; the amplitude of the ground water level fluctuation in range 2.0 m. The altitudes 450.8-459.4 m are the expected values of maximum groundwater level.

Four lithological units have been determined within the investigated area according to lithologic composition and slump properties at $P=0.3$ MPa, as well as water content.

First lithological unit - loess-type loams; brown, macroporous, moistened, with inclusion of calcareous concretions, with proneness to slump at $P=0.3$ MPa. They are on upper part of geological cross-section up to 5.5-8.5 m. Specific gravity of dry soil ranges between 1.41-1.71 t/m³, at normative value 1.54 t/m³, and specific gravity of saturated soil ranges between 1.70-2.03 t/m³, at normative value 1.87 t/m³ and computed values are: $\rho_{II} = 1.85$ t/m³; $\rho_I = 1.83$ t/m³. Slump properties of soils are characterised by the values of relative slump proneness at $P=0.3$ MPa from 0.011 to 0.031. At normal pressure the soils have relative slump proneness. The relative slump at P_{nor} changes from 0.003 до 0.017.

Initial pressure of slump proneness changes from 0.12 to 0.25 MPa. The type of soil properties according slump proneness (Building code KMK 2.02.01-98) is the first type. Initial, final water content for slump proneness and water content at total water saturation are: $W_{sl.} = 0.155$ $W_{eq.} = 0.183$ $W_{sat.} = 0.239$. Strength properties of soils of the first lithological unit are characterised by the value of cohesion at natural state 15.0-35.0 kPa, and internal friction angle is 27° - $29^{\circ}54'$. Normative and computed values of these characteristics are: $C_{II} = 21.5$ kPa; $\varphi_{II} = 28^{\circ}33'$, $C_{II} = 10.5$ KPa; $\varphi_{II} = 26^{\circ}14'$, $C_I = 3.4$ kPa; $\varphi_I = 24^{\circ}42'$.

Strength properties of soils of the first lithological unit are characterized by the value of cohesion at saturated state (and consolidation) 9.0-18.0 KPa and internal friction angle is $24^{\circ}54'$ - $28^{\circ}22'$. Normative and computed values of these characteristics are: $C_{II} = 14.3$ KПа; $\varphi_{II} = 27^{\circ}22'$, $C_{II} = 6.9$ KПа; $\varphi_{II} = 25^{\circ}49'$, $C_I = 2.1$ KПа; $\varphi_I = 24^{\circ}47'$.

According to laboratory data the deformation properties of soils are characterised by the values of compression module of deformation 2.6-11.9 MPa, at the normative value 6.1 MPa. At water saturation of soils the value of deformation module ranges between 1.5-7.4 MPa, at the normative value 3.8 MPa. The variability degree of soil compressibility for the first lithological unit is equal to: $\alpha_E = 6.1 / 3.8 = 1.6$.

Second lithological unit - loess-type loams, brown, macroporous, moistened and water saturated, lying on lower part of cross-section starting from 5.5-8.5 m in depth (up to groundwater level), have not proneness to slump at $P=0.3$ MPa. These soils, according to liquidity index, have solid - liquid-plastic consistencies. Specific gravity of dry soil ranges between 1.39-1.68 t/m^3 , at normative value 1.59 t/m^3 . Specific gravity of saturated soil ranges between 1.65-2.12 t/m^3 , at normative value 1.96 t/m^3 and computed values are: $\rho_{II} = 1.94$ t/m^3 ; $\rho_I = 1.92$ t/m^3 . Strength properties of soils of the second lithological unit are characterised by the value of cohesion at natural state 4.0-19.0 KPa, and internal friction angle is $26^{\circ}34'$ - $29^{\circ}15'$. Normative and computed values of these characteristics are: $C_{II} = 11.4$ kPa; $\varphi_{II} = 27^{\circ}48'$, $C_{II} = 7.9$ kPa; $\varphi_{II} = 27^{\circ}07'$, $C_I = 5.8$ kPa; $\varphi_I = 26^{\circ}40'$.

Strength properties of soils of the second lithological unit are characterised by the value of cohesion at saturated state (and consolidation) 3.0-13.0 kPa and internal friction angle is $25^{\circ}24'$ - $28^{\circ}22'$. Normative and computed values of these characteristics are: $C_{II} = 8.5$ kPa; $\varphi_{II} = 27^{\circ}00'$, $C_{II} = 5.4$ kPa; $\varphi_{II} = 26^{\circ}22'$, $C_I = 3.6$ kPa; $\varphi_I = 26^{\circ}00'$.

According to laboratory data the deformation properties of soils are characterised by the values of compression module of deformation 2.4-5.6 MPa, at the normative value 4.3 MPa. At water saturation of soils the

value of deformation module ranges between 2.3-5.6 MPa, at the normative value 4.3 MPa. The variability degree of soil compressibility for the second lithological unit is equal to: $\alpha_E = 4.3 / 3.9 = 1.1$.

Third lithological unit - loess-type loams, brown, water saturated, lying on lower part of cross-section under the ground water level, up to 13.0-30.0 m in depth. According to liquidity index these soils have tight-plastic - plastic consistencies. Specific gravity of dry soil ranges between 1.60-1.65 t/m^3 , at normative value 1.62 t/m^3 . Specific gravity of saturated soil ranges between 1.98-2.06 t/m^3 , at normative value 2.01 t/m^3 and computed values are: $\rho_{II} = 2.0$ t/m^3 ; $\rho_I = 1.98$ t/m^3 . Strength properties of soils for third engineering-geopolitical element are characterised by the value of cohesion at natural state 12.0-14.0 kPa, and internal friction angle is $27^{\circ}01'$ - $27^{\circ}42'$. Normative and computed values of these characteristics are: $C_{II} = 13.0$ kPa; $\varphi_{II} = 27^{\circ}20'$, $C_{II} = 10.5$ kPa; $\varphi_{II} = 26^{\circ}40'$, $C_I = 8.6$ kPa; $\varphi_I = 26^{\circ}10'$.

Strength properties of soils for third lithological unit are characterised by the value of cohesion at saturated state (and consolidation) 12.0-12.7 KPa and internal friction angle is $26^{\circ}06'$ - $27^{\circ}28'$. Normative and computed values of these characteristics are: $C_{II} = 12.3$ kPa; $\varphi_{II} = 26^{\circ}40'$, $C_{II} = 9.8$ kPa; $\varphi_{II} = 25^{\circ}50'$, $C_I = 7.2$ kPa; $\varphi_I = 25^{\circ}00'$.

According to laboratory data the deformation properties of soils are characterised by the values of compression module of deformation 4.6-5.8 MPa, at the normative value 5.2 MPa. At water saturation of soils the value of deformation module ranges between 4.2-5.2 MPa, at the normative value 4.7 MPa. The variability degree of soil compressibility for the third lithological unit is equal to: $\alpha_E = 5.2 / 4.7 = 1.1$.

Fourth lithological unit - gross soils with loamy filling. Loamy soil - brown colour, water saturated with tight-plastic consistency. Gross are represented by fragments of metamorphic rocks with diameter $d = 2-20$ mm. They are lying on lower part of cross-section in depth 13.0-30.0 m.

CONCLUSIONS

The site investigation consisted of boreholes and geotechnical laboratory tests, combined with geophysical tests in field (see Kholmatov et al. 2009) were carried out on Landfill Ahangaranskaya located in Tashkent Region, Uzbekistan. The basic findings are:

- The type of soil properties according to slump proneness corresponds to the first type according to Building code KMK 2.02.01-98.
- The groundwater level within the investigated area is on altitudes 448-458 m.

- The seismicity of the region (according to Building code KMK 2.01.03-96) is estimated to be ca. MSK 8, and the category of soil by seismic properties is III, the seismicity of investigated area is about MSK 9.
- Maximal depth of seasonal soil freezing is 0.66 cm (Building code KMK 2.01.01-94).
- Constructional category of soil at operation (by machines) should be accepted according to their density values (Building code KMK 4.05.01-96):
 - for fill-up soil - 1.85 t/m³;
 - for loamy soils - 1.87 t/m³.

The landfill construction and operations of the Landfill Ahangaranskaya are of a high standard in comparison with most landfill sites in Central Asia. However, there are still some weaknesses in landfill construction like: insufficient compaction and no proper placement of wastes and soil in layers. In such a situation, there might be geotechnical hazards related consolidation (subsidence) of landfills in case of large earthquakes because it is located in seismic active zone. As there is no liner at the base of landfill, there is a greater chance of contamination of the underlying soil and groundwater.

Since the site is located in flat terrain, the risk of slope failure of the landfill due to earthquake is low. But because of the low density of waste, there is high risk of localized consolidation of the landfill surface in the mid to long term. The operation buildings on the landfill should be safe against earthquake. Otherwise there is a risk for the people working on the landfill due to the possible collapse of the buildings during an earthquake. The already applied compaction of the disposed waste and the installation of intermediate cover help to stabilize the landfill body. Additionally the slopes of the landfill should be flattened and compacted to prevent their collapse and currently unused areas should be temporarily covered. In the fresh landfill site use of liner/geomembrane is suggested to avoid ground contamination and to control leachate.

ACKNOWLEDGEMENTS

The NISMIST project (Contract 516732) is funded by the EU Sixth Framework Programme within the International Cooperation (INCO) especially for Russia and New Independent States (Call identifier FP6-2003-INCO-Russia + NIS-1).

REFERENCES

- Building code KMK 2.02.01-98 - Foundation of constructions and buildings.
- Building code KMK 2.01.03-96 - Construction in seismic active regions.
- Building code KMK 2.01.01-94 - Climatic and physical-geological data for engineering.
- Building code KMK 4.05.01-96 - Volume № 1. Earthworks.
- Braja M Das (2005). Fundamentals of Geotechnical Engineering, ISBN 0-534-49294-0.
- Erdik M, Rashidov T, Safak E, Turdukulov A (2005). Assessment of seismic risk in Tashkent, Uzbekistan and Bishkek, Kyrgyz Republic, Soil Dynamics and Earthquake Engineering, 25, 473-486.
- Interstate Standard 30416-96 - Soils. Laboratory testing. General requirements.
- Interstate Standard 25100-95 - Soils. Classification.
- Interstate Standard 12248-96 - Soils. Laboratory methods for determining the strength and strain characteristics.
- Interstate Standard 20522-96 - Soils. Statistical treatment of the tests result.
- Kholmatov K, Khashimova D, Wang X, Webb S, Wu W (2009). Geophysical site characterization of landfill in Uzbekistan, Proc. of International Symposium on Geoenvironmental Engineering ISGE2009, Sep. 8-10, 2009, Zhejiang University, Hangzhou, China (submitted).
- State Standard 12248-78 - Soils. Laboratory methods for determining the shear strength.

AMBIENT NOISE SITE INVESTIGATION OF A REPRESENTATIVE MSW LANDFILL IN BISHKEK, KYRGYZSTAN

Thiep DOANH¹, Xue-Tao WANG², Stephen WEBB³ and Wei WU⁴

ABSTRACT: This paper explores the possibilities offered by the ambient noise vibration technique to evaluate some dynamic characteristics of the waste and the underlying loess deposit of a representative municipal solid waste (MSW) landfill site in Bishkek, Kyrgyzstan. The paper demonstrates that the ambient noise technique provides the source for a simple and low-cost in-situ dynamic characterization of landfill site. The result can be of great benefit for many developing countries.

KEYWORDS: site investigation, landfill, dynamic characterization

INTRODUCTION

This paper presents the partial results of the geophysical site investigation carried out under the NISMIST project (Management of environmental risks associated with landfills in seismically active regions in the New Independent States (NIS) of Central Asia project) to determine the dynamic characteristics and hazard potential of a representative municipal solid waste landfill site in Bishkek, Kyrgyzstan. The ambient noise vibration technique is used to evaluate some dynamic characteristics of the waste and the underlying loess deposit of Bishkek landfill. This in-situ site investigation is supplemented by some geotechnical, hydrogeological and geoenvironmental surveys.

In the literature of Municipal Solid Wastes (MSW), the usefulness of spectral ratio technique for the characterisation of wastes is reported by Guéguen et al. (2000). In many cases, however, the dynamic properties of wastes are inadequately documented. A very limited number of landfills in the world are permanently instrumented with geophysical equipments as mentioned in Morozhnik et al. (1998). In this context, the present geophysical site investigation of MSW landfill using ambient noise technique (which is low cost and simple) may be of great importance to many developing countries to understand the dynamic characteristics of solid wastes.

SITE DESCRIPTION

Site Description

The landfill is located at a former quarry site, about 10 km north of the Bishkek City, at 42°57.6377' N latitude and 74°35.2118' E longitude. The landfill area extends about 1 km in the north-south and 0.3 km in the east-west direction and occupies a contiguous area of about 30 ha of agricultural land. The landfill is surrounded by an access road, visible in the aerial view of about 1 km width in Fig. 1 (provided by Google Earth software). A water reservoir is located in the eastern part of the landfill site.

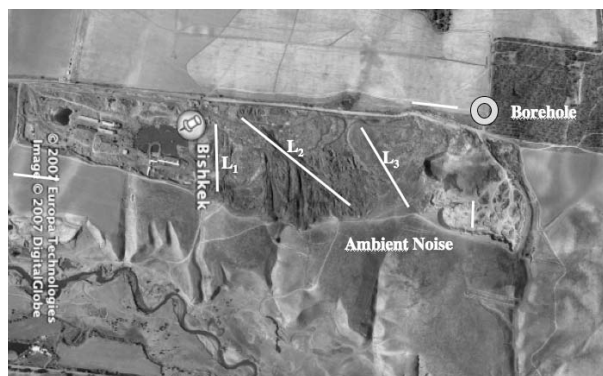


Fig. 1 Ambient noise measurement lines at Bishkek landfill site

¹ Professor, Laboratoire Geomatériaux, Ecole Nationale des Travaux Publics de l'Etat, Vaulx en Velin Cedex, France. Email: Thiep.DOANH@entpe.fr

² MSc., Institute of Geotechnical Engineering, Universität für Bodenkultur Wien, Austria. Email: xuetao.wang@boku.ac.at

³ Dr., Institute of Geotechnical Engineering, Universität für Bodenkultur Wien, Austria. Email: stephen.webb@boku.ac.

⁴ Professor, Institute of Geotechnical Engineering, Universität für Bodenkultur Wien, Austria. Email: wei.wu@boku.ac.at

Geological Setting

Bishkek region is situated in the central part of Chui basin. The city of Bishkek is located on foothill plain of Kyrgyz Mountains with altitudes ranging from 725 m to 800 m above sea level. There are large areas of massive loess and loess-like deposits in the vicinity of Bishkek. The landfill area is located in the northern part of Chui valley. The altitudes range from 678 m (north side) to 691 m (south side). The site has the characteristics of gentle slopes in alluvial - pluvial plain.

The existing boreholes indicate that the ground water table varies from 8 to 14 m below ground surface. Previous site investigations of the landfill area showed three quaternary loess strata below the ground surface. The first thick layer is about 80 – 120 m thick of loam loess including lenses of sandy gravel and boulder deposits of less than 10 m in thickness, the second layer is about 500 m thick of pluvial and alluvial loam with pebble stones, the third layer is a rock substratum with unknown thickness.

Seismicity

Bishkek region lies on the north central of Kyrgyzstan, bordered by the northern foot of the North Tien Shan Mountains often considered as one of the seismically most active region of Central Asia. This high level of seismicity results from the collision of the Indian subcontinent with Eurasia (Erdik et al. 2005). In contrast with other major cities of Central Asia, Bishkek has not experienced any major earthquake during the 20th century.

However, according to seismic zoning maps of Kyrgyz Republic the probability of an earthquake with the magnitude 6.5 - 7.0 on the Richter scale for the next 20 years is rather high for Bishkek,. The well-known Yssyk-Alta fault, delimiting the Chui basin and the foothill terraces of Kyrgyz Mountains, lies in the vicinity of the city. To estimate the seismic hazard at the regional level, Peak Ground Acceleration (PGA) maps of the whole East Asia with 10 % of probability of exceedance in 50 years return period was produced within the Global Seismic Hazard Assessment Program (GSHAP). A large PGA value of about 4.8 m/s² is expected for Bishkek region.

Landfill Characteristics

The landfill was put into operation in 1978 with a projected lifetime of about only 10 years. However, it has been in operation for more than 30 years. The waste is typically unsorted household refuse, construction and metal waste. Organic waste content appears to be relatively low. This landfill was founded on an existing

excavated pit and further developed to a final simple trapezoidal embankment of waste deposits above the ground. The landfill was designed initially without geomembrane base liner, with neither gas nor leachate collection system. Intermediate or final protective cover is also missing.

AMBIENT NOISE SITE INVESTIGATION

As the site investigation is the first step to assess the seismic vulnerability of MSW landfill in Central Asia, the ambient noise technique is selected as the preferred geophysical method to evaluate some dynamic properties in Bishkek landfill. The geophysical site investigation was conducted by T. Doanh (ENTPE) with the help of local scientists. Using noise ambient technique the landfill site was investigated for different material characteristics. The whole waste body including underlying natural loess was investigated. This investigation was aimed at evaluating some dynamic characteristics of waste and loess deposits, mainly for the determination of fundamental resonance frequency and seismic amplification.

The low-cost of this technique, the availability of digital ambient noise instrumentation, the difficult identification of waste properties in laboratory due to inadequate representative volume element of heterogeneous waste materials have contributed to the early adoption of the ambient noise technique in geophysical surveys at the Bishkek landfill site.

Ambient Noise Method

The landfill site is artificially separated into north and south zones along a depression nearly in the middle of landfill. These two zones are oriented approximately to the north. Three measurement lines were arranged (line L₁, line L₂ and line L₃ in Fig. 1) inside the main landfill area, totally 16 double measurement points. Seven additional double measurement points on 3 short measurement lines were also performed on natural loess outside the landfill area, at the base of the excavated area in the northern part and near the water reservoir outside the landfill.

The empirical horizontal-to-vertical spectral ratio (HVSr) method was first introduced by Japanese scientists to evaluate the dynamic characteristics of soft sedimentary deposits. The HVSr method is based on the propagation of surface waves. This technique is further developed and frequently applied in the investigation of the local site response due to its low-cost and fast surveys (Nakamura et al. 1989). In the case of MSW landfill, the fundamental period (f_0) of soil deposits can be estimated, and the shear wave velocity (V_s) evaluated if the thickness of the waste layer is known from landfill records.

Testing Equipment

Two Trominos, digital seismic noise measurement systems (tomography) from Micromed, were used. Each digital tomography consists of one portable high-resolution electrodynamic sensor with 3 orthogonal components, one integrated high resolution digital data acquisition and pre-processor. The three vibration components (EW, NS and UD) were measured nearly simultaneously at a sampling rate of 128 Hz on two data acquisition systems during at least 16 minutes with the same gain level, as recommended by Sesame guidelines (2004). The sensors were installed directly on the loess ground or on top of the waste column. The measurement at each point was simultaneously performed with two tomographies to check the validity of ambient noise measurements.

ANALYSIS AND INTERPRETAION

Following the recommendations of the SESAME project, all measurements were analysed using SESAME (European research project) criteria (2004). The conditions for reliability and stability of the measurements require three criteria, and that of clear peak identification six criteria most of which are fulfilled in the analysis and interpretation of measurements.

Spectral Ratio on Loess

Typical ambient noise responses at point P17 on natural loess in the excavated zone are presented in Fig. 2 - Fig. 5. The thick red line in Fig. 2 represents the average spectral ratio whereas two thin black lines represent confidence limits of 95 % in a semi-logarithmic scale. The Fig. 3 represents the power spectral of the three components, EW, NS and UD separately. The Fig. 4 shows the directional dependency of the HVSR from 0° to 180° and Fig. 5 shows the time history over the whole recording duration.

The measurement data were analysed with 10 % smoothing and triangular window to smooth the spectra with removal of some disturbed windows (black region on the time history graph). The Fig. 2 shows a relatively small and rounded HVSR peak f_0 at about 1.09 ± 0.06 Hz. The amplitude AH/V (f_0) at peak is only 2.2 and there is a narrow amplification which ranges from 0.9 to 1.3 Hz. Note that the peak is not clearly identified since the amplitude is not decreasing rapidly on each side. The second peak at high frequency is probably associated with a very shallow structure, characterized by an inversion in the power spectral graph (Fig. 3). The vertical UD component is above the two horizontal NS, EW components in a large frequency range (from 2 Hz to 80 Hz).

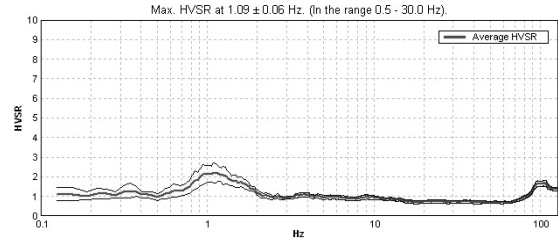


Fig. 2 Average spectral ratio (red line) together with 95 % of confidence limits (black lines) at P17 on natural loess in the excavated zone

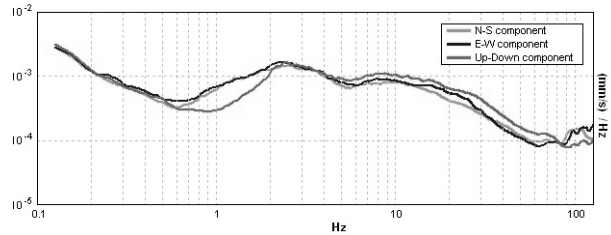


Fig. 3 The power spectral of the EW, NS and UD components at P17 on natural loess

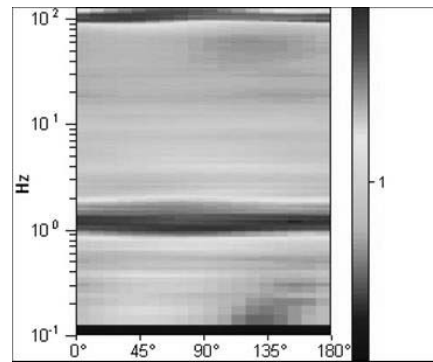


Fig. 4 The directional dependency of the HVSR at point P17

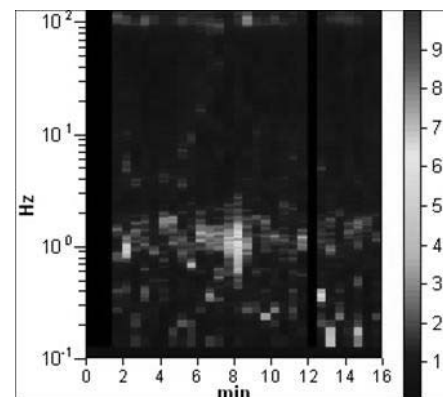


Fig. 5 Time history over the whole recording duration of point P17 on natural loess in the excavated zone

The directional dependency graph (Fig. 4) shows that the identified peak is almost uniform in the whole angular domain with colours varying from orange (3 in

the HVSR colour scale) to red (4). Globally, an isotropic response on loess is observed from this graph and from the similarity between the power spectral responses of two horizontal directions. The time history graph (Fig. 5) indicates the consistency of the peak (light blue zone) at 1.0 Hz over the whole duration of recording (16 minutes) except some disturbances (red colour) in the first minute. Spectral ratio on waste Typical ambient noise responses at point P5 of line L1 on old waste are presented in Fig. 6 - Fig. 9. A unique resonance frequency of about 0.91 ± 0.03 Hz can be clearly identified in Fig. 6. A peak amplification of magnitude 2.5 and amplitude ranging from 0.9 to 1.4 Hz can also be observed in the graph.

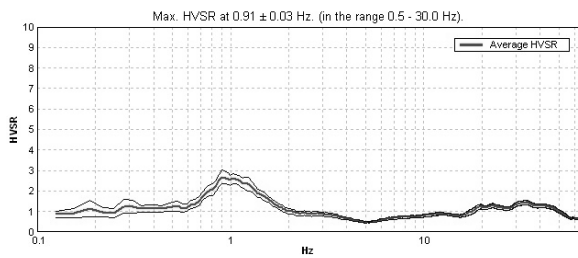


Fig. 6 Average spectral ratio (red line) together with 95 % of confidence limits (black lines) at point P5 of line L1 on wastes

The peak amplitude of 2.5 means a low impedance contrast between the waste and underlying loess layer. Therefore the peak is represented consistently during the whole recording period in the time history graph. A closer look at the HVSR graph reveals numerous peaks at higher frequencies with smaller amplitudes.

The power spectral graph shown in Fig. 7 indicates a clear separation of the two horizontal components below 3 Hz and the directional graph in Fig. 8 shows a HVSR peak around 1 Hz (y-axis) and 90 Hz (x-axis). This means an anisotropic behaviour of the waste deposit and the horizontal component responsible for the peak acted perpendicularly to the sensor's main direction. It seems that this Bishkek landfill has complex underground structures.

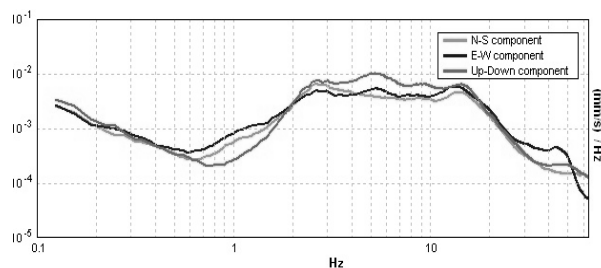


Fig. 7 The power spectral of the EW, NS and UD components at point P5 of line L1 on wastes

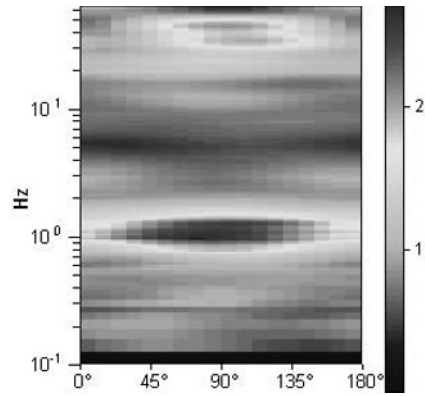


Fig. 8 The directional dependency of the HVSR at point P5 on older wastes

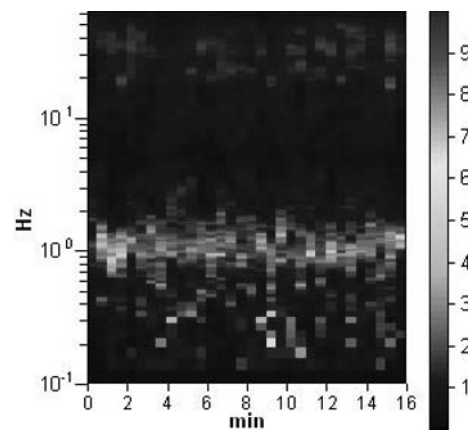


Fig. 9 Time history over the whole recording duration of point P5 of line L1 on older wastes

The ambient noise response on younger waste at point P8 of line L2, right in the central part of the landfill are shown in Fig 10 - Fig. 13. The ambient noise response at this point corroborates the previous observations at point P5. This measurement point generates a resonance frequency of about 1.25 ± 0.06 Hz with amplitude of about 2.5 in the range from 0.9 to 1.5 Hz. The observed anisotropic effect is still visible in the power spectral and directional dependency graphs shown in Fig. 12 and Fig. 13. Similar results are obtained along the three main measurement lines, L1 to L3, inside the waste body.

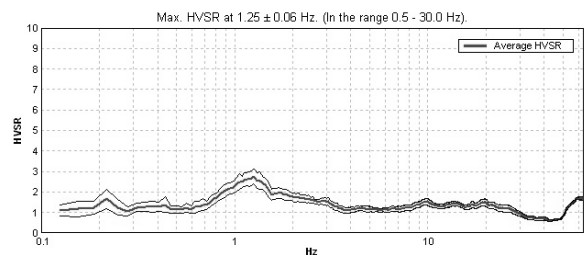


Fig. 10 Average spectral ratio (red line) together with 95 % of confidence limits (black lines) at point P8 of line L2 on younger wastes

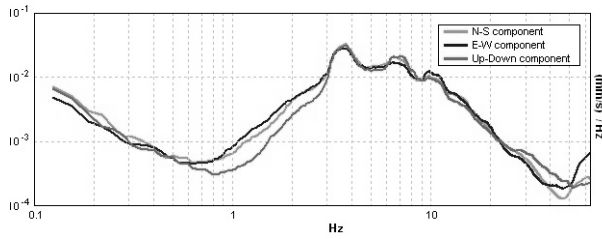


Fig. 11 The power spectral of the EW, NS and UD components at point P8 of line L2 on younger wastes

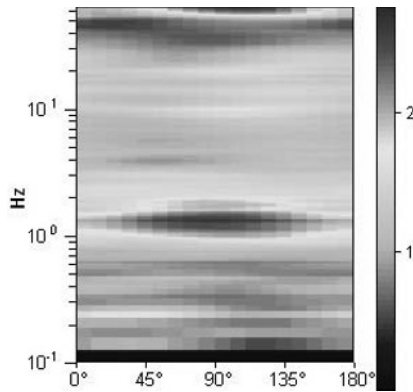


Fig. 12 The directional dependency of the HVSr at point P8 on younger wastes

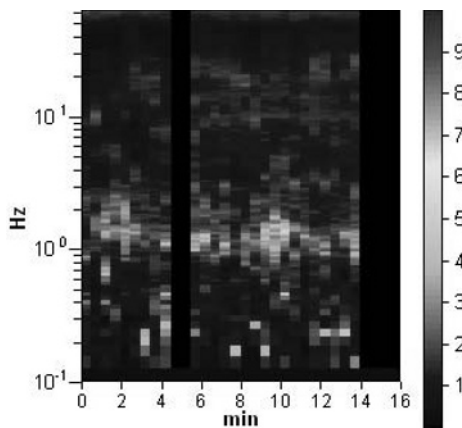


Fig. 13 Time history over the whole recording duration of point P8 of line L2 on older wastes

As mentioned earlier, during the analysis and interpretation of ambient noise tests, all three criteria recommended by SESAME are fulfilled. According to these criteria, the measurements should have more than 10 significant cycles in each analysed window (criterion 1); the total number of significant cycles should be larger than 200 (criterion 2) and the standard deviation of H/V peak frequency should be exceeded by 0 out of 44 times (criterion 3). The present measurements are satisfactory in terms of stability due to a satisfactory level of standard deviation. Concerning the identification of the first

resonance frequency f_0 , five out of six Sesame criteria for an ideal clear H/V peak frequency are fulfilled.

SUMMARY AND CONCLUSIONS

Using the ambient noise vibration technique, a comprehensive geophysical site investigation of a representative municipal solid waste (MSW) landfill site in Bishkek, Kyrgyzstan was carried out within the framework of NISMIST project. The main objective of this site investigation is to determine the dynamical characteristics of the landfill materials along with underground soil. The dynamic properties of material obtained from the site investigation will be used in the dynamic analysis of landfills under seismic loading to investigate the landfill seismic hazards. This paper also shows the possibilities offered by the simple, low-cost and relatively modern ambient noise vibrations technique to be used for geophysical site investigation for a reliable dynamic characterization of MSW landfills.

The ambient noise results obtained are comparable with the results of other conventional geophysical site investigation methods; vertical electrical sounding and the seismic refraction. The applicability and the viability of the ambient noise method as an alternative to conventional geophysical method to characterize MSW landfill is justified with the results of this site investigation at Bishkek. This is the first ambient noise site investigation with the use of modern digital tomography on a landfill in Central Asia. A more detailed analysis of the site can be done by combining the results of geological, geotechnical and hydro-geological site investigations.

ACKNOWLEDGEMENTS

The NISMIST project (Contract 516732) is funded by the EU Sixth Framework Programme within the International Cooperation (INCO) especially for Russia and New Independent States (Call identifier FP6-2003-INCO-Russia + NIS-1).

REFERENCES

- Erdik M, Rashidov T, Safak E, Turdukulov A (2005), Assessment of seismic risk in Tashkent, Uzbekistan and Bishkek, Kyrgyz Republic, *Soil Dynamics and Earthquake Engineering*, 25(7):473-486.
- Guéguen G, Chatelain JL, Guiller B, Yepes H (2000). An indication of the soil topmost layer response in Quito (Ecuador) using noise H/V spectral ratio, *Soil Dynamics and Earthquake Engineering*, 19(2):127-133.

- Kavazanjian E, Jr (1998). Mechanical properties of municipal solid waste, In Proc. 8th Int. Waste Management and Landfill Symposium, Cagliari, Italy: 415-424.
- Morochnik V, Bardet JP, Hushmand B (1998). Identification of dynamic properties of OII landfill, Journal of Geotechnical and Geo-environmental Engineering, ASCE, 124(3): 186-196.
- Nakamura Y (1989). A method for dynamic characteristics estimation of subsurface using microtremor on the ground surface, Quarterly Report of Railway Technical Research Institute, 30(1): 25-33.
- SESAME (Site EffectS assessment using AMbient Excitations) (2004). Guidelines for the implementation of the H/V spectral ratio technique on ambient vibrations, Technical Report, SESAME European Research Project.

ANALYSES ON APPLICABILITY OF ET COVERS IN HUMID AREAS

Wen-Jie ZHANG¹ and Yun-Min CHEN²

ABSTRACT: Evapotranspiration (ET) covers offer a number of potential advantages over conventional covers, however, they are mainly used in arid and semi-arid areas. Analysis on applicability of ET covers in humid climates becomes interesting. Numerical analyses were carried out to simulate the water movements in ET covers. Influences of cover thickness, soil type, LAI and capillary break on performance of ET covers were investigated. The combination of these parameters that can minimize percolation was obtained. ET covers with these design parameters were analyzed considering 20-years period precipitations of Suzhou city in the Yangtze River delta region, China. The results show that final percolation decreases with an increasing cover thickness and an increasing LAI. Cover soils with a large storage capability and a moderate hydraulic conductivity are most effective to minimize percolation. Capillary barriers are more efficient than monolithic barriers. Feasibility analysis shows that ET cover can be used in Yangtze River delta region.

KEYWORDS: ET covers, humid areas, applicability, numerical analyses

INTRODUCTION

Final cover systems are used at landfills to control moisture and percolation, minimize erosion, prevent direct exposure to the waste, control gas emissions and odors, and meet aesthetic and other end-use purposes. Final covers are intended to fulfill these functional requirements for an extended period of time with minimal maintenance. A conventional final cover containing a compacted clay layer is considered susceptible to differential settlement, desiccation cracking and root penetration. A composite cover contains a geomembrane layer, which can cause slippage even being constructed at a small slope angle. Therefore, the use of alternative ET covers is becoming increasingly popular (Zornberg et al. 2003). An ET cover typically consists of a thick layer of fine-grained soil, such as silty sand or sandy clay, that is capable of supporting vegetation (US EPA, 2003). An ET cover acts not as a barrier, but as a reservoir that stores moisture during precipitation events and subsequently returns it to the atmosphere as evapotranspiration.

While ET covers have been installed at a number of landfills, performance data and design guidance for these covers are limited (Benson et al. 2001). Lysimeter tests have been carried out by many researchers (Dwyer, 2003; Roesler et al. 2002) to evaluate the performance of ET covers. However, lysimeter test is time-consuming and expensive. Furthermore, lysimeter conditions may not be

representative of prototype conditions because geomembrane in lysimeter cut off the heat and moisture flux from landfill below. So, the use of lysimeter test for ET cover evaluation is suspect (Kavazanjian, 2001). Zornberg et al. (2003) and Kavazanjian et al. (2006) used water balance models to evaluate the performance of ET covers. Gross (2005) described factors that affect the accuracy of water balance analyses. All these researches are focused on ET covers in arid or semi-arid areas. Whether ET covers are applicable in humid climate still needs to be investigated.

Parametric analyses and applicability analyses are carried out in this paper. Influence of cover thickness, soil type, LAI and capillary break on the performance of ET covers are analyzed. Considering 20-years period precipitations of Suzhou city in the Yangtze River delta region, China, performance of ET covers are analyzed and the applicability in humid areas is discussed.

NUMERICAL MODEL

Net Infiltration

According to the hydrologic water balance on the surface of an ET cover, the net infiltration into the cover can be expressed as:

$$INF = P - R - INT - ES - ET \quad (1)$$

¹ Ph.D, Department of Civil Engineering, Shanghai University, China. Email:wjzhang2008@gmail.com

² Professor, Department of Civil Engineering, Zhejiang University, China. Email:chenyunmin@zju.edu.cn

in which INF = net infiltration; P = precipitation; R = surface runoff; INT = interception of rainfall by vegetation; ES = evaporation of water from soil; ET = evapotranspiration by vegetation. Penman-Monteith formula is used to calculate the potential evapotranspiration, and the actual evapotranspiration is calculated based on the potential evapotranspiration and the actual distribution of water content in the cover soil. The rainfall-runoff process is modeled using the SCS curve-number method for it is computationally efficient and widely accepted (Schroeder et al. 1994). A description of these calculations can be found in Zhang et al. (2009) and is not detailed here because attentions of this paper is focused on parametric analyses. The net infiltration corresponding to various weather and design data is calculated and input into an unsaturated-saturated flow model to simulate the water movement in ET covers.

Governing Equation and Boundary Conditions

A one-dimensional numerical model is used to calculate the percolation through an ET cover. The governing equation used is expressed as:

$$\frac{\partial \theta}{\partial t} = \frac{\partial}{\partial z} \left[k_{\psi} \frac{\partial \psi}{\partial z} \right] - \frac{\partial k_{\psi}}{\partial z} \tag{2}$$

where t is time, z is vertical coordinate, θ is volumetric water content, ψ is matric suction, k_{ψ} is hydraulic conductivity. Volumetric water content and hydraulic conductivity are both taken as functions of matric suction. The relationship between volumetric water content and matric suction can be described by the soil water characteristic curve (SWCC) and in this paper it is defined using the following equation, reported by van Genuchten (1980):

$$\theta = \theta_r + (\theta_s - \theta_r) \left[\frac{1}{1 + (\alpha \psi)^n} \right] \tag{3}$$

where θ_r is the residual water content, θ_s is the saturated water content, and α and n are curve fitting parameters.

The unsaturated hydraulic conductivity k_{ψ} is defined by the van Genuchten equation, the parameters θ_r , θ_s , α and n in Eq.3, and the saturated hydraulic conductivity k_s :

$$k_{\psi}(\Theta) = k_s \Theta^0 \left[1 - (1 - \Theta^{\frac{1}{n}})^n \right]^2 \tag{4}$$

In Eq.4, Θ is the dimensionless water content, which is defined as

$$\Theta = \frac{\theta - \theta_r}{\theta_s - \theta_r} \tag{5}$$

The initial condition of the unsaturated flow model can be defined as:

$$\theta(z, t) = \theta(z), \quad t = 0 \tag{6}$$

where θ is initial water content of the cover soils.

The upper boundary of the numerical model is defined as a flux boundary:

$$\left[k_{\psi} \frac{\partial \psi}{\partial z} - k_{\psi} \right]_{z=0} = INT(t), \quad t \geq 0 \tag{7}$$

The flux boundary may be an inflow boundary or an outflow boundary according to the net infiltration, INF , calculated by Eq.1.

The boundary at the bottom of the numerical model is defined as a free drainage boundary:

$$\left[k_{\psi} \frac{\partial \psi}{\partial z} \right]_{z=H} = 0, \quad t \geq 0 \tag{8}$$

Parameters

Omaha in Nebraska, U.S.A., with an average annual precipitation 760mm, is regarded as a typical humid area. Daily climatologic data such as precipitation, mean temperature, and solar radiation are necessary to calculate INF . These parameters are obtained from historical statistics and are shown in Fig. 1.

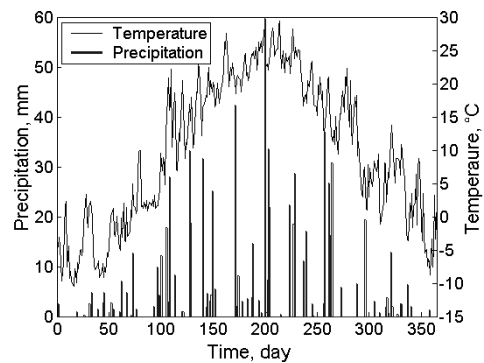


Fig. 1 Precipitation and temperature of Omaha used in the parametric analyses

Three types of soils are chosen as vegetative soils of ET covers. Hydraulic properties of these soils are reported by Roesler et al. (2002). These parameters were defined using van Genuchten equation and are given in Table 1. Soils A, B, C and D are clayey sand, clayey silt, lean clay and sand, respectively. Soils A, B and C are used as vegetative layers, whereas soil D is used in a capillary barrier in this paper. SWCCs of the four soils are shown in Fig. 2. It can be seen that water content of soil D decreases dramatically after the matric suction has exceeded a small value, e.g. about 2 kPa. Matric suction

lines of 33 kPa and 1500 kPa are displayed on Fig. 2, for the volumetric water content at these two matric suctions are assumed to be field capacities, θ_c , and wilting points, θ_w , of these soils, respectively (Hillel, 1998). The storage capacity, or the amount of available water that can be removed by vegetation, is represented by $\theta_c - \theta_w$. The storage capacity corresponding to soils A, B and C are 0.17, 0.24 and 0.36, respectively.

Table 1 Hydraulic parameters of cover soils

Soils	θ_r	θ_s	α kPa ⁻¹	n	k_s cm/s	θ_0
A	0	0.37	0.065	1.26	4.0×10^{-4}	0.12
B	0	0.46	0.0176	1.29	1.9×10^{-5}	0.18
C	0	0.44	0.0039	1.97	6.1×10^{-6}	0.19
D	0.05	0.41	0.35	7.22	2.0×10^{-2}	0.06

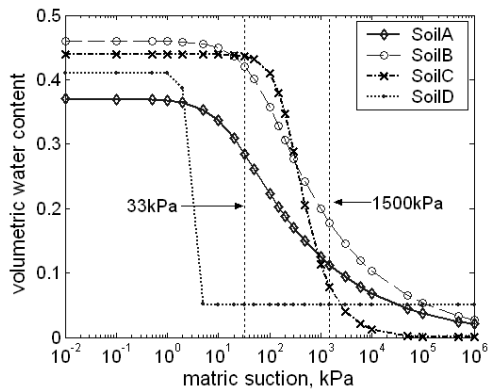


Fig. 2 SWCCs of soils used in the analyses

Leaf area index (LAI) and evaporative zone depth are used in this paper to characterize the capability of vegetative evapotranspiration. The LAI is assumed to reach its maximum 30 days after the germination date, remain at 2.0 throughout most of the growing season, and to decrease linearly 30 days prior to the end of the growing season. For Omaha site, a maximum LAI of 2.0 is used. Growing season starts from the 113rd day and end at the 280th day (Julian date). Evaporative depth is assumed to equal the thickness of the vegetative cover. This may be the actual case for ET covers because trees and shrubbery can be planted and the roots may reach several meters deep.

PARAMETRIC ANALYSES

Thickness of Vegetative Cover

Soil B is used here. Slope of the cover surface is 5% and the corresponding runoff curve number is 85. The

first analyzed thickness is 600 mm. The calculated daily net infiltration is shown in Fig.3. It is input cyclically into the unsaturated flow model as boundary condition. In order to reflect the long-term performance, the ET covers are being simulated for 5 years.

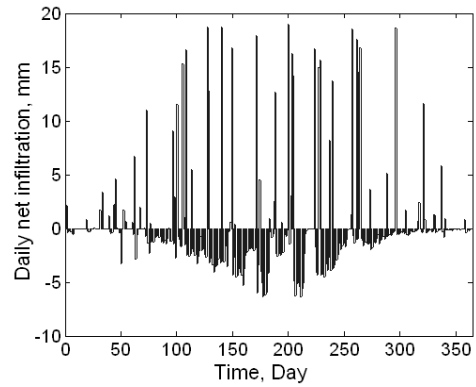


Fig. 3 Daily net infiltration of the 600 mm cover, soil B

The annual percolation in the five years is calculated to be 0.11 mm, 13.07 mm, 31.57 mm, 34.29 mm and 35.11 mm, respectively. The increases in annual percolation arise from relatively low initial water content of the cover soil. The simulated cover in the 5th year is considered representative of the long-term performance and is analyzed hereafter.

Daily percolation together with the volumetric water content of bottom soils is shown in Fig. 4. It can be seen that percolation mainly happens from the 50th day to the 150th day. And in this period of the year, the volumetric water content of the bottom soils exceeds its field capacity. This is because that the growing season has not start, so the evaporation and evapotranspiration is low. In subsequent period, the evapotranspiration becomes considerable and volumetric water content decreases till the end of the growing season.

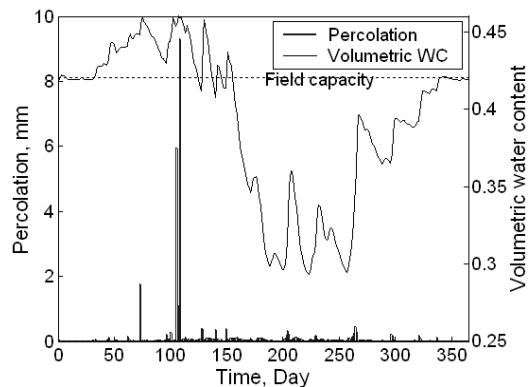


Fig. 4 Daily percolation and volumetric water content of bottom soils of the 600 mm cover, soil B

Percolation is the final criteria to evaluate a landfill cover. Though there is no regulation that specifies the

allowable percolation of an ET cover, an annual percolation of 35.11 mm is still too much, considering percolation can usually be controlled below 1 mm in arid and semi-arid areas. Therefore, covers with the thickness of 800 mm, 1000 mm and 1200 mm are simulated under the same circumstance. The annual percolation corresponding to the 5th year is 29.67 mm, 10.37 mm and 0.05mm, respectively. This illustrate that percolation decrease as the vegetative thickness increases, and that a 1200 mm thick vegetative cover constructed with soil B can satisfy the requirement of percolation control in this area. It should be noted that the above result are obtained in ideal situation. As preferential flow induced by desiccation, freeze-thaw cycling and biota intrusion may happen in field scale, the needed cover thickness should be increase.

Soil Types

ET covers with soils A, B and C (named cover A, B and C hereafter) are compared. Only the calculated final percolation is given here for simplicity. Annual percolations of these covers corresponding to various cover thickness are shown in Fig.5. For cover A, percolation firstly decreases with the increasing cover thickness. However, when the thickness exceeds 1200 mm, the decreasing trend becomes unobvious, and sometimes a little increase in percolation happens as the thickness increases. Even the thickness reaches 2000 mm, there is still 20.24 mm percolation in a year. This illustrate that cover A is not applicable in these area. For cover C, the calculated percolation corresponding to thickness 400 mm, 600 mm and 800 mm is only 0.023mm/yr, 0.017 mm/yr and 0.014 mm/yr, respectively. The great difference in performance of these covers mainly arise from the difference in storage capacity, $\theta - \theta_s$, as mentioned early. So, soil with a high storage capacity is recommend in humid areas.

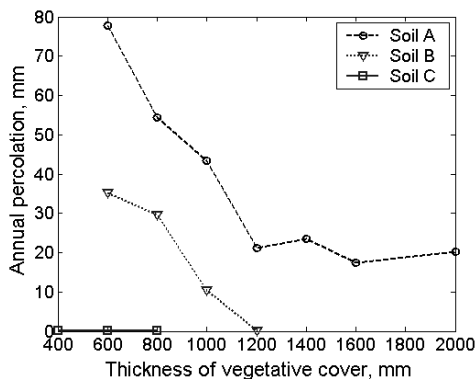


Fig. 5 Annual percolations of covers A, B and C corresponding to various cover thickness

In order to further analyze the influence of k_s on the performance of ET covers, SWCC of soil B is assumed

unchanged whereas k_s is assumed 1.9×10^{-4} cm/s, 1.9×10^{-5} cm/s and 1.9×10^{-6} cm/s. Only 600mm thick cover is analyzed here. The calculated annual percolations are 55.58mm/yr, 35.11mm/yr and 0.01mm/yr, respectively. It is concluded that percolation will decrease with k_s . However, as requirement for vegetation growth is concerned, soil with a very low k_s is not recommended in vegetative use.

LAI

Cover B with the thickness 800 mm and 1000mm are taken as examples to demonstrate the influence of LAI on the final percolation. LAI = 5 means that there is excellent stand of grass on the cover surface and it is used in the calculations to compared with the previously used LAI = 2. In circumstance LAI = 5, the calculated annual percolations corresponding to thickness 800 mm and 1000 mm are 26.03 mm and 1.62 mm, respectively. This means that the more flourishing the vegetation, the less the percolation may happen. However, it should be noted that the maximum LAI = 2 used earlier is taken from field investigation (Rosler, 2002). And an LAI as large as 5 is impossible at this location, because after all surface soils are shallow and only provide little moisture storage for vegetation growth in dry period. To maintain a high LAI, irrigation is suggested in these periods.

Monolithic and Capillary Barriers

Two common ET cover designs are monolithic and capillary barriers. A capillary barrier consists of finer textured layer overlying a coarse-grained soil. Soil B and D are used here. The thickness of soils B and D is assumed 800 mm and 300 mm, respectively. The calculated annual percolation is only 0.003 mm. Contrasted with the annual percolation 29.67 mm of the foregoing 800 mm thick monolithic cover, it is conclude that capillary barriers is more efficient. The volumetric water content of soils near the B-D soil interface is shown in Fig. 6. It can be seen that volumetric water content upside the interface sometimes exceeds field capacity, but volumetric water content underside the interface remain unchanged. The contrast in unsaturated hydraulic properties between the two layers in a capillary barrier forms a capillary break that limits downward water movement..

From the above analyses, a combination of these parameters that can reduce the furthest percolation is obtained. Further analyses will be done to find out its applicability in more humid areas such as Yangtze River delta region, China.

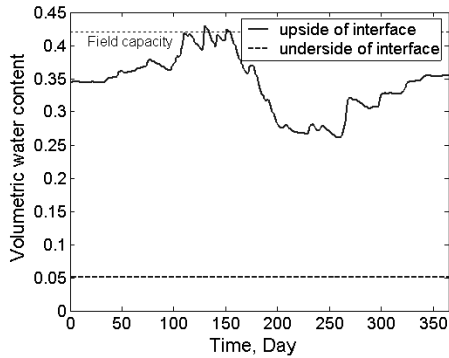


Fig. 6 Volumetric water content near the soil interface in a capillary barrier

APPLICABILITY IN YANGTZE RIVER DELTA REGION

According to CJJ17-2004-China (ECPS-PRC, 2004), the hydraulic design of a landfill can be carried out based on the maximum precipitation in 20 years. The statistical maximum annual precipitation, 7-day precipitation and daily precipitation in a 20-year period in Suzhou city are 1500 mm, 390 mm and 195 mm, respectively. The daily precipitation is generated based on the statistical monthly precipitation and the aforementioned 20-years condition and is shown in Fig. 7. The precipitation during the 192nd day and 197th day is 390 mm, and precipitation on the 195th day is 195 mm. Also shown in Fig. 7 is the average daily temperature generated based on the statistical average monthly temperature. Average humidity is 75% in spring and winter, 80% in summer and autumn in this area. Growing season starts from February and end at November. As shrubbery and trees is considered, LAI = 5 is used and the evaporative depth is assumed to equal the thickness of the vegetative cover.

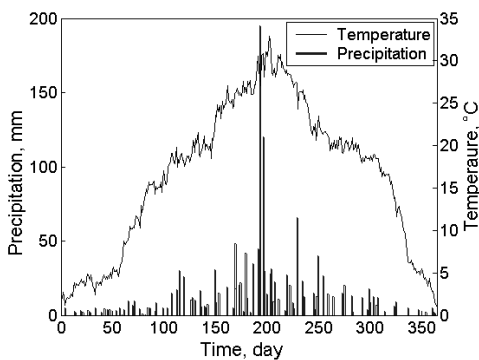


Fig. 7 Precipitation and temperature of Suzhou used in the applicability analysis

A 1000 mm thick monolithic cover made up of Soil C is investigated. As preferential flow in vegetative cover is considered, the saturated hydraulic conductivity of soil C is enlarged to 3.05×10^{-5} cm/s. The calculated

annual percolation is 42.63 mm, i.e. about 2.84% of the annual percolation. Whether this is acceptable is doubtful.

Furthermore, a capillary barrier consists of Soil C and D is analyzed. The vegetative cover is 1000 mm thick and the coarse layer is 300 mm thick. The calculated annual percolation is 0 mm. This shows without doubt that the cover can satisfy the requirement of percolation control in this area. The maximum and minimum volumetric water content at various depths during a year is given in Fig. 8. It can be seen that the range of possible volumetric water content is wide in shallow depth, means intense absorb and release of water. Sometimes the minimum value is very low, corresponding to a dry period. Sometimes the maximum value reaches 0.44, means saturation at that time. The range becomes narrow and remains at about 8% under the depth of 200 mm, corresponding to deeper store and release of water. The water content in sand layer does not change during the year. The capillary break at the soil interface enables the upper layer to store more water for subsequent transpiration, and therefore minimize percolation. Capillary force can hold the water in the fine-grained layer until the soil near the interface approaches saturation.

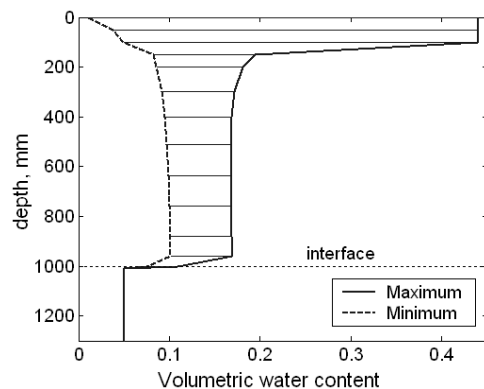


Fig. 8 The range of possible volumetric water content at various depths

The above analyses show that ET cover can be used in Yangtze River delta region, China. Considering the field performance, interim cover and root barrier layer is necessary. Further more, evergreen grass, shrubbery and trees are recommended and irrigation is suggested in dry periods.

CONCLUSIONS

Parametric analyses and applicability analyses of ET covers are carried out in this paper. Conclusions can be drawn as follows.

- 1) Percolation usually decreases with an increasing cover thickness, except when an inapplicable cover soil is use.

2) The bigger the storage capacity, $\theta - \theta_s$, the less the percolation will happen through the cover.

3) Percolation decreases with an increasing LAI. To maintain a high LAI, shrubbery and trees are recommended and irrigation is suggested in dry periods.

4) Capillary barriers are more efficient than monolithic barriers.

5) As 20-years period precipitation circumstances are considered, percolation through the analyzed ET cover is 0 mm. ET cover is applicable in Yangtze River delta region, China.

ACKNOWLEDGEMENTS

This work was supported by the Scientific Research Foundation for Outstanding Young Teacher of Shanghai, China. Thanks are also owed to the reviewers for their patient review.

REFERENCES

- Benson CH, Abichou T, Albright WH, et al. (2001). Field evaluation of alternative earthen final covers. *International Journal of Phytoremediation*. 3(1): 105-127.
- Dwyer SF (2003). Water balance measurements and computer simulations of landfill covers. New Mexico: University of New Mexico.
- Editorial Committee of Professional Standards, People's Republic of China. (ECPS-PRC). (2004). Technical code for sanitary landfill of municipal solid waste (CJJ17-2004). Beijing: China Architecture and building Press.
- Environmental Protection Agency (EPA), US. (2003). Evapotranspiration landfill cover systems fact sheet. EPA 542-F-03-015, <http://clu.in.org/products/altcovers>.
- Gross BA (2005). Water balance evaluations for monitored evapotranspirative cover systems at three sites in the semi-arid and arid Southwest U.S.. Dissertation, U. Texas, Austin, Texas.
- Hillel D (1998). *Environmental Soil Physics*. Academic Press, New York.
- Kavazanjian EJ (2001). Design and performance of evapotranspirative cover systems for arid region landfills. *Proceeding of the 36th Annual Engineering Geology and Geotechnical Engineering Symposium*, Las Vegas.
- Kavazanjian EJ, Beth AG, Tarik HH (2006). Unsaturated flow flux assessment for evapotranspiration cover compliance. *The 4th International Conference on Unsaturated Soils*, ASCE: 634-645.
- Roesler AC, Benson CH, Albright WH (2002). Field Hydrology and Model Predictions for Final Covers in the Alternative Cover Assessment Program-2002. University of Wisconsin-Madison. *Geo Engineering Report No. 02-08*. September 20.
- Schroeder PR, Dozier TS, Zappi PA, Aziz NM (1994). The Hydrologic Evaluation of Landfill Performance (HELP) Model: Engineering Documentation for Version 3. EPA/600/R-94/168b, September 1994, U.S. Environmental Protection Agency Office of Research and Development, Washington, DC.
- Van Genuchten R (1980). Closed-form equation for predicting the hydraulic conductivity of unsaturated soils. *Soil Science Society of America Journal*. 44(5): 892-898.
- Zhang WJ, Qiu ZH, Zhu CR, et al. (2009). Evaluation of evapotranspiration covers of landfills in Yangtze River Delta Region. *Chinese Journal of Geotechnical Engineering*. 31(3): 384-389.
- Zornberg JG, Lafountain L, Caldwell JA (2003). Analysis and design of evapotranspirative cover for hazardous waste landfill. *Journal of Geotechnical and Geoenvironmental Engineering*, 129(5): 427-438.

IN-SITU TESTS AND SLOPE STABILITY ANALYSIS OF MUNICIPAL SOLID WASTE LANDFILL

Hsin-Yu SHAN¹ and Tsuo-Hsien FAN²

ABSTRACT: Due to the limitation of population density and availability of land, a large portion of the landfills of Taiwan, China are located in mountainous area. Current regulations do not require slope stability analysis for these landfills. As a result, almost all of the landfills were not designed to maintain a suitable factor of safety against failure. The composition of Taiwan's solid waste differs considerably from that of the United States or any other country in the world. However, the lack of data of local solid waste poses a great limitation to engineers. The objectives of this research are to collect shear strength data from in-situ tests and perform a series of stability analyses. The results show that the cohesion and friction angle of the MSW at Chu-nan and Hu-kou landfills are 34.9 kPa and 37.9°, 33.6 kPa and 32.1°, respectively. In addition, the coefficients of subgrade reaction, kv, are 875.25 kN/m³ and 494.33 kN/m³, respectively. Results of 2-D and 3-D slope stability analyses show that the factor of safety increases with lower height of wastes, longer length of waste body, smaller slope angle of the back of the excavation, and steeper face slope of final cover. In addition, 3-D analysis indicates that the factor of safety decreases with the widening of the mouth of the landfills on slopes.

KEYWORDS: landfill, in-situ test, shear strength, compressibility, slope stability

INTRODUCTION

Prior to 1980's when direct disposal in landfill was the only appropriate method allowed, there were more than 300 landfills in operation at the same time. There are still more than 130 landfills in use currently although incineration has become the major approach for treating municipal solid wastes (MSW). These active landfills receive nonhazardous industrial wastes along with bottom ash and stabilized fly ash generated by the incinerators. In 2008, more than 4 million tons of MSW was incinerated, which generated about 1.2 million tons of incinerator ash, and approximately 240,000 tons was directly disposed in landfills. Over the time, more landfills will be close while the ones still operates will be limited to the landfills that located in distant rural areas where incineration is inhibited by high cost and those that solely used for disposal of incinerator ash. The closed landfills will be covered with low permeability soil and top soil for vegetation. The Environmental Protection Administration encourages redevelopment of the closed landfills as public recreational facilities such as parks, basketball courts, golf training courses, and croquet courts.

However, a large portion of the landfills in Taiwan

are located in hilly area due to the difficulty in finding suitable locations for landfills as a result of the NIMBY effect. Furthermore, many landfills are dumped with much more MSW than they were designed. Therefore, it is very common for these landfills to experience slope failures of various magnitude in the typhoon season, where accumulation of leachate should be the trigger of such failures.

The objective of this study is to investigate the stability of the landfills with shear strength parameters determined by large scale in-situ tests and 2D/3D slope stability analysis. The results of the study will provide valuable information for future design and operation of the MSW landfills.

BACKGROUND

Unit Weight of MSW

The unit weigh of MSW can be determined by a range of approaches including field methods such as filling a large measuring box with MSW, excavating a test pit, estimation by the weight of MSW dumped and the resulted

¹ Associate Professor, Department of Civil Engineering, National Chiao Tung University, Taiwan, China. Email:hyshan@mail.nctu.edu.tw

² Former graduate student, Department of civil engineering, National Chiao Tung University, Taiwan, China. Email:woodguy1007@yahoo.com.tw

volume, and laboratory methods such as determining the unit weight of remolded MSW (Merz and Stone, 1962; Schumaker, 1972; Sower, 1973; Bromswell, 1978; Dvinoff and Munion, 1986; Sargunan et al. 1986).

The unit weight of MSW ranges from 3.92 to 8.83 kN/m³ depending on the degree of compaction (Table 1) (Dixon and Jones, 2004). The unit weight measured in the field fell between 4.91 and 6.87 kN/m³.

In Taiwan, China the average unit weight of MSW is approximately 1.60±0.05 kN/m³ according to limited data (Taiwan EPA, 2005). This value is much smaller than those listed in Table 1, since the method for measuring the unit weight is different from those used in geotechnical studies.

Table 1 Unit weight of municipal solid wastes (Dixon and Jones, 2004)

Country	Unit Weight (kN/m ³)	Notes	Literature
United Kingdom	5.98	Compacted by 21-ton hammer falling from 2 m above ground	Watts and Charles (1990)
	8.04	Compacted by 21-ton hammer falling from 0.6 m above ground	
Belgium	5.00~10.01	Various degree of compaction	Manassero et al. (1996)
France	6.97	Freshly buried MSW	Gourc et al. (2001)
United States	5.98~6.97	Freshly buried MSW	Kavazanjian (2001)
	14.03~20.01	Highly decomposed	

The data collected by Kavazanjian et al. (1995) showed that the unit weight of MSW near the surface of the fill was about 6 kN/m³ and increased with depth to around 13 kN/m³ at a depth of 80 m. Fassett et al. (1994) showed that the unit weight of MSW near the ground surface to be approximately 3.53 to 6.47 kN/m³ and increased with depth to about 12.5 kN/m³ and remained relatively constant after the depth reached 50 m.

Shear Strength of MSW

The shear strength parameters of MSW are difficult to determine given the wide variety of the type of materials in it and the variation of composition with time due to bio- and/or chemical degradation. The shear strength of MSW has been obtained by large scale direct shear tests or triaxial tests in the laboratory, in-situ direct shear tests, and back-analysis from slope failures. Shear strength parameters available from the literatures are listed in Table 2.

Landva and Clark (1990) conducted large-scale direct shear tests on crushed and shredded MSW in the laboratory and the resultant cohesion and friction angle ranged between 0 to 23 kPa and 24 to 42°, respectively.

Table 2 Shear strength parameters of MSW (Sadek and Manasseh, 2004)

Shear Strength Parameters		Literature	Shear Strength Parameters		Literature
<i>c</i> (kPa)	ϕ (°)		<i>c</i> (kPa)	ϕ (°)	
Direct Shear (LAB)			Back analysis		
19	42	Landva and Clark (1986)	29	22	Pagotto and Rimoldi (1987)
19	38		78	0	Singh and Murphy (1990)
10	33.6		80	8.5	
16	33	Landva and Clark (1990)	60	15	Singh and Murphy (1990)
19	39		57	3	
22	24		40	13	
35	0	Singh and Murphy (1990)	0	35	
70	20		0	38	
65	3		35	14	
0	38		20	20	
0	42		18	20	
15	31		27	19.5	
0	39		Misc.		
0	53	0	35	Martin and Genthe (1993)	
0	41	Golder Assoc.(1993)	10	25	Cowland (1993)
7	42	Jessberger et al. (1994)	15	35	Singh and Murphy (1990)
28	26.5		23.5	20	
50	35	Pelkey (1997)	0	35	Fasset et al. (1994)
27.5	20	Gabr & Valero (1995)	10	23	
0	39		10	32	
0	26	Kavazanjian et al. (1999)	7	38	Jessberger et al. (1994)
43	31		0	30	
24	18	Mazzucato et al. (1999)	0	40	Kolsh (1995)
In-situ tests			15	15	
			18	22	
80	0	Singh and Murphy (1990)	5	25	Jones et al. (1997)
100	0	Richardson and Reynolds (1991)	0-50	35	Eid et al. (2000)
10	18	Whitiam et al. (1995)	Triaxial tests(LAB)		
10	43		100	0	Gabr & Valero (1995)
10	30		40	0	
22	18.2		Thomas et al. (2003)	16.8	34

Singh and Murphy (1990) determined shear strength of MSW by laboratory tests, in-situ tests, and back-calculation and concluded the shear strength $c = -2.35\phi$ (°) +81±17 kPa. Kavazajian et al. (1995) suggested an MSW shear strength envelop where cohesion is 24.0 kPa and friction angle is 0 when normal stress is less than 30.0 kPa and cohesion is 0 and friction angle is 33° when normal stress is greater than 30.0 kPa.

Eid et al. (2000) concluded from the results of large-scale direct shear tests and back-analysis on landfill slope failure that the cohesion and friction angle of MSW to be 25.0 kPa and 35°, respectively. Furthermore, based on the data presented by Eid et al. (2000), Kavazajian et al. (2001) suggested that when normal stress is greater than 150 kPa friction angle of MSW

decreased significantly, such that it is not appropriate to use a straight line for the failure envelope of MSW.

In addition, the stress-strain behavior of MSW is very different from that of soil. Results of triaxial compression tests showed that shear stress continued to increase even after axial strain had already reached 30% (Singh and Murphy, 1990; Machado et al. 2002).

Three-Dimensional Effect of Slope Stability

It is generally believed that the factor of safety resulted from three-dimensional slope stability analysis is often larger than that from two-dimensional analysis. Chang (2005) has quantified the 3D effect of slope stability by the index E_3 , which is defined as:

$$E_3 = (F_3 - F_2) / F_2 \quad (1)$$

where F_2 and F_3 are the factor of safety determined by 2D and 3D stability analysis, respectively. He concluded that 3D effect depends on geometric parameters such as the width to height ratio of the sliding mass, the opening and dipping angles of the slope on the two sides. When the mouth of the slope opens wider than the rest of the slope, 3D analysis gives a smaller factor of safety than 2D analysis. In addition, 3D effect is more pronounced for slopes with width to height ratio less than 5 to 10.

METHODOLOGY

Landfills Selected for Study

Two MSW landfills were selected for this study (Figs. 1 and 2). In-situ direct shear tests and plate load tests were conducted at both landfills, but only the Huko landfill was analyzed for slope stability.

The Huko landfill is located in Hsinchu County. The landfill was in service during 1993 to 2007, which was a year after the in-situ tests were conducted at the site. The Huko landfill covers an area of 3.96 hectare and situated on a mild slope of approximately 10 - 15°. The solid wastes disposed in Huko landfill include MSW and nonhazardous industrial wastes and averaged amount was 40 ton per day.

On the other hand, Chunan landfill is a landfill constructed on flat ground. Concrete and reinforced retaining walls had been constructed as the containing structure of the wastes. The total area of Chunan landfill facility was 31.5 hectare but only a quarter of the area is actually used for disposal of solid wastes. Chunan landfill has been in service since 1987. Nowadays, it only receives around 100 tons of incombustible wastes and 200 tons of nonhazardous industrial waste per day.



(a) General view



(b) Reinforced retaining wall at the toe of slope

Fig. 1 Huko landfill



Fig. 2 Chunan landfill

Physical Properties of MSW

The unit weight of undisturbed MSW samples were measured with a metal sampling box of 500 mm×500 mm×400 mm. Care was taken when trimming samples into the box. Once the samples had been obtained, they were removed from the sampling box and weighed. The samples were taken back to the laboratory to determine their water content.

The compositions of the MSW samples were determined after they were oven dried. Combustible wastes were categorized into plastic, paper, wood and bamboo, and fiber; while non-combustible wastes were categorized into metal, glass, and miscellaneous materials.

In-Situ Tests of MSW

In order to obtain the shear strength parameters of undisturbed MSW samples, large-scale in-situ direct shear tests were conducted. The tests were conducted in

accordance with the inclined load direct shear test suggested by ISRM for testing of weak interface of rock (Lama and Vutukuri, 1978; Brown, 1981) and ASTM D4554-90. Four specimens of 800 mm×800 mm×400 mm were sheared under various normal stresses.

Plate load tests were performed to determine the compressibility of the MSW. Steel plate with a diameter of 750 mm was used as the footing. The tests were conducted following the procedures suggested by ASTM D1194-72.

Slope Stability Analysis

The 3D slope stability analysis was carried out with the software program CLARA-W developed by O. Hungr Geotechnical Research, Inc. The program allows the user to choose from the following methods for analysis: Bishop’s simplified method, Janbu Simplified, method, Spencer’s method, and Morgenstern-Price method.

Four types of 3D failure surface can be selected: ellipsoid, wedge, general, and composite.

RESULTS AND DISCUSSION

Physical Properties of MSW

The unit weight of MSW of Huko landfill ranges between 4.41 – 5.40 kN/m³ with an average of 5.02 kN/m³. The most significant component of the wastes is plastics, which accounts for 72% of the total weight.

On the other hand, the average unit weight of MSW of is 6.37 kN/m³ while the maximum value reaches 7.36 kN/m³. The most significant component is also plastics, which reaches for 26%. The rest of the portion consists of construction debris, food wastes, household wastes, papers, and miscellaneous materials.

Shear Strength and Deformation Properties of MSW

The stress-strain curves of MSW of Huko and Chunan landfills are shown in Figs. 3 and 4, respectively. The normal stresses labeled in the figures are the normal stresses at the start of the tests. The normal stress at failure was computed as the vertical component of shear force increased as shearing took place. It can be seen that the shear stress kept increasing with the shear strain, especially for MSW specimens subject to lower normal stress. For some specimens the shear stress continued to increase even when the shear strain reached 25%. Part of the increase of shear stress can be accounted for by the elevated normal stress, while the majority of the increase should be the result of continuous compaction of MSW during the shearing process. Since the MSW was very loose, dilatancy effect had not been observed.

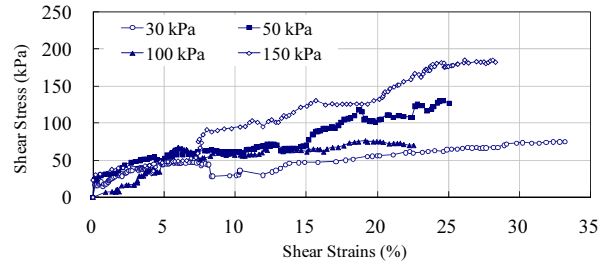


Fig. 3 Stress-strain curves of MSW of Huko landfill

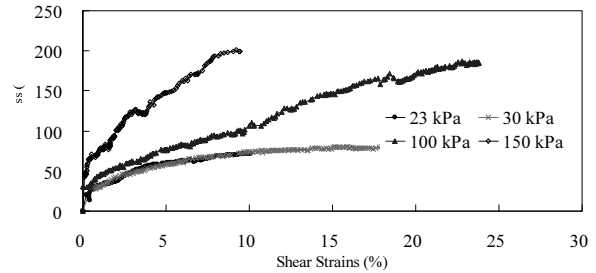


Fig. 4 Stress-strain curves of MSW of Chunan landfill

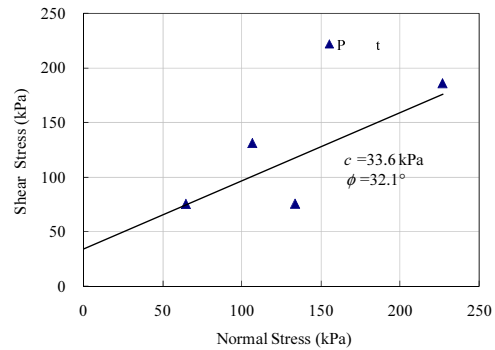


Fig. 5 Failure envelope of MSW of Huko landfill

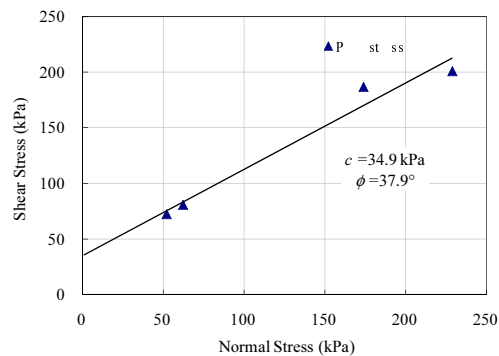


Fig. 6 Failure envelope of MSW of Chunan landfill

The Mohr-Coulomb failure envelopes of the MSW are shown in Figs. 5 and 6. The cohesion and friction angles of MSW of Huko and Chunan landfills are 33.6 kPa and 32.1° and 34.9 kPa and φ=38.0°, respectively. It is likely that the cohesion is an artifact of linear regression. For linear failure envelopes with zero cohesion, the friction angle of Huko and Chunan MSW

are 39.9° and 44.5°, respectively. These shear strength parameters are on the higher side when compared with those tabulated in Table 2.

The load-settlement curves of plate load tests are shown in Figs. 7 and 8. It is difficult to determine the ultimate bearing capacity of the MSW with the relatively linear relationships between settlement and loading. The MSW of Chunan landfill is less compressible and the settlement curve starts to level off after the settlement reached 180 mm. Nevertheless, by following the procedure of data reduction suggested by ASTM D1194 and establish the bearing capacity as loading corresponds to a settlement of 0.5 in., the ultimate bearing capacity, q_{us} of MSW of Huko and Chunan landfills are 5.69 and 11.87 kPa, respectively. These bearing capacity values correspond to those of loose sand and soft clay.

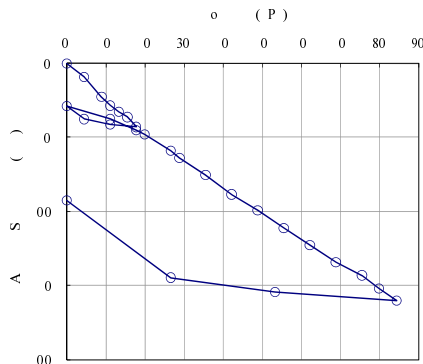


Fig. 7 Load-settlement curve of MSW of Huko landfill

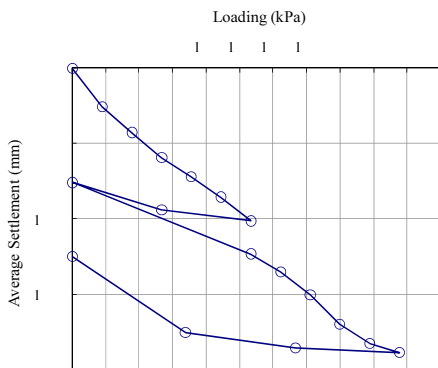


Fig. 8 Load-settlement curve of MSW of Chunan landfill

3D Slope Stability Analysis

The 3D models of the Huko landfill just after construction and before final closure are shown in Fig. 9. The horizontal distance from the geogrid-reinforced retaining wall at the toe of the slope to the top of the slope is approximately 150 m. (Y direction) The width of the landfill is about 100 m (X direction). The maximum height of the MSW approaches 15 m. The height of the retaining wall ranges varied from 6 to 7 m from south to north.

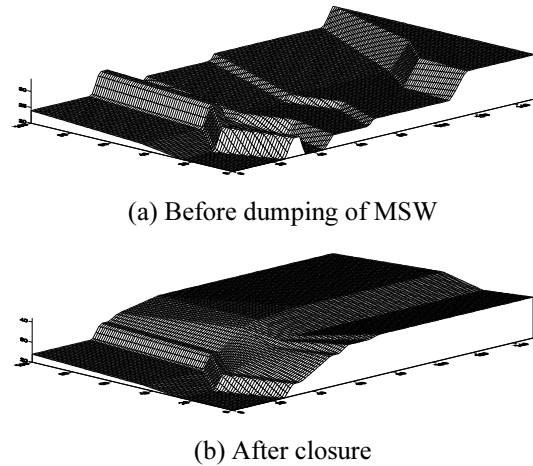


Fig. 9 3D Model of Huko landfill

The factor of safety against slope failure were computed by setting the center of the failure ellipsoidal surface at the profile of minimum and maximum slope, which are $X = 25$ m and $X = 50$ m (from northern boundary), respectively. Factors of safety for ellipsoidal failure surface of various ellipticity, R_e , which is defined as the ratio of major axis to minor axis (X axis/Y axis), were computed. The shear strength parameters were assumed based on the results of in-situ tests with c and ϕ being 30 kPa and 30°. The unit weight was assumed to be 10 kN/m³ in order to take the effect of consolidation in the future into account.

As tabulated in Table 3, the steepest cross-section of the landfill has a lower factor of safety. It is also interesting to find that for the $X = 25$ m cross-section with a rather flat slope 3D analysis gave a lower factor of safety. On the contrary, 3D analysis gave a higher factor of safety for the steepest slope at $X = 50$ m.

Table 3 Factor of safety against slope failure

3D Analysis							
Re	X	25 m	50 m	Re	X	25 m	50 m
1.0		2.52	2.67	2.4		2.42	2.72
1.2		2.43	2.64	2.6		2.43	2.72
1.4		2.43	2.64	2.8		2.45	2.70
1.6		2.37	2.66	3.0		2.52	2.69
1.8		2.41	2.66	4.0		2.49	2.68
2.0		2.40	2.69	100.0		2.60	2.60
2.2		2.42	2.71				
2D Analysis		2.63	2.27				

The index E_3 is listed in Table 4. For steeper slopes, the shear resistance at the lateral boundary has a positive effect on the factor of safety. In contrast, for gentler slopes the smaller normal stress on the 3D slip surface might lead to a lower shear resistance and thus a low factor of safety.

Table 4 3D effect on factor of safety (E_3)

Re \ X	25 m	50 m	Re \ X	25 m	50 m
1.0	-3.82	17.62	2.4	-7.63	19.82
1.2	-7.25	16.30	2.6	-7.25	19.82
1.4	-7.25	16.30	2.8	-6.49	18.94
1.6	-9.54	17.18	3.0	-3.82	18.50
1.8	-8.02	17.18	4.0	-4.96	18.06
2.0	-8.40	18.50	100.0	-0.76	14.54
2.2	-7.63	19.38			

RESULTS AND DISCUSSION

After conducting large-scale in-situ tests in two MSW landfills in Taiwan and performing slope stability analysis, the following conclusions can be drawn from the results. Firstly, the unit weight of MSW in Taiwan's landfills is in agreement with those obtained in landfills worldwide provided that the MSW characteristics might differ significantly. The shear strength parameters obtained from this study are slightly higher than those found from the literatures. The most likely reasons for the difference could be the high percentage of plastic wastes found in the two landfills and the large shear strain reached in the direct shear tests. Furthermore, the compressibility determined with plate load tests is very large and exhibits a linear load-settlement relationship even at very large settlement. In addition, it is difficult to determine the ultimate bearing capacity from the results of the tests. Finally, 3D effect on factor of safety of slope stability may reach as large as 20%. For landfill cross-sections on steeper slopes, factor of safety of 2D analysis is on the conservative side.

ACKNOWLEDGEMENTS

This research is sponsored by Taiwan National Science Council (NSC, China) through grant NSC 95-2221-E-009-201. The authors express their thanks for the support.

REFERENCES

- Bromswell LG (1978). Properties, Behavior, and Treatment of Waste Fills. Seminar Series on Methods of Soil Improvement, Metropolitan Section, ASCE, New York.
- Chang MH (2005). 3D Effect of Slope Stability. Journal of Chinese Institute of Civil and Hydraulic Engineerin. 17(2): 195-204.

- Dixon N & Jones DRV (2004). Engineering Properties of Municipal Solid Waste. Engineering Properties of MSW.
- Dvinoff AH & Munion DW (1986). Stability Failure of Sanitary Landfill. *Proceeding*, International Symposium on Environmental Geotechnolgy. 25-36.
- Eid HT, Stark TD, Evans WD, Sherry PE (2000). Municipal Solid Waste Slope Failure. I: Waste and foundation soil properties. Journal of Geotechnical and Geoenvironmental Engineering, ASCE. 126(5): 397-407.
- Fassett J, Leonards GA, Repetto P (1994). Geotechnical Properties of Municipal Solid Wastes and their Use in Landfills. WASTETECH '94.
- Kavazanjian E, Jr, Beech JF, Matasovic N (2001). *Discussion*. Journal of Geotechnical and Geoenvironment Engineering, ASCE. 127(9): 1126.
- Kavazanjian E, Jr, Matasovic N, Bonaparte R, Schmertmann GR (1995). Evaluation of MSW Properties for Seismic Analysis. In: Geoenvironment 2000, ASCE Geotechnical Special Publication. 46(2): 1126.
- Landva AO & Clark J I (1990). Geotechnics of Waste Fill. Geotechnics of Wastefills—Theory and Practice, ASTM STP 1070: 86–103.
- Machado SL, Carvalho MF, Vilar OM (2002). Constitutive Model for Municipal Solid Waste. Journal of Geotechnical and Geoenvironmental Engineering, ASCE. 128(11): 940-951.
- Merz RC & Stone R (1962). Landfill Settlement Rates. Public. 93(9).
- Sadek SM & Manasseh CG (2004). A Large Direct Shear Apparatus for Testing-Liner Interfaces. (unpublished), [http://webfea.fea.aub.edu.lb/faculty/sal/ah/papers/\[28\]-Sadek%20et%20al.-ASTM-GTJ-Submittal.pdf](http://webfea.fea.aub.edu.lb/faculty/sal/ah/papers/[28]-Sadek%20et%20al.-ASTM-GTJ-Submittal.pdf).
- Sargunan A, Mallikarjun N, Ranapratap K (1986). Geotechnical Properties of Refuse Fills of Madras, India. *Proceeding International Symposium on Environmental Geotechnolgy*: 197-204.
- Schumaker NB (1972). Construction Techniques for Sanitary Landfill. Waste Age, March/April.
- Singh S & Murphy B (1990). Evaluation of the Stability of Sanitary Landfills. Geotechnics of Solid Waste Fills: Theory and Practice. Arvid Landva and G. David Knowles, eds. Philadelphia: American Society for Testing and Materials: 240-258.
- Sowers GF (1973). Settlement of Waste Disposal Fills. *Proceeding 8th ICSMFE, Moscow*, 22: 207-210.
- Taiwan EPA. (2005). Project Report of Sampling and Analysis of Municipal Solid Wastes, EPA-94Z102-02-101.

EFFECT OF MUNICIPAL SOLID WASTE COMPOSITION ON PERMEABILITY

Harris RAMLI¹, Mastura AZMI¹, F. AHMAD² and M. M. ALI²

ABSTRACT: Rapid growth in major cities of the world would make a piece of land cost a fortune to be developed. It might undeniably important to fully utilize every available soil in a city. This includes development of reclamation landfill site for maybe housing or commercial project. However the main concerned is that landfill areas are suffering degradation of environment quality as well as unpredictable consolidation settlement if one tries to reclaim these areas. With the development of improving in landfill leachate quality management by using semi-aerobic landfill concept or well known as Fukuoka landfill method which has been developed more than 20 years ago, next step, it is essential to predict whether this type of landfill method can improve in consolidation settlement during reclamation works. One approach to understand consolidation of a municipal solid waste is from the element of hydraulic coefficient of the waste itself. A falling head test was conducted on 3 days old domestic municipal solid waste taken from compactor unit garbage truck. From the test it is found those wastes that have a higher void ratio, would have a higher permeability as well. However, the higher content of organic waste would reduce the hydraulic conductivity in municipal solid waste. By understanding the characteristic that affect the hydraulic coefficient of a domestic municipal solid waste, consolidation settlement rate of landfill site can be predicted more accurately. Hence landfill site reclaim can be achieved in lesser time by using proper ground improvement method.

KEYWORDS: Municipal Solid Waste Composition; Permeability

INTRODUCTION

Since ancient time practice, man buried any unwanted stuff or so-called garbage, trash, refuse or waste in the ground to ensure that there is no unpleasant odour comes from the garbage that will be the cause most of the disease. As human intellectual evolved, disease vector research started to produce more finding about those human unwanted stuff. It is seem the degradation of the waste and the decompose process of organic waste that would create many pathogen that cause several diseases.

Thus landfill was introduced to solve the waste problem and so far, it does solve it. However there is another problem inferred from this solution, like basic physic laws that mass cannot be destroyed, but only the condition change. Waste inside landfill also cannot avoid this law, as the degradation process taken place inside landfill, leachate and methane gas created.

These are two main sources that become the main cause of environmental degradation in landfill surrounding area that have to be controlled continuously by landfill operator. The gas pressure at the bottom of a landfill has been measured at levels ranging from less than one inch

of water column to as high as 4 atmospheres (Prosser & Janecek 1995).

However, leachate, methane gas control and environmental aspect are not the only considerations that have to be taken into account by landfill operator. There are several other aspects that need serious attention since planning stage like area size, accessibility, ownership, physical characteristic and adjacent land uses (Ayala Misgav 2001) that will have implication to the waste management cost. It was estimated that waste collection and disposal cost were as high as 60% to 80% of total solid waste management cost (Tchobanoglous et al. 1997). With an unstable fuel market price, waste disposal cost increases every year and this would become one of the main concerns in managing waste disposal.

As part of waste management cost planning, most of landfill operator opened landfill at optimal distance to the area served. However with the rapid growth in economic condition, more land are utilized and developed. As most of town growth in widespread trend, sooner or later development would come to the operated landfill area. The utilization of landfill site to be developed will be such a great advantage in land use.

¹ Lecturer, School of Civil Engineering, University Science Malaysia, Penang, Malaysia. Email: cemhr211@gmail.com

² Associate Professor, School of Civil Engineering, University Science Malaysia, Penang, Malaysia. Email: cemmali@eng.usm.my

However due to the environmental and geotechnical aspect, this vision would be far from reach.

Currently there are 5 types of landfill which are Anaerobic, Sanitary, Sanitary Anaerobic, Semi-Aerobic and Aerobic. This paper focused on semi-aerobic andfills since this system provides better air supply to the landfill body. This is because conceptually with the provided air supply will have effect on porosity and void ratio as well as permeability of MSW. Furthermore the leachate recirculation system practical under aerobic conditions, utilize oxygen as nutrient to promote a higher rate of waste decomposition and settlement (Hudgins 1998). With this facts, the time taken for one landfill to finish its secondary settlement due to the waste decomposition will be reduce.

MSW is known for its complexity due to its heterogeneous condition. Because of this condition, the composition of MSW varies dramatically between one location and another as well as standard of living (kathirvale et al. 2003). However, despite this variation, there is a trend in waste composition which is similar to the most of the major city around Asia. It is appeared that organic waste is the main composition with more than 50% of average wet weight for MSW in Indonesia, Dhaka, Kathmandu, Bangkok, Hanoi (Stegmann et al. 2007) and Kuala Lumpur (Nasir & Yosuff 1998). With relation to the above statement, this paper focused on organic waste and paper waste.

The EXPERIMENTAL WORK

Unlike soil or other material that is normally involve in engineering experimental work, MSW could be consider as one of the most difficult sample to work with. It is not just about the intense odor coming from decomposition of organic waste or even our perception from the physical appearances which lead to our psychomotor that this is really a difficult experiment. As far as experiment is concerned, it is more related to the quality of the samples that was used for the entire experimental program as MSW is in heterogeneous condition. Thus each of the steps in experimental program must have a relationship and continuity between one and another. During testing, special attentions had to be made on the collected samples to prevent biodegradation as well as leachate build-up, so that the test results reflect the properties of fresh MSW.

MSW Sample Collection

In this study, waste samples were taken from compactor unit garbage truck at the Batu Maung transfer station in Penang, Malaysia. It is placed with lightly hand compacted until full in 0.03465 m^3 box container,

all 5 of them. The sample is actually from two sources, 2 container boxes from one garbage truck and 3 container boxes from another truck. The sample was 3 days old domestic municipal solid waste originates from landed house. The approach of waste taken from compactor unit garbage truck is to ensure that the sample is well compacted as it would reflect the actual condition in landfill site.

MSW Sample Compositions

After collecting the sample in all 5 boxes containers, each of the container weight was recorded. Furthermore, samples inside the container were separated within its composition group and weight.

MSW Permeability

In determination of MSW permeability, falling head test were conducted on all 5 containers according to procedure on BS1377. For each of the container, 3 permeability tests were conducted on 10.575 cm diameter by 12.615 cm height mould. Samples were compacted in 3 layers for every test. One of the reasons falling head test were chosen for this study because there are some of the field study on MSW shows that the field hydraulic conductivity are around $9.2 \times 10^{-4} \text{ cm/sec}$ to $1.0 \times 10^{-3} \text{ cm/sec}$ (Oweis et al. 1990), (Qian Xuede et al. 2002). Furthermore, the sample condition was high in organic waste by weight percentage and by this the expected result would probably be very small. Falling head test was considered suitable when the permeability of sample expected to be less than $1.0 \times 10^{-3} \text{ cm/sec}$ (Bardet 1997).

But before samples were placed in the mould, the weight of each sample was recorded according to its composition group so that the composition effect can be traced. In order to get an accurate data of MSW composition that affect the permeability, the sample testes for the entire experimental work are limited only to two main compositions in domestic MSW. The composition chosen was organic waste and paper waste. Data accuracy and highest percentages in most samples collected were the reasons why two compositions were selected.

MSW Volumetric-Gravimetric Relationship

Volumetric test was also conducted to the samples of two MSW compositions, which were organic waste and paper. The test was conducted based on BS1377. From the test, value of water content, dry weight, void ratio and degree of saturation was obtained. Through this value, dry unit weight of MSW can be calculated. For each of the sample box container, 3 volumetric tests were conducted to get an average value.

RESULT AND DISCUSSION

Waste Composition

Since the collected MSW sample were 3 days old, the establishment of the waste composition is important for this study, especially to identify the trend or effect of each composition to the permeability. In order to sustain the properties of fresh MSW, each of the sample compositions were weighed on the same day to ensure that there was no additional leachate generation which lead to additional weight and several other changes to the sample properties.

During sample collection, it was found that it was really hard to find a recyclable material inside the compactor unit. Information gathered from personal communication with the garbage truck worker, in Penang most of the recyclable material was gathered or sorted out during the waste collection before the waste plastic bag were thrown into the compactor. These recyclable materials were sold before wastes sent to the transfer station.

As a result of that, a very low percentage of glasses and metal were found in the samples collected. However both of these materials still can be found in the samples, but in small pieces. That would probably be the reason why it was still available there. Thus in the waste composition only waste group from paper, plastic, organic and textile were recovered. Because the percentages of glass and metal were quite low, both of these compositions are group as others. As expected throughout all 5 containers, organic waste is the highest composition of all, as shown in Fig. 1.

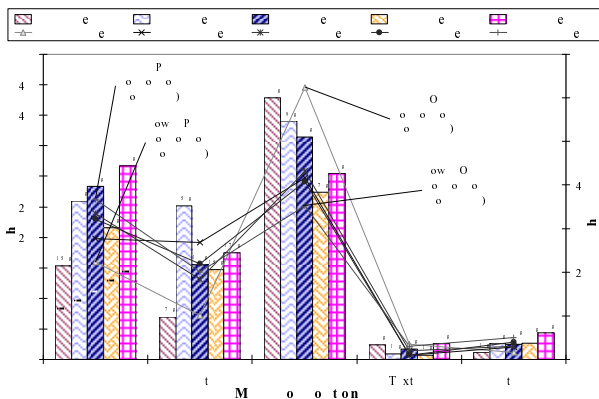


Fig. 1 Distribution of samples taken from compactor unit garbage truck by weight for each waste composition base on kilogram and percentage for all 5 container box

For ease of further discussion in this paper, the container label has been re-arranged based on organic-paper composition by weight percentage ratio. From all

5 containers, only container number 1 shows 62% of organic waste, which was very high, thus reducing the rest of other composition percentage. Whereas organic waste for others, ranges from 35% to 45% based on total weight of the MSW sample. The ratios between organic wastes to paper for container 1 to container 5 were 0.36, 0.66, 0.77, 0.79 and 1.05 respectively. The plastic waste composition ranges from 20% to 25%, except container 1 which was only 10%.

All first 4 compositions shown were considered as compressible component of MSW. These compressible components content has significant effect on the compressibility of MSW (Dixon & Lager 2006). A well-compacted MSW condition is very important to the landfill management because it has an effect to the landfill volume capacity. Achieving a very well compacted and high density of MSW will be considered as positive milestone for landfill operator, but however this is not fully applied for land reclamation purpose. Compressibility of MSW is interrelated with porosity and void ratio in which has a direct effect to the hydraulic conductivity in which affect consolidation settlement of the MSW.

From visual observation, it was found that the waste inside the compactor unit was in very well compacted condition, either inside its original plastic bag or not. Although with this condition, from the observation during sampling work, it was found that the samples were break-up when transferred from compactor unit to container, thus reducing the overall bulk density properties. Such condition happened maybe because of unlike soil, which have cohesion that react as a binder in soil, MSW does not have this cement-like properties in between waste composition. The changes of density condition in the MSW will rely only on rearrangement of waste composition during the mechanical compaction process in the compactor unit. Thus in order to have a better understanding of this condition, a further study is needed on density condition from each stage as well as its effect on MSW properties.

In addition to the field observation, it could be seen that most of the plastic bag that originally covered the waste was torn. As we know that ceramic, glass and metal are among of the compositions in MSW. These materials are considered as incompressible component in MSW (Dixon & Langer 2006). These materials are probably the reason that helps puncture of the plastic bag. This is maybe because of puncture effect that occurs due to the sharp surface of the waste with the help of mechanical force during the waste compaction.

However not all of the plastic bag were torn because some of the plastic bag materials quality varies between thin to thick. So for the waste covered in large plastic bag, in which would normally have stronger and thicker plastic, it would be very less possible to torn if there

were no sharp surface waste around it in the compacter.

As we know that plastic is one of the materials that can provide a smooth surface, this also affect the flow of liquid on top of the waste plastic bag surface. Due to the condition that not all of waste plastic bag was torn, if we look into hydraulic coefficient aspect of the waste, it would appear to be an advantage. The available leachate would be drained out from the landfill body and recirculation it back to the top as in semi-aerobic method, more rapidly. Even during the recirculation, leachate can finish its cycle more rapidly and give better leachate quality as the overall permeability of the waste is higher due to presents of the plastic material.

However if we look into the environmental geotechnic aspect, with the present of these condition, the stability of waste inside landfill cannot be fully achieve. The waste decomposition can practically result in settlement of 15% (Boni et al. 2006) and 20% (Oweis 2006) of landfill thickness. The differential settlement would varies greatly even with the same age of waste in landfill layer. This is due to a significant differential in decomposition rate for waste within the plastic bag and outside the plastic bag.

Waste Permeability and Void Ratio

As permeability is one of the component in consolidation settlement mechanism, a better understanding of this parameter in MSW would increase the understanding of the consolidation settlement behavior for MSW during landfill reclamation work. For this study purpose, falling head test were conducted on paper and organic waste of the 3 days old MSW. The paper-organic waste content for each test conducted were almost similar to its original percentage in sample container if only 2 waste constitution taking into consideration instead of 5 composition. The percentages of paper-organic waste content for each test are as shown in Fig. 2. The range in paper-organic waste distribution content of the sample would reflect from high content of organic waste to normal condition.

From the observation on sample condition, paper waste is still in damp condition, which means the leachate generation is still in small quantity. Furthermore, condition of organic waste also still in its original condition, in which can be identified. Falling head and volumetric test were conducted on these samples, and the permeability as well as void ratio value is shown in Fig. 3.

Results shows on permeability of paper-organic waste are range between 1.57×10^{-4} cm/sec to 3.23×10^{-4} cm/sec and the void ratio is from 4.47 to 4.83. The result shown value almost similar to the permeability obtain by other researcher in which between 10^{-2} cm/sec to 10^{-4} cm/sec as publish by Oweis I. S. (1998).

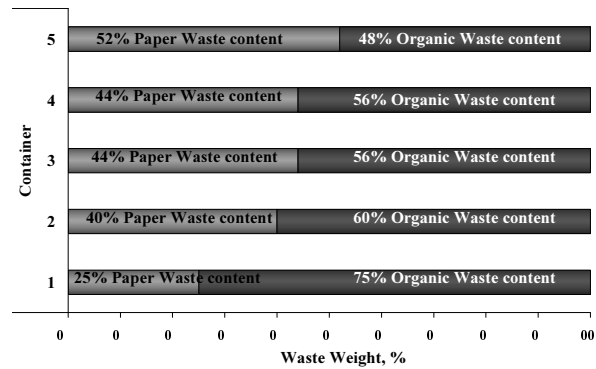


Fig. 2 Distribution of sample’s weight for paper-organic waste base on percentage that had been used for falling head test and volumetric test

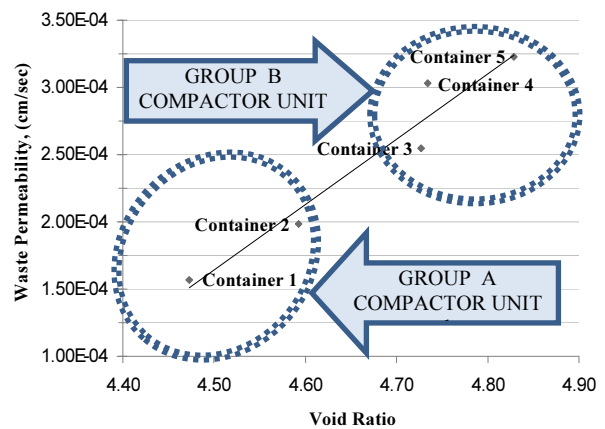


Fig. 3 Relationship between average permeability and void ratio for paper-organic waste sample taken from compactor unit 1 and compactor unit 2

It can be seen that there are two group of condition based on void ratio and permeability, which is container 1 and 2 in Group A, whereas container 3, 4 and 5 are in Group B. This is maybe due to the fact that Group A comes from the same garbage truck and Group B from another garbage truck. Both of it is from different location, thus the weather condition and garbage storage might play important role in the MSW properties. This can be shown on Table 1 where the same groups have similar value in degree of saturation and unit weight. Samples moisture content and saturation degree within same group also demonstrate the close value range.

Careful examination on permeability value trend and sample composition revealed that composition of waste does played important role in waste permeability. It can be shown that with the higher value of organic composition, sample permeability is reduced. This maybe due to the compaction effect that organic waste able to rearrange itself to become denser is better rather than paper waste. Because density of waste will have effect on void ratio and permeability.

Table 1 Relationship of sample saturation degree and unit weight as well as its value range similarity for the sample taken from the same compactor unit

Sample	Average Saturation Degree, %	Average Unit Weight, (kN/m ³)		
		Dry	Mass	Saturated
Box 1	42.7	4.84	8.26	12.86
Box 2	41.6	4.74	8.09	12.79
Box 3	85.2	4.62	11.52	12.72
Box 4	85.0	4.62	11.51	12.72
Box 5	83.4	4.54	11.32	12.67

The permeability of paper-organic waste is increasing with increment in void ratio as the higher void ratio, the higher permeability will be. Void ratio in paper-organic waste shows a higher value compared than soil, maybe due to the fact that waste is heterogeneous. The shape of each waste within the same or different composition is different between one and another. The biodegradation of organic waste also affect the void ratio of MSW. Thus as the void ratio in waste higher, the porosity that allowed liquid flow in waste medium also will be higher and this will increase the permeability value.

However the actual void ratio and porosity of fresh MSW in landfill site would depend on initial compaction of the MSW. This is the fact that porosity of MSW depending on the compaction and composition of the waste (Qian et al. 2002). Compressibility of MSW could also affect the permeability as the more it is compacted, the lower the permeability would be. Hence this condition would increase the consolidation time for one landfill to achieve at least 90% degree of consolidation.

With the concept used in semi-aerobic system (Fukuoka method) in which ambient air flows into the waste body naturally through leachate collection pipe, the reduction of porosity as well as void ratio could be decelerate as MSW having a consolidation settlement. As the decreasing in void ratio with increase in density will resulting decreasing in permeability (Hossain et al. 2009). Thus with continuous air supply, the reduction of MSW permeability can decelerate, and consolidation time would be lesser. Furthermore during the waste decomposition, porosity value would increase (Liang Bing 2008).

In addition to that, semi-aerobic landfill concept approach also will improve the leachate quality as well as gas venting systems. This will result less environmental quality degradation of the landfills site thus creating a more feasible land to be reclaimed for development.

CONCLUSION

Falling head test and volumetric test were conducted on three days old paper-organic waste taken from compactor unit garbage truck. From the laboratory test result, four conclusions can be made.

First, waste composition of sample by weight percentage shows similarity of MSW in most of major cities in Asia. Organic waste remain as a highest percentage, followed by paper, plastic, textile and other. Secondly, waste taken from different place will shown different geotechnical properties but remain the same for the waste from the same place. The geotechnical properties that have these similar trends are degree of saturation, dry unit weight, mass unit weight, saturated unit weight, void ratio and permeability.

Thirdly, the higher value of organic composition, the lower permeability of the sample will becomes. This is mainly due to the sample compressible condition that affects the sample void ratio and permeability. Finally, the permeability of waste will increase as void ratio increase. Thus with better understanding in permeability relationship with compaction, porosity and void ratio will enhance the advantage of semi-aerobic landfill systems and settlement prediction for future landfill reclamation work.

ACKNOWLEDGEMENTS

The author would like to acknowledge Firwan Merican Company, particularly Firdaus Merican for supporting field activities, including MSW sampling. The assistance of Chong Aik Yong, Dziauddin Zainol Abidin and Ahmad Helmi Ghazali in MSW sampling, characterization and laboratory work is appreciated. Finally, author would also like to express gratitude on the incentive grants received from Universiti Sains Malaysia.

REFERENCES

- Ayala Misgav, Noa Perl, Yoram Avnimelech (2001). Selecting a compatible open space use for a closed landfill site. *Landscape and Urban Planning*. Elsevier. 55: 95-111.
- Bardet JP (1997). *Experimental Soil Mechanics*. Prentice Hall: 202-203.
- Boni MR, Chiavola A, Sbaffoni S (2006). Pretreated waste landfilling: Relation between leachate characteristic and mechanical behavior. *Waste Management*. 26(10): 1156-1165.
- Dixon N & Langer U (2006). Development of a MSW classification systems for the evaluation of the

- mechanical properties. *Waste management* 26, 220-232.
- Hossain MS, Penmethsa KK, Hoyos L (2009). Permeability of Municipal Solid Waste in Bioreactor Landfill with Degradation. *Geotechnical and Geological Engineering*. Springer. 27(1): 43-51.
- Hudgins M (1998). Successful Application of An Aerobic Municipal Solid Waste Landfill Bioreactor. *Waste Tech* 98. National Solid Waste Management Association.
- Kathirvale S, Yunus M, Sopian K, Samsuddin AH (2003). Energy potential from municipal solid waste in Malaysia. *Renewable Energy*. 29: 559-567.
- Liang B, Liu L, Xue Q, Zhao Y (2008). Porosity Prediction with settlement and biodegradation in Municipal Landfill. *Bioinformatics and Biomedical Engineering*, 2008. ICBBE 2008. The 2nd International Conference on. IEEE Xplore: 1289-1292.
- Nasir H & Yusoff K (1998). Issues and problems of solid waste management in Malaysia. National review of environmental quality management in Malaysia. Towards the next two decades. Lestari, University Kebangsaan Malaysia.
- Oweis IS (2006). Estimate of landfill settlement due to mechanical and decomposition process. Technical notes. *Journal of Geotechnical and Geoenvironmental Engineering*. 132(5): 644-650.
- Oweis IS & Khera RP (1998). *Geotechnology of Waste Management*. Second Edition. PWS Publishing Company. 133-135.
- Oweis IS, Smith DA, Allwood RB, Greene DS (1990). Hydraulic Characteristics of Municipal Refuse. *Journal of Geotechnical Engineering*. ASCE. 16(4): 539-533.
- Prosser R & Janecek A (1995). Landfill Gas and Groundwater Contamination. *Landfill Closures- Environmental Protection and Land Recovery*, ASCE, Geotechnical Special Publication. 53: 258-271.
- Qian XD, Robert MK, Donald HG (2002). *Geotechnical Aspects of Landfill Design and Construction*. Prentice Hall. 90:188-189.
- Stegmann IKR, Norbu CVT, Gadia RCT, Awang M, Abdul Aziz A, Hassan MN, Chong TL, Ming CT (2007). Solid waste management in Asia. Teaching and training modules for higher education in the waste management sector. http://www.tu-harburg.de/awa/asia_link/module.html. Published by the TUHH, Hamburg University of Technology, Institute of Waste Resources Management, Germany.
- Tchobanoglous G (1977). *Solid Waste: Engineering Principle And Management Issue*. McGraw Hill.

STUDY ON THE DUNCAN-CHANG MODEL PARAMETERS OF STRESS COMPRESSION FOR MUNICIPAL SOLID WASTE

Zhen-Ying ZHANG¹, Chang-Fu WU² and Yun-Min CHEN³

ABSTRACT: The Duncan-Chang model parameters are studied by laboratory test and theory analysis for municipal solid waste. The method is very simple, practical, and the model parameter is easy to obtain. The results show that the damage ratio is 0.55 to 0.65; The parameter k is decreased by the initial void ratio increased, and the relationship between k and initial void ratio is linear, and the slope of the line is 5.0; The parameter n is about 1.05; The parameter G is between 0.3 and 0.4, and the relationship between G and initial void ratio is linear; The parameter F is between 0 and 0.1, and the relationship between F and initial void ratio is linear too.

KEYWORDS: municipal solid waste, stress compression, Duncan-Chang model, parameters

INTRODUCTION

The settlement study are one of the most important research topics in the research of the use of municipal solid waste landfill (Morris & Woods 1990). Landfill settlement mainly composed by two major parts: one part is the settlement caused by the compression stress of waste (including the rolling load, self-weight stress and creep, etc.), the other part is the settlement caused by the biodegradation of organic compounds in the waste. Study (O'leary & Tansel 1986) shows that: the total settlement of the landfill is about 25% -50% of the initial landfill height and Coduto & Huitric (1990) consider that the settlement caused by the biodegradation of organic compounds may reach a high level of 18% -24%. Landfill settlement possibly induces the landfill gas collection pipe distortion failure and hydraulic system breakage, and the asymmetry settlement may possibly induce the capping system impervious layer tear which will cause leakage and affect the use of the land. In this paper, we mainly researched the compression stress-related problems of the waste, and firstly studied the Duncan-Chang model parameters of the municipal solid waste. Feng (2005) conducted a large-scale triaxial test of large-sized solid waste sample, obtained the same conclusion that the waste stress-strain relationship accord with the Duncan-Chang model and gained the Duncan-Chang model parameters of the waste. Using Duncan-Chang model we can do two-dimensional finite element compress stress analysis of municipal solid waste, which lay the foundation for the landfill settlement

analysis. However large-scale triaxial test which cost so much is a heavy work. Although it takes a lot of manpower, material and financial resources, it is difficult to apply it in engineering.

In order to overcome the above problem, in this paper we obtain the Duncan-Chang model parameters through certain theory calculation adopting the simple direct shear test and compression test of the solid waste. By comparing the result with large-scale test, Duncan-Chang model parameters under different initial void ratio are obtained.

DETERMINING DUNCAN-CHANG MODEL PARAMETERS BY DIRECT SHEAR TEST AND COMPRESSION TEST

Duncan-Chang model parameters are generally obtained from triaxial test, however, large-scale triaxial test are very complex, requires a very long time and also are more expensive. In this paper, we consider a simple and practical test method to obtain these parameters: namely, determining Duncan-Chang model parameters through certain theoretical calculation using the test parameters obtained by direct shear test and municipal solid waste compression test.

Determination of Parameters c and ϕ

Using the slow shear test of direct shear test, according to the study of Feng (2005), when shear strain

¹ Professor, Department of Civil Engineering, Zhejiang Sci-Tech University, China. Email: zhangzhenyinga@163.com

² Associate Professor, Department of Civil Engineering, Zhejiang Sci-Tech University, China. Email: wuchangfu@163.com

³ Professor, Department of Civil Engineering, Zhejiang University, China. Email: chenyunmin@zju.edu.cn

is 10%, we take the c and φ as the approximation of Duncan - Chang model parameters c and φ .

Determination of Parameter R

According to the research of Feng(2005), the parameter R increases with the axial strain ε . Under the same strain there is different damage ratio R which should take the average value proposed by Duncan-Chang(Duncan & Chang 1990) with different confining pressure σ . From Fig. 1 which shows the relationship between damage ratio R and axial strain ε , we can see that damage ratio R increase with the strain ε in a hardening increasing trend. Considering the possible waste slop instability after large deformation and the cushion shear caused by large strain impacting the environmental effects, est. we take $\varepsilon=10\%$ as the waste damage standard. It is recommended that the damage ratio $R = 0.55 - 0.65$ without triaxial test data.

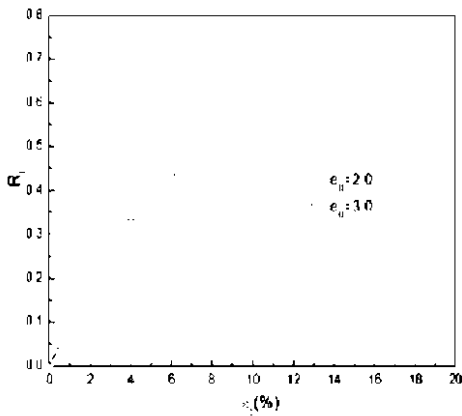


Fig.1 Relationship between R and ε

Determination of Parameters K and n

According to Janbu’s research (Janbu 1963), the initial tangent modulus E and confining pressure σ have the following relations

$$E = Kp \left(\frac{\sigma}{p}\right)^n \tag{1}$$

where K and n are the test parameters, and p is the atmospheric pressure (kPa).

Taking logarithm of the two sides of Eq. (1)

$$\lg\left(\frac{E}{p}\right) = \lg K + n \lg\left(\frac{\sigma}{p}\right) \tag{2}$$

In the Cartesian coordinate system, Eq. (2) is a straight line in which $\lg K$ is the intercept and n is the

slope. That is the method to determine the Duncan-Chang model parameters for the use of triaxial test.

According to the research of Wang (2004), when the soil is under the state of none lateral deformation in uniaxial compression test, the static coefficient of earth pressure is K .

$K = 1 - \sin \varphi$ (Sandy soil); $K = 0.95 - \sin \varphi$ (clay), and the corresponding Poisson's ratio is:

$$\mu = \frac{K}{1+K} \tag{3}$$

The waste compression curve is divided into a number of increments, for a certain load level increment of Δp :

$$\begin{aligned} \Delta\sigma &= \Delta p \\ \Delta\sigma &= K \Delta p \\ \Delta\sigma &= K \Delta p \end{aligned}$$

By the generalized Hook's law, the axial strain is that:

$$\Delta\varepsilon = \frac{\Delta\sigma - 2\mu \Delta\sigma}{E} \tag{4}$$

where: E and μ are the elastic modulus and Poisson's ratio under the state of K , respectively.

There is no lateral strain in uniaxial compression test, so axial strain is therefore the volumetric strain, then:

$$\Delta\varepsilon = \frac{\Delta e}{1+e} \tag{5}$$

where e is the initial void ratio, and Δe is the void ratio change based on a certain level load on the waste compression curve, defined by

$$\Delta e = e - e$$

From Eq. (4) and Eq. (5) the soil modulus E under the state of K can be obtained as that:

$$E = \frac{(1+e)(1-2K\mu)\Delta p}{\Delta e} \tag{6}$$

where Δp is the certain level load increment on the waste compression curve, defined by $\Delta p = p - p$.

According to the study of Duncan-Chang model (Duncan & Chang 1990), initial elastic modulus E can be express by tangent elastic modulus E as Eq. (7) under the soil state of K .

$$E = \frac{E}{(1-R S)} \tag{7}$$

where S is the stress level under the conditions of none lateral deformation.

$$S = \frac{(\frac{1-K}{K})\sigma_3(1-\sin\phi)}{2C \cdot \cos\phi + 2\sigma_3 \sin\phi} \tag{8}$$

where σ is the lateral pressure of the waste.

Substituting Eqs. (6) and (8) in Eq. (7), the initial tangent modulus E under different stress state can be obtained. Then parameters K and n can be obtained by straight-line fitting with the points (E, σ) in the $\lg(\frac{E}{p}) \sim \lg(\frac{\sigma}{p})$ Cartesian coordinate system.

Determination of Parameters G and F

According to the study of Duncan-Chang, the initial Poisson's ratio μ and confining pressure σ have the following relations

$$\mu = G - F \lg(\frac{\sigma}{p}) \tag{9}$$

According to the study of Daniel(Daniel & Olson 1974), tangent Poisson's ratio can be expressed as Eq. (10).

$$\mu = \mu + (\mu - \mu)S \tag{10}$$

Under the state of K , according to Daniel's tangent Poisson's ratio formula, the waste tangent Poisson's ratio μ can be expressed as Eq. (11).

$$\mu = \mu + (\mu - \mu)S \tag{11}$$

$$\mu = \frac{\mu - \mu S}{1 - S} \tag{12}$$

where μ is Poisson's ratio when the waste failure.

The parameters G and F can be obtained by straight-line fitting with the points (μ, σ) in which μ is calculated with different confining stress σ by Eq. (12). Then initial Poisson's ratio μ can be obtained under arbitrary confining pressure with the use of parameters G and F . Parameter G is the intercept of the straight line and F for the slope.

DUNCAN-CHANG MODEL PARAMETERS WITH DIFFERENT INITIAL VOID RATIO

The solid waste parameters c and ϕ can be obtained by slow-shearing shear test, taking the value when the strain is 10%, damage ratio $R = 0.55-0.65$. In this paper,

we mainly establish the Duncan-Chang model parameters, namely, K, n, G and F .

Determination of Parameters K and n .

According to the simplified calculation method and the experimental data of Zhang (2005), Table 1 shows the relation between E and σ under initial void ratio.

Fig. 2 shows the relation between $\lg(\frac{E}{p})$ and $\lg(\frac{\sigma}{p})$.

We compared the simplified calculation method and large-scale triaxial tests data in Fig. 3. Table 2 shows parameters K and n with different initial void ratio, and the relation between them is shown in Fig. 4.

Fig.3 shows that simplified calculation method is closer to the large-scale triaxial tests results. However, parameter k is less and n is bigger.

Table 1 Relationship between E and σ

Initial Void Ratio	σ (kPa)	E (kPa)
1.5	100	2377
	200	3280
	300	8074
3.0	100	1305
	200	3430
	300	4856
	400	5952
3.7	100	1004
	200	2193
	300	3438
	400	4188
4.3	100	690
	200	1810
	300	2892
	400	4277

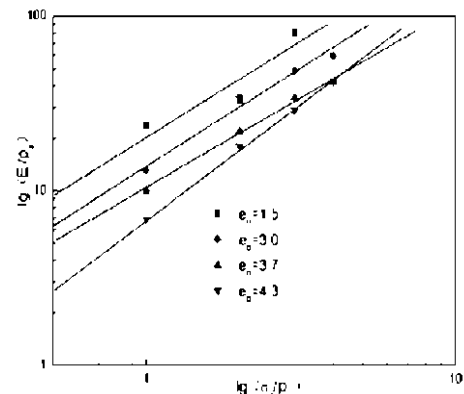


Fig.2 Relationship between $\lg(\frac{E}{p})$ and $\lg(\frac{\sigma}{p})$

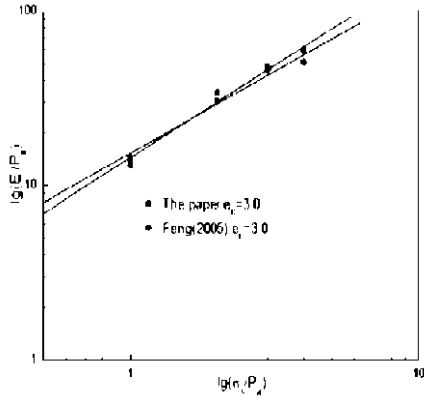


Fig. 3 Curves of the results of the simplified calculation and the tests ($e_0=3$)

Table 2 Model parameters K and n of Duncan-Chang

Initial Void Ratio	K	n
1.5	21.0	1.083
3.0	14.0	1.107
3.7	10.5	1.034
4.3	7	1.326

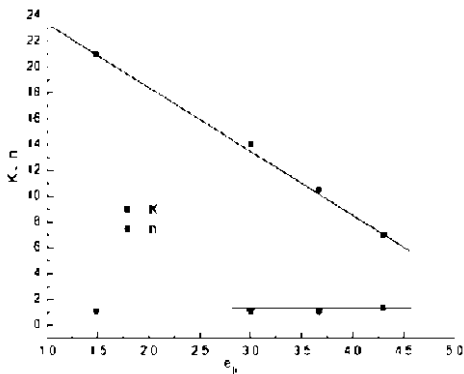


Fig. 4 Relationship between K , n and e_0

We can see from Fig. 4 that the parameter k decreases with the initial void ratio, and it can be fitted with a straight line as the following:

$$K = a - be \tag{13}$$

where: a , b are parameters, taking 28.52 and 5 respectively. Parameter n changes little with initial void ratio with the value about 1.05.

Determination of Parameters G and F

According to the above simplified method and the experimental data of Zhang (Zhang 2005), Table 3 shows the relation between μ and σ under different void ratio, also Fig. 5 shows the relation between μ and

$\lg(\frac{\sigma}{P})$. We compared the simplified calculation method and large-scale triaxial tests in Fig. 6, taking the waste parameters G and F with different void ratio in Table 4, and the relationship between them are shown in Fig. 7.

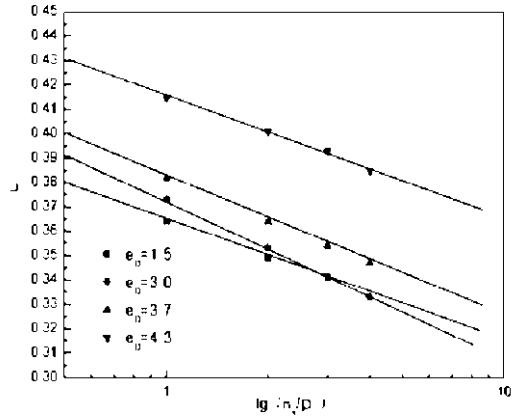


Fig. 5 Relationship between μ and $\lg(\frac{\sigma}{P})$

Table 3 Relationship between μ and σ

Void Ratio	σ (kPa)	μ
1.5	100	0.364
	200	0.349
	300	0.341
3.0	100	0.373
	200	0.353
	300	0.341
3.7	100	0.382
	200	0.364
	300	0.354
4.3	100	0.415
	200	0.401
	300	0.393
	400	0.385

Fig. 6 shows that the results of simplified calculation method are more evenly, while the large-scale triaxial test results are discrete. The reason may be that operation in triaxial test is more complex than uniaxial compression test and the uniaxial compression test is not easily bringing error for its simple operation.

We can see from Fig. 7 that the parameter G varies between 0.3 and 0.4, and is approximately linear relationship. Parameter F which can also be fitting with a straight line varies between 0 and 0.1. $G=0.3\sim 0.4$ is recommended when there is no triaxial experiment data.

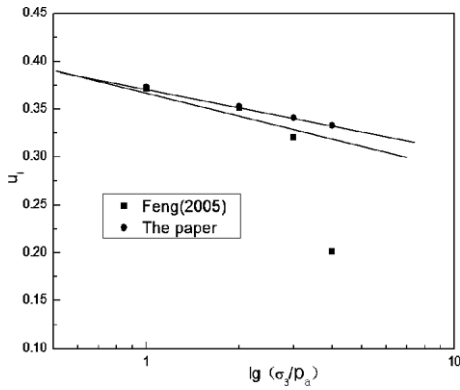


Fig. 6 Curves of the results of the simplified calculation and the tests ($e_0=3$)

Table 4 Model parameters G and F of Duncan-Chang

Initial Void Ratio	G	F
1.5	0.364	0.048
3.0	0.373	0.066
3.7	0.382	0.058
4.3	0.415	0.045

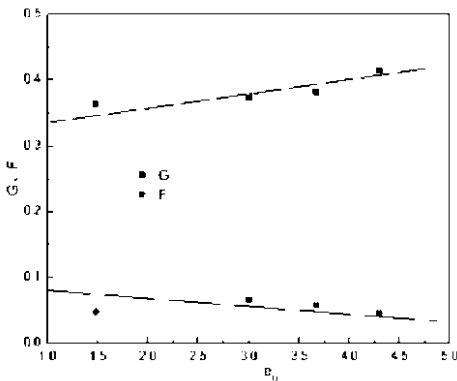


Fig. 7 Relationship between G 、 F and e_0

CONCLUSIONS

Because of the complexity of large-scale triaxial test, taking a lot of manpower, material and financial resources during the experiment and the inconvenience in engineering application, we research a simplified calculation method. And the Duncan-Chang model parameters can be obtained through simple direct shear test and lateral compression test. Comparing the results with large-scale triaxial test, the main conclusions are as follows

- 1) $R = 0.55 - 0.65$ is recommended when there is no triaxial experiment data.
- 2) A simplified calculation method is proposed and the suggest value of Duncan-Chang model parameters

are obtained. Parameter k decrease with initial void ratio and can be fitted with a straight line such as $K = a - be$; parameter n changes little with initial void ratio with the value about 1.05; parameter G varies between 0.3 and 0.4, and is approximately linear relationship with initial void ratio; parameter F varies between 0 and 0.1, and also can be fitted with a straight line.

3) The study shows that the results of the simplified calculation is very close to that of the large-scale triaxial test, so that we can sublimated it for large-scale triaxial test.

ACKNOWLEDGEMENTS

This work is funded by National Natural Science Foundation of China under Contract No.50778164, No.50878197, and Key Projects Foundation from Department of Education of Zhejiang(No.20050744).

REFERENCES

Coduto DP & Huitric R (1990). Monitoring landfill movements using precise instruments. Geotechnics of waste fill-theory and practice: ASTMSTP 1070, American Soc. for Testing Materials, Philadelphia: 358-370.

Daniel DE & Olson RE (1974). Stress-strain properties of compacted clay. Proc. ASCE, JGTD, v100, GT10, 1123.

Duncan JM & Chang CY (1990). Nonlinear analysis of stress-strain for soil. Proc. ASCE, v96, SM5, 1629.

Morris DV & Woods CE (1990). Settlement and engineering considerations in landfill final cover design. Geotechnics of waste fill-theory and practice: ASTMSTP 1070, ASTM Philadelphia: 9-21.

Janbu N (1963). Soil compressibility as determined by oedometer and triaxial tests. Proc. European Conf. on Soil Mech. & Found. Engrg. N1, 19.

O’leary P & Tansel B (1986). Landfill closure and long-term care, Waste Age. 17(10): 53-54,58,60,64.

Feng SJ (2005). Static and dynamic strength properties of municipal solid waste and stability analysis of landfill. Ph.D. Thesis, Zhejiang Univ. China.

Zhang ZY, Wu SM, Chen YM (2000). Experimental research on the parameter of life rubbish in city. Chinese Journal of Geotechnical Engineering. 22(1): 35-39.

Zhang ZY (2005). Study on compressibility and settlement of landfill for municipal solid waste. Ph.D. Thesis, Zhejiang Univ. China.

Wang ZL (2004). Settlement prediction and calculation of embankment on soft ground. Ph.D. Thesis, Hehai Univ. China.

STUDY ON PARAMETER SENSITIVITY OF THE COMBINATION FAILURE OF LANDFILL WITH A DAM

Fan TU¹, Fang-Qiang CHANG², Zhao-Yun XIAO³ and Xiao-Jie WU⁴

ABSTRACT: Combination failure of a solid waste landfill is one of main failure mechanisms. Based on the force limit equivalence theory, one formulae to calculate the factor of safety of the combination failure of landfill with a dam was derived in this article, and then the sensitivities of parameters to influence landfill stability were analyzed. The parameters with the greatest influence on combination failure are the landfill angle α , θ and β , followed by the internal friction angle of solid waste Φ_{sw} , then the interface friction angle of landfill liner system δ , and H_2 , H_1 , δ_D , B and γ are the last. From the point of stability and economy of landfills, the front angle α of landfill is most important. The compaction of solid waste could improve the internal friction angle and choosing of liner with high internal friction are conducive to the stability of landfills.

KEYWORDS: landfill, combination failure, sensitivity analysis, rotational failure, translational failure

INTRODUCTION

The stability of modern sanitary landfill is receiving more and more concerns in society. As for the failure mode, most studies focus on the internal rotational failure of solid waste (Chen et al. 2000; Zhu et al. 2002) and translational failure along the liner interface (Qian et al. 2003; Qian and Koerner, 2004; Feng, 2005; Feng, 2007; Wu, 2008; Gao et al. 2007). However, as for one possible failure mode, named combination failure that fails along the internal solid waste and liner interface, combined the rotational failure and translational failure, no any research on this topic has been published yet. The parameters that influence the landfill stability may play different influence degree on the failure. In order to understand the influence degrees, parameter sensitivity analysis is necessary, and it is also conducive for landfill optimization design, construction, experiment and operational management.

A combination failure model of landfill was briefly introduced firstly, and then parameter sensitivity on combination failure was analyzed which is the main focus of this paper. The failure mode of combination failure of landfill with a dam has two mechanisms, one is failure along internal solid waste, then the landfill base and dam back, the other is along the internal solid waste, then the landfill base and dam base, as shown in Fig. 1.

The parameters to influence landfill stability include geometries of landfill and dam, engineering properties of solid waste, interface shear performance of combined liner, leachate distribution, construction and operational management etc. Through an example, the factors of safety were calculated with one single parameter being changed and the other unchanged. Then the sensitivity of parameter was ranked according to the increase range between factors of safety and the parameters.

COMBINATION FAILURE ANALYSIS OF LANDFILL WITH A DAM

Introduction of Combination Failure Analysis Model

The surface of combination failure is composed by an arc and a broken line. The failure surface could be determined by the position of the cut-off point formed by failure arc and the angle between the string and the tangent. The failure surface approximates arc when the cut-off point is near the heel of the waste dam, and approximates translational failure when the cut-off point is near the heel of side slope of landfill. The failure along arc (internal solid waste) is often analyzed by Slice Method (Lu et al. 2005), such as REAME program (Chen et al. 2000; Zhu et al. 2002) introduced in book

¹ Professor, Department of Civil Engineering, Huaqiao University, China. Email: ftu@hqu.edu.cn

² Lecturer, Department of Civil Engineering, Huaqiao University, China. Email: malcme@126.com

³ Lecturer, Department of Civil Engineering, Huaqiao University, China. Email: zyxiao@hqu.edu.cn

⁴ Assistant Engineer, Maunsell Consultants (Shenzhen) Co., Ltd. Email: wxjtao@163.com

(Huang, 1983). And translational failure along interface between liners and base or back of waste dam, could be analyzed by the Wedge Method (Feng, 2005; Feng, 2007; Wu, 2008; Gao et al. 2007). The Slice Method and the Wedge Method are combined to establish the combination failure model in this article. From the cut-off point and heel of waste dam, slide body was divided

into three wedges, namely active, middle and passive wedges, in which the active part was sliced as shown in Fig. 2 and Fig. 3. According to the force equivalence analysis of the slice and wedge, the formulae to calculate factor of safety of combination failure was derived. For simplification, the cohesion of solid waste and liners was neglected and the leachate level was not considered.

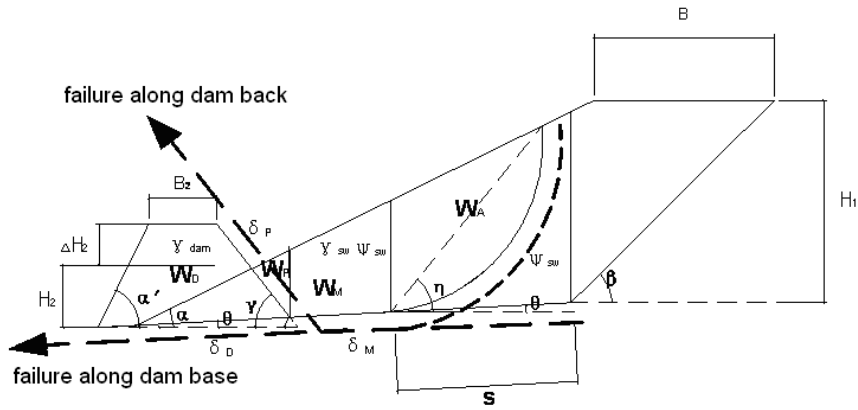


Fig. 1 Schematic diagram of combination failure

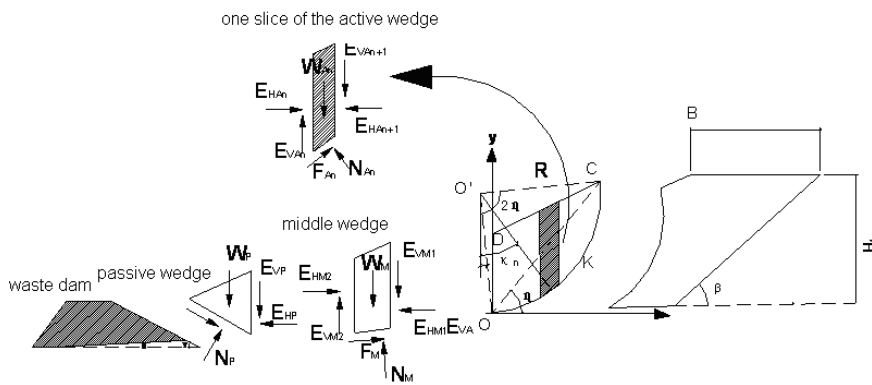


Fig. 2 Forces acting on three adjacent wedges for translational failure along the back of waste dam

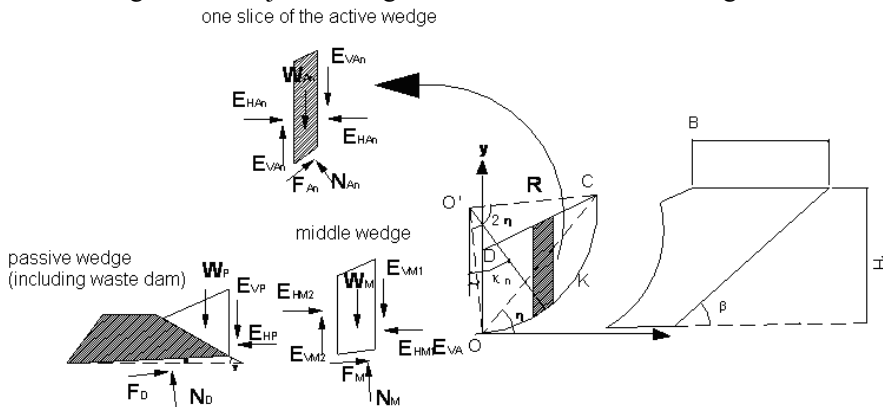


Fig. 3 Forces acting on three adjacent wedges for translational failure along the base of waste dam

The forces acted on slice and wedge in Fig. 2 and Fig. 3 could be shown in Fig. 4:

Firstly, the force limit equivalence of the slice and wedge could be analyzed as following.

According to force equivalence at Y direction ($\sum F_Y = 0$):

$$W + E_1 = N \cos \theta + F \cdot \sin \theta + E \tag{1}$$

In which,

$$F = N \tan \delta / FS \tag{2}$$

$$E_1 = E_1 \tan \varphi / FS \tag{3}$$

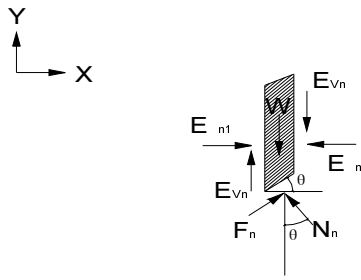


Fig. 4 The forces acted on slice and wedge

$$E = E \tan \varphi / FS \tag{4}$$

Suppose,

$$m = \tan \varphi / FS \tag{5}$$

Substitute Eq. (5) into Eq. (3),

$$E_1 = E_1 m \tag{6}$$

Substitute Eq. (5) into Eq. (4),

$$E = E m \tag{7}$$

Substitute Eqs. (2), (6) and (7) into Eq. (1),

$$W + E_1 m_s = N \cos \theta + (N \tan \delta / FS) \cdot \sin \theta + E m_s \tag{8}$$

According to force equivalence at X direction ($\sum F = 0$),

$$E_1 + N \sin \theta_n = E + F \cos \theta \tag{9}$$

Substitute Eq. (2) into Eq. (9),

$$N = \frac{E - E_2}{\cos \theta \tan \delta / FS - \sin \theta} \tag{10}$$

Substitute Eq. (10) into Eq. (8),

$$\Delta E_H = E_{H1} - E_{H2} = \frac{W (\cos \theta_n \tan \delta / FS - \sin \theta_n)}{\cos \theta_n + \sin \theta_n \tan \delta / FS - m_s \cos \theta_n \tan \delta / FS + m_s \sin \theta_n} \tag{11}$$

Then, the equations of limit equivalence of slice and wedge can be established as following.

As the plus of forces of the whole slide body in X direction is zero, so

$$\Delta E_{H1} + \Delta E_{H2} + \Delta E_{H3} + \dots + \Delta E_{Hn} = 0 \tag{12}$$

$$\sum_{n=1}^N \frac{W (\sin \theta_n FS - \cos \theta_n \tan \varphi_s)}{(\cos \theta_n + m_s \sin \theta_n) FS + (\sin \theta_n - m_s \cos \theta_n) \tan \varphi_s} = 0 \tag{13}$$

At the stable state, the wedges meet the strength criteria, that is, the average shear stress is less than the

average shear strength, assuming that the safety factors of all wedges are the same.

$$FS_1 = FS_2 = \dots = FS = FS \tag{14}$$

Substitute Eq. (14) into Eq. (13) and simplify the formulae,

$$\sum_{n=1}^N \frac{W (\sin \theta FS - \cos \theta \tan \varphi)}{(\cos \theta + m \sin \theta) FS + (\sin \theta - m \cos \theta) \tan \varphi} = 0 \tag{15}$$

The factor of safety could be derived from the Eq. 15.

Factor of Safety Solution

For the above two modes of failure, the factors of safety (FS_V) of wedges are unknown, so the m_{sw} is also unknown, the true factor of safety FS_{true} can't be solved. According to the paper (Qian, 2003, 2004), the maximum and minimum factors of safety could be calculated at extreme conditions, and average factor of safety FS_{ave} could be used instead of FS_{true} , and the error was usually permitted.

Search of the Most Dangerous Failure Surface

In view of the large-scale of modern sanitary landfill, the ratio of the projection lengths of side slope and base slope is very small, so the possibility of whole combination failure induced by side slope failure is low, and only one case of failure surface that the arc and bottom has a cut-off point was considered. In Fig. 5, the failure arc OKC has a cut-off point with the side slope and base, so $\angle KO'P = \beta$, $\angle OO'P = \theta$. As $\angle AO'O = \angle AO'K$, so $\angle AO'O = (\beta - \theta) / 2$. In Right angle, $\triangle AO'O$, $S = \overline{AO} = \overline{OO'} \tan \angle AO'O = R \tan[(\beta - \theta) / 2]$ is the minimum value of S , $T = FA$ is the maximum value of S . Suppose $2\eta \leq 90^\circ$, as $\eta > (\alpha - \theta)$, so, $(\alpha - \theta) < \eta \leq 45^\circ$. For safety factor of all possible failure surface, S lies between (T, S_0) , and angle η lies between $((\alpha - \theta), 45^\circ)$. The minimum value of FS is the safety factor of the combination failure of landfill, and the corresponding surface is the most dangerous failure surface.

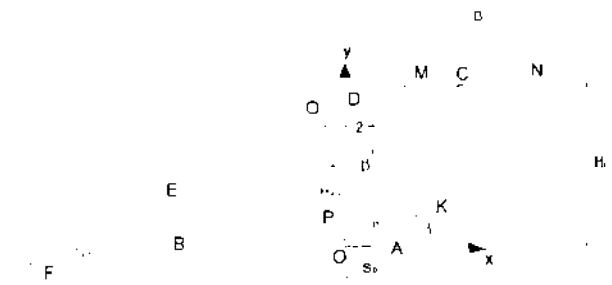


Fig. 5 The definition of the dangerous failure surface

PARAMETER SENSITIVITY ANALYSIS OF COMBINATION FAILURE

In order to study the influence degree of various parameters on the stability, factors of safety of landfill were calculated with only one of these parameters being changed and the rest being unchanged. Finally, the sensitivities of parameters were ranked.

Qian and Koerner (2004) give a landfill example. According to the example, the angles of the side slope β , the front slope α and the base slope θ are 18.4° (1:3), 15.9° (1:3.5) and 1.1° (2%), respectively. Landfill height $H_1=50\text{m}$, top width $B=109.8\text{m}$. The unit weight γ_{sw} and internal friction angle Φ_{sw} of the solid waste are 10.2kN/m^3 and 30° . The minimum angle of interface friction between the liners at base and side slope δ_M and δ_A are all 13° . As Qian and Koerner (2004) did not consider the influence of waste dam, in light of Feng (2005), the following parameters about dam are added: the minimum friction angle δ_P of interfaces at the dam back is 13° , the friction angle δ_D between the dam and base is 28° and the unit weight γ_{dam} of dam is 20.0kN/m^3 . Since the geometry parameters of dam could be considered in the formulae established in this paper, the following parameters about dam are assumed: The height H_2 of waste at the back of dam, the distance ΔH_2 between the tops of waste and dam, the top width B_2 , front angle α' and back angle γ are 9m, 1m, 7m, 60° and 25° respectively. The safety factor of combination failure was calculated and parameter sensitivity to safety factor was analyzed.

In this case, the length of base slope $T=95.92\text{m}$ and $\alpha-\theta=14.8^\circ$. The factors of safety for all possible failure surfaces are drawn in Fig. 6, in which the FS_{base} and FS_{back} are the factors of safety that fail along the base and back of dam separately. When $S=17\text{m}$ and $\eta=40^\circ$, the landfill has the minimum factor of safety, that is 1.765.

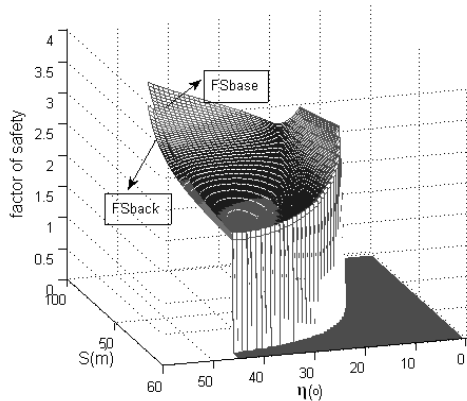


Fig. 6 The relationship between factor of safety and S, η

The Influence of Internal Friction Angle of Solid Waste

As for the internal failure of solid waste, the internal friction angle Φ_{sw} of solid waste is the most important factor (Zhu et al. 2002), and only this parameter is considered in the landfill rotational failure analysis. For the two kinds of combination failures (failures along the back and base of the dam), the relationship between factor of safety and Φ_{sw} was shown in Fig. 7. The factors of safety increase linearly with increase of Φ_{sw} , and the lines are basically parallel. So the change of Φ_{sw} has significant impact on the landfill combination failure.

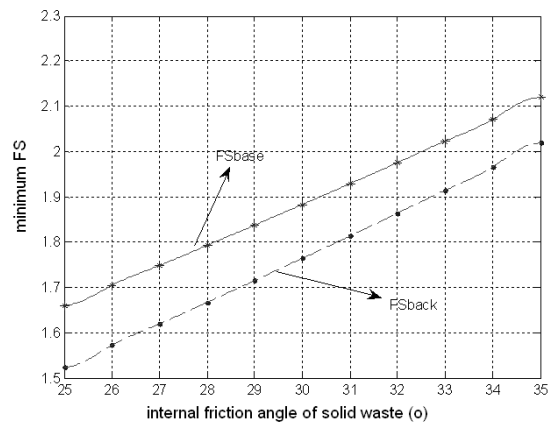


Fig. 7 The relationship between factor of safety and internal friction angle of solid waste

The Influence of Shear Properties Between Liners and Friction Angle Between Dam and Base

The relationship between friction angle of liner interfaces δ and factor of safety was shown in Fig. 8. With the increase of δ , the safety factors of the two failure modes increase linearly, and the lines are also basically parallel. When the friction angle δ_D between the dam and base increases, the factors of safety that fail along the dam base increase linearly, however, the factors of safety that fail along the dam back keep constant, as shown in Fig. 9.

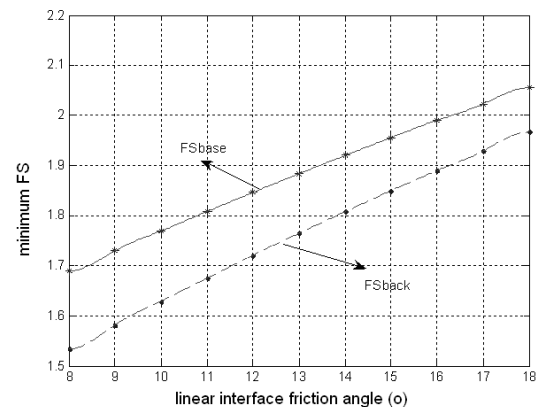


Fig. 8 The relationship between safety factor and friction angle of liner interfaces

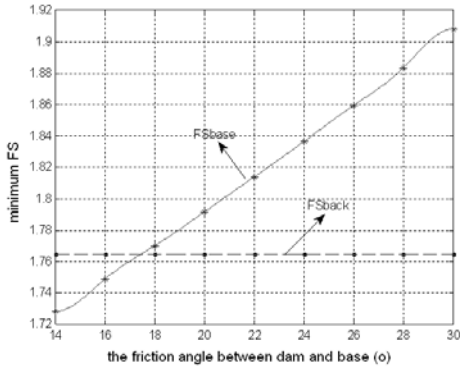


Fig. 9 The relationship between safety factor and friction angle between dam and base

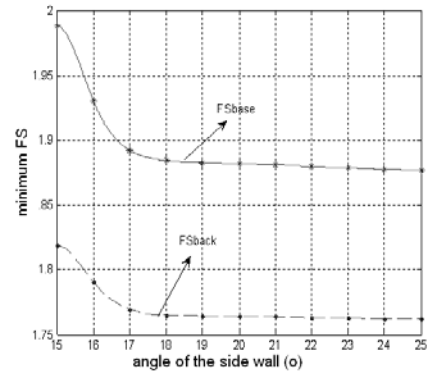


Fig. 11 The relationship between factor of safety and angle of the side slope

The Influence of Geometric Characteristics of Landfill

The influences of geometric parameters of landfill α , β , θ , γ , B , H_1 and H_2 to the safety factor of two failure modes are shown in Figs. 10~16. As the increasing of parameters α , β and θ , the factors of safety reduce, and the reduction trends of the two failure modes are basically the same. When the parameter β reaches a certain value, such as 18° shown in Fig. 11, the factors of safety would be more stable as the increase of β . According to the Fig. 11, when $\beta \leq 18^\circ$, the average increase range $i \approx -0.0478/1^\circ$, when $\beta > 18^\circ$, $i \approx -0.0143/1^\circ$. In generally, β is over 18° , so $i \approx -0.0143/1^\circ$ is taken as the representative value of the sensitivity of β . As the increase of γ , the factor of safety FS_{base} , the failure occurs at the base of dam, would reduce while the factor of safety FS_{back} , the failure occurs at the back of dam, would increase. The increases of B and H_1 lead to the reduction of safety factors of the two failure modes. When B and H_1 reach certain values, such as 100m and 60m shown in Figure 14 and 15, the factors of safety would not reduce obviously. When $H_1 \leq 60$, $i \approx -1.53/1m$, when $H_1 > 60$, $i \approx 0.08/1m$, and when $B \leq 100$, $i \approx -0.64/1m$, when $B > 100$, $i \approx 0.05/1m$. In the filling sequences of waste, H_1 and B increased slowly, so, $i \approx -1.53/1m$ and $i \approx -0.64/1m$ are taken as the representative values of sensitivity of H_1 and B . The factor of safety would increase as the increase of H_2 , as shown in Fig. 16.

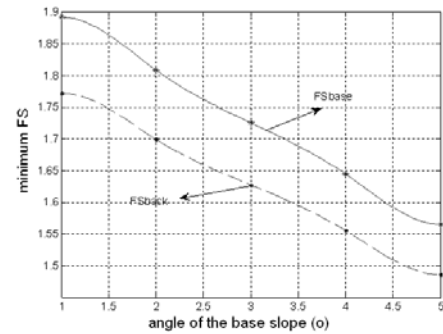


Fig. 12 The relationship between factor of safety and angle of the base slope

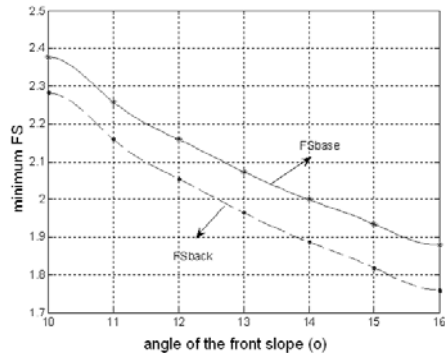


Fig.10 The relationship between factor of safety and angle of the front slope

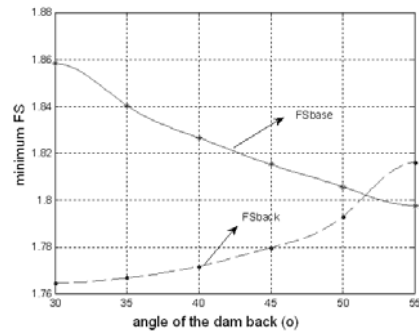


Fig. 13 The relationship between factor of safety and angle of the dam back

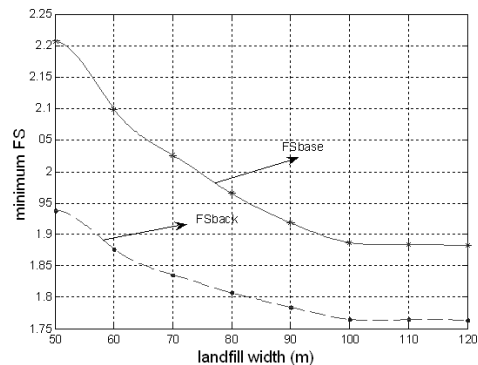


Fig. 14 The relationship between factor of safety and the landfill width

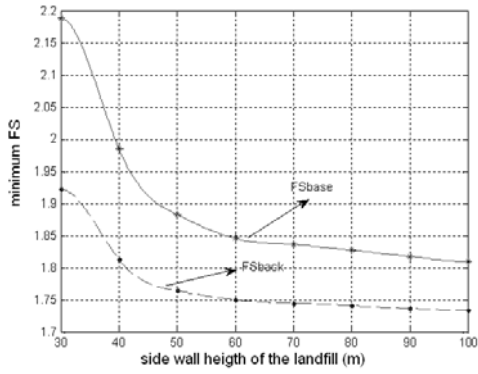


Fig. 15 The relationship between factor of safety and the landfill height

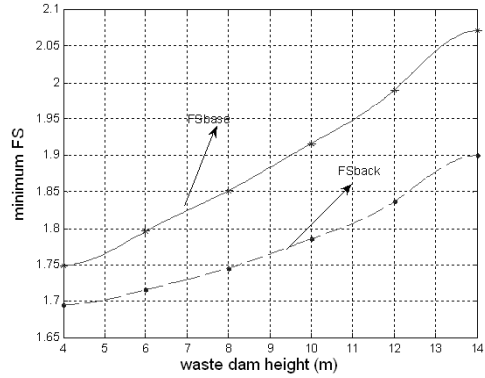


Fig. 16 The relationship between factor of safety and dam height

Table 1 The summary of parameters sensitivity on combination failure

Parameter	Failure mode*	Value of scope	Factor of safety	Increase of FS/%	Sensitivity rank	remarks
$\alpha(^{\circ})$	base	10~16	1.878~2.377	-8.32/1 $^{\circ}$	1	—
	back		1.759~2.283			
$\theta(^{\circ})$	base	1~5	1.577~1.891	-7.85/1 $^{\circ}$	2	—
	back		1.476~1.773			
$\Phi_{sw} (^{\circ})$	base	25~35	1.667~2.124	+4.57/1 $^{\circ}$	4	—
	back		1.534~2.025			
$\delta_A=\delta_M=\delta_P (^{\circ})$	base	8~18	1.689~2.055	+3.66/1 $^{\circ}$	5	—
	back		1.533~1.967			
$H_2(m)$	base	4~14	1.750~2.072	-3.22/1m	6	—
	back		1.695~1.900			
$H_1(m)$	base	30~100	1.811~2.189	-1.53/1m	7	Ranked according to $H_1 \leq 60$
	back		1.734~1.923			
$\beta(^{\circ})$	base	15~25	1.877~1.988	-1.43/1 $^{\circ}$	3	Ranked according to $\beta > 18^{\circ}$
	back		1.762~1.819			
$\delta_D(^{\circ})$	base	14~30	1.728~1.908	+1.13/1 $^{\circ}$	8	—
	back		1.765~1.765			
$B(m)$	base	50~120	1.883~2.207	-0.64/1m	9	Ranked according to $B \leq 100$
	back		1.765~1.938			
$\gamma(^{\circ})$	base	30~55	1.798~1.859	-0.24/1 $^{\circ}$	10	—
	back		1.765~1.816			

Note: “base” means combination failure along dam base, and “back” means combination failure along dam back.

Table 2 The ranks of parameter sensitivity to failure of landfills

	α	θ	β	Φ_{sw}	δ	H_2	H_1	δ_D	B	γ	γ_{sw}	c_{sw}	c
Translational failure (Cui, 2008; Tu and Cui, in pressing)	2	7	1	3	6	4	5	8	—	—	—	—	—
Combination failure	1	3	4	6	9	—	—	—	2	5	7	8	10

The Summary of the Sensitivity Analysis

The influence degrees and sensitivity ranks of various parameters are summarized in Table 1. When the average degree of increase is used to identify the parameter sensitivity, there is a certain degree of error

for those non-linear curves, such as H_1 and B . According to Table 1, the parameters that the greatest influence on combination failure are the landfill angle α and θ , followed by the internal friction angle of solid waste Φ_{sw} , then the friction angle between interfaces of liner system δ , and the last is the $H_2, H_1, \beta, \delta_D, B$ and γ .

From the point of stability and economy, the value of front angle of landfill α is of great importance in the design and management of landfills. The setting of the landfill base angle θ that changes in a small scope is for leachate drainage. The compaction of solid waste that could improve the internal friction angle and choosing of liner system with high internal friction performance are conducive to the stability of landfills.

Discussions

For the translational failure mode, Qian et al. (2003), Qian and Koerner (2004), Feng (2005), Feng et al. (2007), Wu (2008) and Gao et al. (2007) analyzed the sensitivity of single parameter changed, and Cui (2008), Tu and Cui (in pressing) analyzed the sensitivity of multi-parameters simultaneously changed by orthogonal test method. For the combination failure, no research results have been published yet. For comparing the parameter sensitivity of different failure modes, the results in this paper are compared with those in paper (Cui, 2008; Tu and Cui, in pressing), as summarized in Table 2.

In the paper of Cui (2008), Tu and Cui (in pressing), the angle of dam back γ , waste height at the dam back H_2 and the friction angle δ_D between dam and base were not considered since the waste dam in the analysis formulae was not accounted. And the angles of side and base slope β and θ were assumed as the certain values. In this paper, the cohesions of solid waste and liners were neglected, and waste gravity γ_{sw} was assumed as a certain value. As for the parameters in Table 2, the ranks of parameter sensitivity of the translational failure and combination failure are as follows: δ , α , H_1 , B , Φ_{sw} and α , Φ_{sw} , δ , H_1 , B , respectively.

For the translational failure analysis, the friction angle between liner interfaces δ ranks at No.1 and the internal friction angle Φ_{sw} of solid waste ranks at the last, as this mode of failure happens along the liner interface, and internal friction angle is not considered in analysis. For the combination failure, both the friction angle between liner interfaces δ and the internal solid Φ_{sw} are considered, so these two parameters are ranked as No.2 and 3, respectively.

The angle of front slope is important for the modes of translational failure and combination failure, ranks at No.1 and 2 respectively.

The parameter H_1 has higher sensitivity than B , means that the H_1 should be more concerned in the design, management and volume expansion of landfills.

CONCLUSIONS

Based on the force limit equivalence theory, one

formulae to calculate the factor of safety of combination failure of landfill was derived. Through analysis of an example, the parameter sensitivity to combination failure of landfill was gotten. The main conclusions are as following:

(1) According to the sensitivity analysis of parameter on combination failure of landfill, the parameters with the greatest influence are the landfill angle α , θ and β , followed by the internal friction angle of solid waste Φ_{sw} , then the friction angle between interfaces of liner system δ , and H_2 , H_1 , δ_D , B and γ are the last.

(2) From the point of stability and economy of landfills, the choosing of value of landfill front angle α is of great importance. The compaction of solid waste that could improve the internal friction angle and choosing of liner with high internal friction performance are conducive to the stability of landfills.

(3) According to the comparison with the translational failure, the rotational failure is mainly controlled by the strength of waste while translational failure is mainly controlled by the minimum friction angle of liner interfaces. As for the combination failure, the parameter H_1 has higher sensitivity than B , means that the H_1 should be more concerned in the design and management of landfills.

(4) The combination failure model established in this paper does not take cohesions of solid waste and liners as well as the leachate into account, which causes a certain degree of error with the actual case, need to be studied fatherly.

ACKNOWLEDGEMENTS

This study is supported by Natural Science Foundation of Fu Jian Province (Contract No. E0710019)

REFERENCES

- Chen YM, Wang LZ, Hu YY, et al. (2000). Stability analysis of a solid waste landfill slope. *Journal of Civil Engineering*. 23(3): 92-97.
- Cui GQ (2008). The study of stability evaluation of landfill, Master Degree Thesis. Huaqiao University
- Feng SJ (2005). Static and dynamic strength properties of municipal solid waste and stability analysis of landfill. Ph.D.Thesis. Zhe Jiang University.
- Feng SJ, Chen YM, Gao GY, et al. (2007). Effects of retaining wall and interface strength on transnational failure of landfill along underlying liner system. *Chinese Journal of Rock Mechanics and Engineering*. 26(1): 149-155.
- Gao D, Zhu B, Chen YM (2007). Three-part wedge method for translational sliding analysis of landfills

- retained by a toe dam. Chinese Journal of Rock Mechanics and Engineering. 26(add 2): 4378-4385
- Huang YH (1983). Stability Analysis of Earth Slopes, New York, VNR
- Lu TH, Liu ZD, et al. (2005). Advanced Soil Mechanics. Beijing: Machinery industry press
- Qian XD, Koerner RM, Gray DH (2003). Journal of Geotechnical and Geoenvironmental Engineering. 129(6): 506-519.
- Qian XD & Koerner RM (2004). Effect of apparent cohesion on translational failure analysis of landfills. Journal of Geotechnical and Geoenvironmental Engineering. 130(1): 71-80.
- Tu F & Cui GQ (in pressing). An Sensibility Analysis Of Factor Affecting Stability Of Waste Landfill On Neural Network. Rock and Soil Mechanics.
- Wu ZL (2008). Translational failure analysis of stability on sanitary landfill and experimental research on the density of rubbish. Master Degree Thesis. Huaqiao University.
- Zhu XR, Wang CH, Fang PF (2000). Study on feasibility of enlarging capacity in Tianziling waste landfill. Journal of Geotechnical and Geoenvironmental Engineering. 24(3): 281-285.

MODEL TESTS ON DEFORMATION BEHAVIOR OF BENTONITE MIXED SOIL LAYER SUBJECTED TO A LOCAL SUBSIDENCE IN LANDFILL

Shigeyoshi IMAIZUMI¹, Yasuto SHINOZAKI², Kengo KUDO² and Takuya YOSHINAO³

ABSTRACT: Compacted soil mixed with bentonite having a low hydraulic conductivity of less than 10^{-6} cm/s is commonly used as barrier layer in waste landfill in Japan. But it is afraid that the bentonite mixed soil may have cracks when the base ground experiences a local subsidence. The authors conducted trap door tests of bentonite mixed soil under a surcharge pressure of 107.8kN/m^2 . The sizes of the compacted soil layer mixed with 10 % bentonite are 800 mm in length, 200 mm in width and 100 or 200 mm in thickness. The width of trap door was changed as 30, 40 and 50 cm. The rate of lowering the door was 1.0 mm/day. It was found that bentonite mixed soil had a crack in the middle height of soil layer when the trap door subsided between 12 and 13 mm. And then the crack reached at top and bottom surfaces when the door was lowered between 13 and 27 mm. Therefore the shear crack is predominant than bending crack. In the study the image analysis for the tests with a lowering rate of 0.5 mm/min was also conducted by recording the deformation on the video. The amount of calculated shear strain at the cracked position was larger than 20%.

KEYWORDS: barrier system in landfill, bentonite mixed soil, shear behavior, trap door tests

INTRODUCTION

The barrier system in landfills is very important to prevent the leachate from infiltrating into the ground water around the site. In Japan, two-layers barrier system consisting of geomembrane and compacted clay liner has been commonly used since 1998. As the condition to be used, the compacted clay layer is required to have a hydraulic conductivity of less than 10^{-6} cm/s and a thickness of larger than 50 cm. Since, however, there is little natural clay with such low permeability in Japan, the compacted clayey soil that is made by mixing the bentonite into sandy soil (BMS) has been used.

When the compacted clay layer used as top cover system in landfill experienced local subsidence, it was reported that the cracks appeared on the surface. (Viswanadham B.V.S. and Senguputa S. 2005, Camp S. et al. 2007).

The BMS used as bottom layer may subside locally when the soils around underground water collection pipes underlying BMS is eroded by sucking. In this situation, it is afraid that the BMS layer has cracks.

In this paper, the authors conducted trap door tests for BMS layer to know allowable local subsidence till the BMS be damaged. The deformation behavior was

recorded on digital video and the image analysis was also conducted to estimate amount of shear strain.

MATERIALS AND BMS LAYER

Bentonite and Sand

The bentonite used in this study is sodium one produced in U. S. A.. Its particle density is 2.86 g/cm^3 , free swelling is 38 ml/2g, pH is 9.8, Liquid Limit is 581 % and Plastic Limit is 38 %

The sand used as parent material of BMS is the fine crushed rock. Table 1 shows properties of grains. The sand has a maximum particle size of 9.5 mm and well graded soil. It is classified as Sand with Fine-soil (SF) according to the Method of Japanese Classification of Geomaterials for Engineering Purpose (JGS 2000).

Bentonite Mixed Soil (BMS)

BMS was made by mixing sodium bentonite with a ratio of 10 % in dry mass into the sand. The compaction tests using a mould with a volume of 1000 cm^3 and a hammer with a mass of 2.5 kg and drop-height of 30 cm

¹ Professor, Graduate School of Engineering, Utsunomiya University, Japan. Email:timaizumi@cc.utsunomiya-u.ac.jp

² Graduate Student, Graduate School of Engineering, Utsunomiya University, Japan.

³ Technical officer, Faculty of Engineering, Utsunomiya University, Japan

resulted in the maximum dry density ρ_{dmax} of 1.88 g/cm³ and the optimum water content w_{opt} of 10.7 %.

The BMS with a designed water content of 15% was first compacted statically in the steel box using oil jack to be a degree of compaction (D_c) of 95 %. Then it was extruded from the box and was trimmed to become 800 mm in length, 200 mm in width and 100 (or 200) mm in thickness (Kato H. et al. 2007).

Table 1 Particle size and density of the sand

Max. Particle Size (mm)	9.5
Gravel (%)	33.4
Sand (%)	50.5
Silt (%)	7.1
Clay (%)	9.0
Uniformity Coefficient U_c	200.0
Coefficient of Gradation U_c'	7.0
Particle density (g/cm ³)	2.70

TEST APPARATUS AND PROCEDURE

Apparatus

Fig. 1 and Fig. 2 show the model setup and the cross section of the trap door apparatus. The steel container has an inside size of 800 mm in length, 200 mm in width and 350 mm in depth. Its bottom consists of fixed steel plates and separated steel plate. The latter is supported by two screw jacks and can be lowered, that is called trap door.

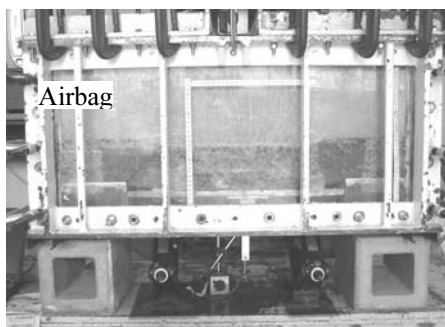


Fig. 1 Experimental setup of trap door tests

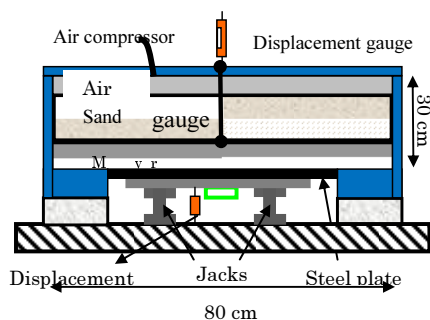


Fig. 2 Cross section of trap door apparatus

Testing Cases

The thickness of the BMS layer was changed as 100 mm and 200 mm. And three types of width of trap door were prepared such as 300 mm, 400 mm and 500 mm. In total, six trap door tests were conducted under the condition shown in Table 2.

Table 2 Condition of the trap door tests

No.	Thickness of BMS layer (mm)	Width of trap door (mm)	Degree of compaction (%)	Rate of lowering the door
1	100	300	95.7	1 mm/day
2	100	400	94.0	1 mm/day
3	100	500	95.5	1 mm/day
4	200	400	95.3	1 mm/day
5	200	500	96.1	1 mm/day
6	200	500	97.1	0.5mm/min

Procedure

The trimmed compacted BMS layer was placed on the bottom plate of the container and then was overlaid by protective sand having a thickness of 200 mm. The airbag placed on the sand functions to apply uniformly distributed pressure on the compacted BMS layer through the protective sand. The amounts of subsidence of BMS layer are measured through the displacement gauges tied to a thin steel plate placed on the top and bottom center of the BMS liner (see Fig. 2).

The trap-door was lowered by the jacks at a rate of 1 mm per 24 hours. During the tests, the airbag had pressured the BMS layer with 107.8 kN/m².

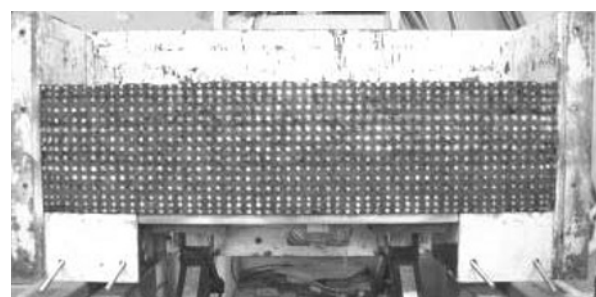


Fig. 3 Markers placed on the side of BMS layer

In the case of No.6 that the deformation behavior was recorded by digital video camera and induced shear strain was calculated by image analysis, it was lowered at a rate of 0.5 mm per min. Fig. 3 shows the markers placed on the front side of BMS layer to recognize the movement.

Calculation of Shear Strain From the Digital Image

The average strains, ϵ_x , ϵ_y and γ_{xy} of triangular element formed by three markers of i, j , and k was calculated as follows.

$$\begin{Bmatrix} \epsilon_x \\ \epsilon_y \\ 2\gamma_{xy} \end{Bmatrix} = [B] \{ u_i \ v_i \ u_j \ v_j \ u_k \ v_k \}^T \quad (1)$$

where, u_i, u_j, u_k are x-direction displacement of markers i, j, k

v_i, v_j, v_k are y-direction displacement of markers i, j, k

$$[B] = \frac{1}{\Delta} \begin{bmatrix} y_j - y_k & 0 & y_k - y_i & 0 & y_i - y_j & 0 \\ 0 & x_k - x_i & 0 & x_i - x_j & 0 & x_j - x_k \\ x_j - x_k & y_j - y_i & x_k - x_i & y_k - y_j & x_i - x_j & y_j - y_k \end{bmatrix}$$

$$\Delta = \begin{vmatrix} 1 & x_i & y_i \\ 1 & x_j & y_j \\ 1 & x_k & y_k \end{vmatrix}$$

TEST RESULTS

Occurrence of Cracks

Fig. 4 shows variation of the amount of subsidence of the BMS layer and trap door in case of No.3, with a layers thickness of 10 cm and trap door width of 50 cm. Fig. 5 shows the cracks appeared on the side of BMS layer at finishing the test. When the center of top surface of the BMS layer subsided by 12.0 mm, the cracks (A ,

B) had taken place in the middle height of the BMS just above the edge of the trap-door. These cracks proceeded upward and downward as trap door subsided more. When the center of top surface of the BMS layer subsided by 13.0 and 15.5 mm, crack A reached the top and bottom surfaces of the layer, respectively. And when the top displacement gauge showed 17.0 and 19.0 mm, crack B reached the top and bottom surfaces, respectively.

Cracks C and D appeared on the bottom of BMS layer when the top surface subside 19 mm. These two cracks were thought as bending ones.

Fig. 6 and Fig. 7 show the variation of the amount of subsidence in case of No.5 with a layers thickness of 20 cm and trap door width of 50 cm and the cracks appeared on side of the BMS layer at finishing.

When the center of the top surface of BMS layer subsided by 12.0 and 13.0 mm, cracks A and B had taken place on the bottom surface of the BMS layer just above the fixed bases. These cracks proceeded upward as the trap door subsided more and reached the top surface when the center of top surface subsided by 24.5 and 27.0 mm, crack A and crack B , respectively. These cracks were thought to be induced by shearing.

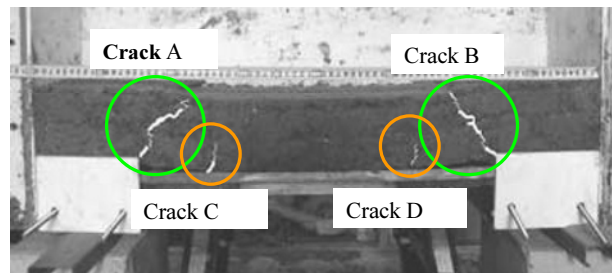


Fig. 5 Observed cracks at a subsidence of 21mm in case of No.3

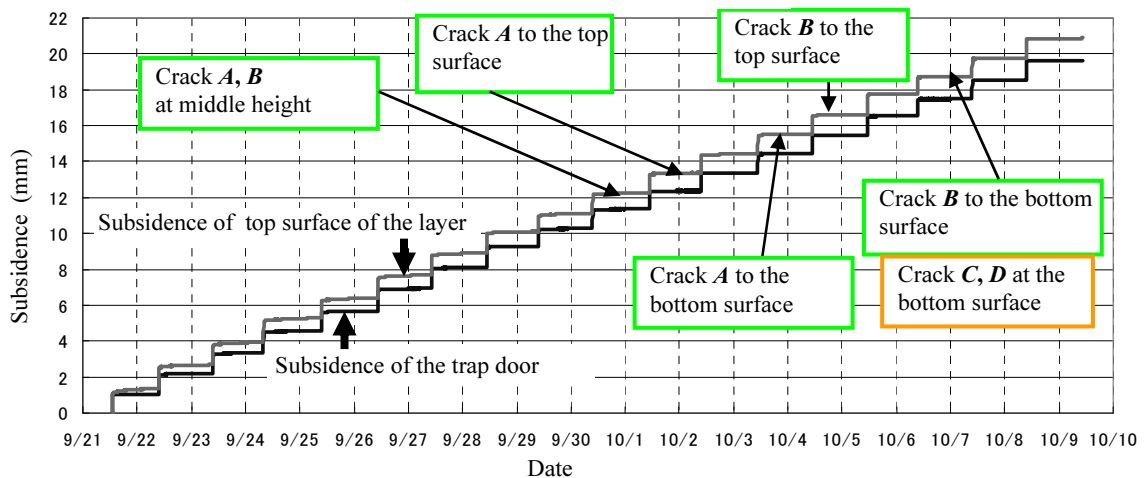


Fig. 4 Amount of subsidence in case of No.3 (Thickness of 10 cm, width of 50 cm)

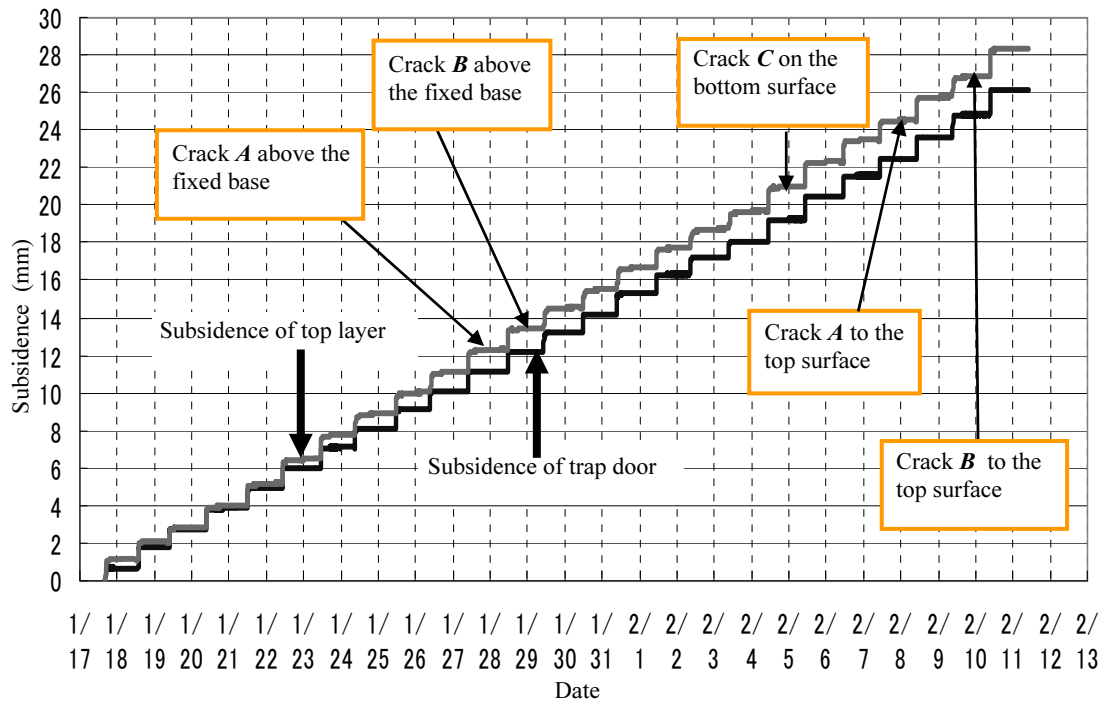


Fig. 6 Amount of subsidence in case of No.5 (Thickness of 20 cm, Width of 50 cm)

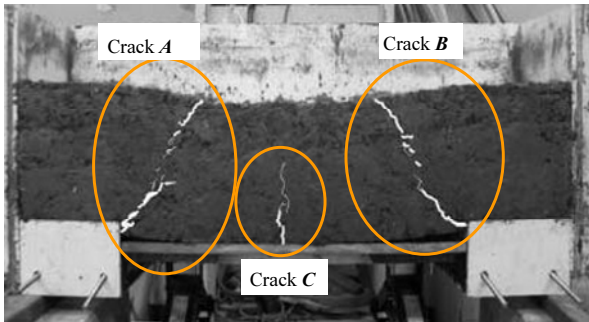


Fig. 7 Observed cracks at a subsidence of 28mm in case of No.5

Table 3 Summary of trap door tests

No.	Ratio of width to thickness	Subsidence at first crack	Position of first crack	Average Angle of crack direction
1	3.0	None	None	-
2	4.0	12 mm	Middle height	55
3	5.0	12 mm	Middle height	50
4	2.0	None	None	-
5	2.5	12.5 mm	Bottom surface	55
6	2.5	25 mm	Bottom surface	52

The bending crack C took place on the center of bottom surface of BMS layer when the top surface subsided by 21.0 mm.

Table 3 shows the summary of the results. In cases of No.1 with a layers thickness of 10 cm and a trap door width of 30 cm and No.4 with a layers thickness of 20 cm and a trap door width of 40 cm, no crack was appeared under a vertical pressure of 107.8 kN/m² and 157 kN/m².

From Table 3, it can be said that the amount of subsidence when the crack was recognized visually was about 12mm and was bit larger as the thickness increased and the cracks was induced by shearing not bending.

In the Table 3, average angle of crack direction against horizontal plane was also presented. Assuming that this angle equals to (45+ frictional angle / 2). the frictional angle can be estimated as about 10 to 20 degrees.

Distribution of Calculated Shear Strain

Fig. 8 shows the distribution of the calculated shear strain in the zone which locates just above the fixed based and is within the dotted line in Fig. 9 . The model elements corresponding to the cracked area indicate a shear strain of lager than 20%. As the element gets from the cracked area, the amount of shear strain decreases.

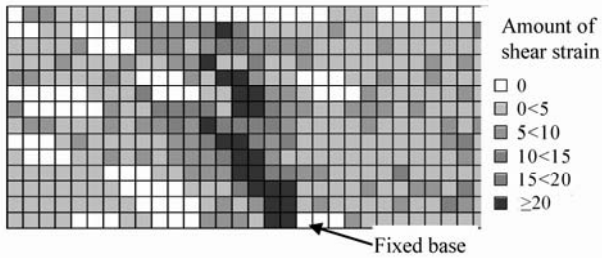


Fig. 8 Distribution of the calculated shear strain

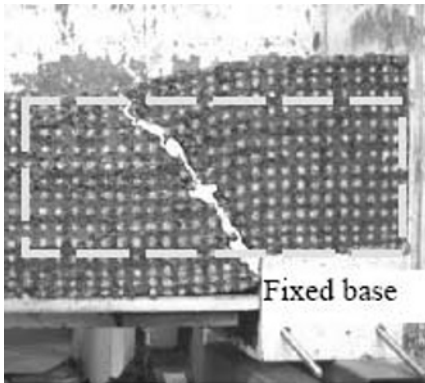


Fig. 9 Zone for estimating the shear strain

SUMMARY

The trap door tests for bentonite mixed soil under a surcharge pressure of 107.8 kN/m^2 were conducted to know how much local subsidence of the base can be permitted. The main results obtained from this study are as follows.

- (1) When the BMS liner deformed under the constant applied pressure of 107.8 kNm^2 , it had a crack in the middle height of soil layer or just above the corner of fixed base when the trap door subsided between 12 and 13 mm.

- (2) Then the crack reached at top and bottom surfaces when the trap door was lowered between 13 and 27 mm.
- (3) The shear crack was predominant than bending crack. The shear strain was thought to be more than 20 %.
- (4) It is thought that the landfill would be designed safely for local subsidence by conducting the trap door tests.

ACKNOWLEDGMENT

This study was financially supported by a grant from Specific Research Program at Utsunomiya University.

REFERENCE

- Camp S, Gourc JP, Ple O, Marchiol A, Round C (2007). Field Tests on Landfill Clay Barrier Submitted to Local Subsidence. Proc. of the 11th International Waste Management and Landfill Symposium, CD-ROM E-10.
- The Japanese Geotechnical Society (2000). Method of Classification of Geomaterials for Engineering Purposes. Japanese Standards for Geotechnical and Geoenvironmental Testing Methods: 215-221 (in Japanese)
- Kato H, Usami S, Imaizumi S, Kudo K, Matsuyama S, Furuichi T, Hanashima M (2007). Experimental Study and Analysis on Deformation of Bentonite Mixed Soil Liner. Proc. of the 11th International Waste Management and Landfill Symposium, CD-ROM. PF.
- Viswanadham BVS & Sengupta S (2005). Deformation Behaviour of Compacted Clay Liners of Landfills in a Geocentrifuge. Proc. of the 10th International Waste Management and Landfill Symposium, CD-ROM No.367.

FACTORS AFFECTING SLOPE STABILITY OF LANDFILL COVERS

Manoj DATTA¹

ABSTRACT: Landfills have to be provided with steep cover slopes to maximize the quantity of waste which can be accommodated. Low interface shearing resistance between components of cover systems limits the steepness of such slopes. This paper examines the influence of various parameters, including soil thickness, seepage forces, seismic forces, height between berms, geomembrane roughness, provision of reinforcing element, provision of geocomposite drain etc. on the stability of slopes. The study reveals that in a cover system, the provision of a geomembrane influences the stability of the cover alongside slopes. The interfaces between the geomembrane and the clay beneath it or the geotextile above/below it are the weak locations at which slippage are likely to occur. Seepage force parallel to the geomembrane during monsoon as well as horizontal seismic loading during earthquakes also causes the factor of safety to reduce significantly. Provision of reinforcement in the soil above the geomembrane, and use of textured geomembrane, improves the stability of slope. Provision of berms at intervals of low heights also helps in increasing the stability of the cover system. Reducing the thickness of the soil above the geomembrane improves the stability of covers which have reinforcement.

KEYWORDS: geosynthesis, landfills, covers, stability

GEOENVIRONMENTAL ENGINEERING IN INDIA

The Indian landscape is dotted with numerous solid waste disposal sites in the form of municipal solid waste landfills, hazardous waste landfills, tailings ponds, coal ash ponds and other waste mounds & dumps.

Till the 1980s, waste disposal in India was mostly in the form of dumping in low-lying areas or in un-engineered mounds with no liners and nominal top covers. In the 1990s, the pollution control authorities were engaged in the formulation of various regulatory measures. By early 2000, design guidelines for solid waste disposal facilities were published by Ministry of Urban Affairs (MUA 2000) as well as the Central Pollution Control Board of the Ministry of Environment and Forests (CPCB 2000, CPCB 2002). This led to the adoption of engineered landfills for municipal and hazardous waste as well as environment-friendly construction of slurry ponds and waste mounds.

Over the next decade, several dozen new landfills, slurry ponds and integrated treatment & disposal facilities are expected to be developed in the country for disposal of municipal and hazardous solid waste. In addition, steps are being taken to close old waste dumps. At several locations in metropolitan cities in India, old and un-engineered waste mounds have reached heights of 15 to 25 meters. Such mounds have either been

abandoned or are still under operation. These have to be closed in a manner that minimizes their harmful impact on the environment. This involves installation of a low-permeability cover system as well as cut-off walls wherever necessary, to minimize formation of leachate and release of green house gases from the waste mound.

In this paper, the influence of various parameters on the cover stability is discussed.

LINERS AND COVERS

The liner and cover configurations for landfills in India, as per the guidelines issued by the regulatory authorities (CPCB 2000, CPCB 2002, MUA2000), are shown in Figs. 1 and 2 for municipal solid waste (MSW) and hazardous waste (HW) for single liner system respectively.

The cover system for a MSW landfill has five components as shown in Fig. 1, including a single barrier of 0.6m thick compacted clay. A HW landfill cover comprises of the same five components but includes a geomembrane as the sixth component which is a part of a composite barrier as shown in Fig. 2. For MSW landfills in which gas collection for energy recovery is envisaged, a geomembrane is incorporated in the cover system, making it akin to a HW cover system.

¹ Director, Punjab Engineering College (Deemed University), Chandigarh, India. Email: director@pec.ac.in, mdatta55@gmail.com

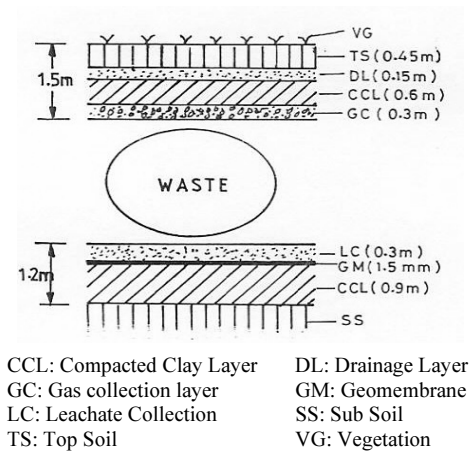


Fig. 1 Components of MSW landfill

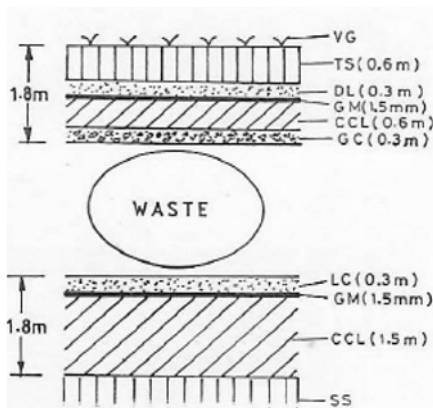
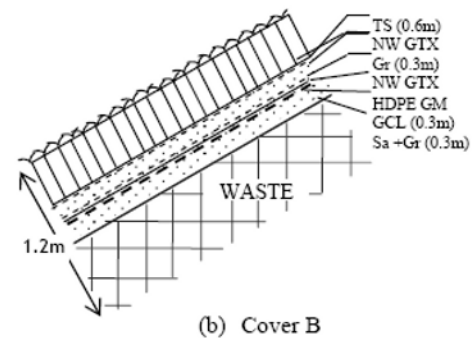
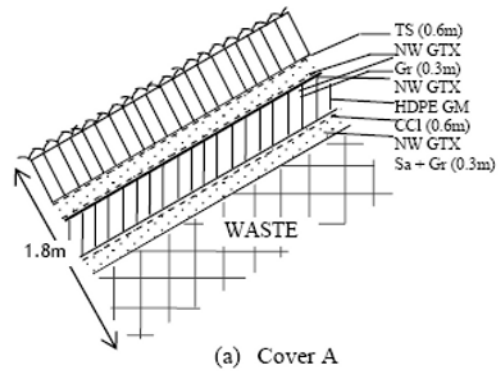


Fig. 2 Components of HW landfill



TS: Top Soil HDPE GM: HDPE Geomembrane
Gr: Gravel NW GTX: Non-woven Geotextile
Sa: Sand GCL: Geosynthetic Clay Liner
CCI: Compacted Clay Layer

Fig. 3 Cover system

To close old waste dumps, no guidelines relating to the cover systems have been issued by regulatory authorities in India. The cover systems are expected to be more stringent than those adopted for new landfills because old waste dumps do not have a liner system at base. Such cover systems also incorporate a geomembrane in the cover making them akin to HW landfill cover systems.

STABILITY OF COVER SYSTEMS

In the present study, to begin with, two cover systems (Fig. 3) were considered for analysis.

Cover A corresponds to the guidelines for HW landfills. In Cover B the compacted clay layer is replaced by a geosynthetic clay liner (non-woven, needle punched with adequate peel strength). The attempt was to arrive at the steepest slope with adequate factor of safety, so that maximum volume of waste could be accommodated. Four cases were considered critical for slope stability and these along with minimum acceptable factor of safety (min FOS) in each case, are listed below:

(a) long term case of dry slope under static loading (min FOS = 1.5);

- (b) short term case, during monsoon, of slope with seepage flow in drainage layer parallel to the outer slope having submergence ratio of 0.5 (min FOS = 1.3);
- (c) short duration case of slope under earthquake loading (pseudostatic approach with horizontal seismic coefficient of 0.1) (min FOS = 1.1);
- (d) rare case of slope with seepage flow and earthquake loading occurring simultaneously (min FOS = 1.0).

Stability analysis was performed for failure along interfaces parallel to outer slope (Qian et al. 2002, Koerner and Daniel 1997). The factors of safety were evaluated for each of the four cases cited above.

Data on interface shearing resistance used in the analysis is listed in Table 1. From this table, it becomes evident that geomembrane-clay interface is a weak interface in Cover A. Textured geomembrane gives better interface resistance than a smooth one. Further, when a GCL replaces the clay layer, as in Cover B, the weakest interface becomes the geomembrane – geotextile interface.

Four sets of results of slope stability are presented hereafter, namely:

- (a) Smooth HDPE geomembrane interface with NW(non-woven), NP(needle punched) geotextile ;

Table 1 Interface shear strength parameters

Base Material	Underlying/Overlying Material	Peak Parameters		Residual Parameters	
		c_a (kPa)	δ (deg)	c_a (kPa)	δ (deg)
Smooth HDPE Geomembrane	Saturated clay	0	11	0	9
Textured HDPE geomembrane	Saturated clay	0	18	0	14
Smooth, HDPE Geomembrane	Non woven, needle punched Geotextile	0	11	0	9
Textured HDPE Geomembrane	Non woven, needle punched Geotextile	0	25	0	17
Textured HDPE Geomembrane	Non woven, needle punched Geosynthetic Clay Liner	0	32	0	20
Textured HDPE Geomembrane	Geocomposite drain	0	24	0	17

(b) Textured HDPE geomembrane interface with NW, NP geotextile ; and

(c) Textured HDPE geomembrane interface with NW, NP geotextile with the presence of a geogrid reinforcement.

(d) Stability after replacing gravel drainage layer above geomembrane by a geocomposite drain

Stability Along Smooth Geomembrane - Geotextile Interface

Stability analysis was conducted at the interface between smooth geomembrane and geotextile using both peak and residual parameters. Table 2 presents the results of analysis for stability along interface of smooth HDPE geomembrane and NW, NP geotextile interface, for various inclinations and slope heights between berms using peak interface strength parameters. It is observed that both for peak parameters (Table 2) and residual parameters, the factors of safety remain below acceptable values indicating that the slopes are not stable. Slope height between berms does not influence the factor of safety. The reason for this is the low angle of interface shear between the smooth geomembrane and the geotextile.

Table 2 Results of stability analysis at interface of HDPE geomembrane (smooth) – geotextile (NW, NP) (Peak Parameter, $c_a = 0$, $\delta = 11^\circ$)

Slope H : V	Height Between Berms (m)	FOS (Without Reinforcement)			
		Static	Seepage	E.Q.	E.Q + Seepage
3 : 1	5.00	0.58	0.49	0.43	0.40
	10.00	0.58	0.49	0.43	0.40
3.5: 1	5.00	0.68	0.58	0.49	0.45
	10.00	0.68	0.58	0.49	0.45
4 : 1	5.00	0.78	0.67	0.54	0.50
	10.00	0.78	0.67	0.54	0.50
5 : 1	5.00	0.97	0.85	0.63	0.59
	10.00	0.97	0.85	0.63	0.59

Stability Along Textured Geomembrane - Geotextile Interface

If a textured geomembrane is used instead of smooth geomembrane in the cover system, the interface shear strength parameters are larger (see Table1). The results of stability along the textured geomembrane – geotextile interface are presented in Tables 3 and 4. The factors of safety are higher than those for the smooth case. For peak strength parameters (Table3), slopes of 3.5: 1 or flatter are observed to be stable. However, for residual strength parameters, slopes are stable for an inclination of 5: 1 (except for EQ + seepage).

Correct choice of interface strength parameters is critical for arriving at reliable results from stability analysis. The use of residual values is recommended when one cannot rule out the possibility of development of large strains due to relative movement during the construction stage.

Stability Along Textured Geomembrane – Geotextile Interface with Geogrid Reinforcement above the Geotextile

To achieve stability of slopes steeper than 5: 1 (for residual parameters), it is necessary to install reinforcing elements in the form of geogrids in the cover system, just above the geotextile. Table 5 presents the results of stability analysis of cover system for slippage along the interface of textured HDPE geomembrane and NW, NP geotextile with geogrid reinforcement over the geotextile.

The geogrid reinforcement is able to oppose the driving stresses upto a value equal to its long term tensile strength. This helps increase the factor of safety of the cover slope. The higher the long term strength, the greater is the improvement in factor of safety.

One notes from the table that a slope of 4.0: 1 with berms at 5.0m interval is suitable when a geogrid with a long-term tensile strength of 30 kN/m is used. Fig. 4 shows the anchor trench arrangement required for holding the geogrid in position under this tensile force, which is likely to develop during earthquake or monsoon.

Table 3 Results of stability analysis at interface of HDPE geomembrane (textured) – geotextile (NW, NP) (Peak Parameter, $c_a = 0$, $\delta = 25^\circ$)

Slope H : V	Height Between Berms (m)	FOS (Without Reinforcement)			
		Static	Seepage	E.Q.	E.Q + Seepage
3 : 1	5.00	1.40	1.20	1.04	0.96
	10.00	1.40	1.20	1.04	0.96
3.5: 1	5.00	1.63	1.41	1.17	1.09
	10.00	1.63	1.41	1.17	1.09
4 : 1	5.00	1.87	1.63	1.30	1.20
	10.00	1.87	1.63	1.30	1.20
5 : 1	5.00	2.33	2.06	1.52	1.42
	10.00	2.33	2.06	1.52	1.42

Table 4 Results of stability analysis at interface of HDPE geomembrane (textured) – geotextile (NW, NP) (Residual Parameter, $c_a = 0$, $\delta = 17^\circ$)

Slope H : V	Height Between Berms (m)	FOS (Without Reinforcement)			
		Static	Seepage	E.Q.	E.Q + Seepage
3 : 1	5.00	0.92	0.78	0.68	0.62
	10.00	0.92	0.78	0.68	0.62
3.5: 1	5.00	1.07	0.92	0.77	0.71
	10.00	1.07	0.92	0.77	0.71
4 : 1	5.00	1.22	1.06	0.85	0.78
	10.00	1.22	1.06	0.85	0.78
5 : 1	5.00	1.53	1.34	1.00	0.92
	10.00	1.53	1.34	1.00	0.92

Table 5 Results of stability analysis at interface of HDPE geomembrane (textured) – geotextile (NW, NP) with geogrid reinforcement (Residual Parameter, $c_a = 0$, $\delta = 17^\circ$)

Slope H : V	Height Between Berms (m)	FOS (Without Reinforcement) Long Term Tensile Strength T=30kN/m			
		Static	Seepage	E.Q.	E.Q + Seepage
3:01	5	1.65	1.45	1.04	0.95
	7.5	1.3	1.15	0.88	0.81
	10	1.18	1.04	0.82	0.75
3.5: 1	5	1.93	1.69	1.15	1.06
	7.5	1.52	1.34	0.99	0.91
	10	1.38	1.22	0.92	0.85
4:01	5	2.2	1.93	1.25	1.15
	10	1.57	1.39	1.01	0.93

Stability after Replacing Drainage Layer (Gravel) by Geocomposite Drain

To increase stability further, the 0.3m thick gravel layer (drainage layer) above the geomembrane is replaced by a 5 mm thick geocomposite drain (geonet sandwiched between non-woven geotextiles). This causes the factors of safety to increase further because the driving stresses on account of the weight of the soil become smaller. As shown in Table 6, a slope of 3.5:1 with berm spacing of 7.5m is observed to be stable.

Table 6 Results of stability analysis at interface of geomembrane (textured) – geotextile ($\delta = 17^\circ$) with geogrid reinforcement and geocomposite drain (5mm))

Slope (H:V)	Height between berm (m)	FOS with reinforcement Long term tensile strength T= 30kN/m			
		Dry	Seepage	E.Q	E.Q + Seepage
2:1	5.0	2.24	1.63	1.23	1.01
	7.5	1.19	0.93	0.81	0.68
	10.0	0.96	0.77	0.69	0.58
2.5 : 1	5.0	2.80	2.04	1.40	1.17
	7.5	1.48	1.17	0.96	0.81
	10.0	1.20	0.96	0.83	0.70
3:1	5.0	3.36	2.45	1.55	1.31
	7.5	1.78	1.40	1.09	0.93
	10.0	1.44	1.15	0.95	0.81
3.5:1	5.0	3.92	2.86	1.67	1.43
	7.5	2.08	1.63	1.20	1.03
	10.0	1.68	1.34	1.05	0.91
4:1	5.0	4.47	3.26	1.77	1.54
	7.5	2.37	1.86	1.30	1.13
	10.0	1.92	1.54	1.15	1.00

CONCLUSIONS

This paper highlights the factors which influence the stability of cover systems on steep slopes of waste mounds.

- The interface between the geomembrane and the clay beneath it or the geotextile above / beneath it is a weak interface at which slippage can occur.
- The choice of strength parameters – residual or peak – should be made taking into account the possibility of the development of large strain during installation; this has an important influence on results of stability analysis.
- Seepage force parallel to the geomembrane during monsoon as well as horizontal seismic force during earthquakes causes the factor of safety to reduce significantly.

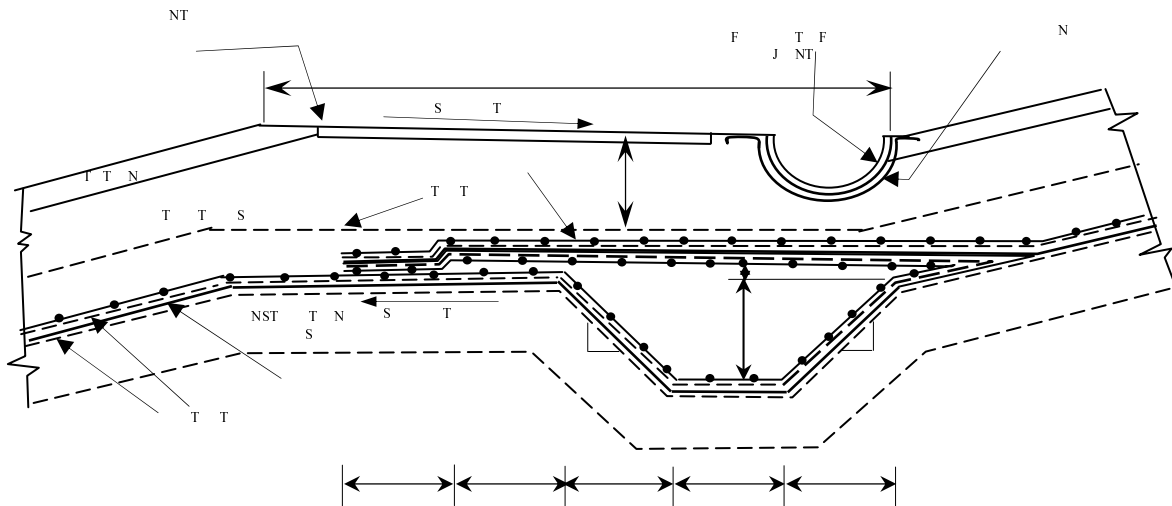


Fig. 4 Wrap – around anchor trench arrangement

- (d) Stability of cover systems improves with provision of textured geomembranes, geogrid reinforcement, berms at low intervals and replacement of drainage layer by geocomposite drain.

REFERENCES

- CPCB (2000). Criteria for hazardous waste landfills. Central Pollution Control Board, New Delhi.
- CPCB (2002). Manual for design, construction and quality control for liners and covers of hazardous waste landfills. Central Pollution Control Board, New Delhi.
- Datta M (2003). Geotechnical study for hydraulic barrier system at tailings pond. ASCE Practice Periodical for Hazardous, Toxic and Radioactive Waste. 7(3): 163-169.
- Datta M (2006). Geotechnical aspects of landfills and old waste dumps – some case studies. Proceedings IGC 2006, Chennai, India: 221-228.
- Hausmann MR (1990). Engineering principles of ground modification. McGraw Hill, New York.
- Koerner RM & Daniel DE (1997). Final covers for solid waste landfills and abandoned dumps. ASCE Press, Virginia, USA.
- MUA (2000). Manual for municipal solid waste management. CPHEEO, Ministry of Urban Affairs, New Delhi.
- Qian X, Koerner RM, Gray DH (2002). Geotechnical aspects of landfill design and construction. Prentice Hall, New Jersey, USA.

ONE-DIMENSIONAL SETTLING BEHAVIOR OF A GROUP OF SOIL MATERIALS IN STATIC WATER ASSUMING COASTAL LANDFILL

Shuichi NAGAOKA¹, Yuta NABESHIMA², Kenichi SATO³, Shotaro YAMADA⁴,
Tomoaki HACHIMURA⁵ and Tetsuya MIYAHARA⁶

ABSTRACT: There are a number of cases that coastal landfill is constructed at the port area where suburbs of the nation's largest metropolitan areas and the cities are located on the alluvial plain. The seabed alluvial clay layer is, therefore, often utilized as an impervious layer for coastal landfill. Thus, it is required to prevent the degradation of impervious function of seabed clay layer by reducing the impact of poured wastes on clay layer. However, the technical data and knowledge concerning this landfill method are currently quite limited. The purpose of this study is to establish the waste pouring method which does not harm seabed. As a first step of this research, one-dimensional settling behaviour of a group of soil samples in static water has been examined using thirty centimetre diameter cylindrical container in this paper. Influential factors selected in this research are shown as follows: 1) Effect of the difference of the fluid in the cylindrical container between the tap water and the sea water. 2) Effect of the difference of grain size, amount of pouring, pouring height and the density of pouring samples on the settling behavior.

KEYWORDS: waste, landfill, settling velocity, impervious layer

INTRODUCTION

Recently, the annual total amount of general waste has been reducing by the increase of recycling. However, the remaining landfill capacity is still on a downwards trend. Since it is getting difficult to secure the onshore (ground-based) landfill site, coastal landfill is one of the predominant solutions to be expected. There are a number of cases that coastal landfill is constructed at the port area where suburbs of the nation's largest metropolitan areas and the cities are located on the alluvial plain. The seabed alluvial clay layer is, therefore, often utilized as an impervious layer for coastal landfill. Thus, it is required to prevent the degradation of impervious function of seabed clay layer by changing the waste pouring position and reducing the impact of poured wastes on clay layer. However, the technical data and knowledge concerning this landfill method are currently quite limited. In the meantime, the wastes which density is large such as slag are also landfilled. In addition, thickness of impervious layer regarding coastal landfill is non-uniform. The landing of poured wastes such as slag on the clay layer

will cause the dents and fling up the clay particles. In case that such phenomenon occurs at the place where the thickness of clay layer is relatively thin, the deterioration of the impermeable function is concerned.

The purpose of this study is to establish the waste pouring method which does not harm seabed. As a first step of this research, the effect of the difference of grain size, amount of pouring, pouring height and the density of soil samples on the one-dimensional settling behavior of a group of soil samples in static water has been examined using cylindrical containers in this paper.

EXPERIMENTAL METHODS AND APPARATUS

Test Samples

In order to investigate the effect of the difference of grain size on the settling behavior, the geotechnical samples that have four patterns of grain size were utilized in this study. Test samples are absolute dry Tagawa decomposed granite soil which density is $\rho_s=2.60\text{g/cm}^3$ and the range

¹ Ph.D Student, Department of Civil Engineering, University of Dundee, UK. Email: s.z.nagaoka@dundee.ac.uk

² Master Course Student, Graduate School of Fukuoka University, Japan. Email: td084014@cis.fukuoka-u.ac.jp

³ Professor, Department of Civil Engineering, Fukuoka University, Japan. Email: sato@fukuoka-u.ac.jp

⁴ Assistant Professor, Department of Civil Engineering, Fukuoka University, Japan. Email: s-yamada@fukuoka-u.ac.jp

⁵ West Branch Office, Japan Environmental Sanitation Center, Japan. Email: tomoaki_hachimura@jesc.or.jp

⁶ West Branch Office, Japan Environmental Sanitation Center, Japan. Email: tetsuya_miyahara@jesc.or.jp

of grain size is $0.85 < d < 2.0$ (mm), and gravels which range of grain size is $4.75 < d < 9.5$, $9.5 < d < 13.2$ and $13.2 < d < 19.0$ (mm) and mixed samples that 4 patterns of soil samples were mixed together. To investigate the effect of the difference of density on the settling behavior, incineration bottom ash ($\rho_s = 2.37 \text{ g/cm}^3$) that range of grain size is $0.85 < d < 13.2$ (mm) is used in this study.

Test Apparatus

Test apparatuses used in this study are shown in Fig. 1. To investigate the restraint effect of wall surface, the two acrylic cylindrical containers which diameter is 19 and 30 cm are used in this research. At first, the tap water or sea water was prepared in these containers so that the water height became 120cm. Next, the bottom open type pouring device shown in Fig. 2 was used in the experiments to eliminate human error as much as possible. This device was fixed on the top of the cylindrical container then the pouring of samples was carried out under the initial velocity $v=0 \text{ cm/sec}$ conditions.

Test Conditions

Test conditions are shown in Table 1. The amount of pouring is determined three patterns such as $m=200$, 500 and 1000g. The pouring of the samples were conducted at $h_p=0$, 10, 20, 30 and 50cm above the water surface. The settling behavior of soil samples was recorded by video camera and the settling velocity to the depth direction was measured. Here, the settling velocity was calculated using the time that the principal forefront of a group of samples spent to settle each 30cm section. The difference of the settling behavior under each condition was examined by the comparison of the settling velocity.

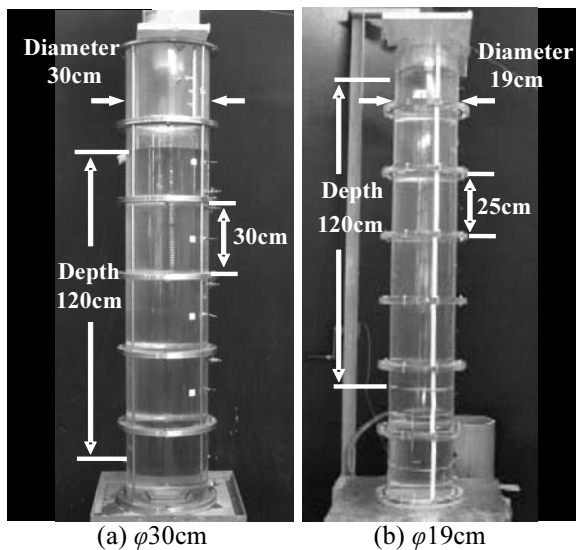


Fig. 1 Cylindrical containers

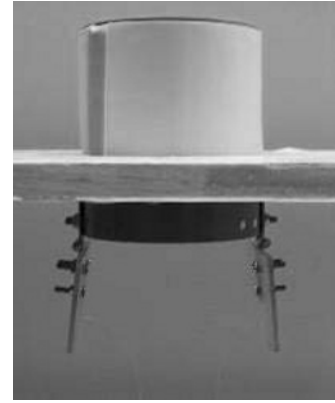


Fig. 2 Bottom open type pouring device

RESULTS AND DISCUSSIONS

Effect of the Difference of Fluid in the Cylindrical Container

Fig. 3 is a settling velocity distributions of gravel ($d=13.2 \text{ mm}$) measured at each water depth under given conditions such as the pouring height $h_p=50 \text{ cm}$ and amount of pouring $m=1000 \text{ g}$ that compares between tap water and sea water. In the results, the settling velocity is similar at any water depths therefore there is nearly no effect due to the fluid difference. From the reasons mentioned above, the tap water is used as the fluid in the containers.

Effect of the Difference of Grain Size

Fig. 4 shows the settling velocity distributions at each water depth under given conditions such as the amount of pouring $m=1000 \text{ g}$ and pouring height $h_p=30 \text{ cm}$ that compares the effect of the grain size difference. The settling velocities of all grain sizes are similar at the water depth of $z=15 \text{ cm}$. The effect of the difference of grain size appears at deeper than $z=45 \text{ cm}$ in water depth. In addition, it is clear from this figure that larger grain size gives faster terminal velocity and shorter the settling distance that the samples reach the terminal velocity. As one of the contributing factors, it is conceived that the larger particles experience the larger resistance force from fluid then the settling velocity is reduced.

Effect of the Amount of Pouring Difference

Fig. 5 demonstrates the settling velocity distributions at each water depth under given conditions such as the amount of pouring $m=200 \text{ g}$ and pouring height $h_p=30 \text{ cm}$ that compares the effect of the grain size difference. By comparison between Fig. 4 and Fig. 5, the settling velocity at the water depth of $z=15 \text{ cm}$ is greatly decreased in case that the amount of pouring is $m=200 \text{ g}$.

Table 1 Test conditions

Diameter ϕ , cm	Fluids	Soil materials	Grain size d , mm	Density ρ_s , g/cm ³	Amount of pouring m , g	Pouring height h_p , cm
		Tagawa decomposed granite soil	$0.85 < d < 2.00$			0
19	Tap water	Gravel	$4.75 < d < 9.50$	2.66	200	10
or	or		$9.50 < d < 13.2$			or
30	Sea water		$13.2 < d < 19.0$			or
		Mixed samples	$0.85 < d < 13.2$		1000	30
		Incineration bottom ash	$0.85 < d < 13.2$	2.37		or
						50

*The grain sizes indicated in boldface represent nominal diameter of each grain size.

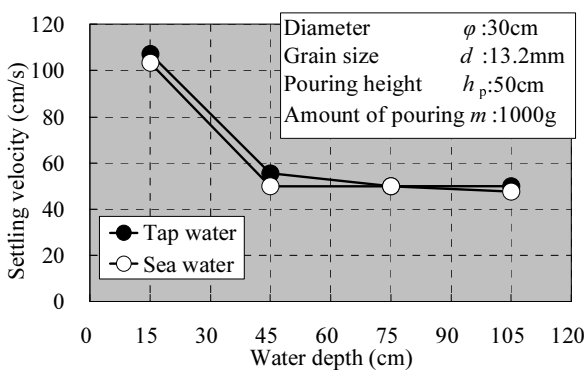


Fig. 3 Effect of difference of fluid

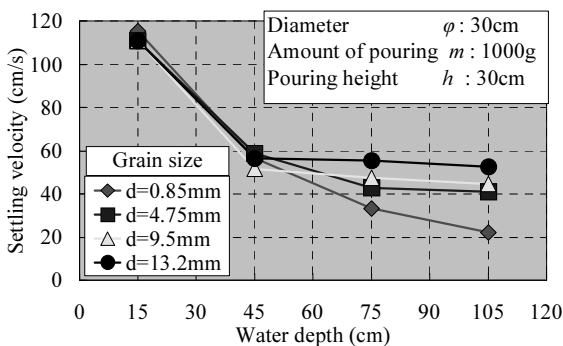


Fig. 4 Effect of difference of grain size

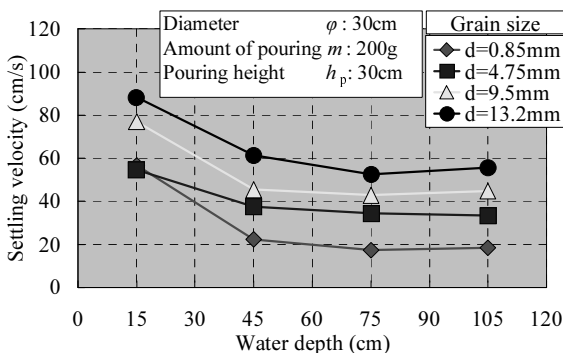


Fig. 5 Effect of the amount of pouring difference

This is thought to be due to the difference of energy to the direction of gravitational force when the samples

land on the water, that is, the difference of the amount of pouring. Paying attention to the settling velocity at the water depth deeper than $z=45$ cm, the difference due to the each grain size can be observed distinctly. Therefore, it is obvious that the settling velocity is susceptible to the grain size in case that the amount of pouring is low. Besides, the settling distance that the samples reach the terminal velocity is shortened with the reduction of the amount of pouring, about the samples except the one which diameter is $d=13.2$ mm. Especially, the difference is appeared prominently in the sample which diameter is $d=0.85$ mm. As observed above, the settling behavior at the water depth between $z=15$ cm and $z=75$ cm is influenced notably by the amount of pouring. However, the settling velocity at the water depth of $z=105$ cm is quite similar to that in Fig. 4. That is, the difference of amount of pouring does not effect to the terminal velocity.

Effect of the Difference of Poring Height

Fig. 6 indicates the settling velocity distributions at each water depth under given conditions such as the amount of pouring $m=1000$ g and pouring height $h_p=0$ cm in order to compare the effect of pouring height difference. By comparison between Fig.4 and Fig. 6, it is obvious that the difference of the pouring height influences to the settling velocity at the water depth of $z=15$ cm. It is assumed that the settling velocity is decreased from the water depth of $z=105$ cm and reach the terminal velocity, expect the samples which diameter is $d=0.85$ mm. As above, it is clear that the difference of the pouring height also influences to the settling distance that is required to reach the settling velocity, as well as the difference of the amount of pouring. Furthermore, the settling velocity of the samples which diameter is $d=0.85$ mm is not decreased at the water depth of $z=45$ cm, compared with others. It seems reasonable to suppose that the group of soil particles settles in clump right after the landing on the water because the grain size is small such as $d=0.85$ mm. In addition, at the water depth of $z=105$ cm, the settling

velocities of each grain size particle are almost same each other regardless of the pouring height.

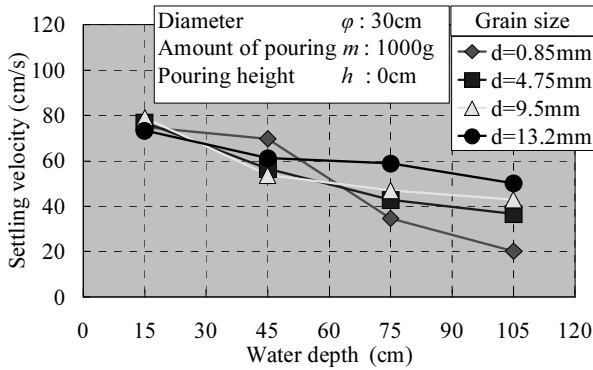


Fig. 6 Effect of the difference of poring height

Effect of the Difference of Container Diameter

For the comparison of the effect of the container diameter between $\phi 19\text{cm}$ and $\phi 30\text{cm}$, the settling velocity distributions of samples ($d=0.85\text{mm}$ and $d=13.2\text{mm}$) measured at each water depth under given conditions such as the amount of pouring $m=1000\text{g}$ and pouring height $h_p=0\text{cm}$ are shown in Fig. 7. It can be observed that the settling velocity at the water depth of $z=15\text{cm}$ in the $\phi 19\text{cm}$ container is slower than that in the $\phi 30\text{cm}$ one. However, at the water depth deeper than $z=75\text{cm}$, there is almost no difference due to the difference of the container diameter. It is conceived that the difference of settling behavior at the water depth of $z=15\text{cm}$ is due to the turned resistance force to the settling direction.

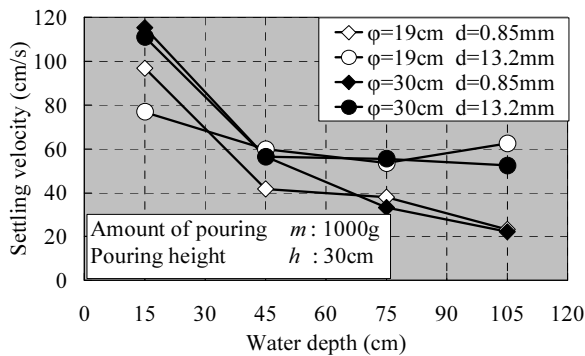


Fig. 7 Effect of the difference of diameter of container

Effect of the Samples Difference

The settling velocity distributions of mixed samples and incineration bottom ash at each water depth are demonstrated in Fig. 8. For the comparing with the results of the maximum grain size of incineration bottom

ash, the results of gravels that grain size is $d=9.5\text{mm}$ are shown here. As the figure indicates, the settling velocity of incineration bottom ash is clearly slower at any water depth because the density is smaller than that of the gravel. Besides, compared with the settling velocity of each diameter samples in Fig.4, this incineration bottom ash has the terminal velocity that nearly equal to the gravel that diameter is $d=4.75\text{mm}$.

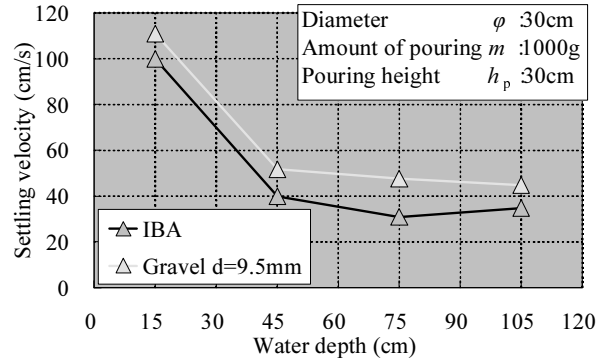


Fig. 8 Effect of the difference of material

CONCLUSIONS

From what has been mentioned above, it should be concluded as follows.

- (1) Under the testing conditions in this research, the effect of the fluid density difference is quite small compared with that of grain size difference.
- (2) The difference of the amount of pouring, pouring height and the restraint effect of the container influence the settling velocity around the water depth of $z=15\text{cm}$.
- (3) The settling behavior is more likely to be influenced by the effect of grain size as the amount of pouring is few.
- (4) Under the constant density conditions, each diameter samples have specific terminal velocity.
- (5) At the same time, the terminal velocity in accordance with the density of samples exists.

REFERENCES

Nabeshima Y, Nagaoka S, Yamada S, Sato K, Hachimura T, Miyahara T (2009). One-dimensional settling behavior and the effect on bottom clayey layer of a group of soil materials in static water for sea-based waste landfill. Proceeding of 8th Environmental geotechnical engineering symposium, submitted (in Japanese).

EXPERIMENTAL STUDY ON THE NONLINEAR CHANGE OF SATURATED HYDRAULIC CONDUCTIVITY OF WASTE SOIL

Ying ZHAO¹, Qiang XUE², Bing LIANG³ and Lei LIU⁴

ABSTRACT: The experiment for studying the nonlinear change law of the saturated hydraulic conductivity of municipal solid waste (MSW) was developed based the self-developed experimental instrument, the effect law of filling time and porosity on the nonlinear evolution process of saturated hydraulic conductivity was discussed, the limitations of using Freeze-Carman formula to describe the nonlinear relationship between saturated hydraulic conductivity and porosity was proved, and based on the analysis and fitting of experimental results the nonlinear constitutive models between the saturated hydraulic conductivity and the porosity at different filling time were put forward. The experimental results showed that the saturated hydraulic conductivity presented an exponential type increasing trend with porosity; the self-defined exponential function could describe the nonlinear relationship between saturated hydraulic conductivity and porosity well, and the correlation coefficient were all more than 0.92; and the effects of filling time on saturated hydraulic conductivity were significant, especially when the porosity was larger.

KEYWORDS: landfill, saturated hydraulic conductivity, porosity, nonlinear constitutive model, experimental study

INTRODUCTION

Permeability of landfill waste soil is the main influence factor on permeation process and distribution law of leachate, which is the key problem in the application of landfill technology. MSW landfill as a kind of porous media, the nonlinear change of its saturated hydraulic conductivity directly affects the transportation and transformation of landfill leachate. Therefore, the study on the permeability of waste soil, especially on the nonlinear change of saturated hydraulic conductivity has important theoretical significance and practical application value on the design of the recirculation parameter of landfill leachate and the seepage controlling and collecting system.

Waste permeability is closely related with properties and porosity. During the stabilization process, municipal solid waste should be considered as a kind of deforming porous medium. Constantly change of waste composition and porosity leads to the change of permeability. However, the researches on the simulation and prediction about landfill leachate transportation and transformation reported in related literature are mostly carried out based on the hypothesis that the saturated hydraulic conductivity is constant. The time and space change of saturated hydraulic conductivity in the process of settlement deformation and organic matter degradation for landfill

is not considered. So the numerical prediction result usually has relatively large errors. In view of these problems, the constitutive relation of saturated hydraulic conductivity and porosity in waste soil is described as Freeze-Carman formula in the numerical procedure by some researchers (Ertan Durmusoglu et al. 2006). But the authors find that using Freeze-Carman formula to describe the nonlinear relationship between saturated hydraulic conductivity and porosity of waste soil also has obvious limitations.

Therefore, the nonlinear relationship between saturated hydraulic conductivity and filling time and porosity of landfill waste was studied based on the laboratory experiment in this paper. The nonlinear constitutive model between saturated hydraulic conductivity and porosity at different filling time was put forward. It will provide the necessary constitutive relation between model parameters for the study on the numerical prediction of leachate quality and quantity.

EXPERIMENTAL PROCESSES

Experimental Device and Method

The schematic diagram of the experimental instrument is showed in Fig. 1. It consists of the inner container and the outer one. The outer container is designed for heating,

¹ Assistant Professor, Institute of Rock and Soil Mechanics, The Chinese Academy of Sciences, Wuhan Hubei. 430071.

² Professor, Institute of Rock and Soil Mechanics, The Chinese Academy of Sciences, Wuhan. Email: qiangx@whrsm.ac.cn

³ Professor, College of Mechanics and Engineering, Liaoning Technical University, Fuxin. 123000.

⁴ Assistant Professor, Institute of Rock and Soil Mechanics, The Chinese Academy of Sciences, Wuhan Hubei. 430071.

and controlling the temperature of the waste in the column. The inner container is used for filling waste, and water outlet and water inlet with 0.6cm in diameter are set on its upper and the lower, respectively. Their spacing is 51cm. A piezometric tube is set above the water inlet every 17cm for observing the change of the water head. The other end of the water inlet is connected with an elevated water tank.

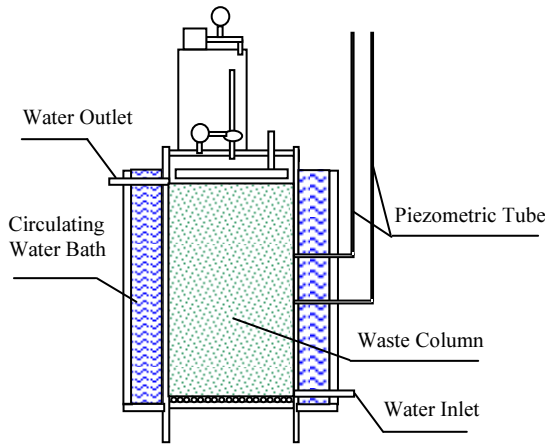


Fig. 1 Schematic Diagram of Experimental Instrument

The constant head method is used for determining the saturated hydraulic conductivity in this study. It is calculated by using Darcy law based on hydraulic gradient and outlet flow rate. From Darcy’s law it can be known that

$$Q = K \times A \times \frac{\Delta H}{\Delta L} \tag{1}$$

where, Q is the discharge, K is the saturated hydraulic conductivity, A is the wetted cross section, ΔH is the water level difference between outlet and inlet, ΔL is the height of column, and $\Delta H / \Delta L$ is the hydraulic gradient.

So the calculation formula of saturated hydraulic conductivity is

$$K = \frac{Q}{A} \times \frac{\Delta L}{\Delta H} \tag{2}$$

Write down the values of discharge Q and the hydraulic gradient $\Delta H / \Delta L$, and the values of saturated hydraulic conductivity K , can be calculated by Eq. (2).

Experimental Materials and Sheme

Preparation of Experimental Materials

The waste used in this study was self-perpetrated by referring to the investigation results about the Wuchang area and Hongsan area in 2006 (Central South Municipal Engineering Design Institute, 2006). Its composition was

shown in Table 2. One part of the perpetrated waste was used to experiment immediately, and the other part was sealed and stored. It would be used to the experiment of mildew waste.

Table 1 Material composition of MSW in Wuchang (W) and Hongshan (H) of Wu Han city (wet weight)

		Organic compounds								
		Food	Fruit	Paper	Wood	Fiber	Plastic	Rubber	Bone	Total
W		31.22	18.50	9.24	2.15	1.22	16.79	2.26	2.01	83.40
H		30.83	30.17	9.91	2.26	2.02	17.06	1.09	3.17	96.50
		Inorganic compounds								
		coal ash	Metal	Glass	ceramic	Total				
W		13.41	0.77	2.07	0.36	16.60				
H		0.00	0.50	2.68	0.32	3.50				

Table 2 The material composition in the experiment

		Organic compounds							
Composition		Food	Fruit	Paper	Wood	Fiber	Plastic	Total	
Proportion		30	19	10	3	2	18	82	
		Inorganic compounds							
Composition		Soil	Metal	Glass	Total				
Proportion		14	2	2	18				

Experimental Shame and Method

This experiment was divided into three groups, and fresh waste and mildew waste which was stored 90 days and 180 days were used in every group, respectively. In every group, 16 experiments were done with the porosities 0.30, 0.32, 0.34, 0.36, 0.38, 0.40, 0.42, 0.44, 0.46, 0.48, 0.50, 0.52, 0.54, 0.56, 0.58 and 0.6. The waste porosity was controlled by the filling mass. The filling volume is invariable, and the particle density of waste could be determined by experiment, so the filling mass corresponding to porosity φ is

$$m = \rho (1 - \varphi)V \tag{3}$$

where, m is the filling mass, ρ is the particle density, φ is the porosity, V is the filling volume.

If the hydraulic gradient is too large, the waste particles will be entrained and transport with water, the redistribution of smaller particles will lead to the clog of smaller pore and make the pore structure changed significantly, and it leads to the higher experimental error fatherly. Meanwhile considering the hydraulic gradient which leads to the flow of landfill leachate under the unsaturated condition is 1. So the gradient in this study was controlled about 1. For avoiding the experimental error due to the instability of water flow, the reading of data must be done after the water flow is stable. Five groups of data must be collected in every

group of experiment, and average value will be used to the calculation of saturated hydraulic conductivity.

EXPERIMENTAL RESULTS AND ANALYSES

Some researchers have carried out studies on the constitutive relationship between K and ϕ at present, and corresponding empirical formulas have been given. The commonly used one is Freeze-Carman formula (Freee R A et al. 1979).

$$K = \frac{g}{\nu} \cdot \frac{d_g}{1.80 \times 10^4} \cdot \frac{\phi^3}{(1-\phi)} \tag{4}$$

where, g is the acceleration of gravity, ν is dynamic viscosity of water, d_g is the geometric mean diameter of particles.

During engineering calculation, the change of dynamic viscosity of water is usually neglected. And the geometric mean diameter of particle is considered as a constant. So the above formula can be simplified as Kozeny-Carman formula (Bear, J. et al. 1972):

$$K = C \frac{\phi^3}{(1-\phi)^2} \tag{5}$$

where, C is constant. In practical calculation, it was calculated by using a known porosity value and its corresponding saturated hydraulic conductivity value. So C is dependent on ϕ and K . If the ϕ or K used in calculation deviates from the practice, it will lead to the error of constitutive model. Taking the saturated hydraulic conductivity experiment of 180-day waste for example, the Kozeny-Carman curves corresponding to the C which was calculated by using two group of ϕ and K , were plotted in Fig. 2. It indicated that the difference of these three empirical curves obtained by using different ϕ and K is significant. It can't be determined which accords with the practical situation better if there is no comparison of other experimental data.

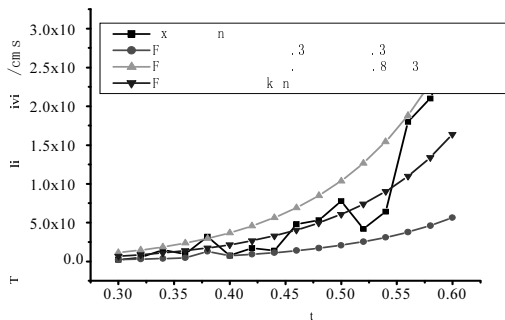


Fig. 2 Curves derived from Freeze-Carman formula with different ϕ and K_s values and comparison with experimental data

The C values calculated by using sixteen groups of ϕ and K_s values in every group of experiment were shown in Fig. 3. The three curves indicated that the variation of C values was significant, and the range were about 2.96×10^{-4} - 3.56×10^{-3} , 4.34×10^{-4} - 2.76×10^{-3} and 4.17×10^{-4} - 2.24×10^{-3} .

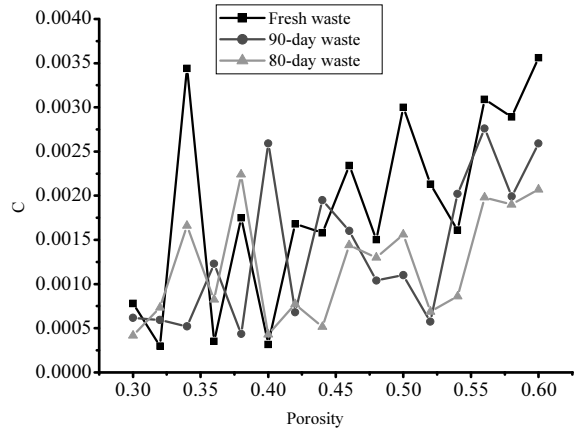


Fig. 3 The values of C with different ϕ and K_s values

Considering the above limitation of Kozeny-Carman formula, the constitutive relationship between saturated hydraulic conductivity K and porosity ϕ will be obtained by the fitting method in this study. In this method the calculation result isn't only dependent on a certain experimental data. It's determined by all data. So the deviation of calculation results caused by experimental errors can be avoided better. Three groups of experimental data were plotted in Fig. 4. It indicated that the saturated hydraulic conductivity presented an exponential type increasing trend with porosity. It accords with the reports in related literature (Zhang Wenjie, 2007; Ran Long, 2005; Ke Han et al. 2006; Stegman R et al. 1989). In this study, the self-defined exponential function was used to fit the experimental data. It's

$$K = A \cdot e^{\overline{B - \phi}} - A \cdot e^B \tag{6}$$

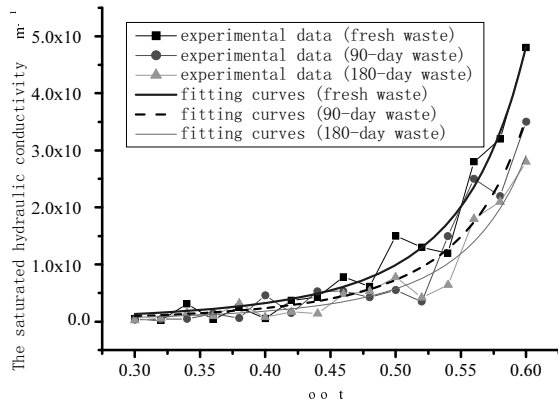
where, A and B are fitting parameters.

From Eq. (6) it can be known that no matter how the data changes, it always exists that when $\phi=0$, $K=0$, and when $\phi=1$, K is infinite. It accords with the practical relationship between porosity and saturated hydraulic conductivity. The fitting parameters for three kinds of waste were shown in Table 3, and the fitting results were shown in Fig. 4.

Table 3 and Fig. 4 indicated that the self-defined exponential function could fitting the experimental data well, and the correlation coefficient were all more than 0.92.

Table 3 The fitting results of the experimental data

Type of waste	A	B	R
Fresh waste	2.1475×10^{-6}	0.32365	0.96651
90-day waste	1.5348×10^{-6}	0.32211	0.92394
180-day waste	1.0462×10^{-6}	0.31494	0.94473

**Fig. 4** The experimental data and fitting curve of K_s for three kinds of MSW

Meanwhile, it can be seen in Fig. 4 that under the smaller porosity, although the size and connection degree of the porosity were different significantly, the saturated hydraulic conductivities with the same porosity and different filling time are similar. But under the larger porosity, they were different obviously. It was because the shorter the degradation time is, the more the large particles have. And it will lead to the worse homogeneity and the formation of channel flow. The channel flow leads to the obvious increase of permeability further. So when the porosity was larger, the saturated hydraulic conductivity of fresh waste was greater than the one of 90-day waste and the one of 180-day waste was the least.

CONCLUSIONS

The experimental study on the nonlinear change law of saturated hydraulic conductivity of waste soil was carried out based on the self-developed test system. The effect law of filling time and porosity on the nonlinear evolution process of saturated hydraulic conductivity was discussed, and the nonlinear constitutive models between the saturated hydraulic conductivity and the porosity were put forward. The main conclusion is as follows

(1) Based on the comparison between calculation results and experimental data, the limitations of using Freeze-Carman formula to describe the nonlinear relationship between saturated hydraulic conductivity and porosity was proved;

(2) The saturated hydraulic conductivity of waste soil presented an exponential type increasing trend with

porosity, so a self-defined exponential function was used to fit the experimental data, and the fitting results showed that this function could describe the nonlinear relationship between saturated hydraulic conductivity and porosity well, and the correlation coefficient were all more than 0.92;

(3) Under the smaller porosity, the saturated hydraulic conductivities with the same porosity and different filling time are similar, and under the larger porosity, they were different obviously. It indicated that the filling time had important effect on the saturated hydraulic conductivity of waste soil.

ACKNOWLEDGEMENTS

This investigation was financially supported by the National Natural Science Foundation of China (50874102), National Fund Key Eleventh-five National Key Technology R&D Program (2006bac06b02), Natural Science Foundation of Hubei Province for Distinguished Young Scholars (2007ABB039) and the Key Technologies Programs of Hubei Province (2008AC008), the Key Technologies Research and Development Program of Wuhan (200860423196).

REFERENCES

- BEAR J (1972). Dynamics OF FLUIDS IN POROUS MEDIA. NEW YORK: ELSEVIER.
- Central South Municipal Engineering Design Institute (2008). Preliminary Design for Wuhan Jiangxia Changshankou MSW Landfill Project. Wuhan: Central South Municipal Engineering Design Institute, 41-42.
- Ertan Durmusoglu M, Yavuz Corapcioglu, Kagan Tuncay (2006). Modeling of Settlement in Saturated and Unsaturated Municipal Landfills. International Journal of Geomechanics, ASCE, 269-278.
- Freeae RA, Cherry JA (1979). Groundwater. Prentice-Hall, Englewood Cliffs, NJ.
- Ke H, Ran L, Chen YM, Feng SJ (2006). Study on MSW filtration experimentation and landfill hydrologic analysis. Chinese Journal of Geotechnical Engineering, 28(5): 631-634.
- Ran L (2005). Study of Compression and Filtration Behaviors of MSW and Hydraulic Behaviors of Landfills. Zhejiang University.
- Stegman R, Ehrig H-J (1989). Leachate Production and quality-results of landfill processes and operation. Proceeding of 2nd international Landfill symposium, Sardinia Italy, XXVII: 1-16.
- Zhang WJ (2007). Experimental and Numerical Study on Water/Leachate Transport in Landfill of Municipal Solid Waste. Zhejiang University.

LANDFILL GAS GENERATION AND TRANSPORT IN BIOREACTOR LANDFILL

Qi-Lin FENG¹, Lei LIU², Qiang XUE³ and Ying ZHAO⁴

ABSTRACT: The activation gas and water flow each other in Bioreactor Landfill. Based on the porous media seepage and bio-degradation theory, the coupling mathematics model considered the effect of water and waste components decomposition for describing landfill gas flow have been developed, and the simulation cells are performed. The simulation results show: the gas moves almost horizontally when it collected by the well, and it transport towards the atmosphere continuous. The gas pressure was released by pumping in landfill. The landfill surface cover system increase the gas pressure, and it can effective restrains gas disorderly leaking and increases the gas flow rate. In the earlier, the flow rate is approximately decreased linear with time during the pumping process. The variation law is identical to the testing data. And the reliability of the coupling model was validated. It will provide the theoretical evidence and technological support to LFG pollution control and reuse on the study of gas flow law for Bioreactor Landfill.

KEYWORDS: bioreactor landfill, landfill gas, transport, mathematics model

INTRODUCTION

With the increasing of amount of waste, gases movement from landfill sites to be a serious safety fault and environment problem have been noticed. Now, reusing and reducing of the landfill gas has been a focus. Landfill gas movement from sites is a complex dynamics process. In addressing these problem, it is often important to know the capability of waste degradation of different components that leading to gas generation characteristic (Angelos et al. 1979; Arigala et al. 1995; Vigneault et al. 2004).

The law of gas generation is one of the very important index of simulation of LFG extraction. On the other hand, the matrix contain a large of water (Liu 2007). The moisture content have a constantly variation as a results of the ambient conditions, including the permeability of the soil, and so on. The whole process of gases generation and transport through the landfill is concomitant with the change of the water contents. Therefore, the flux of the gas well prediction veracious is the foundation and reason of the law of gas transport in bioreactor Landfill. In such cases, the waste is regard as the unsaturated transmit media. The non-linear coupling mathematical model of gas flow combined with the refuse degradation and moisture content. The dynamic state of sucking rate and pressure profile have instructed. The analysis of the model's predictions and the effect of

final soil are then presented. Compared with the simulation results and field testing results of the sucking rate. The reliability of model is examined. It will provide the theoretical evidence and technological support to pollution control and reuse of landfill gas in bioreactor Landfill.

MATHEMATIC MODEL

As a large bioreactor system of landfill, the physical and chemical and biotic reaction were depend on internal factors. The model of gas generation is very complex. It is very difficult to imply to practical engineering. In general, the first order dynamic model could be used to represent the organic degradation rate. The landfill waste was composed of three classes: One that consists of readily biodegradable wastes such as foodstuff; a second class which consists of moderately biodegradable materials such as wood and garden waste, and a third class that includes the least biodegradable materials (Mehrdad Hashemi 2002).

The biodegradation of the three different types of waste is modeled as (USEPA 1997):

$$F_g = \sum_{i=1}^3 LA \lambda e^{-\lambda t} \quad (1)$$

¹Professor, Wuhan Environmental and Sanitation Scientific Research & Design Institute, Wuhan, Hubei. 430015

²Assistant, Institute of Rock and Soil Mechanics, The Chinese Academy of Sciences, Wuhan, Hubei. 430071

³Professor, ditto. Email: qiangx@whrsm.ac.cn

⁴Assistant, ditto.

where, F_g is the generation rate of gas in kg/m^3 of MSW per year. $i=1,2,3$, respectively, biodegradable, moderately biodegradable, and the slowly biodegradable fractions. L is the total gas generation potential of gas i in kg/m^3 . A_i is the constant, is the fraction of MSW corresponding to component i . λ_i is the gas generation constant corresponding to A_i in yr^{-1} . T is the time measured since the first layer of refuse was placed in the landfill, is defined by

$$T = T + Y \frac{T}{D} + T \tag{2}$$

where D is the total landfill depth, T the time elapsed since the landfill was capped, T is the total time to fill the landfill, and T is the current compute time to compute over.

The governing equation of landfill gas flow in Bioreactor Landfill can be written as:

$$\frac{\partial(n\rho S)}{\partial t} + \nabla(\rho_a v_a) = F_g \tag{3}$$

where, ρ is the gas density; S is the gas saturation; F_g is the source phase; v is the gas flow velocity, defined as:

$$v = -\frac{kk}{\mu}(\nabla P + \rho g\eta) \tag{4}$$

where, k is the intrinsic permeability; k is the gas relative permeability. More, landfill gas as the mixture, assumed that it accounts for the four major components of LFG, namely, CH_4 , CO_2 , N_2 and O_2 . At the same time, the total gas pressure P is quoted:

$$P = \sum_{i=1}^4 P_i \tag{5}$$

where the viscosity of gas mixture, we use (USEPA 1996):

$$\mu = \frac{\sum \mu_i}{1 + \sum \psi_i \frac{\chi_i}{\chi}} \tag{6}$$

Where ψ is dimensionless constant, χ being the mole fraction of the gas i .

And the pressure described by the ideal gas state law:

$$P = \frac{RT}{M} \rho \tag{7}$$

where R is the universal gas constant, M is the mean molecular weight of gas mixture, T is the gas absolute

temperature.

Wetting phase flow equation:

$$\frac{\partial(n\rho S)}{\partial t} + \nabla(\rho v) = 0 \tag{8}$$

where ρ is the wetting phase density, θ is the wetting phase moisture content, and the compressibility of wetting phase as shown in the following (USEPA 1996):

$$\rho = \rho_0 e^{\beta(\theta - \theta_0)} \tag{9}$$

where ρ_0 is the water reference density, β is the compression coefficient. The water flow can be described by Darcy law:

$$v = -\frac{kk}{\mu}(\nabla P + \rho g\eta) \tag{10}$$

where k is the relative permeability of wetting phase, μ is the viscosity of wetting phase.

The gas and water in the waste matrix, driving each other, the characteristic is intrinsic and have not effect on organic degradation and chemical reaction. Therefore, the physics relation has the important effects of the fluid, the $K-S-P$ model can describe the driving process (Popov & Power 2000):

$$P = \frac{1}{\sigma}[(S) - S_r] \tag{11}$$

here P is the capillary pressure, S is the effective saturation, given by

$$S = \frac{S - S_r}{S - S_r} \tag{12}$$

where S is the reality saturation, S_r is the residual saturation.

More, the relative permeability can be written by the effective saturation:

$$k_r(Se) = Se^2 [1 - (1 - Se)]^2 \tag{13}$$

$$k_r(Se) = (1 - Se) (1 - Se) \tag{14}$$

MODEL APPLICATION

The landfill gas transport have disposed by one well pumping system in MSW. The landfill depth is 15m, the well depth with 70% of the landfill depth. The bottom is assumed the non-infiltration boundary. The final soil thickness of 1m. Table 1 lists all input landfill parameters for the model (Xue et al. 2007, 2002; Chen et al. 2003). The simulation results in Fig. 2-6.

Table 1 Values of Model parameter

Landfill data	Value
residual saturation	0.03
reaction rate λ_1 (year)	0.1386
reaction rate λ_2 (year)	0.0231
reaction rate λ_3 (year)	0.017328
waste density kg/m^3	880
m	0.11
n	1.12
σm^{-1}	5.0
k_v/k_h	1/3
gas absolute temperature K	310
permeability in the horizontal direction m^2	3.0×10^{-12}
permeability of final soil m^2	1.0×10^{-13}
viscosity of gas mixture $Pa \cdot s$	1.54×10^{-15}

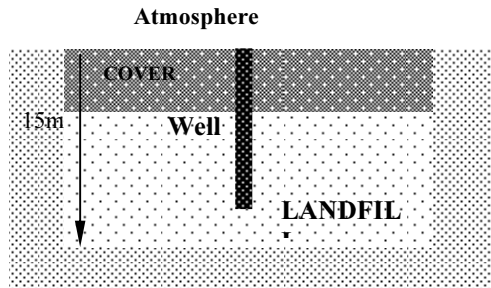


Fig. 1 Single-well pumping system in landfill

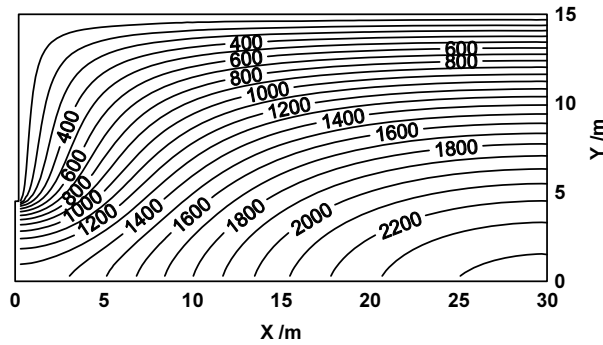


Fig. 2 Contour of LFG pressure on pumping

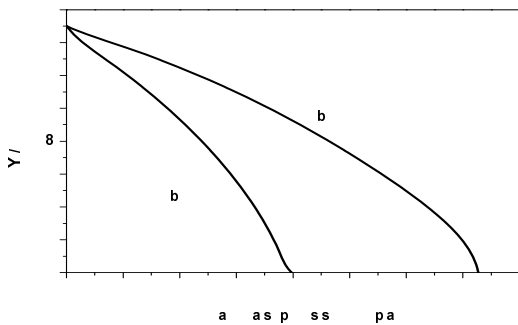


Fig. 3 Effect of the cover's thickness on the total gas pressure

The pressure field is plotted in Fig. 2. The results show that the gas pressure lines near the well are close to each other and the curves stand almost vertically. This indicates that the gas moves almost horizontally and will be collected by the well. With the distance from the shaft top is increased, the interval between two curves will increase quickly and the slope of the curve decline quickly. This implies that the capability of controlling the gas far-away landfill decays quickly with the increase of the radial distance from the well in the passive pumping system.

The final layer of landfill after filling over is to prevent the filtrate infiltration and the landfill gas emission to the atmosphere. The effect of the final soil cover thickness, respectively 0 and 1m, were assigned to illustrate the gas movement law. The simulation results show that in Fig. 3 the gas pressure in landfill increases with increasing final soil thickness.

This is because the permeability of final soil is much smaller than that of the refuse, the increase of the final soil thickness will increase the flow resistance for the gas to go through the final soil layer. Therefore, the better sealing of landfill is more adapt to control and collect the gases.

The variation of sucking rate of gases with pumping time presented in Fig. 4. It shows that the flow rate gradually decays when time is longer. The law of gas sucking rate from well is accord with the practice instance.

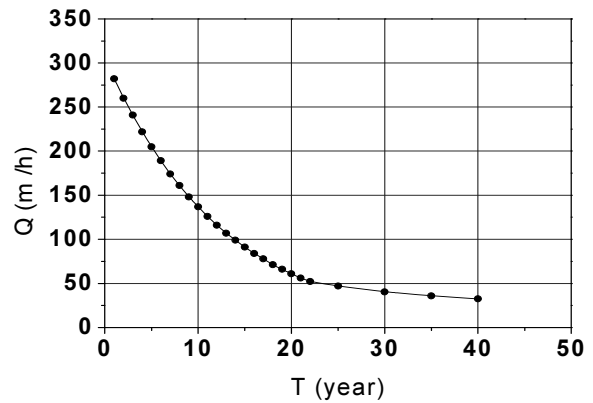


Fig. 4 The variation of LFG flow rate with time (yr)

In order to verify the of the reliability of the mathematical mode in this paper, the simulation result and monitoring result data of the flow rate from pumping well were compared, the profiles showed in Fig. 5. The monitoring result was tested at JinKou landfill of WuHan in 2005.

The testing data is close to linear concordance with the simulation result. And the testing data is less than the simulation result. It is mainly because that the simulation result was completed based on the content of methane is not losing. Then, the testing in field do not reach the perfect cases.

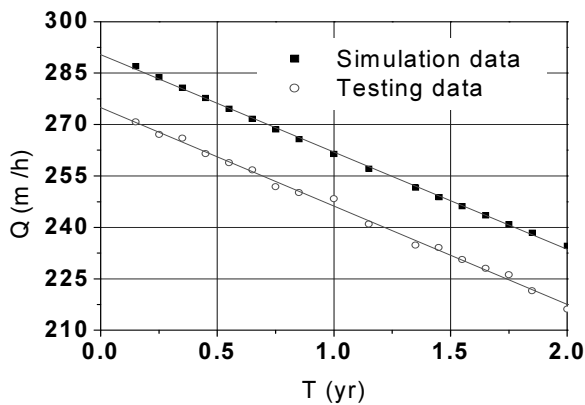


Fig. 5 Comparison of simulation and testing of LFG flow rate

CONCLUSIONS

The coupling mechanism between the landfill gas and moisture content within waste was proposed. The mathematic model of gas transport with waste component degradation and moisture content have been developed. The simulation prediction of landfill collection are performed.

The simulation results show that the lateral direction movement is the main way of gas flow. The gas pressure within landfill was released by extraction system. At the same time, a small amount gases migrate to the atmosphere. The final layer on top of landfill can be effective to prevent the gas flow out. The key of prediction of sucking rate from gas well is the optimization of the simulation parameters. The reliability of the coupling model is verified by contrast analysis of testing result.

ACKNOWLEDGEMENTS

This work was supported by the fundation from National Natural Science Foundation of China (50874102) and National fund Key Eleventh-five National Key Technology R&D Program (2006bac06b02) and a grant from Natural Science Foundation of HuBei Province for Distinguished Young Scholars (2007ABB039) and a

grant from the Key Technologies Programs of HuBei Province (2008AC008) and Science and Technique Foundation from Municipal Manage Agency of WuHan.

REFERENCES

- Angelos N Findikakis & James O Leckie (1979). Numerical Simulation of Gas Flow in Sanitary Landfills. *J. Envir. Engrg.*, 105(E5): 927-945.
- Arigala SG, et al. (1995). Gas Generation, Transport, and Extraction in Landfill. *J. Envir. Engrg.*, 121 (1): 33-44.
- Vigneault H, Lefebvre R, Nastev M (2004). Numerical Simulation of the Radius of Influence for Landfill Gas Wells. *Soil Science Society of America*, 3: 909-916.
- Liu L (2007). Numerical Simulation of Landfill Gas Migration with Water. Liaoning technical university.
- Mehrdad Hashemi, Halil IK, Theodore TT, Muhammad S (2002). Computer simulation of gas generation and transport in landfills—I: quasi-steady-state condition *Chemical Engineering Science*. 57 (13) : 2475-2501.
- USEPA (1997) EIIIP, Landfills, Volume III: Chapter 15 (Emission Inventory Improvement Program).
- USEPA (1996). Section4, Method 2E: Determination of Landfill Gas; Gas Production Flow Rate. 1996, 40 CFR 60 Appendix A 61: 9929.
- Popov V & Power H (2000). Numerical analysis of efficiency of landfill venting trenches. *J. Environ.Eng.*, 126(1): 32-38.
- Xue Q, Liu L, Liang B, et al. (2007). A gas-hydraulic-solid coupling dynamics model with landfill settlement. *Chinese Journal of Rock Mechanics and Engineering*, Sup.1, 26: 3473-3478
- Xue Q, Liang B, Liu XL (2002). Research of unsteady seepage coupling mathematical model and gas migration in landfill. *Rock and Soil Mechanics*, 23(2): 191-195.
- Chen YC, Chen KS, Wu CH (2003). Numerical simulation of gas flow around a passive vent in a sanitary landfill. *Journal of Hazardous Materials*, 100: 39-52.

DEVELOPMENT OF A COMPUTER SOFTWARE FOR PREDICTING LANDFILL SETTLEMENT AND ITS STORAGE CAPACITY

Yao-Shang WANG¹, Han KE², Tony L. T. ZHAN³, Xue-Chen BIAN⁴, Yun-Min CHEN⁵ and Zhe FU⁶

ABSTRACT: Settlement is one of the most obvious phenomenon of MSW Landfills. The prediction of settlement is very important for landfill operation, management and post-closure reclamation. This paper gives a brief introduction to the development of a computer software for predicting landfill settlement and capacity throughout the landfill life. The overall structure and main features of the computer software are presented. An illustrative analysis is used to demonstrate the functions of the software.

KEYWORDS: settlement, computation model, software

INTRODUCTION

Landfill MSW is different from common soil by its high compressibility and degradability. Because of these characteristics, an MSW landfill can take in much more waste than its designed volumn. Therefore, it is important to accommodate landfill storage capacity and expansion rate of volume in landfill design. Compared to manual calculation, computer program provides a better simulation of the real three-dimensional terrain and is more reliable.

In addition, post-construction differential settlement of the landfill may cause the pad in the bottom to fail and the pipes in the bottom to deform, undermining landfill stability.

In sum, settlement prediction is significant for the design and construction of landfill. Developing a software for landfill storage capacity and settlement computation will be of great help for engineers in their design and analysis.

FEATURES AND FUNCTIONS OF THE SOFTWARE

Characteristics of Software

Topographic map of landfill can be produced easily. Topographic maps can be in DXF (Drawing Exchange Format), a CAD data file format developed by Autodesk

for enabling data interoperability between AutoCAD and other programs. So the original topographic map only needs to be slightly modified and used by the software.

A number of typical computing models are integrated which utilize various physical parameters of MSW obtained from test.

Settlement data of each section can be exported. A compatible stability analysis program can analyse section stability and determine the possibility of landslide.

Software's Function Module

Calculating the volume expansion rate of landfill. Using the terrain data and the plan for waste filling, the program calculates the physical storage capacity of landfill, the total weight of intake waste and the volume expansion rate of landfill.

Calculating the post-construction settlement of landfill. The software can predict post-construction settlement of landfill in 20 years and can provide 3D topographical changes of landfill in 20 years. Through partitioning profile users can view settlement change with time. They can also export section data to a stability analysis program to check the section stability.

Assisting in Pipeline design. Landfill drainage system is prone to clogging. One of the reasons is that differential settlement of the landfill lead to the phenomenon that downstream elevation of the pipe is higher than

¹ Master Student, MOE Key Laboratory of Soft Soils and Geoenvironmental Engineering, Zhejiang University, China

² Associate Professor, MOE Key Laboratory of Soft Soils and Geoenvironmental Engineering, Zhejiang University, China

³ Professor, MOE Key Laboratory of Soft Soils and Geoenvironmental Engineering, Zhejiang University, China

⁴ Professor, MOE Key Laboratory of Soft Soils and Geoenvironmental Engineering, Zhejiang University, China

⁵ Professor, MOE Key Laboratory of Soft Soils and Geoenvironmental Engineering, Zhejiang University, China. Email: chenyunmin@zju.edu.cn

⁶ Undergraduate Student, Shanghai JiaoTong University, China

upstream. Leachate siltation is thus ensued. The software can predict the shape of drainage pipe after final settlement and assist in the sloping design of the pipe.

Output Format

The one-dimensional output shows the process of waste filling at a point in the landfill, as in Fig. 1. The figure includes four parts. From the figure we know the filling process of that point and elevation change over time.

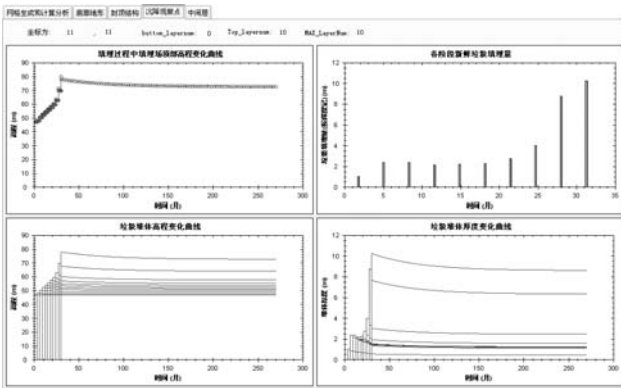


Fig. 1 The One-dimensional output

Fig. 2 shows a section of landfill. From the figure of the terrain profile, we can get the settlement information of each stage.

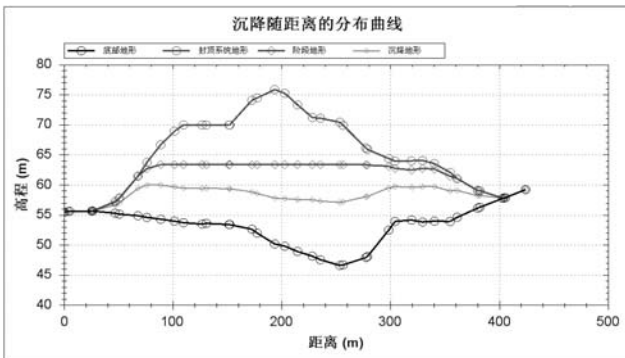


Fig. 2 The two-dimensional output

We can see 3D topographic map of landfill in Fig. 3 with the process of settlement at each stage.

DESIGN OF THE SOFTWARE

Overall Structure

We used the Visual C#. Net development environment. Visual C# is Microsoft's implementation of the C#

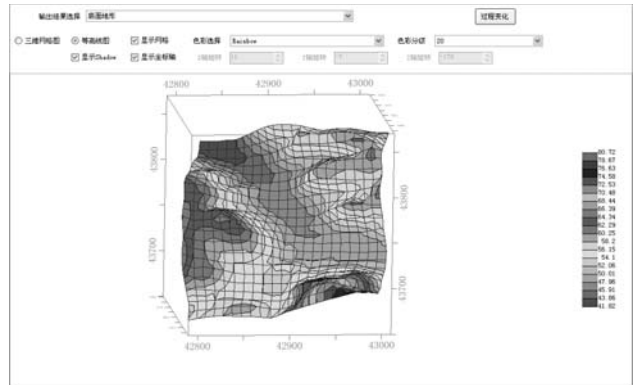


Fig. 3 The three-dimensional output

programming language specification. It is based on the ECMA/ISO specification of the C# language, which Microsoft also created. The software is divided into five modules: topographic data, computing module, one-dimensional analysis, two-dimensional analysis, and three-dimensional analysis. The overall structure is shown in Fig. 5.

Importing Data

The required data in software calculation include topographic data of landfill, physical parameters of the waste and a timetable for landfill. Timetable is a Landfill filling process schedule.

Topographic data include site monitoring data, landfill boundary contour data, and Contour lines data of the landfill top design. The software is compatible with a variety of CAD metafile formats.

There are three ways to develop a timetable for landfill. First, users may manually input the elevation data corresponding with time. Second, users may set a fixed filling rate for the process, for instance, 1.5m per month. The last one is pursuant to the data of the volume of waste received over time. With these data and the terrain of landfill, the program will calculate the useful life of landfill and the elevation of each stage, and a timetable developed by software is shown in Fig. 4

Settlement Calculation Method

Settlement generally includes primary settlement, secondary settlement and decomposition settlement. Primary settlement is often modeled as a consolidation type analysis used in soil mechanics (Sowers 1973; Morris and Woods 1990; Oweis and Khera 1998) which lasts for a limited period of time after the application of load. Secondary settlement occurs over a long period of time in response to self-weight and externally applied loads. Decomposition settlement is primarily ensued by biochemical decay and lasts for a long period. Coduto

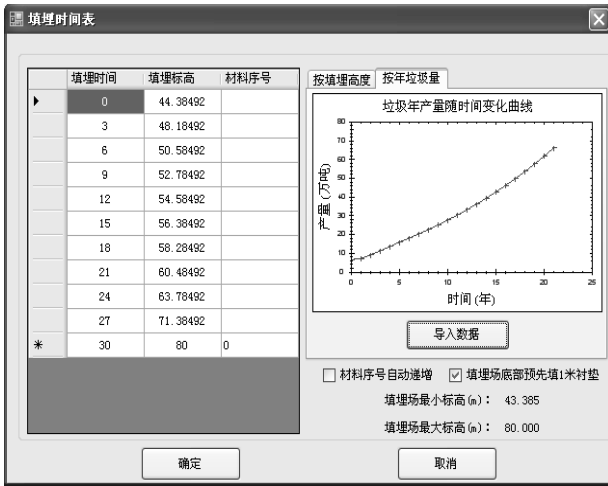


Fig. 4 timetable for landfill

and Huitric (1990) stated that settlement due to biological decomposition is probably 18-24% of total MSW thickness.

Layer wise summation method is used for calculating primary settlement where the total compression is equal to the sum of each layer. MSW degradation as well as

the impact of changes of water level are also taken into account. The main compression is calculated as:

$$\epsilon = C' * \log\left(\frac{P + \Delta P}{P}\right) \tag{1}$$

where ϵ_p = primary compression strain of this layer, C =compression index, P =initial vertical stress, ΔP =change in vertical stress.

The software integrates several secondary settlement computing models which employ a variety of physical parameters of MSW. Take Sowers Model as an example. This method combines secondary settlement and decomposition settlement and is written as:

$$\epsilon = C'_a * \log(t / t_1) \tag{2}$$

where ϵ_s = secondary compression strain of this layer; C'_a = secondary compression; t_1 =starting time for secondary compression and t_2 =ending time for secondary compression.

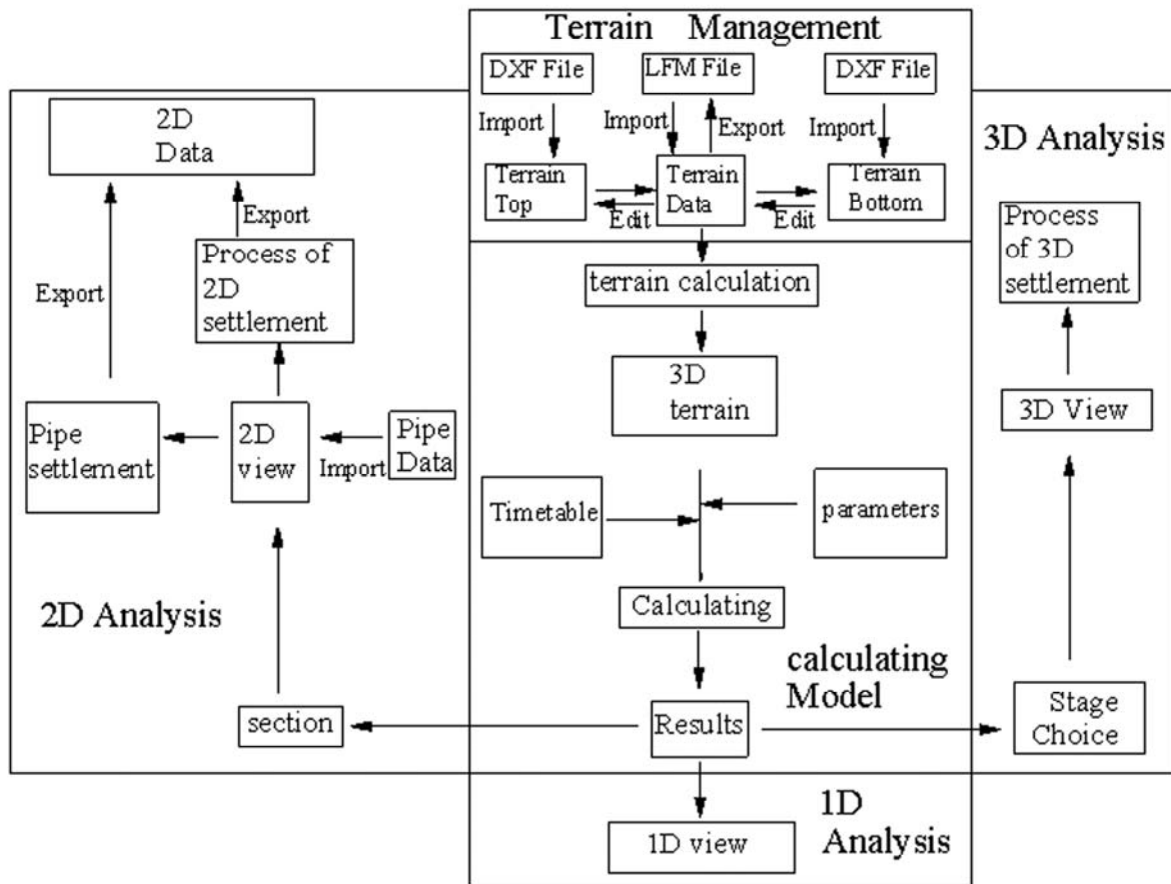


Fig. 5 Structure of the software

EXAMPLE ANALYSIS

Suppose there is a small valley landfill with known terrain data and physical parameters of MSW. We can produce a three-dimensional terrain map by importing terrain data into the program, as shown in Fig. 6

The program develops a landfilling schedule through terrain data and the volume of waste intake over time. Then users import physical parameters of waste and the software begins to calculate. By Sowers Model, the volume expansion rate of landfill is 15.7%, and post-construction settlement at the center of landfill is 24.73% for total MSW thickness.

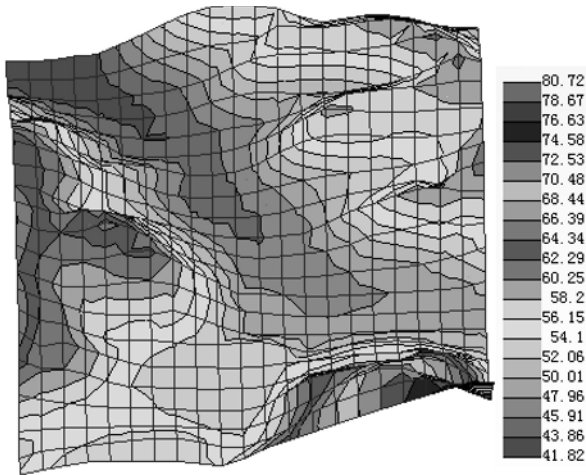


Fig. 6a Bottom of three-dimensional terrain

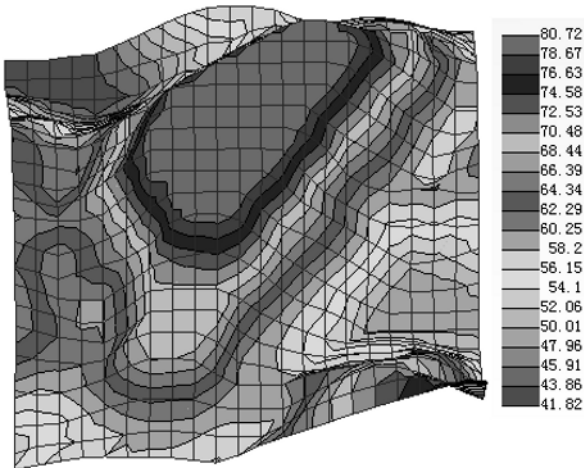


Fig. 6b Top of three-dimensional terrain

CONCLUSIONS

To make use of some common settlement calculation models, the software simplifies filling process as a sequence of discrete, instant load applications after a certain “silence” period. But in reality, waste is filled into landfill everyday. The simplification thus generates considerable error. This software can facilitate the prediction of landfill capacity and volume expansion rate, but physical parameters of waste in the landfill can only be obtained from the surrounding area where waste composition is similar, leading to error in prediction. The software can be of great help in calculating the settlement of landfill. Three different viewing modes offer users more in-depth understanding of the settlement behavior of the whole landfill.

ACKNOWLEDGEMENTS

This work were supported by the funding from National Natural Science Foundation (research grant: 50538080; 50508039), and financial support from Bureau of Science and Technology of Suzhou (research grant: SS0733).

REFERENCES

Christian Nagel, Bill Evjen, Kay Glynn. Professional C# 2005 with. NET 3.0. Tsinghua University Press 2007, 12 (in Chinese).

Issa S Oweis (2006). Estimate of Landfill Settlements Due to Mechanical and Decompositional Processes. Journal of geotechnical and geoenvironmental engineering MAY.

Sowers GF (1973). Settlement of waste disposal fills. Proc., 8th Int. Conf. on Soil Mechanics and Foundation Engineering, Moscow.

Zhang ZY & Chen YM (2004). Settlement model of municipal solid waste landfill. Mining and Metallurgical Engineering, Sep.16-19.

INFLUENCE OF RAINFALL PATTERN ON THE INFILTRATION INTO LANDFILL EARTHEN FINAL COVER

Guan-Wei JIA¹, Tony L.T. ZHAN², Yun-Min CHEN³ and D. G. FREDLUND⁴

ABSTRACT: Rainfall pattern is an important factor that affects the infiltration process into earthen final covers of landfills. In this paper, six typical rainfall patterns present in nature were sorted out. Then the rainfall patterns were used as the infiltration boundaries of an earthen final cover model, and numerical simulations of the infiltration process were carried out by the use of the commercial software SVFlux. The numerical simulation model was firstly verified by experimental data. A parametric study was performed to investigate the influence of rainfall patterns on the infiltration process in the silty soil cover. The numerical simulation results indicate that the rainfall pattern can significantly affect the infiltration process and cumulative infiltration under the same total amount of precipitation. The peak rainfall intensity occurs earlier, the cumulative infiltration will be larger. The advanced pattern (A1) will generate the largest amount of infiltration compared to other patterns. The numerical analyses also suggest that rainfall pattern should be taken into account in the performance assessment of earthen final covers.

KEYWORDS: Rainfall pattern, Earthen final cover, Infiltration, Numerical simulation

INTRODUCTION

Landfill covers were primarily designed to prevent or control the infiltration of precipitation into the waste, so the generation of leachate can be reduced. The earthen final cover is an alternative cover for the traditional landfill covers, such as compacted clay covers and composite covers. The earthen final cover systems use water balance to minimize percolation into the waste. These cover systems can store the infiltrated water until it is either transpired through vegetation or evaporated from the soil surface. The amount of infiltration should be accurately calculated in the design of earthen final covers to carry out the water balance analysis.

When rain falls on the ground surface, a portion of the total rainfall infiltrate into the soil, and the deficit will be the runoff on the surface. The infiltrated water will increase the water content and then reduce the matric suction at the ground surface. The infiltration capacity will decrease as the rainfall advances. There have been numerous rainfall-runoff models to predict the

amount of runoff during rainfall event, such as the Green-Ampt (1911) model, Horton model (1938), Holtan model (1961), Mein-Larson model (1973). The parameters for these models used in geotechnical engineering are mostly obtained empirically. The predicted infiltration capacity of these models can't vary with the rainfall pattern, so it is not in accordance with the practical situation. These rainfall-runoff models are not suitable in the accurate analysis of the infiltration into the earthen final covers.

Numerical simulations are widely used in the analysis of earthen final cover. The commercial software used in numerical simulations includes SEEP/W, HYDRUS, UNSAT-H, Vadose/W and SVFlux (Scanlon 2002). The software use different ways to deal with the ground surface boundary conditions. It is assumed that when the rainfall intensity is smaller than the saturated permeability, all the rainfall will infiltrate into the ground surface and when the rainfall intensity is larger than the saturated permeability of the soil the flux boundary switches to zero pressure head boundary in SEEP/W (GEO-SLOPE

¹ Ph.D Student, MOE Key Laboratory of Soft Soils and Geoenvironmental Engineering, Zhejiang University, China. Email: jiaguanwei@zju.edu.cn

² Professor, MOE Key Laboratory of Soft Soils and Geoenvironmental Engineering, Zhejiang University, China. Email: zhanlt@zju.edu.cn

³ Professor, MOE Key Laboratory of Soft Soils and Geoenvironmental Engineering, Zhejiang University, China. Email: chenyunmin@zju.edu.cn

⁴ Professor, MOE Key Laboratory of Soft Soils and Geoenvironmental Engineering, Zhejiang University, China. Email: unsaturatedsoil@yahoo.com

2004). For SVFlux, if the pore water pressure at the surface is negative, all the rainfall will infiltrate into the ground, if the pore water pressure at the surface reaches zero, the infiltration flux will be equal to the saturated permeability when the rainfall intensity is higher than the saturated permeability (SoilVision 2006). Runoff may take place when the value of the rainfall intensity is larger than the saturated permeability, so runoff must be computed in an interactive manner. The upper boundary condition switches between the flux boundary and hydraulic head boundary depending on the rainfall intensity and the matric suction at the ground surface.

In the previous numerical analysis, it is assumed that the rainfall intensity is uniform in one day (Scanlon 2002). But in fact, the rainfall intensity varies with time. The assumption will affect the process and the amount of infiltration. This paper will perform numerical analysis focus on the influence of rainfall pattern on the process and the amount of infiltration.

THE NUMERICAL MODEL AND ITS VERIFICATION

The Geometry and Boundary Condition of the Numerical Model

The commercial software SVFlux is employed to do the numerical analysis. One dimensional analysis was conducted to investigate the influence of rainfall pattern on the process and the amount of infiltration. Albright et al. (2004) summarized the covers used in the Alternative Cover Assessment Project (ACAP). The thickness of earthen final covers in ACAP project is around 1.5m, so the thickness of 1.5m was chosen as the vertical depth of the numerical model (Fig. 1).

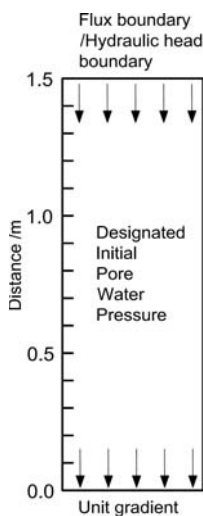


Fig. 1 The geometry and boundary condition of the numerical model

The lower boundary condition of the numerical model is unit gradient boundary. The unit gradient boundary means that there's only gravity gradient acting at the lower boundary and velocity of flow is equal to the soil permeability at the lower boundary. As mentioned previously, for the upper boundary condition, if the pore water pressure at the surface is negative, all the rainfall will infiltrate into the ground, if the pore water pressure reaches zero, the infiltration capacity will be equal to the saturated permeability. The upper boundary condition switches between the flux boundary and hydraulic head boundary.

Rainfall Patterns and Soil Properties

Fig. 2 shows six representative rainfall patterns of 24h duration considered in the paper. They consist of four basic types of rainfall patterns: advanced type (A1 and A2), central-peaked type (C), delayed type (D1 and D2), and uniform type (U) (Ng et al. 2001; Tsai 2008). The advanced patterns have relatively high rainfall intensity during early part of the rainfall event, whereas the delayed type is just the opposite. The central-peaked pattern has relatively high rainfall intensity in the center part, while the uniform type reveals constant rainfall intensity throughout the rainfall duration.

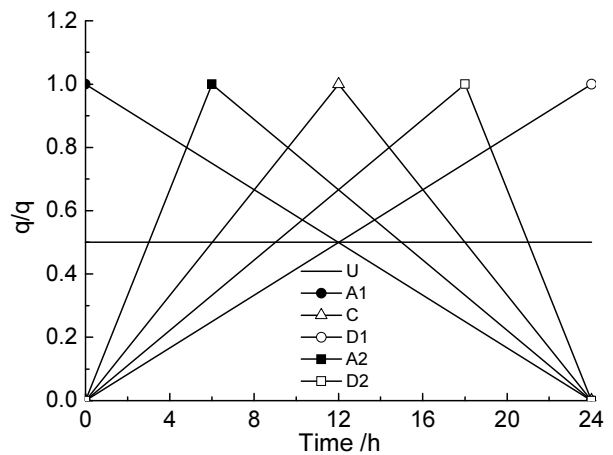


Fig. 2 Representative rainfall patterns used in analysis

Roesler et al. (2002) summarized the hydraulic properties of soils used in the ACAP project. Silt with sand was chosen as the soil used to construct the earthen final cover in the paper. Fig. 3 shows the soil-water characteristic curve of silt with sand. Fig. 4 shows the soil permeability of silt with sand. The soil-water characteristic curve and permeability function were described by van Genuchten equation (van Genuchten 1980).

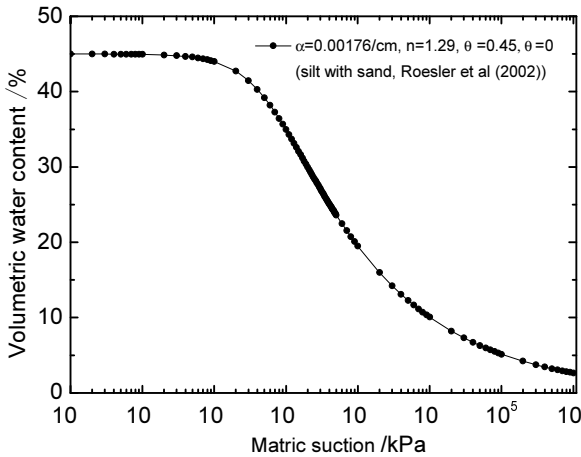


Fig. 3 The soil-water characteristic curve of silt with sand

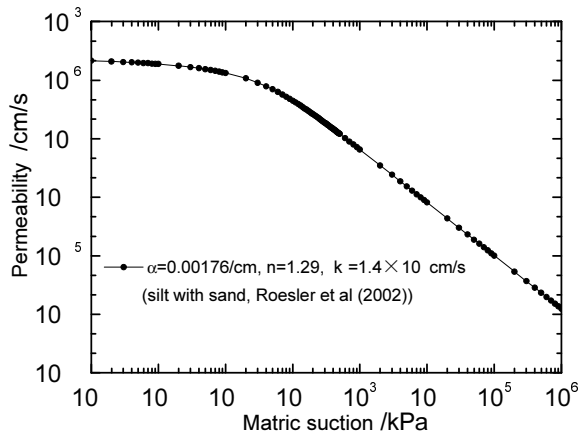


Fig. 4 The permeability curve of silt with sand

Verification of the Numerical Model

Zhu (2006) conducted column infiltration tests to study the process of rainfall infiltration. A numerical analysis was performed by SVFlux to simulate Zhu’s column test. The simulation results are shown in Fig. 5. The trend of the numerical results is consistent with the experimental data obtained by Zhu (2006). It indicates that the numerical model is reasonable and can be used in the parametric studies.

The Program of Parametric Study

The saturated permeability of silt with sand is 1.4×10^{-5} cm/s (i.e. 0.012m/d). In the analysis, it is assumed that the total amount of rainfall in one day is 0.048m, which is four times of the saturated permeability. The total amount of rainfall will distribute according to the six typical rainfall patterns. The initial matric suction of the one dimensional column is 100 kPa.

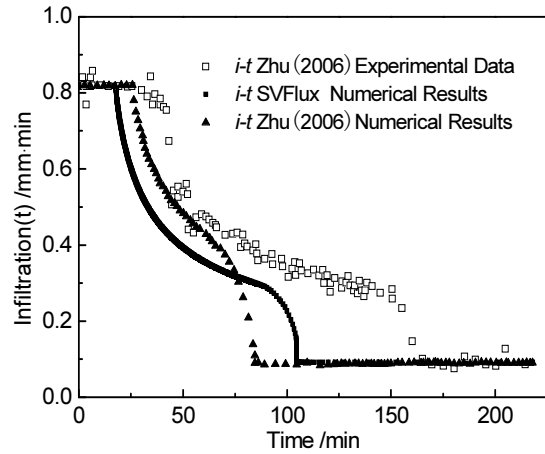


Fig. 5 Infiltration results between the column test and numerical simulations

RESULTS AND DISCUSSION

The Influence of Rainfall Pattern on Infiltration Process

The infiltration process is controlled by many variables, including the soil types, rainfall characteristics, and the initial conditions and so on. Fig. 6 shows the rainfall intensity and the corresponding infiltration rate under six representative rainfall patterns. The rainfall intensity minus the infiltration rate is the runoff rate. The peak rainfall intensity occurs earlier, the runoff will occur earlier. As time elapsed, the rainfall intensity tends to be smaller, there will be no runoff generated and all the rainfall will infiltrate into the ground surface.

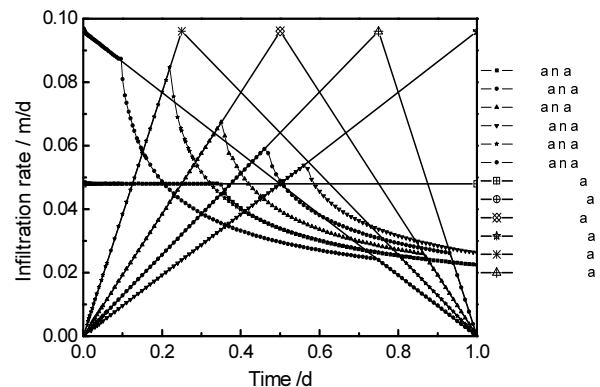


Fig. 6 Rainfall intensity and the corresponding infiltration rate under six representative rainfall patterns

The infiltration process is quite complex. It is primarily influenced by both the hydraulic conductivity and the hydraulic gradient at the ground surface zone. If the ground surface zone is dry, when rainfall on the ground surface, the surface becomes wet, then there will be a great matric suction gradient between the surface and the dry zone, so all the rainfall will infiltrate into the ground.

As rainfall advances, the wetted zone deepens. Then when rainfall falls on the surface, the matric suction gradient becomes smaller. If the surface zone is saturated, the matric suction gradient will diminish and only the gravity gradient act. The infiltration capacity continues to decrease during the rainfall period as the infiltrating water reduces the ground surface matric suctions. Eventually, the infiltration capacity is equal to the saturated permeability of the soil.

The peak rainfall intensity of A1 pattern occurs earliest and the peak rainfall intensity of D1 pattern occurs latest. When the ground surface is dry, the infiltration capacity can be high because of the steep matric suction gradient, so all the rainfall infiltrate into the ground surface though the rainfall intensity is high. Therefore for A1 pattern, when the rainfall intensity is high, the infiltration capacity still exceeds the rainfall intensity and there's no runoff generated. For other non-uniform rainfall patterns, since the rainfall intensity is small in the initial period, when the peak rainfall intensity occurs, the infiltration capacity is less than the rainfall intensity, so runoff occurs. Because the peak rainfall intensity can infiltrate into the ground for A1 pattern, the ground surface can absorb more water during the rainfall period.

Influence of Rainfall Pattern on Cumulative Infiltration

Fig. 7 shows the cumulative infiltration under six representative rainfall patterns. It indicates that the rainfall pattern significantly influence the cumulative infiltration under the same total amount of rainfall. The total amount of rainfall is 0.048m. The cumulative infiltration of A1 pattern is 0.0364m and the cumulative infiltration of D1 pattern is 0.03108m. The infiltration of uniform pattern is 0.03623m. Fig. 7 shows that the advanced pattern (A1) will generate the largest amount of infiltration compared to other patterns. The delayed pattern (D1) will generate the smallest amount of infiltration compared to other patterns. The difference of infiltration between the A1 pattern and D1 pattern is

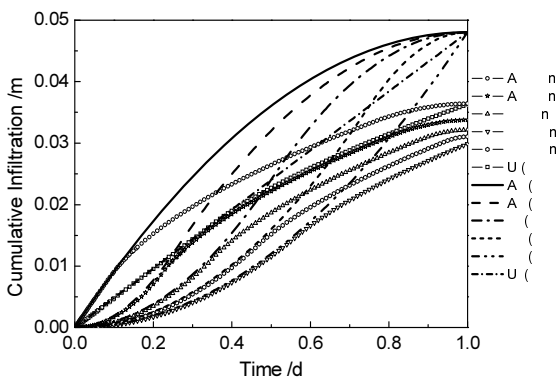


Fig. 7 The cumulative infiltration under six representative rainfall patterns

0.00532m, which is up to 11% of the total amount of rainfall depth. The difference of infiltration between different rainfall patterns is quite high. Therefore, the rainfall pattern should be taken into account to calculate accurate infiltration and then percolation.

CONCLUSIONS

The numerical simulation results indicate that the rainfall pattern can significantly affect the infiltration process and cumulative infiltration under the same amount of precipitation. The peak rainfall intensity occurs earlier, the cumulative infiltration will be larger. The advanced pattern (A1) will generate the largest amount of infiltration compared to other rainfall patterns. The rainfall pattern should be considered in the numerical analysis of landfill earthen final cover to obtain accurate amount of infiltration. If the real time metrological data is available, it will be much better to be used in the landfill earthen final cover design analysis.

ACKNOWLEDGEMENT

The authors would like to acknowledge the financial support from the National Key Technology R&D Program funded by the Ministry of Science and Technology of China (2006BAJ06B02) and research grants (50878194) provided by the National Natural Science Foundation of China (NSFC).

REFERENCES

Albright W, Benson C, Gee G, Roesler A, Abichou T, Apiwantragoon P, Lyles B, Rock S (2004). Field water balance of landfill final covers. *J. Environ. Qual.* 33 (6): 2317-2332.

GEO-SLOPE International Ltd. (2004). Seepage modelling with SEEP/W, user's guide version 6.16. GEO-SLOPE International Ltd., Calgary, Alta.

Green WH & Ampt CA (1911). Studies on soil physics: flow of air and water through soils. *J Agric Sci* 4:1-24

Holtan HN (1961). A concept of infiltration estimates in watershed engineering. ARS41-51, U.S. Department of Agricultural Service, Washington, DC.

Horton RI (1938). The interpretation and application of runoff plot experiments with reference to soil erosion problems. *Soil Science Society of America Proceedings.* 3: 340-349.

Mein RG & Larson CL (1973). Modeling infiltration during a steady rain. *Water Resour Res.* 9(2):384-394.

Ng CWW, Wang B, Tung YK (2001). Three-dimensional

- numerical investigations of groundwater responses in an unsaturated slope subjected to various rainfall patterns. *Canadian Geotechnical Journal*. 38(5): 1049-1062.
- Roesler AC, Benson CH, Albright WH (2002). Field Hydrology and Model Predictions for Final Covers in the Alternative Assessment Program-2002. *Geo-Engineering Report No. 02-08*, University of Wisconsin, Madison, WI. 279 pp. [Online]. Available at: <http://www.acap.dri.edu/>
- Scanlon BR, Christman M, Reedy RC, Porro I, Simunek J, Flerchinger GN (2002). Intercode comparisons for simulating water balance of surficial sediments in semiarid regions, *Water Resour. Res.* 38(12): 1323-1339.
- SoilVision Systems Ltd. (2006). *SVFlux User's Manual*. Saskatoon, Saskatchewan, Canada.
- Tsai TL (2008). The influence of rainstorm pattern on shallow landslide. *Environ Geol.* 53:1563-1569.
- van Genuchten M Th (1980). A closed form equation for predicting the hydraulic conductivity of unsaturated soils. *Soil Science Society of America Journal*. 44 (5): 892-898.
- Zhu W, Chen XD, Zhong XC (2006). Observation and analysis of rainfall infiltration. *Rock and Soil Mechanics*. 27(11): 1873-1879.

MUNICIPAL SOLID WASTE MANAGEMENT AFTER WENCHUAN EARTHQUAKE

Hua TAO¹

ABSTRACT: The massive debris are created by a disaster. A survey on municipal solid waste (MSW) management was conducted after Wenchuan Earthquake on May 12, 2008. As the results, separated collection as early as possible, construction waste reuse and recycling as much as possible are the effective and feasible measures on MSW management in the period of disaster relief and reconstruction. Landfills are light damaged by an earthquake and available for MSW disposal in the period of disaster relief even without artificial bottom liner system.

KEYWORDS: municipal, solid, waste, management, disaster

INTRODUCTION

Natural disasters affect the local and regional society and economy. On 26 December, 2004, the earthquake measured 9.0 on the Richter scale under the Indian Ocean and resulted in a powerful tsunami. The Tsunami caused extraordinary damage. Death toll was put at roughly 187,000, with nearly 43,000 missing and many hundreds of thousands injured. Debris and waste were scattered widely (http 2).

On 29 August 2005, Hurricane made landfall first in Florida and left a trail of heartbreaking devastation and human suffering. Katrina wreaked staggering physical destruction along its path, flooded New Orleans, ultimately killed over 1,300 people. Hurricane Katrina is the most destructive natural disaster in US history and caused damage of approaching US\$100 billion mark (Townsend 2006).

On 12 May, 2008, there was the earthquake measured 8.0 on the Richter scale at Wenchuan County, Sichuan Province, China.

After two weeks of the earthquake, the field study on municipal solid waste management in the earthquake worst-hit areas such as Dujiangyan, Pengzhou, Shifang and Mianzhu cities, was conducted. Later, the field study covered the whole earthquake-hit areas in Sichuan Province.

MAIN PROBLEMS

After disasters, such as the earth quakes, floods, hurricanes and typhoons, how to deal with MSW and

debris created by disasters is main challenge for the governments and residents. Townsend (2006) listed "environmental hazards and debris removal" is one of 17 critical challenges from Hurricane Katrina

The situation was similar to Hurricane Katrina after Wenchuan Earthquake. The main problems on MSW management in the earthquake-hit areas were:

Infrastructures Destroyed/Damaged

Almost all infrastructures, such as roads, bridges, telecommunication, drinking water supply system, electric power supply system, landfills, incineration plants, composting plants, et al. were destroyed and/or damaged by the earthquake. There were not enough facilities nor capacities to appropriately handle MSW.

MSW Dumped

MSW was not collected daily as usually nor disposed properly since the facilities and equipment were destroyed and/or damaged, and cleaning workers were hurt or died.

Massive Construction Waste Created

It was reported that 300 million tons of construction waste was created by Wenchuan Earthquake occurred in Sichuan Province, China on 12 May 2008 (http1). If lanfilled the construction waste, much land would be used. The other facts were how to manage the traffic and vehicles which needed for removal.

¹ Senior Engineer, Vice President and Secretary General, China Association of Urban Environmental Sanitation, 9 San Li He Road, Beijing 100835, China. Email:harry_taohua@yahoo.com

RESULTS

MSW Quantity and Composition

Table 1 shows the MSW generation from cities before the earthquake. The average generation of MSW was 0.8~1.0 kg/d per capita. It was estimated that the generation of MSW in first two months after the earthquake, was 70% to 80% less than that before

Table 1 Amount of MSW collection in 2007

Cities	Amount of collected MSW (t)	Average generation (kg/d.p)
Wenchuan	11000	0.98
Dujiangyan	111200	0.8
Pengzhou	71000	0.87
Shifang	61500	0.9
Mianzhu	53000	0.95
Jiangyou	54000	0.8

Table 2 shows MSW composition from the earthquake-hit areas before the disaster. The organics was about 28~40% of MSW, inorganic 35%~48%, including bricks and ashes.

After the earthquake, the composition of MSW was changed so much comparison to typical composition (Table 2). It was found that the main contents in MSW were packaging materials, like plastics, card board, bottles, and food waste

As the results of the quantity and composition of

Table 2 Typical MSW composition

Cities	Brick & ash	Organ-ics	Plast-ics	Paper	Textile	Metal	Glass	Others
Quake-hit areas	35~48	28~40	3~5	2~4	1~3	1~3	1~3	6~10
Shanghai	1.2	61.52	19.79	9.23	2.76	0.31	2.93	2.26

Source: Qin 2007

Table 3 Damage of MSW disposal facilities

Cities	Facilities	Capacity (t/d)	Damage of facilities	category of quake-hit
Wenchuan	Landfill	75	Bottom liner, office building, fence around site	Worst-hit area
Dujiangyan	Landfill	200	Leachate collection tank	Worst-hit area
Pengzhou	Landfill	150	Fence around leachate collection tank	Worst-hit area
Shifang	Incineration	200	Incinerators, flow gas treatment devices, chimney, office building, fence around the plant	Worst-hit area
Mianzhu	Incineration	200	Incinerators, chimney, workshops, fence around the plant	Worst-hit area
Jiangyou	Landfill	150	Leachate treatment devices, leachate collection pipes, ditch around site	Heavy-hit area

MSW changed so much, less amount and concentration of leachate was generated by less organics degraded. Therefore simplified landfill, without artificial bottom liner system, leachate collection and treatment system, might be available for MSW disposal nearby in the period of disaster relief if landfill is not located at water sources.

It was helpful to separate MSW into two types, packaging materials and food waste as the result of quantity and composition changed heavily. It was seen that MSW was separated already in some temporary shelters.

It was important to collection MSW regularly from streets, houses and all temporary shelters. In Dujiangyan City, near Chengdu, the capital of Sichuan Province, the clean worker who came from Chengdu swept the streets and collected MSW three days after the earthquake.

Facilities Damage Comparison

Landfills are the most common method to dispose the municipal solid waste (MSW) in China. By the end of 2007, there was about 152.1 million tons of MSW generated from 655 cities. 94.4 million tons of MSW was disposed, 82% by landfill (MOHUR, 2008).

In the earthquake-hit areas there were 35 MSW disposal facilities, including 29 landfills, 6 incineration plants and composting plants. Almost all facilities were damaged at different level and a few destroyed by the earthquake.

Comparing the damage, it shows that the damage of landfill is less than that of incineration plant in the same quake-hit area (Table 3). Landfills were used after repaired

in short time. The reasons are that there are more buildings, equipment and devices in incineration plants than in landfills.

Although MSW disposal facilities damaged and/or destroyed by the earthquake in cities and towns, actually MSW was simply disposed by landfill near the resident areas in the earthquake-hit areas. But it was not allowed to landfill MSW at waster sources. The simplified landfills mean they have neither any article bottom liner system, leachate collection system nor treatment system. According to the Chinese Technical Code for MSW Sanitary Landfill (CJJ 17-2004/J 302-2004), a sanitary landfill should have not only those systems, but also landfill gas collection system (MOC, 2004).

In the period of disaster relief, it is feasible to control underwater pollution from leachate generated by MSW landfill, since the biodegradable organics were much less than before. On the other hand, the environmental capacity of bottom clay makes leachate dilution and degradation.

Construction Waste

The massive construction waste or debris is created by a disaster. Townsend (2006) estimated that Hurricane Katrina created 118 million cubic yards of debris, and it took five months to remove 71 million cubic yards of debris.

After two weeks of the earthquake, more and more construction waste was collected and removed from damaged and/or destroyed buildings. Some construction waste was being or would be used for road construction, most dumped onto land for the post-earthquake reconstruction.

It was seen that some residents, particular farmers, had spontaneously separated the irons and steels, woods, bricks from the debris of their houses for reconstruction at that time.

CONCLUSIONS

Based on the field survey from Wenchuan Earthquake, MSW management might be emphasized on followings after disaster:

Collection and Separation

In the period of disaster relief, the generation of MSW

is 70% to 80% less than before. The main contents are packaging materials, like plastics, paper and card board. Consequently, it is possible to separate MSW at source into two types, packaging materials and food waste, for pollution control.

It is important to re-operate MSW collection as early as possible in disaster-hit areas, in both villages and cities.

Landfilled MSW

The damage of landfills is much less than that of incinerations, and composting. It is also easy to repair and re-operate, landfills are available to handle MSW in disaster areas even without bottom liner system and leachate collection system. The natural environmental capacity and dilution could be used as much as possible in the period of disaster relief.

ACKNOWLEDGEMENTS

Appreciate those colleagues who participated in the field study at the earthquake-hit areas in Sichuan Province although aftershocks occurred frequently at that time.

REFERENCES

- Qin F (2007). Composition of Municipal Solid Waste in Shanghai City. In: Yearbook 2005 of China City-Appearance & Environmental Sanitation. China Urban Press, Beijing.
- Department of Integrated Finance of the Ministry of Housing and Urban-Rural Development of PR China (MOHUR) (2008). China Urban Construction Statistical Yearbook 2007. China Architecture & Building Press, Beijing.
- Ministry of Construction (MOC) (2004). Technical Code for Municipal Solid Waste Sanitary Landfill (CJJ 17-2004/J 302-2004). China Architecture & Building Press, Beijing.
- Townsend F (2006). The Federal Response to Hurricane Katrina: Lessons Learned. White House Report, Washington DC.
- [http1://big5.xinhuanet.com/gate/big5/news.xinhuanet.com/politics/2008-06/27/content_8450457.htm](http://big5.xinhuanet.com/gate/big5/news.xinhuanet.com/politics/2008-06/27/content_8450457.htm)
- <http2://www.globaleducation.edna.edu.au/globaled/go/pid/2258#Section1>

FIELD INVESTIGATION ON THE FEASIBILITY OF LEACHATE RECIRCULATION IN CHENGDU MSW LANDFILL, CHINA

Ji-Wu LAN¹, Tony Liang-Tong ZHAN², Yun-Min CHEN³, Han KE⁴, Zhao LIU⁵ and Guo-Qing LU⁶

ABSTRACT: The paper presents a field investigation on the feasibility of recirculating concentrated leachate into the Chengdu landfill of municipal solid wastes. The field investigation included borehole investigation of the hydro-geological conditions and in situ simulation tests of leachate recirculation. Two kinds of facilities, i.e., open pits and vertical wells, were established to carry out the simulation tests. The borehole investigation revealed that the leachate level within the landfill was very high, being at a depth of 1~3m below the landfill surface. The results from the simulation tests indicated that the steady-state recharge capacity into the open pit and vertical well were 24 m³/d and 5 m³/d, respectively, and the hydraulic-conductivity of waste was calculated to be 6.3×10^{-6} m/s. The low recharge capacity was mainly attributed to the high leachate level. Preliminary numerical analyses demonstrated that a drawdown of leachate level will result in an increase in the recharge capacity.

KEYWORDS: leachate recirculation, landfill, field study, leachate level, open pits, vertical wells

BACKGROUND

Leachate recirculation has been in widespread use for a range of purposes for many decades since some researchers have begun to suggest its beneficial use in 1970s (EA 2008). There are many legitimate reasons for undertaking leachate recirculation, such as flow balancing for leachate, accelerating settlement and stimulating gas generation, accelerating degradation of organic waste and leachate, treatment of concentrated leachate or other organic liquid etc. Certainly, there are a lot of risks in the landfill undertaken leachate recirculation, including risk of slope instability, build up of water head in landfill, clogging of basal drainage layer, flooding of gas well (EA 2008; Townsend et al. 2008; Khire et al. 2006; Hossain et al. 2008). In developed countries, more and more attentions were paid to the engineering practice because its multiple use in landfill operation, and after many years of research and practice, a wide range of different leachate recirculation systems, such as low pressure surface application system (EA 2008; Miller & Emge 1997; Haydar & Khire 2005), systems immediately below top liner (EA 2008; Khire & Haydar 2007), structures at depth within wastes (EA 2008; Haydar & Khire 2007) and vertical wells or

trenches (EA 2008; Jain et al. 2005), have been proved to be suitable systems to different situations.

Since 1980s, researchers and designers tried to study and design leachate recirculation systems as aim of balancing and decreasing the volume of leachate in China, but the effectiveness have rarely been good because of high precipitation and the bad daily operation of landfills. After 1990s, the related research and study reduced sharply. Until 2000s, more and more studies about leachate recirculation were carried on as one part of research on bioreactor landfill. These studies carried on by environmental scientist put emphasis on accelerating degradation of organic waste and leachate, but little related study was made on recirculation infrastructure and the influence of recirculation to landfill site (FENG et al. 2009; LIU et al. 2008). Till recent years, when the new national code of leachate treatment was implemented, leachate treatment plants with RO or MBR treatment technology began to be built and operated, leading to more and more concentrated leachate generated, because there is no cost-effective way to treat the concentrated leachate expected to recirculation, then more attentions were put on the recirculation technology and infrastructures suit to Chinese landfill (LUO et al. 2003).

¹ PhD student, MOE Key Laboratory of Soft Soils and Geoenvironmental Engineering, Zhejiang University, Hangzhou, China

² Professor, ditto. Email: zhanlt@zju.edu.cn

³ Professor, ditto.

⁴ Associate Professor, ditto.

⁵ Mphil student, ditto.

⁶ Senior Engineer, North China Municipal Engineering Design and Research Institute, Tianjin, China

This study, focus on study of the feasibility of concentrated leachate recirculation in Chengdu MSW landfill was carried out just in this background. Two issues should be concerned about the feasibility of concentrated leachate recirculation in the study, one is the recharge capacity of the disposed waste, the other is the slope stability of waste mass after a long-term leachate recirculation . To answer the two concerns, site investigation, lab test and numerical analysis work were carried on to investigate the properties of waste such as hydraulic conductivity, shear strength etc. Slope stability of disposed waste after recirculation was further evaluated based on the properties measured. Some advices about system choice and design were given after the investigation and analysis. This paper focus on the site investigation and the preliminary analysis of site investigation results, and the other issues will be discussed in other papers.

SITE INVESTIGATION

Site Description

Chengdu MSW landfill (Fig. 1), 25km away from Chendu city, located in a “U” shape valley at Chang’An village. The landfill site was developed in two Phases, Phase 1 site and Phase 2 site. Phase 1 site, constructed in 1993, with area of 33 ha and 11,000,000 m³ air space, will be finished soon, and Phase 2 site, expansion on base of Phase 1, is now in design stage. One new leachate treatment plant with treatment scale of 1000 m³/d in NF and RO treatment process is being constructed in this landfill, and 20%~25% , about 260 m³ concentrated leachate will be generated in operation. Recirculation is

selected as the treatment process by the owner after considering the cost and technical factors.



Fig. 1 Panoramic photographs of Chengdu MSW landfill

Fig. 2 shows the main cross-section of the landfill as of December 2008, when the field investigation was carried out. The landfill consists of waste pile with average depth of about 30 meters at different embankment slope from 1.5H/1V to 4H/1V, and a stone masonry gravity dam retains the waste in lowest position. Waste has been buried on bottom without liner system, directly on eluvium of quaternary system and mudstone. No complete and well-designed leachate drainage system was constructed on the bottom of landfill, and the simple system was clogged with a period of operation, so the water head is so high that can be found in 1~3 meters below the slope surface in our investigation area, and water exit point even can be found on the lower of the waste slope.

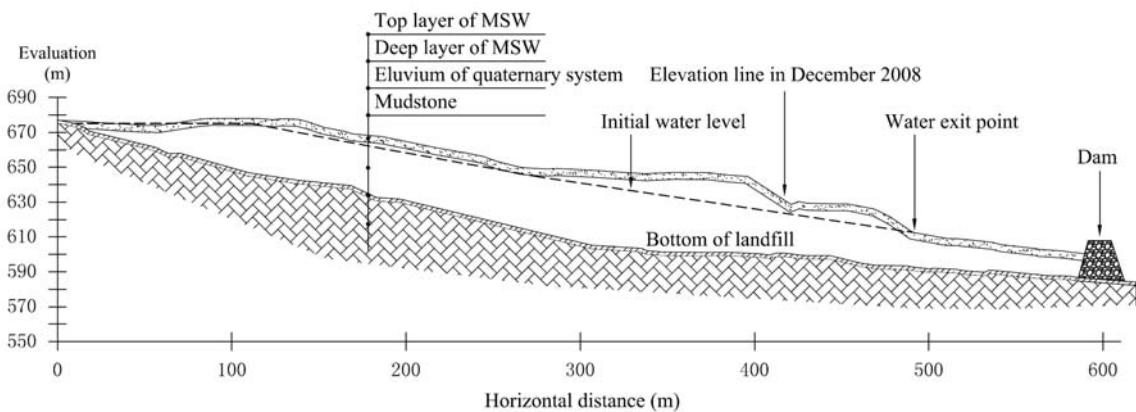


Fig. 2 Main cross-section of Chengdu MSW landfill, phase 1 Site

Investigation on Hydro-geological Conditions of the Landfill

A field study was carried out on the existing landfill to assess hydro-geological conditions of Chengdu MSW

landfill. The field study consisted of borehole investigations, sampling of the waste materials, monitoring of water level in boreholes. In experimental area 1, 7 boreholes (a1 to a3, b1, b2, c1, 1# vertical well) were drilled (see Fig. 3 & Fig. 4). The depth of boreholes ranged from

6.5m to 16.5m. The boreholes were drilled without an introduction of mud and liquids. The diameter of six boreholes is little large than 75mm, a 75mm perforated galvanized steel pipe wrapped with non-woven textile was installed after investigation as the monitoring wells in the following recirculation experiment. The other one borehole, with 500mm diameter in the upper 6m and 300mm diameter under 6m, installing a 270mm perforated galvanized pipe wrapped with textile, also with surrounded gravel layer in the upper 6m, was the recirculation vertical well in experiment. Five boreholes (d1, e1, e2, f1, 2# vertical well) with depth of 10m to 11.6m were drilled in experimental area 2 with the same size and structure (see Fig.3 & Fig. 5). Same as experimental area 1, four ones were monitoring well and one was recirculation vertical well. In process of drilling, MSW samples for lab testing were taken using heavy-wall samplers at an interval of 2.5m, and 1# open recirculation pit and 2# open recirculation pit was also dig out.

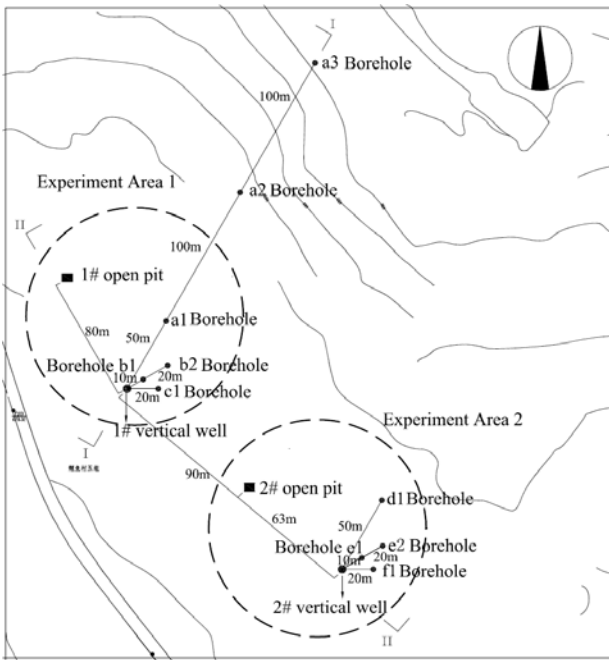


Fig. 3 Plan view of site investigation boreholes and experimental recirculation system

Fig. 4 and Fig. 5 shows the two cross-sections of field study and also the experimental area. The 1-1 cross-section (Fig. 4), indicate the hydro-geological conditions in experimental area 1. From 1-1 cross-section, it can be found that the depth of waste near experimental area 1 is 11~30m, thinner in upstream of the slope, and the initial water level is very high, from 2.42 to 6.39m to the evaluation line. The 2-2 cross-section (Fig. 5) shows the hydro-geological conditions in experimental area 1 and experimental area 2. From the section, it can be indicated that the depth of waste of experimental area is about 10m,

and the initial water level is very high, from 1.1 to 3.0m down the evaluation line. It can also be found that the water level of experimental area 2 is higher than that of experimental area 1, which may lead to the less recirculation volume during experiment.

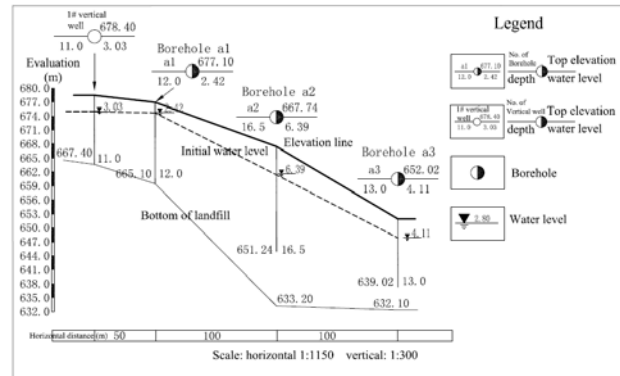


Fig. 4 1-1 Cross-section of field study area

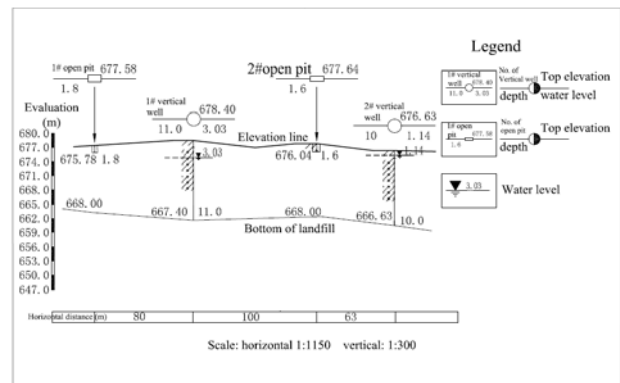


Fig. 5 2-2 Cross-section of field study area

EXPERIMENTAL PROGRAM FOR LEACHATE RECIRCULATION

Layout of Experimental Areas

As shown in Fig. 3 to Fig. 5 and described before, based on the site conditions an experimental leachate recirculation system was installed in the middle-capped area near the top of Phase 1 waste pile. The system consists of two virtually independent experimental areas, recirculation area1 and recirculation area2 with the nearest distance of 90m. Open pit 1 and vertical well 1 (built based on the investigation borehole) located in experimental area 1, open pit 2 and vertical well 2 (built based on the investigation borehole) located in experimental area 2, and the distance of open pits and vertical wells is considered to be far enough to avoid disturbed by each other during experiment. In each experimental area, some monitoring wells (built based on

the investigation boreholes) were installed in different distance apart from recirculation vertical well (Fig. 3). In experimental area 1, the distance of a1, a2, a3 monitoring well is respectively 50m, 150m, 250m away from the 1# vertical well, b1, b2 monitoring well is 10m, 30m away from 1# vertical well, and for c1, the distance is 20m. In experimental area 2, the distance of d1 monitoring well is 50m away from the 1# vertical well, e1, e2 monitoring well is 10m, 30m away from 1# vertical well, and for f1, the distance is 20m.

Set up of Leachate Recirculation System and Operation

As described before, 1# open pit and 1# vertical well were included in experimental area 1. The 1# open pit (Fig. 6) was dig out in plan view size of 6.2m×6m, with depth of 2m, and the 1# vertical well was built in diameter of 270mm, with depth of 11m. The 2# open pit was dig out in plan view size of 6.0m×5.6m, with depth of 1.6m, and the 2# vertical well was built in diameter of 270mm, with depth of 10m. All the monitoring wells are in diameter of 75mm with depth ranged from 6.5m to 16.5m.



Fig. 6 Photograph of 1# open Pit

During recirculation experiment, leachate was pumped to open pits 2~3 times/day to make sure that the water level in pits is more than 0. The vertical wells had to be supplied for 4~9 times to maintain the water level higher than initial natural head. Water level in pit and wells was measured and recorded every one hour, and before and after every water supply process. Volume applied of leachate was also recorded each time. During experiment, water head of every monitoring well was measured and recorded 1 times/day.

Instrumentation and Monitoring Program

A pump powered by diesel motor was used to supply the recirculation leachate, with a rotor water gauge to measure the total flow volume. The water head in

recirculation vertical wells, open pits, and monitoring wells was measured by an electric contact water level gauge.

EXPERIMENTAL RESULTS AND DISCUSSION

Infiltration Capacity of Waste in Experiment

From 2008.12.6~2008.12.20, the experimental recirculation was carried out for 15 days. 1# open pit was injected for 14 days with the total recirculation volume of 612 m³. 1# vertical wells was injected for 10 days with the total recirculation volume of 60 m³. 2# open pit was injected for 12 days with the total recirculation volume of 339 m³. 2# vertical wells was injected for 8 days with the total recirculation volume of 34 m³. The total applied volume of 2# open pit and 2# vertical well proved to be less than the open pit and vertical well in experimental area1 because of the higher water level. In the following, results of 1# open pit and 1# vertical well would be discussed and analyzed carefully, and the detailed experimental results from area 2 would be discussed in other paper.

Daily applied volume of 1# open pit was shown in Fig. 7. During the 12 days experiment, the applied volume of 1# open pit varies from 162 m³/d to 21 m³/d (average 39 m³/d, to be 32 m³/d if exclude the data of the first day, tends to be 24m³/d in the end), and decreases quickly in the first few days, tending to be steady in the last days. Daily applied volume of 1# open pit was shown in Fig. 8. During experiment, the applied volume of 1# vertical well varies from 7 m³/d to 4 m³/d (average 5 m³/d, tends to be 5m³/d in the end), and decrease slowly in the first few days, tending to be steady in the last few days.

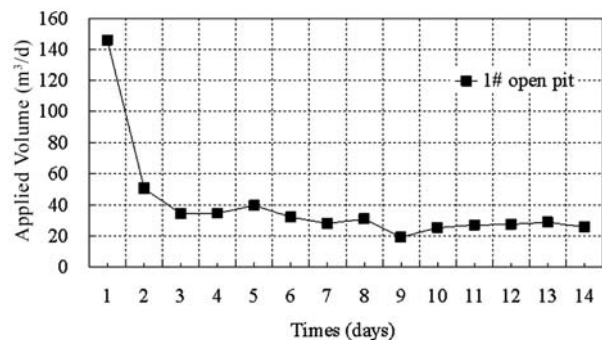


Fig. 7 Daily applied volume of 1# open pit

Through analysis of the daily water head in monitoring wells, it can be found that the radius of influence of this experiment would be about 50m for open pits, and 10m~30m for vertical wells.

In this study, FEMWATER module of GMS 6.0 is used to make back-analysis for Hydraulic conductivity of

waste and to predict the long-term recirculation ability for open pits and vertical wells. A 3D model was constructed as the actual soil layers revealed by engineering investigation within radius of 50m around 1# open pit in GMS 6.0 (Fig. 9), and 1# open pit, in size of 6m×6m, with depth of 2m, was placed in the same position as actual. The initial water level in the model was assigned as the measured data of 1# vertical recirculation well and monitoring wells.

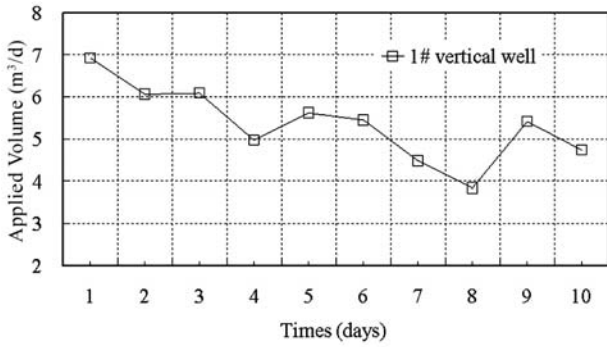


Fig. 8 Daily applied volume of 1# vertical well

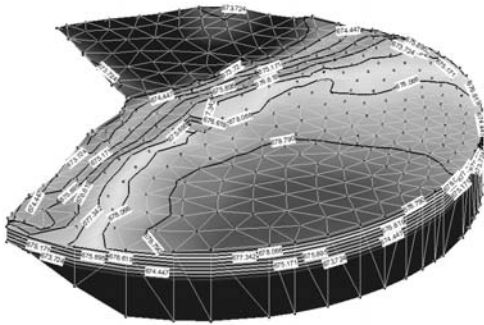


Fig. 9 3D Model of 1# Open Pit Recirculation Area

In process of back-analysis calculation, water level in 1# open pit was assigned as the measured data, and soil-water characteristic curve came from another similar landfill in china, then the only pending parameter is the hydraulic conductivity of waste in site. Referred to the coefficient of permeability of MSW in other landfills in china, three values, which are $3.5 \times 10^{-6} \text{m/s}$, $6.0 \times 10^{-6} \text{m/s}$ and $7.5 \times 10^{-6} \text{m/s}$ were chosen to try in Case1, Case 2 and Case 3. The recirculation volume in three calculation cases were recorded and compared to the measured data to decide the suitable hydraulic conductivity of the waste.

The results of three calculation cases and the measured data are shown together in Fig. 10. It can be found that the result of case 3, variation from 102 m³/d to 25 m³/d (average 31 m³/d if exclude the data of the first day), is similar to the measured data of experiment, so the hydraulic conductivity value is chosen to be $7.5 \times 10^{-6} \text{m/s}$. And considering the seepage of concentrated leachate in

practice will be more difficult than the experimental leachate because of higher coefficient of viscosity, based on the related calculation methods, the hydraulic conductivity of $6.3 \times 10^{-6} \text{m/s}$ was chosen in the following numerical calculation.

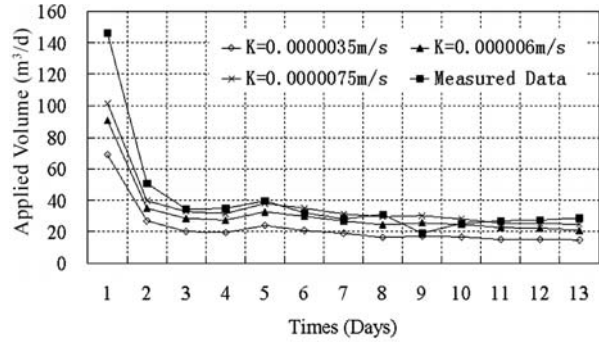


Fig. 10 Analysis of Relationship between Applied Volume and Waste Hydraulic-conductivity of 1# Open Pit

The results of three calculation cases and the measured data are shown together in Fig.10. It can be found that the result of case 3, variation from 102 m³/d to 25 m³/d (average 31 m³/d if exclude the data of the first day), is similar to the measured data of experiment, so the hydraulic conductivity value is chosen to be $7.5 \times 10^{-6} \text{m/s}$. And considering the seepage of concentrated leachate in practice will be more difficult than the experimental leachate because of higher coefficient of viscosity, based on the related calculation methods, the hydraulic conductivity of $6.3 \times 10^{-6} \text{m/s}$ was chosen in the following numerical calculation.

Influence of Water Head on Long-Term Recirculation Volume of 1# Open Pit

On base of the result of previous result of hydraulic-conductivity of waste, the long-term steady recirculation volume of 1# open pit was calculated, as showed in Table 1. In general, the recirculation volume of 1# open pits increase as the raising of water head, from 9 m³/d at 3m water head to 35 m³/d at 6m water head. When water ahead is 3m, the long-term applied volume is 9 m³/d, and when the water head changes to 4m, the long-term applied volume increase quickly to 29m³/d, that may mean that when recirculation in 1# open pit area, to bring down one meter leachate level can get a remarkable increase of daily applied volume. The applied volume in case of 5 m water head is nearly the same as that in 6m water head. The reason may be the taper structure of terrain in 1# open pit recirculation area, when leachate level gets down and water head get higher, the seepage area may decrease quickly.

Table 1 Influence of leachate head on applied volume of 1# open pit (long-term performance)

Items	Water	Water	Water	Water
	head is 3m	head is 4m	head is 5m	head is 6m
Applied volume(m ³ /d)	9	29	35	35

CONCLUSION AND SUGGESTION

The hydro-geological conditions of Chengdu MSW landfill was revealed in the field study. In the experimental area, the depth of waste ranged from 10m to 30m, with very high initial leachate level, which may bring about bad effect to long-term recirculation. The results from the simulation tests indicated that the steady-state recharge capacity into the open pit and vertical well were 24 m³/d and 5 m³/d, respectively, and through analysis of the measured data by GMS6.0, the hydraulic conductivity of waste in Chengdu landfill is suggested to be 6.3×10^{-6} m/s. By further analysis, the discipline was indicated that to bring down the leachate level can make the daily recirculation volume increase.

The high leachate level not only cause to difficulty of construction and operation of recirculation facilities, but also leads to problems of slope instability, so it is suggested that the leachate level in waste should be brought down before operation of recirculation system, and further the sustainable leachate level control system should be included in the recirculation system.

Referred to the experiences of leachate recirculation system construction and operation in China and broad, the clogging of infrastructure in long-term operation should be considered.

ACKNOWLEDGEMENTS

The authors would like to acknowledge financial support from research grants (50538080 and 50878194) provided National Natural Science Foundation of China (NSFC), and the research funding from the Science and Technology Department of Zhejiang Province (2007C23038).

REFERENCES

- Assessment of issues relating to leachate recirculation, Environmental Agency, 2008.05.
- Pradeep Jain, William M Farfour, Sreeram Jonnalagadda et al. (2005). Performance Evaluation of Vertical Wells for Landfill. GSP142 Waste Containment and Remediation, 2005: 1-10.
- Dwight E Miller & Stephen M Emge (1997). Enhancing Landfill Leachate Recirculation System Performance. Practice Periodical of Hazardous, Toxic and Radioactive Waste Management, July 1997: 113-119.
- Timothy G Townsend, Ravi Kadambala, Sendhil Kumar et al. (2008). In-Situ Measurements of Pore Water Pressures in Landfilled Waste in Response to Liquids Addition. GeoCongress 2008: 104-111.
- Milind V Khire & Mazen M Haydar (2007). Leachate Recirculation in Bioreactor Landfills Using Geocomposite Drainage Material. Journal of Geotechnical and Geoenvironmental Engineering, February 2007: 166-174.
- Mazen M Haydar & Milind V Khire (2005). Leachate Recirculation Using Horizontal Trenches in Bioreactor Landfills. Journal of Geotechnical and Geoenvironmental Engineering, July 2005: 837-847.
- Mazen M Haydar & Milind V Khire (2007). Leachate Recirculation Using Permeable Blankets in Engineered Landfills. Journal of Geotechnical and Geoenvironmental Engineering, April 2007: 360-371.
- Milind V Khire, Mazen Haydar, and Moumita Mukherjee (2006). Liquid Head on Landfill Liners Due to Leachate Recirculation. GeoCongress 2006: 1-6.
- Sahadat Hossain MD, Kiran Kumar Penmethsa, and Laureano Hoyos (2008). Permeability of Municipal Solid Waste (MSW) in Bioreactor Landfill with Degradation. GeoCongress 2008: 120-127.
- Feng XM, Jiang JG, Zhang C, et al. (2009). Study of Design Parameters of Leachate Recirculation System In Old Landfills. Industrial Safety and Environmental Protection, January 2009: 30-32 (In Chinese).
- Liu YP, Li XJ, Wang BZ et al. (2008). Study of RO Concentrated Leachate Recirculation. Environmental Engineering, August 2008: 89-93 (In Chinese).
- Luo CY, Chen YM, Tang XW et al. (2003). Study in Theory of Recirculation Design Parameters. Environmental Engineering, August 2003, 13-15 (In Chinese).



Sludge and Dredging Soils

REUSE OF POND SEDIMENT BY MIXING WITH STABILIZERS AND SHREDDED PAPER

Yasuyuki NABESHIMA¹ and Seishi TOMOHISA²

ABSTRACT: Hyogo Prefecture has many irrigation ponds. Sediment in the ponds is removed during agricultural off-season. Because pond sediment has high water content, it is usually stabilized with stabilizers such as cement and lime. Stabilized soil has brittle shear behavior therefore it is quite different from natural soils. The fiber reinforced soil was able to improve the mechanical properties of soft soil. To improve brittle shear behavior of stabilized soils, the authors carried out a series of mixing test of soft clays with cement and shredded paper as a fiber. And unconfined compression tests of cement stabilized clays mixed with shredded paper were performed. As the result, by mixing with shredded paper, the unconfined compression strength of cement stabilized clays increases and the shear deformation behavior is improved.

KEYWORDS: pond sediment, reuse, shredded paper, soil improvement

INTRODUCTION

Many irrigation ponds exist in Hyogo prefecture, the number of irrigation ponds is more than 43,000 and it is the biggest number in Japan. Sediment at the bottom in the ponds is removed during agricultural off-season because of the agricultural and environmental reasons. Huge amount of pond sediment is disposed without reuse. Pond sediment has high water content, so it is difficult to reuse as a geotechnical material without any treatments. Cement stabilization is one of popular techniques to improve soil strength of soft soil, however pond sediment was hard to stabilize because of high water content and high organic.

In this paper, authors applied a new technique to reuse the pond sediment by mixing with cement and shredded paper. To improve shear and deformation characteristics of pond sediment, a series of mixing tests with cement and shredded paper is carried out. Because the amount of cement can be reduced by mixing with shredded paper, the mixing treatment with shredded paper gives economical and environmental benefits. Shredded paper has a high water absorption performance, mixing of shredded paper causes to decrease water content of the pond sediment. And a series of unconfined compression tests is performed. Unconfined compression strength of pond sediment mixed with cement and shredded paper is compared with that of pond sediment improved by cement stabilizer alone. Based on the test

results, unconfined compression strength is compared, shear modulus and failure strain are also compared. It is discussed to reuse the pond sediment from viewpoints of strength and deformation characteristics.

SHREDDED PAPER

After the enforcement of the Act for Protection of Personal Information in 2005, the amount of shredded paper dust from public and business offices rapidly increases. The shredded paper is non-recyclable as the recycled paper because the fiber of shredded paper is too short to regenerate the paper. Thus, total amount of waste paper reached about 5.5 million ton per year in Japan and it was disposed or incinerated without reuse every year.

Many kinds of paper shredder machine were produced in Japan. Also, the shape of shredded paper is quite different. Noodle cut, cross cut and spiral cut were typical shapes of the shredded paper as shown in Fig.1. Fig.1 shows the shapes of the shredded paper of noodle cut, cross cut and spiral cut types. Cross cut type is the most popular among three types of shredded paper. The cross cut shape of shredded paper gradually became small and short after the Act for Protection of Personal Information. Fig.2 shows the frequency distribution of length of shredded paper in Akashi National College of Technology (ANCT). In our campus, there is no paper

¹ Associate Professor, Civil Engineering, Akashi National College of Technology, Japan. Email:nabesima@akashi.ac.jp

² Professor, Civil Engineering, Akashi National College of Technology, Japan. Email:tomohisa@akashi.ac.jp

shredder machine of noodle cut type. As we expected, the cross cut type was predominant. Although the width of shredded paper was about 3 millimeter which was almost constant regardless of shredder machines, the length of shredded paper was scattered from 1.7 to 3.1 centimeter. The mean length of shredded paper was 2.3 centimeter. In this study, shredded paper with around 2.3 centimeter in length was used.

Paper fiber of copy paper is a good quality and it has high tensile strength, and absorbs water. A ground improvement technique using waste paper chips was proposed in Japan (Bon terrain Committee, 2005). Therefore, we expected that it is a good ground improvement material by mixing with soft clay.



(a) noodle cut type



(b) cross cut type



(c) spiral cut type

Fig. 1 Three types of shredded paper pieces

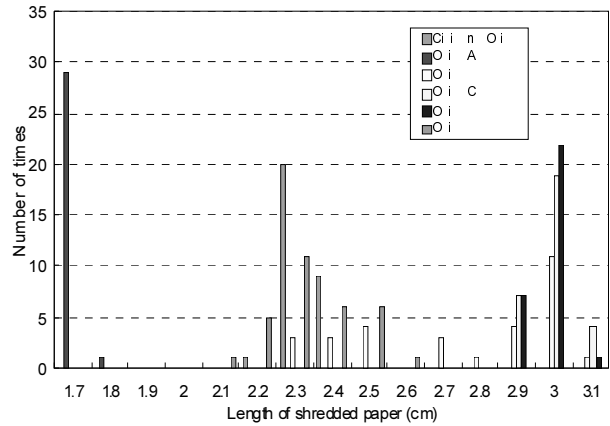


Fig. 2 Distribution of length of shredded paper

TEST PROCEDURES

To investigate shear behavior of cement stabilized soil mixed with shredded paper, a series of unconfined compression test is carried out followed by the mixing test.

Test soil was taken from the bottom of irrigation pond in Inami town near ANCT. Soil properties of test soil were summarized in Table 1. Natural water content at soil sampling was higher than liquid limit, which means very soft and weak. Its water content decreased to 88.5 % during keeping in the storage box. Test soil was mixed with shredded paper and ordinary Portland cement with predetermined mixing rate. Three specimens were made by tamping method in the steel mold which has 50 millimeter in inner diameter and 100 millimeter in height. Shredded paper made by the paper shredder machine in our office was used. Mass of the original paper was about 33.3 kg/m². The average length of shredded paper was about 23 millimeter and thickness about 0.088 millimeter. A series of unconfined compression test were carried out.

Table 1 Soil properties of test soil

Natural water content	123.8 %
Liquid limit	114.5 %
Plastic limit	40.7 %
Plasticity index	73.8
Soil particle density	2.48 g/cm ³
Gradation	
Sand	5 %
Silt	36 %
Clay	59 %

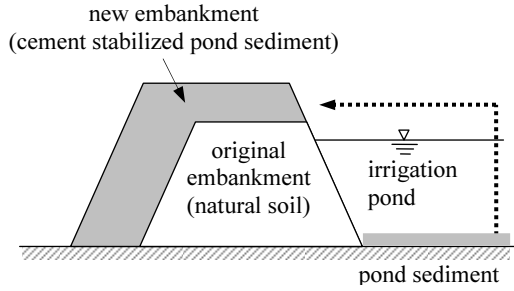


Fig. 3 Application of pond sediment as a pond embankment

In this study, to reuse the pond sediment as an embankment of the irrigation pond as shown in Fig. 3, the unconfined compression strength of the stabilized soil is necessary to strengthen beyond the specified strength of 100 kN/m². It was decided in the Japanese regulation for the reuse of surplus soil and sludge.

TEST RESULTS AND DISCUSSION

Soil Improvement by Mixing with Shredded Paper

Soil improvement mechanism by mixing test soil with shredded paper is demonstrated and discussed. Fig.4 shows a variation of unconfined compression strength with mixing rate of shredded paper. A kinked solid line shows an average value of three unconfined compression strength at every mixing rate. Original unconfined strength of test soil was around 6 kN/m². It gradually increases as the mixing rate of shredded paper increases. The unconfined compression strength at 5% of the mixing rate of shredded paper reached about 15 kN/m². However, the increment of unconfined compression strength by mixing test soil with only shredded paper was very small, some stabilizers such cement are necessary to improve unconfined compression strength until the specified strength.

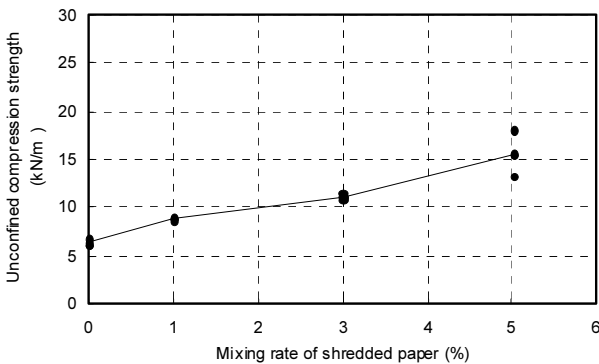


Fig. 4 Unconfined compression strength with mixing rate of shredded paper

Fig. 5 shows a variation of unconfined compression strength with water contents, which were measured at 1 and 7 days after mixing test soil with shredded paper. Water contents in all cases were decreased from original water content of 88.5 % by mixing with shredded paper (SP). It shows that the shredded paper absorbed water from test soil and the decrease in water content became larger as the mixing rate of shredded paper and elapsed days increased. Therefore, the absorption of water from test soil is a major soil improvement mechanism by mixing with shredded paper.

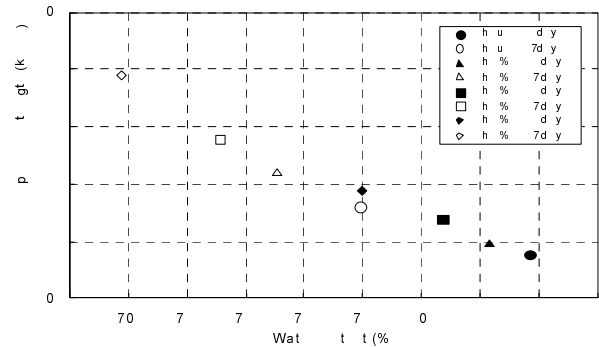


Fig. 5 Unconfined compression strength with water content after 1 and 7days

Because the mixing of pond sediment with shredded paper alone was not enough to improve shear characteristics, the pond sediment was stabilized by mixing with ordinary Portland cement. To determine appropriate additive rate of cement, a series of preliminary unconfined compression test was carried out. Additive rate of cement was determined as 1, 3 and 5 %. Fig. 6 shows a variation of unconfined compression strength and additive rate of cement. A kinked solid line shows an average value of three unconfined compression strength at every additive rate of cement. Unconfined compression strength increases as additive rate of cement increases. Unconfined compression strength at 3 % was much lower than the specified strength and the unconfined compression strength at 5 % was appropriate in the preliminary tests.

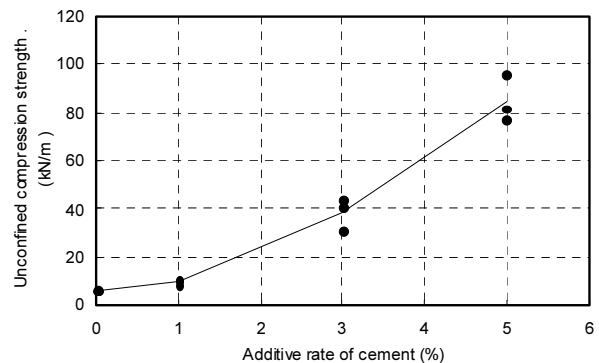


Fig. 6 Unconfined compression strength with additive rate of cement

Soil Stabilization by Mixing with Stabilizers and Shredded Paper

Based on the preliminary test results, the additive rates of cement and magnesia were fixed on 5 %, and the soil stabilization effect of mixing with shredded paper was investigated. Fig.7 shows a relationship between unconfined compression stress and axial strain of cement stabilized pond sediment with/without shredded paper. Open circles show the cement stabilized pond sediment without mixing with shredded paper and solid circles show the cement stabilized soil mixed with shredded paper at 5 %. Unconfined compression strength of cement stabilized pond sediment with shredded paper becomes bigger than that without shredded paper as shown in Fig.7. It was confirmed from Fig.4 that the relationship between unconfined stress and axial strain was improved by mixing of shredded paper. It was similar behavior to that of fiber reinforced soil (e.g. Kohata and Kato 2006, Makiuchi et al. 2007 and Minegishi and Makiuchi 2006).

Fig.8 shows variations of unconfined compression strength of cement stabilized soil with shredded paper under different additive rates of cement. Three solid straight lines show average values of three unconfined compression strength at different additive rates. Solid circles mean additive rate of cement 1 %, solid triangles 3% and solid square symbols 5 %. Unconfined compression strength increases as the mixing rate of shredded paper increases regardless of the additive rate of cement. The increment ratio of unconfined compression strength at the additive rate of cement 5% is bigger than that of 3 %. It means that the effect of mixing with shredded paper is clear in the higher additive rate of cement (Nabeshima and Tomohisa, 2008). It was different from that of fiber reinforced soil because internal friction angle was not improved by mixing with fiber (Makiuchi et al. 2007, Minegishi and Makiuchi 2006).

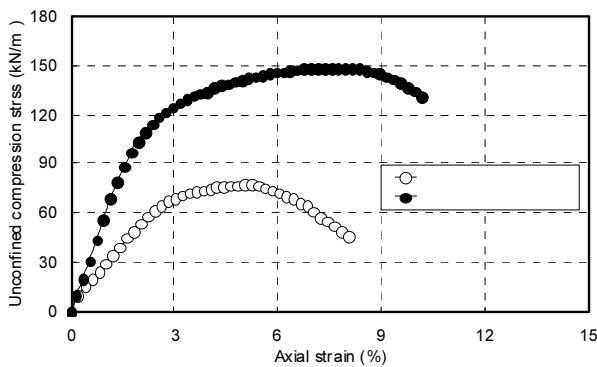


Fig. 7 Relationship between unconfined compression stress and axial strain of cement stabilized soil with/without shredded paper

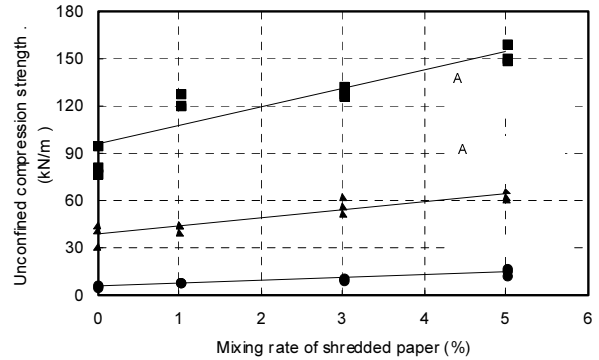


Fig. 8 Unconfined compression strength of cement stabilized soil with shredded paper under different additive rates of cement

Difference between deformation behaviors of materials is very important in case of the hybrid embankment as shown in Fig. 3. Cement stabilized soil usually has very brittle deformation behavior, which is quite different deformation behavior of natural soil. For the application of pond sediment as an embankment material, it is necessary to improve deformation behavior of cement stabilized soil to that of natural soil (Nabeshima and Tomohisa 2008).

Fig.9 shows variations of failure strain with different mixing rate of shredded paper. Failure strain of cement stabilized pond sediment was shown in the same figure. Kinked solid and broken lines show average values of three failure strains of cement stabilized pond sediment at every mixing rate of shredded paper. Increment rate of failure strain was small in this. Thus, the increase in failure strain of cement stabilized soils was due to the mixing of shredded paper.

Fig. 10 shows the failure surface of cement stabilized pond sediment mixed with shredded paper. It was confirmed from Fig. 10 that the shredded paper pieces were uniformly mixed and they were workable as short fiber reinforcements. Any breakage of shredded paper pieces can not be observed in this case.

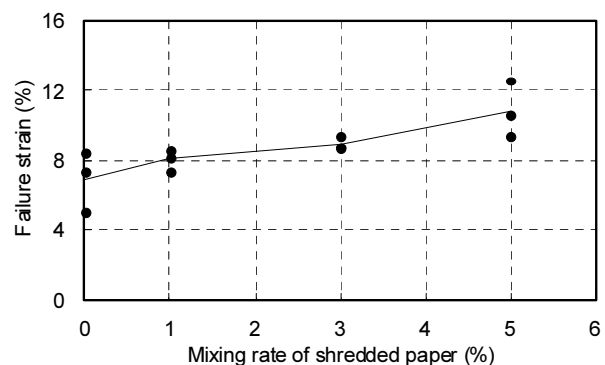


Fig. 9 Failure strain and mixing rate of shredded paper of cement stabilized soil with shredded paper



Fig. 10 Failure surface of cement stabilized pond sediment mixed with shredded paper

As the result, by mixing with shredded paper, the unconfined compression strength of cement stabilized pond sediment increased and its shear behaviors were improved to be tenacious. This means that pond sediment is effectively applicable as a pond embankment material.

ACKNOWLEDGEMENTS

This research was financially supported by a project grant in Akashi National College of Technology. Authors express our profound apology.

CONCLUSIONS

In this paper, a series of unconfined compression tests of cement stabilized pond sediment mixed with shredded paper was performed to investigate its shear behavior. Main conclusions in this study can be summarized as follows:

1. The absorption effect was a major soil improvement

mechanism by mixing with shredded paper.

2. Unconfined compression strength of stabilized pond sediment increased as the mixing rate of shredded paper increased regardless of the additive rate of cement.
3. By mixing with shredded paper, unconfined compression strength of cement stabilized pond sediment with additive rate of 5% was larger than 100 kN/m^2 regardless of mixing rate of shredded paper.
4. Increment ratio of unconfined compression strength by mixing with shredded paper was clear in the higher additive rate of cement.
5. Shear behaviors of cement stabilized pond sediment were improved to be tenacious by mixing with shredded paper.

REFERENCES

- Bon Terrain Committee (2005). Bon Terrain Method, Nikkei Construction 2005.5.13: 74-75.
- Kohata Y & Kato Y (2006). Study on toughness improvement of liquefied stabilized soil in triaxial compression test, Proc. 41st Japan Geotechnical Engineering Conference: 721-722.
- Makiuchi K, Minegishi K, Umemura K, Yoshino E (2007). Shear characteristics of short-fiber reinforced soil for method of slope engineering, Proc. 42nd Japan Geotechnical Engineering Conference: 567-768.
- Minegishi K & Makiuchi K (2006). Effect of reinforcement material on mechanical properties of ribbed short fiber reinforced soil, Proc. 41st Japan Geotechnical Engineering Conference: 681-682.
- Nabeshima Y & Tomohisa S (2008). Shear behavior of cement stabilized clay with shredded paper, Proc. International Symposium on Lowland Technology: 312-314.

LABORATORY STUDY ON ELECTROKINETIC DEWATERING OF SEWAGE SLUDGE

Yuan FENG¹, Tony L. T. ZHAN², Yun-Min CHEN³ and Quan-Fang ZHANG⁴

ABSTRACT: This paper presents a laboratory study on the use of electrokinetic technique to dewater the sludge collected from a wastewater treatment plant. Simulation tests were carried out on the specimens accommodated in a purposely-designed cylindrical cell. Voltage gradient ranging from 2 to 8 V/cm was applied to drive the movement of water within sludge towards the cathode. Results showed that a linear relationship exists between electroosmotic flow and current. Both the electroosmotic flow and current decreased gradually during the dewatering process as a result of an increase in the electrical resistance of the specimens. The residual water content of sludge showed a non-uniform distribution along the direction from anode towards cathode. A lowest water content of 62% was obtained at the anode, and the dewatering extent is proportional to the electric intensity.

KEYWORDS: sludge, electrokinetic dewatering, electroosmotic flow, current, residual water content

INTRODUCTION

Sewage sludge is a typical class of waste products derived from wastewater treatment processes. Reducing sludge volume is of necessity to decrease its detrimental impact and disposal cost. Basically sludge is dispersions of organic residue and solid particles in water. Originally produced sludge has only 1%-5% solids on a mass basis that water contributes majority of its volume, therefore dewatering turns into the critical step to achieve volume reduction.

Mechanical means such as centrifugation and belt pressing have been widely used for sludge dewatering by which free water inside the sludge could be removed effectively. However they are inefficient on removing interstitial water through narrow pore channels in sludge. In China the water content (the ratio of water to total weight of sludge) of sludge generated after mechanical treating is generally around 80% that there is still considerable quantity of water left and a method for further dewatering is necessary.

Electrokinetic dewatering is an emerging technology which applies DC voltage across the sludge by a pair of electrodes, then utilizes the electrical current caused phenomena of electroosmosis which is the movement of aqueous phase towards the negative (cathode) electrode to remove water. Electrokinetic dewatering has the

advantage to remove interstitial water compared with mechanical methods because electroosmosis occurs at inter-particle pore channels of the treated sludge. Its feasibility has been proven through laboratory scale test and field trial in the past (Glendinning et al. 2007).

The interpretation of electroosmosis had been proposed in Helmholtz-Smoluchowski theory, basing on which the electroosmotic volumetric flow rate under an imposed voltage gradient could be described by the equation (Acar et al. 1993):

$$q_e = k_e i_e A \quad (1)$$

where k_e , i_e and A are the electroosmotic permeability coefficient, voltage gradient and cross-sectional area respectively, while k_e is dependent on the permittivity of the fluid (ϵ), the zeta potential of the particle (ζ), the viscosity of the fluid (η), the porosity (n) and tortuosity (τ) of the sample as described by the following equation:

$$k_e = \frac{-\epsilon \zeta n}{\eta \tau^2} \quad (2)$$

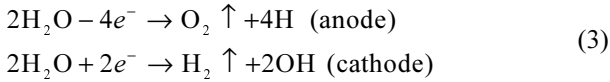
The electrolysis reactions will occur at the electrodes during the electrokinetic dewatering continuously as following:

¹ Ph.D Student, MOE Key Laboratory of Soft Soils and Geoenvironmental Engineering, Zhejiang Univ., China. Email: fy_zju@yahoo.com.cn

² Professor, ditto. Email: zhanlt@zju.edu.cn

³ Professor, ditto. Email: chenyunmin@zju.edu.cn

⁴ Engineer, ditto. Email: zqf@zju.edu.cn



The generated H^+ and OH^- as well as other ions inside the electrolyte would move towards the corresponding electrode under an electric field, what would develop PH and ionic concentration gradients across the sample. Zeta potential is highly dependent upon PH and ionic concentration (Vane and Zang 1997), what make zeta potential a changing variable, as well as the q_e according to Eqs. 1&2. The removing of water towards the cathode would decrease the water content of sludge, which also influences the q_e (Gray and Mitchell 1967). Theoretically, the electroosmotic flow is not constant in the dewatering process. Yang et al. (2005) reported a decrease of electric current and electroosmotic flow during the electrokinetic dewatering of sludge. Yuan and Wen (2003) obtained uneven residual water content across the sludge specimen after electrokinetic dewatering. Hence, electroosmotic flow behaves variably on time and space. In this study, sewage sludge sample was treated in electrokinetic method. The objective of this research was to investigate the electroosmotic flow and the dewatering effect in electrokinetic treating process.

MATERIAL AND EXPERIMENTAL METHOD

Sludge

The sludge used in this research was output after belt pressing from a local wastewater treatment plant. The fundamental characteristics of the sample were listed in Table 1.

Table 1 The physicochemical properties of the sludge

Characteristics	Values
Water content(%)	82.1
Organics(%)	12.7
Density(kg/L)	1.05
Sludge PH	6.89

Electrokinetic Experiments

A series of electrokinetic experiments were conducted in cylindrical cell made of organic glass shown in Fig. 1. A pair of 1mm thick stainless steel disks punched with 3mm diameter holes around were used as the electrodes. Two pieces of 2mm thick geotextiles were attached on the inner sides of the electrodes to separate the sludge from the filtrate. Both the anode and cathode were

connected with air. The tested sludge was placed into the cell under density control. Direct voltage was applied to the sludge. All experimental conditions are listed in Table 2. The effluent electroosmotic flow was collected and measured every minute through a tube connected with the cathode reservoir to calculate the flow rate, simultaneously electric current was monitored. After the experiments, residual water content profiles along the specimen were measured.

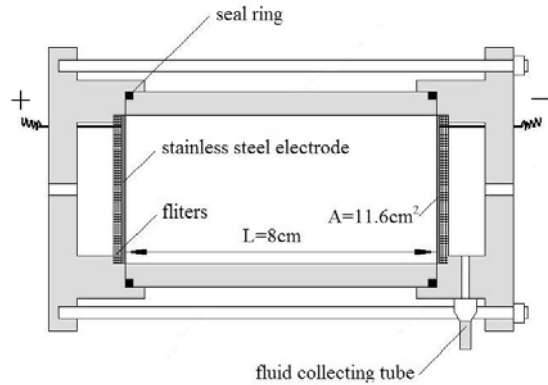


Fig. 1 Electrokinetic experiments apparatus

Table 2 The experimental conditions

Test no.	Potential gradient (V/cm)	Processing time (min)
1	2	160
2	4	140
3	6	100
4	8	100
5	2	40
6	4	40

RESULTS AND DISCUSSION

Electroosmotic Flow Rate

Four levels of voltage had been applied to observe the electrokinetic dewatering process and compare the electroosmotic flow rate under different driving force. The lasting time for test 1-4 varied from 100 to 160 minutes as the experiments had been stopped when the flow rate got close to 0.05ml/min, which was too small to monitored. The variation of current and flow rate throughout test 1-4 are depicted in Fig. 2 & 3.

A distinct current decreasing and coinstantaneous drop of flow rate were shown in all the tests. Both the current and flow rate got a same trend to decrease rapidly at the beginning of the process then reached a relatively constant value gradually. Their reduction behaved increasingly more sharply higher the loaded

voltage was. A gently change of current and flow rate was captured in 16V test while the values for 64V test even dropped below the 16V's after 80 minutes treating.

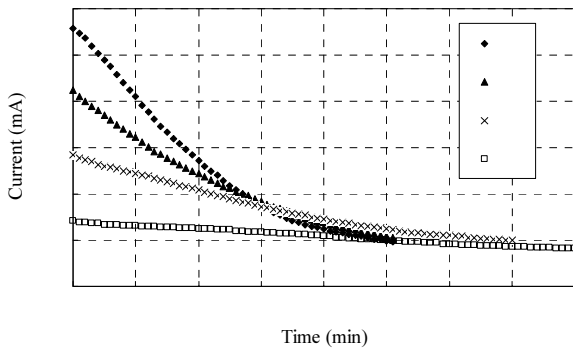


Fig. 2 Variation in current with time for tests 1-4

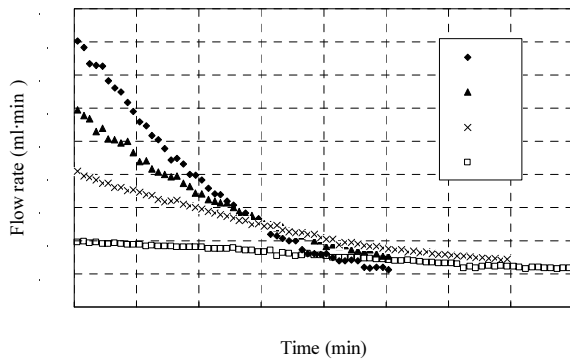


Fig. 3 Variation in flow rate with time for tests 1-4

A linear relationship existed between the flow rate and current as shown in Fig.4, in which all the data in test 1-4 were included. The linearity validates that the current affected the flow rate directly. As the water moved out of the sludge through electroosmosis, electric resistance of the sample would increase causing a current decrease as well as a reduction of flow rate for their linear relationship. Higher voltage would produce faster flow rate what accelerated the resistance increasing, making the current drop more sharply.

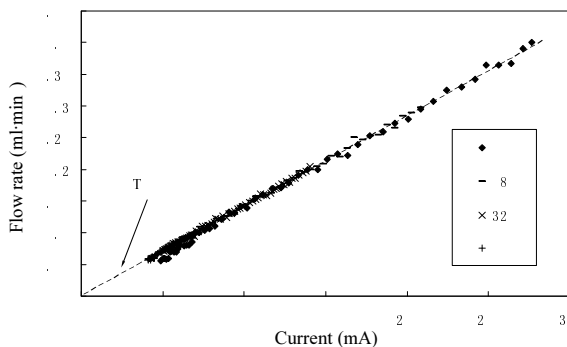


Fig. 4 The relationship between flow rate and the current

Water Removal Effect

Sludge near anode and cathode after electrokinetic treatment were displayed in Fig.5. It's obvious that the sludge was dewatered especially around the anode area, where the sample was rather dry with a mass of crevices. The residual water content profiles along the sludge for test 1-6 are shown in Fig.6.



Fig. 5 The relationship between flow rate and the current

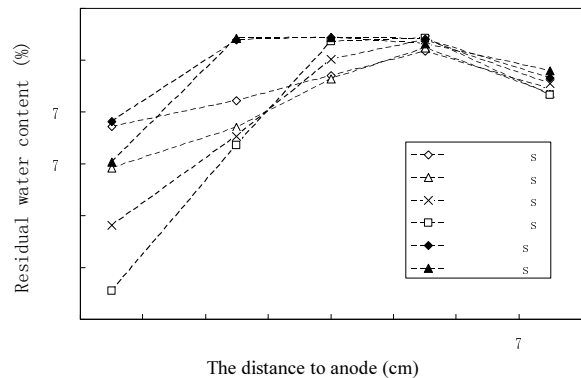


Fig. 6 The residual water content profiles in sludge for tests 1-6

The water removal effect was gradually weakened from anode to cathode. There were apparent reduction of water content at both the anode and cathode. The latter was partly attributed to the water electrolysis reaction at the cathode. Besides, according to Eq.3, the PH value would increase during the process at the cathode what would enhance the zeta potential (Acar and Alshwabkeh 1993) as well as the q_e , this partial reaction might promote the removing of water near the cathode. While at the anode, the residual water content decreased along with the enhancement of the voltage applied, a proportional relationship could be detected between the residual water content near the anode and the electric power as shown in Fig.7, indicating that the dewatering extent lies on the electric intensity.

Comparing the data from test 1&4, the water content at the anode was reduced to 75% after 40 minutes treating, the result hadn't been further reinforced in a 160

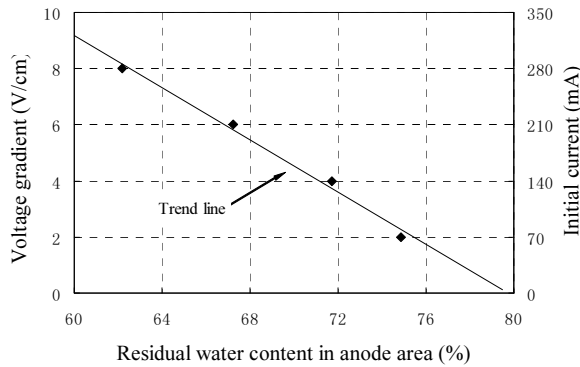


Fig. 7 The relationship between electric power and the residual water content at anode

minutes test. At the second spot beside the anode, the water hadn't been removed at all during the first 40 minutes, and then the water content fell to 77% after 160 minutes treating. The similar rules could be found from test 2 & 6, it represents that the longer treating time wouldn't supply extra dewatering effect at the anode while sludge was dewatered from anode to cathode gradually along with the increasing treating time.

For the reason that electricity dominates the electroosmotic flow rate and the dewatering extent, once the sludge at anode had been dewatered to a certain degree, the decreasing current wouldn't further react on this part effectively. It could be interpreted as the invalidation of the extended treating time. In addition, the dewatering extent for the sludge away from the anode was decreased owing to the current decline, causing inhomogeneous water removal effect from anode to cathode. Therefore the current is the key factor whose change influences the dewatering process dramatically.

CONCLUSIONS

The following conclusions were drawn based on the results of the electrokinetic dewatering experiments:

1. Both the electric current and electroosmotic flow rate decreased as the time increased. The decreasing rate would become more significant as the applied voltage increased.
2. The electroosmotic flow rate was correlated to the

current in a linear relationship.

3. There was a proportional relationship between the dewatering extent (residual water content) and electric intensity.
4. The sludge was dewatered from anode to cathode gradually. The dewatering effect would be weakened spatially as the decline of the current.

ACKNOWLEDGEMENTS

This work was supported by the funding from National Natural Science Foundation (research grant: 50538080), and financial support from Bureau of Science and Technology of Suzhou (research grant: SS0733).

REFERENCES

- Acar YB & Alshawabkeh AN (1993). Principles of electrokinetic remediation. *Environ. Sci. Technol.* 27: 2638-2647.
- Acar YB, Alshawabkeh AN, Gale RJ (1993). Fundamentals of extracting species from soils by electrokinetics. *Waste Management*, 13: 141-151.
- Gray DH & Mitchell JK (1967). Fundamentals aspects of electro-osmosis in soils. *Journal of Soil Mechanics and Foundation Division, ASCE* 93 (SM6): 209-236.
- Stephanie Glendinning, John Lamont-Black, Colin JFP Jones (2007). Treatment of sewage sludge using electrokinetic geosynthetics. *J.Hazard. Mater.* A139 491-499.
- Leland M Vane & Gwen M Zang (1997). Effect of aqueous phase properties on clay particle zeta potential and electro-osmotic permeability: Implications for electro-kinetic soil remediation processes. *J.Hazard. Mater.*, 55: 1-22.
- Yuan C & Weng C (2003). Sludge dewatering by electrokinetic technique: effect of processing time and potential gradient. *Adv. Environ. Res.* 7 (2003): 727-732.
- Lin Yang, George Nakhla, Amarjeet Bassi (2005). Electro-kinetic dewatering of oily sludges. *J.Hazard. Mater.*, B125: 130-140.

HYDRAULIC CONDUCTIVITY EVALUATION OF VERTICAL CUTOFF WALLS BEARING FILTER CAKE FROM SLUG TEST ANALYSIS

The-Bao NGUYEN¹, Chulho LEE², Yonghoon AHN³ and Hangseok CHOI⁴

ABSTRACT: The hydraulic conductivity of a vertical cutoff wall can be estimated through a slug test analysis. A filter cake is a thin and impervious layer formed on the interface between the vertical cutoff wall and the natural soil formation. The conventional line-fitting methods for a slug test analysis have never considered the presence of the filter cake. Therefore, results of a slug test analysis using the line-fitting methods for the vertical cutoff wall is believed to be inaccurate due to the effect of the filter cake. In this study, the hydraulic conductivity of the filter cake was evaluated using a modified fluid loss test. The result of the test indicated that a very low hydraulic conductivity is an important characteristic of the filter cake. The slug test analysis with the consideration of the filter cake in the line-fitting method was then employed to estimate the hydraulic conductivity of the cutoff wall in a case study. Result of the case study proves the significance of the filter cake in the estimation of the hydraulic conductivity of a vertical cutoff wall through a slug test.

KEYWORDS: slug test, cutoff wall, filter cake, hydraulic conductivity, line-fitting method

INTRODUCTION

The slug test has been used to evaluate hydraulic conductivity of aquifers and aquitards (Hyder et al. 1994, Butler 1998). In a slug test analysis, line-fitting method is widely used due to its simplicity and effectiveness. There are two conventional line-fitting methods for analyzing the result of a slug test: (1) The Hvorslev method (Hvorslev 1951); (2) the Bouwer and Rice method (Bouwer and Rice 1976).

The hydraulic conductivity of vertical cutoff walls can also be estimated by the slug test using a single well set up in the wall (Britton et al. 2002, Choi and Daniel 2006a,b). However, the conventional line-fitting methods cannot be directly used for analyzing a slug test result in a vertical cutoff wall because they do not account for the boundaries of the wall, which can be located close to the well intake section, or they do not consider the compressibility of the backfill material. Recently, Choi and Daniel (2006a,b) proposed the modified line-fitting method to analyze the results of slug test in vertical cutoff walls. In this work, the Chirlin's (1989) suggestion was adopted to introduce a modified effective radius, R_e' , for compressible aquifer.

The engineering charts of reduction factor, f , of cutoff walls were developed using the numerical program *Slug_3D*. This program can simulate the slug test in the vertical cutoff wall with consideration of compressible materials, of boundaries between the vertical cutoff wall and the surrounding formation, and of variable hydraulic properties with a change of effective stress (Choi 2007).

In a vertical cutoff wall construction, bentonite-water slurries have been used to effectively prevent the collapse of the trench excavations, which are constructed for vertical cutoff walls. The stability of trench excavations is maintained by the lateral pressure exerted by the slurry. Further, a thin and impervious bentonite layer called filter cake can be formed on the interface between the vertical cutoff wall and the natural soil formation. Formation of bentonite filter cake during the construction of vertical cutoff walls has been observed and reported by Filz et al. (1997) and Henry et al. (1998).

However, the filter cake has not been considered in slug test analyses for vertical cutoff walls. Because the filter cake has a very low hydraulic conductivity and exists between the cutoff wall and the natural soil formation, it directly influences the boundary conditions of the wall. Therefore, the role of filter cake in slug test

¹ Ph.D Student, School of Civil, Architectural, and Environmental Engineering, Korea University, R.O. Korea.
Email: nguyenthebao@korea.ac.kr

² Ph.D Student, ditto. Email: cryfreer@korea.ac.kr

³ Graduate Student, ditto. Email: dream726@korea.ac.kr

⁴ Associate Professor, ditto. Email: hchoi2@korea.ac.kr (corresponding author)

analyses to evaluate hydraulic conductivity of a cutoff wall needs to be considered carefully.

In this study, the authors first measured the hydraulic conductivity of the filter cake in laboratory and then examined the effect of filter cake on the slug test result in vertical cutoff walls with the aid of the program Slug_3D. Based on the study on the effect of filter cake, the boundary conditions of the model of cutoff wall were modified to the no-flux condition to consider the filter cake in the analysis. The line-fitting method proposed by Choi and Daniel (2006a,b) were also modified and utilized to reanalyze the case study that had been performed by Choi and Daniel (2006a). Discussion on the comparison between previous and current results highlights the importance of considering filter cake in practice.

FORMATION AND HYDRAULIC CONDUCTIVITY OF FILTER CAKE

A trench is excavated to be ready for the backfilling process of a vertical cutoff wall construction. Bentonite-water slurry is then used to maintain trench stability. Because of a higher fluid pressure inside the trench, the slurry tends to permeate the walls of the trench. Consequently, a filter cake can be formed on the excavation surface and may remain intact even after the construction is finished. More detailed information on filter cake formation is referred to Filz et al. (1997).

The hydraulic conductivity of filter cake may have an important effect on the behavior of cutoff wall in controlling lateral spreading of ground water. With a range of hydraulic conductivity from 3×10^{-11} m/s to 2×10^{-10} m/s (Henry et al. 1998), the filter cake is supposed to be a relatively impermeable membrane unexpectedly altering the characteristic of the boundary of a cutoff wall. A representative thickness of 0.5 cm was reported and used for interpretation of the in situ hydraulic conductivity test results by Britton (2001).

A fluid loss test is to evaluate fluid loss properties of a clay layer deposited on a filter paper at a certain applied pressure. Then, the hydraulic conductivity of the bentonite filter cake can be obtained from the measurement of fluid loss (ASTM D 5891 - 2002). Chung and Daniel (2008) modified the fluid loss test to estimate the hydraulic conductivity of filter cake effectively. The modified fluid loss test can reproduce the practical condition of filter cake formation in the construction of vertical cutoff wall. The slurry used in the test is the same type as being used in the construction. The applied pressures in the test correspond to those that are possibly exerted during filter cake formation in a vertical cutoff wall.

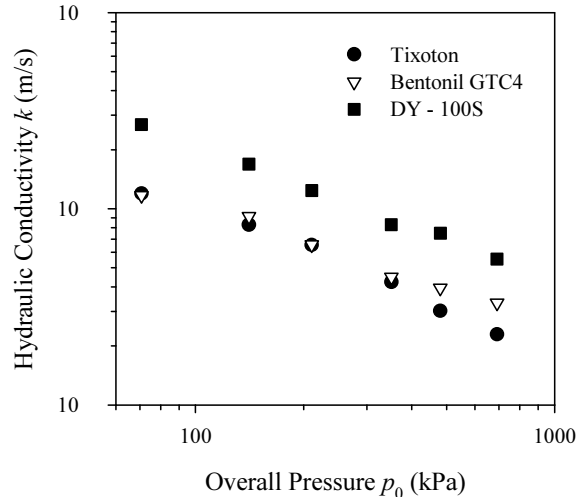


Fig. 1 Hydraulic conductivity – overall pressure relation of Tixoton, Bentonil GTC4, and DY – 100S

In the modified fluid loss test, 5 or 6 filtrate volumes are measured within a certain period of time (typically one hour). The pressure inside the cell must be maintained constant. The bentonite filter cake is carefully detached from the filter paper to measure water content after removing slurry suspension at the top of the cake. The average void ratio of the filter cake is calculated from the measured water content and the specific gravity of solids with the assumption of complete saturation. The filtrate-time relation and the void ratio of filter cake are used to calculate the hydraulic conductivity of filter cake. Three types of bentonite including Tixoton, Bentonil GTC4, and DY – 100S produced by Sud-Chemie Korea Co. and DY Bentonite Industry Co., were used in this experiment.

Results of the experiment are presented in Fig. 1. The range of hydraulic conductivities of the three bentonite filter cakes is from 2×10^{-11} m/s to 2.6×10^{-10} m/s (Nguyen et al. 2008). This range is very similar to the ranges reported by Henry et al. (1998) and Chung and Daniel (2008). With the measured hydraulic conductivities of the filter cakes and of the backfill material, the equivalent hydraulic conductivity of the cutoff wall construction can be calculated for cutoff wall performance evaluation.

INFLUENCE OF FILTER CAKE IN SLUG TEST

The very low hydraulic conductivity and location of the filter cake significantly influence the performance of the cutoff wall. It could enhance the cutoff wall performance to control lateral spreading of ground water with less permeable filter cake layers. The filter cake is believed to alter the boundary condition of the cutoff wall unexpectedly. It is valuable to compare the result of a slug test with consideration of the filter cake to the

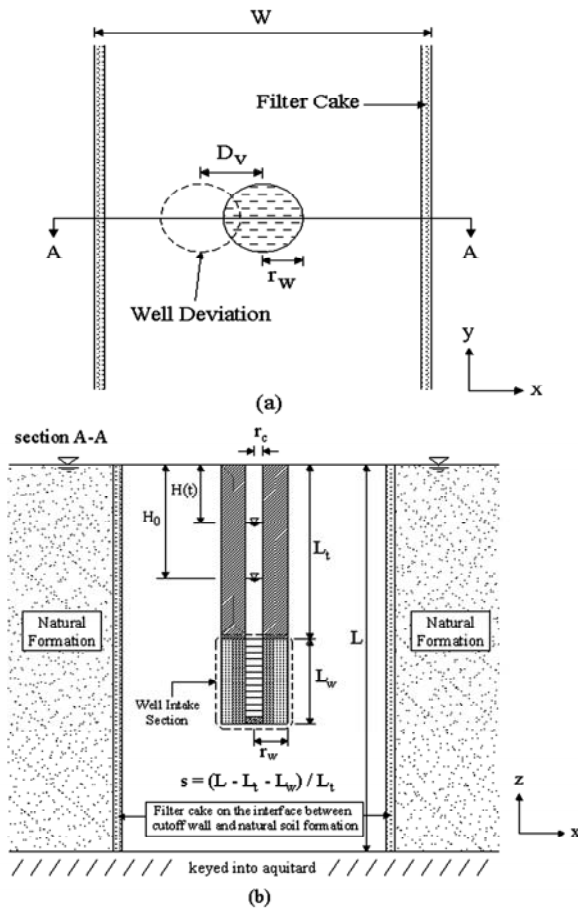


Fig. 2 Slug test configuration in vertical cutoff wall: (a) Plan view and (b) vertical cross section A-A and the locations of filter cakes

results of the slug tests with various boundary conditions of cutoff walls.

Fig. 2 shows a geometrical configuration of a rising-head slug test in the vertical cutoff wall with the presence of filter cake layers. In the plan view, the width of the cutoff wall is denoted as W . The symbols of r_w and r_c represent the outside radius of the filter pack and the inside radius of the well casing, respectively. To consider the deviation of the well from the center of the cutoff wall, the distance between the center of the cutoff wall and the center of the eccentric well is denoted as D_v . The well deviation is expressed non-dimensionally as $2D_v/(W-2r_w)$ in operating the program *Slug_3D*. In practice, the length of a vertical cutoff wall in the y -direction is much larger than the width in the x -direction. Therefore, *Slug_3D* considers only half of a full three-dimensional model of the slug test configuration in the vertical cutoff wall considering a symmetric condition of the model in the y -direction (Choi and Daniel 2006a). In the vertical cross section A-A, it is assumed that the cutoff wall is to be keyed into an aquitard. The depth of the cutoff wall is denoted as L , while L_t and L_w indicate the distance from the water table to the top of the well

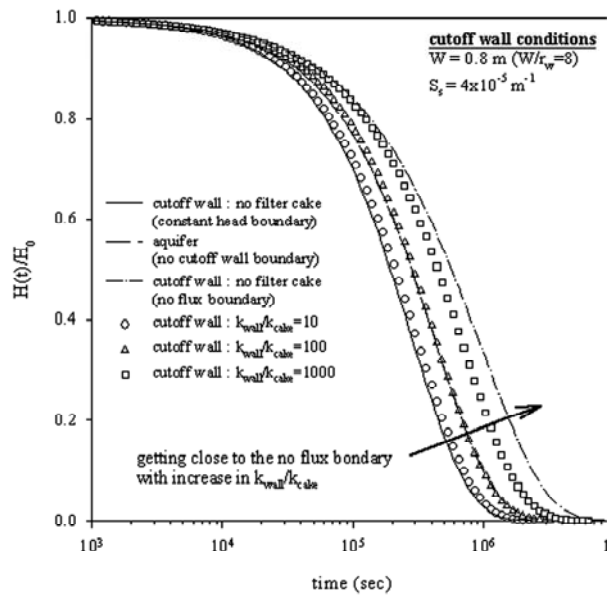


Fig. 3 Filter cake effect on various interface boundary conditions in cutoff walls

intake section and the length of the filter pack, respectively. To indicate the vertical position of the well intake section relative to the depth of the cutoff wall, the value of s is introduced as the formula in Fig. 2 and ranges from zero to infinity. The well intake section is at the mid-depth of the wall when s equals one. Fig. 2 also shows the location of the filter cakes in the configuration of the slug test in the vertical cutoff wall and the thickness of the filter cake is scaled up for higher resolution. The program *Slug_3D* simulates a rising-head slug test with an initial hydraulic head drop denoted as H_0 . The initial hydraulic head drop then reduces gradually with time. The hydraulic head drop at a certain time, denoted as $H(t)$, finally equals zero at the end of the test. To describe hydraulic head recovery data of a slug test, a normalized head drop of $H(t)/H_0$ is used in slug test analyses.

By using *Slug_3D*, Choi and Daniel (2006b) numerically investigated the filter cake effect on the slug test analysis with various interface boundary conditions of cutoff walls. The dimensionless compressibility parameter $\alpha_p (= S_s L_w r_w^2 / r_c^2)$ is 0.001 in these cases. Fig. 3 shows that the response data curves have a tendency getting close to the no-flux-boundary response data with an increase in the hydraulic conductivity ratio (k_{wall} / k_{cake}). The case of $k_{wall} / k_{cake} = 1000$ becomes close to the no flux boundary condition. Accordingly, if a relatively impermeable filter cake forms on the interface, the no-flux boundary condition should be a better alternative to represent a cutoff wall boundary condition in slug test analyses. The program *Slug_3D* was modified to employ the no-flux boundary condition on the interface between the vertical cutoff wall and the natural soil formation.

MODIFIED LINE-FITTING METHOD IN SLUG TEST ANALYSIS WITH CONSIDERATION OF FILTER CAKE

Useful background information about the conventional line-fitting methods for aquifer cases is provided by Hvorslev (1951) and Bouwer and Rice (1976). The modified line-fitting method originally developed by Choi and Daniel (2006a) has the advantage of considering the compressibility of the aquifer. In this method, hydraulic conductivity of an aquifer can be determined using the following formula:

$$k = -\frac{r_c^2 \ln\left(\frac{R_e'}{r_w}\right)}{2L_w} \cdot \frac{1}{t} \ln\left(\frac{H(t)}{H_0}\right) \quad (1)$$

This formula requires the geometry of a well system and the slope of slug test data plotted on the $\ln(H(t)/H_0)$ versus t graph. The effective radius R_e' is the modified equivalent radial distance over which the head change is dissipated. The effective radius R_e' is dependent on the compressibility of the aquifer and on the geometry of the well systems. Choi and Daniel (2006a) and Choi et al. (2008) extended Chirlin's (1989) approach to calculate R_e' in terms of $\ln(R_e'/r_w)$. Fig. 4 provides a set of $\ln(R_e'/r_w)$ for aquifer cases considering the compressibility of the aquifer.

The modified line-fitting method can be used for estimating the hydraulic conductivity of a cutoff wall in a slug test analysis. For the case of no filter cake on the interface between the cutoff wall and the natural soil formation, Choi and Daniel (2006a) developed a procedure to estimate the hydraulic conductivity of cutoff walls through a slug test analysis by introducing a reduction factor, f . The reduction factor is equal to the ratio of $\ln(R_e'/r_w)_{\text{cutoff wall}}$ to $\ln(R_e'/r_w)_{\text{aquifer}}$. The value of $\ln(R_e'/r_w)$ is defined as $2\beta_{p,0.37}$ ($\beta_p = kL_w t/r_c^2$), where the dimensionless time parameter $\beta_{p,0.37}$ is in correspondence with $H(t)/H_0 = 0.37$ according to Hvorslev's basic time lag formula (Hvorslev 1951).

In this study, a modification was made for applying the modified line-fitting method to consider the presence of a filter cake. The modification factor, f^* , is introduced to consider the no-flux boundary condition. In this case, the no-flux boundary reduces the rate of head recovery as discussed previously, and thus the time for head recovery is longer compared to that of the infinite-boundary aquifer. This leads to a larger $\beta_{p,0.37}$ in the cutoff wall case compared to that in the aquifer case. Hence, for the sake of illustration, the modification factor, f^* , is defined as the ratio of $\ln(R_e'/r_w)_{\text{aquifer}}$ to $\ln(R_e'/r_w)_{\text{cutoff wall}}$, which is always less than or equal to

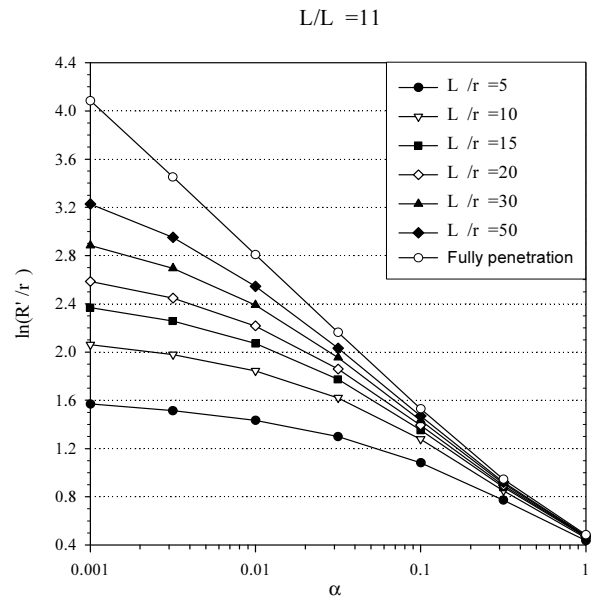


Fig. 4 Values of $\ln(R_e'/r_w)$ for aquifer case

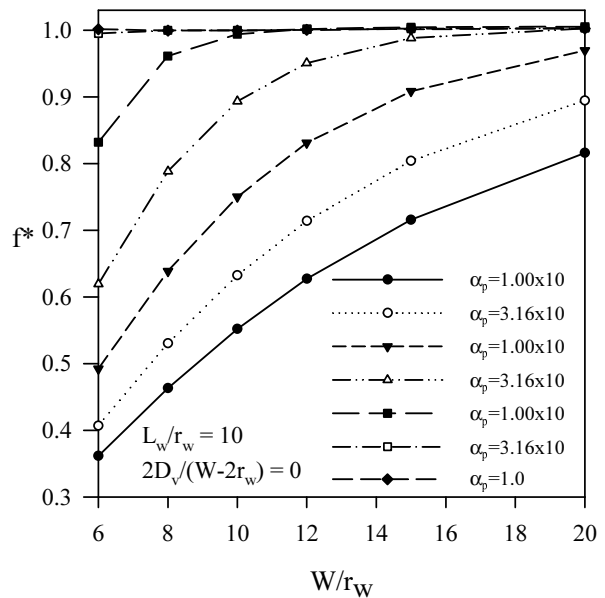


Fig. 5 Typical modification factors f^* for the case of the existence of filter cake ($L/L_w = 11$ and $s = 1$)

unity. Because of a slower hydraulic head recovery caused by the no-flux boundary condition in the vertical cutoff wall, the value of $\ln(R_e'/r_w)$ needs to be modified by f^* in calculating the hydraulic conductivity of the cutoff wall as expressed in Eq. (2).

$$k = \frac{r_c^2 \left[\ln\left(\frac{R_e'}{r_w}\right) / f^* \right]}{2L_w} \cdot \frac{1}{t_{0.37}} \quad (2)$$

Some modification factors are plotted in Fig. 5 for the case of $2D_v/(W-2r_w) = 0$ and $L_w/r_w = 10$. Other modification factors for any geometric combinations of

cutoff walls were made using the program Slug_3D (Nguyen 2007). Similarly, the procedure for using the modified line-fitting method for vertical cutoff walls (Choi and Daniel 2006a) can be utilized to determine the hydraulic conductivity except that Eq. (2) is used in place of the previously proposed equation.

CASE STUDY

A case study from EMCON (1995) had been performed by Choi and Daniel (2006a) without the consideration of a filter cake. The report from EMCON (1995) did not mention the presence of a filter cake. In this study, the modified line-fitting method for estimating hydraulic conductivity of a cutoff wall with the consideration of the filter cake was applied to reanalyze the previous case study. The case study uses the slug test data from the cutoff walls constructed in the early 1990s at the West Contra Costa Sanitary Landfill in Richmond, California. Geometrical approximations made by Choi and Daniel (2006a) are used for the slug test simulations in reanalyzing the case study.

An example of the slug test data and analysis procedure is presented in Fig. 6 for Case 93-1 in the M-11/15 cutoff wall. The analysis results are summarized in Table 1. The basic time lag was first determined as $t_{0.37} = 1.2 \times 10^4$ sec for Case 93-1 in the M-11/15 cutoff wall. The value of $\ln(R_e'/r_w)$ was determined from Fig. 4 along with the obtained value of αp . The value of the modification factor was then selected from Fig. 5. Finally, the hydraulic conductivity was calculated using formulation c in Table 1. Note that formulation d was used for the case where no consideration was taken of the filter cake (Choi and Daniel 2006a). Table 1 also presents EMCON's original results, in which the Bouwer and Rice method had been adopted without considering the compressibility and wall geometric effects. The previous results obtained by Choi and Daniel (2006a) without the consideration of the filter cake were also reported in Table 1 for comparison.

The estimates of hydraulic conductivities in the modified line-fitting method with the consideration of a filter cake are about 65 to 165% higher than the previous results presented by Choi and Daniel (2006a), which do not consider a filter cake (see Table 1). This discrepancy shows the necessity to consider the filter cake in a slug test analysis.

The Bouwer and Rice method, which is a conventional line-fitting method used to estimate the hydraulic conductivity of aquifers, was used in EMCON (1995). The hydraulic conductivities estimated by EMCON (1995) are 25 to 125% lower than those

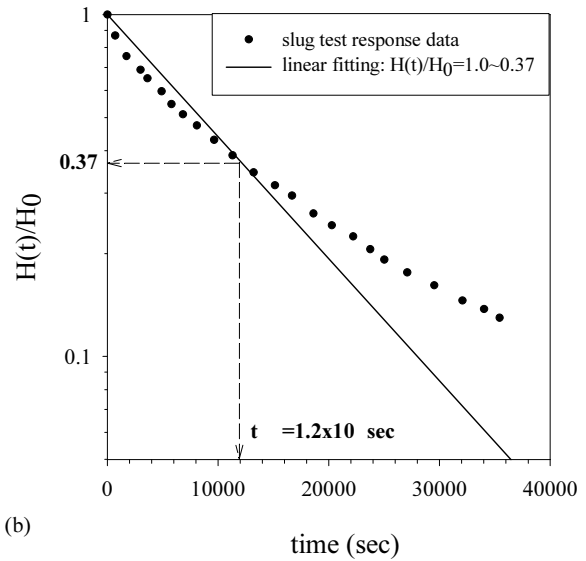


Fig. 6 Case 93-1 in the M-11/15 vertical cutoff wall with the consideration of the effect of filter cake

estimated using the modified line-fitting method. This difference can be explained by the fact that the Bouwer and Rice method is unable to consider the compressibility of a backfill material as well as the role of cutoff wall boundaries.

CONCLUSION

The findings obtained from this study are summarized as follows:

1. The range of hydraulic conductivities of the three bentonite filter cakes is from 2×10^{-11} m/s to 2.6×10^{-10} m/s. This range is very similar to the ranges reported by Henry et al. (1998) and Chung and Daniel (2008). With the measured hydraulic conductivities of the filter cakes and of the backfill material, the equivalent hydraulic conductivity of the cutoff wall construction can be calculated for cutoff wall performance evaluation.

2. The modified line-fitting method for evaluating the hydraulic conductivity of a vertical cutoff wall originally proposed by Choi and Daniel (2006a) has been improved along with the numerical program Slug_3D (Choi 2007) in order to consider the presence of a filter cake in the vertical cutoff wall. The proposed method seems to be relevant for exclusively estimating the hydraulic conductivity of backfill materials that can be used for evaluating the overall hydraulic performance of a vertical cutoff wall system.

3. The results from the case study prove the significance of a filter cake in estimating hydraulic conductivity through a slug test. The hydraulic conductivity of the cutoff wall will be significantly underestimated in a slug test analysis if the filter cake is not properly considered.

Table 1 Case study results of vertical cutoff walls

Case	Modified line-fitting method				EMCON's original results	
Analysis with consideration of filter cake						
Case	$t_{0.37}$ (s)	$\ln(R_e'/r_w)$	f^*	k^c (m/s)	S_s (lab. test) (m^{-1})	k (Bouwer & Rice) (m/s)
93-1 (M-11/15)	1.2×10^4	1.89	0.63	6.8×10^{-8}	2.5×10^{-2}	3.0×10^{-8}
94-15 (M-17/21)	3.0×10^4	2.13	0.82	4.9×10^{-8}	2.5×10^{-2}	4.0×10^{-8}
Analysis without consideration of filter cake (Choi and Daniel 2006a)						
Case	$t_{0.37}$ (s)	$\ln(R_e'/r_w)$	f	k^d (m/s)		
93-1 (M-11/15)	1.2×10^4	1.15	0.98	2.6×10^{-8}		
94-15 (M-17/21)	3.0×10^4	1.71	0.92	3.1×10^{-8}		

$${}^a k = \frac{r \left[\ln\left(\frac{R'}{r}\right) / f^* \right]}{2L} \cdot \frac{1}{t}$$

$${}^b k = \frac{r \left[f \times \ln\left(\frac{R'}{r}\right) \right]}{2L} \cdot \frac{1}{t}$$

ACKNOWLEDGEMENTS

This research was financially supported in part by the Korea Research Foundation, Grant No. D00477, and by BK21 Global Leaders in Construction Engineering.

REFERENCES

- ASTM D5891 (2002). "Standard Test Method for Fluid Loss of Clay Component of Geosynthetic Clay Liners", American Society for Testing and Materials.
- Bouwer H and Rice RC (1976). A slug test for determining hydraulic conductivity of unconfined aquifer with completely or partially penetrating wells. *Water Resour. Res.*, 12(3): 423-428.
- Britton JP (2001). Soil-bentonite cutoff walls: hydraulic conductivity and contaminant transport. Ph.D. thesis, Virginia Polytechnic Institute & State Univ., Blacksburg, Va.
- Britton JP, Filz GM and Little JC (2002). Shape factors for single-well tests in soil-bentonite cutoff walls. *Proc., 4th Int. Congress on Environmental Geotechnics*: 639-644.
- Butler J J (1998). The design, performance, and analysis of slug tests, Lewis, Boca Raton, Fla.
- Chirlin GR (1989). A critique of the Hvorslev method for slug test analysis: The fully penetrating well. *Ground Water Monit. Rev.*, 9(2): 130-138.
- Choi H (2007). Numerical model for analyzing slug tests in vertical cutoff walls. *J. Geotech. Geoenviron. Engrg. ASCE*. 133(10): 1249-1258.
- Choi H and Daniel DE (2006a, b). Slug test analysis in vertical cutoff walls. I: Analysis Methods. and II: Applications. *J. Geotech. Geoenviron. Eng.*, 132(4): 429-447.
- Choi H, Nguyen TB, and Lee C (2008). Slug test analysis to evaluate permeability of compressible materials. *Ground Water*, 46(4): 647-652.
- EMCON. (1995). M-11/15, M-17/21, and M-26/E-29 slurry walls postconstruction performance evaluation, West Contra Costa Sanitary Landfill, Richmond, Ca.
- Filz GM, Boyer RD, and Davidson RR (1997). Bentonite-water slurry rheology and cutoff wall trench stability. *Proc., In Situ Remediation of the Geoenvironment*, GSP No. 71: 139-153.
- Henry L B, Filz, GM, and Davidson RR (1998). Formation and properties of bentonite filter cakes, GSP No. 78, ASCE: 69-88.
- Hvorslev MJ (1951). Time lag and soil permeability in ground-water observation. *Bulletin No. 36*, Waterways Experiment Station, United States Army Corps of Engineers, Vicksburg, Miss.
- Hyder Z, Butler JJ, McElwee CD, and Liu W (1994). Slug tests in partially penetrating wells. *Water Resour. Res.*, 30(11): 2945-2957.
- Nguyen TB (2007). Slug test analysis in vertical cutoff walls with consideration of filter cake. Master thesis, Korea University, Seoul, R. O. Korea.
- Nguyen TB, Lee, C, Yang J, and Choi, H (2008). Evaluation of hydraulic conductivity of bentonite filter cake using modified fluid loss test. *Proc., KGS Fall National Conference*, Kwangju, Republic of Korea.

FILTRATION PERFORMANCE OF TWO-LAYERED NONWOVEN GEOTEXTILES

Li-Fang LIU¹, Lian-Ying JI², Fa-Wen GUO³, Qian-Li WANG⁴ and Xiao-Jie YANG⁵

ABSTRACT: Nonwoven geotextiles have been widely used for separation, filtration, reinforcement and drainage systems. The filtration and drainage functions are especially attractive in the construction of soil structures. In this paper, five two-layered nonwoven geotextiles with different needling density have been developed to study their filtration performance. The experimental results show that needling density has obvious effects on the filtration performance of nonwoven geotextiles. Regarding the five samples in this study, the one with needling density of 470 p/cm² has the best filtration performance.

KEYWORDS: two-layered nonwoven geotextiles, needling density, pore size, permeability, filtration

INTRODUCTION

Nonwoven geotextiles have been widely used for separation, filtration, reinforcement and drainage systems (Faure et al. 1990; 1999; 2006; Fischer et al. 1990; Iryo & Rowe 2003). Especially two-layered geotextile that combine two individual layers made of fibers with different diameter has been developed quickly in recent years (Ji et al. 2009; Liu 2007). The two individual layers have different functions, the one consisted of finer fiber makes geotextile have good filtration property; the other consisted of coarser fiber makes geotextile have good mechanical strength. Therefore, the two-layered geotextile can have excellent filtration property as well as enough mechanical strength. In this paper, a two-layered nonwoven geotextile was studied to analyze the relation between its filtration property and needling density.

EXPERIMENT

Experimental Materials

Specimen

Five two-layered nonwoven geotextiles were designed at the same mass per unit area in this study, marked as geotextile 1~5, respectively. The five samples were fabricated with the same two layers: one was made of 3d polyester staple fibers and the other was 8d; however,

they were needle punched at different needling density, as shown in Table 1.

Table 1 Needling density of five samples

Sample	Needling density (p/cm ²)
geotextile 1	300
geotextile 2	350
geotextile 3	420
geotextile 4	470
geotextile 5	520

Test method

(1) The pores size

The method of dry sieving of sand was proposed in this study to evaluate the pores size of two-layered nonwoven geotextiles. Measurements were repeated at three times for each specimen.

(2) The permeability

The vertical permeability coefficient that obtained by permittivity tester was introduced here to express the permeability of two-layered nonwoven geotextiles. The permeability value was determined by averaging the experimental results of three specimens.

(3) The filtration

The filtration test was carried on an apparatus created by authors, as shown in Fig. 1. The experiment was made according to the following procedures (Liu & Chu 2006):

Cut off a round geotextile sample with diameter of

¹ Associate professor, The Key Lab of Textile Science & Technology, Ministry of Education, Donghua University, China. Email: lifangliu@dhu.edu.cn

² Ph.D Student, College of Textiles, Donghua University, Email: jilianyong@mail.dhu.edu.cn

³ Senior Engineer, Shandong Hydraulic Engineering Corporation, Email: lifangliu@dhu.edu.cn

⁴ Ph.D Student, College of Textiles, Donghua University, Email: wang_qianli@mail.dhu.edu.cn

⁵ Ph.D, School of Materials Science and Engineering, Tongji University, China. Email: yangxiaojie@mail.tongji.edu.cn

14.5mm, weigh and then put it into water till fully saturation, so as to drive off air from it.

Put the sample onto the center of the ground-platform, and then put a round rubber blanket with outer and inner diameter of 14.5cm and 14cm on it, so as to avoid water seeping from the sample edge. Put the top-cylinder just on the rubber blanket, i.e. the sample, rubber blanket and top-cylinder are homocentric. Screw on the six nuts and bolts that evenly distributing along the edge of top-cylinder and ground-platform respectively to clamp sample and rubber blanket to avoid water seep from the edge.

According to the soil density and the inner diameter of the apparatus, weigh about 191g dry soil. Put the soil into a beaker and pour some water to make slurry. Then pour the slurry onto the sample in the apparatus, and add some free-air water till the water have a height of 13cm, and remain the height during whole experiment as shown in Fig. 1 (keep adding water to ensure the height, for water will drop down through samples continually).

Stir the slurry constantly. Stop stirring and adding water after 3h; let water in the apparatus drop freely.

After the water on the sample fully dropping down, take out the sample and the remained soil on it, dry and weigh, then calculate the mass of soil particles passing through the sample.

The average value of filtration was calculated for the two specimens tested.

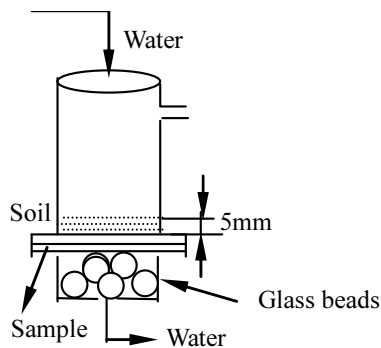


Fig. 1 Schematic diagram of filtration tester

RESULTS AND DISCUSSION

Table 2 summarizes the testing results of pore size, permeability and filtration, which are expressed by O_{90} that means 90% of the pores are smaller than that size, the vertical permeability coefficient K and mass of soil particles passing through per unit area of specimen G , respectively.

The Pores Size

As illustrated in Fig. 2, the pore size first decreases and then increases with the increasing of needling

density, which reaches the minimum value at the needling density of 470 p/cm². This mainly results from the geotextile structure changing with needling density. Firstly, with the increase of needling density, geotextile structure becomes more and more compactness, leading to increase in number of fibers in unit volume of geotextile, so pore size becomes smaller. However, when the needling density continually increases above 470 p/cm², the density of geotextile couldn't increase accordingly. Moreover, penetration holes can be made in geotextile because some fibers are cut off, which can lead to larger pores size.

Table 2 Experimental results of geotextiles

Sample	O_{90} (mm)	K (cm/s)	G (g/ m ²)
geotextile 1	0.132	0.64	506
geotextile 2	0.125	0.58	457
geotextile 3	0.112	0.55	387
geotextile 4	0.087	0.52	310
geotextile 5	0.097	0.57	456

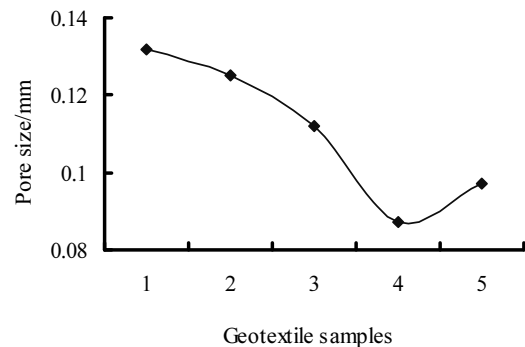


Fig. 2 Pore size O_{90} of five geotextiles

The Permeability Property

Fig. 3 illustrates the vertical permeability coefficient of five two-layered nonwoven geotextiles. As shown in Fig. 3, with the increase of needling density, the vertical permeability coefficient of geotextiles first decreases and then increases, demonstrating the same trend with pore size as shown in Fig. 2. The permeability of geotextile is regarded as to be in direct proportion with the fourth power of the pore size. Therefore, the vertical permeability coefficient shows the same type of trend with pore size. Especially when the needling density reaches 520 p/cm², some fibers are broken down and so penetration holes can be caused, leading to the appearance of some extreme large pores. Therefore, the vertical permeability coefficient increases significantly.

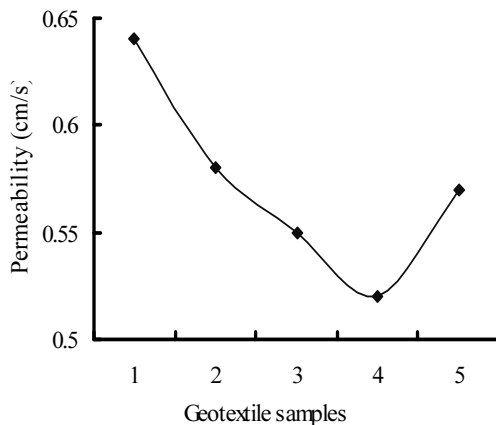


Fig. 3 Pore size O_{90} of five geotextiles

The Filtration Property

Comparison of the five samples in Fig. 4 shows that, with the increasing of needling density soil mass passing through unit area of geotextile firstly decreases and then increases, reaching the smallest value at 470 p/cm^2 . Because increasing needling density can result in a more tangle structure, thereby reducing the pore size of geotextile, so decreasing the soil mass passing through; while needling density reaching 470 p/cm^2 and increasing more, the barbs will cause fibers to break and make the entanglement of fiber more difficult, ultimately, causing larger penetration holes, so increasing the soil mass passing through.

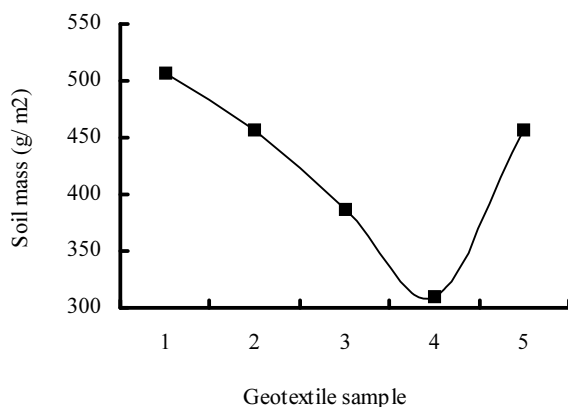


Fig. 4 Soil mass passing through per unit area of samples

CONCLUSIONS

The Permeability and filtration performance of two-

layered nonwoven geotextiles are discussed in this paper. The experimental results show that with the increase of needling density ranging from 300 to 470 p/cm^2 , the pore size, vertical permeability coefficient and soil mass passing through per unit area geotextile are gradually reduced. However, when the needling density reaches 520 p/cm^2 , the three parameters are all increased. Regarding the five samples discussed in this study, the one with needling density of 470 p/cm^2 has the best soil retention performance.

ACKNOWLEDGEMENT

The support of National Natural Science Foundation of China (Project 50809016) is gratefully acknowledged.

REFERENCES

- Faure YH, Gourc JP, Gendrin P (1990). Structural study of porometry and filtration opening size of geotextiles. In: Peggs, I.D. (Editors), *Geosynthetics: Microstructure and Performance*. American Society for Testing and Materials, U.S.A
- Faure YH, Farkouh B, Delmas P, Nancey A (1999). Analysis of geotextile filter behaviour after 21 years in valcros dam. *Geotext. Geomembran.* 17:353-370.
- Faure YH, Baudoin A, Pierson P, Plé O (2006). A contribution for predicting geotextile clogging during filtration of suspended solids. *Geotext. Geomembran.* 24(1): 11-20.
- Fischer GR, Christopher BR, Holtz RD (1990). Filter criteria based on pore size distribution. In: *Proceedings of the Fourth International Conference on Geotextiles Geomembranes and Related products*. The Hague, The Netherlands.
- Iryo T & Rowe RK (2003). On the hydraulic behavior of unsaturated nonwoven geotextiles. *Geotext. Geomembran.* 21: 381-404.
- Ji LY, Yu JY, Liu LF (2009). Filtration behavior of an original two-layered nonwoven geotextile. *International Conference on Fibrous Materials, China*.
- Liu LF & Chu CY (2006). Modeling the slurry filtration performance of nonwoven geotextiles. *Geotext. Geomembran.* 24: 325 - 330.
- Liu LF (2007). Theoretical model on mass of soil particles passing through two-layered nonwoven geotextile. *Indian J Fibre & Textile Res.* 32(6): 207-213.

REASONABLE CONSTRUCTION MANAGEMENT IN FILL LOADING WITH VACUUM CONSOLIDATION METHOD BASED ON FEM ANALYSES

Mohammad SHAHIDUZZAMAN¹, Yoshihiko TANABASHI², Hiroshi KAWABATA³, Yujing JIANG⁴
and Satoshi SUGIMOTO⁵

ABSTRACT: Vacuum consolidation method (VCM) is one of the recent methods for the improvement of soft ground. This method can forcibly drain pore water, and increase ground strength by loading of the vacuum pressure. A fill loading with vacuum consolidation method (FLVCM) is considered to be able to control lateral flow and upheaval of surrounding area during the rapid fill construction. However, the behavior of this combination on the ground deformation is not fully clarified on FLVCM, fill design and site management is depending on the experienced technique. In this study, numerical simulation has been carried out by finite element method (FEM) for the quantitative evaluation of the deformation suppression effect of FLVCM on the soft grounds of ariake clay, Japan. The utility of FLVCM was confirmed from comparison with the observed and the analytical ground deformation. In addition, the numerical simulation have been carried out under the various conditions of vacuum pre- and post-loading pressures and fill speeds, and it is suggested that the reasonable construction management index can be easily obtained by the site measurement of deformation.

KEYWORDS: Lateral displacement, Rational site management index, Settlement, Soft clay, Vacuum consolidation method.

INTRODUCTION

In Japan civil structures are often constructed on the soft ground because of the limited usable land area. Therefore, a variety of soft ground improvement method have been developed which also widely using all over in the world.

The vacuum consolidation was first introduced by Kjellman (1952) to improve the strength of soft grounds and used to soft clayey deposits⁵. In recent years, many successful field applications have been reported in the vacuum consolidation, including the use of vacuum preloading in a land reclamation project in china (Shang et al. 1998). It is demonstrated the effectiveness of vacuum preloading consolidation in eliminating excessive settlement under static and dynamic loads on a airport runway (Tang et al. 2000). Chu et al. (2000) presented a successful case study whereby vacuum preloading was used to improve the soil strength at an oil storage station. Terzaghi's consolidation theory is revisited by vacuum and surcharge combined loading on

the soft ground (Mohamedelhassan et al. 2002). Especially in that case, vacuum consolidation is a soft grounds consolidation promotion method that applying vacuum pressure generates pore water pressure along the horizontal drain of the soil surface and along the length of a vertical drain installed in the soil, water and air has been exhausted compulsorily under the ground and increased soil strength, stability of the soft ground respectively, thereby reducing the time for attaining the ultimate ground settlement (Indraratna et. al 2004). In other word, vacuum consolidation generally induces inner lateral displacement and can cause cracks in the surrounding surface area due to inward of the ground induced by application of the vacuum pressure (Chai et al. 2005, 2006).

Many researchers have carried out their research work only on a particular vacuum consolidation method (VCM) while actually in the field quality and the type of fill consolidation constructions vary from pressure to pressure and fill speeds. This is attempted method that pore water drainage compulsorily, and increased ground

¹ Ph.D Student, Graduate School of Science and Technology, Nagasaki University, Japan.
Email:mohammad@stu.civil.nagasaki-u.ac.jp

² Professor, Graduate School of Science and Technology, Nagasaki University, Japan. Email:tanabasi@nagasaki-u.ac.jp

³ Employee, Yachiyo Engineering Co. Ltd, Japan. Email:hr-kawabata@yachiyo-eng.co.jp

⁴ Professor, Department of Civil Engineering, Nagasaki University, Japan. Email: jiang@civil.nagasaki-u.ac.jp

⁵ Assistant Professor, Department of Civil Engineering, Nagasaki University, Japan. Email: sugimoto@civil.nagasaki-u.ac.jp

strength by loading of the vacuum pressure. Rapidly fill construction and during the fill construction by control of lateral conception behavior and upheaval of surrounding area have been carried out on fill loading with vacuum consolidation method (FLVCM) that the fill construction and VCM is applied together measurement of the ground improvement. Therefore, in some cases, the combination of vacuum pressure and fill speed may provide well overall ground improvement. However, the ground deformation behavior is not clarified enough on FLVCM, and it has not arrived at a reasonable design method and site management is depending on the experienced technique.

In this study, numerical simulation has been executed by finite element method (FEM) that general fill construction, VCM, and FLVCM has been reproduced on the soft grounds of Ariake clay, Japan. The utility of FLVCM was confirmed from comparison with the observed and the analytical ground deformation. In addition, the numerical simulation with the various vacuum pre- and post-loading pressures and fill speeds have been executed, and proposed a reasonable construction management index which can be easily obtain by the site measurements of ground deformation.

LABORATORY TESTING

The soil materials used in the present study were collected from Ariake (undisturbed) in Saga prefecture. The physical properties in the samples were identified by laboratory soil tests. Table 1 shows the result of laboratory soil tests such as particle density, water content, void ratio, degree of saturation, unconfined compressive strength and composition of grain degree for the various depth soil samples on the soft ground respectively. The pore water pressure, settlement, and lateral displacement in the soil samples were identified by triaxial vacuum consolidation test. The detailed procedure is described by Tanabashi et al. (2002).

NUMERICAL ANALYSIS OF FLVCM

Analysis Technique

In this analysis, Sekiguchi-Ohta model are applied as a soil behavioral model of soft clay behavior. Fill construction and VCM are reappeared by FEM analysis of the soil and water coupled. For express to the vacuum consolidation that the drainage boundary has been setting on the connected part of the vertical and horizontal drains. Moreover, the pore water pressure of the improvement area is compulsorily decreased with increasing of hydraulic head of the drainage boundary according to the vacuum pressure, and consolidation is to be advanced. When the vacuum pump was operated, vacuum pressure was given to top of the drain parts corresponded of the hydraulic head, and it was stopped, than condition of un-drain boundary was given.

Model Analysis and Input Parameters

In this research, the plane strain condition was assumed, and the general boundaries as well as the 2D finite element method of a half section of the single improvement area (area 17.6m×187m, depth about 12m) that had been objected by the previous research (Tanabashi et. al 2002) in the field test constructed area shows the analysis model Fig. 1. It is necessary to put the vertical drain up to - 11.0m in depth at intervals of 0.8m respectively. The shape of the fill is assumed to be width 8.8m in the under, 3.8m in the above, and fill height 5.0m respectively. Drainage boundary was setting on the head of the vertical drain according to the vacuum pressure. Moreover, Table 2 shows the input analytical parameters. Surface soil, clay, and silty clay layer are respected on Sekiguchi-Ohta model materials and fill, sand mat and sandy silt layer are respected on the linear elasticity behavior model as a shown material by modeled respectively. The indoor soil test results (table 1) of the sample collected from spot of the field test construction is used for the parameters setting.

Table 1 Result of laboratory soil tests

Depth GL-m	Density ρ_s (g/cm ³)	Water content W (%)	Void ratio e	Degree of Saturation S _r (%)	Unconfined compressive strength q _u (kN/m ²)	Component (%)				Classification of soil
						Gravel	Sand	Silt	Clay	
2.00~2.90	2.609	147.1	3.816	100	21.1	0	1.5	36.2	62.3	Clay
3.00~3.90	2.639	136.3	3.585	100	26.5	0	9.6	33.7	56.7	Silt
4.00~4.90	2.663	107.2	2.875	99.2	28.3	0.2	36.4	26.9	36.5	Silt
5.00~5.90	Sand layer, coefficient of permeability k=1×10 ⁻⁴ cm/sec									Sand
6.00~6.90	2.627	119.2	3.132	100	45.1	0	5.7	40.8	53.5	Silt
7.00~7.90	2.641	125.7	3.318	100	38.5	0	2.5	39.9	57.6	Silt
8.00~8.90	2.617	115.1	3.008	100	48.9	0	4.2	37.5	58.3	Silt
9.00~9.90	2.656	116.5	3.008	100	44.1	0.1	1.9	35	63	Clay
10.00~10.90	2.684	90	2.444	98.9	64.7	0	10.3	37.5	52.5	Silt
11.00~11.90	2.647	67.4	1.782	100	60.7	0.2	11.2	32.8	55.8	Silt

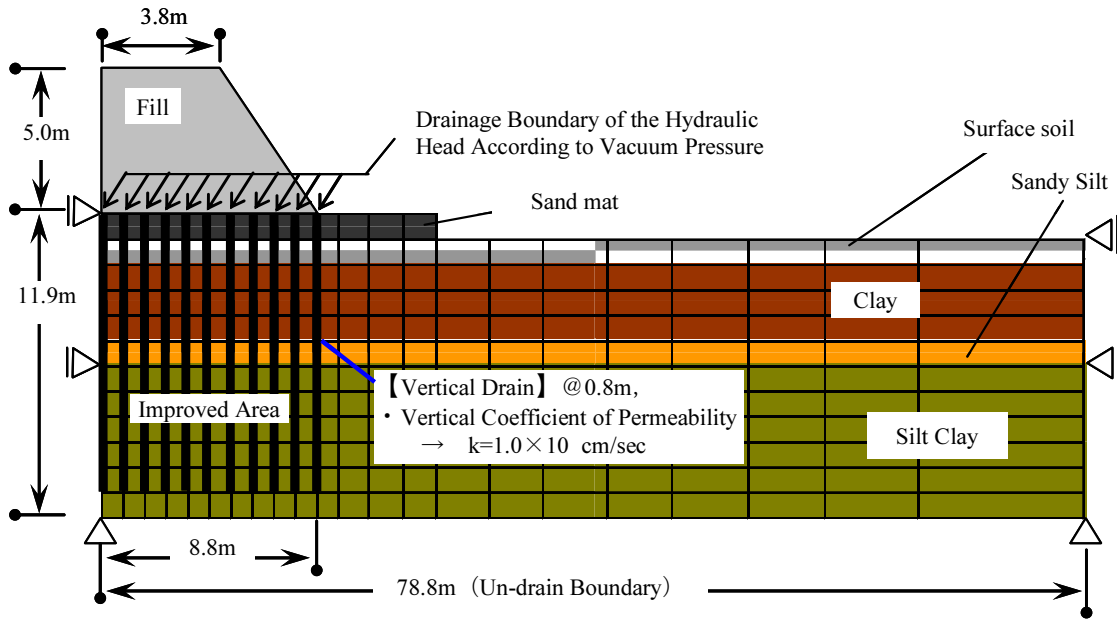


Fig. 1 Two-dimensional plane strain finite element analysis model

Analytical Cases

Table 3 shows construction method of analytical cases. There are three methods with compared to difference of deformation behavior of the ground such as fill construction method (FCM), VCM and FLVCM respectively. FCM and FLVCM have been assumed each of two cases according to the fill speed such as 20 cm/day and 50 cm/day respectively. Another, a single case has assumed without fill construction respectively by VCM. Total five cases are executed in this analysis. It is assumed that fill construction has been setting on the

fill height 5m, fill rest (vacuum pressure releases) 360 days respectively. Overall in this analysis -69kPa loading of vacuum pressure is applied according to pore water pressure.

RESULTS AND DISCUSSION

Comparison with Field Test and Numerical Analyses

Field test and the numerical analysis of achievement field test construction are executed by using the above-

Table 2 Analytical model and input parameters

Name of layer	Depth (GL-m)	Model	ϕ (deg)	ν	D	Λ	M	K_0	$k(\text{cm/sec})$
Fill	-	L.E	46.6	0.300	-	-	-	-	1.0×10^{-2}
Sand Mat	0.0~1.0	L.E	30.3	0.300	-	-	-	-	1.0×10^{-3}
Surface Soil	1.0~2.0		-	0.387	0.093	0.481	0.842	0.631	3.1×10^{-7}
Clay	1	S.O	-	0.387	0.133	0.480	0.840	0.631	3.1×10^{-7}
	2		-	0.378	0.088	0.514	0.900	0.608	2.9×10^{-7}
	3		-	0.361	0.092	0.579	1.013	0.566	2.5×10^{-7}
Sandy Silt	5.0~5.5	L.E	21.3	0.300	-	-	-	-	1.0×10^{-3}
	1		-	0.374	0.092	0.532	0.931	0.596	1.3×10^{-7}
	2		-	0.378	0.116	0.516	0.903	0.607	2.6×10^{-7}
Silty Clay	3	S.O	-	0.377	0.096	0.518	0.907	0.605	2.0×10^{-7}
	4		-	0.379	0.120	0.512	0.895	0.610	4.4×10^{-7}
	5		-	0.364	0.139	0.568	0.995	0.573	2.0×10^{-7}
	6		-	0.361	0.107	0.581	1.016	0.565	8.7×10^{-8}

Note: L.E.: Linear Elasticity, S.O.: Sekiguchi Ohta, ϕ : Friction Angle, ν : poisson Ratio, D : Coefficient of Dilatancy, Λ : Nonreciprocal Ratio, M: Ratio of Limitation, K_0 : Coefficient of Earth Rest, k : Vertical coefficient of permeability

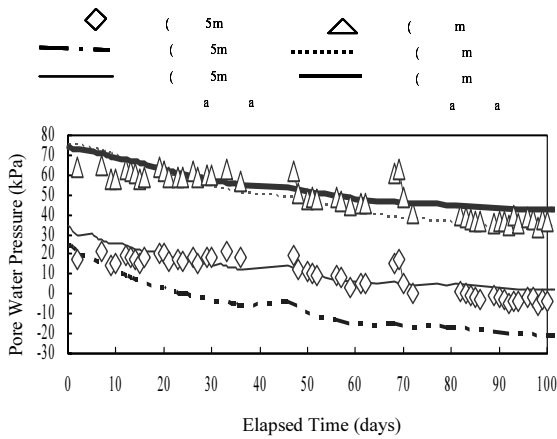


Fig. 2 Plotted for pore water pressure against elapsed time

mentioned physical properties of each layer, analytical model and the input parameters. In this paper, field test samples and numerical analytical points are taken out of equal depth as GL-3.5m and GL-8.5m, respectively.

Fig. 2 plotted for pore water pressure against elapsed time at various depths for the vacuum consolidation test. The data were recorded by field data and model analyses according to 4.9m hydraulic head at depths of GL-3.5m and GL-8.0m respectively. There are approximately similar tendency of the pore water pressure in this figure. It is thought that the behavior of the pore water pressure can be caught from figure by the analysis and also the mechanism of the VCM in which it decreases in the pore water pressure because of action of the vacuum pressure is to be expressed by the analysis roughly. Moreover, it is put that an analytical value of hydraulic head (positive hydraulic head) has 3.5m given for the more similar to the actual field value, respectively.

Fig. 3 shows relation ship between amount of ground settlement and elapsed time. From figure, 2.4m distance from the center of improvement area’s model value is similar to actual field value but center of model value is larger than 2.4m distance from the center of the field value. Maximum settlement is the center according to the analytical result of the total improvement area. It is also thought that increased the distance from center with decreasing the amount of ground settlement.

Table 3 Analytical methods

Construction method	Fill Speed (cm/day)	Fill height (m)	Vacuum pressure (kPa)	Period of vacuum pressure (day)
FCM	20	5	0	0
	50	5	0	0
VCFLM	20	5	-69	25
	50	5	-69	10
VCM	0	0	-69	25

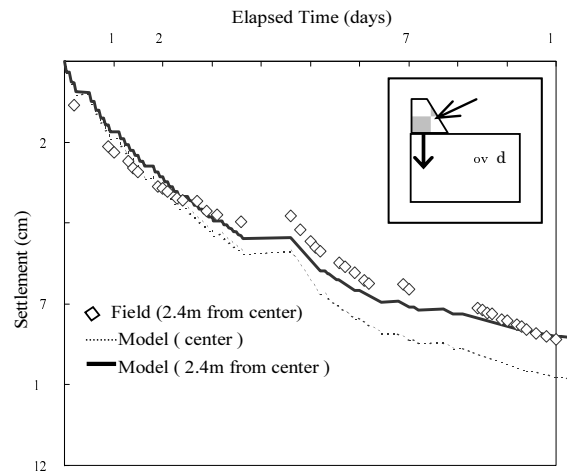


Fig. 3 Shows relationship between amount of ground settlement and elapsed time

Fig. 4 shows the distribution depth of lateral displacement measured by field and model test. Lateral displacement has been showing in here 10.1m distance from center of the improvement area and this displacement is 98 days of elapsed time from starting of the construction. From figure, it has become small increased with increasing the hydraulic head of drainage boundary. In this analysis became a result that the difference with the field data extends into after and before correction of the hydraulic head but it is thought that the lateral shrinkage in the improvement area by the influence of vacuum consolidation is roughly express by the model.

Figs. 2, 3 and 4 show field with compare model test both are similar changing tendency in here. It is thought that assuming the model and soil parameters has been using appropriate, is discussed focus in terms of the relation of the model test to the settlement and lateral displacement, and is indicated to be the overall index management accounting for the fill construction method in this analysis.

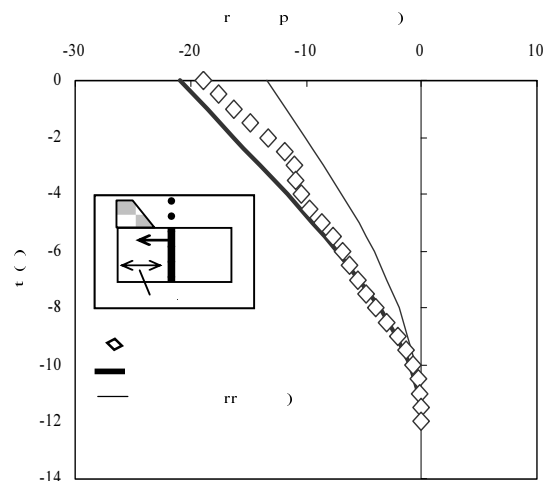


Fig. 4 Shows the distribution depth of lateral displacement measured by the field and model test

Numerical Analyses

As follows, result discussion in here that there are two cases of the 20 cm/day fill speed such as FCM and FLVCM, another a single is VCM respectively. Those cases are compared with pore water pressure and settlement behavior for the period of fill construction.

Moreover, Fig.5 shows the pore water pressure versus ground distributions depth at the center of improvement region. It is shown that pore water pressure has been distributed of initial stage and each cases after 25 days and 375 days elapsed from starting of the fill construction. From fig., fill construction is occurred excess pore water pressure about 50kPa after 25 days elapsed time from starting of the fill construction, oppositely decreasing the pore water pressure could be seen about -30kPa~-20kPa into VCM respectively. At that time, excess pore water pressure has been generated in the low layer on the boundary of -5.0m in depth of the loading of vacuum pressure and compare with the fill construction is become controlled in this result. Moreover, after 375 days elapsed time from starting the construction that only one case of the fill construction is shown higher pore water pressure distribution than initial stage, and the scatter of the excess pore water pressure is late. Fig. 6 shows the amount of settlement versus elapsed time at -4.0m depth center of the ground improvement area. In this fig., it is become result of maximum settlement due to loading of vacuum pressure according to the period of fill loading.

It is thought that settlement behavior is excellent than influences of both parties of the loading of vacuum pressure and loading fill respectively. However, the FCM has become maximum settlement in the fill rest period, and rebound phenomenon has been generated in vacuum consolidation. It is thought that the residual settlement and the rebound behavior can be control by combination of FCM with VCM during the fill construction.

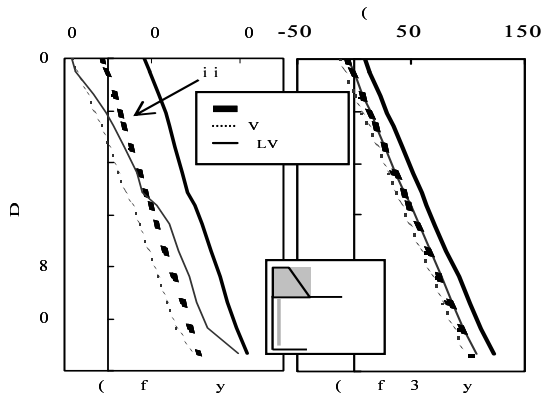


Fig. 5 Shows the pore water pressure versus ground distributions depth

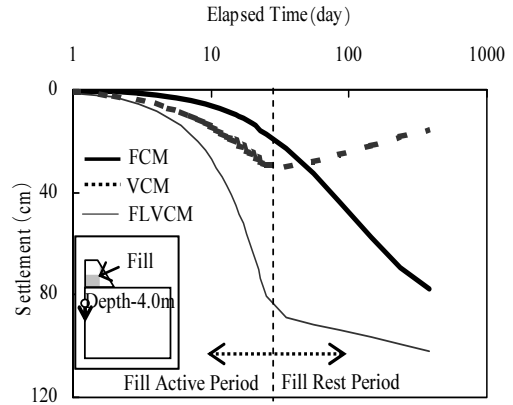


Fig. 6 Shows the amount of settlement versus elapsed time at -4.0m depth from center of the ground improvement area

APPLICATION AND PROPOSAL OF CONSTRUCTION MANAGEMENT INDEX TO DEFORMATION BEHAVIOR

Amount of Soil Settlement and Lateral Flow

Fig. 7 shows one of the deformation ground is assumed for definition ground of amount of soil settlement and lateral flow that it has been proposed the fill construction management index to understand the deformation behavior of the ground. Assumed for definition ground of width and length are 10.1m and 11.9m respectively. Amount of soil settlement (V_s) and amount of soil lateral flow (V_δ) is calculated according to following equation

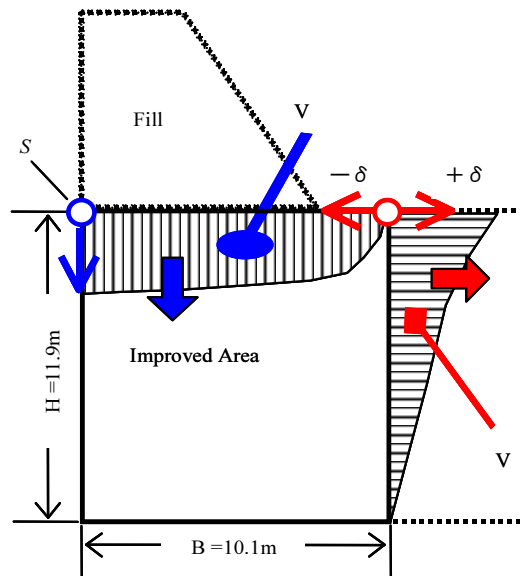


Fig. 7 Assumed for definition ground of amount of soil settlement and lateral flow

$$V_s = \sum \left\{ \frac{1}{2} \times (S_i + S_{i-1}) \times \Delta S \right\} \quad (1)$$

$$V_\delta = \sum \left\{ \frac{1}{2} \times (\delta_i + \delta_{i-1}) \times \Delta \delta \right\} \quad (2)$$

where, V_s : Amount of soil settlement, V_δ : Amount of soil lateral flow, S_i : Amount of settlement in i node, δ_i : Amount of lateral displacement in i node, ΔS : Node distance in vertical direction, $\Delta \delta$: Node distance in horizontal direction

Amount of soil settlement (V_s) and amount of lateral flow (V_δ) values calculated above by Eqs. 1 and 2 and plotted Fig. 8 according to FCM and FLVCM due to fill speed 20 cm/day and 50 cm/day respectively. In this fig., the dotted line is un-drained response that shows the deformation stage of the ground where $V_s = V_\delta$ is satisfied. Un-drain response in closer behavior is shown in the FCM cases and also case 50cm/day is more remarkable compare to another cases and is understood that the cases with fill construction shows deforming behavior like the neighborhood shearing deformation as an un-drain response. Observation in here, the period of fill rest that means after filling both cases are shown strong rebound tendency with increases amount of settlement because is not occurred consolidation, usually after fill soft ground tendency becomes to initial stage without consolidation pressure. But as for the result of VCM is understand of the appearance that V_δ increased the minus axis with increasing the settlement and it is understand that relation of $V_s > -V_\delta$ is occurred superior settlement behavior with lateral shrinkage of the ground deformation. However, FLVCM cases tendency of $V_s > V_\delta$ relation is stronger than FCM cases and also it is understand from fig. settlement behavior more superior in deformation mode. Moreover, it is estimated that the ground tendency has been shrunk rapidly according to the period of fill rest and fill is executed with 50cm/day, respectively.

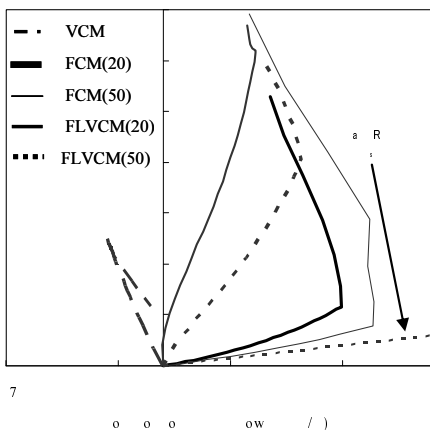


Fig. 8 Plotted for the amount of soil settlement and amount of lateral flow according to fill method

Presumption of the Ground Behavior by Amount of Settlement and Lateral Displacement

The settlement record on the surface of the basic ground and the measurement of the depth direction distribution of the lateral displacement are needed as follows previous condition that calculation V_s and V_δ described in the foregoing paragraph. However, these types of various deformations have some ground where the measurement becomes difficult according to the site. In that situation, usually, the amount of settlement (S) is measured on the site of the fill center, amount of horizontal displacement (δ) of the ground surface in the out of improvement area is applied according to the Fig. 7 and it was tried to calculation the amount of soil deformation by following eq.

$$V_s' = S \times B \quad (3)$$

$$V_\delta' = \delta \times \frac{H}{2} \quad (4)$$

where, V_s' : Amount of soil settlement, V_δ' : Amount of soil lateral flow, S : settlement in the center, δ : Lateral displacement on the ground surface, B : Width of improvement area, H : Thickness of improvement area.

Fig. 9 shows the relation between amount of soil settlement (V_s') and amount of soil lateral flow (V_δ') according to the eqs. 3 and 4 with shown together V_s versus V_δ relation (during the fill construction) respectively. It is seen that correspondence between V_s versus V_δ (during the fill construction) and V_s' versus V_δ' (calculated Fig. 7) relation calculated amount of soil deformation, the strong tendency of ground deformation depends on settlement in center (S) and lateral displacement on the ground surface (δ) is determined. Therefore, it is thought that deformation behavior is possible to manage by settlement in center (S) and lateral displacement on the ground surface (δ) according to the FLVCM.

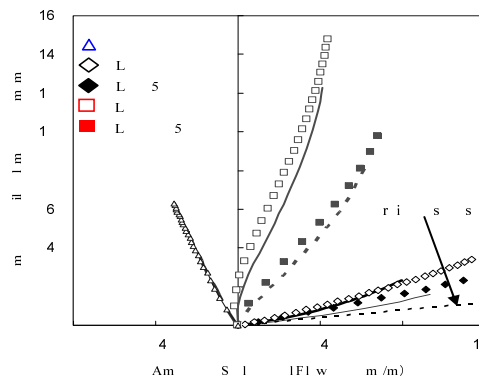


Fig. 9 Shows the relationship between amount of soil settlement (V_s') versus amount of soil lateral flow (V_δ')

Analysis that Attention to Loading of Vacuum Pressure

In this section, it is discussed about the influence that the loading of vacuum pressure and the fill speed caused on the deforming behavior of the soft ground. Fill speed is 20cm/day and 50cm/day and fill height is 5m respectively. Range of vacuum pressures -20kPa to -90kPa is changed that loading of vacuum pressure has been setting up on the model. A part of an analytical case is shown in Table 4. An analytical model and the input parameters are similar as well as the above-mentioned as for this analysis. In this analysis, the ground behavior is evaluated by relation of settlement (S) and lateral displacement (δ) that discuss above. As a criterion, it was taken standard value ($\Delta\delta/\Delta t \leq 15\sim 20\text{mm/day}$) of horizontal displacement speed of edge point of the fill slope by VCM technological material (addition 2004). However, it was assumed that amount of lateral displacement of the ground surface in a point of 1.3m away from edge point of the fill slope or 10.1m away from center of the fill as follows Fig. 7 is used in this analysis. Fig. 10 shows relationship between horizontal displacement speed and elapsed time during fill construction to each case of FLVCM. The cases V-20(50) and V-40(50) that means fill speed 50mm/day and vacuum pressure less than -60kPa are exceeded 15mm/day of the maximum horizontal displacement speed, standard value has not been fulfilled in this figure. Moreover, the maximum horizontal displacement speed is shown 15.4mm/day as a case of V-60(50) that standard value has been satisfied or not in this analysis. Since, fill speed 50cm/day and vacuum pressure less than -60kPa cases are exceeded standard line but fill speed 20cm/day and all vacuum pressure cases are satisfied the standard line. Moreover, V-60(50) is a standard case that the approximation straight line is pulled as a satisfied the standard during the fill construction on the Fig. 11 plotted for settlement (S) versus lateral displacement (δ). In this Fig., V-60(50) case is introduced on the approximation line as a lateral flow allowance line. It is understood that V-20(50) V-40(50) and V-60(50) cases are becoming on the deformation mode with especial superior lateral flow behavior according to S versus δ relation. Moreover, it can be determined that other cases has been shown stable behavior of $S > \delta$ strong tendency.

Thus, it is proposed a stable construction management index concerning the lateral spreading by using S- δ relationship and the standard line in this research.

CONCLUSIONS

Numerical simulation by FEM when FCM, VCM, and FLVCM intended for the soft ground were executed.

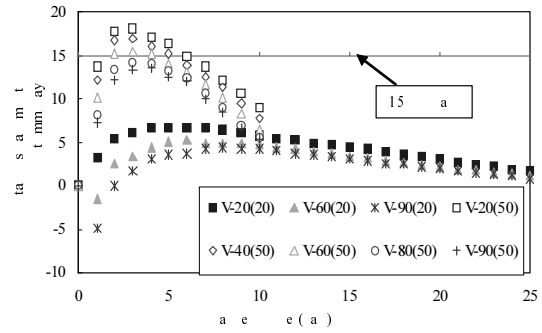


Fig. 10 Plotted for horizontal displacement speed versus elapsed time

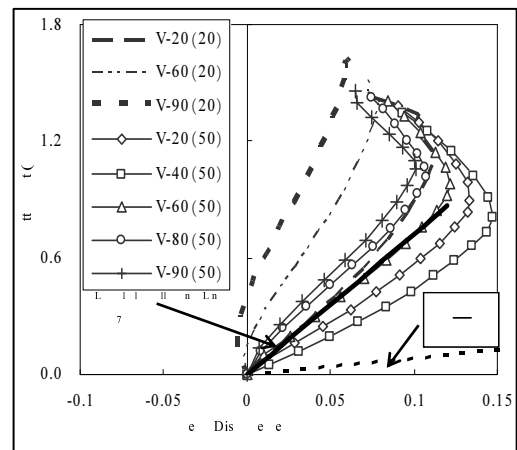


Fig. 11 Plotted for settlement versus lateral displacement

Table 4 Loading of vacuum pressure cases

Cases	Vacuum Pressure (kPa)	Fill Speed (cm/day)	Fill Height (m)	Period of Vacuum Pressure
V-20(20)	-20			25
V-60(20)	-60	20		25
V-90(20)	-90			25
V-20(50)	-20		5	10
V-40(50)	-40			10
V-60(50)	-50	50		10
V-80(50)	-80			10
V-90(50)	-90			10

It is proposed construction management index to examine the utility of FLVCM by comparison with deformation ground behavior to obtain according to those analytical results. Moreover, numerical analysis to which attention was carried out to loading of vacuum pressure in also construction condition of FLVCM, deforming ground behavior was evaluated based on the proposed construction management index, and considered to influence that loading of vacuum pressure exerted on ground deformation behavior.

Ground deformation behavior is clarified points such

as effect of excess pore water pressure's generation is controlled during the fill construction, residual settlement is reduced for the period of fill rest, effect of rebound phenomenon is controlled by FLVCM during the fill construction. Moreover, it is suggested that the deformation behavior of the ground is able to be understood by measuring the amount of settlement at the center of fill and the amount of lateral displacement on the out of improvement area during the application of FLVCM. Especially, the validity is examined with the introduction of the standard concerning the lateral spreading behavior.

REFERENCES

- Chai JC, Carter JP, Hayashi S (2006). Vacuum consolidation and its combination with embankment loading, *Can. Geotech. J.* 43: 985-996.
- Chai JC, Carter JP, Hayashi S (2005). Ground deformation induced by vacuum consolidation, *Journal of Geotechnical and Geoenvironmental Engineering*, 131(12): 1552-1561.
- Chu J, Yan SW, Yang H (2000). Soil improvement by the vacuum preloading method for an oil storage station, *Geotechnique* 50(6): 625-632.
- Indraratna B, Bamunawita C, Khabbaz H (2004). Numerical modeling of vacuum preloading and field applications, *Can. Geotech. J.* 41: 1098-1110.
- Kjellman W (1952). Consolidation of clay soil by means of atmospheric pressure, *Proc. of conf. On soil stabilization*, Massachusetts institute of technology, Boston: 258-263.
- Mohamedelhassan E & Shang JQ (2002). Vacuum and surcharge combined one- dimensional consolidation of clay soils, *Can. Geotech. J.* 39: 1126-1138.
- Shang JQ, Tang M, Miao Z (1998). Vacuum preloading consolidation of reclaimed land: a case study. *Can. Geotech. J.* 35:740-749.
- Technological material (2004). Koushinku N&H method –Vacuum consolidation method, *kairyogata-*, association of vacuum consolidation technology: 185-186
- Tanabashi Y, Shiono T, Jiang Y, Xiao J, Shinohara T, Uehara T (2002). Field investigation and model test for clarifying compaction effect of CVC (compact vacuum consolidation) method, *Proceedings of Saga International Symposium on Lowland Technology*: 169-174.
- Tang M & Shang JQ (2000). Vacuum preloading consolidation of Yaoqiang airport runway, *Geotechnique*, 50(6): 613-623.

FINITE ELEMENT NUMERICAL ANALYSIS TO INTERACTION OF BURIED SPIRAL STEEL PLASTIC COMPOSITE PIPE WITH SURROUNDING SOILS

Xiang-Yong ZENG¹, An-Fu DENG², Bing ZHENG³ and Xiao-Dong GUO⁴

ABSTRACT: With the development of sewage treatment business in China, buried spiral steel plastic composite pipe has been applied in the sewage pipeline construction of many big cities in recent years because it is relatively cheap, convenient in site installation, beneficial to environment and more perdurable as a substitute to traditional concrete sewage pipe. But as a structure of new type, its interaction behavior with surrounding soils still needs investigation because its application period is not long. Finite element method is used for numerical analysis to the interaction of buried spiral steel plastic composite pipe with surrounding soils. Analysis procedure and results can be references to corresponding engineering practice.

KEYWORDS: buried spiral steel plastic composite pipe, interaction of pipe with surrounding soils, finite element analysis

INTRODUCTION

In the past, reinforced concrete pipe used extensively in the underground drainage domain of China. Now many drainage pipeline engineering have used large caliber high-density polyethylene (HDPE) spiral steel rib plastic pipe as a substitute for traditional reinforced concrete pipe. Product shape of buried spiral steel plastic composite pipe is shown as Fig. 1. Compared with reinforced concrete pipe, HDPE buried spiral steel plastic composite pipe is relatively cheap, convenient in site installation, beneficial to environment and more perdurable. Thus the prospect of HDPE buried spiral steel plastic composite pipe is broad (e.g. Hu 2005; Li & Shi 2006; Fang et al. 2005).



Fig. 1 Product of buried spiral steel plastic composite pipe

Because the structure of HDPE spiral steel plastic composite pipe is relatively complicated, traditional analytical mechanic method can not analysis its interaction behavior of pipe with surrounding soils (e.g. Ren et al. 2002). Finite element method is used to analysis the problem. Accordingly such pipe's mechanical behavior in the soils can be cognized more intensively.

COMPUTATION MODEL

In the finite element analysis, buried HDPE spiral steel plastic composite pipe computation model is simplified from the engineering practice real product as Fig. 2. Internal diameter of the pipe is 1.2m. And 2.5m high soils are on the top of the pipe. Steel ribs circle on the outer surface of the pipe as spiral form. Surface of the pipe has 300mm far from sand boundary. And out of the sand, there is soft clay (see Fig. 2). HDPE plastic tube of the pipe has 25mm wall thickness. Spiral steel rib simulated as rectangular section and its width is 5mm and height is 50mm. Spiral steel rib simplified as equal space between closed hoop and its space between is 100mm. Finite element computation model is shown as Fig. 3. In Fig. 3, center point of the pipe has 1.9m distance far from the bottom boundary and 3.0m distance

¹ Ph.D Associate Professor, College of Civil Engineering, Chongqing University, China. Email: zeng_xiangyong@126.com

² Professor, Doctoral Advisor, College of Civil Engineering, Chongqing University, China. Email: danganfu@163.com

³ Ph.D Student, College of Civil Engineering, Chongqing University, China. Email: zhengbing@zzu.edu.cn

⁴ Engineer, ATON Plastics (Chongqing) CO., LTD., China. Email: cqsy01@163.com

far from left and right hand boundary and 3.1m distance far from the top surface of the model.

Boundary restrictions are applied on the boundary surfaces as every node on the surface has no displacement in the normal direction to the surface exclude the top surface of computation model.

In finite element analysis, steel rib is simulated by 2-nodes beam elements, HDPE plastic pipe is simulated by 4-nodes shell elements, soils are simulated by 10-node space tetrahedron (e.g. Wang & Shao 1997).

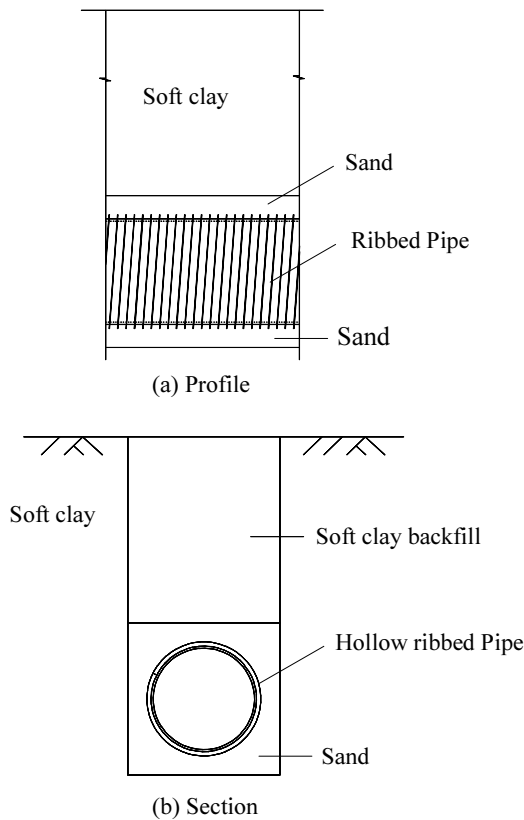


Fig. 2 Engineering example of buried spiral steel plastic composite pipe

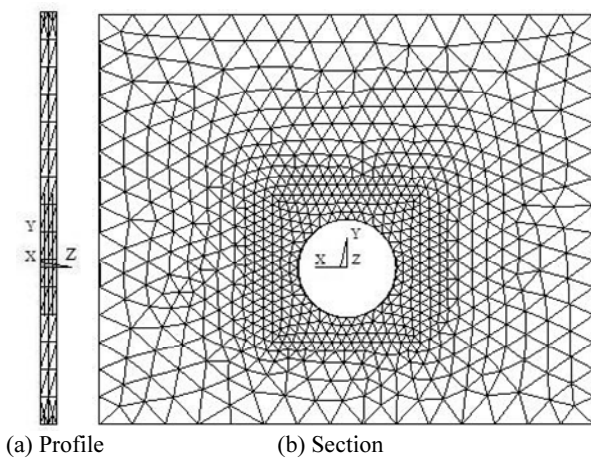


Fig. 3 Finite element computation model of buried spiral steel plastic composite pipe

MATERIAL PROPERTY AND PARAMETER

Uniaxial σ - ϵ relationship curves of HDPE plastic tube of the pipe and spiral steel rib are shown as Fig. 4 and Fig. 5. Related mechanical parameters are shown as table 1 (e.g. Ren et al. 2002)

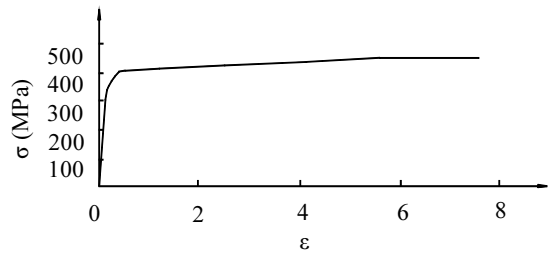


Fig. 4 Uniaxial σ - ϵ relationship curve of steel rib

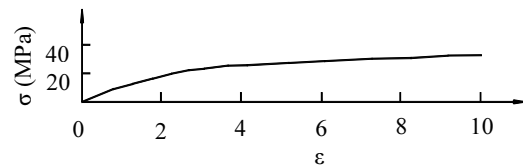


Fig. 5 Uniaxial σ - ϵ relationship curve of HDPE (high-density polyethylene)

Table 1 Material parameters of spiral steel rib and high-density polyethylene

Material	Poisson's ratio	Young's modulus (MPa)	Elastic limit strength (MPa)	Limit strength (MPa)
Spiral steel rib	0.3	1.73×10^5	349.9	452.4
HDPE	0.2	958	9.58	32.64

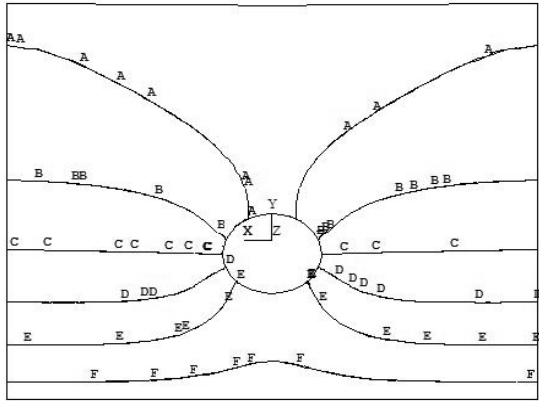
Von Mises elastoplastic constitutive model is used for the mechanical properties simulation of steel rib and HDPE plastic tube of the pipe. Two materials' stress-strain relationships use the above Fig. 4 and Fig. 5 curves. Parameters of two soils are shown as table 2 (e.g. Zhang & Liu 2001). Both of the soils use Drucker-Prager elastoplastic constitutive model in finite element analysis (e.g. Gong 1999)

Table 2 Material parameters of soils around the pipe

Soils	Sand	Soft clay
Weight (kN/m^3)	20	18
Poisson's ratio	0.25	0.35
Deformation modulus (MPa)	7.25	2.58
Cohesion (kPa)	0	15
Internal friction angle ($^\circ$)	30	9

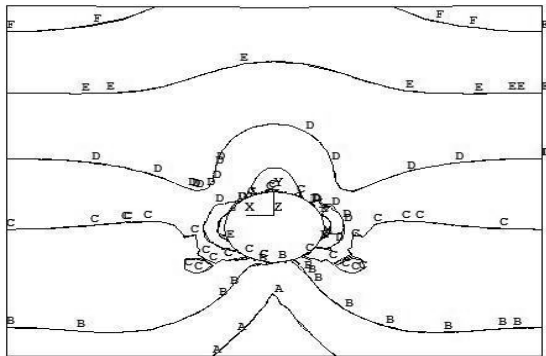
RESULTS OF FINITE ELEMENT ANALYSIS

Load of the pipe comes from surrounding soils' weight. Deformation of pipe and surrounding soils after loading is shown in Fig. 6. Fig. 7 shows the horizontal and vertical normal stress of pipe and surrounding soils. Fig. 8 shows the plastic strain of soils around the pipe.



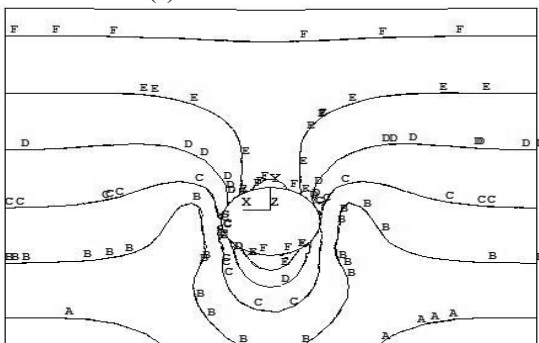
A=-0.059195, B=-0.048432, C=-0.037669
D=-0.026907, E=-0.016144, F=-0.005381

Fig. 6 Vertical displacement of buried spiral steel plastic composite pipe and surrounding soils by FEM (m)



A=-49312, B=-39491, C=-29670
D= -19849, E=-10027, F=-205.992

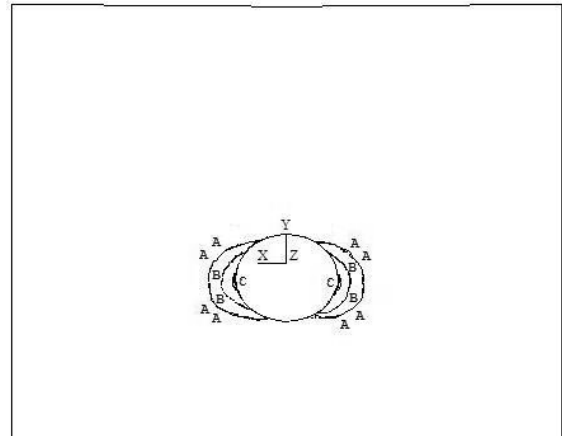
(a) Lateral normal stress



A=-86150, B=-70347, C=-54544
D= -38742, E=-22939, F=-7136

(b) Vertical normal stress

Fig. 7 Normal stress of buried spiral steel plastic composite pipe and surrounding soils by FEM (Pa)



A=0.007078, B=0.021235, C=0.035391

Fig. 8 Plastic strain distribution of soils around the pipe by FEM

CONCLUSIONS

Through the above finite element numerical analysis, conclusions can be summarized as the following:

- (1) Finite element method is useful in buried spiral steel plastic composite pipe mechanical analysis.
- (2) Interaction behavior of pipe and soils can be analyzed by the procedure used above. Results of analysis can be references to corresponding engineering practice.

ACKNOWLEDGEMENT

The authors are grateful for the research support of Chongqing Science & Technology Commission through contract 2008AC7090 (Science and Technology Development Project of CQ CSTC).

REFERENCES

Hu XJ (2005). Application of large caliber HDPE spiral pipe in drainpipe engineering. Chinese Journal of Engineering Plastics Application. 33(11): 38-40.

Li YM & Shi ZY (2006). Development and application of steel strip reinforced plastic buried pipe. Chinese Journal of Chemical Materials for Construction. 22(6): 18-20.

Fang YZ, Wang XL, Zhu YP (2005). Testing Study on HPDE spiral pipe used in soft soil area of shanghai. Chinese Journal of Rock Mechanics and Engineering. 24(5): 889-897.

Ren ZM, Ren DY, Liu KL, Liu JT (2002). The finite element analysis of steel wire frame reinforced plastic pipes. China Plastics. 16(11): 40-42.

Wang XC & Shao M (1997). Basic theory of the finite element method and numerical method. Tsinghua University press. Beijin.
Zhang KG & Liu SY (2001). Soil mecs. China

Architecture & Building Press. Beijin.
Gong XN (1999). Soil plastic behavior mechanics. Zhejiang University Press. Hangzhou.

EXPERIMENTAL STUDY ON ENGINEERING PROPERTIES OF A DREDGED SEDIMENT SOLIDIFIED BY COMMON CEMENTITIOUS MATERIALS

Ping CHEN¹ and Bang-Min QIN²

ABSTRACT: This paper presents an orthogonal experimental program for investigating the effectiveness of using common cementitious materials for solidification of a soft dredged sediment. Three kinds of solidification additives including Portland cement, fly ash and lime were chosen for the experimental study. The water content and mechanical properties of the solidified sediment were measured, and the influence of each solidification additive on the solidification was analyzed. The experimental results revealed that fly ash was the most cost-effective to reduce free water in the sediment, and increase the strength and elastic modulus. It was found that both the strength and water resistance of solidified sediment were enhanced. The experimental results provide an implication to the selection of cost-effective solidification additive for the reuse of the dredged sediment in civil engineering.

KEYWORDS: dredged sediment, water content, strength, cementitious materials

INTRODUCTION

Sediments at the bottoms of seas, rivers, and lakes are more or less contaminated. In order to restore the ecosystem of water bodies, or to keep the waterways and harbors navigable, or to prevent rivers from flooding, a large amount of sediments are dredged every year in China. In general, dredged sediments is a kind of very soft soils which have higher water contents (>80%) and low shear strengths ($c_u < 50$ kpa). (Zhu et al. 2007). Existing disposal techniques for dredged sediments have concentrated on ocean disposal and land disposal. Because of the presence of contaminants, ocean disposal poses a potential threat to water quality and aquatic life. Land disposal is gradually limited because the regions along river and coastal line are short of land. One of the most advanced disposal approaches is to treat the dredged materials into construction materials. (Yamasaki et al. 1994; Zhu et al. 2007). The treatment generally involves a solidification technique. This paper presents experimental study on the effectiveness of using common cementitious materials for solidification of a soft dredged sediment. The solidification additives include fly ash, lime and Portland cement.

EXPERIMENT SCHEME

Materials

In this study the dredged sediments were taken from

the bottom of Ningbo harbor in East China. The sediments had a specific gravity of 2.687g/cm³ and an initial water content over 80%. According to grain-size distribution test and Atterberg limits test, the sediments mainly consisted of silty clay, with 34% of grains sized less than 0.005mm.

The candidate solidification additives included Portland cement, fly ash, lime and plaster. Stabilization of fly ash with lime and cement has been investigated. (Usmen et al. 1990), (Linn et al. 1988). Cost-effectiveness and environmental concerns favored more fly ash over Portland cement. Initially, plaster and lime were considered as activator for fly ash. Comparative study found a better solidification of dredged sediments resulting from using lime. Lime could enlarge the grain size of the sediment, and quicklime could also absorb water and give off heat in its curing process which was good for solidification. All these considered, ground quicklime was selected as one of the solidification additives.

For fly ash we used mixed ash from Hangzhou Banshan Heat-engine Plant and for Portland cement we used ordinary Portland 42.5 from Qianchao Cement Plant.

Sample Preparation and Test Method

An orthogonal experiment program of three factors at three different levels was used, details of which is shown in Table 1.

¹ Associate Professor, Department of Civil Engineering, Zhejiang Sci-tech University, China. Email: zhanchen9608@sina.com

² Engineers, Nanjing Water Planning and Designing Institute, Ltd., China. Email: njslyah@126.com.

Table 1 Experiment scheme

Sample No.	Factors and levels		
	Portland cement (C)	Quicklime(L)	Fly ash(F)
CLF1	1	1	1
CLF2	1	2	2
CLF3	1	3	3
CLF4	2	1	3
CLF5	2	2	1
CLF6	2	3	2
CLF7	3	1	2
CLF8	3	2	3
CLF9	3	3	1

Note: Levels 1, 2 and 3 for Portland cement denote 1%, 2% and 3% of cement in the dry weight of sediments, respectively. Levels 1, 2 and 3 for fly ash denote 1%, 2% and 3% of fly ash in the dry weight of sediments, respectively. Levels 1, 2 and 3 for quicklime denote 1%, 2% and 3% of quicklime in the dry weight of sediments, respectively.

1) Water content test

Additives were mixed into the dredged sediments proportionately, disturbed and put into air-tight containers. They were cured in the lab under a temperature of 15~20°C for 7d, 14d, 21d and 28d before they were sampled and tested. Test samples collected at different curing ages were put into aluminum box and oven-dried at 100~105°C for 24h.

2) Unconfined compression test

Fully mixed dredged sediments were put into rigid moulds sized 70.7mm*70.7mm*70.7mm, vibrated, trimmed and cured at a temperature of 15~20°C. Three samples were made for each mixture ratio and were cured for 28d.

3) Water test of solidified dredged sediments

Water test was conducted for solidified samples with different mixture ratios at curing ages of 7d, 14d, 21d and 28d.

EXPERIMENT RESULT AND ANALYSIS

Influence of Chemical Solidification on the Water Content of Dredged Sediments

Water content influences the physical and mechanical properties of dredged sediments. Chemical solidification is essentially a hydration reaction, in which free water and adsorbed water of the sediments are converted into bound water. The amount of conversion largely reflects the amount of mass produced in the

solidification and the change of mechanical properties of the sediments.

Water content test was conducted for samples with different mixture ratios and curing ages, as seen in Table One. The curing ages were 7d, 14d, 21d and 28d, respectively. The influence of mixture ratio on the conversion of water was studied by an orthogonal experiment table as seen in Table 2.

Table 2 Experiment results of water content test of solidified sediments

Sample No.	water content (%)			
	7d	14d	21d	28d
CLF1	67.58	65.97	63.42	61.05
CLF2	59.79	57.68	55.84	54.75
CLF3	54.18	52.1	49.98	49.40
CLF4	55.62	54.91	54.28	52.53
CLF5	70.32	66.68	61.11	59.23
CLF6	53.36	52.12	51.40	50.22
CLF7	59.9	57.5	56.00	54.83
CLF8	52.52	52.15	50.74	50.42
CLF9	63.47	60.94	58.75	58.39

The initial water content of the dredged sediments was 80%, including mainly free water and absorbed water. Effect of hydration on the reduction of water was pronounced. The orthogonal analysis shows that the ranges of influence of Portland cement, quicklime and fly ash at 7d curing age are 5.66, 12.09 and 39.05, respectively. The ranges of influence of Portland cement, quicklime and fly ash at 14d curing age are 5.16, 13.22 and 34.43. The ranges of influence of Portland cement, quicklime and fly ash aged at 21d are 3.34, 13.57 and 23.15. The ranges of influence of Portland cement, quicklime and fly ash aged at 28d are 3.22, 10.4 and 26.32, respectively. The optimal mixture ratio was C3L3F3 for all ages, which indicates that the addition any of the three, be it Portland cement, quicklime or fly ash, will result in the decrease of water. Among them, fly ash is the most effective, seconded by quicklime and Portland cement.

Influence of Chemical Solidification on Compressibility of Dredged Sediments

The results of compression test and deformation test are shown in Table 3.

Orthogonal analysis shows that the ranges for the influence of Portland cement, quicklime and fly ash on unconfined compression test are 157, 38 and 213,

respectively. The ranges for the influence of Portland cement, quicklime and fly ash on compression deformation are 107.3, 20.9 and 55.2, respectively. The ranges for the influence of Portland cement, quicklime and fly ash on elastic modulus are 0.898, 0.283 and 1.007, respectively. The addition of fly ash increases the strength most, seconded by Portland cement and quicklime. Portland cement influences compression deformation most, seconded by fly ash and quicklime. Fly ash influences elastic modulus of the solidified dredged sediments most, seconded by Portland cement and quicklime.

Table 3 Experiment results of compressibility of solidified sediments

Sample No.	Unconfined compression strength σ (kPa)	Ultimate strain ϵ ($\times 10^{-3}$)	Elastic modulus E ($\times 10^4$ kPa)
CLF1	172	77.2	0.223
CLF2	208	91.5	0.227
CLF3	220	66.6	0.330
CLF4	272	40.1	0.678
CLF5	211	60.0	0.352
CLF6	274	48.6	0.564
CLF7	239	43.3	0.552
CLF8	255	30.0	0.850
CLF9	151	54.7	0.276

Water Soaking Tests of Solidified Dredged Sediments

Solidified sediments at curing ages of 7d, 14d, 21d and 28d with different mixture ratios were selected for the water soaking test. It was found that the water resistance increased with curing age and is positively related with unconfined compression strength.

The sediment samples were air-dried, i.e., physically dewatered before water soaking test. It was found that these physically-dewatered samples swelled easily with water and the lower the initial water content, the quicker the adsorbing process. Some samples even collapsed at a sudden and lost strength. The reason is that the proportion of clay particles was high in samples which had not gone through chemical solidification. With high water-absorbing capacity the samples would swell dramatically, with a large portion of water encapsulating clay particles, undermining inter-particle force. So samples lost strength

and collapsed. On the other hand, dredged sediments that went through chemical solidification improved tremendously on water resistance and retained certain strength even after a couple of days without collapsing. This implies that some cohesive force was formed by chemical solidification. Chemical solidification also enlarged particle size, reduced clay proportion as well as water absorbing-capacity and improved strength and thus engineering property.

CONCLUSIONS

a) The effect of Portland cement, quicklime and fly ash on compressibility varied. The addition of fly ash changed solidified sediments most, in terms of strength and elastic modulus, seconded by Portland cement and quicklime. Portland cement changed compressibility most, seconded by fly ash and quicklime.

b) Fly ash reduced free water and absorbed water in the sediment samples most, seconded by quicklime and Portland cement.

c) There were a lot of clay particles in the dredged sediments. Samples solidified by physical dewatering such as air-drying and mechanical drying lost strength when absorbing a lot of water. Chemical solidification, on the other hand, could increase strength and water resistance. Chemical solidification reduced the amount of clay particles and improved the engineering properties for dredged sediments to be used as backfill material.

REFERENCES

- Zhu W, Zhang CL, Abraham, Chiu CF (2007). Soil-Water Transfer Mechanism for Solidified Dredged Materials, *Journal of geotechnical and geoenvironmental engineering*, 5: 588-598.
- Shoichi Yamasaki, Hiroshi Yasui, Masaharu Fukue (1994). Development of Solidification Technique for Dredged Sediments, *Dredging, Remediation, and Containment of Contaminated Sediments*: 136-144.
- Usmen MA & Chou CP (1990). Stabilization of Class F Fly Ash with Lime and Cement, *Proceedings of the 22nd Mid-Atlantic Industrial Waste Conference*: 171-192.
- Linn David, Mark M, Symons G (1988). Lime-fly Ash Stabilization of Fine-Grained Soils, *Australian Road Research*, 18(3):153-161.

IMPROVING SOFT GROUND AND SLUDGE BY OVER-PRESSURE VACUUM CONSOLIDATION SYSTEM

Ya-Wei JIN¹ and Ben NIU²

ABSTRACT: Sludge is one of the most important sources of COD in Taihu Lake. This paper presents a new method of improving soft clay and sludge soil ground by over-pressure vacuum, which could effectively increase soil strength and reduce consolidation time. Small model tests are performed, suggesting it a promising technique.

KEYWORDS: sludge, Taihu Lake, OVCS

INTRODUCTION

Algae have become the biggest problem in Taihu Basin in recent year. Two major issues are concerned in Taihu Lake contamination, including: 1) Pollutant released from adjacent factories. 2) The deposited pollutant in sludge. Sludge is one of the most important sources of COD in Taihu, which causes a great pollution (Fan et al. 1998; Jin et al. 1999; Gao et al. 2006; Zhang et al. 2006).



Fig. 1 Taihu Lake polluted by algae

Nowadays, yet the emission of high COD containing water has been ceased, the polluted water still exists in the sludge.



Fig. 2 Canal in Taihu Basin polluted by algae

Strength requirement and consolidation time are major issues and the keys to success in soft clay disposal and Taihu Lake sludge treatment projects. Sludge is highly compressed soft clay, with organic content over 3.8% (sometimes even over 6.3%) and permeability less than 10^{-7} cm/s. Sludge properties specified above imply that Taihu Lake, in large area, is not properly exploited.

There are mainly three methods consolidating soft clay and sludge grounds: the chemical consolidation method, consolidation with electroosmosis and drainage consolidation method. Up till now, consolidating the sludge is supposed to be a most efficient way disposing the soils. This paper introduces a new system improving soft ground and sludge by over-pressure vacuum consolidation system (OVCS). We have indicated the new system a proper and scientific way to treat Taihu sludge.

¹ General Manager, Yixing XinTai Earthwork Materials Co., Ltd, Yixing, China. Email: yxxintai@126.com

² Ph.D Student, MOE Key Laboratory of Soft Soils and Geoenvironmental Eng., Zhejiang Univ., China. Email: nbote@163.com

INTRODUCTION OF OVCS

The OVCS consists of two components: the core pipe system and the vacuum system. The former is formed by lateral pressure pipe connecting with the PVC pipe. The latter mainly consists of three parts: the anti-block PVD, the creative hand-connect, and the PVC vacuum pipe.

The mechanism of the OVCS is listed as follows:

1. The vacuum inside the PVC vacuum pipe make the pore water run faster out of the soil.
2. The core pipe gives an enhancement of the positive pressure in the centre of the soil, so the pressure differences increase and the compressed positive pressure in the core pipe make the pore water flow right along the direction set by the designer. In this way, the strength of the soil are greatly enhanced in the consolidation process. The whole system is shown in Figs. 3 and 4.

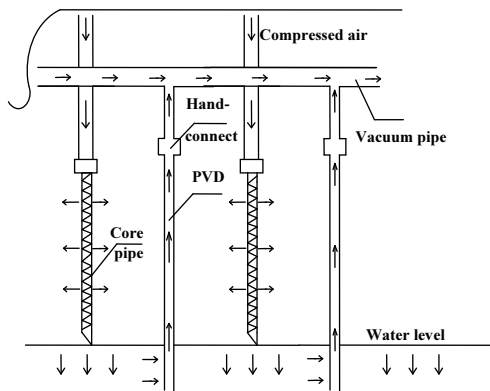


Fig. 3 Vertical profile of OVCS

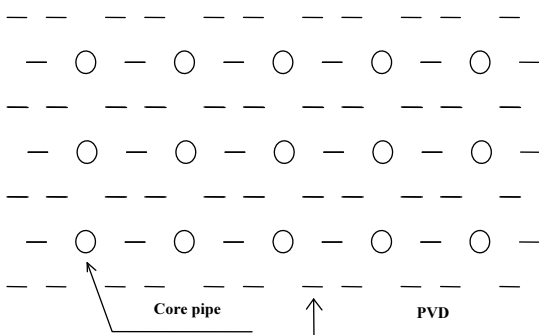


Fig. 4 Layout of the system

IMPROVING SOFT GROUND

This new method is conducted in in-situ test in Zhoushan, Zhejiang, China, with a field of 2,700m² area in August, 2007, which showed a good result. Besides, in November, 2008, at Lingang Industrial Zone, Tianjin, another test in large-area of 150,000m² is performed. The layout is shown in Fig.5 and Fig. 6. The curves of pore pressure in Lin Gang are listed in Fig. 7.



Fig. 5 Layout of the in-situ test at Lingang Industrial Zone, Tianjin, China



Fig. 6 Overview of the in-situ test at Lingang Industrial Zone, Tianjin, China

In Fig. 7, only by 2 months' time (from 08-10-14 to 08-12-13), even at the deepest point, 17m from the ground surface, the pore pressure reduces nearly 80kpa. The big decrease of the pore pressure during such a short time proves that the new method is efficient.

IMPROVING SLUDGE

Three groups of samples are prepared from the in-situ test. The distance the samples away from the core pipe is 5cm, 10cm, 15cm, respectively. After taken out of the ground, samples are made into 5cm×5cm×5cm

cubic to get loaded.

The test was carried out this way:

1. Make a tank with dimensions of 5m×2m×0.6m for the sludge; install the OVCS into the tank;
2. The ground was consolidated for one month to obtain enough strength to plant the reeds, then we grow reeds in the ground;

3. After about 2 months, the reeds grew up to the height as shown in Fig. 8.

4. We cut the reeds, take samples from the field and then the samples are loaded until damage to obtain the yield strength.

The procedure of the test is shown in Figs. 8-12 and the change of water contents is shown in Table.1.

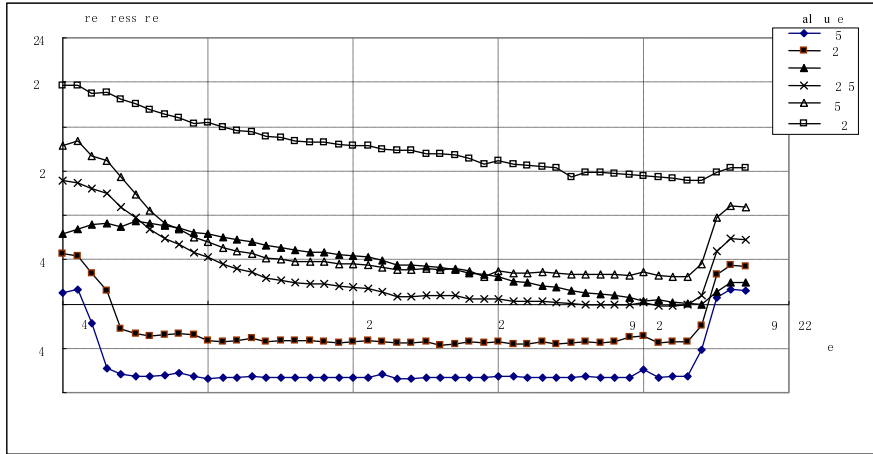


Fig. 7 Pore pressure dissipation curve



Fig. 8 Strength test field—before the weeds cut



Fig. 10 Taking samples out of the test field



Fig. 9 Strength test field—after the weeds cut



Fig. 11 Sludge without consolidation

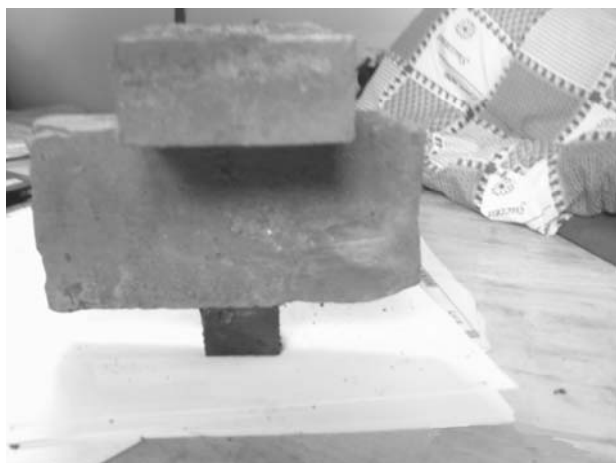


Fig. 12 The strength test

Table 1 The change of water contents.

Distance away from the core pipe (cm)	1 month after consolidation	Samples
	Water content (%)	Water content (%)
5	105	28
10	105	30
15	105	32

Water content decreased greatly. One month after consolidation, water content of the sludge was 105%, then after another two month, the water content decreased to about 30%, which is a huge improvement of the sludge soil. Besides, the result in Table 1 shows, the further the samples are, the higher the water content remained. It is because pressure, which passes on to the deeper soil, becomes less against distance, namely, more dissipation occurs within further soil, leading to less water remained.

The strength of the sludge increased greatly. Comparison between Figs.11 and 12 shows how greatly the strength of the sludge has been enhanced. In Fig.11, the sludge is soft, with nearly no strength, while after consolidation, in Fig.12, it could bear a loading of two

bricks. The OVCS gives the sludge a good treatment and a great increase in strength.

SUMMARY

Years of research has been put in improving technology on enhancing the strength of the soil and improving the environment around the Taihu Lake. Now, a whole new system with a set of creative equipments finally comes to reality. So many outstanding advantages make the system special:

1. The original creation of the accessories, and the unique over-loading method out of the whole Geotechnique world, these give a brand-new concept to everyone's mind.

2. By using OVCS, the consolidation time of the sludge has been evidently shortened, and the soil strength is significantly increased.

In-situ test has proved the efficient of the OVCS, with more projects go on, the OVCS will experience a bright future.

REFERENCES

- Fan CX, Chen YW, Yang LY, Sun Y (1998). Preliminary Analysis on Apparent Dynamics of Organic Pollutantson the Decline in the South of Meiliang Bay, Taihu Lake. *Journal of lake sciences* 10: 48-52.
- Jin XC, Ye C, Yan CZ, Ren BX, Zhang YC, Wang XQ, Wang YB (1999). Comprehensive Treatment Plan for Key-Polluted Regions of Lake Taihu. *Research of Environmental Science* 12: 1-5.
- Gao Y, Mao XW, Xu WD (2006). Aimlysis of the Influence on the Taihu Lake and the Area Around: Diversion from the Yangtze River to the Taihu Lake. *Journal of China Hydrology* 26: 92-94.
- Zhang XF, Lin YS, Yu F, Xu YG, Hu L, Li M (2006). The Change of TN, TP and COD in Representative Water Body of Tai-Ge valley. *Jiangsu Environmental Science and Technology* 19: 1-3.

CHANGING IN THE PHYSICAL PARAMETERS OF DUMPS OF THE COAL-MINING INDUSTRY OF KANSK-ACHINSK (SIBERIAN) COAL FIELD AND POSSIBILITY OF THEIR REMEDIATION

E.V. STANIS¹, E.N. OGORODNIKOVA² and E.A. KARPUKHINA³

ABSTRACT: While opencast mining of coal a large amount of dumps consisting of surface rocks, coal and other materials are formed. In the Kansk-Achinsk brown coal field the disposal areas occupy a large territory. The result of this is the loss of the agricultural and forest lands. The dumps consist of technogenic rocks, whose properties are differed from the properties of natural rocks. Further use of such disturbed lands is impossible without their remediation with the use of different plant species. The remediation of dumps cannot be successful without accounting changes in their physical properties in time. Our studies showed that the properties of technogenic rocks change in a similar way independently of the way of their formation. The following parameters change: skeleton density, humidity, the angle of internal friction, cohesion, the modulus of deformation. For the technogenic rocks of dumps it is possible to distinguish the stage of progressive lithogenesis (about 5 years) and then the stage of regressive lithogenesis (about 20 years).

KEYWORDS: dumps, technogenic soils, remediation

INTRODUCTION

The Central-Siberian basin holds considerable brown coal reserves. These reserves have been extracted by the open-cut method. In 2006, the coal mining in the basin has exceeded 40 m. tones per year. The Nazarovsky open-cast coal mine is included into top 10 of the largest coal cuts. A various waste of the coal-mining industry is stored on the surface. It was discovered that for the Nazarovsky open-cast mine artificial soils go through different stages of soil condition: consolidation and decompaction, and lithogenous transformations. Such processes change their physicommechanical properties. Change of properties results from consolidation under body weight, weight of overlying filled layers and dehydration, and also under the influence of the secondary processes occurring in the formed file.

As an example we will consider temporal changes in properties of non-transportable and transportable dumps of the Nazarovsky open-cast mine.

Non-transportable dumps accumulate quaternary loams and terrigenous deposits of Jurassic period. During formation of dumps, large fragments roll down downwards on slopes and form a horizon consisting of large not broken fragments with a small amount of dispersed filler in the basis of each floor. Broken rocks

with insignificant portion of small-size fragments prevail in the top part of a cut in each circle of dumps. During maintenance of each ground portion those rocks which fall the first and those laying below are consolidated to the greatest degree.

Moreover, rocks dump consolidates under their body weight. Thus rocks dump are non-uniform in structure and properties. Such indicators as skeleton density, cohesion, deformation module have the general tendency to increase with depth. In addition, fluctuations connected with change in ratio of plastic material and filler and a presence of recondensed layers in each circle are imposed. Spatial variability of rock properties in non-transportable dumps is connected, mainly, with the massif age. The dumps sediments traversed by wells, had the following age: 1 week, 0.5 year, 5 years, and approximately 20 years. The most widespread lithogenous type of soils is yellow-grey loams with fragments of aleurolites and inclusions of other stripping rocks (Ogorodnikova & Stanis 2005).

Dumps with age of 7 days, are characterized by humidity of 17 % that corresponds to humidity of the drained rocks of the open-cast mine east board. The density of rocks was 1,49 g/sm³, the skeleton density was 1,27/sm³. Such parameters define their low compactness and low durability. Soils of non-

¹ Professor, Chief of the department of Geoecology, Russian People's Friendship University, Moscow. Email: estanis@mail.ru

² Professor of the department of Geoecology, Russian People's Friendship University, Moscow. Email: estanis@mail.ru

³ Professor of the department of System ecology, Russian People's Friendship University, Moscow. Email: nemorum@mail.ru

transportable dumps of six months age had no differences in lithogenous structure comparing to what is described above. However, these soils were in more condensed condition and with the skeleton density about $1.40/\text{sm}^3$. Increase in density with time testifies new structural cohesions, and growth of cohesive forces in soils. For non-transportable dumps at the age of 5 years the density of a skeleton of a ground was $1.58 \text{ g}/\text{sm}^3$, and greater humidity, than for those soils described (0,22). Higher strength properties testify that consolidation of

rocks under a body weight occurs before 5-year-old age. Swelling is common for technogenic soil dumps of such age. The degree of swelling is 10.3 %, humidity of swelling of 30%, and is not observed in younger or later soil formations.

In time the skeleton density of dumps decreases and at the age of 5 years is $1.58 \text{ g}/\text{sm}^3$ and at the age of 20 years $-1.44 \text{ g}/\text{sm}^3$.

Humidity increases, the angle of internal friction, cohesion, the modulus of deformation decrease (Table 1).

Table 1 Physicomechanical properties of non-transportable dumps rocks (yellow-grey loams with fragments of aleurolites and inclusions of other stripping rocks)

Dump age	Physicomechanical properties						
	Density of solid phase, g/cm^3	Humidity	Density of rock, g/cm^3	Plasticity number	Angle of internal friction	Cohesion, MPa	Modulus of deformation, MPa
1 week	2,70 (5)*	0,17 (5)	1,49 (5)	0,11 (5)	22 (5)	0,027 (5)	-
0,5 year	2,69 (11)	0,18 (12)	1,66 (11)	0,13 (11)	24 (12)	0,045 (12)	12,5 (12)
5 years	2,69 (11)	0,22 (26)	1,93 (21)	-	23 (13)	0,089 (13)	12,4 (13)
20 years	2,7 (9)	0,28 (8)	1,85 (7)	0,16 (9)	26 (7)	0,065 (7)	10,8 (5)

* Numbers of measurings is given in brackets

It possible to explain the decreasing of physicomechanical properties values at the age of 20 years with swelling and decompaction.

Technogenic permafrost is formed in dumps.

It is formed while the rocks are put on snow cover in winter or spring time especially in relief depressions. The thickness of frozen rocks is 10-15m, thickness of ice lenses is 1m and more. If the thickness of overlaying soils is rather small, the permafrost degradation begins in 2-3 years after the formation. When the permafrost degrades deep gaps (up to 5m) are being formed on the dump surface. Since frozen soils and ice are laying on various depth, the permafrost degradation and accompanying processes occur in different time. The temperature of the frozen layers varies from 0°C to -1°C . Annually new plots (several hectares by area) with specific relief are formed on the dump surface.

Tehnogenic soils of transportable dumps have more complicated composition and structure, than non-transportable dumps. Lower layers (thickness 2-3m) of transportable dumps consists of broken rocks without small-size fragments.

The most wide-spread lithological variants of transportable dumps are loams, argillaceous sand with fragments of argillites, solid aleurolites, sandstone of Jurassic period age and coal.

The age of studied transportable dumps was 20 years,

20, 18 and 5 years, 3, 1, 0,5, 1 weeks. The data analysis shows that soil characteristics within each lithological type change in time. Before 5-year-old age the skeleton density increasing under comparatively constant meanings of humidity results in growing of solidity and deformation parameters. At this age the sample of soils are characterized with maximum values of swelling degree. Presence of swelling is indicative of instability of structural bindings formed as a result of consolidation under body weight. The decrease and stabilization of physico-mechanical parameters is observed for dump soils of 20-year-old and more age. At the same time the humidity increases and the swelling decreases. The general trend of changes in density, solidity, swelling for transportable dumps remains the same as for non-transportable dumps.

The dump soils are very sensitive for different external influences (natural and anthropogenic). Changes in temperature and humidity regimes can result in thermal subsidence of rock, swelling and other negative processes. It is necessary to take into consideration these features of dump soils in case of remediation and subsequent using. of During the remediation in the territory of Kansk-Achinsk coal field the surface of dumps is often covered black earth (chernozem). In this case the intensity of thermal subsidence of rock increases. The subsidence makes the protection forest plantations in

course of remediation work rather complicated. The positive feature of dumps in the region is their non-toxicity for plants. That is why we recommend on the first stage of remediation to create the upper layer of native black soils 10-15cm and to plant herbs and bushes (such as *Caragana arborescens* Lam., *Crataegus sanguinea* Pall., *Rosa acicularis* Lindl., *Spiraea* sp.). Creating of forest plantations is recommended only after the surface stabilization (more than 20-year-old dumps).

Thus for the technogenic rocks of dumps it is possible to distinguish the stage of progressive lithogenesis (about 5 years) and then the stage of regressive lithogenesis (about

20 years). This fact influences the possibility of dump remediation.

REFERENCE

Ogorodnikova EN & Stanis EV (2005). Lithogenetic transformations of coal-mining industry tailing /Bulletin of Russian People's friendship University, series Ecology and Life Safety 1(11): 57-62 (Russian).

DYNAMIC REACTION ANALYSIS OF TAILING DAMS UNDER EARTHQUAKE

Bao-Lin XIONG¹, Xi-Liang WANG² and Chun-Jiao LU³

ABSTRACT: The nonlinear idiosyncrasy of soil in tailings dam with viscous damping can be simplified as oscillation system of equivalent viscoelasticity. By this means, dynamic reaction of tailings dam during earthquake is analyzed. Then peak acceleration of ground motion in base rock, predominant period and equivalent times of cyclic action are investigated. Acceleration reaction and isoline of principal stress of representative cross section during earthquake are discussed. The preliminary results show that dynamic reaction of dam during earthquake rests on earthquake inputting of base rock and mechanical specialty of tailings dam materials.

KEYWORDS: tailings dam, earthquake, dynamic analysis, acceleration, base rock

INTRODUCTION

Grain of tailing is thin, fine-graded, low density, great clay grain content, difficult drained consolidation and easy liquidation under earthquake. The quasi statics method is adopted for the normal calculating of anti-earthquake stability of tailings dam, which is a kind of special construction for metal or non-metal mine, but not enough because of the difference between the actual condition and the hypothesis in this method for the form and mechanism of dam damage (Harper et al. 1992). So it is necessary to conduct the dynamic analysis. Thereby dynamic reaction of tailing dam and ash yard is analyzed by seismic intensity of field. The method and steps of the analysis are introduced with project example.

DYNAMICAL NONLINEAR METHOD OF DAM UNDER EARTHQUAKE

Dynamic analysis of structure during earthquake is adopted by time domain method or frequency domain method (Harder and Stewart 1996). Time domain method applies integration method to solve nonlinear dynamic equation and gains displacement, acceleration of dam. When motion equation or wave equation is solved by frequency domain method, ground motion and dynamic reaction of soil is considered as steady process. Motion equations are transformed into sum of harmonic motions by Fourier switch. Then motion equation or wave equation is solved to gain steady solution. Finally

dynamic reaction of soil is obtained by Fourier reverse switch.

According to equivalent linear method, nonlinear specialty of soil in tailings dam with viscous damping is simplified as oscillation system of equivalent viscoelasticity (Newmark 1965). Movement equation of dam under earthquake is:

$$[M]\{\delta''\} + [K]\{\delta'\} + [C]\{\delta\} = -\{E\}_x u_{g,x}(t) - \{E\}_y u_{g,y}(t) \quad (1)$$

where $[M]$ is mass matrix, $[K]$ is whole rigidity matrix of dam and $[C]$ is damping matrix. According to regulation of Raleigh damping, damping matrix is linear combination of mass matrix and rigidity matrix, viz. $[C] = \alpha[M] + \beta[K]$, $\alpha = \xi\omega$, $\beta = \xi/\omega$. ξ is damping ratio. ω is minimum circle frequency of natural dam. $\{\delta\}$, $\{\delta'\}$, $\{\delta''\}$ are displacement, velocity, acceleration respectively. $\{E\}_x$ and $\{E\}_y$ are mass vector of X-direction and Y-direction respectively.

Original condition of equation is $\{\delta''\}_= = 0$ and $\{\delta'\}_= = 0$. Boundary condition of surface on base rock is $\{\delta\}_{,x=0} = 0$.

The dynamical equation (1) is solved by Wilson- θ method (θ is 1.4). Displacement, velocity, acceleration are solved. According to strain-displacement determined by displacement shape function, dynamic strain of

¹ Doctor, Department of Civil Engineering, Shijiazhuang Railway Institute, China. Email: xiongbao77@163.com

² Professor, Department of Civil Engineering, Shijiazhuang Railway Institute, China

³ Assistant, Department of Architecture and Art Design, Shijiazhuang Railway Institute, China

element is gained. Dynamic stress of element is solved by stress-strain relationship of plane strain condition.

Equivalent linear method considers dynamic nonlinear property of soil. According to original value of shear modulus G_0 and damping ratio ξ_0 . Wave theory of time domain or frequency domain estimates dynamic reaction of soil. Effective strain γ_{eff} of soil element is confirmed. γ_{ff} is usually 0.65 of maximum shear strain γ_{max} . Then curve of $G \sim \gamma$ and $\xi \sim \gamma$ of soil are gained by test. The dynamic parameter with effective strain γ_{eff} is estimated. Linear analysis goes through again. The final computing result is regarded as nonlinear dynamic reaction.

DYNAMICAL PARAMETER OF BASE ROCK UNDER EARTHQUAKE

Dynamic reaction and liquefaction of dam during earthquake relate not only geometrical specialty of dam and mechanical characteristics of soil, but also

composing specialty of ground motion. Before dynamic analysis, reasonable parameter of ground motion is ascertained by local fatalness result of earthquake. The design of ground motion includes temporal processes of base rock, peak acceleration of ground motion in base rock, predominant period and equivalent times of cyclic action.

According to relation of ground motion of base rock with magnitude and epicenter distance established by Seed and Martin (Seed1966), maximum acceleration of earthquake is 0.05 g, equivalent oscillation times are ten times, predominant period is 0.35s, endurance time of oscillation is 2s (Ishihara et al. 1980).

GRID SUBDIVISION OF FINITE ELEMENT

Representative cross section A-A of main dam in Waitoushan tailings dam and D-D of auxiliary dam are used to analyze dynamical reaction of earthquake, as shown in Figs.1 and 2. Parameters of material are shown in Table 1.

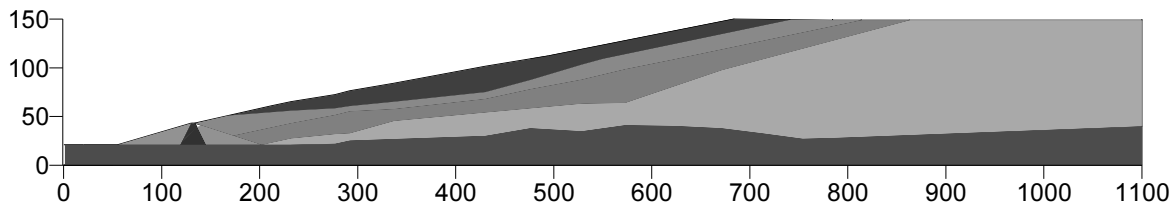


Fig. 1 Cross section A-A of main dam

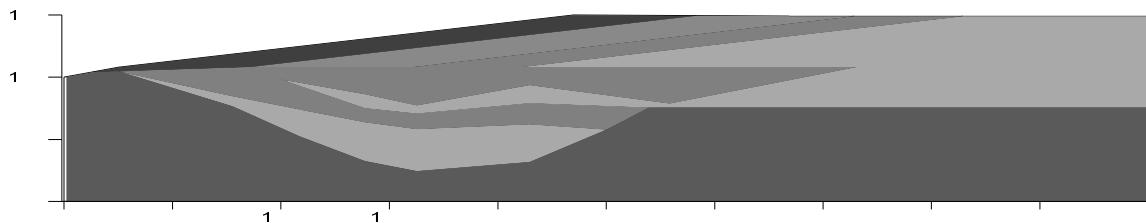


Fig. 2 Cross section D-D of auxiliary dam

Table 1 Parameters of material

Material name	Natural bulk density (kN/m ³)	Saturated bulk density (kN/m ³)	Dry state		Saturated state		Dynamical state	
			c _{cq} (kPa)	φ _{cq} (°)	c _{cq} (kPa)	φ _{cq} (°)	c _{cq} (kPa)	φ _{cq} (°)
Tailing mealy sand	21.7	21.7	0	27.1	0	27.1	1.7	15.8
Tailing silt	20.7	20.7	0	26.7	0	26.7	2.2	15.0
Tailing slime	20.5	20.5	0	18.3	0	18.3	2.3	14.8
Tailing sand	19.4	19.4	9	22.0	9	22.0	4.0	8.0
silty clay	19.5	19.5	27	19.0	27	19.0	6.0	7.5
clay	19.7	19.7	40	22.0	40	22.0	6.6	10.1
Base rock	20.0	20.0	22	34	22	34.0	5.0	30.0

Each part of dam is wholly considered. Surface on base rock is thought as fixed boundary. Element is plane isoparametric element of 4-node. Grid subdivision is automatically accomplished by computing program.

Considering load combination of dynamic analysis and operation of tailing dams, length of dry beach is 100m and drainage is normal.

RESULTS OF DYNAMICAL ANALYSIS

Dynamic reaction of dam during earthquake rests on earthquake inputting of base rock and structural specialty of dam. If frequency of earthquake is closer to natural frequency of dam, Dynamic reaction of dam becomes more strongly.

Fig.3, Fig.4, Fig.5 and Fig.6 are acceleration reaction of representative cross section during earthquake.

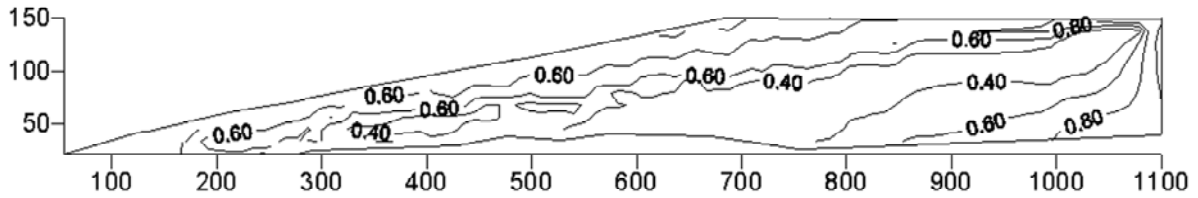


Fig. 3 Acceleration isoline of X-direction in Cross section A-A

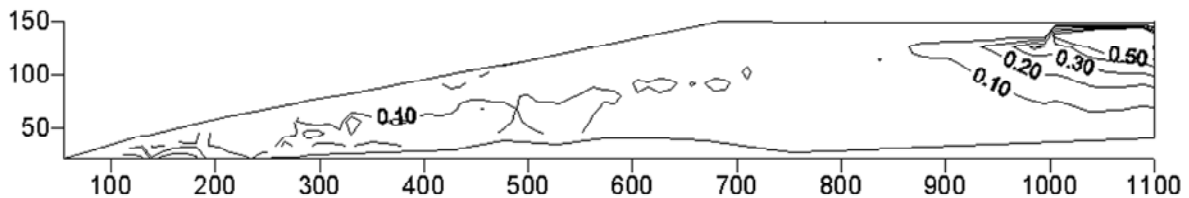


Fig. 4 Acceleration isoline of Y-direction in Cross section A-A

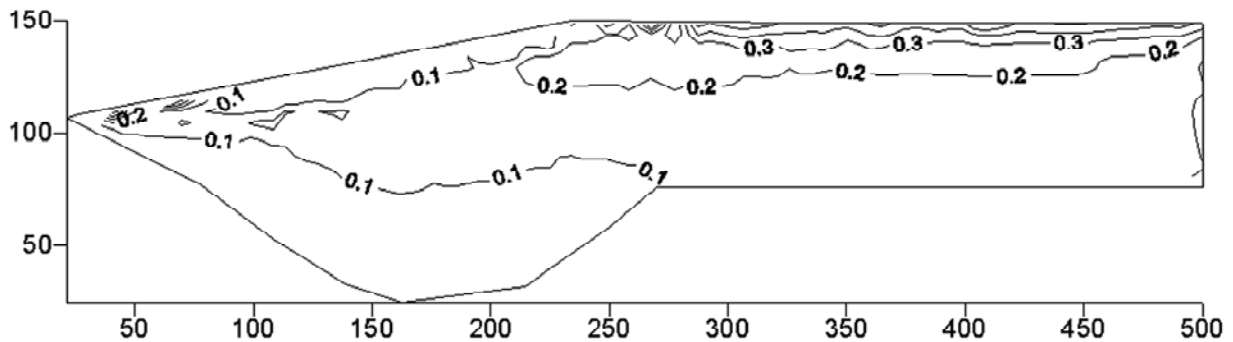


Fig. 5 Acceleration isoline of X-direction in Cross section D-D

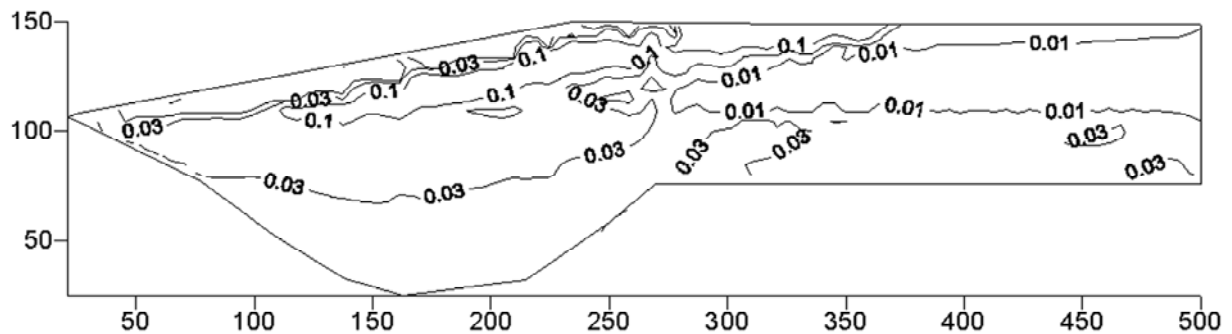


Fig. 6 Acceleration isoline of Y-direction in Cross section D-D

From the above figures, level acceleration is maximum on the top of tailing dam. The level acceleration of the main dam is about $0.8m/s^2$ and the level acceleration of the auxiliary dam is about $0.3m/s^2$. The plumb acceleration of the dam is small and the

plumb acceleration of the auxiliary dam is less than $0.1m/s^2$.

Fig.7, Fig.8, Fig.9 and Fig.10 are isoline of principal stress σ_1 and σ_3 of representative cross section during earthquake.

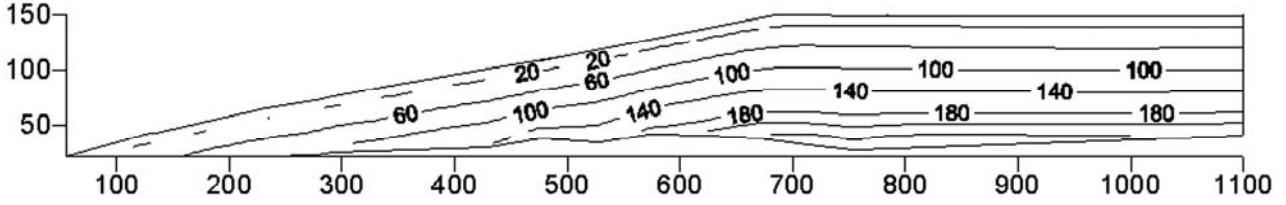


Fig. 7 Isoline of big principal stress σ_1 in cross section A-A

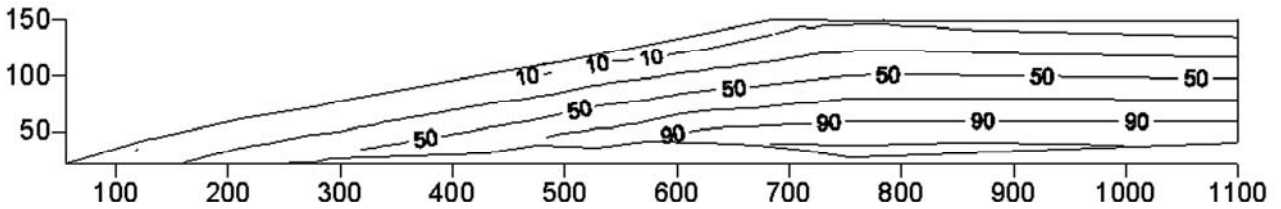


Fig. 8 Isoline of small principal stress σ_3 in cross section A-A

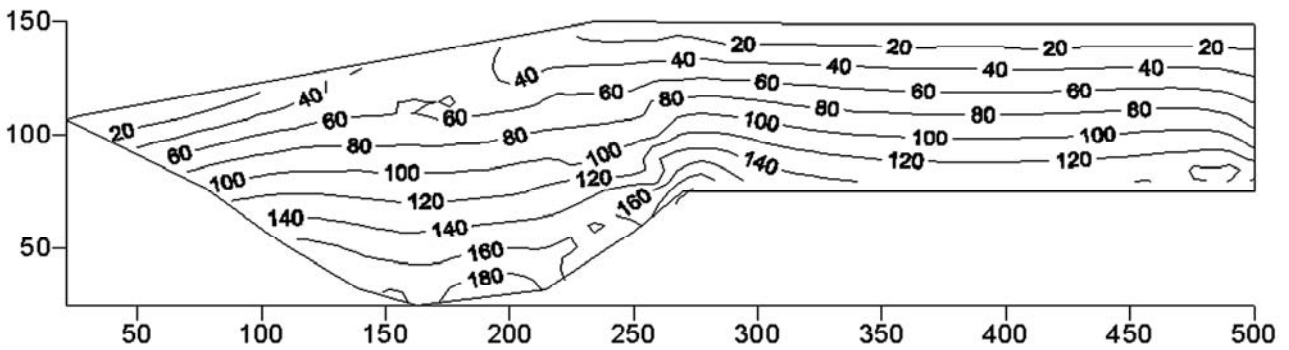


Fig. 9 Isoline of big principal stress σ_1 in cross section D-D

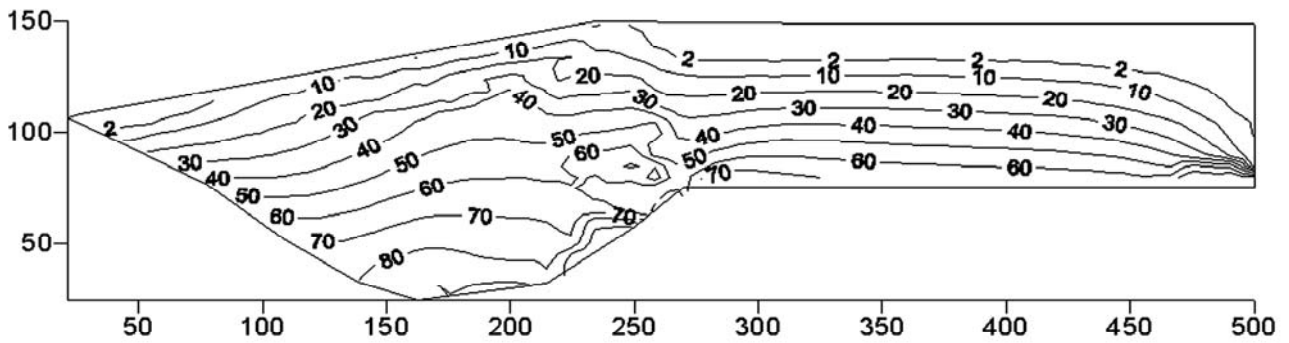


Fig. 10 Isoline of small principal stress σ_3 in cross section D-D

From the above figures, maximum of big principal stress σ_1 in cross section A-A is closely 200kPa. Maximum of small principal stress σ_1 in cross section A-A is closely 90kPa. Maximum of small principal stress σ_1 in cross section D-D is closely 200kPa. Maximum of small principal stress σ_1 in cross section D-D is closely 80kPa. Distributing region of maximum value in cross section A-A lies at the bottom of dam. But distributing region of maximum value in cross section D-D lies at the bottom of tailing mud.

CONCLUSIONS

(1) Dynamical nonlinear method of tailings dam can well consider nonlinear specialty and viscosity of stress-strain relationship on soil.

(2) Dynamic reaction of dam during earthquake relates not only geometrical specialty of dam and

mechanical characteristics of soil, but also composing specialty of ground motion.

PREFERENCES

- Harper T, Meleod H, Davies M (1992). Seismic assessment of tailings dams. *Civil Engineering*, 12: 64-66.
- Harder JLF & Stewart JP (1996). Failure of Tapo Canyon tailings dam. *Journal of Performance of Constructed Facilities*, 10(3): 109-114.
- Newmark NM (1965). Effects of earthquakes on dams and embankments. *Geotechnique*, 15(2): 139-160.
- Seed HB & Martin GR (1966). The seismic coefficients in earth dam design. *Journal of the Soil Mechanics and Foundations Division, ASCE*, 92(3): 25-58.
- Ishihara K, Tmncoso J, Kawase Y (1980). Cyclic strength characteristics of tailings materials[J]. *Soils and Foundations*, 20(4): 127-142.



**Geotechnical Reuse of
Industrial Wastes**

USE OF RECYCLED COPPER SLAG IN CEMENT-TREATED SINGAPORE MARINE CLAY

S. H. CHEW¹ and S. K. BHARATI²

ABSTRACT: Copper slag is a by-product obtained during the matte smelting and refining of copper. Singapore imports huge amount of copper slag to be used as abrasive material for ship clearing and repairing, and resulting in used copper slag as waste material. It has been estimated that 300,000 tonnes of copper slag needs to be disposed annually. Singapore being an island country and having shortage of landfill space, hence copper slag disposal becomes an environmental problem. The objective of this research is to study the possible pozzolanic property of this used copper slag to see if it can be effectively used as a partial cement substitute and partial soil replacement in cement-treated soft clay. If so, it will be solving environmental problem on one hand, and strengthening soft clay at the same time.

In this paper the effect of copper slag on strength characteristics of cement-treated Singapore marine clay is studied by varying the percentage of copper slag at 100% water content and constant workability of cement-clay mix. The results show that when workability of cement-treated clay with and without copper slag is kept constant, the unconfined compressive strength at 28 days curing time is observed to be constant. Therefore it seems to suggest that copper slag can be used in treating soft marine clay with less amount of cement and yet no reduction in strength can be achieved.

KEYWORDS: copper slag, pozzolanic property, cement-treated clay, strength

INTRODUCTION

For every ton of copper metal production about 2.2 tonnes of slag is generated and each year, approximately 24.6 million tonnes of copper slag is generated from world copper production. The major copper slag producing regions with quantities are given in Table 1. Copper slag application in Singapore is mainly on sand blasting for ships, therefore there are huge amount of copper slag accumulated. It has been estimated that 300, 000 tonnes of copper slag needs to be disposed annually (Lim and Chu, 2006). Singapore being an island country, dumping or disposal of such huge quantities of slag causes environmental and space problems.

Consequently, there is an urgent need to find possible solutions to use the copper slag. One such option is to utilize copper slag for engineering practices. There have been some researches on the possible utilization of copper slag in construction-related applications (e.g. for preparation of mortar and concrete) (Madany et al. 1991; Toshiki et al. 2000). Some researches shows that copper slag exhibits pozzolanic properties (Douglas and Mainwaring, 1985; Pavez et al. 2004) and may be used as partial or full replacement of cement (Gorai et al. 2003). However, Lim and Chu (2006) stated that copper

slag has no observable pozzolanic property. Hence, the present research aim to clarify the possible pozzolanic property of this used copper slag in cement-treated clay.

Table 1 Copper slag generation (after Gorai et al. 2003)

Regions	Copper slag (in million tonnes/annum)
Asia	7.26
North America	5.90
Europe	5.56
South America	4.18
Africa	1.23
Oceania	0.45

Cement treatment of soft clay has been widely used to improve the engineering properties of the clayey soils (Tatsuoka and Kobayashi, 1983; Chew et al. 2004; Lee et al. 2005). It is well known that there are two major chemical reactions which are induced by the addition of cement to clay and govern the soil cement stabilization process: the primary hydration reaction of the cement and water, and the secondary pozzolanic reactions between Ca(OH)_2 and the clay minerals. The hydration reaction leads to the initial gain in strength because of

¹ Assistant Professor, Department of Civil Engineering, National University of Singapore, Singapore. Email: cvecsh@nus.edu.sg

² Ph.D Student, Department of Civil Engineering, National University of Singapore, Singapore. Email: g0600364@nus.edu.sg

the formation of primary cementitious products. In pozzolanic reaction, silica and alumina from the clays react with the Ca^{2+} ions, forming calcium silicate hydrate (CSH) and calcium aluminate hydrate (CAH), which are the secondary cementitious products. These compounds crystallize and harden with time, thereby enhancing the strength of the soil cement mixes. If copper slag contains sufficient and suitable silica and alumina, and exhibits the pozzolanic property, then it will help in pozzolanic reaction and contribute to increase in strength in cement-treated clay. Copper slag can thus be used as partial cement substitute in cement-treated soft clay with solving the environmental and space shortage problems.

EXPERIMENTAL INVESTIGATION

Singapore Upper Marine Clay, Ordinary Portland Cement (OPC) and copper slag are used in the preparation of unconfined compression test samples in this study. The Singapore Upper Marine Clay is obtained from 4 to 5m depth, at an offshore dredge site near Pulau Tekong, Singapore. Its index properties are given in Table 2. The copper slag used in this study is from JPL industries Pvt. Ltd., Singapore. The particles are black and shape of particle ranged from partially rounded to angular. The chemical composition and index & engineering properties of copper slag are given in Table 3 & 4 respectively.

Table 2 Index properties of Singapore marine clay

Properties	Results
Liquid limit, %	87
Plastic limit, %	45
Plasticity index, %	42
Specific gravity	2.7
Grain size distribution:	
• Sand size (%)	2
• Silt size (%)	33
• Clay (%)	55

To study the effect of copper slag on strength characteristics of cement-treated clay, two series of mixes are prepared with varying percentage of copper slag (0 to 30%). For first series of mixes, the water content of mixes (defined as total weight of water over total weight of soil solid, dry cement and dry copper slag) is kept constant (in this case kept at 100%). For second series of mixes, the workability of mixes is kept constant. The range of the cement content and the water content are representative of that used in jet grouting and deep mixing methods in treating marine clay (Lee et al. 2005;

Chew et al. 1997). A summary of the laboratory testing program is shown in Table 5.

Table 3 Chemical composition of copper slag

Elements	Unit (% w/w)
Si	13.80
Ca	5.21
K	0.76
Fe	38.05
Al	2.75
Mg	0.78
Na	ND
Zn	0.80
Cu	1.02
Cd	ND
Cr	< 0.10
Pb	< 0.10
As	0.19
Hg	ND

Table 4 Index and engineering properties of copper slag

Properties	Results
Specific gravity	3.57
Grain size distribution:	
• Sand size (%)	88
• Silt size (%)	12
pH value	7.50
Shear strength parameter : (loose state)	
• ϕ_{peak}	33 ⁰
• ϕ_{residual}	30 ⁰

Table 5 Summary of the laboratory testing program

Mix no.	c/s	Cus/s	w	Workability
I	10 & 30%	0 to 30%	100%	Varying
II	30%	0 to 30%	Varying	Constant

In Table 5, Apparent Cement Content (c/s) is defined as the ratio of the weight of dry cement (c) to the weight of dry soil (s); Apparent Copper Slag Content (Cus/s) is defined as the ratio of the weight of dry copper slag (Cus) to the weight of dry soil (s); and Water Content (w) is defined as the ratio of the total weight of water to total weight of soil solid, dry cement and dry copper slag.

TEST RESULTS AND ANALYSIS

- (a) Unconfined compressive strength of cement-treated clay with copper slag at 100% water content

Figs. 1 and 2 show the stress-strain curves obtained from unconfined compression test (UCT) on cement-treated SMC with 10% apparent cement content and varying apparent copper slag content. It can be seen in the figures that all samples show clear peak value of unconfined compressive strength (q_u). Fig. 3 shows the effect of apparent copper slag content on unconfined compressive strength (q_u) of cement-treated SMC at both 7 & 28 days curing time. This plot shows that as apparent copper slag content increases, the unconfined compressive strength decreases, for both 7 & 28 days curing time.

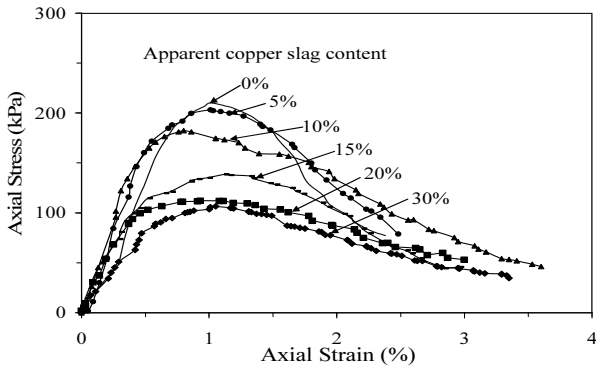


Fig. 1 Effect of copper slag on stress-strain behavior of cement-treated SMC (c/s = 10%, and curing time = 7 days)

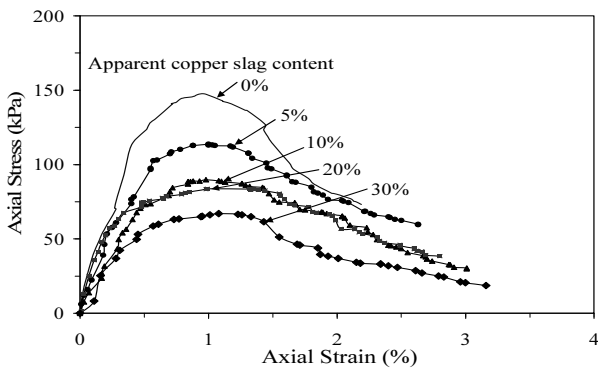


Fig. 2 Effect of copper slag on stress-strain behavior of cement-treated SMC (c/s = 10%, and curing time = 28 days)

(b) Unconfined compressive strength of cement-treated clay with copper slag at constant workability

Studies of mixes at 100% water content show that as apparent copper slag content increases, the mix of copper slag-cement-clay becomes more slurry. Thus the workability of mix increases as apparent copper slag content increases. The increase in workability can be inferred from falling cone penetration test used in liquid limit (LL) determination. The test results are shown in Fig. 4. However for comparison of strength for different copper slag-cement-clay mixes, it is important to keep the “workability” to be constant. Hence, workable range for particular case of apparent cement content of 30% is

determined as shown in Fig. 5 (the workability range is determined by the method adopted by Chew et al. (1997)) and a cone penetration value of 24 mm is selected as “reference workability” so that the mixes with this same workability value will be compared. This cone penetration value (24 mm) is selected because it corresponds to the penetration of cement-clay mix without copper slag at 100% water content as shown in Fig. 6. It is also noted that the line is parallel to LL line.

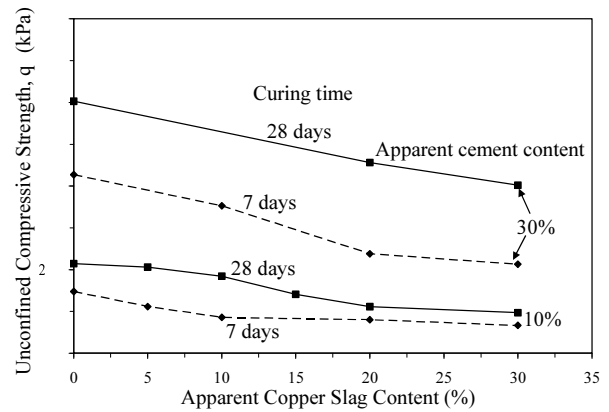


Fig. 3 Effect of copper slag on q_u of cement-treated SMC ($w_i = 100\%$)

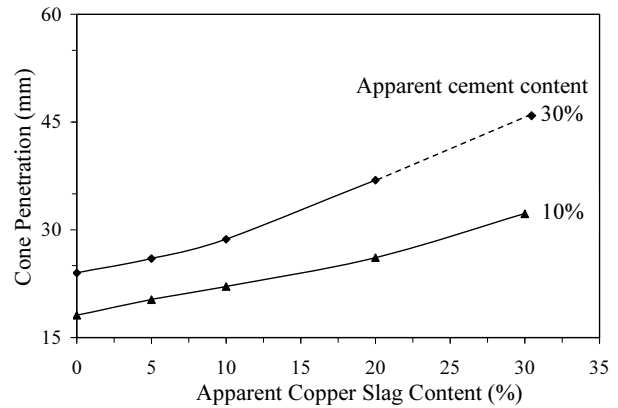


Fig. 4 Effect of copper slag on cone penetration of fresh slurry of cement-treated SMC (c/s = 10% & 30% and $w_i = 100\%$)

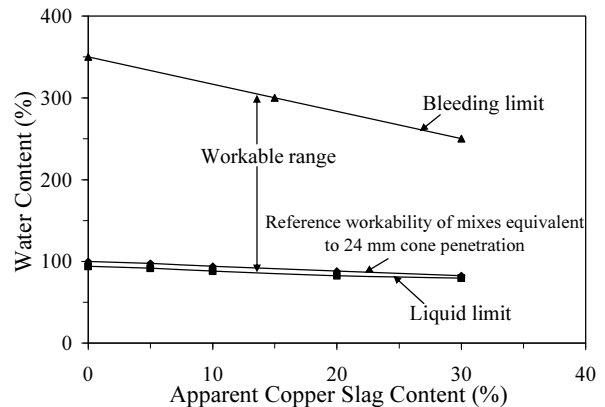


Fig. 5 Workable range of fresh cement-clay mix with varying apparent copper slag content (c/s = 30%)

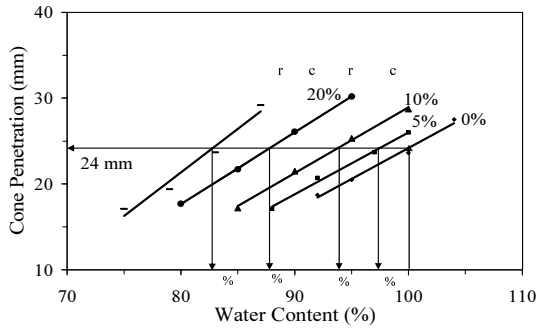


Fig. 6 Water content of cement-treated SMC with varying apparent copper slag content at “reference workability” equivalent to 24 mm cone penetration

Figs. 7 & 8 show the stress-strain curves obtained from unconfined compression test on cement-treated clay with and without copper slag for samples at “reference workability” equivalent to 24 mm cone penetration. With the inclusion of upto 30% apparent copper slag content, the general stress-strain behavior remains about the same shapes. The peak value (q_u) varies slightly, while the failure strain are all about 1 to 1.5%. Fig. 9 shows the q_u value at various apparent copper slag contents. This figure shows that as apparent copper slag content increases the unconfined compressive strength slightly decreases at 7 days curing time, whereas

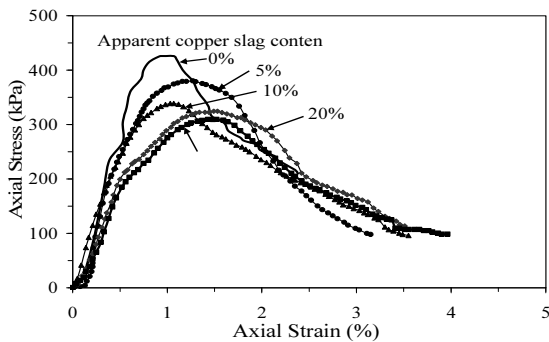


Fig. 7 Effect of copper slag on stress-strain behavior of cement-treated SMC at “reference workability” equivalent to 24 mm cone penetration (c/s = 30% & curing time = 7 days)

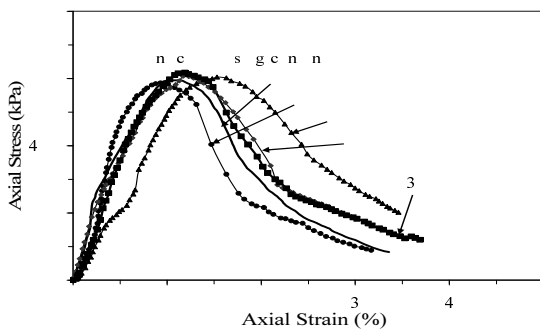


Fig. 8 Effect of copper slag on stress-strain behavior of cement-treated SMC at “reference workability” equivalent to 24 mm cone penetration (c/s = 30% & curing time = 28 days)

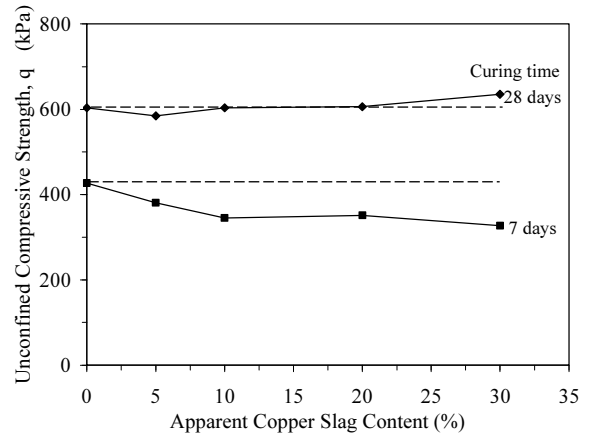


Fig. 9 Effect of copper slag on q_u of cement-treated SMC at “reference workability” equivalent to 24 mm cone penetration

at 28 days curing time, strength of cement-treated clay with copper slag is approximately constant.

Due to the lower water absorption, higher specific gravity and smaller specific surface area of copper slag than that of cement and clay particles, the addition of copper slag into cement-treated clay will result in lower water to solid ratio, if the workability is kept constant. This will then give rise to higher shear strength. This is termed “Physical effect” of copper slag.

The cementitious action of copper slag under activation of sufficient Ca(OH)_2 leads to the increase of the strength of cement-treated clay. This is termed “Chemical effect” of copper slag.

On the other hand, as apparent copper slag content increase, “actual” amount of cement per total solid (dry clay + dry copper slag + dry cement) weight (i.e. actual cement content) is reduced as shown in Fig. 10. Hence, the strength arising from the chemical reaction between the cement and other solid will reduce as increasing apparent copper slag content. Here copper slag is assumed to function as “soil”.

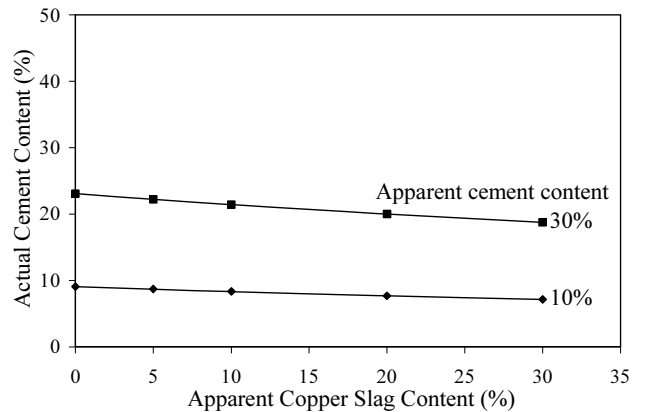


Fig. 10 Effect of copper slag on “actual” cement content of copper slag-cement-clay mix

If it is assumed that the strength gain in cement-treated clay with copper slag is due to cement-“soil” reaction (γ) and physical effect (α) & chemical effect (β) of copper slag. As indicated in Fig. 11, α is the strength component due to physical effect of copper slag, assumed to be same at 7 & 28 days curing time; β_7 is the strength component due to chemical effect of copper slag at 7 days curing time; γ_7 is strength component due to cement-“soil” reaction at 7 days curing time; γ_{28} is strength component due to cement-“soil” reaction at 28 days curing time; β_{28} is strength component due to chemical effect of copper slag at 28 days curing time. The relative amount of various components assumed is for indication only. As explained earlier, γ_7 and γ_{28} should be reduced as apparent copper slag content increases.

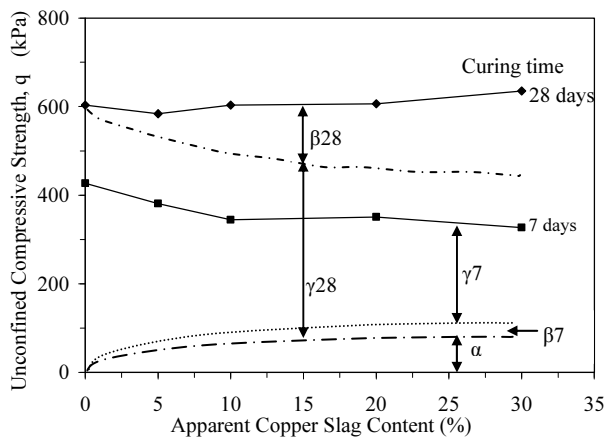


Fig. 11 Different components of strength

At 7 days curing time, the strength of cement-treated clay with copper slag is sum of value of α , β_7 and γ_7 as can be seen in Fig. 11. The sum of value of α , β_7 and γ_7 decreases as apparent copper slag increases. Thus it seems that the “strength gain” by physical effect (α) and chemical effect (β_7) of copper slag at 7 days curing time is less than the reduction of strength due to decrease in “actual” cement content.

At 28 days curing time, the strength of cement-treated clay with copper slag is sum of value of α , β_{28} and γ_{28} . The results show that the 28 days strength remain constant at various percentage of copper slag added. Hence, it can be observed from Fig. 11 that it is the larger value of β_{28} as compared β_7 that made the 28 days strength stay constant. The gain in strength with time from the copper slag (i.e. β_{28} vs β_7) is probably due to the activation of the more cementitious action of copper slag in longer curing period. This suggests that the copper slag may exhibits the pozzolanic property when added into cement-treated clay.

CONCLUSIONS

The following conclusions are warranted regarding the use of copper slag in cement-treated clay:

- (1) At 100% water content of mixes, the strength of cement-treated clay sample decreases as apparent copper slag content increases. However the workability of mixes increases as apparent copper slag content increases.
- (2) At constant workability of mixes and for 28 days curing time, the strength of cement-treated clay samples is found to be approximately constant as apparent copper slag content increases. Therefore it can be suggested that copper slag can be used in treating soft marine clay with less amount of cement and yet no reduction in strength can be achieved.
- (3) The strength decreases at constant workability with apparent copper slag content at 7 days curing time but remains almost constant at 28 days curing time. The gain in strength with time (i.e. $\beta_{28} > \beta_7$) is probably due to the activation of the more cementitious action of copper slag in longer curing period. This suggests that the copper slag may exhibits the pozzolanic property when added into cement-treated clay.
- (4) At 28 days curing time, the strength of cement-treated clay sample with copper slag is observed to be about constant. This suggests that the gain in strength by physical and chemical effect of copper slag is about the same as reduction in strength due to decrease in “actual” cement content of copper slag-cement-clay mix sample.

REFERENCES

- Chew SH, Kamruzzaman AHM, Lee FH (2004). Physico-Chemical and Engineering Behaviour of Cement-Treated Clays. *J. Geotech. Geoenviron. Eng. ASCE*, 130(7): 696-706.
- Chew SH, Lee FH, Lee Y (1997). Jet Grouting in Singapore Marine Clay. *Proceedings of the 3rd Asian Young Geotechnical Engineering Conference*, Singapore: 231-238.
- Douglas E & Mainwaring PR (1985). Hydration and pozzolanic activity of nonferrous slag. *American Ceramic Society Bulletin*, 64: 700-706.
- Gorai B, Jana RK, Premchand (2003). Characteristics and utilization of copper slag-a review. *Resources Conservation and Recycling*, 39: 299-313.
- Lee FH, Lee Y, Chew SH, Yong KY (2005). Strength and Modulus of Marine Clay-Cement Mixes. *J. Geotech. Geoenviron. Eng., ASCE*, 131(2): 178-186.
- Lim TT & Chu J (2006). Assessment of the use of spent copper slag for land reclamation. *Waste Management*

- & Research, 24: 67-73.
- Madany IM, Al-Sayed MH, Raveendran E (1991). Utilization of copper blasting grit waste as a construction material. *Waste Management*, 11: 35-40.
- Pavez O, Rojas F, Palacios J, Nazer A (2004). Pozzolanic activity of copper slag. Proceedings of the VI international conference on clean technologies for the mining industry, University of Concepcion, Chile.
- Tatsuoka F & Kobayashi A (1983). Triaxial Strength Characteristics of Cement-Treated Clay. Proc. 8th ECSMFE, Helsinki: 8(1): 421-426.
- Toshiki A, Osamu, K, Kenji S (2000). Concrete with copper slag fine aggregate. *Journal of the Society of Materials Science*, 49(10): 1097-1102.

EXPERIMENTAL STUDY ON THE ENGINEERING PROPERTIES OF TWO INCINERATION BOTTOM ASH OF MUNICIPAL SOLID WASTES

Jian-Ming ZHANG¹, Min-Yun HU² and Si-Fa XU³

ABSTRACT: For the sake of safe disposal and re-utilization of incineration bottom ash of municipal solid wastes, two kinds of incineration bottom ash, which were from typical grate incinerator and fluidized bed incinerator respectively, were tested in laboratory. According to the grading character, compaction, shearing strength and compression property, engineering properties of the two incineration bottom ash were analyzed and compared. Also, the properties were compared with data from other areas, which may offer a reference to incineration bottom ash's utilization as road bed fill.

KEYWORDS: municipal solid waste; incineration bottom ash; compaction test; compression test; direct shear test

INTRODUCTION

Incineration is one of the major methods that were used to dispose the municipal solid waste in China. Especially in comparatively developed area, incineration develops rapidly. For example, more than half municipal solid wastes were disposed by incineration in Zhejiang province. At present, the most widely used and representative incinerators for municipal solid wastes disposal were grate type incinerator, fluidized bed incinerator and rotary kiln incinerator. As the rotary kiln incinerator is mainly used for the disposal of poisonous waste and industrial waste, grate type incinerator and fluidized bed incinerator were commonly used. Unfortunately, whatever incineration methods may leave residues after incineration which need further disposal.

Shi AJ et al. (2004) consider that the incineration residues generally take a percentage of 20% to 30% of the weight of the initial wastes. The municipal solid waste incineration residues can be divide into two kinds, incineration bottom ash and incineration fly ash, according to the location where it is collected. The incineration bottom ash weighs 80 percent of the weight of the incineration residues, which account for the majority of incineration residues. As the incineration fly ash has toxic heavy-metal elements, generally it is used for landfill disposal.

For the sake of offering references in the disposal and re-utilization of the incineration bottom residue of municipal solid waste, the writer respectively gathered

the incineration bottom ashes which were from two typical incinerations of municipal solid waste, and made comparative analysis of their physical, chemical and engineering properties by the results from tests in laboratory.

MATERIAL AND METHODS

Sampling

In order to test and compare two different kinds of bottom ashes, samples were taken from grate type incinerator and fluidized bed incinerator, respectively, from typical incineration plants in Zhejiang province. The tested properties of samples were shown in Table 1. The grate type incinerator was marked as LP, and its bottom ash was marked as LP-B; the fluidized bed incinerator was marked as LH, and its bottom ash was marked as LH-B. The two samples were collected from two different commercial cities with similar climate and geographical environment. They are in equivalent scale and with similar level of development. The initial wastes were municipal solid wastes without being classified and without pre-disposal.

Items and Methods

For the sake of the safe disposal of incineration bottom ash and resource utilization, it is necessary to analyze the physical, chemical characteristics of incineration

¹ Graduate, College of Architecture and Civil Engineering, Zhejiang University of Technology, Email: jianming2815@163.com

² Associate Prof, College of Architecture and Civil Engineering, Zhejiang University of Technology, Email: huminyun@ziut.edu.cn

³ Associate Prof, College of Architecture and Civil Engineering, Zhejiang University of Technology, Email: xy20038@hotmail.com

Table 1 Description of the incineration bottom ash samples

Incineration furnace type	Auxiliary fuel	Numbering	Color	Smell	Shape
LP	None	LP-B	Dark brown	Pungent	Granular aggregate
LH	Add coal	LH-B	Brown	Minor pungent	Blocky

bottom ash. Therefore we do the following tests with samples of bottom ashes. (1) Physical properties: tests for the water content, water absorption, grain composition and the proportion of the two types of incineration bottom ash; (2) Engineering properties: compaction test, compression test, direct shear test.

RESULTS AND ANALYSIS

The Physical Properties of Incineration Bottom Ash

The screening tests results were shown in Fig. 1, which gives the grain composition of the two different incineration bottom ashes. The particle size related indexes of the bottom ash were shown in Table 3. From the test results, in LP-B, the content of the particle size between 0.075mm and 2mm takes a percentage of 82.94%, while in LH-B, takes a percentage of 57.65%. Therefore, both in LP-B and in LH-B, the particle size between 0.075mm and 2mm were in majority, which were similar with the sand particle distribution in classification of particles group. Particles above 5mm in LH-B were mainly composed of metal, ceramic fragment and glass fragment, which should be removed before being used for engineering purpose.

Uneven coefficient C_u and curvature coefficient C_c are two kinds of indexes which reflected the distribution of relative particle size of soil. They are also applied to the incineration bottom ash. C_u reflects the distribution shape of particles size in the curve; C_c reflects the shape of distribution of particles in the curve. Soil which meet the condition $C_u \geq 5$ and the condition $C_c = 1 \sim 3$ together is called good gradation soil.

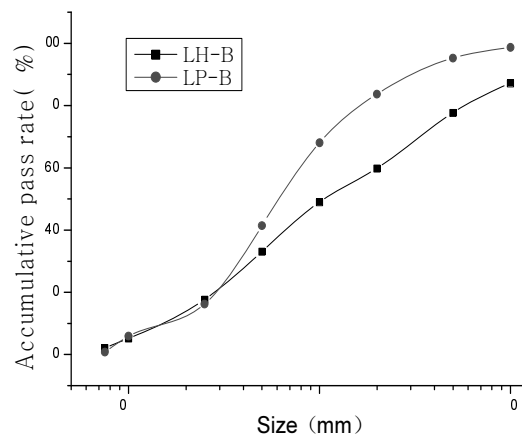


Fig. 1 Grain composition curves of the incineration bottom ash samples

Table 2 Physical properties of the incineration bottom ash samples

Sample	Water content	Water absorption	uneven coefficient C_u	Curvature coefficient C_c	Proportion d_s
LP-B	24.90%	43.3%	5.88	1.19	1.94
LH-B	5.86%	34.6%	11.76	0.52	2.30
Standard	—	—	≥ 5	1 ~ 3	—

From Table 2 we know, LP-B is good gradation, and LH-B is bad gradation. If the incineration bottom ash can be used as filler, the incineration bottom ash LP-B is more valuable than LH-B. When the incineration bottom ash is released, generally it needs water to cool down, and the quantity of water is not constant, so the incineration bottom ash has unsteady water content. From the proportion d_s of the incineration bottom ash, we can see it is lower than the sand which has proportion d_s between 2.65 and 2.69.

Compaction Test

The compaction test can help us understand the

compaction characteristics which can provide information on soil compaction for engineering design and roller compaction of field construction. Sand filling roadbed must be compacted in order to have sufficient strength and stability. Through the compaction test we can obtain the maximum dry density and optimum water content of materials, it can be used to guide the construction and check the quality of compaction on site. The equipment of the test is proctor compaction test device, original samples go though 5mm sieve, the particles more than 5mm of LP-B sample take a percentage of 18.46 of weight, the particles of LH-B take 24.80%, they are both less than 30% of the total mass of the sample, so maximum dry density and optimum water content are

needed to be corrected. The test based on “Soil Engineering Test Manual”, use the light compaction device, the quality of the hammer is 2.5kg, the diameter of the hammer is 51mm, the drop height is 305mm, the inner diameter is 102mm, the tube is 116mm high, with a volume of 947.4cm³, the number of hammer is three with 25 hit of each layer, the compaction work of unit volume is 592.2kJ/m³. From the Fig. 2 we know:

(1) The optimum water content of LP-B $W_o = 27\%$, maximum dry density $\rho = 1.49\text{g/cm}^3$. The optimum water content of LH-B $W_o = 26\%$, maximum dry density $\rho = 1.48\text{g/cm}^3$.

(2) The LH-B curve is flat, indicating that LH-B water stability is good and its mechanical properties was less affected by the water content, that is, the dry density has a small fluctuation when water content changes. LP-B has a certain degree of viscosity. LH-B is closer to the sand.

(3) Optimal water content and maximum dry density of LP-B and LH-B are very close, which is helpful to mixture applications in engineering.

(4) They can have a larger density in a larger range of water content, showing good performance of the compaction.

(5) The water content curve of LP-B is much steep after the optimum water content.

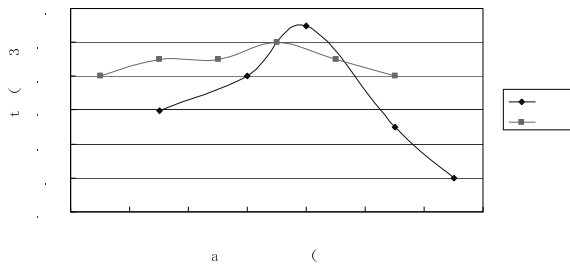


Fig. 2 Compaction curves of the incineration bottom ash samples

Compression Test

The compression characteristics of soil have a direct impact on foundation settlement. It is needed to study on the compression characteristics of the incineration bottom ash, considering it as a foundation material for filling. The compression curve reflects the compression characteristics of soil after being compressed. Compressibility is one of the important indexes of soil compression. The steeper the E-p curve is, the greater of ‘a’, and then the compression character is higher of the soil. As the E-p curve is usually not a straight line, the compressibility is not a constant even if the same soil. It will decrease when the initial pressure increases. In order to comparison in engineering, it is accustomed to employ the soil compressibility between 100kPa and 200kPa to express the level of compression properties. In this paper, we do a conventional compression test with LP-B which compaction coefficients were 0.95 and 0.90, and has a water content W of 27%. And with LH-B which compaction coefficients were 0.95 and 0.90, has a water content W of 26%. Before the test, the incineration bottom ash has been gone through the 5mm sieve. The load grade level is respectively 50, 100, 200, 300, 400, 800, 1600kpa, and the time space of loading is 24h, the results were shown in Table 3 and Fig. 3.

From Table 3 we know,

(1) When the compaction coefficients were 0.95 and 0.90, optimum water content, the a_{1-2} compressibility of LH-B is 0.133 and 0.150, is lower than the LP-B which compressibility is 0.160 and 0.181. The LP -B and LH-B are equivalent to middle-low compression of soil.

(2) Under the same compaction condition, LH-B has a lower compressibility and a higher modulus of compressibility than LP-B. From this point, LH-B is more favorable in engineering.

(3) Under the optimal water content, the modulus of compressibility increased with the improving of the compaction coefficient, but compressibility will turn lower.

Table 3 Compression test of the incineration bottom ash samples

Sample	compaction coefficient	Water content /%	E_{S1-2} / MPa	E_{S3-4} / MPa	a_{1-2} / MPa ⁻¹	a_{3-4} / MPa ⁻¹
LP-B	0.95	27	8.543	12.760	0.160	0.105
LP-B	0.90	27	7.694	12.014	0.181	0.111
LH-B	0.95	26	12.297	24.082	0.133	0.067
LH-B	0.90	26	10.848	14.843	0.150	0.108

Direct Shear Test

In the real project, when calculating the bearing capacity and evaluating the stability of the foundation, we shall always use the shear strength index. Therefore, it is great significance to test the shear strength of soil in engineering.

The test is based on the “Soil Engineering Test Manual”, which respectively prepares samples with the LP-B and LH-B; each contains 27% and 26% of optimal water content. And we choose samples with compaction coefficient of 0.95, carrying out the direct shear test to the LP-B and LH-B respectively, in which the vertical load is 50, 100, 150, 200, 300, 400kPa respectively. The

results of the experiments were on the pictures From Fig.4. We make a straight line to these points, and get the data of the LP-B and LH-B-cohesion C. The C values ranged were 15.23kpa and 2.33kpa, and the friction angle ϕ values ranged were 23.11° and 27.29°.

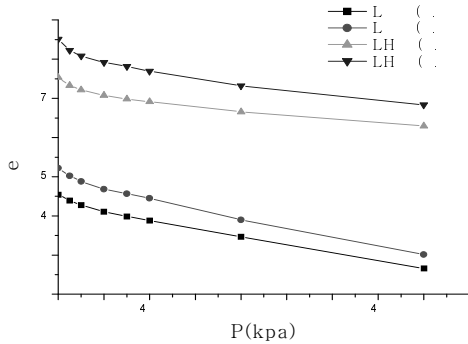


Fig. 3 Compression curves of the incineration bottom ash samples

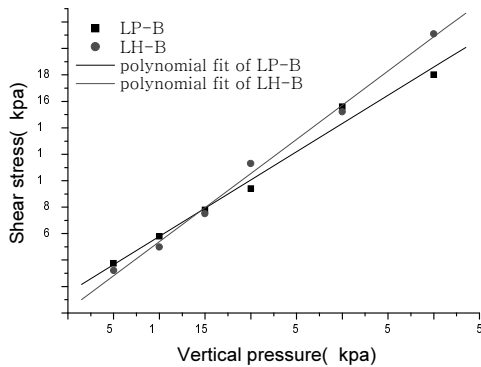


Fig. 4 Direct shear curves of the incineration bottom ash samples

From Fig.4 we know,

(1) The shear strength of the LP-B and LH-B is small, with C of 15.23kpa、 2.33kpa respectively. The friction angle is similar to each other, with ϕ of 23.11°、 27.29° respectively.

(2) The LH-B C = 2.33kpa, the cohesive strength is very small, which close to the sandy soil of 0.

CONCLUSIONS

(1) Incineration bottom ash on physical properties. Measured by the test, the water content of bottom ash is between 5% and 25%, and the water content of LP-B is higher. The range of particle size of incineration bottom

ash mostly is 0.1 ~ 5.0 mm, and effective grain size is about 0.15mm. According to the characteristics of the particles, the incineration bottom ash and sandy soil have a similar property. Li-Han. LI et al. (1999) and Ai-Juan SHI et al. (2004) suggest that particle size distribution, aggregate gradation good compaction prone to a high load-bearing capacity of the state, and the shear capacity of high frost resistance, and stability. Some studies show that Aggregates with uniform distribution of particle size and good gradation can be compacted to a high load-bearing capacity of the state. The aggregates are also with a high shear capacity, high frost resistance and good stability. These experimental results show that LP-B is good gradation. If the incineration bottom ash can be used as filler, the incineration bottom ash LP-B is more valuable than LH-B.

(2) The optimal water content and maximum dry densities of the LP-B and LH-B ash are very close, which is conducive to work on the mixed use of the two types of ash. Optimal water content and maximum dry densities of LP-B and LH-B are very close, which is a condition for the mixed use of two types of bottom ash.

(3) Compaction coefficient of the bottom residues has important implications for the strength, the higher the compaction coefficient is, the lower the compressibility, the higher the compression modulus. The compressibility of LH-B is lower than the LP-B. The LP -B and LH-B are equivalent to middle-low compression of soil.

(4) The cohesion of LH-B is lower than LP-B, because LP-B has a low level of clay and meanwhile a high level of sand. Therefore, the cohesion of LH-B is smaller than LP-B, because LH-B has less clay and more sand. Both of them lead to lower shear strength. In order to improve its shear strength, it should be mixed with the other soil in engineering.

REFERENCES

Gong XN (2002). Soil Mechanics. China Architecture Building Press.
 Li LH & Zhang NL (1999). Road Building Materials. Shanghai: Tongji University Press.
 Shi AJ, et al. (2004). Engineering Characteristics of Cinder from Municipal Domestic Refuse Incinerator. Environmental Engineering. 22(1):47-50.
 Yang ZQ & Zhou SQ (2005). Investigation Development on the Control of Heavy Metals from MSW Incineration Flue Gas Ash. Environmental Sanitation Engineering. 13(4):36-42.

UTILIZATION OF COAL ASH AS RECYCLING MATERIAL OPTIONS IN VIEW POINT OF GEOENVIRONMENT

Ahmad RIFA'I¹, Noriyuki YASUFUKU², Kiyoshi OMINE³ and Kazuyoshi TSUJI⁴

ABSTRACT: Disposed coal ash is result from the residual of coal refinery processes and become environmental important issues. Coal ash consists of bottom ash and fly ash. The number of coal ash production is abundant, and can be considered as waste material if it is not effectively reused or recycled for other application. In engineering practice, utilization of fly ash as additive materials is limited and in small quantity while the disposal of fly ash is quite high. The major aim of this paper is to stress the characterization, classification and utilization of coal ash as recycling structural material in view point of geoenvironment. Also, to prove of coal ash contribution in geotechnical engineering, give benefit in engineering practice and also become as part of engineering material that is environmental friendly. Material characteristics involve physical, mechanical, mineral composition and chemical properties, including environmental aspect by laboratory tests are presented. Uniaxial test, CBR test, sulphate resistance test and leaching test of heavy metal contents of coal ash as recycling structural material were also conducted to ensure environmentally acceptable based on Indonesian standard SNI. Fly ash is grouped in F class. Based on SNI-03-2460-1991, fly ash sample is available as additive material in concrete. Mix design of coal ash paving block is conducted toward several mixes, different volumes of coal ash and cement to grasp optimum utilization of coal ash and qualify minimum standard requirement of Indonesian standard SNI 03-0691-1996. Coal ash paving block with quality B, i.e. has compression strength 200 kg/cm² can be mixed with fly ash adding 30% maximum as additive, or use of 50% fly ash as substitution with cement content is kept or using fly ash 30% and bottom ash 40%. Coal ash paving block samples resist to sulphate. Effect of addition of fly ash, bottom ash and lime on physical and mechanical properties can improve the index properties of soft soil sub grade layer, increases bearing capacity, as well as decreases swelling potential. Coal ash-soil mixture contains some heavy metals, but concentration values is still under boundary threshold of government act PP No. 20, 1990 about criteria of water quality in group D.

KEYWORDS: coal ash, recycling material, geoenvironment, engineering properties, environmental friendly, mix design.

INTRODUCTION

Disposed coal ash is result from the residual of coal refinery processes and become environmental important issues. Coal ash consists of bottom ash (5-15%) and fly ash (85-95%) (JCOAL, 2008). In engineering practice, utilization of fly ash as additive materials is limited and in small quantity while the disposal of fly ash is quite high. It also occurs at companies in Indonesia.

Fly ash is the fine powder formed from the mineral matter in coal, consisting of the non-combustible matter in coal plus a small amount of carbon that remains from incomplete combustion. Fly ash is generally light tan in color and consists mostly of silt-sized and clay-sized

glassy spheres. This gives fly ash a consistency somewhat like talcum powder. Properties of fly ash vary significantly with coal composition and plant-operating conditions. Each fly ash from different place has different quality, where quality requirements for fly ash vary depending on the intended use.

The number of fly ash production is abundant, and can be considered as waste material if it is not effectively reused or recycled for other application. Currently there are various applications of fly ash utilization by sector consist of cement or concrete, structural fills, soil stabilization and agriculture. The major aim of this paper is to stress the characterization, classification and utilization of coal ash as recycling structural material in

¹ Associate Professor, Dept of Civil and Environmental Engineering, Faculty of Engineering, Gadjah Mada University, Indonesia. Email: ahmad.rifai@tsipil.ugm.ac.id

² Professor, Dept of Civil and Structural Engineering, Kyushu University, Japan. Email: yasufuku@civil.kyushu-u.ac.jp

³ Associate Professor, Dept of Civil and Structural Engineering, Kyushu University, Japan. Email: oomine@civil.kyushu-u.ac.jp

⁴ President Director, PT Toray Trading Indonesia, Indonesia. Email: kazuyoshi_tsuji@ina.toray.co.id

geoenvironment point of view. Study and analysis of addition of fly ash and bottom ash on physical and mechanical properties of recycling structural material are described and discussed. Also, to prove of coal ash contribution in geotechnical engineering, give benefit in engineering practice and also become as part of engineering material that is environmental friendly.

EFFECTIVE COAL ASH UTILIZATION AND CHARACTERISTICS

In Indonesia, coal is used as fuel in several industries, included electric power plant and chemical industries. Coal ash generation increases with the increased demand for energy source and economic growth, but coal ash utilization is still low in Indonesia. The task of expanding its effective uses is a critical one.

Several countries have developed coal ash utilization well. In Japan, coal ash is produced from electric power plants and general industries. The ratio of fly ash production is relatively stable every year. An electric power utility is average 75% and 25% from general industries. In year 2006, the ratio of effective utilization was reached about 97%. Coal ash utilization by sector in Japan is 68.2% for cement, 13.2% for public work, 3.7% for construction works, 1.5% for agriculture fields and others is 13.3% (JCOAL, 2008).

One of effective utilization of coal ash in Japan is Hi-Beads material. Hi-Beads is used as materials alternative to sea sands. It is granular with diameter less than 10 mm, and use fly ash as main ingredients. Hi-Beads have sufficient strength as sand compaction pile and sufficient drain capacity as sand drain. Fig. 1 shows material comparison of hi-beads, bottom ash and fly ash. Production of Hi-Beads at electrical power plant in Japan is shown in Fig. 2.



Fig. 1 Grain size of Hi-Beads, bottom ash and fly ash



Fig. 2 Production of Hi-Beads at electrical power plant in Japan

There are four most relevant characteristic of fly ash quality for that must be investigated i.e. loss on ignition (LOI), fineness, chemical composition, and uniformity. LOI is a measurement of unburned carbon (coal) remaining in ash and is a critical characteristic of fly ash, especially for concrete applications.

Fineness of fly ash is most closely related to the operating condition of the coal crusher and the grind ability of the coal itself. For fly ash use in concrete application, fineness is defined as the percent by weight of the material retained on the 0.044 mm (No. 325 sieve). A coarser gradation can result in a less reactive ash and could contain higher carbon contents. Some non-concrete application, such as structural fills are not affected by ash fineness. However, other applications such as asphalt filler are greatly dependent on the fly ash fineness and its particle size distribution.

Chemical composition of fly ash relates directly to the mineral chemistry of the parent coal and any additional fuels or additives used in the combustion or post combustion processes. The pollution control technology that is used also affect the chemical composition of the fly ash. From the chemical composition, the fly ash can be classified as class C or class F.

Uniformity of fly ash characteristic from shipment to shipment is imperative in order to supply a constant product. Fly ash chemistry and characteristics are typically known in advance so concrete mixes are designed and tested for performance.

Class C fly ash are generally derived from sub-bituminous coals and consist primarily of calcium alumina-sulphate glass, as well as quartz, tri calcium aluminates, and free lime (CaO). Class C is also referred to as high calcium fly ash because typically contains more than 20 percent CaO. Class F ashes are typically derived from bituminous and anthracite coals and consist primarily of alumina-silicate glass, with quartz, mullite, and magnetite present. Class F, or low calcium fly ash has less than 10 % CaO.

Based on ASTM C 618-78, class C fly ash has minimum content of SiO₂, Al₂O₃ and Fe₂O₃ about 50% and maximum LOI about 6%, while class F has minimum content of SiO₂, Al₂O₃ and Fe₂O₃ about 70% and maximum LOI about 12%. Class C can be used as stand-alone material while Class F is commonly blended with lime or cement. Therefore, fly ash from a certain location needs to be studied further of physical and chemical characteristics to get more effective and more efficient in utilization. Also, to ensure that utilization coal as recycling material options is not environment load to ensure environmentally acceptable based on Indonesian standard.

MATERIAL AND RESEARCH METHOD

Research material is disposed coal ash and taken from chemical industry around Jakarta, Indonesia. Fly ash and bottom ash materials are shown in Fig. 3. Scope works of this research involves physical, mechanical and chemical properties and mineral composition, including environmental aspect by laboratory tests.

Main test consist of index properties test, mineral composition test using XRD as shown in Fig. 4, uniaxial test, permeability test, sulphate resistance and leaching test of heavy metal contents. Standard test method is adopted from ASTM and SNI.

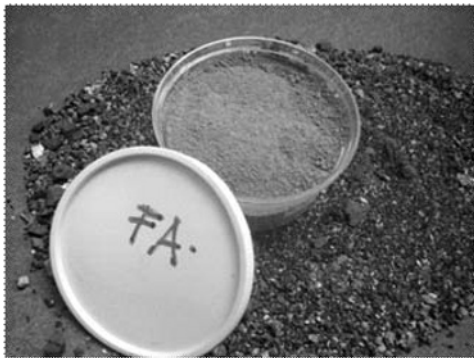


Fig. 3 Sample of coal ash: fly ash and bottom ash



Fig. 4 XRD equipment

Mix design test is conducted with variation of coal ash adding on recycling structural material for road applications. Fig. 5 shows fabrication of coal ash paving block.



Fig. 5 Coal ash paving block

CHARACTERIZATION AND CLASSIFICATION OF COAL ASH

Result of mineral composition of coal ash is summarized in Table 1. Index properties of fly ash such as water content is about 2.8%, spesific gravity G_s= 2.77 and fineness by weight of the material retained on No. 325 sieve is 17.2%.

Table 1 Mineral composition of coal ash

Mineral composition	Fly ash (%)	Bottom ash (%)
Silica (SiO ₂)	50.03	63.67
Alumina (Al ₂ O ₃)	3.68	13.43
Calcium Oxide (CaO)	3.80	5.46
Magnesium Oxide (MgO)	4.01	2.46
Iron Oxide (Fe ₂ O ₃)	32.88	11.41
Potash (K ₂ O)	0.32	1.03
LOI (Loss on Ignition)	3.99	0.84
SiO ₂ active	30	-

It shows that fly ash contains SiO₂ + Al₂O₃ + Fe₂O₃ = 86.6% (min70 %), LOI = 3.99% (max 6%) and retained sieve # 325 = 17.2% (max 34 %). Based on ASTM C 618-78, fly ash is grouped in F class. Fly ash sample is available as additive material in concrete based on SNI-03-2460-1991.

MIX DESIGN AND PERFORMANCE OF COAL ASH PAVING BLOCK

Fabrication of specimen is carried out to obtain the job mix formula. Mix test of coal ash paving block is conducted toward several mixes, different volumes of fly

ash, bottom ash and cement to grasp optimum utilization of coal ash and qualify minimum standard requirement of Indonesian standard SNI 03-0691-1996 as shown Table 2. Compressive strength is evaluated using uniaxial compression test. Durability is measured using abrasion test. Water absorption and sulphate resistant test also were conducted.

Table 2 Technical specification of paving block based on SNI 03-0691-1996

Quality	Compression (kg/cm ²)		Abrasion (mm/minute)		Water absorp. Max. (%)
	Average	Min	Average	Min	
A	400	350	0,090	0,103	3
B	200	170	0,130	0,149	6
C	150	125	0,160	0,184	8
D	100	85	0,219	0,251	10

Uniaxial compressive strength of coal ash paving block with fly ash variation at age 28 days is presented in Fig. 6. It shows sea water act as an accelerator to reaches the peak strength of paving block, but it will affect porosity due to chemical reaction. Coal ash paving block with quality B (use for pedestrian, parking area) can be mixed with fly ash adding 30% maximum as additive. Also, use of 50% fly ash as substitution with cement content is kept, gave compression strength equal B quality based on SNI 03-0691-1996. Another composition is using fly ash 30% and bottom ash 40% also gave B quality compressive strength, i.e average uniaxial compressive strength about 200 kg/cm².

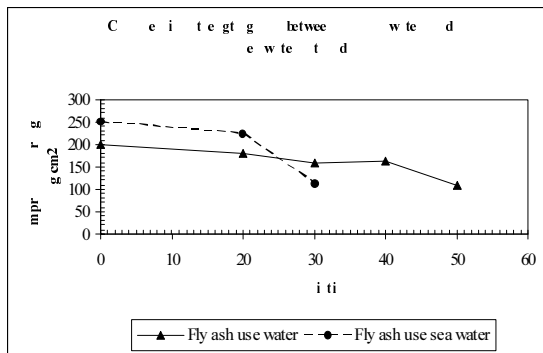


Fig. 6 Uniaxial compressive strength of coal ash paving block age 28 days

Coal ash paving block samples resist to sulphate attack and still under boundary threshold of SNI- 03-0691-1996 as shown in Fig. 7. The average dry weight loss of paving block with fly ash substitution is 0.8%.

Sample number 3,4,7 and 8 used sea water. It seen that coal ash paving block is less resistance to sulphate attack than conventional paving block up to 28 age days. Also, the utilization of sea water decrease sulphate resistance of coal ash paving block.

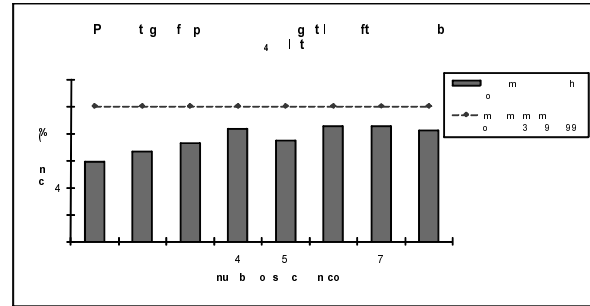


Fig. 7 Sulphate resistance of coal ash paving block

EFFECT COAL ASH ON STABILIZATION OF SUBGRADE

Utilization of coal ash on subgrade stabilization is performed by analysis of consistency limit parameter, swelling potential, California Bearing Ratio (CBR) value and leaching test of heavy metal on coal ash-soil mixture. Engineering properties of soil as subgrade layer is summarized in Table 3. It shows soil has high plasticity, fat clay, very poor as sub base and high activity. It indicates that soil has high swelling potential.

Table 3 Engineering properties of subgrade soil

No.	Parameters	Value
1.	Water content, w	54,77%
2.	Specific gravity, G _s	2,634
3.	Liquid limit, L _L	82,86%
4.	Plastic limit, P _L	28,33%
5.	Plasticity index, P _I	54,53%
6.	Shrinkage limit, S _L	10,06%
7.	Fines fraction	92,39%
8.	Coarse fraction	7,61%
9.	USCS classification	CH
10.	AASHTO classification	A-7-6
11.	Activity	2,48

Evolution of consistency limit with variation of coal ash content on soil mixture is shown in Fig. 8 and 9. Fig. 10 shows effect of coal ash content on swelling potential of coal ash-soil mixture. Evolution of CBR values of coal ash-soil mixture also is presented in Fig. 11. It shows that the increasing of coal ash cause the decreasing of liquid limit and plasticity index. Also, the

increasing of coal ash cause decreasing of swelling potential. The significant change of swelling potential of coal ash-soil mixture is using mixing of fly ash, bottom ash and lime. CBR value is also increasing with increase of coal ash content in soil mixture. Effect of addition of fly ash, bottom ash and lime on physical and mechanical properties can improve the index properties of soft clay, increases bearing capacity, as well as decreases swelling potential.

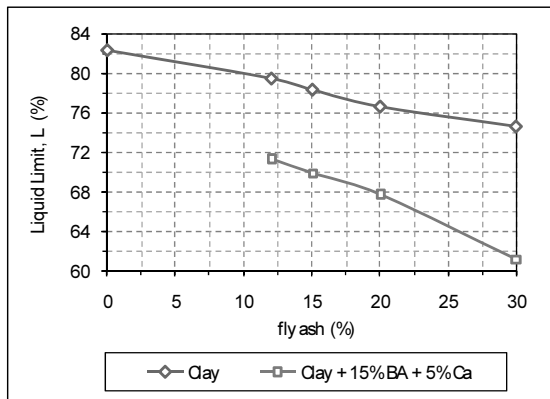


Fig. 8 Liquid limit value of coal ash -soil mixture

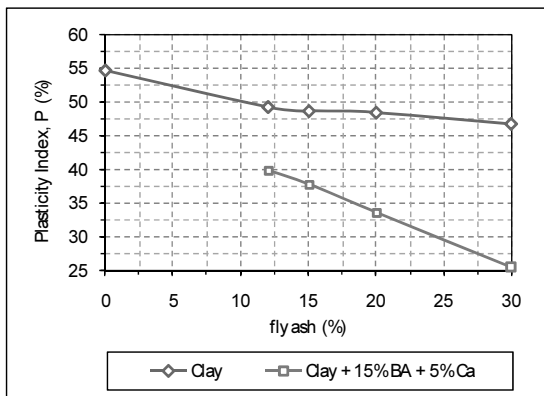


Fig. 9 Plasticity index of coal ash -soil mixture

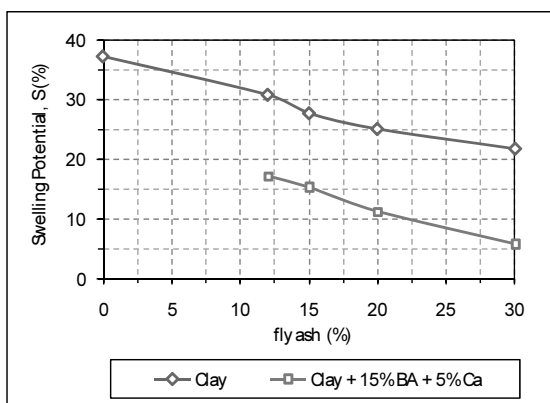


Fig. 10 Swelling potential of coal ash -soil mixture

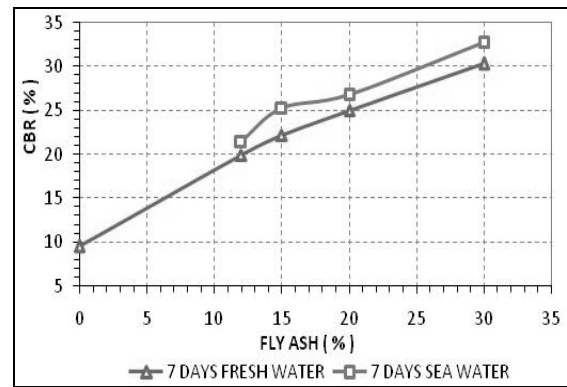


Fig. 11 CBR values of coal ash -soil mixture

Leaching test of heavy metal content on coal ash-soil mixture is conducted using Atomic Absorption Spectrophotometer (AAS) method. Based on leaching test, coal ash-soil mixture contains some heavy metals, but concentration values is still under boundary threshold of government act (PP) no. 20, 1990 about criteria of water quality in group D (irrigation use, industri and electricity power plant).

CONCLUSIONS

Characterization, classification and utilization of coal ash as recycling material options in geoenvironment point of view are presented and discussed. Mineral composition of coal ash by XRD test is presented. Based on ASTM C 618-78, fly ash is grouped in F class. Based on SNI-03-2460-1991, fly ash sample is available as additive material in concrete.

Coal ash paving block with quality B, application for pedestrian, street and parking area use can be mixed with fly ash adding 30% maximum as additive. Also, use of 50% fly ash as substitution with cement content is kept, gave compression strength equal B quality based on SNI 03-0691-1996. Another composition is using fly ash 30% and bottom ash 40% also gave B quality compressive strength, i.e average uniaxial compressive strength about 200 kg/cm². Coal ash paving block samples resist to sulphate attack and still under boundary threshold of SNI- 03-0691-1996. Utilization of sea water decrease sulphate resistance of coal ash paving block.

Coal ash is also used on subgrade layer stabilization. Analysis of consistency limits parameter, swelling potential, California Bearing Ratio (CBR) value and leaching test of heavy metal on coal ash-soil mixture are discussed. Effect of addition of fly ash, bottom ash and lime on physical and mechanical properties can improve the index properties of soft clay, increases bearing capacity, as well as decreases swelling potential. Based on leaching test, coal ash-soil mixture contains some heavy metals,

but concentration values is still under boundary threshold of government act (PP) no. 20, 1990 about criteria of water quality in group D (irrigation use, industri and electricity power plant).

ACKNOWLEDGEMENTS

The authors expresses their thanks to PT Toray Trading Indonesia and Hi-Link project for financial support. Then, the authors would like to thanks to colleagues of Department of Civil and Environmental Engineering, Gadjah Mada University who were very helpful and full of spirit in conducting laboratory test.

REFERENCES

- ASTM (2003). Annual Book of ASTM Standards, Section 4, Vol. 04.02, 04.08& 04.09, West Conshohocken.
- Bowles JE (1984). Physical and Geotechnical Properties of Soils, Mc. Graw Hill, Singapore.
- Budiono A & Triwulan (1993). Seminar Nasional Hasil Terbaru Penelitian Bahan, Pusat Antar Universitas Ilmu Teknik Universitas Gadjah Mada, Yogyakarta.
- Chugoku Electric Power Co., Inc. (2003). Civil Engineering of The Chugoku Electric Power, Sanko Inc., Japan.
- Das BM (1994). Principles of Geotechnical Engineering, PWS Publishing Comp., Boston, USA.
- Day RW (2000). Geotechnical Engineer's Portable Handbook, Mc Graw Hill, New York.
- Departemen Pekerjaan Umum (1982). Persyaratan Umum Bahan Bangunan di Indonesia, Pusat Penelitian dan Pengembangan Pemukiman, Departemen Pekerjaan Umum, Bandung.
- Departemen Pekerjaan Umum (1987). Pemanfaatan Abu Terbang Untuk Pekerjaan Beton, Pusat Penelitian dan Pengembangan Pemukiman, Departemen Pekerjaan Umum, Bandung.
- Departemen Pekerjaan Umum (1996). Standar Nasional Indonesia Bata Beton (Paving block), Pusat Penelitian dan Pengembangan Pemukiman, Departemen Pekerjaan Umum, Bandung.
- Herman (2005). Studi Potensi Limbah Pembakaran Batu Bara PLTU Sijantang Untuk Stabilisasi Lempung Ekspansif, Master Thesis, Graduate Program, Gadjah Mada University, Yogyakarta.
- Holtz DR & Kovacs WD (1981). An Introduction to Geotechnical Engineering, Prentice-Hall, Inc., Englewood Cliffs, N.J. 07632, USA.
- JCOAL (2008). Japan Coal Energy Center, www.jcoal.or.jp/coaltech_en/coalash/, 2008/04/10.
- Liu C & Evett JB (2003). Soil Properties: Testing, Measurement, and Evaluation, 5th Ed., Prentice Hall, New Jersey.
- Mulyani S (2006). Stabilisasi Tanah Lempung dengan Menggunakan Abu Terbang dan Kapur, Master Thesis, Graduate Program, Gadjah Mada University, Yogyakarta.
- Saito T (2002). Coal Ash Utilization Technology at Chugoku Electric Power.
- Syawal (2004). Identifikasi Potensi dan Tekanan pengembangan Tanah Lempung Ekspansif Dengan Alat Oedometer, Master Thesis, Graduate Program, Gadjah Mada University, Yogyakarta.
- Tjokrodimuljo K (1996). Teknologi Beton, Nafiri, Yogyakarta.
- Waller (1993). Coal bottom Ash/ Boiler Slag-Material Description 2000, <http://www.google.com>., Download 15 May 2008 at 19.00 WIB.

STUDY ON THE ENGINEERING PROPERTY OF MIXED-SOIL FLY ASH

Ya-Sheng LUO¹, Jing LI² and Andrew CHAN³

ABSTRACT: Fly ash is a byproduct dumped out of thermal power plants which use coal as one kind of fuel. It is urgent to consider how the vast quantity of harmful fly ash resources can be utilized. There are a large number of potential solutions to this problem, an effective disposal method is to use it as a fill material for dam construction or filled ground. Fly ash is a uncompacted lightweight material with a lot of pores. On one hand, it has a superior engineering capability in many aspects; On the other hand, pure fly ash lacks any necessary cohesion so that it has a very sensitive reaction with water which is an undesirable effect on the safe operation of the project which employs pure fly ash. Based on above considered, the engineering performance of the fly ash can potentially be enhanced by mixing different quantity of clay into fly ash, therefore the study on mechanical properties of fly ash mixed with different quantities of clay could help to promote the engineering application of fly ash. In this paper, fly ash from the Xianyang Weihe thermal power plant is the object of study, and different quantity of loess it is used to obtain the mixed-soil fly ash, then the engineering characteristics of fly ash with different quantity of soil mixed are studied via compaction test, compression test, and direct shear test as well as triaxial compression test. Furthermore, the trends of influence of different quantity of soil mixed on deformation and strength characteristics of fly ash are also obtained. The research results in this paper will offer the basis for both the effective utilization of fly ash and the improvement of its engineering property.

KEYWORDS: fly ash, mixtures, engineering property, experiment study

INTRODUCTION

Fly ash is a by-product from the burning of coal in thermal power plants and the amount produced is enormous and is increasing year by year. In China, the amount of fly ash produced annually by coal-burning power plants was already more than 170 million tons in 2003. It is urgent to find ways to utilize the vast quantity of harmful fly ash resources (Lu & Zhu, 2005). At present, there are a large number of potential solutions to this problem, one of the effective disposal methods is to use it as a fill material for dam construction or filled ground (ZHANG Ai-jun et al. 2004; K. Kayabal et al. 2000; Bumjoo Kim et al. 2005). Fly ash is an uncompacted lightweight material with a lot of pores. Its particles form was found to be granular, and its colors is between off-white and deep gray. Generally, fly ash is well graded, ranging from mostly silt to fine sand sizes. A majority of the sizes occurred in a range between 0.005 and 0.5 mm on the curve of grain size analysis, and there are a few particles with a size more than 2 mm occasionally. Fly ash has a superior engineering capability in many aspects,

and the outcomes of a lot of studies on the mechanical characteristic and application of fly ash have been reported also (FENG Hai-ning et al. 2002; Shenbaga et al. 2004; B. R. Phani Kumar et al. 2004; FENG Mei-guo et al. 2007). Pure fly ash lacks any necessary cohesion so that it has sensitive reaction with water, and this could be a hinderance to the safe operation of the project that uses pure fly ash. Researches had been carried in order to improve the engineering performance of fly ash by mixing it with other materials (Shenbaga R. Kaniraj et al. 1999; LIN Tong et al. 2003; Shenbaga. R. Kaniraj et al. 2003). According to the above researches, the engineering performance is enhanced potentially by mixed different quantities of clay into fly ash, and a study on the mechanical property of fly ash mixed with different quantity of clay will help to promote the engineering application of fly ash.

In this paper, fly ash from Xianyang Weihe thermal power plant is the object of study, and different quantities of loess were mixed into it in order to obtain the mixed-soil fly ash. Then the engineering characteristics of fly ash with different quantity of soil are studied via

¹ Professor, Northwest A&F University, China. Email: lyas1967@nwsuaf.edu.cn

² Professor, Northwest A&F University, China. Email: lijinglee@tom.com

³ Professor, Civil Engineering, School of Engineering, University of Birmingham, U.K. Email: a.h.chan@bham.ac.uk

compaction test, compression test, and direct shear test as well as triaxial compression test. Furthermore, the trends of influence of different amount of clay on the deformation and strength characteristics of fly ash are obtained. The research results in this paper will offer the bases for both the effective utilization of fly ash and the improvement of its engineering property.

TEST MATERIALS AND PROGRAM

Test Materials

In this paper, the weight ratios of fly ash to loess used are 1.0:0.0, 0.9:0.1, 0.8:0.2, 0.7:0.3 respectively. The fly ashes used in tests were collected from Xianyang Weihe thermal power plant near Xi'an. Table 1 shows the physical property indexes of fly ash. The loess used in the test was collected from Weihe two-stage terrace at Yangling District, Shaanxi Province at depth from 3.5 m to 5.0 m. The loess was the Loess of Q3. The natural water content is 17.8% obtained using drying method. Its natural dry density is 1.26 g/cm³, its natural void ratio is

1.151, and its natural degree of saturation is 41.9%. Table 2 shows the basic physical properties of loess.

Test Program

In this study, tests performed include compaction test, direct shear test and compression test as well as triaxial shear test. All of them were performed according to Specification of Soil Test SL237-1999, the industry standard of P.R China. The dry density used in this study is 0.95 of the degree of compaction multiplied by the maximal dry density of mixed-soil fly ash under different loess content obtained using the compaction tests respectively. Saturated samples are used in all the direct shear tests, compression tests and triaxial shear tests. The samples are formed by method of dry compaction. The saturated samples used in direct shear tests and triaxial shear tests are saturated by the vacuum method. The other saturated samples used in compression test are saturated directly in the apparatus. For the triaxial shear tests, the consolidated untrained triaxial compression (CU) test was employed. Table 3 shows the test program.

Table 1 Physical property indexes of fly ash

specific gravity G _s	constrained diameter /mm			Coefficient of uniformity C _u	Coefficient of curvature C _c	composition of particles /%		
	d ₆₀	d ₃₀	d ₁₀			2-0.075 mm	0.075-0.005 mm	<0.005 mm
2.07	0.055	0.19	0.005	11.00	1.31	27.0	63.0	10.0

Table 2 Indexes of physical property of loess

Specific gravity G _s	Liquid limit w _l / %	Plastic limit w _p / %	Plasticity index I _p / %	Classification according to plasticity chart	composition of particles /%			Classification according to composition of particles
					>0.05 mm	0.05~0.005 mm	<0.005 mm	
2.71	30.5	18.6	11.9	CI	6.5	61.4	32.1	Silty clay

Table 3 Tests program

loess content / %	Samples amount under different tests			
	compaction test	triaxial shear test	compression test	direct shear test
0	6	4	4	4
10	6	4	4	4
20	6	4	4	4
30	6	4	4	4

Test Methods and Purpose

The purpose of compaction test is to measure the

relations between density and water content of soil, thereby obtaining the relationship between maximum dry density and optimum water content of soil so that the test density can be found for the other three sets of tests.

For the direct shear tests, four groups of samples are loaded by horizontal shear force under different vertical pressures respectively. From the shear stress measured, the parameters of shear strength of soil (angle of internal friction ϕ and cohesion c) can be found according to Coulomb's law. The direct shear tests used in this study is the consolidated quick direct shear test (CQ) test.

The purpose of compression test is to obtain the relationship between deformation and pressure or the

relationship between deformation and time under the conditions of constrained lateral deformation and axial drainage.

The triaxial shear test is used to measure shear strength of soil. Generally, three to four cylindrical soil samples are loaded by axial load to shear until failure under different constant confining pressures. From these test results, the parameters of shear strength of soil (angle of internal friction ϕ and cohesion c) can be found according to the Mohr-Coulomb theory. The triaxial shear tests used is the consolidated undrained triaxial compression (CU) test, and the parameter of effective shear strength c' , ϕ' can be obtained.

TEST RESULTS

Compaction Test

Fig.1 shows the compaction curves of mixed-soil fly ash with four different amount of loess. The relationships of different quantity of loess mixed and the maximum dry density and optimum water content are shown in Figs. 2 and 3 respectively.

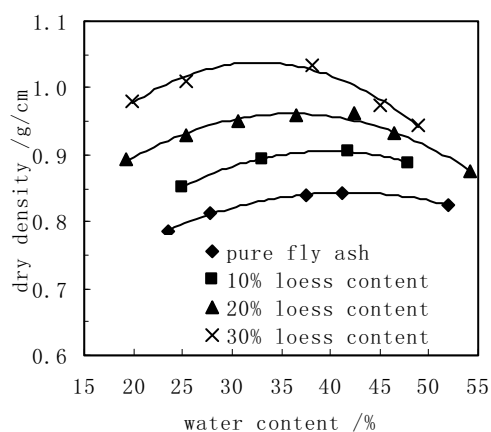


Fig. 1 The compaction curves of mixed-soil fly ash

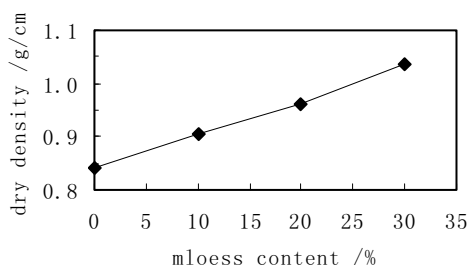


Fig. 2 The relation curves of loess content and the maximum dry density

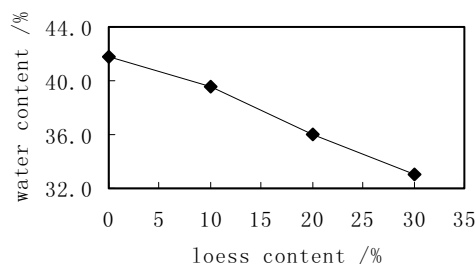


Fig. 3 The relation curves of loess content and optimum water content

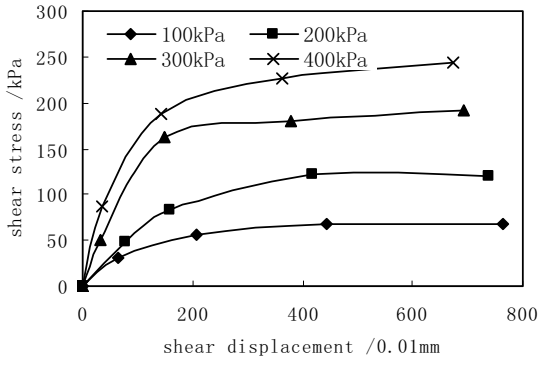
From these graphs, it can be noted that, as the amount of loess increased from 0 to 30%, the maximum dry density increased in an approximately linear fashion, while the optimum water content decreased. At a higher loess content, the compaction curve of mixed-soil fly ash has value of higher level, and its relative sensitivity of maximum dry density to optimum water content increases also.

The maximum dry density of mixed-soil fly ash with 30% loess content is at least 23% better than the maximum dry density of pure fly ash, but its optimum water content was reduced by at least 21%. Therefore, it can be concluded that, by mixing an appropriate quantity of loess into fly ash, it not only increases the maximum dry density therefore improving the stress condition in dam, but also using the amount of water required for the construction can be reduced sharply.

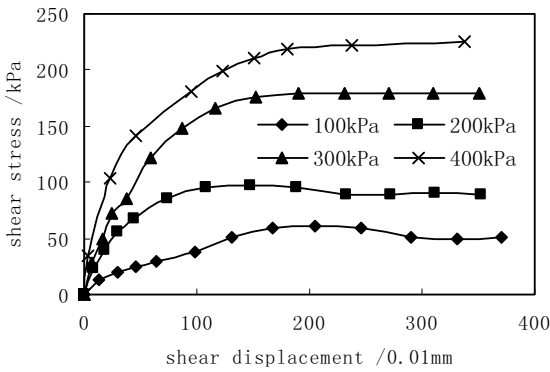
Direct Shear Test

The relationship of shear stress and shear displacement of fly ash with different quantity loess are given in Fig. 4 with the corresponding curves of shear strength and vertical pressure shown in Fig.5. The cohesion of mixed-loess fly ash, which were measured using direct shear tests, are all very close to zero. When the loess content are 0, 10%, 20%, 30%, the angles of internal friction of fly are 31.79°, 29.49°, 29.48°, 31.13°, respectively. Compared with pure fly ash, the shear strength of the other three groups reduces by 8.77%, 8.81% and 2.58% respectively. The curve of the angles of internal friction and the loess content is shown in Fig.6.

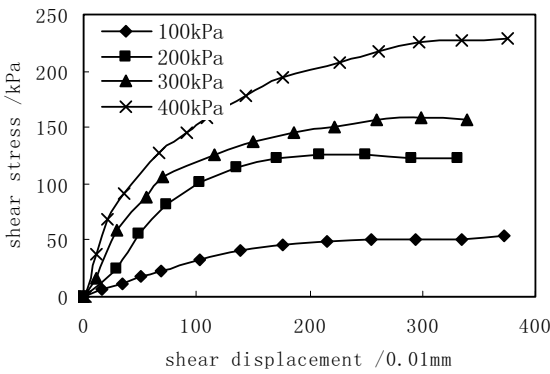
The results show that the shear strength of mixed-loess fly ash all reduces in comparison with pure fly ash, but the reduction is much lower. The shear strength firstly reduces with weight of loess added, and then picks up. When the loess content reaches 30%, the shear strength of mixed-loess fly ash is close to the shear strength of pure fly ash.



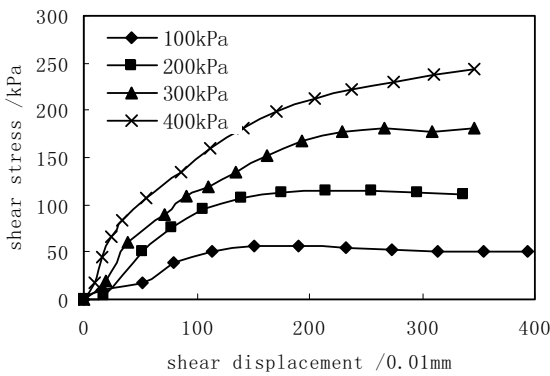
a) pure fly ash



b) fly ash with 10% loess content



c) fly ash with 20% loess content



d) fly ash with 30% loess content

Fig. 4 Curves of shear stress and shear displacement of fly ash

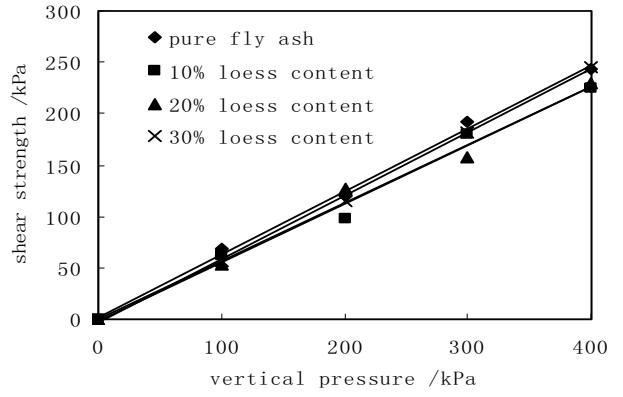


Fig. 5 Corresponding curves of shear strength and vertical pressure

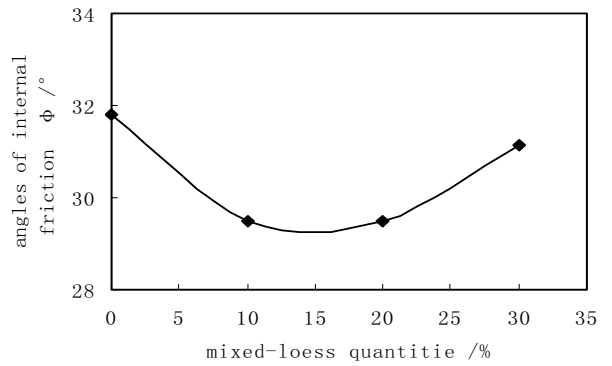


Fig. 6 Curve of the angles of internal friction and the loess content

Compression Test

The compression curves of fly ash mixed with four different quantities of loess are shown in Fig.7.

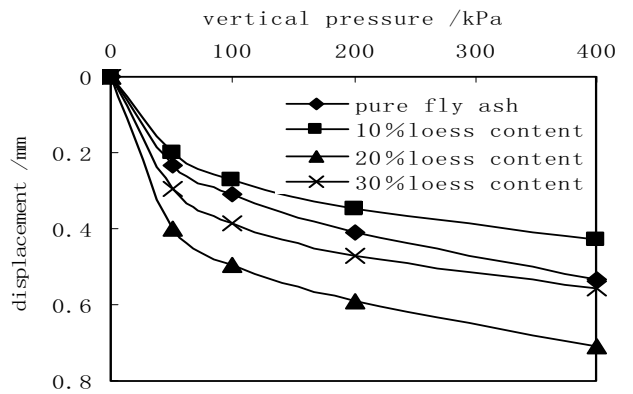


Fig. 7 Compression curves of fly ash mixed with different loess content

Fig. 7 shows that under the same pressure, the trend between the deformation of the fly ash and the loess content is not evident. The deformation of the fly ash

with 10% loess content is the smallest which is followed by pure fly ash, and the deformation of the fly ash with 20% loess content is the largest. In general, the maximum deformations of fly ash mixed with four different quantities of loess are between 0.4 mm and 0.8 mm, and the vertical confined deformation ratio is less than 4%, showing good characteristics of resistance to compression deformation.

Triaxial Shear Test

Through the tests, the curves of stress and strain of mixed-soil fly ash with different quantities of loess can be obtained. Fig.8 shows the curves of stress and strain of mixed-soil fly ash with 10% loess, and Fig.9 shows the corresponding curves of pore water pressure and strain. Then the Mohr-Coulomb strength envelopes of triaxial shear tests were drawn, as shown in Fig.10. The shear strength indexes of fly ash with different loess content are listed in Table 4.

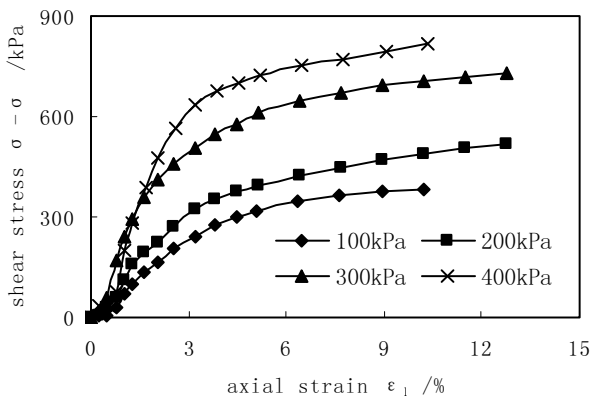


Fig. 8 Curves of stress and strain of mixed-soil fly ash with 10% loess content

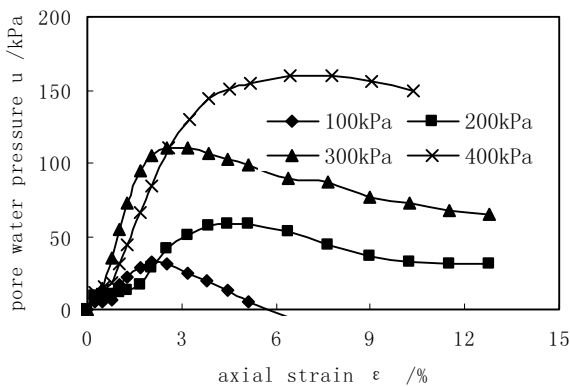
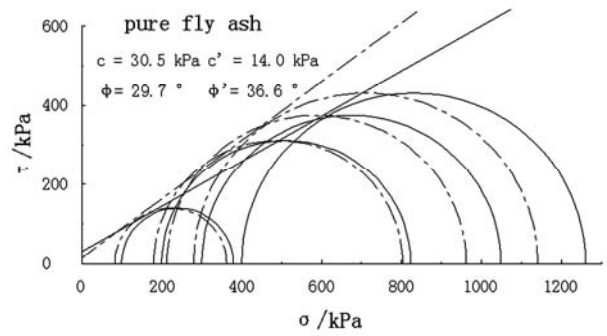
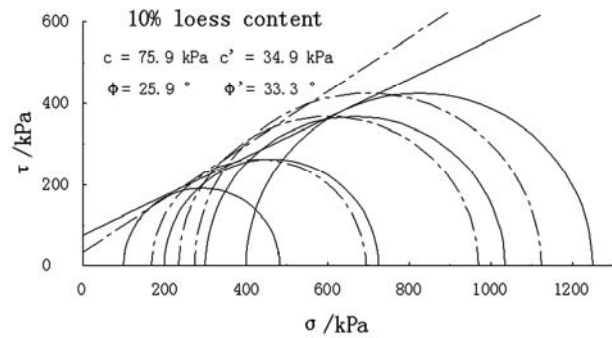


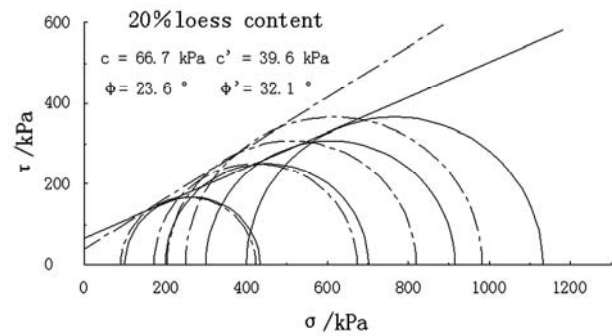
Fig. 9 Curves of pore water pressure and strain of mixed-soil fly ash with 10% loess content



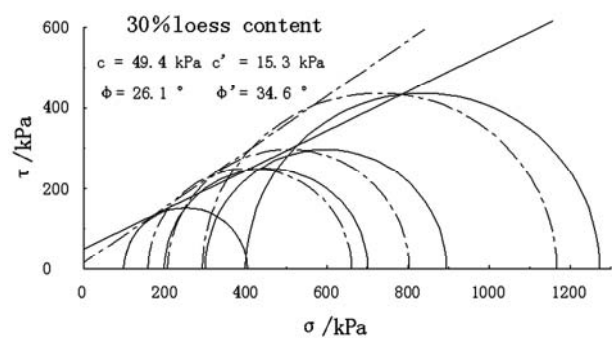
a) pure fly ash



b) 10% loess content fly ash



c) 20% loess content fly ash



d) 30% loess content fly ash

Fig. 10 Mohr-Coulomb strength envelopes of triaxial shear tests

Table 4 Shear strength indexes of fly ash with different loess content

loess content / %	Total stress index		Effective stress index	
	c /kPa	ϕ / °	c /kPa	ϕ / °
0	30.5	29.7	14.0	36.6
10	75.9	25.9	34.9	33.3
20	66.7	23.6	39.6	32.1
30	49.4	26.1	15.3	34.6

Shear strength indexes of fly ash with different quantities of loess as given in Table 4 showed that when mixed with a small volume of loess, first increase and then decrease and the angle of internal friction first decreases and then increases with the amount of loess added. The cohesion of pure fly ash is the smallest, while its angle of internal friction is the biggest. However, the change in total stress index is bigger than the effective stress index. Compared to pure fly ash, the cohesions increased significantly by 18.9kPa for 30% to 45.4kPa for 10% and the angles of internal friction decrease by 3.60 to 6.10 for the total stress index. On the other hand, the cohesions increase by 1.3kPa to 25.6kPa and the angles of internal friction decrease by 2.0 to 3.30 for the effective stress index. Considering both the increase of cohesions and the decrease of angles of internal friction, fly ash mixed with 10% loess content reflects good characteristics of shear strength. However, by considering only the angle of internal friction, the property of fly ash mixed with 30% loess is close to pure fly ash, and this confirms the trend obtained from the direct shear test.

CONCLUSIONS AND SUGGESTIONS

Compaction tests, direct shear tests, compression tests and triaxial shear tests were carried out on fly ash with different quantity of loess, and the effects of loess quantity on the engineering properties of fly ash were been studied. The results show that:

a) With the increase of loess mixed, the maximum dry density is more sensitive to the moisture content and it increases more-or-less linearly, and at same time, the corresponding optimum moisture content decreases linearly;

b) Compared with pure fly ash, the shear strength of mixed-loess fly ash, which is measured by direct shear test, all reduces slightly. It firstly reduces with the weight of loess added, and then picks up. When the loess content reaches 30%, the shear strength of mixed-loess fly ash is close to the shear strength of pure fly ash;

c) Under the same pressure, the trend between the

deformation of the fly ash and the loess content is not evident. The total deformation is small, and the mixed-loess fly ash showed good characteristics of resistance to compression deformation;

d) Shear strength indexes of fly ash with different loess content as shown in Table 5 show that when mixed with a small quantity of loess, firstly increase with the amount of loess mixed and then decrease and the angle of internal friction firstly decreases and then increases. The cohesion of pure fly ash is the smallest, while its angle of internal friction is the largest. However, the change in total stress index is larger than the effective stress index. Considering both the increase in cohesion and the decrease of angle of internal friction, fly ash mixed with 10% loess by weight shows good characteristics of shear strength. However, considering only from the point of view of the angle of internal friction, fly ash mixed with 30% loess has property close to pure fly ash, which is consistent with the trend obtained from direct shear test.

When mixed with a small volume of loess, the density and cohesion of fly ash improve significantly, and its good characteristics of resistance to compression deformation and shear failure are also maintained. So in the fly ash dam projects which have higher requirement of density and cohesion, it would be beneficial to use the fly ash mixed with some amount of soil. This not only can ensure the strength of the material used, but can also save spaces which may be required to store large volume of fly ash.

ACKNOWLEDGEMENT

This research was supported by China Education Ministry New Century Excellent Intelligent Fund Program (NECT-06-0864).

REFERENCES

- Lu XY & Zhu XY (2005). Present situation and developing prospect of comprehensive utilization of fly ashes, *J. of Liaoning Technical Univ.*, 24(2):295-298.
- Zhang AJ, Luo YS, Li P (2004). Analysis of consolidation characteristics in construction of hydraulic filling fly ash dam, *Chinese Journal of Northwest A&F University (Natural Science Edition)*, 32(11): 138-142.
- Kayabal K & Bulus G (2000). The usability of bottom ash as an engineering material when amended with different matrices, *Engineering Geology*, 56: 293-303.
- Bumjoo Kim, Monica Prezzi, Rodrigo Salgado (2005).

- Geotechnical properties of fly and bottom ash mixtures for use in highway embankments, *Journal of Geotechnical and Geoenvironmental Engineering*, July 2005: 914-924.
- Feng HN, Yang YH, Gong XN (2002). Test research on engineering characteristic of fly ash, *Chinese Journal of Rock and Soil Mechanics*, 23(5): 579-582
- Shenbaga R Kaniraj & Gayathri V (2004). Permeability and consolidation characteristics of compacted fly ash, *J. Energy Engineering*, April 2004: 18-43.
- Phani Kumar BR, Radhey S, Sharma MASCE (2004). Effect of fly ash on engineering properties of expansive soils, *Journal of Geotechnical and Geoenvironmental Engineering*, July 2004: 764-767.
- Feng MG, Chen SX, Yu S, Jia MA (2007). Laboratory study on water stability of flyash-treated expansive soil, *Chinese Journal of Rock and Soil Mechanics*, 28(9): 1889-1893.
- Shenbaga R Kaniraj & Vasant G Havanagi (1999). Compressive strength of cement stabilized fly ash-soil mixtures, *Cement and Concrete Research*, 29: 673-677.
- Lin T & Liu ZD (2003). Study on indoor tests of fly ash and quick lime improving soft soils, *Chinese Journal of Rock and Soil Mechanics*, 24(6): 1049-1052.
- Shenbaga R Kaniraj & Gayathri V (2003). Geotechnical behavior of fly ash mixed with randomly oriented fiber inclusions, *Geotextiles and Geomembranes*, 21: 123-149.

EXPERIMENTAL STUDY ON TREATMENT OF OVER-WETTED CLAYS USING CALCIUM CHLORIDE

Ying-Ying ZHANG¹, Yan-Jun DU², Song-Yu LIU³ and Fan ZHANG⁴

ABSTRACT: In the highway construction in the south of Jiangsu Province, China, over-wetted clays are commonly encountered. Since this type of soil has higher water content than the optimum water content, it needs to be properly treated before being used as embankment filling material. Binders like lime, Portland cement, and fly ash are commonly used to stabilize the over-wetted soils. In this paper, a new treatment method using solid calcium chloride, which is a chemical reaction product from waste calcium carbides, is proposed. A series of laboratory experiments were carried out to investigate the treatment effectiveness of calcium chloride additive with content of 0.5%-12%. The test results show that with a relatively high content of calcium chloride additive, the water content of the treated soil could be reduced by 42% and the unconfined compressive strength (UCS) of the treated soil with varying contents of calcium chloride increased by 22%-82%, compared to the untreated case. Besides, the maximum dry density increased while the optimum water content decreased, which is similar to the phenomenon by increasing compaction energy. It is also found that when the content of calcium chloride was over 8%, UCS decreased, which indicates there is likely to exist an optimum content value. It is expected that the solid calcium chloride can be used as a binder to treat the over-wetted soils.

KEYWORDS: over-wetted clays, waste calcium carbides, solid calcium chloride, experimental study

INTRODUCTION

In the highway construction in the south of Jiangsu Province, China, over-wetted clays are commonly encountered. This type of soil has relatively high water content and will easily become elastic soil under an imposing compaction. Using untreated over-wetted clay as embankment filling material will be likely to cause an excessive settlement, cracking or instability of subgrade and pavement under vehicle load when the highway construction is completed (Zhang 2006). The key points of treatment of over-wetted soils can be concluded as two aspects: one is to reduce the water content within a short time so that soils can be appropriately compacted to obtain sufficient strength and stability. Another is to increase the strength to meet the design requirement.

This paper presents a new treatment method for over-wetted soils using solid calcium chloride (CaCl_2), which is a chemical reaction product from waste calcium carbides and is different from conventional inorganic additives such as Portland cement, lime, fly-ash and lime mixtures. A series of laboratory tests including

heavy compaction test, water change test, and unconfined compressive strength test were performed to investigate the effectiveness of solid CaCl_2 for improving over-wetted soils.

BACKGROUND

Saylak et al. (2008) indicated that solid calcium chloride has high water-absorbing performance. At a relative humidity of 95%, solid CaCl_2 can absorb 16.6 times its weight of water. Even in a relatively low humidity environment of 30%, it can absorb almost equal to its own weight water. In addition, calcium chloride dissociates into Ca^{2+} ions in the presence of water which will lead to ion exchange reactions with Na^+ and K^+ ions initially adsorbed on the clay particle surface. As a result, the thickness of double diffusion layer (DDL) of soil particles will be reduced and soil particle aggregates will form (Mitchell 1993). Consequently, the soil plasticity will decrease and strength will increase (Rajasekaran 2005).

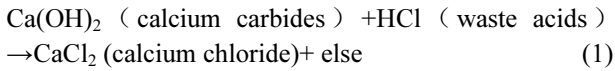
¹ M.S. candidate, Institute of Geotechnical Engineering, Southeast University, China. Email: yinggyinggg@126.com

² Professor, Institute of Geotechnical Engineering, Southeast University, China. Email: duyanjun@seu.edu.cn

³ Professor, Institute of Geotechnical Engineering, Southeast University, China. Email: liusy@seu.edu.cn

⁴ M.S. Student, Institute of Geotechnical Engineering, Southeast University, China. Email: fightmanzone@163.com

Solid CaCl₂ can be obtained from the industrial wastes, calcium carbides, which are byproducts of acetylene factory. Currently in China, these calcium carbides are usually open stocked without any covering material, which has caused serious environmental pollution problem at rain season. However, calcium carbides can be reused to produce solid CaCl₂ through following chemical reaction:



Here, Ca(OH)₂ is the main component of calcium carbides and HCl is a kind of waste acids produced from iron or steel factory. At this moment, CaCl₂ isn't solid, and it needs heating and drying to be in solid state.

By doing so, calcium carbides can be reused and its impact on surrounding environment can be reduced. The validity of Eq. (1) has been approved in preliminary series of laboratory tests. It is found that through chemical reaction as described by Eq. (1), up to 0.85 kg solid CaCl₂ can be obtained from 1 kg calcium carbides, implying that the source of solid calcium carbides could be guaranteed in engineering practice.

MATERIALS AND EXPERIMENTS

Materials

In this study, the over wetted clay is defined as the clay has much higher water content than its optimum water content while less than the liquid limit. The soil used in this study was sampled from Changzhou City of Jiangsu Province, China. The main engineering properties are shown in Table 1. Waste calcium carbides were procured from Changzhou Acetylene Manufacturing Company. The chemical analysis indicated that the main components of waste calcium carbides were 85% calcium oxide (CaO), 10% insoluble impurities (coke, other poorly soluble ores), and 5% soluble ferric salts. The solid anhydrous CaCl₂ additive used is a commercial product with white color and granular shape. The average diameter of the granular CaCl₂ is 3 mm. The purity was analytically pure level.

Table 1 Properties of sampled over-wetted soil

w (%)	w _L (%)	w _p (%)	CF (%)	SLF (%)	ρ _{dmax} (g/cm ³)	w _{opt} (%)
13.4	32.3	20.4	34.1	64.9	1.88	12.8

Note: w=Natural water content; w_L=Liquid limit; w_p=Plastic limit; CF=Clay content; SLF=Silt content; ρ_{dmax}=Maximum dry density; w_{opt}= Optimum water content.

Experiments

All the experimental programmes were conducted according to the China Test Methods of Soils for Highway Engineering (JTG E40-2007). To assess the treatment effectiveness of solid calcium chloride for the over-wetted clays, contents of additive which was arranged as 0.5%, 1%, 2%, 4%, 8%, and 12%. were subjected to water content change test, soil consistency test, heavy compaction test, and unconfined compressive strength test, based on JTG E40-2007 standard methods T0103-1993, T0118-2007, T0137-2007, and T0148-1993, respectively. For water content change test, water contents were adjusted so that the soil consistency index w_c (w_c = (w_L-w)/I_p) were in a range of 0.1, 0.25, 0.5, 0.75, and 1.0.

RESULTS AND DISCUSSIONS

Water Content Change Test

To investigate the water absorption capacity of solid CaCl₂, the soils were grinded and sieved firstly. The initial water contents with the corresponding soil consistency index are listed in Table 2. The contents of CaCl₂ additive were 0.5%, 1%, 2%, 4%, 8%, and 12%.

Table 2 Water content of different consistencies soils

Consistency index (w _c)	0.1	0.25	0.5	0.75	1.0
Water content (%)	31.1	29.3	26.4	23.4	20.4

From Figs. 1 to 4, it can be seen that for any particular consistency, with an additive of 0.5% to 4% solid CaCl₂, the change of water content is marginal and the greatest water content reduction is only 4%. However, with a relatively high content (6%-12%) of CaCl₂ additive, there is a considerable decrease in water content. For example, for the soil with the consistency of 0.25 and 12 % CaCl₂ additive under 1 day curing time, the water content even reduced by 42%.

There are several reasons to explain this phenomenon. Firstly, the addition of solid CaCl₂ increased the total weight of soil. Since the density of solid CaCl₂ is 2.15g/cm³, which is much higher than the soil, thus the soil water content was lowered. Secondly, because of the great water absorption ability of solid CaCl₂ mentioned before, the anhydrous calcium chloride turned into calcium chloride crystalline hydrates upon adding to the soil. This increased the solid portion and reduced the

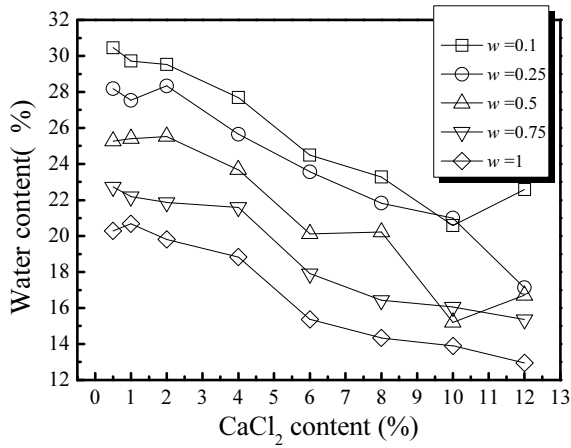


Fig. 1 Water content of treated soil with different consistency index and different contents of solid CaCl_2 at 1 day curing time

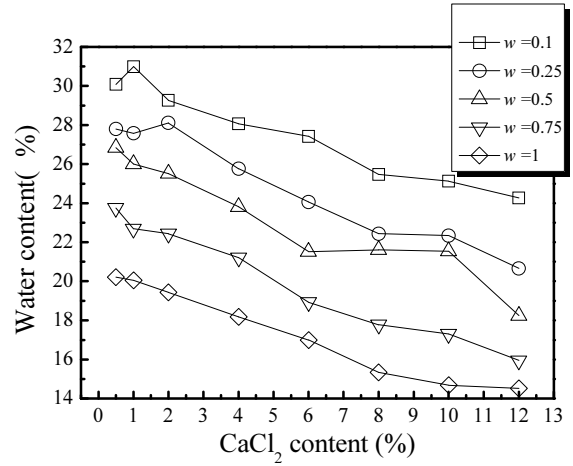


Fig. 4 Water content of treated soil with different consistencies and different contents of solid CaCl_2 at 14 days curing time

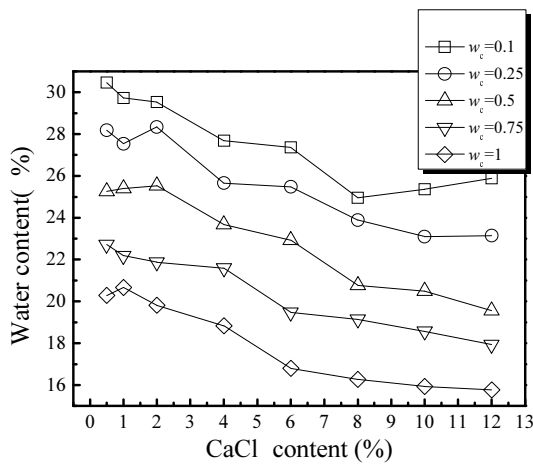


Fig. 2 Water content of treated soil with different consistencies and different contents of solid CaCl_2 at 3 days curing time

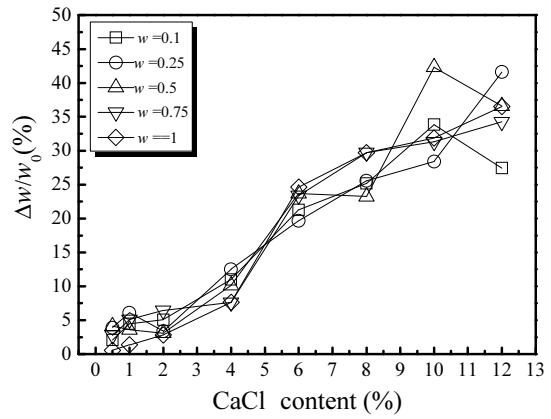


Fig. 5 Change ratio of water content of treated soil with different consistencies and different contents of solid CaCl_2 at 1 day curing time

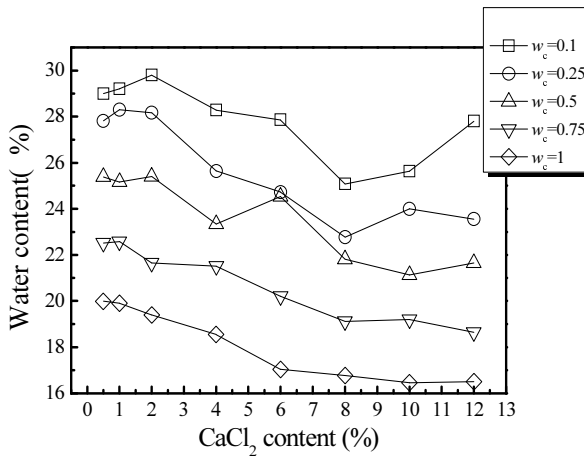


Fig. 3 Water content of treated soil with different consistencies and different contents of solid CaCl_2 at 7 days curing time

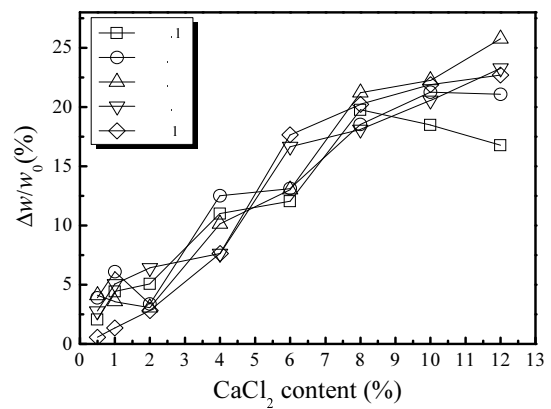


Fig. 6 Water content rate of treated soil with different consistencies and different contents of solid CaCl_2 at 3 days curing time

measured water content. Thirdly, the mixture of solid CaCl_2 and soil is an exothermic process which had accelerated the water evaporation.

It can be seen from Figs. 5 and 6 that the influence of initial water content on the change ratio of water content for the CaCl_2 treated soils can nearly be neglected, since these curves are almost parallel to each other. Moreover, from the water content variations of soil specimens with the same additive content while different curing time, it can be seen that the curing time did not significantly change the water content (see Figs. 1 to 4). These observed phenomena imply that in engineering practice, testing of the water content variation in a short term (e.g., 1 d curing time) is suggested when the CaCl_2 additive content is high.

Soil Consistency Test

The part results of untreated and treated over-wetted soils are shown in Table 3.

Table 3 Effect of CaCl_2 additives on the soil consistency

CaCl_2 content (curing time)	w_L (%)	w_p (%)	I_p
0%	33.5	21.3	12.2
0.5% (7d)	32.4	20.8	11.6
1% (7d)	32.4	20.9	11.5
2% (7d)	31.4	19.8	11.6
4% (7d)	30	19.7	10.3
6% (7d)	30.7	19	11.7
8% (7d)	29.9	18.9	11
10% (7d)	28.6	16.2	12.4
12% (7d)	27.3	16	11.3

As shown in Table 3, generally, both the plastic limit and liquid limit of treated soil decreased with the increase of CaCl_2 content. For the plasticity index, its change is relevant to additive content, but the influence is not remarkable. It is found that when the CaCl_2 additive content is less than 4%, the plasticity index decreased with additive content increment. When the content exceeds 4%, the decrease of the plasticity index with the increase of CaCl_2 content is marginal. The change in plasticity index is thought to be mainly due to

the exchange of dissolved calcium ions with the readily exchangeable cations like Na^+ and K^+ ions that were initially adsorbed on the soil particle surface (Ding 2001, Rajasekaran 2005). The cation exchange reaction resulted in a reduction in the thickness of the diffused double layer (DDL) of soil particles, and induced flocculation and aggregation of soil particles, which consequently lowered soil plasticity and improved soil stability (Wang 2007).

Heavy Compaction Test

Heavy compaction test results and corresponding moisture-density relationships of untreated and calcium chloride treated soils are shown in Table 4 and Fig.7 respectively.

Table 4 Heavy compaction test results of untreated and CaCl_2 treated soils

Soil samples	Maximum dry density (g/cm^3)	Optimum water content(%)
Untreated soil	1.88	12.8
Treated soil with 0.5% solid CaCl_2	1.90	12.6
Treated soil with 1% solid CaCl_2	1.92	10.6
Treated soil with 2% solid CaCl_2	1.94	10.4
Treated soil with 4% solid CaCl_2	1.93	9.6
Treated soil with 8% solid CaCl_2	1.97	9.1
Treated soil with 12% solid CaCl_2	1.95	9.5

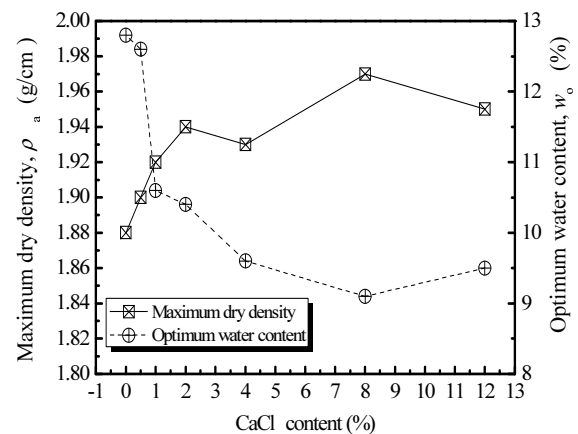


Fig. 7 Change of maximum dry density and optimum water content with solid CaCl_2 additive content

It is observed from the testing results that the addition of solid CaCl₂ to soils resulted in increase of maximum dry density and decrease of optimum water content. When the additive content is less than 4%, the changes of above mentioned parameters are significant. However, when the additive content exceeded 4%, the changes became slightly. Both parameters reached the peak when the additive content reached 8%. The observed phenomenon is illustrated in Fig. 8a, which is similar to the effect of the increased compactive effort on the compaction curve (see Fig. 8b). From Fig. 8, it can be seen that within a certain range of CaCl₂ additive content, the increased additive content and the increased compactive effort have the same effect on the compaction curves of treated over-wetted soils. The reasons for the observation presented in Fig. 8a are mainly due to three aspects: 1) The density of solid CaCl₂ is nearly 2.15, which is higher than that of most compacted soils. As a result, maximum dry density increased with the increment of CaCl₂ additive content; 2) The thickness of DDL reduced due to the cation exchange of dissolved Ca²⁺ and the readily exchangeable cations like Na⁺ and K⁺ initially adsorbed on the soil particle surface. With the increase in CaCl₂ additive content, the cation exchange reaction became greater and its effect on thickness of DDL was more considerable. Consequently, repulsive force between soil particles decreased (Sridharan et al. 1973). As a result, soils could be easily compacted at a relatively high density under the same compactive effort; and 3) solid CaCl₂ could absorb certain amount of free soil pore water and these pore water were transmitted into crystalline water. Therefore, the measured water content of treated soils decreased, which reduced lubricating effect between soil particles. As a result, air phase existed in the pore space could be easily compacted and resulted in a relatively high soil density.

It is observed that when the CaCl₂ content exceeds 8%, the maximum dry density tended to decrease with the increase in CaCl₂ content. This result implies that there would be an optimum CaCl₂ additive content for treating over-wetted soils under the conditions presented in this study. It seems that 8 % of the CaCl₂ additive content could be an optimum value.

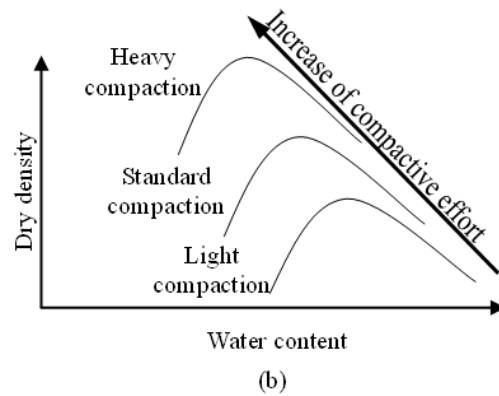
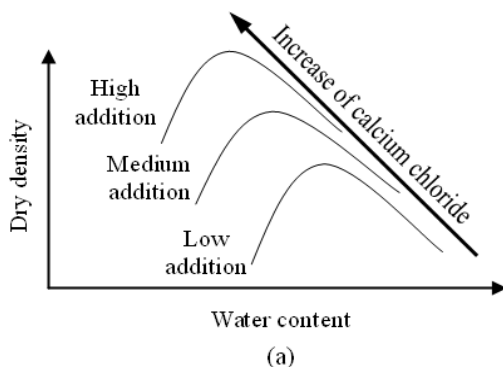


Fig. 8 Similarity comparison: a) effect of CaCl₂ additive content on compaction curve of treated soils; b) effect of compactive curve on compaction curve of soils

Unconfined Compression Test

Table 5 shows the results of unconfined compression test.

It can be seen that compared to the untreated soils, the strength of treated soils at 7 days curing time is generally greater except for the case of 12% CaCl₂ content. This proves that the solid calcium chloride could enhance the soil strength. Besides, the increase in CaCl₂ additive content results in an initial increase (less than 8% CaCl₂) followed by a remarkable decrease (more than 8% CaCl₂) in unconfined compressive strength (UCS). The result is consistent with the results of heavy compaction test, indicating that there exists an optimum CaCl₂ additive content.

Table 5 Unconfined compressive strength (UCS) of treated soil with different CaCl₂ additive contents (7 days curing time)

CaCl ₂ contents (%)	0	2	4	8	12
UCS (MPa)	0.68	1.24	0.83	1.18	0.61
Water content (%)	12	10	10.1	8.2	9.3
Dry density (g/cm ³)	1.91	1.92	1.87	1.95	1.97

IMPLYCATION TO PRACTICE

The main component of waste calcium carbides is calcium hydroxide whose content is over 60%. With

simple chemical reaction and heating treatment, it is relatively easy to extract solid calcium chloride. Preliminary laboratory investigation shows that 1 ton calcium carbides can extract 0.85-0.9 ton calcium chloride by chemical reaction with waste hydrochloric acid (HCl). The cost is estimated about 330-400 per ton, which is equivalent to lime and Portland cement. Furthermore, the utilization of calcium carbides could mitigate the environmental pollution caused by the open-dumped calcium carbides at industry factories during a rainfall season. Hence, utilization of calcium carbide extracted CaCl_2 to treat over-wetted soil is both cost-effective and environment-friendly. It is expected that solid CaCl_2 can be used in engineering practice. Further studies need to be carried out to investigate the durability and long-term performance of CaCl_2 treated over-wetted soils.

CONCLUSIONS

In this paper, experimental tests on the application of solid calcium chloride to the treatment of over-wetted clayey soils were presented. Based on the test results, following conclusions can be drawn.

(1) Addition of CaCl_2 to the over-wetted clays resulted in decrease of water content and plasticity index.

(2) When the content of CaCl_2 is less than 8%, the maximum dry density increased with the increase of additive content whereas the optimum water content decreased, which is contrary to the case when CaCl_2 content exceeded 8%. The unconfined compressive strength test results also have the same tendency. It is concluded that 8% additive content is the optimum design value under the conditions presented in this study.

(3) Using calcium carbides extracted solid CaCl_2 to treat over-wetted clayey soils is both cost-effective and environment-friendly. It is expected that CaCl_2 can be applied in engineering practice to treat over-wetted soils.

ACKNOWLEDGEMENT

This study is part of the Jiangsu Provincial Transport Project titled Treatment of over-wetted clays using solid calcium chloride (No. 8821006034), which is financially supported by Jiangsu Provincial Communications Department. The authors thank for the graduate students who have been involved in the related laboratory tests.

REFERENCES

- Sridharan A & Venkatappa Rao G (1973). Mechanisms controlling volume change of saturated clays and the role of the effective stress concept. *Geotechnique* 23: 359-382.
- Don Saylak, Surendra K Mishra, Gleb G Mejeoumov, Shon Chang-Seon (2008). Fly ash - Calcium Chloride Stabilization in Road Construction, TRB 2008 Annual Meeting CD-ROM.
- Sulphate G Rajasekaran (2005). Attack and Ettringite Formation in the Lime and Cement Stabilized Marine Clays, *Ocean Engineering* 32: 1133-1159.
- Wang GC (2007). Embankment construction technique of dealing with over-wetted soil by using quicklime powder. *ShanXi Science & Technology of Communications*, No.4, Aug.2007 (in Chinese).
- Zhang LY (2006). Application of HAS curing agent in the hardening of over-wetted earth subgrade, *Highway Engineering*:27-31 (in Chinese).
- Susan D Rafalko, George M Filz, Thomas L Brandon, James K Mitchell (2007). Rapid Chemical Stabilization of Soft Clay Soils, TRB 2007 Annual Meeting CD-ROM.
- Ding ZY (2001). The improvement and treatment of over-wetted Soils, *Journal of Pingyuan University*, 18(2) (in Chinese).

MECHANICAL AND CHEMICAL PROPERTIES OF ASH MOLTEN SLAG MIXED WITH BENTONITE

Fujio IGARI¹ and Shigeyoshi IMAIZUMI²

ABSTRACT: Since 2000, the number of facilities to produce the ash molten slag has rapidly increased in Japan. But, the place where the ash molten slag is used as construction material is limited such a municipality as ash molten slag facility is located. So, it is necessary to establish effective uses other than aggregate in base course of a road or as aggregate in ready mixed concrete for building, etc.

In this research, physical properties of ash molten slag were studied by conducting sieving tests, density tests, compaction tests. The elution tests and the content tests on four typical heavy metals, such as Pb, Cd, As and Cr⁶⁺, were also conducted to confirm its safety. Then the ash molten slag was mixed with bentonite changing the addition ratio in dry mass. The compacted ash molten slag mixed with bentonite was tested to get its maximum density, optimum water content, unconfined compression strength, shear strength parameters and coefficient of permeability.

As a result, it was found that the bentonite mixed molten slag can be used as alternative soil materials for barrier course in waste landfill.

KEYWORDS: ash molten slag, ash molten slag mixed with bentonite, waste landfill, compacted soil barrier systems, permeability.

INTRODUCTION

Since 2000, the number of facilities to produce the ash molten slag has rapidly increased in Japan. The reason is thought such that this facility dose not discharge dioxin and the resultant molten slag can confine the heavy metals in it. It is also thought the volume of molten slag will be about one fifth that of the incinerated ash and therefore the life of landfill will extend.

According to The Japan Society of Industrial Machinery Manufacturers (2007), the production of ash molten slag from garbage was about 520,000 tons in 2004 and will increase to be about one million tons in 2013. But, today, the place where ash molten slag can be used is limited such a municipality as ash molten slag facility is located. Therefore, it is expected to extend the area where ash molten slag is steadily used.

Since the standardization of the quality of ash molten slag was established in July of 2006 for a road materials (Japan Industrial Standards (JIS A 5032) and for a ready mixed concrete materials (JIS A 5031), the ash molten slag was commonly used as aggregate in base course of a road or as aggregate into ready mixed concrete for building.

On the other side, in Japan, the barrier system of waste landfill is required to have double liner including

barrier sheet and compacted impermeable soil with a coefficient of permeability of less than 10^{-6} cm/s. But, in Japan, it is difficult to obtain quality natural clay having such low-permeability and high-strength from the surrounding of planned waste landfill site. So, the soil barrier course is commonly constructed by mixing the bentonite with the purchase sand.

In this research, first, physical properties of ash molten slag were studied by conducting sieving tests, density tests, compaction tests. The elution tests and the content tests on four typical heavy metals, such as Pb, Cd, As and Cr⁶⁺, were also conducted to confirm its safety. Then the ash molten slag was mixed with bentonite changing the addition ratio in dry mass. The compacted ash molten slag mixed with bentonite was tested to get its maximum density, optimum water content, unconfined compression strength, shear strength parameters (angle of friction and cohesion) and coefficient of permeability.

PHYSICAL PROPERTIES OF ASH MOLTEN SLAG

The ash molten slag produced from garbage at the facility in Yokohama was extracted. The particles passing through the sieve with an open-size of 20mm were used

¹ Leader of Group, OYO Corporation, Japan. Email: igari-fujio@oyonet.oyo.co.jp

² Professor, Graduate School of Engineering, Utsunomiya University, Japan. Email: imaizumi@cc.utsunomiya-u.ac.jp

as sample in this research. Photo 1 shows microphotograph of particles taken by SEM. It is found that the shape of ash molten slag is angular.

Fig. 1 shows the grain size distribution curves, where the curve tested after compaction test is also presented. Table 1 shows the texture, the density of the soil particle, and the Atterberg characteristic.

From Fig.1 and Table 1, it can be said that ash molten slag contains fine particle with less than 1% and is "well graded" soil having both $U_c=14.3$, $U'_c=2.3$ before compaction tests and $U_c=13.3$, $U'_c=1.4$ after compaction tests. And it is classified as "Sandy gravel (GS)" based on Japanese Standard.

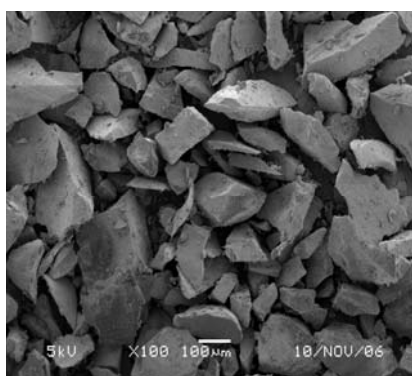


Photo 1 Photograph of particles

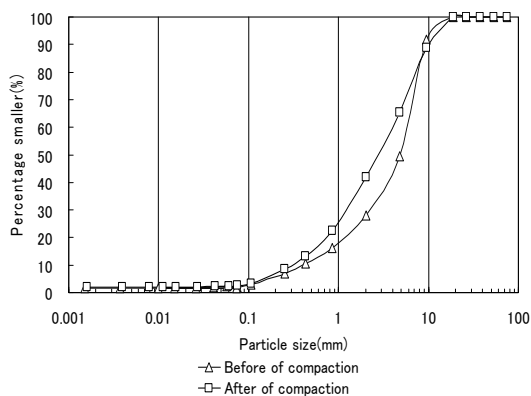


Fig. 1 Grain size distribution curves

Table 1 Mechanical properties

Item	Ash molten slag
Gravel(%)	73
Sand(%)	26
Fine particle(%)	1
Coefficient of uniformity U_c	14.3
Coefficient of curvature U'_c	2.3
Density of the soil particle (ρ g/cm ³)	2.734
Liquid limit W_p (%)	NP
Plastic limit W_L (%)	NP
Percentage of absorption(%)	0.333

In addition, it is also found that the ash molten slag is such material that can easily crushes by compaction, because the ratio of particles between 2.0 and 5.0mm increases by about 10% after compaction tests.

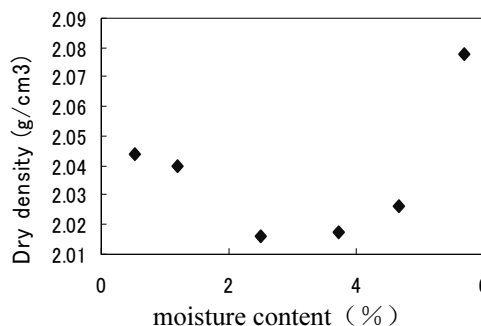


Fig. 2 Compaction curve

Fig. 2 shows the results of the compaction test done according to the A-c method of JIS A 1210. It can be seen that there is no relationship between the moisture content and the dry density, and therefore the optimum moisture content and maximum dry density can not be decided. It is thought as a reason that the particle of ash molten slag doesn't contain water as shown in Table 1. Then, there seems to be possibility of improvement of the characteristic as the soil material by adding the bentonite into ash molten slag particles.

CHEMICAL SAFETY OF ASH MOLTEN SLAG

As ash molten slag is originated from garbage, it can contain the solubility salts and some harmful heavy metals. Therefore, it is necessary to investigate the environmental impact of ash molten slag on underground water and the ground.

According to previous research (JSIM 2007), four heavy metals, that is Cd, Pb, As, Cr^{6+} , were chosen as typical harmful ones to elute easily. The heavy metal content test (Ministry of the Environment 2002), the heavy metal elution test (Ministry of the Environment 2003), oxidation added elution tests (Geo-Environmental Center 2008) and alkali added elution tests (Public Works Research Institute 2007) for the ash molten slag were conducted based on environmental standards related to the pollution of the soil. The oxidation added elution test immersed the ash molten slag into dissolvent with pH=4.5 and the alkali added elution test into dissolvent with pH=10.5.

The results are shown in Table 2. On heavy metal elution tests, all four heavy metals satisfy the environmental standards value. On the oxidation added elution test, however, measurements of the lead are a bit higher than that obtained from the official elution test. On the alkali added elution tests, measurements of the Cr^{6+} test are

higher than that of the official method. This is thought due to the fact that ionization potential of each element is very sensitive to pH.

Table 2 Results of content tests, elution tests, oxidation added solution tests and alkali added solution tests

Item	Content tests		Elution tests		Oxidation added elution tests pH=4.5	Alkali added elution tests pH=10.5
	Standards for Soil Pollution Standard Values(mg/kg)	Measurements (mg/kg)	Environmental Quality Standards for Soil Pollution Standard Values(mg/l)	Measurements (mg/l)	Measurements (mg/l)	Measurements (mg/l)
cadmium	<150	<1	<0.01	<0.001	<0.001	<0.001
lead	<150	<10	<0.01	<0.001	0.002	<0.001
arsenic	<150	<10	<0.01	<0.001	<0.001	<0.001
chromium (VI)	<250	<1	<0.05	<0.005	<0.005	0.01

Table 3 Results of oxidation added elution tests and alkali added elution tests

Item	Environmental Quality Standards for Soil Pollution Standard Values(mg/l)	Oxidation added elution tests (pH=4.5) Soaking period/(mg/l)				
		1 day	7 days	1 month	2 months	15 months
cadmium	<0.01	<0.001	<0.001	<0.001	<0.001	<0.001
lead	<0.01	<0.001	<0.001	<0.001	<0.001	<0.001
arsenic	<0.01	<0.001	<0.001	<0.001	<0.001	<0.001
chromium (VI)	<0.05	<0.005	<0.005	<0.005	<0.005	<0.005
total mercury	<0.0005	-	-	-	-	<0.0005
selenium	<0.01	-	-	-	-	<0.001
Oxidation reduction potential (mV)	-	-	-	-	-	+108

Item	Environmental Quality Standards for Soil Pollution Standard Values(mg/l)	Alkali added elution tests (pH=10.5) Soaking period/(mg/l)				
		1 day	7 days	1 month	2 months	15 months
cadmium	<0.01	<0.001	<0.001	<0.001	<0.001	<0.001
lead	<0.01	<0.001	<0.001	<0.001	<0.001	<0.001
arsenic	<0.01	<0.001	<0.001	<0.001	<0.001	<0.001
chromium (VI)	<0.05	0.005	0.005	0.007	0.008	<0.005
total mercury	<0.0005	-	-	-	-	<0.0005
selenium	<0.01	-	-	-	-	<0.001
Oxidation reduction potential (mV)	-	-	-	-	-	+59

It is afraid that the heavy metals may dissolve out from molten slag if the duration of soaking continues longer. So the tests in which the duration was changed as 7 days, 1 month, 2 months and 15 months were conducted. Table 3 shows the results. From the Table 3, it is found that all four heavy metals of the oxidation added elution tests (pH=4.5) satisfy the environmental standards value. On the other hand, in the alkali added elution tests (pH=10.5), measurements of Cr⁶⁺ were a bit larger though it still satisfies the environmental standards. This is due to the nature that Cr⁶⁺ can easily elute on the alkali side.

When soaking period passed for 15 months, Cr⁶⁺ was not detected. It is thought as a reason that the Cr⁶⁺ had changed to Cr³⁺ and remained in a more stable state of Cr₂O₃, because Oxidation Reduction Potential was 59 mV, which means a bit reduced state (National Institute of Advanced Industrial Science and Technology 2005)

MECHANICAL PROPERTIES OF ASH MOLTEN SLAG MIXED WITH BENTONITE

Compaction Characteristics

The Na-type bentonite produced in United States Wyoming was mixed into ash molten slag, changing addition ratio α , such as 5, 10, 15, and 20% in dry mass. Then the compaction tests were conducted according to A-c method of JIS A 1210, which uses a mould with 1000 cm³, and drop hammer with 2.5 kg. Drop height was 30 cm and blowing number was 25 for each layer.

Fig. 3 shows the resultant compaction curves. The optimum moisture content and the maximum dry density estimated for each addition ratio curve are summarized in Table 4. The optimum moisture contents range from 10% to 14% and show the tendency to increase as the addition ratio increase.

The other side, the maximum dry densities range from 1.86 to 2.01 g/cm³ and show a tendency to decreases. It is also found that the compaction characteristic is greatly improved by adding a small amount of bentonite, just as mentioned previously.

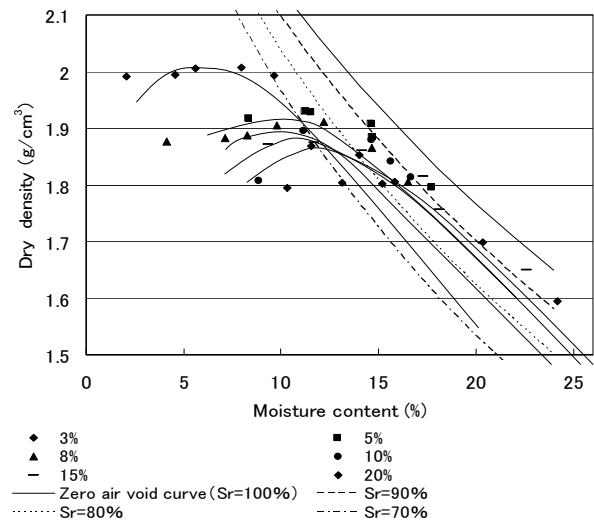


Fig. 3 Compaction curves of ash molten slag mixed with bentonite

Table 4 Results of compaction tests

Addition ratio of bentonite α (%)	3	5	8	10	15	20
Maximum dry density ρ_{dmax} (g/cm ³)	2.01	1.93	1.91	1.90	1.87	1.86
Optimum water content W_{opt} %	8.0	11.3	11.5	11.9	12.5	13.0

Calculation of Critical Bentonite Addition

Relating to a bentonite mixed soil, it was said that the coefficient of permeability decreases with increasing the bentonite addition ratio and has almost steady value

beyond some addition ratio of bentonite. This was called critical bentonite addition. The design critical ratio can be estimated based on the idea of macro void ratio (Ohtsuka 2006).

The macro void ratio e_m was calculated by the following equation (1), substituting the values of dry density and the maximum dry density for each addition ratio of bentonite shown in Table 4.

$$e_m = \rho_s \left(\frac{1 + \alpha/100}{\rho_{d\max\alpha}} - \frac{\alpha/100 \cdot \beta}{\rho_b} \right) - 1 \quad (1)$$

where, α : Addition ratio of bentonite (%), β : Swelling ratio of bentonite, ρ : Density of the molten slag particle (g/cm^3), ρ_b : Density of bentonite (g/cm^3), $\rho_{d\max\alpha}$: Maximum dry density of ash molten slag with addition ratio α of bentonite .

The relation between the addition ratio α and the calculated macro void ratio e_m is shown in Fig. 4. The macro void ratio decreases as the addition ratio of bentonite increases. Here, the addition ratio of bentonite corresponding to the macro void ratio of 0 in Fig. 4 can be defined as the calculated critical addition ratio of bentonite α_{cr} . Then, in this study, the calculated critical addition ratio of bentonite of the ash molten slag used is estimated as 9 %.

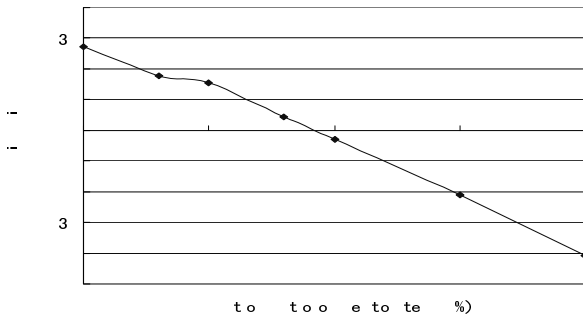


Fig. 4 Calculated macro void ratio versus addition ratio of bentonite

Unconfined Compression Strength

Unconfined compression tests were conducted under the condition of a strain rate of 1% per minute in accordance with JIS A 1216. The test specimen was made by compacting bentonite mixed molten slag with optimum water content. Fig. 5 shows stress-strain curves at each addition ratio of bentonite. The initial curve shows concave. This is due to insufficient contact of the loading piston with the upper surface of the specimen. Then, deformation modulus E_{50} is calculated after initial strain was corrected. Relating to ash molten slag with a addition ratio of bentonite of 0 %, test specimen could not be made because it had no cohesion.

Table 5 shows the estimated averages of deformation modulus E_{50} and unconfined compression strength q_u for each addition ratio of bentonite. The values of the deformation modulus range from 2.2 to 2.5 MN/m^2 though that of the addition ratio 15% is a bit larger.

Fig. 6 shows the relation between addition ratio of bentonite and unconfined compression strength. It can be seen that unconfined compression strength increases gradually with addition ratio of bentonite. But it is also found that there are not so many differences of unconfined compression strength between an addition ratio of 15% and 20%.

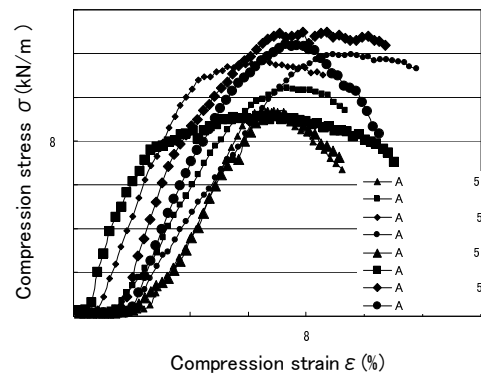


Fig. 5 Stress-strain curve on addition ratio

Table 5 Average of unconfined compression strength and deformation modulus

Addition ratio of bentonite α (%)	5	10	15	20
Average of unconfined compression strength q_u (kN/m)	93.39	97.71	122.99	121.86
Average of deformation modulus E_s (MN/m)	2.14	3.34	4.17	3.06

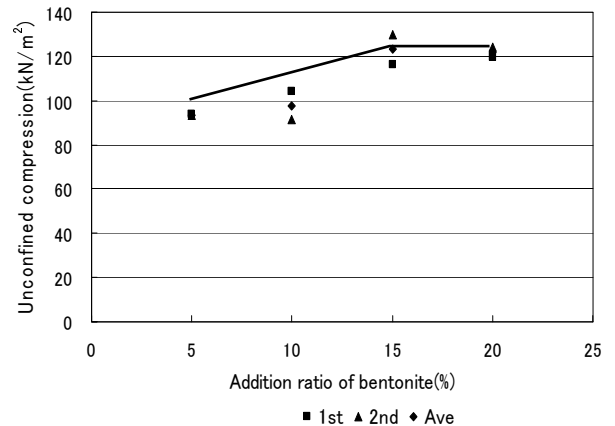


Fig. 6 Unconfined compression strength versus addition ratio of bentonite

From Fig. 6, unconfined compression strength corresponding to an addition ratio of 8%, which is critical

addition ratio of bentonite as described previously, is about 100 kN/m².

In Japan, the trafficability of ground is commonly judged based on cone index q_c (kN/m²). Table 6 shows the necessary value of cone index for various vehicles to work. Assuming that a relation between cone index q_c and unconfined compression strength q_u can be expressed as $q_c=5q_u$ (The Japanese Geotechnical Society 2004), cone index (q_c) of 500 kN/m² can be obtained for ash molten slag with an addition ratio of bentonite of 8%. Referring to Table 6, it is said that ash molten slag with an addition ratio of 8% can carry 15-tons class bulldozer.

Table 6 Indicator of trafficability (Japan Road Association 1986)

Kind of construction machinery	Cone index q (kN/m ²)
Super-marsh bulldozer	200over
Marsh bulldozer	300over
Usualbulldozer (15ton class)	500over
Usualbulldozer (21ton class)	700over
Scrapedozer	600over 400over)
Type of scrapedozer to be pulled	700over
Self-propelled scrapedozer	1,000over
Dump track	1,200over

Shear Strength Parameters

Consolidated Undrained (CU) triaxial compression tests was conducted under the condition of a confining pressure of 49, 98 and 196 kN/m² for the specimen with addition ratio of bentonite 5%. In the tests, pore pressure during the axial loading was measured through strain-gauge type indicator. Table 7 shows the condition of the specimen used.

Table 7 Condition of specimen (Addition ratio of Bentonite 5%)

Consolidation stress (kN/m ²)	49	98	196
Mass of sample (g)	420.1	429.8	416.6
Moisture content w (%)	10.7	12.3	10.6
Wet density of specimen ρ (g/cm ³)	2.167	2.178	2.155
Dry density of specimen ρ (g/cm ³)	1.958	1.939	1.948
Degree of compaction	101.4	100.5	101.0

Fig. 7 shows the Mohr circles which were expressed in terms of effective stress. From the Mohr-Coulomb's Failure line in Fig. 7, the values of angle of friction ϕ' and cohesion c' can be estimated as 43.0° and 0 kN/m², respectively.

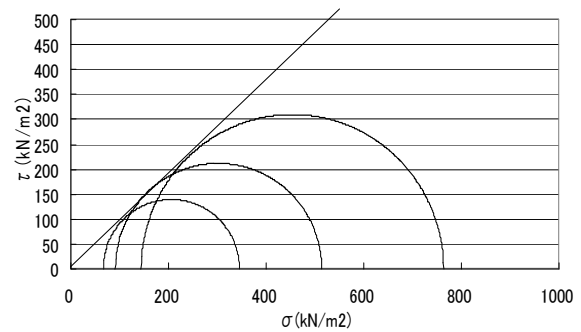


Fig. 7 Mohr circles

Coefficient of Permeability

The permeability tests were conducted using flexible wall permeameter (Imaizumi et al. 2008) for the test specimen with an addition ratio of bentonite of 3, 5 and 8%. These addition ratio were smaller than the critical addition ratio described previously. The specimen was compacted to become the maximum dry density with optimum water content. The test for the specimen with an addition ratio of bentonite of 0% was also conducted. Table 8 shows the condition of the specimen at each addition ratio of bentonite.

Table 8 Condition of specimen with each addition ratio of bentonite

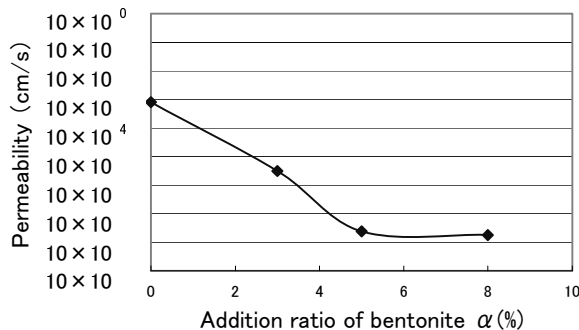
Addition ratio of bentonite α (%)	0	3	5	8
Macro void ratio e'	0.27	0.18	0.15	0.04
Dry density of specimen ρ (g/cm ³)	2.04	2.00	1.96	1.93
Maximum dry density ρ (g/cm ³)	2.06	2.01	1.93	1.91
Moisture content w (%)	0.98	7.51	11.85	12.06
Optimum moisture content W_{opt} (%)	-	8	11.3	11.9

After the specimen was fully saturated, the variation of head was measured and the coefficient of permeability was calculated. The hydraulic gradient was kept as 5 for the specimen with an addition ratio of bentonite of 3, 5, and 8% and 20 for the specimen with an addition of 0%. The calculated coefficient of permeability decreased gradually with elapsed time and kept a steady value. Table 9 and Fig. 8 show the steady value of coefficient of permeability against addition ratio of bentonite.

From Fig. 8, it can be seen that the coefficient of permeability decreases with increasing the addition ratio of bentonite up to about 5% and keeps a constant value of about 2×10^{-8} cm/s. This addition ratio of 5% can be said as experimental critical addition ratio of bentonite. In this study, the calculated critical ratio of bentonite, 9% is a bit larger than the experimental critical addition of bentonite.

Table 9 Coefficient of permeability

Addition ratio of bentonite α (%)	0	3	5	8
Permeability k (cm/s)	7.96×10^{-4}	3.14×10^{-4}	2.41×10^{-4}	1.82×10^{-4}

**Fig. 8** Coefficient of permeability versus addition

It is also found that the ash molten slag with a addition ratio of bentonite beyond 3.5 % have a coefficient of permeability of 1×10^{-6} cm/sec that is the standard value required for compacted soil barrier layer in waste landfill in Japan.

CONCLUSIONS

The main conclusions obtained from this study are followings.

- 1) Ash molten slag produced from garbage having a maximum particle size of 20 mm and a particle density of 2.734 g/cm^3 was classified as Sandy gravel (GS) from engineering point of view.
- 2) Gravel sized ash molten slag is material that crushes easily. It became sandy particles but not down to fine particles.
- 3) The measurements of heavy metals, Cd, Pb, As and Cr^{6+} from elution test, content test, oxidation-added elution tests and alkali-added elution tests satisfied the environmental standards value on the soil. But, Cr^{6+} seems to elute a bit on the alkali side.
- 4) The calculated critical addition ratio of bentonite was 9 % and is bit larger than a experimental critical ratio of 5 %.
- 5) Well compacted ash molten slag with 10 % addition ratio of bentonite has an unconfined compression strength of about 100 kN/m^2 . Therefore it is expected to carry 15 tons class bulldozer.
- 6) Well compacted ash molten slag with 5 % addition ratio of bentonite has an angle of friction of 42.3° and a cohesion of 0 kN/m^2 .

7) Well compacted ash molten slag with addition ratio of bentonite of more than 3.5% has a coefficient of permeability less than 1×10^{-6} cm/s that is a standard value of the compacted soil barrier layer in Japan.

As described above, ash molten slag mixed with bentonite can be used as the materials for compacted soil barrier layer. However, it seems necessary to conduct further elution tests for crashed slag.

ACKNOWLEDGMENT

This study was financially supported by a grant from Specific Research Program at Utsunomiya University.

REFERENCES

- Geo-Environmental Protection Center (2008). URL: <http://www.gepc.or.jp/reference/report.html>
- Imaizumi S, Wataru M, Takahashi N, Doi Y (2008). Estimation of Critical Ratio of Bentonite Addition, Proc. of the Fifth Asia-Pacific Landfill Symposium, CD-ROM, 3B-1.
- Japan Road Association (1986). Road navy-Soil exploration Indicator (in Japanese).
- Ministry of the Environment (2002). No.19 of the Ministry of the Environment notification: (in Japanese).
- Ministry of the Environment (2003). No.18 of the Ministry of the Environment notification: (in Japanese).
- National Institute of Advanced Industrial Science and Technology (2005). Research material, Figure ATLAS 8(Eh-pH): 80 (in Japanese).
- Ohtsuka S, et al. (2006), Permeability property of bentonite mixed with tuff- sandstone crushing sand, 33th Civil Engineering association Kanto branch symposium (in Japanese).
- Public Works Research Institute (2007). Manual for heavy-metal contamination of natural origin on the construction work: 90 (in Japanese).
- The Japanese Geotechnical Society (2004). Japanese Standards for Geotechnical and Geoenvironmental Investigation Methods. –Standards and Explanations: 293 (in Japanese).
- The Japan Society of Industrial Machinery Manufacturers (2007). Current state and data of eco-slag for effective use: 2-26 (in Japanese).
- The Japan Society of Industrial Machinery Manufacturers (2007). Current state and data of eco-slag for effective use : 130-146 (in Japanese).

AN APPLICABILITY OF DEHYDRATED CAKE PRODUCED FROM QUARRY TO IMPERMEABLE MATERIAL WITH HEAVY METAL ADSORPTION

Ryo SUETAKE¹, Kenichi SATO², Miyako TAKEDA³ and Morimoto TATSUO⁴

ABSTRACT: For impermeable materials for landfill constructed at intermountain region, clayey materials supplied homogeneously and stably are required. Authors have paid attention to the dehydrated cakes mainly produced from quarry at intermountain region. Then, new impervious material with an additive which allows absorbing heavy metals has been developed. According to the previous studies, it was confirmed that the landfill standard regarding sealing work could be secured by the compaction of two kind of different dehydrated cakes with the constant condition of water content. Now, there are approximately 1,500 quarries in Japan and each lithological character is different. Whether such differences of lithological character are problematic to the usage as impermeable materials is an important issue to be examined. Moreover, this paper describes the results of the examination in terms of the following three points. (1) The water content and the degree of compaction on the trafficability and permeability properties, (2) Evaluation of long-time durability (3) This material have the heavy metal adsorption ability.

KEYWORDS: dehydrated cake, impermeable material, permeability, heavy metal adsorption

INTRODUCTION

Regarding the double bottom seepage control work at the controlled type final landfill site in Japan, the landfill often faces the problem of leaching from wastes due to the geo-membrane damage. The bentonite mixed soil has been generally used as an impermeable material so far. Bentonite mixed soil has self-sealing capability and low hydraulic conductivity with swelling effect. (Mizuno et al. 2005). Moreover, regulation for impermeable material in Japan is 50cm and a hydraulic conductivity is less than 1×10^{-6} cm/sec. (IGS, 2000). We have been developing a new type impermeable material with heavy metal adsorption. The heavy metal can be absorbed by mixing the dolomite, zeolite and hydrotalcite with the dehydrated cake. First of all this study, a physical property of 10 kinds of dehydrated cakes is evaluated. Next, the required capability, long-term durability and heavy metal adsorption capability of impermeable material were evaluated using two kind of dehydrated cakes.

SOIL PROPERTIES

We used dehydrated cakes produced at a macadam factory as a form of sludge. Now, there are approximately

1,500 quarries in Japan. The dehydrated cake produced at quarry has different properties of each. This study used ten kinds of dehydrated cakes from different quarries. The material was evaluated by examining each physical characteristic, and using the plasticity chart. The physical properties of these dehydrated cakes A~J with different localities are summarized in Table 1. Fig.1 shows the grain size distribution curves of the dehydrated cakes. The density of the soil particle of each dehydrated cake is in the range of about $\rho_s = 2.6 \sim 2.9$ (g/cm³), and it is resulted from the difference of the lithological characteristic.

Table 1 Physical properties of the dehydrated cakes with different lithological characters

	De si fs i i es)	i i i i w	s i i i w	s i i i ex	x i i s i e ()
A	2.631	39.9	25.4	14.5	100.0
B	2.946	42.2	28.2	14.0	99.0
C	2.785	34.2	21.3	12.9	96.6
D	2.722	31.3	18.7	12.6	87.5
E	2.791	23.7	18.7	5.0	95.9
F	2.683	56.7	34.9	21.8	88.9
G	2.734	34.7	19.5	15.2	95.4
H	2.691	40.6	23.4	17.2	97.7
I	2.775	32.9	19.4	13.5	94.9
J	2.780	29.9	46.2	16.2	92.9

¹ Master Course Student, Department of Civil Engineering, Fukuoka University, Japan. Email:td084008@cis.fukuoka-u.ac.jp

² Professor, Department of Civil Engineering, Fukuoka University, Japan. Email:sato@fukuoka-u.ac.jp

³ Miss., ASTEC Co.,Ltd, Japan. Email:m.takeda@astec-geo.co.jp

⁴ Mr., ASTEC Co.,Ltd, Japan.

All dehydrated cakes are composed of the fine-grained fraction. Fig.2 shows the plasticity chart of the dehydrated cakes used in this study. In this chart, compressibility is defined by the B line ($w_L=50\%$). In addition, the modulus of volume change, permeability, toughness and tolerance for dryness can be judged by the A line ($I_p=0.73(w_L-20)$). As this figure demonstrates, most of dehydrated cakes used in this study are at the position of (CL), and low-plastic and low-compressible cohesive soil. According to the previous studies, it was confirmed that the landfill standard regarding sealing works could be secured by the compaction of two kind of different dehydrated cakes A and B with constant conditions of water content (Takeda et al. 2007). The eight kinds of dehydrated cakes newly examined this time have almost same physical properties as dehydrated cake A and B. It is believed that these materials can secure the permeability and trafficability required as an impermeable material.

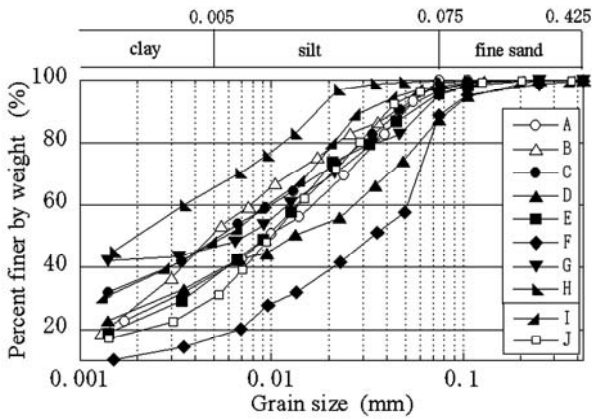


Fig. 1 Particle-size distribution curves for dehydrated cakes with different lithological characteristic

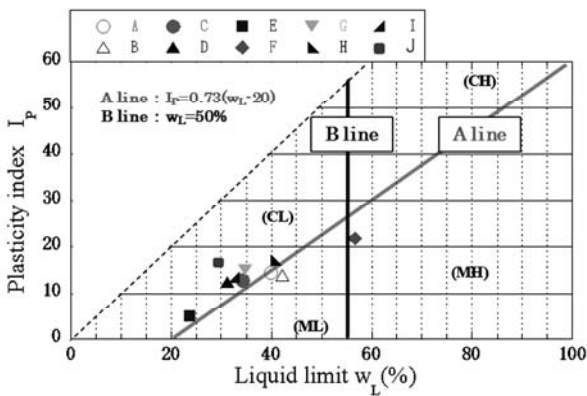


Fig. 2 Plasticity chart

These eight samples will be examined on the permeability and trafficability hereafter. Then, the examination will be carried out on the basis of the

evaluation method concerning bentonite mixed soil using consistency index suggested by Mizuno et al. (2004)

EXPERIMENTAL TARGETS

The additive was mixed with each dehydrated cake and the basic mixing rate is the dolomite 2%, zeolite 2%, and hydrotalcite 5%. The density management of the test piece was carried out on the basis of each impermeable material shown in Fig.3. The items compaction curve of to be examined are as follows.

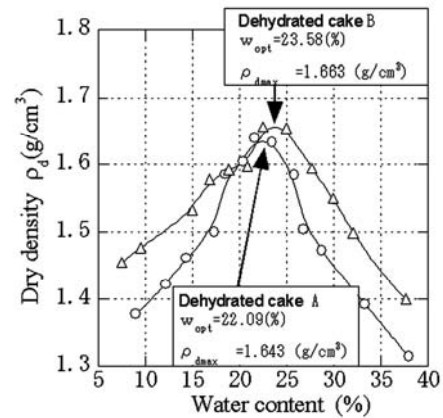


Fig. 3 Results of compaction test

(1) Performance of the impermeable material

It is important for the construction of sealing works to secure the trafficability and a regulated coefficient of using permeability. The cone index test was conducted to examine the trafficability and the permeability test was performed the flexible wall type method (ASTM 5084). The test specimens examined in this research were prepared under the conditions that the degree of compaction $D=80, 90,$ and 95% obtained from the dry densities in Fig.3.

(2) Evaluation of long-time durability

Since the dolomite as an additive has hydraulic property, it is inferred that the strength and permeable characteristics of the impermeable material will change with time. Then, the cone penetration test was conducted to investigate the long-term strength characteristic of the impermeable material. In addition, the longitudinal permeability test was performed to examine the change in permeable characteristics with time.

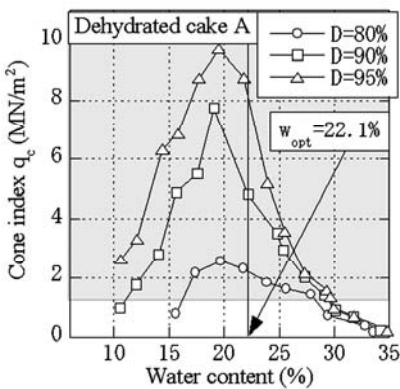
(3) The heavy metal adsorption ability

To investigate the longitudinal stability about the heavy metal adsorption of the target impermeable material in this research, the equilibrium adsorption test and column test to lead, Pd and hexavalent chromium, Cr (VI).

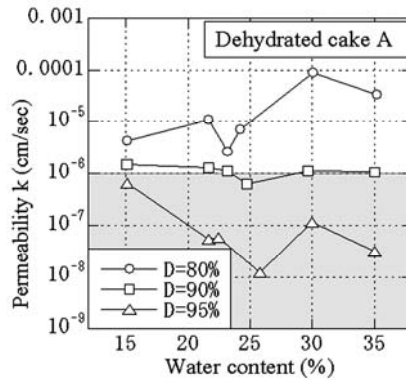
PERFORMANCE OF THE IMPERMEABLE MATERIAL

At first, the cone index $q_c=1200\text{kN/m}^2$ required for a dump truck is determined as performance requirement value of the impermeable material. Fig.4 shows the relations between the cone index and water content of different dehydrated cakes. The increase of cone index associated with the increase of degree of dump truck. Besides, in case of $D=95\%$ conditions, it is also clear that conditions that water content is less than 30% to obtain the trafficability required for a run of dump truck. That is, the control of initial water content on construction is very important for the dehydrated cake that has high water content. Fig.5 shows the relationships between the coefficient of permeability index and water content of dehydrated cake A and B. The regulation for the impermeable material in Japan less than or equal to $k=1.0\times 10^{-6}\text{cm/sec}$ in the coefficient of impermeability (IGS, 2000). It is obvious that the coefficient of permeability becomes small if the degree of compaction

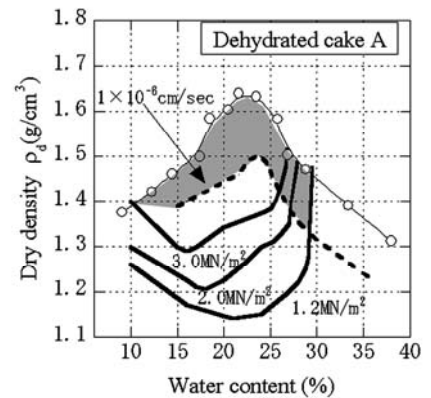
becomes high in both dehydrated cakes. Additionally, it is clear that the regulated coefficient of permeability can be secured under the $D=95\%$ condition in both dehydrated cakes. In case of 15% water content, however, the coefficient of permeability grows to around $1.0\times 10^{-6}\text{cm/sec}$. Moreover, in case that the degree of compaction $D=90\%$ of the dehydrated cake B, when the water content becomes less than or equal to 25%, the coefficient of permeability becomes large rapidly. Judging from the above, it is preferable for both dehydrated cakes to be undertaken under the conditions such as the degree of compaction is 95% and water content is more than or equal to 20%. The strength (1.2, 2.0, 3.0MN/m²) and permeability ($1\times 10^{-6}\text{cm/sec}$) contours drawn in the compaction curves for the dehydrated cake A and B are demonstrated in Fig.6 respectively. Using this kind of chart allows understanding the ranges that satisfy the regulations at the constructions of the impermeable material by the water content and compacting conditions.



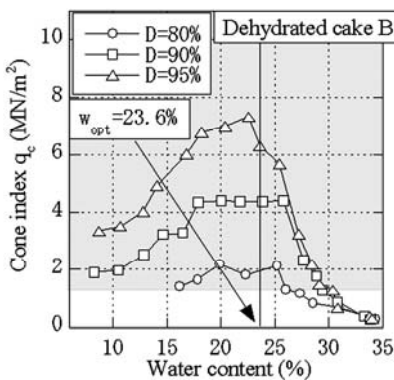
(i) Dehydrated cake A



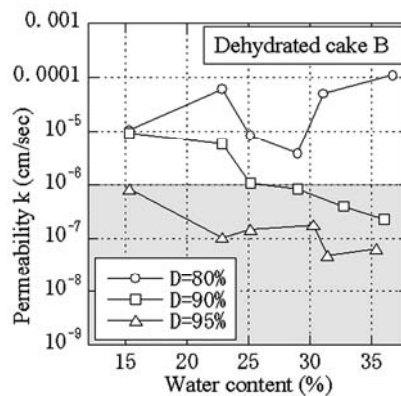
(i) Dehydrated cake A



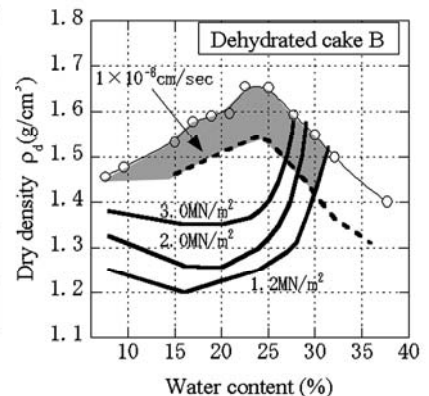
(i) Dehydrated cake A



(ii) Dehydrated cake B



(ii) Dehydrated cake B



(ii) Dehydrated cake B

Fig. 4 Relationships between cone index and water content

Fig. 5 Relationships between permeability and water content

Fig. 6 Summary of results

EVALUATION OF LONG-TIME DURABILITY

The experimental results of long-term cone and permeable indexes obtained using the specimens that degree of compaction is 95% and the water content is optimum conditions are indicated in Fig.7 and Fig.8. The cone index exhibited the considerable increase, especially until seven curing days. This can be regarded as the hydraulic effect of dolomite. It is thought that this is hydraulic property of the dolomite. Thereafter, the strength increases gradually until 186 curing days, even though the strength varies slightly. Accordingly, it is revealed that this material has stable strength. Besides, it is revealed that the coefficient of permeability has decreased. This target impermeable material has sufficient trafficability and impermeability.

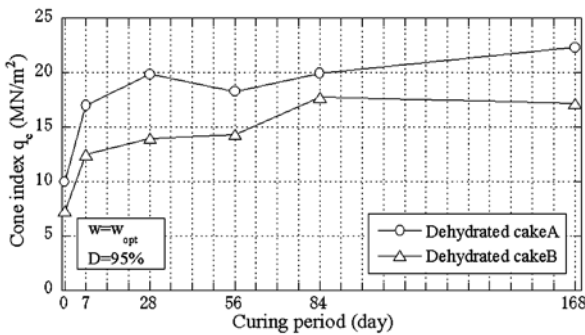


Fig. 7 Relationships between cone index and curing period

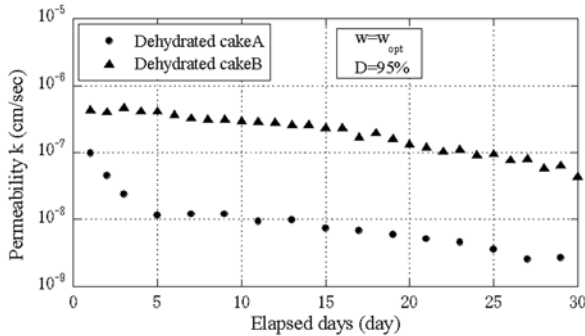


Fig. 8 Relationships between permeability and elapsed days

VALUATION OF DURABILITY HEAVY METAL ADSORPTION

The equilibrium adsorption test was conducted using dehydrated cake A to confirm the effect of heavy metal adsorption ability. Fig.9 and 10 show the results of equilibrium adsorption test for Pb and Cr (VI). Since both adsorption abilities can be increased by the additives, it is clearly evidenced that the additives are effective to the increase of heavy metal adsorption. The

results of calculations about the sustained years of Cr (VI) are shown in Fig.11 and 12. These results highlight that the heavy metal adsorption of the dehydrated cake A is greater than that of the dehydrated cake B. Additionally, if the concentration of Cr (VI) and coefficient of permeability are less than or equal to 0.1mg/L and 1.0×10^{-6} cm/sec respectively, the sustained years of Cr (VI) adsorption can be more than or equal to fifty years. That is, sufficient heavy metal adsorption ability is proved. As a result, if the required performance about impermeable materials is filled, the heavy metal adsorption ability is also able to be satisfied.

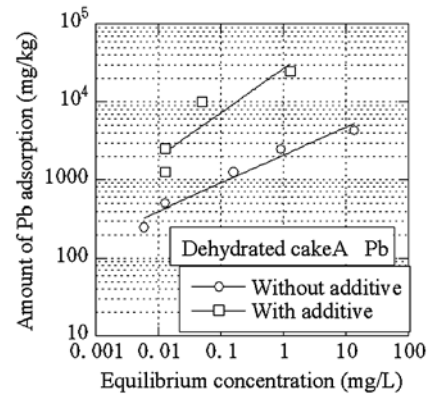


Fig. 9 Results of equilibrium adsorption test about Pb

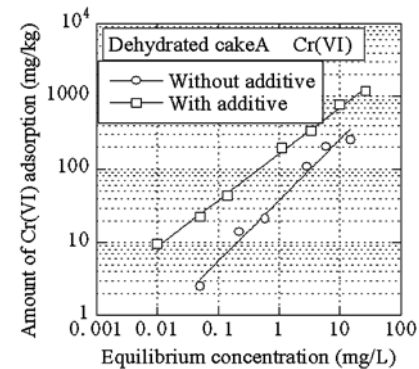


Fig. 10 Results of equilibrium adsorption test about Cr (VI)

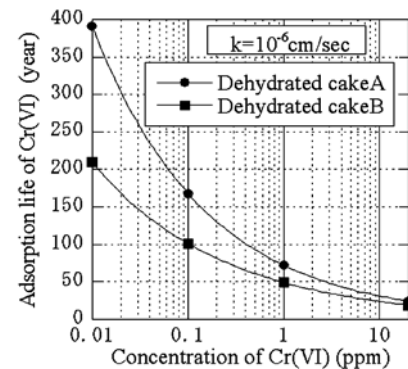


Fig. 11 Relationships between Cr (VI) concentration and durable years

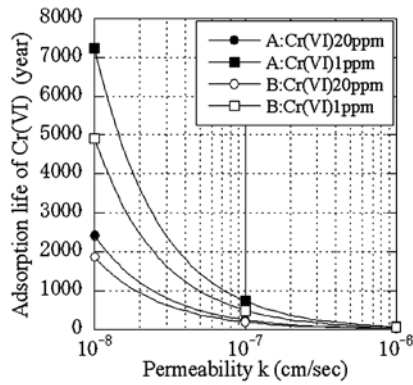


Fig. 12 Relationships between Cr (VI) concentration and permeability

CONCLUSIONS

Since newly investigated ten kinds of dehydrated cakes have almost similar physical properties, it is thought that the performance requirements as impermeable material can be secured.

The ranges that satisfy the regulations at the constructions of the impermeable material can be clarified by the water content and compacting conditions.

Judging from the examination of long-term strength and permeable characteristics of this target impermeable

material, the improvement of impermeability can be expected.

The heavy metal adsorption ability of this impermeable material, the improvement of impermeability can be expected.

REFERENCES

- Mizuno K, Endo K, Hongo T, Fujiwara T, Kamon M, Iwasaki Y (2005). Quality control of bentonite mixed soil as clay-liner for waste landfill. The Proceeding of the 10th International Landfill Symposium (Sardinia 2005): 383-384, in Cagliari, Italy.
- Japan Chapter of International Geosynthetic Society (2000). Geomembrane technology committee, Design and construction of waste repository hand book-seepage control work technology: 202, in Japanese.
- Takeda M, Sato K, Yamada S, Fujikawa T, Morimoto T, Kuchibune A (2007). Study on workability of new type clay liner with heavy metal adsorption. The proceedings of the 7th Environmental geotechnical engineering symposium: 173-176, in Japanese.
- Mizuno K, Okada T, Fujiwara T, Endo K, Nsigaki M, Kamon M (2004). The proceedings of the 15th Japan society of waste management experts: 1169-1171, in Japanese.

UNCONFINED COMPRESSIVE STRENGTH OF MIXTURE OF PHOSPHOGYPSUM-FLY ASH-LIME-CLAY

Zhi-Hong QI¹, Xue-Yuan XU², Mi-Lin ZHU³ and Yang HU⁴

ABSTRACT: In this paper, the unconfined compressive strength test of mixture of phosphogypsum-fly ash-lime-clay for 7days and 28days curing period is based on 16 kinds of mix design method for orthogonal analysis, the optimum mix of phosphogypsum-fly ash-lime-clay is obtained by the unconfined compressive strength test at the same time. Combined with practice, the application of phosphogypsum to the subgrade and pavement is studied for its feasibility and practicality, and the result shows that phosphogypsum is not only a kind of the best roadbed filler but also a type of the road base course with the excellent performance.

KEYWORDS: phosphogypsum, mixture of phosphogypsum, method for orthogonal analysis, unconfined compressive strength

INTRODUCTION

With the development of China's chemical industry, waste and industrial by-product known as phosphogypsum is produced. As a result, phosphogypsum has seriously polluted the environment and it will get worse with the progressing of chemical industry if without any measures. Therefore, how to reuse phosphogypsum is a big challenge we are facing in China.

This paper will illustrate the experiment and application on waste industrial phosphogypsum produced by the phosphate fertilizer plant in Yancheng. Through the trial study, with the method for orthogonal analysis, it takes the unconfined compressive strength test by phosphogypsum – fly ash – lime – clay of 16 kinds of mix. According to the result, the optimum mix is presented by the unconfined compressive strength test.

EXPERIMENT AND METHOD

Plan of Orthogonal Analysis

Research on the law of the strength of mixture, changed with the content of phosphogypsum mixed into the roadbed materials in highway construction, combined with the actual situation, the factor levels of mixture are got shown in the following tables:

Table 1 Factor levels of mixture

levels	Influencing factors		
	A. Phosphogypsum	B. Fly ash	C. Lime
1	0%	10%	6%
2	10%	15%	8%
3	15%	20%	0%
4	20%	25%	(0%)

In table 1 it can be seen, lime dose is expanded from three levels to the four levels: 6%, 8%, 0%, (0%) (proposed level).

Note: All materials are accounted for the percentage of the total weight of mixture.

The results of compaction test of 16 kinds of mix are in table 2.

The project has three factors with four levels, the results shown in Table 2 are selected for the unconfined compressive strength test.

Test Conditions

According to the code for unconfined compressive strength test of Ministry of Transports of the People's Republic of China, 16 kinds of samples of mixture (Φ5.0

¹ Engineer, College of Architectural & Civil Engineering, Jinling Institute of Technology, China. Email:qzh@jit.edu.cn

² Lecturer, College of Civil Engineering, Yancheng Institute of Technology, China. Email:xyy@ycit.cn

³ Lecturer and Engineer, College of Architectural & Civil Engineering, Jinling Institute of Technology, China. Email:zml@jit.edu.cn

⁴ Lecturer, College of Architectural & Civil Engineering, Jinling Institute of Technology, China. Email:huyang@jit.edu.cn

× 5.0cm³) are made respectively. 16 groups of samples are obtained, 10 parallel samples in each group, 160 samples in all, cured for 7days and 28days in a standard curing chamber (under a temperature of 25°C ± 2°C, a relative humidity of more than 90%), finally, the unconfined compressive strength tests (each curing period for 5 parallel samples) are carried out respectively. The samples without any restrictions in the side conditions bear the maximum axial stress (i.e., unconfined compressive strength).

Table 2 Method for orthogonal analysis

Serial number	Phosphogypsum content (%)	Fly ash content (%)	Lime content (%)	Clay content (%)
1	0	10	6	84
2	0	15	8	77
3	0	20	0	80
4	0	25	0	75
5	10	10	8	72
6	10	15	6	69
7	10	20	0	70
8	10	25	0	65
9	15	10	0	75
10	15	15	0	70
11	15	20	6	59
12	15	25	8	52
13	20	10	0	70
14	20	15	0	65
15	20	20	8	52
16	20	25	6	49

Test Results

Analyze the results of test of the unconfined compressive strength of mixture of phosphogypsum - fly ash - lime - clay, and the results are shown in Table 3. (Table 3 in Page 3)

Analyze the unconfined compressive strength of mixture with method for orthogonal analysis. Select the unconfined compressive strength as evaluation indexes of 16 kinds of mix, fill the unconfined compressive strength of 16 kinds of mix for 7d and 28d curing period in Table 4. (Table 4 in Page 3)

In Table 4, the sum of compressive strength (i.e.,K1, K2, K3 and K4) and the average compressive strength (i.e.,AK1, AK2, AK3 and AK4), as well as the Range in the four tests are calculated as follows:

The K_i and the values of K_i for factor A (as an example to 7d curing period):

$K1 = 0.387 + 0.482 + 0.476 + 0.125 = 1.472$ (the sum of the unconfined compressive strength of test NO.1,2,3,4);

$K2 = 0.117 + 0.123 + 0.127 + 0.148 = 0.516$ (the sum of the unconfined compressive strength of test NO. 5,6,7,8);

$K3 = 0.214 + 0.229 + 0.479 + 0.423 = 1.344$ (the sum of the unconfined compressive strength of test NO.9,10,11,12);

$K4 = 0.270 + 0.168 + 0.311 + 0.438 = 1.188$ (the sum of the unconfined compressive strength of test NO.13,14,15,16);

$AK1 = K1 / 4 = 0.368$, $AK2 = K2 / 4 = 0.129$, $AK3 = K3 / 4 = 0.366$, $AK4 = K4 / 4 = 0.297$.

The Range of $AK1$, $AK2$, $AK3$ and $AK4$ (or $K1$, $K2$, $K3$ and $K4$) is obtained by the large numbers minus the small ones. For example, the first Range (for factor A) = $0.368 - 0.129 = 0.107$, and the rest calculations are the same with the first one.

The law of the unconfined compressive strength of 16 kinds of mix for 7d and 28d curing period, changed with the content of various factors are shown in Figs.1 and 2.

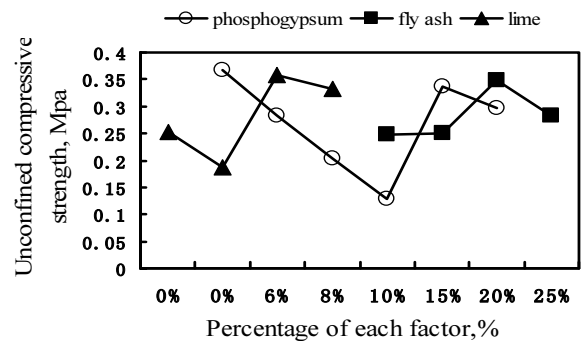


Fig. 1 Law of unconfined compressive strength of mixture for 7d curing period, changed with the content of various factors

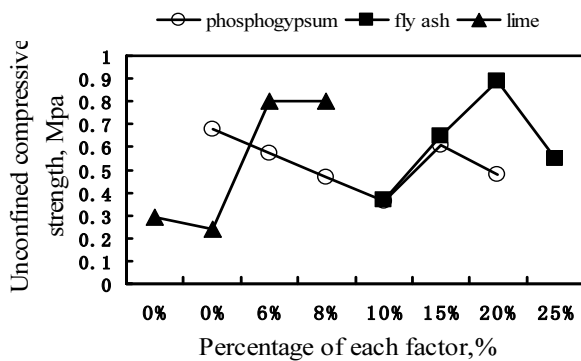


Fig. 2 Law of unconfined compressive strength of mixture for 28d curing period, changed with the content of various factors

Table 3 Test results of the unconfined compressive strength of mixture of phosphogypsum - fly ash - lime – clay

Serial number	Mixing proportion	Compressive strength (MPa)	
	Phosphogypsum: fly ash: lime: clay	R7	R28
1	0: 10: 6: 84	0.387	0.87
2	0: 15: 8: 77	0.482	1.11
3	0: 20: 0: 80	0.476	0.50
4	0: 25: 0: 75	0.125	0.24
5	10: 10: 8: 72	0.117	0.13
6	10: 15: 6: 69	0.123	0.95
7	10: 20: 0: 70	0.127	0.19
8	10: 25: 0: 65	0.148	0.17
9	15: 10: 0: 75	0.214	0.32
10	15: 15: 0: 70	0.229	0.35
11	15: 20: 6: 59	0.479	0.98
12	15: 25: 8: 52	0.423	1.08
13	20: 10: 0: 70	0.270	0.17
14	20: 15: 0: 65	0.168	0.17
15	20: 20: 8: 52	0.311	0.89
16	20: 25: 6: 49	0.438	0.70

Table 4 Unconfined compressive strength of mixture of 16 kinds of mix for 7d and 28d curing period for orthogonal analysis

Test number	A.Phosphogypsum (%)	B. Fly ash (%)	C. Lime (%)	Evaluation indexes (MPa)	
				7d	28d
	1	2	3	5	6
1	1(0%)	1(10%)	1	0.387	0.87
2	1	2(15%)	2	0.482	1.11
3	1	3(20%)	3	0.476	0.50
4	1	4(25%)	4	0.125	0.24
5	2(10%)	1	2	0.117	0.13
6	2	2	1	0.123	0.95
7	2	3	4	0.127	0.19
8	2	4	3	0.148	0.17
9	3(15%)	1	3	0.214	0.32
10	3	2	4	0.229	0.35
11	3	3	1	0.479	0.98
12	3	4	2	0.423	1.08
13	4(20%)	1	4	0.270	0.17
14	4	2	3	0.168	0.17
15	4	3	2	0.311	0.89
16	4	4	1	0.438	0.70
K ₁	1.472/2.72	0.988/1.49	1.428/3.2	The sum of (K ₁ , K ₂ , K ₃ and K ₄):	
K ₂	0.516/1.44	1.004/2.58	1.332/3.21		
K ₃	1.344/2.44	1.392/2.26	1.008/1.16		
K ₄	1.188/1.92	1.136/2.19	0.752/0.952		
AK ₁	0.368/0.68	0.247/0.373	0.357/0.8	4.52/8.52	
AK ₂	0.129/0.36	0.251/0.645	0.333/0.803		
AK ₃	0.336/0.61	0.148/0.565	0.252/0.290		
AK ₄	0.297/0.48	0.284/0.548	0.188/0.238		
Range	0.107/0.20	0.136/0.097	0.189/0.562		

Note: the left data of the oblique line (/) are the values of the unconfined compressive strength for 7d curing period ; and the right ones are the values of the unconfined compressive strength for 28d curing period .

CONCLUSIONS AND APPLICATION

Conclusions

In Table 4, compare the average compressive strength (i.e. AK1, AK2, AK3 and AK4), (AK1 cannot be considered because the level of AK1 is 0%, and it is inconsistent with the purpose of this research), such as the first AK3 (for factor A) = 0.336, is greater than AK2 = 0.129 and AK4 = 0.297, which approximately shows that the influence on the unconfined compressive strength of mixture for the incorporation of 15% phosphogypsum is greater than those of the incorporation of 10% and of 20%. By analogy with the other two factors, the optimum mix is for A₃B₃C₁ (that is, the incorporation of phosphogypsum is 15%, of fly ash is 20% and of lime is 6%).

From Figs. 1 and 2 it can be seen:

1. After mixing phosphogypsum, the unconfined compressive strength of mixture for 7d and 28d curing period all decline, but with the increased content of phosphogypsum, the unconfined compressive strength gradually increase. When the incorporation of phosphogypsum is 15%, the greatest strength of mixture is obtained, and with the increased incorporation of phosphogypsum, the strength of mixture decline.

2. When mixing lime, the unconfined compressive strength of mixture for 7d and 28d curing period obviously increase, and the incorporation is 6%, the unconfined compressive strength of mixture is the greatest, with the increased incorporation, the strength of mixture decline slightly.

3. With the increased content of fly ash, the unconfined compressive strength of mixture for 7d and 28d curing period increase, and with the incorporation of fly ash more than 20%, the strength of mixture begin to decline.

4. With the increased curing period, the unconfined compressive strength of mixture increase.

Application

A few years ago, in Yancheng, the project of widening the Yan-Jin Road, tried to apply the phosphate fertilizer to the roadbed filler. The phosphate fertilizer, which is divided into two levels compaction in the section of the Yan-Jin Road nearly 1.1 km long with 2 meters width, is applied as the roadbed filler. The thickness is nearly 30 cm after compaction. The practice shows that the effect of applying the phosphate fertilizer to the roadbed filler is satisfied. Mixture of phosphogypsum has been done well in the application to the road base course construction. It shows that phosphogypsum is not only a kind of the best roadbed filler but also a type of the road base course with the excellent performance.

ACKNOWLEDGEMENTS

This paper comes from the project (YK2006208), which is sponsored and established in 2006 by Yancheng Technology Bureau.

REFERENCES

- Ding JW, Shi ML, Liu WZ (2009). Reusing test study and application of phosphogypsum-lime solidified soil in road base course. *Journal of Southeast University (Natural Science Edition)*. 39(1): 121-125 (in Chinese).
- Fan YR, Huang YB, Tang JP (2008). Feasibility study on application of ardealite in rural road pavement construction. *Technology of Highway and Transport* (5): 11-12,20 (in Chinese).
- Gaylarde CC, Ribas Silva M, Warscheid Th (2003). Microbial impact on building materials: an overview. *Materials and Structures / Matériaux et Constructions*. 36: 342-352.
- Potgieter SS, Potgieter JH, Panicheva S (2004). Investigation into methods of chloride analysis of South African cement and cement-related materials with low chloride concentrations. *Materials and Structures / Matériaux et Constructions*. 37:155-160.
- Pugazhendhi Thayumanavan & Peter ONelson (2005). Application of whole effluent toxicity test procedures for ecotoxicological assessment of industrial wastes used as highway construction materials. *Handb Environ Chem*. Vol.5, Part F, 2: 111-131.
- Shen WG, Jiang J, Zhang L, Wang K, Zhou MK (2008). A study on properties of phosphogypsum modified lime-fly ash road base materials. *Highway* (1):141-144 (in Chinese).
- Shen WG, Zhou MK, Zha J, Zhao QL (2005). Research on the proportion design of phosphogypsum modification lime fly-ash road base material. *Journal of Wuhan University of Technology*. 27(10): 19-22 (in Chinese).
- Suphaphat Kwonpongsagoon, Hans-Peter Bader, Ruth Scheidegger (2007). Modelling cadmium flows in Australia on the basis of a substance flow analysis. *Clean Techn Environ Policy*. 9:313-323.
- Xu XY, Xu YZ, Chen GS, Yu XJ (2004). Testing study on engineering characteristics of phosphogypsum. *Chinese Journal of Rock Mechanics and Engineering*. 23(12) : 2096-2099 (in Chinese).
- Zhao Y & Shi ML (2007). Research on reusing phosphogypsum-fly ash-lime solidified mixtures. *Rock and Soil Mechanics*. 28 Supp.: 98-102 (in Chinese).

ADSORPTION BEHAVIOR AND MECHANISM OF Cu(II) ON ACTIVATED FIRMIANA SIMPLEX LEAF

Qiang TANG¹, Xiao-Wu TANG², Man-Man HU³, Yun-Min CHEN⁴, Yan WANG⁵ and Nai-Yu KOU⁶

ABSTRACT: Copper pollution has caused serious public health problems recently, and activated Firmiana Simplex Leaf has proved effective to remove Cu(II) from aqueous solution. Factors affecting the adsorption of Cu(II) include: dosage, solution pH, temperature and duration. The thermodynamic behavior reveals the endothermic and spontaneous nature of the adsorption, and the max adsorption capacity calculated by Langmuir model is 66.721 mg g⁻¹. The adsorption mechanism is further studied with the assistance of FT-IR test.

KEYWORDS: Firmiana Simplex Leaf, activated leaf, Cu(II), adsorption kinetic, adsorption equilibrium

INTRODUCTION

The presence of heavy metals in environment during the last decade aroused considerable public concern since their increasing discharge, toxic nature and other adverse effects on water resources. What is worse, toxic heavy metals cause DNA damage, and their mutagenic ability will probably cause carcinogenic effects in animals and humans (Knasmüller et al. 1998; Hartwig 1995). Copper is an essential trace element for healthy growth of living creatures, but at elevated level, it is potentially toxic. It causes stomach and intestinal distress, kidney damage, and anemia (Carson et al. 1986). Cu(II) contained wastewater is commonly produced during electroplating, PCB processing, mining, metallurgy, and battery manufacture (Gulnaz and Saygideger 2005). Besides, high concentrations of Cu(II) in landfill leachate also can be observed (Fan et al. 2006). According to statistics, by the early 1990s, the worldwide annual release had reached 954,000 tons for copper (Kovalchuk et al. 2001).

The conventional methods for heavy metal removal from wastewater include precipitation, ion exchange, adsorption, coagulation, evaporation, redox and extraction. But in practice, adsorption has been proved to be an economical, effective and environmentally friendly method for heavy metals removal (Tran et al. 1999; Peterlene et al. 1999). Firmiana Simplex is distributed in almost the entire district with monsoon climate of medium latitudes,

such as Europe, the USA, Japan and China. Arising from the large production, the limited capacity of landfills and harmful emissions by incinerations, it is necessary to develop new treatment. Therefore, the adsorbent conducted in this study is Firmiana Simplex Leaf (FSL). The adsorption behaviors of Cu(II) on FSL are investigated in this paper.

MATERIALS AND METHODS

Preparation of Adsorbent

The FSL studied in this paper was collected in October, 2008 then pulverized into powder. Afterwards, the leaf was placed into an oven which temperature was regulated at 250°C, then pertained for 5 h. There was no gas supply into the oven during the calcination process. The product was cooled to room temperature after equilibrates, and the obtained activated ashes were collected.

Characterization

FT-IR spectra of AL (activated leaf) and Cu(II) laden leaf were recorded using Nexus-670 (Nicolet, USA). The Cu(II) laden leaf sample was prepared by centrifuging the mixture (equilibrated 400 mg AL with 40 mL 5 g L⁻¹ Cu(II) solution for 24 h at 55°C) at 3000 rpm for 5 min.

¹ MA Student, MOE Key Laboratory of Soft Soils and Geoenvironmental Eng., Zhejiang Univ., China. tangqiang85@hotmail.com

² Prof., MOE Key Laboratory of Soft Soils and Geoenvironmental Eng., Zhejiang University, China. Email: tangxiaowu@zju.edu.cn

³ Ph.D Student, MOE Key Laboratory of Soft Soils and Geoenvironmental Eng., Zhejiang Univ., China. Email: jsgyhmm@gmail.com

⁴ Prof., MOE Key Laboratory of Soft Soils and Geoenvironmental Eng., Zhejiang Univ., China. Email: chenyunmin@zju.edu.cn

⁵ Ph.D Student, MOE Key Laboratory of Soft Soils and Geoenvironmental Eng., Zhejiang Univ., China. wangyan850407@163.com

⁶ MA Student, MOE Key Laboratory of Soft Soils and Geoenvironmental Eng., Zhejiang Univ., China. kounaiyu19870210@163.com

Experiment

Dosage effect: the adsorbent dosage (AL) in the aqueous solution was increased from 0.5 to 1, 2, 5, 10 and 20 g L⁻¹ in order to determine the most appropriate one. Initial Cu(II) concentration was set at 50 mg L⁻¹ and after mixing with the adsorbent, the flasks were put into a thermostated agitator (25°C) for 24 h at 180 rpm. At the end, the mixture was separated by centrifuging at 3000 rpm for 5 min. The supernatant was collected and the equilibrium Cu(II) concentration was determined by AAS (Atomic Absorption Spectrophotometer).

Adsorption kinetics: the adsorbent dosage was fixed 10 g L⁻¹ and the initial solute concentrations were set 100 mg L⁻¹ with temperature maintained at 25°C. The test was stopped after specific times that increased from 3 to 6, 9, 12, 15, 20, 40, 80, 120, 180, 240, 300 and 1440 minutes. The supernatant and equilibrium Cu(II) concentration was determined with the above method.

Adsorption isotherms and thermodynamics: the AL (10 g L⁻¹) was blended with eight sets of copper chloride solution (initial solute concentration ranged from 25 to 600 mg L⁻¹) at increasing temperature from 5 to 55°C. All samples were equilibrated for 24 h in the controlled temperature agitator and the equilibrium Cu(II) concentrations were measured by AAS.

pH effect: the same amount of AL (400 mg) and Cu(II) solution (100 mg L⁻¹, 40 mL) were mixed and put into nine pretreated conical flasks. Then pH_i (the initial solution pH) of these nine samples was ranged from 2.0 ± 0.2 to 10.0 ± 0.2 with an increment of 1.0. The samples were then placed into a thermostated agitator (25°C) for 24 h. The supernatant and equilibrium Cu(II) concentration was determined with the above method.

RESULTS AND DISCUSSIONS

Effect of Adsorbent Dosage

The effect of adsorbent dosage is shown in Fig. 1. It is apparent that the unit adsorption amount of the AL

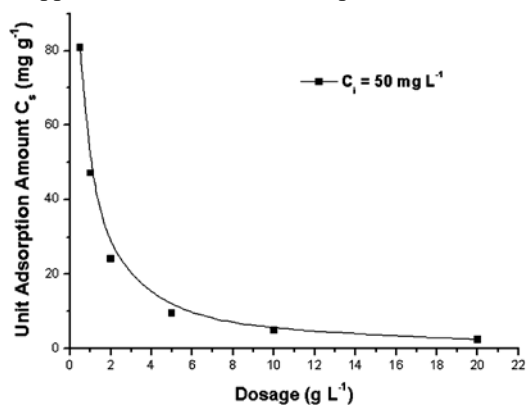


Fig. 1 Dosage effect on unit adsorption amount

decreased continually, but this trend was not linear, as the sharp decrease at the first stage and what followed became flat gradually at higher dosage. Dosage (10 g L⁻¹) is find the optimum adsorbent dosage to satisfy both total Cu(II) uptake and adsorption efficiency. Thus, this dosage was fixed in subsequent study.

Adsorption Kinetics

Fig. 2 plots C_s of Cu(II) as a function of equilibration durations. From the chart, it is obvious that the unit adsorption amount of Cu(II) reaches a relative high value within a fairly short time (less than 3 min) and then slowly increases until it reaches a plateau after 40 min.

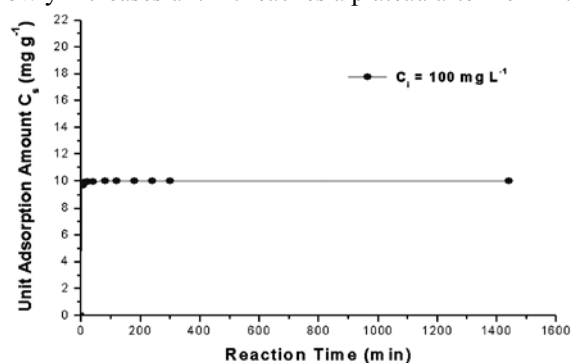


Fig. 2 Duration effect on the unit adsorption amount

Adsorption Isotherms at Different Temperatures

Fig. 3 shows adsorption isotherms of Cu(II) on AL at 55°C. The unit adsorption amount of Cu(II) shows a gradual ascending trend and eventually achieved a maximum adsorption amount at increased equilibrium solute concentrations. Three general isothermal equations, including the Langmuir, Freundlich, and D-R models, were applied to evaluate the test results in order to poke more information on adsorption mechanisms.

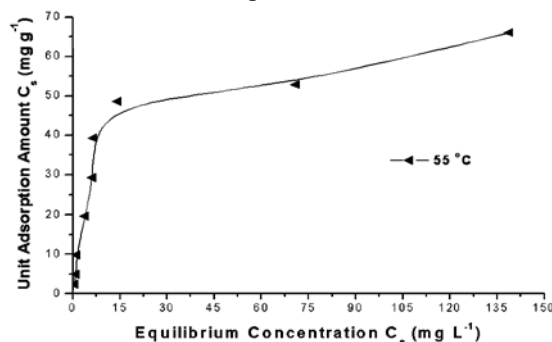


Fig. 3 Isothermal adsorption line

The Langmuir isotherm can be written as (Do 1998):

$$\frac{1}{C_s} = \frac{1}{Q^0} + \frac{1}{bQ^0C} \quad (1)$$

where C_e is the equilibrium concentration of solute solution (mg L⁻¹), Q^0 represents the maximum adsorption

capacity of the adsorbent (mg g^{-1}), and b (L mg^{-1}) the Langmuir constant.

The Freundlich model assumes the surface heterogeneity and exponential distribution of active sites, provides an empirical relationship between the adsorption capacity and equilibrium constant of the adsorbent. The Freundlich isotherm can be expressed as:

$$C = K C^n \quad (2)$$

where K_F (mg g^{-1}) indicates the adsorption capacity and strength of the adsorptive bond, and n represents the heterogeneity factor. The values of R^2 are regarded as a measure of goodness-of-fit of experimental data to the isotherm models.

The D-R model is written as:

$$\ln C_s = \ln q_m - k\varepsilon^2 \quad (3)$$

where q_m is the maximum adsorption capacity (mol g^{-1}), k a model constant related to the free sorption energy and ε the Polanyi potential, which is written as:

$$\varepsilon = RT \ln(1 + (1/C)) \quad (4)$$

The mean free energy of adsorption (E) is:

$$E = -\frac{1}{\sqrt{2k}} \quad (5)$$

The results of predicted isothermal constants for the adsorption of Cu(II) were gathered in Table 1. The Langmuir model was found to show the best-fit to the test data based on calculated correlation coefficients, and the maximum Cu(II) adsorption capacities of AL were estimated to be 66.721 mg g^{-1} .

The adsorption capacities estimated by D-R model were $242.533 \text{ mg g}^{-1}$, higher than those obtained with the Langmuir model since the inherent assumption in the D-R model that all micropores are filled with solute. However, this ideal state is difficult to realize in practice.

Table 1 Predicted constants of isothermal models for Cu(II) adsorption (55°C)

Langmuir model			
Q^0	b	R^2	
66.721 mg g^{-1}	0.142 L mg^{-1}	0.967	
Freundlich model			
K_F	n	R^2	
16.746 mg g^{-1}	3.821	0.844	
D-R model			
q_m	k	E	R^2
$242.533 \text{ mg g}^{-1}$	0.004	-11.323	0.858
	$\text{mol}^2 \text{ kJ}^{-2}$	kJ mol^{-1}	

Thermodynamics

For studying the thermodynamic behaviors of Cu(II) adsorption, thermodynamic considerations were evaluated. Thermodynamic parameters such as enthalpy change (ΔH^0), Gibbs free energy change (ΔG) and entropy change (ΔS) can be estimated with the following Gibbs free energy equations:

$$\Delta G^0 = -RT \ln K \quad (6)$$

$$\Delta G = \Delta H - T\Delta S \quad (7)$$

where R is the ideal gas constant ($8.314 \text{ J mol}^{-1}\text{K}^{-1}$), T the absolute temperature (K), K_D is the distribution coefficient of the solute between the adsorbent and the solution in equilibrium C_s/C_e (mL g^{-1}).

Eqs. 6 and 7 can be written in a linearized form between $\ln K_D$ and $1/T$ as:

$$\ln K = \frac{\Delta S^0}{R} - \frac{\Delta H^0}{RT} \quad (8)$$

ΔH and ΔS can be determined from the slope and the intercept of the plot between $\ln K_D$ versus $1/T$ (Tewari et al. 2005).

Table 2 Thermodynamic parameters for adsorption

C_i (mg L^{-1})		25	
T	$1/T$	$\ln K_D$	G^0 (kJ mol^{-1})
278	0.0035	4.249	-9.822
288	0.0034	7.357	-17.615
298	0.0033	4.589	-11.370
308	0.0032	7.468	-19.124
318	0.0031	8.015	-21.190
328	0.0030	8.311	-22.663
ΔS^0 ($\text{J mol}^{-1} \text{K}^{-1}$)		235.951	
ΔH^0 (kJ mol^{-1})		54.529	
R		0.757	

The predicted constants of thermodynamics shown in Table 2 can be determined through linearization of the test data. The Gibbs free energy was negative, suggesting that the adsorption process was spontaneous and could be promoted by the increasing temperature. The change of enthalpy was $54.529 \text{ kJ mol}^{-1}$ and the change of entropy was $235.951 \text{ J mol}^{-1} \text{K}^{-1}$, which implies an endothermic character to the adsorption process and increasing disorder in the system.

Effect of pH

Fig. 4 plots Cu(II) adsorption percent on AL versus

the initial solution pH (pH_i). A sharp pH-adsorption edge could be observed between pH 2.0 and 5.0, while the percentage Cu(II) removal boosts from about 30% to more than 80%, the curve then plateaus with continuously increasing pH_i .

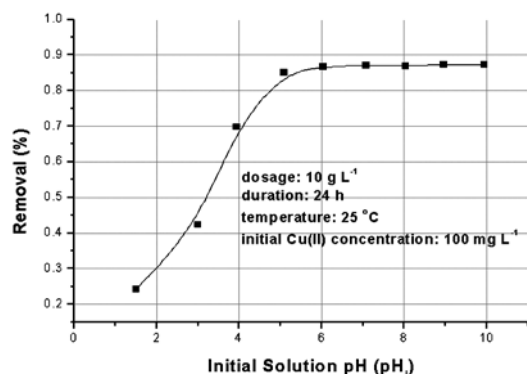


Fig. 4 Variation of Cu(II) removal percentage with varied initial solution pH (pH_i)

DISCUSSION

In the FT-IR spectra of AL before and after adsorption process as shown in Fig. 5, the bands at 1319 cm^{-1} in Cu(II) laden leaf shown in Fig. 5(b) could be assigned to the vibration of N-H group. The high affinity of amine towards Cu(II) would contribute to the adsorption of Cu(II) on AL. Furthermore, the N-H IR intensities were significantly weakened during the Cu(II) adsorption process as shown in Fig. 5.

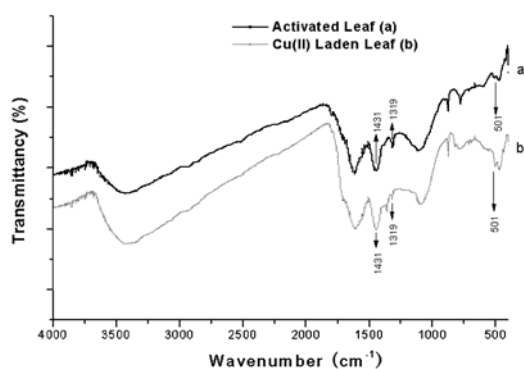
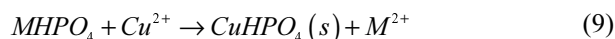


Fig. 5 IR spectra of activated leaf and Cu(II) laden leaf (a. Activated Leaf; b. Cu(II) laden leaf)

The band at 1431 cm^{-1} in the IR spectrum of AL was assigned to carbonate component, which maybe the preferred adsorption site for Cu(II). However, as to AL, the intensity of the band relevant to carbonate had no obvious change after Cu(II) adsorption, suggesting that the carbonate contained in AL was not the dominant adsorption site for Cu(II).

Phosphate was also observed in original AL (Somya

et al. 2009). The presence of phosphate would also contribute to the adsorption of Cu(II) in the form as follows:



The activated Firmiana Simplex Leaf has relatively high Cu(II) adsorption capacity and the fastest rate of reaction. Besides, as a widely planted tree, the Firmiana Simplex provides a locally available cheap source of adsorbent. The activation method provided here proves effective and appears promising in the heavy metals removal from wastewaters.

REFERENCES

- Carson BL, Ellis V, McCann JL (1986). Toxicology and Biological Monitoring of Metals in Ilumans, 71. Lewis Publishers, Chelsea, Michigan: p. 133.
- Do DD (1998). Adsorption Analysis: Equilibrium and Kinetics. Imperial College Press, London.
- Fan HJ, Shu HY, Yang HS, Chen WC (2006). Characteristics of landfill leachates in central Taiwan, China. Sci. Total Environ. 361(1-3): 25-37.
- Hartwig A (1995). Current aspects in metal genotoxicity. BioMetals 8: 3-11.
- Knasmüller S, Gottmann E, Steinkellner H, Fomin A, Pickl C, Paschke A, Göd R, Kundi M (1998). Detection of genotoxic effects of heavy metal contaminated soils with plant bioassays. Mutat. Res. 420: 37-48.
- Kovalchuk O, Titov V, Hohn B, Kovalchuk L (2001). A sensitive transgenic plant system to detect toxic inorganic compounds in the environment. Nature 19: 568-572.
- Peterlene WS, Winkler-Hechenleitner AA, Pineda EAG (1999). Adsorption of Cd(II) and Pb(II) onto functionalized formic lignin from sugar cane bagasse. Bioresour. Technol. 68: 95-100.
- Somya A, Rafiquee MZA, Varshney KG (2009). Synthesis, characterization and analytical applications of sodium dodecyl sulphate cerium (IV) phosphate: A new Pb (II) selective, surfactant-based intercalated fibrous ion exchanger. Colloids and Surfaces A: Physicochem. Eng. Aspects 336: 142-146.
- Tewari N, Vasudevan P, Guha BK (2005). Study on biosorption of Cr(VI) by Mucor hiemalis. Biochemica Engineering Journal 23: 185-192.
- Tran HH, Roddick FA, O'Donnell JA (1999). Comparison of chromatography and desiccant silica gels for the adsorption of metal ions-I. Adsorption and kinetics. Water Res. 33: 2992-3000.



**Contaminated Land and
Remediation Technology**

PURIFICATION OF Cr(VI)-CONTAMINATED SOIL BY FERMENTATION OF ORGANIC MATTER

Kiyoshi OMINE¹, Noriyuki YASUFUKU² and Kazuya TAMURA³

ABSTRACT: This paper describes a purification method of Cr(VI)-contaminated soil with low environmental load using fermentation of organic matter. There are several remediation technologies and these are usually high cost. A remediation method by using aerobic or anaerobic fermentation is applied. The effect of composting with aerobic or anaerobic fermentation was discussed based on the test results. It is concluded that the anaerobic fermentation with organic matter, effective microorganisms resources, and leaf mold is very effective for remedying the contaminated soil with hexavalent chromium.

KEYWORDS: contaminated soil, hexavalent chromium, fermentation, organic matter, microorganism

INTRODUCTION

Recently, many contaminated soils containing heavy metals have been detected in Japan, because the pollution investigation on vacant sites of factories and groundwater investigation are promoted based on the Soil Contamination Countermeasures Law. It is said from the investigation of the soil environmental center that 320,000 places of contaminated sites are needed to purify in our country. A brownfield place remaining untouched due to high cost of soil remediation becomes social problem. It is therefore that a low cost purification technique with low environmental load is required.

In this study, a fundamental study on purification effect of contaminated soil with hexavalent chromium is performed based on the test results. From a viewpoint of composting of organic matter, the aerobic and anaerobic fermentation are used for purification of the contaminated soil (Omine et al. 2009).

AEROBIC AND ANAEROBIC FERMENTATIONS

A lot of autonomous communities are recommended to reduce amount of garbage by composting which is a fermentation based on a metabolism of microorganisms. There are two kinds of fermentations under aerobic and anaerobic conditions. Composting of livestock excreta by dairy farmer is usually made in the anaerobic condition because of efficient production for a large

amount of organic matter. On the other hand, the anaerobic fermentation is also used for the disposal of general household garbage, because it is easy to treat and not susceptible to corrosion for reducing a moisture. The organic matter with the anaerobic fermentation becomes an acid in pH and after that it have to do the aerobic fermentation or lie in a soil about a few weeks for making perfect compost.

Photo 1 shows a micrograph of the organic matter on agar after the aerobic and anaerobic fermentations.



Photo 1 Microscopical observation of microorganisms cultivated on agar after the aerobic and anaerobic fermentations

¹ Associate Professor, Department of Civil Engineering, Kyushu University, Japan. Email:oomine@civil.kyushu-u.ac.jp

² Professor, Department of Civil Engineering, Kyushu University, Japan. Email: yasufuku@civil.kyushu-u.ac.jp

³ Master student, Department of Civil Engineering, Kyushu University, Japan. Email: soil35@civil.kyushu-u.ac.jp

It was observed that several microorganisms are generated on the organic matter. It is considered that a filamentous bacterium appears in the early stage of composting under the aerobic condition.

PURIFICATION OF Cr(VI)-CONTAMINATED SOILS

Mechanism of Purification of Hexavalent Chromium

Valence of chromium enables to change trivalent or hexavalent. Stainless steel is an alloy with iron and chromium, and it is a stable and resistant to corrosion. A film of chromium is used in a lot of plated ware of domestic articles. There exists generally a conformation of trivalent chromium or chromium without valence widely in a soil on the earth. The trivalent chromium is a stable and harmless whereas the hexavalent chromium has a strong toxicity. In general, hexavalent chromium is generated artificially by burning trivalent chrome for high heat. Hexavalent chromium dissolves in water as unstable material and oxidizes an organic matter in an acid condition, and then it resolves itself into trivalent chromium. It is said that a humus material affects an oxidation-reduction of chromium (Nakayasu et al. 1999).

It is also reported that concentration of hexavalent chromium in a chrome slag ruin was restrained largely by disseminating wood vinegar or bran vinegar (Watanabe 2008). It is therefore considered that harmless of hexavalent chromium may be possible by reduction action of various organic matters. As one of the methods, anaerobic fermentation used in compost of organic matters is applied in this study. The anaerobic fermentation is usually promoted by mixing organic matters, leaf mold and microorganisms resource and it changes acid condition. It is expected that the anaerobic fermentation has an effect on the reduction of hexavalent chromium for the contaminated soil.

Samples and Test Method

An artificial contaminated soil was prepared by

mixing a hexavalent chromium standard solution ($K_2Cr_2O_7$) into granite decomposed soil. The standard solution with concentration of 50 mg/L is used and the hexavalent chromium of 5 g in weigh is added into the granite decomposed soil of 500 g.

Before investigating an effect of fermentation, a preliminary test using bamboo vinegar was performed. Because it is reported that leaching of hexavalent chromium from a chrome slag ruin was restrained largely by disseminating wood vinegar or bran vinegar. A soil sample mixed with bamboo vinegar offered commercially was used. The bamboo vinegar diluted in 10 times by distilled water was mixed. It is considered that the bamboo vinegar is a similar property to wood vinegar or bran vinegar.

Test conditions of samples with aerobic and anaerobic fermentations are listed in Tables 1 and 2. Mowed weed is used as an organic matter. Case 1 is the artificial contaminated soil without treatment and Case 2 is a soil sample mixed with leaf mold only into the contaminated soil. Case 3 is a soil sample with the aerobic fermentation carried out by mixing the mowed weed and rice bran into the contaminated soil. Case 4 is a soil sample with the anaerobic fermentation carried out by mixing the mowed weed and EM (effective microorganisms) resources offered commercially into the contaminated soil in a sealed plastic bag during a week. After that, this sample was fermented by opening the plastic bag in the aerobic condition. Photo 2 shows the state of each sample before blending. Photos 3 and 4 show the conditions of the soil samples with mowed weed before and after the aerobic fermentation, respectively.

After the fermentation, a sample of 50 g was taken from each soil and leaching test was performed according to Notification No. 46 of the Japan Environmental Agency. The test fluid was prepared with a solid-liquid ratio of 1:10 and agitated for 6 h to leach the contaminants in the specimen. The mass of the hexavalent chromium released from the soil sample was measured using portable spectrophotometer (DR2800).

Table 1 Composition of samples

Sample	Soil(g)	Leaf mold(g)	Mowed weed(g)	Rice bran(g)	EM resources(g)	Remarks
Case 1	500	-	-	-	-	Contaminated soil
Case 2	500	50	-	-	-	Mixing only leaf mold
Case 3	500	50	50	25	-	Aerobic fermentation
Case 4	500	50	50	-	5	Anaerobic fermentation

Table 2 Test conditions on content of hexavalent chromium for samples with 500 g

Hexavalent chromium	C1	C2	C3
Weight (mg)	0.25	0.50	0.75
Content (mg/kg)	0.5	1.0	1.5

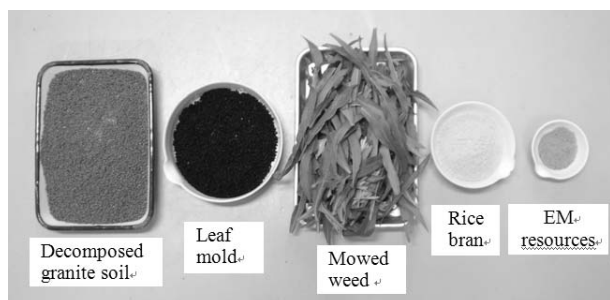


Photo 2 Each sample used in the tests

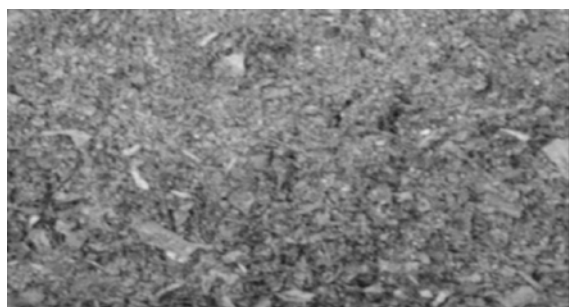


Photo 3 Sample before the fermentation (Case 4)

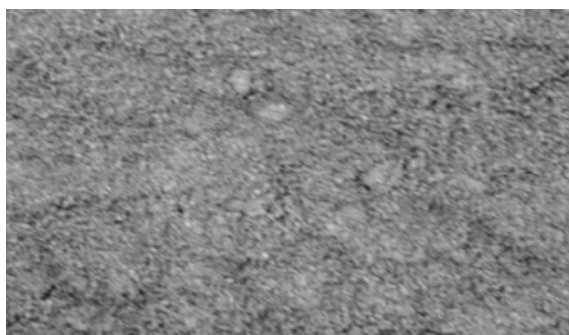


Photo 4 Sample with the anaerobic and aerobic fermentations after degradation of mowed weed (Case 4)

Test Results and Discussions

Effect of bamboo vinegar

Bamboo vinegar is a nature product which is extracted from bamboo and obtained by cooling off and gathering smoke from a charcoal kiln of bamboo charcoal. It includes a lot of tannin which is a type of polyphenol as well as wood vinegar or bran vinegar.

Cr(VI) concentration obtained from the leaching test on the contaminated soil with or without the bamboo vinegar is shown in Table 3. Although the value of Cr(VI) on the contaminated soil without the bamboo vinegar was 0.110 mg/L, it decreased to 0.064 mg/L. It is suggested that the bamboo vinegar has any effect on reduction of Cr(VI). However, it could not control it in less than 0.05 mg/L of the environmental quality standards for soil contamination in this condition.

Table 3 Concentration of Cr(VI) from the contaminated soil without treatment and with bamboo vinegar

Hexavalent chromium	Without treatment	Mixing bamboo vinegar
Concentration (mg/L)	0.110	0.064

Effect on aerobic and anaerobic fermentations

Table 4 shows the results of leaching and pH tests on the contaminated soil with aerobic or anaerobic fermentation for the different content of Cr(VI). In comparison, the results in the case of the contaminated soil without treatment or mixed with leaf mold only are also shown in the table. Although pH in Case 1 and Case 2 is in a range of 7~8, the value in Case 4 decreases slightly due to the condition of anaerobic fermentation. Fig. 1 shows the concentration of Cr(VI) for each soil sample under the initial condition of Cr(VI) content of 1.0 mg/kg in which the maximum concentration of Cr(VI) is 0.10 mg/L. The result using the bamboo vinegar is also shown in the figure. The concentration of Cr(VI) in Case 1 without treatment exceeds 0.10 mg/L and it is considered that the value has a margin of error. The value decreases in sequence of bamboo vinegar, leaf mold, aerobic fermentation, and anaerobic fermentation. The concentration in Case 5 with the anaerobic condition was not detected in the lower limit of 0.01 mg/L.

The results of leaching test on the samples with different initial content of Cr(VI) are shown in Fig. 2. As shown in the figure, in the case of low content of Cr(VI), the concentration can be controlled less than 0.05 mg/L by mixing only the leaf mold. Furthermore, large reduction effect of Cr(VI) is obtained for the aerobic and anaerobic fermentations. In each Cr(VI) content, the concentration level of Cr(VI) is in a sequence of control, leaf mold, aerobic fermentation, and anaerobic fermentation.

It is therefore said that the anaerobic fermentation with organic matter, effective microorganisms resources, and leaf mold is very effective for remedying the contaminated soil possessing hexavalent chromium. In the further study, effects of organic content and fermentation period should be also clarified.

Table 4 Concentration of Cr(VI) from the contaminated soil without treatment and with bamboo vinegar

	Sample	Case 1	Case 2	Case 3	Case 4
Concentration of hexavalent chromium (mg/L)	C1	0.084	0.021	0.015	N.D.
	C2	0.113	0.048	0.031	N.D.
	C3	0.141	0.070	0.066	0.028
pH	C1	7.67	7.08	7.73	6.94
	C2	7.97	7.22	7.18	6.98
	C3	8.04	7.36	7.27	7.06

N.D.: Non-detected (< 0.01 mg/L)

Effect of microorganisms

Sterilization by autoclave

It is confirmed that the concentration of Cr(VI) can be reduced somewhat by mixing only the leaf mold. In order to investigate the effect of microorganisms existing in the leaf mold, an autoclave is applied for the contaminated soil mixed with the leaf mold. The autoclave means to sterilize equipment and supplies by subjecting samples to high pressure steam at 121° C or more.

Two samples were prepared, one is the contaminated soil without treatment and another one is the contaminated soil with the autoclave. After the autoclave, the leaching test was performed immediately. It is considered that the microorganism does not exist in this condition. The result of the leaching test is shown in Table 5. As shown in the table, a difference of the concentration between the samples with and without the autoclave does not appear clearly. It is considered that the humus material in the leaf mold may affect on the oxidation-reduction reaction of chromium.

Measurement of a quantity of microorganisms

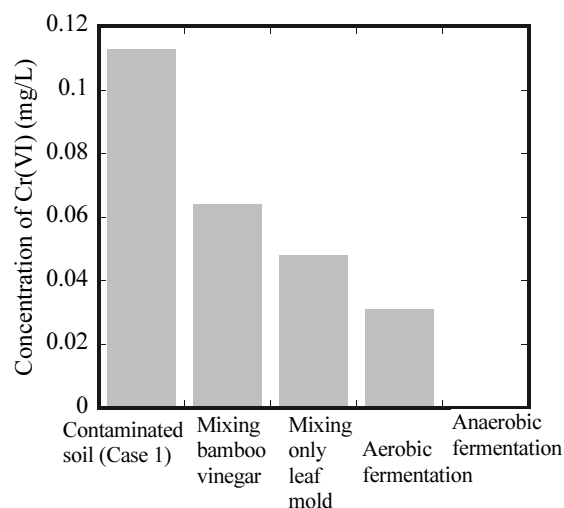
Relationship between the reduction effect of Cr(VI) and a quantity of microorganisms on each sample is discussed here.

It is said that adenosine triphosphate (ATP) is a multifunctional nucleotide, and plays an important role in cell biology as a coenzyme that is the "molecular unit of currency" of intracellular energy transfer. A quantity of microorganisms is estimated by measuring ATP. Kikkoman's Lumitester C-110 was used for the measurement of ATP. This method makes use of luciferase, an enzyme derived from fireflies. The values of ATP are shown in Table 6 and Fig. 3. The ATP value was measured on the sample with the aerobic or anaerobic fermentation only for five days and on the sample with both fermentations from the anaerobic condition to the aerobic condition for more five days. As shown in Table 6, amount of ATP increases considerably after the fermentations. Particularly, the sample with the

aerobic fermentation only indicates highest value of ATP. This sample contains the rice bran. It is considered that this is due to the effect of rice bran with rich nutrition. However, the anaerobic fermentation is more effective for the reduction of Cr(VI). It is suggested that the effect depends on not only the amount of ATP but also kind of the microorganisms. In other words, the anaerobic microorganisms is effective for the reduction of Cr(VI) in comparison with the aerobic microorganisms.

Table 5 Concentration of Cr(VI) from the contaminated soil without treatment and with autoclave

Hexavalent chromium	Without treatment	Autoclave
Concentration (mg/L)	0.120	0.110

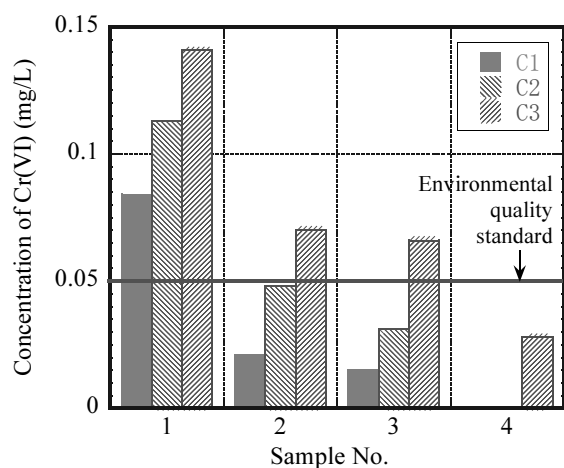
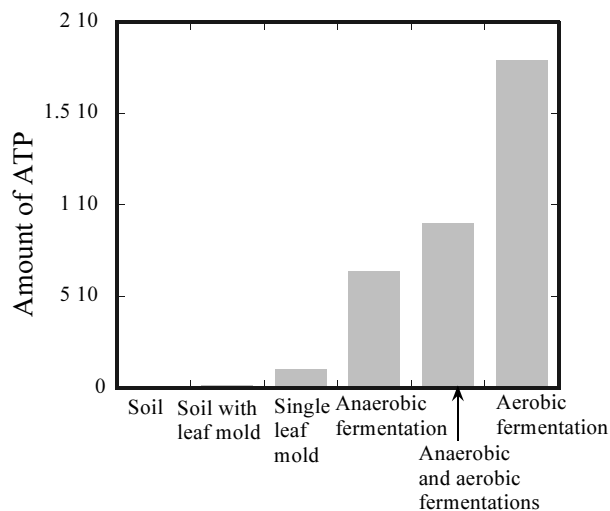
**Fig. 1** Reduction effect of Cr(VI) for leaching of the contaminated soils

CONCLUSIONS

A fundamental study on the purification effect of contaminated soil possessing hexavalent chromium was

Table 6 Amount of microorganisms (ATP) for each sample

Sample	Granite decomposed soil	Soil mixed with only leaf mold	Single leaf mold	Soil with anaerobic fermentation	Soil with aerobic and anaerobic fermentations	Soil with aerobic fermentation
Amount of microorganisms (ATP)	867	1,600	9,933	63,773	90,300	179,367

**Fig. 2** Concentration of Cr(VI) on the contaminated soil with different initial contents**Fig. 3** Amount of ATP for each sample

performed by the laboratory test. Especially, an effect of composting with aerobic or anaerobic fermentation was discussed based on the test results. Main conclusions obtained from this study are as follows:

1) The anaerobic fermentation with organic matter, effective microorganisms resources, and leaf mold is very effective for remedying the contaminated soil possessing hexavalent chromium.

2) It is suggested that the reduction effect of Cr(VI) depends on not only the amount of ATP (adenosine triphosphate) but also kind of the microorganisms.

REFERENCES

- Nakayasu K, Fukushima M, Sasaki K, Tanaka S, Nakamura H. Comparative studies of the reduction behavior of Chromium (VI) by humic substances and their precursors, *Environmental Toxicology and Chemistry*, 18(6): 1085–1090, 1999.
- Omine K, Yasufuku N, Kobayashi T, Tamura K. Purification effect of Cr(VI)-contaminated soil by metabolic of microorganism, *Proceedings of Workshop for underground water / soil contamination and prevention countermeasure*, CD-ROM, 2009 (in Japanese).
- Watanabe N. Strong reduction effect of wood vinegar and barn vinegar -purification of hexavalent chromium contaminant-, *Reader for utilization of wood, bamboo and bran vinegars*, Noubunkyou: 186-187, 2008 (in Japanese).

AN OVERVIEW OF STABILIZATION/SOLIDIFICATION TECHNIQUE FOR HEAVY METALS CONTAMINATED SOILS

Yan-Jun DU¹, Song-Yu LIU², Zhi-Bin LIU³, Lei CHEN⁴, Fan ZHANG⁵ and Fei JIN⁵

ABSTRACT: Recently, in-situ and ex-situ stabilization/solidification of heavy metals contaminated soils (HMCS) using lime, cement, and other binders has been widely adopted in geoenvironmental engineering practice. In this paper, the mechanisms of heavy metal-soil-binder interaction are overviewed based on literature studies. The performance of various leaching test standards for solidified HMCS is reviewed and the difference between these standards is compared in terms of soil grain size, soil-solution contact time, soil-solution ratio, rotary method, and solution type. The performance requirements for the HMCS under different engineering scenarios are presented. It also presents the shear strength properties and influencing factors including soil type, metal concentration, and curing time. The methods for analyzing environmental impact of HMCS to surroundings are addressed. The long-term performance of HMCS under conditions of infiltration of rainfall acid infiltration is discussed. Finally, the HMCS program undergoing at the Institute of Geotechnical Engineering, Southeast University is briefly introduced.

KEYWORDS: stabilization, heavy metal, leaching, strength

INTRODUCTION

Recently, solidification/stabilization (*S/S*) technology has been widely used to treat contaminated lands and landfill waste incinerations. Compared with other remediation technology like soil fusing, chemical treatment, bio-remediation, and thermal deposition, *S/S* has the merits of relatively low cost, ease of use, comprehensive strength, and high resistance to biodegradation (Al-Tabbaa 2005, Shi and Spence 2004). Due to these merits, both geotechnical engineers and researchers are concerning this technology. For example, based on the report of US PEA (2004), *S/S* has been identified as the best demonstrated available technology for 57 Resource Conservation and Recovery Act (RCRA) listed hazardous wastes. It has been used in nearly 24% of superfund remediation action sites in USA (US EPA 2004). In France, *S/S* technology is mostly related to the solidification of the industry wastes being disposed to landfill, and it is the only treatment of industry wastes for landfill disposal (UK EA 2004). In UK, *S/S* technology is prescribed as the treatment method for industry wastes and contaminated dredged materials (UK EA 2004, Al-Tabbaa 2005). In Asian regions, Japan Geotechnical Society has selected *S/S* technology as a key

and priority research topic in the twenty-one century (JGS 2005). In China, urban land contamination caused by the less strictly controlled discharge of industrial pollutants (e.g. heavy metals and organic pollutants) becomes a serious environment pollution problem. Due to the limited space in urban areas, most of these contaminated lands need to be re-developed for residential housing and mercantile occupancy. However, by far there are no legacies related to remediation of contaminated urban lands. Researches and engineering practice on this issuing are very few in China. Such an undesirable condition has greatly retarded economy develop and caused serious problems to human health and ecosystem. Therefore, it is much necessary to advocate and address the key issues of *S/S* remediation technology in China.

This paper presents an over-view of following aspects: 1) mechanisms controlling *S/S* binder and contaminant interactions; 2) criteria for assessment of *S/S* performance; 3) comparison of various leaching tests; 4) factors controlling the shear strength of *S/S* treated contaminated clays. Finally, the *S/S* testing program at the Institute of Geotechnical Engineering, Southeast University is briefly introduced.

¹ Professor, Institute of Geotechnical Engineering, Southeast University, China. Email: duyanjun@seu.edu.cn

² Professor, Institute of Geotechnical Engineering, Southeast University, China. Email: liusy@seu.edu.cn

³ Lecturer, Institute of Geotechnical Engineering, Southeast University, China. Email: seulzb@seu.edu.cn

⁴ PhD student, Institute of Geotechnical Engineering, Southeast University, China. Email: clove.chenlei@gmail.com

⁵ Master student, Institute of Geotechnical Engineering, Southeast University, China. Email: fightmanzone@163.com, lhjf@163.com

INTERACTIONS OF BINDER AND HEAVY METAL CONTAMINANTS

Binders that have been used in the *S/S* of contaminated soils include cement, blast furnace slag, fly ash, lime, modified clay (e.g. organo-clay), and some waste products (Al-Tabbaa and Perera 2005). *S/S* has been mostly used to treat inorganic contamination but recently there are successful treatment cases of some organic contamination (Conner 1990, Al-Tabbaa and Stegemann 2005). In *S/S* process, the immobilization of contaminants occurs by three main mechanisms (Paria and Yuet 2006): 1) chemical fixation of contaminants by interactions between hydration products of binders and contaminants; 2) Physical adsorption of contaminants on the surface of various binder hydration products; and 3) physical encapsulation of contaminants. In engineering practice, *S/S* processes can be using in-situ processing and ex-situ processing (Wiles 1987, Paria and Yuet 2006).

There are number of investigations of interaction between binders and inorganic contaminants including heavy metals. Conner (1990) mentioned that for contaminants like iron compounds and lead compounds would lead to the curing acceleration and curing retardation of treated contaminated soil matrix. Shi and Spence (2004) indicated that since the solubility of heavy metals like Cd, Cr, Cu, Pb, Ni, and Zn decreases with increasing pH up to 10, the variation of solubility of these metals is an important factor affecting the leaching behavior of the *S/S* treated heavy metal contaminated soils (HMCSs). Boardman et al. (1999, 2004) found that for *S/S* treated Pb contaminated soils using lime binder, Pb concentration in leachate decreased with the increasing lime content. They also concluded that pozzolanic reaction of Pb contaminated bentonite was retarded due to the presence of Pb. However, the general shear strength was not greatly affected. Fuessle and Taylor (2004) indicated that immobilization effect of Pb was great when leachate pH exceeded 12, whereas the immobilization effect was much less when leachate pH decreased to 4 to 5. Halim et al. (2004) indicated that immobilization mechanism of Pb in *S/S* process was not only due to physical encapsulation but also the even distribution to CSH matrix. Fuessle and Taylor (2004), Halim et al. (2004) found that for *S/S* treated Cd contaminated soils using cement binder, low Cd concentration in TCLP extracts when curing time is short. However, when the curing time is longer than 1 year, Cd concentration became high. Halim et al. (2004) also found that Cd was mainly fixed mainly by adsorption on CSH matrix surface. For *S/S* treated As contaminated soils, it is found that the solidification effect in terms of Cd concentration in the leachate, would be enhanced with the pretreatment by oxidizers like H_2O_2 and $FeSO_4$ (Fuessle and Taylor 2000, Miller 2000). However, it

seems difficult to apply such a pre-treatment in reach practice due to time consuming and cost-ineffective. Fatta et al. (2004) and Balkan and Kocasoy (2004) indicated that Cu could be effectively immobilized using cement-based *S/S* treatment. They found that the predominant immobilization mechanisms in terms of Cu concentration in leachate was precipitation/dissolution which was mainly affected by leachate pH.

Several main findings can be concluded from aforementioned literature studies:

1) In the *S/S* treated HMCSs, immobilization of heavy metals are much affected by their solubility, which is mainly controlled by pH of soil pore fluid. A too high (e.g. $pH > 12-13$) or too low ($pH < 6$) value will suppress the *S/S* treatment efficiency.

2) Physical encapsulation is not the only mechanism that controls the immobilization of Cu and Pb in *S/S* processing, the distribution in CSH matrix also controls the immobilization mechanisms. For the case of Cd, the primary immobilization mechanism will be its adsorption on CSH surface in the cementitious system.

3) For the case of soils contaminated by multi-heavy metals, the immobilization mechanisms in the *S/S* processing is not clear.

ASSESSMENT CRITERIA FOR *S/S* PERFORMANCE

There is a range of tests available for assessing performance of *S/S* treated HMCSs including unconfined compressive strength (UCS) test, durability test (e.g. freeze-thaw, wet-dry) test, setting time test, expansion/shrinkage test, hydraulic conductivity test, and chemical leaching test (Al-Tabbaa and Perera 2005). Perhaps the mostly common tests are unconfined compressive test, leaching test, durability, and hydraulic conductivity test (in the case of cut-off wall).

A value of greater than 350 kPa of USC has been issued by US EPA for the *S/S* treated wastes being disposed to landfills (US EPA 1986). In other countries like the Netherlands and France, a value of 1 MPa is suggested for landfill disposal (Mulder 2002, UK EA 2002). For the *S/S* treatment of HMCSs, few requirements have been published with regard to the minimum value of UCS. Evans (2000) recommended a minimum bearing capacity of 150 kPa for the *S/S* treatment of a contaminated site. However, so far no administrative guideline has been issued with respect to the minimum requirement of UCS for *S/S* treated HMCSs.

There are several types of leaching tests available for evaluating the concentrations of heavy metals leached from leachates under specific management scenarios. These tests can be subdivided into three main categories: (1) extraction test including The Toxicity Characteristic Leaching Procedure (TCLP) (US EPA

2003a) and The Synthetic Precipitation Leaching Procedure (SPLP) (US EPA 2003b); 2) semi-dynamic test like ANS 16.1 (ANS 1986); and 3) dynamic test like CEN monolithic Tank test (CEN/TC292), ASTM column extraction method (ASTM D4874-95 2001), and European standard column test (prEN14405 2002). The main parameters and simulated field scenarios of these standard tests are summarized below:

1) The management scenario of TCLP test is mainly to evaluate a *S/S* treated waste that can be disposed to landfills with municipal wastes (Perera et al. 2005). Due to the presence of organic acid in landfill, the test uses acetic acid (pH = 4.93 or 2.88) and crushed wet material (maximum size < 9.5 mm) at a liquid/solid (L/S) ratio of 20:1 for a continuous mixing duration of 18 hrs. Although this method has been criticized since it does not consider management scenarios other than landfill disposal (Perera et al. 2005), TCLP is still used to evaluate performance of *S/S* treated HMCSs in most literatures.

2) The SPLP is developed as an alternative solution for situations where disposal is outside of landfill. The maximum size of material, L/S ratio, and mixing duration of SPLP test are the same with those of TCLP test. However, the liquid is sulfuric/nitric acids (pH = 4.2 or 5) in SPLP test. Pereta et al. (2005) argued that SPLP test could reflect the alkaline property of *S/S* materials which have high acid buffering capacity whereas TCLP test failed to not have such a performance.

3) In the ANS 16.1 semi-dynamic leaching test, an intact sample and distilled water (volume/sample surface area = 10/1) are used. In the test, the cylindrical shaped sample is preferred. The leachant is periodically replaced by the same amount of distilled water. Moreover, the effective diffusion coefficient can be determined from the target contaminant concentration in the accumulated leachant.

4) In the column leaching test, an upward flow of liquid (usually distilled water) through sample is used to simulate a scenario where steady advective transport is occurred. Unlike TCLP and SPLP tests, intact sample (either undisturbed or remolded) with specified size is used. However, the column leaching test uses rigid wall container without overburden pressure on sample, which may result in a leakage at the interface between the container and the sample with monolithic shape. The unit of the column leaching test result is expressed as mg/kg dry sample, which is different from the unit of mg/L as used in the TCLP, SPLP, and ANS 16.1 tests. In this sense, column leaching test result represents the case of maximum leached quantity of mass, whereas TCLP, SPLP, and ANS 16.1 tests represent the case of the maximum leached concentration.

5) Other test methods designed particularly for *S/S* treated contaminants (e.g. wastes and HMCSs) are

developed (van der Sloot and Dijkstra 2004). van der Sloot and Dijkstra (2004) indicated that factors controlling the leaching test results could be concluded as material shape (e.g. granular or monolithic), leachant composition, liquid/solid ratio, contact time, temperature, and leachant pH.

As for the hydraulic conductivity of *S/S* treated wastes, US EPA (1989) recommended that the value should be at least two orders of magnitude less than surrounding materials. However, for *S/S* treated HMCSs, there is no prescribed or suggested value.

STRENGTH PROPERTIES OF *S/S* TREATED HMCSs

There are number of actors affecting the shear strength of *S/S* treated HMCSs. The primary factors can be summarized as binder composition, heavy metal type, and curing condition (i.e., time, curing temperature, curing condition) (Al-Tabbaa et al. 2005). Boardman (1999) reported that for Pb contaminated two clayey soils, bentonite and natural clay, with the increase in lime content, the shear strength of treated soils increased. He found that compared to un-contaminated soils (i.e., the content of Pb is zero), the lime-treated soils have lower shear strength than the case of Pb contaminated soils. In his research, he also found that this observation is more significant for bentonite. He then attributed this phenomena to the cation exchange between dissolved calcium cations released from hydrated lime and sodium cations that were initially adsorbed on the soil particle surface, and the different cation exchange capacities of bentonite and natural clay. However, he did not clarify why the presence of low amount of Pb could enhance the shear strength. Hamilton and Sammes (1999) and Yin et al. (2006) also reported the similar results on the effect of presence of Pb on shear strength of Pb contaminated cement mortar and Pb contaminated soils, respectively. However, opposite results were found in the experimental work of Park (2000), Asavapisit et al. (2000), and Lee et al. (2005). Park (2000) indicated that the presence of heavy metal would retard the hydration of cementitious materials of *S/S* treated HMCSs, implying that shear strength could decrease. Asavapisit et al. (2000) and Lee et al. (2005) found that the presence of Pb would reduce the shear strength of *S/S* treated soils by cement even after a relatively long curing time (56 days). Moreover, Lee et al. (2005) indicated that with the increase in the content of Pb, the shear strength of *S/S* treated HMCSs would decrease. Conner (1990) suggested that the presence of heavy metals would retard the hydration of *S/S* treated HMCSs, which implies that the shear strength of *S/S* treated HMCSs would decrease. He indicated that the extent of the hydration retardation was much

depending on the charge and hydrated radius of heavy metals.

Several main findings can be summarized from aforementioned literature studies with respect to the investigation of *S/S* treated HMCSs:

1) The presence of heavy metal would retard the hydration of cementitious materials in the *S/S* treated HMCSs.

2) The presence of heavy metal would affect the shear strength of *S/S* treated HMCSs. However, the existed researches revealed that there is a conflicting observation on this effect.

3) Further research needs to be conducted to thoroughly investigate the effect of types of heavy metals and contents of heavy metals on the development of *S/S* treated HMCSs.

4) The cation exchange capacity (CEC) would considerably affect the *S/S* treatment of HMCSs in terms of development of shear strength. Therefore, caution should be exercised when *S/S* technology is applied for soils with low CEC.

LONG-TERM PERFORMANCE OF *S/S* TREATED HMCSS

UK EA (2004) stated that a long-term monitoring of *S/S* treated HMCSs is likely to be required for a management scenario where treatment is near to or over a sensitive water body. Generally, the long-term performance of *S/S* treated HMCSs usually include the shear strength, leaching properties, hydraulic conductivity, and pH variation on some occasions. The public report of long-term performance of *S/S* treated HMCSs is very limited, perhaps due to the lack of appropriate monitoring sites and the lack of specific monitoring specifications.

Al-Tabbaa (2005) reported a case study of *S/S* treated heavy metals contaminated land site. The mechanical and chemical properties of the sampled cores of the treated soils were examined in terms of UCS, pH, and leached heavy metals concentrations up to a long time of 5 years. The results show that after 5 years, the pH value of treated soils decreased from initial 10 to 11 to averagely 6.5. Al-Tabbaa (2005) attributed this phenomenon to the continued carbonation process during 5 years. The UCS increased by nearly 2 times as compared with the initial 28 days after treatment. However, the use of unconfined compressive strength test has been questioned by Ikegami et al. (2005) since this testing method could not reflect the change of strength at the peripheral side of the mixed soil-cement columns, whereas the needle penetration test method could reflect this change. Indeed, at the peripheral side, the strength would be lower than that in the middle of the in-situ mixed column. This strength variation is mainly due to the diffusion of

calcium ions (Ca^{2+}) from soil-cement columns to surrounding soils driven by the concentration difference between the column and surrounding soils (Ikegami et al. 2005). Al-Tabbaa (2005) indicated that as compared with the case of over-lapped columns, the single column had higher shear strength mainly due to the non-uniform mixing of the former one. The hydraulic conductivities of several treated soils including natural sand, gravel, and artificial ground, were found to be nearly constant even after 5 years. The TCLP leaching test results revealed that the for the short-term (28 days), the concentrations of heavy metals were well below the prescribed safe limit values, whereas at a long-term (5 years), the concentrations of heavy metals increased significantly and was even greatly higher than safe limit values. The reason was attributed to the decreased pH value of the samples.

In China, environmental pollution caused by the acid rainfall is becoming a serious problem in the Southern provinces. In these regions where *S/S* treatment is conducted on heavy metal contaminated soils, acid rainfall will infiltrate into the ground, and react with *S/S* treated HMCSs. With the infiltration of acid rainfall, the soil pH may decrease due to the presence of large amount of hydrogen ions. Consequently, the solution ability of initially fixed heavy metals will increase, leading to the increase in the released concentrations of heavy metals upon the seepage of the ground water. Moreover, due to the mass reaction, H^+ will replace Ca^{2+} adsorbed on soil particles, which will decrease the saturation degree of calcium hydroxide ($\text{Ca}(\text{OH})_2$) existing in the cementitious matrix. Both of the decrease in pH and saturation degree of $\text{Ca}(\text{OH})_2$ will enhance the dissolution of calcium silicate hydrate (CSH), which is the primary contribution to the development of strength of cement-solidified materials. As a result, the shear strength of *S/S* treated HMCSs will decrease. The aforementioned chemical dynamic reactions have been suggested by Kamon et al. (1996) for the lime and cement stabilized clayey soils under the infiltration of acid rainfall. However, so far in China, very few investigations have been reported with respect to the effect of infiltration of acid rainfall on the long-term performance of *S/S* treated HMCSs. Therefore, an uncertainty is existing on the long-term performance of *S/S* treated HMCSs under the presence of acid rainfall infiltration.

Several findings can be summarized from aforementioned literature studies and assumed management scenarios:

1) The shear strength of *S/S* treated HMCSs in terms of unconfined compressive strength at a relatively long-term would increase, while pH value would decrease resulting in much higher concentration of released heavy metals.

2) There is an argument on the appropriate testing method for evaluating long-term strength of *S/S* treated HMCSs. The use of unconfined compressive strength testing method may not correctively reflect the change of strength of in-situ stabilized HMCSs.

3) Complicated environmental variation like infiltration of acid rainfall in *S/S* treated HMCSs would cause the degradation of the shear strength in a long term. Further research needs to be carried out to investigate this aspect.

PROGRAM OF *S/S* TREATED HMCS UNDERGOING AT IGE SEU

From 2008, Institute of Geotechnical Engineering, Southeast University (herein called IGE SEU) has started the laboratory investigation on *S/S* treatment of HMCSs using cement and other additives. The current program is undergoing to understand the shear strength of cement stabilized kaolin/sand mixture contaminated by lead. It is assumed that the contaminated clay is stabilized together with sand for the reuse as construction material (e.g. road embankment fill).

The performance of the *S/S* treated lead contaminated soil is investigated in terms of unconfined compressive strength and concentration of released lead. The main findings can be summarized as following:

1) At present stage, it is found that the factors influencing the soil strength include the lead concentration, cement content, water content, and curing time.

2) Particularly, with the increase in the lead concentration, there is a peak value of soil strength. At the low concentration of lead, soil strength increased with the increase in the lead concentration, while at high concentration of lead, soil strength decreased with the increase in the lead concentration. This peak value increased with the increase in the cement content. However, so far, no reasonable reason is available to explain this observation.

3) Moreover, when the lead concentration was up to 3%, the strength became much low both at a short time and long time, indicating that high concentration of lead has a strong effect in suppressing the development of *S/S* treated soil.

4) A new parameter titled water content change ratio is proposed to reflect the influence of lead content on the hydration retardation of *S/S* treated soils. It is found that the proposed parameter has a good relation with both the lead concentration and the unconfined compressive strength.

5) The leaching test results show that with the increase in cement content and curing time, the concentration of released lead ions decreased. The electrical resistivities of the *S/S* treated samples were measured. It is found that with the increase in the lead concentration, the electrical

resistivity increased. Moreover, the electrical resistivity was found to have a good relation with the unconfined compressive strength. It is expected that the electrical resistivity measurement method can be applied to the field practice as a quick and non-destructive method to evaluate the *S/S* treatment effectiveness.

CONCLUSIONS

This paper presents an over-view of the application of *S/S* technology for the remediation of heavy metal contaminated soils. Several conclusions can be drawn:

1) The primary immobilization mechanisms of heavy metals in a solidified/stabilized cementitious matrix include physical encapsulation, sorption on CSH matrix, and distribution to CSH matrix. However, for multi-heavy metals contaminated soils, the immobilization mechanisms of heavy metals are not clear.

2) There are various types of leaching tests with different management scenarios. Caution should be exercised when an appropriate leaching test is selected for assessing the performance of the *S/S* treated HMCSs.

3) The presence and concentration of heavy metals have significant effects on the development of strength of *S/S* treated HMCSs. However, there is a conflicting result on this effect in the existed researches.

4) The long term performance of *S/S* treated HMCSs under the condition of infiltration of acid rain is still not clear. Further research needs to be carried out on this aspects.

5) The effect of presence of lead has played much different role in affecting the strength of HMCSs depending on the lead concentration, according to the laboratory tests conducted at IGE SEU.

ACKNOWLEDGEMENTS

This study is financially supported by the National Nature Science Foundation of China under Grant No. 50878052 & 40802065, Science Found of the Laboratory of Geotechnical and Underground Engineering, Tongji University under Grant No. KLE-TJGE-0801, and the National Science Found of Southeast University under Grant No. 9221001483.

REFERENCES

- Al-Tabbaa A (2005). State of Practice Report – Stabilisation/Solidification of contaminated materials with wet deep soil mixing. Proc. Deep Mixing2005: 697-731.
- Al-Tabbaa A & Stegemann JA (2005). Stabilisation/

- Solidification Treatment and Remediation. Proceedings of International Conference on Stabilization/Solidification Treatment and Remediation, Cambridge: 485.
- Al-Tabbaa A & Perera ASR (2005). Stabilisation/solidification treatment and remediation. Part II: Binders and technologies-research. Proceedings of the International Conference on Stabilisation/Solidification Treatment and Remediation, Cambridge: 387-397.
- Asavapisit S, Boonjam M, Polprasert C (2000). Effects of lead and chromium hydroxides on cement-based solidified waste properties, *Int. J. Sc. Tech.*, 5(3): 1-9.
- Boardman DJ (1999). Lime stabilization: clay-metal-lime interactions. Ph.D. Thesis, Civil and Building Engineering, Loughborough University, United Kingdom.
- Boardman DJ, Glendinning S, Rogers CDF (2004). The influences of iron (III) and lead (II) contaminants on lime-stabilised clay. *Geotechnique*, 54(7): 467-486.
- Conner JR (1990). Chemical Fixation and Solidification of Hazardous Wastes. Van Nostrand Reinhold, New York.
- Evans CW (2000). Cleaning up the store. *Contract Journal Supplement*: 22-23.
- Fatta D, Papadopoulou A, Stefanakis N, Loizidou M, Savvides C (2004). An alternative method for the treatment of waste produced at a dye and a metal-plating industry using natural and/or waste materials. *Waste Manage. Res.* 22: 234-239.
- Fuessle RW & Taylor MA (2004). Stabilization of arsenite wastes with prior oxidation. *J. Environ. Eng.* 130(9): 1063-1066.
- Halim CE, Amal R, Beydoun D, Scott JA, Low G (2004). Implications of the structure of cementitious wastes containing Pb(II), Cd(II), As(V), and Cr(VI) on the leaching of metals. *Cem. Concr. Res.* 34(7): 1093-1102.
- Hamilton IW & Sammes NM (1999). Encapsulation of steel foundry bag house dusts in cement mortar. *Cement and Concrete Research*: 29(1): 55-61.
- Ikegami M, Ichiba T, Ohishi K, Terashi M (2005). Long-term properties of cement treated soil 20 years after construction. *Proc. 16th Int. Conf. Soil Mech. Geotech. Engrg.*, Rotterdam, Millpress Science Publishers: 1199-1202.
- Kamon M, Ying C, Katsumi T (1996). Effect of acid rain on lime and cement stabilized soils. *Soils and Foundations*, 36(4): 91-99.
- Lee D, Waite TD, Swarbrick G, Lee S (2005). Comparison of solidification/stabilization effects of calcite between Australian and Korea(R. O.) cements. *Cement and Concrete Research* 35(11): 2143-2157.
- Miller J, Akhter H, Cartledge FK, McLearn M (2000). Treatment of arsenic-contaminated soils. II Treatability study and remediation. *J. Environ. Eng.* 126(11): 1004-1012.
- Mulder E, Feenstra L, Brouwer JP, Frenay JW, Bos S (2005). Stabilisation/solidification of dredging sludge containing polycyclic aromatic hydrocarbons. In: A. Al-Tabbaa and J.A. Stegemann (Editors), *Stabilisation/solidification treatment and remediation: advances in S/S for waste and contaminated land*, Balkema, London: 241-247.
- Ouki SK & Hills CD (2002). Microstructure of Portland cement pastes containing metal nitrate salts. *Waste Management*, 22(2): 147-151.
- Lin SL, Lai JS, Chian ESK (1995). Modifications of sulfur polymer cement (SPC) stabilization and solidification (S/S) process, *Waste Management*, 15(6): 441-447.
- Paria S & Yuet PK (2006). Solidification/stabilization of organic and inorganic contaminants using Portland cement: a literature review. *Environmental Reviews*. 14(4): 217-255.
- Park CK (2000). Hydration and solidification of hazardous wastes containing heavy metals using modified cementitious materials. *Cement and Concrete Research*, 30(3): 429-435.
- Perera ASR, Al-Tabbaa A, Reid JM, Stegemann JA (2005). State of practice report UK Stabilisation/Solidification Treatment and Remediation Part IV: Testing and Performance Criteria. Proceedings of the International Conference on Stabilisation/Solidification Treatment and Remediation, Cambridge: 415-435.
- Shi C & Spence R (2004). Designing of cement-based formula for solidification/stabilization of hazardous, radioactive, and mixed wastes. *Critical. Review in Environmental Science and Technology*. 34(4): 391-417.
- United Kingdom Environment Agency (UK EA) (2004). Review of scientific literature on the use of stabilisation/solidification for the treatment of contaminant soil, solid waste and sludges. Science Report SC98003/SR2. Environment Agency, Aztec West, Bristol.
- US EPA (1986). Method 9100: saturated hydraulic conductivity, saturated leachate conductivity, and intrinsic permeability. In: EPA SW-846: test methods for evaluating solid waste, physical/chemical methods. Bristol.
- US EPA (1989). Stabilization/solidification of CERCLA and RCRA wastes, EPA/625/6-89/022.
- US EPA (2003a). Method 1311: Toxicity characteristic leaching procedure. SW846 Online test methods for evaluation of solid wastes, physical chemical methods.
- US EPA (2003b). Method 1312: Synthetic precipitation leaching procedure. SW846 Online test methods for evaluation of solid wastes, physical chemical methods.

- US EPA (2004). Treatment technologies for site cleanup: annual status report (Eleventh Edition), EPA-542-R-03-009.
- van der Sloot HA & Dijkstra JJ (2004). Development of horizontally standardized leaching tests for construction materials: a material based or release based approach? Identical leaching mechanisms for different materials. ECN-C-04-060, Energy Research Centre of the Netherlands.
- Wiles CC (1987). A review of solidification/stabilization technology. *J. Hazard. Mater.* 14(1): 5–21.
- Yin CY, Mahmud HB, Shaaban MG (2006). Stabilization /solidification of lead-contaminated soil using cement and rice husk ash. *Journal of Hazardous Materials*, 137(3): 1758–1764.

CASE STUDY ON INFLUENCES OF OIL CONTAMINATION ON GEOTECHNICAL PROPERTIES OF COASTAL SEDIMENTS IN THE YELLOW RIVER DELTA

Yong-Gang JIA¹, Qiong WU², Xiang-Mei MENG³, Xiu-Juan YANG⁴,
Zhong-Nian YANG⁵ and Geng-Cheng ZHANG⁶

ABSTRACT: With the process of large-scale exploitation of coastal and offshore oil, coastal soils have encountered oil pollution due to the historical waste from oil drilling, related tanker navigations and accidents in recent years. Therefore, it is important to find out geotechnical properties of oil-contaminated coastal sediments for engineering and environmental purposes. In a certain clayey beach of an oil-contaminated intertidal zone in the Hai-gang region of Yellow River Delta, some groups of coastal soil were sampled and their geotechnical properties were studied in a lab. The testing on contaminated soil samples included basic physical properties test, grain size analysis, Atterberg limits, compaction, direct shear test and a micro-structure scan. Oil content in the samples was analyzed by ultraviolet-spectrophotometer assay. The results show that heavily-polluted soil has higher clay particle content, liquid and plastic limit, and compression coefficient than light-polluted soil. Compression modulus is lower for heavily-polluted soil, while cohesion force and internal friction angle have no notable correlation with oil content. According to micro-structure scan, soil particles are finer and surrounded by oil particles in the heavily-polluted samples.

KEYWORDS: Yellow River Delta, oil-contaminated coastal soil, geotechnical properties, samples and analyses

INTRODUCTION

In the petroleum industry near coastal areas, oil contamination of soils has been the subject of extensive research over the last few years due to the increasing rate of its occurrence. When oil spill or leakage occurs, soils might be contaminated by the leakage and it would be very harmful to marine ecosystem and coastal engineering. In these cases, field investigation mechanism and evaluation of oil pollution are crucial. Major tasks are required to determine the geotechnical properties of the oil-contaminated soil, determining the effect on the existing structures, remediation and reclamation of the contaminated sites.

In recent years, there has been a substantial increase in investigations on geotechnical properties of contaminated soils; however, most of them focus on artificially contaminated sand with different contamination percents, while few focus on in-situ oil-contaminated soil (Zhu & Liu 2007, Chen et al. 2003).

Mashalah Khamehchiyan and colleagues (2007) carried out an extensive laboratory testing program to determine the effects of crude oil contamination on some

of the geotechnical properties of clayey and sandy soils such as CL, SM and SP sampled from the southern coastal plain of Iran at the Persian Gulf. The testing included basic properties, Atterberg limits, compaction, direct shear, uniaxial compression and permeability tests on clean and contaminated soil samples at the same densities. The contaminated samples were prepared by mixing the soils with crude oil in the amount of 2%, 4%, 8%, 12%, and 16% by dry weight.

Al-sarawi et al. (1998) made measurements on 60 samples to determine the physical properties of the soil profiles contaminated with oil lakes in AlAhmadi and Burgan oil fields which include 80% of the Greater Burgan oil wells in southern Kuwait. The two soil profiles were contrasted in fluvial origin and eolian origin, which have similar saturation percentages, field capacities, and wilting coefficients, low available water capacities due to stratification and very low matric potential, and high bulk densities due to compaction by vehicle wheels. Aiban (1998) undertook an investigation to evaluate the effect of temperature on strength, permeability, and compressibility of an oil-contaminated sand obtained from eastern Saudi Arabia. The sand was

¹ Professor, College of Environmental Sciences and Engineering, Ocean University of China. Email: yonggang@ouc.edu.cn

² Ph.M. candidate, College of Environmental Sciences and Engineering, Ocean University of China. Email: wuqiong0401@163.com

³ Ph.D. candidate, College of Environmental Sciences and Eng., Ocean University of China. Email: xiangmeimeng@yahoo.com.cn

⁴ Ph.D. candidate, College of Environmental Sciences and Engineering, Ocean University of China. Email: yliny@163.com

⁵ Ph.M. candidate, College of Environmental Sciences and Engineering, Ocean University of China. Email: zhnyang110@163.com

⁶ Ph.M. candidate, College of Environmental Sciences and Engineering, Ocean University of China. Email: qingfangcun@126.com

artificially contaminated with different grades and percentages of crude oil.

The Yellow River Delta is a well known near-shore submarine delta which is dominated by river sedimentation. Large-scale of oil exploitation has led to the contamination of part of coastal sediments in the area. In this study, a research was carried out in laboratory to determine contamination effects on soils of one oil-contaminated beach in the Hai-gang region of Yellow River Delta. The main physical mechanical properties indexes of the oil-contaminated soil were valued by conventional geotechnical tests, including grain size analysis, Atterberg limits, compaction, direct shear tests, a micro-structure scan on contaminated soil samples. Additionally, different oil content in the samples was analyzed by ultraviolet-spectrophotometer assay. The effects of pollution on a variety of the geotechnical properties of the offshore sediments were discussed. Finally, some useful conclusions are summarized.

METHODS

Overview of the Study Area

Located on the west coast of the Bohai Sea and covering a land area of 5500 km², the modern Yellow River Delta has been building since 1855 when a major switch in its lower course took place. In this study, we obtain a core in an oil-contaminated intertidal zone of Hai-gang lobe (Fig.1), which is in the Diao-kou deltaic lobe formed from 1964 to 1976. The investigated area, 120m in length and 80m in width, offers one such classical case wherein point source contamination resulted in degradation of soil to an extent of non-uniform layered distribution. 5 survey lines and 25 test points were arranged regularly, which were of 30m at transverse interval and 20m at longitudinal interval. Attempts were made to check further lateral migration of contaminants by way of field investigation, including digging test pits, field observations and collecting soil samples.

Analysis Method and Process in Laboratory

The testing programs used here included water content, grain size analysis, Atterberg limits, compaction, direct shear, micro-structure scan tests for understanding the effects of crude oil contamination on geotechnical properties of the selected soil samples. In the lab, the samples were divided into three groups artificially on the basis of their oil content to determine their properties' parameters. If oil content was less than 0.1mg/g in lab tests, the samples were labeled light-polluted (L). Samples containing more than 1mg/g were labeled

heavily-polluted samples (H), while medium-polluted samples (M) fell between them. Measurement of oil content was made by ultraviolet-spectrophotometer assay method.

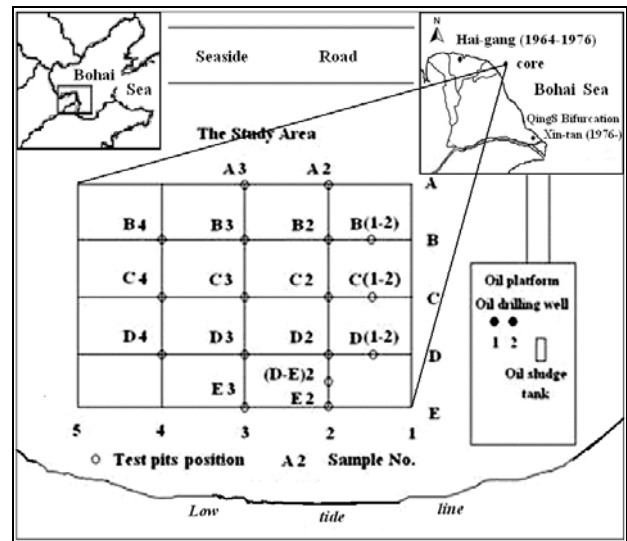


Fig. 1 Sketch map of the study area

RESULTS AND DISCUSSIONS

Geological Properties and Oil Content of Coastal Sediments

In order to describe regional variations in the physical properties of the natural sediments and considering the short core lengths (up to 35~40cm), the respective values for each considered property were averaged along the entire length for the purpose of this discussion. The samples were called silty soil on the basis of grain size analysis and plasticity index. The fundamental geotechnical properties of coastal sediment samples are shown in table 1.

Influence of Oil Contamination on Geological Properties of Coastal Sediments

Grain Size Analysis

Grain size analysis of soil samples concern relative content of every grain group in the soil. Fig.2 shows the grain size distribution curves for three different kinds of soil samples. The results show that the clay grain (<0.005) content in heavily-polluted soil samples is higher than ones in light-polluted soil samples. There are some colloids in the soil, such as organic and inorganic composite colloids, free oxide colloid sand and soluble salts. When the soil mass was corrupted by those pollutants, and these colloids dissolved, resulting in a strong link between soil grains weakened or disappeared

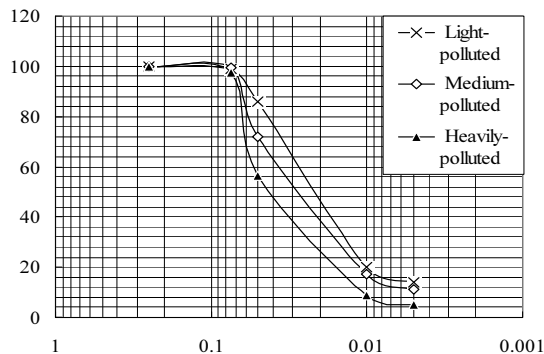
Table 1 The geotechnical properties of coastal sediments samples

S No.	O /mg/g	Physical Properties			Grain Size Distribution /mm				
		W/%	D/g/cm ³	e	>0.075	0.075-0.05	0.05-0.01	0.01-0.005	<0.005
C4-1	0.021	24.0	1.99	0.682	1.5	36.3	53.2	2.3	6.7
C3-1	0.031	24.7	1.98	0.700	2.1	51.9	40.6	0.3	5.1
C4-2	0.058	25.2	2.02	0.673	0.4	47.0	38.4	4.9	9.3
C(1-2)	0.138	25.9	2.00	0.700	0.4	28.0	57.1	6.4	8.1
C3-2	0.368	27.4	2.01	0.711	1.7	18.1	65.7	7.4	7.1
B3	0.471	—	1.96	—	3.0	45.1	42.2	2.8	6.9
D3	0.927	24.2	1.98	—	1.8	17.9	63.9	7.1	9.3
B2	1.912	26.1	2.02	0.685	3.2	30.5	57.0	4.1	5.2
D(1-2)	2.734	27.8	1.95	0.770	2.1	31.6	53.6	5.4	7.3
D2	3.529	32.0	1.94	0.837	0.8	13.3	63.6	8.9	13.4
A2	4.736	25.6	2.02	0.679	2.0	10.0	67.2	6.5	14.3
(D-E)2	14.017	37.6	1.670	1.438	1.2	16.2	59.7	8.3	14.6

Table 1 (continued)

Atterberg Limits			Compression Test		Direct Shear Test		Contamination Grade Ranking
Wp/%	Wl/%	Ip	a/Mpa ⁻¹	E/Mpa	C/Kpa	Φ/°	
17.9	25.7	7.8	0.151	11.14	3.0	22.8	Light-polluted
—	—	—	0.188	9.04	10.0	25.2	Light-polluted
19.6	27.2	7.6	0.162	11.22	18.0	16.8	Light-polluted
18.2	27.0	8.8	0.213	8.06	14.0	16.1	Medium-polluted
18.2	26.8	8.6	0.160	10.69	10.0	26.6	Medium-polluted
20.6	27.7	7.1	0.157	10.92	30.0	12.5	Medium-polluted
18.5	27.8	9.3	0.187	10.61	16.0	20.3	Medium-polluted
22.6	28.8	6.2	0.163	10.34	14.0	20.3	Heavily-polluted
18.4	26.3	7.9	0.159	11.13	8.0	18.8	Heavily-polluted
20.7	28.8	8.1	0.680	2.70	8.0	17.3	Heavily-polluted
19.5	29.2	9.7	0.393	4.27	17.0	19.4	Heavily-polluted
21.7	38.8	17.1	1.629	1.43	—	—	Heavily-polluted

※ S No.— Sample Number. O— Oil content. W— Water content. D— Density. e— Void ratio. Wp— Plastic limit. Wl— Liquid limit. Ip— Plastic index. a— Compression coefficient. E— Compression modulus. C— Cohesion. Φ— Internal friction angle.

**Fig. 2** Grain size distribution curve for soil samples

(Mitchell 2005). Hence, most of the soil grains were dispersed easily, and the clay grain content was seen to be much higher in the heavily-polluted soil samples.

Atterberg Limits

Atterberg limits are characterized by plastic and liquid limits as well as plasticity index. Although these limits are easily determined and their qualitative correlations with soil composition and physical properties have been quite well established, the fundamental interpretation of the limits and quantitative relationships between their values and compositional factors is more complex (Mitchell 2005).

The results show an increase in Wl (liquid limit), Wp (plastic limit), Ip (plasticity index) with increasing oil contamination, and the trend is expressed in a fitted line of correlation coefficient R (Fig.3). This increment in Atterberg limits can be explained by the viscous nature of the pore fluid. In saturated fine-grained soils, pore fluid fills the pores of the fabric and a thin layer of fluid exists between mineral contacts. It acts as a lubricant, causing particles to attain a closer packing. Lubrication at particle contact is caused by the viscous nature of the pore fluid. An increase in pore fluid viscosity changes the properties of mineral-to-pore fluid contacts, so the consistent state of soil samples will become difficult to change, presented as an increment in Atterberg limits.

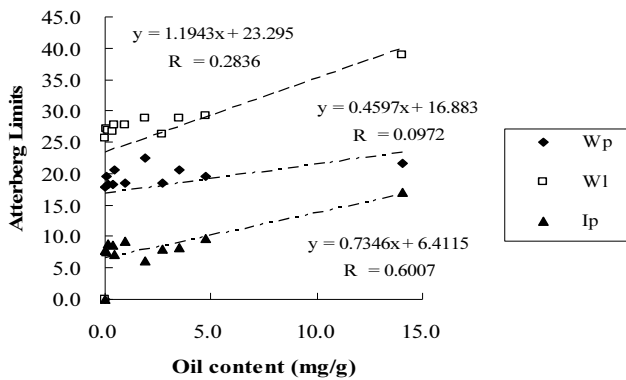


Fig. 3 Influence of oil content on Atterberg limits

Compaction Test

A compaction test was carried out under laterally constrained compression with cyclic loading; this test reflects the variety of the pores and structure when subjected to an external force in the geological environment (Da-Xiong Tang et al. 1999). From the results (Fig.4), compression coefficient (a) increases greatly, and heavily-polluted samples have become high compression other than medium compression in the light-polluted samples. Contrarily, compression modulus (E) decreases with the same trend. It may be caused by the variety of pores and structure properties. When soil was corrupted by oil contamination, the texture link between grains was weakened, with the result that the pores become more numerous and the structure becomes loose, thereby displaying softening of stress-strain behavior.

Direct Shear Tests

Direct shear tests were carried out to find the effect of oil contamination on strength parameters of soils. Under loads of 50, 100, 150, and 200, the present results show no correlation between oil content and internal friction angle (Φ) and cohesion (C) in these samples with a degree of oil contamination (Fig.5). Perhaps it is the

result of viscosity and inherent cohesion of oil. Shear strength of fine-grained soil mainly depends on cohesion of soil and to a lesser degree on friction angle, and it performs on texture link in soil (Da-Xiong Tang et al. 1999). Although the texture link was weakened in oil-contaminated soil samples, viscosity and inherent cohesion of oil particles filling in soil pores made a contribution to the shear strength of soil samples, thereby displaying combined effects.

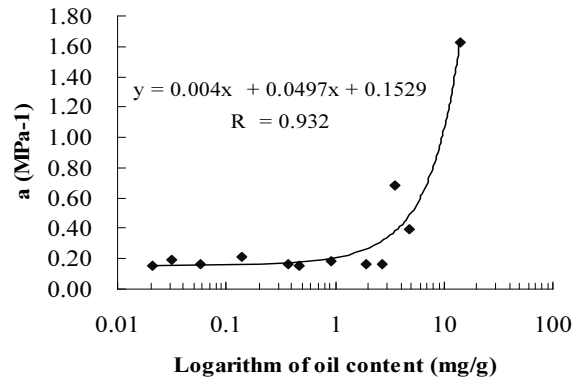


Fig. 4 The relation between oil content and compression coefficient

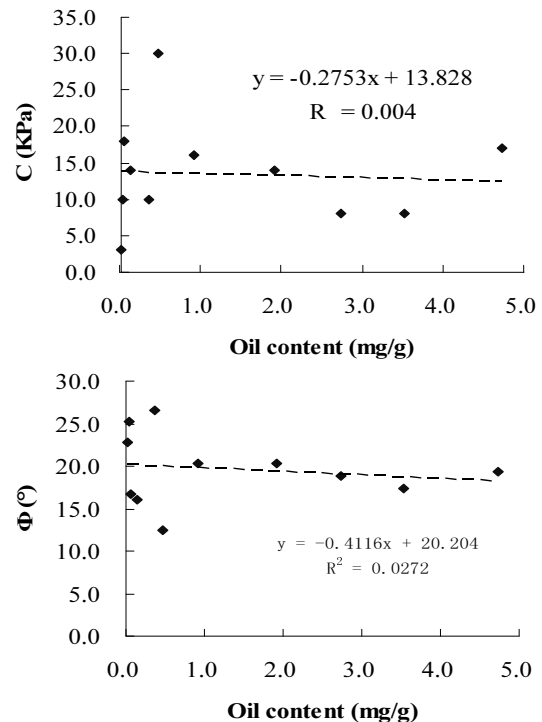


Fig. 5 Influence of oil content on shear strength parameters

However, in-situ Penetration test results (Fig.6) show the strength of soil mass reduces with increase of oil contamination. In a heavily-polluted area, it is less than 30KPa. Most of the study area is located in an intertidal zone, with the result that the soil is saturated and the

draining consolidation process becomes very slow, so the strength of the saturated soil decreases with increasing water content instead of being a function of viscosity and the inherent cohesion effect of oil (Da-Xiong Tang et al. 1999).

Micro-structure characters

Oil contamination in soil causes adverse effects on its basic geotechnical properties. The variety is essentially caused by the change of the micro-structure character in soil samples. Therefore, in this study, a microscope was used for observing the micro-structure character of soil samples. The pictures, magnified by 180 times, of light-polluted, medium-polluted and heavily-polluted samples are shown in Fig.7a, 7b and 7c.

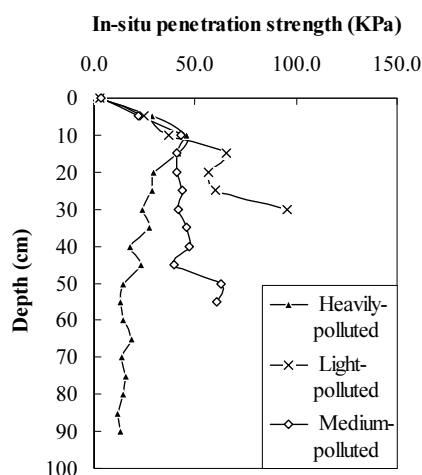


Fig. 6 Influence of oil content on in-situ penetration strength in the study area

For light-polluted soil samples, it is evident from the picture that soil grains of particle-particle contact look cleaner, and there are many pores between the grains which liquid can transverse freely. The pores are filled with oil molecules and the grains become finer because of corrosion contamination with increasing oil content. Granular matter and the honeycomb structure of high compression appear in the heavily-polluted samples; the pores are invisible in the magnified pictures. To a lesser or greater degree, these changes cause the weakness of geotechnical properties of oil-contaminated soil samples.

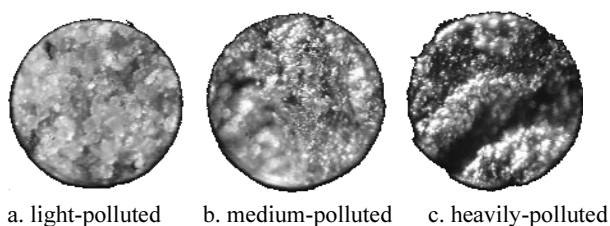


Fig. 7 The micro-structure pictures of soil samples (180times)

CONCLUSIONS

In this study, fuel oil contamination caused deleterious effects to the basic geotechnical properties of coastal sediments. It is noteworthy to point out that oil has a complex composition, and the mechanism of variable properties in an intertidal zone is different from the mechanism in land. The following conclusions are based on these tests:

The clay grain (<0.005) content in heavily-polluted soil samples is higher than that in the light-polluted soil samples, as is shown in the micro-structure pictures the grain size is smaller in heavily-polluted samples. Atterberg limits increase with increasing oil contamination in soil samples.

Compression coefficients (a_{1-2}) of soil samples increase greatly, and heavily-polluted samples became high compression instead of medium compression in the light-polluted samples. Additionally, in-situ penetration test show the decrease in the strength of sediments.

ACKNOWLEDGEMENTS

This study was joint supported by Natural Science Foundation of China (Contract No. 40876042) and National High Technology Program (863) (Contract No. 2008AA09Z109).

REFERENCES

- Al-Sarawi M, Massoud MS, Wahba SA (1998). Physical properties as indicators of oil penetration in soils contaminated with oil lakes in the greater Burgan oil fields, Kuwait. *Water, Air, and Soil Pollution* 102 (1-2): 1-15.
- Zhu CP & Liu HL (2007). Study on engineering properties of polluted soil. *Rock and Soil Mechanics*, 28 (3): 625-630.
- Tang DX, et al. (1999). *Rock and Soil Engineering*. Beijing, China: 61-67, 102-105.
- Liu HL, Zhu CP, Zhang XL (2008). Fundamental physical properties of soil polluted by acid and alkali in laboratory. *Chinese Journal of Geotechnical Engineering*, 30 (8): 1213-1217.
- Khamehchiyan Mashalah, Charkhabi Amir Hossein, Majid Tajik (2007). Effects of crude oil contamination on geotechnical properties of clayey and sandy soils. *Engineering Geology*, 89: 220-229.
- Mitchell JK (2005). *Fundamental of Soil Behavior*. New Jersey, John Wiley & Son: 288-290.
- Saad A Aiban (1998). The effect of temperature on the engineering properties of oil-contaminated sands. *Environment International*, 24(1-2): 153-161.
- Chen XH & Tan HM (2003). The current situation and prospect of contaminated soil research. *Geology and Prospecting*, 39 (1): 77-80.

BIOREMEDIATION OF WATER CONTAMINATED WITH BTEX, TPH AND TCE UNDER DIFFERENT ENVIRONMENTAL CONDITIONS

C.K. LEI¹, J. H. LI², S.S. DONG³ and H. SHIM⁴

ABSTRACT: Many studies have been done about the biodegradation for benzene, toluene, ethylbenzene, and xylenes (collectively known as BTEX), total petroleum hydrocarbons (TPH), or chlorinated aliphatic hydrocarbons (CAHs), as they are among the most commonly found environmental contaminants. Since many sites are contaminated with mixtures of these compounds, this research was performed to find out more about their interactions during the bioremoval process, using water artificially contaminated with the mixtures of BTEX, TPH, and trichloroethylene (TCE) as a representative CAH under different environmental (temperature and pH) conditions. One microbial isolate obtained from the potentially contaminated site was grown aerobically for the bioremoval of these mixtures, with BTEX and TPH provided as substrates for the co-metabolic removal of TCE.

KEYWORDS: BTEX, TPH, TCE, bioremoval, interaction

INTRODUCTION

In recent decades, following the industrialization widespread worldwide and the increased use of organic compounds, the accidental spillage and leaking of these compounds as environmental contaminants is unavoidable (Chang and Lin 2006). Accordingly, the cleanup of these leaked or spilt toxic chemicals is of concern intensively.

Total petroleum hydrocarbons (TPH) such as gasoline and diesel compounds are among the most frequently found environmental contaminants, which include benzene, toluene, ethylbenzene, and three isomers (*ortho*-, *meta*-, and *para*-) of xylene (collectively known as BTEX). These chemicals, in addition to their environmental contamination, can also cause hazardous effects to humans since most of them are known carcinogenic. Trichloroethylene (TCE), on the other hand, is a widely used industrial and cleaning solvent and is also suspected carcinogenic (ATSDR 1997). Furthermore, no microorganism has been found capable of growing on TCE as a sole carbon or energy source (Hyman et al. 1995). In comparison, only several aerobic bacteria are known to co-metabolize TCE as a non-specific enzymes synthesized in the presence of a growth substrate (Kocamemi and Cecen 2007).

Among all those remediation technologies available to remove contaminants from water and soil, bioremediation is considered one of the most economical and environmentally sound and sustainable treatments (Kota et al. 2004). In this study, using a microbial isolate obtained from the site near a gas station in Xiamen,

In this study, we isolated indigenous microorganisms from high potentially contaminated soil in different places, Macau and Xiamen, China. Then set up one China, potentially contaminated with gasoline compounds, the interactions among BTEX, TPH, and TCE during their bioremoval were studied in lab-scale batch experiments at different temperatures and pHs, and their bioremoval efficiencies were evaluated.

MATERIALS AND METHODS

Chemicals

Benzene (purity, 99.7%), toluene (purity, 99%), ethylbenzene (purity, 99%), *ortho*-xylene (purity, 99%), *meta*-xylene (purity, 99%), and *para*-xylene (purity, 99%) were purchased from the International Laboratory

¹ M.S. Student, Department of Civil and Environmental Engineering, Faculty of Science and Technology, University of Macau, Macau SAR, China. Email: chengkeng.lee@gmail.com

² Ph.D Student, Department of Civil and Environmental Engineering, FST, University of Macau. Email: ya87410@umac.mo

³ B.S. Student, Department of Civil and Environmental Engineering, FST, University of Macau. Email: da52821@umac.mo

⁴ Associate Professor, Department of Civil and Environmental Engineering, FST, University of Macau. Email : hjshim@umac.mo (Corresponding author)

(USA). TCE (purity, 99%) was purchased from Da Mao Chemical Manufacture in Tianjin (China). The TPH stock solution was prepared using the 1:1 ratio (v/v) of unleaded gasoline and diesel, purchased from the Caltex Company in Macau Special Administrative Region (SAR) (China).

Soil Sample Collection

Several indigenous microorganisms were isolated from the soil samples, potentially contaminated with petroleum compounds and obtained from a construction site nearby a gas station in Fai Chi Kei in Macau SAR and the site near a gas station in Xiamen. Soil samples were stored in a freezer until use.

Enrichment and Isolation

The microbial pure cultures were enriched and isolated from the soil samples. Soil samples (5%, w/w) from two locations were first added into the nutrient broth (contained 3.0 g/L beef extract and 5.0 g/L peptone) in a serum bottle, and then 150 mg/L toluene was added as a substrate for the microbial growth. After the serum bottles were covered with stoppers (90% teflon/10% silicone) and aluminum crimp sealed, they were inverted and placed on an orbital shaker (IKA) at 150 rpm and 25°C. Then, 10% (v/v) inocula from these bottles were aseptically inoculated into the mineral salt medium (MSM contained KH_2PO_4 1.0 g/L; K_2HPO_4 1.0 g/L; NH_4NO_3 1.0 g/L; $\text{MgSO}_4 \cdot 7\text{H}_2\text{O}$ 0.2 g/L; $\text{Fe}_2(\text{SO}_4)_3$ 0.5 g/L; and CaCO_3 0.02 g/L.) containing 150 mg/L toluene as a sole substrate. After several weeks of subculturing, pure cultures were isolated from the bottles by using nutrient agar (NA) plates. The pH of medium was adjusted by adding HNO_3 or NaOH solution. All the instruments and media were autoclaved (HIRAYAMA) after preparation.

Several microbial colonies with different morphologies were chosen from the NA plates and transferred to test tubes with MSM aseptically, which contained 150 mg/L toluene. After the tubes were incubated on the shaker at 150 rpm and 25°C, one microbial pure culture from each soil sample, which showed higher turbidities by measuring optical density (OD) at 600 nm and higher toluene removal efficiencies, were chosen for further experiments. The selected pure cultures were further transferred, 10% (v/v), into the newly prepared MSM containing BTEX and TPH in mixture.

Bioremoval of Mixture

After subculturing for a few weeks, the pure cultures were added (10% v/v) to the fresh MSM containing

different concentrations of BTEX/TPH/TCE mixtures at different pHs and temperatures. Three pHs (5, 7, and 9) and two temperatures (25 and 35°C) were chosen as growth conditions. The indigenous microorganism isolated from the Xiamen soil sample was further tested with the mixture of toluene and *ortho*-xylene (ToX) as substrates at 150 and 350 mg/L and TCE at 15 and 30 mg/L at three different pHs and two different temperatures. The microbial isolate obtained from the Macau soil sample, on the other hand, was further inoculated to serum bottles containing MSM with the mixture of BTE_oX (350 mg/L), TPH (1,000 mg/L), and TCE (15 mg/L) at different pHs and temperatures.

After the serum bottles were sealed with stoppers and aluminum crimps, they were inverted to minimize the volatilization of these compounds and incubated on the shaker at 150 rpm. Bottles containing MSM with these compounds but without microorganisms served as controls. At specific intervals, sample aliquots were withdrawn from the bottles and analyzed for the microbial growth as OD at 600 nm, and the concentrations of BTEX, TPH, and TCE, and chloride as a mineralization product from the TCE bioremoval were measured.

Analytical Methods

The concentrations of BTE_oX, TPH, and TCE were measured using a gas chromatograph (Agilent, 6890N, Agilent Technologies Co., Ltd, China) equipped with a flame ionization detector (FID) and a capillary column (HP-5; 30 m × 0.53 μm I.D. with a stationary-phase film thickness of 0.88 μm). One microliter of liquid samples was injected by the autosampler injector (7638 Series, Agilent Technologies Co., Ltd, China) equipped with a tapered microsyringe (5181-1267, Hamilton Company, USA). Nitrogen gas was used as a carrier gas. The magnitude of OD was measured at 600 nm using a spectrophotometer (DR 2800, Hach Company, USA). The concentration of chloride was measured by using an ion chromatograph (Dionex ICS 2500, Dionex Corporation, USA) equipped with separator column (IonPac AS11-HC), guard column (IonPac AG11-HC), GP50 gradient pump, suppressor (ASRS-ULTRA II 4-mm), AS50 autosampler, and ED50 electrochemical detector.

RESULTS AND DISCUSSION

Bioremoval of ToX/TCE Mixture

Mixture of ToX (150 mg/L) and TCE (0-30 mg/L)

When the indigenous microbial isolate obtained from the Xiamen soil sample was tested for the bioremoval of the mixture of ToX (150 mg/L) and TCE at different pHs

and temperatures, the highest bioremoval efficiency for ToX (81.8%) was observed at pH 7 and 35°C but without TCE, whereas the lowest ToX bioremoval efficiency (55.1%) was observed at pH 9 and 25°C with 30 mg/L TCE (Table 1), implying the inhibitory effect of TCE on the ToX bioremoval. The TCE concentration, however, was not shown that much significant in terms of inhibiting the ToX bioremoval. On the other hand, at 15 mg/L TCE, its bioremoval efficiencies were observed the highest at pH 5 and 35°C (71.6%) and the lowest at pH 9 and 25°C (50.8%), whereas at 30 mg/L TCE, the highest bioremoval efficiency at pH 9 and 35°C (54.4%) and the lowest at pH 9 and 25°C (47.5%), with chloride generated from the mineralization of TCE accordingly. In addition, at the higher TCE concentration of 30 mg/L, its bioremoval efficiencies (47.5-54.4%) were not significantly affected by pH and temperature. In general, TCE was more biologically removed through co-metabolism for this microbial isolate at the lower concentration at 15 mg/L, implying the concentration of ToX as substrates might not be enough for the respective co-metabolism of TCE.

Table 1 Removal efficiencies (%) for ToX (150 mg/L)/TCE (0-30 mg/L) mixtures and chloride generated (mg/L). (Averages for duplicates)

pH	Removal	ToX (150 mg/L)			
		TCE (0mg/L)	TCE (15mg/L)	TCE (30mg/L)	
25°C	5	Biotic	67.5	72.9/54.6	68.9/53.8
		Abiotic	4.1	3.4/5.3	3.1/1.5
		Total	71.6	76.3/59.9	72.0/55.3
		Chloride	-	7.6	9.8
	7	Biotic	66.2	70.5/54.6	66.7/50.0
		Abiotic	0.8	2.2/13.8	1.3/2.7
		Total	67.0	72.7/68.4	68.0/52.7
		Chloride	-	5.8	5.6
	9	Biotic	58.6	59.5/50.8	55.1/47.5
		Abiotic	3.7	1.3/6.5	3.6/2.2
		Total	62.3	60.8/57.3	58.7/49.7
		Chloride	-	8.9	11.0
35°C	5	Biotic	70.2	73.2/70.5	69.2/50.5
		Abiotic	1.8	1.4/1.1	1.5/3.6
		Total	72.0	74.6/71.6	70.7/54.1
		Chloride	-	7.2	13.0
	7	Biotic	81.8	81.4/64.6	73.6/52.7
		Abiotic	1.7	1.5/5.9	3.7/1.4
		Total	83.4	82.9/70.5	77.3/54.1
		Chloride	-	8.6	10.1
	9	Biotic	62.0	67.9/59.7	67.7/51.9
		Abiotic	8.2	3.3/10.6	1.3/2.5
		Total	70.3	71.2/70.3	69.0/54.4
		Chloride	-	7.6	8.0

Mixture of ToX (350 mg/L) and TCE (0-30 mg/L)

Table 2 shows the bioremoval efficiencies for the mixture of ToX at 350 mg/L and TCE at 0-30 mg/L. Different from the previous results when the ToX

mixture concentration was 150 mg/L, the highest ToX removal efficiency (87.8%) was at pH 7 and 35°C but with the presence of TCE at 15 mg/L, whereas the lowest ToX removal efficiency (57.1%) was at pH 9 and 25°C with 15 mg/L TCE. This implies the bioremoval of ToX mixture stimulated by the presence of TCE at 15 mg/L under this specific environmental condition (pH 7 and 35°C), compared to the ToX bioremoval without TCE. The Xiamen microbial isolate was also shown with higher overall ToX removal efficiencies at the higher temperature when the ToX concentration was higher and TCE not present, regardless of pH.

Table 2 Removal efficiencies (%) for ToX (350 mg/L)/TCE (0-30 mg/L) mixtures and chloride generated (mg/L). (Averages for duplicates)

pH	Removal	ToX (350 mg/L)			
		TCE (0mg/L)	TCE (15mg/L)	TCE (30mg/L)	
25°C	5	Biotic	72.9	74.4/58.4	74.5/54.9
		Abiotic	2.2	2.1/2.5	6.5/1.2
		Total	75.1	76.5/60.9	75.9/56.1
		Chloride	-	7.1	11.3
	7	Biotic	67.5	69.5/63.4	68.8/43.9
		Abiotic	0.4	3.2/5.4	0.7/12.6
		Total	67.9	72.7/68.4	69.5/56.5
		Chloride	-	7.0	5.7
	9	Biotic	59.6	57.1/43.6	58.3/47.7
		Abiotic	1.3	2.9/7.3	12.6/3.2
		Total	60.9	60.0/50.9	59.9/50.9
		Chloride	-	8.2	10.9
35°C	5	Biotic	80.9	76.8/76.2	59.6/50.2
		Abiotic	1.9	1.8/1.8	9.7/2.2
		Total	82.8	78.6/78.0	69.3/52.4
		Chloride	-	7.6	12.1
	7	Biotic	83.9	87.8/76.5	77.2/53.5
		Abiotic	2.2	1.8/6.5	0.6/3.9
		Total	86.1	89.6/83.0	77.8/57.4
		Chloride	-	8.6	9.8
	9	Biotic	72.2	68.2/64.9	67.7/51.9
		Abiotic	8.1	3.3/6.5	1.3/2.5
		Total	80.3	71.5/71.4	69.0/54.4
		Chloride	-	7.6	9.1

On the other hand, at 15 mg/L TCE, its bioremoval efficiencies were observed the highest at pH 7 and 35°C (76.5%), whereas the lowest at pH 9 and 25°C (43.6%), similar to when the ToX concentration was lower (150 mg/L). In comparison, at 30 mg/L TCE, the highest bioremoval efficiency was at pH 5 and 25°C (54.9%) and the lowest at pH 7 and 25°C (43.9%), with chloride generated from the mineralization of TCE accordingly. Similar to the previous experiments, the TCE bioremoval efficiencies (43.9-54.9%) were not significantly affected by pH and temperature at 30 mg/L and TCE was more biologically removed through co-metabolism at the lower concentration of 15 mg/L.

Bioremoval of BTE_oX/TPH/TCE Mixture

The microbial isolate obtained from the Macau soil sample was tested for the bioremoval of BTE_oX (350 mg/L)/TPH (1,000 mg/L)/TCE (15 mg/L) mixture at different pHs (5, 7, and 9) and temperatures (25 and 35°C), and the results are shown in Table 3.

Table 3 Removal efficiencies (%) for BTE_oX (350 mg/L)/TPH (1,000 mg/L)/TCE (15 mg/L) mixtures. (Averages for duplicates)

	pH	Removal	BTE _o X	TPH	TCE
25°C	5	Biotic	13.1	16.4	28.4
		Abiotic	8.5	8.3	9.4
		Total	21.6	24.7	37.8
	7	Biotic	60.8	30.7	35.2
		Abiotic	27.7	13.1	13.2
		Total	88.5	43.8	48.4
	9	Biotic	55.2	45.7	43.6
		Abiotic	23.1	17.2	9.3
		Total	78.3	62.9	52.9
35°C	5	Biotic	47.8	14.3	28.8
		Abiotic	23.2	12.0	16.4
		Total	71.0	26.3	45.2
	7	Biotic	71.2	35.5	37.2
		Abiotic	20.7	15.4	13.7
		Total	91.9	50.9	50.9
	9	Biotic	70.8	42.6	50.3
		Abiotic	23.4	14.6	12.8
		Total	94.2	57.2	63.1

Effect of pH

Regardless of temperatures, this microbial isolate was shown with lower overall bioremoval efficiencies for the mixture at pH 5 compared to pH 7 and 9, and all three compounds (BTE_oX, TPH, and TCE) were shown the lowest bioremoval efficiencies at pH 5. At pH 5, the bioremoval efficiencies for BTE_oX, TPH, and TCE ranged 13.1-47.8%, 14.3-16.4%, and 28.4-28.8%, respectively. TPH and TCE were shown the highest bioremoval efficiencies at pH 9 (45.7% and 50.3%, respectively), and BTE_oX with the highest bioremoval efficiency at pH 7 (71.2%) but not that much different from the bioremoval efficiency at pH 7 (70.8%). This further suggests the microbial isolate preferring neutral or slightly alkaline conditions for the bioremoval of mixture.

Effect of temperature

As shown in Table 3, the higher temperature in general was shown preferred by the microbial isolate for the bioremoval of this mixture, especially for BTE_oX. The bioremoval efficiencies for BTE_oX, TPH, and TCE in mixture ranged 13.1-60.8%, 16.4-45.7%, and 28.4-43.6%, respectively, at 25°C and 47.8-71.2%, 14.3-42.6%, and 28.8-50.3%, respectively, at 35°C. This also

suggests the bioremoval of TPH and TCE in this mixture not significantly affected by temperature. While the highest TPH bioremoval efficiency was observed at 25°C (pH 9), the highest bioremoval efficiencies for BTE_oX and TCE in mixture were at 35°C.

CONCLUSIONS

Two microbial pure cultures isolated from the regional soil samples potentially contaminated with gasoline compounds were shown with various responses in terms of bioremoval efficiencies toward mixtures of ToX (150-350 mg/L)/TCE (0-30 mg/L) and BTE_oX (350 mg/L)/TPH (1,000 mg/L)/TCE (15 mg/L) at different pHs (5-9) and temperatures (25-35°C). The microbial isolate from the Xiamen soil sample was shown the highest bioremoval efficiency for ToX at pH 7 and 35°C, regardless of the presence of TCE. However, at 150 mg/L ToX the highest bioremoval efficiency was without TCE, whereas at 350 mg/L ToX, with the presence of 15 mg/L TCE. In case of the bioremoval of BTE_oX/TPH/TCE mixture by the microbial isolate from the Macau soil sample, the highest bioremoval efficiencies for mixture was at pH 9. However, the highest bioremoval efficiencies for BTE_oX and TCE was at 35°C, whereas for TPH at 25°C.

Even though lots of studies have been done with the removal of BTEX (singly and in mixtures), TPH, or TCE (singly and in mixtures with other chlorinated aliphatic compounds, using such substrates as toluene for the enzymes toluene-*ortho*-monooxygenase and toluene dioxygenase, *ortho*-xylene for toluene/*ortho*-xylene monooxygenase, and methanol for methane monooxygenase) individually, unfortunately almost no study seems dealing with the interaction (stimulatory or inhibitory to each other's removal) among BTEX, TPH, and TCE when they exist in mixtures, especially under different environmental conditions. The results from this study further show some contradictory interaction results among BTEX, TPH, and TCE when they existed in mixtures at different pHs and temperatures. Since this study is just preliminary toward the interactions among these very commonly found organic environmental contaminants present in mixtures, further studies are warranted to find out more exact interactions among them, due to their co-existence at many actual contaminated sites.

ACKNOWLEDGEMENTS

This study was supported by research grants from the University of Macau Research Committee and the Macau Science and Technology Development Fund.

REFERENCES

- ATSDR (Agency for Toxic Substances and Disease Registry) (1997). Toxicology Profile for Trichloroethylene. Atlanta, Georgia.
- Chang JL & Lin C-C (2006) A Study of Storage Tank Accidents. *Journal of Loss Prevent.* 19: 51-59.
- Hyman MR, Russell SA, Ely RL, Williamson KJ, Arp DJ (1995). Inhibition, Inactivation, and Recovery of Ammonia-oxidizing Activity in Cometabolism of Trichloroethylene by *Nitrosomonas europaea*. *Appl. Environ. Microbiol.* 61(4): 1480-1487.
- Kocameci BA & Cecen F (2007). Kinetic Analysis of the Inhibitory Effect of Trichloroethylene (TCE) on Nitrification in Cometabolic Degradation. *Biodegradation.* 18: 71-81.
- Kota S, Barlaz MA, Borden RC (2004). Spatial Heterogeneity of Microbial and Geochemical Parameters in Gasoline Contaminated Aquifers. *Practice Periodicals of Hazardous, Toxic, and*

HYSTERETIC RETENTION OF Pb(II) IN KAOLIN COLUMN

Zhen-Ze LI¹, Yun-Min CHEN², Xiao-Wu TANG³, Yan WANG⁴ and Qiang TANG⁵

ABSTRACT: The leaching behavior of metals in soil is key to in-depth understanding of the remediation target and relevant measures for polluted soil. This paper investigated the leaching of Pb(II) from Kaolin column. Solution pH, Pb(II) concentration were recorded and analyzed with a decaying transport theory, separately. The obtained model constants were discussed with emphasis on the hysteretic retention of metal in soil column. The tailing effect of Pb(II) release from polluted soil seems critical to the longterm pollution and requires careful treatment in engineering practices.

KEYWORDS: heavy metal, pollution, kaolin, leaching

INTRODUCTION

Heavy metal pollution has been widely reported in developing countries recently. The polluted soil always requires proper remediation treatment to improve the soil quality as well as the environmental safety. The leaching behavior of metals in soil is thus becoming a key to in-depth understanding of the remediation target and relevant measures.

Kamon et al. (2000) showed that the legislations about the leaching test scheme in different countries varied from each other. However, the reported attentions are always paid to the level of contaminant that is able to be leached from the polluted soil rather to the desorption characteristics during the leaching process. Ishimori et al. (2005) reported the evaluation of the desorption curves of phosphate from sand column using numerical backward analysis method. Although the fitted curve is close to the observed result, the affecting factors were merely restricted on adsorption patterns while many others not mentioned.

In this study, the leaching behavior of Pb(II) from Kaolin column was investigated. The desorption process was successively fitted with a decaying transport equation which speculates and verifies a slow release process of Pb(II) varied with elapsed time. Discussions emphasize the chronic and longterm pollution caused by the gradually released pollutant.

BACKGROUND

Decaying Transport Function

The fate of inert solute in soil is mainly in form of sorption, diffusion and hydraulic dispersion. As to the reactive solute whose transport in soil involves chemical reactions, i.e. biological decomposition, precipitation and dissolution etc., a function describing the decaying behavior of solute with time will be applicable (Bauer et al. 2001; Genuchten, 1981):

$$R \frac{\partial C}{\partial t} = \frac{\partial}{\partial x} \left(D \frac{\partial C}{\partial x} \right) - v \frac{\partial C}{\partial x} - \lambda C \quad (1)$$

where R_d is the retardation factor, D_e the effective diffusion coefficient, v the infiltration velocity, λ is the decaying factor relevant to the change of solute concentration in pore liquid:

$$C(t) = C_0 e^{-\lambda t} \quad (2)$$

where C_e is the solute concentration in pore liquid, C_{e0} the initial concentration, t the time.

With the following boundary and initial conditions,

$$\begin{aligned} C(0, t) &= C_0 \\ C(x, 0) &= C \\ \lim_{x \rightarrow \infty} C(x, t) &= 0 \end{aligned} \quad (3)$$

¹ Ph.D, MOE Key Laboratory of Soft Soils and Geoenvironmental Eng., Zhejiang University, China. Email: lazyhero@126.com

² Professor, ditto. Email: chenyunmin@zju.edu.cn

³ Professor, ditto. Email: tangxiaowu@zju.edu.cn

⁴ Ph.D Student, ditto. Email: wangyan850407@163.com

⁵ Ph.D Student, ditto. Email: tangqiang85@hotmail.com

the analytical solution of Eq. (1) could be written as (column length is L, break through curve at exit end of column) (Li, 2009):

$$\frac{C(L,t)-C}{C-C_0} = \frac{1}{2} e^{-\frac{\lambda}{Dv}} \left[e^{-\sqrt{\frac{\lambda}{Dv}} \left(\frac{L}{2\sqrt{Dt}} - \sqrt{\frac{v}{4RD} + \frac{\lambda}{R}} t \right)} + e^{\sqrt{\frac{\lambda}{Dv}} \left(\frac{L}{2\sqrt{Dt}} + \sqrt{\frac{v}{4RD} + \frac{\lambda}{R}} t \right)} \right] \quad (4)$$

MATERIALS AND METHODS

Purified Kaolinite mineral was obtained from a mineral deposit in Huaibei, Anhui Province. XRD spectrum showed no other mineral occurred in the sample and confirmed the purity of the mineral.

Table 1 shows some preparation parameters for Pb(II) laden soil. The kaolin (100 g) was first equilibrated with Pb(II) solution (2.00 g/L, 500 mL) in a beaker. The Batch adsorption was conducted at 300 rpm with a magnetic stirrer for 2 days. Afterwards, the slurry was separated by centrifuging at 300 rpm. The obtained slurry was used to prepare the soil column while the supernatant was sampled to determine the equilibrium Pb(II) concentration.

Table 1 Preparation parameters for Pb(II) laden Kaolin

Preparation process	Parameter	Value	Unit
Batch adsorption	Soil weight	100	g
	Initial Pb(II) conc.	2.00	g/L
	Volume of solution	500	mL
Column leaching	Pressure head	100	kPa
	Initial Pb(II) conc.	534.2	mg/L
	Adsorbed Pb(II)	7.329	mg/g

Table 2 Properties of Kaolin column

Parameters	Value	Unit
Soil weight	100.0	g
Pore ratio <i>e</i>	1.722	
Specific gravity	2.75	
Dry density	1.010	g/cm ³
Total volume	99.0	cm ³
Column length	4.51	cm
Cross section	22.0	cm ²
Pore volume	62.64	mL

The soil column was prepared through hydraulic consolidation method. The obtained column was in 4.51

cm length with dry density at 1.01 g/cm³. In the following leaching test, tap water was utilized as the leaching agent and the pressure head was fixed at 100 kPa. The leachate at the end of the column was collected separately for Pb(II) concentration determination.

RESULTS AND DISCUSSION

Fig. 1 shows the test conditions. The pressure head was fixed at 100 kPa and the infiltration velocity was in the range of 0.3-0.6 mL/min. The uniform velocity indicates that the kaolin column was uniform in dry density and in pore structure, which verified the successive preparation of soil column.

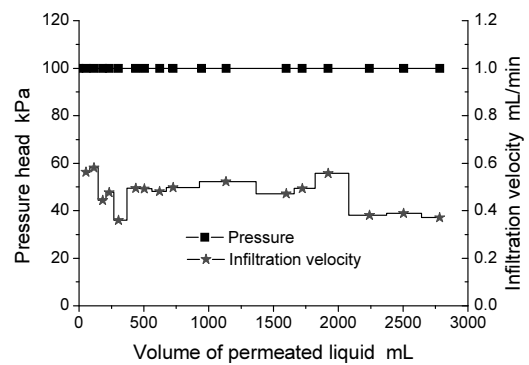


Fig. 1 Test conditions

Fig. 2 shows the variation of Pb(II) concentration on Kaolin and desorption amount with leachate volume. When the leachate volume was less than 233 mL, the adsorption amount *C_s* decreased significantly from 7.33 to 6.36 mg/g. Further leaching did not obviously give rise to the decrease in *C_s* (reach 6.282 mg/g at 2783 mL). The desorption amount has a similar trend: a flexion was found at 233 mL with 96.78 mg Pb(II) desorbed. Further 10.9 times increase in leachate volume just increase 7.88 mg desorption. This may be caused by the fact that most of the dissolved Pb(II) in pore liquid was removed from the kaolin column at the initial stage. The following

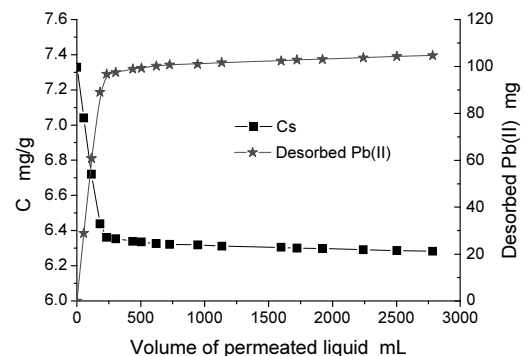


Fig. 2 Variation of Pb(II) concentration on Kaolin and desorption amount with leachate volume

desorption of Pb(II) was caused by the gradual and slow transport of Pb(II), which was fixed on the mineral surface, from the solid phase to the liquid phase. It is obvious that the desorption process is very difficult to be accomplished in terms of dilution effect.

Fig. 3 shows the variation of Pb(II) concentration with leachate volume. The exit Pb(II) concentration was observed decreasing sharply from 534.2 to 9.9 mg/L with leachate volume increasing to 305 mL. Further leaching resulted in slow release of Pb(II) with the equilibrium concentration ≥ 1.348 mg/L, higher than the Chinese Drinking Water Standard (<0.05 mg/L). It is shown that the previously sorbed Pb(II) could be retained by the clay mineral and thus lead to long term chronic pollution to the ground water. For clays with high sorption affinity, this effect will not be obvious. The authors have investigated the leaching performance of Pb(II) from loess column and found that the final equilibrium concentration of Pb(II) in leachate was about half of that obtained from Kaolin column (Li, 2009).

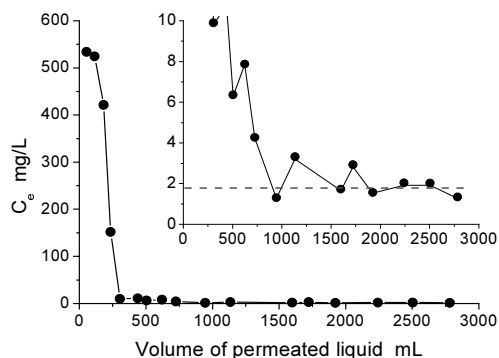


Fig. 3 Variation of Pb(II) concentration with leachate volume

Fig. 4 shows the variation of pH with Pb(II) concentration in leachate. The pH was found increased with decreasing solute concentration. The change in pH could be considered to be caused by the change in Pb(II) concentration which would affect the acid-alkaline balance in aqueous solution. The relationship between pH and Pb(II) concentration C_e was fitted linearly as ($R=0.929$)

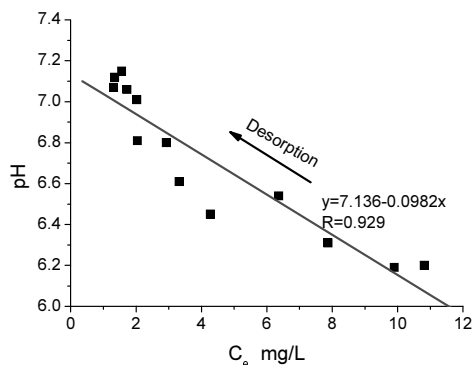


Fig. 4 Variation of pH with Pb(II) concentration in leachate

$$pH = 7.136 - 0.0982 * C \quad (5)$$

Fig.5 shows the breakthrough curve of Pb(II) in Kaolin column. The testdata were fitted by decaying transport equation as shown in Eq. (4). The fitted parameters were shown in Table 3. With different set of decaying factor λ , the testdata were separately simulated. It is found that both linear and decaying transport could successively fit the test result with correlation coefficients > 0.9995 . The obtained model constants were similar to each other with regarding retardation factor (2.12) and effective diffusion coefficient ($0.0923-0.0945$ cm^2/h).

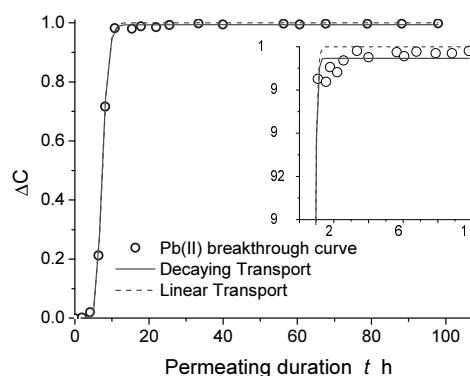


Fig. 5 Breakthrough curve of Pb(II) in Kaolin column (leaching velocity 1.29 cm/h, column length 4.5 cm)

Table 3 Transport parameters of Pb(II) in Kaolin column

Parameters	Value	
	Linear transport	Decaying transport
R_d	2.12	2.12
D_e cm^2/h	0.0945	0.0923
λ	0	0.00193
R^2	0.9995	0.9997

However, the tailing effect could not be predicted by linear transport theory. Instead, the decaying transport theory could successively predict the tailing effect. It is thus shown that the decaying effect exists in the desorption of Pb(II) from kaolin column. That is to say, the desorption was a dynamic process and was governed by first order kinetics. Tailing effect was widely reported in heterogeneous natural soils with abundant crevice and uneven pore sizes (Pang et al. 2003; Srivastava et al. 2004; Luo et al. 2006). The formation of soil aggregates results in solute diffusion inward the dead pores aside from the transport in connected pores. Therefore, the solute contained in the dead space will continually migrate toward the connected pore where they are easy to 1) be taken out of the soil by soil flush and 2) cause

tailing phenomenon.

The retardation factor R_d in this test was determined at 2.12, which is about half of that determined by column diffusion test ($R_d = 5.55-6.31$) (Li, 2009). The decreased retardation factor in leaching test compared to the pollution test indicates the hysteretic retention of Pb(II) on kaolin. This effect greatly increase the remediation cost for polluted kaolin. Although this study was merely about kaolin, it is certain that the hysteretic behavior commonly exists in the environment and requires specific attention when encountered in engineering practices.

CONCLUSIONS

- 1) Pb(II) is hard to be leached from kaolin using tapwater.
- 2) Pb(II) concentration in leachate remains ≥ 1.348 mg/L above the drinking water standard in China.
- 3) The pH increased with decreasing solute concentration in the leachate.
- 4) The decaying transport theory could successively predict the tailing effect.
- 5) Hysteretic retention of Pb(II) in Kaolin was obvious and requires careful treatment in engineering practices.

REFERENCES

Srivastava P, Singh B, Angove M (2005). Competitive

- adsorption behavior of heavy metals on kaolinite. *Journal of Colloid and Interface Science* 290: 28-38.
- Bauer P, Attinger S, Kinzelbach W (2001). Transport of a decay chain in homogenous porous media: analytical solutions. *Journal of Contaminant Hydrology* 49: 217-239.
- Genuchten MTV (1981). Analytical solutions for chemical transport with simultaneous adsorption, zero-order production and first-order decay. *Journal of Hydrology*. 49: 213-233.
- Ishimori H, Katsumi T, Htanaka K, et al. (2006). Effects of adsorption/desorption phenomenon on pump-and-treat remediation for groundwater contaminated with chemical substances. *Mitigation and Coustermeasures of Ground Environment*: 73-79.
- Kamon M, Hartlen J, Katsumi T (2000). Reuse of waste and its environmental impact. *GeoEng2000*, 1: 1095-1123.
- Luo J, Cirpka OA, Kitanidis PK (2006). Temporal-moment matching for truncated breakthrough curves for step or step-pulse injection. *Advances in Water Resources*. 29: 1306-1313.
- Li Z (2009). Mechanism of Sorption, Desorption, Diffusion and Remediation of Heavy Metals in Soils. PhD thesis. Zhejiang University: Hangzhou, China.
- Pang L, Close M, Goltz M (2003). Application of the method of temporal moments to interpret solute transport with sorption and degradation. *Journal of Contaminant Hydrology* 60: 123-134.

EXPERIMENTAL STUDY ON THE MECHANISM OF ACTION OF IONIC SOIL STABILIZER ON RED CLAY OF WUHAN

Wei XIANG¹, De-Shan CUI² and Fei AI³

ABSTRACT: The reinforcement of cement and other traditional stabilizer not only waste aggregates, but also pollute the environment. New Ionic Soil Stabilizer (ISS) was used to reinforce the red clay in Wuhan. X-Ray Diffraction (XRD), Fourier Transfer Infra Red spectroscopy (FTIR), Cation Exchange Capacity (CEC), BET Surface Area (BET) and Zeta potential were performed before and after treatment with ISS. The test results indicated that (1) d_{001} of clay mineral becomes broad with smaller intensity, that (2) the strong adsorbed water film thins, that (3) CEC is reduced, that (4) BET surface area decreases. Finally the mechanism of action of Ionic Soil Stabilizer on red clay of Wuhan is analyzed from the aspects of CEC, the electric double layer and the adsorbed water.

KEYWORDS: red clay, Ionic Soil Stabilizer, cation exchange capacity, electric double layer, adsorbed water

INTRODUCTION

Red clay of Quaternary in Wuhan is formed by alluvial-diluvial. Experimental study demonstrates that the conflicts between bad physical property and well mechanical character were mainly determined by the adsorbed water and structure of clay particles. The strength of red clay decreases as the thickness of adsorbed water increases. The characteristic morphological structure of the clay provides a significant reinforcing action (Deng et al. 2009).

In China, the special engineering property of red clay is arising more attention. Because of the shrinkage and water sensitivity of red clay, the slope destroys, the ground distorts in asymmetry and the road crazes. Therefore, the experimental and theoretical studies are urgently needed (Zhao et al. 2003).

The red clay in Wuhan shows high strength in dry. But when meeting water, it will swell and soften. Take the cement and fly-ash to reinforce the red clay, not only the time is long and the cost is high, but also the sand and stone are largely needed. How to decrease the consumption of sand and stone under the premise of ensuring the quality of the road engineering, and how to decrease the environment destruction, are problems to be necessarily resolved.

A new kind of economic and suitable Ionic Soil Stabilizer (ISS) to reinforce the red clay was studied, not only short of construction period, low-cost, but also

environmental protection. Even more value is that the red clay directly used at the site as a raw material can dispense with the expensive excavation and ex-situ material costs. Therefore, it will be widely used in road and environment engineering.

TEST MATERIALS AND METHODS

Red Clay

The undisturbed red clay was taken from Wuhan. The depth of sampling is from 0 to 3 meters. The basic physical and mechanical indicators of red clay are shown as Table 1.

Table 1 Basic property of the red clay

Items	
Moister water content (%)	25.67
Density (g/cm ³)	1.98
Specific gravity	2.72
Liquid limit (%)	33.87
Plastic limit (%)	15.47
Plasticity index	18.40
Cohesive strength (kPa)	30.95
Inner friction angel(°)	24.72

¹ Professor, Faculty of Engineering, China University of Geosciences, China. Email:xiangwei@cug.edu.cn

² Ph.D Student, Faculty of Engineering, China University of Geosciences, China. Email:cuideshan2008@yahoo.com.cn

³ Ph.D Student, Faculty of Engineering, China University of Geosciences, China. Email:starry_2004@163.com

Ionic Soil Stabilizer

ISS is a kind of liquid surfactant composite of active ion, which is suitable to reinforce various clay soil whose clay fraction percent is more than 25% (Dong et al. 2004). The hydrophilic group and hydrophobic group of ISS can significantly reduce the surface tension of water. The molecular weight is from 5×10^4 to 20×10^4 . The cation exchange capacity is from 5 to 6 mg/100g.

Methods

X-Ray diffraction

After removing the impurities, the red clay mud was dropped in the ceramic chip. Glue the ceramic to the sample holder. The sample holder was then placed in a Siemens D5000 X-Ray diffractometer and analyzed between angles 2° to 30° . Identification of red clay structure by X-ray diffraction is based on the fact that each solid mineral crystal has its own characteristic atomic structure which diffracts X-rays in a characteristic pattern (Mercier et al. 2008). The recognition of the pattern establishes uniquely the diffracting substance before (a) and after (b) treatment with ISS.

Fourier transfer infra red spectroscopy (FTIR)

FTIR techniques were used to distinguish between different types of clay minerals and to derive information concerning their structure, composition and structural changes upon chemical modification (Madejova 2003). An important aspect of the present study is to determine the effect of ISS on the degree of hydration of red clay particles. The degree of hydration is related to the swelling and engineering property. FTIR is most suited for strong adsorbed water film investigation. Therefore a reduction in the H-OH bonds/Si-O-Si bonds is an evidence of adsorbed water decrease.

BET surface area

BET surface area analysis, by nitrogen adsorption, was used to measure the specific surface area of the red clay before and after treatment to determine effect of ISS. The method is based on measuring the amount of nitrogen gas adsorbed (physically) on the surface of the red clay at 77.32K (-196°C) and calculates the specific surface area using the Brunauer, Emmett and Teller (BET) method of adsorption of an inert gas. (Dogan et al. 2006).

Zeta potential

Red clay consists mainly of plate-like particles, which when meeting water, usually have negatively charged faces. Variation in pH alters the zeta (zeta) potential of soils (Kaya 2005). The physical properties of

red clay-water systems such as swelling are extremely sensitive to the nature of the electric double layer around the particles. Zeta potential measurements provide particularly relevant information regarding swelling. Zeta potential was measured by the Zetasizer Nano ZS90 of Malvern.

RESULTS AND DISCUSSION

X-Ray Diffraction (XRD)

The influence of ISS on the mineral composition of red clay is confirmed by the XRD patterns before and after treatment (Fig.1). The main clay minerals are kaolin, illite and chlorite. The patterns of each clay mineral exhibits there is no new crystallization after treatment with ISS. The peaks become broad with smaller intensity and shifts to a smaller angle after treatment. The appearance of such broad, small intensity peak coupled with the shrinkage of the interlayer spacing is indicative of the exchangeable interlayer cations.

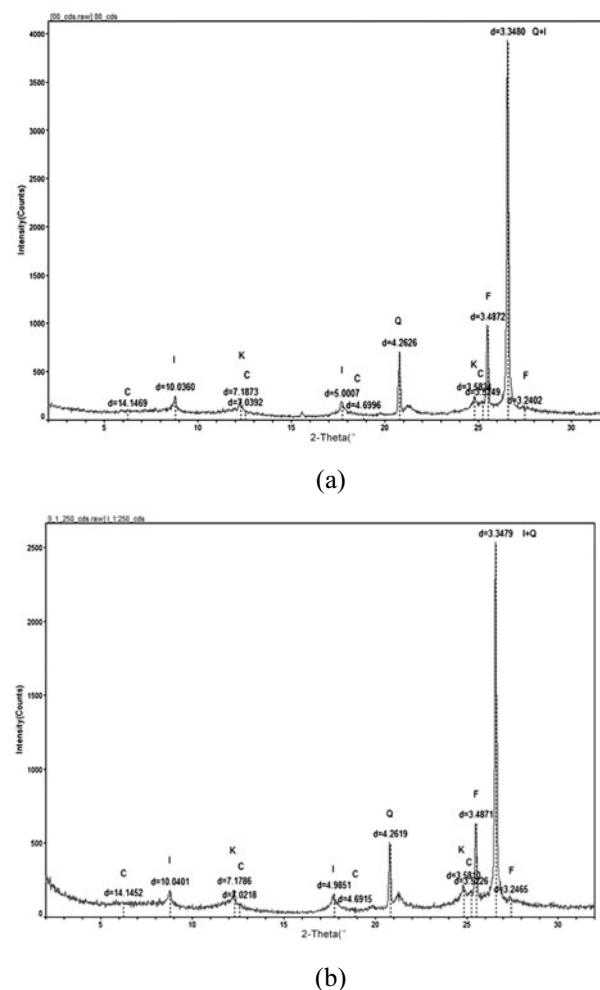


Fig. 1 XRD of red clay before (a) and after (b) treatment with Ionic Soil Stabilizer

Fourier Transfer Infra Red spectroscopy (FTIR)

The FTIR spectra of the treated and untreated samples are presented in Fig. 2. A clear diminution in the intensity of the 3400 cm^{-1} (H-OH) band is reflecting the change of strong adsorbed water. The persistence of the 1040 cm^{-1} band indicates that the Si-O-Si linkages were not removed. Because the cause and geography of red clay determine its silicate content, two non-overlapping absorption peaks can be chosen to analyze the relative content of strong adsorbed water. The decrease in ratio of H-OH/Si-O-Si reflects the reduction of strong adsorbed water film (Table 2). But it has been established that strong adsorbed water surrounding the clay particles are not all removed. The reduction in the intensity of (H-OH) band after treatment is indicative of the lower water content at the outer surface of clay particles and of the release of water that was originally "bound" in the soil-water matrix.

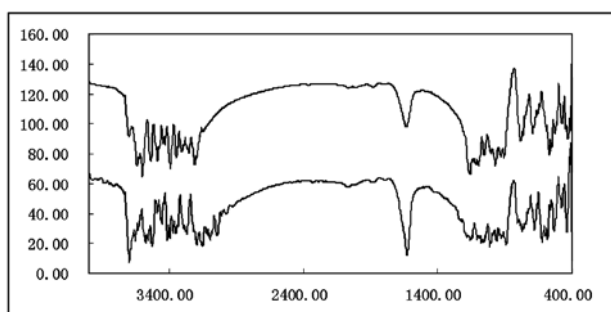


Fig. 2 FTIR of red clay before (up) and after (down) treatment with ionic soil stabilizer

Table 2 The ration of two pecks of red clay

Sample	3400 cm^{-1}	1040 cm^{-1}	Ratio of two pecks
Before treatment	41.69	21.24	1.96
After treatment	28.56	23.98	1.19

Cation-Exchange Capacity (CEC)

The CEC is influenced by lots of factors. The operation must be strictly controlled for getting the credible results. According to the Standard for Soil Test Method of PRC Industry Standard (SL237-1999), it takes the method of BaCl_2 buffer solution to determine the CEC of red clay (Table 3).

The CEC of red clay decreases after treatment. The CEC of clay is not only decided by the mineral component of clay, but also determined by the percent of clay fraction and time. The smaller the percent of clay

fraction is, the less the CEC of clay is. As time increases, CEC decreases. The CEC of red clay was found to be 23.02 cmol/kg and after treatment with ISS for 2 weeks, it drops to 10.32 cmol/kg . For 4 months, CEC decreases more. This is an indication of the decrease of expansive power after treatment with ISS and of the effect of ISS reinforcing as the time.

Table 3 Cation-Exchange Capacity of red clay

ISS: Water	CEC (cmol/kg)	
	4 months	2 weeks
1: 50	16.19	17.17
1: 100	12.71	12.79
1: 150	10.13	10.32
1: 200	10.27	14.64
1: 250	10.27	13.44
1: 300	6.96	15.47
1: 350	18.38	12.28
1: 400	19.09	18.38
0	20.17	23.02

BET Surface Area (BET)

Nitrogen adsorption technique was used to determine effect of ISS on the specific surface area of red clay particles. The specific surface area of untreated red clay is $27.30\text{ m}^2/\text{g}$. After treatment with ISS, the specific surface area decreases to $22.27\text{ m}^2/\text{g}$ (Table 4). This can be explained that due to the decrease of adsorbed water and flocculation of ISS, red clay particle becomes flocs in the function of molecular bond and hydrogen bond.

Table 4 BET Surface Area of red clay

ISS: Water	BET $\text{S}/\text{m}^2\cdot\text{g}^{-1}$	Linear fit	Slope coefficient	Intercept
1: 50	24.631	0.998	0.172	0.005
1: 150	22.270	0.995	0.186	0.009
1: 200	24.166	0.997	0.173	0.007
1: 250	25.745	0.998	0.164	0.005
0	27.304	0.999	0.156	0.004

Zeta Potential

The red clay particles less than 2000 nm are prepared. The Zetasizer Nano ZS90 of Malvern is taken to analyze the zeta potential of red clay before and after treatment with ISS (Table 5). The change value of zeta potential of red clay is not disciplinary after treatment. But the zeta potential decreases after treated by ISS. Commonly, the

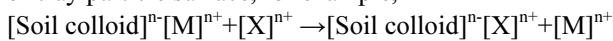
higher the ionic valence is, the better the exchange ability is (Tan et al. 2006). The strong ion of ISS is easy to make the electric double layer thin, the zeta potential of red clay decrease. Zeta potential was found to be -31.03 mV before treatment and it dropped to -18.6 mV after treatment.

Table 5 Zeta potential of red clay

ISS:Water (Volume)	Zeta potential mV	Conductivity mS/cm
1: 50	-28.8	0.0615
1: 100	-26.7	0.0388
1: 150	-18.6	0.0256
1: 200	-21.7	0.0377
1: 250	-21.9	0.0334
1: 300	-20.1	0.0366
1: 350	-19.7	0.0363
1: 400	-19.0	0.039
0	-31.03	0.0826

The Mechanism of ISS Reinforcing Red Clay

ISS is a kind of surfactant consisting of some strong ion, which can exchange the cation of clay particle surface. ISS is an electrolyte dissolving in water, which can electrolyze to cation $[X]^{n+}$ and anion $[Y]^{n-}$. The cation electrolyzed from the ISS can exchange the cation of clay particle surface, for example,



In the function of hydrophobic group of ISS, the anion can decrease the surface tension of adsorbed water, and make adsorbed water to free water (Fig. 3).

That means the function of ISS is to drive away the surface and easy hydration cations.

ISS can quickly ionize diluted, which can decrease the charge property of soil particle surface. The force of soil and water change from attraction to repulsion, the electric chemical bond is opened, which can release the adsorbed water in electric double layer, and decrease the zeta potential of soil particle surface.

The reaction is not a reversible reaction. When the red clay is disposed by ISS, it cannot come back to the primary unbalance state. ISS will firmly adhere to the soil particles surface and interlayer, change the property of hydrophilic to hydrophobic, decrease the thickness of the adsorbed water film and pair-electricity layer, and reduce the cation exchange capacity.

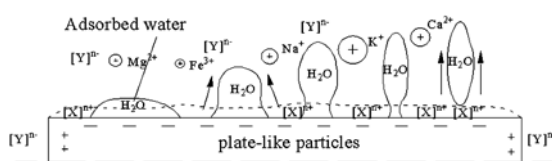


Fig. 3 Model of ISS reducing adsorbed water

CONCLUSIONS

As one kind of new material, ISS is applied in China traffic engineering departments at the initial development stage. After experimental study, the following conclusions can be drawn:

(1) The treatment processes are irreversible and the interlayer spacing is reduced and the surface cations are exchanged.

(2) The strong adsorbed water film thins.

(3) The CEC of red clay was 23.02 cmol/kg and after treatment with ISS, it drops to 10.32 cmol/kg.

(4) After treatment with ISS, the BET surface area decreases to 22.27 m²/g, due to the flocculation of small particles into flocs.

(5) Zeta potential was -31.03 mV before treatment and it dropped to -18.6 mV after treatment.

For the disaster aroused by red clay, the adsorbed water is commonly the important factor that influence the quality of road engineering. The study of ISS is in the beginning, especially the mechanism of reaction. Although the cation exchange capacity, zeta potential of treatment can be measured, the quantification study of the adsorbed water film is not enough. The questions of how the microstructure and the osmosis ways changes after treatment are needed to be demonstrated.

ACKNOWLEDGMENT

The authors acknowledge the support of the National Natural Science Foundation of China, project No. 40672188.

REFERENCES

- Deng H, Ao NJ, Yan T, et al. (2009). The Reinforcement of Red Clay on Natural Rubber and Its Reinforcing Mechanism. *Journal of applied polymer science*, 112(6): 3418-3422.
- Dogan M, Dogan AU, Yesilyurt FI, et al. (2007). Baseline studies of The Clay Minerals Society special clays: Specific surface area by the Brunauer Emmett Teller (BET) method. *CLAYS AND CLAY MINERALS*, 55(5): 534-541.
- Dong J, Wei T, Li G, et al. (2004). A new way of sanitary landfill with ionic soil stabilizer (ISS) for domestic refuse. *Proceedings of 1st Symposium of CGFGE*: 71-76.
- Kaya A & Yukselen Y (2005). Zeta potential of clay minerals and quartz contaminated by heavy metals. *CANADIAN GEOTECHNICAL JOURNAL*, 42(5): 1280-1289.
- Madejova J (2003). FTIR techniques in clay mineral

- studies.VIBRATIONAL SPECTROSCOPY. 31(1): 1-10
- Mercier PHJ, Patarachao B, Kung J, et al. (2008). X-ray diffraction (XRD)-derived processability markers for oil sands based on clay mineralogy and crystallite thickness distributions.ENERGY & FUELS,22(5): 3174-3193.
- Tan LR & Kong LW (2006). Special geotechnical engineering soil sciences. Sciences Press, Beijing..
- Zhao YW, Kong LW, Guo AG, et al. (2003). Mechanical Behaviors and Water-Sensitive Properties of Intact Guangxi Laterite. Rock and Soil Mechanics (in Chinese), 24(4): 568-572.

EFFECTS OF SURFACE-ACTIVE AGENT ON MECHANICAL BEHAVIORS OF LOESS

Nai-Yu KOU¹, Xiao-Wu TANG², Quan-Fang ZHANG³, Yun-Min CHEN⁴ and Qiang TANG⁵

ABSTRACT: The surface-active agent is common in the environment and its effect on the engineering properties of soil remains unclear up to date. The surface-active agent, Sodium Dodecyl Benzene Sulphonate was found able to cause obvious changes in mechanical behaviors of Chinese loess. The shear strength behavior decreased in the SDBS-polluted loess. The effect of the pollutants on the shear strength of loess is found to be similar to that of moistening, and the influence of pollutants gets more and more weak with increasing the degree of saturation. The microstructure was investigated to explain the experimental observations. It is proposed that the presence of SDBS in loess and other soils should be tested and the relevant influences should be evaluated in engineering practices in the future.

KEYWORDS: Chinese loess, surfactant pollution, shear strength, SEM

INTRODUCTION

Detergents are manufactured in large quantities, about 1.5-2 million ton per year, and disposed into the environment after household use (Ying, 2006). Linear Alkyl benzene Sulphonate (LAS) is the main surface-active agent used in detergents throughout the world because of its effectiveness, versatility and cost/performance ratio (Olf & Feijtel, 1998). Nevertheless, surface-active agents may be introduced into soil by various routes and will remain stable and resist decomposition, resulting in persistent and negative impacts on the engineering properties of affected soils.

Loess is a soil that is widely distributed in arid and semiarid areas in northern and western China. It has a low natural bulk density and is sensitive to water content as it has volume collapsibility potential. (Assallay et al. 1997). The Chinese government has proposed a strategic plan for westward development including the large scale development of key infrastructure such as highways and railways. These developments will pass through the areas polluted by surface-active agents. The construction of high road banks, which require a great deal of borrow soil as a basement material, raise the question of whether the soils at the sites are suitable fill material. The effects of the surface-acting agents on the mechanical properties of soil remain unclear.

The interactions between clay minerals and surface-acting agents have been investigated with respect to the

adsorption behavior (Rao & He, 2006), and rheological and colloidal properties of bentonite-cationic surfactant slurry (İşçi et al. 2005), and the micro-structural change (Lee et al. 2005) and adsorption behavior (Sanchez-Martin et al. 2006) of montmorillonite modified by cationic surfactant. These studies on surface-acting agents are focused on soil chemistry and environmental science. However, few studies are available on the changes in the mechanical behavior of soils as a result of the addition of surface-acting agents, particularly anionic surface-acting agents.

The mechanical behaviors of soils with organic components have been widely studied. The effect of organics on the mechanical behavior of soil is complicated because it depends on both the type of soil and that of organic additive. Coop and Willson (2003) examined the behavior of hydrocarbon reservoir sands and sandstones, and found that the presence of hydrocarbons weakened the shear strength of sands. Natural organic materials can make farmland soils soft and prone to compaction (Hamza & Anderson, 2005). However, Moo-Young and Zimmie (2003) found that the addition of paper mill sludge can increase the strength of soils and thus it can be used as landfill cover. Fibrous organic soil was also reported with strengthened nonlinear dynamic properties (Wehling et al. 2003). The question remains: "What is the possible effect of anionic surface-acting agents on the mechanical behaviors of loess?"

¹ MA Student, MOE Key Laboratory of Soft Soils and Geoenvironmental Eng., Zhejiang Univ., China. Email:kouny0210@hotmail.com

² Professor, MOE Key Laboratory of Soft Soils and Geoenvironmental Eng., Zhejiang Univ., China. Email:tangxiaowu@zju.edu.cn

³ Engineering, ditto. Email:zqf@zju.edu.cn

⁴ Professor, ditto. Email:chenyunmin@zju.edu.cn

⁵ MA Student, ditto. Email:tangqiang85@hotmail.com

The objective of this research was to investigate the difference in mechanical behavior between crude loess and loess polluted with a surface-active agent. Sodium DodecylBenzene Sulphonate (SDBS), a typical LAS, was selected as the pollutant. Following the Chinese Standard of Soil Test (NSAC, 1999), consolidated quick direct was conducted to investigate the impact of LAS pollution on the mechanical behaviors of loess. With the assistance of a scanning electron microscope (SEM) (Cambridge Stereoscan 260, UK), the relevant mechanism was also investigated.

MATERIAL AND EXPERIMENTAL PROGRAM

Soil samples were taken from a construction site in a suburban area of Xi'an, China, located at 2.5 m below the ground surface level. The main physical and chemical parameters are shown in Table 1. The samples of crude loess (CL) were air-dried, ground to pass through a 2 mm sieve, oven dried at 105 °C and then preserved in plastic bags.

Table 1 Physical and chemical parameters of loess

Physical parameters	Value
Original bulk density (g/cm ³)	1.44
Specific gravity	2.71
Natural soil water content (%)	4.5

Sodium Dodecylbenzene Sulphonate (SDBS), a common component of detergent that is widely used in daily life (Shen et al. 2004), was selected as the targeted pollutant. The SDBS-loaded loess (SLL) was prepared by thoroughly blending SDBS powder with dry crude loess powder with a mechanical blender. The mass ratio of SDBS to crude loess was adjusted during the preparation process to investigate the effect of pollutant concentration on the mechanical behaviors of loess.

For the shear test, loess samples with various SDBS concentrations (0, 1%, 2% and 10%), were prepared. The water content of each group was adjusted to 15%, 19%, 23% and 25.5% (saturated). Consolidated quick direct shear tests were conducted to obtain the strength parameters.

Figs. 1(a-b) show the shear test sample of SLL with the water content of 15% and 25.5%. The sample with the water content of 25.5% is more smooth than that with the water content of 15%.

In order to further understand the differences in the microscopic structure of the different loess samples, photomicrography of original loess, saturated CL, compacted

CL and SLL with Standard Proctor energy was taken by SEM (JEOL 6335 F-SEM, Japan).



Fig. 1(a) Shear test sample of SLL at w=15%



Fig. 1(b) Shear test sample of SLL at w=25.5%

RESULTS AND DISCUSSION

Figs. 2(a-d) show the results of consolidated quick direct shear tests. Both the cohesion and the friction angle of loess were reduced proportionately with increasing water content and SDBS concentration respectively. The effect of SDBS is like that of water that made the cohesion and the friction angle of loess reduce. In the lower water content, the downward trend changed fast. When the water content increased up to some level, continue increasing the SDBS concentration didn't result in further weak.

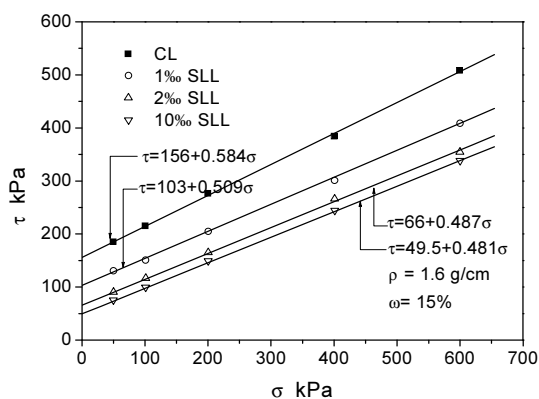


Fig. 2(a) Changes in shear strengths for CL and SLL at w=15%

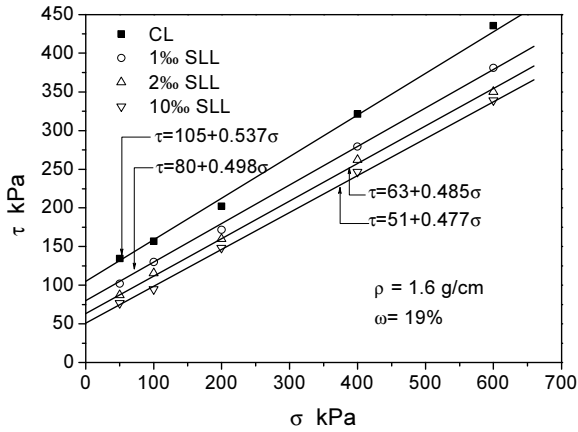


Fig. 2(b) Changes in shear strengths for CL and SLL at w=19%

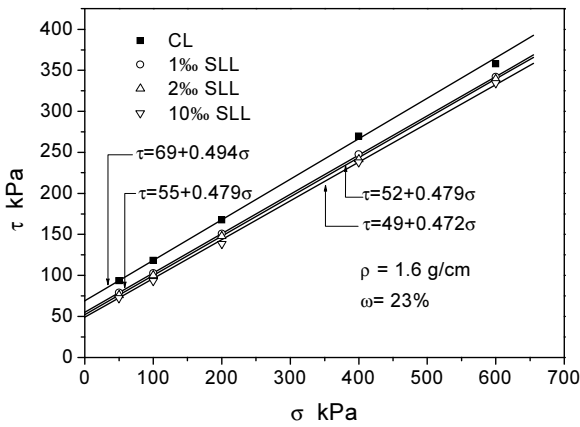


Fig. 2(c) Changes in shear strengths for CL and SLL at w=23%

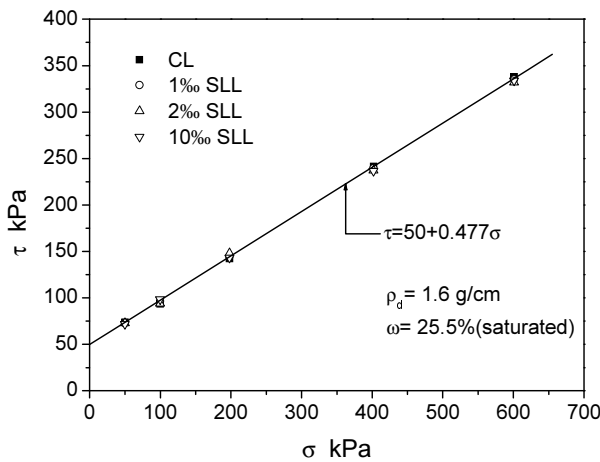


Fig. 2(d) Changes in shear strengths for CL and SLL at saturation

It was interesting to find that 1% SDBS resulted in a similar effect to 100% water saturation on the shear strength parameters of loess. The shear strength parameters did not change with varying water content at 1% SLL or change with SDBS concentration in the saturated state.

The surface-active agent may obviously let down the tension of the different interface including the cohesion and the friction angle so that the solid tiny grain easily changes liquid phase. The crumb structure of loess breaks bring about soil dispersion. The clay particle ingredient losses the cementing property cause that the soil losses the cohesion on the view of macroscopic.

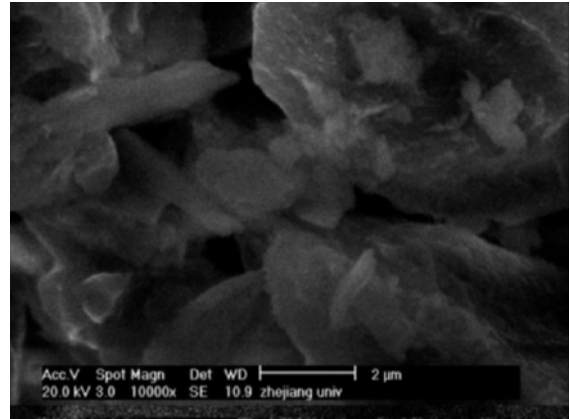


Fig. 3 SEM photograph of original loess sample

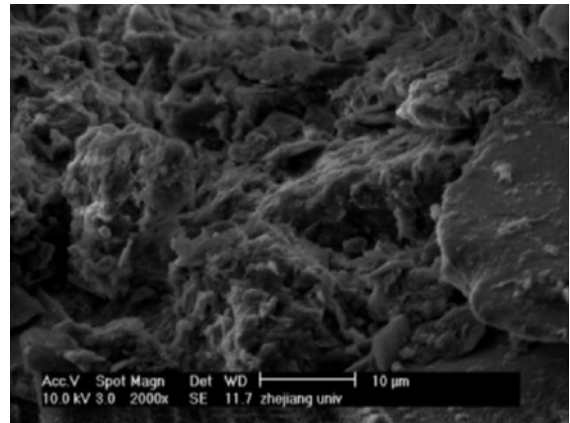


Fig. 4(a) SEM photograph of CL after water immersion

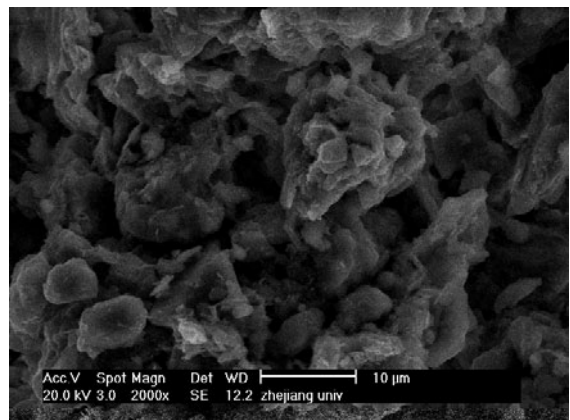


Fig. 4(b) SEM photograph of SLL after water immersion

The SEM photographs of loess are shown in Figs. 3 and 4. Fig. 3 shows the microstructure of the original loess sample with occluded fusiform particles and large pores. Fig. 4 (a) shows the microstructure of saturated crude loess where the particles are glued together and form a dense body but changed. Fig. 4 (b) shows the microstructure of the polluted loess. The separate soil particles are loosely contacted in a manner of point-connection. The cohesive aggregates are dispersed and divided into small particles due to the surface active effect of the SDBS (Shen et al. 2004).

The SEM photographs prove the SDBS changes the structure of loess. The structure of loess is susceptible to destroy, so the effect of the surface-active agent is not to be sneezed at.

CONCLUSIONS

The loess polluted by the surface-active agent, SDBS, exhibited obvious changes in mechanical behaviors when compared to crude loess. The shear strengths of loess decreased with both increasing water content and SDBS concentration until 1% SDBS and 100% saturation where the shear strength parameters approached each other.

The effect of surface-active agent on the shear strength of loess is found to be similar to that of moistening, and the influence of surface-active agent pollutants gets weaker with increasing the degree of saturation.

SEM photos indicated that the dispersive effect of a surface active agent on soil particles was essential to the increase in compressibility and the decrease in shear strength.

The presence of SDBS in loess and other soils should be tested and the relevant influences including the permeability, the compressibility, the collapsibility, etc. should be evaluated in engineering practices in the future.

ACKNOWLEDGEMENTS

The authors would like to express their sincere gratitude to the Key Project of National Science Foundation of China (NSFC) (grant 50538080) for their financial support of this study. Professor Zengyu Guo from Xi'an University of Technology (China) is also appreciated for his help in loess sampling works.

REFERENCES

- Assallay AM, Rogers CDF, Smalley IJ (1997). Formation and collapse of metastable particle packings and open structures in loess deposits. *Engineering Geology* 48(1-2): 101-115.
- Coop MR & Willson SM (2003). Behavior of hydrocarbon reservoir sands and sandstones. *J. Geotech. Geoenviron. Eng.* 129(11): 1010-1019.
- İşçi S, Güner FS, Ece ÖI, Güngör N (2005). Investigation of rheological and colloidal properties of bentonitic clay dispersion in the presence of a cationic surfactant. *Prog. Org. Coat.* 54: 28-33.
- Hamza MA & Anderson WK (2005). Soil compaction in cropping systems—A review of the nature, causes and possible solutions. *Soil Till. Research* 82(2): 121-145.
- Lee SY, Cho WJ, Hahn PS, Lee M, Lee YB, Kim KJ. (2005). Microstructural changes of reference montmorillonites by cationic surfactants. *Applied Clay Sci.* 30: 174-180.
- Moo-Young HK & Zimmie TF (1996). Geotechnical properties of paper mill sludge for use in landfill covers. *J. Geotech. Eng.* 122(9): 768-775.
- NSAC (1999), Chinese Standard of Soil Test, GB/T 50123-1999, China Railroad Press, Beijing, P.R. China.
- Olf W de & Feijtel T (1998). Terrestrial risk assessment for linear alkyl benzene sulophate (LAS) in sludge-amended soils. *Chemosphere* 36: 1319-1343.
- Rao PH & He M. (2006). Adsorption of anionic and nonionic surfactant mixtures from synthetic detergents on soils. *Chemosphere* 63: 1214-1221.
- Sanchez-Martin MJ, Rodriguez-Cruz MS, Andrades MS, Sanchez-Camazano M (2006). Efficiency of different clay minerals modified with a cationic surfactant in the adsorption of pesticides: influence of clay type and pesticide hydrophobicity. *Applied Clay Sci.* 31: 216-228.
- Shen Z, Zhao ZG, Wang GT (2004). *Colloid and Surface Chemistry*, 3rd Ed., Chemistry Industry Press, Beijing, P.R. China (in Chinese).
- Wehling TM & Boulanger RW, Arulnathan R, Harder LF, Jr, Driller MW (2003). Nonlinear dynamic properties of a fibrous organic soil. *J. Geotech. Geoenviron. Eng.* 129(10): 929-939.
- Ying GG (2006). Fate, Behavior and effects of surfactants and their degradation products in the environment. *Environ. Intern.* 32: 417-431.

EDTA-ENHANCED ELECTROKINETIC EXTRACTION OF CADMIUM FROM A NATURAL CLAY OF HIGH BUFFER CAPACITY

Ying-Ying GU¹, Albert T. YEUNG² and Hong-Jiang LI³

ABSTRACT: Electrokinetic extraction of contaminants from soils is a promising *in-situ* remediation technology. During the process, protons generated at the anode enhance the dissolution of metals into the solution phase. However, development of the low pH environment by the process alone is often difficult for natural soils of high buffer capacities. Enhancement agents are thus being used to promote desorption of heavy metals from soil particle surfaces. In this study, EDTA was used to remove cadmium from a natural clay of high buffer capacity from Shanghai, China. Batch experiments and an electrokinetic extraction experiment were conducted to investigate the effectiveness of EDTA in extracting cadmium from the soil. The results of batch tests indicate that it is practically very difficult to solubilize the cadmium sorbed on soil particle surfaces when the soil pH is above 7.0 without enhancement. With the addition of EDTA, more than 90% of the sorbed cadmium can be dissolved into solution in the pH range of 2.0-11.0. The results of the electrokinetic experiment indicate that the spiked cadmium was transported towards the anode when the final soil pH was increased to 7.8 at the anode and 11 at the cathode. However, a significant amount of cadmium was accumulated in a narrow zone near the anode after 20 hours of electrokinetic treatment.

KEYWORDS: electrokinetic extraction, cadmium contamination, natural clay, buffer capacity, EDTA

INTRODUCTION

Heavy metal contamination of soil is a worldwide environmental problem, posing great threats to public health and the environment. Cadmium is a toxic heavy metal in the environment due to its high water solubility and its ability to cause the *itai-itai* disease (Nogawa and Kido 1993). In Shanghai, China, the crop, paddy and natural soils in many sites are contaminated by cadmium (Yao et al. 2005; Shen et al. 2006).

Electrokinetic extraction is a promising *in-situ* remediation technology for metal-contaminated soils of low hydraulic conductivity because of its high removal efficiency when the environmental conditions are favorable (Stichnothe et al. 1996; Yeung et al. 1996; Yeung 2006a, 2009). It has been experimentally proven to be effective in removing heavy metals from Georgia kaolinite of low buffer capacity by many researchers. However, the removal efficiency is low in natural soils of high buffer capacities, where the generation a low pH environment in the soil by the process alone is difficult. Enhancement agents are thus essential to enhance the

contaminant extraction process in these soils.

In this study, ethylenediaminetetraacetic acid (EDTA) was selected to be the enhancement agent to remove cadmium from a natural clay of high buffer capacity from Shanghai, China. Batch desorption tests and an electrokinetic extraction experiment were performed to evaluate the efficiency of EDTA in extracting cadmium from the soil.

MATERIALS AND METHODS

Soil

The soil used in this study was collected from Shanghai, China. The soil was air-dried, pulverized, passed through a 2-mm sieve, homogenized, and saved for later use. The soil is classified as CL according to the Unified Soil Classification System. The pH of the soil (mass:volume 1:1) is 8.3. The organic content and electrical conductivity of the soil are 0.18% and 0.339 dS/cm, respectively. The background concentration

¹ Research Assistant, Department of Civil Engineering, University of Hong Kong, Pokfulam Road, Hong Kong Special Administrative Region, China. Email: yeungat@hku.hk

² Associate Professor, Department of Civil Engineering, University of Hong Kong, Pokfulam Road, Hong Kong Special Administrative Region, China. Email: guyhjlee@hku.hk

³ Engineer, ShenZhen Environment Project Service Center, Block 5, No. 50, Street One, Honggui Road, Shenzhen 518008, Guangdong Province, China. Email: hongjianglee@yahoo.com.cn

of cadmium in the soil is negligible relative to the high cadmium concentration spiked into the soil in this study. Detailed discussion of the soil properties are given by Gu et al. (2009).

Buffer Capacity of the Soil

The pH-dependent buffer capacity of the soil was determined using the technique of potentiometric titration developed by Yeung et al. (1996), and Yeung and Hsu (2005). In this experiment, 1.5 g of dry soil and 30 mL of deionized water were placed in each centrifuge tube to prepare a soil mixture. The soil mixtures were thoroughly mixed for 24 hours using a wrist action shaker at 25°C. An accurately measured quantity of 1 M H₂SO₄ or 1 M NaOH was then added to each soil-water mixture in duplicates. The mixtures were shaken again for another 24 hours for equilibration and the pH of each duplicate mixture was measured to ensure reproducibility of results for the determination of the buffer capacity of the soil.

Desorption Characteristics

Desorption edge experiments were conducted using the method described by Torrens et al. (1998). Firstly, 10 mL of 0.5 mM Cd(NO₃)₂ solution was added to 1 g of air-dried soil to prepare each soil mixture and the mixtures were shaken for 24 hours. The soil mixtures were centrifuged. The cadmium concentration in the supernatant was measured using a Perkin Elmer Analyst 300 flame atomic absorption spectrometer to determine the total cadmium sorbed on soil particle surfaces. The supernatant was then replaced by 10 mL of EDTA solution of different concentrations. A series of control tests were also conducted using 10 mL of deionized water as the desorption solution. The pH of the mixture solution was adjusted to pre-determined values by the adding 1 M NaOH or 1 M HNO₃. The soil mixtures were shaken for 24 hours and then centrifuged. The final pH levels and cadmium concentrations of the supernatants were measured in duplicate specimens.

Electrokinetic Extraction of Cadmium

Experimental setup

The experimental apparatus was modified from that of Yeung et al. (1997) to better simulate field conditions. It includes an electrokinetic cell, hollow graphite electrodes, electroosmotic flow volume and gas volume measurement devices, a dc power supply, and current and voltage measurement devices. The cell is 50×50 mm in cross-section and made of plexiglass. Six porous graphite tubes were inserted at the ends of the cell in two rows separated by a distance of 120 mm to serve as

power electrodes as shown in Fig. 1. The porous graphite tubes were warped by a stainless steel mesh to prevent intrusion of soil particles into the hollow electrodes, as the electrodes were also used to add enhancement agents to the soil and collect gases generated by the process. Another 6 graphite tubes were inserted into the soil as passive electrodes for voltage distribution measurements. Six burettes were connected to the power electrodes for gas volume measurements. The fluid levels at the anode and the cathode were kept at the same level to eliminate any hydraulic gradient.

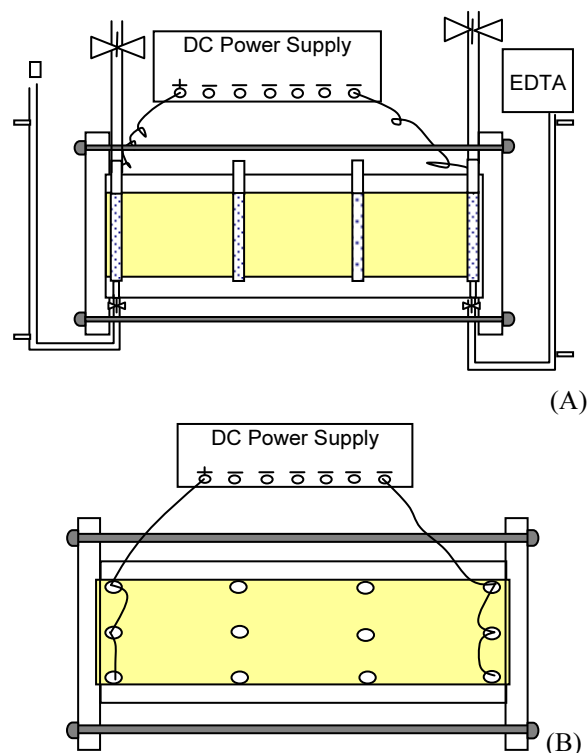


Fig. 1 Experimental setup for electrokinetic extraction: (A) Elevation; and (B) Plan

Soil specimen preparation

Approximately 315 mL of 3.0 mM Cd solution was added to 440 g of air-dried soil to prepare a contaminated slurry specimen. The soil slurry was thoroughly mixed and allowed to equilibrate for 48 hours. It was then loaded into a consolidation cell consisting of a rectangular Lucite specimen cell encapsulated by a base plate and a collar. The specimen was consolidated using a unconfined compression apparatus as shown in Fig. 2. The final porosity of the specimen after consolidation was approximately 0.5, a typical value in natural silt and clayey soil (Domenico and Schwartz 1990).

Electrokinetic extraction

After consolidation, the specimen was dismantled from the consolidation cell and assembled in the electrokinetic cell shown in Fig. 1. The volume measurement

tubes were connected to the power electrodes, the reservoirs were filled with 100 mM EDTA solution, and the valves at the top of the burettes were closed to collect the gases generated. The electrokinetic extraction experiment was conducted by applying a constant dc potential of 22 V across the soil specimen for 20 hours continuously. During the electrokinetic experiment, voltage distribution along the specimen, current passing through the specimen, and fluid levels were monitored as a function of time.

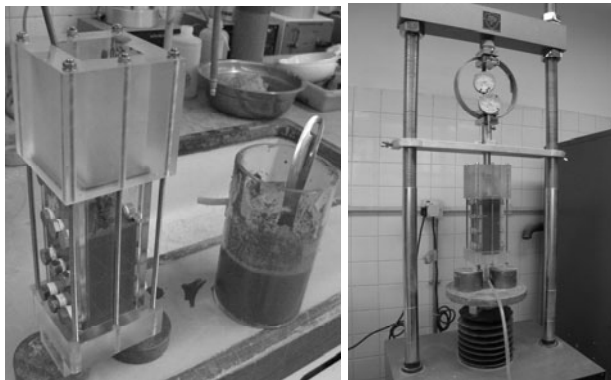


Fig. 2 Soil slurry preparation and consolidation

Chemical analyses of the specimen

After the extraction process, the dc power source was removed and the Lucite electrokinetic cell was dismantled from the setup. The soil specimen was removed from the Lucite electrokinetic cell and sliced into 6 2-cm thick sections along its longitudinal axis. The soil pH and Cd concentration in each section of the soil specimen were measured in duplicate. The measurement methods follow those reported by Yeung et al. (1996).

A control soil specimen was cut into 8 1.5-cm thick sections along its longitudinal axis after consolidation. Water content, soil pH, and cadmium concentration of the consolidated soil were also measured to establish the viability of the specimen preparation procedure and the initial conditions of the specimen.

RESULTS AND DISCUSSION

Acid/base Buffer Capacity

The acid/base buffer capacity of the soil as a function of pH is presented in Fig. 3. The soil used in this study has a very high buffer capacity compared to many other soils such as Georgia kaolinite and Milwhite kaolinite (Hsu 1997). A total volume of 700 μL of 1 M H_2SO_4 is required to lower the pH level of the soil suspension from 8.3 to 5.5. Therefore, it is practically very difficult to lower the soil pH to below 5.5 in practice, an environment essential to solubilize the sorbed cadmium into the pore fluid for removal in this soil without any enhancement agent as shown in Fig. 4.

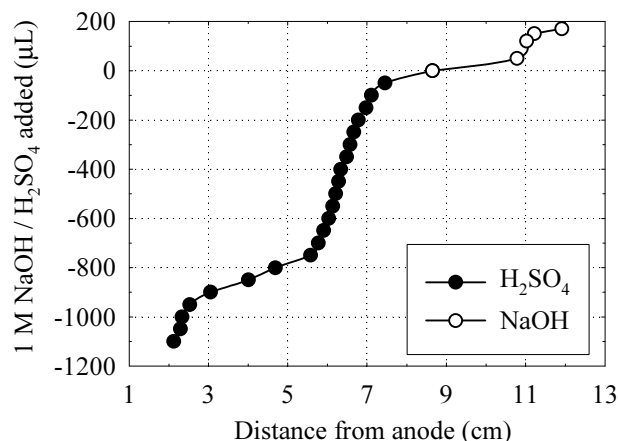


Fig. 3 Acid-base titration curve of soil after 24 hours of contact time

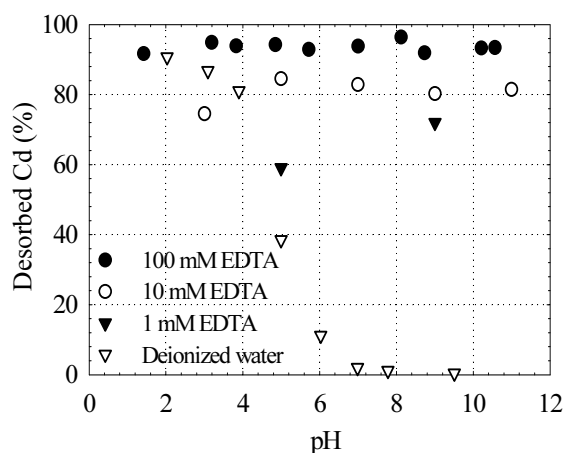


Fig. 4 Desorption edge curves of the soil

Batch desorption Tests of Cadmium with EDTA

Desorption tests of cadmium with desorption solutions of different EDTA concentrations in the pH range of 2.0-11.0 were performed to evaluate the cadmium desorption characteristics of the clay at different pH levels. The desorption edge curves of the soil using EDTA solutions and deionized water are presented in Fig. 4. It should be noted that nearly all the cadmium was sorbed on soil particle surfaces initially after the sorption process under a slightly alkaline natural environment before adjustment of soil pH.

The proportion of cadmium desorbed from the soil using deionized water decreases sharply with increase in pH. For the pH range of 2.0 to 4.0, more than 80% of cadmium sorbed on soil particle surfaces is solubilized by deionized water. However, when the soil pH is higher than 4.0, the proportion of desorbed cadmium decreases almost linearly with increase in pH. Cadmium on soil particle surfaces cannot be desorbed by deionized water at all when soil pH is above 7.0.

It can be observed that the EDTA solution changes the cadmium sorption characteristics of the soil drastically.

The desorption of cadmium is primarily due to the formation of water-soluble strongly negatively charged 1:1 complexes. At all pH levels, EDTA is very efficient in solubilizing cadmium from soil particle surfaces. The proportion of desorbed cadmium increases with concentration of EDTA solution. When 1 mM of EDTA was added, 60 to 70% of cadmium in the sorbed phase was desorbed at pH levels of 5.0 to 9.0. The proportion was increased to 75 to 85% at pH levels of 3.0 to 11.0 when 10 mM EDTA was used. It was further increased to more than 90% when the EDTA concentration was increased to 100 mM.

The results obtained from batch desorption tests establish the viability of enhanced electrokinetic extraction of cadmium from soils of high buffer capacities. The results of desorption tests using deionized water indicate that less than 20% of the sorbed cadmium can be solubilized when the soil pH is higher than 5.5 without enhancement. As the soil has a high buffer capacity, the removal efficiency of cadmium by electrokinetic extraction alone may be unacceptably low. The addition of EDTA greatly enhances the desorption of cadmium from the soil in a wide range of pH levels, making the contaminant mobile for electrokinetic extraction. Therefore, EDTA may be an effective enhancement agent for cadmium-contaminated soil of high buffer capacity during electrokinetic extraction.

Electrokinetic Extraction of Cadmium

Soil specimen preparation

The water content, soil pH, and initial cadmium concentration in the control soil specimen were measured after consolidation of soil slurry to examine the uniformity of the soil specimen so prepared. The results are presented in Figs. 5, 6, and 7.

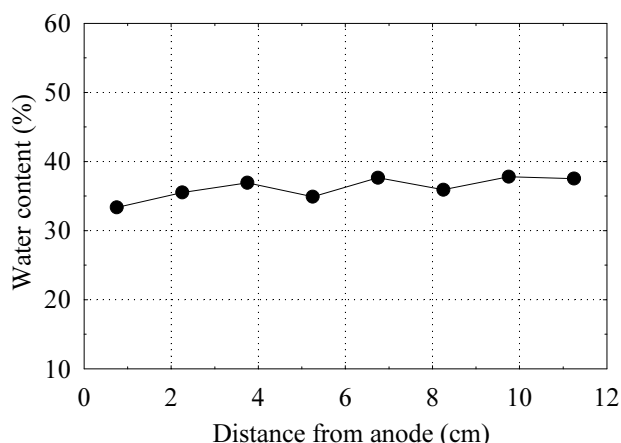


Fig. 5 Water content distribution in the specimen

The water content of the soil specimen was in a narrow range of 33 to 38% throughout the specimen as shown in Fig. 5. It can be determined from the water content and void ratio of the specimen that the soil

specimen was fully saturated. A uniform initial pH of approximately 7.6 was measured throughout the soil specimen as shown in Fig. 6. The initial concentration of cadmium in the specimen extracted using 8.0 M HNO₃ was in the range of 225 to 244 mg/kg as shown in Fig. 7. It is evident from Figs. 5 to 7 that the initial conditions of the soil specimen prepared were quite homogeneous.

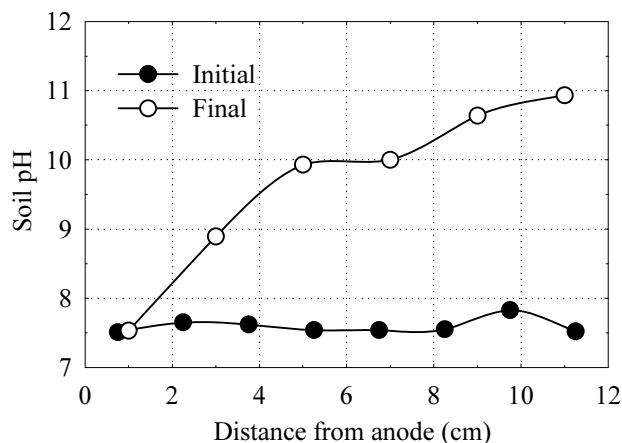


Fig. 6 Soil pH distributions

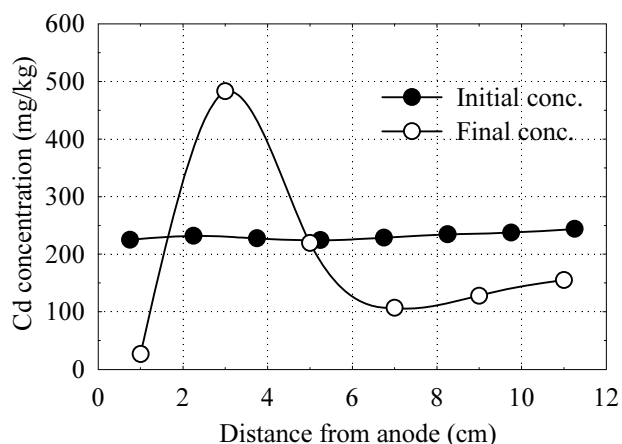


Fig. 7 Cd concentration distributions

Electrokinetic extraction

The final soil pH distribution after electrokinetic extraction is also shown in Fig. 6 with the initial soil pH distribution. It can be observed that the pH level in most parts of the soil specimen rose. While the soil pH at the anode has not changed significantly, the soil pH at the cathode has increased to approximately 11. There may be two reasons for the phenomenon observed: (1) the EDTA solution added to the specimen was alkaline, with pH higher than 8.0; and (2) the soil has a very high buffer capacity, preventing acidification of soil by the hydrogen ions generated at the anode. In accordance with the results of desorption tests of cadmium shown in Fig. 4, almost none of the cadmium sorbed on soil particle surfaces can be solubilized and removed from the soil by electrokinetic extraction when the final soil pH is above 7.5 without the use of enhancement agents.

Initial concentration of cadmium in the soil specimen was 231 mg/kg on average. After completion of the 20-hour extraction process, cadmium concentration was measured as a function of space. The final cadmium concentration distribution after the electrokinetic extraction is presented in Fig. 7 together with the initial cadmium concentration distribution in the control soil specimen. It can be observed that the injection of 100 mM EDTA into the specimen could effectively solubilize the cadmium sorbed on soil particle surfaces. The cadmium concentration in approximately 75% of the soil specimen was significantly reduced as shown in Fig. 7. However, only approximately 23% of the initial concentration of cadmium in the specimen was removed from the specimen. A significant amount of Cd initially spiked to the specimen was transported towards the anode and accumulated within a narrow zone near the anode. The Cd concentration in the vicinity of the anode was approximately twice that of the initial concentration. The results are in agreement with those reported by Giannis and Gidarakos (2005), and Yeung and Hsu (2005).

The accumulation of cadmium near the anode in this study may be attributed to the fact that the forward electroosmotic flow hinders the electromigration of negatively charged Cd-EDTA complexes. However, the rate of electromigration of Cd-EDTA complexes is higher than that of the electroosmotic flow. As a result, negatively charged cadmium species were transported towards the anode. As the duration of electrokinetic extraction was only 20 hours, there may not be enough time for cadmium to be extracted from the soil specimen. Higher cadmium removal efficiency may be able to be achieved for longer extraction duration.

During electrokinetic extraction, the variation of electrical current passing through the specimen and the voltage distribution along the specimen were monitored using a data logger as a function of time.

The electrical current was recorded at 15-minute intervals. It fluctuates around a mean value of approximately 8 mA with time as shown in Fig. 8. In contrary to the observation by Yeung (2006b), there is no significant decay of electrical current with time. However, the results are in good agreement with the volume of O₂ produced at the anode. The fluctuation of electrical current may be attributed to the variation of soil resistance caused by electroosmotic flow of pore fluid, electromigration of ions, electrophoresis of fines, and/or formation and bursting of bubbles at the electrodes, etc. under the influence of the imposed dc electric field.

Two rows of passive electrodes were inserted into soil as shown in Fig. 1 to monitor the voltage distribution during the process. Voltage distributions along the centerline of the soil specimen as a function of time are depicted in Fig. 9. It can be observed that the voltage

distribution in the specimen was practically linear throughout the electrokinetic extraction process.

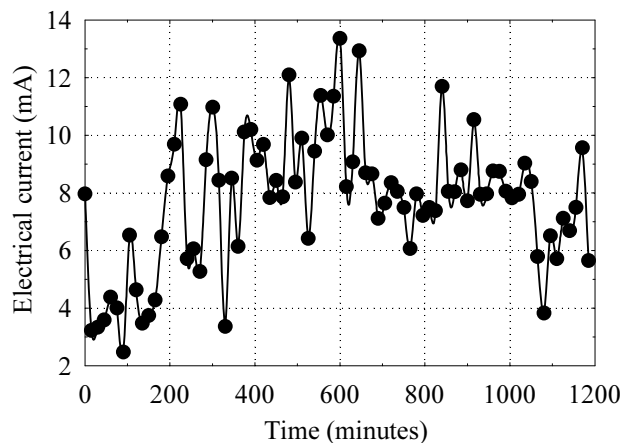


Fig. 8 Variation of electrical current with time

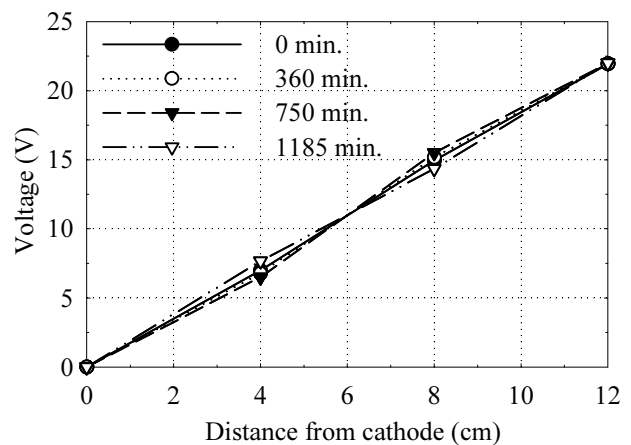


Fig. 9 Voltage distribution in the soil specimen

The electroosmotic inflow rate at the anode and the outflow rate at the cathode during electrokinetic extraction are presented in Fig. 10. It can be observed that the direction of electroosmotic flow during treatment is always forward, i.e., from the anode towards the cathode. The observation is consistent with the soil pH distribution in the specimen (Yeung 2006b). The magnitude of electroosmotic flow rate is relatively steady throughout the process. The coefficient of electroosmotic conductivity is in the range of 1.2×10^{-9} to 2.4×10^{-9} m²/V-s which is within the typical range of soils (Yeung 1994).

According to the Helmholtz-Smoluchowski theory, the electroosmotic flow rate is mainly determined by the zeta potential of soil particle surfaces (Yeung 2006, 2009). The results of our previous study on the effects of enhancement agents on the zeta potential of soil particle surfaces indicate that the zeta potential of soil particle surfaces is not significantly affected by the addition of EDTA and Cd in the pH range of 8 to 11 (Gu et al. 2009). As a result, the electroosmotic flow rate is relatively steady during the electrokinetic extraction process.

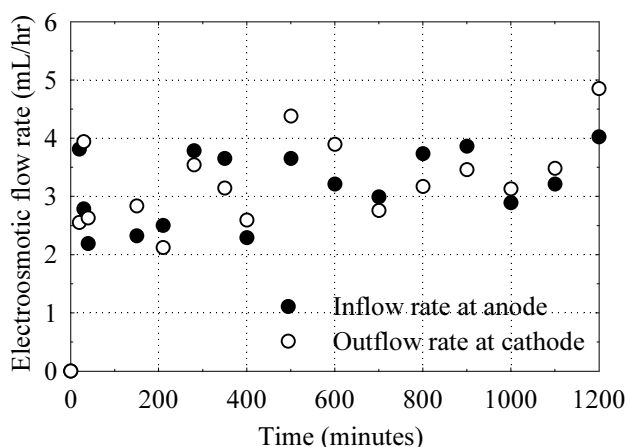


Fig. 10 Electroosmotic flow rates during electrokinetic extraction

The electroosmotic inflow rate at the anode is consistent with the outflow rate at the cathode, indicating that the soil specimen has been kept saturated through the treatment process.

CONCLUSIONS

Several conclusions can be drawn from this experimental study on EDTA-enhanced extraction of cadmium from a natural clay of high buffer capacity.

Desorption of cadmium from the soil without enhancement is pH-dependent. The proportion of Cd desorbed by deionized water decreases dramatically with the increase of pH. However, more than 90% of cadmium can be desorbed from soil particle surfaces with the addition of 100 mM EDTA solution in a wide range of pH levels.

The results of the electrokinetic extraction experiment indicate that cadmium is accumulated to a narrow zone near the anode after remediation process. It may be due to the combined effects of forward electroosmotic flow towards the cathode and electromigration of the negatively charged Cd-EDTA complexes towards the anode.

Soil pH at the anode has not been changed significantly and the pH at the cathode has been increased due to the alkalinity of the EDTA added and the high buffer capacity of the soil.

REFERENCES

Domenico PA & Schwartz FW (1990). Physical and chemical hydrogeology. John Wiley & Sons, New York, New York.

Giannis A & Gidaracos E (2005). Washing enhanced electrokinetic remediation for removal cadmium from real contaminated soil. *Journal of Hazardous*

Materials, 123(1-3):165-175.

Gu Y-Y, Yeung AT, Koenig A, Li H (2009). Effects of chelating agents on zeta potential of cadmium-contaminated natural clay. *Separation Science and Technology*, 44(10):2203-2222.

Hsu CN (1997). Electrokinetic remediation of heavy metal contaminated soils. PhD Thesis, Texas A&M University, College Station, Texas.

Nogawa K & Kido T (1993). Biological monitoring of cadmium exposure in itai-itai disease epidemiology. *International Archives of Occupational and Environmental Health*, 65(Supplement 1):S43-S46.

Shen G, Xie Z, Qian X, Huang L, Guo C, Wang M, Shan Z. (2006). Investigation and analysis of heavy metal accumulation in the soil of vegetable cropland in Shanghai. *Journal of Agro-environmental Science*, 25(z1):37-40 (in Chinese).

Stichnothe H, Czediwoda A, Schönbacher A (1996). Electrokinetic removal of cadmium from fine-grained soil. *Proc., 3rd Int'l. Symposium on Environmental Geotechnology*, San Diego, 780-785.

Torrens JL, Herman DC, Miller-Maier RM (1998). Biosurfactant (rhamnolipid) sorption and the impact on rhamnolipid-facilitated removal of cadmium from various soils under saturated flow conditions. *Envir. Sci. & Technology*, 32(6):776-781.

Yao C, Chen Z, Zhang J, Hou J (2005). Heavy metal pollution assessment of vegetables in Pudong zone of Shanghai. *Journal of Agro-environmental Science*, 24(4):761-765 (in Chinese).

Yeung AT (1994). Electrokinetic flow processes in porous media and their applications. *Advances in Porous Media*. Corapcioglu M.Y., Editor, Elsevier, Amsterdam, the Netherlands, 2;309-395.

Yeung AT (2006a). Contaminant extractability by electrokinetics. *Envir. Engrg. Science*, 23(1):202-224.

Yeung AT (2006b). Fundamental aspects of prolonged electrokinetic flows in kaolinites. *Geomechanics and Geoengineering*, 1(1):13-25.

Yeung AT (2009). Geochemical processes affecting electrochemical remediation. *Electrochemical remediation technologies for polluted soils, sediments and groundwater*. Reddy K.R. and Cameselle C., Editors, John Wiley & Sons, New York, N.Y., in press.

Yeung AT & Hsu CN (2005). Electrokinetic remediation of cadmium-contaminated clay. *Journal of Environmental Engineering*, ASCE. 131(2):298-304.

Yeung AT, Hsu CN, Menon RM (1996). EDTA-enhanced electrokinetic extraction of lead. *Journal of Geotechnical Engineering*, ASCE. 122(8):666-673.

Yeung AT, Scott TB, Gopinath S, Menon RM, Hsu C (1997). Design, fabrication, and assembly of an apparatus for electrokinetic remediation studies. *Geotech. Test. J., ASTM*, 20(2):199-210.



**Applications of Geosynthetics in
Geoenvironmental Engineering**

APPLICATIONS OF GEOGRID REINFORCED SOIL RETAINING WALL WITH WRAP-AROUND FACING IN RAILWAY

Guang-Qing YANG¹, Qiao-Yong ZHOU², Bao-Jian ZHANG³ and Jun-Xia DING⁴

ABSTRACT: The geogrid reinforced soil retaining wall with wrap-around facing on China's railway line was built and monitored during construction and the first 1.5 years after construction. The reinforcement strains were measured using flexible displacement sensors, and the soil stresses were recorded using vibrating-wire load cells. The maximum vertical foundation pressure along the wall's reinforcements occurs at the central point of the reinforcement, gradually decreasing toward the front and back ends of the wall. The measured lateral earth pressure within the reinforced soil wall is non-linear along the height, and the value is less than the active lateral earth pressure. The distribution of tensile strain on the geogrid reinforcements within the upper portion of the wall is at a single peak value, but the distribution of tensile strain along the reinforcements within the lower portion of the wall have double-peak values. The potential failure plane within the wall closely follows the active Rankine Earth Pressure Theory. The results presented in this paper are useful in advancing the understanding of the behavior of reinforced soil walls with wrap-around facing.

KEYWORDS: geosynthetics, wrap-around facing, geogrid, reinforcement soil retaining wall, field test

INTRODUCTION

This paper records our field test of the 12.2-metre-high geogrid reinforced retaining wall with wrap-around facing along the Gan-Long Railway of China. The test examines the vertical foundation stress, lateral earth pressure within the wall, and reinforcement strains. The test data from the beginning of construction through 1.5 years after construction will be analyzed in this paper.

The geogrid reinforced soil retaining wall with wrap-around facing is located along the segment GDK144+100~GDK144+130 of the Gan-Long Railway, south of the Changting County railway station in the Fujian province of China. The reinforced soil retaining wall was designed according to the Code for design of retaining structures on railway subgrade (TB10025-2006 2006). For a photo of the geogrid reinforced soil retaining wall with wrap-around facing, see Fig. 1.

The upper portion of the wall is filled with rammed clay. The 7.5-m length reinforcements, placed horizontally and spaced 0.50 m apart vertically, are high-density polyethylene (HDPE) uniaxial geogrids with tensile-strength values of 65 kN/m (EG65R). The lower portion of the wall is reclaimed gravel soil. The 12.2 m length reinforcements, also placed horizontally and

spaced 0.50 m apart, vertically, are HDPE uniaxial geogrids with tensile-strength values of 130 kN/m (EG130R). The bearing capacity of the slope wash, cohesive soil-supporting ground, is 250 kPa, with a backfill degree of compaction at 93%. Each level of reinforcement will wrap around the closed-grain geotextile gravel bags at the front of the wall. The wall facing, using soil bags wrapped with reinforcements, is environmentally friendly and can be made green by planting grass (Yamamoto and Jin 2008). Furthermore, human labor alone can construct the soil bags without



Fig. 1 Photo of the geogrid reinforced soil retaining wall with wrap-around facing

¹ Professor, School of Civil Engineering, Shijiazhuang Railway Institute, China. Email: gtsyang@163.com

² Lecturer, School of Civil Engineering, Shijiazhuang Railway Institute, China. Email: zhouqy_007@163.com

³ Assistant professor, School of Civil Engineering, Shijiazhuang Railway Institute, China. Email: zbj1911@163.com

⁴ Lecturer, School of Civil Engineering, Shijiazhuang Railway Institute, China. Email: ytgcx@sjzri.edu.cn

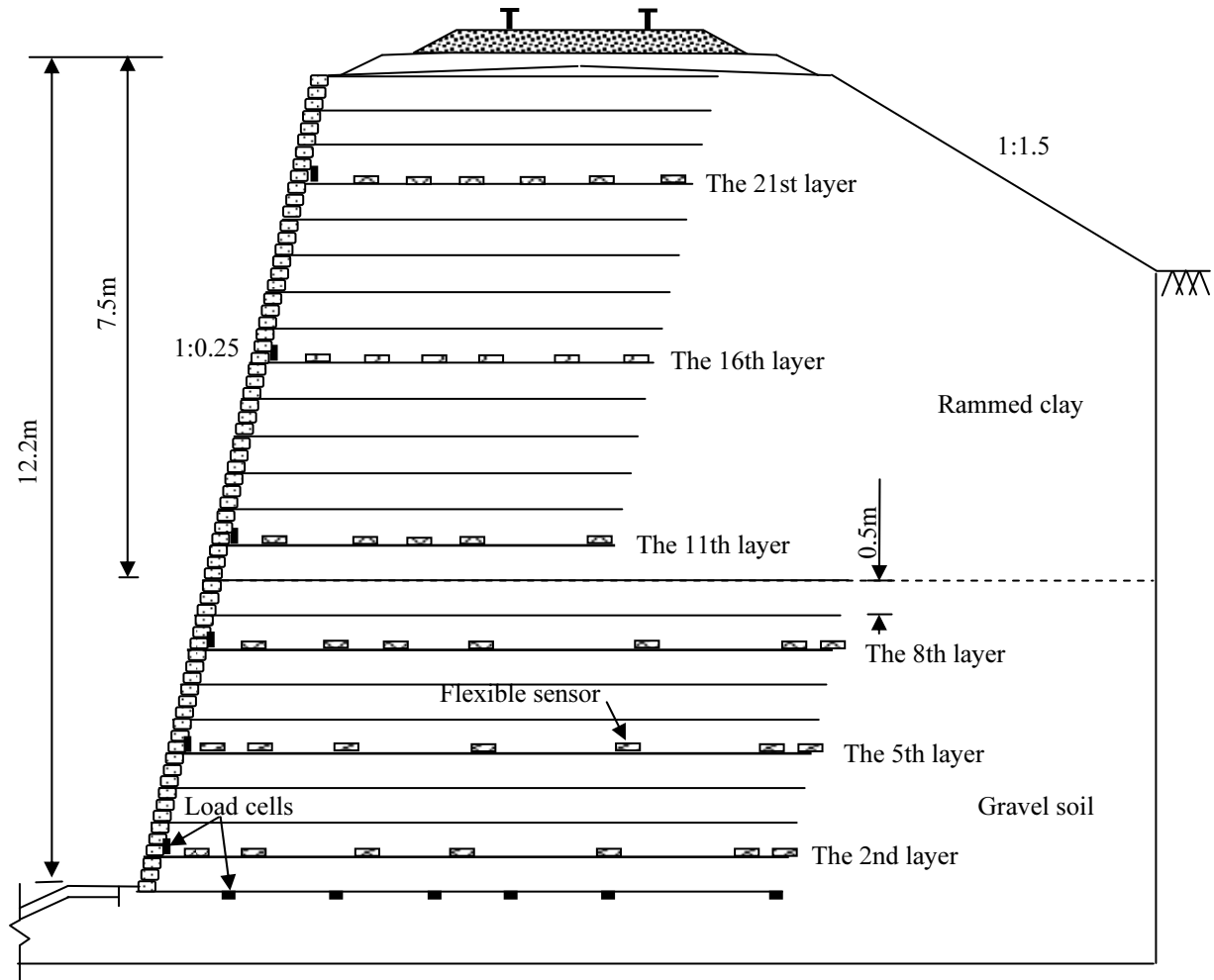


Fig. 2 Cross-sectional arrangement of the instrumental section

Table 1 Arrangement of the measuring points along the testing section

Item	Location	Distance to the wall facing(m)
Flexible displacement sensor	the 2nd layer	0.5, 1.0, 2.0, 4.0, 6.0, 8.5, 11.7
	the 5th layer	0.8, 1.3, 2.3, 5.8, 8.8, 11.7
	the 8th layer	2.0, 3.0, 4.0, 5.0, 8.0, 10.5, 11.7
	the 11th layer	1.7, 3.2, 4.2, 5.2, 6.2, 7.3
	the 16th layer	1.8, 3.3, 4.3, 5.3, 6.3, 7.3
	the 21st layer	1.6, 3.1, 4.1, 5.1, 6.1, 7.3
Vertical load cell	The first layer	1.5, 3.0, 5.0, 6.5, 8.5, 12.0

special equipment. The bags are cheap and easy to acquire.

ARRANGEMENT SCHEME OF MEASURING POINTS

The monitored wall cross section is at GDK144+120. The monitoring devices used and their positions are represented in Fig. 2. The monitoring devices' characteristics and their location along the wall were

selected based on published, monitored case histories (e.g. Benjamim et al. 2007; Tatsuoka et al. 2007).

The geogrid reinforcement strains were measured at six reinforcement levels using the JMDL-2405A inductive flexible displacement sensors. Refer to Table 1 to see the spacing of the monitoring sensors on each reinforcement level. This arrangement makes it possible to determine the strain distribution throughout the reinforcement length as well as the position of maximum tension.

The vertical foundation and lateral stresses were recorded using vibrating-wire load cells. There were six cells at the first reinforcement level, and six placed vertically behind the soil bags. A data-acquisition instrument measured the reinforcement strain values and earth stress.

The test began with the initial construction. After finishing each geogrid reinforcement level, the baseline data from the flexible sensors and load cells were read. Post-construction, readings were conducted once a month.

ANALYSIS OF OBSERVATION RESULTS

Characteristics of Vertical Foundation Stress

Fig. 3 and Fig. 4 show the distribution curves of the vertical foundation pressure along the reinforcement length during construction and at different times after construction.

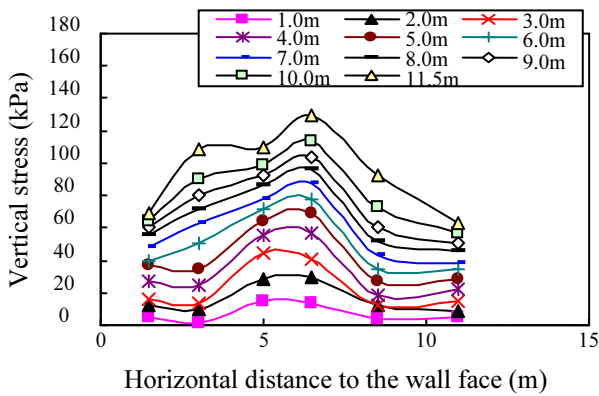


Fig. 3 Distribution of vertical foundation pressure for different heights above the first reinforcement layer during construction

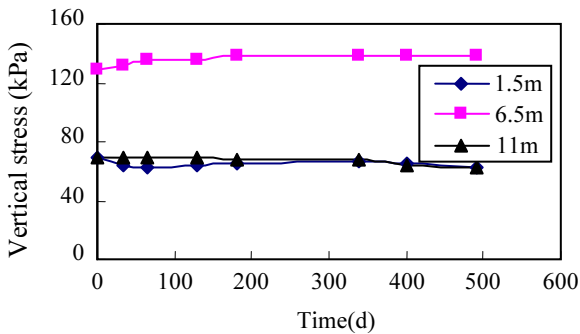


Fig. 4 Distribution of the vertical pressure of different distances to the wall face post-construction

As the wall height increases, the vertical foundation stress gradually increases as well. The distribution of the vertical foundation stress is not identical to the linear distribution used in the current standard (e.g. BS8006 1995; Christopher et al. 1989; TB10025-2006 2006).

The distribution of the vertical foundation stress along the length of the geogrid reinforcement appears non-linear, with the location of the maximum stress value near the middle of the reinforcement and gradually decreasing toward the wall face and the wall's end. The maximum value is larger than the theoretical value of $\sigma = \gamma \cdot h$ (γ indicates the soil unit weight and h denotes the vertical distance to the wall top). Theoretically, the largest vertical earth pressure should occur close to the wall, while the minimum value should appear at the end of the geogrid reinforcement. But in practical engineering, the vertical foundation pressure closest to the wall facing will decrease.

Post-construction, the ground appears to settle because of the hefty weight of the high, reinforced soil-retaining wall, and the soil-arching effect at the leading and tail ends of the reinforcement. All these factors can lead to a decrease in the vertical foundation pressure and an increase near the central part of reinforcement.

Characteristics of Lateral Earth Pressure

Fig. 5 represents the test results of lateral earth pressure upon the retaining wall.

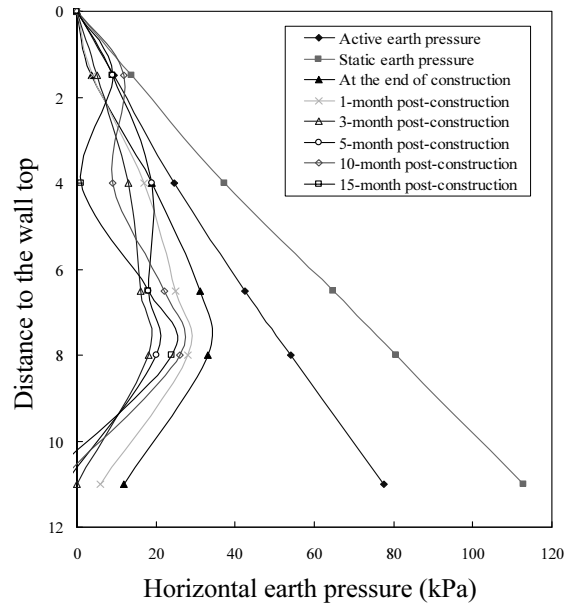
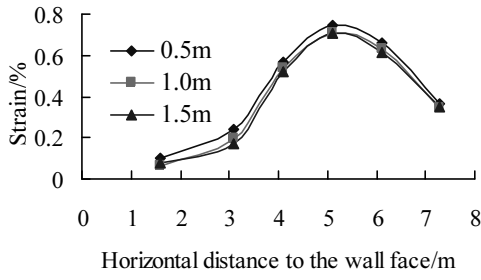


Fig. 5 Lateral earth pressure along wall height

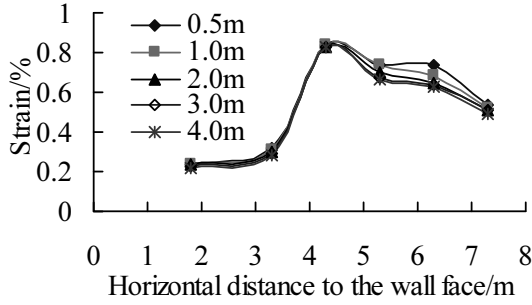
The distribution of lateral earth pressure is nonlinear along the wall height. Below the central part of the wall, the lateral earth pressure decreases gradually (Miyata and Bathurst 2007; Bathurst et al. 2008) and nears zero at the foot of the wall.

After construction, the lateral earth pressure will decrease over time. This is mainly because the horizontal deformation will gradually increase, reducing the vertical stress near the wall caused by foundation settlement.

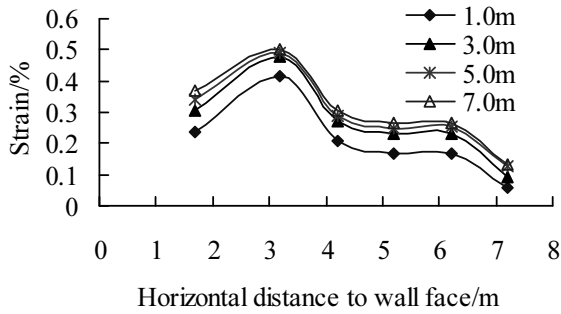
(a) The 21st layer



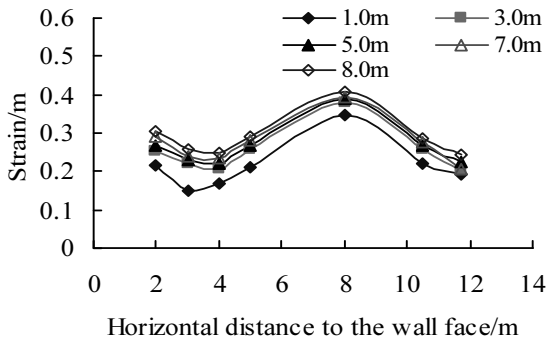
(b) The 16th layer



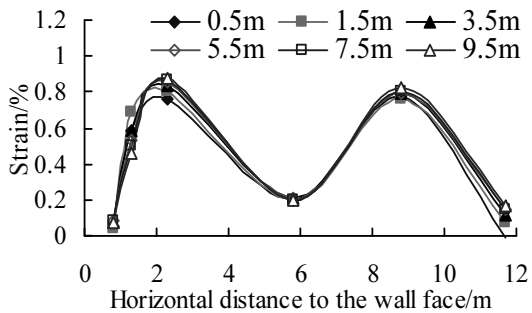
(c) The 11th layer



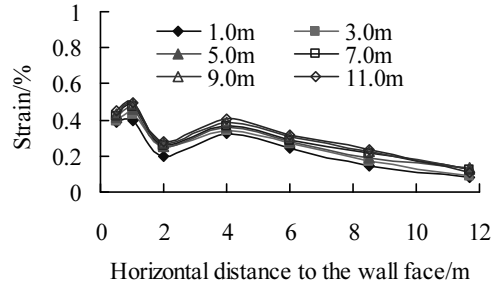
(d) The 8th layer



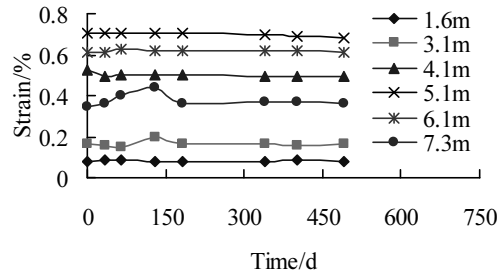
(e) The 5th layer



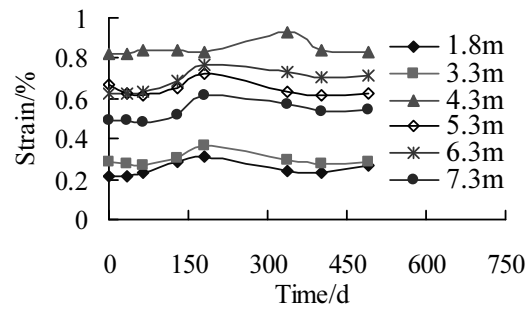
(f) The 2nd layer



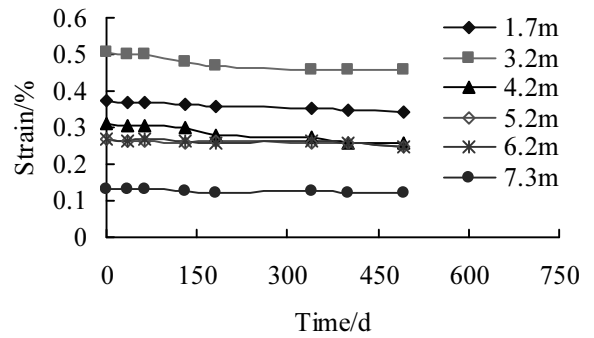
(g) The 21st layer



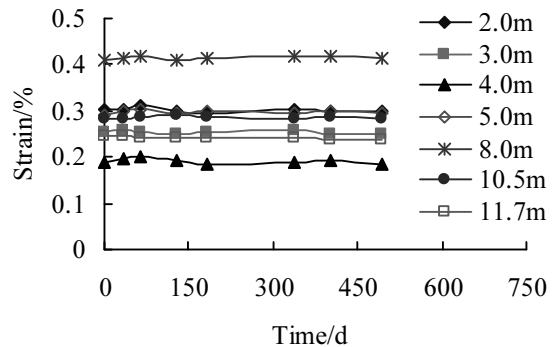
(h) The 16th layer



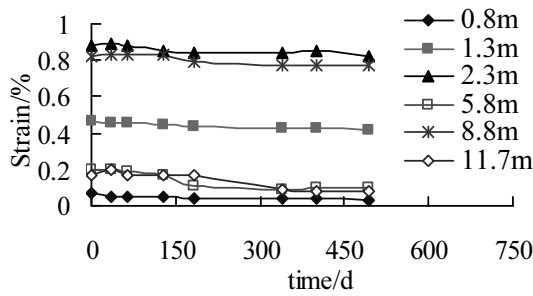
(i) The 11th layer



(j) The 8th layer



(k) The 5th layer



(l) The 2nd layer

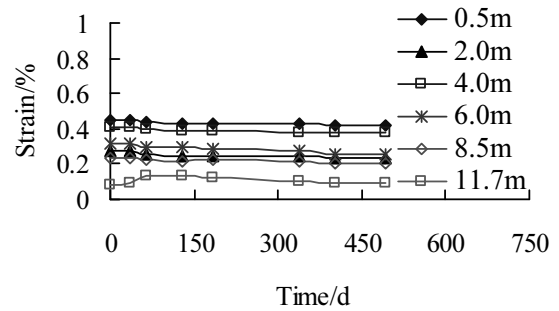


Fig. 6 Strain of the various geogrid layers

(a)-(f) The strain of different heights above the testing reinforcement layer during construction; (g)-(l) The strain of different distances to the wall face with time passage post-construction.

Characteristics of Geogrid Reinforcement Strain

Fig. 6 shows the strain curve of the reinforcements on different layers as the wall height increases and time passes post-construction.

With an increase of wall height, the reinforcement strain of each layer will also increase. The strain range of the tested, short reinforcements in the upper clay backfill is 0.10% to 0.97%. The stress-strain relationship of the geogrid should consider the strain rate and the confine pressure. The range of actual geogrid loads is 1.74 kN/m to 8.72 kN/m, which is only 2.5 % to 12.5 % of the ultimate tensile strength (69.17 kN/m). The measured strain along the geogrid reinforcement in gravel-fill materials within the reinforced soil ranged between 0.16% and 0.88%. The range of actual loads in the geogrid is from 5.23 kN/m to 17.41kN/m, which is only 3.8% to 12.4% of the ultimate tensile strength (139.83 kN/m). Therefore, the actual forces experienced within the two types of geogrid were far less than the design value. Creeping deformation under this low tension is very small. This conclusion can be confirmed by observing the curves showing stress curves on each reinforcement layer as time passes post construction.

The reinforcement strain in the upper wall shows a single-peak appearance. The peak strain is farther away from the facing slab at the top of the wall, and gradually gets closer to the slab with increasing distance to the wall top. The reinforcement strain of the lower wall portion shows the emergence of a double peak. The first-strain peak value near the facing slab may be due to lateral earth pressure, while the second one is likely the result of the weight of the fill materials, frictional resistance between fill materials, and reinforcement.

The reinforcement strain within the upper portion of the wall increases appreciably while the measured reinforcement strain within the lower portion of the wall remains constant with time after construction. Quite possibly, the major movement of the wall occurs during construction.

Characteristics of the Potential Slide Surface

Connecting the largest testing reinforcement strain location, we can analyze the location of the potential slide surface from Fig. 7.

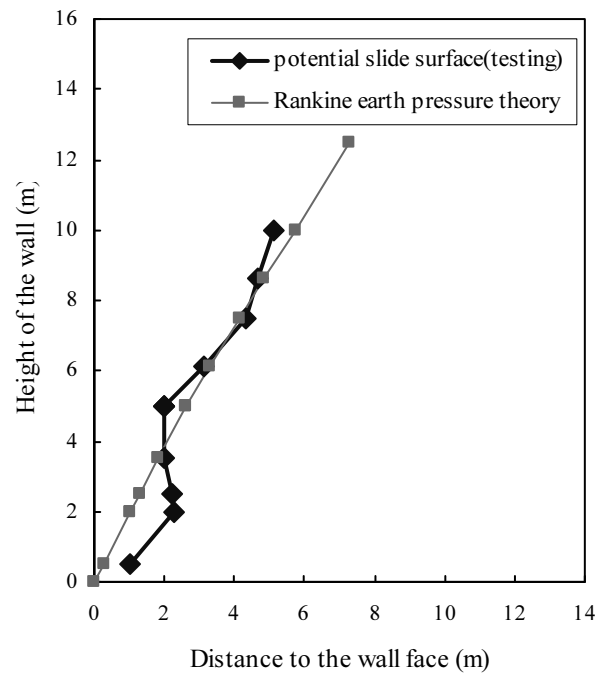


Fig. 7 Potential slide surface of the wall

As far as the whole wall height is concerned, the tested potential slide surface presents a curve distribution. The shape of the wall is relatively close to the Rankine Earth Pressure Theory.

CONCLUSIONS

Significant observational data has been achieved through the field test of the geogrid reinforced soil retaining wall with wrap-around facing both during and

after construction. The characteristics of the structure and of this data are described in detail throughout this paper. From the data, we can draw the following conclusions:

(1) The maximum vertical foundation pressure along the reinforcement occurs at the central part of the reinforcement, and gradually decreases toward the wall face and the back end of the reinforcement. Post-construction, the vertical foundation stress near the wall will decrease, and will increase near the reinforcement central portion.

(2) The measured lateral earth pressure is less than the active earth pressure value. The lateral earth pressure appears to demonstrate a decreasing trend with the passage of time after construction.

(3) Strain within the upper reinforcement shows a single-peak distribution, while the distribution of measured strain within the lower reinforcement has a double peak.

(4) The potential slide surface within the geogrid-reinforced soil retaining wall is relatively close to the Rankine Earth Pressure Theory.

REFERENCES

- Iizuka A, Kawai K, Kim ER, Hirata M (2004). Modeling of the confining effect due to the geosynthetic wrapping of compacted soil specimens, *Geotextiles and Geomembranes*, 22(5): 329-358
- Bathurst RJ, Miyata Y, Nernheim A, Allen AM (2008). Refinement of K-stiffness Method for geosynthetic-reinforced soil walls, *Geosynthetics International*, 15(4): 269-295
- Benjamin CVS, Bueno BS, Zornberg JG (2007). Field monitoring evaluation of geotextile-reinforced soil-retaining walls, *Geosynthetics International*, 14(2): 100-118
- BS8006 (1995). Code of Practice for strengthened/reinforced soils and other fillings, British Standards Institute, London, England
- Christopher BR, Gill SA, et al. (1989). Reinforced soil structures Vol.1.Design and construction guidelines and reinforced soil Vol.2.Summary of research and systems information, Federal Highway Administration. FHWA-RD-89-043, Washington, USA
- Miyata Y & Bathurst RJ (2007). Development of the K-stiffness method for geosynthetic reinforced soil walls constructed with c-soils, *Canadian Geotechnical Journal*, 44: 1391-1416
- Tatsuoka F, Tateyama M, Moltri Y, Matsushima K (2007). Remedial treatment of soil structure using geosynthetic-reinforcing technology, *Geotextiles and Geomembranes*, 25(4-5): 204-220
- TB10025-2006 (2006). Code for design on retaining engineering structures of railway subgrade, Beijing, China (in Chinese)
- Wetzel RA, Buttry KE, McCullough ES (1995). Preliminary results from instrumented segmental retaining wall, *Proceedings of Geosynthetics'95*, Nashville, USA: 133-146.
- Won MS & Kim YS (2007). Internal deformation behavior of geosynthetic-reinforced soil walls, *Geotextiles and Geomembranes*, 25(1):10-22.

TEST STUDY ON ENGINEERING PROPERTIES OF GABION STRUCTURES

Guo-Lin YANG¹, Xiang-Jing HUANG² and Yu-Liang LIN³

ABSTRACT: In order to study mechanical characteristic of gabion meshes, engineering properties of reinforced gabion retaining wall and green reinforced gabion retaining wall, tests including air tensile tests of gabion meshes, fatigue and aseismic tests on gabion structures were carried out. The main tensile mechanical indexes of gabion meshes, fatigue property and seismic behavior of these two gabion structures were obtained. Test results showed: Air tensile curves of gabion mesh showed a zigzag shape; Main factors influencing the dynamic deformation behavior of gabion structures were amplitude of dynamic load, vibration times and so on, and vibration frequency had no significant influence; In fatigue tests, the maximum accumulated lateral deformation occurred in the third layer for reinforced gabion retaining wall, and the fifth layer for green reinforced gabion retaining wall; Accumulated deformation ratios of gabion structures were less than 1% under fatigue load; Both of these two gabion structures were excellent aseismic structures, and they could bear earthquake action with seismic intensity of eight.

KEYWORDS: engineering property, air tensile test, fatigue test, seismic test, gabion mesh, gabion structure

INTRODUCTION

Gabion mesh, of double twisted hexagonal shape, is a new reinforcement in China. Gabion structures mainly include reinforced gabion structures, green reinforced gabion structures and composite structures. At present, gabion structures, as new reinforced earth structures, have been used in west line of Xiangtan to Hengyang highway in Hunan province. Although some researches have been made on dynamic behavior and seismic property of reinforced earth retaining wall (Yang et al. 2003; Ling et al. 2005; Liu 2008), there were very few researches on gabion structures. Therefore, researches on gabion structures became necessary.

Based on reinforced gabion retaining wall and green reinforced gabion retaining wall in Xiangtan to Hengyang highway, air tensile tests of gabion meshes, fatigue tests and aseismic tests on gabion structures were carried out. During the tests, several influencing factors could be taken into consideration, and fatigue and seismic behaviors of gabion structures were studied effectively. Main tensile mechanical indexes of gabion meshes were obtained successfully. Test results were not only of great significance for construction of gabion structures, but also provided a reference for gabion structures research.

AIR TENSILE TESTS ON GABION MESHES

Experimental

2.2 mm gabion mesh and 2.7 mm gabion mesh were chosen. Five parallel air tensile tests were carried out for each gabion mesh. To limit lateral deformation of gabion meshes, special clamps were adopted (as showed in Fig.1). Every mesh was orderly and tightly fixed in every hole of two same clamps by bolt. During the test, one end of the specimen was fixed, and the other end was drawn by MTS actuator at a uniform speed of about 20 mm/min, which could meet the provision about wide strip tensile test of "Test Methods of Geosynthetics for Highway Engineering (JTG E50-2006)", as showed in Fig.2. Tensile load could distribute on gabion meshes uniformly.

Test Results and Analysis

Air tensile test results are shown in Table 1. The typical curve between tension of unit width (T/L) and unit elongation is showed in Fig.3. Test results show: Tensile strength of 2.7 mm gabion meshes is about 1.44 times as much as that of 2.2 mm gabion meshes; Air tensile curves of both 2.2 mm gabion mesh and 2.7 mm gabion mesh show a zigzag shape.

1 Professor, School of Civil Engineering and Architecture, Central South University, China. Email: yangguolin6301@163.com

2 Senior Engineer, Hunan Provincial Communications Planning, Surveying and Design Institute. Email: hncshxj@163.com

3 Ph.D Student, School of Civil Engineering and Architecture, Central South University, China. Email: linyuliang11@yahoo.com.cn

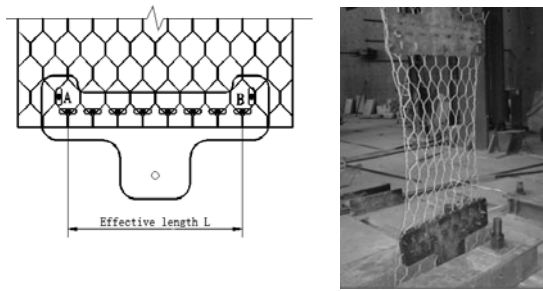


Fig. 1 Clamping system **Fig. 2** Tensile device



Fig. 3 Typical air tensile curve of gabion mesh

FATIGUE TESTS ON GABION STRUCTURES

Nowadays, the long-term action of vertical traffic load on subgrade structure is attracting more and more attention, especially in high-speed railway. Although based on the project in highway, if the simulated test load is selected based on train load, the test results can not only guide the construction of gabion structures and guarantee the safety of project, but also provide an important basis for the question whether the gabion structures can be used in railway system or not.

Experiment

Special test box was made. The dimension of the box was 3 m×0.86 m×2 m (3 m in length, 0.86 m in width and 2 m in height). Both of reinforced gabion retaining wall and green reinforced gabion retaining wall were filled by red sandstone with the compactness of 95%. The main physical and mechanical characteristics of red sandstone were shown in Table 2. The filling ratio of gabion cage of reinforced gabion retaining wall was about 70%. Gabion structures were constructed at a proportion of 1:2.5 compared with that in construction site. There were five layers in total, and each layer was 0.4 m in height. The diameters of reinforced gabion component and green reinforced gabion component were both 2.7 mm. During the tests, lateral and vertical deformation was measured by dial indicators. As showed in Fig.4 and Fig.5.

MTS servo-actuator was used to simulate trainload. The magnitude of trainload and speed of the train could

be reflected by the output of the amplitude and frequency of input load. For reinforced gabion retaining wall, frequencies (HZ) of 2, 4, 6, 8 and 10 were imposed, and the amplitudes of dynamic load (kPa) were 40~80, 50~100 and 60~120 respectively. For green reinforced gabion retaining wall, frequencies (HZ) were 4, 6, 8 and 10, and the amplitudes (kPa) were 30~60, 40~80, 50~100 and 60~120 respectively. The input dynamic load coincided with the tested dynamic loads in Datong-Qinhuangdao line, Chengdu-Kunming line and Baoji-Chengdu line, as showed in Table 3. Table 4 showed loading rules of gabion structures in fatigue tests.

Test Results and Analysis

Curves of Accumulated lateral deformation and vertical deformation (settlement) changing with vibration times of gabion structures are showed in Fig.6 and Fig.7 respectively.

According to the tests, the following conclusions can be drawn:

(1) The main factors influencing the dynamic deformation behavior of gabion structures are amplitude of dynamic load, vibration times, and so on. Vibration frequency has no significant influence. In addition, the filling ratio of gabion cage influences deformation behavior of reinforced gabion retaining wall.

(2) With the increase of dynamic load amplitude, more vibration times are needed for deformation to achieve stability and the deformation value increases. The dynamic deformation increases during the proceeding of vibration, first rapidly, and then slowly.

(3) Under the same amplitude and the times of vibration, vertical deformation is much greater than lateral deformation of the same layer.

(4) After 2 million vibrations, the maximum accumulated lateral deformation occurs in the third layer for reinforced gabion retaining wall, and the fifth layer for green retaining gabion retaining wall. The maximum accumulated vertical deformation (settlement) occurs in the fifth layer of gabion structures.

(5) When the amplitude of dynamic load (kPa) reaches 60~120, accumulated lateral and vertical deformation of gabion structures change obviously. In addition, about another 0.3~0.4 million vibrations later, the deformation approaches stability. Therefore, it can be regarded as a critical condition of yield failure when analyzing the dynamic behavior of gabion structures.

(6) Define accumulated deformation ratio as the ratio of accumulated deformation to the height of retaining wall. Accumulated lateral and vertical deformation ratios of gabion structures are less than 1%. Gabion structures show good engineering behavior under fatigue load.

Table 1 Air tensile test results of gabion meshes

Mechanical indexes	Double twisted hexagonal gabion mesh	
	2.2 mm gabion mesh	2.7 mm gabion mesh
Mesh type	8 mm×10 mm	8 mm×10 mm
Diameter of marginal wire (mm)	2.7	3.4
Tensile strength of 5% unit elongation (kN/m)	19.9	21.1
Tensile strength of 10% unit elongation (kN/m)	26.4	30.2
Tensile strength at rupture (kN/m)	34.7	49.8
Unit elongation under maximum load (%)	17.5	22.1

Table 2 Basic physical indexes of red sandstone

Specific gravity	Liquid limit (%)	Plastic limit (%)	Cohesion (kPa)	Internal friction angle (°)	Optimum moisture content (%)	Maximum dry density (g/cm ³)
2.74	41.78	25.14	25	21	18.13	1.73

Table 3 Distributed scope of dynamic load in roadbed

Test place	Da-Qin Line	Bao-Cheng Line	Cheng-Kun Line	Reinforced gabion retaining wall	Green reinforced gabion retaining wall
Amplitude of dynamic stress (kPa)	20~110	30~120	40~100	40~100	30~120

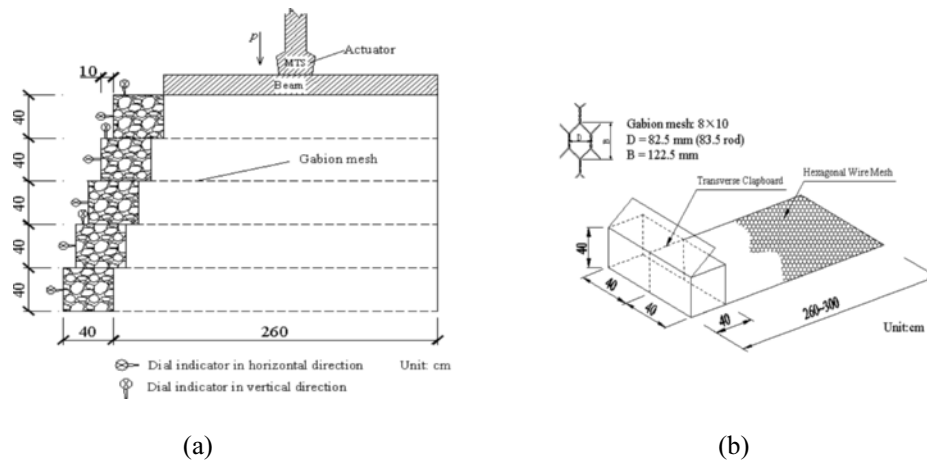


Fig. 4 (a) Reinforced gabion retaining wall; (b) Reinforced gabion component

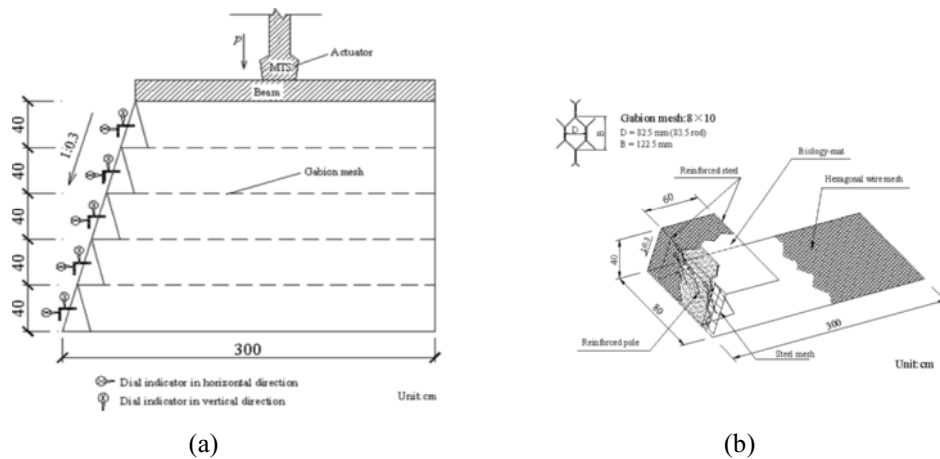


Fig. 5 (a) Green reinforced gabion retaining wall; (b) Green reinforced gabion component

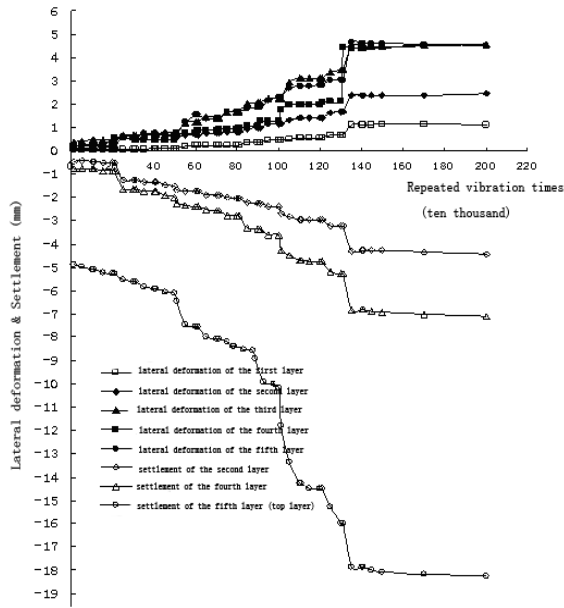


Fig. 6 Curves of accumulated lateral deformation and settlement changing with vibration times of reinforced gabion retaining wall

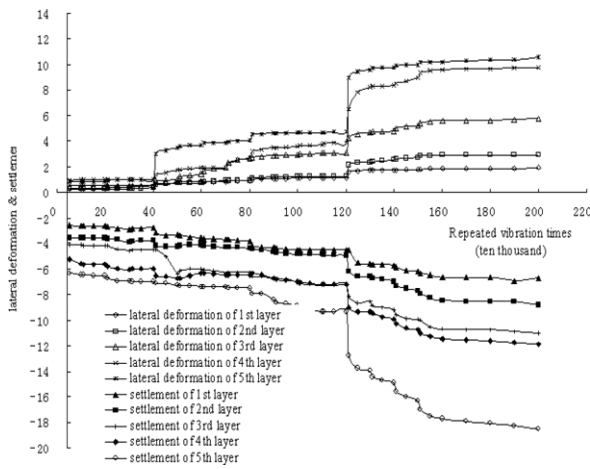


Fig. 7 Curves of accumulated lateral deformation and settlement changing with vibration times of green reinforced gabion retaining wall

SEISMIC TESTS ON GABION STRUCTURES

Experimental

Both of reinforced gabion retaining wall and green reinforced gabion retaining wall were constructed as the same as fatigue tests. MTS was used to input seismic wave. Seismic waves of ELCETRO (ELCE, 1940, NS) and HACHINOHE (HACHI, 1968, EW) were adopted.

In most cases, horizontal acceleration is bigger than vertical acceleration, and it may cause great damage to structures. Therefore, in order to study dynamic response of gabion structures to horizontal seismic wave of different acceleration peaks, ELCE_NS with acceleration peaks of 0.17 g, 0.34 g, 0.51 g and 0.68 g and HACHI_EW with peaks of 0.09 g, 0.18 g, 0.27 g and 0.36 g were input.

Six 941B geophones (in horizontal and vertical direction) were placed at the height of 0.4 m, 1.2 m and 2.0 m to measure acceleration and displacement response. Several dynamic earth pressure cells were placed at 0.5 m, 1.0 m and 1.5 m to study dynamic stress response of gabion structures. As showed in Fig.8 and Fig.9.

Table 4 Loading rules of gabion structures ($\times 10^4$)

Amplitude (kPa)	Frequency (HZ)	Reinforced gabion retaining wall	Green reinforced gabion retaining wall
30-60	4	—	10
	6	—	10
	8	—	10
	10	—	10
	Subtotal	—	40
40-80	2	10	—
	4	10	10
	6	10	10
	8	10	10
	10	10	10
Subtotal	50	40	
50-100	2	10	—
	4	10	10
	6	10	10
	8	10	10
	10	10	10
Subtotal	50	40	
60-120	2	10	—
	4	10	10
	6	10	10
	8	10	10
	10	60	50
Subtotal	100	80	
Total vibration times		200	200

Results and Analysis

Peaks of acceleration and displacement response of gabion structures are showed in Table 5 and Table 6.

Peaks of dynamic earth stress response are showed in Table 7, Table 8, Fig.10 and Fig.11. According to the test, following conclusions can be drawn:

(1) Gabion structures are provided with excellent aseismatic behavior. Under the seismic action of more than 0.6 g, the structures don't destroy. Therefore, it can be inferred that gabion structures can bear earthquake action with seismic intensity of eight.

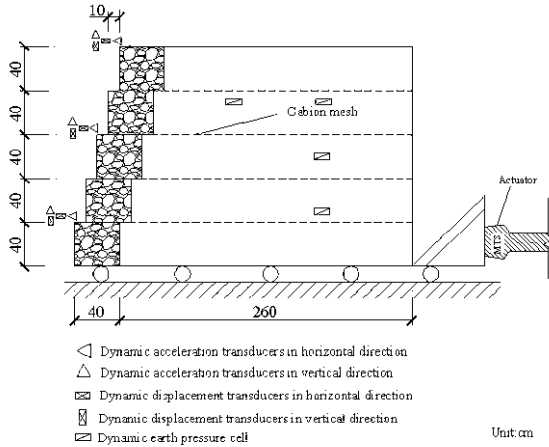


Fig. 8 Seismic test of reinforced gabion retaining wall

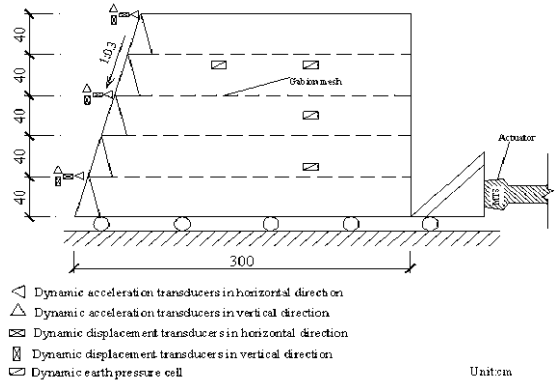


Fig. 9 Seismic test of green reinforced gabion retaining wall

(2) Gabion structures have magnifying function on input horizontal acceleration. For reinforced gabion retaining wall, the magnification of horizontal acceleration is 1.0~1.88 to ELCE_NS and 1.0~2.78 to HACHI_EW. For green reinforced gabion retaining wall, the magnification is 1.0~1.86 to ELCE_NS and 1.0~2.12 to HACHI_EW, as showed in Table 5 and Table 6. Horizontal acceleration response differs greatly under different seismic waves.

Table 5 Peaks of acceleration and displacement response of reinforced gabion retaining wall

Seismic wave	Peaks of input seismic wave (g)	Test position (m)	Horizontal acceleration response (g)	Horizontal displacement response (mm)	Vertical acceleration response (g)	Vertical displacement response (mm)
ELCE_NS	0.17	2.0	0.32	43.52	0.08	1.30
		1.2	0.27	44.32	0.07	2.43
		0.4	0.28	44.25	0.07	3.87
	0.34	2.0	0.62	82.67	0.16	3.90
		1.2	0.53	84.36	0.15	4.02
		0.4	0.55	88.57	0.16	6.65
	0.51	2.0	0.91	108.64	0.27	4.12
		1.2	0.78	106.85	0.26	4.04
		0.4	0.82	108.32	0.26	7.45
	0.68	2.0	1.14	106.45	0.36	4.15
		1.2	0.99	105.65	0.35	5.26
		0.4	1.06	118.69	0.35	7.86
HACHI_EW	0.09	2.0	0.25	45.58	0.04	1.39
		1.2	0.18	44.37	0.05	1.42
		0.4	0.17	47.25	0.04	4.08
	0.18	2.0	0.48	90.67	0.10	2.52
		1.2	0.36	84.36	0.10	2.45
		0.4	0.33	87.55	0.09	6.48
	0.27	2.0	0.69	101.64	0.15	2.86
		1.2	0.49	105.81	0.14	3.56
		0.4	0.47	106.22	0.14	6.54
	0.36	2.0	0.84	110.42	0.20	2.84
		1.2	0.63	108.66	0.18	2.73
		0.4	0.59	120.55	0.19	6.89

Table 6 Peaks of acceleration and displacement response of green reinforced gabion retaining wall

Seismic wave	Peaks of input seismic wave (g)	Test position (m)	Horizontal acceleration response (g)	Horizontal displacement response (mm)	Vertical acceleration response (g)	Vertical displacement response (mm)
ELCE_NS	0.17	2.0	0.32	45.42	0.08	0.98
		1.2	0.22	48.92	0.06	1.40
		0.4	0.23	49.38	0.07	2.45
	0.34	2.0	0.62	86.53	0.18	2.48
		1.2	0.46	73.10	0.14	1.79
		0.4	0.45	92.58	0.14	5.17
	0.51	2.0	0.90	102.84	0.32	2.85
		1.2	0.68	101.71	0.27	2.18
		0.4	0.66	109.07	0.30	6.06
	0.68	2.0	1.14	109.59	0.42	2.91
		1.2	0.88	108.44	0.32	3.91
		0.4	0.87	116.80	0.40	5.75
HACHI_EW	0.09	2.0	0.19	47.35	0.04	1.41
		1.2	0.12	49.50	0.03	1.40
		0.4	0.13	49.30	0.04	2.97
	0.18	2.0	0.37	91.13	0.10	2.40
		1.2	0.24	92.63	0.09	2.09
		0.4	0.25	95.80	0.08	5.24
	0.27	2.0	0.53	101.38	0.14	2.73
		1.2	0.36	86.94	0.12	3.13
		0.4	0.35	105.00	0.15	5.30
	0.36	2.0	0.65	111.76	0.25	2.66
		1.2	0.47	79.65	0.18	2.58
		0.4	0.45	117.64	0.22	5.48

Table 7 Peaks of dynamic earth stress response of reinforced gabion retaining wall

Position of dynamic earth pressure cells /m	Peaks of dynamic stress response to ELCE_NS (kPa)				Peaks of dynamic stress response to HACHI_EW (kPa)			
	0.17 g	0.34 g	0.51 g	0.68 g	0.09 g	0.18 g	0.27 g	0.36 g
1.5	78.6	120.1	189.3	374.5	66.5	99.2	286.3	370.5
1.0	32.4	63.2	145.6	146.8	67.7	90.4	172.5	212.8
0.5	36.8	82.7	218.8	192.5	66.8	98.7	288.6	240.6

Table 8 Peaks of dynamic stress response of green reinforced gabion retaining wall

Position of dynamic earth pressure cells /m	Peaks of dynamic stress response to ELCE_NS (kPa)				Peaks of dynamic stress response to HACHI_EW (kPa)			
	0.17 g	0.34 g	0.51 g	0.68 g	0.09 g	0.18 g	0.27 g	0.36 g
1.5	81.4	115.3	179.0	368.8	67.8	97.1	261.5	364.9
1.0	33.5	60.9	132.6	142.4	67.3	87.9	189.8	236.6
0.5	34.5	88.9	221.9	186.0	67.0	98.2	289.9	243.9

(3) The magnification of horizontal acceleration decreases as input acceleration increasing. In fact, the magnification should be a constant for an ideal system of linear elasticity and linear damping. Therefore, it can be inferred that the modulus of soil decreases and damping

ratio increases with the shear strain increasing during the test, and the soil shows obvious nonlinear behavior.

(4) Vertical acceleration response is much smaller than horizontal acceleration response. For reinforced gabion retaining wall, the peak of vertical acceleration

response is about 47%~53% of input ELCE_NS acceleration, and 44%~56% of HACHI_EW. For green reinforced gabion retaining wall, it is about 47%~64% of ELCE_NS, and 44%~69% of HACHI_EW.

(5) Vertical displacement decreases along the wall height and the maximum value appears in the bottom.

The horizontal displacement increases as the input acceleration increasing.

(6) The peaks of the dynamic stress response increase as the input acceleration increasing. The minimum value appears at 1/2 H, and the maximum value appears at 3/4 H. As showed in Table 7, Table 8, Fig.10 and Fig.11.

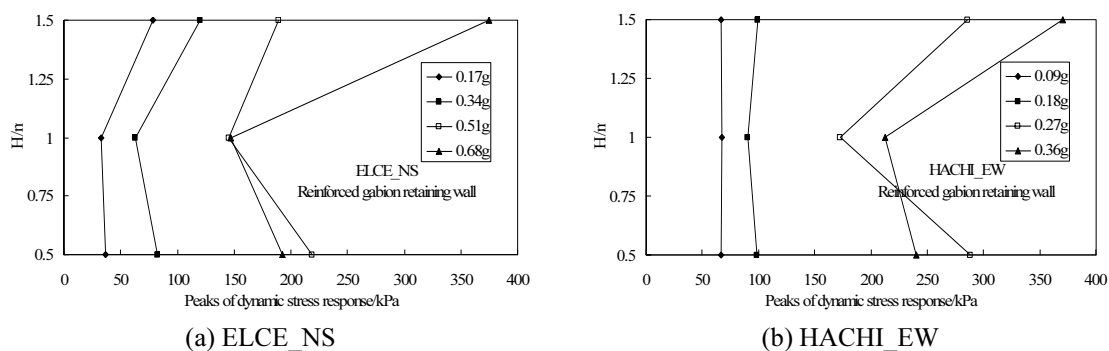


Fig. 10 Peaks of dynamic stress response along wall height of reinforced gabion retaining wall

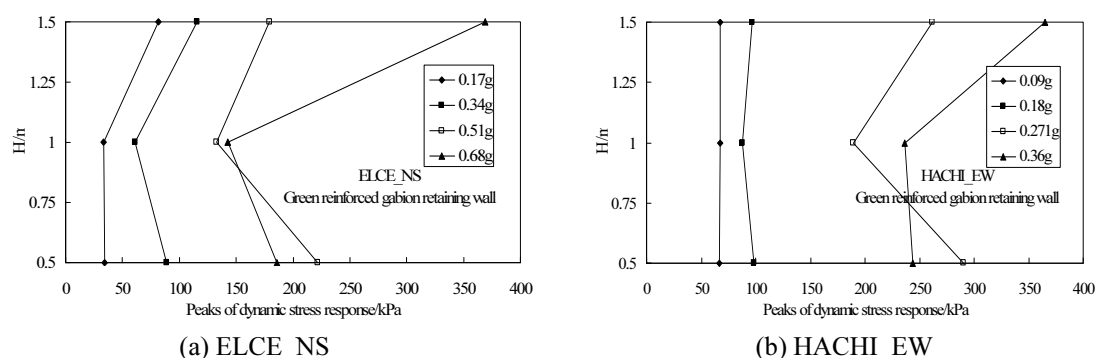


Fig. 11 Peaks of dynamic stress response along wall height of green reinforced gabion retaining wall

CONCLUSIONS

(1) Tensile strength of 2.7 mm gabion meshes is about 1.44 times as much as that of 2.2 mm gabion meshes. Air tensile curves of gabion meshes show a zigzag shape.

(2) Main factors influencing dynamic deformation behavior of gabion structures are amplitude of dynamic load, vibration times, and vibration frequency has no significant influence. In addition, filling ratio of gabion cage influences dynamic deformation behavior of reinforced gabion retaining wall.

(3) The maximum accumulated lateral deformation occurs in the third layer for reinforced gabion retaining wall, and the fifth layer for green reinforced gabion retaining wall. Accumulated deformation ratios of gabion structures are less than 1% under fatigue load.

(4) Both of reinforce gabion retaining wall and green reinforced gabion retaining wall are excellent aseismatic structures, and they can bear earthquake action with seismic intensity of eight.

REFERENCES

- Ling HI, Liu H, Mohri Y (2005). Parametric studies on the behavior of reinforced soil retaining walls under earthquake loading. *Journal of Engineering Mechanics*, ASCE, 131(10): 1056-1065.
- Liu HB (2008). Internal stability analysis of segmental geosynthetic-reinforced soil retaining walls subjected to seismic loading. *Chinese Journal of Geotechnical Engineering*, 30(2): 278-283.
- Yang GL, Li HS, Wang YH (2003). Model test on reinforced earth retaining wall under cyclic loading. *China Civil Engineering Journal*, 36(6): 105-110.

PULLOUT TEST STUDY ON INTERFACE FRICTION CHARACTERISTICS OF REINFORCEMENTS WITH RED SANDSTONE AS FILLER

Yu-Liang LIN¹, Guo-Lin YANG², Yun LI³ and Xiang-Jing HUANG⁴

ABSTRACT: In order to study interface friction characteristics between reinforcements and red sandstone, pullout tests were carried out. Three reinforcements were chosen: 2.2 mm gabion mesh, 2.7 mm gabion mesh and 70RE geogrid. The pullout coefficient, cohesion and friction angle of these three reinforcements were obtained. The curves of pullout friction coefficient and normal stress, shear stress and pullout displacement were established. Test results showed: Pullout friction coefficient decreased nonlinearly with the increase of normal stress; When the pullout displacement reached a certain value, shear stress tended to be stable, and most of which presented a peak value; Pullout coefficients of different reinforcements differed greatly; Double twisted hexagonal gabion mesh had better interface friction characteristic than geogrid; The smaller the diameter of gabion mesh was, the better the interface friction characteristic would be; In general, the pulling-out process of reinforcements could be divided into three stages: initial stage, developing stage and yield stage. During the test, special clamping system was installed to limit lateral deformation of specimen.

KEY WORDS: interface friction characteristics; pullout test; gabion mesh; geogrid; red sandstone

INTRODUCTION

Green reinforced gabion retaining wall can promote environmental reconstruction and micro-ecological balance by planting or semination. Combining with plants, the structure is capable of absorbing high-strength sound, and the gaps of stones in gabion cage can reduce noise effectively. Gabion structure can be taken as one of ideal solutions to geoenvironmental engineering problems. Gabion is a new reinforcement while the geogrid is widely used in China. At present, both gabion and geogrid have been used in west line of Xiangtan to Hengyang highway in Hunan province. The interface friction characteristic between reinforcements and filler is a key point for application of reinforced structure. When the interface between reinforcement and filler becomes a weak interface, the friction characteristic directly determines the internal stability of structure. Consequently, researchers and designers should carry out friction characteristic test to provide a basis for stability and deformation analysis of reinforced structure.

Until now, researches on interface friction characteristics of geogrid and filler were widely carried out both in home and abroad (Yang et al. 2001; Xu et al. 2004; Yang et al. 2006; Zhang et al. 2007), but only a

few scholars started the gabion mesh researches (Bergado et al. 2001; Bergado et al. 2003; Nicola et al. 2006a; Nicola et al. 2006b). The methods taken were mainly pullout test and direct shear test. In this paper, based on the project in Xiangtan to Hengyang highway, pullout tests on gabion meshes and geogrid with red sandstone as filler were carried out. Pullout test results are not only of great significance for construction of reinforced structures, but also provide a reference for relative research.

EXPERIMENT

Test Device

Pullout tests were carried out in model box, as showed in Fig.1. The dimension of the model box was 3 m×0.86 m×2 m (3 m in length, 0.86 m in width and 2 m in height). One 3.0 m × 2.0 m face was made by organic glass for observation, and two free faces: a 3.0 m×0.85 m one at the top of box for imposing vertical load, the other of 0.85 m × 2.0 m at fore-end for pulling out the reinforcements. The other three faces were welded by steel plate. Reinforcements were laid in model box,

1 Ph.D Student, School of Civil Engineering and Architecture, Central South University, China. Email: linyuliang11@yahoo.com.cn

2 Professor, ditto. Email: yangguolin6301@163.com

3 Ph.D Student, ditto. Email: liyun2007@mail.csu.edu.cn

4 Senior Engineer, Hunan Provincial Communications Planning, Surveying and Design Institute. Email: hncshxj@163.com

every 0.2 m a layer and 6 layers in total. The filler was red sandstone with the compaction of about 95% as required in construction site. Two MTS actuators were used for imposing loads, and pullout-tension was imposed by strain-controlled setting with the speed of 3 mm/min, which met the specification of “Test Method of Geosynthetics for Highway Engineering” (JTG E50-2006). As showed in Fig.2.

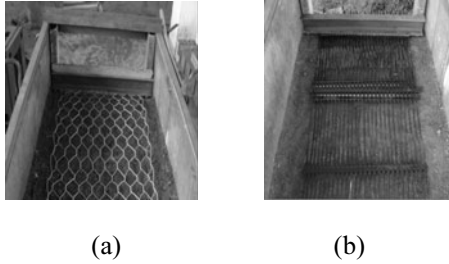


Fig. 1 Gabion mesh (a) and 70RE geogrid (b) used in test

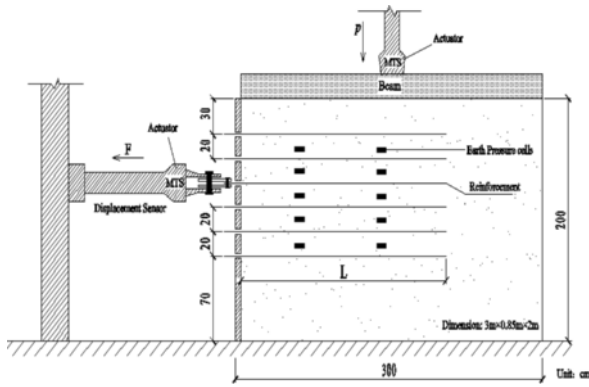


Fig. 2 Pullout device used in tests

During the test, vertical load might be partly consumed by friction resistance of inner wall of model

box, which would result in smaller normal stress along reinforcements. This consumption was affected by the dimension of model box, specimens size, the position in box, and so on. Consequently, on one hand, the model box should be big enough and lubricating oil could be spread on inner wall if possible. On the other hand, the width ratio of specimen to box should be strictly controlled. In the tests, lubricating oil was spread and two earth pressure cells were laid in each layer to test normal stress along reinforcement. Therefore, the loss of normal stress could be avoided.

Reinforcements in Test

Three reinforcements were chosen: 2.2 mm gabion mesh, 2.7 mm gabion mesh and 70RE geogrid. Gabion mesh, of double twisted hexagonal shape, was galvanized and covered by PVC for anti-corrosion. The main technical indexes of gabion meshes and geogrid were showed in Table 1 and Table 2 respectively. The dimensions of reinforcements in test were determined according to normal stress and the mechanical properties of reinforcements, obeying the principle of being able to be pulled out. Red sandstone was taken from construction site. For the characteristics of low strength, water softening and dehydration crack, red sandstone was considered to be ill roadbed filler. The main basic physics indexes of red sandstone were showed in Table3.

Clamping System

Test results were greatly influenced by clamping system. If reinforcement was left outside with too much free-length, the free deformation would result in lager pullout displacement, and necking phenomenon would occur for gabion mesh.

Table 1 Technical indexes of geogrid

Reinforcement	Dimension (Length × Width)	Elongation at rupture	Fracture force	Long-term creep strength	Tensile strength of 2% elongation
70RE geogrid	1200 mm × 60 mm	<12%	≤100 KN/m	≤32 KN/m	≤24 KN/m

Table 2 Technical indexes of gabion meshes

Reinforcements	Mesh type	Dimension (Length × Width)	Fringe wire diameter	Tensile strength
2.2 mm gabion mesh	8 mm×10 mm	600 mm × 680 mm	2.7 mm	34.7 KN/m
2.7 mm gabion mesh	8 mm×10 mm	800 mm × 680 mm	3.4 mm	49.8 KN/m

Table 3 Basic physical indexes of red sandstone

Specific gravity	Liquid limit (%)	Plastic limit (%)	Cohesion (kPa)	Internal friction angle (°)	Optimum moisture content (%)	Maximum dry density (g/cm ³)
2.74	41.78	25.14	25	21	18.13	1.73

The special clamping system in tests was shown in Fig. 3. Every mesh was orderly and tightly fixed in every hole of two same clamps by bolt. There were two lateral holes at each side of clamp (A and B), which can effectively limit the horizontal deformation of specimen. The other end of clamp was rooted in horizontal MTS actuator. Load could distribute on reinforcement uniformly.

70RE geogrid was fixed by two clamps similarly. Ribs of geogrid were restricted by each hole of clamps. A steel bar covered with earthwork cloth was used to fix the ribs. Load could distribute on every rib uniformly.

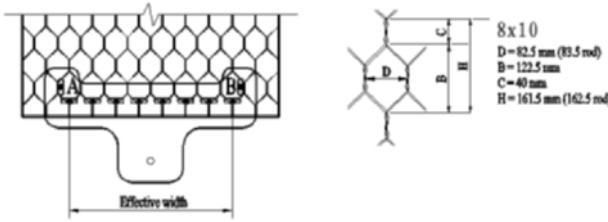


Fig. 3 Clamping system for reinforcements

TEST RESULTS AND ANALYSIS

As a quantitative index, pullout friction coefficient f is usually used to describe interface friction characteristic between reinforcement and filler. f can be calculated by following formula:

$$f = \frac{\tau}{\sigma} = \frac{T_x}{2bl \cdot \sigma} \tag{1}$$

In which, T_{max} is the maximum tension (kN); τ is shear stress (kPa); σ is normal stress (kPa); b, l are the width and length of reinforcement respectively (m). Pullout friction coefficient f is affected by the length of specimen, compaction of filler, overburden pressure, trait or type of reinforcements, and so on. Fig.4 shows the curves between pullout friction coefficient f and normal stress σ . As can be seen, f decreases non-linearly as σ increasing. Therefore, this phenomenon should be concerned much especially for high reinforced retaining wall.

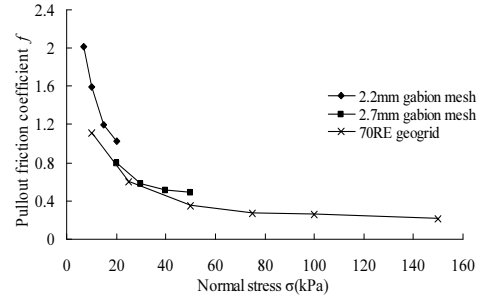


Fig. 4 The curves between pullout friction coefficient f and normal stress σ

To illustrate the effect of reinforcement on the strength of filler, pullout coefficient K can be defined as:

$$K = \tan \varphi / \tan \varphi = f / \mu \tag{2}$$

In which, φ is friction angle between reinforcement and filler; φ is friction angle of filler; f is friction coefficient between reinforcement and filler, and $f = \tan \varphi$; μ is friction coefficient of filler, and $\mu = \tan \varphi$. K reflects the interaction between reinforcement and filler.

Pullout test results are showed in Table 4. Pullout test curves of 2.2 mm gabion mesh, 2.7 mm gabion mesh and 70RE geogrid are showed in Fig.5~7 respectively. According to the tests, following conclusions can be drawn:

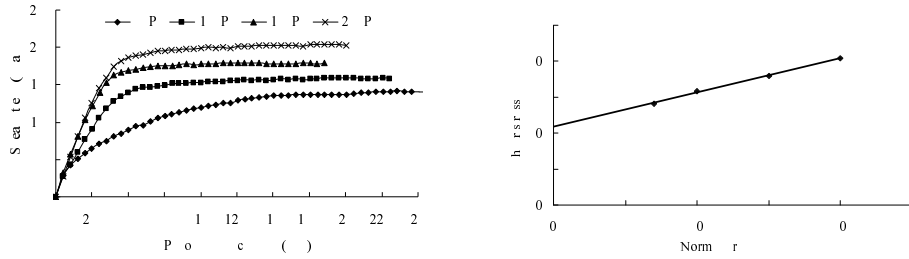
(1) The curves between pullout displacement and shear stress under different normal stress show similar shape for each reinforcement. When the pullout displacement reaches a certain value, the curves turn gentle, and most of which present shear stress peak.

(2) Pullout coefficients of different reinforcements differ greatly. They are 2.2 mm gabion mesh, 2.7 mm gabion mesh and 70RE geogrid arranging from high to low, with the ratio of 3.15:1.97:1.

(3) With red sandstone as filler, the friction angel of 70RE geogrid is just 8.6°. The cohesions of gabion meshes and geogrid are small but stable. Therefore, it is proposed to taken the impact of cohesion into consideration when calculating anchorage length.

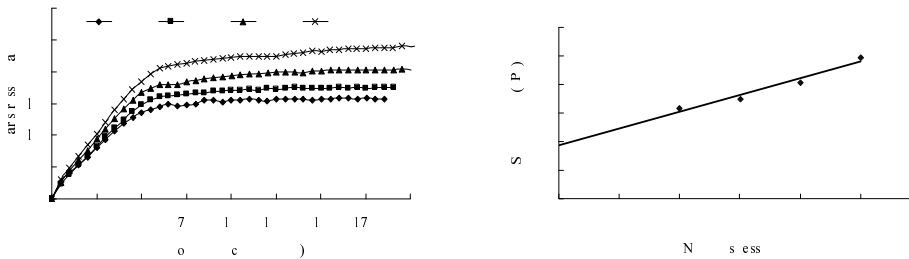
Table 4 Pullout test results of reinforcements

Reinforcements	Cohesion C (kPa)	Friction angel φ_{sg} (°)	Friction coefficient f_{sg}	Pullout coefficient K
2.2 mm gabion mesh	10.9	25.3	0.47	1.23
2.7 mm gabion mesh	9.3	16.4	0.29	0.77
70RE geogrid	10.3	8.6	0.15	0.39



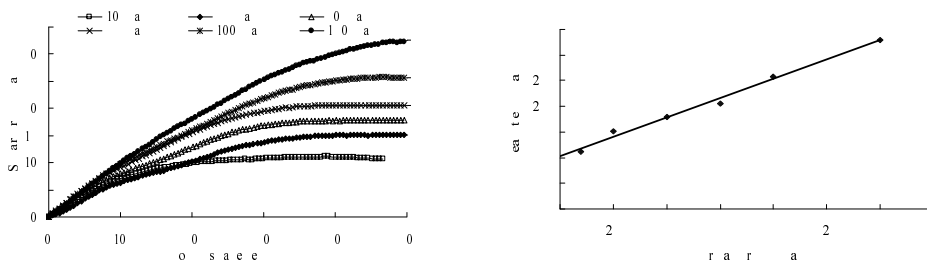
(a) Curves between pullout displacement and shear stress (b) Curve of normal stress and shear stress

Fig. 5 Curves of pullout test of 2.2 mm gabion mesh



(a) Curves between pullout displacement and shear stress (b) Curve of normal stress and shear stress

Fig. 6 Curves of pullout test of 2.7 mm gabion mesh



(a) Curves between pullout displacement and shear stress (b) Curve of normal stress and shear stress

Fig. 7 Curves of pullout test of 70RE geogrid

(4) The cohesions for three reinforcements are nearly the same, but the friction angles of gabion meshes are much bigger than geogrid. Therefore, it implies double twisted hexagonal gabion mesh has better interface friction characteristic than geogrid.

(5) The smaller the diameter of gabion mesh is, the bigger the cohesion and friction angle are.

(6) Under the same normal stress, the smaller the diameter of gabion mesh is, the bigger the shear stress peak will be. In the tests, when normal stress is 20kPa, shear stress peak is 20.4 kPa for 2.2 mm gabion mesh, and 15.5 kPa for 2.7 mm gabion mesh. The former is 1.36 times as much as the latter, as showed in Fig.8. It may imply the gabion mesh of smaller diameter can provide more pullout resistance under the same normal stress.

Further analysis and discussion on test results are made as follows:

(1) Interface friction angle between reinforcement and filler consists of two parts: the first part is caused by friction between reinforcement and filler. The other is caused by passive earth stress along the transverse rib for the filler is embedded in reinforcement. These two parts real exist for both geogrid and gabion mesh. For the little

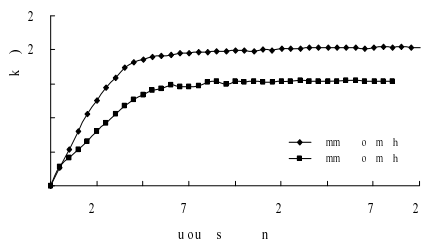


Fig.8 Displacement-shear curves of two gabion meshes under $\sigma = 20$ kPa

contact area, the effect of first part is usually small, and the second part always plays a leading role. Meanwhile, the second part is significantly affected by the shape and the dimension of reinforcement, the grain composition of filler, and so on. During the test, red sandstone can be embedded in double twisted hexagonal gabion mesh easily, but the gaps between adjacent ribs of geogrid are too small and the embedding effect is not so obvious. That is a good explanation for why double twisted hexagonal gabion mesh has better interface friction characteristic than geogrid of strip shape.

(2) It can be seen that the diameter of wire affects interface friction characteristic of gabion mesh. The smaller the diameter of gabion mesh is, the better the interface friction characteristic will be. This is mainly because the filler can be embedded in gabion mesh easily when the wire diameter is smaller, and therefore, cohesion function and embedding effect are more obvious. In order to get more information about how the diameter of gabion mesh affects the interface friction characteristics, further study may be needed.

(3) The development of pullout resistance can be divided into three stages with the increase of pullout displacement. (a) Initial stage. When pullout displacement is small, pullout resistance (consists of bite force, friction force and adhesive force) doesn't develop completely and it increases with pullout displacement increasing. Pullout resistance near clamps is the biggest and it decreases along the reinforcement. And some parts of reinforcement buried in fillers are in free-state. In this stage, the curves between pullout resistance and pullout displacement show two important features: On one hand, working areas of reinforcement are growing; On the other hand, resistance in working areas is increasing with pullout displacement increasing, and the total pullout resistance increases rapidly. (b) Developing stage: With the increase of pullout displacement, micro-cracks of filler develop along the reinforcement. Pullout resistance increases gradually until reaches a peak value. (c) Yield stage: with the development of micro-cracks of filler, the whole reinforcement tends to be in residual resistance state. Pullout resistance doesn't increase even if pullout displacement increases and it reaches residual resistance finally.

CONCLUSIONS

(1) The clamping system used in test can effectively limit the lateral deformation of specimen and reduce necking effect. The tension can distribute on reinforcement uniformly.

(2) Pullout friction coefficient f decreases nonlinearly as σ increasing. This phenomenon should be concerned

much especially for high reinforced retaining wall.

(3) The curves between pullout displacement and shear stress under different normal stress show similar shape. When the pullout displacement reaches a certain value, the curves turn gentle, and most of which present shear stress peak.

(4) With red sandstone as filler, pullout coefficients of different reinforcements differ greatly. Consequently, pullout coefficient should be determined by pullout tests for different reinforced structures.

(5) The cohesions of gabion meshes and geogrid are small but stable. Therefore, it is proposed to taken the impact of cohesion into consideration when calculating anchorage length.

(6) Double twisted hexagonal gabion mesh has better interface friction characteristic than geogrid

(7) The smaller the diameter of gabion mesh is, the better the interface friction characteristic will be.

REFERENCES

- Bergado DT, Youwai S, Teerawattanasuk C, Visudmedanukul P (2003). The interaction mechanism and behavior of hexagonal wire mesh reinforced embankment with silty sand backfill on soft clay. *Computers and Geotechnics*, 30:517-534.
- Bergado DT, Voottipruex P, Srikongsri A, Teerawattanasuk C (2001). Interaction between hexagonal wire mesh reinforcement and silty sand backfill. *Canadian Geotechnical Journal*, 24: 26-41.
- Nicola M & Domenico G (2006). A simple method to evaluate the pullout resistance of extruded geogrids embedded in a compacted granular soil. *Geotextiles and Geomembranes*, 24:116-128.
- Nicola M & Piergiorgio R (2006). Factors affecting the pullout behaviour of extruded geogrids embedded in a compacted granular soil. *Geotextiles and Geomembranes*, 24: 220-242.
- Xu C, Zhao CF, Ye GB (2004). Research on Interface between Soil and Geosynthetics. *Journal of Tongji University*. 32(3): 307-311.
- Yang GL & Wang YH (2001). Study of engineering characteristic of material used reinforced earth. *China Journal of Highway and Transport*, 14(3): 11-16.
- Yang GQ, Li GX, Zhang BJ (2006). Experimental studies on interface friction characteristics of geogrids. *Chinese Journal of Geotechnical Engineering*, 28(8): 948-952.
- Zhang WH, Wang BT, Zhang FH, Li SD (2007). Test study on interaction characteristics between two-way geogrids and clay. *Rock and Soil Mechanics*, 28(5):1031-1034.

APPLICATION OF GEOMEMBRANE AS CARBON CAPTURE AT PALM OIL MILL

Andryan SUHENDRA¹ and Amelia MAKMUR²

ABSTRACT: Global warming is the most important issue in last decade that causes a climate change. Global warming is triggered by greenhouse effect, whereas the process by absorption and emission of infrared radiation by atmospheric gases increases the temperature. Methane is one of the gases, which contribute to increase the greenhouse effect and predicted 20 times larger than Carbon Dioxide potential impact. However, methane can be used as alternative resources energy such as biogas. Methane is produced from organic waste like biomass, animal and human waste, also the palm oil mill's waste. In West Indonesia where the expansions of palm oil fields grow faster, the increasing methane gases become a serious matter. One of the alternative solutions to minimize that methane's impact is by using an aerobic bio-digestion process. HDPE geomembrane, one of the geosynthetics products can be used to captures the methane gases and led in them by using a pipeline to the biogas converter. The installation processes of geomembrane are including patterning, deploying, anchoring and seaming of HDPE geomembrane. As a carbon capture in Palm Oil mill, HDPE geomembrane contribute to reduce the greenhouse effect, provide an alternative energy and for the future hopefully will save our environment.

KEYWORDS: global warming, methane, carbon capture, HDPE geomembrane, biogas, anaerobic bio-digestion process

INTRODUCTION

The spectacular expansion of palm oil mill in Indonesia; especially in West Indonesia, not only generate income for inhabitant in that the region, but in the other hand it's also left a serious problem behind with the palm oil mill's waste. That waste potent to produce the methane gases (CH_4), which predict will be increasing the greenhouse gases effect 20 times larger than Carbon Dioxide. Contribution of several gases to increase the greenhouse effect is shown on the figure below.

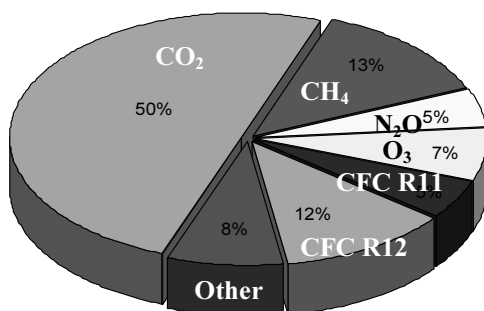


Fig. 1 Percentage contribution of several gases that increasing the greenhouse effect

Palm Oil Mill effluent as known as POME is a liquid waste of palm oil mill, which has 100 times potential as a pollutant waste than another municipal waste. That potential effect will increase the greenhouse effect, if there is no action to treat that entire palm oil mill's waste. The Biological Oxygen Demand of untreated POME average 25,000 mg/liter (Ojonoma & Nnennaya, 2007). Anaerobic biodigestion system can solve the problem of greenhouse gases effect of palm oil mill effluent and also give several benefits:

- Re-use the POME as an alternative source energy
- Create an electricity power
- Reduce the unpleasant odor
- Re-use the POME as a fertilizer
- Reduce the impact of greenhouse gases

Based on the research, 50 million tons of biomass has 1.4 trillion cubic meters potential of biogas or equivalent to 337 MW electrical power generations.

POME TREATMENT SYSTEM

The conventional treatment system of POME is use biological system, by utilizing the microbe to reduce BOD and neutralizing the acidity of POME.

¹ Lecturer of Bina Nusantara University, Jakarta. Member of Indonesian Society of Geotechnical Engineering (ISSMGE) and International Geosynthetic Society Indonesia Chapter (INA-IGS). Email:andryan@geosinindo.co.id

² Lecturer of Bina Nusantara University, Jakarta. Member of Indonesian Society of Geotechnical Engineering (ISSMGE) and International Geosynthetic Society Indonesia Chapter (INA-IGS). Email:amelia1935@binus.edu

This conventional system need open lagoon with size depend on the volume of POME will be treated. These are 3 phases of POME Treatment, such as:

Preliminary Treatment

This phase consist of de-oiling and acidifying pond.

At first phase, POME from fat-pit delivers to de-oiling pond, and then transferred to acidifying pond. The temperature and acid density at acidifying pond is kept constant in high condition to ensure the oil content at the POME surface still liquid.

The POME will be remained at acidifying pond during 4 to 5 days to increase the acid density for making easier the next process.

Anaerobic Biodigestion Treatment

The purpose of this treatment is to change the complex organic mass into the simple one.

There are 2 phases on an-aerobic biodigestion treatment i.e. primary and subsequent anaerobic alternation lagoon.

Primary alternation lagoon

In this pond, the complex organic mass will be changed to volatile acid by using an acid bacterial. BOD and COD will be decreased in neutral condition at lagoon during 40 days.



Fig. 2 Primary Lagoon

Subsequent anaerobic alternation lagoon

In this lagoon, the volatile acid changes into an acetate acid and then it will become the gases of CO, CH₄, H₂S, and H₂O.

Further Treatment

The further treatment of POME consists of 2 lagoons: facultative and aerobic lagoon.

Facultative lagoon

The aerobic oxidation occurs at the surface and in that time the an-aerobic fermentation of sedimentation is also occurred, as a consequence the value of BOD and COD will be decreased.

Aerobic lagoon

Bacterial need oxygen for proliferating, so in this place they will get it and all the process will decrease BOD and COD value.



Fig. 3 Subsequent Lagoon

BIOGAS

The biggest component of biogas, which produced from POME treatment, is methane gas; for 600 kg – 700 kg of POME can produce biogas approximately 20 m³ (Goenadi, 2006).

The process of methane can be divided into 3 stages: hydrolysis, aetogenesis (dehydrogenesis) and metanogenesis (Sorensen, 2004).

At first phase (hydrolysis phase), the complex biomass is decomposited to a simple glucose by using microorganism enzyme as catalyst. The important thing in this process is the result of a simpler chemistry for the next phase.

The second phase will change glucose into an acetate acid and broken off the long acid chain become the short one finally it will produce an acetate acid as a final product.

The third phase is the changing process of biogas from acetate acid by using fermentation of metanogenic bacterial.

As an illustration, in case of palm oil mill process 100 ton of fresh fruit bunches (FFB) per hour, will produce 50 m³/hour of POME (assumed 55% of FFB with unit weight 1.1g/cm³, Kartiman, 2008). If the mill operates 10 hours/day, the volume of POME will be

1,000 m³ per day with characteristic as shown at table 1.

With assumption of the POME temperature shall be decreased up to 40°C, the process run at temperature of 50°C and expected of degradation rate is 80% (Budiarto & Agung, 2009), the biogas production per hour can be estimated as follow:

$$50 \text{ m}^3 \times 112.5 \text{ kg COD/m}^3 = 5,625 \text{ kg COD}$$

$$5,625 \text{ kg COD} \times 0.45 \text{ m}^3 \text{ biogas/kg COD} = 2,531.25 \text{ m}^3 \text{ biogas}$$

Table 1 Characteristic of POME for mill capacity of 100 ton of fresh fruit bunches and operation time of 10 hours/day (Sixt, 1994 & Sa'id, 1996)

Parameter	Unit	Volume
BOD	mg/l	50,000 – 75,000
COD	mg/l	87,500
		112,500
Solid Solution	mg/l	70,000
Total Solid	mg/l	120,000
Total Nitrogen	mg/l	262.5
Phosphate	mg/l	540
Oil/Fat	mg/l	3,750 – 5,000
pH	-	4

The calorie of methane gas (biogas) is approximately 35.882 MJ/m³ (Sydgas AB, 1998) and the efficiency of generation is 25%, the output of biogas as power potential is as follow:

$$2,531.25 \text{ m}^3 \text{ biogas} \times 35.882 \text{ MJ/m}^3 = 25.25 \text{ MW(t)h}$$

$$25.25 \text{ MW(t)h} \times 0.25 = 6.3125 \text{ MW(e)h}$$

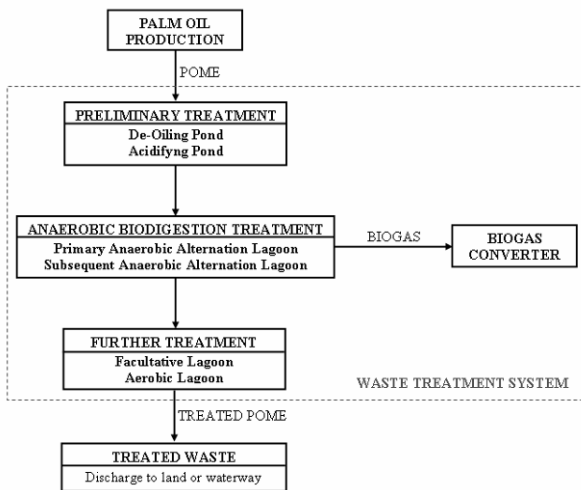


Fig. 4 Flow diagram of POME treatment process

A methane gas, which is produce from the anaerobic lagoon, shall be captured by using impermeable liner so that the gases will not be released to open air.

One of the impermeable liners that suitable for this application is geomembrane. The geomembrane will be

installed to cover the open lagoon and capture the methane gas.

GEOMEMBRANE

According to ASTM D4439, a geomembrane can be defined as a very low permeability synthetic membrane liner or barrier that will be used with any geotechnical engineering material so as to control (or gas) migration in a human-made project, structure or system.

Geomembranes are made from continuously polymeric sheets, or impregnation of nonwoven geotex-tiles with bitumen.

Although the polymeric geomembrane are not absolutely impermeable, with the value of permeability as measured by water-vapor transmission in range of 1 x 10⁻¹² to 1 x 10⁻¹⁵ m/s, the geomembranes are more impermeable compared to clay soil.

The polymeric geomembrane can be made from polymer of Polyethylene (PE), Polypropylene (PP) or Polyvinyl Chloride (PVC).

Selection procedure of the suitable geomembrane including the thickness applied for this application shall consider several aspects such as:

- durability of geomembrane against chemical content of POME
- survivability requirements when packing, handling, and installation process
- geometric consideration including the anchorage of geomembrane.

Table 2 General chemical resistance of some geomembranes (After Vandervoort)

Chemical	Geomembrane Type			
	HDPE		PVC	
	38°C	70°C	38°C	70°C
General				
Allphatic hydrocarbons	√	√		
Aromatic hydrocarbons	√	√		
Chlorinated solvents	√	√		
Oxygenated solvents	√	√		
Crude Petroleum solvents	√	√		
Alcohols	√	√	√	√
Acids				
Organic	√	√	√	√
Inorganic	√	√	√	√
Heavy Metals	√	√	√	√
Salts	√	√	√	√

Note: √ = generally good resistance

Table 3 Recommended minimum properties for general geomembrane installation survivability (Koerner, 2005)

Property & Test Method	Requirement Properties			
	Low	Medium	High	Very High
Thickness (D1593) (mm)	0.63	0.75	0.88	1.00
Tensile (D882) (kN/m)	7	9	11	13
Tear (D1004 Die C) (N)	33	45	67	90
Puncture (D4833) (N)	110	140	170	200
Impact (D3398 mod.) (J)	10	12	15	20

Note: Low, Medium, High, Very High indicates the risk degree shall be taken by geomembrane.

Base on the requirement and geomembrane properties, HDPE geomembrane is the best choice if it is compared to PVC geomembrane and it is usually recommended by the experts as a lagoon cover and carbon capture.

INSTALLATION OF GEOMEMBRANE

The installation processes of Geomembrane are:

Patterning

To minimize the waste of material, the layout shall be designed and the prefabrication needs to be considered if the condition of work is possible.



Fig. 5 Fabrication work

Deploying

Generally geomembrane panels are put in the same direction with maximum slope (not in the cross direction of slope)

Anchoring

To ensure the position of geomembrane during

construction and service time, the geomembrane shall be anchored well.



Fig. 6 Geomembrane deployment

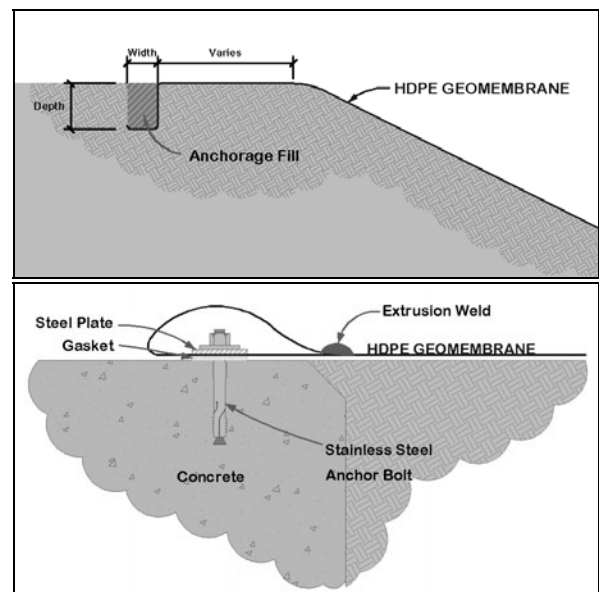


Fig. 7 Anchoring type of geomembrane

Seaming

Seaming usually carried out as soon as geomembrane panels deployment attempted.

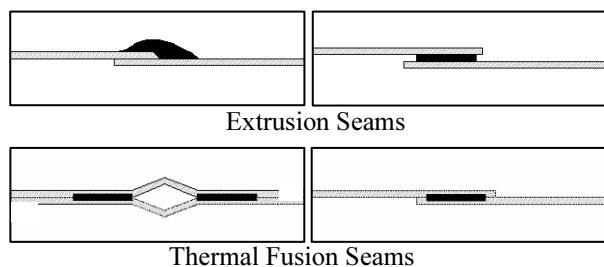


Fig. 8 Seaming type of geomembrane

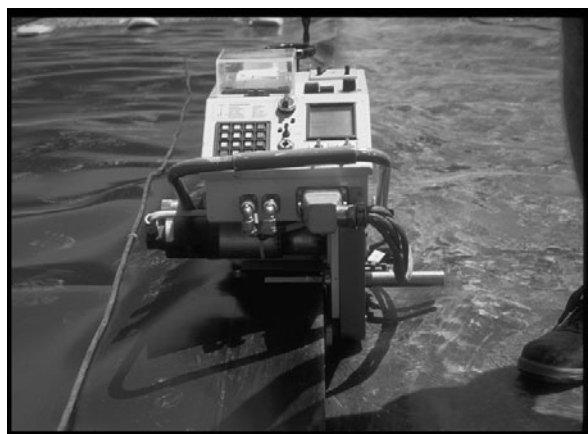


Fig. 9 Seaming work



Fig. 10 The HDPE geomembrane as carbon capture show the good performance

CONCLUSION

Palm oil mill produce a lot of waste such as a solid waste and a liquid waste (known as palm oil mill effluent – POME).

POME will produce methane gas, which cause the greenhouse effect; therefore the treatment of that waste is significantly needed.

The right treatment of palm oil mill effluent not only is able to minimize the environmental pollution, but it also can contribute to produce be use as an alternative energy or power.

To capture the methane gas during anaerobic biodegestion process, the HDPE geomembrane which covered open lagoon had already proven the good performance as a carbon capture.

ACKNOWLEDGEMENT

The authors would like to convey our sincerely gratitude and thank to PT Tetrasa Geosinindo (Indonesian Geosynthetics Specialist) and also to Civil Engineering Department—Bina Nusantara University for their great support.

REFERENCES

- Ahmad A, Ismail S, Bhatia S (2003). Water recycling from palm oil mill effluent (POME) using membrane technology. *Desalination*, 157:87- 95.
- Budiarto & Agung (2009). *Potensi Energi Limbah Pabrik Kelapa Sawit*, Universitas Gajah Mada Yogyakarta.
- Koerner RM (2005). *Designing with Geosynthetics*, 5th edition, Pearson Prentice Hall.
- Metclaf & Eddy (1991). *Wastewater Engineering, treatment disposal, reuse*. Third edition. Mc GrawHill, inc.
- Ojonoma & Nnennaya (2007). The environmental impact of palm oil mill effluent (POME) on some physico-chemical parameters and total aerobic bioload of soil at a dump site in Anyigba, Kogi State, Nigeria, *African Journal of Agricultural Research* 2 (12): 656-662.
- Tobing PL (1997). *Minimalisasi dan Pemanfaatan Limbah Cair-Padat Pabrik Kelapa Sawit dengan Cara Daur Ulang*, PPKS, Medan.

INTERFACE FRICTIONAL PROPERTY BETWEEN SAND AND GEOMEMBRANE

Jun-Li GAO¹, Meng-Xi ZHANG² and Wen-Jie ZHANG³

ABSTRACT: Interface instability between HDPE geomembrane and sand is a main reason for landfill structural failure on lining interface. Though frictional coefficient of textured geomembrane is large, it is easy to be split by the huge tension force accumulated on the landfill lined slope. A novel concept of reinforced HDPE geomembrane is proposed in this paper. A series of direct shear tests were carried out to investigate interfacial characteristics between sand/geomembranes (reinforcement and unreinforcement) and sand/textured geomembrane. The results show that the peak shear strength of the reinforced HDPE geomembrane is larger than that of smooth HDPE geomembrane under the same normal stress, and reinforced HDPE geomembranes have advantages over textured geomembranes on rupture strength.

KEYWORDS: direct shear test, geomembrane, shear stress, reinforcement

INTRODUCTION

Landfills used for the containment control of solid waste serve a variety of functions: e.g. maximization of waste storage per unit area, isolation of waste from the surrounding environment, gas generation for power utilization, and conversion opportunities for post closure land uses.

Unfortunately, stability is an issue that sometimes has been overlooked. On March 9, 1996, the largest slope failure at a municipal solid waste (MSW) landfill in the United States, based on volume of waste involved (approximately 1.2 million m³), occurred, and it provides the industry with some lessons for the operation, expansion, and stability of landfill slopes (Seed et al. 1990; Byrne et al. 1992).

Composite liners containing soil and geosynthetic materials provide effective isolation of waste and leachate from the environment. High-density polyethylene (HDPE) and polyvinyl chloride (PVC) geomembranes are widely used in the modern municipal solid waste containment system (Koerner & Daniel 1997). And the majority of geomembranes are placed under CCLs to act as composite liners within landfill bottom liner and cover systems. Since these applications typically involve side slopes, interface instability between HDPE geomembranes and soil is a main reason for landfill structural failures on lining interface.

However, the shearing force at soil-geosynthetic and geosynthetic-geosynthetic interfaces is often low, and low interface strength has led to slippage and slope

failures (Koerner & Soong 2000). Though the shear strength of soil/geosynthetic interface has been investigated by conducting other tests, such as tilt table tests (Wu et al. 2008), direct shear test is still the most common testing method. Research involving the interface of soil and geomembrane under different conditions can be found in (Fishman & Pal 1994; Hsieh & Hsieh 2003; Fleming et al. 2006; Zabielska-Adamska 2006; Wu et al. 2008; Vukelic et al. 2008). Though frictional coefficient of textured geomembrane is large, it is easy to be split by the huge tension force accumulated on the landfill lined slope. A novel concept of reinforced HDPE geomembrane is proposed in this paper. A series of direct shear tests were carried out to investigate the interface between sand/geomembrane (reinforcement and unreinforcement) and sand/textured geomembrane. The details of these tests are presented in this paper. The characteristics of overall geomembranes/sand interface shear resistance are reported.

EXPERIMENTAL PROCEDURE

Test Device

The size of the shearing device can influence the direct shear test results. Several parts of the large pullout direct shear apparatus have been reconstructed in order to meet the demand of experiments. Technical parameters of this device are as follows: the effective length, width, and thickness of the upper shear box is 200mm, 200mm,

¹ Ph.D Candidate, Department of Civil Engineering, Shanghai University, China. Email: susan_jl@staff.shu.edu.cn

² Professor, Department of Civil Engineering, Shanghai University, China. Email: mxzhang@staff.shu.edu.cn

³ Ph.D Department of Civil Engineering, Shanghai University, China. Email: zhwjlyl@163.com

100mm, respectively. The effective length, width of the lower shear plate is 270mm, 250mm, respectively. A minimum sand thickness of 50mm in the upper shear box is recommended so as to ensure the reproduction of normal pressures at the shearing plane when a rigid load plate is used for applying the normal load. This device fulfills this requirement, because thickness of sand in the upper box is 100mm. Beneath the lower shear plate, some thin-plates are placed, which thickness are from 1 mm to 3mm and can be adjusted according to reinforcement height. The movement of the lower shear box in the horizontal direction is controlled by a steel pole which is mobilized by an electric motor. The vertical loading applied by an air compressor is transferred through the rigid reaction frame and added on a rigid load plate which is placed on top of the sand in the upper shear box.

The horizontal displacement of the lower shear box during the shear tests is collected by a linear variable displacement transformer (LVDT) and the shear stress is collected by a load cell. These data are recorded by a data acquisition system and then transformed to a linked computer. The system is capable of applying a normal stress up to 600 kPa and shear velocity up to 3.5mm/s. The capacity for horizontal LVDT is 30 mm. Fig. 1 shows a frontal view of a large scale direct shear device used in this study. The device reaches the international advanced level, so it has the wide application market and developing future, and meets with design specifications and current experiment specifications.



Fig. 1 Large scale pullout direct shear apparatus.

Test Material

Sand

Uniform, clean, quartz beach sand from shores was used. Table 1 lists the grain size distribution of sand, while Table 2 shows their physical characteristics. To reduce influence of water content, dry sand was used in the tests.

Table 1 Grain size distribution of sand.

Grain composition /%				
10-5	5-2	2-0.5	0.5-0	<0.25
3.45	14.93	52.47	22.35	6.90

Table 2 Lists the physical characteristics of sand.

Property	Specific gravity	Unit weight (kN/m ³)	Moisture content (%)	Void ratio
Sand	2.643	16.74	0.15	0.5890

Geomembrane

This study uses smooth HDPE geomembrane and textured geomembrane, and they are denoted as SM and TM respectively. The geomembranes used in the tests are commercially available products in landfills and from the same manufacture (Jiangsu Jinba Limited Company). Table 3 lists the physical characteristics of these geosynthetics.

Table 3 Geosynthetic characteristics

Material	SM	TM
Thickness (mm)	1.5	1.5
Minimum density (g/cm ³)	0.939	0.939
Yield strength (N/mm)	22	22
Rupture strength (N/mm)	40	16
Injection molded (%)	12	12
Elongation at break (%)	700	100

Test Procedure

The sand used for the large scale pullout direct shear is compacted from the initial sand to the target unit weight within the shear box. The sand is compacted in three layers. The compaction of dense sand is conducted by using a steel plate which dimension is the same with style. The geomembrane is put in the lower shear plate and is fixed on the four edges of the lower shear box by some aligned bolts and four steel bars. Testing apparatus are symbolized in Fig. 2.

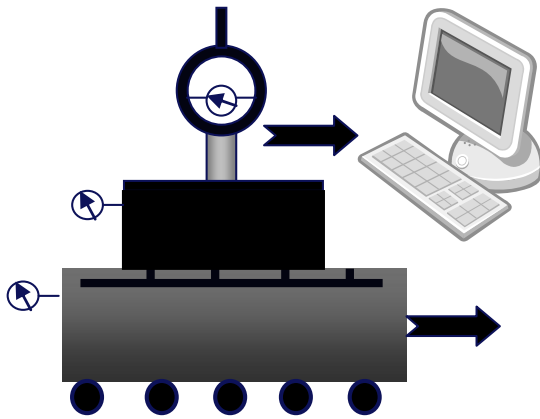


Fig. 2 Testing machine

A total of 51 shear tests were carried out to investigate the effects of test parameters. Experimental cases are shown in Table 4. The test parameters mainly include: space of reinforcement, material property and normal stress. A summary of these test parameters are as follows:

- (1) Different configurations of reinforcements (Fig. 3).
- (2) Type of materials: smooth HDPE geomembrane and textured geomembrane.
- (3) Four normal stress (100, 200, 300 and 400 kPa). According to ASTM D5321, a shear rate of 1 mm/min is used in this test. The test stops when the shear displacement reaches about 15 mm. The direct shear tests for sand/geosynthetic were conducted under the same normal stress and the same testing procedure for the sake of comparison.

Table 4 Experimental cases

Case	Type of reinforcing	Space (mm)	Normal stress (kPa)
1	SM	---	100,200,300,400
2	RM-1	---	
3	RM-2	80	
4	RM-3	60	
5	TM	---	

TEST RESULTS AND DISCUSSIONS

Shear Behavior of Sand/Geosynthetic Interface

To discuss the shear stress-shear displacement behavior of sand/geosynthetics interface, the results of direct shear

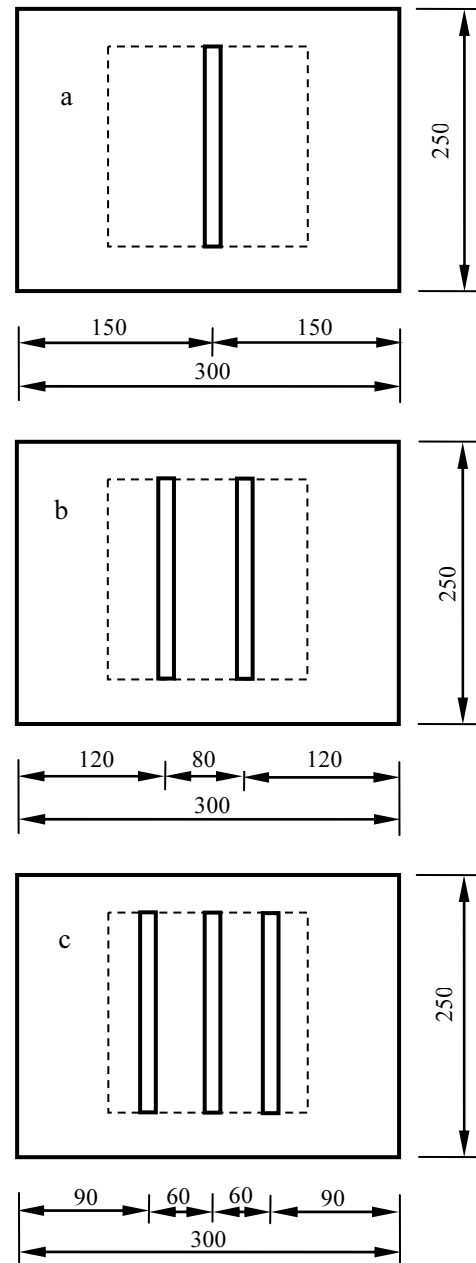


Fig. 3 Configurations of reinforcements (Unit: mm)

tests under four normal stress are presented in Fig. 4. At the initial stage, as the shear displacement is small, usually is lesser than 2mm, variation tendency of geosynthetics/sand under different normal stress is relatively uniform. Curvature of shear stress-shear displacement increases with increment of shear displacement. The results also show that there is a well-defined peak shear strength observed for smooth geomembrane/sand and reinforced geomembrane/sand interface. However, to textured geomembrane/sand, interface. However, to textured geomembrane/sand, there is no well-defined peak shear strength. In general, a peak shear stress is reached at a small shear displacement

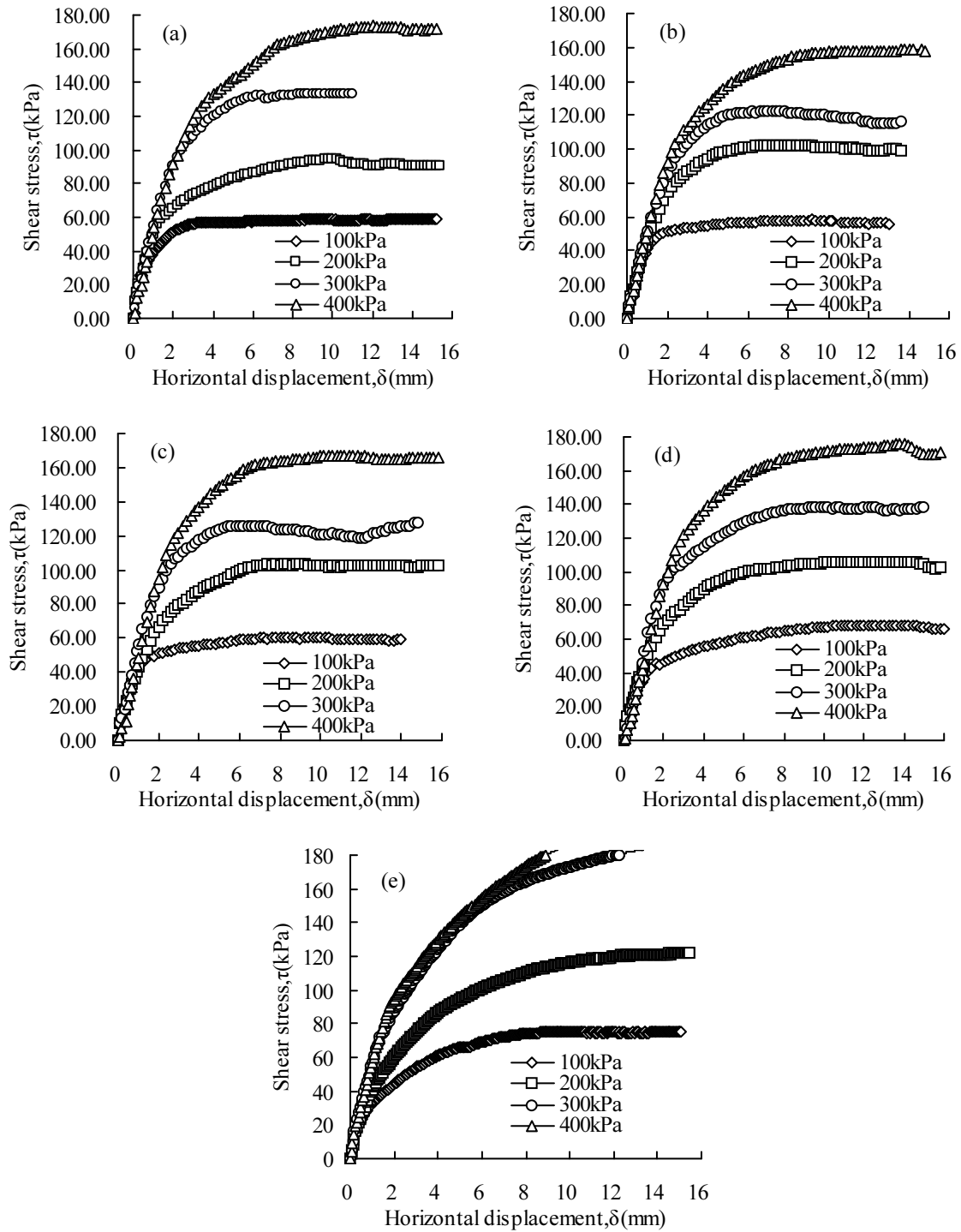


Fig. 4 Shear stress-horizontal displacement curves for: (a) SM/S; (b) RM-1/S; (c) RM-2/S; (d) RM-3/S; (e) TM/S

(usually less than 10 mm). The shear stress of the sand/textured geomembrane interface continues to increase.

Typical photographs of failed specimens are shown in Fig. 6. A close examination of the failed specimens reveals that reinforced specimen was always dropped off between reinforced geomembrane/sand, and smooth geomembrane and textured geomembrane was always drawn breakage.

Peak Shear Strength of Soils and Sand/Geosynthetic Interfaces

Fig. 7 shows the peak shear strength for sand/smooth geomembrane and sand/reinforced geomembrane interface. The best-fit line for each category is also plotted to show the general trend. The trend lines show an apparent cohesion and internal frictional angle. The peak shear strength of sand/smooth geomembrane

interface is significantly lower than the peak shear strength of sand against three-strip reinforced geomembrane under different normal stress.

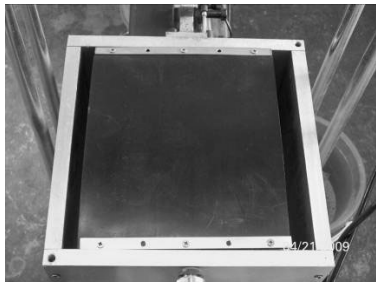


Fig. 5 Specimen in test

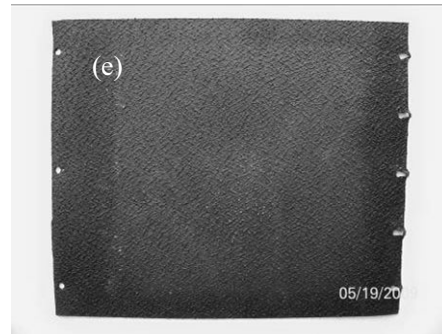
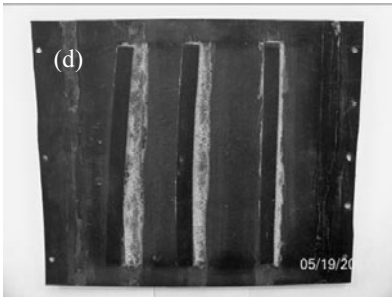
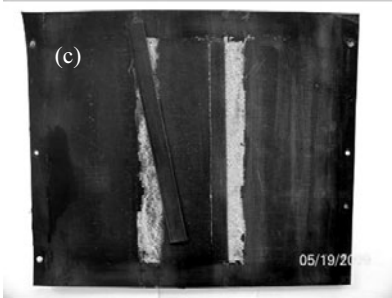
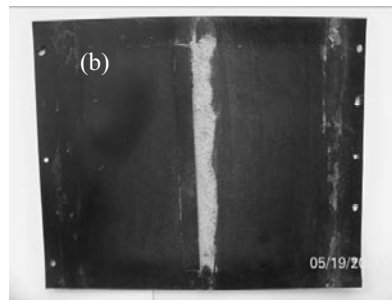
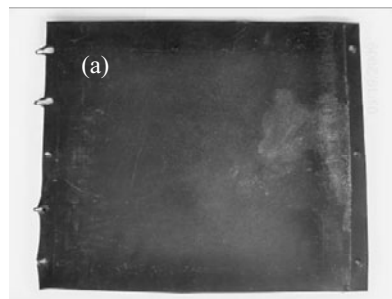


Fig. 6 Typical photographs of failed specimens: (a) SM/S; (b) RM-1/S; (c) RM-2/S; (d) RM-3/S; (e) TM/S

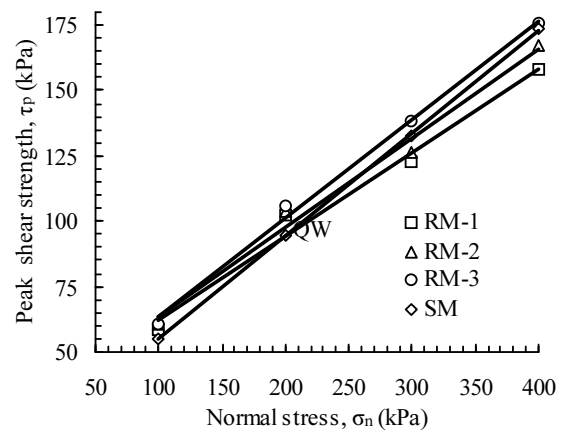


Fig. 7 Peak shear strength of sand/ geosynthetic interface under different normal stress

Reinforcing Effects

From the results of the direct shear tests about the geomembrane reinforced with strip, some conclusions can be obtained as follows:

- (1) For geomembrane reinforced with strip, the more the amount of reinforced strips, the greater is the increase in shear strength in comparison with smooth geomembrane.
- (2) With the same space of reinforcement, the shear strength of reinforced geomembrane and sand will generally be decreased with the decrease of normal pressure. So the reinforcements are also more effective under lower normal stress, as is the case for the conventional horizontal reinforcement.

CONCLUSIONS

In this paper, a new concept of geomembrane reinforced with strip was proposed. In order to study interface mechanism, a series of large direct shear tests were carried out on sand and geosynthetics. The following conclusions can be drawn:

(1) Compared with smooth HDPE geomembranes, the shear strength of reinforced geomembranes can be increased much more. And compared with textured geomembranes, rupture strength of reinforced geomembranes is higher.

(2) The test results show that there is a well-defined peak shear strength observed for the sand/smooth geomembrane and sand/reinforced geomembrane interface. However, there is no well-defined peak shear strength observed for the sand/ textured geomembrane.

(3) As the space of the horizontal reinforcements decreases, the peak shear strength of reinforced geomembrane increases.

ACKNOWLEDGEMENTS

This work was supported by the National Natural Science Foundation of China (50678100). Thanks are also owed to the reviewers for their patient review.

REFERENCES

- ASTM D5321 (2002). Standard test method for determining the coefficient of soil and geosynthetic or geosynthetic and geosynthetic friction by the direct shear method. ASTM Designation: D5321-02, ASTM, USA.
- Byrne RJ, Kendall J, Brown S (1992). Cause and mechanism of failure Kettleman Hills Landfill B-19, Unit IA. Proc. ASCE Spec. Conf. on Performance & Stability of Slopes & Embankments-II, 1188-1215.
- Hsieh C, Hsieh MW (2003). Load plate rigidity and scale effects on the frictional behavior of sand/geomembrane interfaces. *Geotextiles and Geomembranes*, 21(1):25-47.
- Fishman KL, Pal S (1994). Further study of geomembrane/cohesive soil interface shear behavior. *Geotextiles and Geomembranes*, 13(9): 571-590.
- Koerner RM, Daniel DE (1997). Final covers for solid waste landfills and abandoned dumps. ASCE Press, Virginia, USA. MUA.
- Koerner RM, Soong TY (2000). Leachate in landfills:the stability issues. *Geotextiles and Geo- membranes*, 18(5):293-309.
- Seed RB, Mitchell JK, Seed HB (1990). Kettleman Hills Waste Landfill slope failure. II: Stability analyses. *Geotech. Engrg, ASCE*, 116(4):669-690.
- Vukelic A, Szavits NA, Kvasnicka P (2008). The influence of bentonite extrusion on shear strength of GCL/geomembrane interface. *Geotextiles and Geomembranes*, 26(1): 82-90.
- Wu W, Wick H, Ferstl F, Aschauer F (2008). A tilt table device for testing geosynthetic interfaces in centrifuge. *Geotextiles and Geomembranes*, 26(1): 31-38.
- Zabielska A. (2006). Shear strength parameters of compacted fly ash-HDPE geomembrane interfaces. *Geotextiles and Geomembranes*, 24(1): 91-102.

COVERED ANAEROBIC LAGOONS WITH HDPE GEOMEMBRANE: EXPERIENCES IN DEVELOPING ASIAN COUNTRIES

Hoe-Boon NG¹, Chang-Wei QI² and Xiao-Ming TAN³

ABSTRACT: Polyethylene geomembrane, particularly HDPE is gaining widespread popularity as a sealing system in cover and bottom liner system of sludge and wastewater facilities, anaerobic/aerobic treatment ponds and evaporation ponds in animal waste facilities, etc. An HDPE floating cover system provides a more cost-effective alternative to steel or concrete storage containers. With its water-tightness and outstanding performance in various aspects, HDPE geomembrane is a suitable material that meeting the Kyoto-driven greenhouse gas emission restrictions as well as for Carbon Trading. The paper summarizes the experiences in developing Asian countries that installed floating covers on waste lagoons to achieve benefits of using Polyethylene geomembranes (HDPE or LLDPE) for biogas collection and recovery, energy production, fume and odor control, protection against evaporation and contamination of groundwater. The paper discusses the manufacturing quality assurance and quality control program, floating cover design and installation concerns. Successful case histories on the application of the polyethylene geomembranes as the floating membrane cover for anaerobic covered lagoons are also presented.

KEYWORDS: geosynthetics liner, HDPE geomembrane, wastewater, floating cover, anaerobic, methane gas

INTRODUCTION

Since its introduction in the mid 1980's, geosynthetic lining system has been extensively adopted particularly for containment in liquid and wastewater containments, sanitary landfill facilities, etc. Geomembranes have been widely accepted as standard components of geosynthetic lining systems in many containment structures. They isolate leachates generated by waste to prevent groundwater contamination, contain valuable products to prevent loss into the ground, prevent rain water from becoming leachate and avoid the contamination of groundwater. Among the plastic materials utilized for geomembranes purpose, high density polyethylene (HDPE) with its superior hydraulic and mechanical properties in combination with its greater chemical resistance and ultra violet light degradation resistance is the most widely used geosynthetic lining materials adopted for various containments applications. HDPE geomembranes serve as essentially impermeable barriers to stop or limit the migration of liquids and chemicals out of the containment.

This paper presents the application of HDPE geomembrane on wastewater treatment system. HDPE geomembrane was introduced as bottom liner system and floating membrane cover with the objectives: (i) to

enhance the anaerobic digestion activity by exclusion of air (oxygen); (ii) to enable the collection of methane gas which can be used as an alternative fuel; (iii) to reduce the effect of odor from anaerobic activity. The paper focuses on the wastewater treatment aspects based on the use of geomembrane component to provide treatment plants for wastewater and animal wastes. The two successful case studies are the covered anaerobic lagoons for animal waste ponds in Thailand and a sanitary landfill leachate treatment pond in China, which were covered with HDPE geomembrane to control odor, to prevent rodents and/or to generate electricity using the biogas (methane) collected from the waste ponds.

GEOMEMBRANE FLOATING COVER: AN INNOVATIVE SOLUTION

Today, flexible geomembrane floating cover has evolved into a proven technology for protecting water resources from evaporation, contamination and algae growth. Taylor et al. (1993) highlighted that a thorough analysis of specific site and performance-related requirements of the lining materials is needed prior to specifying an appropriate cover design. HDPE

¹ Technical Manager, GSE Lining Technology Co., Ltd., Bangkok, Thailand. Email: hermannn@gseworld.com

² Sales Manager, GSE Lining Technology Co., Ltd.- Shanghai Office, China. Email: qic@gseworld.com

³ Chief Sales Manager, GSE Lining Technology Co., Ltd. - Shanghai Office, China. Email: tanx@gseworld.com

geomembranes have been extensively used on wastewater system as substitutes for conventional materials, and working efficiently since 1980s. The significant advantages of HDPE geomembrane includes not only on its low permeability, excellent long term weathering performance and chemical resistance, but its outstanding performance in many aspects also promote it becomes an excellent liner for wastewater facilities inclusive of floating cover system. An important aspect for a floating cover system is to keep the liquid and gases contained in the pond and keep rainwater and other contaminants out, it is therefore essential that the geomembrane liner used has very low hydraulic conductivity, low gas and water vapor transmission rate. Thus, HDPE geomembrane is a well-suited candidate among the geomembrane used for floating cover system.

Practically a rigid roof structure could be constructed over the reservoirs, but the costs involved are usually high (Koerner, 1997). The use of HDPE geomembrane can be a more cost-effective solution. Herman (1999) reported that geosynthetic covers are one-eighth the cost of metal covers and feature a longer life expectancy. The HDPE geomembrane cover has a density lower than water density, floated on the surface of reservoir or liquid containment, and no infrastructure is needed to support the geomembrane, hence ease for installation. Flexible geomembrane floating covers were first installed in 1950s (Herman, 1999). However, in the past few decades, applications and installations of these geomembrane systems have increased significantly. The US Environmental Protection Agency estimated that 70% of animal residual comes from 5% of operations in US (Olsta et al. 2000). As agribusiness issues become more prominent, the foul smell manure becomes a pungent problem, since most animal waste is dumped into open pits; the environmental issues are concerned about groundwater contamination as well as odor. Encapsulating manure lagoons with a floating cover can provide a decent solution (Herman, 1999). Three direct benefits resulting from covering the animal residual pond are the odor control, rodents prevention, and the electricity generated from the biogas in the animal waste containment. At the peak time, one farmer can capture enough gas to meet 70% of his farm's electricity needs (Herman, 1999). Sadlier et al. (1994) reported that treatment systems based on geosynthetic anaerobic lagoon covers provide potential solutions to process and odor problems based on his experience in both municipal and industrial wastewater treatment facilities by utilizing HDPE geomembrane as floating cover to improve the anaerobic efficiency and allow capture of methane gas for a clean energy. Zhou et al. (2005) reported on the successfully constructed of HDPE geomembrane floating cover system for large scale leachate treatment lagoons in sanitary waste landfills of mainland China.

MANUFACTURING QUALITY ASSURANCE

HDPE geomembrane is a flexible synthetic liners manufactured from polyethylene resin with a small amount of carbon black, UV stabilizers and antioxidants. A thorough quality assurance program is needed to be established prior to the manufacturing process to ensure consistent production of quality materials that meeting the project specifications. The manufacturing quality assurance (MQA) program consists of three stages, which starts with proper selection of highest quality raw materials. All the raw materials have to meet the geomembrane manufacturer's specifications and pass the acceptance of conformance tests prior to their utilization. The resins used in HDPE geomembrane requires to exhibit remarkable oxidation degradation and stress crack resistances. Heat and UV stabilizers are normally blended with the virgin polyethylene resin to improve the longevity of the material in exposed condition. During the manufacturing process, an electrical spark detector is necessary to provide immediate notification of pinholes and defects in the finished product. No fillers and leach-able additives are allowed as to ensure the HDPE geomembrane maintains excellent resistance to brittleness that may occur over time when plasticizers are used. A series of laboratory conformance tests shall be conducted to form the final examination on the finished products meeting the project specifications. The finished products are sampled for laboratory conformance tests as per the test frequency stipulated in the project specification and in compliance with the manufacturer's established minimum test frequency. All the geomembranes must pass through various industry standards on laboratory quality conformance tests, meeting manufacturer's minimum requirements and project specifications.

CASE HISTORIES

This section describes case histories on the application of HDPE geomembranes as floating cover system in developing countries include animal waste lagoons of a hog farm located in Thailand and a large scale leachate treatment ponds of municipal solid waste (MSW) landfill in mainland China.

Animal Waste Lagoon in Thailand

In this case study, two existing open animal waste ponds in a hog farm located at Chonburi province, Thailand were covered with HDPE floating covers with objective to control odor, prevent rodents and to generate electricity using the biogas collected from the waste ponds. The farm at that time had more than 2000 hogs in barns, which can produce large quantity of animal waste.

There are two existing open waste ponds (WP1 and WP2) of 130 m by 45 m (WP1) and 220 m by 24 m (WP2), to contain the excretion. One side of the waste ponds are two Evaporation Ponds constructed to contain the degraded overflow from the waste ponds. On the other side there are pig barns, where the animal residual is supplied to the waste ponds. The pungent smell from the two open impoundments and heavy fly concentration resulted in complaints from the neighbors. Considering the neighbors' complaints and the potential of utilizing biogas for electricity, the farm owner decided to cover the waste ponds with geomembrane floating covers.

As shown in Fig. 1, the animal waste pond is 7 m deep with designed slope angle of 45°. The perforated gas collection pipe was installed around the edge of the pond, its diameter is 100 mm. The cross section of the anchor trench is 500 mm by 500 mm in square with one meter long runoff from the pond edge and was backfilled with soil for anchoring purpose.

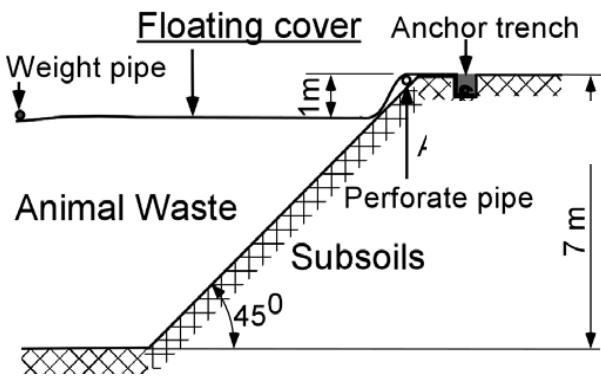


Fig. 1 Cross section of waste pond with adequate anchor trench design

The layout of the geomembrane cover of WP1 is shown in Fig. 2. There are 20 panels seamed together to cover the pond of 130 m by 45 m in dimension. On the surface of the floating cover are the weight pipes (e.g. storm water weight pipes and lateral weight pipes). The storm water weight pipes were 3.0 m long each, with a diameter 150 mm; they are HDPE pipes filled with sand and are very flexible. The storm water weight pipes are one of the most important parts in the floating cover system (Zimmel, 2000). These pipes are located such that they can most effectively maintain tension in the cover while taking out the slack material. The storm water weight pipe takes the slack out by forming a trench in the cover as shown in Fig. 3 for WP1. The trench also serves as water collection passage on the cover. The storm water weight pipes are positioned along the central axis of the pond. An important function of the floating cover on the waste pond is the containment and transport of generated biogas in this project.

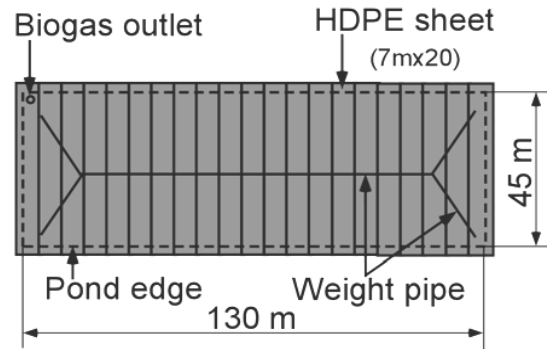


Fig. 2 Layout plan of floating cover system for WP1



Fig. 3 Storm water weight pipe (Top) and connection pipe from the excretion pond (Down)

The gas collected from the perforated pipe is transferred to the biogas generator to generate electricity through the gas extraction pipe as shown in Fig. 3. Gas extraction from the waste basin is accomplished through a single pipe fitting in the cover. The pipe is connected to the generator. Two biogas generators were installed on this project to serve the two pig waste ponds respectively. Similarly, WP2 waste pond was installed with the HDPE floating cover, where 33 panels were seamed together to form the floating cover. The installation was successfully completed by local experienced geosynthetic liner installer in Thailand. Besides that, the floating cover application in this project has been put into operation of generating electricity. The electricity is used to heat water for the farming operations. The pungent odor is effectively controlled by the cover, and it also cut off the access of the rodents to live on and in the waste

ponds, eliminating the risk of the disease from rodents to the livestock.

Sanitary Landfill Leachate Treatment Pond in China

The project site is the largest MSW landfill located in Shanghai, the largest city in China and is the centre of the Chinese economy. The high economic growth in China has been rapidly increasing the country's electricity demand, causing a serious power supply shortage, primarily in coastal regions. In view of this, the Government of China is promoting the twin goals of the development of the energy sector and energy saving. In terms of energy development, the main focus is placed on the development of power sources, development of alternative and renewable energies. Meanwhile, the vigorous consumption accompanying the rapid expansion of industrial production and economic development has made the issue of waste (pollution by solid waste) a serious problem. In urban areas, the generated volume of solid waste has been increasing at an average annual rate of more than 8%. According to World Bank Report (2005), until 2007 Chinese municipalities generate about 190 million tons of solid waste per year and, by 2030, this is expected to increase up to 480 million tons, nearly double the amount the United States is projected to produce over the same period. At most landfill sites in China, methane gas is produced from waste, causing not only a serious impact on global warming but also worsening the local environment in terms of bad odor and fire hazard. This project aims at collecting landfill gas, the main constituent of which is methane, and using this landfill gas for power electricity generation. The project was conceived and planned to improve environment using landfill gas as a clean energy source and to contribute to the sustainable development of the project through environmental and economic benefits.

The methane gas collection and utilization project is a type of CDM project which is given priority by the Government of China. Hence, the project of the collection and utilization of landfill gas for power generation at the project site matches the CDM policy of China. Located at Laogang town, Nanhui district, about 60 km from the city center, the Shanghai Laogang MSW landfill site has an area of some 600 ha and some 6,000 tons of waste are currently disposed of at this site per day. The project aims at collecting landfill gas, which is a green house gas produced at waste landfill sites with the main constituent of methane gas, and utilized this landfill gas for power generation. Under the CDM Project, landfill gas collection wells will be installed at the site and the collected methane gas will be fed to a gas engine for power generation after pre-treatment by a gas adjuster. The generated electric will be sold except for the portion used by the landfill site and the surplus gas

will be burned by flaring. In this case study, the leachate treatment pond for one of the landfill cells in Shanghai Laogang MSW Landfill was covered with floating covers using HDPE geomembrane of 2.0mm in thickness with the objective to enhance the anaerobic digestion activity, and to collect the biogas from the waste leachate ponds. The floating cover geomembrane was deployed successfully by a local experienced geosynthetic liner installer. Fig. 4 shows the completed geomembrane floating cover system with floats design.



Fig. 4 A Completed HDPE Geomembrane Floating Cover System in Shanghai, China

DEPLOYMENT AND FIELD QUALITY ASSURANCE

The installation of geomembrane floating cover requires experienced installer and welders. Generally, the installation involves: (i) Anchor trenches to be excavated around the existing ponds (refer to Fig. 1); (ii) the floating cover is arranged and placed into position. HDPE floating covers are generally deployed and seamed on the empty ponds. But in the case where the existed waste ponds are fully functioning, an alternative installation was adopted. HDPE geomembrane can be cut into the required dimensions and the panels were seamed on land with an overlap seaming width of about 150 mm. With assistance of a floating bamboo raft or pontoon on the waste, pulling by a mechanical device, the floating cover was positioned as predetermined; (iii) the floating cover can be anchored in the anchor trench with an optional of anchor nails at a close spacing (1m to 2.5m) around the pond, and the trench is then backfilled with soils or concretes. (iv) weight pipes are allotted on the floating cover as per the design (See Fig. 2).

A proper geomembrane installation and associated construction quality assurance (CQA) is crucial to the long-term performance of lining system. A CQA plan is usually developed before construction and used during construction to guide observation, inspection, testing and documentation of all field records. The prevailing wind

problem is usually the major concern during installation. After deployment, the liners were left in place and sandbags were arranged on the edges as ballast and counterweight. Extra caution is necessary on windy site to prevent a blow-out situation, which may cause serious damage and injury to site personnel. In common practice, at the end of a shift, or in any area that will be left with an open edge, at least one continuous row of sandbags shall be placed on the leading edge of the liner.

A series of construction quality assurance (CQA) program is important to ensure the leak-proof and long term performance of the floating cover. It is necessary to be extra careful during the installation process as to prevent equipment or personnel from damaging the liner. The seaming of polyethylene geomembrane always requires well-trained personnel and suitable welding equipments. It is also necessary to ensure the materials to be welded shall be wiped clean of moisture, dust and debris prior to the field welding. During the deployment of the initial geomembrane rolls, trial welds are usually conducted on the same type of materials used on this project. This is mainly to verify the seaming conditions are similar to operation condition and to ensure that the equipment functions properly. The trial welds are then subjected to field destructive tests to qualify the welding and the equipment used before the actual field seaming works. After the seaming works, a series of installation quality assurance tests include non-destructive and destructive weld tests, are carried out in order to ensure the welding quality at site fully compliance with the design requirements and the equivalent recognized testing standards. The most common methods of non-destructive seam testing adopted in the field are air pressure testing and vacuum-box tests.

The primary welding technique using thermal wedge welder creates a double-track weld, leaving an air channel in between these two weld tracks, which can then be used to non-destructively air pressure test the integrity of the seam. When the seam is completed, both ends of the air channel are sealed off and the seam is pressure-tested to determine its continuity. The non-compliance seams shall then be patched with extrusion welding techniques before retesting. The non-destructive vacuum-box testing is used to check the continuity of wedge weld seam, extrusion weld seams, repairs and patches that is not practical to conduct air pressure test. Fig. 5 shows the non-destructive air pressure test is in progress.

Destructive seam testing is used to evaluate bonded seam strength, which involves cutting out a section of the seam and tested until failure is attained. Test strips are cut from the section and tested on site. The destructive samples are tested for shear-strength and peel-strength values, carried out in accordance to ASTM D 6392. The sampling frequency can be referred to

method of attributes as described in GRI-GM14 in order to minimize the samples taken and cut-off from the proper welded seams. The destructive shear test involves application of a tensile stress from the edge of one sheet, through the weld to the edge of the adjoining sheet. For peel test, the overlapping portions of the sheet are pulled in opposite directions to observe weld separation behavior. Fig. 6 shows the specimens for destructive tests of seam shear strength and peel strength tests



Fig. 5 A Non-destructive air pressure test is in progress.

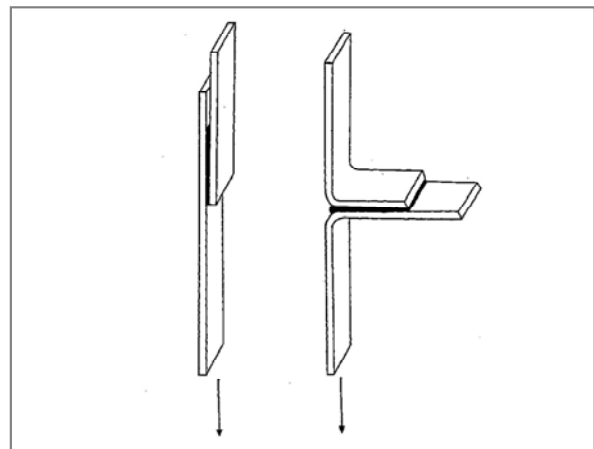


Fig. 6 Field destructive seam test specimens for: (i) Shear strength, and (ii) Peel strength tests

DISCUSSIONS AND CONCLUSIONS

With the fast-growing of carbon development mechanism projects for the sake of reducing emissions of greenhouse gases and to improve the global environment by using a clean energy source, many investors have focused on the abundant resources of carbon market in Asia. A more environmentally friendly alternatives of treating and releasing waste products than a traditional compacted clay liner has become a new

trend in this century. To prevent the environmental pollution such as algae blooms and groundwater contamination, HDPE geomembranes are gaining widespread popularity as a sealing system in floating cover system of sludge and wastewater facilities, anaerobic/aerobic treatment ponds and evaporation ponds in animal waste facilities. With its outstanding performance in various aspects, impermeable HDPE geomembrane provides a more cost-effective alternative to other storage containers and is a well-suited material that meeting the Kyoto-driven greenhouse gas emission restrictions.

The paper summarizes the Asian's experiences of using HDPE geomembranes to serve as lagoon gas containment and collection, odor control, and protection against evaporation or contamination of groundwater. Two case histories on the application of HDPE geomembranes as floating cover system for anaerobic lagoons of a MSW landfill leachate treatment pond and for the animal waste ponds that enable methane gas collection for an alternative electric power generations in Asia are presented in the paper. Since different covers suit different types of lagoons, it is important to conduct a complete evaluation and diagnosis of the critical factors for geomembrane installation and the operational requirements specific to floating covers. It is therefore recommended that a competent and experienced designer be consulted to review the design and application. A proper selection of high quality geomembrane liner and engage suitable geomembrane specialist contractor associated with a proper construction quality assurance (CQA) program are always crucial to the long term performance of geomembrane floating cover system.

From the successful case studies in the developing Asian countries at recent years, it can be concluded that with strong motivation and support from carbon trading and the trend of utilizing renewable energy source as a cost-effective global climate change mitigation, these can be of great economic value and environmentally sound in promoting the applications of HDPE bottom liners and floating cover system in the anaerobic waste lagoons that are capable of controlling the odor problem, offer potential for improved anaerobic activity and biogas utilization in an energy conscious century.

ACKNOWLEDGEMENTS

The author would like to express his greatest appreciation to Mr. Newby M. of Golder Associates

(HK) Ltd., Mr. Wang Y. of Shanghai Municipal Engineering Design General Institute, Mr. Zhou X. and Mr. Wang Y. of Shenzhen Shengyi Environmental Co., Ltd., China, VES-CITIC Pacific Co., Ltd. Consortium-Shanghai Chengtou Environmental Industries Dev. Co., Ltd. JV, Genesis Geo-Technical Co., Ltd., Thailand, Dr. You G. of University of Ballarat, Victoria, Australia, Mr. Boonchai D. and Mr. Suwit J. of GSE Lining Technology Co., Ltd. for their contribution in this paper.

REFERENCES

- Herman A (1999). Floating Covers Usage for Tanks Is Growing, *Geotechnical Fabrics Report*, 17(7):26-29.
- Ivy N & Corrigan C (2000). Animal Waste Containment Using Geosynthetics, *Geotechnical Fabrics Report*, 19(5): 30-33.
- Koerner RM (1997). *Designing with Geosynthetics* (4th edition), Prentice Hall, Upper Saddle River, New Jersey 07458.
- Olsto JT, Fishman S, Wright G (2000). GCLs for Animal Waste Containment, *Geotechnical Fabrics Report*, 18(5): 30-33.
- Sadlier MA, Russell J, Harris M (1994). Innovative Geosynthetic-Based Waste Water Treatment Systems, *Proceeding of Fifth International Conference on Geotextiles, Geomembranes and Related Products*, Singapore: 1057-1062.
- Taylor RT & Schader LR (1993). *Geomembrane Floating Covers: Technology for the Nineties*, *Geosynthetics '93 Conference Proceedings*, Vancouver, Canada, IFAI: 1161-1172.
- World Bank Report (2005). *Waste Management in China: Issues and Recommendations Solid Waste*, <http://siteresources.worldbank.org/INTEAPREGTOP/URBDEV/Resources/China-Waste-anagement1.pdf>
- Zhou X, Yang X, Yuan Z, Yang H, Xu Y (2005). An Introduction on Floating Cover System for Sanitary Landfill Leachate Treatment Pond, *Shenzhen Shengyi Technical Literatures on Sanitary Landfills*: 37-39. (In Chinese)
- Zimmel E (2000). *Floating Cover Design*, GSE Interior Technical Notes.

LESSONS LEARNED FROM THE NUMERICAL MODELLING OF A RETAINING WALL WITH NON-UNIFORM REINFORCEMENTS

Xiang-Jing HUANG¹, Ze LIU² and Vicari M³

ABSTRACT: A research program focused on the performance of a full scale test on a wrapped-face retaining wall reinforced by two types of reinforcement materials embedded in sand is presented. To evaluate the complex behavior of such structure, a 3.6 m high retaining wall was constructed and instrumented, then loaded to failure. Plane-strain numerical analysis have been performed using FLAC in order to model the reinforced soil structure taking into account the sequential bottom-up construction of the wall facing, soil, reinforcement and surcharge. This allowed to evaluate whether the measured stress-strain and collapse behavior of the wall can be fitted by the conventional limit-state equilibrium methods or if a more sophisticated method which takes into account the different linear stiffness of the reinforcements, such as the Displacements Method, must be used. To this purpose a new software has been developed and validated to perform reinforced walls stability analysis using different types of reinforcements and complex design scenarios. This research provides guidance to the design of retaining wall with non-uniform reinforcements.

KEYWORDS: a retaining wall with non-uniform reinforcements, numerical modeling, Displacements Method, full scale instrumented walls

INTRODUCTION

The use of reinforcements with different mechanical properties (i.e. strength and stiffness) allows engineers to obtain more economical designs, as they can benefit from positive aspects of both materials, thus reducing the cost of reinforcement while maintaining adequate internal stability. However, as pointed out by Hatami et al. (2001) the use of reinforcement layers of different deformability may give rise to load concentrations in the stiffer layers that must be carefully checked in order to avoid unforeseen overstressing of the reinforcements.

To the present this kind of mixed structures have been the subject of numerical analysis to investigate their structural response, but no reliable results are available in the literature on full scale instrumented walls reinforced with materials having different linear stiffness.

The results of this study are aimed the two following objectives: to check the influence of the different reinforcements deformability both in design and collapse conditions; to evaluate whether the conventional limit equilibrium methods can be applied to non-uniformly reinforced structures or if a more sophisticated approach (i.e. kinematic compatibility concepts: Lemonnier et al.

1998) such as the so called "Displacement Method" proposed by Gourc et al. (1986) should be used.

WALL TEST FACILITY

The first test model had been constructed in the Static Tests Facility of the Civil Engineering Laboratory of ENEL-HYDRO in Sierate, Italy, and the second model for further research was constructed in Center South University, China. The internal dimensions of the rigid test tank were 2130×5100×4000 mm.

Soil and reinforcements

The soil adopted as fill material was a medium uniformly graded natural silica sand whose strength and deformability parameters are:

peak friction angle $\phi'_p = 43^\circ$

drained cohesion $c = 0$

constant volume friction angle $\phi = 34^\circ$

small strain shear modulus $G = 0.7kPa$

¹ Senior Engineer, School of Building, South Central University, China
 Hunan Provincial Communications Planning, Survey & Design Institute, China. Email: hncshxj@163.com

² Ph.D Student. School of Building, South Central University, China. luckzeliu@163.com

³ Technical Cooperation with Subsidiaries. Officine Maccaferri S.P.A. Italy. marco.vicari@maccaferri.com

The sand was subjected to direct shear tests in a large direct shear box in order to determine the direct sliding interaction coefficient (α_{ds}) from both soil to reinforcement and soil to soil direct shear tests (Vicari and Duran da Silva, 2003). The two adopted reinforcements are:

- (1) a double-twisted steel wire mesh;
- (2) a polyester geogrid.

Model Instrumentation

A wrapped-face wall 2.0 m wide has been constructed up to a total height of 3.6 m consisting of 6 reinforcement layers alternatively placed: the bottom layer is made with woven wire mesh, over which a layer made with geogrid is laid and so on (Fig.1 and Fig.2). The wall is battered with a 20° sloping face angle from the vertical.



Fig. 1 Test model

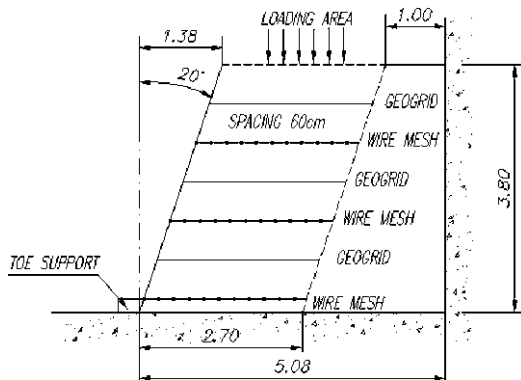


Fig. 2 Cross section of the model

The loading was applied through a steel plate 1.9×1.1 m, further loading was applied by a hydraulic system acting on the plate through a spherical joint. A total of 70 instruments were deployed in the model wall.

The analysis of all measurements gathered during loading phase and the observations of the integrity of the reinforcements after material removing at the end of the test, allowed for the determination of the failure surface (Fig. 5).

FLAC^{2D} NUMERICAL MODELLING

Numerical modelling of both the pullout tests and the wall was carried out by means of a two-dimensional finite difference code (FLAC^{2D}).

A sub-routine was added to the commercial version of the code in order to implement a new non-linear constitutive law for granular soils.

The adopted numerical model consists of the following three elements: soil, reinforcements and interface between soil and reinforcement; their constitutive relationships are described hereafter.

Soil, Reinforcements and Interface

Soil model adopted for silica sand is a non-linear elastic model associated to a Mohr-Coulomb failure criterion with allowance for dilatancy and post-peak softening.

Non linear stress-strain behaviour is taken into account by means of a shear modulus degradation law of the hyperbolic type.

Both reinforcements were modelled through a linear elastic, one-dimensional axial element (cable) with no flexural rigidity and yielding only in tension, characterised by the following tensile strength T_{ult} and linear stiffness J :

Wire mesh: $T_i = 50kN/m$, $J = 500kN/m$;

Geogrid: $T = 30kN/m$, $J = 186kN/m$.

The interface has been modelled through “grout” elements represented by “spring-slider” systems located at the nodal points (Fig. 3).

The shear behaviour of the “grout” elements during the relative displacement between reinforcement and soil is numerically described by a linear elastic, perfectly-plastic relationship (Fig.4) characterised by the following parameters:

K_b : interaction (bonding) stiffness coefficient;

τ_b : ultimate (bonding) shear strength.

Furthermore a purely frictional model (i.e. zero cohesion) has been assumed for τ_b according to the expression $\tau = \sigma \alpha \tan \varphi$, where α_b is the interaction (bonding) strength coefficient.

Values of α_b and K_b were evaluated from back-analysis of pullout tests at best fit of the load-displacement curves obtained in such tests.

FLAC Analyses

A 4 nodes grid made of 3656 elements, 3800 mm in height, 5400 mm (at the base) and 3800 mm (top) in length, was adopted in FLAC calculations (Fig. 3).

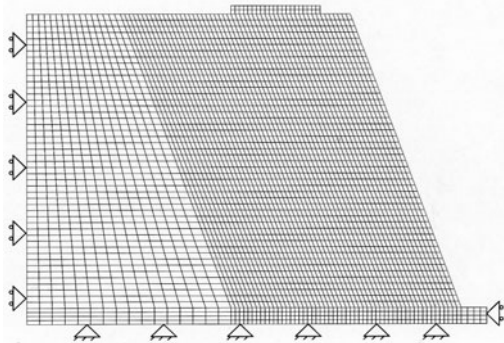


Fig. 3 FLAC wall modelling

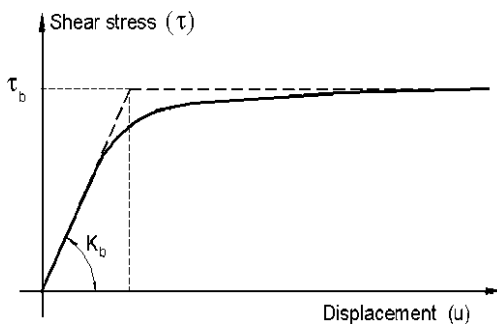


Fig. 4 Shear behaviour of the grout elements

Side walls were considered to be rigid and perfectly smooth, while the wall bottom is blocked. The load plate is modelled through a series of very stiff elements, free to sustain plane displacements and rotations, connected to the soil through a purely frictional interface, characterised by a friction coefficient $f = 0.7 \tan \phi$

Reinforcements within the soil were modelled through horizontal “cable” elements; for those of the facing, the interface parameters (f_b , K_b) have been halved in order to take into account that the soil-reinforcement contact only occurs on one face; this device was also used where reinforcements were overlapped.

The end of the wall construction has been assumed to start the load steps modelling. The initial tensional state has been evaluated by considering for the soil its Proctor density ($\gamma = 15.6 \text{ kN/m}^3$), while the compaction effect has been taken into account by modelling the variation of the effective horizontal stress with the soil depth, through a bilateral law.

The following loading phase has been divided into 18 load steps of 314 kN each, except for the last one set to 98 kN. At the beginning of each load step, the initial

tensional state was set to the value resulting from the previous step, together with the parameters related to the tensional and/or deformative state (G, ϕ, K).

The numerical analysis started from the completely executed wall; at the beginning of each load step the tensile loads in the reinforcements were checked not to exceed their nominal breaking load. While the dilatancy angle δ' has been taken equal to 17° , the analysis covered two cases in terms of soil peak friction angles ϕ'_p :

$$\phi = 47^\circ \text{ in triaxial conditions}$$

$$\phi = 53.5^\circ \text{ in plane strain conditions}$$

FLAC RESULTS WITH ϕ'_{pp}

Failure Surface and Settlements

Fig.6 shows the calculated surface of the maximum soil plastic shear deformations vs. the surface of the highest reinforcement tensions; the good correspondence with the measured surface (Fig.5) suggests that the modeled failure surface is slightly longer than the experimental one. It cannot be excluded that at the end of the loading phase the experimental wall did not reach a definitive collapse, thus originating a not completely developed failure surface: the modeled curve is substantially coincident with the experimental one but for the zone between layers 2 and 3.

Apart from the last load step, the calculated settlements of the load plate are very close to the measured ones, both along the plate edges and at its centre. The differences between measured and calculated values are equal to 13% at the plate centre and 10% at the upper edge.

Calculated and measured settlements along the reinforcements plane show a very good correspondence, especially those located close to the load plate (reinforcements 5 and 6), where differences are not greater than 17 %.

Lower reinforcements show higher differences (30-35%) and this is basically due to the lower precision caused by the very small deformations to be measured.

Tensile Forces in the Reinforcements

Fig. 6 shows the tensile forces in the reinforcements at the last load step: as a general rule it appears that wire mesh elements are more loaded than geogrids. The analysis of the central sections, where stresses are higher for both reinforcements, gave the following calculated forces:

$$\text{wire mesh: } T_w = 42 \text{ kN/m};$$

$$\text{geogrid: } T = 19 \text{ kN/m}$$

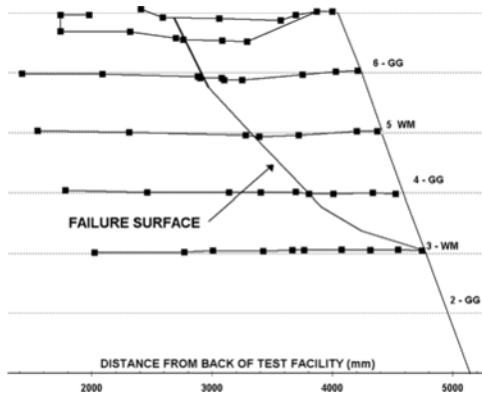


Fig. 5 Measured failure surface

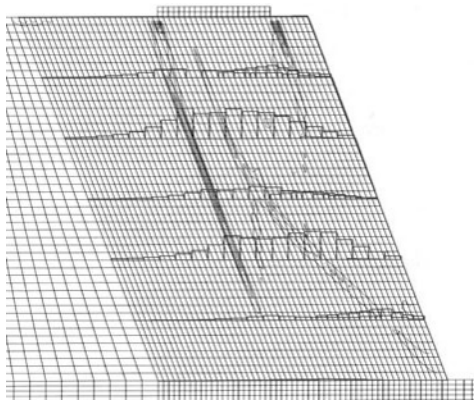


Fig. 6 Modelled soil plastic shear deformations and reinforcement loads.

The ratio T_w / T is equal to 2.26, which is in accordance with the corresponding ratio between the reinforcements linear stiffness modulus $J_w / J = 2.69$. Therefore, the maximum calculated longitudinal deformations are respectively 9% for the wire mesh and 10 % for the geogrid, which are close to the breaking values also measured in the experimental wall.

FLAC RESULTS WITH ϕ'_{pt}

Fig.7 shows the soil plastic shear deformations obtained with ϕ' at the last load step: the critical surface is very close to the corresponding ϕ' one shown in Fig.6.

As per the deformative state, however, the calculated values are considerably higher (65 to 75 %) than the corresponding ϕ'_{pp} ones and those measured in the experimental wall.

This is in accordance with the recent findings based upon a back-analysis on a large number of reinforced

soil structures and indicating that the peak plain strain friction angle controls the internal capacity of geosynthetic structures (Allen e Bathurst , 2001).

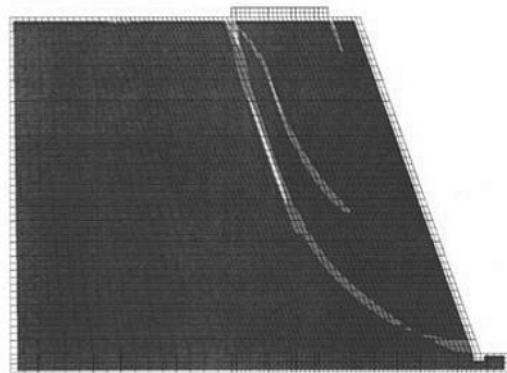


Fig. 7 Plastic shear deformations with ϕ'_{pt}

THE DISPLACEMENTS METHOD

The Principle of Displacements Method

Under the hypothesis of Limit Equilibrium, the slope stability analysis takes into account the reinforcements as concentrated forces situated along the considered surface, at the intersection between the reinforcement and the surface itself.

The module of these forces is taken as the minimum between the breaking load of the reinforcement and the pullout one, both reduced through appropriate safety factors that depend upon the adopted standard.

This approach is based on the implicit hypothesis that all reinforcements always work in a synchronic way, whatever is their geometric configuration and their linear stiffness.

These hypothesis are convenient because strongly simplify the computation procedure, but from a mathematical point of view it is coarse and not protective. In fact, to assume the synchronic loading of the reinforcements located along the given surface, means to take into account the configuration which maximize the stabilizing forces given by the reinforcements.

A more restrictive approach (see par. 4.3), points out that the different stiffness of the reinforcements imply a non-uniform distribution of the forces, which are taken at first by the stiffer reinforcements and then by the weakest ones.

In technical literature a computation method called “Displacement Method” is available, which can evaluate the varying reinforcement performances caused by different stiffness even in conditions of rigid equilibrium. Therefore, the Displacement Method is not a calculation method to evaluate the slope stability: it is a procedure

used to define the strength pattern, along the considered sliding surface, simulating the presence of reinforcements.

The stability analysis is made in rigid equilibrium conditions so that even the classical formulations (Bishop, Janbu, etc.) remain unchanged. The limit of the Displacement Method is the need of circular sliding surfaces. The procedure to evaluate the forces simulating the presence of reinforcements in the stability analysis is shown hereafter:

Once defined the sliding surface for which the safety factor has to be found, a rigid rotation along the surface itself is applied.

This rotation causes in each point of the sliding surface a movement $\delta = R d\alpha$, where R is the radius of the sliding surface and $d\alpha$ is the rotation angle. If the movements are very little, and this is acceptable for slope stability analysis, the δ movement can be taken as straight.

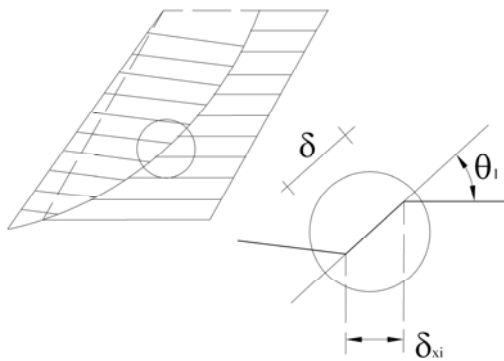


Fig. 8 Horizontal component δ_{xi} of the elongation of the reinforcement

This movement δ corresponds to the elongation of the reinforcement in a tangential direction to the sliding surface, therefore only the horizontal component δ_x is the cause of the reacting forces;

The effective component for the reinforcement can be calculated as $\delta = \delta_x \cos \theta$, where θ is the angle between the reinforcement and the tangent line to the sliding surface at the intersection with the reinforcement (Fig.8); knowing δ_x for all reinforcements and their linear stiffness K_i , it is eventually possible to determine the relevant force $f = K \delta$ thus defining the reinforcements strength pattern along the sliding surface.

A new software has been developed in compliance with the previous premises and, apart from the conventional limit equilibrium approach (Bishop, Janbu), allows to automatically adjust the pullout stiffness of the reinforcement layers according to the actual failure surface considered in the stability analysis.

The Result of Displacements Method Analysis

By assigning the failure surface and step-loading the structure. The main results of the Displacements Method analysis are: the experimental collapse conditions (FS=1; $q=784$ kPa) have been obtained with a value of the friction angle close to φ , in accordance with the FLAC results; the calculated vertical settlements are almost the same as the measured ones and tend to be higher only when the applied load is close to collapse (Fig. 9); the maximum value of FS is achieved for all the load steps by imposing a strain in the wire mesh reinforcements equal to 18%; the condition FS=1 is achieved for $q=650$ kPa, at which corresponds a vertical settlement of the wall top front equal to 40 mm.

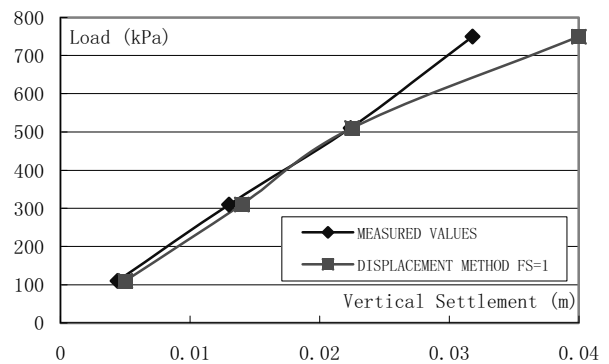


Fig. 9 Macstars vs. measured settlements

In conclusion the Displacements Method implemented has shown a very good capability in modelling the design conditions, that is far from the collapse conditions, which is the normal case the designers have to deal with.

On the contrary, the plasticizations occurring both in the soil and in the reinforcements before collapse do not allow the software to fully reproduce the experimental conditions at failure.

CONCLUSIONS

A full scale test on a locally surcharged non-uniformly reinforced soil structure has been carried out to evaluate the stress-strain response of the two adopted reinforcement materials with different linear stiffness (double-twisted steel wire mesh and polyester geogrid).

The combined analysis of the measured deformations (within and outside the reinforced soil structure), and that of the visual inspection on the reinforcements sheets during the exhumation of the wall, allowed for the thorough determination of the failure surface.

The interpretation of the results and the numerical modeling activity has allowed to evaluate whether the calculation methods normally used for analyzing the stability of the reinforced walls can be applied also to non-uniformly reinforced soil structure or if more sophisticated approaches (such as the Displacement Method or other similar ones based on kinematic compatibility concepts) which take into account the different linear stiffness of the reinforcements should be used.

The software, implemented with the Displacements Method, has shown to be able to provide reliable information about soil settlements, stress and strain pattern of the reinforcements and safety factor without the need of a more time consuming numerical analysis such as the FLAC one.

This demonstrates that a simpler tool can be successfully used to know the actual behavior (i.e. stress and strain pattern) of a reinforced wall with non-uniform reinforcements in design conditions.

A more exhaustive validation of the software shall be obtained in the next future, after the completion of the analysis of different real non-uniformly reinforced, variable in geometry, load conditions and reinforcements pattern.

REFERENCES

- Allen TM & Bathrust RJ (2001). Prediction of Soil Reinforcement Loads in Mechanically Stabilized Earth (MSE) Walls. Final Research Report prepared for Washington DOT (USA).
- Ghionna VN, Fioravante V, Vicari M (2002). Full scale test on a retaining wall with non-uniform reinforcements. 7th ICG, Nice..
- Gourc JP, Ratel A, Delmas P (1986). Design of fabric retaining walls: The displacement method, 3rd International Conference On Geotextiles, II: 289-294, Vienna.
- Hatami K, Bathrust RJ, Di Pietro P (2001). Static Response of Reinforced Soils Retaining Walls with Non-uniform Reinforcements. The International Journal of Geomechanics: Volume 1, Number 4' 477-506.
- Lemonnier P, Soubra AH, Kastner R (1998). Variational displacement method for geosynthetically reinforced slope stability analysis: I. Local stability, Geotextiles and Geomembranes 16: 1-25, Elsevier
- Vicari M & Duran da Silva J (2003). Interpretation of direct shear and pullout tests on double-twisted steel wire mesh reinforcements. Geosinteticos 2003, Porto Alegre.

EXPERIMENTAL STUDIES OF ARCHING EFFECT AND GEOSYNTHETIC DEFORMATION IN LOCAL SUBSIDENCE PROBLEM

Deng GAO¹, Bin ZHU², Yun-Min CHEN³, Tony L. T. ZHAN⁴ and Xiang-Zhi WANG⁵

ABSTRACT: For vertical landfill expansion, high-strength geosynthetic reinforcement is being applied to minimize the deformation of a composited liner system caused by local subsidence in the existing landfill. In this study, a small-scale test device was developed to model the local subsidence problem. A kind of PVC geomembrane (GM) was used to simulate the geosynthetic reinforcement in the composite liner system. A total of six tests were conducted to evaluate the effect of filling height and GM stiffness on the soil arching and the GM deformations. The test results shown that the filling height and GM stiffness have little influence on the final pressure acted on the deflected GM. The GM stiffness can heavily influence its deformation in a certain range, while the influence decreases with the increase of the GM stiffness. Finally, the tests results were compared with those calculated by the current design method.

KEYWORDS: landfill, composite liner system, geomembrane, arching effect, strain

INTRODUCTION

The expansion of the existing landfills is presently being undertaken in many cities of China due to the social and political problems associated with identifying new landfill sites (Zhan et al. 2008). According to new regulations in China (CJJ 17-2004), a composite liner system involving sealing materials must be installed at the bottom of the expanded landfill. However, voids or local subsidence are often created by progressive degradation and collapse of large objects buried in the existing landfill. The voids can cause "localized" deformations and strains of the composite liner system. If the induced tensile strain in the liner system exceeds the tensile capacity of the sealing materials, tension cracks or tensile failure will be made. The tension cracks will reduce the effectiveness of the liner as a hydraulic barrier by providing a direct flow path through the composite liner system (Jang and Montero, 1993).

At present, high-strength geosynthetic reinforcement is being applied to minimize the deformation of a composited liner system caused by local subsidence in the existing landfill. The design method is based on a worst-case scenario assumption that a void is located immediately underneath the composite liner, and was

developed considering soil arching theory for the fill materials overlying the reinforcement with the tensioned membrane theory (Giroud et al. 1990, Qian et al. 2001, Kuo et al. 2005). However, these design methods are rather theoretical. It is well known that the degree of soil arching is dependent on the various factors, such as geosynthetic stiffness, overburden height, direction of deformation, soil characteristics, etc. Many experiments have been conducted to study the soil arching effect in the trap-door problems or reinforced piled embankments in the past (Terzaghi, 1943; McNulty, 1965; Hewlett and Randolph, 1988; Tanaka and Sakai, 1993; Chen et al. 2008), while few tests focused on the arching effect and geosynthetic deformation in the local subsidence problem have been seen.

In this study, a small-scale test device was developed to model the local subsidence problem in the existing landfill. A kind of PVC geomembrane (GM) was used to simulate the geosynthetic reinforcement in the composite liner system. A total of six tests were conducted to study the effect of filling height and GM stiffness on the soil arching and the GM deformations. The GM strains are evaluated by Digital Image Analysis (DIA). Finally, the tests results were compared with those calculated by the current design method.

¹ Ph.D Student, Department of Civil Engineering, Zhejiang University, China. Email:gaodengdeng@zju.edu.cn

² Associate Professor, Department of Civil Engineering, Zhejiang University, China. Email:binzhu@zju.edu.cn

³ Professor, Department of Civil Engineering, Zhejiang University, China. Email:chenyunmin@zju.edu.cn

⁴ Professor, Department of Civil Engineering, Zhejiang University, China. Email:chenyunmin@zju.edu.cn

⁵ Engineer, Suzhou Bureau of Urban Environment and Sanitary, China. Email: wangxiangzhi@126.com

MODEL TEST

Test Device

As shown in Fig 1, the test device consisted of a bricked base, a subsidence simulator and a tank. The subsidence simulator is 200 mm wide and could move up and down. Toughened glasses were used in the front and back walls of the tank to allow observation. Steel plates were used in the right and left walls and the surfaces were lubricated with epikote to limit frictional effects. The system was 1200 mm long, 1000 mm wide and 2000 mm high.

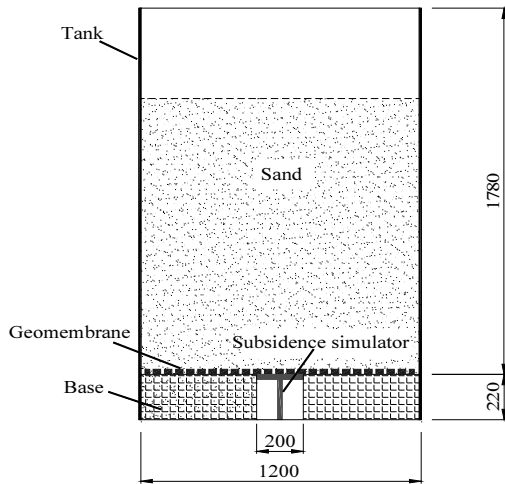


Fig. 1 Layout of test device (Unit, mm)

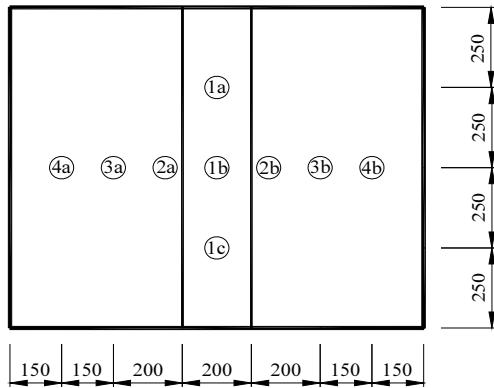


Fig. 2 Layout of soil pressure transducer (Unit, mm)



Fig. 3 Soil pressure transducer (SPT)

To investigate the variation of vertical pressure applied on the GM during the local subsidence, nine soil pressure transducers (SPT) were placed on the subsidence zone and the nearby static zone (see Fig. 2). These transducers are 67 mm in diameter, 13 mm in thickness (see Fig. 3). The calibration of these transducers has been performed before tests. Due to the considerable amount of data collected during the test, a data acquisition system (Fluke 2680) was used. The digital signal can be transmitted to the computer for storage and analysis.

The test program is detailed in Table 1. Tests 1~4 were performed to study the effect of filling height on the soil arching and GM deformations. Tests 4~6 formed a series to investigate the effect of GM stiffness on the soil arching and GM deformations.

Table 1 Test details

Test no.	Filling height (mm)	Geosynthetic stiffness (kN/m)
1	400	4.7
2	800	4.7
3	1200	4.7
4	1600	4.7
5	1600	9.4
6	1600	14.1

Material Properties

The sand used in the model tests was from Qiantang River Beach, China. The specific gravity $G=2.65$, the coefficient of uniformity $C_u=1.82$. Other characteristics were $D_{10}=0.088\text{mm}$, $D_{60}=0.16\text{mm}$, $e_{\text{max}}=1.01$, $e_{\text{min}}=0.52$. The sand was pluviated at a relative density of 60% with a dry unit weight equivalent to 14.09 kN/m^3 . The friction angle for the sand is measured from direct shear tests as 34.16° at about 60% relative density.

A kind of PVC GM was used in the model with biaxial tensile strengths 4.7 kN/m at 10% axial strain. One layer of GM was placed in Tests 1~4, while Test 5 and Test 6 needed two and three layers of GMs, respectively.

Test Procedure

After installation of the test set-up, the GM was placed above the bricked base and anchored at the edge of the static zone, which means that the GM elongation in the static zone was not considered (Giroud et al. 1990). Eleven markers were glued on the GM to calculate the GM strain. A thin layer of wet sand was placed in between the GM and the front wall. This is because considerable necking will happen during the GM deformation, and the overlying dry sand will drop into

the gap and some markers will be covered. Comparison tests has been carried out which shown that the thin layer of wet sand had negligible effect on the final GM deformation. Then, nine SPTs were placed on the GM, as shown in Fig. 2.

When the filling height was arrived, the subsidence simulator was dropped down in several stages and the readings of SPTs were recorded after stable. The GM locations were also recorded by video camera.

TEST RESULTS

Soil Pressures

Fig. 4 shows the variation of soil pressures acted on the deflected GM for different filling height. The curves were drawn using the average values of SPT1a, SPT1b and SPT1c. It can be seen that the soil pressure drops rapidly when the GM deflection y is less than 2 mm. With the development of GM deflection, the soil pressure decreases slowly and seems to reach a stable value finally. The final pressure is 0.96 kPa ($H=400$ mm), 1.15 kPa ($H=800$ mm), 1.20 kPa ($H=1200$ mm), 1.04 kPa ($H=1600$ mm), respectively. Thus, it may be concluded that the filling height has little effect on the final pressure acted on the deflected GM, on condition that the filling height is sufficient to form the soil arching. The soil arching has an ability of transfer soil pressures. The larger is the filling height, the more pressures will be transferred from the subsidence zone to the nearby zone.

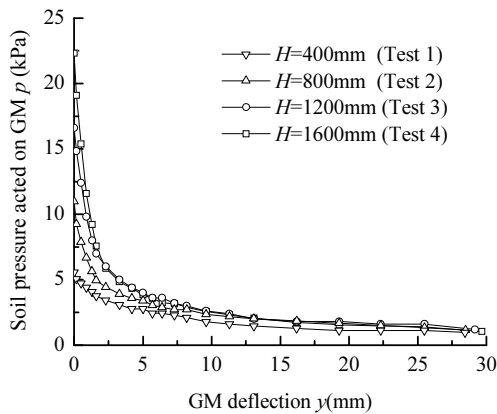


Fig. 4 Soil pressures acted on the deflected GM for different filling height

Fig. 5 shows the variation of soil pressures acted on the deflected GM for different stiffness. The three curves are quite similar and the soil pressure reaches a minimum value finally. The final soil pressure is 1.04 kPa ($Et=4.7$ kN/m), 1.19 kPa ($Et=9.4$ kN/m), 0.88 kPa ($Et=14.1$ kN/m), respectively. Thus, for the GM stiffness in the tests, the final pressure applied on the deflected

GM is independent of its stiffness. It is thought that the soil archings are fully formed in all the three cases, since the GM deflections are sufficient. However, in an extreme case in which the GM is perfectly rigid, there is no deflection that leads to stretching of the GM. As such, there will be no soil arching and the soil pressure acted on the GM will be equal to the self-weight stress.

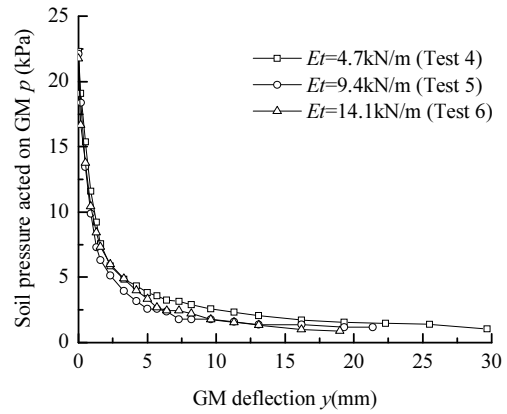


Fig. 5 Soil pressures on the deflected GM for different GM stiffness

GM Deflections and Strains

As shown in Fig. 6, the filling height has little influence on the final deflected shape of GM. The maximum deflection is 28.45 mm($H=400$ mm), 28.50 mm($H=800$ mm), 29.17 mm($H=1200$ mm), 29.69 mm($H=1600$ mm), respectively. According to the tensioned membrane theory (Giroud et al. 1990), a GM will deform equally under the same pressure. Thus, Fig 6 approves that the final pressure applied on the deflected GM is independent of the filling height from another point of view.

Fig 7 shows the effect of GM stiffness on the final deflected shape of GM. The maximum GM deflection is 21.38 mm($Et=9.4$ kN/m) and 19.00 mm($Et=14.1$ kN/m), respectively. Thus, the stiffness can heavily influence the GM deformation in a certain range, and the influence will decrease with the increase of the GM stiffness. Fig. 8 shows the final deflected shape of GM (Test 5). As anticipated, sliding has not happened in the two markers at the edge of subsidence zone, which shows good anchorage.

The strain distribution of the GM was evaluated by Digital Image Analysis (DIA) (Zornberg and Arriaga, 2003; Viswanadham and Mahajan, 2007). Eleven handmade markers were glued on the GM in the tests (see Fig 9). The strain between two markers can be calculated by comparing their initial distance and final distance. Consider two adjacent markers with initial coordinates $C(x_i, y_i)$ and $D(x_{i+1}, y_{i+1})$. These two markers will be displaced to new positions after subsidence, with final coordinates $C(x'_i, y'_i)$ and $D(x'_{i+1}, y'_{i+1})$. Thus, the

strain of section CD can be expressed as follows

$$\epsilon = \frac{\sqrt{(x_+ - x) + (y_+ - y)}}{\sqrt{(x_+ - x) + (y_+ - y)}} - 1 \quad (1)$$

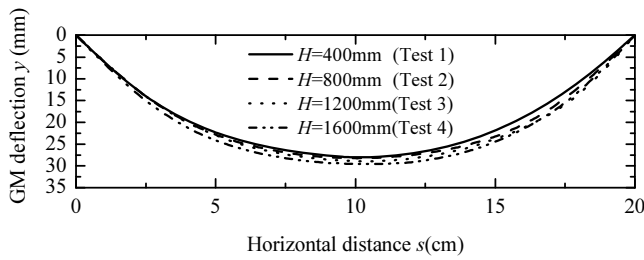


Fig. 6 Soil pressure on the deflected GM for different filling height

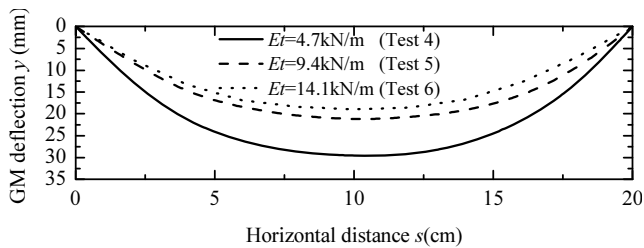


Fig. 7 Soil pressure on the deflected GM for different GM stiffness

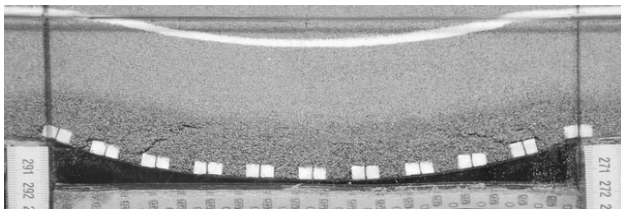


Fig. 8 Final deflected shape of GM (Test 6)

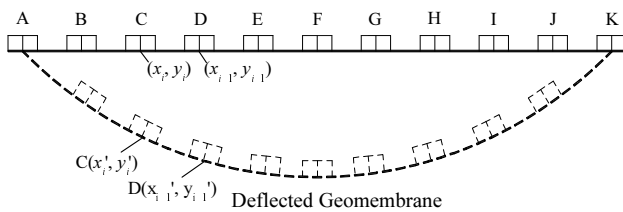


Fig. 9 Soil pressure on the deflected GM for different GM stiffness

The calculated GM strains by Digital Image Analysis are shown in Table 2, Fig 10 and Fig 11. In general, the strains at the edge of GM are much larger than those in the middle part, while the Giroud et al. (1990) method assumes that the strains are uniform throughout the deflected GM. With the increase of filling height, the average GM strains are quite similar. The maximum GM strain ranges from 8.58% to 9.88%. These values have reached or exceeded the allowable strains of many

sealing materials such as HDPE GM. With the increase of GM stiffness, both the average strain and the maximum strain reduce obviously. Thus, the importance of geosynthetic reinforcement in the composite liner system in expanded landfills is evident.

Table 2 Calculated GM strains by DIA (Unit, %)

Strain	Test 1	Test 2	Test 3	Test 4	Test 5	Test 6
ϵ_{AB}	7.77	9.88	7.97	9.55	6.4	3.81
ϵ_{BC}	5.47	5.39	4.81	6.48	4.45	2.3
ϵ_{CD}	4.78	4.04	4.13	6.12	2.27	2.84
ϵ_{DE}	4.68	4.31	6.38	3.94	2.29	1.06
ϵ_{EF}	2.91	3.94	4.37	6.71	2.33	0.52
ϵ_{FG}	4.72	3.71	6.61	4.43	3.48	2.16
ϵ_{GH}	5.78	4.75	4.9	4.39	1.12	2.65
ϵ_{HI}	2.3	5.22	4.79	6.79	1.13	1.1
ϵ_{IJ}	6.00	3.32	4.6	3.64	1.79	1.29
ϵ_{JK}	8.58	9.53	9.08	7.56	6.72	3.63
ϵ_{ave}	5.30	5.41	5.76	5.96	3.2	2.14
ϵ_{max}	8.58	9.88	9.08	9.55	6.72	3.81

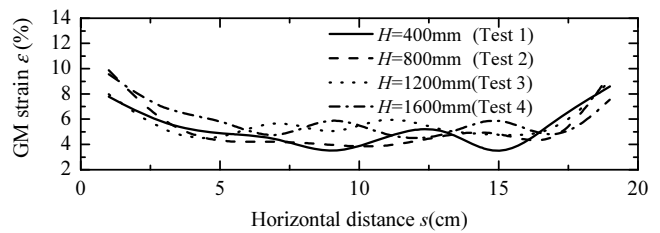


Fig. 10 GM strains for different filling height

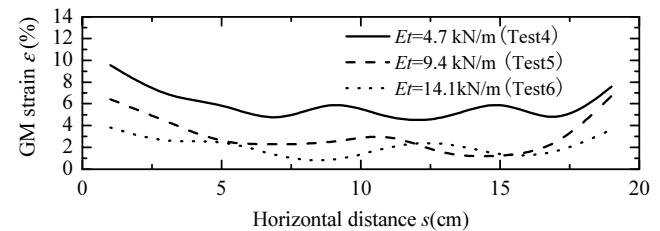


Fig. 11 GM strains for different GM stiffness

COMPARISONS

The design method has been developed considering arching theory for the fill materials overlying the reinforcement with the tensioned membrane theory (Giroud et al. 1990). The calculation formulas were expressed as follows

$$p = \frac{\gamma b}{2K \tan \phi} (1 - e^{-2 \cdot t \cdot \phi \cdot b}) \quad (2)$$

$$T = Et\epsilon = pr\Omega \quad (3)$$

where p is soil pressure acted on the reinforcement over the void, T is tensile load of reinforcement, γ is unit weight of waste contained above the composite liner, K is coefficient of lateral earth pressure, ϕ is friction angle of waste, H is thickness of waste contained above the lining system, b is width of the infinite long void, Ω is dimensionless factor related to reinforcement deflection y or strain ε .

$$1 + \varepsilon = 2\Omega \sin^{-1} [1/2\Omega] \tag{4}$$

Eq. 2 is the classical expression of Terzaghi(1943) loosen soil pressure. However, since the stress state of the soil in the arching zone is not fully understood by now, various values of K are available. Marston and Anderson(1913) assumed K to be equal to the active pressure coefficient K_a . Terzaghi (1943) referred to K as “an empirical coefficient” and suggested that K is equal to one, while Giroud et al. (1990) preferred the Handy’s K (Handy, 1985), which is defined the follows equation

$$K = 1.06(\cos^2 \theta + K \sin^2 \theta) \tag{5}$$

where $\theta = 45^\circ + \phi/2$. When $\phi \geq 20^\circ$, $K \tan \phi \approx 0.25$. Thus, Eq. 2 can simplified as follows

$$p = 2\gamma b(1 - e^{-\dots b}) \tag{6}$$

Fig. 12 shows the comparison of soil pressure acted on deflected GM by different methods. The soil pressures calculated by Eq. 2 or Eq. 6 are much larger than the test results. Thus, it may be concluded that the soil pressure based on Terzaghi’s arching theory is over conservative, which was also shown by other experiments (Evans, 1983; Adachi et al. 2003).

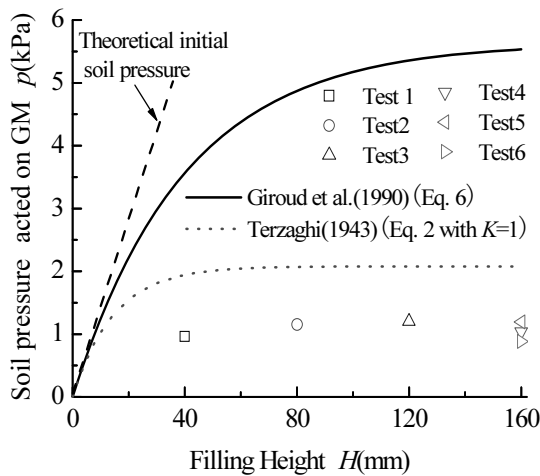


Fig. 12 Comparison of soil pressures

Combining Eq. 3 with Eq. 4, the following equation

can be obtained

$$Et[2\Omega \sin^{-1} (1/2\Omega) - 1] = pb\Omega \tag{7}$$

when the values of p , Et and b are known, the dimensionless factor Ω can be calculated by Eq. (7). Then the GM strain ε can also be obtained by Eq. (4). The average soil pressure p acted on the deflected GM in Test 1~Test 6 is

$$p = \frac{1.04 + 1.20 + 1.15 + 0.96 + 1.19 + 0.88}{6} = 1.07 \text{ kPa} \tag{8}$$

Fig. 13 shows the comparison of GM strains by different methods. The calculated GM strains by tensioned membrane theory (Giroud et al. 1990) are consistent with the average strains in the six tests. However, this theory can not predict the maximum GM strains well. A safe design of landfill liner system requires that the maximum tensile strain is lower than the allowable tensile strains of geosynthetics, especially for the sealing materials such as GMs and GCLs. Thus, the assumption of uniform strain in the tensioned membrane theory may be non-conservative from this point of view.

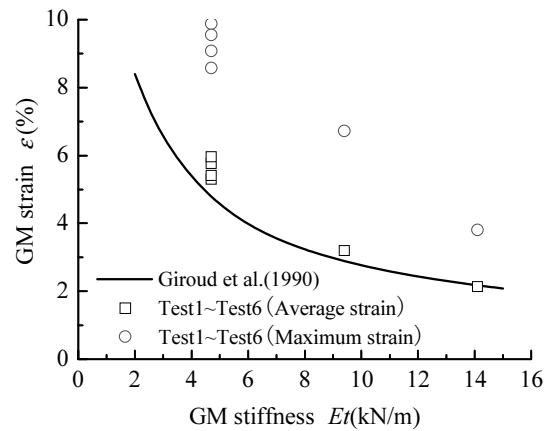


Fig. 13 Comparison of GM strains

CONCLUSIONS

- (1) The filling height has little effect on the final pressure acted on the deflected GM. The larger is the filling height, the more pressures will be transferred from the subsidence zone to the nearby stable zone.
- (2) For the GM stiffness considered in the tests, the final pressure applied on the deflected GM is independent of its stiffness.
- (3) The filling height has little influence on the final deflected shape of GM. The GM stiffness can heavily

influence the GM deformation in a certain range, and this influence will decrease with the increase of the GM stiffness.

(4) The strains are not uniform throughout the deflected GM. The strains at the edge of GM are much larger than those in the middle part.

(5) The calculated soil pressure based on Terzaghi's arching theory is over conservative. The calculated GM strains by tensioned membrane theory are consistent with the average strains in the six tests. However, this theory can not predict the maximum GM strains well.

ACKNOWLEDGEMENTS

This work were supported by the key fund of the National Natural Science Foundation (research grant: 50538080), National Distinguished Young Scientist Foundation of China (research grant: 50425825) and financial support from Bureau of Science and Technology of Suzhou (research grant: SS0733).

REFERENCES

- Zhan TLT, Chen YM, Lin WA (2008). Shear Strength Characterization of Municipal Solid Waste at the Suzhou Landfill, China. *Eng. Geol.* 97:97-111.
- CJJ 17-2004. (2004). Technical Code for Municipal Solid Waste Sanitary Landfill. Ministry of Construction P. R. China, Beijing.
- Jang DJ & Montero C (1993). Design of liner systems under vertical expansions: an alternative a geogrids. *Proceeding of geosynthetics*, 3: 1487-1510.
- Giroud JP, Bonaparte R, Beech JF, et al. (1990). Design of soil layer-geosynthetic systems overlying voids. *Geotex. Geomembr.* 9:11-50.
- Qian XD, Koerner RM, Gray DH (2001). Geotechnical aspects of landfill design and construction. Prentice Hall, Upper saddle River, NJ.
- Kuo SS, Desai K, Rivera L (2005). Design method for municipal solid waste landfill liner system subjected to sinkhole cavity under landfill site. *Practice Periodical of Hazardous, Toxic, and Radioactive Waste Management.* 9(4):281-291.
- Terzaghi K (1943). *Theoretical soil mechanics.* John Wiley and Sons, Inc, New York: 37-42.
- McNulty JW (1965). An Experimental Study of Arching in Sand, Ph.D. Thesis in Civil Engineering, University of Illinois.
- Hewlett WJ & Randolph MF (1988). Analysis of Piled embankments. *Ground Engineering.* 21(3): 12-18.
- Tanaka T & Sakai T (1993). Progressive failure and scale effect of trap-door problems with granular materials. *Soils and Foundations.* 33(1):11-22.
- Chen YM & Cao WP (2008). An experimental investigation of soil arching within basal reinforced and unreinforced piled embankments. *Geotex. Geomembr.* 26:164-174.
- Zornberg JG & Arriaga F (2003). Strain distribution within geosynthetic-reinforced slopes. *J. Geotech. Geoenviron. Eng.* 129(1):32-45.
- Viswanadham BVS & Mahajan RR (2007). Centrifuge model tests on geotextile- reinforced slopes. *Geosynthet. Int.* 14(6): 365-378.
- Marston A & Anderson AO. The theory of loads on pipes in ditches and tests of cement and clay drain tile and sewer pipe. Iowa Engrg. Experiment Station Bull, Iowa State Coll., Ames, Iowa, 1913.
- Handy RL (1985). The arch in soil arching. *J. Geotech. Eng.* 111(3): 302-318.
- Evans CH (1983). An Examination of Arching in Granular Soils, M.S. Thesis, MIT.
- Adachi T, Kimura M, Kishida K (2003). Experimental study on the distribution of earth pressure and surface settlement through three-dimensional trapdoor tests. *Tunnelling and Underground Space Technology.* 18: 171-183.

A LARGE-SCALE RAMP MODEL TEST ON COMPOSITE LINER SYSTEMS

Wei-An LIN¹, Tony L. T. ZHAN², Yun-Min CHEN³ and Sheng HE⁴

ABSTRACT: Composite liner systems comprising geosynthetics are widely used in landfills. In this paper, a large-scale ramp model test was carried out to simulate the sliding along the interface of GT/GM liner. The simulation test was performed by using a purposely-design set-up in the Zhejiang University large model box for foundation and slope engineering. The composite liner laid on a sloping foundation was loaded to a vertical stress level of 75 kPa, and a sliding along the GT/GM interface was successfully simulated by removing the lateral support. The softening behavior of the GT/GM interface during the sliding process was revealed. The experimental results of GT/GM liner system show that when the shear stress induced by the vertical loading exceeds the peak shear strength of the GT/GM interface, the GT/GM interface quickly fell into a residual shearing condition, and the tension stress in GT would increase sharply.

KEYWORDS: composite liner systems, a large-scale ramp model test, GT, GM

INTRODUCTION

Composite liner systems comprising geosynthetics are widely used in landfills. They offer the particular advantage of being easy to install compared with traditional solutions and provide an interesting alternative from the economic point of view. These systems are composed of a geosynthetic complex comprising one or several layers of geosynthetics with layers of granular soil above and below it.

Geosynthetics placed on side slopes of a landfill can experience tension due to various factors (Thusyanthana, 2007). For example, during construction of the liner systems, wind up-lift on uncovered areas, movement of heavy vehicles such as bulldozers and frictional forces from the cover soil can all cause tension in the geomembrane. After the closure of a landfill, the down-drag caused by settling waste (Jones and Dixon, 2005) also induces tension in the geosynthetics.

Ramp tests have been performed by several researchers on different combinations of apparatus characteristics, soils and materials to study the tension in geosynthetics (Giroud et al. 1990; Palmeira et al. 2002, 2003). Generally, in these works the area of the interface tested varied between 0.005 and 1 m² and the typical stress level applied to the interface only between 1 and 5 kPa. In spite of the rather large number of works with the ramp test, the authors are not aware of such tests being performed for the investigation of the effects of strain-

softening to increase the tension transferred to geosynthetics. In this paper, a large-scale ramp model apparatus on the composite liner system was developed with a higher stress level. The stability test on the GT/GM single-interface was studied.

THE LARGE-SCALE RAMP MODEL APPARATUS FOR COMPOSITE LINER SYSTEMS

The apparatus shown in Fig. 1 is mainly composed of a sloping ground, reinforced concrete base board and transmission board, framework, the relative displacement measurement system, the tension measurement system; the sliding control systems, and sand bags. The various components of the design and use are introduced as following:

Reinforced Concrete Base Board and Transmission Board

Base board and transmission board are both made of reinforced concrete. The base board is 4.95 m long×1.7 m wide×0.2 m thick (weigh 40kN), and would placed on the sloping ground filling with gravel. It is used to support the entire test system. The transmission board is 4.5 m long×1.35 m wide (the lower surface is 1 m wide)×0.2 m thick (weigh 28.8 kN). Since the framework would takes a considerable amount of space, the cross-

¹ Ph.D, Department of Civil Engineering, Zhejiang University, China. Email:linxi@zju.edu.cn

² Professor, Department of Civil Engineering, Zhejiang University, China. Email:zhanlt@zju.edu.cn

³ Professor, Department of Civil Engineering, Zhejiang University, China. Email:chenyunmin@zju.edu.cn

⁴ Engineer, Suzhou Bureau of Urban Environment and Sanitary, China. Email: szesa@126.com

section of the transmission board is design as a T-shape, and the upper surface is 1.35 m width or the lower surface is 1 m width. Ten steel plate with a size of 0.1m×0.1m×0.01m would be embedded in the edge of the upper surface, used for welding the vertical steel pipe of the framework and the board together. The lower surface of the transmission board must be roughened in order to increase the interface shear strength of transmission board/GT. The rough surface is used to prevent sliding along the transmission board/GT interface.

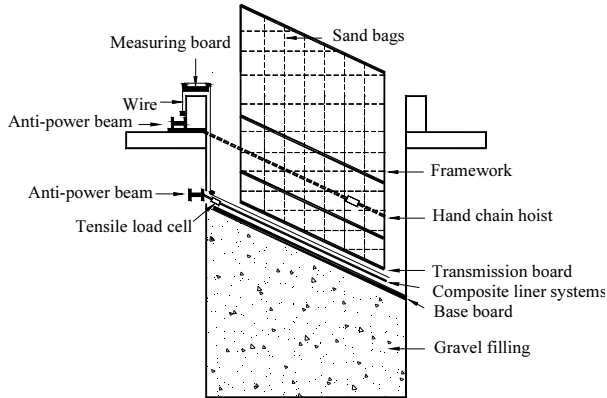


Fig. 1 The large-scale ramp test apparatus

Framework

Framework is made of scaffolding structures and used for filling sand bags, shown in Fig. 1. To meet the mechanical requirements, the framework are designed as follows: (1) vertical steel tube and embedded steel plate were welded together; (2) vertical steel tube and the horizontal steel tube steel are arranged 0.5 m intervals, the cross would be connected by vertical jig; In order to safeguard the stability of the whole framework structure, six inclined strut are set up;

The Relative Displacement Measurement System

The relative displacement measurement system is composed of 1 mm diameter wires, measuring board as well as pulley wheels, as shown in Fig. 2. Pairs of fishhooks were glued to each of the geosynthetics, and a stainless wire was attached to the fishhooks to measure the relative displacement (Dniel et al. 1998; Frownes et al. 2007). Each wires extended from the fishhooks run, via two pulley wheels, over displacement measuring boards (Fig. 2) with each tensioned using a 300 g static weight. The fishhooks were attached to each of the geosynthetics at five locations along the slope.

Tension Measurement System

Tension measurement system is composed of clamps, load cells, and the anti-power beam. The tension acting

on the geosynthetics at the anchorage were measured by tensile load cells between clamp and the anti-power beam.

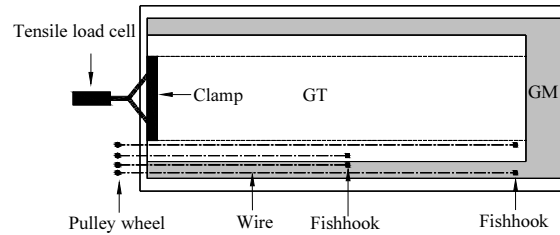


Fig. 2 Tension and displacement measure systems

Sliding Control Systems

Sliding control systems is composed of two hand chain hoists, a tensile load cell (50 kN limit), a steel cable (20 mm diameter), a steel plate and a anti-power beam, which was used for controlling slippage of the entire system along a interface. The hand chain hoists are the core of this system, which was connected by the steel cable. The two hand chain hoists were released in step to control the framework movement. The tensile load cell was positioned between the steel cable and the hand chain hoist to measure the tension in the hand chain hoists. If the vertical steel tubes were directly surrounded by the connecting steel cable, the vertical steel tubes were easily damaged due to stress concentration. Therefore, a steel plate (120 cm long × 50 cm wide × 1 cm thick) was employed. Channel steel is used for keeping the steel cable in a fixed location. Three steel tubes were welded on the steel plate back, making it possible to fix the steel plate to the framework.

Sand Bags

For convenience, sand bags were adopted for loading. In order to achieve a maximum normal stress 75kPa desired on the interface, approximately 700 sand bags (total weight of 350 kN) were needed.

PROCEDURE FOR GT/GM SINGLE-INTERFACE TEST

GT/GM single-interface test was adopted a liner system only composed of GT and GM geosynthetics, as shown in Fig. 3.

GT specimen (4.7 m×1.3 m) was cut in the machine direction during production. The additional 0.2 m long portion of GT specimen was used for clamping the specimens and the additional 0.3 m wide portion of GT specimen was used for the relative displacement measurement. GM specimen (5 m×1.6 m) was cut oriented in the machine direction. To maintain a constant contact

area during sliding, the GM specimen is 5 m long (i.e., 0.5 m longer than the GT specimen). Also the additional 0.6 m wide portion of GM specimen was used for the relative displacement measurement.

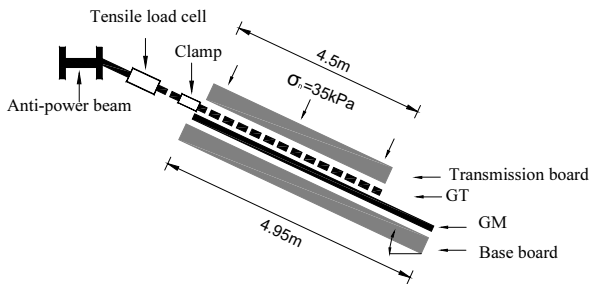


Fig. 3 GT/GM single-interface test

In order to protect GT from tensile failure, a normal stress of 35kPa was selected for the GT/GM single-interface test. According to the shear strength of GT/GM interface changes with the normal stress, to ensure that slippages along the GT/GM interface would occurs when loaded to 35kPa, slope angle of 35° was adopted.

The procedures were described by Lin (2009) and are not presented here.

RESULTS FOR GT/GM SINGLE-INTERFACE TEST

Results During the Loading Process

Fig. 4 shows that the tension at the GT anchorage and in the hand chain hoist varied with the total weight during loading process, as well as the sum of them. In the initial phase, the tension of GT and hand chain hoist almost keep at zero. When loaded to 113kN, the tension had a mutation, which the tension at the GT anchorage increased from 0.059kN to 0.112kN and the tension in the hand chain hoist increased from 0.074kN to 0.41kN. With the weight continuing to increase, both of the tension had an increasing trend. At the weight of 160kN both tension declined. Finally, when the total weight achieve to 180kN, namely to achieve 35kPa normal stress, the tension in GT and the hoist were 2.12 kN/m and 0.44 kN/m, respectively.

Fig. 5 shows that the displacement near the GT anchorage and at the top of the transmission board varied with the total weight. The variation could be divided into two stages. At the initial stage, the displacement remained almost unchanged, and when loaded to 113 kN, the displacement near the GT anchorage and at the top of the transmission board arrived at 0.5 cm. Finally, the displacements were both 2.2 cm.

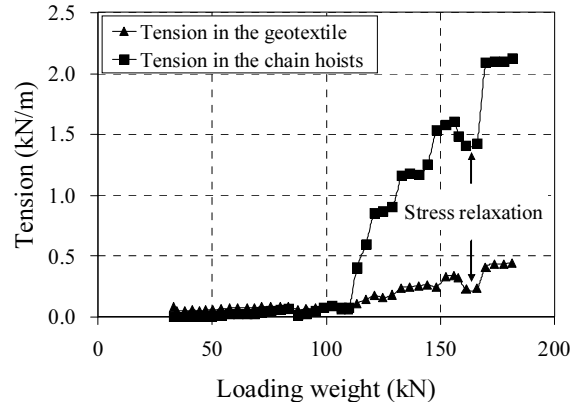


Fig. 4 The tension in the GT and the hand chain hoist varied with the total weight during loading process

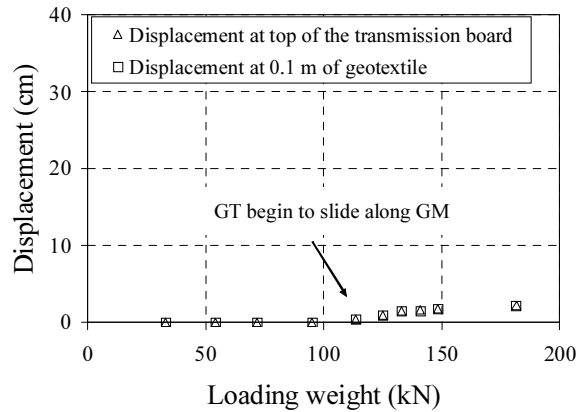


Fig. 5 The displacement near the GT anchorage and at the top of board varied with the total weight during loading process

Results during the Sliding Process

Fig. 6 shows that the tension at the GT anchorage and in the hand chain hoist varied with the controlled displacement during sliding process, as well as the sum of them. There is an initial increase in tension of GT as soon as displacement starts, with a rapid increase in GT tension with increasing displacement, followed by decrease, at last the tension is 16.71 kN/m. The tension in hand chain hoist decreased in the initial stage, when the displacement arrived at 5.8 cm, the tension reached the minimum value of 0.96 kN/m. After that, the tension gradually increased, and ultimately achieved 3.6 kN/m. The sum of the two tension stresses varied similar as the tension in GT, when the displacement arrived at 17.8 cm, the sum reached the maximum value of 21.56 kN/m.

Fig. 7 shows that the displacement of the five different positions on GT with the controlled displacement during sliding process. In the initial phase, the displacement at 0.1 m increases with the controlled displacement. When the controlled displacement reached at 14.8 cm, the displacement at 0.1 m almost kept unchanged. The displacement at 0.7 m also increased with the increase of the controlled displacement. But when the controlled

displacement reached at 20.8 cm, since the fishhook at this point was drawn off from GT caused by horizontal deformation of GT, the displacement at 0.7 m could not gained subsequently. The displacement at 1.24 m, 3.31 m and 4.35 m almost kept the same as the controlled displacement.

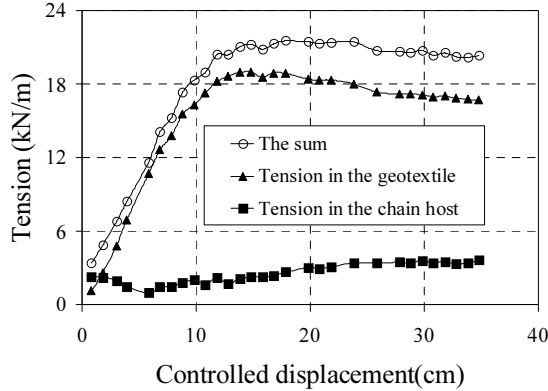


Fig. 6 The tension in the GT and the hand chain hoist varied with the displacement during sliding process

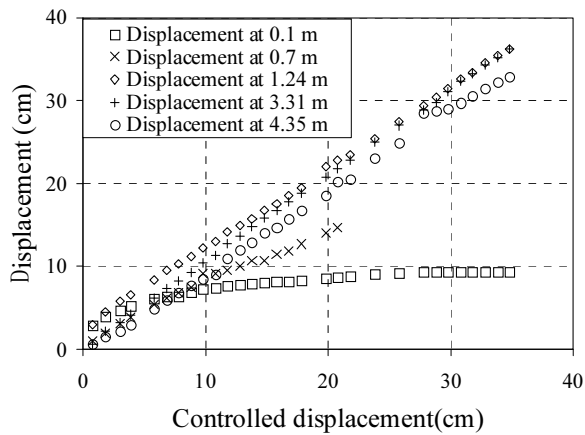


Fig. 7 The displacement near the GT anchorage and at the top of board varied with the displacement during sliding process

Discussion

From the results during the loading process, it could be seen that when the load weight is less than 113 kN, the peak shear strength of GT/GM interface is greater than the external shear stress, the shear strength of GT/GM interface was still in elastic stage. When the load weight is more than 113 kN, the peak shear strength of GT/GM interface is less than the external shear stress, the shear strength of GT/GM interface could not balance the external shear stress, the tension in GT and chain host were generated to keep a balance. From the results during the sliding process, it could be seen that the shear strength of GT/GM interface gradually become smaller with strain-softening. When the controlled displacement was greater than 14.8 cm, the GT/GM interface began to play a residual strength.

SUMMARY

This paper presents the large-scale ramp model test set-up purposely-designed for the simulation of sliding along a composite liner system. A sliding along the GT/GM interface was successfully simulated by the use of the set-up. The softening behavior of the GT/GM interface during the sliding process was revealed. The experimental results of GT/GM liner system show that when the shear stress induced by the vertical loading exceeds the peak shear strength of the GT/GM interface, the GT/GM interface quickly fell into a residual shearing condition, and the tension stress in GT would increase sharply.

ACKNOWLEDGEMENTS

This work were supported by the key fund of the National Natural Science Foundation (research grant: 50538080), National Distinguished Young Scientist Foundation of China (research grant: 50425825) and financial support from Bureau of Science and Technology of Suzhou (research grant: SS0733).

REFERENCES

Daniel DE, Koerner RM, Bonaparte R, Landreth RE, Carson DA, Scranton HB. Slope stability of geosynthetic clay liner test plots. *Journal of Geotechnical and Geoenvironmental Engineering*, 1998, 124(7): 628-637.

Fowmes GJ, Dixon N, Jones DRV. Validation of a numerical modeling technique for multilayered geosynthetic landfill lining systems. *Geotextiles and Geomembrane*, 2008, 26(2): 109-121.

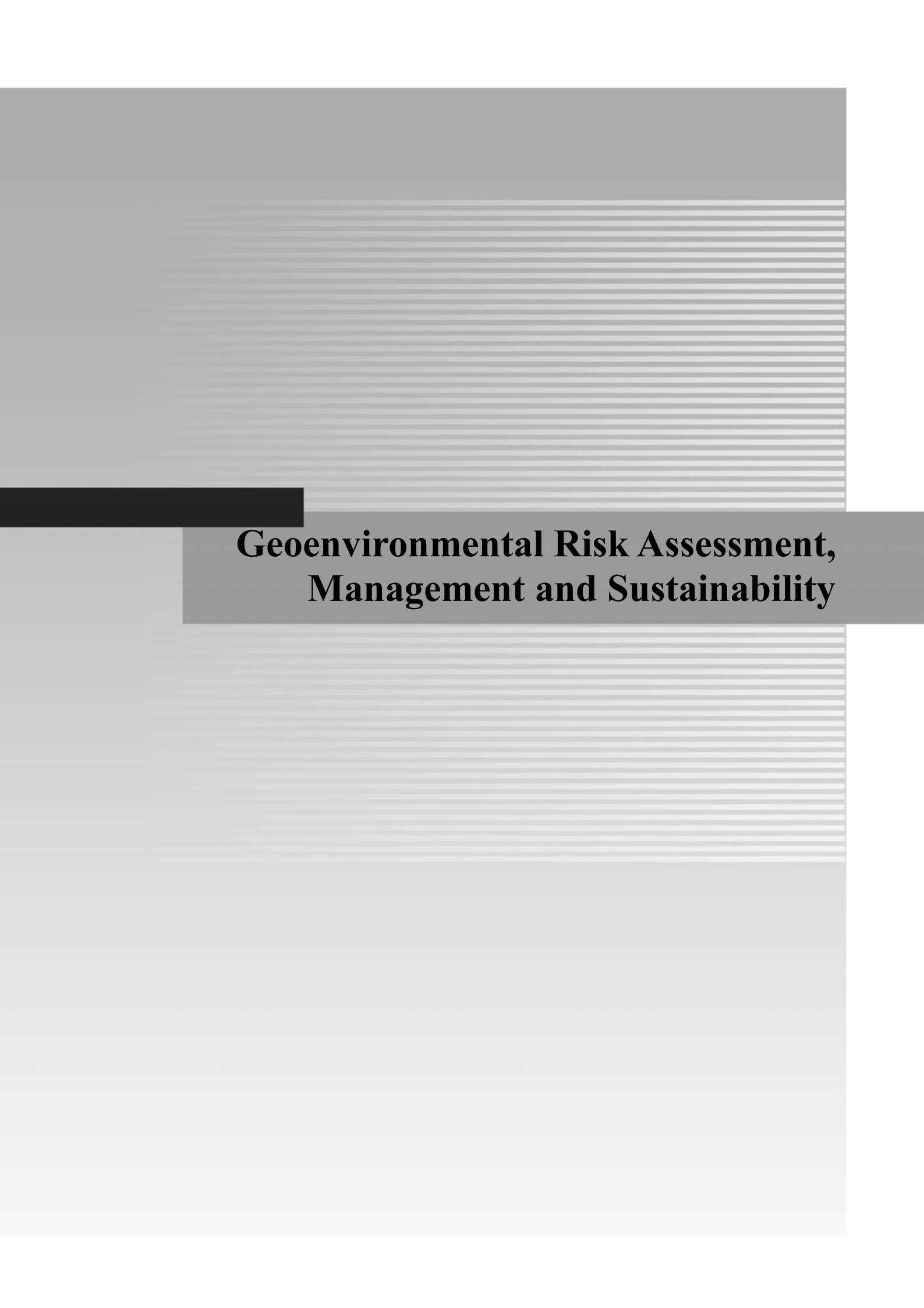
Jones DRV & Dixon N. Landfill lining stability and integrity: the role of waste settlement. *Geotextiles and Geomembranes*. 2005, 23(1): 27-53.

Palmeira EM, Lima NR, Jr, Mello LGR. Interaction between soils and geosynthetic layers in large-scale ramp tests. *Geosynthetic s International*, 2002: 9(2): 149-187.

Palmeira EM & Viana NL. Effectiveness of geogrids as inclusions in cover soils of slopes of waste disposal areas *Geomembrane and geotextile*, 2003, 21: 317-337

Lin WA. Shear stress transfer, strength characteristics and safety control of composite liner systems. PhD dissertation, Zhejiang University, Hangzhou, 2009

Thusyanthana NI & Madabhushia SPG, Singh S. Tension in geomembranes on landfill slopes under static and earthquake loading- Centrifuge study. *Geotextiles and Geomembranes*, 2007, 25: 78-95.



**Geoenvironmental Risk Assessment,
Management and Sustainability**

URBAN NIGHT SOIL TRANSPORTATION AND TREATMENT IN CHINA

Ting LIU¹, Zhu-Lei CHEN² and Lie YANG³

ABSTRACT: With the growth of population, night soil had become an important influencing factor for ecological environment of China. The situation of urban night soil transportation and treatment in China was investigated and described. Depending on the China Urban Construction Statistical Yearbooks and other references, relative data of urban night soil are statistically treated. By correlation analysis and variance analysis, the chronological changes and their relations with other factors of the night soil transportation and treatment were studied. Over the last twenty two years, urban night soil transportation quantity was affected by the urban non-agricultural population and latrines. Urban night soil non-hazardous treatment quantity had significant positive correlation with the urban night soil transportation quantity. Urban night soil transportation quantity of Eastern region was higher than that of Central region and Western region, and urban night soil non-hazardous treatment quantity of Eastern region was highest. The urban night soil treatment model of China is diverse, co-treating night soil with sewage or establishing separate night soil treatment plant, but the level of technology is below that of some developing countries. Due to lack of enough urban environmental sanitation funds, large amount of urban night soil were untreated, and most untreated night soil had been discharged directly, which caused environmental pollution. The problems of urban night soil system of China were also discussed.

KEYWORDS: urban night soil, transportation, treatment, China

INTRODUCTION

Night soil refers to human feces and urine which as a manure or soil conditioner had been in use since ancient times in China. With the growth of population, night soil had become an important influencing factor for ecological environment of China. Night soil was collected and used as manure after anaerobic digestion, and the practice is still followed in most rural areas in China now. China's urban night soil transportation and treatment had developed since 1950s, and urban night soil collection, transportation and treatment system had formed the last decade.

With development of the urban sanitation, three squares septic tank was the most widely used in China, and solids were removed by both physical and biological processes in these systems. Flush water and night soil went to septic tanks, and the supernatant together with household waste water discharged to drain pipes and then transported to the urban sewage treatment plant.

Septic tank night soil was transported to sewage treatment plant or the separate night soil treatment plant by vacuum tank truck regularly. Since the mid 1990s, night soil had been treated in new processing model in more and more cities. The model was that night soil was dehydrated beforehand and then the liquid were transported to sewage treatment system and dregs were transported to sludge treatment system or a system of landfill or compost. In this stage more than 30 night soil treatment plants had been built in this model in China.

Differing from developed countries, urban night soil is one kind of municipal solid waste in China. China has issued a series of laws and regulations on solid waste, such as the "Law on Prevention and Control of Environmental Pollution Caused by Solid Waste of PRC", the "City Appearance and Environmental Sanitary Management Ordinance". The ministry of construction of PRC has issued a series of standards on night soil transportation and treatment, such as the "Sanitary standard for the non-hazardous treatment of night soil"

¹ Ph.D, Institute of Environmental Science & Engineering, Huazhong University of Science and Technology, Wuhan 430074, China. Email: xianglt@263.net

² Professor, Institute of Environmental Science & Engineering, Huazhong University of Science and Technology, Wuhan 430074, China. Email: chenzhulei@263.net

³ Ph.D student, Institute of Environmental Science & Engineering, Huazhong University of Science and Technology, Wuhan 430074, China. Email: yanglie612@163.com

(GB7959-87), the “Vacuum sewer cleaner-Classifications”, the “Vacuum sewer cleaner-Specifications”, the “Vacuum sewer cleaner-Methods of performance test”, the “Vacuum sewer cleaner-methods of reliability test”, the “Specific equipments for municipal environmental sanitation-Cleaning, collecting and transporting”, the “Code for design of urban night soil treatment works”, and the “Technical Specification for operation, maintenance and safety of urban night soil treatment”. The last two standards was issued in 1995 and 1999 respectively, and amended in 2008.

Like other municipal solid waste, night soil is managed by municipal and district Environmental Sanitation Bureaus which have charge of the planning of MSW facilities and implementation of MSW policies in the respective city. Environmental Sanitation Stations are responsible not only for municipal solid waste collection but also for night soil collection and transportation, and there is at least one environmental sanitation station for each district.

The last few years, urban night soil transportation and treatment system presented new tendency in China, this paper aimed to elucidate the changes of transportation and treatment of urban night soil in China in recent years. We believe that the findings from this research will add first hand information to the very scanty data of urban night soil situation of China.

DATA SOURCE AND ANALYSIS

‘Night soil transported’ data and other correlated data were cited from the China Urban Construction Statistical Yearbooks and other references. Continuous ‘night soil treatment facilities’ data were lacking, so changes of night soil treatment facilities and treatment capacity are hard to estimate base on current data.

In order to find influencing factors of urban night soil transportation quantity, urban population, urban non-agricultural population, urban sewer length, latrines and environmental sanitation special vehicles were selected to analyze the effect on urban night soil transportation quantity. Expenditure of urban environmental sanitation fund was selected to analyze with urban night soil non-hazardous treatment. The statistical package SPSS 11.5 for Windows (SPSS Inc., Chicago, USA) was used for the pearson correlation analysis.

According to the China Urban Construction Statistical Yearbook of 2004, China was divided into three macro-regional development zones (the Eastern region, the Central region, and the Western region). Urban night soil transportation and treatment of three macro-regional development zones were described.

RESULTS AND DISCUSSION

Variation of Urban Night Soil Transportation

In the last twenty years with the expansion of the city scale and the acceleration of urbanization, urban night soil transportation quantity presented increasing tendency. Fig. 1 shows annual variation of urban night soil transportation quantity of the last twenty two years (1986-2007). In the late of 1980s urban night soil transportation quantity was about 24 million tons/year, and in the early of 1990s, urban night soil transportation quantity was increased obviously. Then urban night soil transportation quantity decreased slowly in the mid and late 1990s. From 2001 to 2005 urban night soil transportation quantity increased straightly again, and reached a highest volume of 38 million tons. It is surprising that urban night soil transportation quantity decreased to 21.3 million tons in 2006.

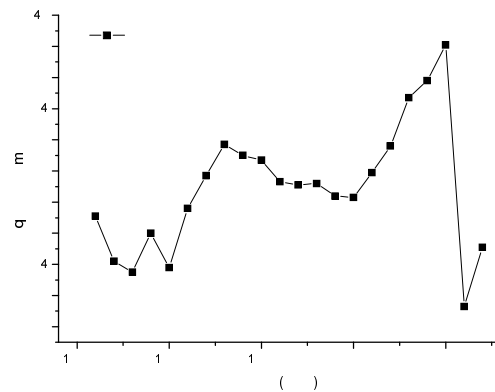


Fig. 1 Annual variation of urban night soil transportation quantity (1986 ~ 2007) Source: China Urban Construction Statistical Yearbook (2008)

In the early of 1990s, with the popularization utilization of vacuum tank truck, urban night soil transportation quantity was increased obviously. Then utilization of chemical fertilizers and pesticides led to shrinkage of agricultural manure market and night soil utilization in trouble, so urban night soil transportation quantity decreased slowly in the mid and late 1990s. From 2000 to 2005, migrant workers from rural areas increased quickly, and they might made contributions to increase of urban night soil.

In 2006, urban night soil transportation quantity decreased in most of provinces, especially decreased largely in Jiangsu, Zhejiang, Shandong, Guangdong, and Shanxi Provinces. Therefore total urban night soil transportation quantity of the country decreased to 21.3 million tons.

Influence Factors of Urban Night Soil Transportation

Urban population includes urban agricultural population and urban non-agricultural population. Fig. 2 shows that annual variation of urban population and urban non-agricultural population. Urban night soil transportation quantity had no significant correlation with the urban population ($r = 0.407, p > 0.05, n = 22$), and had significant positive correlation with urban non-agricultural population ($r = 0.8, p < 0.01, n = 20$).

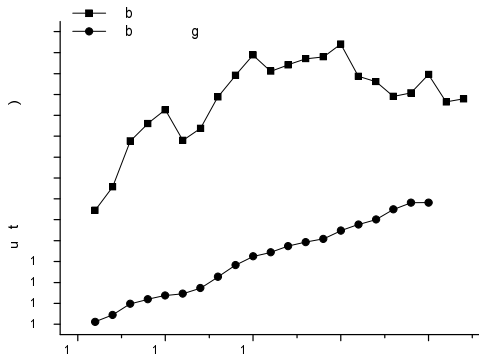


Fig. 2 Annual variation of urban population and urban non-agricultural population in China (1986 ~ 2007)
Source: China Urban Construction Statistical Yearbook (2008)

22). As lack of continuous national statistical data of night soil transportation vehicles, the data of environmental sanitation special vehicles were used to replace them for evaluating the situation of mechanization transportation quantity. Urban night soil transportation quantity had no significant correlation with special vehicles ($r = 0.365, p > 0.05, n = 22$). The mechanization level of night soil transport was still low, night soil transport special vehicles seriously inadequate and need to be increase.

The growth rate of urban sewer pipes was higher than the growth rate of urban night soil transportation quantity. Commonly, with the increase of urban sewer length, urban night soil transportation decreased, because more night soil was flushed into sewer pipes and into wastewater treatment plants. However, from 1986 to 2005, urban night soil transportation quantity had not decreased with increase of urban sewer pipes, the reasons might lie in: increase of urban non-agricultural population, latrines and environmental sanitation special vehicles made urban night soil transportation quantity increased; water toilets increased which made night soil concentration decreased and volume increased. As urban night soil transportation quantity did not decrease with increase of urban sewer length, it is difficult to say what extent the urban sewer length developing should make night soil transportation decline significantly.

In the last two years, urban night soil transportation quantity decreased largely, and had the opposite trend to that of urban sewer length, latrines and environmental sanitation special vehicles. However, the decrease of urban night soil transportation quantity may be not because of the increase of urban sewer length. Urban night soil transportation quantity decreased mainly in Jiangsu, Zhejiang, Shandong, Guangdong, and Shanxi Provinces, and urban night soil transportation quantity of other provinces was not decreased largely.

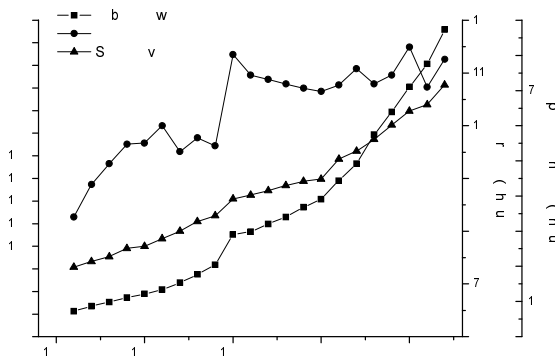


Fig. 3 Annual variation of urban sewer length, latrines and special vehicles in China. Source: China Urban Construction Statistical Yearbook (2008)

Fig. 3 shows that annual variation of urban sewer length, latrines and environmental sanitation special vehicles. Urban night soil transportation quantity had no significant correlation with urban sewer length ($r = 0.288, p > 0.05, n = 22$). Urban night soil transportation quantity was mainly collected from latrines and septic tanks, and variation of urban latrines was important. Urban night soil transportation quantity had significant positive correlation with latrines ($r = 0.450, p < 0.05, n =$

Urban Night Soil Non-hazardous Treatment

Annual urban night soil non-hazardous treatment quantity and urban night soil non-hazardous treatment rate had the same trend during 1999 to 2007 (Fig. 4), both increased from 2000 to 2005, and linear decreased in 2006. Urban night soil non-hazardous treatment quantity had the same trend to urban night soil transportation quantity, and had significant positive correlation with the latter ($r = 0.978, p < 0.01, n = 9$).

Urban night soil non-hazardous treatment was decided by urban night soil treatment financial input. There was no special data of expenditure of urban night soil treatment, so expenditure of urban environmental sanitation fund was used in analysis (Fig. 5). Expenditure of urban environmental sanitation fund was including expenditure of municipal garbage, night soil treatment and others projects. Expenditure of urban

environmental sanitation fund continually slow increased before 2000, and fast increased later. Urban night soil non-hazardous treatment quantity had no significant correlation with the expenditure of urban environmental sanitation fund ($r = 0.571, p > 0.05, n = 9$).

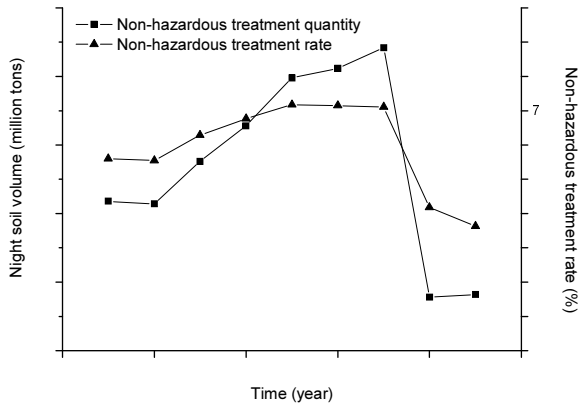


Fig. 4 Annual variation of urban night soil non-hazardous treatment quantity and non-hazardous treatment rate in China (1999 ~ 2007) Source of “non-hazardous treatment quantity” data: China Urban Construction Statistical Yearbooks (2000-2008)

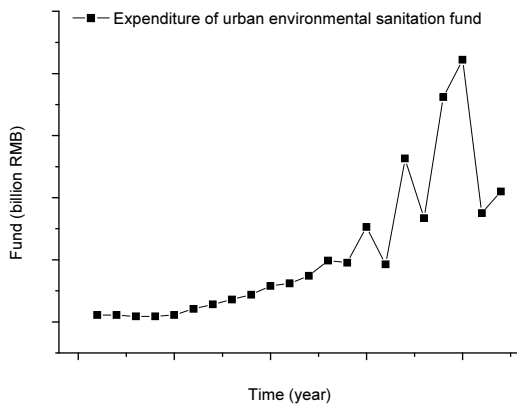


Fig. 5 Expenditure of urban environmental sanitation fund in past years (1986-2007) Source: China Urban Construction Statistical Yearbook (2008)

For historical reasons, the government departments paid much attention to the garbage treatment and neglected the night soil treatment in cities, so most expenditure of urban environmental sanitation fund was used for garbage treatment. According to data of some cities, the expenditure of urban night soil transportation and treatment was less than 5% of all expenditure of urban environmental sanitation fund (Chen et al. 2007). With insufficient fund input, it was hard to change the backward situation of urban night soil non-hazardous treatment in China.

Night Soil Transportation and Treatment in Different Geographical Regions

The night soil transportation quantity of Eastern region and Central region increased before 2006 and decreased in 2006, in contrast the night soil transportation quantity of Western region was almost stable in these years (Fig. 6). The urban night soil transportation quantity of Eastern region was higher than that of Central region and Western region, and the gap of Western region and Central region and Eastern region was very obvious. Fig. 7 and Fig. 8 respectively show that night soil non-hazardous treatment quantity and treatment rate in Eastern, Central and Western region in China. Urban night soil non-hazardous treatment quantity of Eastern region was highest, that related to the night soil transportation and treatment model. The cities and population of Eastern region were large, caused large night soil transportation quantity. In addition, night soil was considered to be waste in Eastern region early and night soil disposal facilities were fairly complete. However, city scale of Central and Western region was smaller and population less, so night soil transportation quantity was low. At the same time, disposal facilities of Central and Western region were relatively backward.

Differences of the per capita night soil transportation quantity between different geographical regions were significant, that caused by the local economic and technological level, environmental sanitation-related capital investment, sewer length and special vehicles, etc. Caused by the socio-economic development level of the region, difference of night soil transportation mechanization between different geographical regions was obvious, and mechanization level was higher in higher development level cities.

Model of Night Soil Transportation and Treatment in China

The western model of night soil transportation and treatment is that toilets flush water is directly connected to sewer pipes and sewerage systems, and the model is the dominant night soil treatment model in some developed countries. Unlike the western model, there are several treatment models in Asia countries. In Japan, night soil is mainly treated in the night soil treatment plants of centralized systems, and in the sewerage systems or johkasous for flushed toilet waste water (Katoh et al. 2005). Night soil collection and treatment systems in Bangkok can be classified into two groups, one type is based on Thai-style toilet, whose flush water goes to leaching cesspools, and only a part of supernatant is then discharged to drain pipes or surface water bodies, the other type is the same as western-style toilets, whose flush water is directly connected to sewer

pipes and men treated (Giri et al. 2005). In China, urban night soil is mainly treated in the septic tanks, the sewerage systems, and the night soil treatment plants of centralized systems. Actually, there are often various night soil treatment systems in developing countries.

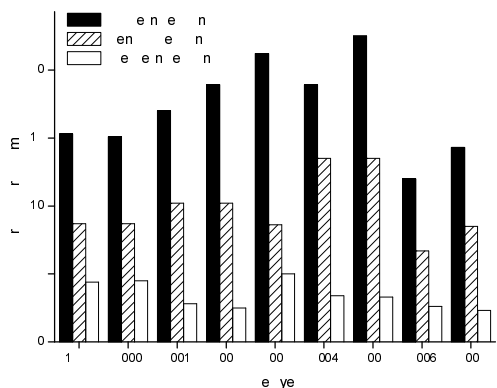


Fig. 6 Night soil transportation quantity in different geographical region in China

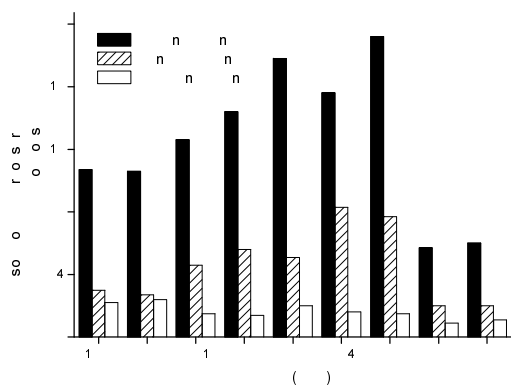


Fig. 7 Night soil non-hazardous treatment quantity in different geographical region in China

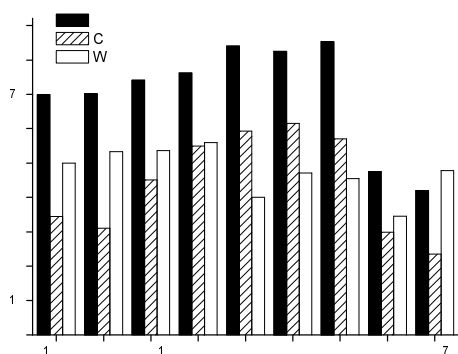


Fig. 8 Night soil non-hazardous treatment rate in different geographical region in China

The western model of sewage treatment is still the dominant one leading the environmental technological development over the world (Kuai et al. 1999). Western

industrial countries spend about 160 years in developing framework of night soil and sewage co-treatment system. However, China cannot fully duplicate the western developed country system. Night soil treatment can not heavily depend on urban sewage system in China recently and in the near future. Some researches show that current night soil treatment facilities are shortage and the level of technology is still low in most cities of China (Chen et al. 2007). Therefore, large-scale night soil transportation and treatment system will be long-standing in China. How to treat a great amount of night soil properly, the government should attach great importance and should be made in the strategic choice for sustainable development.

Problem of Urban Night Soil System

In 2006 there were about 0.37 billion urban population in China, if use the median of Narain (2002), there were about 0.27 billion tons faeces and 1.53 billion tons urine generated. Approximately all urban housing units in China have septic tank systems, urine was flushed to septic tank and then into drainpipe, and faeces was intercepted in septic tank. Septic tank can remove as high as 65% of the TSS generally (Bounds, 1997). Approximately 21.3 million tons urban night soil (mainly was faecal matter) was transported in 2006, after septic tank system, the rest 87.8 million tons faeces and 1.53 billion tons urine went to sewage system. About 52% night soil transported was not treated and about 45% waste water was not treated in 2006, as a result, about 50.6 million tons faeces and 0.69 billion tons urine discharged to surface water bodies without treatment.

Direct discharge of night soil into local waters endangers the hygienic quality, and it is generally assumed that the direct discharge of raw night soil is responsible for a high risk of infectious disease transmission in many developing countries (Schertenleib, 1995). According to the Organization for Economic Cooperation and Development (2007), China's many water courses, lakes and coastal waters are severely polluted as a result of agricultural, industrial and domestic discharges.

In China septic tank is still considered to be a common technology of night soil non-hazardous treatment, almost all urban housing units have septic tank systems. Though urban night soil of latrines and septic tanks are transported by Environmental Sanitation Stations, many septic tanks of residential areas still are not cleaned timely. In some cities, urban night soil transportation was operated by local environmental sanitation companies, and the operations of the company were affected by market demands. In many conditions, managers of residential areas did not call up local environmental sanitation companies for septic tanks

cleaning until septic tanks were full. Most septic tanks of old residential areas, which had been built more than 20 years and lacked of management, were full and could not stop and anaerobic digest night soil. Moreover, the old septic tanks bring many problems such as methane gas which maybe accumulated in septic tank system is both explosive and suffocative. Yao (2007) estimated that about 3.75 thousand tons methane are emitted from septic tanks of Chinese cities every year. As a greenhouse gas, methane has 21 times more global warming potential than the equivalent amount of CO₂ (The World Bank, 2005). Now some coastal cities in East China decide to cancel septic tank in newly built district, such as Shanghai City, Hangzhou City and Guangzhou City (Lu et al. 2007). This will be a help to reduce problems of septic tank.

CONCLUSION

Over the last twenty years urban night soil transportation quantity and treatment quantity increased in different degree, but both decrease largely in 2006. Urban night soil transportation was affected by the urban non-agricultural population and latrines, and night soil transportation quantity had significant positive correlation with urban non-agricultural population and latrines. Urban night soil non-hazardous treatment quantity had significant positive correlation with the urban night soil transportation quantity. The urban night soil transportation quantity of Eastern region was higher than that of Central region and Western region, and urban night soil non-hazardous treatment quantity of Eastern region was highest.

Chinese urban night soil treatment model is diverse, co-treating night soil with sewage or establishing separate night soil treatment plant, but the level of technology is below that of some developing countries. Night soil treatment can not heavily depend on urban sewage system in China recently and in the near future.

ACKNOWLEDGMENTS

The authors are grateful to the Funding for this study provided by the Eleventh Five-year National Technology Supporting Plan Program (No. 2006BAC06B02), Project (No. 20080430967 and No. 0128110004) of Postdoctor Fund of China. Great thanks are extended to Dr. Adey So for his help in language editing.

REFERENCES

- Bounds TR(1997). Design and Performance of Septic Tanks: Site Characterization and Design of Onsite Septic Systems. In: Bedinger, M.S., Johnson, A.I., Fleming, J.S. (Eds.). American Society of Testing Materials, Philadelphia. ASTM STP 901.
- Chen ZL, Zheng SS, Li YY, Zhang X, Huang LJ, Chu Y, Shi BF (2007). Development of urban night soil treatment technology in China. Proceedings of China Association of Urban Environmental Sanitation Annual Congress 2007: 263-277.(in Chinese).
- Giri RR, Takeuchi J, Ozaki H (2005). Influence of night soil contamination on activated sludge microbial communities in Bangkok, Thailand. *Ecological Engineering*. 25: 395-404.
- Katoh H, Watanabe T, Ohmori H, Kawamura K, Makino Y (2005). Carbonization of johkasou sludge using batch-type equipment. *J Mater Cycles Waste Manag.* 7: 55-64.
- Kuai L, Kerstens W, Phu Cuong N, Verstraete W (1999). Treatment of domesticwastewater by enhanced primary decantation and subsequent naturally ventilated trickling filtration. *Water, Air, and Soil Pollution*. 113: 4-62.
- Lu SM, Yin YP, Zhang ZD, Yu N (2007). Feasibility study of Abolish the Septic Tank in old urban area of Guangzhou. *Environmental Science and Technology*. 30(10): 53-57 (in Chinese).
- Narain S (2002). The flush toilet is ecologically mindless. *Down To Earth*, 28: 28-38.
- Schertenleib R (1995). 'Improved Traditional Nightsoil Disposal in China – An Alternative to the Convention Sewerage System?'. *Sandec News*.1: 17-19.
- The Ministry of Construction of PRC (2000 to 2008). *China Urban Construction Statistical Yearbook*. China Architectrue and building press, Beijin.
- The Organization for Economic Cooperation and Development. (2007). *Environmental Performance Reviews China (Chinese version)*. Chinese Environmental Science Press, Beijin.
- The World Bank (2005). *Waste management in China: issues and recommendations*. Working Paper No. 9. Urban Development Working Papers. East Asia Infrastructure Department, May, Washington, DC.
- Yao GH (2007). Abolish the Septic Tank and Reduce the Emission of Greenhouse Gas. *Sichuan Architecture*. 27(4): 45-46.

STUDY ON THE RELATIONSHIP BETWEEN LANDSLIDES, DEBRIS FLOWS AND THE MODERN RIVER GEOLOGICAL PROCESSES

Ming-Xin ZHENG¹

ABSTRACT: In this paper, the development and distributing regularity of landslides, debris flows along Qingyi River in Sichuan province, is the study object. Then, the relationship between hazards and the river geological processes is discussed. By the reflection analysis, the conceptual model of mass motion and stop of slope materials is set up. Moreover, on the basis of utilizing super entropy-theory, the assessment method of stability of the total or segment river is put forward, which provides a new way for prediction of regional geological hazards.

KEYWORDS: modern river geological processes, narrow and wide valley, reflection analysis, super entropy

INTRODUCTION

The development and distribution of geological hazards, such as landslides, debris flows is controlled by the dynamic geological process, such as stratum, geological structure, topography, precipitation and earthquake. Among the factors, topography is the result of comprehensive ex-behalves process; and the river geological process is the intrinsic controlling process in the change of terrain or topography (Zheng 1994; Alan 1995).

On the basis of analysis on the longitudinal profile and map feature of river, which represent the characteristics of river geological process, the location of geological hazards, such as landslide, debris flows will be judged. Using the reflection, the developing and distributing regularity of geological hazards are discussed.

RELATIONSHIP BETWEEN LANDSLIDES, DEBRIS FLOWS AND THE CHARACTERISTICS OF RIVER SHAPE

In fact, the river includes a series of segments of narrow and wide valley. The wide valleys, e.g. the basins, like string beads in the map of river. By analyzing the longitudinal profile, there is a series of steep valley interval mitigative valley, see as Fig. 1.

In general, the landslides always develop in the section where the transition from narrow valley to the wide valley and the debris flows in the transition section from width valley to narrow valley. If we incorporate

landslide and debris flow into a broad slope, we can set up a conceptual model of mass motion, stop of slope materials.

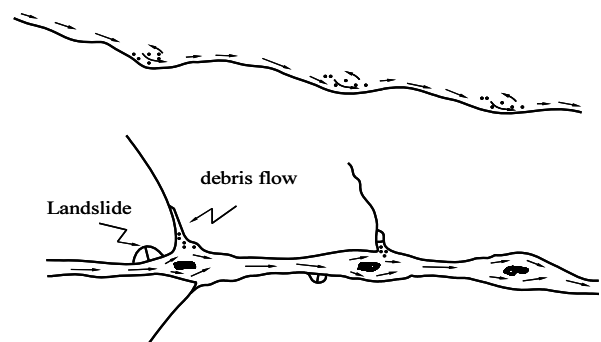


Fig. 1 Sketch of river's vertical section (upper) and map of river (lower)

Reflection Analysis of Landslides, Debris Follows and the Longitudinal Profile of the Qingyi River

Using reflection analysis, the correlation between landslides, debris flows and the environmental background can be discussed.

Analysis of characteristics of river

Characteristics of river illustrate in Fig. 2. It shows that:

(1) Gradient of longitudinal profile of river (GLP) and gradient of shore slope (GSS) decrease gradually as the grade of river becomes big, according the 1:500000 terrain maps. See as Table 1.

¹ Professor, Institute of Bridge & Road and Geotechnical Engineering, East China Jiaotong University, Nanchang, China. Email: zhengmx2002@yahoo.com.cn

Table 1 Reflection analysis between river grade and landslides, debris flows

Grade of river	GLP %	GRB %	Number of landslide	Number of debris flow
III	14~52	50~90	15	25
IV	3~18	32~110	7	12
V	1~4	14~38	10	3

(2) The river is made of a series steep and mitigate segments about 35~40Km length, therefore, there is a lot of basin as string beads in map. Most landslides often develop in the section where the narrow valley transits to wide valley. For example, at the steep and mitigate valley of Yaoji, there are 3 landslides developing in the narrow section of river where the gradient of longitudinal profile of river (GLP) is 30~40‰ and gradient of shore slope (GSS) is 80~92%. On the other hand, there are 6 debris flows develop in the wide section of river, which GLP is 13~17‰ and GSS is 56~76%. In addition, in the section of Feixianguan~Ya'an narrow and wide valley, 1 landslide develops at narrow valley, where GLP is 4~16‰ and GSS is 52~64%; 5 debris flows develop at the wide valley, where GLP is 2.6~4.2‰ and

GSS is 18~34%. See as Fig. 2.

Reflection analysis

(1) Debris flows always develop in the mitigate section of river. The reasons include A and B.

A: Debris flow has character of resurrection. It needs a large amount of debris materials accumulated for a long time under the mitigate wide basin.

B: The location of debris flow valley situates in basin, like a string bead, where there are a lot of streams distributing at the two shores, so the terrain is wide, and GSS is mitigate. By the regressive analysis of GLP and GSS, it shows that GLP is positive correlation to GSS.

(2) Landslide always develops in steep shore of river.

A: Landslide always develops in steep bank because the gravity potential energy is accumulated. So it makes slopes easy to deform and failure.

B: Riverbed of steep bank always has seriously vertical erosion and lateral erosion. So the slope deformation is along with the riverbed.

(3) Results of river geological process reflects the characteristics of stratum and lithology, geological tectonics, even locate climate. For example, the river always develops along the fault or soft stratum; accumulative stream is always controlled by the garben basin; and eroded stream is always controlled by the geological structure.

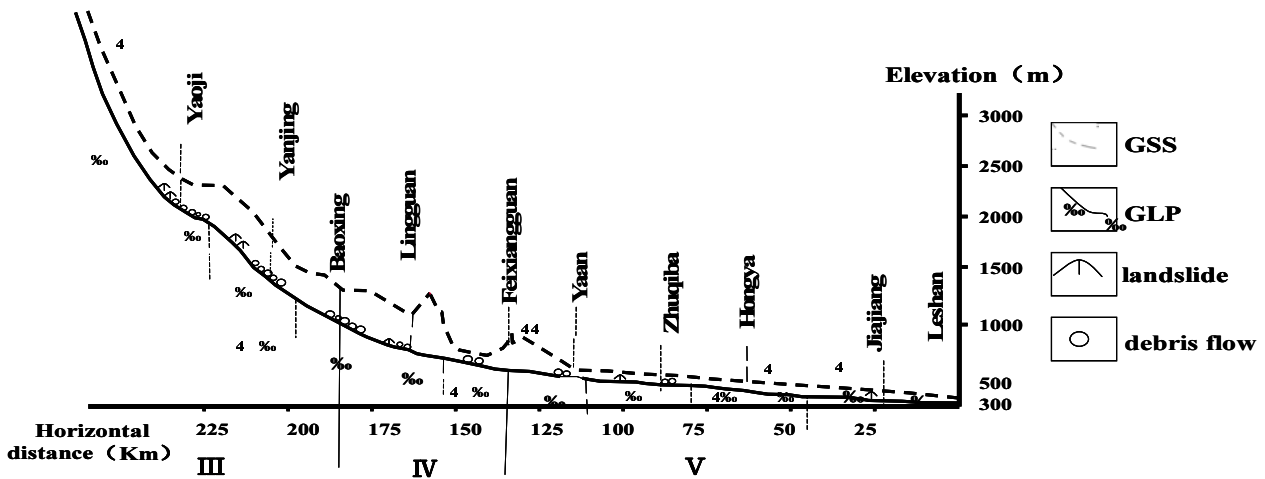


Fig. 2 Reflection analysis sketch of river vertical section and the landslides, debris flows in Qingyi River

RELATIONSHIP BETWEEN THE SLIDE, FLOW, ACCUMULATION OF SLOPE MATERIALS AND GRADIENT OF LONGITUDINAL PROFILE OF STREAM

In order to predict and control the hazards, it is important to master the regularity of sliding, flowing and accumulation of slope materials. According to the investigation of two tributaries on upper-stream of

Qingyi River, a conceptual model of slope movement is given in the follows.

(1) LiuLuo tributary: It is a slope-type debris flow. The average of gradient of longitudinal profile (GLP) is 438.5‰ or 23.5°. The GLP of upper-stream (formation zone of debris flow) is bigger than 25°, gradient of shore slope (GSS) is bigger than 35°, GLP of middle-stream (passage zone) is 12°~25°, and GLP of downstream is 5°~8°(or less than 10°).

(2) HePing tributary: It is a gully-type debris flow. The length of main gully is 7.5 Km, and the average of GLP is 173~225‰ (or 10°~13°). GLP of upper-stream is 220~466‰ (or 12.5°~25°), GLP of middle-stream is 148~250‰ (or 9.5°~14°), and GLP of down-stream is 75~110‰ (or 4.5°~7°). See as Fig. 3

From the two debris flows, we can derived that debris flow always develops in mountain tributary where the average of GLP is more than 15°, and landslide or collapse always develops at the GSS more than 30°. The sediment zone always develops at the GSS less than 10°, e.g. the wide stream or mitigate zone.

(3) When the landslide without the high speed sliding or far distance sliding, the gradient of landslide's tongue is about 30°~38°. This conclusion is derived by the field investigation about gradient of tongue of falling or landslide accumulation along the upper-stream of Qingyi River. See as Table 2.

According to the above analysis, a conceptual model of the broad slope, which incorporates landslide and debris flow into an entirely slope failure model of sliding—flowing—accumulations, is set up. See as Fig. 3.

Table 2 The gradients of falling, sliding accumulations along Qingyi Rive

Gradient	<20°	20°~30°	30°~40°	>40°
Number of Landslide (rockfall)	3	10	32	1

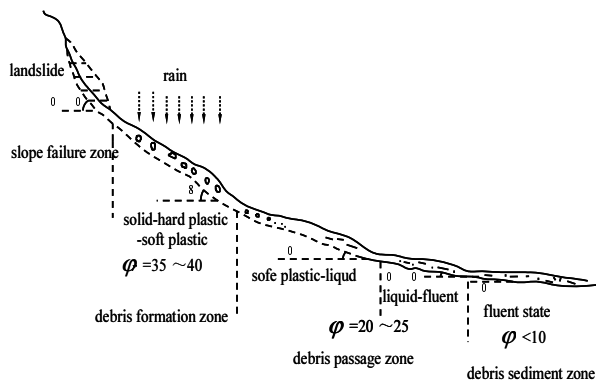


Fig. 3 Conceptual model of the failure pattern of general slope

RELATIONSHIP BETWEEN LANDSLIDE, DEBRIS FLOW AND THE SUPER-ENTROPY OF DRAINAGE BASIN

The Super-Entropy of Drainage Basin

AI (1987) proves that the curve of Strahler(A.N. Strahler,1963, ALAN E,1995) represents the shape

characteristics at equilibrium when drainage basin's balance of en-energetic and ex-energetic process. Then he induces the linear balance entropy to study the drainage basin. For most of drainage basin, which is in a far balance energetic system, is a structure of consumption. Furthermore, he discussed the differentiate index of stability of drainage basin system with super-entropy (AI, 1993).Then he sets up a formula of super-entropy about the nonlinear and unstable state. As for a certain drainage basin, the formula of super-entropy is:

$$\partial P = \frac{-\beta N (N - 1)(N + 1)}{N (-\beta - 1) - 3} \tag{1}$$

where N, β are the factors of Strahler's curve (or curve of GLP) under unbalance state. It can express with the function:

$$f(x) = (1 - x)^N \text{ or } f(x) = (1 - x)^{\frac{1}{1+\beta}} \tag{2}$$

This formula expresses the characteristics of riverbed and the evolving stage of river.

When $\partial P > 0$, the system of river is stability; $\partial P = 0$, in critical state; and $\partial_x P < 0$, instability.

Classification with Drainage Basin Super-Entropy

First, analysis on a drainage basin with rectangular map, and the equation of its GLP is:

$$\frac{h}{H} = \left(\frac{l}{L}\right) \tag{3}$$

Correspondingly, the curve of GLP is:

$$\frac{h}{H} = \left(\frac{a}{A}\right) = \left(\frac{l}{L}\right) \tag{4}$$

where: h is the high disparity and l is the length of section river from the river ends to the study points; a is the basin area of section river from the river ends to the study point.

H, L and A is the high disparity, length and basin area of entirely river, respectively.

N is the shape index of river GLS.

From Eq. (2),

$$N = 1 - \frac{2}{1 + \beta}, \text{ or } \beta = \frac{1 + N}{1 - N} \tag{5}$$

Therefore, the super-entropy of rectangular map of drainage basin is:

$$\partial P = \frac{N^3 (N + 1) (N + 1)}{3 - N} \tag{6}$$

From the equation we can drive out:

(1) The fan-shape drainage basin
The equation of its GLP is:

$$\frac{h}{H} = \left(\frac{l}{L}\right)^N$$

Then, the super-entropy of fan-shape drainage basin is:

$$\partial P = \frac{N(N-4)(N+2)}{32(6-N)} \tag{7}$$

(2) The leaf shape drainage basin:
The equation of its GLP is:

$$\frac{h}{H} = \left(\frac{l}{L}\right)^{-N}$$

Then, the super-entropy of leaf-shape drainage basin is:

$$\partial P = \frac{N(N-2.25)(N+1.5)}{9.59375(4.5-N)} \tag{8}$$

(3) The narrow-fan drainage basin :

$$\frac{h}{H} = \left(\frac{l}{L}\right)^{-3N}$$

Then, the super-entropy of leaf-shape drainage basin is:

$$\partial P = \frac{N(N-9)(N+3)}{243(9-N)} \tag{9}$$

The curve of $N-\partial P$ and the stage of stability is illustrated in Fig. 4.

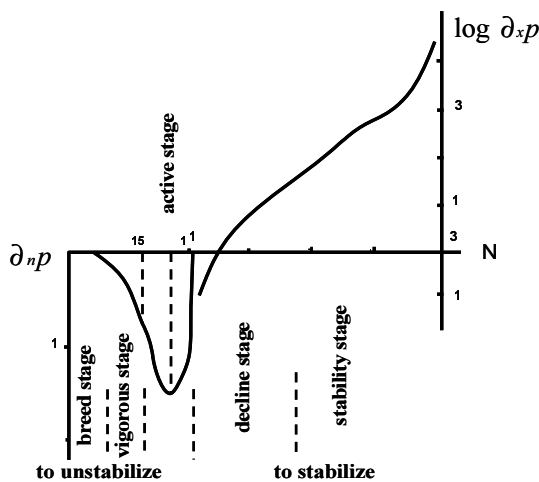


Fig. 4 Values of N of rectangular basin and ∂P with the developing stage of river

In it: When $\partial P = -0.151$, the drainage basin is at the utmost instability;

$-0 \rightarrow -0.0979$ the developing of landslide and debris flow of drainage at breeding stage;

$-0.0979 \sim -0.0151 \rightarrow 0$, at the vigorous stage, hazards happen frequently;

$0 \sim 38.85$, in decline stage; $38.85 \rightarrow +\infty$, at stability situation.

From the results we can see: In a confined system, the value of N shows the stage of erosion cycle; And in an opening system, it shows the degree of antagonism between en-factors and ex-factors. When N is small, the function of en-factors is more than that of ex-factors; conversely, ex-factors is less than that of en-factors.

A broad slope is being critical when the function of ex-factors equal to the function of ex-factors, and the drainage basin being at its utmost instability. So we can use super-entropy $\partial P(N)$ to analyze the stability of the drainage basin.

STABILITY EVALUATION TO QINGYI RIVER BASIN USING SUPPER-ENTROPY THEORY

The Trunk of Qingyi River

The river can be divided into 7 narrow and wide valleys (see as Fig. 1). We can measure the value of h, l, H and L of narrow and wide valley is measured, respectively. Then, according to the kind of shape, the value of N is calculated by regression analysis; Furthermore, the value of is calculated by the formula (6)~(9). See as Table 3.

From table 3 we can draw the conclusions as follows:

(1) To the total drainage basin of entirely river, it is suitable to use the leaf drainage basin to evaluate. In fact, the drainage basin is a leaf shape; and the geological hazards are less than that of historical period. At present, the river is being stable, e.g. the development of landslide and debris flow is decrease. The stability state is in the decline period because $\partial P(2N/3) = 6.683 > 2.8$. On the contrary, the landslide and debris flow are developing in the upper-stream.

(2) As to the section of river, it is suitable to evaluate downstream using rectangular shape, middle-stream using leaf shape and upper-stream using fan shape.

① Specifically, in the downstream, Jiajiang to Yaan, there are 4 narrow and wide valleys, which caters to use the rectangular shape to evaluate.

Hongya ($\partial P = 1.25$) and Wucunba ($\partial P = 0.1247$, only 1 old landslide), are being in the decline stage; and the section of Hongya is more stable than that of Wucunba Feixianguan to Ya'an section Hongya ($\partial P = 1.25$) and Wucunba ($\partial P = 0.1247$, only 1 old landslide), are being in the decline stage; and the section of Hongya

Table 3 The results of $\partial P - N$ of Qianyi River

Segment stream of drainage basin		∂P (Rectangular)	∂P (Leaf)	∂P (Fan)
Jiajiang	Upstream	-0.037	-0.0105	-0.00425
	Downstream	0	-0.1176	-0.0562
	Whole stream	-0.10816	-0.0355	-0.0142
Hongya	Upstream	-0.106	-0.0316	-0.0519
	Downstream	-0.049	-0.11	-0.0519
	Whole stream	1.25	-0.1506	-0.098
Wucunba	Upstream	-0.092	-0.029	-0.0118
	Downstream	-0.0077	-0.0021	-0.009
	Whole stream	0.1247	-0.1293	-0.0646
Feixianguan-Ya'an	Upstream	-0.0834	-0.0257	-0.0105
	Downstream	1.3045	-0.15	-0.0998
	Whole stream	-0.1319	-0.0892	-0.0398
Baoxing--Ling'guan	Upstream	1.8762	-0.144	-0.109
	Downstream	10.72	0.135	-0.150
	Whole stream	0.6113	-0.1477	-0.084
Yanjing	Upstream	-0.15	-0.0731	-0.0316
	Downstream	0.285	-0.1384	-0.0724
	Whole stream	1.144	-0.151	0.0968
Yaoji	Upstream	28.85	0.8626	0.129
	Downstream	1.8817	-0.1443	-0.109
	Whole stream	8.5963	0.0557	-0.1473
Drainage of Qingyi		91.925	6.683	-0.1246

is more stable than that of Wucunba Feixianguan to Ya'an section ($\partial P = -0.13179$), developing several landslides and debris flows, especially debris flows have happened in the last two decades), are in active stage. Section of Jiajiang ($\partial P = -0.108163$), because of accumulation sediment and vertical erosion by the river, several landslides have happened in the steep bank recently. This section is more instable than that of FeiXianGuan to Ya'an.

② In middle-stream, there are 2 narrow and wide valleys. The section of Lingguan to Baoxing ($\partial P = -0.1477$) and section of Yanjing ($\partial P = 0.151$), it is suitable to use leaf shape to evaluate. The landslides and debris-flows are developing in the active stage ($-0.0979 \sim -0.151 \rightarrow 0$), especially in the section stream of Yanjing.

③ In upper-stream, for the section stream of Yaoji, which belongs to grade III basin according to 1:500000 topography map, is suitable to use fan shape to evaluate ($\partial P = -0.1473$), which is at the active stage. In 1987, 1989 and 1990, 7 debris flows happened and made a great hazard.

(3) From all the narrow and wide valleys, the former (downstream) are suitable using rectangular basin to evaluate; the later (upper-stream) is suitable using leaf shape. According to the Table 4, developing landslides are often happened in the transition from middle-stream

to downstream; the slope is more instable from middle-stream to upper-stream.

Branch River of Heping Tributary

Moreover, the value of $\partial P - N$ of Heping tributary and its section stream is calculated respectively. See as Table 4.

Table 4 The analysis result of $\partial P - N$ in Heping valley

Segment stream of drainage basin	Down stream	Middle stream	Up stream	Whole stream
Rectangular (N)	1.112	0.8472	0.964	1.3936
Leaf (2N/3)	-0.12148	-0.0788	-0.10857	-0.142
Fan (N/2)	-0.00756	-0.03446	-0.0506	-0.126

By the site investigation, the area of drainage basin is 18.5Km² and it belongs to the leaf shape. Table 4 shows that the upper-stream and downstream are unstable, where the accumulation and scouring are seriously in downstream; On the contrary, the middle-stream is stable.

CONCLUSIONS

(1) From the case of Qingyi River, the relationship between the developing location of landslides, debris flows and modern river geological process is very intimate. The shape characteristics of river imply the stability of drainage basin and the evolving regularity of drainage basin, which is a comprehensive, behave of ex-energetic and en-energetic geological process.

(2) There is inherit correlation between the landslides, debris flows and the characteristics of river shape, the hazards always develop in a particular river section. In order to predict the developing location of hazard, reflection analysis between the landslides, debris flows and the characteristics of river shape figure out. On the basis of reflection analysis in the river basin of Qingyi, it shows that landslides always develop at the segment from narrow to wide valley; and debris flows always develops at the transition section from wide to narrow valley, especially at downstream of wide river.

(3) According to the relationship between the mass motion, stop of slope materials and the longitudinal profile of river, a conceptual model of broad slope about deformation and failure is set up, which provides a stretching concept about the integration system of slide and debris flow.

(4) By analyzing the shape index N of longitudinal profile, the stability of drainage basin is evaluated by the super-entropy theory, which makes an important and

effective method. It caters to use rectangular shape to evaluate the stability of large drainage basin. As to the segment of river, it is necessary to choose a corresponding basin shape to evaluate the stability of stream.

Still, there are two problems such as: N only represents the river shape characteristics of drainage basin, while it does not considering of rainfall, lithology, geological structure and human activity, etc.

ACKNOWLEDGEMENTS

The author wishes to express his gratitude to Chinese Council of Scientific Research for financial support for his work. He would also like to acknowledge to Professor Wang Lan-Sheng, who's from Chengdu University of Technology.

REFERENCES

- Ai NS (1987). The information entropy of the erosional drainage basin. *Journal of Natural Environment Reservation (Chinese)*, 1(2): 1-8.
- Ai NS (1993). On dynamics of drainage evolution. *The Chinese Journal of Geological Hazard and Control*. 4(3): 26-34.
- Alan E K (1995). *Geology for engineering and environmental scientists*. Prentice Hall, Englewood Cliffs, New Jersey: 395-441.
- An S (1963). Hyposometric (area-altitude) analysis of erosional topography. *Geol. Soc. Am. Bull*: 1117-1142.
- Zheng MX (1994). A primary research on the relationship between landslide and present geological process of river. 4(5): 40-47.

SEISMIC DAMAGE CHARACTERISTICS OF RURAL ADOBE-WOOD BUILDING IN GANSU PROVINCE INDUCED BY THE WENCHUAN GREAT EARTHQUAKE

Ai-Lan CHE¹, Zhi-Jian WU², Jun-Jie SUN³ and Jing-Hua QI⁴

ABSTRACT: The Wenchuan great earthquake, which measured at Ms8.0 and Mw7.9, occurred on May 12, 2008 in Sichuan Province of China, caused enormous death toll and economic loss. The buildings, lifeline engineering and infrastructures were damaged badly, and secondary disasters were serious and wide, and the rural adobe-wood buildings in rural regions were damaged severely. In order to investigate the damage characteristics and mechanism of buildings induced by the earthquake, and to service reconstruction, the disaster investigations and simulation were practiced. The results shows that the reasons of fragilities in the earthquake of abode-wood building are insufficient component capacity, weakness in joint and connection, instabilities of structural framework, etc. Those results will be useful for serving the reconstruction after the earthquake.

KEYWORDS: adobe-wood building, Wenchuan Great Earthquake, seismic characteristics

INTRODUCTION

The Ms8.0 Great Earthquake occurred at the Longmen Mountain Fault, Sichuan Province on May 12, 2008. Gansu and Shaanxi were the two provinces suffered damage less than Sichuan Province, which was the most seriously quake-hit area by the Earthquake. The huge earthquake affected the whole area of Gansu Province and damaged 52 counties (districts) of 10 cities, in which more than 600 villages in 46 counties (districts) of 8 cities was damaged seriously. The whole disaster area spread 110,000 km², there were 15,169,131 people and about 203,640,395 families affected, 369 people died and 10171 people injured. The earthquake caused great damages to rural houses, educational and healthy buildings, and lifeline engineering, meanwhile, it also caused serious secondary geotechnical disasters.

The casualties and destruction caused were mainly caused by the collapse of houses, in which the adobe-wood buildings were most destroyed significantly. Part of agricultural home in many areas are still used adobe load-bearing wall, especially the livestock loop, firewood room, kitchen and so on are even used the typical form of the adobe structure. Those structures had poor seismic performance and are non-antiseismic design, and which

was the main collapsed structure in the quake-hit area of Gansu Province.

In order to clarify the seismic characteristics and damage mechanisms of rural adobe-wood building, the investigation in Gansu earthquake disaster region were performed and a series of dynamic simulations were conducted. The results is used to recommend a much better way serving the reconstruction after the earthquake.

HAZARDS INVESTIGATION IN RESEARCH AREA

The hazards investigation on the damage to buildings in the quake-hit areas of Gansu Province was conducted by the Lanzhou Institute of Seismology after the earthquake from May 23 to 30 in 2008. The typical towns, buildings and secondary geotechnical disaster regions were selected as key investigated objects. The building investigation covered rural and urban buildings in Wudu district, Wen County, and the other counties of the Longnan City, the damages to the buildings of Tianshui City and Yaodu town in Qingchuan County of Sichuan Province were investigated as well. The methods in buildings investigation includes damage-suffering characteristics, and photos taken for damage

¹ Key Laboratory of Geological Hazards on Three Gorges Reservoir Area, Ministry of Education, Three Gorges University China Associate professor, School of Naval Architecture, Ocean and Civil Engineering, Shanghai Jiaotong University, China. Email: alche@sjtu.edu.cn

² Associate professor, Lanzhou Institute of Seismology, China Earthquake Administration (CEA), China. Email: zhijianlz@163.com

³ Assistant professor, Lanzhou Institute of Seismology, China Earthquake Administration (CEA), China. Email: sunnunj@163.com

⁴ Doctor, School of Naval Architecture, Ocean and Civil Engineering, Shanghai Jiaotong University, China. Email: qijinghua@sjtu.edu.cn

features.

The main building constructues of the rural citizens at the quake-hit areas in Gansu Province are brick-wood building and adobe-wood building, which occupy 65%—80% of the rural citizen’s buildings in Gansu (Wang, 2005) (Table 1). There are two kinds of buildings of adobe-wood buildings, the wall load-bearing building, brick column load-bearing building, which occupy 45%—55% of the rural citizen buildings.

Table 1 Occupation ratio of rural citizen buildings at the quake-hit area of Gansu Province

Type of Building	Brick-concrete building	Wood-frame building	Brick-wood building	Adobe-wood building		Other building
				Wall load-bearing	Brick column load-bearing	
Occupation Ratio	≤10%	15%	20-25%	45-55%		≤5%

In Gansu Province, the intensity degrees caused by the great earthquake are from V to IX degree at different regions. The different types buildings had different performances at different intensity degree areas (Yuan, 2008). At the IX degree area of Gansu, south of Longnan City, the brick-concrete buildings were damaged seriously, generally, penetrative and shear fractures appeared on the walls and the precast slabs Fig. 1). Figs. 2, 3 and 4 show that the brick-wood building and adobe-wood building were completely collapsed, however, parts of the wood-frame buildings kept standing and the walls collapsed. At the VIII degree area, shear fractures appeared on the walls of the brick-wood buildings (Fig. 5). However, most of the Adobe-wood buildings were collapsed (Fig. 6). At the VII degree area, the adobe-wood buildings were damaged seriously, and lengthways fractures were usually appered at the joint of wall and brick column of the brick column load-bearing houses (Fig. 7). Fig.8 shows that the adobe-wood building was damaged on the wall at the VI degree area.



Fig. 1 A brick-concrete building at Bikou Village, Wenxian County, Gansu Province. (IX degree)



Fig. 2 A brick-wood house collapsed, Jiulongzhen Town, Mianzhu City, Sichuan Province. (IX degree)



Fig. 3 A village, which houses were adobe-wood buildings, was destroyed at Zhongmian, Wenxian County, Gansu Province. (IX degree)



Fig. 4 A wood-frame house was damaged seriously at Kongjiashan Village, Wenxian County, Gansu Province. (IX degree area)



Fig. 5 Damages to brick-wood building in Haoping Village of Wudu District, Gansu Province(VIII degree)



Fig. 6 Damages of adobe-wood building in Yingzhuang Village of Xihe-County(VIII degree area)



Fig. 7 Lengthways fracture on joint of the wall and brick column of Leiba Village hospital of Lixian County, Gansu Province.(VII degree area)



Fig. 8 Damage to the adobe-wood house at the Wudang Village of Zhangxian County, Gansu Province. (VI degree)

STRUCTURAL CHARACTERISTICS OF RURAL ADOBE-WOOD BUILDING

Masonry Technology of Adobe Wall

The masonry technology of adobe wall in Gansu province is mainly vertical masonry. There are casually one or multi-storey horizontal masonry. Fig. 9 shows the typical masonry technology of adobe wall.



(a) 1-vertical and 2-horizontal



(b) 4-vertical and 1-horizontal

Fig. 9 Typical masonry technology of adobe wall.

The Structural Type of Traditional Adobe-Wood Building

It can be divided into the following types of rural adobe-wood building at the quake-hit area in Gansu Province.

(1) Wall load-bearing building (Fig. 10): The adobe walls act as the main load-bearing, and the beam or sub-purlin directly hang over the load-bearing wall. There are no fixed measures between beam or sub-purlin with load-bearing walls, and the wall bears the full loads of the roof system;

(2) Brick column load-bearing building (Fig. 11): The brick columns act as the main load-bearing, and the adobe walls use as envelope and partition wall. There are extended riveting strokes for reinforcement and no fixed measures between structural frames with load-bearing walls. The connection measures between the brick columns with adobe walls are lack.



Fig. 10 A wall load-bearing building.



Fig. 11 A Brickcolumn load-bearing building

The material strength of adobe walls and rammed earth wall is low, the pointing material (grass mud or plaster) strength of stuffing wall with broken (gravel) rock is insufficient, and there are almost no effective extended joint measures, then the overall of the structure is poor (Qiu, 2009). It is easy to be collapsed of the wall and roof, and separated vertical horizontal wall with horizontal one.

DYNAMIC ANALYSIS OF TRADITIONAL ADOBE-WOOD BUILDING

Time domain dynamic analysis method is applied to typical traditional adobe-wood building to obtain the dynamic characteristics. The dynamic behavior of the structure, the dynamic stress and strain is evaluated.

Modeling

As shown in Fig. 12, a 3-dimensional FEM model is created as possible as being approximate to the typical masonry of adobe wall. The foundation is considered to be rigid, and the property constants of the structure are listed in Table 2.

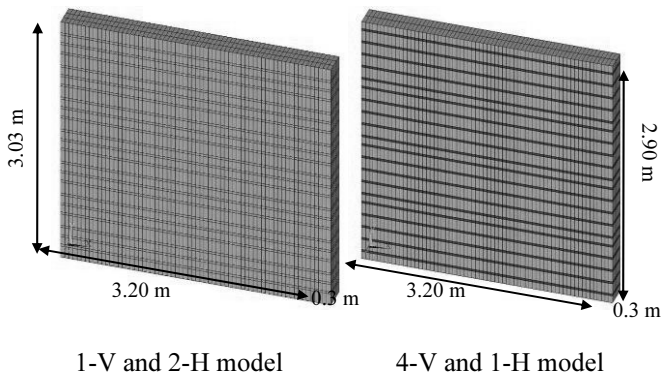
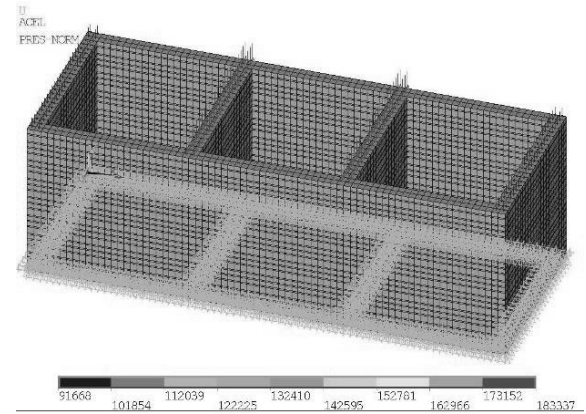


Fig. 12 A 3-dimensional FEM model of adobe wall

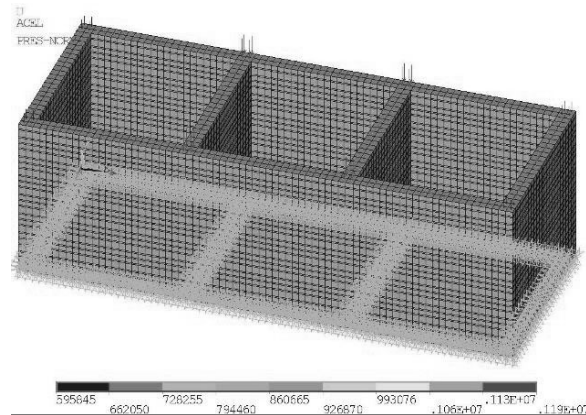
Table 2 Property constants of the structure

Material	Density (kg/m ³)	Elastic modulus (Pa)	Poisson's ratio
Adobe	1627	2.1342×10 ⁸	0.28
Interlayer mud	1422	9.712×10 ⁷	0.3

According to the structural type of traditional adobe-wood building, a 3-dimensional FEM model is created as wall load-bearing type and brick (wooden) column load-bearing type with 3 rooms, which is 6-8 m length, 3.6 m width, and 3.3 m height. The 4-vertical and 1-horizontal type of adobe wall is used (Fig. 13). The roof loads are acted at horizontal walls in brick (wooden) column load-bearing type model.



(a) Wall load-bearing type model



(b) Brick (wooden) column load-bearing type model

Fig. 13 A 3-dimensional FEM model of traditional adobe-wood building

Seismic Loads

The aftershock data of Wenchuan Great Earthquake is used (Fig. 14). The maximum acceleration is 100 gal, and the dominant frequency is 2.5 Hz and 5.0 Hz, respectively.

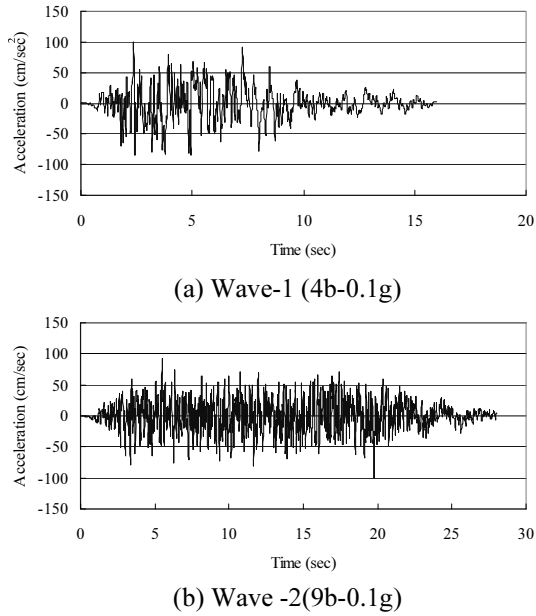


Fig. 14 Aftershock data of Wenchuan Great Earthquake

Results

Dynamic characteristics of adobe wall

Numerical simulation results of the seismic response of the adobe wall show that the maximum response of 4-vertical and 1-horizontal model is great than that of 1-vertical and 2-horizontal as shown as Table 3.

Table 3 Numerical simulation results of the seismic response of the adobe wall

Maximum response	Wave-1(4b-0.1g)		Wave -2(9b-0.1g)	
	1-V 2-H model	4-V 1-H model	1-V 2-H model	4-V 1-H model
Displacement (mm)	0.7	1.9	1.0	3.6
Shear stress (kPa)	2449	5592	3192	13094
Strain (μ)	65.2	80	110	348

Dynamic characteristics of traditional adobe-wood building

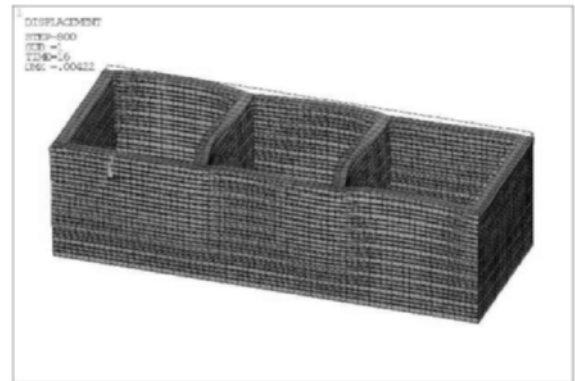
(1) Response of displacement

Response of displacement is shown as Fig. 15. The structure shows shear behaviors due to earthquake. The maximum displacement is 4.2 mm in the wall load-bearing type model and 2.2 mm in the brick (wooden) column load-bearing type model, respectively.

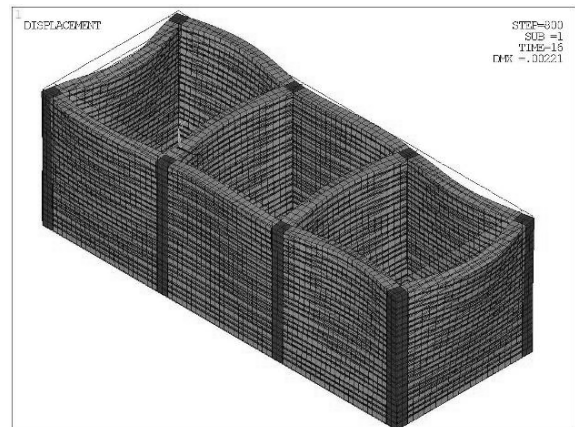
(2) Response of shear stress

Figs. 16-17 shows the distribution of principal stress and shear stress response in the end of the earthquake. It is shown that the maximum shear stress is concentrated on the joint between vertical and horizontal wall in the middle room which is 1.2×10^5 kPa and the maximum

principal stress is concentrated on the horizontal walls in the middle room which is 2.5×10^5 kPa in the wall load-bearing type model; the maximum shear stress is concentrated on the joint between horizontal wall and columns which is 1.14×10^6 kPa and the maximum principal stress is concentrated on the columns in the middle room which is 1.2×10^6 kPa in the brick (wooden) column load-bearing type model. Therefore, the maximum stress of brick (wooden) column load-bearing type model is 10 times than that of wall load-bearing type model.

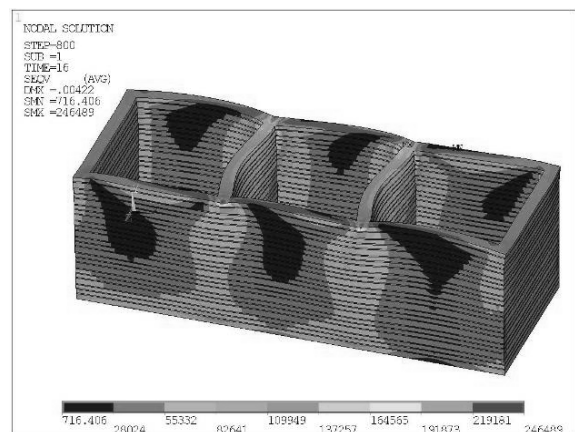


(a) Wall load-bearing type model

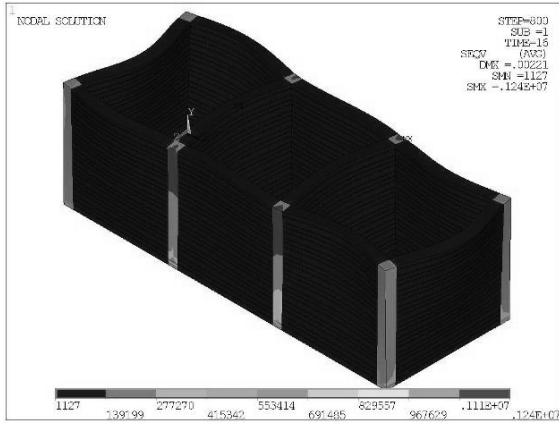


(b) Brick (wooden) column load-bearing type model

Fig. 15 Response of displacement of traditional adobe-wood building

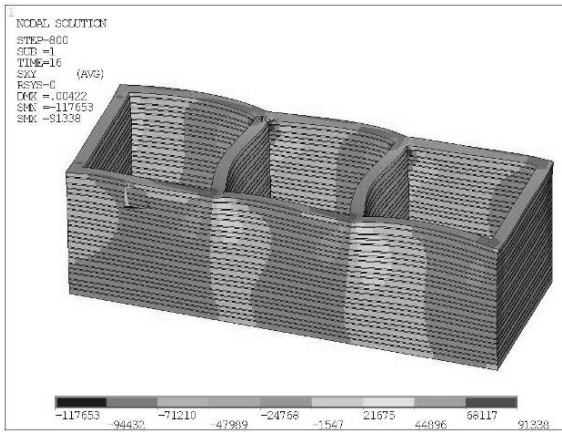


(a) Wall load-bearing type model

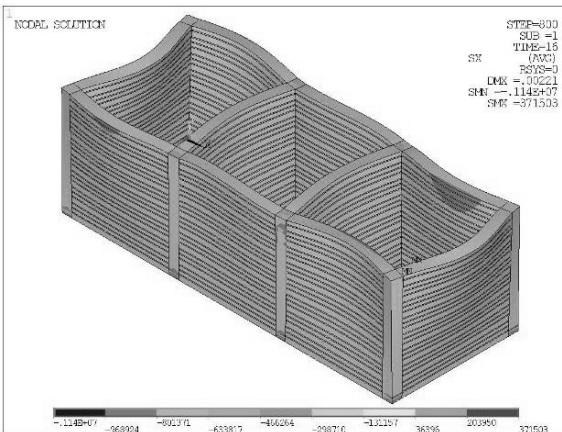


(b) Brick (wooden) column load-bearing type model

Fig. 16 Distribution of principal stress response in the end of the earthquake



(a) Wall load-bearing type model



(b) Brick (wooden) column load-bearing type model

Fig. 17 Distribution of shear stress response in the end of the earthquake

(3) Response of acceleration

Fig. 18 shows the time history of the structure. It is shown that the acceleration is increasing from the bottom to top of the structure. The maximum acceleration is appeared on the horizontal wall in the middle room which is 888 gal in the wall load-bearing type model; it

is appeared on the columns in the middle room which is 1350 gal in the brick (wooden) column load-bearing type model. Moreover, the composition of earthquake is absorbed by the structure.

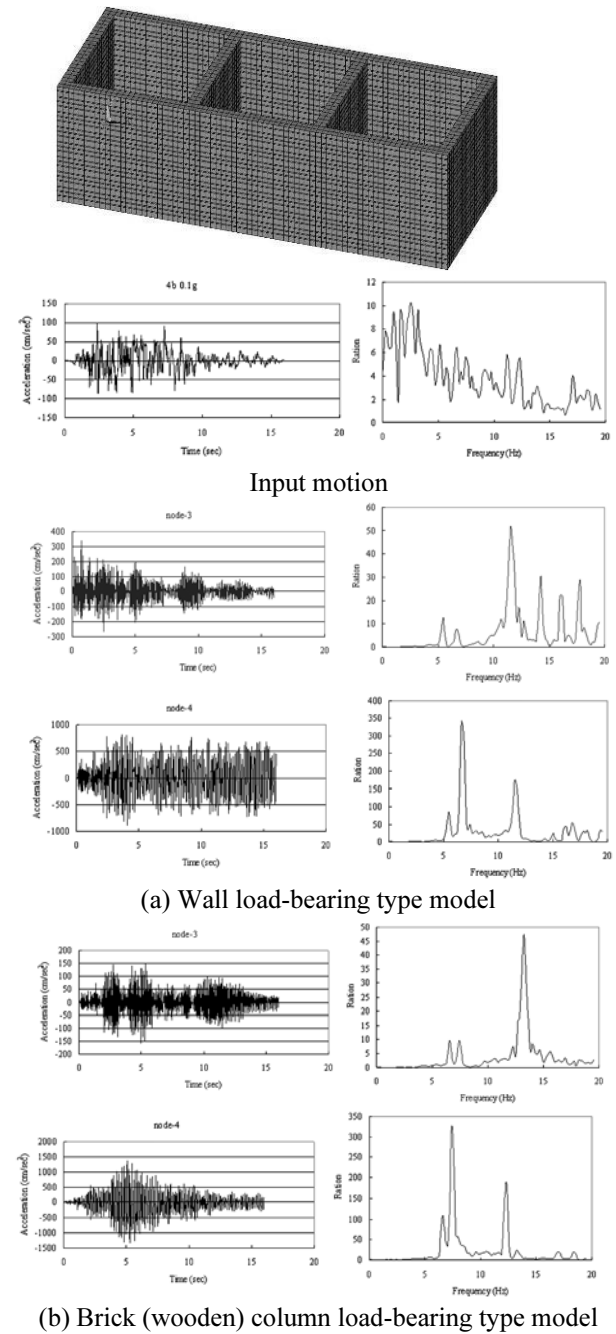


Fig. 18 Time history of the structure

CONCLUSIONS

The investigation in Gansu earthquake disaster region and a series of dynamic simulations were conducted to clarify the seismic characteristics and damage mechanisms of traditional adobe-wood building, the results are as follows:

(1) The structure shows shear behaviors due to earthquake.

(2) The response of brick (wooden) column load-bearing type model is great than that of wall load-bearing type model. Both of maximum shear stress and principal stress are concentrated on the connection between columns and walls in the middle room, and the weak point of brick (wooden) column load-bearing type model is the joint between columns and walls. Therefore the reinforce of the joint between columns and walls is the point of increasing the seismic resistance of traditional adobe-wood building.

(3) Acceleration is increasing from the bottom to top of the structure, and the composition of earthquake is absorbed by the structure.

ACKNOWLEDGEMENTS

This work was supported by the grant of the Western

Project of the Chinese Academy of Sciences (No. KZCX2-XB2-10) and the basic research fund of the Earthquake Predict Institute, CEA.

REFERENCES

- Wang LM, Yuan ZX, Lin XW (2005). Survey and an alysis on the seismic vulnerability of rural buildings in Gansu Province. *World Earthquake Engineering, China*. 21(4): 16-25.
- Yuan ZX, Tan M, Ma ZH (2008). Damages on Brick—concrete Rural Buildings in Qingchuan County , Sichuan Province, during the Great Wenchuan Earthquake. *Northwest Seismological Journal, China* 30(4): 317-325.
- Qiu RD, Yuan ZX, Wang Q (2009). Earthquake damages of earth-wood buildings during the Wenchuan Ms 8.0 Earthquake. CRC Press, Taylor & Francis Group (Balkema), Japan.

EFFECTIVE FACTORS ON AMPLIFICATION IN CHABAHAR CITY, SOUTHEAST OF IRAN

Ahmad ADIB¹ and Kobra HEYDARZADEH²

ABSTRACT: Amplification factor identify effect of soil characteristics on wave acceleration in ground surface. Some factors affect on amplification factor. This paper analyzes this object. ground response analysis in Cabahar city, south eastern of Iran, gained by using numerical method (one dimensional) and soil equivalent linear behavior and by EERA program. Resulted amplification factors separated according Iran building design against earthquake code, standard 2800, and analyzed. According the analysis, it is found that amplification factor nearly increased from more to less competent ground type (i to iii) but this trend don't observe in some sites. to research the reason of this complexity we analyzed another effective factor on amplification, such as impedance ratio. it is found that impedance ratio between bedrock and surface layer and also between layers of any site, is one of the effective factors on amplification. According to the impedance ratios, the reason of the low and high amplification in some sites identified whereas they have less and more competent ground type, respectively.

KEYWORDS: amplification, impedance ratio, ground type

INTRODUCTION

Amplification factor or transfer function are ratio of the ground surface to bedrock fourier spectrum. this factor is an important of the factors used in seismic geotechnic microzonation, to identify increasing ground surface to bedrock acceleration.

This factor, as told above, obtain from seismic geotechnic microzonation study. Seismic microzonation has different methods (such as one, two and three dimensional and by using linear, equivalent linear and nonlinear behavior). In every these methods, soil geotechnic properties should be identified to can obtain results of applying wave from bedrock to soil layers in the ground surface according to these properties as told in definition of this factor, it is result of devide of ground surface into bedrock fourier spectrum is representative wave frequency content (Kramer 1996). Then frequency is one important factors that affect amplification. Soil thickness and shear wave velocity affect it, too. Indeed, hardness or softness of ground type in any sites affect it.

Chabahar city has located in southeast of Iran, in beach margin of Oman sea. This region according to geology division is located in Makran subduction zone and on its accretionary prism (Fig. 1). Beach margin of Oman sea involve alluvium terraces that the study region is located on Qt1 alluvium terraces (Fig. 2).

STUDY METHOD

In this study, amplification factor presented based on seismic geotechnic microzonation of chabahar city (Heydarzadeh, 2008) that ground response analysis in it, obtained using numerical method (one dimentional with equivalent linear soil behaviour) and by EERA software (Bardet et al. 2000).

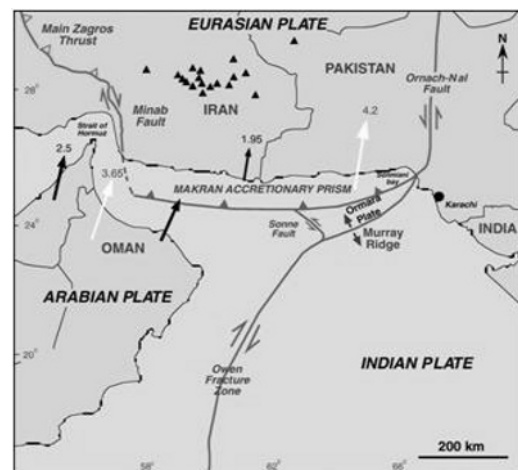


Fig. 1 Tectonic map of the Arabian, Indian and Eurasian plates showing the location of the Makran accretionary prism of southeastern Iran and southern Pakistan (After Grando & McClay 2007)

¹ Islamic Azad university, South Tehran Branch, Iran. Email: dr_a_adib@yahoo.co.uk

² Zaminkav Research Group, Iran. Email: k.heydarzadeh@yahoo.com

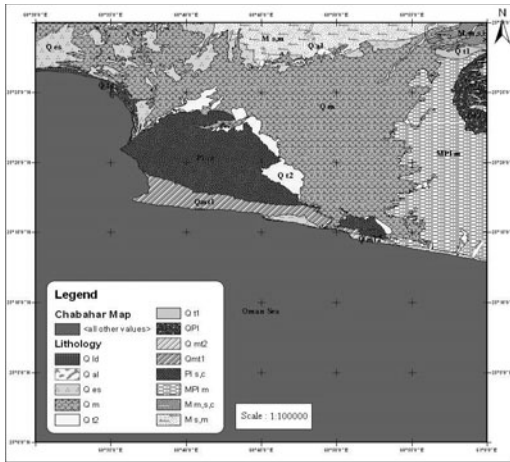


Fig. 2 Geology map of 1:100000 Chabahar sheet, Chabahar city indicated in Black rectangular (Samadian, 1993-1999)

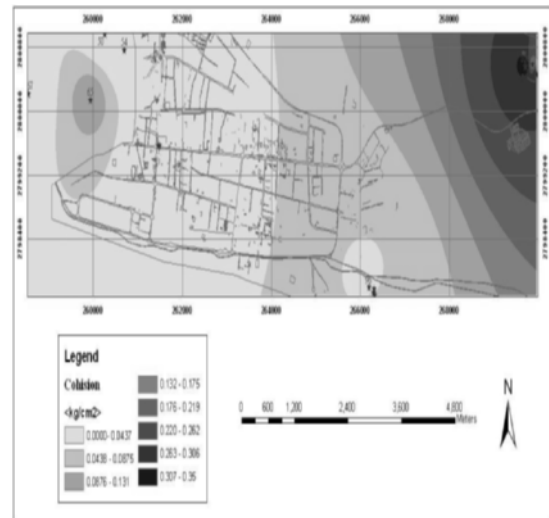


Fig. 3 Cohesion map of city in depth 0-8m (Heydarzadeh 2008)

DISCUSSION

To analyze soil behavior, definition of all layers of the soil profile and properties of primary motion operated to the profile is necessary. Most important parameters of the soil profile to approximate soil behavior in dynamic state are thickness, natural density, maximum shear modulus, ground gravity acceleration in the location of boreholes and soil type (Seed et al. 1986). Seismic characteristic and shear wave velocity of the site determined by downhole test and seismic profiles.

Geotechnic Properties of the Site

General materials of deposits of the site are SM and SP-SM, there is some where compact clay. Density, generally, is without large variation in the region and its values are about 1.7-1.8 (Kg/cm³) in different depth. Cohesion increases from east to west in depth 8-39m, but from west to east at the surface to depth 8m (Figs. 3 and 4). Mean shear wave velocity is maximum in the margins into another parts of the site (Fig. 5).

Ground Response Analysis

As said, in this study, ground response analysis evaluated using equivalent linear as one dementional. Ground response evaluated for 18 station and using 3 accelerograms for recurrent period 75,475 and 2475 year. The results include maximum ground surface acceleration, amplification factor, amplification frequency and period. In this paper, just amplification factor presented that resulted by applying Taftan accelerogram and for recurrent period 475 year in different stations. Gained amplification factors in every stations presented in Table 1 and Fig. 6.

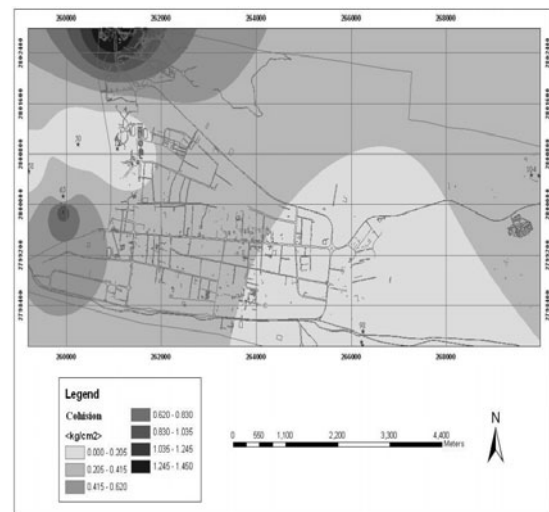


Fig. 4 Cohesion map of city in depth 8-14m (Heydarzadeh 2008)

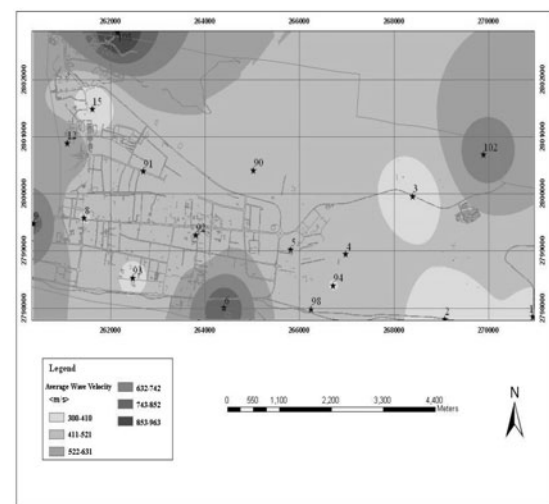


Fig. 5 Vs(30) map of the city (Heydarzadeh 2008)

Table 1 Amplification factors in all stations of the site

Site	Amplification factor	Site	Amplification factor
1	2.74	15	3.81
2	2.98	90	1.69
3	3.30	91	1.94
4	2.90	92	1.96
5	2.85	93	2.25
6	1.51	94	2.29
8	3.03	98	2.52
9	1.52	102	2.43
12	1.51	108	1.21

To separate and study obtained amplification factors all stations classified based on ground classification of Iran building design against earthquake code, standard 2800. In this classification, ground type divided based on mean shear wave velocity to depth 30km, and soil thickness (Table 2). Amplification factors presented in Table 3 and Fig. 7 comparing to ground type.

Amplification factor histograms versus their frequency is drawn in ground variety that is illustrated in Fig. 8. According to histograms, amplification factors are frequent in ground type Ia in range 1-2, in type Ib in range 2-3 (but range 1-2 has significant frequency by

applying Bandarkhamir and Deyhook accelerogram) in type IIb in ranges 1-2 and in type IIIb in range 3-4.

Table 3 Ground classification of the site based on Iran Standard 2800

site	V_s^{30} (m/s)	Standard 2800 classification
1	400.43	Ib
2	353.28	IIIb
3	335.88	IIIb
4	453.61	Ib
5	453.61	Ib
6	840	Ia
8	404.02	Ib
9	764.35	Ia
12	592.66	IIb
15	300	IIIb
90	486.31	IIb
91	455.27	IIb
92	454.11	Ib
93	389.41	IIb
94	406.60	IIb
98	471.76	Ib
102	697.93	Ib
108	963.32	Ia

Table 2 Ground classification of Iran Standard 2800

Ground type	Deposits description	V_s^{30} (m/s)
I	a) Igneous rocks (with fine and coarse texture), hard and very competent sedimentary rocks and massive metamorphism rocks (Gneiss, crystalline Silicate rocks)- Conglomerate beds.	More than 750
	b) hard soil (dense Gravel and Sand, very hard Clay) with thickness less than 30 m.	$750 > V_s \geq 375$
II	a) Loose igneous rocks (such as Tuff), loose sedimentary rocks, foliated metamorphism rocks and generally all rocks that are loosed under weathering and foliation (declare and destroy) situation.	$750 > V_s \geq 375$
	b) hard soils (dense Gravel, Sand, very hard Clay) with thickness more than 30 m.	$750 > V_s \geq 375$
III	a) weathered rocks	$375 > V_s \geq 175$
	b) Moderate dense soils, Gravel and Sand with intergranular connection and moderate dense Clay.	$375 > V_s \geq 175$
IV	a) Soft deposits with high moisture because of high elevation of ground water surface.	Less than 175
	b) Any soil profile including minimum 6 m Clay with plastic index more than 20% and moisture more than 40%.	

As defined from isoamplification map (Fig. 6), the region divided two parts that the east part has high amplification factor into the west part except around boreholes 8 and 15. According to this figure (Fig. 6), maximum amplification exists in two station around boreholes 3 and 15 that have ground type IIIb. Now, we analyze amplification factor in every ground type:

Type Ia: amplification factor has minimum value (1.21-1.73).

Type Ib: amplification factor varies from low (1.73-2.25) to medium (2.25-2.77). one exception exists around borehole 8 with high amplification (3.29-3.81) that is because of its high impedance ratio (see next section).

Type IIb: amplification factor varies from very low (1.21-1.73) to medium (2.25-2.77). Large variations are because of their different impedance ratios (see next section).

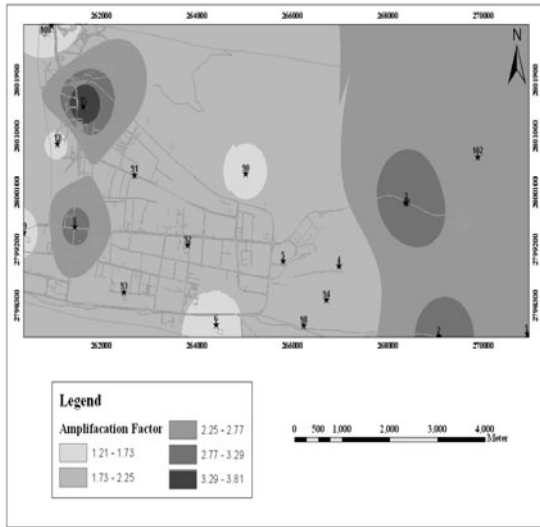


Fig. 6 Map of amplification factor in the city

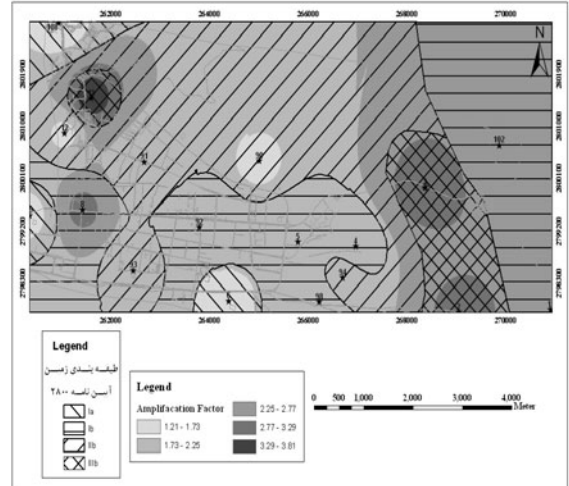


Fig. 7 Amplification factor map with ground classification (Heydarzadeh 2008)

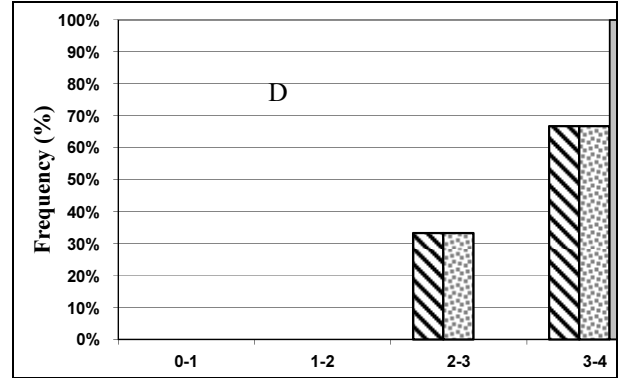
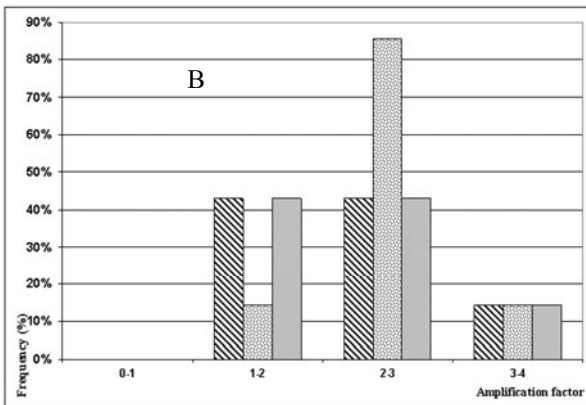
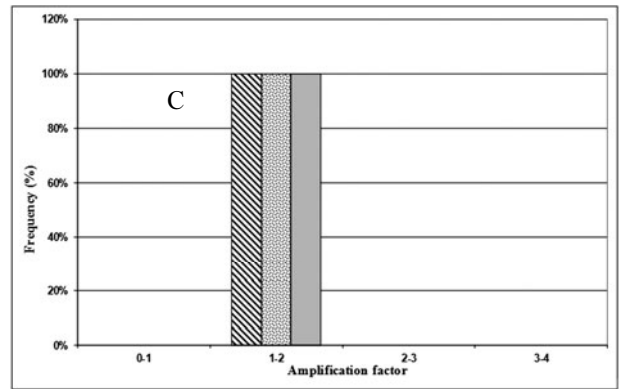
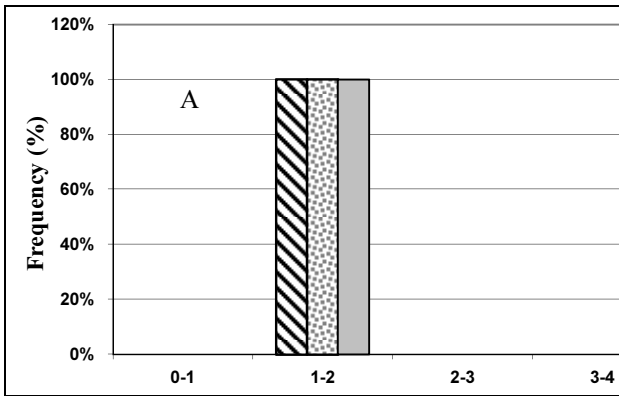


Fig. 8 Histograms of amplification factors in the four ground type of the site, A: Ia, B: Ib, C: IIb, D: IIIb

Type IIIb: amplification factor is high (2.77- 3.29) to very high (3.29-3.81).

According to these results, amplification factors accommodate with ground type as Ia is rock type and then its amplification is low, Ib and IIb are hard soil and

looser than Ia then amplification is higher than Ia and lower than IIIb, and in IIIb because of medium dense soil and looser ground than another type, amplification is higher.

Effect of Impedance Ratio on Amplification Factor

As told, different factors affect amplification factor. One of the these factors is ground type that studied in previous section. Another factor that affect amplification, is impedance ratio (Tucker et al. 1994).

Impedance ratio represents hardness of two invironments or layers into one another. Table 4 presented impedance ratio between bedrock and surface layer ($\rho_2 V_{s2} / \rho_1 V_{s1}$ where bedrock is 2 and 1 is surface layer), in all stations. In this table, values of amplification factor sorted from low to high and their impedance ratio written in front of them. According to the table, one can observe amplification factor increases with increasing impedance impedance ratio, except stations 91,92, 93, 94 and 98, means whatever hardness variation between bedrock and surface layer is more, amplification factor is higher, too (ground type has effect on it, too). But boreholes 4, 5 and 91 to 98 have lower amplification factor despite their very high impedance ratio. This matter is because of lower impedance between (any) layers of these stations presented in Tables 5 to 11.

According these tables, impedance ratios between layers, in these stations, don t arrive even upto two as just one interlayering impedance ratio of them should be high (like another stations), because of their high impedance ratio between bedrock and surface layer (Table 4). In fact, the difference between interlayering and their bedrock/surface layer impedance ratios are more than 1.5, means that impedance ratios between layers are very less than impedance ratio between bedrock and surface layer whereas in other boreholes, this difference is less than 1.5 and bedrock /surface layer and interlayering impedance ratios correspond with together (Table 12).

Table 4 Impedance ratio values in the all stations of the site

Site	X	Y	Impedance	Ampli (Average)	Class
108	260966	2802783	1.8	1.21	Ia
9	260376	2799482	2.45	1.51	Ia
6	264409	2798009	2.05	1.52	Ia
12	261088	2800890	2.19	1.52	IIb
90	265033	2800414	2.53	1.6	IIb
91	262701	2800398	3.67	1.73	IIb
93	262477	2798532	4.33	1.83	IIb
4	266987	2798942	3.89	1.91	Ib
94	266719	2798404	5.22	1.93	IIb
92	263814	2799278	3.13	1.96	Ib
98	266252	2797993	4.41	1.97	Ib
5	265822	2799020	3.64	2.02	Ib
102	269897	2800683	3.11	2.48	Ib
1	270942	2797862	2.71	2.75	Ib
2	269077	2797814	2.96	3	IIIb
8	261449	2799575	3.53	3.05	Ib
3	268398	2799958	3.46	3.33	IIIb
15	261621	2801485	3.85	3.81	IIIb

Table 5 Impedance ratio values between layers of site 91

Layer	Density	Vs	I
1	18.80	234.4	1.33
2	16.80	348.4	1.12
3	16.40	398.5	1.04
4	16.20	419.3	1.16
5	17.60	447.9	1.03
6	17.00	477.9	0.86
7	14.20	492.2	1.06
8	14.35	518.5	1.15
9	15.60	546.5	1.21
10	17.00	605	1.11
11	17.00	672	1.07
12	17.00	718	1.11
Bedrock	18.00	750	

Table 6 Impedance ratio values between layers of site 92

Layer	Density	Vs	I
1	16.90	234.1	1.45
2	16.20	354.5	1.25
3	15.50	462	1.38
4	17.00	582	1.12
5	16.50	674.4	1.08
6	16.50	726.3	1.03
bedrock	16.50	750	

Table 7 Impedance ratio values between layers of site 93

Layer	Density	Vs	I
1	18.25	185	1.29
2	18.25	238.2	1.24
3	18.25	296.25	1.23
4	18.25	365	1.28
5	18.75	454	1.16
6	19.00	520	1.18
7	19.50	600	1.25
Bedrock	19.50	750	

Table 8 Impedance ratio values between layers of site 94

Layer	Density	Vs	I
1	14.80	170	1.43
2	14.80	243	1.65
3	16.70	355	1.33
4	17.10	461	1.17
5	17.00	543	1.20
6	17.50	635	1.12
7	17.50	712	1.05
Bedrock	17.50	750	

Table 9 Impedance ratio values between layers of site 98

Layer	Density	Vs	I
1	15.62	190.7	1.49
2	15.62	283.2	1.30
3	15.62	368	1.35
4	16.75	462.3	1.16
5	17.20	522.5	1.08
6	17.20	565	1.16
7	17.50	643.8	1.13
8	17.50	725.4	1.03
Bedrock	17.50	750	

Table 10 Impedance ratio values between layers of site 4

Layer	Density	Vs	I
1	15.50	275	2.12
2	18.06	500	1.06
3	19.13	500	0.99
4	19.00	500	1.74
Bedrock	19.50	850	

Table 11 Impedance ratio values between layers of site 5

Layer	Density	Vs	I
1	16.75	275	1.88
2	17.33	500	1.03
3	17.82	500	1.88
Bedrock	19.75	850	

Table 12 Impedance ratio values between layers of site 98

Site	Impedance ratio (bedrock/surface layer)	Max Impedance ratio (interlayering)	Difference
108	1.8	1.61	0.19
9	2.45	1.61	0.84
6	2.05	2.05	0
12	2.19	1.74	0.45
90	2.53	1.19	1.34
91	3.67	1.33	2.34
93	4.33	1.29	3.04
4	3.89	2.12	1.77
94	5.22	1.65	3.57
92	3.13	1.45	1.68
98	4.41	1.49	2.92
5	3.64	1.88	1.76
102	3.11	2.94	0.17
1	2.71	2.37	0.34
2	2.96	2.55	0.41
8	3.53	1.28	0.74
3	3.46	2.79	0.67
15	3.85	3.6	0.25

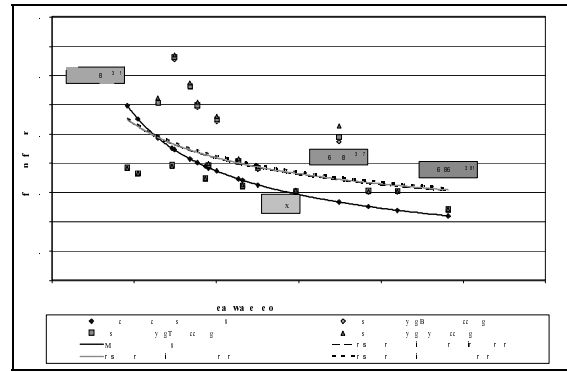


Fig. 9 Relation between V_s^{30} and amplification factor in the site

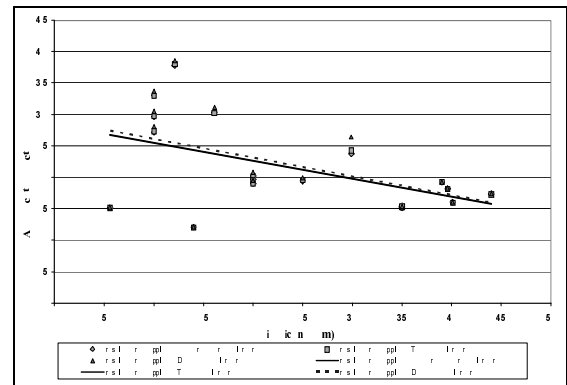


Fig. 10 Relation between thickness and amplification factor in the site

CONCLUSIONS

Here, the parameters that affect amplification factor are: ground type (soil thickness and mean shear wave velocity) and impedance ratio. According to results division based on ground type, amplification factor increases from high to low hardness and from rock to soil type of stations (from Ia to IIIb) (relation of amplification factor with shear wave velocity imply this matter, Fig. 8). Of course in type IIb, range 1-2 is more frequent than range 2-3, that doesn't accord with this trend (relation of amplification with soil thickness that is decreasing, imply this matter, Fig. 9).

In addition to ground type, impedance ratio between bedrock and surface layer and also between layers of any stations affect amplification factor, as high amplification (such as stations 15, 3, 8, ...) are associated with high impedance ratio except stations 4, 5, 92, 98 (ground type Ib) and 91, 93, 94 (ground type IIb) that whatever their impedance ratios between bedrocks and surface layers are very high but impedance ratios between their layers are very low and this cause to lower amplification in this stations. According to impedance ratios, cause of low amplification in some stations despite their loose ground

(IIb type) such as stations 12, 90, 91, 93, 94 and cause of high amplification in another stations despite their hard ground (Ib type) such as station 8, 1 and 102 is identified.

REFERENCES

- Bardet JP, Ichii K, Lin CH (2000) EERA: A computer program for Equivalent-Linear Earthquake site Response Analyses of Layered Soil Deposits, University of southern California, Department of civil engineering.
- Grando G & McClay K (2007). Morphotectonics domain and structural styles in the Makran accretionary prism, offshore Iran, *Sedimentary Geology*, 196: 157-179
- Heydarzadeh K (2008). Seismic Microzonation of Chabahar city, M. S. Thesis, Geology department (Tectonics) Shahid Beheshti University, Iran, in Persian.
- Iran Building & Housing Research Center (1999) Building Design against earthquake Code, 2800 standard, 2nd Ed, BHHRC, Tehran.
- Kramer S (1996) *Geotechnical Earthquake Engineering*, Prentice Hall, Upper Saddle River, New Jersey.
- Samadian MR scientific Supervisor (1993-1999) Maps & Geology Reports of Kahir, Bandiny, Chabahar, Zarabad & Peersohrab 1:100000 sheet, Geological survey of Iran.
- Seed HB, Wong RT, Idriss IM, and Tokimatsu K (1986). Module and damping factors for dynamic analyses of cohesionless soils, *Geotechnical engineering*, ASCE, 112(11): 1016-1032.
- Tucker BE, Edrik M, Hwang Ch (1994) *Issues in Urban Earthquake Risk*, Springer, p. 329.

POST DISASTER INFORMATION MANAGEMENT: ISSUES RELATED TO MITIGATION ACTIVITIES IN IRAN

Ahmad ADIB¹ and Vahid Hosseini JENAB²

ABSTRACT: The primary objective of an emergency information system is to improve the capacity of decision makers to take needed action. Effective information management system is the key, although also a very difficult aspect of the emergency management. Emergency information management is defined as the collection, consolidation, analysis and dissemination of the information and to be effective, it needs to be planned, organized and controlled to insure that information is given to the right decision maker at the right time to satisfy their needs to know. The goal of this study was to analyze the importance of information management for increasing the efficiency of post-disaster and also mitigation activities. In this study, 50 managers and experts who are active in the field of disaster management were interviewed regarding their viewpoints about the defects that have adverse impact on effectiveness of their efforts to manage a crisis. The interviewed group included a group of 40 men with average age of 36 and 10 women with average age of 28, all experienced in disaster management, among which 30 had bachelor degree, 10 had masters and 10 had PHD degrees in related fields. The list of the defects included factors such as the engineering measures, physical planning, institutional management, social/economic barriers and lack of efficient information management system. In this article, we are having a look at these defects especially the lack of efficient information management system and will provide solutions to overcome this problem through activities such as for providing data required for contingency planning in pre-disaster phase, operation planning during disaster response and creation of reports and utilization of best practices in post-disaster phase.

KEYWORDS: Disaster, Information management, Mitigation

INTRODUCTION

Emergency information management- defined as the collection, consolidation analysis and dissemination of the information – requires that the emergency manager be fully cognizant of the need of the eventual users of the information. Effective emergency information management requires concerted planning, organizing, controlling, and influencing of human, material, and information resources to ensure that information is disseminated to the right decision – makers at the right time to satisfy those needs.

An effective information system provides selective information relevant to the user's needs, clarifies particular problem and available option, and helps the user to make reasonable choices. It does not drown the decision maker's activities. It provides a whole picture. An emergency information management system is no different: it, too, must select from and organize the various data collected and disseminated by what is likely to be a multitude of emergency respondents the system must process that data to enable the development and implementation of a clear plan of action in response to

the emergency.

Such a system may be viewed as a cycle starting with the identification of user needs and continuing through the feed back of lessons learned (institutional memory) in to program design or modification.

The starting point in the design of any information management system is the identification of the eventual users of the system and their particular need.

The users of information in most disaster situations are numerous. Each is likely to have specific information need which the designer of the disaster information management system should consider in advance. These users will include some or all of the following:

- The affected population
- Private donors (individuals, corporation, and foundations)
- Public donors (taxpayers and government funding agencies)
- Government response organization (national, regional, and local authorities)
- Military forces and civil defense units
- UN organization
- Non-governmental organization (both international and local)

¹ Natural Disaster Research Institute, Iran. Email: dr_a_adib@yahoo.co.uk

² Natural Disaster Research Institute, Iran. Email: vahidjenab46@yahoo.com

- Religious institutions
- The media (international and local)
- Clearly, with such a varied list of users, perceptions of information needs will vary greatly.

The information needs of a particular user also differ according to the phases of the disaster of concern to that user.

The primary objectives of an emergency information system are to improve the capacity of decision-makers to take needed action. Effective information management and telecommunications system are keys.

INFORMATION NEEDS: PRE-CRISIS

Information Needs for Contingency Planning

Most emergency managers, in preparing for disaster, follow early warning signs and at least informally consider the contingency scenarios that might occur.

In identifying these information needs, it is critical to understand the links between the early warning system and the contingency planning process.

Emergency management responsible for contingency planning must first consider the types of hazards to which their area of concern may be subject. They must then make decisions concerning the particular hazards and the phase(s) of the disaster to which their organization can realistically be expected to respond.

Emergency managers responsible for contingency planning must first consider the types of hazards to which their area of concern may be subject. They must then make decisions concerning the particular hazards and the phase(s) of the disaster to which their organization can realistically be expected to respond.

This essential process of winnowing forces the manager to reduce a universe of great uncertainty to a smaller more manageable group of realistic contingencies. No longer faced by an overwhelming number of potential events, the manager can begin to identify the information needed to monitor those contingencies; he or she can select the indicators that should be tracked to warn that one or more of these contingency scenarios is likely to occur.

In short, prior to the emergency situation, an effective emergency information management system monitors and provides warning information to feed an ongoing contingency planning process which, in turn, aims to establish a realistic view of the organization's capacity to respond to emergencies. The information system, prior to the actual crisis, helps the organization to make choices about its potential future responses and, where needed, set realistic limits.

Vulnerability Analysis

Emergency planners increasingly use information on differences in vulnerability to fine-tune their contingency

planning scenarios. Vulnerability analyses ideally provide indications of where the effects of disaster are likely to be the most pronounced (by region and population), and to assist managers with future targeting decisions. Data ideally are gathered from organized surveys. Where feasible, precise, data are sought on specific locales or segments of a larger population.

Most vulnerability analysis is performed using national data sets such as censuses, and income and expenditure surveys, which are then geographically disaggregated to the extent possible.

Those wishing to use vulnerability analysis to help make decisions about future emergency responses should be aware that analyses based on existing national data sets often cannot be performed at a low-enough administrative level to assist actual targeting needs.

INFORMATION NEEDS: WITH ONSET OF CRISIS

Information needs for operations planning: With the onset of an actual emergency, just as the various contingency scenarios anticipated by managers are reduced to one actuality, the information needs of the various respondent seem to increase exponentially. In preparing operations plans to deal with this new reality, emergency managers must strive to add specificity to the planned response in terms of composition (demographics), needs, and numbers of affected, locations, targets, and resources.

Where emergency conditions prevail, an effective information system shows great flexibility in responding to the changing needs of its users. Information gathered by assessment, monitoring, and (on occasion) ongoing evaluation teams is fed into the system and analyzed with the aim of identifying needed changes in the response. Ideally, the system provides decision makers with a clear understanding of whether or not planned objectives are being met and, even more importantly, whether these objectives are still the essential ones.

INFORMATION NEEDS POST- CRISIS

Rehabilitation and recovery: Emergency response organizations involved in the later phases of the disaster response should, ideally, begin planning their longer-term activities even before emergency conditions stabilize. The information needed for this process will vary with the type of disaster and the intended response.

In general, a decision to begin longer-term activities requires information on the damage generated by the disaster and the longer-term needs inflicted upon the population. A grasp of the longer-term political, economic, social, and environmental changes brought about by the disaster is also needed, as is an understanding of the coping mechanisms which the affected population still maintains.

In complex emergency situation, security is generally the major concern of those beginning to plan and implement longer-term activities.

Other information which managers need before deciding to implement rehabilitation or recovery programs includes: the level of political will and resource availability for longer-term activities; and the existence of other "more pressing" emergencies which could place demands on scarce needed by the rehabilitation or recovery programs.

Mitigation activities: Mitigation strategies, whose aim is to reduce losses in the event of a future hazard occurrence, encompass a wide range of activities, from infrastructure development- such as stronger and more rigorously enforced building codes; flood- engineering improved structural resistance to high winds and earthquakes in non-engineered structures- to measures such as improved detection systems and public education.

There are many different stakeholders in mitigation activities, including the affected population; the business community; political representatives and decision makers; the development and urban and rural planning communities. Each of these groups needs to draw upon a common pool of information, and each also has its own specialized information requirements. Major contributions are made by engineers, technicians and scientists; the insurance industry; the banking and investment industries; and the individual activists and promoters of mitigation and preparedness measures who are often drawn from all these groups and who advocate for improvements in safety.

METHODS

The goal of this study was to analyze the importance of information management for increasing the efficiency of post- disaster and also mitigation activities.

In this study, 50 managers and experts who are active in the field of disaster management were interviewed regarding their viewpoints about the defects that have adverse impact on effectiveness of their efforts to manage a crisis.

The interviewed group included a group of 40 men with average age of 36 and 10 women with average age of 28, all experienced in disaster management, among which 30 had bachelor degree, 10 had masters and 10 had PHD degrees in related fields.

MITIGATION ACTIONS

- 1- Engineering and construction measures.
 - Map and inventory of non-engineered, disaster-prone buildings.
 - Design standards, building codes. Performance specifications.
 - Listing of existing or potential incentives for construction

of disaster- resistant structures or retrofitting of disaster-prone structures (e.g. Reduced insurance rates. Preferential loan packages, land title or tenants rights agreements).

2- Physical planning measures

- Land use and zoning regulations.
- Map and inventory of lifeline facilities (e.g. hospitals, water treatment and pumping stations, power generating and transmission structures, telecommunications facilities, etc.)
- Degree of concentration or dispersion of lifeline facilities.
- Location of population concentrations.
- Design of supply and transport networks.

3- Economic measures

- Unemployment, income distribution, poverty levels.
- Degree of diversification of economic activities.
- Taxation policies.
- Availability of, access to insurance and cost of premiums.

4- Management and institutional measures

- Degree of authorities' political will to implement mitigation measures.
- Understanding of government structures established to plan, implement mitigation and preparedness activities.
- Availability of human and material resources for training.

5- Societal measures

- Degree of commitment (ie, resources and time) devoted to public education (radio broadcasts. Posters, etc.) and drills.
- Degree of inclusion of disaster education in public schools, meetings or other for a.
- Degree of participation of community in decisions about mitigation activities.

DISCUSSION

It is clear that emergency managers have an obvious stake in mitigation planning. Those activities which are likely to reduce the impact of future hazards on emergency lifeline services- such as measures to strengthen the hazard- resistance of telecommunications, medical, and transport systems—clearly help to ensure a more timely, effective emergency response. Mitigation planners and emergency managers can have much positive impact by sharing information on the types of hazards likely to affect particular regions of the country and the state of essential lifeline system in those regions which may strengthening.

Data-gathering is a continuous emergency management function, it is conducted before (warning,) during (assessment and monitoring) and after (evaluation) the emergency operation to ensure that decision makers can stay abreast of changing conditions.

Decisions concerning the particular techniques to be used in gathering data depend primarily upon availability of financial resources, expertise, and time. Decisions

about the frequency of data gathering also depend upon these factors, although, ideally, "the frequency of data collection and reporting must match the rate of change in the situation being assessed".

Without a carefully planned, well-organized approach to data-gathering, the information flow in an emergency can slow to a trickle with decision makers forced to take actions based in minimal information.

Emergency managers, confronted with a deluge unfiltered data, often tend to react more from personal experience than from any useful insights sub-mitted by field staff.

What decision makers clearly need is not sheer volume, but well-reasoned, insightful finding and conclusions accompanied by recommendations for action and clear statements from data analysis on how particular conclusions were drawn.

Emergency managers generally obtain data from a wide range of sources, including the findings submitted by assessment or monitoring teams, situation reports from field staff, minutes from meetings with colleagues and counterpart organizations, and media reports- With increasing access to the Internet and the world wide web, second-hand sources are today practically without limit, every disaster seems to spawn a new set of web sites, on-line documents, and Internet-based organization.

This proliferation of sources had increased the need for data cross- checking and verification. Staff responsible for data analysis must quickly but systematically collate and cross- check data against reports received from other sources.

Analysts should be prepared to rate the information's accuracy according to scale acceptable to the particular organization: e.g.: confirmed by other sources, probable, doubtful, improbable, cannot be judged.

The early stages of an emergency response are often characterized by very fast moving events and high levels of stress on operational staff. Mechanisms for filtering information are essential. Those responsible for filtering and prioritizing information are essential. Those responsible for filtering and prioritizing information for decision makers must be concerned with the following:

-Translating and structuring incoming messages:

Filtering

Prioritization

Corroboration

Reliability

-Presentation formats are important insofar as they assist decision makers to grasp a situation more quickly. GIS maps, prepared situation report formats, commodity pipeline analyses- these are all essential tools for decision- making.

-Emergency managers seeking software support for decision-making should always consider the availability

of ongoing software support- particularly in remote areas where expertise may be lacking.

-Emergency managers should never assume that information finds its way to those who need it. Procedures for the dissemination of information to the decision makers and media who are positioned to set the wheels of the disaster response in motion should be planned in advance. Planning should take into account the geographical, political, and organizational location of those eventual users.

ORGANIZATIONAL PROTOCOLS

-An organization's "normal" information dissemination channels are often inadequate to engender a quick, effective response.

-Organizational protocols which should be developed well in advance of a crisis include the following concerns:

Levels of transparency

Identifying the recipients

An emphasis on reporting

-Use of coordination structures for information dissemination.

-Use of media in information dissemination

-The internet and the World Wide Web

CONCLUSIONS

At the heart of effective information management is a capacity to use "institutional memory" -i.e., the recording and feedback into program design of the organization's emergency response experience. Despite ready acknowledgment by all managers of the need to develop such a capacity, maintenance and use of institutional memory continue to be among the most neglected areas of emergency information management.

Building a real capacity for institutional memory requires a firm commitment by top management, a detailed plan, and a funded, operating budget.

REFERENCES

- Emergency Information Management and Telecommunications: Disaster Management Training Program; UNDP & DHA; 2008.
- Emergency Management, Michael K Lindell, etal: Wiley pub; 2007.
- Disaster Response & Recovery: David A. Mc Entire; Wiley pub; 2007.

ANALYSIS AND EVALUATION ON HYDROFRACTURE FAILURE IN AN ASPHALT CONCRETE CORE ROCK-FILL DAM: A MAOPINGXI DAM CASE

Xin-Hua ZHOU¹ and Xi-Bao RAO²

ABSTRACT: Whether hydrofracture failure is likely to occur in an asphalt concrete core rock-fill dam or not is one of hotspot problems widely concerned by the engineering community. In this paper, the authors adopt effective stress method to analyze the stress deformation in the core wall of Maopingxi dam and evaluate the hydrofracture problem in dam's core wall in the light of evaluation criteria that minor principal stress in the core wall is no less than relevant water pressure. Calculation results show that there is little possibility of hydrofracture failure in asphalt concrete core wall of the Maopingxi dam.

KEYWORDS: Asphalt concrete core wall, hydrofracture, stress deformation analysis

INTRODUCTION

Since it is characterized by best antiseepage performance, strong compatibility with deformation, nice earthquake-resistant behavior, thin thickness, smaller quantities, fast construction speed and mechanized construction in an all-round way, simple structure as well as the simple and reliable connection with rigid structures including bedrock and bank slope concrete etc., the asphalt concrete core wall began to be gradually utilized in the 1970s in the antiseepage system of earth-rockfill dams, especially in medium to high earth-rockfill dams, and it was rapidly developed; especially in areas with scarce clay material. So, it, together with concrete face rockfill dam, has been favored by designers. According to incomplete statistics, there are 12 currently under-construction or existing rolled asphalt concrete earth-rockfill dams in China, of which earth-rockfill dam of Zhile hydropower project under-construction with a dam height of 125m is highest; the existing Maopingxi asphalt concrete rock-fill dam with a height of 104m has at present been impounded to El.135m, and is about to impound to El.154m. With the construction of Maopingxi, Zhile and Nierji high asphalt concrete core rock-fill dams, the advantages of asphalt concrete as rock-fill dam's core wall has been continuously further realized by designers, so this technology will have a relatively wide development perspective and spreading value.

But as the only antiseepage barrier of water retaining

dam, safety problems existed in asphalt concrete, e.g. hydrofracture failure, stress deformation characteristics, durability and ageing resistance etc., are still problems extensively concerned by the engineering community, especially hydrofracture failure problem occurred in the asphalt concrete core wall under a high head action.

In this paper, taking Maopingxi asphalt concrete core rock-fill dam as an example, the authors adopt finite element calculation method to analyze the stress-strain of asphalt concrete core wall and discuss the hydrofracture failure problem as a focal point, providing a reference to the selection and decision-making of the dam's impounding scheme.

AN INTRODUCTION TO THE MAOPINGXI ROCK-FILL DAM

Maopingxi dam is an asphalt concrete core rock-fill dam. Located between Chenjiachongkou to Banqiao and Hanjiazui, Yichang, Hubei province, it is a part of Three Gorges Project. The dam in grade, the same as the main structures of Three Gorges Project, is a Grade-I structure. The axial line of antiseepage system for the dam has an overall length of 1,840m. The dam with a maximum height of 104.0m has a crest elevation of 185.0m. The core wall with a maximum height of 93.0m has crest and bottom levels of 184.0m and 91.0m. Core wall's thickness is gradually increased from 0.5m at crest level to 1.2m at El.94.0m; core wall at bottom is connected

¹ Senior engineer, Yangtze River Scientific Research Institute, China. Email: zzh728728@tom.com

² Professor, Yangtze River Scientific Research Institute, China. Email: raoxibao8899@126.com

with the concrete base through a 3.0m high gradually-expanded section. The asphalt concrete core wall is located at concrete base within which it is equipped with a grouting gallery. The dam body's cross section and materials' zoning is shown in Fig. 1.

The dam has a normal pool level of 175m with a check flood level of 180.4m and a dead water level of 135.0m. The dam was completed at the end of 2003 and finally accepted in 2004. In June 2003, the reservoir

began to impound; at present the reservoir water level has reached up to about El.135.0m, and is about to impound to El.154m.

In order to insight into the dam's operating behavior and monitor the safety of the dam, the deformation, seepage, stress-strain and temperature monitoring systems were arranged within the dam body, of which stress-strain monitoring system is mainly located at the maximum cross section 0+700.

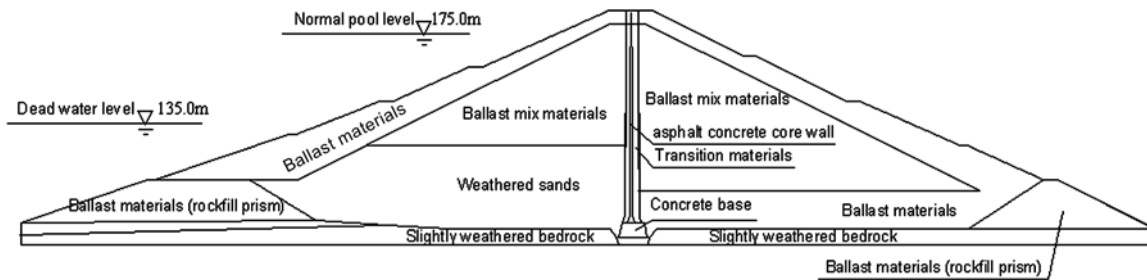


Fig. 1 The dam's maximum cross section (0 + 700) and materials' zoning map

STANDARD TO JUDGE HYDROFRACTURE FAILURE

Hydrofracture refers to a physical phenomenon occurred when due to the rise in water pressure, the stress state of soil body or antiseepage body reaches up to its limit tensile strength under its internal pore pressure and surface pressure action. For example, the longitudinal cracking of Jiatuluha core rock-fill dam completed in 1965 in Indonesian was induced owing to construction settlement, it was found through hydraulic pressure test that water would loss when water pressure in holes reaches to a certain value (Rao & Gong 2005); for Badehei narrow earth core rock-fill dam completed in 1965 in England, vertical pressure in the core wall was less than the weight of overburden soils due to arching effect, when the reservoir in early 1966 was impounded to its maximum water level, a larger extent of erosion damage within the core wall occurred, thereby making a sudden increase in the quantity of seepage. Especially the sudden failure of Teton dam in United States in 1976 during its initial impoundment period (Seed & Duncan, 1981) was reviewed by several eminent scholars as the consequence caused by a hydrofracture (Penman 1986, Sherard 1986). Since then, the hydrofracture problem occurred in the earth-fill dam has become a widely-noticed thesis. Since the cracks due to hydrofracture are expanded and visible only under the condition of pressure existed within cracks after reservoir impoundment, technicians cannot directly observe and validate whether a hydrofracture phenomenon within the dam body or antiseepage body truly occurs or not. In

examples that earth-rockfill dam's failure are asserted in the past to be caused by hydrofracture, these conclusions are obtained mainly by testing, analysis and presumption.

Hydrofracture failure may occur in different media, e.g. rock, earth-rockfill dam's core wall and mining well floor etc. As to the problem of standard to judge the hydrofracture, since experimental study and calculation analysis on different media are utilized by different ways, results obtained are different. Main results in experimental aspect include as follows.

(1) Haimwon (1968) showed through water pressure test in rock borehole that the minor principal stress is normal to the impervious rock along hole axis, the water pressure leading to the hydrofracture is equal to the sum of rock's tensile strength and twice minor principal stress, i.e. $U_{if} = 2\sigma_{\min} + |\sigma_t|$, and the relationship among U_{if}^* , the water pressure causing the hydrofracture of pervious rock, U_{if} , and σ_{\min} is:

$$U_{if} > U_{if}^* > \sigma_{\min} \quad (1)$$

(2) Vaughan (1971) recommended that the discriminant of hydrofracture by water pressure (or water injection) tests in on-site boreholes is:

$$U_{if} = m\sigma_{\min} + |\sigma_t| \quad (2)$$

where $m = 1-2$;

(3) Jawoski, Duncan & Seed (1981) carried out hydrofracture test by using undisturbed and remolding soils from Teton dam to make 203mm cubic samples and

respectively apply water pressure within boreholes perpendicular to compacted bedding plane, and studied the influences of soil composition, density, moisture content, tensile strength and testing duration on hydrofracture. They believed that water pressure leading to hydrofracture U_{if} can be expressed as the linear function of lateral minor principal stress:

$$U_{if} = m\sigma_H + \sigma_{ta} \quad (3)$$

where m is a gradient of regression line at testing point, depending on stress distribution around the boreholes and soil's total stress line, value ranging 1-2, experimental value is 1.5-1.8; σ_{ta} is an intercept, it is related to σ_{ta} , test conditions, loading speed and borehole size;

(3) Yang et al. (1985) utilized triaxial compression, tension, torsion shear instruments to conduct hydrofracture tests under complex stress conditions including different ambient pressure and different stress ratios etc. Results show that seepage action may not only cause the tension failure form due to σ_{\min} reaching to tensile strength σ_t , but also can lead to shear plastic flow governed by Moll-Coulomb theory, which must be depended upon the ratio of sample's major principal stress to minor principal stress σ_1/σ_3 . Whether hydrofracture failure in samples occurs or not cannot be judged by whether internal water pressure value U_i is more than the sum of σ_{\min} and σ_t under starting condition or not, but hydrofracture can occur only after minimum effective principal stress σ_{\min} reaches to σ_t .

(4) Huang & Ding et al. (1982) conducted exploration and preliminary analysis on hydrofracture mechanism. Mr. Huang Wenxi in view of the hydrofracture problem in earth-rockfill dam pointed out: "if the pore water pressure at any point in the core wall make the effective value of minor principal stress at this point less than the tensile strength value of core wall's soil material, hydrofracture in the core wall would happen along this minor principal stress plane". Water pressure includes pore static water pressure and excess pore water pressure induced by roll-compaction during construction process. As for dam shell filled with coarse materials, since pore water pressure caused by roll-compaction process during construction period is dissipated relatively quickly, the authors consider that the static water pressure at upstream edge of the core wall during impoundment period can be directly utilized as an evaluation reference.

In numerical calculation aspect, Duncan et al. adopted total stress method to conduct stress deformation

analysis on the failed Teton dam and believed that the stress at the core wall of Teton dam was reduced due to the presence of arching effect, thereby inducing hydrofracture failure. Shen et al. (1994) simulated the destructive process of Teton dam through a centrifugal model test and conducted the calculation analysis on effective stress; testing and calculated results have not proven the presence of any hydrofracture phenomenon, therefore, they considered that the conclusion that the failure of Teton dam is assessed to be caused due to hydrofracture by using total stress method is not necessarily correct, and popular total stress discriminant method overestimates the occurrence possibility of hydrofracture (Shen & Yi, 1994).

At present, Mr. Huang Wenxi's research result (Zhang & Yu, 2003) is mainly referred as the standard to assess the hydrofracture failure in the core wall of earth-rockfill dam in China; at the same time, due to the layered placement and roll-compaction construction, horizontal layer become a weak plane; since its seepage path is shorter, water pressure could lead to the tension cracking of hidden cracks, it can also make the core wall in tension reach up to its limit tensile strength and produce new cracks at weak planes. If arching effect from the core wall is obvious and static water pressure at upstream side is more than core wall's vertical pressure, it can also cause hydrofracture failure. Core wall's vertical stress is slightly smaller than major principal stress, but in value, it is obviously larger than minor principal stress. The use of the ratio of minor principal stress to water pressure as a standard to judge hydrofracture failure is a relatively conservative practice; if a hydrofracture failure does not occur under this standard, this shows that the core wall is safe.

Finite-element method can analyze the stress distribution of dam body and antiseepage body under various conditions, so it is very intuitive and convenient when this method is applied to assess whether hydrofracture failure in dam body or antiseepage body could occur or not. This paper adopts effective stress method to analyze stress deformation of Maopingxi asphalt concrete core rock-fill dam, and evaluate the occurrence possibility of hydrofracture failure in the core wall of Maopingxi dam according to the hydrofracture failure standard proposed by Mr. Huang Wenxi (Zhang & Yu 2003) for earth-rockfill dam.

STRESS-STRAIN CALCULATION FOR ASPHALT CONCRETE CORE WALL

Calculation Principle and Method

Duncan-Chang $E-\mu$ nonlinear elastic model is adopted for fill materials of dam body and asphalt concrete core

wall.

The increment tangent modulus of deformation E_t and tangent Poisson ratio μ_t for Duncan-Chang $E-\mu$ hyperbolic stress-strain model can be expressed as follows:

$$E = KP_a \left(\frac{\sigma}{P_a}\right) (1 - S_t R) \tag{4}$$

$$\mu = \frac{G - F \lg(\sigma / P)}{[1 - D(\sigma_1 - \sigma) / E (1 - R S)]^2} \tag{5}$$

where the stress level S_t to measure the shear force of materials is:

$$S = \frac{(\sigma - \sigma_3)(1 - \sin \varphi)}{2(C \cdot \cos \varphi + \sigma_3 \sin \varphi)} \tag{6}$$

Modulus of deformation E_{ur} when unloading and reloading is:

$$E = K P \left(\frac{\sigma_3}{P}\right)^n \tag{7}$$

Contact elements of Duncan-Chang hyperbolic pattern are provided between asphalt concrete core wall and transition materials.

Tangent shear stiffness showing the relationship between shear stress and relative displacement at contact plane is:

$$K = K \gamma_w \left(\frac{\sigma}{P}\right) \left(1 - \frac{\tau.R}{\sigma \lg \delta + C}\right)^2 \tag{8}$$

Calculation Parameters

Parameters for fill materials of dam body are analyzed and determined according to monitoring feedback results of dam's stress deformation (as shown in Table 1), and the feedback analysis process is not described here. Five set of parameters for asphalt concrete core wall are selected in the light of laboratory experiments and on-site core wall drilling results as shown in Table 2. Model parameters for both linear-elastic materials (such as bedrock, concrete base etc.,) and contact planes are shown in Table 3.

Table 1 Parameters for dam body's fill materials obtained through analysis

Name of fill materials	$\rho(\text{kN/m}^3)$	k	n	R_f	G	F	D	Φ (°)	C (MPa)
Weathered sands	21.0	800	0.5	0.8	0.27	0.282	0.084	39.0	0.045
Transition materials	22.5	1678	0.55	0.75	0.472	0.176	5.413	39.0	0.12
Rockfill prisms as well as bottom ballast materials	22.5	1500	0.65	0.85	0.295	0.33	0.219	40.0	0.1
Ballast materials	22.2	1188	0.612	0.848	0.295	0.33	0.219	40.0	0.1
Ballast mix materials 1	21.5	1150	0.55	0.8	0.3	0.33	0.22	39.5	0.1
Ballast mix materials 2	21.0	850	0.5	0.7	0.3	0.33	0.22	38.0	0.08

Table 2 Parameters for asphalt concrete

No.	$\rho(\text{kN/m}^3)$	k	n	R_f	G	F	D	Φ (°)	C (MPa)	Shaping method
1	24.4	241.3	0.175	0.722	0.488	0.008	0.090	35.9	0.160	Compacted shaping
2	24.5	292.2	0.367	0.565	0.478	0.005	0.142	35.2	0.203	Compacted shaping
3	24.3	413.0	0.249	0.574	0.387	0.129	11.660	35.5	0.196	Core taking on-site
4	24.3	522.8	0.551	0.485	0.396	0.059	9.030	36.2	0.329	Static compression shaping

Table 3 Parameters for linear materials and contact planes

Parameters for linear materials				Parameters for contact planes					
Materials	$\rho(\text{kN/m}^3)$	$E(\text{MPa})$	μ	Contact plane	Δs	$C_s(\text{kPa})$	R_{fs}	K_s	n_s
Concrete base	26.0	25,000	0.17	Impervious wall and bedrock	30.2	3.4	0.75	2500	0.65
Slightly weathered bedrock	24.0	20,000	0.27						

Table 4 Statistics of maximum deformation values at different locations of dam body obtained by Scheme 1

Locations	During completion period			At 175.0m normal pool level		
	Horizontal displacement (cm)		Settlement (cm)	Horizontal displacement (cm)		Settlement (cm)
	Upstream	Downstream		Upstream	Downstream	
Dam body	11.6	7.6	69.7	7.01	13.9	68.0
Core wall's upstream side	7.2	0.0	68.2	0.0	12.6	64.5
Core wall's intermediate point	6.6	0.0	68.3	0.0	12.1	64.4
Core wall's downstream side	5.8	0.0	68.0	0.0	12.8	64.0
Upper transition material	10.7	0.0	68.4	3.0	11.8	63.9
Downstream transition material	4.3	1.5	67.6	0.0	13.0	63.7

Calculation Cross Section and Calculation Scheme

Maximum cross section 0+700 is used as a calculation cross section, and its cross section structure and material zoning are shown in Fig.1. There are in total 1,323 profile elements, of which 167 are for asphalt concrete core wall. Since the core wall is the key to the dam, element subdivision is relatively denser, namely bounded by El.157.0m, above which are two rows of elements and below which are three rows of elements. 126 contact elements are provided between core wall and transition materials. Loading in levels simulates on-site construction process, 29 levels loading in total, 1-24 levels are for construction period, 25-29 levels are for impoundment period.

Calculation schemes are divide into four ones in the light of asphalt concrete's characteristics.

CALCULATION RESULTS AND ANALYSIS

Deformation

Calculation results show that deformation rule of asphalt concrete, transition materials and dam body obtained by using four schemes are the same; differences in value are calculated in mm, which indicates that dam's deformation is mainly controlled by fill materials within dam body, and core wall's deformation develops

concertedly with dam body.

Maximum deformation values for dam body, core wall and transition materials obtained by Scheme 1 (modulus base number for asphalt concrete is 241.3) are shown in Table 4. It follows that core wall deformation is controlled by dam deformation, and vertical settlement is slightly more than that of transition materials at two sides.

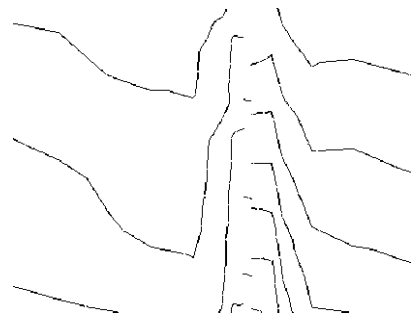
Stress at Asphalt Concrete Core Wall

Calculation results indicate that major principal stress at dam body distributed between core wall and transition materials shows significant discontinuity, core wall's principal stress at the same elevation is smaller than that of transition materials at two sides, and principal stress within transition materials is also obviously more than that at two sides of dam body. The locally-enlarged layout of principal stress distribution is shown in Fig. 2. Monitoring results show that compressive stress value measured at core wall's bottom is smaller than stress caused by self-weight, and also smaller than value measured by earth pressure gauges in upstream and downstream transition materials at the same elevation. The analysis indicates that since settlement deformation of asphalt concrete core wall is more than that of transition materials, transition materials share some load of the core wall, i.e. transition materials exert passive earth pressure on the core wall to a certain extent. Compressive stress graph shows that the compressive

stress at core wall's bottom is continuously increased with the arising of the core wall elevation, and its rising rule is well in agreement with the arising condition of core wall elevation. Calculation results are consistent with stress deformation results obtained from monitoring Maopingxi dam, which indicates that stress deformation within the core wall has rather apparent arching effect.



(a) During completion period

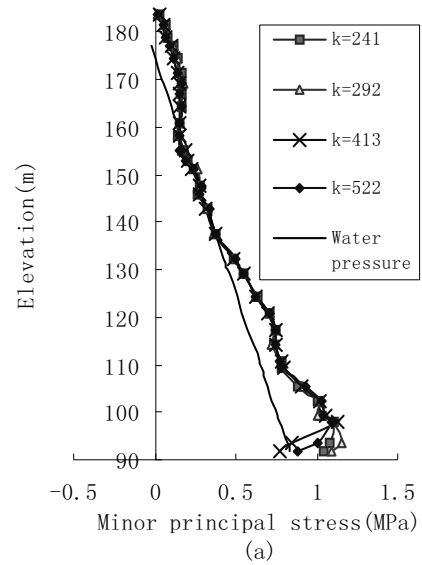


(b) At 175.0m normal water level

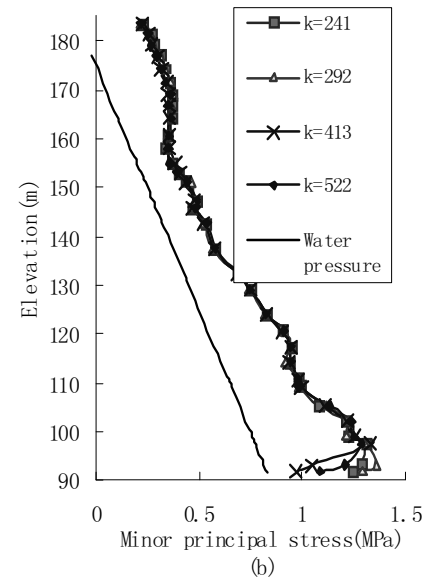
Fig. 2 Partially-enlarged layout of dam body's major principal stress distribution at core wall and transition materials

Since the standard to evaluate the hydrofracture failure of asphalt concrete is associated mainly with minor principal stress, the distribution of core wall's minor principal stress is only analyzed here. The distribution rule of asphalt concrete core wall's minor principal stress and water pressure against elevation under 175m normal water level operating condition by using different schemes are shown in Fig. 3.

Distribution rule of minor principal stress is the same as the gravity, and basically increases with an increase in depth. Due to great difference between modulus of asphalt concrete and transition materials, there exists arching effect within the core wall to a certain extent. According to the standard of minor principal stress being no less than relevant water pressure (mainly taking into account static water pressure), without considering asphalt concrete's tensile strength, if core wall's minor principal stress at location ranging from El.135m to El.160m and at core wall bottom is slightly smaller than its relevant water pressure, a hydrofracture failure probably occurs. The Yangtze River Scientific Research



(a) Without considering asphalt concrete's tensile strength



(b) Considering asphalt concrete's 0.2MPa tensile strength

Fig. 3 Distribution plan for core wall's minor principal stress vs. elevation at upstream side obtained by using different calculation schemes (at 175.0m normal water level)

Institute adopted circular cylinder and circular plate samples to conduct experimental studies on hydrofracture of asphalt concrete core wall in Maopingxi dam. Results show that whether it is under a confined condition or under an unconfined condition, hydrofracture for asphalt concrete sample occurs only in case of the presence of pressure difference between internal and external water pressures and after a given amount of radial deformation are produced, so they are radial hydrofracture. The stress from radial tension can amount to more than 0.2MPa

(Shen Zhujiang, 1994). After considering the asphalt concrete with a tensile strength of 0.2MPa, core wall's minor principal stress is more than its corresponding water pressure, this indicate that the core wall is safe when asphalt concrete's modulus base number is no less than 241, so the occurrence possibility of hydrofracture failure in the core wall is little.

CONCLUSION

Core wall's stress deformation calculated by total stress method is used to evaluate whether a hydrofracture failure would occur in a core wall. Although this method is somewhat conservative, due to the invisibility of hydrofracture failure, at present there are still no better, no more intuitive method to judge them, therefore, finite element calculation and analysis method can be still accepted as an effective and intuitive evaluation method.

Calculation analysis results above answer the question proposed by the engineering community about whether a hydrofracture failure could occur in the core wall of Maopingxi asphalt concrete core rock-fill dam, and if core wall's modulus base number is no less than 240, the occurrence possibility of hydrofracture failure in the core wall is less.

REFERENCES

- Rao XB & Gong BW (2005). Model Experimental Study on Asphalt Concrete Hydrofracture. Practice and Development of Geotechnical Testing Technology. Proceedings of the 24th National Symposium on Geotechnical Testing.
- Seed HB & Duncan JM (1981). The Teton Dam Failure: A Retrospective Review. 10th Int. Conf. SMFE. 4: 219-239.
- Penman (1986). Twenty-Sixth Rankine Lecture on the Embankment Dam. Geotechnique. 36(3).
- Sherard J (1986). Hydraulic Fracturing of Embankment Dams. Journal of Geotechnical Engineering Division. ASCE. Vo1.112, No. 10.
- Shen ZJ & Yi JD (1994). Centrifuge Model Test of Dam's Hydrofracture and its Analysis. Journal of Hydraulic Engineering, No.9
- Zhang BY & Yu YZ (2003). Several Key Technical Problems in High Earth-Rockfill Dam. Proceedings of the Ninth Symposium on Soil Mechanics and Geotechnical Engineering, Chinese Society of Civil Engineers, Beijing.
- Shen ZJ (1994). Feedback Analysis on Deformation in Lubuge Core Rock-Fill Dam. Journal of Geotechnical Engineering. 16(3): 1-13.

GEOENVIRONMENTAL RISK ASSESMENT IN ALBANIA

L. BOZO¹ and G. J. IKONOMI²

ABSTRACT: During the last 15-19 years in Albania were evidenced many dangerous phenomena's which are tied with tailing dams, deformation of mine areas, contaminated lands ect. In this paper we would like to present our work about the evaluation of geoenvironmental risk, and our purposes' for the remediation of the situation in Ohrid lake.

KEYWORDS: lake, contamination, pollution, engineering measures, geoenvironmental

INTRODUCTION

Albania is a rich country with minerals. Albania had a developed mineral industry and consequently many tailing dams, which served as deposits for residue from the mineral industry. During the last 20 years these tailing dams have been a dangerous factor for the contamination of the geoenvironment. In the other hand, over the coal mines near Tirana and Memaliaj cities were constructed 2-3 floor houses, which were damaged by the enormous deformation of the ground. One part of our territory near the chemical factories which w abandoned during this last 20 years, was contaminated with very dangerous elements like arsenic, sulfur, phosphate ect. We want to reveal the risk that menaces the geoenvironment from the causes mentioned above, to make the evaluation of this danger and to predict the measures for the minimization of danger.

EVALUATION OF GEOENVIROMENTAL RISK IN ALBANIA

Before 1990 in Albania there was a big development of the industries like the: Industry of extraction of minerals: Cr, Cu, Fe, Ni, C Industry of treatment and enrichment of minerals as metallurgic and siderurgic works. Construction of tailing dams. Chemical industry particularly for fertilizers in Lac, Fier, Durres cities. After 1990 this industries stopped their activities completely or partially. Most of them where abandoned without having their effects in the environment monitored, they weren't maintained and the worst of all was that they got permissions to construct buildings and to create urban areas in this zone. It is evidenced that the geoenvironment is threatened from this event in three

ways: Contamination of soils and of the underground water which influences the development of flora and fauna. The population takes the dangerous elements from the plants and animals that grow in these zones. The danger for serious or incurable maladies which can affect the inhabitants that have constructed their houses in the contaminated zones. To protect the geoenvironment and the live of the people we think that we must take some defensive measures as: To inform and to prepare the population for the danger that these zones have, their health and their lives. The regulation of the existing legislation so that they will not permit any more constructions in this environment. The monitoring of the degree of the contamination and the determination of the scale of danger for the health and the lives of the people that live there. The taking of some measures for the rehabilitation of the situation and the return of these zones in their normal state.

THE CASE OF OHRID LAKE

Ohrid lake is 2-3 million years old and is one of the oldest lakes in the world. It is situated 695m over sea level, is surrounded by mountains 2000m high, has a surface of 537km² and is 289m deep. The basin that collects water in the Ohrid lake is 1487km². The lake of Ohrid is the biggest biological reserve in Europe with a very rich and uncial flora and fauna. For this reason at 1980 it was decolorized by UNESCO as a territory with natural and cultural inheritance. The zone around the lake has a population of 100.000 habitants who are divided in three cities Ohrid, Struga, Pogradec and many villages. Near Ohrid lake is developed a huge mineral activity which has a major impact in the surrounding environment disturbing the ecological balance of the

¹ Professor, Geotechnical Department of Civil Engineering Faculty Tirana, Albania. Email:Luljeta_bozo@yahoo.com

² Associate Professor, Environment Department of Civil Engineering Faculty Tirana, Albania

lake basin and the surrounding areas. The population of the lake is result of: Mineral-rich residues that come from the production process which are estimated 30/100% of the mineral production (Cr, Fe-Ni, Cu, and C). Another important source of pollution is the technological wastes of the mine activity coming to the lake through the hydrological system of surface water. The chemical analysis and compounds of the stockpile of some of the mines resulted as the following chemical elements (Table 1).

Table 1 Chemical analysis and compounds of the stockpile of some of mines

Chemical elements	Fine inert	Rude inert
Fe	14,92%	30,03%
Ni	0,27%	0,95%
Co	0,01%	0,08%
Cr	0,72%	0,24%
SiO ₂	18,10%	11,74%

Untreated wastewater from the inhabited areas and the dirty water from the plants. A significant amount of the solid material is transported from the streams coming from the slopes of the mountains with mineral activity. Transportation and exploitation tracks and stockpile of residues are probably significant values for the volume and the surface that they have. The filtration of the contaminated waters as a result of the geological and tectonic construction.

Shed sewage. From the measurements and the sample analysis in 1998 we have compiled the following graph (Fig. 1).

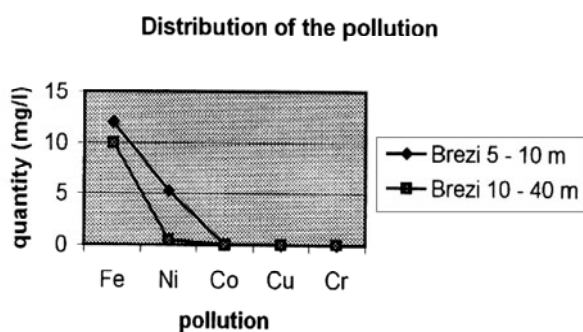


Fig. 1 Distribution of the pollution

The Ohrid lake has special and particular characteristics, it is one of the most preferable touristic place for foreign and Albanian tourists. For this reason the problem of protection of the lake for pollution the protection of the natural resources and ecological balance are very important problems.

GEOENVIRONMENT OF OHRID LAKE

From the geological point of view: Triassic and Jurassic deposits consist in carbonate formation, Ultrabasic and ofiolitice. Also we have discovered deposits of Oligocene, Tortonian and Pliocene are presented by conglomerates, sands, and alevrolites and clay Quaternaries deposits with thickness 60-160m and with marsh-lake origin.

From the hydrological point of view: We have three water bearer complexes the first of Cretan carbonates, the second Triassic carbonates and the third is the Ultra basic rocks.

From the geological study results that, in this zones are present three categories of soils: hard, medium and weak soils. Also here are present the geodynamic phenomena as: New tectonics, phenomena tied with atmospheric changes, slope instabilities, abrasion phenomena, important settlements ect.

From the seismological study results that this zone has high seismic activity. From the statistical elaboration of the data in this zone is probable to happen an earthquake with $M > 5.9$ every 50years.

From the study of the water balance-sheet results that the total volume of flowing created in the basin of Ohrid lake is $570 \cdot 10^6$ m³ with module 14L/s*km².

From the thermic study results that the difference of temperature in upper water layer (h=130m) is 22o-5.7oC while in the bottom water layer (h=130-264m) there isn't any more temperature difference and it stays at about 5.5oC.

The chemical composition of the water of the lake shows that it has a few salts (200-250mg/L). In this salts predominate HCO₃⁻, Ca⁺⁺, Mg⁺⁺ and their quantity are HCO₃⁻ > Cl⁻ > SO₄⁻⁻ ; Ca⁺⁺ > Mg⁺⁺ > Na⁺ > K⁺.

THE CAUSES OF THE MISS BALANCE OF THE GEOENVIRONMENT

During the 20 last years we have observed the disorder of the ecological and geoenvironment balance in some directions. This is very dangerous for the ecological value of Ohrid lake because it damages the geoenvironment by creating problems for the development of this zone and for the health of the habitants. The mines of Chrome in Pojska and Memëlisht, the mines of Iron-Nickel in Gradisht, Çervenak, Guri I Kuq, and the mines of coal in Alarup, Vërdovë, and Pretush ECT are in a distance 2-2.5km from Ohrid lake. The ecological miss balances are caused by man activities which are made in three directions: Shedding of the sewerage directly in the lake causes the augmentation of the percentage of the organic material. Flowing of the contaminated industrial waters and water from mines

including the toxic substances, heavy metals from stockpiles of Chrome minerals (114000m³), Iron-Nickel (228000m³) and Coal (206000m³). Shedding of the solid residue of the streams from slopes with mineral activity. It results that the solid material which is transported in the lake is from 5000m³/year until 40000m³/year. In this solid material we can find heavy metals as: Fe = 10-12 mg/L, Ni = 5.26 mg/L, Co = 0.07 mg/L, Cu = 0.0215 mg/L, Cr = 0.01 mg/L. Shedding of water from plants, from the process of erosion ect.

MEASURES PROSED FOR THE REMEDIATION OF THE SITUATION (CONCLUSIONS)

The preservation of the ecological balance of Ohrid lake and their surrounding zones needs some engineering measures, the creation of the monitoring system and the management of the data's or information. The engineering measures are tied with: Construction of purification plants for the sewerage. Isolation of the flows from the tankers that have dangerous material in them. Engineering protecting measures for erosion phenomena. Regulation of the surface water by different drains, canals with different levels ect. The monitoring system of Ohrid lake intends to persevere the biodiversity and their ecological functions. We think that for the monitoring system some institutes must be created which will have the following responsibilities: They should assign a frequency of the monitoring from one month to

10 years. To determinate the percentage of the phosphor, nitrogen, organic materials, carbon, oxygen, chlorophyll, heavy metals, pesticides, physical and biological parameters ect. They have to determinate the mechanism for the data exchanging. They should organize the receiving of the samples. They must analyze the samples. They must determine the local pollution and contamination. They must determine the used methods. The management of the data's or information from the monitoring system must be done from the local or central authorities for some purposes: To inform the public for the situation. To take the necessary measures for the neutralization of the dangers or the miss balances of the geoenvironment. To take the engineering measures which will defend the geoenvironment from their degradation and destruction.

REFERENCES

- Bozo L & Gogo K (2004) The problems related to the construction and exploitation of the tailing dams in Albania. Proc. Int. Conference in Soil Mechanics and Geotechnical engineering Prague.
- Bozo L, Shkodrani N, Muceku Y (2005) Landslide risk assessment on roads in Albania. Proc. Int. Conference on Landslide Risk Management Vancouver Canada.
- Fetahu K (2000) Mineral activity in Pogradec region. Int. Seminar Ohid Macedonia.
- Ikonomi GJ & Xhelepi S (2004) Monitoring of Ohrid lake. Monograph Tirana Albania.

STUDY ON DEBRIS FLOW HAZARD DISCRIMINANT ANALYSIS AND ZONING OF ONE DUMP

Shi-Guo SUN¹, Shao-Jie FENG², Ting-Ting JIANG³, Hua XIAO⁴ and Sheng-Hua ZHANG⁵

ABSTRACT: Due to the dump consists of a large number of loose materials and it is located at the hillside, the dump with bad engineering geological condition is likely to constitute a composite slope mass. During the rainy season, those constitute necessary condition of landslide and debris flow. Therefore, this paper reference assessment methods of the mountain debris flow hazard degree, aiming at the characteristics of environmental engineering geological condition of one dump, establish hazard degree discrimination method of collaborative failure of hillside and dump then induce debris flow. Accordingly, we can obtain discrimination results of Yichang limestone mine dump hazard area.

KEYWORDS: dump, debris flow, hazard degree discrimination, hazard zoning

INTRODUCTION

The dump safety issue is not only relates to the mine production safety, but also involves surrounding environment and nearby residents safety. However, for those which dump with bad engineering geological conditions, how to ensure the dump safety, which is very difficult, and during the rainy season once landslides is likely to induce debris flow, because of loose and rich gravel soil, the rainy weather have continuous heavy rain, as well as bad environmental engineering geological conditions, constitute the debris flow induced by the necessary and sufficient conditions, however, less research in this field, so urgent to solve such problems (Kuang 2006, Dang 2007).

THE ZONING METHOD AND PRINCIPLE OF DEBRIS FLOW

The Zoning Principle of Debris Flow

In general case, There are three main methods of the debris flow hazard zoning. One is the direct indicator method, which uses status of activities within the region, gully density, the frequency, the scale and other indicators to zoning; Second is indirect indicator method, which uses background conditions of the intra-regional debris flow development, such as topography, geology,

vegetation, precipitation and other indirect indicator to zoning; Third, it is combining method of the direct and indirect indicator. As the dump in study area is built up in recent years, there is no historical record of the occurrence of debris flow, therefore using the indirect indicator method.

The debris flow hazard zoning model is a core, which to ensure reliability of the zoning result, in this paper, extension model is used for debris flow hazard zoning in dump area.

According to the quantitative zoning principle, firstly, it's need to establish a quantitative region model. However, the debris flow hazard zoning classification is no clear boundaries, in order to scientifically and systematically express such limits, in this paper, we adopt fuzzy mathematics method to process. so, introduce spatial data mining technology from extension theory, then establish extension model of the debris flow hazard zoning, determine the quantitative zoning indicator system, finally, zone the debris flow hazard degree in whole dump area.

The Basic Principles and Methods of Extension Model

Assume that i factors $X_i (i = 1, 2, 3 \dots n)$, and under different states of n factors, $B (j = 1, 2, 3 \dots m)$ event may be occurred. In order to determine what B events

¹ Professor, Department of Civil Engineering, North China University of Technology. Email: ssg918@163.com

² Assistant, Department of Civil Engineering, North China University of Technology. Email: fsjje@163.com

³ Postgraduate, Department of Civil Engineering, North China University of Technology. Email: jtt-8491@163.com

⁴ Senior Engineer, Huaxin (Yichang) CO. LTD. Email: xiaohua@huaxincem.com

⁵ Senior Engineer, Huaxin (Yichang) CO. LTD. Email: zhangshenghua@huaxincem.com

will have occurred in combination states of factor $R(X, X, X \dots X)$, first, construct the standard matter-element model of the event B_j occurrence for Eq.1.

$$R = \begin{pmatrix} B & X & x \\ & X & x \\ & X & x \end{pmatrix} \tag{1}$$

where x_1, x, x respectively is the value of the factor X, X, X .

And then calculate the state of R and the corresponding relational level of the event B in standard matter-element model, determine the event B occurring according to correlation degree.

Assume that $X = (a, b), X = (c, d), X_0 \subset X$, and no public endpoint, let be

$$K(x) = \rho(x, X_0) / D(x, X_0, X) \tag{2}$$

Among them:

$$\rho(x, X) = |x - (a + b) / 2| - 1 / 2(b - a)$$

$$D(x, X, X) = \begin{cases} \rho(x, X) - \rho(x, X), x \notin X \\ -1, x \in X \end{cases} \tag{3}$$

According to Eq.3, we can calculate the relational level between factor X of the event B occurring in standard matter-element model with factor X of the state R , as the following Eq. 4.

$$K_j(V_i) \quad (j=1,2,\dots,m; i=1,2,\dots,n) \tag{4}$$

Then, the relational level of the state R on the event B as the following Eq. 5.

$$K(P) = \sum_{v=1}^n \alpha K(v) \tag{5}$$

If $K(P) = \max_{v \in \{1\}} K_j(P)$, then, determine the event

B occurring under the state R .

As for debris flow zoning in dump, judge the debris flow hazard degree in different conditions at different areas according to the standard matter-element model of debris flow hazard degree. firstly, we should choose several influential factors of debris flow, that is debris flow hazard zoning indicator, Then, construct debris flow matter-element model and the extension model of debris flow hazard zoning. Lastly, judging debris flow hazard degree in this area.

Hazard Zoning Indicator

How to choose the factors for hazard zoning indicator is very important, and the main factors in debris flow development are environmental engineering conditions, characteristics of loose fragmental material and water sources.

Geological conditions

Geological conditions affect debris flow development at two aspects, That is relative height and gradient. Relative height provides the energy conditions for debris flow development, and is also the basic condition for debris flow happening as well. And the gradient condition is essential for potential energy turning to kinetic energy. Using the statistical units zoning debris flow hazard area and the same size of each unit, the horizontal distance could be the same in the statistical sense, and there are the good relevance and the strict positive correlations exist between relative height and gradient. In order to be convenient to get the data, we could choose the gradient as the geological indicator for debris flow hazard zoning and reflect the energy conditions for debris flow development.

Dump conditions

According to the terrain condition and environmental engineering geological condition, we can divide the dump and the adjacent hills into four areas as Fig.1. Because there are a lot of accumulated soil and gravel soil in area A, so the hazard degree level is higher, and the quantitative value is 0.85. There are bedrock in area B and C, and the quantitative value is 0.4. D area is cultivated land, and the quantitative value is 0.6.

Precipitation indicator

If terrain condition and loose soil are prepared, the precipitation condition would be the exciting factors of debris flow occurrence. Because the debris flow always occurs in rainstorm condition, we using precipitation condition as the evaluation indicator for debris flow hazard zoning. Although the rainfall is a complex indicator because of the good positive correlation between precipitation and rainstorm condition, we choose the precipitation from August to September as the evaluating indicator.

The Establishment of Extension Model of Hazard Zoning

The determination of statistics unit in hazard zoning

In order to zoning the debris flow hazard area, we have to mesh the entire area into the same size unit so that we could use the same standard to zoning it. We can determine the units' size base on the debris flow area. If

the units' size is too big, it is easy to ignore the small area with characteristics, and the ultimate result would be unreal. If the units' size is too small, the factors in the units couldn't reflect the actual situation of debris development and the ultimate result would be too discrete. According to the similar degree of gradient, we divide the area into 4 parts, and the units' size are $500 \times 500 \text{ m}^2$. Because the gradient could be changed in the same unit, we use average gradient to calculate the average elevation (as Fig. 1).

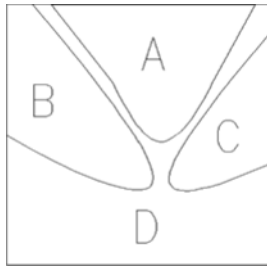


Fig. 1 Debris flow hazard degree zoning graph

Zoning evaluation system and the grade division of zoning indicator system

There are several evaluation systems in debris flow hazard zoning, such as 5 level evaluation system, 3 level evaluation system and multi-level evaluation system. Because the research area is small, we pick 3 level evaluation system out, that is we divide the debris flow hazard degree into serious, moderate and mild. The standard of zoning indicator level is as what Table 1 shown.

Table 1 Grading standard of debris flow hazard degree zoning evaluation indicator

	High hazard degree	Middle hazard degree	Low hazard degree
relative height (mm)	> 200	$200 > h > 100$	< 100
geology	$1 - 0.7$	$0.7 - 0.3$	< 0.3
precipitation (mm/h)	> 100	$50 - 100$	< 50

Hazard degree assessment on standard matter-element model

Topography, geology and precipitation is selected as the evaluation indicator of debris flow hazard degree assessment, and the level standard of various indicators in different hazard zoning was given, Hereby, it can be constructed to describe environmental background of the debris flow development in each unit, That is the matter-

element model of debris flow hazard degree, as follow Eq. 6.

$$R = \begin{pmatrix} \text{debris flow hazard area} & T & x_1 \\ & G & x_2 \\ & J & x_3 \end{pmatrix} \quad (6)$$

Where T is topographic indicator, G is geologic indicator, J is precipitation indicator, x_1 , x_2 and x_3 respectively for quantitative indicator of topography, geology and precipitation.

In order to determine the classification of the statistical each unit matter-element, the classification knowledge must be modeling of matter-element, as a measure condition of matter-element classification. According to the classification results of each indicator and evaluation system of the debris flow hazard zoning in the research area, construct standard matter-element model of each hazard level. As shown in Table 2.

Regionalization indicator weight coefficient

when evaluating an object, there are differences between the importance of the all measuring conditions, generally, weight coefficient used to express the importance of measuring conditions, it's value has a decisive influence for evaluation results.

The weight of topography, geology and precipitation in debris flow sonority commenting expressed by $\alpha = (0.45, 0.35, 0.2)$, according to the natural conditions of debris flow development.

Evaluation model

Determine debris flow hazard zoning district indicators, evaluation system, the weight coefficient for each indicator. and construct standard matter-element model of debris flow hazard zoning, then it will be able to establish a debris flow hazard zoning extension model. Extension model is the use of the correlation degree to characterize the thing of its value. Firstly, we calculate the correlation degree $K(X)$ of each district indicators for each unit and the evaluation level of the hazard area, in which $j = 1, 2, 3, 4; i = 1, 2, 3, 4$.

Then introducing each factor weight coefficient α , the correlation degree of statistical unit P with respect to debris flow hazard degree evaluation level expressed by Eq.7.

$$K(P) = \sum_{i=1}^n \alpha K(x_i) \quad (7)$$

The correlation degree of debris flow hazard degree of statistical unit P and three hazard level respectively for

Table 2 Standard matter-element model

Regional type	Regional characteristics	Regional standard matter-element
Low hazard degree area	1. Topography: $T < 100$ 2. geology: $G < 0.3$ 3. precipitation: $J < 50$	$R = \begin{pmatrix} \text{Low hazard area} & T(0, 100) \\ & G(0, 0.3) \\ & J(0, 50) \end{pmatrix}$
Middle hazard degree area	1. Topography: $100 < T < 200$ 2. geology: $0.3 < G < 0.7$ 3. precipitation: $50 < J < 100$	$R = \begin{pmatrix} \text{Middle hazard area} & T(100, 200) \\ & G(0.3, 0.7) \\ & J(50, 100) \end{pmatrix}$
High hazard degree area	1. Topography: $T > 200$ 2. geology: $G > 0.7$ 3. precipitation: $J > 100$	$R = \begin{pmatrix} \text{High hazard area} & T(200, 299) \\ & G(0.7, 0.99) \\ & J(100, 199) \end{pmatrix}$
Controlled field of each indicator in region		$R = \begin{pmatrix} \text{Region} & T(0, 300) \\ & G(0, 1) \\ & J(0, 200) \end{pmatrix}$

Table 3 D area hazard degree calculation results

D area	$\rho(x, X_0)$	$\rho(x, X)$	$\rho(x, X, X)$	$K(x)$	$K_j(P)$	K_{j_0}
Low hazard degree area	1(50) $X_0 = (0, 100)$ -50	$X = (0, 300)$ -50	-1	50		
	2(0.6) $X_0 = (0, 0.3)$ 0.3	$X = (0, 1)$ -0.4	-0.7	-0.43	22.4	
	3(91) $X_0 = (0, 50)$ -9	$X = (0, 200)$ -91	-82	0.1		
middle hazard degree area	1(50) $X_0 = (100, 200)$ 50	$X = (0, 300)$ -50	-100	-0.5		
	2(0.6) $X_0 = (0.3, 0.7)$ -0.1	$X = (0, 1)$ -1	-1	0.1	-0.01	22.4
	3(91) $X_0 = (50, 100)$ -9	$X = (0, 200)$ -1	-1	9		
high hazard degree area	1(50) $X_0 = (200, 300)$ 150	$X = (0, 300)$ -50	-200	0.75		
	2(0.6) $X_0 = (0.7, 1)$ 0.1	$X = (0, 1)$ -0.4	-0.5	-0.2	0.25	
	3(91) $X_0 = (100, 200)$ 9	$X = (0, 200)$ -91	-100	-0.09		

$K_1(P)$, $K_2(P)$, $K_3(P)$ and $K_4(P)$. According to maximum membership degree law, the hazard degree level of statistical unit P is maximum, such as Eq.8. Then debris flow hazard level of being evaluated units is corresponding to j through this evaluation model, it can evaluate each of the debris flow hazard level.

$$K_j(P) = \max_{j \in \{1, 2, 3, 4\}} K_j(P) \tag{8}$$

Dump hazard zoning results

According to Eqs. 2-5 obtains calculation results, as follows:

D area quantitative indicator is respectively $T = 40$, $G = 60$, $J = 91$, The results shown in Table 3, of which $K_{j_0} = 22.4$, then *D* area and low hazard degree obtained maximal correlation degree, therefore it belong low hazard degree area. Other areas also use this calculating method. *C* area quantitative indicator is respectively $T = 60$, $G = 40$, $J = 91$, The calculation results $K_{j_0} = 210.95$, *C* area and low hazard degree obtained maximal correlation degree, therefore it belong low hazard degree area. *B* area quantitative indicator is respectively $T = 110$, $G = 0.4$, $J = 91$, The calculation results $K_{j_0} = 8.75$, *D* area and middle hazard degree obtained maximal correlation degree, therefore it belong middle hazard degree area. *A* area quantitative indicator is respectively $T = 250$, $G = 0.85$, $J = 91$, The calculation results $K_{j_0} = 22.5$, Comprehensive analysis and discriminant, *A* area and high hazard degree obtained maximal correlation degree, therefore it belong high hazard degree area.

CONCLUSIONS

According to the engineering geological condition of a limestone mine dump, explore collaborative failure mechanism between soft rock basement and the dump, as well as conditions of the dump landslide into a debris flow; Apply fuzzy mathematics methods and spatial data mining technology of extension theory, establish extension model of debris flow hazard zoning, determine the quantitative zoning indicator system, zoning and discriminate the dump which induce debris flow, thus

provides a scientific basis for dump safety.

ACKNOWLEDGEMENTS

The authors are grateful to the support of Beijing Municipal Education Commission Project (KM200710009007), Geotechnical Graduate Education project (PXM2009-014212-076740), and Beijing Research Base and Innovation Platform project (PXM2008-014212-053940).

REFERENCES

- Kuang LH, Xu LR, Liu BC (2006). Debris flow hazard assessment based on extension method. *China Railway Science*, 27(5):1-10.
- Dang RT (2007). Apply gray theory to predict the risk coefficient of debris flow occurrence, *Technology of Soil and Water Conservation*, 1: 15-17.
- Liu JL, Lu XK, Liu GY (2001). Fuzzy comprehensive evaluation method to evaluate debris flow hazard degree, *Geological Science and Technology Information*, 20:87-88.
- Ai NS (1987). Comentropy in erosional-drainage-system, *Journal of Soil and Water Conservation*, 1(2): 1-7.
- Ai NS & Yue TX (1988). Second discussion of the comentropy of drainage-system, *Journal of Soil and Water Conservation*, 2(4): 1-7.
- Wang XP, Pan M, Ren QZ (2006). Hazard assessment of debris flow based on geomorphic information entropy in catchment, *Journal of Peking University (natural science edition)*, 1(3):1-9.



**Ecological Techniques and
Case Histories**

SUSTAINABLE DESIGN BASED ON NEAR NATURE CONSTRUCTION METHOD —A CASE STUDY

Huat-Yoo CHUA¹, Hsiao-Chou CHAO² and Chung-Tien CHIN³

ABSTRACT: To meet the demands in both flood control and nature conservation, near nature construction method was adopted for the river restoration on downstream of Fazih River. The project was performed following the procedures: (1) ecology investigation, (2) basic hydrological information collection, (3) riverbed and embankment design, (4) nature conservation design, and (5) construction. Special features include guiding river flow with low jetties to generate fish habitat, using Ryushikou method to build revetment covered with densely populated vegetation, afforestation for heron nesting. A rough post construction evaluation showed satisfactory results are achieved thus far.

KEYWORDS: river restoration, revetment, embankment, ecosystem, habitat

INTRODUCTION

Conventional river work was flood control oriented within which eco-environmental issues usually was not a primary concern. It is apparent the aquatic ecosystem throughout the island has been degraded by various development activities where engineering played an important role over the past decades. As the value of natural resource conservation gradually recognized by the public in recent year, people started to demand better ecological environment aside from the function and performance of civil engineering infrastructures. Under the circumstance, river management became a multi-objective work within which the role of nature conservation is at least equivalently as important as the other factors (e.g. Nakamura et al. 2006). This article presents a case study in which the methods of near nature river engineering were modified and adopted in building flood control facilities and restoring the ecological environment of the river corridor along the downstream of Fazih River.

BACKGROUND

The project site is located along the Fazih River between the Chung-Chang Expressway and the Taiwan high speed Rail on the northeast proximity of Wurih Station of Taiwan High Speed Rail as shown in Fig.1. The drainage system of the Fazih River is shown in Fig.

2. As a plain river with total length of approximately 21km flows through the western suburban of Taichung County where most lands are still used for agriculture and small-scale industries, the Fazih River is able to keep its abundant flora and fauna resources. Although polluted moderately, record of biota shows alongside the river still inhabit a variety of wildlife species.

As most rivers in Taiwan, China the Fazih River is prone to rapid rises and drops in water level after rainfall. In 2001, a heavy rainstorm brought by Toraji typhoon caused part of the levees along downstream collapse. Flood flowed over the surrounding area resulted severe life loss and economic damage. This event along with other large-scale construction activities underway including Taiwan High Speed Rail, the Chung-Chang Expressway and a new interchange across the Fazih River between the Wurih Station of Taiwan High Speed Rail and the Chung-Chang Expressway made the rehabilitation an urgent action. Because the awareness in environmental issues grew stronger at the time, people once again started to recognize the importance the ecology balance, natural landscape and good living conditions. Effective flood control and improvements of the river environment at same time became a common demand for the public. However, this brought a new challenge to the rehabilitation work aftermath.

In response to the challenge, the concept of “design with nature” (McHarg 1992) and the methods of “near nature” river engineering or “nature-oriented” river works (e.g. Yamawaki 2000) aimed to conserve or

¹ Principal Engineer, Taichung MRT Special Project, Moh And Associates, Inc., Taiwan, China. Email: hy.chua@maaconsultants.com

² Senior Geotechnical Engineer, Moh And Associates Inc., Taiwan, China. Email: hsch.chao@maaconsultants.com

³ Vice president, Moh And Associates Inc., Taiwan, China. Email: ct.chin@maaconsultants.com

restore the ecosystem of river corridor were introduced into this project. Important characteristics of near nature river works include it uses as much natural materials such as boulders, logs or vegetations as possible and uses nature oriented devices with the help of nature to manage river flow or generate wildlife habitat (Nakamura 2003). Fig. 3 illustrates the formation of near nature river work and general river work. As can be seen, rather than flat riverbed, narrow and deep riverbed that is able to provide a better habit for fishes are basic elements in near nature river work.



Fig. 1 Satellite image of the project site (Source: Google earth)

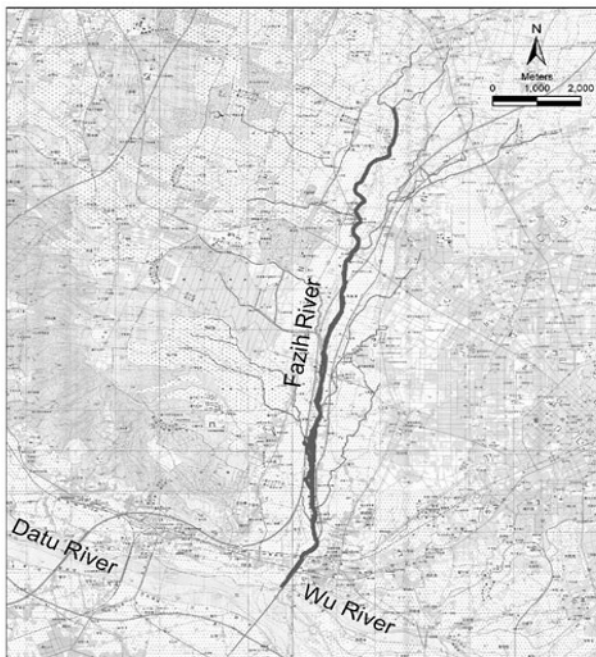


Fig. 2 The Fazih river drainage system

RIVER RESTORATION

To bring back the balance of the eco-environment of Fazih river, the objectives of river restoration in the rehabilitation are focused on (1) regenerating habitat for diverse species (e.g. fish, aquatic insects, birds, other wildlife), (2) reducing riverbank erosion, and (3) achieving a self-sustaining river system with minimized requirements of periodic dredging or construction of additional flood control facilities. To achieve these objectives, the following works were conducted prior to start of design: (1) ecology investigation, (2) establish baseline information.

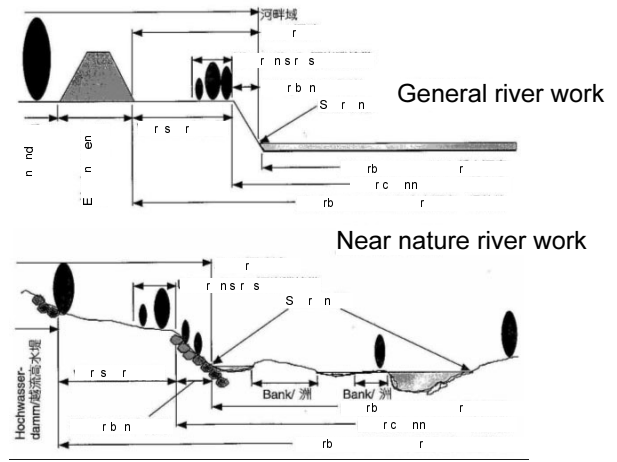


Fig. 3 General and near nature river works

Ecology Investigation

Results of the ecology investigation indicated along the Fazih River from upstream to downstream within the project site has at least 67 species of Vascular plant, mostly dicotyledon. While revetments on low banks are primarily covered with the *Humulus scandens* (L.) err. and *Celosia argentea*, on high banks covers primarily with *Bidens pilosa* L. var. *radiata* Sch and *Ipomoea indica* (Burm. F.) Merr.

It also showed at least 70 species of birds, 2 species of mammals, 3 species of reptiles, 3 species of amphibians, 23 species of butterflies and 2 species of dragonflies were found in this region. Seven species of fishes are aboriginal. The dominant bird species is White Java Sparrow and other 3 species of herons. As the population of the dominant bird species along the river corridor is in stable condition, research also revealed species diversity can be recovered by restoring the habitat for those lived alongside the shallow water area.

Basic Hydrological Information

To provide a baseline for restoration design, the following hydrological and planning information need to

be established:(1) strong flow thrust points and moderate flow zones during flood, (2) normal water level and thalweg, (3) sites appropriate for waterfront parks and thick vegetation cover. Baseline information was established here by rough estimation. Fig. 4 illustrates the estimated thalweg or strong flow route during flooding periods.

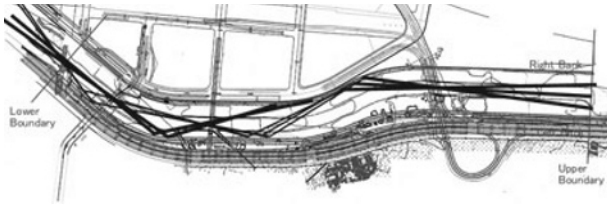


Fig. 4 Estimated thalweg or strong flow route during flood

The key design results for river restoration, riverbed and revetment, developed based on the techniques of near nature river work are presented herein

Riverbed

As illustrated in Fig. 5, guide spurs, or low jetties are installed in three places to guide river flow and protect riverside from scouring. Guide spurs are structures extending to water in the path of flood flow submerged during flood. They are used to guide flow into the thalweg line of the river. Local scouring resulted by the concentrated flow could change the riverbed morphological features and generates deep, narrow and sometimes meandering habitat for fishes and benthic invertebrates.

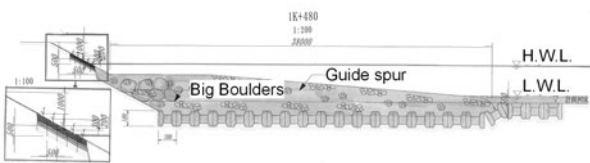


Fig. 5 Schematic of guide spur

The ground-sill is a structure built to pass water to a lower elevation while control the energy and velocity of the water as it passes over. It is installed in 3 places along the river. Layout of guide spurs and ground-sills are shown in Fig. 6.

As also shown in Fig. 9, three tentative bed consolidation works were designed to keep the riverbed elevation as planned and protect the riverbed near the bridge piers. Because constant scouring as a result of flow along thalweg line tend to undercut the bank on a curve of the river, several pools are expected to be formed in due time. These pools would provide good

habitat for fish if the heels of the embankments can be well protected. Expected locations of pools are shown in Fig. 7.

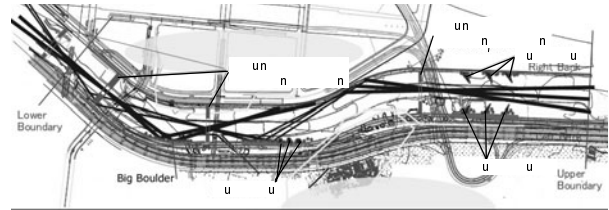


Fig. 6 Layout of guide spurs and ground-sills

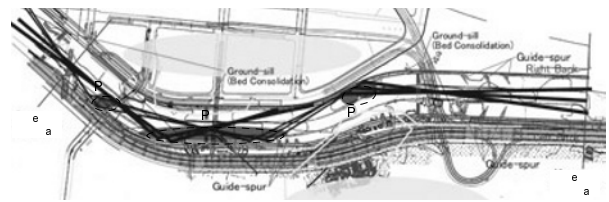


Fig. 7 Pools expected to be formed in due time

Revetment

River revetments are sloping structures placed on banks to absorb the energy of incoming water. They are usually built to preserve the shoreline and to protect the slope, as defense against erosion. Combination measures of using gabion, box-gabion, big boulders, stairs-like, rip-rap, and the newly introduced Ryushikou revetment were evaluated based on the consideration of possible thalweg line, river shape, thrust power of river flow, pool-rifle configuration, locations of waterfront park and thick riparian vegetation zone. To select appropriate types of revetments, two-dimensional depth averaged model of river hydrodynamic and fish habitat analyses were performed using River-2D software (Steffler P. and Blackburn J. 2002).

Results of revetment design are summarized in Table 1. For demonstration, revetment layout form 0k+260 to 1k+300 is shown in Fig. 8. The cross sections of box-gabion and stairs-like gabion revetments are shown in Figs. 9 and 10, respectively.

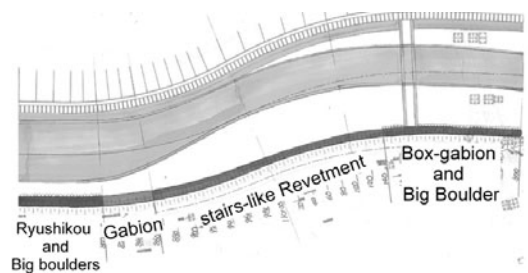


Fig. 8 Layout of revetment (0k+260 to 1k+300)

Table 1 Results of Revetment Design

Section		Revetment type	H (m)	B (m)	V (m/s)	
From	To					
0K+000	0K+100	Box-gabion	5.08	3.00	3.58	5.81
0K+100	0K+260	Box-gabion & Big boulders	4.63	3.00	4.60	6.90
0K+260	0K+440	Ryushikou & Big boulders	4.55	6.60	4.38	5.94
0K+440	0K+620	Gabion & Boulders	4.00	4.00	4.97	7.08
0K+620	0K+800	Ryushikou & Big boulders	4.59	6.60	4.10	5.64
0K+800	0K+860	Gabion	3.38	4.00	4.83	6.75
0K+860	1K+140	Stair-like	4.03	4.00	4.31	6.15
1K+140	1K+300	Box-gabion & Big boulders	3.26	6.60	4.38	6.06
1K+300	1K+520	Jetty & Ryushikou	3.25	6.60	4.51	5.54
1K+520	1K+800	Riprap	3.53	-	3.81	4.11

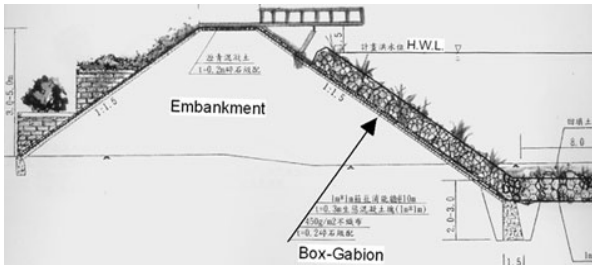


Fig. 9 Cross section of embankment with box gabion revetment

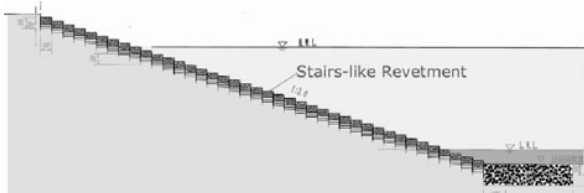


Fig. 10 Cross section of embankment with stairs-like revetment

The new introduced “Ryushikou” technique uses log-framed-stone structure available on site or nearby areas with living Willow, to be the stake. As Willows grow up in due course, their root system provides extra stiffness to strengthen the embankment structure regardless the log frames are decayed. The Willows form vegetation cover as the habitat for wildlife and shelter for fish in flooding periods. The cross section of Ryushikou revetment is shown in Fig. 11.

The so-called “Ryushikou” technique is not commonly used in Taiwan thus far. Nevertheless, the “near nature” characteristics of this construction method make it one of the better ways for creating wildlife habitat, vegetation recovery. The “porous” surface acts as damping device for energy brought by flood wave to dissipate. However, it should be noticed the plants on

“Ryushikou” revetment could be detrimental to the embankment structure if they are uprooted during flood. Hence, maintenance measures such as clipping, paring or pruning are required every 2 to 3 years to keep the vegetation from growing too tall.

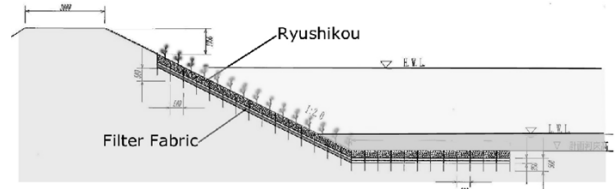


Fig. 11 Cross section of embankment with Ryushikou revetment

SAFETY OF THE EMBANKMENT

With regard to safety of the embankments, various failure modes such as sliding, overturning, bearing capacity were analyzed. Liquefaction potential and piping failure were also examined. Computer software SLOPE/W was used for slope stability analyses in which the critical states at (1) completion of the embankment construction, (2) stable infiltration and seepage, and (3) rapid water level drawdown were analyzed under the conditions of earthquake with horizontal acceleration of 0.33g and 100-year flood level. The safety factor of 1.5 was adopted in the analyses. Fig. 12 demonstrates results of the analyses.

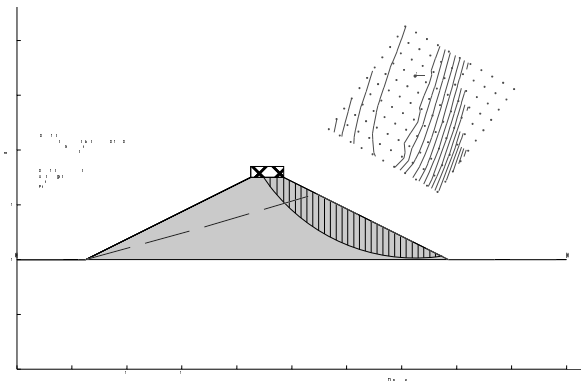


Fig. 12 Results of slope stability analysis

NATURAL CONSERVATION

Heron Habitat

In addition to the riparian forest along the river, a heron forestry at the slip circle is planned. Various species of plant attracting heron to build their nest are arranged and planted as shown in Fig. 13.

Fish Pool

The formulation of fish pool is shown in Fig 14. According to the results of slope stability and safety evaluation for the revetment, it was determined to have big boulders placed on the heel of the embankment slope such that both the possible fish habitat and protective shelter can be created.

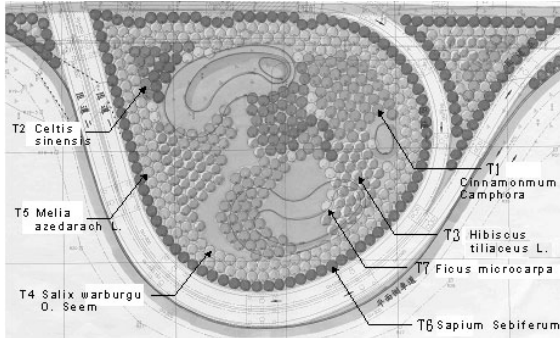


Fig. 13 Vegetation on heron conservation site

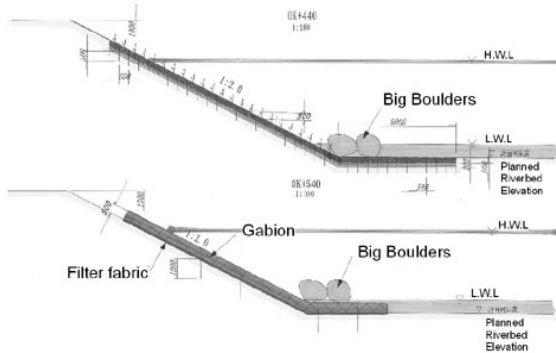


Fig. 14 Fish pool formulation

POST-CONSTRUCTION EVALUATION

Construction of the embankment started in October 2003 and completed in December 2004. The constructions of the stairs-like and Ryushikuo revetments were shown in Figs. 15 and 16, respectively.



Fig. 15 Stairs-like revetment under construction



Fig. 16 Ryushikou revetment under Construction

Fig. 17 shows the site condition in 2008, about 4 years after completion of the project. As can be seen, revetment built by Ryushikou method had been covered by densely populated Willows. The effectiveness of wildlife habitat together with fish habitat generation will be evaluated in the near future. As for the woods in the slip circle designed for heron’s habitat, the expected height and density of the plants have not been reached and thus further evaluation has not scheduled yet. For the revetments and embankments alongside the river, it is evident they are able to meet flood control requirements thus far after struck by several severe rainstorms since 2005.



Fig. 17 Current condition of the embankment with box gabion and Ryushikou Revetments along the river

CONCLUSION

Although intuitively contradictory, this case study showed nature conservation and flood control can be integrated to a certain level. Because of the constant residential, commercial and industrial growth in urban and suburban areas of Taichung metropolitan, river could be the last remaining open space for amenity and recreation in the future. Thus, the importance of careful and appropriate use of engineering measure for river work cannot be overstressed.

ACKNOWLEDGEMENTS

The Authors are grateful to Dr. Za-Chi Moh for his support in preparation of the manuscript and to all the colleagues who have contributed their efforts to the planning and design of this project. Assistances from Prof. Tseng C. and Prof. S. Nakamura for guiding ecology investigation and river-work planning are gratefully acknowledged.

REFERENCES

Nakamura K, Tockner K, Amano K (2006). River and

- Wetland Restoration: Lessons from Japan, *Bioscience*, May 2006, 56(5).
- McHarg IL (1992). *Design with Nature*, John Wiley and Sons, Garden City, N.Y.
- Yamawaki M (2000). *Naturnaher Wasser und Strassenbau* (in Japanese). Tokyo Shinzansya Sci-tech.
- Nakamura S (2003). Design with Nature in nature-oriented river works in Japan, *Int. WS for Eco-hydraulics & Eco-rivers Engineering*, Taiwan, China.
- Steffler P & Blackburn J (2001). *River2D: Two-Dimensional Depth Averaged Model of River Hydrodynamics and Fish Habit*, University of Alberta, Edmonton, Alberta, Canada.

ENGINEERING GEOLOGICAL PROPERTIES OF THE SATURATED CLAY FOUNDATION AT THE SOUTHERN EDGE OF MU US DESERT IN CHINA

Sheng-Rui SU¹ and Fang-Qiang SUN

ABSTRACT: In order to investigate the engineering geological properties of the saturated clay foundation along the Jingbian-Wangquanliang expressway, *in-situ* and laboratory tests had been done, including *in-situ* standard penetration test, cone penetration test and geotechnical tests in the laboratory. According to test results, the physical and mechanical properties of the saturated clay foundation are studied. It is found that most of the ground does not exhibit the characteristics of soft soil in the studied area, but the variation of the consolidation coefficient is relatively large, between 0.05 and 0.33 MPa⁻¹, which may result in inhomogeneous settlement. The soft ground within the depth of 12 m shows slight salinization and serious liquefaction. Friction angle of the saturated clay is 30° and its cohesion is 10kPa. Bearing capacity of the foundation is less than 100kPa in the depth less than 3 m and less than 140 kPa within the depth less than 5 m.

KEYWORDS: saturated clay foundation, salinized soil, silt soil, liquefaction, bearing capacity of foundation

INTRODUCTION

With the rapid development of economy in China, the scale and range of expressway construction are increasing constantly, and the quantity of expressway built on saturated clay foundation is getting more and more. The main problems in the engineering constructed on the saturated clay foundation are the lower bearing capacity, larger deformation and stronger liquefaction when shocked by earthquakes (Lu 2004), (Ren et al. 2007), (Yasuda 1992), (Finn et al. 2002) which often can not meet the needs of project designing. Therefore, saturated clay foundation must be reinforced(Wu 2000), (Arulanandan 2000), (Martin1995). The Jingbian-Wangquanliang expressway passes through the saturated clay foundation at the southern edge of Mu Us Desert. It has important economic meaning and practice value to investigate the engineering geological properties of the saturated clay and to put forward the effective and economical measure for the treatment of the saturated clay foundation.

ENGINEERING GEOLOGICAL CONDITION

Geological Background

The engineered area of the expressway is located in the Ordos depression of the western part of north China

plate. The basement in the area is composed of Mesozoic monoclinical strata with little joints and faults and the surface is Quaternary sands and loess.

Topography and Geomorphology

The engineered area lies at the border between the loess plateau in the south and the Mu Us desert in the north. The north part is a flat terrain with sand dunes, salt meadows, sand beaches (Fig.1) and salt lakes. The south part is low loess hills with a mean elevation of 1200-1600 meters.

Hydrological Geology

The main rivers are Hongliu River and Lu River of the upstream of Wuding River in the east part of the area. Their discharge magnitude is very small, especially in the dry seasons. In summer, small lakes are often formed. However, they often get dry in winter and spring. Most of the perennial lakes are salt ponds.

As the area belongs to arid and semiarid monsoon climate, the climate varies greatly in four seasons. In winter, it is very cold and there is almost no snow due to the effect of Siberian cold air. When spring comes, cold and warm air appears subsequently, the temperature changes greatly between day and night. It is very common to form cold wave and frost along with heavy wind and sand storm. While in summer, it is hot and

¹ Professor, Department of Geological Engineering Chang'an University, Xi'an, China. Email: dcsusr@chd.edu.cn

rainy accompanied by drought and most of the rain is storm. In autumn, the temperature declines sharply, frost and flood happens frequently, and the temperature gap between day and night is large due to the effect of the desert.



Fig. 1 Sand beach

The main groundwater type in the area is phreatic water in Quaternary deposits. The groundwater level is about 10m at the higher part of the area, and about 0.5-3 m at the lowest part.

General Properties of the Strata

The main strata are low liquid limit clay and silt of Q_4^{al+pl} and Q_3^{al+pl} . Low liquid limit clay and silt of Q_4^{al+pl} show horizontal stratification, and contain humus. They are in semi-hard to hard plastic state above the groundwater level, have a relatively higher pore ratio and show collapsibility characteristic. Near and below the groundwater level, it is soft and in plastic flow state. Low liquid limit clay and silt of Q_3^{al+pl} mainly contain Fe-Mn nodules and a small amount of humus with horizontal stratification, and most of them are in the hard plastic state.

PHYSICAL PROPERTIES OF THE SATURATED CLAY FOUNDATION

In order to investigate the engineering geological properties of the saturated clay foundation, test work was done at four sections of the expressway, that is, K74+002 to K75+380, K104+300 to K105+960, K136+600 to K138+200 and K140+000 to K141+500. The statistics of the physical and mechanical index is shown in Table 1. The chemical properties of soluble salts for the saturated clay foundation are also investigated in the corresponding locations and the result is shown in Table 2.

Table 1 Statistics of the Physical and Mechanical Index

Index	Num	Max	Min	Mean Value	Standard Deviation
$\omega_0(\%)$	20	27.0	13.8	21.7	3.5
$\rho(g/cm^3)$	20	2.17	1.79	1.99	0.11
e	20	0.86	0.44	0.63	0.12
Sr(%)	20	100	55.2	90.2	13.3
$W_L(\%)$	20	27.9	20.1	23.9	1.98
$W_P(\%)$	20	19.9	15.5	17.1	1.3
I_P	20	8.8	3.9	7.1	1.2
$a_{1-2}(MPa)^{-1}$	19	0.33	0.05	0.18	0.07
$E_s(MPa)$	19	28.17	5.65	10.36	5.01
δ_s (0.2MPa)	19	0.014	0	0.003	0.004
C(MPa)	11	12.9	0	6.5	5.0
$\phi(^{\circ})$	11	38.95	25.9	31.9	3.24

Table 2 Result of chemical properties of soluble salts

Statistical index	Sample number	Max	Min
$Ca^{2+}(\%)$	22	0.051	0.004
$Mg^{2+}(\%)$	22	0.041	0.003
$K^+Na^+(\%)$	22	0.171	0.005
$SO_4^{2-}(\%)$	22	0.055	0.005
$Cl^-(\%)$	22	0.324	0.004
$HCO_3^-(\%)$	22	0.178	0.000
$SO_4^{2-}(\%)$	22	0.078	0.003
Salt content (%)	22	0.609	0.047
PH	22	10.4	9.0
Cl^-/SO_4^{2-}	22	5.89	0.80

From Table 1 and Table 2, it may be seen that, for the saturated clay foundation, the water content is between 13.8% and 27.0%, the liquid limit is between 20.1% and 28.1%, and water content is less than liquid limit. The pore ratio is 0.6 and the maximum is 0.860, the minimum is 0.443. The degree of saturation is between 55.2% and 100%, and its mean value is 90.2%, showing the feature of saturated soil. The compressibility factor is between 0.05 and $0.33MPa^{-1}$ showing relatively stronger variation. According to the compressibility factor, most part of saturated clay foundation does not have the characteristic of soft soil. The coefficient of collapsibility is relatively small, that is, the foundation does not have the collapsibility characteristic. Salt content in the saturated clay foundation is lower relatively with the maximum 0.609 %, and the minimum 0.047 %, showing characteristic of slight salinization. Most of the salinized soil is sulfite saline soil, and the other is chlorine saline soil.

The variation of shear strength of the saturated clay is relatively small, and its cohesion is 10kPa with the maximum 15kPa and the minimum 1.14kPa. The friction angle is about 30°, and its maximum is 38.95°, minimum is 20.5°. It is notice that the friction angle of the clay is related with the water content. The relationship between water content and friction angle are shown in Table 3. As shown in Table 3, when the degree of saturation (St) are the same or close, the larger the pore ratio (e) is, the larger the water content (W) is. However, the friction angle (ϕ) decrease with the increase of as water content, which indicate that the with the pore ratio increasing, the cohesive force of the soil is weakened, and the shear strength decrease.

LIQUEFACTION PROPERTIES OF THE SATURATED CLAY FOUNDATION

Macroscopic Judgment of Liquefaction Potential

The grain-size of soil samples from different locations is analyzed. Grain-size of the soil distributes between 0.25 and 0.074(Fig. 2) and shows strong heterogeneity, which indicates that the foundation are easier to produce liquefaction. Moreover, because most of the soils at the shallower depth are silt sand and silt soil which lie in relatively lower less-discharged terrain, such as meadow, beach, or salt lake, liquefaction is even much easy.

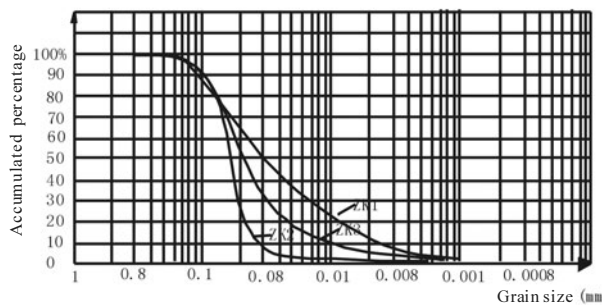


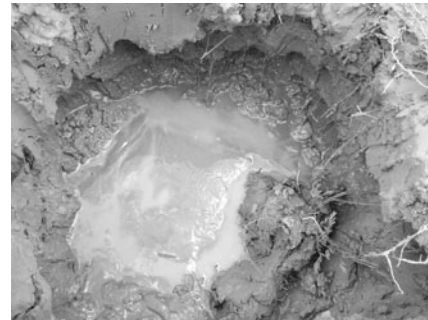
Fig. 2 Grain-size distribution curve of the soil

Fig. 3 shows the liquefaction process of a test pit. The soil in the pit starts to disintegrate after the pit is formed for several minutes, and the diameter of the hole expands gradually. The self-stability of the soil at the wall of the pit is quite poor and liquefaction is serious, therefore, it is difficult to form deep test pit. Fig. 3 also indicates that the burying depth of groundwater in the area is quite shallow.

As a whole, according to the preliminary judgment from the burying depth of groundwater, the discharge condition site liquefaction phenomena, liquefaction may be produced easily in the area.



a. Test pit is formed



b. Disintegration of the pit after three minutes



c. Twenty-four minutes after the pit is formed



d. Eighty-four minutes after the pit is formed

Fig. 3 Liquefaction process in a test pit

Microscopic Judgment of Liquefaction Potential

In order to further confirm the liquefaction characteristic of the saturated clay foundation, in-situ standard penetration test was done. Among the seven test

points, four points may produce liquefaction, and the depth of these easily-liquefied layer is less than 12m deep. Thus, the foundation clay at the depth less than 12 m is easier to produce liquefaction.

MECHANICAL PROPERTIES OF THE SATURATED CLAY FOUNDATION

Cone penetration test was done in typical locations of the saturated clay foundation in order to investigate mechanical properties of the bearing capacity of foundation. The result of cone penetration test is shown in Table 4. It could be seen that the specific penetration resistance is relatively small in the shallow strata. To gather the specific penetration resistance and bearing capacity of the foundation, empirical formula is used to calculate the bearing capacity of the soft foundation. It is found that the bearing capacity is quite small, it is less than 100kPa in the depth less than 3 m and less than 140kPa within the depth less than 5 m. Therefore, the foundation must be treated to satisfy the project designing requirement of road construction.

Table 4 Result of cone penetration test

Test point	Test depth(m)	specific penetration resistance PS(MPa)	Bearing capacity f ₀ (kPa)
1-1	0-2.9	0.8	80
	3-3.6	5.33	261
	3.7-4.9	1.17	94.8
1-2	5-6.6	3.95	206
	0-4.6	1.36	102
2-1	0-3.6	1.18	95.2
	3.7-4.8	2.18	135
2-2	0-2.9	0.71	76.4
	3-4.2	2.28	139
3-1	0-2.3	0.93	85.2
	2.4-3.5	2.23	137
3-2	0-2.8	1.07	91

CONCLUSIONS

(1) For the saturated clay foundation in the studied area, the water content is less than liquid limit, the mean value of saturation degree is 90.2%, the variation of the compressibility factor is large, and the variation of shear strength is low.

(2) The saturated clay foundation has salinization characteristic, but its salt content is lower, and most of the salt is sulfite saline soil, the other is chlorine saline soil.

(3) Liquefaction is serious and may occur easily at the depth less than 12 m.

(4) The bearing capacity is quite small in studied area, and the bearing capacity of foundation is less than 100 kPa in the depth less than 3m and less than 140 kPa within the depth less than 5m.

REFERENCES

- Arulanandan K, Li X, Sivathasan K (2000). Numerical simulation of liquefaction-induced deformations. *Geotechnique and Geoenvironment Engineering*, 7(126): 657- 666.
- Finn WDL & Fuiita N (2002). Piles in liquefiable soils: seismic analysis and design issues. *Soil Dynamics and Earthquake Engineering*, (22):731 - 742.
- Lu XB (2004). Liquefaction and Displacement of Saturated Sand under Water Pressure Oscillation. Beijing: Science Press, 23(19).
- Martin GR, Finn WDL, Seed HB (1975). Fundamentals of liquefaction under cyclic loading *Journal of the Geotechnical Engineering Division, ASCE*, 101(5): 423-438.
- Ren HM, Lu XL, Li PZ (2007). Advances in liquefaction research on saturated soils. *Journal of Earthquake Engineering and Engineering Vibration*, 27(6), 166-175.
- Yasuda S, Nagase H, Kiku H, et al. (1992). The mechanism and a simplified procedure for the analysis of permanent ground displacement due to liquefaction. *Soils and Foundations*, 32(1) : 149- 160.
- Wu SM (2000). *Soil Dynamics*. Beijing: Chinese Construction Industry Press.

GEOLOGY CONSIDERATION INFLUENTIAL IN URBAN DEVELOPMENT AND VULNERABILITY OF THE GORGAN REGION (NE IRAN)

Naser EBADATI¹, Ahmad ADIB² and Reza MAGSOODLORAD³

ABSTRACT: Investigation of the outcomes of natural disasters considering the regional situation of paramount importance, because of many of the requirements and necessities will be distinguished in advance and direct the trend of urban development in order to face the least possible risk in cause of critical situations. Gorgan is a ancient city in north east of Iran , although this region is located the distance from coastal ground of Caspian sea , but the many of region for urban development to place on grain size sediments and result geotectonic investigation show the much thickness of soils and sediment of grounds are kinds of SM, ML, CL group . Considering the potentiality to generate earthquake and ground water situation can to result. There are related phenomenon earth movement, landslide and liquefaction.

Loess sediments of Gorgan are the mayor deposit that covered in the most of area and geotechnic characteristic of loess caused to become more in fluent and natural disasters. The part events for example flood, slumping on slop are the mayor parts of Gorgan, that to develop city and industrial zone. Therefore recognition of vulnerable zones, are important, and the damages resulting from floods, slides is in a close relation with the population density the amount of investment infra structural affairs and level of city and in dustrial development of loess sediment areas. Consequently preventing from erosion of soil and controlling the deposits using establishment of structures along the foothills can be taken as preventive measures. The results of the studies indicate and rate of erosion has brought about unsuitable conditions in the region. the steep un stable geological layers have accelerated the erosion for estimating earth movement geomorphologic and geotechnic factors have been taken in to account and their relation with tectonic a activities and fault scarps have been recognized and indicate movements.(too long)

KEYWORDS: Gorgan region, loess, development, earth movement

INTRODUCTION

Golestan Province is about two million acres with latitude of 52,30' – 56,30' & longitude of 36,30' – 38,10'. Regarding topography , its altitude is around – 27 to 3750 m & due to this point , it has various climates and plants. The climates include cold, mountainous weather to dry and semi – dry one. The amount of rain in this area is around 150-800 mm. 27 percent of the area is located in mountainous or high zones (over %40 slope) and 20 percent of the area is in the middle steep (between 12-40 percent) and 53 percent is placed in plains (less than 12 percent steep) .

GEOALOGY OF THE AREA

The oldest and the newest formation of Geology can be seen in this area. Gorgan's schists are the oldest

formations of Geology in this area which in average their steepness is about 15-50 percent toward north. They have been affected by the tectonic movements and folding for several times and the above and bottom border are mostly the faults.

Loess one of the youngest formations that are seen as the hilly region in Geological maps in different areas & in southern part of Gorgan is the quaternary loess with no stratification. A low land of 100 km is seen from Bandar Torkaman to the east which has stretched from Gonbad knows along Gorganrood valley.

Main part of this area is covered by the sand wind sediments, regarding sedimentology, they are the clastic sediment which are left from the silt and sands, loess. Also from the beginning of Gorganrood River and far area from it there are lots of alluvial that are seemed to be like loess sediments and mostly have formed the farming lands; here one can say that there has happened

¹ Ph.D, Islamic Azad University, Islamshahr Branch, Iran. Email: drebadati@yahoo.com

² Ph.D, Islamic Azad University, South Tehran Branch , Iran. Email: dr_a_adib@yahoo.co.uk

³ M.S, Gorgan University

the river sediment forming by thick of 5-6 m along with mass movements of loess.

In different dies dispersions the thickness of loess sediments varies from 5 to 40 m. In the north part of Gorgan's holes the sediments have widespread which mostly include sandy loess sediments. Generally

Speaking, 20 percent of all lands & farms in Golestan province have been covered by loess sediments and weak formation.

The height of the loess sediments up to 400m from the sea level in southern Gorgan indicates that in the time of sediment forming, due to the old condition of dry forest climates, they went backward to this height and then the humid and wood covered climate has developed in the whole parts of the area. The brown horizons in various depths of the loess sediments confirm this issue.

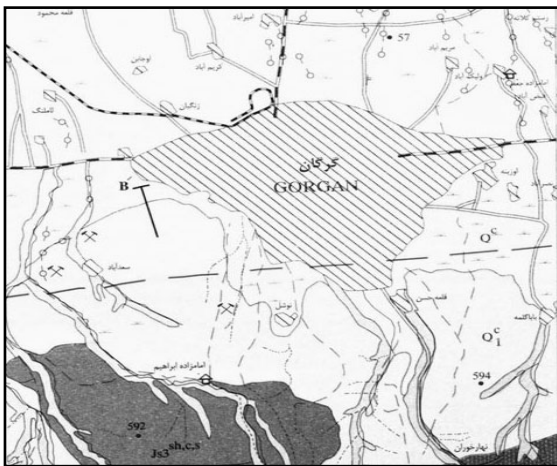


Fig. 1 Geological Map of Gorgan
Q₁^c: Loess Q₁^c: Quaternary sediment

The chemical and physical analysis along with age finding in the style of carbon 14 show that the loess sediments of Holocene period in Iran have been laid on loose Conglomerates material in result of a heavy rain period. The pedology of this era indicates humid, warm climate and in general the soils belong to three period warm & humid climates that are interrupted by 4 periods of warm and dry climates together with loess sediments (pashayee, 1996). In the lands of Gorgan & the plain, the chronology of the civils states a civilization in 3800 B.C. and in different times many residential parts for human being have been established here and more than 300 ancient hills in various areas to Torkmanestan farms have been recognized.

The function of young faults has caused some cuts in southern rivers in Gorgan & Gonbad which in Gonbad in the altitude of 30-50 m, the loess and folder travertine are recognizable. Also toward the southern & south western parts of the area to Behshahr & Neka the folding faults can be seen and that is the sign of over thrust &

other pressing forms. Along with the Alborz tectonic lineation toward East, the right – turning movements is recognizable .Following is the most action fault land.

NORTHERN ALBORZ FAULT

As pointed out , this fault is one of the most active ones in the area and in a form of reverse fault has spread from Aliabad in Gorgan to near Tonekabon. With steepness toward south Eastern is till south western. Regarding the fact that centers of several earthquakes have been located in this fault in recent times & in twenty century especially. This fault is considered to be one of the quaking faults.

Reverse faults of Minoodasht and Moravehtappeh. These faults have stretched along the North Eastern part of the northern Alborz fault to the border of Iran Torkmanestan. They have main role in earthquakes of the history and especially in 20th century in Gorgan. The center point of the earthquakes is in South Easterpart of intersection of Robatgharehbill faults, Minoodasht and Moraveh tappeh fault.

KHAZAR & BEHSHAR FAULT

These faults are placed from Lahijan fault to Gorgan southern parts in a length of 210 km. The destructive earthquakes of the history have taken place in this region and probably they have been due to activity of part of Khazar fault. Additionally the North Eastern – South Western Behshahr fault has caused several destruction earthquakes in cities like Behshahr, Sary, Babol & etc.

GORGAN FAULT

This fault is a thrust one in the direction of East – West crossing Northern Gorgan. Disastrous earthquakes in Gorgan have been related to the activity of this fault or to the intersection of Minoodasht and Northern Alborz faults. Therefore special attention should be paid to the server movements of the earth in this area due to quaking aptitude of the zone. On the other hand, Geological feature of the area that was pointed out before are somehow certain about the non – liner movement of soil, looseness and various quakes in several regions.

The presence of alluvial sediments, sandy loess, clay middle layers , high level of mineral water , heavy amount of rain have put the area in danger of earthquake and continues earth movements .

The pervious earthquake in Gorgan region can be considered from two view points. The earthquakes happened due to materials weight, their transportation in

result of pressure of water and instability of the steeps and those slides taken place with regard to the kind of the earth influenced during earthquake or after that.

The amount of cracks and cuts in steepy layers of loose & loessy grounds will increase fact in result of amount of annual rain up to 800 mml & sudden heavy rains in special seasons.

- In lower borders, the soft & sandy sediments together with older & firm formations (regarding the level of mineral water) may cause the incident of slumping and slide with thickness of around 5-10 m and generally may affect the wind sediments.

- Close or change on the way of streams sub-layer gullies in steeps may happen in result of earthquakes and therefore in the next rains they might increase the pressure of pores.

- cutting layers would come up in steepy masses due to earthquakes. This will cause break in many weaker surfaces at the time of earthquake.

- Constructing buildings in loess areas with unsmooth and steepy ground may cause destruction & increase in chance of slide at the end of growth and spread of waste to the mass of soil. One of these slides happened in Mohtasham in Gorgan in (2006).

GEOTECHNICAL FEATURES

As pointed out, part of Gorgan & its neighboring towns and areas have been built on loess sediments & loose grounds. Instability of the natural & artificial steeps has caused great loss in finance and lives of people during these years.

Due to poor construction and weak cement of these formation, the resistance of soil and sediments in the area in the manipulated from is much less than the natural form. Sometimes in natural forms.

However, these high and sharp steeps would start to slide due to overcoming the factor of motivation.

That is the result of plants roots decay together with the initial fabric and construction is considered to be the weak point of these soils.

The stability of the foothills is mostly based on the kind and litological features , for instance , the foothill that are made of vapping & clay Minerals would be less stable because of the process of dissolution, Swell ability and their impenetrable ability to Mass of water.

The factors like earthquake. Increase in sediment, weight, streams washing the foothills & the loading growth of foothills in residential areas will boost the danger of earth drive. Research shows that the layer of the natural cut of ground and holes in various areas & the under construction wells indicate the high stability of these sediment & the non-continuity of tectonic like joint and fault in layer of earth are indistinguishable.

In North Eastern part of the area, regarding the development of this kind of sediment, field analysis and the sampling show that the main kind of soil here includes CL, ML or CL-ML & in Northern parts of the lone they have mainly SM.

The dry special weight of the samples varies around 1.35 to 1.55 KN / M3 and the special density of Mass soil GS varies about 2.4 to 2.6.

The more we go toward south and southwestern , the smaller the of sediments would be and in Northern part and in ending areas of Iran- Torkamanestan border the amount of sandy and silty grains will in crease .

In regard of the change in temperature and Topographical conditions of the lone, depth of ice here would be around 50-60 CM.

Geotechnical analysis in loessy areas state that the kind of earth here is of III to IV type (Iran’s standard 2008) that is for designing the buildings against the earthquakes, TS, 0.7 and, S is equal to 1.75.

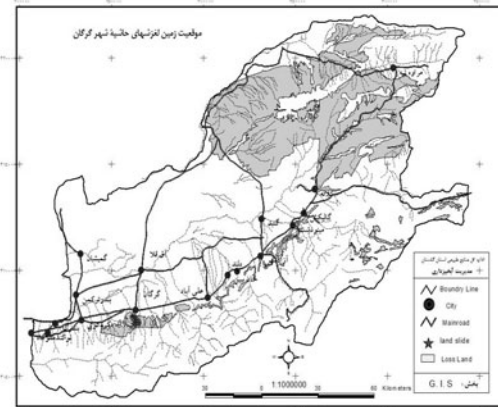


Fig. 2 Distribution of land slides and loess in region

Ascribing to what has Mentioned above , one can say that Sedimental and Geotechnical features of the earth that are called as geological influences are high in intensifying the movement and slide of the ground that is caused by local conditions. Based on categories (Midorikava–1987) the damping coefficient is around 2-3.

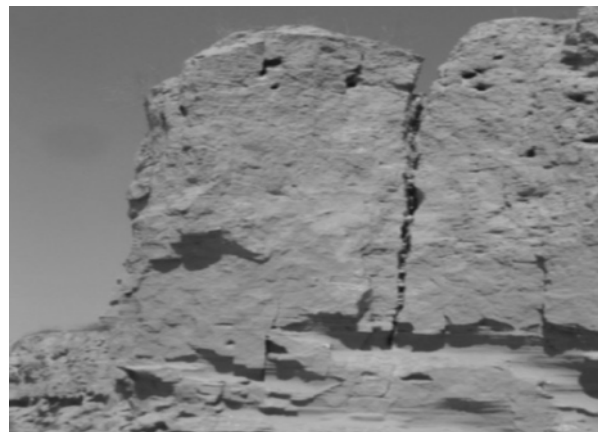


Fig. 3 Cut of loess sediments



(a)



(b)

Fig. 4 Sample of land slides

CONCLUSION

Generally 20% of the land in Golestan province is

covered by loess and clay sediments which are somehow high in this regard. Unfortunately a main part of the residential area of this province is based on this land. Therefore, the hazard will increase. So firstly, designing civil development should be seriously cared about due to highly destructive feature of them on loose and irresistible lands. Secondly, regarding the changes in topographical steeps, the slide zonation and gravity movement of mass of soil in this area are probable. Thirdly, the status of seismo tectonic of the area shows the high rate of quakability and acceleration of earth slides in the time of earthquake. Earth slides in the time of earthquakes are considered to be one of the greatest disasters of the area and it is suggested that in the future researches the complete and precise studies be done on seismic geotechninc zonation for important projects.

REFERENCES

- Berberian M & Yeats R (2001). contribution of archeological data of earthquakes history in Iranian plateau , *Journal of Structural Geology* , 23: 563-584.
- Bronger A, winter R, Heinkele T (1998). Pleistocene climatic history of East and central Asia based on paleopedo logical, indicators in loess–paleosol sequences, *catena*, 34: 1-17.
- Jackson J & Mckenzie D (1984). Active Tectonic of the Alpine- Himalayan Belt BiTween western turkey and Pakistan, *Geophy, J, R, Astr*, 11: 185-264.
- Komak panah A, Montazer ghaem S, chodani A (1992). Landslide Hazard Zonation in Iran, *landslides and a Review on landslides in Iran. IIEES pub. No, 73-94-5, Iran*, p. 65.
- Mirmohammad Hoseini S, Arefpour B, Ghassemi A (1999) . *Manual for zonation on seismic geotechnical Hazards.* Pub: IIEES, No 99-98-1, Iran, 172.

PROTECTION TECHNOLOGY AND APPLICATIONS OF GABION

Guo-Lin YANG¹, Zhe-Zhe LIU², Gui-Lin XU³ and Xiang-Jing HUANG⁴

ABSTRACT: A gabion is a box-shaped container filled with soil or rock which can be used to prevent soil erosion and keep slope stable. New material and modern manufacturing technology revitalize gabion type structure which has a long history. The use of gabion type system is nowadays a common practice which enables engineers to provide effective protections to a wide range of structures. An overview of some applications of the gabion type system is presented in this paper, as well as several engineering examples, in order to highlight the main advantages of this system, together with their functional characteristics.

KEYWORDS: gabion, mattress, flexibility, eco-friendly structure

INTRODUCTION

A gabion is a rectangular, columniform or mattress-shaped container filled with soil or rock which can be used to protect bank or build retaining wall (Fig. 1). Gabions have been used for several millennia in Egypt and China. But for a long time, gabions were constructed with plant materials, which severely limited their useful life. In about 1879, a firm in Italy is thought to have first used wire mesh in the construction of gabion baskets (Freeman et al. 2000). Since then, gabions have experienced much progress by taking advantage of modern technology.

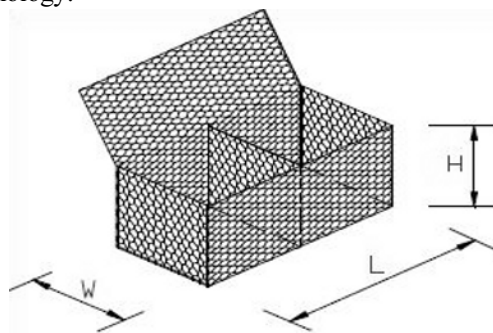


Fig. 1 Gabion basket unit

MATERIAL OF GABION

The gabion discussed in this paper is flexible cage made of hexagonally woven double twisted wire mesh.

The welded diamond mesh gabion is beyond the scope of this paper as it is of such inferior strength and flexibility.

The wire diameter varies but it is typically 2.7 or 3.0 mm (2.2 mm for mattresses) and presents an anti-corrosion treatment based on a Zn-Al alloy, whose durability characteristics are higher than the traditional heavy zinc coating. The plastic coating, originally Polyvinyl Chloride (PVC), has been recently converted to a cross-linked polyethylene (XLPE), with higher mechanical characteristics and longer life. The diameter of XLPE protected wires is 2.7/3.7 mm (2.2/3.2 mm for mattresses), guaranteeing therefore a good mechanical resistance (Vicari et al. 2002). According to the requirement of BS1052: 1980(1986), the tensile strength of the steel wire should be in the range of 380~500Mpa and the minimum elongation rate at failure should be 12%. The double twisted hexagonally woven mesh configuration ensures that the force can be distributed evenly to the steel wire and if one wire was to accidentally break, the mesh would not unravel (Fig. 2)(Maccaferri China Pty Ltd).

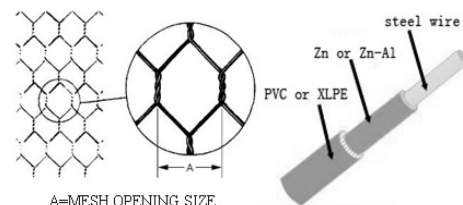


Fig. 2 Details of hexagonal mesh and coated steel wire

¹ Professor, Department of Civil Engineering and Architecture, Central South University, China. Email: yangguolin6301@163.com

² M.E, Department of Civil Engineering and Architecture, Central South University, China. Email: asukazhezhe@126.com

³ M.E, Department of Civil Engineering and Architecture, Central South University, China. Email: xuguilin606@163.com

⁴ Ph.D, Design Institute of Traffic Planning and Survey of Hunan Province, China. Email: hncshxj@163.com

FILL FOR GABION

The rock fill should be clean, hard and not show any sign of weathering as well as not disintegrate on exposure to water during service life. It should be evenly graded, be angular to provide interlock and have a specific gravity (SG) of at least $2.4t/m^3$. Rock with an SG less than $2.4t/m^3$ can be used, provided further stability analyses and weathering tests are carried out. The rock shall be large enough to prevent individual pieces from passing through the mesh opening. A rock fill size between 1.5D to 3D is recommended to limit the void ratio and maximize productivity (Chaychuk 2005). In all cases the rock sizes shall allow for the placement of three or more layers of rock within the each gabion compartment and two or more layers of rock within each mattress compartment (Vicari et al. 2002).

WORKING PRINCIPLE OF GABION SYSTEM

Flexible gabion type protection acts as one monolithic homogeneous structure as it was made of granular material fastened (laced) by woven steel wire mesh. The gabion strength comes from a double twisted hexagonal mesh of steel wire which is reinforced by selvages of heavier wire running along the edges and by transverse diaphragms. The double twisted wire will not unravel, even when cut. This system can utilize the weight of the granular material as well as the characteristic of high strength and flexibility of woven wire mesh.

ADVANTAGES OF GABION SYSTEM

There are many advantages of the gabion type system over conventional protections that make it an appealing solution to prevent soil erosion and keep slope stable.

Durable Structures

The durability of the gabion type system depends to a great extent on the durability of the wire mesh. The present technology of zinc coated plus the external revetment with a PVC or XLPE coating guarantee the durability of gabion type structure. Galfan (Zn-5% Al-MM) coated reno mattress produced by Maccaferri has been certified by independent international body BBA to offer a design life of over 60 years and when plus PVC the design life extends to 120 years.

Flexible and Monolithic Structures

Gabions and Reno mattresses easily accommodate curves, transitions and abrupt changes of direction. If

required, they may be cut on site to fit into existing structures. Gabion walls may include woven mesh reinforcement extending from the rear wall face into fill to create a soil reinforced structure significantly reducing the cost of traditional gravity gabion walls.

The fastening procedure ensures units acts as one monolithic homogeneous structure. The same cannot be said for loosely placed rock armour where each rock acts individually and therefore needs to be excessively large.

Permeable Structures

Rigid (semi-rigid) structure such as precast concrete plate and cast-in-place concrete plate is always impermeable (semi-impermeable). Once local water erosion damage occurred, the scope of damage would expand ceaselessly, even result in the failure of whole structure. In contrary, the gabion type structure are approximately 30% voided, pore water pressures are easily dissipated through the structure without build up of hydrostatic pressures (Chaychuk 2005). This inherent benefit ensures that the natural banks are not isolated from the river.

Convenient and Economical Structures

Gabions and Reno mattresses are ease of installation in any environment, without the aid of specialized equipment or personnel, reducing costs. Future modification of the structure is straightforward; e.g. new layers can be installed to increase the height of the structure (provided structural stability is verified). Gabion structures also have the benefits of immediate performance following installation and ease of maintenance.

Eco-friendly Structures

Special gabion units are available that allow filling at the front face with soils to provide a vegetated solution to slope stabilization. The opportunity to combine live plants with a high sound absorption capability, make gabion structures ideal solutions to balance engineering and environmental needs (Maccaferri Pty Ltd 2003).

APPLICATIONS OF GABION

In the past more than one hundred years, hexagonally woven double twisted wire mesh has been used in civil engineering and hydraulic engineering successfully.

Retaining Structures

Soil subjected to dynamic or static loading must be stabilized to ensure equilibrium of the surrounding

environment. When soil is confined or loaded, distributing forces are set up that may give rise to sliding, overturning and bearing failures. To withstand these effects, retaining structures may be required. Tried and tested for well over a century, traditional rock filled wire mesh gabions remain one of the most economical ways to construct gravity retaining structures. Fig. 3 shows that a fill slope retaining wall was constructed in 1974 to supporting a railroad embankment at Coalcliff, near Sydney. The structure has a maximum height of 6.50 m and it is built of PVC coated gabions. More than thirty years after its completion it still appears in good conditions (Maccaferri Pty Ltd 2008).



Fig. 3 Gabion retaining wall

Hydraulic Structures

Management of catchment areas requires protection and stabilization of riverbanks, reducing erosion of slopes, conveyance of water around infrastructure in a controlled manner and the protection of human settlements from the impact of floods.

Longitudinal structures

Constructed parallel to a watercourse, longitudinal structures correct and control the flow of water preventing flooding of towns and cities, and erosion of stream beds and edges of banks. Fig. 4 presents a bank protection structure of a 2 m high gabion structure resting on a 300 mm thick Reno mattress spanning a total length of 160 m (Maccaferri SA Pty Ltd 2007 a).

Gabion or reno mattress units can be made in a wide range of sizes and weights and may be placed in accordance with the shape of the bank or streambed. The main characteristic of gabions and reno mattresses is their capability to remain flexible even in low temperatures, thus being able to constantly mould itself to the bank or streambed modifications.

Groynes

Gabion groynes are purpose built structures used for the protection and recouping of eroded banks by

deflecting the flow in a watercourse away from the bank. Groynes, constructed some distance into the watercourse perpendicular to the direction of flow, create and form a series of backwater zones that allows for the deposition of the sediment (Fig. 5). Anchored into the bank, gabions and Reno mattresses are ideal products for these types of structures where construction is in phases and, in most cases, in water.



Fig. 4 Gabion & reno mattress longitudinal structure



Fig. 5 Gabion groyne

Culverts

Structures built from double twist hexagonal wire mesh gabions and reno mattresses are a valid and effective technical solution in the design and maintenance of culverts and low-level river crossings (Fig. 6) (Maccaferri SA Pty Ltd 2007 b).



Fig. 6 Reno mattress culvert

In inlet works it is necessary to guide the flows into the culvert, thus avoiding dangerous uncontained flows. In restoration work, one should be aware of erosion of riverbeds and banks which may undermine the structure. In the case of deeply cut watercourses, it is advisable to create structures capable of both containment and support. When the riverbed is not well defined it is good practice to extend the wing walls of the culverts to protect the flanks.

Dams and spillways

Overflow spillways are constructed as part of embankment dams. The spillway section is lower than the other sections of the dam allowing water to flow over its top and down its front face when the storage capacity of the dam is reached (Fig. 7) (Chaychuk 2008).



Fig. 7 Gabion spillway

Due to the steepness of the embankment slopes or the poor limit velocities of the bed material, severe erosion can take place. Reno mattresses or gabion cascade structures are effective ways of reducing those velocities and therefore limiting erosion.

Bridge protection

Erosion at the foot of the bridge foundations is a serious problem in road engineering. Bridge abutments and bridge piers often collapse as a consequence of scour around and under the foundation from the erosive power of flowing water. Gabions and Reno mattresses provide the ideal protection to the foundation of the piers and abutments and the terrain around the bridge structure. In remote areas, gabions themselves can be used to support the bridge deck structure (Fig. 8) (Maccaferri SA Pty Ltd 2007 c).

Marinas

Marinas, moorings and small ports demand well thought out construction processes due to the presence of continual flow and wave action. Pre-filled gabions and

mattresses, which are easily placed in the presence of water, constitute an excellent solution when compared to the more traditional approach, as they are able to function immediately upon placement. Moreover, they are able to accommodate changing field conditions, differential settlements and consolidation without cracking.



Fig. 8 Gabion bridge pier protection

Thesen Islands development is an ambitious and technically complicated project where the 960,000 m² Thesen Island is master planned into an estate of 19 islands surrounded by wide tidal waterways linked by bridges (Fig. 9). Seventeen kilometers of pristine water front property needed to be protected in the most environmentally friendly way possible against the erosive forces of fluctuating tide levels and associated wave action to ensure that the islands were developed in harmony with the Knysna Estuary environment.



Fig. 9 Aerial view of Thesen Islands

Gabion and Reno mattress combinations were selected as the most appropriate solution because of their flexibility to meet with the geometrical constraints of the canal embankments, durability under harsh marine environments and ability to lend themselves favorably to environmental rehabilitation (Maccaferri SA Pty Ltd 2007 d).

Coastal Protection

Coastal environments are subject to aggressive hydraulic forces generated from tidal and wave action. Erosion energy in the coastal and estuarial environment is substantially greater than that encountered inland. Coastal vegetation and sand dunes are continually being eroded by natural forces and human activity.

The recovery and protection of coastal zones and beaches necessitate versatile structures that are easily constructed and able to resist the constant dynamic forces resulting from wave action. Traditionally, layers of large stone or riprap have been used for coastal protection as they provide a rough surface to dissipate erosion energy. Encapsulating stones within gabions or mattresses thereby stopping it moving, increases the resistance of the revetment, and is a more efficient use of stone (Fig. 10). Encapsulated stone mattresses also often have added ecological value.



Fig. 10 Gabion coastal protection

There are also Longitudinal structures, like groyne, in the form of gabions and mattresses. Groynes are a series of structures built perpendicular to the beach to protect and recoup the eroded shore. These structures, anchored into the bank are constructed some distance into the sea, transversely to the current direction.

CONCLUSION

This paper has briefly introduced gabion type system and presented some applications of it. There are many advantages of gabion type system over conventional protections that make it an appealing solution to prevent soil erosion and keep slope stable. Gabion system has a broad developing prospect as an important protection technology. Thus the material of gabion as well as coating should be improved and the working mechanism is worthy to be further studied.

REFERENCES

- British Board of Agrément (1995). Maccaferri hexagonal mesh for civil engineering [DB/OL]. http://www.bbacerts.co.uk/PDF/3141i2_web.pdf. 199 5-06-30.
- BS1052 (1980). Specification for mild steel wire for general engineering purposes [S].
- Dale Chaychuk (2005). The Use of Gabions and Reno Mattresses in River and Stream Rehabilitation. [EB/OL].
- Dale Chaychuk (2008). Dam Spillway Protection [EB/OL]. <http://www.maccaferri.com.au/webfiles/MaccaferriAu/files/CS-ArmidaleFarm-DamSpillway.pdf>
- Gary E Freeman & Craig Fischenich (2000). Gabions for Streambank Erosion Control [DB/OL]. <http://www.stormingmedia.us/30/3048/A304873.htm> 1. 2000-05.
- Maccaferri China (Pty) Ltd. Maccaferri solutions [EB/OL]. <http://www.maccaferri-china.com/maccaferri%20solutions.pdf>. (in Chinese). www.maccaferri.com.au/webfiles/MaccaferriAu/files/SIAPaper_Final_Rev.pdf. 2005-04-21.
- Maccaferri Pty Ltd (2003). Road Works-Problems and Solutions-Gravity Earth Retaining Structure [EB/OL]. http://www.maccaferri.com.au/webfiles/MaccaferriAu/files/Gravity_Earth_Retaining_Structures-Brochure_2003-AUS.pdf.
- Maccaferri SA (Pty) Ltd (2007 a). Inkongweni River Bank Protection [EB/OL]. <http://www.africangabions.co.za/files/casehistory/ZAF-CH-019-InkongweniRiver-Eng-Rev03.pdf>
- Maccaferri SA (Pty) Ltd (2007 b). Drie Bruddies. [EB/OL]. <http://www.africangabions.co.za/files/casehistory/ZAF-CH-035-InkongweniRiver-Eng-Rev03.pdf>
- Maccaferri SA (Pty) Ltd (2007 c). Gabions for Erosion Control [EB/OL]. <http://www.africangabions.co.za/files/casehistory/ZAF-CH-036-InkongweniRiver-Eng-Rev03.pdf>
- Maccaferri SA (Pty) Ltd (2007 d). Thesen Island Marina [EB/OL]. <http://www.africangabions.co.za/files/casehistory/ZAF-CH-015-Thesen-Eng-Rev03.pdf>. 2007-11-03.
- Maccaferri Pty Ltd (2008). Coalcliff Gabion Wall [EB/OL]. <http://www.maccaferri.com.au/webfiles/MaccaferriAu/files/CS-Coalcliff-GabionWalls.pdf>. 2008-02-20.
- Marco Vicari, Massimo Branzanti (2002). Bituminous mattresses and plastified gabions for the protection and ballasting of sealines and outfalls: case histories and applications [M/CD]. "MWWD Collection" DVD (ISBN 9944-5566-1-0).

A PARAMETRIC STUDY ON EVALUATION OF STABILITY OF COLUMN TYPE DM IMPROVED GROUND

Masaki KITAZUME¹

ABSTRACT: The deep mixing method, an in-situ soil stabilization technique using cement and/or lime as a binder, is often applied to improve soft ground. The group column type improvement is extensively applied to stabilize foundation of embankment or lightweight structure. An improved ground design method is established in Japan mainly for reinforcing embankment, in which two failure patterns related to external and internal stabilities are assumed. The author conducted a research project on the failure mechanism and stability of the group column type improved ground subjected to embankment loading. The project involves investigating the failure criteria of two stabilities and the failure mode related to the external and internal stability. These studies have revealed that the current design method may overestimate the stability of improved ground because inadequate failure modes are assumed. However, as far as the author knows, there have been few cases recorded of serious failure or large deformation in the group column type improved ground under embankment loading. This is a discrepancy against the overestimation in the current design method. In this paper, a parametric calculation on evaluation of the stability of column type DM improved ground was carried out to investigate the characteristics of the current and the proposed design methods.

KEYWORDS: deep mixing soil stabilization, design, deformation, embankment, failure, soft ground, stability

INTRODUCTION

The deep mixing method (DMM), an in-situ soil stabilization technique using cement and/or lime as a binder, is often applied to improve soft soils in Japan and foreign countries (Coastal Development Institute of Technology, 2002). A group column type improvement is extensively applied to stabilize foundation of embankment or lightweight structure. An improved ground design method is established in Japan based on a composite ground concept mainly for reinforcing embankment (Public Works Research Center, 2004), in which two failure patterns related to external and internal stabilities are assumed. For the external stability, the possibility of sliding failure mode is evaluated, in which the DM columns and the clay between are assumed to show horizontal displacement on a stiff layer without any rearrangement of columns. For the internal stability, the possibility of rupture breaking failure is evaluated by a slip circle analysis.

The author conducted a research project on the failure mechanism and stability of group column type improved ground subjected to embankment loading. The project involves investigating the failure criteria of two stabilities and the failure mode related to the external and internal stabilities. Based on the researches, three

more failure modes and criteria are proposed and compared with centrifuge model tests and FEM analyses (Kitazume and Maruyama, 2006 and 2007). These studies have revealed that the current design method may overestimate the stability of improved ground because inadequate failure modes are assumed.

In this paper, a parametric calculation on evaluation of the stability of column type DM improved ground was carried out to investigate the characteristics of the current and the proposed design methods.

FAILURE MODES ASSUMED

In the current design method, two failure modes are assumed: sliding failure mode in external stability and slip circle failure mode in internal stability (PWRI, 2004). In the sliding failure mode, the DM columns and the clay between are assumed to show horizontal displacement on a stiff layer without any rearrangement of columns. In the slip circle failure mode, the improved ground consisted of the DM columns and the clay layer is assumed as a composite ground and to fail with circle shaped failure plane. The stability is evaluated by the slip circle analysis with an average shear strength of the improved ground.

¹ Distinguish Researcher, Port and Airport Research Institute, Japan. Email:kitazume@pari.go.jp

In the researches (Kitazume and Maruyama, 2006 and 2007), three more failure modes were proposed: collapse failure mode in the external stability and shear failure and bending failure modes in the internal stability. In the collapse failure mode, the DM columns and the clay between are assumed to deform as simple shear due to the imbalance between active and passive earth pressures acting on the side boundaries of the improved area. In the shear failure mode, the DM columns and the clay between are assumed to be sheared along a horizontal plane. In the bending failure mode, the improved area above an assumed failure plane are assumed to deform as simple shear.

CHARACTERISTICS OF DESIGN METHOD

Ground Condition Studied

A trapezoid shape embankment on the column type DMM ground is studied for the current and the proposed design procedures, as shown in Fig. 1. The ground condition here is referenced in the design manual on DMM (PWRI, 2004), and their soil properties are summarized in Table 1 (Kitazume, 2008).

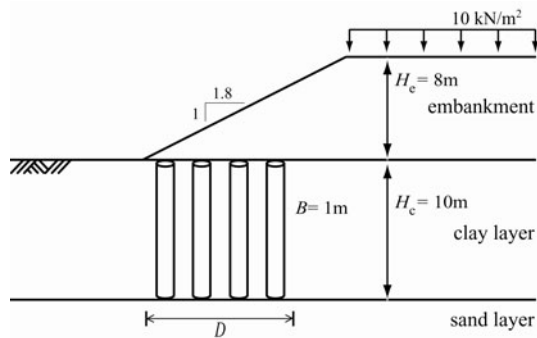


Fig. 1 Ground condition studied

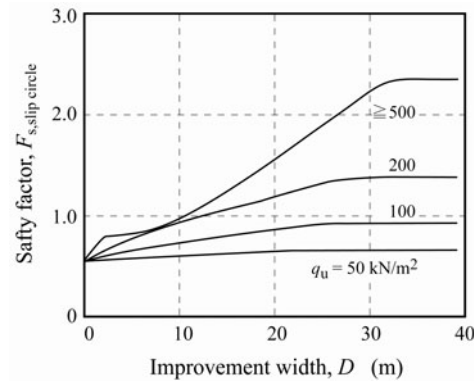
Table 1 Soil properties of ground

Embankment	
Unit weight, γ	14 kN/m ³
Internal friction angle, ϕ	30
Clay layer	
Unit weight, γ	4 kN/m ³
Shear strength profile	10 + 1.5 z kN/m ²
Strength increment ratio, c_u/p	0.3
Sand layer	
Unit weight, γ	9 kN/m ³
Internal friction angle, ϕ	35
DM column	
Unit weight, γ	9 kN/m ³
Diameter, B	1 m
Strength ratio, σ'_v/q_u	0.28
Improvement area ratio, a_s	50%

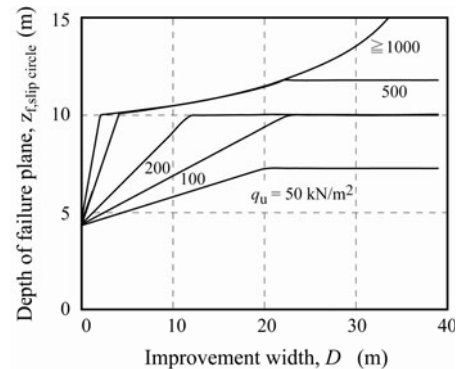
Characteristics of Slip Circle Analysis

A series of slip circle analyses was carried out to investigate the effect of column strength, $q_{u,column}$, and the improvement width, D , for the improvement area ratio, a_s , of 50%. The calculated safety factor, $F_{s,slip\ circle}$, is plotted along D in Fig. 2(a). In the case of $q_{u,column}$ of 50 kN/m², $F_{s,slip\ circle}$ increases slightly with increasing D and reaches a constant value at D of about 25 m. A similar phenomenon can be seen in the cases of $q_{u,column}$ of 100 and 200 kN/m². In the case of $q_{u,column}$ of 500 kN/m², on the other hand, $F_{s,slip\ circle}$ climbs very quickly at D of about 2 m, and then increases gradually with increasing D to a constant value. The same relationship is found in the case of $q_{u,column}$ higher than 500 kN/m².

The depth of failure plane, $z_{f,slip\ circle}$, where the slip circle passes, is plotted in Fig. 2(b) for various $q_{u,column}$. The $z_{f,slip\ circle}$ for $q_{u,column}$ of 50 kN/m² increases linearly with increasing D to a constant value of 7.4 m, which means that the slip circle always passes through the improved area. A similar phenomenon can be seen for $q_{u,column}$ of 100 and 200 kN/m², while the slip circle passes underneath the improved area for a large D value.



(a) Improvement width and $F_{s,slip\ circle}$



(b) Improvement width and depth of failure plane

Fig. 2 Slip circle analyses (a_s of 50%)

In the case of $q_{u,column}$ of 500 kN/m² or higher, $z_{f,slip\ circle}$ continuously increases with increasing D , which indicates that the size of slip circle increases with

increasing D and passes underneath the improved area.

Another slip circle calculations were carried out changing a_s and $q_{u,column}$. $F_{s,slip\ circle}$ almost coincides and increases with increasing the average undrained shear strength of the improved area at its bottom, $c_{u,ave}$, to a constant value of about 150 kN/m^2 irrespective of the combination of a_s and $q_{u,column}$. This value is almost of the same order as the shear strength mobilized in the bottom sand layer, $\sigma_v * \tan \phi_s$, where σ_v is the vertical stress on the sand layer and ϕ_s is the internal friction angle of the sand layer. This clearly shows that the slip circle passes through the improved area as long as the average shear strength of the improved area is lower than the shear strength mobilized in the sand layer. The column strength in a field is highly dependent upon the type and amount of binder to be mixed with the soil. The general Japanese practice is to set the design column strength as 400 to 500 kN/m^2 to assure uniformity in column strength. The magnitude of a_s is usually set as 50% or higher. As $c_{u,ave}$ is about 200 kN/m^2 or higher, it can be concluded that the slip circle does not pass through the improved area but through the sand layer under practical conditions. This indicates that the slip circle analysis in the current design procedure for evaluating internal stability practically evaluates the sliding failure mode in the external stability. In many cases, column strength is not determined by the slip circle analysis.

Characteristics of Sliding, Collapse, Shear and Bending Failure Modes and Comparison to Slip Circle Analysis

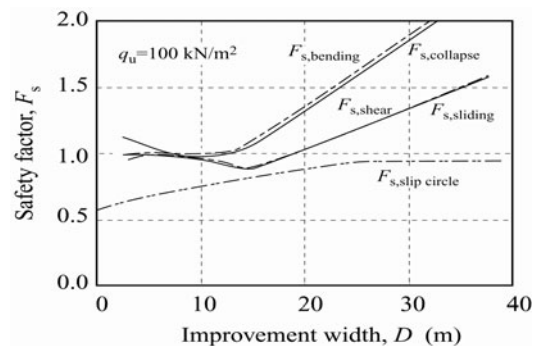
In investigating the sliding, collapse, shear and bending failure modes, the active earth pressure of the embankment is calculated by the Coulomb theory in which the maximum earth pressure is obtained by changing the assumed slip line passing through the embankment. Here, two parameters, column strength and improvement area ratio on the stability of the improved ground are investigated.

Effect of column strength

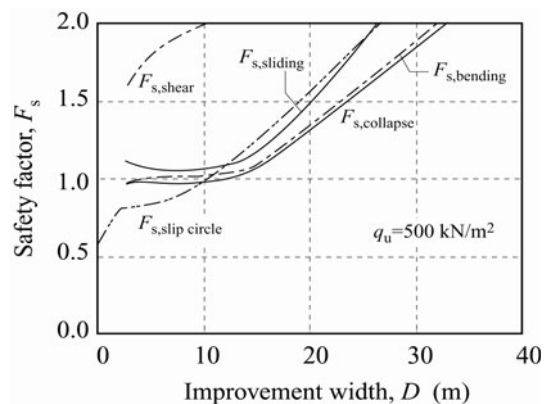
Fig. 3 shows the relationship between the improvement width, D , and safety factors for column strength, $q_{u,column}$, of 100 and 500 kN/m^2 in the case of improvement area ratio, a_s , of 50% and stress concentration ratio, n , of 3 . In the case of $q_{u,column}$ of 100 kN/m^2 , Fig. 3(a), the safety factor for the sliding failure mode, $F_{s,sliding}$, and the shear failure mode, $F_{s,shear}$, almost coincide, and that for the collapse failure mode, $F_{s,collapse}$, and bending failure mode, $F_{s,bending}$, also almost coincide. $F_{s,sliding}$ and $F_{s,shear}$ decrease gradually and $F_{s,collapse}$ and $F_{s,bending}$ remain almost constant when D is smaller than about 15 m , because the active earth pressure acting on the improved area increases with the increase in embankment height

with increasing D . However, when D exceeds about 15 m , all the safety factors increase linearly with increasing D . $F_{s,sliding}$ and $F_{s,shear}$ are lower than $F_{s,collapse}$ and $F_{s,bending}$ when D is larger than about 10 m . This indicates that the improved ground fails either by sliding or shear failure mode rather than by collapse or bending failure mode. As the depth of failure plane for the shear failure mode is 10 m at the bottom of the improved area, as later shown in Fig. 4(a), it can be concluded that the sliding failure mode takes place instead of the shear failure mode. In the figure, $F_{s,slip\ circle}$ is also plotted. $F_{s,slip\ circle}$ increases almost linearly with increasing D , but $F_{s,slip\ circle}$ reaches a constant value at D of about 30 m .

As $q_{u,column}$ increases, the magnitude of $F_{s,sliding}$ and $F_{s,shear}$ becomes higher. However, the magnitude of $F_{s,collapse}$ and $F_{s,bending}$ remains constant irrespective of D . In the case of $q_{u,column}$ of 500 kN/m^2 , Fig. 3(b), $F_{s,collapse}$ and $F_{s,bending}$ almost coincide and are more or less higher than $F_{s,sliding}$. However, $F_{s,shear}$ is considerably higher than the other three, a result of the role played by the shear strength of columns, F_{rf} . As later shown in Fig. 4(b), the failure depth for the bending failure mode is 10 m . These findings indicate that the improved ground fails by collapse failure mode. $F_{s,slip\ circle}$ continuously increases with increasing D , which is quite a different phenomenon from that described in Fig. 3(a).



(a) $q_{u,column}$ of 100 kN/m^2



(b) $q_{u,column}$ of 500 kN/m^2

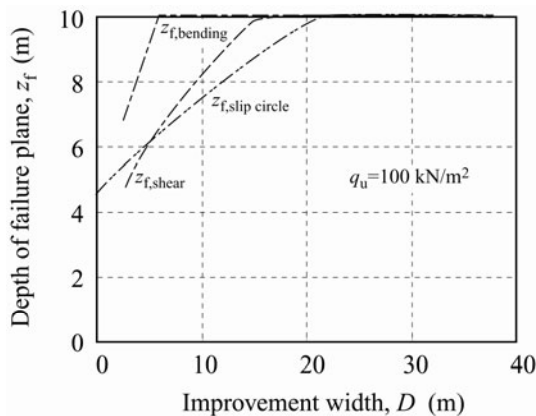
Fig. 3 Effect of column strength on improvement width and safety factor relation

It can be concluded that the failure mode of the improved ground is highly dependent upon the column strength: the sliding failure mode when $q_{u,column}$ is of a relatively low order of 100 kN/m^2 and the collapse failure mode when $q_{u,column}$ is of a relatively high order of 500 kN/m^2 . This phenomenon is confirmed irrespective of the improvement area ratio.

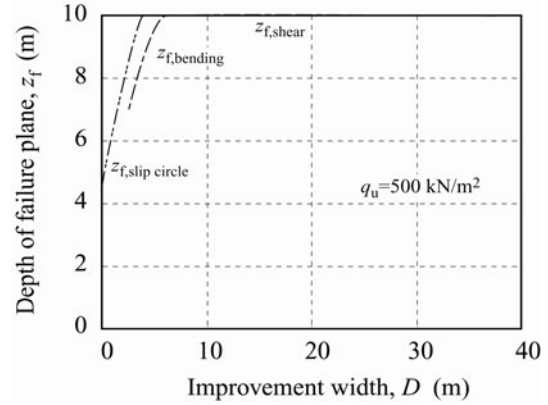
Drawing a comparison, the magnitude of $F_{s,slip \text{ circle}}$ is always the lowest in the case of $q_{u,column}$ of 100 kN/m^2 , but not in the case of $q_{u,column}$ of 500 kN/m^2 . As described above, the current design method has two criteria: the sliding failure mode in the external stability and the slip circle calculation in the internal stability. Regarding to the ground conditions studied, the current design method gives the lowest safety factor in the case of relatively low column strength of the order of 100 kN/m^2 , but an overestimation in the case of relatively high column strength of the order of 500 kN/m^2 .

Figs. 4(a) and 4(b) show the relationship between D and failure depth, z_f , for various $q_{u,column}$ values. In the case of $q_{u,column}$ of 100 kN/m^2 , Fig. 4(a), $z_{f, \text{shear}}$ and $z_{f, \text{bending}}$ increase with increasing D , and reach a constant value of 10 m at D of about 5 m and 15 m, respectively. This indicates that neither bending failure mode nor shear failure mode takes place after that. As $q_{u,column}$ increases, the magnitude of $z_{f, \text{shear}}$ increases, while $z_{f, \text{bending}}$ remains constant, as shown in Fig. 4(b). In the case of $q_{u,column}$ of 500 kN/m^2 , $z_{f, \text{slip circle}}$ reaches 10 m at quite a small D value of about 3 m. This indicates that the slip circle analysis does not evaluate the internal stability under practical conditions.

The required improvement width should be determined so as to ensure that the safety factor for all the failure modes is higher than the allowable F_s value. Here, the allowable F_s value is simply assumed as 1.25, which is the value adopted in the slip circle analysis in the current design method (PWRI, 2004). Fig. 5 shows the required improvement width, $D_{req.}$, along with $q_{u,column}$. The $D_{req.}$ for the shear failure mode, $D_{req., \text{shear}}$, decreases very rapidly with increasing $q_{u,column}$ and reaches zero at



(a) $q_{u,column}$ of 100 kN/m^2 .



(b) $q_{u,column}$ of 500 kN/m^2

Fig. 4 Effect of column strength on improvement width and depth of failure plane relation

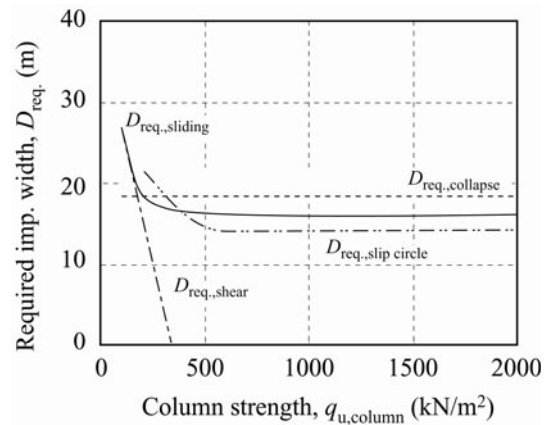


Fig. 5 Column strength and required improvement width relation

$q_{u,column}$ of about 300 kN/m^2 , which means that the shear failure mode can't be a critical factor under practical conditions. The $D_{req.}$ for the slip circle, $D_{req., \text{slip circle}}$, decreases rapidly with increasing $q_{u,column}$ and reaches an almost constant value when $q_{u,column}$ is about 500 kN/m^2 . The $D_{req.}$ values for the collapse failure mode, $D_{req., \text{collapse}}$, and bending failure mode, $D_{req., \text{bending}}$, almost coincide and decrease very slightly with increasing $q_{u,column}$. The $D_{req.}$ should be adopted as the maximum among all the failure modes, and be determined for the slip circle failure mode when $q_{u,column}$ is lower than about 300 kN/m^2 and for the collapse failure mode when $q_{u,column}$ exceeds about 300 kN/m^2 . The effect of the $q_{u,column}$ on the $D_{req.}$ is highly dominant when $q_{u,column}$ is lower than about 300 kN/m^2 , but is negligible when $q_{u,column}$ exceeds about 300 kN/m^2 .

Effect of improvement area ratio

As discussed above, the failure mode of the improved ground is highly dependent upon the column strength: sliding failure mode for relatively low column strength and collapse failure mode for high column strength. Here,

the effect of improvement area ratio, a_s , is discussed for two separate cases of column strength.

For $q_{u,column}$ of 100 kN/m², the effect of a_s on the relationship between D and F_s is shown in Fig. 6. In the case of a_s of 25%, Fig. 6(a), $F_{s,collapse}$ and $F_{s,bending}$, and $F_{s,sliding}$ and $F_{s,shar}$ almost coincide throughout D . All the safety factors decrease slightly when D is lower than about 15 m, but increase linearly with increasing D for further D . The increasing ratio of $F_{s,collapse}$ and $F_{s,bending}$ is larger than that of $F_{s,sliding}$ and $F_{s,shar}$. In the figure, $F_{s,slip\ circle}$ is plotted together. It can be seen that $F_{s,slip\ circle}$ increases almost linearly and reaches a constant value of about 20 m. It can also be seen that $F_{s,slip\ circle}$ is the lowest throughout D . Even with increasing a_s , Fig. 6(b), $F_{s,collapse}$ and $F_{s,bending}$, and $F_{s,sliding}$ and $F_{s,shar}$ still almost coincide throughout D , and $F_{s,slip\ circle}$ increases with increasing D to a constant value, which is a similar phenomenon to the case of a_s of 25%.

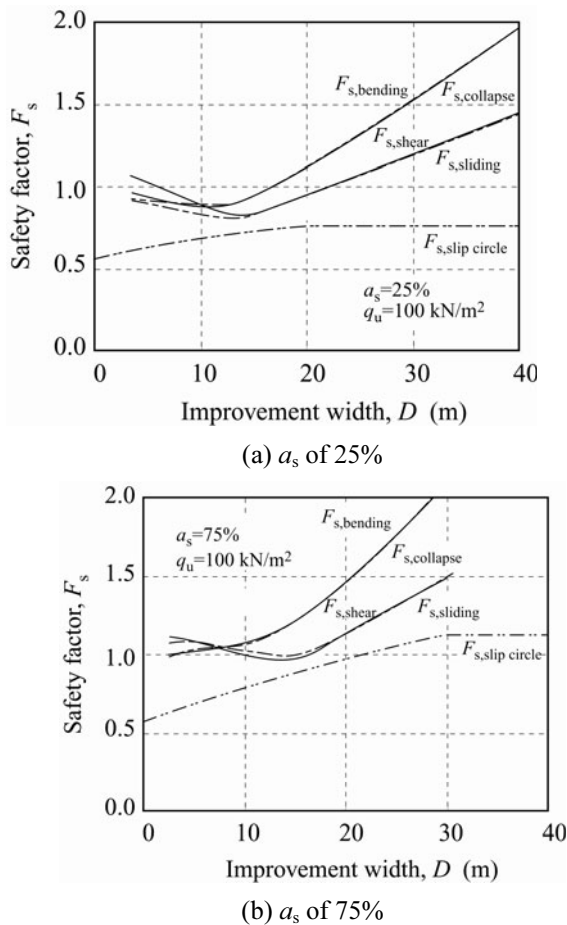


Fig. 6 Effect of improvement area ratio on improvement width and safety factor relation ($q_{u,column}$ of 100 kN/m²)

Comparing the figures, the magnitude of all the factors becomes higher with increasing a_s . As $F_{s,sliding}$ is always lower than $F_{s,collapse}$ for a wide range of D , it can be concluded that the improved ground fails by sliding failure mode rather than by collapse failure mode. It was

found that $F_{s,slip\ circle}$ is the lowest throughout D irrespective of a_s , which indicated that the current design method, gives a reasonable evaluation. In order to investigate the effect in more detail, $F_{s,sliding}$ and $F_{s,collapse}$ are plotted in Fig. 7 along with a_s for D of 15 m and 20 m, in which the F_s value is close to the allowable value of 1.25. $F_{s,sliding}$ increases slightly with increasing a_s irrespective of D , while $F_{s,collapse}$ increases more rapidly compared with $F_{s,sliding}$. In the figure, $F_{s,slip\ circle}$ is also plotted. Drawing a comparison, $F_{s,slip\ circle}$ gives the lowest value, and increases slightly with increasing a_s .

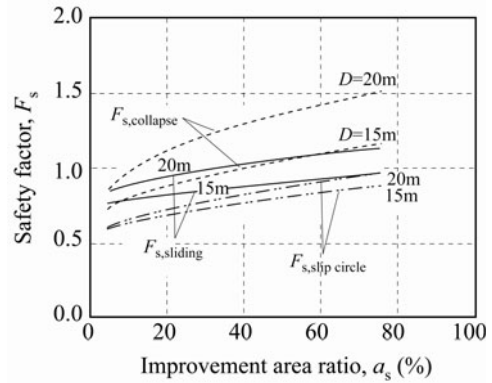


Fig. 7 Improvement area ratio and safety factor relation ($q_{u,column}$ of 100 kN/m²)

Fig. 8 shows $F_{s,sliding}$ and $F_{s,collapse}$ along with a_s for D of 15 and 20 m. $F_{s,sliding}$ and $F_{s,collapse}$ increase rapidly at first and then slowly with increasing a_s irrespective of D . In the figure, $F_{s,slip\ circle}$ is also plotted along with a_s , drawing a comparison, $F_{s,slip\ circle}$ is higher than $F_{s,collapse}$ irrespective of D and a_s . This indicates that the current design method gives an overestimation.

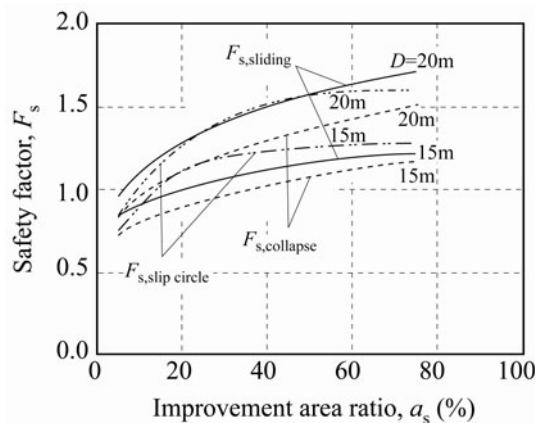


Fig. 8 Improvement area ratio and safety factor relation ($q_{u,column}$ of 500 kN/m²)

Figs. 9(a) and 9(b) show D_{req} for ensuring F_s of 1.25 along with a_s for $q_{u,column}$ of 100 and 500 kN/m², respectively. In the case of $q_{u,column}$ of 100 kN/m², as

$F_{s, \text{slip circle}}$ is always lower than unity irrespective of D , $D_{\text{req., slip circle}}$ can't be obtained. $D_{\text{req., sliding}}$ and $D_{\text{req., collapse}}$ decrease with increasing a_s , while $D_{\text{req., sliding}}$ is always larger than $D_{\text{req., collapse}}$. $D_{\text{req.}}$ is determined by the criteria of the sliding failure mode. In the case of $q_{u, \text{column}}$ of 500 kN/m^2 , $D_{\text{req., sliding}}$ and $D_{\text{req., collapse}}$ decrease with increasing a_s . $D_{\text{req., slip circle}}$ decreases rapidly at first and then more slowly with increasing a_s . The $D_{\text{req., collapse}}$ is always the largest throughout a_s .

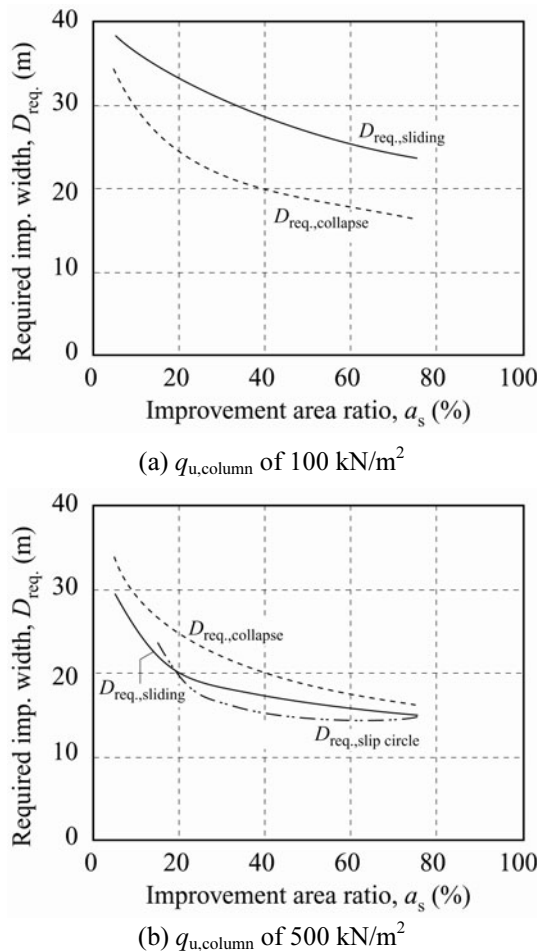


Fig. 9 Improvement area ratio and required improvement width relation

CONCLUSIONS

A parametric calculations on evaluation of stability of column type DM improved ground was carried out to investigate the characteristics of the current design method and the proposed design method. The major

conclusions derived in this study are as follows:

- 1) The failure pattern of the column type improved ground is highly dependent upon column strength and column diameter. The improved ground fails by shear failure mode for relatively low column strength and by collapse failure mode for relatively high column strength.
- 2) The slip circle calculation, which is used for evaluating the internal stability in the current design method, in fact evaluates the external stability of the improved ground with increasing $q_{u, \text{column}}$ of the order of 500 kN/m^2 . This means that there are no criteria for determining the required column strength from the viewpoint of stability analysis.
- 3) The effect of the improvement area ratio is dominant, where the safety factors for the sliding and collapse failure modes increase rapidly with increasing improvement area ratio.
- 4) The current design method provides reasonable agreement with the proposed design as long as the column strength is a relatively low value where the improved ground is expected to fail by shear failure mode. However, when the column strength increases where the improved ground is expected to fail by collapse failure mode, the current design method overestimates compared to the proposed method.

REFERENCES

- Coastal Development Institute of Technology (2002). The Deep Mixing Method - Principle, Design and Construction, A.A. Balkema Publishers, 123p.
- Kitazume M (2008). Stability of Group Column Type DM Improved ground under Embankment Loading, Report of the Port and Airport Research Institute, 47 (1): 1-53.
- Kitazume M & Maruyama K (2006). External Stability of Group Column Type Deep Mixing Improved Ground under Embankment Loading, Soils and Foundations, 46(3): 323-340.
- Kitazume M & Maruyama K (2007). Internal Stability of Group Column Type Deep Mixing Improved Ground under Embankment Loading, Soils and Foundations, 47(3): 437-455.
- Public Work Research Center (2004). Design and construction manual on deep mixing method for inland construction, 326p. (in Japanese).

CASE STUDY ON GEOENVIRONMENTAL EFFECTS OF PRESS-IN PILES INSTALLATION

Jian-Xue SONG¹, Tong-He ZHOU² and Yuan-Cheng GUO³

ABSTRACT: The press-in pile has become one the most frequently used piles in weak soil. However, there are some geoenvironmental problems in the course of installation. The press-in pile belongs to the soil-squeezing pile, and the soil surrounding the pile will be pressed during the process of construction, which leads to the excessive pore water pressure, and that may destroy the surrounding buildings, pipe lines and other civil works. Based on a practical case study, the geoenvironmental effects of press-in piles are investigated, and the excessive pore water pressure is measured day by day. Then, the spatial distribution and the time domain development tendency are summarized. The ratio of pore water pressure to the soil stress caused by the weight of upper layer soil may be used as the control criterion for the installation rate, and it may be set as 0.6 in order to avoid the geoenvironmental failure.

KEYWORDS: geoenvironment, excessive pore water pressure, press-in pile, case study

INTRODUCTION

During the process of press-in pile installation (especially in the saturated soft soil), the excessive pore water pressure comes into being, which may destroy the surrounding soil and civil works. After the installation, the excessive pore water pressure dies out, and the soil consolidates again. The geoenvironmental effect of press-in pile is rather complicated, and it changes with the geological background and the pile installation scheme. For the time being, precise prediction of effect deduced by excessive pore water pressure is still difficult. Field continually monitoring provides direct data for surrounding assessment and environment protection. For the more, the data may be used in the future theoretical analysis and modeling of prediction.

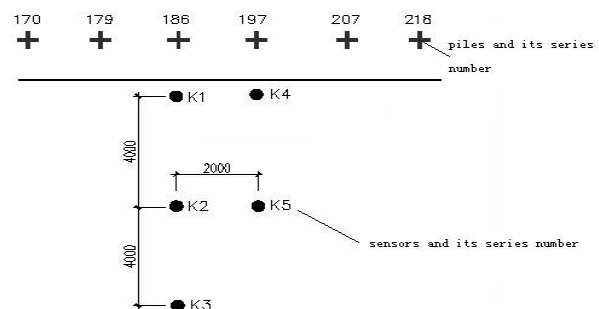
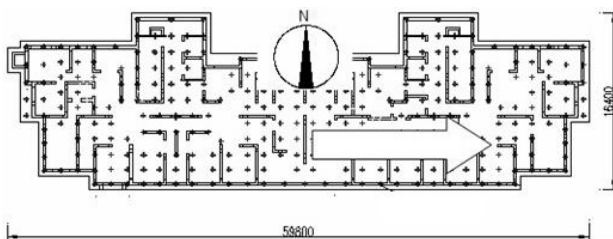


Fig. 1 Site plan and the setting of sensors

Table 1 Parameters of soil

NO.	name	thickness (m)	Water content (%)
1	fill soil	0.7-2.1	
2	Silt	1.5-5.4	19.9
3	silty clay	0.5-3.5	23.6
4	Silt	0.5-5.9	23.2
5	silty clay	1.0-5.6	25.5
6	silt	1.3-4.1	26.0
7	silty clay	1.3-3.5	29.8
8	silty sand	1.4-4.0	24.6
9	fine sand	7.0-12.5	20.6

¹ Professor, Civil Engineering School, Zhengzhou University, China. Email: jxsong@zzu.edu.cn

² Professor, Design Institute, Zhengzhou University, China. Email: zth1964@126.com

³ Professor, Civil Engineering School, Zhengzhou University, China. Email: guoyc@zzu.edu.cn

A case study is carried out in Zhengzhou, the capital city of Henan province, in the center of China, and just on the bank of the Yellow River. The excessive pore water pressure is observed in two schemes, one aims at the process of whole project, since the first pile pressing-in to the final pile installation; and the other focuses on a single pile installation. The features of excessive pore water pressure are summarized and a kind of criterion of pile installation rate control is suggested.

ENGINEERING BACKGROUND

There are five residential buildings being built in a certain area in Zhengzhou, which are all high-rising shearwall structures, with 32 stories over the ground and 2 stories beneath the ground. The bottom of foundation is 8 meters (from the nature ground level). The end opened Pre-stressed High-strength Concrete (PHC) pipe pile is employed to support the raft, with the diameter as 500mm. The installation method is pressing-in. No. 1 building is chosen as the specimen, which is located on the furthest south end of the area. There are 289 piles being pressed-in. The soil parameters are shown in Table-1. The 9th layer fine sand is chosen as the bearing bottom of pile. The length of pile is 13.5m, and at least 2m pressed into the bearing layer. The space between piles ranges from 1.5m to 3.6m. When the piles under No. 1 building begin to be installed, the construction pit for the neighboring No. 2 building is excavated to the bottom. The ground water is about -11.4m after being pumped.

EXPERIMENT DESIGN

Sensors

Due to the objective and the duration of the experiment, the vibrating wire sensors and corresponding read out unit are employed. For the convenience of analysis, the frequency modulus is measured.

$$P = K(F - F_0) + B \quad (1)$$

Where:

- P —pore water pressure (MPa);
- K —calibration constant of sensor (MPa/F);
- F_0 —datum of frequency modulus (F);
- F —field read out frequency modulus (F);
- B —amendment constant of sensor (MPa).

Setup of Sensors

Holes with diameter as 150mm are bored to the design depth, then, sensors are installed into the holes.

For sure of the readings, only one sensor is installed into a hole. Five sensors are shown in Fig 2. According to the experiment design, sensor-1, sensor-2 and sensor-3 are arranged on the normal direction of the pit side and the depth is 15m; the space between either two holes is 4m. Sensor-1 and sensor-4 are located on the parallel line of pit side, and the depth of them is 15m and 20m respectively. The space between sensor-1 and sensor-4 is 2m. Arrangement of sensor-5 is similar to sensor-4.

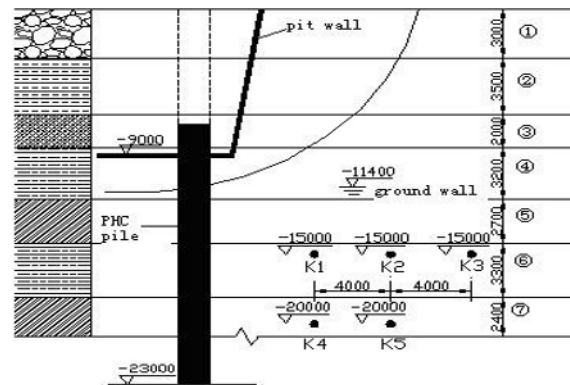


Fig. 2 Vertical Arrangement of Sensors

Monitoring Scheme

Monitoring on excessive pore water pressure begins one week before the installation of PHC piles, so as to obtain the datum pore water pressure. Two kinds of monitoring schemes are set: the first one aiming at the entire period of project, i.e. Scheme-1; the other aiming at the period of single pile installation, i.e., Scheme-2. For Scheme-1, monitoring on pore water pressure is carried out at the same time once a day, until nine days after all the piles have been pressed-in, and at that time the construction pit begins to be excavated. When piles are pressed-in near the sensors, Scheme-2 is carried out: during the pressing-in process, the pore water pressure is detected continuously. At the same time, the length of pile that already penetrates into the soil is recorded simultaneously.

RESULTS AND ANALYSIS

Results of Scheme-1

Traditionally, field excessive pore water pressure is measured only once every day, and the chart of excessive pore water pressure is used to feature the process of pile installation. However, the excessive pore water pressure varies significantly during a single pile penetrating course, and it is also different with the variation of distance to the monitor, and with different geological background.

Fig 3 shows the general tendency of pore water pressure during the whole procedure of pile pressing-in, and the total period is about 20 days. In Scheme-1, the pore water pressure is measured once a day at the same time in a day. Fig 3 indicates that the two peak values come into being on 2008-5-18 and 2008-5-26. The project ratio (percentage of installed piles to the total number of piles) corresponding to the peak values are 15% and 85% respectively. Further investigation shows that on the peak value day, the pressing piles are in the nearest and second nearest rows to the sensors, i.e., the furthest south row and the second furthest row. It reveals that the excessive pore water pressure is mainly affected by the distance of the installation location.

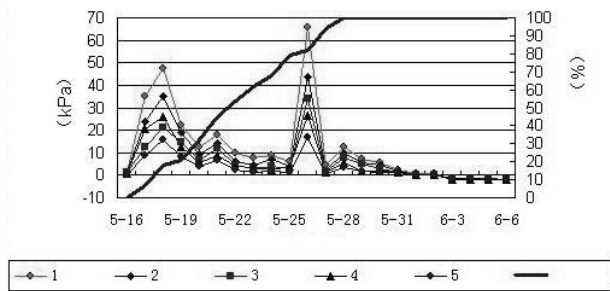


Fig. 3 The time-domain pore pressure distribution

In Scheme-2 (2008-5-26), the excessive pore water pressure is detected continuously during No. 186 pile being pressed-in. It is found that the maximum value only last for a few seconds. Therefore in Scheme-1, some peak values may be missed, and the chart in Fig 3 may be inadequate to assess the effects of pressing-in pile installation.

There is another interesting phenomenon. Since 2008-6-2, the excessive pore water pressure changes into negative. Usually, the excessive pore water pressure, or the increment of water pressure to the static one, can not be negative. During the procedure of PHC pile installation, the pressure rises up, when the installation is over, the excessive pore water pressure dies out, until the pore water pressure equals to the static one. However, in the case project, the interregna period after pile installation is almost null. The whole process of pressing-in is ended on 2008-5-28, and the entire load is removed on the same day. The construction pit is excavated on the next day. The excavation removes the upper load of soil, and may cause the resilience of soil. The pore volume of soil expands, which results in the negative value of excessive pore water pressure.

Results of Scheme-2

The summation pore water pressure includes the static one and the excessive one. During the procedure of pile pressing-in, the static one is regarded as constant,

and the effect of soil and water driven by the pile is mainly manifests by the varying of excessive pore water pressure. In the field test, the excessive pore water pressure is determined by the increment of pore water pressure while the pile is pushed in. Fig 4 and Fig 5 show the summation pore water pressure and the excessive pore water pressure in the course of pressing-in of Pile-186 respectively.

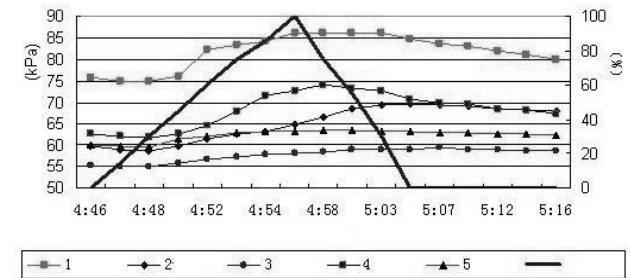


Fig. 4 Summation pore water pressure and the percentage of single pile penetrating into soil

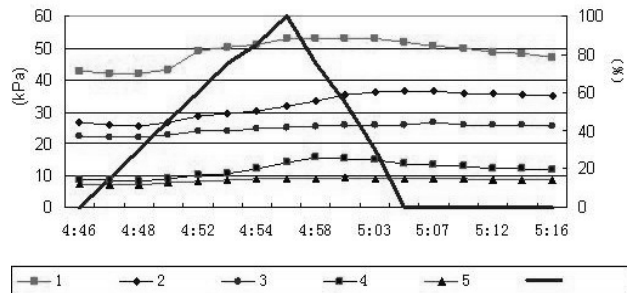


Fig. 5 Excessive pore water pressure and the percentage of single pile penetrating into soil

(1) After a single pile has been pressed to the design position, while the follower pile is being drawn out, the maximum pore water pressure emerges. The maximum pore water readings appear in sensors one after another in the sequence of sensor-4, 5, 1, 2, and 3. For this very single pile, the depth of pile is 20.5m, and sensor-4 and sensor-5 are almost on the same level of the bottom of pile-186. Further more, sensor-4 is nearer to pile-186. It is found that the maximum reading in sensor-4 comes into being only several seconds after pile-186 is pressed to the bottom position.

Generally, the maximum readings in a pore water pressure sensor appear while the follower pile is pulled up to the same level as the sensor locating.

(2) The sensors are divided into two groups: group A, i.e., sensor 1-2-3, and group B, i.e., sensor 4-5. For both groups, when the sensors' code numbers are listed in the descending sequence of pore water pressure variation magnitude, the sequence in group A is 1-2-3, and the sequence in group B is 4-5. In group A, the pore water pressure difference of 1-2 is greater than that of 2-3, which discloses the tendency of pore water pressure

attenuation, i.e., with the distance increases, the pore water pressure attenuates at an increasing rate.

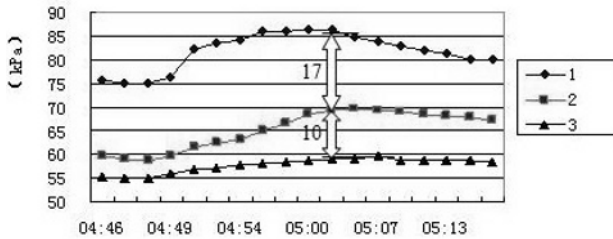


Fig. 6 Pore water pressure variation in Group A

(3) The summation pore water pressure decreases at the initial stage of a single pile pressing-in, then it increases with the penetration of pile, at the final stage, it descends once more. This is the colligate effects of group piles pressing-in. At the initial stage, the pore water pressure induced by the previous installed piles descends faster than the increment caused by the just pressing-in one, so the summation pore water pressure declines; however, with the penetration of pile, the increase of pore water pressure is the dominant factor, so it increases; at the final stage, the pore water pressure diffuses mainly, so it drops again.

(4) Some general tendency may be summarized in the excessive pore water pressure chart (Fig 5). The variation scope of excessive pore water pressure in sensor-1 is greater than that of sensor-4, although their distance to the boundary is the same. It indicates that the upper sensor varies greater than the deeper one. The same tendency can be found when comparing sensor-2 and sensor-5.

(5) For sensor-3, the maximum increment of pore water pressure is 4.6kPa, which may be neglected in practical project. According to the general concept, if the excessive pore water pressure is smaller than 5kPa, the geoenvironment effect may be neglected. So, for the case project, the geoenvironment affecting area by press-in pile installation is about 30 times D, where D stands for the diameter of the pile. It is rather smaller than the previous reported one.

Control Criterion

According to the fundamental principles of soil mechanism, the stress in soil is the sum of pore water pressure and the effective soil stress. During the course of pile pressing-in, the weight leading to stress in soil remains the same, and on the spot of sensor, the load of pressing-in machine may be neglected, so the stress may be regarded as constant. Therefore, when the pore water pressure increases, the effective stress in soil decreases. When the pore water pressure equals, or even greater than the effective soil stress, the soil is damaged. Therefore, the ratio of pore water pressure to the soil

stress caused by weight of upper layer soil may be used as a control criterion for the installation rate. In the case project, the alarm value for the ratio is set as 0.6. In the whole installation process, the detected ratio is smaller than the criterion (Table-2), and no surrounding soil destroy is found.

Table 2 Maximum pore water pressure/soil stress caused by weight

No	K1	K2	K3	K4	K5
Depth (m)	15	15	15	20	20
ratio	0.31	0.21	0.15	0.12	0.07

CONCLUSIONS

Based on the field monitoring data and corresponding analysis, some conclusions are drawn as following.

(1) If the excessive pore water pressure is measured only once a day, the maximum value may be missed, and the real varying course can not be traced. So, in the situation with important buildings and pipe lines surrounding the construction area, the excessive pore water pressure caused by the pressing-in pile installation should be monitored continuously.

(2) The summation pore water pressure decreases at the initial stage of pile pressing-in, then it increases with the penetration of pile, at the final stage, it descends again. The maximum reading appears while the follower pile is pulled up to the same level as the sensor locating.

(3) The geoenvironmental affecting area by pressing-in pile installation is about 30 times D, where D stands for the diameter of pile.

(4) The ratio of pore water pressure to the soil stress caused by the weight of upper layer soil may be used as the control criterion for the installation rate, and it may be set as 0.6, so as to avoid the geoenvironmental failure.

REFERENCES

Lu Q, Gong XN, Ma M, et al. (2007). Observation and analysis on a case project of pressing-in pile installation. Bulletin of Science and Technology. 23(2): 232-236.

Standardization Society of Chinese Civil Engineering Construction (1993). Code on pore water pressure monitoring. CECS55: 93 [S], Wuhan.

Tang SD, Wang YX, et al. (2003). The excessive pore water pressure caused by group piles pressing-in to the saturated soft soil. Journal of Tongji University, 31(11): 1290-1294.

A CONSTRUCTION CASE OF RAMPS LOCATED ON THE EXPANSIVE SOIL FOR HIGHWAY INTERCHANGE

He-Ping YANG¹, Xiao NI² and Jie XIAO³

ABSTRACT: The Baise basin in Guangxi Zhuang Autonomous Region is one of the famous areas for the wide distribution of expansive soil in China. Two highways, Baise-Longlin and Nanning-Baise, meet in the east of Baise city. The ramps of the interchange are completely located on the expansive soil. Therefore, the arrangement of interchange ramps and the stability of the cut slopes became big technological problems for the design and construction of the interchange. Based on the analysis of the engineering geological characteristics and properties of Baise expansive soil and the application of physical treatment technology on expansive soil subgrade, the original design was altered in the light of local conditions: the center-island was leveled in order to reduce the quantities of cut slopes; the excavated expansive soil was directly used to fill the embankments; and all the cut slopes of ramps were treated with the flexible supporting measure. Through the design changes in three aspects, the problems of building ramps in expansive areas are solved safely, economically and effectively. This paper can provide a great example and reference for the construction of similar projects.

KEYWORDS: expansive soil, interchange ramp, construction case, flexible supporting, center-island

INTRODUCTION

As one part of the Shantou-Kunming highway under construction, the Baise-Longlin highway in northwestern Guangxi Zhuang Autonomous Region is an important section connecting China-ASEAN free trade area. Its initial point lies in the Baise basin that is famous for the distribution of expansive soil in China. The whole section traverses expansive soil area more than 20 kilometers. The Sitang interchange at the east of Baise city connecting two highways, Baise-Longlin and Shantou-Kunming, is entirely located on the typical Baise expansive soil and it is the first time to build interchange ramps on expansive soil for highway construction in China. Because of the importance of the project and the fact that cut slopes used to be bound to landslide, embankments used to be bound to collapse and soil erosion used to occur during the construction of highway in expansive soils area, great attention should be paid to the construction of interchange ramps on expansive soil by the builders. Based on the study on geologic characteristics and properties of Baise expansive soil/rock, the right design and the rational engineering treatment approach should

ensure the process of project construction successful and be adopted to prevent the repeated instability of subgrade, serious economic loss and ecological damage during the construction of highway on expansive soil.

PROPERTIES OF SITANG EXPANSIVE SOIL (ROCK)

Five groups of undisturbed samples were collected from different locations in the ramps with depths from 3m to 8m. Their properties were tested by the Institute of Geology and Geophysics, Chinese Academy of Sciences. The average results were shown in Table 1&2.

As seen from Table 1&2, the expansive soil/rock in Sitang belongs to Tertiary expansive weathered mudstone, which is a type of hard soil/soft rock with high clay content, high liquid limit, and great free expansion ratio. For the same index, the difference between samples from various positions is small. The main clayey mineral is I/S (illite/montmorillonite) mixed layer mineral with a high ratio of 45%. The expansive soil/rock has high physicochemical activity due to the effective montmorillonite content (16.58%) and exchangeable cations (mainly Ca²⁺

¹ Professor, School of Traffic and Transportation Engineering, Changsha University of Science&Technology. China. Email: cscuyang@163.com

² Postgraduate student, School of Traffic and Transportation Engineering, Changsha University of Science&Technology. China. Email: nixiao919@yahoo.com.cn

³ Ph.D Student, School of Traffic and Transportation Engineering, Changsha University of Science&Technology. China. Email: xiaojie324@sina.com

and Mg^{2+}). Based on the results and the treatment experience of expansive soil cut slopes of NanYou highway in Guangxi Zhuang Autonomous Region (Yang et al. 2004), the speed of ramp construction should be as fast as possible to prevent the slope from damage caused by discharging, drying shrinkage and wetting expansion

during the period of the ramp building. The effective full closure measures of flexible supporting should be used instead of rigid supporting. In addition, the expansive soil should not be used as embankment filler without chemical improvement, according to the existing subgrade design criterion.

Table 1 Properties and particle composition of SiTang Paleogene expansive weathered mudstone

Moisture Content (%)	Bulk Density (%)	Particle Size Distribution (%)				Void Ratio	LL (%)	PI (%)	Fs (%)	A
		>0.75	0.075-0.005	<0.005	<0.002					
20.60	2.092	0.10	52.02	47.88	45.20	0.59	56.26	34.89	82	0.77

Note: LL=Liquid Limit; PI= Plasticity Index; Fs = free swelling ratio; A=Activity

Table 2 Chemical properties of SiTang Paleogene expansive weathered mudstone

SSA (m^2/g)	Relative Clayey Mineral Content (%)				Mixed Ratio (%S)	EMC (%)	Exchange Capacity of Cation ($meq/100g$)	Changeable Cation ($meq/100g$)			
	I/S	I	K	C				Ca^{2+}	Mg^{2+}	K^+	Na^+
130.77	54	22	24	1	45	16.58	17.86	12.47	4.16	0.23	0.77

Note: SSA =Specific Surface Area; ECM = Effect Content of Montmorillonite

ORIGINAL AND MODIFIED DESIGNS FOR SITANG INTERCHANGE

The Sitang interchange contains four ramps named A, B, C and D. Its detailed layout is shown in Fig. 1.

For the original design, there are sixteen cut slopes with height ranging from 6 to 12 m and the most slope ratios (horizontal to vertical) are 1:2. The treatment approach of slopes is using a toe wall associated with grid skeleton. Within the scope of the interchange, the designed excavation wastes are more than 500, 000 m^3 and the needed embankment fills that must be brought from nine kilometers away are about 200,000 m^3 . Several expansive soil slopes of Nanning-Youyiguan highway deformed and damaged in less than one year after construction. Learning from this case as well as recognizing the engineering properties of Baise expansive soil, the author concluded that the long-term stability of cut slopes would be a big problem for the original design; the total project cost would increase due to huge earthwork without using the excavation soil to fill the embankments; the wastes would result in serious eco-environmental damage and it would be difficult to accomplish the engineering as scheduled. Therefore, the original design was modified based on the treatment experience in Ningming expansive soil from western expansive soil project (Yang et al. 2005), (Yang et al. 2006a), (Yang et al. 2006b), (Yang et al. 2008a), such as amendment of overall layout, improvement of the

technical ideas on the treatment of ramps built on expansive soil and its corresponding construction technique. The detailed modifications are as follows:

1. According to the physical treatment technology on expansive soil embankment in Nanning-Youyiguan highway, the excavated expansive soil from ramp is used to fill embankment as more as possible to reduce borrow and spoil earth. The Sitang expansive soil as embankment filler is feasible based on test results, so the excavated expansive soil is directly filled in the embankment in the main line from k176+135 to k176+410 in Baise-Longlin highway, which may reduce the soil erosion during construction.

2. Minimize the number of excavation slopes. Four ramps, A, B, C and D, intersect at the main line in the initial point of Baise-Longlin highway. In the original design, there is a long-narrow center-island between BC ramps at the start point (Fig. 1). For the two high-long cut slopes, there are a large amount of works treated by the measure of toe wall associated with grid skeleton and the driving sight distance will be poor after construction. In order to improve the landscape of the original design and to radically eliminate the potential dangers of expansive soil cut slopes, the center-island is leveled in which grasses and trees are planted to be a green belt. Meanwhile, the excavated soil is used to fill subgrade of the main line. The aforementioned operations will not only improve the overall ramp layout but also gain good eco-environmental benefits.

3. Effectively guarantee the stability of the cut slopes. The practice of Nanning-Youyiguan highway has proven

that the flexible supporting with geogrid which has been awarded a national invention patent can effectively solve the problem about the stability of expansive soil cut slopes. It is economical, friendly environmental and convenient for construction to directly use expansive soil

as reinforced body filler. The slope ratio of 1:2 in the original design is changed into 1:1.5, which will reduce the amount of excavated expansive soil. Therefore, the rigid supporting in original design is altered to flexible supporting and all the ramp slope ratios are 1:1.5.

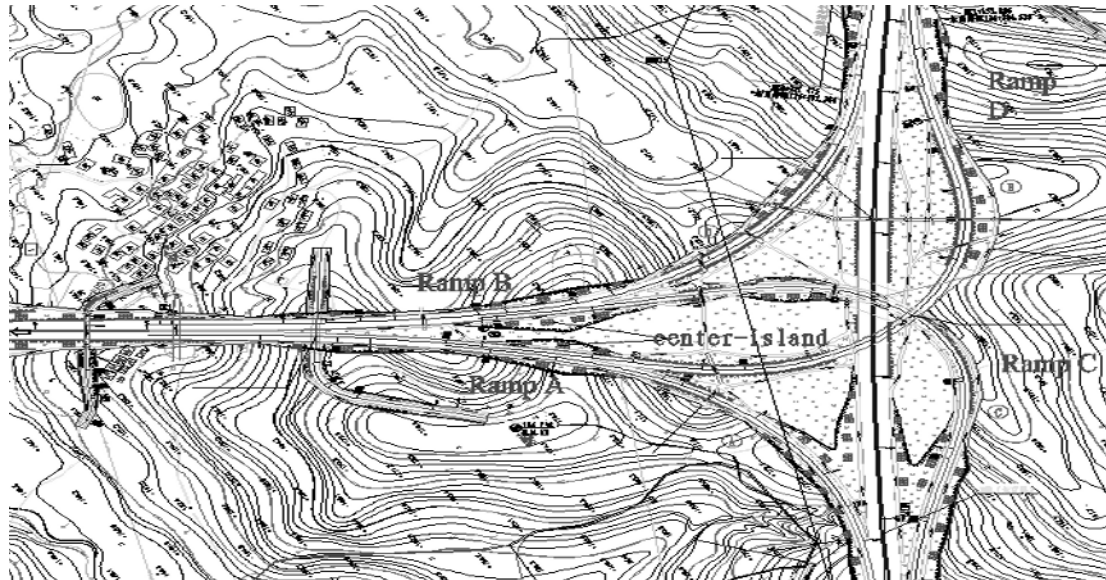


Fig. 1 General layout of SiTang interchanges

Through the aforementioned changes in the design and optimization, the decrease in excavated expansive soil is about 10,000 m³ and the expansive soil rationally used is 200,000 m³. In particular, leveling the center-island reduces the number of cut slopes and adopting flexible supporting instead of rigid supporting in the original design to treat the cut slopes can guarantee the safety and reliability of the engineering and shorten the construction time. Meanwhile, it may save the project cost of about 5,000,000 Yuan by preliminary budget.

IMPLEMENTING SITUATION OF THE MODIFY DESIGN

Directly Fill Embankment with Excavated Expansive Soil

Experiment argumentation of expansive soil as filler

Some requirements about strength and water-stability should be met in order to use expansive soils as embankment filler. According to the Specifications for Design of Highway Subgrades (JTGD30-2004), (JTGF10-2006), the standard CBR test values must be greater than or equal to 3% and the total rate of swelling-shrinkage should not exceed 0.7%. Through a large number of engineering practices and related test study, the existing specification for evaluation of expansive soil as embankment filler is questioned by the author. The classification

method with three indexes that is accordance with actual engineering conditions for expansive soils is established based on the modified CBR test method. The physical treatment technology, using expansive soils to directly fill the under embankment, is put forward (Yang et al. 2007), (Yang et al. 2009a), (Yang et al. 2009b). In order to determine the feasibility of using SiTang expansive soil as embankment filler, the conventional CBR tests and the modified CBR tests were carried out. The results are shown in Table 3.

From Table 3, it can be seen that the standard CBR value of expansive soil is less than 2%, which does not satisfy the requirement on the minimum value of 3% for expansive soil as embankment filler in the Specifications for Design of Highway Subgrades. However, the modified CBR testing results with CBR value of 4% and swelling ratio of 4.93% and the natural consistency value all satisfy the requirement on the III class filler proposed by the author (Yang et al. 200a). Therefore, this kind of expansive soil could be directly used to fill subgrade if the right technical measures are adopted.

Filling embankment under the main line

Considering that SiTang expansive soil can only meet the lowest criteria as embankment filler and the height of embankment at main line of Baise-Longlin highway, k176 +135- k176 +410, is 13 m, the technology program of enveloping both slope sides with non-expansive clay is adopted based on the experiences in successful

constructions of numerous highway embankment sections in the past. The distinct influencing depth of dry-wet cycle for expansive soil in Baise is also taken into consideration. With the purpose of maintaining the moisture content of expansive soil stable, stabilizing embankments, and reducing post-construction settlement, the non-expansive clay wrapping width of 3.5 m and “sandwiches” method are utilized. The “sandwiches” method is that one non-expansive soil layer is laid upon 2 or 3 expansive soil layers in turns after the completion of non-expansive soil basement. According to the wet heavy compaction standard and the requirement of special soil prescribed in the Specifications for Design of Highway Subgrades, the actual measured degree of compaction for each layer should be more than 90%. Currently, the height of embankment containing expansive soil in the main line has reached 5m. Actually,

14 expansive soil layers were filled in the core of embankment. The consumption of excavated expansive soil is about 35,000 m³. Fig. 2 gives a photo of embankment construction.



Fig. 2 Construction of expansive soil embankment by the enveloping method

Table 3 Results of road performance of SiTang expansive soil

Moisture Content (%)	w _{opt} (%)	Maximum Dry Density (g/cm ³)	LL (%)	PI (%)	CBR (%)	CBR δ _c (%)	MCBR (%)	MCBR δ _c (%)	Natural Consistency
19.73	17.31	1.80	54.68	30.24	1.98	5.35	4.11	4.925	1.16

Note: LL=Liquid Limit; PI= Plasticity Index; CBR=California Bearing Ratio; δ_c = soaking swelling ratio
w_{opt} = the optimum moisture content according to the wet heavy compacted standards

Ramp Slope Cutting Project Implementation.

Excavated center-Island

The maximum length and height of the wedge-shaped center-island are 250 m and 9 m, respectively. According to the revised design, leveling the center-island will excavate expansive soil of nearly 50,000 m³, most of which are filled in the core of embankment in K176+135 -K176+410 section of the main line. Excavating the center-island has already begun (Fig. 3).



Fig. 3 Partly excavation of center-island

Flexible supporting method for cut slopes

Fig. 4 illustrates the design of the flexible supporting method. The basic technical principals are “full closure of the slope surface”, “maintaining the moisture content stable” and “conquering the expansion with the

flexibility” (Yang et al. 2008b). The basic processes of construction are listed as follows: 1. Overexcavate the designed slope to get a certain extra width; 2. Construct the drainage layer at the foot of slopes; 3. Place geogrid horizontally and fix it with nails of “U” type; 4. Back-fill and compact expansive soil layer by layer; 5. Back-envelop the compacted soil with geogrids; 6. Connect the geogrids of upper and lower layers with a connecting rod to make the reinforced body as a whole; 7. Repeat 3-6 until the height of slope reaches the designed height; 8. Envelope the top of slope with two layers of earthwork cloth and a layer of geo-membrane; 9. Cover the slope with planting soils on which grasses and trees are planted.

Fig. 5 shows the flexible supporting under construction for the A ramp slope.

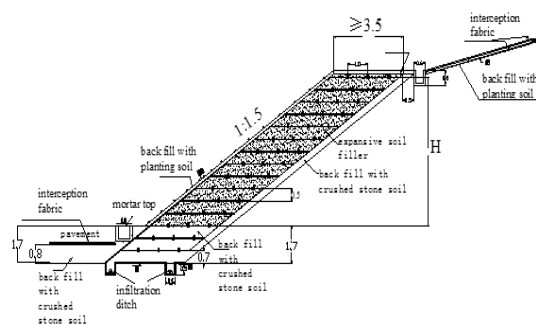


Fig. 4 Design of slope treated with flexible supporting



Fig. 5 Implementation of flexible supporting for ramp slopes

CONCLUSIONS

The treatment of expansive soil subgrade is a worldwide technical problem. The optimal design and construction technology provided by this case is a new exploration of the treatment of expansive soil engineering, especially for constructing interchange ramps in expansive soil. Because of the large quantity of the whole project and the long construction period, the project is still under construction and the revised design is not completed entirely. However, it is sure that the optimized program, taking the security, economy, and environmental protection into account, will provide significant benefits for the ramp construction in Baise-Longlin highway and an excellent engineering reference to the construction of other similar projects.

REFERENCES

- Industry Standard of the People's Republic of China, Specification for Design of Highway Subgrades. (JTGD30-2004). Beijing, China Communication Press.
- Industry Standard of the People's Republic of China, Technical Specification for Construction of Highway Subgrades. (JTGF10-2006). Beijing, China Communication Press.
- Jiang ZX, Qin XL, Li M (1995). The Research Development of Nankun Railway Expansive Soil (Rock) and Its Treatment. *The Chinese Journal of Geological Hazard and Control*. 6:1-8.
- Jiang ZX & Li M (1999). Cutting Slop Engineering Tests of Expansion Mudstone. *Subgrade Engineering*. 5:35-42.
- Feng YY, Zhang YS, Qu YX (2001). Mechanism of Embankment Defects Caused by Expansive Soils in Baise Basin, Nankun Railway. *Chinese Journal of Geotechnical Engineering*. 23(4).
- Yang HP & Zheng P (2004). Geological Investigation and Reflection on the Expansive Soil in Nanning-Youyiguan Highway. *Journal of Changsha University of Science and Technology (Natural Science)*. 1(1): 14-19.
- Yang HP & Zhang GF (2008a). The appropriate wrapping width of expansive soil fill embankment built by the enveloping method. *Journal of Highway and Transportation Research and Development*. 25(7): 37-42.
- Yang HP & Zheng JL (2005). The Engineering Treating Technique of Expansive Soil Embankments in Nanning~Youyiguan Highway in Guangxi Province. *The Annual Academy Proceedings of China Road Association in 2005*: 156-163.
- Yang HP, Zheng JL, Zhang R (2006a). Addressing Expansive Soils. *Civil Engineering (ASCE)*. 77: 62-69.
- Yang HP & Zheng JL (2006b). The New Engineering Treatment Techniques Of Expansive Soil Subgrade For GuangXi Nanning—Youyi Guan Highway. *Unsaturated Soil*. 1: 439-450.
- Yang HP, Zhao PC, Zheng JL (2007). Suggestion and Verification on Modified CBR Test Method for Expansive Soils filler. *Chinese Journal of Geotechnical Engineering*. 12: 1751-1757.
- Yang HP, Zhao PC, Zheng JL (2009a). Research on Classification Scheme of Expansive Soils Used as Embankment Fill. *Chinese Journal of Geotechnical Engineering*. 2: 194-202.
- Yang HP, Zhang GF, Zheng JL (2009b). Physical Treating Techniques of Highway Embankment Filled With Expansive Soils. *Chinese Journal of Geotechnical Engineering*. 4.
- Yang HP, Xiao J, Wang S (2008b). Treat cut slopes with expansive soils adopting geogrid-reinforced technique, *Proceeding of the 4th Asian Regional Conference on Geosynthetics*.

ANALYSIS OF THE DEEP-SEATED CONCRETE SLAB FOR SETTLEMENT CONTROL AT BRIDGE APPROACH EMBANKMENT

Yun SUN¹, Yi-Qiang XIANG², Dong-Mei GUO³ and Ting-Ting ZHANG⁴

ABSTRACT: The deep-seated reinforced concrete slab, which is different from the traditional reinforced concrete slab for settlement control at bridge approach embankment, can avoid the complaints about the reinforced concrete slab cracking with the long-term impact action of vehicle. A simplified two-dimensional plane strain finite element model for bridge-approach, in which soil parameters are selected from the geological prospecting data, is proposed. The comparison between field experiment and theoretical results shows the characteristics of subsidence of bridge-approach overlaying the deep-seated concrete slab. Parametric analysis is also performed to investigate the influence factors of disposal effect of the deep-seated reinforced concrete slab. The results indicate that the deep-seated concrete slab has more advantages on the settlement control and alleviating vehicle bouncing at the bridge approach.

KEYWORDS: deep-seated concrete slab, finite element model, vehicle bouncing at the bridge approach, parametric analysis

INTRODUCTION

Bridge approach is normally constructed with reinforced concrete slab connecting the bridge deck with the road paved roadway to prevent the differential settlement. However, many complaints about the ride quality of bridge approach still need to be resolved, for instance, concrete slab cracking with the long-term impact action of vehicle, or the settlement under the slab, which will bring the adverse effect for the bridge head riding comfort and the security. So it is necessary to research and discuss the new method in processing vehicle bouncing at the bridgehead.

A great number of articles have been reported on the research of traditional bridge approach slab how to alleviate vehicle bouncing of the bridgehead. Shi & Cai (2003, 2008) established regression equation on approach slab force and deformation in different disengaging sizes and the vehicle-bridge dynamical system to analyze dynamic response under the vehicle load. Roy et al. (2007) adopted the nonlinear finite element analysis to obtain the development of concrete approach slab crack in different dimensions, foundation coefficients and local disengaging size. Wong (1994) placed the bridge approach slab to the abutment with a certain inclined angle to do the experimental research indoors; Wang et al. (1996)

made a nonlinear finite element analysis on force characteristics of the inclined bridge approach slab and influencing factors; Gu et al. (1996) made a monographic study on structure, size, force and reinforcement of bridge approach slab; Zhang (1999) adopted the spline subdomain method to solve the bridge approach slab's internal force and compared with experimental results on indoor model; Zhou (2004) made the internal force analysis of the bridge approach slab on different supporting conditions and different moving loads; Yu (2006) used the finite element software considering the coupling of the force and the deformation to analyze the force characteristic and the applicability of the approach slab; Huang (2003) and Xu et al. (2005) improved the design on the traditional bridge approach slab in the practical engineering.

In this paper, a new method is proposed to process the vehicle bouncing at bridgehead, in which the bridge approach slab combined with the light-weight backfill is seated in the certain depth. A theoretical analysis and an experimental study are performed combined with engineering case.

The deep-seated reinforced concrete slab is different from the traditional ones, because the deep-seated reinforced concrete slab not only provides a smooth transition between the bridge deck and the roadway

¹ Ph.D Student, Department of Civil Engineering, Zhejiang University, China. Email: yvettesun@zju.edu.cn

² Professor, Department of Civil Engineering, Zhejiang University, China. Email: xiangyiq@zju.edu.cn

³ Ph.D Student, Department of Civil Engineering, Zhejiang University, China. Email: guodongmei_2004@126.com

⁴ Post-graduate Student, Department of Civil Engineering, Zhejiang University, China. Email: mayzhangtingting12@163.com

pavement, but also will not crack by the long-term impact action of vehicle.

ENGINEERING BACKGROUND

The bridge approach abutment as a typical test on the soft foundation is located at national highway No.104 in Huangyan district in Taizhou of Zhejiang Province without any foundation treatment before. The cumulative settlement between bridge and road pavement was even more than 40 centimeter. After several maintenances, the pavement of the bridge approach still became rugged because of the bad geology. Geological prospecting data is shown in Fig. 1.

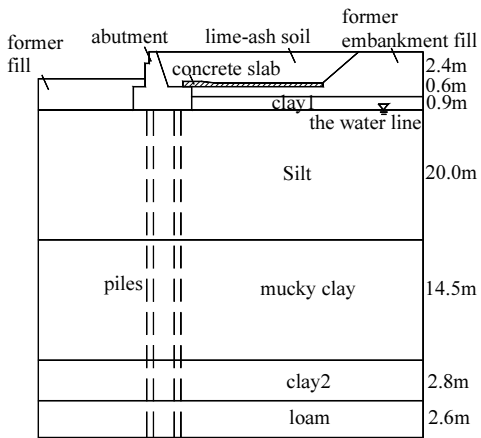


Fig. 1 Soil distribution under the embankment approaching the bridge

The reinforced concrete slab dimensions are: thickness of 0.3 m and length of 10.6 m. Its width is equal to the roadwidth. The planting steel bars with PVC tubes are used to connect concrete slab and bearing platform, in order to assure that the slab can rotate around the connective end (Fig. 2). Lime-ash soil (lime: fly ash: cinder = 9: 21: 70) was paved above the concrete slab after laying-curing.

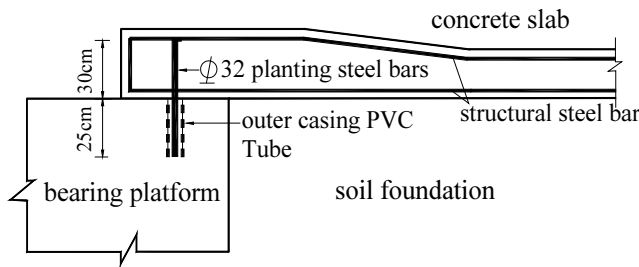


Fig. 2 The schematic diagram of planting steel bar into bearing platform

FINITE ELEMENT MODEL

Geometric Modeling

According to bridge approach condition and the deformation feature, 2D plane strain analytical model about bridge vertical section of soft road embankment behind the abutment is built. Some material properties and mechanical characteristics of the soil are simplified as follows: Non-saturated property of back fill materials and former embankment fill are ignored; rigid elements are used to simulate the bearing platform in finite element model due to its large stiffness; the vehicle load is simplified as the uniformly distributed load of 11Kpa.

Based on geological prospecting data and the size of bearing platform, the size of calculation model is determined (the thickness of road pavement is 0.65m, the height of embankment fill is 1.75m and the thickness of the concrete slab is 0.3metre). In the whole model the height in vertical direction (z direction) is 43.8m from the top of road pavement to the bottom of loam layer, and along the length of longitudinal direction is 65m. The length behind the expansion joint is 37.8m.

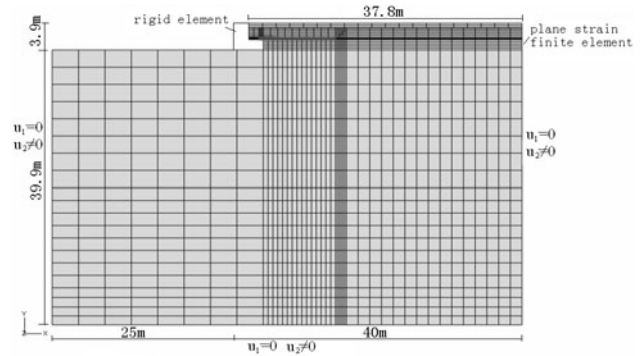


Fig. 3 A simplified FEM model of the deep-seated concrete slab behind the abutment

Construction process of pouring approach slab, backfilling lime-ash soil and paving road pavement are simulated and consolidation calculation is carried out after applying vehicle load. Loading history is showed in Fig. 4.

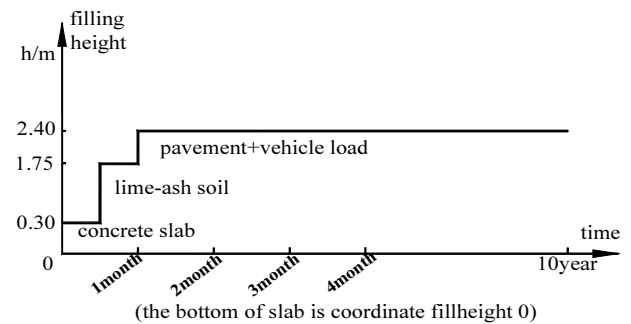


Fig. 4 The history of step loading

Boundary Condition

The left and right boundary are horizontal restraint ($u_1 = 0, u_2 \neq 0$); bottom boundary is constraints in all directions ($u = 0, u = 0$); the boundary between slab and bearing platform is constraints in all directions ($u = 0, u = 0$) and the top surface is free. In consolidation calculation, model's top surface is free drainage, and other interface is non-drainage.

Constitutive Relation

In finite element calculation, different constitutive relations are chosen to describe the actual deformation on the basis of varied material's actual characteristics. Linear elastic model is used to describe pavement, embankment fill, concrete slab, lime-ash soil, clay layer and loam layer; Mohr-Coulomb plastic model is used to describe silt and silt clay; all the materials are assumed to have the same permeability coefficient in each direction. The parameters of the model are referred to Tables 1 and 2.

In order to reflect action relations between the slab and the clay, between abutment and backfill, between the pavement and the soil, between the bottom of the abutment and the silt clay, contact relationships are set up between the contact elements above.

Table 1 Parameters of linear elasticity model

Material	γ /(KN·m ⁻³)	E /KPa	ν	K /(m·d ⁻¹)
Lime-ash soil	13.7	2E4	0.3	3.00E-5
Concrete slab	25	3E7	0.167	2.00E-8
Road pavement	23	1.6E6	0.2	2.00E-8
Embankment fill	18	2E4	0.3	3.42E-6
Clay1	17.5	4010	0.3	9.42E-6
Clay2	17.8	3360	0.3	2.18E-5
Loam clay	20.1	6800	0.3	3.00E-5

Table 2 Parameters of Mohr-Coulomb model

Material	γ /(KN·m ⁻³)	E /KPa	C /kPa	ϕ /(°)	ν	k /(m·d ⁻¹)
Silt clay	19.87	1730	18	10	0.3	2.67E-5
Mucky clay	11.52	2080	22	13	0.3	3.80E-5

CALCULATION ANALYSIS

Settlement Analysis

Observation points on pavement are located at road center-line and driveway edge-line. Fig. 5 shows the comparison curve of the measured value and the calculating result by finite element model of surface settlement points along the driveway center-line. As the road operating time increases, surface settlement increases gradually under the repeated action of the vehicle load in the bridgehead. When the traffic operating time is 304 days, surface settlement is 7-17mm, but the surface settlement above the slab free end is a little larger. The calculating result of the finite element in Fig. 5 is based on the traffic operating time which is 10 years later; the settlement is up to 54mm and the changing slope is 0.54% at the bridge approach. Additionally, the free end of slab is supported by the sleeper beam in site construction, while sleeper beam model is not considered in finite element calculation. As a result, the finite element calculation is large in the free end.

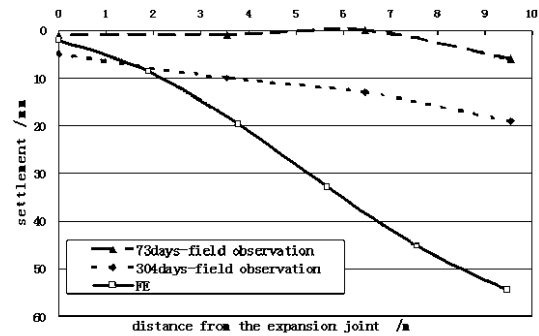


Fig. 5 Longitudinal distribution of settlements of pavement

Length of Approach Slab

On the basis of the calculation model mentioned above, how the approach slab length influences the surface settlement value and the road line is studied. Lime-ash soil is filled back above the concrete slab. Six different finite element models are built, with the slab length being 0m, 3m, 6m, 8m, 12m and 15m respectively.

In Fig. 6, the variation of the approach slab's length has a great influence on the surface line. When there is no concrete slab, the surface settlement and the change of slope are great; when L (the slab length) is larger than 10m, the surface settlement above the slab free end and the change of bridge approach slope appear obviously; when L is less than 6m, the weight of approach slab decreases as the size being smaller and the corresponding lime-ash soil filling begins to play a major role in controlling the settlement; when L is in the range of

8~10m, the free end of approach slab links up the non-treated area smoothly, and the vehicle will not bump again.

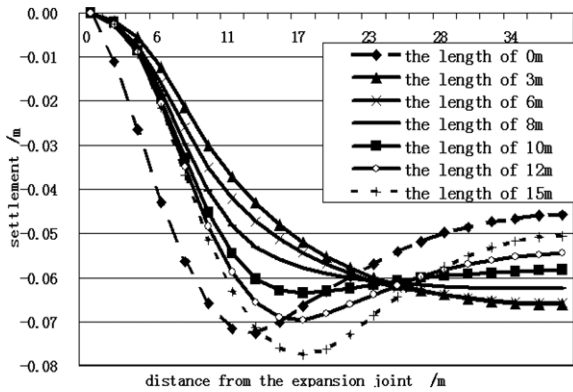


Fig. 6 The variation of surface settlement with length of concrete slab along road centerline

Length of Approach Slab

Increasing the thickness of approach slab properly may enlarge the stiffness of the entire bridge approach embankment, and make the road longitudinal line of the bridge approach smoothly. In Fig. 7, if the thickness of approach slab is between 15-20cm, the settlement controlling effect is inferior to the thicker slab for length of 10m; During designing the thickness of slab, it is considered that increasing the approach slab volume or inner reinforcement quantity lead to an increase in the slab dead-weight, which increases the stress of original structure especially for the bearing platform.

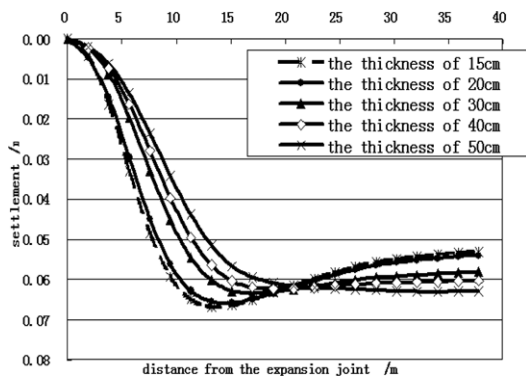


Fig. 7 The variation of surface settlement with thickness of concrete slab along road centerline

CONCLUSIONS

A new foundation treatment called the deep-seated concrete slab for controlling settlement at bridge approach embankment, combined with engineering case,

is proposed in the paper. Some factors, which include the location, the depth of concrete slab, the size of concrete slab and so on, should be taken into consideration in this method. The effectiveness of concrete slab for settlement control, which can improve the stress distribution and deformation of the embankment near the bridge, has been verified by field experimental study, and its control of the different settlement of bridge approach embankment is discussed.

(1) The deep-seated reinforced concrete slab for settlement control at bridge approach embankment proved an effective control of the settlement difference and can alleviate vehicle bump at bridge head since the road was open to traffic.

(2) During design of the deep seated concrete slab, the influence of the length, thickness and the reinforcement on the self weight should be considered. The motive of the deep-seated concrete slab is to increase the rigidity of bridge approach embankment by concrete slab. Unfavorable settlement difference is uniformly distributed. So if the strength of slab's bending and shearing is adequate, the slab length, thickness and the reinforcement ratio should not be too large. It is suggested that the length of slab should be chosen in the range of 6-10 m under level-A load; slab thickness should be taken in the range of 30-40 cm, if the bearing capacity of foundation under the slab is allowable; the connection between the bearing platform and concrete slab should be between hinged and fixed connections.

(3) Compared with the method of filling soil, the result shows that the deep-seated concrete slab for settlement control at bridge approach embankment can effectively control settlement difference and it is another good choice to maintain and reinforce existing bridge approach embankment.

REFERENCES

Ankum P, Koga K, Segeren WA, Luijendeijk J (1988). Lessons from 1200 years impoldering in the Netherlands. Proc. Int. Symposium on Shallow Sea and Lowland, Institute of Lowland Technology, Saga Univ. Saga: 102-108.

Shi XM & Cai CS (2004). Finite Element Analysis of Concrete Approach Slab on Soil Embankment. Geotechnical Engineering for Transportation Projects: 393-402.

Cai CS & Shi XM (2005). Structural Performance of Bridge Approach Slabs under Given Embankment Settlement. Journal of Bridge Engineering.10(4): 482-489.

Shi XM, Cai CS, Chen SR (2008) .Vehicle Induced Dynamic Behavior of Short-Span Slab Bridges

- Considering Effect of Approach Slab Condition. *Journal of Bridge Engineering*.13 (1): 83-92.
- Roy S & Ganesh T (2007). Nonlinear Finite-Element Analysis of Reinforced Concrete Bridge Approach Slab. *Journal of Bridge Engineering*.12(6): 801-806.
- Wong H (1994). Effect of Orientation of Approach Slabs on Pavement Deformation. *Journal of Transportation Engineering*.120(4): 590-602.
- Wang SB & Lai GL (1996). Analysis of Behavior of Skew Approach Slabs. *China Journal of Highway and Transport*.9 (3): 47-61.
- Gu F, Shao RG, Pei SB (1996). The Design of concrete slab at bridge approach.*Highway*:1-5.
- Zhang W (1999). The Application of Spline Subdomain Method to Analyzing Approach Slabs. *Journal of Taiyuan University of Technology*.30(5): 532- 536.
- Zhou YM & Tan ZM (2004). Structural Analysis of Approach Slab . *Highway*.(1):82-86.
- Yu YH, Xie YL, Yang XH (2006). Mechanics property and adaptability of approach slab. *Journal of Traffic and Transportation Engineering*.6(3): 51- 56.
- Huang B (2003).The Improvement Design of Concrete Slab in Highway. *Highway*. (1):132-134.
- Xu B, Wang W, Xu HF (2005). The Improvement Design of Approach Slab.*Journal of China & Foreign Highway*.25(1):28-31.
- Shen Z & Huang XM (2007). Analysis on Post-construction Settlements and Differential Settlement of Solidified Fly Ash Backfills Adjacent to Abutment on Soft Clay Foundation. *Journal of Highway and Transportation Research and Developmen*.24 (5): 53-56.
- Liu MC & Huang XM (2004). Numerical Analysis of Post-construction Settlements of Backfills Adjacent to Abutment on Soft Clay Foundations.*Journal of Highway and Transportation Research and Developmen* : 21(12): 22-26.

APPLICATION OF GEOCELL IN THE ECOLOGICAL PROTECTION OF ROCK SLOPE

Xin-Jun ZOU¹ and Ming-Hua ZHAO²

ABSTRACT: Based on the available ecological protection techniques of slope and new problems associated with the protection of rock slope especially in southern cities, a new kind of ecological protection method by using geocell was advised. And in order to study the interaction between the geocell and rock slope, numerical analysis by the finite element method (FEM) was completed, from which the bearing behavior and stabilization mechanism of the present method were discussed in detail. Finally, regulations as well as construction techniques for the geocell ecological protection method of rock slope was drawn and applied to an engineering practice with favorable social and economical benefit obtained.

KEYWORDS: rock slope, ecological protection, geocell, finite element method, interaction

INTRODUCTION

During the construction of roads or residential quarters with the development of city, a mass of rock slope are being formed inevitably. Traditional methods, such as mortar rubble masonry pavement and shotcrete covering, are still being used to protect these rock slopes (ZHOU and ZHANG 2003). By doing so, the stability of slope may be met. However, besides enormous manpower and delayed construction period, bad visual or environmental protection effect has become the most disadvantageous shortcoming. Moreover, the growing and living environment for nature and human beings will deteriorate gradually till unrecoverable, which are also against the current environmental protection and people oriented policies the world over. Therefore, how to protect these kinds of rock slope ecologically to fit the circumstance has become a new and important subject or task for geotechnical engineers.

Based on the current slope ecological protection methods (GRAY and Sotir 1996; YE 2007) and the engineering features of rock slope, a new kind of ecological protection technique by using geocell was advised for rock slope especially in cities. And numerical analysis by the finite element method was carried out to study the working mechanism and behavior of the present method. According to the analysis result, regulations as well as construction techniques for the advised ecological protection method by using geocell (a new kind of three-dimensional geotextile) were drawn and applied to an engineering practice to verify its feasibility.

FEATURES OF ROCK SLOPE IN CITY

Compared with general rock slope met in the construction of mine, highway or irrigation works, not only the slope stability should be assured, but the environmental protection and ecological effect should also be considered, between which differences mainly consist the following fields (Guangxi Highway Bureau and Hunan University, 2002):

1) Firstly, because of the costly and limited land in city, the rock slope usually has to be shaped as high and abrupt as possible, which results in a higher demand of safety especially considering the running vehicles or passerby. Of course, these kinds of problems can also be solved by available analysis and calculation methods (CHEN et al. 2001).

2) The second various aspect, however, is still a difficult problem being solved by geotechnical engineers the world over. As the protection of this kind of rock slope in city should also consider environmental protection and ecological effect to make the environment around us more delightful and habitable (ZHAO et al. 2004; YANG et al. 2007).

THE ECOLOGICAL PROTECTION TECHNIQUE OF ROCK SLOPE BY USING GEOCELL

Remaining Soil Methods

After reliable supporting structures used to ensure the slope stability, effective remaining soil methods should

¹ Associate Professor, Ph.D, College of Civil Engineering, Hunan University, China. Email: xjzouhd@yahoo.com

² Professor, Ph.D, College of Civil Engineering, Hunan University, China. Email: mhzhaohd@yahoo.com

also be adopted for the ecological protection. As the soil needed by the growing of plant tend to be eroded and washed away by rainwater (WAGN et al. 2007), quite a few kinds of remaining soil methods have been found out and used in practice, such as the three-dimensional geotextile net, the geocell and the rhombic wire netting. In this paper or study, the geocell (a new kind of three-dimensional geotextile) was adopted to remain the soil and achieve ecological protection effect.

The geocell is constructed by high molecular polymers through welding and has a three-dimensional net structure with high bearing capacity and tensile strength, as shown in Fig.1. Among the cell, soil as well as grass seeds or plant may be filled to form fixed elastic body, which will enhance the integrity effect and resist deformation.

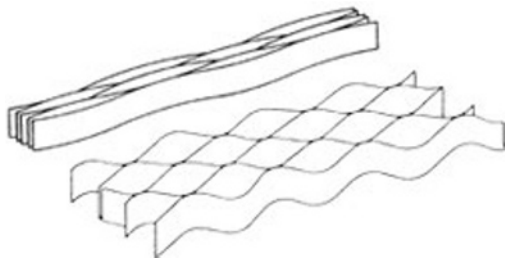


Fig. 1 Structure of geocell

Numerical Analysis by the Finite Element Method

In order to study the behavior of geocell used in ecological protection of rock slope theoretically, numerical modeling test by the finite method was carried out as follows.

Analysis model

The analysis model consists of rock slope, geocell, soil (filled in the geocell), and interface between the slope and the geocell layer, as shown in Fig.2. In the analysis model, a total number of 4 260 elements were used to disperse the slope body with the height of 10.0m, top width of 5.0m, and inclination angle of 50.

Due to the difference between the rock mass and geocell layer, interface elements were set along the interface to stimulate the sliding or opening deformation. As for the constitutive relation, linearly elastic model and elastoplastic model were chosen for the geocell layer and rock mass, respectively. And linearly Mohr-Coulomb yield criterion was used to judge and simulate the failure of rock mass during the course of stepped loading (CHEN et al. 2006).

While the physical and mechanical parameters of these materials are listed in Table 1.

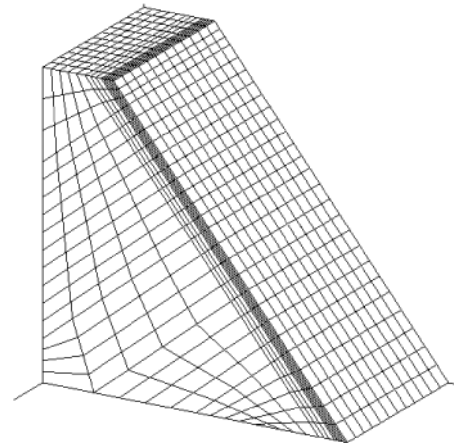


Fig. 2 Numerical analysis model of rock slope by using geocell

Table 1 Caption of table should be left justified

Name of material	elastic modulus /MPa	Poisson's ratio	Density /kN.m ⁻³	Shear strength /MPa	Friction angle /°
Rock	3000	0.18	27.0	3.00	45
Soil	30	0.30	18.0	0.03	20
Geocell	300	0.25	18.0	3.00	30
Interface	0.03	0.40	18.0	0.03	10

Result analysis

As shown in Fig.3 and Fig.4, the vertical deformation of geocell is almost equal to zero. Although larger vertical deformation was observed in the small part of soil over the geocell layer, obvious reduction was caused by the restriction of geocell and anchors (which were used to fix the geocell layer).

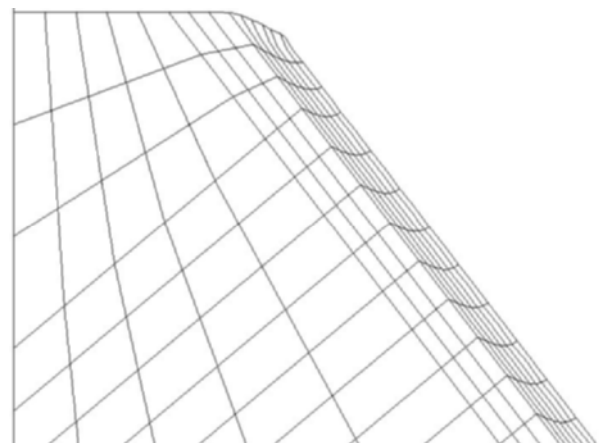


Fig. 3 Deformation of the model without geocell

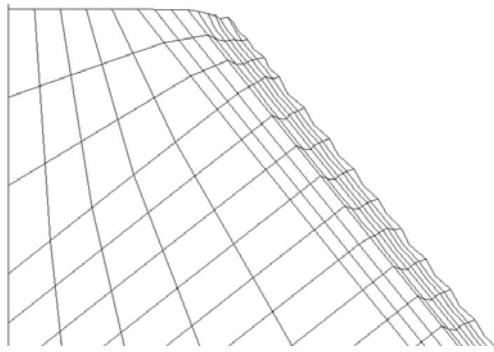


Fig. 4 Deformation of the model without geocell

In order to discuss the influence by the geocell on the horizontal displacement at the slope top, a set of curves were shown in Fig.4. From the figure, we can see that, the top horizontal displacement increases gradually from the central line to the bottom. Due to the favorable effect by the geocell, the value of horizontal displacement is always smaller than that without geocell.

As for the effect by the height of geocell layer on the horizontal displacement of slope bottom, influencing curves under 3 groups of different thickness of geocell layer (i.e., 0.1m, 0.2m, 0.3m) were obtained. The rules reflected show obviously that, the changing tendency is same under various thicknesses of geocell layer, and the horizontal displacement value under each condition with geocell is all smaller than that without geocell. While the influencing rules by different thicknesses of geocell layer on the vertical displacement or settlement at the slope top show that, the thickness of geocell layer has little effect on the top settlement. Therefore, to increase the thickness of geocell layer to cut down the settlement of slope top is not advisable.

Construction Techniques

Based on the above analysis result and indoor model test data (not given here limited by the length of paper), regulation or construction techniques for the present rock slope ecological protection by geocell were drawn as follows to guide the engineering practice.

1) Construction preparations. Before construction, three kinds of preparation work should be done, i.e., checkout of raw and processed materials, cleanup of slope surface, and drainage establishment both at the top and bottom of slope to prevent washout by rainwater.

2) Spread out the geocell net adequately and fix it onto the slope with short anchored bars.

3) Connect adjacent geocell net with special bolts.

4) Fill in the cell with nutritious soil under an order down from the top to the bottom.

5) Spray and plant grass seed. Generally, the density of grass seed is no smaller than 0.009 kg/m^2 . And the seed should be fixed with fertilizer, water absorbent and

other assistant material in advance. After planted, geotextile layer should be covered until an outgrowth of 30~50 mm grass.

6) Maintenance. After above working procedures, watering and fertilization should be continued until the outgrowth of grass. Generally, during the first few months, the nutritious soil filled in the cell is enough for the need of grass seeds. But afterward, appropriate fertilizer (slow-acting fertilizer with a content of nitrogen no more than 50%, and spray density of $5\sim7 \text{ kg/m}^2$) has to be added. Moreover, weed or pest should also be cleaned ever and again.

APPLICATIONS

During the construction of the 3rd ring road of Changsha, quite a few rock slopes with a diverse height of 10.0~45.0m were shaped and had to be protected ecologically. According to the present method in this paper, climate conditions in Changsha and properties of



(a) Construction (spreading geocell)



(b) The first month (2007.1)



(c) Three month later (2007.4)

Fig. 5 Ecological protection of rock slope of the 3rd ring road by geocell

the slope rock mass, a combination of grass species, such as Bermuda-grass, *Paspalum notatum* and ryegrass, was chosen to protect the slope. And the nutritious soil full of organic matter, nitrogen, kalium and other components with a dry density of $0.8\sim 0.9\text{kN/m}^3$ was maintained both by the rhombic wire netting and geocell. After treated by the present method, good ecological protection effect was achieved, which was verified by the pictures in Fig.5 from site investigations.

CONCLUSIONS

In order to protect the rock slope met in city construction safely and ecologically, some meaningful work was carried out as follows.

1) The engineering features of rock slope in city were analyzed and summarized. And based on the available methods, a new kind of rock slope ecological protection technique was advised.

2) The interaction working mechanism between rock slope and geocell layer, bearing and deforming behavior of the geocell layer were studied by a nonlinear finite element numerical analysis, from which quite a few influencing curves or rules were obtained.

3) Construction techniques or regulation for the present method were drawn and used to guide an engineering example with good environmental and ecological protection effect achieved.

REFERENCES

Zhou DP & Zhang JY (2003). Slope protection by Vegetation. Beijing: China Communication Press.

Gray DH & Sotir RB (1996). Biotechnical and soil bioengineering slope stabilization. John Wiley & Sons.

Ye JJ (2007). Discussion on several problems in the projects of slope ecological protection engineering. Research of Soil and Water Conservation, 14(5): 333-335.

Guangxi Highway Bureau & Hunan University (2002). Research report of treatment and bio-engineering protection technology of Rock slope. Changsha: Hunan University.

Chen ZY, Mi HL, Wang XG (2001). A three-dimensional limit equilibrium method for slope stability analysis. Chinese Journal of Geotechnical Engineering, 23(5):525-529.

Zhao MH, Jiang DS, Chen CF, et al. (2004). Research on the spot and Indoor washing-out tests of ecological protection of rocky slopes. Journal of Hunan University: Natural Sciences, 31(5):77-80.

Yang HH, Zhao MH, Liu XP (2007). Analysis of the mechanics of bio-engineering protection of rock slope and its application. Central South Highway Engineering, 32(1):47-51.

Wang L, Yang JJ, Liu Q, et al (2007). Study on surface seepage effects on stability of borrowed soil in ecological slope. Rock and Soil Mechanics, 29(6): 1440-1445.

Chen CF, Liu HX, Li YP (2006). Experiment Investigation On Reinforcement Mechanism And Strength Criterion Of Grass Roots Reinforced Soils. Central South Highway Engineering, 31(2):2-6.